

Advances in Science, Technology & Innovation
IEREK Interdisciplinary Series for Sustainable Development



Zakaria Hamimi · Hassan Khozyem · Thierry Adatte ·
Fadi H. Nader · Francisca Oboh-Ikuenobe ·
Mohamed K. Zobaa · Haytham El Atfy *Editors*

The Phanerozoic Geology and Natural Resources of Egypt

Advances in Science, Technology & Innovation

IEREK Interdisciplinary Series for Sustainable Development

Editorial Board

Anna Laura Pisello, Department of Engineering, University of Perugia, Italy

Dean Hawkes, University of Cambridge, Cambridge, UK

Hocine Bougdah, University for the Creative Arts, Farnham, UK

Federica Rosso, Sapienza University of Rome, Rome, Italy

Hassan Abdalla, University of East London, London, UK

Sofia-Natalia Boemi, Aristotle University of Thessaloniki, Greece

Nabil Mohareb, Faculty of Architecture—Design and Built Environment,
Beirut Arab University, Beirut, Lebanon

Saleh Mesbah Elkaffas, Arab Academy for Science, Technology and Maritime Transport,
Cairo, Egypt

Emmanuel Bozonnet, University of La Rochelle, La Rochelle, France

Gloria Pignatta, University of Perugia, Italy

Yasser Mahgoub, Qatar University, Qatar

Luciano De Bonis, University of Molise, Italy

Stella Kostopoulou, Regional and Tourism Development, University of Thessaloniki,
Thessaloniki, Greece

Biswajeet Pradhan, Faculty of Engineering and IT, University of Technology Sydney,
Sydney, Australia

Md. Abdul Mannan, Universiti Malaysia Sarawak, Malaysia

Chaham Alalouch, Sultan Qaboos University, Muscat, Oman

Iman O. Gawad, Helwan University, Egypt

Anand Nayyar , Graduate School, Duy Tan University, Da Nang, Vietnam

Series Editor

Mourad Amer, International Experts for Research Enrichment and Knowledge Exchange
(IEREK), Cairo, Egypt

Advances in Science, Technology & Innovation (ASTI) is a series of peer-reviewed books based on important emerging research that redefines the current disciplinary boundaries in science, technology and innovation (STI) in order to develop integrated concepts for sustainable development. It not only discusses the progress made towards securing more resources, allocating smarter solutions, and rebalancing the relationship between nature and people, but also provides in-depth insights from comprehensive research that addresses the **17 sustainable development goals (SDGs)** as set out by the UN for 2030.

The series draws on the best research papers from various IEREK and other international conferences to promote the creation and development of viable solutions for a **sustainable future and a positive societal** transformation with the help of integrated and innovative science-based approaches. Including interdisciplinary contributions, it presents innovative approaches and highlights how they can best support both economic and sustainable development, through better use of data, more effective institutions, and global, local and individual action, for the welfare of all societies.

The series particularly features conceptual and empirical contributions from various interrelated fields of science, technology and innovation, with an emphasis on digital transformation, that focus on providing practical solutions to **ensure food, water and energy security to achieve the SDGs**. It also presents new case studies offering concrete examples of how to resolve sustainable urbanization and environmental issues in different regions of the world.

The series is intended for professionals in research and teaching, consultancies and industry, and government and international organizations. Published in collaboration with IEREK, the Springer ASTI series will acquaint readers with essential new studies in STI for sustainable development.

ASTI series has now been accepted for Scopus (September 2020). All content published in this series will start appearing on the Scopus site in early 2021.

Zakaria Hamimi • Hassan Khozyem •
Thierry Adatte • Fadi H. Nader •
Francisca Oboh-Ikuenobe •
Mohamed K. Zobaa •
Haytham El Atfy
Editors

The Phanerozoic Geology and Natural Resources of Egypt

Editors

Zakaria Hamimi
Department of Geology
Faculty of Science
Benha University
Benha, Egypt


Hassan Khozyem
Department of Geology
Faculty of Science
Aswan University
Aswan, Egypt

Thierry Adatte
Lausanne, Switzerland

Fadi H. Nader
IFP Energies Nouvelles
Rueil-Malmaison, France

Francisca Oboh-Ikuenobe
Department of Geoscience
Missouri University of Science and Technology
Missouri, MO, USA

Mohamed K. Zobaa
Department of Geoscience
University of Texas Permian Basin
Odessa, TX, USA

Haytham El Atfy 
University of Tübingen
Tübingen, Germany

Geology Department, Faculty of Science
Mansoura University
Mansoura, Egypt

ISSN 2522-8714 ISSN 2522-8722 (electronic)
Advances in Science, Technology & Innovation
IEREK Interdisciplinary Series for Sustainable Development
ISBN 978-3-030-95636-3 ISBN 978-3-030-95637-0 (eBook)
<https://doi.org/10.1007/978-3-030-95637-0>

© The Editor(s) (if applicable) and The Author(s), under exclusive license to Springer Nature Switzerland AG 2023, corrected publication 2023

This work is subject to copyright. All rights are solely and exclusively licensed by the Publisher, whether the whole or part of the material is concerned, specifically the rights of translation, reprinting, reuse of illustrations, recitation, broadcasting, reproduction on microfilms or in any other physical way, and transmission or information storage and retrieval, electronic adaptation, computer software, or by similar or dissimilar methodology now known or hereafter developed.

The use of general descriptive names, registered names, trademarks, service marks, etc. in this publication does not imply, even in the absence of a specific statement, that such names are exempt from the relevant protective laws and regulations and therefore free for general use.

The publisher, the authors, and the editors are safe to assume that the advice and information in this book are believed to be true and accurate at the date of publication. Neither the publisher nor the authors or the editors give a warranty, expressed or implied, with respect to the material contained herein or for any errors or omissions that may have been made. The publisher remains neutral with regard to jurisdictional claims in published maps and institutional affiliations.

Cover illustration: The interaction between history and geosciences is a unique character of the Egyptian territory. The cover photo captures one of these exceptional examples. The Mortuary Temple of Hatshepsut, the masterpiece of ancient architecture, where its three massive terraces rise above the Paleocene (Esna Formation) desert floor and into the cliffs of Deir el-Bahari (or Dayr al-Bahri) that includes the type locality of the Egyptian Eocene sediments (Thebes Formation), Luxor, Egypt. Photo by Atef Moatamed A. Mohamed.

This Springer imprint is published by the registered company Springer Nature Switzerland AG
The registered company address is: Gewerbestrasse 11, 6330 Cham, Switzerland

This book is dedicated to Earth Scientists victims of the Corona virus (COVID-19) pandemic, especially Mohamed Ragaie El-Tahlawy, Hassan Abdel Hameed, Samir Mohamed Khawasik, Ahamed Abdelaziz El Kammar, Kamal Abdelazim Dahab, Abdelaaty Badr Salman, Soliman Mahmoud Soliman, Moustafa Gharib, Mamdouh Abdeen, Mohamed Hassaan Awad, Adam El-Shahat, Tarek El-Sahaby, Mohamed El-Askalani, Abdelaziz Abdelwareth, Hassan Mohamed Yosef El-Shayeb, Medhat Said Abdelghany, Eid Abdelhalim Abdelmajid, Adel Waheed Felesteen and Esam A. Abd El-Gawad, for their pioneering research in the geology of Egypt. The book is also dedicated to the well-known late Algerian Scientist Asia Harbi for her pioneering role in promoting geosciences in the Arab World.

Preface

Why This Book?

The Phanerozoic Geology and Natural Resources of Egypt includes a series of chapters written by a highly qualified group of researchers whose expertise is recognized and appreciated not only in Egypt, but also globally. The chapters span a wide range of geological sub-disciplines including tectonics, paleogeography, stratigraphy, sedimentology, paleontology, groundwater and energy resources, just to name a few. In this regard, the book provides the reader with ample knowledge about the different facets of the fascinating and always intriguing geology of Egypt since the Precambrian time. For a junior researcher or a geoscience student, the book is a comprehensive, multidisciplinary one-stop resource that they will continue to reference and rely on for years to come. For a more experienced scientist, the book summarizes the current state of knowledge, highlights the magnitude of complexity of the geology of Egypt and northeast Africa and reveals potential areas where future research should be directed. The book is written in simple, easy to understand English language and contains very useful high-quality illustrations. Last but not least, *The Phanerozoic Geology and Natural Resources of Egypt* has been reviewed and edited by world class, highly ranked geoscientists from Egypt, Europe and USA.

Contents

The book consists of two parts; The first part covers the *Phanerozoic Geology of Egypt*, and the second part reports the *Natural Resources in Egypt*, including mineral resources, hydrocarbon potentialities and water resources. The following scientists (arranged in Alphabetical order) contributed to the two parts (Abdelgalil Hewaidy, Abdou Abouelmagd, Adam El-Shahat, Ahmed Heneish, Ahmed Mohamed, Ahmed. E. Radwan, Amr A. Metwally, Andre Jasper, Asmaa A. Taha, Atef Moatamed A. Mohamed, Bahay Issawi, Bandar I. Ghassal, Basma M. H. Mansour, Brahimsamba Bomou, Clément Coiffard, Dieter Uhl, Edoardo Dallanave, Fadi H. Nader, Felix J. Augustin, Felix J. Augustin, François Baudin, Gad El-Qady, Galal El-Habaak, Gehad M. Saleh, Gerta Keller, Hamdy M. Abdalla, Hassan Khozyem, Haytham El Atfy, Hesham Elasmr, Hiroharu Matsueda, Jorge E. Spangenberg, Josephina Hartung, Kamel H. Mahfouz, Mahmoud Abdel-Hakeem, Maria-Fernanda Romero-Sarmiento, Mohamed Abdel Zaher, Mohamed H. Geriessh, Mohamed K. Zobaa, Mohamed Yossef, Mohammad Abdelfattah Sarhan, Mortada Mourad Taha ElAref, Mounir H. El-Azabi, Nageh A. Obaidalla, Panagiotis Kampouridis, Panagiotis Kampouridis, Ralf Littke, Salah Y. El Beialy, Samah Elbarbary, Samer Bou Daher, Sebastian Grohman, Sherif Farouk, Shunso Ishihara, Tarek Anan, Thierry Adatte, Uwe Kirscher, Valerian Bachtadse, Wael Hagag, Yebo Liu, Zakaria Hamimi). We would like to thank all of them for accepting our invitation and for their valuable contributions. Special thanks are also extended to the Egyptian National Committee for Earth Sciences, Academy of Scientific Research and Technology, for great support and fruitful discussion during the preparation the final version of this volume.

The first part of this book comprises 17 chapters. The first four chapters (overall paleogeographic and geodynamic evolution) addresses the overview and tectonic framework, the Phanerozoic geomorphology and the paleoposition and paleogeography of Egypt during the Phanerozoic Era. The fifth chapter (Paleozoic) deals with the Precambrian life and Cambrian revolution. The Mesozoic sedimentary succession, Mesozoic oceanic anoxic events and the associated black shale deposits as a potential source of Energy, the evolution of vegetation through the Cretaceous of Egypt, dinosaur faunas of Egypt—the terrestrial Mesozoic vertebrate record, Cretaceous wildfires in Egypt: Inferences to paleoecology and paleoenvironment and paleoenvironmental and paleontological study of the Gabal Ekma section (Egypt) throughout the Coniacian-Santonian boundary are treated in the next chapters (sixth to eleventh). The twelfth to seventeenth chapters address the climatic and environmental changes during the Paleocene–Eocene Thermal Maximum in Egypt: an overview, the standard Sequence Stratigraphic Scheme for the Maastrichtian-Ypresian Successions of the Southern and Central Western Desert, Egypt, the Eocene–Oligocene vertebrate assemblages of the Fayum Depression, the Oligocene palynology and paleoclimates of northern Egypt as recorded in the Dabaa Formation, the Quaternary environmental and climatic changes and the evolution of the River Nile through time.

In the second part, nine chapters of the book (chapters eighteenth to twenty-sixth) are dedicated to the issue of natural resources in Egypt. The eighteenth to twentieth chapters examine the Phanerozoic Stratabound/Stratiform Ore Deposits of Egypt, the potential exploitation of the Phanerozoic Glauconites, and the Phanerozoic Rare Earth Elements in Egypt. The twenty-first and twenty-second chapters revisit the major groundwater reservoirs and the geothermal potential in Egypt. The twenty-third chapter is devoted to the petroleum Source Rocks of Egypt—an Integrated Palynological and Organic Geochemical Approach. The last chapters (twenty-fourth to twenty-sixth) systematically describe the hydrocarbon potential of carbonate rocks, the Western Desert petroleum sources and reservoirs and the offshore East-Mediterranean Mesozoic-Cenozoic Petroleum Systems.

Benha, Egypt

Aswan, Egypt

Lausanne, Switzerland

Rueil-Malmaison, France

Missouri, USA

North Dakota, USA

Tübingen, Germany

Zakaria Hamimi

Hassan Khozyem

Thierry Adatte

Fadi H. Nader

Francisca Oboh-Ikuenobe

Mohamed K. Zobia

Haytham El Atfy

Acknowledgements

The guest editors would like to thank the following reviewers (arranged in alphabetical order) for their valuable comments that significantly improved the submitted manuscripts: Abbas Mansour, Abdalla Abu Hamad, Abd El-Hamid El-Shater, Abd El-Hay El-Shafey, Adam T. Halamski, Ahmed E. Radwan, Ahmed Ismail, Ahmed Reda El Younsy, Alan kehew, Ali Bakr, Ali M. A. Abdallah, Andreas Matzke, Ashraf A. Mostafa, Becky Briant, Danial Stanley, David Bord, David Sibley, Dimiter Ivanov, Elsayed Abdelaziz Youssef, Esam Abdelgawad, Fekri Hassan, Francisca Oboh-Ikuenobe, François Roure, Gouda Ismail Abdel Gawad, Guillaume Charbonnier, Hamdalla Wanas, Hans-Georg Herbig, Hany Shalaby, Hassan Khozyem, Haytham El Atfy, Isabelle Moretti, Jean-Daniel Stanley, Jihan El-Bakry, Jim Rose, Jiří Kvaček, John Pigott, Khairy Zaki, Lawrence H. Tanner, Mahmoud Faris, Mahmoud Kora, Mahmoud Lotfy Leila, Massimo Mattei, Martin Pickford, Michael W. Maisch, Michael Wagreich, Moataz El-Shafeiy, Mohamed Abdelfattah Ebeid, Mohamed Ahmed, Mohamed Aljahdali, Mohamed Boukhary, Mohamed Elnady, Mohamed El-Sharkawy, Mohamed Metwaly, Mohamed Zobaa, Mohammed Hail Hakimi, Mona Kaisar, Mostafa Yosef, Oussama Himid, Ramadan Abu Zeid, Sebastian Luening, Sevket Sen, Sherif Fawzy, Tesfaye Kidane Birke, Thierry Adatte, Wafaa Afify, William Harrison, Yasser Safori.

Contents

Phanerozoic Geology of Egypt	
An Overview of the Phanerozoic Geology in Egypt	3
Bahay Issawi and Sherif Farouk	
Phanerozoic Structural Setting and Tectonic Evolution of Egypt	27
Mohamed Yousef, Zakaria Hamimi, Ahmed Heneish, Wael Hagag, and Tarek Anan	
Phanerozoic Geomorphology in Egypt	83
Atef Moatamed A. Mohamed	
Paleoposition and Paleogeography of Egypt During the Phanerozoic Era	123
Uwe Kirscher, Edoardo Dallanave, and Valerian Bachtadse	
Precambrian Life and Cambrian Revolution	133
Abdel Galil Hewaidy	
Mesozoic Sedimentary Succession in Egypt	169
Nageh A. Obaidalla, Kamel H. Mahfouz, and Amr A. Metwally	
Mesozoic Oceanic Anoxic Events and the Associated Black Shale Deposits as a Potential Source of Energy	221
Tarek Anan and Adam El-Shahat	
The Evolution of Vegetation Through the Cretaceous of Egypt	235
Clément Coiffard and Haytham El Atfy	
Dinosaur Faunas of Egypt—The Terrestrial Late Cretaceous Vertebrate Record	253
Felix J. Augustin, Josephina Hartung, and Panagiotis Kampouridis	
Cretaceous Wildfires in Egypt - Inferences for Palaeoecology and Palaeoenvironments	285
Haytham El Atfy, Dieter Uhl, and André Jasper	
Palaeoenvironmental and Palaeontological Study of the Gabal Ekma Section (Egypt) Throughout the Coniacian-Santonian Boundary	291
Brahimsamba Bomou, Thierry Adatte, and Jorge E. Spangenberg	
Climatic and Environmental Changes During Paleocene-Eocene Thermal Maximum in Egypt: An Overview	305
Hassan Khozyem, Thierry Adatte, and Gerta Keller	
A Standard Sequence Stratigraphic Scheme for the Maastrichtian-Ypresian Successions of the Southern and Central Western Desert, Egypt	339
Mounir H. El-Azabi and Sherif Farouk	

The Eocene–Oligocene Vertebrate Assemblages of the Fayum Depression, Egypt	373
Panagiotis Kampouridis, Josephina Hartung, and Felix J. Augustin	
The Oligocene Palynology and Palaeoclimates of Northern Egypt as Recorded in the Dabaa Formation	407
Salah Y. El Beialy, Ahmed Mohamed, Mohamed K. Zobia, Asmaa A. Taha, Dieter Uhl, and Haytham El Atfy	
Quaternary Environmental and Climatic Changes in Egypt: Proxies from Sedimentary Records	425
Hesham M. El-Asmar	
Evolution of the Nile River Through Time	491
Bahay Issawi and Sherif Farouk	
Natural Resources in Egypt	
The Phanerozoic Stratabound/Stratiform Ore Deposits of Egypt: Their Mode of Occurrence and Formation in Accordance with the Phanerozoic Geological Evolution	501
Mortada Mourad Taha El Aref	
Potential Exploitation of the Phanerozoic Glauconites in Egypt	565
Galal El-Habaak and Mahmoud Abdel-Hakeem	
Phanerozoic Rare Earth Element Resources of Egypt: Metallogenic and Mineral Exploration Constraints	581
Hamdy Mahmoud Abdalla, Hiroharu Matsueda, Gehad M. Saleh, and Shunso Ishihara	
Major Groundwater Reservoirs of Egypt	613
Mohamed H. Geriesh, Abdou Abouelmagd, and Basma M. H. Mansour	
Geothermal Potentiality of Egypt: Review and Updated Status	637
Mohamed Abdel Zaher, Gad El-Qady, and Samah Elbarbary	
Petroleum Source Rocks of Egypt: An Integrated Spatio-temporal Palynological and Organic Geochemical Studies Within the Phanerozoic	649
Haytham El Atfy, Bandar I. Ghassal, and Ralf Littke	
Hydrocarbon Potential of Carbonate Rocks in Egypt	675
Mohammad Abdelfattah Sarhan	
Western Desert Petroleum System: New Exploration Opportunities and Challenges	691
Ahmed E. Radwan	
A Review of the Offshore East Mediterranean Mesozoic-Cenozoic Petroleum Systems	719
Fadi H. Nader, Sebastian Grohmann, Bandar I. Ghassal, Haytham El Atfy, Maria F. Romero-Sarmiento, Samer Bou Daher, François Baudin, and Ralf Littke	
Correction to: The Phanerozoic Stratabound/Stratiform Ore Deposits of Egypt: Their Mode of Occurrence and Formation in Accordance with the Phanerozoic Geological Evolution	C1
Mortada Mourad Taha El Aref	

Editors and Contributors

About the Editors



Zakaria Hamimi is a structural geologist who has spent much of his academic career at Benha University (Egypt), in addition to some years at Sana'a University (Yemen) and King Abdulaziz University (Saudi Arabia). He graduated with a B.Sc. degree (1984) from Assiut University (distinction with honors), and holds a M.Sc. (1988) degree from Zagazig University (Egypt) and a Ph.D. (1992) in structural geology and tectonics from Cairo University. His research interests focus on structural geology, microstructures and tectonics. He has worked in many field-related sub-disciplines of Earth Sciences including geologic mapping, microstructural analysis, strain analysis, paleostress reconstruction, active tectonics, tectonic geomorphology, crustal deformation, and image processing. He used all these fields to study key areas in the Arabian-Nubian Shield, and to decipher their deformation history. He has been the president and one of the founding team members of the Arabian Geosciences Union since its founding in 2012.

Professor Hamimi received the medal of the Egyptian Geological Society of Egypt in 2015, and the medal of the Arab Mining and Petroleum Association in 2016. He has co-published 90 research articles in national and international indexed and refereed journals and authored several books. He has considerable editorial and publishing experience, having started in the *Egyptian Journal of Geology* in 1998–2002. He has been An Associate editor of the *Arabian Journal of Geosciences* (since 2016) and *Journal of African Earth Sciences* (since January 2022). He is a member of the Egyptian Universities Promotion Committee of the Supreme Council for Universities (SCU, Egypt, 2016–2019). In addition, he was nominated as a Secretary of the Egyptian National Committee for Geological Sciences of the Academy of Scientific Research and Technology, and designated as the IUGS-Representative for Egypt to the Gondwana 16 International Conference in Bangkok, Thailand. In September, 2020, he was nominated as the President of this same committee.



Hassan Khozyem is an associate professor in the Geology Department, Faculty of Sciences, Aswan University (Egypt). He received a Ph.D. (2013) degree in geosciences and environments from Lausanne University (Switzerland). He works mainly on the geochemistry and sedimentology of Paleogene sediments in Egypt, India, and Spain. His research interests focus on global climatic and paleoenvironmental changes associated with warming events using high-resolution bio-, and chemostratigraphy. In 2015, he was awarded the state Prize of Encouragement from the Egyptian government (Egyptian Science and Technology Academy) in geosciences that was followed by the first-class concession provided by the Egyptian President in 2017. His work is largely the result of interdisciplinary collaborations with an international team of scientists and students. Recently, he was as a member of the National committee of Geological Science (Egyptian Academy of Scientific Research and Technology). Hassan Khozyem was a former director of the Quality Assurance Unit in the Faculty of Science, Aswan University as well as the Vice-Chairman of the International Ranking Committee at the same University.



Thierry Adatte is Professor and head of the geochemistry and mineralogy sedimentary laboratory at the Institute of Earth Sciences of the University of Lausanne, Switzerland. He received his Ph.D. in Mineralogy and Sedimentary Geology from the University of Neuchâtel, Switzerland. 1989–1990: Postdoctoral fellow (FNS), Mexican Petroleum Institute (IMP). 1990–1993: Postdoctoral fellow (FNS), Universidad Autonoma de Nuevo Leon, Mexico and Neuchâtel University, Switzerland. 1993–2004: Maître assistant (“Assistant professor”), head of the Mineralogical and Geochemical Laboratory, Geological Institute, Neuchâtel University, Switzerland. 2004–2012: Associate Professor, “Chargé de cours et d’enseignement” (paleontology, sedimentary-environmental mineralogy, general geology), Geological Institute, Neuchâtel University, Switzerland. 2008–2018:

Researcher at the Institute des Sciences de la Terre (ISTE), Lausanne University, Head of the geochemistry sedimentary lab (XRD, CHN-Rock-Eval, Phosphorus). 2017–2018: Privat Docent at the Institute des Sciences de la Terre (ISTE), Lausanne University 2018–: Professor remplaçant at the Institute des Sciences de la Terre (ISTE), Lausanne University. His research interests are in the fields of global environmental change and extinction events, and his involvement in the deciphering of the events around the Cretaceous-Tertiary boundary event is documented by a series of publications (from 1997 to 2019). He also explored the sedimentary documents of the PETM the Paleocene-Eocene boundary event (from 2000 to 2019). He is also involved in the study of oceanic anoxic event (from 2001 to 2018). His interests are in the use of geochemical and mineralogical proxies, such as stable carbon and oxygen isotopes, organic matter, clay

minerals and recently also trace metal distributions as indicators of environmental and climatic change at the time of the extinction events. One of his main actual interest is the link between LIPS activity and mass extinction events, in particular during the K/Pg mass extinction. His team provided the most accurate dating of the Deccan activity and highlighted its crucial role in the K/Pg extinction. The use of mercury as a tracer of volcanic activity is also part his research. Acidification linked with these events is also one of his recent interest, more particularly for the K/Pg mass extinction. Since 1987, active participation (oral presentations and posters) of nearly 1112 meetings and symposia (GSA, AGU, EUG, IAS, SNOWBIRD, réunion spécialisées SGF) Convenor and co-convenor of sessions on Mass Extinctions, Volcanism, Impacts, and Catastrophic Environmental Changes at EGU Meetings since 2013 to 2018. Convenor and coconvenor of sessions on mass extinctions at GSA meetings in 2009, 2016 and 2017.



Fadi H. Nader is currently a project leader and geosciences expert at IFP Energy nouvelles (IFPEN, France) and chaired professor of “Multiscale Fluid-Rock Interactions” at Utrecht University (the Netherlands). He graduated from the American University of Beirut (Lebanon) in Geology (B.Sc. 1994, M.Sc. 2000), received a Ph.D. in 2003 from the KU Leuven University (Belgium) and HDR (Habilitation de Direction de la Recherche) from the Paris-Sorbonne University (France) in 2015. He is an expert in sedimentology, characterization and modeling of sedimentary basins and reservoirs/aquifers (clastics and carbonate rocks, fluid flow, diagenesis), integrated stratigraphy, and seismic interpretation. He is very active in several international scientific and professional societies, such as the International Union of Speleology (UIS), the Geological Society, London (GSL), the American Association of Petroleum Geologists (AAPG, Europe and Middle East), and the International Lithosphere Program (ILP—IUGS-IUGG).



Francisca Oboh-Ikuenobe is a professor and past interim chair in the Department of Geosciences and Geological and Petroleum Engineering Rolla, MO, USA. She obtained a Ph.D. degree in Geology from the University of Cambridge through a Commonwealth Scholarship, and M.S. and B.S. (First Class) degrees from the University of Ife (now Obafemi Awolowo University) in Ile-Ife, Nigeria. Dr. Oboh-Ikuenobe teaches courses about the evolution of the earth, stratigraphy, basic and advanced paleontology, and paleoclimatology. She uses her training in sedimentology to conduct research in palynology, a sub-discipline of paleontology that uses organic-walled microfossils such as pollen, spores, dinoflagellates and acritarchs, to unravel the history of the Earth.

Dr. Oboh-Ikuenobe is an elected Fellow of the American Association for the Advancement of Science (AAAS) and the Geological Society of America (GSA), and a 2019 Albert Nelson Marquis Lifetime Achievement inductee. She is an active member of several professional associations, serving as a director of the Association for Women Geoscientists Foundation, member of several GSA committees (including co-chairing the Diversity in the Geosciences Committee 2 which introduced the On To The Future Scholarships), and as President of the AASP—The Palynological Society. A Fulbright Specialist Roster Candidate from 2010 to 2015, Dr. Oboh-Ikuenobe is an African Scientific Institute Fellow and member of the International Geoscience Programme (IGCP) Scientific Board (Global Change Group) of UNESCO/International Union of Geological Sciences. She is the recipient of more than 30 professional and civic awards and honors.



Mohamed K. Zobaa is an assistant professor at the University of Texas Permian Basin (USA). He received a Ph.D. degree in geology and geophysics from Missouri University of Science and Technology (USA). He leads the palynology and sedimentary organic matter research group at his institution, focusing primarily on the accumulation, distribution, and diagenesis of organic matter in time and space, and how they can be used to characterize petroleum systems through the interpretation of depositional paleoenvironments, kerogen type, and organic thermal maturity. He has over 20 years of research experience studying the stratigraphy, palynology, and sedimentary organic matter content of some of the world's most important hydrocarbon-generating provinces (e.g., Gulf of Mexico, the Permian Basin in Texas, the San Juan Basin in New Mexico, the Williston Basin in North Dakota, and the North Western Desert of Egypt). He is the recipient of the prestigious University of Texas System's Rising STARS Award (\$500,000) which he used to establish his Sedimentary Organic Matter and Hydrocarbon Source-Rock Research Laboratory, the first of its kind in the Permian Basin area that provides comprehensive research and development support to the local hydrocarbon exploration and production operators.



Haytham El Atfy is an associate professor at Mansoura University (Egypt) from where he received a B.Sc. degree in geology and an M.Sc. in palynology. He received a Ph.D. in geosciences (palynology and organic geochemistry) from Goethe University, Frankfurt (Germany) in 2014, and PD (Habilitation) from the University of Tübingen (Germany) in 2022. He acquired experience in industrial palynology through work with GUPCO (BP), Egypt. Haytham has been a Research Fellow of the Alexander von Humboldt Foundation at the University of Tübingen (Germany) since 2019. He was recently a visiting scientist at the Senckenberg Research Institute, Germany. His research interests span all aspects of palynology and its applications in dating, palaeoenvironmental

and palaeoclimatical reconstructions, and hydrocarbon exploration, particularly of the Mesozoic and Cenozoic and, to a lesser extent, the Palaeozoic. He has more recently become involved in organic geochemistry. He is a member of the AASP—The Palynological Society, the Micropalaeontological Society (TMS), Arbeitskreis für Paläobotanik und Palynologie (APP), and the Paleontological Society of Egypt (PSE). He is a recipient of many awards, including the Bernd Rendel Prize from the German Science Foundation (DFG), Egyptian State Incentive Award, and the First-Class Excellence Concession that is provided by the Egyptian president.

Contributors

Hamdy Mahmoud Abdalla Nuclear Materials Authority, Cairo, Egypt

Mohamed Abdel Zaher National Research Institute of Astronomy and Geophysics (NRIAG), Helwan, Cairo, Egypt

Mahmoud Abdel-Hakeem Department of Geology, Faculty of Science, South Valley University, Qena, Egypt;
Remote Sensing and Applied Geology Lab, South Valley University, Qena, Egypt

Abdou Abouelmagd Geology Department, Faculty of Science, Suez Canal University, Ismailia, Egypt

Thierry Adatte Institute of Earth Sciences (ISTE), University of Lausanne, Geopolis, Lausanne, Switzerland

Tarek Anan Geology Department, Faculty of Science, Mansoura University, Mansoura, Egypt

Felix J. Augustin Department of Geoscience, Eberhard Karls University of Tübingen, Tübingen, Germany

Valerian Bachtadse Department of Geo- and Environmental Sciences, Ludwig-Maximilians University, Munich, Germany

François Baudin ISTeP, Sorbonne Université, Paris, France

Salah Y. El Beialy Geology Department, Faculty of Science, Mansoura University, Mansoura, Egypt

Brahimsamba Bomou Institute of Earth Sciences (ISTE), University of Lausanne, Geopolis, Lausanne, Switzerland

Clément Coiffard Structural and Functional Plant Diversity Group, Institute of Biology, Freie Universität Berlin, Berlin, Germany

Samer Bou Daher Division of Global Solutions, Beicip-Franlab, Paris, France

Edoardo Dallanave Faculty of Geosciences, University of Bremen, Bremen, Germany

Mortada Mourad Taha El Aref Department of Geology, Faculty of Science, Cairo University, Giza, Egypt

Haytham El Atfy Department of Geosciences, University of Tübingen, Tübingen, Germany;
Geology Department, Faculty of Science, Mansoura University, Mansoura, Egypt

Hesham M. El-Asmar Geology Department, Faculty of Science, Damietta University, New Damietta, Egypt

Mounir H. El-Azabi Geology Department, Faculty of Science, Cairo University, Giza, Egypt

Galal El-Habaak Department of Geology, Faculty of Science, Assiut University, Assiut, Egypt

Gad El-Qady National Research Institute of Astronomy and Geophysics (NRIAG), Helwan, Cairo, Egypt

Adam El-Shahat Department of Geology, Mansoura University, Mansoura, Egypt

Samah Elbarbary National Research Institute of Astronomy and Geophysics (NRIAG), Helwan, Cairo, Egypt

Sherif Farouk Exploration Department, Egyptian Petroleum Research Institute, Nasr City, Egypt;
Egyptian Petroleum Research Institute, Cairo, Egypt

Mohamed H. Geriesh Geology Department, Faculty of Science, Suez Canal University, Ismailia, Egypt

Bandar I. Ghassal EXPEC Advanced Research Center, Saudi Aramco, Dhahran, Saudi Arabia

Sebastian Grohmann Institute of Geology and Geochemistry of Petroleum and Coal, Energy and Mineral Resources (EMR), RWTH Aachen University, Aachen, Germany

Wael Hagag Geology Department, Faculty of Science, Benha University, Benha, Egypt

Zakaria Hamimi Geology Department, Faculty of Science, Benha University, Benha, Egypt

Josephina Hartung Department of Geoscience, Eberhard Karls University of Tübingen, Tübingen, Germany

Ahmed Heneish Geology Department, Faculty of Science, Zagazig University, Zagazig, Egypt

Abdel Galil Hewaidy Geology Department, Faculty of Sciences, Al-Azhar University, Cairo, Egypt

Shunso Ishihara Hokkaido University, Sapporo, Japan

Bahay Issawi Egyptian Geological Survey, Cairo, Egypt

André Jasper Programa de Pós-Graduação em Ambiente e Desenvolvimento, Universidade do Vale do Taquari - UNIVATES (PPGAD/UNIVATES), Lajeado, Rio Grande do Sul, Brazil

Panagiotis Kampouridis Department of Geoscience, Eberhard Karls University of Tübingen, Tübingen, Germany

Gerta Keller Department of Geosciences, Princeton University, Princeton, NJ, USA

Hassan Khozyem Department of Geology, Faculty of Sciences, Aswan University, Aswan, Egypt;
Institute of Earth Sciences (ISTE), University of Lausanne, Lausanne, Switzerland

Uwe Kirscher Department of Geosciences, Eberhard Karls University of Tübingen, Tübingen, Germany;
Earth Dynamics Research Group, The Institute for Geoscience Research (TIGeR), School of Earth and Planetary Sciences, Curtin University, WA, Bentley, Australia

Ralf Littke Energy and Mineral Resources Group (EMR), Institute of Geology and Geochemistry of Petroleum and Coal, RWTH Aachen University, Aachen, Germany

Kamel H. Mahfouz Geology Department, Faculty of Science, Al-Azhar University, Assiut, Egypt

Basma M. H. Mansour Geology Department, Faculty of Science, Suez Canal University, Ismailia, Egypt

Hiroharu Matsueda Hokkaido University, Sapporo, Japan

Amr A. Metwally Geology Department, Faculty of Science, Assiut University, Assiut, Egypt

Ahmed Mohamed Geology Department, Faculty of Science, Mansoura University, Mansoura, Egypt

Atef Moatamed A. Mohamed Geography Department, Faculty of Arts, Cairo University, Giza, Egypt

Fadi H. Nader IFP Energies Nouvelles, Earth Sciences and Environmental Technologies, Paris, France

Nageh A. Obaidalla Geology Department, Faculty of Science, Assiut University, Assiut, Egypt

Ahmed E. Radwan Faculty of Geography and Geology, Institute of Geological Sciences, Jagiellonian University, Kraków, Poland

Maria F. Romero-Sarmiento IFP Energies Nouvelles, Earth Sciences and Environmental Technologies, Paris, France

Gehad M. Saleh Nuclear Materials Authority, Cairo, Egypt

Mohammad Abdelfattah Sarhan Geology Department, Faculty of Science, Damietta University, New Damietta, Egypt;
Center of Space Research and Applications (CSRA), Damietta University, New Damietta, Egypt

Jorge E. Spangenberg Institute of Earth Surface Dynamics (IDYST), University of Lausanne, Geopolis, Lausanne, Switzerland

Asmaa A. Taha Geology Department, Faculty of Science, Mansoura University, Mansoura, Egypt

Dieter Uhl Senckenberg Forschungsinstitut und Naturmuseum Frankfurt, Frankfurt am Main, Germany

Mohamed Yousef Geology Department, Faculty of Science, Ain Shams University, Cairo, Egypt

Mohamed K. Zobia Department of Geosciences, University of Texas Permian Basin, Odessa, TX, USA

Phanerozoic Geology of Egypt



An Overview of the Phanerozoic Geology in Egypt

Bahay Issawi and Sherif Farouk

Abstract

Egypt is located in northeastern portion of Africa and extends into the Asian near East. It is susceptible to many local and global tectonic events with sea-level changes during deposition of the Phanerozoic sediments. The Paleozoic history of Egypt showed that the sediments were meagerly comparing with the Mesozoic and Cenozoic. The most important structures which had a great effect on the stratigraphy of Egypt stretched from the northern shores of Egypt to its extreme southern part. The controlling factor in the development and distribution of the Paleozoic is rolled by several high arcs which stretch from south to north, irregularity with Pre-Cambrian and Paleozoic plumes ($541\text{--}431 \pm 20\text{--}30$ Ma). Important glaciation sediments were recorded during the infra-Cambrian of the Hammamat sediments and Late Ordovician–Early Silurian Gabgaba Formation at southeast Egypt and Al Gilf Kebir which stretching from the northwestern part of Africa to the Arabian Plate. The Mesozoic deposits in Egypt are very unequally distributed. Marine Triassic is only known from the Arif El Naga dome in northeast Sinai, where continental Triassic covers more areas in Egypt. Marine Jurassic deposits were recorded from the north and northeast Sinai as well as from the western side of the Gulf of Suez. The best and most complete section of the Jurassic is exposed at Gebel Maghara North Sinai. On the other hand, Jurassic fluvio-marine and fluvial sections were mapped from the southern parts of the country as far as lat. $23^{\circ} 30'$ N. Subsurface marine and continental sequences were identified in the subsurface of the north Western Desert. The transition from Jurassic to Cretaceous history was marked by a major and widespread hiatus in Egypt due to Cimmerian Event. Cretaceous

deposits are widely distributed on the surface and subsurface covering about 40% of the total area of Egypt extending from north Sinai to the Egyptian–Sudanese border. Remarkable facies and thickness variations are noted in Egypt. Where Egypt was covered by a thin blanket of Mesozoic sediments in paleo-high areas, thick sections were deposited in trough areas in-between the arcs. The Early Cenozoic marine transgression covered most of Egypt and even penetrated inside Sudan. The history of the Cenozoic in Egypt witnessed three major events named: (1) closure of the Neo-Tethys; (2) rifting of the Gulf of Suez associated with the gradual uplift of the Red Sea Basement Mountains; and (3) Messinian Crises leading to the desiccation of the Mediterranean.

Keywords

Global events • Phanerozoic • Paleozoic arcs • Cimmerian event • Messinian crises • Neo-Tethys

1 Introduction

Africa was a part of Gondwana during the end of the Precambrian period, and the South Pole was placed just north of where the African Plate is now. The plate moved northward over and away from the South Pole throughout the Phanerozoic (Siegesmund et al., 2018). This was succeeded by a period of relative stability with the only slow rotation of the plate at about the same latitude for the past ~ 200 m.y. as neighboring plates within Gondwana dispersed (Burke et al., 2003). The end of the Pan-African orogenic events rendered present-day African Plate was positioned inside of Gondwana, bordered to the west by the South American Plate and to the east by Arabia, India, Madagascar, and Antarctica. Therefore, only regions of the African Plate that were at the boundaries of Gondwana, i.e., the far northern and far

B. Issawi
Egyptian Geological Survey, Cairo, Egypt

S. Farouk (✉)
Egyptian Petroleum Research Institute, Cairo, Egypt
e-mail: geo.sherif@hotmail.com

southern sections, are registered for subsequent orogenic events during the Phanerozoic (Bumby & Guiraud, 2005).

The evolution of African basins must be considered in view of periodic plumes rising under the African Plate and also the climate that changed with sea-level changes accompanying the northward drift of the supercontinent during the transgressions–regressions Phanerozoic cycles, which have a direct influence on basin fill. The majority of the Phanerozoic tectonism and magmatism within the African Plate can be considered to have occurred along broad lineaments, which represent the reactivation and exploitation of earlier Late Proterozoic Pan-African sutures (Merdith et al., 2017; Unrug, 1997). Several Phanerozoic magmatic events have been identified (Issawi & Gayed, 2011; Fig. 1) as postdating the Precambrian (620–570 Ma) Dokhan Volcanics in different parts of Egypt, including the Paleozoic cycle I ($541\text{--}431 \pm 20\text{--}30$ Ma) in southwestern Egypt known as the Katherina event. The Permian–Triassic–Jurassic cycle II ($216\text{--}145 \pm 5\text{--}3$ Ma), a rejuvenation of cycle I, has also been identified in southwestern Egypt as a circle extending eastward. Eruptions of the same age were also recorded in the Eastern Desert and Sinai. The Cretaceous cycle III ($14,274 \pm 3$ Ma) has been identified in many parts of Egypt where new eruptions took place rejuvenating the older cycle and in new areas. Cycle IV ($46\text{--}22 \pm 1$ Ma) occurred in the Cenozoic and has been recorded across most of Egypt, including the areas of the Cretaceous cycles.

Although the spatial distribution, the fauna, and sedimentological characteristics of the Phanerozoic deposits are well scrutinized in Egypt, their integration in the global framework and the events which prevailed before and during the Phanerozoic are lacking. One of the targets, which the present study aims at, is to fit Egypt's Phanerozoic history into a regional picture as far as the global changes in the sea level, the rifting episodes, the history of the global events, and their effect on Egypt's sedimentation sequences and the main magmatic events are concerned. As many stratigraphic sequences are adopted by different groups working on the Phanerozoic sequences, the result is a labyrinth of formation names, which confuse the younger generations who have the stamina for developing and enriching the geology of Egypt. Enough has been given on the identification of a formation and the interest in the following pages is focused on the global events, which had a great bearing on the history of the Phanerozoic geology of Egypt.

2 Paleozoic Arcs and Basins

The large number of faults that crosscut the Precambrian Shield regions of the Gondwana supercontinent in general, and Egypt in particular, is the controlling factor in the Paleozoic sedimentation.

The faults led to the uplift of several plutonic arcs that crossed Egypt in a general northeast–southwest direction and along the margins of the intracratonic basins. The larger arcs, within the covered basement rocks, dissect Egypt into several high narrow blocks and between-blocks low areas, which became sites of thick sedimentation. The Phanerozoic section accumulated conformably and unconformably in thin to thick sequences characterized by facies shifts between the highs (arcs) and lows (basins). The identification of the arcs helps in solving many of the tectonostratigraphic problems in Egypt. Many arcs dissecting Egypt into multiple highs and lows, trending generally northeast–southwest during the Pan-African and Paleozoic times, were covered by a thin blanket of Mesozoic sediments, and thick sections were deposited in trough areas between the arcs. The most important arcs in Egypt during the Paleozoic were the Umbark, Sharib–Shiba, Uweinat–Bahariya–Port Said, Tarfawi–Qena–southern Sinai, Chephren–Kom Ombo, El Nashfa–El Balliyna, Suez–Cairo–Dabaa, and Gharib–Raqaaba–Taba (Fig. 2). However, intracratonic basins related to stresses within the shield are also important in Egypt; for instance, they include the many small basins within the Red Sea Mountains.

In Egypt, the Pan-African tectonics produced a geologic setting characterized by a crescent-shaped exposure of basement rock, a basin filled with sedimentary deposits, and extruded volcanics to the north and west of the outcropping basement, amounting to a total cumulative thickness assumed to be 25 km. The frequent rejuvenation of these faults was also control for local or regional tectonic evolution, with various behaviors in magmatic eruptions, delineation of the basin size coupled by rise and fall of sea-level change.

Deposits of the Precambrian–Cambrian transition are distinguished by a bedded clastic sequence, locally including a conglomerate bed and unmetamorphosed sediments except near a granitic intrusion (e.g., Gebel Umm Had in the central Eastern Desert and at Wadi Lithi in southwestern Sinai). U–Pb ages of the Hammamat Series refer to 585 ± 13 Ma (Wilde & Youssef, 2002). Deposition of the Hammamat Series occurred from braided alluvial-fan streams with some marine paleoenvironment pulses (indicated by microfossils together with the mineral chamosite) (Grothaus et al., 1979; Khalifa et al., 1988; Wilde & Youssef, 2002). The fluvial conditions of the Hammamat end phase continued through the Cambrian. The Infracambrian Hammamat sediments are coarse-grained clastics, which could be partly coeval with the Taba Formation in Sinai west of the Gharib–Raqaaba–Taba arc. The 8-m-thick Hammamat here consists of conglomerate, sandstone, and minor siltstone. The Hammamat and the feldspathic sandstone of the Araba Formation are known to be deposits overlying basement along the east and south sides of the Egyptian Basin.

Paleozoic deposition took place in intracratonic basins delineated by basement-exposing high arcs, which generally crossed Egypt in a north-northeast–south-southwest direction.

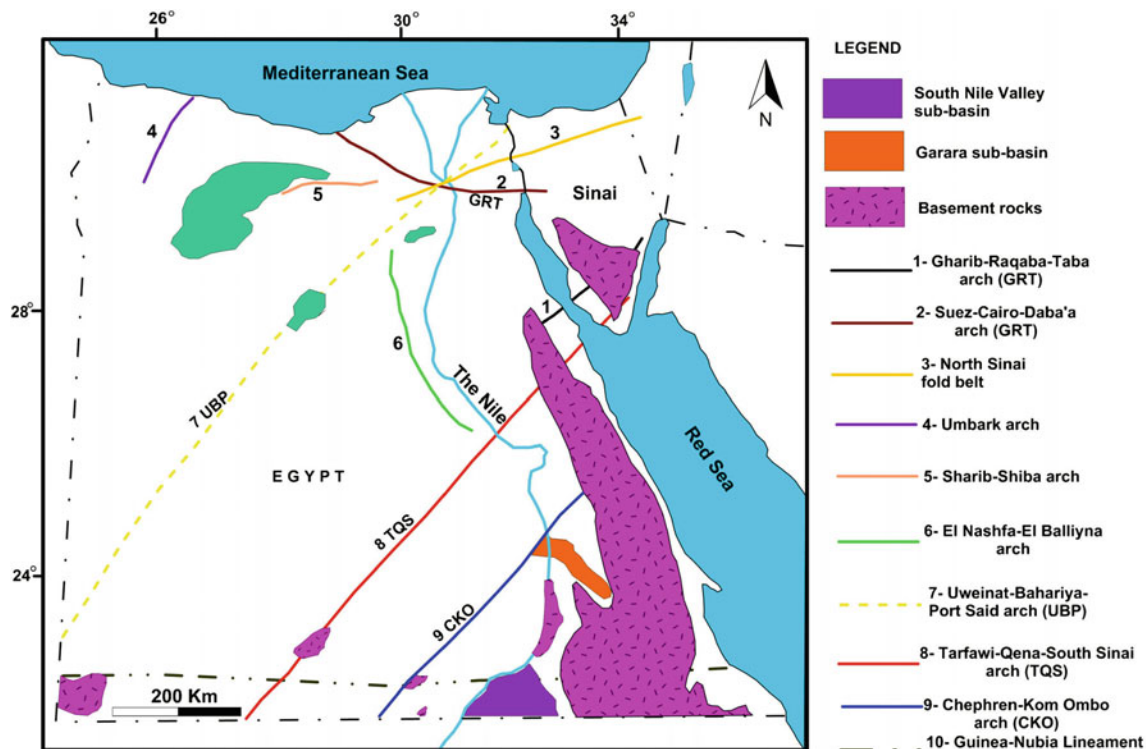


Fig. 1 Paleozoic arcs in Egypt (Issawi et al., 2009)

Sedimentation was influenced by global climate, sea-level changes, and periodic flooding by the Paleo-Tethys Ocean southward over newly assembled northern Africa. Generally, braided river deposits in the south (southern Nile and Dakhla Basins) pass into tidal and shallow-marine facies toward the north (Gulf of Suez, Sinai, and Siwa Basins) where the Paleo-Tethys Ocean had transgressed: (1) the southern Nile Basin including the Araba, Gabgaba, Naqus, Wadi Malik, and Gilf Formations; (2) the Dakhla Basin (including the Araba, Naqus, Wadi Malik, and Abu Ras Formations); (3) the Gulf of Suez Basin (including the Araba, Naqus, Rod El Hamal, Abu Darag, Aheimer, and Qiseib Formations); (4) the Sinai Basin including the Taba, Araba, Naqus, Wadi Malik, Um Bogma, Ataqa, Abu Durba, and Aheimer Formations; (5) the Siwa Basin including the Shifa, Kohla, Basur, Zeitoun, Desouqy, Dahiffan, and Safi Formations. Figure 3 shows the coeval units in different basins.

2.1 The Cambrian Deposits

In the subsurface Siwa Basin, the 300–1500-m-thick Cambrian Shifa Formation consists of heterogeneous sandstones with interbedded conglomerate, claystone, and commonly dolomitized skeletal carbonate (Keeley, 1989). The Shifa is coeval with the Araba Formation which recorded in different parts of Egypt (Fig. 3). The middle part of the Araba

Formation contains *Cruziana* and *Skolithos* ichnofacies, which refer to the Cambrian (Elicki et al., 2013; Khalifa et al., 2006; Wanas, 2011).

The pediplain, which dips away from central, northeastern, and western African orogens and over which the Cambrian was deposited, started to rise during the Cambrian–Ordovician transition (Sardinian and pre-Caradoc) tectonic event (Table 1). During both times, this event was responsible for the limited accumulation of sediments and hence the many unconformities. Thick deposits are found only on the passive margin of northern Africa (Siwa Basin), with the exception of an area in the northeast part of the Egyptian Basin that was blocked by the Turkish Plate. For this reason, the Lower Paleozoic pedimentation in this part of the Egyptian Basin was quite limited.

2.2 The Ordovician Deposits

The low sea level during the Early Ordovician coupled with a general uplift of Egypt along the arcs generally reflected the Taconic movement in northern Africa (Table 1). Ordovician marine sediments are almost totally absent, although they are found on both sides of Egypt as well as in Libya and Saudi Arabia. The Taconic movement was well recorded in Wadi Gabgaba, where the tilting of the Cambrian Araba Formation is as described in southwestern Libya (in the Uweinat area); in

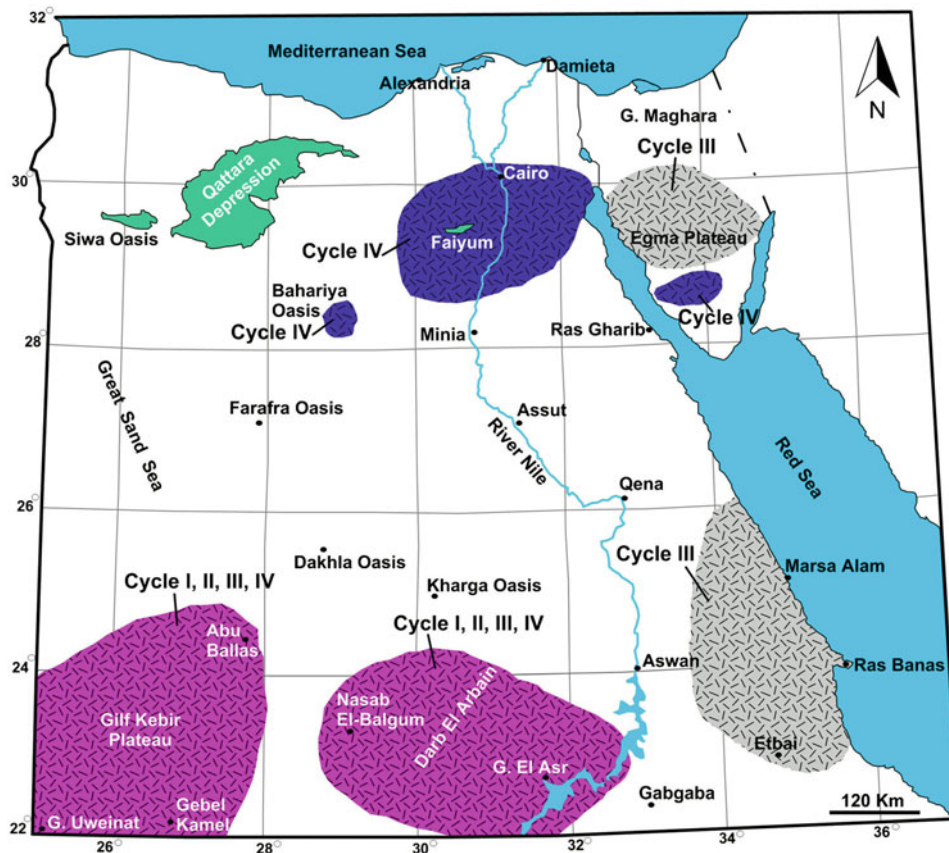


Fig. 2 Anogenic and orogenic plumes in Egypt (Issawi & Gayed, 2011)

the Gilf Kebir in Egypt, two faults bound its scarp on the west side (Issawi et al., 2009). By the Late Ordovician, Gondwana had drifted northward over the South Pole, which was then located in an interior position in what is now northwestern Africa. Late Ordovician glacial deposits (sandstone and tillite) are thus widespread through northern Africa. By correlation with similar facies in Arabian Plate (e.g., Saudi Arabia, Jordan, Iraq), a fluvioglacial mode of deposition is substantiated for the Naqus Formation in Egypt. The Naqus Formation lies unconformably on top of the Araba Formation separated by a paleosol layer. A fluvioglacial origin of the Naqus Formation depends largely on the presence of dropstones or erratic pebbles (Issawi et al., 2009).

The fissures, cracks, and faults in the Gabgaba area led to degradation and deepening of the wadis at the base of the Archean igneous and metamorphic units in the hills bordering the east side of the wadis. These paleovalleys later were the sites of deposition of the Gabgaba Formation, glaciogene conglomerates that resulted from the Ordovician glaciation (Issawi, 2000). The next phase in the glaciation history was the complete melting of the ice and the deposition of the Naqus Formation during the Early Silurian. Glaciogene diamictite deposits are common in many parts of Egypt extending from Sinai through Wadi El Dakhli in the

northern Eastern Desert to Wadi Gabgaba in the southern Eastern Desert to Gilf Kebir in the southern Western Desert. Issawi's (2005) detailed study of Gabgaba geology revealed four glacial phases and four interglacial paleosol layers. The Ordovician unit in the Siwa Basin is the 80–600-m-thick Kohla Formation, which consists of fluvioglacial tidal-flat sandstone and mudstone deposits.

2.3 The Devonian–Silurian Deposits

The Late Caledonian uplifts during the Early Devonian were accompanied by the continuous regression of the sea and by progradation of braided plains over large areas in southern Egypt. The Late and Early Devonian registered a brief marine transgression during the Emsian with the deposition of the ~ 750-m-thick Zeitoun Formation as shallow-marine sandstone and offshore marine mudstone all along the northern Africa platforms (Carr, 2002) and conglomerate in the Siwa Basin. In southern Egypt, erosion of the high land as a result of the Caledonian movement resulted into significant thinning of the outcropping clastic parts of the Devonian Wadi Malik Formation (80–100 m) in the Dakhla Basin near the west side of the Gilf Kebir; in Sinai, the Wadi

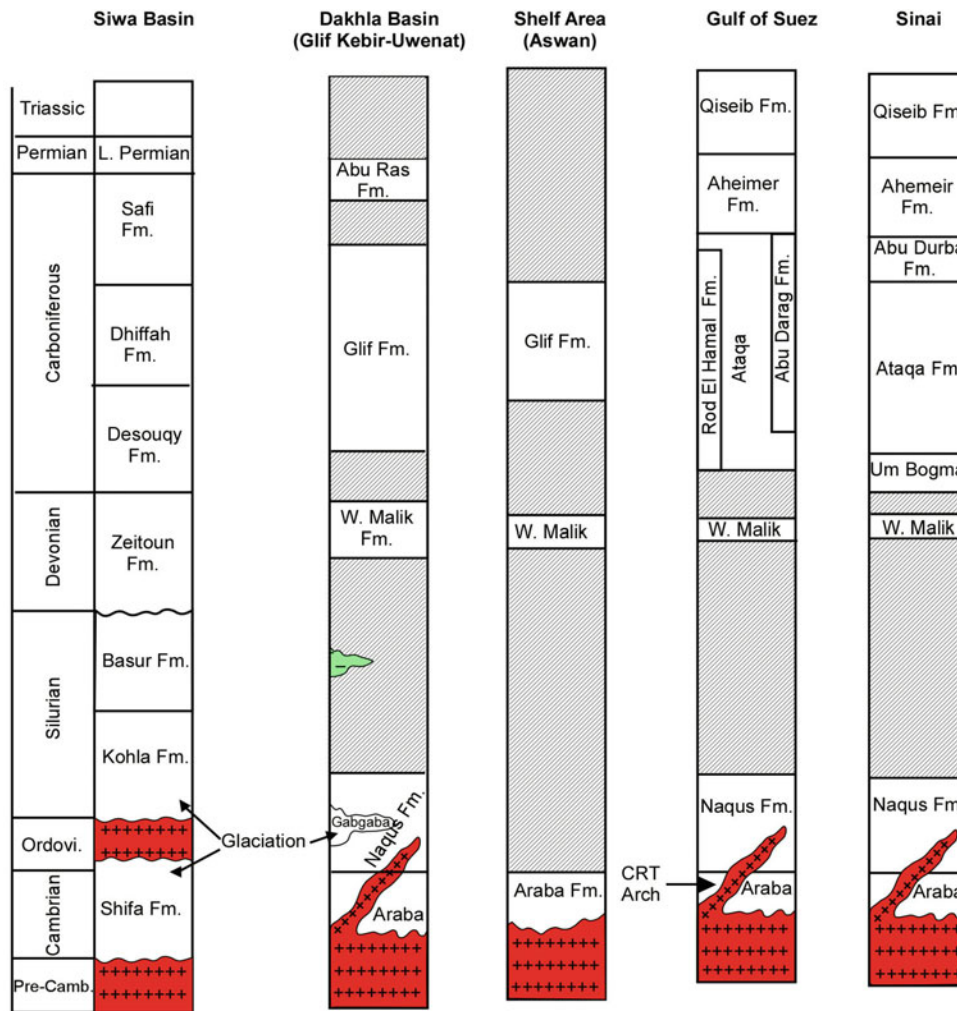


Fig. 3 Paleozoic rock units in Egypt

Malik section is only 15 m thick and consists of sandstone. Devonian rocks are also of record in eastern Aswan at Wadi Abu Agag, in southeastern Aswan at Wadi Gabgaba, and in southwestern Aswan at Um Shagir Hill. On the basis of subsurface data from both the Hurghada oilfield and the Zaafrana drillhole, Devonian sediments are likely extend below the confirmed Carboniferous section.

In Wadi Gabgaba, Late Ordovician Gabgaba conglomerates and the Naqus Formation were tilted 10–35°, indicating a second uplift reflecting the Erian phase of the Caledonian orogeny. The Devonian sediments were again tilted in response to the Late Devonian–Early Carboniferous uplift known as the Bretonian or Late Acadian movement representing the first phase of the Hercynian orogeny. Block tilting of the Carboniferous sediments, domal uplift, and folding are clearly evident in the Lower Paleozoic sediments in Sinai, in the Wadi Gabgaba area, and in the Gilf–Uweinat stretch. Minor deformation in northern Africa strata in the Late Devonian (the Bretonian event) is associated with the initial northward subduction of the Paleo-Tethys.

During the Late Silurian, the deposition of the 400–700-m-thick Basur Formation (sandstone, minor interbedded siltstone, and conglomerate) occurred in the Siwa Basin (Issawi et al., 2009; Keeley, 1989; Fig. 3). The Silurian hot shale rich in organic matter provided good sources for the petroleum systems adjacent to Egypt—the Libya–Algeria basins to the west and the Arabian basins to the east. Because the Turkish Plate dammed the northern shores, no rich organic matter of marine origin comparable to that in the surrounding countries has been found in Egypt.

2.4 The Carboniferous–Permian Deposits

The Early Carboniferous witnessed globally high sea levels and warm temperatures with the sea invading northern Africa over the pre-Carboniferous deformed surface. Although deformation led to the inversion of the Siwa Basin, in other parts of this basin, thick deposits of sediments accumulated, thereby forming the 100–300-m-thick Tournaisian–Early

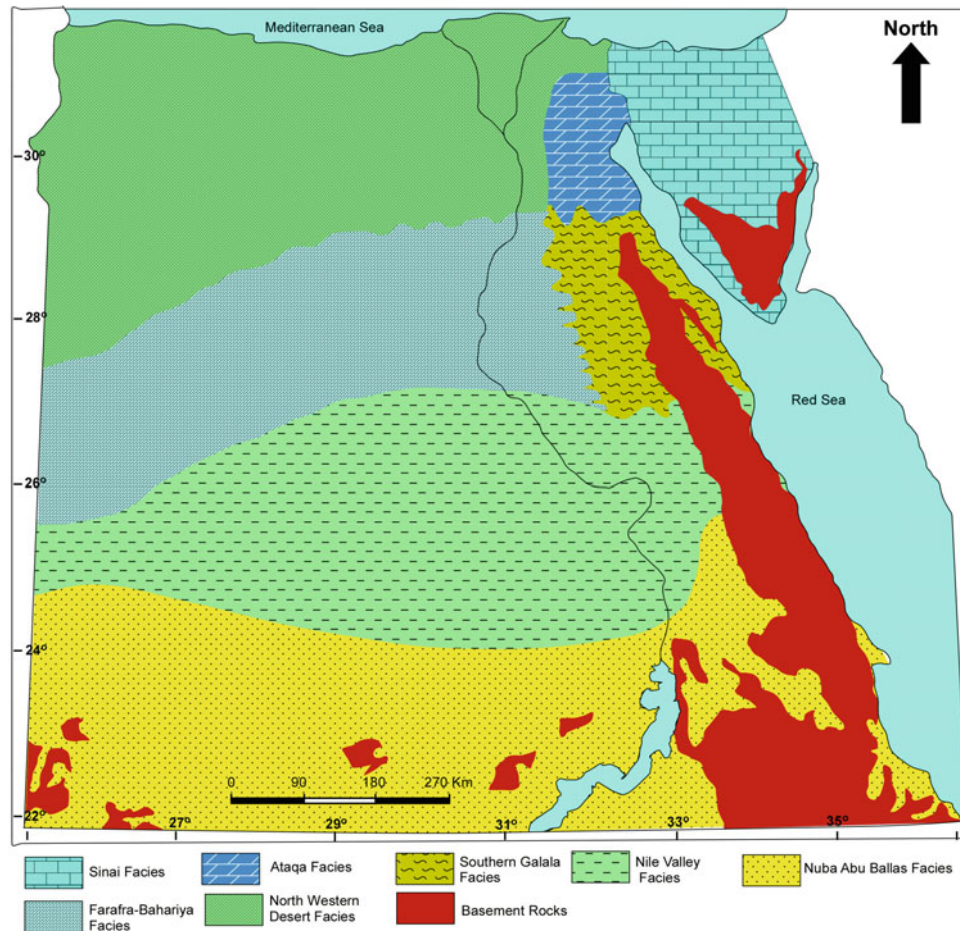


Fig. 4 Different cretaceous facies in Egypt (after Issawi et al., 2009)

Visean Desouqy Formation (bedded sandstone with minor intercalated siltstone). To the south, in the Uweinat–Gifl Kebir stretch, the Gifl Formation unconformably overlies older Paleozoic units in an area stretching from the southern Western Desert to the high basement rocks of the present Red Sea Hills.

In Sinai, the area north of Gharib–Raqaba–Taba received a thick succession of Carboniferous deposits including the Um Bogma and the Abu Durba Formations, mainly clastics and minor carbonates that host the well-known manganese–iron ore deposit. South of the arc, the inversion of the basin during post-Naqus Formation time continued in response to the Hercynian–Variscan orogeny. The Hercynian orogeny, which dates back to 350–280 Ma (Early Carboniferous–Early Permian) (Coward & Ries, 2003), was responsible for intraplate deformation throughout the entire Sahara platform (Haddoum et al., 2001), often by reactivation along the Pan-African suture zones such as the northeast–southwest-trending arcs crossing Egyptian basins. All these features involve Paleozoic sediments, but most of the Mesozoic units (Triassic and Jurassic) are missing or are represented by continental lithofacies.

Sea-level oscillation in the Late Carboniferous was associated with the early stages in the opening of the central Atlantic Ocean and resulted in lithofacies changes varying from shallow to deep marine in northern Egypt. The many unconformities within the Carboniferous marine section were due to these transgression–regression phases as well as the many deformations resulting from the Westphalian–Stephanian Asturian event of the Variscan orogeny and generally may have been synchronous with or may have postdated a rapid cooling phase in the global climate, which reached its maximum during the Late Carboniferous–Early Permian glaciation (Klitzsch, 1983). At the time, most of Egypt was paleo-highs except probably its northern part, where the Aheimer Formation formed. Inland, the 30–40-m-thick Abu Ras Formation (conglomerate) unconformably overlies the Carboniferous Gifl Formation. Both the Aheimer and the Abu Ras Formations are considered to be Upper Carboniferous to Permian (Kora, 1998).

The progressive fragmentation of Gondwana began during the Late Carboniferous–Early Permian and continued through the Early–Middle Mesozoic. In the first stage of rifting, consequent escape structures resulting from

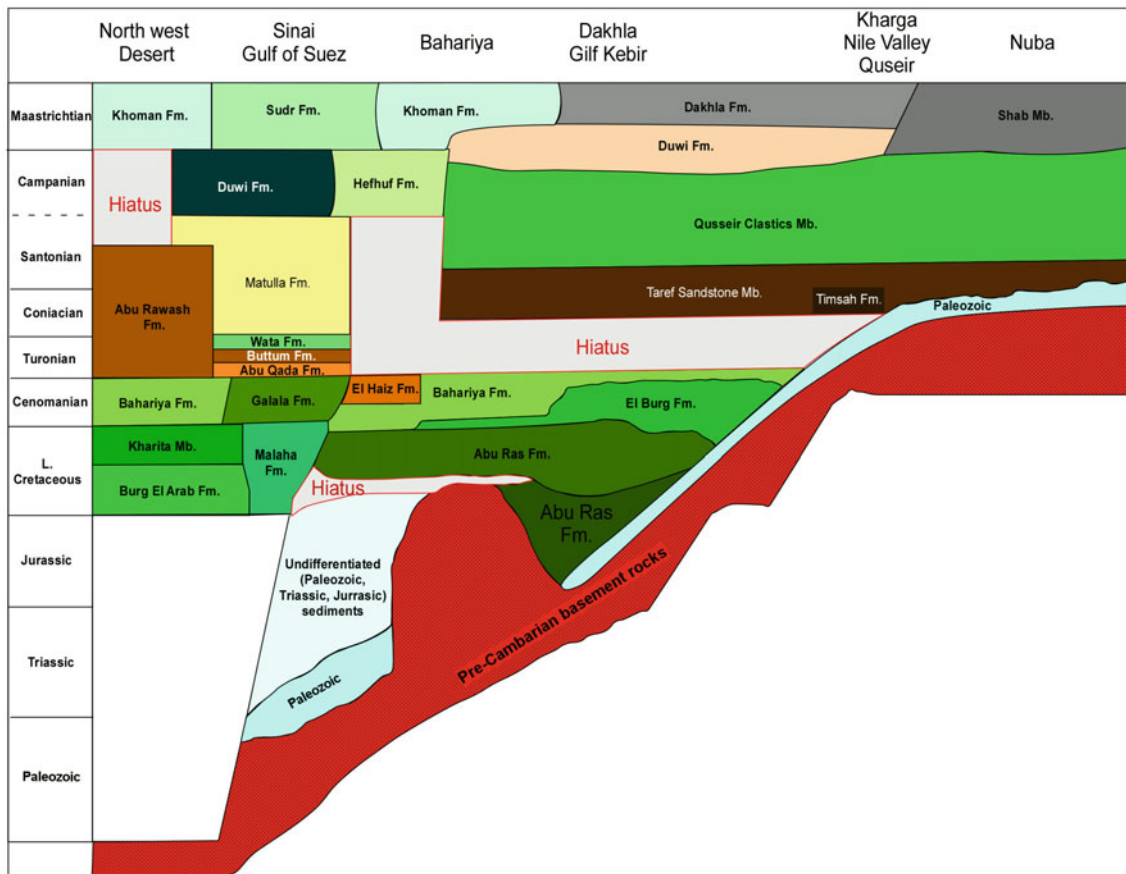


Fig. 5 Cross sections and distribution of Cretaceous rock units in Egypt (after Issawi et al., 2009)

fragmentation processes (or vice versa), the northern and eastern margins of Africa, were greatly affected.

2.5 The Permian / Triassic Transition

The northern margin of Africa changed from being a convergent margin associated with the closure of the Paleo-Tethys Ocean to a passive margin during the Permian and Triassic, as the Neo-Tethys began to open (Wilson et al., 1998). Rifting occurred by reactivation of Hercynian faults under a purely extensional regime along the passive margin (Pique et al., 2002). Large-scale transcurrent fault zones, such as the Newfoundland-Azores-Gibraltar and Guinea-Nubia fracture zones, which acted as northern and southern transform faults, respectively, enclosing the central Atlantic during crustal separation, allowed for the opening of the central Atlantic (Bumby & Guiraud, 2005). The clockwise rotation of Africa (Fairhead et al., 2013) during the process of separation of South America from Africa led to the positioning of the southern rift of the northern fracture zone to be in northern Africa. The zone includes the Syrian Arc System and associated structures, such as along the northern Egypt

fracture zone (Issawi et al., 2009) between Taba (on the north end of the Gulf of Aqaba) and Suez and through Cairo to the Mediterranean. Farther west, the presence of sinistral strike-slip faulting and associated flower structures in parts of the Atlantic trough attests to this transgressive movement (Pique et al., 2002). However, the passive margin of Egypt's African Plate seems to have not been much affected by the suturing phase of the plates, and the Triassic heralded the onset of thick Jurassic and Cretaceous sediments in the northern Egyptian Basin, together with subsidence that affected the eastern Mediterranean margin in conjunction with the opening of the Neo-Tethys (Stampfli & Boreál, 2002).

2.6 The Triassic Deposits

The Triassic section at Arif El Naga (northeastern Sinai) comprises the 50-m-thick basal Anisian Qiseib Formation (fine- and coarse-grained clastics), which is overlain successively by the 19-m-thick Anisian Arif El Naga Formation (lumachels in a gypseous or marly matrix) and the 50-m-thick Ladinian-Carnian Abu Nusra Formation (fossiliferous massive limestone and dolomite with interbedded

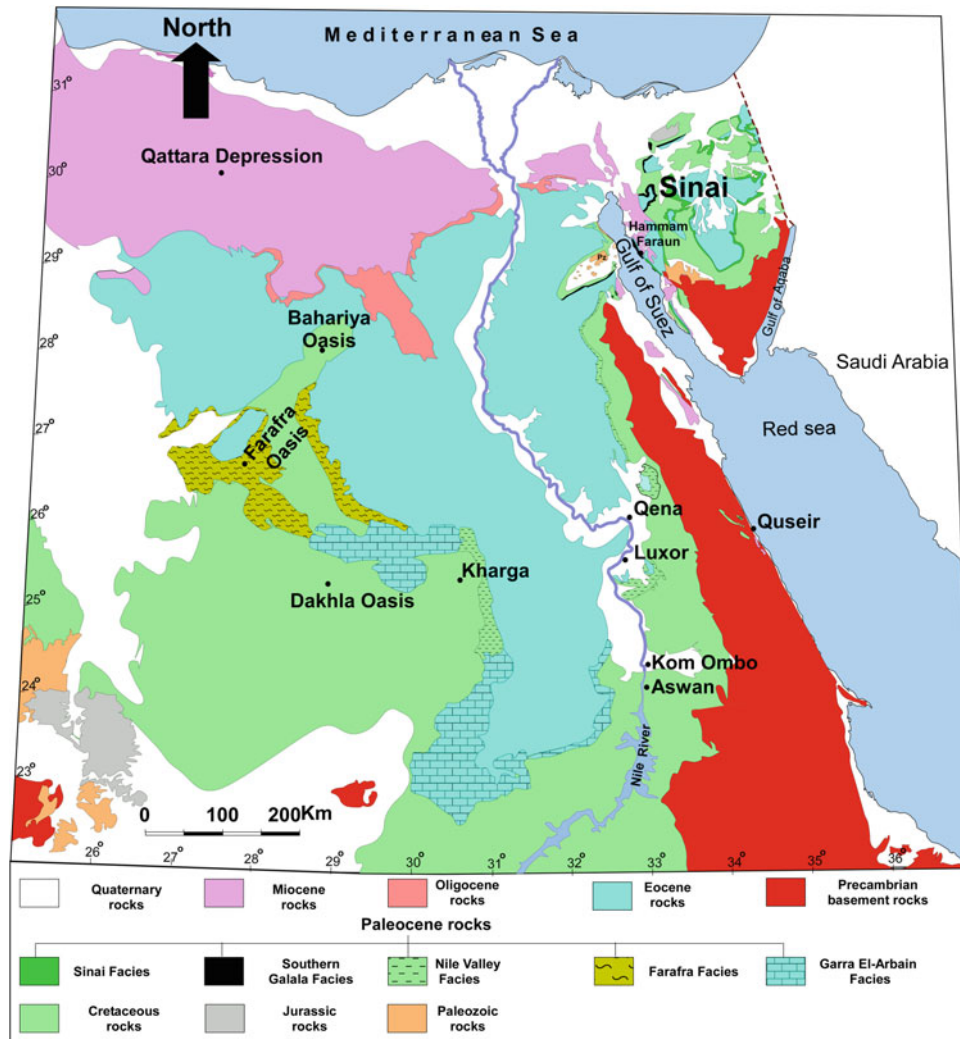


Fig. 6 Paleocene facies distribution in Egypt (Farouk, 2016)

gypsaceous clay and marl). The marine Triassic sediments are known from most wells drilled in northern Sinai between Arif El Naga and the Gulf of Suez, whereas continental conditions prevailed in the high area south of Lat 30°N in both the Eastern Desert and Sinai.

In the northern Western Desert, the subsurface sandstones above the Carboniferous and below the Jurassic might belong to both the Permian and the Triassic, while in the southern Western Desert, the 50-m-thick Abu Ras Formation (sandstone, shale, and grit) is thought to be of Triassic age. Volcanic activity peaked at ~ 200 Ma (Guiraud, 1998), which is near the Triassic–Jurassic contact, when extensive alkaline basalt flows were emplaced in northern and central Africa and in the Levant, preceding the separation between northern Africa and Europe (Table 1).

2.7 The Triassic–Jurassic Transition

A major unconformity representing the Triassic–Jurassic transition is known from the Egyptian successions and in Sinai is marked by a gypsaceous clay and conglomerate horizon at the top of the Triassic section. The hiatus followed the rifting and basin-development episode, which was terminated by volcanic eruptions. Tectonic instability had increased from Middle Triassic time and was underscored by block tilting and local uplifts along the Africa–Arabia Neo-Tethys margins, as reported by frequent unconformities and hiatus in the Triassic–Jurassic sediments and also by the complete lack of Triassic marine deposition apart from the Arif El Naga area. These deformations represent the distal effect of the Eo-Cimmerian orogenic event.

Location		Fayum	Bahariya Farafra	Nile Valley - Cairo			Helwan	Sinai	
Age									
Upper Eocene	Priabonian	Qasr El Sagha Fm.	Up. Hamra Fm.	Maadi Fm.			Wadi Hof Fm.	Tayiba Fm.	
	Late Bartonian	Birket Qarun Fm.		Mereir Fm.		Schaibon Fm.	W. Garawi Fm. Qurn Fm.		
Middle Eocene	Early Bartonian	Gehannam Fm.	L. Hamra Fm.	Beni Suef Fm.	Sannor Fm.	Observotry Fm.	Giushi Fm.	Tanka Fm.	
	Late Lutetian	G. Hof Fm.		G. Hof Fm.					
	Middle Lutetian	Rayan Fm.		Mokattam Fm.		Qarara Fm.		Khaboba Fm.	
	Early Lutetian	Samalut Fm.			Maghagha Fm.		Sheikh Fadl Fm.		Darat Fm.
					Minia Fm.				
Lower Eocene	Ypresian		Qazzun Fm.						
			Naqb Fm.	Dungul Fm.	Thebes Fm.			Egma Fm.	
			Farafra Fm.					Thebes Fm.	

Fig. 7 Distribution of eocene rock units in Egypt

2.8 The Jurassic Deposits

In northern Sinai, Jurassic sediments attained a thickness of > 1800 m through three marine and three continental sedimentary-facies cycles, each of which incorporated a minor cycle of the other facies (Al-Far, 1966). The Gebel Maghara Facies characterize the sediments into three marine and three continental cycles. Each cycle carried a minor second-order cycle, and thus, the marine cycle has a minor representation of the continental facies vice versa. The Gebel Maghara Facies started at base with the continental Mashaba Formation followed by the Marine Rajabiah, Continental Shusha, marine Bir Maghara, continental Safa, and marine Masajid Formation at top. Though the Safa Formation includes coal beds, it is hard to apply the term cyclotheming to the whole section; it may be referred to as “poor cyclotheming.”

However, in Khashm El Galala exposed section on the west side of the Gulf of Suez has the same Gebel Maghara units but is much reduced in thickness (220 m). The line along which the Gebel Maghara Sinai Facies changes to Khashm Facies is now the Gulf of Suez. The continual sinking of Sinai and rising of Khashm during the Jurassic led to the initiation of the Gulf of Suez.

Guiraud et al.’s (2005) interpretation of the geodynamic events during the Jurassic does not fit with field observations. We do not concur with a high sea level in the Late Kimmeridgian, the reduced intracontinental fluviatile-lacustrine basins, and the development of the alkaline anorogenic intrusions in Nubia. The Kimmeridgian Masajid Formation is a shallow-marine unit, both in the subsurface of the Western Desert (Hantar, 1990) and in the Gebel Maghara section (Al-Far, 1966); the Dakhla Basin is distinguished by its fluviatile and shallow-marine Jurassic sediments (Issawi et al., 2009); and the Jurassic intrusive rocks in Nubia, southern Egypt, are of minor importance relative to the Oligocene volcanics extending from west of the Nile to Gilf-Uweinat in the far west.

The subsurface Jurassic sediments in the northern Western Desert are assumed to be as thick as 1524–1828 m, but they average 600 m farther south; in the Dakhla and Kom Ombo Basins, the Jurassic comprises mainly clastics, as proven by drilling in the western Kom Ombo area. The Late Jurassic–Early Cretaceous Abu Ballas Formation is exposed in the Dakhla Basin as a 20–53-m-thick unit of sandstone and clay. The sandstone in Kharga Oasis was described in part by palynological studies of drill core. Also, palynology

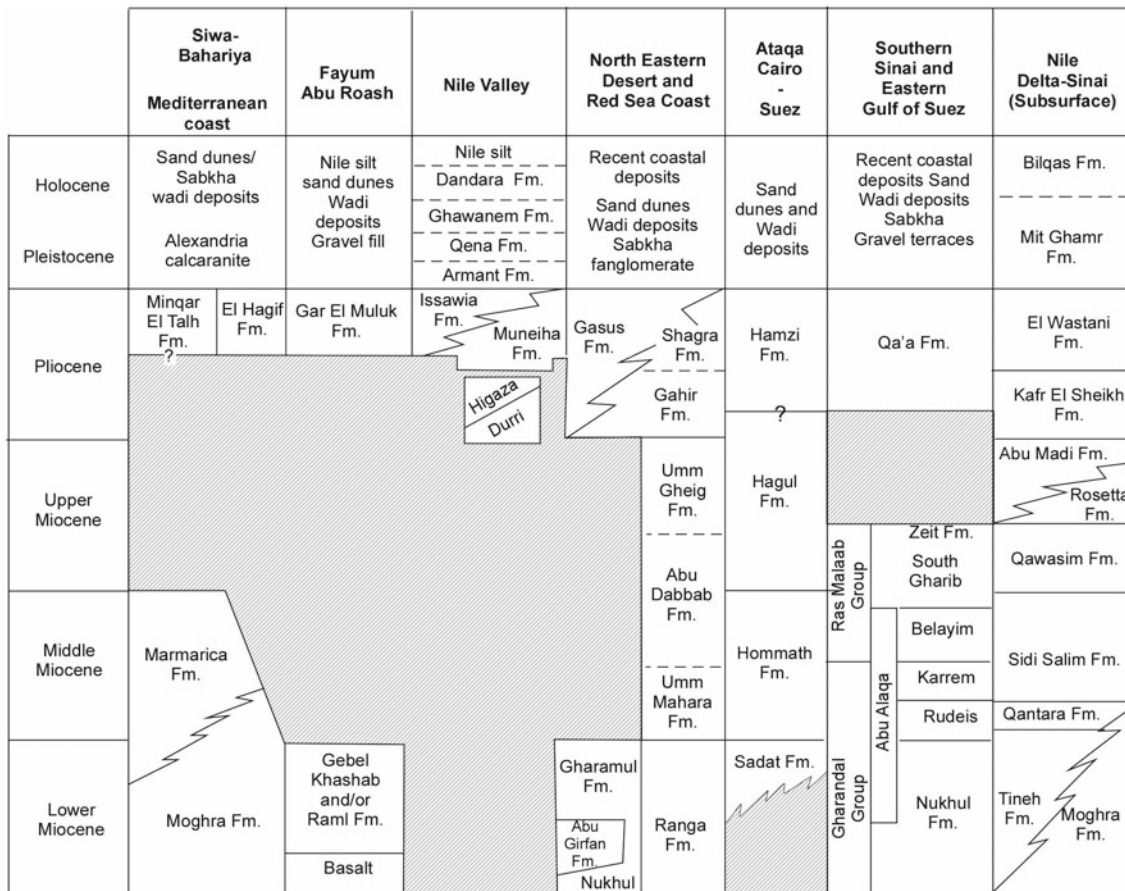


Fig. 8 Distribution of the Neogene rock units in Egypt

studies of the sandstones in Foram-1 and Ammonite-1 wells in the west-central Western Desert revealed 273 m and 105 m thicknesses, respectively (Schrank, 1987). A Jurassic 120-m-thick marine-sediments section, composed of interfingering limestones and sandstones, was cored in the Nile Delta (Schlumberger, 1984).

2.9 The Jurassic–Cretaceous Transition

Within many basins in north, west, and central Africa, the Jurassic–Cretaceous transition exhibits hiatuses and unconformities associated with Late Tithonian sharp drop in sea level and also with uplift, block tilting, and slight folding caused by local transpression from the tectonic Cimmerian event near the end of the Late Jurassic that has been throughout much of the Middle East (Fourcade et al., 1993). These deformations represent the distal effect of strong tectonic activity, including thrusting that occurred in southeastern Europe, known as the mid-Berriasian orogenic event (Nikishin et al., 1998). Stresses during these events caused many rift stages in eastern and northern Africa margins and in the eastern Mediterranean in general, with

many east–west-trending rifts, especially along the northern margins of Egypt. These rifts' depocenters in the main Egyptian Basin became wider and larger, ready to be covered by Cretaceous seas and thick Cretaceous deposits. The Jurassic–Cretaceous transition was marked by a major and widespread hiatus in Egypt. The top beds of the Masajid Formation in the Gebel Maghara Facies belong to the Barthonian–Kimmeridgian, whereas the overlying Malha Formation is commonly dated as Aptian–Albian; the top-most Jurassic (Tithonian) and the basal Cretaceous (Berriasian to Barremian) are missing in most of the sections analyzed. However, Aboul Ela et al. (1989–1991) identified 25 species of pollen and spores from the kaolin bands within the Malha Formation from the west side of the Gulf of Suez, which relegates the lower part of this unit to the Barremian or possibly older.

The buildup of many domes along the Syrian Arc belt started by rifting and initiation of the basins in northern Egypt in general, during the Triassic–Lias associated with the widening of the Neo-Tethys. The main structural configuration of this belt developed in the Late Jurassic through the Cimmerian event and continued intermittently during the Cretaceous, reaching its acme during the Santonian.

In southern Egypt, the opening of the Indian Ocean around the Horn of Africa happened ~ 156 Ma (Middle–Late Oxfordian) (Rabinowitz et al., 1983), and most probably, the resulting escape structures mobilized to southern Egypt intracratonic basins, which have different orientations: northwest–southeast (Garara and Kom Ombo Basins) and northeast–southwest (southern Nile and Dakhla Basins). Among the structural features that are considered to be more important in the geologic history of Egypt are the widening of the Gulf of Suez, the renewable uplift of the Pan-African arcs that generally trend northeast–southwest, and the northward movement of the Arabia–Nubia block. This second stage of Late Jurassic–Early Cretaceous rifting followed a Late Carboniferous–Middle Jurassic initial stage of rifting and strongly affected the development of Karoo Basin, which stretches from southern Africa to Kenya–Somalia and Ethiopia in the north (Bumby & Guiraud, 2005). The first stage of rifting was the initial movement stage in the breakup of Gondwana at ~ 180 Ma, which separated West Gondwana (Africa, Arabia, and South America) from East Gondwana (India, Madagascar, Antarctica, Australia, and New Zealand). Both of these rifting phases and a third Late Eocene–Early Miocene rifting phase resulted in the gradual breakup of Gondwana, the beginning of the opening of the Neo-Tethys, basin development on this supercontinent, and the activation of Pan-African sutures and arcs. Because these events corresponded to a general sea-level rise and fall, both widespread marine-sediment accumulation through transgressions and accumulation hiatuses occurred within the basins. These effects were most important on the high arcs in the Egyptian Basin. During the Jurassic–Cretaceous within the African Plate, superimposed on the main regime of extensional tectonics were compressional events believed to have been linked to a change in the spreading direction and rate within the Indian and Atlantic Oceans.

3 The Cretaceous Deposits

A bird's eye view over Egypt makes it possible to identify the following seven facies: (1) Sinai (including Aptian–Albian Malha, Cenomanian Galala, Lower Turonian Abu Qada, Middle Turonian Buttum, Middle to Lower Turonian Wata, Coniacian–Santonian Matulla, Campanian Duwi, Early Maastrichtian Qadiera, and Maastrichtian Sudr Formations); (2) Ataq (including Malha, Galala, Turonian Maghra El Hadida, Santonian–Campanian Adabiya, and Maghra El Bahari Formations); (3) Southern Galala (Malha, Galala, Abu Qada, Wata, Matulla, Southern Galala, and Sudr Formations); (4) Nile Valley (including Nubia Formation, Taref Sandstone Member, Qusseir Clastic Member, Duwi, and Dakhla Formations); (5) Nuba Abu Ballas (including Abu Ballas, Burg, Timsah, Taref Sandstone,

Qusseir Clastic, and Shab Members); (6) Farafra–Bahariya (including Bahariya, Heiz, Hefhuf Formations, and Khoman Chalk); and (7) subsurface northern Western Desert Facies (including: Burg El Arab Formation, Alam El Bueb Clastic, Alamein Dolomite, Dahab Shale, Kharita Clastic Members, Bahariya, Abu Roash, and Khoman Chalk). Each of these facies is further classified into several rock units, and some of the units cross over to another facies type. The differentiation between the facies is controlled by the surface of depositional basins, the degree of marine flooding, and structural deformation before and during deposition. Figures 4 and 5 show the coeval units in different basins.

Marine incursions covered northern Egypt depositing sediment units that vary by lithology and thickness. Transgression reached southern Egypt in the Dakhla Basin and in extreme southeastern Egypt (Abraq), where the Abu Ballas Formation is found and is assumed to be in the subsurface of the Garara Basin. Deposition of this unit took place as a reflection of the Middle to Late Aptian and Albian dextral-transform movement along the Equatorial Atlantic fractural system (Gulf of Guinea). The escape structures of this movement led to widening (resulting in pull-apart basins) and subsiding of subbasins within the Egyptian Basin, and the movement certainly was accelerated by the constant opening of the Indian Ocean.

The final separation between Africa and South America occurred during 105–100 Ma (Albian–Cenomanian), although the Atlantic was completely opened in the Santonian (Nurnberg & Muller, 1991; Jolivet et al., 2016), coinciding with the closure of the Neo-Tethys. These movements resulted in seafloor spreading in western Africa and in intracratonic basins, the Cenomanian high sea-level stand, and the establishment of a marine connection between the Neo-Tethys and the Gulf of Guinea (Atlantic Ocean). Because the Cenomanian sea-level rise covered all of Egypt, Cenomanian marine beds are known from the southern Aswan Abu Rawash near Cairo. Over the high arcs, the Cenomanian is poorly represented or partly absent, but the high seawater masked all the structures in the Egyptian Basin. The widespread Cenomanian over Africa is an expression of the Cretaceous Normal Magnetic Quiet Zone recorded worldwide that was initiated at ~ 120 Ma (Early Aptian) and ended at 83.5 ± 0.5 Ma (latest Santonian) (Ziegler, 1990, 1992). The Turonian events that are by far the most active in Cretaceous time occurred during the closure of the Neo-Tethys, although it probably was initiated during the Cenomanian (Guiraud et al., 2005; Issawi et al., 2009). The huge volcano mountain in southeastern Egypt, the presence of a 15-m-thick gypsum section of Buttum Formation, the Turonian section in Sinai, the northward retreat of the Turonian shoreline from the Cenomanian shoreline (~ 400 km between $22^\circ 30' N$ and $26^\circ 30' N$), and the closure of the trans-African seaway connecting the

Tethys with the Atlantic are among the important events characterizing this stage.

This rather-uneventful period was interrupted by the development of two major regional unconformities, one of them Albian–Cenomanian and the other Turonian. The duration of these hiatuses, maturation of the paleokarst features, and the presence of kaolin both in western Sinai and on the west side of the Gulf of Suez (northwest of Zaafarana) point to exposure that was not just brief or transient. Thus, unconformities were tectonically rather than eustatically controlled (Farouk, 2015; Farouk et al., 2017).

In Egypt, the Cenomanian sediments are mostly clay and limestone, but sandstone and clay with rare carbonate (increasing northward) are found in the area south of 26°N. In Gebel Halal, the Cenomanian consists of a 350-m-thick limestone. Shallowing conditions of deposition dominated during the Turonian, but generally the sediments are shales and marls in Sinai with gypsum in the middle and carbonate at the top. The Turonian is missing south of Qena and farther west, in Farafra and Bahariya Facies. Accessed by drilling, the subsurface of the Western Desert was found to include an 1800–1900-m-thick Turonian–Senonian section of fine-grained clastics and clean carbonates.

The Coniacian, which is not well defined in Egyptian stratigraphy, consists mostly of sandstone of the Nubia Formation in the southern and middle latitudes of Egypt. Mountains in southeastern Egypt provided felsic-volcanic source rock for this unit; the volcanogenic sediments were brought to the basins by rivers mostly flowing from these high mountains toward the north, east, and west in a centripetal drainage system. The Nubia Formation is divided into the Taref Sandstone Member at the base (~ 80–150 m thick; Coniacian–Santonian), the Qusseir Clastic Member in the middle, and the 54-m-thick Shab Clastic Member. Found only in extreme southwestern Egypt, the Shab is coeval with the Maastrichtian–Early Paleocene Dakhla Shale in the north. In the Farafra–Bahariya Facies, the Campanian is represented by 120-m-thick Hefhuf Formation (dolomitic limestone at the top and base and argillaceous sandstone in the middle). Turonian–Santonian strata are missing in these facies.

The most important unit in the Late Cretaceous is the Upper Campanian Duwi Formation as it includes Egypt's economically viable phosphate beds, extending from the Red Sea (Safaga–Qusseir) through the Nile Valley (Qena to Edfu) and farther west within the Kharga–Dakhla stretch up to the Libyan–Egyptian border through the Sand Sea (Ahmad et al., 2014). The phosphate horizon in southern Egypt forms the south boundary of the Upper Cretaceous marine sedimentary units in the north and the north boundary of the Upper Cretaceous continental sedimentary units in the south.

The Santonian events are clearly reflected in the inversion of the Syrian Arc basins forming many domes in northern

Sinai through constant rifting and drifting, uplift, gliding of the mostly Cenomanian upper carbonate units, and steeply tilting the half domes (Issawi et al., 2009). Dipping of the Santonian Matulla Formation together with the angular unconformity between the Matulla and the overlying Duwi and Sudr Formations is proof of the Santonian inversion of these features.

The Africa–Arabian Plate's strong rotation in an anti-clockwise direction resulted in collision with the Eurasian Plate (Reilinger & McClusky, 2011). The collision is expressed in northern Egypt by increased faulting and accentuation of the old structures on the surface or in the subsurface of the northern Western Desert. The activated northeast–southwest arcs in the Egyptian Basin exhibit well-defined courses, especially in Bahariya Oasis, where the Cenomanian Bahariya and Heiz Formations are steeply tilted with an angular unconformity. The overlying units (Turonian, Coniacian, and Santonian sediments) are not present in the Bahariya Oasis. In the Eastern Desert, the Santonian is missing in Gebel Shabrawet and in most of Gebels Ataqa and Northern Galala but is found in Southern Galala (Farouk, 2015). Active block movements started before the Santonian and became more pronounced with time until the Middle Miocene opening of the Red Sea.

The Campanian transgression reached south–southwestern Aswan, where the Duwi Formation (a clastic phosphate–carbonate unit) was deposited; the Duwi gradually reflects deeper marine conditions northward and is part of the Southern Galala and Sinai Facies. Also representing the Campanian transgression is the Hefhuf Formation in Bahariya. The shallow conditions prevailing over much of the Egyptian basins, associated with tranquil tectonic events, gave way to more marine transgression during the Early Maastrichtian, when the basal part of the Dakhla Formation was deposited as far south as Lat 23° N and northward in Sinai; it is also found at the surface and in subsurface sections of the northeastern and northern western deserts. The Maastrichtian Dakhla Shale is well exposed above the Duwi Formation east and west of the Nile, along the Sin El Kaddab scarp, through Darb El Arbain to the Kharga–Dakhla oases and Lat 26° 45' N (Hatyet El Sheikh Marzouk south of Farafra Oasis but gradually changing to Khoman Chalk to the north). In the northern Western Desert, the chalk reaches a considerable thickness (1814 m), as observed in the Betty well and in many oil wells in the northern Egyptian basins. Issawi and Osman (2002) consider the Farafra Oasis latitude to be a boundary between platform (Dakhla Shales) and ramp (Khoman Chalk) environments of deposition. Such platform–ramp conditions extended eastward to where, in the southern Galala Facies, deeper conditions of deposition prevailed during the Maastrichtian and the ~ 88-m-thick Sudr Chalk (chalky limestone) formed, and in the Ataqa Facies, because block faulting caused a

disturbance in the depositional regime in the north, the 80-m-thick Maastrichtian Maghra El Bahari Formation (sandstone, marl, limestone, and conglomerate). The high sea level during the Maastrichtian penetrated the high uplifted blocks in the north, thereby causing a reversal of the ramp–platform relationship.

In southern Egypt, in the Nuba–Abu Ballas Facies, the Campanian Duwi Phosphate is largely missing; It is represented only by thin fossiliferous phosphatic lenses along Darb El Arbain (Issawi et al., 2009). The Maastrichtian Dakhla is replaced by minor shale beds (Shab Clastic Member at the top of the Nubia Formation; Fig. 5). Repeated major sedimentary cycles from continental and marine facies were observed at least three times from the Late Jurassic through the Late Cretaceous in southern Egypt. Each of these cycles (as follows, from top to base) includes basal continental sediments overlain by transitional deltaic rocks and marine deposits: The Nubia Formation includes the Santonian Qusseir Clastic Member (dominantly shallow-marine to deltaic facies) and the Coniacian Taref Sandstone Member (dominantly continental facies). The Early Senonian Timsah Formation consists mainly of iron-bearing beds, clay, and sandstone of lacustrine and deltaic facies intercalated with marine sediments. The Albian–Cenomanian Burg Formation consists mainly of fluviatile and deltaic continental deposits on-lapped with sediments from marine incursions, such as the Upper Cenomanian Heiz or Maghrabi Formation (shallow-marine facies). The Lower Cenomanian Bahariya or Sabaya Formation consists of shallow-marine to continental and deltaic facies (Catuneanu et al., 2006.). The Lower Cretaceous (Aptian) Abu Ballas Formation consists of continental sediments at the base (named Six Hills Formation by the Germans), overlying Upper Jurassic shallow-marine deposits (called the Abu Ballas Formation by the Germans). The end of the Cretaceous in Egypt is marked by a retreat of the sea, with a wide unconformity representing the Cretaceous–Paleogene boundary.

4 Cenozoic

After the closure of the Neo-Tethys at the end of the Mesozoic, the Cenozoic witnessed two major events, with many structural and stratigraphic consequences: the appearance of the Red Sea in the Middle Miocene and the desiccation of the Mediterranean during the Messinian. These occurred as brief but very important events in the geologic history of Egypt, which were unequaled by any events during earlier times.

Along the northern African–Arabian Plate, the basins recorded strong subsidence through rifting during the Paleocene–Early Eocene, a continuation of the general subsidence during the Jurassic and the Cretaceous. Strong faulting

and folding happened in Egypt from the Syrian Arc System in the north to the Guinea–Nubia lineament far to the south; compression collision occurred in the Zagros and the Oman Mountains in the northeast; folding happened along the Central African Rift System and the Horn of Africa in the south and southwest; and deformation occurred in north-western Africa. The effects in Egypt manifested as a general Cretaceous–Paleogene unconformity (between the Dakhla and Kurkur conglomerates), the gradual upheaval of southern Egypt associated with block faulting (especially in the Gulf of Suez and in Sinai), and the extensive folding along the northeast-oriented arcs dissecting the Egyptian Basin.

4.1 The Paleocene–Eocene Successions

The Paleocene five age-coeval facies associations from south (shallower) to north (deeper) are: (1) Garra El Arbain; (2) the Nile Valley; (3) Farafra; (4) Galala; and (5) Sinai (Fig. 6). The Paleocene reefal Kurkur Formation in southern Egypt gave way to the more marine Tarawan Formation in the middle latitudes, overlying deep-marine facies of the Dakhla Formation, which extends from the Red Sea in the east to the Sand Sea in the west. The uneven Cretaceous surface over which the Cenozoic sediments were deposited displayed several facies varying from quiet deep marine (Nile Valley Facies) in the eastern and central parts of Egypt to reefal facies in the southern and western parts (Garra El Arbain Facies), where many Cretaceous–Lower Paleocene unconformities were recorded in the top strata.

The sea-level stand reached southern Egypt and penetrated a few hundred kilometers into Sudan during the Paleocene and Early Eocene. Deposits during these times overlie a very irregular surface caused by the above-mentioned movements; as a result, units are quite variable in thickness and are commonly missing altogether. The Paleocene is totally missing in Bahariya area in spite of the northern location (where Paleocene sediments are common), 500 km to the south (in Sin El Kaddab scarp) and 35 km north of the Egypt–Sudan border (Lat 22°N) at Bargat El Shab.

In the northern Farafra area, the Paleocene Tarawan Chalk is only 2.5 m thick, and an unconformity separates the underlying Khoman Chalk; also, the Paleocene gradually thins out toward the north Farafra Oasis owing to the effects of the Syrian Arc System (Farouk, 2015; Farouk et al., 2019). In the Red Sea area, the Paleocene transgression reached Lat 26° N, most probably owing to sea-level rise rather than structural conditions as in the Nile Valley and the Western Desert, where the sea covered more areas toward the south. The most-probable explanation relates to the beginning of the uplift of the Red Sea Mountains and the consequent westward tilting of the Egyptian basins.

In the northern Eastern Desert, many unconformities are known from the Paleocene–Lower Eocene sequence, together with lateral facies changes (Farouk, 2016). This evidence plus the idea presented earlier that the Gulf of Suez formed during the Jurassic indicates that the Red Sea and the Gulf of Suez opened from north to south. Since the Paleozoic tectonic pulses led to the uplift of the Red Sea Mountains. This area also has witnessed active block movements recorded along the Wadi Gabgaba in southwestern Egypt.

In Sinai, the Paleocene is represented by the 40–50-m-thick Esna Shale unconformably overlain by 200-m-thick Lower Eocene limestone with chert. To the north, at the Syrian Arc fold belt, the Paleocene is generally missing (Farouk, 2016). In the subsurface of the northern Western Desert, different thicknesses were recorded for the Paleocene–Eocene sediments in oil wells drilled in the many subbasins or depocenters of the Egyptian basins which reflect the interaction among and instability of the blocks. Since the Late Cretaceous, the Farafra Oasis area stood on the downward edge of the continental slope of the Egyptian basins. It is in this area that the Maastrichtian Dakhla Shale is replaced by thick Khoman Chalk in the subsurface of the northern Western Desert. The Paleocene in the subsurface is commonly made up of limestone alternating with thin shale layers in the deeper parts of the subbasins. The undivided Eocene Apollonia Formation (550–1788-m-thick limestone) is generally unconformably overlain by the Tarawan Formation and the thick Paleocene–Eocene Ain Dalla Formation. To the south (Farafra), deeper sediments of the Paleocene–Eocene are replaced by a shallow facies comprising the Esna and the Farafra Formations. This supports the assumption that the Farafra area was a transition zone between a platform in the south and a ramp in the north during Late Cretaceous–Early Eocene time (Hewaidy et al., 2006, Farouk et al., 2019). To the north, in the Bahariya eastern scarp, the Lower Eocene Farafra Formation (limestone) is interdigitated with the 68-m-thick Naqb Formation (limestone), which makes up the Bahariya eastern and northern scarps and part of the western scarp and also covers many of the isolated hills in the northern part of the depression (Fig. 7). The Naqb Formation conformably underlies the 32.7-m-thick Qazzun Formation (limestone) deposited during the Late Ypresian under relatively quiet conditions in contrast to the oscillating and turbulent conditions during Naqb time (Issawi et al., 2009).

A conglomerate bed forms the contact between the Middle–Upper Eocene Lower–Upper Hamra Formations (together 63 m thick) and the underlying Qazzun Formation. The Lower Hamra Formation is Bartonian in age while the Upper Hamra Formation is Priabonian; the Lutetian is totally missing, indicating an uplift pulse in the Uweinat–Bahariya–Port Said arc, reflecting Late Lutetian Pyrenean movement. The 45-m-thick Qazzun Formation is of record to the north

and northwest of El Quss Abu Said in the Farafra depression, reflecting a major detour in the sea north, west, and south of Bahariya Oasis. The Qazzun Formation consists of a sequence of marl and limestone including abundant chert pebbles and reworked carbonates with a 4-m-thick gypseous shale layer at the top. The shale is highly fossiliferous; *Nummulites cailliaudi* is most common in the formation at Bahariya in the northern plateau, although patches of *N. gizehensis*-bearing limestones were recorded from the west-central part of the Bahariya depression. The limited Eocene section in the vicinity of Bahariya slopes and dips eastward toward the Nile Valley, where very thick units are known, besides some newly discovered units that outcrop in places within the Lutetian gap to the west.

In the Nile Valley between Qena and Cairo, the Lower Eocene Esna Shale is overlain by a 200-m-thick Paleocene–Lower Eocene limestone (Farouk, 2016). A 1-m-thick chert-bearing conglomerate bed is found at Darb Gaga west of the Nile opposite Qena between the Esna and Ypresian Thebes Formations (El-Azabi & Farouk, 2011). Farther north, at the latitude of Minia, the 80-m-thick Minia Formation (limestone) from the top of the Ypresian is overlain by the 80-m-thick Lower Lutetian Samalut Formation (limestone bearing *N. gizehensis*), which underlies the Middle Lutetian Mokattam or the coeval Rayan Formation (Fig. 7). This sedimentary sequence comprises 100-m-thick sand and sandy-clay beds, which unconformably overlie the 50-m-thick Lower Bartonian Giushi Formation or the coeval 80-m-thick Observatory Formation, both of which are fossiliferous limestones with marl and dolomite intercalations (Fig. 7).

In the Mokattam area, the Giushi Formation and the coeval Wadi Hof Formation are unconformably overlain by the Priabonian Maadi Formation, which is coeval with the Qasr El Sagha Formation in the Faiyum area (Issawi et al., 2009). To the south, in the Helwan area, the basal 97-m-thick Qaurn (limestone) and the overlying 25-m-thick Wadi Garawi Formation (clay and marl) are considered Late Bartonian (although unconfirmed, pending further paleontological work) (Fig. 7). These two units are coeval with the well-dated Birket Qarun Formation in Faiyum. The Garra El Arbain Facies in southern Egypt comprise the ~ 100-m-thick Late Paleocene–Ypresian Upper Garra beds (limestone), overlain by the 127-m-thick Ypresian Dungal Formation (limestone on top of shale) (El-Azabi & Farouk, 2011).

In northeastern Egypt, many unconformities distinguish the Paleocene–Eocene section from Wadi Qena in the south through southern and northern Galala and the Ataqa and Shabrawet Mountains. A 90-m-thick Lower Eocene limestone unconformably underlies Middle Eocene limestone with a 20-m-thick conglomerate bed between the two units in the St. Paul area on the southern Galala Plateau; Upper Eocene beds have not been confirmed in the area.

Table 1 Summary of global events during the Phanerozoic showing the resulting features and the response in Egypt

Global events	Resulting features	Response in Egypt
Major craton forming events in the Archean followed by a complex history of mountain building and rifting that culminated with the Pan-African Orogeny	Tectonic magmatic episodes of Late Proterozoic–Early Paleozoic age. The resulting basement rocks are classified into several units: gneisses and migmatites to younger granitoids and post-granitic dykes. Uprising of acidic magma. In Egypt, the oldest rocks in Gebel Ouwinat are 2656 ± 71 Ma; the rocks become younger eastward extended between 1000 and 550 Ma	– Emplacement of the main basement rocks and their faults and arcs along the Red Sea and South Western Desert. – Faults and arcs delineated the troughs in-between which became later the main basins in Egypt during the Phanerozoic. – The arcs were either due to plumes along fracture zones or due to normal tectonic movements marking the plates and subplate boundaries
Cambrian–Ordovician–Pre-Caradoc tectonism; Early Caledonian Orogeny	Uplifting of the main orogenic belts in west, central, and south Africa associated with faulting and compressive stresses	<ul style="list-style-type: none"> • Uplifting and igneous intrusions in most regions in Southern Sinai and southern Egypt (especially arcs areas) • Unconformities, cracks, faults in most sedimentary successions during this period
Late Ordovician–Early Silurian Taconic Orogeny	Low sea level spread of glaciers from west Africa to Saudi Arabia and Iran passing by Egypt. South pole located offshore of Algeria (west Gondwana)	<ul style="list-style-type: none"> • Thick conglomerate diamictic glaciogene sediments in the cracks along the present Wadi Cabgaba (Gabgaba Formation) • Second pulse in the rising Red Sea Hills in south Egypt
<ul style="list-style-type: none"> • Late Silurian–Erian; last phase of the Caledonian Orogeny • High sea level 	Acadian collision between Gondwana and Laurasia–Deposition of rich graptolitic shale in Libya and Saudi Arabia; petroliferous source rocks	<ul style="list-style-type: none"> • Stream deposits of the Naqus Formation • Four glacial periods were identified in Gabgaba area, separated by 3 interglacial periods plus a fourth one at the base of the section • Third pulse in the rising Red Sea Hills in southern Egypt. Each pulse is represented by an angular unconformity in the basal unit
<ul style="list-style-type: none"> • Early Devonian • Rapid marine transgression • Bretonian (Late Acadian) first phase of Hercynian Orogeny 	<ul style="list-style-type: none"> • Deformation, plutonic, and metamorphic events in Laurasia, prolonged over a more extended period dated 330 and 360 Ma. The Acadian had best been regarded, not a single orogenic episode, but as an orogenic era • Northward subduction of Paleo-Tethys • Subsidence and rifting along the plate margins 	<ul style="list-style-type: none"> • Inversion of Siwa basin and the basin south of GRT in south Sinai • Thick unit in the north sub-basin of the Egyptian Basin (Siwa) duo to rifting • Tilting of pre-Carboniferous (Cb) sediments in Cabagaba area • Uplifting in south Egypt and deflation of much of Devonian sediments • Gulf of Suez basin received Devonian sediments, kept intact by block movement
<ul style="list-style-type: none"> • Early Carboniferous • High sea level • Austrian Event (Orogeny) • (Westphalian–Stefanian) 	Transgression–regression phases in the marine section along the North Africa–Arabia plate	<ul style="list-style-type: none"> – Deposition of marine-continental section in north Egypt, and fluvial section in the south – In Gabgaba area, the Carboniferous Gifl Formation overlaps older Paleozoic units with pronounced unconformities
<ul style="list-style-type: none"> • Late Carboniferous–Early Permian • Variscan Orogeny • Drop in sea level and glaciation • Early stages in the opening of the Paleo-Tethys closing and opening the Neo-Tethys 	<ul style="list-style-type: none"> • Sharp cooling associated with drop in sea level. Progressive fragmentation of Gondwana • Rifting occurred as escape structure for this fragmentation along the north African–Arabian Plate • Clockwise rotation of Africa 	<ul style="list-style-type: none"> Major uplift of most Egyptian basins associated with low marine transgression – Continental sediments are common with fluvio-marine intercalations – Initiation of the Syrian Arc folded belt in response to the opening of the Central Atlantic and the rotation of Africa
<ul style="list-style-type: none"> • Permian–Triassic • Break up of Gondwana • Neo-Tethys was born • Eo-Cimmerian Events • Transit process 	<ul style="list-style-type: none"> – Rifting increased along N. Africa passive margin and in general in the Tethys domain Rifling. Propagated rapidly from the N. Arabian Plate westward – Plates accreted to EuroSLA, detached from African Gondwana (transit process) 	<ul style="list-style-type: none"> – Marine and continental sediments were deposited in NE Sinai and in the subsurface of the Western Desert – Tectonic instability increased from Mid Tr., underscored by block tilting and local uplifts; a distal effect of the EO-Cimmerian Events

(continued)

Table 1 (continued)

Global events	Resulting features	Response in Egypt
Triassic–Jurassic transition	<ul style="list-style-type: none"> • Break in sedimentation • Volcanic extrusions terminated basins development 	<ul style="list-style-type: none"> • A major unconformity is known in between the Triassic and Jurassic – Continental sediments represent this transition time and even extended through the Early Jurassic time in the N. Western Desert subsurface sections • Rifting continued and the north basins kept widening • Volcanic extrusions were dominated
Middle Jurassic Separation between north Africa and Europe	<ul style="list-style-type: none"> – Along the NW margin of Africa, rifting continued. – Rifting terminated with the more crustal separation between Africa and S. America around 180–175 Ma: Toarcian/Bajocian – Rift-related magmatism peaked within Central Tethys during Late Triassic /Early Jurassic (Morocco, Algeria, and Libya) 	<ul style="list-style-type: none"> • Rifting in the north Egypt led to the accentuation and extension of the old basins which were filled by Jurassic and Cretaceous sediments • Deposition of thick Upper Jurassic marine section alternates with three continental units • Magmatic intrusions
<ul style="list-style-type: none"> • Late Jurassic–Early-Cretaceous Cimmerian Event: the distal effect of the stronger Mid-Berriassian Orogenic event • Continuous opening of Central and South Atlantic Oceans • Split of Gondwana into western and eastern parts. – Opening of Indian Ocean during the Oxfordian • Tithonian drop in sea level 	<ul style="list-style-type: none"> • Second stage rifting, uplifting, and block tilting initiated at the transition from Late Jr. to Early Cretaceous following the Mid-Jurassic separation between Northern Africa and Europe • Rifting affected large areas including the South and Equatorial Atlantic margins, the West and Central African Rift Systems, and the Northern Africa margin from Tunisia to Egypt • Atlantic rift system propagated southward in the S. hemisphere and northward in the N. Hemisphere toward a land bridge created by the Pan-African orogenic belt in the equatorial region 	<ul style="list-style-type: none"> • Omission of the Upper Jurassic sediments in south Egypt. Activation of the Garara basin which was received Upper Jurassic and Cretaceous sediments • Widening and activation of highs of the south subbasins
<ul style="list-style-type: none"> – Neocomian–Early Aptian – Progressive northward crustal separation between Africa and S. America and sea floor spreading in the newly opened S. Atlantic – Early Aptian Normal Magnetic Quiet Zone 	<ul style="list-style-type: none"> – Rifting was accentuated inside Africa leading to the development of internally rigid continental blocks within the African Plate namely West Austral and Arabia-Nubia; the latter could be separated into central and eastern blocks. The boundaries between the blocks correspond to zones of crustal weakness inherited from the Pan-African Orogeny – Beginning of the closure of the Neo-Tethys 	<ul style="list-style-type: none"> • Northern Western Desert basins were more developed in some of them Late Jurassic magmatic phases preceded the rifting. In the Eastern Desert: the Lower Cretaceous sediments are partly marine with thick continental sediments
End of Aptian till Late Albian Rapid opening of Equatorial Atlantic Ocean. Differential rates of sea floor spreading	<ul style="list-style-type: none"> • Very active strong phase of magmatic activity. -Linking of the Central and South Atlantic ○ Rejuvenation of the crustal weakness zones in Africa (those between the blocks) ○ Important lateral displacements along these zones ○ Basins were pulling apart in response to dextral and sinistral or strike slip movements • Basins continued to evolve 	<ul style="list-style-type: none"> ○ Rejuvenation of the old arcs—hence the adjacent basins become more widespread receiving more sediment. The unequal filling of basins led to their pull apart and in response to the movements which accentuated the uplift of the arcs ○ Basins continued to evolve in north Egypt as anticipated from the following thick Up. Cretaceous section • Intrusion of syenite, gabbro, and basalt in the Eastern Desert took place as huge (in area and thickness) ring complexes, dykes, and silts • Polyphase rifting was common during many episodes in the Cretaceous

(continued)

Table 1 (continued)

Global events	Resulting features	Response in Egypt
<ul style="list-style-type: none"> • Late Cretaceous (Laramide = Getic movement) • Collision between Africa and Europe • High stand of sea level during the Cenomanian, a connection was established between the Tethys and the Gulf of Guinea • Late Santonian: end phase of the Normal Magnetic Quiet Zone and the collision between African, Arabian, and European plates 	<ul style="list-style-type: none"> • Compressional forces leading to shortening in N. Africa and South Europe, during the Santonian (Guiraud et al. 1992) or during the Cenomanian (Philip, 1993) • Major hiatus within the Up. Cretaceous sediments, associated with structure features • The continuous development of Syrian Arc System along the North Africa margin • Polyphase rifting, folding, and basins inversion along Africa margin and inside the continent associated with many volcanic eruptions 	<ul style="list-style-type: none"> ○ Deposition of thick Cenomanian marine section in North Egypt, continental on the arcs (Bahariya Formation) with thin marine incursions • A major hiatus at the Cenomanian / Turonian contact in Egypt, uplift in South Egypt leading to the missing of Turonian beds and very shallow conditions dominated in Sinai (Buttum Formation) ○ Santonian carbonates were still high and received clastics-fine and coarse (Qusseir Clastic Member of the Nubia Formation) ○ Campanian carbonates in north Egypt are shallow in central Egypt giving rise to phosphate beds and neritic carbonates, continental in South Egypt (Nubia Formation)
<ul style="list-style-type: none"> • Campanian relaxation of global tectonics which extended through the Early Maastrichtian 	<ul style="list-style-type: none"> ○ Rifting episode followed the Santonian folding event • Several rift basins rejuvenated or were initiated by the Campanian–Maastrichtian times; some of them carrying on through the Paleocene 	<ul style="list-style-type: none"> • Development of the phosphate basin stretching between the Red Sea and the Libyan border
<ul style="list-style-type: none"> ○ Late Maastrichtian • The Mediterranean Seuil carrying on through the Paleocene 	<ul style="list-style-type: none"> • Many basins along African–Arabian Plate margin in the Palmyrides, the Abu Gabra, the Muglad, the White Nile, the Blue Nile, and many others inside Africa and along its northern western and eastern margins were reactivated, some of them carrying on through the Paleocene 	<ul style="list-style-type: none"> ○ Injection of quartz vein in the phosphate bed at Darb El Arbain • Unconformities within many parts of Egypt • Missing of the Paleocene in Bahariya area, and partly missing in east Farafra along the Uweinat–Bahariya–Port Said arc
<ul style="list-style-type: none"> • Late Ypresian–Lutetian • Drop in sea level and tectonics paleo-highs 	<ul style="list-style-type: none"> Retreat of the Early Eocene sea towards the north 	<ul style="list-style-type: none"> – Moving of the shore-lines during the Lutetian, Bartonian, and Priabonian reaching its acme during the Oligocene – Facies of different became younger north ward – Unconformities are known from the Eocene section, e.g., the Lutetian missing in Bahariya area, in Ataqa, and in many parts in Sinai and along the Gulf of Suez
<ul style="list-style-type: none"> • The Late Lutetian • Pyrenean Atlasic compression event 	<ul style="list-style-type: none"> Dextral transpression along Africa, Arabia, Eurasia plate frontiers—Opening of NNW to NNE Oligocene rifts 	<ul style="list-style-type: none"> ○ Activation of the Guinea–Nubia Lineament ○ Uplift of basement rocks in south Egypt through the thin sedimentary cover, developing centroclinal folds ○ Development of Trans North Egypt Fracture Zone with eastwest faults • Many dome and basin structures along fault planes
<ul style="list-style-type: none"> Oligocene uplift in east Egypt with basalt plumes during the initial rifting of the Gulf of Suez 	<ul style="list-style-type: none"> • Gradual rise of the Red Sea Hills in pulses started in the Priabonian • Developing of many Oligocene rifts along the Mediterranean and inland. Volcanic eruptions were common 	<ul style="list-style-type: none"> ○ Reversal of slopes of the main part of Egypt—nearly south of latitude 29° 0' N • Development of hinges along the western side of the uplifted basement rocks • Many fissures and cracks developed parallel to wadis • Deposition of dominantly fluvial continental section in the inland rifts with some marine sediments especially in the northerly developed basins. The Fayium delta with vertebrate fossils

(continued)

Table 1 (continued)

Global events	Resulting features	Response in Egypt
<ul style="list-style-type: none"> – Early Miocene to Middle Miocene the Red sea came into existence – Collision of Alpine and Himalayan plates – Plume activities preceded the breakup of E. Mediterranean 	<ul style="list-style-type: none"> Faults along the Red Sea coast rifts developed creating local basins in the Red Sea mega-rift and along the Mediterranean coast – Reorganization of the convection system within the upper mantle across the Africa, Arabia, and Europe margins 	<ul style="list-style-type: none"> Deposition of thick Miocene sediments in the rift basins in the sea and the Mediterranean and of shallow continental, shallow marine, and evaporites on the shoulders of the rift. Evaporite was also common in the rift – Hot brines gushed along the axis of the Red Sea. – Volcanic eruptions in many parts of Egypt
<ul style="list-style-type: none"> – The place of the present Nile Delta began to build up during the Early Miocene 	A thick section in the place of the Nile Delta, sediments brought from inland by northerly flowing rivers most probably emanating from northeast high plateaus, e.g., Gebel Ataqa and Northern Galala. The southern Galala-Minia high area formed a water divide between north and central Egypt, where some rivers, e.g., Tarfa, flowed southward. Migration of the Oligocene Fayium delta to Moghra area in the northeast	
<ul style="list-style-type: none"> – Messinian desiccation of the Mediterranean 	Formation of saltwater lagoons in the Qattara, forming a Salt Mesa at m depth, means that the Qattara was hewed to this depth between the Serravallian—the last sea transgression—and the Messinian—the time of the Salt Mesa, i.e., between 11.7 and 7.1 Ma; Tortonian time	
<ul style="list-style-type: none"> – Zanclean transgression 	Transgression of the Mediterranean through the many gorges along its southern coast, in case of Egypt, transgression reached Aswan and Wadi Haifa in Sudan. Marine sediments were deposited in the deep part of the estuary, cascading sediments were known from the foot of the eastern cliffs bordering the estuary. Continental sediments were recorded inland away from the Pliocene Gulf. The main delta of Egypt took its present shape, supplied by local Egyptian rivers and marine sediments. Third location of the main Egyptian delta	
<ul style="list-style-type: none"> – Piacenzian regression 	Rivers started to adjust their courses to cope with the new base level in the Mediterranean. The welding of the many rivers along the present Nile, the course took place only when the Pliocene Gulf invaded Egypt. Though the E- W rivers resumed their courses during the Piacenzian regression, the drastic changes in the climate of Egypt from wet to dry gradually changed these rivers from being active to sluggish which were easily captured by the flood of the Ethiopian waters during the Middle to Late Pleistocene	

In Sinai, the 200-m-thick Lower Eocene Egma Formation (chert-bearing limestone) shows varied gradation including siliceous, dolomitic, chalky, and marly limestones. The Egma is overlain by the 98-m-thick Darat Formation (green and brown shale, marl, and limestone), which in turn is topped by the 93-m-thick Khaboba Formation. The Darat and Khaboba are coeval with the Middle Lutetian Rayan or Mokattam Formation (the Early Lutetian is missing). The 180-m-thick Middle–Late Eocene Tanka Formation consists of clayey limestone and salty dark shale at its base, which is Late Bartonian; the top beds might be Late Eocene in age, whereas the overlying 20-m-thick Tayiba Formation (marl and clay) is Priabonian. The Tayiba Formation is unconformably overlain by Miocene sediments along the east coast of the Gulf of Suez. The many unconformities in the Paleocene–Eocene sediments in general and the uplift in southern Egypt associated with the continuous retreat of the Paleocene–Early Ypresian seas off Egypt from south to north led to the many facies described above. The sea regression coupled with the activation of the northeastern arcs in many parts of southern and eastern Egypt (especially in the vicinity of the Red Sea and the Gulf of Suez and in Sinai) reflected the Pyrenean–Atlasic compression event. This represents a major stage in the collision of Arabia–Nubia and European plates as a result

of the changes in the rate and direction of the opening of the central, southern, and northern Atlantic Ocean (Fairhead et al., 2013). The activation of block movements in north-eastern Egypt is clearly evident in the interplay and hierarchy among the blocks in this area, resulting in the total absence of the Lutetian in Gebel Ataqa and also probably in Shabrawet. The unconformity there is represented by 5-m-thick paleosol between the Ypresian Suez Formation and the overlying Middle Bartonian Ramiya Formation (Osman, 2003).

The interior basins among the basement rocks in Safaga and the southern Qusseir stretch (e.g., Mohamed Rabah, Wasif, Hamrawein, Duwi, and Hamadat) were dragged eastward toward the Red Sea (in the Safaga area) or westward (in the Qusseir area) forming very asymmetric synclines. The longer flank with the Thebes massive limestone at the top was tilted eastward (or westward), gliding on the underlying shale of the Esna and Dakhla, which lubricated the movement for considerable distances (2–4 km) before another short flank (a few hundred meters in length) overrode the basement rocks while dipping in the opposite direction to that of the longer flank. The movement is certainly post-Ypresian and probably related to the Pyrenean–Atlasic movement. After this movement, volcanic eruptions through the Oligocene and younger sediments were very common.

In Sinai, along the trans-Egypt fracture zone, a number of significant highly tilted domal structures are found between Taba in the east (on the Gulf of Aqaba) and Cairo in the west, especially in the Sudr El Heitan area, east of the Gulf of Suez, and along the Suez–Cairo stretch. The area of Sudr El Heitan is probably one of the most structurally complicated areas in Egypt. The dominantly Cretaceous and Eocene rocks involved in this area are related to the Lutetian Pyrenean–Atlasic movement.

4.2 The Eocene/Early Oligocene Transition

The Late Eocene–Early Oligocene transition witnessed the rise of the Red Sea Hills, most probably coinciding with the opening of Gulf of Aden. This rifting developed large basins along the gulf and also inside the Africa Lakes region, which resulted in the gradual separation and the northward drift of the Arabian subplate, enabled by sinistral movement along the Dead Sea–Levant transform fault.

The constant movement of the Red Sea Hills during the Oligocene formed escape structures for the northward-moving Arabia subplate and the widening of the Gulf of Aden. The resulting uplift in eastern Egypt changed the slopes in the region to be east–west rather than south–north and, coupled with 1500-mm rainfall during the Oligocene, caused major wadis to become important rivers in the Egyptian geomorphic landscape. The master stream was the Qena River, initiated along the cracks and faults that resulted from the uplift movements. The southern Galala Plateau became a high catchment area for the Qena River headwaters and formed a water divide where from which the Qena flowed southward and the Bown and Karus Rivers flowed westward to the Faiyum depression, thereby building a huge fan with fluvial and deltaic deposits in which lived various vertebrates since the Late Eocene and the Oligocene. The area is now considered to be one of the biggest graveyards for these animals in Africa and probably in the world.

4.3 The Oligocene Deposits

The main Oligocene deposits in Egypt are of fluvial and deltaic origin. The marine sediments are confined to far northern Egypt along an exposed strip extending from Risan Aneiza in northern Sinai and passing by El Arag south of the Qattara Depression to Siwa Oasis in the far west. Most noteworthy among the deltaic Oligocene units is the 340-m-thick Gebel Qatrani (sandstone, sandy mudstone, limestone, and shale) north of Faiyum, where important and unique vertebrate fossils are very common. Other Oligocene units include the 50-m-thick fluvial section (vividly

colored sandstone) known as the Gebel Ahmar Formation, near Cairo; the 120-m-thick Nakheil Formation (coarse-grained breccia and conglomerate) in the Qusseir–Safaga stretch; and the 40-m-thick Radwan Formation (ferruginous sandstone) in the Bahariya Oasis. The subsurface 1086-m-thick Tineh Formation (shale and sandstone, as observed in Qantra-1 well) has been drilled through east of the Nile Delta and in northern Sinai; the top of the Tineh is Early Miocene. On the Mediterranean coast, the Daba'a well penetrated the 442-m-thick Daba'a Formation (shale and limestone).

The 60-m-thick Oligocene Wadi El Arish Formation in Risan Eneiza (Kuss & Boukhary, 2008) consists of basal marine sandstone, clay in the middle, and massive limestone at the top. At El Arag, this formation (only 7-m-thick) comprises sandy calcareous clay and limestone. In the Gulf of Suez, drilling opposite the Northern Galala Plateau revealed a thick Oligocene section: 690-m-thick shales interbedded with sandstones and limestones overlying 300-m-thick argillaceous limestones, shales, and sandstones. Associated with the Red Sea uplift were 31–23.2-Ma flood basalts on the rift shoulders along the coast and also inland (Abu Zaabal, Bahariya, El Bahnassa, and many other areas).

4.4 The Oligocene–Miocene Transition

The Oligocene–Miocene transition involved significant movements in the Mediterranean region from its far west end in southern Spain to the Levant passing by all of northern Africa. In the Levant and Anatolia, collision among African, Arabian, and Eurasian plates significantly intensified from the very Early Miocene when the Arabian Plate constantly moved northward along the Dead Sea Transform where the northern part of this plate crops out in southeastern Turkey (Kissel et al., 2003). In Egypt, as a result of the tectonic events briefly summarized above, linear topographic scarps and deeply incised valleys developed along active faults. The Red Sea Mountains kept rising during the Miocene, while the east–west-trending rivers (especially in the Qena System) deepened their channels, and the two main plateaus of central Egypt became conspicuous geomorphic features. Minor thrusts have been recorded in Sinai (Issawi et al., 2009) and along the still-active Kalabsha Fault in southern Egypt, which is part of the reactivated Guinea–Nubia lineament (Bumby & Guiraud, 2005). Strong magmatism predated and accompanied the rift tectonics, mostly along the Red Sea shoulder in the Nubia area, along the reactivated northeast-trending arcs (Bahariya, trans-northern Egypt fracture zone, and in Suez–Cairo areas). The stresses exerted by the Oligocene–Miocene tectonics favored extension by weakening the lithosphere (Bosworth, 2015).

4.5 The Miocene Deposits

The Miocene sediments in Egypt are classified into Red Sea, Mediterranean, and Inland Facies. The Early Miocene Red Sea Facies protorift sedimentation started with a continental sequence: sandstone, siltstone, grit, and coarse-grained fanglomerate in the 70-m-thick Ranga, 37-m-thick Gebel El Russas, and 40-m-thick Abu Gerfan Formations. Northward at the foot of Gebel Ataqa, the marine unit coeval with these formations is the 52-m-thick Sadat Formation (Fig. 8).

Facies of the Lower–Middle Miocene basin include the basal 460–490-m-thick Nukhul Formation (calcareous shale, marl, and limestone) and the overlying 600–800-m-thick Rudies Formation (shale and sandy shale, with minor limestone). The Gharmoul Formation in the Eastern Desert and the Qabeliyat Formation in Sinai are shallow-marine equivalents capped by the Rudies in the basinal area.

The Serravallian Kareem Formation consists of 120–135-m-thick Rahmi evaporite overlain by 186–221-m-thick Shager open-marine sediments (calcareous sandstone and shale). The overlying Belayim Formation comprises the Baba (a 54–126-m-thick evaporite), the Sidri (a 9–100-m-thick open-marine shale, the Feiran (a 40–60-m-thick evaporite), and the Hammam Faraun (a 44–84-m-thick open-marine phase including shale, marl, and sandstone). The ~ 50-m-thick Abu Dabbab (or Gypsum) Formation is coeval with the Kareem Formation that is exposed along the Red Sea coast along the Egypt–Sudan border (almost 800 km to the north). Overlying the Abu Dabbab Gypsum is the 35-m-thick Samh Formation (marl, shale, and sandstone), the topmost middle unit along the Red Sea coast (Fig. 8).

In Sinai, the 120-m-thick Sarbut El Gamal Formation (conglomerate and limestone) forms the top of the Middle Miocene section and is coeval with the Qabeliyat Formation. Both these are coeval with the 6–12-m-thick Upper Burdigalian–Langhian Gharmoul Formation (sandy and argillaceous dolomitic limestones) exposed along the east coast of the Gulf of Suez. The overlying sediments are classified into the 0–1650-m-thick South Gharib Formation (anhydrite with shale bands) and the overlying 27–900-m-thick Zeit Formation (shale with thin intercalated anhydrite lenses). The 22-m-thick Upper Miocene Hagul Formation at the entrance of the Gulf of Suez consists of shale overlain by a chalk bed.

Differences in thickness locally are explained by the absence of some units. For instance, the range of thickness of the South Gharib (0–1650 m) is in part attributable to the absence of units such as the Rahmi Anhydrite Member, which is missing in the Morgan-1 well. This contributes to the very uneven surface of the floor of the Gulf of Suez, which is also due to the (210-m-thick) Kareem Formation carbonates' unconformably overlying basement rocks in the

central part of Gebel El Zeit Bay. Another factor is the havoc imposed by the many blocks in the gulf owing to faulting, which also explains many unconformities among the units.

Messinian sedimentation was a fluvial phase in many parts along the Red Sea and the Gulf of Suez coasts, where sand section rich in fossil wood and gravels covers the older Miocene units. This section is widespread as patchy outcrops unconformably overlying Oligocene and Eocene sediments along the Suez–Cairo road. In the Mediterranean Facies, a 200-m-thick Miocene section includes clastics with minor carbonates and conglomerates as well as lenses of gypsum; the unit is known as the Moghra Formation and belongs to the Aquitanian–Burdigalian. The top 70–160-m-thick Marmarica Formation (Langhian–Serravallian) consists of limestone and calcarenite beds that change laterally to 6–10-m-thick gypsum at the Hagif scarp. The Tertiary section drilled offshore from the Mediterranean revealed a 287-m-thick Early–Middle Miocene shale unit.

The desiccation of the Mediterranean Sea during the Messinian led to many salt layers in dry depressions across the dry seabed. In the Qattara Depression, the southwestern parts of the Salt Mesa are at a 100-m depth, which means that the depression formed during the period between the last marine transgression over the area, i.e., in the Serravallian (11.2 Ma), and the time of the Salt Mesa. Thus, the depression was excavated to a depth of 100-m below sea level during the Tortonian. The subsurface basal Miocene section in the Nile Delta is composed of the 300-m-thick Moghra Formation (open-marine shale) overlain by the 130-m-thick Langhian–Tortonian Sidi Salem Formation (shale, dolomitic marl, and rare sandstone). Above that is the 280-m-thick Tortonian–Messinian Qawasim Formation (conglomerate and sandstone), which in turn is overlain by the 2040-m-thick Rosetta Anhydrite in the eastern and northern Nile Delta but is missing in the western part of the delta. Where present, the Rosetta is an expression of the general desiccation of the Mediterranean during the Messinian. The uppermost Miocene in the delta subsurface is represented by the 222-m-thick Abu Madi Formation, which formed by continuous deposition during the Messinian to the Zanclean and laterally is coeval with the Rosetta Anhydrite.

In the Sinai subsurface, the 1086-m-thick Oligocene–Miocene Tineh Formation (shale and sandstone) is overlain by the 533-m-thick Burdigalian–Langhian Qantara Formation (intercalated marl and sandstone) (Farouk et al., 2014). The Qantara Formation in turn is successively overlain by the 552-m-thick Langhian–Tortonian Sidi Salem Formation (banded shale and sandstone), the 185–258-m-thick Qawasim Formation, and the 992–1400-m-thick Abu Madi Formation (Farouk et al., 2014). The Gebel El Khashab Formation is represented by the 40–90-m-thick (sandstone and gypseous clay) in the northern Western Desert (Fig. 8).

The rate of tectonic activity in the Red Sea and the Gulf of Suez rifts was reduced considerably since the Late Miocene (Segev et al., 2017; Steckler, 1985) concurrently with the dislocations and cracks along the Gulf of Aqaba. However, the connection of this Gulf with the Red Sea never happened except during the Pleistocene contrary to what many foreign scholars believe. The axial basins in the place of the Gulf of Aqaba and its margins kept extensively lowered and uplifted, respectively, most probably as escape structures to what we're happening in the Red Sea and the Gulf of Suez plus of course the northward moving of the Arabian Plate.

The drop in the Atlantic Ocean water and the close of Gibraltar during the Messinian led to a break in communication between the Ocean and the Mediterranean Sea, hence the desiccation and disintegration of the sea into a number of isolated sea lakes which became the sites of the Messinian Rosetta Anhydrite.

4.6 The Pliocene Deposits

During the Early Pliocene, a major transgression of the Mediterranean through the many gorges along its southern coast, in case of Egypt, transgression reached Aswan and Wadi Haifa in Sudan (Table 1). Marine sediments were deposited in the deep part of the estuary; cascading was the opening of Gibraltar and the filling of the sea in which the water level was 110–120 m above the present sea level. The sea thence transgressed inside Africa and Europe filling the Late Miocene degraded channels which the rivers in response to the lower base level during the Messinian. The seawater invaded Egypt to south Aswan crossing a water divide in the area of South Galala and a promontory coming down the western scarp in southwest Faiyum area (Issawi et al., 2009). That incident represents the first time for a continuous water body located at the place of the present Nile River. The cracks and faults in this part of the country were formed in consequence to the uplift of the Red Sea basement rocks. The contact between the base of Gar El Muluk Fm. (Zanclean) with the underlying Miocene Raml Fm. and Gebel El Khashab Formation is marked by 2.5 m conglomerate composed of angular quartz and chert gravels. This unconformity was named Mikheimin conglomerates after a locality carrying the same name west of Wadi El Natrun. The unconformity is believed to have more than local significance since it recorded from Sinai.

In the deeper part of the Pliocene Gulf, which has a width of 60 km north of the water divide or what is known as the neck, 1458 m thick Lower Pliocene shale section was deposited and known as Kafr El Sheikh Fm. South of the neck at El Minshah, south of Sohag, the formation is 12 shales and limestone at top; the base was not exposed. At the

subsurface in Aswan, the Lower Pliocene marine section is montmorillonitic clay with lenses of fine-grained micaceous sands including ostracodes. When the Gulf marine waters reached -21 m below the present sea level, the Gar El Muluk Fm. was deposited at the area of Wadi El Natrun, consisting of 27 m deltaic and lacustrine gypseous sandstones, clays, and minor limestones. The section includes both freshwater vertebrate faunae and marine ostracodes.

The Middle and Late Pliocene witnessed a retreat of the Gulf marine waters to the north. During this phase, the water halted in Kom El Shelul area of the neck depositing the formation with the same name. This formation is made of \approx 25 m coquina limestone and sandstone highly laden with pelecypod shells. In the east side of the Gulf where high mountains are common with fluvial drainages, the marine water cascaded over the Gulf bank and both marine and freshwaters fill topographic low depressions. In there, Umm Raqaba Formation (23.85 m) was deposited composed of alternating conglomerate and sandstone beds. The inland continental Pliocene sediments in the Upper Nile Valley are known as the Muneiha Fm. (14.6 m sandstones) at the latitude of Kom Ombo area and the Issawia Fm., 15 m brecciated limestones, east of Sohag. Both units belong to the Middle Pliocene.

In the Red Sea near Mersa Alam, the Pliocene section is divided into Gahir Fm. (944 m sandstone, marls, and conglomerates) of Early Pliocene age and the overlying Shagra Fm. (80 m sandstones, marls, and reefal limestones) dated Middle Pliocene to Pleistocene. In Safaga area, both units, Gabir and Shagra, are lumped together under the name Gasus Formation with the Samh Formation (late Miocene) at base. In Sinai, the undifferentiated Pliocene sediments in the west are described under the Qa'a Fm. (52 m grits, sandstones, anhydrite, and shelly limestones). The formation is 100 m in the drilled oil wells.

In the Nile Delta basin, the Pliocene–Pleistocene succession starts by the sandy deposits of the upper part Abu Madi Formation and followed by fine clay deposits of the Kafr El Sheikh Formation and attains about Kafr El 120–259 m in the oil wells in the Nile Delta, only 23 km south of Giza, represented by sandstones and clay pockets. The Pleistocene section in Nile Delta and Mediterranean Sea consists of fluvial-deltaic the Wastani, Mit Ghamr, and Bilqas Formations which consist dominantly of thickly bedded silty sands with clay streaks, overlying the El Wastani Formation (Fig. 8).

5 Surface Water Resources in Egypt

During the Phanerozoic, Egypt was a rainy country and many older rivers were flowed into present-day deserts. This was best recorded in southeast Egypt at Abraha and Hodain

where freshwater fossils were recorded during the Mesozoic and Cenozoic (Issawi et al., 2009). Also, at Bahariya and Kharga oases, dinosaur fossils were described from the Upper Cretaceous deposits. In Faiyum, a major collection of Oligocene freshwater fossils was collected by many scientists (Simons & Rasmussen, 1990). One of the oldest major rivers in Egypt was the Qena river as a result of the uplift of the Red Sea Mountains in pulses, during the Late Eocene up to the Early Miocene. The Qena River collected all the Egyptian waters from the Southern Galala Plateau to the extreme southwest of Egypt. The Pleistocene deposits of the Nile Valley are represented by lower Pleistocene conglomerates of the Armant Formation and Middle Pleistocene sands of the Qena Formation which represented the oldest Quaternary deposits in the Nile Valley resulted from the Qena River (Issawi et al., 2009). The Pleistocene oldest sediment is the Qena Sand which has a suite of minerals specific to Egypt's Eastern Desert including opaque minerals rich in zircon and epidote with a relatively high abundance of amphiboles (Omar, 1996). To the south in Egypt, in the Gabgaba area, the Gabgaba River started its course in Sudan near the Dungola loop and flowed northward along cracks developed on the west side of the hills exposing basement in southern Egypt. The Gabgaba then joined the Allaqi River and the system is now known as the Gabgaba–Allaqi River; flowing northward and westward, it was captured by the Qena River flowing from the north to the southwest below the westward-diminishing Sin El Kaddab scarp. Thus, a huge amount of water was flowing in southwestern Egypt, including now-defunct streams that were braided in some places and had conspicuous banks in others, all covered by thick deflated sands during the arid phases that have been dominant across Egypt in the Middle-Late Quaternary. This drainage system, known as the Radar Rivers or the trans-African drainage system, reached the Atlantic during the Oligocene and later times. Another older river, the Gilf, was also important during the Oligocene; it was formed in the north and flowed through southwestern Egypt while building the Siwa deltaic sediments.

The Nile River is applied to the south-north a river which has its upstream from two locations: Victoria Lake (Uganda, the White Nile) and Tana Lake (Ethiopia, Blue Nile). Both Niles meet at Khartoum. The important diagnostic characteristics distinguishing Nile sediments from other riverine systems are their inclusions with an Ethiopian heavy minerals suite (e.g., pyroxenes mainly augite, amphiboles, strongly dwindled zircon accompanied by an intermediate epidote contents). These heavy minerals are only recognized in the Dandara Formation which is well exposed in both banks of the Nile in Upper Egypt. It is believed that the sediments of the Dandara Formation are the first deposits of a river coming into Egypt from Ethiopia heading toward the Mediterranean. In between both units, i.e., Qena and

Dandara Formations, the Ghawanem Formation was recorded including both minerals of Qena and Dandara Formations with the Egyptian and Ethiopian suites indicating that the Qena System was partly active even when the Ethiopian water reached Egypt. The top third of the Dandara Formation is 210 ka which gives an approximate age for the Ethiopian water with its special mineral suite at least $\frac{1}{2}$ million years—the age of the present Nile. The presence of Nilotic fishes and crocodile remains in Tarfawi, Sahara area 300 km west of the Nile, is a proof for a connection between the Nile and the site of the fauna. The age of the fauna is 174 ka and elevation is ca 247 m a.s.l. With this connection, water must have covered a huge stretch in the south Western Desert. Remnants of this water can be seen in the many and extensive playas south of Sin El Kaddab and at Bir Tarfawi–Bir Sahara stretch. The playas down the Darb El Arbian, Kharga, and Dakhla scarps have elevation less than 200 m a.s.l. This tells that the Nile water once flowed into these depressions during the Late Pleistocene.

The most important problem facing many African countries north of the equator is the lack of freshwater taken with construction of dams from upstream countries with a rapid increase in population, which could lead to increased death rates and the lack of enough water to sustain irrigation and economy. Such limited water inevitably leads to conflicts such as the tribal war in Darfur and the confrontation between Sudan and Chad, not to mention the dispute between Ethiopia on the side and Sudan and Egypt on the other, about construction of a huge dam on the Blue Nile just upstream from the Sudan border, in a seismically active region close to the Ethiopian rift. It is surprising, therefore, to realize that large amounts of water originating in Central Africa and Congo were trapped in the swamps of the Bahar El Gebel and Bahar El Zaraf depressions in west South Sudan. This suggests that the channels of the ancient Cenozoic river system, which flowed naturally from the southern region across what is now the Sahara Desert could be used with relatively little expense to transport freshwater to the populated territories of northeastern Africa. Some of the northern feeders of the Congo River near Buta, or near Ueley further north, are low-gradient streams that could be reversed to flow into these natural collectors. From here, the old Radar Rivers' channels could transport water to the sand-filled Gilf River channel, or further west into the ancient Chad-Libya mega system. The main trunk of the rejuvenated channel would run from the swampy areas in western South Sudan to Darfur near El Fasher, and further north through Lagiet Arbain and Lagiet Omran to reach the Wadi Magrur and Wadi Howar. At Merga, 100 km further north, a reservoir could be developed to supply two main systems, the paleo-Gilf flowing into Egypt across the Sudan border east of Gebel Kamel and the paleo-Kufra flowing past west Gebel Uweinat into north Chad and south Libya. In all

these swathes, the suggested new canals would take advantage of the existing excavation provided by the ancient river systems, to develop a new life in a dead desert.

References

- Aboul Ela, N. M., El Saadawy, W. E., & Darwish, M. H. (1989–1991). Lower cretaceous microflora from Abu Darag area, western side of the Gulf of Suez. *Egypt Journal of Geology*, 33, 1–2, 347–362.
- Ahmad, F., Farouk, S., & Abdel Moghny, M. W. (2014). A regional stratigraphic correlation for the upper Campanian phosphorites and associated rocks in Egypt and Jordan. *Proceedings of the Geologists' Association*, 125, 419–431.
- Al-Far, D. M. (1966). Geology and coal deposits of Gebel Al Maghara North Sinai, Egypt. *Journal of Geology Survey Egypt*, 37.
- Bosworth, W. (2015). Geological evolution of the Red Sea: historical background, review, and synthesis. In *The Red Sea* (pp. 45–78). Berlin, Heidelberg: Springer.
- Bumby, A. J., & Guiraud, R. (2005). The geodynamic setting of the Phanerozoic basins of Africa. *Journal of African Earth Sciences*, 43 (1–3), 1–12.
- Burke, K., MacGregor, D. S., & Cameron, N. R. (2003). Africa's petroleum systems: Four tectonic 'Aces' in the past 600 million years. *Geological Society, London, Special Publications*, 207(1), 21–60.
- Catuneanu, O., Khalifa, M. A., & Wanas, H. A. (2006). Sequence stratigraphy of the lower cenomanian bahariya formation, Bahariya Oasis, Western Desert Egypt. *Sedimentary Geology*, 190, 121–137.
- Carr, I. D. (2002). Second-Order sequence stratigraphy of the Palaeozoic of North Africa. *Journal of Petroleum Geology*, 25(3), 259–280.
- Coward, M. P., & Ries, A. C. (2003). Tectonic development of North African basins. *Geological Society, London, Special Publications*, 207(1), 61–83.
- El-Azabi, M. H., & Farouk, S. (2011). High-resolution sequence stratigraphy of the Maastrichtian-Ypresian succession along the eastern scarp face of the Kharga Oasis, south Western desert, Egypt. *Journal of the International Association of Sedimentology*, 58, 579–617.
- Elicki, O., Khalifa, M. A. G., & Farouk, S. M. (2013). Cambrian ichnofossils from northeastern Egypt. *Neues Jahrbuch für Geologie Und Paläontologie, Abhandlungen*, 270, 129–149.
- Fairhead, J. D., Green, C. M., Masterton, S. M., & Guiraud, R. (2013). The role that plate tectonics, inferred stress changes and stratigraphic unconformities have on the evolution of the West and Central African rift system and the Atlantic continental margins. *Tectonophysics*, 594, 118–127.
- Farouk, S. (2015). Upper Cretaceous sequence stratigraphy of the Galala Plateaux, western side of the Gulf of Suez Egypt. *Marine and Petroleum Geology*, 60, 136–158.
- Farouk, S. (2016). Paleocene stratigraphy in Egypt. *Journal of African Earth Sciences*, 113, 126–152.
- Farouk, S., Ahmad, F., & Powell, J. (2017). Cenomanian-Turonian stable isotope signatures and depositional sequences in northeast Egypt and central Jordan. *Journal of Asian Earth Sciences*, 134, 207–230.
- Farouk, S., Khalifa, M., Abu El-Hassan, M., Papazzoni, C., Fabrizio, F., Coccioni, R., & Zaky, A. (2019). Upper Paleocene to lower eocene microfacies, biostratigraphy, and paleoenvironmental reconstruction in the northern Farafra Oasis, Western desert (Egypt). *Micropaleontology*, 65, 5381–5406.
- Farouk, S., Ziko, A., Eweda, S. A., & Said, A.E. (2014). Subsurface Miocene sequence stratigraphic framework in the Nile delta, Egypt. *Journal of African Earth Sciences*, 91, 89–109.
- Fourcade, E., Azema, J., Cecca, F., Dercourt, J., Guiraud, R., Sandulescu, M., Ricou, L. E., Vrielynck, B., Cottreau, N., & Petzold, M. (1993). Late Tithonian (138 to 135 Ma). Atlas Tethys Palaeoenvironmental Maps. Explanatory notes. In Gauthier-Villars (Ed.), Paris, pp. 113–134.
- Grothaus, B., Eppler, D., & Ehrlich, R. (1979). Depositional environment and structural implications of the Hammamat Formation, Egypt. *Annals of the Geological Survey of Egypt*, IX, 564–590.
- Guiraud, R. (1998). Mesozoic rifting and basin inversion along the northern African Tethyan margin: An overview. *Geological Society, London, Special Publications*, 132(1), 217–229.
- Guiraud, R., Binks, R. M., Fairhead, J. D., & Wilson, M. (1992). Chronology and geodynamic setting of Cretaceous-Cenozoic rifting in West and Central Africa. *Tectonophysics*, 213(1–2), 227–234.
- Guiraud, R., Bosworth, W., Thierry, J., & Delplanque, A. (2005). Phanerozoic geological evolution of Northern and Central Africa: An overview. *Journal of African Earth Sciences*, 43(1–3), 83–143.
- Haddoum, H., Guiraud, R., & Moussine-Pouchkine, A. (2001). Hercynian compressional deformations of the Ahnet-Mouydir Basin, Algerian Saharan Platform: Far-field stress effects of the Late Palaeozoic orogeny. *Terra Nova*, 13(3), 220–226.
- Hanter, G. (1990). North western desert. In *The Geology of Egypt* (pp. 239–319). Rotterdam: Brookfield, Balkema.
- Hewaidy, A. A., El-Azabi, M. H., & Farouk, S. (2006). Facies associations and sequence stratigraphy of the upper cretaceous-lower Eocene succession in the Farafra Oasis, Western desert, Egypt. In *8th International Conference of Arab world, Cairo University II*, pp. 569–599.
- Issawi, B. (2000). Northern Gondwana early paleozoic glaciation. In *Fifth International Conf. Arab World, Cairo University* (Vol. 3, pp. 1243–1250).
- Issawi, B. (2005). Archean-Phanerozoic birth and development of the Egyptian land. In *Geology of the Tethys. Proceedings of the First International Conference on the Geology of the Tethys, Cairo University* (Vol. 2, pp. 339–380).
- Issawi, B., & Gayed, B. (2011). Anogenic and orogenic plumes in Egypt. *Annals of the Geological Survey of Egypt*, XXXI, 521–539.
- Issawi, B., Francis, M.H., Youssef, E.A., & Osman, R.A. (Ed). (2009). *The phanerozoic geology of Egypt: a geodynamic approach* (vol. 81, p. 571). Ministry of Petroleum and the Egyptian Mineral Resources Authority Special Publication.
- Issawi, B., & Osman, R. A. (2002). Geological history of NE Egypt during the Paleozoic and Mesozoic as anticipated from lithofacies-isopach maps. In *The Geology of the Arab World, Cairo University, Sixth International Conference II*, pp. 451–468.
- Jolivet, L., Faccenna, C., Agard, P., Frizon de Lamotte, D., Menant, A., Sternai, P., & Guillocheau, F. (2016). Neo-Tethys geodynamics and mantle convection: from extension to compression in Africa and a conceptual model for obduction. *Canadian Journal of Earth Sciences*, 53(11), 1190–1204.
- Keeley, M. L. (1989). The palaeozoic history of the western desert of Egypt. *Basin Research*, 2(1), 35–48.
- Khalifa, H., Omran, A. M., & Higazy, H. A., (1988). Microfossils from Late Proterozoic (Hammamat Group) Eastern Desert, Egypt. *Bulletin of the Faculty of Science, Assiut University*, 12, 1–29.
- Khalifa, M., Soliman, H., & Wanas, H. A. (2006). The Cambrian Araba formation in northeastern Egypt: Facies and depositional environments. *Journal of Asian Earth Sciences* 27, 873–884.
- Kissel, C., Laj, C., Poisson, A., & Görür, N. (2003). Paleomagnetic reconstruction of the Cenozoic evolution of the Eastern Mediterranean. *Tectonophysics*, 362(1–4), 199–217.

- Klitzsch, E. (1983). Paleozoic formations and a Carboniferous glaciation from the Gifl Kebir-Abu Ras Area in southwestern Egypt. *Journal of African Earth Sciences* (1983), 1(1), 17–19.
- Kora M. (1998). The Permo-Carboniferous outcrops of the Gulf of Suez region, Egypt: stratigraphic classification and correlation. *Geodiversitas*, 20(4).
- Kuss, J., & Boukhary, M. A. (2008). A new upper Oligocene marine record from northern Sinai (Egypt) and its paleogeographic context. *GeoArabia*, 13(1), 59–84.
- Merdith, A. S., Williams, S. E., Müller, R. D., & Collins, A. S. (2017). Kinematic constraints on the Rodinia to Gondwana transition. *Precambrian Research*, 299, 132–150.
- Nikishin, A. M., Cloetingh, S. A. P. L., Brunet, M. F., Stephenson, R. A., Bolotov, S. N., & Ershov, A. V. (1998). Scythian platform, Caucasus and Black Sea region: Mesozoic-Cenozoic tectonic history and dynamics. *Peri-Tethys Memoir*, 3, 163–176.
- Nürnberg, D., & Müller, R. D. (1991). The tectonic evolution of the South Atlantic from late Jurassic to present. *Tectonophysics*, 191(1–2), 27–53.
- Omar, A., (1996). *Geological, mineralogical and geochemical studies on the Neogene and Quaternary Nile Basin deposits, Qena—Assiut Stretch, Egypt*. [Ph.D. Thesis] (324 pp). South Valley University.
- Osman, R. (2003). Contribution to the stratigraphy of El Arag depression, N. Western desert Egypt. *Journal Sedimentol Egypt*, 11, 157–168.
- Philip, J. (1993). Late cenomanian palaeoenvironments (94–92 Ma). Atlas Tethys palaeoenvironmental maps, explanatory notes.
- Piqué, A., Tricart, P., Guiraud, R., Laville, E., Bouaziz, S., Amrhar, M., & Ouali, R. A. (2002). The mesozoic-cenozoic atlas belt (North Africa): An overview. *Geodinamica Acta*, 15(3), 185–208.
- Rabinowitz, P. D., Coffin, M. F., & Falvey, D. (1983). The separation of Madagascar and Africa. *Science*, 220(4592), 67–69.
- Reillinger, R., & McClusky, S. (2011). Nubia–Arabia–Eurasia plate motions and the dynamics of Mediterranean and middle east tectonics. *Geophysical Journal International*, 186(3), 971–979.
- Schlumberger, R. F. (1984). Well evaluation conference, Egypt, geology of Egypt. *Schlumberger Middle East SA, EGPC*
- Schrank, E. (1987). Biostratigraphic importance of microfloras from the late cretaceous clastic series of northwestern Sudan. *Cretaceous Research*, 8(1), 29–42.
- Segev, A., Avni, Y., Shahar, J., & Wald, R. (2017). Late Oligocene and Miocene different seaways to the Red Sea-Gulf of Suez rift and the Gulf of Aqaba-Dead Sea basins. *Earth-Science Reviews*, 171, 196–219.
- Siegesmund, S., Basei, M. A., Oyhantçabal, P., & Oriolo, S. (Eds.). (2018). *Geology of Southwest Gondwana*. Springer.
- Simons, E. L., & Rasmussen, D. T. (1990). History of research, faunal review and future prospects. In R. Said (Ed.), *The Geology of Egypt* (pp. 627–638). Balkema.
- Stampfli, G. M., & Borel, G. D. (2002). A plate tectonic model for the Paleozoic and Mesozoic constrained by dynamic plate boundaries and restored synthetic oceanic isochrons. *Earth and Planetary Science Letters*, 196(1–2), 17–33.
- Steckler, M. S. (1985). Uplift and extension at the Gulf of Suez: Indications of induced mantle convection. *Nature*, 317(6033), 135–139.
- Unrug, R. (1997). Rodinia to Gondwana: The geodynamic map of Gondwana supercontinent assembly. *GSA Today*, 7(1), 1–6.
- Wanas, H. A. (2011). The Lower Paleozoic rock units in Egypt: An overview. *Geoscience Frontiers*, 2(4), 491–507.
- Wilde, S., & Youssef, K. (2002). A re-evaluation of the origin and setting of the late precambrian hammamat group based on SHRIMP U-Pb dating of detrital zircons from Gebel Umm Tawat, North Eastern Desert Egypt. *Journal of the Geological Society*, 159(5), 595–604.
- Wilson, M., Guiraud, R., Moreau, C., & Bellion, Y. C. (1998). Late Permian to recent magmatic activity on the African-Arabian margin of Tethys. *Geological Society, London, Special Publications*, 132 (1), 231–263.
- Ziegler, P. A. (1990). Geological atlas of western and central Europe. Geological Society of London.
- Ziegler, P. A. (1992). Plate tectonics, plate moving mechanisms and rifting. *Tectonophysics*, 215(1–2), 9–34.



Mohamed Bahay Issawi graduated with B.Sc. (1955) and M.Sc. (1964) degrees from Cairo University, and also holds a Ph.D. in Stratigraphy and Structures (1968) from the same institution. His work in the Western Desert is extensive where he conducted extensive field work and aerial-photo mapping over many years. He discovered the Abu Tartur phosphate deposits, iron ore deposits of the Bahariya Oasis, and the Kalabsha kaolin deposits south of Aswan. He contributed covered a large array on the geology of Egypt, in addition to some. He has written several books on the Phanerozoic geology of Egypt.



Sherif Farouk is a professor at the Exploration Department of the Egyptian Petroleum Research Institute, Cairo. He obtained a Ph.D. degree from Al-Azhar University (Egypt). He worked for the Geological Survey of Egypt from 1996 until 2007. He is a specialist in high-resolution stratigraphy, paleoenvironmental analysis, sequence stratigraphic studies, and paleontological applications. He has published about 101 scientific articles in several international journals on Phanerozoic stratigraphy, especially of Egypt, Jordan, Saudi Arabia, Iraq, United Arab Emirates, and Tunisia.



Phanerozoic Structural Setting and Tectonic Evolution of Egypt

Mohamed Yousef, Zakaria Hamimi, Ahmed Heneish, Wael Hagag, and Tarek Anan

Abstract

The study of the Phanerozoic structural setting and tectonic evolution in Egypt has gained more attention during the last three decades. The present work reviews the characteristic tectonic/structural features of this succession, with emphasis on different structural geometries and styles. The chapter is divided into three main parts, highlighting the Paleozoic, Mesozoic, and Cenozoic structures of Egypt. Unlike the Mesozoic and Cenozoic structures, the Paleozoic structures are not well understood in Egypt, due to limited exposures and insufficient subsurface data. However, this chapter attempts to present the available data, even if limited. Following the introduction (Sect. 1), the main outline of part one includes: the Precambrian-Cambrian transition, the distribution of Paleozoic sediments, glacial/fluvioglacial deposits, and Paleozoic structural framework (Paleozoic arches and basins). In part two, the Mesozoic structures in Egypt are dealt with in terms of Jurassic-Early Cretaceous rifts, Cretaceous rifts, Late Cretaceous to Recent inverted structures (northern Western Desert, northern Eastern Desert, and North Sinai inverted structures), and Late Mesozoic–Early Tertiary structures in central and southern Egypt (the Bahariya Depression and southern Western Desert inverted structures). The Cenozoic structures in Egypt are discussed in part three throughout the following

main topics: Cretaceous-Paleogene (K/P) boundary, Paleocene-Eocene transition, the Oligocene–Miocene rifting (magmatism, the Red Sea and Gulf of Suez Rift System, Cairo-Suez District), the opening of the Gulf of Aqaba, and the Quaternary and neotectonics.

Keywords

Western Desert • Eastern Desert • Sinai • Red Sea • Gulf of Suez • Cairo-Suez District • Paleozoic structures • Santonian inversion • Magmatism • Rifting

1 Introduction

Egypt and neighboring regions lie along the passive margins of the Palaeotethys, Neotethys, and Mediterranean Sea, throughout different epochs, at the northern border of the Greater Gondwana (or Pannotia). The Greater Gondwana itself resulted from the fragmentation and breakup of Pangaea which represents the latest supercontinental assembly throughout the history of Earth. Such unique geographic position, together with the eustatic sea-level changes and the prolonged tectonic setting, greatly influenced the facies distribution, not only in Egypt but also in the adjacent areas. The Phanerozoic paleogeography was dominated by the development of marine slopes and carbonate, and mixed-marine platforms in the present-day north, giving way to clastic facies in the south (Guiraud et al., 2001). The pre-existing Neoproterozoic deep crustal structures, intracratonic faulting/shearing, and tectonic sagging/collapse of the underlying cratonized rocks and Pan-African crystalline basement complex also significantly contributed to the Phanerozoic tectonostratigraphic phases, basin evolution and dynamics, and structural fabrics. Distinct phases of Syrian Arc compressional deformation, and the development of extensional basins associated with the rifting of the Red Sea and the Gulf of Suez, interrupted the impact of subsidence

M. Yousef (✉)
Geology Department, Faculty of Science, Ain Shams University,
Cairo, 11566, Egypt
e-mail: mohamed.yousef@sci.asu.edu.eg

Z. Hamimi · W. Hagag
Geology Department, Faculty of Science, Benha University,
Benha, 13518, Egypt

A. Heneish
Geology Department, Faculty of Science, Zagazig University,
Zagazig, Egypt

T. Anan
Geology Department, Faculty of Science, Mansoura University,
Mansoura, Egypt

on the Egyptian continental margin, which in turn created a distinctive structural imprint throughout the Phanerozoic basin evolution (Keeley, 1989). The NNW-SSE (Clysmic or Erythrean), NE-SW (Syrian Arc or Aualitic), and WNW-ESE (Tethyan) structural fabrics recorded in the Phanerozoic succession are regarded to represent reactivated preexisting weak zones or structural elements in the basement to accommodate strain.

This chapter is an attempt to review and summarize the structural framework and tectonic evolution of the Phanerozoic succession of Egypt. This evolution has a direct relation to the tectonics of the Neoproterozoic Arabian-Nubian Shield and the history of the southern margin of the Palaeotethys and Neotethys. The Arabian-Nubian Shield structural fabrics have been reactivated as high strain zones throughout the Phanerozoic. Moreover, the polyphase tectonic phases that impacted the African-Arabian plate throughout the Phanerozoic resulted in post-depositional deformation and erosion of most of the basins in Egypt and its environs.

2 Paleozoic Structures in Egypt

2.1 Precambrian-Cambrian Transition and the Hammamat Sediments

The pre-Paleozoic regional tectonic framework of the Egyptian Nubian Shield (e.g., Fowler & Hamimi, 2020, 2021; Hamimi et al., 2019, 2020, 2021a, 2021b; Hamimi & Fowler, 2021) had a great influence on the deposition of Paleozoic succession in Egypt, and their geographic distribution, lithology, and thicknesses. The setting was also affected by the position of the plate and plate-boundaries of the Paleotethys realm. The basement complex of Egypt (Fig. 1) is well exposed along the Red Sea hills and extends to the east of the Nile Valley underneath the Phanerozoic cover. To the west of the Nile Valley, the basement has limited exposures at Uweinat and Gebel Kamil, while the rest of the basement is exposed along Uweinat-Aswan uplift but masked by the sedimentary cover which prevents the exploration of the general characteristics of the shield and their relationship to the overlying Paleozoic rocks. The sedimentation of Paleozoic in Egypt is highly controlled by the great number of major, as well as many minor faults, which cut across the Precambrian Shield and led to the uplift of several plutonic arches trending mainly NE-SW and flanking intra-cratonic Paleozoic to Mesozoic sedimentary basins. The Pan-African structural trends controlled the Paleozoic basins in the NE-SW, E-W, and NW-SE directions, while the N-S trend has had a minor effect. Rejuvenation of these faults/shear belts was responsible for the regional and local tectonic evolution of such basins with various effects on the magmatic eruptions, basin extension, and the limitations of

transgression and regression. The result was the formation of an uneven basement surface controlling the overlying sediments, where the Paleozoic section had echoed the change in basement relief before and during basin fill. Furthermore, the opening of Neotethys in the Late Carboniferous-Permian and the breaking up of Gondwanaland from the Carboniferous time up to the Cretaceous contributed to the structural discontinuities affecting the Paleozoic sequence in Egypt. In Egypt, the volcanic rocks were injected within the Paleozoic section following the old structural trends such as in Gebel Kamil (Schandelmeir & Reynolds, 1997) and Gebel Uweinat (Issawi, 1978), as well as at the subsurface (in drill holes, Dardir, 1981; Issawi, 1996). The intrusion of granite in the Lower Paleozoic sediments at Wadi Lithi in Sinai (El Kelany, 2000) and at Gebel Babein (Egyptian-Libyan border) (Schandelmeir et al., 1983) may extend the evolution of the Pan-African events to the Early Paleozoic time (Issawi et al., 2009).

The post-orogenic Hammamat molasse sediments represent the early cycle of deposition within the Arabian-Nubian Shield. These sediments are composed mainly of conglomerates and siltstones and were accumulated mainly in intra-cratonic basins, grabens, and sag areas over old crystalline basement units (Fig. 2). The structural setting of the Hammamat basins is not unified and change locally from area to another. From a stratigraphic point of view, the Hammamat sediments are the first true bedded (Akaad, 1972) and unmetamorphosed sediments except near granitic intrusions (e.g., Hassan & Hashad, 1990). The bedding and lithologic characteristics (especially the conglomerates at the base of the section), beside their deposition in paleovalleys below the higher scarps of crystalline basement rocks, could possibly mean that these sediments are glaciogene sediments deposited a bit earlier in the Early Paleozoic time (i.e., younger than 590 Ma). This argument can be supported by the assumption that the southern pole was located just off what is now the north coast of Africa during the latest Precambrian time, and the stratigraphy of the Precambrian-Cambrian interval is not well identified in Egypt. The type of Cambrian strata in Sinai, southern Eastern Desert, and southern Western Desert are not relatively far from the lithology of the Hammamat sediments, where these Early Cambrian units are composed mainly of sandstones rich in quartz pebbles (dropstones) unconformably overlying the Precambrian basement rocks. The only difference is that the former Cambrian strata (e.g., Araba Formation in Sinai) contains some primitive fossils. However, Issawi et al. (2009) documented the microfossils within the Hammamat sediments from Wadi Iqla and Wadi Semna in the central Eastern Desert, where some species of algal microflora and oncolites have been recorded. Few archaeocyathids from Wadi Semna were also identified. An approximate age of Late Neoproterozoic-Early Cambrian

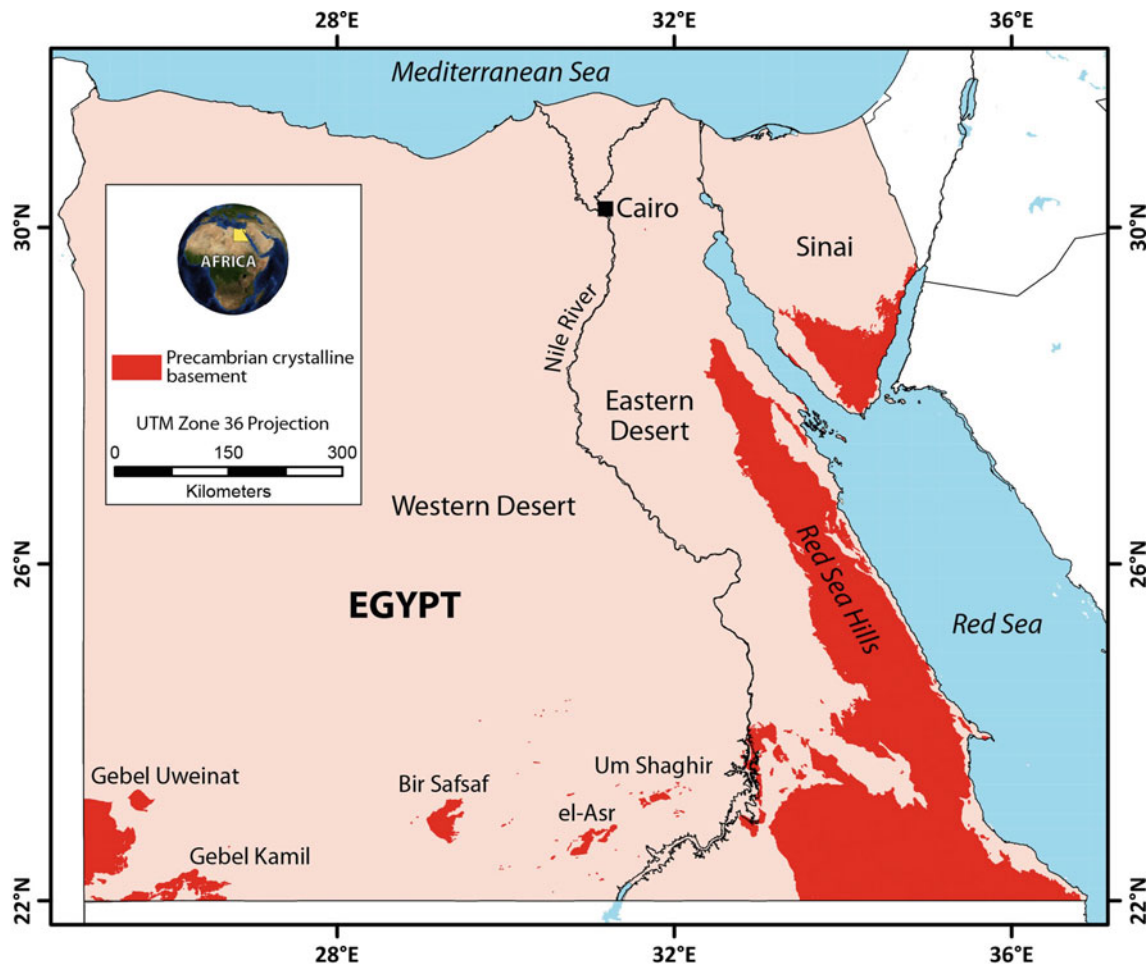


Fig. 1 Location map showing the distribution of Precambrian crystalline basement exposures in southern Sinai, Eastern Desert, and southern Western Desert, Egypt

can be suggested based on the presence of these fossils. The marine microorganisms documented by Khalifa et al. (1988) from the Late Proterozoic Hammamat Group in the Eastern Desert suggest some marine incursions during the deposition of these sediments instead of the nonmarine origin which is widely believed. El-Habbak and Mahmoud (1994) also recorded the first microfossil remains occurring in the Banded Iron Formation of Wadi Kareem in the Eastern Desert. The Hammamat sediments is often thought of as the earliest depositional cycle exclusively occurring within the Eastern Desert of Egypt. So, further stratigraphic and sedimentologic studies are needed to accurately pinpoint the age and environment of deposition of such sediments.

2.2 Distribution of Paleozoic Sediments Allover Egypt

The surface exposures of the Paleozoic rocks (Fig. 3) are relatively limited on the geologic map of Egypt. The

Paleozoic rocks in Egypt are well exposed along the Gulf of Suez in northeast Egypt, in Sinai and in the remote areas between Gebel Uweinat and Abu Ras plateau (~ 1000-m-thick Paleozoic section west of Gilf Kebir; Klitzsch, 1978; Klitzsch & Lejal-Nicol, 1984) at the southwestern corner of the Western Desert. In the subsurface of northern Western Desert, a great section of Paleozoic sediments (several kilometers in thickness) is known. Until the works of Picard (1942), Omara and Conil (1965), Omara (1972), and Weissbrod (1969) in Sinai and Said (1981) in southwest Egypt, the Pre-Carboniferous deposits were not clearly identified. The thickness of Paleozoic strata in Egypt regionally varies from thick subsurface sequences in north-western Egypt to relatively reduced and incomplete sections in Sinai, Gulf of Suez, and southwest Egypt. Over the remaining parts of Egypt, the Paleozoic section is minor or completely missing. Identifying the Paleozoic strata in Egypt proves challenging, because of the similarity of sedimentary environments and the lack of index fossils, besides the high dependence on trace fossils.

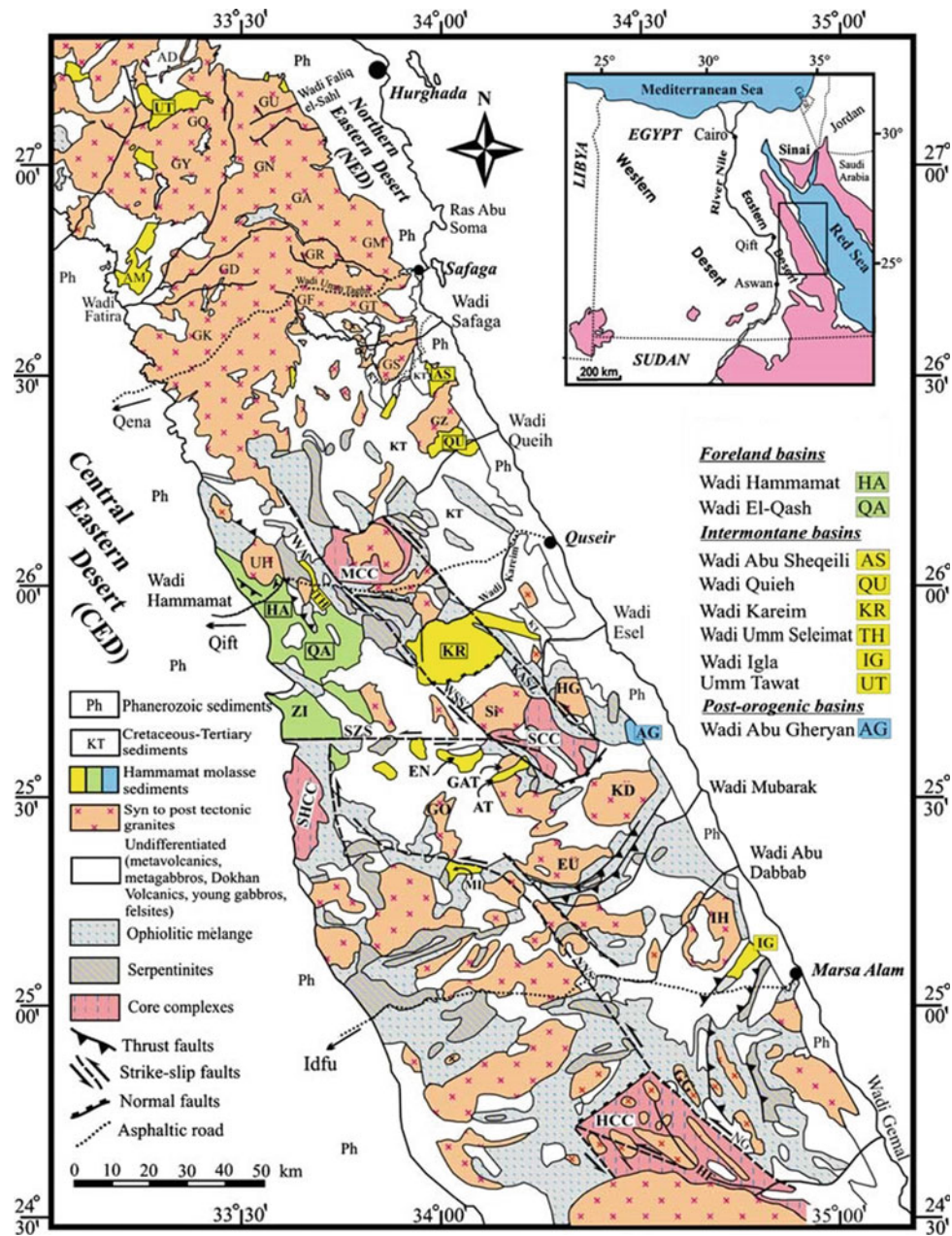


Fig. 2 Simplified geologic map showing the structural framework of the central Eastern Desert of Egypt and the distribution of the Late Neoproterozoic-Early Phanerozoic? Hammamat Molasse sediments (after Abd El-Wahed, 2010). HCC: Hafafit, HF: Wadi Hafafit, NG: Wadi Nugrus, GG: Gebel Nugrus, IG: Wadi Igla, IH: Igl al-Ahmar monzogranite, GX: G. Um Nagat, NNS: Um Nar-Nugrus shear zone, EU: Gebel el-Umra older granite, MI: el-Miyah, KD: Kadabora monzogranite, SHCC: el-Shalul, AT: Atawi, GAT: Gebel Atawi granite, EN: Andiya, AG: Abu Gheryan, SCC: Sibai, WSSZ: Wadi Sitra, KASZ: Kab Ahmed, HG: Homrat Ghaunam granite, ZI: Wadi Zeidoun, SZS: Wadi Zeidoun-Wadi el-Shush, QA: Wadi el-Qash, KR: Kareim, TH: Um Esh-Um Seleimat, HA: Hammamat, UH: Um Had granite, WA: Wadi Atalla, MCC: Meatiq, QU: Wadi Quieh, AS: Abu Sheqeili, GZ: Um Zarabit, GK: Kafari, GS: Gasus, GD: el-Dob, GF: Abu Furad, GT: Um Taghir, GR: Ras Barud, GM: el-Magal, GA: Um Anab, GY: Shayib el-Banat, GQ: Qattar, GU: Um Araka, UT: Um Tawat, AD: Gebel Dokhan

Cambrian sediments are recorded in Sinai at Um Bogma area and in places between Abu Durba and Wadi Feiran. They were regarded as the lower part of the Carboniferous sequence until Omara and Conil (1965), Weissbord (1969), and Omara (1972) proved their Cambrian age. Similar strata are exposed between northern Wadi Qena and Wadi Dakhl (Klitzsch, 1986).

The Cambrian strata are also recognized in oil wells between Bahariya and Qattara depressions. In southwest Egypt, the Cambrian sediments were early recorded by Buroillet (1963), Conant and Goudarzi (1964), and Said (1971).

Late Ordovician strata are exposed in Sinai, southwestern Egypt (northeast of Gebel Uweinat; Klitzsch & Lejal-Nicol,

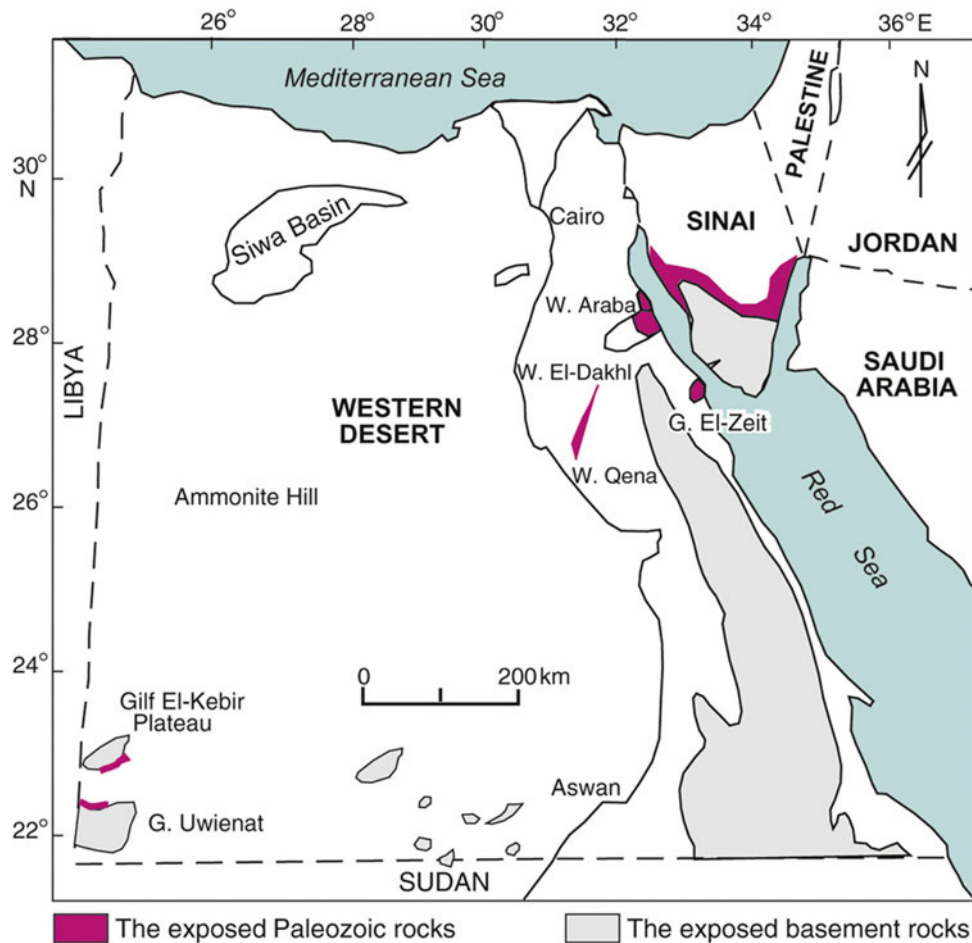


Fig. 3 Distribution of the Paleozoic rocks in Egypt (after Wanas, 2011)

1984), at Wadi Gabgaba in southern Eastern Desert (Issawi, 2005) and recognized in the subsurface of northern Western Desert (Keeley, 1989). The subsurface Silurian rocks were reported in the northern Western Desert (Hantar, 1990; Schrank, 1984), while their surface exposures cover large tracts in southwest Egypt at Gebel Uweinat-Abu Ras area west of Gilf Kebir Plateau (Klitzsch & Lejal-Nicol, 1984).

A small section (15-m thick) of Devonian strata was recognized in western Sinai by Issawi and Jux (1982). They stated that the section might be coeval with the Devonian section in southwest Egypt. In the Gulf of Suez area, no Devonian sediments have been identified, except the interpretation of Issawi et al. (2009) based on the works of Kora (1992, 1995) and Kora and Mansour (1992), where they suggested to lower down a bit most of the Upper Paleozoic section in Block (IV) comparable with the section on the western side of the Gulf. In contrast, a thick subsurface Devonian section (700-m thick) was reported by oil companies (Hantar, 1990; Keeley, 1989; McGarva, 1986; Schrank, 1984) in northwest Egypt. In southern Egypt, Osman et al. (2002) assigned the section composing the

eastern scarp of Wadi Gabgaba as Devonian in age, while Issawi and Jux (1982) identified a 70-m section of Devonian sediments northeast of Uweinat area. Further to the north of the area of Issawi and Jux, a thick Devonian succession (up to 200 m) which is covered northward by the well-defined Carboniferous strata was mapped by (Said & Mehdi, 2000).

The Carboniferous strata were the first to be identified and the most discussed. They are exposed in several areas in Sinai (Wadi Feiran, Abu Durba, and Um Bogma areas), Gulf of Suez, and in southwest Egypt. The Carboniferous of the Gulf of Suez-Sinai area was first described in detail by Walther (1890) and reviewed by Said (1962) and in many early research endeavors (Abdallah & Adindani, 1963; Hassan, 1967; Hermina et al., 1983; Kora, 1984; Kora & Jux, 1986; Omara, 1965, 1971; Omara & Conil, 1965; Omara & Schultz, 1965; Said, 1971; Said & Eissa, 1969; Soliman & El Fotouh, 1970; Weissbrod, 1969). In the western side of the Gulf of Suez, Carboniferous strata are well exposed and largely represented in the South Galala Plateau (between northern Wadi Qena and Wadi Dakhl), and further north in Wadi Araba and in the eastern and southern

footslopes of North Galala Plateau (e.g., Abdallah & Adindani, 1963). The stratigraphy of Carboniferous sediments in southwest Egypt (Abu Ras—Gebel Uweinat area) was studied by Klitzsch (1979, 1983) and Klitzsch and Lejal-Nicol (1984). In addition, the subsurface Carboniferous section in the northern Western Desert was identified by Said (1962) and later discussed by Hantar (1990).

The Permian strata were recorded by Abdallah and Adindani (1963) from Wadi Malha in the North Galala Plateau. These strata are also identified from Wadi Araba between Zaafarana and St. Antony (Lejal-Nicol, 1986). In Sinai, similar strata were recognized in Um Bogma area and between Gebel Araba and Wadi Feiran. The Permian strata in the subsurface of northwest Egypt is represented by the topmost Paleozoic unit (Late Carboniferous-Early Permian) identified by Keeley (1989) from Siwa area. In southwest Egypt, the 30- to 50-m-thick strata (Issawi & Jux, 1982) overlying the Carboniferous rocks in Uweinat area (at Gilf Kebir and Abu Ras plateaus) belong to the Permian or to the Permo-Triassic. Klitzsch and Lejal-Nicol (1984) also recognized a similar section below the Early Mesozoic sediments to the northeast of Gebel Uweinat.

2.3 Glacial/Fluvioglacial Deposits in Egypt

During the Late Ordovician–Silurian time, the glaciers advanced from the South Pole to North Africa (Husseini, 1991; Mahmoud et al., 1992; McGillivray & Husseini, 1992), Fig. 4. The glacial ice was recorded in Algeria, Tunisia, Libya, Jordan, Syria, Turkey, Oman, and Iran (e.g., Bellini & Massa, 1980; Beuf et al., 1971; Hughes Clarke, 1988; Lababidi & Hamdan, 1985; Powell, 1989; Stocklin, 1972; Wolfart, 1981). Glaciogene, periglacial, and glaciofluvial clastic strata were accumulated within the deeply incised paleovalleys, overlying the old shallow marine to siliciclastic sediments, including pebbles and cobbles of Precambrian, Cambrian, and Early Ordovician rocks, commonly igneous and sandstones embedded in a glacial till diamictite. By the mid-Early Silurian (Rhuddanian-Aeronian), glaciers started to retreat due to the abrupt rise in sea level (Fig. 5), synchronous with the melting of ocean ice during the periglacial phase. The melting ice released sediments that infilled the paleovalleys during the periglacial, fluviglacial, and fluvial phases. Subsequently, the outwash sands and gravels formed extensive non-channelized fluviglacial deposits. Owing to the constant rising in sea level during the Silurian, the glaciogenic and periglacial clastics in North Africa and Arabia were overlain by black shales rich in organic matter, while in Egypt a wide hiatus including most of the Middle and Late Silurian above the glacial sediments was recorded (e.g., Issawi et al., 1999).

The glacial deposits in Egypt were first documented in southwest Egypt (Beall & Squyres, 1980) and in several sections from Sinai, the Galala Plateaus, northern Wadi Qena, and southern Eastern and Western Deserts (Issawi & Jux, 1982). The authors were able to recognize the dropstones or erratic stones (glacial features) in the siliciclastic sequences. The observations of the work of Issawi and Jux (1982) were later supported by the trace fossils and graptolites identified in the study of Keeley (1989). In Keeley's study, up to 600 m of fluviglacial sandstone and mudstone intercalated with marine claystone (the Kohla Formation) was documented from the subsurface section of the northern Western Desert. The glacial to fluviglacial deposits in Egypt are represented by the Naqus Formation in Sinai and northern Egypt and the Gabgaba Formation in the South Nile Basin.

The Naqus Formation (Hassan, 1967 and Said, 1971) is composed essentially of snow-white sandstones which developed in general in East Sinai (e.g., Wadi Saal). Upon first glance, the formation seems chalky in appearance. The lower part of the formation is composed of coarse-grained sandstones (includes erratic stones and affected by magmatic intrusions) and a section of fine-grained sandstone at the top. Stratigraphically, the basal coarse sandstone section of the Naqus Formation in Sinai is correlated with the Gabgaba Formation in southern Egypt (South Nile Basin), e.g., El Kelany (2000). The age of the formation is Late Ordovician (for the basal part) to Early Silurian (for the upper sandstone section). The glaciofluvial origin of the Naqus Formation is substantiated based on two aspects: the presence of the egg-shaped quartz pebbles randomly distributed in a sandstone section (e.g., dropstones) and by the correlation with the similar facies in Jordan (Abed et al., 1993; Powell, 1989; Powell et al., 1994) as well as in Saudi Arabia (Husseini, 1991; Mahmoud et al., 1992). The formation may be formed where the outwash sands were deposited over a wide area and then erratic pebbles that were held by the ice sheets slumped into the loose sands before lithification.

The Gabgaba Formation (Issawi, 2005) is composed of a thick section of poorly sorted and striated conglomerates, with pebbles representing a wide variety of rocks. The conglomerates are interbedded with thick bands of cross-bedded sandstone and breccia. These conglomerates were interpreted as diamictites filling the paleovalleys during the periodical melting of the ice sheets covering the high lands overlooking the valleys. Warm episodes were also recorded as some paleosol layers were detected at intervals. The type section of the formation is in Wadi Gabgaba at the southern Eastern Desert and the section is Late Ordovician in age. In the Gabgaba area, Issawi (2000, 2005) and Osman et al. (2002) indicated that the Paleozoic section has been affected by tectonic movements during the deposition, where

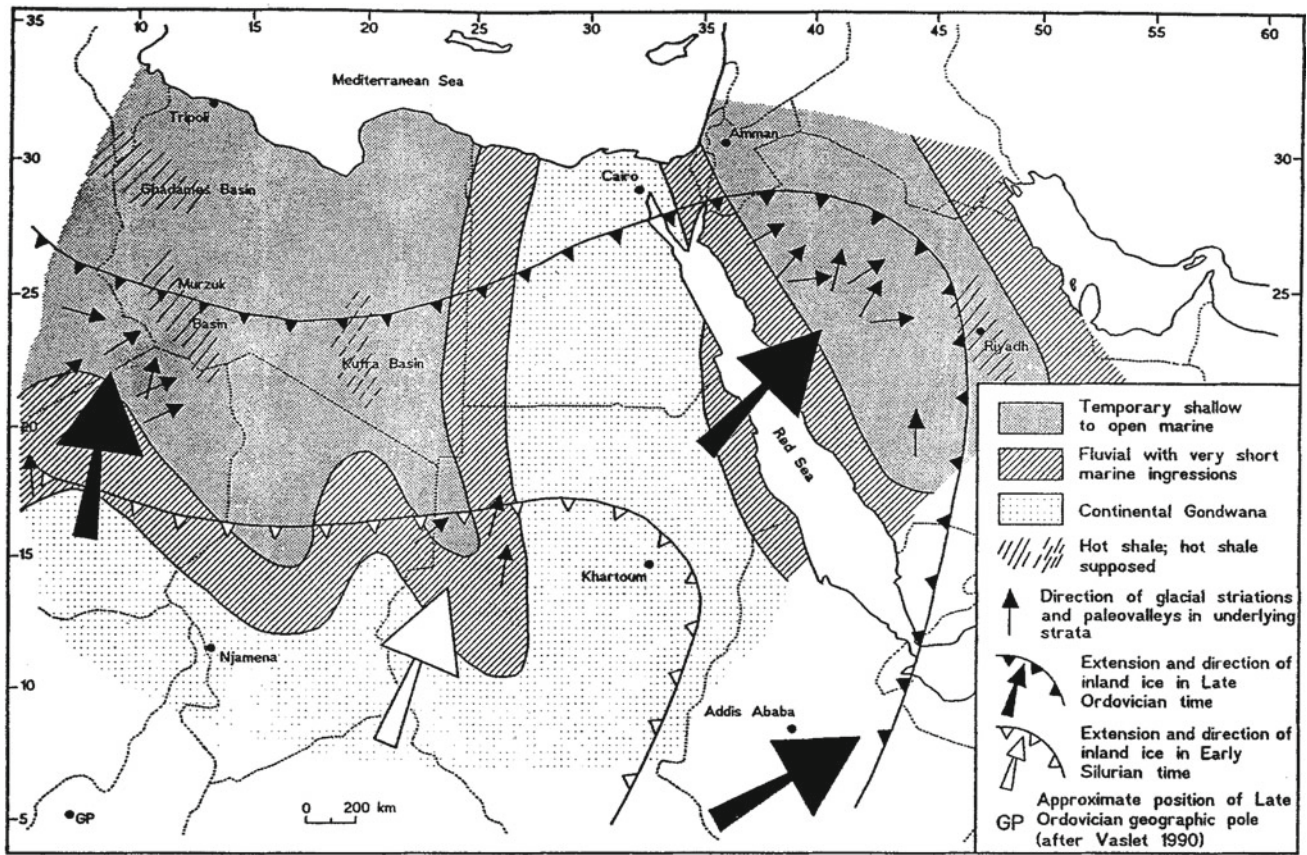


Fig. 4 Paleogeography, extension, and direction of inland ice during the Ordovician and Silurian (after Semtner & Klitzsch, 1994)

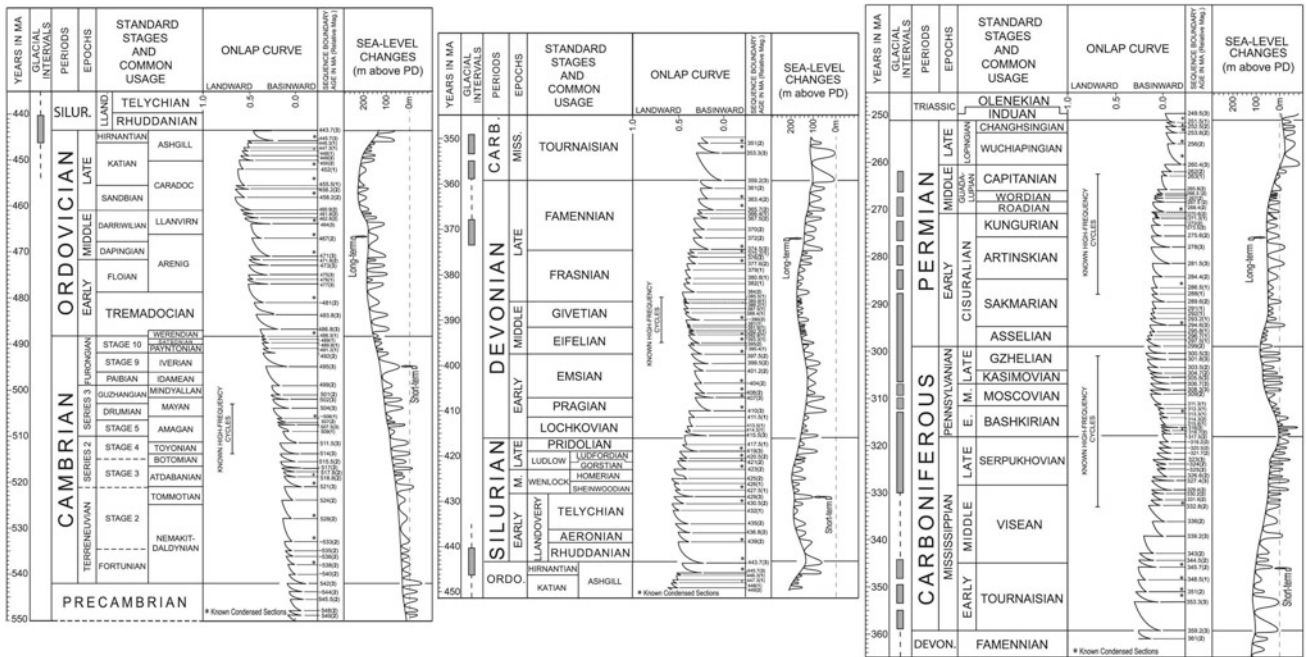


Fig. 5 Sea-level changes during the Paleozoic (after Haq & Stephen, 2008)

the crystalline basement by the latest Cambrian was uplifted forming several cracks and deep valleys that were later filled by the glaciogene deposits.

2.4 Paleozoic Structural Framework of Egypt

2.4.1 Paleozoic Arches

The Paleozoic sediments in Egypt form an extensive platform covering the Precambrian basement and increase in thickness toward the north and west. Older Paleozoic strata crop out near the contact with the basement in Sinai and northern Eastern Desert, while in southern Eastern and Western Deserts, the Paleozoic rocks are exposed over a vast denuded tableland of highly eroded surfaces that came after periods of rigorous uplifting and exposition in southern Egypt. As discussed earlier, the pre-Paleozoic regional tectonic framework highly affected the formation and the deposition of the Paleozoic basins and other Phanerozoic basins as well. The basement arches dissect Egypt into narrow uplifted blocks bounding several low areas in between, the sites where Paleozoic sequences were deposited and experienced many unconformities and vertical and horizontal facies change. The paleogeographic and paleotectonic features that controlled the deposition of the Paleozoic epochs in Egypt and the surrounding areas have been described on maps in Fig. 6 (Guiraud et al., 2001). Nine Paleozoic arches (Fig. 7), bounding the Paleozoic basins, were recognized by Issawi (1996) and Issawi et al. (1999, 2009) and will be described below.

Uweinat-Bahariya arch (Keeley, 1989)—It is oriented NE-SW including the Farafra and Bahariya highs, passing by the western bank of Lake Qarun before it continues to Cairo and reaches the Mediterranean coast immediately to the south of Port Said. This arch was named Uweinat-Bahariya-Port Said arch (UBP) by Issawi et al. (2009).

Tarfawi-Qena-South Sinai arch (TQS)—This arch crosses the Tarfawi basement complex at Bir Tarfawi and includes some basement knobs to the south of Kharga Oasis. Then, it continues to the north of Qena bend and further northeast to Hurghada before it heads to the basement complex at South Sinai.

Chephren-Komombo arch (CKO)—It passes by the basement complex at Chephren Quarries and heads to the north of Komombo plain, where it then disappears in the lineament swarms in the central Eastern Desert.

Umbark arch (Keeley, 1989)—It is a short arch of NE trend and is located in the Siwa Basin. On the isopach maps, Paleozoic sediments were not recorded along the arch (Moussa, 1986).

Suez-Cairo-Dabaa arch (SCD)—This arch strikes WNW-ESE and links between Suez and Cairo, where it is responsible for many structural highs and volcanic flows along the Cairo-Suez road. The arch reaches the Mediterranean Sea near Dabaa.

The North Sinai Fold Belt (Syrian Arc)—It is believed to overlie a series of basement (deep-seated) faults striking ENE-WSW and that were rejuvenated several times during the Phanerozoic. This arc is located in North Sinai and represents a segment of the NE- to ENE-oriented Syrian Arc structures.

Sharib-Sheiba High (Moussa, 1986)—It is located to the north of Abu Gharadig Basin. This arch trends E-W and extends between the Siwa Basin in the west and Fayium Depression in the east. It is also called the Qattara Ridge.

El-Nashfa-El-Balliyna arch—This ridge strikes N to NNW and extends for about 400 km, west of the Nile Valley, from northwest Qena to the south of Fayium area. This arch is known from the drill holes (Nashfa and el-Balliyna wells), where Paleozoic section is nearly missing in most of drilled wells there.

2.4.2 Paleozoic Basins

The early fill of the NE- to ENE-oriented Phanerozoic basins in Egypt, which were located in the vicinity of the Pan-African linear and shear zones, where they first experienced local mechanical subsidence that was rapidly followed by regional thermal subsidence (e.g., Coward & Ries, 2003). These basins were infilled during the Early Paleozoic time which resulted in the formation of well-developed clastic sequences composed mainly of coarse sandstones, rich in quartz, characterizing the basal Paleozoic sections. The contribution of fine-grained clastics and carbonate beds was minor in Egypt, while in neighboring regions (Libya and Saudi Arabia) limited carbonates and fine clastics are common in the Lower Paleozoic rocks. The stratigraphic data in Egypt substantiate the occurrence of a large sedimentary basin covering most of the Egyptian territory and extends to the west and north of the Red Sea Hills (i.e., overlying and flanking the basement complex). Smaller intra-cratonic basins (Fig. 8) do occur within such Egyptian basin, representing the depocenters that depicted that the structural movements took place in different times during the Phanerozoic history of the Egyptian craton. So, the main Egyptian basin is complex and composite (Clifford, 1970). These basins include extensional basins (Gulf of Suez), marginal basins (Siwa and Abu Gharadig), and interior basins (Dakhla and South Nile Valley). Sinai is an exceptional structural basin since it was rejuvenated in many periods during the Phanerozoic time. In the following paragraphs, the

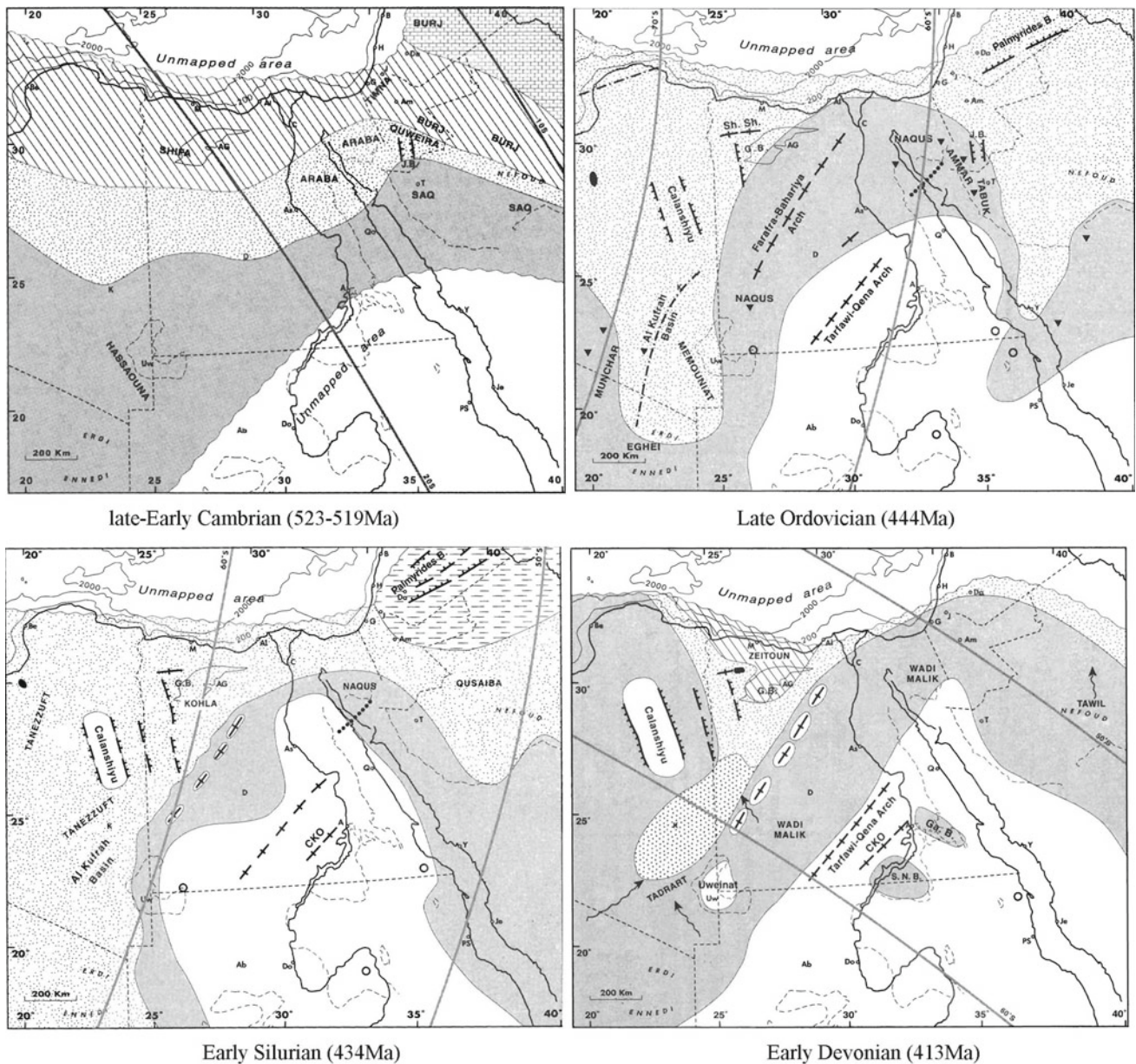


Fig. 6 Paleogeographic/Paleotectonic maps of the Paleozoic epochs (after Guiraud et al., 2001). 1: deep basin, 2: carbonate platform, 3: mixed platform, 4: evaporitic platform, 5: terrigenous platform, 6: fluvatile-deltaic environment, 7: fluvatile-lacustrine environment, 8: exposed land, 9: volcanics, 10: alkaline anorogenic complex, 11: dykes, 12: depocenter, 13: uplifted arch, 14: active normal fault, 15: unspecified active fault, 16: mid-oceanic ridge, 17: direction of sediment supply from paleoriver, 18: tillite, 19: paleomeridian, 20: present-day shoreline, 21: present-day Precambrian basement-sedimentary cover limit, 22: state boundary. A, Aswan; Ab, Djebel Abiod; Al, Alexandria; Am, Amman; As, Assyut; AG, Abu Gharadig; B, Beirut; Be, Benghazi; C, Cairo; D, Dakhla; Da, Damascus; Do, Dongola; G, Gaza; H, Haifa; J, Jerusalem; Je, Jeddah; JB, Jafri Basin; K, al-Kufrah; Kh, Khartoum; M, Matruh; Q, Quseir; PS, Port Sudan; T, Tabuk; Uw, Uweinat; Y, Yambu

Paleozoic Siwa, Dakhla, Abu Gharadig, South Nile, Sinai, and Gulf of Suez basins will be discussed in detail.

Siwa Basin

It was named by Keeley (1989) as Ghazalat Basin. The basin is located in northwestern Egypt occupying the boundary between Egypt and Libya, as well as it opens out along the

Mediterranean coast. From the south, the basin is bounded by the Qattara Depression, while eastward it is limited by the Suez-Cairo-Dabaa arch (SCD). This basin is structurally controlled by E-W-oriented faults where the maximum thickness of the sedimentary fill attains 4700 m. For the description of stratigraphic section and associated lithologic formations, see Keeley (1989) and Issawi et al. (2009) (Fig. 9).

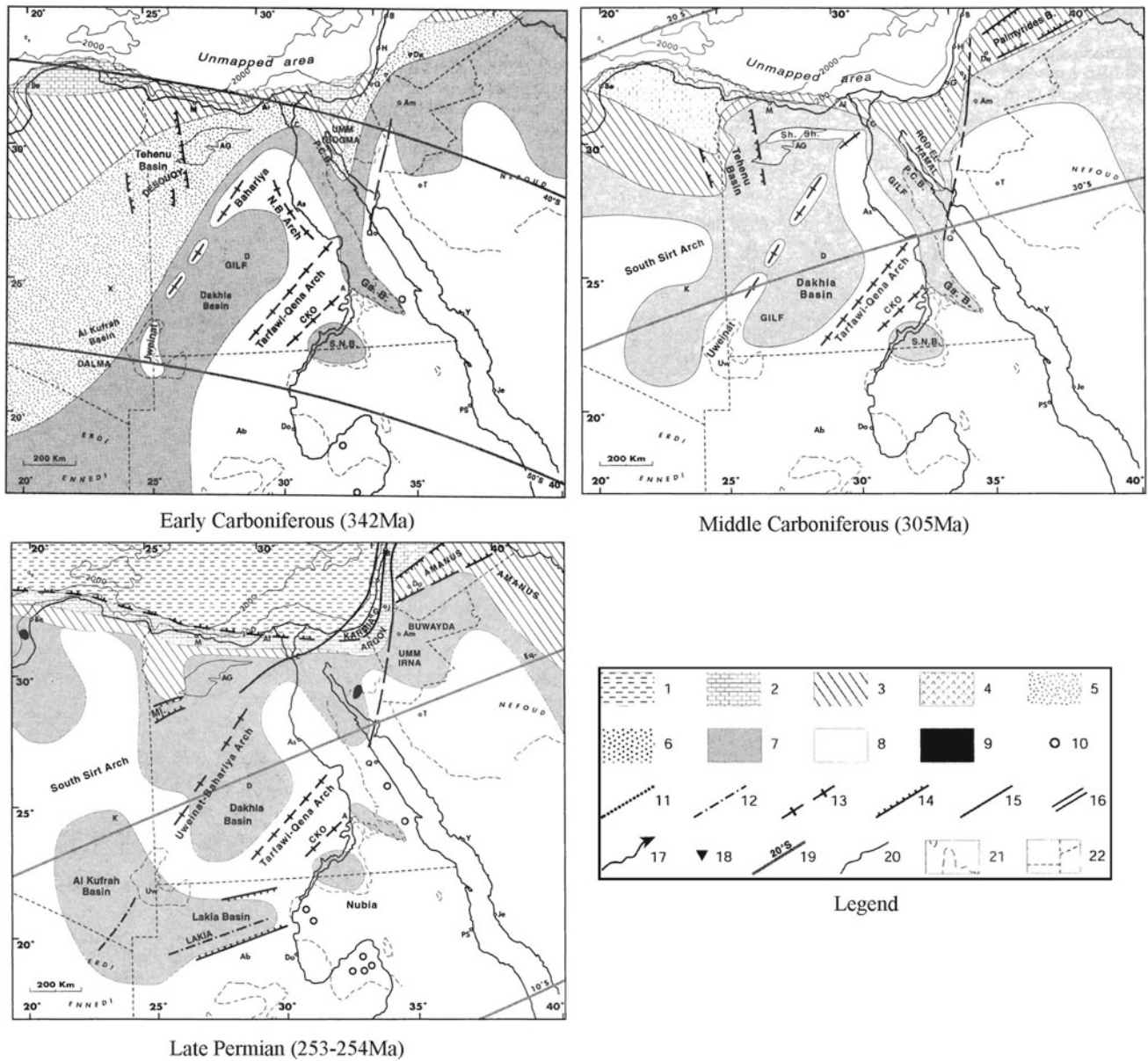


Fig. 6 (continued)

Dakhla Basin

It is a NE-SW-oriented basin, which was recognized from the structural contour map of the Dakhla Oasis (Hermina et al., 1961) and was later extended southward by Issawi (1981) to include most of the Gilf Plateau and the area in its eastern vicinity. This basin is delineated from the south by Gebel Uweinat and Gebel Kamil, while from the east and southeast the basin extended following the Tarfawi-Qena-South Sinai arch (TQS). The Paleozoic–Mesozoic section of the basin is covered by the Cretaceous and younger deposits to the north. The reactivation of the Precambrian E-W faults of the Nubia-Guinea lineaments and

the uplifting of the basement rocks at Uweinat area were responsible for the exposition of the Paleozoic sediments within the basin. The outcrops of the Paleozoic strata are clear on the eastern and western scarps of the Gilf Kebir Plateau and also between the plateau and Gebel Uweinat. The total thickness of Paleozoic strata in the Dakhla Basin is about 1–2 km, where it is approximately missing near or along the TQS arch.

South Nile Basin

This basin is bounded from the east and west by the basement rocks of Red Sea Hills and lies immediately to the west of the

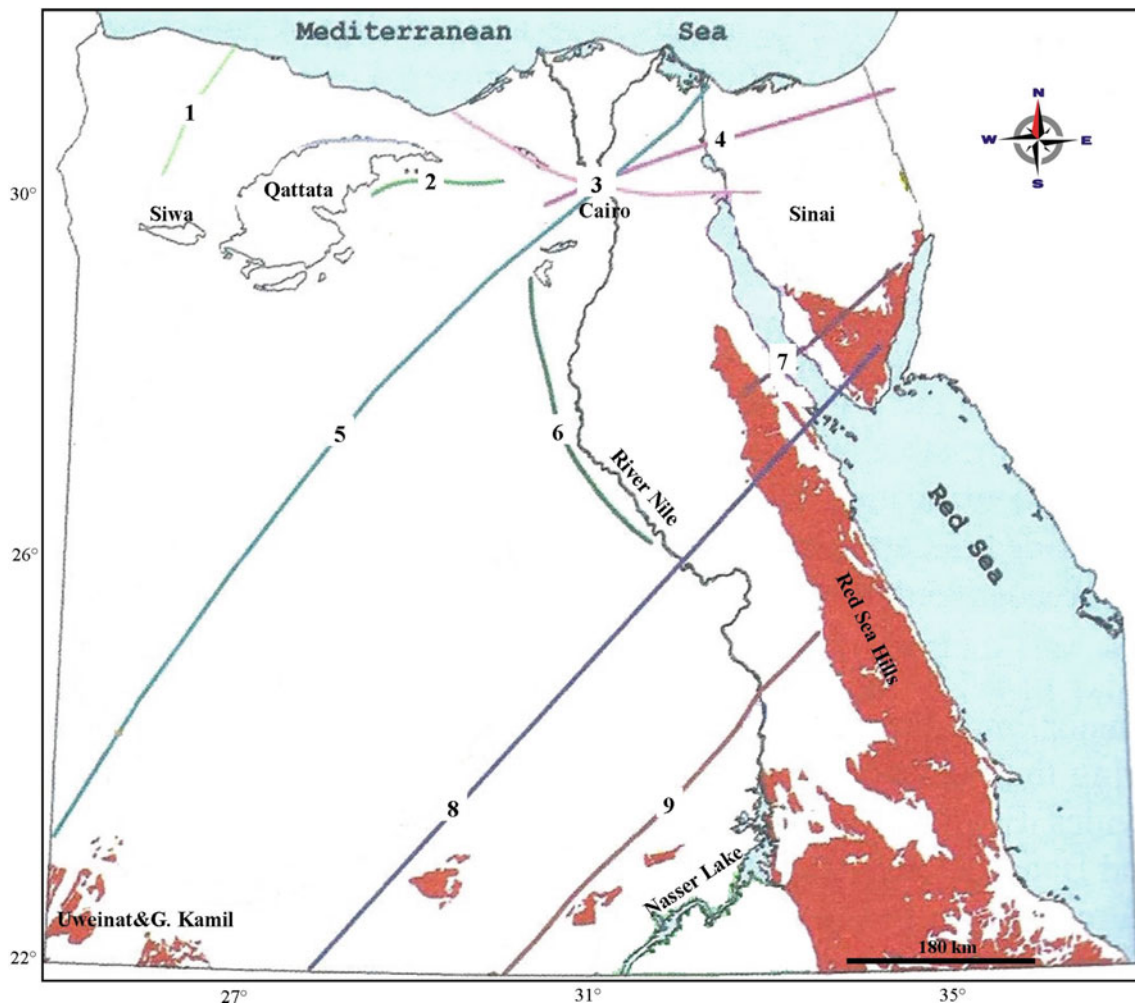


Fig. 7 The distribution of Paleozoic arches in Egypt (modified from Issawi et al., 2009). 1: Umbark arch, 2: Sharib-Shiba arch, 3: Suez-Cairo-Dabaa arch, 4: North Sinai Syrian Arc, 5: Uweinat-Bahariya-Port Said arch, 6: el-Nashfa- el-Balliyana arch, 7: Gharib- Ragaba-Taba arch, 8: Tarfawi-Qena-South Sinai arch, 9: Chephren- Komombo arch

Chephren-Komombo arch (CKO), where Wadi Gabgaba and Korosko Plateau are the main features in this area. Northward, the basin extends until the southern scarps of Sin el-Kaddab Plateau and the Kalabsha Fault. From the south, the basin is bounded by the Egyptian-Sudanese border and may continue to the south within the Sudan. The basin fill is characterized by conglomerates and sandstones with minor paleosol bands, with total thickness assuming 760 m. Most of the sediments in the basin belong to the Paleozoic, unconformably overlying the basement and covered by the Cretaceous and Quaternary rocks. The Paleozoic succession in the basin includes: The Araba (33 m), Gabgaba (447 m), Naqus (15 m), Wadi Malik (40 m), and Gilf (227 m) formations.

Sinai Basin

A large basin located within central Sinai. It was delineated by Issawi et al. (1994) on their Paleozoic map. About

80-m-thick Paleozoic section above the basement rocks was recorded in drill holes at the core of Araif el-Naqa Anticline in eastern Sinai, while westwards at least 500 m of Paleozoic strata were revealed at Nekhl and Kontella. The distribution of the Paleozoic rocks in Sinai basin is discussed in Sect. (2). The Paleozoic succession there attains 1000 m and includes: Taba (8 m), Araba (40–250 m), Naqus (200–300 m), Wadi Malik (15 m), Um Bogma (50 m), Ataqa (35–150 m), Abu Durba (60–180 m), and Aheimer (35–60 m) formations (Issawi et al., 2009).

The Gulf of Suez Basin

The early work of Abdallah and Adindani (1963) described the exposed Paleozoic section on the western shoulder of the Gulf of Suez rift in the Wadi Araba and in the eastern escarpments of North Galala Plateau. The Paleozoic section in these areas ranges in age from Rod el-Hamal Formation

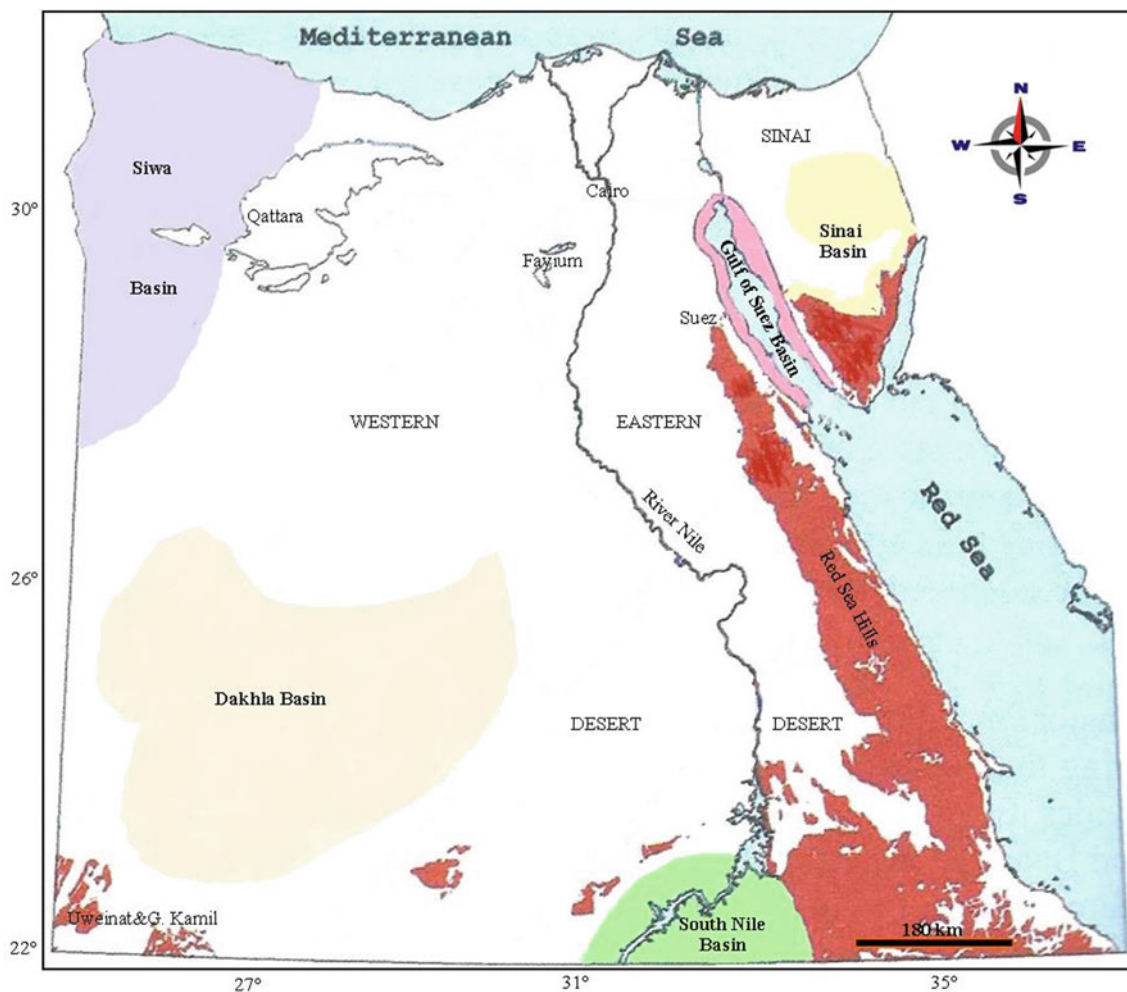


Fig. 8 The distribution of Paleozoic basins in Egypt (modified from Issawi et al., 2009)

(Early Carboniferous, 360 m) passing by Abu Darag Formation (Early-Late Carboniferous), Aheimer Formation (Late Carboniferous-Early Permian) to Qiseib Formation (Permian-Triassic, 52 m). In Issawi et al. (2009), a Paleozoic section was described along a profile covering five faulted blocks at the western coast of the Gulf of Suez stretched from Wadi Esh el-Mallaha on the Red Sea coast to the North Galala Plateau (Fig. 10). Virtually, the profile gives a regional image about the distribution of subsurface and surface Paleozoic rock units. In Block (I), the Araba and Naqus formations were unconformably overlain by the Lower Cretaceous sediments; in Block (II), the Naqus Formation is completely missing, and Lower/Middle Carboniferous sediments overlie the Araba Formation; in Block (III) at St. Paul area, no Paleozoic sediments crop out; in Block (IV) at Wadi Araba, the Paleozoic is represented by latest Devonian and Lower to Upper Carboniferous strata; and Block (V) is almost Carboniferous in age.

3 Mesozoic Structures in Egypt

3.1 Jurassic-Early Cretaceous Rifts

Sometime during the Permian to Early Jurassic, the Neotethys began opening (Fig. 11), and Pangea started breaking up, resulting in the formation of intra-cratonic rift basins in North Africa (Şengör, 1979; Stampfli et al., 2001; Garfunkel, 2004; Guiraud et al., 2005; Yousef et al., 2019) and affected parts of the Arabian plate, where most of the Jurassic source rocks were deposited. The onset of Jurassic rifting (Tethyan rifting) is marked by characteristic rock assemblages of red clastics, a thin evaporitic section, and alkali magmatic intrusions (Bartov et al., 1980a; El Shazly, 1977; Meneisy, 1986).

During these times, the northern passive margin of Gondwana including northern Egypt was subjected to N-S

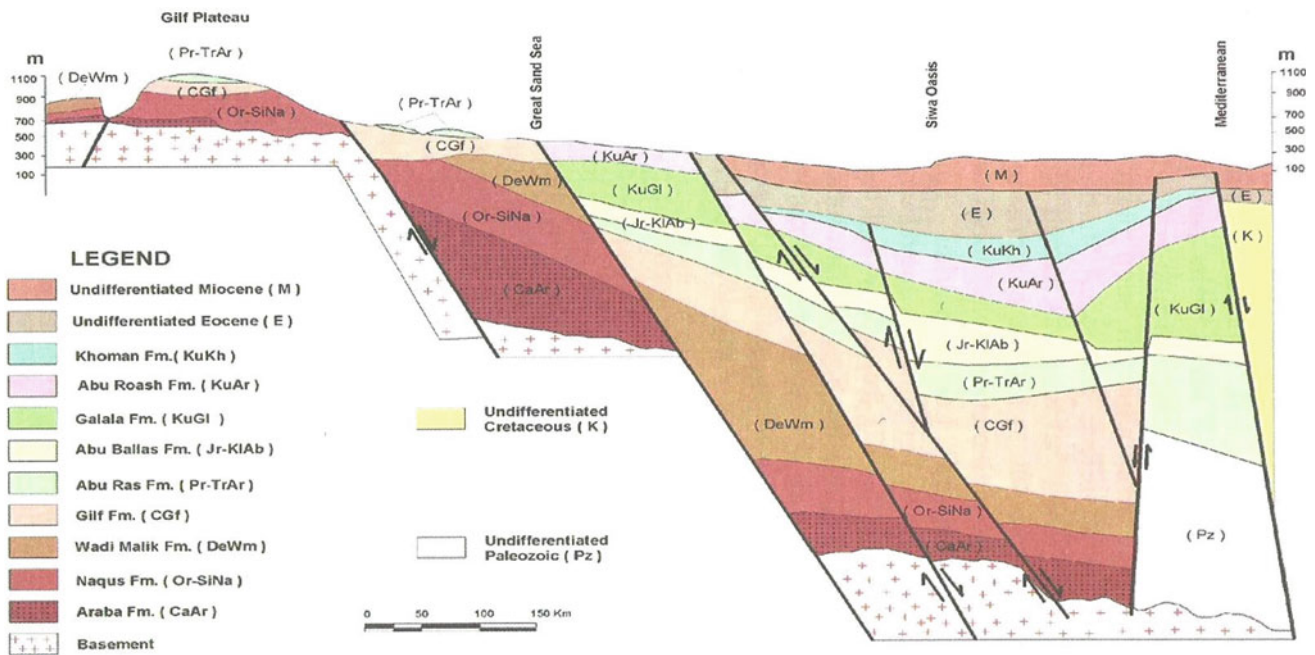


Fig. 9 N-S regional geologic cross-section between the Gifl Kebir Plateau and the Mediterranean showing the distribution of the Paleozoic units within the structurally controlled Siwa Basin (after Issawi et al., 2009)

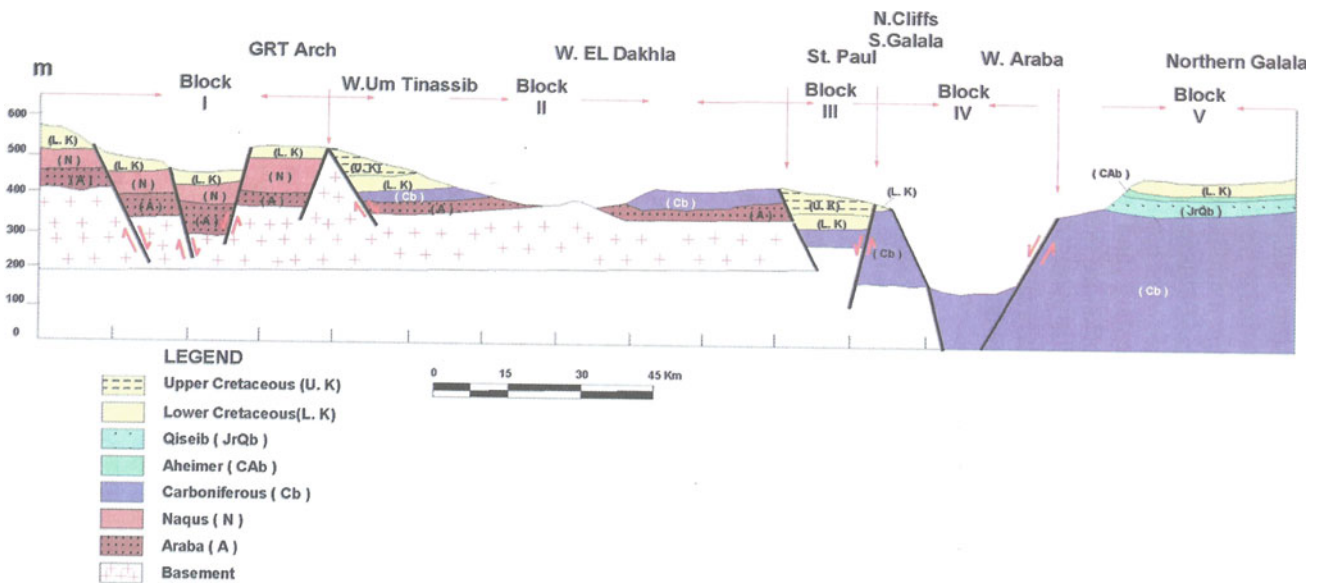


Fig. 10 N-S regional geologic cross-section along the western shoulder of the Gulf of Suez rift (from G. el-Zeit-Esh el-Mallaha to the North Galala Plateau) showing the faulted blocks and GRT arch influencing the deposition and distribution of Paleozoic units (after Issawi et al., 2009)

extension. However, seismic (reflection and refraction), magnetic, and gravity data indicate a WNW-ESE opening direction of the eastern Mediterranean (Fig. 12) developing a left-lateral transform boundary that has separated the oceanic crust of the southern Neotethys from the northern Egypt continental crust (Garfunkel, 1998, 2004; Longacre et al., 2007; Meshref, 1990).

Tethyan rifting resulted in the development of NE-SW- and ENE-WSW-oriented interior rift basins in northern Egypt (Fig. 13), as well as similarly oriented normal faults in central Western Desert (e.g., Bahariya Depression) and southern Western Desert (e.g., Nubia Fault System) (Dolson et al., 2014; Moustafa, 2008, 2020). The only exception is Matruh Basin in northern Western Desert, which is oriented

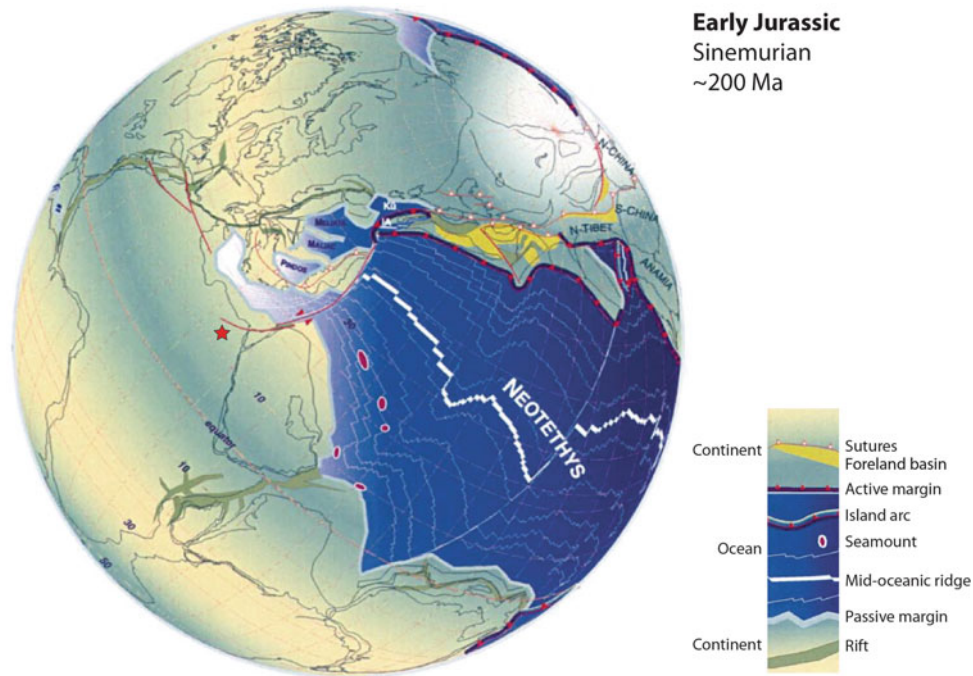


Fig. 11 Paleogeographic reconstructions of the Tethyan area during the Early Jurassic (~ 200 Ma) showing the breakup of Neotethys in relation to the northern margin of Gondwana (compiled from Stampfli & Borel, 2002). Red star represents the location of Egypt

NNE-SSW, most likely due to the influence of the reactivation of deep-seated basement structures (Moustafa et al., 2002). This means that the present structures of the Western Desert of Egypt are superimposed on an intricate system of rift basins of Mesozoic age (Bosworth et al., 2008; Dolson et al., 2014; Guiraud, 1998; Keeley & Wallis, 1991), that links to basins of the same age in Libya to the west, Sinai and Levant to the east, and enclosing the Nubian Shield to the south (Bosworth, 1994; Bosworth et al., 2015; Guiraud, 1998; Guiraud et al., 2005).

Detailed subsurface data shows that red clastics are widespread at the base of the Jurassic section at some localities in the Western Desert, accompanied by thin coal beds (Hantar, 1990; Keeley et al., 1990). In the northeastern side of the Western Desert, an anhydrite section of Early Jurassic age was documented in several wells (Hantar, 1990). This Jurassic section thickens significantly toward the north but shows thinning to the west and south of the Western Desert (Bosworth & Tari, 2021). Minor magmatic activity, accompanied by deposits of fluvial and lacustrine environments, also characterizes this Early Jurassic rifting phase in the northern Western Desert (Moustafa et al., 2002).

During the Late Jurassic, rifting was accompanied by a phase of magmatism that mainly affected the Western Desert (Abbas et al., 2019) and was also recorded in the nearby Sirt Basin in Libya. In Egypt, this rifting phase is generally marked by fluvial and lacustrine deposition, accompanied by estuarine and marine facies (Keeley & Wallis, 1991).

During the transitional stage from the Jurassic to the Cretaceous, northern Egypt witnessed a slight and short-lived compressional event, accompanied by remarkable unconformities in many localities in the Western Desert, North Sinai, and the eastern Mediterranean. Several studies interpreted this phase of deformation as the remote effects of the 'Cimmerian' tectonic event that took place in southeastern Europe (Bosworth et al., 2020; Guiraud et al., 2005; Nikishin et al., 2001; Stampfli et al., 2001; Yousef et al., 2010b). The impact of this event is noticeable in some localities in Faghur (Fig. 14) and East Abu Gharadig (Fig. 15) basins, where Early Cretaceous inversion was interpreted on some of the ENE–WSW-striking faults (Bosworth & Tari, 2021).

During the Early Cretaceous and shortly after the Cimmerian event, rifting witnessed a dramatic increase across most of Gondwana. As in the Jurassic, extension stayed mostly N-S resulting in the fastest phase of subsidence in many basins across northern Egypt (Fig. 16; Bosworth et al., 2020; Yousef et al., 2010b). Fluvial and estuarine siliciclastic deposits prevailed during the Early Cretaceous in the basins of eastern North Africa. Moving northward, these facies first change into shallow marine carbonates and shale before they completely change to deep marine facies (Keeley et al., 1990; Norton, 1967).

Geometrically, Early Mesozoic rift basins in the Western Desert are half grabens tilting NNW and are bounded by normal faults on the NW sides (Fig. 17). However, the

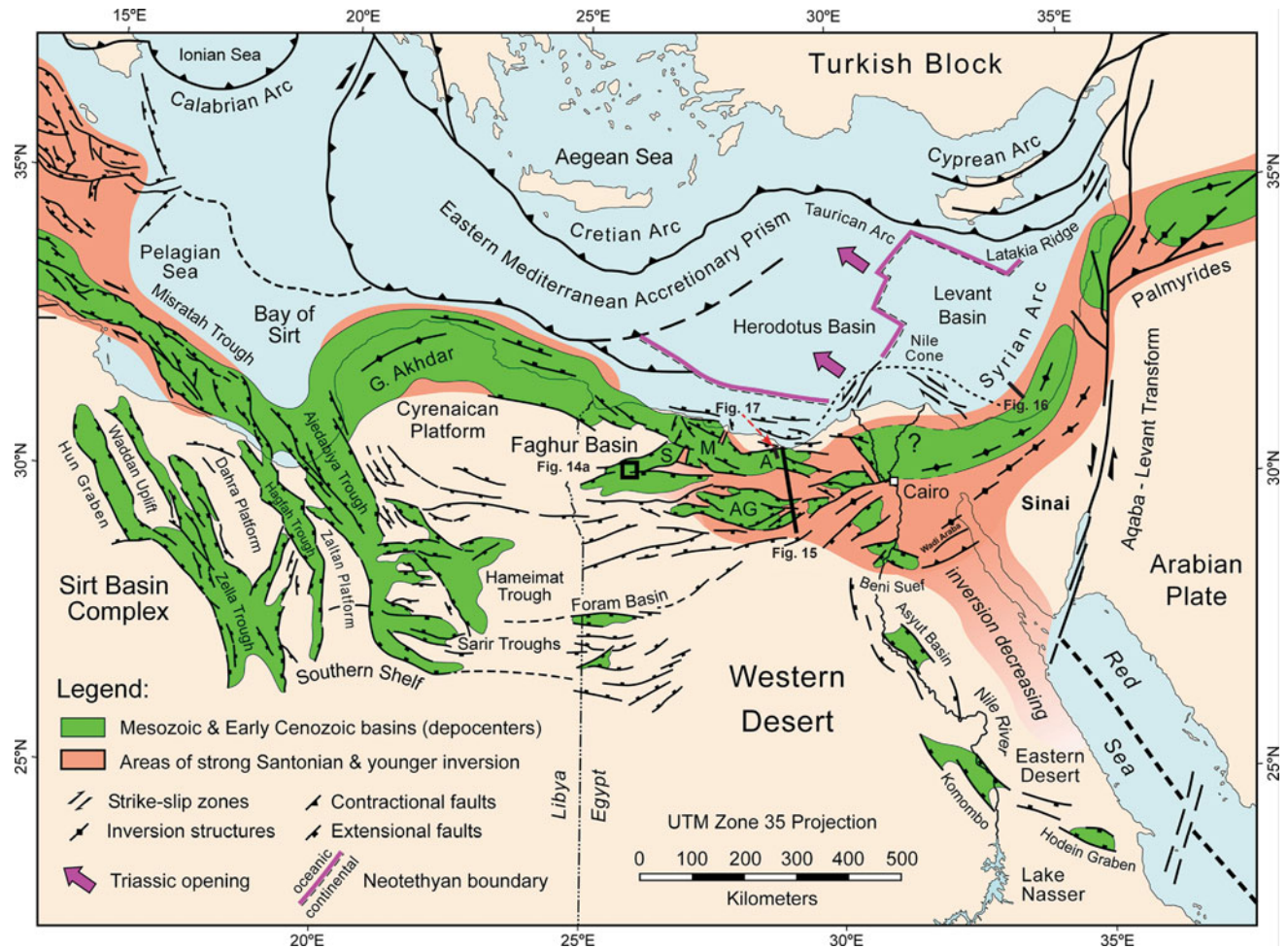


Fig. 12 Regional geologic setting of northeast Africa and eastern Mediterranean (after Bosworth & Tari, 2021). A: Alamein Basin; AG: Abu Gharadig Basin; M: Matruh Basin; S: Shushan Basin. Triassic opening direction and Neotethyan oceanic–continental crustal boundary after Longacre et al. (2007)

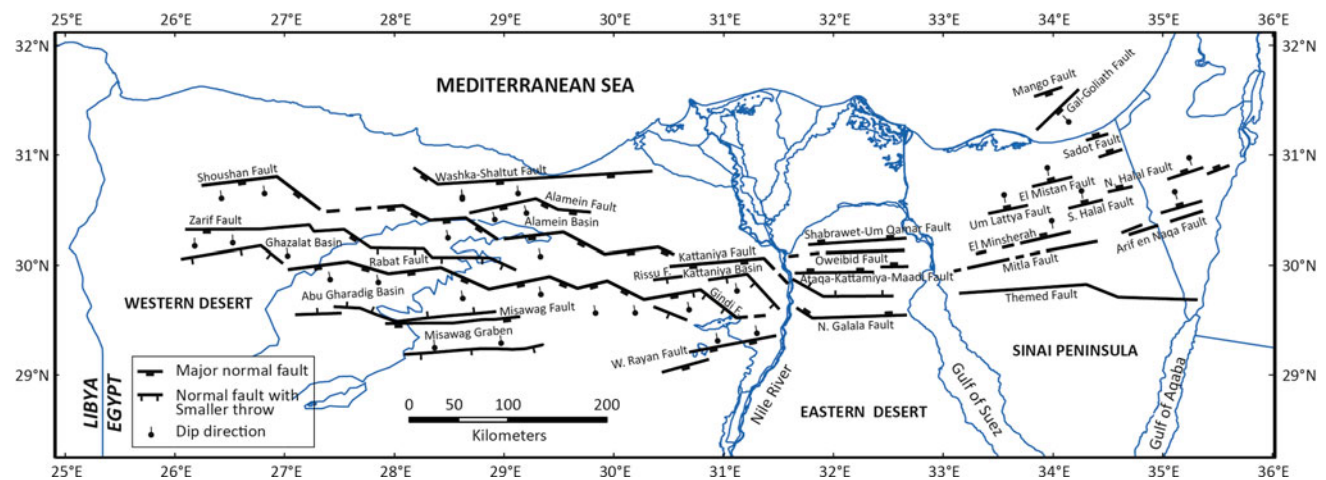


Fig. 13 NE-SW- and ENE-WSW-oriented Jurassic-Early Cretaceous rift basins in northern Egypt (redrawn after Moustafa et al., 1998). Offshore North Sinai structures are after Yousef et al., (2006a, 2006b; 2010b)

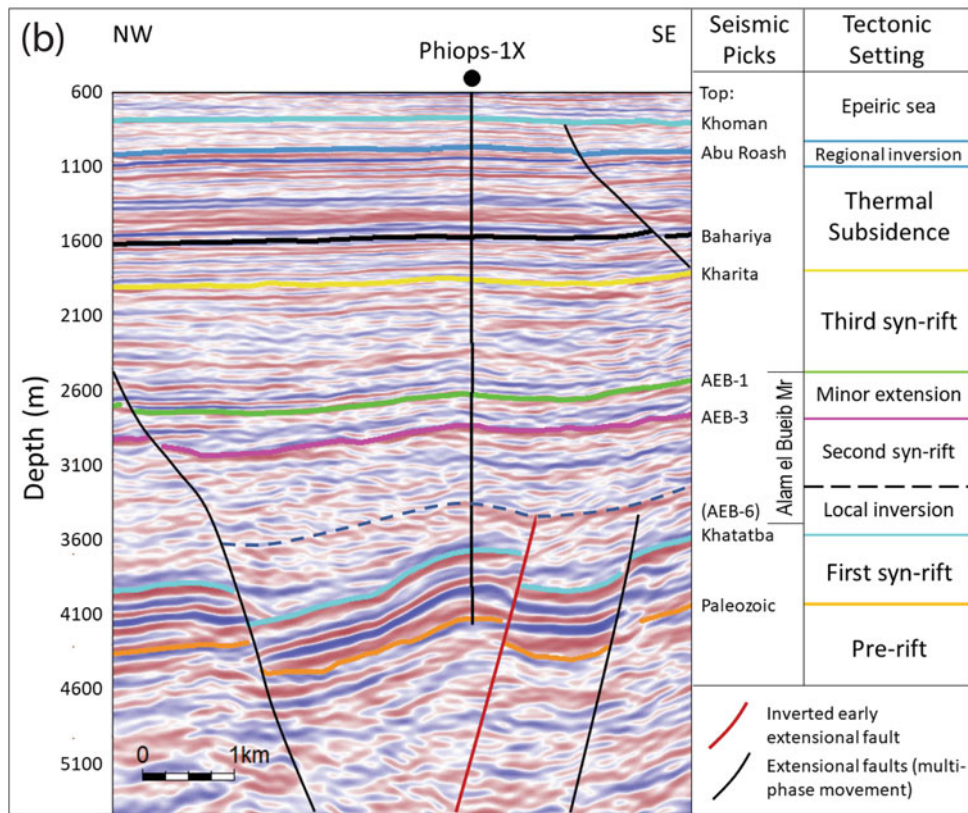
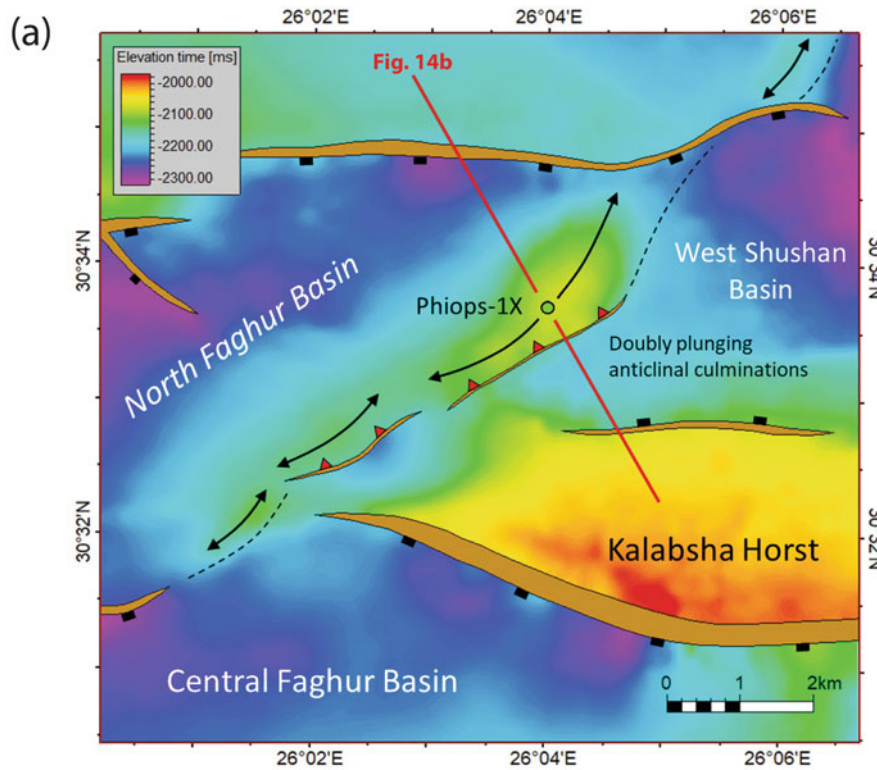


Fig. 14 a Time-structure map of top Khatatba Formation (Middle Jurassic) showing the Phiops inverted structure in eastern North Faghur Basin. See Fig. 12 for location. b NW-SE seismic section crossing the inversion anticline at Phiops field. See Fig. 14a for location (after Bosworth & Tari, 2021)

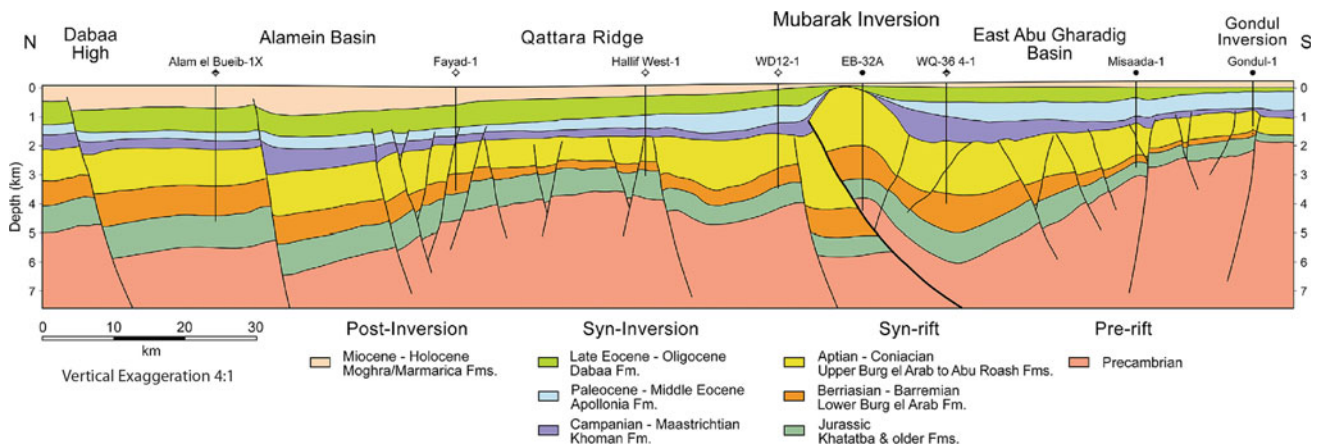


Fig. 15 N-S regional geoseismic section through the eastern area of the Western Desert showing the Mubarak inverted structure. See Fig. 12 for location (after Bosworth et al., 2008)

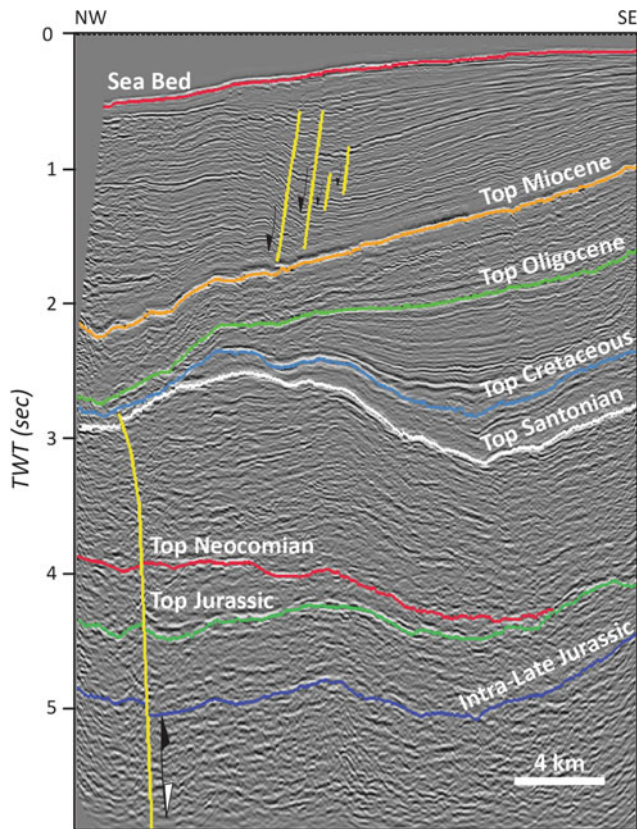


Fig. 16 NW-SE seismic section through Mango inverted half graben (offshore North Sinai) showing Early Cretaceous syn-rift basin fill. See Fig. 12 for location (after Yousef et al., 2010b)

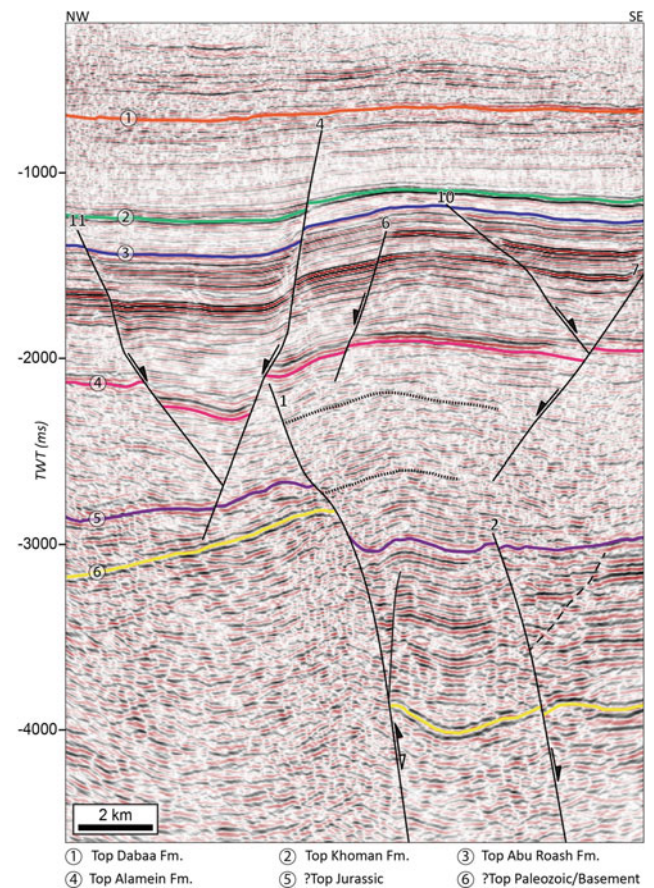


Fig. 17 NW-SE seismic section through Horus inverted half graben (Alamein Basin). The half graben is tilting NNW and bounded at its NW side by the ENE-WSW-striking Horus Fault. See Fig. 12 for location (after Yousef et al., 2019)

extension of these basins into the Eastern Desert and northern Sinai displays a change in polarity (Fig. 13), where these basins are similarly oriented, but their bounding normal faults lie on the opposite sides of the basins (Moustafa et al., 1998). Detailed subsurface data confirm that Jurassic and Lower Cretaceous rocks were deposited in these half

grabens, with a characteristic syn-rift deposition (Abd El Aziz et al., 1998; Guiraud, 1998; Yousef et al., 2010b, 2019).

3.2 Cretaceous Rifts

Following the previous Jurassic-Early Cretaceous rifting phases (~ 130 Ma), extension orientation throughout most of northern Gondwana changed to a NE-SW direction (Guiraud, 1998; Guiraud & Bosworth, 1999; Guiraud et al., 2005). During the Aptian-Albian (~ 125 Ma) and after a maximum marine flooding event, Egypt witnessed the impact of the far-field stress caused by the onset of the South Atlantic rifting (Fig. 18), which in turn initiated a remarkable rifting phase in northern Gondwana that created several NW-SE to WNW-ESE rift basins in Egypt (Fig. 19) with a predominant fluvial and shallow marine conditions (Bosworth et al., 2020; Norton, 1967; Said, 1962). Mid-Cretaceous intercalated volcanic rocks and siliciclastic sediments are found in several localities in the Western Desert and the Eastern Desert, as well as in the nearby Sirt Basin in Libya (Meneisy & Kreuzer, 1974a, 1974b;

Bosworth et al., 2020). However, during the Cenomanian-Turonian, a rise in sea level created another maximum flooding event that affected the Western Desert, establishing a phase of tectonic quiescence (Bosworth & Tari, 2021; Kerdany & Cherif, 1990; Said, 1962).

Cretaceous rift basins in Egypt are Beni Sueif and Asyut basins in central Egypt, and Komombo Basin in southern Egypt (Fig. 20). Abu Gharadig Basin in the northern Western Desert is also a Cretaceous rift basin. However, some of its sub-basins witnessed their rifting onset during the Late Jurassic. Subsurface data show that these basins/sub-basins are bounded by NW-SE- to WNW-ESE-striking normal faults, against which syn-rift successions of Cretaceous age thicken. All four of these basins are of half graben geometry, except Beni Sueif Basin, which is a graben (Fig. 20; Salem & Sehim, 2017). While Abu Gharadig and Komombo basins (Fig. 21) tilt northward, Beni Sueif and Asyut basins tilt southward.

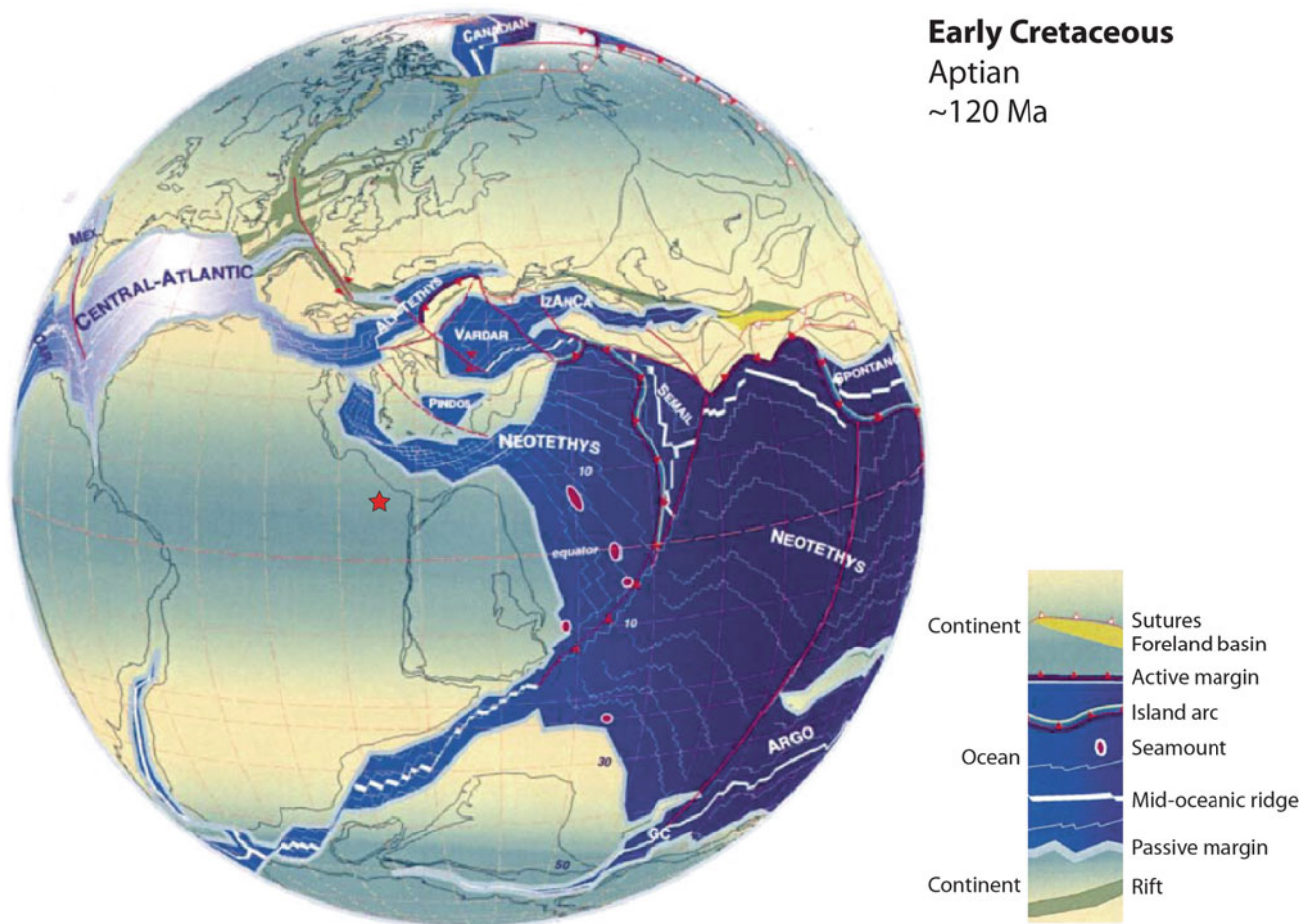


Fig. 18 Paleogeographic reconstructions of the Tethyan area during the Early Cretaceous (~ 120 Ma) showing the onset of the South Atlantic rifting (compiled from Stampfli & Borel, 2002). Red star represents the location of Egypt

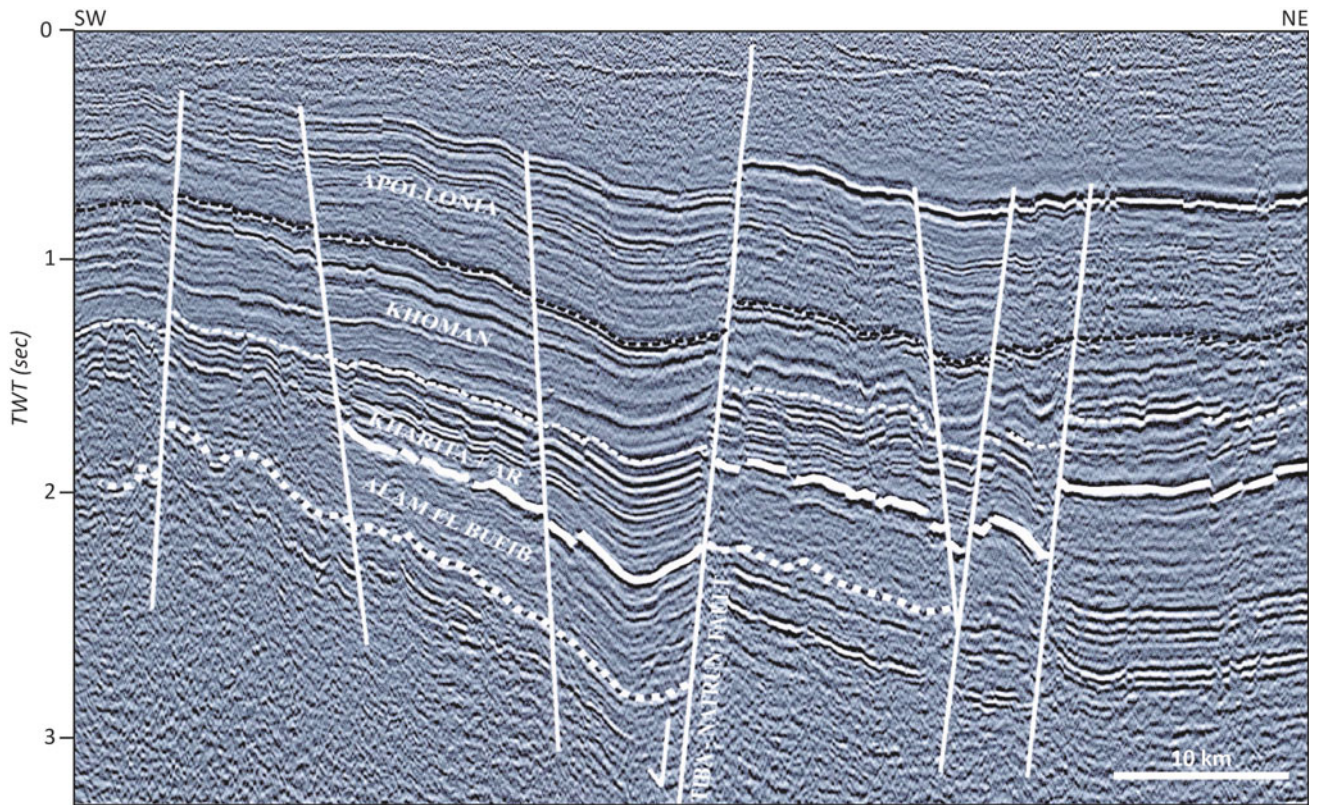


Fig. 19 NE-SW seismic section showing the Cretaceous rifting in the northern Western Desert. Rift-bounding faults are striking WNW-ESE (after Moustafa, 2008)

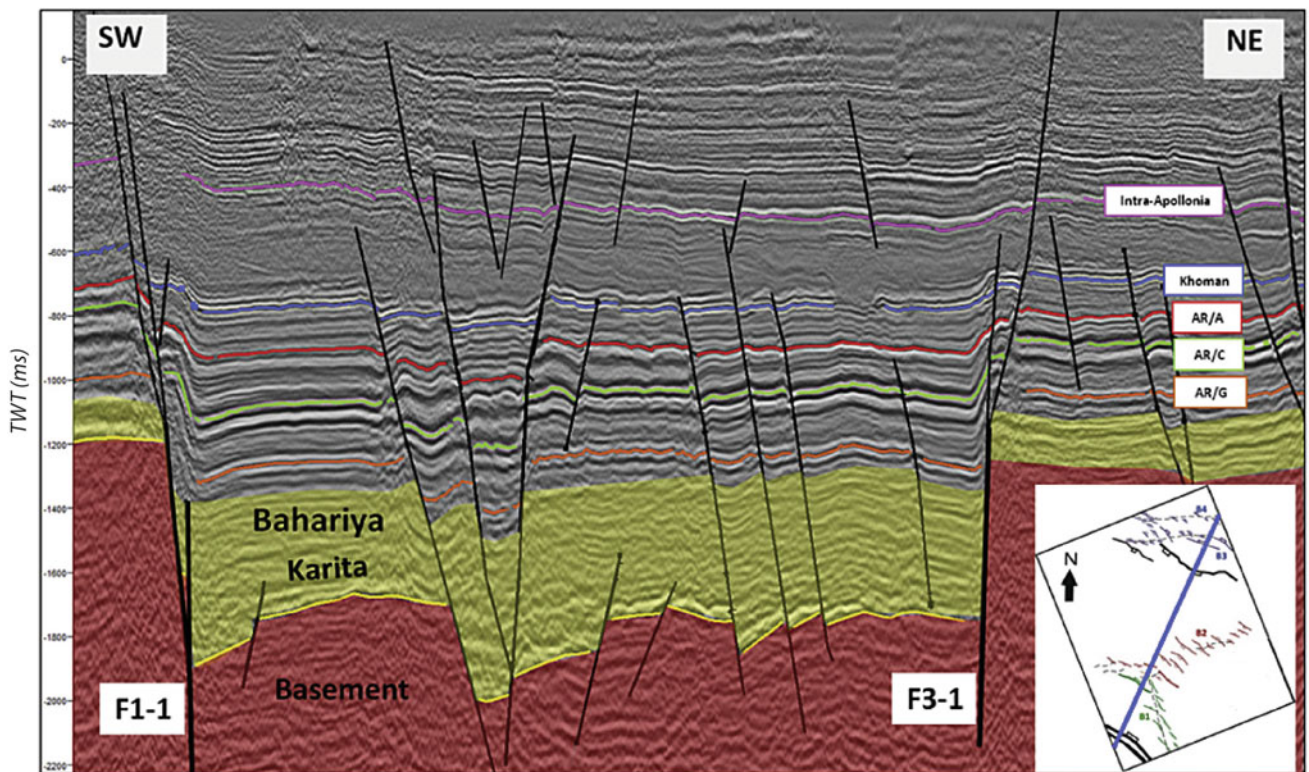


Fig. 20 NE-SW seismic section through East Beni Suef Basin showing the graben geometry (after Salem & Sehim, 2017)

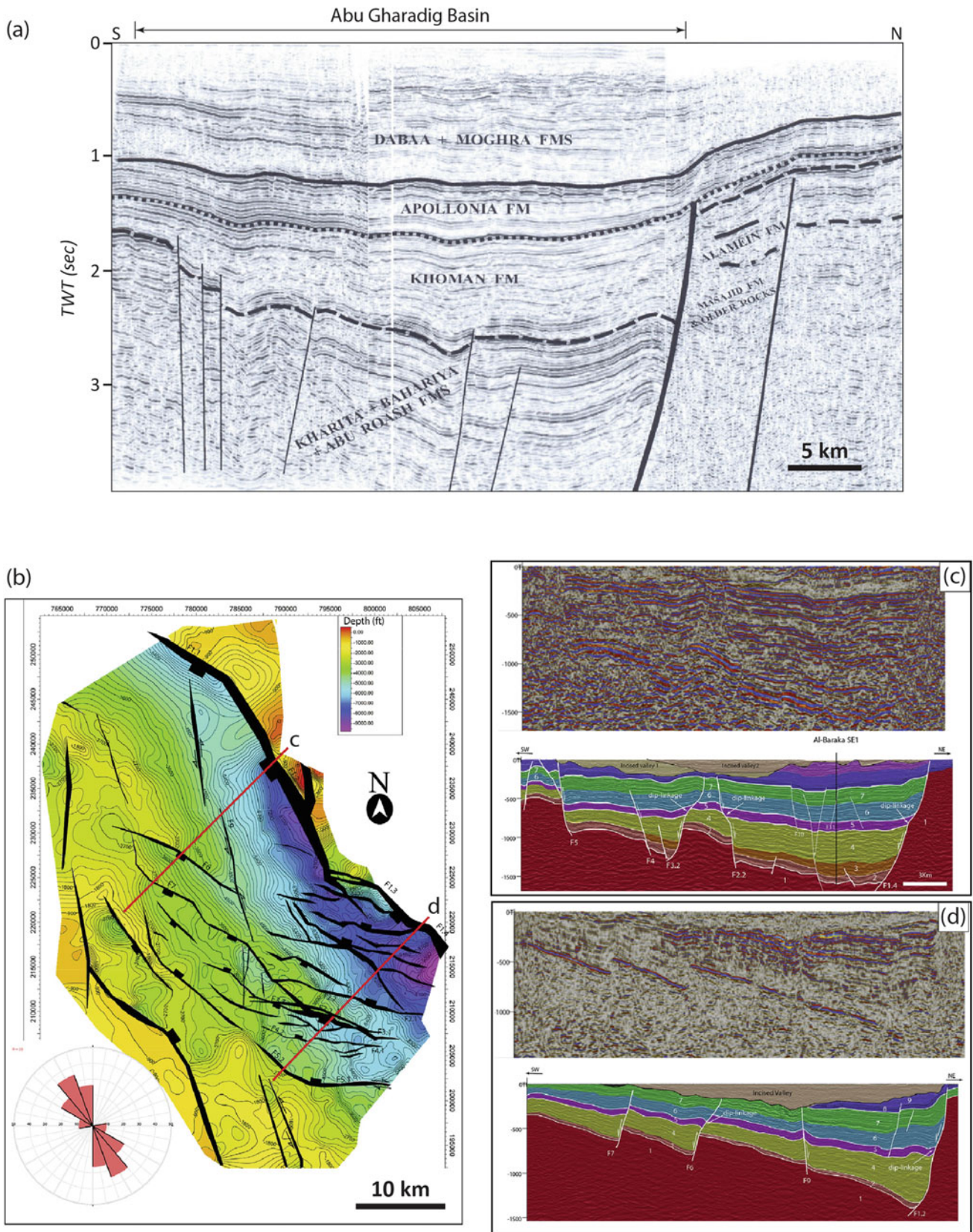


Fig. 21 a N-S seismic section through Abu Gharadig Basin showing the northward tilt of the half graben (after Moustafa, 2008). b Depth-structure map of top crystalline basement, southern Komombo Basin showing the northeast tilt of the half graben (after Said & Sakran, 2020). c and d Uninterpreted and interpreted NE-SW seismic sections (see Fig. 21b for location) across the southern Komombo Basin (after Said & Sakran, 2020)

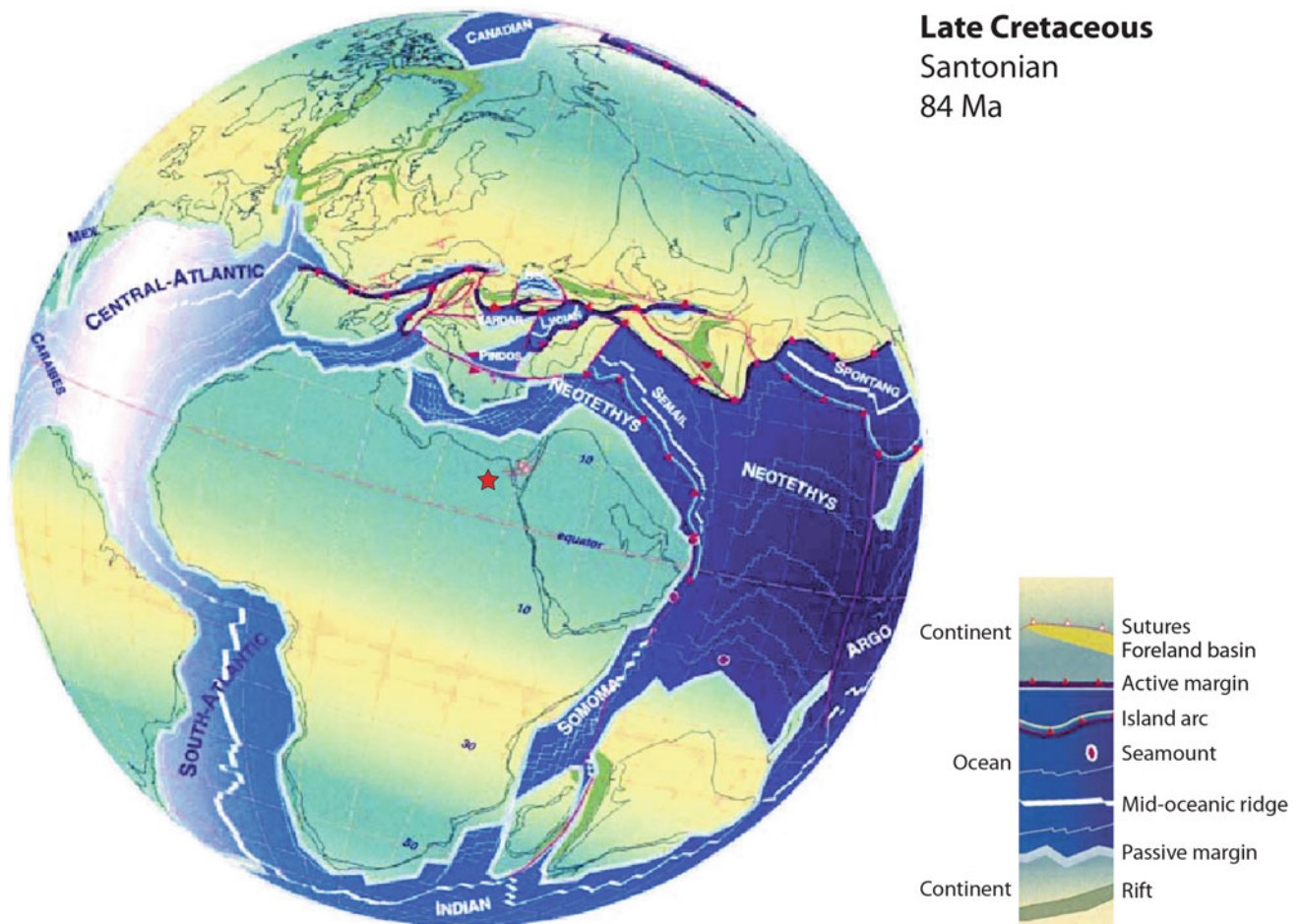


Fig. 22 Paleogeographic reconstructions of the Tethyan area during the Late Cretaceous (84 Ma) showing the closure of Neotethys and the convergence of Afro-Arabian and Eurasian plates (compiled from Stampfli & Borel, 2002). Red star represents the location of Egypt

3.3 Late Cretaceous to Recent Inverted Structures

In the Late Cretaceous (84 Ma), Egypt witnessed the direct effects of major plate rearrangements, known as the ‘Santonian event’, resulting from the drastic change in the Afro-Arabian and Eurasian plate movements (Fig. 22) from divergence across the Neotethys to convergence that continues to the present day in select localities (Smith, 1971; Guiraud & Bosworth, 1997; Bosworth et al., 2008; Bevan & Moustafa, 2012; Abd El-Fattah, 2021). Even though other compressional phases affected Egypt during the Phanerozoic, this event remains the most prominent and impactful compressional tectonic event (Bosworth & Tari, 2021; Bosworth et al., 2020). This is synchronous with what has become to be known as the Cretaceous Normal Magnetic Quiet Zone, which suggests that the crustal deformation caused by this event can be associated with internal processes of the lower mantle and core (Guiraud & Bosworth, 1997).

The Santonian event, though short lived, is considered the most impactful far-field compressional event affecting northern Gondwana to date (Abd El-Fattah, 2021; Bosworth et al., 2020). It is mainly responsible for the closure of the Neotethys, which in turn caused a change in regional stress regime, across the Afro-Arabian plate, from extension to N-S to NW–SE compression (Bosworth et al., 2020; Guiraud & Bosworth, 1997; Yousef et al., 2010b), resulting in the formation of the ‘Syrian Arc’ structures of Krenkel (1925), Fig. 12. This involves thrusting to the west in the Atlas fold belts of Morocco, Algeria, and Tunisia (Ben Ferjani et al., 1990; Letouzey & Trémolières, 1980). Moving eastward, the effects of the Santonian event include the inversion of the Cyrenaica Basin in Libya, as well as the inversion of several Jurassic half grabens and the formation of inversion folds that extend across northern Egypt and into the Palmyrides in Syria (Bartov et al., 1980a; Patton et al., 1994; Sehim, 1993).

At the Egyptian-Libyan border, the magnitude of Late Cretaceous inversion is very gentle to almost absent. This

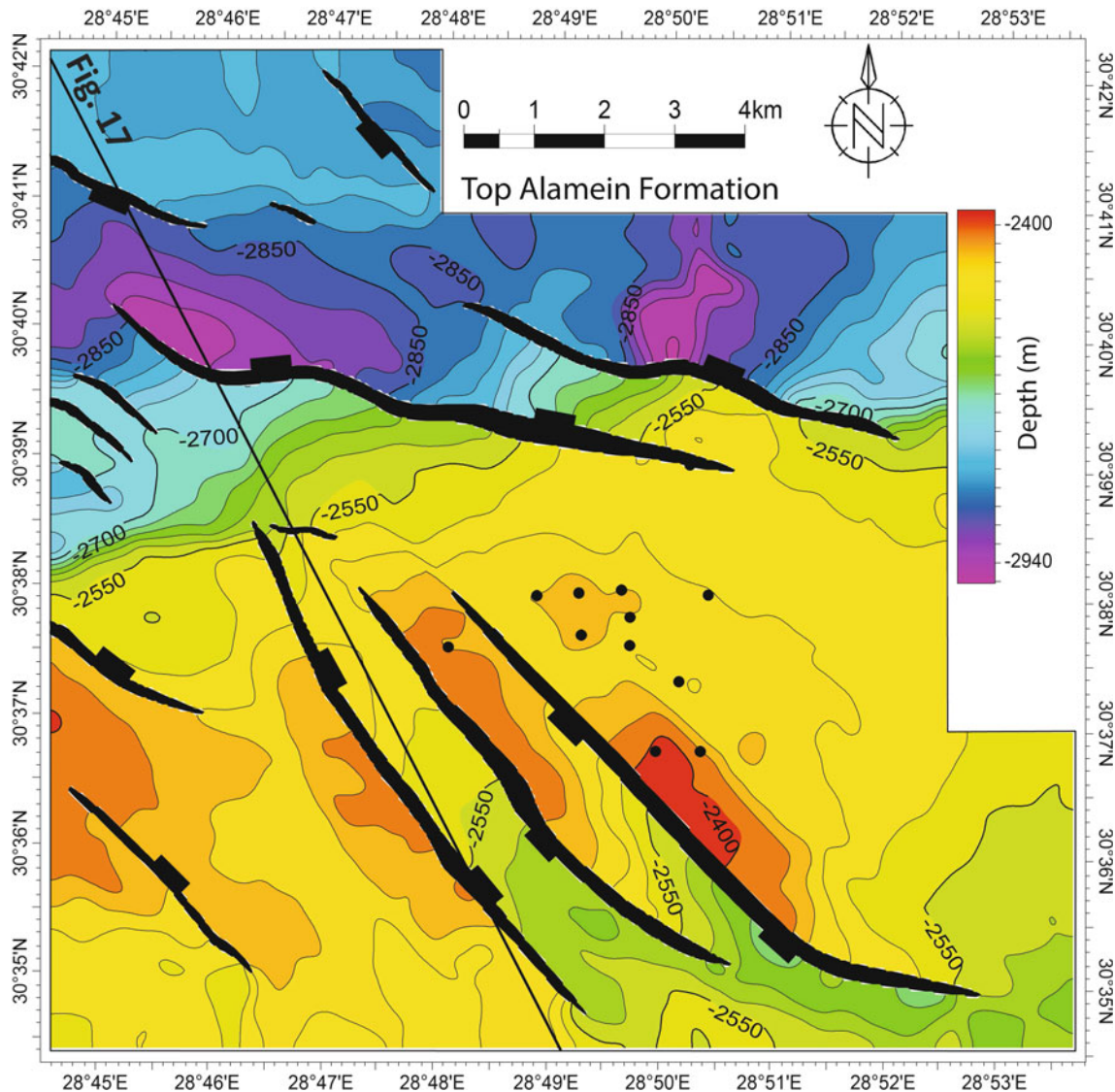


Fig. 23 Depth-structure map of top Alamein Formation (top Aptian) showing the left-stepping en echelon WNW-ESE-striking normal faults dissecting the NW steep flank of the major inversion anticline in Horus field, Alamein Basin (after Yousef et al., 2019). Position of Fig. 17 is indicated

could be interpreted that the indentation of Cyrenaica in Libya absorbed most of the effect of the Afro-Arabian-Eurasian convergence resulting in milder inversion south of Cyrenaica (Bosworth et al., 2008).

A common claim among the available early literature is that the Jurassic to Early Cretaceous rift basins of northern Egypt underwent positive structural inversion resulting from pure compression (Ayyad & Darwish, 1996; Bevan & Moustafa, 2012). However, other studies interpreted some inverted structures in specific localities (e.g., Abu Roash outcrop, Mitla pass (North Sinai), and the Themed Fault (central Sinai), among others) to have undergone wrench deformation (Moustafa, 1988, 2013; Sehim, 1993). However, detailed surface/subsurface mapping indicate that inversion was dominantly compressional with a minor

component of strike-slip (Moustafa, 2010; Yousef et al., 2010a, 2019). Moving southward, the impact of this compressional event can be observed as the ENE-striking faults of the Bahariya Depression, as well as the southern part of the Western Desert, were reactivated by dextral transpression (Issawi, 1968; Sakran & Said, 2018).

Recent studies informed by detailed seismic and borehole data confirmed that certain inverted structures were formed by transpression that is dominantly compressional, with a minor component of strike-slip. In Alamein Basin, Late Cretaceous-Early Cenozoic left-stepping en echelon WNW-ESE-striking normal faults, which are not aligned normal to the inversion anticline, dissect its steep flank (Fig. 23; Yousef et al., 2019). In BED 17 field (Abu Gharadig Basin), inversion caused the reactivation of preexisting

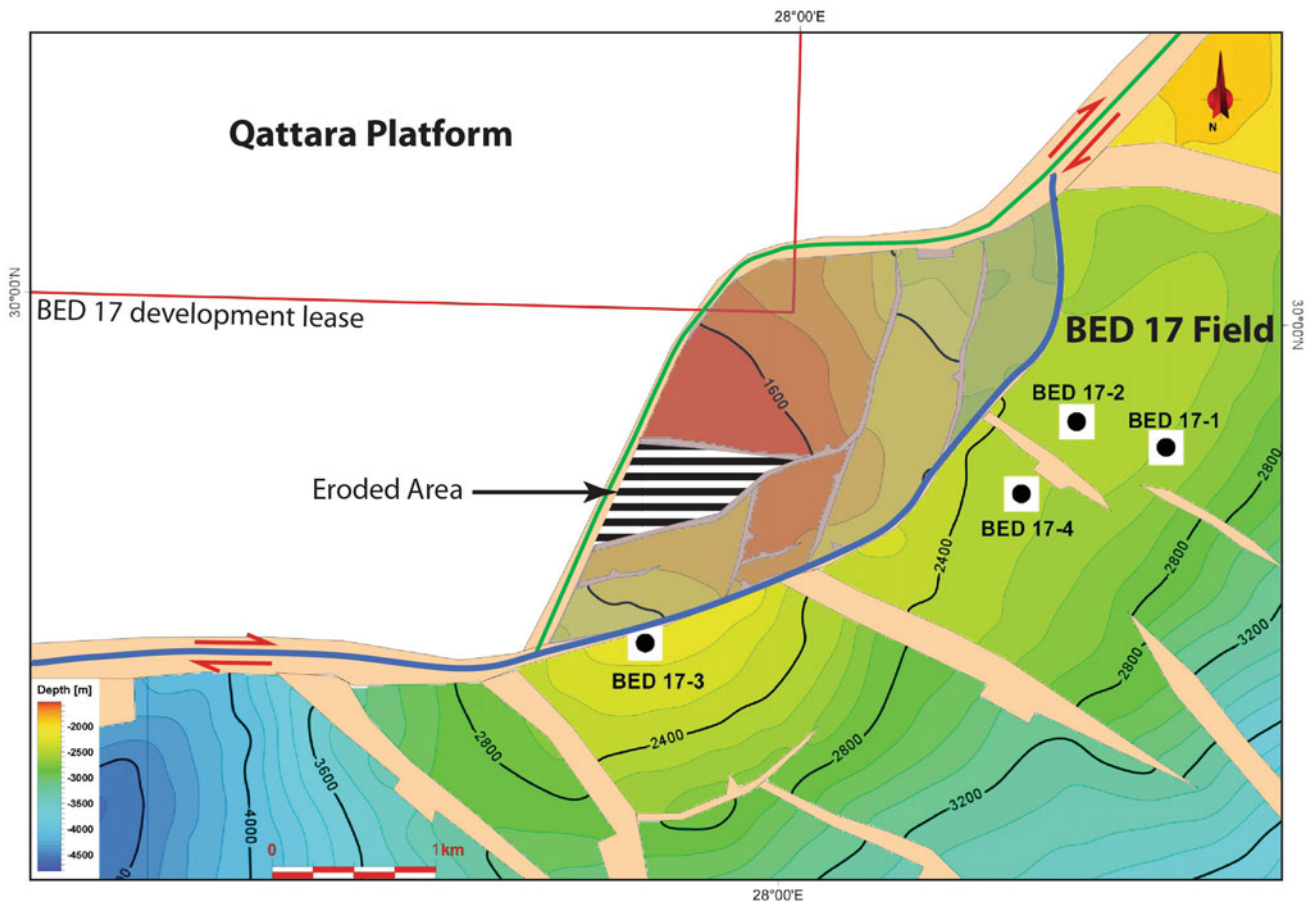


Fig. 24 Depth-structure map of top Abu Roash “C” Member showing a pop-up inversion structure developed by the transpressional reactivation of preexisting E-W-striking normal faults in BED 17 field, Abu Gharadig Basin (after Salah et al., 2014)

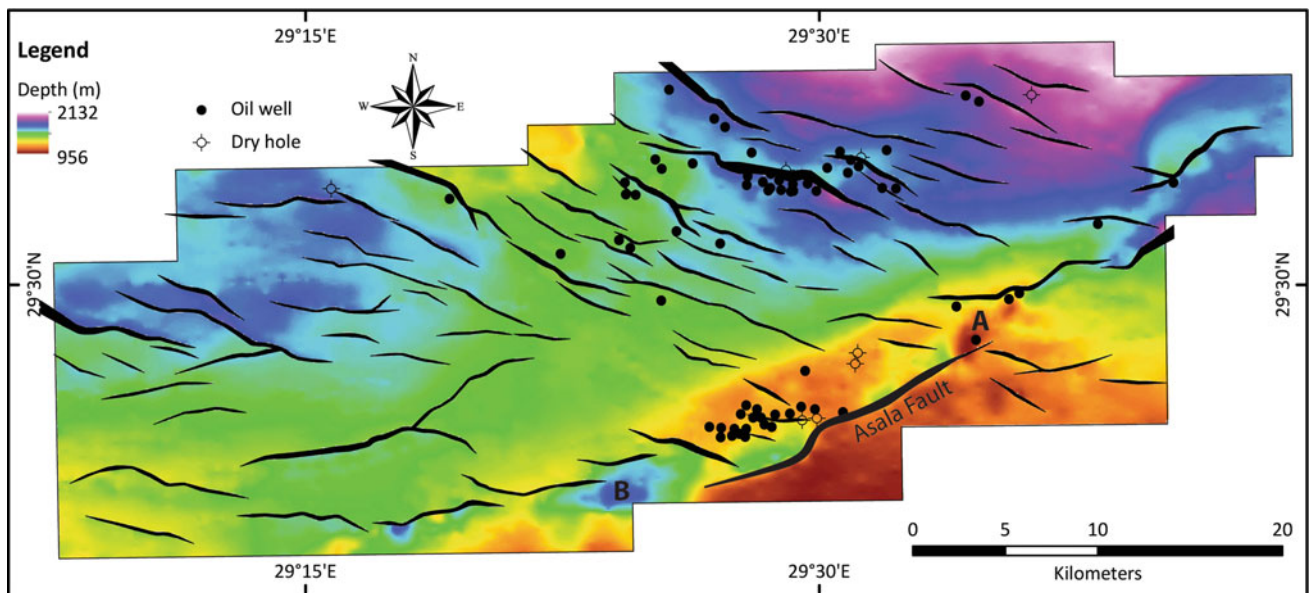


Fig. 25 Depth-structure map of top Coniacian in East Bahariya concession (eastern Abu Gharadig Basin). Area marked by letter A represents a pop-up structure lying between two left-stepping en echelon segments of Asala Fault, whereas area marked by letter B represents a pull-apart structure lying between two right-stepping en echelon segments of Asala Fault (after Yousef et al., 2009, 2010a)

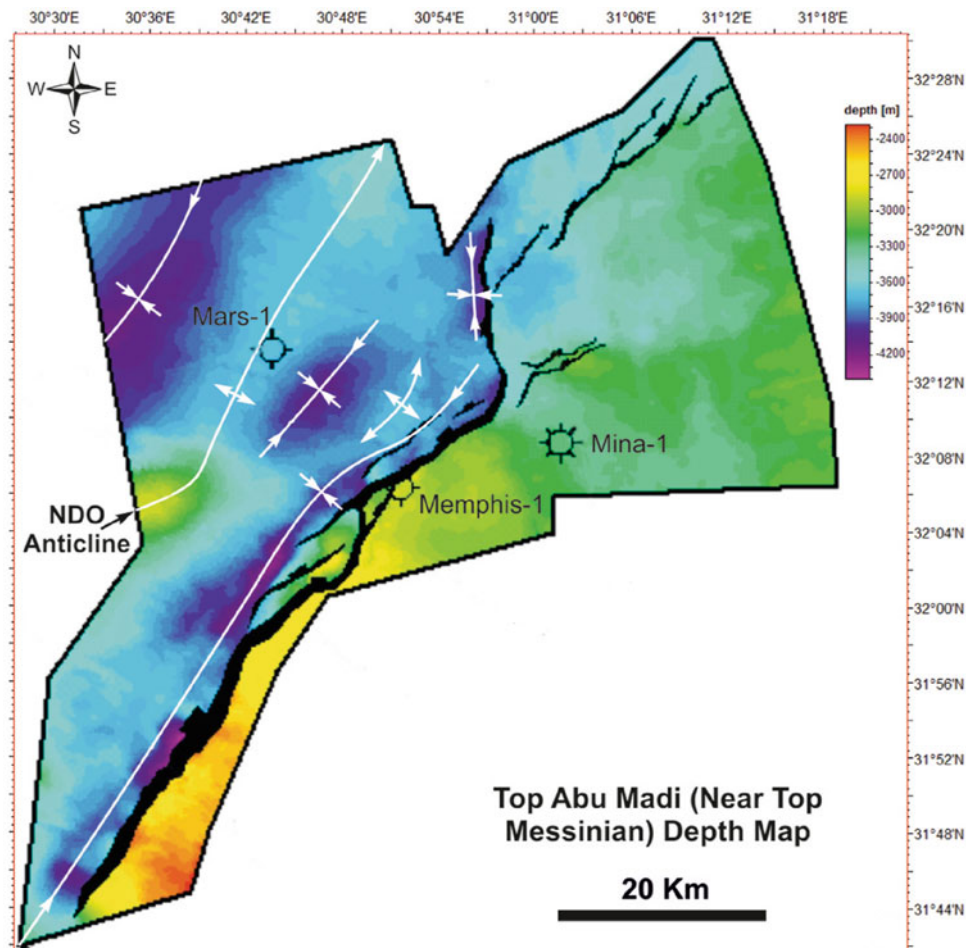


Fig. 26 Depth-structure map of top Abu Madi Formation (near top Messinian) showing NE-SW-oriented folds in the hanging-wall of Rosetta Fault, western offshore Nile Delta (after Abd El-Fattah et al., 2021)

E-W-striking normal faults, resulting in the formation of a pop-up structure and a NE-oriented asymmetric fold (Fig. 24; Salah et al., 2014). Oblique-slip reactivation of the Asala Fault created a similar pop-up structure in East Bahariya concession, eastern Abu Gharadig Basin (Fig. 25; Yousef et al., 2009, 2010a).

A recent study by Abd El-Fattah et al. (2021) revealed that northern Egypt is still witnessing the effects of the continuous African and Eurasian plate convergence to the present day, as indicated by the reactivation of the Rosetta Fault in the western offshore Nile Delta by sinistral transtension, and the formation of NE-SW-oriented folds in the Herodotus Basin at present time (Fig. 26).

Inversion anticlines across northern Egypt are mostly NE-SW oriented, except in some localities where they change orientation slightly due to the difference in basin-bounding faults orientation. The NE-SW-oriented inversion folds are dissected by NW-SE-striking normal faults. Moustafa (2008) believes that these faults were formed as

the result of NE-SW extension contemporaneous with the NW-SE compression associated with basin inversion.

Ayyad and Darwish (1996) reported that Jurassic to Early Cretaceous basins of northern Egypt underwent positive inversion during the Late Cretaceous compressional phases, which continued into the Early Cenozoic time, in concurrence with the closure of the Neotethys. However, recent studies disputed this belief considering new detailed subsurface data. Yousef et al. (2019) concluded that inversion continued until the Oligocene-Early Miocene in Horus field (Alamein Basin), Fig. 17. Bevan and Moustafa (2012) also observed that the Late Cretaceous-Eocene rocks vary in thickness in the vicinity of the elevated core of the Mubarak inverted structure. They concluded that inversion extended into the Miocene as well (Fig. 15). Yousef et al. (2006a, 2006b; 2010b) observed a similar timing of positive inversion in offshore north Sinai, where the inversion was synchronous with or shortly after the deposition of Oligocene succession and continued to the top Langhian (Middle

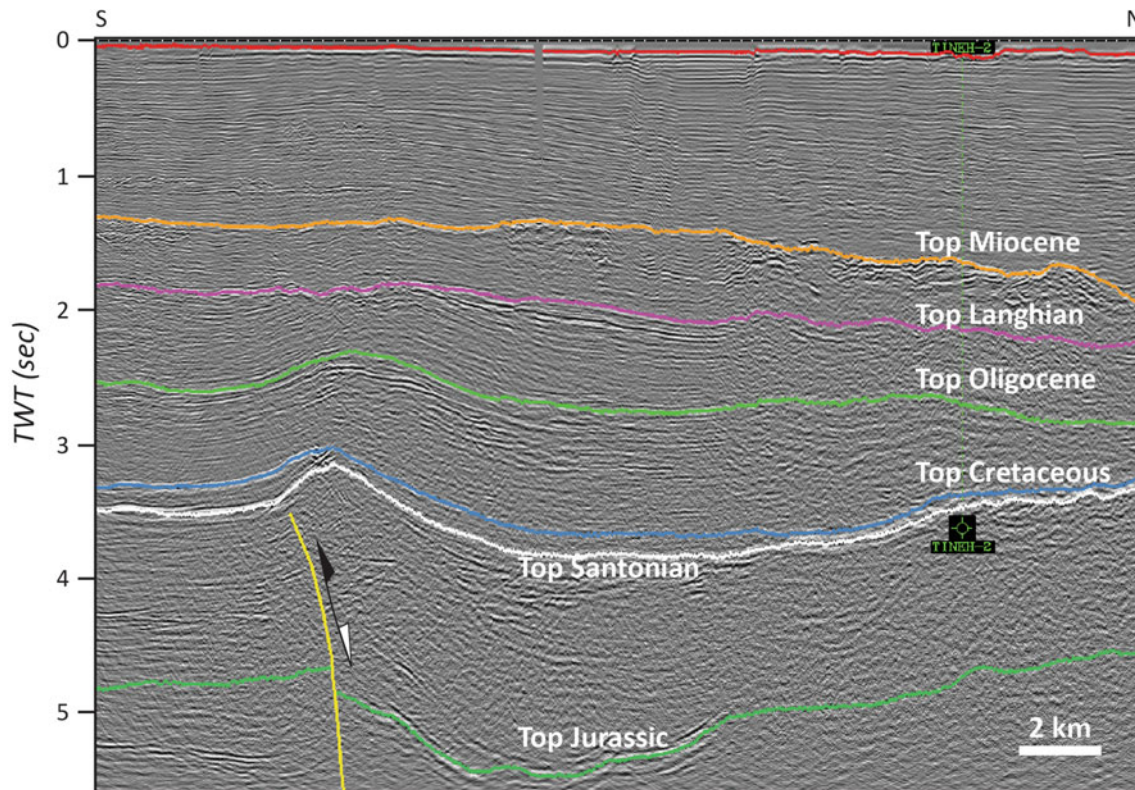


Fig. 27 N-S seismic section showing top Langhian (Middle Miocene) unconformity resulting from the positive inversion in offshore North Sinai (after Yousef et al. 2006a, 2006b)

Miocene), Fig. 27. In the following paragraphs, a detailed account of the inverted structures of northern Egypt will be discussed.

3.3.1 Northern Western Desert Inverted Structures

During the Late Cretaceous, the positive inversion of Jurassic-Early Cretaceous rift-bounding faults resulted in the formation of asymmetric doubly plunging inversion folds in the northern Western Desert that are oriented NE-SW, except for Shoushan-Matruh Basin where they are NNE-SSE oriented, due to the control of preexisting structural trends (Moustafa et al., 2002).

Kattaniya inverted structure—Lying in the eastern part of the northern Western Desert, and slightly extending across the Nile River into the Eastern Desert, Kattaniya Basin is a completely inverted basin (Fig. 28). This Jurassic-Early Cretaceous NW-dipping half graben underwent Late Cretaceous inversion, which resulted in the formation of a large NE-SW-oriented asymmetric anticline, often referred to as the Kattaniya High (Abd El-Aziz et al., 1998; Nemeč, 1996). This inversion created a foredeep basin (Gindi Basin), to the southeast of the Kattaniya Basin, where thick syn-inversion stratigraphic units of Paleocene-Eocene age were deposited (Fig. 28).

Mubarak inverted structure—To the southwest of the Kattaniya inversion anticline lies the Mubarak structure of Bevan and Moustafa (2012), which is another inversion anticline that lies to the east of Abu Gharadig Basin (Fig. 15). This NE-SW-oriented inversion anticline shows a relatively milder inversion than its neighboring Kattaniya anticline (Moustafa, 2020). This structure shows signs of inversion up until the latest Oligocene, as indicated by Campanian to Eocene syn-inversion units (Bevan & Moustafa, 2012).

Alamein inverted structure—Lying to the northwest of Kattaniya Basin, Alamein Basin is a partially inverted Jurassic-Early Cretaceous half graben, with a NE-striking main bounding fault on its northwestern side (Figs. 15 and 17). The available seismic reflection data suggest that this basin could either contain a series of en echelon NE-oriented doubly plunging inversion anticlines, or one large asymmetric inversion anticline (Moustafa, 2008). The basin was subjected to a mild magnitude of inversion, which did not allow for the main bounding fault to propagate through the post-rift rocks, resulting in a fault-propagation fold lying above the inverted fault (Yousef et al., 2019). Earlier studies of this basin suggested that this huge anticline is the result of wrench deformation (Bakr & Helmy, 1990; El-Shaarawy et al., 1992). However, recent studies suggested that it is an

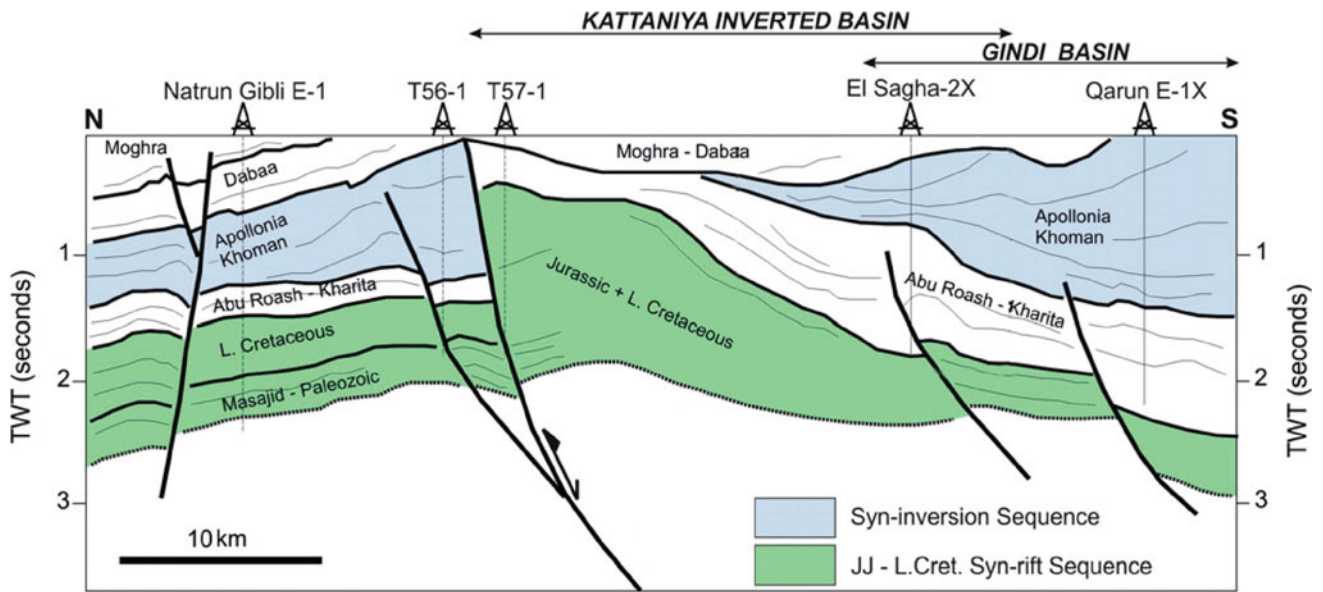


Fig. 28 Geoseismic section of the Kattaniya inverted structure (after Moustafa, 2020)

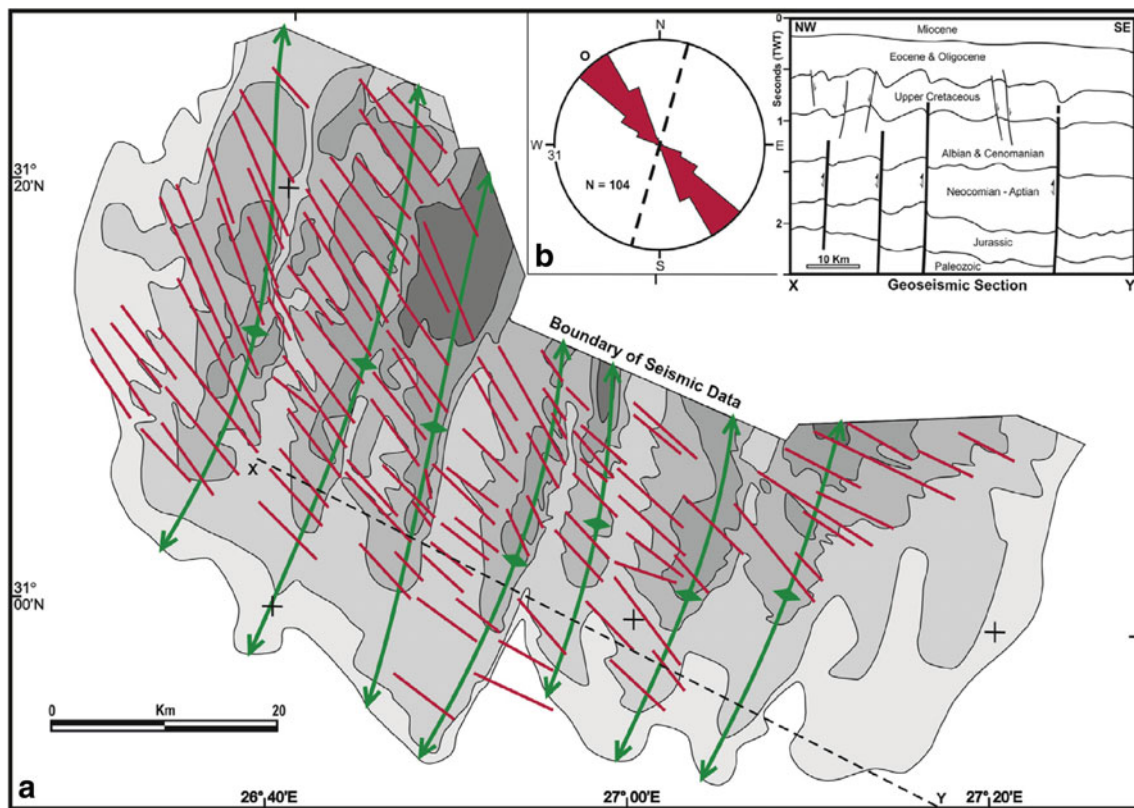


Fig. 29 Matruh Basin inversion anticlines. **a** Time-structure map of top Turonian inversion anticlines in Matruh Basin. Shading represents elevation with the darkest representing the highest. **b** Rose diagram showing the trend of the faults dissecting the anticlines. The bold dashed line represents the average trend of the anticlines (after Moustafa et al., 2002)

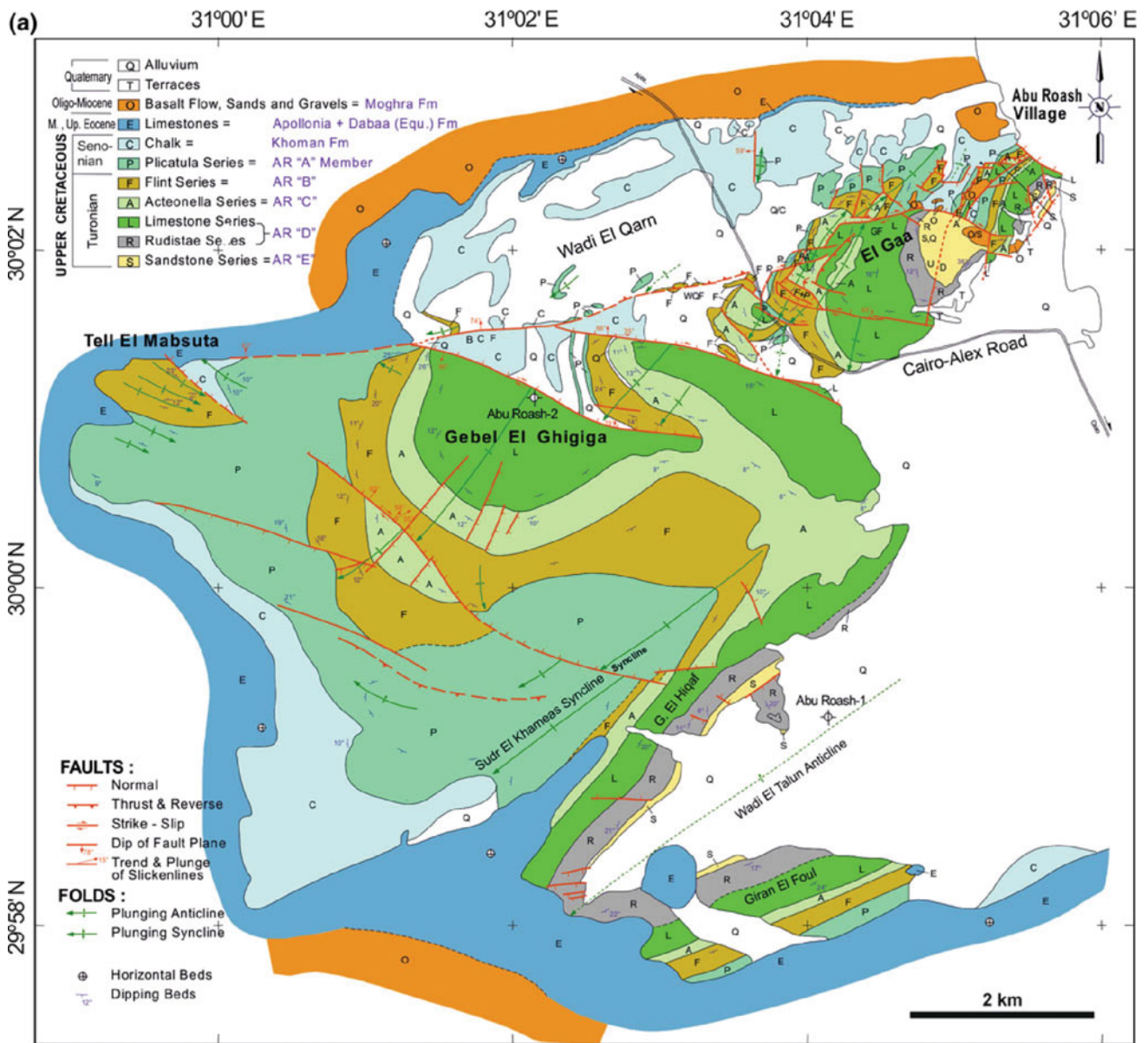


Fig. 30 a Detailed geologic map of Abu Roash area (after Moustafa, 1988). b 3D model showing the development of pop-up structures in the area (after Moustafa, 2020)



Fig. 31 Landsat TM image of North Sinai showing the Sinai Hinge Belt separating the inversion anticlines of Gebels Mahgara, Yelleg, Halal, and the Hamayir–Amrar area from the central Sinai gently folded area. Black arrow represents the compressive stress direction at Late Cretaceous–Cenozoic time (after Moustafa, 2010)

inversion anticline (Ayyad & Darwish, 1996; Darwish & Tewfik, 2008). This was later confirmed by a study supported by 3D seismic and borehole data by Yousef et al. (2015, 2019), who indicated that the formation of this Late Cretaceous–Miocene inversion anticline was not the result of pure compression but involved a minor strike-slip component.

Shoushan–Matruh inverted structures—Shoushan–Matruh Basin is located in the northwestern part of the Western Desert (Fig. 12). Seven Late Cretaceous–pre-Late Eocene NNE-oriented asymmetric inversion anticlines with E vergence exist in Matruh Basin (Fig. 29) and are controlled by preexisting Jurassic–Early Cretaceous NNE–SSW-striking normal faults (Metwalli & Pigott, 2005; Moustafa et al., 2002; Tari et al., 2012). Moving westward, inverted fault trends in Shoushan Basin change to ENE–WSW and NE–SW.

Abu Gharadig inverted structures—Abu Gharadig Basin is a rift basin tending in an E–W direction that lies in the

central part of the northern Western Desert (Figs. 12 and 21a), bounded to the north by E–W, NE-, and NW-striking fault segments (El Saadany, 2008). While this rift basin is of Cretaceous age, some of its NE–SW-oriented sub-basins opened during the Jurassic rifting. Santonian–Oligocene inversion led to the rejuvenation of the Jurassic–Early Cretaceous extensional faults, creating three main inverted structures: the Abu Sennan Anticline, the Abu Gharadig Anticline, and the Mid-Basin Arch (Moustafa, 2020). Inversion in this basin was most likely accompanied by dextral slip displacement on the main bounding fault segments, forming a pop-up structure between the left-stepping E–W-striking faults (Said et al., 2014; Salah et al., 2014). At the southeastern part of Abu Gharadig Basin lies the Jurassic–Early Cretaceous Asala Fault in the East Bahariya concession (Fig. 25). This fault was reactivated by Santonian oblique-slip inversion, forming the Asala anticline and pop-up and pull-apart structures at the ends of en echelon fault segments (Yousef et al., 2009, 2010a).

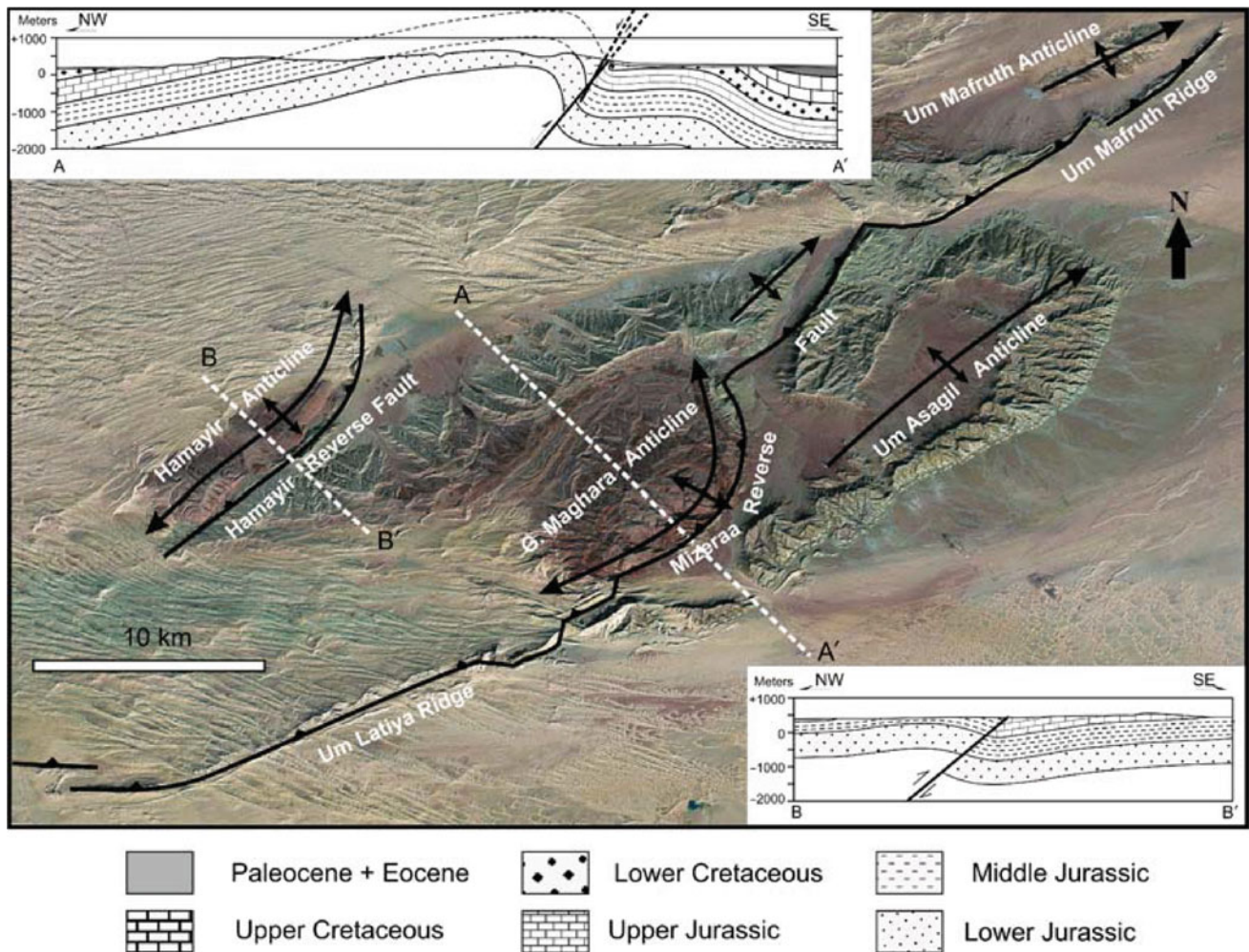


Fig. 32 Landsat TM image of the Gebel Maghara inverted structure (after Moustafa, 2005, 2010). A-A' and B-B' are two NW-SE cross-sections across the structure

Abu Roash inverted structures—Abu Roash lies to the southwest of Cairo. Its structures consist of three main NE-SW-oriented folds (Fig. 30; Moustafa, 1988). They are interpreted to be a large pop-up structure formed as a result of dextral strike-slip displacement on left-stepping en echelon faults striking in an E-W direction (Moustafa, 1988). The largest anticline in the area is NE-SW oriented and dissected by WNW-striking left-stepping en echelon dextral strike-slip faults, enclosing small plunging anticlines, that are considered pop-up structures (Moustafa, 1988). These smaller pop-up structures were formed as a result of the inversion that took place in Abu Roash area like some localities in the adjacent Abu Gharadig Basin.

3.3.2 Northern Eastern Desert Inverted Structures

Late Cretaceous inversion can be observed in the northern Eastern Desert in two localities: Wadi Araba and Gebel Shabraweit, with a remarkable angular unconformity, where

Campanian carbonates rest unconformably on Santonian clastics (Moustafa & Khalil, 1995).

Wadi Araba inverted structure—Santonian inversion most likely resulted in an ENE-WSW-oriented large asymmetric anticline with a breached core in Wadi Araba in the northern Eastern Desert, in between the North and South Galala Plateaus (Fig. 12). Its NW flank is gently dipping, whereas its SE flank is steeply dipping, reaching a nearly vertical attitude. This anticline is thought to be a fault-propagation fold, where the SE steep flank overlies a high-angle NW-dipping reverse fault (Moustafa, 2020). Moustafa and Khalil (1995) suggested that this anticline extends further east into the offshore area of the Gulf of Suez.

Gebel Shabraweit inverted structure—North of Wadi Araba, lies another Santonian to pre-Middle Eocene inversion ENE-WSW-oriented anticline, known as the Gebel Shabraweit Anticline (Al-Ahwani, 1982; Faris & Abbass,

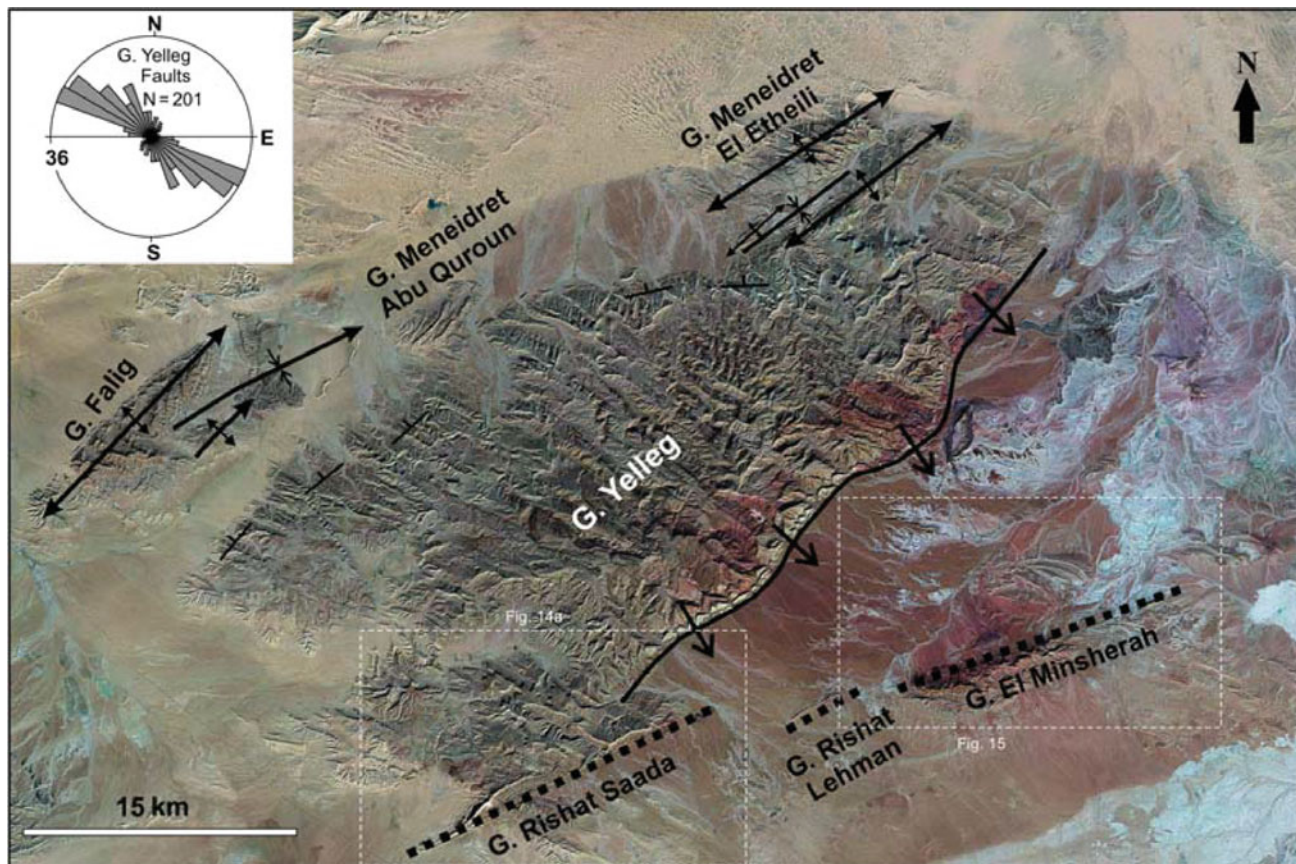


Fig. 33 Gebel Yelleg inverted structure (after Moustafa, 2010). **a** Landsat TM image of the structure. **b** Rose diagram showing the trend of the mapped faults

1961). Its SE flank is overturned and bounded by a reverse fault which is dipping in a NW direction (Moustafa & Khalil, 1995). Moustafa (2020) suggests that the southern side of an inverted basin lies beneath this anticline to the north of Gebel Shabraweit.

3.3.3 North Sinai Inverted Structures

The surface inversion folds of onshore North Sinai (Moustafa, 2010) resemble those in the subsurface of northern Western Desert in geometry and structural style, except that the folds of Sinai are of the opposite vergence (Moustafa, 2013). North Sinai includes a strongly folded area (Yelleg, Halal, and Maghara folds), whereas north-central Sinai encloses a gently folded area (Moustafa, 2010; Shata, 1959). A wide fault zone of ENE-WSW-striking right-stepping en echelon strike-slip faults and associated folds, termed the Sinai Hinge Belt by Shata (1959), separates the two areas (Fig. 31). Moustafa et al. (2014) interpreted that the faults of this belt were reactivated by Late Cretaceous to Early Tertiary dextral transpression.

Gebel Maghara inverted structure—Four NE-oriented, asymmetric anticlines, which are bounded on their SE flanks by inverted reverse faults, constitute the Gebel Maghara

structure (Fig. 32; Moustafa, 2014). This inverted structure is breached at its core exposing a thick Jurassic section. These anticlines are crossed by steeply dipping normal faults (Moustafa, 2013). The anticlines are situated above an inverted Jurassic half graben, bounded by the right-stepping en echelon segments of Um Asagil Fault (Fig. 32), which could be a strong indication of Santonian-Middle Eocene transpressional inversion (Moustafa, 2020).

Gebel Yelleg inverted structure—A Late Cretaceous NE-SW-oriented doubly plunging anticline of SE vergence represents the inverted structure of the Gebel Yelleg area (Fig. 33). Its NW flank is gently dipping, while its SE flank is steeply dipping and bounded by an unexposed high-angle reverse fault (Moustafa & Fouda, 2014). The anticline is cut by steep NW-striking normal faults (Moustafa, 2013). Seismic data indicate that this anticline is a fault-propagation fold resulting from the inversion of the underlying Jurassic asymmetric graben (Moustafa, 2020).

Gebel Halal inverted structure—The Gebel Halal inverted structure is a Late Cretaceous NE-oriented doubly plunging anticline of SE vergence (Fig. 34; Abd-Allah et al., 2004).

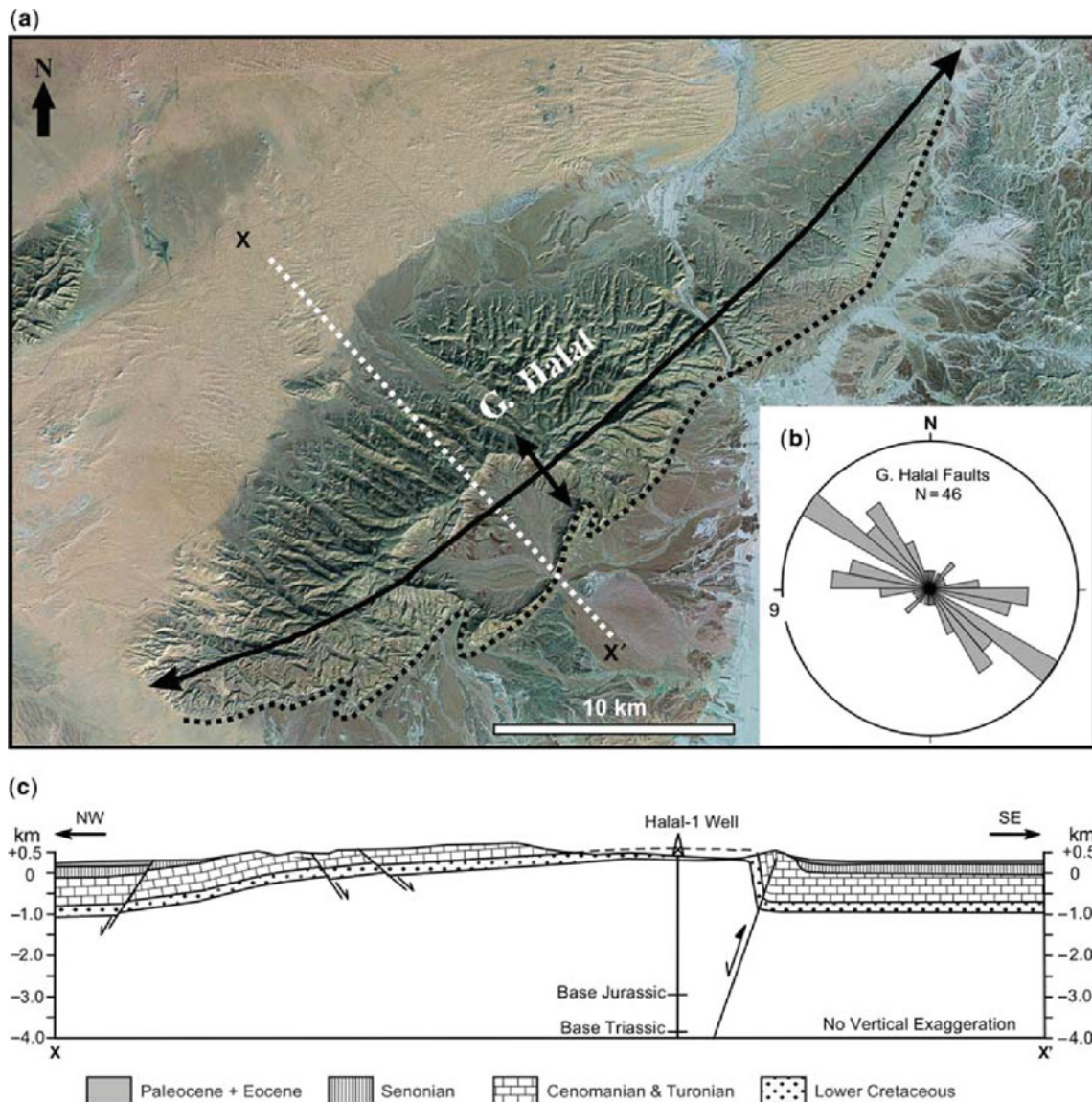


Fig. 34 Gebel Halal inverted structure (after Abd-Allah et al., 2004; Moustafa, 2010). **a** Landsat TM image of the structure. **b** Rose diagram showing the trend of the mapped faults. **c** Structural cross-section

Its NW flank is gently dipping, while its SE flank is vertical to overturned, overlying a NE-striking reverse fault, consisting of right-stepping en echelon segments. This anticline is crossed by high-angle NW-SE-striking normal faults (Moustafa, 2013). Inversion of this anticline took place during the Late Santonian. The current geometry of this anticline is interpreted to have been the result of the transpressional inversion of the underlying NE-SW-oriented Triassic-Jurassic half graben.

Offshore North Sinai inverted structures—Five doubly plunging inversion anticlines were mapped by Yousef et al., (2006a, 2006b, 2010b) in offshore North Sinai using detailed subsurface data (Fig. 35). The area was subjected to post-Santonian positive inversion, extending into the

Miocene times (Yousef et al., 2010b). The Mango, North Sinai 21, and Tineh anticlines are NE oriented with NW steeper flanks. The Mango asymmetric anticline has a breached crest (Fig. 16). Both the Goliath and Gal anticlines are NNE oriented, of which Goliath has a steeper NE flank and is bounded by a NNE-striking inverted fault, whereas Gal has a steeper SE flank (Yousef et al., 2010b).

3.4 Late Mesozoic–Early Tertiary Structures in Central and Southern Egypt

Said (1962) believed that the areas lying south to the inverted basins of northern Egypt (central and southern Egypt) belong to what he termed the ‘stable shelf’ region,

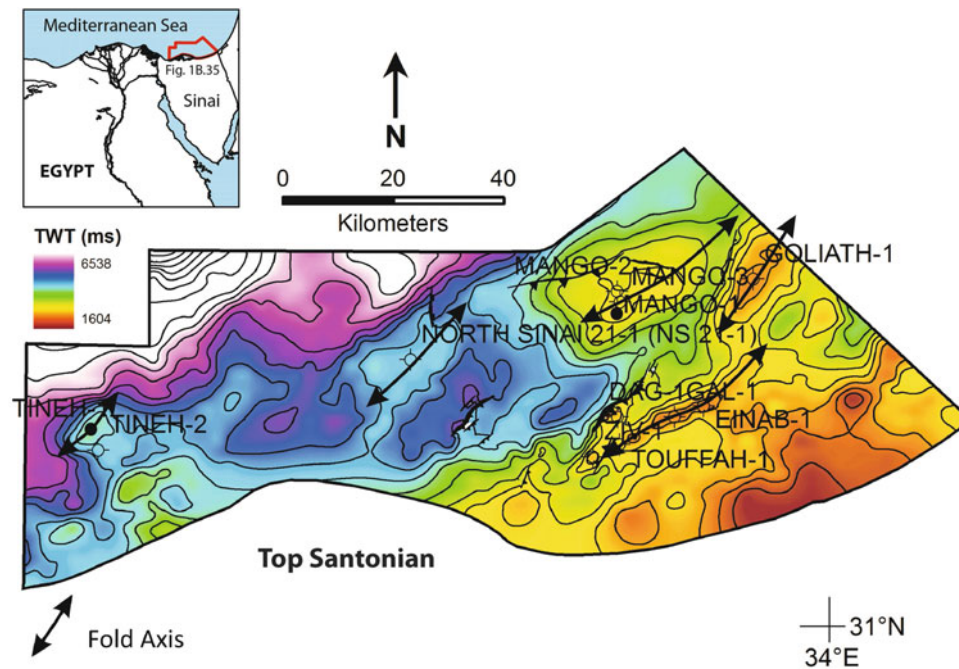


Fig. 35 Time-structure map of top Santonian, offshore North Sinai. Contour interval is 200 ms (after Yousef et al., 2010b)

which did not witness the impact of the Late Cretaceous-Recent convergence of the Afro-Arabian and Eurasian plates. However, recent studies confirm that these areas were affected by the Santonian far-field compressional stress, resulting in multiple compressional structures (Bosworth et al., 1999; Sakran & Said, 2018; Yousef, 2003).

3.4.1 The Bahariya Depression Inverted Structures

The Bahariya Depression in the central Western Desert is considered a breached inversion anticline, which was mapped and termed the Bahariya Swell by Moustafa et al. (2003), Fig. 36. The inversion is marked by an unconformity synchronous with the Santonian event. Affected by the Late Cretaceous-post-Middle Eocene NW compression, three ENE-oriented structural belts of small right-stepping en echelon folds and left-stepping en echelon normal faults, were formed due to the oblique-slip reactivation of ENE-WSW deep-seated normal faults (Moustafa et al., 2003).

3.4.2 Southern Western Desert Inverted Structures

The southern part of the Western Desert is characterized by two fault belts (Fig. 37). These belts were formed due to fault reactivation by Santonian-Late Eocene dextral transpression (Guiraud & Bosworth, 1999). This resulted in the formation of growth folds affecting the Upper Cretaceous-Lower Eocene strata. The first is a belt of pervasive E-W- to ENE-WSW-striking faults and small-scale en echelon folds, in comparison to the folds of northern Egypt, termed the

Nubia Fault System by Moustafa (2020), and first mapped by Issawi (1968 and 1971). This belt comprises several faults such as the Kalabsha Fault which consists of ENE-striking right-lateral strike-slip fault segments, lying to the south of Sin el-Kaddab Plateau (Fig. 37). The pop-up structure of Kalabsha fault is the result of right-lateral strike-slip movement on left-stepping en echelon fault segments and consists of basement-cored doubly plunging anticlines (Abdeen & Gaballah, 2013; Sakran & Said, 2018).

The Seyial Fault is another fault that belongs to this belt. It is also an ENE-striking right-lateral strike-slip fault located to the north of the Kalabsha Fault (Fig. 37). It consists of four left-stepping en echelon ENE-striking right-lateral strike-slip fault segments. These fault segments are linked by restraining fault bends. These restraining bends are associated with ENE-NE-trending folds affecting the Upper Paleocene and Lower Eocene strata. The Abu Bayan Fault crosses the western scarp of the Sin el-Kaddab Plateau (Fig. 37) and also belongs to this belt. It consists of two ENE-striking right-lateral strike-slip fault segments interconnected by a restraining fault bend, which is associated with two ENE-trending doubly plunging asymmetrical anticlines.

This belt is accompanied by a second belt of N-S- to NNE-SSW-striking faults, associated with N-S belts of left-stepping en echelon doubly plunging folds (Ghobrial, 1967). Sin el-Kaddab Fault is an example of NNE-striking left-lateral strike-slip faults affecting the Eocene rocks of the Sin el-Kaddab Plateau (Fig. 37). It consists of right-stepping en echelon fault segments forming characteristic restraining right stepovers. Such restraining stepovers are associated

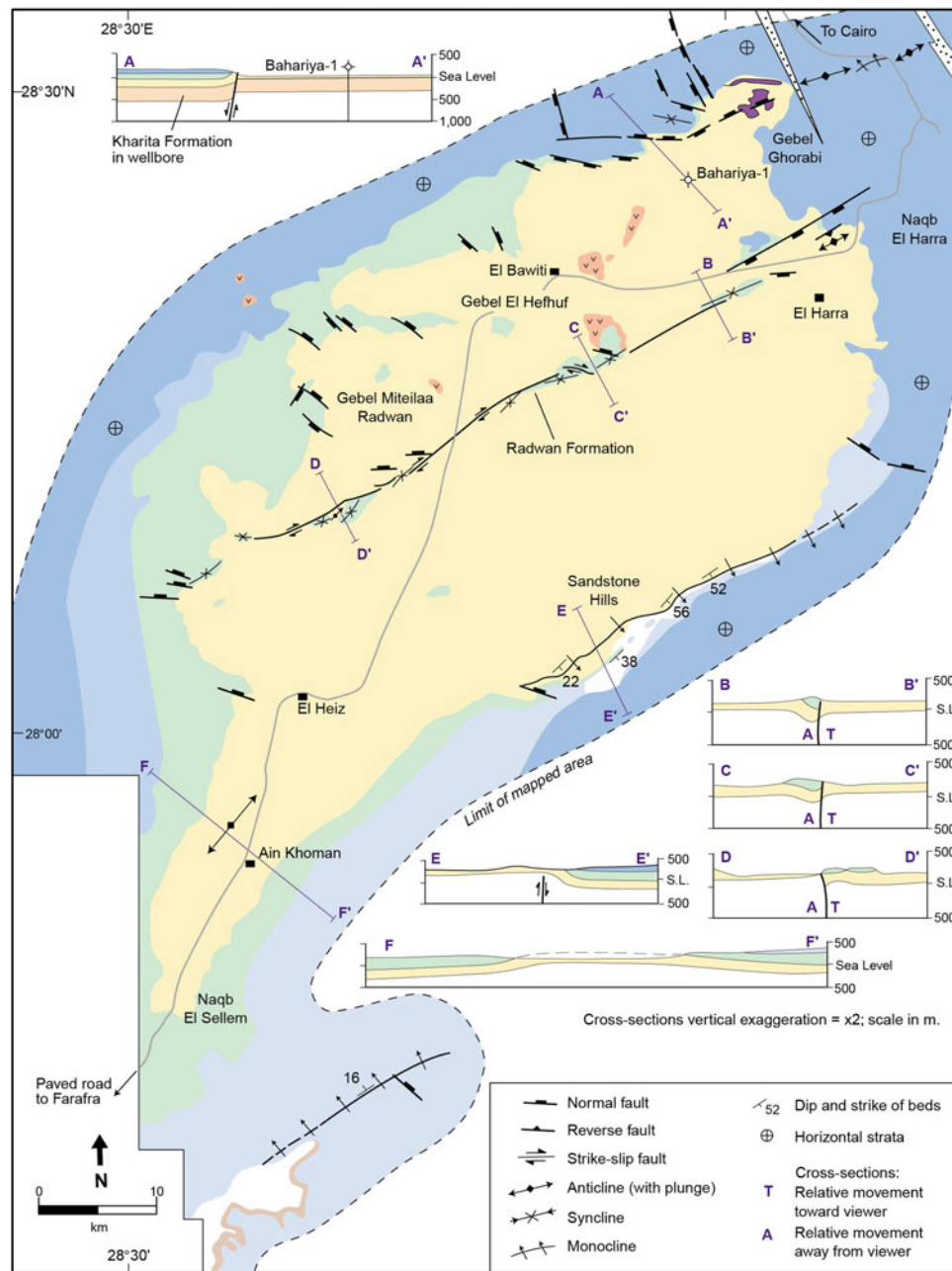


Fig. 36 Geologic map and cross-sections of the Bahariya Depression (after Moustafa et al., 2003)

with en echelon folds with NE-NNE-trending axes. Negative and positive flower structures on seismic sections indicate strike-slip movement on the fault segments (Fig. 38).

4 Cenozoic Structures in Egypt

4.1 Cretaceous/Paleogene (K/P) Boundary

The Cretaceous/Paleogene (K/P) boundary is characterized by the most recorded mass extinction through the

Phanerozoic Eon (Alvarez et al., 1980). The boundary witnessed environmental changes, global warming, and extinction of various groups of biota. Planktonic foraminifera, calcareous nannoplankton, ostracods, ammonites, and inoceramid bivalves were nearly wiped out (Bernaola & Monechi, 2007; Olsson & Liu, 1993). However, benthic foraminifera, diatoms, radiolarian, brachiopods, and gastropods were come across the boundary with minor effect (Culver, 2003). Various opinions have dealt with the causes of this event. Mclean (1978) revealed that the CO₂ poisoning is the cause. Alvarez et al. (1980) believed that extraterrestrial

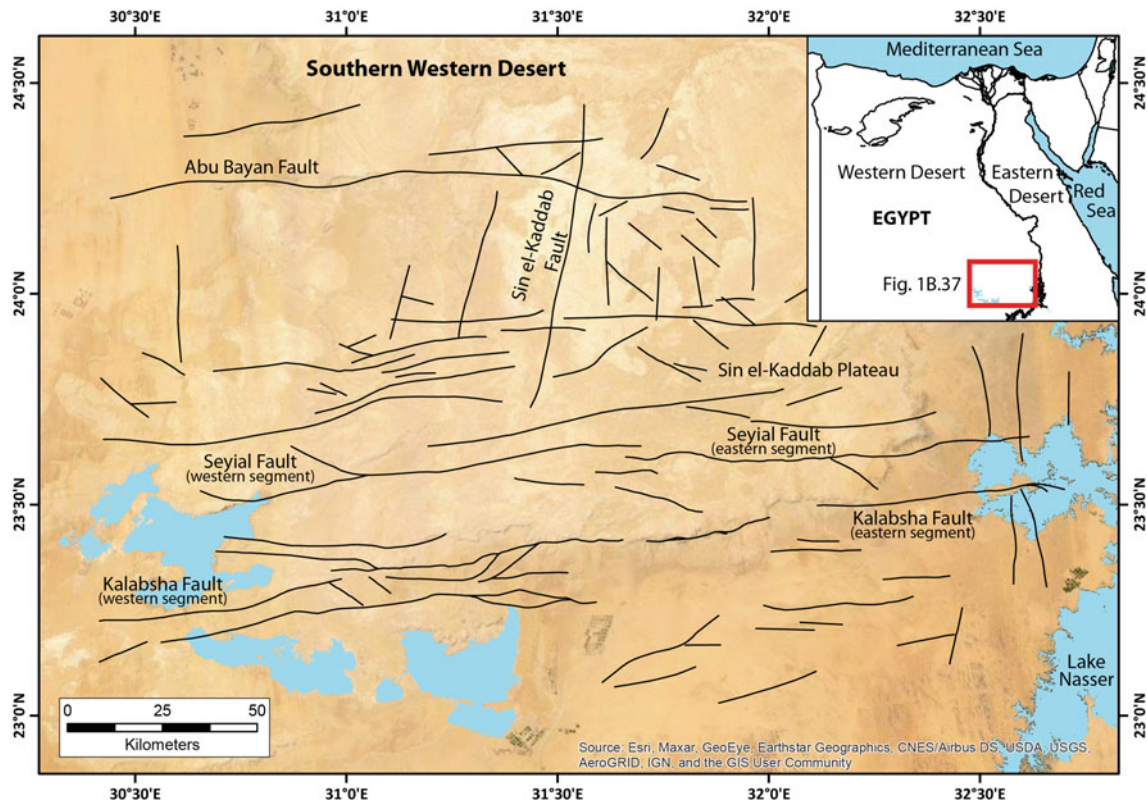


Fig. 37 Detailed fault map of the Nubia Fault System, (redrawn after Sakran & Said, 2018)

bolide impact was the reason. Officer and Lyons (1993) considered that volcanism was responsible for this event. Finally, Adatte et al. (2002) believed that sea level fluctuations, climate change, and bolide impact were the reasons. Numerous studies were focused on the K/P boundary in Egypt (e.g., Issawi, 1972; Obaidalla & Kassab, 2000; Said, 1962; Shahin & Kora, 1991). All of them stated that there are global and local hiatuses of different duration at the K/P boundary. The K/P boundary in northern Egypt lies within the uppermost part of Sudr chalk, whereas in southern Egypt it occurs within the lower part of the Dakhla Shale.

4.2 Paleocene-Eocene Transition

The Paleocene-Eocene boundary was a catastrophic event that lasted for about 22,000 years (Röhl et al., 2000; Westerhold et al., 2009) at ca. 55.8 my ago. This event is considered to be the warmest event in the Cenozoic (Bornemann et al., 2009). During this event, most of the deep-sea benthic foraminifera were wiped out (Tjalsma & Lohmann, 1983). This benthic turnover is associated with a sudden shift in $\delta^{13}\text{C}$, which indicates a hiatus between the Paleocene and Eocene rocks (Khozyem et al., 2013, 2015). Through the Early Paleogene, Egypt was located at the southern Tethyan margin. The Global Standard Stratotype-

section and Point (GSSP) for the boundary between the Paleocene and Eocene is located above the base of Dababiya Quarry Member of the Esna shale at Dababiya section, Egypt (Dupuis et al., 2003). Richness of calcareous nannoplanktonic assemblages characterizes the Paleocene-Eocene sediments in the central parts of Egypt (Youssef, 2016). The Paleocene-Eocene Thermal Maximum (PETM) interval in Egypt is marked by limestones and laminated phosphatic shales (Dupuis et al., 2003). By the Early Eocene, the Dababiya Quarry Member began with calcareous shale containing bone fragments and teeth (Anan & Shahin, 2021). This period of global warming was accompanied by a rapid turnover of planktonic foraminifera.

4.3 Oligocene–Miocene Rifting

4.3.1 Magmatism

The Late Oligocene–Early Miocene registered the initiation of extension in the Red Sea as well as the Gulf of Suez. Together, the Red Sea and Gulf of Suez started as continental rifts at the early stages of separation of Arabia from the African plate (Fig. 39). Magmatic activity took place during early rifting stages at Afar and northern Egypt. The Afar flood basalts (31–30 Ma) were synchronous with the beginning of Gulf of Aden rifting and the plume was hence a

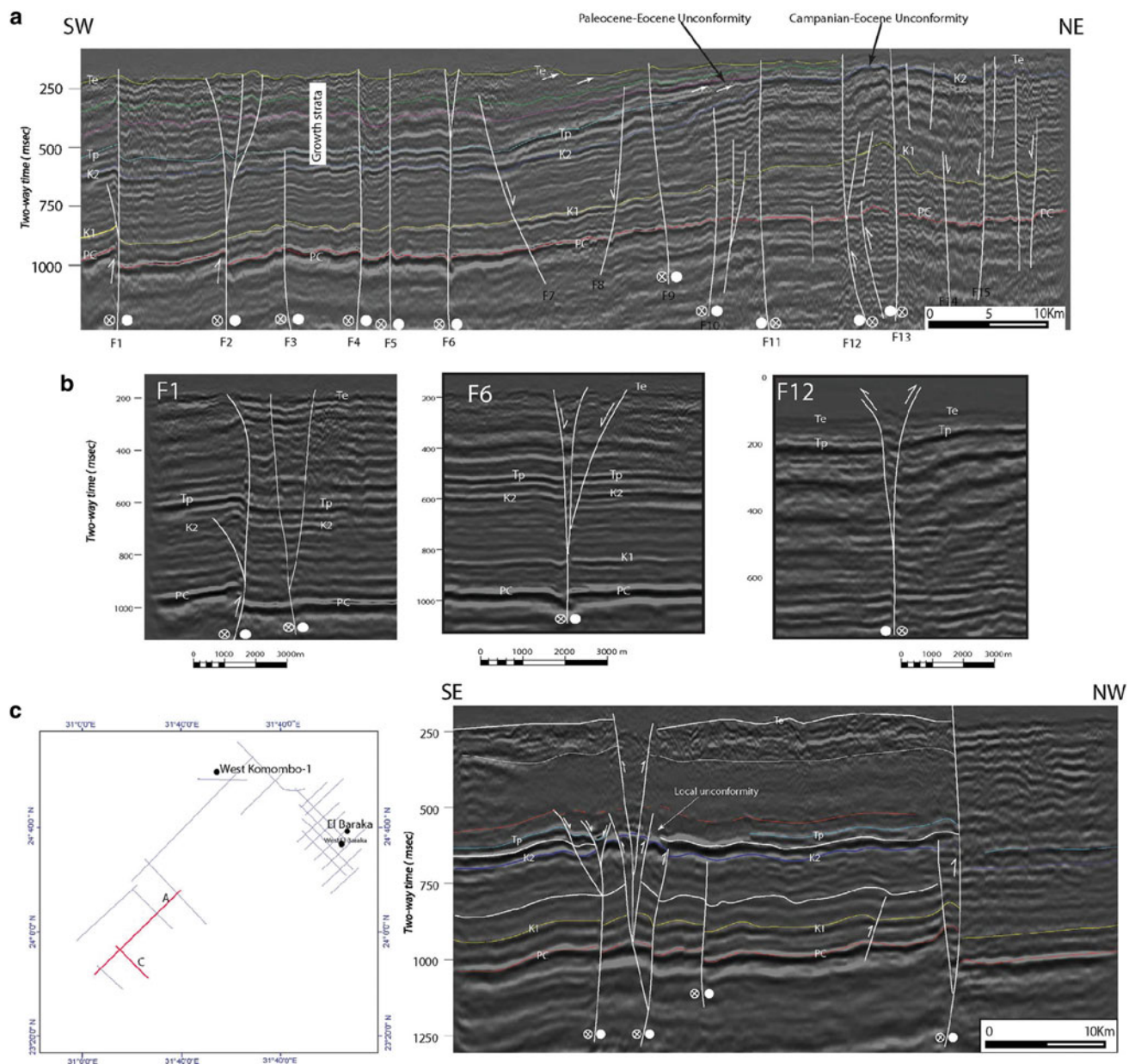


Fig. 38 Seismic sections through the Nubia Fault System showing negative and positive flower structures (after Sakran & Said, 2018)

cause for rifting (Bosworth et al., 2005; Courtillot et al., 1999). Basaltic flows as well as intrusions took place in several structural lows and through fault zones (Figs. 40, 41 and 42). A large Oligo-Miocene basalt field exists in northern Egypt mainly near Cairo City. Such field has many exposures at the northern Eastern Desert (e.g., Attwa & Henaish, 2018; Gamal et al., 2021; Hagag, 2016; Henaish & Kharbush, 2020; Khalaf et al., 2015), northern Western Desert (Mazzini et al., 2019), and Sinai (e.g., Baldrige et al., 1991; Perrin et al., 2009).

Basalts of northern Egypt have been dated by many authors to be of Late Oligocene-Early Miocene age (e.g., Bosworth et al., 2015; Meneisy & Abdel Aal, 1984; Meneisy & Kreuzer, 1974a, 1974b; Steen, 1982). Age dating of basalt samples from northern Egypt revealed that volcanism took place over less than 2 Ma at the Oligocene–Miocene boundary (23 Ma), also, such basalts are similar in composition to those of the Afar. Surface and subsurface studies by Bosworth et al. (2005) revealed a volcanic center which is called the Cairo mini-plume that is volumetrically smaller

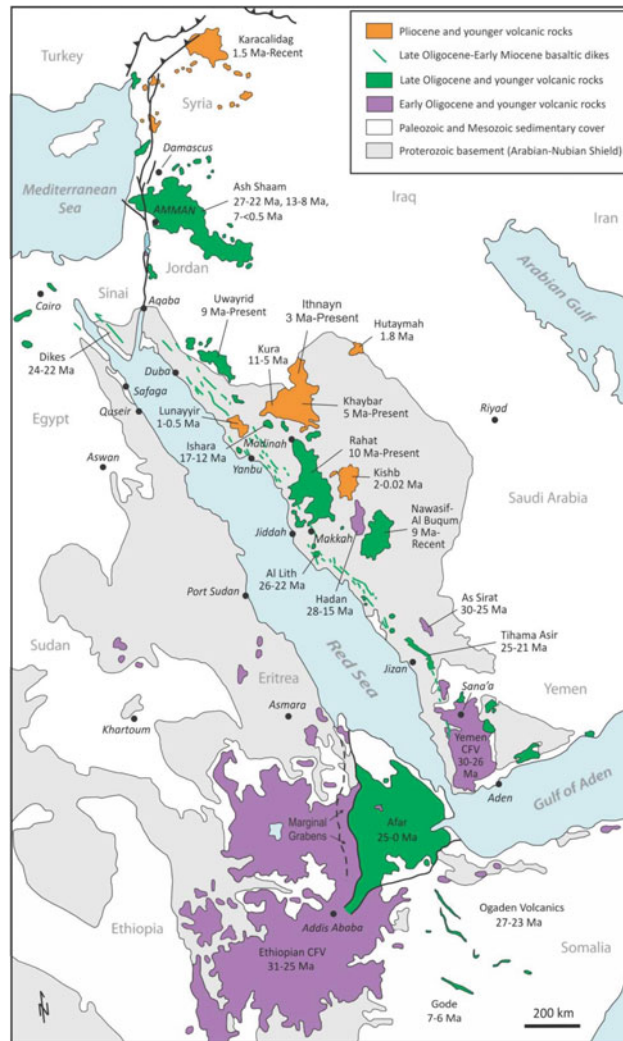


Fig. 39 Distribution of northeast Africa and Arabia Cenozoic volcanism (after Bosworth & Stockli, 2016)



Fig. 40 Field view of basaltic flows accumulation through a graben structure at the eastern margin of the Gulf of Suez

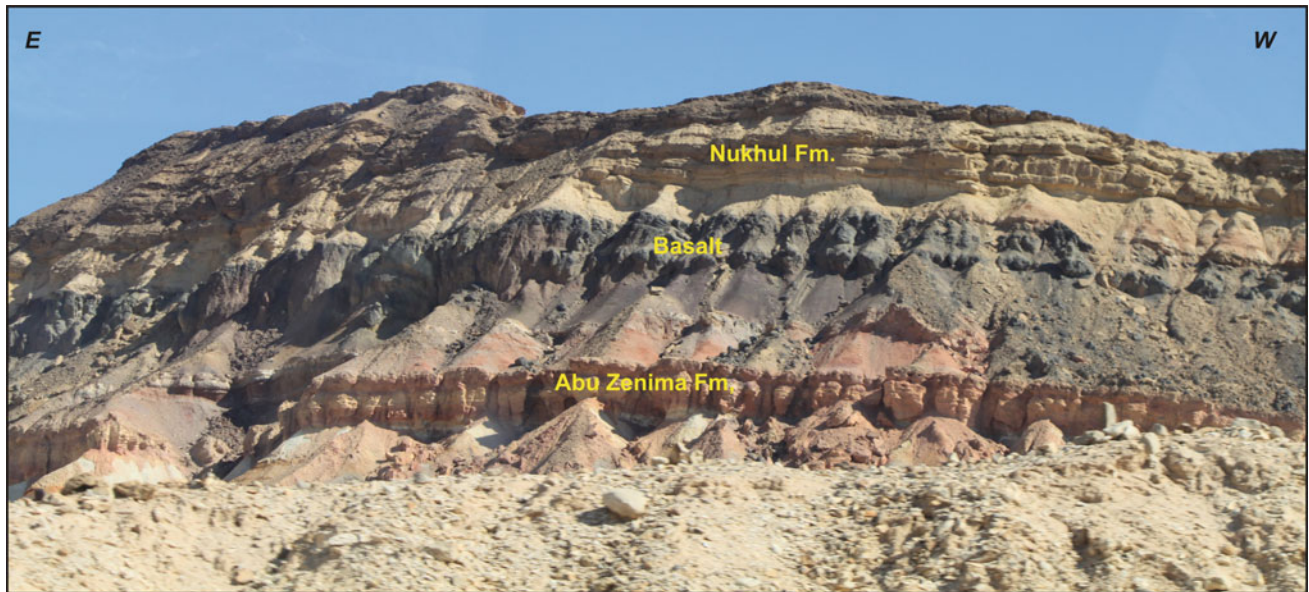


Fig. 41 Field photo at the eastern margin of the Gulf of Suez (Wadi Tayiba) showing early rift (Abu Zenima Formation) overlain by Early Miocene basalt flow and Lower Miocene Nukhul Formation



Fig. 42 Field photo at the Bahariya Depression (Gebel Mandisha) showing the Oligo-Miocene basalt flow

than that of Afar and played a similar role as a trigger for a large-scale rift event (Fig. 43).

4.3.2 The Red Sea and Gulf of Suez Rift System

The divergence of the Arabian plate away from the African plate in a NE direction led to the opening of the Red Sea and the Gulf of Suez rift. The Red Sea was formed by extensional splitting of the Precambrian crystalline basement starting in the Late Paleogene. In the southern Red Sea, sea floor spreading commenced about five Ma (e.g., Roeser, 1975), and the central and northern Red Sea is currently experiencing the transition from continental to oceanic rifting (e.g., Cochran et al., 1991; Guennoc et al., 1990). The Gulf of Suez is the

northwestern continuation of the Red Sea rift system (Fig. 44). The Oligo-Miocene Gulf of Suez rift between the African plate and the Sinai microplate is more than 300 km long and inactive at the moment. (Garfunkel & Bartov, 1977).

The Gulf of Suez and northern Egyptian Red Sea consist of tilted fault blocks that extend over several kilometers and are bounded by NW-striking extensional faults (Fig. 44). The structural style of the Gulf of Suez rift basin is characterized by three major half grabens. These half grabens, 'dip provinces' of Moustafa (1976), are separated by two accommodation zones. The Zaafarana Accommodation Zone separates the northern SW-dipping half graben from the central NE-dipping half graben, which is also separated

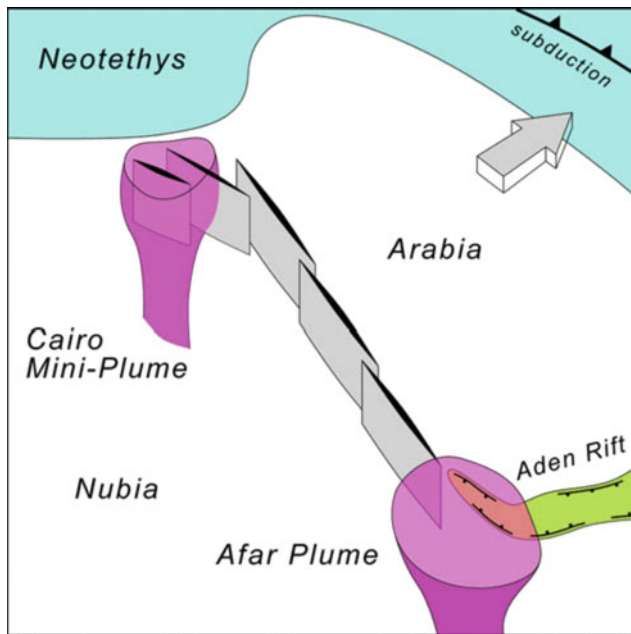


Fig. 43 Two-plume model for the origin of the Red Sea continental rift (after Bosworth et al., 2015)

from the southern SW-dipping half graben by the Morgan Accommodation Zone. Such dip provinces are represented both onshore and offshore by several tilted blocks (e.g., Moustafa, 2002; Patton et al., 1994).

The NW margin of the Red Sea consists of two major dip provinces namely, the northern Safaga dip province and the southern Quseir dip province (e.g., Khalil & McClay, 2002). The Safaga dip province includes several SW-dipping tilted blocks bounded by major normal faults dipping in a NE direction, whereas the Quseir dip province is characterized by NE-dipping tilted blocks bounded by SW-dipping normal faults. The change of fault polarity happens throughout the Duwi Accommodation Zone (e.g., Jarrige et al., 1990; Khalil & McClay, 2009).

Large-scale faults of the Gulf of Suez and northwestern Red Sea have been grouped by Patton et al. (1994) into four major populations based on their orientations (Fig. 45). These four main trends are rift-parallel or Clysmic, north-oblique, west-oblique, and cross fault sets. These deduced fault sets control the geometry of rift blocks boundaries and the rift shoulders, which in turn leads to a distinguishable zigzag fault geometry. Also, dip angles of the rift faults are controlled by both fault age and orientation relative to the direction of block rotation. Hence, block rotation affects Clysmic as well as west-oblique faults the most, whereas cross faults are the least affected by this rotation (Fig. 46).

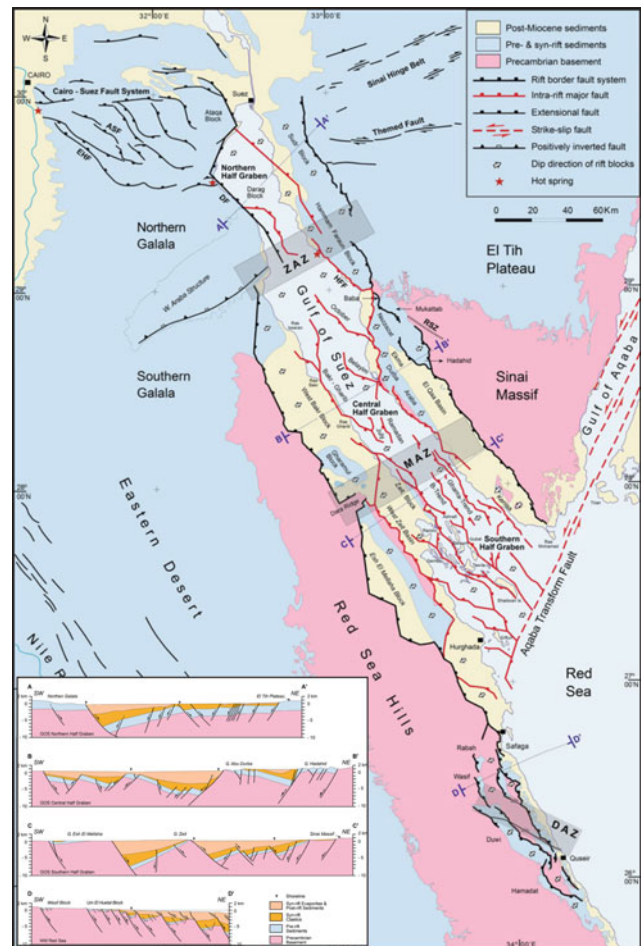


Fig. 44 Simplified structural map and structural cross-sections (compiled from Moustafa & Khalil, 2020; Patton et al., 1994; Thiriet et al., 1986) showing the rift blocks of the Gulf of Suez and northwestern Red Sea and the accommodation zones between the half grabens (Zafarana (ZAZ), Morgan (MAZ), and Duwi (DAZ) accommodation zones). Abbreviations designate: Rihba Shear Zone (RSZ), Hammam Faraun Fault (HFF), Darag Fault (DF), Abu Shama Fault (ASF), and el-Hai Fault (EHF)

Many outcrop examples are well exposed along the margins of the Gulf of Suez and northwestern Red Sea which have been mapped and studied by many authors (e.g., Khalil, 1992; Mostafa et al., 2015; Moustafa, 2002; Sakran et al., 2016a, 2016b). Structural mapping and analysis of the surface exposures of the Gulf of Suez represent analogs for the oil and gas structural traps in the subsurface. Among these outcrops, Gebel el-Zeit area represents one of the most unique examples of exposed rift blocks along the western margin of the Gulf of Suez rift (Mostafa et al., 2015), Fig. 47. The outcrops at Gebel el-Zeit provide important constraints on the geometry of the rift coastal faults and fault block rotation in the southern Gulf of Suez. In addition,

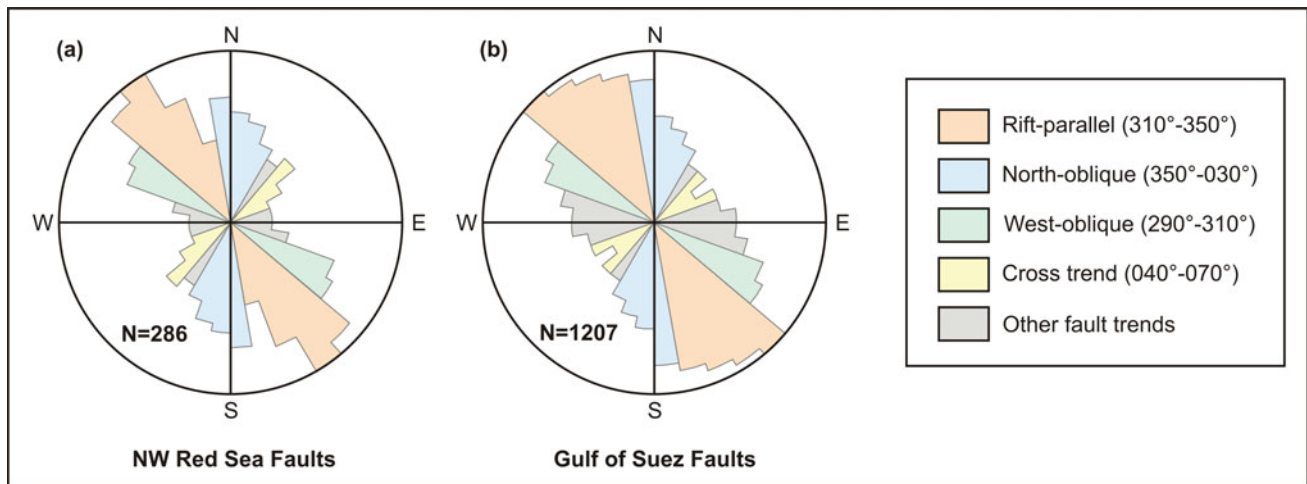


Fig. 45 Rose diagrams of the faults in onshore areas of the Gulf of Suez rift (a) and the northwestern Red Sea (b). Modified from Patton et al., (1994) and Moustafa & Khalil, (2020)

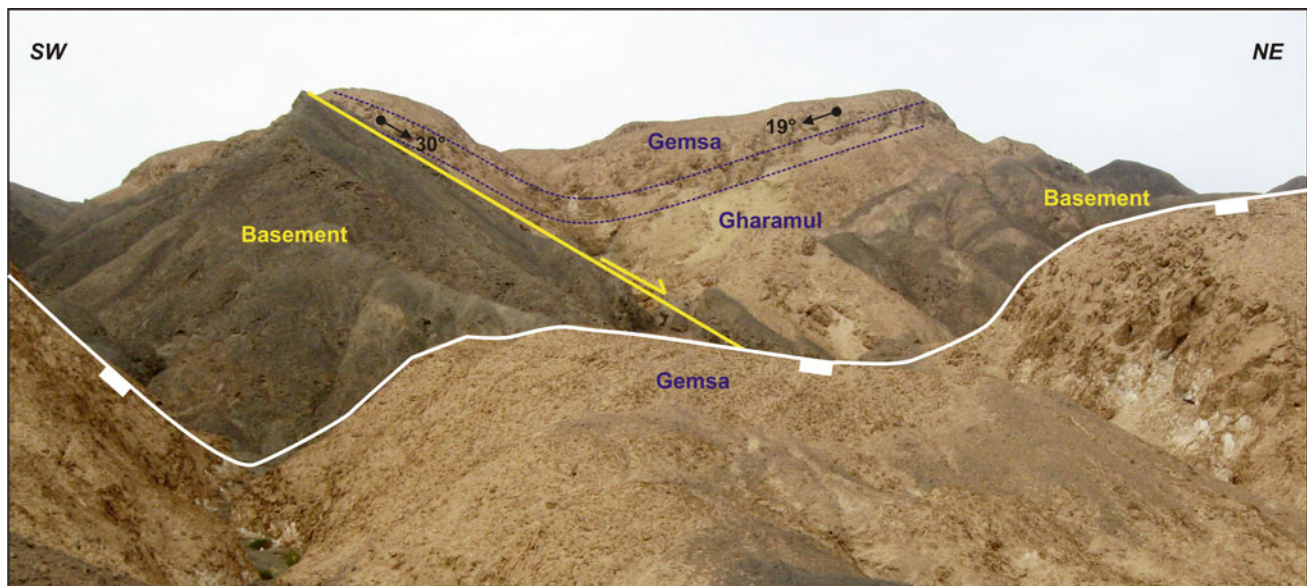


Fig. 46 Field photo of a Clysmic-trending normal fault (yellow) that intersect a cross-trending normal fault (white) at southern Gebel el-Zeit. The lower-middle Miocene Gharamul Formation and the middle Miocene Gemsa formation are folded due to drag along the hanging-wall of the clysmic trend fault

subsurface data provide insight into the large-scale geometry of the main fault systems (Mostafa et al., 2015; Mayhoub et al., 2017 and 2019). The regional structural architecture of the southern part of the Gulf of Suez is controlled by five main fault populations (Sakran et al., 2016a, 2016b), Fig. 47. The most extensively drilled fault trend in the southern Gulf of Suez lies in the subsurface east of Ashrafi, Gubal, and Shadwan Islands (Bosworth, 1995). This is commonly known as the B-trend (Khalil, 1992). The

regional structural style of the southern Gulf of Suez is shown in three regional cross-sections in Fig. 48.

4.3.3 The Cairo-Suez District

The Cairo-Suez District (Fig. 49) represents one of the most prominent structural provinces at the northern Eastern Desert that covers an area for about 12,000 km². It extends from Cairo City to Suez City for about 127 km long. Moreover, it has a width of 95 km where it extends northerly from the

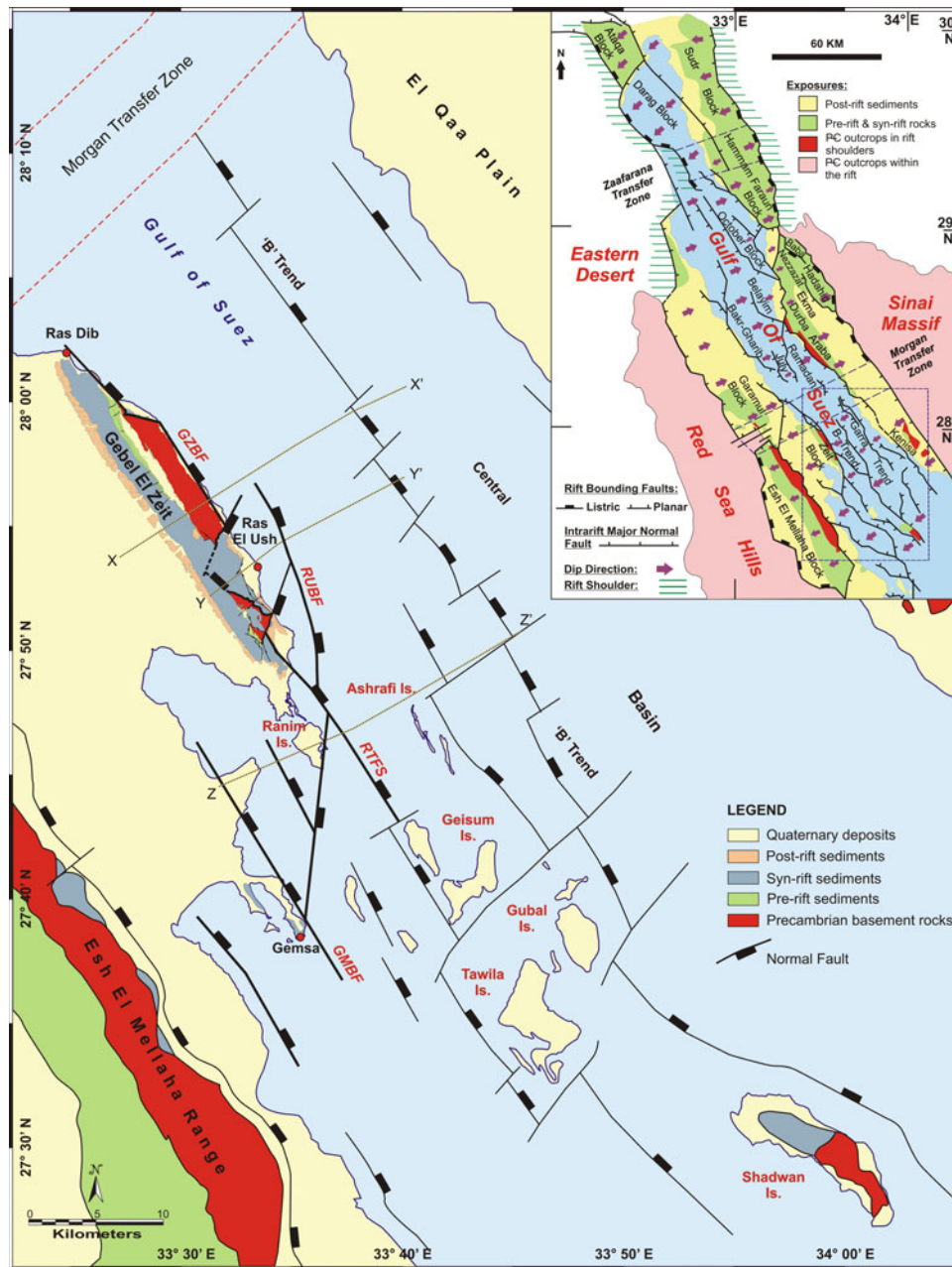


Fig. 47 Location map of the studied areas and surface projections of major faults: Gebel el-Zeit Boundary Fault (GZBF), Little Zeit Boundary Fault (LZBF), Ras el-Ush Boundary Fault (RUBF), Ranim-Tawila Fault System (RTFS), and Gemsa Boundary Fault (GMBF), in the southern Gulf of Suez (compiled from Bosworth, 1995; Sakran et al., 2016b). The inset shows the tectonic setting, major rift blocks and fault trends of the Gulf of Suez rift (after Moustafa, 2002)

Great Bitter Lake and ends southerly at the northern scarp of the North Galala Plateau. The northern part of Cairo-Suez District is represented by Cretaceous, to Miocene faulted and folded exposures (e.g., G. Hamza; G. Um Raqm; G. Oweibed; G. Shabraweit). However, the southern part of the Cairo-Suez District consists of multiple distinct fault blocks of Eocene age (e.g., G. Qattamiya; G. Abu Treifiya; G. Abu Shama; G. Ataqa). Nine belts of en echelon faults have been mapped along the Cairo-Suez District (Gamal et al., 2021),

Fig. 49. A zigzag fault pattern was created when the E-W fault belts were hard-linked with the NW-striking normal faults.

The Cairo-Suez District encompasses the area that lies northwest of the Gulf of Suez. The throw on the faults in the northern part of this Oligo-Miocene rift was transferred into the nearby Cairo-Suez District because the Gulf of Suez rift was unable to extend north of Suez City (Moustafa & Abd-Allah, 1992). The movement on these faults was

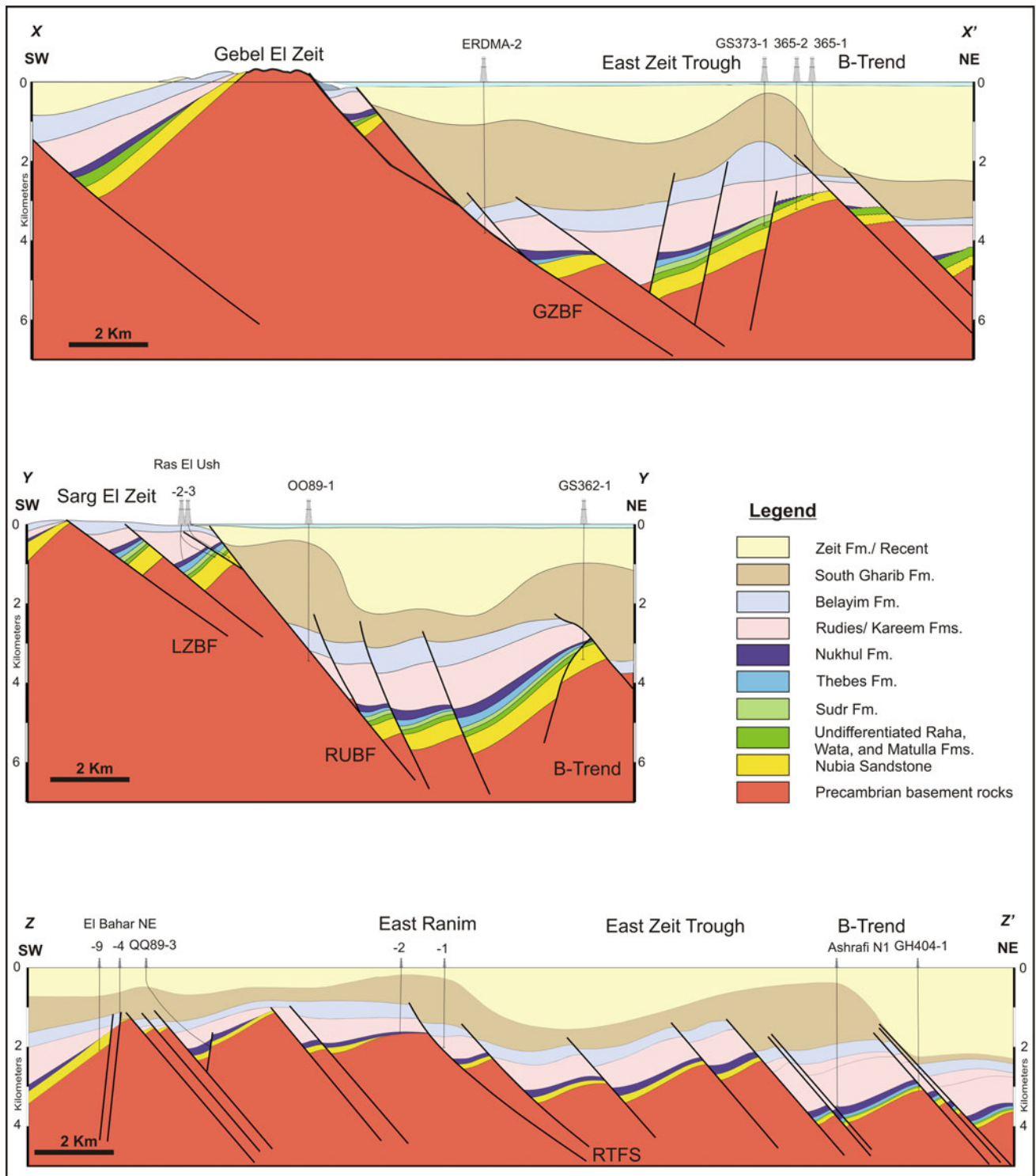


Fig. 48 Regional cross-sections through the southern Gulf of Suez Basin (compiled from Atta, 1994; Bosworth, 1995; Sakran et al., 2016a). Locations are given in Fig. 47

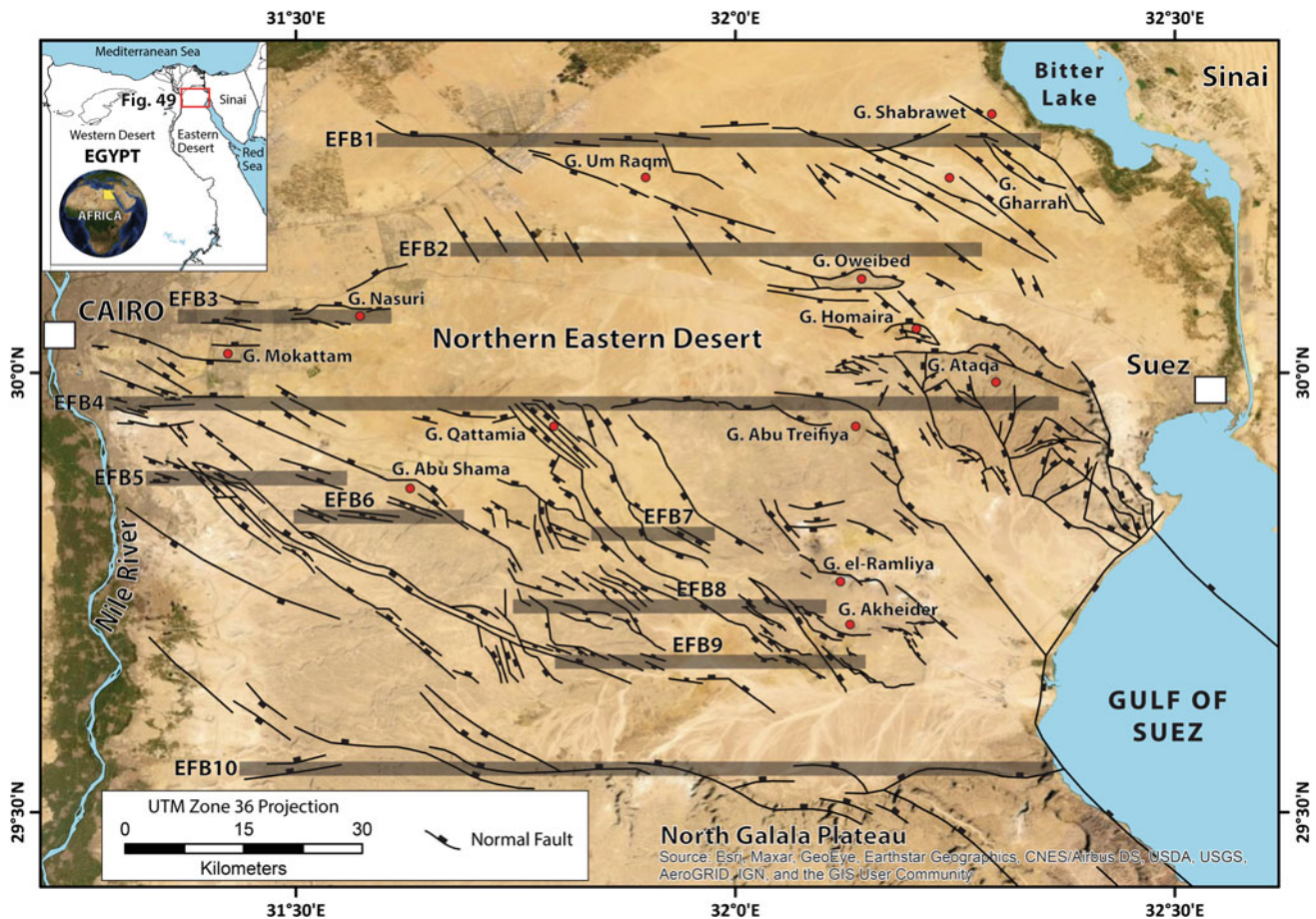


Fig. 49 Detailed structural map of the Cairo-Suez District (after Maqbool et al., 2014, 2016; Moustafa et al., 1985, Moustafa & Abd-Allah, 1992, Moustafa et al., 1998; Henaish, 2018a, 2018b; Gamal et al., 2021). E-W-elongated left-stepping en echelon fault belts (EFBs) are numbered from north to south and highlighted in gray. UTM—Universal Transverse Mercator

transferred through the deep-seated E-W-striking faults, which caused their rejuvenation by right-lateral tension. This is what formed the aforementioned E-W-elongated fault belts (Gamal et al., 2021).

The Cairo-Suez District is a well-known locality of different structural geometries and linkage styles of fault arrays (e.g., Attwa et al., 2020; Gamal et al., 2021; Henaish, 2018a). In addition, transfer zones are well represented at the outcrop level in several localities that attracted many authors (Attwa et al., 2020; Gamal et al., 2021; Henaish & Attwa, 2018; Henaish, 2018b; Moustafa, 2002). Six types of transfer zones have been suggested by Henaish and Kharbush (2020) along Cairo-Suez District which belong to soft- as well as hard-linkage transfer zones (Fig. 50). An extensive recent study by Gamal et al. (2021) also mapped several transfer structures and linked fault systems at the south-central part of the Cairo-Suez District. The study relied on detailed field mapping, a constructed high-resolution Digital Elevation Model, and displacement profiles to delineate and study in detail the structural

geometry and evolution of relay ramps, curved fault traces, conjugate relay zones, transfer faults, and what the study called ‘accommodation folds’, Fig. 51. Other folds and domal structures are well outcropped along the Cairo-Suez District in many localities at various scales (Fig. 52). Several mechanisms have been proposed for the formation of folded structures along the Cairo-Suez District (e.g., Gamal et al., 2021; Hagag, 2016; Henaish & Kharbush, 2020; Henaish, 2018a, 2018b; Moustafa & Khalil, 1995) including inversion (e.g. Gebel Shabraweit), drag (e.g., Gebel Eweibed and Gebel Nasuri), or as transfer structures between the overlapped fault segments (e.g., Gebel Um Raqm and the area to the southwest of Gebel Akheider).

4.4 The Opening of the Gulf of Aqaba (Miocene-Pliocene)

During the Miocene time, the activity on the Dead Sea Transform took place, which in turn terminated extension in

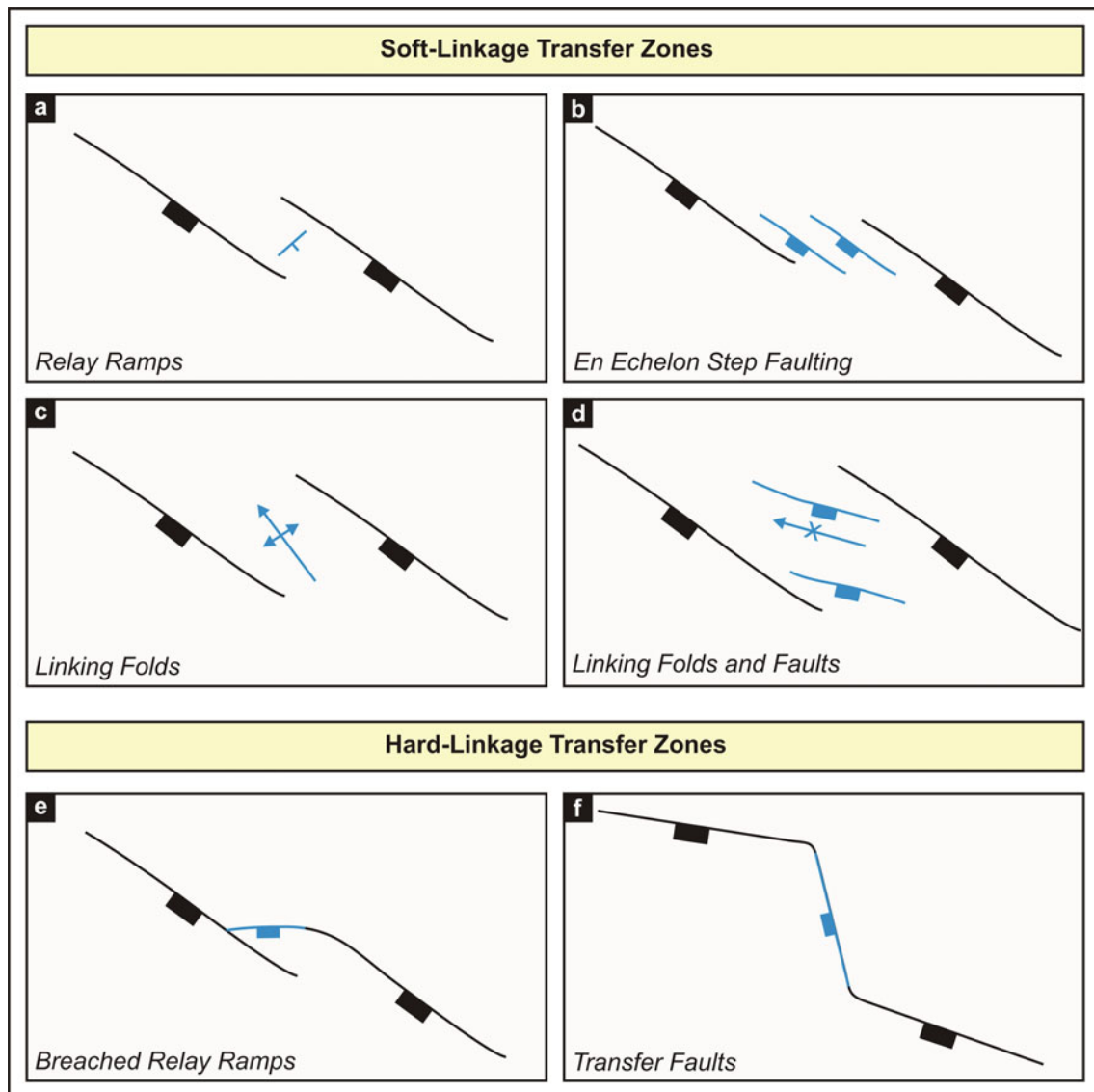


Fig. 50 Different types of transfer zones in Cairo-Suez District (after Henaish & Kharbish, 2020)

the Gulf of Suez Rift and led to continued opening of the Red Sea Basin (Bosworth & McClay, 2001; Cochran, 2005; Eyal et al., 1981; Freund et al., 1970; Garfunkel & Bartov, 1977; Patton et al., 1994; Robson, 1971). Sinistral slip on the Dead Sea Transform resulted in the opening of the Gulf of Aqaba a group of linked pull-apart basins.

The Gulf of Aqaba was formed at the southernmost end of the Dead Sea Transform and is considered its principal depression. The Gulf of Aqaba consists of three NNE-trending elongated en echelon fault-bounded pull-apart basins, which include several distinct deeps (Fig. 53).

Numerous N-S- to NNE-SSW-striking oblique faults are exposed along the Gulf of Aqaba in the Sinai margin. Bartov

et al. (1980b) first combined the displacement along these faults to suggest sinistral offset of more than 20 km. However, Eyal et al. (1981) suggested that the spatial distribution of the N-S-striking faults in eastern Sinai is such that the lateral offset along them seems to be continuous rather than cumulative. Interaction between the terminations of the N-S- to NNE-SSW-striking faults led to the formation of many pull-apart grabens along the eastern side of Sinai (e.g., Wadi el-Ghaib and Kid). Extraordinary recumbent folding is exposed at the western margin of the Gulf of Aqaba in the area north of Nuweibaa City. These folds are thought to be formed due to gravitational sliding by Hildebrand et al. (1974) and Abdel-Khalek et al. (1993).

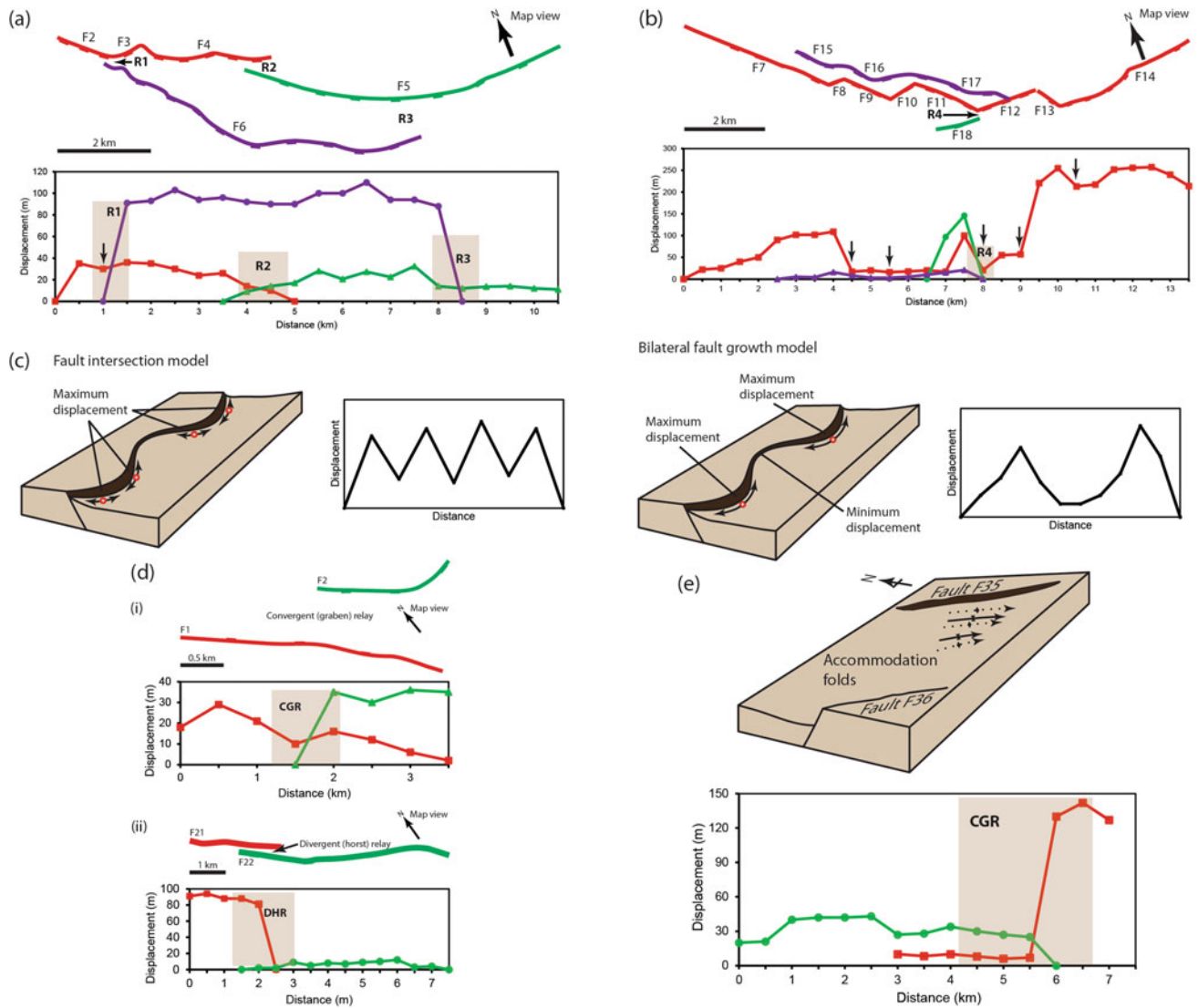


Fig. 51 Examples of transfer structures and linked fault systems at the south-central part of the Cairo-Suez District (compiled from Gamal et al., 2021). **a, b** Simplified fault trace maps and fault displacement profiles showing variations of displacement along fault strike, delineating relay ramps and transfer faults, respectively. R = Relay ramp. Black arrows points to displacement minima indicating fault linkage. **c** Fault growth models of curved fault traces and schematic fault displacement profiles (based on Gamal et al., 2021; Wu & Bruhn, 1994). **d** Simplified fault trace maps and fault displacement profiles showing variations of displacement along fault strike, representing conjugate relay zones. (i) CGR = Convergent graben relay. (ii) DHR = Divergent horst relay. Shaded area indicates area of fault overlap and interaction. **e** Schematic block diagram showing the accommodation folds enclosed between overlapping conjugate normal faults. Fault displacement profile showing variations of displacement along strike. CGR = Convergent graben relay

4.5 The Geology of the River Nile (Pliocene)

Please refer to chapter 4G for a detailed discussion in a separate chapter of this volume.

4.6 Quaternary and Neotectonics

Quaternary deposits are distributed along Egypt overlying the older rock units. Continental facies are dominant and

mainly represented by alluvial fan, braided stream, dune, and sabkha accumulations (e.g., Said, 1990). However, frequent concordant series are preserved at many localities in Egypt, including the Nile Delta area, the Gulf of Aqaba, the Gulf of Suez, and the Red Sea.

According to Guiraud and Bosworth (1999), active Quaternary fault zones in Egypt are distributed in several localities including: (1) the Nile Delta area in the form of E-W- to NW-SE-striking, normal, or dextral transpressive faults, (2) Helwan and Aswan E-W dextral, transpressive

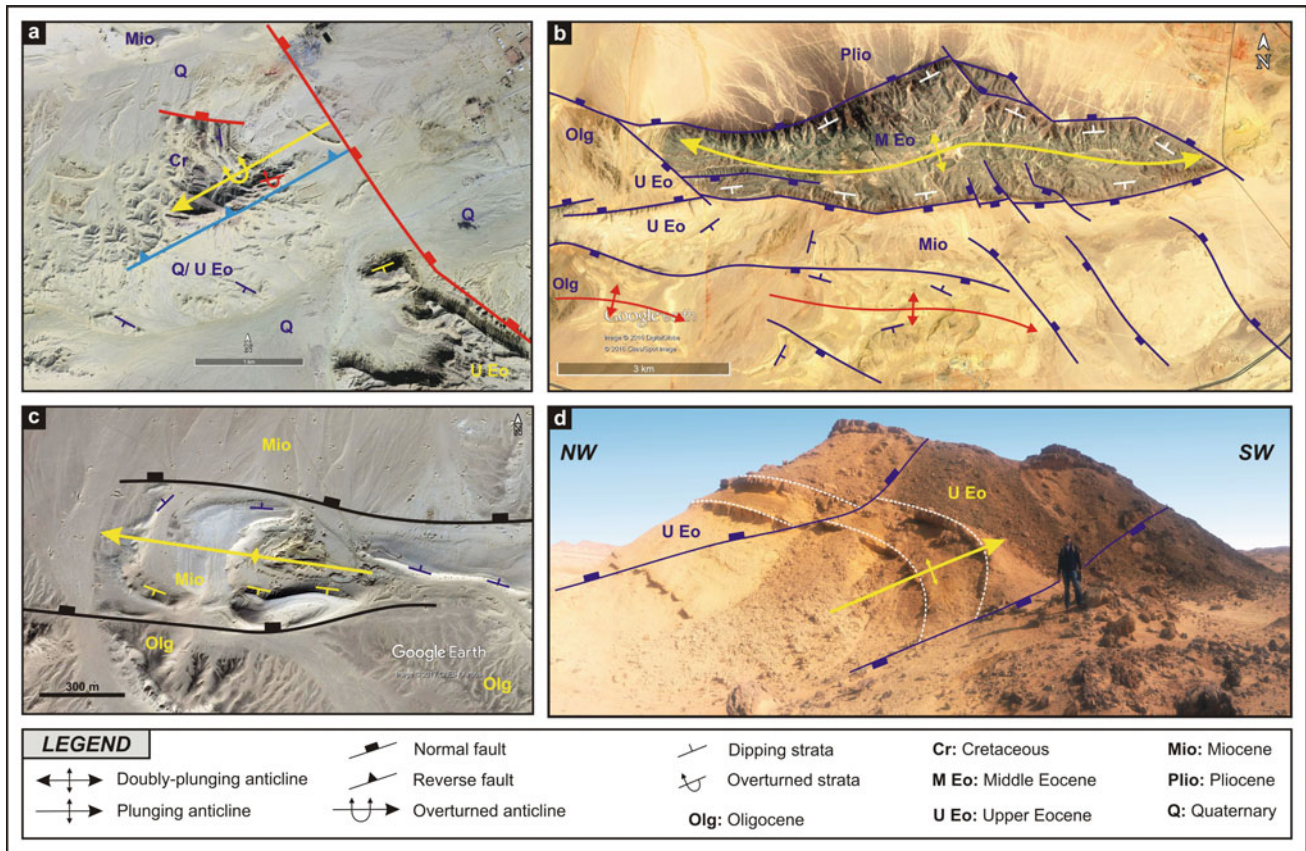


Fig. 52 Different types of fault-related folds in Cairo-Suez District. **a** Gebel Shabraweit. **b** Gebel Oweibed. **c** Gebel Um Raqm. **d** Gebel Nasuri

fault zones, (3) the Gulf of Suez and the Red Sea comprising NW-SE faults delimiting tilted blocks and rift shoulders, and (4) the Gulf of Aqaba-Dead Sea fault zone representing the ~ N-S sinistral, transpressive faults.

It is important to take into account the seismotectonics and current stress field in Egypt, when analyzing the activity of Gulf of Aqaba, the Red Sea, and Gulf of Suez, and the effects of the Eastern Mediterranean subduction zone on the North African passive continental margin (Fig. 54). Although the occurrences of the earthquakes in 2200 B.C. are unconfirmed (Ambrasyses et al., 1994), there is no historical data on the consequences of earthquakes prior to that time. Data on earthquakes comes from the macroseismic impacts of big or damage shocks during the beginning of the twentieth century. Badawy (1999) reports that there have been 83 historical earthquakes up to 1900, including unconfirmed ones. The historical earthquakes, which were documented in Egypt, are shown in Fig. 55.

Borehole breakout analysis from four-arm caliper logs was carried out for 30 exploratory wells that were mainly located in the Gulf of Suez area (compiled from Badawy, 2001;

Heidbach et al., 2008), Fig. 55. Applying the World Stress Map project quality ranking scheme, 19 of the total observations were ranked as a B-Quality (63.3%), 9 were of C-Quality (30%), and 2 were of D-Quality (6.7%). This analysis reflected a breakout mean azimuth (S_H) of 107.5° (Fig. 56).

Uplifted coral reefs and associated beach rocks, back-lagoonal sands, and shore gravels crop out extensively along both margins of the Red Sea and the Gulf of Suez rifts, thus facilitating neotectonic studies of this rift basin (Andres & Radtke, 1988; Dullo, 1990; Gvirtzman, 1994; Hoang & Taviani, 1991; Strasser et al., 1992). The best represented reefal complex along the Gulf of Suez rift belongs to the last interglaciation period with an age of ~ 125 ka (Lambeck & Nakada, 1992; Martinson et al., 1987). Andres and Radtke (1988), Reyss et al. (1993), Choukri et al. (1995), Bosworth and Taviani (1996), and Plaziat et al. (2008) have uranium-series dated corals and sea urchin spines from several of the Pleistocene reef terraces at Gebel el-Zeit. Bosworth and Taviani (1996) demonstrate that the maximum uplift for Gebel el-Zeit, after subtracting 6 m of eustatic sea-level change, is at least 0.1 m/kilo-year.

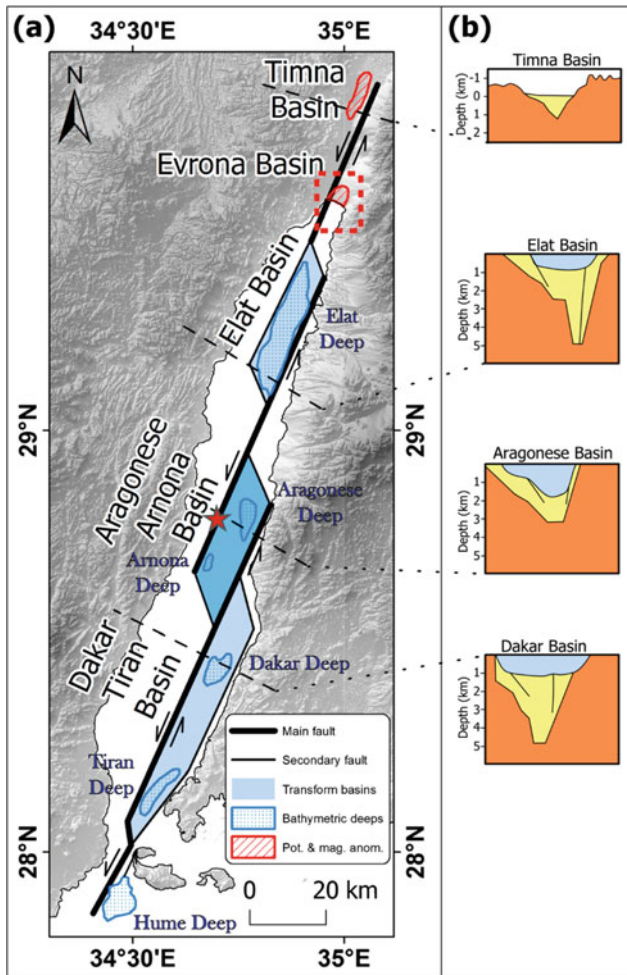


Fig. 53 Generalized tectonic setting and distribution of main deeps of the Gulf of Aqaba (after Hartman et al., 2014). Note that the Hume deep, south of the Tiran Island, connects the Gulf of Aqaba with the axial depression of the Red Sea

5 Commentary on the Main Topics Highlighted in this Chapter

The following are the main topics discussed in the present reviews of the Phanerozoic tectonic evolution and structural history of Egypt:

- The pre-Paleozoic regional tectonic framework of the Egyptian Nubian Shield had a great influence on the deposition of the Paleozoic succession in Egypt, the geographic distribution of Paleozoic units, and their lithology and thicknesses.
- The preexisting Pan-African structures controlled the Paleozoic basins in NE-SW, E-W, and NW-SE directions, while the N-S trend has had a minor effect. Rejuvenation of these Neoproterozoic faults/shears was responsible for the regional and local tectonic evolution of such basins with

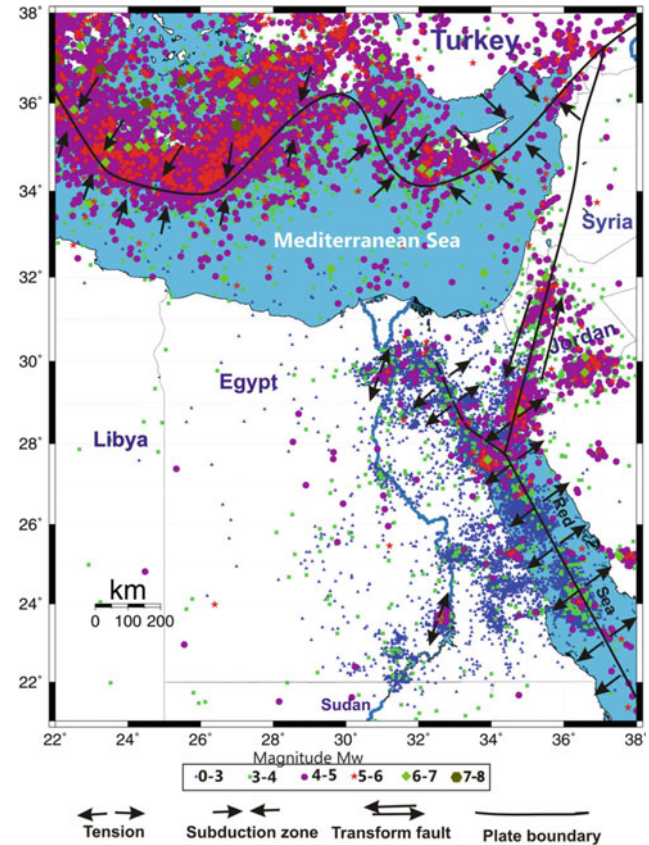


Fig. 54 Distribution of seismic activity from 1900 to 2014 and the main tectonic boundaries around Egypt (after Abd El-Aal et al., 2020)

various effects on the magmatic eruption, basin extension, and the limitations of transgression and regression.

- The surface exposures of the Paleozoic rocks are remarkably limited on the geological map of Egypt, being restricted to the Gulf of Suez in northeast Egypt, Sinai and the remote area between Gebel Uweinat and Abu Ras Plateau at the southwestern corner of Western Desert. In the subsurface of northern Western Desert, a great section of Paleozoic sediments (several kilometers in thickness) is known.
- The glaciogenic dropstones (erratic fragments and blocks) were documented by many authors in several siliciclastic sections from Sinai, Galala Plateaus, northern Wadi Qena, and southern Eastern and Western Deserts.
- The glacial to fluvio-glacial deposits in Egypt are exemplified by the Naqus Formation in Sinai and northern Egypt, and the Gabgaba Formation in the South Nile Basin.
- The Paleozoic arches are typified in Egypt by Uweinat-Bahariya-, Tarfawi-Qena-South Sinai- Chephren-Komombo-, Umbark- Suez-Cairo-Dabaa-, and el-Nashfa-el-Balliyna arches, along with the North Sinai Syrian Arc Fold Belt, and the Sharib-Sheiba high.
- Siwa-, Dakhla-, South Nile-, Sinai-, and Gulf of Suez basins are examples of Paleozoic basins in Egypt. These

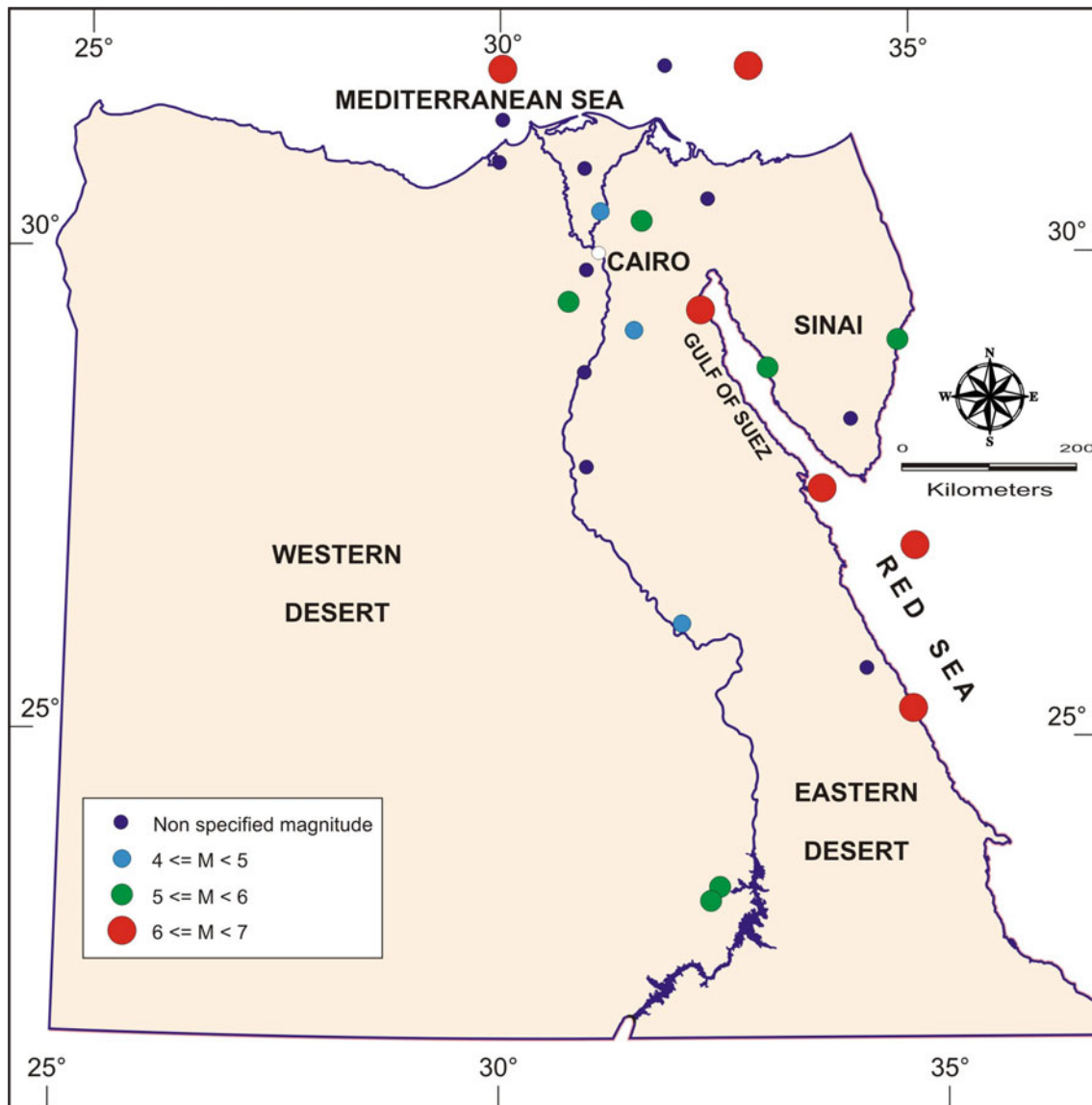


Fig. 55 Locations of the historical earthquakes from 2200 B.C. to 1900 A.D. (the data is compiled from Ambraseys et al., 1994; Poirer & Taher, 1980; Maamoun et al., 1984)

- basins lie in the vicinity of the Pan-African linear and shear zones, and include extensional basins (Gulf of Suez), marginal basins (Siwa and Abu Gharadig), and interior basins (Dakhla, and South Nile Valley).
- The Tethyan rifting resulted in the development of NE-SW- and ENE-WSW-oriented interior rift basins in northern Egypt, as well as similarly oriented normal faults in central Western Desert (e.g., Bahariya Depression) and southern Western Desert (e.g., Nubia Fault System).
 - The NNE-SSW-oriented Matruh Basin in northern Western Desert is an exceptional case, where it was regarded to be the influence of the reactivation of deep-seated basement structures.
 - Cretaceous rift basins in Egypt are represented by Beni Sueif and Asyut basins in central Egypt, Komombo Basin in southern Egypt, along with Abu Gharadig Basin in the northern Western Desert.
 - During the Late Cretaceous (84 Ma), Egypt witnessed the direct effects of major plate rearrangements, known as the 'Santonian event', resulting from the drastic change in the Afro-Arabian and Eurasian plate movements from divergence across the Neotethys to convergence that continues to the present day in select localities.
 - The Santonian far-field compressional stress resulted in the formation of multiple compressional structures in the areas lying south to the inverted basins of northern Egypt (central and southern Egypt).

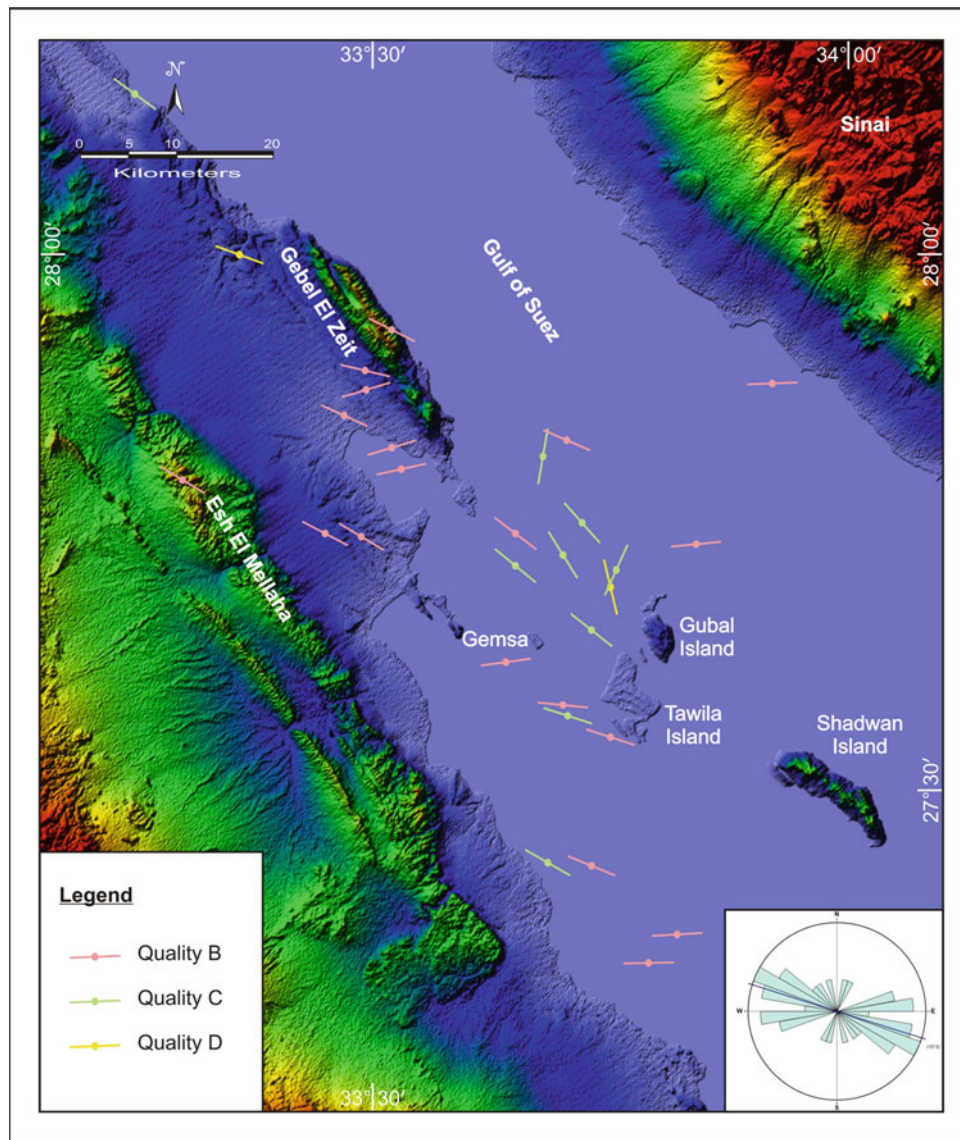


Fig. 56 Maximum horizontal stress directions from borehole breakouts for the southern part of the Gulf of Suez with rose diagram of S_H with a mean vector of 107.5° (compiled from Badawy, 2001; Heidbach et al., 2008; Henaish, 2015)

- The dissection of the NE-SW-oriented inversion folds by NW-SE-striking normal faults led some researchers to believe that these faults were formed as the result of NE-SW extension contemporaneous with the NW-SE compression associated with basin inversion.
- During the Late Cretaceous, the positive inversion of Jurassic-Early Cretaceous rift-bounding faults resulted in the formation of asymmetric doubly plunging inversion folds in the northern Western Desert.
- Late Cretaceous inversion was documented in the northern Eastern Desert of Egypt in two localities: Wadi Araba and Gebel Shabraweit.
- The Nubia Fault System in the southern part of the Western Desert exhibits two main fault belts: E-W to ENE-WSW and N-S. This system was formed due to fault reactivation by Santonian-Late Eocene dextral transpression.
- The Red Sea and Gulf of Suez Rift System was formed by extensional splitting of the Precambrian basement, initiated in the Late Oligocene because of the upwelling of Afar plume.
- Active Quaternary fault zones in Egypt are distributed in several localities, including (1) the Nile Delta area in the form of E-W- to NW-striking, normal, or dextral transtensive faults; (2) Helwan and Aswan E-W dextral, transpressive fault zones; (3) the Gulf of Suez and the Red Sea comprising NW-SE faults delimiting tilted blocks and rift shoulders; and (4) the Gulf of Aqaba-Dead Sea fault zone representing the \sim N-S sinistral, transtensive faults.

- It is important to take into account the seismotectonics and current stress field in Egypt, when analyzing the activity of Gulf of Aqaba, the Red Sea, and Gulf of Suez, and the effects of the Eastern Mediterranean subduction zone on the North African passive continental margin.

References

- Abbas, I., Guinn, S., Afify, W., Ramadan, Y., Jennette, D., & Gharieb, A. (2019). Impact of Jurassic volcanic rocks on hydrocarbon exploration, North Western Desert, Egypt. In *14th Offshore Mediterranean Conference and Exhibition, Ravenna, Italy, extended abstract*.
- Abdallah, A. M., & Adindani, A. (1963). *Stratigraphy of Upper Paleozoic rocks, western side of Gulf of Suez*. Egypt Geology of Survey, paper 25, 18pp.
- Abd-Allah, M. A., Moustafa, A. R., & Hashem, W. A. (2004). Structural characteristics and analysis of the Gebel El Halal fold, Northeast Sinai Egypt. *MERC, Ain Shams University, Earth Science Series, 18*, 1–26.
- Abdeen, M. M., & Gaballah, H. M. (2013). Utilization of open source imagery data in delineating active faults, SE Western Desert Egypt. *Geological Society of America Abstracts with Programs, 45*(7), 160.
- Abd El-Aal, A. E. -A. K., Hagag, W., Sakr, K., & Saleh, M. (2020). Seismicity, seismotectonics and neotectonics in Egypt. In Z. Hamimi, A. El-Barkooky, J. Martinez Frias, H. Fritz & Y. Abd El-Rahman (Eds.), *The Geology of Egypt* (pp. 375–413). Springer International Publishing. https://doi.org/10.1007/978-3-030-15265-9_10
- Abd El-Aziz, M., Moustafa, A. R., Said, S. E. (1998). Impact of basin inversion on hydrocarbon habitat in the Qarun Concession, Western Desert, Egypt. In *Proceedings of 14th EGPC Exploration and Production Conference, Cairo*, (Vol. 1, pp. 139–155).
- Abd El-Fattah, B. K., Moustafa, A. R., & Yousef, M. (2021) A new insight into the structural evolution of Rosetta Fault, eastern margin of Herodotus Basin, East Mediterranean. *Marine and Petroleum Geology, 105161*. <https://doi.org/10.1016/j.marpetgeo.2021.105161>
- Abdel Khalek, M. L., Abdel Wahed, N., & Sehim, A. A. (1993). Wrenching deformation and tectonic setting of the northwestern part of the Gulf of Aqaba. *Geological Society Egypt Special Publication, 1*, 409–444.
- Abd El-Wahed, M. (2010). The role of the Najd Fault system in the tectonic evolution of the Hammamat molasse sediments, Eastern Desert Egypt. *Arabian Journal of Geosciences, 3*, 1–26. <https://doi.org/10.1007/s12517-008-0030-0>
- Abed, M. A., Issa, M. M., Anihre, B. S., & Khalil, B. (1993). Upper Ordovician glacial deposits. *Episodes, 16*(1,2), 316–328.
- Addate, T., Keller, G., & Stinnesbeck, W. (2002). Late Cretaceous to Early Paleogene climate and sea-level fluctuations: The Tunisia record. *Palaeogeography, Palaeoclimatology, Palaeoecology, 178*, 165–196.
- Akaad, M. K. (1972). A contemplation and assessment of 1960–1961 classification of rocks of the central Eastern Desert Egypt. *Annals of the Geological Survey of Egypt, 2*, 19–45.
- Al-Ahwani, M. M. (1982). Geological and sedimentological studies of Gebel Shabrawet area, Suez Canal district—Egypt. *Annals of the Geological Survey of Egypt, 12*, 305–381.
- Alvarez, L. W., Alvarez, W., Asaro, F., & Michel, H. V. (1980). Extraterrestrial cause for the Cretaceous-Tertiary extinction. *Science, 208*, 1095–1108.
- Ambraseyes, N. N., Melville, C. P., & Adams, R. D. (1994). *The seismicity of Egypt, Arabia and Red Sea, a historical review*. King AbdulAziz City for Science and Technology (pp. 1–137). Cambridge University Press.
- Anan, T., & Shahin, A. (2021). Biostratigraphy and depositional environments of the Palaeocene-Eocene succession at Um El Huwaitat area, Eastern Desert Egypt. *Geological Journal, 56*, 1795–1820.
- Andres, W., & Radtke, U. (1988). Quartäre Strandterrassen an der Kilüste des Gebel Zeit (Golf von Suez/Agypten). *Erdkunde, 42*, 7–16.
- Atta, M. (1994). *Geological study of the Gebel El Zeit-Esh El Mellaha basin, with special emphasis on geochemical evolution* [M.Sc. Thesis], Cairo University, Egypt.
- Attwa, M., & Henaish, A. (2018). Regional structural mapping using a combined geological and geophysical approach—A preliminary study at Cairo-Suez district Egypt. *Journal African Earth Sciences, 144*, 104–121.
- Attwa, M., Henaish, A., & Zamzam, S. (2020). Hydrogeologic characterization of a fault-related dome using outcrop, borehole and electrical resistivity data. *Natural Resources Research, 29*, 1143–1161.
- Ayyad, M. H., & Darwish, M. (1996). Syrian arc structures: A unifying model of inverted basins and hydrocarbon occurrences in north Egypt. In *EGPC 13th Petroleum Conference Egypt* (Vol. 1, pp. 40–59).
- Badawy, A. (1999). Historical seismicity of Egypt. *Acta Geodaetica et Geophysica Hungarica, 34*, 119–135. <https://doi.org/10.1007/BF03325564>
- Badawy, A. (2001). Status of the crustal stress in Egypt as inferred from earthquake focal mechanisms and borehole breakouts. *Tectonophysics, 343*, 49–61.
- Bakr, A., & Helmy, M. (1990). Wrench faulting and its implication on hydrocarbon accumulations: Alamein- Yidma area, Western Desert, Egypt. In *Proceedings of 10th EGPC Petroleum Exploration and Production Conference* (Vol. 2, pp. 257–289).
- Baldrige, W. S., Eyal, Y., Bartov, Y., Steinitz, G., & Eyal, M. (1991). Miocene magmatism of Sinai related to the opening of the Red Sea. *Tectonophysics, 197*, 181–201.
- Bartov, Y., Lewy, Z., Steinitz, G., & Zak, I. (1980a). Mesozoic and Tertiary stratigraphy, paleogeography and structural history of the Gebel Areif en Naqa area, eastern Sinai Israel. *Journal of Earth Sciences, 29*, 114–139.
- Bartov, Y., Steinitz, G., Eyal, M., & Eyal, Y. (1980b). Sinistral movement along the Gulf of Aqaba. *Nature, 285*, 220–222.
- Beall, A. O., & Squyres, C. H. (1980). Modern frontier exploration strategy, a case history from Upper Egypt. *Oil and Gas Journal, 4*, 106–110.
- Bellini, E., & Massa, D. (1980). A stratigraphic contribution to the Paleozoic of the southern basins of Libya. In M. J. Salem & M. T. Buserwil (Eds.), *The geology of Libya* (Vol. 1, pp. 3–56). London: Academic Press.
- Ben Ferjani, A., Burolet, R. F., & Mejri, F. (1990). Petroleum geology of Tunisia: ETAE Tunis, 160 pp.
- Bernaola, G., & Monechi, S. (2007). Calcareous nannofossil extinction and survivorship across the Cretaceous-Paleogene boundary at Walvis Ridge (ODP Hole 1262C, South Atlantic Ocean). *Palaeogeography, Palaeoclimatology, Palaeoecology, 255*, 132–156.
- Beuf, S., Biju-Duval, B., de Charpal, O., Ragnon, P., Gariel, O., & Bennacef, A. (1971). Les gres du Paleozoique inferieur au Sahara. In Technip (Ed.), *Sedimentation et discontinuite, Evolution Structurale d'un craton* (480pp). Paris: College of Science Et Technology Du Petrole.
- Bevan, T. G., & Moustafa, A. R. (2012). Inverted rift-basins of Northern Egypt. In D. G. Roberts & A. W. Bally (Eds.), *Regional geology and tectonics: phanerozoic rift systems and sedimentary basins* (Vol. 2, pp. 483–507). Elsevier

- Bornemann, A., Schulte, P., Sprong, J., Steurbaut, E., Youssef, M., & Speijer, R. (2009). Latest Danian carbon isotope anomaly and associated environmental change in the southern Tethys (Nile Basin, Egypt). *Journal of Geological Society of London*, *166*, 1135–1142.
- Bosworth, W. (1994). *A model for the three-dimensional evolution of continental rift basins, northeast Africa: Geologische Rundschau* (Vol. 83, pp. 671–688). <https://doi.org/10.1007/BF00251067>
- Bosworth, W. (1995). A high strain rift model for the southern Gulf of Suez, Egypt. In J. Lambiase (Ed.), *Hydrocarbon habitat in rift basins* (Vol. 80, pp. 75–102). Journal of Geological Society of London, Special Publications.
- Bosworth, W., & McClay, K. R. (2001). Structural and stratigraphic evolution of the Suez rift, Egypt: a synthesis. In P. A. Zeigler, W. Cavazza, A. H. F. Robertson & S. Crasquin-Soleau (Eds.), *Peri-Tethyan rift-wrench basins and passive margins* (pp. 567–606). Musee Nationale Hist Natural.
- Bosworth, W., & Stockli, D. F. (2016). Early magmatism in the greater Red Sea rift: Timing and significance. *Canadian Journal of Earth Sciences*, *53*, 1158–1176.
- Bosworth, W., & Tari, G. (2021). Hydrocarbon accumulation in basins with multiple phases of extension and inversion: Examples from the Western Desert (Egypt) and the western Black Sea. *Solid Earth*, *12* (1), 59–77. <https://doi.org/10.5194/se-12-59-2021>
- Bosworth, W., & Taviani, M. (1996). Late Quaternary reorientation of stress field and extension direction in the southern Gulf of Suez, Egypt: Evidence from uplifted coral terraces, mesoscopic fault arrays, and borehole breakouts. *Tectonics*, *15*, 791–802.
- Bosworth, W., Guiraud, R., & Kessler, L. G. (1999). Late Cretaceous (Ca. 84 Ma) compressive deformation of the stable platform of northeast Africa (Egypt): Far-field stress effects of the “Santonian event” and origin of the Syrian arc deformation belt. *Geology*, *27*, 633–636.
- Bosworth, W., Stockli, D. F., & Helgeson, D. E. (2015). Integrated outcrop, 3D seismic, and geochronologic interpretation of Red Sea dike-related deformation in the Western Desert, Egypt—The role of the 23 Ma Cairo “mini-plume.” *Journal of African Earth Sciences*, *109*, 107–119.
- Bosworth, W., El-Hawat, A. S., Helgeson, D. E., & Burke, K. (2008). Cyrenaican “shock absorber” and associated inversion strain shadow in the collision zone of northeast Africa. *Geology*, *36*(9), 695–698.
- Bosworth, W., Huchon, P., & McClay, K. (2005). The Red Sea and Gulf of Aden basins. *Journal of African Earth Sciences*, *43*, 334–378.
- Bosworth, W., Lučić, D., & Stockli, D. F. (2020). North African Phanerozoic. In D. Alderton & S. A. Elias (Eds.), *Encyclopedia of Geology* (2nd edn, pp. 244–258). Oxford: Academic Press. <https://doi.org/10.1016/B978-0-12-409548-9.12454-6>
- Burollet, P. F. (1963). Reconnaissance géologique dans le sud-est du bassin de Kufra. *Review Institut Français Pétrole*, *18*, 219–227.
- Choukri, A., Reyss, J. L., & Plaziat, J. C. (1995). Datations radiochimiques des hauts niveaux marins de la rive occidentale du Nord de la Mer Rouge au moyen de radioles d'oursin. *Comptes Rendus De L'academie Des Sciences. Serie III, Sciences De La Vie*, *321*, 25–30.
- Clifford, T. N. (1970). The structural framework of Africa. In T. N. Clifford & I. G. Gass (Eds.), *African magmatism and tectonics* (pp. 1–23). Oliver and Edinburg.
- Cochran, J. R. (2005). Northern Red Sea: Nucleation of an oceanic spreading center within a continental rift. *Geochem-Geophys-Geosyst*, *6*, Q03006. <https://doi.org/10.1029/2004gc000826>
- Cochran, J. R., Gaulier, J. M., & LePichon, X. (1991). Crustal structure and the mechanism of extension in the northern Red Sea: Constraints from gravity anomalies. *Tectonics*, *10*, 1018–1037.
- Conant, L. C., & Goudarzi, G. H. (1964). Geological map of the Kingdom of Libya. *US Geological Survey*, *1*(2)
- Courtillot, V., Jaupart, C., Manighetti, I., Tapponnier, P., & Besse, J. (1999). On causal links between flood basalts and continental breakup, Earth Planet. *Science Letter*, *166*, 177–195.
- Coward, M. P., & Ries, A. C. (2003). Tectonic development of North African basins. *Geological Society, London, Special Publications*, *207*, 61–83.
- Culver, S. (2003). Benthic foraminifera across the Cretaceous-Tertiary (K-T) boundary: A review. *Marine Micropaleontology*, *47*, 177–226.
- Dardir, A. A. (1981). Basement rocks of the Gilf-Uweinat area. *Annals Geological Survey of Egypt*, *11*, 67–78.
- Darwish, M., & Tewfik, N. (2008). Sequence stratigraphy and facies of the Jurassic-Lower Cretaceous rift systems in NE Africa. In M. Salem, A. El-Arnauti & A. Saleh (Eds.), *3rd Symposium on the Sedimentary Basins of Libya* (Vol. 1, pp. 345–368). The Geology of East Libya.
- Dolson, J. C., Atta, M., Blanchard, D., Sehim, A., Villinski, J., Loutit, T., & Romine, K. (2014). Egypt's future petroleum resources: a revised look into the 21st century. In L. Marlow, C. Kendall & L. Yose (Eds.), *Petroleum systems of the Tethyan region* (Vol. 106, pp. 143–178). AAPG Memoir
- Dullo, W. C. (1990). Facies, fossil record, and age of Pleistocene reefs from the Red Sea (Saudi Arabia). *Facies*, *22*, 1–46. Evidence from uplifted coral terraces, mesoscopic fault arrays, and borehole breakouts. *Tectonics*, *15*, 791–802.
- Dupuis, C., Aubry, M. -P., Steurbaut, E., Berggren, W., Ouda, Kh., Magioncalda, R., Cramer, S., Kent, D., Speijer, R., & Heilmann-Clausen, C. (2003). The Dababiya quarry section: Lithostratigraphy, clay mineralogy, geochemistry and paleontology. *Micropaleontology*, *49*, 41–60.
- El Habaak, G. H., & Mahmoud, S. (1994). Carbonaceous bodies of debatable organic provenance in the banded iron formation of the Wadi Kareim area, Eastern desert Egypt. *Journal of African Earth Sciences*, *19*, 125–133.
- El Kelany, A. (2000). Lithostratigraphy and petrology of the Paleozoic sequence in Sinai, Egypt. [Ph.D. Thesis] (208pp). Al Azhar University.
- El Saadany, M. (2008). Structural style and tectonic evolution of the central part of the northern Western Desert, Egypt. [Ph.D. dissertation] (267pp). Ain Shams University.
- El Shazly, E. M. (1977). The geology of the Egyptian region. In A. E. M. Nairn, W. H. Kanes, & F. G. Stehli (Eds.), *The Ocean Basins and Margins*, vol. 4(A) (pp. 379–444). Plenum Press.
- El-Shaarawy, O. A., Abdel Aal, A., & Papazis, P. (1992). Tectonic setting of the Razzak oil field, northern Western desert of Egypt. In *Proceedings of 11th EGPC Petroleum Exploration and Production Conference* (vol. 3, pp. 310–323).
- Eyal, M., Eyal, Y., Bartov, Y., & Steinitz, G. (1981). The tectonic development of the western margin of the Gulf of Elat (Aqaba) rift. *Tectonophysics*, *80*, 39–66.
- Faris, M. I., & Abbass, H. L. (1961). The geology of Shabrawet area. *Ain Shams University of Science Bulletin*, *7*, 37–61.
- Freund, R., Garfunkel, Z., Zak, I., Goldgerg, M., Weissbrod, T., & Derin, B. (1970). The shear along the Dead Sea rift. *Philosophical Transactions of the Royal Society of London. Series A*, *267*, 107–130.
- Gamal, N., Yousef, M., Moustafa, A. R., & Bosworth, W. (2021). Spatiotemporal evolution of transfer structures and linked fault systems in an extensional setting: Southwest Gebel Akheider, Cairo-Suez District, Egypt. *Marine and Petroleum Geology*, *133*, 105260 <https://doi.org/10.1016/J.MARPETGEO.2021.105260>
- Garfunkel, Z. (1998). Constrains on the origin and history of the Eastern Mediterranean basin. *Tectonophysics*, *298*(1–3), 5–35.
- Garfunkel, Z. (2004). Origin of the Eastern Mediterranean basin: A reevaluation. *Tectonophysics*, *391*, 11–34. <https://doi.org/10.1016/j.tecto.2004.07.006>

- Garfunkel, Z., & Bartov, Y. (1977). The tectonics of the Suez rift. *Bulletin Geological Survey of Israel*, 71, 1–84.
- Ghobrial, M. G. (1967). The structural geology of the Kharga Oasis. *Geological Survey of Egypt paper*, 43, 39.
- Guennoc, P., Pautot, G., Le Quentric, M. F., & Coutelle, A. (1990). Structure of an early oceanic rift in the northern Red Sea. *Oceanologica Acta*, 13, 145–155.
- Guiraud, R. (1998). Mesozoic rifting and basin inversion along the northern African-Arabian Tethyan margin: an overview. In MacGregor, Moody, Clark-Lowes (Eds.), *Petroleum Geology of North Africa* (vol. 133, pp. 215–227). Geological Society, London, Special Publication. <https://doi.org/10.1144/GSL.SP.1998.132.01.13>
- Guiraud, R., & Bosworth, W. (1997). Senonian basin inversion and rejuvenation of rifting in Africa and Arabia: Synthesis and implications to platescale tectonics. *Tectonophysics*, 282, 39–82. [https://doi.org/10.1016/S0040-1951\(97\)00212-6](https://doi.org/10.1016/S0040-1951(97)00212-6)
- Guiraud, R., & Bosworth, W. (1999). Phanerozoic geodynamic evolution of northeastern Africa and the northwestern Arabian platform. *Tectonophysics*, 315, 73–108. [https://doi.org/10.1016/S0040-1951\(99\)00293-0](https://doi.org/10.1016/S0040-1951(99)00293-0)
- Guiraud, R., Bosworth, W., Thierry, J., & Delplanque, A. (2005). Phanerozoic geological evolution of Northern and Central Africa: An overview. In Catuneanu, O., Guiraud, R., Eriksson, P., Thomas, B., Shone, R., & Key, R. (Eds.) *Phanerozoic Evolution of Africa. Journal of African Earth Sciences* (vol. 43, pp. 83–143). Elsevier.
- Guiraud, R., Issawi, B., Bosworth, & W. (2001). Phanerozoic history of Egypt and surrounding areas. In P. A. Zeigler, W. Cavazza, A. H. F. Robertson & S. Crasquin-Soleau (Eds.), *Peri-Tethys Memoir 6, Peri-Tethys Rift/Wrench Basins and Passive Margins* (Vol. 186, pp. 469–509). de Paris: Memoir Museum National d’Histoire Natur.
- Gvirtzman, G. (1994). Fluctuations of sea level during the past 400 000 years: The record of Sinai, Egypt (northern Red Sea). *Coral Reefs, Heidelberg*, 13, 203–214.
- Hagag, W. (2016). Structural evolution and Cenozoic tectonostratigraphy of the Cairo-Suez district, north Eastern Desert of Egypt: Field-structural data from Gebel Qattamiya-Gebel Um Reheiat area. *Journal of African Earth Sciences*, 118, 174–191.
- Fowler, A., & Hamimi, Z. (2020). Structural and tectonic framework of neoproterozoic basement of Egypt: From gneiss domes to transpression belts. In Z. Hamimi, A. El-Barkooky, J. Martínez Frías, H. Fritz & Abd El-Rahman, Y. (Eds.), *The Geology of Egypt, Regional Geology Reviews* (pp. 81–129). Springer Nature Switzerland, 762p https://doi.org/10.1007/978-3-030-15265-9_2
- Fowler, A., & Hamimi, Z. (2021). Post-amalgamation depositional basins in the Arabian-Nubian Shield: The Hammamat Basins of Egypt. In Z. Hamimi, A. -R. Fowler, J. -P. Liegeois, A. Collins, M. Abdelsalam & M. Abd El-Wahed (Eds.), *The Geology of the Arabian-Nubian Shield, Regional Geology Reviews book series (RGR)* (pp. 451–483), Springer Nature Switzerland, 786p. <https://doi.org/10.1007/978-3-030-72995-0>
- Hamimi, Z., Abd El-Wahed, M., Gahlan, H. A., & Kamh, S. Z. (2019). Tectonics of the Eastern desert of Egypt: Key to understanding the Neoproterozoic evolution of the Arabian-Nubian Shield (East African Orogen). In A. Bendaoud, Z. Hamimi, M. Hamoudi, S. Djemai & B. Zoheir (Eds.), *Geology of the Arab World- An Overview* (pp. 1–81). Springer Geology, Springer Geology. https://doi.org/10.1007/978-3-319-96794-3_1
- Hamimi, Z., El-Barkooky, A., Martínez Frías, J., Fritz, H., & Abd El-Rahman, Y. (Eds.) (2020). *The geology of Egypt, regional geology reviews*. Springer Nature Switzerland, 762p. https://doi.org/10.1007/978-3-030-15265-9_2
- Hamimi, Z., & Fowler, A. (2021). Najd shear system in the Arabian Nubian shield. In Hamimi, Z., Fowler, A. -R., Liegeois, J. -P., Collins, A., Abdelsalam, M., Abd El-Wahed, M. (Eds.), *The Geology of the Arabian-Nubian Shield, Regional Geology Reviews Book Series (RGR)* (pp. 359–392). Springer Nature Switzerland, 786p. <https://doi.org/10.1007/978-3-030-72995-0>
- Hamimi, Z., Arai, S., Fowler, A., & El-Bialy, M. Z. (Eds.) (2021a). The geology of the Egyptian Nubian Shield. In *Regional Geology Reviews Book Series (RGR)*. Springer Nature Switzerland, 700p. <https://doi.org/10.1007/978-3-030-49771-2>
- Hamimi, Z., Fowler, A.-R., Liegeois, J. -P., Collins, A., Abdelsalam, M., & Abd El-Wahed, M. (Eds.) (2021b). The geology of the Arabian-Nubian Shield. In *Regional Geology Reviews Book Series (RGR)*. Springer Nature Switzerland, 786p. <https://doi.org/10.1007/978-3-030-72995-0>
- Hantar, G. (1990). North Western desert. In R. Said (Ed.), *The Geology of Egypt*. (Vol. 15, pp. 293–319). Balkema, Chapter.
- Haq, B. U., & Stephen, R. S. (2008). A chronology of Paleozoic Sea-level changes. *Science*, 322, 64–68.
- Hartman, G., Niemi, T. M., Tibor, G., Ben-Avraham, Z., Al-Zoubi, A., Makovsky, Y. E., Akawwi, E., Abueladas, A., & Al-Ruzouq, R. (2014). Quaternary tectonic evolution of the Northern Gulf of Elat/Aqaba along the Dead Sea transform. *Solid Earth*, 119, 9183–9205.
- Hassan, A. A. (1967). A new Carboniferous occurrence in Abu Durba, Sinai, Egypt. In *6th Arab Petroleum Congress Baghdad* (pp. 1–8).
- Hassan, M. A., & Hashad, A. (1990). Precambrian of Egypt. In R. Said (Ed.), *The geology of Egypt* (pp. 201–248). Balkema.
- Heidbach, O., Tingay, M., Barth, A., Reinecker, J., Kurfess, D., & Mueller, B. (2008). The 2008 database release of the world stress map project. *Deutsches GeoForschungsZentrum GFZ*. <https://doi.org/10.1594/GFZ.WSM.Rel2008>
- Henaish, A. (2015). Neotectonics and structural geology controls of hydrocarbon seepages in the southern part of the Gulf of Suez, Egypt [Ph.D. Thesis] (209pp). Zagazig University.
- Henaish, A. (2018a). Fault-related domes: Insights from sedimentary outcrops at the northern tip of the Gulf of Suez rift Egypt. *Marine and Petroleum Geology*, 91, 202–210.
- Henaish, A. (2018b). Soft-linkage transfer zones: Insights from the Northern Eastern desert Egypt. *Marine and Petroleum Geology*, 95, 265–275.
- Henaish, A., & Kharbish, S. (2020). Linkage style of rift-associated fault arrays: insights from central Cairo-Suez district, Egypt. *Carpathian Journal of Earth and Environmental Sciences*, 15(1), 189–196.
- Hermine, M. H., Ghobrial, M. G., & Issawi, B. (1961). The geology of the Dakhla area. *Geological Survey of Egypt*, 33.
- Hermine, M. H., Wassef, A., El Tahlawy, A., Kamel, A., (1983). The subsurface Paleozoic section of Wadi Araba, Egypt. *Annals of the Geological Survey of Egypt*, 13, 257–269.
- Hildebrand, N., Shirav, M., & Freund, R. (1974). Structure of the western margin of the Gulf of Elat (Aqaba) in the Wadi El Quseib-Wadi Himur area, Sinai. *Israel Journal of Earth Sciences*, 23, 117–130.
- Hoang, C., & Taviani, M. (1991). Stratigraphic and tectonic implications of Uranium-series-dated coral reefs from uplifted Red Sea Islands. *Quaternary Research*, 35, 264–273.
- Hughes Clarke, M. W. (1988). Stratigraphy and rock unit nomenclature in the oil producing area of interior, Oman. *Journal Petroleum Geology*, 11, 5–60.
- Husseini, M. I. (1991). Tectonic and depositional model of the Arabian and adjoining plates during the Silurian-Devonian. *Bulletin American Association of Petroleum Geologists*, 57(1), 108–120.
- Issawi, B. (1968). The geology of Kurkur Dungul area. *Geological Survey of Egypt, Paper*, 46, 102.
- Issawi, B. (1971). Geology of Darb El-Arbain, Western Desert. In R. Said & M. Y. Meneisy (Eds.), *Annales of the Geological Survey of Egypt* (Vol. 1, pp. 53–92).
- Issawi, B. (1972). Review of upper cretaceous-lower tertiary stratigraphy in central and Southern Egypt. *Bulletin of the American Association of Petroleum Geologists*, 56, 1448–1463.

- Issawi, B. (1978). New findings on the geology of uweinat-gilf Kebir. *Annals Geological Survey of Egypt*, 8, 27–293.
- Issawi, B. (1981). Geology of the South Western Desert of Egypt. *Annals Geological Survey of Egypt*, 11, 57–66.
- Issawi, B. (1996). Tectono-sedimentary synthesis of the Paleozoic basins in Egypt. In *13th Petroleum Conference, Egyptian General Petroleum Corporation, Cairo* (Vol. 1, pp. 1–24).
- Issawi, B. (2000). Northern Gondwana Early Paleozoic glaciation. In *International Conference Geology of Arab World, Cairo University* (Vol. 3, pp. 1243–1250).
- Issawi, B. (2005). Archean-Phanerozoic birth and development of the Egyptian land. In *1st International Conference Geology of Tethys, Cairo University* (Vol. 2, pp. 339–352).
- Issawi, B., & Jux, U. (1982). Contribution to the stratigraphy of the Paleozoic rocks in Egypt. *Geology of Survey Egypt, Paper*, 64, 24.
- Issawi, B., El Hinnawi, M., Francis, M., & Mazhar, A. (1999). The Phanerozoic geology of Egypt: A geodynamic approach. *Egypt Geology Survey Paper*, 76, 462.
- Issawi, B., Francis, M., Youssef, E., & Osman, R. (2009). The Phanerozoic geology of Egypt, a geodynamic approach. In *Special Publication* (Vol. 81, 589pp). EMRA, Egypt.
- Issawi, B., Osman, R., Yehia, M., & El Defitar, T. (1994). The delineation of Sinai water basins by using lithofacies isopach and structural contour maps. In *2nd Conference Geol Arab World, Cairo University*, pp. 48–497.
- Jarrige, J. J., Ott d'Estevou, P., Burollet, P. F., Montenat, C., Prat, P., Richert, J. P., & Thiriet, J. P. (1990). The multistage tectonic evolution of the Gulf of Suez and northern Red Sea continental rift from field observations. *Tectonics*, 9, 441–465.
- Keeley, M. L. (1989). The Paleozoic history of the Western Desert of Egypt. *Basin Research*, 2, 35–48.
- Keeley, M. L., Dungworth, G., Floyd, C. S., Forbes, G. A., King, C., McGarva, R. M., & Shaw, D. (1990). The Jurassic System in northern Egypt: I. Regional stratigraphy and implications for hydrocarbon prospectivity. *Journal Petroleum Geology*, 13, 397–420.
- Keeley, M. L., & Wallis, R. J. (1991). The Jurassic system in northern Egypt: II. Depositional and tectonic regimes. *Journal of Petroleum Geology*, 14, 49–64.
- Kerdany, M. T., & Cherif, O. H. (1990). Mesozoic, chap. 22, In R. Said & A. A. Balkema (Eds.) *The Geology of Egypt, Rotterdam, The Netherlands*, pp. 407–438.
- Khalaf, E. A., Abdel Motelib, A., Hamed, M. S., & El Manawi, A. H. (2015). Volcano-sedimentary characteristics in the Abu Treifiya Basin, Cairo-Suez District, Egypt: Example of dynamics and fluidization over sedimentary and volcanoclastic beds by emplacement of syn-volcanic basaltic rocks. *Journal of Volcanology and Geothermal Research*, 292, 1–28.
- Khalifa, H., Omran, A. M., Higazy, H. A. (1988). Microfossils from Late Proterozoic (Hammamat Group) Eastern Desert, Egypt. *Bulletin Faculty Science Assiut University*, 12, 1–29.
- Khalil, M. (1992). The structural evolution of the 'B' trend and its significance for hydrocarbon exploration in offshore Gulf of Suez, Egypt. In *Proceedings 11th Explore Conference EGPC*, pp. 64–78.
- Khalil, S. M., & McClay, K. R. (2002). Extensional fault-related folding, northwestern Red Sea Egypt. *Journal Structural Geology*, 24, 743–762.
- Khalil, S. M., & McClay, K. R. (2009). Structural control on syn-rift sedimentation, northwestern Red Sea margin Egypt. *Marine and Petroleum Geology*, 26, 1018–1034.
- Khozyem, H., Adatte, T., Spangenberg, J., Keller, G., Tantawy, A., & Ulianov, A. (2015). New geochemical constraints on the Paleocene-Eocene thermal maximum: Dababiya GSSP Egypt. *Palaeogeography, Palaeoclimatology, Palaeoecology*, 429, 117–135.
- Khozyem, H., Adatte, T., Spangenberg, J., Tantawy, A., & Keller, G. (2013). Palaeoenvironmental and climatic changes during the Palaeocene-Eocene Thermal Maximum (PETM) at the Wadi Nukhul section, Sinai Egypt. *Journal of Geological Society of London*, 170, 341–352.
- Klitzsch, E. (1978). Geologische Bearbeitung Südwest Ägyptens. *Geology of Rundschau*, 67, 509–520.
- Klitzsch, E. (1979). Zur Geologie des Gilf Kebir Gebietes in der Ostsahara. *Clauth Geology Abhandlungen*, 30, 113–132.
- Klitzsch, E. (1983). Geological research in and around Nubia. *Episodes*, 3, 15–19.
- Klitzsch, E. (1986). Plate tectonics and cratonic geology in northeast Africa (Egypt/Sudan). *Geology Rundschau*, 75, 755–768.
- Klitzsch, E., & Lejal-Nicol, A. (1984). Flora and fauna from a strata in southern Egypt and northern Sudan (Nubia and surrounding areas). *Berlin Geowiss Abhandlungen*, 50(A), 47–79 (1942).
- Kora, M. (1984). The Paleozoic outcrops of Um Bogma area, Sinai, [Ph.D. Thesis] (253pp). Mansoura University, Mansoura.
- Kora, M. (1992). Carboniferous macrofauna from Wadi khaboba west central Sinai Egypt. *Geology Et Paleontology*, 26, 13–27.
- Kora, M. (1995). Lower Carboniferous calcareous microfossils from the Gulf of Suez region Egypt. *Geology Et Paleontology*, 29, 217–231.
- Kora, M., Jux, U. (1986). On the Early carboniferous macrofauna from the Um Bogma Formation, Sinai. *Neues Jahrbuch für Geologie und Paläontologie, Monatshefte*, 2, 85–98.
- Kora, M., & Mansour, Y. (1992). Stratigraphy of some Permo-Carboniferous successions in the Northern Galala, Gulf of Suez region Egypt. *Neues Jahrbuch für Geologie und Paläontologie, Abhandlungen*, 185(3), 377–394.
- Krenkel, E. (1925). *Geologie der Erde, Geologie Afrikas, volume I*. Gebrüder Borntraeger, 461 p.
- Lababidi, M. M., & Hamdan, A. N. (1985). Preliminary lithostratigraphic correlation study in OAPC member countries. *Organization Arabian Petroleum Exposure Countries, Energy Resource Department*, 171.
- Lambeck, K., & Nakada, M. (1992). Constraints on the age and duration of the last interglacial period and on sea-level variations. *Nature*, 357, 125–128.
- Lejal-Nicol, A. (1986). Decouverte d'une flora à Callipteris dans la région du Suez (Egypte). C.R. 111eme. *Congress Nature Society of Servey*, 2, 9–22.
- Letouzey, J., & Tre'molie' res, P. (1980). Paleo-stress fields around the Mediterranean since the Mesozoic derived from microtectonics: comparisons with plate tectonic data. In J. Aubouin, J. Debelmas & M. Latreille (Eds.), *Geology of the Alpine chains born of the Tethys* (Vol. 115, pp. 261–273), Me'm. B.R.G.M.
- Longacre, M., Bentham, P., Hanbal, I., Cotton, J., & Edwards, R. (2007). New crustal structure of the Eastern Mediterranean Basin: detailed integration and modeling of gravity, magnetic, seismic refraction, and seismic reflection data. In *EGM 2007 International Workshop: Innovation in EM, Grav and Mag Methods: A New Perspective for Exploration, Capri, Italy, 15–18 April 2007*, 4 pp.
- Maamoun, M., Megahed, A., & Allam, A. (1984). *Seismicity of Egypt. HIAG Geophys. Bull.*, 4, 109–160.
- Mahmoud, N. M., Vaslet, D., & Hussein, M. I. (1992). The lower Silurian Qalibah formation of Saudi Arabia. *Bulletin American Association of Petroleum Geologists*, 63(10), 1491–1506.
- Maqbool, A.-R., Moustafa, A. R., Dowidar, H., & Yousef, M. (2014). Structural setting of Gebel Ataqa area, Gulf of Suez, Egypt: Implications for rift-related fault array. *Egyptian Journal of Geology*, 58, 205–221.
- Maqbool, A.-R., Moustafa, A. R., Dowidar, H., & Yousef, M. (2016). Architecture of fault damage zones of normal faults, Gebel Ataqa area, Gulf of Suez rift, Egypt. *Marine and Petroleum Geology*, 77, 43–53.
- Martinson, D. C., Pisias, N. G., Hays, J. D., Imbrie, J., Moore, T. C., Jr., & Shackleton, N. J. (1987). Age dating and the orbital theory of

- the ice ages: Development of a high resolution 0 to 300,000-year chronostratigraphy. *Quaternary Research*, 27, 1–29.
- Mayhoub, A. A., Moustafa, A. R., Yousef, M., & Zalat, S. M. (2017). Subsurface structural setting of Al Amir and Geyad fields, southwestern part of the Gulf of Suez rift, Egypt: Bulletin of the Faculty of Science. *Zagazig University*, 39, 229–243.
- Mayhoub, A. A., Moustafa, A. R., Yousef, M., & Zalat, S. M. (2019). Cyclo-sequence stratigraphy of the Miocene syn-rift succession, Al Amir and Geyad fields, southwestern part of the Gulf of Suez rift. *Journal of African Earth Sciences*, 157, 103504.
- Mazzini, A., Lupi, M., Sciarra, A., Hamed, M., Schmidt, S. T., & Suessenberger, A. (2019). Concentric Structures and Hydrothermal Venting in the Western Desert Egypt. *Frontiers Earth Science*, 7, 266.
- McGarva, R. M. (1986). Sedimentology, petrography and diagenesis of the Zeitoun Formation (Devonian) of the Western Desert, Egypt. In *8th Petroleum Conference Egyptin Petroleum Corporation, Cairo*.
- McGillivray, G., & Hussein, M. I. (1992). The Paleozoic petroleum geology of Central Arabia. *Bulletin American Association of Petroleum Geologists*, 76(10), 1473–1490.
- McLean, D. M. (1978). A terminal Mesozoic “Greenhouse”: Lessons from the past. *Science*, 201, 401–406.
- Meneisy, M. Y. (1986). Mesozoic igneous activity in Egypt. *Qatar University of Bulletin of V, Science*, 6
- Meneisy, M. Y., & Kreuzer, H. (1974a). Potassium-argon ages of Egyptian basaltic rocks. *Geologisches Jahrbuch*, D9, 21–31.
- Meneisy, M. Y., & Kreuzer, H. (1974b). Potassium-argon ages of nepheline syenite ring complexes in Egypt. *Geologisches Jahrbuch*, D9, 33–39.
- Meneisy, M. Y., & Abdel Aal, A. Y. (1984). Geochronology of phanerozoic volcanic rocks in Egypt. *Ain Shams Scientific Bulletin*, 25(24B), 163–176.
- Meshref, W. (1990). Tectonic framework. In R. Said, (Ed.), *The geology of Egypt* (734 p). Balkema Pub., Netherlands.
- Metwalli, F. I., & Pigott, J. D. (2005). Analysis of petroleum system criticals of the Matruh-Shushan Basin, Western Desert Egypt. *Petroleum Geoscience*, 11, 157–178.
- Moussa, S. (1986). Evolution of the sedimentary basins of north Western Desert, Egypt. In *8th Petroleum Conference Egypt General Petroleum Corporation, Cairo*, 14 pp
- Moustafa, A. M. (1976). Block faulting in the Gulf of Suez. In *Proceedings of 5th Egyptian General Petroleum Corporation Exploration Seminar, Cairo*, 35 pp.
- Moustafa, A. R. (1988). Wrench tectonics in the north Western Desert of Egypt (Abu Roash area, Southwest of Cairo). *MERC Ain Shams University Earth Science Service*, 2, 1–16.
- Moustafa, A. R. (2002). Controls on the geometry of transfer zones in the Suez rift and northwest Red Sea: Implications for the structural geometry of rift systems. *AAPG Bulletin*, 86, 979–1002.
- Moustafa, A. R. (2005). Structural architecture of Late Cretaceous–Early Tertiary inverted structures in northern Sinai (Gebel Maghara area): abstract. In *43rd Annual Meeting of the Egyptian Geological Society, Cairo, December 2005*.
- Moustafa, A. R. (2008). Mesozoic-Cenozoic basin evolution in the northern Western Desert of Egypt. In: M. Salem, A. El-Arnauti & A. Saleh (Eds.), *3rd Symposium on the Sedimentary Basins of Libya* (Vol. 3, pp. 29–46). The Geology of East Libya.
- Moustafa, A. R. (2010). Structural setting and tectonic evolution of north Sinai folds, Egypt. In C. Homberg & M. Bachmann (Eds.), *Evolution of the Levant Margin and Western Arabia Platform Since the Mesozoic* (Vol. 341, pp. 37–63). Geological Society of London Special Publication.
- Moustafa, A. R. (2013). Fold-related faults in the Syrian Arc belt of northern Egypt. *Marine and Petroleum Geology*, 48, 441–454.
- Moustafa, A. R. (2014). Structural architecture and tectonic evolution of the Maghara inverted basin, Northern Sinai Egypt. *Journal of Structural Geology*, 60, 80–96.
- Moustafa, A. R. (2020). Mesozoic-Cenozoic Deformation History of Egypt. In Z. Hamimi, A. El-Barkooky, J. Martínez Frías, H. Fritz, & Y. Abd El-Rahman (Eds.), *The Geology of Egypt* (pp. 253–294). Cham: Springer International Publishing. https://doi.org/10.1007/978-3-030-15265-9_7
- Moustafa, A. R., & Abd-Allah, M. A. (1992). Transfer zones with en echelon faulting at the northern end of the Suez rift. *Tectonics*, 11, 499–509.
- Moustafa, A. R., & Fouda, H. G. A. (2014). Structural architecture and tectonic evolution of the Yelleg inverted half graben, northern Sinai Egypt. *Marine and Petroleum Geology*, 51, 286–297.
- Moustafa, A. R., & Khalil, M. H. (1995). Superposed deformation in the northern Suez rift, Egypt: Relevance to hydrocarbon exploration. *Journal of Petroleum Geology*, 18, 245–266.
- Moustafa, A. R., & Khalil, S. M. (2020). Structural setting and tectonic evolution of the Gulf of Suez, NW Red Sea and Gulf of Aqaba rift systems. In Z. Hamimi, A. El-Barkooky, J. Martínez Frías, H. Fritz & Y. Abd El-Rahman (Eds.), *The Geology of Egypt* (pp. 375–413, 295–342). Springer International Publishing. https://doi.org/10.1007/978-3-030-15265-9_10.
- Moustafa, A. R., El Badrawy, R., & Gibali, H. (1998). Pervasive E-ENE oriented faults in northern Egypt and their effect on the development and inversion of prolific sedimentary basins. In *14th Proceedings of Petroleum Conference Cairo* (Vol. 1, pp. 51–67). Egyptian General Petroleum Corporation.
- Moustafa, A. R., Yehia, M. A., & Abdel Tawab, S. (1985). Structural setting of the area east of Cairo, Maadi and Helwan. *Middle East Research Center at Ain Shams University Science Research Services*, 5, 40–64.
- Moustafa, A. R., El-Barkooky, A. N., Mahmoud, A., Badran, A. M., Helal, M. A., Nour El Din, M., & Fathy, H. (2002). Matruh basin: hydrocarbon plays in an inverted Jurassic-Cretaceous rift basin in the northern Western Desert of Egypt. In *AAPG International Meeting, Cairo, Oct 2002, Abstract*.
- Moustafa, A. R., Salama, M. E., Khalil, S. M., & Fouda, H. G. (2014). Sinai Hinge Zone: A major crustal boundary in NE Africa. *Journal of the Geological Society of London*, 171, 239–254.
- Moustafa, A. R., Saoudi, A., Moubasher, A., Ibrahim, I. M., Molokhia, H., & Schwartz, B. (2003). Structural setting and tectonic evolution of the Bahariya Oasis, Western Desert Egypt. *Georabia*, 8, 87–120.
- Mostafa, A., Sehim, A., & Yousef, M. (2015). Unlocking subtle hydrocarbon plays through 3D seismic and well control: A case study from West Gebel El Zeit District, Southwest Gulf of Suez, Egypt. In *Offshore Mediterranean Conference and Exhibition: Ravenna, Italy, Offshore Mediterranean Conference* (p. 14).
- Nemec, M. C. (1996). Qarun oil field, Western Desert, Egypt. In *Proceedings of 13th EGPC Petroleum Conference, Cairo* (Vol. 1, pp. 140–164).
- Nikishin, A. M., Ziegler, P. A., Panov, D. I., Nazarevich, B. P., & Brunet, M. F. (2001). Mesozoic and Cainozoic evolution of the Scythian platform-Black Sea-Caucasus domain. *Mémoires Du Muséum National D'histoire Naturelle*, 186, 295–346.
- Norton, P. (1967). *Rock-stratigraphic nomenclature of the Western Desert, Egypt* (p. 557). International Report of GPC.
- Obaidalla, N. A., & Kassab, A. S. (2000). Biostratigraphy of the Khoman Formation, Bahariya Oasis, Western Desert, Egypt. An approach to the K/T boundary. *Egyptian Journal of Geology*, 44(2), 443–453.
- Officer, C. B., & Lyons, J. B. (1993). A short note on the origin of the yellow glasses at the Haiti Cretaceous/Tertiary sections. *Earth and Planetary Science Letter*, 118, 349–351.
- Olsson, R. K., & Liu, C. (1993). Controversies on the placement of Cretaceous-Paleogene boundary and the K/P mass extinction of planktonic foraminifera. *Palaios*, 8, 127–139.

- Omara, S. (1965). A micropaleontological approach to the stratigraphy of the Carboniferous exposures of the Gulf of Suez region. *Neues Jahrbuch für Geologie und Paläontologie Monatshefte*, 6, 409–419.
- Omara, S. (1971). Early Carboniferous tabulate corals from Um Bogma area, southwestern Sinai Egypt. *Rivista Italiana di Palaeontologia e Stratigrafia*, 77, 141–154.
- Omara, S. (1972). An Early Cambrian outcrop in southwestern Sinai, Egypt. *Neues Jahrbuch für Geologie und Paläontologie Monatshefte*, 5, 306–314.
- Omara, S., & Conil, R. (1965). Lower Carboniferous foraminifers from southwestern Sinai Egypt. *Annals of the Societe Geologique Belgique*, 5, 221–242.
- Omara, S., & Schultz, G. (1965). A Lower Carboniferous microflora from southwestern Sinai. *Palaeontographica*, 117(A), 47–58.
- Osman, R., Ahmed, S. M., & Khater, T. (2002). The stratigraphy and facies of Wadi Gabgaba and its surroundings with an emphasis on the Lower Paleozoic glaciation. In *6th International Conferences on Geology of the Arab World, Cairo University Egypt* (Vol. 2, pp. 469–482).
- Patton, T. L., Moustafa, A. R., Nelson, R. A., & Abdine, A. S. (1994). Tectonic evolution and structural setting of the Suez rift. In S. M. Landon (Ed.), *Interior rift basins* (Vol. 59, pp. 9–55). AAPG Memoir.
- Perrin, M., Saleh, A., & Alva-Valdivia, L. (2009). Cenozoic and Mesozoic basalts from Egypt: A preliminary survey with a view to paleointensity. *Earth, Planets and Space*, 61, 51–60.
- Picard, L. (1942). New Cambrian fossils and Paleozoic problematica from the Dead Sea and Arabia. *Bulletin Geology Department Hebrew University*, 3.
- Plaziat, J. C., Reyss, J. L., Choukri, A., & Cazala, C. (2008). Diagenetic rejuvenation of raised coral reefs and precision of dating. The contribution of the Red Sea reefs to the question of reliability of the Uranium-series datings of middle to late Pleistocene key reef-terraces of the world. *Carnets de Géologie/Notebooks on Geology, Article 2008/04* (CG2008_A04).
- Poirer, J. P., & Taher, M. A. (1980). Historical seismicity in the Near and Middle East, North Africa and Spain from Arabic documents (VIIth–XVIIth century). *Bulletin of the Seismological Society of America*, 70, 2185–2201.
- Powell, J. H. (1989). Stratigraphy and sedimentation of the Phanerozoic rocks in central and southern Jordan. Part A. Ram and Khreim Groups. *Jordan Resource Authentication Geology Division Bulletin*, 11, 72.
- Powell, J. H., Mohamed, B. K., & Masri, A. (1994). Late Ordovician–Early Silurian glaciofluvial deposits preserved in paleovalleys in South Jordan. *Sedimentary Geology*, 89, 303–314.
- Reyss, J., Choukri, A., Plaziat, J., & Purser, B. (1993). Datations radiochimiques des récifs coralliens de la rive occidentale du Nord de la Mer Rouge, premières implications stratigraphiques et tectoniques. *Comptes Rendus De L'Académie Des Sciences, Paris*, 317, 487–492.
- Robson, D. A. (1971). The structure of the Gulf of Suez (clysmic) rift, with special reference to the eastern side. *Journal of the Geological Society of London*, 127, 242–276.
- Roeser, H. A. (1975). A detailed magnetic survey of the southern Red Sea. *Geologisches Jahrbuch*, 13, 131–153.
- Röhl, U., Bralower, T. J., Norris, R. D., & Wefer, G. (2000). New chronology for the late Paleocene thermal Maximum and its environmental implications. *Geology*, 28, 927–930.
- Said, R. (1962). *The Geology of Egypt* (p. 377). Elsevier Pub Co.
- Said, W. S., Yousef, M., El-Mowafy, H. Z., & Abdel-Halim, A. (2014). Structural geometry and evolution of BED 17 field, Abu El Gharadig basin, northern Western Desert of Egypt: An example of restraining stepovers in strike-slip fault systems. AAPG Search & Discovery Article # 20266, 22 pp.
- Said, M. M., & El Mehdi, B. O. (2000). Explanatory booklet, sheet: Jabal Asbah, NF 35–1, scale 1: 250 000. *Geology Survey Egypt and Industrial Research Center Libya*, 84.
- Said, R. (1971). Explanatory notes to accompany the geological map of Egypt. *Egyptian Geology Survey Paper*, 56, 123.
- Said, R. (1981). *The geological evolution of the River Nile* (151pp). Springer.
- Said, R. (1990). The geology of Egypt. In A. A. Balkema (Eds.), Rotterdam, 729 pp.
- Said, R., & Eissa, R. (1969). Some microfossils from Upper Paleozoic rocks of western coastal plain of Gulf of Suez region, Egypt. In *Proceedings of the 3rd African Micropaleontological Colloquium Cairo* (pp. 337–384).
- Said, S. M., & Sakran, S. (2020). Structural analysis and tectonic evolution of the Komombo basin, south Egypt; an example of interior Cretaceous rift. *Journal of African Earth Sciences*, 162, 103719. <https://doi.org/10.1016/j.jafrearsci.2019.103719>
- Sakran, S., & Said, S. M. (2018). Structural setting and kinematics of Nubian fault system, SE Western Desert, Egypt: An example of multi-reactivated intraplate strike-slip faults. *Journal of Structural Geology*, 107, 93–108.
- Sakran, S. M., Nabih, M., Henaish, A., & Ziko, A. O. (2016a). Structural regime and its impact on the mechanism and migration pathways of hydrocarbon seepage in the southern Gulf of Suez rift: An approach for finding new unexplored fault blocks. *Marine and Petroleum Geology*, 71, 55–75.
- Sakran, S. M., Nabih, M., Henaish, A., & Ziko, A. O. (2016b). Fracture reopening by micro-earthquakes, a mechanism for oil seepage in mildly active rifts: A Case study from Gemsa oil field, the southern Gulf of Suez rift Egypt. *Arabian Journal of Geosciences*, 9(5), 1–17.
- Salah, W., Yousef, M., Abdel-Halim, A., El-Mowafy, H. Z., & Kamel, D. (2014). Structural setting and hydrocarbon potential of BED-17 field, Abu Gharadig Basin, northern Western Desert Egypt. *Egyptian Journal Geology*, 58, 121–136.
- Salem, E., & Sehim, A. (2017). Structural imaging of the East Beni Sueif basin, north Eastern Desert Egypt. *Journal of African Earth Sciences*, 136, 109–118.
- Schandelmeir, H., & Reynolds, P. O. (1997). Paleogeographic-Paleotectonic Atlas of North-Eastern Africa. *Arabia, and Adjacent Areas (late Neoproterozoic to Holocene)*. Rotterdam-Balkema, 160.
- Schandelmeir, H., Richter, A., & Franz, G. (1983). Outline of the geology of magmatic and metamorphic units between Gebel Uweinat and Bir Safsaf (SW Egypt/NW Sudan). *Journal of African Earth Sciences*, 1(3/4), 275–284.
- Schrank, E. (1984). Paleozoic and Mesozoic palynomorphs from the Foram-1 well (Western Desert, Egypt). *Neues Jahrbuch für Geologie und Paläontologie-Monatshefte*, 2, 95–112.
- Sehim, A. (1993). Cretaceous tectonics in Egypt. *Egyptian Journal of Geology*, 37, 335–372.
- Semtner, A. K., & Klitzsch, E. (1994). Early Paleozoic paleogeography of the northern Gondwana margin: New evidence for Ordovician–Silurian glaciation. *Geologische Rundschau*, 83, 743–751.
- Sengör, A. M. C. (1979). Mid-Mesozoic closure of Permo-Triassic Tethys and its implications. *Nature*, 279, 590–593. <https://doi.org/10.1038/279590a0>
- Shahin, A., & Kora, M. (1991). Biostratigraphy of some Upper Cretaceous–Early Tertiary succession in the eastern central Sinai. *Neues Jahrbuch für Geologie und Paläontologie, Monatshefte, H* (11), 671–692.
- Shata, A. (1959). Structural development of the Sinai Peninsula (Egypt). In *Proceedings of the 20th International Geological Congress, Mexico* (pp. 225–249).
- Smith, A. G. (1971). Alpine deformation and the oceanic area of the Tethys, Mediterranean and Atlantic. *Geological Society of American Bulletin*, 82, 2039–2070.
- Soliman, S. M., & El Fotouh, M. A. (1970). Carboniferous of Egypt, isopach and lithofacies maps. *Bulletin—American Association of Petroleum Geologists*, 54, 1918–1930.

- Stampfli, G. M., & Borel, G. D. (2002). A plate tectonic model for the Paleozoic and Mesozoic constrained by dynamic plate boundaries and restored synthetic oceanic isochrons. *Earth and Planetary Science Letters*, 196(1), 17–33. [https://doi.org/10.1016/S0012-821X\(01\)00588-X](https://doi.org/10.1016/S0012-821X(01)00588-X)
- Stampfli, G. M., Mosar, J., Favre, P., Pillecuit, A., & Vannay, J. C. (2001). Permo-Mesozoic evolution of the western Tethys realm: the Neo-Tethys East Mediterranean Basin connection. In P. A. Ziegler, W. Cavazza, A. H. F. Robertson & S. Crasquin-Soleau (Eds.), *Peri-Tethys Memoir 6: Peri-Tethyan Rift/Wrench Basins and Passive Margins* (Vol. 186, pp. 51–108). Mémoires du Muséum National d'Histoire Naturelle de Paris
- Steen, G. (1982). Radiometric age dating and tectonic significance of some igneous rocks, Gulf of Suez. Gupco Report, Er 82/2 (23 pp.).
- Stocklin, J. (1972). Iran: Lexique Stratigraphique International, 3, Asie, 283pp.
- Strasser, A., Strohmenger, C., Davaud, E., & Bach, A. (1992). Sequential evolution and diagenesis of Pleistocene coral reefs (South Sinai; Egypt). *Sedimentary Geology*, 79, 59–79.
- Tari, G., Hussein, H., Novotny, B., Hannke, K., & Kohazy, R. (2012). Play types of the deep-water Matruh and Herodotus basins, NW Egypt. *Petroleum Geoscience*, 18, 443–455.
- Thiriet, J., Burollet, P., Montecat, C., & Ott d'Estevou, P. (1986). Evolution tectonique et sédimentaire Neogène à la transition du Golfe de Suez et de la Mer Rouge: La secteur de Port-Safage (Egypte). *Dot Et Trav IGAL*, 10, 93–116.
- Tjalsma, R. C., & Lohmann, G. P. (1983). Paleocene-Eocene bathyal and abyssal benthic foraminifera from the Atlantic Ocean. *Micro-paleontology, Special Publication*, 4, 1–90.
- Walther, J. K. (1890). Über eine Kohlenkalk Fauna aus der ägyptischen-Arabischen Wüste. *Zeitschrift Deutsche Geologische Gesellschaft*, 42, 419–449.
- Wanas, H. A. (2011). The Lower Paleozoic rock units in Egypt: An overview. *Geoscience Frontiers*, 2(4), 491–507.
- Weissbrod, T. (1969). The Paleozoic of Israel and adjacent countries: Part I, The subsurface Paleozoic stratigraphy of S. Israel. *Bulletin Geological Survey of Israel*, 47, 1–25; Part II, the Paleozoic outcrops in SW Israel and their correlation with those of S Israel. 48, 1–32.
- Westerhold, T., Rohl, U., McCarren, H. K., & Zachos, J. C. (2009). Latest on the absolute age of the Paleocene-Eocene Thermal Maximum (PETM): New insights from exact stratigraphic position of key ash layers +19 and -17. *Earth Planetary Science Letters*, 287, 412–419.
- Wolfart, R. (1981). Lower Paleozoic rocks of the Middle East. In C. H. Holland (Ed.), *Lower Paleozoic of the Middle East, Eastern and Southern Africa and Antarctica* (pp. 6–130). New York: Wiley.
- Wu, D., & Bruhn, R. L. (1994). Geometry and kinematics of active normal faults, South Oquirrh Mountains, Utah: implication for fault growth. *Journal of Structural Geology*, 16(8), 1061–1075. [https://doi.org/10.1016/0191-8141\(94\)90052-3](https://doi.org/10.1016/0191-8141(94)90052-3)
- Youssef, M. M. (2003). Structural setting of central and south Egypt: An overview. *Micro-paleontology*, 49(1), 1–13. (text figures 1–6).
- Youssef, M. (2016). Calcareous nannofossils and paleoenvironments of the Paleocene-Eocene thermal maximum (PETM) interval in central Egypt. *Journal of African Earth Sciences*, 114, 203–219.
- Yousef, M., Moustafa, A. R., & Shann, M. (2006a). The Petroleum Play Systems in the Mango—Tineh area: Offshore North Sinai, Egypt. In *The 8th International Conference on the Geology of the Arab World, Cairo, Egypt (Abstract)*.
- Yousef, M., Moustafa, A. R., & Shann, M. (2006b). Tectonic evolution of Mango-Tineh area: offshore North Sinai, Egypt. In *The 44th Annual Meeting of the Geological Society of Egypt, Cairo, Egypt (Abstract)*
- Yousef, M., Moustafa, A. R., Bosworth, W., & Helgeson, D. (2009). Three-dimensional structural model and fault trap analysis of East Bahariya concession, northern Western Desert, Egypt. In *Geological Society of Egypt, Cairo, Egypt (Abstract)*.
- Yousef, M., Moustafa, A. R., Bosworth, W., & Helgeson, D. (2010a). Structural and tectonic evolution of East Bahariya concession, northern Western Desert, Egypt, Egyptian. *The Journal of Geology*, 54, 1–16.
- Yousef, M., Moustafa, A. R., & Shann, M. (2010b) Structural setting and tectonic evolution of offshore North Sinai, Egypt. *Geological Society Special Publication*, 341. <https://doi.org/10.1144/SP341.4>
- Yousef, M., Sehim, A., & Yousef, M. (2015). Structural style and evolution of inversion structures. In *Horus oil field, Alamein basin, north Western Desert: The 8th International Conference on the Geology of the Middle East, Cairo, Egypt, Abstract*.
- Yousef, M., Yousef, M., & Sehim, A. (2019). Structural style and evolution of inversion structures of Horus field, Alamein Basin, northern Western Desert of Egypt. *Marine and Petroleum Geology*, 110, 55–72. <https://doi.org/10.1016/j.marpetgeo.2019.07.009>



Mohamed Yousef received M.Sc. (2006) and Ph.D. (2010) degrees in structural geology from Ain Shams University (Egypt) where he is currently an associate professor. His research has focused on the structural and tectonic evolution of sedimentary basins in the northern Western Desert, Suez rift, Nile Delta, and

offshore North Sinai of Egypt. This includes the study of extension, inversion, strike-slip, and thrust terrains. His research integrates field studies and the interpretation of 2D and 3D seismic datasets, with a special focus on structural restoration and fault analysis. He has co-supervised 20 M.Sc. and Ph.D. theses and dissertations.



Zakaria Hamimi is a structural geologist who has spent much of his academic career at Benha University (Egypt), in addition to some years at Sana'a University (Yemen) and King Abdulaziz University (Saudi Arabia). He graduated with a BSc degree (1984) from Assiut University (distinction with honors), and holds

a M.Sc. (1988) degree from Zagazig University (Egypt) and a Ph.D. (1992) in structural geology and tectonics from Cairo University. His research interests focus on structural geology, microstructures and tectonics. He has worked in

many field-related sub-disciplines of Earth Sciences including geologic mapping, microstructural analysis, strain analysis, paleostress reconstruction, active tectonics, tectonic geomorphology, crustal deformation, and image processing. He used all these fields to study key areas in the Arabian-Nubian Shield, and to decipher their deformation history. He has been the president and one of the founding team members of the Arabian Geosciences Union since its founding in 2012. Prof. Hamimi received the medal of the Egyptian Geological Society of Egypt in 2015, and the medal of the Arab Mining and Petroleum Association in 2016. He has co-published 90 research articles in national and international indexed and refereed journals and authored several books. He has considerable editorial and publishing experience, having started in the Egyptian Journal of Geology in 1998–2002. He has been An Associate editor of the Arabian Journal of Geosciences (since 2016) and Journal of African Earth Sciences (since January 2022). He is a member of the Egyptian Universities Promotion Committee of the Supreme Council for Universities (SCU, Egypt, 2016–2019). In addition, he was nominated as a Secretary of the Egyptian National Committee for Geological Sciences of the Academy of Scientific Research and Technology, and designated as the IUGS-Representative for Egypt to the Gondwana 16 International Conference in Bangkok, Thailand. In September, 2020, he was nominated as the President of this same committee.



Ahmed Heneish is an associate professor of structural geology at Zagazig University (Egypt). He obtained M.Sc. and Ph.D. degrees in structural geology from Zagazig University. His research interests include surface and subsurface structural modeling and analysis. He has several publications, including

some on the structure and tectonics of the Suez Rift, Gulf of Aqaba, and northern Egypt.



Wael Hagag is an associate professor of structural geology at Benha University (Egypt). His main research interest is in the structural and tectonic processes deforming the upper and lower crustal levels on both local and regional scales, using structural-field work and applying the modern techniques such as remote sensing, anisotropy of magnetic susceptibility (AMS), in addition to microstructural/microtectonic investigations.



Tarek Anan is a sedimentologist who has spent the majority of his academic career at the Geology Department, Faculty of Science, Mansoura University (Egypt). He graduated from Mansoura University with B.Sc. (1999) and MSc degrees (2005), and Ph.D. (2011) in sedimentary rocks and sequence stratigraphy (joint supervision between Mansoura University and Western Michigan University, USA). His research interests include the sedimentology, stratigraphy and sequence stratigraphy of mixed carbonate-siliciclastic and carbonate depositional systems. His work focuses on the determination of depositional environments, reconstructing depositional models, diagenetic alterations of carbonate rocks, and the sedimentological history of carbonate rocks in terms of sequence stratigraphy. Recently, he has been focusing on the determination of oceanic anoxic events and global warming events using a combination of sedimentologic and geochemical approaches.



Phanerozoic Geomorphology in Egypt

Atef Moatamed A. Mohamed

Abstract

The current paper gives an outlook of some major lineaments of Egypt's landforms during the Phanerozoic Eon. Egyptian lands have been exposed for all geological episodes that affected the global earth's crust. Phanerozoic geomorphology in Egypt is heavily affected by the succession stages of Tethys sea transgression and regression, the largest one was in Early Eocene, covering most of Egypt up to the White Mountain in Northern Sudan. In the Oligocene, a dramatic change has occurred in Egypt's geological evolution with the formation of rifting and drifting system. This paper adopted the thesis concluded by Issawi et al. (The phanerozoic geology of Egypt: A geodynamic approach. Ministry of Petroleum, Cairo, 2009) concerning the development of Egyptian lands during the Phanerozoic. In this thesis, Egypt is composed of tectonic arcs (positive relief) separated in between by lowlands or huge depressions. In the current review, the author depends on his field trips across Egypt during the last three decades and summarizing, at the same time, the conclusions of the previous works. The paper consists of two principal items: (1) the physiographic regions which include the generic units of Nile valley, Delta, and the three deserts of the Eastern Desert, Sinai Desert and the Western Desert; and (2) the geomorphological evolution of paleo-fluvial systems.

Keywords

Phanerozoic Eon • Geomorphology • Physiography • Paleo-fluvial systems • Landforms

1 Introduction

Along ten degrees of latitudes (22–32° N) and more than twelve degrees of longitudes (25–37° E), Egypt holds an area exceeds 1 million km² (Fig. 1). Thanks to River Nile, Egypt hardly escaped the deterministic destiny of being lost oases in the Great Sahara. Since the onset of the modern geographical thought (see Ball, 1942), Egypt was usually the optimum example resembling the well-known dichotomy of “River vs. Desert.” In ancient Egypt, fertile lands of Nile valley were known as “Kemet” meaning “black lands,” while the rocky and sandy deserts beyond the Nile had been named “Deshret” means “the red one.”

The idiographic character of Egypt's geography is emulated by the geological uniqueness. The idea of considering Egypt's geography as a simple scholastic lesson has dominated across the first half of the twentieth century, John Ball (1938), for example, stated that:

The general outline of the cultivated portion of Egypt has been not inaptly likened to that of a lotus-plant, the Nile valley representing the stem, the delta the flower, and the faiyum a bud.

Egyptian lands have been exposed for all geological episodes that affected the global earth's crust. Phanerozoic geomorphology in Egypt is heavily affected by the succession stages of Tethys sea transgression and regression. The largest sea transgression over Egyptian lands was in Early Eocene, covering most of Egypt up to the White Mountain in Northern Sudan (See Issawi et al., 2009; Klitzsch, 1984). During the Oligocene, Tethys Sea retreated northward gradually, till a dramatic change has occurred in Egypt's geological evolution with the formation of rifting system. Hills of the Red sea started to rise in early Miocene, and in late Miocene, a great network of Paleo-Rivers has been developed in a prior system to the Nile valley.

While Miocene deposits cover the Red Sea hills, the un-roofing geological processes have affected the many rock formations, which tilted in both sides of the erected summits.

A. M. A. Mohamed (✉)
Geography Department, Faculty of Arts, Cairo University, Giza,
Egypt
e-mail: atefoov@gmail.com

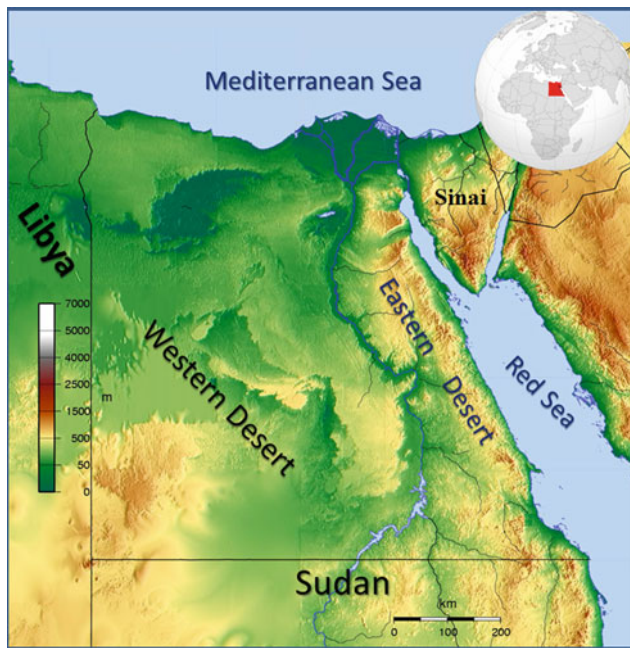


Fig. 1 General view of Egyptian topography

Over these igneous and metamorphic basement rocks, thick layers of sedimentary veneers had been deposits across millions of past years; these “Phanerozoic” episodes of sedimentation, marine and/or continental, give Egypt very diverse landscapes, ranging from mountainous lands, with summits exceeds 2500 m above sea levels, to lowlands and depressions beneath the sea level.

2 Physiographic Regions

2.1 The Nile Valley

Along its 1350 km in the Egyptian lands, from Nubia to the Mediterranean Sea, the river Nile receives no single active tributary. All the side valleys and paleo-streams, from both the Western and the Eastern deserts, have no perennial flow. Hence, water resources in Egypt are heavily dependent on external sources from equatorial and Abyssinian regions. The fertile flood plains of the Nile widen northward from Aswan to Cairo, with an average width of 10 km. For different geological and hydrological reasons, Nile course tends to occupy the eastern side of its valley, washing the eastern desert cliffs and creating, on the meantime, vast cultivatable lands on the western side. The course of the Nile valley does not follow a straightforward from south to north, but it bends, sinuous and meanders as a result of different geological controls, where Qena bend is the most prominent feature. The river course widens from south to north, reaching an average width of $\frac{3}{4}$ km. The stream itself is

sinuous and dotted with tens of islands. The cluster of granitic islands in Aswan called “the cataract” and still represents the spectacular landscape even though after the adjustment of river hydrology with the constructions of successive dams. Figures 2, 3, 4 and 5 give different views of the River Nile from the most spectacular sector lying between Edfu (Gebal El-Silsila) to Aswan Cataract.

Since the establishing of Aswan Dam in 1902, and the High Dam of Aswan and Lake Nasser in the late 1960s, the hydrological system of the Nile has been changed and the Nubian environmental characteristics had been dramatically altered. The Nile valley represents a longitudinal corridor, hardly connected with the other regions in Sahara. Since the last three decades, great efforts are in progress to redistribute the population across the country in order to achieve the geographic “exodus” from the siege of the historical “sticking in” the Nile flood plains and deltaic soils. Cutting its way to the Mediterranean, the Nile Valley runs through different rock types. Its Nubian sector, from Wadi Halfa to Aswan, is composed mainly of basement rocks (granite) with intercalation of sandstone. Throughout the Aswan-Esna sector, the basement rocks give place to sandstone, while the rest of the valley from Esna to Cairo is composed of limestone rocks.

Northward of Cairo for some 20 km, the Nile valley opens out forming the Delta cone, with its two parallel branches: Rosetta and Damietta. Till the 1930s, only half of the total area of the Nile delta was cultivated (22,000 km²). Nowadays, this area has been doubled as a result of land reclamation on both eastern and western fringes, in addition to discharging of swamps in the northern part of the deltaic margins, bounding the Mediterranean coastal belt, which consists of shallow lakes, swampy wetlands and coastal vegetated and bare dunes. Although Faiyûm is geographically a desert depression lying 60 km. southwest of Cairo, it is highly connected with the cultivation history of the Nile valley via the semi-natural channel of “Bahr Yousuf.” Faiyûm depression is cut in the limestone rocks with an area of 2000 km² and attains a level of – 45 m. While the southeastern portion of Faiyûm depression is covered by alluvium and highly cultivated, the northwestern portion is filled with the remnants of an old vast lake called “Mories,” the nowadays “Birket Qarûn.” A southern smaller depression called “El-Rayan” had been used since the 1990s as a discharging outlet for the excessive amount of irrigation in the proper Faiyûm depression.

2.2 Eastern Desert and Sinai

Egypt is described usually as a fluvial environment with a geographic stereotype based on the imagination of muddy black soils in featureless landscapes. In fact, Egypt is a rocky

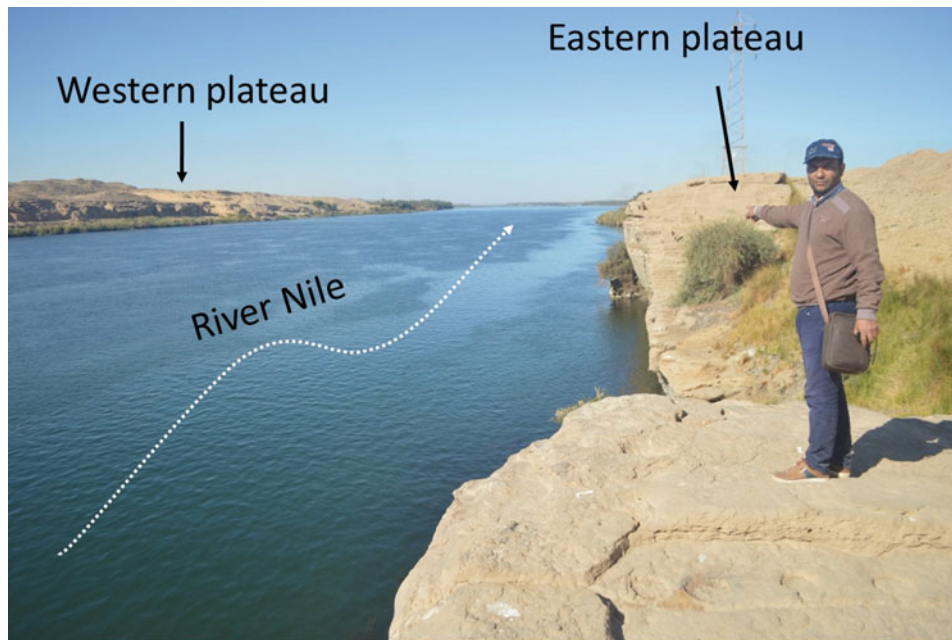


Fig. 2 Nile Valley in El-Silsila sector-Northern Aswan; both sides are composed of Sandstone

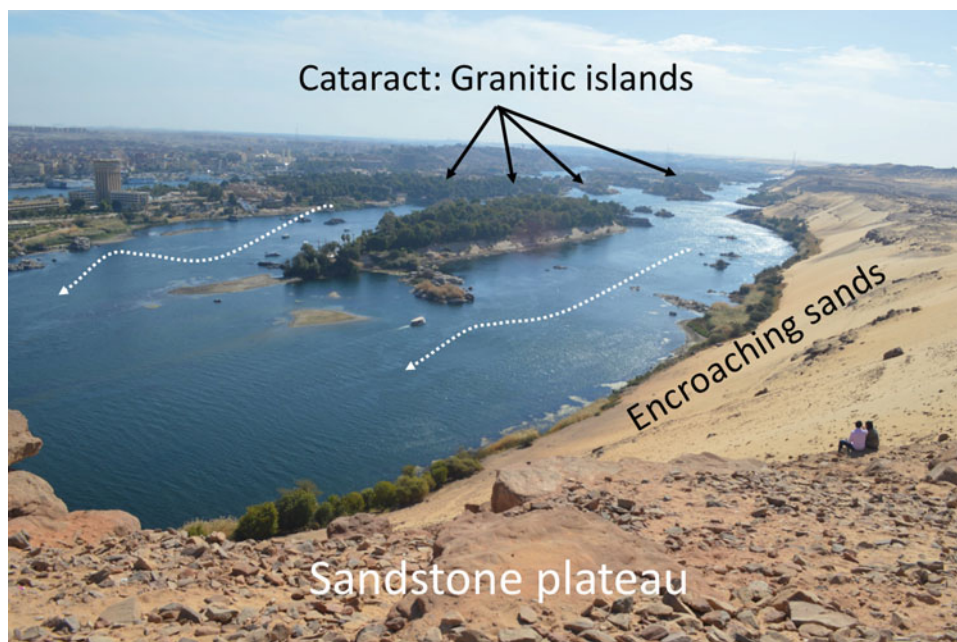


Fig. 3 Western Nile plateau, Cataract area, Aswan region

country in its most area. The spectacular mountainous regions extend basically in the Eastern Desert and Sinai, which occupies about one-third of Egyptian land (220,000 km²) and looks like a great triangle (see Figs. 6, 7 and 8), its base on the borderline with the Sudan and its apex on southeastern delta. The backbone of this desert is a range of pyramid-like mountains run parallel to the Red sea for

more than 700 km at a short distance inland from the coastline (see Mohamed 2001).

More than 100 peaks dotted the Eastern Desert, forming what might be named “Badlands” with steep, rugged slopes that have been formed in a structurally controlled terrain dissected by oblique faults. The highest one is Gebel El-Sheyib (2185 m above sea level). The most famous



Fig. 4 Western Nile plateau, Qubat Al Hawa, Aswan region



Fig. 5 Dune encroachments along western side of River Nile–Gharb Suhail, Aswan Sector

mountains from south to north are: Elba (1435 m), Mishbih (1385 m), Faraid (1366 m), Ras El-Kharit (1661 m), Hamata (1978 m), Zabara (1361 m), Nugrus (1505 m), Um Negat (1310 m), Mi'tig (1118 m), Abu Dokhan (1662 m), Ghareb (1751 m) and Um Tanassib (1104 m). The coastal belt of Gulf of Suez in the Eastern desert has longitudinal ridges of Miocene formation affected by the tectonic movements during that geological rifting system. Some of the geomorphic units in this sector are well-preserved in the inner ridges of E'sh El-Mallaha. The local name "Mallaha"

means "salt wetland" as the seasonal flash floods is hindered by the volcanic-limestone ridges, impeding the floods from reaching the Red Sea (Gulf of Suez). A dense wetland covered by a thin veneer of salts and salt flats is forming in between the successive ridges of Eish El-Mallaha (Figs. 9 and 10). The effect of volcanic activity on deforming the Miocene sedimentation is ideally obvious in Wadi Bili in the same region of E'sh El-Mallaha, as shown in Fig. 11. Tectonic activity in forming and deforming landforms in the coastal belts of Red Sea is much demonstrated in the Wadi

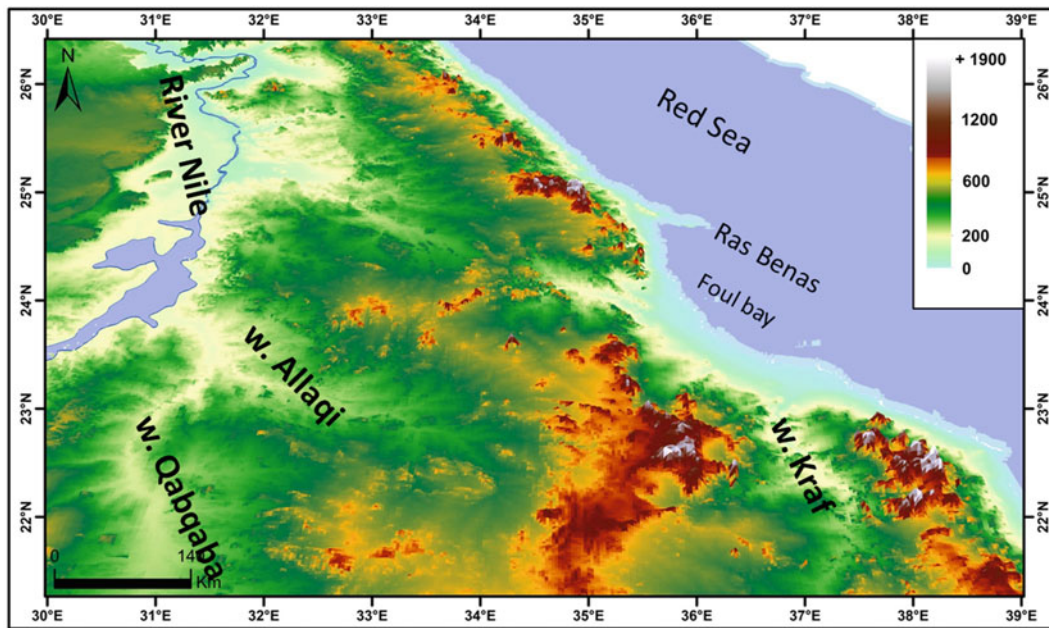


Fig. 6 Southern portion of the Eastern Desert of Egypt

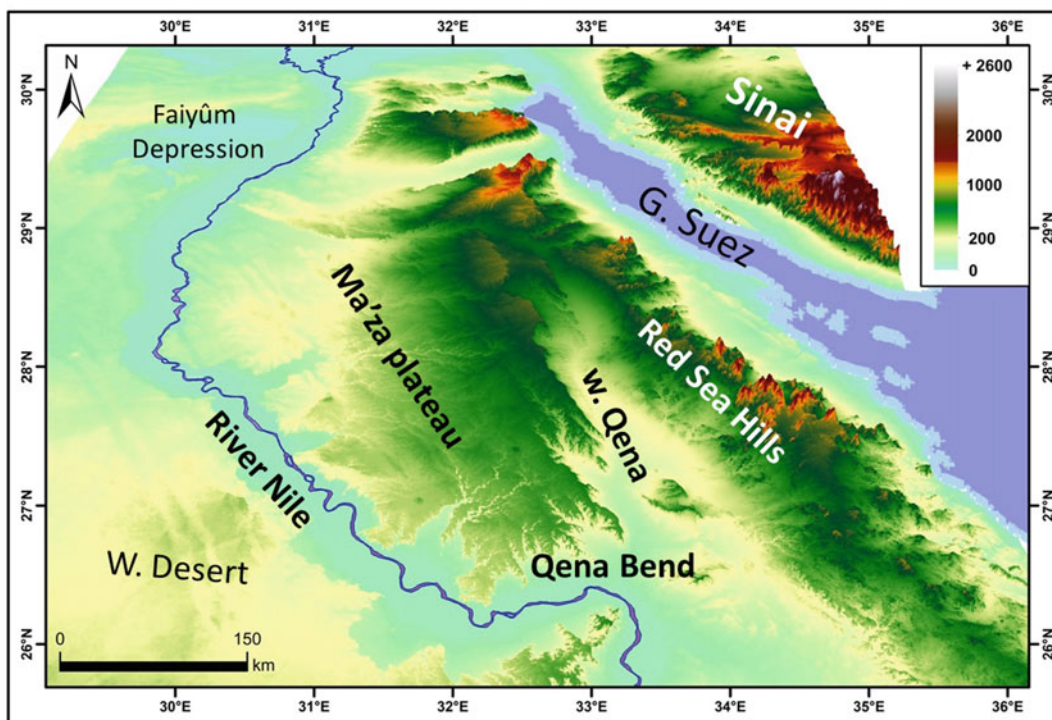


Fig. 7 Northern portion of the Eastern Desert of Egypt

El Gemal area as shown in Fig. 12 for Ranga area and Fig. 13 for the Abu Ghusun area. In fact, the northern extension of basement complex exceeds Um Tanassib Mt. onto more northern locations to Wadi El-Dakhl, where

granitic rocks, extend side by side with the sandstone and limestone outcrops. The average height of Egyptian mountains in the Eastern Desert is 1500 m. Northward of these mountains, semi-detached blocky limestone tablelands

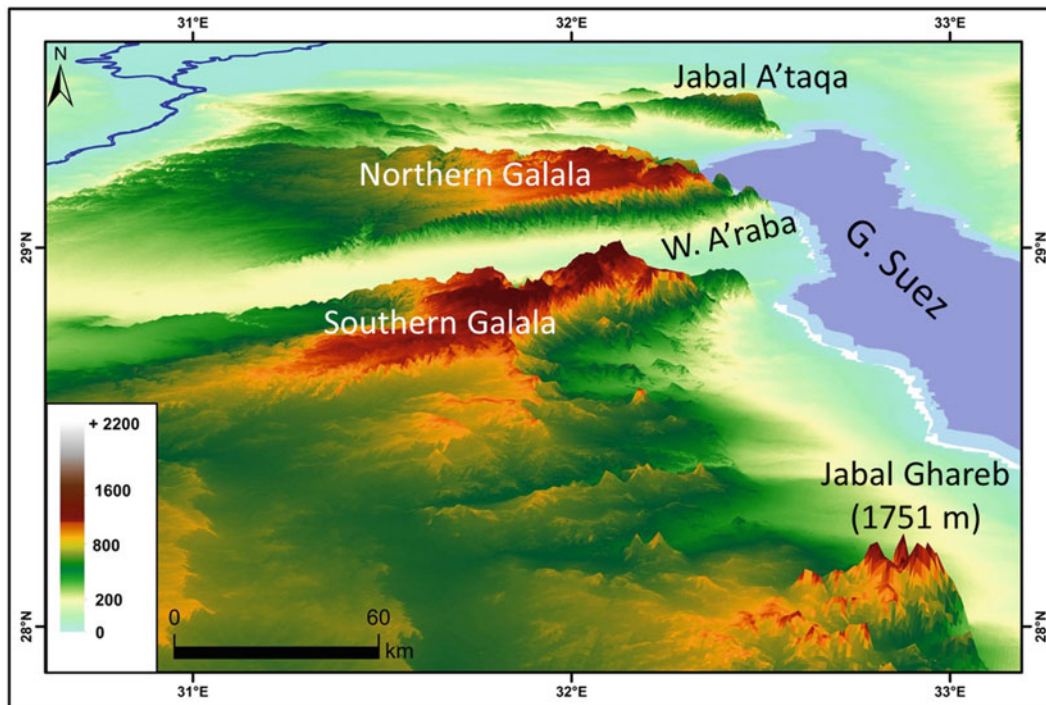


Fig. 8 Plateaus of the northern portion of the Eastern Desert (Southern and Northern Galala)

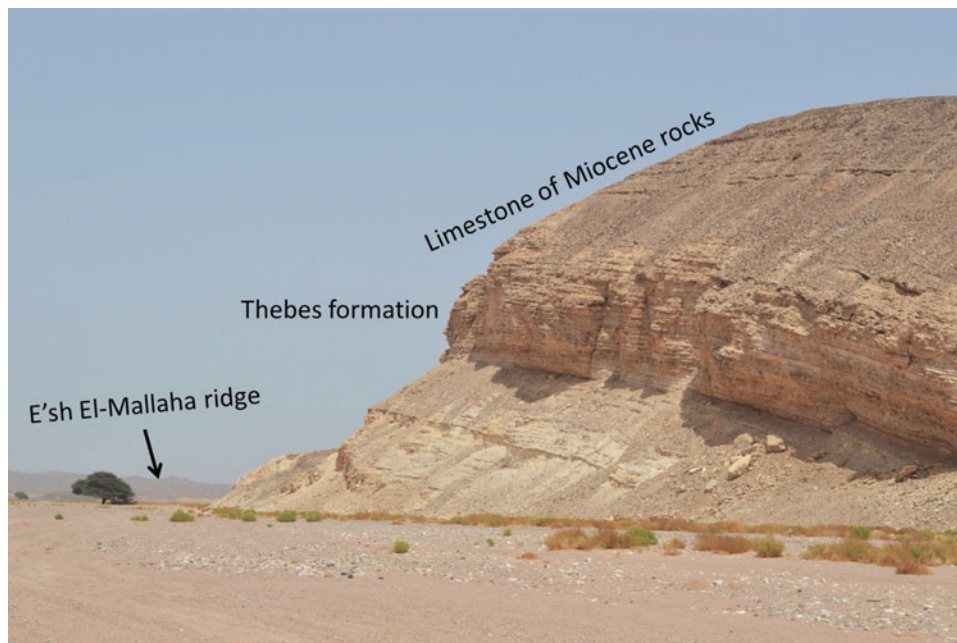


Fig. 9 Valley Side in Wadi Abu Marwat, the inner ridges of E'sh El-Mallaha, Gulf of Suez

extend parallel to Gulf of Suez, including the Southern and Northern Limestone Galala plateaus and Gebel Ataqa, with an elevation does not exceed 1000 m.

The Red Sea pyramid-like peaks represent a water-divide for hundreds of dry valleys (Wadies), but two principal

wadies are the most important: Qena and Qabqaba. Numerous short valleys run to the Red Sea bringing torrential floods. The most prominent, from south to north, are Shelal, Sermatai, Dieb, Hodein, Gemal, A'mbagi, Queh, Safaga, Bili, Abu Marwa, Abu Had, Dara, Hawashih, Araba,



Fig. 10 Wetlands of E'sh El-Malaha, Red Sea, Gebel Abu Sha'r El-Qebly

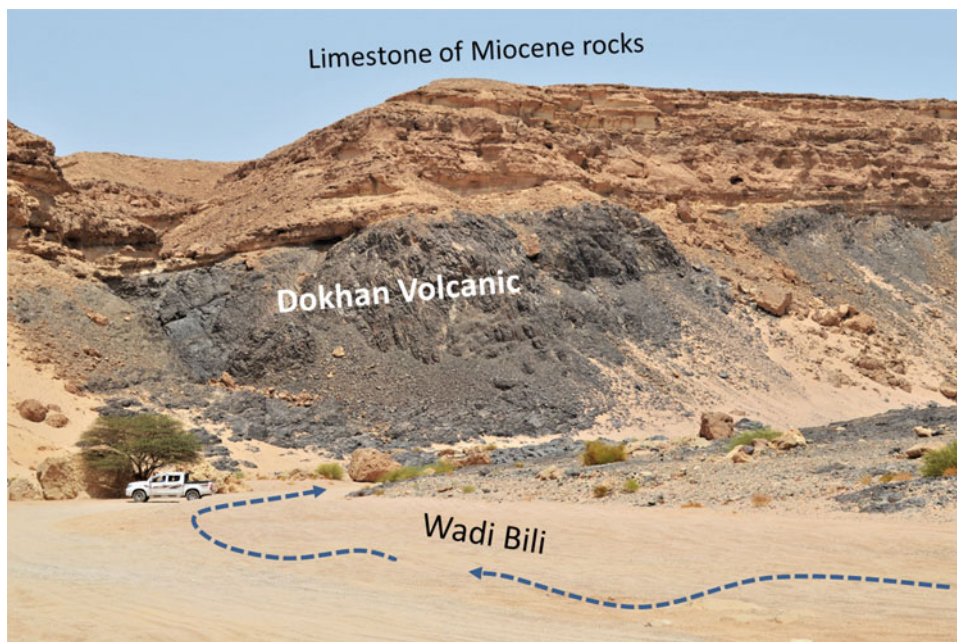


Fig. 11 Succession of volcanic and sedimentary rocks, Wadi Bili

Ghweiba, Hagul and Ashra. On the other hand, longer and larger valleys cut these mountain ranges from east to west, reaching the River Nile and crossing sedimentary plateaus in between. The remarkable examples of these wadis, from south to north, are: Allaqi, Garrara, Natash, Shait, Khurit, Abbad, Hammamat, Qena, El-Asyuti, Tarfa, Sennur and El-Gafra. On both sides of mountainous terrains, the natural

vegetation spots delineate wadis' beds. The riparian vegetation system is well preserved in many of these drainage systems. Some karstic springs are abundant as Bir Abu Sha'r (Fig. 14). The Sinai Peninsula is a good resembling model of Egyptian geography, with its 60,000 km² (1/16 of Egypt's total area). In Ras Gharb along the Gulf of Suez, Sinai's coastline with some peaks of famous mountains is clearly



Fig. 12 Ranga field of sulfur ores extraction from Miocene limestone low hills, Wadi El-Gemal region, Red Sea, Southeastern Egypt

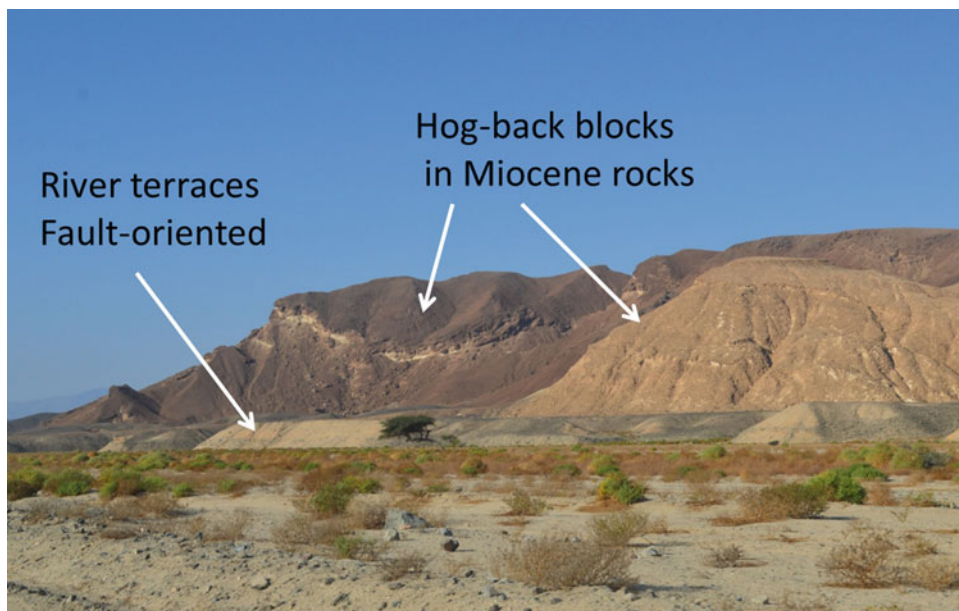


Fig. 13 Mouth of Wadi Abu Ghosoun into the Red Sea

seen (Fig. 15). For that reason, since the ancient Egyptian time, Sinai and Eastern Desert, via Gulf of Suez, were closely connected with sea shipping and ancient ports on both sides (see Figs. 16 and 17).

The Sinai Peninsula is composed of two different geomorphic units; the southern portion is a basement complex, mainly of high mountains, while the northern portion is a sedimentary one basically of plateaus and sandy plains. West-Central Sinai is a conjunctive zone between the Precambrian triangle and the Phanerozoic landforms. Abu

Zneima in the West-Central zone is a complex of sub geomorphic zone, acting different roles of many tectonic geomorphology and exogenesis factors. As shown in Fig. 18, the structurally controlled coastal cliffs (150 m a.s.l) of Upper Eocene (limestone and marl) are the major landforms on this coastal plain, with sediments are enriched here by fluvial flash floods from Wadi Taiba. Most of the Southern portion of Sinai extends in a type of the badlands (Fig. 19). It is Southern Sinai, which has the highest peak in all Egypt, Mt. Catherine (2639 m), in addition to the other summit as

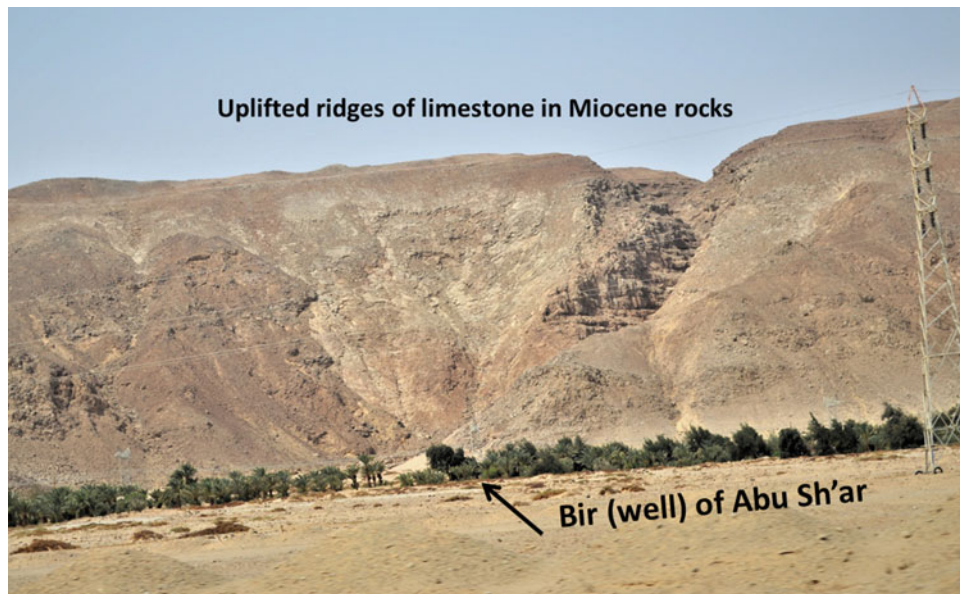


Fig. 14 Southern cliffs of Jebel Abu Sha'r El-Qibli, Gulf of Suez

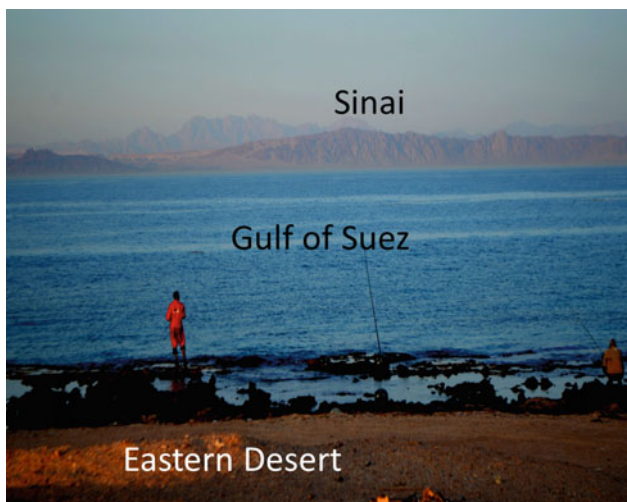


Fig. 15 Ras Ghareb area, a view toward Sinai Peninsula

Um Shomer (2586 m) and El-Thebt (2439 m). Northward of this mountainous terrain, The Sinai Peninsula slopes toward the Mediterranean Sea in a plateau-like landscape. While the mountainous region in South Sinai is dissected by fluvial actin, the northern portion of Sinai is dissected by large and shallow tributaries of W. Al A'resh. The Gulf of Aqaba represents a complex geomorphological sub-unit, in some places, like Nuweib'a area, the Pre-Phanerozoic and Phanerozoic landscapes are mutually overridden as a result of the tectonic history of uplifting and sliding) see Fig. 20). Gulf of Aqaba exhibits one of the unique cases in all Egypt, where overturned and recumbent Cretaceous folds occurred (Fig. 21).

At the head of Gulf of Aqaba, Jabal el-A'safier represents a prominent faulted block hogback composed mainly of sandstone/limestone and surrounded by pre-Phanerozoic basement badlands (Fig. 22). The same degree of complexity of Precambrian with Cambrian rocks is well illustrated in Western Sinai, where archeological findings confirmed ancient Egyptian metallurgic activities for copper melting in the area of Wadi Nasab (Fig. 23). The area of Jebel El Naqus in Southwestern Sinai is an ideal example of Sandstone formation related to Cambrian age (Fig. 24). One of the spectacular valleys in western Sinai is Wadi Araba which cut through some of the oldest rock types of the Phanerozoic geology of Egypt (Fig. 25). Cambrian rock types are also well preserved in West-Central Sinai, as in Um Bogma area (Fig. 26).

2.3 The Western Desert

Westward from the Nile valley (see Fig. 27), a great territory of desert geomorphology represents two-thirds of Egypt (680,000 km²). Sand seas cover the proper masses of this desert which composed of a series of sandstone/limestone plateaus, sloping northward to the Mediterranean Sea. The sandy plains are stretching here side by side with bare dissected terrains. The two depressions of Kharga and Dakhla (Fig. 28) could be treated as one geomorphic region (see for details Brooks, 1993; Mohamed, 2021). The southeastern corner of the Western Desert usually knows as Darb Al Arba'in. This subgeomorphic region is distinguished by the paleo-erosive actions of both paleo-river system and karstification in the white limestone, especially in the *Mesharsher*



Fig. 16 Geoaerchological excavations of ancient Egyptian ports in Wadi El-Garf area, a view from the Eastern Desert toward Sinai Peninsula across the Gulf of Suez

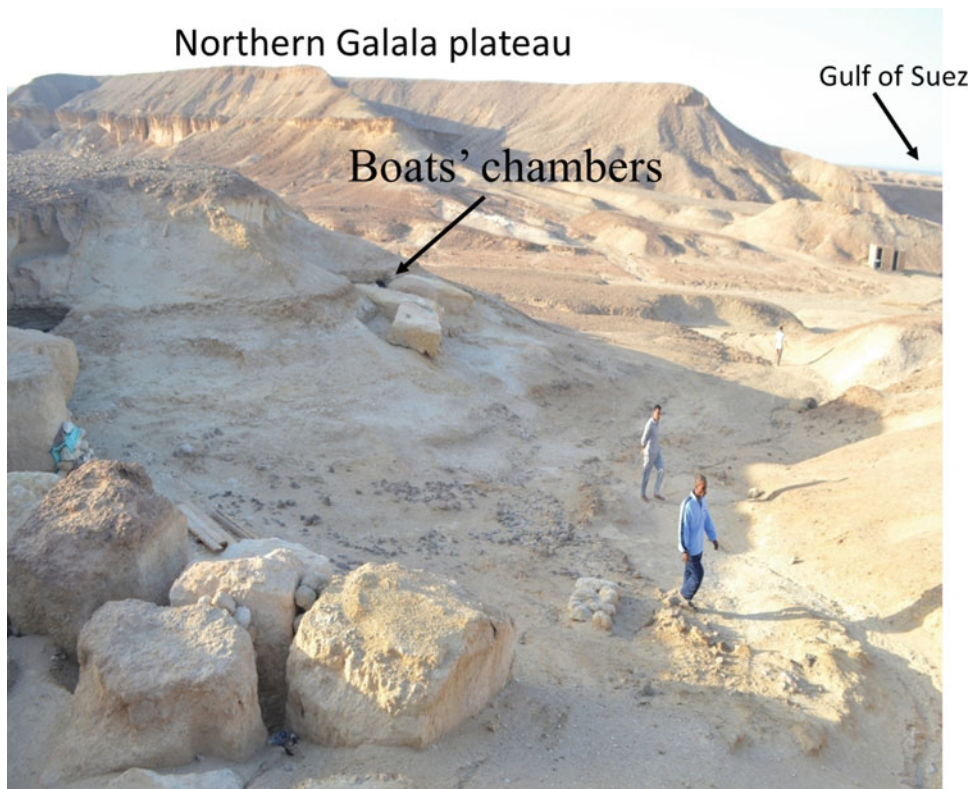


Fig. 17 Geoaerchological excavations of ancient Egyptian port, northern Galala plateau



Fig. 18 Coastal cliffs in Abu Zneima area, west-central Sinai

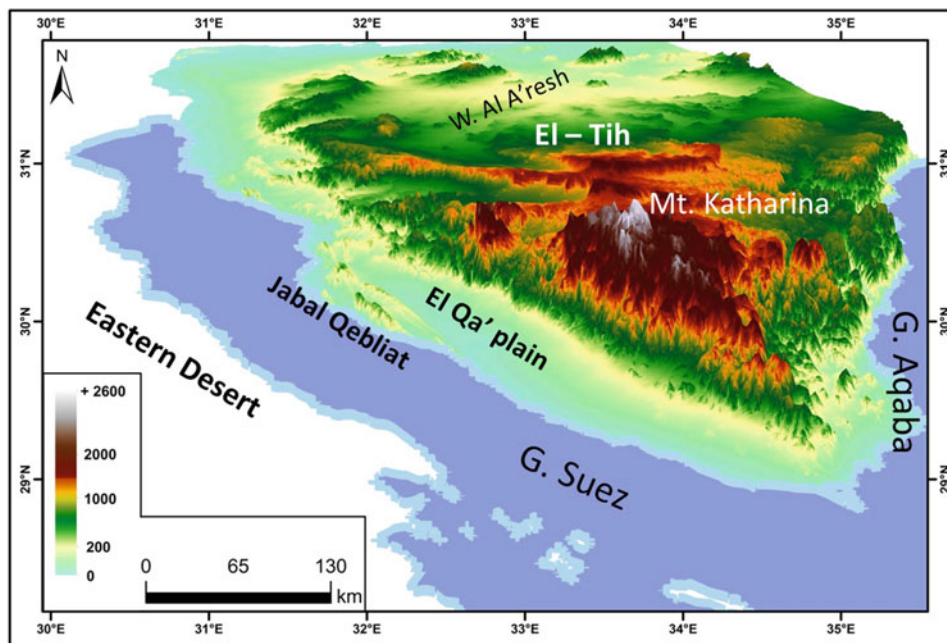


Fig. 19 Elevation map of southern Sinai

area. *El Mesharsher* is the Arabic local name which gives a good toponymical significance, since it means “saw-like” ridges. In recent times, a paved road was established to connect Aswan and Abu Simbel on the Nile with Kharga, Bares and East of El-O’uinat in the Western Desert. All of these roads are superimposed over ancient caravan routes

which were very active till early twentieth century. The caravan trade routes of Darb El Arba’in were watered from natural springs (tiny palm oasis) scattered in a 50–80 km distance across the area. The most important springs were: Kurkur, Dunqul, El-Nekhela, El Shab and many others. Unfortunately, most of these natural springs have been

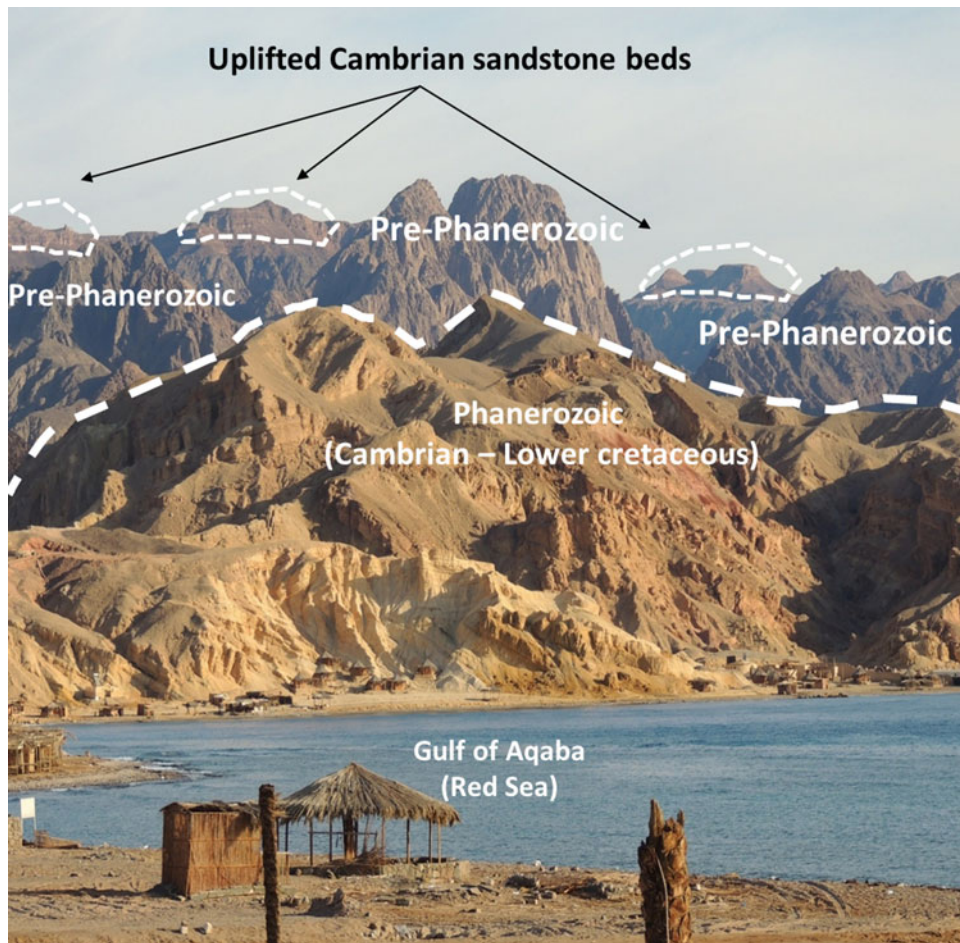


Fig. 20 Pre-Phanerozoic and Phanerozoic landscapes in Eastern Sinai, Gulf of Aqaba, North of Nuweib'a

depleted as a result of excessive pumping of underground water and consistence aridity (see Fig. 29). Amid these peneplains of Darb Al Arba'in, composed principally of Upper Cretaceous/lower Eocene of sandstone, limestone and shale, three inselbergs of old Granite are erected along the historical road (See Haynes, 1984). The three have a common name of Abu Bian (meaning in Arabic “the landmark”). This name expresses the role of inselberg morphology along the featureless route of Darb El Arba'in. The three names are Abu Bian Al-Bahary (the northern one), Abu Bian Al-Wastani (the central one) and Abu Bian A-Qibly (the southern one).

3 Geomorphological Evolution

3.1 Fluvial Systems

In late Eocene, tectonic movements had uplifted the Red Sea hills, creating very intensive system of faulting, responsible for major paleo-river drainage networks, prior to the Nile

(see Issawi et al., 2009; Omar & Steckler, 1995). They are as follows:

- Wadi Qena
- Wadi Qapqapa, the major tributary of Wadi Al-A'llaqi
- Wadi Al-A'llaqi
- Wadi El-Tarfa
- Radar rivers in Libyan Deserts
- Al-Arish valley.

Issawi et al. (2009) supposed that the two rivers of Qena and Allaqi-Qabqaba had been met in an area coincides with nowadays central Qena bend. Qabqaba is the largest tributary of Allaqi River, and both of them were formed as a result of the Eocene–Oligocene tectonic movements. Because Qena river system was mightier than Allaqi-Gabqaba, the first succeeded in capturing the latter and the three tributaries formed one mega river, which had been pushed southwestward into the Libyan Desert, and probably was one of the tributary of the great “radar rivers” suggested by previous literatures (see McCauley et al., 1982; Issawi

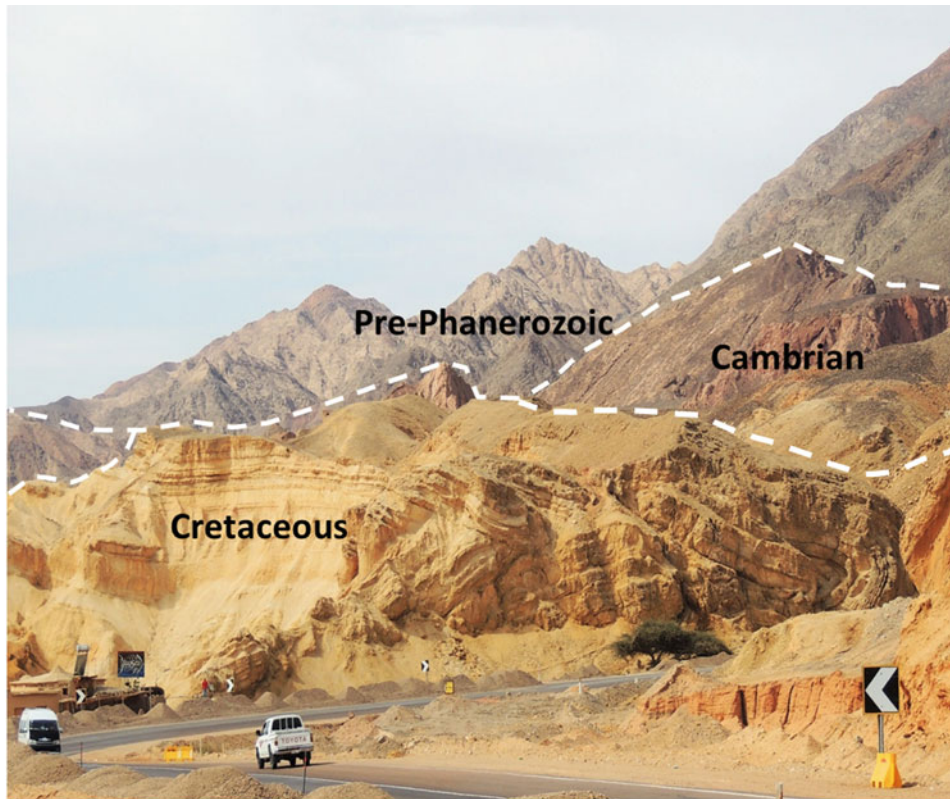


Fig. 21 Overturned and recumbent Cretaceous folds, North of Nuweib'a

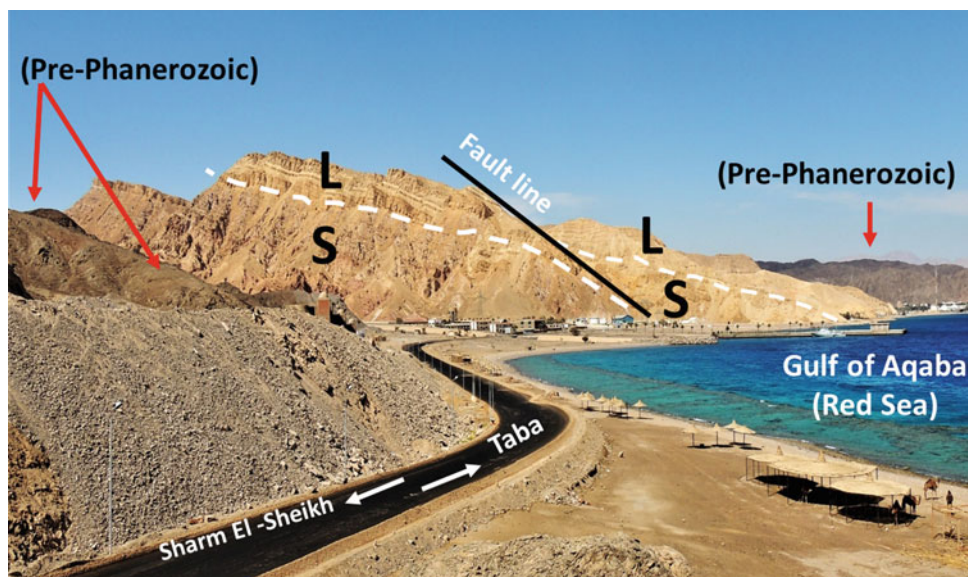


Fig. 22 Pre-Phanerozoic and Phanerozoic landscapes in Eastern Sinai, Gulf of Aqaba, Jabal el-A'safir area—Taba where S = Sandstone (Cambrian to lower cretaceous) L = Limestone (upper cretaceous)

et al., 2009). Moreover, El Deftar et al. (1978) have concluded that amid the Phanerozoic of limestone deposits in the Western Desert of Egypt, relics of gravels leached from Precambrian of the Eastern desert had been spread in

isolated locations separated from its sources by the Quaternary rivers of the Nile. The very good example of that is opposite to Wadi El-Tarfa in central Egypt. Precambrian gravels have been brought to the Western Desert in a prior

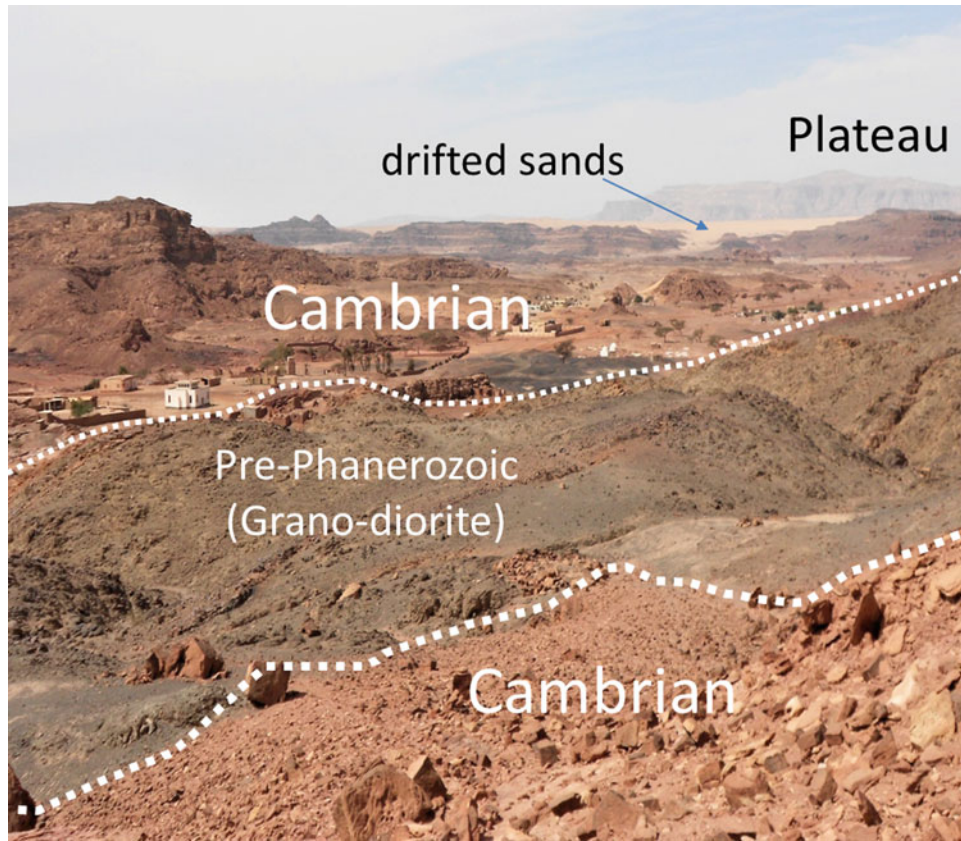


Fig. 23 High plateau of Cambrian sandstone–Western Sinai



Fig. 24 The type locality of the Naqus Formation, Cambrian age, Western Sinai

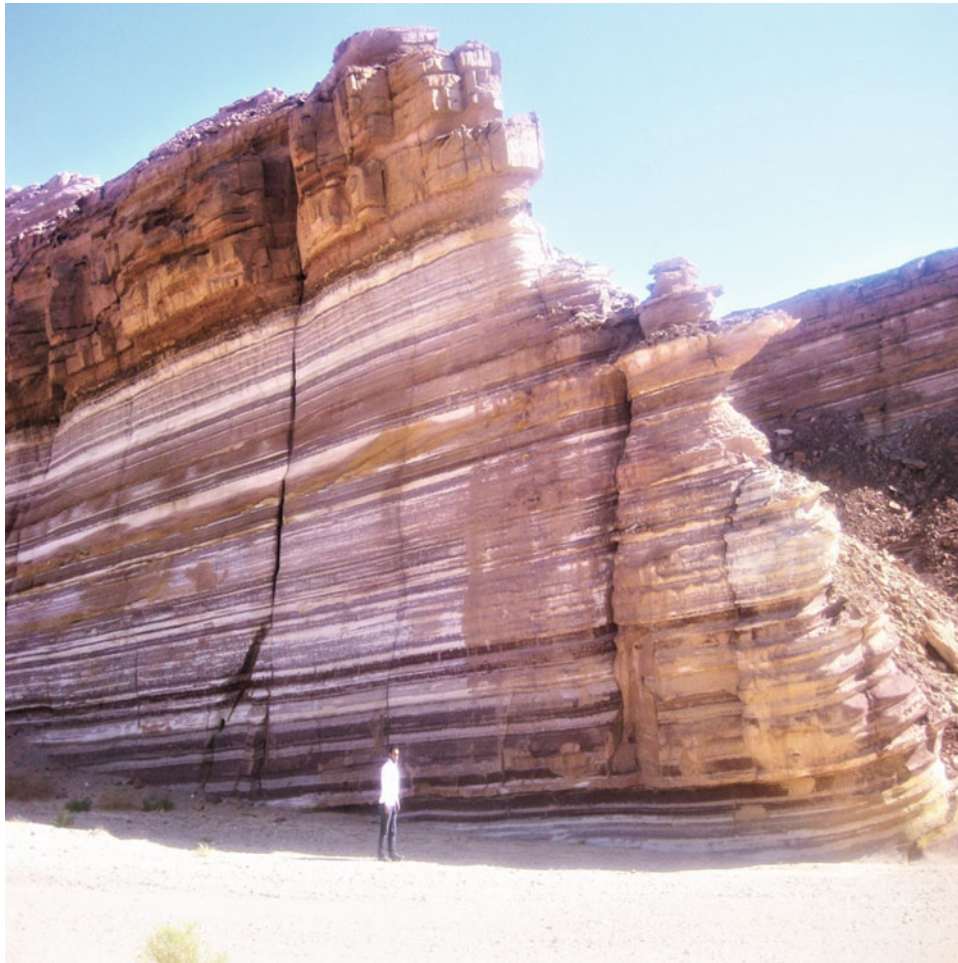


Fig. 25 A typical view of the Cambrian sediments in Western Sinai; the Araba Formation

river system preceded the Nile, e.g., since late Eocene and through the Oligocene and Miocene. While Wadi El-Tarfa runs in a Phanerozoic plateau in the Eastern Desert, its head tributaries, as Wadi Ragala, run in Precambrian rocks. The tectonic uplifting movements of the Red Sea during Eocene–Oligocene has changed the fluvial system orientation to be East–West; hence tens of valleys have been formed, e.g.: Khorit, Shu'it, Abbad, Al-Asyuity and Sinur.

Issawi and Youssef (2016) had shed more lights upon the buried fluvial channels across the Sahara landscape (see Fig. 30) during Late Paleogene and the Neogene. (For more details, see Said et al. 1994, and Mohamed, 2021).

Wadi Al-A'resh collects most of the drainage basins of central Sinai limestone plateaus. Previous literatures have mentioned to the canyon channel system in the Lower basin of Wadi Al-A'resh, where tens of meters deep and 150 m wide, has been formed in the hilly obstacles of Jebal El-Halal. After passing the narrow neck of El-Halal obstacle, Wadi El-Arish spreads out forming its tiny delta into the Mediterranean.

In northern Sinai, El Halal and other hills (Fig. 31) have been formed as a folding belt in late cretaceous. Sea-level retreating since that geological time has forced the fluvial system to cut northward and run through this folding belt and make their gorge-like channels in three successive canyons, e.g.: Khoriem, Tal'et El-Badan and El Daiqa. On the other hand, numerous previous literatures have concluded that the present-day valley of the River Nile has been cut during Late Miocene. Prior to this epoch of geological time, sedimentological evidences, on surface and subsurface, have indicated that there are old independent fluvial systems preceded the Nile. The most famous known system is that river which drained the elevated Egyptian lands in a western corridor parallel to the Present-Nile, with a major delta, 300–500 m thick. This paleo-delta coincides in nowadays with Fayum region and adjacent areas in northern Egypt, where a marine gulf was receiving fluvial sediments (sands and gravels) belong to Late Eocene–Early Oligocene, very rich in vertebrates. As Said (1981) have clarified, extensive gravel and sand spreads are overlying early late

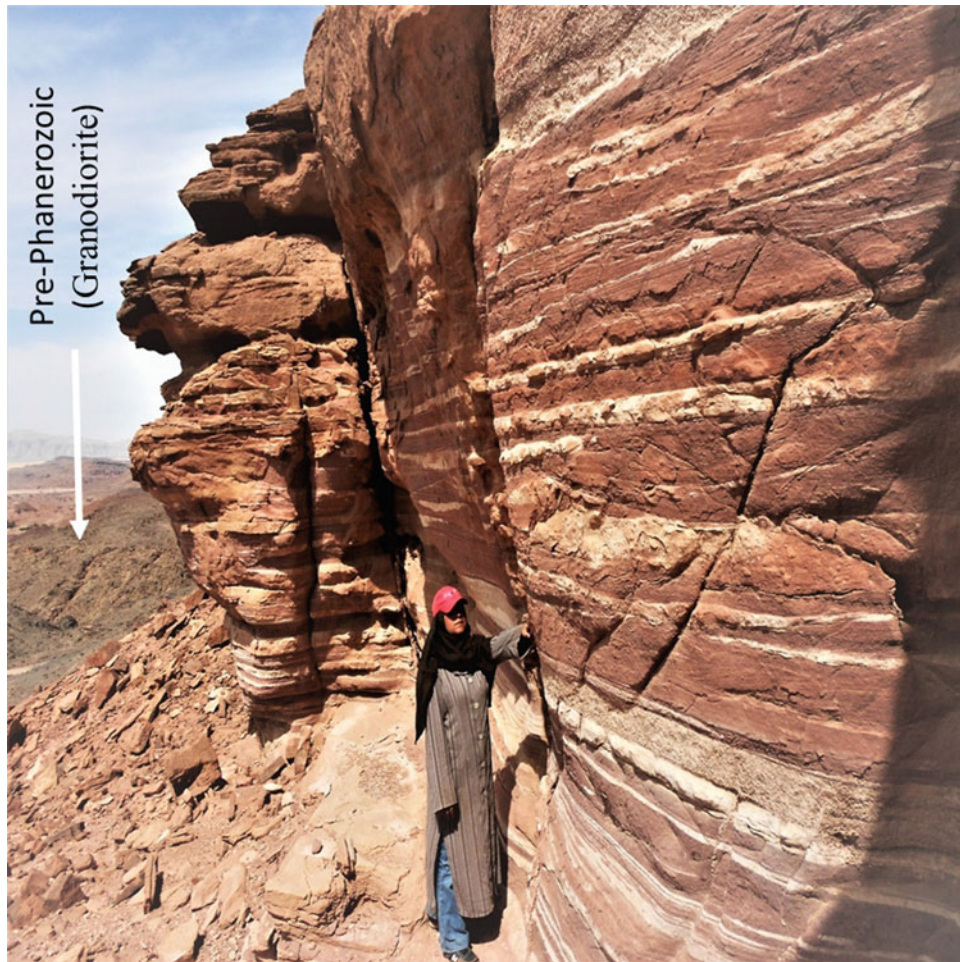


Fig. 26 Free-slope in Cambrian sandstone rocks, Um Bogma region, Western Sinai

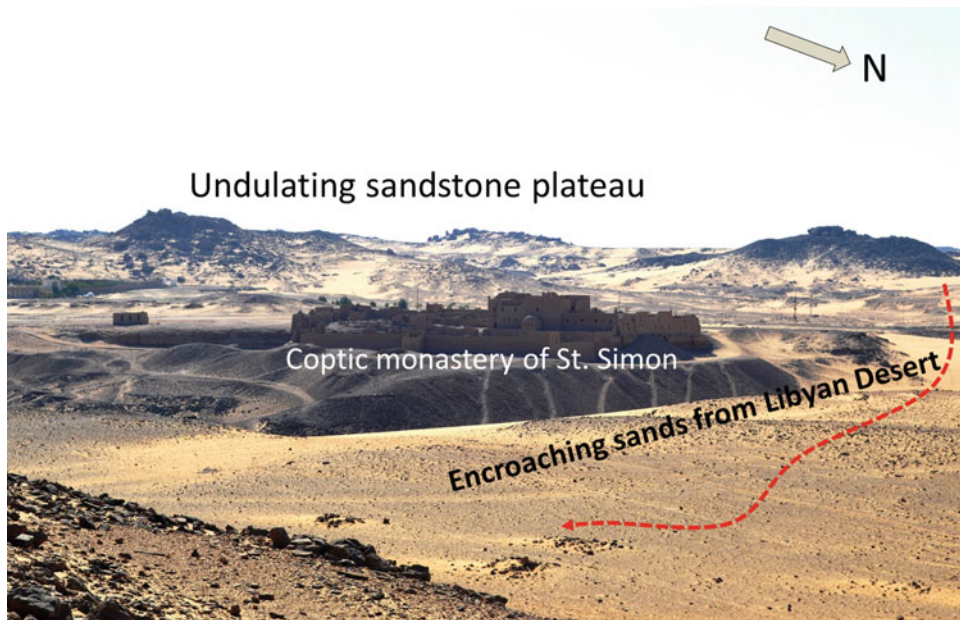


Fig. 27 Western Nile plateau, Aswan region

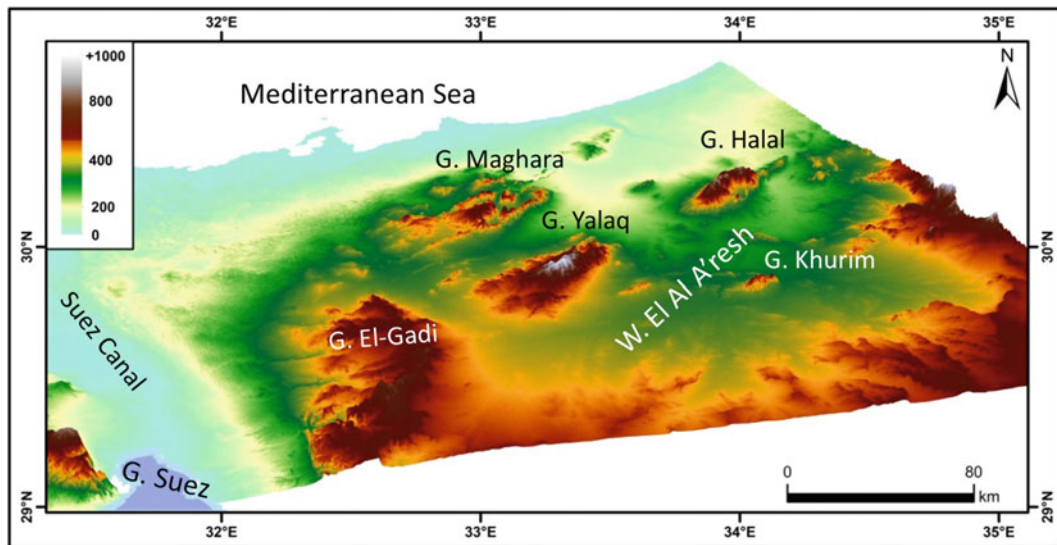


Fig. 28 Wadi El-A'resh among the folded arc system on Northern Sinai

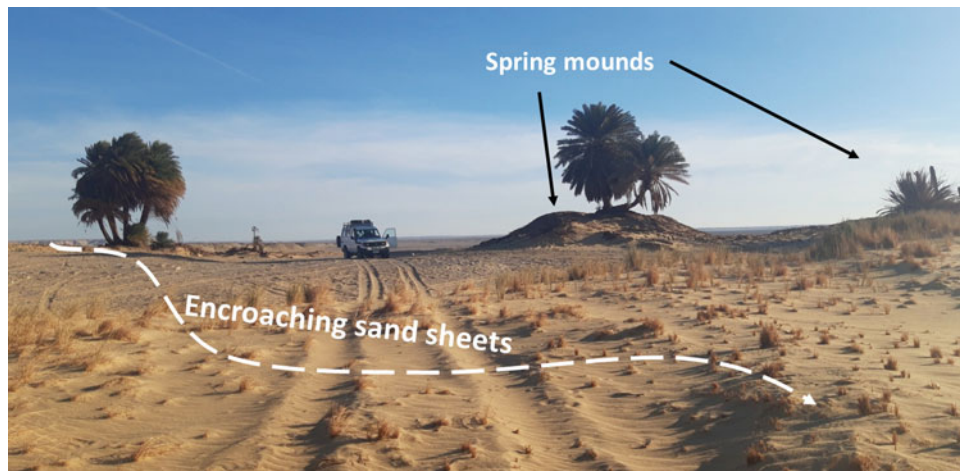


Fig. 29 Karstic springs in the high surface plateau of Darb El-Arba'in, Western Desert of Egypt

Eocene/Oligocene river system. These deposits of gravels extend upon the western desert plateau between Minia and Bahariya Oasis in a northwestern direction. These fluvial gravels and sands probably belong to a river system that had formed a huge delta system in Moghra Oasis.

The Nile has been formed through successive episodes given by Said (1981) as follows:

1. *Eonile* represents the late Miocene period, when it was cutting a deep valley canyon, as a result of the Messinian crises which was a period of sea regression and heavy erosion in northern Africa and a desiccation in the Mediterranean. These global events led to fluvial vertical erosion as a result of lowering sea level by several hundred meters. It has been found that there is a lack of
2. *Paleonile*, with the end of Messinian crises, sea level had been raised in early Paleocene era. The ingression of sea level had flooded the Nile Pliocene canyon forming what Ball (1938) named "the Pliocene Gulf," an elongated gulf extended southward up to the latitude of nowadays Aswan. Hence, the *Paleonile* is actually the "*Paleocene-nile*." The absence of African tropical fauna from *Paleonile* suggests that *Paleonile* had no connection with the drainage sources in Central Africa or Ethiopia. Remnants of these Pliocene sediments still obvious in many sectors in Upper Egypt as in Qena region.



Fig. 30 Radar River–Libyan Desert (modified after Issawi & Youssef, 2016)

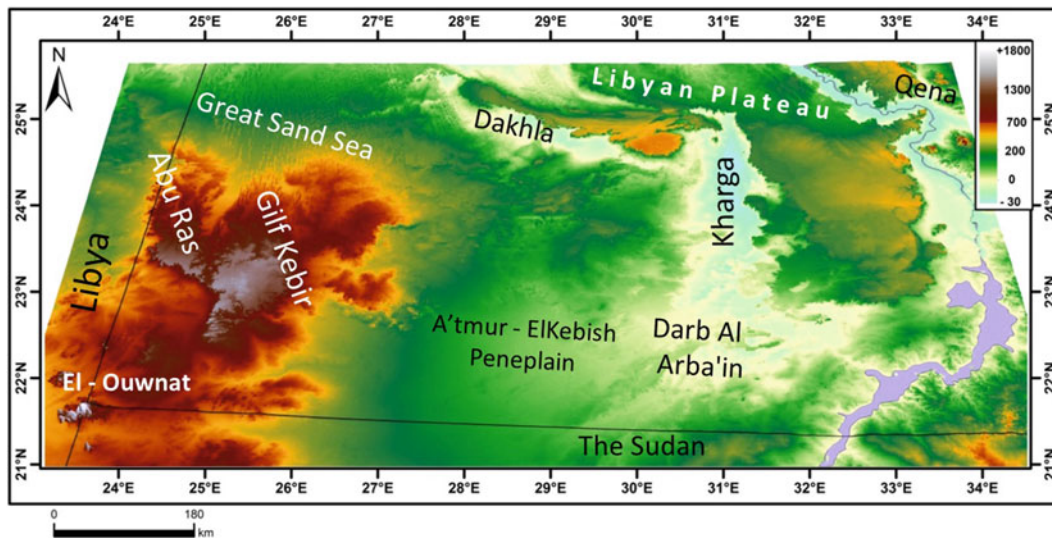


Fig. 31 Southern portion of Western Desert of Egypt

3. The Quaternary Rivers of the Nile. This is the third type of the Nile, actually the recent one. It lies fully in Quaternary and have been developed across three stages: *Protonile*, *Prenile*, *Neonile*.

3.2 Plateaus

Analysis of Phanerozoic geological structure clarifies that Egypt looks like a huge plateau dissected by tectonic controls and fluvial factors into many sub-regions:

- (1) The two plateaus of Sinai:
 - El-Tih
 - El-E'gma
- (2) The three plateaus of the Eastern Desert:
 - Northern Galala (including Jebal A'taqa)
 - Southern Galala
 - Ma'zaa
- (3) The three plateaus of the Western Desert:
 - The Libian plateau
 - El-Gilf-Abu Ras
 - Marmarica.

While El-Gilf-Abu Ras is the only plateau composed of Paleozoic (Carboniferous) and Mesozoic (Cretaceous), the rest of all plateaus in Egypt is covered by Paleogene (e.g., Eocene) and Neogene (e.g., Miocene). Issawi et al. (2009) concluded a reasonable thesis of Phanerozoic evolution in Egypt. In this thesis, Egypt is composed of tectonic arcs (positive relief) separated in between by lowlands or huge depressions. During the Paleozoic and Mesozoic, deposition was filling gradually these regional basins. These depressions were filled basically by thick deposits of Cretaceous-Eocene ages. For a tectonic reason, in the early to middle Miocene, lowland areas had been inverted to form positive relief (e.g., plateaus). Omar and Steckler (1995) suggested

that this inversion had been occurred as a gradual uplifting in syn-rifting processes.

3.2.1 The Two Plateaus of Central Sinai

In Central Sinai, El-E'gma plateau consists, mainly, of Eocene limestone rocks, with an average elevation of 1000 m. It is highly dissected by fluvial systems running into three water bodies: (1) The Gulf of Aqaba, as in W. Watir; (2) the Gulf of Suez as in W. Gharandel; (3) to the Mediterranean as in W. Al-A'rish. This plateau is merged to the north with a tableland called "El-Tih," with an average elevation of 600 m. Figure 32 gives a good example of piedmont zone and cliff-slope of El-Tih Plateau, which consists, mainly, of sandstone of Triassic age. Northward of El-E'gma/El Tih tabular geomorphology, the inversion processes mentioned above had affected the Jurassic- Cretaceous basins that had been inverted to form a cluster of hills belonging to what called "the Syrian arc system."

3.2.2 The Two Plateaus of Galala (Northern and Southern)

Northern Galala (El Galala El-Baharia) is overlooking Gulf of Suez, comprising both A'taqa and Kahliya blocks, in addition to minor hills. With an average elevation of 700–1100 m, the surface geology is composed of Middle Eocene,



Fig. 32 Piedmont zone and free-slope of El-Tih Plateau



Fig. 33 Wadi Askhar, a major tributary to Wadi Araba, Northern Galala



Fig. 34 Old spring in the piedmont of Northern Galala, Gulf of Suez (the Eastern Desert of Egypt)



Fig. 35 Wadi El-Garf, cave gallery in Northern Galala plateau



Fig. 36 Karst roof gallery–Sinur cave, the Eastern Desert of Egypt



Fig. 37 Fault line in Sinur cave with an outlet to the exterior



Fig. 38 Different columns in Sinur cave, Sinur cave



Fig. 39 Southern flank of El-Galala El Baharia plateau, Gulf of Suez, Red Sea

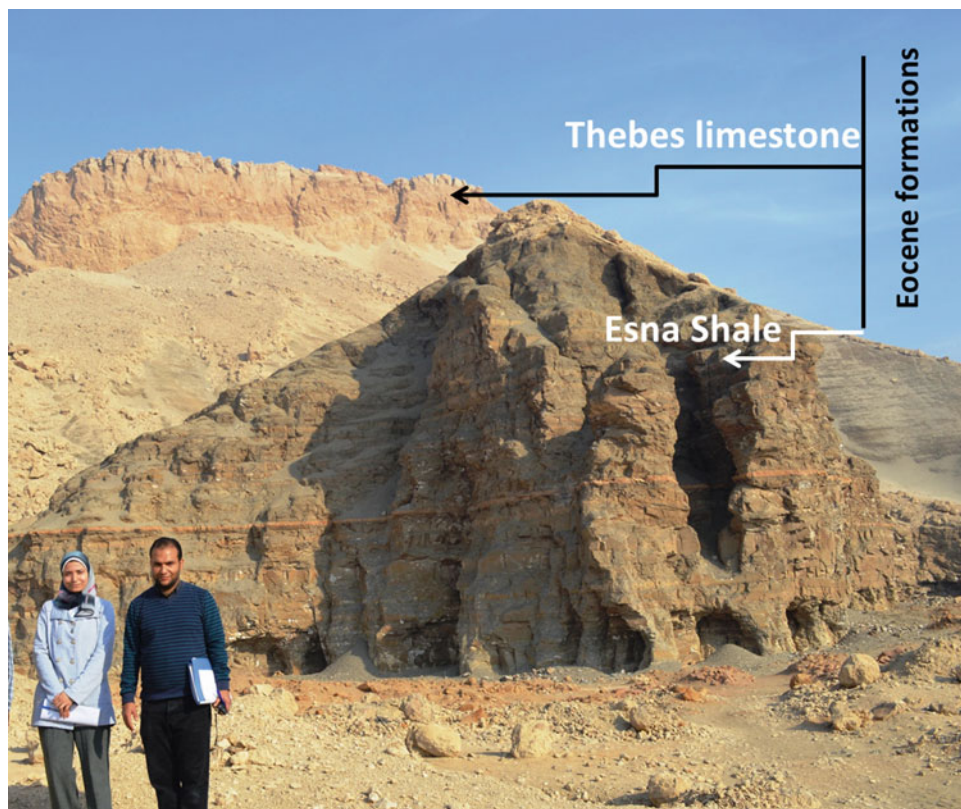


Fig. 40 Al-Dababia, El Shaghab area, East Nile Plateau, Luxor region



Fig. 41 Western cliff of Ma'zaa plateau, Antenenopolis (El-Sheikh E'bada) El-Minya region

while the cliff slopes of the Gulf of Suez show Paleozoic strips of reddish sandstone, which belong to Carboniferous-Permian times. As a cuesta-like plateau, northern Galala extends east–west for more than 75 km, overlooking the Nile valley. On the other hand, the cuesta-like plateau of southern Galala is tectonically matched with its northern counterpart. Wadi Araba, a 90 km long, running from west to east, is a superimposed valley debouching in the Gulf of Suez and occupying the corridor in between the two plateaus. The upper basin of that valley is fed by torrential streams (Fig. 33) as resembling by Wadi Askhar (the “Rocky valley” in Arabic), where small relics of Paleozoic sandstone is outcropping. There are numerous relic features of paleo-karst and springs in the deep valleys of Northern Galala, as in Wadi Abu Hulify (Fig. 34). Moreover, a gorge-like valley called Wadi El-Garf shows a very good example of typical paleo cave system (Fig. 35). On the other hand, Wadi Sinur, a 100 km long and runs from east to west is debouching into the Nile Valley. Paleokarst geomorphology presents new discovered landforms in this plateau, as in the impressive cave of Sinur (Figs. 36, 37 and 38). The

Limestone cliffs of the Eocene in southern Galala lie in direct contact with sandstone hills of the Paleozoic and lower cretaceous and Precambrian inselbergs southwards to Ma'zaa as well as with the Precambrian outcrops as shown in Fig. 39.

3.2.3 Ma'zaa

Wadi El-Tarfa represents the boundary line between Southern Galala and what called Ma'zaa plateau. Ma'zaa has an average elevation of 700 m, extending southwards for more than 250 km until Wadi El-Qiryia. Although the Ma'zaa plateau is conventionally and ethnographically ends in Qena bend region, it actually extends, geologically, southwards for more than 100 km till other Eocene dissected blocks (600–700 m. high) such as El Shaghab, El-Nezzy, Al-Rakhmya, Al-O'wayniai. Ma'zaa plateau is highly dissected by faulting axes superimposed by numerous valleys debouche to the Nile, the most important from north to south are: El Tarfa, Qena, El Assuity, Abu Shih, Qasab, Abu Nafukh, Gurdi (a north–south tributary of Wadi Qena). El Shaghab area, southeast of Luxor, has a worldwide importance in the geological records, as it contains



Fig. 42 Ancient quarries in limestone cliffs, Eastern Plateau, Minya region

the missed link in Paleocene-Eocene geologic succession (Thanetian/Ypresian, 55.8 million years ago). It was declared a national protected area, and it is nominated to become part of the UNESCO's World Heritage (Fig. 40). The Eocene Ma'zaa plateau is geologically matched with the Libyan Desert, as the Nile has excavated its valley in post-Eocene period, e.g., late Miocene for the *Eonile*. A good example could be seen in El-Minya region (see Figs. 41, 42 and 43).

3.2.4 The Libyan Plateau

This great plateau is bounded by cliffs from all sides: toward the Nile in the east (as shown in Fig. 44), or toward large depressions in the west and southwest, and to the north is bounded by the southern cliffs of a relatively recent, Miocene age of Marmarica (El-Difa) tableland. The Libyan plateau exhibits many geomorphic processes, especially karstic and Aeolian processes.

The transitional area between the two depressions of Dakhla and Kharga (Fig. 45) is a good example of peneplain. Other sub-regions, as in northern Kharga, are fault-oriented valley-like corridors, encroached by sand sheets (Fig. 46).

3.2.5 El-Gilf-Abu Ras

El-Gilf-Abu Ras plateau lies in the southwestern portion of Egypt. While all the previous mentioned plateaus are composed of Eocene limestone depositions, this older plateau has been deposited during the Paleozoic (Silurian, Devonian and Carboniferous) and Mesozoic (from Late Jurassic to late Cretaceous). The major rock types here are fluvial sandstone and shallow marine siltstone or shale (see Said, 1990 and Embabi, 2018). This plateau is the highest one all over the western desert, with elevation exceeds 1000 m and the average elevation is 600 m. Grolier and Schultejann (1982) identified 33 volcanic exposures, some of which extend for more than 4 km and in an irregular form. Elevations vary between 40 and 100 m (Embabi, 2018). Basaltic lava eruptions are widespread in other parts of the Western Desert; the prominent example is Bahariya Depression as shown in Figs. 47, 48 and 49. El-Gilf-Abu Ras plateau is dissected by vertical and canyon-like valleys, and most of them are inaccessible. The most famous wadies are El-Diyag (the narrow valley), El-Wassa' (the wide valley). Many evidences of the paleoclimate are inherited in dried lake and playa. The whole area is encroached by sand dunes, sand



Fig. 43 Dissolution caves in the eastern side of the Nile Valley in El-Minia, Upper Egypt

sheets and successive waves of the Great Sand Sea (Fig. 50 for example).

3.2.6 Marmarica

Marmarica is a triangular-shape tableland. The Bedouin Arabic name for this plateau is “*El-Diffa*” referring to the reddish loamy soils of this region, which usually host shrubs and arable patches (Falls, 1915). With an average elevation of 200 m, Marmarica has steep slopes from both northern and southern sides. It overlooks the Mediterranean coastal cliffs, leaving only very narrow coastal strips in many sectors. The southern slopes overlook many depressions; the most famous are Siwa and Qattara. While the plateau is high and steep in the western portion, it dies into wide undulating coastal plains in the eastern portion of Maryut, with its 25 km wide. Maryut region represents undulated plains, composed mainly of a series of coastal limestone bars, marine deposits at base and Oolitic limestone from Aeolian origin at top (El-Asmar, 1991; Mohamed, 1997).

3.3 Depressions

Egyptian lands are dotted by tens of depressions; all are exclusively in the Western Desert. Various explanations have been introduced to understand the mechanism of formation. Conclusions of previous studies have suggested that fluvial and karstic actions, controlled in many cases by tectonic forces, are the major factors. Wind erosion and Aeolian processes are secondary sources of formations. Morphometric analysis of these depressions shows that they range in areas between 3000 km² (Bahariya) to more than 45,000 km² (Qattara). Most of them are below sea level (– 145 m. in Qattara, – 64 m in W. El Rayan). Embabi (2004, 2018) had classified depressions, according to their size, depth and areas, into five categories: mega, large, small, micro and minute. The research of (Mohamed, 2021) gives a detailed geomorphological analysis of Dakhla depression. Across these depressions, there are very good indications of karstic processes (see El-Aref et al., 1987) old springs



Fig. 44 Caves and paleokarst in limestone cliffs, Nile Valley, Western Plateau in Qena region, Upper Egypt



Fig. 45 Western Kharga peneplain in what called “Red Desert”



Fig. 46 The corridor valley of Ain Um El-Dabadeb, the sandstone of the Turonian age is heavy oriented by fault line axes across Gebel El-Taref (northern Kharga Depression)



Fig. 47 The what called "Black Desert" in Southern Bahariya Depression, volcanic thick sheets of basalt upon sedimentary rocks. (see for more details, Meneisy, 1990)

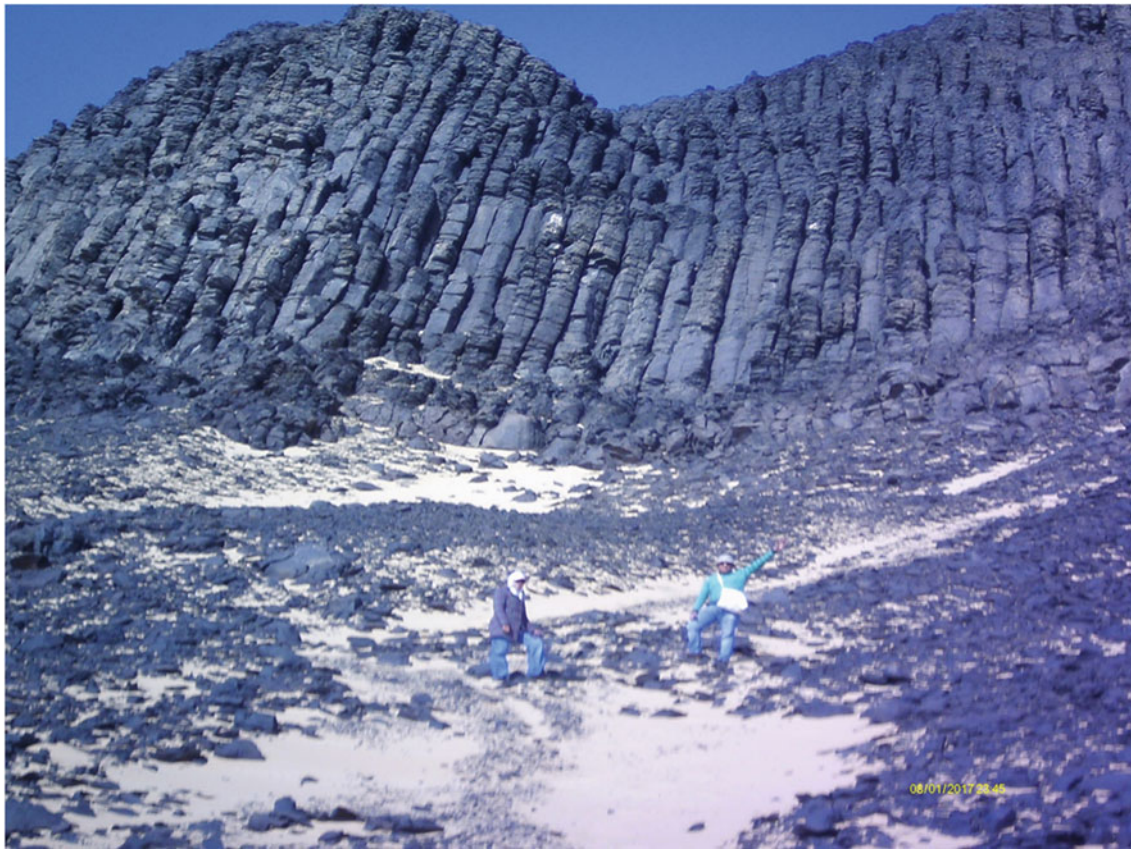


Fig. 48 Columnar basaltic hills, Bahariya Oasis

(Fig. 51) paleokarst processes (Figs. 52, 53 and 54) and tufa deposits (Fig. 56). After examining different depressions walls, the current author considers the vertical walls of Kharga depression as an ideal example of examining many paleo and current geomorphic processes and landforms in this upper cretaceous/lower Eocene escarpment. Along these walls, 200 m high, it is easily to delineate the following typical landforms:

1. Detached and attached hills, affected by faulting system and karstification. The most famous ones are the two hills of Jebal Um El-Ghanaim and Jebal Ghanima (Fig. 55). The same feature is obvious in Bahariya as shown in (Fig. 56) in the detached limestone hill of El-Maghrafa on the northwestern slope.
2. Differential weathering activities and erosional processes along the soft marine shale of upper cretaceous and the hard limestone rocks of the lower Eocene. Marine shale of the Upper Cretaceous/Lower Eocene in this area is very rich in some fossils like *Amonite* (Fig. 57) and *Exogyra Overwigi* (Fig. 58).
3. Hanging valleys which associated with rejuvenated points and paleowaterfalls. Most of these valleys have been used across history as pathways connecting the Nile

with the Kharga-Dakhla depressions. These pathways known locally as Naqb (pl. Nuqub)

4. High-altitude springs have been active in the paleoclimate, and they are now mere relics on the free escarpments (e.g., A'in Tafnis El Jebal, eastern Kharga). The analysis of satellite images and field study accomplished by the author have clarified that many of these springs are connected through the subsurface with dolines and dissolution holes over the plateau.
5. Encroaching sand dunes from the northerly direction which form vast fields of invasive climbing dunes and transverse types crossed the depression into Nile valley and Lake Nasser. Some examples of these dunes are shown in Figs. 59, 60, 61 and 62.
6. On the other hands, inside the depressions there are minor features as springs, spring mounds and dolines.

In a previous study (Mohamed, 2021), the current author listed from different topographic maps in Dakhla depression more than 2150 springs (*A'yn*, pl. *A'youn*) and Wells (*Bir*, pl. *Abar*). However, there is no active natural spring in Dakhla-Kharga region, except A'in Amur, in the backward of Abu Tartur southern escarpment. According to Adelsberger (2008), there are numerous spring mounds in Dakhla



Fig. 49 Disintegration of basaltic blocks, Bahariya Oasis

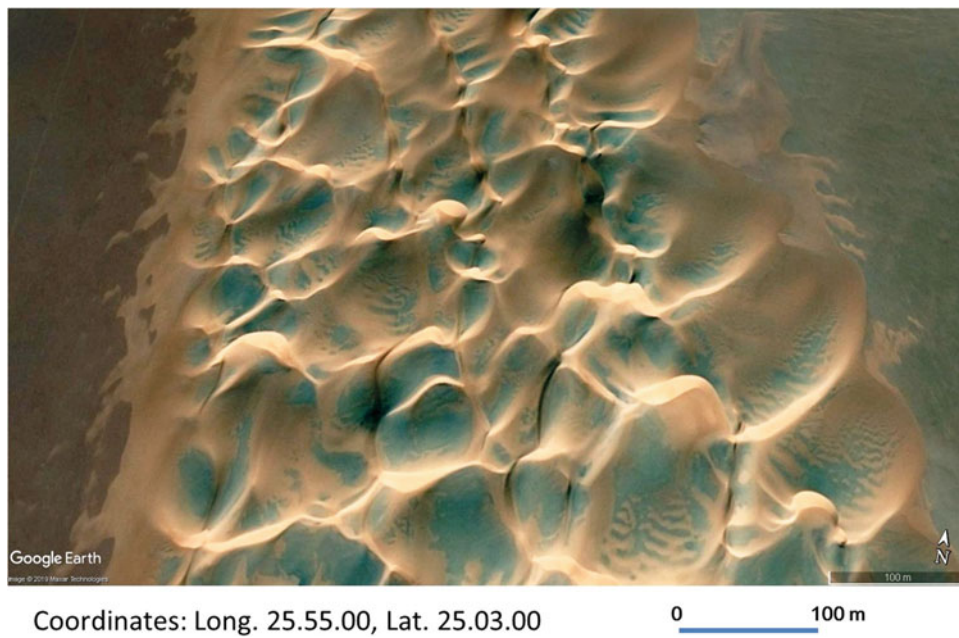


Fig. 50 Part of the Great Sand Sea complex dune fields, what called Qaret El-Hanash area



Fig. 51 El-Bishmo Karstic spring, Bahariya Oasis, Western Desert of Egypt



Fig. 52 Collapsed karstic arches, 5 m high, the northern plateau of Farafra oases, the Western Desert of Egypt



Fig. 53 *Terra Rosa* in Eocene plateau—the Western Desert, Sohag area, Upper Egypt



Fig. 54 Tufa deposits on steep slope of Naqb El Moudawara area, east of Kharga



Fig. 55 Jebal Um El-Ghanaem, a detached hill from Eastern Kharga plateau



Fig. 56 The Detached limestone hill of El-Dist, Bahariya Depression

oasis associated with the contact between Taref Formation sandstones and Quseir Formation shales, as well as with faults and uplifted sandstone units associated with the Tawil Anticline. However, Playa, dried lakes and sebkhas are the most spectacular landforms in depressions' floor. Siwa depression for example has many of these lakes and associated landforms/land use. In recent times, hyperevaporation

in eastern Siwa lakes has enhanced salt extractions for commercial and international trading. Siwa undergoes a severe problem of discharging the excess water lodging in agricultural lands. Many suggestions have been introduced to solve these problems, including out-of-depression solution. In the middle of *Libyan* plateau lies Farafra depression which undergoes a vast sand dune encroachment, especially



Fig. 57 Ammonite fossils, upper cretaceous, Kharga Oasis, Western Desert of Egypt



Fig. 58 *Exogyra overwegi*, Jebal El-Tir, Kharga depression



Fig. 59 Lee dunes–Northern Kharga depression



Fig. 60 Barchanoid dunes–Western Kharga depression



Fig. 61 An ideal example of Barchan dune, Doush area, Kharga Oasis, Western Desert

on its eastern side. Many indications showed that this depression has been shifted into dryness after a period of wetness (Barich et al., 2014). Playa and playa's deposits are scattered in many sub-regions in the Western Desert of Egypt. Some good examples are shown in Figs. 63, 64 and 65.

4 Conclusions

- The Nile valley represents a longitudinal corridor, hardly connected with the other regions in Sahara. Since the last three decades, some efforts are in progress to redistribute the population across the country in order to achieve the geographic "exodus" from the siege of the historical "sticking in" the Nile flood plains and deltaic soils.
- The Eastern Desert occupies about one-fifth of Egyptian land (220,000 km²) and looks like a great triangle, with its base on the borderline with the Sudan and its apex on southeastern delta. More than 100 peaks dotted the Eastern Desert forming what might be named "Badlands" with steep rugged slopes that have been formed in a structurally controlled system of dissected terrains by oblique faults.
- The Sinai Peninsula is a model of Egyptian geography and geomorphology. It is composed of two different geomorphic zones: the southern portion is a basement complex mainly of high mountains, while the northern portion is a sedimentary one basically of plateaus and sandy plains.
- In late Eocene, some tectonic movements were responsible for the uplifting of Red Sea hills. Results of this uplifting is the very intensive system of faulting which formed paleo-river system, prior to the Nile, especially Wadi Qena, Allaqi-Qabqaba, El-Tarfa Al-Arish, in addition to what called "Radar rivers."
- Since the Middle Eocene, the modern Nile has been formed through five episodes: Eonile, Paleonile, Protonile, Prenile and Neonile.
- Analysis of Phanerozoic geological structure clarifies that Egypt looks like a huge plateau dissected by tectonic and fluvial factors into many sub-regions: the two plateaus of Sinai (El-Tih and El-E'gma); the three plateaus of the



Fig. 62 Previous Barchan dune in Fig. 61, a view from crest toward the two horns



Fig. 63 Vast playa–Southeastern portion of Kharga depression



Fig. 64 Playa deposits, El-Sherka plain, Kharga depression, Western Desert



Fig. 65 Playa deposits, rich in plant roots. El-Sherka plain, Kharga depression, Western Desert

Eastern Desert, (Northern Galala, Southern Galala and Ma'zaa); the three plateaus of The Western Desert (the Libyan plateau, El-Gilf-Abu Ras and Marmarica).

References

- Adelsberger, K. (2008). *Geoarchaeology, geomorphology and sedimentology of Paleolithic landscapes in Egypt*. (Unpublished Ph.D. thesis). Washington University, Department of Earth and Planetary Sciences.
- Ball, J. (1938). *Contributions to the geography of Egypt*.
- Ball, J. (1942). *Egypt in the classical geographers*. Survey of Egypt.
- Barich, B., Lucarini, G., Hamdan, M., & Hassan, F. (Eds.). (2014). *From lake to sand: The archaeology of the Farafra Oasis, Western desert, Egypt*. Edizioni All'Insegna del Giglio.
- Brooks, I. (1993). Geomorphology and quaternary geology of the Dakhla oasis. *Quaternary Science Reviews*, 12, 529–552.
- El Deftar, T., Issawi, B., & Abdallah, A. M. (1978). Contributions to the Geology of Abu Tartur and adjacent areas, the Western desert of Egypt. *Annals of the Geological Survey of Egypt*.
- El-Aref, M., Abou Khadra, A., & Lotfy, Z. (1987). Karst topography and karstification processes in the Eocene Limestone Plateau of El Bahariya oasis, Western desert, Egypt. *Zeitschrift fur Geomorphologie*, 31, 45–64
- El-Asmar. (1991). *Old shorelines of the Mediterranean coastal zone of Egypt in relation with sea level changes* (Unpublished Ph.D. thesis) Mansura University, Faculty of Science.
- Embabi, N. (2004). *The geomorphology of Egypt: Vol. 1, the Nile Valley and the Western desert*. The Egyptian Geographical Society.
- Embabi, N. (2018). *Landscapes and landforms of Egypt*. Springer.
- Falls, J. C. (1915). Three years in the Libyan desert: Travels, discoveries and excavations of the Menas expedition (Kaufmann expedition).
- Grolier, M., & Schultejan, P. (1982). Geology of the southern Gilf Kebir plateau and vicinity, Western Desert, Egypt. In F. El-Baz & T. Maxwell (Eds.), *Desert landforms of Southwest Egypt: a basis for comparison with Mars*. Washington D.C.: NASA
- Haynes, C. (1984). *Western desert quaternary studies, preliminary report on the 1984 field season*. US Geological survey.
- Issawi, B., Francis, M., Youssef, E., & Osman, R. (2009). *The phanerozoic geology of Egypt: A geodynamic approach*. Ministry of Petroleum.
- Issawi, B., & Youssef, E., (2016). Rejuvenation of old dry channels in NE Africa. *Annals Geological Survey Egypt*, XXXIII, 1–32.
- Klitzsch, E. (1984). Northwestern Sudan and bordering areas. Geological development since Cambrian time. *Berliner geowiss. Abh. (A)*, 50 Berlin.
- McCauley, J., Schaberi, G., Breedi, C., Grolieri, M., Haynes, C., Issawi, B., Elachi, C., & Blom, R. (1982). Subsurface valleys and geoarcheology of the eastern Sahara revealed by shuttle radar science.
- Meneisy, M. Y. (1990). Vulcanicity. In R. Said (Ed.), *The geology of Egypt*. CRC Press
- Mohamed, A. M. A. (2021). Geomorphology of Dakhla depression. In E. Iwasaki, A. M. Negm & S. F. Elbeih (Eds.), *Sustainable Water Solutions in the Western Desert, Egypt: Dakhla Oasis*. Springer Nature.
- Mohamed, A. (1997). *The Geomorphology of Arabs' bay gulf, west of Alexandria* (Unpublished M.A thesis). Cairo University, Department of Geography. Faculty of Arts.
- Mohamed, A. (2001) *The Geomorphology of Halaib area, Southeastern Egypt* (Unpublished Ph.D. thesis). St. Petersburg University, Faculty of Geography. Faculty of Arts.
- Omar, G., & Steckler, W. (1995). Fission track evidence on the initial rifting of the Red Sea: Two pulses, no proportion. *Sciences*.
- Rizzini, A., Vezzani, F., Coccette, V., & Milad, G. (1978). Stratigraphy and sedimentation of neogene quaternary section in the Nile Delta, Egypt. *Marine Geology*.
- Said, M., Oweiss, K., El Mandi, B., Sweisy, Kh., Turki, S., Diaf, A., & El Tagory, A. (1994). A note on the preliminary reconnaissance field trip to Al Uwaynat area. *Annals of the Geological Survey of Egypt*, XIX, 549–569.
- Said, R. (Ed.). (1990). *The geology of Egypt*. Balkema.
- Said, R. (1981). *The geological evolution of the River Nile*. Springer.



Atef Moatamed A. Mohamed is a professor of physical geography, Cairo University (Egypt). He received a Ph.D. degree in 2001 from the Department of Paleogeography and Geomorphology, Faculty of Geography, St. Petersburg University (Russia). He has pursued a diverse international scientific collaboration network with Rennes University (France), Freie Universität Berlin (Germany), University of Belo Horizonte (Brazil), Spiru Haret University (Romania), and Slovenian Academy of Science. As supervisor for more than 20 Ph.D. and M.A. students, he has carried out extensive fieldtrips across Egyptian deserts. From 2014 to 2016, he served as Cultural Attaché and the Director of the Egyptian Culture Center at the Egyptian Embassy in Moscow, Russia.



Paleoposition and Paleogeography of Egypt During the Phanerozoic Era

Uwe Kirscher, Edoardo Dallanave, and Valerian Bachtadse

Abstract

The paleogeographic position of Egypt through the Phanerozoic is tightly connected to the motion of the African continent. Paleogeographic studies using paleomagnetism of rock samples from Egypt range back to the 70s and 90s of the last century, but they also continued until very recent times. Paleomagnetic data generally confirm that Egypt was part of Africa in the last ~150–200 Ma. Before that, high-quality paleomagnetic data from Egypt are sparse and possibly affected by remagnetization. Using the master apparent polar wander path of Africa and continental reconstructions, we reviewed the paleoposition of Egypt throughout the Phanerozoic. The general trend is a location of Egypt near the paleo-South Pole during the early Paleozoic, followed by a northward motion accompanied by rotational movements.

Keywords

Egypt • Paleogeography • Paleomagnetism • Gondwana

1 Introduction of Paleomagnetic Work in Egypt

Paleomagnetic work in Egypt started in the 1970s involving scientists mostly from Egypt, Germany, and the Czech Republic (El Shazly & Krs, 1971, 1973; Saradeth et al., 1987; Schult et al., 1978, 1982). Most paleomagnetic studies were related to paleogeography trying to establish the paleoposition of Egypt during the Cenozoic and the Mesozoic. The second major focus is related to Cenozoic magmatism (e.g., Resselar et al., 1981). Paleomagnetic poles determined from these early studies indicate that Egypt did not go through major movement between ~200 and 100 Ma and roughly place the position of Egypt near the paleo-equator (El Shazly & Krs, 1973). A more recent collaboration between scientists from the USA and Belgium resulted in paleomagnetic data from Paleocene–Eocene sediments indicating pervasive remagnetization overprinting the primary magnetic signal (Kent & Dupuis, 2003). Other studies including a publication on Neoproterozoic dikes confirm the presence of widespread remagnetization affecting various rock formations in Egypt (Saleh, 2020). Other studies reveal primary magnetic signals, which show a counterclockwise rotation of Egypt between the Cretaceous and the present day (Lotfy, 2015). Recently, Perrin and Saleh (2018) obtained new high-quality data and also presented a review of Cretaceous to Cenozoic paleomagnetic data including calculation of an apparent polar wander path (APWP) for Egypt. They pointed out some discrepancy between the Egyptian data compared with the master APWP from Africa and proposed different explanations for this: (1) inclination flattening of paleomagnetic directions, (2) age uncertainties, or (3) remagnetization. We present a review of the paleomagnetic data of Egypt for the entire Phanerozoic and the corresponding paleogeographic position for Egypt during that time. We furthermore present a mean APWP calculated using the Egyptian data and a comparison with African and Gondwanan data compilations.

U. Kirscher (✉)

Department of Geosciences, Eberhard Karls University of Tübingen, Tübingen, Germany
e-mail: uwe.kirscher@uni-tuebingen.de

Earth Dynamics Research Group, The Institute for Geoscience Research (TIGeR), School of Earth and Planetary Sciences, Curtin University, WA 6102 Bentley, Australia

E. Dallanave
Faculty of Geosciences, University of Bremen, Bremen, Germany

V. Bachtadse
Department of Geo- and Environmental Sciences,
Ludwig- Maximilians University, Munich, Germany

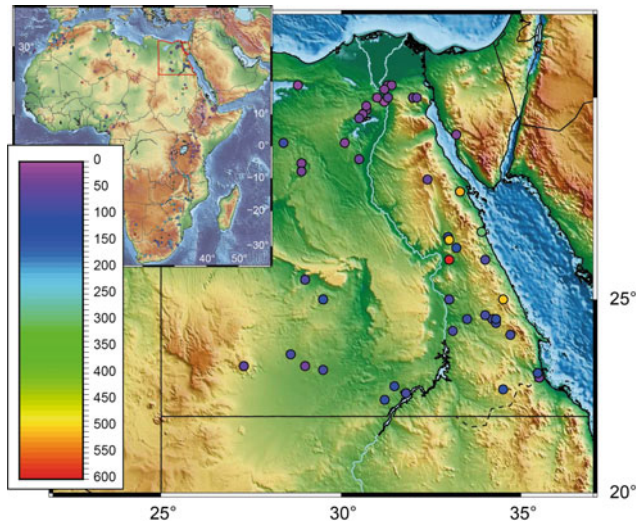


Fig. 1 Topographic map of Africa (small) and Egypt (large) including locations of paleomagnetic studies color coded by age. Ages of color bar are in Ma. Maps generated using Generic Mapping Tools (Wessel & Luis, 2017) and topographic dataset ETOPO1 (Amante & Eakins, 2009)

2 Material and Methods

To assess the paleoposition of Egypt throughout the Phanerozoic, we took a rather straightforward approach. First, we present a compilation of available paleomagnetic data for the entire Phanerozoic (Fig. 1) without considering potential remagnetization. Subsequently, a mean APWP was calculated adopting 50 Ma windows, eventually compared to the global synthetic APWP (GAPWP) of Torsvik et al. (2012). This includes global entries classified by using the quality criteria of Van der Voo (1990) and rotated into African coordinates by using the relative fits listed in Torsvik et al. (2008). To account for the Benue rift (Benkhelil, 1989), paleomagnetic data older than ~ 200 Ma were rotated into a West African and subsequently South African reference frame using rotation parameters of Kidane et al. (2013) and Torsvik et al. (2012). After that, a continental paleogeographic model was used to obtain paleogeographic maps for the entire Phanerozoic (Torsvik et al., 2014). To reconstruct the continents of the world including northern Africa, we used the software GPlates (Müller et al., 2018)

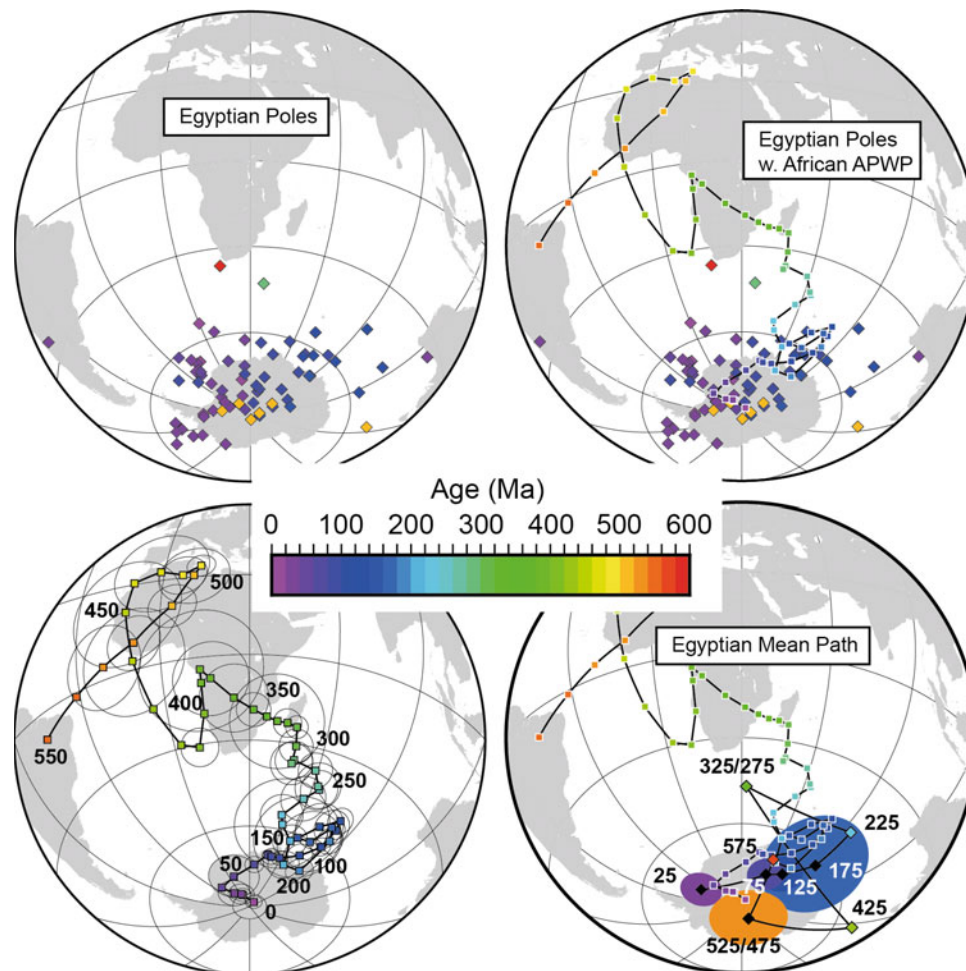


Fig. 2 Paleomagnetic data of Egypt (top left) color coded by age. Top right: Egyptian data together with the master APWP of Africa (Torsvik et al., 2012). Bottom left: master APWP with according error intervals. Bottom right: mean APWP of Egyptian data together with master APWP of Africa. Egyptian data were rotated into a South African reference frame using rotation parameter of Torsvik et al., (2012) for ages younger than 200 Ma and older than 50 Ma. Mean data older than 200 Ma were rotated first into a West African reference frame accounting for the Benue rift and subsequently into a South African frame using parameters of Kidane et al. (2013) and Torsvik et al. (2012). Mean path is labeled with median age (e.g., 75 represents 50–100 Ma interval)

and the Generic Mapping Tools (Wessel & Luis, 2017). For the topographic data, we used the ETOPO1 dataset of Amante and Eakins (2009).

3 Results

As expected from previous studies (e.g., Perrin & Saleh, 2018), the general trend of the GAPWP is also visible in the Egyptian APWP (Fig. 2). In present coordinates, the Egyptian APWP between 25 and 225 Ma moves from Antarctica toward Australia. This supports the proposed counterclockwise rotation of the African continent between the early Cretaceous and the present day (Lotfy, 2015). Prior to the 200–250 Ma window, the data get extremely sparse, but all poles lie within $\sim 50^\circ$ from the present-day South Pole.

This is likely the consequence of remagnetization of all older rocks related to Mesozoic or Cenozoic magmatism (Saleh, 2020). This is particularly evident for the 450–500 Ma and 500–550 Ma intervals, which plot very close to the South Pole and in proximity of the 0–50 Ma and 50–100 Ma poles.

4 Paleogeographic Evolution

To illustrate the paleogeographic evolution, we present reconstruction snapshots every 50 Ma (except for the 35 Ma reconstruction; Figs. 3, 4, and 5) based on a deep-mantle-structure reference frame (Torsvik & Cocks, 2016; Torsvik et al., 2014). Figure 3 shows snapshots of 250, 200, 150, 100, 35 Ma, and present day (0 Ma).

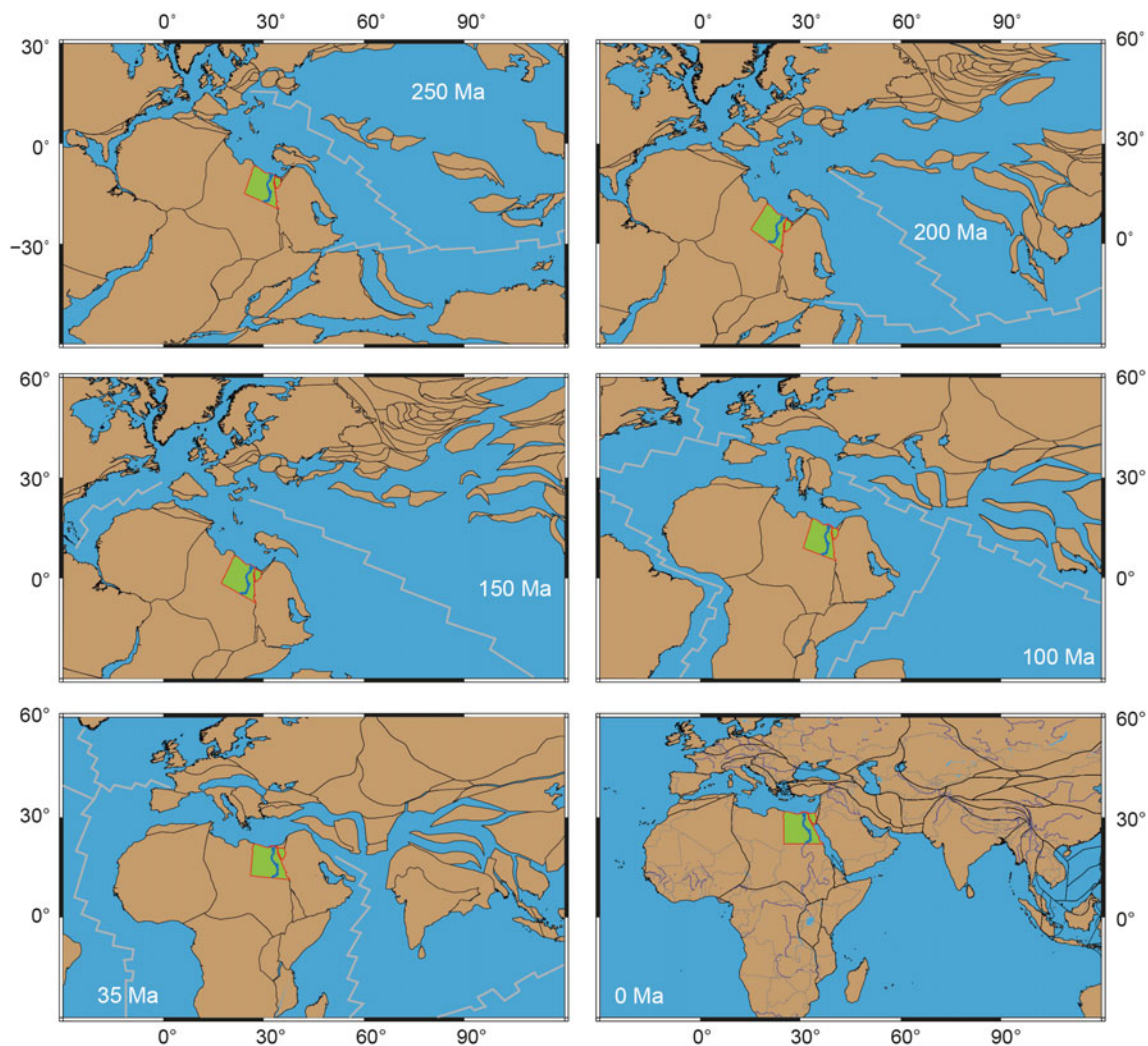


Fig. 3 Paleogeographic reconstructions for distinct time slices based on continental models of (Torsvik et al., 2014). Reconstructions were made using GPlates (Müller et al., 2018) and GMT (Wessel & Luis, 2017). Egypt is highlighted with red contour and green fill color. Reconstructed mid-ocean ridges are indicated based on Stampfli and Borel (2002)

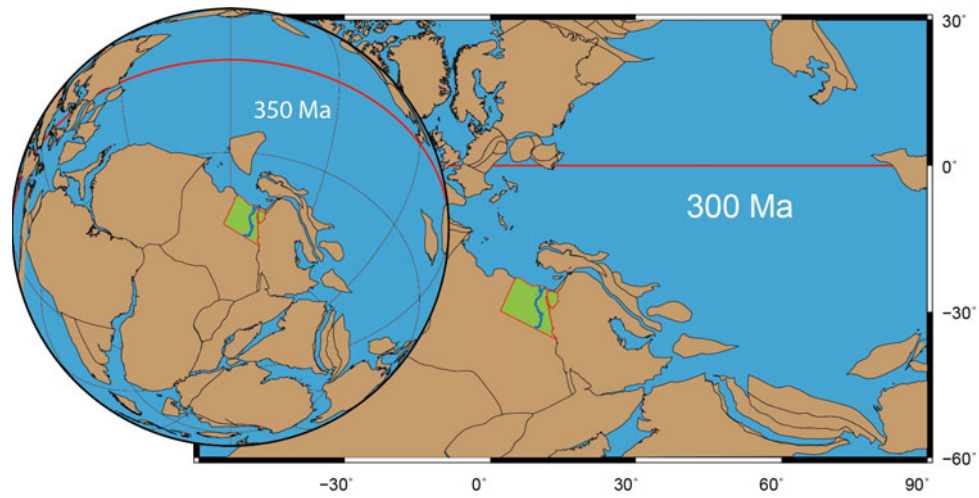


Fig. 4 Paleogeographic reconstructions similar as in Fig. 3 for 300 and 350 Ma. Red line shows paleo-equator



Fig. 5 Paleogeographic reconstructions for 400–540 Ma similar as in Fig. 3. Red line shows paleo-equator

4.1 Mesozoic–Present

Between 250 and 200 Ma, the main paleogeographic feature is a northward movement of Gondwana, which starts at ~ 220 Ma and ceases at about 190 Ma (Le Pichon et al., 2021). A minor southward movement follows, which puts Egypt close to the paleo-equator at ~ 160 Ma (Fig. 3). Between ~ 160 and 100 Ma, a counterclockwise rotation took place, which stopped roughly at the same time when the Central Atlantic started to open around 100 Ma (Granot & Dyment, 2015). After that, the paleogeographic position of Egypt is modulated by the closure of the Neotethys and the evolution of the Mediterranean (e.g., Stampfli & Borel, 2002, Fig. 3). The slow counterclockwise rotation accompanying the closure of the Neotethys brought Egypt from equatorial positions toward its present-day latitude of $\sim 30^\circ\text{N}$.

4.2 Paleozoic

The Paleozoic evolution (Figs. 4 and 5) of Egypt, which is not supported by primary paleomagnetic data from Egypt itself, is characterized by the peculiar paleogeographic evolution of Gondwana (Evans, 2003; Kirschvink, 1978; Wu et al., 2021a). Gondwana underwent several periods of counterclockwise and clockwise rotations during the whole Paleozoic. Between the beginning of the Phanerozoic at 541 and ~ 500 Ma, Gondwana rotates counterclockwise, which translates Egypt from a position slightly south of the

paleo-equator toward $\sim 30^\circ\text{S}$ (Fig. 5). Subsequently, Gondwana went through a prolonged, stepwise period of clockwise rotation until ~ 360 Ma with a rotation pole that brings Egypt as far south as 60° at ~ 400 Ma. This was also the time when the formation of Pangea initiated via orthogonal convergence of Laurussia and Gondwana (Wu et al., 2021b). This evolution brought Egypt again toward the paleo-equator at the end of the Paleozoic (Fig. 4).

5 Paleolatitudinal Evolution

To investigate the latitudinal evolution of Egypt through the Phanerozoic, the paleopoles of Africa calculated from the GAPWP (Torsvik et al., 2012), single-locality poles from Egypt (this study) and the derived mean poles of Egypt (this study) were transferred into paleolatitudes using a reference location in the center of Egypt (Lat = 27° and Long = 30° ; Fig. 6). The resulting graphs indicate again a good agreement of the Egyptian data with the expected values based on the Africa APWP between 250 Ma and the present (Fig. 6). Additionally, the 250–300 Ma interval matches well with the expected values, whereas between 400 and 550 Ma, remagnetization is most likely. Missing paleolatitude evolution details between 100 and 150 Ma might be related to insufficient number of studies (Fig. 6). Individual results based on Cambrian rocks (Table 1, Fig. 6) might reflect primary signals or at least remagnetization prior to 100 Ma, but more data are needed to verify this.

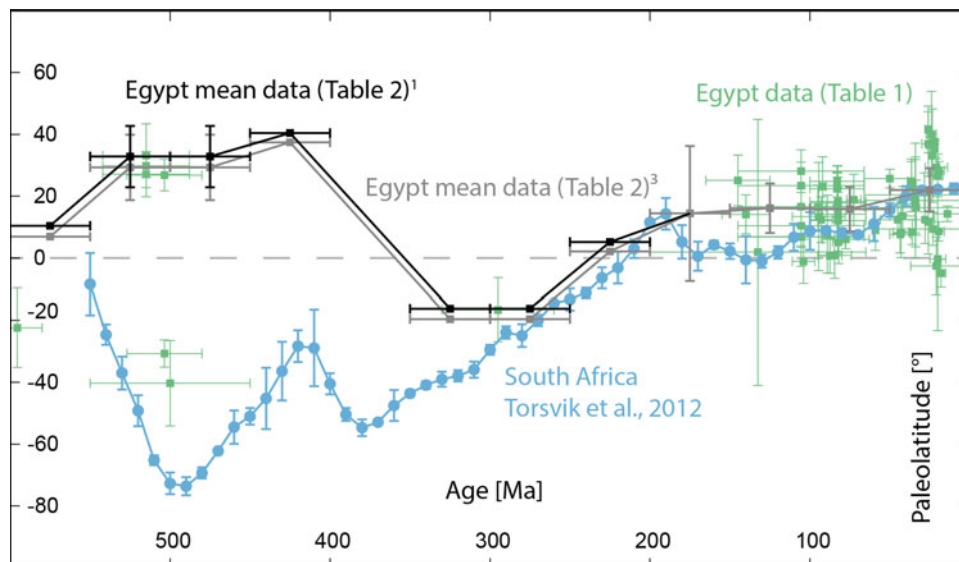


Fig. 6 Paleolatitude versus age plot for Egyptian raw and mean data. All paleolatitude data are calculated for a site of Lat = 27° and Long = 30° within Egypt. Green data represent paleolatitudes for Egyptian raw data (Table 1). Blue curve represents data based on the APWP of Gondwana in South African coordinates (Torsvik et al., 2012). Gray and black data represent the mean data of the Egyptian paleomagnetic dataset. Black data points refer to data rotated into South African coordinates, whereas gray indicates the additional rotation related to the Benue rift (see also Table 2)

Table 1 Paleomagnetic data for Egypt. **Caption:** age: median age estimate; Unc: age uncertainty; Slat and Slong: site coordinates with latitude and longitude; Plat and Plong: paleopole position with respective A_{95} ; paleolatitude (λ) and corresponding α_{95} based on a site within Egypt (Lat = 27°, Lat = 30°); Ref: respective reference

Age	Unc	Slat	Slong	Plat	Plong	A_{95}	λ	α_{95}	Reference
3.5	1.5	29.9	31.2	81.4	144.7	5.3	23.2	5.6	Abdeldayem (1999)
14.0	9.0	30.3	28.8	77.0	198.0	2	14.3	2.5	Abdeldayem (1996)
18.0	3.0	28.4	28.9	54.0	180.0	3.2	- 4.9	4.5	Perrin and Saleh (2018)
19.5	3.5	30.0	31.0	66.0	167.0	2.3	8.6	3.1	Lotfy et al., (1995)
19.5	3.5	30.0	31.0	76.0	111.0	3.0	28.3	2.9	Lotfy et al., (1995)
20.0	5.0	28.2	28.9	62.6	206.0	16.3	- 0.3	23	Schult et al., (1982)
20.0	3.0	30.0	32.0	79.0	119.0	7	26.7	6.9	Perrin and Saleh (2018)
21.0	16.0	28.4	28.9	58.2	186.7	6.6	- 2.6	9.3	Hussain et al., (1979)
21.0	7.0	30.0	32.0	76.0	107.0	3	29.3	2.8	Perrin and Saleh (2018)
22.0	0.0	30.3	31.3	68.0	92.0	3	35.3	2.5	Perrin and Saleh (2018)
22.0	0.0	30.3	31.4	70.0	83.0	1	37.6	0.8	Perrin et al., (2009)
23.0	43.0	30.0	32.0	66.0	164.0	4	9.4	5.3	Perrin and Saleh (2018)
23.5	0.5	29.6	30.6	66.9	98.5	17.2	33.1	15.1	Abdeldayem (1999)
24.0	3.0	29.1	33.2	75.0	57.2	17.9	40.1	13.8	Wassif (1991)
25.0	2.0	29.7	30.7	66.0	90.0	3	36.6	2.5	Perrin et al., (2009)
26.0	4.0	29.8	30.7	72.7	81.0	12.7	36.9	10.4	Schult et al., (1982)
26.0	2.0	30.2	31.2	63.5	79.6	10.0	41.6	7.5	El Shazly and Krs (1971)
26.0	2.0	28.5	30.5	68.0	161.0	8	11.7	10.4	Perrin and Saleh (2018)
28.0	6.0	28.9	30.1	68.0	158.0	6	12.4	7.7	Lotfy and Van der Voo (2007)
28.5	5.5	29.6	30.6	79.6	152.2	5.7	21.2	6.3	Abdeldayem (1999)
33.5	31.5	23.3	29.0	74.1	159.8	7.4	16.3	8.9	Hussain and Aziz (1983)
34.0	32.0	23.0	35.5	83.0	190.0	11	20.4	12.3	Niazi and Mostafa (2002)
34.0	32.0	23.0	35.5	50.0	22.0	10	66.2	5.5	Niazi and Mostafa (2002)
34.0	32.0	23.0	35.5	34.0	305.0	16	18.6	18.5	Niazi and Mostafa (2002)
34.0	2.0	23.0	35.5	25.0	112.0	12	17.7	14.1	Niazi and Mostafa (2002)
36.0	2.0	30.0	32.0	64.0	162.0	3	8.4	4.0	Perrin and Saleh (2018)
36.5	2.5	28.2	28.9	83.5	138.6	7.0	24.8	7.2	Schult et al., (1982)
36.5	2.5	28.2	28.9	81.5	145.2	7.6	23.1	8.1	Schult et al., (1978)
42.0	8.0	30.0	31.3	78.1	162.8	3.9	18.6	4.5	Abdeldayem (1999)
42.0	8.0	29.5	30.5	70.0	159.0	4	13.6	5.0	Lotfy and Van der Voo (2007)
43.0	5.0	28.5	30.5	61.0	156.0	6	8.2	8.1	Perrin and Saleh (2018)
43.5	6.5	30.0	32.1	69.4	189.4	4.4	7.6	6.0	Hussain et al., (1979)
45.0	11.0	28.0	32.4	69.0	161.0	3.5	12.4	4.5	Perrin and Saleh (2018)
50.0	16.0	26.0	33.0	88.0	159.0	3	25.7	3.0	Kent and Dupuis (2003)
59.0	2.0	23.3	27.3	72.0	204.0	5	9.1	6.7	Lotfy (2015)
72.5	4.5	25.5	29.0	81.5	225.0	7.2	18.8	8.3	Saradeth et al., (1987)
77.5	14.5	26.0	34.0	63.0	252.3	2.2	6.0	3.0	Ressetar et al., (1981)
82.0	4.0	24.5	34.3	67.0	229.0	5	5.1	6.9	Lotfy (2011)
82.5	17.5	23.6	28.6	77.2	259.0	9.8	18.3	11.4	Hussain and Aziz (1983)
82.5	17.5	23.2	29.5	67.8	268.8	9.6	14.2	12.0	Hussain and Aziz (1983)
82.5	17.5	25.0	33.0	80.4	227.0	4.1	17.8	4.8	Schult et al., (1978)
82.5	17.5	25.0	33.0	79.3	220.0	4.0	16.5	4.8	Schult et al., (1978)
82.5	17.5	24.2	33.1	75.0	203.2	8.3	12.1	10.7	El Shazly and Krs (1973)
83.0	17.0	25.0	29.5	66.0	141.0	9	16.6	10.8	El-Shayeb et al., (2013)

(continued)

Table 1 (continued)

Age	Unc	Slat	Slong	Plat	Plong	A ₉₅	λ	α ₉₅	Reference
83.0	17.0	22.6	31.8	83.0	283.0	5	24.8	5.1	Mostafa et al., (2016)
83.0	17.0	22.6	31.8	78.0	280.0	5	22.4	5.4	Mostafa et al., (2016)
84.5	10.5	24.1	34.7	61.1	237.6	5.3	0.9	7.5	Ressetar et al., (1981)
87.5	7.5	24.5	34.2	63.5	217.9	4.0	0.7	5.7	El Shazly and Krs (1973)
89.0	2.0	24.6	34.0	59.1	266.0	9.3	7.7	12.6	Ressetar et al., (1981)
92.0	2.0	24.5	34.3	86.0	223.0	9	23.1	9.6	Lotfy (2011)
93.0	7.0	24.4	34.3	69.3	258.1	5.8	12.4	7.4	Schult et al., (1982)
94.5	16.5	24.5	33.5	75.7	228.3	13.8	13.4	17.5	Ressetar et al., (1981)
95.0	5.0	28.9	28.4	71.0	151.0	6	16.3	7.2	Odah (2004)
104.0	7.0	24.5	34.3	55.0	250.0	5	- 1.1	7.1	Lotfy (2011)
105.5	39.5	23.12	35.46	59.0	273.0	4.9	10.4	6.5	Perrin and Saleh (2018)
105.5	39.5	23.12	35.46	57.0	302.0	7.2	23.4	7.6	Perrin and Saleh (2018)
105.5	39.5	22.78	31.48	64.0	252.0	2.5	6.8	3.4	Perrin and Saleh (2018)
105.5	39.5	22.43	31.21	62.0	258.0	7.0	6.9	9.6	Perrin and Saleh (2018)
105.5	39.5	26.57	32.97	87.0	323.0	7.2	28.1	6.9	Perrin and Saleh (2018)
105.5	39.5	26.57	32.97	48.0	295.0	4.9	16.6	5.9	Perrin and Saleh (2018)
132.5	67.5	26.3	33.2	44.9	273.0	30.4	1.9	42.9	Hussain et al., (1979)
140.0	15.0	22.7	34.5	68.0	268.0	5	14.1	6.3	Abd El-All (2004)
145.0	20.0	25.0	29.5	78.0	294.0	8	25.1	8.2	El-Shayeb et al., (2013)
295.0 ³	35.0	26.7	33.9	42.7	216.2	8.6	- 16.6	10.3	Nairn et al., (1987)
500.0 ³	50.0	26.0	33.0	- 53.5	147.0	18.0	- 40.3	13.8	Davies et al., (1980)
503.5 ³	23.5	26.5	33.0	- 87.3	124.2	4.8	- 30.7	4.4	Davies et al., (1980)
503.5 ³	23.5	25.0	34.5	85.1	165.7	5.2	26.8	5.1	Davies et al., (1980)
515.0 ³	27.0	27.7	33.3	87.3	25.9	11.8	33.1	10.3	Abdullah et al., (1984)
515.0 ³	27.0	27.7	33.3	81.6	120.8	4.1	29.8	3.8	Abdullah et al., (1984)
515.0 ³	27.0	27.7	33.3	82.7	273.5	7.4	27.1	7.3	Abdullah et al., (1984)
595.5 ³	15.5	26.0	33.0	36.1	197.1	11.9	- 22.4	12.8	Davies et al., (1980)

Table 2 Paleomagnetic mean data for Egypt. **Caption:** Age: median age bin for paleomagnetic mean data; Long/Lat: longitude and latitude of mean paleopole for respective age bin with according paleolatitude (λ) and α₉₅ based on a site within Egypt (Lat = 27°, Lat = 30°); mean paleopoles are based on paleomagnetic data from Egypt in the same Northeast African (NEA) reference frame and rotated into South African (SA using rotation parameter of Lat = 40.5°, Long = - 61.4°, angle = - 0.7°, Torsvik et al., 2012), West African (WA, rotation parameters of Lat = 19.2°, Long = 352.6°, angle = - 6.3°, Kidane et al., 2013), and into West and subsequent South African reference frame (WA-SA, rotation parameters of WA, see latter, and to SA of Lat = 33.6°, Long = 26.0°, angle = 2.3°, Torsvik et al., 2012)

Age	NEA					To SA ¹				To WA ²		To WA-SA ³			
	Long	Lat	A ₉₅	λ	α ₉₅	Long	Lat	λ	α ₉₅	Long	Lat	Long	Lat	λ	α ₉₅
25	139.9	77.0	6.4	22.0	7.0	139.9	77.0	22.0	7.0						
75	244.5	76.5	5.9	15.7	7.2	244.7	76.6	15.8	7.2						
125	260.0	73.3	6.6	15.7	8.0	261.0	73.6	16.1	8.0						
175	274.9	64.0	17.5	14.0	21.9	275.5	64.2	14.4	21.8						
225	273.0	44.9	-	1.9	-	273.0	45.1	2.1	-	272.1	51.0	274.3	49.2	5.2	
275	216.2	42.7	-	20.1	-	215.8	43.2	19.6	-	209.1	46.6	212.4	46.8	- 16.6	
325	216.2	42.7	-	- 20.1	-	215.8	43.2	- 19.6	-	209.1	47.0	212.4	46.8	- 16.6	
425	327.0	53.5	-	37.3	-	327.2	53.2	37.4	-	332.8	55.5	332.5	54.0	40.4	
475	322.3	84.8	11.3	28.9	10.8	327.0	84.6	29.3	10.6	27.6	84.0	11.0	83.8	32.8	9.9
525	322.3	84.8	11.3	28.9	10.8	327.0	84.6	29.3	10.6	27.6	84.0	11.0	83.8	32.8	9.9
575	244.0	65.9	68.1	6.5	93.7	244.2	66.3	6.9	93.3	236.2	71.8	242.2	70.8	10.4	-

6 Summary

In summary, due to the pervasive remagnetization suffered by several rock formations and the absence of primary paleomagnetic data from Paleozoic rocks, the autochthonous Egyptian dataset is not ideal to establish the paleogeographic evolution of Egypt throughout the whole Phanerozoic. However, for the last 150–200 Ma, the available data are in good agreement with each other and also with rotated data from other areas of Africa. Using most recent continental paleogeographic reconstructions, the evolution of Egypt went from a position close to the paleo-equator at the beginning of the Phanerozoic toward $\sim 60^\circ\text{S}$ at ~ 400 Ma and back toward $\sim 30^\circ\text{N}$ at present day. This evolution is related to rotational movements of Gondwana, the northward motion of Pangea, and the closure of the Neotethys.

Acknowledgements We thank the editors of this book Zakaria Hamimi, Hassan Khozyem, and Haytham El Atfy for giving us the possibility to provide this chapter. We furthermore thank two constructive reviews by Massimo Mattei and Tesfaye Kidane Birke, whose comments led to a significant improvement of the chapter.

References

- Abd El-All, E. (2004). Paleomagnetism and rock magnetism of El-Naga ring complex South Eastern Desert, Egypt: NRIAG. *Journal of Geophysics*, 3(1), 1–25.
- Abdeldayem, A. (1996). Palaeomagnetism of some Miocene rocks, Qattara depression, Western Desert, Egypt. *Journal of African Earth Sciences*, 22(4), 525–533.
- Abdeldayem. (1999). Palaeomagnetism of some Cenozoic sediments. *Cairo-Fayum Area, Egypt: Physics of the Earth and Planetary Interiors*, 110(1–2), 71–82.
- Abdullah, A., Nairn, A., Savino, D., & Sprague, K. (1984). Paleomagnetic study of some of the dikes from the Esh El Mellaha Range, Eastern Desert, Egypt. *Journal of African Earth Sciences* (1983), 2(3), 267–275.
- Amante, C., & Eakins, B. W. (2009). ETOPO1 Global Relief Model converted to PanMap layer format. *PANGAEA*.
- Benkhelil, J. (1989). The origin and evolution of the Cretaceous Benue Trough (Nigeria). *Journal of African Earth Sciences (and the Middle East)*, 8(2–4), 251–282.
- Davies, J., Nairn, A., & Resselar, R. (1980). The paleomagnetism of certain late Precambrian and early Paleozoic rocks from the Red Sea Hills. *Eastern Desert, Egypt: Journal of Geophysical Research: Solid Earth*, 85(B7), 3699–3710.
- El Shazly, E., & Krs, M. (1973). Paleogeography and paleomagnetism of the Nubian Sandstone eastern desert of Egypt. *Geologische Rundschau*, 62(1), 212–225.
- El-Shayeb, H., El-Hemaly, I., Aal, E. A., Saleh, A., Khashaba, A., Odah, H., & Mostafa, R. (2013). Magnetization of three nubia sandstone formations from central western desert of Egypt: NRIAG Journal of *Astronomy and Geophysics*, 2(1), 77–87.
- Evans, D. A. D. (2003). *True Polar Wander and Supercontinents: Tectonophysics*, 362(1–4), 303–320.
- Granot, R., & Dyment, J. (2015). The Cretaceous opening of the South Atlantic Ocean. *Earth and Planetary Science Letters*, 414, 156–163.
- Hussain, A. G., & Aziz, Y. (1983). Paleomagnetism of Mesozoic and Tertiary rocks from East El Owenat Area, southwest, Egypt. *Journal of Geophysical Research: Solid Earth*, 88(B4), 3523–3529.
- Hussain, A. G., Schult, A., & Soffel, H. (1979). Palaeomagnetism of the basalts of Wadi Abu Tereifiya, Mandisha and dioritic dykes of Wadi Abu Shihat, Egypt. *Geophysical Journal International*, 56(1), 55–61.
- Kent, D. V., & Dupuis, C. (2003). Paleomagnetic study of the Paleocene-Eocene Tarawan chalk and Esna Shale: dual polarity remagnetizations of Cenozoic sediments in the Nile Valley (Egypt). *Micropaleontology*, 49(Suppl_1), 139–146.
- Kidane, T., Bachtadse, V., Alene, M., & Kirscher, U. (2013). Palaeomagnetism of Palaeozoic glacial sediments of Northern Ethiopia: A contribution towards African Permian palaeogeography. *Geophysical Journal International*, 195(3), 1551–1565.
- Kirschvink, J. L. (1978). The Precambrian-Cambrian boundary problem: Paleomagnetic directions from the Amadeus Basin. *Central Australia: Earth and Planetary Science Letters*, 40, 91–100.
- Lofy, H., & Van der Voo, R. (2007). Tropical northeast Africa in the middle-late Eocene: Paleomagnetism of the marine-mammals sites and basalts in the Fayum province, Egypt. *Journal of African Earth Sciences*, 47(3), 135–152.
- Lofy, H. I. (2011). Active concomitant counterclockwise rotation and northwards translation of Africa during the Albian-Campanian time: A paleomagnetic study on the Wadi Natash alkaline volcanic province (104–78 Ma). *South Eastern Desert, Egypt: Palaeogeography, Palaeoclimatology, Palaeoecology*, 310(3–4), 176–190.
- Lofy, H., Van der Voo, R., Hall, C., Kamel, O., & Aal, A. A. (1995). Palaeomagnetism of Early Miocene basaltic eruptions in the areas east and west of Cairo. *Journal of African Earth Sciences*, 21(3), 407–419.
- Lofy, H. (2015). Early Cretaceous counterclockwise rotation of Northeast Africa within the equatorial zone: Paleomagnetic study on Mansouri ring complex. *Southeastern Desert, Egypt: NRIAG Journal of Astronomy and Geophysics*, 4(1), 1–15.
- Mostafa, R., Khashaba, A., El-Hemaly, I., Takla, E., Abdel Aal, E., & Odah, H. (2016). 1st paleomagnetic investigation of Nubia Sandstone at Kalabsha, south Western Desert of Egypt. *NRIAG Journal of Astronomy and Geophysics*, 5(1), 254–262.
- Müller, R. D., Cannon, J., Qin, X. D., Watson, R. J., Gurnis, M., Williams, S., Pfaffelmoser, T., Seton, M., Russell, S. H. J., & Zahirovic, S. (2018). GPlates: Building a virtual earth through deep time. *Geochemistry Geophysics Geosystems*, 19(7), 2243–2261.
- Naim, A., Perry, T., Resselar, R., & Rogers, S. (1987) A paleomagnetic study of the Dokhan Volcanic formation and younger granites, eastern desert of Egypt. *Journal of African Earth Sciences* (1983), 6(3), 353–365.
- Niazi, H., & Mostafa, M. (2002). A paleomagnetic study of the Tertiary basaltic lava flows around Wadi Hudayn Shalatayn area, south Eastern Desert, Egypt. *Annals Geological Survey, Egypt*, 429–442.
- Odah, H. (2004). Paleomagnetism of the Upper Cretaceous Bahariya Formation, Bahariya Oasis, Western Desert, Egypt. *Journal of Applied Geophysics*, 3(2), 177–187.
- Perrin, M., Saleh, A., & Alva-Valdivia, L. (2009). Cenozoic and Mesozoic basalts from Egypt: A preliminary survey with a view to paleointensity. *Earth, planets and space*, 61(1), 51–60.
- Perrin, M., & Saleh, A. (2018). Cenozoic to Cretaceous paleomagnetic dataset from Egypt: New data, review and global analysis. *Earth and Planetary Science Letters*, 488, 92–101.
- Le Pichon, X., Jellinek, M., Lenardic, A., Şengör, A. C., & İmren, C. (2021). Pangea Migration. *Tectonics*, 40(6), e2020TC006585.
- Resselar, R., Nairn, A., & Monrad, J. (1981). Two phases of cretaceous—tertiary magmatism in the eastern desert of Egypt: Paleomagnetic, chemical and K-Ar evidence. *Developments in geotectonics* (Vol. 17, pp. 169–193). Elsevier.
- Saleh, A. (2020). Paleomagnetism of Late Neoproterozoic African Dike Swarms from the South Eastern Desert and the Paleoneoproterozoic dataset from Egypt. *Pure and Applied Geophysics*, 177(11), 5251–5262.
- Saradeth, S., Soffel, H., & Schult, A. (1987) Paleomagnetic and rockmagnetic studies in SW-Egypt and N-Sudan: contributions to the African polar wander path.
- Schult, A., Soffel, H., & Hussain, A. (1978). Palaeomagnetism of Cretaceous Nubian sandstone, Egypt. *Journal of Geophysics*, 44(4), 333–340

- Schult, A., Hussain, A., & Soffel, H. (1982). Palaeomagnetism of Upper Cretaceous volcanics and Nubian sandstones of Wadi Natash. *SE Egypt and Implications for the Polar Wander Path for Africa in the Mesozoic: Journal of Geophysics*, 50(1), 16–22.
- El Shazly, E. M., & Krs, M. (1971) Magnetism and palaeomagnetism of Oligocene basalts from Abu Zaabal and Qatrani, northern Egypt. *Geolysi Kalai Sbornik*, 19(356), 261–270
- Stampfli, G. M., & Borel, G. (2002). A plate tectonic model for the Paleozoic and Mesozoic constrained by dynamic plate boundaries and restored synthetic oceanic isochrons. *Earth and Planetary Science Letters*, 196(1–2), 17–33.
- Torsvik, T. H., Muller, R. D., Van der Voo, R., Steinberger, B., & Gaina, C. (2008). Global plate motion frames: Toward a unified model. *Reviews of Geophysics*, 46(3).
- Torsvik, T. H., van der Voo, R., Preeden, U., Mac Niocaill, C., Steinberger, B., Doubrovine, P. V., van Hinsbergen, D. J. J., Domeier, M., Gaina, C., Tohver, E., Meert, J. G., McCausland, P. J. A., & Cocks, L. R. M. (2012). Phanerozoic polar wander, palaeogeography and dynamics. *Earth-Science Reviews*, 114, 325–368.
- Torsvik, T. H., & Cocks, L. R. M. (2016). *Earth history and palaeogeography*. Cambridge University Press.
- Torsvik, T. H., van der Voo, R., Doubrovine, P. V., Burke, K., Steinberger, B., Ashwal, L. D., Trønnes, R. G., Webb, S. J., & Bull, A. L. (2014). Deep mantle structure as a reference frame for movements in and on the Earth. *Proceedings of the National Academy of Sciences*, 111(24), 8735–8740.
- Van der Voo, R. (1990). *The Reliability of Paleomagnetic Data: Tectonophysics*, 184(1), 1–9.
- Wassif, N. A. (1991). Palaeomagnetism and opaque mineral oxides of some basalt from west central Sinai, Egypt. *Geophysical Journal International*, 104(2), 319–330.
- Wessel, P., & Luis, J. F. (2017). *The GMT/MATLAB Toolbox: Geochemistry Geophysics Geosystems*, 18(2), 811–823.
- Wu, L., Huang, W., Liang, H., Brendan Murphy, J., Kirscher, U., Mitchell, R. N., Hawkins, L. M. A., Halverson, G. P., Gu, Y. J., Zhang, J., & Liu, X. (2021a). Paleomagnetism of the Guanyang Devonian sedimentary successions in Guangxi province, South China. *Gondwana Research*.
- Wu, L., Murphy, J. B., Quesada, C., Li, Z.-X., Waldron, J. W., Williams, S., Pisarevsky, S., & Collins, W. J. (2021b). The amalgamation of Pangea: Paleomagnetic and geological observations revisited. *Bulletin*, 133(3–4), 625–646.



Edoardo Dallanave is a paleomagnetist with a background in stratigraphic geology. He obtained an M. Sc degree from the University of Milan (Italy) in 2004, and a Ph.D. from the University of Padova (Italy) in 2010. From 2012 to 2018, he worked as a research associate at the Ludwig-Maximilians University in Munich (Germany), before moving to the University of Bremen (Germany) where he now works. His research interest is in paleomagnetism and rock-magnetism applied to different chronologic and paleogeographic problems, particularly during the Cenozoic.



Valerian Bachtadse is a geologist/geophysicist who spent the majority of his scientific career applying paleomagnetism to reconstruct the distribution of the continents before, during and after the Hercynian orogeny. After receiving a doctorate degree in 1984 from Johannes-Gutenberg-University, Mainz, Germany, supervised by Alfred Kröner, he moved on to a research professor position at the University of Michigan (USA) where he started working with Rob van der Voo on Paleozoic sediments in South Africa. In 1986, he received a research fellow position at Oxford University where he and

Jim Briden were part of a major BP-funded research project studying the paleomagnetism of Paleozoic rocks from eastern and northern Africa. In 1990, he moved on to Ludwig-Maximilians-University in Munich (Germany) where he worked on the Paleozoic of Europe and Central Asia. In addition, he studied the Proterozoic of the Baltic shield, the Permian of southern Europe and northern Africa as well as the Cretaceous/Paleogene boundary and the Quaternary of Armenia and Georgia. In 2020, he retired from his position as a senior research professor.



Uwe Kirscher is a paleomagnetist with a background in geophysics, who received his Ph.D. degree in 2015 from the Ludwig-Maximilians University in Munich (Germany). Thereafter, he spent three years at Curtin University in Australia, after which he worked at Tuebingen University (Germany) between 2019 and 2022. Since early 2023 he is works again at Curtin University in Perth, Australia. His research interests focus on the usage of paleo- and rock magnetic techniques in paleogeography, chronology and Earth's evolution studies. Some of his main fields of interest include human evolution, supercontinent cycles, and paleoclimate studies.



Precambrian Life and Cambrian Revolution

Abdel Galil Hewaidy

Abstract

The Precambrian or Cryptozoic Eon represents about 88% of the Earth's geologic time. It is subdivided into Hadean (4543–4000 mya), Archean (4000–2500 mya), and Proterozoic (2500–541 mya) eons. Life originated on Earth according to the theory of organic evolution in the mid-oceanic ridges through a sequence of chemical reactions between carbon, hydrogen, oxygen, and nitrogen under electrical charge to produce amino acids that joined together to form proteins and nucleic acids, and these must be transformed into living, self-replicating structures, in oxygen-free environment at the Late Hadean to Early Archean time. The Precambrian in general is distinguished by the poverty of its life compared to the succeeding Phanerozoic. Furthermore, the Archean is greatly poorer than the Proterozoic. Archean life witnessed the change from the abiologic evolution to biologic evolution. All Archean life was pelagic prokaryotes including methanogens, bacteria, and cyanobacteria (blue-green algae). The oldest known fossils on Earth were recorded in the chert of the banded iron formations in the greenstone belt terranes in Canada, Greenland, Australia, and South Africa. The oldest Archean life records are organic carbon and graphite preserved as microbial mats in stromatolites included in the greenstone belt of Nuvvuagittuq in Quebec, Canada, and Isua in southwest Greenland dated at about 3700–3800 mya. The Archean oldest cellular life is recorded in Fig Tree Formation or Group in South Africa and the North Pole area in Western Australia at about 3500 mya. Methanogens are suggested to maybe as a link to the earliest forms of life. The prokaryote's fossil records of Proterozoic are comparatively abundant, relative to that of the Archean.

The Gunflint Chert algae from the Gunflint Iron Formation of Ontario, Canada, is the first Precambrian microflora to be described. It is dated to about 2 billion years and represents the evidence for diversity of prokaryotic life at that time. It is diverse and includes thread-like, rod-like, and spheroidal, star-shaped, and umbrella-shaped species identical in form to present-day bacteria and blue-green algae. Pelagic single-celled eukaryotic acritarchs appeared in about 1500 mya. Bitter Springs fauna in Australia gives evidence for diversification of eukaryotes and evolution of sexual reproduction. The Ediacaran fauna is soft-bodied with calcareophosphatic shells appeared in the Late Proterozoic Ediacaran Period between 635 and 541 Mya after the Cryogenian glaciation. In Egypt, an Ediacaran algal microfloral assemblage was described from the Iгла Formation, Hammamat Group, cropping out in Wadi Iгла, west Marsa Alam, Eastern Desert. This assemblage includes seven species related to phylum Cyanophyta and one species phylum Pyrrophyta. These in addition to microfossils (oncolites) of cyanobacterial growth and other unnamed forms of probable algal affinities have also been reported. The transition from Precambrian at the end of the Ediacaran Period with soft-bodied fossils to Cambrian with appearance of the first assemblages of shelly faunas is known as the Cambrian Explosion. This major event in Earth's history spans about 13–25 million years after 541 mya and led to the emergence of most modern metazoan phyla. This event is passed in three stages: low diversity, moderate diversity (Tommotian Stage), and high diversity (Atdabanian Stage). The last stage witnessed the first appearance of *Trilobites*. In Egypt, a rare microfossil assemblage including some archaeocyathids, sponge spicules, and the algal *Bactrophyucus oblongum* Zhang was recorded in the Iгла Formation, Hammamat Group, cropping out in Wadi Semna, near Safaga, Eastern Desert. These in addition to seven agglutinated foraminiferal species following four genera recorded from the

A. G. Hewaidy (✉)
Geology Department, Faculty of Sciences, Al-Azhar University,
Cairo, Egypt
e-mail: ahewaidy@azhar.edu.eg

same Igla Formation in Wadi Semna may indicate a Lower Cambrian age for that formation in Wadi Semna. The Araba Formation is the oldest Paleozoic sedimentary unit exposed in southwest Sinai and northern part of the Eastern Desert. The lower part of the Araba Formation includes a limestone bed with body fossils of stromatolites and archaeocyathid elements of probable Early Cambrian age. The Araba Formation is found ichnofossil bearing, and about 20 species of these trace fossil species were recorded from the middle unit of the Araba Formation and ensured its Lower Cambrian age. The Burgess Shale fauna is a middle Cambrian exceptional assemblage of more than 170 species representing at least eight known phyla of animals of soft-bodied and biomineralized organisms. It affords a profoundly informative picture for the Cambrian post-explosion world. All oxygen in the Earth's atmosphere was produced in Early Proterozoic time by photosynthesis of the cyanobacteria. This released oxygen in the atmosphere and the shallow oceans experienced an oxygen rise leading to the oxygen revolution at approximately 2400–2000 Mya which killed major part of the living prokaryotes.

Keywords

Prokaryotes • Oxygen revolution • Ediacaran fauna • Cambrian revolution • Burgess Shale fauna

1 Introduction

The Precambrian or the Cryptozoic Eon—that immensely long interval of geologic time preceding the appearance of abundant megafossils in the Cambrian—covers approximately seven-eighths {4541–541 mya} of the Earth's entire time of existence. The Hadean, Archean, and Proterozoic eons are subdivisions of the main informal Precambrian unit of the geologic time scale. The Precambrian straddles from the establishment of Earth about 4.6 billion years ago (Ga) to the start of the Cambrian Period, about 541 million years ago (Ma), when creatures with hard skeleton first appeared in high abundance. Hadean Eon spans from 4.6 to 4.0 Ga, Archean Eon spans from 4.0 to 2.5 Ga, and Proterozoic spans from 2.5 Ga to 541 million years ago.

Until 1950s, this major part of the Earth's history was believed to be barren of any fauna, and the oldest known fossil was the *Trilobites*. No logic interpretation for this absence of life during this very long time interval. During the last seven decades, a lot of discoveries, experiments, radiometric dating, and scientific hypotheses tried to throw lights on this Precambrian life history and their evolutionary steps.

During this very long time interval, life developed very slowly from its first appearance at about 4000 mya as pelagic non-skeletal single-celled bacteria and cyanobacteria to pelagic skeletal metazoan life at the start of the Cambrian time.

At the beginning of the Hadean at about 4543 Ma, the Earth accumulated from material scattered in orbit around the Sun and may have been impacted by a very huge (Mars-sized) planetesimal shortly after it formed. Moon was formed from the scattered material of this impact. The oldest Earth's crust was apparently in place by 4433 Ma, since zircon crystals from Western Australia have been dated at 4404 ± 8 Ma. Hydrosphere and atmosphere are formed during this Hadean time and soon after the formation of the Earth at 4543 mya. Life originated nearly at the Late Hadean to Early Archean and takes the time interval of the Archean (4000–2500 mya) and Proterozoic (2500–541 mya) to diverse and widespread.

The Phanerozoic fossil record is richer than that of the preceding Precambrian, where the Precambrian fossils (e.g., stromatolites) are of restricted biostratigraphic usage. This can be explained by one of the following three reasons: (1) Many Precambrian rocks are heavily metamorphosed, which obscures their origins, (2) many Precambrian rocks have been destroyed by erosion, and (3) vast areas of Precambrian rocks have been deeply buried beneath Phanerozoic strata.

The main feature of the Earth is the distribution of life on its surface and preservation of its remains in its layers. This life may be biochemically originated before 3800 mya in the mid-oceanic ridges which have the favorable conditions for formation of the first cells. The evolution and extinction are the main features of that life. Evolution is the process by which life has developed from single-celled prokaryotic organisms to the present complex animals and plants during the Earth's history. That life was affected during its long history on Earth by many catastrophic events including the oxygen revolution event at 2400 million years ago, snowball Earth at the late Proterozoic glaciation events, and the five great extinction events in the Phanerozoic Eon. These catastrophic events lead to major extinctions in the life content on the Earth.

2 Origin of Life

2.1 Definition and Characteristics of Life

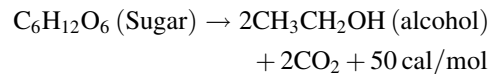
Earth is the only astronomical entity known to harbor life. This is for its suitable size and temperature. The suitable size should be large enough to have sufficient gravity, to retain an oxygen atmosphere and small enough to allow hydrogen to escape. The suitable temperature is in the range of 0–100 °C.

Based on geological and geochemical evidence, Earth is believed to be formed over 4.54 billion years, and life may have appeared as early as 4.1 billion years ago. Life appeared in the oceans and began to play main role in changing Earth's atmosphere and surface, resulting in propagation of anaerobic and, later, aerobic organisms. Since then, the combination of Earth's distance from the Sun, physical criteria, and geological context have permitted life to advance and thrive. During the last 200 years, the fossil record provides a tremendous increase in our knowledge about history of life and amazing changes in types of organisms that have populated the Earth. Various scientific hypotheses are used to explain the observed changes in life with time and account for the life origin. The meaning of life and how it may have originated are two critical and debatable questions about the life which is the fascinating and important phenomenon of our Earth.

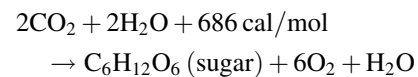
Life is defined as the circumstance that discriminates animals and plants from inorganic materials, including the ability for growth, reproduction, functional activity, and continual change preceding death. Life is marked by the following characteristics:

- Organisms are distributed on Earth in areas where water occurred in a liquid state, as water is vital for support of living organisms.
- Solar radiation into the Earth surface, temperature of the land surface, and chemical composition of the atmosphere and hydrosphere are other important environmental conditions influencing the ability of organisms to exist in the biosphere.
- Living systems are recognized by particular diagnostic characteristics and essentially represent chemical factories that consist primarily of four elements—carbon, hydrogen, nitrogen, and oxygen—that combine to form organic molecules. These elements also combine with lesser amounts of about 20 other elements to provide a large number of complex molecules.
- Organisms consist of one or more cells that are capable of reproducing themselves by chemical replication of a wide variety of complex organic molecules.
- Individual organisms undergo many other chemically related activities such as metabolism, excretion, and growth.
- Important metabolic reactions in cells are:
 - Fermentation is the process of splitting organic compounds such as sugar to release energy, carbon dioxide, and alcohol. Organism using this process depends on an external supply of organic molecules and is heterotrophic as yeast. It is an anaerobic process that produces alcohol and releases about 50 cal of heat

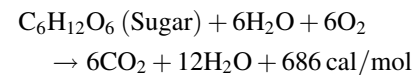
energy. This reaction goes according to the following equation.



- Photosynthesis is a process that green plants and certain other organisms employ to convert light energy into chemical energy. During photosynthesis in green plants, light energy is utilized to convert water, carbon dioxide, and minerals into energy-rich organic compounds (e.g., sugar), and oxygen is liberated as a by-product. This free-produced oxygen is a poison to life. Organism using this process manufactures their own food and is autotrophic as plants, algae, and cyanobacteria. Photosynthesis is an aerobic process and provides a much larger amount of heat energy. This reaction goes according to the following equation.



- Respiration is the process by which cells combine sugars and oxygen to produce energy, water, and carbon dioxide. Organism using this process depends on an external supply of organic molecules and is heterotrophic as animal-like organisms. It is an aerobic process and provides a much larger amount of heat energy. This reaction goes according to the following equation.



- Organisms are able to move or cause motion in water or air.
- Individuals, whether unicellular or multicellular, have a boundary layer such as a cell membrane, cell wall, or skin that permits selective exchange of gases and liquids with the environment.
- All life as we know it has the characteristic ability to adapt to environmental changes, whether by physiological response to small-scale seasonal changes or by genetic change of successive generations through a longer interval of time.

Living organisms should possess all of these characteristics. Paleontologists recognize that fossils are the remains or traces of once-living organisms, so we may assume that such fossilized organisms also possessed these characteristics when they were living.

2.2 The Origin of Life

In summary, the formation of life probably began with formation of amino acids. Amino acids can be produced by electrical discharge in a mixture of water, methane, ammonia, and hydrogen, or of carbon monoxide, carbon dioxide, and nitrogen. To form life, amino acids must join to form proteins and nucleic acids, and these must be transformed into living, self-replicating structures. This could form only in oxygen-free environment and in oceans. Fossil bacteria and cyanobacteria (blue-green algae) are found in rocks as old as 3500 million years ago. The first organisms with sexual reproduction are green algae 1000 Ma in Australia. The evolution began about 1400 Ma.

Life on Earth originated by a sequence of chemical reactions that produced aggregates of organic molecules under environmental conditions significantly different from those existing on the planet today within the early hydrosphere during pre-Archean to Early Archean time. This model provides a logical complement to the theory of organic evolution, in that they suggest that many of the same mechanisms that control populations today—competition, replication of molecules, and natural selection—influenced the development of non-living, or abiologic organic molecules that preceded the first living cells.

In 1870, Huxley discussed the idea that biological systems evolved from abiologic molecules in primitive oceans resembling dilute organic soup, but he was at a loss to explain the method by which this may happen. Oparin and Haldane in the 1930s supported hypotheses that life began on Earth as a result of chemical reactions in oxygen-deficient environments. These ideas stimulated a number of laboratory experiments in which attempts were made to duplicate conditions thought to exist on primitive Earth.

The key experiment of Urey in the 1950s had suggested that in the early stages of Earth's history, its atmosphere consisted of ammonia and methane and thus was a reducing atmosphere. The graduate student of Miller constructed an apparatus containing these gases and water and energized the mixture with electrical discharge, Fig. 1. Within a short time, a variety of organic molecules had formed, including many types that occur in living organisms. This experiment provided strong evidence for a method by which complex organic molecules and possibly living cells could develop from simple chemicals in appropriate environments.

- Life on Earth may originate in mid-oceanic ridges for the following causes:
 - The great volume of these ridges gives a wide range of temperatures needed for organic evolution.
 - Chemical compounds needed to originate life are dissolved in the hot water around these ridges.

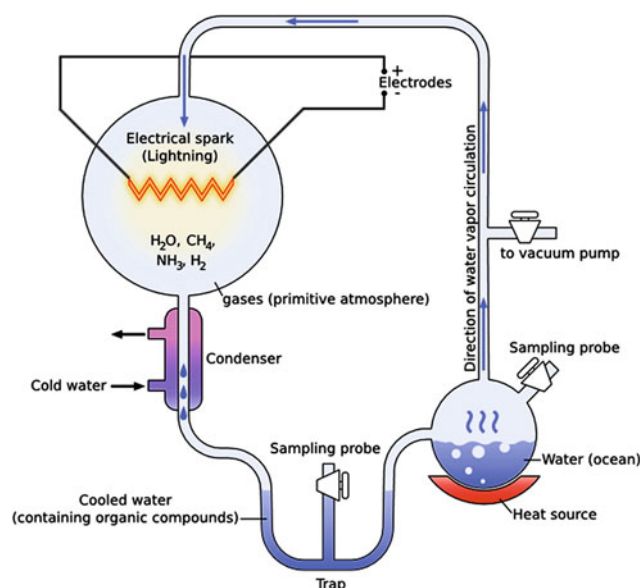


Fig. 1 Miller apparatus. Methane, ammonia water vapor, and hydrogen gas were circulated in a system sealed off from the atmosphere and subjected to electric charge. Amino acids formed in a relatively short time and collected in the trap (Miller experiment in Wikipedia)

- The common occurrence of phosphorus is a basic request for building living cells.
- Zinc and nickel which are needed by small amounts are existing with minor amounts and needed for all organisms.
- Early composed molecules and reactions may have been bound up within clay minerals, either in the oceans or in hot springs. In this situation, the atomic structure of the clay may have acted as template for the development and restructuring or replication of developing organic molecules.
- The absence of oxygen helped simple organisms to start chemical reactions and give organisms their energy requirements.
- From a series of abiologic evolutionary processes during pre-Archean or Early Archean time. In this time, Earth was probably with an atmosphere of CO_2 , CO , H_2O , N_2 , H_2 , oceans of water, and sedimentation processes occurring. This evolutionary process consisted of a number of progressively more complex chemical reactions which involved pre-biologic molecules within the early hydrosphere.
- The reactions involved the four main chemical building blocks of carbon, hydrogen, nitrogen, and oxygen and led to the formation of organic compounds into more complex **organic macromolecules**.
- These macromolecules responded to environmental changes by undergoing various reactions, Fig. 2.

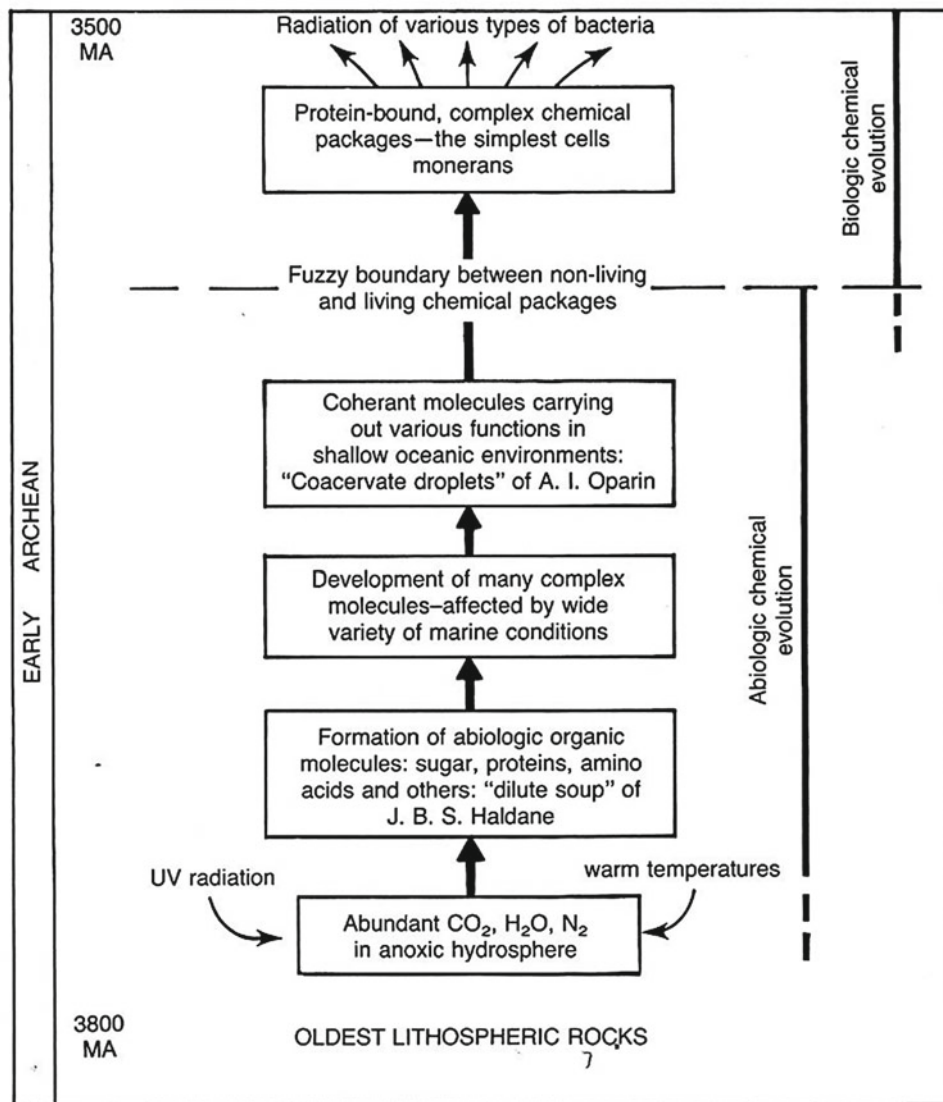


Fig. 2 Synthesis of hypotheses for the origin of life. Most significantly, these ideas support an origin through gradual chemical evolutionary steps occurring within some part of Earth's hydrosphere over a significant length of Early Archean time. Living systems (cells) represented a change from inorganic chemical evolution to organic chemical evolution (Cooper et al., 1990)

- A combination of macromolecules formed that possessed a combination of characteristics which fit our definition of life, and so the simplest living system, **the cell**, appeared on Earth.
- Laboratory experiments and studies of remaining Early Archean rocks give a wide range of information about the origin of life. This information suggests that living organisms developed (a) by a sequence of successively more complex chemical reactions, (b) during an unknown length of geologic time after formation of the lithosphere, atmosphere, and hydrosphere, and (c) within an anaerobic hydrosphere and atmosphere, lacking an ozone layer, that allowed high levels of ultraviolet radiation to reach the surface.
- Life originally formed from chemicals that underwent a succession of many different reactions. These chemical combinations and recombinations may have taken place over a reasonably short time interval. The reactions may have occurred in the primitive hydrosphere, because the various properties of water would have provided appropriate environments for necessary chemical reactions and would have provided some protection from ultraviolet radiation.
- As the organic molecules became more complex, the clay mineral templates were eliminated and the newly formed molecules could have gradually migrated to the oceans.
- This model for the origin of life is maintained by several evidences in the Early Archean rock record:

- These rocks indicate a lack of free oxygen in the Earth's early atmosphere as no oxidized iron minerals are preserved in the sedimentary and metasedimentary rocks of this time.
- These rocks composed predominantly of detrital particles, and nonterrestrial rocks such as limestone and dolostone are very rare. This scarcity of nonterrestrial (chemical) rocks is explained by the existence of low pH values in the primitive oceans.
- Many of these old rocks contain unstable minerals, such as uraninite and pyrite that could not have survived in the presence of oxygen.
- These rocks contain carbon that in some instances appears to have been derived from an organic source. At few localities, micro-sized structures have been found which are interpreted to represent carbonized organic remains of simple cells. These structures have been recognized only since the 1950s and considered to represent bacteria and cyanobacteria (blue-green algae).
- This organically derived carbon and microfossils indicate that life had originated in the Early Archean or Late Hadean time.

3 Precambrian Life

The Precambrian interval is paleontologically characterized, then, by pelagic microfossils of monerans first and by monerans and one-celled protistans later. Benthic stromatolites produced by blue-green algae occur throughout, but are far more common during its latter half. Megafossils of the larger multicellular animals or metazoans are not recorded throughout almost the entire Precambrian.

The Precambrian well-preserved remains of microfossils have been found in sedimentary rocks billions of years old. Such preservation is possible mainly because of the physical properties of the mineral chert, which in pure form is silicon dioxide (SiO₂). This material precipitates rapidly as nodules or thin beds in seawater, hardens quickly, and becomes a very durable, noncompressible rock; therefore, this mineral is ideal for the preservation of simple, semirigid organisms such as bacteria and fungi. Microfossils in these cherts are examined in thin sections under high magnification microscopes. Evidences of this Precambrian life were recorded in different continents.

In the early 1950s, Tayler made a startling discovery that started a new dimension in our understanding of early life on the Earth. This was the first definitive evidence of life in the Precambrian. This is the Gunflint microbiota of 2000 million years old. This includes prokaryotic fossils including bacteria and cyanobacteria. Prior to Tyler's discovery, the only

described Precambrian fossils were the megascopic pillar-like and mound-shaped laminated structures called stromatolites. In 1965, Barghoorn and Schopf collected rod-shaped, thread-like filaments and spherical microorganisms of bacteria and cyanobacteria of Fig Tree Formation in South Africa, which dated to about 3400 million years ago. Schopf and Barghoorn also identified unicellular eukaryotes (microorganisms with a cell nucleus) from the chert of the Bitter Springs Formation in Northern Australia of about 900 million years ago.

Thus, during the 1950s and 1960s, major discoveries not only provided evidence in Precambrian, but also shed light on the crossing of three major evolutionary thresholds.

- The Fig Tree Formation microfossils were evidence that the transition from chemical evolution to organic evolution had been crossed prior to 3400 million years ago;
- The Gunflint Formation microbiota was evidence of the crossing of the threshold of diversity at least 2000 million years ago; and
- The Bitter Springs Formation eukaryotes were evidence that the greatest of all thresholds had been crossed—the evolution of nucleated cell. Once the nucleated cell evolved, the chromosomes and the DNA and RNA molecules could be confined and organized, paving the way to sexual reproduction and emergence of the multicellular life.

3.1 The Archean Life

Archean life preserved in rocks of that time can be difficult to distinguish as they have been altered totally over its very long time period of about 3.5-billion-year history. The cell wall structure may be preserved, but the original composition alters over time due to mineralization. Six criteria must be approved in a certain microstructure to be considered a microfossil:

- Acquiring an abundant occurrence.
- True microfossils should be of carbonaceous composition, if mineralic, or be biologically precipitated (for example, some bacteria form pyrite due to metabolic processes).
- Exhibiting a distinguishable biological morphology.
- Occurrence in a geologically reasonable context (for instance, microfossils cannot be present in igneous rock, as living organisms cannot dwell in molten lava).
- Fitting within a logic evolution system (for instance, complex microfossils are implausible to found at 3.5 Ga, where they have not emerged from their more simple cellular ancestors yet).

- Clear distinction from carbonaceous matter of the non-biogenic origin.

43 groups of assumed Archean fossils had been documented from 30 sedimentary units. Almost, all of these Archean fossil records have been questioned as true fossils at one time or another. The Archean terranes of southern Africa and Western Australia represent the most promising targets for Archean fossils. Older microorganisms were recorded in Nuvvuagittuq Greenstone Belt (NGB), Northern Quebec, and Isua Greenstone Belt, southwest Greenland, but these two records are controversially interpreted as putative organic remains.

These records are described in some detail in the following lines arranged in chronological order as follows:

3.1.1 Abiologic Chemical Evolution

• Nuvvuagittuq Greenstone Belt (NGB) life

The earliest life on Earth is represented by microstructures that occur in the form of hematite tubes and filaments, comparable in shape and size to structures formed at present by the action of bacteria inhabiting subsea hydrothermal vents. These microstructures are thought to have been produced by “biological activity” and afford clues for the hypothesis that abiogenesis began near hydrothermal vents. This earliest microfossil life on Earth existed during the Hadean-Eoarchean Era when the Earth’s crust had become cool and hardened after the molten Hadean Eon. This earliest physical record so far found comprises microfossils in the Nuvvuagittuq Greenstone Belt (NGB). This belt is a succession of metamorphosed mafic to ultramafic volcanic and sedimentary rocks, which is called a greenstone belt, situated on the eastern shore of Hudson Bay, 40 km southeast of Inukjuak, Northern Quebec, Canada, Fig. 3. These rocks have experienced impressive metamorphism and signify some of the oldest rocks on Earth. This finding is found in banded iron formation rocks of at least 3.77 Ga (possibly 4.28 Ga), which suggest that life had initiated immediately after oceans formed.

• Isua Greenstone Belt life

The Isua Greenstone Belt includes another evidence on the earliest life on our Earth. This record is represented by remains of complex stromatolite microbial colonies that display wavy and dome-shaped forms of a typically 1–4 cm high. It is preserved in iron and magnesium-rich dolomites that had recently been recovered by snow melting. In other portions of the Isua supracrustal belt, graphite inclusions enclosed within garnet crystals refer to the other elements of

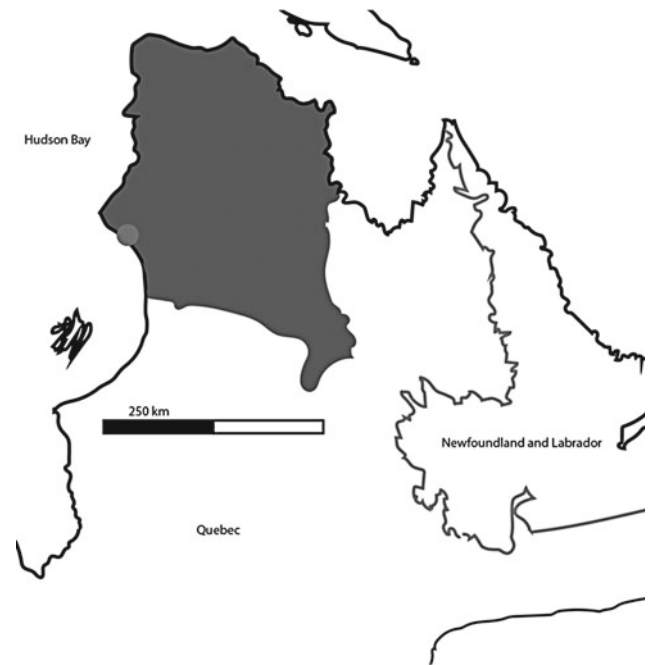


Fig. 3 Location of the Nuvvuagittuq Greenstone Belt (NGB) shown in light gray

life: oxygen, nitrogen, and possibly phosphorus, indicating additional signal for life at 3.7 Gya. The complex structure of the Isua stromatolites proposes a somewhat sophisticated life, and the earliest life on Earth probably emerged over 4 Ga. Isua Greenstone Belt is distributed in Akilia Island, near the Isua supracrustal belt in southwestern Greenland. It is an Archean greenstone belt with metamorphosed mafic and sedimentary rocks. It has shown biogenic carbon isotopes, dated to 3.7–3.8 Gya. Therefore, it has long been the target of studies dedicated to explore the signatures of early terrestrial life (Fig. 4).

3.1.2 Biologic Chemical Evolution

The second main phase in the evolution of life on Earth following the abiologic evolution is the cellular evolution. The fossil evidences of that stage are recorded in Fig Tree Formation in the Barberton Greenstone Belt exposed in eastern South Africa and in Pilbara Craton of Western Australia. The existence of these records denotes that cellular life evolved prior to that time, and a window of about one billion years for cellular life to evolve on a lifeless Earth.

The abovementioned cratons have remarkably similar early Precambrian lithostratigraphic and chronostratigraphic structural sequences between 3.5 and 2.7 Ga. Paleomagnetic records from two ultramafic complexes in the cratons revealed that at 3.87 Ga the two cratons might have been part of the Vaalbara supercontinent (Fig. 5). In the following, some notes on these two localities.

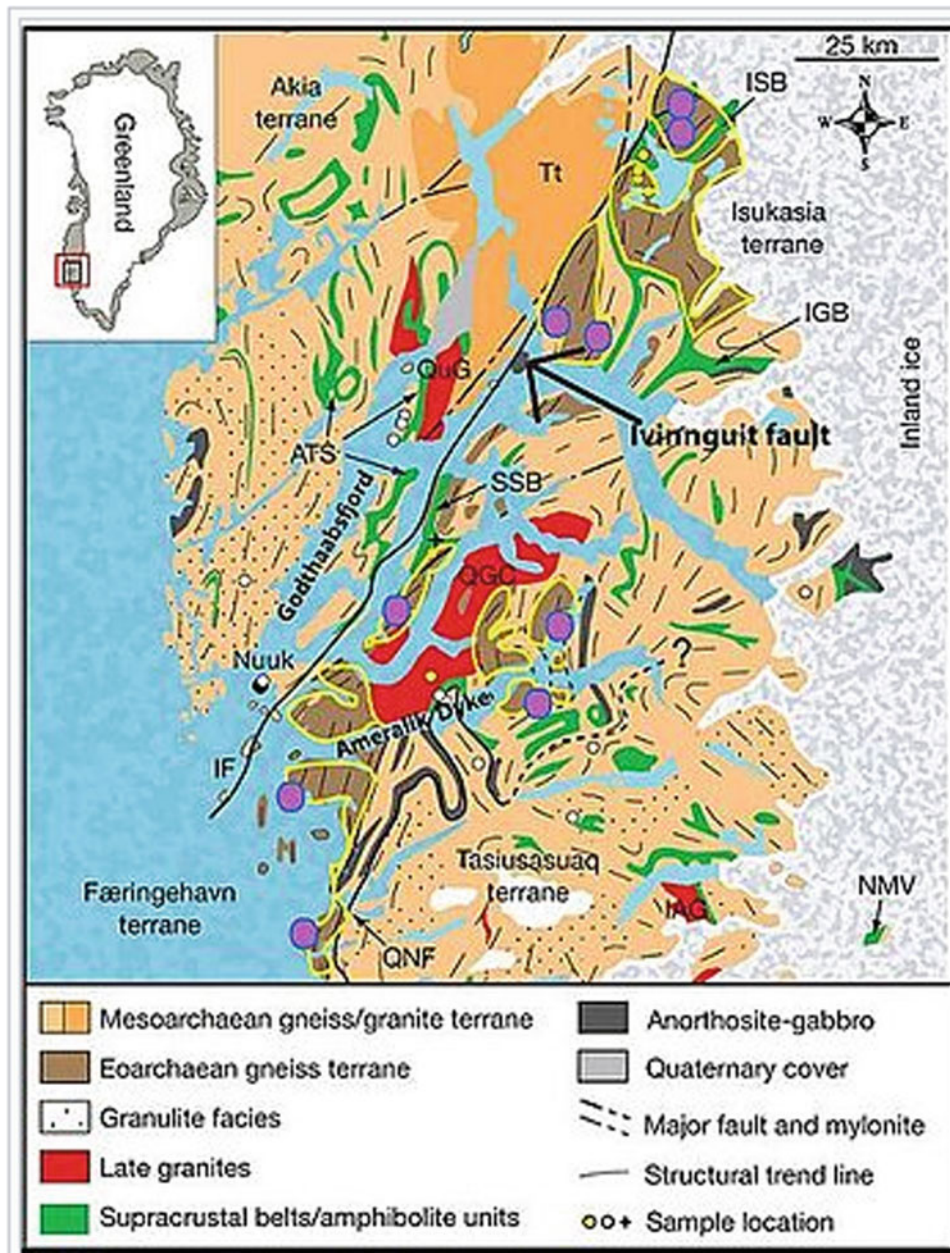


Fig. 4 Isua Greenstone Belt (in Wikipedia)

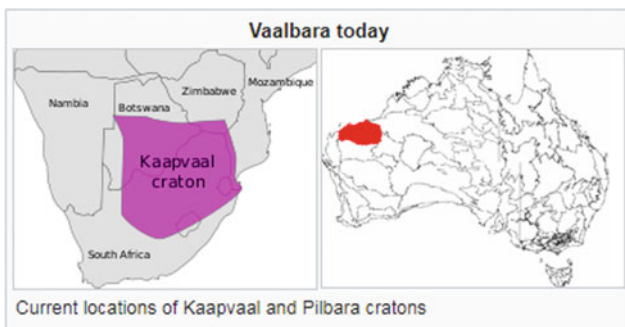


Fig. 5 Vaalbara today (in Wikipedia)

• Fig Tree and Onverwacht Groups in South Africa

The Kromberg and Hooggenoeg formations, which belong to the Onverwacht Group, include the oldest microfossils in the South African Barberton Greenstone belt. These formations are mostly composed of igneous rock and partly metamorphosed sedimentary rocks that still promising to locate some microfossils in chert. The microfossil content of these cherts is represented by microbial mats and stromatolites. Evidence for this hypothesis is preserved in both chert and lithified stromatolites.

Stromatolites are large colonies of microorganisms, produced by cyanobacteria, consisting of sediment layers alternated with microbes. Stromatolites denote shallow-water settings in the fossil record, as inferred from the necessity of microbes to exist in the photic zone of water. Stromatolites are usually composed of filamentous microfossils, Fig. 6. The oldest stromatolites have been formed at approximately 3.5 Ga in the Archean. They are the most striking and characteristic group in the Proterozoic, while their abundance started to decrease around 1000 Ma, slowly at first and then devastatingly around the culmination of the Proterozoic. The most accepted explanation for the stromatolites deterioration is the appearance of organisms that either competed with stromatolites for space on the shallow sea floor (seaweeds developed around the same time) or fed on the microbial mats.

Microfossils recovered from the Barberton chert extend recordist age back to 3.5 Ga. Chert can have different colors,

but microfossils commonly associate black cherts, where the dark color specify organic material. The recorded fossils include a *Huronia* an algal-like form and *Eubacterium*, a bacterium, Fig. 7.

These microstructures are considered organic upon the following five principal arguments:

- Are within the size range of modern prokaryotes.
- Form a bell-shaped or polymodal size distribution with a limited range of 1–4 μm and have a diagnostic size like that of modern prokaryotes.
- Exhibit a variety of shapes: flattened, wrinkled, and folded as well as spherical.
- Preserved in approximately various phases of cell division.
- The C_{12} : C_{13} ratios are too high for inorganic origin and even suggest carbon fixed by the process of photosynthesis.

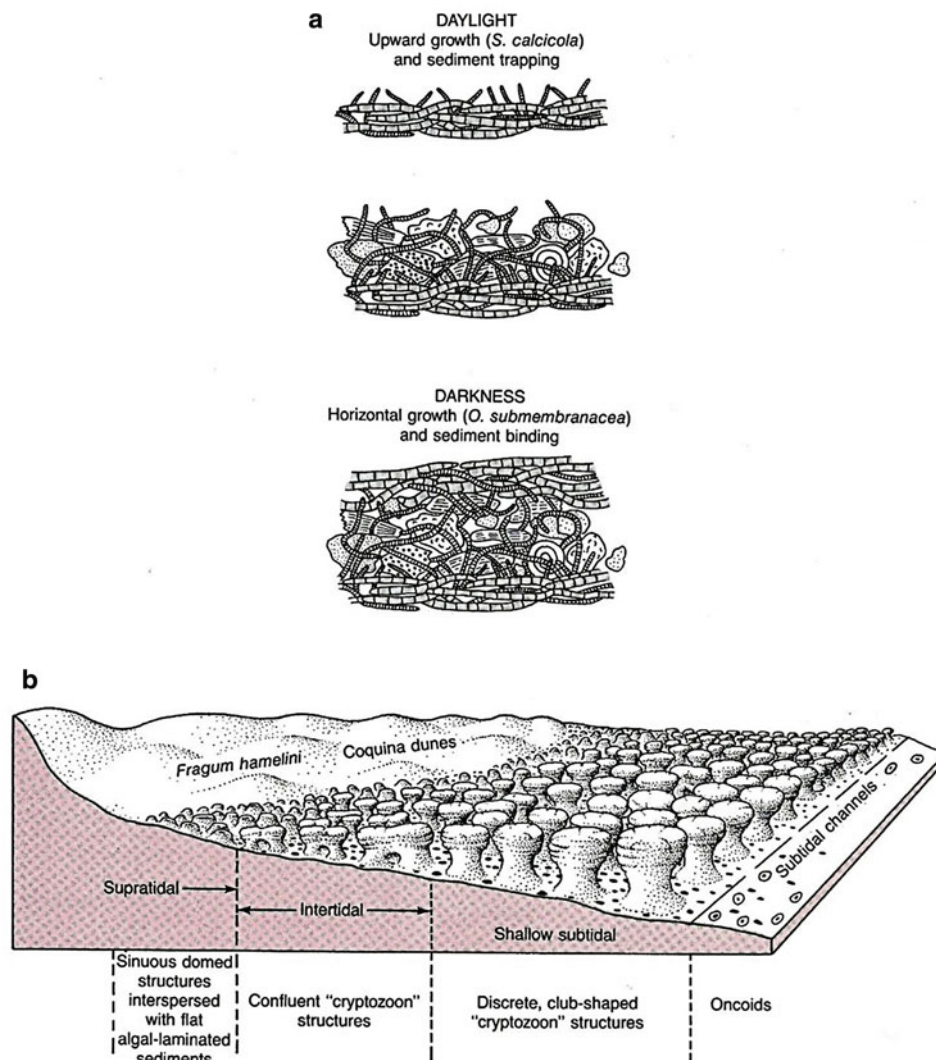


Fig. 6 a Day-night accretion cycle in stromatolites. b Idealized from zonation of stromatolites at Shark Bay, Western Australia (Cooper et al., 1990)

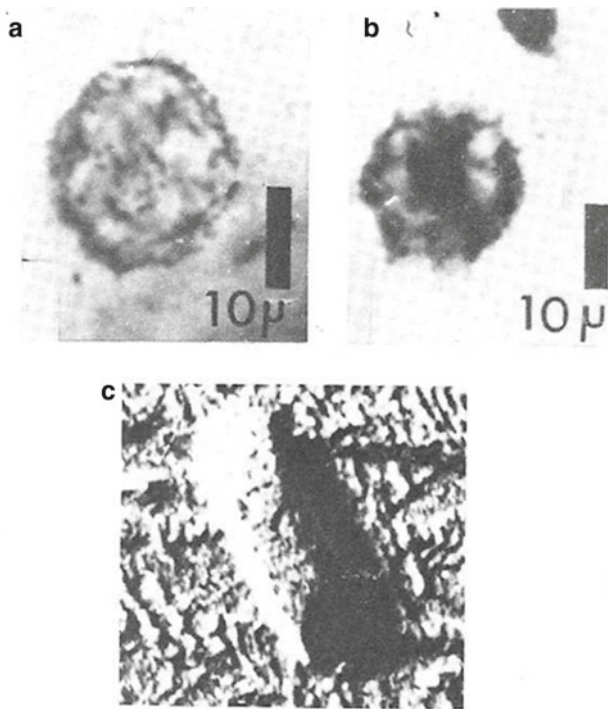


Fig. 7 Fig Tree group fossils. **a, b** *Huronia* an algal-like form; **c** *Eubacterium*, a bacterium (Mintz, 1981)

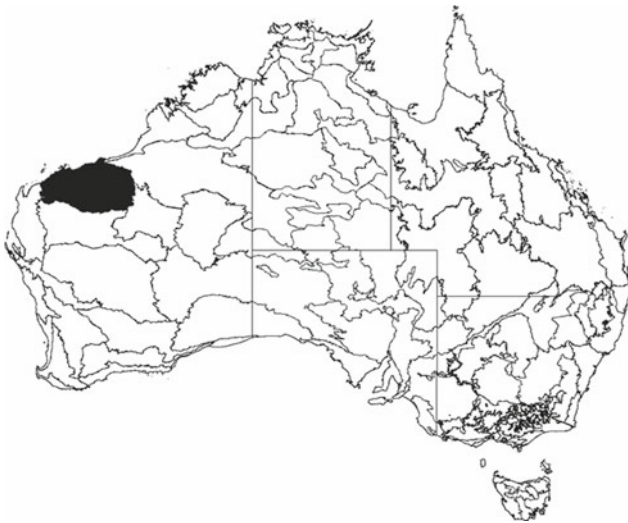


Fig. 8 Map of Australia with the Pilbara region highlighted in black

- **Warrawoona Group, North Pole dome region of the Pilbara block, Western Australia**

The Pilbara Craton represents the stable part of the continental lithosphere situated in Pilbara, Western Australia, Fig. 8. It is of Archean age (3.6–2.7 billion years ago).

The Pilbara region of Western Australia comprises some exposures for the oldest rocks preserved on Earth. It includes

another evidence of early life. This record is represented by rounded tubular cells that oxidized sulfur by photosynthesis in oxygenless conditions, Fig. 9, found in pyrite-bearing sandstone in a fossilized beach. Another fossil record is stromatolites-layered structures of 3.48 Ga in the undeformed hydrothermal-sedimentary strata of the Dresser Formation which show textural criteria suggestive for biogenic origins, Fig. 10. Major evolutionary events in the Archean are shown in Table 1.

3.1.3 Methanogens

Methanogens are suggested to may be as a link to the earliest forms of life. Methanogens are a distinct group of prokaryote microorganisms which grow by oxidizing hydrogen and reducing CO_2 to methane (CH_4). They are anaerobic; they die in the presence of oxygen and confined to unusual oxygen-free environments such as deep hot springs and fetid mud bottoms of stagnant ponds. They have a unique RNA nucleotide sequencing. As the Earth's original atmosphere was devoid of oxygen and rich in CO_2 , the very conditions under which methanogens thrive and under which the Earth's original life might have evolved. All prokaryotes including methanogens, bacteria, and cyanobacteria have had a common ancestor and had the same RNA sequence at one point in their past. Thus, a major radiation of methanogens predated the Fig Tree and North Pole organisms.

3.2 Proterozoic Life

3.2.1 Prokaryotes

- Methanogens, bacteria, and cyanobacteria (blue-green algae) are of nonnucleated cells and belong to the superkingdom Prokaryote.
- Prokaryotic Archean fossil record is very limited compared to that of the abundant Proterozoic that includes about 300 species recorded from both shales and cherts in a large number of localities. This prokaryotes fossil record increased in abundance and became widely dispersed by about 2100 Ma. The major part of these species is of cyanobacterial affinity.
- The Gunflint Chert algae and fungi from the Gunflint Iron Formation of Ontario, Canada, discovered in 1954 is a much more extensive assemblage and the first Precambrian microflora to be described. It is dated to about 2 billion years by radiometric means. The flora is diverse and includes thread-like, rod-like, and spheroidal, star-shaped, and umbrella-shaped species identical in form to present-day bacteria and blue-green algae. Eight new genera with large number of species have been named from the Gunflint Formation, Fig. 11.

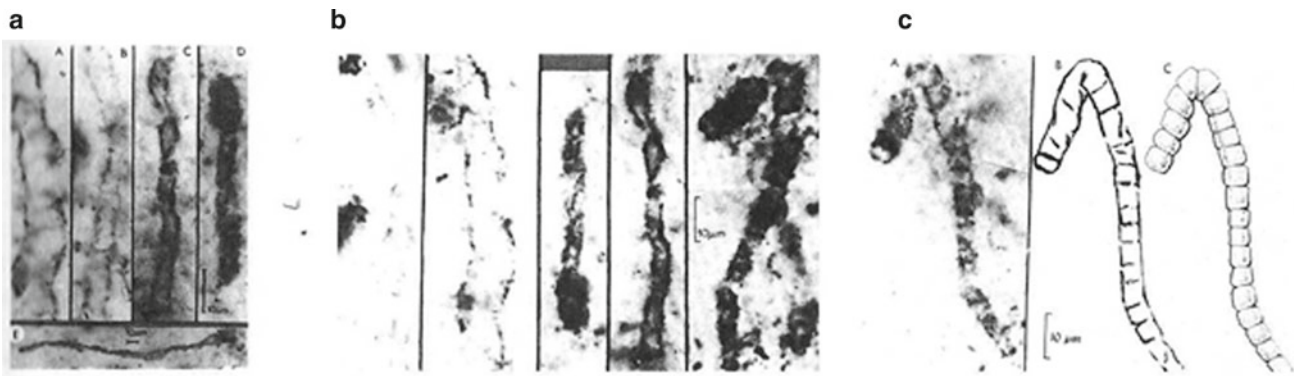


Fig. 9 Microfossils from carbonaceous chert, Early Archean Warrawoona Group, North Pole dome region of the Pilbara block, Western Australia. **a** Tubular or partially flattened bacterial or cyanobacterial sheaths. **b** Elongate, rod-shaped, apparently nonseptate fossil bacteria. **c** Unbranched, septate, apparently somewhat tapering filamentous fossil prokaryote shown in petrographic thin section (Cooper et al., 1990)

3.2.2 Eukaryotes (The Greatest Evolutionary Step)

- Organisms whose cells have nuclei are called eukaryotes. The major difference between the two is the extent to which they tolerate oxygen. Oxygen requirements are quite different among the prokaryotes. Some are totally anaerobic; others can tolerate small amounts of oxygen, and some are fully aerobic. On the other hand, eukaryotes have an absolute requirement for oxygen. Eukaryotes arose only after a significant quantity of oxygen had accumulated in the atmosphere.
- These conditions made possible the evolution of the more efficient and complex eukaryotic cell of protists.
- The Neoproterozoic, which spanned from 1000 million years ago (Ma) to 541 Ma at the beginning of the Cambrian, was a very exciting time in the evolution of the Earth's life history. (1) Eukaryote, which is metabolically and structurally advanced relative to prokaryote, was arisen, and (2) Supercontinent Rodinia was assembled and then break up and dispersed. The prokaryotic cells differ greatly from the eukaryotic cells. Both have a cell wall or membrane vary in composition and structure, in order to separate the cell contents from the external world. Eukaryotic cells are actually less complicated than Prokaryotic cells. Both types of cells are filled with cytoplasm, Fig. 12. The essential distinctions between the two cell kinds lie mostly in the internal composition and structure. In prokaryotic cells, the genetic material is scattered within the cytoplasm instead of being captured within the nucleus. Eukaryotic cells encompass numerous types of specialized structures termed organelles. The most distinctive eukaryotic organelle is, indubitably, the nucleus, in which the genetic information is enclosed. Table 2 summarizes the main differences between prokaryotic and eukaryotic cells.
- The earliest acritarchs that can be considered with some confidence eukaryotic are the oldest recorded fossils of that group. Acritarchs are organic-walled microfossils with a central cavity surrounded by an organic single or multi-layered wall. They have a generally globular shape with diameters ranging from few ten micrometers up to two hundred micrometers. The Acritarch walls are either smooth or have spine-like protrusions and complex surface ornamentations. Acritarch's cell wall is tough and durable and made up of various organic compounds, Fig. 13. Acritarch fossils are known as far back as 1800–1900 Ma (from a special locality in China) and become common since 1000 Ma. The earliest acritarchs resemble, in overall morphology, the undisputed later acritarchs, which date back to about 1400 Ma.
- The earliest development of the eukaryotes appears to occur in a very slow rate.
- The diversity of eukaryotes, both unicellular (mostly acritarchs) and multicellular (mostly algae), increased greatly during the Neoproterozoic.
- Bitter Springs Formation in the northern Terrain of Australia dated at about 1000 Ma has a well-preserved assemblage of plants preserved as organic residues in laminated black chert. This assemblage includes fossil of green algae that differs from cyanobacteria (blue-green algae) in having sexual reproduction, and some of the fossils recovered from this chert show cell division. Blue-green algae are abundant, and colonial bacteria, fungus-like filamentous organisms, spheroidal green algae, and other cellular forms are also present. Fossil evidence indicates that the first eukaryotic organisms developed from certain prokaryotic cells about 1.5 billion years ago. The Bitter Springs cherts have yielded thirty new species of plant microfossils. Over half of these are blue-green algae and no animal life have been recognized, Fig. 14.

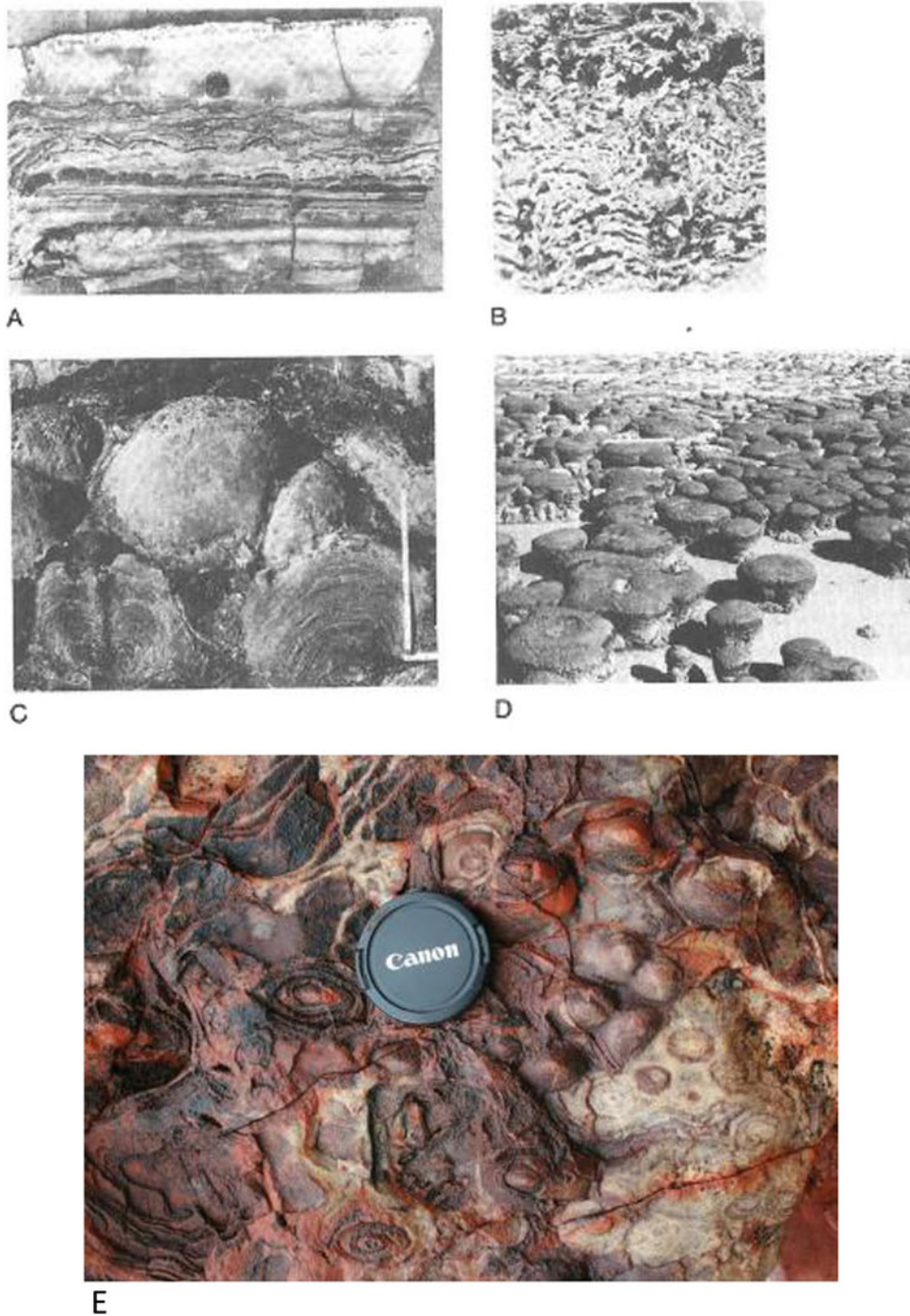


Fig. 10 Ancient and modern stromatolites. **a** Possible stromatolites from 3500 Ma Warrawoona Group, Western Australia. **b** Similar-looking, modern-day crinkly laminated stromatolite from Hamelin Pool, Shark Bay, Western Australia. **c** Domal morphology and cross-sections of 1900 Ma stromatolites from near east arm of Great Slave Lake, Canada. **d** Holocene domal stromatolites exposed at low tide, Hamelin Pool, Shark Bay, Western Australia (Cooper et al., 1990). **e** Pilbara stromatolites

- These relatively complex microfossils from Proterozoic strata are recorded in China, France, USA, Poland, Scotland, Sweden, Russia, and elsewhere.
- Simple sexual reproduction had evolved by perhaps 1000 million years ago.
- Eukaryotic unicellular microfossils are rare or absent in rocks older than 1500 million years old, while these become increasingly more abundant in rocks younger than that.

Table 1 Major evolutionary events in the Archean (Cooper et al., 1990)

Major evolutionary events during first half of Earth's history			
Age in Ma	Eon	Event	Evidence
2000	PROTEROZOIC	7 Advent of significant O ₂ in atmosphere	7 Earliest major development of red beds
2200		6 Major development of aerobic photosynthesis; rapid evolution of cyanobacteria	6 Major development of banded iron formations (B.I.F.) and widespread, diverse stromatolites
2400			
2600	ARCHEAN	5 Beginning of aerobic photosynthesis; early evolution of cyanobacteria	5 Oldest definitive stromatolites
2800			
3000		4 Early diversification of anaerobic bacteria; first primitive anaerobic photosynthesis; simple prokaryotes	4 Oldest definitive evidence of life on Earth: moderately diverse prokaryotes in Warrawoona Group, Western Australia; Fig Tree and Onverwacht Groups in South Africa
3200			
3400			
3600	3 Formation of primitive lithosphere, atmosphere, hydrosphere, biosphere	3 Oldest dated rocks on Earth (Isua supracrustal terrane of southwest Greenland, ~3800 Ma); indicates time of metamorphism of sedimentary sequences and plutonic igneous rocks; presence of possible organic carbon and B.I.F.	
3800			
4000			
4200	2 Major volcanism and meteoric impact	2 Lunar craters and rocks	
4400			
4600	1 Formation of the Earth	1 Age of meteorites; Pb-evolution curves	

- The moderately diverse Gunflint microbiota at about 2000 Ma is exclusively prokaryotic; thus, it would seem that eukaryotes first evolved sometime between about 2000 and 1500 Ma; 1500 Ma also is close to the time of abundant occurrence of red beds.
 - Increase in atmospheric O₂ and CO₂.
 - Increase in carbonate rocks.
 - Formation and stabilization of the ozone layer.
 - Rise of sexual reproduction.
- The prokaryotes evolved mainly during the time when environmental oxygen concentration in the atmosphere changed from “inconsistently essentially zero” to “consistently slight.” However, by the time the eukaryotes appeared, the atmospheric oxygen increased and was conducive to respiration, which is the central metabolic process of organisms having nucleated cells.
- During the first 2000 million years in the history of life, only the simple prokaryotic level was involved.
- The emergence of superkingdom Eukaryota needs many evolutionary biogeochemical consequences as:
 - The first three underscore the profound influences that life exerted on the total environment. Sexuality and increasing atmospheric oxygen levels to perhaps 6–10% present atmospheric level (PAL) may have provided the critical evolutionary triggers that promoted Late Proterozoic eukaryotic diversification and ultimately the evolutionary emergence of multicellular organisms about 700 million years ago.
 - Life as we know it could not have arisen in the presence of oxygen, but it also could not have evolved beyond

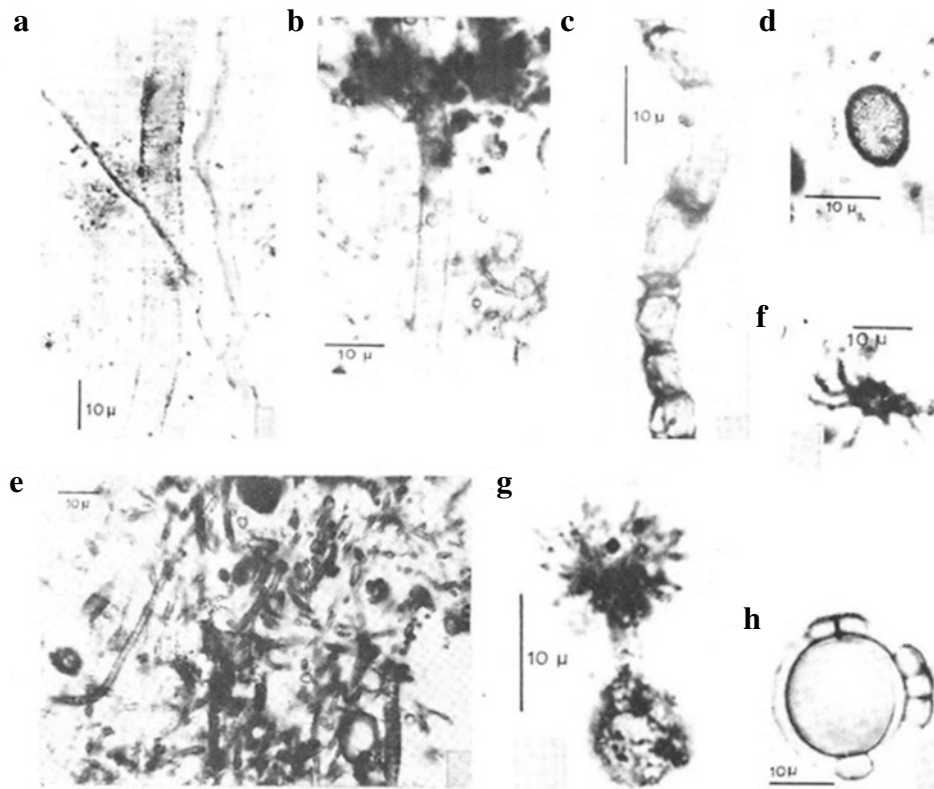


Fig. 11 Gunflint Chert Fossils. **a–c** Blue-green algae, *Animikia*, *Entrospheroides*, and *Gunflintia*; **d** *Huroniospora*, and algal spore; **e** *Gunflintia* and *Huroniospora*; **f** *Euastrian*, a bacterium; **g** *Kakabekia*; **h** *Eosphaera* (Mintz, 1981)

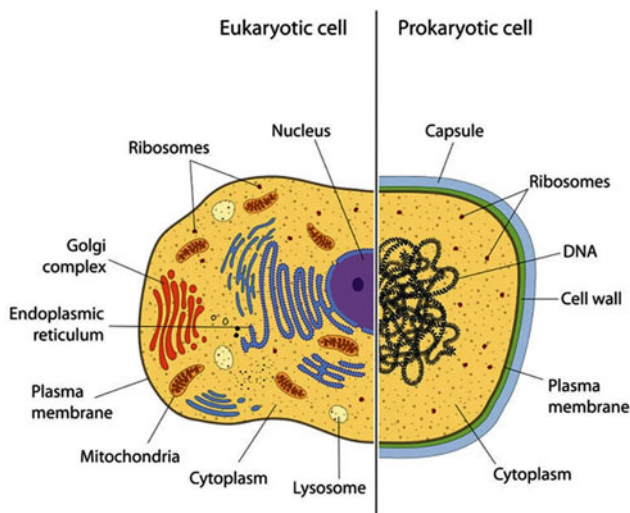


Fig. 12 Prokaryotic cell versus eukaryotic cell (in Wikipedia)

bacteria without it. Major evolutionary events during Proterozoic are shown in Table 3 and summary of major evolutionary events in the Precambrian is shown on Table 4.

4 Oxygen Revolution

The Oxygen Revolution spans from 2.4 to 2.0 Ga within the Paleoproterozoic era, when the oxygen significantly increased in the Earth's atmosphere and the shallow oceans for the first time. Chemical and geological (isotopic) evidences propose that biologically induced molecular oxygen (dioxygen O_2) began to accumulate in Earth's atmosphere and altered it from a slightly reducing to oxidizing, which drives extinction of many species existing on Earth. The event was caused by cyanobacteria generating the oxygen which supported the following development of multicellular forms.

This early atmosphere devoid of oxygen can be indicated by evidences come from certain sedimentary minerals from greenstone belts. These minerals are very unstable and might reflect the concentration of free oxygen at the time they were deposited:

- Grains of the mineral uraninite are readily oxidized and dissolved in the presence of oxygen. Uraninite probably could not have accumulated in Archean deposits if there

Table 2 Features distinguishing eukaryotes from prokaryotes (Cooper et al., 1990)

Distinguishing characteristics	Unicellular organisms	
	Prokaryotes	Eukaryotes
Cell size	Very small; generally 1–10 μm	Larger; generally 20–100 μm
Cell wall	Present	Present
Cell organization	Poor	Organized
Nucleus	Absent	Present
Organelles	Absent	Mitochondria and chloroplasts
Genetic organization	Loop of DNA in cytoplasm	DNA organized in chromosomes within nucleus
Oxygen requirements	Intolerance to tolerance	Oxygen required
Metabolism	Anaerobic to aerobic	Aerobic
Energy production	Fermentation or respiration	Respiration
Reproduction	Binary fission	Mitosis or meiosis
Organisms represented	Bacteria, methanogens, cyanobacteria	Protists

**Fig. 13** Acritarch (in Wikipedia)

had been an appreciable concentration of atmospheric oxygen (as much as 1% of present atmospheric level).

- Significant amounts of unoxidized pyrite also support the notion of anoxic conditions.

In the rock record, the Banded Iron Formations (BIFs) include the evidence for the timing of the transition from an oxygenless to an oxygen-rich atmosphere. They are distinct sedimentary rock units composed of alternated bands of iron oxides and iron-poor chert, Fig. 15. Nearly all of these sedimentary units are of Precambrian age (Early Proterozoic between 2400 and 2000 Ma). The rich prokaryotic microbiota of the Gunflint Formation occurs in a banded iron formation approximately 2000 Ma. Free oxygen released during this time joined with dissolved ferrous iron (Fe and Fe^{2+}) to produce insoluble ferric iron

(magnetite $\text{Fe}^{2+}\text{Fe}^{3+}\text{O}_4$), which precipitated at the substrata of the shallow seas to form BIFs. Thus, the BIFs represent the deposits of “oxygen sinks.” The time interval of the most abundant banded iron formation development coincides with a major development of carbonate rocks and stromatolites in the geologic record.

- Stromatolites are known from rocks 3100 and 2800 million years old in South Africa and Rhodesia, and perhaps from rocks as old as 3500 million years old at North Pole, Western Australia. However, the Early Proterozoic represents a tremendous explosion in stromatolite development, and with it, a major build-up of oxygen produced by the photosynthetic activity of abundant and widespread mats of cyanobacteria. Thus, the record of major oxygen release is provided by the BIFs, and the record of the oxygen-releasing agent is provided by the stromatolites.
- Red beds are another kind of iron-rich deposit that includes detrital sediments whose particles are coated with iron oxides, mostly the mineral hematite (Fe_2O_3). Red beds are common in many sedimentary sequences younger than about 2000 million years ago, but rare in older ones. Banded iron formations are unknown in rocks younger than about 2000–1800 Ma. There is some stratigraphic overlap between these two different kinds of iron-rich sedimentary rocks (one chemical, the other detrital), red beds essentially supplement banded iron formations after about 1800 million years ago. Iron-stained red sediments are attributed to oxidation of iron by free oxygen in the atmosphere and are most common in non-marine (subaerially exposed) environments. The onset of red beds and disappearance of BIFs

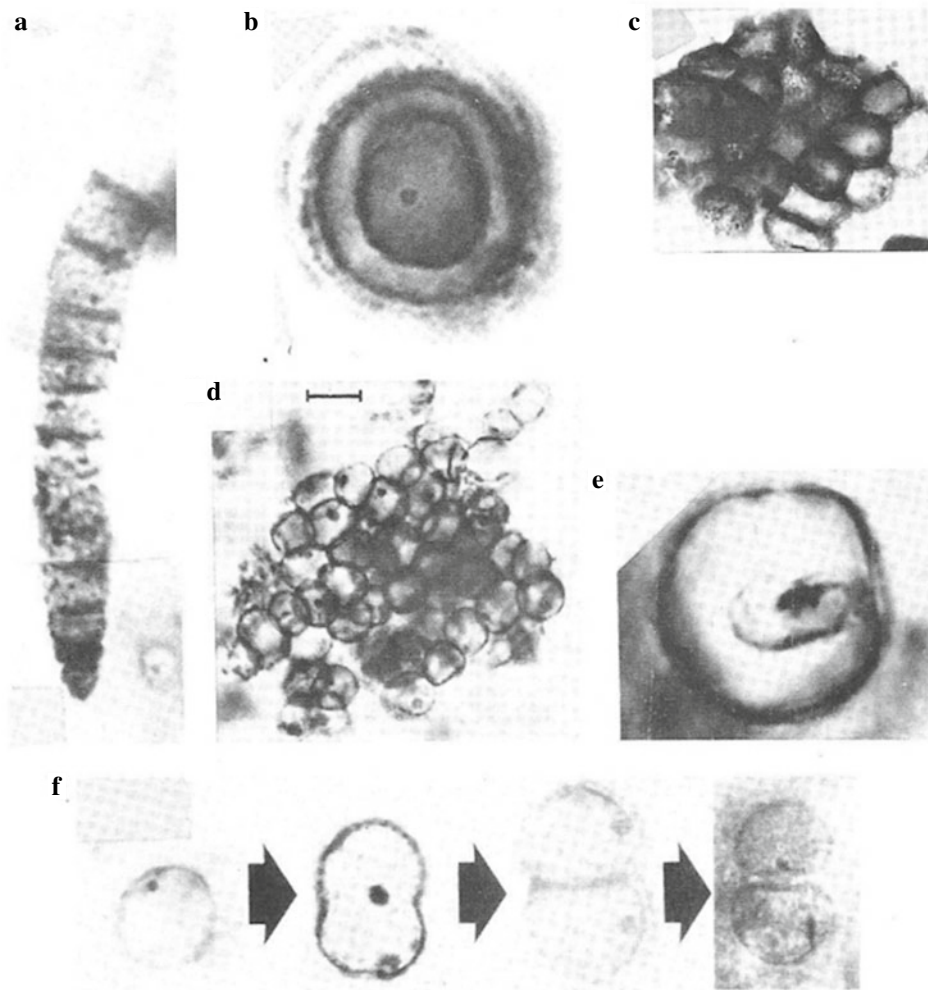


Fig. 14 Bitter Springs Chert Fossils. **a, c, d** Blue-green algae: *Cephalophytarion*, *Myxococcoides*, and *Palaeonacytis*; **b** ?Dinoflagellate *Gloeodiniopsis*, and **e, f** green algae *Caryosphaeroides*, *Glenobotrydion* (Mintz, 1981)

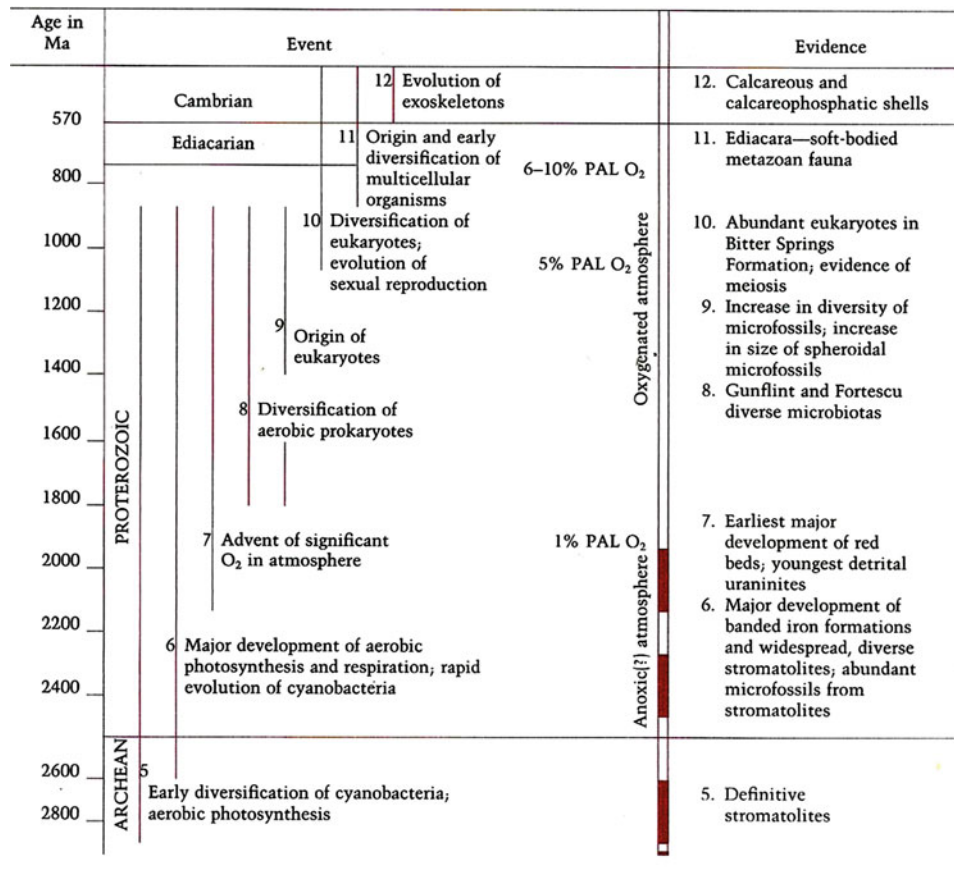
in the geologic record signals the initial build-up of oxygen in the atmosphere after the oxygen sinks were filled up at about 2000 million years ago.

- Evolution of life is directly connected to different physical and chemical conditions prevailing on Earth. Life first appeared in an oxygen-free atmosphere. Oxygen was released in the Early Proterozoic time by photosynthesis of the cyanobacteria and at later times by cyanobacteria and other more complex plants. Earth's history is divided into five stages of Earth's atmosphere. Stage 1 (3.85–2.45 Ga): Basically, no O₂ is found in the atmosphere. The oceans were largely anoxic with likely exception of O₂ in the shallow oceans. Stage 2 (2.45–1.85 Ga): O₂ produced, increasing to values of 0.02 and 0.04 atm, but consumed by absorption in oceans and seabed rock. Stage 3 (1.85–0.85 Ga): O₂ starts to release out of the oceans, but is absorbed on land surfaces. No substantial change in

oxygen concentration. Stage 4 (0.85–0.54 Ga) and stage 5 (0.54 Ga–present): Other O₂ reservoirs filled, gas accumulates in atmosphere, Fig. 16.

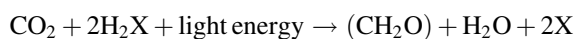
5 Photosynthesis

Organisms can be classified into **autotrophic** or **heterotrophic**. An autotrophic organism manufactures its own organic materials through conversion of simple inorganic components, making use of a variety of external energy sources. A heterotrophic organism gets its nutrients from preexisting organic substance (or abiotic organic molecules). Autotrophs can be classified as being either chemoautotrophic or photoautotrophic depending on the form of energy utilized. Chemoautotrophic organisms utilize

Table 3 Major evolutionary events during latest Archean and Proterozoic (Cooper et al., 1990)

chemical energy to fuel the biochemical synthesis. Such organisms survive today in the deep ocean, especially in the areas around hydrothermal vents accompanying mid-ocean ridges. Photoautotrophic organisms use energy from the solar radiation in their processes of synthesis.

Photosynthesis is a complex biochemical process, in which the organism utilizes the solar radiation as source of energy and chlorophyll as a reaction catalyst to oxidize the relatively reduced compounds that are stable in the natural environment. The general reaction can be written as



The oxygen is represented by element “X” in this reaction. By photosynthesis, the organism splits the water molecule (which consumes a lot of energy) and combines the emitted hydrogen with carbon dioxide to produce carbohydrate material (represented here by the simplest form of carbohydrate; the carbohydrate sucrose, heavier but still simple, has the molecular formula C₆H₁₂O₆) and free molecular oxygen.

That’s known as oxygenic photosynthesis, and the organisms that do it are termed oxygenic photoautotrophs. These are called aerobic or oxic and essentially produced all of the free oxygen in our atmosphere. This type of photosynthesis is performed by cyanobacteria, algae, and higher plants, Fig. 17. Essentially all of the oxygen produced during the early stages of oxygen revolution was by stromatolitic communities of cyanobacteria.

Organisms that have no chlorophyll cannot adopt oxygen for the “X” in photosynthesis. These are some bacteria-encompassing components catalytically resembling chlorophyll that makes them able to use hydrogen sulfide (H₂S), as the raw material. That method of photosynthesis, called anoxygenic photosynthesis, yields free sulfur instead of oxygen as the by-product. The organisms that adopt this method are termed anaerobic or anoxic photoautotrophs.

Early photic autotrophs (oxygenic photoautotrophs) might have lived in mat-like communities in shallow water, but under conditions of comparatively low light intensity,

Table 4 Summary of major events during the Precambrian (Cooper et al., 1990)

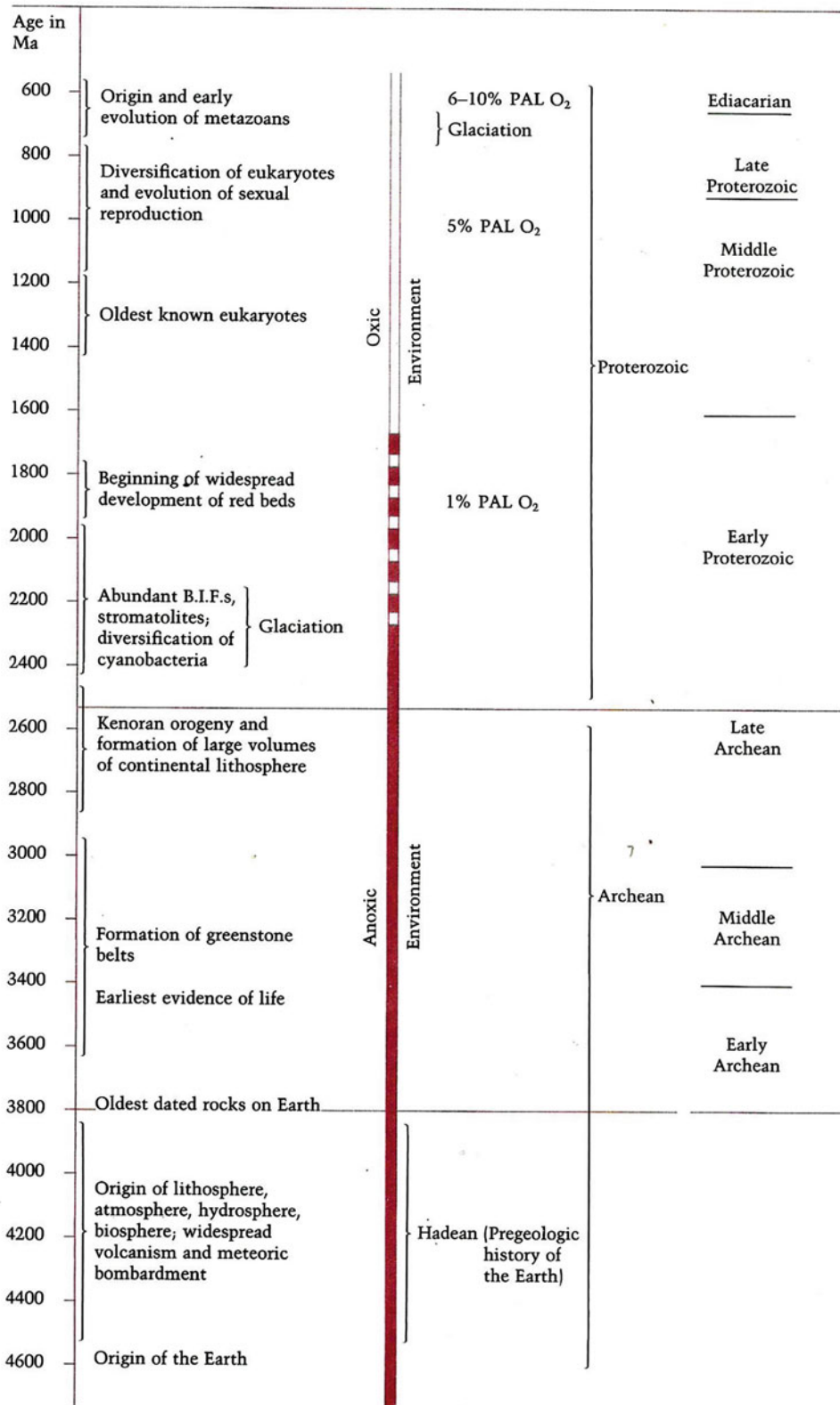




Fig. 15 Banded iron formation (in Wikipedia)

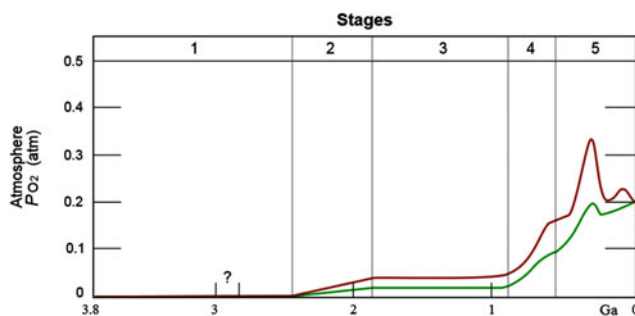


Fig. 16 O_2 build-up in the Earth's atmosphere (red and green lines represent the range of the estimates while time is measured in billions of years ago (Ga)) ("History of Earth" in Wikipedia)

which was controlled by the cloudy, CO_2 -rich, Venus-like atmosphere. Somewhat later, the quantity and range of light reaching the ocean surface improved, and water-splitting accelerated oxidation (water-splitting is the photochemical breaking of the water molecule into hydrogen and free oxygen).

Under these conditions, primitive prokaryotes probably gave rise, as a mutant strain, to the first organisms capable of aerobic photosynthesis; these organisms were the ancestors of modern cyanobacteria.

This type of photosynthesis was more efficient as a means of energy and nourishment; however, the molecular oxygen released was a toxin that no doubt poisoned many kinds of anaerobic organisms. Anaerobic photosynthesis was very likely going on during deposition of the Fig Tree and Warrawoona beds 3400 million years ago.

The cyanobacteria spread rapidly and dominated virtually all accessible habitats by the beginning of the Proterozoic. And with them, the rise of aerobic photosynthesis about 2000 million years ago introduced a change in the global environment that was to profoundly influence all subsequent evolution.

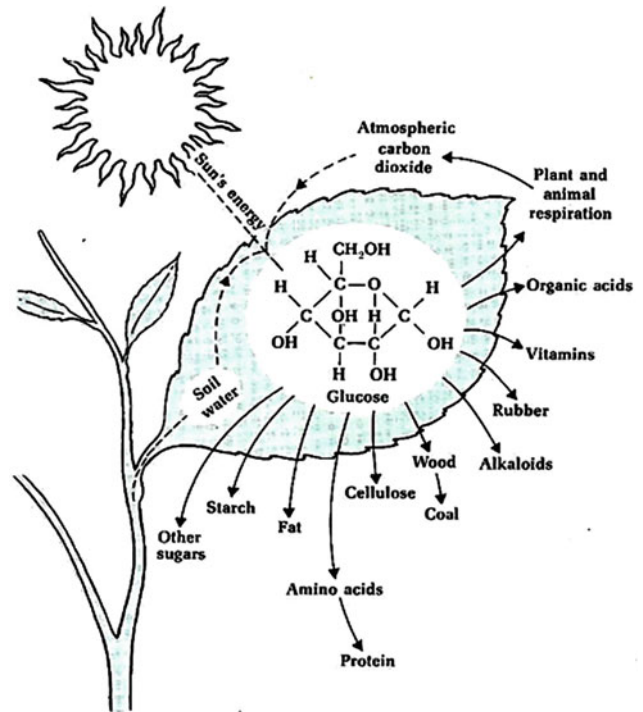


Fig. 17 The green plant uses the energy of the sun to produce many valuable products ("Photosynthesis" in Wikipedia)

6 Ediacaran Biota

The Ediacaran biota or Ediacara fauna is a unique soft-bodied assemblage consisting of all life forms preserved globally as impressions of fossil in sandstone beds during the Ediacaran Period (ca. 635–541 Mya). They signify a significant advancement in the evolution of life on Earth, as they precede the explosion of life forms at the commencement of the Cambrian Period 541 Ma called Cambrian Revolution. These were encompassing enigmatic tubular and frond-shaped, generally immovable organisms. Trace fossils of these organisms have been recorded globally and denote the earliest recognized specialized multicellular organisms.

Ediacaran biota may have experienced evolutionary radiation following the culmination of the Cryogenian Period's widespread glaciations. This biota was largely wiped out consistently with the rapid biodiversity increase of the Cambrian Revolution. Most of body plans of animals existing today firstly appeared in the Cambrian instead of the Ediacaran. For macro-organisms, the Cambrian biota seem to have entirely replaced the Ediacaran surviving organisms, even though relationships are still a matter of argument. The Ediacaran Period organisms first appeared around 600 Ma and flourished till the Cambrian onset at 541 Ma, when these distinctive communities of fossils were wiped out.

Ediacaran Biota from their type locality in the Ediacara Hills at Pound Quartzite located in Adelaide Basin, South Australia, includes 30 species including 20 genera. These were classified into two-thirds as coelenterates, about one-quarter as annelid worms, and about one-twentieth as arthropods. Coelenterates include abundant and moderately diverse jellyfish-like plans as genera *Charodiscus* and *Cyclomesusa*. The annelids are represented by small worm-like forms as *Spriggina* and *Dickinsonia*. Primitive arthropod-like animals are represented by *Parvancorina*. The disk-shaped *Tribrachidium* is possibly a primitive echinoderm. Trace fossils represented by feeding trails, possibly made by worm-like creatures, are also present, Fig. 18.

Most of the specimens are preserved as casts or molds of soft-bodied organisms on the bottom surfaces of sandstone beds. No biomineralization, to yield hard skeletal materials, was included. The sedimentological evidences of the enclosing deposits clearly indicate that these organisms were surviving mostly in shallow ocean waters, where light was available. These strange organisms comprised the world's first known animal community and inaugurated the age of metazoan life.

In general, the Ediacara fauna are large bag-like and sheet-like organisms, with extremely variable body plans but

with certain common traits. They were apparently without mouth and gut, and lacking respiratory organs.

Trace fossils first appeared in the Ediacaran. In the beginning, the traces were simpler: represented by millimeter-wide tracks on the surface of sediment. As time went on, the traces complexed gradually and become more advanced, where the burrows and the surface tracks appeared. Presumably, the sophisticated soft-bodied organism burrowed through the sediment instead of creeping over the sediment surface. The trace's abundance and complexity increased up into the lowermost Cambrian, even after the disappearance of the fossil record of the Ediacaran. The formal base of the Cambrian is now delineated based on the appearance of one particularly distinctive burrowing trace fossil, known as *Treptichnus pedum*, an arcuate horizontal burrow from which branches grow up to probe at the sediment surface, Fig. 19.

7 Neoproterozoic Microfossils of Egypt

The oldest fossil assemblage in Egypt was recorded from the Neoproterozoic (Ediacaran) Igla Formation, Hammamat Group in Wadi Igla Eastern Desert, Egypt (Khalifa et al.,

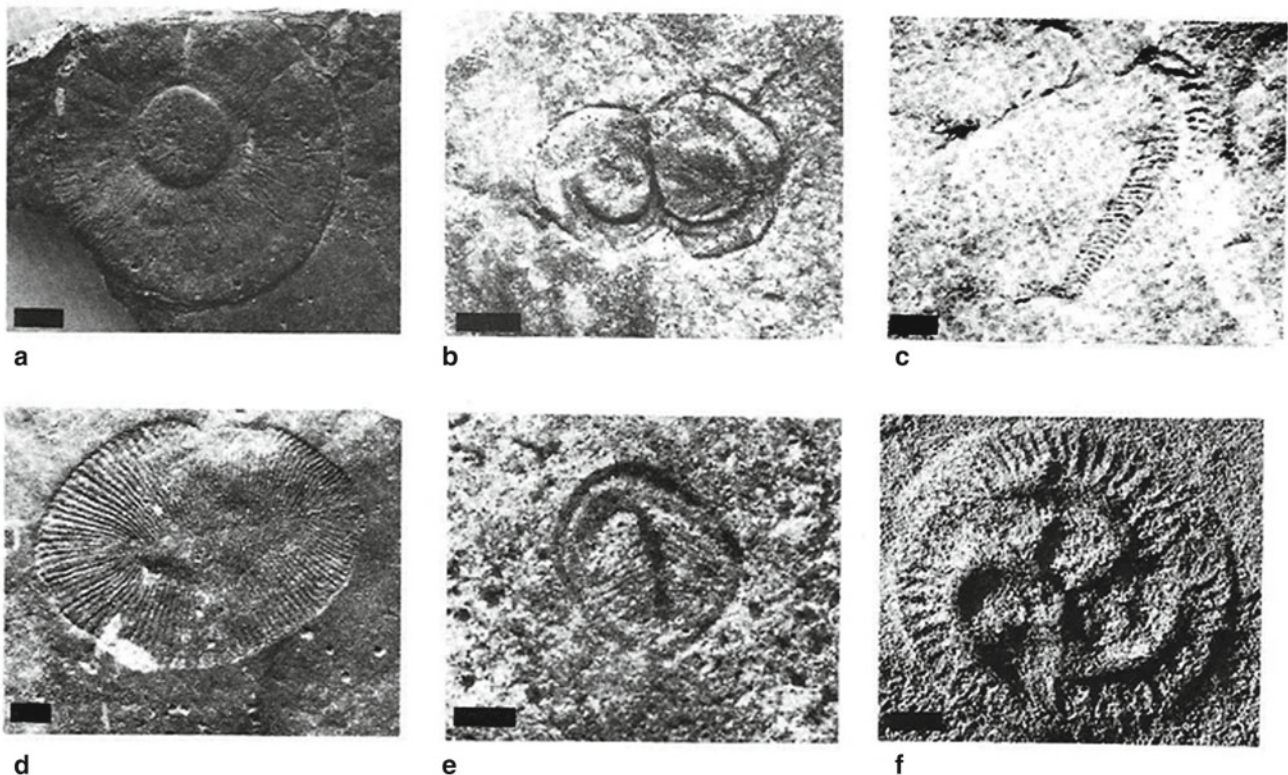


Fig. 18 Ediacaran fauna. Primitive coelenterates: **a** *Charodiscus*; **b** *Cyclomedusa*. Primitive annelid flatworms: **c** *Spriggina floundersi*; **d** *Dickinsonia costata*. Primitive arthropod (?): **e** *Parvancorina minchami*. Primitive echinoderm (?): **f** *Tribrachidium*. Bars = 1 cm (Cooper et al., 1990)



Fig. 19 The base Cambrian trace marker fossil *Treptichnus pedum* (Seilacher, 1955)

1988). The Precambrian igneous and metamorphic Basement Complex of Egypt covers about 10% of the Egyptian surface (about 100,000 km²) mainly in the Eastern Desert and South Sinai, and some restricted areas in the south Western Desert, Fig. 20. The oldest rocks in Egypt are recorded in G. Uweinat-G. Kamel inlier that belong to the Saharan

Metacraton and dated to the Archean (about 3.1 Ga), while the basement rocks of the Eastern Desert and South Sinai are related to the Pan African Event of Neoproterozoic (900–550 Ma) crust of the Arabian-Nubian Shield.

7.1 The Hammamat Group

The Hammamat Group comprises a thick clastic sediment succession that represents the youngest unit of the layered sequences of the basement complex of Egypt. The Hammamat is taken its name from the type area of that unit in Wadi El Hammamat, approximately 70 km west-southwest of Qoseir, Fig. 21. According to Akaad and Noweir (1980), The Hammamat Group includes two formations: the Igla Formation below and the Shaximiao Formation above. The Igla Formation consists of sandstones, siltstones, and silty mudstones with a basal conglomerate. The Shaximiao Formation is composed of conglomerates, greywackes, and sandstones. Each formation was further subdivided into members.

The Hammamat sediments are exposed in separate outcrops distributed mostly in the central and northern Eastern

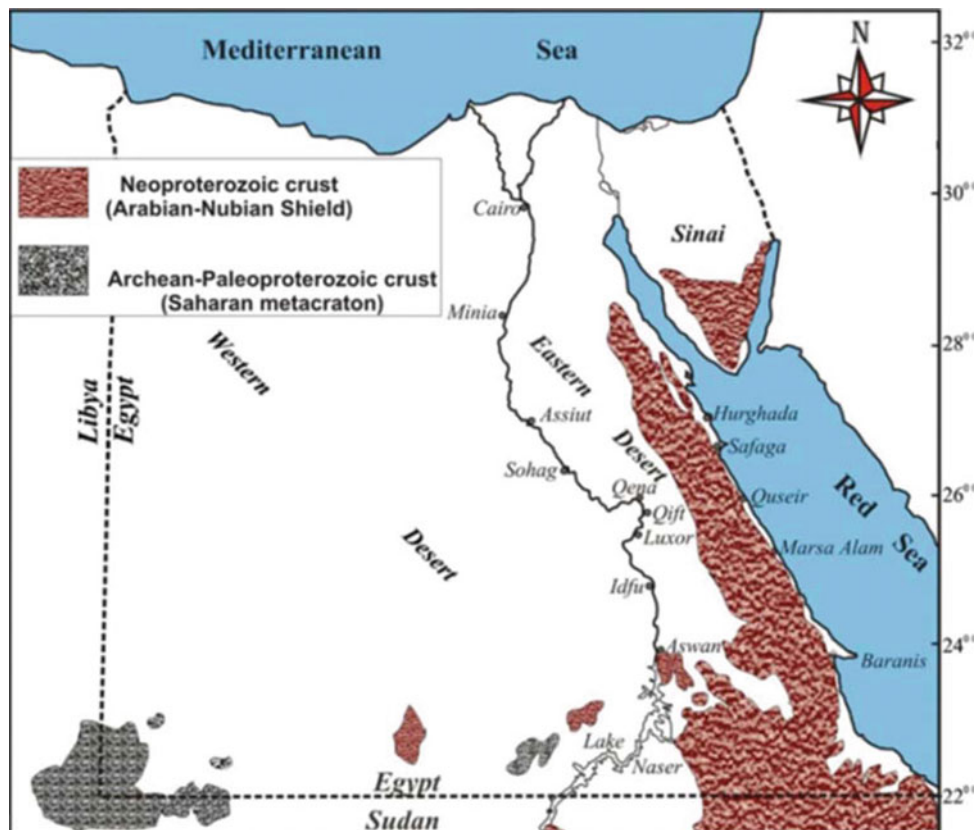


Fig. 20 Distribution of Precambrian rocks in Egypt

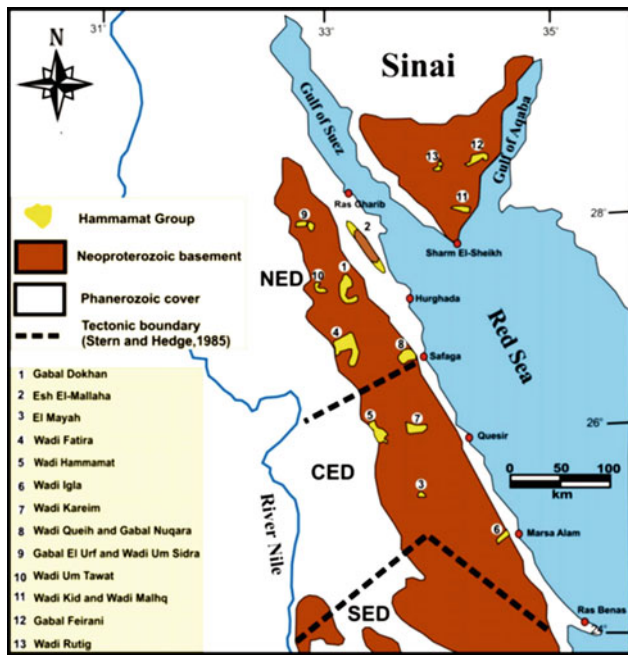


Fig. 21 A map showing the distribution of the major Hammamat basins in the Eastern Desert and Sinai (modified after Abd El-Wahed, 2010 and references therein)

Desert. They attain a thickness of about 4000 m in their type area (Akaad & Noweir, 1980). The Hammamat crops at the surface in down-faulted blocks or in topographic lows. They overlay older units unconformably with a basal conglomerate and are intruded locally by younger granitoids and later intrusives (Hassan & Hashad, 1990).

The Hammamat sediments are composed of totally immature to semi-immature sediments including conglomerates, greywackes, sandstones, and slates, with characteristic green, purple, and gray colors (Hassan & Hashad, 1990). These sediments are considered as post-orogenic molasse deposited in disconnected intermountain basins as a result of rapid uplift and erosion.

These sediments are supposed to may be deposited in an alluvial fan-braided stream complex. The detritus shed from the uplifted terrain was deposited adjacent to the uplifts. The finer-grained facies are thought to have been accumulated in two different environments. The thinner siltstone units indicate cutoff channel deposits within braided streams, whereas the much thicker units are viewed as playa or lake sediments.

7.2 Ediacaran Microfossils of the Hammamat Group

Eight algal microfloral species were recorded from the Neoproterozoic Hammamat Group exposed in Wadi Igla,

central Eastern Desert, Egypt. These include seven species belonging to phylum Cyanophyta and one species belonging to phylum Pyrrophyta, these in addition to microphytolites (oncolites) of cyanobacterial growth, and other unnamed forms of probable algal affinities. Ediacaran microfossils are recorded from the Hammamat Group in Wadi Igla, Central Eastern Desert, Egypt.

Wadi Igla is located west to southwest of Marsa Alam (longitudes $34^{\circ} 41' 2''$ – $34^{\circ} 53' 3''$ N and latitudes $25^{\circ} 2'–25^{\circ} 10' E$), Fig. 22. The Hammamat sediments in Wadi Igla is composed of stratified succession striking generally NE–SW and dipping gently to the east. The succession is composed mainly of hematitic siltstone, greywackes, arenites, mudstone, and polymictic conglomerates. The different lithofacies occur as thin laminae to beds several meters thick. These rocks lie unconformably above older metavolcanics in the southern part and metagabbroic rocks in the western part, Fig. 23. They are overlain unconformably to the east by Miocene sediments. These immature clastic sediments are characterized by the frequent occurrence of polymictic conglomerate layers.

• Microfossil Assemblages

A wide variety of microfossils are identified from the Hammamat molasse clastics of Wadi Igla. Most of the detected microfossils are characterized by soft bodies without hard parts. Morphologically, fossil microorganisms embedded in clastic sediments are well preserved compared to those included in carbonates. The preserved organic remains range in size from 2 to 190 μm in most cases. Under the microscope, the preserved microfossils are commonly outlined by dark brown to red brown coloration. Some forms, however, display more or less distinctive extracellular pigmentation denoting individual cell envelopes, sheaths, or entire colonies.

The original pigmentation of the organic remains may be entirely lost, and it is substituted by a uniform coloration relying on the preservation circumstances, rather than the nature of the microfossils.

The microfossils comprise algal microflora. The microflora constitutes the majority of all microfossils embedded in the studied thin sections compared to other microfauna. The microflora include four species of Cyanophyta and three monotypic species tentatively referred to this phylum: *Siphonophycus kestron* Schopf, *Siphonophycus inornatum* Zhang, *Sphaerophycus wilsonii* Knoll, *Myxococcoides inornata* Schopf, *Tenuofillum septatum* Schopf, *Caudiculophycus revulariodes* Schopf, and *Bactrophycus oblongum* Zhang. One species of Pyrrophyta, namely *Gloeodiniopsis gregaria* Knoll and Golubic, has been recorded, Figs. 24, 25 and 26.

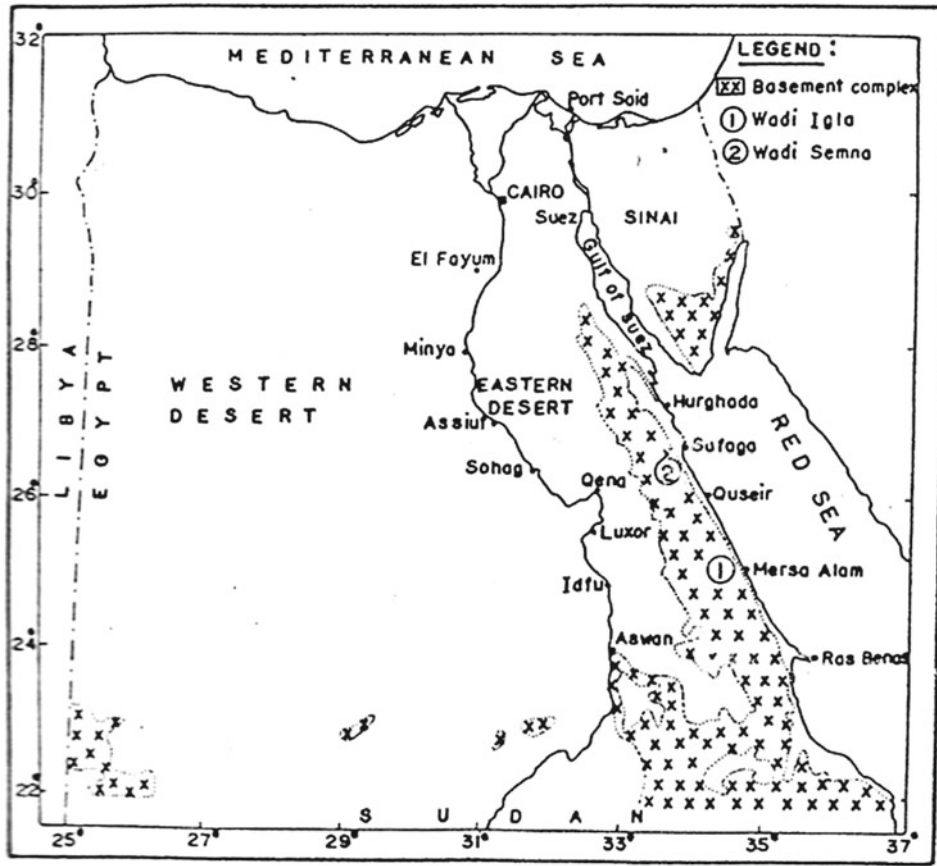


Fig. 22 Location map of Wadi Iгла and Wadi Semna, Eastern Desert, Egypt (after Khalifa et al., 1988)

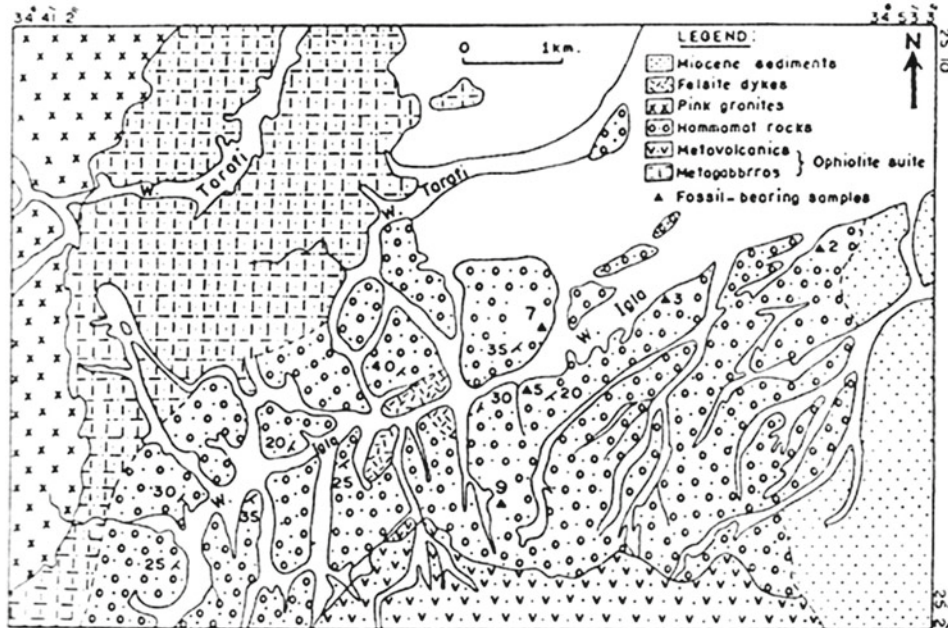


Fig. 23 Fossil-bearing samples, Wadi Iгла (after Khalifa et al., 1988)

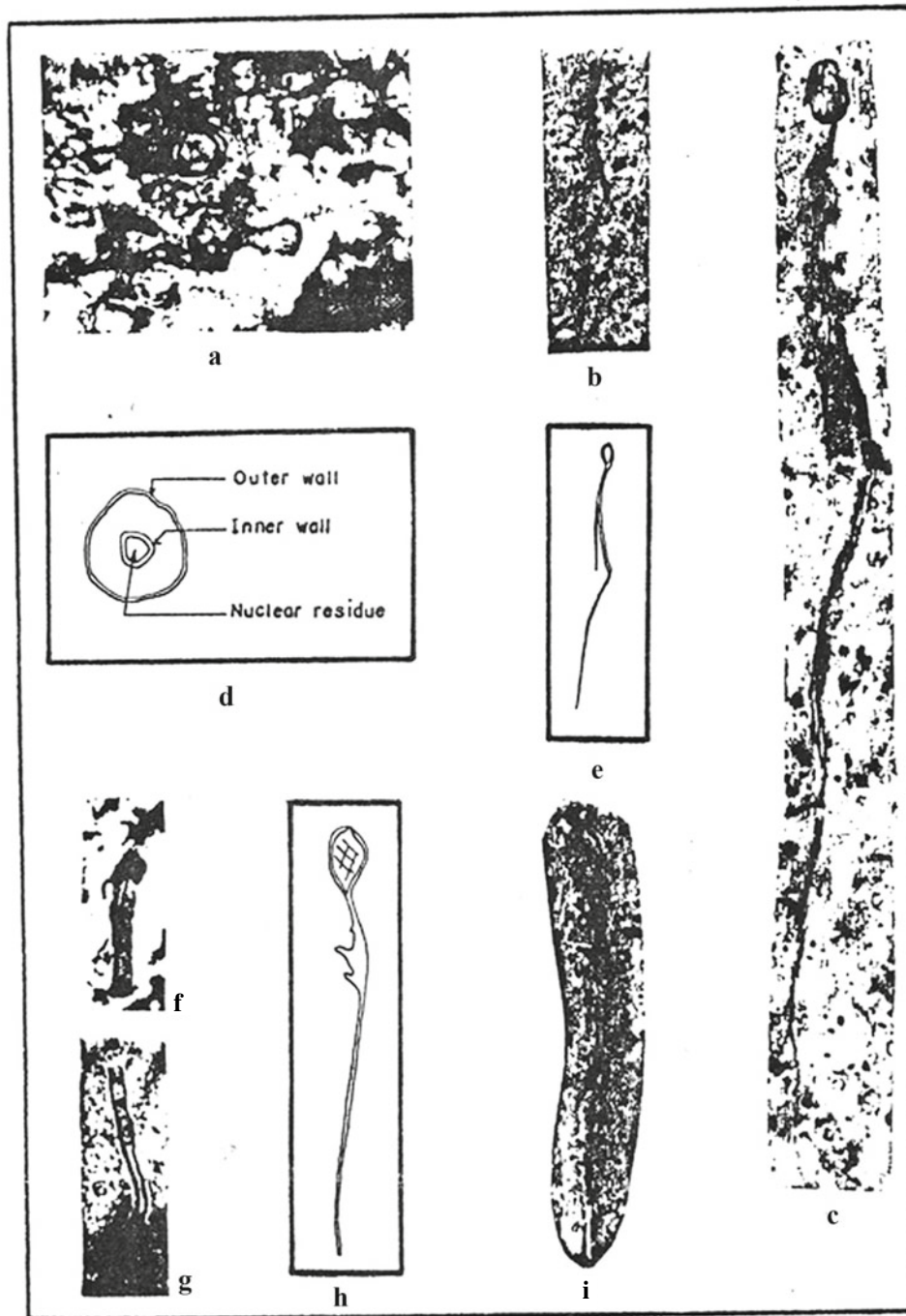


Fig. 24 a, d *Gloeodiniopsis gregaria* Knoll and Golubic. 4. Generalized drawing of a typically preserved cell. a X 1250, d X 2500; W. Iglá. b, c, e, h, i *Tenuofilum septatum* Schopf. 3. Composite photomicrograph; 5, 8. Generalized drawing of the photomicrograph. b, e, h, i X 340, c X 1420. W. Iglá. f *Siphonophycus kestron* Schopf. X 1000. W. Iglá. g *Siphonophycus inornatum* Zhang. X 1000. W. Iglá (all photos after Khalifa et al., 1988)

Microphytolite (oncolites) grains and other unnamed forms, probably of algal affinities, have also been encountered. They are genetic composites encompassing bacterial

or cyanobacterial growth and mineralization processes, inorganic precipitation, periodic rip-up abrasional or erosive events, and neomorphic processes.

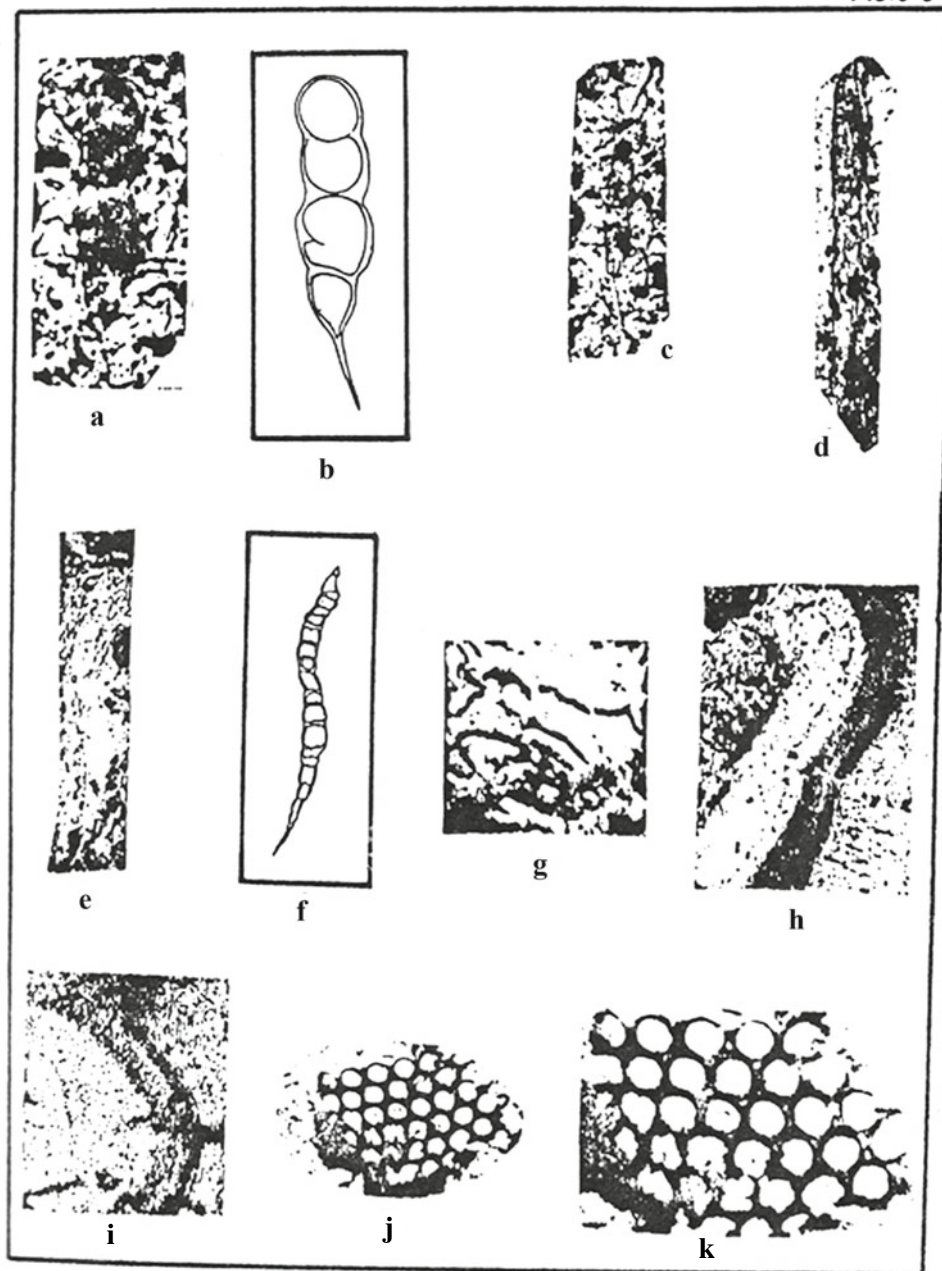


Fig. 25 a–c, e, f *Caudiculophucus revulariodes* Schopf. X 450. W. Igla. d Fragment of sheathed algal filament. X 450. W. Igla. g–i Archaeocyathid fragment. X 2000. W Igla. j, k *Myxococcoides inornata* Schopf. j X 500, k X 750. W. Igla (all photos after Khalifa et al., 1988)

• Age Assignment

The age of the Hammamat clastics is based mainly here on the detected microfossil assemblages compared to similar fossil microorganisms from other parts of the world. Known from several stratigraphically well-studied localities in North America, Australia, and Saudi Arabia, *Tenuofilum septatum* Schopf, *Siphonophycus kestron* Schopf, *Sphaerophycus*

wilsonii Knoll, and *Gloeodiniopsis gregaria* Knoll and Golubic first appeared near the close of the Late Proterozoic (Knoll & Vidal, 1980; Schopf, 1968).

The microphytolites (oncolites) are well represented geographically and lithologically in the latest Proterozoic successions of different parts of the world. Consequently, they act as index fossils for worldwide biostratigraphic correlation (Milstein & Golovanov, 1979).

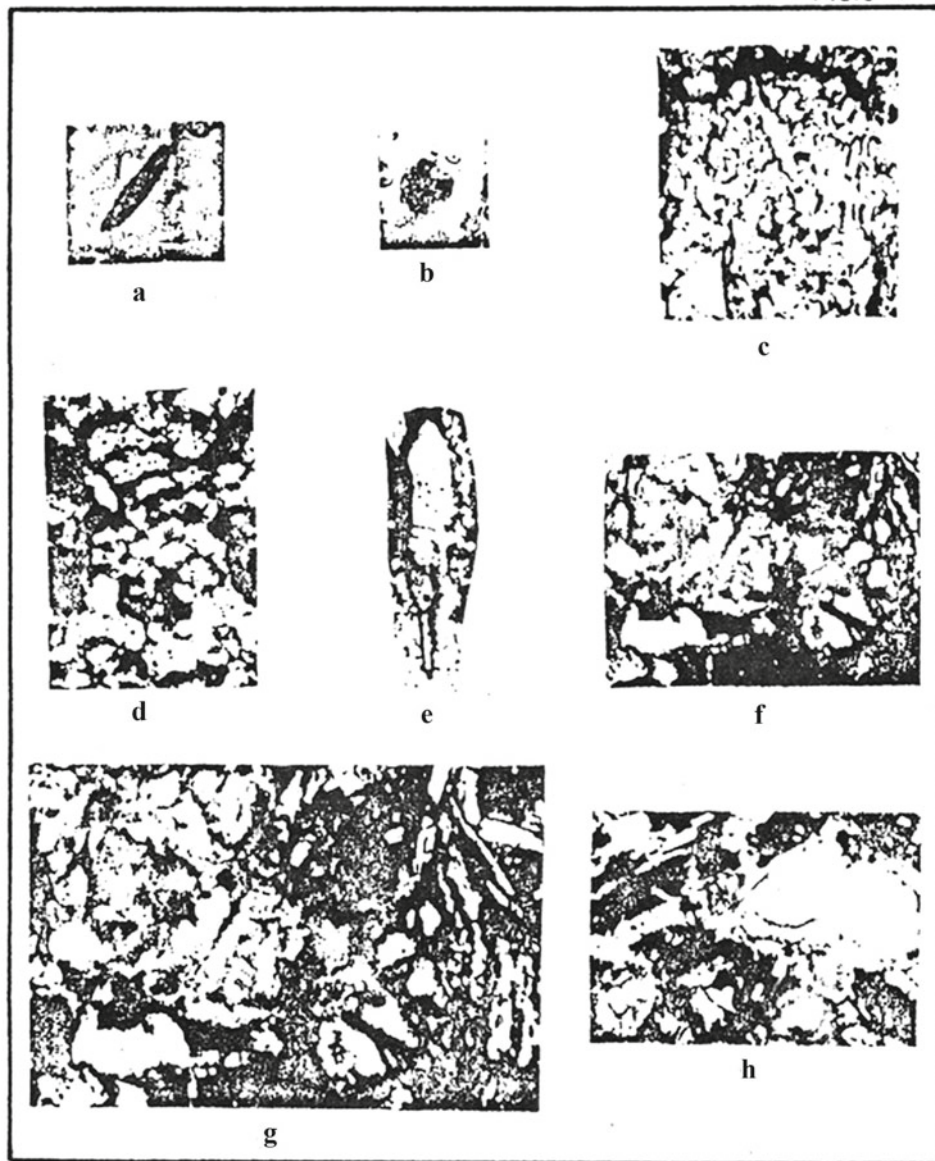


Fig. 26 a *Bactrophyucus oblongum* Zhang. X 400. W. Semna. b *Sphaerophycus wilsonii* Knoll. X 2000. W. Igla. c-e Probably blue-green algae. X 300. W. Igla. f-h Microphytolites (oncolites). X 200. W. Igla (all photos after Khalifa et al., 1988)

It is clear from the abovementioned data that the Hammamat sediments exposed in Wadi Igla are of Late Proterozoic (Ediacaran Period) age.

Radiometrically, the Hammamat sediments are dated between 616 ± 9 and 590 ± 11 Ma. These two ages are Rb/Sr whole rock ages. The first age is of calc-alkaline volcanic rocks in Wadi Sodmein (believed to be equivalent to Dokhan volcanic) which underlines unconformably the Hammamat sediments. The second age is for Umm Had granite that intruded the Hammamat sediments in their type area in Wadi El Hammamat (Ries et al., 1983).

• Depositional Environment

The Hammamat sediments occur in several, often enormous isolated outcrops, predominantly in the central Eastern Desert between Safaga and Marsa Alam. The abovementioned microfossil assemblages recorded in the Hammamat molasse type facies include mainly algal microflora of Cyanophyta (blue-green algae) and Pyrrophyta which indicate that the algal mats of the identified species have been accumulated subtidally in a quiet, shallow marine environment, perhaps a lagoon separated from the open sea by some

type of barrier. The recorded microfossils specify current conditions intermediate between low energy conditions, in which microbial mats might be formed, and the more continuously turbulent environments (Khalifa et al., 1988).

8 Cambrian Revolution

The Cambrian revolution or Cambrian explosion was an event at the beginning of the Cambrian about 541 Ma when practically all major animal phyla began appearing in the fossil record. It spanned for about 13–25 million years and caused the divergence of most modern metazoan phyla. The event was supplemented by great diversification in other organisms.

Most organisms were simple (unicelled, or small multi-celled) occasionally grouped into colonies before the Cambrian revolution. As the rate of diversification consequently hastened, the variety of life started to bear a great resemblance to that of today. Nearly all existing animal phyla made their first appearance during this period.

The Ediacaran time interval represents **Phase I** in the transition from Precambrian to Cambrian. **Phase II** in this transition began about 570 Ma (± 30 million years) with the extinction of the Ediacaran soft-bodied fauna and the appearance of the first assemblages of shelly faunas of low diversity, in which about 5 species of shelled animal are found together. These are small, chitinous, calcareous, and phosphatic metazoan fossils of mostly problematic affinity. Genus *Prothertzia* is an example of this early shelly, small (a few mm in length), phosphatic, tusk-shaped fossil,

Figs. 27 and 28. *Anabarites* is another taxon of this phase and is small tube-shaped, with three distinct interior ridges, composed of calcium carbonate fossil. *Cloudina* and *Sinotubulites* are the first shelly fossils, composed of calcium carbonate and associated with Ediacaran soft-bodied fossils.

Phase III in the transition from Precambrian to Cambrian and which lasted for about 10–20 million years is characterized by shelly faunas of moderate diversity in which more than 5, but generally fewer than 15, species of shelled animals are found together. This fauna of tiny shelled fossils underlies the lowermost trilobite-bearing strata in different regions of the world. The stratigraphic interval comprising Phase III is generally referred to as the Tommotian Stage. This stage marks the first appearance of the archaeocyathids, a group of unusual, vase-shaped, double-walled calcium carbonate-shelled creatures. Other described taxa from Tommotian Stage comprise hyolithids, monoplacophorans, inarticulate brachiopods, possible gastropods, sponges, and protoconodonts, Fig. 29.

During the time interval in which overlying strata were deposited that are clearly of transitional Cambrian age (the Atdabanian Stage), the geographic range of archaeocyathids expands greatly, and trilobites, those hallmarks of Cambrian faunas, appeared for the first time and diversified rapidly. Both Phase II and Phase III shelly faunas also partly fill the gap between the Precambrian and Cambrian, thus further reducing the apparent abruptness of appearance of the first trilobites.

Major skeletonized faunas made their appearance over an interval of perhaps 20–30 million years and this constitutes a

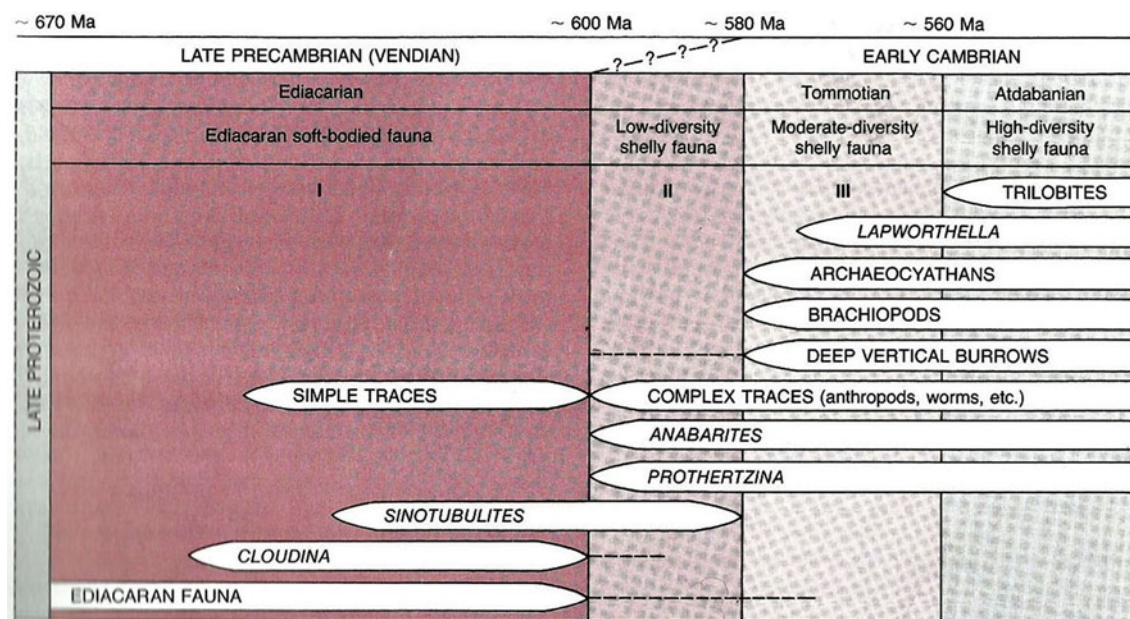


Fig. 27 Late Proterozoic-Early Cambrian time scale illustrating the evolutionary phases in the transition from Precambrian to Cambrian (Cooper et al., 1990)

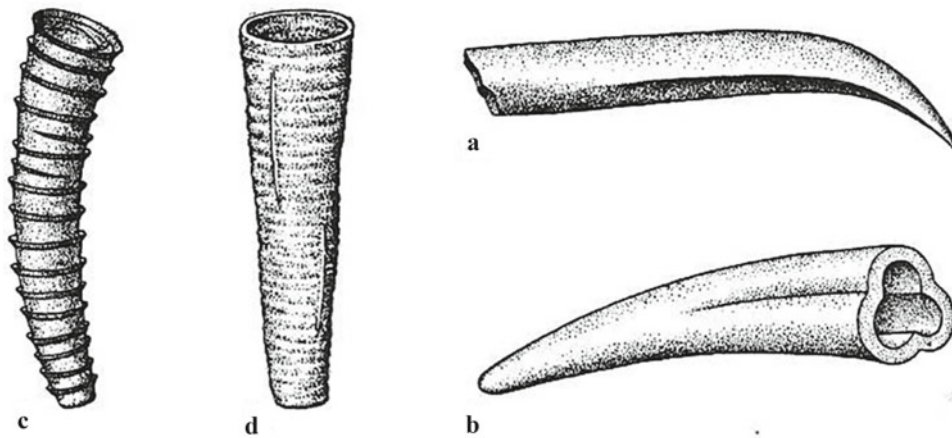


Fig. 28 Early skeletonized fossils from Phases I and II of the Precambrian–Cambrian transition. **a** *Prothertzina*, the probable calcium phosphate grasping spine of an early predator. **b** *Anabarites*, a common associate of *Prothertzina* in Phase II assemblages. **c** *Cloudina* and **d** *Sinotubulites*, tube-shaped fossils of calcium carbonate composition representing the earliest known skeletonized organisms (Cooper et al., 1990)

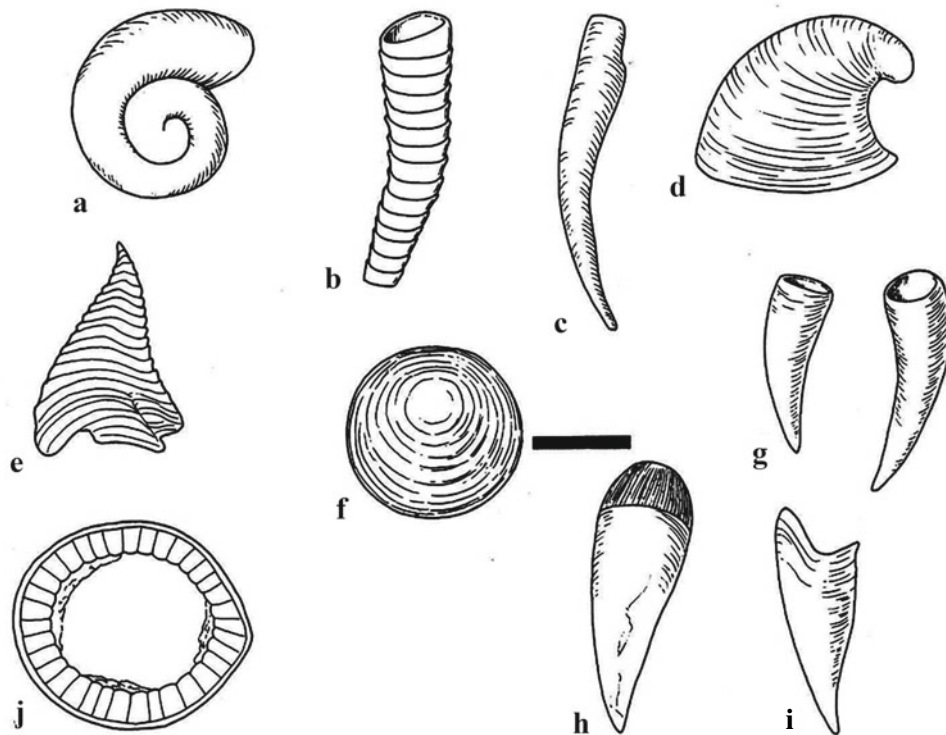


Fig. 29 Enigmatic earliest shelly fossils from Tommotian strata. **a–i** Mollusk-like calcareous cone and coiled shells. **j** Transverse section of archaeocyathid showing double-walled structures. Bar is 1 cm (Cooper et al., 1990)

major adaptive radiation. This dramatic faunal radiation is shown in the number of high-level taxa, representing radically different kinds of organisms, that made their appearance in such a short time interval. This appearance of natural new phyla and classes occurred at a scale and rate that has not been matched since, Fig. 30.

The metazoan adaptive radiation probably was related to a combination of factors, including rising atmosphere oxygen levels, continued continental fragmentation and flooding of continental shelves by transgressing seas, and ecological interactions within the biosphere. More oxygen allowed for more complex anatomical grades, Fig. 31. Land-sea changes

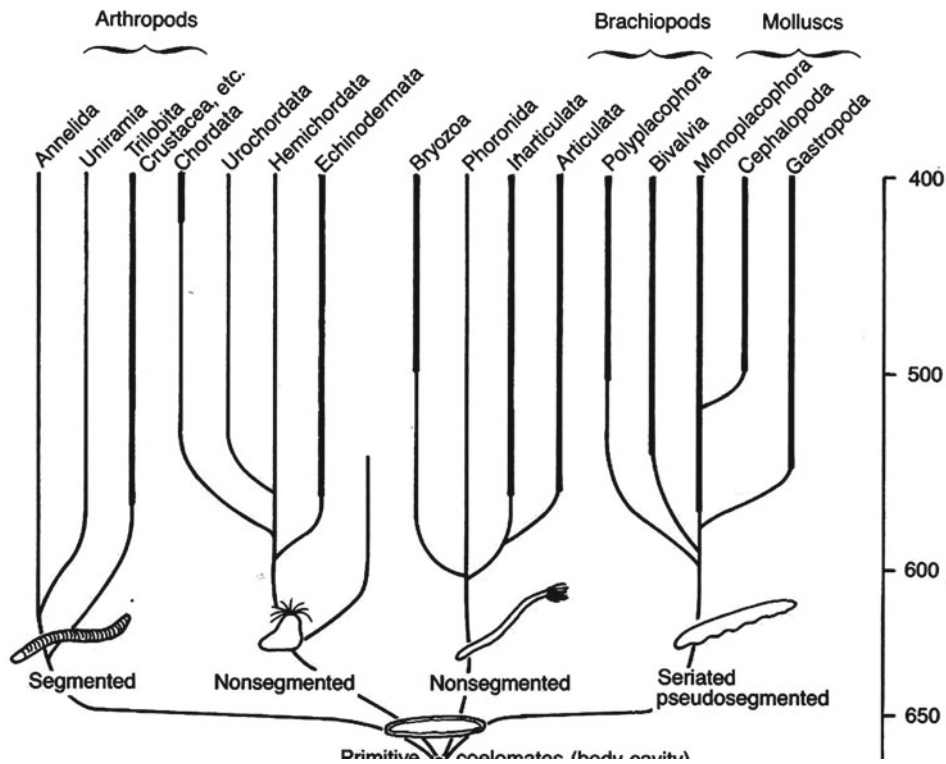


Fig. 30 Evolution of the metazoan phyla. Heavier lines indicate that the lineage of the phylum had acquired a mineralized skeleton (Cooper et al., 1990)

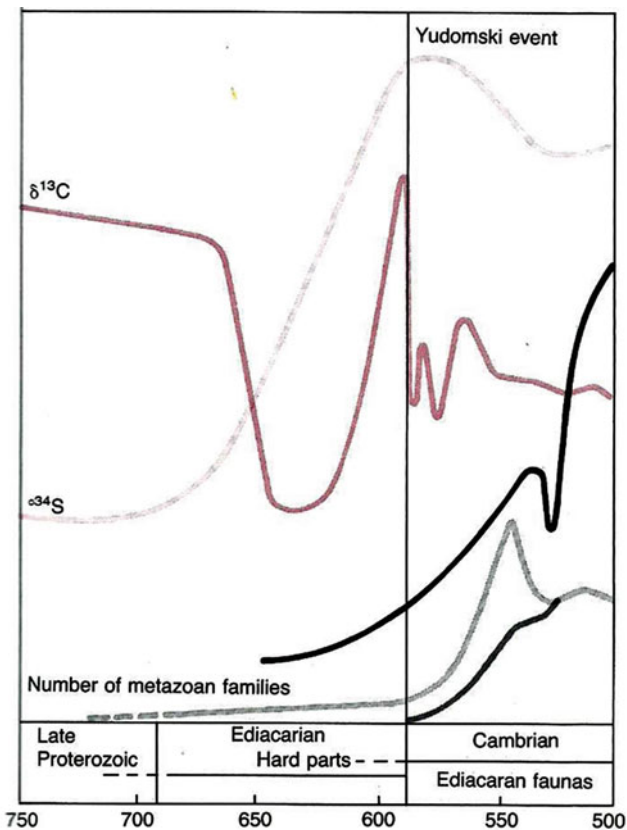


Fig. 31 Combination of geochemical, geological, and paleobiological data that contribute to understanding the events that occurred during the Precambrian–Cambrian transition interval (Cooper et al., 1990)

created a greater diversity of shallow marine habitats and niches, which were rapidly filled by opportunistic, unique kinds of metazoans. Continental separation also produced more genetic isolation and may also have triggered changes in ocean chemistry, both of which influenced biological development. Relative sea level rise and marine transgression drowned low-relief continental margins, producing new tracts of shallow-water habitats.

9 Cambrian Fauna of Egypt

Cambrian sediments comprise two main facies types: the Igla Formation of the Hammamat Group in Wadi Semna, west of Safaga as part of the Egyptian basement complex, and the Araba Formation exposed in north Eastern Desert, and in southwest Sinai. At southwest Sinai, the Araba Formation is exposed at Um Bogma, Wadi Feiran, and Abu Durba, while it is also exposed in the Eastern Desert at Wadi Qena, between there and south of the western end of Wadi Dakhel and at G. Zeit. Some Archaeocyathids and few sponge spicules are recorded in the Lower Cambrian Igla Formation in Wadi Semna (Khalifa et al., 1988). Soliman and Habib (1974) recorded a Paleozoic foraminiferal assemblage in the Igla Formation in Wadi Semna, Eastern Desert. Body and trace fossils were recorded in the Lower Cambrian exposures

in southwest Sinai and north Eastern Desert by Omara (1972), Said (1980), Jenkins (1990), Klitzsch (1990), Seilacher (1990), and Elicki et al. (2013).

9.1 Cambrian Fauna of the Iгла Formation, Hammamat Group, Wadi Semna, Central Eastern Desert

Wadi Semna is located west of Safaga (longitude $33^{\circ} 35' 2''$ – $33^{\circ} 38' 7''$ N and latitudes $26^{\circ} 0' 28''$ – $26^{\circ} 31' 55''$ E), Figs. 22 and 32. The clastic Hammamat sediments occupy an elongated strip, covering an area of about 8 km^2 . They are represented mainly by arenites, polymictic conglomerates, greywackes, siltstones, and mudstones in decreasing order of abundance. These rocks appear to have been deposited unconformably above the older metavolcanics to the east and west and metagabbros to the south (El-Gaby & Habib, 1982). It is clear that the western contact dips eastwards in harmony with the bedding plane of the sequence. The Iгла Formation, Hammamat Group in Wadi Semna, includes microfossil archaeocyathids, sponge spicules, and benthic agglutinated foraminifera.

9.1.1 Cambrian Microfossil Assemblage Other Than Foraminifera of Wadi Semna

Khalifa et al. (1988) identified microfaunal assemblage comprising few specimens of *Bactrophyucus oblongum* Zhang (Fig. 26) and Phylum Archaeocyathids beside primitive sponge spicules (Fig. 33) and. Though archaeocyathids are few in the studied samples yet their occurrence is of prime importance as a clue for the age of the Hammamat Group in Egypt.

• Age assignment of the Iгла Formation in Wadi Semna

The oldest known species of Archaeocyathids came from the Tommotian Stage in Russia (Raaben, 1981). They are diversified in subsequent stages of the Early Cambrian. Species are few in the Middle Cambrian. They have been recorded by Omara (1972) from southwestern Sinai, Egypt, and by Basahel et al. (1984) from the Fatima Formation, western Saudi Arabia. Early Cambrian age has been suggested to the Archaeocyathids yielding sediments in the aforementioned localities. Thus, an Early Cambrian age is proposed for the Iгла Formation in Wadi Semna.

• Depositional environment of the Iгла Formation in Wadi Semna

The occurrence of Archaeocyathids indicates marine environment which had moderate turbidity current and warm

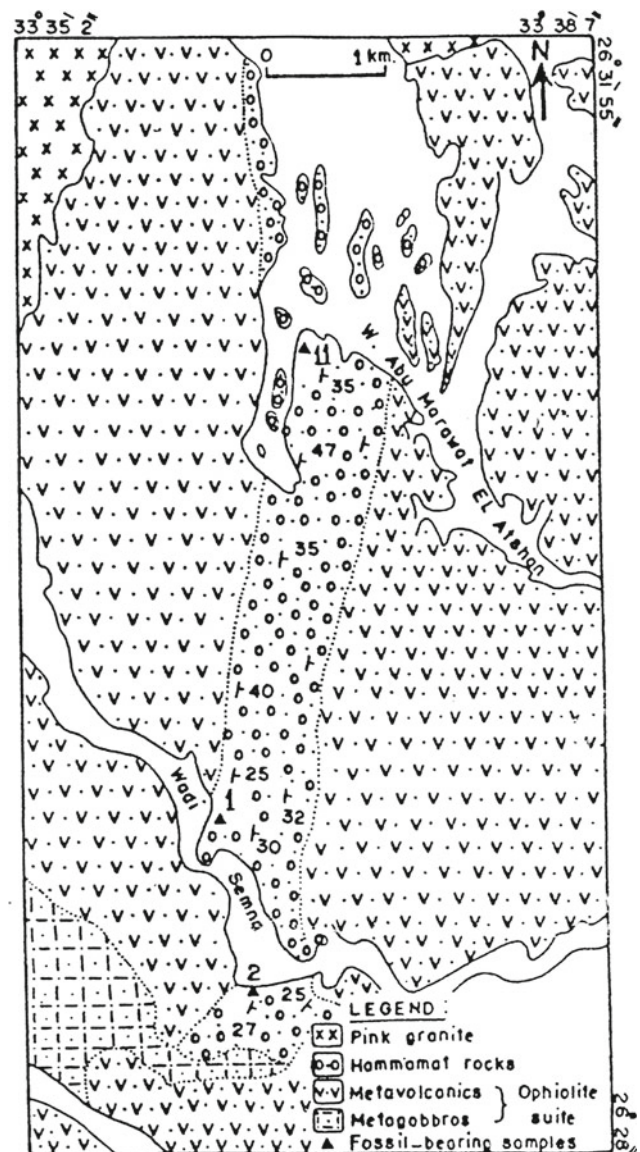


Fig. 32 Fossil-bearing samples, Wadi Semna (Khalifa et al., 1988)

water (25°) at shallow depths of 20–50 m. This indicates that the largely non-marine Hammamat clastics include marine intercalations containing marine microfossils and chamosite, which implies marine incursion or incursions in a sequence of non-marine clastics (Khalifa et al., 1988).

9.1.2 Foraminiferal Fauna of the Iгла Formation at Wadi Semna

The Iгла Formation, Hammamat Group of the Basement complex, Eastern Desert was found containing some foraminifera in Wadi Semna, west Safaga, Eastern Desert, Egypt. Soliman and Habib (1974) identified four benthic agglutinated foraminiferal genera including seven species in the hematitic arenites, siltstones, and greenish

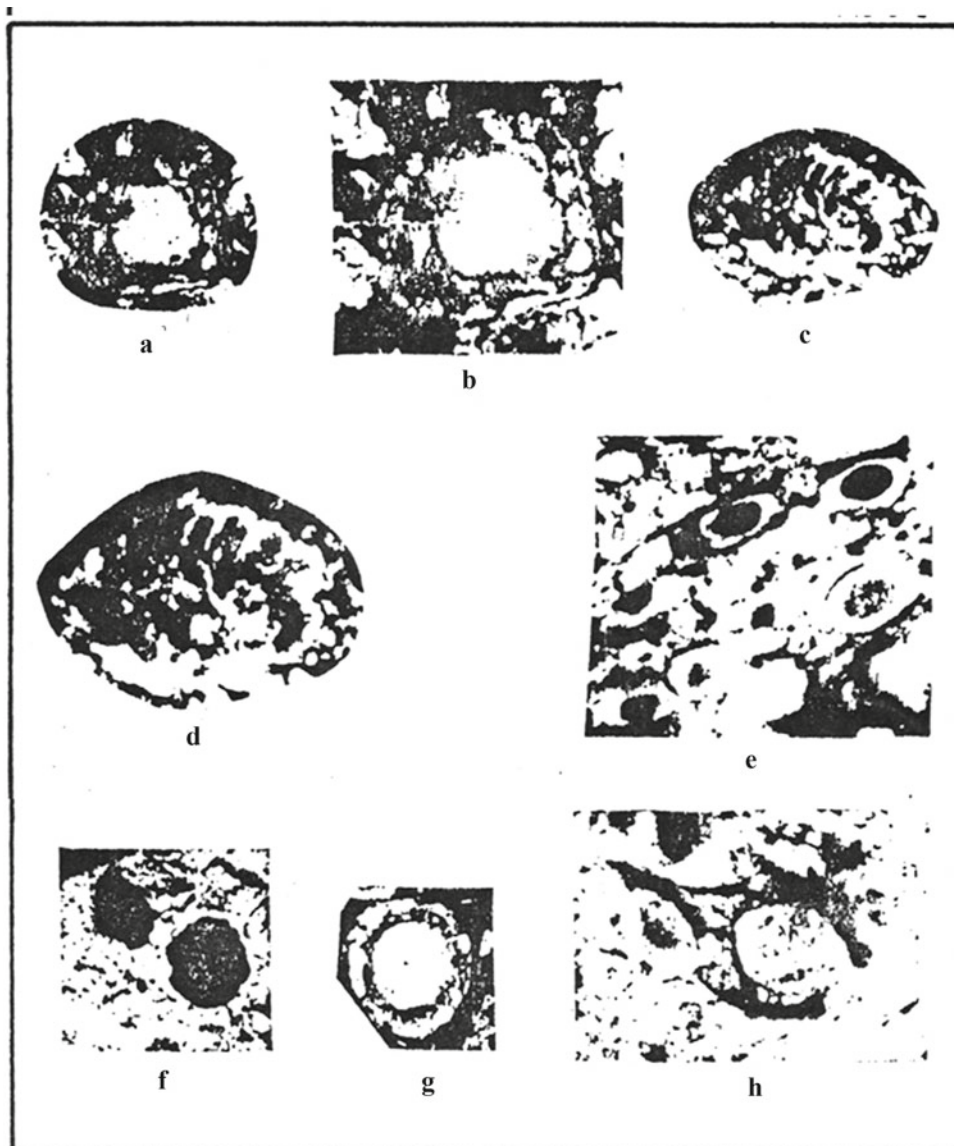


Fig. 33 a, b Transverse section of archaeocyathid. a X 300, b X 420. W. Semna. c, d Transverse section of archaeocyathid shows septa, but wall are recrystallized. c X 300, d X 420. W. Semna. e Tangential section of archaeocyathid shows outer porous wall. X 500. W. Semna. f Organic wall. X. 2000. W. Iglá. g Fragment of archaeocyathid cup shows porous outer and inner walls. 1 X 250. W. Semna. h Sponge spicule. X 250. W. Semna (all photos after Khalifa et al., 1988)

mudstone bands of the Iglá Formation in thin sections and separated specimens. These are *Hyperammia glabra* Cushman and Waters, *Hyperammia bulbosa* Cushman and Waters, *Haplophragmoides margus* Harlton, *Haplophragmoides ciscoensis* Harlton, *Ammobaculites stenomecus* Cushman and Waters, *Ammobaculites suttonensis* Cushman and Waters, and *Trochammia ridus* Cushman and Waters, Fig. 34. They compared this

foraminiferal fauna with similar assemblages described by Cushman and Waters (1927) and others and considered the Iglá Formation in Wadi Semna is of Paleozoic age and not of Precambrian age. This Paleozoic age was verified as Early Cambrian by Khalifa et al. (1988) based on the presence of Archaeocyathids, sponge spicules, and *Bactrophyucus oblongum* Zhang in the Iglá Formation in Wadi Semna.

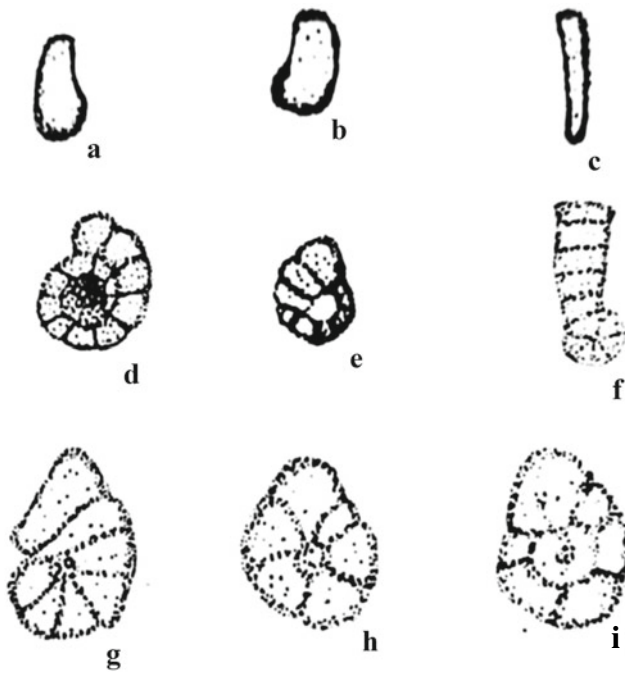


Fig. 34 a, b *Hyperammina bulbosa* Cushman and Waters, X 25; c *Hyperammina glabra* Cushman and Waters, X 25; d *Haplophragmoides ciscoensis* Harlton, X 40; e *Haplophragmoides margus* Harlton, X 35; f *Ammobaculites stenomecus* Cushman and Waters, X 50; g *Ammobaculites suttonensis* Cushman and Waters, X 50; h, i *Trochammina rudis* Cushman and Waters, X 50 (all photos after Soliman & Habib, 1974)

Abu Durba areas in southwest Sinai, while in north Eastern Desert it is exposed in G. Zeit, and north Wadi Qena, Fig. 35. In all the above mentioned areas, the Araba Formation overlies directly the Precambrian basement. The Araba Formation consists of fluvatile to shallow marine, cross-bedded sandstone, and minor conglomerates at its base. It can be subdivided into three discrete units. The basal unit includes basal conglomerate and fluvatile, cross-bedded sandstone. The middle unit comprises shallow marine, dark red silt, and fine sandstone. This is the ichnofossil-bearing unit. The upper unit is predominated by trough cross-bedded sandstone. The Araba Formation attains up to 190 m thick.

In Abu Durba area, the lower part of the Araba Formation includes some meters of limestone holding stromatolites and archaeocyathids of Early Cambrian age (Omara, 1972). Said (1980) reports a carbonate bed at that area that yielded algal stromatolites which have been identified as belonging to the species *Vetella ushbasica* known from the lower Cambrian of Kazakhstan. This Lower Cambrian age is supported by Klitzsch (1990) and Seilacher (1990) based on ichnofossil assemblages, but the body fossils identified by Omara (1972) are doubted by Elicki et al. (2013).

The Araba Formation includes a rich ichnofossil content of Lower Cambrian age. This content was previously studied in detail by Klitzsch (1990), Seilacher (1990), and later by Elicki et al. (2013).

In these studies, 20 Cambrian ichnofossil species are described. These are 9 ichnofossil species specific to the Eastern Desert, 7 ichnofossil species specific to Sinai, and 4 ichnofossil species recorded in both the Eastern Desert and Sinai. The specific species to the Eastern Desert are *Diplichnites* isp., *Dimorphichnus* cf. *quadrifidus* (Seilacher, 1990), *Diplocraterion* isp., *Arenicolites* isp., *Teichichnus rectus* (Seilacher, 1955), *Planolites montanus* (Richter, 1937), *Helminthopsis tenuis*, isp. indet. (?*Dydimaulichnus*, ?*Archaeonassa*), and biomat structures. The specific species to Sinai are *Rusophycus burjensis* (Hofmann et al., 2012), *Cruziana* isp., *Dimorphichnus quadrifidus* (Seilacher, 1990), *Dimorphichnus* cf. *obliquus* (Seilacher, 1955), *Bergaueria sucta* (Seilacher, 1990), ?*Bergaueria* isp., and *Fucusopsis* isp. The ichnofossil species reported from both the Eastern Desert and Sinai are *Rusophycus aegypticus* (Seilacher, 1990), *Cruziana salomonis* (Seilacher, 1990), and *Skolithos* isp. and *Palaeophycus tubularis* (Hall, 1847), Figs. 36 and 37.

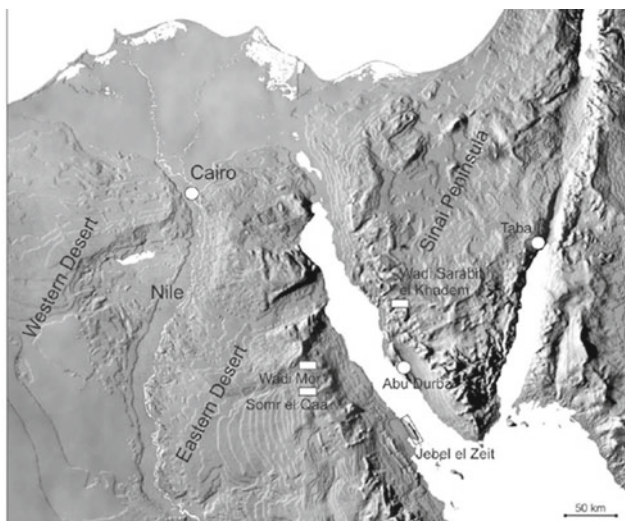


Fig. 35 Location of areas of exposures of the Araba Formation in northeastern Desert and southwest Sinai (after Elicki et al., 2013)

9.2 Cambrian Fauna of Sinai and Eastern Desert

The oldest Cambrian unit in southwest Sinai and north Eastern Desert of Egypt is the Araba Formation. The Araba Formation is exposed in Um Bogma, Wadi Feiran, and

9.3 Burgess Shale Fauna

The Middle Cambrian Burgess Shale is one of the most unique fossil assemblages in the geologic archives, which

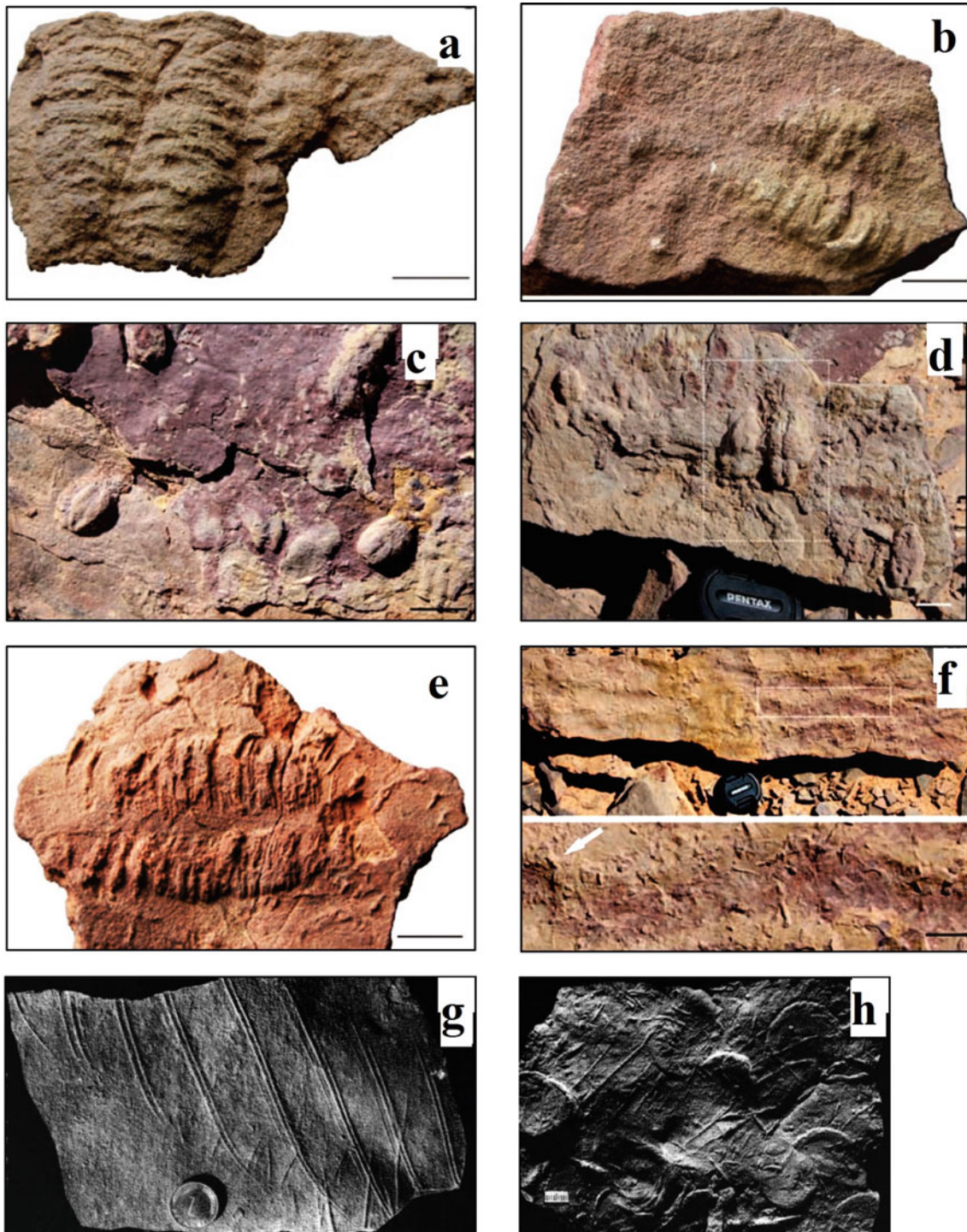


Fig. 36 a, b *Rusophycus burjensis* Hofmann, scale bar = 2 cm; c, d *Rusophycus aegypticus* (Seilacher, 1990), scale bar = 2 cm; e *Cruziana salomonis* (Seilacher, 1990), scale bar = 2 cm; f *Planolites montanus* (Richter, 1937), scale bar = 2 cm; g *Dimorphichnus* cf. *obliquus* (Seilacher, 1955); h *Bergaueria sucta* (Seilacher, 1990) (a–f after Elicki et al., 2013, g, h after Seilacher, 1990)

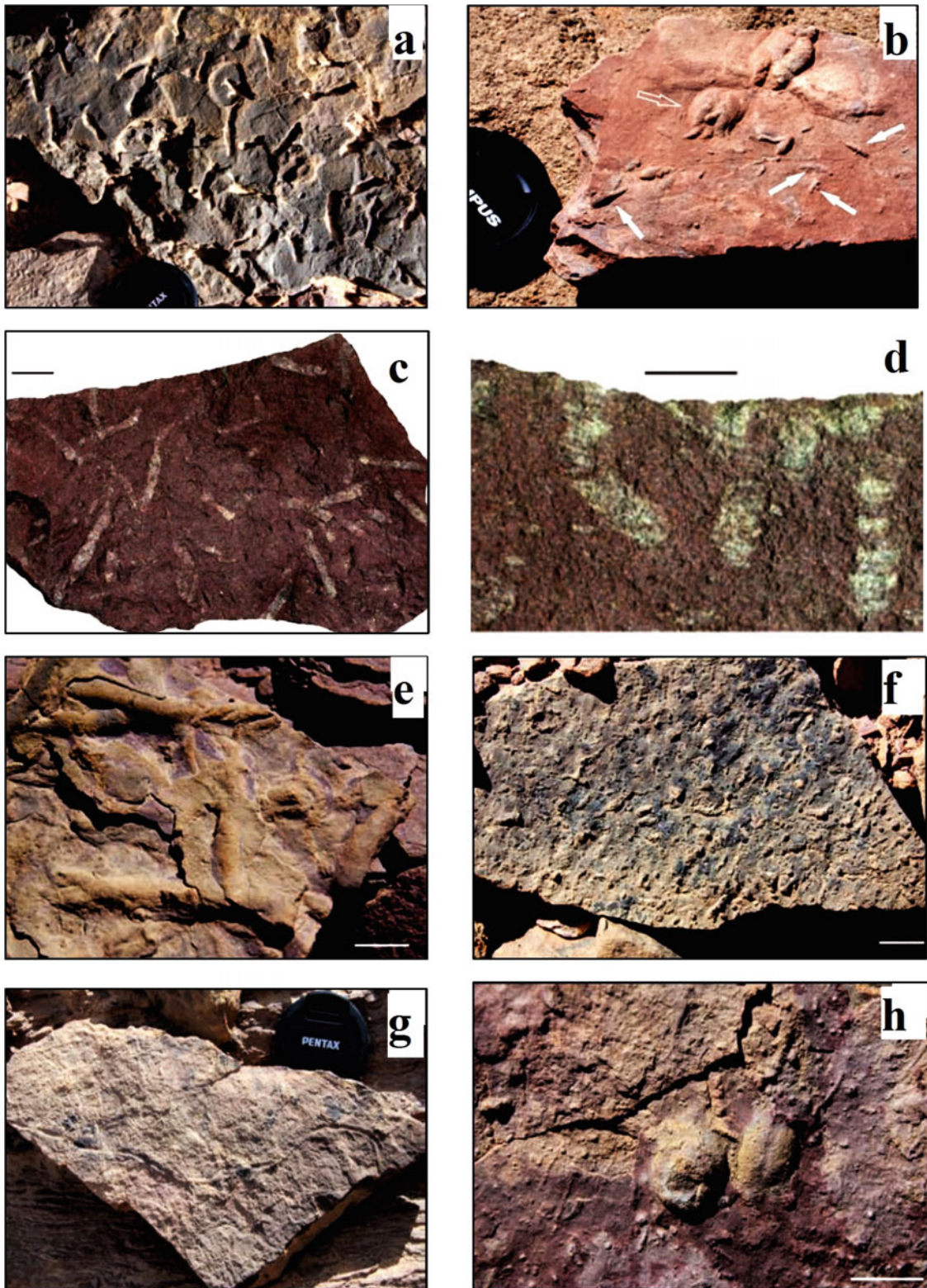


Fig. 37 **a** *Diplocraterion* isp., diameter of lenscap 6.5 cm; **b** *Arenicolites* isp., diameter of lenscap 4 cm; **c**, **d** *Teichichnus rectus* (Seilacher, 1955), scale bar = 1 cm; **e** *Palaeophycus tubularis* (Hall, 1847), scale bar = 1 cm; **f** *Planolites montanus* (Richter, 1937), scale bar = 3 cm; **g** *Helminthopsis tenuis*, diameter of lenscap 6.5 cm; **h** *Skolithos* isp., poorly preserved *Rusophycus aegypticus* (Seilacher, 1990), scale bar = 1 cm (all figures after Elicki et al., 2013)

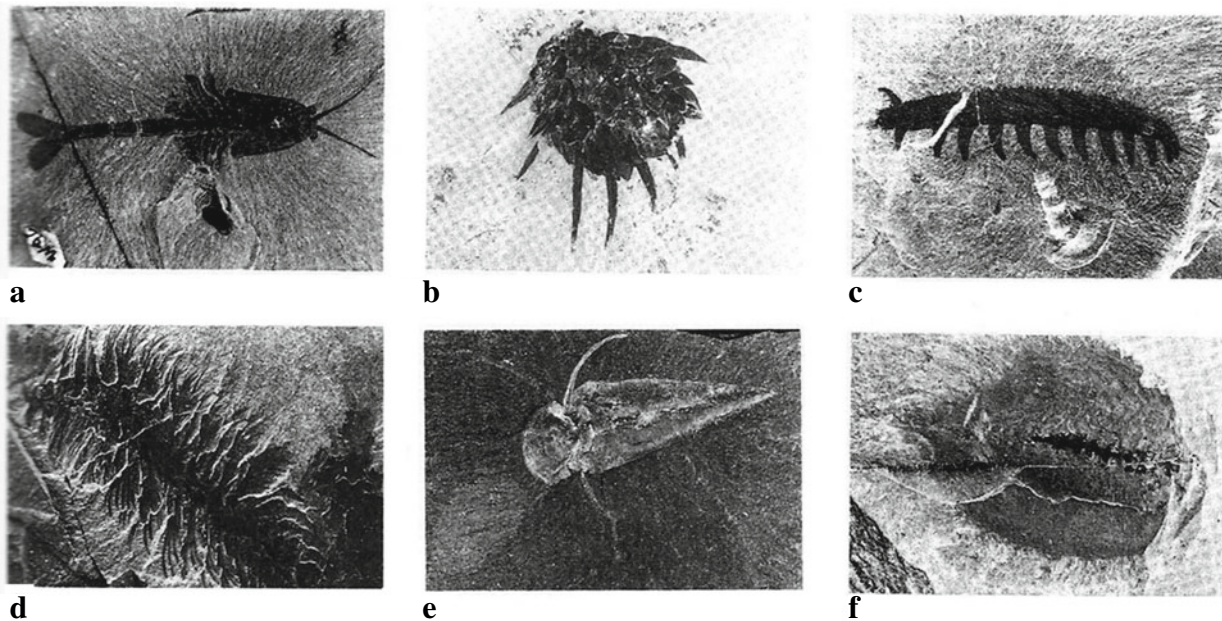


Fig. 38 Burgess Shale fossils. **a** *Waptia fieldensis*, an arthropod. **b** *Wiwaxia corrugate*, affinity uncertain. **c** *Aysheaia pedunculata*, an arthropod. **d** *Canadia irregularia* an annelid worm. **e** *Hyolithes carinatus*, a mollusk (?). **f** *Naraoia spinifer*, an arthropod (Cooper et al., 1990)

includes more than 170 species representing at least eight known and perhaps even more previously unknown phyla. Most of the fossils are unique to the single locality and represent taxa that went into extinction by the end of the Cambrian. The Burgess Shale is a fossil-bearing deposits cropping out in the Canadian Rockies of British Columbia, Canada.

The Burgess Shale encompasses a remarkable assemblage of fossils of soft-bodied organisms, many of them were not recognized from nowhere else, accompanied by biomineralized organisms. It gives the most complete glimpse of Lower Paleozoic life. The Burgess Shale faunal assemblage includes trilobites, many worm phyla as annelids, and several groups of soft-bodied arthropods transitional in structure between the trilobites and the modern arthropod groups, jellyfish and sea anemones, a particular scaly mollusk, a holothurians echinoderm, an ancestral chordate, and several representatives of totally extinct groups, Fig. 38. The Burgess Shale soft-bodied fossils are preserved as flattened carbonaceous films along the bedding planes of the shale in amazing detail.

This black shale deposit apparently formed at the base of a steep algal reef where unstable muds slid down into a deeper basin which was a toxic, hydrogen sulfide-generating environment excluding bacteria and scavengers. As a result, organisms which were swept into or swam into the area were asphyxiated, died, and were buried without being destroyed.

References

- Abd El-Wahed, M. A. (2010). The role of the Najd fault system in the tectonic evolution of the Hammamat molasse sediments, Eastern Desert, Egypt. *Arabian Journal of Geosciences*, 3, 1–26.
- Akaad, M. K., & Noweir, A. M. (1980). Geology and lithostratigraphy of the Arabian Desert orogenic belt of Egypt between latitudes 25° 35' and 26° 30' N. *Bulletin Institute of Applied Geology, King Abdul Aziz University, Jeddah*, 3(4), 127–134.
- Basahel, A. N., Bahafzallah, A., Omara, S., & Jux, U. (1984). Early Cambrian carbonate platform of the Arabian Shield. *Neues Jahrbuch für Geologie und Paläontologie—Monatshefte*, 1984(2), 113–128.
- Cooper, J. D., Miller, R. H., & Patterson, J. (1990). *A trip through time* (2nd ed.). Merrill Publishing Company, A Bell & Howell Information Company.
- Cushman, J. and Waters, T. (1927). Arenaceous Paleozoic Foraminifera from Texas. *Contributions from the Cushman Laboratory for Foraminiferal Research*, 3(2), 146–155.
- El-Gaby, S., & Habib, M. (1982). The eugeosynclinal filling of Abu Ziran Group in the area SW of Port Safaga, Eastern Desert, Egypt. *Bulletin Institute of Applied Geology, King Abdul Aziz University, Jeddah*, 3(4), 134–142.
- El-Gaby, S., List, F. K., & Tehrani, R. (1990). The basement complex of the Eastern Desert and Sinai. In R. Said (Ed.), *The geology of Egypt* (pp. 75–184). Balkema.
- Elicki, O., Khalifa, M. A., & Farouk, S. (2013). Cambrian ichnofossils from northeastern Egypt. *Neues Jahrbuch für Geologie und Paläontologie—Abhandlungen*, 270(2), 129–149.
- Hall, J. (1847). *Paleontology of New York. Vol. 1. Containing descriptions of the organic remains of the lower middle division of the New York System (equivalent in part to the Lower Silurian rocks of Europe)*. 338p Albany (C. van Benthuyssen).

- Hassan, A. M. (1967). A new Carboniferous occurrence in Abu Durba, Sinai, Egypt. In Sixth Arab Petroleum Congress, *Baghdad*, 39(B-3), 8.
- Hassan, M. A., & Hashad, A. H. (1990). Precambrian of Egypt. In R. Said (Ed.), *The geology of Egypt* (pp. 201–248). Balkema.
- Hofmann, R., Mangano, G., Elicki, O., & Shinaq, R. (2012). Paleoecologic and biostratigraphic significance of trace fossils from Middle Cambrian shallow- to marginal -marine environments of Jordan. *Journal of Paleontology*, 86(6), 931–955.
- Jenkins, D. A. (1990). North and Central Sinai. In R. Said (Ed.), *The geology of Egypt* (pp. 361–380). Balkema.
- Khalifa, H., Omran, A. M., & Hegazy, H. A. (1988). Microfossils from Late Proterozoic (Hammamat Group), Eastern Desert, Egypt. *Bulletin of the Faculty of Science, Assiut University*, 17(1-F), 131–159.
- Klitzsch, E. (1990). Paleozoic. In R. Said (Ed.), *The geology of Egypt* (pp. 393–406). Balkema.
- Knoll, A. H., & Vidal, G. (1980). Protistan microfossils in phosphate nodules from the Late Precambrian Visingsö beds of Central Sweden. *Geologiska Föreningen i Stockholm Förhandlingar*, 102(3), 207–211.
- Milstein, V. E., & Golovanov, N. P. (1979). Upper Precambrian microphytolites and stromatolites from Svalbard. *Norsk Polarinstittut Skrifter*, 167, 219–224.
- Mintz, L. W. (1981). *Historical geology* (3rd ed.). Merrill Publishing Company, A Bell & Howell Information Company.
- Omara, S. (1972). An Early Cambrian outcrop in southwestern Sinai, Egypt. *Neues Jahrbuch für Geologie und Paläontologie—Monatshefte*, 1972(5), 306–314.
- Raaben, M. (Ed.). (1981). *The Tommotian Stage and the Cambrian lower boundary problem*. Amerind Publishing.
- Richter, R. (1937). *Marken und Spuren aus allen Zeiten*, I-II. Senckenbergiana, Vol. 19, pp. 150–169.
- Ries, A. C., Shackleton, R. M., Graham, R. H., & Fitches, W. R. (1983). Pan-African structures, ophiolites and melange in the Eastern Desert of Egypt: A traverse at 26°N. *Journal of the Geological Society of London*, 140, 75–95.
- Said, R. (1990). *The Geology of Egypt*. p. 731, Balkema.
- Schopf, J. W. (1968). Microflora of the Bitter Springs Formations, Late Precambrian, Central Australia. *Journal of Paleontology*, 42, 651–688.
- Seilacher, A. (1955). Spuren und Lebensweise der Trilobiten. In: Schindewolf, O.H. & Seilacher, A. (Eds.): *Beitrag zur Kenntnis des Kambriums in der Salt Range (Pakistan)*. Abhandlungen der Akademie der Wissenschaften und der Literatur in Mainz, mathematisch-naturwissenschaftliche Klasse, Vol. 10, pp. 342–399.
- Seilacher, A. (1990). Paleozoic trace fossils. In R. Said (Ed.), *The geology of Egypt* (pp. 649–722). Balkema.
- Soliman, H. A., & Habib, M. F. (1974). Discovery of Paleozoic Foraminifera in the Iqla Formation of Semna, Eastern Desert, Egypt. *Bulletin of the Faculty of Science, Assiut University*, 3(2), 89–97.



Abdel Galil Hewaidy is a professor and former head of the Geology Department, Faculty of Science, Al-Azhar University, Cairo, Egypt. He received a Ph.D. (1983) degree in micropaleontology and stratigraphy from Al-Azhar University, Egypt. His research interests integrate systematic paleontology, biostratigraphy, paleoecology, sea-level fluctuations and sequence stratigraphy in Jurassic, Cretaceous, Paleogene and Neogene successions in Egypt, Saudi Arabia, and Qatar. During the last 40 years, he has published 105 research papers in local and international journals, five geologic books written in Arabic, as well as the Glossary of illustrated

terms in geology and environmental geology (English-Arabic) published in 2020. He has described 67 new foraminiferal, ostracod, molluscan and vertebrate species. Prof. Abdel Galil Hewaidy has supervised more than 55 M.Sc. and Ph.D. theses and dissertations. A former editor of the Egyptian Journal of Paleontology (2001–2015), he has been a consultant for the Ministry of Environmental Affairs since 2016. He is member of the National Committee of the Geological Sciences of the Academy of Scientific Research and Technology (2020–2023). In 2006, he received the “Kuwait Foundation for the Advancement of Sciences” prize for the “best scientific book written in Arabic” and the medal of the Egyptian Ministry of Environmental Affairs (2016) for his efforts in the protection and maintenance of the environment.



Mesozoic Sedimentary Succession in Egypt

Nageh A. Obaidalla, Kamel H. Mahfouz, and Amr A. Metwally

Abstract

The three Mesozoic divisions (Triassic, Jurassic, and Cretaceous) are represented in Egypt by sedimentary rocks on the surface and subsurface areas by different percentages in the different geographic provinces of Egypt. Generally, the Triassic and the Jurassic sedimentary successions confined to the northern part of Egypt, while the Cretaceous sedimentary rocks are well represented all over the Egyptian geographic provinces. The distribution of the Mesozoic sedimentary rocks may be related to the intensive erosion following the regional uplifting of the most parts of Egypt due to several tectonic events such as the Pan-African Orogeny at the end of the Proterozoic Era, the collision of the Gondwana and Laurasia at the end of the Paleozoic Era, the formation of the Central Atlantic Ocean during the Late Jurassic (rifting of Laurasia from Gondwana), the South Atlantic rifting during the Late Cretaceous (breakup of Africa from South America), and finally, the formation of Syrian Arc Structure at the end of the Cretaceous. The Cretaceous strata are characterized by different facies in the different localities of Egypt, due to the impact of the rifting of Africa and South America continental plates at this time and the deformation of the Syrian Arc Event which led to the rejuvenation of old faults and form several sedimentary basins. The northern region of Egypt shows more or less complete Mesozoic sedimentary successions, but the central and southern regions show missing for the Lower Mesozoic strata

(Triassic, Jurassic, and several strata of the Lower Cretaceous sedimentary succession).

Keywords

Mesozoic successions • Proterozoic Era • Syrian Arc Structure • Egypt

1 Introduction

The Mesozoic sedimentary rocks in Egypt are differentiated into three systems which are arranged from older to younger into Triassic, Jurassic, and Cretaceous. These rocks are distributed by different percentages on the surface (exposed rocks) and subsurface (unexposed rocks) in the different geographic provinces (Western Desert (WD), Eastern Desert (ED), and Sinai (SN)) of Egypt (Fig. 1). The Triassic and Jurassic successions represent the minor percentage of the Mesozoic sedimentary rocks, but the Cretaceous strata represent the major percentage at both the surface and subsurface geographic provinces of Egypt. The Triassic and Jurassic sedimentary rocks are mainly restricted to the northern parts of Egypt, while they are missing in the other parts of Egypt (Figs. 2 and 3). This missing may be linked to the intensive erosion following the regional uplifting of the most parts of Egypt due to the Pan-African Orogeny at the end of the Proterozoic Era, the collision of the Gondwana and Laurasia at the end of Paleozoic Era, the formation of the Central Atlantic Ocean during the Late Jurassic (rifting of Laurasia from Gondwana), the formation of the South Atlantic Ocean during the Late Cretaceous (rifting of Africa from South America), and the deformation of Syrian Arc Event at the end of the Cretaceous (Fig. 4). The final event continued until the Eocene Epoch (Morgan, 1990). In these parts of Egypt, the sedimentary rocks of the Early and/or Late Cretaceous age overlie the Precambrian rocks, especially in the south parts of Egypt. This indicates that these parts were high positive

N. A. Obaidalla (✉) · A. A. Metwally
Geology Department, Faculty of Science, Assiut University,
Assiut, 71516, Egypt
e-mail: nageh@ aun.edu.eg

A. A. Metwally
e-mail: amr.metwally@ aun.edu.eg

K. H. Mahfouz
Geology Department, Faculty of Science, Al-Azhar University,
Assiut Branch, Assiut, 71524, Egypt
e-mail: kamel.mahfouz@ azhar.edu.eg

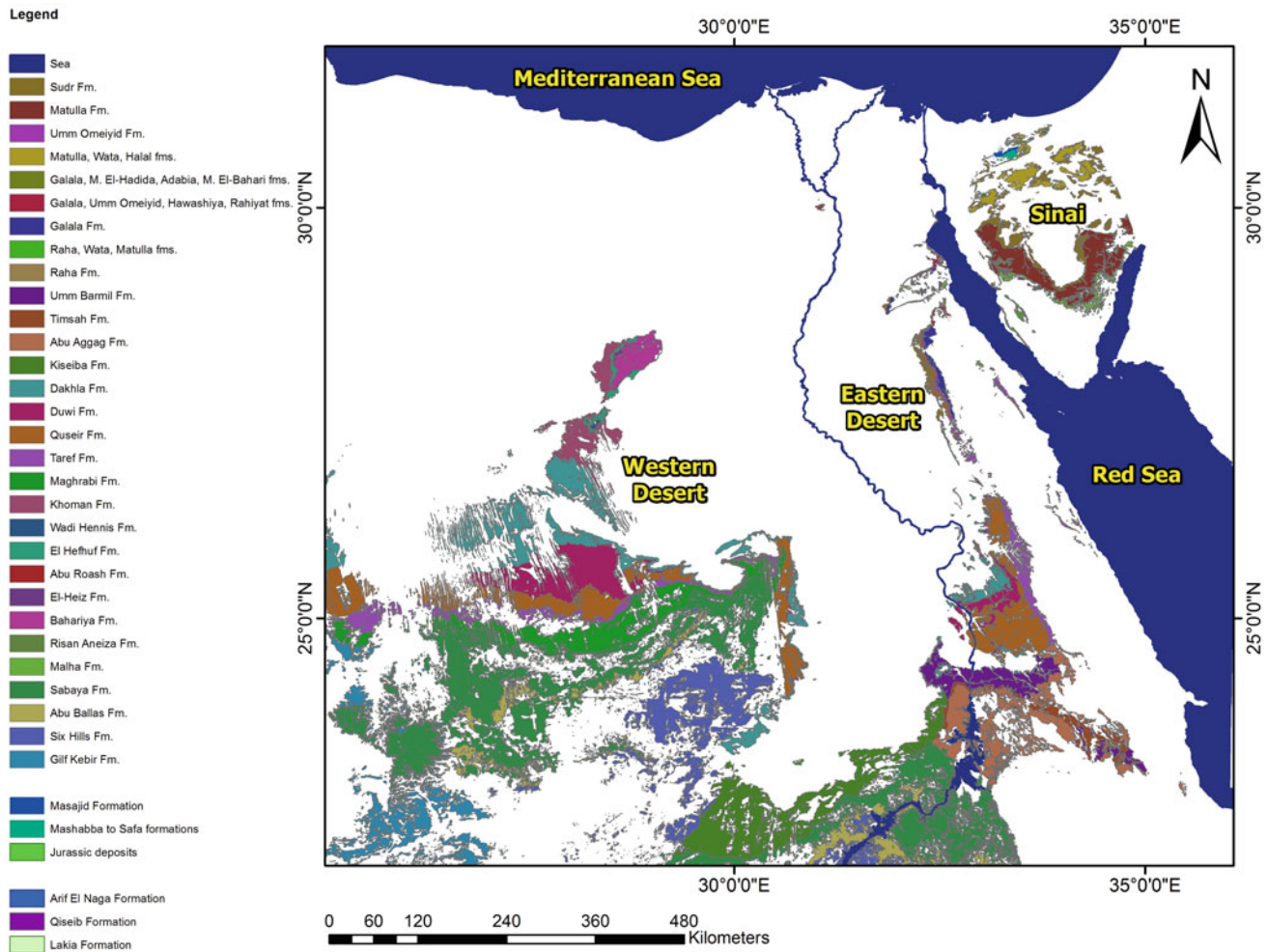


Fig. 1 Geological map of the Mesozoic sedimentary rock units in Egypt (modified after Conoco, 1987)

structural over long time after the orogeny. Moustafa (2020) believed that the missing of the almost Triassic and Jurassic sedimentary rocks may be due to the effect of a phase of deformation started in the Middle-Late Triassic (divergent motion of the Eurasian and Afro-Arabian Plates).

On the contrary, the Cretaceous sedimentary rocks are widely distributed in Egypt covering ~ 40% (Fig. 5). The sedimentary rocks of the Cretaceous are characterized by different facies due to the formation of several sedimentary basins in the different localities of Egypt. These sedimentary basins were controlled by the fragmentation of Gondwana Continent due to the formation of the Atlantic Ocean.

The northern parts of Egypt (e.g., SN and north ED) reveal approximately complete surface Mesozoic sedimentary sequences from Triassic to Cretaceous. Also, in the northern WD, these complete sequences are well documented from the subsurface data of the activities of the petroleum companies. On the other hand, the southern parts of Egypt are only represented by the Cretaceous sedimentary rocks.

The Mesozoic sedimentary successions in Egypt have been great attention by many authors such as Kerdany and Cherif (1990) and Issawi et al. (2009). Also during the last century, a lot of the stratigraphic works were carried out, several works on the Mesozoic sedimentary rocks in the different localities in Egypt on specific time intervals (e.g., Abdallah et al., 1963; Abdel-Gawad et al., 2011; Abed et al., 1996; Al Far, 1966; Awad & Ghobrial, 1965; EGPC, 1992; El-Naggar, 1970; El Nakkady, 1955; Ghorab, 1961; Hantar, 1990; Hermina et al., 1989; Kerdany & Cherif, 1990; Khalifa & Abu El-Hassan, 1993; Klitzsch, 1978, 1990; Kora et al., 1994; Luger, 1985; Norton, 1967; Obaidalla & Kasab, 2000; Obaidalla et al., 2018, 2020; Sadek, 1926; Said, 1961, 1962, 1971; Saber et al., 2009; and others). The accumulated results of these publications and other published works, especially in the last two decades, need to link with the other to summarize and simplified the different rock units of the Mesozoic sedimentary rocks. At the same time, the vertical and lateral relationship between almost Mesozoic

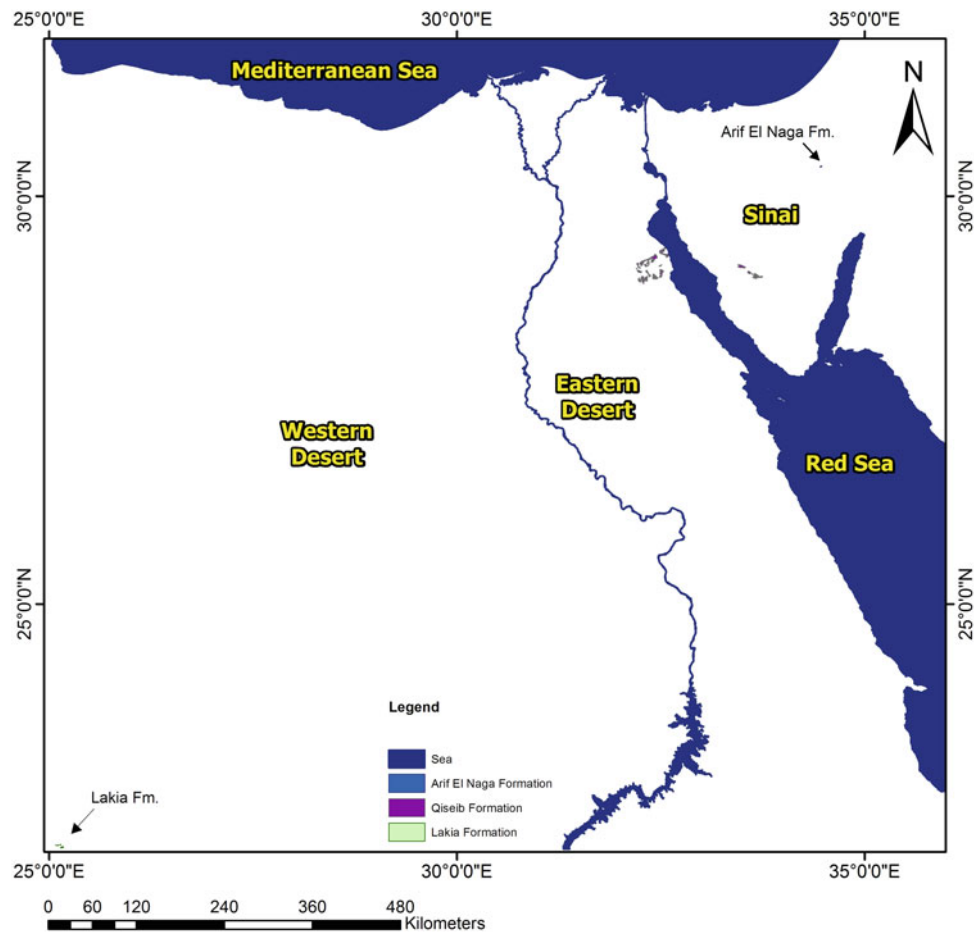


Fig. 2 Geological map of the Triassic sedimentary rock units in Egypt (modified after Conoco, 1987)

rock units needs more investigation to be clearer for the readers. So, the main aims of the present work are as follows: (1) trace the main tectonic events which effect on the formation of the Mesozoic sedimentary succession, (2) merge and simplify the similar rock units upon the priority, and (3) define the vertical and lateral rock units relationship. The sedimentary successions of the three systems of the Mesozoic (Triassic, Jurassic, and Cretaceous) are discussed in the following paragraphs.

2 The Triassic Successions

The Triassic sedimentary rocks are mainly of tidal flat and deltaic sedimentation, and the marine one was deposited only on a limited place at the extreme northeast part of Egypt at the Arif El Naga Domal Structure (Fig. 6). This indicates that the Triassic marine was restricted to the northeast part of Egypt and most of the Egyptian places were positively exposed area. This may be due to the Pan-African Orogeny at the end of the Proterozoic Era or the collision of the Gondwana and Laurasia plates at the end of the Paleozoic Era. Also, the first phase of the

fragmentation of the Gondwana Continent was at the end of the Triassic Period and was represented by the drifting of the Cimmeria Blocks (Turkey, Iran, and Tibet). The impact of the Pan-African Orogeny is documented by the nonconformity relationships between the Precambrian basement rocks and Early and/or Late Cretaceous sedimentary rocks at the south of Egypt such as: Barramiya area along the Idfu-Meras Road, west Fawakher, Wadi (W.) Hamamat and Gebel (G.) Duwi along the Qift-Qusier Road, W. Quieh near the Red Sea coast, W. Shait east of Kom Ombo, W. Haudian (Abraq area) northwest of Shalatin (Fig. 7). The impact of the collision of the Gondwana and Laurasia plates is documented by the occurrence of disconformity between the Late Paleozoic sedimentary rocks and the Jurassic and/or the Cretaceous strata (Abrams et al., 2016; Klitzsch et al., 1979, 1990; Wycisk, 1984).

The marine strata at Arif El Naga dome are of Middle Triassic, which indicates that the Tethys Ocean covered this area of Egypt at that time (Fig. 8). The Triassic fluvio-marine rocks are recorded in four localities: (1) Central SN at Nekhl, Hamra, and Ayun Musa regions and southwest SN at Um Bogma (Qiseib Formation (Fm.)), (2) Northern ED (W. Araba and Abu El Darag), (3) southwest Egypt at Abu Ras

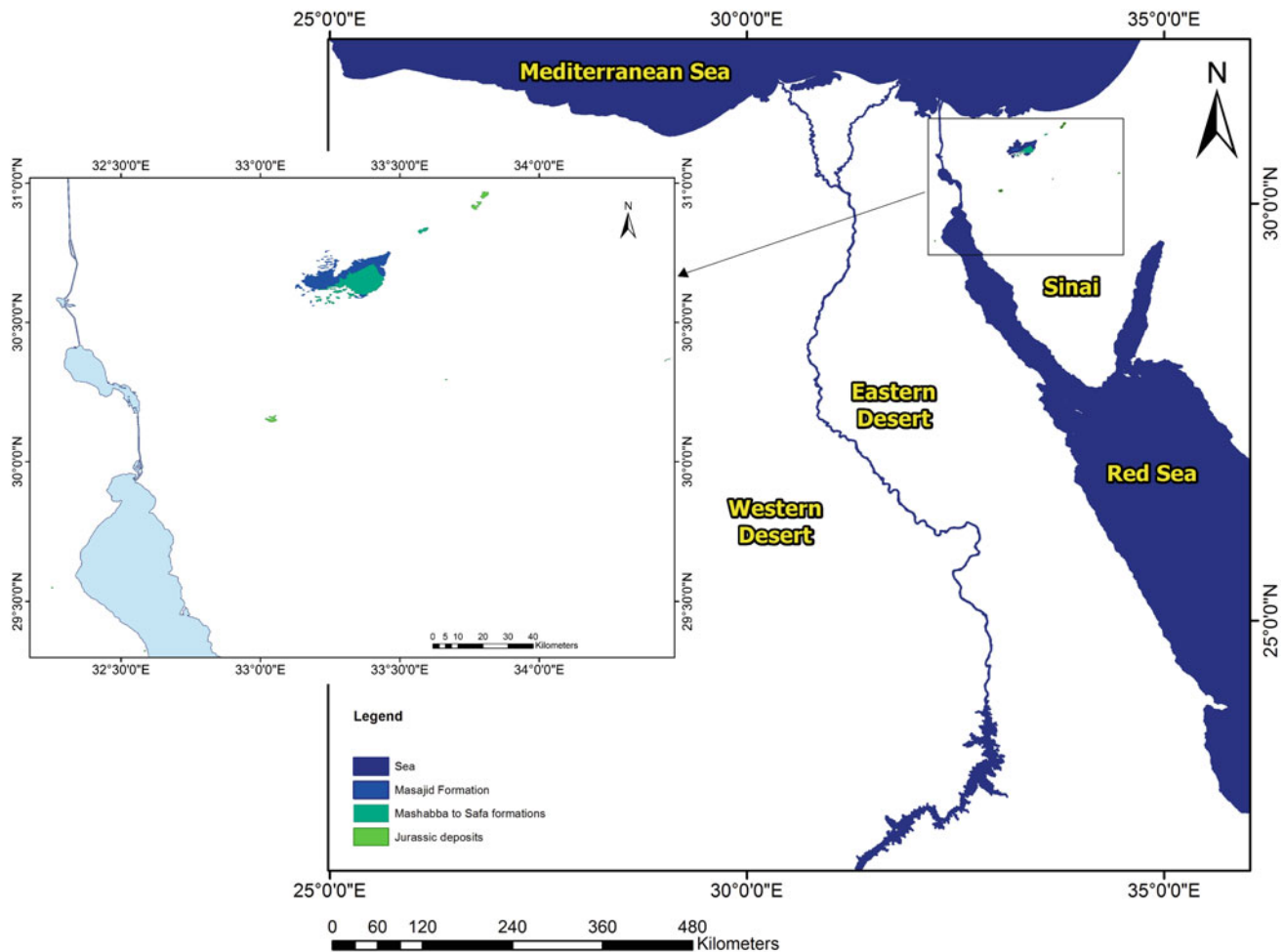


Fig. 3 Geological map of the Jurassic sedimentary rock units in Egypt (modified after Conoco, 1987)

Plateau (Abu Ras or Lakkia Fm.), and (4) North WD at Alamein, Faghur, and Abu Gharadig (Eghei Group).

The distribution of the Triassic rock units is restricted in the north of Egypt. This distribution indicates that the facies of the Triassic strata are changed from continental (fluvial) to shallow-deep marine facies from south to north (Fig. 9).

2.1 The Arif El Naga Formation

Awad (1946) described this formation at G. Arif El Naga Domal Structure (Fig. 6). Said (1971) and Abed et al. (1996) assigned the Arif El Naga Fm. at the type locality to the Middle Triassic age. G. Arif El Naga Domal Structure locates at the extreme northeast of Egypt; ~ 10 km west of the eastern Egyptian border and ~ 40 km SSE of the El-Qusaima region. Said (1971) subdivided the Arif El Naga Fm. into three informal units:

- A. **The Arif El Naga (A) Unit:** It composes of fluvial to fluvio-marine strata of ~ 50 m thick, which subdivided into basal part of ~ 23 m thick of non-fossiliferous varicolored, medium-grained quartzite sandstone with minor claystone, the upper part is ~ 27 m thick and consists of sandstone, limestone, and claystone beds carrying vertebrate remains, plant imprints, and fossil wood. Also, this part contains bivalves fossil such as *Trigonodus tenuidentatus* and *Unionites fassaensis*.
- B. **The Arif El Naga (B) Unit:** It measures ~ 18 m thick of argillaceous limestone and claystone beds with the ammonite *Beneckia levatina* and the bivalve *Neoschizodus orbicularis*. The age of both (A) and (B) units is Middle Triassic. They were deposited in tidal flats-shallow neritic settings.
- C. **The Arif El Naga (C) Unit:** It is ~ 117 m thick of fossiliferous limestones, marls, and shales. The age of the "C" beds is late Middle-early Late Triassic. Zak (1964)

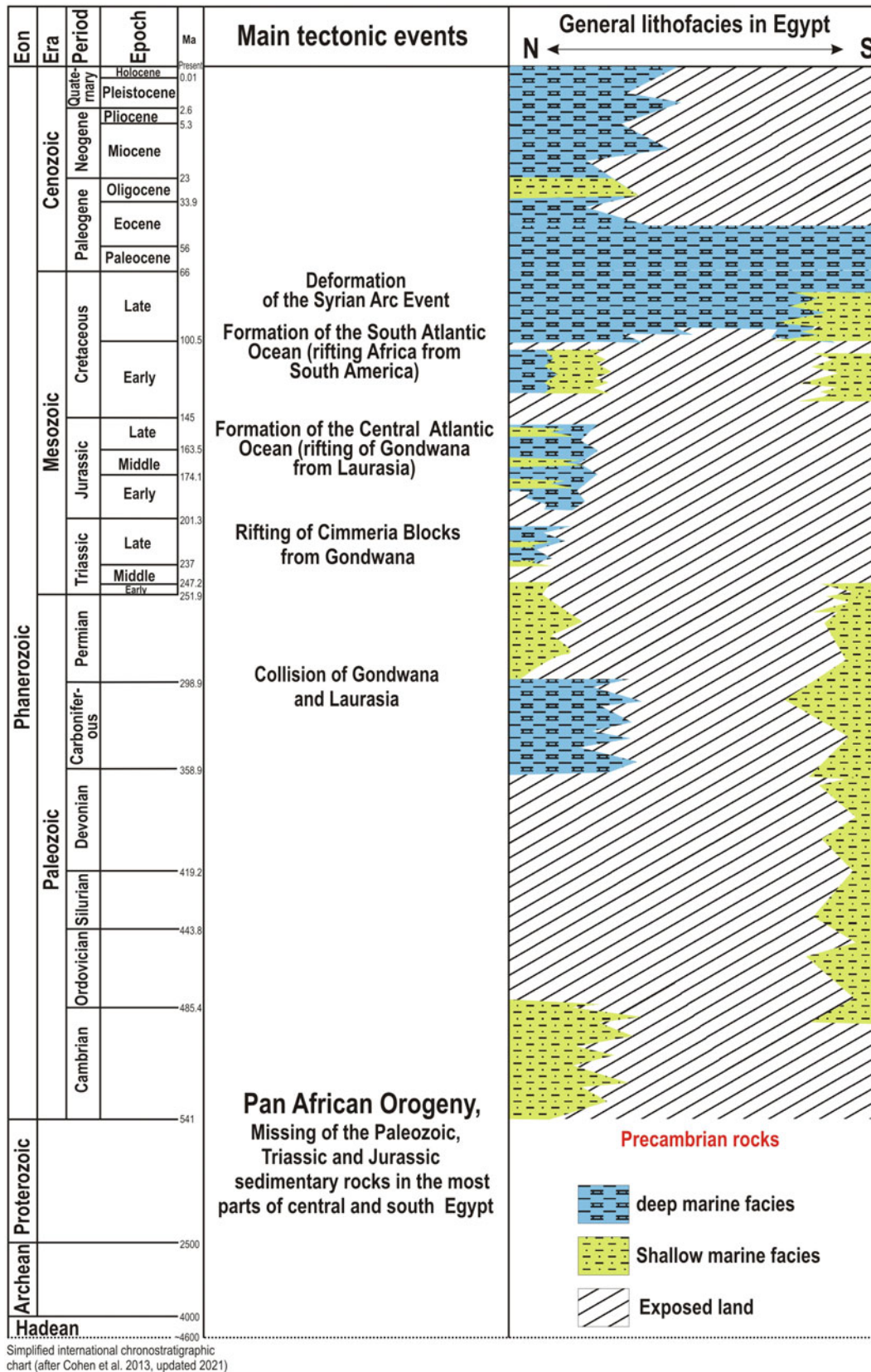


Fig. 4 Main tectonic events affected on the distribution of the Mesozoic sedimentary successions in Egypt

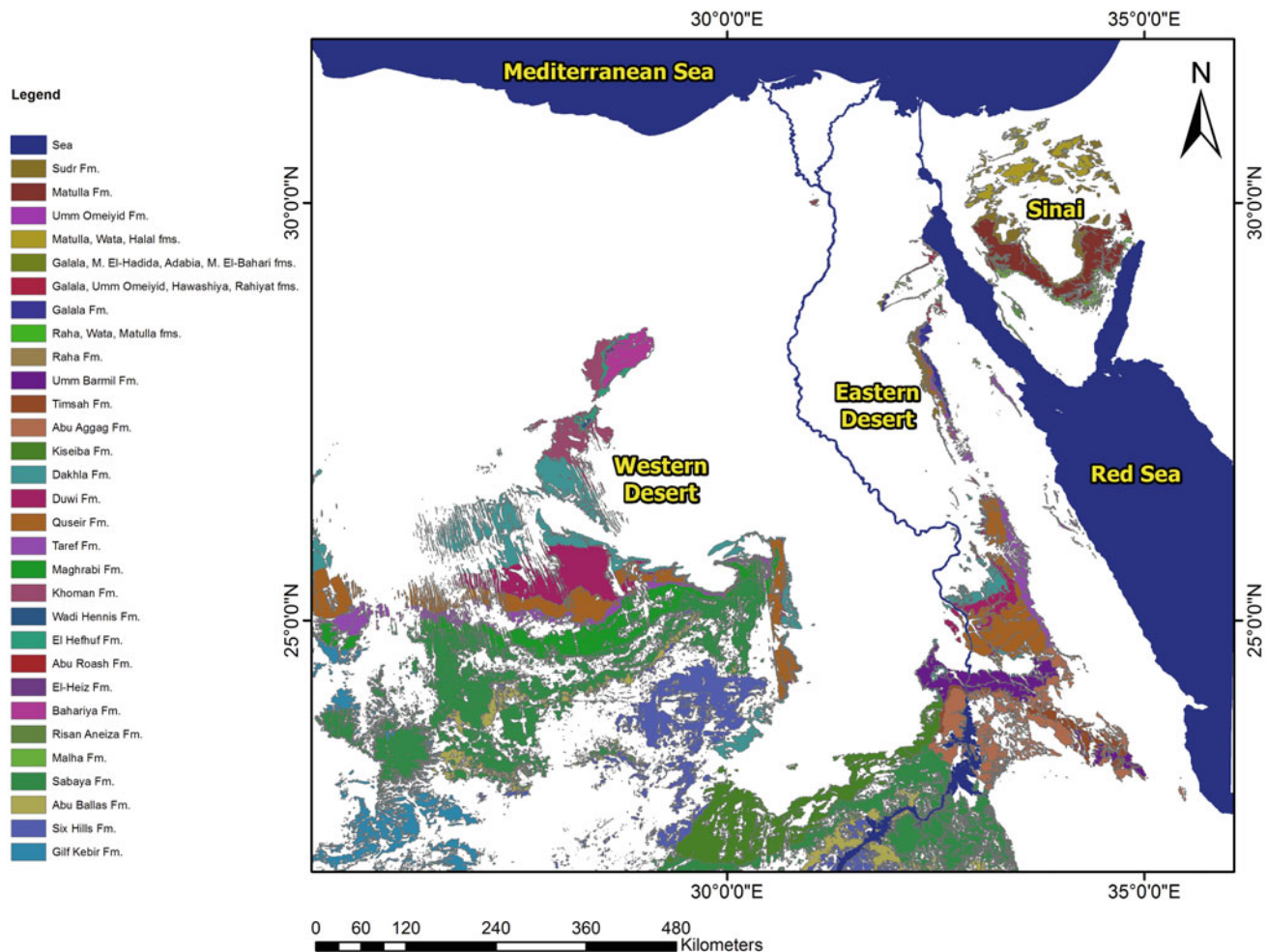


Fig. 5 Geological map of the Cretaceous sedimentary rock units in Egypt (modified after Conoco, 1987)

classified this unit into three parts from base to top as: basal unit is ~ 35 m thick of fossiliferous limestone (e.g., *Paraceratites binodosus*, *Gevanites inflatus*, and *Gevanites awadi*) cutting by an olivine basalt dike; the middle part is ~ 31 m thick of limestone and marl with the ammonite *Gevanites epigonus*, bivalve *Pseudoplacunopsis fossistriata*, and vertebrate remains; the upper part consists of ~ 51 m thick limestone and gypsum with many dolomite and marl intercalations. It contains some poorly preserved nautilids, gastropods, crinoid stems, echinoid spines, and the marker conodont *Pseudofurnishius murcianus* of the late Middle Triassic. This indicates shallow marine setting with local hypersaline conditions.

El-Azabi and El-Araby (2005) subdivided Arif El Naga Fm. into two facies: the lower clastic facies (Early-Middle Triassic age) deposited under continental to shallow subtidal setting. But the upper carbonate facies (Late-Middle–earliest Late Triassic age) deposited under intertidal to shallow

subtidal settings. They (op. cit.) demonstrated unconformity relationship between Arif El Naga Fm. and the Jurassic Mashabba Fm.

2.2 The Qiseib Formation

Qiseib Fm. was introduced by Abdallah and Adindani (1963) at W. Qiseib, north ED. It belongs to the Permo-Triassic age (Klitzsch, 1990; Wanas & Soliman, 2018). The Qiseib Fm. overlies the Upper Carboniferous Aheimer Fm. and underlies the Lower Cretaceous Malha Fm. at W. Qiseib, north ED. The Qiseib Fm. is ~ 43 m thick in the type locality, but it reaches ~ 140 m thick at W. Araba and ~ 100 m thick at central SN. The lower part of the Qiseib Fm. contains red beds mainly variegated brown, purple, and gray shale and siltstone and minor sandstone. At W. Araba, this lower part contains tree trunks fossil and other plant remains of the Permian age (Klitzsch, 1990), while the upper part composes of thin carbonate clastic beds,

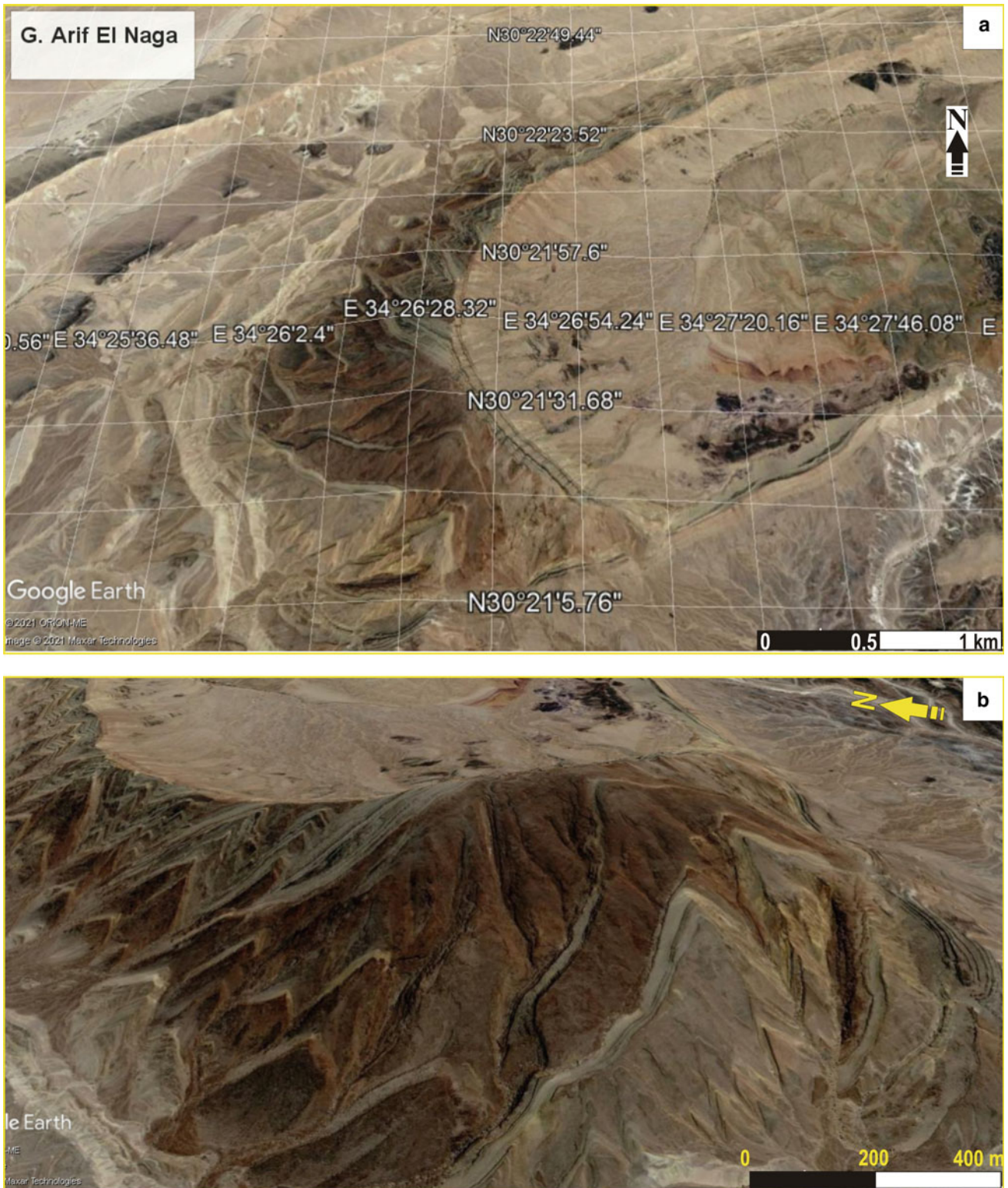


Fig. 6 a general view of the G. Arif El Naga; b 3D view shows the Domal Structure of the G. Arif El Naga (Google Earth Images)



Fig. 7 Nonconformity between the Precambrian basement rocks and the Lower Cretaceous Nubian sandstone

which contain marine fossils of Middle Triassic age. At Abu Darag area, the upper part belongs to the Middle Triassic; it contains the gastropod *Naticopsis* and the pelecypods *Hoernesia* and *Pleuromya* spp. (Weissbrod, 1969).

The subsurface Qiseib Fm. was recorded in many wells such as Abu Hamth-1, Nekhl-1, Hamra-1, and Ayun Musa-2. It reaches ~ 376 m thick at Abu Hamth-1 well, which consists of lower clastic red beds of an Early to Middle Triassic age including many thin coal seams. Horowitz (1970) defined the palynomorphs *Sulcatisporites krauseli*, *Verrucosisporites applanatus*, *Corollina meyeriana*, *Cyathidites minor*, and *Concavisporites juriensis*. These lower clastic beds are capped with ~ 36 m of limestones rich in Middle Triassic marine fossils (Druckman, 1974).

2.3 The Lokia Formation

The Lokia Fm. was presented by Klitzsch and Léjal-Nicol (1984) northeast G. Uweinat, southwest Egypt. It lies above the Late Carboniferous Northern W. Malik Fm. which represented by a thick succession of ~ 350–400 m of coarse-bedded clayey sandstone and mudstone. The age of

the Lokia Fm. is of Permian–Triassic age (Klitzsch, 1990). The middle and upper parts of Lokia Fm. contain fossilized wood trunks of the Triassic age. The lower part of this section is of Permian age (Klitzsch, 1990). The Lokia Fm. is equivalent to the Abu Ras Fm. (Issawi et al., 1999), which contains fluvial and lacustrine strata at the northwestern side of the Gilf Kebir Plateau, southwest Egypt. This formation was formed due to the erosion of the older strata in large places of south and central Egypt due to the uplift of these places. Wycisk (1993) proposed the Permo-Triassic–Early Jurassic age for the Lokia Fm. in NW Sudan.

2.4 The Egheh Group

This rock unit is only recorded from the subsurface Triassic rocks in the northern WD. Its type section is at G. Egheh, SE Libya (Norton, 1967). The Egheh Group composes of red Nubian Magna facies conglomerate, massive cross-bedded arkose sandstone, siltstone, and shale. Keeley et al. (1990) believed that the Egheh Group is unconformably overlain by the Jurassic Mashabba Fm. (G. Maghara, northern SN) and the Jurassic Bahrein and Ras Qattara/Wadi Natrun fms. in

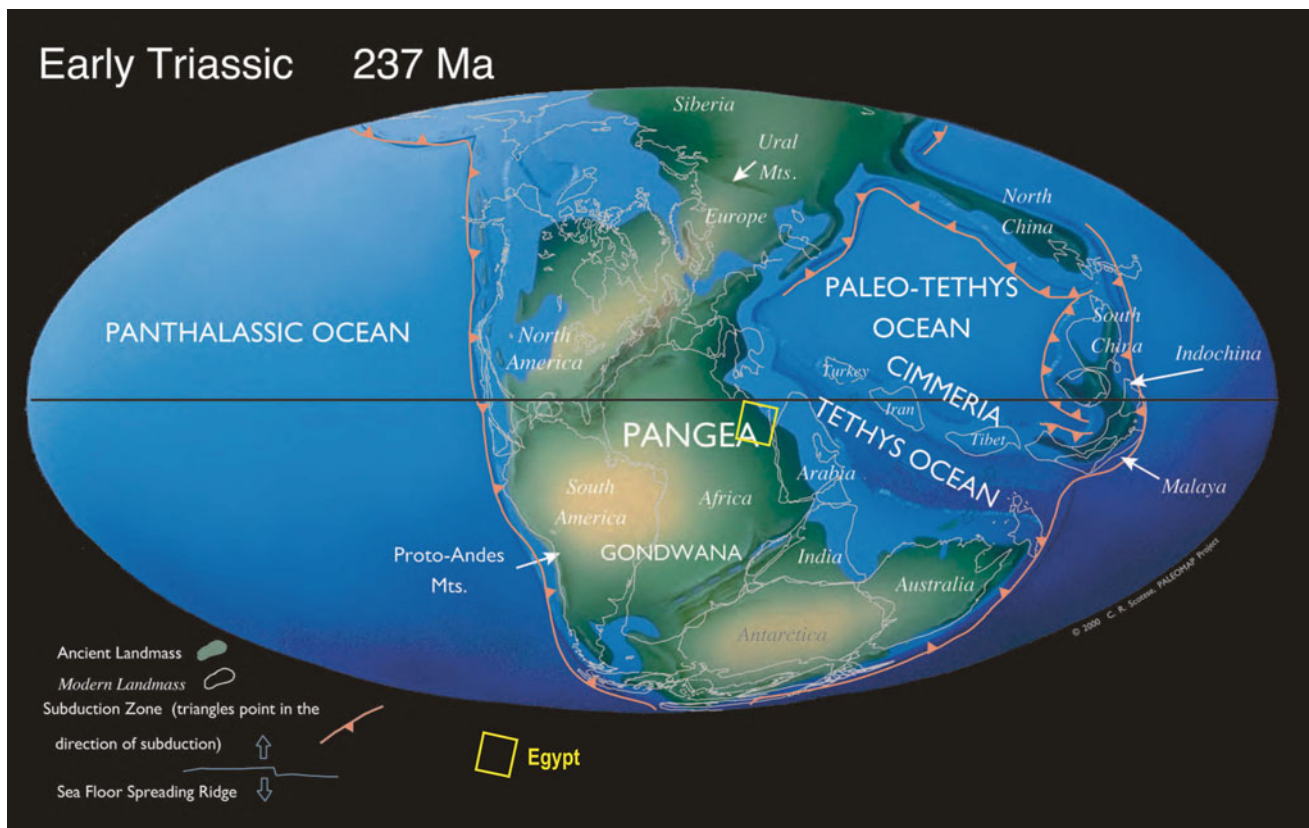


Fig. 8 Paleogeographic map for the continents during the Triassic Period (after Scotese, 2001)

the northern localities of Egypt (El Nady, 2015; Keeley et al., 1990). The Eghei Group is stratigraphically equivalent to the Fadda Fm. of the Ramon Group, Fadda Borehole-1, northern SN, Egypt (Gwin & Nasr, 1940). The Fadda Fm. forms of sandstone intercalated with dolomite and shale with some coal seams.

3 The Jurassic Successions

The Jurassic sedimentary rocks are represented in the northern places of Egypt. They are exposed in northern ED (Khashm El-Galala, Sadek, 1926) and SN (Maghara, Al Far, 1966; Barthoux & Douvillé, 1913; Minsherah, Farag & Shata, 1954; Arif El Naga, Bartov et al., 1980). In the northern parts of the WD, the Jurassic strata are only recorded in the petroleum boreholes as subsurface sequences. On the other hand, the Jurassic rocks are missing as the Triassic ones due to the impact of the Pan-African Orogeny or the collision of the Gondwana and Laurasia plates. By the end of the Jurassic, the Gondwana Continent was separated from the Laurasia due to the formation of Central Atlantic Ocean (Fig. 10). The marine strata in the northern localities indicate that the Tethys Ocean covered this area of Egypt at that time. The Jurassic rock units are well distributed

(Fig. 11) toward the north places of Egypt. The facies of the Jurassic rocks are dominated by shallow-deep marine facies, especially toward northern localities (surface strata in north SN, north ED and subsurface one in the northern WD) of Egypt (Fig. 12). These marine facies were interrupted by continental facies (fluvio-marine). The thickest and most complete surface Jurassic rocks (~ 1900 m) in Egypt are that of the G. Maghara (Fig. 13), northern SN, Egypt (Al Far, 1966). The stratigraphic succession of the G. Maghara consists of six rock units (formations). These are three fluvial formations (Mashabba, Shusha, and Safa) alternative to three marine ones (Rajabiah, Bir Maghara, and Masajid). The Safa Fm. (Figs. 14, 15 and 16) contains cross-bedded sandstone, siltstone, shale, and economic coal beds (Adindali & Shakhov, 1970). The rock units of G. Maghara are as follows.

3.1 The Jurassic Rocks of the Gebel Maghara

3.1.1 The Mashabba Formation

It was introduced by Al Far (1966) to describe the oldest Jurassic strata (W. Sadd El Mashabba, G. Maghara). The lower part of this rock unit is unexposed. The exposed rocks compose of ~ 100 m thick of fluvio-marine, pale sandstone,

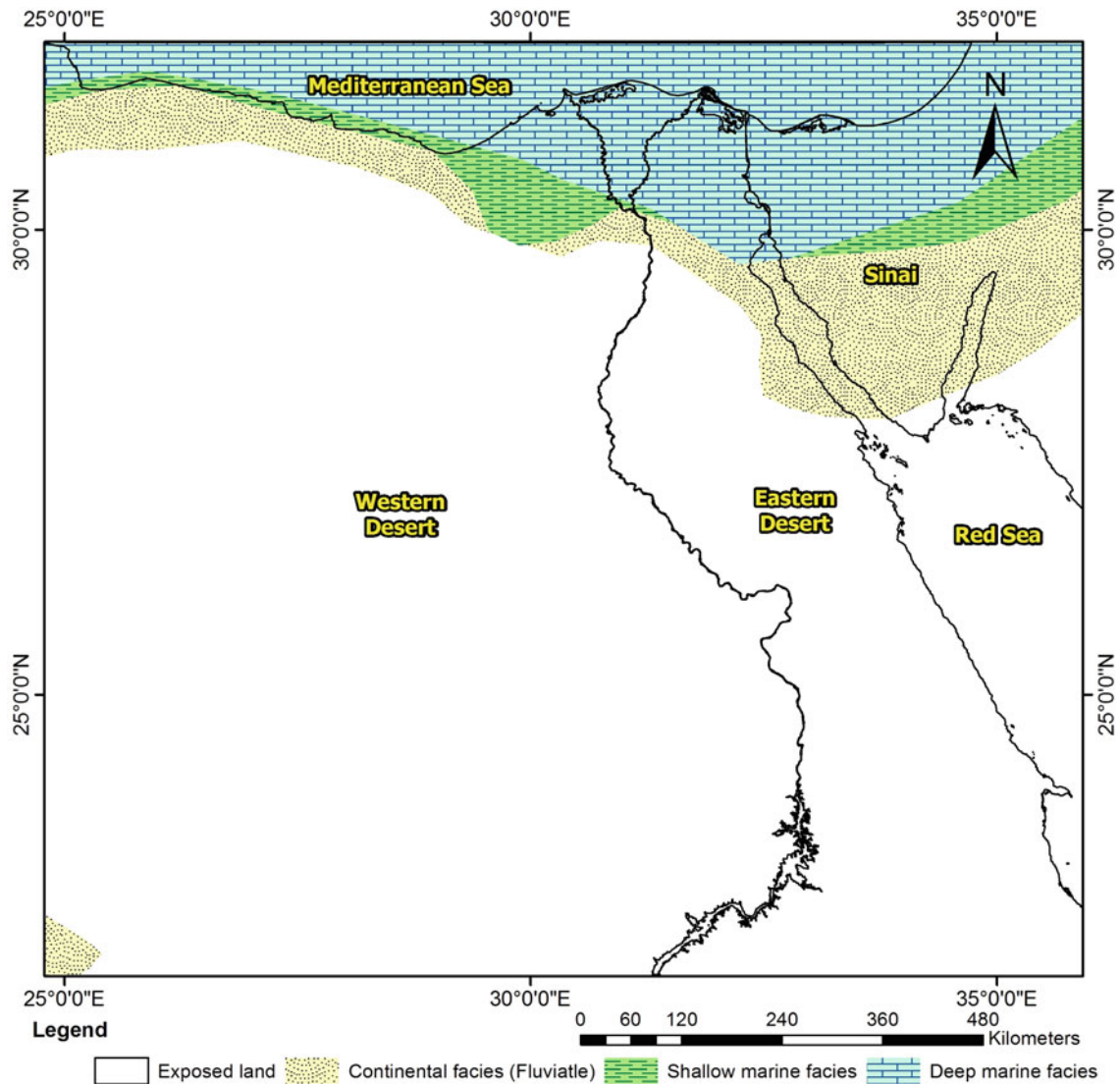


Fig. 9 Facies distribution of the Triassic sedimentary rocks in Egypt (modified after Guiraud & Bosworth, 1999)

thickly bedded, with thin interbeds of fossiliferous claystone and marine limestone. The limestone beds contain corals, bivalves, and algae, while the clay layers contain plant fossils such as *Equisitites* sp., *Gleichenites* sp., *Lacopteris* sp., and *Weichseilia* sp. Keeley et al. (1990) suggested latest Pliensbachian/earliest Toarcian for the Mashabba Fm. It is overlain by Rajabiah Fm. at G. Maghara. Zak (1964) and Bartov et al. (1980) described about 21 m thick of ferruginous silty shale, alternating with limestone, dolomite, marl, and variegated sandstone beds, with basal silty pisolitic, ferruginous shale at G. Arif El Naga and believed that these strata represent the oldest Jurassic rocks (Toarcian age). These strata probably represent the initial Jurassic transgression phase which peaked in the Toarcian age and reflects deposition in shallow shelf marine environment probably saline or brackish lagoon environment (Bartov et al., 1980;

Zak, 1964). These strata were recorded in the subsurface boreholes at Nekhl-1 and Hamth-1, Hamra-1, Halal-1, Tineh-1, and Ayun Musa-2 (Jenkins, 1990). On the other hand, Abed et al. (1996) demonstrated that the Jurassic strata at G. Arif El Naga are absent due to the occurrence of a hiatus at this time. The Mashabba Fm. is equivalent to the Jurassic successions at Khashm El-Galala (Sadek, 1926). Also, Farag (1948) recorded the Jurassic rocks at Ras El-Abd (~ 4 km southern Khashm El-Galala). Moreover, El Nakkady (1955) defined a surface Jurassic rocks near the Northern Galala Plateau.

3.1.2 The Rajabiah Formation

It was also designated by Al Far (1966) to define ~ 292 m thick of grayish, stylolitic, hard, coralline, and algal limestone of shallow marine reefal depositional conditions. It lies

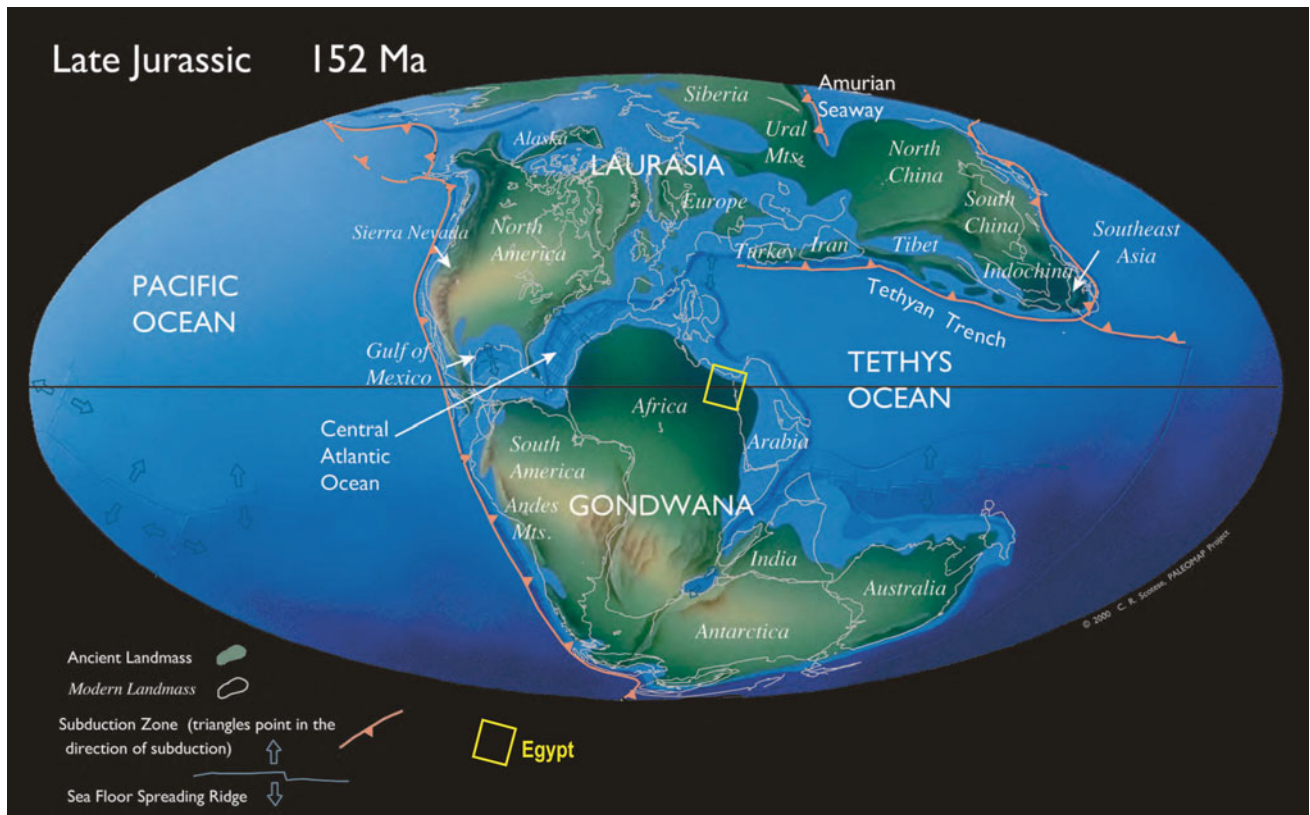


Fig. 10 Paleogeographic map for the continents during the Jurassic Period (after Scotese, 2001)

Time units		North Western Desert (Subsurface rock units)	Gulf of Suez (Khashm El-Galala) (Abd-Elshafy 1988)	North Sinai (G. Maghara) (Al Far 1966)	North Sinai (G. Maghara) (Abdelhady 2014)
Mesozoic	Upper	Kimmeridgian	Sidi Barrani Fm.	Ras El-Abd Fm.	Masajid Fm.
		Oxfordian	Masajid Fm.	Masajid Fm.	Tauriat Fm.
	Middle	Callovian	Khatatba Fm.		Arousiah Fm.
		Bathonian			Kehailia Fm.
		Bajocian		Rieina Fm.	Safa Fm.
		Aalenian	Bahrein Fm.		Bir Maghara Fm.
	Lower	Toarcian	Wadi Natrun Fm.		Mahl Fm.
			Ras Qattara Fm.		Shusha Fm.
				Shusha Fm.	
				Rajabiah Fm.	
			Mashabba Fm.		
				Not studied	

The base unexposed

Fig. 11 Simplified sketch shows the vertical and lateral relationships of the Jurassic sedimentary rock units in the G. Maghara, Gulf of Suez, and north WD, Egypt

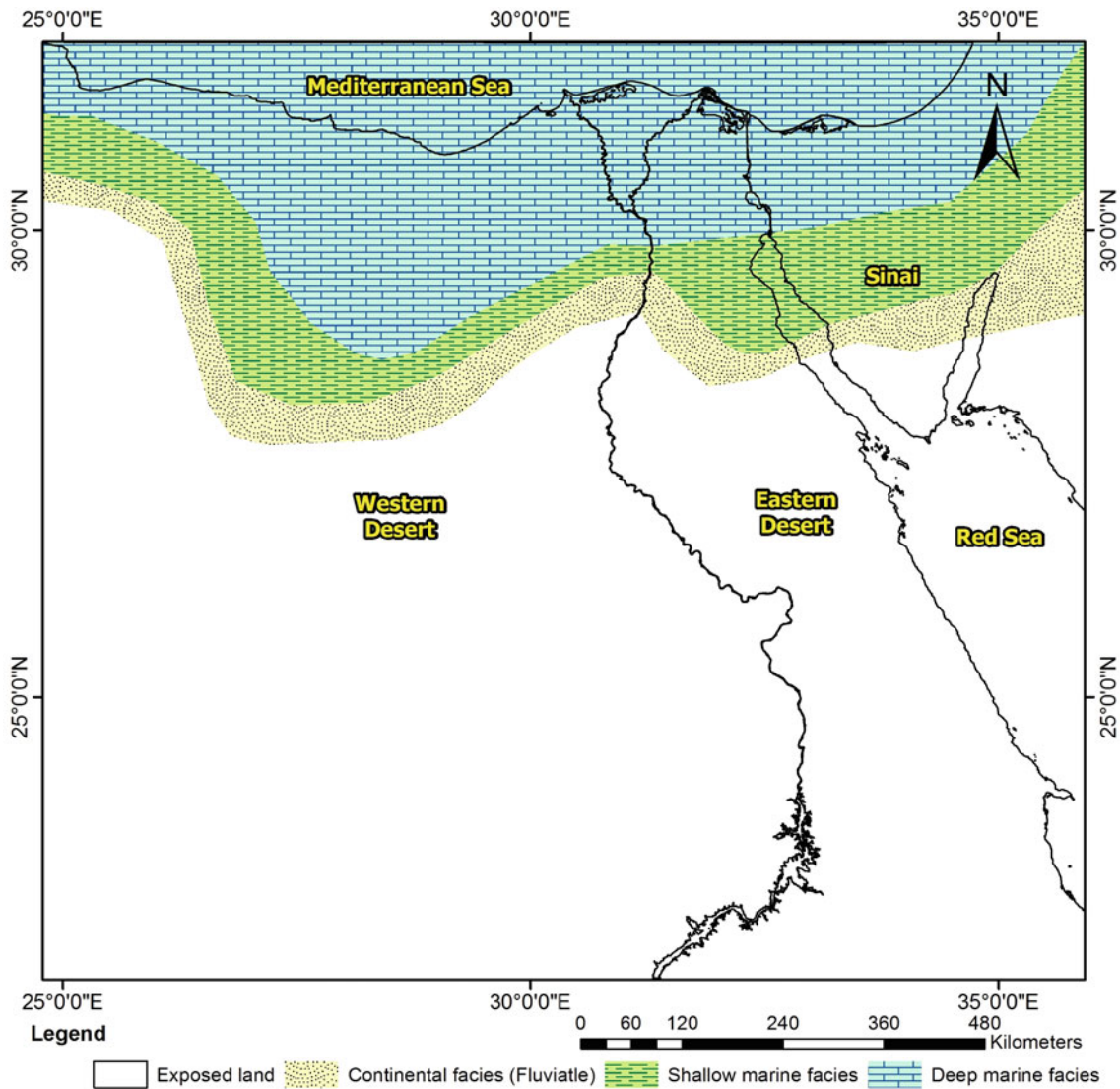


Fig. 12 Facies distribution of the Jurassic sedimentary rocks in Egypt (modified after Guiraud & Bosworth, 1999)

between Shusha Fm. at top and Mashabba Fm. at bottom at W. El Rajabiah, G. Maghara. This formation represents the oldest marine deposits in the G. Maghara. The uppermost part (~ 9 m thickness) of the Rajabiah Fm. composes mainly of limestone and yields the earliest ammonite (*Grammoceras*) in the succession which is assigned to the Toarcian age (Arkell, 1952, 1956). Keeley et al. (1990) assigned the Rajabiah Fm. to the latest Toarcian/Early Aalenian to Late Pliensbachian age. Also, this formation contains abundant genera of bivalve fossils such as: *Trigonia*, *Nucula*, *Lapha*, *Mactromya*, *Cuspidaria*, *Barbatia*, *Astarte*, and *Protocardia* (Al Far, 1966). This rock unit is unconformably overlain by the Shusha Fm.

3.1.3 The Shusha Formation

Al Far (1966) described ~ 271 m thick of tidal flat-deltaic-fluvio-marine sandstone and siltstone with shale, limestone, and coal beds with abundant ironstone concretions, at the Shushet El Maghara, south of Bir Maghara, G. Maghara. The Shusha Fm. is relatively rich in plant remains through the shale beds such as *Marathiopsis anglica*, *Stachypteris turkestanica*, *Eboracia lobifolia*, and *Thinfieldia rhomboidalis* (Al Far, 1966; Issawi et al., 2009). Also, corals, brachiopods, and bivalves (*Nucula* sp.) are occurring within the limestone beds (Al Far, 1966). There is a controversy in the assignment of the accurate age of this formation. For examples, Keeley et al. (1990) assigned the



Fig. 13 Panorama field view of G. Maghara Domal Structure

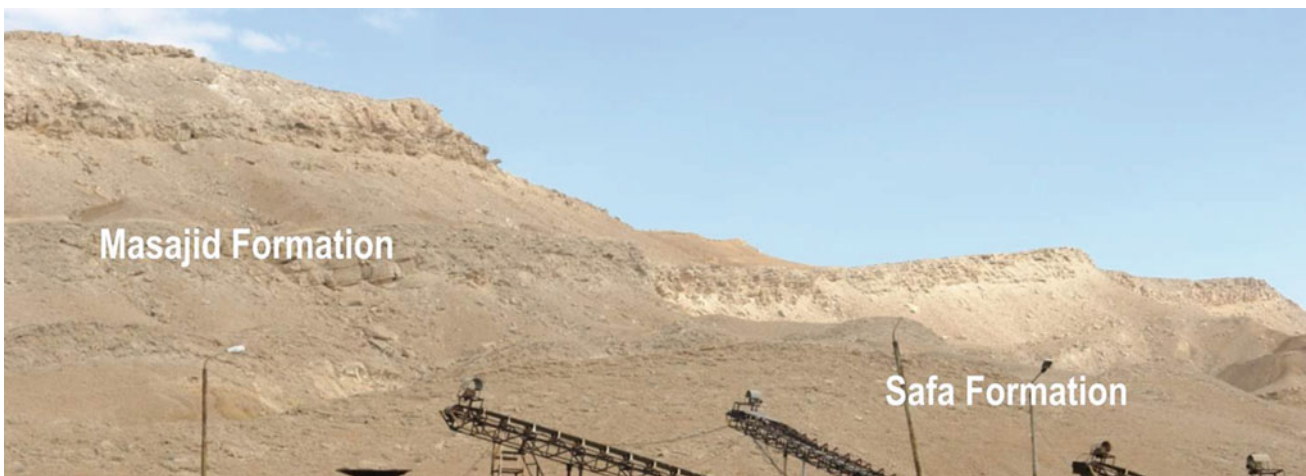


Fig. 14 Field view of the Safa and Masajid fms. at the G. Maghara Domal Structure shows the remnants of the extracted coal ore

Shusha Fm. to latest Toarcian/Early Aalenian. While Kerdany and Cherif (1990) assigned it to Aalenian, the Shusha Fm. shows a sharp contact with the underlying Rajabiah and the overlying Bir Maghara fms.

3.1.4 The Bir Maghara Formation

Al Far (1966) designated this formation to describe a thick massive limestone, with thin sandstone, shale, and rarely coal beds at Bir Maghara and Bir Moweirib. According to Al

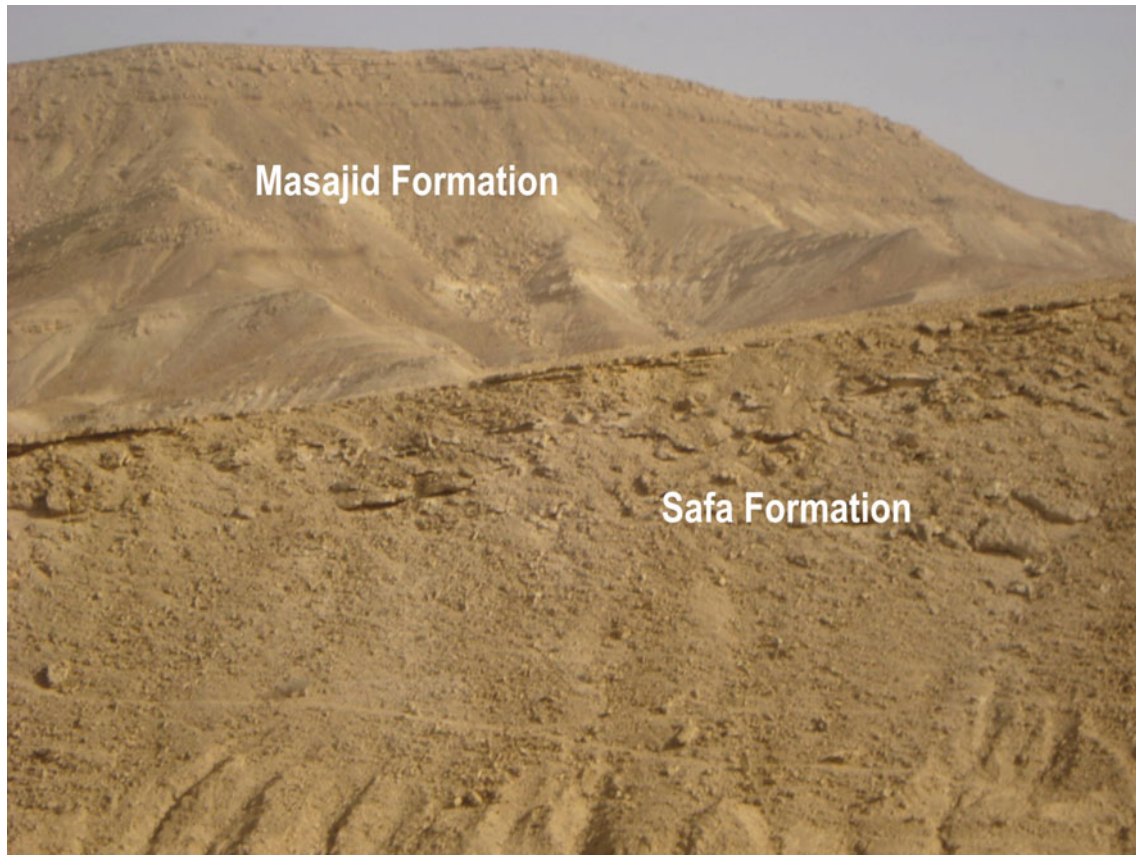


Fig. 15 Field view of the Safa and Masajid fms. at the G. Maghara Domal Structure



Fig. 16 Field view of the Bir Maghara, Safa, and Masajid fms. at the G. Maghara Domal Structure

Far (1966), it is classified into three formal rock units as follows:

- A. **The Mahl Member:** It consists of ~ 93 m thick hard coralline fossiliferous massive limestone intercalated by marly limestone and claystone beds at W. Mahl. The lowermost part of Mahl Member is marked by the occurrence of high amount of pyrite, while the uppermost part composed of algal grit-like limestone. Picard and Hirsch (1987) raised the stratigraphic rank of this member to formation.
- B. **The Moweirib Member:** It attains about ~ 133 m thick of alternating claystone and limestone beds intercalated with sandstone beds at Bir Moweirib. The claystone beds are silty and calcareous and contain ironstone concretions. The top ~ 10 m of this member contains fossiliferous marl beds which grading upward to ripple-mark, concretionary, and ferruginous sandstone.
- C. **The Bir Maghara Member:** It consists of ~ 216 m thick of fossiliferous claystone, marl, limestone, and sandstone beds.

In our point of view, the International Stratigraphic Code prevents the duplications in the nomenclature of the rock units. So, our opinion is to merge this member (Bir Maghara Member) to the Moweirib Member, because there is similarity in the lithology of the two members.

Middle Bajocian age was given to the rocks of Moweirib and Mahl members by Al Far (1966) due to the occurrence of the index ammonite *Dorsetensia* sp. and *Otoites* sp., while the Bir Maghara Member was assigned to the Late Bajocian due to the occurrence of the index ammonite, such as: *Telermoceras*, *Normannites*, *Kosmoceras*, *Leptosphinctes*, and *Thamboceras*. The present member also contains brachiopods, pelecypods, and gastropods fossils. The lithology and faunal content of the Bir Maghara Fm. point to shallow marine environment (continental shelf, inner-shallow outer shelf setting).

3.1.5 The Safa Formation

Al Far (1966) defined ~ 215 m deltaic, coastline, and fluvio-marine rocks at W. Safa, G. Maghara. The Safa Fm. composes of sandstone (cross-bedded, ripple-marked), alternating with siltstone and coal beds (especially at the lower part), which contains shale and limestone interbeds (Figs. 14 and 15). These beds contain several plant fossils including *Pitlophyllum cutchens*, *Cycadites karatubensis*, *Zamites feneconis*, and *Otozamites* sp. (Issawi et al., 1999). The lowermost beds of the Safa Fm. carry species of ammonoidea (e.g., *Thambites*) which assigns this formation to the Early

Bathonian age. This formation also includes many benthonic foraminiferal species such as: *Haplophragmoides* spp., *Nodosaria dolioligera*, *Glomospira compacta*, and *Quinqueloculina compressa* of inner shelf environment. Keeley et al. (1990) assigned the Safa Fm. to the Bathonian.

Unconformable relationship marked the contact between the Safa Fm. and the underlay Bir Maghara Fm. This surface is characterized by the abrupt facies change between the carbonate facies of Bir Maghara Member (upper part of Bir Maghara Fm.) and the swampy terrigenous facies of the lower part of Safa Fm. Farag and Omara (1955) described about 80 m thick of sandstone, marl, and limestone rocks containing *Rhynchonella* spp. at G. Minshireh. The lithology and faunal contents of the Safa Fm. indicate swamp-fluvial environment with some interruption of marine invasions at different occurrences.

3.1.6 The Masajid Formation

Al Far (1966) defined Masajid Fm. as a younger one of the G. Maghara rock units. Al Far (1966) described a total thickness of ~ 575 m thick of shallow marine shelf limestone beds at W. Masajid, G. Maghara. Al Far (op. cit.) classified the Masajid Fm. into two formal rock units (members) as follows:

- A. **The Kehailia Member:** It represents that the lower part of Masajid Fm. encompasses ~ 132 m thick of alternating sandstone, claystone beds, marly, and glauconitic limestone which is partly coralline and algal.
- B. **The Arousiah Member:** It marks the upper part of Masajid Fm. and represents marine environmental depositional setting. It comprises ~ 443 m thick-bedded limestone intercalated with claystone and sandstone beds. The middle part of Masajid Fm. (lower part of Arousiah) carries ammonite *Erymnoceras* fauna (Callovian), while the upper part of this member yields the Oxfordian *Euaspidoceras* fauna. The Kimmeridgian is missing at the G. Maghara. Moreover, Abdelhady (2014) and Abdelhady and Fürsich (2015) introduced the Tauriat Fm. which is equivalent to the upper part of the Masajid Fm. of Al Far (1966). Meantime, they (op. cit.) changed the lithostratigraphic ranking of the Kehailia and Arousiah (Al Far, 1966) from member to formation. So, they subdivided the Jurassic succession in the G. Maghara which overlay the Shusha Fm. into seven formations in stratigraphic order (Fig. 11): the Mahl (Aalenian), the Bir Maghara (Bajocian), the Safa (Early Bathonian), the Kehailia (Middle-Late Bathonian), the Arousiah (Callovian), the Tauriat (Oxfordian), and the Masajid (Early Kimmeridgian).

3.2 The Jurassic Rocks of the Gulf of Suez

It was firstly described by Barthoux and Douvillé (1913). Subsequently, Sadek (1926) described ~ 220 m thick of the Jurassic rocks between G. Ataqa and El-Galala El-Bahariya. The lower part of this measured succession is non-fossiliferous, while the upper part was assigned to Bathonian (Sadek, 1926). Also the Jurassic successions were recorded at Ras El-Abd and Khashm El-Galala, which is described as follows.

3.2.1 The Jurassic Rocks at Ras El-Abd

The Jurassic rocks were subdivided into three informal units (Darwish et al., 1984). The lower unit consists of varicolored sandstone. The middle unit attains ~ 72 m thick of shale intercalated with limestone and minor sandstone beds. This unit contains brachiopods, bivalves, and gastropods shell. Also, flora and benthic foraminifera contents were recorded (e.g., Abd-Elshafy & El-Saadawi, 1982). This part is assigned to Bathonian age as suggested by Hegab and Aly (2004). The upper unit consists of intercalation of sandstone and shale beds that underlie the sandstone Malha Fm. (Lower Cretaceous).

3.2.2 The Jurassic Rocks at Khashm El-Galala

It was subdivided into two formations according to Abd-Elshafy (1988) and Abu El-Hassan and Wanas (2003). These formations are Rieina at base and Ras El-Abd at top (Fig. 11). This classification was also followed by Sallam and Wanas (2019) and Ruban et al. (2019).

A. The Rieina Formation

It ranges from ~ 70 m at Ain Sukhna section to ~ 10 m at Ras El-Abd section. It consists of varicolored cross-bedded sandstone intercalated with several ledges of hard sandstone, which is capped by claystone bed (~ 1.5 m) that contains plant-leaf imprints. A bed of *Thalassinoides* burrows (~ 0.5 m) marks the contact between the Rieina Fm. and the overlying Ras El-Abd Fm. (Ruban et al., 2019). The Rieina Fm. is of Bajocian age.

B. The Ras El-Abd Formation

According to Ruban et al. (2019), it consists mainly of intercalated shale and carbonate (limestone and dolostone) beds. It ranges from ~ 100 m to ~ 150 m at Ras El-Abd and Ain Sukhna, respectively. Two remarkable coquina and rhynchonellid limestone beds are marked this formation. The lower coquina limestone bed varies in thickness between ~ 4 and ~ 7 cm and contains bivalve shells (e.g., *Nicaniella pisiformis*, *Modiolus* sp.) The rhynchonellid bed is

subdivided into two beds. The lower bed (~ 1 m thick) contains *Globirhynchia concinna* and *Echyrosia expansa* along with bivalve shells such as *Pholadomya orientalis*, *Neocrassina (Coelastarte) excavatus*, and *N. pisiformis*. Also, gastropods are present, which are represented by *Buckmanina laevis* and *Amphitrochus mogharensis*. The upper bed (~ 8–14 cm) includes *Globirhynchia triangulata* and *E. expansa* (El-Qot et al., 2009). The Ras El-Abd Fm. is of Bathonian-Oxfordian age.

3.3 The Subsurface Jurassic Successions

Thick sequences of subsurface Jurassic sedimentary rocks were recorded in the north WD by the activities of petroleum exploration. These rocks were introduced and mentioned by several petroleum specialized workers such as Hantar (1990), Wever (2000), Moretti et al. (2010), El Nady (2015), and El Diasty et al. (2016). The different sedimentary Jurassic rock units are summarized in the following (Fig. 11).

3.3.1 The Bahrein Formation

WEPCO Petroleum Company introduced this formation to describe the sedimentary continental (fluvial) Jurassic strata which underlie the marine Jurassic rocks in many parts of the north WD at the Betty-I well (29° 40' N and 27° 45' E) between 3888 and 4437 m. The name was introduced to replace the Eghei Group (see the Triassic successions, the same chapter), which was proposed by Norton (1967) for the continental section above the Carboniferous strata. Bahrein Fm. consists of red color clastic sandstone with thin pebble, siltstone and shale, occasionally carbonaceous or pyritic. Also, anhydrite beds are recorded. The Bahrein Fm. unconformably overlies the Triassic rocks (El Nady, 2015; Moretti et al., 2010). It unconformably lies below the Jurassic marine Khatatba Fm. The Eghei/Bahrein boundary is very difficult, according to the similarity in the lithologic character and the lacking of index fossils. On the other hand, the Bahrein/Khatatba formational boundary easily defined at the vertical facies change from the continental clastic of the Bahrein and the marine carbonate facies of the Khatatba Fm. In some boreholes in the north WD, there is a huge hiatus between the Early Jurassic Bahrein Fm. and the Early Cretaceous Alam El Bueib Fm.

El Nady (2015) and El Diasty et al. (2016) replaced Bahrein Fm. by the non-Marine (fluvial/lacustrine) siliciclastic rocks the Ras Qattara Fm. The Ras Qattara Fm. consists of non-marine massive sandstone with some shale interbeds, especially toward the top.

In the eastern parts of the north WD, Bahrein Fm. changes laterally into the marine carbonate Wadi Natrun Fm. (Fig. 11). The maximum thickness of the Bahrein Fm. was

recorded in Betty-I where it reaches ~ 550 m thick. The Bahrein Fm. was assigned to early Middle (?) Jurassic age (Moretti et al., 2010). It might be correlated with the outcropped Mashabba Fm. at the G. Maghara, north SN.

3.3.2 The Wadi Natrun Formation

It was suggested by Norton (1967) to describe the marine limestone strata, which are equivalent to the fluvial rocks of the Bahrein Fm. The age of this formation is Toarcian-Bajocian (Hantar, 1990; Kerdany & Cherif, 1990). The limestone strata are dolomitic toward the upper part. The type locality was recorded in the W. Natrun-I Borehole throughout the interval between 3594 and 4056 m (Norton, 1967). The carbonate of the type locality (W. Natrun-I Borehole) is mostly dolomitic. The Wadi Natrun Fm. is unconformably overlain the Eghei Triassic Group (EGPC, 1992; El Diasty, 2015; El Nady, 2015). The Wadi Natrun Fm. is conformably overlain by Khatatba Fm. The contact between these two formations is easily defined either by paleontological evidence or by lithostratigraphic characteristics. Wadi Natrun Fm. could be equivalent to the surface Rajabiah Fm. The Wadi Natrun Fm. is known only in the eastern part of the north WD and has ~ 833 m at Natrun T-57-1 well (Hantar, 1990). Shallow marine and low energy depositional setting characterize Wadi Natrun Fm. (e.g., Hantar, 1990; Ibrahim et al., 2001).

3.3.3 The Khatatba Formation

It was introduced by Norton (1967) to describe the sandstone and shale subsurface beds in the north WD. The upper part of this formation in the eastern and northeastern parts of the WD contains limestone beds (Keeley et al., 1990; Shalaby et al., 2011). Its type section is at Khatatba-I Borehole (30° 13' 44" N and 30° 50' 07" E) of the north WD. Issawi et al. (1999) believed that the carbonate beds of Khatatba Fm. could be equivalent to the lower part of Bir Maghara Fm. in G. Maghara. The Khatatba Fm. rests over the Wadi Natrun or Bahrein fms. (Fig. 11) in some parts of the WD (EGPC, 1992; Hantar, 1990). Also, it rests over the Ras Qattara Fm. in some places of the WD such as Shushan Basin (Shalaby et al., 2011). Also, Khatatba Fm. underlies Masajid Fm. in most area except in the south where it underlies unconformably the Lower Cretaceous Burg El-Arab Fm. Khatatba Fm. was deposited in deltaic to shallow marine settings (Hantar, 1990; Shalaby et al., 2011).

3.3.4 The Masajid Formation

It was described by Al Far (1966) as mentioned earlier at the W. Masajid, G. Maghara, north SN. This formation represents the younger rock units of Jurassic subsurface section in the north WD. The Masajid Fm. composes of a massive limestone succession which is cherty toward the northeast and central parts of the north WD. While shale beds dominate

at the base and top toward the northern and eastern parts of the area. The Masajid Fm. overlies the Khatatba Fm. and underlies the Lower Cretaceous Alam El Bueib Fm. The Masajid Fm. thickness reaches ~ 450 m in the W. Natrun area (W. Natrun-I Borehole). It attains ~ 840 m in Nile delta (Q-72-1 Borehole). It was deposited in an inner-middle neritic settings (Hantar, 1990; Schlumberger, 1984; Tawadros, 2011). The age of the Masajid Fm. is assigned to Oxfordian to Kimmeridgian (Gentzis et al., 2018; Hantar, 1990).

3.3.5 The Sidi Barrani Formation

Hantar (1990) introduced Sidi Barrani Fm. to define a thick dolomitic limestone bed which lies between ~ 1899 and ~ 4301 m in Sidi Barrani Borehole (30° 41' 39" N, 25° 28' 0" E). It attains ~ 2404 m in Sidi Barrani-I well. The lower part of this formation consists of sandstone, shale, and anhydrite. The Jurassic part of Sidi Barrani is equivalent to Masajid Fm., while its upper part is comparable to the Lower Cretaceous Alam El Bueib Fm. It overlies the Khatatba Fm. and underlies the Alam El Bueib Fm. The Sidi Barrani Fm. has a limited occurrence at the northwestern portion in the north WD. It was recorded in some wells which are located between Matruh and Sidi Barrani district. The Sidi Barrani Fm. is deposited in a quite open marine environment. This is evidenced by the scarcity of the clastic and the abundance of organic material (Hantar, 1990). The geologic age of Sidi Barrani Fm. is Middle Jurassic–Early Cretaceous.

4 The Cretaceous Successions

The Cretaceous strata cover the most areas (~ 40%) of the different regions of Egypt (Fig. 5). The Cretaceous was characterized by the important episode fragmentation of the Great Gondwana Continent, especially the drifting of South America away from Africa due to the opening of South Atlantic Ocean (Fig. 17). Also, at the end of this period (Turonian, Scheibner et al., 2003), Egypt, especially the northern parts, was deformed by the Syrian Arc Event (Fig. 4).

This continental rifting was associated with a major phase of intercontinental rifting in parts of west and central Africa and to a less degree in east Africa (Issawi et al., 2009). Rifting also occurred in some small zones such as southeast Sirt in Libya and northwest of Egypt (Guiraud & Bosworth, 1999). Active rifting was also concentrated further southwards within the interpolate domain, where some large rift basins were formed (e.g., the Blue Nile in Sudan, Guiraud & Bellion, 1995). The final fragmentation between Africa and South America occurred at ~ 100–105 Ma (e.g., Albian–Cenomanian, Issawi et al., 2009; Moustafa, 2020). The Atlantic Ocean was completely opened in the Santonian age

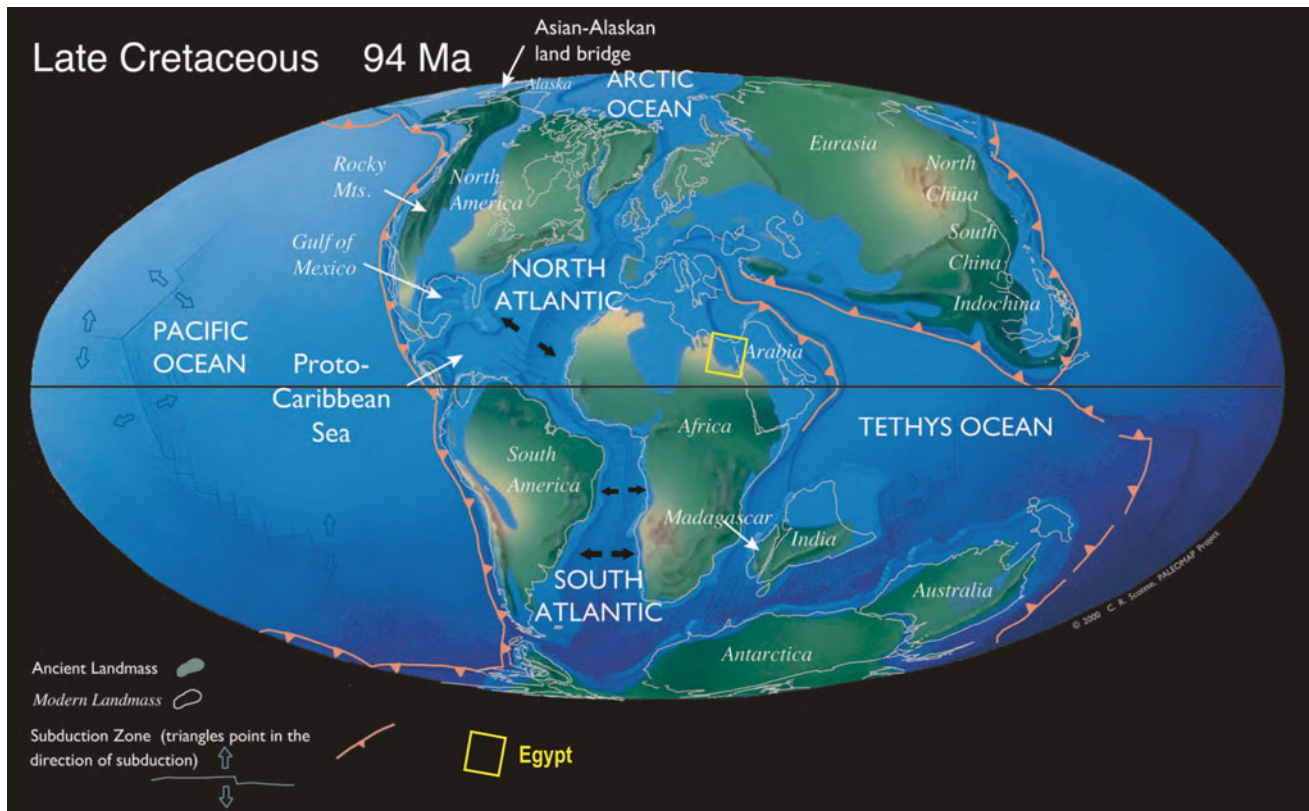


Fig. 17 Paleogeographic map for the continents during the Cretaceous Period shows the formation of Atlantic Ocean and the rifting of Gondwana Continent (after Scotese, 2001)

(Masclé et al., 1988). At the same time, the Tethys Ocean began to close during the Turonian age (Guiraud & Bosworth, 1997). The closure of the Tethys Ocean triggered multiple phases of rifting resulting from the multiple phases of this ocean closure along the African–Arabian Plate (Issawi et al., 2009). The closure episodes of the Tethys were associated with N–S shortening and the collision between north Africa and Europe (Argyriadis et al., 1980; Sengor et al., 1984). This event led to the formation of Syrian Arc Mountains, which extend from northwestern Libya to Syria passing by northern Egypt. Maghara, Yelleg, Halla, Arif El Naga, and Minsherah mountains are examples for this event in north SN, Egypt.

Generally, the Cretaceous Period is characterized by Tethys transgression over Egypt during Early Cretaceous (Aptian age). The surface Cretaceous successions are well distributed all over the Egyptian geographic regions (Fig. 5). These successions cover the most areas of Egypt from south to north and from east to west and reflect a lateral variation in the lithology from one place to other at different geologic ages (Fig. 18). These variations led to the occurrence of several names for the Cretaceous rock units of same geologic age (e.g., Six Hills and Gilf El Kebir, Galala and Raha; Rakkiyat and Matulla, Abu Qada and Maghra El-Hadida).

Moreover, the Cretaceous rock units change laterally and interfinger with the equivalent ones from north to south (e.g., Sudr or Khoman and Dakhla; Halal and Raha) and from east to west (e.g., Halal or Raha and Bahariya and Maghrabi). In the oases of the WD (e.g., Baris, Kharga, Dakhla, Farafra, Bahariya), the Cretaceous sedimentary successions build the walls of the scarps surrounding the depressions. At the ED, the Cretaceous strata are well represented at both south and north parts. At SN, the Cretaceous sedimentary rocks are well distributed.

The facies distribution of Lower Cretaceous rock units indicates that the major areas of Egypt (central and southern Egypt) were represented by continental facies (Fig. 19). On the other hand, the marine facies dominated the north parts of Egypt, especially during the Aptian–Albian age. The Late Cretaceous Epoch is characterized by a major transgressive phase all over Egypt, which led to form proper marine facies. During the Cenomanian–Turonian age, the marine facies cover the most parts of north Egypt, where these marine facies are changing to continental one toward the south (Fig. 20). In contrast, the Coniacian–Santonian age is characterized by restricted marine facies in the northern parts of Egypt, whereas the main areas are represented by continental facies or were positive parts (Fig. 21). This may be due to the

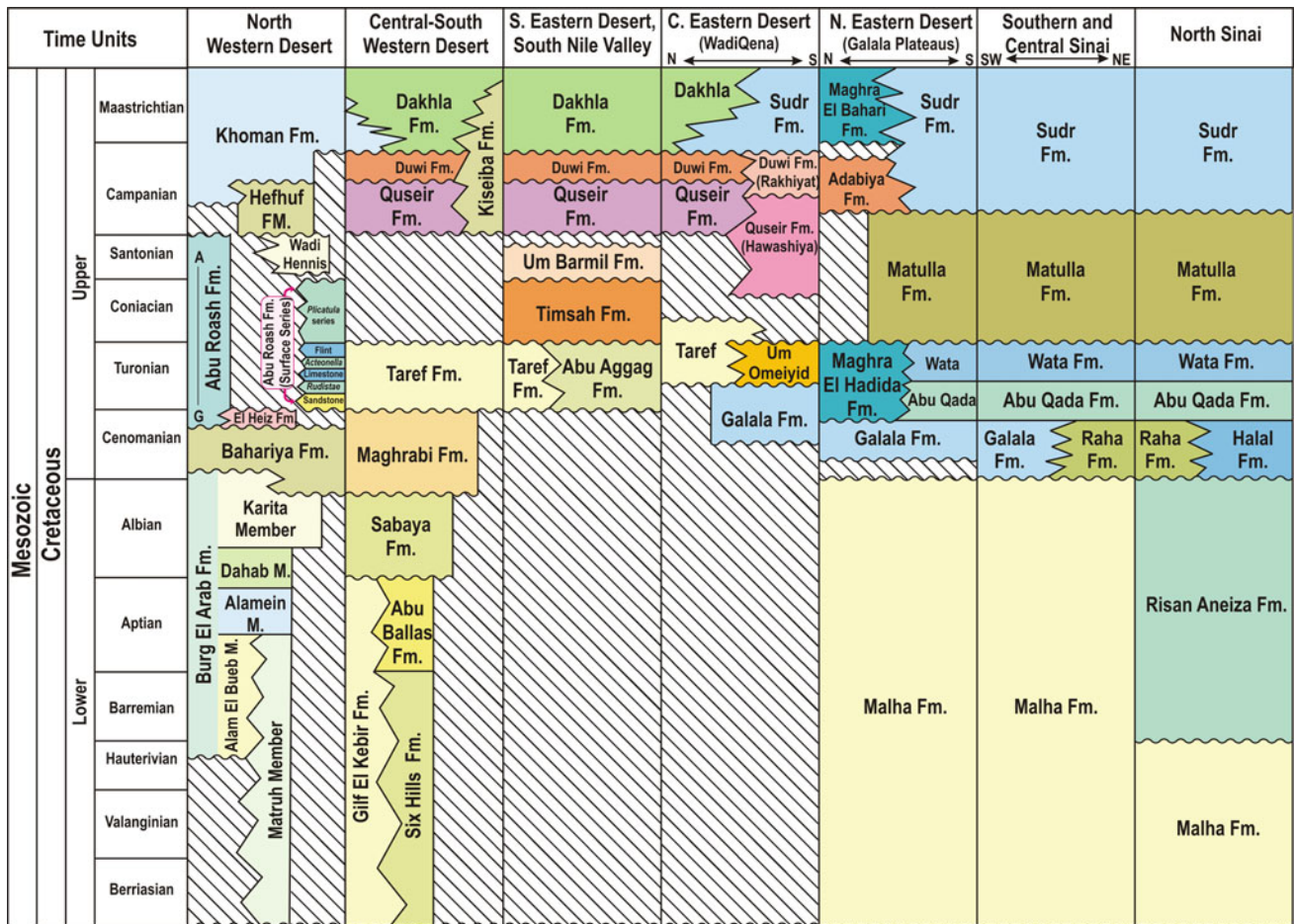


Fig. 18 Simplified sketch shows the vertical and lateral relationships of the Cretaceous sedimentary rock units in Egypt

intensive impact of the Syrian Arc Event on the most provinces of Egypt. At Late Cretaceous (Campanian–Maastrichtian age), the Tethys covers mostly all areas of Egypt (Fig. 22). This age was characterized by the dominated deep marine facies all over Egypt except for the southern parts which were covered by fluvatile-shallow marine facies. The Cretaceous sedimentary rocks are here classified depending on the different geographic provinces as follows:

4.1 The Surface Lower Cretaceous Sedimentary Rocks

4.1.1 The South Western Desert

A. The Gilf El Kebir Formation

In southern Egypt at the Gilf El Kebir Plateau, there are undifferentiated thick clastic sedimentary rocks (~ 250 m thick), which was described by Klitzsch et al. (1979). This

formation is made up of fluvatile, deltaic sandstone rests unconformably over the Late Paleozoic strata (Wadi Malik Fm. of Carboniferous Period). Stratigraphically, Wycisk (1984) assigned Gilf El Kebir Fm. to the Early Cretaceous (Berriasian–Berremian age) at the G. Kamil near Sudanese/Egyptian border, where Gilf El Kebir Fm. rests unconformably over the Carboniferous strata, according to the occurrence of plants imprints. The formation is the lateral comparable to Six Hills and Abu Ballas fms. (Klitzsch et al., 1979).

B. The Six Hills Formation

It was originally designated by Barthel and Boettcher (1978) to describe the Early Cretaceous strata at WD. It reaches about 500 m thick at its type locality near the Mut-Bir Tarfawi road and G. Nusba El-Balgum northeast of Tarfawi, WD. It was also named by Klitzsch (1978) and Klitzsch et al. (1979) as an informal rock unit “Basal clastic unit” or Desert rose unit, respectively. It forms of ill-sorted grained sandstone. Its upper part is made up of multi-color ill-sorted sandstone (Klitzsch et al., 1979). These strata are

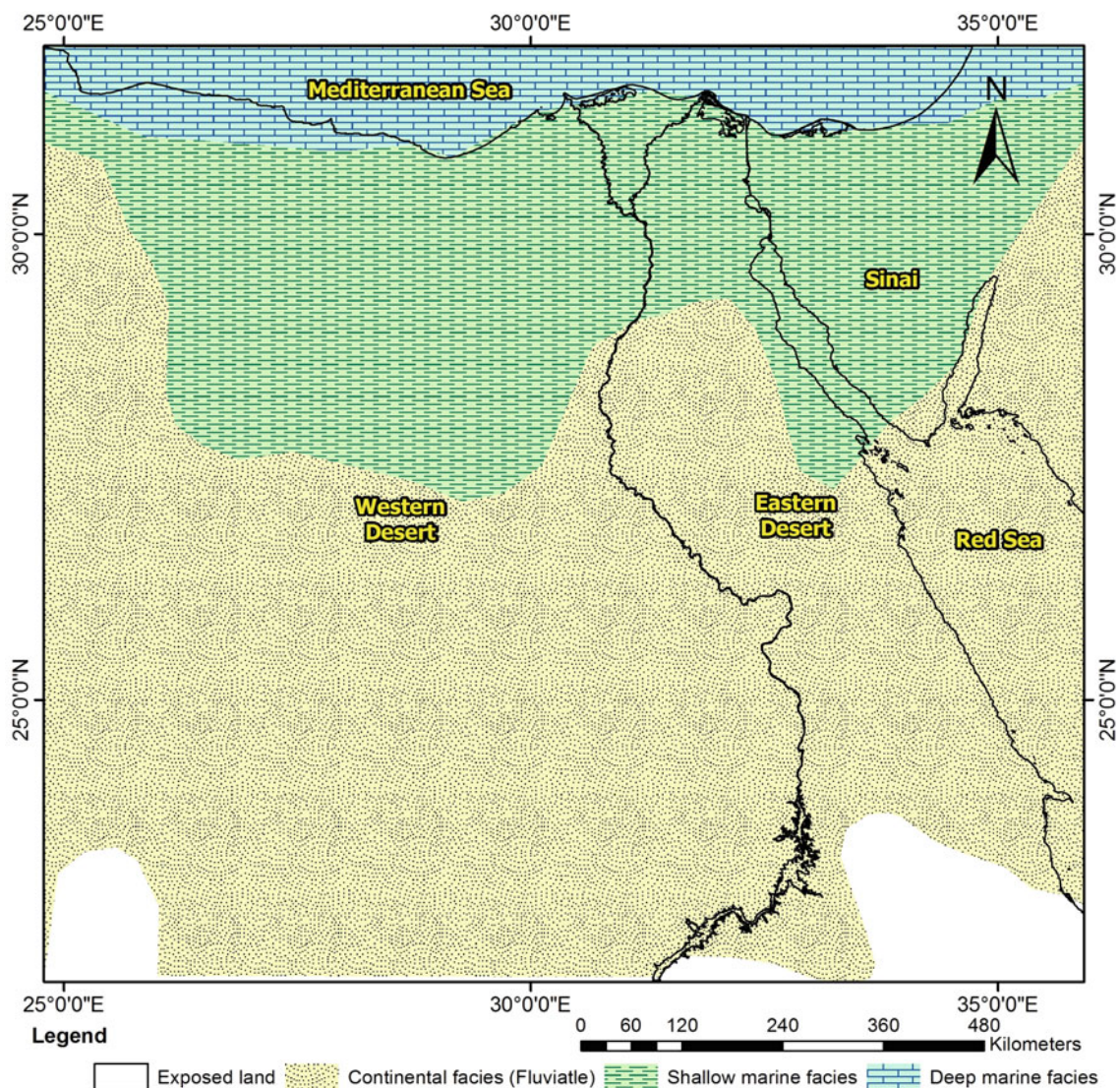


Fig. 19 Facies distribution of the Lower Cretaceous sedimentary rocks in Egypt (modified after Guiraud & Bosworth, 1999)

characterized by a large-scale cross-bedding with some massive, horizontally beds, small-scale ripple siltstone and sandstone. Klitzsch (1986) used Abu Simbil Fm. (~ 200 m thick) instead of the Six Hills Fm. near Lake Nasser. The Six Hills Fm. is unconformably overlying Precambrian rocks and conformably overlain by Abu Ballas Fm. (Hermina et al., 1989). Six Hills Fm. was deposited in a fluvial-dominated flood-plain environment (Hendriks & Kallenbach, 1986).

C. The Abu Ballas Formation

It was originally suggested by Barthel and Boettcher (1978) to describe marine sandstone which lies at ~ 200 km southwest of the Dakhla Oasis, WD. It was also named by Klitzsch et al. (1979) as an informal unit "Lingula shale

unit". The strata of Abu Ballas Fm. contain some fossils of brachiopods, pelecypods, and gastropods which indicated a shallow marine environment (Barthel & Boettcher, 1978). They (op. cit.) attributed the Abu Ballas Fm. to Late Jurassic to Early Cretaceous and believed that the strata of Abu Ballas Fm. were deposited in a shallow, partially intertidal, estuarine environment. Schrank (1982) suggests Aptian age based on the occurrence of abundant plant remains. It was changed upwards from lower and middle clay beds to upper silty to sandy beds (Klitzsch et al., 1979). Boettcher (1982) subdivided Abu Ballas Fm. into three claystone and four siltstone and sandstone units. He (op. cit.) thought that this reflects a transgression-regression sea level. Its thickness ranges from a few meters to ~ 100 m (Klitzsch et al., 1979). Klitzsch (1986) used Lake Nasser Fm. instead of the Abu Ballas Fm. around Lake Nasser. The Abu Ballas Fm. is

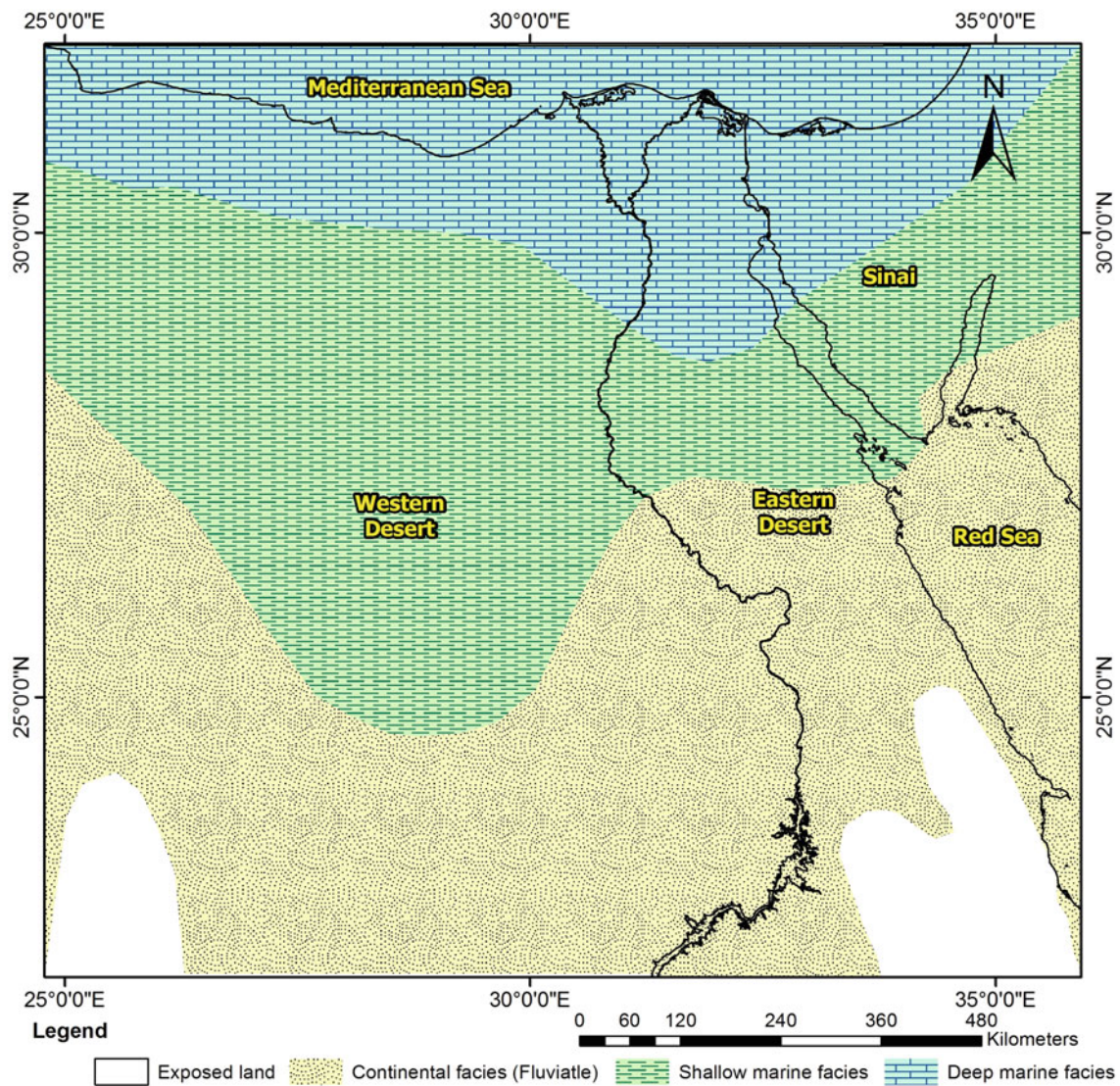


Fig. 20 Facies distribution of the Cenomanian–Turonian sedimentary rocks in Egypt (modified after Guiraud & Bosworth, 1999)

conformably overlying the Six Hills Fm. and conformably overlain by the Sabaya Fm.

D. The Sabaya Formation

It was proposed by Klitzsch et al. (1979) to describe a ~ 30–300-m-thick succession which overlies the sedimentary rocks of Abu Ballas Fm. The type locality is at G. Qulu El-Sabaya, Abu Tartur Plateau, about 90 km west-southwest of Kharga Oasis along the road to Mut. The Sabaya Fm. has a wide surface extension in the WD from the Gilf El Kebir in the south toward the Dakhla and Kharga oases toward the north. It composes of fluvial, sandstone, and conglomeratic sandstone with cross-bedding, especially at the basal part. The lower strata of the Sabaya Fm. generally are formed by rivers in a flood-plain environment (Hendriks &

Kallenbach, 1986). They (op. cit.) suggested that the Sabaya Fm. was truncated by several paleosols which reflect intense vegetation around the rivers and incision of laterally migrating stream channels into the flooding-plain sediments. Sabaya Fm. is assigned to an Albian age and laterally comparable to the marine Kharita Member, northern WD (Kerdany & Cherif, 1990).

4.1.2 The Sinai and the Northern Eastern Desert

A. The Malha Formation

Abdallah et al. (1963) described the strata of the Malha Fm. at the western side of Gulf of Suez. Malha Fm. unconformably overlies the Precambrian in some places such as

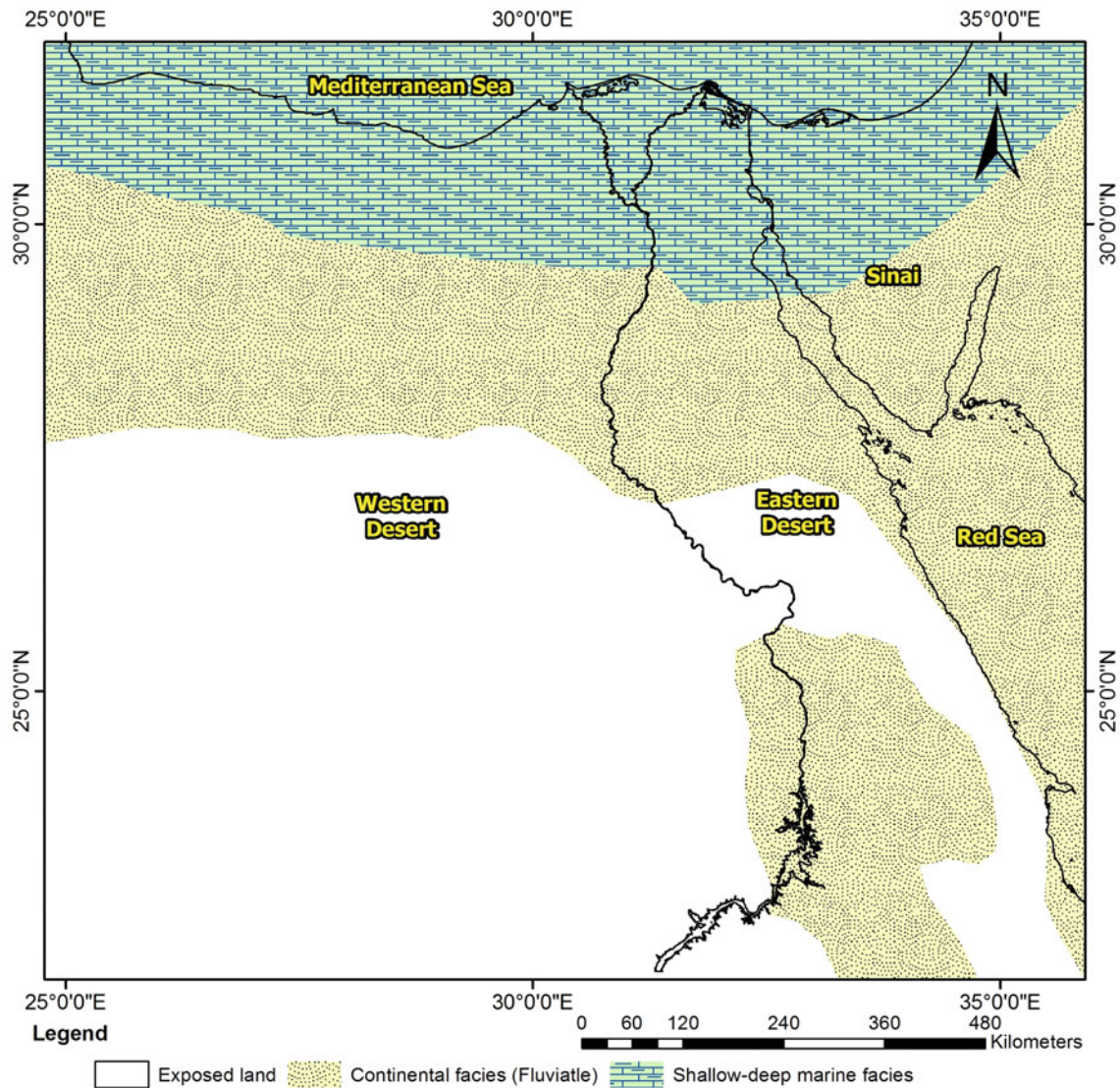


Fig. 21 Facies distribution of the Coniacian–Santonian sedimentary rocks in Egypt

W. Feiran, west southern SN (Fig. 23). Also, it unconformably overlies the Paleozoic rocks in others (Klitzsch et al., 1990). Malha Fm. consists of fluvial sandstone, kaolinite (Fig. 24), cross-bedding intercalated with local conglomeratic beds, and paleosols. It is overlain in the most places by marine strata of the Raha (Fig. 25) or its equivalent Galala fms. Darwish (1992) assigned Jurassic–Early Cretaceous to the sandstone of Malha Fm. in the Northern Galala Plateau. Klitzsch et al. (1990) defined Wadi Qena Sandstone in the north of W. Qena and the W. Dakhil as an equivalent rock unit to the Malha Fm. The Wadi Qena Sandstone rests unconformably over the Precambrian basement rocks (Klitzsch et al., 1990). Allam and Khalil (1988) described ~ 160– ~ 180 m thick of the Malha Fm. at the Arif El Naga area. It composes of white and variegated cross-bedded poorly sorted ferruginous sandstone with

siltstone and shale intercalations. Mostly, the Malha Fm. at north SN unconformably overlies Jurassic rocks and conformably underlies Cenomanian Halal Fm. (Fig. 26). El-Azabi (1999) described mottled, red, brown, purple, violet, black, and white sandstone as the Malha Fm. at G. Shabrawet. Also, Soliman (2001) described ~ 74 m thick of sandstone, siltstone, and kaolinitic claystone at the same area. The sandstones are poorly to medium sorted and varicolored (white, gray, yellow, red, violet, and brown). The siltstone and claystone dominate its upper part. Soliman (2001) assigned it to the Barremian–Early Aptian.

B. The Risan Aneiza Formation

It was originally proposed by Said (1971) for the marine succession at Bir Lagma, northern of G. Maghara, north SN.

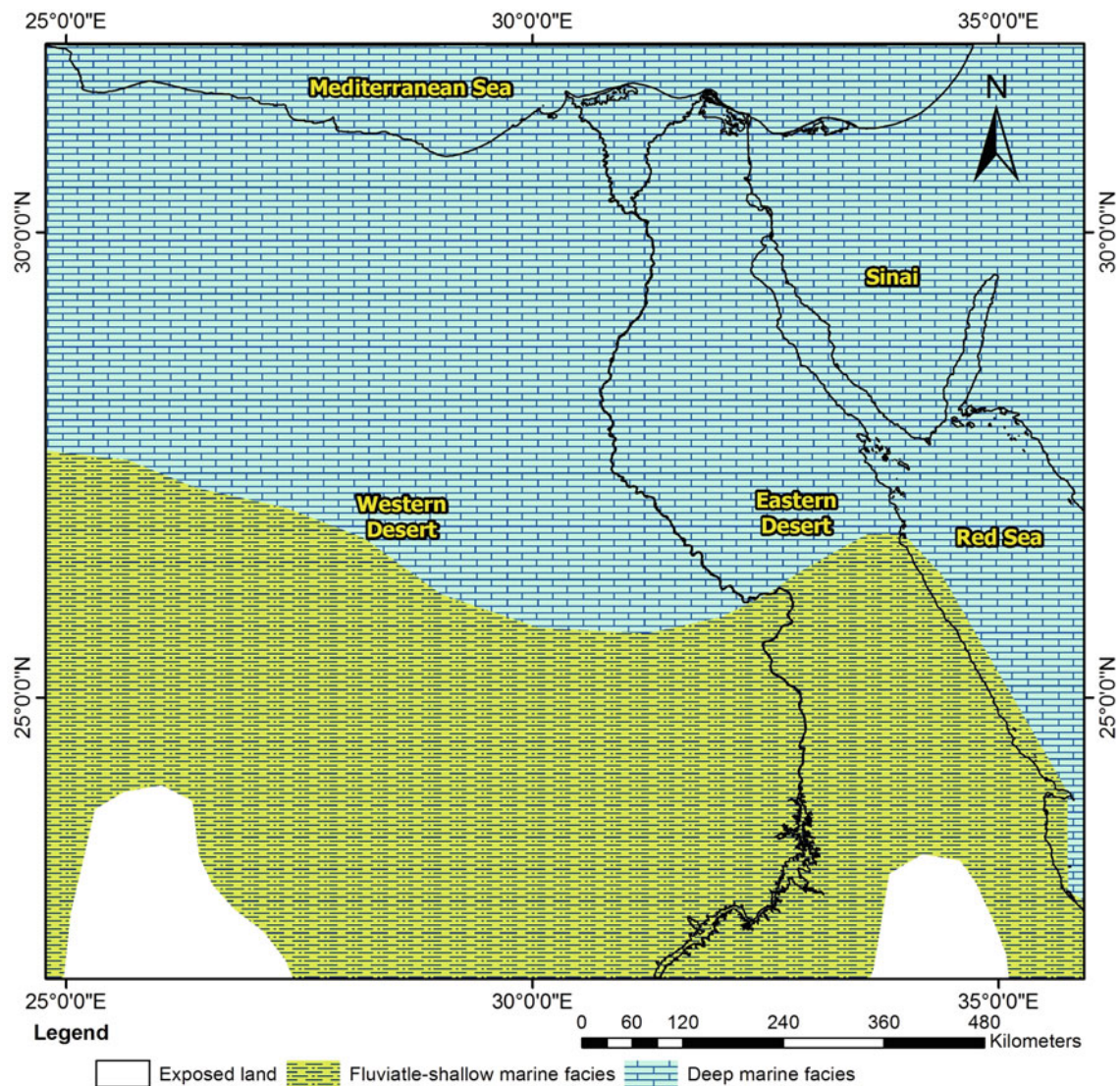


Fig. 22 Facies distribution of the Campanian–Maastrichtian sedimentary rocks in Egypt (modified after Guiraud & Bosworth, 1999)

It composes of ~ 110 m thick of a sequence of sandstone and calcareous sandstone intercalated with fossiliferous limestone and marl. Said (1971) assigned it to the Aptian–Albian age. Abdel-Maksoud (2006) assigned the age of the Risan Aneiza Fm. to Barremian–Albian age according to the occurrence of ammonite fossils (Figs. 27, 28, 29 and 30). El-Azabi (1999) described the Risan Aneiza Fm. at G. Shabrawet west the Suez Canal and subdivided the formation into the lower carbonate/clastic unit of Aptian age and the upper carbonate-dominated unit of Albian age.

Moreover, Soliman and Wanas (2004) described the Risan Aneiza Fm. at G. Manzour, east G. Maghara, and subdivided it into two parts A and B. Part A composes of about 92 m thick of sandstone, claystone, and limestone beds. The

sandstones are fine to coarse-grained, yellow, and brown, ferruginous, dolomitic, siliceous, and gypsiferous. Part B consists of ~ 48 m thick of sandstone, claystone, and limestone interbeds with increasing of carbonate rocks upwards. Part B rests conformably over part A. The sandstone of part B is fine to coarse-grained, calcareous, or dolomitic. Recently, Salama et al. (2018) described ~ 230 m thick of shallow marine (homoclinal ramp) deposits of Risan Aneiza Fm. from G. Raghawi (north SN). They (op. cit.) assigned it to Late Barremian–Middle Albian depending on the occurrence of orbitolina, rudists, and ammonites fauna. Also, Salama et al. (2021) recoded the Risan Aneiza Fm. at base of G. Manzour, G. El Tour Kumanyia, and G. Minsherah and assigned the Aptian–Early Albian age for it.



Fig. 23 Field photo for the basement rocks (Precambrian) and the Malha (Early Cretaceous) at W. Feiran, southern Sinai



Fig. 24 Mines of kaolinite within the Malha Fm. at the W. Budra and Abu Zeinema area, southwestern Sinai

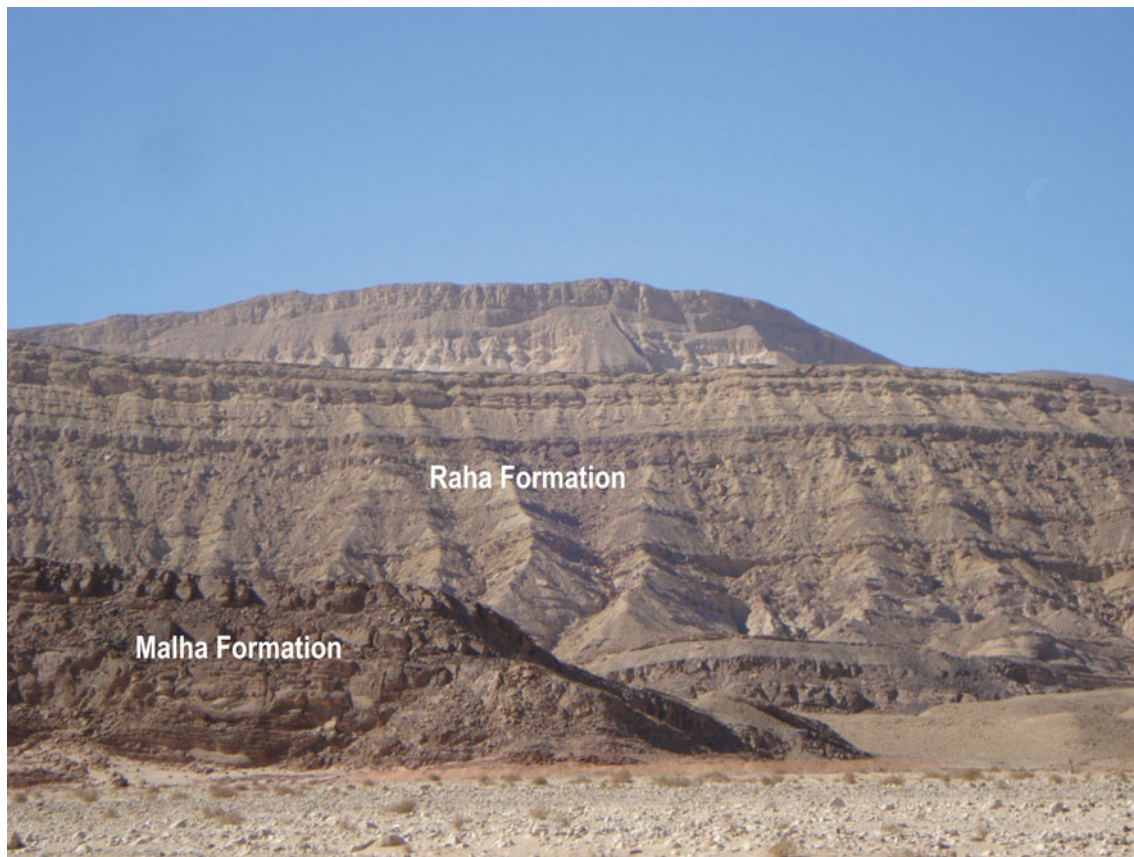


Fig. 25 Field photo of the Malha (Early Cretaceous) and Raha (Late Cretaceous) rock units. at the W. Feiran, southwestern Sinai

4.2 The Subsurface Lower Cretaceous Sedimentary Rocks

The subsurface Lower Cretaceous strata are represented in the south of Egypt at the west and east of the river Nile in Kom Ombo provinces (e.g., Kom Ombo Basin) and in the northern portion of the WD, such as: Matruh and Abu Gharadig basins. These strata were defined by the petroleum companies which worked there.

4.2.1 The Kom Ombo Basin

The subsurface Lower Cretaceous sedimentary rock units at the Kom Ombo Basin (Upper Egypt) are represented by the same surface Lower Cretaceous successions in the south of Western Egypt (see details about these rock units in the previous part). These rock units in a stratigraphic order are Six Hills, Abu Ballas, and Sabaya fms. Issawi et al. (2016) described about 150 and 250 m thick of Six Hills and Abu Ballas fms., respectively, at Kom Ombo-3 Borehole (west of the River Nile). Meantime, Issawi et al. (2016) described these formations from the east side of the River Nile at the Nukra-1 and Kharit-1 boreholes and measured 550 and 400 m thick for the Six Hills Fm. and 300 and 150 m thick

for the Abu Ballas Fm., respectively. They (op. cit.) believed that Sabaya Fm. is missing at all boreholes.

4.2.2 The Northern Western Desert

A. The Burg El-Arab Formation

There are several sedimentary basins in the north of the WD such as Matrouh, Shoushan, Faghur, Alemein, and Abu Ghardig. The Lower Cretaceous rocks in this part of Egypt are represented by Burg El-Arab Fm., which was subdivided into four members. Its type locality lies at the Burg El-Arab well (30° 55' 20" N, 29° 31' 28" E), the interval from ~ 4054 to ~ 2305 m depth. This formation overlies conformably the Late Jurassic carbonate Masajid Fm. (Hantar, 1990; Shalaby et al., 2011). At some places, it unconformably overlies the Wadi Natrun/the Bahrein strata (Early-Middle Jurassic age) or the Paleozoic or the Precambrian rocks. Burg El-Arab Fm. conformably underlies Bahariya Fm. Hantar (1990) subdivided this formation into four members, namely in stratigraphic order are: Alam El Bueib/Matruh, Alamein, Dahab, and Kharita (Fig. 18).

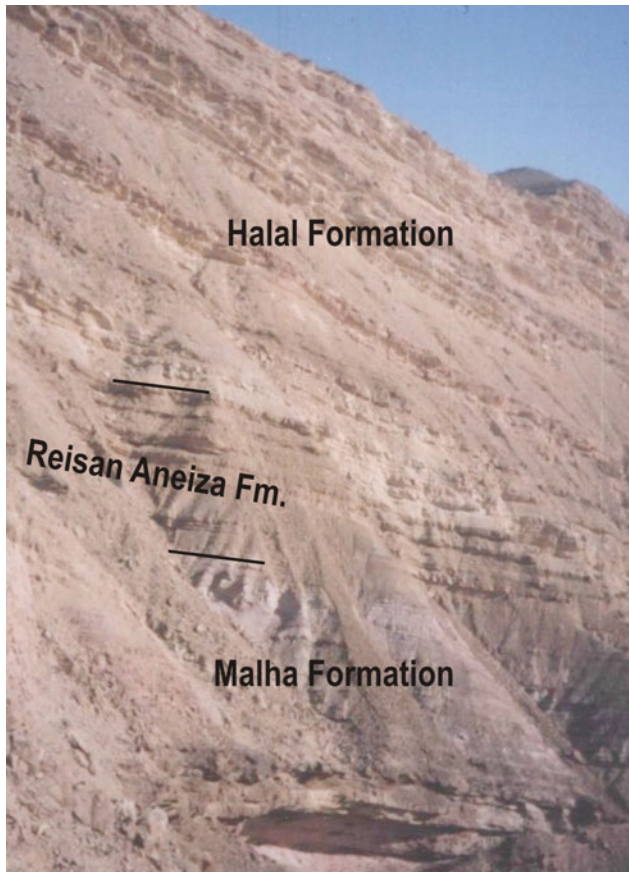


Fig. 26 Field photo of the Malha, Risan Aneiza, and Halal fms. at the G. Halal, northern Sinai

– The Alam El Bueb Member

It consists of sandstone with frequent shale and limestone beds in the lower and upper parts, respectively. The type locality of this member lies at Alam El Bueb-I well (30° 38' 39" N, 29° 08' 37" E), the interval from ~ 4297 to ~ 3927 m depth.

In some boreholes, the Alam El Bueb Member was named in different rock units by different petroleum companies such as Matruh and Shaltut (El Diasty, 2015; El Nady, 2015; Gentzis et al., 2018; Moretti et al., 2010). The lower part of this unit was sometime named by the Betty Fm. (El Diasty, 2015; El Nady, 2015; Gentzis et al., 2018; Hantar, 1990; Moretti et al., 2010). This member reaches its maximum thickness at Alamein-I Borehole (~ 1820 m). It ranges from Barremian to Aptian (El Diasty, 2015; El Nady, 2015; Gentzis et al., 2018; Moretti et al., 2010). El Atfy et al. (2019) assigned this member to the Late Hauterivian–Early Barremian age. It is marked by shallow marine setting with continental influence toward the south (Hantar, 1990).

– The Matruh Member

It composes of pyritic calcareous shale which includes carbonaceous layers in its upper part with few carbonate and sandstone interbeds. This unit is stratigraphically equivalent to the Alam El Bueb Member. The type locality is at the Mersa Matruh-I Borehole at the interval from ~ 4572 to ~ 4297 m depth.



Fig. 27 Field photo of the Risan Aneiza Fm. at Risan Aneiza Village, northern Sinai



Fig. 28 Field photo of the Risan Aneiza and Halal fms. at Naquib Ouda, Maghara area, northern Sinai



Fig. 29 Field photo of the Risan Aneiza Fm. at G. Manzour, Maghara area, northern Sinai

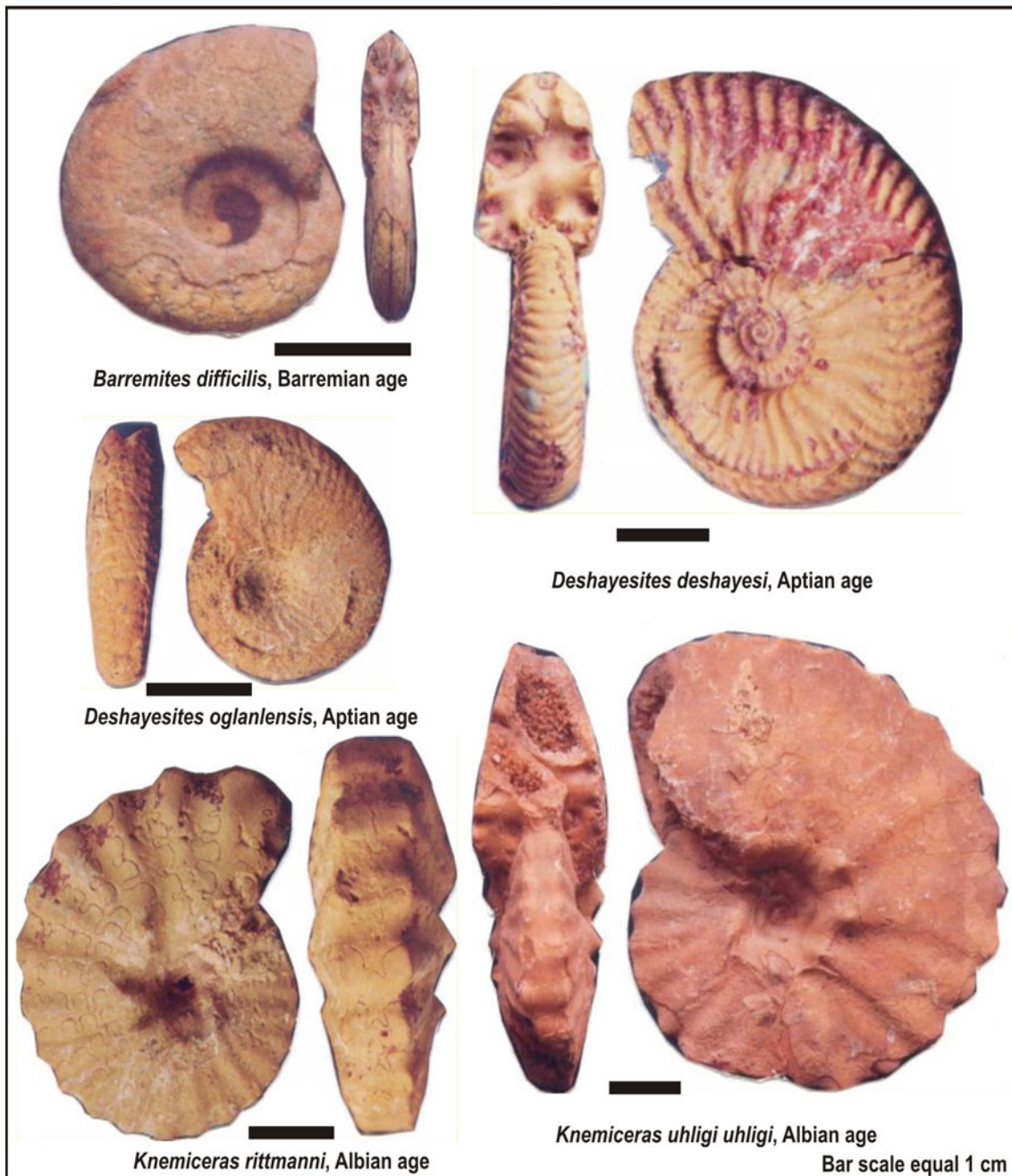


Fig. 30 Barremian–Albian ammonites fossils of Risan Aneiza Fm., Risan Aneiza Village, northern SN, Egypt (after Abdel-Maksoud, 2006)

~ 2585 m depth. The base of this unit was recorded in Siqueifa-I Borehole, where it rests unconformably over the Middle Jurassic Sidi Barrani Fm. Hantar (1990) assigned Matruh Member to Neocomian–Aptian that deposits in shallow marine with continental influence near the top.

– The Alamein Member

This member is widely distributed all over the Northern WD (El Atfy et al., 2019; El Diasty, 2015; El Nady, 2015;

Gentzis et al., 2018; Moretti et al., 2010). It composes of microcrystalline dolomite with shale beds. This member overlies Alam El Bueb and underlies the Dahab members with sharp contact. The type locality of this member was recorded at the Alamein-I well (30° 36' 39" N, 28° 43' 52" E) between the intervals from ~ 2573 to ~ 2489 m depth. The Alamein Member grades laterally into shale toward the north in the Matruh area (Hantar, 1990). Generally, the thickness of this member ranges from ~ 20 to ~ 80 m thick all over the northern WD. On the other hand, in some

places its thickness reaches about 92–97 m thick at Alamein-1 and Kanayis-1, respectively. Bosworth and Tari (2021) believed that this member was deposited in a shallow marine setting and gave it Aptian to Albian age.

– The Dahab Member

It forms of a gray shale with siltstone and sandstone beds. It rests conformably over Alamein Member and under the Kharita Member with sharp contact. The type locality of this member is at the Dahab-I Borehole (30° 48' 24" N, 28° 45' 25" E) at the interval from ~ 3354 to ~ 3180 m depth. The age of the Dahab Member is Aptian–Early Albian (Bosworth & Tari, 2021; Hantar, 1990). A shallow marine setting characterizes this member (Bosworth & Tari, 2021).

– The Kharita Member

The Kharita Member composes of sandstone with shale and carbonate beds. Its type locality of this member is at the Kharita-I Borehole (30° 33' 48" N, 28° 35' 32" E) at the interval from ~ 2890 to ~ 2501 m depth. This member rests conformably over the Dahab Member or unconformably over the older sedimentary rock units of the Mesozoic Era or

the basement rocks of the Precambrian Eon. It underlies conformably all over the northern WD the famous Bahariya Fm. It reaches ~ 1100 m at Mersa Matruh-I Borehole. The Kharita Member was assigned to Albian–Cenomanian age (Bosworth & Tari, 2021; El Diasty, 2015; El Nady, 2015; Gentzis et al., 2018; Moretti et al., 2010). It was deposited under fluvial conditions (Norton, 1967; Said, 1962). On the other hand, El Diasty (2015) suggested shallow marine setting for Kharita Member at Abu Ghardig Basin. Moreover, Shehata et al. (2018) recorded this member at the west of the Beni-Suef Basin and believed that the strata of this member were deposited under fluvial conditions.

4.3 The Surface Upper Cretaceous Sedimentary Rocks

4.3.1 North Western Desert Successions

A. The Bahariya Formation

Said (1962) introduced this formation to describe the continental friable, false-bedded sandstone, claystone, and



Fig. 31 Field photo shows the type section of the Bahariya Fm. at the G. El Dist, Bahariya Oasis, WD, Egypt

ferruginous with fine siltstone bands in the north part of the WD. Its type section lies in G. El Dist, Bahariya Oasis (Fig. 31). Bahariya Fm. covers the floor and scarps of this oasis with strata range in thickness from few meters to ~ 170 m thick (Moustafa, 1980). In the drilling boreholes (Box-1), the thickness of Bahariya Fm. reaches about 705 m thick. It reaches maximum thickness (~ 1143 m) at the Kattaniya-1 borehole (Issawi et al., 2009). This formation builds the most isolated hills in the central and southern parts of the Bahariya Depression. Soliman and Khalifa (1993) described Bahariya Fm. and subdivided it into three informal units in the central part of the depression: the lower interbedded siltstone and sandstone, the middle cross-bedded sandstone, and the upper ferruginous sandstone. The Bahariya Fm. was dated as Cenomanian age in the type section (Hataba & Ammar, 1990; Said, 1962; Soliman & Khalifa, 1993; Soliman et al., 1970). It unconformably overlies the Kharita Member or directly covers the basement rocks (El-Bassyouny, 1970). The Bahariya Fm. unconformably underlies the Heiz (Late Cenomanian) Fm. (Khalifa & Abu El-Hassan, 1993) or El-Naqb (Early-Middle Eocene) Fm. (El-Bassyouny, 2004). Bahariya Fm. includes vertebrate remains (iconic dinosaurs) such as the carnivorous *Carcharodontosaurus*, and *Spinosaurus*, and the herbivorous *Aegyptosaurus*, and *Paralititan* (Nothdurft et al., 2002; Smith et al., 2001). El-Akkad and Issawi (1963) interpreted the Bahariya Fm. as a deltaic paleoenvironment with marine sea incursions. Issawi et al. (2009) indicate that the fluvial and marine environments setting alternated over the Bahariya region, where the fluvial setting was prevailing in the lower parts and decreasing upwards and the marine setting increased gradually upward with time.

B. The Heiz Formation

Heiz Fm. was defined by El-Akkad and Issawi (1963) to describe the mainly carbonate units with clastic interbeds, including dolomitic sandstone bed at the base and dolostone bed at the top of ~ 30 m thick at the Bahariya Oasis. It unconformably overlies Bahariya Fm. and unconformably underlies Hefhuf Fm. Heiz Fm. is widely distributed in the Bahariya Depression and represents the upper escarpment face that overlies the Bahariya Fm. in the central and southern parts of the oasis, while it is absent northward in the Naqb of the Bahariya Oasis. Its thickness ranges from ~ 5 to ~ 24 m thick (Khalifa & Abu El-Hassan, 1993). They contributed that the Heiz Fm. consists of sedimentary cycles from claystone at the base to dolostone at the top, which deposited in an inner shelf paleoenvironment setting in the central and southwestern of the oasis, changed to the outer shelf paleoenvironment setting in the northeastern portions of the depression. Heiz Fm. contains *Heterodiadema libyca*,

Hemiaster fournelli, *Dosinia delectrei*, *Exogyra plecifera*, *Ostrea nicasei*, *Ostrea mermeti*, *Ostrea flabellata*, and *Ostrea africana* of the Late Cenomanian age (El-Akkad & Issawi, 1963).

C. The Abu Roash Formation

Norton (1967) proposed this formation to describe the mainly rocks consist of carbonate limestone interbeds with clastic shale and sandstone. Norton (op. cit.) described the rocks of this formation from the subsurface rocks at Mubarak-1 well (north WD), which unconformably overlies Bahariya Fm. and underlies Khoman Fm. It was subdivided into seven informal rock units from the base to the top: G, F, E, D, C, B, and A. These units could be distinguished lithologically due to the alternatives between the clastic (G, E, C, and A) and the pure carbonate units (F, D, and B). The thickness of the formation ranges between 250 and 750 m thick. The exposure deposits of this rock unit were described by Beadnell (1902) at G. Abu Roash (type section), west Giza Pyramids. Its base is unexposed and unconformably underlies the Eocene succession (Faris, 1948). Abu Roash Fm. was subdivided into six informal rock units by Jux (1954). These units in a stratigraphic order are: the Sandstone, *Rudistae*, Limestone, *Acteonella*, Flint, and *Plicatula* Series (Fig. 18). Abdel-Gawad et al. (2011) assigned the lower series (Sandstone, *Rudistae*, Limestone) to the Middle Turonian and the *Acteonella*, the Flint Series to the Upper Turonian, and the *Plicatula* Series to the Middle Coniacian. Said (1962) assigned the Abu Roash Fm. to the Late Cenomanian to Santonian age. Recently, Salama et al. (2017) assigned G unit to Late Cenomanian, while the remainder units are of Turonian to Coniacian age.

D. The Hefhuf Formation

It was defined by El-Akkad and Issawi (1963) at the type section in the G. Hefhuf, Bahariya Oasis. It was named Ain El Wadi Limestone by Omara et al. (1970). This formation occurs in the Bahariya and Farafra oases. It attains ~ 120 m thick and is made up of dolostone with intercalation of sandstone, shale, and phosphatic beds. It unconformably overlies Heiz Fm. and underlies Khoman Fm. Khalifa (1977) and Khalifa et al. (2002) revised the term the Hefhuf Fm. and separated the upper phosphatic member from the Hefhuf Fm. and redefined it as an independent rock unit named the Ain Giffara Fm., assigned to the Campanian–Maastrichtian age. Khalifa (1977) subdivided the Hefhuf Fm. into three informal units: the lower dolostone, middle dolostone-claystone, and the upper claystone-sandstone. The Hefhuf Fm. is rich in macrofossils such as *Ostrea dichotoma*, *Protocardia mobitica*, *Isocardia chargensis*, and *Cardium* spp. of Campanian

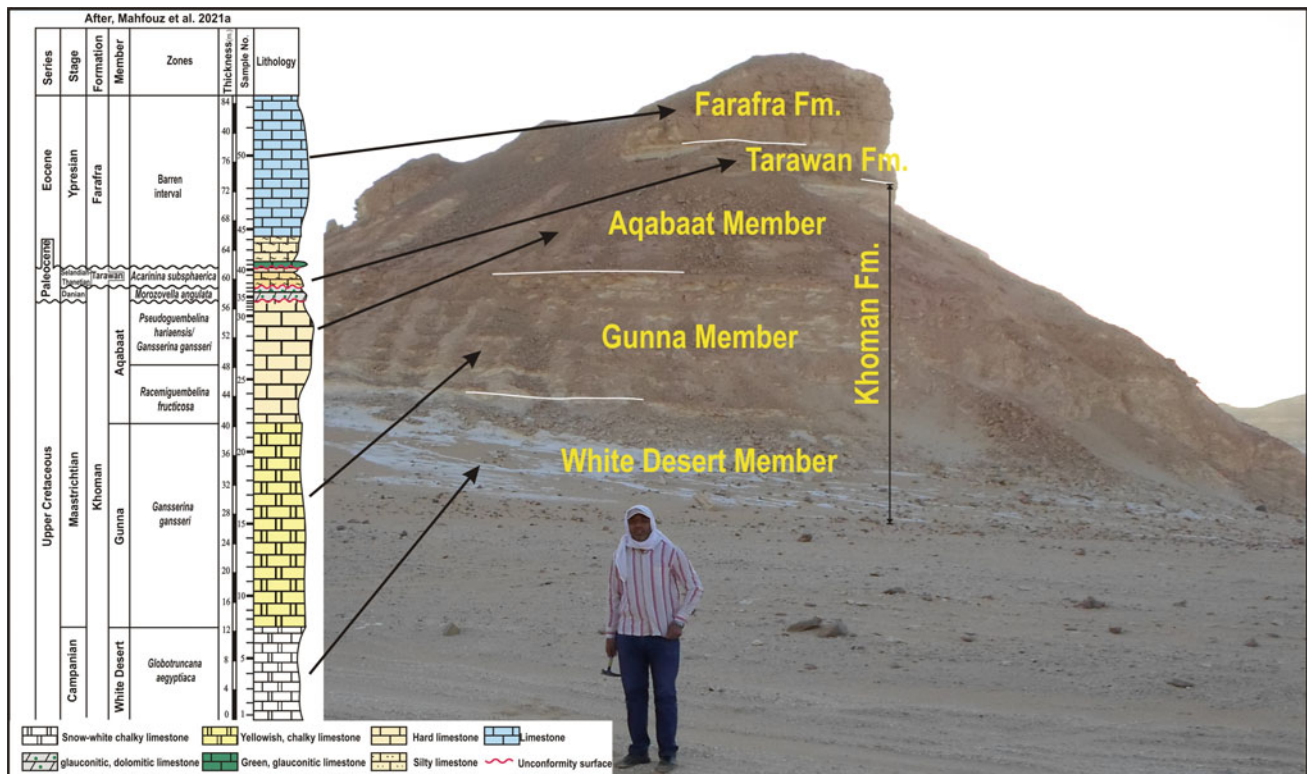


Fig. 32 Field photo shows the Khoman Fm. at the Farafra Oasis, WD, Egypt

age (Youssef & Abdel Aziz, 1971). Khalifa and Tanner (2017) believed that the strata of Hefhuf Fm. were deposited in shallow marine environment ranging from supratidal to subtidal setting and gave them Turonian–Santonian age.

E. The Wadi Hennis Formation

It was introduced by Dominik (1985) to describe the clastic sequence at Wadi Hennis, northeast to the Farafra Depression. It composes of bituminous claystone and glauconitic sandstone. It unconformably underlies the Khoman Fm. (Obaidalla et al., 2020) or the Hefhuf Fm. (Dominik, 1985). Obaidalla et al. (2020) considered the Wadi Hennis Fm. to be of the Santonian age due to its stratigraphic position below the lowermost Campanian *Globotruncanita elevata* Zone that recorded in the basal part of the Khoman Fm. Hermina (1990) assigned this formation to the Lower Campanian age and believed that it is equivalent to Quseir Fm. In Farafra area, the Wadi Hennis Fm. is the oldest exposed succession with limited extent in the core of the northeast-southwest anticline within the area between W. Hennis and Ain El Maqfi (Hermina, 1990). Obaidalla et al. (2020) believed that Wadi Hennis Fm. was mainly deposited under continental environment (fluvial).

F. The Khoman Formation

Kerdany (1968) described the subsurface chalky limestone at Ain Khoman, southern Bahariya Oasis, as the Khoman Fm. This formation is exposed as surface rocks between the southern parts of Bahariya to Farafra depressions. Also, it is exposed at Abu Roash area, near Pyramids Plateau. It unconformably overlies Hefhuf or Abu Roash or Bahariya fms. and unconformably underlies the Apollonia or Dabaa or Naqb or Tarawan or the upper part of the Dakhla fms. At Aqabaat area (Fig. 32), Mahfouz et al. (2021a) stratigraphically subdivided ~ 59 m of the exposed Khoman Fm. into three members: the White Desert, the Gunna, and the Aqabaat. These members are represented by the planktonic foraminiferal zones from the *Globotruncana aegyptiaca* to *Igorina pusilla*, which cover the Campanian to Danian time interval. At the subsurface, the Khoman Fm. attains ~ 144 m thick at Sahl Baraka borehole (Obaidalla et al., 2020), which is represented by planktonic foraminiferal zones from *G. elevata* to *Praemurica uncinata* that cover the Campanian to Danian time. Tassy et al. (2015) assigned the age of the Khoman Fm. to the Coniacian–Maastrichtian age. They (op. cit.) believed that the Khoman Fm. is unconformably overlain Abu Roash Fm. and underlain Apollonia

Fm. Obaidalla et al. (2020) evidenced that the carbonate facies chalky limestone rocks of the Khoman Fm. were intertonguing with the siliciclastic facies shale of the Dakhla Fm. at Sahl Baraka borehole (Fig. 18) with shale interbeds. At WD-7-1 borehole, the Khoman Fm. has its maximum thickness ~ 1644 m (Hantar, 1990). The Khoman Fm. is missing completely toward the south at Abu Minqar and Dakhla areas. Khoman Fm. was deposited under proper marine environment, from outer shelf to upper bathyal settings (Mahfouz et al., 2021a; Obaidalla et al., 2020).

4.3.2 South Western Desert Successions

A. The Maghrabi Formation

The Maghrabi Fm. was defined by Barthel and Herrmann-Degen (1981). It attains about 60 m thick of fine-grained, bioturbated marine sandstone and claystone. Maghrabi Fm. unconformably overlies Early Cretaceous (Albian) Sabaya Fm. Its type section lies in the southern portion of the WD at Dakhla Basin along Kharga-Dakhla Road. The Maghrabi Fm. is of Cenomanian age (Hendriks, 1986). The basal sandstone parts are marked by abundant plant remains (mainly leaves of angiosperms), while the upper parts are composed of shale and sandy glauconitic beds including abundant pelecypod shells as well as fish teeth. South of Ammonite hill, remains of a dinosaur were found in the Maghrabi Fm. (Kerdany & Cherif, 1990). Maghrabi Fm. changes laterally toward the north of the WD to the Bahariya Fm. At the same time, it is laterally changed to non-fossiliferous sandstone and claystone toward the south and west of the Dakhla Depression, where the Maghrabi Fm. represents by a continental sandstone sequence, almost devoid of fossils.

B. The Taref Formation

It was defined by Awad and Ghobrial (1965) at G. Taref (type section), northern Kharga Oasis. The Taref Fm. consists of fine coarse-grained, cross-bedded sandstone with a conglomeratic base. Generally, it is distributed in the central and southern parts of Egypt, covering the central parts of the WD from the Kharga region and extended westwards and southwestwards. In addition, it is distributed in the central ED (Issawi et al., 1978). Taref Fm. unconformably overlies the basement rocks or Maghrabi Fm. and underlies Quseir Fm. Attia (1955) stratigraphically subdivided the Taref Fm. (Turonian–Santonian) into three rock units, the Abu Aggag, Timsah, and Um Barmil. El-Naggar (1970) separated these three units into formal lithostratigraphic units (formations). The Taref Fm. is ~ 100 m thick at the G. Taref (Kharga Oasis, Awad & Ghobrial, 1965). It attains ~ 130 m thick along Red Sea coast, ~ 150 m at the downstream side of

W. Qena, ~ 200 m at W. El-Mashash (Issawi et al., 1978), 60–80 m at Sabaya–Mahamid area, and ~ 13 m at Kom Ombo Graben, whereas it measures ~ 120 m at G. Silsila at the upthrow side of the northern fault limiting the Kom Ombo Graben, ~ 100 m in W. Abad east of Idfu and ~ 150 m at the plains south of Dakhla Oasis (Issawi et al., 2009). In the subsurface, its average thickness reaches ~ 110 m increasing to the south of the Dakhla Depression (Ghoubachi, 2001). Awad and Ghobrial (1965) believed that Taref Fm. was mainly deposited under continental environment (fluvial) with near shore marine intercalations. This formation is of Turonian age (Hermina, 1990).

C. The Quseir Formation

The Quseir Fm. was firstly defined by Ghorab (1956) to describe the variegated, vividly colored shale alternating with sandstone beds. Youssef (1957) introduced the Quseir Variegated Shale at G. Atshan, Quseir region. In the WD (Dakhla and Kharga oases), this formation was named informally “purple shale” by Beadnell (1909) and “variegated shale” by Said (1962) and Awad and Ghobrial (1965). Also, Barthel and Herrmann-Degen (1981) named it formally as the Mut Fm. Omara et al. (1976) subdivided Quseir Fm. into two members, the Mut (red claystone) at the base and the Hindaw (varicolored, gypsiferous shales, claystones, argillaceous sandstone, and siltstone with some sandstone lenses) at the top. The type locality of the Mut Member is at the Mut Region and unconformably rests on the Taref Fm., whereas the type locality of the Hindaw Member is at the Hindaw Village, and it is overlain by Duwi Fm.

Generally, Quseir Fm. is widely distributed all over the Egyptian geographic regions. Said (1990) mentioned that this formation contains Campanian ammonites index fossils (e.g., *Canadoceras cottreaui* and *Manambolites pivetaui*). This formation deposits in very shallow marine (tidal flats), but the basal strata of it contain remains of freshwater reptiles, gastropods, terrestrial plant debris, and dinosaur skeletons (Hendriks et al., 1984). Dominik (1985) believed that the Quseir Fm. is equivalent to the Wadi Hennis Fm. The Quseir Fm. includes some vertebrate fossils as *Corax bosanii*, *Lamma appendiculata*, and *Schizoria stromeri* (El Nakkady, 1951). It was considered of Campanian age (Youssef, 1957). Recently, Sallam et al. (2018) recorded and described the sauropod dinosaur *Mansourasaurus shahinae* gen. et sp. nov., from Quseir Fm. in Dakhla Oasis.

D. The Duwi Formation

Duwi Fm. was defined by Youssef (1957) to describe the varying thickness of phosphatic beds alternating with claystone, siltstone, marl, oyster limestone, and sandstone beds



Fig. 33 Field photo of the Duwi Fm. at the G. Duwi, Quseir area, Red Sea coast, Egypt

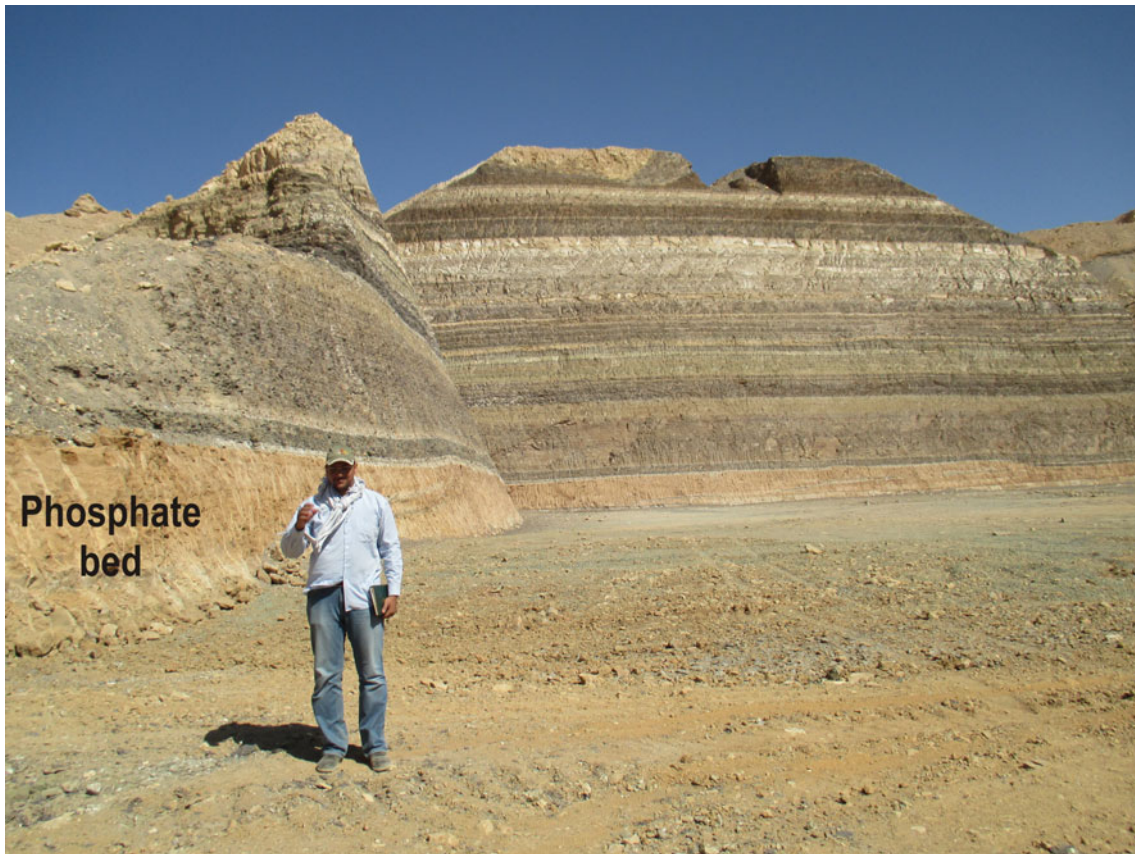


Fig. 34 Field photo shows the Duwi Fm. at Abu Tartur area, WD, Egypt



Fig. 35 Field photo shows the Dakhla Fm. at El Qasr area, Dakhla Oasis, WD, Egypt

rich in glauconite at the type section in the G. Duwi, Quseir area, Red Sea coast. The strata of this formation were named Phosphate Fm. (by Said, 1962, 1971). It unconformably overlies Quseir Fm. and underlies Dakhla Fm. The Duwi Fm. is formed a belt in Egypt, where it is represented in the Red Sea (Quseir–Safaga region, Fig. 33), Nile Valley (Mahamid–Sebaiya–Qena region), and New Valley (Kharga–Dakhla region, Fig. 34). It occurs as phosphatic bearing units (beds or lenses). The deposit of the Duwi Fm. indicates reworking and disturbed deposition with clear unconformity evidence, which indicates high-energy shallow marine with a highly oscillating bottom (El Ayyat, 2015). Also El Ayyat (2015) described black shale strata within the Duwi Fm. at Abu Tartur, WD. It is equivalent to Hefhuf Fm. (El-Akkad & Issawi, 1963) in Bahariya and Farafra regions.

Hendriks et al. (1987) introduce Rakhayat Fm. at the central W. Qena to describe ~ 85 m thick of shale intercalated with phosphate beds. He (op. cit.) believed that it is equivalent to the Quseir and Duwi fms. The lower and middle parts are characterized by the presence of phosphatic intraformational conglomerate sandstone, siltstone, marl, and limestones beds, which are indicated a repeated change of low- and high-energy deposition due to tidal influence as well as to syn-sedimentary tectonism. The upper part of

Rakhayat Fm. consists of shale deposited in low energetic conditions (Hendriks & Luger, 1987).

E. The Dakhla Formation

Said (1961) introduced it to describe the siliciclastic facies shale strata at Rasheda Village at the north of Mut area, the Dakhla Oasis. It unconformably overlies Duwi Fm. and unconformably underlies Tarawan or Kurkur fms. Dakhla Fm. attains ~ 230 m thick, which consists of dark shale, marl, and interbeds of siltstone, sandstone, and limestone. Awad and Ghobrial (1965) subdivided Dakhla Fm. into three members: Mawhoob (black shale rocks) at base, Baris (oyster mudstone rocks) at middle, and Kharga (gray shale rocks) at top (Fig. 35). The Kharga Shale Member was informally subdivided by Luger (1985) into Lower Kharga Shale and Upper Kharga Shale units. The contact between these two units marked the Cretaceous/Paleogene boundary, which is characterized by the occurrence of conglomerate bed (disconformity) within the Kharga Member (Mahfouz & Metwally, 2020). The Dakhla Fm. changes laterally northwards at Farafra-Bahariya oases, WD into Khoman Fm. (Obaidalla et al., 2020). El-Naggar (1970) defined the Sharawna (shale intercalated by marl beds) Fm. equivalent to the Dakhla Fm.

In the Nile Valley (W. Hamama–G. Qrieya) and the Red Sea (Quseir–Safaga) regions, Dakhla Fm. was subdivided into two members: the Hamama (pink marl–chalky limestone rocks) at the base and the Beida (black to gray shale rocks) at the top (Abdel Razik, 1972). Obaidalla et al. (2017) considered that the Hamama Member at the G. Qrieya represents a tongue of the Sudr Fm., according to the similarity on the lithology and facies. Also, they (op. cit.) considered that the Hamama Member is equivalent in the geologic age to the Late Campanian–Maastrichtian. Dakhla Fm. covers the Maastrichtian–Paleocene time interval (Mahfouz et al., 2021b). It changed laterally northwards at the north ED and SN into the Sudr Fm. (El Ayyat & Obaidalla, 2013).

At these localities (ED and WD), the Dakhla Fm. represents a tongue, where it overlies the Khoman or the Sudr Fm. by its the upper part of the Danian age. The rocks of the Dakhla Fm. were deposited under proper marine environment, in outer shelf settings at the ED (El Ayyat & Obaidalla, 2013). In the WD, Dakhla Fm. was deposited in

shallow marine ranging from inner shelf to outer shelf settings (Metwally et al., 2021; Obaidalla et al., 2006).

F. The Kiseiba Formation

It was defined by Klitzsch and L  jal-Nicol (1984) and Hendriks et al. (1984) at the type section in the escarpment of Bir Kiseiba, south WD. It was named Quseir Clastic Member and Shab Clastic Member by Issawi (1973). It is of the Campanian–Maastrichtian age. Luger (1988) correlated the Kiseiba Fm. with the Mut, Duwi, and lower part of the Dakhla fms. The Kiseiba Fm. unconformably overlies the basement rocks and underlies the Paleocene Kurkur Fm. It consists of fine-grained sandstone, flaser, and small-scale cross-bedding with intercalation of shale, siltstone with phosphatic, and bones beds at a different level of this section. The thickness ranges from ~ 150 to ~ 300 m (Hendriks et al., 1987). Tantawy (1994) defined the Kiseiba Fm. at G. El Kaddab, Kurkur Oasis, and G. El Barga instead of the Dakhla Fm.



Fig. 36 Field photos show: **a** the contact between the Abu Aggag Fm. and basement rocks, Abra q area; **b** the paleosol layer at the contact between the Cenomanian Abu Aggag Fm. and Precambrian basement rocks



Fig. 37 Field photo shows the remnants of the basement (Precambrian) rocks at the base of the Abu Aggag Fm., Abraha area, Egypt

4.3.3 The South Eastern Desert Successions

A. The Abu Aggag Formation

The Abu Aggag Fm. was proposed by El-Naggar (1970) to describe the fluvial strata at W. Abu Aggag, northeast of Aswan. It attains ~ 30–40 m thick of basal conglomerates, upgraded into violet to red, coarse-grained, cross-bedded, and kaolinitic sandstone with many paleosol layers in the uppermost parts (El-Naggar, 1970). It unconformably overlies Precambrian (basement) rocks (Figs. 36 and 37) and conformably underlies the Timsah Fm. The formation is distributed in the Aswan area, Lake Nasser, the W. Timsah–G. Dif region, and Abraha area northwest Shalatin, Red Sea, Egypt. The Abu Aggag Fm. is characterized by rare fossils, fluvial environment with poorly preserved plant fossils (Kerdany & Cherif, 1990). The Abu Aggag thickness increases north and northeastwards at W. Natash (~ 120–155 m, Said et al., 1976) and Deir El Kanaieess (~ 175–250 m, Abdel Razik, 1972). Kerdany and Cherif (1990) assigned the geologic age of Abu Aggag Fm. to Turonian (?).

B. The Timsah Formation

This formation was described by El-Naggar (1970). It consists of claystone and siltstone which are rich in organic

matter at some levels, especially toward the top. Also, it is intercalated with fine sandstone beds, which are cross bedded and bioturbated especially at the base and contain oolitic iron ore bands toward the top. Its type section lies at the G. Timsah, northeast of Aswan. Timsah Fm. unconformably underlies the Um Barmil Fm. It is of Coniacian age (Kerdany & Cherif, 1990). Its thickness ranges from ~ 5 to ~ 130 m and it attains ~ 40 m thick at the type section. It is distributed in the northeast of Aswan at the W. Timsah and G. Dif. Also, it is recorded in the other localities such as Kalabsha, Garf Hussein, Korosko, Abu Simbil, and Abraha, northwest Shalatin, Red Sea, Egypt. The rocks of the Timsah Fm. are deposited in fluvio-marine environment.

C. The Umm Barmil Formation

Umm Barmil Fm. was introduced by El-Naggar (1970) at G. Umm Barmil, northeast of Aswan to describe the cross bedded medium-coarse-grained sandstone. It correlates with Taref Fm. (Klitzsch, 1984). The thickness of the strata of this rock unit is ~ 86 m. Kerdany and Cherif (1990) believed that the rocks of this formation are deposited under continental (fluvial) environment conditions. The Umm Barmil Fm. unconformably underlies the Kiseiba Fm. around Aswan and the Dakhla Fm. westward of Aswan. Klitzsch (1986) and Hendriks et al. (1987) assigned Umm Barmil Fm.



Fig. 38 Quarry of SN Cement Company shows the Halal Fm. at G. Lebni, east of Maghara area, north SN, Egypt

to the Santonian–Early Campanian, where some beds of this formation contain small lamellibranches and *Ostrea rouvillei*.

4.3.4 The North Eastern Desert and Sinai Successions

A. The Halal Formation

Said (1971) introduced the Halal Fm. to describe ~ 450 m thick of the white to light gray hard crystalline limestone and dolomite with few marl bands at the G. Halal, east Maghara area, north SN. The upper part of the Halal Fm. is mainly interbedded with chalky white fossiliferous limestone. Saber et al. (2009) described the strata of the Halal Fm. at G. Yelleg (~ 420 m thick), G. Maaza (~ 270 m thick), and G. Minsherah (~ 220 m thick). They (op. cit.) demonstrated that the upper part of Halal Fm. contains ammonite's fossils. Also, it occurs at G. Lebni, east Maghara area, north SN (Fig. 38). Bachmann et al. (2003) and Aly et al. (2005) stated that Halal Fm. unconformably overlies Risan Aneiza and unconformably underlies Wata Fm. At G. Halal (type

locality), the Halal Fm. unconformably overlies Risan Aneiza Fm. (Fig. 26). The rocks of this formation contain the Late Cenomanian *Neolobites vibrayeanus* (d'Orbigny) in the middle part and *Calycoceras* spp., *Vascoceras cauvini* Chudeau, and *Metengonoceras dumbli* (Cragin) in the uppermost part (Saber et al., 2009). Also, it includes common bivalves such as *Ceratostreon flabellatum* (Goldfuss), *Ilymatogyra africana* (Lamarck), *Gyrostrea delettrei* (Coquand), and *Costogyra olisiponensis* (Sharpe); gastropods such as *Strombus incertus* (d'Orbigny) and *Nerinea gemmifera* Coquand; coralline sponges such as *Steineria* sp., and *Actinostromarianina* sp. (Abdel-Gawad, 2001; Abdel-Gawad & Gameil, 1995). The geologic age of the Halal Fm. is of the Cenomanian (Abdel-Maksoud, 2006; Saber et al., 2009). Generally, the rocks of Halal Fm. were deposited under marine conditions, from middle to outer shelf setting.

B. The Raha Formation

Ghorab (1961) introduced it to describe the marls, varicolored gypsiferous and glauconitic shale, marly limestone, and sandstone strata at the Raha Plateau, west-central SN, Egypt. The thickness of the exposed Raha Fm. differs from one



Fig. 39 Field photo shows the Raha Fm. at W. Feiran, southwestern Sinai, Egypt

locality to others at SN such as: ~ 100 m thick at the Sheikh Attiya, east SN (Kerdany & Cherif, 1990); ~ 140 m thick at W. Feiran, west SN (Obaidalla & Kassab, 2000); and ~ 190 m thick along the Tih escarpment (Kerdany & Cherif, 1990). It unconformably overlies the Malha Fm. at W. Feiran, southwestern SN (Fig. 39). The geologic age of the Raha Fm. is Cenomanian (Kora et al., 1994). This age was conformed according to the occurrence of the Cenomanian index megafossils such as: echinoids (*Hemiaster cubicus*) and oyster (*C. flabellatum* and *I. africana*). Kassab and Obaidalla (2001), according to the integrated study of the index fossils of the ammonite and the planktonic foraminifera, assigned the age of the Raha Fm. at W. Feiran to the Cenomanian–earliest Turonian age. In the subsurface, the Raha Fm. consists of an interbedded carbonate and clastic rocks intercalated with carbonate one with a great thickness of ~ 310, ~ 316, and ~ 326 m at the Darag, Nekhl, and Abu Hamth boreholes in the central SN, respectively. The siliciclastic facies of the Raha Fm. changes laterally toward the north SN to the carbonate facies of the Halal Fm. (Fig. 18). Obaidalla (2002) believed that the strata of the lower part of Raha Fm. at W. Feiran were deposited in a restricted environment (lagoon), but the middle and upper strata of this formation were deposited under continental shelf (inner-middle shelf) environment.

C. The Galala Formation

Abdallah and Adindani (1963) defined it to describe the sedimentary rocks in the western coast of the Gulf of Suez

along Galala Plateaus and southwards until the middle part of the W. Qena. It reaches ~ 180 m thick and differentiated into two informal lithostratigraphic units: the lower clastic unit (interbedded marl, shale, and sandstone) and the upper carbonate unit (limestone and dolomite). The Galala Fm. was assigned to the Middle-Late Cenomanian age by Wilmsen and Nagm (2013) and Nagm and Bamoussa (2020) especially at the Northern Galala Plateau, according to the occurrence of *N. vibrayeanus* and *V. cauvini* ammonite index fossils. Southwards, at Southern Galala Plateau, W. Hawashiya, and northern W. Qena, Nagm (2015) believed that the geologic age of Galala Fm. is of Upper Cenomanian–Early Turonian according to the occurrence of the Late Cenomanian and Early Turonian ammonites index fossils. Galala Fm. unconformably overlies Malha Fm. (Early Cretaceous) at the Galala Plateaus and W. El-Dakhl, or the Paleozoic Naqus Fm. southward at W. Hawashiya and northern W. Qena region (Nagm & Bamoussa, 2020). Galala Fm. unconformably underlies the Maghra El-Hadida Fm. at the North Galala Plateau and conformably underlies Abu Qada Fm. at the Southern Galala (Nagm, 2015; Wilmsen & Nagm, 2013). Also, they (op cit.) added that the Galala Fm. unconformably underlies Umm Omeiyid Fm. at W. Hawashiya and northern W. Qena. Recently, Nagm et al. (2021) believed that the age of the Galala Fm. at W. Um-Artah and W. Hawashiya is latest Cenomanian according to the occurrence of calcareous nannofossil index fossils (e.g., *Axopodorhabdus albianus* and *Helenea chiastia*). They (op. cit.) added that Galala Fm. is characterized by the presence of Cenomanian molluscan fossils (e.g., *Ostrea*



Fig. 40 Field photo shows the Turonian ammonite fossils within the marly limestone of the Abu Qada Fm. at W. Abu Qada, west-central Sinai, Egypt

olisiponensis, *O. africana*, *O. flabellata*, *Periaster oblongus*, *Tylostoma elatius*, *Diplopodia variolaris*, *Heterodiadema libycum*, *Nerinea bicatenata*, and *Exogyra olisoponesis*). The strata of the Galala Fm. were deposited under continental shelf (inner-shallow outer shelf) environment (Nagm & Bamoussa, 2020; Nagm et al., 2021). The Galala Fm. is equivalent to Halal and Raha fms. at north and south SN (Fig. 18).

D. The Abu Qada Formation

It was introduced by Ghorab (1961) to describe the alternating green-gray soft shale and hard yellowish marly limestone at W. Abu Qada, west-central SN, Egypt. Said (1962) described an Early Turonian ammonites bed at the central and southwest SN and the west bank of Gulf of Suez areas. At W. Abu Qada, the strata of Qada Fm. are rich in the Turonian ammonites fossils (Fig. 40). In the east-central SN, Kora and Genedi (1995) described the Abu Qada Fm. at W. El Ghaib (~ 26 m), G. Gunna (~ 39 m), G. Dhalal (~ 58 m), Sheikh Attia (~ 79 m), and W. Taba (~ 23 m). It contains large-sized oysters and ammonites. They (op. cit.) assigned Abu Qada Fm. to Late Cenomanian–Early Turonian age, due to the presence of Late Cenomanian oyster fossils in its lower part and the Early Turonian ammonites fossils at its upper part such as: *Vascoceras douvillei* and *Choffaticeras segne*. At W. Feiran, based on the study of ammonite and planktonic foraminifera, Kassab and Obaidalla (2001) assigned the age of this formation to the Early

Turonian. At west bank of the Gulf of Suez (W. El-Dakhl), the Abu Qada Fm. assigned to the latest Cenomanian–Early Turonian age (Nagm, 2015) according to the presence of latest Cenomanian ammonite fossils, *V. cauvinii* and the Early Turonian *Vascoceras proprium*, *Choffaticeras* spp., and *Wrightoceras munieri*. Nagm and Bamoussa (2020) assigned the age of the Abu Qada Fm. to the Early Turonian at W. Irkas and W. Abu Rimth according to the presence of the characterized ammonite fossil *C. segne*. Obaidalla (2002) and Nagm et al. (2021) noted that the strata of Abu Qada Fm. were deposited under middle-outer shelf environment. The Abu Qada Fm. conformably overlies Galala Fm. at the west bank of the Gulf of Suez (Nagm, 2015; Nagm & Bamoussa, 2020) and the Raha Fm. at W. Feiran, west-central SN (Kassab & Obaidalla, 2001). Generally, an Oceanic Anoxic Event (OAE2) globally marked the Cenomanian/Turonian (C/T) boundary (e.g., Mort et al., 2008; Voigt et al., 2006). On the other hand, this boundary in Egypt is marked by a hiatus (Kassab & Obaidalla, 2001; Wilmsen & Nagm, 2013) which led to the absence of the signal of the Cenomanian/Turonian anoxic event.

E. The Wata Formation

Ghorab (1961) introduced this formation to describe ~ 102 m thick hard cliff massive limestone and dolomite, with very minor clastic facies (marl and shale beds) at W. Wata, west-central SN. Kora and Genedi (1995) described the strata of the Wata Fm. as a well-bedded dolomitic



Fig. 41 Field photo shows the Wata Fm. at W. Feiran, southwestern Sinai, Egypt

limestone and rudist limestone with minor chert concretions at east-central SN (~ 44 m thick at G. Dhalal, ~ 70 m thick at G. Gunna, ~ 19 m thick at W. El-Ghaib, and ~ 12 m thick at Taba). Wata Fm. conformably overlies Abu Qada Fm. and unconformably underlies Matulla Fm. (Fig. 41). In the northern SN, Saber et al. (2009) described the Wata Fm. at the G. Minsherah (~ 80 m) and G. Yelleg (~ 115 m). They (op. cit.) assigned it to the Turonian age according to the occurrence of the index ammonite fossils such as: *Pseudaspidoceras flexuosum*, *C. segne*, and *Mammites nodosoides* of Early-Middle Turonian at the lower part, and Late Turonian index ammonite fossils such as: *Coilopoceras requienianum* at the uppermost part of the formation. Furthermore, Saber et al. (2009), the upper part of Wata Fm. carries the gastropod *Nerinea requieniana* and yielded rudist assemblage of *Distefanella cf. lombricalis*, *Praeradiolites ponsianus*, *Durania arnaudi*, *Durania gaensis*, and *Radiolites sauvagesi*. Kassab and Obaidalla (2001) at W. Feiran assigned the age of this formation to the Late Turonian according to the ammonite and the planktonic foraminifera studies. Wata Fm. at W. Feiran was deposited in the middle shelf environment (Obaidalla, 2002).

F. The Maghra El-Hadida Formation

It was originally defined by El-Akkad and Abdallah (1971) to describe the strata (~ 142 m thick) that consist of hard, dolomitic limestone, dolomite varicolored marls, and sandstone beds at W. Maghra El-Hadida, southeast of G. Ataq,

near Suez district. This formation is distributed at G. Ataq area, Galala Plateaus, and northern W. Qena. The lower parts of this formation are rich in the Turonian ammonites. It unconformably overlies Galala Fm. and underlies Matulla. Maghra El-Hadida Fm. is equivalent to Abu Qada and Wata fms. at SN (Nagm, 2009). In addition, Saber et al. (2009) used the Wata Fm. at the SN region as the time-equivalent strata of Maghra El-Hadida Fm. At W. Araba, Nagm et al. (2010a, 2010b) assigned its age to Late Cenomanian–Late Turonian age, according to the occurrence of the latest Cenomanian index ammonites (e.g., *Metoicoceras geslinianum* and *V. cauvini*) and the Turonian index ammonite (e.g., *V. proprium*, *Choffaticeras* spp., *W. munieri*, *C. requienianum*). In the Northern Galala, Nagm and Bamousa (2020) assigned the Maghra El-Hadida Fm. (~ 65 m thick) to the latest Cenomanian–Early Turonian. They traced the C/T boundary within Maghra El-Hadida Fm. Maghra El-Hadida Fm. was deposited in shallow marine conditions (inner-middle shelf setting).

G. The Um Omeiyid Formation

It was introduced by Klitzsch and List (1980) to describe ~ 56-m-thick cross-bedded, continental sandstone at W. Umm Omeiyid, north ED, Egypt. Wilmsen and Nagm (2013) assigned Um Omeiyid Fm. to the Middle-Late Turonian at W. Qena district. This is because its stratigraphic position overlain the Late Cenomanian–Early Turonian Galala Fm. Um Omeiyid Fm. unconformably overlies Galala Fm. (Wilmsen & Nagm, 2013). Hermina et al. (1989)



Fig. 42 Field photo shows the uppermost part of the Matulla Fm. underlies the Sudr Fm. at Abu Qada, southwestern Sinai, Egypt

restricted Um Omeiyid Fm. to the Turonian age and they believed that the strata of this formation were deposited under continental conditions.

H. The Matulla Formation

Matulla Fm. was proposed by Ghorab (1961) to describe ~ 170 m of clastic facies sandstone and shale intercalated with limestone and marl at W. Matulla, west-central SN. Kora and Genedi (1995) described the Matulla Fm. in the east-central SN at Sheikh Attia (~ 89 m thick), W. El Ghaib (~ 62 m thick), G. Dhalal (~ 22 m thick), and W. Taba (~ 22 m thick) and assigned its age to the Coniacian–Santonian age according to the occurrence of the Coniacian–Santonian index megafossils (e.g., *Heterotissotia neoceratites*, *Plicatula ferryi*, *Crassostrea heinzi*). It unconformably overlies Wata Fm. and underlies Sudr Fm. Obaidalla and Kassab (2000) assigned the age of Matulla Fm. at SN to Coniacian–Santonian age according to the integrated study of the ammonite and the planktonic foraminiferal fossils. Abdel-Gawad et al. (2007) described Matulla Fm. at southern Galala Plateau, north ED, and

assigned its age to the Coniacian–Early Campanian (?) according to the occurrence of the index megafossils *Gyrostrea thevestensis*, *Nicaiolopha tissoti*, and *Nicaiolopha nicaisei*. Obaidalla et al. (2018) described the upper part of the Matulla Fm. at five stratigraphic sections: Sudr Al-Hitan, W. Sudr, Abu Qada, Ain-Markha, and W. Feiran. They concluded that the uppermost part of Matulla Fm. is of Campanian age (Fig. 42). Obaidalla et al. (op. cit.) traced the Santonian–Campanian boundary within the uppermost part of the Matulla Fm. at the base of the organic-rich black shale which indicates a dysoxic-anoxic oceanic event during the earliest Campanian age. Kallenbach and Hendriks (1986) at central W. Qena, NE of Masak El-Rakhiyat and south of W. Um Omeiyid used the Hawashiya Fm. instead of the Matulla Fm.

I. The Sudr Formation

It was defined by Ghorab (1961) at its type section in the W. Sudr (~ 247 m), west-central SN. It consists of snow-white chalky limestone which vertically changes into marly limestones. The Sudr Fm. is commonly distributed in SN and



Fig. 43 Field photo shows the Paleocene Dakhla Fm. above the Campanian–Maastrichtian Sudr Fm. at W. Nukhul, Abu Zeinema, southwestern Sinai, Egypt

north ED. It unconformably overlies Matulla Fm. and underlies Dakhla Fm. (Figs. 43 and 44). Generally, the basal part of Sudr Fm. in Egypt is marked by the occurrences of rich phosphatic materials (Fig. 45). The Sudr Fm. is of Campanian–Maastrichtian age (Faris et al., 2018; Mahfouz et al., 2018; Salman et al., 2021). It is very rich with oyster fossils such as *Pycnodonte vesicularis* especially at the lower part (Fig. 46). It also contains bivalves fossils such as *Pecten farafereces* (El Ayyat & Obaidalla, 2013) heteromorph ammonites (Abdel-Gawad, 1990). At the same time, this formation is rich within the microfossils especially the planktonic foraminiferal taxa of Campanian–Maastrichtian age such as: *G. elevata*, *Gansserina gansseri*, and *Plummerita hantkeninoides* (Mahfouz et al., 2018; Salman et al., 2021). The rocks of the Sudr Fm. were deposited under marine environment ranging from middle shelf to lower continental slope (El Ayyat & Obaidalla, 2013). El-Akkad and Abdallah (1971) and Abdallah and Eissa (1971) introduced the Adabiya and the G. Thelmet fms. west the Gulf of Suez instead of the Sudr Fm. The similarity in the lithology of the Adabiya and the G. Thelmet fms. with the Sudr Fm. lead to gathering these formations in one name, the Sudr Fm. according to the priority. Ismail and Boukhary (2001) used the name G. Thelmet Fm. at the Southern Galala and

assigned it to the Campanian age. Moreover, the petroleum company geologists used Brown Limestone Beds in the Gulf of Suez as informal rock unit for the phosphatic limestone beds. On our point of view, these beds represent the basal strata of the Sudr Fm. This is evidenced by the presence of brown phosphatic strata at the base of the Sudr Fm. at almost localities in north ED and SN (Fig. 45).

J. The Maghra El Bahari Formation

Maghra El Bahari Fm. was defined by El-Akkad and Abdallah (1971) to describe the clastic beds at W. Maghra El Bahari, G. Ataq, west Gulf of Suez. Maghra El Bahari Fm. unconformably overlies Adabiya Fm. at G. Ataq and unconformably overlies Maghra El-Hadida Fm. at G. Shabrawet. It attains ~ 80 m thick and is composed of unfossiliferous sandstone (continental red beds) with minor claystone, marl, and conglomerate intercalations. The Maghra El Bahari Fm. is of Maastrichtian–Early Paleogene (?). Wanas and Abu El-Hassan (2006) subdivided Maghra El Bahari Fm. into two informal units: the lower clastic unit (unfossiliferous sandstone, siltstone, and silty claystone) and the upper carbonate and evaporate deposits which indicate alluvial and lacustrine environments.



Fig. 44 Field photo shows the Paleocene Dakhla Fm. above the Campanian–Maastrichtian Sudr Fm. at W. Tarfa, north ED, Egypt

4.4 The Subsurface Upper Cretaceous Sedimentary Rocks

4.4.1 The Western Desert Successions

Mostly, all the surface WD sedimentary rock units are well represented as subsurface successions with different thickness. These rock units were recorded by several workers such as: Schrank and Mahmoud (1998), El Beialy et al. (2010), Moretti et al. (2010), Shalaby et al. (2011, 2016), El Nady (2013, 2015), El Diasty (2015), El Diasty et al. (2016), Gentzis et al. (2018) and Bosworth and Tari (2021).

4.4.2 The Eastern Desert Successions

Several surface formations of the ED and SN are recorded as subsurface sequences by the activities of the petroleum companies, especially in Gulf of Suez (e.g., Awad & Serag El Din, 2009; Elhossainy et al., 2021). Also, the Quseir,

Duwi, and Dakhla fms. were documented in the WD (Kom Ombo and Dakhla basins) due to the activities of the petroleum and underground water companies (e.g., Issawi et al., 2016; Schrank & Mahmoud, 1998).

5 Conclusions

The studies which carried out on the Mesozoic sedimentary successions in Egypt suggest that the creation of these rocks was controlled by different types of global tectonic events. The important tectonic events are: the Pan-African Orogeny (end of the Proterozoic Era), the collision of the Gondwana and Laurasia plates (end of the Paleozoic Era), the rifting of the South Atlantic Ocean due to the fragmentation of African Plate from South American Plate (Late Cretaceous), and finally, the deformation of Syrian Arc Event



Fig. 45 Field photo shows the phosphatic materials within the lower part of the Sudr Fm. at the W. Taref, north ED, Egypt

(termination of Cretaceous). Due to the effect of these tectonic events, the Triassic and Jurassic sedimentary rocks are missed in the most provinces of Egypt and confined to the north parts, where they are represented in the surface and subsurface boreholes in the north ED and north WD, respectively. The sedimentary facies of these two periods are characterized by continental to marine facies. On the other hand, the Cretaceous sedimentary rocks are well dis-

tributed all over the geographic provinces of Egypt. These rocks are well represented in the surface and subsurface with different lateral and vertical change in the sedimentary facies due to the formation of numerous sedimentary basins. The Cretaceous rocks are characterized by proper marine facies approximately all over the different provinces in Egypt, with some fluvial-shallow marine facies at the south places of Egypt.



Fig. 46 Field photo shows the oyster bank of the *Pycnodonte vesicularis* fossils at the lowermost part of the Sudr Fm. at W. Tarfa, north ED, Egypt

Acknowledgements Thanks are due to the editors for their kind invitation to contribute the present Springer's book volume. The authors are grateful to Professor Mohamed Boukhary (Ain Shams University), Professor Gouda Abdel-Gawad (Beni-Suef University), and Professor Abd El-Hamid El-Shater (Sohag University) for their reviews which further enhanced the chapter impressively.

References

- Abdallah, A. M., & Adindani, A. (1963). Stratigraphy of upper Paleozoic rocks, western side of Gulf of Suez. *Geological Survey of Egypt*, 25, 18 pp.
- Abdallah, A. M., & Eissa, R. A. (1971). The Campanian rocks of the Southern Galala. *Bulletin of the Faculty of Science, Cairo University*, 44, 259–270.
- Abdallah, A. M., El Adindani, A., & Fahmy, N. (1963). Stratigraphy of the Lower Mesozoic rocks, western side of the Gulf of Suez. *Geological Survey and Mineral Research Department of the United Arab Republic*, 27, 1–23.
- Abdel-Gawad, G. I. (1990). Some gastropods from the Upper Campanian of the Middle Vistula Valley, Central Poland. *Acta Geologica Polonica*, 40(1–2).
- Abdel-Gawad, G. I. (2001). Some Upper Cretaceous coralline sponges from Egypt. *Egyptian Journal of Paleontology*, 1, 299–325.
- Abdel-Gawad, G. I., El Qot, G. M., & Mekawy, M. S. (2007). Macrobiostratigraphy of the Upper Cretaceous succession from Southern Galala, Eastern Desert, Egypt. In *Second International Conference of the Tethys* (pp. 329–349). Cairo University.
- Abdel-Gawad, G. I., & Gameil, M. (1995). Cretaceous and Paleocene coral faunas in Egypt and Greece. *Coral Research Bulletin*, 4, 1–36.
- Abdel-Gawad, G. I., Saber, S. G., El Shazly, S. H., & Salama, Y. F. (2011). Turonian Rudist Facies from Abu Roash area, North Western Desert, Egypt. *Journal of African Earth Sciences*, 59, 359–372.
- Abdelhady, A. A. (2014). *Palaeoenvironments and palaeoecology of the Middle and Upper Jurassic succession of Gebel Maghara (Sinai)* [Ph.D. thesis]. Friedrich-Alexander-Universität Erlangen-Nürnberg.
- Abdelhady, A. A., & Fürsich, F. T. (2015). Quantitative biostratigraphy of the Middle to Upper Jurassic strata of Gebel Maghara (Sinai, Egypt). *Newsletters on Stratigraphy*, 48, 23–46.
- Abdel-Maksoud, N. A. (2006). *Integrated biostratigraphy of the Lower Cretaceous successions, Northern Sinai, Egypt* [Unpublished Ph.D. thesis]. Assiut University, Assiut, Egypt.
- Abdel Razik, T. M. (1972). Comparative studies on the Upper Cretaceous-Early Paleogene sediments on the Red Sea Coast, Nile Valley and Western Desert, Egypt. In *Proceedings of the 8th Arab Petroleum Congress* (Vol. 71, No. B-3, pp. 1–23). Algiers.
- Abd-Elshafy, E. (1988). On some problematic Mesozoic exposures on the western side of the Gulf of Suez, Egypt. *Bulletin of Faculty of Science, Zagazig University*, 10, 53–78.
- Abd-Elshafy, E., & El-Saadawi, W. (1982). Macroflora from the Jurassic of Ras El Abd, Gulf of Suez, Egypt. *Bulletin of Faculty of Science, Zagazig University*, 4, 33–40.

- Abed, M. M., Ayyad, S. A., & Abu Zied, R. H. (1996). Stratigraphic classification of Triassic-Cretaceous rocks of Gebel Arif El-Naga, Northeastern Sinai, Egypt. *Newsletters on Stratigraphy*, 33(3), 117–131.
- Abrams, M., Greh, M. D., Collister, J. W., & Thompson, M. (2016). Egypt far Western Desert basins petroleum charge system as defined by oil chemistry and unmixing analysis. *Marine and Petroleum Geology*, 72, 54–74.
- Abu El-Hassan, M. M., & Wanas, H. A. (2003). Dolomitization of the Jurassic carbonate sediments at Khashm El-Galala and Abu Darag, western side of the Gulf of Suez, Egypt. In *The Third International Conference on the Geology of Africa*, Assiut, Egypt (Vol. 3, pp. 485–497).
- Adindali, A., & Shakhov. (1970). The occurrence of coal and some geological features of the Mesozoic and Paleozoic sediments of Egypt. In O. Moharram, et al. (Eds.), *Studies on some mineral deposits of Egypt* (pp. 67–86). Geological Survey of Egypt.
- Al Far, D. M. (1966). Geology and coal deposits of Gebel Al Maghara, North Sinai, Egypt. *U.A.R. Geologic Survey*, 37, 1–59.
- Allam, A. M., & Khalil, I. (1988). Geology and stratigraphy of the Arif El-Naga area, Sinai, Egypt. *Egyptian Journal of Geology*, 32, 199–218.
- Aly, M. F., Abdel-Gawad, G. I., & Gaber, A. (2005). Uppermost Albian-Basal Cenomanian ammonites from north Sinai, Egypt. *Egyptian Journal of Paleontology*, 5, 347–385.
- Argyriadis, I., De Graciansky, P. C., Marcoux, J., & Ricou, L. E. (1980). The opening of the Mesozoic Tethys between Eurasia and Arabia-Africa. *Memoire du Bureau de Recherches Geologiques et Minieres*, 115, 199–214.
- Arkell, W. J. (1952). Jurassic ammonites from Jebel Tuwaiq, Central Arabia, with R. A. Bramkamp; M. Steineke with stratigraphical introduction. *Philosophical Transactions of the Royal Society of London, Series B*, 633(236), 241–314.
- Arkell, W. J. (1956). *Jurassic geology of the world* (p. 806). Oliver and Boyd.
- Attia, M. I. (1955). Topography, geology and iron-ore deposits of the district east of Aswan. *Geological Survey of Egypt*, 262.
- Awad, G. H. (1946). On the occurrence of marine Triassic (Muschelkalk) deposits in Sinai. *Bulletin de l'Institut d'Egypte*, 27, 397–429.
- Awad, G. H., & Ghobrial, M. G. (1965). Zonal stratigraphy of the Kharga Oasis. *Ministry of Industry, General Egyptian Organization for Geological Research and Mining, Geological Survey, Cairo*, 34, 1–77.
- Awad, M. H., & Serag El Din, S. (2009). Micro-zonation and characterization of the pre-Miocene reservoirs in Ras Budran oil field, Gulf of Suez, Egypt. *Journal of Geology and Mining Research*, 1(9), 180–194.
- Bachmann, M., Bassiouni, M. A. A., & Kuss, J. (2003). Timing of mid-Cretaceous carbonate platform depositional cycle, northern Sinai, Egypt. *Palaeogeography, Palaeoclimatology, Palaeoecology*, 200, 131–162.
- Barthel, K. W., & Boettcher, R. (1978). Abu Ballas Formation: A significant lithostratigraphic unit of the former "Nubian Series." *Mitteilungen der Bayerischen Staatssammlung für Paläontologie und Historische Geologie*, 18, 155–166.
- Barthel, K. W., & Herrmann-Degen, W. (1981). Late Cretaceous and Early Tertiary stratigraphy in the Great Sand Sea and its SE margins (Farafra and Dakhla Oases), SW Desert, Egypt. *Mitteilungen der Bayerischen Staatssammlung für Paläontologie und Historische Geologie*, 21, 141–182.
- Barthoux, J. C., & Douvillé, H. (1913). Le Jurassique dans le desert à l'est de l'Isthme de Suez. *Comptes Rendues de l'Academie des Sciences*, 175, 265p.
- Bartov, Y., Levy, Z., Steinitz, G., & Zak, I. (1980). Mesozoic and Tertiary stratigraphy, paleogeography and structural history of the Gebel Areif en Naqa area, eastern Sinai 1. *Israel Journal of Earth Science*, 29, 114–139.
- Beadnell, H. J. L. (1902). *The Cretaceous region of Abu Roash near the Pyramids of Giza, Egypt* (p. 48). Survey Department.
- Beadnell, J. L. (1909). *An Egyptian oases; An account of the Oasis of Kharga of the Libyan Desert* (p. 284). Murray.
- Boettcher, R. (1982). Die Abu Ballas Formation (Lingula Shale) (Apt?) der Nubischen Gruppe Sudwest Agyptens. *Berliner Geowissenschaftliche Abhandlungen*, 39(A), 1–145.
- Bosworth, W., & Tari, G. (2021). Hydrocarbon accumulation in basins with multiple phases of extension and inversion: Examples from the Western Desert (Egypt) and the western Black Sea. *Solid Earth*, 12, 59–77.
- Conoco. (1987). *Geologic map of Egypt*. Egyptian General Authority for Petroleum (UNESCO Joint Map Project). Scale (1:500,000).
- Darwish, M. (1992). Facies development of the Upper Paleozoic-Lower Cretaceous sequences in Northern Galala Plateau and evidences for their hydrocarbon reservoir potentiality, Northern Gulf of Suez, Egypt. In *Proceeding of 1st International Conference Geology of Arab World* (Vol. 1, pp. 175–214).
- Darwish, M., Abdallah, A. M., & Hassanein, A. M. (1984). Contributions to the petrography and diagenesis of the Jurassic exposures, Gulf of Suez, Egypt. *Annals of the Geological Survey of Egypt*, 14, 173–192.
- Dominik, W. (1985). Stratigraphie und Sedimentologie (Geochemie Schwimneralanavse) der Oberkreide von Bahariya aund ihre Korrelation zum Dakhla Becken (Western Desert, Ägyptten). *Berliner Geowissenschaftliche Abhandlungen*, 62(A), 1–173.
- Druckman, Y. (1974). The stratigraphy of the Triassic sequence in southern Israel. *Bulletin Geological Survey of Israel*, 64, 1–92.
- EGPC (Egyptian General Petroleum Corporation). (1992). Western Desert, oil and gas fields (a comprehensive overview). In *EGPC 11th Petroleum Exploration and Production Conference*, Cairo, Egypt (p. 431).
- El-Akkad, S., & Abdallah, A. M. (1971). Contribution to geology of Gebel Ataqa area. *Annals of the Geological Survey of Egypt*, 1, 21–42.
- El-Akkad, S., & Issawi, B. (1963). Geology and iron ore deposits of the Bahariya Oasis. *Geological Survey and Mineral Research Department, Egypt*, 18, 301.
- El Atfy, H., Mostafa, A., Maher, A., Mahfouz, K., & Hosny, A. (2019). Early Cretaceous biostratigraphy and palaeoenvironment of the northern Western Desert, Egypt: An integrated palynological and micropalaeontological approach. *Palaeontographica B*, 299, 103–132.
- El Ayyat, A. M. (2015). Lithostratigraphy, sedimentology, and cyclicity of the Duwi Formation (late Cretaceous) at Abu Tartur plateau, Western Desert of Egypt: Evidences for reworking and redeposition. *Arabian Journal of Geosciences*, 8(1), 99–124.
- El Ayyat, A., & Obaidalla, N. A. (2013). Stratigraphy, sedimentology and tectonic evolution of the Upper Cretaceous/Paleogene succession in north Eastern Desert, Egypt. *Journal of African Earth Sciences*, 81, 35–59.
- El-Azabi, M. H. (1999). Facies analysis and paleoenvironmental interpretation of Gabal Shabraweet Lower/Middle Cretaceous (Barremian-Cenomanian) succession and its sequence stratigraphic applications, north Eastern Desert, Egypt. In *4th Conference on Geology of the Arab World (GAW4)* (pp. 643–683). Cairo University.
- El-Azabi, M. H., & El-Araby, A. (2005). Depositional facies, environments and sequence stratigraphic interpretation of the Middle Triassic-Lower Cretaceous (pre-Late Albian) succession in

- Arif El-Naga anticline, northeast Sinai, Egypt. *Journal of African Earth Sciences*, 41(1–2), 119–143.
- El Bassyouny, A. A. (1970). *Geology of the area between Gara El Hamra of Ball-Qur Lyons and Ghard El Moharrik, and its correlation with El Harra area, Bahariya Oasis, Egypt* [Unpublished M.Sc. thesis] (p. 180). Cairo University.
- El Bassyouny, A. A. (2004). Stratigraphy of El-Harra area, Bahariya Oasis, Western Desert, Egypt. *Sedimentary Egypt*, 12, 207–232.
- El Beialy, S. Y., El Atfy, H. S., Zavada, M. S., El Khoriby, E. M., & Abu-Zied, R. H. (2010). Palynological, palynofacies, paleoenvironmental and organic geochemical studies on the Upper Cretaceous succession of the GPTSW-7 well, North Western Desert, Egypt. *Marine and Petroleum Geology*, 27(2), 370–385.
- El Diasty, W. Sh. (2015). Khatatba Formation as an active source rock for hydrocarbons in the northeast Abu Gharadig Basin, north Western Desert, Egypt. *Arabian Journal of Geosciences*, 8(4), 1903–1920.
- El Diasty, W. Sh., El Beialy, S. Y., Littke, R., & Farag, F. A. (2016). Source rock evaluation and nature of hydrocarbons in the Khalda Concession, Shushan Basin, Egypt's Western Desert. *International Journal of Coal Geology*, 162, 45–60.
- Elhossainy, M. M., Salman, M. A., Sarhan, M. A., & Al-Areeq, N. M. (2021). Sequence stratigraphic analysis and depositional evolution of the Upper Cretaceous deposits in Ras Budran oil field, Gulf of Suez, Egypt. *Arabian Journal of Geosciences*, 14(13), 1104.
- El Nady, M. M. (2013). The volumetric calculation of hydrocarbons generation of source rocks in the Gulf of Suez, Egypt. *Petroleum Science and Technology*, 31(3), 310–320.
- El Nady, M. M. (2015). Evaluation of the nature, origin and potentiality of the subsurface Middle Jurassic and Lower Cretaceous source rocks in Melleiha G-1x well, North Western Desert, Egypt. *Egyptian Journal of Petroleum*, 24(3), 317–323.
- El-Naggar, Z. R. M. (1970). On a proposed lithostratigraphic subdivision for the late Cretaceous early Paleogene succession in the Nile Valley, Egypt. In *7th Arab Petroleum Congress*, Kuwait.
- El Nakkady, S. E. (1951). Zoning the Mesozoic-Cenozoic transition of Egypt by the Globorotallidae. *Bulletin of the Faculty of Science*, 1, 45–50.
- El Nakkady, S. E. (1955). The stratigraphy and geology of the district between the Northern and Southern Galala Plateaus. *Bulletin de l'Institut d'Égypte*.
- El-Qot, G. M., Abdel-Gawad, G. I., & Mekawy, M. S. (2009). Taphonomy of Middle Jurassic (Bathonian) shell concentrations from Ras El Abd, west Gulf of Suez, Egypt. *Journal of African Earth Sciences*, 54, 31–36.
- Farag, I. A. M. (1948). Deux nouveaux eisements de Bathoniei fossilifere sur la rive occidentale du Golf de Suez. *Compte Rendu Sommaire des Séances de la Société Géologique de France*, 1948, 109–110.
- Farag, I. A. M., & Omara, S. (1955). On the occurrence of marine Jurassic deposits at Gebel El Minshera. *Bulletin de l'Institut du Désert d'Égypte*, 5(1), 165–172.
- Farag, I. A. M., & Shata, A. P. (1954). Detailed geologic survey of El Minshera area. *Bulletin de l'Institut du Désert d'Égypte*, 4(2), 5–82.
- Faris, M. I. (1948). Contribution to the stratigraphy of Abu Rauwash and the history of the Upper Cretaceous in Egypt. *Bulletin Faculty of Science, Cairo University*, 27, 221–239.
- Faris, M., Obaidalla, N. A., Metwally, A. A., Salman, A., & Zaky, A. S. (2018). Late Cretaceous-Early Paleogene tectonic events at Farafra-Abu Minqar Stretch, Western Desert, Egypt: Results from calcareous plankton. *Arabian Journal of Geosciences*, 11, 1–18.
- Gentzis, T., Carvajal-Ortiz, H., Deaf, A. S., & Tahoun, S. S. (2018). Multi-proxy approach to screen the hydrocarbon potential of the Jurassic succession in the Matruh Basin, North Western Desert, Egypt. *International Journal of Coal Geology*, 190, 29–41.
- Ghorab, M. A. (1956). A summary of a proposed rock-stratigraphic classification of the Upper Cretaceous rocks in Egypt. Presented at the Meeting of the Geological Society of Egypt, Abstract.
- Ghorab, M. A. (1961). Abnormal stratigraphic features in Ras Gharib oil field. In *Proceedings of the 3rd Arabian Petroleum Congress* (Vol. 2, pp. 1–10).
- Ghoubachi, S. Y. (2001). *The hydrogeological characteristics of the Nubia sandstone system aquifer in the Dakhla Depression, Western Desert, Egypt* [M.Sc. thesis] (p. 261). Faculty of Science, Ain Shams University.
- Guiraud, R., & Bellion, Y. (1995). Late Carboniferous to recent, geodynamic evolution of the West Gondwanian, cratonic, Tethyan margins. In A. Nairn, L. E. Ricou, B. Vrielynck, & J. Dercourt (Eds.), *The ocean basins and margins 8, the Tethys Ocean* (pp. 101–124). Plenum Press.
- Guiraud, R., & Bosworth, W. (1997). Senonian basin inversion and rejuvenation of rifting in Africa and Arabia: Synthesis and implications to plate-scale tectonics. *Tectonophysics*, 282, 39–82.
- Guiraud, R., & Bosworth, W. (1999). Phanerozoic geodynamic evolution of northeastern Africa and the northwestern Arabian platform. *Tectonophysics*, 315, 73–108.
- Gwin, J. W., & Nasr, S. N. (1940). *The Ramon anticline, petroleum development (Palestine) limited* (Geological Report 155).
- Hantar, G. (1990). North Western Desert. In R. Said (Ed.), *The geology of Egypt* (pp. 293–319). A.A. Balkema.
- Hataba, H., & Ammar, G. (1990). Comparative stratigraphic study on the Upper Cenomanian-lower Senonian sediments between the Gulf of Suez and Western Desert, Egypt. In *10th Petroleum Exploration and Production Conference*, Cairo, Egypt (p. 16).
- Hegab, A. A. A., & Aly, M. F. (2004). Contribution to the Middle Jurassic Brachiopoda (Rhynchonellida) from Gulf of Suez, Egypt. *Egyptian Journal of Paleontology*, 4, 183–198.
- Hendriks, E. (1986). The Maghrabi formation of the El-Kharga area (SW Egypt): Deposits from a mixed estuarine and tidal-flat environment of Cenomanian age. *Journal of African Earth Sciences*, 5(5), 481–489.
- Hendriks, F., & Kallenbach, H. (1986). The offshore to backshore environments of the Abu Ballas Formation of the SE Dakhla Basin (Western Desert, Egypt). *Geologische Rundschau*, 75, 445–460.
- Hendriks, F., & Luger, P. (1987). The Rakhayat Formation of the Gebel Qreiya area: Evidence of Middle Campanian to Early Maastrichtian synsedimentary tectonism. *Berliner Geowissenschaftliche Abhandlungen*, 75(A), 83–96.
- Hendriks, F., Luger, P., Bovitz, J., & Kallenbach, H. (1987). Evolution of the depositional environments of SE Egypt during the cretaceous and lower tertiary. *Berliner Geowissenschaftliche Abhandlungen*, 75(A), 49–82.
- Hendriks, F., Luger, P., Kallenbach, H., & Schroeder, J. H. (1984). Stratigraphical and sedimentological framework of the Kharga-Sinn el-Kaddab stretch (western and southern part of the Upper Nile Basin), Western Desert, Egypt. *Berliner Geowissenschaftliche Abhandlungen*, 50, 117–151.
- Hermina, M. (1990). The surroundings of Kharga, Dakhla and Farafra oases. In R. Said (Ed.), *The geology of Egypt* (pp. 259–292). Balkema.
- Hermina, M., Klitzsch, E., & List, F. K. (1989). *Stratigraphic lexicon and explanatory notes to the geological map of Egypt 1:500,000* (p. 264). Conoco/E.G.P.C.

- Horowitz, A. (1970). Palynostratigraphy of the upper Triassic-lower Mesozoic sequence in Zohar-8 borehole (southern Israel). *Geological Survey of Israel*, 70, 1–9.
- Ibrahim, M. I. A., Aboul Ela, N. M., & Kholeif, S. E. (2001). Palynostratigraphy of Jurassic to Lower Cretaceous sequences from the Eastern Desert of Egypt. *Journal of African Earth Sciences*, 32, 269–297.
- Ismail, A. A., & Boukhary, M. (2001). Campanian larger foraminifera of Gebel Thelmet Formation (stratotype), Southern Galala, Eastern Desert, Egypt. *Revue de Paleobiologie*, 20(1), 77–90.
- Issawi, B. (1973). Nubia sandstone: Type section. *American Association of Petroleum Geologists Bulletin*, 57(4), 741–745.
- Issawi, B., El-Hinnawi, M., Francis, M., & Mazhar, A. (1999). The Phanerozoic of Egypt: A geodynamic approach. *Egyptian Geological Survey, Cairo*, 76, 462.
- Issawi, B., Francis, M. H., Youssef, E. A. A., & Osman, R. A. (2009). *The Phanerozoic geology of Egypt: A geodynamic approach* (2nd ed., p. 589). Special Publication 81. Ministry of Petroleum, The Egyptian Mineral Resources Authority.
- Issawi, B., Hassan, M. Y., & Attia, S. A. N. (1978). Geology of Abu Tartur plateau, Western Desert, Egypt. *Annals of the Geological Survey of Egypt*, 8, 91–127.
- Issawi, B., Sallam, E., & Zak, S. R. (2016). Lithostratigraphic and sedimentary evolution of the Kom Ombo (Garara) sub-basin, southern Egypt. *Arabian Journal of Geoscience*, 9, 420.
- Jenkins, D. (1990). North and Central Sinai. In R. Said (Ed.), *The geology of Egypt* (pp. 361–380). A.A. Balkema.
- Jux, U. (1954). Zur Geologie des Kreidegebietes von Abu Roash bei Kairo. *Neues Jahrbuch für Geologie und Paläontologie*, 100(2), 159–207.
- Kallenbach, H., & Hendriks, F. (1986). Transgressive and regressive sedimentary environments of Cretaceous to Lower Tertiary age in upper Egypt: A case study from central Wadi Qena. In *12th International Sedimentological Congress*, Canberra, Abstracts (p. 158). International Association of Sedimentologists.
- Kassab, A. S., & Obaidalla, N. A. (2001). Integrated biostratigraphy and inter-regional correlation of the Cenomanian–Turonian deposits of Wadi Feiran, Sinai, Egypt. *Cretaceous Research*, 22(1), 105–114.
- Keeley, M. L., Dungworth, G., Floyd, C. S., Forbes, G. A., King, C., McGarva, R. M., & Shaw, D. (1990). The Jurassic system in northern Egypt: I. Regional stratigraphy and implications for hydrocarbon prospectivity. *Journal of Petroleum Geology*, 13, 397–420.
- Kerdany, M. T. (1968). Note on planktonic zonation of the Miocene in the Gulf of Suez region. *Proceedings of the Committee of Mediterranean Neogene Stratigraphy, Giornale di Geologia*, 35, 157–166.
- Kerdany, M. T., & Cherif, O. H. (1990). Mesozoic. In R. Said (Ed.), *The geology of Egypt* (pp. 407–438). A.A. Balkema.
- Khalifa, M. A. (1977). *Geological and sedimentological studies of El Hefhuf area, Bahariya Oasis, Western Desert, Egypt* [Unpublished M.Sc. thesis] (p. 181). Cairo University.
- Khalifa, M. A., & Abu El-Hassan, M. M. (1993). Lithofacies, diagenesis, cyclicity and depositional environment of the Upper Cenomanian El-Heiz Formation, Bahariya Oasis, Western Desert, Egypt. *Journal of African Earth Sciences*, 17, 555–570.
- Khalifa, M. A., Soliman, H. E., & Abu El Hassan, M. (2002). Lithostratigraphy and sequence stratigraphy of the Turonian-Santonian rocks; Bahariya Oasis, Western Desert, Egypt. In *6th Conference of the Geological Arab World* (Vol. II, pp. 483–500). Cairo University.
- Khalifa, M. A., & Tanner, L. H. (2017). High frequency peritidal cycles in the lower member of the Late Cretaceous (Turonian, Coniasian-Santonian) El Hefhuf Formation, Bahariya Oases, Western Desert, Egypt. *Journal of African Earth Sciences*, 130, 223–237.
- Klitzsch, E. (1978). Geologische Bearbeitung Südwest-Ägyptens—Programm und erste Ergebnisse. *Geologische Rundschau*, 67(2), 509–520.
- Klitzsch, E. (1984). Northwestern Sudan and bordering areas; geological developments since Cambrian time. *Berliner Geowissenschaftliche Abhandlungen*, 50(A), 23–45.
- Klitzsch, E. (1986). Plate tectonics and cratonic geology in Northeast Africa (Egypt/Sudan). *Geologische Rundschau*, 75(3), 753–768.
- Klitzsch, E. (1990). The Paleozoic. In R. Said (Ed.), *The geology of Egypt* (pp. 393–406). Balkema.
- Klitzsch, E., Groeschke, M., & Herrmann-Degen, W. (1990). Wadi Qena: Paleozoic and pre-Campanian Cretaceous strata. In R. Said (Ed.), *The geology of Egypt* (p. 734). A.A. Balkema.
- Klitzsch, E., Harms, J. C., Lejal-Nicol, A., & List, F. (1979). Major subdivisions and depositional environments of Nubia strata, southwestern Egypt. *American Association of Petroleum Geologists Bulletin*, 63, 974.
- Klitzsch, E., & Léal-Nicol, A. (1984). Flora and fauna from strata in southern Egypt and northern Sudan (Nubia and surrounding areas). *Berliner Geowissenschaftliche Abhandlungen*, 50(A), 47–79.
- Klitzsch, E., & List, F. K. (1980). *Geological interpretation map of Egypt, a preliminary edition, 1: 500 000, sheets 2827 and 3127*.
- Kora, M. A., & Genedi, A. (1995). Lithostratigraphy and facies development of Upper Cretaceous carbonates in east central Sinai, Egypt. *Facies*, 32, 223–236.
- Kora, M., Shahin, A., & Semiet, A. (1994). Biostratigraphy and paleoecology of some Cenomanian successions in west central Sinai, Egypt. *Neues Jahrbuch für Geologie und Paläontologie Monatshefte*, 10, 597–617.
- Luger, P. (1985). Stratigraphie der marinen Oberkreide und des Alttertiärs in südwestlichen Oberrhein-Becken (SW-Ägypten) unter besonderer Berücksichtigung der Mikropaläontologie, Paläökologie und Paläogeographie. *Berliner Geowissenschaftliche Abhandlungen (A)*, 63, 1–151.
- Luger, P. (1988). Campanian to Paleocene agglutinated foraminifera from freshwater influenced marginal marine (deltaic) sediments of southern Egypt. *Abhandlungen der Geologischen Bundesanstalt*, 41, 255–263.
- Mahfouz, K. H., El-Sheikh, I., Obaidalla, N. A., & Shreif, A. (2021a). New insights into stratigraphy and paleoenvironment of the Upper Cretaceous-Eocene succession, Farafra Oasis, Western Desert, Egypt. *Journal of African Earth Sciences*, 175, 104096.
- Mahfouz, K. H., Hewaidy, A., Mostafa, A., & El-Sheikh, I. (2018). Resolution enhancement of foraminiferal biostratigraphy of the Campanian/Maastrichtian interval: A case study from the Eastern Desert, Egypt. *Journal of African Earth Science*, 145, 215–226.
- Mahfouz, K. H., & Metwally, A. (2020). Maastrichtian-Paleocene successions at Kharga-Dakhla stretch, Western Desert, Egypt: Paleoenvironmental and basin evolution interpretations. *Journal of African Earth Sciences*, 162, 103731.
- Mahfouz, K. H., Obaidalla, N. A., Hewaidy, A. A., Mostafa, A., & El-Sheikh, I. (2021b). Evolution of the Maastrichtian-Paleocene sedimentary basin in the Safaga-Quseir region, Red Sea Coast, Egypt. *Marine Micropaleontology*, 169, 102039.
- Masce, J., Blarez, E., & Marhino, M. (1988). The shallow structure of the Guinea and Ivory Coast-Ghana transform margins: Their bearing on the Equatorial Atlantic Mesozoic evolution. *Tectonophysics*, 155, 193–209.
- Metwally, A. A., Soliman, H. A., Obaidalla, N. A., & Thabet, A. G. (2021). Maastrichtian-Paleocene sequences at Dakhla-Abu Minqar District, Western Desert, Egypt: Stratigraphical and

- paleoenvironmental framework. *Arabian Journal of Geosciences*, 14(1), 1–21.
- Moretti, I., Kerdraon, Y., Rodrigo, G., Huerta, F., Griso, J. J., Sami, M., Said, M., & Ali, H. (2010). South Alamein petroleum system (Western Desert, Egypt). *Petroleum Geoscience*, 16, 121–132.
- Morgan, P. (1990). Egypt in the framework of global tectonics. In R. Said (Ed.), *The geology of Egypt* (pp. 91–111). Balkema.
- Mort, H., Adatte, T., Keller, G., Bartels, D., Föllmi, K., Steinmann, P., Berner, Z., & Chellai, E. H. (2008). Organic carbon deposition and phosphorus accumulation during Oceanic Anoxic Event 2 in Tarfaya, Morocco. *Cretaceous Research*, 29, 1008–1023.
- Moustafa, A. R. (1980). *Subsurface geological and hydrogeological study on El-Bahariya Oasis, Western Desert, Egypt* [M.Sc. thesis] (p. 200). Faculty of Science, Assiut University
- Moustafa, A. R. (2020). Mesozoic-Cenozoic deformation history of Egypt. In Z. Hamimi, A. El-Barkooky, J. Martínez Frias, H. Fritz, & Y. Abd El-Rahman (Eds.), *The geology of Egypt* (pp. 253–290). Regional Geology Reviews. Springer.
- Nagm, E. (2009). *Integrated stratigraphy, paleontology and facies analysis of the Cenomanian–Turonian (Upper Cretaceous) Galala and Maghra El Hadida formations of the western Wadi Araba, Eastern Desert, Egypt* [Ph.D. thesis]. Universität Würzburg.
- Nagm, E. (2015). Stratigraphic significance of rapid faunal change across the Cenomanian-Turonian boundary in the Eastern Desert, Egypt. *Cretaceous Research*, 52, 9–24.
- Nagm, E., & Bamousa, A. O. (2020). Factors controlling facies distribution during the early Late Cretaceous in the Eastern Desert of Egypt: Paleoenvironmental reconstruction and relationship to sequence stratigraphy. *Journal of African Earth Sciences*, 169, 103877.
- Nagm, E., Jain, S., Mahfouz, K. H., El-Sabbagh, A., & Abu Shama, A. (2021). Biotic response to the latest Cenomanian drowning and OAE2: A case study from the Eastern Desert of Egypt. *Proceedings of the Geologists' Association*, 132(1), 70–92.
- Nagm, E., Wilmsen, M., Aly, M., & Hewaidy, A. (2010a). Cenomanian-Turonian (Cretaceous) ammonoids from the western Wadi Araba area, Eastern Desert, Egypt. *Cretaceous Research*, 31, 473–499.
- Nagm, E., Wilmsen, M., Aly, M., & Hewaidy, A. (2010b). Bio-stratigraphy of the Upper Cenomanian-Turonian (lower Upper Cretaceous) successions of the western Wadi Araba, Eastern Desert, Egypt. *Newsletters on Stratigraphy*, 44, 17–35.
- Norton, P. (1967). *Rock stratigraphic nomenclature of the Western Desert* (Internal Report). Pan-American Oil Company.
- Nothdurft, W., Smith, J. B., Lamanna, M. C., Lacovara, K. J., Poole, J. C., & Smith, J. R. (2002). *The lost dinosaurs of Egypt* (p. 242). Random House.
- Obaidalla, N. A. (2002). Planktic foraminifera, paleoenvironment and relative sea-level changes in the Cenomanian-Turonian of the Wadi Feiran, southwestern Sinai, Egypt. *Neues Jahrbuch für Geologie und Paläontologie-Abhandlungen*, 275–297.
- Obaidalla, N. A., El-Ayyat, A. M., & Kassab, A. (2006). Biostratigraphical and sedimentological studies on the Upper Cretaceous/Paleogene sequence, Western Desert, Egypt. *Assiut University Journal of Geology*, 35, 141–207.
- Obaidalla, N. A., El-Sheikh, I., Mahfouz, K. H., Salman, A. M., Soliman, M. F., & Abdel-Aleem, F. E. M. (2020). Upper Cretaceous–lower Paleocene subsurface sequence, Farafra Oasis, Western Desert, Egypt: Stratigraphical and paleoenvironmental inferences. *Arabian Journal of Geosciences*, 13, 957.
- Obaidalla, N. A., El-Younsi, A. R., Philobos, E. R., & Salman, A. M. (2017). Impact of the African/Arabian and Eurasian plates collision on the evolution of the upper cretaceous-lower Paleogene sedimentary basin, Eastern Desert, Egypt. *International Journal of Ecological Science and Environmental Engineering*, 4(5), 51–71.
- Obaidalla, N. A., & Kassab, A. S. (2000). Biostratigraphy of the Khoman Formation, Bahariya Oasis, Western Desert, Egypt: An approach to the K/T boundary. *Egyptian Journal of Geology*, 44(2), 443–453.
- Obaidalla, N. A., Mahfouz, K. H., Soliman, M. F., & Moghawry, A. (2018). Stratigraphical studies on the Matulla/Sudr formational boundary, western Sinai, Egypt. *Assiut University Journal of Geology*, 47(2), 23–40.
- Omara, S., Hemid, I. A., & Sanad, S. (1970). Structure and hydrogeology of Farafra Oasis, Western Desert, UAR. In *7th Arab Petroleum Congress*, Kuwait, Paper 65 (B-3) (p. 15).
- Omara, S., Philobos, E. R., & Mansour, H. H. (1976). Contribution to the geology of the Dakhla Oasis area, Western Desert, Egypt. *Bulletin of the Faculty of Science, Assiut University, Assiut, Egypt*, 5, 319–339.
- Picard, L., & Hirsch, F. (1987). *The Jurassic stratigraphy in Israel and adjacent countries* (p. 106). The Israel Academy of Sciences and Humanities.
- Ruban, D. A., Sallam, E. S., & Wanas, H. A. (2019). Middle–Late Jurassic sedimentation and sea-level changes on the northeast African margin: A case study in the Khashm El-Galala area, NE Egypt. *Journal of African Earth Sciences*, 156, 189–202.
- Saber, S. G., Salama, Y. F., Scott, R. W., Abdel-Gawad, G. I., & Aly, M. F. (2009). Cenomanian–Turonian rudist assemblages and sequence stratigraphy on the North Sinai carbonate shelf, Egypt. *GeoArabia*, 14(4), 113–134.
- Sadek, H. (1926). The geography and geology of the district between Gebel Ataqa and El-Galala El-Bahariya (Gulf of Suez). *Geological Survey and Mineral Research Department of Egypt*, 40, 1–140.
- Said, R. (1961). Tectonic framework of Egypt and its influence on distribution of foraminifera. *American Association of Petroleum Geologists, Bulletin*, 45, 198–218.
- Said, R. (1962). *The geology of Egypt* (p. 377). Elsevier.
- Said, R. (1971). Explanatory notes to accompany the geological map of Egypt. *Geological Survey of Egypt*, 56, 123.
- Said, R. (1990). Cretaceous paleogeographic maps. In R. Said (Ed.), *The geology of Egypt* (pp. 439–449). A.A. Balkema.
- Said, R., Sabkt, A. H., Zalata, A. A., Teiniakov, V. A., & Pokryshkin, V. I. (1976). A review of theories on the geological distribution of bauxite and their application for bauxite prospecting in Egypt. *Annals of Geological Survey of Egypt*, 6, 6–32.
- Salama, H., Darwish, M., Wahdan, M., & El-Batal, A. (2017). Identify re-development concepts to enhance Abu Roash “C” oil reservoir productivity Sitra Area, Abu Gharadig Basin, Western Desert, Egypt. *Egyptian Journal of Petroleum*, 26(2), 235–267.
- Salama, Y. F., Al-Hashim, M. H., Grammar, M. G., Gahlan, H. A., Al-Asmar, H., & Abd El-Gaied, I. M. (2021). Palaeoecology and facies analysis of benthic communities in mid-Cretaceous successions in the Sinai platform, Egypt. *Journal of African Earth Sciences*, 175, 104091.
- Salama, Y. F., Grammar, M. G., Saber, S., El-Shazly, S., & Abdel-Gawad, G. (2018). Sequence stratigraphy and rudist facies development of the Upper Barremian-Lower Cenomanian platform, Northern Sinai, Egypt. *Acta Geologica Sinica (English Edition)*, 92(1), 286–310.
- Sallam, E. S., & Wanas, H. A. (2019). Petrography and geochemistry of the Jurassic siliciclastic rocks in the Khashm El-Galala area (NW Gulf of Suez, Egypt): Implication for provinces, tectonic setting and source area paleoweathering. *Journal of African Earth Sciences*, 160, 103607.
- Sallam, H. M., Gorscak, E., O'Connor, P. M., El-Dawoudi, I. A., El-Sayed, S., Saber, S., Kora, M. A., Sertich, J. J. W., Erik, R.,

- Seiffert, E. R., & Lamanna, M. C. (2018). New Egyptian sauropod reveals Late Cretaceous dinosaur dispersal between Europe and Africa. *Nature Ecology & Evolution*, 2, 445–451. <https://doi.org/10.1038/s41559-017-0455-5>
- Salman, A. M., Mahfouz, K. H., El-Sheikh, I., Obaidalla, N. A., & Metwally, A. A. (2021). Facies analysis, cyclicity and biostratigraphy of the Upper Cretaceous Sudr Formation, Wadi El Dakhl, West Gulf of Suez, Egypt: Implications for sea-level changes and tectonics. *Carbonates and Evaporites*, 36, 68.
- Scheibner, C., Reijmer, J. J., Marzouk, A. M., Speijer, R. P., & Kuss, J. (2003). From platform to basin: The evolution of a Paleocene carbonate margin (Eastern Desert, Egypt). *International Journal of Earth Sciences*, 92, 624–640.
- Schlumberger. (1984). *Well evaluation conference, Egypt*. Schlumberger Middle East Surface.
- Schrank, E. (1982). Kretazische Pollen und Sporen aus dem 'Nubischen Sandstein' des Dakhla Beckens (Ägypten). *Berliner Geowissenschaftliche Abhandlungen*, 40(A), 87–109.
- Schrank, E., & Mahmoud, M. S. (1998). Palynology (pollen, pores and dinoflagellates) and Cretaceous stratigraphy of the Dakhla Oasis, central Egypt. *Journal of African Earth Sciences*, 26, 167–193.
- Scotese. (2001). *Atlas of earth history*. PALEOMAP Project, Arlington, Texas (p. 52).
- Senogur, A. M. C., Yilmaz, Y., & Sungurulu, O. (1984). Tectonics of the Mediterranean Cimmerides: Nature and evolution of the western termination of Palaeo-Tethys. In J. E. Dixon & A. H. F. Robertson (Eds.), *The geologic evolution of the eastern Mediterranean* (pp. 77–112). The Geological Society. Special Publication No. 17.
- Shalaby, M. R., Hakimi, M. H., & Abdullah, W. H. (2011). Geochemical characteristics and hydrocarbon generation modelling of the Jurassic source rocks in the Shoushan Basin, north Western Desert, Egypt. *Marine and Petroleum Geology*, 28(9), 1611–1624.
- Shalaby, M. R., Hakimi, M. H., Abdullah, W. H., & Islam, M. D. A. (2016). Implications of controlling factors in evolving reservoir quality of the Khatatba Formation, Western Desert, Egypt. *Geology Scientia Bruneiana Special Issue*, 129–146.
- Shehata, A. A., El Fawal, F. M., Ito, M., Abdel Aal, M. H., & Sarhan, M. A. (2018). Sequence stratigraphic evolution of the syn-rift Early Cretaceous sediments, West Beni Suef Basin, the Western Desert of Egypt with remarks on its hydrocarbon accumulations. *Arabian Journal of Geosciences*, 11, 331.
- Smith, J. B., Lamanna, M. C., Lacovara, K. J., Dodson, P., Smith, J. R., Poole, J. C., Giegengack, R., & Attia, Y. (2001). A giant sauropod dinosaur from an upper cretaceous mangrove deposit in Egypt. *Science*, 292, 1704–1706.
- Soliman, H. E. (2001). Lithostratigraphy and sedimentology of the Lower Cretaceous succession at Gabal Shabrawet, North Eastern Desert, Egypt. *Scientific Journal of Faculty of Science, Minufiya University*, XV, 209–235.
- Soliman, H. E., & Khalifa, M. A. (1993). Stratigraphy, facies and depositional environments of the Lower Cenomanian Bahariya Formation, Bahariya Oasis, Western Desert, Egypt. *Egyptian Journal of Geology*, 37, 193–209.
- Soliman, H. E., & Wanas, H. A. (2004). A contribution to the lithostratigraphy and sedimentology of the Lower Cretaceous succession at Gabal Manzour, Maghara area, North Sinai, Egypt. *Scientific Journal of Faculty of Science, Minufiya University*, XVII, 63–94.
- Soliman, S. M., Faris, M. I., & Badry, O. E. (1970). Lithostratigraphy of the Cretaceous Formations in the Bahariya Oasis, Western Desert, Egypt. In *Seventh Arab Petroleum Congress*.
- Tantawy, A. A. (1994). *Paleontological and sedimentological studies on the Late Cretaceous–Early Tertiary succession at Wadi Abu Ghurra–Gabal El-Kaddab Stretch, South Western Desert, Egypt* [M.Sc. thesis]. Aswan Faculty of Science, Assiut University.
- Tassy, A., Crouzy, E., Gorini, C., Rubino, J., Bouroullec, J., & Sapin, F. (2015). Egyptian Tethyan margin in the Mesozoic: Evolution of a mixed carbonate-siliciclastic shelf edge (from Western Desert to Sinai). *Marine and Petroleum Geology*, 68, 565–581.
- Tawadros, E. (2011). *Geology of North Africa* (p. 930). CRC Press.
- Voigt, S., Gale, A. S., & Voigt, T. (2006). Sea-level changes, carbon cycling and palaeoclimate during the Late Cenomanian of northwest Europe; an integrated palaeoenvironmental analysis. *Cretaceous Research*, 27, 836–858.
- Wanas, H. A., & Abu El-Hassan, M. M. (2006). Paleosols of the Upper Cretaceous–Lower Tertiary Maghra El-Bahari Formation in the northeastern portion of the Eastern Desert, Egypt: Their recognition and geological significance. *Sedimentary Geology*, 183, 243–259.
- Wanas, H. A., & Soliman, H. E. (2018). Permo-Triassic Qiseib Formation, western side of the Gulf of Suez, Egypt: A link of fluvial facies with sequence stratigraphy. *Journal of Geology & Geophysics*, 7, 333.
- Weissbrod, T. (1969). The Paleozoic of Israel and adjacent countries: Pan 11, The Paleozoic outcrops in south western Sinai and their correlation with those of southern Israel. *Bulletin Geological Survey of Israel*, 48, 1–32.
- Wever, H. E. (2000). Petroleum and source rock characterization based on C₇ star plot results: Examples from Egypt. *American Association of Petroleum Geologists Bulletin*, 84(7), 1041–1054.
- Wilmsen, M., & Nagm, E. (2013). Sequence stratigraphy of the lower Upper Cretaceous (Upper Cenomanian–Turonian) of the Eastern Desert, Egypt. *Newsletters on Stratigraphy*, 46(1), 23–46.
- Wycisk, P. (1984). Depositional environment of Mesozoic strata from northwestern Sudan. *Berliner Geowissenschaftliche Abhandlungen*, 50(A), 81–97.
- Wycisk, P. (1993). Outline of the geology and mineral resources of the southern Dakhla Basin, SW Egypt. In B. Meissner & P. Wycisk (Eds.), *Geopotential and ecology—Analysis of a desert region*. *Catena* (Supplement 26), 67–97.
- Youssef, M. I. (1957). Upper Cretaceous rocks in Kosseir area. *Bulletin Institution Desert Egypt*, 7(2), 35–54.
- Youssef, M. I., & Abdel Aziz, W. (1971). Biostratigraphy of the Upper Cretaceous–Lower Tertiary in Farafra Oasis, Libyan Desert, Egypt. In L. C. Gary (Ed.), *Symposium on the Geology of Libya*, Faculty of Science, Libya University (pp. 227–249).
- Zak, I. (1964). The Triassic of Arayif en Naqa, Sinai. *Geological Survey of Israel*, 1/64, 28.



Nageh A. Obaidalla is a professor of stratigraphy and micropaleontology in the Faculty of Science, Assiut University (Egypt) from where he earned M.Sc. (1988) and Ph.D. (1993) degrees. He was a member of the student training scholarship from DAAD, the Germany Academic Exchange Service in 1984 and was a researcher at Rikkyo University, Tokyo, Japan (1991–1992). In 2008, he received training on remote sensing and geographic information system at Vrije University, Brussels (Belgium). He worked with the international team on the GSSP of the Paleocene/Eocene (P/E) boundary from 1999 to 2003. His fields of interest are the integrated stratigraphy, global correlation, tectonic events, stage boundaries and sedimentary basin analysis. He is also interested in the micropaleontology (foraminifera) and paleoenvironments of the Mesozoic and Cenozoic sedimentary successions.



Kamel H. Mahfouz is an associate professor of stratigraphy and micropaleontology in the Geology Department, Faculty of Science, Al-Azhar University (Assiut Branch, Egypt), where he graduated in 2002 with a B.Sc. degree (distinction with honor). He holds an M.Sc. (2008) from Al-Azhar University, Cairo and obtained a Ph.D. (2013) in stratigraphy and micropaleontology from Assiut University (Egypt). His main field of research is event stratigraphy, micropaleontology (especially the

use of the planktonic foraminiferal species for biostratigraphy) and paleo-environmental studies. He is also interested in syn-sedimentary tectonic events and their impact on the evolution of sedimentary basins.



Amr A. Metwally is an associate professor of stratigraphy and micropaleontology in the Geology Department, Faculty of Science, Assiut University (Egypt). He received a M.Sc. (2011) degree from the University of the Witwatersrand (Bernard Price Institute for Palaeontological Research), Johannesburg (South Africa) and Ph.D. (2014) in stratigraphy and micropaleontology from Assiut University. His research focuses on stratigraphy and micropaleontology, particularly the calcareous nanofossils. He utilizes

nanofossils in interpreting past environmental changes associated with the boundary events throughout the Late Cretaceous-early Paleogene time interval.



Mesozoic Oceanic Anoxic Events and the Associated Black Shale Deposits as a Potential Source of Energy

Tarek Anan and Adam El-Shahat

Abstract

Oceanic anoxic events (OAEs) are considered as periods of oxygen deficiency in many oceans; accompanied by accumulation of organic-rich black shales. Mesozoic anoxic events were recognized based on the presence of black shales that are rich in organic matter. The most significant anoxic events during the Mesozoic are the Early Toarcian, the Early Aptian, and the Cenomanian–Turonian. The less significant events are the Valanginian–Hauterivian, the Hauterivian–Barremian, the Aptian–Albian, the Late Albian, the Albian–Cenomanian, and the Coniacian–Santonian. The recognized OAEs in Egypt are the Early Aptian (OAE 1a), the Aptian–Albian (OAE 1b), the Late Albian (OAE 1c), the Albian–Cenomanian (Breistroffer, OAE 1d), and the Cenomanian–Turonian (Bonarelli Event, OAE 2). However, the most widely recorded event is the OAE 2. The Cretaceous oceans hosted huge amounts of organic-rich black shales that sufficient to source all of the hydrocarbons. Black shales are considered as the most important source of hydrocarbons. The exploitation of black shales to generate hydrocarbons becomes a vital substitutional resource for energy. Such utilization of black shales may compensate the shortage of hydrocarbons in Egypt. Detailed field work and analytical data are required before final estimation of black shale resources in Egypt.

Keywords

Mesozoic • Anoxic events • Black shales • Organic matter • Cenomanian–Turonian • Valanginian–Hauterivian

1 Introduction

Oceanic anoxic events (OAEs) were first described by Schlanger and Jenkyns (1976). These events are global-scale periods of marine anoxia that associated with a widespread accumulation of organic carbon-rich fine sediments. The responsible factors for this phenomenon remain problematic. However, the general assumption was that during some intervals in the geological time, intensified oxygen minimum horizons prevailed in many oceans. Schlanger and Jenkyns (1976) concluded that the essential factor leading to enhanced organic carbon accumulation was reducing oxygen content in ocean bottom waters (less than 1.0 ml O₂ per 1.0 L H₂O). Oxygen deficiency was formed due to two factors: (i) water column stratification and (ii) increases in primary productivity. OAEs were believed to be accompanied by major fluctuations in the global carbon cycle. Carbon isotope excursions have been reported across pelagic and shallow-water marine carbonate successions (Danelian et al., 2004; Farrimond et al., 1990; Karakitsios et al., 2010; Kemp et al., 2005; Schouten et al., 2000).

Oceanic anoxic events were recorded in different geologic periods, such as Early to Middle Paleozoic, end Permian, and Mesozoic events. Varved black shales in the Cambrian (Zhuravlev & Wood, 1996), graptolite shales in both the Ordovician and Silurian (Berry & Wilde, 1978) or Devonian and Carboniferous black shale deposits point to deposition from oxygen deficient deep water during the Early and Middle Paleozoic times. The end-Permian oceanic anoxic event was widespread and indicated by the presence of laminated organic black shales that contain abundant pyrite and was deposited in shallow to deep water settings (Wignall & Twitchett, 2002). The Mesozoic anoxic events are widespread and can be correlated globally.

Leckie et al. (2002) declared that most oceanic anoxic events are associated with extensive volcanism that accompanied by the release of methane hydrates (Beerling et al., 2002). During these circumstances, CO₂ content increases

T. Anan (✉) · A. El-Shahat
Department of Geology, Mansoura University, Mansoura, 35516,
Egypt
e-mail: atarek@mans.edu.eg

and causes global warming (Fig. 1). These situations lead to intensive chemical weathering on the continents that in turn will enhance nutrient discharge to the oceans (Fig. 1). Finally, this will lead to increase the production of organic matter in the oceans (Jenkyns, 2010). In addition, during most oceanic anoxic events, the water became euxinic (i.e., the water is anoxic and sulfidic) (Jenkyns, 1988; Westermann et al., 2013).

This chapter aims to shed some light on the presence of OAEs during the Mesozoic, the accumulation of organic-rich black shales during these events, the occurrence of OAEs in Egypt, and the utilization of such black shales as a source of energy.

2 Mesozoic Oceanic Anoxic Events

Mesozoic oceanic anoxic events are determined based on the presence of black shales that are rich in organic carbon. These black shales contain huge amounts of carbon

sufficient to source the majority of the petroleum and natural gas (Schlanger & Cita, 1982). Multiple periods of widespread anoxic conditions (Fig. 2) have been recorded in the Mesozoic Era (Schlanger & Jenkyns, 1976). The events have durations varying between a few hundreds of thousands of years and up to a million years. During the Mesozoic Era (Fig. 2), oceanic anoxic events of global significance are: (1) the Early Toarcian Event (Posidonien-schiefer event, T-OAE, Mazzini et al., 2010), (2) the Early Aptian Event (Selli event, OAE 1a, Malinverno et al., 2010), and (3) the Cenomanian–Turonian Event (Bonarelli Event, OAE 2). The less significant oceanic events (Fig. 2) in the Mesozoic Era are: (1) the Valanginian-Hauterivian Event (Weissert Event), (2) the Hauterivian-Barremian Event (Faraoni Event), (3) the Aptian-Albian Event (OAE 1b, Paquier Event), (4) the Late Albian (OAE 1c), (5) the Albian-Cenomanian Event (OAE 1d, Breistroffer Event), and (6) the Coniacian-Santonian Event (OAE 3). Description of the most widespread oceanic events (Early Toarcian, Early Aptian, and Cenomanian–Turonian) will be discussed in the following sections.

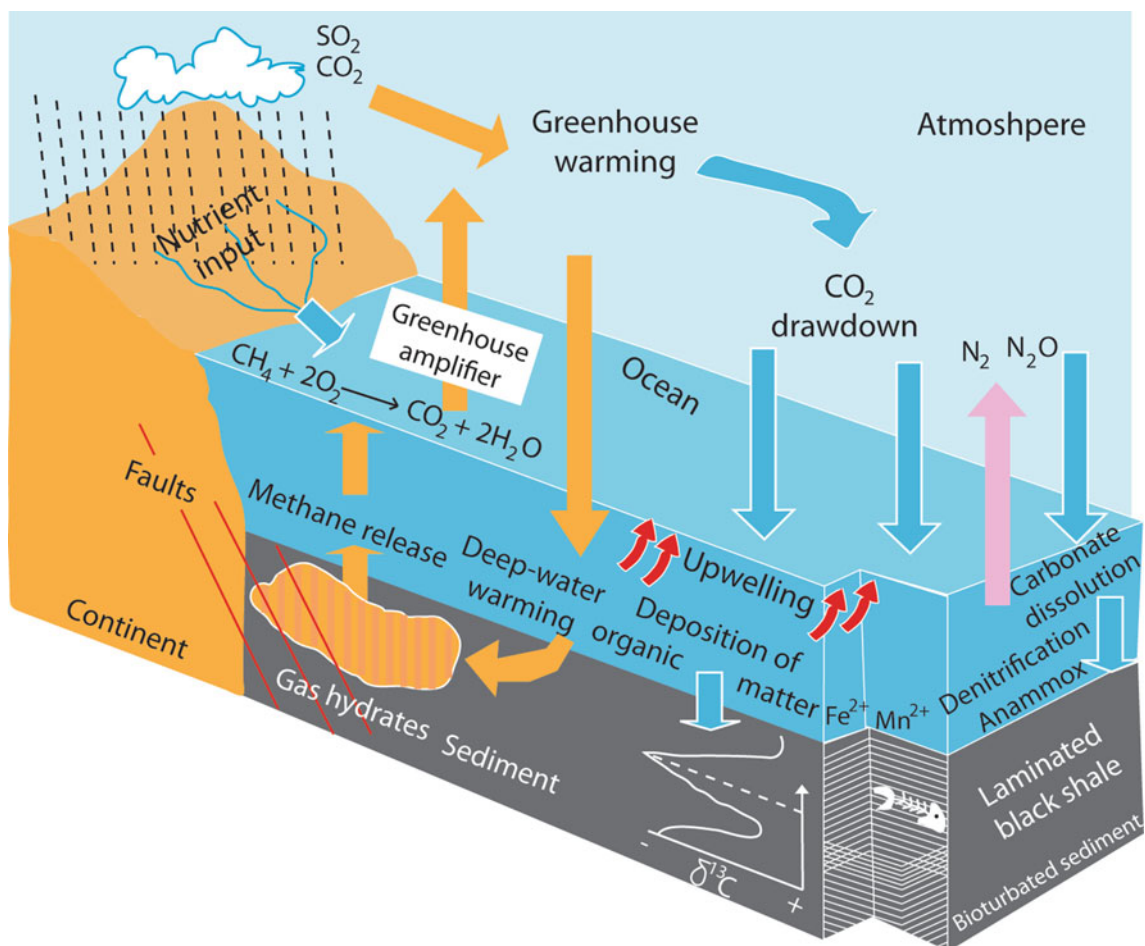


Fig. 1 Illustration of the various geochemical processes that are associated with OAEs, after Jenkyns (2010)

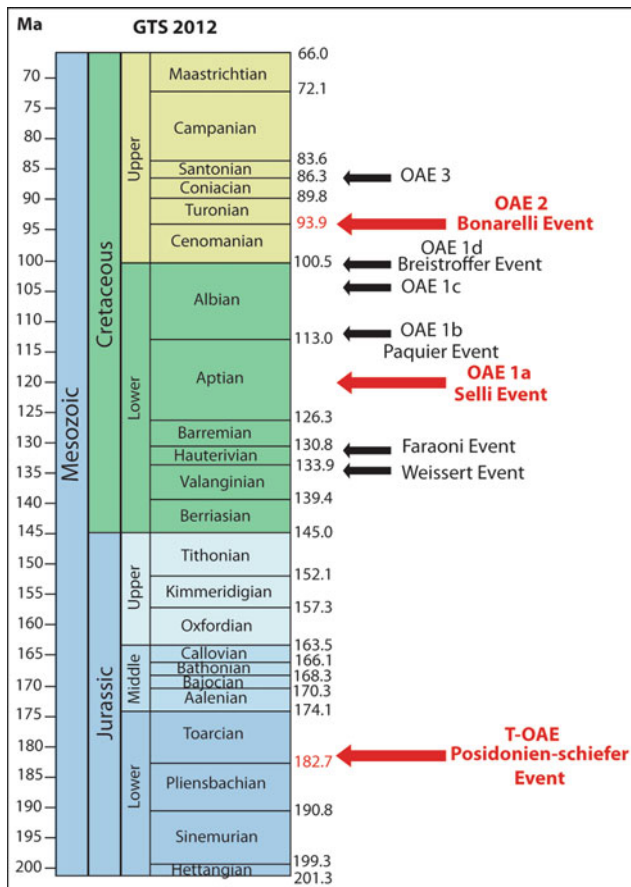


Fig. 2 The position of the different Mesozoic OAEs. Red arrows denote the most significant events. Figure after Jenkyns (2010). The geological time scale (GTS 2012) is given in Gradstein et al. (2012)

2.1 The Early Toarcian (T-OAE)

This event is considered as the earliest OAE in the Mesozoic. It is associated with a mass extinction (eastern Tethyan, Wignall et al., 2006) and accumulation of organic carbon (Jenkyns et al., 2001). The Early Toarcian Event showed increased organic carbon sequestration. The total organic carbon (TOC) of black shales of this event varies between 0.60 and 19 wt% (Jenkyns, 1988, 2010; Jenkyns et al., 2002). Such variation is interpreted to be a result of water depth, different redox conditions, and degree of organic productivity. Carbon isotope content of bulk organic matter during this event drops below -30% from background levels of generally -26 to -27% . However, the carbon isotope content of carbonates fluctuates due to diagenetic alterations (the Pindos Zone, Greece, Kafousia et al., 2010). Fluctuations in the global carbon cycle were recorded in the T-OAE (Remírez & Algeo, 2020). In the Northwest European Shelf, T-OAE displays large organic carbon isotope excursion (-5 to -7%) and high TOC content ($\sim 10\%$) (Remírez & Algeo, 2020).

2.2 The Early Aptian (OAE 1a, Selli Event)

It is the earliest major OAE in the Cretaceous period. Like the Early Toarcian event, the Selli Event is characterized by the global accumulation of black shales in continental shelves and marginal environments (Gröcke et al., 1999; Heimhofer et al., 2004). In addition, the Selli Event is associated with pronounced turnover in calcareous nannoplankton (Erba, 1992) and severe extinction of siliceous and calcareous plankton (Heimhofer et al., 2004). Palaeotemperature data showed an abrupt increase in sea surface temperature of about $8\text{ }^{\circ}\text{C}$ in the OAE 1a that in turn followed by a cooling trend (Ando et al., 2008). Recently, Percival et al. (2021) studied the OAE 1a at different localities; Pacific, Tethyan, Arctic, and South Atlantic areas. They stated that volcanic carbon emissions accompanied by magmatic degassing are the trigger of the OAE 1a.

2.3 The Cenomanian–Turonian (OAE 2, Bonarelli Event)

The Cenomanian–Turonian OAE 2 is the most extensively studied event among the all OAEs throughout the geologic times. During this event, global accumulation of organic-rich fine sediments was recorded (Schlanger & Jenkyns, 1976; Tsikos et al., 2004). In addition, a positive carbon isotope excursion in marine carbonates of 2–3‰ and in bulk organic matter of 4–6‰ was recorded. Jenkyns et al., (2007) recognized the highest carbon isotope excursions in and around the Atlantic Ocean where huge amounts of black shales were deposited. According to the orbital time scale of Sageman et al. (2006), the time span of the OAE 2 is about 600 ka.

During the OAE 2, the mid-Atlantic oceanic rift had created a basin of about 4000–5500 km² in the Northern Hemisphere. This basin is known as the proto-North Atlantic during the Cenomanian–Turonian times. Many researchers (e.g., Algeo & Rowe, 2012; Hetzel et al., 2009) have reported that the proto-North Atlantic was a semi-closed and restricted basin with steep slopes. During the mid-Cretaceous, sea-level transgression occurred and led to the formation of an epicontinental sea across the North American continent (Fig. 3) (Haq et al., 1987; Miller et al., 2005). This sea is called the Western Interior Seaway. Hancock and Kauffman (1979) stated that during this interval, Europe turned into an archipelago resulting from Late Cenomanian transgression. Through the OAE 2, substantial amounts of organic-rich sediments were globally accumulated. This in turn led to enhanced burial of organic carbon that resulted in a ¹³C enriched global carbon reservoir. So, there is a positive excursion in the stable carbon isotope ($\delta^{13}\text{C}$) (Fig. 4) of both organic matter and carbonate rocks (e.g., Arthur et al., 1988; Tsikos et al., 2004). Such positive excursion in $\delta^{13}\text{C}$ is



Fig. 3 Palaeogeographic reconstruction of the Cretaceous denoting section locations: Colorado, Western Platform, Tarfaya, Eastbourne, Gongzha, Tappu, Mangaotane B, and Sawpit Gully (modified after Gangl et al., 2019; Zhou et al., 2015)

considered as a global phenomenon and may be used in correlation of different OAE 2 successions (Voigt et al., 2008).

3 Oceanic Anoxic Events in Egypt

The Early Toarcian rocks in north Sinai (the Mashabba Formation) contain black shales in its lower part. This shale contains abundant plant remains such as *Equisitites* sp., *Gleichenites* cf. *cycadina* (Schrank), *Laccopteris* cf. *densa* (Edwards), and *Weichselia* sp. (Al Far, 1966). The Mashabba Formation was deposited in shallow marine conditions with fluvial and deltaic settings (Al Far, 1966), so the Early Toarcian OAE is not recorded. There are no isotopic data from the Mashabba Formation. The recorded Mesozoic OAEs in Egypt are; the Early Aptian (OAE 1a), the Aptian-Albian (OAE 1b), the Late Albian (OAE 1c), the Albian-Cenomanian (Brestroffer, OAE 1d), and the Cenomanian-Turonian (Bonarelli Event, OAE 2). The most widely distributed event in Egypt is the OAE 2.

The Early Aptian Event (OAE 1a, Selli Event)

The Early Aptian event has a limited distribution in Egypt; only recorded in north Sinai. Salama and Abdel-Gawad (2018) subdivide the Late Barremian-Late Albian succession at Gabal Raghawi, north Sinai into 22 characteristic carbon

segments (C1–C22). They recognized the OAE 1a below the Early-Late Aptian boundary at Gabal Raghawi. This event corresponds to the Early Aptian ammonite *Deshayesites forbesi* Zone.

The Aptian-Albian Event (OAE 1b)

Like the OAE 1a, this event is recorded only in north Sinai. Salama and Abdel-Gawad (2018) reported the OAE 1b event above the ammonite *Acanthohoplites nolani* horizon at Gabal Raghawi, north Sinai. The negative carbon isotope excursion (CIE) of the carbon segments (C11–C12) is interpreted as the onset of the OAE 1b.

The Late Albian Event (OAE 1c)

This event has a limited distribution; only recorded at Gabal Raghawi, north Sinai (Salama & Abdel-Gawad, 2018). The beginning of negative CIE between the carbon segments (C16–C17) refers the presence of OAE 1c.

The Albian-Cenomanian Event (OAE 1d, Brestroffer)

The OAE 1d event was determined at Gabal Raghawi, north Sinai by Salama and Abdel-Gawad (2018). It was accompanied by a positive carbon isotope shift at the Albian-Cenomanian boundary within the ammonite *Mortonicerias inflatum* Zone.

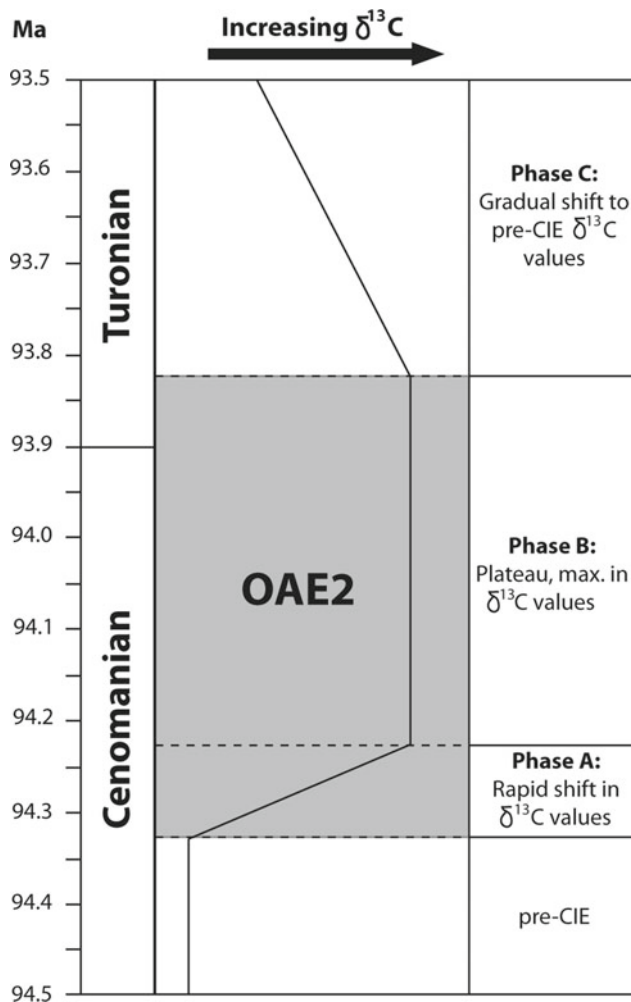


Fig. 4 Schematic representation of the for OAE 2 characteristic positive carbon isotope excursion (CIE). Timescale after Meyers et al. (2012). Figure after Kuypers et al. (2002)

The Cenomanian–Turonian Event (OAE 2, Bonarelli Event)

This event is considered as the most extensive oceanic anoxic event that has been studied in Egypt (Fig. 5). Different sections from Sinai Peninsula were chosen to study the presence of the OAE 2. These sections are: Gabal Nezzazat (Shahin, 2007), Wadi El-Ghaib (Gertsch et al., 2010), Wadi Feiran (El-Sabbagh et al., 2011), Gabal Musabaa Salama, Gabal Ekma, and Gabal Qabaliat (Anan et al., 2013). In the Eastern Desert, El-Sabbagh et al. (2011) recognized the presence of OAE 2 at Wadi Dakhli, whereas Nagm et al. (2014) determined this event at Wadi Qena. In the north Western Desert, Zobaa et al. (2011) recorded the Cenomanian–Turonian oceanic anoxic event in the Razzak oil field. Recently, Kassem et al. (2020) recorded this event from subsurface samples in the October oil field, Gulf of Suez.

Shahin (2007) recorded the OAE 2 in Gabal Nezzazat, west central Sinai. He observed a dark shale layer in the Abu Qada Formation below the Cenomanian–Turonian boundary. In addition, he defined this event on the basis of foraminiferal content and high positive $\delta^{13}\text{C}$ excursions in both the bulk carbonate samples and oyster shells. He recorded two high positive $\delta^{13}\text{C}$ excursions; 3.88 and 5.06‰ during this event. Gertsch et al. (2010) recognized the OAE 2 in the restricted shallow settings at Wadi El-Ghaib, Sinai. The oceanic anoxia/dysoxia conditions in these shallow marine settings are delayed because anoxic waters carried to shorelines during transgression. Zobaa et al. (2011) recorded a positive $\delta^{13}\text{C}_{\text{org}}$ excursion (2.01‰), and they believed this is correlated to the OAE 2. They identified this event within the organic-rich shaley limestone in the basal part of the Abu Roash “F” member.

Anan et al. (2013) determined OAE 2 in the Cenomanian–Turonian Abu Qada Formation in three sections in west central Sinai (Gabal Musabaa Salama, Gabal Ekma, and Gabal Qabaliat, Fig. 5). Lithologically, the OAE 2 bearing sequence consists mainly of argillaceous limestone and dark shale (Fig. 6) containing planktonic foraminifera, calcispheres, thin-shelled bivalves, in addition to ammonites. This horizon was deposited during periods of sea-level rise between the Cenomanian and Turonian. The observed $\delta^{13}\text{C}$ excursions are 3.04, 3.99‰ in Gabal Musabaa Salama, 4.51, 5.14‰ in Gabal Ekma, and 4.22, 5.24‰ in Gabal Qabaliat. These high positive excursions in $\delta^{13}\text{C}$ are associated with highly negative values of $\delta^{18}\text{O}$. A shift to more negative $\delta^{18}\text{O}$ values may be the result of warming and diagenetic alterations. Kassem et al. (2020) recorded positive $\delta^{13}\text{C}$ excursion (1.8‰) in the dark gray shale of the Abu Qada Formation. At the Cenomanian–Turonian boundary, they attributed the abrupt increase in organic matter (3.75 wt%) to a depletion in the oxygen level and in turn increase in the preservation of organic carbon.

Nagm et al. (2014) recognized the Cenomanian–Turonian boundary event (OAE 2) in shallow marine succession at Wadi Qena, Eastern Desert. The positive $\delta^{13}\text{C}$ excursion of the studied interval reaches 6.5‰. The positive carbon isotope excursions at Wadi Qena show the proceeding of the oceanic event into the shallow-water succession. In northeast Egypt, the OAE 2 was determined in shallow neritic environments (Wadi Dakhli, El-Sabbagh et al., 2011). Anoxic conditions that are associated with the OAE 2 are delayed until the beginning of the Early Turonian in shallow shelf successions.

4 Black Shale of the Oceanic Anoxic Events

North (1979) concluded that the Cretaceous oceans deposited large amount of organic-rich black shales. However, today, organic-rich and/or sulfur-rich shales accumulate in

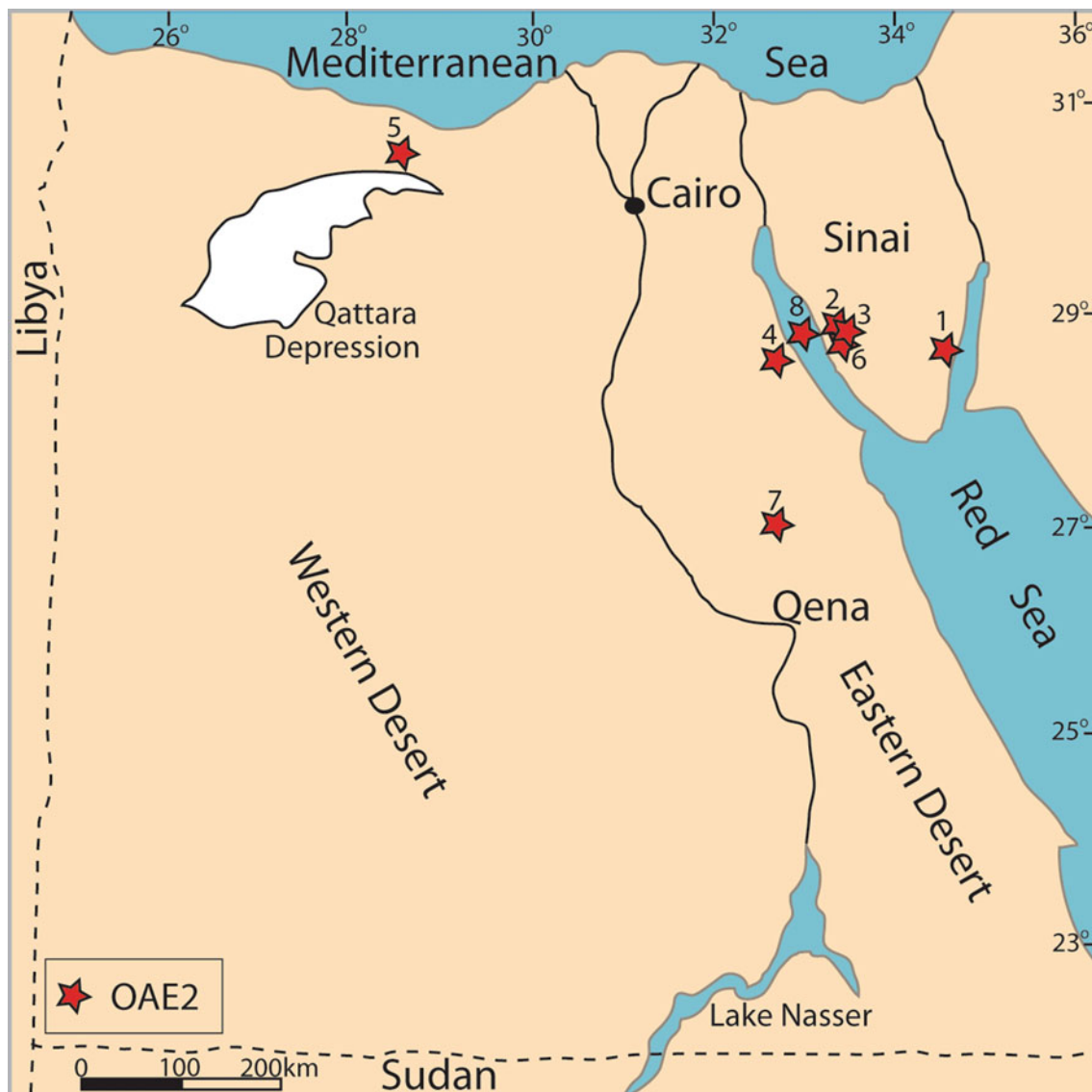


Fig. 5 Location of the OAE 2 in different parts of Egypt. (1) Gabal Nezzazat (Shahin, 2007), (2) Wadi El-Ghaib (Gertsch et al., 2010), (3) Wadi Feiran (El-Sabbagh et al., 2011), (4) Wadi Dakhli (El-Sabbagh et al., 2011), (5) Razzak oil field, Western Desert (Zobaa et al., 2011), (6) Gabal Musabaa Salama, Gabal Ekma and Gabal Qabaliatie (Anan et al., 2013), (7) Wadi Qena (Nagm et al., 2014), and (8) October oil field, Gulf of Suez (Kassem et al., 2020)

the Black Sea (Kaiser et al., 2017). Schlanger and Jenkyns (1976) highlighted that the OAEs contain widespread deposition of black shale. These intervals correspond to major sea-level rise. OAEs are associated with fluctuations in the global carbon cycle (Schlanger & Jenkyns, 1976). Such fluctuations are associated with positive and/or negative carbon isotope excursions in both pelagic and shallow marine organic-rich fine sediments (black shale) (Farrimond et al., 1990; Kemp et al., 2005). Black shales of the OAEs in the Mesozoic were widely deposited in the Pacific Ocean (Takashima et al., 2010), the Atlantic Ocean (Lipinski et al., 2003), and the Tethys Ocean (Wang et al., 2001) (Fig. 7). Among all OAEs, the Cenomanian–Turonian event (OAE 2)

is associated with widespread accumulation of black shales (Gangl et al., 2019). Deposition of black shale in OAE 2 commenced in the Southern North Atlantic Ocean and the Western Interior Seaway and spread to the North Atlantic Ocean and the Tethys Ocean (Kuroda & Ohkouchi, 2006). Black shales reserve huge quantities of carbon that sufficient to source the majority of the hydrocarbons. Schlanger and Cita (1982) stated that the highest ratio of hydrocarbon source rocks accumulated during the times of oceanic anoxic events.

If oxygen is abundant in any depositional environment, decomposition of organic matter occurs, and the CO_2 is returned to the water. As oxygen becomes limited,



Fig. 6 Field photographs showing the Cenomanian–Turonian Abu Qada Formation. **a** Dark gray shale of the Abu Qada Formation in Gabal Ekma, West Sinai (after Anan, 2010). **b** Close up view of the black shale of the Abu Qada, Gabal Nezzazat, West Sinai. Geologic hammer for scale is 32.5 cm (after Anan, 2014)

deposition of organic matter will be protected from aerobic decomposition. Such oxygen deficiency prevailed during the OAEs. Oceanic anoxic events are considered as extremely narrow time intervals, where the majority of the world's oceans transformed from carbon oxidizing to carbon storing system (Schlanger & Cita, 1982). The rate of burial and preservation of organic matter in marine environment depends up on the rate of production, the rate of bulk sedimentation, and the rate of organic decomposition (Arthur & Sageman, 1994; Sageman & Lyons, 2003).

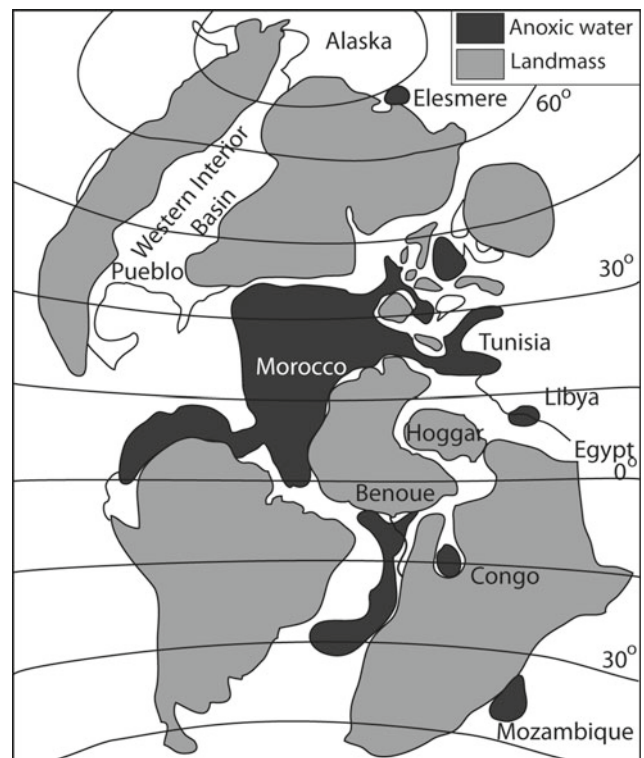


Fig. 7 Distribution of organic-rich fine sediments through the Cenomanian–Turonian boundary in the Atlantic and adjacent areas (modified after Graciansky et al., 1986)

Organic-rich black shale is a characteristic feature through the OAE 2 especially in deeper waters of the North Atlantic, Tethyan, and surrounding margins (Mort et al., 2008; Voigt et al., 2006). On the other hand, in shallow marine settings, these black shales are generally missing, either because they were not deposited or not preserved (El-Sabbagh et al., 2011; Lüning et al., 2004). Different lithologies that are associated with the OAEs contain elevated TOC values compared with their interbedded sediments. Huge amounts of organic-rich fine sediments occur on the eastern margins of the Atlantic and along shelf margins (Jenkyns, 1985). Black shales of the Atlantic contain benthic bivalve *Inoceramus* that was deposited in dysoxic rather than truly anoxic conditions (Thiede & van Andel, 1977).

5 Black Shale Associated with the OAEs in Egypt

In Egypt, the black shales are extensively distributed. They are widespread in different stratigraphic successions and different ages (El-Kammar, 2008). As far as the writers are aware, very little is known about the properties and organic geochemistry of the black shales in Egypt. Most of the

previous detailed studies are concerned with black shales which are not associated with the OAEs. The first study of the Egyptian black shales was achieved by Said (1962) when he studied the carbonaceous black shale horizons of the Paleozoic Rod El-Hammal Formation at Wadi Araba, Eastern Desert. After that, Mustafa and Ghaly (1964) studied the black shale of the Quseir area, Eastern Desert. Troger (1984) estimated the black shale resources in Egypt. He declared that the resources in Quseir-Safaga and Abu Tartur areas are $4500 \times (10^6)$ bbls and $1200 \times (10^6)$ bbls, respectively. The Upper Cretaceous organic-rich fine sediments in both the Duwi Formation and Dakhla Shale contain potential oil shale accumulations with estimated resources of approximately 15 billion tons (El-Kammar, 2008, 2017). The lithofacies of the Campanian–Maastrichtian succession include black shales, limestones, phosphates, glauconites, and dolostone. The recorded black shales contain a substantial amount of organic matter.

The unconventional petroleum reserves in black shales are currently one of the most important and underutilized energy resources. In Egypt, the knowledge about exploitation of these black shales is very limited where the black shale exploration endeavors are still very immature.

5.1 The Aptian Stage

During the Aptian time, marine transgression took place and north Sinai and southern Western Desert were covered by shallow sea (Said, 1990). In northern and southern Egypt, the Alamein and Abu Ballas formations were deposited, respectively. In northern parts of Sinai, the Risan Aneiza Formation is composed mainly of delta front and prodelta sediments, whereas in northern Western Desert, marine conditions dominated, and carbonate and shale were deposited (Said, 1990). The Abu Ballas Formation is composed mainly of red and green fossiliferous shales. The Aptian rock units may include the Early Aptian Event (OAE 1a).

5.2 The Albian Stage

During the Albian, the sea level regressed northward. Shallow marine sediments were deposited in the northern Western Desert above the Dahab Shales (Said, 1990). The Aptian–Albian event (OAE 2b) was traced at Gabal Raghawi, north Sinai (Salama & Abdel-Gawad, 2018).

5.3 The Cenomanian–Turonian Stages

The marine Cenomanian–Turonian rocks are well-exposed in the northeastern part of Egypt in Sinai and the Eastern

Desert (Said, 1990). In central and east Sinai, the Cenomanian rocks are unconformably overlain by gray green shale, dark gray shale, marl, and argillaceous limestone beds that are rich in ammonites. Ghorab (1961) named this succession the Abu Qada Formation. The average thickness of the Abu Qada Formation is 35 m, whereas in northeastern part of Sinai, the thickness reaches 50 m. This formation includes the Cenomanian–Turonian boundary event. El-Shinnawi and Sultan (1973) stated that the Abu Qada Formation is composed of dark gray to blackish gray succession dominated by *Heterohelix globulosa*. The Abu Qada Formation can be traced in Sinai from north to south. The ammonite bed that marks the Cenomanian–Turonian boundary occurs in northern and central Sinai. This bed is absent in the southern localities; Gabal Mukattab and Gabal Qabaliat.

Kora et al. (1993) placed the Cenomanian–Turonian boundary in west Sinai within the middle part of the Abu Qada Formation as the boundary between the oyster *Exogyra (Costagyra) olisiponensis* and the ammonite *Mammites nodosoides* zones. Ismail (2002) determined the OAE 2 within the Abu Qada Formation in Wadi Feiran, south western Sinai in a black shale unit yielding planktonic foraminifera. A clear warming trend is recorded by Khalil (2007) from the latest Cenomanian to the earliest Turonian; based on the increased diversification of the ammonites. Gertsch et al. (2010) studied the Cenomanian–Turonian succession in the Wadi El-Ghaib, east Sinai. The studied succession reflects shallow nearshore environment that became deeper around the Late Cenomanian–Late Turonian. Around Cenomanian–Turonian, the Abu Qada Formation consists of red laminated, fossiliferous shales, and marls with ammonites.

El-Sabbagh et al. (2011) studied the Cenomanian–Turonian in Eastern Desert and in west Sinai. In the two studied locations, the Abu Qada Formation is well developed and consists of shales, marls, nodular marls, limestones, and oyster-rich limestone beds. Zobia et al. (2011) studied the Cenomanian–Turonian boundary in the Razzak #7 oil well, Razzak oil field (in north Western Desert) and reported a positive excursion in the $\delta^{13}\text{C}_{\text{org}}$ within the basal part of the Abu Roash “F” member. The lithology in this horizon is composed of predominantly organic-rich, black shaley limestone.

Anan (2014) described the Cenomanian–Turonian rock units in west central Sinai. He recorded the Cenomanian–Turonian boundary in the Abu Qada Formation that is dominated by dark gray shale. Thickness of this formation varies between 26 m in Gabal Esseilah to 47 m in Gabal Nezzazat, West Sinai. In the Eastern Desert, Nagm et al. (2014) studied the Cenomanian–Turonian boundary in Wadi Qena. Such boundary is placed in the Galala Formation between the Late Cenomanian *Vascoceras cauvini* and the Early Turonian Vascoceratid zones. The recorded lithology

in the C/T boundary is shale and marly limestone. Kassem et al. (2020) studied the Cenomanian–Turonian boundary event in October oil field, central Gulf of Suez, and they reported dark gray calcareous shale that is a characteristic feature for the abrupt redox conditions of the OAE 2. In addition, they reported a good to very good source rock maturity of the Abu Qada Formation.

6 Properties of Black Shale

Black shales are composed mainly of four components: clastics, carbonates, organic matter, and pyrite (Röhl et al., 2001). The content of organic matter ranges from 0.5 to 50 wt% of the whole rock. If the organic matter content is below 10%, black shales are called bituminous mudstones; whereas oil shales contain more than 10% organic matter (Röhl et al., 2001). The content of hydrogen in organic matter from black shales is much higher than that found in other fossil fuels (Zhang et al., 2012). In addition, black shales are characterized by low caloric value, low cohesiveness, high ash, and the high volatiles.

Black shales contain trace contents of some metals such as vanadium, molybdenum, uranium, arsenic, zinc, and antimony (El-Kammar, 2017). Moreover, depositional basins of the black shales may receive exceptional amounts of detrital materials, some elements such as zirconium, thorium, and rare earth elements are enriched. Sources of metals in black shales include seawater-derived material (Slack et al., 2015), hydrothermal and/or multiple metal sources (Young et al., 2013), post-depositional diagenetic and metamorphic processes (Rimstidt et al., 2017), and organic compounds and biomineralization (Rimstidt et al., 2017). In addition, sulfate-reducing bacteria may cause the deposition of sulfide minerals (Greenwood et al., 2013). Parviainen and Loukola-Ruskeeniemi (2019) choose eight black shale samples (from Finland, China, Canada, Poland and Germany, Zambia, Sweden, South Korea, and USA) for analyses. The studied black shales contain > 1% organic carbon and over 1% sulfur. In addition, Parviainen and Loukola-Ruskeeniemi (2019) recorded the abundance of sulfide minerals in these black shales such as pyrite, pyrrhotite, chalcopyrite, sphalerite, galena, molybdenite, marcasite, bornite, vaesite, wurtzite, melnicovite, ullmannite, stannite, and millerite.

Next to coal, organic content in black shales is more enriched in hydrogen and therefore is comparatively more liable to produce oil (Lille, 2003). Unlike lignite and bituminous coal, the organic matter of black shales has a higher hydrogen and lower oxygen content (Dyini, 2003). In black shales, organic matter degradation is incomplete due to oxygen depletion or even lack of oxygen. Such situations cause enrichment of organic matter in black shales (Dyini,

2003). Hence, preservation of organic matter in black shales is excellent.

Black shales contain non-clay minerals such as calcite, dolomite, glauconite, quartz, apatite, and pyrite. The recorded non-clay minerals are diverse in their origin. For example, dolomite is diagenetic. The minor non-clay minerals include ankerite, Mg-calcite, and marcasite. Due to the action of weathering, some minerals like gypsum, anhydrite, hematite, and halite are recorded (El-Kammar, 2017). High content of kaolinite in the black shales of the Dakhla Shale is a result of extensive weathering (El-Shafeiy et al., 2014; Keller et al., 2002). In addition, black shales contain smectite that shows a strong tendency to form complexes with organic molecules. El-Kammar (1993) determined that discrete illite is not detected in the black shales, however, it may interstratify with the smectite layers. Chlorite has a limited distribution in the studied black shales.

7 Black Shale as a Source of Energy

Energy demand increases continually and the International Energy Agency (IEA) predicts that this demands in 2030 will be more than two times in 1990 (Zhang et al., 2012). This growing demand is the main reasons to seek for alternative fuel sources such as black shales. The total resources of black shales in the world is 409 billion tons (Dyini, 2006). Extensive exploration will for sure add more billions the estimated resources. Huyck (1990) defined black shales as the rock that contain > 0.5% organic carbon. Other researchers stated that black shales contain > 1% of both organic carbon and sulfur.

Black shales are of tremendous economic value as they store the majority of the world's hydrocarbons (Wignall, 1994). Recently, black shale is considered as the most important source of hydrocarbons. Successful exploitation of black shale was recorded in the USA, Canada, and South America. The exploitation of black shales to generate hydrocarbons becomes a vial substitutional resource for energy (Xie et al., 2020).

Besides their importance in crude oil production, black shales can be used in generating electricity and a source of other valuable chemicals. Through the nineteenth century, thermal processing of black shales started in Australia, USA, Germany, Brazil, and Scotland. During the twentieth century, black shales processing started in China. Nowadays, significant quantities of black shales are mined in Estonia, Russia, China, Brazil, and Germany (Dyini, 2003). Black shales act as source rocks for oil and gas that will cover the most of energy needs in modern societies. The exploitation of oil shale from 1880 to 2010 is shown in Fig. 8. The major part of production comes from Estonia. Much smaller quantities come from Russia, China, and Brazil (Clerici & Alimonti, 2015).

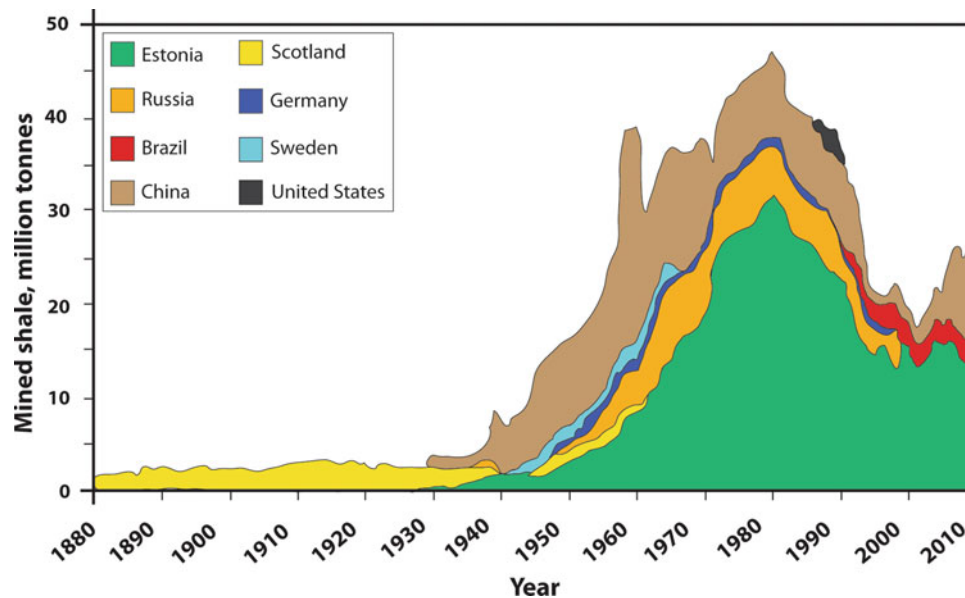


Fig. 8 Black shales world production in millions of metric tons (after Clerici & Alimonti, 2015). The major production comes from Estonia

8 Utilization of Black Shale

According to Zhang et al. (2012), there are two ways to exploit the black shales; combustion to generate energy and retorting to extract oil. During the twentieth century, black shales were used alone or mixed with coal for generating power by combustion. The retorting technique includes the distillation of kerogen by pyrolysis at temperatures > 700 °C (Zhang et al., 2012). The utilization of black shales includes two main processes; direct combustion and oil distillation process. Finally, the low-grade black shale can be used in cement industry (El-Kammar, 2017).

8.1 Direct Combustion

The older method of combustion is called pulverized combustion, and it was first used in Estonia with a high-grade black shale. To use a low-grade black shale (as low as 900 kcal/kg), a new technique was invented. This technique is called fluidized bed combustion. The combustion process includes three stages; the aerosol combustion, the fluid bed combustion, and the circulation fluid bed combustion Zhang et al. (2012).

8.2 Oil Distillation Process

In this process, a heat treatment method can be used to extract oil from black shales. The essential step here is to isolate the oil shale under the airless conditions and heat

up to temperature range (450–600° C), and then, the physicochemical reaction occurs. The final products are shale oil, coal gas, and semi-coke. The shale oil can be used as a fuel directly, whereas the byproduct is taken as waste such as coal gas and semi-coke Zhang et al. (2012).

8.3 Cement Industry

Low-grade black shales are in most cases suitable as raw materials in cement industry (El-Kammar, 2017). Recently, black shales are used by cement factories in the south Nile Valley. The usage of black shales may be part of the energy required for clinker production and that depends on the kerogen content.

9 Economic Analysis

Figure 9 illustrates the material and energy balance of black shale exploitation, the productivity value that contain the shale oil, semi-coke, and ash slag (Zhang et al., 2012). The outcome shows that the mass utilization of black shale includes oil distillation process and electricity generation. The investment in black shale industry will include the refinery, the electricity generation, and the production of building materials that can bring great opportunities for society. Moreover, the development of black shale refining industry can compensate for the shortage of petroleum in Egypt. Confrontation of shortage in energy in Egypt (i.e., the contradiction between demand and supply) will hinder the development of our national economy. Hence, seeking for

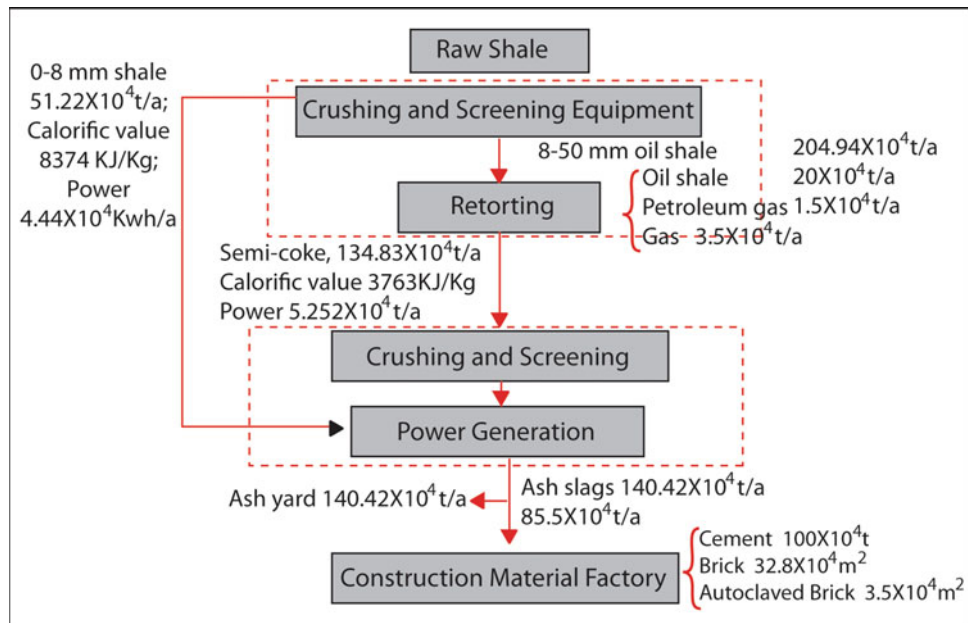


Fig. 9 Material and energy balance of black shale mass exploitation (after Zhang et al., 2012). Huyck, 1990, For the review, we selected eight black shale deposits and occurrences containing > 1% organic carbon and over 1% sulfur. Moreover, microbial activity, specifically sulfate-reducing bacteria, may trigger the precipitation of sulfide minerals, and the accumulation of metals may be promoted by porphyrins that bind metals to form complexes (Greenwood et al., 2013); Malinverno et al. (2010)

new energy resources is the only solution to solve this sophisticated problem.

10 Conclusions

Black shales accumulated through the OAEs in the Mesozoic are widely distributed in the majority of the world oceans. Among all OAEs, OAE 2 is accompanied by extensive accumulation of black shales. Black shales host huge quantities of carbon that are sufficient to source the hydrocarbons. The OAE 2 event is the most widely distributed oceanic anoxic event in Egypt. The marine Cenomanian–Turonian rock units are well-exposed in the northeastern parts of Egypt. The exploitation of black shales to generate hydrocarbons becomes a viable substitutional resource for energy. The mass exploitation of black shales includes direct combustion, oil distillation process, and the low-grade black shale can be used in cement industry. Detailed field work and chemical analyses are very vital to give an accurate estimation of the black shale resources in Egypt.

References

Al Far, D. M. (1966). Geology and coal deposits of Gebel Maghara, north Sinai, Egypt. *Geological Survey of Egypt, paper 37*, 59.

- Algeo, T. J., & Rowe, H. (2012). Paleooceanographic applications of trace-metal concentration data. *Chemical Geology*, 324–325, 6–18.
- Anan, T. (2010). Sedimentology of the Cenomanian–Turonian succession in west central Sinai, Egypt, (p. 171). Unpublished Ph.D Thesis, Mansoura University, Egypt.
- Anan, T. (2014). Facies analysis and sequence stratigraphy of the Cenomanian–Turonian mixed siliciclastic–carbonate sediments in west Sinai. *Egypt. Sedimentary Geology*, 307, 34–46.
- Anan, T., El-Shahat, A., Genedi, A., & Grammer, M. (2013). Depositional environments and sequence architecture of the Raha and Abu Qada formations (Cenomanian–Turonian), west central Sinai. *Journal of African Earth Sciences*, 82, 54–69.
- Ando, A., Kaiho, K., Kawahata, H., & Kakegawa, T. (2008). Timing and magnitude of early Aptian extreme warming: Unraveling primary $\delta^{18}\text{O}$ variation in indurated pelagic carbonates at Deep Sea Drilling Project Site 463, central Pacific Ocean. *Palaeogeography, Palaeoclimatology, Palaeoecology*, 260(3–4), 463–476.
- Arthur, M. A., Dean, W. E., & Pratt, L. M. (1988). Geochemical and climatic effects of increased marine organic-carbon burial at the Cenomanian–Turonian boundary. *Nature*, 335, 714–717.
- Arthur, M. A., & Sageman, B. B. (1994). Marine Black Shales: Depositional mechanisms and environments of ancient deposits. *Annual Review of Earth and Planetary Sciences*, 22, 499–551.
- Beerling, D. J., Lomas, M. R., & Gröcke, D. R. (2002). On the nature of methane gas-hydrate dissociation during the Toarcian and Aptian oceanic anoxic events. *American Journal of Science*, 302, 28–49.
- Berry, W. B., & Wilde, P. (1978). Progressive ventilation of the oceans - an explanation for the distribution of the lower Paleozoic black shales. *American Journal of Science*, 278, 257–275.
- Clerici, A., & Alimonti, G. (2015). Oil shale, shale oil, shale gas and non-conventional hydrocarbons. *The European Physical Journal Conferences*, 98, 03001. <https://doi.org/10.1051/epjconf/20159803001>
- Danelian, T., Tsikos, H., Gardin, S., Baudin, F., Bellier, J. P., & Emmanuel, L. (2004). Global and regional palaeoceanographic changes as recorded in the mid-Cretaceous (Aptian–Albian)

- sequence of the Ionian zone (NW Greece). *Journal of the Geological Society*, 161(4), 703–709.
- Dyni, J. R. (2003). Geology and resources of some world oil-shale deposits. *Oil Shale*, 20, 193–252.
- Dyni, J. R. (2006). Geology and resources of some world oil-shale deposits. *Scientific Investigation Report (2005–5294)* (p. 42). Published by the US Department of the Interior, US Geological Survey, Reston, Virginia.
- El-Kammar, M. M. (1993). Organic and inorganic composition of the Upper Cretaceous-Lower Tertiary black shales from Egypt and their hydrocarbon potentialities, Ph.D. Thesis, Faculty of Sciences, (p. 227). Cairo University.
- El-Kammar, A. (2008). Upper Cretaceous-Lower Tertiary black shales in Egypt: Possible potential source of energy. *Invited Talk. Sedimentology of Egypt*, 16, 1–5.
- El-Kammar, A. (2017). Oil shale resources in Egypt: The present status and future vision. *Arabian Journal of Geosciences*, 10, 439.
- El-Sabbagh, A., Tantawy, A., Keller, G., Khozyem, H., Spangenberg, J., Adatte, T., & Gertsch, B. (2011). Stratigraphy of the Cenomanian-Turonian oceanic anoxic event OAE2 in shallow shelf sequences of NE Egypt. *Cretaceous Research*, 32(6), 705–722.
- El-Shafeiy, M., Birgel, D., El-Kammar, A., El-Barkooky, A., Wagreech, M., Mohamed, M., & Peckmann, J. (2014). Palaeoecological and postdepositional changes recorded in Campanian-Maastrichtian black shales, Abu Tartur Plateau. *Egypt. Cretaceous Research*, 50, 38–51.
- El-Shinnawi, M., & Sultan, I. (1973). Lithostratigraphy of some subsurface Upper Cretaceous sections in the Gulf of Suez area. *Egypt. Acta Geologica Academiae Scientiarum Hungaricae*, 17, 469–494.
- Erba, E. (1992). Calcareous nannofossil distribution in pelagic rhythmic sediments (Aptian-Albian Piobbico core, central Italy). *Rivista Italiana Di Paleontologia e Stratigrafia*, 97, 455–484.
- Farrimond, P., Eglinton, G., Brassell, S. C., & Jenkyns, H. C. (1990). The Cenomanian/Turonian anoxic event in Europe: An organic geochemical study. *Marine and Petroleum Geology*, 7(1), 75.
- Gangl, S. K., Moy, C. M., Stirling, C. H., Jenkyns, H. C., Crampton, J. S., Clarkson, M. O., Ohneiser, C., & Porcelli, D. (2019). High-resolution records of Oceanic Anoxic Event 2: Insights into the timing, duration and extent of environmental perturbations from the palaeo-South Pacific Ocean. *Earth and Planetary Science Letters*, 518, 172–182.
- Gertsch, B., Keller, G., Adatte, T., Berner, Z., Kassab, A. S., Tantawy, A. A., El-Sabbagh, S., & D. (2010). Cenomanian-Turonian transition in a shallow water sequence of the Sinai. *Egypt. International Journal of Earth Sciences*, 99(1), 165–182.
- Ghorab, M. A. (1961). Abnormal stratigraphic features in Ras Gharib oilfields, Egypt. In *3rd Arab Petroleum Congress* (pp. 1–10) Alexandria.
- de Graciansky, P. C., Deroo, G., Herbin, J. P., Jacquini, T., Magni, F., Montadert, I., & Müller, C. (1986). Ocean-wide stagnation episodes in the Late Cretaceous. *Geological Rundschau*, 75, 17–41.
- Gradstein, F. M., Ogg, J. G., Schmitz, M. D., & Ogg, G. M. (2012). *The Geologic Time Scale 2012* (1st ed., p. 1176). UK, Elsevier.
- Greenwood, P. F., Brocks, J. J., Grice, K., Schwark, L., Jaraula, C. M. B., Dick, J. M., & Evans, K. A. (2013). Organic geochemistry and mineralogy I. Characterisation of organic matter associated with metal deposits. *Ore Geology Reviews*, 50, 1–27.
- Gröcke, D., Hesselbo, S. P., & Jenkyns, H. C. (1999). Carbon isotope composition of Lower Cretaceous fossil wood: Ocean-atmosphere chemistry and relation to sea-level change. *Geology*, 27, 155–158.
- Hancock, J. M., & Kauffman, E. G. (1979). The great transgressions of the Late Cretaceous. *Journal of the Geological Society of London*, 136, 175–186.
- Haq, B. U., Hardenbol, J., & Vail, P. R. (1987). Chronology of fluctuating sea levels since the Triassic. *Science*, 235, 1157–1167.
- Heimhofer, U., Hochuli, P. A., Herrle, J. O., Andersen, N., & Weissert, H. (2004). Absence of major vegetation and palaeoatmospheric pCO₂ changes associated with oceanic anoxic event 1a (Early Aptian, SE France). *Earth and Planetary Science Letters*, 223(3–4), 303–318.
- Hetzl, A., Böttcher, M. E., Wortmann, U. G., & Brumsack, H. J. (2009). Paleoredox conditions during OAE2 reflected in Demerara Rise sediment geochemistry (ODP Leg 207). *Palaeogeography, Palaeoceanography, Palaeoecology*, 273(3–4), 302–328.
- Huyck, H. L. (1990). Proposed definition of “black shale” and “metalliferous black shale” for IGCP #254. *Book of Abstracts, 8th IAGOD Symposium* (pp. A183-184). GSC.
- Ismail, A. (2002). The biostratigraphic and sequence stratigraphic applications on the Upper Cretaceous succession of Wadi Feiran, southwestern Sinai. *Egypt. Egyptian Journal of Geology*, 46, 515–533.
- Jenkyns, H. C. (1985). The early Toarcian and Cenomanian-Turonian anoxic events in Europe: Comparisons and contrasts. *Geologische Rundschau*, 74, 505–518.
- Jenkyns, H. C. (1988). The Early Toarcian (Jurassic) anoxic event: stratigraphic, sedimentary, and geochemical evidence. *American Journal of Science*, 288, 101–151.
- Jenkyns, H. C. (2010). Geochemistry of oceanic anoxic events. *Geochemistry, Geophysics, Geosystems*, 11, Q03004.
- Jenkyns, H. C., Gröcke, D. R., & Hesselbo, S. P. (2001). Nitrogen isotope evidence for water mass denitrification during the Early Toarcian (Jurassic) Oceanic Anoxic Event. *Paleoceanography*, 16, 593–603.
- Jenkyns, H. C., Jones, C. E., Gröcke, D. R., Hesselbo, S. P., & Parkinson, D. N. (2002). Chemostratigraphy of the Jurassic system; applications, limitations and implications for palaeoceanography. *Journal of the Geological Society of London*, 159(4), 351–378.
- Jenkyns, H. C., Matthews, A., Tsikos, H., & Erel, Y. (2007). Nitrate reduction, sulfate reduction, and sedimentary iron isotope evolution during the Cenomanian-Turonian oceanic anoxic event. *Paleoceanography*, 22, PA3208.
- Kafousia, N., Karakitsios, V., & Jenkyns, H. C. (2010). Preliminary data from the first record of the Toarcian Oceanic Anoxic Event in the sediments of the Pindos Zone (Greece). *Bulletin of the Geological Society of Greece*, 43(2), 627–633.
- Kaiser, D., Kononov, S., Schultz-Bull, D., & Waniek, J. J. (2017). Organic matter along longitudinal and vertical gradients in the Black Sea. *Deep Sea Research Part I: Oceanographic Research Papers*, 129, 22–31.
- Karakitsios, V., Kafousia, N., & Tsikos, H. (2010). A Review of Oceanic Anoxic Events as recorded in the Mesozoic sedimentary record of mainland Greece. *Hellenic Journal of Geosciences*, 45, 123–132.
- Kassem, A., Sharaf, L., Baghdady, A., & El-Naby, A. (2020). Cenomanian/Turonian oceanic anoxic event 2 in October oil field, central Gulf of Suez. *Egypt. Journal of African Earth Sciences*, 165, 103817.
- Keller, G., Adatte, T., Burns, S., & Tantawy, A. A. (2002). High-stress paleoenvironment during the late Maastrichtian to early Paleocene in central Egypt. *Palaeogeography, Palaeoclimatology, Palaeoecology*, 187, 35–60.
- Kemp, D. B., Coe, A. L., Cohen, A. S., & Schwark, L. (2005). Astronomical pacing of methane release in the Early Jurassic period. *Nature*, 437(7057), 396–399.
- Khalil, H. (2007). Macrostratigraphical, paleoecological and palaeobiographical studies of the Cenomanian/Turonian transition of Wadi Watir (El Sheikh Attia), Sinai. *Egypt. Egyptian Journal of Paleontology*, 7, 245–267.
- Kora, M., Shahin, A., & Semiet, A. (1993). Biostratigraphy and macrofauna of the Cenomanian exposures in west central Sinai. *Egypt. Mansoura Science Bulletin*, 20, 227–260.

- Kuroda, J., & Ohkouchi, N. (2006). Implication of spatiotemporal distribution of black shales deposited during the Cretaceous Oceanic Anoxic Event-2. *Paleontological Research*, 10(4), 345–358.
- Kuypers, M. M., Pancost, R. D., Nijenhuis, I. A., & Sinninghe Damsté, J. S. (2002). Enhanced productivity led to increased organic carbon burial in the euxinic North Atlantic basin during the late Cenomanian oceanic anoxic event. *Paleoceanography*, 17(4), 1051. <https://doi.org/10.1029/2000PA000569>
- Leckie, R. M., Bralower, T. J., & Cashman, R. (2002). Oceanic anoxic events and plankton evolution: biotic response to tectonic forcing during the Mid-Cretaceous. *Paleoceanography*, 17, PA1041.
- Lille, U. (2003). Current knowledge on the origin and structure of Estonian kukersite kerogen. *Oil Shale*, 20, 253–263.
- Lipinski, M., Warning, B., & Brumsack, H. J. (2003). Trace metal signatures of Jurassic/Cretaceous black shales from the Norwegian shelf and the Barents Sea. *Palaeogeography Palaeoclimatology Palaeoecology*, 190, 459–475.
- Lüning, S., Kolonic, S., Belhadj, E. M., Belhadj, Z., Cota, L., Baric, G., & Wagner, T. (2004). Integrated depositional model for the Cenomanian-Turonian organic-rich strata in North Africa. *Earth Science Reviews*, 64, 51–117.
- Malinverno, A., Erba, E., & Herbert, T. D. (2010). Orbital tuning as an inverse problem: Chronology of the early Aptian oceanic anoxic event 1a (Selli Level) in the Cison APTICORE. *Paleoceanography*, 25, PA2203. <https://doi.org/10.1029/2009PA001769>.
- Mazzini, A., Svensen, H., Leanza, H. A., Corfu, F., & Planke, S. (2010). Early Jurassic shale chemostratigraphy and U-Pb ages from the Neuquén Basin (Argentina): Implications for the Toarcian oceanic anoxic event. *Earth and Planetary Science Letters*, 297, 633–645.
- Meyers, S. R., Siewert, S. E., Singer, B. S., Sageman, B. B., Condon, D. J., Obradovich, J. D., Jicha, B. R., & Sawyer, D. A. (2012). Intercalibration of radio isotopic and astrochronologic time scales for the Cenomanian-Turonian boundary interval, Western Interior Basin, USA. *Geology*, 40, 7–10.
- Miller, K. G., Miller, M. A., Browning, J. V., Wright, J. D., Mountain, G. S., Katz, M. E., Sugarman, P. J., Cramer, B. S., Christie-Blick, N., & Pekar, S. (2005). The Phanerozoic Record of Global Sea-Level Change. *Science*, 310, 1293–1298.
- Mort, H. P., Adatte, T., Keller, G., Bartels, D., Föllmi, K. B., Steinmann, P., Berner, Z., & Chellai, E. H. (2008). Organic carbon deposition and phosphorus accumulation during oceanic anoxic event 2 in Tarfaya. *Morocco, Cretaceous Research*, 29, 1008–1023.
- Mustafa, A., & Ghaly, E. L. (1964). Survey of Quseir shales and other carbonaceous shales in Egypt. *Journal of Chemical and Engineering Data*, 9(4), 557–567.
- Nagm, E., El-Qot, G., & Wilmsen, M. (2014). Stable-isotope stratigraphy of the Cenomanian-Turonian (Upper Cretaceous) boundary event (CTBE) in Wadi Qena, Eastern Desert. *Egypt Journal of African Earth Sciences*, 100, 524–531.
- North, F. K. (1979). Episodes of source-sediment deposition (1). *Journal of Petroleum Geology*, 2, 199–218.
- Parviainen, A., & Loukola-Ruskeeniemi, K. (2019). Environmental impact of mineralised black shales. *Earth-Science Reviews*, 192, 65–90.
- Percival, L. M. E., Tedeschi, L. R., Creaser, R. A., Bottini, C., Erba, E., Giraud, F., Svensen, H., Savian, J., Trindade, R., Coccioni, R., Frontalini, F., Jovane, L., Mather, T. A., & Jenkyns, H. C. (2021). Determining the style and provenance of magmatic activity during the Early Aptian Oceanic Anoxic Event (OAE 1a). *Global and Planetary Change*, 103461.
- Remírez, M. N., & Algeo, T. J. (2020). Carbon-cycle changes during the Toarcian (Early Jurassic) and implications for regional versus global drivers of the Toarcian oceanic anoxic event. *Earth-Science Reviews*, 209, 103283.
- Rimstidt, J. D., Chermak, J. A., & Schreiber, M. E. (2017). Processes that control mineral and element abundances in shales. *Earth-Science Reviews*, 171, 383–399.
- Röhl, J., Schmid-Röhl, A., Oschmann, W., Frimmel, A., & Schwark, L. (2001). The Posidonia Shale (Lower Toarcian) of SW-Germany: An oxygen-depleted ecosystem controlled by sea level and palaeoclimate. *Palaeogeography Palaeoclimatology Palaeoecology*, 165, 27–52.
- Sageman, B. B., & Lyons, T. W. (2003). Geochemistry of fine-grained sediments and sedimentary rocks. In MacKenzie, F. (Ed.), *Treatise on Geochemistry* (Vol. 7, pp. 115–158). Elsevier.
- Sageman, B. B., Meyers, S. R., & Arthur, M. A. (2006). Orbital time scale and new C-isotope record for Cenomanian-Turonian boundary stratotype. *Geology*, 34, 125–128.
- Said, R. (1962). *The Geology of Egypt* (p. 377). Elsevier.
- Said, R. (1990). *The Geology of Egypt* (p. 729). Elsevier.
- Salama, Y., & Abdel-Gawad, G. (2018). Early Cretaceous Oceanic Anoxic Events in Rudist-Bearing Succession, North Egypt. In Boughdiri, M., Bádenas, B., Selden, P., Jaillard, E., Bengtson, P., & Granier, B. (Eds.), *Paleobiodiversity and Tectono-Sedimentary Records in the Mediterranean Tethys and Related Eastern Areas. Proceedings of the 1st Springer Conference of the Arabian Journal of Geosciences (CAJG-1)* (pp. 183–185).
- Schlanger, S. O., & Cita, M. B. (1982). *Nature and Origin of Cretaceous Carbon-rich Facies* (p. 229). Academic Press.
- Schlanger, S. O., & Jenkyns, H. C. (1976). Cretaceous oceanic anoxic events: Causes and consequence. *Geologie En Mijnbouw*, 55(3–4), 179–184.
- Schouten, S., Van Kaam-Peters, H. M. E., Rijpstra, W. I. C., Schoell, M., & Sinninghe Damsté, J. S. (2000). Effects of an oceanic anoxic event on the stable carbon isotopic composition of Early Toarcian carbon. *American Journal of Science*, 300, 1–22.
- Shahin, A. (2007). Oxygen and carbon isotopes and foraminiferal biostratigraphy of the Cenomanian-Turonian succession in Gabal Nezzazat, southwestern Sinai. *Egypt. Revue De Paléobiologie, Genève*, 26, 359–379.
- Slack, J. F., Selby, D., & Dumoulin, J. A. (2015). Hydrothermal, biogenic, and seawater components in metalliferous Black Shales of the Brooks Range, Alaska: Syndimentary metal enrichment in a carbonate ramp setting. *Economic Geology*, 110, 653–675.
- Takahima, R., Nishi, H., Yamanaka, T., Hayashi, K., Waseda, A., Obuse, A., Tomosugi, T., Deguchi, N., & Mochizuki, S. (2010). High-resolution terrestrial carbon isotope and planktic foraminiferal records of the upper Cenomanian to the lower Campanian in the Northwest Pacific. *Earth and Planetary Science Letters*, 289(3–4), 570–582.
- Thiede, J., & van Andel, T. H. (1977). The palaeo- environment of anaerobic sediments in the late Mesozoic South Atlantic Ocean. *Earth and Planetary Science Letters*, 33, 301–309.
- Troger, U. (1984). The oil shale potential of Egypt. *Berliner Geowissenschaftliche Abhandlungen (a)*, 50, 375–380.
- Tsikos, H., Jenkyns, H. C., Walsworth-Bell, B., Petrizzo, M. R., Forster, A., Kolonic, S., Erba, E., Premoli Silva, I., Baas, M., Wagner, T., & Sinninghe Damsté, J. S. (2004). Carbon-isotope stratigraphy recorded by the Cenomanian-Turonian Oceanic Anoxic Event: Correlation and implications based on three key localities. *Journal of the Geological Society of London*, 161, 711–719.
- Voigt, S., Erbacher, J., Mutterlose, J., Weiss, W., Westerhold, T., Wiese, F., Wilmsen, M., & Wonik, T. (2008). The Cenomanian—Turonian of the Wunstorf section (north Germany): Global stratigraphic reference section and new orbital time scale for oceanic anoxic event 2. *Newsletters on Stratigraphy*, 43, 65–89.
- Voigt, S., Gale, A. S., & Voigt, T. (2006). Sea-level change, carbon cycling and palaeoclimate during the Late Cenomanian of northwest Europe; an integrated palaeoenvironmental analysis. *Cretaceous Research*, 27, 836–858.

- Wang, C. S., Hu, X. M., Jansa, L., Wan, X. Q., & Tao, R. (2001). The Cenomanian-Turonian anoxic event in southern Tibet. *Cretaceous Research*, 22(4), 481–490.
- Westermann, S., Stein, M., Matera, V., Fiet, N., Fleitmann, D., Adatte, T., & Föllmi, K. B. (2013). Rapid changes in the redox conditions of the western Tethys Ocean during the early Aptian oceanic anoxic event. *Geochimica Et Cosmochimica Acta*, 121, 467–486.
- Wignall, P. (1994). *Black Shales* (p. 127). Clarendon Press.
- Wignall, P. B., Hallam, A., Newton, R. J., Sha, J. G., Reeves, E., Mattioli, E., & Crowley, S. (2006). An eastern Tethyan (Tibetan) record of the Early Jurassic (Toarcian) mass extinction event. *Geobiology*, 4(3), 179–190.
- Wignall, P. B. & Twitchett, R. J. (2002). Extent, duration, and nature of the Permian-Triassic superanoxic event. In Koeberl, C. & Leod, K. G. (Eds.), *Catastrophic Events and Mass Extinctions: Impacts and beyond* (Vol. 356, pp. 395–413). Geological Society of America Special Paper.
- Xie, X., Li, M., Xu, J., Snowdon, L. R., & Volkman, J. K. (2020). Geochemical characterization and artificial thermal maturation of kerogen density fractions from the Eocene Huadian oil shale. *NE China. Organic Geochemistry*, 144, 103947.
- Young, S., Loukola-Ruskeeniemi, K., & Pratt, L. (2013). Reactions of hydrothermal solutions with organic matter in Palaeoproterozoic black shales at Talvivaara, Finland: Evidence from multiple sulfur isotopes. *Earth Planetary Science Letters*, 367, 1–14.
- Zhang, L., Zhang, X., Li, S., & Wang, Q. (2012). Comprehensive utilization of oil shale and prospect Analysis. *Energy Procedia*, 17, 39–43.
- Zhou, X., Jenkyns, H. C., Owens, J. D., Junium, C. K., Zheng, X. Y., Sageman, B. B., Hardisty, D. S., Lyons, T. W., Ridgwell, A., & Lu, Z. (2015). Upper ocean oxygenation dynamics from I/Ca ratios during the Cenomanian-Turonian OAE 2. *Paleoceanography*, 30, 510–526.
- Zhuravlev, A. Y., & Wood, R. A. (1996). Anoxia as the cause of the mid-Early Cambrian (Botomian) extinction event. *Geology*, 24, 311–314.
- Zobaa, M., Oboh-Ikuenobe, F., & Ibrahim, M. (2011). The Cenomanian/Turonian oceanic anoxic event in the Razzak Field, north Western Desert, Egypt: Source rock potential and paleoenvironmental association. *Marine and Petroleum Geology*, 28, 1475–1482.



Tarek Anan is a sedimentologist who has spent the majority of his academic career at the Geology Department, Faculty of Science, Mansoura University (Egypt). He graduated from Mansoura University with B.Sc (1999) and M.Sc degrees (2005), and Ph.D (2011) in sedimentary rocks and sequence stratigraphy

(joint supervision between Mansoura University and Western Michigan University, USA). His research interests include the sedimentology, stratigraphy and sequence stratigraphy of mixed carbonate-siliciclastic and carbonate depositional systems. His work focuses on the determination of depositional environments, reconstructing depositional models, diagenetic alterations of carbonate rocks, and the sedimentological history of carbonate rocks in terms of sequence stratigraphy. Recently, he has been focusing on the determination of oceanic anoxic events and global warming events using a combination of sedimentologic and geochemical approaches.



Adam El-Shahat was an emeritus professor at Mansoura University (Egypt), and previously Head of the Geology Department. As a sedimentologist, he spent much of his academic career at the Geology Department, Faculty of Science, Mansoura University, as well as five years at Constantine University (Algeria). He earned an M.Sc (1969) degree from Ain Shams University (Egypt) and a Ph.D (1977) from Southampton University (England). His research interests focused on carbonate sedimentology, diagenesis, geochemistry, and depositional environments. Recently, besides some geophysical tools, he focused on archaeology using his vast experience in sedimentology and geology as well. Sadly, Prof. El-Shahat passed away in 2021 during the COVID pandemic.



The Evolution of Vegetation Through the Cretaceous of Egypt

Clément Coiffard and Haytham El Atfy 

Abstract

This work summarizes the results of previous investigations on the plant fossil remains since the last century within the Egyptian strata, exclusively from the Cretaceous. Most of these data are often dispersed across many poorly accessible sources or not written in English. Cretaceous floras of Egypt are known from different localities mainly in the Western Desert, as well as small localities in southern Egypt and the Eastern Desert. The plant-bearing successions were deposited mostly in fluvial and shallow marine settings. The oldest floras from the Aptian Abu Ballas (Kilf Kebir) Formation are dominated by gymnosperms and free-sporing plants. Starting from the Albian-early Cenomanian of the Sabaya Formation, followed by the Bahariya Formation (early Cenomanian), the Timsah Formation (Coniacian-Santonian), and ending with the youngest assemblage of the Campanian Mut Formation, turned into angiosperm-dominated communities. These assemblages are mostly well preserved and comprise diverse lineages of macroflora, as well as palynoflora. Our work focussed not only on previous records, but also on localizing many curated specimens while enhancing the available data on their palaeoecology and palaeoenvironment.

Keywords

Plant fossil remains • Cretaceous floras • Abu Ballas Formation • Palynoflora • Palaeoecology

1 Introduction

Although there is an emerging consensus on the global climate patterns during the Cretaceous, details about the climate in North Africa, including Egypt, are currently poorly resolved and estimates for terrestrial climate remain incomplete. A careful appraisal of the previous contributions focussed on megaflores and palynology within this time window in Egypt was essential and showed that many issues concerning the climate and vegetation remain equivocal. This motivated us to carry out this study as a step in a trial to deduce and ultimately provide a clear understanding of the vegetation and climate changes during the Cretaceous of Egypt.

The Cretaceous strata host the richest fossil flora in Egypt, not only macroflora but also palynomorphs. The recorded floral assemblages from the Cretaceous in Egypt are generally well preserved and encompass diverse groups of macrofloral as well as microfloral algae, spores, and pollen. They are known from different localities mainly in the Western Desert, as well as a few localities in southern Egypt and the Eastern Desert (Fig. 1). As previously outlined by the recent appraisal of El-Saadawi et al. (2020), the Cretaceous strata host the most diverse palaeoflora in Egypt, not only macroflora but also palynomorphs. Most of these assemblages were described in poorly accessible sources or even written in non-English languages, this motivated the authors to undertake an overview that will certainly be valuable for palaeobotanists working on the Cretaceous all over the world. The main aim of this work is not only to review previous records, but also to localize many curated specimens as well as introduce more data about their

C. Coiffard (✉)

Structural and Functional Plant Diversity Group, Institute of Biology, Freie Universität Berlin, 14195 Berlin, Germany
e-mail: ccoiffard@zedat.fu-berlin.de; clement.coiffard@berlin.de

H. El Atfy

Institut für Geowissenschaften, Eberhard Karls Universität Tübingen, 72076 Tübingen, Germany

Geology Department, Faculty of Science, Mansoura University, Mansoura, 35516, Egypt

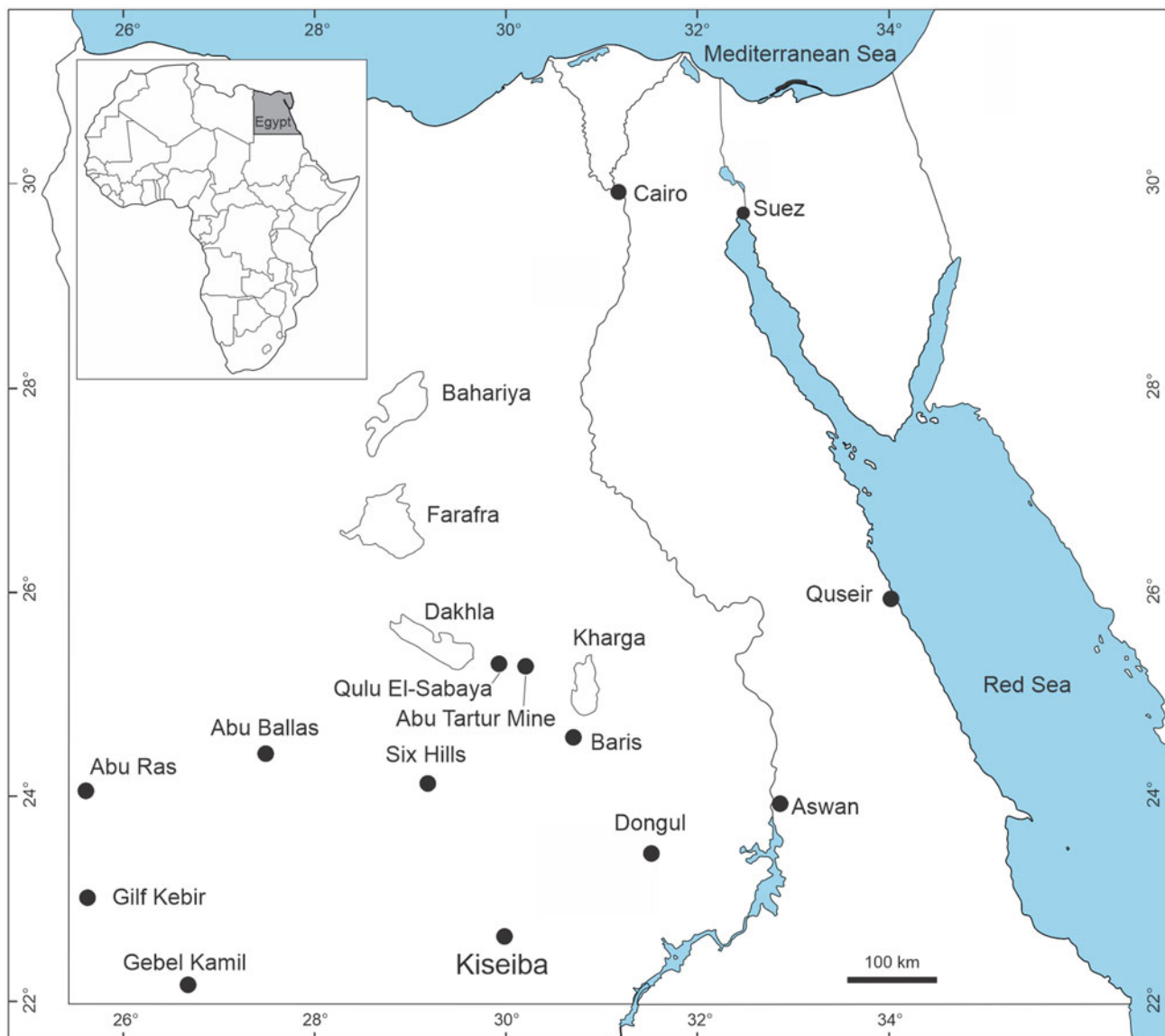


Fig. 1 Location map of Egypt showing the plant-bearing sites

palaeoecology and palaeoenvironment. This will be carried out through descriptions of plant megafossils together with palynomorph taxa from different spatial and temporal Cretaceous windows in Egypt (Fig. 2).

2 Abu Ballas Floras and Its Allies

The Abu Ballas Formation (Barthel & Böttcher, 1978) is synonymous to the *Lingula* Shale of Klitzsch (1978). At its type section at Abu Ballas Scarp in southern Egypt, it is made of a highly fossiliferous 44-m thick silty shale, which includes *Lingula* sp. and many others of invertebrates, including lamellibranchiata, gastropoda, echinoidea, brachiopoda, arthropods, as well as vertebrate remains

(Böttcher, 1982). Based on previous fossil content as well as abundant plant remains and palynomorphs, the Abu Ballas Formation has been dated as Aptian (Klitzsch & Hermina, 1989).

To the best of our knowledge, the oldest-known Cretaceous megafloral assemblages from Egypt come from the Gifl Kebir and the Abu Ballas Formations. Both are partly lateral equivalents and hence will be considered together to avoid stratigraphic inconsistency around the Gifl Kebir Formation. However, a few assemblages dated as Jurassic-Early Cretaceous were previously described and discussed earlier, see El-Saadawi et al. (2020).

Fossil leaves from the so-called Gifl Kebir Formation (pre-Aptian) were first mentioned by Lejal-Nicol (1981a) from the Akaba area, further assemblages are also



Fig. 2 Correlation chart of the Cretaceous rock units (surface-exposed) in Egypt, compiled after Klitzsch and Hermina (1989). Age of the Cretaceous stages follow Gale et al. (2020)

recognized in Klitzsch and Lejal-Nicol (1984), Klitzsch and Wycisk (1987), and Lejal-Nicol (1987). These assemblages are dominated by the fern taxon *Weichselia reticulata* (Stokes and Webb) Fontaine (Fig. 3e), accompanied by another fern determined as *Phlebopteris* Brongniart (Fig. 3f), less frequent remains of conifers (*Pagiophyllum*, *Frenelopsis*), and other gymnosperms (*Pterophyllum*, *Podozamites*, and *Ginkgoites*) and the fern *Cladophlebis*. Lejal-Nicol (1981a, 1987) identified most of the recorded taxa to the species level but one must keep in mind that these fossils are imprints in sandstones, which usually lack detailed anatomical features of the gross morphology so that even a generic identification can be contentious, such as the case for *Frenelopsis*.

Secondly, fossil leaves from the Abu Ballas Formation (Aptian) were first mentioned by Barthel and Böttcher (1978) from various localities in south Western Desert. In contrast to the Gilf Kebir assemblages, these fossils come from fine-grained sediments (silts and clays). *W. reticulata* (Fig. 3d) is also frequent in these assemblages, as well as *Phlebopteris* (Fig. 3a) (Barthel & Böttcher, 1978). Nevertheless, two assemblages display aquatic plants of possible angiospermous affinities. The first and best-known assemblage comes from coastal sediments (Lejal-Nicol, 1981b) and include *Klitzschophyllites aegyptiacum* Lejal-Nicol (Fig. 3b), first determined as *Hausmannia* in Barthel and Böttcher (1978), as well as *W. reticulata*, *Leguminocarpon abuballense* Lejal-Nicol (a possible gnetalean), and other Gymnosperms (Lejal-Nicol, 1981b). The second assemblage, coming from an oxbow lake deposit, was described by Böttcher (1982) and contains *W. reticulata*, *Phlebopteris* sp. and a single tiny, peltate leaf (Fig. 3c), similar to *Plouffolia* (Sender et al., 2010).

On the western side of the Gulf of Suez, El-Saadawi and Kedves (1991) described a presumably Lower Cretaceous flora containing, among others, ferns, *Otozamites*, and *Araucaria*. The persistent occurrence of *W. reticulata*, a xeromorphic fern, in most of the assemblages suggest a rather dry climate for the period. A palynological investigation carried out by Aboul Ela et al. (1989) did not offer a detailed age dating for such an Early Cretaceous assemblage and did not exclude Jurassic-Early Cretaceous age.

The flora of Gebel Dirra from the Sudan (Edwards, 1926; Watson, 1983; Schrank, 1999) is very similar to the Gilf Kebir Formation assemblages, containing *W. reticulata*, *Frenelopsis silfloana*, *Pseudofrenelopsis parceramosa*, and *Cladophlebis* sp. Similarly, the Crato flora of the Aptian age (Coiffard et al., 2019 and references therein) is also alike to both of the Gilf Kebir and Abu Ballas assemblages, displaying *Klitzschophyllites*, *Frenelopsis*, and various gnetophytes with a physiognomy similar to *Podozamites*. Nevertheless, it lacks *W. reticulata* and pinnate gymnosperm foliage (e.g. *Pterophyllum*) and is also characterised by the

occurrence of various angiosperms. This difference can be attributed to taphonomy, as well as facies control or climate.

Palynological results from the Dakhla Basin (Western Desert) reveal that the transition from the Barremian (to early Aptian?) non-marine Six Hills Formation to the overlying Aptian shallow marine Abu Ballas Formation is characterised by a rise in the abundance of the early angiosperm palynomorphs from 3 to 4% in the Six Hills to about 30% in the Abu Ballas Formation. According to Schrank (1982, 1983), the most conspicuous angiosperm element in the Abu Ballas Formation is the pollen genus *Brenneripollis* (*Retimonocolpites peroreticulatus-reticulatus* group of Schrank, 1982). In addition to the co-occurrence of *Afropollis*, *Asteropollis*, *Clavatapollenites*, and *Retimonocolpites* (*Schrankipollis mawhoubensis* Schrank that provide reliable dating data for the Abu Ballas Formation, gymnosperms were also defined comprising xerophytic elements of *Ephedripites* and *Claspollis* that denote arid climate.

3 Sabaya Formation, the First Angiosperm-Dominated Assemblage

The Sabaya Formation (Barthel & Böttcher, 1978) was also known as the Desert Rose Bed (Klitzsch et al., 1979) of Albian to possibly early Cenomanian age (Kora et al., 1988). Its type area is the group of hills at Qulu El-Sabaya, south of Abu Tartur Plateau at the road between El Kharga and El Dakhla, where it overlies the Abu Ballas Formation and is overlain by the Plant Bed (Maghrabi Formation). It represents a lateral equivalent to Facies 1 of van Houten et al. (1984) and the basal part of the Nubia Sandstone in the central Eastern Desert (Ward & McDonald, 1979). However, Klitzsch (1987) restricted the Sabaya Formation to those sediments located south of Aswan to the area between Abu Simbel and Selima. Lithologically, the Sabaya Formation is composed of white, grey, yellowish brown and red, fine- to coarse-grained, occasionally conglomeratic sandstone. In its type locality, it comprises 60-m thick of fluvial sediments (Klitzsch & Hermina, 1989).

Fossil leaves from the Sabaya Formation were first revealed by Barthel and Böttcher (1978). This rock unit is marked by the appearance of the first angiosperm-dominated assemblages. Such an assemblage was collected at Plant Hill in channelled sandstones (number 161177-1 of the Technical University of Berlin 'TU' collection), a few metres above the base of the Sabaya Formation (Barthel & Böttcher, 1978). It comprises four angiosperm taxa (Böttcher, 1982; Klitzsch & Lejal-Nicol, 1984; Kahlert et al., 2009): (1) *Eucalyptophyllum sabayense* Kahlert, Rufflé, and Gregor, corresponding to the *Rogersia*-type and the *Ficophyllum*-type of former publications (Fig. 4a), (2) *Araliaephyllum*-type (Fig. 4c), (3) cinnamomoid-type (Fig. 4b), (4) *Vitiphyllum*-like (Fig. 4

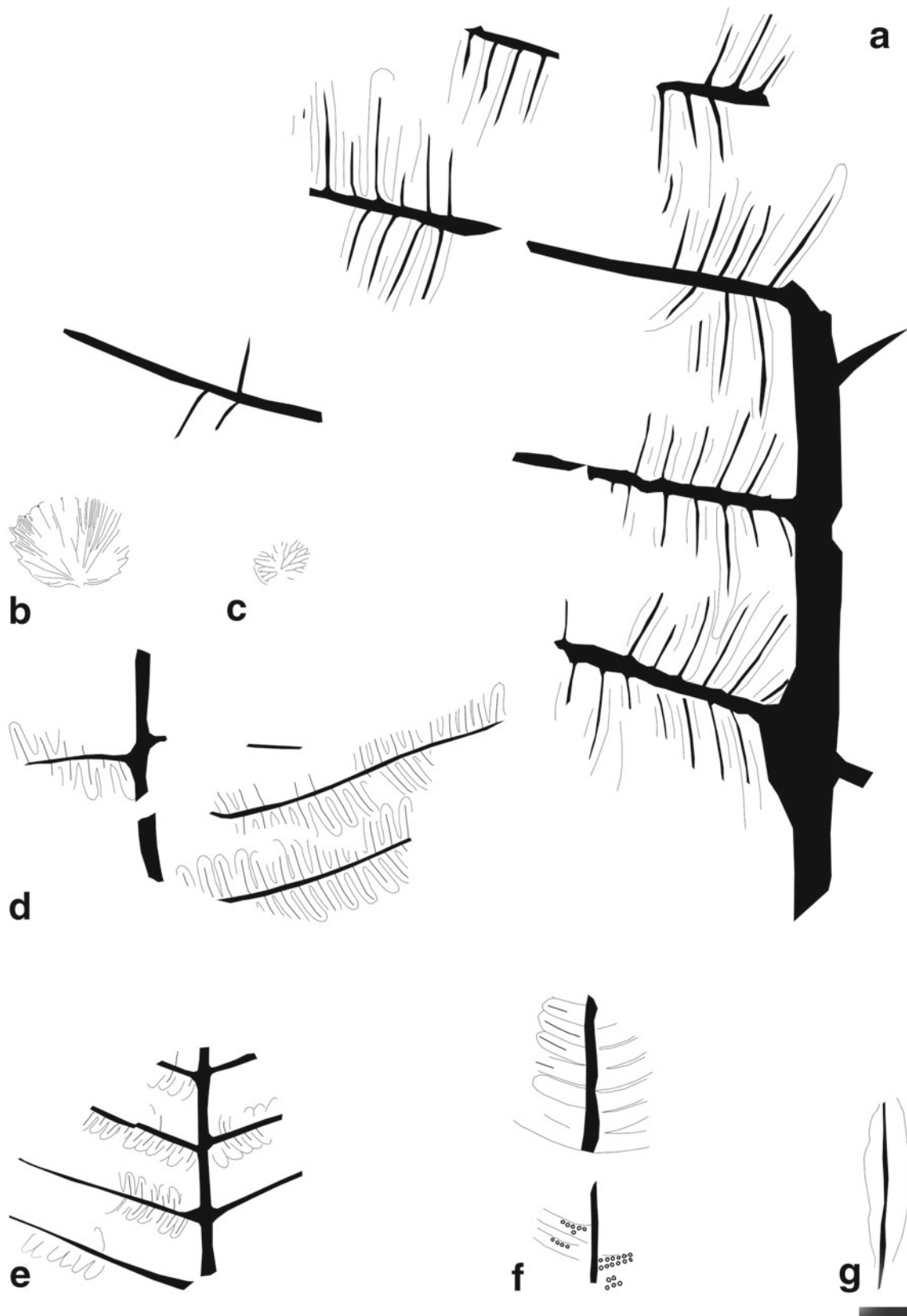


Fig. 3 Line drawing of leaves from the Abu Ballas (a–d) and Gilf Kebir (e–g) Formation. **a** *Phlebopteris* sp., **b** *Klitzschophyllites aegyptiacum* Lejal-Nicol, **c** peltate leaf, **d**, **e** *Weichselia reticulata* (Stokes and Webb) Fontaine, **f** *Phlebopteris* sp., **g** leaf identified as *Sagenopteris* sp. Scale bar is equal to 1 cm

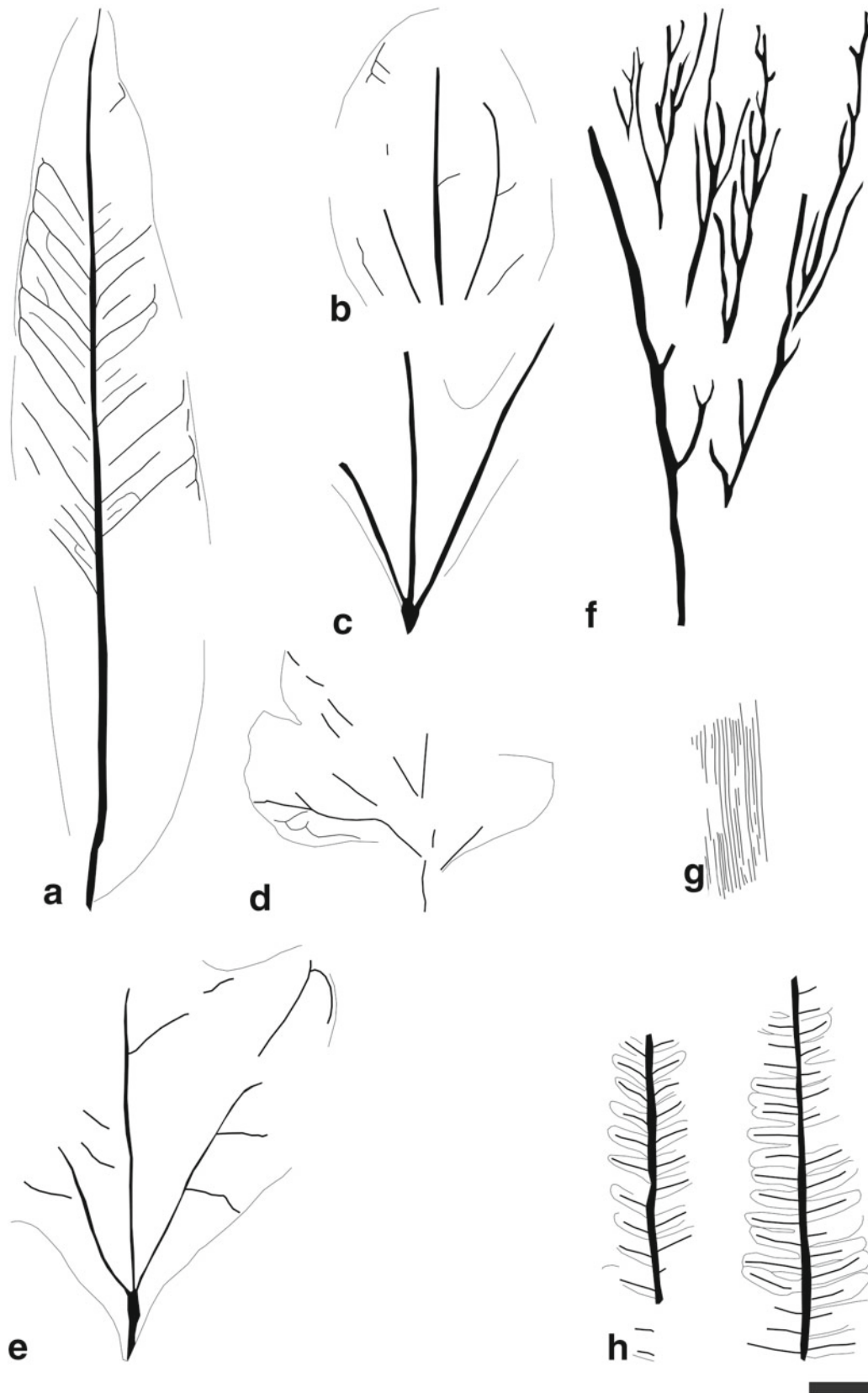


Fig. 4 Line drawing of leaves from the Sabaya Formation. **a** *Eucalyptophyllum sabayense* Kahlert, Rüffle and Gregor, **b** cinnamomoid-type, **c** *Araliaephyllum*-type, **d** *Vitiphyllum*-type, **e** *Araliaephyllum*-type, **f** *Frenelopsis* sp., **g** unidentified parallel-veined leaves, **h** *Weichselia reticulata* (Stokes and Webb) Fontaine. Scale bar is equal to 1 cm

d). All those leaves are micro- to notophyllous. Another assemblage (090279-1) embraces one *Araliaephyllum*-like leaf (Fig. 4e) and a *W. reticulata* pinna (Fig. 4h). In contrast, other assemblages from the same unit contain only ferns and gymnosperms such as those from 201077-7, located about 40 m above the base (Barthel & Böttcher, 1978). From this assemblage, Klitzsch and Lejal-Nicol (1984) identified *Phlebopteris* sp., *Frenelopsis* sp. (Fig. 4f), *Araucaria* sp., *Brachyphyllum* sp., and *W. reticulata* as well as unidentified parallel-veined leaves (Fig. 4g). Two further localities southward of the type area and on the Upper part of Gebel Kamil were mentioned by Klitzsch and Lejal-Nicol (1984), the first one containing *Paradoxopteris stroemeri* Hirmer and *Phlebopteris* sp. Brongniart and the second one *Frenelopsis* aff. *parceramosa* Fontaine and *F.* aff. *ramosissima* Fontaine (non-angiosperm, especially conifers poorly preserved).

The lack of accurate sedimentological description of the localities precludes further understanding of the distribution of angiosperms. It is however clear that at least two kinds of plant associations existed in a fluvial context during the Albian, one dominated by ferns and gymnosperms, similar to the Aptian assemblages and to the older vegetation, and one nearly exclusively dominated by angiosperms. Furthermore, Kora et al. (1988) outlined the occurrence of silicified wood and other badly preserved plant fragments within the Sabaya Formation in the Darb El Arbain area, Southern Egypt and northern Sudan. However, the lack of illustrations hinders a better discussion of the recovered plant assemblages.

To the authors' knowledge, no previous palynological contributions have focussed on the Sabaya Formation, which could be attributed to sampling bias as there are no enough surface sections or even subsurface wells targeting it. The megafloal assemblages of the Negev (Krassilov & Schrank, 2011) and Jordan (Abu Hamad et al., 2016) share some similarities to the assemblages of Egypt. The assemblages IQ2 from the Negev (Krassilov & Schrank, 2011) exhibit a mixture of ferns, gymnosperms and micro- to notophyllous angiosperms. Nevertheless, the Near-East assemblages are characterised by quite a common occurrence of *Sapindopsis* leaves, which presently remain unknown from Egypt. Furthermore, the other assemblages described from the Negev (Krassilov & Schrank, 2011) and Jordan (Hu & Taylor, 2014; Abu Hamad et al., 2016) come from fine-grained sediments. Despite these lithofacies differences, *W. reticulata* is common in both Egyptian and Near-Eastern assemblages.

4 Bahariya Formation and Its Equivalents (Angiosperms-Dominated Flora)

In the northern Western Desert, the Cenomanian deposits are named the Bahariya Formation after El Akkad and Issawi (1963). Its type section occupies the floor and scarps of the

oasis depression around Gebel Dist and has an exposed thickness of 170 m to more than 300 m underlying the El-Hefhuf Formation (Dominik, 1985). It is composed of sandstone, mudstone, and limestone, its upper part is richer in shale than the lower one. The sandstones and mudstones are tan, greenish grey, and glauconitic in parts, with many trace fossils. According to Dominik (1985), the Bahariya Formation was divided into two rock units: the lower Gebel Ghorabi Member, represented by fluvial sandstone. The upper Gebel Dist Member (estuarine-shallow marine), which is composed of intercalations of sandstone, siltstone, and claystones, that are partly glauconitic. It is strongly tide-influenced with some intercalations of lagoonal inputs. Some workers (e.g. Dominik, 1985) treated the overlying El Heiz Formation as a third member, which comprised calcareous or siliceous sandstones and claystones that characterize gradual regression of lagoonal and supratidal origin. Though, in this work, we consider it separately as El Heiz Formation, following the widely accepted nomenclature of El Akkad and Issawi (1963) and others. The Bahariya Formation is of early Cenomanian age, based on foraminifera (Barakat et al., 1974). The fossil content of the Bahariya Formation is highly diverse, including not only plant macrofossil, but also terrestrial aquatic such as lungfishes, turtles, crocodiles, and dinosaurs, plus marine vertebrate fauna such as sharks, plesiosaurs, and the sea serpent *Symoliophis* sp., besides lamellibranchiate, ammonites, and mangrove-dwelling crabs (e.g., Dominik, 1985; Werner, 1989; Smith et al., 2001; Schweitzer et al., 2003). Dominik (1985) concluded that the Bahariya Formation was deposited first under fluvial conditions, then under estuarine conditions and finally under lagoonal conditions based entirely on lithological and palaeontological evidence.

In addition to wood, the first record of plant megafossils in the Bahariya Formation is initiated by Seward (1935), followed by Stromer (1936) and Kräusel (1939) who described *Macclintockia cretacea* Heer (closely resembles a Nelumbonaceae), from Gebel Ghorabi as well as *W. reticulata* and *Nelumbites schweifurthii* Fritel (Kräusel) from Gebel El Dist.

Between 1980 and 1982, additional material was collected from the Bahariya area which was first mentioned by Dominik (1985) and then described in Lejal-Nicol and Dominik (1987, 1990). This material comprises mainly *W. reticulata* associated with *P. stroemeri* Hirmer as well as two angiosperms-dominated assemblages. Furthermore, the first angiosperm-dominated assemblage comes from the Bahariya Formation from Naqb El Farafra corresponding to fluvial sandstone channel deposits. This assemblage consists mostly of mesophyllous, simple, entire-margined leaves, identified by Lejal-Nicol and Dominik (1990) as various species of *Cornophyllum* (Fig. 5a), *Laurophyllum* (Fig. 5e), *Magnoliaephyllum* (Fig. 5b), *Rogersia* (Fig. 5d), and *Liriophyllum*

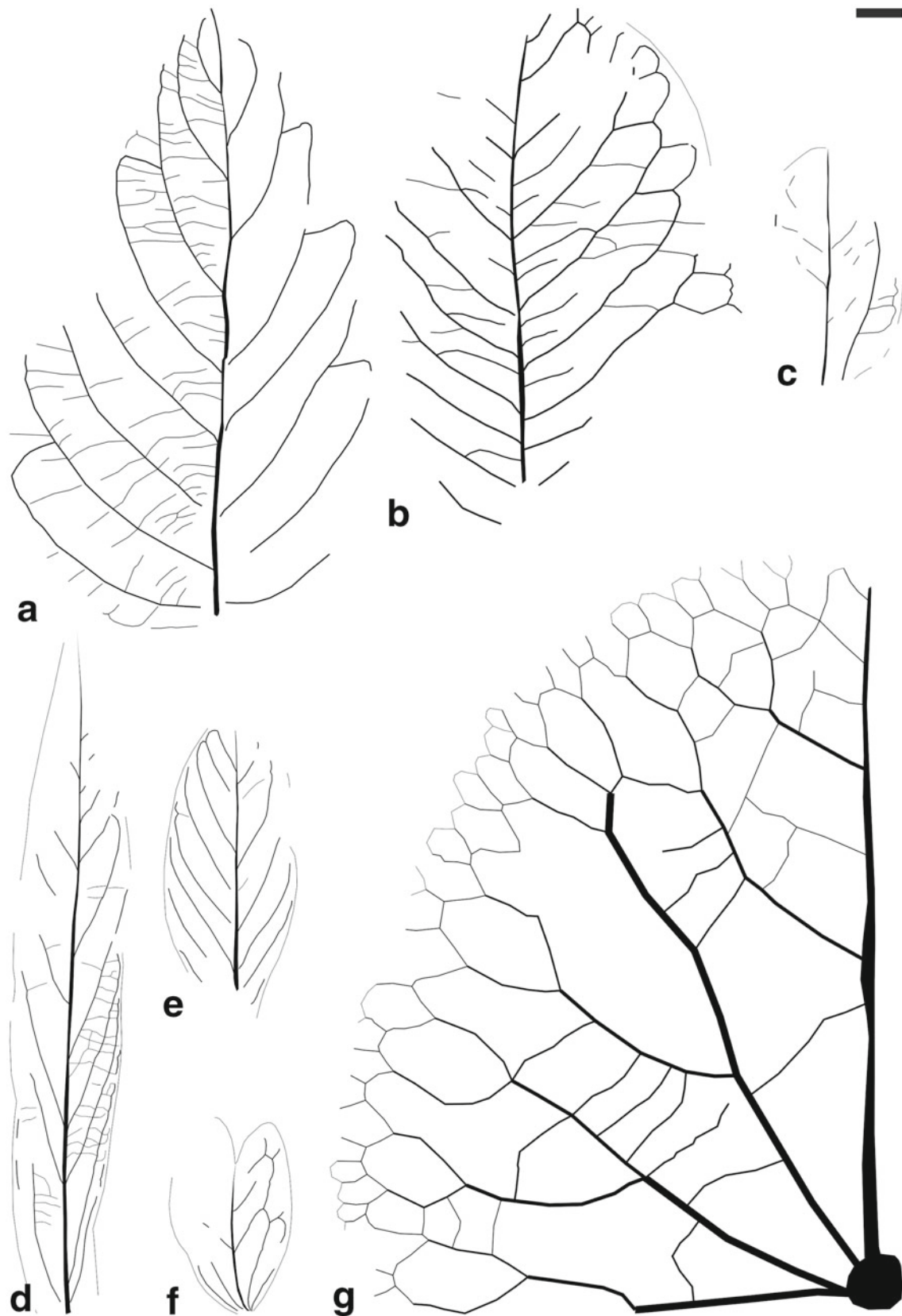


Fig. 5 Line drawing of leaves from the Bahariya Formation. **a** *Cornophyllum*, **b** *Magnoliaephyllum*, **c** cinnamomoid-type, **d** *Rogersia*, **e** *Laurophyllum*, **f** *Liriophyllum*, **g** *Nelumbites giganteum* Lejal-Nicol and Dominik. Scale bar is equal to 1 cm

(Fig. 5f), the latter being characterised by its emarginate apex. In addition to these land plants, this assemblage also contains *Nelumbites giganteum* Lejal-Nicol and Dominik, an aquatic plant with nymphaealean affinities (Fig. 5g).

Another angiosperm-dominated assemblage comes from the El Tibnia locality which represents swamp clay sediments. This assemblage contains terrestrial plants identified as a *Vitiphyllum* Fontaine by Lejal-Nicol (1990) and some cinnamomoid-type leaves (Fig. 5c), as well as the aquatics *N. schweifurthii* Fritel (Kräusel) and possibly *N. giganteum* Lejal-Nicol and Dominik and various monocot-like leaves (e.g. cf. *Typhaephyllum*). The *W. reticulata* specimens described by Lejal-Nicol and Dominik (1990) are embedded in grey siltstone deposits differing from both the sediment of Naqb El Farafra (ferruginous sandstones) and El Tibnia (brown claystones). Concerning the ecology of this species in the Bahariya Formation, it is interesting to note that Schweitzer et al. (2003) reported it from a mangrove palaeosol.

Later, Lyon et al. (2001), mentioned the occurrence of 30 morphotypes, of which 25 are angiosperms, while Darwish and Attia (2007), mentioned more than 62 morphotypes, unfortunately without detailed description and enough illustrations of these morphotypes.

Further south, the equivalent Maghrabi Formation (Fig. 2) yielded an angiosperm-dominated assemblage quite similar to the assemblages reported from the Bahariya Formation (Klitzsch et al., 1979; Klitzsch & Lejal-Nicol, 1984).

Outside of Egypt, the flora of the Umm Badda Member of the Omdurman Formation (Sudan) is quite similar to the Bahariya assemblage, being dominated by angiosperms of mesophyllous size (Hassan, 1973), but further taxonomic revision is required for a better understanding of their affinities. In contrast to the assemblages of Egypt and the Sudan, the assemblages from Lebanon and Morocco are dominated by ferns and gymnosperms (Krassilov & Bacchia, 2000, 2013). Angiosperms of these assemblages are of nano- to microphyllous size. This suggests the existence of different vegetation belts between the tropics, the Egyptian and Sudanese assemblages being close to the paleoequator and wetter, while Moroccan and Jordanian assemblages being closer to the tropics and dryer.

According to El Atfy et al. (2023), palynological assemblages from the Bahariya Formation, mainly from subsurface materials, are diverse and mostly dominated by ferns, conifers products and angiosperm that represented mostly by *Afropollis* (Winteraceae; Schrank, 2001). Ferns are mainly represented by Filicopsida; Cyathaceae (*Cyathidites*), Lygodiaceae (*Triplanosporites*), Matoniaceae (*Cibotiumspora jurienensis* (Balme) Filatoff, *Concavisporites*, *Trilobosporites*, *Matonisporites*), Anemiaceae (*Cicatricosisporites*), and Incertae Sedis (*Leptolepidites*), aquatic ferns include Marsileaceae (*Crybelosporites*

pannuceus Srivastava, *Gabonisporis vigourouxii* Boltenhagen), and Salviniaceae (*Ariadnaesporites*). Non-gnetalaeen gymnosperms comprised Erdtmanitheceae (*Eucommiidites*), Cycadales, Ginkgoales, and Bennettitales (*Cycadospites*, *Exesipollenites*, *Monosulcites*), and Conifers. Among the conifers, representatives of the Cheirolepidiaceae (*Classopollis*) are by far the most abundant, followed by Araucariaceae (including *Araucariacites* and *Balmeiopsis*). Gnetalaeen gymnosperms are represented by Elaterate Complex (*Elaterocolites*, *Elateroplicites*, *Elaterosporites*, *Senegalosporites*, *Sofrepites*) and Ephedroides (*Ephedripites*, *Equisetosporites*, *Steevesipollenites*). Angiosperms, except for *Afropollis*, are relatively infrequent but show a progressive increase in diversity comprising eudicots, monocots, and dicots. However, the most numerous elements are winteraceous angiosperms (*Afropollis*). This contradicts the macroflora yield and could be attributed to sampling or even spatial or even temporal differences among the surface exposures and subsurface counterparts.

Microfloral elements described from the north Western Desert were initially described from the Gebel Dist, Bahariya Oasis and yielded early Cenomanian microflora (Soliman & Sultan, 1976), however, a late Cenomanian age may be assumed for this likely angiosperm-dominated microflora that contains most advanced angiosperms triporates and perhaps also a periporate pollen related to *Cretacaeiporites* (Pl. 1–6 therein). Within the subsurface, previous microfloral records (see review in El Atfy et al., 2023), did not exhibit marked spatial differences among different boreholes, except for variable distributions amid the recorded palynomorphs. Of special importance here is to highlight peaks of *Afropollis jardinus* (Brenner) Doyle, Jardiné and Doerenkamp (El Atfy et al., 2023) have been repeatedly recognized in Egypt (e.g. 11–64%: El-Beialy, 1994; 31–60%: Schrank & Ibrahim, 1995; 24–62%: Deaf et al., 2014). This *A. jardinus* peak has been interpreted by Schrank (2001) to be controlled by local humid conditions, as the parent plant (alleged Winteraceae) is thought to favour humid and coastal plains.

The Albian-Cenomanian (Maghrabi Formation) microflora of the Dakhla Oasis (Schrank & Mahmoud, 1998) is characterized by ferns (including Salviniaceae), dominant *Araucariacites* and angiosperms, namely tricolpates (*Foveotricolpites*), tetracolpates (*Tetracolpites*), and tricolporates (*Tricolporopollenites*, *Nyssapollenites*). It is possible that the studied material from the Kharga 1 borehole, at 28 and 12 m (Saad & Ghazaly, 1976), represent Maghrabi equivalents younger than Albian to early Cenomanian. The presence of a triporate (*Proteacidites* Type A Saad & Ghazaly, 1976; zone III) would be consistent with age not older than late Cenomanian. However, similarity with the Maghrabi palynofloras of Schrank and Mahmoud (1998), e.g. presence of *C. pannuceus* Srivastava, combined with the

scarcity of triporates and absence of typical Coniacian-Santonian markers probably favour an age older than Santonian-Campanian, the age originally proposed for zone III by Saad and Ghazaly (1976), which is also comparable with middle assemblage zone of Abdel Mohsen (1992) from the Bulaq 15 well, south of Kharga Oasis. However, Mahmoud and Essa (2007) studied the palynomorph composition from three samples (El Nom borehole, near Gebel Abraç area, SE Aswan), belonging to the so-called Timsah Formation, which is considered by the authors as an equivalent to the Maghrabi Formation, though we think it is younger. Their results document the presence of 48% fungal spores, 25% angiosperms, 14% gymnosperms, 11% spores, and 2% freshwater algae. Pteridophytic spores consist almost exclusively of *Deltoidospora* and *Triplanosporites*. *C. pannuceus* Srivastava (spore of a marsilean water fern), *Balmeisporites*, and *Ariadnaesporites* (salvinealean spores) were also observed, as well as a single occurrence of *Cicatricosisporites*, in addition to foveolate, echinate and poorly preserved verrucate spores. Angiosperms comprise mainly *Foveotricolpites gigantoreticulatus* Schrank, small monocolpates, and tricolpates, however, *Rousea delicipollis* Srivastava, reticulate tricolpates are rare. Gymnosperms are not as common as angiosperms.

From a palynological context, the most significant floral criterion of the Maghrabi Formation is the absence of elaterrates, which was also the case for a few microfloral assemblages recovered from the Bahariya Formation (see El Atfy, 2021 and references therein). This could correspond to the megafloras, maybe a kind of wet phase.

5 Timsah Formation Floral Assemblage

East of Aswan, at Wadi Abu Aggag, the sandstone section on top of the basement complex includes rich iron beds, which was classified by Attia (1955) into three units: an upper group above the iron beds, which are included in his middle group and a lower group below the iron beds (Issawi et al., 2009). Later, El-Naggar (1970) named these groups in a descending order Um Barmil, Timsah, and Abu Aggag Formation. The Timsah Formation (El-Naggar, 1970), which is equivalent to Middle Group of Attia (1955), grey and red shale and thin sandstones of Ward and McDonald (1979) and to Facies 2 of van Houten et al. (1984), has been described from its type section in Gebel Timsah area southeast of Aswan (Klitzsch & Hermina, 1989). Lithologically, it is made up of near-shore marine to deltaic silt and fine-grained sandstone with thick shale intercalations. The Timsah Formation is underlain by the Abu Aggag Formation and disconformably overlain by the fluvial Umm Barmil Formation (Klitzsch & Hermina, 1989).

Fossil leaves from the Timsah Formation were first mentioned by Barthoux and Fritel (1925), who identified *Weichselia* sp., *Cycadomyelon fourtaui* Fritel (a putative cycadeoid wood), and several angiosperms. These fossils come from a ferruginous sandstone lens near Aswan.

Among the angiosperms, Barthoux and Fritel (1925) described four monocots. Although *Zosterites* sp., *Arundinites* aff. *groenlandica* Heer, and *Rhizocaulon* sp. display a clear parallel venation, what these authors consider a palm is from material that is so poorly preserved that it remains highly contentious. Concerning the dicot leaves, the fragmentary nature of some specimens raises doubts about their identification and only six morphotype can be distinguished (i.e. *Laurus cailliaudi* Fritel, *Cinnamomum humei* Fritel, *Magnolia barthouxi* Fritel, *Magnolia obtusata* Heer, *Nelumbium schweinfurthi* Fritel, and *Phyllites rozierii* Fritel). In terms of physiognomy, these leaves are mostly notophyllous, thus they are smaller than the leaves from the Bahariya Formation.

In 1987, Germann et al. recognized another assemblage from silt- and claystones overlying the horizon B of the Timsah Formation, unfortunately without mentioning any collection number. Following Lejal-Nicol identifications mentioned in Germann et al. (1987), this assemblage should contain *Celastrophyllum latifolium* Fontaine, cf. *Ficophyllum* sp., *Magnoliaephyllum bahariyense* Lejal-Nicol and Dominik, *Paulliniacarpon* n. gen. (sic., a nomen nudum), *Rogersia* aff. *angustifolia* Fontaine, *Rogersia aegyptiaca* n. sp. (sic.), *Tiliaephyllum* sp., and *Ulmocarpon* sp.

Assemblages from the Negev and the Sudan share some similarities to the Egyptian Timsah assemblages and even more similarities between them, probably due to the higher number of specimens. *Dewalquea*-like leaves are found in both the Negev (Krassilov et al., 2005) and the Sudan (Schrank & Ruffle, 2003) and are also found in the TU collection (Fig. 6b). Furthermore, their leaflets fit with the venation and obovate shape of *M. obtusata* Heer described by Barthoux and Fritel. *Celtidophyllum* sp. from Gebel Mudaha (Schrank & Ruffle, 2003) is also similar to *P. rozierii* Fritel while *L. cailliaudi* Fritel was also identified there. The specimen B1378 identified as *Ulmiphyllum* cf. *brookense* displays a tertiary venation similar to the specimens shown in Fig. 6a, especially the epimedial tertiaries running parallel to the secondaries. Some leaves of *Eocercidiphyllites glandulosus* Krassilov from the Negev are similar to *C. humei* Fritel. Surprisingly, such taxa are probably the only linkage to northern mid-latitude assemblages since they also occur in Europe (e.g. Halamski & Kvaček, 2016). This is also noticed with the occurrence, despite rarity of Normapolles pollen (Fig. 8r) from the equivalent subsurface rock units (Abu Roash Formation) within the north Western Desert, however, no other

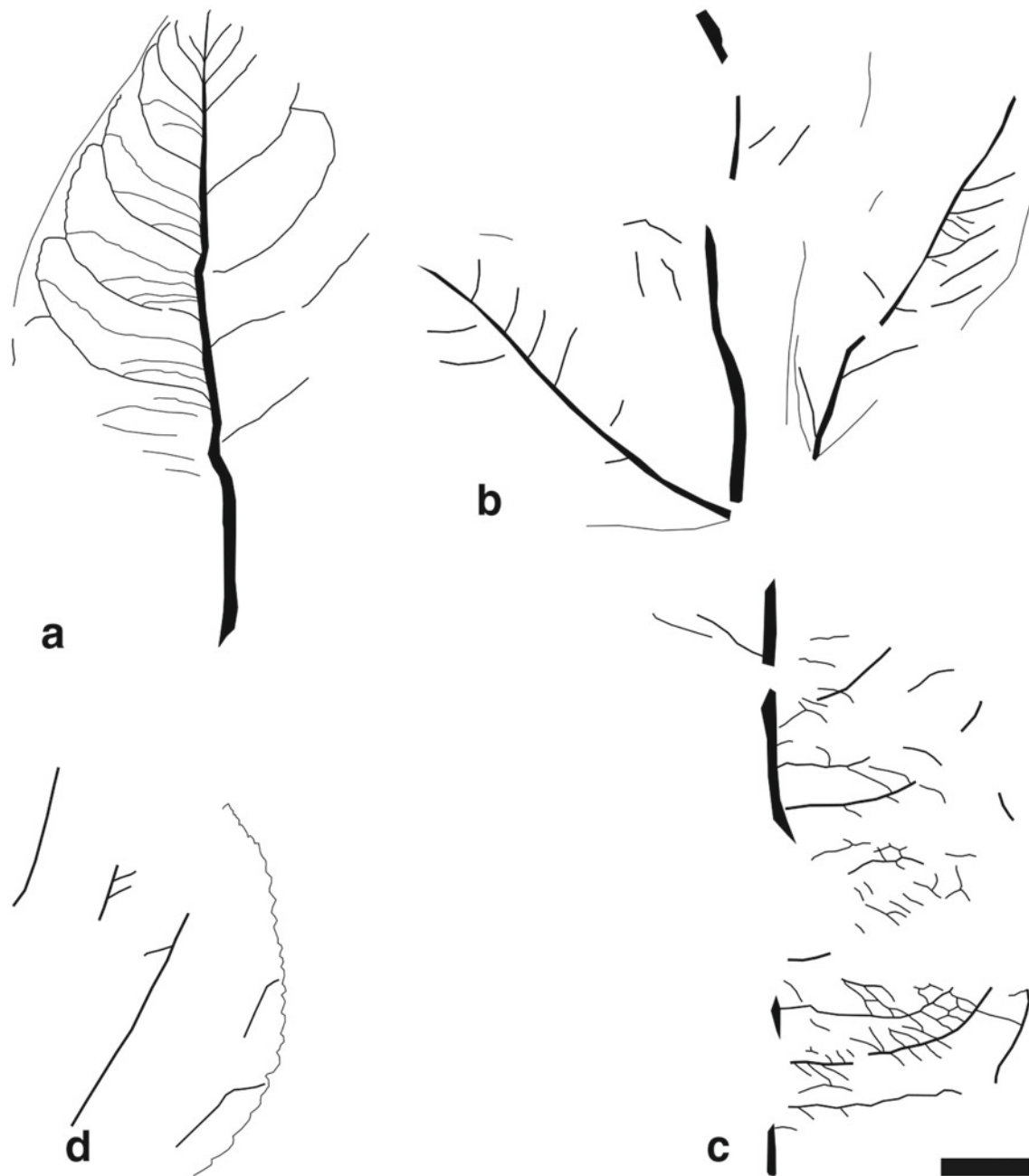


Fig. 6 Line drawing of leaves from the Timsah Formation. **a** Unidentified leaf, **b** *Dewalquea*-like leaf, **c** unidentified leaf, **d** unidentified leaf. Scale bar is equal to 1 cm

published information is available about the occurrence of this pollen group in southern Egypt.

In contrast to older floras, the vegetation seems to have been rather homogeneous between the Sudan and the Levant. The physiognomy of these assemblages has been compared to tropical seasonally dry climate vegetation (Schrank & Rüffle, 2003) or to Mediterranean vegetation (Krassilov et al., 2005).

Palynologically, Sultan (1985) described microflora of the Timsah Formation (described there as Nubia Sandstone). The palynological content, especially from El Khalsab section, consists of the diagnostic pollen *Droseridites senonicus* Jardiné and Magloire (Fig. 8q), a taxon which occupied 8% of the total yield and very characteristic within the Coniacian-Santonian (El Atfy, 2021 and references therein). In addition, relatively common ephedroid pollen (13%),

20% *Sphaeripollenites* (Cheirolepidiaceae?) that represent xerophilic element, 3% pteridophytic spores and the most dominant angiosperm which engrossed 39% of the total palynomorph recovery. The palynological and leaf physiognomic characteristics, together speak for a seasonally dry paleoclimate.

6 Mut Formation Flora and Its Counterparts

The Mut Formation (Barthel & Hermann-Degeen, 1981), Quseir Formation (Youssef, 1957), and Variegated Shales (Said, 1962) have been used for the same stratigraphic sequence in the surroundings of Dakhla and Kahrqa Oases (Klitzsch & Hermina, 1989). According to Barthel and Hermann-Degeen (1981), the Mut Formation reference area at the lowest scarps along the road from Mut to El-Rashda comprised vermilion to brick-red clays. This colour may vary to grey and green near leaching horizons, near its top but also within it, sandstones may occur rather frequently. These strata attain more than 150 m thick (Klitzsch & Schandelmeier, 1990). The depositional environment of the Mut Formation was possibly fluvial to brackish and restricted marine, as is indicated by the presence of glauconite in variegated shales and sands below El-Hindaw Formation in the Ammonite I well (Barthel & Hermann-Degeen, 1981).

The fossil flora from the Mut Formation (= Quseir Variegated Shale) was first described by Kahlert et al. (2009). It contains a highly diverse assemblage with 25 angiosperm taxa, a high proportion of monocots (seven taxa) and rare ferns (3 taxa, not mentioned in the original publication). A partial revision of the monocots of these assemblages revealed the occurrence of seven Alismatales taxa (e.g. *Cobbania pharao* Coiffard and B.A.R. Mohr; Fig. 7a), including two terrestrial Araceae with affinities with modern tropical rainforest taxa. It further highlighted the need of a robust revision of this collection since Kahlert et al. (2009) only mentioned two Alismatales. In addition to the Alismatales, this assemblage is characterized by the common occurrence of *Nelumbo* (Fig. 7b), *Salvinia* (Fig. 7c), and mesophyllous, entire-margined leaves referred as *Ficus* (Fig. 7f) or *Dipterocarpophyllum* (Fig. 7d), as well as other monocots (Fig. 7e, g). The latter taxon was first defined from Egypt by Seward (1935) from the Nubia Sandstone from Wadi Zeraib and comprised *Dipterocarpophyllum humei* Seward and *Dipterocarpophyllum zeraibense* Seward, beside other two angiosperms of *Dicotylophyllum balli* Seward and *Dicotylophyllum egyptiacum* Seward. These leaves are mostly notophyllous and, interestingly, the last taxa are trifoliolate and display similarities with the *Dewalquea*-like taxa. Furthermore, *Dipterocarpophyllum* has been

also described by from the Kiseiba Formation (southern Egypt) and from Jebel Abyad (North Sudan) by Lejal-Nicol (1987). Other assemblages from the Mut Formation come from Qena (Schränk, 1992). It shares with Baris the occurrence of *Salvinia* and simple, parallel-veined monocots (*Typhaephyllum*).

The Kiseiba Formation which is, in part, a local equivalent of the Mut Formation (Fig. 2) produced two assemblages near Bir Kiseiba. The first assemblage (Lejal-Nicol, 1987) displays *Nelumbo*, and a leaf corresponding to *Ficus celtidifolia* Berry from Baris. In contrast to the above-mentioned assemblage which preserved in claystones, the second assemblage from Bir Kiseiba (Lejal-Nicol, 1987) comes from ferruginous sandstones. According to Lejal-Nicol (1987), it contains *Credneria* sp., *Ficophyllum* sp., *Cassiaephyllum aegyptiacum* Lejal-Nicol, and cf. *Rogersia angustifolia* Fontaine, without evidence of aquatics.

Outside Egypt, Campanian–Maastrichtian fossil assemblages are restricted to the Sudan, probably due to the transgression which covered the Levant of North Africa. In Gebel Abyad, the Kababish Formation produced an assemblage (Barazi, 1985; Lejal-Nicol, 1987; Coiffard & Mohr, 2015) from siltstones which contains among other *Lejalia* and *Typhaephyllum*-like leaves also found in Baris. Three assemblages were also collected in the Nukeila-Bir Atrun area (Klitzsch & Wycisk, 1987; Lejal-Nicol, 1987). One assemblage comes from claystones comprising *Nelumbo*, *Salvinia*, and *Typhaephyllum*-like leaves as well as dicot leaves, and is similar to the assemblage from Baris. Two other assemblages come from sandstones and display mesophyllous, entire-margined leaves reminding the second assemblage from Bir Kiseiba.

Considered together, the Campanian assemblages from North-eastern Africa fall in two groups: the assemblages from claystones, corresponding to paludal-lacustrine palaeoenvironments, display a mix of dicot leaves with a high proportion of monocots and the occurrence of *Nelumbo* and *Salvinia*. The second assemblages from sandstones, corresponding to fluvial conditions, consist exclusively of dicot leaves, mostly mesophyllous and entire margined.

Palynological data from the equivalent Quseir Formation also point to a flora dominated by angiosperms, although pteridophytes and gymnosperms are abundant, but not diverse (Mahmoud, 2003). Based on the composition and diversity of the palynoflora, as well as data from palynofacies analysis, Mahmoud (2003) interpreted the source habitats of the palynomorphs as a fluvio-lacustrine landscape with abundant moist and aquatic habitats and subordinately drier habitats (i.e. with *Araucariacites*, ephedroids, and other gymnosperms) in the hinterland, in which the plants grew under a warm and humid, tropical to subtropical, palaeoclimate.

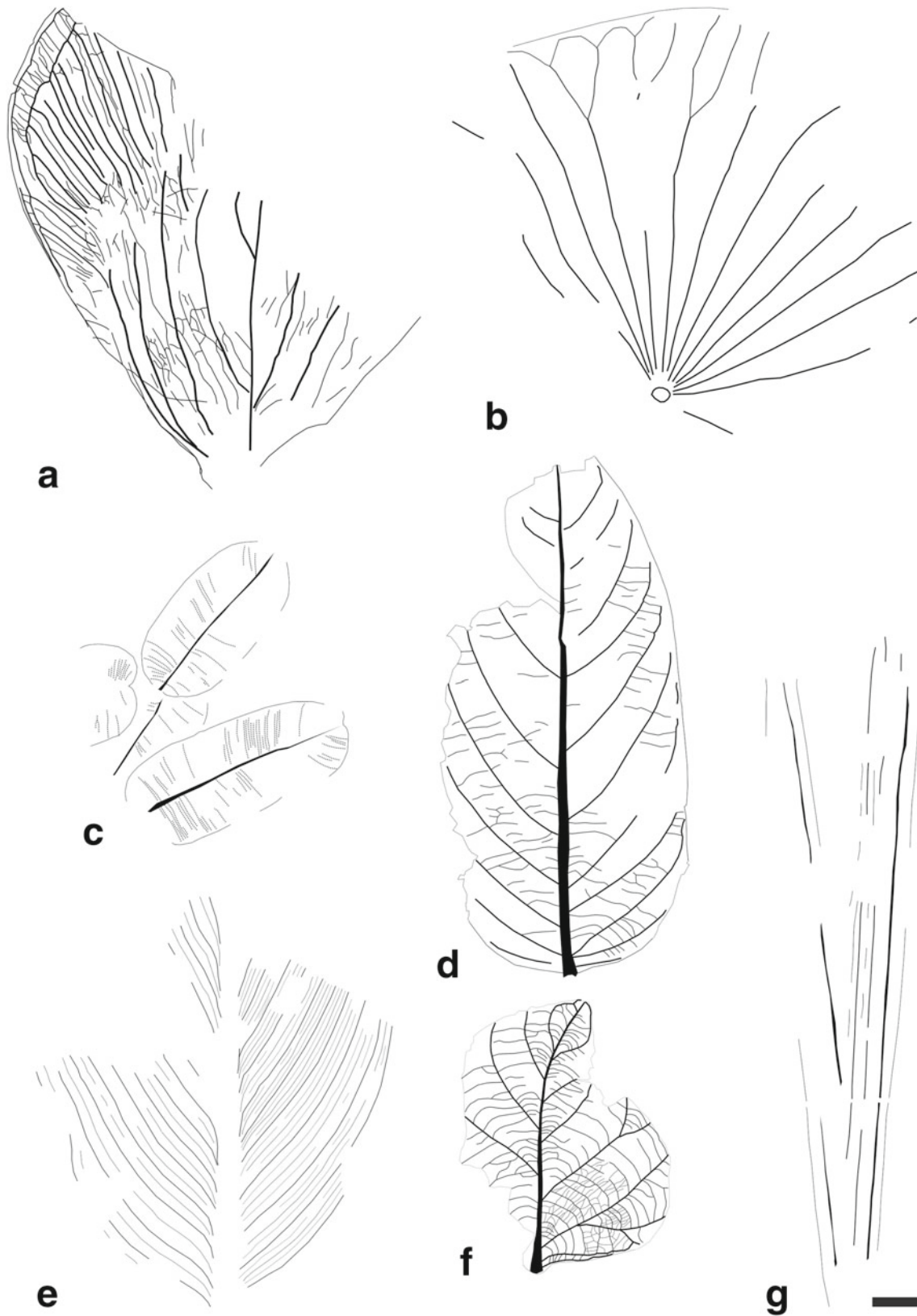


Fig. 7 Line drawing of leaves from the Mut Formation. **a** *Cobbania pharao* Coiffard and B.A.R. Mohr, **b** *Nelumbo* sp., **c** *Salvinia* sp., **d** *Dipterocarphyllum* sp., **e** Zingiberales leaf, **f** *Ficus* sp., **g** monocotyledon leaves. Scale bar is equal to 1 cm

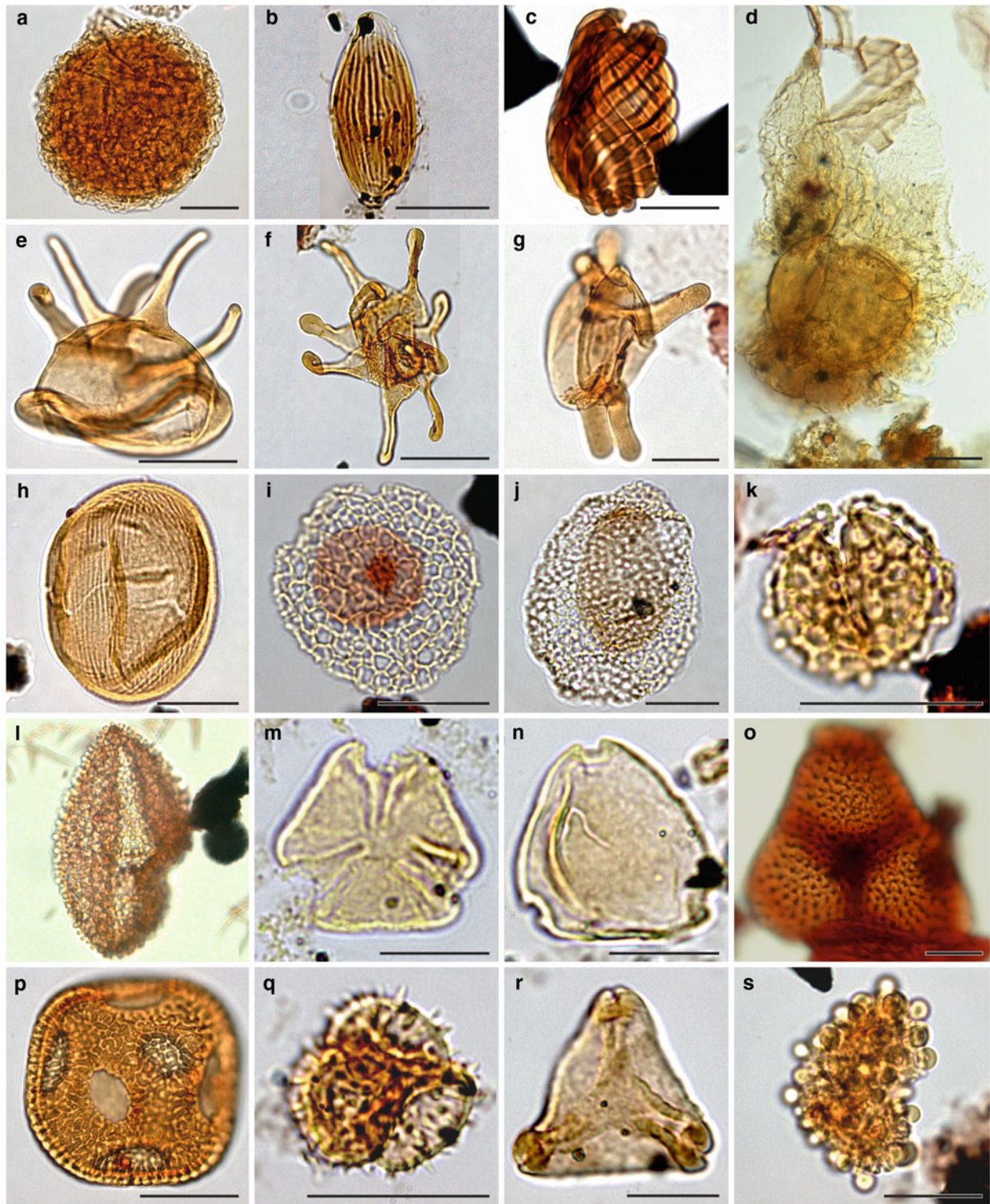


Fig. 8 Photomicrographs represent examples of taxa among the most significant Cretaceous palynomorphs recorded from Egypt; **a, d** water ferns, **b, c** *Ephedra*, **e–g** elaterates, **h** *Classopollis*, **i–r** angiosperms, **s** incertae sedis. Scale bar is equal to 20 μm : **a** *Crybelosporites pannuceus* (Brenner) Srivastava, **b** *Equisetosporites ambiguus* (Hedlund) Singh, **c** *Ephedripites jansonii* (Pocock) Muller, **d** *Ariadnaesporites* sp., **e** *Elaterosporites klaszii* (Jardiné and Magloire) Jardiné, **f** *Elaterocolpites castelainii* Jardiné and Magloire, **g** *Sofrepites legouxae* Jardiné, **h** *Classopollis brasiliensis* Herngreen, **i** *Afropollis jardinus* (Brenner) Doyle, Jardiné and Doerenkamp, **j** *Afropollis kahramanensis* Ibrahim and Schrank, **k** *Dichastopollenites ghazalatensis* Ibrahim, **l** *Stellatopollis* sp., **m** *Nyssapollenites* sp., **n** *Scabratrporites simpliformis* van Hoeken-Klinkenberg, **o** *Integritradites porosus* Schrank and Mahmoud, **p** *Cretacaeiporites densimurus* Schrank and Ibrahim, **q** *Droseridites senonicus* Jardiné and Magloire, **r** *Plicapollis* sp., **s** *Reyrea polymorphus* Herngreen

7 Vegetation and Floristic Composition and Palaeoclimate: Concluding Remarks

The fossil flora record (mainly leaves and palynoflora) of Egypt offers a unique opportunity to follow the vegetation changes in the tropics throughout the Cretaceous. The following remarks are of special importance:

1. The oldest assemblages from the Abu Ballas (Kilf Kebir) Formation (Aptian) are dominated by gymnosperms and free-spring plants and demonstrate a dominance of xeromorphic taxa such as *W. reticulata* and frenalopsids. These assemblages seem to be dominated by ferns, suggesting an open vegetation, maybe similar to what is known in Europe (Coiffard et al., 2012), perhaps in relation to a seasonally dry climate (and wildfire?). Similar to European assemblages, this assemblage introduces the earliest evidences of angiosperms in Egypt.
2. The plant megafossils assemblages from the Sabaya Formation (Albian to possibly early Cenomanian) are only known by fluvial assemblages and some are already dominated by angiosperms. The co-occurrence of non-angiosperm- and angiosperm-dominated assemblages may be due to lateral variations of the vegetation. The majority of micro- to notophyllous angiosperms as well as the common occurrence of *W. reticulata* suggest a (seasonally) dry climate.
3. The assemblages from the Bahariya Formation (early Cenomanian) reveal the next change in the vegetation with nearly complete disappearance of Mesophytic forms, only *W. reticulata* being recorded. In this stage, palustrine/lacustrine assemblages took a modern appearance with the dominance of Nelumbonaceae and various monocots (*Typhaephyllum*) which will remain more or less unchanged till at least the end of the Cretaceous. *W. reticulata* occurs in nearly monodominant assemblages interpreted as mangrove. The fluvial assemblages consist of angiosperms displaying mesophyllous, entire-margined leaves suggesting a (sub) humid tropical climate.
4. The Timsah Formation (Coniacian-Santonian) assemblages are the less known and display strong singularities compared to older (Bahariya) and younger (Mut) assemblages. *W. reticulata* make its last appearance while the fluvial assemblages display strong similarities with contemporaneous assemblages from the Negev and the Sudan suggesting a certain homogeneity of the vegetation between the equator and the tropics. This vegetation was characterized, among others, by trifoliate to pedately compound leaves usually attributed to the genus *Dewalquea*. Surprisingly, such taxa are possibly the only

link to northern mid-latitude assemblages since they also occur in Europe (e.g. Halamski & Kvaček, 2016). This is also noticed with the occurrence, despite the rare advent of Normapolles pollen within the north Western Desert. In terms of physiognomy, these assemblages are dominated by notophyllous taxa, suggesting that the climate was dryer than both older and younger stages and probably (seasonally) dry. The palustrine/lacustrine assemblages are very similar to the older Bahariya assemblages.

5. The youngest Cretaceous assemblages of the Mut Formation (Campanian) and its equivalents are characterized by the full dominance of angiosperms. It is characterized with the appearance of derived monocots, mostly Araceae giving, then a modern appearance. In contrast to the Timsah assemblages, a shift to bigger leaf size (mesophyllous and bigger) and the nearly disappearance of toothed leaves. This suggest a much wetter climates, even wetter than the Bahariya assemblages.

Acknowledgements We appreciate the Editors' interest and proposal that produced this chapter. H.E. acknowledges the financial support by the Alexander von Humboldt Foundation, Germany (EGY—1190326—GF-P). Insightful reviews by Jiří Kvaček and Adam T. Halamski enabled an improved presentation of this work. We are indebted to Gerardo Antonio Cordero for improving the English of the manuscript.

References

- Abdel Mohsen, S. A. (1992). Cretaceous plant microfossils from the subsurface of Kharga Oasis, Western Desert, Egypt. *Journal African Earth Sciences*, 14, 567–577.
- Aboul Ela, N. M., El-Saadawi, W. E., & Darwish, M. H. (1989). Some Lower Cretaceous microfloras from Abu Darag area, Western Side of the Gulf of Suez. *Egyptian Journal of Geology*, 33(1–2), 347–361.
- Abu Hamad, A. M. B., Amireh, B., Jasper, A., & Uhl, D. (2016). New palaeobotanical data from the Jarash Formation (Aptian–Albian, Kurnub Group) of NW Jordan. *The Palaeobotanist*, 65, 19–29.
- Attia, M. I. (1955). Topography, geology and iron-ore deposits of the district east of Aswan. *Geological Survey of Egypt*, 262.
- Barakat, M. G., Sadek, A., & Arafa, A. A. (1974). Planktonic foraminiferal zonation of early Upper Cretaceous in Mersa Matruh well n°1, Western Desert, Egypt. *Revista Española de Micropaleontología*, 6, 111–125.
- Barazi, N. (1985). Sedimentologie und Stratigraphie des Abyad-Beckens (NW Sudan). *Berliner Geowissenschaftliche Abhandlungen A*, 64, 1–85.
- Barthel, K. W., & Böttcher, R. (1978). Abu Ballas Formation (Tithonian/Berriasian; Southwestern Desert, Egypt) a significant lithostratigraphic unit of the former “Nubian Series.” *Mitteilungen Bayerische Staatssammlung Paläontologie Historische Geologie*, 18, 153–166.
- Barthel, K. W., & Hermann-Degeen, W. (1981). Late Cretaceous and Early Tertiary stratigraphy in the Great Sand Sea and its SE Margins (Farafra and Dakhla Oases), SW Desert, Egypt. *Mitteilungen der*

- Bayerischen Staatssammlung für Paläontologie und Historische Geologie, 21, 141–182.
- Barthoux, J., & Fritel, P. H. (1925). Flore Crétacée du Grès de Nubie. *Mémoires Présentés à l'Institut Egyptien*, 7, 65–119.
- Böttcher, R. (1982). Die Abu Ballas Formation (Lingula Shale) (Apt?) der Nubischen Gruppe Südwest-Ägyptens. *Berliner Geowissenschaftliche Abhandlungen A*, 39, 1–145.
- Coiffard, C., Gomez, B., Daviero-Gomez, V., & Dilcher, D. L. (2012). Rise to dominance of angiosperm pioneers in European Cretaceous environments. *Proceedings of the National Academy of Sciences*, 109(51), 20955–20959.
- Coiffard, C., Kardjilov, N., Manke, I., & Bernardes-de-Oliveira, M. E. (2019). Fossil evidence of core monocots in the Early Cretaceous. *Nature Plants*, 5(7), 691–696.
- Coiffard, C., & Mohr, B. A. (2015). *Lejalialia sagenopteroides* gen. nov. et comb. nov.: A new tropical member of Araceae from Late Cretaceous strata of northern Gondwana (Jebel Abyad, Sudan). *Taxon*, 64(5), 987–997.
- Darwish, M. H., & Attia, Y. (2007). Plant impressions from the mangrove-dinosaur unit of the Upper Cretaceous Bahariya Formation of Egypt. *Taekholmia*, 27, 105–125.
- Deaf, A. S., Harding, I. C., & Marshall, J. E. A. (2014). Cretaceous (Albian–early Santonian) palynology and stratigraphy of the Abu Tunis 1x borehole, northern Western Desert, Egypt. *Palynology*, 38, 51–77.
- Dominik, W. (1985). Stratigraphie und Sedimentologie (Geochemie, Schwermineralanalyse) der Oberkreide von Bahariya und ihre Korrelation zum Dakhla-Becken (Western Desert, Ägypten). *Berliner Geowissenschaftliche Abhandlungen A*, 62, 1–173.
- Edwards, W. N. (1926). Fossil plants from the Nubian Sandstone of eastern Darfur. *Quarterly Journal of the Geological Society*, 82(1–4), 94–100.
- El Akkad, S., & Issawi, B. (1963). *Geology and iron ore deposits of the Bahariya Oasis* (United Arab Republic Geological Survey and Mineral Research Department. Paper no. 18, p. 301).
- El Atfy, H. (2021). Palynofacies as a paleoenvironment and hydrocarbon source potential assessment tool: An example from the Cretaceous of north Western Desert, Egypt. *Palaeobiodiversity and Palaeoenvironments*, 101, 35–50.
- El Atfy, H., Coiffard, C., El Beialy, S. Y., & Uhl, D. (2023). Vegetation and climate change at the southern margin of the Neo-Tethys during the Cenomanian (Late Cretaceous): Evidence from Egypt. *PlosOne* <https://doi.org/10.1371/journal.pone.0281008>
- El-Beialy, S. Y. (1994). Palynostratigraphy and palynofacies analysis of some subsurface Cretaceous formations in the Badr El Dein (Bed 1–1) borehole, North Western Desert, Egypt. *Neues Jahrbuch für Geologie und Paläontologie*, 192, 133–149.
- El-Naggar, Z. R. M. (1970). On a proposed lithostratigraphic subdivision for the late Cretaceous-early Paleogene succession in the Nile Valley, Egypt. In *7th Arabian Petroleum Congress*, Kuwait. Paper n. 64 (B-3).
- El-Saadawi, W. E., & Kedves, M. (1991). Palaeobotanical investigations on plant impressions and sporomorphs from Egypt. *Plant Cell Biology and Development*, 2, 8–33.
- El-Saadawi, W. E., Nour-El-Deen, S., El-Noamani, Z. M., Darwish, M. H., & Kamal El-Din, M. M. (2020). Fossil flora of Egypt. In Z. Hamimi, A. El-Barkooky, J. Martínez Frías, H. Fritz, & Y. Abd El-Rahman (Eds.), *The geology of Egypt* (pp. 495–520). Springer. Regional Geology Reviews.
- Gale, A. S., Mutterlose, J., Batenburg, S., Gradstein, F. M., Agterberg, F. P., Ogg, J. G., & Petrizzo, M. R. (2020). The Cretaceous period (Chap. 27). In F. M. Gradstein, J. G. Ogg, M. D. Schmitz, & G. M. Ogg (Eds.), *Geologic time scale 2020* (Vol. 2, pp. 1023–1086). Elsevier.
- Germann, K., Mocke, A., Doering, T., & Fischer, K. (1987). Late Cretaceous laterite-derived sedimentary deposits (oolitic ironstone, kaolin deposits, bauxite) in Upper Egypt. *Berliner Geowissenschaftliche Abhandlungen A*, 75(3), 727–758.
- Halamski, A. T., & Kvaček, J. (2016). The Coniacian leaf flora from the northeastern part of the Bohemian Cretaceous Basin. *Bulletin of Geosciences*, 91, 297–318.
- Hassan, M. H. (1973). Fossil flora of Umm Badda, Omdurman. *Sudan Notes and Records*, 54, 153–167.
- Hu, S., & Taylor, D. W. (2014). Floristics and paleoecology of an Early Cretaceous flora from Jordan. *Bulletin of the Peabody Museum of Natural History*, 55(2), 153–170.
- Issawi, B., Francis, M. H., Youssef, E. A. A., & Osman, R. A. (2009). *The Phanerozoic geology of Egypt. A geodynamic approach* (2nd ed). Ministry of Petroleum, The Egyptian Mineral Resources Authority, Special Publication 81.
- Kahlert, E., Ruffe, L., & Gregor, D. H. J. (2009). *Die Oberkreide-Flora (Campanian) von Baris (Ägypten) und ihre ökologisch-geographischen Beziehungen unter plattentektonischen Aspekten* (Documenta Naturae 178). Verlag Documenta Naturae.
- Klitzsch, E. (1978). Geologische Bearbeitung Südwest-Ägyptens. *Programm und erste Ergebnisse. Geologische Rundschau*, 67, 509–520.
- Klitzsch, E. (1987). The paleogeographic development of NE Africa. In G. Matheis & H. Schandlmeier (Eds.), *Current research in African earth sciences* (pp. 159–164). Balkema.
- Klitzsch, E., Harms, J. C., Lejal-Nicol, A., & List, F. K. (1979). Major subdivisions and depositional environments of Nubia strata, south-western Egypt. *AAPG Bulletin*, 63(6), 967–974.
- Klitzsch, E., & Hermina, M. (1989). The Mesozoic. In M. Hermina, E. Klitzsch, & F. List (Eds.), *Stratigraphic Lexicon and explanatory notes to the geologic map of Egypt 1:500,000* (pp. 77–139). Conoco Inc.
- Klitzsch, E., & Lejal-Nicol, A. (1984). Flora und fauna from strata in southern Egypt and northern Sudan. *Berliner Geowissenschaftliche Abhandlungen A*, 50, 47–79.
- Klitzsch, E., & Schandlmeier, H. (1990). South Western Desert. In R. Said (Ed.), *The geology of Egypt* (pp. 249–325). Balkema.
- Klitzsch, E., & Wycisk, P. (1987). Geology of the sedimentary basins of northern Sudan and bordering areas. *Berliner Geowissenschaftliche Abhandlungen A*, 75, 97–136.
- Kora, M., Issa, G., & El-Sherbini, M. (1988). Petrology of the Sabaya Formation, Darb El Arbain area, Southern Egypt and Northern Sudan. *Bulletin of the Faculty of Science, Mansoura University*, 15, 473–490.
- Krassilov, V., & Bacchia, F. (2000). Cenomanian florule of Nammoura, Lebanon. *Cretaceous Research*, 21, 785–799.
- Krassilov, V., & Bacchia, F. (2013). New Cenomanian florule and a leaf mine from southeastern Morocco: Palaeoecological and climatological inferences. *Cretaceous Research*, 40, 218–226.
- Krassilov, V., Lewy, Z., Nevo, E., & Silantjeva, N. (2005). *Late Cretaceous (Turonian) flora of Southern Negev, Israel* (p. 252). Pensoft Publishers.
- Krassilov, V., & Schrank, E. (2011). New Albian macro- and palynoflora from the Negev (Israel) with description of a new gymnosperm morphotaxon. *Cretaceous Research*, 32, 13–29.
- Kräusel, R. (1939). Ergebnisse der Forschungsreisen Prof. E. Stromers in den Wüsten von Ägypten. IV. Die fossilen Floren Ägyptens. 3. Die fossilen Pflanzen Ägyptens. E. Vorbemerkungen, F. Nachträge zu B–D, G. Angiospermae Dicotyledoneae, H. Allgemeine Betrachtungen, J. Bestimmungstabelle für die fossilen Laubhölzer Ägyptens und einiger anderer afrikanischer Fundorte, K. Schriftenverzeichnis, L. Tafelerklärungen. *Abhandlungen der Bayerischen Akademie der Wissenschaften, Mathematisch-naturwissenschaftliche Abteilung Neue Folge*, 47, 1–140.

- Lejal-Nicol, A. (1981a). A propos de nouvelles flores paléozoïques et mésozoïques de l'Égypte du sud-Ouest. *Comptes Rendus de l'Académie des Sciences de Paris*, 292(Série II), 1337–1340.
- Lejal-Nicol, A. (1981b). Nouvelles empreintes de la "Lingula Shale Unit" dans la région d'Abu Ballas (Égypte). In *Comptes Rendus du Congrès National de la Société des Savantes* (Vol. 106, pp. 15–27) Perpignan 1.
- Lejal-Nicol, A. (1987). Flores nouvelles du Paléozoïque et du Mésozoïque d'Égypte et du Soudan septentrional. *Berliner Geowissenschaftliche Abhandlungen A*, 75, 151–248.
- Lejal-Nicol, A. (1990). Fossil flora. In R. Said (Ed.), *The geology of Egypt* (pp. 615–625). Balkema.
- Lejal-Nicol, A., & Dominik, W. (1987). Plant cover and palaeoenvironment during the Cenomanian in Bahariya basin (Egypt). In *14th International Botanical Congress*, Berlin (Abstract) (p. 402).
- Lejal-Nicol, A., & Dominik, W. (1990). Sur la paléoflore à Weichseliaceae et à angiospermes du Cenomanien de la région de Bahariya (Égypte du Sud-Ouest). *Berliner Geowissenschaftliche Abhandlungen A*, 120, 957–992.
- Lyon, M. A., Johnson, K. R., Wing, S. L., Nichols, D. J., Lacovara, K. J., & Smith, J. B. (2001). Late Cretaceous equatorial coastal vegetation: New megaflora associated with dinosaur finds in the Bahariya Oasis, Egypt. In *Geological Society of America, Annual Meeting*. Abstracts with Programs—Geological Society of America (Vol. 33, No. 6, p. 198).
- Mahmoud, M. S. (2003). Palynology and palaeoenvironment of the Quseir Formation (Campanian) from central Egypt. *Journal of African Earth Sciences*, 36, 135–148.
- Mahmoud, M. S., & Essa, M. A. (2007). Palynology of some Cretaceous mudstones from southeast Aswan, Egypt: Significance to regional stratigraphy. *Journal of African Earth Sciences*, 47, 1–8.
- Saad, S. I., & Ghazaly, G. (1976). Palynological studies in Nubia Sandstone from Kharga Oasis. *Pollen et Spores*, 18, 407–470.
- Said, R. (1962). *The geology of Egypt* (p. 377). Elsevier Publ. Co.
- Schrank, E. (1982). Kretazische Pollen und Sporen aus dem "Nubischen Sandstein" des Dakhla-Beckens (Ägypten). *Berliner Geowissenschaftliche Abhandlungen A*, 40, 87–109.
- Schrank, E. (1983). Scanning electron and light microscopic investigation of angiosperm pollen from them Lower Cretaceous of Egypt. *Pollen et Spores*, 25, 213–242.
- Schrank, E. (1992). Nonmarine Cretaceous correlations in Egypt and northern Sudan: Palynological and palaeobotanical evidence. *Cretaceous Research*, 13, 351–368.
- Schrank, E. (1999). Mesozoic Floren aus Nordost-Afrika und ihre Beziehungen zum Klima am Paläoäquator. *Deutsche Forschungsgemeinschaft*, 1999, 137–166.
- Schrank, E. (2001). Paleocological aspects of *Afropollis*/elaterates peaks (Albian–Cenomanian pollen) in the Cretaceous of Northern Sudan and Egypt. In D. K. Goodman & R. T. Clarke (Eds.), *Proceedings of the IX International Palynological Congress* (pp. 201–210). AASP Foundation.
- Schrank, E., & Ibrahim, M. I. A. (1995). Cretaceous (Aptian–Maastrichtian) palynology of foraminifera-dated wells (KRM-1, AG-18) in northwestern, Egypt. *Berliner Geowissenschaftliche Abhandlungen A*, 177, 1–44.
- Schrank, E., & Mahmoud, M. S. (1998). Palynology (pollen, spores and dinoflagellates) and Cretaceous stratigraphy of the Dakhla Oasis, Central Egypt. *Journal of African Earth Sciences*, 26, 167–193.
- Schrank, E., & Rüffle, L. (2003). The Late Cretaceous leaf flora from Jebel Mudaha, Sudan. *Courier Forschungsinstitut Senckenberg*, 241, 119–129.
- Schweitzer, C. E., Lacovara, K. J., Smith, J. B., Lamanna, M. C., Mandela, M. A., & Attia, Y. (2003). Mangrove-dwelling crabs (Decapoda: Brachyura: Necrocarcinidae) associated with dinosaurs from the Upper Cretaceous (Cenomanian) of Egypt. *Journal of Paleontology*, 77, 888–894.
- Sender, L. M., Gomez, B., Diez, J. B., Coiffard, C., Martin-Closas, C., Villanueva-Amadoz, U., & Ferrer, J. (2010). *Ploufolia cerciforme* gen. et comb. nov.: Aquatic angiosperm leaves from the Upper Albian of north-eastern Spain. *Review of Palaeobotany and Palynology*, 161, 77–86.
- Seward, A. C. (1935). *Leaves of dicotyledons from the Nubian Sandstone of Egypt* (p. 21). Government Press.
- Smith, J. B., Lamanna, M. C., Lacovara, K. J., Dodson, P., Smith, J. R., Poole, J. C., Giegengack, R., & Attia, Y. (2001). A giant sauropod dinosaur from an upper Cretaceous mangrove deposit in Egypt. *Science*, 292, 1704–1706.
- Soliman, H. A., & Sultan, I. (1976). Spores et pollen des Grès de Baharia, Désert Ouest, Égypte. *Revue de Micropaléontologie*, 19, 108–111.
- Stromer, E. (1936). Ergebnisse der Forschungsreisen Prof. E. Stromers in den Wüsten Ägyptens, VII. Baharije-Kessel und-Stufe mit deren Fauna und Flora eine ergänzende Zusammenfassung. *Abhandlungen der Bayerischen Akademie der Wissenschaften, Mathematisch-naturwissenschaftliche Abteilung Neue Folge*, 33, 3–102.
- Sultan, I. Z. (1985). Palynological studies in the Nubia Sandstone Formation, East of Aswan, Southern Egypt. *Neues Jahrbuch für Geologie und Paläontologie Monatshefte*, 10, 605–617.
- Van Houten, F. B., Bhattacharyya, D. P., & Mansour, S. E. I. (1984). Cretaceous Nubia Formation and correlative deposits, eastern Egypt: Major regressive-transgressive complex. *Geological Society of America Bulletin*, 95, 397–405.
- Ward, W. C., & McDonald, K. C. (1979). Nubia Formation of central Eastern Desert, Egypt—Major subdivisions and depositional setting. *AAPG Bulletin*, 63, 975–985.
- Watson, J. (1983). A new species of the conifer *Frenelopsis* from the Cretaceous of Sudan. *Botanical Journal of the Linnean Society*, 86 (1–2), 161–167.
- Werner, C. (1989). Die Elasmobranchier-Fauna des Gebel Dist Member der Bahariya Formation (Obercenoman) der Oase Bahariya, Ägypten. *Palaeo Ichthyologica*, 5, 112.
- Youssef, M. I. (1957). Upper Cretaceous rocks in Kosseir area. *Bulletin Institution Desert Egypt*, 7, 35–54.



Clément Coiffard is a botanist at the Freie Universität Berlin (Germany). He obtained a doctoral degree in 2006 from the Lyon I University (France) working on the evolution of European vegetation during the Cretaceous with Bernard Gomez. After the Ph.D., Clément studied the systematics and phylogeny of Cretaceous tropical early angiosperms. Later, he worked on Upper Cretaceous tropical vegetation, which involved fieldworks in Sudan. He is involved in projects on the taxonomy, phylogeny, palaeoenvironmental reconstruction, and vegetation dynamics in the Cretaceous of Europe, Brazil, and Northeastern Africa.



Haytham El Atfy is an associate professor at Mansoura University (Egypt) from where he received a B.Sc. degree in geology and an M. Sc. in palynology. He received a Ph. D. in geosciences (palynology and organic geochemistry) from Goethe University, Frankfurt (Germany) in 2014, and PD (Habilitation) from the University of Tübingen (Germany) in 2022. He acquired experience in industrial palynology through work with GUPCO (BP), Egypt. Haytham has been a Research Fellow of the

Alexander von Humboldt Foundation at the University of Tübingen (Germany) since 2019. He was recently a visiting scientist at the Senckenberg Research Institute, Germany. His research interests span all aspects of palynology and its applications in dating, palaeoenvironmental and palaeoclimatical reconstructions, and hydrocarbon exploration, particularly of the Mesozoic and Cenozoic and, to a lesser extent, the Palaeozoic. He has more recently become involved in organic geochemistry. He is a member of the AASP—The Palynological Society, the Micropalaeontological Society (TMS), Arbeitskreis für Paläobotanik und Palynologie (APP), and the Paleontological Society of Egypt (PSE). He is a recipient of many awards, including the Bernd Rendel Prize from the German Science Foundation (DFG), Egyptian State Incentive Award, and the First-Class Excellence Concession that is provided by the Egyptian president.



Dinosaur Faunas of Egypt—The Terrestrial Late Cretaceous Vertebrate Record

Felix J. Augustin, Josephina Hartung, and Panagiotis Kampouridis

Abstract

Egypt has yielded some of the richest and most spectacular records of Mesozoic terrestrial vertebrates from Africa. Certainly, the best-known and most diverse of these are the vertebrate assemblages of the Upper Cretaceous Bahariya Formation (Cenomanian), which includes numerous different taxa of fishes, abundant remains of turtles and crocodyliforms, as well as several different theropod and sauropod dinosaurs. Originally discovered early in the twentieth century by famous German palaeontologist Ernst Stromer von Reichenbach and fossil collector Richard Markgraf, most of the material has subsequently been destroyed during the Second World War. Aside from the high diversity, the Bahariya Formation also yielded some of the most bizarre and iconic dinosaurs such as the giant theropods *Spinosaurus* and *Carcharodontosaurus* or the enormous sauropod *Paralititan*. Although the Bahariya Oasis has yielded by far the most diverse and extensive remains of Mesozoic terrestrial vertebrates from Egypt, other localities from the Turonian, Campanian and Maastrichtian offer additional important—albeit much less complete—insights into the composition and evolution of African Late Cretaceous terrestrial ecosystems. Some of these assemblages, especially the latest Cretaceous Quseir Formation, have just begun to reveal the richness and diversity of their vertebrate fauna, often with spectacular results, and certainly have the potential to yield further significant insights into the evolution of the Cretaceous life on land. In this chapter, we provide a summary of the terrestrial Mesozoic vertebrate record of Egypt and thus an overview of these remarkable dinosaur faunas.

Keywords

Egypt • Dinosauria • Crocodyliformes • Testudinata • Bahariya Formation • Quseir Formation

1 Introduction

Egypt has yielded one of the richest records of terrestrial vertebrates from the Mesozoic of the African continent. All Egyptian continental Mesozoic vertebrate assemblages are Late Cretaceous in age, spanning from the beginning of that period (Cenomanian) up to the latest Cretaceous (Maastrichtian), representing the final days of the dinosaur era. Although the Mesozoic record of terrestrial ecosystems from Africa is generally extensive, the Cretaceous, and especially the Late Cretaceous, is poorly documented (Rauhut & Werner, 1997; Russell, 1995; Weishampel et al., 2004). Therefore, the Egyptian Late Cretaceous vertebrate assemblages play a key role in our understanding of the evolution of terrestrial ecosystems in Africa during the Cretaceous. Moreover, the Egyptian vertebrate assemblages yielded some of the most astonishing and bizarre land vertebrates, including the large-sized and potentially semi-aquatic carnivorous theropod *Spinosaurus* (Ibrahim et al., 2014, 2020b; Stromer, 1915) or the enormous sauropod *Paralititan*, one of the largest terrestrial animals ever to walk the earth (Smith et al., 2001).

The most famous of these Egyptian terrestrial vertebrate assemblages is the fauna from the Upper Cretaceous (Cenomanian) of the Bahariya Oasis (Fig. 1), which was discovered early in the twentieth century by German palaeontologist Ernst Stromer von Reichenbach and fossil collector Richard Markgraf. Over the course of three years (1912–1914) a diverse array of vertebrates was recovered, including numerous fishes, turtles, crocodyliforms, as well as sauropod and theropod dinosaurs (Stromer, 1936). Although the Bahariya Oasis has yielded by far the most diverse and extensive remains of terrestrial vertebrates, other

F. J. Augustin (✉) · J. Hartung · P. Kampouridis
Department of Geosciences, University of Tübingen,
Hölderlinstraße 12, 72074 Tübingen, Germany
e-mail: felix.augustin@uni-tuebingen.de

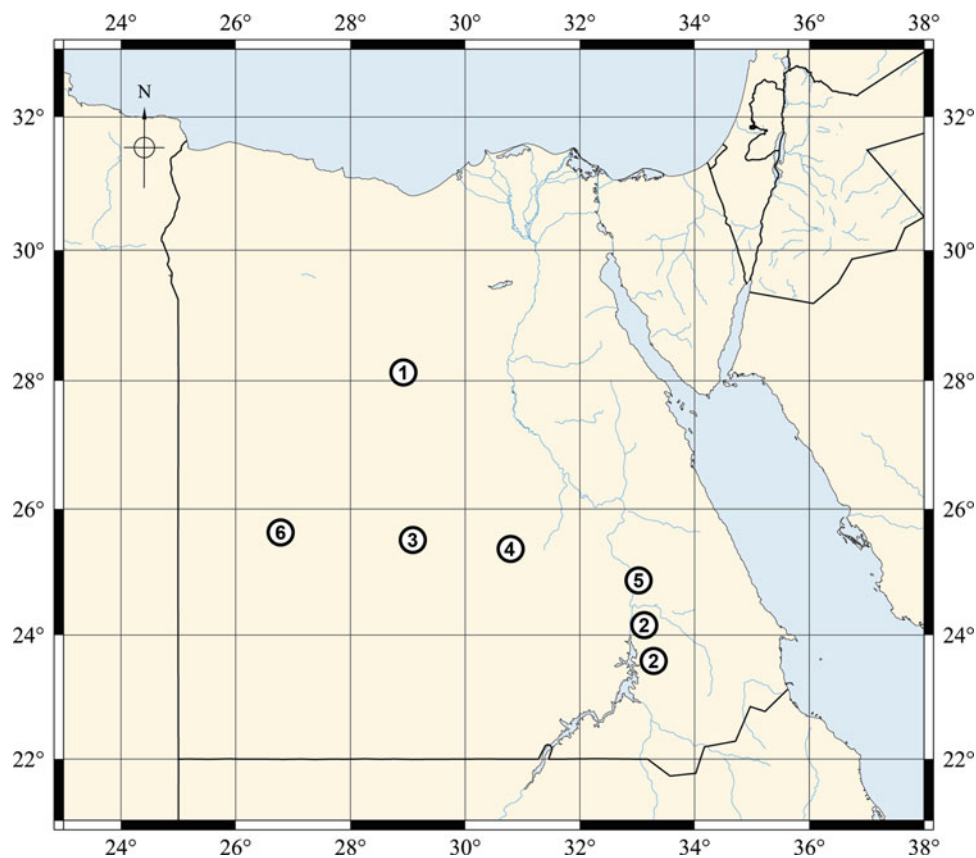


Fig. 1 Map of Egypt with the location of vertebrate-yielding sites from the Cretaceous. 1 Bahariya Oasis (Bahariya Formation); 2 track-sites near Aswan (Abu Agag Formation), 75–80 km south of Aswan and 15 km south of Aswan respectively; 3 Dakhla Oasis (Quseir Formation); 4 Kharga Oasis (Quseir Formation); 5 Nile Valley near Idfu (Quseir Formation); 6 Ammonite Hill Member of the Western Desert (Dakhla Formation). The map was created with GMT6 (Wessel et al. 2013)

localities from the Turonian (Demathieu & Wycisk, 1990), Campanian (Saber et al., 2018; Salem et al., 2021; Sallam et al., 2016, 2018) and Maastrichtian (Rauhut & Werner, 1997; Smith & Lamanna, 2006) offer additional important—albeit sparse—insights into the composition and evolution of African Late Cretaceous terrestrial ecosystems.

In this chapter, a summary of the Cretaceous terrestrial vertebrate assemblages from Egypt is provided. After an overview of the research history of Mesozoic terrestrial vertebrates from Egypt (especially the early phase), each of the different vertebrate assemblages is reviewed, starting with the oldest fauna from the Cenomanian (Bahariya Formation) and ending with the youngest one from the Maastrichtian (Dakhla Formation). As a conclusion, the importance of the Egyptian Mesozoic vertebrate assemblages for our understanding of past terrestrial ecosystems is shortly discussed.

2 Historical Overview

The early research history of the terrestrial Mesozoic vertebrates of Egypt is closely connected to two men, Ernst Stromer von Reichenbach and Richard Markgraf (Fig. 2),

who uncovered and studied the rich vertebrate fauna from Bahariya, certainly the most important Mesozoic vertebrate locality from Egypt. Ernst Freiherr Stromer von Reichenbach was a nobleman of an old aristocratic family from the medieval city of Nuremberg and a German palaeontologist. He was a student of the famous German palaeontologist Karl Alfred von Zittel, who conducted some of the first palaeontological fieldwork in Egypt (see below) during expeditions with the famous explorer of Africa Gerhard Rohlfs (Zittel, 1883). Stromer travelled three times to Egypt (1902, 1903 and 1910) to discover new fossil sites and collect vertebrate specimens. During his first two expeditions, Stromer primarily collected mammal fossils from the Palaeogene of the Fayum Depression (Kampouridis et al., [this volume](#)). During his second and third expedition to Egypt, Stromer was accompanied by fossil collector Richard Markgraf. Richard Markgraf was an Austro-German musician who joined a travelling musical group when he was young, finally ending up sick and impoverished in Cairo. In 1897, he met German palaeontologist Eberhard Fraas, who hired him because of his knowledge in Arabian to assist him in his fieldwork. Fraas trained Markgraf in fossil collection and, after recognising his talent and skills, hired him to

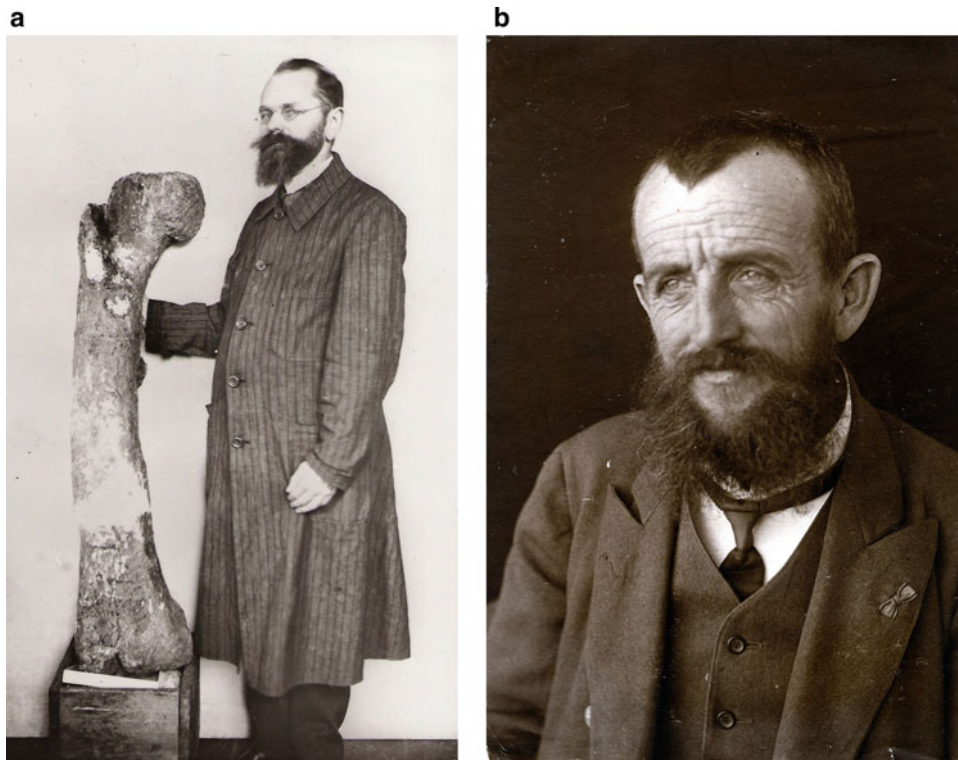


Fig. 2 The German palaeontologist Ernst Stromer von Reichenbach (a) and the Austro-German fossil collector Richard Markgraf (b), who collected the vast majority of the fossil vertebrates from Bahariya

continue collecting fossils for the Natural History Museum of Stuttgart, Germany. Markgraf was one of the most significant fossil collectors in Egypt, though he did not receive any real fame or fortune for his accomplishments and lived a very simple life.

Originally, the main purpose of Stromer's third expedition to Egypt was the collection of mammal fossils in Wadi el Natrun and in the Nile Valley. Stromer was not able to collect the quantity of fossils he hoped and when his companion Markgraf fell sick in winter 1910, Stromer had to return to Cairo and hire a new guide. In January 1911, he and his new guide travelled to the Bahariya Oasis for the first time, where Stromer was not able to find any mammal fossils but made another awe-inspiring discovery: he found the first dinosaur fossils from Egypt. After Markgraf's recovery, Stromer entrusted him with collecting more fossils from the Bahariya Oasis. In the years 1912–1914 Markgraf continued his work there, gathering an incredibly rich collection of fossils, which he sent to Munich, Germany, to be studied by Stromer and comprising the famous gigantic theropod dinosaur *Spinosaurus* (Stromer, 1915), among others. Markgraf himself collected almost all fossils, that were later published by Stromer and his colleagues, including several new genera and species. Unfortunately, he was unable to continue his fossil collection after 1914, because of the First World War. Due to his sickness, Markgraf died in January

1916 in his home in Sinnuris, in Fayum (Stromer, 1916). The last fossils that Markgraf collected in 1914 were not sent to Stromer in Munich until 1922 (Stromer, 1926). This material comprised several new species, including the dinosaurs *Carcharodontosaurus saharicus* and *Aegyptosaurus baharijensis* (Stromer, 1931, 1934b), as well as the fishes *Markgrafia libyca* and *Stromerichthys aethiopicus*, which were named in honour of collector Markgraf and researcher Stromer, respectively (Weiler, 1935). Unfortunately, during the Second World War almost all of Stromer's material from the Bahariya Oasis that was stored in Munich was destroyed on 24 April 1944 during a bombardment by the Allied Royal Air Force, and only few specimens survived, including the holotypes of *Libycosuchus* and *Aegyptosuchus* among others (Smith et al., 2006).

More recent field activities with the aim to uncover fossil vertebrates from the Mesozoic continental deposits of Egypt have demonstrated the potential of these strata to yield further spectacular and important material. One of the most important among these is probably the field activities of the Technical University of Berlin (1970s and 1980s) that studied the stratigraphy, sedimentology and palaeontology of the Bahariya and Dakhla formations (see below) among others. The Bahariya Dinosaur Project of the University of Pennsylvania continued the search for dinosaurs and other vertebrates in the Upper Cretaceous Bahariya Formation and

recovered significant new material, most importantly the holotype of an enormous sauropod dinosaur, *Paralititan stromeri* (for an overview, see Nothdurft & Smith, 2002). More recently, extensive fieldwork was conducted by the Mansoura University in the Bahariya Formation (Salem et al., 2018), and primarily in the latest Cretaceous Quseir Formation (Saber et al., 2018; Sallam et al., 2016, 2018) with spectacular results, including a new sauropod dinosaur (*Mansourasaurus*) and a new crocodylian (*Wahasuchus*) that have important palaeobiogeographic implications.

3 The Vertebrate Fauna of the Bahariya Formation (Cenomanian)

The Bahariya Formation yielded by far the most diverse and richest vertebrate assemblage from the Mesozoic terrestrial deposits of Egypt. The fauna from this formation has been known for more than a century (see above) and is famous for the presence of multiple large-sized carnivorous theropod dinosaurs that lived among gigantic sauropods, several different crocodyliforms, turtles and numerous chondrichthyan and osteichthyan fishes. Unfortunately, most of the fossil vertebrates that were collected in the first half of the twentieth century have been destroyed due to the allied bombing of Munich during the Second World War. Thus, our knowledge of this vertebrate assemblage is largely based on the original descriptions by Stromer. However, more recent fieldwork in the Bahariya Formation has offered important new insights into this unique ecosystem, highlighting the potential of these strata to yield significant new discoveries (Lamanna et al., 2000; Salem et al., 2018; Schweitzer et al., 2003; Smith et al., 2001; Tumarkin-Deratzian et al., 2004).

Vertebrate assemblages that are remarkably similar to that of the Bahariya Formation are relatively widespread in Northern Africa and roughly coeval continental deposits with a comparable vertebrate fauna are known from Algeria (Benyoucef et al., 2015; de Lapparent, 1960), Morocco (Cavin et al., 2010; Ibrahim et al., 2020a; Sereno et al., 1996), Niger (Sereno et al., 2004), Tunisia (Benton et al., 2000; Fanti et al., 2012) and Sudan (Buffetaut et al., 1990; Rauhut, 1999; Werner, 1994). These Upper Cretaceous strata are often referred to the ‘Continental Intercalaire’, an informal unit comprising mostly Lower Cretaceous to Upper Cretaceous continental deposits (de Lapparent, 1960; Kilian, 1931; Lavocat, 1954; Taquet, 1976). Perhaps the most important of these Upper Cretaceous continental deposits in terms of vertebrate diversity is the Kem Kem beds of southern and southeastern Morocco, which yielded remains of chondrichthyan and osteichthyan fishes, amphibians, turtles, squamates, crocodylians, pterosaurs, sauropods and theropods (for a recent overview of the geology and palaeontology of the Kem Kem beds, see Ibrahim et al., 2020a).

3.1 Geological and Palaeoenvironmental Setting

The vertebrate fossils from the Bahariya Formation were collected in the eponymous Bahariya Oasis, a large depression in the Western Desert of Egypt, 320 km southwest of Cairo (Fig. 1). The rocks of this lithostratigraphic unit are well exposed, forming the floor of the Bahariya Oasis and most of the surrounding slopes (Fig. 3). The exposed thickness of the formation varies between 90 m in the central part of the Oasis and about 190 m in the northern parts (Catuneanu et al., 2006; Khalifa & Catuneanu, 2008). The Bahariya Formation has been regarded as Cenomanian in age since the beginning of its research history (Stromer, 1914a), and that age was later corroborated based on ammonite biostratigraphy (Luger & Gröschke, 1989), and comparative studies of vertebrate and plant material (Lejal-Nicol & Dominik, 1990; Schaal, 1984; Werner, 1990). The Bahariya Formation mainly consists of mudstones, siltstones and sandstones that were deposited on a low-gradient, low-energy coastal plain at the southern shore of the Tethys ocean (Khalifa & Catuneanu, 2008; Kirscher, this volume; Lacovara et al., 2003). Most finds of terrestrial vertebrates, including most dinosaurs, were collected from the base of the exposed sequence.

The depositional environments of the Upper Cretaceous sedimentary rocks of the Bahariya Formation range from braided and meandering river systems to coastal floodplains, tidal flats and channels, lagoons, mangrove forests and oyster reefs (Khalifa & Catuneanu, 2008; Lacovara et al., 2003). Several different groups of plants inhabited these extremely productive coastal environments, as evidenced by abundant plant remains of ferns, gymnosperms and angiosperms in the Bahariya beds (Coiffard & El Atfy, this volume; El Atfy et al., 2023; Lejal-Nicol & Dominik, 1990). The coastal areas were colonised by mangrove vegetation dominated by the tree fern *Weichselia*, which probably formed extensive mangrove forests (Lacovara et al., 2003). Recently, evidence for repeated wildfires during the deposition of the Bahariya Formation has been identified (El Atfy et al., 2019). Moreover, invertebrates, such as small decapod crabs, have been found within these mangrove habitats (Schweitzer et al., 2003). The palaeoclimate during the deposition of the Bahariya Formation has been reconstructed as warm and humid (Khalifa & Catuneanu, 2008; Lacovara et al., 2003).

3.2 Fishes

The Bahariya Formation contains an extremely rich and diverse fish fauna with up to twenty species of cartilaginous and more than ten species of bony fish. They are by far the

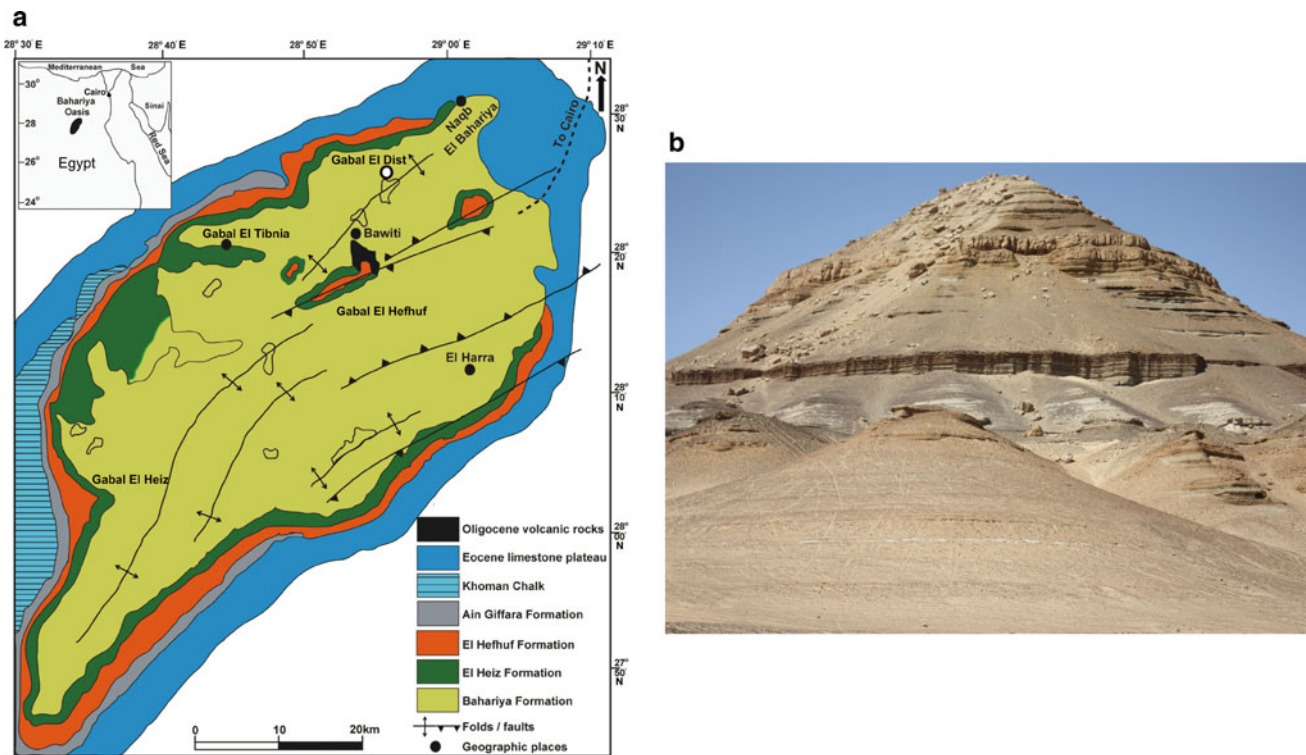


Fig. 3 Geological map of the Bahariya Formation (a) and field photo of Gebel El Dist (b), from where many important vertebrate specimens have been collected. Geological map modified after El Atfy et al. (2019). Photo of the Gebel El Dist locality kindly provided by Haytham El Atfy

most diverse and abundant vertebrate group in the Bahariya Formation, thus certainly playing a crucial role in this palaeoecosystem, and as such deserve special consideration here.

3.2.1 Chondrichthyes

Cartilaginous fishes are represented by Elasmobranchii, specifically Euselachii, which comprise sharks and rays. Among euselachians, hybodontiform sharks are well-known from their isolated teeth and vertebrae, as well as their large morphological variety of fin spines (Stromer, 1927, 1936; Weiler, 1935). Besides a comprehensive overview of the taxonomy of the Bahariya elasmobranchian fauna, Stromer (1927), as one of the most detailed studies, investigated the microstructure of these hybodontiform fin spines using thin sections (e.g. Stromer, 1927: pl. III, Figs. 1–14). He furthermore erected two new species of hybodontiform sharks based on material from Bahariya. The fauna also contains a rich and diverse assemblage of neoselachians assigned to Selachimorpha (modern sharks) and Batoidea (rays, skates, and sawfish). Selachimorpha are represented by Lamniformes (mackerel sharks) like *Scapanorhynchus*, *Squalicorax*, *Cretodus*, *Cretalamna* (Murray, 2000; Slaughter & Thurmond, 1974; Smith et al., 2006; Stromer, 1927; Vullo et al., 2007;

Werner, 1989, 1990) and *Haimirichia*, which was previously also classified as *Odontaspis*, *Serratolamna* and *Carcharias* (Cavin et al., 2010; Vullo et al., 2016).

Among batoids, Sclerorhynchidae are very similar but not closely related to extant sawfishes. They share an elongated rostrum with lined, lateral protruding, barbed, and hook-like teeth. The family is represented by several different species, like, for example, *Peyeria* and *Markgrafia* (Stromer, 1927; Weiler, 1935). The most extensively studied and best-known taxon is the peculiar sclerorhynchid *Onchopristis numidus* (Fig. 4). Well-preserved, articulated remains of a rostrum, including teeth, were described and figured by Stromer (1917). Isolated teeth are also very abundant in the Kem Kem beds of Morocco (Ibrahim et al., 2020a; Villalobus-Segura et al., 2021). Recent size estimations using the rostrum length revealed a total body length of up to four meters (Villalobus-Segura et al., 2021). Other unusual sclerorhynchid sawfishes are *Schizorhiza* (Stromer and Weiler, 1930) and *Squatina*, the ‘angelshark’ (Slaughter & Thurmond, 1974). The Bahariya batoids also include the enigmatic groups Myliobatidae (eagle rays), represented by *Rhinoptera*, *Hypolophites* and *Trygon* (Stromer, 1927; Weiler, 1935) and Myliobatiformes (butterfly ray) such as *Gymnura* (Weiler, 1935; Werner, 1989).

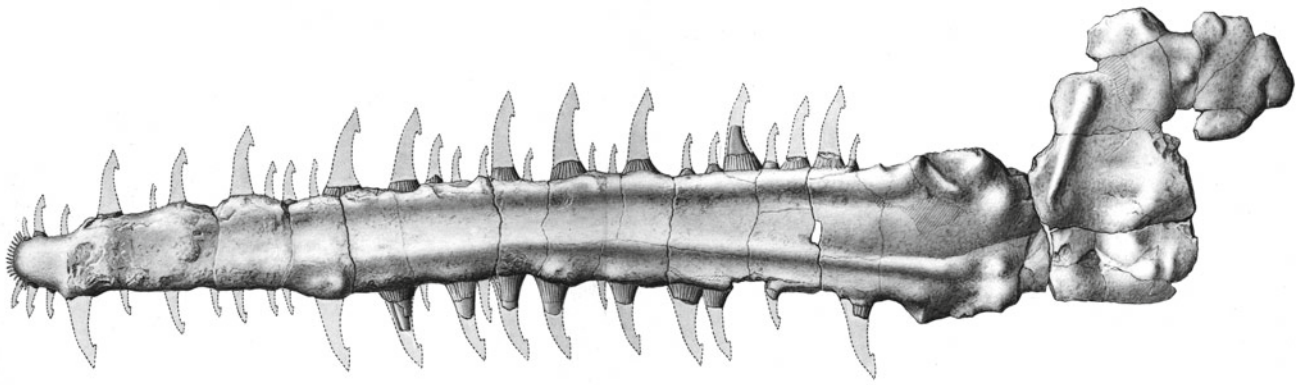


Fig. 4 Rostrum and partial cranium of the large sawfish *Onchopristis numidus* from the Upper Cretaceous Bahariya Formation. Modified after Stromer (1925)

3.2.2 Osteichthyes

Bony fishes are almost as diverse as chondrichthyans in the Bahariya Formation. Actinopterygii (ray-finned fishes) are represented by several taxa such as *Bawitius*, an archaic looking, giant, polypterid bichir (Grandstaff, 2006; Grandstaff et al., 2012; Smith et al., 2006; Stromer, 1936), *Coelodus*, a pycnodontid (Stromer, 1936), and *Enchodus*, an aulopiform (Stromer, 1936; Weiler, 1935). Furthermore, *Lepidotes* (Stromer, 1936; Weiler, 1935) is assumed to occur in the Bahariya Formation based on scales and few isolated teeth (Weiler, 1935: pl. II, Figs. 5–8 and 13). However, the material is probably referable to polypterids such as *Bawitius* (Grandstaff, 2006, 2012; Smith et al., 2006; Stromer, 1936), although *Lepidotes* is a well-known taxon, of which complete skulls are known from the Kem Kem beds of Morocco (Forey et al., 2011). Another actinopterygian is the predatory *Stromerichthys*, known from articulated cranial remains (Stromer, 1936; Weiler, 1935), and named by Weiler (1935) in honour of Ernst Stromer von Reichenbach.

There are three actinopterygian fishes that are under nomenclatural debate such as *Paranogmius* (Cavin & Forey, 2008; Stromer, 1936; Weiler, 1935), which is known from cranial remains and a partial vertebral column (Weiler, 1935; Fig. 4). The specimens, like many other, were destroyed during the Second World War and today it is assumed to be conspecific with *Concavotectum moroccensis* (Cavin & Forey, 2008). The second taxon is *Saurodon*, which was identified by Stromer (1936). Saurodontids were already mentioned by Weiler (1935) based on isolated teeth. Weiler (1935) and Stromer (1936) furthermore mentioned another possible ichthyodectid, *Portheus*, but only few conical teeth were potentially identified. The third taxon is *Plethodus* (Cavin & Forey, 2001; Stromer, 1914a, 1936; Weiler, 1935). Two species were identified based on teeth and palatal remains, but the holotypes were destroyed during the Second

World War. Today, some species of *Plethodus* are believed to belong to *Palaeonotopterus* (Cavin & Forey, 2001).

Although Osteichthyes are not as diverse as cartilaginous fishes, they are represented by some peculiar groups such as lungfishes and coelacanth. Both are often referred to as ‘living fossils’ and belong to Sarcopterygii (lobe-finned fishes). Lungfishes (Dipnoi) exhibit a basal sarcopterygian bauplan and retained the ability to breathe air. They are represented by the well-known and abundant *Ceratodus* (Churcher & Iuliis, 2001; Stromer, 1914a, 1914b, 1936), which has an almost worldwide distribution ranging from the early Triassic (Romano et al., 2016) to the earliest Eocene (Cione et al., 2011). *Ceratodus* from Bahariya was studied in detail by Peyer (1925) and Churcher and Iuliis (2001) based on the typically isolated tooth plates. Besides *Ceratodus*, several authors (Churcher & Iuliis, 2001; Slaughter & Thurmond, 1974) reported remains of *Neoceratodus* from the Bahariya Formation and Churcher and Iuliis (2001) suggest that some specimen of *Neoceratodus* belong to another genus, *Retodus* (Churcher et al., 2006). *Ceratodus* probably lived in a freshwater habitat in the Bahariya Formation as Dipnoi are known to live in freshwater environments during the Mesozoic (Cavin et al., 2007). Another freshwater inhabitant is *Mawsonia lybica*, a giant coelacanth, the holotype of which was also lost during the Second World War (Grandstaff, 2006; Stromer, 1936; Weiler, 1935). The number of North African species of *Mawsonia* is currently under debate (Carvalho & Maisey, 2008; Cavin & Forey, 2004). *Mawsonia* is otherwise well-known from the Early Cretaceous of Brazil and could reach up to 6.5 m in body length (e.g. Carvalho & Maisey, 2008). Fossil remains of this genus are very abundant in the Bahariya Formation, especially cranial material, and therefore, it represents one of the most characteristic faunal elements of the Bahariya assemblage (Grandstaff, 2006; Weiler, 1935).

3.3 Testudinata

Turtle remains are numerous in the Upper Cretaceous sedimentary rocks of the Bahariya Formation but usually incomplete and poorly preserved (Stromer, 1934a). Only one genus and species has been named from these deposits to date, *Apertotemporalis baharijensis* (Stromer, 1934a). Additional material was described by Stromer (1934b) and referred to the Pleurodira. This includes several purported pleurodiran carapacial and plastral fragments from Gebel El Dist and Gebel Mandische (Stromer, 1934a). A partial femur, previously described as a testudinid humerus by Daqué (1912), from the upper part of the Gebel El Dist section was tentatively assigned to the Pelomedusidae by Stromer (1934b). Moreover, Stromer (1934b) referred a large cervical vertebrae and fragments of a large carapax, both collected from a basal level near Gebel Majesre, to the Pleurodira, noting some similarities with the Chelidae. Interestingly, the well-known Kem Kem beds of Morocco have also exclusively yielded pleurodiran turtle remains to date (Ibrahim et al., 2020a).

3.3.1 *Apertotemporalis baharijensis*

The genus and species *Apertotemporalis baharijensis* (Fig. 5) was erected for three fragmentary cranial remains discovered at Gebel El Dist (Stromer, 1934a). The specimens were found close to each other in a greyish sandy mudstone layer at the base of the exposed section. Two of them show a perfect fit and together comprise the partial braincase and the ear regions. The third element probably is part of the anterior part of the skull (Stromer, 1934a). Stromer (1934b) noted similarities to several cryptodiran and pleurodiran turtles but did not conclude to which higher taxon the new genus and species belonged. Subsequent studies generally classified *Apertotemporalis* as a bothremydid pleurodiran (de Lapparent de Broin, 2000; Pérez-García, 2017; Zalmout et al., 2005).

3.4 Crocodyliformes

Crocodylian remains are numerous in the Bahariya Formation and belong to at least three, possibly up to five different taxa: *Libycosuchus brevirostris*, *Stomatosuchus inermis* and *Aegyptosuchus peyeri*, as well as two indeterminate genera. These taxa differ markedly from each other in some cases, ranging from small and probably terrestrial forms (*Libycosuchus*) to very large, semi-aquatic and probably piscivorous animals (*Stomatosuchus*).

3.4.1 *Libycosuchus brevirostris*

The first crocodylian described from the Bahariya Formation was *Libycosuchus brevirostris* (Fig. 6), which was founded

on a well-preserved skull and lower jaws, as well as three dorsal vertebrae and one caudal vertebra, all assignable to one individual (Stromer, 1914b). The material was collected in 1911 from the lower-most horizon at Gebel El Dist in the northern part of the Bahariya depression. Stromer (1914b) erected the new family Libycosuchidae for the genus, which he presumed to be most closely related to *Notosuchus* and *Theriosuchus* (Stromer, 1914b, 1933, 1936). Stromer reconstructed *Libycosuchus* as a terrestrial carnivorous animal (Stromer, 1914b, 1936), a notion also supported by later studies (Buffetaut, 1976). In contrast to most other vertebrate material described by Stromer, the holotype specimen of *Libycosuchus* survived the Second World War (Serenó & Larsson, 2009; Tumarkin-Deratzian et al., 2004). Additional material of *Libycosuchus* was collected during the early 2000s from the Bahariya Formation, including articulated dentaries and two associated vertebrae from two separate localities (Tumarkin-Deratzian et al., 2004). In general, libycosuchids were a family of small, short-snouted and likely terrestrial predatory crocodylians with a wide distribution across the Cretaceous of northern Africa (Buffetaut, 1976). Recent phylogenetic analyses place *Libycosuchus* (and the family Libycosuchidae) within the Notosuchia, a very successful group of terrestrial crocodyliforms, primarily known from the Cretaceous of Gondwana (Larsson & Sues, 2007; Pol et al., 2014).

3.4.2 *Stomatosuchus inermis*

The holotype of *Stomatosuchus inermis* (Fig. 7) comprises a partial skull, the right lower jaw, as well as a fragmentary cervical and sacral vertebra of one individual (Stromer, 1925). The holotype specimen represents a very large crocodylian, with an estimated skull length of almost 2 m when complete (Stromer, 1925). Aside from the huge size, the cranium of *Stomatosuchus* is also remarkable for its peculiar anatomy, including the long, flat and broad skull, very small teeth and the weak symphysis of the lower jaws (Stromer, 1925). Additional cranial material of the genus was described by Stromer (1933). Due to the peculiar anatomy of the genus, Stromer (1925) erected the new family Stomatosuchidae to encompass this genus, the phylogenetic relationships of which, however, remaining unclear for decades, also because the remains of *Stomatosuchus* were destroyed during the Second World War. Recently, a very similar crocodyliform genus, *Laganosuchus*, has been described based on mandible remains from the Echkar Formation of Niger (*Laganosuchus thaumastos*) and the Kem Kem beds of Morocco (*Laganosuchus maghrebensis*) (Serenó & Larsson, 2009). Like *Stomatosuchus*, *Laganosuchus* is a member of Stomatosuchidae, which was placed within Neosuchia by Sereno and Larsson (2009). Stomatosuchids were reconstructed as semi-aquatic crocodyliforms hunting for fish in shallow water (Serenó &

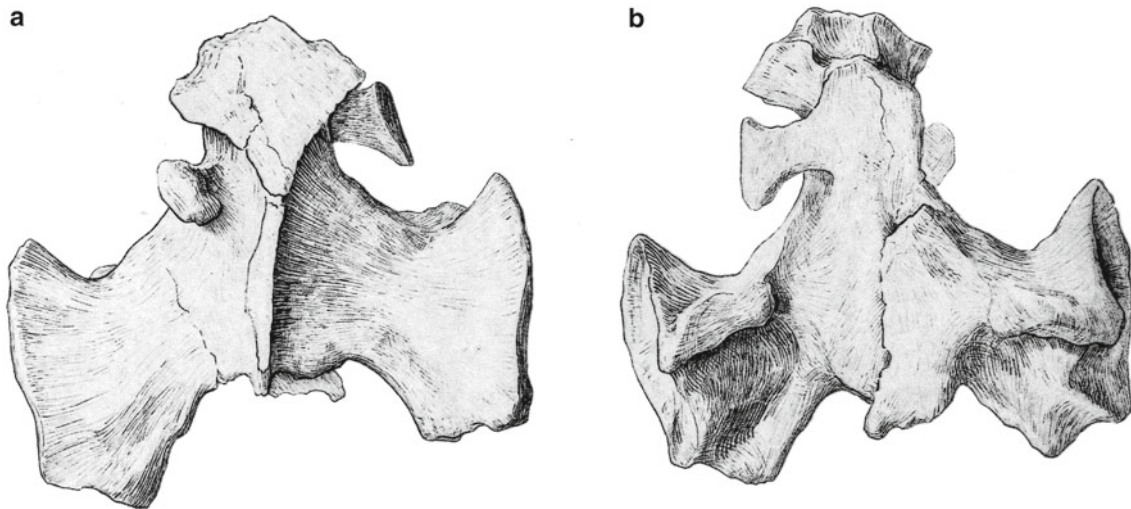


Fig. 5 Holotype partial cranium of the turtle *Apertotemporalis baharijensis* from the Upper Cretaceous Bahariya Formation in dorsal (*1a*) and ventral view (*1b*). Modified after Stromer (1934a)

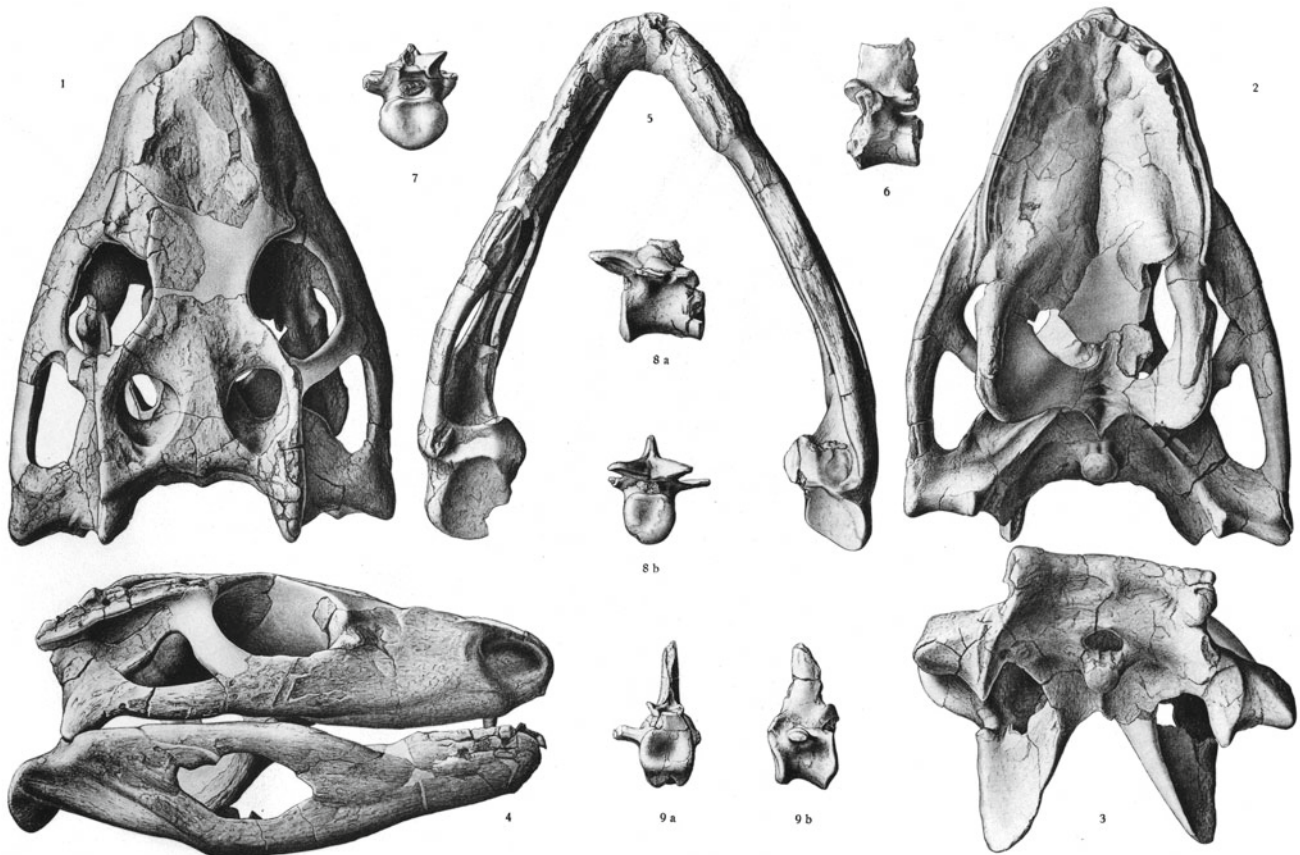


Fig. 6 Holotype material of the crocodyliform *Libycosuchus brevirostris* from the Upper Cretaceous Bahariya Formation. 1–4 Cranium in dorsal (1), ventral (2), posterior (3) and right lateral view (4); 5 lower jaw in dorsal view; 6–8 three dorsal vertebrae in right lateral (6), posterior (7), right lateral (8a) and posterior view (8b); 9 caudal vertebra in posterior (9a) and left lateral view (9b). All to the same scale, cranium about 165 mm long. Modified after Stromer (1914b)

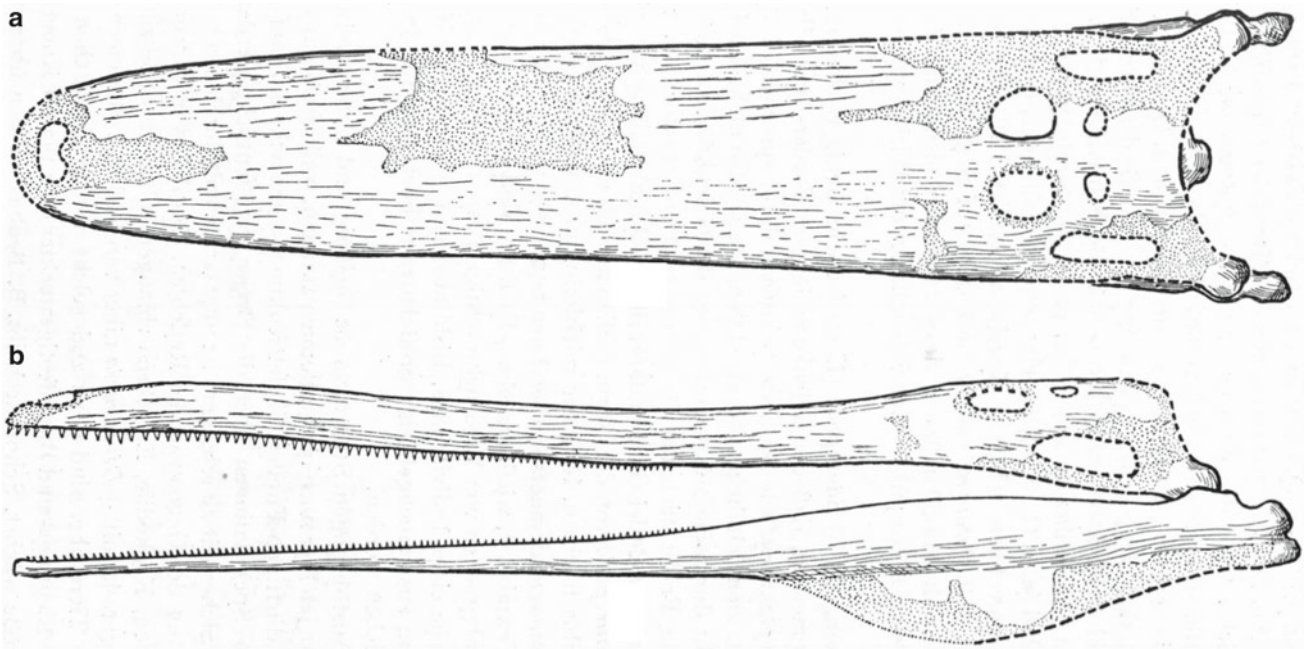


Fig. 7 Reconstruction of the holotype skull of the crocodyliform *Stomatosuchus inermis* from the Upper Cretaceous Bahariya Formation in dorsal (a) and left lateral view (b). The skull has a length of almost 2 m. Modified after Stromer (1936)

Larsson, 2009; Stromer, 1936); it has even been suggested that *Stomatosuchus* possessed a pelican-like gular pouch below the lower jaw (Nopcsa, 1926; Stromer, 1933), though there is currently no evidence for this (Serenó & Larsson, 2009).

3.4.3 *Aegyptosuchus peyeri*

A partial skull, comprising the braincase and skull roof as well as several isolated teeth discovered in 1912 at Gebel El Dist several meters above the basal-most dinosaur layer, were the basis for the erection of a new genus and species, *Aegyptosuchus peyeri* (Stromer, 1933). Additional referred material includes an articular, and several cervical, dorsal and caudal vertebrae, a coracoid, scapula, ilium, ischium, pubis, femur and a metatarsal (Stromer, 1933). However, Stromer (1933) cautioned that the referral of these postcranial specimens to *Aegyptosuchus* is somewhat speculative. The holotype of *Aegyptosuchus* was one of the few remains that survived the Allied bombing of Munich during the Second World War. Like for the other peculiar crocodyliform taxa from the Bahariya Formation, Stromer (1933) erected a distinct family for the genus, Aegyptosuchidae. Recent cladistic phylogenetic analyses recovered *Aegyptosuchus* as a derived eusuchian, most closely related to *Aegisuchus* from the Upper Cretaceous Kem Kem beds of Morocco (Holliday & Gardner, 2012). Notably, Ibrahim et al. (2020a) suggested that *Aegyptosuchus* is almost indistinguishable from *Stomatosuchus* based on the preserved elements and that the former might turn out to be a

junior synonym of the latter; the same might then be true for *Aegisuchus* and *Laganosuchus*, respectively (Ibrahim et al., 2020a). In this case, the family Aegyptosuchidae would be synonymous with Stomatosuchidae (Ibrahim et al., 2020a).

3.4.4 Indeterminate Crocodyliforms ('Krokodilier G and F')

Due to the fragmentary nature of most crocodylian remains from the Bahariya Formation and an associated lack of overlapping material, Stromer (1933) discussed the difficulties of deciding how many crocodyliforms were really present in the assemblage. He concluded that a minimum of five genera are probably represented by the material: *Libycosuchus brevirostris*, *Stomatosuchus inermis* and *Aegyptosuchus baharijensis*, as well as two indeterminate crocodyliforms (Stromer, 1933, 1936). The two indeterminate forms are Stromer's 'Krokodilier (crocodylian) G' and 'Krokodilier F', which differ significantly from all the other known crocodylians of the Bahariya Oasis (Stromer, 1933). 'Krokodilier G' is based on a partial lower jaw from an unknown locality of the Bahariya Oasis (Stromer, 1933). 'Krokodilier F' is known too from a fragmentary lower jaw that was collected three kilometres east of Ain Gedid (Stromer, 1933). Stromer (1933) noted that 'Krokodilier F' is overall similar to *Bottosaurus* from the Upper Cretaceous of North America but, based on some noteworthy anatomical differences and the spatio-temporal separation of the two forms, he concluded that they are probably not congeneric (Stromer, 1933). Later, Kuhn (1936) erected two genera,

Stromerosuchus and *Baharijodon*, which he based on fragmentary and indeterminate material of Stromer; these are, however, nowadays considered to represent nomina dubia (e.g. Nothdurft & Smith, 2002).

3.5 Dinosauria

At least five different genera of dinosaurs have been identified in the Cenomanian deposits of the Bahariya Formation, including three theropods and two sauropods: *Spinosaurus aegyptiacus*, *Carcharodontosaurus saharicus* and *Bahariasaurus ingens*, as well as *Aegyptosaurus baharijensis* and *Paralititan stromeri*. Furthermore, additional but indeterminate mid- to large-sized theropods and two more sauropods were possibly present in the faunal assemblage of the Bahariya Formation (see below). The vertebrate fauna is thus characterised by the presence of three (possibly up to five) large-bodied carnivorous theropods. This rather unusual faunal composition, also known as ‘Stromer’s Riddle’ (McGowan & Dyke, 2009), has also been observed in some other North African localities, most famously the Kem Kem Beds of Morocco (Ibrahim et al., 2020a). Despite early reports to the contrary (Stromer, 1914a, 1914b), ornithischians are apparently absent from the Bahariya Formation. Evidence of ornithischians is extremely rare in the contemporaneous well-known (and better sampled) Kem Kem beds of Morocco, consisting of one fragmentary tooth crown and a footprint (Ibrahim et al., 2020a).

3.5.1 *Spinosaurus aegyptiacus*

Spinosaurus (Figs. 8, 9 and 10) is probably the most famous Egyptian dinosaur and one of the most iconic dinosaurs in general, mostly owing to its bizarre anatomy and the enormous size of the animal as well as its inferred palaeoecological adaptations. The type material of this genus was found in 1912 by Richard Markgraf approximately 3 km north of Gebel El Dist in the northern part of the Bahariya Oasis and described by Stromer in 1915. The material was recovered from a white muddy sandstone layer situated at the base of the Gebel El Dist profile near the floor of the Bahariya Oasis (Stromer, 1914a, 1915). The bones were found close to each other but were disarticulated, randomly arranged and some of them suffered minor distortion and breakage (Stromer, 1915). The type material comprises the left and right partial mandibles with teeth but missing the posterior parts, a left angular, a fragment of the left maxilla, more than a dozen isolated teeth, two cervical vertebrae, seven dorsal vertebrae, three sacral vertebrae, one anterior caudal vertebra, fragmentary dorsal ribs and several gastralia, all belonging to one individual (Stromer, 1915). Later, Stromer (1933) questioned the assignment of the caudal vertebra to the holotype individual. More recently, the

referral of the holotype material to one individual was also questioned by Rauhut (2003), though most authors agree with Stromer’s (1915) interpretation of all the holotype material being derived from one individual (Dal Sasso et al., 2005; Evers et al., 2015; Ibrahim et al., 2020a). The specimen was probably exposed to surficial weathering before discovery as indicated by the bleached and cracked appearance of some bones; most bones are, however, well-preserved with delicate processes and laminae being present (Stromer, 1915). Interestingly, the right dentary exhibits a weak thickening, likely representing a pathology caused by injury (Stromer, 1915).

Stromer (1915) noted that *Spinosaurus* likely had a long and narrow snout, conical teeth and exceptionally long spinal processes (up to eight times higher than the centrum). He rejected the idea of these extremely elongated spinal processes having functioned as attachment sites for muscles or as a fatty hump, and compared them to pelycosaur and extant lacertilians concluding that they instead likely formed a narrow sail (Stromer, 1915); later, he suggested them to be akin to display structures (Stromer, 1936). Based on the holotype description of *Spinosaurus*, Stromer (1915) erected the Spinosauridae, a diverse family now including several different genera from South America, Africa, Asia and Europe (for an overview of spinosaurid diversity, see Evers et al., 2015; Hone & Holtz, 2017). Additional remains probably also referable to the type species *S. aegyptiacus* comprising vertebrae, teeth and ribs are known from a similar horizon near Gebel El Dist and from Gebel Maisara to the south (Stromer, 1915).

Another specimen comprising isolated teeth, five cervical and dorsal vertebrae, and a series of seven caudal vertebrae from Gebel El Harra was referred to ‘*Spinosaurus B*’, differing from the type material and perhaps representing another species (Stromer, 1934b). Russell (1996) referred ‘*Spinosaurus B*’ to the new genus and species *Sigilmassasaurus brevicollis*, which he based on isolated material from the Kem Kem beds of Morocco; in the same paper, he also erected a new species of *Spinosaurus*, *Spinosaurus maroccanus*, for material from Morocco (Russell, 1996). Alternatively, the material pertaining to ‘*Spinosaurus B*’ was also referred to *C. saharicus* (Sereno et al., 1996). For a detailed discussion of ‘*Spinosaurus B*’ and its systematic affinities (including a potential synonymy with *S. aegyptiacus* or *Sigilmassasaurus*), see Evers et al. (2015) and Ibrahim et al. (2020a). In addition, Stromer (1934a) described further postcranial material, including a femur and tibiae that he referred to ‘*Spinosaurus B*’. Although the *Spinosaurus* remains described by Stromer have been destroyed during the Second World War in Munich, they are still among the best-preserved and most complete specimens of the genus.

Additional material discovered since then in Algeria, Tunisia and most prominently a partial skeleton from the

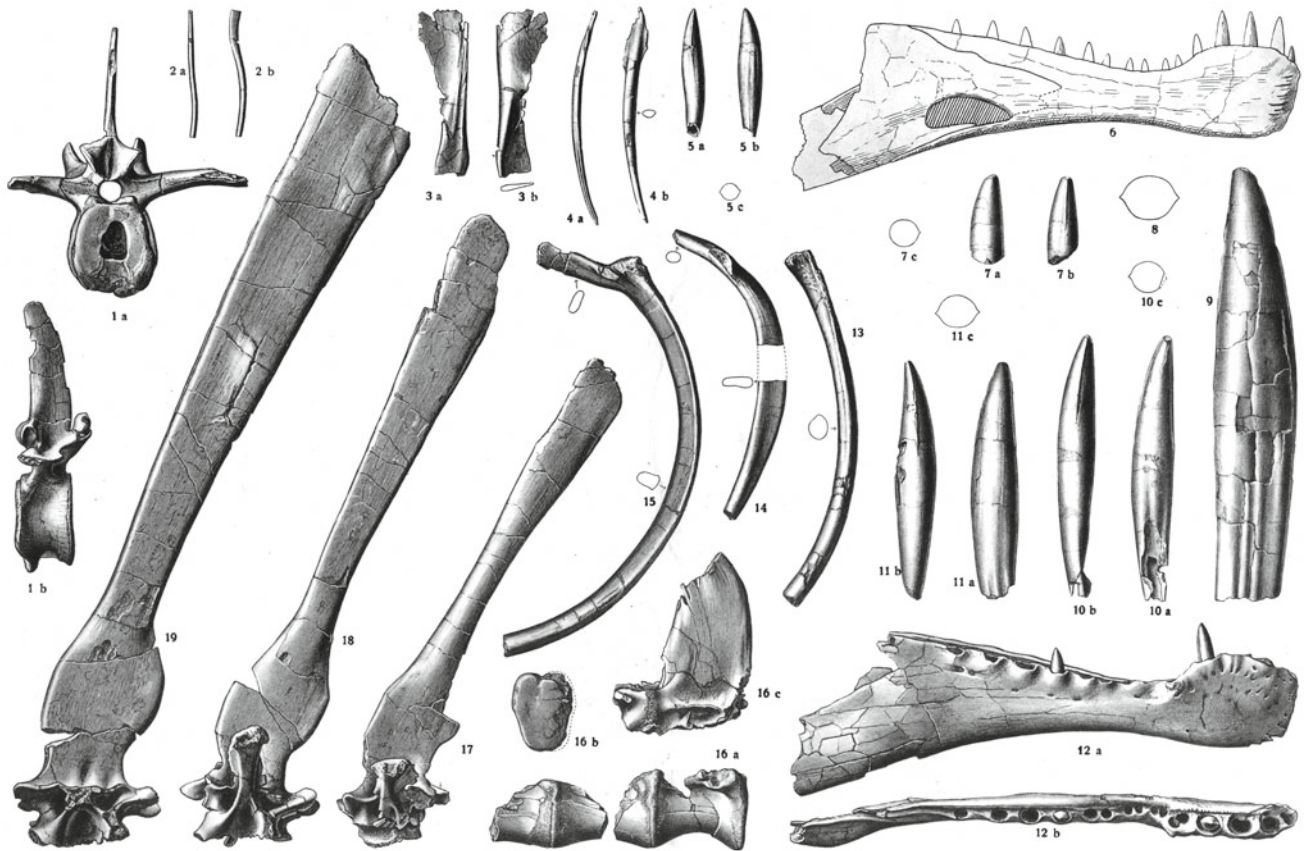


Fig. 8 Holotype material of the theropod dinosaur *Spinosaurus aegyptiacus* from the Upper Cretaceous Bahariya Formation. 1 Anterior caudal vertebra in posterior (1a) and right lateral view (1b); 2 fragmentary gastral rib; 3 left angular in external (3a) and internal view (3b); 4 gastral rib; 5 smallest tooth; 6 left lower jaw in internal view; 7 first left tooth of the lower jaw; 8 second largest isolated tooth from the right upper jaw; 9 largest isolated tooth from the right upper jaw; 10–11 two medium-sized teeth from the posterior part of the upper jaw; 12 right lower jaw in external and dorsal view; 13–15 three fragmentary ribs; 16 three sacral vertebrae in right lateral view (16a), anterior view of sacral vertebra (16b), and neural arch of sacral vertebra in right lateral view (16c); 17–19 neural arch and spinal processes of anterior dorsal vertebrae in right lateral view. Figures 1–4, 6 and 12–19 as well as 5 and 7–11 to the same scale, respectively. Modified after Stromer (1915)

Kem Kem beds of Morocco (Ibrahim et al., 2014, 2020b; this specimen was also suggested as a neotype for the genus, but see Evers et al., 2015 for an alternative view on the association of the material), have shed new light on the anatomy and palaeoecology of *Spinosaurus*. Especially the partial skeleton from Morocco has been interpreted as showing several features (e.g. weakly developed hind limbs and a unique tail anatomy indicating a propulsive function in water) that indicate semi-aquatic habits of *Spinosaurus* (Ibrahim et al., 2014, 2020b), a notion independently confirmed by stable isotope data of spinosaurid bones and teeth (Amiot et al., 2010a), as well as taphonomical data (Beever et al., 2021). This interpretation has been questioned recently, however, based on taphonomical, biomechanical and anatomical considerations (Evers et al., 2015; Henderson, 2018; Hone & Holtz, 2019, 2021). Concordant with a presumed semi-aquatic habit, *Spinosaurus* and related genera have been interpreted as (at least partially) piscivorous animals based on a gut content (Charig & Milner, 1997),

biomechanical modelling (Cuff & Rayfield, 2013) and stable isotope analysis (Amiot et al., 2010a; Hassler et al., 2018); this idea of a fish-eating *Spinosaurus* has also been proposed already by Stromer (1936: 71). Moreover, based on these new specimens (primarily a partial snout from Morocco), it has been shown that *Spinosaurus* was among the largest of all theropod dinosaurs (Dal Sasso et al., 2005).

3.5.2 *Carcharodontosaurus saharicus*

The second theropod genus that was described from the Bahariya deposits is *Carcharodontosaurus saharicus* (Figs. 11 and 12), an extremely large-sized carnivorous dinosaur, rivalling the famous *Tyrannosaurus* in size (Serenio et al., 1996). The holotype of this genus was collected in 1914 by Richard Markgraf from a basal marl horizon at Gebel Harra (Stromer, 1931). The holotype comprises two femora, a left fibula, both pubes, a left ischium, three cervical vertebrae, a caudal vertebra, a fragmentary rib and chevron as well as a fragmentary cranium including the

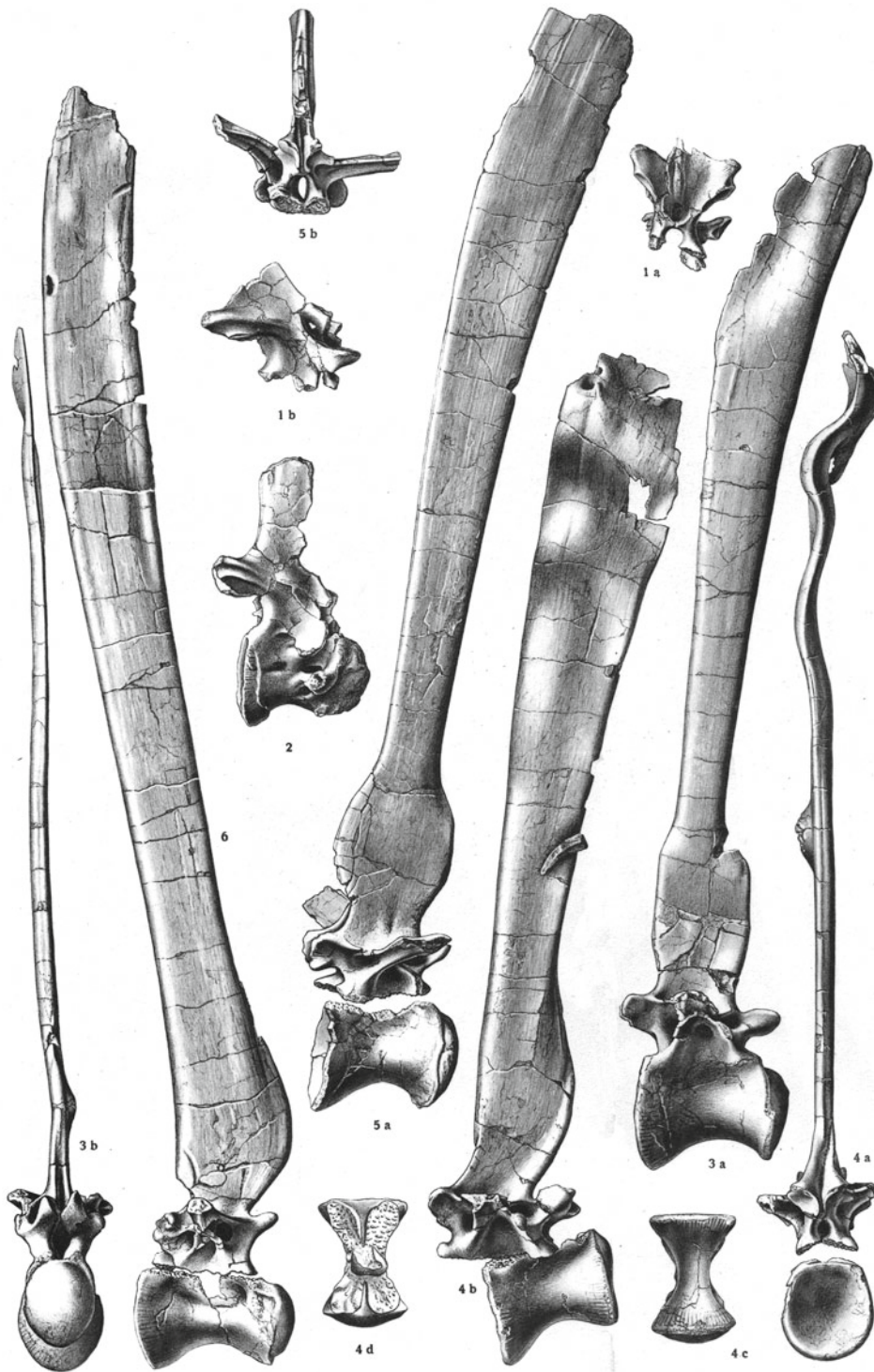


Fig. 9 Holotype material of the theropod dinosaur *Spinosaurus aegyptiacus* from the Upper Cretaceous Bahariya Formation. 1 Neural arch of an anterior cervical vertebra in posterior (1a), and right lateral view (1b); 2 middle or posterior cervical vertebra in right lateral view; 3 middle dorsal vertebra in right lateral (3a), and anterior view (3b); 4 middle dorsal vertebra in posterior (4a), right lateral (4b), ventral (4c) and dorsal view (4d); 5 posterior dorsal vertebra in right lateral (5a) and posterior view (5b); 6 posterior dorsal vertebra in right lateral view. All to the same scale. Modified after Stromer (1915)

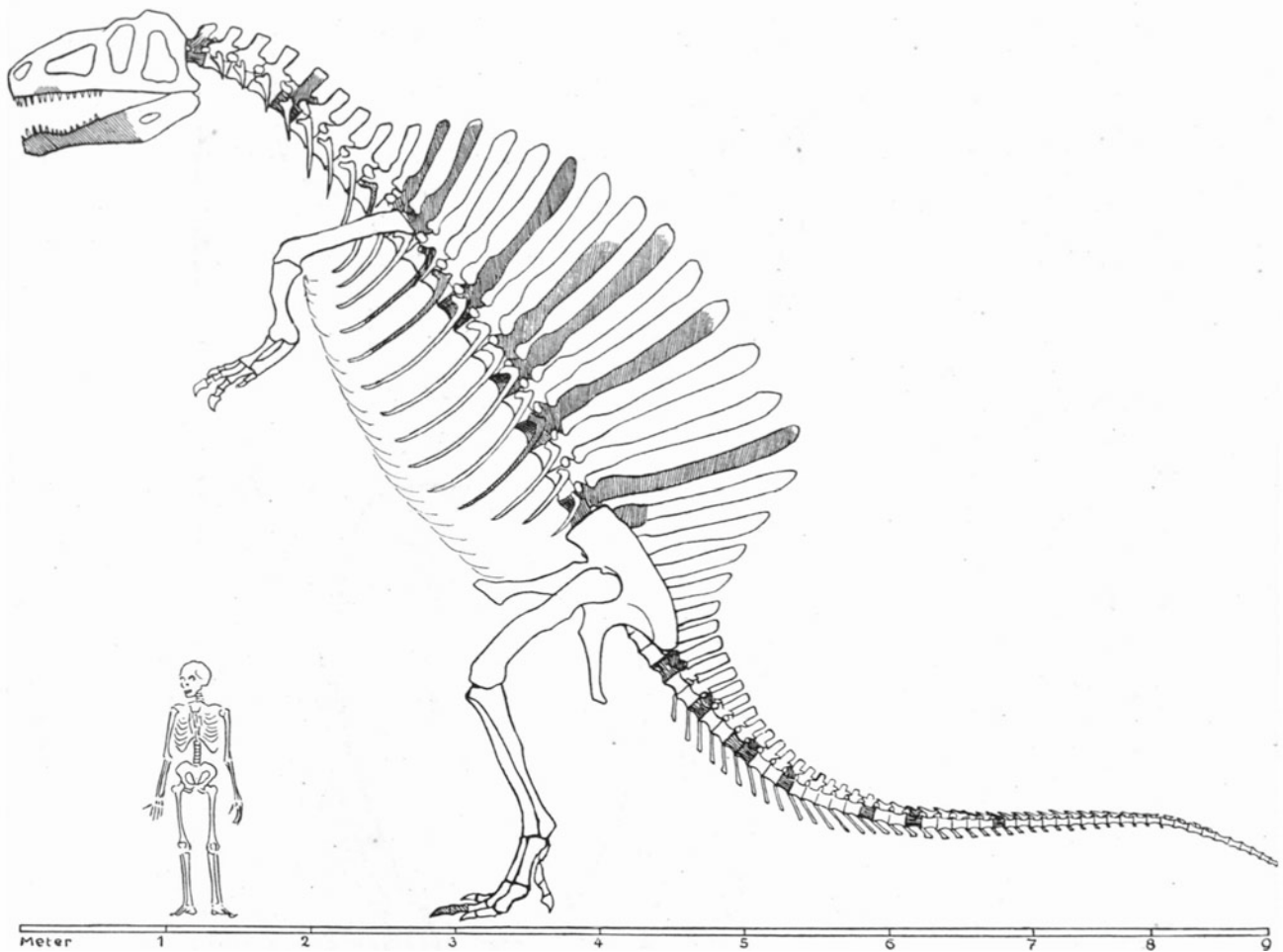


Fig. 10 Reconstruction of the skeleton of *Spinosaurus aegyptiacus*. The parts of the skeleton that were known to Stromer are shaded. Modified after Stromer (1936)

braincase, frontals and parietals, nasals, maxilla and teeth (Stromer, 1931). Based on the resemblance of the teeth to those of the shark genus *Carcharodon*, Stromer (1931) named the new theropod *Carcharodontosaurus*. He also referred teeth from the ‘Continental Intercalaire’ of Algeria to this genus, originally described as *Megalosaurus sahariensis* (Deparet & Savornin, 1925). Based on the description of this material, Stromer (1931) coined the family Carcharodontosauridae, a highly successful family of very large carnivorous dinosaurs, mainly known from the Cretaceous of Gondwana (for an overview of carcharodontosaurid diversity, see Novas et al., 2005, 2013). Additional remains, including a right ilium, from the lower-most level at Gebel el Dist were later assigned to *Carcharodontosaurus* (Stromer, 1934b), though their referral to this genus is questionable (Rauhut, 1995).

Carcharodontosaurus seems to have been relatively widespread in the Upper Cretaceous of Northern Africa, remains of this genus having been recovered from Algeria

(Benyoucef et al., 2015), Morocco (Serenio et al., 1996), Niger (Brusatte & Sereno, 2007) and Tunisia (Fanti et al., 2012). As for *Spinosaurus*, especially spectacular discoveries in the Kem Kem beds of Morocco, including a well-preserved skull missing the lower jaws, have greatly improved our understanding of this taxon (Serenio et al., 1996). This skull, which was also proposed to serve as the neotype for the genus (Brusatte & Sereno, 2007), has an estimated total length of 1.6 m, which is longer than that of the famous *Tyrannosaurus rex* from North America, making *C. sahariensis* one of the largest meat-eating land vertebrates of all time (Serenio et al., 1996). More recently, cranial remains from the Upper Cretaceous (Cenomanian) Echkar Formation of Niger were designated as the holotype of a new species of *Carcharodontosaurus*, *C. iguidensis* (Brusatte & Sereno, 2007). In contrast to *Spinosaurus*, *Carcharodontosaurus* is regarded as a terrestrial animal preying mostly upon large-sized land vertebrates (Amiot et al., 2010a, 2010b; Beevor et al., 2021; Hassler et al., 2018; Stromer, 1936).



Fig. 11 Holotype material of the theropod dinosaur *Carcharodontosaurus saharicus* from the Upper Cretaceous Bahariya Formation. 1 Isolated tooth; 2 unerupted anterior tooth from the left maxilla; 3 cross-section of a right unerupted maxillary tooth; 4 cranium in right lateral (4a), dorsal (4b), and posterior view (4c); 5 endocast of the brain cavity in right lateral (5a) and dorsal view (5b); 6 left maxilla in internal (6a) and external view (6b); 7 right nasal in dorsal and external (7a) and internal (7b) view; 8 axis in anterior view; 9 anterior cervical vertebra in left lateral view; 10 anterior caudal vertebra in right lateral (10a) and anterior view (10b); 11 chevron in right lateral (11a), anterior (11b) and dorsal view (11c); 12 left ischium; 13 left pubis (13a) with cross-sectional views of the shaft (13b–c); 14 left femur in anterior view (14a) and reconstructed ventral view of the right femur (14b); 15 left fibula in anterior view (15a) and cross-sectional views (15b–d). Figures 1–3 and 4–15 to the same scale, respectively

3.5.3 *Bahariasaurus ingens* and *Deltadromeus agilis*

The third large-bodied theropod dinosaur from Bahariya is the enigmatic and rather poorly known *Bahariasaurus ingens* (Figs. 13 and 14). The holotype material of this genus has been recovered from a mudstone horizon at Gebel Ghorabi near the northern margin of the Bahariya depression (Stromer, 1934b). The material comprises two dorsal vertebrae, a neural arch, ribs, three coalesced sacral vertebrae, a right ischium and both pubes, all attributable to one individual (Stromer, 1934b). Moreover, Stromer (1934a) referred several additional specimens to this taxon, including a cervical vertebra and two dorsal vertebrae discovered 4 km south of Gebel Ghorabi, a left and right pubis from Gebel Ghorabi, a right scapula from Ain Murun in the north-western part of the depression, a right ischium discovered 2.5 km east of Gebel El Dist, two caudal vertebrae and two small conjoined pubes discovered 3.5 km east of Gebel El Dist, a small right ischium discovered 1 km south of Gebel

El Dist, as well as three dorsal vertebrae, two caudal vertebrae, a neural arch, a left and right femur, and a left fibula from Gebel El Dist. In addition, he assigned a cranial fragment, nine caudal vertebrae, a left scapula and a left coracoid from Gebel El Dist to this genus (Stromer, 1934b). Like *Spinosaurus* and *Carcharodontosaurus*, *Bahariasaurus* was an extremely large-sized theropod (Stromer, 1934b), the right femur from Gebel El Dist being only slightly shorter than that of *T. rex* (Serenó et al., 1996).

In light of the poor preservation and the size differences of the material mentioned above, Stromer (1934a) cautioned that the material might pertain to more than one species or even genus. In fact, the classification and taxonomic status of *Bahariasaurus* has proven to be especially challenging. Although Stromer (1934a) did not regard *Bahariasaurus* as being closely related to the other theropod genera of the Bahariya Formation, Rauhut (1995) suggested that both *Bahariasaurus* and *Carcharodontosaurus* might in fact belong to the Carcharodontosauridae. Some of the material

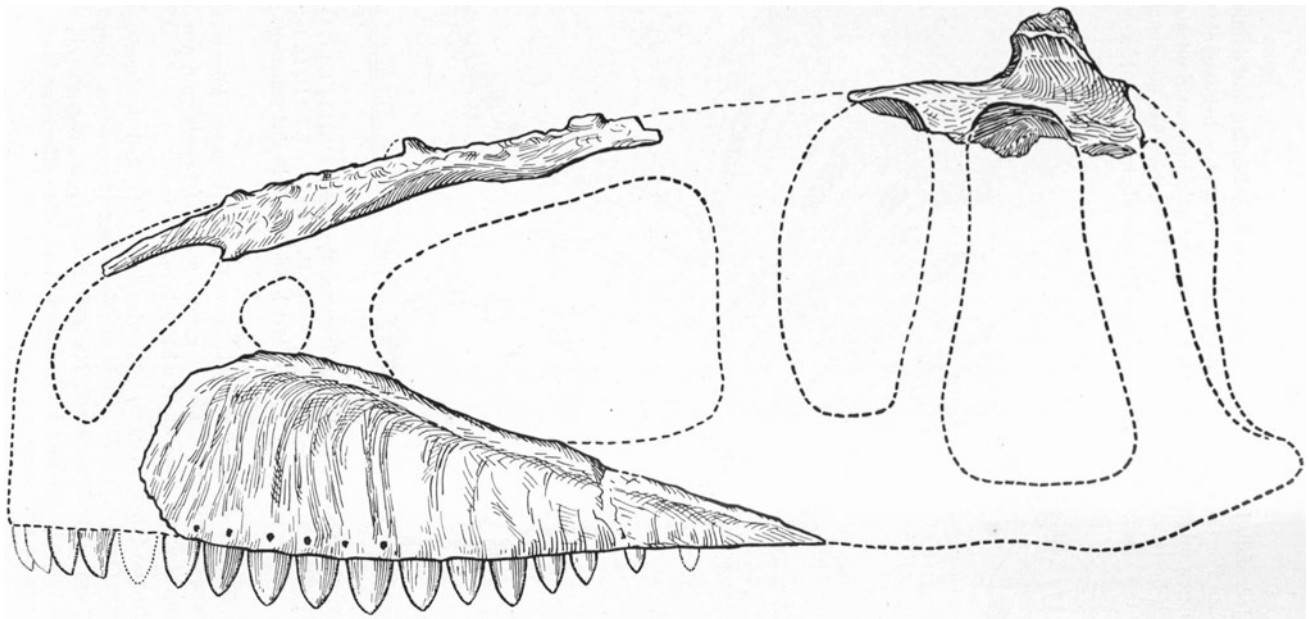


Fig. 12 Reconstruction of the holotype cranium of *Carcharodontosaurus saharicus* in left lateral view. Modified after Stromer (1936)

(including left coracoid, pubes, right tibia, left fibula, right femur), referred to *Bahariasaurus* by Stromer (1934a), was later assigned to *Deltadromeus agilis*, which was founded on a partial skeleton from the Kem Kem beds of Morocco (Serenio et al., 1996). Recently, *Bahariasaurus* was even regarded as a nomen dubium, while several elements assigned to it were referred to *Deltadromeus* (Ibrahim et al., 2020a), thus agreeing with the classification of Sereno et al. (1996). *Deltadromeus* in turn has been classified as a basal coelurosaur (Serenio et al., 1996), as being closely related to ornithomimosaur (Rauhut, 2003), as a noasaurid (Serenio et al., 2004), a basal ceratosaur (Carrano & Sampson, 2008; Chiarenza & Cau, 2016) or a neovenatorid, and thus closely related to *Carcharodontosaurus* (Apesteguía et al., 2016). In yet another recent study, *Bahariasaurus* was considered as a valid taxon distinct from *Deltadromeus*, but closely related to the latter and both, together with *Aoniraptor* from South America, forming the Bahariasauridae, a family (originally coined by von Huene, 1948) of megaraptoran theropods (Motta et al., 2016). Therefore, at least three, but possibly five (if *Bahariasaurus* and *Deltadromeus* as well as *S. aegyptiacus* and ‘*Spinosaurus B*’ are indeed distinct), different large-bodied theropods were likely present in the Bahariya faunal assemblage. Remains of *Bahariasaurus*, including six caudal vertebrae, have also been found in the ‘Continental Intercalaire’ of Niger (de Lapparent, 1960).

3.5.4 Indeterminate Theropods (aff. *Erectopus sauvagei* and cf. *Elaphrosaurus bambergi*)

Stromer (1934a) referred the distal part of a right femur to aff. *Erectopus sauvagei* (Fig. 14), a taxon originally known from

the Lower Cretaceous of France (von Huene, 1932). The femur was recovered in 1912 from a basal mudstone horizon at Gebel El Dist (Stromer, 1934b). A proximal tibia found in approximately the same horizon from Ain Murun was referred to the same taxon as the femur (Stromer, 1934a). A third element, a much smaller distal tibia, from Gebel Mandische was also tentatively assigned to aff. *E. sauvagei*, though likely representing a younger individual than the other two elements (Stromer, 1934a). All the material referred to aff. *E. sauvagei* most probably represents an indeterminate theropod (Weishampel et al., 2004). Two tibiae from Gebel El Dist were referred to aff. *Elaphrosaurus bambergi* (Fig. 14) (Stromer, 1934b), a taxon originally known from the famous Upper Jurassic dinosaur beds of Tendaguru, Tanzania (Janensch, 1920). Stromer (1934a) also assigned a right femur from Gebel Mandische to this taxon, that he initially classified as an ornithopod dinosaur (Stromer, 1914a). It should be noted that Stromer (1934a: 43–44) cautioned that the elements are overall similar to *Elaphrosaurus*, but do show significant differences and thus—together with the markedly different age—they certainly represent a different species but might be related to *Elaphrosaurus*. Like the other indeterminate theropod material mentioned above, the specimens referred to cf. *Elaphrosaurus* likely represent an indeterminate theropod dinosaur (Weishampel et al., 2004). Recently, the presence of an indeterminate abelisaurid has been preliminarily reported based on a cervical vertebra (Salem et al., 2018; Salem et al., 2022).

3.5.5 *Aegyptosaurus baharijensis*

The first sauropod remains described from the Bahariya Formation were unearthed in 1911 by Richard Markgraf

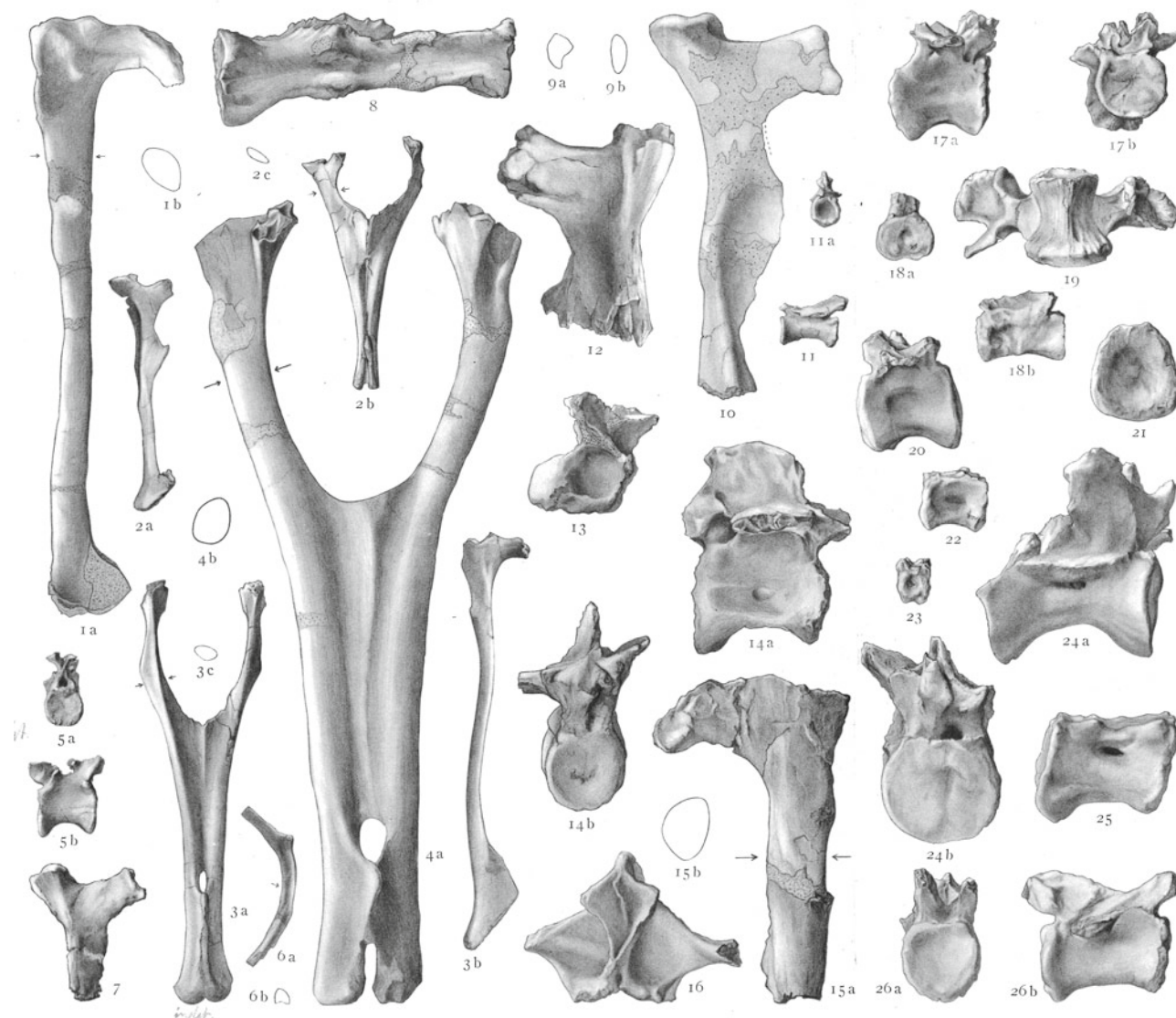


Fig. 13 Material of the theropod dinosaur *Bahariasaurus ingens*, including the holotype (4, 9, 10), and indeterminate theropods from the Upper Cretaceous Bahariya Formation. 1 Pubes of *Bahariasaurus* in left lateral view (1a) and in cross-sectional view (1b); 2 pubes of an indet. theropod in left lateral (2a), posterior (2b), and cross-sectional view (2c); 3 pubes of *Bahariasaurus* in posterior (3a) and cross-sectional view (3b); 4 pubes of *Bahariasaurus* in posterior (4a) and cross-sectional view (4b); 5 dorsal vertebra of an indeterminate theropod in posterior (5a) and right lateral view (5b); 6 fragmentary rib of an indeterminate theropod; 7 right ischium of *Bahariasaurus*; 8 three sacral vertebrae of *Bahariasaurus* in ventral view; 9 rib of *Bahariasaurus*; 10 right ischium of *Bahariasaurus*; 11 middle caudal vertebra of *Bahariasaurus* in posterior (11a) and left lateral view (11b); 12 left ischium of *Bahariasaurus*; 13 posterior cervical vertebra of *Bahariasaurus* in left lateral view; 14 posterior dorsal vertebra of *Bahariasaurus* in right lateral (14a) and anterior view (14b); 15 right pubis of *Bahariasaurus* in right lateral (15a) and cross-sectional view (15b); 16 neural arch of an anterior caudal vertebra of *Bahariasaurus* in posterior view; 17 anterior caudal vertebra of *Bahariasaurus* in left lateral (17a) and anterior view (17b); 18 posterior caudal vertebra of *Bahariasaurus* in anterior (18a) and left lateral view (18b); 19–23 posterior caudal vertebrae of indeterminate theropods in ventral (19), right lateral (20), anterior (21), right lateral (22) and anterior view (23); 24 posterior dorsal vertebra of *Bahariasaurus* in right lateral (24a) and anterior view (24b); 25 anterior caudal vertebra of *Bahariasaurus* in right lateral view; 26 middle caudal vertebra of *Bahariasaurus* in anterior (25a) and right lateral view (25b). All to the same scale. Modified after Stromer (1934b)

at Gebel El Dist (Stromer, 1932). The material comprises a dorsal vertebra, two caudal vertebrae, a left fragmentary scapula, left humerus, both ulnae, both radii, both femora and the left tibia, all belonging to one individual. Upon this material Stromer (1932) erected the new genus and species *Aegyptosaurus baharijensis* (Fig. 15), which he

referred to the Titanosauridae, a relatively widespread family of sauropods from the Cretaceous known primarily from Gondwana. Additional material belonging to a much smaller individual was tentatively assigned to this taxon by Stromer (1932), including an indeterminate vertebra, one caudal vertebra and two cervical vertebrae from



Fig. 14 Material of theropod dinosaurs from the Upper Cretaceous Bahariya Formation. 1 Left tibia of cf. *Elaphrosaurus* in anterior (1a) and cross-sectional view (1b); 2 left tibia of cf. *Elaphrosaurus* in anterior (2a) and cross-sectional view (2b); 3 left fibula of *Bahariasaurus* in medial (3a) and cross-sectional view (3b–c); 4 left tibia of aff. *Erectopus* in anterior (4a) and cross-sectional view (4b); 5 right femur of *Bahariasaurus* in anterior (5a), lateral (5b) and cross-sectional view (5c–d); 6 right proximal femur of cf. *Elaphrosaurus* in lateral view; 7 partial astragalus of an indeterminate theropod dinosaur in anterior (7a) and dorsal view (7b); 8 right proximal tibia of aff. *Erectopus* in dorsal (8a) and lateral view (8b); 9 right distal femur of aff. *Erectopus* in posterior (9a) and ventral view (9b); 10 right proximal femur of an indeterminate theropod in dorsal (10a) and posterior view (10b); 11 phalanx of an indeterminate theropod in right lateral (11a) and dorsal view (11b); 12 ungual phalanx of an indeterminate theropod in right lateral (12a) and dorsal view (12b); 13 left scapula of *Bahariasaurus* in lateral view; 14 left coracoid of *Bahariasaurus* in medial view; 15 right ilium of *Carcharodontosaurus* in medial view; 16 left proximal humerus of an indeterminate theropod in anterior (16a) and cross-sectional view (16b–d); 17 left humerus of an indeterminate theropod in posterior (17a) and cross-sectional view (17b–e); 18 right metatarsal IV of an indeterminate theropod in posterior (18a), dorsal (18b) and ventral view (18c). All to the same scale. Modified after Stromer (1936)

Gebel El Dist. Moreover, an isolated ungual phalanx of a large-sized sauropod (comparable in size to the holotype specimen) found at Gebel El Dist was referred to *Aegyptosaurus* (Stromer, 1932). Subsequently, fragmentary material from the ‘Continental Intercalaire’ of Niger has been referred to *Aegyptosaurus* by de Lapparent (1960), comprising caudal vertebrae, a partial rib and proximal portions of two metatarsals; this material might, however, represent indeterminate sauropod remains (Weishampel et al., 2004). More recently *Aegyptosaurus* was placed as a basal member of Titanosauria (Upchurch et al., 2004).

3.5.6 *Paralititan stromeri*

The second named sauropod dinosaur from the Bahariya faunal assemblage and the largest animal from this fauna is *Paralititan stromeri* (Smith et al., 2001). In fact, the genus represents the only tetrapod taxon from Bahariya named since Stromer’s descriptions of this vertebrate assemblage. It was founded on a partial skeleton, including two fused sacral vertebrae, two caudal vertebrae, dorsal and sacral ribs, both fragmentary scapulae, both humeri, and the distal part of a metacarpal (Smith et al., 2001). The specimen represents one of the largest known sauropods, with a humeral length of 1.69 m (Smith et al., 2001). A dorsal vertebra from Gebel El

Dist (Fig. 15) originally described by Stromer (1932) was tentatively referred to *Paralititan* (Smith et al., 2001). The initial phylogenetic analysis of Smith et al. (2001) recovered *Paralititan* as a titanosaurid, while later, it was classified as a lithostrotian titanosaur (Upchurch et al., 2004). Recent studies recovered *Paralititan* as a saltasaurid titanosaur together with several other Late Cretaceous titanosaurs (Gorscak & O'Connor, 2019; Sallam et al., 2018). The holotype material of *P. stromeri* was discovered at Gebel Fagga in strata representing tidal channel and tidal flat facies, thus indicating that sauropods habitually entered mangrove environments (Smith et al., 2001). A shed tooth crown of *Carcharodontosaurus* was discovered between the bones of the holotype, indicating that the theropod scavenged on the carcass of *Paralititan* (Smith et al., 2001). Due to a

presumed low water energy at the site, the carcass and the theropod tooth were most likely not transported to this locality, suggesting an autochthonous assemblage (Smith et al., 2001).

3.5.7 Indeterminate Sauropods (cf. *Dicraeosaurus* sp. and an Indeterminate Rebbachisaurid)

A poorly preserved caudal vertebra recovered from an unknown locality was referred to cf. *Dicraeosaurus* sp. by Stromer (1932). *Dicraeosaurus* is originally known from the Upper Jurassic dinosaur beds of Tendaguru, Tanzania (Janensch, 1914). Due to the fragmentary nature of the specimen and the temporal separation from other *Dicraeosaurus* occurrences, however, Stromer (1932) emphasised the tentative nature of this referral. In addition, Smith et al.



Fig. 15 Holotype material of the sauropod dinosaur *Aegyptosaurus baharijensis* (1–9) and an indeterminate sauropod dinosaur (10), both from the Upper Cretaceous Bahariya Formation. 1 Left humerus in anterior (1a) and cross-sectional view (1b–c); 2 right ulna in anterior (2a) and cross-sectional view (2b–c); 3 left radius in posterior (3a) and cross-sectional view (3b); 4 middle caudal vertebra in left lateral (4a), anterior (4b) and posterior view (4c); 5 ungual pedal phalanx in medial (5a) and cross-sectional view (5b–c); 6 left tibia in lateral (6a) and cross-sectional view (6b); 7 left femur in posterior (7a) and cross-sectional view (7b–c); 8 left scapula in lateral view; 9 anterior caudal vertebra in posterior (9a) and right lateral view (9b); 10 dorsal vertebra of an indeterminate sauropod dinosaur (might pertain to *Paralititan stromeri*, see text for explanations and Smith et al., 2001). All to the same scale. Modified after Stromer (1932)

(2001) noted the presence of a possible rebbachisaurid in the Bahariya faunal assemblage based on an isolated scapula. Rebbachisaurid remains are also known from several coeval deposits of northern Africa, including the Kem Kem beds of Morocco (Ibrahim et al., 2020a; Lavocat, 1954), and the ‘Continental Intercalaire’ of Tunisia (Fanti et al., 2012).

3.6 Plesiosauria

Remains of plesiosaurs are relatively common in the deposits of the Bahariya Formation but they mostly occur as isolated and fragmentary specimens (Stromer, 1935). Intriguingly, the fossils of plesiosaurs seem not to occur in the basal-most layers of the Bahariya depression, from which the majority of the vertebrate material was recovered (especially terrestrial ones), but instead they derive from a higher position in the sequence that probably reflects a marine depositional environment (Stromer, 1935). Moreover, the remains of plesiosaurs differ from those of the terrestrial vertebrates (e.g. dinosaurs) in terms of preservation and mostly comprise brownish bones as opposed to the often greyish to whitish bones of the dinosaurs (Stromer, 1935). This is in accordance of the presumed habitat of these predatory marine reptiles (Stromer, 1935, 1936). Similar to the other vertebrate groups, however, the most abundant and best-preserved specimens of plesiosaurs are known from Gebel El Dist (Stromer, 1935).

Although Stromer (1935) expected at least part of the plesiosaur material to belong to previously known species (because of the marine habitat and thus an assumed wider geographic distribution), he was unable to assign any of the material to a pre-existing plesiosaur taxon. Moreover, due to the fragmentary nature of the plesiosaur remains, Stromer (1935) also refrained from erecting a new genus or species based on the available material. Nonetheless, he distinguished at least four, and possibly up to seven, different plesiosaurs (‘Plesiosaurier A–D’) represented by isolated and associated cranial and postcranial material. Stromer (1936) noted that ‘Plesiosaurier D’ closely resembles *Trinacromerum* from the Upper Cretaceous of North America, thus suggesting a possible close relationship to that genus. Stromer (1936) favoured a near-shore and/or brackish habitat for the plesiosaurs of the Bahariya Formation, a hypothesis agreeing well with the presumed distinctiveness of the plesiosaur fauna. Interestingly, plesiosaur remains have not yet been reported from the Kem Kem beds of Morocco (Ibrahim et al., 2020a), despite a high degree of faunal similarity between both the Kem Kem and the Bahariya faunas and plesiosaurs representing a common faunal element in the latter.

3.7 Squamata (*Simoliophis* sp.)

Stromer (1914a, 1914b) reported the remains of a small snake from the Bahariya Formation, which were later described in detail by Nopcsa (1925). The material comprises numerous cervical, dorsal and caudal vertebrae, as well as rib fragments belonging to several individuals (Nopcsa, 1925). The remains were mostly recovered by Richard Markgraf, except for one individual that was collected by Ernst Stromer von Reichenbach (Nopcsa, 1925). Nearly all of the specimens originate from marine strata above the basal-most dinosaur bearing horizon, only one weathered vertebra was collected from this lower-most horizon (Nopcsa, 1925). Both Stromer (1914b) and Nopcsa (1925) referred the material to *Simoliophis* (spelled ‘*Symoliophis*’), otherwise known from the Cenomanian of France and Portugal, and at the time representing the oldest snake in the fossil record. Nopcsa (1925) also erected the family Simoliophidae for this genus. Originally referred to the type species, *Simoliophis rochebrunei*, the material from Egypt probably represents a new unnamed species of *Simoliophis* (Rage & Escuillié, 2003). Moreover, according to Rage and Escuillié (2003), Nopcsa (1925) actually mixed the vertebrae of two distinct snakes, one of them representing an unnamed genus; however, this view was subsequently challenged by Rage et al. (2016), who argued in favour of only one species (*Simoliophis* sp.) being represented by the material from Bahariya.

The dorsal vertebrae and dorsal ribs are remarkably thick and show a dense bone microstructure (pachyostosis), which, together with the predominantly marine depositional setting for most *Simoliophis* remains, led Nopcsa (1925) to conclude that *Simoliophis* inhabited marine environments. This interpretation was recently confirmed by Rage et al. (2016), who regarded *Simoliophis* as a slow swimmer, capable of long but shallow dives and inhabiting shallow marine and brackish environments. The pachyostotic vertebrae and ribs, already noted by Nopcsa (1925), might have been an adaptation to counteract buoyancy caused by the air-filled lungs (Nopcsa, 1925; Rage et al., 2016). The roughly coeval Kem Kem beds of Morocco yielded a diverse snake fauna with five different taxa of snakes, including *Simoliophis* (Ibrahim et al., 2020a). Thus, snakes probably were a common and diverse faunal element in the early Late Cretaceous of North Africa.

3.8 Palaeoecology

The palaeontology of the Bahariya Formation indicates an extremely productive ecosystem, comprising a wide range of

fluvial, brackish, tidal and near-shore marine environments, which supported a diverse vegetation dominated by extensive mangrove forests. The palaeoecosystem of the Bahariya Formation is characterised by a very high faunal diversity of vertebrates and an overabundance of predatory taxa, the latter of which has also been referred to as ‘Stromer’s Riddle’ (McGowan & Dyke, 2009). Like in other roughly contemporaneous North African deposits (see above), aquatic and semi-aquatic taxa dominate the vertebrate assemblage from the Bahariya Formation. Especially numerous and diverse are the fishes with more than 20 taxa of cartilaginous fishes and more than 10 taxa of bony fishes. The fishes are not only taxonomically diverse but also with regard to their palaeoecology—some groups like lungfishes and polypterids likely inhabited freshwater ecosystems, while others such as hybodontid sharks were inhabitants of the marine realm (Stromer, 1936); still others likely lived in brackish environments, like the large coelacanth *Mawsonia* and the huge sawfish *Onchopristis* (Ibrahim et al., 2020a). Many tetrapods of the Bahariya Formation likely were at least partially dependent on this rich fish assemblage. This includes the abundant plesiosaurs, which likely hunted in brackish to near-shore marine environments as originally suggested by Stromer (1936). Moreover, at least three and up to five different crocodyliforms are present in the Bahariya ecosystem, most of which probably had a piscivorous diet. The small and likely terrestrial *Libycosuchus* is a notable exception and likely hunted small prey on land.

The overabundance of large-sized theropods in the local faunal assemblage is one of the most outstanding features of the Bahariya Formation and was originally also noted by Stromer (1936). At least five, and potentially up to eight, different theropods have been reported from the Bahariya Formation, three of which (*Spinosaurus*, *Carcharodontosaurus* and *Bahariasaurus/Deltadromeus*) are among the largest terrestrial carnivores of all time. This peculiarity has also been observed in coeval deposits of Northern Africa, most prominently in the Kem Kem beds of Morocco (Cavin et al., 2010; Ibrahim et al., 2020a; Russell, 1996). Based on the high diversity and abundance of fishes in the early Late Cretaceous of North Africa, it has been suggested that the great majority of carnivorous tetrapods, including the theropods, fed on aquatic prey items (Russell, 1996; Stromer, 1936). This might be particularly true for the spinosaurids from the Bahariya assemblage (*Spinosaurus aegyptiacus* and ‘*Spinosaurus B*’/*Sigilmassasaurus*) which likely subsisted on a fish diet (see above). An alternative theory that has been brought forward to account for the dominance of large carnivorous dinosaurs, is a sampling bias towards large theropods (McGowan & Dyke, 2009); however, this hypothesis has been rejected recently, and thus the overabundance of predators might indeed be real (Ibrahim et al., 2020a).

The abundance of large terrestrial (or semi-aquatic) carnivores contrasts sharply with the rarity of terrestrial herbivores, which so far only comprise sauropod dinosaurs. This includes the large-sized *Aegyptosaurus*, the gigantic *Paralititan* and two indeterminate sauropods (a dicraeosaurid and a rebbachisaurid). Again, this situation is similar to that of other North African vertebrate assemblages of a similar age (Benyoucef et al., 2015; Ibrahim et al., 2020a). One potential reason for this might be the patchy distribution of vegetation in these coastal environments (Ibrahim et al., 2020a). Evidence for theropod dinosaurs feeding on the sauropods exists in the form of a shed tooth crown of the large-sized *Carcharodontosaurus* between the holotype skeleton of *Paralititan* (Smith et al., 2001). Ornithischians, albeit being a common faunal component in most Early and Late Cretaceous Mesozoic terrestrial ecosystems, are completely absent from the Bahariya Formation. Mammals and birds are also completely absent from the Bahariya Formation thus far. Furthermore, neither of them has been described from the well-sampled Kem Kem beds of Morocco, or other contemporaneous deposits of Northern Africa that yielded a similar vertebrate fauna (Ibrahim et al., 2020a). It has been hypothesised that small multicuspate crocodyliforms with a presumed insectivorous and herbivorous diet replaced mammals in the Kem Kem ecosystem (Ibrahim et al., 2020a) and the same might have been true for the Bahariya ecosystem. Other small-sized terrestrial vertebrates are unknown from the Bahariya assemblage as well, the small marine squamate *Simoliophis* being the only exception. Pterosaurs have only recently been reported from the Bahariya Formation based on an isolated first-wing phalanx (Salem et al., 2018), although they are a common faunal element in the very similar Kem Kem beds (e.g. Martill et al., 2020).

4 Tetrapod Trackways from the Abu Agag Formation (Turonian)

The Abu Agag Formation has yielded tetrapod footprints from the Upper Cretaceous (Demathieu & Wycisk, 1990). The tracks were originally discovered in the 1980s during stratigraphical and sedimentological fieldwork by the Technical University of Berlin in southeastern Egypt (Fig. 1) and northern Sudan (Demathieu & Wycisk, 1990). As vertebrate tracks are generally rarely reported in the Cretaceous of Northern Africa and the time interval covered by the Abu Agag Formation is poorly known in the region, these footprints offer important insights into the composition and palaeoecology of these terrestrial ecosystems.

4.1 Geological and Palaeoenvironmental Setting

The fluvial sedimentary rocks of the Abu Agag Formation comprise basal conglomerates that grade up into coarse-grained cross-bedded sandstones and mudstones, directly overlying Precambrian basement (Demathieu & Wycisk, 1990; El Sharkawi & Mesaed, 1996; Klitzsch & Wycisk, 1987). The Abu Agag Formation represents a regressional phase in the area and is in turn overlain by the shallow marine Upper Cretaceous (Coniacian–Santonian) Timsah Formation (El Sharkawi & Mesaed, 1996). The depositional environments of the Abu Agag Formation range from channel lag deposits (basal conglomerates) to distal channels of low sinuosity rivers and braided streams (cross-bedded sandstones), as well as to floodplain deposits with occasional paleosol development (mudstone-dominated facies to the top) (Demathieu & Wycisk, 1990; El Sharkawi & Mesaed, 1996). The age of the formation is considered to be Turonian (El Sharkawi & Mesaed, 1996; Hendriks et al., 1987; Klitzsch & Wycisk, 1987), though it might turn out to be somewhat older due to the lack of conclusive dating for the succession (Demathieu & Wycisk, 1990).

4.2 Tetrapod Trackways

The tracks of the Abu Agag Formation occur in several different stratigraphic horizons at three different locations in Egypt, 75–80 km south and 15–30 km north of Aswan (Demathieu & Wycisk, 1990). The first location, situated 80 km south of Aswan, preserves four different trackways, for which tracemakers could be identified (Demathieu & Wycisk, 1990). The first of these trackways is a small pentadactyl trackway resembling the ichnogenus *Capitosauroides* and probably representing a small amphibian, similar to a salamander with an estimated total length of 40 cm. The second trackway comprises two footprints that are comparable to the ichnotaxon *Rhynchosauroides* and likely were produced by a small lepidosaur, about 20 cm in length. The third trackway shows similarities to *Rotodactylus* and consists of two left footprints of a small quadrupedal animal, probably an archosaur with long limbs. The fourth trackway comprises a manus imprint and two small tridactyl footprints that are comparable to the ichnogenus *Amblydactylus* and were likely made by a very small ornithischian dinosaur. In addition, the site yielded indeterminate tracks that were probably made on wet mud and thus are badly preserved; in contrast, the identifiable tracks were likely produced on dry sediment.

The second locality from the Abu Agag Formation that preserves tetrapod tracks is situated 75 km south of Aswan

(Demathieu & Wycisk, 1990). Although the footprints from this site are generally poorly preserved, two different trackways were identified. Among them is a small trackway that resembles the ichnotaxon *Rhynchosauroides*, and was likely produced by a small lepidosaur with a length of about 40 cm. The second trackway consists of two footprints from a small quadrupedal animal of uncertain affinities, comparable to the ichnogenus *Gallegosichnus*, but it might have been produced by a mammal-like animal. The third location, 15 km north of Aswan, yielded indeterminate tracks that were made in wet mud and thus are badly preserved, as well as one large and well-preserved four-toed footprint resembling *Chirotherium* (Demathieu & Wycisk, 1990). The latter probably represents a large archosaur with an estimated total length of 4–5 m.

The tracks are all preserved in fluvial to lacustrine sedimentary rocks that were laid down in low-energy environments of channel and overbank deposits (Demathieu & Wycisk, 1990). Remarkably, the tracks are mostly assignable to small animals—tracks of large vertebrates are missing with the exception of one footprint of a large-sized archosaur. The local vertebrate assemblage as reconstructed from the ichnites includes amphibians, lepidosaurs, mammal-like animals, small (ornithischian?) dinosaurs, as well as small and large archosaurs of uncertain affinities (Demathieu & Wycisk, 1990). If some of the small tracks from the Abu Agag Formation indeed represent ornithischians, as suggested by Demathieu and Wycisk (1990), this would constitute one of the only (if not the only) record of ornithischians from post-Cenomanian deposits in Africa (see also Lamanna et al., 2004). Similarly, the small tracks potentially produced by mammals (Demathieu & Wycisk, 1990) would represent one of the very few mammalian occurrences in Upper Cretaceous deposits from continental Africa. Unfortunately, the poor preservation of these tracks makes their assignment uncertain (Demathieu & Wycisk, 1990; Lamanna et al., 2004).

5 The Vertebrate Fauna of the Quseir Formation (Campanian)

The Upper Cretaceous Quseir Formation has yielded a diverse fauna of terrestrial vertebrates, representing the second richest Cretaceous continental assemblage from Egypt after the Bahariya Formation (see above). Numerous different groups are known from these deposits, including fishes, turtles, crocodyliforms and dinosaurs. Due to the young age of the formation, this vertebrate fauna offers most important insights into latest Cretaceous (Campanian–Maastrichtian) terrestrial ecosystems of continental Africa, a time period that is extremely underrepresented on this continent.

5.1 Geological and Palaeoenvironmental Setting

The Quseir Formation has a widespread distribution in Egypt but the majority of fossil vertebrate material has been reported from the Dakhla and Kharga Oases in the Western Desert of Egypt as well as from the Nile Valley (Fig. 1). The Quseir Formation is also known as the ‘variegated shale’ of the Nubia Formation (Awad & Ghobrial, 1966; Lamanna et al., 2004; Said, 1962), Baris Formation (Hendriks et al., 1987; Lamanna et al., 2004), Mut Formation (Barthel & Herrmann-Degen, 1981; Mahmoud, 2003), or the upper part of the Nubia Sandstone (Klitzsch et al., 1979; Mahmoud, 2003); the ‘Nubian Sandstones’ (German ‘Nubischer Sandstein’) of Stromer and Weiler (1930) from the Nile Valley are probably also referable to the Quseir Formation. The formation consists of variegated shales, mudstones and siltstone, with occasional phosphatic horizons (Sallam et al., 2016).

The depositional environment, in which these sediments were laid down, ranges from fluvial, to brackish and shallow marine (Sallam et al., 2016). The palaeoflora as reconstructed by studies of the palynomorph assemblage from central Egypt is dominated by angiosperms, but pteridophytes, aquatic plants and freshwater algae seem to have been abundant as well, indicating warm and humid palaeoclimatic conditions (Mahmoud, 2003). Recently, evidence for wildfires in the ecosystems of the Quseir Formation has been mentioned based on the presence of charcoal attributable to gymnosperms (El Atfy et al., 2016). The Quseir Formation has been interpreted to be early to middle Campanian in age (Mahmoud, 2003; Sallam et al., 2016). In addition to the terrestrial (or semi-terrestrial) vertebrates outlined below, the Quseir Formation also yielded diverse but mostly fragmentary remains of elasmobranchians, teleosts and lungfishes (Churcher, 1995; Churcher & Iuliis, 2001; Churcher et al., 2006; Claeson et al., 2014; Stromer & Weiler, 1930), as well as scarce remains of marine reptiles including elasmosaurid sauropterygians and mosasaurs (Churcher, 1995; Stromer & Weiler, 1930).

5.2 Testudinata Indet.

Turtle remains are abundant in the Quseir Formation of the Kharga and Dakhla Oases and mostly consist of isolated shell elements—so far no cranial remains of turtles are known from the Quseir Formation (Sallam et al., 2016). Noteworthy among these turtle remains is a well-preserved and nearly complete shell that comprises both the carapace and plastron, missing most of the peripherals and the

epiplastron (Sallam et al., 2016). The specimen belongs to a medium-sized turtle with an estimated carapace length of 50 cm and was discovered by a team from the Mansoura University south of Kharga Oasis in the basal part of the formation (Sallam et al., 2016). The turtle has been referred to the Pleurodira and shows similarities to Pelomedusoides (Sallam et al., 2016). In addition, four well-preserved and mostly complete turtle shells have been preliminarily reported, three of them comprising a complete plastron with a partial carapace and one comprising a plastron and carapace (Gawad & Abuelkheir, 2018). The specimens were discovered south of Kharga Oasis in the upper part of the Quseir Formation (Sallam et al., 2016). All of them probably belong to bothremydid pleurodires.

5.3 Crocodyliforms

Numerous crocodyliform remains have been collected from the Quseir Formation, comprising both cranial and postcranial remains of at least three different neosuchians (Saber et al., 2018; Sallam et al., 2016). These include an indeterminate dyrosaurid (Lamanna et al., 2004), a gavialoid neosuchian (Saber et al., 2020; Sallam et al., 2016) and the recently described *Wahasuchus egyptensis* (Saber et al., 2018).

5.3.1 *Wahasuchus egyptensis*

The type material of *Wahasuchus* was collected in the early 2000s from the Dakhla Oasis by a team of the Mansoura University (Saber et al., 2018). The holotype consists of a partial skull and a fragmentary left mandible assignable to one individual (Saber et al., 2018). Referred material comprises a partial braincase and skull roof, a partial left maxilla, a partial right premaxilla, a left dentary, a partial right mandible, two dorsal vertebrae, a right femur, a distal right tibia and a proximal left humerus (Saber et al., 2018). *Wahasuchus* probably represents a basal neosuchian that is remarkably different from both Gondwanan and European Late Cretaceous crocodyliforms, pointing to some degree of endemism in the Late Cretaceous terrestrial vertebrate faunas of Northern Africa (Saber et al., 2018). Therefore, Saber et al. (2018) suggested that some representatives of this Late Cretaceous North African fauna may have been regionally adapted to the southern Tethys area. This contrasts with the supposed affinities of other Late Cretaceous vertebrate groups such as titanosaurian sauropods, which show close relationships to members of neighbouring landmasses (South America, Eurasia) and thus suggests some degree of faunal interchange (Sallam et al., 2018). *Wahasuchus* likely was a semi-aquatic generalist preying upon fishes, turtles and terrestrial vertebrates (Saber et al., 2018).

5.3.2 Crocodyliformes Indet.

A left humerus, originally described as pertaining to an ornithischian (Awad & Ghobrial, 1966), was later referred to an indeterminate dyrosaurid crocodylian (Lamanna et al., 2004). The presence of dyrosaurids in the Quseir Formation has previously been also suggested by Churcher and Iuliis (2001). Dyrosaurids are generally regarded as predators of marine to brackish environments with a wide distribution and ranging from the Upper Cretaceous to the Eocene (de Andrade & Sayão, 2014; Khosla et al., 2009). Furthermore, well-preserved cranial remains of a long-snouted neosuchian crocodylian are known from the Kharga Oasis near Baris (Sallam et al., 2016). The largely complete skull probably pertains to a ‘thoracosaur’ gavialoid and thus might represent the oldest member of the Gavialoidea (Saber et al., 2020; Sallam et al., 2016). Stromer and Weiler (1930) reported on isolated crocodylian teeth and a partial femur from the ‘Nubian Sandstone’ of the Nile Valley that they referred to the Goniopholidae. Interestingly, these goniopholid teeth seem to be different from those described by Gemmellaro (1921) from the overlying Duwi Formation of the Nile Valley (see below).

5.4 Dinosauria

Dinosaur remains are relatively common in the deposits of the Quseir Formation, belonging to both theropod and sauropod dinosaurs (Salem et al., 2021; Sallam et al., 2016). Recently, a reasonably complete and well-preserved sauropod, *Mansourasaurus shahinae*, has been described from this formation representing the first named dinosaur taxon from the post-Cenomanian of Egypt (Sallam et al., 2018). Ornithischian remains mentioned by Awad and Ghobrial (1966) were later shown to represent a dyrosaurid crocodylian, thus limiting the occurrence of ornithischians to pre-Turonian times in continental Africa (Lamanna et al., 2004).

5.4.1 Theropoda Indet.

Theropods are represented mostly by isolated, fragmentary and indeterminate remains. Two isolated teeth that were found in 1993 near El Atrun in the Kharga Oasis by Dale Russell and Charles Churcher were tentatively referred to *Spinosaurus* and *Carcharodontosaurus* but were never described in detail (Churcher, 1995). An indeterminate partial caudal vertebra and a proximal fibula were recovered during expeditions of the Mansoura University from the Dakhla and Kharga Oasis respectively (Salem et al., 2021). The fibula described by Salem et al. (2021) resembles those of abelisaurids and might indicate the presence of this theropod family in the Quseir Formation. Abelisaurids are in general poorly documented from the Upper Cretaceous of

Africa (for an overview, see Salem et al., 2021); a tooth from the overlying Duwi Formation of the Nile Valley near Idfu (see below) has also been referred to the Abelisauridae by Smith and Lamanna (2006). A small proximal theropod tibia from the ‘Nubian Sandstones’ of the Nile Valley was described by Stromer and Weiler (1930), and might potentially also belong to an abelisaurid (Smith & Lamanna, 2006).

5.4.2 *Mansourasaurus shahinae*

Mansourasaurus has a special role in the vertebrate assemblages of Egypt as it represents the best-known terrestrial vertebrate from the post-Cenomanian of the entire African continent (excluding Madagascar) and as such offers unique insights into the relationships of Egyptian Late Cretaceous ecosystems (Sallam et al., 2018). The holotype of *Mansourasaurus* comprises cranial fragments, both dentaries, cervical and dorsal vertebrae, ribs, scapulocoracoid, sternal plate, both humeri, a radius, metacarpal III, three metatarsals, osteoderms and indeterminate fragments, all pertaining to one individual (Sallam et al., 2018). This partial skeleton was discovered during an expedition of the Mansoura University in the upper part of the Quseir Formation in the Dakhla Oasis (Sallam et al., 2018). A phylogenetic analysis performed by Sallam et al. (2018) recovered *Mansourasaurus* as a saltasaurid titanosaurian and, more specifically, as the sister taxon of the Late Cretaceous European titanosaur *Lohuecotitan*. This clade (*Mansourasaurus* and *Lohuecotitan*), in turn, is closely related to Late Cretaceous titanosaurs from central Asia (*Nemegtosaurus* and *Opisthocoelicaudia*) and Europe (*Ampelosaurus* and *Paludititan*) (Sallam et al., 2018).

Therefore, *Mansourasaurus* offers new insights into the palaeobiogeography of African terrestrial vertebrates during the Late Cretaceous, providing evidence for a latest Cretaceous dispersal between Europe and northern Africa (Sallam et al., 2018). This theory has been previously proposed by several authors, although the exact timing and nature of these dispersals have remained controversial (for an overview of Late Cretaceous biogeographical relationships between Europe and Africa, see Buffetaut & Le Loeuff, 1991; Csiki-Sava et al., 2015; Gheerbrant & Rage, 2006; Pereda-Suberbiola, 2009; Rabi & Sebők, 2015). *Mansourasaurus* provides additional and important evidence for a close biogeographic connection between Africa and Europe (Sallam et al., 2018).

5.4.3 Sauropoda Indet.

Aside from the well-preserved holotype specimen of *Mansourasaurus shahinae*, the Quseir Formation has yielded two more partial skeletons of titanosaur sauropods. Both of them have been recovered from the Kharga Oasis, but neither of them has been properly described in detail yet (Lamanna

et al., 2017; Salem et al., 2020). The first was discovered in the 1970s by a team of the Technical University of Berlin and comprises five dorsal vertebrae, and several appendicular elements (Díez Díaz et al., 2017; Lamanna et al., 2017). This specimen was only described in an unpublished thesis thus far, but a detailed study of the material is currently ongoing (Lamanna et al., 2017). The second skeleton was discovered in 2017 by a team from the Mansoura University and includes a cervical vertebra, five dorsal vertebrae, a caudal vertebra, and the articulated right tibia and astragalus (Salem et al., 2020). Work is currently in progress to describe this specimen as well (Salem et al., 2020). The preliminary results point to the presence of at least two different titanosaur sauropods in the Quseir Formation of Egypt (Salem et al., 2020).

In addition, several indeterminate sauropod remains have been described from the Quseir Formation recently. This includes a partial left femur from the Kharga Oasis, and the associated proximal parts of both the right tibia and fibula from the Dakhla Oasis, all referable to titanosauriform sauropods (Salem et al., 2021). Moreover, Salem et al. (2021) described a partial titanosauriform cervical vertebra from the Kharga Oasis, and two isolated titanosaurian caudal vertebrae from the Dakhla Oasis. Interestingly, one of the isolated caudal vertebrae exhibits a camellate internal morphology that is also found in saltasaurine titanosaurians and thus might suggest affinities of at least one sauropod from the Dakhla Oasis to this clade of Late Cretaceous South American titanosaurs (Salem et al., 2021). The sauropod dinosaurs from the Quseir Formation thus possibly show affinities to both South American and Laurasian titanosaurs (see above), indicating more complex biogeographical relationships of the Late Cretaceous dinosaurs from this region than previously thought.

5.4.4 Mammalia? Indet.

Stromer and Weiler (1930) reported a very small tooth from the ‘Nubia Sandstone’ of the Nile Valley that was discovered near Mahamid. The tooth has a preserved length of 5 mm, but the lower part (at least 3 mm) was lost during excavation (Stromer & Weiler, 1930). The tooth is elongated and flat with an oval cross-section at the base and a chisel-like morphology near the apical part (Stromer & Weiler, 1930: pl. I, Fig. 4a–e). Due to its peculiar morphology that is uncommon in reptiles, Stromer and Weiler (1930) referred it tentatively to an indeterminate mammal. At the same time, however, they stress that this referral should be viewed with caution due to the fragmentary preservation of the tooth and its peculiar morphology. Although the assignment of the tooth to a mammal is far from certain, it deserves a notion here, being the only report of a Mesozoic mammalian from Egypt.

6 The Vertebrate Fauna of the Duwi Formation (Campanian–Maastrichtian)

Fragmentary remains of abelisaurid theropods and crocodyliforms are known from the uppermost Cretaceous Duwi Formation of the Nile Valley (Fig. 1) (Gemmellaro, 1921; Smith & Lamanna, 2006). This represents one of only two occurrences of terrestrial vertebrates from the Maastrichtian of Egypt, the other being sauropod and turtle remains from the overlying Dakhla Formation (see below).

6.1 Geological and Palaeoenvironmental Setting

The Duwi Formation has a widespread distribution in central and southern Egypt, including the Dakhla and Kharga Oases as well as the Nile Valley. It is underlain by the Quseir Formation and overlain by the Dakhla Formation (El-Younsy et al., 2017), both of which also yielded terrestrial vertebrates, including dinosaurs (see above and below). The formation mainly consists of shales, limestones and phosphates and several massive oyster layers (Abdelhady et al., 2020; El-Ayyat & Kassab, 2004). The sediments were deposited in a shallow marine setting and marked the onset of fully marine conditions in Egypt following the late Cretaceous marine transgression of the region (El Ayyat, 2015; El-Ayyat & Kassab, 2004). The Duwi Formation is considered to be late Campanian to early Maastrichtian in age (El Ayyat, 2015; El Beialy, 1995; Hamama & Kassab, 1990; Kassab & Mohamed, 1996). The ‘Phosphates’ (German ‘Phosphate’) of Stromer and Weiler (1930) from the Nile Valley between Mahamid and Edfu (= Idfu) are probably referable to the Duwi Formation based on: (i) their distinctive richness in phosphatic layers; (ii) the abundance of oyster shell layers; and (iii) the ‘Phosphates’ are overlying the ‘Nubian Sandstone’ (the latter likely representing the Quseir Formation, which underlies the Duwi Formation, see below).

The marine deposits of the Duwi Formation have yielded a fauna of relatively low diversity, including invertebrates (El-Ayyat & Kassab, 2004; Hamama & Kassab, 1990; Kassab & Mohamed, 1996), osteichthyan and chondrichthyan fishes (Holloway et al., 2017; Salama et al., 2021; Sallam et al., 2016; Stromer & Weiler, 1930), and marine tetrapods such as sauropterygians (plesiosaurs) and mosasaurs (Churcher & Iuliis, 2001; Gemmellaro, 1921; Sallam et al., 2016). Terrestrial vertebrates are represented only by the presence of isolated and fragmentary crocodyliform and theropod remains (Gemmellaro, 1921; Smith & Lamanna, 2006). Isolated teeth of crocodyliforms were referred to the marine dyrosaurid *Dyrosaurus phosphaticus* and to an

indeterminate member of the Goniophoridae (Gemmellaro, 1921). The terrestrial vertebrates (theropod dinosaurs and the semi-aquatic goniopholid crocodyliforms) were likely washed into the sea and thus offer insights into the faunal composition of the nearby coast. The low faunal diversity of the Duwi Formation and the occurrence of autochthonous oyster beds probably are the result of stressed environmental conditions (Abdelhady et al., 2020); additionally, the oyster shell layers are indicative of repetitive storm events (Abdelhady et al., 2020). The palaeoclimate was probably humid and tropical as evidenced by the palynomorph assemblage (El Beialy, 1995).

6.2 Abelisauridae Indet.

Gemmellaro (1921) reported the occurrence of several isolated theropod tooth crowns and an ungual phalanx that were recovered from Upper Cretaceous strata of the Nile Valley near Idfu (for details, see also Smith & Lamanna, 2006). Originally, the teeth were assigned to '*Megalosaurus*' *crenatissimus* (Gemmellaro, 1921), a theropod known from the Upper Cretaceous of Madagascar (Depéret, 1896), which was later referred to the new genus *Majungasaurus* *crenatissimus* (Lavocat, 1955). Subsequent discoveries of more complete skeletal material from Madagascar showed *Majungasaurus crenatissimus* (= '*Majungatholus*' *crenatissimus*) to be a derived abelisaurid theropod (Krause et al., 2007; Sampson et al., 1998). More recently, Smith and Lamanna (2006) re-evaluated the affinities of the theropod teeth from the Duwi Formation, showing that one tooth almost certainly belongs to an abelisaurid theropod (Smith & Lamanna, 2006). Although it is unlikely that the tooth indeed belongs to *Majungasaurus crenatissimus* due to the isolation of Madagascar prior to the Late Cretaceous, the study demonstrates that it represents a derived (instead of a more basal) abelisaurid (Smith & Lamanna, 2006). The presence of a derived abelisaurid in uppermost Cretaceous (post-Cenomanian) deposits from continental Africa has important biogeographic implications, suggesting connections between Africa and South America (where these derived abelisaurids likely originated) until the Late Cretaceous and thus weakens the hypothesis that Cretaceous African land vertebrates developed in isolation (Smith & Lamanna, 2006).

7 The Vertebrate Fauna of the Dakhla Formation (Maastrichtian–Palaeocene)

The Maastrichtian strata of the Dakhla Formation have yielded an isolated but well-preserved sauropod femur (Rauhut & Werner, 1997) that is one of only two

Maastrichtian occurrences of terrestrial vertebrates from Egypt (Fig. 1)—the other being isolated theropod and crocodyliform remains from the slightly older Duwi Formation of the Nile Valley near Idfu (see above). In addition, abundant and diverse remains of marine turtles are known from the same strata of the Dakhla Formation (Ammonite Hill Member) as the sauropod femur (de Lapparent de Broin & Werner, 1998). Although earlier fieldwork in the region conducted by the famous German palaeontologist Karl Alfred von Zittel from the University of Munich already led to the discovery of marine reptiles and turtles, the material was unfortunately destroyed during the Second World War, similar to the famous Bahariya collection of Ernst Stromer von Reichenbach (see above). Subsequent expeditions of the Technical University of Berlin recovered a rich vertebrate assemblage, including the sauropod femur and most of the turtle remains.

7.1 Geological and Palaeoenvironmental Setting

The Dakhla Formation consists of dark grey shales that are often intercalated with fossiliferous siltstones and sandstones (Tantawy et al., 2001). The age of the Dakhla Formation ranges from the Campanian–Maastrichtian boundary to the early Palaeocene based on macrofossil (bivalves, ammonites) and microfossil (foraminifera, calcareous nannofossils) biostratigraphy (Tantawy et al., 2001). The sauropod femur described by Rauhut and Werner (1997) was found in the Ammonite Hill Member of the Dakhla Formation, which crops out only in the westernmost margin of the Dakhla Basin and comprises a lower Maastrichtian and an upper Palaeocene part (Rauhut & Werner, 1997). The Ammonite Hill Member consists of highly fossiliferous mudstones, siltstones, sandstones and limestones that represent an interfingering of distal alluvial to deltaic shallow marine depositional settings (Barthel & Herrmann-Degen, 1981; Rauhut & Werner, 1997). The palaeoclimate as inferred from clay minerals during the time of the deposition has been reconstructed as tropical to subtropical with seasonal humid conditions (Tantawy et al., 2001).

The fauna of the Ammonite Hill Member includes numerous invertebrate groups (bioturbation trace fossils of crustaceans, ammonites, bivalves, gastropods, echinoids, corals), plant remains (fruits of the mangrove plant *Nypa*), fishes (osteichthyans, elasmobranchians), as well as marine and terrestrial tetrapods (Barthel & Herrmann-Degen, 1981; Hedeny et al., 2021; Rauhut & Werner, 1997). Among the marine tetrapods are fragmentary remains of mosasaurs (*Prognathodon*), and elasmosaurid plesiosaurs (Rauhut & Werner, 1997; Werner & Bardet, 1996). Additionally, abundant and diverse remains of marine to brackish turtles

were collected from the Ammonite Hill Member, probably representing at least six different species (de Lapparent de Broin & Werner, 1998). A sauropod femur is the only definitive representative of the terrestrial vertebrate fauna and indicates near-shore conditions (Rauhut & Werner, 1997).

7.2 Testudinata

Turtles are the most abundant vertebrates from the Ammonite Hill Member of the Dakhla Formation (de Lapparent de Broin & Werner, 1998). The material ranges from isolated remains to nearly complete skulls and shells, belonging to at least six different species (de Lapparent de Broin & Werner, 1998). The vast majority of the turtle specimens was collected in 1979 and 1980 by a team from the Technical University of Berlin under the leadership of Werner Barthel. Five different species of bothremydid pleurodirans and one indeterminate cryptodiran (known only from a humerus) are present in the assemblage (de Lapparent de Broin & Werner, 1998). Based on the humerus morphology of the indeterminate cryptodiran that closely resembles extant marine turtles, it was regarded as a marine turtle (de Lapparent de Broin & Werner, 1998). The bothremydids comprise indeterminate forms, *Taphrosphys* sp. and *T. cf. sulcatus*, as well as *Arenila krebsi* and *Zolhafah bella*, the last two of which were newly erected for material recovered from the Ammonite Hill Member (de Lapparent de Broin & Werner, 1998). Due to the marine depositional environment in which their remains have been found and the peculiar shell ornamentation, the bothremydids are likewise interpreted as inhabitants of marine and perhaps brackish environments (de Lapparent de Broin & Werner, 1998).

7.3 Sauropoda Indet.

The sauropod femur from the Dakhla Formation was also recovered in 1980 by the team from the Technical University of Berlin, from the Great Sand Sea of the Western Desert of Egypt, west of the Dakhla Oasis (Rauhut & Werner, 1997). The femur is well-preserved and nearly complete, only the proximal and distal portions are slightly abraded. Based on the presence of a well-developed lateral bulge of the femur, Rauhut and Werner (1997) argue that the femur might belong to either a brachiosaurid or a titanosaur sauropod. Due to the overall greater resemblance to brachiosaurids (and *Brachiosaurus* in particular) than to titanosaurs, the authors favour close affinities to this family and thus refer the femur to a brachiosaurid. The relatively small size of the specimen (proximo-distal length of 724 mm), together with the probable adult ontogenetic stage of the individual as

indicated by the robustness of the shaft, suggests that the sauropod represented by the femur was a comparatively small animal (Rauhut & Werner, 1997). If indeed belonging to a brachiosaurid, the femur would represent the youngest record of the family in the fossil record, providing evidence for the survival of the lineage up to the latest Cretaceous. Moreover, the femur underscores how little is actually known of Late Cretaceous terrestrial ecosystems from continental Africa.

8 The Importance of Egyptian Mesozoic Terrestrial Ecosystems

The Mesozoic terrestrial vertebrate assemblages of Egypt as a whole offer significant insights into the diversity of terrestrial vertebrates in Africa and the evolution of continental Mesozoic ecosystems. Among these assemblages, the Bahariya Formation yielded by far the richest and most diverse vertebrate fauna, including numerous different chondrichthyan and osteichthyan fishes, abundant remains of turtles, several different crocodyliforms, as well as theropod and sauropod dinosaurs. In addition, it was the first well-known Cretaceous vertebrate fauna from Africa and many families that are now known from numerous different localities around the world (especially from Gondwana), have first been established on material from Bahariya. Most prominently, this includes the holotypes of the very large theropods *Spinosaurus* and *Carcharodontosaurus*, serving as the basis for the Spinosauridae and Carcharodontosauridae, respectively. Although similar faunas are now known to have been widespread across Northern Africa, the fauna from the Bahariya Formation represents the first well-studied of these early Late Cretaceous vertebrate assemblages and also yielded some of the best specimens (e.g. the holotypes of *Spinosaurus*, *Carcharodontosaurus*, *Bahariasaurus*, *Aegyptosaurus*) if not the only material of the respective vertebrate taxa known so far (e.g. *Paralititan*, *Libycosuchus*, *Stomatosuchus*).

Despite the sparse and often fragmentary terrestrial vertebrate remains recovered from the other Upper Cretaceous formations of Egypt (i.e. Abu Agag, Quseir, Duwi and Dakhla formations), they nonetheless offer significant insights into the evolution of life on land in the later parts of the Late Cretaceous, including the latest Cretaceous (Campanian, Maastrichtian)—a period, which is extremely poorly represented in continental Africa. Even isolated finds (single teeth and bones) can thus hold valuable information on palaeobiogeography (e.g. the abelisaurid tooth from the Duwi Formation) and the faunal composition of these latest Cretaceous vertebrate faunas (e.g. the sauropod femur from the Dakhla Formation). Some of these formations (especially the Quseir Formation) have just begun to reveal the richness

and diversity of their vertebrate fauna, often with spectacular results—the holotype specimen of *Mansourasaurus* and its implications for the palaeobiogeography of the latest Cretaceous Tethys realm being a prime example. In the future, these rather poorly known vertebrate assemblages from the later part of the Late Cretaceous have a great potential to yield further significant insights into the evolution of the Cretaceous life on land in what is still one of the most enigmatic continents with respect to its vertebrate palaeontology—Africa.

Acknowledgements We would like to thank Haytham El Atfy (Mansoura University, Egypt and University of Tübingen, Germany) for the invitation to write this chapter and thus to contribute to this volume. In addition, it was a great chance to dive deeply into the Mesozoic terrestrial ecosystems of Egypt, which fascinated us for a long time. We would also like to express our gratitude to Zakaria Hamimi (Benha University, Egypt) for the kind assistance during the publication of this book chapter. We are thankful to two reviewers for their helpful comments and critical evaluation of this manuscript.

References

- Abdelhady, A. A., Seuss, B., Fürsich, F. T., Ali, A., Abdel-Raheem, K. H. M., & Mohamed, R. S. A. (2020). Palaeoenvironmental significance of the monospecific biostromes in the Campanian-Maastrichtian Duwi Formation (Eastern Desert, Egypt). *Sedimentary Geology*, *408*, 105772.
- Amiot, R., Buffetaut, E., Lécuyer, C., Wang, X., Boudad, L., Ding, Z., Fourel, F., Hutt, S., Martineau, F., Medeiros, M. A., Mo, J., Simon, L., Suteethorn, V., Sweetman, S., Tong, H., Zhang, F., & Zhou, Z. (2010a). Oxygen isotope evidence for semi-aquatic habits among spinosaurid theropods. *Geology*, *38*, 139–142.
- Amiot, R., Wang, X., Lécuyer, C., Buffetaut, E., Boudad, L., Cavin, L., Ding, Z., Fluteau, F., Kellner, A. W. A., Tong, H., & Zhang, F. (2010b). Oxygen and carbon isotope compositions of middle Cretaceous vertebrates from North Africa and Brazil: Ecological and environmental significance. *Palaeogeography, Palaeoclimatology, Palaeoecology*, *297*, 439–451.
- Apesteiguá, S., Smith, N. D., Valieri, R. J., & Makovicky, P. J. (2016). An unusual new theropod with a didactyl manus from the Upper Cretaceous of Patagonia, Argentina. *PLoS ONE*, *11*, e0157793.
- Awad, G. H., & Ghobrial, M. G. (1966). Zonal stratigraphy of the Kharga Oasis. *General Egyptian Organization for Geological Research and Mining*, *34*, 1–77.
- Barthel, K. W., & Herrmann-Degen, W. (1981). Late Cretaceous and early Tertiary stratigraphy in the Great Sand Sea and its SE margins (Farafra and Dakhla oases), SW desert, Egypt. *Mitteilungen der Bayerischen Staatssammlung für Paläontologie und Historische Geologie*, *21*, 141–182.
- Beever, T., Quigley, A., Smith, R. E., Smyth, R. S. H., Ibrahim, N., Zouhri, S., & Martill, D. M. (2021). Taphonomic evidence supports an aquatic lifestyle for *Spinosaurus*. *Cretaceous Research*, *117*, 104627.
- Benton, M. J., Bouaziz, S., Buffetaut, E., Martill, D., Ouaja, M., Soussi, M., & Trueman, C. (2000). Dinosaurs and other fossil vertebrates from fluvial deposits in the Lower Cretaceous of southern Tunisia. *Palaeogeography, Palaeoclimatology, Palaeoecology*, *157*, 227–246.
- Benyoucef, M., Läng, E., Cavin, L., Mebarki, K., Adaci, M., & Bensalah, M. (2015). Overabundance of piscivorous dinosaurs (Theropoda: Spinosauridae) in the mid-Cretaceous of North Africa: The Algerian dilemma. *Cretaceous Research*, *55*, 44–55.
- Brusatte, S. L., & Sereno, P. C. (2007). A new species of *Carcharodontosaurus* (Dinosauria: Theropoda) from the Cenomanian of Niger and a revision of the genus. *Journal of Vertebrate Paleontology*, *27*, 902–916.
- Buffetaut, E. (1976). Der Land-Krokodilier *Libycosuchus* Stromer und die Familie Libycosuchidae (Crocodylia, Mesosuchia) aus der Kreide Afrikas. *Mitteilungen der Bayerischen Staatssammlung für Paläontologie und Historische Geologie*, *51*, 1–20.
- Buffetaut, E., Bussert, R., & Brinkmann, W. (1990). A new nonmarine vertebrate fauna in the Upper Cretaceous of northern Sudan. *Berliner Geowissenschaftliche Abhandlungen A*, *120*, 183–202.
- Buffetaut, E., & Le Loeuff, J. (1991). Late Cretaceous dinosaur faunas of Europe: Some correlation problems. *Cretaceous Research*, *12*, 159–176.
- Carrano, M. T., & Sampson, S. D. (2008). The phylogeny of Ceratosauria (Dinosauria: Theropoda). *Journal of Systematic Palaeontology*, *6*, 183–236.
- Carvalho, M. S. S., & Maisey, J. G. (2008). New occurrence of *Mawsonia* (Sarcopterygii: Actinistia) from the Early Cretaceous of the Sanfranciscana Basin, Minas Gerais, southeastern Brazil. *Geological Society, London, Special Publications*, *295*, 109–144.
- Catuneanu, O., Khalifa, M. A., & Wanas, H. A. (2006). Sequence stratigraphy of the Lower Cenomanian Bahariya Formation, Bahariya Oasis, Western Desert, Egypt. *Sedimentary Geology*, *190*, 121–137.
- Cavin, L., & Forey, P. L. (2001). Osteology and systematic affinities of *Palaeonotopterus greenwoodi* Forey 1997 (Teleostei: Osteoglossomorpha). *Zoological Journal of the Linnean Society*, *133*, 25–52.
- Cavin, L., & Forey, P. L. (2004). New mawsoniid coelacanth (Sarcopterygii: Actinistia) remains from the Cretaceous of the Kem Kem beds, Southern Morocco. In G. Arratia & A. Tintori (Eds.), *Mesozoic fishes 3—Systematics, palaeoenvironments and biodiversity* (pp. 493–506). Verlag Dr. Friedrich Pfeil.
- Cavin, L., & Forey, P. L. (2008). A new tselatiiform teleost from the Upper Cretaceous (Cenomanian) of the Kem Kem beds, Southern Morocco. In G. Arratia, H.-P. Schultze, & M. V. H. Wilson (Eds.), *Mesozoic fishes 4—Homology and phylogeny* (pp. 199–216). Verlag Dr. Friedrich Pfeil.
- Cavin, L., Suteethorn, V., Buffetaut, E., & Tong, H. (2007). A new Thai Mesozoic lungfish (Sarcopterygii, Dipnoi) with an insight into post-Palaeozoic dipnoan evolution. *Zoological Journal of the Linnean Society*, *149*, 141–177.
- Cavin, L., Tong, H., Boudad, L., Meister, C., Piuze, A., Tabouelle, J., Aarab, M., Amiot, R., Buffetaut, E., Dyke, G., Hua, S., & Le Loeuff, J. (2010). Vertebrate assemblages from the early Late Cretaceous of southeastern Morocco: An overview. *Journal of African Earth Sciences*, *57*, 391–412.
- Charig, A. J., & Milner, A. C. (1997). *Baryonyx walkeri*, a fish-eating dinosaur from the Wealden of Surrey. *Bulletin of the Natural History Museum Geology*, *53*, 11–70.
- Chiarenza, A. A., & Cau, A. (2016). A large abelisaurid (Dinosauria, Theropoda) from Morocco and comments on the Cenomanian theropods from North Africa. *PeerJ*, *4*, e1754.
- Churcher, C. S. (1995). Giant Cretaceous lungfish *Neoceratodus tuberculatus* from a deltaic environment in the Quseir (=Baris) Formation of Kharga oasis, western desert of Egypt. *Journal of Vertebrate Paleontology*, *15*, 845–849.
- Churcher, C. S., & Iuliis, G. D. (2001). A new species of *Protopterus* and a revision of *Ceratodus humei* (Dipnoi: Ceratodontiformes) from the Late Cretaceous Mut Formation of eastern Dakhleh Oasis, Western Desert of Egypt. *Palaeontology*, *44*, 305–323.

- Churcher, C. S., Iuliis, G. D., & Kleindienst, M. R. (2006). A new genus for the dipnoan species *Ceratodus tuberculatus* Tabaste, 1963. *Geodiversitas*, 28, 635–647.
- Cione, A. L., Gouiric-Cavalli, S., Gelfo, J. N., & Goin, F. J. (2011). The youngest non-lepidosirenid lungfish of South America (Dipnoi, latest Paleocene–earliest Eocene, Argentina). *Alcheringa: An Australasian Journal of Palaeontology*, 35, 193–198.
- Claeson, K. M., Sallam, H. M., O'Connor, P. M., & Sertich, J. J. W. (2014). A revision of the Upper Cretaceous lepidosirenid lungfishes from the Quseir Formation, Western Desert, central Egypt. *Journal of Vertebrate Paleontology*, 34, 760–766.
- Coiffard, C., El Atfy, H. (this volume). The evolution of vegetation through the Cretaceous of Egypt. In: Z. Hamimi, H. Khozyem, T. Adatte, F. H. Nader, F. Oboh-Ikuenobe, M. K. Zobia, H. El Atfy (Eds.), *The Phanerozoic geology and natural resources of Egypt*. Springer.
- Csiki-Sava, Z., Buffetaut, E., Ösi, A., Pereda-Suberbiola, X., & Brusatte, S. L. (2015). Island life in the Cretaceous—Faunal composition, biogeography, evolution, and extinction of land-living vertebrates on the Late Cretaceous European archipelago. *ZooKeys*, 469, 1–161.
- Cuff, A. R., & Rayfield, E. J. (2013). Feeding mechanics in spinosaurid theropods and extant crocodylians. *PLoS ONE*, 8, e65295.
- Dal Sasso, C., Maganuco, S., Buffetaut, E., & Mendez, M. A. (2005). New information on the skull of the enigmatic theropod *Spinosaurus*, with remarks on its size and affinities. *Journal of Vertebrate Paleontology*, 25, 888–896.
- Daqué, E. (1912). Die fossilen Schildkröten Ägyptens. *Geologische und Paläontologische Abhandlungen, Neue Folge*, 10, 275.
- de Andrade, R. C. L. P., & Sayão, J. M. (2014). Paleohistology and lifestyle inferences of a dyrosaurid (Archosauria: Crocodylomorpha) from Paraíba Basin (Northeastern Brazil). *PLoS ONE*, 9, e102189.
- de Lapparent, A. F. (1960). Les dinosauriens du “continental intercalaire” du Sahara central. *Mémoires de la Société Géologique de France*, 88A, 1–57.
- de Lapparent de Broin, F. (2000). African chelonians from the Jurassic to the present: Phases of development and preliminary catalogue of the fossil record. *Palaeontologia Africana*, 36, 43–82.
- de Lapparent de Broin, F., & Werner, C. (1998). New late Cretaceous turtles from the Western Desert of Egypt. *Annales de Paléontologie*, 84, 131–214.
- Demathieu, G. R., & Wycisk, P. (1990). Tetrapod trackways from Southern Egypt and Northern Sudan. *Journal of African Earth Sciences (and the Middle East)*, 10, 435–443.
- Deparet, C., & Savornin, J. (1925). Sur la decouverte d'une faune de vertebres albiens a Timimoun (Sahara occidental). *Comptes Rendus de l'Académie des Sciences de Paris*, 181, 1108–1111.
- Depéret, C. (1896). Note sur les dinosauriens sauropodes et théropodes du Crétacé supérieur de Madagascar. *Bulletin de la Société Géologique de France*, 3(24), 176–196.
- Díez Díaz, V., Gorscak, E., Lamanna, M. C., Schwarz, D., & El-Dawoudi, I. (2017). The metatarsus of a Late Cretaceous titanosaur (Dinosauria: Sauropoda) from the Kharga Oasis of Egypt. In *15th Annual Meeting of the European Association of Vertebrate Palaeontologists. Information and Abstracts*.
- El Atfy, H., Anan, T., Jasper, A., & Uhl, D. (2019). Repeated occurrence of palaeo-wildfires during deposition of the Bahariya Formation (early Cenomanian) of Egypt. *Journal of Palaeogeography*, 8, 28.
- El Atfy, H., Sallam, H., Jasper, A., & Uhl, D. (2016). The first evidence of paleo-wildfire from the Campanian (Late Cretaceous) of North Africa. *Cretaceous Research*, 57, 306–310.
- El Atfy, H., Coiffard, C., El Beialy, S. Y., & Uhl, D. (2023). Vegetation and climate change at the southern margin of the Neo-Tethys during the Cenomanian (Late Cretaceous): Evidence from Egypt. *Plos One*. <https://doi.org/10.1371/journal.pone.0281008>
- El Ayyat, A. M. (2015). Lithostratigraphy, sedimentology, and cyclicity of the Duwi Formation (late Cretaceous) at Abu Tartur plateau, Western Desert of Egypt: Evidences for reworking and redeposition. *Arabian Journal of Geosciences*, 8, 99–124.
- El-Ayyat, A. M., & Kassab, A. S. (2004). Biostratigraphy and facies analysis of the Upper Cretaceous oyster storm shell beds of the Duwi Formation, Qusseir District, Red Sea Region, Egypt. *Journal of African Earth Sciences*, 39, 421–428.
- El Beialy, S. Y. (1995). Campanian-Maastrichtian palynomorphs from the Duwi (Phosphate) Formation of the Hamrawein and Umm El Hueitat mines, Red Sea Coast, Egypt. *Review of Palaeobotany and Palynology*, 85, 303–317.
- El Sharkawi, M. A., & Mesaed, A. A. (1996). Stratigraphic setting and paleoenvironment of the Coniacian-Santonian ironstones of Aswan, South Egypt. *Geological Society of Egypt, Special Publications*, 2, 243–278.
- El-Younsy, A. R. M., Obaidalla, N. A., Philobos, E. R., & Salman, A. M. (2017). High-resolution sequence stratigraphy of the Upper Cretaceous-Lower Paleogene succession, Gabal Qreiya area, Upper Egypt. *Arabian Journal of Geosciences*, 10, 531.
- Evers, S. W., Rauhut, O. W. M., Milner, A. C., McFeeters, B., & Allain, R. (2015). A reappraisal of the morphology and systematic position of the theropod dinosaur *Sigilmassasaurus* from the “middle” Cretaceous of Morocco. *PeerJ*, 3, e1323.
- Fanti, F., Contessi, M., & Franchi, F. (2012). The “Continental Intercalaire” of southern Tunisia: Stratigraphy, paleontology, and paleoecology. *Journal of African Earth Sciences*, 73–74, 1–23.
- Forey, P. L., López-Arbarello, A., & MacLeod, N. (2011). A new species of *Lepidotes* (Actinopterygii: Semiontiformes) from the Cenomanian (Upper Cretaceous) of Morocco. *Palaeontologia Electronica*, 14, 1–12.
- Gawad, A. M. K., & Abuelkheir, G. (2018). Quseir Testudines remains from the Late Cretaceous Kharga area, south western desert, Egypt. In *78th Annual Meeting 2018 of the Society of Vertebrate Paleontology. Abstract Volume*.
- Gemmellaro, M. (1921). Rettili maëstrichtiani d'Egitto. *Giornale di Scienze Naturali ed Economiche*, 32, 339–351.
- Gheerbrant, E., & Rage, J.-C. (2006). Paleobiogeography of Africa: How distinct from Gondwana and Laurasia? *Palaeogeography, Palaeoclimatology, Palaeoecology*, 241, 224–246.
- Gorscak, E., & O'Connor, P. M. (2019). A new African titanosaurian sauropod dinosaur from the middle Cretaceous Galula Formation (Mtuka Member), Rukwa Rift Basin, Southwestern Tanzania. *PLoS ONE*, 14, e0211412.
- Grandstaff, B. S. (2006). *Giant fishes from the Bahariya Formation, Bahariya Oasis, Western Desert, Egypt* [Ph.D. thesis] (pp. 1–185). University of Pennsylvania, Philadelphia.
- Grandstaff, B. S., Smith, J. B., Lamanna, M. C., Lacovara, K. J., & Abdel-Ghani, M. S. (2012). *Bawitius*, gen. nov., a giant polypterid (Osteichthyes, Actinopterygii) from the Upper Cretaceous Bahariya Formation of Egypt. *Journal of Vertebrate Paleontology*, 32, 17–26.
- Hamama, H. H., & Kassab, A. S. (1990). Upper Cretaceous ammonites of Duwi Formation in Gabal Abu Had and Wadi Hamama, Eastern Desert, Egypt. *Journal of African Earth Sciences (and the Middle East)*, 10, 453–464.
- Hassler, A., Martin, J. E., Amiot, R., Tacail, T., Godet, F. A., Allain, R., & Balter, V. (2018). Calcium isotopes offer clues on resource partitioning among Cretaceous predatory dinosaurs. *Proceedings of the Royal Society B: Biological Sciences*, 285, 20180197.
- Hedeny, M. E., Kassab, W., Rashwan, M., El-Kheir, G. A., & Gawad, A. M. K. (2021). Bivalve borings in Maastrichtian fossil *Nypa* fruits: Dakhla Formation, Bir Abu Minqar, South Western Desert, Egypt. *Ichnos*, 28, 24–33.

- Henderson, D. M. (2018). A buoyancy, balance and stability challenge to the hypothesis of a semi-aquatic *Spinosaurus* Stromer, 1915 (Dinosauria: Theropoda). *PeerJ*, 6, e5409.
- Hendriks, F. L., Bowitz, J. P., & Kallenbach, H. (1987). Evolution of the depositional environments of SE-Egypt during the Cretaceous and early Tertiary. *Berliner Geowissenschaftliche Abhandlungen A*, 75, 49–52.
- Holliday, C. M., & Gardner, N. M. (2012). A new eusuchian crocodyliform with novel cranial integument and its significance for the origin and evolution of Crocodylia. *PLoS ONE*, 7, e30471.
- Holloway, W., Claeson, K., Sallam, H., El-Sayed, S., Kora, M., Sertich, J., & O'Connor, P. (2017). A new species of the neopterygian fish *Enchodus* from the Duwi Formation, Campanian, Late Cretaceous, Western Desert, central Egypt. *Acta Palaeontologica Polonica*, 62, 603–611.
- Hone, D., & Holtz, T. (2021). Evaluating the ecology of *Spinosaurus*: Shoreline generalist or aquatic pursuit specialist? *Palaeontologia Electronica*, 1–28.
- Hone, D. W. E., & Holtz, T. R. (2017). A century of *Spinosaurids*—A review and revision of the Spinosauridae with comments on their ecology. *Acta Geologica Sinica—English Edition*, 91, 1120–1132.
- Hone, D. W. E., & Holtz, T. R. (2019). Comment on: Aquatic adaptation in the skull of carnivorous dinosaurs (Theropoda: Spinosauridae) and the evolution of aquatic habits in spinosaurids. *Cretaceous Research*, 93, 275–284.
- Ibrahim, N., Sereno, P. C., Varricchio, D. J., Martill, D. M., Dutheil, D. B., Unwin, D. M., Baidder, L., Larsson, H. C. E., Zouhri, S., & Kaoukaya, A. (2020a). Geology and paleontology of the Upper Cretaceous Kem Kem Group of eastern Morocco. *ZooKeys*, 928, 1–216.
- Ibrahim, N., Maganuco, S., Dal Sasso, C., Fabbri, M., Auditore, M., Bindellini, G., Martill, D. M., Zouhri, S., Mattarelli, D. A., Unwin, D. M., Wiemann, J., Bonadonna, D., Amane, A., Jakubczak, J., Joger, U., Lauder, G. V., & Pierce, S. E. (2020b). Tail-propelled aquatic locomotion in a theropod dinosaur. *Nature*, 581, 67–70.
- Ibrahim, N., Sereno, P. C., Sasso, C. D., Maganuco, S., Fabbri, M., Martill, D. M., Zouhri, S., Myhrvold, N., & Iurino, D. A. (2014). Semiaquatic adaptations in a giant predatory dinosaur. *Science*, 345, 1613–1616.
- Janensch, W. (1914). Übersicht über die Wirbeltierfauna der Tendaguru-Schichten, nebst einer kurzen Charakterisierung der neu aufgeführten Arten Sauropoden. *Archiv für Biontologie*, 3, 81–110.
- Janensch, W. (1920). Über *Elaphrosaurus bambergi* und die Megalosaurier aus den Tendaguru-Schichten Deutsch-Ostafrikas. In *Sitzungsberichte Der Gesellschaft Naturforschender Freunde Zu Berlin* (pp. 225–235).
- Kampouridis, P., Hartung, J., & Augustin, F. J. (this volume). The Eocene – Oligocene vertebrate assemblages of the Fayum Depression, Egypt. In: Z. Hamimi, H. Khozyem, T. Adatte, F. H. Nader, F. Oboh-Ikuenobe, M. K. Zoubaa, H. El Atfy (Eds.), *The Phanerozoic geology and natural resources of Egypt*. Springer.
- Kassab, A. S., & Mohamed, A. S. (1996). Upper Cretaceous macrofossils from the Duwi Formation of the Nile Valley, southern Egypt. *Neues Jahrbuch für Geologie und Paläontologie—Abhandlungen*, 259–284.
- Khalifa, M. A., & Catuneanu, O. (2008). Sedimentology of the fluvial and fluvio-marine facies of the Bahariya Formation (Early Cenomanian), Bahariya Oasis, Western Desert, Egypt. *Journal of African Earth Sciences*, 51, 89–103.
- Khosla, A., Sertich, J. J. W., Prasad, G. V. R., & Verma, O. (2009). Dinosaurian remains from the Intertrappean Beds of India and the Late Cretaceous distribution of Tyrosauridae. *Journal of Vertebrate Paleontology*, 29, 1321–1326.
- Kilian, C. (1931). Des principaux complexes continentaux du Sahara. *Comptes Rendus de la Société Géologique de France*, 9, 109–111.
- Klitzsch, E., Harms, J. C., Lejal-Nicol, A., & List, F. K. (1979). Major subdivisions and depositional environments of Nubia Strata, Southwestern Egypt. *AAPG Bulletin*, 63, 967–974.
- Klitzsch, E., & Wycisk, P. (1987). Geology of the sedimentary basins of northern Sudan and bordering areas. *Berliner Geowissenschaftliche Abhandlungen A*, 75, 97–136.
- Krause, D. W., Sampson, S. D., Carrano, M. T., & O'Connor, P. M. (2007). Overview of the history of discovery, taxonomy, phylogeny, and biogeography of *Majungasaurus crenatissimus* (Theropoda: Abelisauridae) from the Late Cretaceous of Madagascar. *Journal of Vertebrate Paleontology*, 27, 1–20.
- Kuhn, O. (1936). Fossilium Catalogus I. Animalia Part 75: Crocodylia. W. Junk, Berlin, 144 pp.
- Lacovara, K. J., Smith, J. R., Smith, J. B., & Lamanna, M. C. (2003). The Ten Thousand Islands Coast of Florida: A modern analog to low-energy mangrove coasts of Cretaceous epeiric seas. In *Proceedings of the 5th International Conference on Coastal Sediments* (pp. 1773–1784).
- Lamanna, M. C., Gorscak, E., Díaz, V. D., Schwarz, D., & El-Dawoudi, I. (2017). Reassessment of a partial titanosaurian sauropod dinosaur skeleton from the Upper Cretaceous (Campanian) Quseir Formation of the Kharga Oasis, Egypt. In *15th Annual Meeting of the European Association of Vertebrate Palaeontologists. Information and Abstracts*.
- Lamanna, M. C., Smith, J. B., Attia, Y. S., & Dodson, P. (2004). From dinosaurs to dyrosaurids (Crocodyliformes): Removal of the post-Cenomanian (Late Cretaceous) record of Ornithischia from Africa. *Journal of Vertebrate Paleontology*, 24, 764–768.
- Lamanna, M. C., Smith, J. B., Lacovara, K. J., Dodson, P., & Attia, Y. (2000). New vertebrate discoveries from the Cretaceous of Egypt. *Journal of Vertebrate Paleontology*, 20, 53A.
- Larsson, H. C. E., & Sues, H.-D. (2007). Cranial osteology and phylogenetic relationships of *Hamadasuchus rebouli* (Crocodyliformes: Mesoeucrocodylia) from the Cretaceous of Morocco. *Zoological Journal of the Linnean Society*, 149, 533–567.
- Lavocat, R. (1954). Reconnaissance géologique dans les hammas des confins algéro-marocains du sud. *Notes et Mémoires Du Service Géologiques*, 116, 1–147.
- Lavocat, R. (1955). Les recherches de reptiles fossiles à Madagascar. *National Malgache*, 7, 203–207.
- Lejal-Nicol, A., & Dominik, W. (1990). Sur la paleoflore a Weichseliaceae et a angiospermes du Cenomanien de la region de Bahariya (Egypte du Sud-Ouest). *Berliner Geowissenschaftliche Abhandlungen A*, 120, 957–991.
- Luger, P., & Gröschke, M. (1989). Late Cretaceous ammonites from the Wadi Qena area in the Egyptian Eastern Desert. *Palaeontology*, 32, 355–407.
- Mahmoud, M. S. (2003). Palynology and palaeoenvironment of the Quseir Formation (Campanian) from central Egypt. *Journal of African Earth Sciences*, 36, 135–148.
- Martill, D. M., Smith, R., Unwin, D. M., Kao, A., McPhee, J., & Ibrahim, N. (2020). A new tapejarid (Pterosauria, Azhdarchoidea) from the mid-Cretaceous Kem Kem beds of Takmout, southern Morocco. *Cretaceous Research*, 112, 104424.
- McGowan, A. J., & Dyke, G. J. (2009). A surfeit of theropods in the Moroccan Late Cretaceous? Comparing diversity estimates from field data and fossil shops. *Geology*, 37, 843–846.
- Motta, M. J., Aranciaga Rolando, A. M., Rozadilla, S., Agnolín, F. E., Chimento, N. R., Brissón Egli, F., & Novas, F. E. (2016). New theropod fauna from the Upper Cretaceous (Huincul Formation) of northwestern Patagonia, Argentina. *New Mexico Museum of Natural History and Science Bulletin*, 71, 231–253.

- Murray, A. M. (2000). The Palaeozoic, Mesozoic and early Cenozoic fishes of Africa. *Fish and Fisheries*, 1, 111–145.
- Nopcsa, F. (1925). Ergebnisse der Forschungsreisen Prof. E. Stromers in den Wüsten Ägyptens. II. Wirbeltierreste der Baharije-Stufe (unterstes Cenoman). 5. Die *Symoliophis*-Reste. *Abhandlungen der Bayerischen Akademie der Wissenschaften, Mathematisch-Naturwissenschaftliche Abteilung, Neue Folge*, 30, 1–27.
- Nopcsa, F. (1926). Neue Beobachtungen an *Stomatosuchus*. *Centralblatt für Mineralogie, Geologie und Paläontologie*, 1926, 212–215.
- Nothdurft, W. E., & Smith, J. (2002). *The lost dinosaurs of Egypt* (1st ed., p. 242). Random House.
- Novas, F. E., Agnolín, F. L., Ezcurra, M. D., Porfiri, J., & Canale, J. I. (2013). Evolution of the carnivorous dinosaurs during the Cretaceous: The evidence from Patagonia. *Cretaceous Research*, 45, 174–215.
- Novas, F. E., de Valais, S., Vickers-Rich, P., & Rich, T. (2005). A large Cretaceous theropod from Patagonia, Argentina, and the evolution of carcharodontosaurids. *Naturwissenschaften*, 92, 226–230.
- Pereda-Suberbiola, X. (2009). Biogeographical affinities of Late Cretaceous continental tetrapods of Europe: A review. *Bulletin de la Société Géologique de France*, 180, 57–71.
- Pérez-García, A. (2017). A new turtle taxon (Podocnemidoidea, Bothremyidae) reveals the oldest known dispersal event of the crown Pleurodira from Gondwana to Laurasia. *Journal of Systematic Palaeontology*, 15, 709–731.
- Peyer, B. (1925). Ergebnisse der Forschungsreisen Prof. E. Stromers in den Wüsten Ägyptens. II. Wirbeltierreste der Baharije-Stufe (unterstes Cenoman). 6. *Ceratodus*-Funde. *Abhandlungen der Bayerischen Akademie der Wissenschaften, Mathematisch-Naturwissenschaftliche Abteilung, Neue Folge*, 30, 1–23.
- Pol, D., Nascimento, P. M., Carvalho, A. B., Riccomini, C., Pires-Domingues, R. A., & Zaher, H. (2014). A new notosuchian from the Late Cretaceous of Brazil and the phylogeny of advanced notosuchians. *PLoS ONE*, 9, e93105.
- Rabi, M., & Sebök, N. (2015). A revised Eurogondwana model: Late Cretaceous notosuchian crocodyliforms and other vertebrate taxa suggest the retention of episodic faunal links between Europe and Gondwana during most of the Cretaceous. *Gondwana Research*, 28, 1197–1211.
- Rage, J.-C., & Escuillié, F. (2003). The Cenomanian: Stage of hindlimbed snakes. *Carnets de Géologie*, 1–11.
- Rage, J.-C., Vullo, R., & Néraudeau, D. (2016). The mid-Cretaceous snake *Simoliophis rochebrunei* Sauvage, 1880 (Squamata: Ophidia) from its type area (Charentes, southwestern France): Redescription, distribution, and palaeoecology. *Cretaceous Research*, 58, 234–253.
- Rauhut, O. W. M. (1995). Zur systematischen Stellung der afrikanischen Theropoden *Carcharodontosaurus* Stromer 1931 und *Bahariasaurus* Stromer 1934. *Berliner Geowissenschaftliche Abhandlungen A*, 16, 357–375.
- Rauhut, O. W. M. (1999). A dinosaur fauna from the Upper Cretaceous (Cenomanian) of northern Sudan. *Palaeontologia Africana*, 35, 61–84.
- Rauhut, O. W. M. (2003). The interrelationships and evolution of basal theropod dinosaurs. *Special Papers in Palaeontology*, 69, 1–213.
- Rauhut, O. W. M., & Werner, C. (1997). First record of a Maastrichtian sauropod dinosaur from Egypt. *Palaeontologia Africana*, 34, 63–67.
- Romano, C., Koot, M. B., Kogan, I., Brayard, A., Minikh, A. V., Brinkmann, W., Bucher, H., & Kriwet, J. (2016). Permian-Triassic Osteichthyes (bony fishes): Diversity dynamics and body size evolution. *Biological Reviews*, 91, 106–147.
- Russell, D. A. (1995). China and the lost worlds of the dinosaurian era. *Historical Biology*, 10, 3–12.
- Russell, D. A. (1996). Isolated dinosaur bones from the Middle Cretaceous of the Tafilalt, Morocco. *Bulletin du Muséum National d'Histoire Naturelle. Section C, Sciences de La Terre, Paléontologie, Géologie, Minéralogie*, 18, 349–402.
- Saber, S., Sertich, J. J. W., El-Kheir, G. A., Ouda, K. A., El-Sayed, S., O'Connor, P. M., Seiffert, E. R., & Sallam, H. M. (2020). The oldest gavialoid crocodyliform ('thoracosaur') from the Campanian Quseir Formation of Baris Oasis, Western Desert, Egypt. In *80th Annual Meeting of the Society of Vertebrate Paleontology. Virtual 2020. Abstract Volume*.
- Saber, S., Sertich, J. J. W., Sallam, H. M., Ouda, K. A., O'Connor, P. M., & Seiffert, E. R. (2018). An enigmatic crocodyliform from the Upper Cretaceous Quseir Formation, central Egypt. *Cretaceous Research*, 90, 174–184.
- Said, R. (1962). *The geology of Egypt* (p. 377). Elsevier.
- Salama, Y., Altoom, N. G., Allam, A. A., Ajarem, J. S., & Abd-Elhameed, S. (2021). Late Cretaceous anacoracid sharks (*Squalicorax*) from Duwi Formation, Gebel Duwi, central Eastern Desert, Egypt: Qualitative and quantitative analyses. *Historical Biology*, 33, 1–9.
- Salem, B. S., El-Kheir, G. A., Lamanna, M. C., Gorscak, E., El-Sayed, S., & Sallam, H. M. (2020). A new titanosaurian sauropod dinosaur partial skeleton from the Late Cretaceous (Campanian) of the Kharga Oasis, Western Desert of Egypt. In *80th Annual Meeting of the Society of Vertebrate Paleontology. Virtual 2020. Abstract Volume*.
- Salem, B. S., O'Connor, P. M., Gorscak, E., El-Sayed, S., Sertich, J. J. W., Seiffert, E. R., & Sallam, H. M. (2021). Dinosaur remains from the Upper Cretaceous (Campanian) of the Western Desert, Egypt. *Cretaceous Research*, 123, 104783.
- Salem, B. S., Sallam, H. M., El-Sayed, S., Thabet, W., Antar, M. S., & Lamanna, M. C. (2018). New fossil diapsid remains from the Upper Cretaceous (Cenomanian) Bahariya Formation, Bahariya Oasis, Western Desert of Egypt. In *The 56th Annual Scientific Meeting. Scientific Program and Abstracts*. The Geological Society of Egypt.
- Sallam, H. M., Gorscak, E., O'Connor, P. M., El-Dawoudi, I. A., El-Sayed, S., Saber, S., Kora, M. A., Sertich, J. J. W., Seiffert, E. R., & Lamanna, M. C. (2018). New Egyptian sauropod reveals Late Cretaceous dinosaur dispersal between Europe and Africa. *Nature Ecology & Evolution*, 2, 445–451.
- Sallam, H. M., O'Connor, P. M., Kora, M., Sertich, J. J. W., Seiffert, E. R., Faris, M., Ouda, K., El-Dawoudi, I., Saber, S., & El-Sayed, S. (2016). Vertebrate paleontological exploration of the Upper Cretaceous succession in the Dakhla and Kharga Oases, Western Desert, Egypt. *Journal of African Earth Sciences*, 117, 223–234.
- Salem, B. S., Lamanna, M. C., O'Connor, P. M., El-Qot, G. M., Shaker, F., Thabet, W. A., El-Sayed, S., & Sallam, H. M. (2022). First definitive record of Abelisauridae (Theropoda: Ceratosauria) from the Cretaceous Bahariya Formation, Bahariya Oasis, Western Desert of Egypt. *Royal Society Open Science*, 9, 220106.
- Sampson, S. D., Witmer, L. M., Forster, C. A., Krause, D. W., O'Connor, P. M., Dodson, P., & Ravoavy, F. (1998). Predatory dinosaur remains from Madagascar: Implications for the Cretaceous biogeography of Gondwana. *Science*, 280, 1048–1051.
- Schaal, S. (1984). Oberkretazische Osteichthyes (Knochenfische) aus dem Bereich von Bahariya und Kharga, Ägypten, und ihre Aussagen zur Paläökologie und Stratigraphie. *Berliner Geowissenschaftliche Abhandlungen A*, 53, 79.
- Schweitzer, C. E., Lacovara, K. J., Smith, J. B., Lamanna, M. C., Lyon, M. A., & Attia, Y. (2003). Mangrove-dwelling crabs (Decapoda:

- Brachyura: Necrocarcinidae) associated with dinosaurs from the Upper Cretaceous (Cenomanian) of Egypt. *Journal of Paleontology*, 77, 888–894.
- Sereno, P. C., Dutheil, D. B., Iarochene, M., Larsson, H. C. E., Lyon, G. H., Magwene, P. M., Sidor, C. A., Varricchio, D. J., & Wilson, J. A. (1996). Predatory dinosaurs from the Sahara and Late Cretaceous faunal differentiation. *Science*, 272, 986–991.
- Sereno, P. C., & Larsson, H. C. E. (2009). Cretaceous Crocodyliforms from the Sahara. *ZooKeys*, 28, 1–143.
- Sereno, P. C., Wilson, J. A., & Conrad, J. L. (2004). New dinosaurs link southern landmasses in the Mid-Cretaceous. *Proceedings of the Royal Society of London. Series B: Biological Sciences*, 271, 1325–1330.
- Slaughter, B. H., & Thurmond, J. T. (1974). A lower Cenomanian (Cretaceous) ichthyofauna from the Bahariya Formation of Egypt. *Annals of the Geological Society, Egypt*, 4, 25–40.
- Smith, J. B., & Lamanna, M. C. (2006). An abelisaurid from the Late Cretaceous of Egypt: Implications for theropod biogeography. *Naturwissenschaften*, 93, 242–245.
- Smith, J. B., Lamanna, M. C., Lacovara, K. J., Dodson, P., Smith, J. R., Poole, J. C., Giegengack, R., & Attia, Y. (2001). A giant sauropod dinosaur from an Upper Cretaceous mangrove deposit in Egypt. *Science*, 292, 1704–1706.
- Smith, J. B., Lamanna, M. C., Mayr, H., & Lacovara, K. J. (2006). New information regarding the holotype of *Spinosaurus aegyptiacus* Stromer, 1915. *Journal of Paleontology*, 80, 400–406.
- Stromer, E. (1914a). Ergebnisse der Forschungsreisen Prof. E. Stromers in den Wüsten Ägyptens. I. Die Topographie und Geologie der Strecke Gharq-Baharije nebst Ausführungen über die geologische Geschichte Ägyptens. *Abhandlungen der Bayerischen Akademie der Wissenschaften, Mathematisch-Physikalische Klasse*, 26, 1–78.
- Stromer, E. (1914b). Ergebnisse der Forschungsreisen Prof. E. Stromers in den Wüsten Ägyptens. II. Wirbeltierreste der Baharije-Stufe (unterstes Cenoman). 1. Einleitung und 2. *Libycosuchus*. *Abhandlungen der Bayerischen Akademie der Wissenschaften, Mathematisch-Physikalische Klasse*, 27, 1–16.
- Stromer, E. (1915). Ergebnisse der Forschungsreisen Prof. E. Stromers in den Wüsten Ägyptens. II. Wirbeltierreste der Baharije-Stufe (unterstes Cenoman). 3. Das Original des Theropoden *Spinosaurus aegyptiacus* nov. gen., nov. spec. *Abhandlungen der Bayerischen Akademie der Wissenschaften, Mathematisch-Physikalische Klasse*, 28, 1–32.
- Stromer, E. (1916). Richard Markgraf und seine Bedeutung für die Erforschung der Wirbeltierpaläontologie Ägyptens. *Centralblatt für Mineralogie, Geologie und Paläontologie*, 11, 287–288.
- Stromer, E. (1917). Ergebnisse der Forschungsreisen Prof. E. Stromers in den Wüsten Ägyptens. II. Wirbeltierreste der Baharije-Stufe (unterstes Cenoman). 4. Die Säge des Pristiden *Onchopristis numidus* Haug sp. und über die Sägen der Sägehaie. *Abhandlungen der Bayerischen Akademie der Wissenschaften, Mathematisch-Physikalische Klasse*, 28, 1–28.
- Stromer, E. (1925). Ergebnisse der Forschungsreisen Prof. E. Stromers in den Wüsten Ägyptens. II. Wirbeltierreste der Baharije-Stufe (unterstes Cenoman). 7. *Stomatosuchus inermis* Stromer, ein schwach bezahnter Krokodilier und 8. Ein Skelettrest des Pristiden *Onchopristis numidus* Haug sp. *Abhandlungen der Bayerischen Akademie der Wissenschaften, Mathematisch-Naturwissenschaftliche Abteilung*, 30, 1–22.
- Stromer, E. (1926). Ergebnisse meiner Forschungsreisen in den Wüsten Ägyptens. *Die Naturwissenschaften*, 14, 353–356.
- Stromer, E. (1927). Ergebnisse der Forschungsreisen Prof. E. Stromers in den Wüsten Ägyptens. II. Wirbeltierreste der Baharije-Stufe (unterstes Cenoman). 9. Die Plagiostomen, mit einem Anhang über käno- und mesozoische Rückenflossenstacheln von Elasmobranchiern. *Abhandlungen der Bayerischen Akademie der Wissenschaften, Mathematisch-Naturwissenschaftliche Abteilung*, 31, 1–64.
- Stromer, E. (1931). Ergebnisse der Forschungsreisen Prof. E. Stromers in den Wüsten Ägyptens. II. Wirbeltierreste der Baharijesteufe (unterstes Cenoman). 10. Ein Skelett-Rest von *Carcharodontosaurus* nov. gen. *Abhandlungen der Bayerischen Akademie der Wissenschaften, Mathematisch-Naturwissenschaftliche Abteilung, Neue Folge*, 9, 1–22.
- Stromer, E. (1932). Ergebnisse der Forschungsreisen Prof. E. Stromers in den Wüsten Ägyptens. II. Wirbeltierreste der Baharije-Stufe (unterstes Cenoman). 11. Sauropoda. *Abhandlungen der Bayerischen Akademie der Wissenschaften, Mathematisch-Naturwissenschaftliche Abteilung, Neue Folge*, 10, 1–21.
- Stromer, E. (1933). Ergebnisse der Forschungsreisen Prof. E. Stromers in den Wüsten Ägyptens. II. Wirbeltierreste der Baharije-Stufe (unterstes Cenoman). 12. Die procölen Crocodilia. *Abhandlungen der Bayerischen Akademie der Wissenschaften, Mathematisch-Naturwissenschaftliche Abteilung, Neue Folge*, 15, 1–55.
- Stromer, E. (1934a). Ergebnisse der Forschungsreisen Prof. E. Stromers in den Wüsten Ägyptens. II. Wirbeltierreste der Baharije-Stufe (unterstes Cenoman). 14. Testudinata. *Abhandlungen der Bayerischen Akademie der Wissenschaften, Mathematisch-Naturwissenschaftliche Abteilung, Neue Folge*, 25, 1–26.
- Stromer, E. (1934b). Ergebnisse der Forschungsreisen Prof. E. Stromers in den Wüsten Ägyptens. II. Wirbeltierreste der Baharije-Stufe (unterstes Cenoman). 13. Dinosauria. *Abhandlungen der Bayerischen Akademie der Wissenschaften, Mathematisch-Naturwissenschaftliche Abteilung, Neue Folge*, 22, 1–79.
- Stromer, E. (1935). Ergebnisse der Forschungsreisen Prof. E. Stromers in den Wüsten Ägyptens. II. Wirbeltierreste der Baharije-Stufe (unterstes Cenoman). 15. Plesiosauria. *Abhandlungen der Bayerischen Akademie der Wissenschaften, Mathematisch-Naturwissenschaftliche Abteilung, Neue Folge*, 26, 1–55.
- Stromer, E. (1936). Ergebnisse der Forschungsreisen Prof. E. Stromers in den Wüsten Ägyptens. VII. Baharije-Kessel und -Stufe mit deren Fauna und Flora. Eine ergänzende Zusammenfassung. *Abhandlungen der Bayerischen Akademie der Wissenschaften, Mathematisch-Naturwissenschaftliche Abteilung, Neue Folge*, 33, 1–102.
- Stromer, E., & Weiler, W. (1930). Ergebnisse der Forschungsreisen Prof. E. Stromers in den Wüsten Ägyptens. VI. Beschreibung von Wirbeltier-Resten aus dem nubischen Sandsteine Oberägyptens und aus ägyptischen Phosphaten nebst Bemerkungen über die Geologie der Umgebung von Mahamid in Oberägypten. *Abhandlungen der Bayerischen Akademie der Wissenschaften, Mathematisch-Naturwissenschaftliche Abteilung, Neue Folge*, 7, 1–42.
- Tantawy, A. A., Keller, G., Adatte, T., Stinnesbeck, W., Kassab, A., & Schulte, P. (2001). Maastrichtian to Paleocene depositional environment of the Dakhla Formation, Western Desert, Egypt: Sedimentology, mineralogy, and integrated micro- and macrofossil biostratigraphies. *Cretaceous Research*, 22, 795–827.
- Taquet, P. (1976). Géologie et paléontologie du gisement de Gado-faoua (Aptien du Niger). *Cahiers de Paléontologie. C.N.R.S.*, 1–191.

- Tumarkin-Deratzian, A. R., Grandstaff, B. S., Lamanna, M. C., & Smith, J. B. (2004). New material of *Libycosuchus brevirostris* from the Cenomanian Bahariya Formation of Egypt. *Journal of Vertebrate Paleontology*, 24, 123A.
- Upchurch, P., Barrett, P. M., & Dodson, P. (2004). Sauropoda. In D. B. Weishampel, P. Dodson, & H. Osmolska (Eds.), *The Dinosauria* (2nd ed., pp. 259–322). University of California Press.
- Villalobus-Segura, E., Kriwet, J., Vullo, R., Stumpf, S., Ward, D. J., & Underwood, C. J. (2021). The skeletal remains of the euryhaline sclerorhynchoid *Onchopristis* (Elasmobranchii) from the 'Mid'-Cretaceous and their palaeontological implications. *Zoological Journal of the Linnean Society*, 20, 1–26.
- von Huene, F. (1932). Die fossile Reptilordnung Saurischia: Ihre Entwicklung und Geschichte. 1 (1932). Borntraeger. *Monographien zur Geologie und Paläontologie*, 1, 1–361.
- von Huene, F. (1948). Short review of the lower tetrapods. *The Royal Society of South Africa Special Publications, Robert Broom Commemorative Volume*, 1, 65–106.
- Vullo, R., Cappetta, H., & Néraudeau, D. (2007). New sharks and rays from the Cenomanian and Turonian of Charentes, France. *Acta Palaeontologica Polonica*, 52, 99–116.
- Vullo, R., Guinot, G., & Barbe, G. (2016). The first articulated specimen of the Cretaceous mackerel shark *Haimirichia amonensis* gen. nov. (Haimirichidae fam. nov.) reveals a novel ecomorphological adaptation within the Lamniformes (Elasmobranchii). *Journal of Systematic Palaeontology*, 14, 1003–1024.
- Weiler, W. (1935). Ergebnisse der Forschungsreisen Prof. E. Stromers in den Wüsten Ägyptens. II. Wirbeltierreste der Baharije-Stufe (unterstes Cenoman). 16. Neue Untersuchungen an den Fischresten. *Abhandlungen der Bayerischen Akademie der Wissenschaften, Mathematisch-Naturwissenschaftliche Abteilung, Neue Folge*, 32, 1–57.
- Weishampel, D. B., Barrett, P. M., Coria, R. A., Loeuff, J. L., Xing, X., Xijin, Z., Sahni, A., Goman, E. M. P., & Noto, C. R. (2004). Dinosaur distribution. In D. B. Weishampel, P. Dodson, & H. Osmolska (Eds.), *The Dinosauria* (2nd ed., pp. 517–606). University of California Press.
- Werner, C. (1989). Die Elasmobranchier-Fauna des Gebel Dist Member der Bahariya Formation (Obercenoman) der Oase Bahariya, Ägypten. *Palaeo Ichthyologica*, 5, 1–112.
- Werner, C. (1990). Biostratigraphical results of investigations on the Cenomanian elasmobranchian fauna of Bahariya Oasis, Egypt. *Berliner Geowissenschaftliche Abhandlungen A*, 120, 43–956.
- Werner, C. (1994). Die kontinentale Wirbeltierfauna aus der unteren Oberkreide des Sudan (Wadi Milk Formation). *Berliner Geowissenschaftliche Abhandlungen E*, 13, 221–249.
- Werner, C., & Bardet, N. (1996). First record of elasmosaurs (Reptilia, Plesiosauroidea) in the Maastrichtian of the Western Desert of Egypt. *Berliner Geowissenschaftliche Abhandlungen E*, 18, 335–343.
- Wessel, P., Smith, W. H. F., Scharroo, R., Luis, J., & Wobbe, F. (2013). Generic Mapping Tools: Improved version released. *Eos*, 94, 409–410.
- Zalmout, I. S., Mustafa, H. A., & Wilson, J. A. (2005). *Karkaemys arabicus*, a new side-necked turtle (Pleurodira, Bothremydidae) from the Upper Cretaceous Wadi Umm Ghudran Formation of Karak, Jordan. *Contributions from the Museum of Paleontology, University of Michigan*, 31, 155–177.
- Zittel, K. A. (1883). Beiträge zur Geologie und Paläontologie der Libyschen Wüste und der angrenzenden Gebiete Ägyptens. *Palaeontographica*, 30, 1–147.



Felix J. Augustin is a paleontologist from Germany who focuses on terrestrial Mesozoic ecosystems. He graduated from the Technical University Freiberg (Germany) in 2016 with a B.Sc. degree and earned an M.Sc. degree from the University of Tübingen (Germany), where he is currently writing his Ph.D. His research interests focus on terrestrial Mesozoic vertebrates, ranging from taxonomy to paleoecology and taphonomy. His research interests span all aspects of vertebrate taxonomy, paleoecology and taphonomy of the Late Jurassic of Germany,

the Late Jurassic and Early Cretaceous of northwestern China and the Late Cretaceous of Romania. He has participated in field trips to and excavations in Germany, Romania, Bulgaria and the United States. The Late Cretaceous vertebrates from Egypt have fascinated him for long, especially the peculiar dinosaur faunas.



Josephina Hartung is a vertebrate paleontologist focusing on Cenozoic mammals and Mesozoic sarcopterygians. Her study on mammals focuses on artiodactyls from the Miocene of Europe. She completed her B.Sc. studies at the Freie Universität Berlin and her M.Sc. at the Rheinische Friedrich Wilhelms Universität Bonn, both in Germany. During her M.Sc. degree, she studied the bovids from the late Miocene hominid locality of Hammerschmiede (Germany) and continued her research on ruminants from this locality as her

Ph.D. project at the University of Tübingen. Together with the University of Bonn, she works on the evolution of Late Triassic coelacanths from Europe and South America.



Panagiotis Kampouridis is a vertebrate paleontologist with his main focus on the study of Old-World mammals. He completed a B.Sc. degree at the National and Kapodistrian University of Athens (Greece) where he focused on the Neogene and Quaternary terrestrial faunas of Greece and the adjacent region, including the world-renowned late Miocene localities of Pikermi and Samos (Greece). During his M.Sc. studies at the University of Tübingen (Germany) he expanded on the study of non-mammalian vertebrates, while

working on the late Miocene hominid locality of Hammerschmiede (Germany). His Ph.D. dissertation focuses on the evolution of the Eurasian rhinocerotid genus *Chilotherium*. During this time, he has also expanded his studies on the Paleogene mammals of the Old-World, including the Eocene-Oligocene fauna of the Fayum (Egypt).



Cretaceous Wildfires in Egypt - Inferences for Palaeoecology and Palaeoenvironments

Haytham El Atfy¹, Dieter Uhl², and André Jasper³

Abstract

Based on numerous findings of fossil charcoal worldwide, the Cretaceous is considered a high-fire period in Earth's history. Macro-charcoal, as direct evidence for the occurrence of palaeo-wildfires during deposition of Cretaceous strata, has so far been reported from three different localities in Egypt: (1) the pre-Aptian Malha Formation of Wadi Budra, Sinai, (2) the early Cenomanian Bahariya Formation at Gebel El Dist at the Bahariya Oasis in the Western Desert and (3) the Campanian Quseir Formation from the Baris Oasis in the south Western Desert. These findings support the view, that the Cretaceous was globally a high-fire world. However, further research on charcoal from additional Cretaceous deposits of Egypt is necessary to offer a more complete picture regarding the interactions between wildfires and vegetation but also dinosaurs and other animals that lived during this important time in the evolution of life.

Keywords

Wildfire • High-fire world • Pre-Aptian • Cenomanian • Campanian

H. El Atfy

Department of Geosciences, University of Tübingen,
72076 Tübingen, Germany
e-mail: El-Atfy@daad-alumni.de

Geology Department, Faculty of Science, Mansoura University,
Mansoura, 35516, Egypt

D. Uhl (✉)

Senckenberg Forschungsinstitut und Naturmuseum Frankfurt,
Frankfurt am Main, 60325, Germany
e-mail: dieter.uhl@senckenberg.de

D. Uhl · A. Jasper

Programa de Pós-Graduação em Ambiente e Desenvolvimento,
Universidade do Vale do Taquari - UNIVATES
(PPGAD/UNIVATES), Lajeado, Rio Grande do Sul, Brazil
e-mail: ajasper@univates.br

1 Introduction

Although wildfires and their immediate destructive effects on ecosystems as well as human economies are often portrayed by the media, as well as politicians, as devastating catastrophic events that should be prevented (Cochrane, 2019), such events represent a natural source of disturbance in many ecosystems, at least since the Silurian Period (Glasspool et al., 2004). After more than 400 million years of co-evolution of the biosphere and wildfires, some biotas depend on the more or less regular occurrence of wildfires (e.g. Scott et al., 2014), to maintain an ecological balance.

On a long (geological) timescale, the occurrence, frequency and severity of wildfires is controlled by the available fuel (vegetational biomass), climatic factors (i.e. temperature, seasonality, rainfall) and the atmospheric oxygen content (e.g. Scott, 2000; Scott et al., 2014). Variability of these factors over time had a profound impact on the frequency and intensity of wildfires, leading to phases with globally few occurrences of wildfires, as well as phases with globally increased fire activities (Diessel, 2010; Jasper et al., 2021; Scott, 2000, 2010; Scott et al., 2014). Both the Permian and the Cretaceous periods have been considered high-fire intervals, where the frequency of such events increased globally (e.g. Brown et al., 2012; Jasper et al., 2021; Scott, 2000; Scott et al., 2014). The Cretaceous Period is of particular interest with regard to the evolution of modern ecosystems. It was during this period that the biosphere experienced an enormous restructuring, with the appearance and radiation of angiosperms in the Early Cretaceous, and the rise of this plant group to dominance in many continental ecosystems (Coiffard et al., 2012)—a dominance that persists today. In recent years, it has become evident that the evolutionary success of angiosperms was very likely linked to fire ecology and that various positive feedback mechanisms between angiosperms and wildfires may have influenced the early radiation and dispersal of this plant group (Belcher & Hudspeth, 2017; Belcher et al., 2021).

2 Cretaceous Wildfires and Their Impact on Ecosystems

Modern plant taxa and vegetation types with origins dating back to the Cretaceous Period probably experienced evolutionary pressures related to fire regimes of increased frequency and possibly intensity (e.g. He et al., 2012, 2016; Lamont & He, 2017). Therefore, the emergence of angiosperms and their initial spread occurred under global high-fire conditions and were most likely had been directly influenced by such events (e.g. Belcher & Hudspith, 2017; Bond & Scott, 2010; Brown et al., 2012). Bond and Scott (2010) argued that angiosperms, that have higher production and reproduction rates than the gymnosperms they were to replace and consequently were able to outcompete the latter under fire regimes that imparted a selective pressure for rapid and opportunistic post-fire recolonization. In turn, this may have fuelled a positive feedback for the gradual replacement of the previously gymnosperm-dominated vegetation by angiosperm-dominated, highly diverse and more fire-prone communities, potentially increasing the incidence and intensity of fire propagation in these environments (e.g. Belcher & Hudspith, 2017; Belcher et al., 2021; Bond & Midgley, 2012). In addition, a novel vertical stratification in plant communities, enabled by angiosperm habitat partitioning may have led to a more efficient connection of the understorey portions to the canopies via ladder fuels. This may have had a significant impact on gymnosperm-dominated canopies with crown fires increasing fire intensity and presenting a greater disadvantage to gymnosperm taxa that had evolved to survive the lower-temperature and less damaging surface fires in these environments (e.g. Belcher et al., 2010; Bond & Scott, 2010).

Fossil charcoal, as direct evidence of palaeo-wildfires, is widely distributed in many deposits worldwide, ranging

from the Silurian Period to the Holocene (Glasspool et al., 2004; Scott, 2000, 2010). This is due to the fact that charcoal, as the product of incomplete combustion of biomass, is chemically almost inert and is thus highly resistant to chemical and biological degradation (Jones & Chaloner, 1991; Scott, 2000, 2010). However, charcoal is brittle and is susceptible to mechanical pressure, which may cause it to shatter into very small pieces during normal compaction of sediments during diagenesis (Itter et al., 2017). Under conditions of reduced compaction, charcoal retains its three-dimensional structure and may exhibit extremely well-preserved anatomical characteristics (Crawford & Belcher, 2014). This, together with its distinctive black colour, black streak when touched, silky lustre, as well as homogenized cell walls (as seen under SEM) provide unique characteristics that are frequently used to identify fossil charcoal (Jones & Chaloner, 1991; Scott, 2000, 2010).

3 Cretaceous Wildfires in Egypt

Cretaceous strata host the richest fossil flora in Egypt (El-Saadawi et al., 2020, Coiffard & El Atfy, *in press*). The floral assemblages are generally well-preserved and encompass diverse macrofloral elements as well as palynofloras. Despite the sporadic nature of the Egyptian fossil record of mesofossils, including fossil charcoal, they play an important role in the interpretation of palaeoenvironmental and palaeoclimatic developments in the continental realm. The charred plant remains represent important components of the North African (Fig. 1) palaeoflora during the Cretaceous (El Atfy et al., 2016).

Fossil charcoal, as direct evidence for the occurrence of palaeo-wildfires is so far known from three different time windows in the Cretaceous of Egypt (Fig. 2).

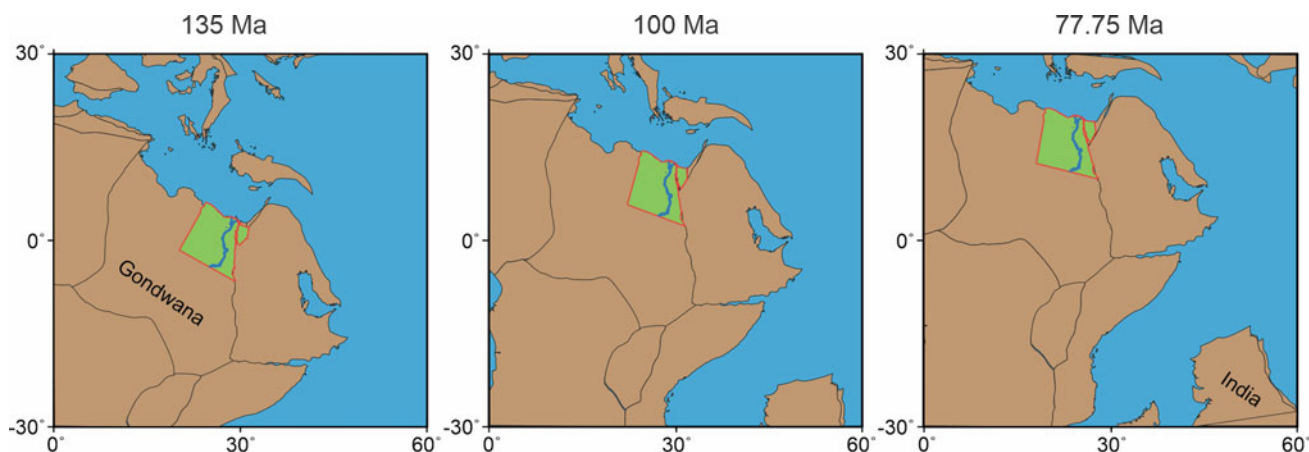


Fig. 1 Palaeogeographic position of Egypt as part of northern Gondwana during the studied periods in the Cretaceous, for more detail see Kirscher et al. ([this volume](#))

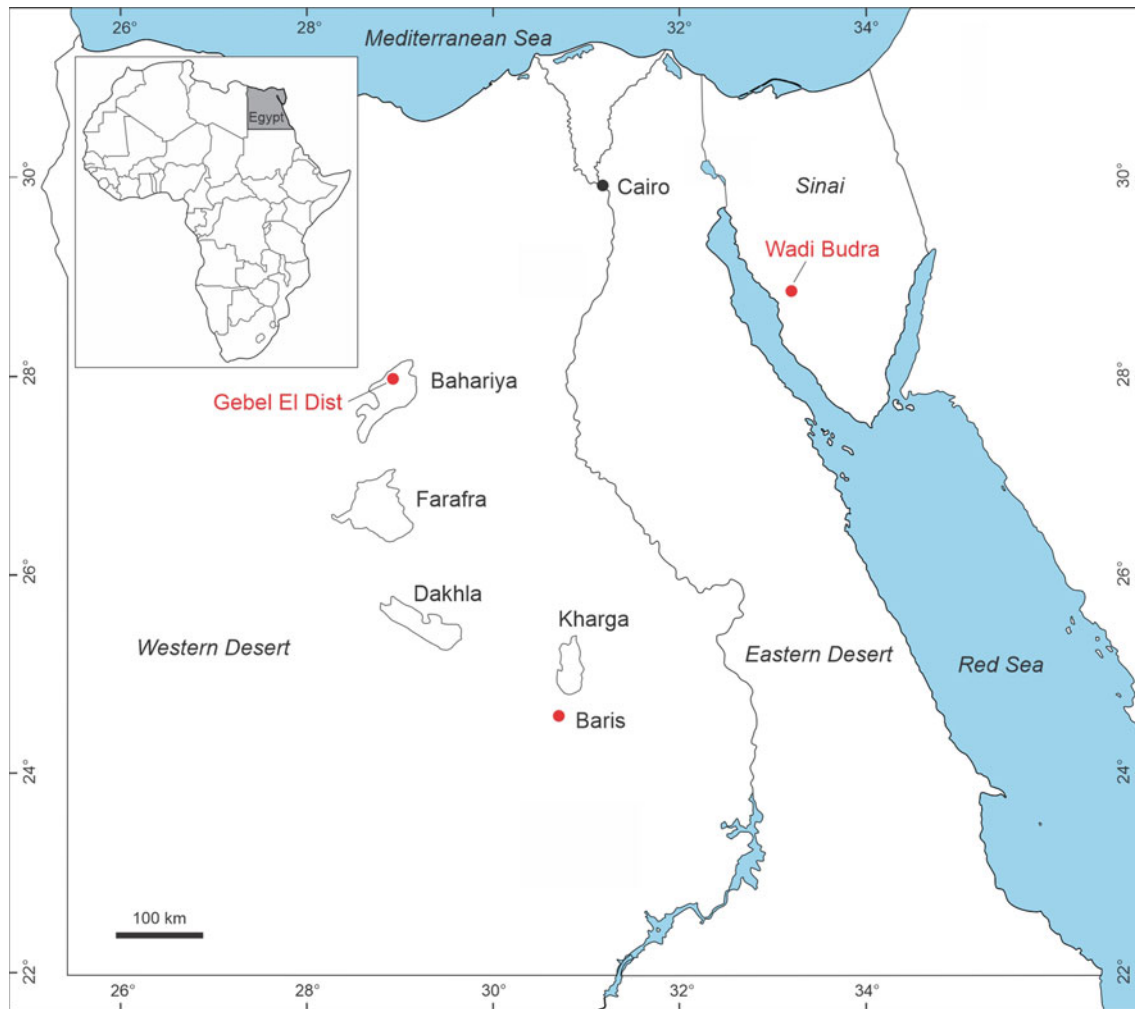


Fig. 2 Map of Egypt showing the position of the localities where Cretaceous macro-charcoal has been documented so far (red dots)

3.1 Malha Formation, Sinai

The oldest known palaeo-wildfire record within the Cretaceous of Egypt comes from a dark grey, kaolinitic shale collected from Wadi Budra, west-central Sinai, Egypt from the pre-Aptian Malha Formation, where gymnospermous charcoal (Fig. 3) provides reliable evidence for the occurrence of wildfires in a typical pre-angiosperm vegetation consisting of pteridophytes and various gymnosperm groups (El Atfy et al., 2022).

3.2 Bahariya Formation, Bahariya Oasis

The second and best-studied charcoal occurrence within the Cretaceous of Egypt comes from the type profile of the Cenomanian Bahariya Formation at Gebel El Dist at the Bahariya Oasis in the Western Desert (El Atfy et al., 2019). Charcoal has been studied in detail from six different

horizons of shale, claystone and sandstone. Gymnosperms, as well as angiosperms and pteridophytes, have been identified from this material (Fig. 3). Of considerable interest is the presence of one horizon dominated by charcoal that can be attributed to ferns, which shows great similarities to *Paradoxopteris/Weichselia*, probably growing in mangrove-like vegetation. These results indicate that the iconic dinosaurs, like the carnivorous *Spinosaurus* and *Carcharodontosaurus*, as well as the herbivorous *Aegyptosaurus* and *Paralititan* (e.g. Nothdurft et al., 2002; Smith et al., 2001; Stromer, 1915, 1931, 1932), which have been found in the Bahariya Formation, dwelled in a landscape frequently affected by wildfires.

3.3 Quseir Formation, Baris Oasis

The third occurrence of fossil charcoal from Egypt, again of exclusively gymnospermous affinity (Fig. 3), is known from

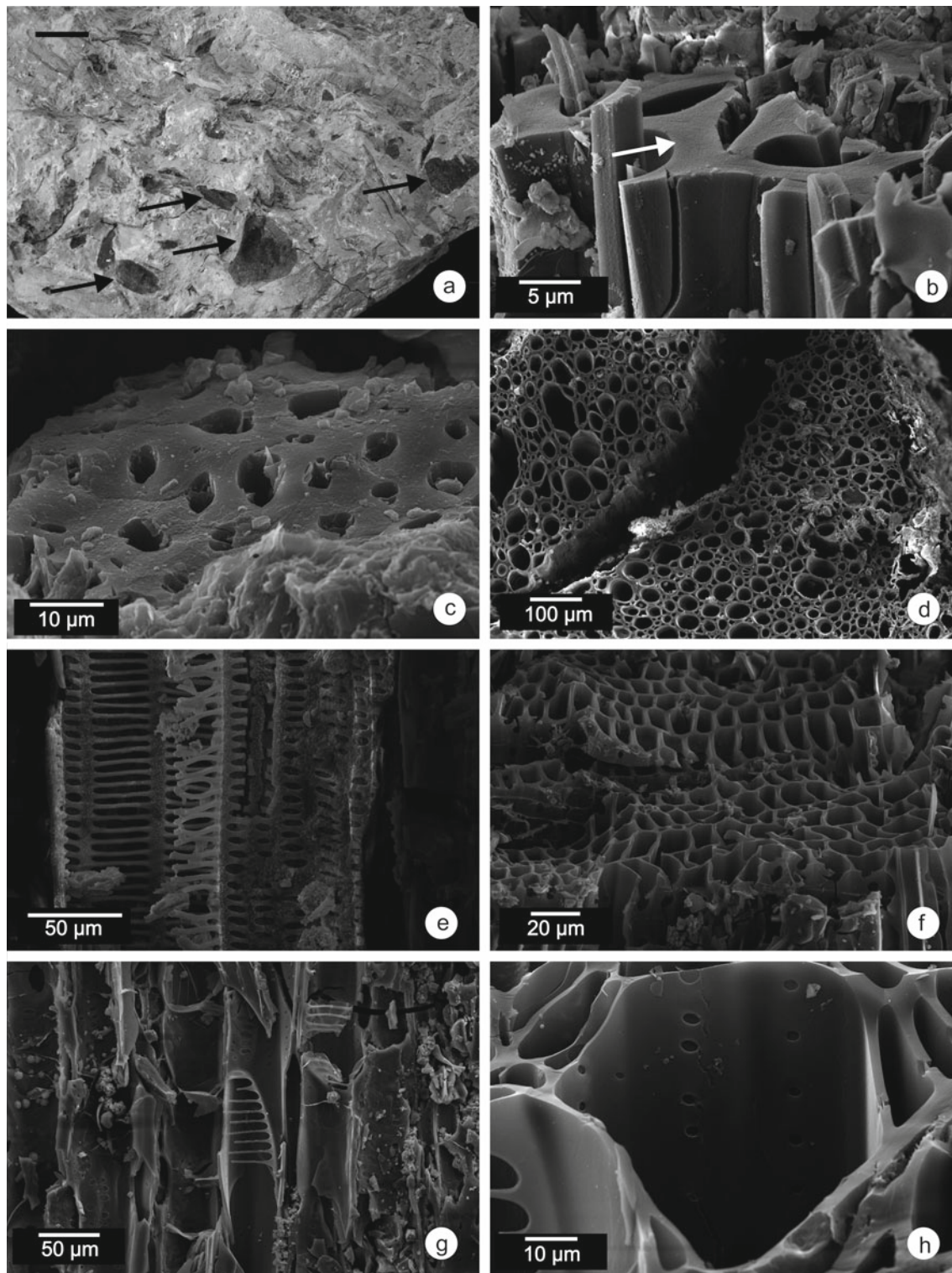


Fig. 3 Examples of Cretaceous charcoal from Egypt. **a** Overview of a split surface of a sample from the pre-Aptian Malha Formation from Wadi Budra, Sinai, exhibiting numerous macro-charcoal fragments (black arrows), scale bar = 2 cm (from El Atfy et al., 2022); **b** SEM image of charcoal from the Malha Formation exhibiting homogenized cell walls (white arrow), a diagnostic character of charcoal (from El Atfy et al., 2022); **c** SEM image of charcoal from the Campanian from Baris area, exhibiting the cross-section of three-dimensionally preserved wood with thick, homogenized cell walls (from El Atfy et al., 2016); **d–h** SEM images of macro-charcoal from the early Cenomanian Bahariya Formation (Gabal El Dist profile at the Bahariya Oasis) (from El Atfy et al., 2019); **d** cross-section of fern xylem; **e** fern tracheid with scalariform pitting; **f** cross-section of gymnosperm wood showing more or less rectangular cross-section of tracheids; **g** angiospermous charcoal exhibiting vessels with scalariform sieve-plate and axial parenchyma; **h** detail of pitting on vessel wall consisting of small uniseriate pits in cell walls shared with tracheids

the Campanian Quseir Formation from the Baris Oasis in the south Western Desert (El Atfy et al., 2016). Here the wildfires probably occurred in a vegetation dominated by angiosperms and pteridophytes, with only minor gymnosperm component, which grew under warm and wet climatic conditions, as demonstrated by previous palynological studies (e.g., Mahmoud, 2003).

All in all, the charcoal data from the Cretaceous of Egypt support the view, that the Cretaceous was globally a high-fire world. However, further research on charcoal from Cretaceous deposits of Egypt is necessary to provide a more complete picture regarding the interactions between wildfires and vegetation, as well as dinosaurs and other animals living during this important period of Earth's history.

Acknowledgements We appreciate the Editors' interest and proposal that produced this chapter. H.E. acknowledges the financial support of the Alexander von Humboldt Foundation, Germany (EGY—1190326—GF-P). A.J. acknowledges funding by FAPERGS, CNPq (Brazil—305938/2019-3) and Alexander von Humboldt Foundation (Germany—3.4–8151/18 025). Insightful reviews by Rose Prevec, Jiří Kvaček and Abdalla M.B. Abu Hamad enabled an improved presentation of this work.

References

- Belcher, C. M., & Hudspeth, V. A. (2017). Changes to Cretaceous surface fire behaviour influenced the spread of the early angiosperms. *Science*, *321*, 1197–1200.
- Belcher, C. M., Mills, B. J. W., Vitali, R., Baker, S. J., Lenton, T. M., & Watson, A. J. (2021). The rise of angiosperms strengthened fire feedbacks and improved the regulation of atmospheric oxygen. *Nature Communications*, *12*, 503.
- Belcher, C. M., Yearsley, J. M., Hadden, R. M., McElwain, J. C., & Rein, G. (2010). Baseline intrinsic flammability of earths' ecosystems estimated from paleoatmospheric oxygen over the past 350 million years. *PNAS*, *107*, 22448–22453.
- Bond, W. J., & Midgley, J. J. (2012). Fire and the angiosperm revolutions. *International Journal of Plant Sciences*, *173*(6), 569–583.
- Bond, W. J., & Scott, A. C. (2010). Fire and the spread of flowering plants in the Cretaceous. *New Phytologist*, *188*, 1137–1150.
- Brown, S. A. E., Scott, A. C., Glasspool, I. J., & Collinson, M. E. (2012). Cretaceous wildfires and their impact on the earth system. *Cretaceous Research*, *36*, 162–190.
- Cochrane, M. A. (2019). Burning questions about ecosystems. *Nature Geosciences*, *12*, 82–87.
- Coiffard, C., & El Atfy, H. (in press). The evolution of vegetation through the Cretaceous of Egypt (Chap. 8). In Z. Hamimi, H. Khozyem, T. Adatte, F. H. Nader, F. Oboh-Ikuenobe, M. K. Zobaa, & H. El Atfy (Eds.), *The Phanerozoic geology and natural resources of Egypt*. Springer.
- Coiffard, C., Gomez, B., Daviero-Gomez, V., & Dilcher, D.L. (2012). Rise to dominance of angiosperm pioneers in European Cretaceous environments. *PNAS*, *109*, 20955–20959.
- Crawford, A. J., & Belcher, C. M. (2014). Charcoal morphometry for palaeoecological analysis: The effects of fuel type and transportation on morphological parameters. *Applications in Plant Sciences*, *2*(8), 1400004.
- Diessel, C. F. (2010). The stratigraphic distribution of inertinite. *International Journal of Coal Geology*, *81*, 251–268.
- El Atfy, H., Anan, T., Jasper, A., & Uhl, D. (2019). Repeated occurrence of palaeo-wildfires during deposition of the Bahariya Formation (early Cenomanian) of Egypt. *Journal of Palaeogeography*, *8*, 28.
- El Atfy, H., Kora, M., Spiekermann, R., Jasper, A., & Uhl, D. (2022). Further evidence for Cretaceous wildfires: Macro-charcoal from the Malha Formation at Wadi Budra, Sinai, Egypt. *South African Journal of Geology*, *125*, 211–216.
- El Atfy, H., Sallam, H., Jasper, A., & Uhl, D. (2016). The first evidence of paleo-wildfire from the Campanian (Late Cretaceous) of North Africa. *Cretaceous Research*, *57*, 306–310.
- El-Saadawi, W. E., Nour-El-Deen, S., El-Noamani, Z. M., Darwish, M. H., & Kamal El-Din, M. M. (2020). Fossil flora of Egypt. In Z. Hamimi, A. El-Barkooky, J. Martínez Frias, H. Fritz, & Y. Abd El-Rahman (Eds.), *The geology of Egypt* (pp. 495–520). Springer. Regional Geology Reviews.
- Glasspool, I. J., Edwards, D., & Axe, L. (2004). Charcoal in the Silurian as evidence for the earliest wildfire. *Geology*, *32*, 381–383.
- He, T., Lamont, B. B., & Manning, J. (2016). A Cretaceous origin for fire adaptations in the Cape flora. *Scientific Reports*, *6*, 1–6.
- He, T., Pausas, J. G., Belcher, C. M., Schwilk, D. W., & Lamont, B. B. (2012). Fire-adapted traits of *Pinus* arose in the fiery Cretaceous. *New Phytologist*, *194*, 751–759.
- Itter, M. S., Finley, A. O., Hooten, M. B., Higuera, P. E. H., Marlon, J. R., Kelly, R., & McLachlan, J. S. (2017). A model-based approach to wildland fire reconstruction using sediment charcoal records. *Environmetrics*, *28*, e2450.
- Jasper, A., Pozzebon-Silva, Â., Siqueira Carniere, J., & Uhl, D. (2021). Palaeozoic and Mesozoic palaeo-wildfires: An overview on advances in the 21st century. *Journal of Palaeosciences*, *70*, 159–171.
- Jones, T. P., & Chaloner, W. G. (1991). Fossil charcoal, its recognition and palaeoatmospheric significance. *Palaeogeography, Palaeoclimatology, Palaeoecology*, *97*, 39–50.
- Kirscher, U., Dallanave, E., & Bachtadse, V. (this volume). Paleoposition and paleogeography of Egypt during the Phanerozoic era (Chap. 4). In Z. Hamimi, H. Khozyem, T. Adatte, F. H. Nader, F. Oboh-Ikuenobe, M. K. Zobaa, & H. El Atfy (Eds.), *The Phanerozoic geology and natural resources of Egypt*. Springer.
- Lamont, B. B., & He, T. (2017). When did a Mediterranean-type climate originate in southwestern Australia? *Global and Planetary Change*, *156*, 48–58.
- Mahmoud, M. S. (2003). Palynology and palaeoenvironment of the Quseir Formation (Campanian) from central Egypt. *Journal of African Earth Sciences*, *36*, 135–148.
- Nothdurft, W., Smith, J. B., Lamanna, M. C., Lacovara, K. J., Poole, J. C., & Smith, J. R. (2002). *The lost dinosaurs of Egypt* (p. 242). Random House.
- Scott, A. C. (2000). The pre-Quaternary history of fire. *Palaeogeography, Palaeoclimatology, Palaeoecology*, *164*, 281–329.
- Scott, A. C. (2010). Charcoal recognition, taphonomy and uses in palaeoenvironmental analysis. *Palaeogeography, Palaeoclimatology, Palaeoecology*, *291*, 11–39.
- Scott, A. C., Bowman, D. M., Bond, W. J., Pyne, S. J., & Alexander, M. E. (2014). *Fire on earth: An introduction*. Wiley.
- Smith, J. B., Lamanna, M. C., Lacovara, K. J., Dodson, P., Smith, J. R., Poole, J. C., Giegengack, R., & Attia, Y. (2001). A giant sauropod dinosaur from an Upper Cretaceous mangrove deposit in Egypt. *Science*, *292*, 1704–1706.

- Stromer, E. (1915). Ergebnisse der Forschungsreisen Prof. E. Stromers in den Wüsten Ägyptens, II. Wirbeltier-Reste der Baharijestufe (unterstes Cenoman), 3. Das Original des Theropoden *Spinosaurus aegyptiacus*. *Abhandlungen der Bayerischen Akademie der Wissenschaften, Mathematisch-naturwissenschaftliche Abteilung Neue Folge*, 28, 1–32.
- Stromer, E. (1931). Ergebnisse der Forschungsreisen Prof. E. Stromers in den Wüsten Ägyptens, II. Wirbeltier-Reste der Baharijestufe (unterstes Cenoman), 10. Ein Skelett-Rest von *Carcharodontosaurus* nov. gen. *Abhandlungen der Bayerischen Akademie der Wissenschaften, Mathematisch-naturwissenschaftliche Abteilung Neue Folge*, 9, 1–23.
- Stromer, E. (1932). Ergebnisse der Forschungsreisen Prof. E. Stromers in den Wüsten Ägyptens, II. Wirbeltier-Reste der Baharijestufe (unterstes Cenoman), 11. Sauroptoda. *Abhandlungen der Bayerischen Akademie der Wissenschaften, Mathematisch-naturwissenschaftliche Abteilung Neue Folge*, 10, 1–21.



Haytham El Atfy is an associate professor at Mansoura University (Egypt) from where he received a B. Sc. degree in geology and an M.Sc. in palynology. He received a Ph.D. in geosciences (palynology and organic geochemistry) from Goethe University, Frankfurt (Germany) in 2014 and PD (Habilitation) from the University of Tübingen (Germany) in 2022. He acquired experience in industrial palynology through work with GUPCO (BP), Egypt. Haytham has been a Research Fellow of the Alexander von Humboldt Foundation at the University of Tübingen (Germany) since 2019. He was recently a

visiting scientist at the Senckenberg Research Institute, Germany. His research interests span all aspects of palynology and its applications in dating, palaeoenvironmental and palaeoclimatical reconstructions and hydrocarbon exploration, particularly of the Mesozoic and Cenozoic and, to a lesser extent, the Palaeozoic. He has more recently become involved in organic geochemistry. He is a member of the AASP, The Palynological Society, the Micropalaeontological Society (TMS), Arbeitskreis für Paläobotanik und Palynologie (APP) and the Palaeontological Society of Egypt (PSE). He is a recipient of many awards, including the Bernd Rendel

Prize from the German Science Foundation (DFG), Egyptian State Incentive Award and the First-Class Excellence Concession that is provided by the Egyptian president.



Dieter Uhl is the head of the Department of Palaeontology at the Senckenberg Research Institute and Natural History Museum in Frankfurt am Main (Germany) and also adjunct professor at Tübingen University (Germany). He was awarded his Diploma in biology in 1994 from the Technical University of Kaiserslautern (Germany) and his Ph.D. (Dr. rer. nat.) in palaeontology in 1999 from the University of Tübingen. After doing research at Münster University (Germany), Utrecht University (The Netherlands)

and Tübingen University (Germany), he joined the Senckenberg Research Institute and Natural History Museum in Frankfurt am Main (Germany) in 2007. He is a member of the International Organisation of Palaeobotany, Paläontologische Gesellschaft and a fellow of the Linnean Society of London. His main research interest is on the use of fossil plants (macroremains and palynomorphs) as palaeoenvironmental proxies. So far, he has published more than 200, mostly peer reviewed, scientific papers and book chapters. His works span a wide variety of topics, stratigraphically ranging from the Carboniferous up to the Pliocene, with a focus on the former supercontinent Gondwana.



André Jasper is a titular professor at Universidade do Vale do Taquari—Univates Lajeado (Brazil). He graduated with a B.S. degree in biological sciences and obtained M.Sc. and Ph.D. degrees in Palaeontology/Palaeobotany, working with Gondwanan palaeofloras since the 1990s. He now researches palaeowildfire evidence through deep time and collaborates with researchers from diverse countries in diverse palaeobotanical studies.



Palaeoenvironmental and Palaeontological Study of the Gabal Ekma Section (Egypt) Throughout the Coniacian-Santonian Boundary

Brahimsamba Bomou, Thierry Adatte, and Jorge E. Spangenberg

Abstract

The Gabal Ekma section, located in the Sinai desert (Egypt), is characterised by shallow marine deposits of mixed siliciclastic/carbonate sediments of the Matulla Formation which includes the Coniacian and Santonian stages. The section exhibits significant accumulation of organic-rich intervals and phosphatic layers associated with fossiliferous vertebrate remains. The Coniacian-Santonian (CS) carbon isotopic patterns appear to be recognised in the Egyptian section and are used to characterise the interval of the CS oceanic anoxic event (OAE 3). However, this latest Cretaceous OAE appears not to be truly important on a global scale but was more dependent on local or regional conditions. These are mainly limited to shallow-water environments and epicontinental seas of the equatorial and South Atlantic basins and the Western Interior Seaway. Based on a weathering index and mineralogy, climate gradually evolved from warm and seasonal climate to arid conditions during the late Coniacian up to the base of the Santonian (Michel Dean Event). Then a significant change to more humid and tropical conditions is observed above the Michel Dean Event (early Santonian), which persisted up to the Buckle Event (base of the late Santonian), coinciding with the organic-rich shales deposits in deeper environments. Fluctuations in total phosphorus (Total-P) contents are clearly independent from detrital input but seem to be controlled by regional anoxia and phosphogenesis. Total-P contents are indeed depleted in the organic-rich interval, suggesting intense P regeneration due to anoxic conditions. This type of P

regeneration may explain the formation of the bone bed located at the C-S boundary characterised by very well-preserved shark teeth and vertebra, associated with phosphatised nodules in a sandy phosphatic matrix.

Keywords

Coniacian-Santonian boundary • OAE3 • Bone-bed • Gabal Ekma section

1 Introduction

During the Cretaceous period, several episodes of climate and palaeoceanographic change dramatically affected marine environments and resulted in a succession of oceanic anoxic events (OAE). They are characterised by major and widespread deposition of laminated sediments enriched in organic matter, which coincide with positive shift in $\delta^{13}\text{C}$ values (Arthur et al., 1990; Jenkyns, 1980; Schlanger & Jenkyns, 1976). The largest OAE took place near the end of the Cenomanian and is known as OAE 2. The OAE 3, of Coniacian to Santonian age, is thought to be the youngest of the Cretaceous OAEs (e.g., Arthur et al., 1990; Hofmann et al., 2003; Jenkyns, 2010). However, associated organic-rich deposits appear to be spatially limited. They are documented from the eastern tropical Atlantic Ocean, Ivory Coast, and Ghana (Hofmann et al., 2003; Holbourn & Kuhnt, 1998; Wagner, 2002), Venezuela (Erlich et al., 1999; Rey et al., 2004), the Brazilian shelf (Mello et al., 1989), Mexico (Sohl et al., 1991), and the Western Interior Seaway of North America (Dean & Arthur, 1998). Deposition of organic-rich sediments appears therefore to represent a regional rather than global event (Wagner, 2002; Wagner et al., 2004; Wagreich, 2009, 2012). Additionally, the organic-rich sediment deposits are rarely synchronous and occur in different time intervals within the Coniacian and Santonian, depending on the palaeo-location of the basin

B. Bomou (✉) · T. Adatte
Institute of Earth Sciences (ISTE), University of Lausanne,
Geopolis, CH-1015 Lausanne, Switzerland
e-mail: brahimsamba.bomou@unil.ch

J. E. Spangenberg
Institute of Earth Surface Dynamics (IDYST), University of
Lausanne, Geopolis, CH-1015 Lausanne, Switzerland

(Locklair et al., 2011). Moreover, carbon isotope records associated with OAE 3 lack major excursions. For example, in the reference record of the English Chalk, the OAE 3 interval is characterised by two minor and gradual positive $\delta^{13}\text{C}$ excursions of only 0.5‰ (Jarvis et al., 2006), culminating in the middle-late Coniacian and middle Santonian, respectively. Interestingly, $\delta^{13}\text{C}$ values decrease across the Coniacian-Santonian boundary in numerous sections like Eastbourne (G.B.), Olazagutia (Spain) or Tingri (Tibet) (Jarvis et al., 2006; Lamolda & Paul, 2007; Wendler et al., 2009). As previously stated by Wagreich (2012), the Coniacian-Santonian interval can therefore not be considered to be a true OAE.

Contrary to the other Cretaceous OAEs, only a few studies have been performed to date the control and the evolution of organic carbon burial during that period (e.g., Davis et al., 1999; Erlich et al., 1999; Hofmann et al., 2003; Jenkyns et al., 1994; Locklair et al., 2011; Wagner, 2002). Recently, Locklair et al. (2011) showed that organic carbon accumulation rates were quite elevated, regardless of the low amplitude of the carbon isotope excursions. Moreover, unlike older OAEs, the burial flux of carbonate was rather high during the Coniacian-Santonian interval, which may explain the absence of a significant $\delta^{13}\text{C}$ excursion.

The focus of the present chapter is to study the palaeoenvironmental and palaeoclimatic evolution recorded in the Gabal Ekma section (Sinai, Egypt), which is characterised by organic-rich sediments and phosphatic bone-bed layers deposited in shallow-water environment, throughout the Coniacian-Santonian interval. Using a multidisciplinary approach based on sedimentology, mineralogy, phosphorus analyses, stable carbon isotopes, and major elements (weathering indices), the main goal of this study is to explore the expression of the OAE 3 in these shallowest environments and better constrained the phosphorus behaviour and the organic-rich deposits in regional anoxia context.

2 Geological Setting and Lithology

The Gabal Ekma (GE) section is located in west-central Sinai, Egypt (GPS: 28° 41' 17.76° N; 33° 17' 21.92° E), along the east coast of the Gulf of Suez (Fig. 1a). The section belongs to the NW-tilted Ekma block, which is part of the Syrian arc folding system which was active during the Turonian-Coniacian interval (El-Azabi & El-Araby, 2007). The Gabal Ekma section comprises mixed siliciclastic/carbonate sediments assigned to the Matulla Formation (El-Azabi & El-Araby, 2007). The Matulla Fm is intercalated

between the Wata Fm (Turonian) and the Sudr Chalk Fm (Campanian–Maastrichtian) and includes the Coniacian and Santonian stages (Fig. 1b, c) (El-Azabi & El-Araby, 2007).

The Matulla Fm was defined for the first time by Ghorab (1961) and described in several sections in Sinai and in the east coast of Egypt. Most of the sections are located in the western part of Sinai as the Gabal Somar, Wadi Sudr, Wadi Abu Qada, Gabal Musala, Wadi Matulla, Gabal Nezzazat, Wadi Feiran, and Gabal Ekma sections (Abdel-Gawad et al., 2004; El-Azabi & El-Araby, 2007; Farouk et al., 2016; Khalil & Mashaly, 2004; Kora et al., 2002; Samuel et al., 2009; Zalut et al., 2012). This formation can be encountered in the eastern part of Sinai close to the Aqaba gulf in the El Sheik Attia sections (Mandur, 2011), and finally in the eastern part of Egypt (Abdel-Gawad et al., 2007). This formation, found primarily in western Sinai, comprises three main units: a lower siliciclastic unit, a middle clastic/carbonate unit of Coniacian age, and an upper predominantly clastic Santonian unit (El-Azabi & El-Araby, 2007; Kora et al., 2002; Obaidalla & Kassab, 2002). The depositional environment evolved from a siliciclastic coastline to a subtidal environment (Fig. 1d; Bauer et al., 2003).

At Gabal Ekma, sediments are very diverse, comprising shale, siltstone, sandstone, limestone, dolostone, and ironstone with a huge accumulation of oysters. The sandstone is often cross-bedded with symmetric ripples due to wave activity. The shale intervals are mainly laminated and are not bioturbated (Fig. 2). Three “bone-bed” intervals comprise abundant vertebrate remains (bones and shark teeth) embedded in a phosphatic matrix (Fig. 2). These lithologies suggest shallow depositional environments ranging from intertidal (e.g., cross-bedded sandstone; Fig. 2, GE 58) to slightly deeper subtidal environment (El-Azabi & El-Araby, 2007).

The first 5 m of the section is characterised by centimetric to metric sandstone beds, with a particular oyster bed at 1 m (GE 4), followed by an 8 m thick interval of finely laminated shale enriched in organic matter (Fig. 2, GE 29), intercalated by two sandstone beds. A change in lithology is observed from 13 to 30 m, with centimetric and metric sandstone beds alternating with metric dolostone beds (GE 54). These levels are enriched in teeth and bones remains (Fig. 2, GE 52; 58). At 30 m, a particularly well-preserved bone bed is observed (GE 58). Above, the lithology changes again to shales and silty shales (Fig. 2, GE 85) which are enriched in organic matter from 30 to 43 m. A succession of metric sandstone beds is alternated with plurimetric interval of marls from 43 to 69 m. The marls interval exhibits plants debris, in particular between 57 and 60 m. The topmost of the section consists of chalk of the Sudr Chalk Fm dating of Campanian (e.g. El-Azabi & El-Araby, 2007).

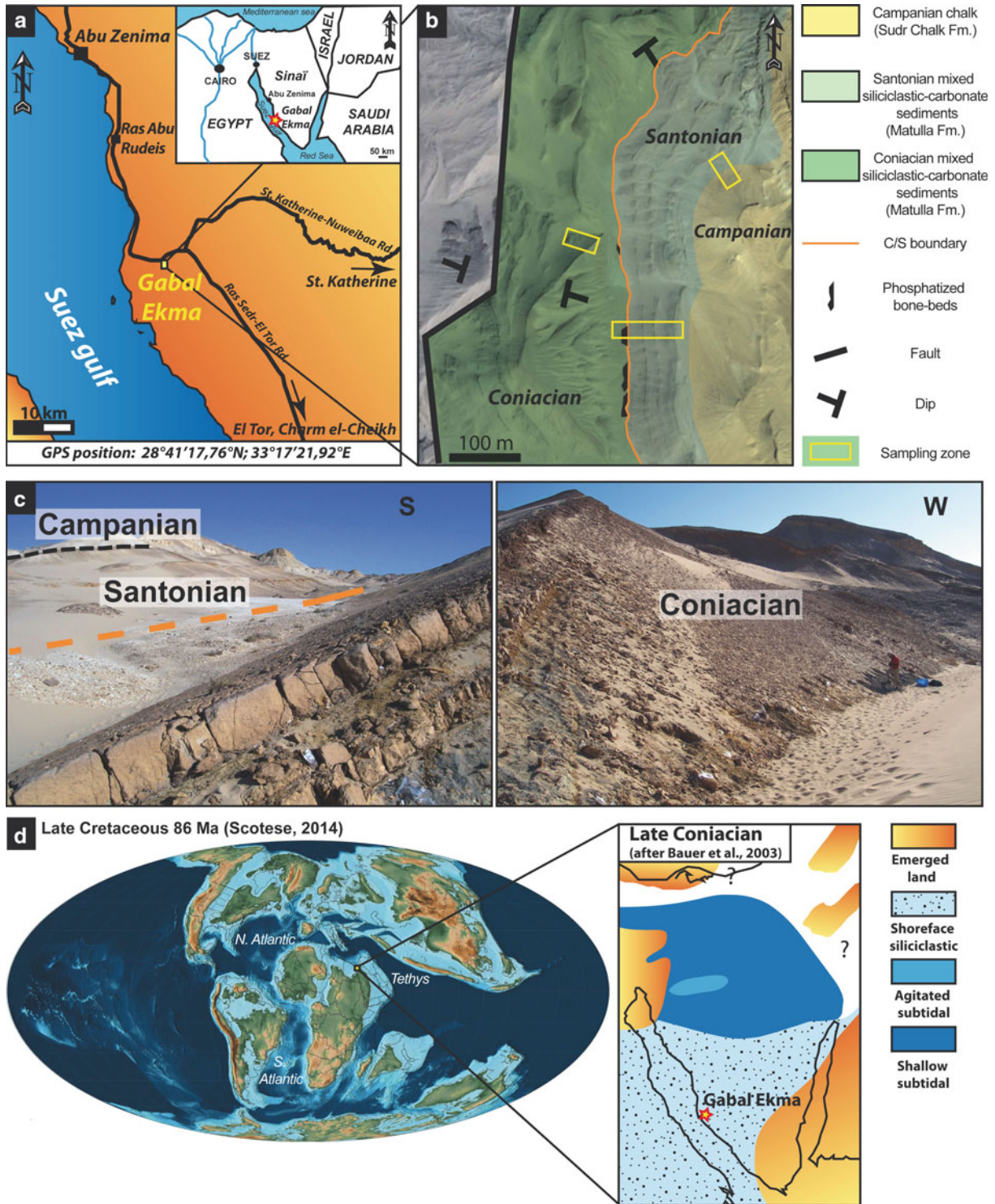


Fig. 1 Location and paleogeographic location of the section of Gabal Ekma section during the late Coniacian

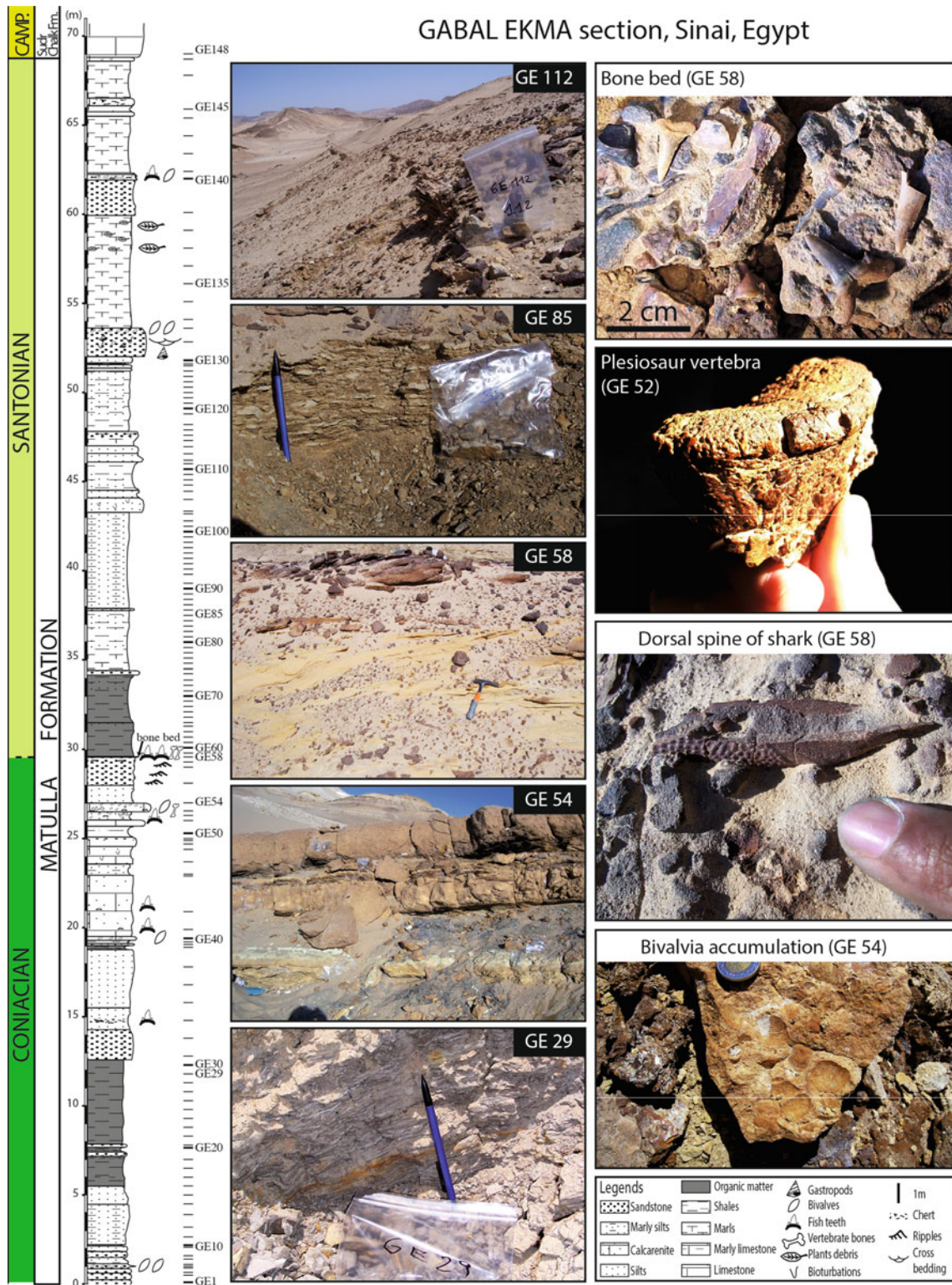


Fig. 2 Lithology of the Gabal Ekma section, Sinai, Egypt

3 Material and Methods

A total of 148 samples were collected throughout the Gabal Ekma section with a resolution of 0.15–1 m. The palaeontological remains were washed and are currently under analysis in the INSEM laboratory of the University of Montpellier (France) for the shark teeth, and in the laboratories of MNHN, Paris (France), and Claude Bernard University Lyon (France) for the vertebrate materials. Altered and recrystallised parts were removed from the collected samples, and the whole-rock powders were ground in a mechanical agate grinder.

Organic carbon stable isotope analyses were achieved at the Institute of Earth Surface Dynamics, University of Lausanne (IDYST-UNIL) on decarbonated bulk rock powders by flash combustion on a Carlo Erba 1108 elemental analyser coupled to an isotope ratio mass spectrometer via a ConFlo II interface (Thermo Fisher Scientific Delta V Plus). The $\delta^{13}\text{C}_{\text{org}}$ values are reported relative to VPDB. The reproducibility was better than 0.1‰ (1 σ).

XRD analyses of the whole rock were carried out for all the samples using a X-TRA Thermo-ARL Diffractometer at the Earth Sciences Institute of the University of Lausanne (ISTE-UNIL). The samples were prepared following the procedure of Kübler (1987) and Adatte et al. (1996). The error fluctuates between 5 and 10% for the phyllosilicates and is 5% for the grain minerals.

Total phosphorus measurements were performed at ISTE-UNIL by applying the ascorbic acid molybdate blue method (Eaton et al., 1995). The blue colour intensity, depending on the phosphorus concentration, was measured with a Perkin Elmer Lambda 25 UV/Vis spectrophotometer. The PO_4 concentration in mg/L was acquired by calibration using internal standard solutions with an precision better than 5%.

Major element concentrations were determined by X-ray fluorescence spectrometry (XRF), employing a Philips PW2400 XRF spectrometer at ISTE-UNIL. Major element analyses were conducted on glass beads after fusion using lithium tetraborate. The detection limits are around 0.01%, and the external reproducibility (1 σ) varies from 0.5 to 5%, depending on the element. The accuracy of the analyses was estimated by analyses of standard reference materials (NIM-G; SDC; BHVO; QLO).

On the basis of major-element concentrations, the Chemical Index of Weathering (CIA) and the Weathering Index of Parker (WIP), were calculated to characterise detrital sources and palaeoclimatic conditions (Fedó et al., 1995, 1997; Nesbitt & Young, 1982; Yan et al., 2010). The Chemical Index of Alteration (CIA; Nesbitt & Young,

1982) has been used to assess the weathering of unstable minerals, while the Weathering Index of Parker (WIP; Parker, 1970) has been used to estimate the degree of chemical weathering by tracing the labile elements mass transfer such as alkali and alkaline earth elements (e.g., Price & Vebl, 2003; Gertsch et al., 2011). However, to use these indices, the CaO molar proportion must be limited to that derived from a silicate mineral (Nesbitt & Young, 1982, 1989; Yan et al., 2010). Due to the occurrence of carbonates (calcite, dolomite) and apatite, an adjustment is required (McLennan, 1993; Yan et al., 2010). After the correction for the phosphates, the remaining content of CaO is still greater than that of Na_2O , thus indicating that the CaO values cannot be used (Yan et al., 2010). As a result, the original formula was adjusted according to formulas (1) and (2), where the CaO content is replaced by the Na_2O content (McLennan, 1993).

The CIA (in molar proportion) is expressed as:

$$\text{CIA} = \text{Al}_2\text{O}_3 \times 100 / (\text{Al}_2\text{O}_3 + \text{Na}_2\text{O}^* + \text{Na}_2\text{O} + \text{K}_2\text{O}) \quad (1)$$

The WIP (in molar proportion) is expressed as:

$$\text{WIP} = 100 \times [(2 \times \text{Na}_2\text{O}/0.35) + (\text{MgO}/0.9) + (2 \times \text{K}_2\text{O}/0.25) + (\text{Na}_2\text{O}^*/0.7)] \quad (2)$$

In both formulas, the Na_2O^* content replacing the CaO content.

4 Results

4.1 Organic Carbon Stable Isotopes

Due to low calcite amounts, carbon stable isotope analyses were performed on organic matter. Values fluctuate mainly between -26 and -24 ‰ with a maximum of -22.5 ‰ (Fig. 3). An overall decreasing trend is observed throughout the section. Despite the scarcity of measurements, some significant positive shifts (up to 3‰) are identified along the section. First one at 6 m (GE 17; -22.5 ‰), then at 29.7 m (GE 58; -22.8 ‰), at 35.1 m (GE 77; -22.7 ‰), at 40.1 m (GE 93; -23.6 ‰) and finally at 49.4 m (GE 121; -24.0 ‰) following by a plateau up to 58 m. Four important negative excursions are also observed at 7.7 m (GE 20; -26.2 ‰), at 29.8 m (GE 59; -25.3 ‰), at 35.7 m (GE 79; -26.1 ‰), and at 62.4 m (GE 141; -26.0 ‰). Unfortunately, between 13 and 29 m, carbon isotope data are not available due to dolomitic lithology and absence of organic matter in the sediment.

Gabal Ekma section, Sinai, Egypt

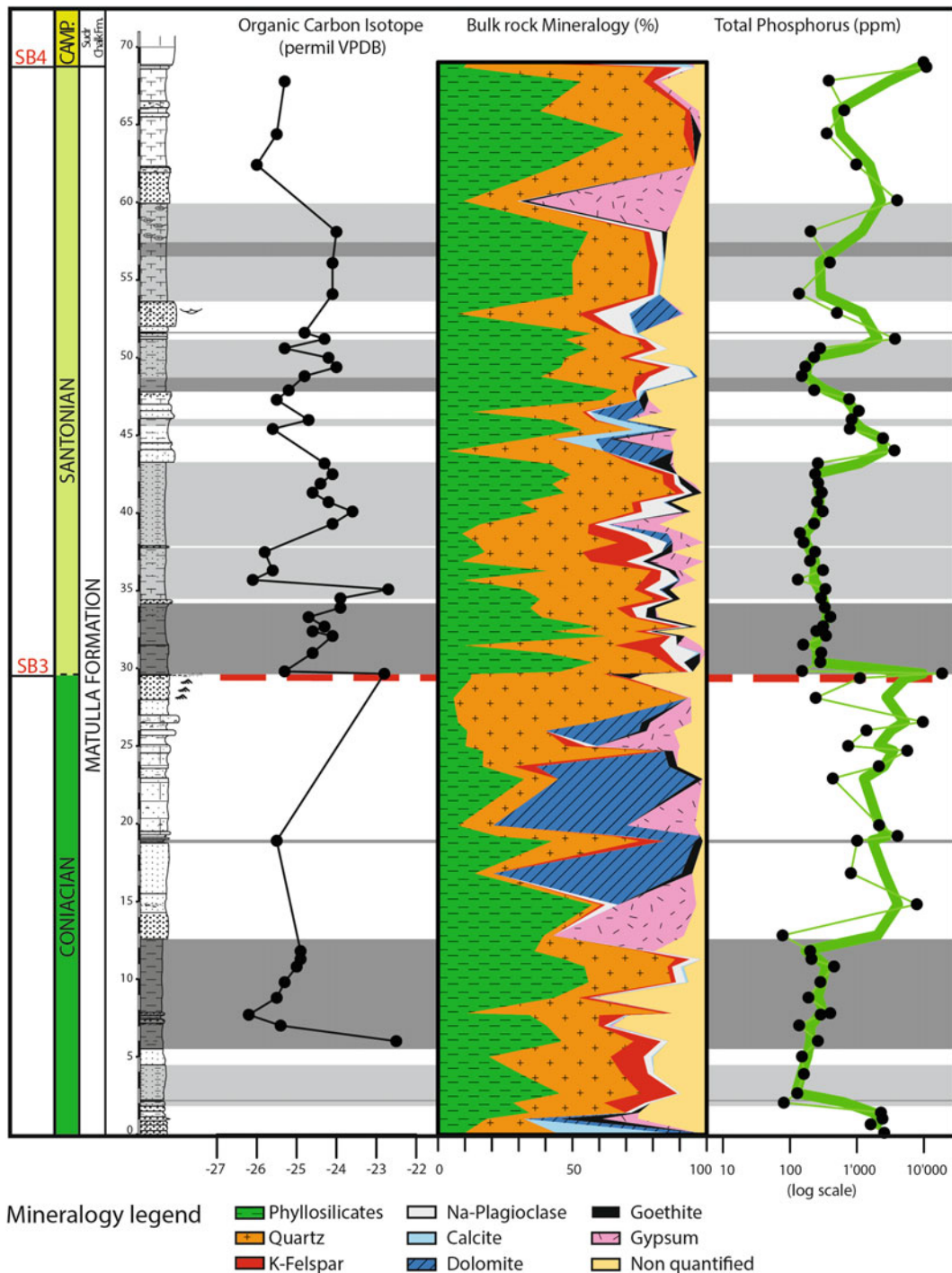


Fig. 3 $\delta^{13}\text{C}$ organic record (in ‰VPDB), bulk-rock mineralogy data (in %) based on XRD analyses and total phosphorus (in ppm on a log scale) of the Gabal Ekma section. Grey intervals correspond to organic-rich shale interval, dark grey for high enrichment in organic matter, and light grey for lesser enrichment

4.2 Bulk-Rock Mineralogy

The great diversity of lithology observed at Gabal Ekma (Fig. 2) is well reflected by the highly variable concentrations

in quartz (3–87%), phyllosilicates (4–69%), K-feldspar (0–26%), plagioclase (0–16%), goethite (0–16%), dolomite (0–70%), gypsum (0–57%), and calcite (0–42%) (Figs. 3 and 4b). The non-quantified phase, which reaches 42%,

corresponds mainly to poorly crystallised minerals such as apatite, goethite, hematite, and phyllosilicates (kaolinite, smectite, and mica).

Gypsum and halite represent secondary minerals, which probably resulted from water table fluctuations under arid conditions. Major minerals (e.g. calcite, phyllosilicates) do not show any significant long-term trend. Quartz increases to the detriment of phyllosilicates in the sandstone intervals and inversely in the shale layers. Phyllosilicates increase from the base to 15 m and then decrease gradually up to the C-S boundary (30 m), above which they abruptly increase. This peak in phyllosilicates occurs in a shale interval, just above the bone-bed level (GE 58). Above, phyllosilicate contents roughly increase up to the top of the section, with lower values corresponding to sandstone levels. Quartz contents relatively mirror the phyllosilicates, except for levels corresponding to sandy-shale intervals (Figs. 3 and 4b). An interval with high dolomite is observed between 15 and 27 m and corresponds to dolostone and calcarenite (Fig. 3 and 4b). A detritus curve (Fig. 4a, b) is calculated, resulting from sum of detrital minerals like Quartz, Phyllosilicates, K-Feldspar, and Na-Plagioclase (Fig. 4b). Significant increases in detritus are observed along the clayed interval deposits enriched in organic matter (Fig. 4, grey interval), alternated with low detritus contents through the dolostone interval of the late Coniacian (17–27 m, Fig. 4b).

4.3 Phosphorus

Total-P contents range from 77 to 18,700 ppm. Total-P reaches very high values, particularly in the bone-bed GE 58 (18,700 ppm), which is characterised by huge accumulation of fish teeth and vertebrate bones (enriched in P) and a phosphatised matrix linked to a hardground composed of a P-rich crust. Low values of total-P (around 100 ppm) are observed in two main intervals (2–13 m and 30–43 m), which correspond to shale enriched in organic matter. Intermediate to higher values (1000–5000 ppm) are associated with shallow sandstone and dolostone lithologies also containing fish teeth debris, particularly in the 13–30 m and the 43–70 m intervals (Fig. 3).

4.4 Major Elements

The most abundant MEs are SiO₂ (13–94%) and CaO (0–27%), followed by Al₂O₃ (1–18.4%), MgO (0–14%), Fe₂O₃ (1–13%) and Na₂O (0–9.5%) (Fig. 12). TiO₂, K₂O, Cr₂O₃, and NiO are present in minor concentrations (< 2%). TiO₂ and Al₂O₃ present the same trend as SiO₂, except for the shale intervals, in which these three elements are not closely coupled (increase both in TiO₂ and Al₂O₃, decrease in SiO₂).

High CaO contents in the intervals between 13 and 25 m and at 47 m are related to the presence of dolomite. The major elements fluctuations are mainly driven by the mineralogical composition (Fig. 4). SiO₂ derived mainly from Quartz content, TiO₂ and Al₂O₃ from Phyllosilicates, MgO and CaO from Dolomite, and the peak at 45 m for CaO from Calcite contents. The links with the other elements are less clear, but a relationship can be made between Fe₂O₃ and Goethite. The similar trends between the detritus curve and SiO₂, TiO₂, Al₂O₃, and K₂O suggest a detrital origin of these elements (Fig. 4a, b).

4.5 Biostratigraphy

The Gabal Ekma section exhibits a scarce and low diversity microfauna due to the nature of the sediments, which mainly consist of sandstone and clay assigned to the Matulla Fm. According to previous analyses in nearby sections located in western central Sinai (Wadi Matulla and Gabal Nezzazat sections), the lower and middle parts of the Matulla Fm is of Coniacian age, and the upper unit is considered to be Santonian, based on ammonites and foraminiferal assemblages (Obaidalla & Kassab, 2002). In western central Sinai, the middle unit of the Matulla Fm corresponds to the middle-late Coniacian *Metatissotia fourneli* and *Subtissotia africana* ammonites zones (Obaidalla & Kassab, 2002) and late Coniacian *Dicarinella concavata* foraminiferal Zone (El-Dawy, 1994). The upper unit of the Matulla Fm contains ammonites indicating the *Texanites texanus* and *Tissotia semmamensis* zones and foraminifera from the *D. asymetrica* and *Sigalia carpatica* zones, indicating a Santonian age. These correlations, including the biostratigraphical and lithostratigraphical data, remain relatively uncertain. El-Azabi and El-Araby (2007), using correlations based on sequence stratigraphy, identified a major sequence boundary (SB3) at the C-S boundary, which may coincide with a phosphatic hardground including a bone-bed (29–30 m, GE 58).

4.6 Systematic Palaeontology

Several levels rich in vertebrate bones and fish teeth, informally termed “bone-beds” were identified throughout the section. The first level located at GE 52 exhibits a fragment of a large vertebra (7 cm of diameter) with well-preserved centrum has been found and present a concave articular facet (Fig. 2; GE 52). Given the size and general shape of the vertebra, this specimen is assigned to a Plesiosauria indet.

Above a particular level enriched in numerous vertebrate remains (at 30 m; Fig. 2, GE 58) were collected from that level and are described herein. Several vertebrae with two

Gamal Ekma Section, Sinai, Egypt

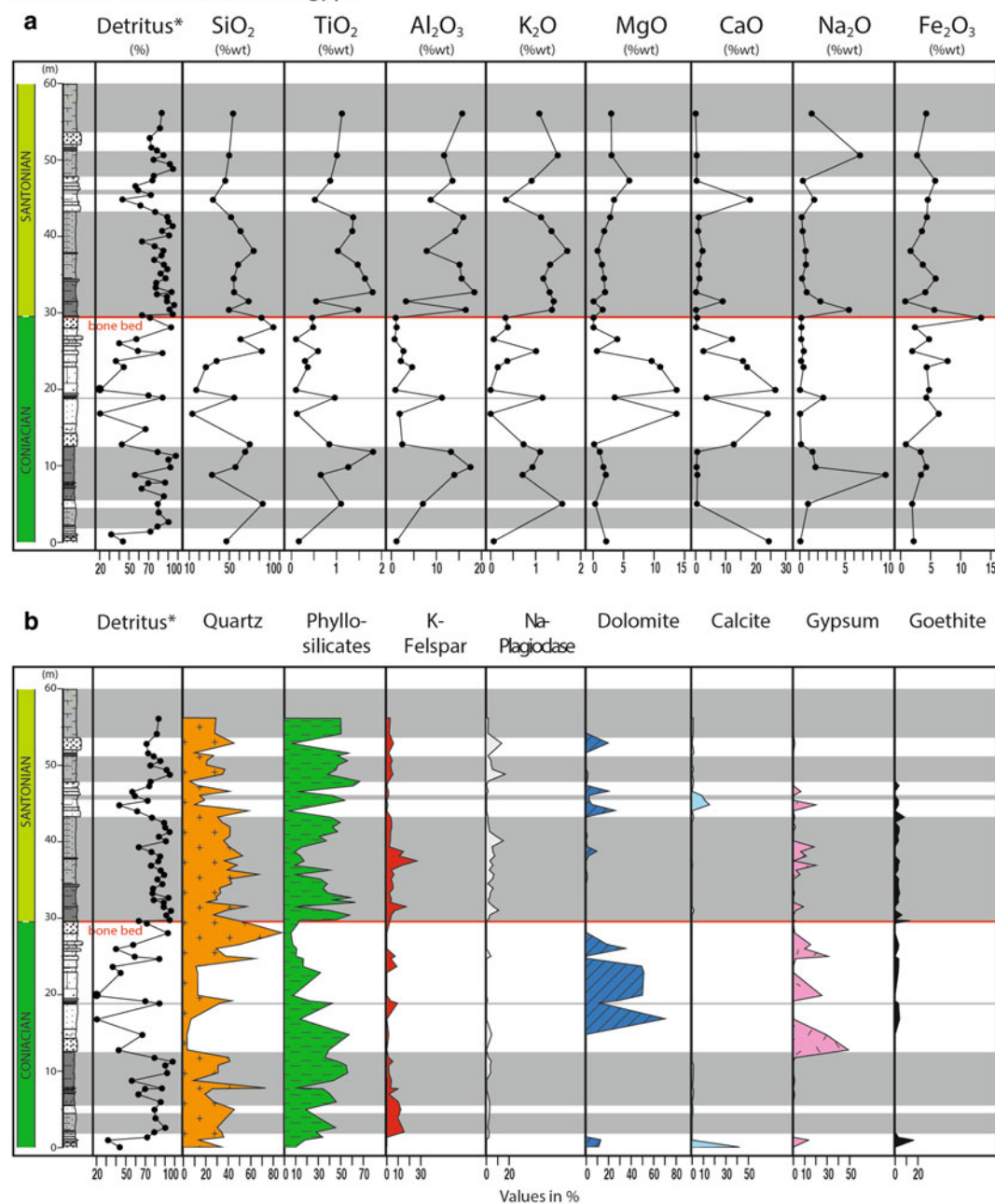


Fig. 4 **a** Major-element contents (% in weight) of the Gabal Ekma section. Grey intervals correspond to organic-rich shale interval. **b** Detritus curve and mineral phases content (in %) based on XRD analyses

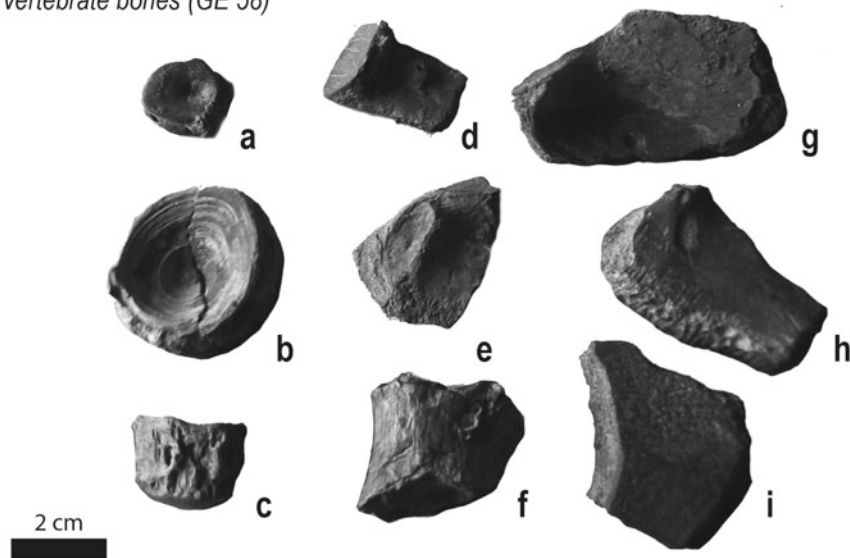
concave articular facets are assigned to bony fish (*Actinopterygii*; Fig. 5a, b). A small vertebra, characterised by a concave anterior articular facet and a convex posterior one, is tentatively attributed to a *Mosasauridae* indet. (Fig. 5c). This is likely a posterior caudal vertebra. Fragmented turtle ventral plastrons are the most abundant remains of tetrapods and are tentatively attributed to

chelonian indet (Fig. 5d, e, g, h, and i). A long bone (humerus or femur), damaged at both extremities is also attributed to an indeterminate chelonian (Fig. 5f).

A large number of teeth of Chondrichthyes (elasmobranchs or selachians, which include sharks, rays, and chimaeras) were also recovered (Fig. 5k, l). The large amount of teeth of various morphologies reveals their great diversity.

Bone-bed assemblages

Vertebrate bones (GE 58)



Fish teeth (GE 58)



Fig. 5 Bone-bed assemblages of level GE 58 (Gabal Ekma section). **a, b** Actinopterygii vertebra; **c** Mosasauridae indet; **d, i** Chelonian indet; **k, l** Chondrichthyes teeth

5 Discussion

5.1 Carbon Isotope Correlations Through Oceanic Anoxic Event 3

The Coniacian-Santonian OAE3 is less clearly expressed than other OAEs (e.g., Selli and Bonarelli events), as is shown by the carbon isotope record (Jarvis et al., 2006), and seems to be a regional event rather than a real global OAE, as was already suggested by Wagreich (2012). However,

small perturbations in $\delta^{13}\text{C}$ are present in several sections around the world, which are not systematically associated with organic carbon deposits (e.g. in Tibet; Wendler et al., 2009). The very low amplitude of the carbon isotope fluctuations can be explained by the high accumulation rate of carbonate relative to organic carbon (Locklair et al., 2011). A relationship between the carbon isotope excursions and sea-level fluctuations has also been suggested (e.g., Jarvis et al., 2006; Jenkyns et al., 1994; Voigt & Hilbrecht, 1997; Wendler et al., 2009), considering that the highest $\delta^{13}\text{C}$ values recorded during C-S events (e.g. White Fall and

Horseshoe Bay events) coincide with substantial sea-level rise.

Despite the weak amplitude of the $\delta^{13}\text{C}$ fluctuations, a tentative correlation is made between the records of the English Chalk reference section (Jarvis et al., 2006) and the Gabal Ekma section (Fig. 6). Several isotope events have been identified in the English Chalk section (Jarvis et al., 2006), suggesting repeated carbon perturbations rather than a major single global event. These carbon isotope events are however globally recognised and used as significant global stratigraphic tool (Jarvis et al., 2006). From the late Coniacian to the late Santonian, ten carbon isotope events are recognised in the English Chalk reference curve: Kingsdown, *k1*, *k2*, Michel Dean, Bedwell, Haven Brow, Horseshoes Bay, Buckle, Hawks Brow, and Foreness (Jarvis et al., 2006). According to the literature (e.g., El-Azabi & El-Araby, 2007), the section of Gabal Ekma includes an interval starting from the middle-late Coniacian up to the late Santonian-early Campanian (Fig. 6).

Due to the absence of calcite content, organic carbon isotopes have been used to tentatively correlate the Gabal Ekma section with the inorganic carbon isotope reference

curve of the English Chalk. $\delta^{13}\text{C}_{\text{org}}$ and $\delta^{13}\text{C}_{\text{carb}}$ values are generally well coupled during the Mesozoic and Cenozoic due to abundant skeleton-forming organisms, which dominate the marine carbon cycle and dampened the isotope response to perturbations (Bartley & Kah, 2004). Significant decoupling or delayed excursions may, however, occur between inorganic and organic carbon due to several parameters such as a change in the organic matter source or excessive carbon burial (Kump & Arthur, 1999). Anyway, $\delta^{13}\text{C}_{\text{org}}$ values measured at Gabal Ekma show fluctuations which can be tentatively correlated with the $\delta^{13}\text{C}_{\text{carb}}$ reference curve established in the English Chalk by Jarvis et al. (2006). Furthermore, a correlation has been extended to a well-documented organic isotopic curve of Yezo Group section, Japan (Fig. 6; Takashima et al., 2019), which is relatively well constrained in term of biostratigraphy and quite well correlated with reference curves (Takashima et al., 2019). However, uncertainty still remains for the Foreness, Buckle, and Bedwell isotopic events (Fig. 6; Takashima et al., 2019). New interpretation is suggested for the Bedwell and Michel Dean events location and seems well correlated with Gabal Ekma and English chalk sections (Fig. 6).

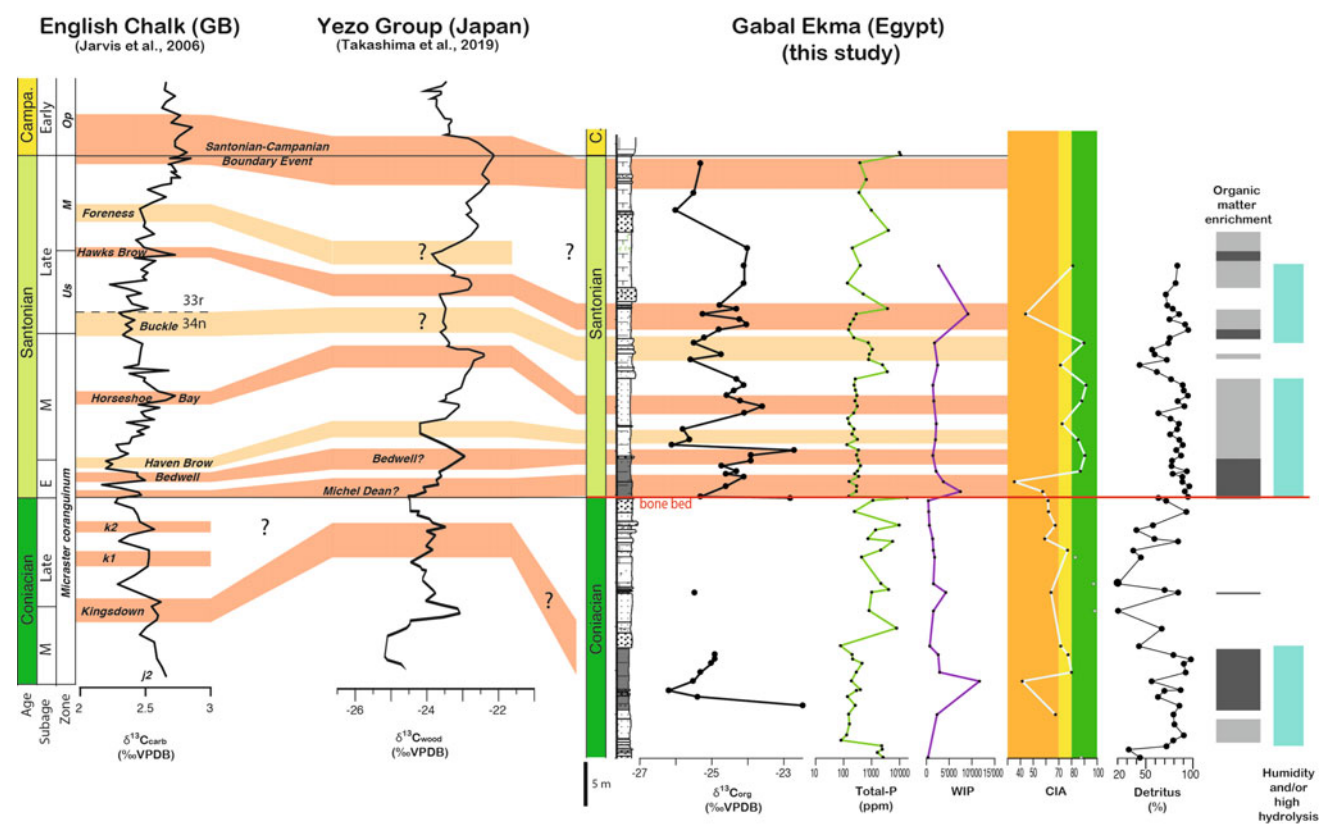


Fig. 6 Synthetic correlation of the Gabal Ekma sections with the $\delta^{13}\text{C}_{\text{wood}}$ Yezo Group, Japan (Takashima et al., 2019) and the $\delta^{13}\text{C}_{\text{carb}}$ reference curve of the English Chalk (Jarvis et al., 2006). Chemical Index of Alteration (CIA and WIP) and Detritus (in %) are based on major-element contents and bulk-rock mineralogy, respectively. For the CIA, the green colour indicates tropical and humid, yellow temperate humid and orange arid conditions. Qualitative enrichment in organic matter is represented by dark grey boxes (strongly enriched) and light grey boxes (less enriched). Intervals of humidity and/or high hydrolysis is marked by blue boxes

Unfortunately, due to lack of data linked to absence of organic carbon, no correlation could be made in the late Coniacian (Fig. 6). At Gabal Ekma, the amplitude of $\delta^{13}\text{C}_{\text{org}}$ shifts is significantly higher (3‰) compared to the $\delta^{13}\text{C}_{\text{carb}}$ values obtained in the English sections, but in the same order with the amplitude of $\delta^{13}\text{C}_{\text{org}}$ shifts of the Yezo Group section (2.5‰). This observation supports the hypothesis of Locklair et al. (2011) suggesting that during OA3, organic carbon burial is not fully represented in the $\delta^{13}\text{C}_{\text{carb}}$ record. The inorganic carbon response to widespread deposition of organic-rich sediment in the equatorial Atlantic may have been dampened by widespread deposition of carbonate carbon (chalk) on flooded shelves during the Coniacian-Santonian interval.

5.2 Links Between Phosphorus, Anoxia and Climatic Changes

The WIP and CIA are weathering indices used to infer weathering processes and climatic fluctuations (Fedó et al., 1997; Nesbitt & Young, 1982; Price & Velbel, 2003). The CIA values varying from 80 to 100 suggest a tropical and humid climatic conditions, a warm and seasonal climate between 60 and 80, and a cold and/or arid climate with values under 60 (Nesbitt & Young, 1982, 1989). The WIP index has been used to assess the weathering profile on the basis of alkali and alkaline earth metals (Na, K, Mg, and Ca), which are favourably leached in areas of intensive chemical weathering (Price & Velbel, 2003). The significant negative correlation between CIA and WIP ($R^2 = -0.61$), suggests that high WIP values indicate periods of increasing physical weathering in an arid climate, while low WIP values indicate intense chemical weathering in a humid climate (Fig. 6). However, 4 points (GE 1, 35, 41, and 43) have been excluded for the CIA interpretation due to the diagenetic nature of the dolomitic beds, strongly enriched in MgO and CaO contents, which decreases the original signal and hampers the palaeoenvironmental interpretation.

During the late Coniacian, from the first organic-rich shales interval (5–12 m) up to the top of the dolostone and calcarenite beds (marked by the bone bed at 30 m), a decreasing trend in the CIA index from warm and seasonal climate to arid climate conditions is observed at Gabal Ekma (Fig. 6). The detritus contents show a similar decreasing trend, in particular during the dolostone and calcarenite beds interval (12–23 m), suggesting a significant hydrolysis reduction (Fig. 6). However, a decoupling phase between the detritus contents and CIA is observed between 23 and 32 m. This interval corresponds to the strong enrichment in quartz versus phyllosilicates contents (Fig. 4b), consistent with lithological change to sandstones beds (Fig. 2). Furthermore, the decreasing trend observed in the detritus curve is also

probably due to dilution by carbonate production (dolostone beds).

During the early Santonian, just above the Michel Dean Event, CIA sharply increases indicating humid and tropical conditions which persisted up to the Buckle Event, associated with high content of detritus which indicates higher hydrolysis (Fig. 6). These humid conditions, which prevailed in Egypt until the earliest late Santonian, coincide with the shale and claystone deposits, enriched in organic matter, and deposited in deeper environments (Fig. 6). Furthermore, this deeper environment interval recorded in the Gabal Ekma section, which corresponds to a maximum flooding surface (El-Azabi & El-Araby, 2007) and to the carbon isotope event Horseshoes Bay, is coinciding to a high sea-level period in England (Jarvis et al., 2006), reinforcing this correlation.

Total-P values show no significant correlation with detrital inputs ($R^2 = -0.25$), suggesting that the main P phase was not derived from detrital input but relative to authigenesis and/or organic matter. Thus, fluctuations in total-P do not seem to be related to detrital input but rather driven by anoxia and also by phosphogenesis during hard-ground formation (Bone-bed levels). Moreover, total-P is strongly depleted in the organic-rich interval, suggesting intense P regeneration due to anoxic conditions, comparable to what is often observed in Cenomanian–Turonian OAE-2 sections (e.g. Kraal et al., 2010; Mort et al., 2007, 2008). However, this anoxia occurring during the Coniacian-Santonian OAE 3 interval seems still regional and limited to restricted basin or shallow epicontinental environment, the organic-rich sediment deposits are indeed rarely synchronous and occur in different time intervals within the Coniacian and Santonian (Locklair et al., 2011). Phosphorus regeneration from sedimentary organic matter may have been used for bone-bed phosphatisation (Suan et al., 2012). These bone-bed levels, probably deposited by storm deposits in shallow shoreface settings, are strongly phosphatised and characterised by very well-preserved shark teeth and vertebra, associated with phosphatised nodules in a sandy phosphatic matrix. This type of P regeneration under anoxic conditions may explain the main source of phosphate required to phosphatised these bone-bed levels located close to the C-S boundary (GE 58), similarly observed in Triassic-Jurassic bone-beds by Suan et al. (2012).

6 Conclusions

The Coniacian-Santonian carbon isotopic curve patterns are partly recognised at the Gabal Ekma section, mainly the Santonian interval, and are used to characterise the interval of the Coniacian-Santonian oceanic anoxic event (OAE 3). Correlations are also proposed between the $\delta^{13}\text{C}_{\text{org}}$ record of

the Gabal Ekma section, the Yezo Group (Japan), and the $\delta^{13}\text{C}_{\text{carb}}$ of the English Chalk reference record. However, this event appears to be local or regional rather than global event, depending mainly on local and regional conditions and restricted mostly to shallow-water settings and epicontinental seas.

Based on the weathering index CIA and WIP and bulk mineralogy, the climate switched gradually from warm and seasonal climate to arid conditions during the late Coniacian up to the base of the Santonian (Michel Dean Event), followed by a new change to more humid and tropical conditions which persisted up to the Buckle Event (base on the late Santonian), coinciding with laminated organic-rich shales and claystone deposition.

Fluctuations in total phosphorus (Total-P) contents appears not driven by detritism, but seem to be controlled by regional anoxia and phosphogenesis. Total-P contents are thus depleted in the organic-rich interval, suggesting intense P regeneration due to anoxic conditions.

The phosphatisation of bone-bed levels is thus explained by huge availability of phosphorus due to the P regeneration under anoxic conditions, allowing the strong accumulation and well preservation of shark teeth and vertebrate remains.

Acknowledgements We warmly thank Peggy Vincent (MNHM, Paris, France), Jeremy E. Martin (ENS Lyon, France) for the vertebrate remains determination, Guillaume Guinot (INSEM, Montpellier, France) for the current study of shark teeth. We warmly also thank Valentina Togni and Alicia Fantasia for their helpful laboratory assistance, Hassan Khozyem for his advice, help in laboratory, and assistance during fieldwork in Egypt, Abdelaziz Tantawy (Aswan University) for his help in the field in Egypt, and Tiffany Monnier and Jean-Claude Lavanchy for the analyses of major element. This research is supported by the Swiss National Science Foundation (Grants 200021-116046/1 and 200020-119943/1).

References

- Abdel-Gawad, G. I., El Sheikh, H. A., Abdelhamid, M. A., El Beshtawy, M. K., Abed, M. M., Fürsich, F. T., & El Qot, G. M. (2004). Stratigraphic studies on some Upper Cretaceous successions in Sinai, Egypt. *Egyptian Journal of Paleontology*, 4, 263–303.
- Abdel-Gawad, G. I., El-Qot, G. M., & Mekawy, M. S. (2007). Macrobiostratigraphy of the Upper Cretaceous succession from Southern Galala, Eastern Desert, Egypt. In *Proceedings of the Second International Conference on the Geology of Tethys* (pp. 329–349). Cairo University, Cairo.
- Adatte, T., Stinnesbeck, W., & Keller, G. (1996). Lithostratigraphical and mineralogic correlations of near K/T boundary clastic sediments in northeastern Mexico: Implications for origin and nature of deposition. In G. Ryder, D. Fastovsky, & S. Gartner, (Eds.), *The Cretaceous-Tertiary event and other catastrophes in earth history. Geological society of America special paper* (Vol. 307, pp. 211–226).
- Arthur, M. A., Jenkyns, H. C., Brumsack, H. J., & Schlanger, S. O. (1990). Stratigraphy, geochemistry and paleoceanography of organic carbon-rich Cretaceous sequences. In R. N. Ginsburg, & B. Beaudoin (Eds.), *Cretaceous resources, events and rhythms. NATO ASI series C* (Vol. 304, pp. 75–119).
- Bartley, J. K., & Kah, L. C. (2004). Marine carbon reservoir, Corg-Ccarb coupling, and the evolution of the Proterozoic carbon cycle. *Geology*, 32, 129–132.
- Bauer, J., Kuss, J., & Steuber, T. (2003). Sequence architecture and carbonate platform configuration (Late Cenomanian–Santonian), Sinai, Egypt. *Sedimentology*, 50, 387–414.
- Davis, C., Pratt, L., Sliter, W., Mompert, L., & Murat, B. (1999). Factors influencing organic carbon and trace metal accumulation in the Upper Cretaceous La Luna Formation of the western Maracaibo Basin, Venezuela. In E. Barrera & C. C. Johnson (Eds.), *Evolution of the Cretaceous Ocean—Climate system. Geological society of America special paper* (Vol. 332, pp. 203–230).
- Dean, W. E., & Arthur, M. A. (1998). Geochemical expression of cyclicity in Cretaceous pelagic limestone sequences: Niobrara Formation, Western Interior Seaway. In W. E. Dean, & M. A. Arthur (Eds.), *Stratigraphy and Paleoenvironments of the Cretaceous Western Interior Seaway, U.S.A. SEPM, Concepts in sedimentology and paleontology* (Vol. 6, pp. 227–255).
- Eaton, A. D., Clesceri, L. S., & Greenberg, A. E. (1995). *Standard methods for examination of water and waste water* (Vol. IXI, pp. 4113–4114).
- El-Azabi, M. H., & El-Araby, A. (2007). Depositional framework and sequence stratigraphic aspects of the Coniacian-Santonian mixed siliciclastic/carbonate Matulla sediments in Nezzazat and Ekma blocks, Gulf of Suez, Egypt. *Journal of African Earth Sciences*, 47, 179–202.
- El-Dawy, M. H. (1994). The Coniacian-Santonian boundary in Wadi El-Seih, west central Sinai, Egypt: Stratigraphy, foraminiferal fauna and sea level changes. *Neues Jahrbuch für Geologie und Paläontologie*, 192(2), 203–219.
- Erlach, R. N., Macsotay, O., Nederbragt, A. J., & Lorente, M. A. (1999). Palaeoceanography, palaeoecology, and depositional environments of Upper Cretaceous rocks of western Venezuela. *Palaeogeography, Palaeoclimatology, Palaeoecology*, 153, 203–238.
- Farouk, S., Ahmad, F., Powell, J., & Marzouk, A. (2016). Integrated microfossil biostratigraphy, facies distribution and depositional sequences of the upper Turonian to Campanian succession in northeast Egypt and Jordan. *Facies*, 62, 8.
- Fedo, C.M., Nesbitt, H.W., Young, G.M. (1995). Unraveling the effects of potassium metasomatism in sedimentary rocks and paleosols, with implications for paleoweathering conditions and provenance. *Geology*, 23, 921–924.
- Fedo, C. M., Young, G. M., & Nesbitt, G. M. (1997). Paleoclimatic control on the composition of the Paleoproterozoic Serpent Formation, Huronian Supergroup, Canada: A greenhouse to icehouse transition. *Precambrian Research*, 86, 201–223. [https://doi.org/10.1016/S0301-9268\(97\)00049-1](https://doi.org/10.1016/S0301-9268(97)00049-1)
- Gertsch, B., Keller, G., Adatte, T., & Bartels, D. (2011). Trace-element geochemistry of Brazos sections, Texas, U.S.A. In G. Keller & T. Adatte (Eds.), *End-Cretaceous mass extinction and Chicxulub impact in Texas* (Vol. 100, pp. 251–280). SEPM Special Publication.
- Ghorab, M. A. (1961). Abnormal stratigraphic features in Ras Gharib oil field. In *Third Arab petroleum congress* (Vol. 2, p. 10). Alexandria, Egypt.
- Hofmann, P., Wagner, T., & Beckmann, B. (2003). Millennial- to centennial-scale record of African climate variability and organic carbon accumulation in the Coniacian-Santonian eastern tropical Atlantic (Ocean Drilling Program Site 959, off Ivory Coast and Ghana). *Geology*, 31, 135–138.
- Holbourn, A. E. L., & Kuhnt, W. (1998). Turonian-Santonian benthic foraminifer assemblages from Site 959D (Côte d'Ivoire-Ghana Transform Margin, Equatorial Atlantic): indication of a late Cretaceous oxygen minimum zone. In J. Mascle, G. P. Lohmann, & M.

- Moullade (Eds.), *Proceeding of the ODP, Scientific Results* (Vol. 159, pp. 375–387). College Station, TX: Ocean Drilling Program.
- Jarvis, I., Gale, A. S., Jenkyns, H. C., & Pearce, A. (2006). Secular variation in Late Cretaceous carbon isotopes: A new $\delta^{13}\text{C}$ carbonate reference curve for the Cenomanian–Campanian (99.6–70.6 Ma). *Geological Magazine*, *143*, 561–608.
- Jenkyns, H. C. (1980). Cretaceous anoxic events: From continents to oceans. *Journal of the Geological Society*, *137*, 171–188.
- Jenkyns, H. C. (2010). Geochemistry of oceanic anoxic events. *Geochemistry, Geophysics, Geosystems*, *11*, Q03004. <https://doi.org/10.1029/2009GC002788>
- Jenkyns, H. C., Gale, A. S., & Corfield, R. M. (1994). Carbon- and oxygen-isotope stratigraphy of the English Chalk and Italian Scaglia and its palaeoclimatic significance. *Geological Magazine*, *131*, 1–34.
- Khalil, H., & Mashaly, S. (2004). Stratigraphy and stage boundaries of the Upper Cretaceous–Lower Paleogene succession in Gabal Musaba Salama area, southwestern Sinai, Egypt. *Egyptian Journal of Paleontology*, *4*, 1–38.
- Kora, M., Hamama, H., & Sallam, H. (2002). Senonian macrofauna from west-central Sinai: Biostratigraphy and palaeobiogeography. *Egyptian Journal of Paleontology*, *2*, 435–458.
- Kraal, P., Slomp, C. P., Forster, A., & Kuypers, M. M. M. (2010). Phosphorus cycling from the margin to abyssal depths in the proto-Atlantic during oceanic anoxic event 2. *Palaeogeography, Palaeoclimatology, Palaeoecology*, *295*, 42–54.
- Kübler, B. 1987. *Cristallinité de l'illite, méthodes normalisées de préparations, méthodes normalisées de mesures*. Cahiers Institut Géologie de Neuchâtel, Suisse, Série AD.
- Kump, L. R., & Arthur, M. A. (1999). Interpreting carbon-isotope excursions: Carbonates and organic matter. *Chemical Geology*, *161*, 181–198.
- Lamolda, M. A., & Paul, C. R. C. (2007). Carbon and oxygen stable isotopes across the Coniacian/Santonian boundary a Olazagutia, northern Spain. *Cretaceous Research*, *28*, 37–45.
- Locklair, R., Sageman, B. B., & Lerman, A. (2011). Marine carbon burial flux and the carbon isotope record of Late Cretaceous (Coniacian–Santonian) Oceanic Anoxic Event III. *Sedimentary Geology*, *235*, 38–49.
- Mandur, M. M. M. (2011). Lithostratigraphy and biostratigraphy of the upper Cretaceous succession of Southeastern Sinai, Egypt. *Egyptian Journal of Petroleum*, *20*, 89–96.
- McLennan, S. M. (1993). Weathering and global denudation. *Journal of Geology*, *101*, 295–303.
- Mello, M. R., Koutsoukos, E. A. M., Hart, M. B., Brassell, S. C., & Maxwell, J. R. (1989). Late Cretaceous anoxic events in the Brazilian continental margin. *Organic Geochemistry*, *14*, 529–542.
- Mort, H. P., Adatte, T., Föllmi, K., Keller, G., Steinmann, P., Matera, V., Berner, Z., & Stüben, D. (2007). Phosphorus and the roles of productivity and nutrient recycling during Oceanic Anoxic Event 2. *Geology*, *35*(6), 483–486.
- Mort, H. P., Adatte, T., Keller, G., Bartels, D., Föllmi, K. B., Steinmann, P., Berner, Z., & Chellai, E. H. (2008). Organic carbon deposition and phosphorus accumulation during oceanic anoxic event 2 in Tarfaya, Morocco. *Cretaceous Research*, *29*, 1008–1023. <https://doi.org/10.1016/j.cretres.2008.05.026>
- Nesbitt, H. W., & Young, G. M. (1982). Early Proterozoic climates and plate motions inferred from major element chemistry of lites. *Nature*, *299*, 715–717.
- Nesbitt, H. W., & Young, G. M. (1989). Formation and diagenesis of weathering profiles. *Journal of Geology*, *97*, 129–147.
- Obaidalla, N. A., & Kassab, A. S. (2002). Integrated biostratigraphy of the Coniacian–Santonian sequence, southwestern Sinai, Egypt. *Egyptian Journal Paleontology*, *2*, 85–104.
- Parker, A. (1970). An index of weathering for silicate rocks. *Geological Magazine*, *107*, 501–504.
- Price, J. R., & Velbel, M. A. (2003). Chemical weathering indices applied to weathering profiles developed on heterogeneous felsic metamorphic parent rocks. *Chemical Geology*, *202*, 397–416.
- Rey, O., Simo, J. A., & Lorente, M. A. (2004). A record of long- and short-term environmental and climatic change during OAE3: La Luna Formation, Late Cretaceous (Santonian–early Campanian), Venezuela. *Sedimentary Geology*, *170*, 85–105.
- Samuel, M. D., Ismail, A. A., Akarish, A. I. M., & Zaky, A. H. (2009). Upper Cretaceous stratigraphy of the Gebel Somar area, north-central Sinai, Egypt. *Cretaceous Research*, *30*, 22–34.
- Schlanger, S. O., & Jenkyns, H. C. (1976). Cretaceous anoxic events: Causes and consequences. *Geologie en Mijnbouw*, *55*, 179–184.
- Sohl, N. F., Martinez, E. R., Salmeron-Ureña, P., & Soto-Jaramillo, F. (1991). Upper Cretaceous. In A. Salvador (Ed.), *The Gulf of Mexico Basin* (pp. 205–244). Geological Society of America, Decade of North American Geology.
- Suan, G., Föllmi, K. B., Adatte, T., Bomou, B., Spangenberg, J. E., & van De Schootbrugge, B. (2012). Major environmental change and bonebed genesis prior to the Triassic–Jurassic mass extinction. *Journal of Geological Society of London*, *169*, 191–200. <https://doi.org/10.1144/0016-76492011-045>
- Takashima, R., Nishi, H., Yamanaka, T., Orihashi, Y., Tsujino, Y., Quidelleur, X., Hayashi, K., Sawada, K., Nakamura, H., & Ando, T. (2019). Establishment of Upper Cretaceous bio- and carbon isotope stratigraphy in the northwest Pacific Ocean and radiometric ages around the Albion/Cenomanian, Coniacian/Santonian and Santonian/Campanian boundaries. *Newsletters on Stratigraphy*, *52* (3), 341–376. <https://doi.org/10.1127/nos/2019/0472>
- Voigt, S., & Hilbrecht, H. (1997). Late Cretaceous carbon isotope stratigraphy in Europe: Correlation and relations with sea level and sediment stability. *Palaeogeography, Palaeoclimatology, Palaeoecology*, *134*, 39–59.
- Wagner, T. (2002). Late Cretaceous to early Quaternary organic sedimentation in the eastern Equatorial Atlantic. *Palaeogeography, Palaeoclimatology, Palaeoecology*, *179*, 113–147.
- Wagner, T., Sinninghe Damste, J. D., Hofmann, P., & Beckmann, B. (2004). Euxinia and primary production in Late Cretaceous equatorial Atlantic surface waters fostered by orbitally driven formation of marine black shales. *Paleoceanography*, *19*, PA4099.
- Wagreich, M. (2009). Coniacian–Santonian oceanic red beds and their links to Oceanic Anoxic Event 3. *SEPM (society for Sedimentary Geology) Special Publication*, *91*, 235–242.
- Wagreich, M. (2012). “OAE 3”—Regional Atlantic organic carbon burial during the Coniacian–Santonian. *Climate of the past*, *8*, 1447–1455. <https://doi.org/10.5194/cp-8-1447-2012>
- Wendler, I., Wendler, J., Grafe, K.-U., Lehmann, J., & Willems, H. (2009). Turonian to Santonian carbon isotope data from the Tethys Himalaya, southern Tibet. *Cretaceous Research*, *30*, 961–979.
- Yan, D., Chen, D., Wang, Q., & Wang, J. (2010). Large-scale climatic fluctuations in the latest Ordovician on the Yangtze block, south China. *Geology*, *38*(7), 599–602.
- Zalat, A. A., Zaid, S. M., Gadallah, M. H., & Abdel-Aziz, Z. A. (2012). Sandstones reservoir quality of the Matulla Formation, Gulf of Suez, Egypt. *Australian Journal of Basic and Applied Sciences*, *6* (12), 511–529.



Brahimsamba Bomou is currently a scientific collaborator at the Institute of Earth Sciences (ISTE), University of Lausanne (Switzerland). He graduated from the University of Rouen (France) and Burgundy University (Dijon, France) in Earth Sciences (B.Sc., 2002; M.Sc., 2007). He received a Ph.D. from the University of Lausanne (Switzerland, 2012) where he focused on phosphorus and carbon burial during Cretaceous Oceanic Anoxic Events and their links with climatic changes. He completed his CV Postdoctoral

researcher (CNRS), Franche-Comté University (Besançon, France), IPGP (Paris, France) and LSCE (Gif-sur-Yvette, France) in 2012-2013. Temporary teaching and research assistant at the University of Corsica Pascal Paoli (Corte, France) in 2014-2016. Substitute Lecturer in Sedimentology at ISTE, University of Lausanne (Switzerland) in 2018-2020. He is an expert in sedimentary geochemistry, specializing in paleoenvironmental and paleoclimatic reconstructions using a multiproxy approach (sedimentology, geochemistry, mineralogy, micropaleontology) in basin and carbonate platform environments. He is member of several geological societies, such as the French Geological Society (SGF), International Association of Sedimentologists (IAS), and European Geosciences Union (EGU).



Thierry Adatte is Professor and head of the geochemistry and mineralogy sedimentary laboratory at the Institute of Earth Sciences of the University of Lausanne, Switzerland. He received his Ph.D. in Mineralogy and Sedimentary Geology from the University of Neuchâtel, Switzerland. 1989-1990: Postdoctoral fellow (FNS), Mexican Petroleum Institute (IMP). 1990-1993: Postdoctoral fellow (FNS), Universidad Autonoma de Nuevo Leon, Mexico and Neuchâtel University, Switzerland. 1993-2004: Maître assistant

(“Assistant professor”), head of the Mineralogical and Geochemical Laboratory, Geological Institute, Neuchâtel University, Switzerland. 2004-2012: Associate Professor, “Chargé de cours et d’enseignement” (paleontology, sedimentary-environmental mineralogy, general geology), Geological Institute, Neuchâtel University, Switzerland. 2008-2018.

Researcher at the Institute des Sciences de la Terre (ISTE), Lausanne University, Head of the geochemistry sedimentary lab (XRD, CHN-Rock-Eval, Phosphorus). 2017-2018: Privat Docent at the Institute des Sciences de la Terre (ISTE), Lausanne University 2018-: Professor remplaçant at the Institute des Sciences de la Terre (ISTE), Lausanne University. His research interests are in the fields of global environmental change and extinction events, and his involvement in the deciphering of

the events around the Cretaceous-Tertiary boundary event is documented by a series of publications (from 1997 to 2019). He also explored the sedimentary documents of the PETM the Paleocene-Eocene boundary event (from 2000 to 2019). He is also involved in the study of oceanic anoxic event (from 2001 to 2018). His interests are in the use of geochemical and mineralogical proxies, such as stable carbon and oxygen isotopes, organic matter, clay minerals and recently also trace metal distributions as indicators of environmental and climatic change at the time of the extinction events. One of his main actual interest is the link between LIPS activity and mass extinction events, in particular during the KPg mass extinction. His team provided the most accurate dating of the Deccan activity and highlighted its crucial role in the KPg extinction. The use of mercury as a tracer of volcanic activity is also part his research. Acidification linked with these events is also one of his recent interest, more particularly for the KPg mass extinction. Since 1987, active participation (oral presentations and posters) of nearly 1112 meetings and symposia (GSA, AGU, EUG, IAS, SNOWBIRD, réunion spécialisées SGF) Convenor and co-convenor of sessions on Mass Extinctions, Volcanism, Impacts, and Catastrophic Environmental Changes at EGU Meetings since 2013 to 2018. Convenor and coconvenor of sessions on mass extinctions at GSA meetings in 2009, 2016 and 2017.



Jorge E. Spangenberg is a laboratory manager, senior research scientist and part-time lecturer at the Organic Geochemistry Institute of Earth Surface Dynamics, University of Lausanne, Switzerland. He obtained two M.Sc. degrees in 1984 and 1991 from the University of the Republic, Montevideo (Uruguay) and the University of Heidelberg (Germany), respectively, and a Ph.D. (1995) in economic geology/geochemistry from the University of Geneva (Switzerland). From 1995 to 1997, he undertook his first post-

doctoral research in stable isotope and organic geochemistry at the University of Virginia in Charlottesville, Virginia (USA). His second postdoctoral research from 1997 to 1999 was at the Institute of Earth Sciences, University of Lausanne (Switzerland) and then because supplant professor of stable isotope geochemistry. He started his career as a research assistant at the University of the Republic, Montevideo, from where he moved to work with the Geological Survey of France (BRGM) at Orleans. He is a specialist in broad interdisciplinary interests, including new analytical methods for bulk and compound-specific stable isotopes in geological and environmental samples, low-temperature stable isotope geochemistry, organic geochemistry, paleoclimate and paleoecology, biogeosciences, sediment-hosted ore deposits, archaeometry, ecology, and the applications of organic and stable isotope techniques and concepts to plant, wine, and food science. His current research topics include biogeochemical studies of Neoproterozoic and Permian-Triassic climate and environmental changes. He has published and participated in more than 600 scientific publications.



Climatic and Environmental Changes During Paleocene-Eocene Thermal Maximum in Egypt: An Overview

Hassan Khozyem, Thierry Adate, and Gerta Keller

Abstract

During the last decades, Egypt became a focal point for studying the climate and paleoenvironmental changes during the late Paleocene early of Eocene that is known as the Paleocene-Eocene Thermal Maximum (PETM). This chapter sheds light on the climatic and paleoenvironmental changes recorded from the Egyptian sedimentary record, based on: biostratigraphy, sedimentology, and geochemistry. We also introduce a complete raw data set of Dababiya Global Stratigraphic Section and Point.

Keywords

GSSP • PETM • Carbon isotopic excursions • Weathering • Hg-anomaly

1 Introduction

In the 1980s, the world's governments paid attention to the problem of climate change in which global temperatures increased, sea levels rose, oceans became more acidic, and many species were extinct. However, these changes are

repeatedly observed in deep-geologic time., similar to what happened on Earth about 56 million years ago (PETM). Therefore, it is a big challenge to understand the climatic and paleoenvironmental changes occurred through that time to better understand the current climatic changes.

The Paleocene–Eocene Thermal Maximum (PETM), alternatively Eocene Thermal Maximum 1 (ETMI), and formerly known as the Initial Eocene Thermal Maximum (IETM) or Late Paleocene Thermal Maximum (LPTM); all of the previous terms refer to a short-term global warming event recorded within the sedimentary rocks of about 56 million years (My) in age. That time was a period of more than 5–8 °C global average temperature rise. This climatic event occurred at boundary interval between the late Paleocene and early Eocene and extended for about 200 ky (Zachos et al., 2001). The observed climatic and environmental changes coincident with rapid shifts in both oxygen and carbon isotopes, and perturbations in the carbon cycle.

Kennett and Stott (1991) documented first observation of these changes when they observed rapid shifts in isotopes ($\delta^{18}\text{O}$ and $\delta^{13}\text{C}$) of specific foraminifera species obtained from ODP-Site 690B (Ocean Drilling Program; Antarctica Coast). Their study comes up with several criteria coinciding with the well-known extinction event in benthic foraminifera; these criteria count as follows:

- Estimated increase in oceanic surface water temperature by 3–4 °C, synchronous with an increase in deep ocean water temperature by about 6 °C.
- abrupt negative carbon isotope shift in benthic and planktic foraminifera (– 2‰ and – 4‰, respectively).
- Evolutionary and reproducible diversity trend of the warm water planktons.
- An increase in kaolinite contents in recorded sediments indicates an increase in detrital input.
- Regression in sea level led to a decrease in the water depth gradient.

Electronic supplementary material

The online version of this chapter (https://doi.org/10.1007/978-3-030-95637-0_12) contains supplementary material, which is available to authorized users.

H. Khozyem (✉)
Department of Geology, Faculty of Sciences, Aswan University,
Aswan, Egypt
e-mail: h.m.khozyem@aswu.edu.eg

H. Khozyem · T. Adate
Institute of Earth Sciences (ISTE), University of Lausanne, 1015
Lausanne, Switzerland

G. Keller
Department of Geosciences, Princeton University, Princeton, NJ
08544, USA

In the terrestrial realm, the PETM event resulted in the branching out of modern mammal species and their migration across the northern hemisphere (Bajpai et al., 2008; Bowen et al., 2002, 2004; Khozyem et al., 2021; Krause & Maas, 1990; Rana et al., 2008; Rodríguez, 1999; Wing et al., 2005). As well as resulted in rapid shifts in plant communities composition as observed in the late Paleocene in the Bighorn Basin and Wyoming plant fossils communities (*Metasequoia occidentalis*, *planicostata*, *Corylites* sp., *Brownia serrata*, *Macginitiea gracilis*, *Ginkgo adiantoides*, *Zizyphoides flabella*, *Davidia antiqua*, *Fagopsphyllum groenlandicum*, *Cercidiphyllum genitrix*; Wing & Currano, 2013).

1.1 Theories Explaining the PETM Event

Based on the data resolution and techniques, the criteria observed by Kennett and Stott (1991) are then modified several times; for example, a similar magnitude of increasing temperature based on the $\delta^{18}\text{O}$ is observed by using the Mg/Ca ratio and ranging between 5 and 8 °C (Thomas et al., 2002; Zachos et al., 2006). Similar magnitude of the temperature increase (from 5 to 8 °C) was also inferred using the biomarker paleothermometer (TEX₈₆ and GDGT), and similar results were obtained (Sluijs et al., 2006; Weijers et al., 2007). The evidence of temperature increase during the PETM is not only approved by marine sediments but also retrieved from analysis of leaf margin, the mammals tooth enamel and calcareous soil nodules (Bowen et al., 2001; Fricke et al., 1998; Fricke & Wing, 2004; Khozyem et al., 2014; Koch et al., 2003; Tremblin et al., 2021; Wing et al., 2005).

Change in temperature is a direct environmental response to carbon cycle perturbations and CO₂ input in both ocean and atmosphere. The increase of CO₂ input in both ocean and atmosphere is due to abnormal oxidation of carbon reservoir, which led to extensive dissolution in deep-ocean carbonate as a result of reducing the ocean water pH (Zachos et al., 2005), as well as extensive silicate weathering as indicated by increasing kaolinite input (Boll et al., 2000, 2001; Khozyem et al., 2013, 2015). Therefore, a leading cause that forces the increase in temperature and its consequences is massive CO₂ input. However, the sources of the enormous CO₂ amounts released during the PETM are still controversial. Five major scenarios were proposed to explain the source of CO₂ during PETM:

- *Methane clathrates destabilization*: the clathrates are associated with the deep continental shelf deposits in a stabilized phase of methane, but due to changes in oceanic physicochemical conditions (Temperature, ocean circulation, and/or slope failure), the clathrate can be destabilized (Dickens et al., 1995, 1997; Katz et al., 1999). When methane clathrate is destabilized, it is

released and oxidized to CO₂. These stored clathrates have negative $\delta^{13}\text{C}$ up to -60‰ (Kvenvolden, 1993).

- *Wildfire*: during the Paleocene, massive peat and coal were accumulated (Khozyem et al., 2021), and due to the latest Paleocene dry conditions, increase in atmospheric O₂ contents and/or orogenic events, the compensation took place and led to an increase in the CO₂ input (Kurtz et al., 2003; Moore & Kurtz, 2008).
- *Thermogenic methane*: burning the organic-rich sediments due to magma injection from the large igneous provinces could explosively release the thermogenic methane, as recorded through Cretaceous-Paleocene organic-rich sediments in the North Atlantic province (Svensen et al., 2004, 2010; Westerhold et al., 2009).
- *Drying epicontinental seas*: the rapid oxidation of organic matter has resulted from drying of tectonically formed epicontinental seas as observed in vast areas of central Asia (Higgins & Schrag, 2006).
- *Permafrost*: DeConto et al. (2010) proposed that during Paleogene, enormous quantities of carbon stored in permafrost and peat could have been rendered, oxidized, and released a vast amount of CO₂.

Among the previous proposed CO₂ sources; methane clathrate destabilization is the most accepted scenario, and recently it is conjugated with the large igneous provinces effect as mean source of heating during end of Paleocene (North Atlantic Igneous Province—NAIP) (Jones et al., 2017a, 2017b, 2019; Keller et al., 2018; Khozyem et al., 2014; Stokke et al., 2020).

1.2 Age and Duration of the PETM Event

The age estimation of the carbon isotope excursion (CIE) onset has recently been designated to 56.011 Ma using radiometric data (Westerhold et al., 2009). Dating based on zircon crystals associated with bentonite layers from the upper part of the CIE indicates age of 56.09 ± 0.03 Ma (Jaramillo et al., 2010). However, the astronomically calibrated cyclostratigraphy indicates duration of 150–220 ka for the CIE (Aziz et al., 2008; Röhl et al., 2007). The calculations based on extraterrestrial ³He fluxes suggests a duration between 120 and 220 ka for the PETM (Murphy et al., 2000).

The accuracy of this determination depends on presence or absence of the uppermost Paleocene dissolution levels.

Cyclostratigraphic studies were used to determine the duration of the initial part of the PETM event, which continued for about 100 ky for both marine and continental environments (Westerhold et al., 2011, 2018; Fig. 1). The duration of the PETM initial period was determined to be 90–110 ky by using the flux of extraterrestrial Helium that

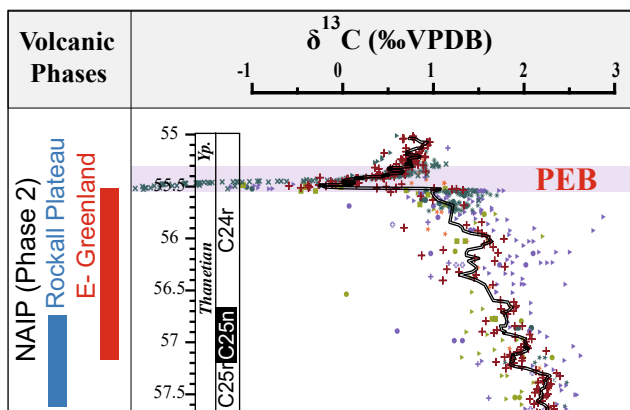


Fig. 1 Time relationship between the Paleocene Eocene Thermal Maximum carbon isotopic excursion (PETM-CIE) and the North Atlantic Igneous Provinces (NAIP) (modified after Westerhold et al., 2011)

matches well with the cyclostratigraphy results (Farley & Eltgroth, 2003; Murphy et al., 2000). The fast and abrupt carbon isotopic excursions were affected mainly by post-depositional alteration, condensation, and/or erosion of the boundary interval sediments, except for few examples of the PETM sections; therefore, tentative estimates from less than 10 ky (marine) to 8–23 ky (continental) have been proposed (McInerney & Wing, 2011).

1.3 Paleoposition Overview

Tethys is a potential region to investigate the causes and mechanisms of the PETM event. During the PETM, Tethys was a semi-restricted basin surrounded by vast numbers of tectonically formed shallow epicontinental seas (Fig. 2)

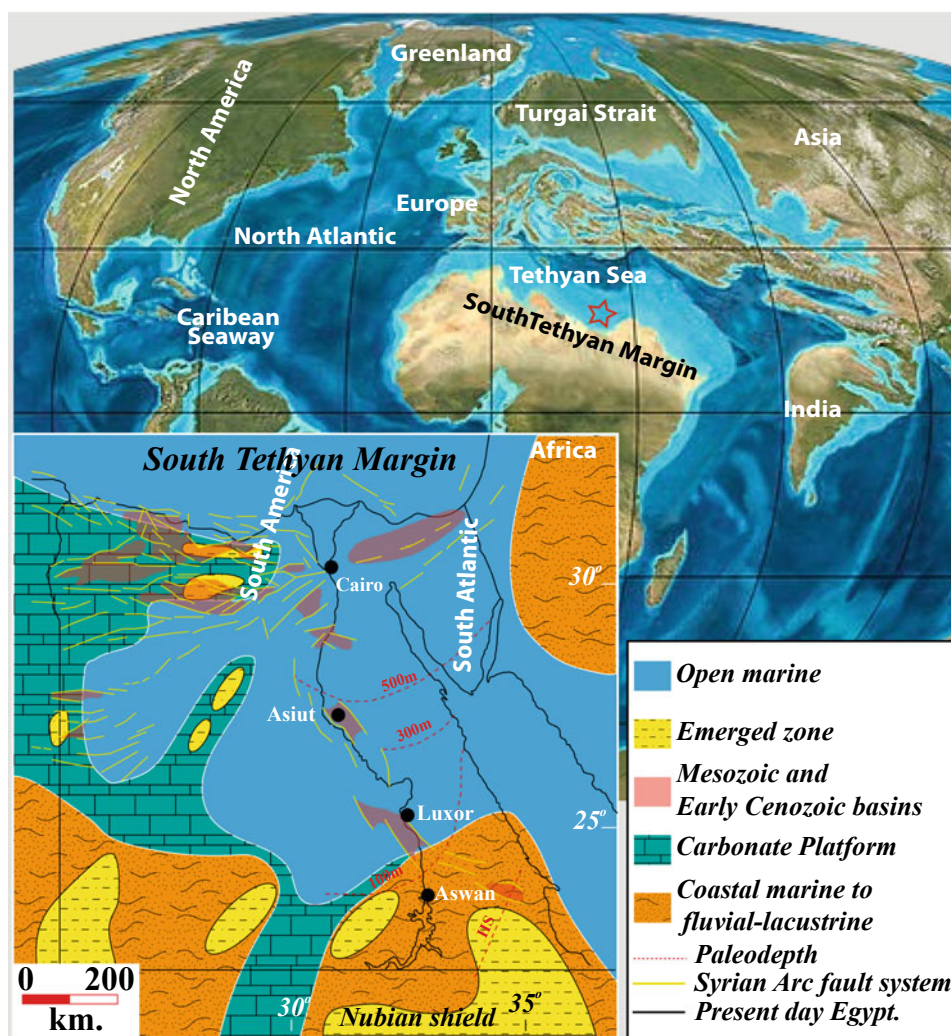


Fig. 2 Paleoposition of Egypt during the late Paleocene-early Eocene; Asterisk refers to the paleoposition of the Dababiya GSSP. The inset map shows the lithostratigraphic and structural lineament map of the Syrian Arc fold system in association with paleodepth (modified after Blakey, 2007; Guiraud & Bosworth, 1999; Speijer et al., 2000)

(Klootwijk et al., 1992; Oberhänsli, 1992; Oberhänsli & Hsü, 1986; Selverstone & Gutzler, 1993). Therefore, it was thought that Tethyan regions were essential organic carbon reservoirs (Raymo & Ruddiman, 1992; Selverstone & Gutzler, 1993) and acts as warm saline deep water bodies that affected ocean circulation during the PETM initial phase (Kennett & Stott, 1990, 1991). From Maastrichtian to Eocene, the Tethyan margins were located in the northern tropical climatic zone. This zone is characterized by repetitive upwelling episodes as recorded by the phosphate deposits of the eastern Mediterranean, North and North-Western Africa, Northern South America, and parts of the Caribbean sea (Föllmi, 1996; Jarvis et al., 1994; Lucas and Prevot-Lucas, 1995; Soudry et al., 2006).

A general overview of North African paleogeography through the late Paleocene to early Eocene revealed formations of shallow marine platforms (Guiraud & Bosworth, 1999). Several E–W trending uplifted blocks were formed along the Northern African Tethyan margin (Fig. 2; Guiraud & Bosworth, 1999). The tectonic instability and active subsidence affected most of northern Egypt (Said, 1990). All the previous factors resulted in the formation of semi-restricted basins, epicontinental seas, and shallow to neritic seas. These deformations may be in solid relation to the “Laramide event” described in Western Europe (Ziegler, 1990). The detailed investigation of semi-restricted basins and epicontinental sections located at the eastern end of this upwelling belt indicates similarities with the coeval deep-sea sections in terms of benthic foraminifers extinctions, planktic foraminifera turnover, as well as calcareous nanofossils (Monechi et al., 2000b; Speijer, 1994; Speijer & Schmitz, 1998; Speijer & Van der Zwaan, 1994; Speijer et al., 1996; Tantawy, 1998).

2 Paleocene Eocene Thermal Maximum in Egypt

As previously mentioned, Egypt was a part of the South Tethyan margin during the late Cretaceous to early Paleogene. The sedimentary successions during that time were deposited within epicontinental seas under unstable shelf conditions and were affected by tectonic instability linked to the Syrian Arc orogeny (Guiraud & Bosworth, 1999; Höntzsch et al., 2011) in the North. In Southern Egypt, the deposition took place on stable shelf that was surrounded by the Arabian Nubian craton (Fig. 2). In Egypt, most of the late Cretaceous–early Paleogene sediments are made of clastic to carbonate platform sediments (Fig. 2) and can be classified into several formations starting at the base with Dakhla Fm, Tarawan Fm, Esna Fm, and capped by Thebes formation (Said, 1990). The Paleocene/Eocene boundary in Egypt is well determined based on the calcareous nanofossils and

planktic foraminifera and placed at the middle to lower third part of Esna Fm. (Fig. 3; Aubry & Salem, 2013). The PETM was determined in Egypt based on several criteria: (1) An abrupt negative shift in both organic and inorganic carbon isotopes as well as nitrogen isotopes (Bolle et al., 2000; Dupuis et al., 2003; Guasti and Speijer, 2007; Khozyem et al., 2013, 2015; Schmitz et al., 1998; Speijer et al., 1997; Tantawy et al., 2000). (2) Abrupt changes in different geochemical proxies include weathering indexes, redox indicators, and paleoproductivity indicators (Ghandour, 2020; Keller et al., 2018; Khozyem et al., 2013, 2014, 2015; Schulte et al., 2011; Soliman, 2003). (3) An abrupt change in mineralogy at the PEB includes increased phyllosilicate, quartz, and Kaolinite content, as well as the presence of Palygorskite and sepiolite (Bolle et al., 2000, 2001; Dupuis et al., 2003; Khozyem et al., 2013, 2014). Figure 4 shows the locations and local names of Egypt’s most extensively studied late Paleocene–early Eocene successions.

In this chapter, we will discuss the nature and tempo of the Paleocene–Eocene Thermal Maximum event, and we will introduce a complete data set with a brief explanation of the PETM characteristics at the Dababiya GSSP.

3 Dababiya GSSP

In 2004, the International Union of Geological Science (IUGS) accepted Dababiya site as the Global Standard-Stratotype Sections and Points (GSSP). The golden spike was placed at the base of Dababiya quarry beds after a recommendation from the Paleocene/Eocene (P/E) working group based on the following criteria:

- The negative shifts in organic and inorganic carbon isotopes.
- Notable extinction of benthic foraminifera (*Stensioina beccariiiformis*).
- Observed transient occurrence of planktic foraminifera (*Acarinina africana*, *A. sibaiyaensis*, *Morozovella allisonensis*) and the calcareous nanofossils (*Rhomboaster* spp. and *Discoaster araneus*) along with the PETM interval.
- High occurrence of dinoflagellate (*Apectodinium*; Aubry et al., 2007).

Dababiya quarry beds are located at the base of Esna formation in the massive quarry that located on the eastern bank of the Nile River, 35 km south of Luxor city. The Dababiya quarry deposits cover the time interval from the late Paleocene to the early Eocene and are represented by Tarawan chalk, Esna shale, and Thebes limestone. The PETM in Dababiya quarry is 3.5 m thick in and consists of five distinctive beds (Dupuis et al., 2003). The basal bed is

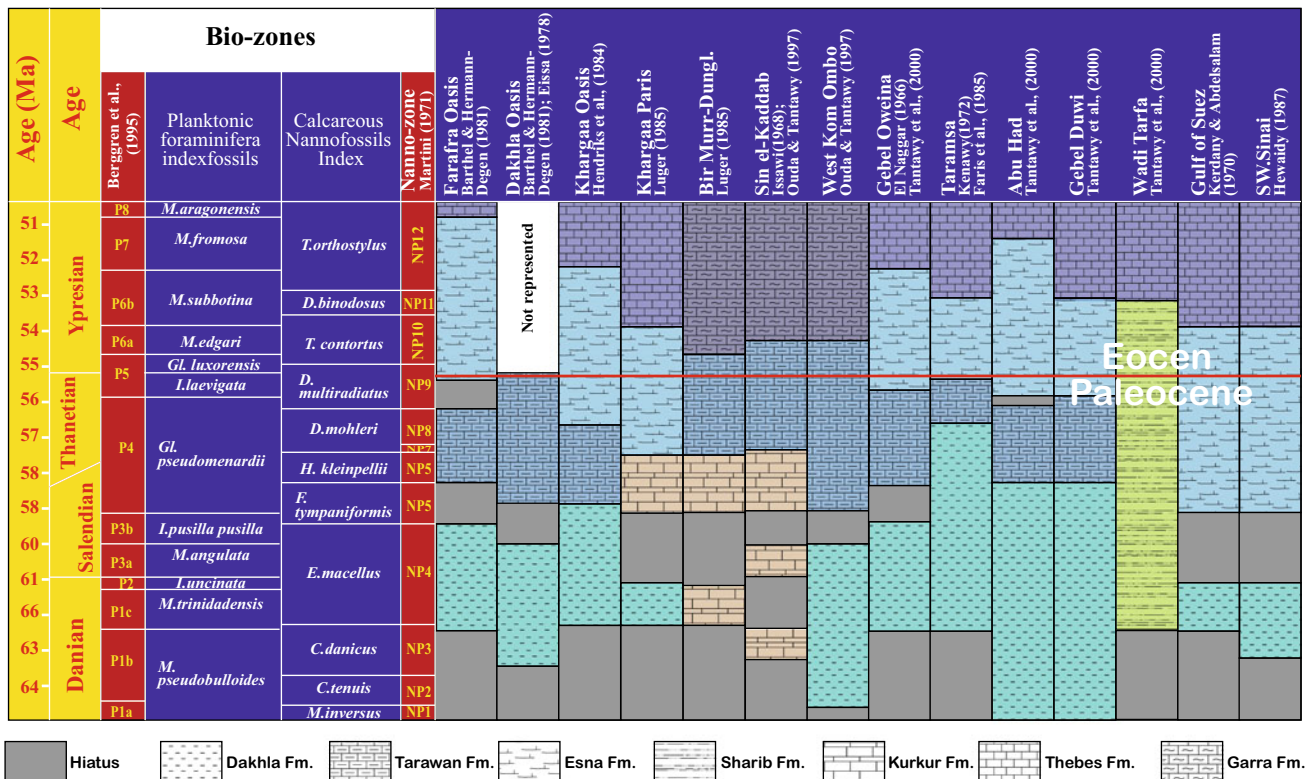


Fig. 3 Correlation of different Paleocene to lower Eocene successions representing the stratigraphically well-studied sections in Egypt (modified after Tantawy et al., 2000)

formed of dark clay representing the PEB, graded upward to shale, and partially silty-shale, overlain by phosphatic shale followed upward by calcareous shale and marl. Although the thickness of the PETM interval in Dababiya GSSP is variable from the northeast to the northwest (Fig. 5), ranging between 2 and 3.5 m, the observed variation in thickness is due to its depositional setting that inferred by several authors to be an asymmetrical submarine channel (Khozyem et al., 2014; Schulte et al., 2011).

3.1 Stable Isotope Profiles

Inorganic carbon ($\delta^{13}C_{carb}$) and organic carbon ($\delta^{13}C_{org}$) isotopes analyzes have been conducted on the Dababiya GSSP samples (sampled by Khozyem et al., 2014; Fig. 5).

At Dababiya, the $\delta^{13}C_{carb}$ shows an expanded $\delta^{13}C_{carb}$ excursion with a gradual onset and recovery (Fig. 6). Throughout the uppermost Paleocene, no changes were observed in the $\delta^{13}C_{carb}$ values, which are relatively stable around 1‰ and correspond to the planktic zone P4c. Within planktic zone P5, a gradual decrease in the $\delta^{13}C_{carb}$ values was observed, reaching its minimum values (− 4‰) 20 cm below the top of planktic zone P5, representing the PEB (Fig. 6). This gradual decrease is referred to as a pre-PEB

decrease. No values recorded for the $\delta^{13}C_{carb}$ at the lower Eocene interval (planktic zone E1) may be due to the absence of carbonate and/or dilution by increased detrital input. Then, initial recovery is occurred at the lower part of planktic foraminifera (zone E2; upper part of Bed-2). The $\delta^{13}C_{carb}$ shift ranges between − 2 and − 3‰ and is followed by rapid increases at Bed-3/Bed-4 contact to 0.39‰. Toward the top of the studied section, no changes in $\delta^{13}C_{carb}$ were observed.

The organic carbon isotope ($\delta^{13}C_{org}$) shows a similar pattern to $\delta^{13}C_{carb}$. During the late Paleocene (zones P4c to middle P5), $\delta^{13}C_{org}$ values are gradually increasing from − 25.8 to − 23.8‰, followed by abrupt decrease across the PEB and reach its minimum value close to the base of zone E2 (upper part of Bed-2; Fig. 6). In zone E2, the $\delta^{13}C_{org}$ gradually increases but is still lower than its mean value observed through the late Paleocene.

3.2 Biostratigraphy

It is well known that any environmental and climatic changes, directly and indirectly, impact the biota. The direct one is recorded as the extinction of species or families of micro and mega organisms. In contrast, the indirect impact can be

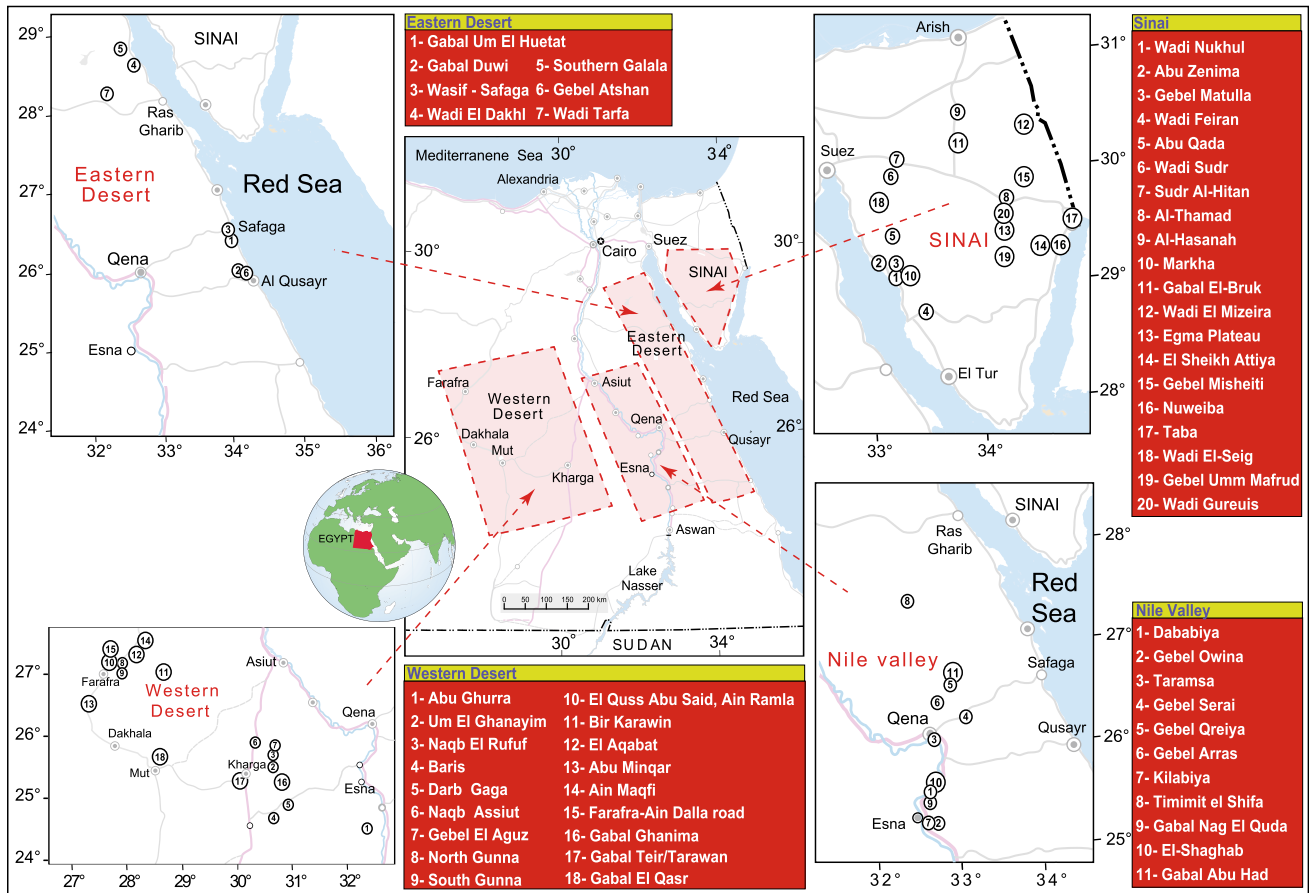


Fig. 4 Plot of the most extensive PETM section studied in Egypt (see references in the supplementary data files)

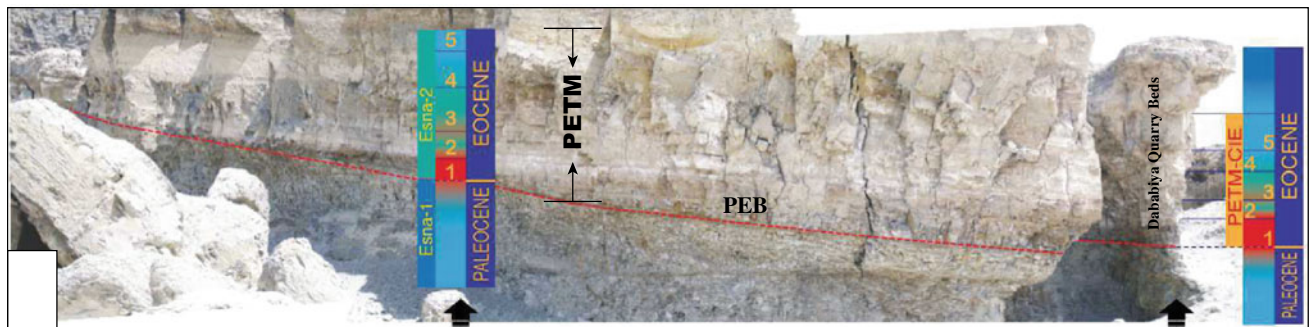


Fig. 5 Field photograph showing the Dababiya quarry beds at Dababiya GSSP and the studied section in the west of the main GSSP (after Khozyem et al., 2014)

observed by changes in the habituated state of the biota. Microorganisms are susceptible to any changes that occur in their environments. During PETM, both terrestrial and marine biota have been affected. In marine environments, extinction took place for benthic organisms, as well a partial extinction event was observed in plankton. In the terrestrial environment, migration and diversification of the biota were the most observed impacts of environmental changes.

Several authors have extensively studied the biostratigraphy of Dababiya GSSP (e.g., Aubry et al., 2007; Berggren & Ouda, 2003; Keller et al., 2018; Khozyem et al., 2014, 2015; Ouda & Berggren, 2003). Biostratigraphy of Dababiya GSSP is studied based on high-resolution planktic foraminifera. The standard biozonation scheme of Olsson et al. (1999) and Pearson et al. (2006) was followed (Fig. 7a). Four planktic foraminifera zones covering the time

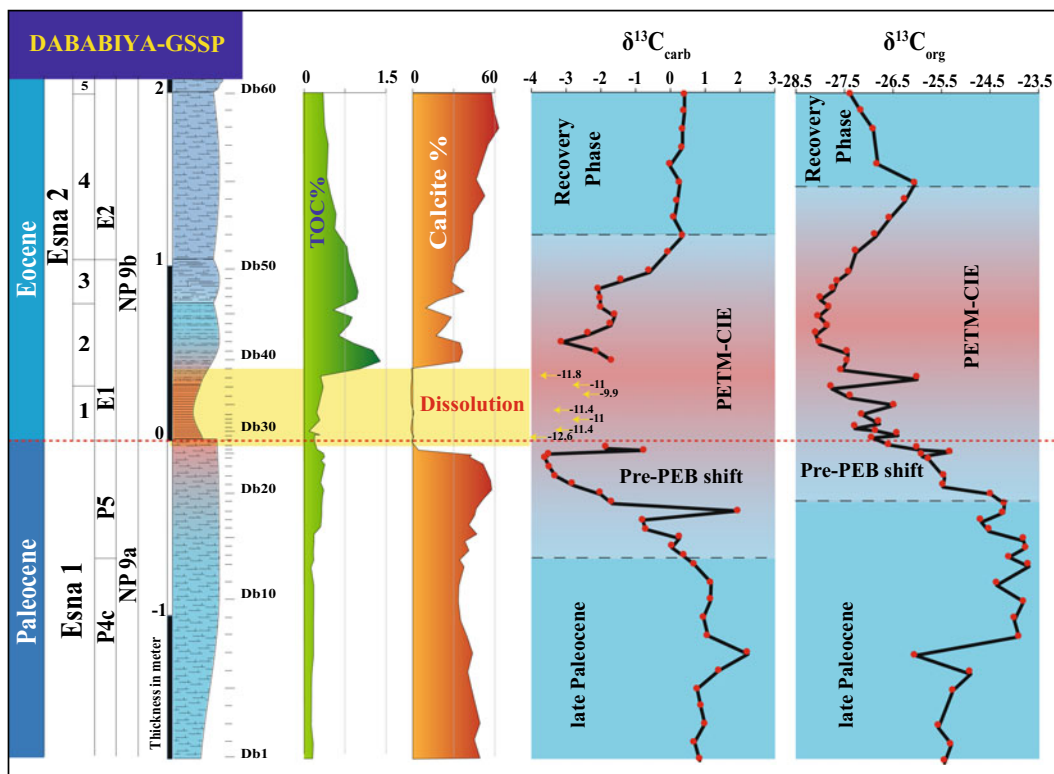


Fig. 6 $\delta^{13}C_{org}$ and $\delta^{13}C_{inor}$ profiles along with a lithostratigraphic illustration of the Dababiya GSSP together with the total organic carbon and carbonate content in percent, note the very negative values of $\delta^{13}C_{inor}$ above the PEB up to middle Bed 2

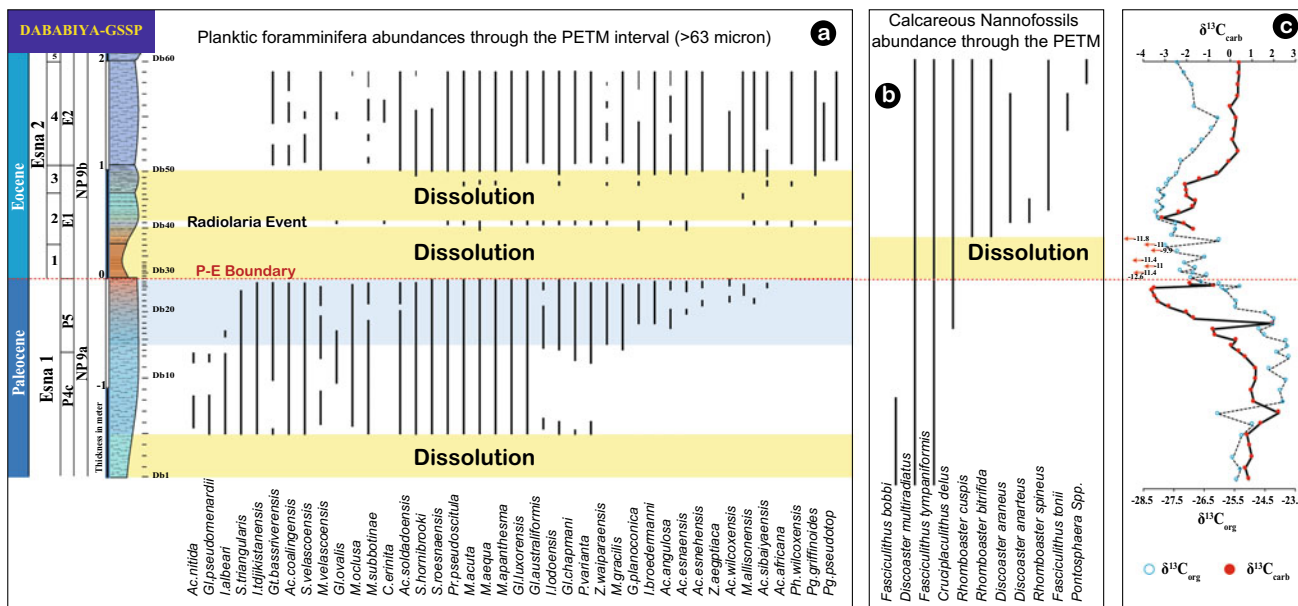


Fig. 7 a Selected ranges of planktic foraminifera, b calcareous nannofossil species from section located at 50 m to the left of the Dababiya GSSP, and c. Carbon isotopes ($\delta^{13}C_{org}$ and $\delta^{13}C_{carb}$). Note that a reduction in species richness in the late Paleocene is offset by a few new species during the gradual decrease in carbon isotopes, and this evolutionary trend increased during the gradual recovery in carbon isotopes in the early Eocene (modified from Keller et al., 2018; Khozyem et al., 2014)

interval from 54.5 to 56.5 Ma were recorded (Keller et al., 2018). The lowermost zone (P4c) is marked by the last appearance (LA) of *Globanomalina pseudomenardii*, and the dominated assemblage are *Igorina tadjikistanensis*, *Acarinina soldadoensis*, *Subbotina hornibrooki*, *Morozovella acuta*, and *M. aequa*. (Fig. 7a). Second observed planktic foraminifera biozone (zone P5) was determined between LA of *Gl. Pseudomenardii* and first appearance (FA) of *Acarinina sibaiyaensis*. This zone represents topmost part of Paleocene. The topmost part of zone P5 is characterized by 40% increase in species diversity and decreased abundance of the dominant species, indicates the onset of the PEB. Above the PEB, zone E1 is observed. It 1 m thick, the lower 42 cm represents barren interval. It is composed of clay devoid of CaCO₃, marking dissolution and/or ocean acidification, followed by 5 cm of thick radiolarian-rich interval associated with the transient PETM fauna (dominated by *A. sibaiyaensis* and *A. africana*. FA of *A. africana* and *Morozovella allisonensis*) followed upward by 50 cm, marking the recovery phase. The second dissolution and/or ocean acidification interval with rare foraminifera in the upper 20 cm was recorded. Contact surface between zone E1 and zone E2 placed at the first continuous occurrence of *Pseudohastingerina wilcoxensis* and coincides with the reappearance of the latest Paleocene existing assemblages (Berggren & Ouda, 2003; Kaiho et al., 2006; Kelly et al., 1996; Khozyem et al., 2014; Lu et al., 1998; Lu & Keller, 1993, 1995; Luciani et al., 2007, 2016). No significant species extinctions were observed even with observed climate warming, decreased productivity, and ocean acidification associated with PETM that could be linked to species migrations into higher latitudes during warming (Keller et al., 2018).

The Paleocene-Eocene boundary in Dababiya GSSP is placed at the contact interval between the calcareous nanofossils biozone (NP9a; Fig. 7b) and spans the late Paleocene and NP9b covers the early Eocene. The calcareous nanofossil assemblages are moderately diversified; the preservation of observed fauna varies from poor to moderate, and the barren/dissolution intervals recorded through Bed-1 and lower part of Bed-2 (Fig. 7b). The dissolution interval is followed by the first appearance of *Rhombaster cuspis* and *R. bitrifida*, *D. araneus*, and *D. anartus*, whereas *C. eodelus* appears earlier in NP9a and *R. spineus*, later in NP9b, similar to the southeast Atlantic (Agnini et al., 2007), and Kharga Oasis, Western Desert, Egypt (Tantawy, 2006).

Most observed calcareous nanofossils species of zone NP9a extinct at the P/E transition; only *Fasciculithus tympaniformis* survived into the lower Eocene, presence of this species, along with *Fasciculithus tonii* in the upper part of Dababiya GSSP (Bed-4), is likely reworked, as they are known to disappear at PETM onset (e.g., Agnini et al., 2007; Monechi et al., 2000a; Raffi et al., 2005; Tantawy, 2006).

3.3 Bulk Rock and Clay Mineralogy

The upper Paleocene sediments at Dababiya GSSP (zone P4c-P5) formed mainly of marl with 43% of calcite, 41% of phyllosilicates, 7% of quartz, and less than 1% of anhydrite with absence of phosphorus bearing minerals (apatite; Table 1; Fig. 8a). Smectite was the significant phyllosilicates mineral at this interval (mean value 68%) associated with 14% of illite, 7% of illite–smectite interstratification, 4% of palygorskite, 4% of kaolinite, and 3% of chlorite.

An abrupt decrease in calcite is observed (less than 5%); it is associated with an increase in phyllosilicates (58%), quartz (8%), anhydrite (7%), and the presence of Ca-apatite (7.5%). Goethite, K, and Na-feldspar are present in tiny amounts (Table 1; Fig. 8a).

Bed 1 and 2 (1.1 m; zone E1 to the base of E2) are marked by an abrupt increase in phyllosilicates, quartz, goethite, and anhydrite, with the presence of K and Na feldspars and low calcite contents. The low Ca-apatite content is due to reworked from underlying sediments with the presence of rare coprolites.

The interval covering E1/E2 zonal boundary is characterized by a sharp increase in calcite content (35%), coincident with a high concentration of Ca-apatite (up 26%), and a relative increase in anhydrite content. This interval is also characterized by an abrupt decrease in smectite content (45%) together with a sharp increase in kaolinite content (up to 10%) and gradual increase in illite (19%), chlorite (12%), illite–smectite (10.8%), and palygorskite (8.8%). Above this level, marl is the primary dominant sediment to the top of the studied section and corresponds to the upper zone E2 (Bed-4 to 5; Table 2; Fig. 8b).

3.4 Organic Matter and Mercury Contents

Dababiya GSSP samples are generally highly degraded poor in organic matter content. Through zone P4c-P5, organic matter content fluctuates between 0.2 and 0.4%; maximum value is observed close to PEB. The OM content decreased from the PE-boundary to 40 cm above and ranged from 0.08 to 0.24%. The TOC is enriched from the top of P5 to the E1/E2 boundary, ranging between 0.59 and 1.3%. The TOC in this interval is represented by Type-III organic matter (Khozyem et al., 2015) derived from continental sources and/or highly weathered marine OM; further to the top, TOC is gradually decreased with an average of 0.43% (Fig. 9).

The mercury profile from the beginning of the section to 20 cm below the PEB (Fig. 9). Mercury shows a low concentration with average values of 51 ppb. The 20 cm below the PEB shows a gradual increase in the Hg content, reaching its maximum at the PEB (value of 201 ppb). From the PEB to the E1/E2 contact, the Hg has high concentration

Table 1 The bulk rock composition of the studied samples (in percentage) together with mineral ratios

Samples	Phyll	Quartz	Feldspar	Calcite	Pyrite	Anhydrit	Apatite	MI ^a	DI ^b	Detritus ^c
DBA-1	43.02	4.64	0.00	47.98	1.84	0.00	0.00	0.90	0.99	47.66
DBA-2	41.04	4.04	0.00	44.01	0.00	0.00	0.00	0.91	1.02	45.08
DBA-3	44.63	5.33	0.00	47.87	0.00	0.78	0.00	0.89	1.04	49.96
DBA-4	41.78	4.63	0.00	44.87	0.00	1.59	0.00	0.90	1.03	46.41
DBA-5	38.92	3.94	0.00	41.87	0.00	2.39	0.00	0.91	1.02	42.86
DBA-6	40.03	5.77	0.00	39.45	0.00	0.00	0.00	0.87	1.16	45.80
DBA-7	38.78	4.80	1.27	42.65	0.00	0.00	0.00	0.86	1.05	44.85
DBA-8	39.22	5.38	0.00	38.90	0.00	0.00	0.00	0.88	1.15	44.60
DBA-9	41.23	6.38	0.00	34.45	0.00	0.00	0.00	0.87	1.38	47.61
DBA-10	51.23	6.57	1.20	32.87	0.00	0.00	0.00	0.87	1.79	59.00
DBA-11	44.23	4.93	0.00	33.17	0.00	0.00	0.00	0.90	1.48	49.16
DBA-12	39.12	6.62	1.58	36.78	1.35	1.07	0.00	0.83	1.29	47.32
DBA-13	45.73	5.66	0.00	33.91	0.00	0.46	0.00	0.89	1.52	51.40
DBA-14	40.32	6.30	0.00	40.13	0.00	2.14	0.00	0.86	1.16	46.62
DBA-15	43.48	5.84	0.00	37.45	0.00	0.00	0.00	0.88	1.32	49.32
DBA-16	40.12	6.75	0.00	45.70	0.00	0.00	0.00	0.86	1.03	46.87
DBA-17	44.34	8.90	0.00	40.12	0.00	0.00	0.00	0.83	1.33	53.24
DBA-18	40.88	7.09	0.00	44.07	0.00	0.00	0.00	0.85	1.09	47.97
DBA-19	40.03	8.34	0.00	45.34	0.00	1.12	0.00	0.83	1.07	48.37
DBA-20	35.09	9.01	0.00	50.03	0.00	0.00	0.00	0.80	0.88	44.10
DBA-21	30.89	9.63	0.00	56.00	0.00	0.00	0.00	0.76	0.72	40.52
DBA-22	27.89	10.88	0.00	55.12	0.00	0.00	0.00	0.72	0.70	38.77
DBA-23	31.49	9.95	0.00	52.58	0.00	0.00	0.00	0.76	0.79	41.44
DBA-24	35.09	9.01	0.00	50.03	0.00	0.00	0.00	0.80	0.88	44.10
DBA-25	40.02	9.59	0.00	47.02	0.00	0.00	0.00	0.81	1.06	49.61
DBA-26	45.55	8.63	0.00	40.74	0.00	1.36	0.00	0.84	1.33	54.18
DBA-27	45.41	9.31	0.00	41.90	0.00	0.00	0.00	0.83	1.31	54.72
DBA-28	57.74	8.21	4.80	5.44	1.19	7.09	7.48	0.82	13.01	70.76
DBA-29	60.33	9.90	3.81	1.28	0.00	16.77	3.98	0.81	58.02	74.04
DBA-30	71.02	14.34	1.80	0.65	0.00	6.44	0.00	0.81	133.97	87.16
DBA-31	72.45	13.05	0.00	2.02	0.00	8.34	0.00	0.85	42.33	85.50
DBA-32	71.53	15.89	3.55	0.92	0.00	7.09	0.00	0.79	99.31	90.96
DBA-33	34.36	2.90	0.86	0.04	0.00	58.90	2.23	0.90	953.00	38.12
DBA-34	70.23	16.03	2.09	0.62	0.00	10.87	0.00	0.79	142.52	88.35
DBA-35	73.02	20.34	1.43	2.02	0.00	0.83	0.00	0.77	47.03	94.79
DBA-36	72.11	20.02	2.49	0.30	0.00	2.34	0.00	0.76	313.47	94.62
DBA-37	66.89	22.23	1.49	0.40	0.00	4.78	0.00	0.74	226.52	90.61
DBA-38	61.45	27.44	1.20	0.86	0.00	3.22	0.00	0.68	105.33	90.09
DBA-39	59.07	22.14	3.12	0.34	0.00	9.08	0.00	0.70	251.53	84.33
DBA-40	35.31	12.43	0.00	33.56	0.00	13.56	0.00	0.74	1.42	47.74
DBA-41	33.56	11.90	0.00	35.78	0.00	8.77	0.00	0.74	1.27	45.46
DBA-42	30.90	10.04	1.93	34.09	0.00	3.60	0.00	0.72	1.26	42.87
DBA-43	22.12	7.52	0.00	17.52	0.00	20.63	25.11	0.75	1.69	29.64
DBA-44	28.34	11.05	1.54	23.54	0.00	6.09	26.09	0.69	1.74	40.93

(continued)

Table 1 (continued)

Samples	Phyll	Quartz	Feldspar	Calcite	Pyrite	Anhydrit	Apatite	MI ^a	DI ^b	Detritus ^c
DBA-45	25.89	8.77	1.48	28.07	0.00	2.58	28.43	0.72	1.29	36.14
DBA-46	22.68	7.58	1.60	10.38	0.00	25.43	25.49	0.71	3.07	31.85
DBA-47	16.90	6.34	0.00	18.32	0.00	30.12	27.87	0.73	1.27	23.24
DBA-48	27.18	8.30	0.00	36.89	0.00	8.57	14.51	0.77	0.96	35.48
DBA-49	21.51	7.59	0.00	28.10	0.00	9.67	30.90	0.74	1.04	29.10
DBA-50	30.12	8.34	0.00	31.34	0.00	3.23	26.09	0.78	1.23	38.46
DBA-51	30.17	5.08	0.00	40.00	0.00	1.51	13.66	0.86	0.88	35.25
DBA-52	38.01	7.45	0.00	42.21	0.00	1.04	10.45	0.84	1.08	45.46
DBA-53	30.87	5.83	1.51	43.12	0.00	0.70	8.90	0.81	0.89	38.22
DBA-54	37.28	5.99	0.00	51.28	0.00	0.00	4.98	0.86	0.84	43.27
DBA-55	28.92	4.05	0.00	45.29	0.00	6.45	7.34	0.88	0.73	32.97
DBA-56	34.45	4.34	0.00	53.51	0.00	0.00	6.92	0.89	0.72	38.79
DBA-57	33.04	5.18	0.00	57.20	0.00	0.00	3.46	0.86	0.67	38.22
DBA-58	31.63	6.02	0.00	60.89	0.00	0.00	0.00	0.84	0.62	37.64
DBA-59	33.96	5.39	0.00	57.34	0.00	0.00	0.00	0.86	0.69	39.35
DBA-60	33.52	5.70	0.00	55.70	0.00	0.00	0.00	0.85	0.70	39.22

^a Maturity index calculated as Phyllosilicate/(Phyllosilicate + total feldspar + Quartz) (Bhatia, 1985)

^b Detrital input calculated as DI = (Phyllosilicate + total feldspar + Quartz)/Calcite (Bolle et al., 2000; Khozyem et al., 2013)

^c Detritus calculated as (Phyllosilicate + total feldspar + Quartz)

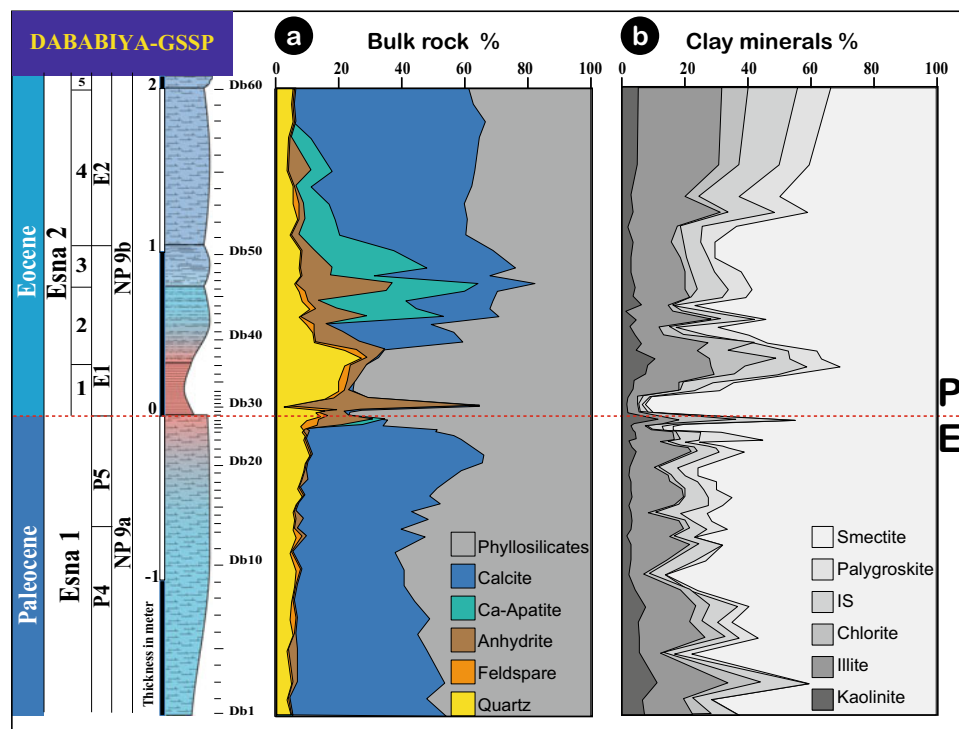


Fig. 8 **a** Bulk rock compositions of the Dababiya GSSP. Note the increased phyllosilicate and quartz with the presence of feldspar in the first 50 cm above the PEB. An increase in Ca-apatite coincides with increased calcite contents and several intervals enriched in anhydrite and **b** Relative of clay minerals. Note the increase in kaolinite, chlorite, IS, and palygorskite to the detriment of smectite at 50 cm above the PEB

contents ranging between 93 and 314 ppb with an average value of 187 ppb. Then it decreased to a mean value of 83.5 ppb.

Generally, the TOC-normalized Hg shows two remarkable enrichments; the first is started from the base of the section to top zone P4c with mean value of 443. The second

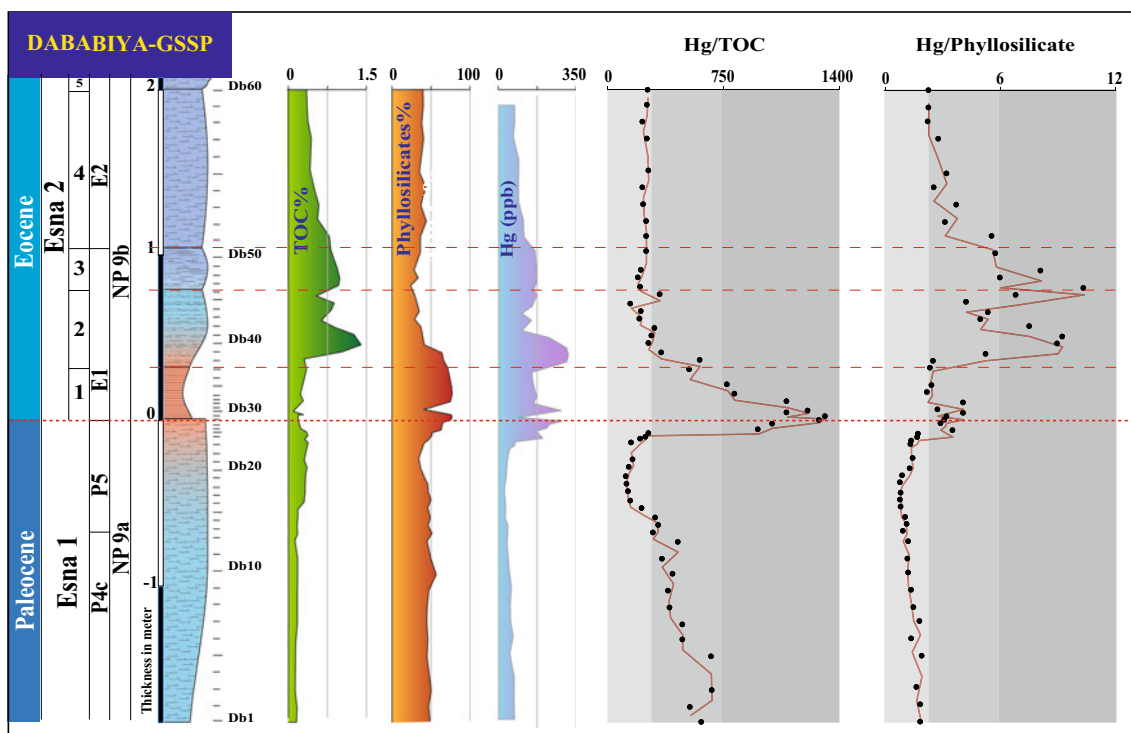
Table 2 Clay contents of the phyllosilicate fraction in the studied samples (in percent)

Sample	Kao	Smectite	Illite	Chlorite	Il-Sm	Palygorskite	Kao/Il + Chl
DBA-1	6.77	62.46	15.51	6.06	9.21	0.00	0.31
DBA-2	5.98	71.28	13.04	3.59	6.11	0.00	0.36
DBA-3	10.67	40.59	22.83	10.73	15.19	0.00	0.32
DBA-4	7.91	59.13	14.79	5.99	9.47	2.73	0.48
DBA-5	5.15	77.66	6.75	1.24	3.75	5.45	0.65
DBA-6	5.17	56.73	20.69	7.21	4.43	5.77	0.19
DBA-7	4.80	64.86	16.58	4.09	5.09	4.58	0.23
DBA-8	6.98	59.57	16.12	5.00	8.65	3.69	0.33
DBA-9	3.82	75.89	14.21	3.87	0.00	2.22	0.21
DBA-10	1.84	86.29	4.41	2.55	4.91	0.00	0.26
DBA-11	2.46	73.36	11.51	2.49	6.53	3.65	0.18
DBA-12	2.24	67.89	18.84	3.43	7.60	0.00	0.10
DBA-13	1.18	76.73	13.81	1.94	6.34	0.00	0.07
DBA-14	2.37	66.69	17.06	2.20	5.33	6.35	0.12
DBA-15	2.55	71.38	15.38	2.02	2.81	5.85	0.15
DBA-16	2.28	73.11	5.43	3.11	8.12	7.95	0.27
DBA-17	1.60	67.92	14.71	1.86	9.61	4.29	0.10
DBA-18	2.74	65.25	16.28	1.19	7.40	7.14	0.16
DBA-19	2.43	70.20	16.51	1.21	5.92	3.72	0.14
DBA-20	2.32	69.99	12.33	2.39	6.92	6.05	0.16
DBA-21	1.56	75.89	12.57	1.45	4.73	3.81	0.11
DBA-22	1.98	75.62	7.78	1.95	6.18	6.49	0.20
DBA-23	3.05	68.42	12.68	2.26	6.43	7.18	0.20
DBA-24	4.11	61.21	17.58	2.57	6.67	7.86	0.20
DBA-25	2.84	66.12	17.73	2.79	6.82	3.69	0.14
DBA-26	2.42	67.89	13.64	2.69	8.61	4.75	0.15
DBA-27	1.87	75.34	10.11	3.00	5.30	4.38	0.14
DBA-28	4.04	53.43	12.08	2.66	5.92	19.86	0.27
DBA-29	3.58	68.47	12.32	1.48	7.65	6.50	0.26
DBA-30	2.92	83.73	6.06	1.15	3.40	2.73	0.40
DBA-31	2.46	83.70	4.71	0.80	5.04	3.29	0.45
DBA-32	3.32	80.30	8.90	3.67	0.98	2.82	0.26
DBA-33	10.91	44.93	6.94	18.44	18.78	0.00	0.43
DBA-34	1.48	89.88	3.29	1.06	2.71	1.59	0.34
DBA-35	1.06	92.49	3.46	1.20	0.97	0.82	0.23
DBA-36	1.49	90.43	2.89	2.68	1.71	0.79	0.27
DBA-37	2.93	69.17	14.69	1.33	4.22	7.67	0.18
DBA-38	3.47	64.74	14.37	1.95	9.18	6.29	0.21
DBA-39	6.90	46.87	22.25	6.83	13.93	3.21	0.24
DBA-40	7.69	30.77	20.52	11.18	19.63	10.22	0.24
DBA-41	10.08	36.77	17.30	22.01	4.33	9.52	0.26
DBA-42	4.06	38.23	19.82	9.91	19.51	8.48	0.14
DBA-43	5.69	53.60	21.28	15.48	0.00	3.96	0.15
DBA-44	3.82	59.90	8.91	7.17	7.13	13.07	0.24

(continued)

Table 2 (continued)

Sample	Kao	Smectite	Illite	Chlorite	Il-Sm	Palygorskite	Kao/Ill + Chl
DBA-45	2.14	69.37	9.32	3.85	2.00	13.32	0.16
DBA-46	4.08	54.11	23.80	3.54	10.95	3.52	0.15
DBA-47	0.60	68.57	15.34	3.36	7.93	4.20	0.03
DBA-48	5.54	76.80	8.97	1.89	0.00	6.80	0.51
DBA-49	2.88	60.86	18.40	1.08	9.80	6.97	0.15
DBA-50	3.71	58.49	16.02	4.58	9.66	7.54	0.18
DBA-51	2.37	61.88	17.34	2.26	7.39	8.77	0.12
DBA-52	2.43	70.60	15.73	2.52	6.98	1.73	0.13
DBA-53	3.09	70.56	12.15	4.41	5.50	4.30	0.19
DBA-54	1.39	63.75	15.78	1.46	7.00	10.62	0.08
DBA-55	2.99	40.85	27.91	3.14	14.78	10.33	0.10
DBA-56	2.24	49.90	17.44	5.07	12.85	12.51	0.10
DBA-57	3.28	45.22	21.73	6.04	12.90	10.85	0.11
DBA-58	4.31	40.54	26.01	7.01	12.95	9.18	0.13
DBA-60	4.73	33.62	26.84	8.82	15.87	10.12	0.13

**Fig. 9** Lithostratigraphic log and geochemical attributes; TOC, Hg, and Hg/TOC together with phyllosilicate and phyllosilicate normalized-Hg through the PETM interval at Dababiya GSSP section (Egypt)

is a very high concentration of Hg/TOC at the interval from 20 cm to top of Bed-1, reaching ~ 1400 . Above, Hg/TOC shows a gradual decrease. The phyllosilicate normalized Hg (Fig. 9) represents two spikes of enrichments covering the intervals of Bed-3 and Bed-4 with values of 9 and 8, respectively.

3.5 Geochemistry

The major elements in Dababiya GSSP (Table 3) correlate to changes in clay content. However, there are no changes observed in major elements through P4C.

Table 3 Raw data of the major elements analyzed for Dababiya GSSP

Sample	SiO ₂	TiO ₂	Al ₂ O ₃	F _e 2O ₃	MnO	MgO	CaO	Na ₂ O	K ₂ O	P ₂ O ₅
DBA-1	33.16	0.45	11.17	4.13	0.03	2.41	19.94	2.32	0.29	0.40
DBA-2	33.40	0.46	11.23	3.75	0.03	2.30	20.43	2.24	0.36	0.49
DBA-3	33.54	0.44	11.09	3.43	0.03	2.27	20.36	2.37	0.32	0.51
DBA-5	33.71	0.43	10.82	3.48	0.04	2.21	20.41	2.34	0.36	0.56
DBA-6	36.04	0.43	11.48	3.62	0.03	2.31	18.67	2.35	0.49	0.53
DBA-7	36.52	0.44	11.50	3.97	0.04	2.34	18.11	2.40	0.54	0.58
DBA-8	37.62	0.44	11.87	3.98	0.03	2.35	16.89	2.43	0.55	0.58
DBA-9	39.22	0.45	12.21	3.97	0.03	2.37	15.90	2.47	0.65	0.57
DBA-10	39.08	0.46	12.22	4.25	0.03	2.43	15.88	2.48	0.61	0.53
DBA-11	38.55	0.46	12.13	4.23	0.03	2.37	16.23	2.45	0.58	0.54
DBA-12	38.71	0.46	11.91	4.22	0.03	2.47	16.14	2.52	0.55	0.54
DBA-13	37.21	0.44	11.36	3.90	0.03	2.44	17.38	2.26	0.53	0.51
DBA-14	35.86	0.42	10.84	4.26	0.04	2.39	18.36	2.38	0.42	0.47
DBA-15	35.03	0.42	10.63	3.91	0.04	2.40	19.68	2.21	0.45	0.47
DBA-16	33.93	0.39	9.95	3.33	0.03	2.35	20.96	2.16	0.34	0.45
DBA-17	34.06	0.39	9.88	3.26	0.03	2.37	21.26	2.13	0.39	0.42
DBA-18	32.76	0.36	9.32	3.04	0.04	2.38	22.71	2.03	0.28	0.41
DBA-19	31.79	0.34	8.66	3.15	0.04	2.38	23.67	1.95	0.21	0.38
DBA-20	30.14	0.32	8.24	2.83	0.04	2.42	25.32	1.85	0.10	0.40
DBA-21	30.59	0.31	7.85	2.76	0.04	2.53	25.37	1.79	0.13	0.42
DBA-22	30.64	0.30	7.70	2.59	0.04	2.56	25.55	1.67	0.14	0.44
DBA-24	30.26	0.30	7.70	2.38	0.03	2.64	25.72	1.65	0.14	0.50
DBA-25	30.36	0.32	7.95	2.53	0.03	2.52	25.24	1.73	0.11	0.56
DBA-26	35.07	0.35	9.11	2.81	0.02	2.42	21.47	2.13	0.32	0.79
DBA-27	33.40	0.33	8.55	2.63	0.02	2.36	23.13	1.85	0.21	0.72
DBA-28	40.41	0.48	12.10	3.88	0.01	2.90	5.48	4.35	1.00	1.26
DBA-29	47.89	0.89	17.48	5.48	0.01	2.95	2.62	3.87	0.63	0.83
DBA-30	54.71	0.87	15.16	5.05	0.01	3.12	1.20	3.52	0.87	0.32
DBA-31	52.66	0.86	15.09	6.36	0.01	3.04	1.49	3.55	1.17	0.56
DBA-32	58.69	0.97	14.80	3.17	0.00	3.26	0.83	3.56	0.79	0.10
DBA-34	57.90	0.92	14.26	3.09	0.00	3.12	1.44	3.57	0.77	0.10
DBA-35	59.12	0.91	14.22	3.60	0.00	3.09	0.57	3.43	0.86	0.14
DBA-36	59.06	0.85	13.81	3.82	0.01	2.88	1.18	3.62	0.86	0.18
DBA-37	58.63	0.72	12.58	5.61	0.01	2.50	1.87	3.17	1.29	0.42
DBA-38	56.50	0.63	10.64	3.69	0.01	2.08	5.42	3.03	1.40	0.36
DBA-39	51.62	0.57	10.52	4.62	0.01	2.18	6.27	3.07	1.70	1.22
DBA-40	32.79	0.32	6.16	5.88	0.01	1.94	23.02	1.70	0.91	1.19
DBA-41	33.85	0.31	6.11	5.74	0.01	1.91	22.62	1.83	0.89	1.13
DBA-42	37.25	0.43	9.39	6.61	0.02	2.36	15.66	2.68	1.29	7.61
DBA-43	28.67	0.30	6.94	4.54	0.01	1.70	27.03	1.76	0.83	7.36
DBA-44	34.13	0.36	8.45	4.47	0.01	1.91	20.58	2.07	0.94	6.54
DBA-45	31.06	0.31	7.39	4.32	0.02	1.78	24.77	1.53	0.70	7.17
DBA-46	28.28	0.31	7.50	8.46	0.02	1.68	24.88	1.91	0.83	6.15
DBA-47	29.19	0.32	7.43	3.25	0.02	1.66	26.52	1.95	0.67	7.01

(continued)

Table 3 (continued)

Sample	SiO ₂	TiO ₂	Al ₂ O ₃	Fe ₂ O ₃	MnO	MgO	CaO	Na ₂ O	K ₂ O	P ₂ O ₅
DBA-48	28.26	0.30	7.27	2.89	0.02	1.63	27.81	1.76	0.43	6.69
DBA-49	28.14	0.29	6.97	3.18	0.02	1.57	27.73	1.60	0.56	7.92
DBA-50	30.29	0.33	7.99	3.40	0.02	1.75	25.41	1.80	0.48	5.81
DBA-51	31.40	0.36	8.68	3.54	0.02	1.85	24.27	1.90	0.42	3.14
DBA-52	31.80	0.35	8.66	3.35	0.02	1.82	24.19	1.79	0.36	2.52
DBA-53	32.03	0.34	8.74	3.43	0.02	1.85	23.88	1.77	0.34	1.80
DBA-54	29.51	0.34	8.44	3.11	0.02	1.75	25.93	1.72	0.20	1.13
DBA-55	27.45	0.31	7.89	2.75	0.02	1.66	28.33	1.42	0.15	1.34
DBA-56	25.81	0.29	7.48	2.60	0.02	1.55	29.82	1.23	0.12	1.58
DBA-58	26.91	0.32	8.02	2.69	0.02	1.58	29.01	1.14	0.12	0.70
DBA-59	25.86	0.32	7.77	2.78	0.02	1.55	29.97	1.14	0.09	0.77
DBA-60	25.86	0.32	7.77	2.78	0.02	1.55	29.97	1.14	0.09	0.77

From the beginning of zone P5 up to the PEB, a gradual decrease in SiO₂, Al₂O₃, TiO₂, Fe₂O₃, Na₂O₃, and K₂O values are observed (mean values are 33%, 9%, 0.4%, 3%, 2%, and 0.3 respectively) and a notable increase in CaO (mean 23%), with no changes in MgO, MnO, and P₂O₅ concentrations. Above the PEB, a level of 40 cm shows abrupt enrichments in MEs (mean values 53% of SiO₂, 13% of Al₂O₃, 0.8% of TiO₂, 5% of Fe₂O₃, 3% of MgO, 3% of Na₂O₃, and 1% of K₂O) coincident with a notable decrease in MnO and CaO (0.01 and 4.28%, respectively). Further to the top, all MEs gradually returned to the mean values observed below the PEB except a rapid increase in P₂O₅ content (mean values of 6%; Table. 3).

Trace element concentrations and its normalized values are used as environmental indicator in marine sediments (Brumsack, 2006; Riquier et al., 2006; Tribouvillard et al., 2006). The Al-normalized trace elements (TEs) of Dababiya have distinctive behavior cross the PETM interval. Cu/Al, Zr/Al, and Pb/Al are enriched just above PEB in zone E1 and suddenly return to pre-PEB values. V/Al, U/Al, Mo/Al, Cd/Al, Ni/Al, and Zn/Al are abruptly enriched, followed by a sudden drop at the E1/E2 zonal boundary.

This drop brings all values of the Al-normalized TEs, almost to the background values observed in the basal Eocene (zone E1) and late Paleocene. Co/Al and Ba/Al represent their minimum values at basal Eocene (zone E1), whereas Co/Al is gradually increased above Bed-1 to the top of the section (Table 4). A vast peak of Cr/Al concentrations is observed in Bed-2 and Bed-3 returning to pre-PEB values in Bed-4.

The REEs concentration of the studied samples is shown in Table 5. The REEs content is normalized to Post-Archaean Australian Shales (PAAS; McLennan, 1989). The REE signatures provide information on secular variations in ancient marine environmental conditions regarding

and oxygenation conditions through the water column (Holser, 1997; Kamber & Webb, 2001). In addition, REE proxies provide crucial information on paleoceanography, marine redox history, and biogenicity of marine precipitates (Bellanca et al., 1997; German & Elderfield, 1990; Holser, 1997; Lawrence & Kamber, 2006; Shields & Webb, 2004; Van Kranendonk et al., 2003; Webb & Kamber, 2000). Therefore, the ratios of $Ce/Ce^* = Ce_{SN}/(0.5 La_{SN} + 0.5 Pr_{SN})$. when the Ce-Anomaly tends to be negative, it expresses the presence of anoxic conditions. The Eu-Anomaly represents Eu/Eu^* where $Eu^* = Eu_{SN}/(0.5Sm_{SN} + 0.5Gd_{SN})$ (Bau & Dulski, 1996; Nothdurft et al., 2004) and its direct proxy for weathering (Table 6).

4 Discussion

Based on the introduced results, we will discuss some critical features associated with PETM events that provide crucial information about the nature and tempo of this event.

4.1 Carbon Isotope Variations and Possible Causes

The carbon isotopic profile across the PETM event is almost globally identical and permits the identification and correlation of this event in marine and terrestrial environments (Keller et al., 2018; Khozyem et al., 2014, 2015). PEB itself is characterized by abrupt (most of the PETM sections) or gradual negative shift (few of the PETM sections; Sluijs & Dickens, 2012). In Dababiya GSSP, both organic and inorganic carbon isotope profiles are identical in trend. Carbon isotope excursion (PETM-CIE) at Dababiya GSSP has three specific intervals: Gradual decrease, CIE minimum, and

Table 4 Raw data of the trace elements analyzed for Dababiya GSSP

Sample	Sc	V	Cr	Co	Ni	Cu	Zn	As	Sr	Y	Zr	Nb	Mo	Cd
DBA-1	13.1	174.7	604.7	12.7	393.0	18.4	225.0	3.9	607.3	31.5	76.7	12.2	20.7	1.2
DBA-2	13.9	187.7	331.7	11.7	153.7	19.1	208.7	3.2	595.0	36.4	79.6	12.2	18.1	1.2
DBA-3	13.7	188.3	538.0	13.7	344.0	22.8	207.3	3.3	602.7	37.6	80.4	12.1	23.7	1.2
DBA-5	13.4	188.7	591.3	16.4	384.0	16.1	196.3	3.4	618.3	38.3	75.9	11.6	28.0	1.2
DBA-6	14.2	192.0	529.0	17.3	362.3	21.3	199.3	3.9	584.0	36.7	81.5	12.0	28.9	1.1
DBA-7	14.0	187.3	461.0	18.7	322.7	24.3	176.7	4.6	563.7	39.3	81.2	11.8	31.6	1.5
DBA-8	14.1	193.0	467.7	20.2	337.7	19.2	194.7	5.4	530.3	38.2	82.5	12.2	32.4	1.3
DBA-9	14.5	195.3	481.0	18.1	340.3	22.4	180.0	5.3	557.7	37.8	83.7	12.7	29.4	1.2
DBA-10	15.1	201.0	688.3	22.3	546.7	20.9	173.0	5.3	563.0	37.0	83.5	12.6	37.1	1.3
DBA-11	15.1	198.7	615.7	18.9	447.7	20.3	157.3	5.0	498.7	38.4	86.9	13.0	37.0	1.7
DBA-12	14.4	190.3	685.3	19.4	527.3	19.5	166.7	5.2	573.7	37.8	85.4	12.7	43.3	1.4
DBA-13	13.6	188.3	897.7	15.2	355.0	23.3	178.3	5.2	535.3	34.6	79.2	12.4	35.3	2.0
DBA-14	12.8	186.0	573.7	17.1	393.0	20.2	185.7	9.3	572.7	33.2	76.8	12.0	51.0	1.8
DBA-15	12.8	182.7	514.7	14.9	351.7	21.5	164.7	6.0	574.3	32.8	75.0	11.7	40.7	2.0
DBA-16	12.5	169.3	434.3	13.7	317.0	19.2	161.3	5.7	659.7	31.8	71.1	11.2	26.8	2.1
DBA-17	12.0	170.0	479.3	13.2	421.0	26.5	349.0	7.1	680.7	29.6	67.5	10.8	27.1	2.6
DBA-18	11.6	172.0	426.0	12.7	376.7	19.2	138.3	6.4	803.7	28.5	65.9	10.3	28.4	2.7
DBA-19	10.7	192.0	685.3	13.1	408.7	17.8	144.3	7.6	763.7	27.6	63.1	9.7	30.6	3.0
DBA-20	10.1	185.3	311.0	10.5	396.0	17.3	124.3	6.1	747.3	27.6	60.8	9.5	21.0	4.0
DBA-21	10.0	183.3	263.3	9.6	298.7	28.3	150.0	7.3	757.3	28.0	59.5	8.8	21.5	4.5
DBA-22	9.8	194.0	138.3	8.0	150.7	16.4	159.3	8.5	740.3	27.9	58.0	8.9	16.9	8.7
DBA-24	10.0	196.3	156.7	7.7	160.7	17.6	193.3	6.9	1176.7	30.2	58.6	8.5	16.7	10.0
DBA-25	9.9	219.9	287.4	8.8	206.6	17.6	239.1	8.1	1003.1	30.6	57.3	8.5	19.1	9.1
DBA-26	11.7	300.6	263.6	8.1	193.7	14.6	268.6	8.3	2197.3	39.4	65.9	9.4	26.7	8.4
DBA-27	11.4	270.2	287.4	7.6	226.2	19.5	307.0	7.3	1841.9	36.3	64.0	8.9	18.0	7.2
DBA-28	13.6	548.8	468.9	10.0	311.7	38.1	116.0	13.1	1885.6	65.9	95.8	12.5	73.4	1.5
DBA-29	12.7	757.7	484.0	9.7	538.3	75.1	653.0	32.3	995.7	48.4	227.3	19.6	65.8	13.7
DBA-30	12.5	2500.0	1133.3	9.2	545.3	106.3	426.0	29.3	730.3	44.2	232.7	17.6	173.7	9.7
DBA-31	13.3	2666.7	571.3	5.6	323.0	113.3	437.0	36.1	1236.7	57.5	236.0	17.6	187.7	10.4
DBA-32	12.6	3033.3	530.7	4.4	287.0	162.0	369.0	12.5	192.3	25.8	265.0	19.6	65.4	7.0
DBA-34	11.6	3183.3	405.3	3.7	240.0	160.7	325.7	15.2	265.7	28.5	260.0	18.6	67.6	5.7
DBA-35	11.4	3533.3	463.7	4.0	336.7	150.7	358.7	11.5	297.3	36.8	261.3	17.9	190.3	9.4
DBA-36	11.4	4420.0	603.0	6.0	435.7	193.3	396.7	14.1	375.0	40.9	244.0	17.0	251.7	7.8
DBA-37	11.9	3006.7	1053.3	4.4	247.7	204.3	552.3	24.8	561.3	36.5	198.7	13.0	323.3	7.8
DBA-38	9.8	4336.7	1316.7	3.3	181.3	200.3	308.7	16.8	879.0	37.6	182.7	11.7	193.3	5.9
DBA-39	10.2	8363.3	1018.3	6.3	538.0	189.3	774.3	34.3	640.0	68.1	168.3	10.7	1150.0	16.8
DBA-40	6.7	9866.7	1076.7	6.2	638.7	184.7	1450.0	24.9	1013.3	47.7	87.4	6.0	1810.0	25.5
DBA-41	6.6	9596.7	1033.3	6.3	616.7	109.7	1413.3	23.5	951.3	46.2	84.8	5.9	1836.7	25.3
DBA-42	10.5	1913.3	2116.7	7.7	433.0	104.0	502.3	19.2	739.0	45.3	92.3	9.5	103.7	5.1
DBA-43	8.4	974.0	1453.3	5.9	281.3	63.2	402.7	13.7	885.3	38.5	63.7	6.9	54.3	11.9
DBA-44	10.1	949.3	1780.0	7.2	329.3	70.0	408.0	16.3	741.3	38.2	77.1	8.8	52.7	7.4
DBA-45	9.0	932.0	1680.0	7.2	336.0	44.7	391.7	13.3	983.3	39.8	65.6	7.5	46.8	10.9
DBA-46	9.5	798.3	1140.0	9.3	285.3	73.0	467.3	149.0	1153.3	37.7	70.7	7.8	90.7	4.3
DBA-47	9.5	630.3	1060.0	7.4	249.3	48.3	319.7	15.2	1010.0	41.5	69.8	8.1	29.1	10.1

(continued)

Table 4 (continued)

Sample	Sc	V	Cr	Co	Ni	Cu	Zn	As	Sr	Y	Zr	Nb	Mo	Cd
DBA-48	9.1	644.7	1213.3	7.6	291.7	33.5	294.3	26.1	1001.7	39.1	60.7	7.7	24.2	8.5
DBA-49	9.0	596.0	1216.7	9.0	404.0	32.5	326.7	12.9	1073.3	40.6	58.9	7.2	36.9	8.8
DBA-50	10.0	450.3	993.7	9.5	343.0	34.8	329.3	12.5	991.0	41.7	64.8	8.4	28.1	6.5
DBA-51	11.0	356.3	686.7	9.1	281.0	32.8	307.3	18.1	835.7	37.3	68.8	9.4	28.9	6.0
DBA-52	10.6	307.3	549.7	8.6	236.0	30.8	308.3	11.9	831.7	35.3	67.1	9.4	28.4	4.4
DBA-53	10.9	277.7	552.7	10.3	306.0	93.7	334.0	10.8	780.3	35.7	67.0	9.3	29.6	3.6
DBA-54	11.1	245.3	387.7	10.3	224.3	29.0	220.0	8.4	766.3	35.9	65.3	9.0	22.2	2.3
DBA-55	10.5	240.3	404.0	8.0	211.7	40.2	198.7	8.1	939.0	40.3	66.0	8.7	24.8	2.9
DBA-56	10.0	215.0	359.7	9.9	214.0	41.6	189.7	5.6	1003.3	42.6	63.1	8.4	15.7	2.5
DBA-58	10.5	217.0	291.3	7.8	145.3	43.5	149.7	5.4	820.0	39.2	67.4	8.9	12.2	1.4
DBA-59	10.4	219.0	315.3	12.7	204.0	48.1	186.0	12.1	874.3	38.6	64.0	8.8	12.9	2.5
DBA-60	10.4	207.3	259.0	12.6	170.8	49.7	161.5	10.7	814.8	38.1	64.7	8.9	6.6	1.8

gradual recovery (Fig. 6). Pre-CIE, the lower interval of the section covered the latest Paleocene, starting from base of the section up to zone P4c/P5, with almost no changes in both carbonate and organic matter contents. That indicates stability in the oceanic and terrestrial carbon cycle (Fig. 6). This stability in the carbon cycle is reflected as no significant changes in isotopic composition. The PETM gradual warming started below the PEB (about 60 cm and 40 cm below the PEB for $\delta^{13}\text{C}_{\text{carb}}$ and $\delta^{13}\text{C}_{\text{org}}$, respectively).

The observed gradual shifts in the $\delta^{13}\text{C}_{\text{org}}$ and $\delta^{13}\text{C}_{\text{carb}}$ below the PEB may be linked to the gradual temperature increase at the latest Paleocene (Bowen & Zachos, 2010) as a consequence of the volcanisms (North Atlantic volcanic province, Caribbean volcanic activity, and mid-ocean ridge volcanism; Courtillot & Renne, 2003; Storey et al., 2007).

Similar gradual $\delta^{13}\text{C}_{\text{org}}$ and $\delta^{13}\text{C}_{\text{carb}}$ decreases have been documented in Alamedilla, Spain (Lu et al., 1996) and Spitsbergen, Norway; the latter is linked to North Atlantic Igneous Province (Bowen & Zachos, 2010; Khozyem et al., 2015; Sluijs et al., 2008; Speijer & Wagner, 2002; Wicczorek et al., 2013). The observed time lag between CIE onset in $\delta^{13}\text{C}_{\text{org}}$ and $\delta^{13}\text{C}_{\text{carb}}$ is one of the essential criteria for this interval, and it is unique for the Dababiya GSSP. The observed time lag can be explained as a delayed terrestrial environmental response to global warming that started from the bottom ocean by releasing the carbon dioxide stored within the continental shelf deposits (clathrate). Therefore, it led to ocean acidification with massive input of light carbon in both ocean and atmosphere that were observed as negative values of the $\delta^{13}\text{C}_{\text{carb}}$ (Bowen & Zachos, 2010; Renssen et al., 2004). Therefore, first pulse of the PETM warming was determined below the PEB, and it was mainly an oceanic event.

Evidence of the gradual decrease in stable isotope ratios (0–2 m below the PEB) in several sections including Spain

(Alamedilla; Lu et al., 1996), Uzbekistan (Aktumsuk; Bolle et al., 2000), Egypt (Dababiya; Aubry et al., 2007), ODP site 690 (Bains et al., 2000), and in pedogenic carbonate from Polecat Bench, Wyoming (Bowen et al., 2001) and Esplugafreda, Spain (Khozyem et al., 2017) is determined to span time interval of about 120 ky before the PEB (Speijer et al., 2000) in marine and terrestrial sections.

Consequently, the released light CO_2 into the atmosphere is exhaled by terrestrial plants during the photosynthetic activities, then back into the ocean sediments through the weathering process and decayed OM. Both $\delta^{13}\text{C}_{\text{org}}$ and $\delta^{13}\text{C}_{\text{carb}}$ CIE- reached their minimum values through middle part of Bed-2 (top zone E1; Note very negative $\delta^{13}\text{C}_{\text{carb}}$ values; Fig. 6) and were followed by gradual recovery. It is noted that $\delta^{13}\text{C}_{\text{carb}}$ was recovered before the $\delta^{13}\text{C}_{\text{org}}$ that reached the recovery at the base part of zone E2. The $\delta^{13}\text{C}_{\text{org}}$ CIE reaches its minimum within onset of the $\delta^{13}\text{C}_{\text{carb}}$ PETM recovery phase" (early zone E2; Bed-3) and is marked by increase in TOC content in the upper part of Bed-3, as well as a significant Ca-apatite increase. TOC appears to be terrestrial in origin that can explain the delayed response of the continental environment to enormous light carbon input into the atmosphere (Khozyem et al., 2015).

Delay in $\delta^{13}\text{C}_{\text{org}}$ CIE-minimum was observed in several Egyptian PETM sections (Khozyem et al., 2013). This delayed recovery of the $\delta^{13}\text{C}_{\text{org}}$ CIE minimum is may be due to gradual exhalation of the light carbon released from volcanic sources and/or methane oxidation by different processes such as: (i) increased continental silicate weathering under hot-humid climate (Bowen & Zachos, 2010; Kelly et al., 1996, 2005); (ii) photosynthetic fixation of the excess atmospheric CO_2 and formation wetlands (Bains et al., 2000; Dickens et al., 1997; Zeebe et al., 2009); and (iii) increase in primary ocean productivity (Torfstein et al., 2010). Globally, the carbon isotope curves show abrupt negative shifts at the

Table 5 Raw data of the rare earth elements analyzed for Dababiya GSSP

Sample	La	Ce	Pr	Nd	Sm	Eu	Gd	Tb	Dy	Ho	Er	Tm	Yb	Lu
DBA-1	31.37	48.07	6.11	24.33	4.52	1.13	4.56	0.64	4.33	0.89	2.53	0.36	2.46	0.37
DBA-2	33.50	50.47	6.62	25.50	5.18	1.17	5.05	0.71	4.67	0.98	2.86	0.40	2.76	0.43
DBA-3	34.13	51.17	6.69	26.60	5.09	1.14	5.15	0.73	4.89	1.12	3.02	0.43	2.93	0.44
DBA-5	33.67	50.60	6.54	26.07	5.06	1.32	5.10	0.74	5.06	1.03	2.98	0.42	3.00	0.47
DBA-6	34.03	51.60	6.63	26.07	5.18	1.20	5.48	0.76	4.90	1.12	3.08	0.45	2.96	0.46
DBA-7	35.20	53.73	6.89	27.67	5.47	1.28	5.34	0.75	5.05	1.10	3.18	0.47	2.97	0.51
DBA-8	35.70	55.13	6.94	28.13	5.66	1.29	5.63	0.75	5.23	1.10	3.12	0.47	3.10	0.52
DBA-9	36.03	56.97	7.10	28.47	5.64	1.25	5.84	0.77	5.29	1.04	3.13	0.42	3.05	0.49
DBA-10	34.97	54.73	6.96	28.07	5.12	1.25	5.29	0.79	4.88	0.99	3.03	0.47	2.93	0.48
DBA-11	35.90	55.63	7.18	27.57	5.44	1.20	5.49	0.80	5.32	1.04	3.16	0.46	3.00	0.49
DBA-12	35.73	54.03	6.76	27.90	5.40	1.20	5.31	0.72	4.80	1.05	2.98	0.46	3.02	0.48
DBA-13	32.37	49.73	6.37	25.30	4.74	1.13	4.79	0.72	4.59	1.06	2.81	0.41	2.77	0.44
DBA-14	31.07	47.50	6.16	24.73	4.76	1.14	4.43	0.66	4.45	0.93	2.62	0.39	2.70	0.42
DBA-15	31.27	47.03	6.02	23.60	4.49	1.09	4.94	0.68	4.30	0.94	2.67	0.39	2.68	0.42
DBA-16	29.67	44.93	5.69	23.03	4.68	1.06	4.77	0.64	4.17	0.83	2.65	0.37	2.61	0.41
DBA-17	28.03	42.77	5.43	22.00	4.14	0.95	4.26	0.57	3.84	0.79	2.37	0.33	2.39	0.36
DBA-18	26.87	40.63	5.37	20.77	4.33	0.97	4.33	0.57	3.79	0.82	2.38	0.35	2.28	0.34
DBA-19	25.70	38.27	5.01	19.77	3.68	0.89	3.91	0.53	3.87	0.80	2.31	0.33	2.30	0.34
DBA-20	25.50	37.23	4.93	19.50	4.00	0.96	3.86	0.54	3.65	0.74	2.28	0.32	2.06	0.34
DBA-21	24.53	35.67	4.81	19.57	3.88	0.90	3.75	0.52	3.60	0.76	2.26	0.32	2.15	0.34
DBA-22	24.97	36.07	4.86	19.27	3.67	0.85	3.73	0.55	3.68	0.79	2.14	0.32	2.19	0.36
DBA-24	25.57	36.03	4.94	19.33	3.82	0.88	3.90	0.57	3.92	0.80	2.49	0.37	2.38	0.37
DBA-25	25.18	35.91	4.97	19.43	3.74	0.96	4.03	0.58	3.88	0.76	2.34	0.35	2.32	0.40
DBA-26	30.41	41.19	5.81	22.84	4.42	1.13	4.46	0.71	4.81	1.06	3.13	0.45	3.15	0.53
DBA-27	28.32	38.80	5.42	21.75	4.32	1.04	4.58	0.69	4.25	0.97	3.01	0.45	3.14	0.50
DBA-28	40.06	51.57	7.60	31.53	6.43	1.65	7.15	1.09	7.81	1.87	5.42	0.82	5.45	0.88
DBA-29	24.13	28.77	4.89	20.97	4.05	1.07	4.78	0.76	5.63	1.28	3.83	0.56	3.77	0.58
DBA-30	28.93	31.97	5.93	24.27	4.68	1.19	5.35	0.76	5.66	1.16	3.33	0.46	3.25	0.51
DBA-31	28.57	28.97	5.64	24.60	5.42	1.25	6.20	0.94	7.08	1.59	4.87	0.74	5.16	0.83
DBA-32	21.83	25.93	4.58	19.87	3.67	0.77	3.35	0.55	3.61	0.77	2.19	0.35	2.70	0.41
DBA-34	26.30	26.23	4.27	16.40	2.98	0.71	3.33	0.51	3.57	0.75	2.43	0.36	2.58	0.42
DBA-35	21.50	22.30	3.50	13.90	2.79	0.63	3.39	0.54	4.20	0.93	2.92	0.45	3.02	0.44
DBA-36	13.40	19.37	2.94	12.00	2.81	0.69	3.61	0.58	4.38	1.10	3.42	0.52	3.67	0.54
DBA-37	22.00	26.87	4.64	19.40	3.43	0.85	3.81	0.61	4.45	1.02	3.19	0.50	3.45	0.52
DBA-38	24.83	29.17	4.80	18.53	3.78	0.83	4.25	0.61	4.10	0.96	2.90	0.41	2.96	0.44
DBA-39	33.53	34.03	6.04	24.07	4.98	1.14	6.16	0.94	6.87	1.65	4.93	0.73	5.05	0.78
DBA-40	24.70	23.17	4.63	18.90	3.76	0.96	4.75	0.71	4.98	1.16	3.52	0.51	3.23	0.54
DBA-41	24.30	22.87	4.42	18.67	3.83	0.94	4.61	0.67	4.78	1.10	3.27	0.49	3.24	0.51
DBA-42	28.90	35.73	5.45	21.90	4.31	0.97	4.86	0.67	5.01	1.12	3.45	0.50	3.65	0.59
DBA-43	25.23	30.37	4.64	18.60	3.61	0.89	4.02	0.58	4.16	0.93	2.95	0.43	2.93	0.48
DBA-44	26.67	33.57	5.07	20.20	3.90	0.97	4.52	0.65	4.38	1.02	3.04	0.45	3.10	0.50
DBA-45	26.83	32.80	4.86	19.93	3.87	0.94	4.08	0.62	4.53	0.99	2.94	0.45	3.05	0.49
DBA-46	26.50	32.87	4.87	19.73	3.93	0.98	4.27	0.63	4.31	0.99	3.01	0.43	2.98	0.49
DBA-47	28.67	35.40	5.43	22.10	4.13	1.10	4.74	0.70	4.86	1.09	3.25	0.46	3.23	0.52

(continued)

Table 5 (continued)

Sample	La	Ce	Pr	Nd	Sm	Eu	Gd	Tb	Dy	Ho	Er	Tm	Yb	Lu
DBA-48	27.90	33.77	5.12	19.87	4.22	1.08	4.43	0.65	4.37	0.98	2.99	0.43	3.05	0.46
DBA-49	27.90	33.67	5.15	20.70	4.01	1.08	4.44	0.65	4.64	1.03	3.06	0.46	3.28	0.47
DBA-50	30.33	37.93	5.67	22.23	4.60	1.10	4.75	0.66	4.92	1.08	3.32	0.45	3.16	0.51
DBA-51	28.67	37.93	5.59	22.90	4.50	1.17	4.61	0.70	4.67	0.98	2.93	0.44	3.00	0.45
DBA-52	27.60	36.83	5.30	21.67	4.32	1.02	4.45	0.64	4.36	0.93	2.85	0.42	2.81	0.44
DBA-53	28.03	37.97	5.66	22.50	4.68	1.07	4.46	0.62	4.44	0.95	2.81	0.42	2.81	0.46
DBA-54	28.37	36.63	5.29	21.20	4.24	1.01	4.69	0.67	4.28	0.99	2.89	0.43	2.87	0.44
DBA-55	30.23	38.20	5.68	23.63	4.77	1.08	4.91	0.71	4.65	1.05	3.14	0.47	3.10	0.46
DBA-56	30.67	38.17	5.69	23.70	4.63	1.11	5.24	0.73	5.18	1.12	3.30	0.48	3.02	0.49
DBA-58	29.47	36.60	5.39	22.10	4.64	1.05	4.90	0.69	4.59	1.08	3.06	0.45	2.91	0.50
DBA-59	29.13	37.57	5.54	21.97	4.43	1.10	4.79	0.64	4.62	0.98	2.98	0.45	3.01	0.50
DBA-60	28.75	36.77	5.39	21.20	4.36	1.08	4.79	0.63	4.60	1.00	2.94	0.44	2.92	0.52

PEB. The abrupt changes in the carbon isotope shift may indicate the presence of hiatus at the PETM onset as observed worldwide, for examples in Egypt (Gebel Duwi and Gebel Aweina; Speijer et al., 2000; Wadi Nukhul, Khozyem et al., 2013), Italy (Forada section; Agnini et al., 2007), Spain (Zumaya section; Schmitz et al., 1998), Uzbekistan (Aktash section; Khozyem et al., *in prep.*; Trabakua section; Bolle et al., 2000), DSDP Sites 401 and ODP Sites 690, 685, 689, 865, 1051, 1263, 1260B, and 1172D (Katz et al., 2003; Mutterlose et al., 2007; Sluijs et al., 2008).

4.2 Weathering Inferred from Mineralogical Composition

The weathering process has a vital role in drawing down atmospheric CO₂ during PETM events. The nature of the weathering process during the PETM event can be studied through a few sections that have the complete PETM sedimentary record (i.e., Dababyia, Egypt; Alamandilla, Spain). In addition, mineralogy and geochemical data can provide us with valuable information on weathering by using specific proxies.

Mineralogically, phyllosilicates are the most abundant minerals in Dababiya GSSP. Below the PEB, the detrital component (Phyllosilicate + total feldspar + Quartz) shows marl composition where its values are around 50%; an abrupt increase in the detrital component is observed above the PEB and extended along the lower part of the CIE (from the BEP to the middle of Bed 2). The increase in detrital input was observed as well as within the detrital index (Table 1; $DI = (\text{Phyllosilicate} + \text{total feldspar} + \text{Quartz}) / \text{Calcite}$; (Bolle et al., 2000; Khozyem et al., 2013). The detrital flux then decreases to the typical background observed below the PEB up to the top of Dababiya GSSP.

The DI shows that the detrital input was derived from the depositional setting in several rapid pulses (Fig. 10) that may correspond to several minor regression/transgression events during the early phase of the PETM events. During these minor events, the sediment derived from the ocean was moderate to highly mature, based on the maturity index ($MI = \text{phyllosilicates} / (\text{phyllosilicates} + \text{quartz} + \text{feldspars})$). MI determines the degree of recycling from a sedimentary/metasedimentary source (Bhatia, 1985). Through PETM-CIE, mineralogical maturity shows two specific intervals; the first, where there is high detrital input, the maturity index is increased, which can be explained by the increased detrital input and recycled upper Paleocene sediment (Table 1; Fig. 11). The second is moderate MI (from top of Bed-1 to middle Bed-2), which can be explained as deriving from fresh weathered materials during the transgression phase. Note that the absence of calcite may be linked to low pH conditions during the early stage of the PETM, but the increased detrital input can be counted as another reason for this dilution.

The first explanation is more reasonable and amplifies the signal from the detrital input. The phyllosilicate assemblage at Dababiya GSSP comprises smectite, kaolinite, illite, illite-smectite, chlorite, and palygorskite. The clay mineral ratios of (Kaolinite/smectite, Kaolinite/illite + chlorite; Table 2; Fig. 10) can improve our knowledge on weathering processes. The relatively high kaolinite/smectite can be explained as an increase in humid conditions. At the same time, the high kaolinite/illite + chlorite reflects the chemical weathering. In the Dababiya GSSP, three notable intervals with high Kaolinite/smectite ratios are observed. Lower one is recorded at basal part within zone P4c, the others are coincident to PEB and the middle of Bed-2 and coincident to with high kaolinite/smectite ratio (Fig. 10) and higher kaolinite, chlorite, illite-smectite, and palygorskite contents

Table 6 Calculations of elemental ratios used as different proxies

Sample	CIA	CIW	ICV	C-value	Sr/cu	Ga/Rb	Eu/Eu*	Mn*	Ce/Ce*	V/Cr	V/(V + Ni)	Porg	Ba(Ef)
DBA-1	69.38	21.89	2.65	0.17	33.01	3.04	1.28	- 0.54	0.80	0.29	0.31	0.31	0.17
DBA-2	69.93	21.56	2.63	0.15	31.21	2.37	1.17	- 0.49	0.78	0.57	0.55	0.39	0.16
DBA-3	68.67	21.40	2.64	0.14	26.47	2.79	1.14	- 0.45	0.78	0.35	0.35	0.41	0.19
DBA-4	68.45	21.18	2.67	0.14	32.40	2.50	1.23	- 0.41	0.78	0.33	0.34	0.44	0.19
DBA-5	68.22	20.95	2.70	0.14	38.33	2.21	1.31	- 0.36	0.78	0.32	0.33	0.47	0.19
DBA-6	68.88	23.51	2.43	0.16	27.38	1.48	1.17	- 0.47	0.79	0.36	0.35	0.44	0.18
DBA-7	68.29	24.09	2.42	0.17	23.23	1.18	1.21	- 0.41	0.79	0.41	0.37	0.49	0.19
DBA-8	68.70	26.01	2.25	0.18	27.57	1.17	1.19	- 0.51	0.80	0.41	0.36	0.48	0.18
DBA-9	68.61	27.76	2.12	0.19	24.86	1.01	1.15	- 0.50	0.82	0.41	0.36	0.46	0.20
DBA-10	68.70	27.79	2.14	0.21	26.98	1.09	1.22	- 0.53	0.81	0.29	0.27	0.43	0.21
DBA-11	68.85	27.21	2.17	0.20	24.61	1.11	1.11	- 0.53	0.80	0.32	0.31	0.44	0.18
DBA-12	68.04	26.95	2.22	0.20	29.42	1.09	1.16	- 0.53	0.80	0.28	0.27	0.44	0.20
DBA-13	69.23	24.63	2.38	0.18	22.94	1.15	1.19	- 0.50	0.80	0.21	0.35	0.41	0.18
DBA-14	67.63	22.80	2.61	0.19	28.40	1.49	1.23	- 0.45	0.79	0.32	0.32	0.38	0.20
DBA-15	68.63	21.26	2.74	0.16	26.67	1.44	1.22	- 0.41	0.79	0.35	0.34	0.38	0.19
DBA-16	68.11	19.18	2.97	0.13	34.30	2.15	1.17	- 0.44	0.79	0.39	0.35	0.36	0.23
DBA-17	68.00	18.86	3.02	0.13	25.65	1.66	1.19	- 0.43	0.80	0.35	0.29	0.33	0.22
DBA-18	68.25	17.03	3.31	0.12	41.79	2.63	1.17	- 0.31	0.78	0.40	0.31	0.33	0.26
DBA-19	67.81	15.46	3.67	0.12	42.90	3.65	1.23	- 0.33	0.78	0.28	0.32	0.31	0.19
DBA-20	68.48	14.00	3.99	0.10	43.20	10.41	1.25	- 0.29	0.76	0.60	0.32	0.33	0.17
DBA-21	67.96	13.39	4.20	0.10	26.79	5.80	1.20	- 0.28	0.75	0.70	0.38	0.35	0.19
DBA-22	68.88	13.10	4.26	0.09	45.05	5.56	1.16	- 0.25	0.75	1.40	0.56	0.37	0.19
DBA-23	69.01	13.06	4.27	0.09	56.02	4.40	1.16	- 0.28	0.74	1.33	0.56	0.41	0.21
DBA-24	69.15	13.02	4.27	0.08	66.98	3.25	1.15	- 0.31	0.74	1.25	0.55	0.44	0.22
DBA-25	69.06	13.61	4.08	0.09	56.83	9.01	1.27	- 0.34	0.74	0.77	0.52	0.49	0.18
DBA-26	66.58	17.51	3.24	0.11	150.77	2.31	1.25	- 0.49	0.71	1.14	0.61	0.71	0.22
DBA-27	68.65	15.60	3.57	0.10	94.37	5.11	1.18	- 0.47	0.72	0.94	0.54	0.65	0.21
DBA-28	55.53	52.49	1.49	0.29	49.55	0.51	1.24	- 1.12	0.68	1.17	0.64	1.15	0.27
DBA-29	67.59	76.93	0.94	0.56	13.26	0.92	1.23	- 1.21	0.61	1.57	0.58	0.68	0.18
DBA-30	65.75	86.33	0.97	0.64	6.87	0.74	1.24	- 1.16	0.56	2.21	0.82	0.19	0.21
DBA-31	64.56	83.54	1.09	0.72	10.91	0.79	1.11	- 1.26	0.52	4.67	0.89	0.44	0.26
DBA-32	65.19	89.86	0.85	0.44	1.19	0.75	1.05	- 1.34	0.60	5.72	0.91	0.00	0.23
DBA-33	64.77	86.51	0.88	0.42	1.42	0.73	1.10	- 1.30	0.58	6.78	0.92	0.00	0.20
DBA-34	64.35	83.16	0.90	0.41	1.65	0.71	1.15	- 1.26	0.56	7.85	0.93	0.00	0.17
DBA-35	64.83	92.55	0.88	0.53	1.97	0.89	1.04	- 1.37	0.58	7.62	0.91	0.02	0.18
DBA-36	63.00	85.42	0.96	0.53	1.94	0.59	1.11	- 1.04	0.71	7.33	0.91	0.07	0.21
DBA-37	62.25	77.12	1.21	0.69	2.75	0.43	1.18	- 1.18	0.61	2.85	0.92	0.32	0.28
DBA-38	58.79	49.55	1.53	0.37	4.39	0.32	1.08	- 1.03	0.61	3.29	0.96	0.27	0.35
DBA-39	57.31	45.62	1.75	0.44	3.38	0.30	1.06	- 1.13	0.55	8.21	0.94	1.13	0.42
DBA-40	58.87	11.81	5.48	0.27	5.49	0.52	1.18	- 1.26	0.50	9.16	0.94	1.14	0.28
DBA-41	57.38	11.89	5.45	0.26	8.67	0.54	1.17	- 1.25	0.51	9.29	0.94	1.08	0.27
DBA-42	58.52	23.07	3.09	0.32	7.11	0.37	1.11	- 0.99	0.65	0.90	0.82	7.53	0.43
DBA-43	61.49	11.38	5.21	0.15	14.00	0.52	1.21	- 1.13	0.64	0.67	0.78	7.30	0.24
DBA-44	62.46	17.03	3.59	0.19	10.59	0.47	1.20	- 1.14	0.66	0.53	0.74	6.47	0.27

(continued)

Table 6 (continued)

Sample	CIA	CIW	ICV	C-value	Sr/cu	Ga/Rb	Eu/Eu*	Mn*	Ce/Ce*	V/Cr	V/(V + Ni)	Porg	Ba(Ef)
DBA-45	66.33	12.99	4.52	0.16	21.98	0.78	1.20	- 0.83	0.66	0.55	0.74	7.11	0.27
DBA-46	61.71	13.10	5.08	0.29	15.81	0.46	1.22	- 1.08	0.66	0.70	0.74	6.08	0.35
DBA-47	61.90	12.29	4.63	0.11	20.90	0.73	1.28	- 0.69	0.65	0.59	0.72	6.94	0.30
DBA-48	64.79	11.55	4.79	0.10	29.93	1.26	1.27	- 0.65	0.65	0.53	0.69	6.63	0.28
DBA-49	64.92	11.16	5.02	0.11	33.06	1.09	1.31	- 0.69	0.64	0.49	0.60	7.86	0.31
DBA-50	66.25	13.59	4.15	0.12	28.45	1.42	1.21	- 0.73	0.66	0.45	0.57	5.74	0.31
DBA-51	67.31	15.16	3.73	0.13	25.45	1.90	1.28	- 0.75	0.69	0.52	0.56	3.06	0.24
DBA-52	68.75	15.18	3.68	0.12	27.03	2.38	1.19	- 0.74	0.70	0.56	0.57	2.44	0.24
DBA-53	69.19	15.47	3.62	0.13	8.33	2.77	1.20	- 0.58	0.69	0.50	0.48	1.73	0.23
DBA-54	69.84	14.00	3.92	0.11	26.46	5.14	1.18	- 0.55	0.69	0.63	0.52	1.06	0.18
DBA-55	72.48	12.22	4.39	0.09	23.34	4.04	1.14	- 0.50	0.67	0.59	0.53	1.27	0.20
DBA-56	74.33	11.15	4.76	0.08	24.14	4.60	1.18	- 0.48	0.66	0.60	0.50	1.52	0.22
DBA-57	75.68	11.65	4.56	0.08	21.50	4.33	1.16	- 0.49	0.66	0.67	0.55	1.07	0.21
DBA-58	77.03	12.15	4.35	0.09	18.87	4.06	1.14	- 0.50	0.67	0.74	0.60	0.63	0.19
DBA-59	76.60	11.47	4.62	0.09	18.18	5.13	1.26	- 0.50	0.68	0.69	0.52	0.70	0.18
DBA-60	76.60	11.47	4.62	0.09	16.39	5.15	1.26	- 0.50	0.68	0.80	0.55	0.70	0.17

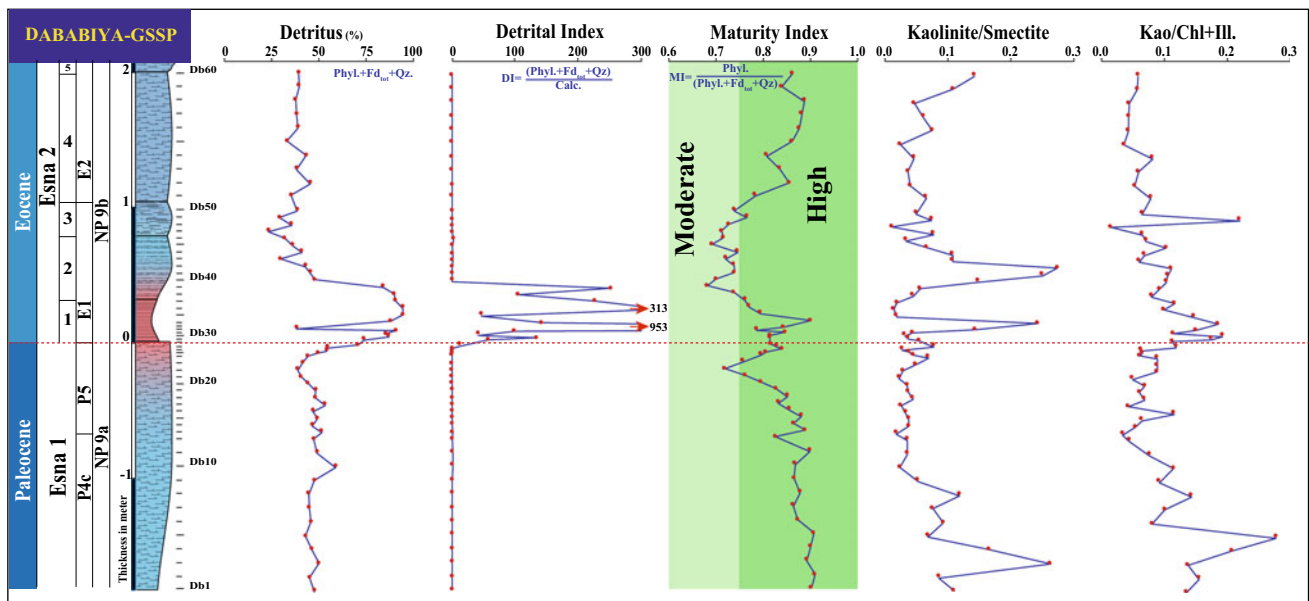


Fig. 10 Represents different mineralogical proxies and ratios (detrital input and mineralogical maturity as well as the humid vs. arid conditions) that can be used to predict the nature of the weathering interval during the PETM

(Fig. 8). This indicates low to medium detrital input under semi-arid conditions at the basal part of the PETM interval and increased detrital input during the upper part as evident by increased quartz contents (Fig. 8), that may due to the increased runoff (Bolle et al., 2000; Khozyem et al., 2013, 2015; Schulte et al., 2011).

4.3 Weathering and Paleoclimatic Conditions Inferred from Geochemistry

The geochemical weathering proxies indicate an increase in continental weathering that led to massive input of Si, Ti, and Zr, and the presence of negative Eu/Eu* anomalies at the

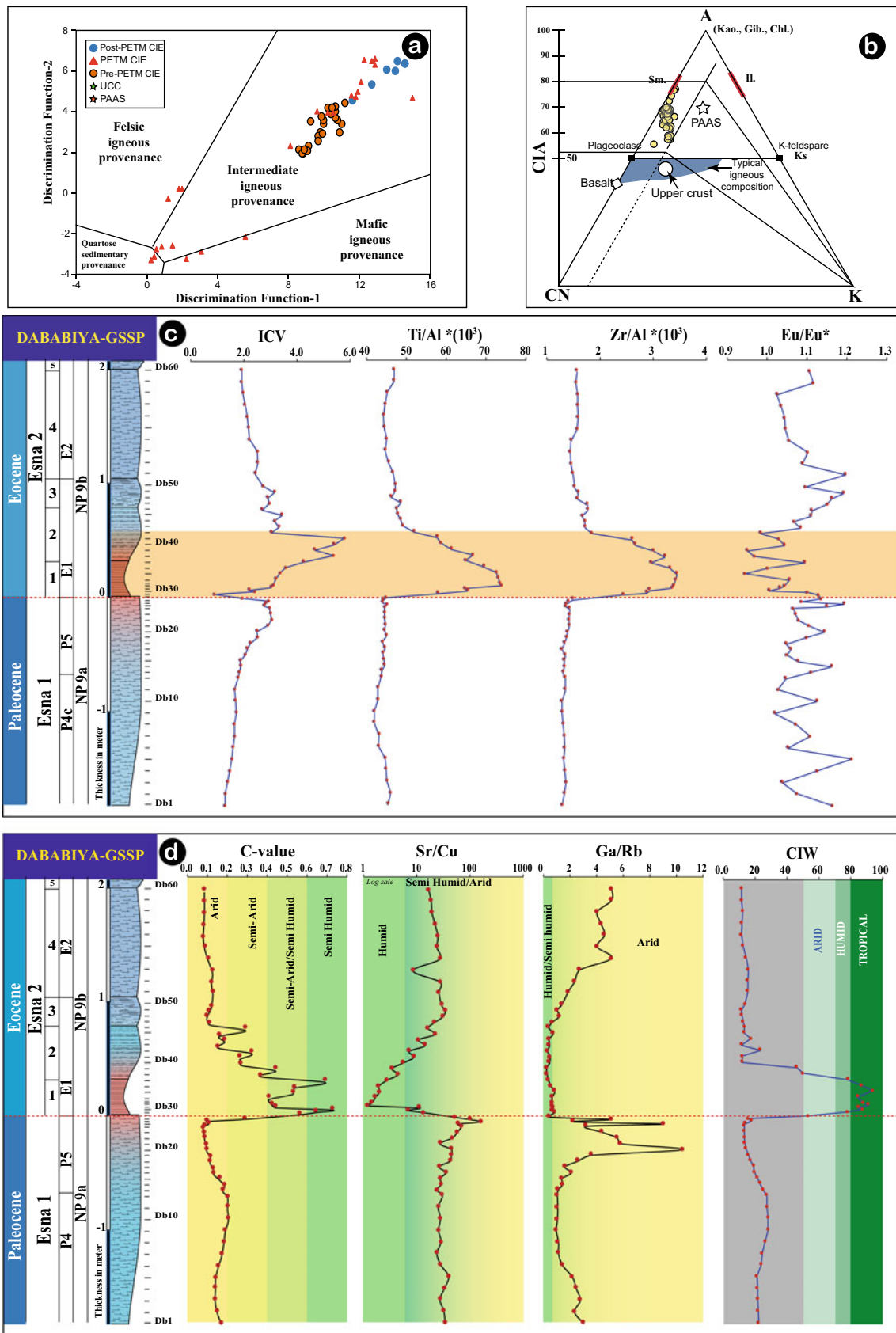


Fig. 11 a Discrimination function diagram (after Roser & Korsch, 1988); b A-CN-K ternary diagram together with CIA values, c different geochemical proxies indicative of the weathering, d sedimentary maturity, and weathering nature based on Eu-anomaly and Chemical index of weathering (CIW). Note that the increase in Ti, Zr, and weathering indexes are associated with a negative Eu/Eu* ratio

CIE interval that coincident with high detrital input level (Fig. 11).

Using the formula of major elements for sedimentary provenance discriminant diagrams proposed by Roser and Korsch (1988) can help to discriminate between the different sources of the sediments

$$\begin{aligned} \text{Discriminant Function 1} &= 0.607\text{Al}_2\text{O}_3 - 1.773\text{TiO}_2 \\ &\quad + 0.760\text{Fe}_2\text{O}_3 - 1.500\text{MgO} + 0.616\text{CaO} \\ &\quad + 0.509\text{Na}_2\text{O} - 1.224\text{K}_2\text{O} - 9.090 \\ \text{Discriminant Function 2} &= 0.445\text{TiO}_2 + 0.070\text{Al}_2\text{O}_3 \\ &\quad - 0.250\text{Fe}_2\text{O}_3 - 1.142\text{MgO} + 0.438\text{CaO} \\ &\quad + 1.475\text{Na}_2\text{O} - 1.426\text{K}_2\text{O} - 6.861. \end{aligned}$$

The cross-plots indicate that the multi-compositional silicate source has been subjected to intensive weathering processes during the PETM, and their weathered products form thick weathering interval at the Dababiya GSSP (Fig. 11a). Several other weathering indexes can be valuable to determine the nature of weathering during the PETM event, among them chemical index of alteration (CIA) and chemical index of weathering (CIW).

CIA of Nesbitt and Young (1982) is based on the relationship between alumina and alkalis following the formula $\text{Al}_2\text{O}_3/(\text{Al}_2\text{O}_3 + \text{CaO}^* + \text{Na}_2\text{O} + \text{K}_2\text{O}) * 100$; CIA values are used to assess chemical weathering degree of provenance. In combination with $\text{Al}_2\text{O}_3-(\text{CaO} + \text{Na}_2\text{O})-\text{K}_2\text{O}$ ternary plot, they are helpful geochemical parameters for studying the provenance and maturity of sedimentary rocks. CaO^* represents CaO in silicate-bearing minerals only, and the CaO from non-silicate minerals (carbonate and phosphate) is excluded using the methodology proposed by McLennan (1989). The content of $\text{CaO}_{\text{rest}} = \text{CaO} - (10/3) * \text{P}_2\text{O}_5$; if $\text{CaO}_{\text{rest}} < \text{Na}_2\text{O}$ then the content of $\text{CaO}^* = \text{CaO}_{\text{rest}}$, otherwise, $\text{CaO}^* = \text{Na}_2\text{O}$.

The CIA values of the CIE interval in Dababiya GSSP (Table 6) range from 55 to 80. This result matches the maturity index results and supports that the sediments in the PETM interval are moderate to high mature. The A-CN-K shows that the mineralogical composition of the PETM in Dababiya GSSP is a mix between fresh weathered materials and highly mature sediments (Figs. 10 and 11b, c). CIW also provides information on the intensity of chemical weathering. Compared to other weathering indices, CIW is a superior method involving a restricted number of well-known components for consistent geochemical behavior during weathering.

CIW formula as expressed by Harnois (1988) is equal $\text{Al}_2\text{O}_3/(\text{Al}_2\text{O}_3 + \text{CaO}^* + \text{Na}_2\text{O}) * 100$ (Table 6). CIW shows abrupt changes between the sequence boundary interval to the middle part of Bed-2 (Fig. 11c). These abrupt changes observed in CIW indicate that the high detrital input in the Dababiya GSSP is linked to intense chemical

weathering under hot, humid conditions, and can reach tropical weathering.

The concentration of some major and trace oxides can infer paleoenvironmental conditions (Cao et al., 2018a; Roy & Roser, 2013; Wang et al., 2017). Fe, V, Cr, Mn, and Ni can be concentrated under humid climatic conditions (Fu et al., 2016). However, the concentrations of Ca, Na, Mg, K, Ba, and Sr prevailed under arid climatic condition and increased alkalinity of water during evaporation processes. Based on the behavior of the previously mentioned two groups; C-values ratios are calculated as $\sum (\text{Fe} + \text{Mn} + \text{Cr} + \text{Ni} + \text{V} + \text{Co}) / \sum (\text{Ca} + \text{Mg} + \text{Sr} + \text{Ba} + \text{K} + \text{Na})$. C-value is considered as paleoclimate proxy (Cao et al., 2018a, 2018b; Feng et al., 2014; Fu et al., 2016; Hu et al., 2016).

The calculated C-values (Table 6; Fig. 11d) are categorized as 0–0.2 (arid), 0.2–0.4 (semi-arid), 0.4–0.6 (semi-arid to semi-humid), 0.6–0.8 (semi-humid), and 0.8–1.0 (humid). The C-value is associated with other ratios of trace elements to categorize paleoclimate, such as Ga, which is generally associated with kaolinite and indicates warm and humid conditions. In contrast, Rb is associated with illite and inferring cold-arid conditions.

Generally, sedimentary rocks with low Sr/Cu and high Ga/Rb ratios are deposited in warm and humid climatic conditions (Black et al., 2017). However, values of more than 5.0 represent hot-arid climatic conditions (Roy & Roser, 2013; Yandoka et al., 2015).

In Dababiya PETM-CIE interval (Fig. 11), the basal part of the CIE (above the PEB to the middle Bed 2). The C-value is increased to the range between 0.4 and 0.8, referring to the semi-humid to humid climatic conditions through Bed-1 and gradually decreased up to Bed-3; both Sr/Cu and Ga/Rb ratios are decreased at the same level indicating the prevailed humid conditions. In Dababiya GSSP PETM-CIE, lower part is linked to intense humid climatic conditions linked to the considerable input of CO_2 during the early stage of the PETM. The climate changes in the recovery direction with a gradual drawdown of CO_2 in the later stage of the PETM (Fig. 11d).

Therefore, all the proxies proved that the general chemical weathering of silicate rocks under hot, humid conditions and that the weathering products derived from the sedimentary basins in several pulses may be linked to the fluvial discharge (Schulte et al., 2011) and or through the several regression/transgression minor events. The gradual recovery trend may be linked to the gradual drawdown of CO_2 .

4.4 Redox Condition and Paleoproductivity During the PETM

The paleoredox conditions can be explained as determining whether conditions were oxidizing or reducing during the

deposition processes, and they can be categorized as oxic–suboxic–anoxic (Tyson & Pearson, 1991). The changes in the redox conditions of bottom water conditions can be emphasized by particular trace, rare earth elements, and their ratios (e.g., V/Sc, V/Cr, Ni/Co, U/Th, V/V + Ni, etc.) as well as the changes in chalcophile Al-normalized elements (e.g., Fe, Mn, U, V, Zn, Pb, Cu, Ni; Algeo & Maynard, 2004; Cruse & Lyons, 2004; Joachimski et al., 2001; Pujol et al., 2006; Rimmer, 2004; Tribovillard et al., 2006). Other proper proxies are Mn* (Cullers, 2002) and Ce-anomaly (Ce/Ce*). Mn* is best expression of Mn concentration linked to redox conditions and can be calculated from as: $Mn^* = \log [(Mn_{\text{sample}}/Mn_{\text{PAAS}})/Fe_{\text{sample}}/Fe_{\text{PAAS}}]$, where Mn²⁺ replaces Ca in Ca-rich sediments during the diagenetic processes and producing the Mn-bearing carbonate. Ce-anomaly is another strong indicator for water column oxygenation. Ce is present in seawater in tiny amounts because Ce can be easily oxidized to its insoluble state (4+) (Holser, 1997; Shields & Stille, 2001). However, the Ce⁴⁺ tends to be depleted under

prevailing anoxic conditions. Ce and Mn behave similarly under both oxic and anoxic water columns.

The Ce/Ce*, Ni/Co, and V/Cr ratios are more sensitive to the changes in the oxygen level in water column. In contrast, the ratios of Mn* and V/V + Ni can explain the general trend of the ocean water oxygenation level.

In Dababiya GSSP, Ce/Ce* shows an abrupt decrease in the PEB (from the mean of 0.9–0.5). This decrease in Ce/Ce* is represented in two specific intervals, the first at base of Bed-1 (zone E1; Table 6; Fig. 12), and the second is at the middle part of Bed-2, and is coincident to the maximum TOC content (Fig. 6). The observed negative Ce intervals were associated with sharp spikes in V/Cr, Ni/Co and V/V + Ni ratios reaching to their maximum values and represent stable anoxic conditions during the beginning of the PETM event. At the same interval, Mn* shows its maximum negative shift. The presence of negative Mn* shift indicates dysoxic bottom water conditions (Bruland, 1983; Landing & Bruland, 1980, 1987).

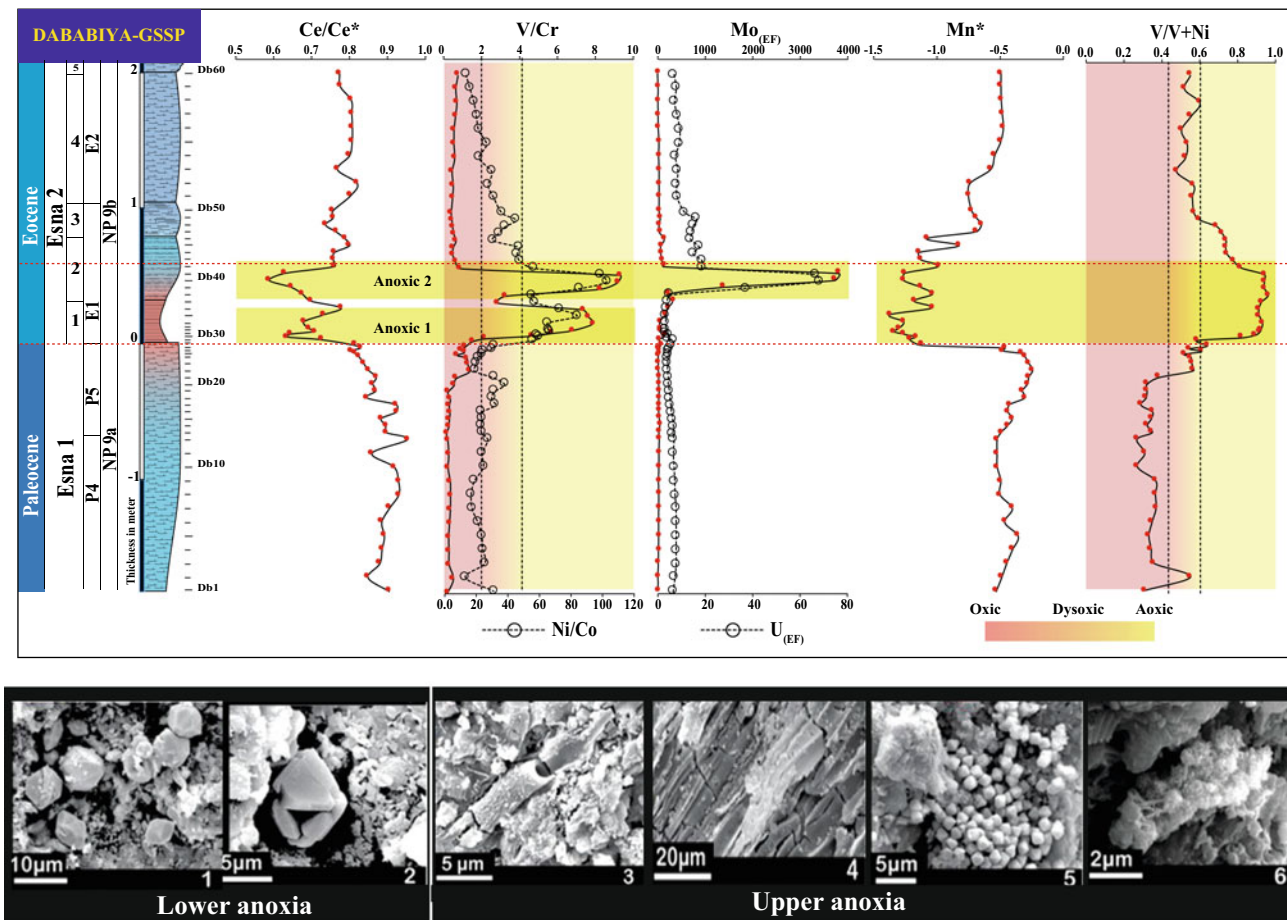


Fig. 12 Represents the different redox condition proxies. Note the presence of a double peak in Ce-anomaly, V/Cr, and Ni/Co that indicates the presence of two anoxic levels. The abrupt increase in the enrichment factors of both Mo and U coincident with the upper anoxic level. The negative shift in Mn* at the same level as the high V/V + Ni ratio starts from the PEB and extends up to the middle of zone E1. The SEM photographs show: 1, 2 the presence of pyrite crystals associated with the lower anoxic interval, 3, 4 different organic matter forms associated with the upper anoxic level, and 5, 6 show the fine-grained framboidal pyrite associated with the upper anoxic level

Anoxic conditions during PETM may be due to oceanic acidification with anhydrite formation. The relation between sulfate reduction and methane hydrate release is well constrained (Khozyem et al., 2015; Whiticar, 1999), when methane released it produces free SO^{+4} . Sulfate can be easily reduced to HS^- under acidic-anaerobic conditions and form pyrite (Fig. 12) in anoxic water column at the anaerobic/aerobic interface (Campbell et al., 1992; Jenkyns, 2010; Whiticar, 1999). Based on these processes; Khozyem et al. (2015) explained the presence of two anoxic intervals as the following: the lower anoxic interval is characterized by an increase in detrital input, pyrite deposition, presence of anhydrite, negative Ce-anomaly, and abrupt increase in V/Cr ratio (Table 6).

The upper anoxic interval is associated with high TOC content, Ce-anomaly, and abrupt increases in V/Cr ratio. In association with high kaolinite content and the presence of framboidal pyrite. In this upper anoxic interval, a considerable concentration of both Mo and U is observed. Both Mo and V are present in seawater in the form of sulfides and oxyhydroxides that can precipitate directly in the water-sediment interface resulting in their enrichments. The weak-to-moderate correlation between the TOC and enrichment factor of both Mo (Mo_{EF}) and U (U_{EF}) ($R^2 = 0.4$ and 0.7 , respectively; Fig. 13) within the PETM-CIE indicates that hygienic phases and high TOC content. These enrichments in Mo and U indicate that strong anoxic conditions prevailed during the beginning of the PETM Recovery Phase.

Therefore, the development of bottom anoxia during the PETM may be linked to: (1) poorly oxygenated water invasion into epicontinental circulation that enhanced upwelling cycle with a massive input of nutrients and increased primary productivity (Speijer & Wagner, 2002), (2) water column stratifications and increased eutrophic conditions (Ghandour, 2020; Khozyem et al., 2015; Schulte et al., 2011) and (3) increased CO_2 dissolved in the ocean

due to the methane hydrate release and results in ocean acidification (Khozyem et al., 2015). In addition, water stratification led to increased surface water productivity and deposition of organic matter, and increased bacterial activities that led to the consumption of bottom oxygen. (Khozyem et al., 2015; Schulte et al., 2011).

Low TOC content is generally related to primary photosynthetic, paleoproductivity, and rate of organic matter deposition. A high TOC concentration zone is associated with enrichment of Cu, Pb, Zn, Ni, Cd, Mo, and V. The metal elements are adsorbed within the OM in the water column electrostatically or via oxygen-containing functional groups of organic matter and fixed into the sediments. Consequently, OM degradation liberates the adsorbed metals and participates in sulfide and vanadium-bearing minerals. TOC contents combined with other specific TE can be used as geochemical proxies to reconstruct the paleoproductivity; among them, organic phosphorus (P_{org}) is the most widely used (Algeo & Ingall, 2007; Brumsack, 2006; Dehairs et al., 1980; Dymond et al., 1992; Ghandour, 2020; Schoepfer et al., 2015).

Under the favoring conditions, the preservation of both P_{org} helps to detect the paleoproductivity conditions during the PETM event (Algeo et al., 2011; Schoepfer et al., 2015). As a result, organic phosphorus fluxes (P_{org}) are estimated as following the formula:

$$P_{\text{org}} = P_{\text{tot}} - P_{\text{terr}} \quad (1)$$

where P_{terr} is the terrigenous part of P that is derived from the sediment with the detrital input and can be calculated as follow:

$$P_{\text{terr}} = \text{Al} \times (P/\text{Al})_{\text{det}} \quad (2)$$

$(P/\text{Al})_{\text{det}}$ ratio is 0.009 based on the upper continental crust's average P and Al concentration (McLennan, 2001).

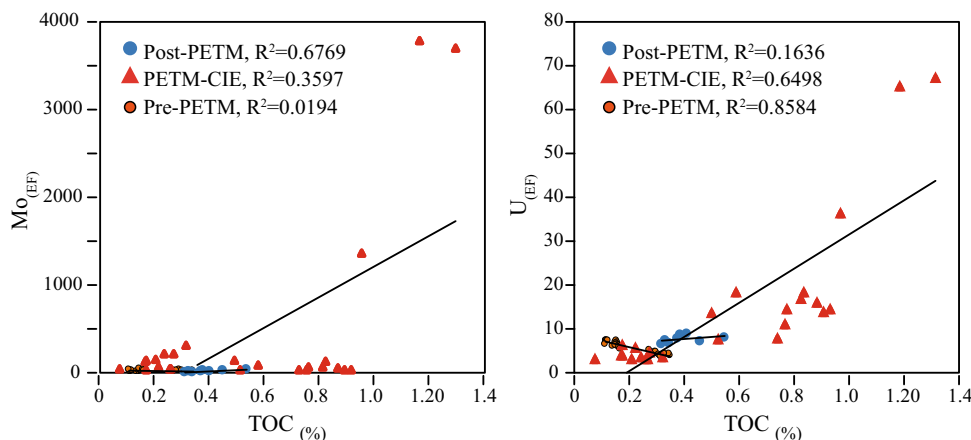


Fig. 13 Cross plots of both Mo and U enrichment factors relative to PAAS against the TOC in percent

From Eqs. (1) and (2).

$$P_{\text{org}} = P_{\text{tot}} - (Al \times (P/Al)_{\text{det}}) \quad (3)$$

Equation (3) is used to assess the amount of the organic P that precipitated during the PETM recovery phase (Fig. 14); P_{org} is enriched in the interval from the top of the second anoxic level that is coincident with the high TOC content, (middle Zone E1 to the base of zone E2). Phosphorus is commonly precipitated from water column into the sediments by assimilation into OM or by forming metal oxyhydroxide complexes (Stein et al., 2011).

Under anoxic conditions, P is remobilized from older sediments and diffused in the above water column (Ingall et al., 2005; Kraal, 2011). Therefore, through the anoxic intervals of PETM in Dababiya GSSP P_{org} shows its minimum concentrations due to the diffusion under anoxic conditions (Fig. 14).

However, it is noted that P_{org} contents start to increase with the upper anoxic level with high pyrite contents and may result from the prevailing upwelling zone in the presence of sulfide oxidizing bacteria. Therefore, the P cannot be removed from the porewater, which leads to concentrating the phosphorus under anoxic conditions (Goldhammer et al., 2010), as noted in the Dababiya GSSP.

In the oxic and/or dysoxic environment (Below the PEB and in the interval middle Zone E1) authigenic phosphate precipitated through adsorption and complexation processes (Kraal, 2011; Schoepfer et al., 2015; Tribouillard et al., 2006). This explanation is due to the low correlation between P_{org} and TOC ($R^2 = 0.3054$; Fig. 14). Also, the low correlation between P_{org} and TOC may be linked to the organic matter types associated with the level enriched in P_{org} (Terrestrial OM). On the other hand, in the interval above PETM-CIE, P_{org} values correlate with the TOC, which may be due to the activation of marine biological activities. This process led to the deposition of P_{org} in the form of polyphosphates, proving the oceans' return to normal productivity conditions after the termination of the PETM event.

4.5 Volcanism Associated with PETM Event

During late Paleocene, two major volcanic events took place and overlapped with the PETM ($\sim 56 \pm 0.2$ Ma; Fig. 1; Westerhold et al., 2009; Wicczorek et al., 2013): (1) the North Atlantic Igneous Province (NAIP), and (2) Central American circum-Caribbean volcanism (Fig. 1). The NAIP

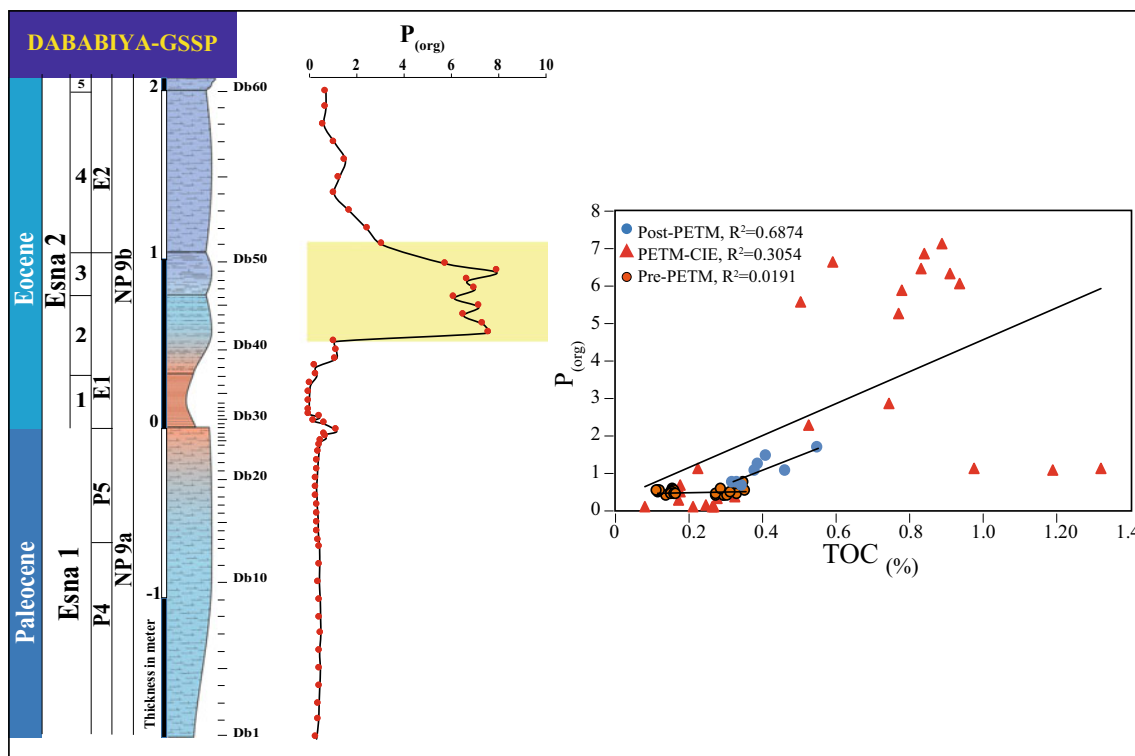


Fig. 14 Plot of the calculated P_{org} against the Dababiya GSSP illustration showing the huge input of the P_{org} associated with the upper part of the PETM-CIE, and cross plot between P_{org} and TOC showing the weak-to-moderate correlation between the two

results from opening the northern part of the North Atlantic ocean at ~ 61 Ma reaching its maximum activity between 57 and 54 Ma (Hirschmann et al., 1997; Storey et al., 2007; Svensen et al., 2004, 2010). The Central American circum-Caribbean volcanism is a tectonically active volcanic province took place around ~ 56 – 55.5 Ma in the proto Great Antilles (Sigurdsson et al., 1997). Therefore, both of these large igneous provinces may be participating in foreseeing the warming that occurred during the PETM event and/ or maybe the leading causes of initial pulse of PETM global warming. Generally, NAIP eruptions were different from the other records of LIPs (Permo-Triassic, Cyprian trap, Cretaceous-Tertiary Deccan volcanism).

In the last few years, Hg-anomaly caught the attention of scientists as a paleoenvironmental proxy that could link volcanic activities to hyperthermal events. Especially the PETM (Jones et al., 2019; Khozyem et al., 2017) and provides further evidence linking NAIP and PETM event as the main reason produce the initial pulses of warming that led to the release of methane hydrate from the continental shelf (Maclennan & Jones, 2006; Svensen et al., 2004, 2010; Wieczorek et al., 2013).

Dababiya GSSP is part of the Tethys south margin, deposited shallow continental margin (100–150 m; Speijer & Wagner, 2002; Fig. 2). Three intervals show Hg enrichment; the lower Hg spike is placed in the top of P5 and NP9a biozones and corresponds to the one observed in Zumaia (Tremblin et al., 2021) and is associated with the pre-PETM gradual shift in both $\delta^{13}\text{C}_{\text{carb}}$ and $\delta^{13}\text{C}_{\text{org}}$. That large Hg-spike can be explained as direct precipitation of atmospheric Hg at the distal area within the sediments with no lithological change (Fig. 9). However, the increased Hg/TOC ratio at the same level reinforces the driving of the Hg with detrital TOC input. Proceeding to the PEB, the second interval enriched in Hg is above the PEB and corresponds to the sharp change in lithology from the marine to clastic sediments (Fig. 9). The low TOC content reveals that the primary source of the Hg is the Hg-bonded to the sediments. This explanation is supported by increasing the Hg/TOC ratio at the same interval, followed by a third Hg enrichment level linked to the anoxic conditions that prevailed within the middle part of the PETM (Khozyem et al., 2014, 2015). At the anxious level, sulfur-reducing bacteria adsorb sulfur for their metabolism, fixing HgS and methyl mercury as byproducts. In the high sulfide interval, HgS precipitated. Therefore, the main trigger for high Hg concentrations in the detrital TOC is typically scavenged by organic matter during the biotic and abiotic processes (Sanei et al., 2012), as observed in deeper section (Wadi Nukhul; Khozyem et al., 2013). The phyllosilicate normalized Hg shows three intervals of Hg-phyllosilicate enrichment. The lower corresponds to the

PEB level (Fig. 9), and the upper two correspond to the upper part of the CIE in which the sediments became mineralogically mature, which can be explained as the fixation of Hg within the fine sediment with the incorporation of marine TOC in the later stage of the PETM. In general, the impact of volcanism can be noticed by increasing the Hg input through the pre-and during the PETM-CIE.

4.6 Complete PETM Scenario Emphasizes from Dababiya GSSP

The geochemical, mineralogical, and paleontological studies on Dababiya GSSP (Khozyem et al., 2015; Fig. 15) emphasized four phases of PETM event; started with: Phase-1, pre-PETM volcanic activities took place during late Paleocene (North Atlantic volcanic province, Caribbean and mid-ocean ridge areas; Courtillot & Renne, 2003; Storey et al., 2007), these volcanic activities foresee the destabilization of Methane clathrate by changing the ocean temperature, as well as the ocean circulation (Dickens et al., 1995, 1997). As a result, gradual release of methane clathrate, both $\delta^{13}\text{C}_{\text{org}}$, and $\delta^{13}\text{C}_{\text{carb}}$, were gradually decreased, reaching Paleocene-Eocene sequence boundary (PEB). Second phase is linked to volcanic activities, which led to thermal expansion, sea-level rise, and complete methane-hydrated destabilization and CO_2 release (Sluijs et al., 2008; Speijer & Wagner, 2002). CO_2 consumed the seawater oxygen contents during its oxidation and produced oceanic anoxic conditions as observed in the sedimentary record of Dababiya GSSP (Khozyem et al., 2015; Schulte et al., 2011), as well as led to shoaling of carbonate dissolution datum (CDD; Zachos et al., 2008). This phase is identified based on a clay-rich layer and a negative Ce-anomaly, negative Mn* associated with an increase in redox element indicators (Khozyem et al., 2015).

Consequently, methane clathrate is completely oxidized at water/atmosphere interface, releasing massive CO_2 amounts to atmosphere that contribute to greenhouse gases. The released CO_2 during phase 3 (Fig. 15) thus, intensified the hot, humid conditions globally. Therefore, phase 3 increases precipitation rates, high silicate weathering, increased kaolinite formation/input, and massive input of terrestrial organic matter into the ocean through the fluvial discharges. The previous elements led to the rise of the second anoxic level observed by presence of different kinds of bacterial activities (SRB and cyanobacteria). The feedback of the biosphere represents direct response to high tropical temperatures (Huber, 2008), introduces seasonal aridity in continental interiors (Wing et al., 2003), and releases less CO_2 to ocean/atmosphere system. Physical

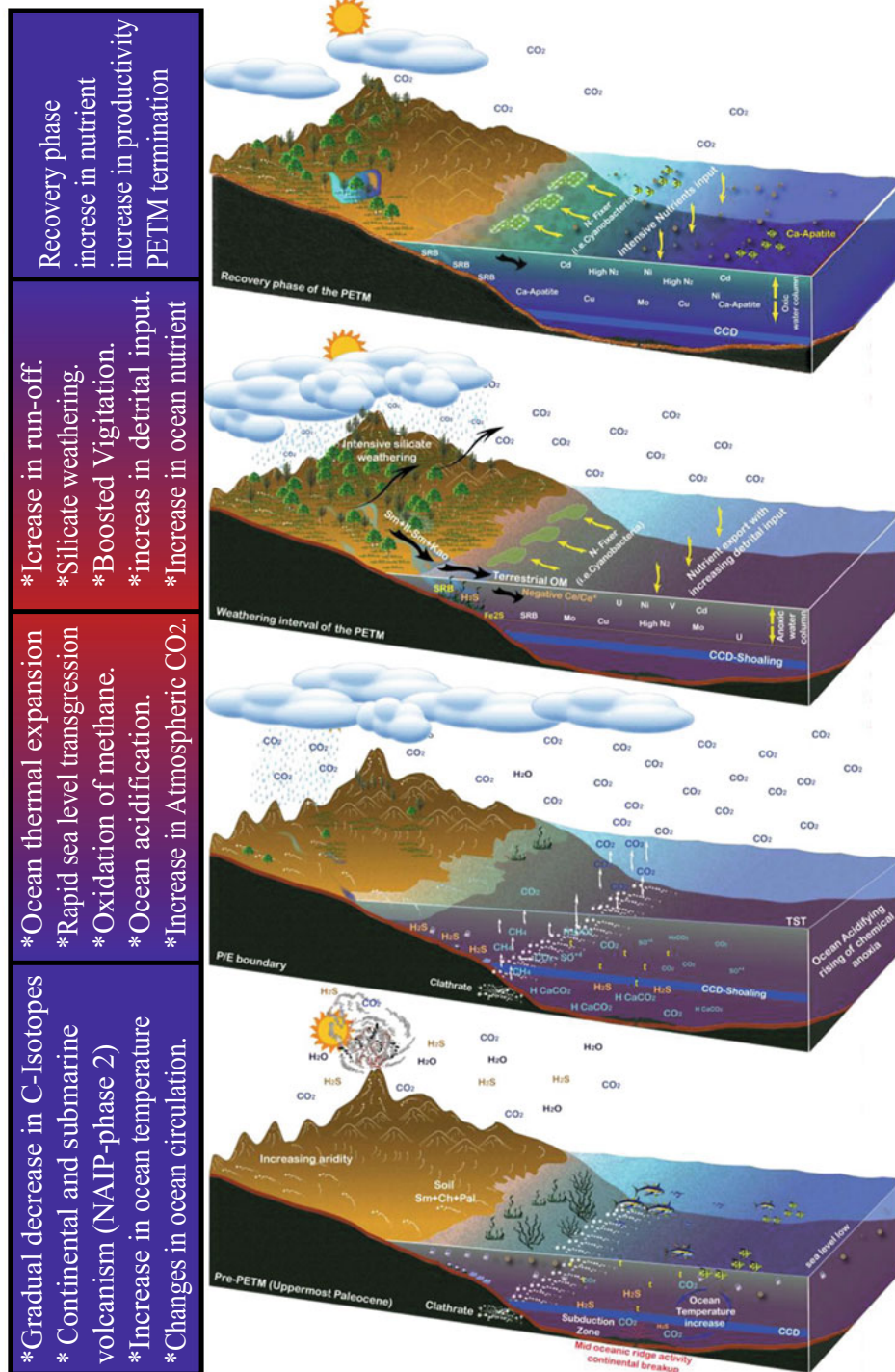


Fig. 15 Illustration of the four main phases of the Paleocene Eocene Thermal Maximum event (modified after Keller et al., 2018; Khozyem, 2020; Khozyem et al., 2015)

recovery occurred in the environmental recovery phase due to increased nutrient flux resulting from intensive continental weathering. It caused increased ocean surface productivity, which was the main reason for increasing the ocean water pH, with an abundance of phosphorous with fixation of Ba due to prevailing oxic conditions.

5 Conclusions

To sum up, PETM is one of the pronounced events to be used as an analog for current warming; therefore, it is extensively studied worldwide, particularly in Egypt. More than 120

section outcrops from different paleoenvironmental settings are very well recognized in Egypt during late Paleocene to early Eocene sedimentary records. Dababiya GSSP represents one of the most complete sections worldwide. PETM event in Dababiya has several unique criteria, including clear weathering profile that represents global environment response to the increased atmospheric CO₂ and its drawdown by silicate weathering and the posted vegetations. The $\delta^{13}\text{C}_{\text{carb}}$ and $\delta^{13}\text{C}_{\text{org}}$ show gradual decrease below the PEB that are recorded in few sections and indicates the gradual increase in temperature pre-PETM initial pulse, although most of the studied records around the world (terrestrial and marine) represent an abrupt negative shift in $\delta^{13}\text{C}_{\text{carb}}$ and $\delta^{13}\text{C}_{\text{org}}$. Presence of two anoxic intervals that cannot be recognized and separated in any known PETM section. The link between PETM and central igneous provinces is well constrained in Dababiya GSSP based on the Hg anomaly.

Acknowledgements The authors would like to express their profound thanks to staff member of the sedimentary mineralogy and geochemistry labs of Lausanne University. The thanks is as well extended to Prof. Dr. Jorge E. Spangenberg for his continuous support and fruitful discussion during the preparation of the manuscript and technical and laboratory facilities that he offers during the analysis of isotopes.

References

- Agnini, C., Fornaciari, E., Rio, D., Tateo, F., Backman, J., & Giusberti, L. (2007). Responses of calcareous nannofossil assemblages, mineralogy and geochemistry to the environmental perturbations across the Paleocene/Eocene boundary in the Venetian Pre-Alps. *Marine Micropaleontology*, *63*, 19–38.
- Algeo, T. J., & Ingall, E. (2007). Sedimentary C_{org}:P ratios, paleocean ventilation, and Phanerozoic atmospheric pO₂. *Palaeogeography, Palaeoclimatology, Palaeoecology*, *256*(3), 130–155. <https://doi.org/10.1016/j.palaeo.02.029>
- Algeo, T. J., Kuwahara, K., Sano, H., Bates, S., Lyons, T., Elswick, E., Hinnov, L., Ellwood, B., Moser, J., & Maynard, J. B. (2011). Spatial variation in sediment fluxes, redox conditions, and productivity in the Permian-Triassic Panthalassic Ocean. *Palaeogeography, Palaeoclimatology, Palaeoecology*, *308*, 65–83.
- Algeo, T. J., & Maynard, J. B. (2004). Trace-element behavior and redox facies in core shales of Upper Pennsylvanian Kansas-type cyclothems. *Chemical Geology*, *206*, 289–318.
- Aubry, M.-P., Ouda, K., Dupuis, C., Berggren, W. A., Van Couvering, J. A., & The Members of the Working Group on the Paleocene/Eocene Boundary. (2007). Global Standard Stratotype-Section and Point (GSSP) for the base of the Eocene series in the Dababiya section (Egypt). *Episodes*, *30*(4), 271–286.
- Aubry, M. P., & Salem, R. (2013). The Dababiya core: A window into Palaeocene to early Eocene depositional history in Egypt based on coccolith stratigraphy. *Stratigraphy*, *9*(3–4), 287–346
- Aziz, H., Kamar, A., & Ariffin, S. (2008). Heavy metals (Cd, Pb, Zn, Ni, Cu and Cr(III)) removal from water in Malaysia: Post treatment by high quality limestone. *Bioresource Technology*, *99*(6), 1578–1583.
- Bains, S., Norris, R. D., Corfield, R. M., & Faul, K. L. (2000). Termination of global warmth at the Palaeocene/Eocene boundary through productivity feedback. *Nature*, *407*, 171–174. <https://doi.org/10.1038/35025035>
- Bajpai, S., Kay, R. F., Killiams, B. A., Dash, D. P., Kapur, V. V., & Tiwari, B. N. (2008). The oldest Asian record of Anthropoidea. *Proceedings of the National Academy of Sciences, USA*, *105*, 11093–11098.
- Bau, M., & Dulski, P. (1996). Distribution of yttrium and rare-earth elements in the Penge and Kuruman iron-formations, Transvaal Supergroup, South Africa. *Precambrian Research*, *79*, 37–55.
- Bellanca, A., Masetti, D., & Neri, R. (1997). Rare earth elements in limestone/marlstone couplets from the Albian-Cenomanian Cison section (Venetian region, northern Italy): Assessing REE sensitivity to environmental changes. *Chemical Geology*, *141*, 141–152.
- Berggren, W. A., & Ouda, K. (2003). Upper Paleocene–lower Eocene planktonic foraminiferal biostratigraphy of the Dababiya section, Upper Nile Valley (Egypt). In K. Ouda & M.-P. Aubry (Eds.), *The Upper Paleocene–Lower Eocene of the Upper Nile Valley: Part 1, stratigraphy. Micropaleontology* (Vol. 49, pp. 61–92).
- Bhatia, M. R. (1985). Rare-Earth element geochemistry of Australian Paleozoic Graywackes and Mudrocks: Provenance and tectonic control. *Sedimentary Geology*, *45*, 97–113. [https://doi.org/10.1016/0037-0738\(85\)90025-9](https://doi.org/10.1016/0037-0738(85)90025-9)
- Black, B. A., Perron, J. T., Hemingway, D., Bailey, E., Nimmo, F., & Zebker, H. (2017). Global drainage patterns and the origins of topographic relief on Earth, Mars, and Titan. *Science*, *356*(6339), 727–731. <https://doi.org/10.1126/science.aag0171>
- Blakey, R. C., (2007). Carboniferous-Permian paleogeography of the assembly of Pangaea. In: Wong, Th. E (Ed.), Proceedings of the XVth International Congress on Carboniferous and Permian Stratigraphy. Utrecht, 10–16 August 2003. Royal Dutch Academy of Arts and Sciences, Amsterdam, pp. 443–456.
- Bolle, M. P., & Adatte, T. (2001). Paleocene-early Eocene climatic evolution in the Tethyan realm: Clay mineral evidence. *Clay Minerals*, *36*, 249–261.
- Bolle, M. P., Tantawy, A. A., Pardo, A., Adatte, T., Burns, S. J., & Kassab, A. (2000). Climatic and environmental changes documented in the upper Paleocene to lower Eocene of Egypt. *Eclogae Geologicae Helveticae*, *93*, 33–51.
- Bowen, G. J., Beerling, D. J., Koch, P. L., Zachos, J. C., & Quattlebaum, T. (2004). A humid climate state during the Paleocene-Eocene thermal maximum. *Nature*, *432*, 495–499.
- Bowen, G. J., Clyde, W. C., Koch, P. L., Ting, S., Alroy, J., Tsubamoto, T., Wang, Y., & Wang, Y. (2002). Mammalian dispersal at the Paleocene/Eocene boundary. *Science*, *295*, 2062–2065.
- Bowen, G. J., Koch, P. K., Gingerich, P. D., Norris, R. D., Bains, S., & Corfield, R. M. (2001). Refined isotope stratigraphy across the continental Paleocene-Eocene boundary on Polecat Bench in the Northern Bighorn Basin. In P. D. Gingerich (Ed.), *Paleocene–Eocene stratigraphy and biotic change in the bighorn and Clarks Fork Basins, Wyoming* (Vol. 33, pp. 73–88). University of Michigan Papers on Paleontology.
- Bowen, G. J., & Zachos, J. C. (2010). Rapid carbon sequestration at the termination of the Palaeocene-Eocene thermal maximum. *Nature Geoscience*, *3*, 866–869.
- Bruland, K. W. (1983). Trace elements in sea water. In J. P. Riiey & R. Chester (Eds.), *Chemical oceanography* (Vol. 8, pp. 157–220). Academic Press.
- Brumsack, H.-J. (2006). The trace metal content of recent organic carbon-rich sediments: Implications for Cretaceous black shale formation. *Palaeogeography, Palaeoclimatology, Palaeoecology*, *232*, 344–361.
- Campbell, I. H., Czamanske, G. K., Fedorenko, V. A., Hill, R. I., & Stepanov, V. (1992). Synchronism of the Siberian traps and the Permian-Triassic boundary. *Science*, *258*, 1760–1763.
- Cao, J., Yang, R., Yin, W., Hu, G., Bian, L., & Fu, X. (2018a). Mechanism of organic matter accumulation in residual bay

- environments: The early cretaceous Qiangtang Basin, Tibet. *Energy & Fuels*, 32, 1024–1037.
- Cao, W., Xi, D., Melinte-Dobrinescu, M. C., Jiang, T., Wise, S. W. Jr., & Wan, X. (2018b). Calcareous nannofossil changes linked to climate deterioration during the Paleocene-Eocene thermal maximum in Tarim Basin, NW China. *Geoscience Frontiers*, 9, 1465–1478.
- Courtillot, V., & Renne, P. R. (2003). On the ages of flood basalt events. *Comptes Rendus Géoscience*, 335, 113–140.
- Cruse, A. M., & Lyons, T. W. (2004). Trace metal records of regional paleoenvironmental variability in Pennsylvanian (Upper Carboniferous) black shales. *Chemical Geology*, 206(319), 345.
- Cullers, R. L. (2002). Implications of elemental concentrations for provenance, redox conditions, and metamorphic studies of shales and limestones near Pueblo, CO, USA. *Chemical Geology*, 191, 305–327.
- DeConto, R. M., Galeotti, S., Pagani, M., Tracy, D., Schaefer, K., Zhang, T., Pollard, D., & Beerling, D. J. (2010). Past extreme warming events linked to massive carbon release from thawing permafrost. *Nature*, 484, 87–91.
- Dehairs, F., Chesselet, R., & Jedwab, J. (1980). Discrete suspended particles of barite and the barium cycle in the open ocean. *Earth and Planetary Science Letters*, 49, 528–550.
- Dickens, G. R., Castillo, M. M., & Walker, J. C. G. (1997). A blast of gas in the latest Paleocene; Simulating first-order effects of massive dissociation of oceanic methane hydrate. *Geology*, 25, 259–262.
- Dickens, G. R., O'Neil, J. R., Rea, D. K., & Owen, R. M. (1995). Dissociation of oceanic methane hydrate as a cause of the carbon isotope excursion at the end of the Paleocene. *Paleoceanography*, 10(6), 965–971.
- Dupuis, C., Aubry, M.-P., Steurbaut, E., Berggren, W. A., Ouda, K., Magioncalda, R., Cramer, B. S., Kent, D. V., Speijer, R. P., & Heilmann-Clausen, C. (2003). The Dababiya Quarry section: Lithostratigraphy, clay mineralogy, geochemistry and paleontology. In K. Ouda & M.-P. Aubry (Eds.), *The Upper Paleocene–Lower Eocene of the Upper Nile Valley: Part 1. Stratigraphy: Micropaleontology* (Vol. 49, pp. 41–59).
- Dymond, J., Suess, E., & Lyle, M. (1992). Barium in deep-sea sediment: A geochemical proxy for paleoproductivity. *Paleoceanography*, 7, 163–181.
- Farley, K. A., & Eltgroth, S. F. (2003). An alternative age model for the Paleocene-Eocene thermal maximum using extraterrestrial (super 3) He. *Earth and Planet Science Letters*, 208, 135–148.
- Feng, X. L., Fu, X. G., Tan, F. W., & Chen, W. B. (2014). Sedimentary environment characteristics of Upper Carboniferous Cameng Formation in Kongkong Chaka Area of Northern Qiangtang Basin, Tibet. *Geoscience*, 28, 953–961.
- Föllmi, K. B. (1996). The phosphorus cycle, phosphogenesis and marine phosphate-rich deposits. *Earth-Science Reviews*, 40, 55–124.
- Fricke, H. C., Clyde, W. C., O'Neil, J. R., & Gingerich, P. D. (1998). Intra-tooth variation in $\delta^{18}\text{O}$ of mammalian tooth enamel as a record of seasonal changes in continental climate variables. *Geochimica et Cosmochimica Acta*, 62, 1839–1851.
- Fricke, H. C., & Wing, S. L. (2004). Oxygen isotope and paleobotanical estimates of temperature and $\delta^{18}\text{O}$ -latitude gradients over North America during the early Eocene. *American Journal of Science*, 304, 612–635. <https://doi.org/10.2475/ajs.304.7.612>
- Fu, X., Wang, J., Chen, W., Feng, X., Wang, D., Song, C., & Zeng, S. (2016). Elemental geochemistry of the early Jurassic black shales in the Qiangtang Basin, eastern Tethys: Constraints for palaeoenvironment conditions. *Geological Journal*, 2016(51), 443–454.
- German, C. R., & Elderfield, H. (1990). Application of Ce anomaly as a paleoredox indicator: The ground rules. *Paleoceanography*, 5, 823–833.
- Ghandour. (2020). Paleoenvironmental changes across the Paleocene–Eocene boundary in West Central Sinai, Egypt: Geochemical proxies. *Swiss Journal of Geosciences*, 113, 3. <https://doi.org/10.1186/s00015-020-00357-3>
- Goldhammer, T., Brüchert, V., Ferdelman, T. G., & Zabel, M. (2010). Microbial sequestration of phosphorus in anoxic upwelling sediments. *Nature Geoscience*, 3, 557–561.
- Guastrini, E., & Speijer, R. P. (2007). The Paleocene-Eocene Thermal Maximum in Egypt and Jordan: An overview of the planktic foraminiferal record. *Special Paper of the Geological Society of America*, 424, 53–67. [https://doi.org/10.1130/2007.2424\(03\)](https://doi.org/10.1130/2007.2424(03))
- Guiraud, R., & Bosworth, W. (1999). Phanerozoic geodynamic evolution of north-eastern Africa and the northwestern Arabian platform. *Tectonophysics*, 315, 73–108.
- Harnois, L. (1988). The CIW index: A new chemical index of weathering. *Sedimentary Geology*, 55, 319–322.
- Higgins, J. A., & Schrag, D. P. (2006). Beyond methane: Towards a theory for the Paleocene-Eocene thermal maximum. *Earth Planetary and Science Letters*, 245, 523–537.
- Hirschmann, G., Duyster, J., Harms, U., Kontny, A., Lapp, M., de Wall, H., & Zulauf, G. (1997). The KTB superdeep borehole: Petrography and structure of a 9-km-deep crustal section. *Geologische Rundschau*, 86, 3–14.
- Holser, W. T. (1997). Geochemical events documented in inorganic carbon isotopes. *Palaeogeography, Palaeoclimatology, Palaeoecology*, 132, 173–182.
- Höntzsch, S., Scheibner, C., Kuss, J., Marzouk, A., & Rasser, M. (2011). Tectonically driven carbonate ramp evolution at the southern Tethyan shelf—the Lower Eocene succession of the Galala Mountains, Egypt. *Facies*, 57, 51–72.
- Hu, J., Li, Q., Li, J., Huang, J., & Ge, D. (2016). Geochemical characteristics and depositional environment of the Middle Permian mudstones from central Qiangtang Basin, northern Tibet. *Geological Journal*, 51, 560–571.
- Huber, M. (2008). A hotter greenhouse? *Science*, 321, 353–354.
- Ingall, E., Kolowith, L., Lyons, T., & Hurtgen, M. (2005). Sediment carbon, nitrogen and phosphorus cycling in an anoxic fjord, Engham Inlet, British Columbia. *American Journal of Science*, 305, 240–258.
- Jaramillo, C., Ochoa, D., Contreras, L., Pagani, M., Carvajal-Ortiz, H., Pratt, L. M., Krishnan, S., Cardona, A., Romero, M., Quiroz, L., & Rodriguez, G. (2010). Effects of rapid global warming at the Paleocene-Eocene boundary on neotropical vegetation. *Science*, 330, 957. <https://doi.org/10.1126/science.1193833>
- Jarvis, I., Burnett, W. C., Nathan, Y., Almbaydin, F. S., Attia, A. K., Castro, L. N., Flicoteaux, R., Hilmy, M. E., Husain, V., Qutawnah, A. A., & Serjani, A. (1994). Phosphorite geochemistry: State of the art and environmental concerns. *Eclogae Geologicae Helveticae*, 87, 643–700.
- Jenkyns, H. C. (2010). Geochemistry of oceanic anoxic events. *Geochemistry, Geophysics, Geosystems*, 11. [https://doi.org/10.1029/2009GC002788\(Q03004\)](https://doi.org/10.1029/2009GC002788(Q03004)).
- Joachimski, M. M., Ostertag-Henning, C., Pancost, R. D., Strauss, H., Freeman, K. H., Littke, R., Sinninghe Damsté, J. S., & Racki, G. (2001). Water column anoxia, enhanced productivity and concomitant changes in $\delta^{13}\text{C}$ and $\delta^{34}\text{S}$ across the Frasnian–Famennian boundary (Kowala Holy Cross Mountains/Poland). *Chemical Geology*, 175, 109–131.
- Jones, D. S., Martini, A. M., Fike, D. A., & Kaiho, K. (2017a). A volcanic trigger for the Late Ordovician mass extinction? Mercury data from south China and Laurentia. *Geology*, 45(7), 631–634.
- Jones, M. T., Augland, L. E., Shephard, G. E., Burgess, S. D., Eliassen, G. T., Jochmann, M., Friis, B., Jerram, D. A., Planke, S., & Svensen, H. H. (2017b). Constraining shifts in North Atlantic plate

- motions during the Palaeocene by U-Pb dating of Svalbard tephra layers. *Nature Scientific Reports*, 7, 6822. <https://doi.org/10.1038/s41598-017-06170-7>
- Jones, M. T., Percival, L. M. E., Stokke, E. W., Frieling, J., Mather, T. A., Riber, L., Schubert, B. A., Schultz, B., Tegner, C., Planke, S., & Svensen, H. H. (2019). Mercury anomalies across the Palaeocene-Eocene thermal maximum. *Climate of the Past*, 15, 217–236. <https://doi.org/10.5194/cp-15-217-2019>
- Kaiho, K., Takeda, K., Petrizzo, M. R., & Zachos, J. C. (2006). Anomalous shifts in tropical Pacific planktonic and benthic foraminiferal test size during the Paleocene-Eocene thermal maximum. *Palaeogeography, Palaeoclimatology, Palaeoecology*, 237, 456–464. <https://doi.org/10.1016/j.palaeo.2005.12.017>
- Kamber, B. S., & Webb, G. E. (2001). The geochemistry of late Archaean microbial carbonate: Implications for ocean chemistry and continental erosion history. *Geochimica et Cosmochimica Acta*, 65 (15), 2509–2525. [https://doi.org/10.1016/S0016-7037\(01\)00613-5](https://doi.org/10.1016/S0016-7037(01)00613-5)
- Katz, M. E., Katz, D. R., Wright, J. D., Miller, K. G., Pak, D. K., Shackleton, N. J., & Thomas, E. (2003). Early Cenozoic benthic foraminiferal isotopes. Species reliability and interspecies correction factors. *Paleoceanography*, 18(2), 1024.
- Katz, M. E., Pak, D. K., Dickens, G. R., & Miller, K. G. (1999). The source and fate of massive carbon input during the Latest Paleocene thermal maximum. *Science*, 286, 1531–1533.
- Keller, G., Mateo, P., Punekar, J., Khozyem, H., Gertsch, B., Spangenberg, J., Bitchong, A., Adatte, T. (2018). Environmental changes during the Cretaceous-Paleogene mass extinction and Paleocene-Eocene thermal maximum: Implications for the Anthropocene. *Gondwana Research*. <https://doi.org/10.1016/j.gr.2017.12.002>.
- Kelly, D. C., Bralower, T. J., Zachos, J. C., Premoli Silva, I., & Thomas, E. (1996). Rapid diversification of planktonic foraminifera in the tropical Pacific (ODP Site 865) during the late Paleocene thermal maximum. *Geology*, 24, 423–426.
- Kelly, D. C., Zachos, J. C., Bralower, T. J., Stephen A., & Schellenberg, S. A. (2005). Enhanced terrestrial weathering/runoff and surface ocean carbonate production during the recovery stages of the Paleocene-Eocene thermal maximum. *Paleoceanography*, 20, 4023. <https://doi.org/10.1029/2005PA001163>
- Kennett, J. P., & Stott, L. (1990). Proteus and Proto-Oceanus: Paleogene Ocean as revealed from Antarctica stable isotopic results. *Proceeding of ODP Scientific Results*, 113, 865–879.
- Kennett, J. P., & Stott, L. D. (1991). Abrupt deep-sea warming, palaeoceanographic changes and benthic extinctions at the end of the Palaeocene. *Nature*, 353, 225–229.
- Khozyem, H. (2020). An overview of paleo-climatic evidences in Egypt. In E. S. E. Omran & A. M. Negm (Eds.), *Climate change impact on agriculture and food security in Egypt*. Springer Water. <https://doi.org/10.1007/978-3-030-41629-4-2>
- Khozyem, H., Adatte, T., Keller, G., & Spangenberg, J. E. (2021). Organic carbon isotope records of the Paleocene-Eocene thermal maximum event in India provide new insights into mammal origination and migration. *Journal of Asian Earth Sciences*, 212, 104736. <https://doi.org/10.1016/j.jseas.2021.104736>
- Khozyem, H., Adatte, T., Keller, G., Tantawy, A. A., & Spangenberg, J. E. (2014). The Paleocene-Eocene GSSP at Dababiya, Egypt-revisited. Episodes 37(2), 78–86.
- Khozyem, H., Adatte, T., Mbabi Bitchong, A., Mahmoud, A., & Keller, G. (2017). The role of volcanism (North Atlantic Igneous province) in the PETM events revealed by Mercury anomalies. *GSA Geological Society of America Abstracts with Programs*, 49(6).
- Khozyem, H., Adatte, T., Spangenberg, J. E., Tantawy, A. A., & Keller, G. (2013). Paleoenvironmental and climatic changes during the Paleocene-Eocene Thermal Maximum (PETM) at the Wadi Nukhul Section, Sinai, Egypt. *Journal of the Geological Society of London*, 170, 341–352. <https://doi.org/10.1144/jgs2012-046>
- Khozyem, H., Adatte, T., Spangenberg, J. E., Keller, G., Tantawy, A. A., & Ulianov, A. (2015). New geochemical constraints on the Paleocene-Eocene thermal maximum: Dababiya GSSP, Egypt. *Palaeogeography, Palaeoclimatology, Palaeoecology*, 429, 117–135. <https://doi.org/10.1016/j.palaeo.2015.04.003>
- Klootwijk, C. T., Gee, J. S., Peirce, J. W., Smith, G. M., & McFadden, P. L. (1992). An early India Asia contact: Paleomagnetic constraints from Ninetyeast Ridge, ODP Leg 121. *Geology*, 20, 395–398.
- Koch, D., Park, J., & DelGenio, A. (2003). Clouds and sulfate are anticorrelated: A new diagnostic for global sulfur models. *Journal of Geophysical Research*, 108(D24), 4781. <https://doi.org/10.1029/2003JD003621>
- Kraal, P. (2011). Redox-dependent phosphorus burial in modern and ancient marine sediments. In *Geologica ultraiectina*. Faculteit Geowetenschappen, Departement Aardwetenschappen: Utrecht, The Netherlands.
- Krause, D. W., & Maas, M. C. (1990). The biogeographic origins of late Paleocene-early Eocene mammalian immigrants to the Western Interior of North America. *Geological Society of America Bulletin. Special Paper*, 243, 71–105.
- Kurtz, A. C., Kump, L. R., Arthur, M. A., Zachos, J. C., & Paytan, A. (2003). Early Cenozoic decoupling of the global carbon and sulfur cycles. *Paleoceanography*, 18, 1090. <https://doi.org/10.1029/2003PA000908>
- Kvenvolden, K. A. (1993). A primer on gas hydrates. In *The future of energy gases*. U.S. geological survey professional paper (Vol. 1570, pp. 279–1008).
- Landing, W. M., & Bruland, K. W. (1980). Manganese in the North Pacific. *Earth and Planetary Science Letters*, 49(1), 45–56.
- Landing, W. M., & Bruland, K. W. (1987). The contrasting biogeochemistry of iron and manganese in the Pacific Ocean. *Geochimica et Cosmochimica Acta*, 51, 29–43.
- Lawrence, M. G., & Kamber, B. S. (2006). The behavior of the rare earth elements during estuarine mixing—revisited. *Marine Chemistry*, 100, 147–161. <https://doi.org/10.1016/J.MARCHEM.2005.11.007>
- Lu, G., Adatte, T., Keller, G., & Ortiz, N. (1998). An abrupt climatic, oceanographic and ecologic changes near the Paleocene-Eocene transition in deep Tethyan basin: The Alamedilla section, southern Spain. *Ecologiae Geologica Helvetica*, 91, 293–306.
- Lu, G., & Keller, G. (1993). Climatic and oceanographic events across the Paleocene-Eocene Transition in the Antarctic Indian Ocean: Inference from planktic foraminifera. *Marine Micropaleontology*, 21, 101–142.
- Lu, G., & Keller, G. (1995). Planktic foraminiferal faunal turnovers in the subtropical Pacific during the late Paleocene to early Eocene. *Journal of Foraminiferal Research*, 25, 97–116.
- Lu, G. Y., Keller, G., Adatte, T., Ortiz, N., & Molina, E. (1996). Long-term (10⁵) or short-term (10³) $\delta^{13}\text{C}$ excursion near the Palaeocene-Eocene transition: Evidence from the Tethys. *Terra Nova*, 8, 347–355.
- Lucas, J., & Prevot-Lucas, L. (1995). Tethyan phosphates and bioproductites. In A. E. Nairn (Ed.), *The Ocean Basins and margins—The Tethys Ocean* (Vol. 8, pp. 367–391). Plenum Press.
- Luciani, V., Dickens, G. R., Backman, J., Fornaciari, E., Giusberti, L., Agnini, C., & D’Onofrio, R. (2016). Major perturbations in the global carbon cycle and photosymbiont-bearing planktic foraminifera during the early Eocene. *Climate of the Past*, 12, 981–1007. <https://doi.org/10.5194/cp-12-981-2016>
- Luciani, V., Giusberti, L., Agnini, C., Backman, J., Fornaciari, E., & Rio, D. (2007). The Paleocene Eocene thermal maximum as recorded by Tethyan planktonic foraminifera in the Forada section

- (northern Italy). *Marine Micropaleontology*, 64, 189–214. <https://doi.org/10.1016/j.marmicro.2007.05.001>
- Maclennan, J., & Jones, S. M. (2006). Regional uplift, gas hydrate dissociation and the origins of the Paleocene-Eocene thermal maximum. *Earth and Planetary Science Letter*, 245, 65–80.
- McInerney, F. A., & Wing, S. L. (2011). The Paleocene–Eocene thermal maximum: A perturbation of carbon cycle, climate, and biosphere with implications for the future. *Annual Review in Earth Planetary Science*, 39, 489–516.
- McLennan, S. M. (1989). Rare earth elements in sedimentary rocks: Influence of provenance and sedimentary process. *Review of Mineralogy*, 21, 169–200.
- McLennan, S. M. (2001). Relationships between the trace element composition of sedimentary rocks and upper continental crust. *Geochemistry, Geophysics, Geosystems*, 2, 1021.
- Monechi, S., Angori, E., & Speijer, R. P. (2000a). Upper Paleocene biostratigraphy in the Mediterranean region: Zonal markers, diachronism, and preservational problems. *GFF. Geologiska Föreningens, Stockholm Förhandlingar*, 122, 108–110.
- Monechi, S., Angori, E., & von Salis, K. (2000b). Calcareous nannofossil turnover around the Paleocene/Eocene transition at Alamedilla (southern Spain). *Bulletin de la Societe Geologique de France*, 171, 477–489.
- Moore, E. A., & Kurtz, A. C. (2008). Black carbon in Paleocene-Eocene boundary sediments: A test of biomass combustion as the PETM trigger. *Palaeogeography, Palaeoclimatology, Palaeoecology*, 267(147), 52.
- Murphy, A. E., Sageman, B. B., Hollander, D. J., Lyons, T. W., & Brett, C. E. (2000). Black shale deposition and faunal overturn in Devonian Appalachian basin: Clastic starvation, seasonal water-column mixing, and efficient biolimiting nutrient recycling. *Palaeoceanography*, 15, 280–291.
- Mutterlose, J., Linnert, C., & Norris, R. (2007). Calcareous nannofossils from the Paleocene Eocene thermal maximum of the equatorial Atlantic (ODP Site 1260B): Evidence for tropical warming. *Marine Micropaleontology*, 65, 13–31. <https://doi.org/10.1016/j.marmicro.2007.05.004>
- Nesbitt, H., & Young, G. M. (1982). Early Proterozoic climates and plate motions inferred from major element chemistry of lutites. *Nature*, 299, 715–717.
- Nothdurft, L. D., Webb, G. E., & Kamber, B. S. (2004). Rare earth element geochemistry of Late Devonian reefal carbonates, Canning Basin, Western Australia: Confirmation of seawater REE proxy in ancient limestones. *Geochimica et Cosmochimica Acta*, 68, 263–283.
- Oberhänsli, H. (1992). The influence of the Tethys on the bottom water of the Early Tertiary ocean. In J. P. Kennett, (Ed.), *The Antarctic paleoenvironment: A prospective on global change: Antarctic research service* (pp. 167–184).
- Oberhänsli, H., & Hsü, K. J. (1986). Paleocene–Eocene paleoceanography. In K. J. Hsü (Ed.), *Mesozoic and cenozoic oceans. American geophysical union geodynamics series* (Vol. pp. 85–100).
- Olsson, R. K., Hemleben, C., Berggren, W. A., & Huber, B. T. (1999). Atlas of Paleocene planktonic foraminifera. *Smithsonian Contributions to Paleobiology*, 85(I–V), 1–252.
- Ouda, K., & Berggren, W. A. (2003). Biostratigraphic correlation of the Upper Paleocene Lower Eocene succession in the Upper Nile Valley: A synthesis. *Micropaleontology*, 49, 179–212.
- Pearson, P. N., Olsson, R. K., Huber, B. T., Hemleben, C., & Berggren, W. A. (Eds.). (2006). *Atlas of Eocene planktonic foraminifera* (pp. 1–513). Cushman Foundation Special Publication.
- Pujol, F., Berner, Z., & Stueben, D. (2006). Palaeoenvironmental changes at the Frasnian Famennian boundary in key European sections: Chemostratigraphic constraints. *Palaeogeography, Palaeoclimatology, Palaeoecology*, 240, 120–145.
- Raffi, I., Backman, J., & Pälke, H. (2005). Changes in calcareous nannofossil assemblage across the Paleocene/Eocene transition from the paleoequatorial Pacific Ocean. *Palaeogeography, Palaeoclimatology, Palaeoecology*, 226, 93–126.
- Rana, R. S., Kumar, K., Escarguel, G., Sahni, A., Rose, K. D., Smith, T., Singh, H., & Singh, L. (2008). An ailuravine rodent from the lower Eocene Cambay Formation at Vastan, western India, and its palaeobiogeographic implications. *Acta Palaeontologica Polonica*, 53, 1–14.
- Raymo, M. E., & Ruddiman, W. F. (1992). Tectonic forcing of late Cenozoic climate. *Nature*, 359(6391), 117–122. <https://doi.org/10.1038/359117a0>
- Renssen, H., Beets, C. J., Fichetef, T., Goosse, H., & Kroon, D. (2004). Modeling the climate response to a massive methane release from gas hydrates. *Palaeoceanography*. <https://doi.org/10.1029/2003PA000968>
- Rimmer, S. M. (2004). Geochemical paleoredox indicators in the Devonian-Mississippian black shales, central Appalachian Basin (USA). *Chemical Geology*, 206(3–4), 373–391.
- Riquier, L., Tribouvillard, N., Averbuch, O., Devleeschouwer, X., & Riboulleau, A. (2006). The Late Frasnian Kellwasser horizons of the Harz Mountains (Germany): Two oxygen deficient periods resulting from contrasting mechanisms. *Chemical Geology*, 233, 137–155.
- Rodriguez, J. (1999). Use of cenograms in mammalian palaeoecology. A critical review. *Lethaia*, 32, 331–347.
- Röhl, U., Westerhold, T., Bralower, T. J., Zachos, J. C. (2007). On the duration of the Paleocene-Eocene thermal maximum (PETM). *Geochemistry, Geophysics, Geosystems*, G3, Q12002.
- Roser, B. P., & Korsch, R. J. (1988). Provenance signatures of sandstone and mudstone suites determined using discriminant function analysis of major-element data. *Chemical Geology*, 67, 119–139.
- Roy, D. K., & Roser, B. P. (2013). Climatic control on the composition of Carboniferous-Permian Gondwana sediments, Khalaspir basin, Bangladesh. *Gondwana Research*, 23, 1163–1171.
- Said, R. (Ed.). (1990). *The geology of Egypt* (p. 734p). Balkema.
- Sanei, H., Grasby, S. E., & Beauchamp, B. (2012). Latest Permian mercury anomalies. *Geology*, 40(1), 63–66. <https://doi.org/10.1130/G32596>
- Schmitz, B., Molina, E., & von Salis, K. (1998). The Zumaya section in Spain: A possible global stratotype section for the Selandian and Thanetian stages. *Newsletters on Stratigraphy*, 36, 35–42.
- Schoepfer, S. D., Shen, J., Wei, H., Tyson, R. V., Ingall, E., & Algeo, T. J. (2015). Total organic carbon, organic phosphorus, and biogenic barium fluxes as proxies for paleomarine productivity. *Earth Science Reviews*, 2015(149), 23–52.
- Schulte, P., Scheibner, C., & Speijer, R. P. (2011). Fluvial discharge and sea-level changes control-ling black shale deposition during the Paleocene–Eocene thermal maximum in the Dababiya Quarry section. *Egypt: Chemical Geology*, 285, 167–183.
- Selverstone, J., & Gutzler, D. S. (1993). Post-125 Ma carbon storage associated with continent-continent collision. *Geology*, 21, 885–888.
- Shields, G. A., & Stille, P. (2001). Diagenetic constraints on the use of cerium anomalies as palaeoseawater redox proxies: An isotopic and REE study of Cambrian phosphorites. *Chemical Geology*, 175, 29–48.
- Shields, G. A., & Webb, G. E. (2004). Has the REE composition of seawater changed over geological time? *Chemical Geology*, 204, 103–107.
- Sigurdsson, H., Leckie, R. M., & Acton, G. (1997). *Proceedings of the Ocean Drilling Program, Initial reports* (Vol. 165, p. 865). College Station, Texas, Ocean Drilling Program.

- Sluijs, A., Brinkhuis, H., Crouch, E. M., John, C. M., Handley, L., Munsterman, D., Bohaty, S. M., Zachos, J. C., Reichart, G.-J., Schouten, S., Pancost, R. D., & Sinninghe Damsté, J. S. (2008). Eustatic variations in the Paleocene–Eocene greenhouse world. *Paleoceanography*, 23. <https://doi.org/10.1029/2008PA001615> (PA4216).
- Sluijs, A., & Dickens, G. R. (2012). Assessing offsets between the $\delta^{13}\text{C}$ of sedimentary components and the global exogenic carbon pool across Early Paleogene carbon cycle perturbations. *Global Biogeochemical Cycles*, 26 (GB4005).
- Sluijs, A., Schouten, S., Pagani, M., Woltering, M., Brinkhuis, H., Damsté, J. S. S., Dickens, G. R., Huber, M., Reichart, G.-J., Stein, R., Matthiessen, J., Lourens, L. J., Pedentchouk, N., Backman, J., Moran, K., & The Expedition 302 Scientists. (2006). Subtropical Arctic Ocean temperatures during the Palaeocene/Eocene thermal maximum. *Nature*, 441(7093), 610–613. <https://doi.org/10.1038/nature04668>
- Soliman, M. F. (2003). Chemostratigraphy of the Paleocene/Eocene (P/E) boundary sediments at Gabal El-Qreiya, Nile Valley, Egypt. *Micropaleontology*, 49(Suppl-1), 123–138. <https://doi.org/10.2113/49.Suppl1.123>
- Soudry, D., Glenn, C. R., Nathan, Y., Segal, I., & Vonderhaar, D. (2006). Evolution of Tethyan phosphogenesis along the northern edges of the Arabian-African shield during the Cretaceous-Eocene as deduced from temporal variations of Ca and Nd isotopes and rates of P accumulation. *Earth-Science Reviews*, 78(2006), 27–57.
- Speijer, R. P. (1994). Extinction and recovery patterns in benthic foraminiferal paleocommunities across the Cretaceous/Paleogene and Paleocene/Eocene boundaries [Ph.D. thesis. University of Utrecht, Netherlands]. *Geologica Ultraieciina*, 124, 1–191.
- Speijer, R. P., & Schmitz, B. (1998). A benthic foraminiferal record of Paleocene sea-level changes and trophic conditions at Gebel Aweina, Egypt. *Palaeogeography, Palaeoclimatology, Palaeoecology*, 137, 79–101.
- Speijer, R. P., Schmitz, B., & Luger, P. (2000). Stratigraphy of late Palaeocene events in the Middle East: Implications for low to middle-latitude successions and correlations. *Journal of the Geological Society of London*, 157, 37–47.
- Speijer, R. P., Schmitz, B., & van der Zwaan, G. J. (1997). Benthic foraminiferal extinction and repopulation in response to latest Paleocene Tethyan anoxia. *Geology*, 25, 683–686.
- Speijer, R. P., & Van der Zwaan, G. J. (1994). The differential effect of the P/E boundary event on extinction and survivorship in shallow to deep water Egyptian benthic foraminiferal assemblages. *Geologica Ultraieciina*, 124, 121–168.
- Speijer, R. P., Van der Zwaan, G. J., & Schmitz, B. (1996). The impact of Paleocene/Eocene boundary events on middle neritic benthic foraminiferal assemblages from Egypt. *Marine Micropaleontology*, 28, 99–132.
- Speijer, R. P., Wagner, T. (2002). Sea-level changes and black shales associated with the late Paleocene thermal maximum: Organic-geochemical and micropaleontologic evidence from the southern Tethyan margin (Egypt–Israel). In C. Koeberl & K. MacLeod (Eds.), *Catastrophic events and mass extinctions: Impacts and beyond*. Geological Society of America, special papers (Vol. 356, pp. 533–549).
- Stein, M., Föllmi, K. B., Westermann, S., Godet, A., Adatte, T., Matera, V., Fleitmann, D., & Berner, Z. (2011). Progressive palaeoenvironmental change during the late Barremian–early Aptian as prelude to Oceanic Anoxic Event 1a: Evidence from the Gorgo a Cerbara section (Umbria–Marche basin, central Italy). *Palaeogeography, Palaeoclimatology, Palaeoecology*, 302, 396–406.
- Stokke, E. W., Morgan, E. W. S., Jessica, T. J., Henrik, E. T., Jessica, H. S., Whiteside, H. (2020). Temperature changes across the Paleocene-Eocene thermal maximum a new high-resolution TEX86 temperature record from the Eastern North Sea Basin. *Earth and Planetary Science Letters*, 544, 116388.
- Storey, M., Duncan, R. A., & Tegner, C. (2007). Timing and duration of volcanism in the North Atlantic Igneous Province: Implications for geodynamics and links to the Iceland hotspot. *Chemical Geology*, 241(3–4), 264–281.
- Svensen, H., Planke, S., & Corfu, F. (2010). Zircon dating ties NE Atlantic sill emplacement to initial Eocene global warming. *Journal of the Geological Society of London*, 167, 433–436.
- Svensen, H., Planke, S., Malthes-Sorensen, A., Jamtveit, B., Myklebust, R., Rasmussen Eidem, T., & Rey, S.S. (2004). Release of methane from a volcanic basin as a mechanism for initial Eocene global warming. *Nature*, 429, 542–545.
- Tantawy, A. A. (1998). *Stratigraphical and paleoecological studies on some Paleocene-Eocene successions in Egypt* [Unpublished Ph.D. thesis]. Faculty of Science, (Aswan), Assiut University, Egypt.
- Tantawy, A. A. (2006). Calcareous nannofossils of the Paleocene-Eocene transition at Qena Region, Central Nile Valley, Egypt. *Micropaleontology*, 52(3), 193–222.
- Tantawy, A. A., Ouda, K., Von Salis, K., & Saad El-Din, M. (2000). Biostratigraphy of Paleocene sections in Egypt. *GFF*, 122:1, 163–165. <https://doi.org/10.1080/11035890001221163>
- Thomas, D. J., Zachos, J. C., Bralower, T. J., Thomas, E., & Bohaty, S. (2002). Warming the fuel for the fire: Evidence for the thermal dissociation of methane hydrate during the Paleocene Eocene thermal maximum. *Geology*, 30, 1067–1070.
- Torfstein, A., Winckler, G., & Tripathi, A. (2010). Productivity feedback did not terminate the Paleocene–Eocene Thermal Maximum (PETM). *Climate of the Past*, 6, 265–272.
- Tremblin, M., Khozyem, H., Adatte, T., Spangenberg, J., Fillon, C., Grauls, A., Hunger, T., Nowak, A., Laeuchli, C., Lasseur, E., Roig, J., Serrano, O., Calassou, S., Guillocheau, F., & Castellort, S. (2021). Mercury evidence for enhanced volcanism during the Paleocene-Eocene thermal maximum (PETM). *Global and Planetary Change* (in review).
- Tribouillard, N., Algeo, J., Lyons, T., & Riboulleau, A. (2006). Trace metals as palaeoredox and palaeoproductivity proxies: An update. *Chemical Geology*, 232, 12–32.
- Tyson, R. V., & Pearson, T. H. (1991). Modern and ancient continental shelf anoxia: An overview. *Geological Society, London, Special Publications*, 58, 1–24.
- Van Kranendonk, M. J., Webb, G. E., & Kamber, B. S. (2003). Geological and trace element evidence for a marine sedimentary environment of deposition and biogenicity of 3.45 Ga stromatolitic carbonates in the Pilbara Craton, and support for a reducing Archaean ocean. *Geobiology*, 1, 91–108.
- Wang, Z., Fu, X., Feng, X., Song, C., Wang, D., Chen, W., & Zeng, S. (2017). Geochemical features of the black shales from the Wuyu Basin, southern Tibet: Implications for palaeoenvironment and palaeoclimate. *Geological Journal*, 2017(52), 282–297.
- Webb, G. E., & Kamber, B. S. (2000). Rare earth elements in Holocene reefal microbialites: A new shallow seawater proxy. *Geochimica et Cosmochimica Acta*, 64, 1557–1565.
- Weijers, J. W. H., Schouten, S., Sluijs, A., Brinkhuis, H., & Sinninghe Damsté, J. S. (2007). Warm arctic continents during the Palaeocene–Eocene thermal maximum: *Earth Planetary Science Letter*, 261, 230–238.
- Westerhold, T., Röhl, U., Donner, B., McCarren, H. K., & Zachos, J. C. (2011). A complete high resolution Paleocene benthic stable

- isotope record for the central Pacific (ODP Site 1209). *Paleoceanography* 26(2).
- Westerhold, T., Röhl, U., Donner, B., & Zachos, J. C. (2018). Global extent of early Eocene hyperthermal events—A new Pacific benthic foraminiferal isotope record from Shatsky Rise (ODP Site 1209). *Paleoceanography and Paleoclimatology*, 33(6), 626–642.
- Westerhold, T., Röhl, U., McCarren, H. K., & Zachos, J. C. (2009). Latest on the absolute age of the Paleocene–Eocene Thermal Maximum (PETM): New insights from exact stratigraphic position of key ash layers +19 and –17. *Earth Planetary Science Letter*, 287, 412–419.
- Whiticar, M. J. (1999). Carbon and hydrogen isotope systematics of bacterial formation and oxidation of methane. *Chemical Geology*, 161, 291–314.
- Wieczorek, R., Fantle, M. S., Kump, L. R., & Ravizza, G. (2013). Geochemical evidence for volcanic activity prior to and enhanced terrestrial weathering during the *Paleocene Eocene Thermal Maximum*: *Geochimica et Cosmochimica Acta*, 119, 391–410. <https://doi.org/10.1016/j.gca.2013.06.005>.
- Wing, S. L., & Curran, E. D. (2013). Plant response to a global greenhouse event 56 million years ago. *American Journal of Botany*, 100(7), 1234–1254.
- Wing, S. L., Harrington, G. J., Bowen, G. J., & Koch, P. L. (2003). Causes and consequences of globally warm climates in the Early Paleogene. In S. L. Wing, P. D. Gingerich, S. Birger, & E. Thomas (Eds.), *Geological society of America special paper* (Vol. 369, pp. 425–440).
- Wing, S. L., Harrington, G. J., Smith, F. A., Bloch, J. I., Boyer, D. M., & Freeman, K. H. (2005). Transient floral change and rapid global warming at the Paleocene-Eocene boundary. *Science*, 310, 993–996.
- Yandoka, B. M. S., Abdullah, W. H., Abubakar, M. B., Hakimi, M. H., & Adegoke, A. K. (2015). Geochemical characterization of Early Cretaceous lacustrine sediments of Bima Formation, Yola Sub-basin, Northern Benue Trough, NE Nigeria: Organic matter input, preservation, paleoenvironment and paleoclimatic conditions. *Marine and Petroleum Geology*, 61, 82–94.
- Zachos, J. C., Dickens, G. R., & Zeebe, R. E. (2008). An early Cenozoic perspective on greenhouse warming and carbon cycle dynamics. *Nature*, 451, 279–283.
- Zachos, J. C., Pagani, M., Sloan, L. C., Billups, K., & Thomas, E. (2001). Trends, rhythms, and aberrations in global climate 65 Ma to present. *Science*, 292, 686–693.
- Zachos, J. C., Röhl, U., Schellenberg, S. A., Sluijs, A., Hodell, D. A., Kelly, D. C., Thomas, E., Nicolo, M., Raffi, I., Lourens, L. J., & McCarren, H. (2005). Rapid acidification of the ocean during the Paleocene-Eocene Thermal Maximum. *Science*, 308, 1611–1615.
- Zachos, J. C., Schouten, S., Bohaty, S., Quattlebaum, T., Sluijs, A., Brinkhuis, H., Gibbs, S. J., & Bralower, T. J. (2006). Extreme warming of mid-latitude coastal ocean during the Paleocene Eocene thermal maximum: Inferences from TEX86 and isotope data. *Geology*, 34(9), 737–740. <https://doi.org/10.1130/G22522.1>
- Zeebe, R. E., Zachos, J. C., & Dickens, G. R. (2009). Carbon dioxide forcing alone insufficient to explain Palaeocene-Eocene thermal maximum warming. *Nature Geoscience*, 2, 576–580. <https://doi.org/10.1038/ngeo578>
- Ziegler, P. A. (1990). *Geological Atlas of Western and Central Europe* (2nd ed., p. 239). Shell International Petroleum Mij. B.V. and Geological Society.



Hassan Khozyem is an associate professor in the Geology Department, Faculty of Sciences, Aswan University (Egypt). He received a Ph.D. (2013) degree in geosciences and environments from Lausanne University (Switzerland). He works mainly on the geochemistry and sedimentology of Paleogene sediments in Egypt, India, and Spain. His research interests focus on global climatic and paleoenvironmental changes associated with warming events using high-resolution bio-, and chemostratigraphy. In 2015, he was awarded the state Prize of

Encouragement from the Egyptian government (Egyptian Science and Technology Academy) in geosciences that was followed by the first-class concession provided by the Egyptian President in 2017. His work is largely the result of interdisciplinary collaborations with an international team of scientists and students. Recently, he was as a member of the National committee of Geological Science (Egyptian Academy of Scientific Research and Technology). Hassan Khozyem was a former director of the Quality Assurance Unit in the Faculty of Science, Aswan University as well as the Vice-Chairman of the International Ranking Committee at the same University.



Thierry Adatte is Professor and head of the geochemistry and mineralogy sedimentary laboratory at the Institute of Earth Sciences of the University of Lausanne, Switzerland. He received his Ph.D. in Mineralogy and Sedimentary Geology from the University of Neuchâtel, Switzerland. 1989–1990: Postdoctoral fellow (FNS), Mexican Petroleum Institute (IMP). 1990–1993: Postdoctoral fellow (FNS), Universidad Autonoma de Nuevo Leon, Mexico and Neuchâtel University, Switzerland. 1993–2004: Maître assistant (“Assistant professor”), head of the Mineralogical and Geochemical Laboratory, Geological Institute, Neuchâtel University, Switzerland. 2004–2012: Associate Professor, “Chargé de cours et d’enseignement” (paleontology, sedimentary-environmental mineralogy, general geology), Geological Institute, Neuchâtel University, Switzerland. 2008–2018.

Researcher at the Institute des Sciences de la Terre (ISTE), Lausanne University, Head of the geochemistry sedimentary lab (XRD, CHN-Rock-Eval, Phosphorus). 2017–2018: Privat Docent at the Institute des Sciences de la Terre (ISTE), Lausanne University 2018-: Professor remplaçant at the Institute des Sciences de la Terre (ISTE), Lausanne University. His research interests are in the fields of global environmental change and extinction events, and his involvement in the deciphering of the events around the Cretaceous-Tertiary boundary event is documented by a series of publications (from 1997 to 2019). He also explored the sedimentary documents of the PETM the Paleocene-Eocene boundary event (from 2000 to 2019). He is also involved in the study of oceanic anoxic event (from 2001 to 2018). His interests are in the use of geochemical and

mineralogical proxies, such as stable carbon and oxygen isotopes, organic matter, clay minerals and recently also trace metal distributions as indicators of environmental and climatic change at the time of the extinction events. One of his main actual interest is the link between LIPS activity and mass extinction events, in particular during the KPg mass extinction. His team provided the most accurate dating of the Deccan activity and highlighted its crucial role in the KPg extinction. The use of mercury as a tracer of volcanic activity is also part his research. Acidification linked with these events is also one of his recent interest, more particularly for the KPg mass extinction. Since 1987, active participation (oral presentations and posters) of nearly 1112 meetings and symposia (GSA, AGU, EUG, IAS, SNOWBIRD, réunion spécialisées SGF) Convenor and co-convenor of sessions on Mass Extinctions, Volcanism, Impacts, and Catastrophic Environmental Changes at EGU Meetings since 2013 to 2018. Convenor and coconvenor of sessions on mass extinctions at GSA meetings in 2009, 2016 and 2017.



Gerta Keller is a professor emerita of paleontology and geology in the Geosciences Department at Princeton University (USA) where she has been employed since 1984. She received a Ph.D. degree from Stanford University in 1978. Her primary research centers on major catastrophes in Earth's history, including the biotic effects of meteorite impacts, major volcanic eruptions, rapid extreme climate changes, ocean anoxia and sea level changes associated with mass extinction and rapid faunal turnovers. Her research inte-

grates quantitative micropaleontology, paleoecology, stratigraphy, sedimentology, and stable isotopes in reconstructing paleoenvironments and exploring cause-effect scenarios. She has over 240 scientific publications in international journals and is a leading authority on catastrophes and mass extinctions, including the biotic and environmental effects of impacts and volcanism. Her work is largely the result of interdisciplinary collaborations with an international team of scientists and students. On June 4, 2021, Gerta Keller received an honorary doctorate degree (*honoris causa*) from the Faculty of Geosciences and Environment, University of Lausanne, Switzerland, for her life-long research contributions to the mass extinction that killed off over 70% of Earth's life 66 million years ago.



A Standard Sequence Stratigraphic Scheme for the Maastrichtian-Ypresian Successions of the Southern and Central Western Desert, Egypt

Mounir H. El-Azabi and Sherif Farouk

Abstract

A standard sequence stratigraphic scheme is proposed for the Maastrichtian-Ypresian deposits in the southern and central Western Desert of Egypt. This is relying on combined stratigraphic, sedimentological and planktic foraminiferal biostratigraphic studies of ten outcrops in the Abu Bayan, Beris, Kharga, Dakhla and Farafra areas. The outcrops signify three different facies associations: Garra El-Arbain, Nile Valley and Farafra, which are widely exposed in the Western Desert. They span the time interval from Maastrichtian to Ypresian. This interval is divided into eight depositional sequences, which are outlined by basin-wide sequence boundaries of different time span. These sequences are successively of early Maastrichtian, late Maastrichtian, mid-late Danian, late Selandian, late Thanetian, late-latest Thanetian, early Ypresian and early-late Ypresian ages. The hiatuses outlining these sequences are compared within Egypt to assess regional tectonic significance; and with Libyan, Tunisian, Arabian Plate, European data and global records for testing eustatic controls. They express the interaction and dual signatures of eustasy and regional tectonics. The latter is most evident in the sediments of the Farafra Oasis, which makes the inferred hiatuses extend for a much longer period than other areas. Thus, the present study enhances the age assignment of the Maastrichtian-Ypresian sequences and their boundaries, affords detailed information to perceive the paleogeographic evolution of the Dakhla Basin, and allows an explanation of its evolution in relation to eustatic sea-level changes.

Keywords

Maastrichtian-Ypresian Successions • Biostratigraphy • Paleoenvironment • Sequence Stratigraphy • Western Desert • Egypt

1 Introduction

Faunal ecology and paleoenvironmental changes of the Tethyan Ocean were described during the Maastrichtian-Ypresian (El-Azabi & Farouk 2011; Farouk et al., 2019a, 2019b; Hewaidy et al., 2019a, 2019b, 2019c; Keller, 2002; Keller et al., 2002; Speijer & Wagner, 2002; Sprong et al., 2009; Tantawy et al., 2001; Zaky et al., 2020). Several hypotheses have been proposed to clarify the origin and causes of Paleocene catastrophic events, including an extraterrestrial bolide effect, hyperthermal events in Earth's history, and eustatic sea-level changes associated with tectonic activities. Although the hyperthermal events in Earth's history occurred far from Egypt, such as the Deccan volcanism in India (Keller et al., 2020), and the North Atlantic Igneous Province centered on Iceland (Stokke et al., 2020; Thomas et al., 2005), these events affected the biotic changes in the entire world. Thus, the hyperthermal events are age coeval and correlate with eustatic sea-level changes and global tectonics. Volcanic activity was generally associated with regional tectonics, which led to changes in paleogeography of the basins and hence in sea level. Therefore, the interplay of eustatic sea-level changes and regional tectonics associated with hyperthermal events, along with changes in clastic supply and climate, greatly affected the faunal, paleoenvironments and spatial distribution of the Maastrichtian-Ypresian sequences.

The southern and central Western Desert was part of the ancient Dakhla Basin. This basin consists of a thick record of the late Jurassic-Eocene in the southeastern part and of the

M. H. El-Azabi (✉)

Geology Department, Faculty of Science, Cairo University, Giza, 12613, Egypt

e-mail: mnelazabi@sci.cu.edu.eg

S. Farouk

Egyptian Petroleum Research Institute, Nasr City, 11727, Egypt

Paleozoic-Eocene in the northwestern part (Hermina, 1990). The Paleozoic rocks stripped away in the southeastern part of the Dakhla Basin during the late Carboniferous-early Jurassic, when uplift, tilting and severe erosion in central Egypt were accompanied by ENE–WSW striking highs and lows due to the re-arrangement of the structural relief of the Precambrian basement complex (Klitzsch, 1986).

The Cretaceous-Eocene deposits of the Dakhla Basin are characterized by pronounced lateral changes in facies, which has complicated the stratigraphy of the Western Desert and hence the understanding of its sedimentary evolution. Three laterally coeval facies associations are recorded, which are termed from north to south: Farafra, Nile Valley and Garra El-Arbain, respectively (Issawi, 1972). The interactions between the three facies associations and their evolution through time largely achieved through the application of high-resolution biostratigraphic and sequence stratigraphic syntheses. These tools provide guides that can be applied locally and regionally to compare the three facies associations. This is important because the Cretaceous-Paleogene deposits are targets for petroleum exploration in the Western Desert. The widespread presence of these deposits affords an analog example of a subsurface stratigraphy.

The southern and central Western Desert has received great attention from many authors, who have contributed to the geology of the Kharga Oasis. They include Hendriks et al., (1984, 1987), Schnack and Luger (1998), and El-Azabi and Farouk (2011). Other authors who have studied the Dakhla Oasis are Issawi (1972), Luger and Schrank (1987), El-Azabi and El-Araby (2000), Tantawy et al. (2001), and Farouk and Jain (2018). Contributions by authors to the Farafra Oasis include Abdel-Kireem and Samir (1995), Ibrahim and Abdel-Kireem (1997), and Hewaidy et al. (2006). Most of the previous work has studied the stratigraphy, biostratigraphy and paleontology from exposures. A few of these authors have studied the sequence stratigraphic framework of the Cretaceous-Eocene successions (e.g., El-Azabi & El-Araby, 2000; El-Azabi & Farouk, 2011; Hewaidy et al., 2006, 2019a, 2019b).

The objectives of the present research are to: (1) study the facies associations and biostratigraphy of the Maastrichtian-Ypresian sediments and their sedimentary environments; (2) present a comprehensive sequence stratigraphic framework; (3) re-assess the nature, extent and time gap of the defined boundaries; (4) correlate the identified sequence boundaries with those of North Africa, the Arabian Plate,

Europe and global records; and (5) accurately reconstruct the sedimentary history of the Dakhla Basin during the Maastrichtian-Ypresian time.

2 Stratigraphic Setting

The Western Desert is a plateau desert that occupies about 65% of the entire area of Egypt (Fig. 1). It is a part of the northeastern continental margin of Africa, which was initiated during the late Triassic-early Jurassic opening of the Neo-Tethys due to the breakup of Pangea (Dercourt et al., 1993). In consequence, two NW–SE trending intra-shelf basins, Dakhla and Assiut, were developed in central Egypt (Flexer & Reymont, 1989; Hendriks et al., 1987). Beris, Kharga, Dakhla and Farafra are important oases in the southern and central parts of the Western Desert (Fig. 1). They are formed of thick, well-defined Maastrichtian-Ypresian sediments with pronounced facies, thickness and faunal changes, and regionally traced hiatuses along their escarp faces (Fig. 2). The escarpments of the Kharga and Dakhla oases begin with fine clastics of the early Middle Campanian Quseir Formation, which succeeded upwards by phosphate-rich facies of the Upper Campanian Duwi Formation (Fig. 3). The latter unconformably overlain by shale and mudstone of the Lower Maastrichtian-Upper Paleocene Dakhla Formation with its three partitions, the Mawhoob Shale, the Beris Mudstone and the Kharga Shale members of Awad and Ghobrial (1965). The Kharga Shale Member is divided into the lower and upper Kharga Shale units (Luger, 1985) with a hiatus representing the Cretaceous/Paleogene (K/Pg) boundary between them. A limestone facies of the Kurkur Formation replace the lower part of the upper Kharga Shale unit in the south Kharga Oasis and the Abu Tartur Plateau (Fig. 3). Another limestone facies attributed to the Upper Paleocene Garra Formation unconformably overlies the Kurkur Formation. The Maastrichtian part of the Dakhla Formation is substituted by chalk of the Khoman Formation in the Farafra Oasis (Fig. 3). The Khoman Formation is followed upwards by shale and limestone that belong to the upper Kharga Shale unit of the Dakhla Formation (Fig. 3b), and then the limestone of the Upper Paleocene Tarawan Formation. Upsection, thick shale with limestone forms the Esna Formation of latest Paleocene-early Eocene age. Planktic foraminifera provide evidence that the Paleocene/Eocene (P/E) contact is found in the lower part of

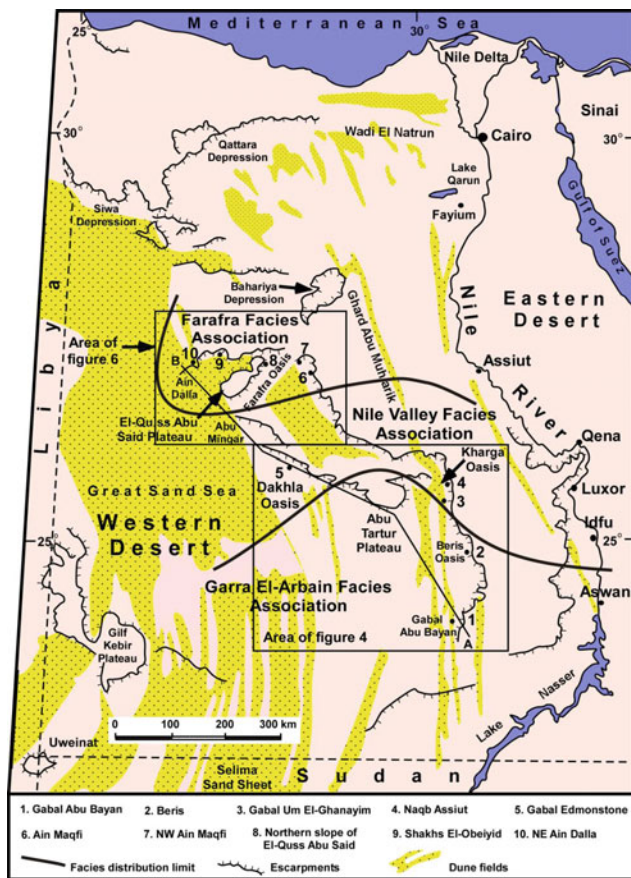


Fig. 1 Location map of the Western Desert of Egypt showing its major physiographic features, the distribution of the major facies associations and the sites of the stratigraphic sections (modified after Brookes, 2003). **a–b** transect is shown in Fig. 3

the Esna Formation (e.g., Berggren & Ouda, 2003). This formation exhibits a conformable contact with the overlying Lower Eocene Thebes Formation. The latter is replaced by the Farafra Limestone in the Farafra Oasis (Fig. 3).

3 Material and Methods

Detailed stratigraphic, sedimentological and planktic foraminiferal biostratigraphic studies were performed on the three facies associations of the southern and central Western Desert. Ten stratigraphic sections were studied (Fig. 1). Among these, two sections were chosen in Abu Bayan and Beris, two sections in the Kharga, one section in the Dakhla and five sections in the Farafra oases. The three sections selected in the Beris and Kharga oases were previously studied by El-Azabi and Farouk (2011). They are revised and paleontologically refined to re-interpret them within the present sequence stratigraphic framework. Re-sampling of many stratigraphic intervals in these sections provided a new precise timing for some of them. In the Dakhla Oasis,

samples were taken from a new section at Gabal Edmonstone, about 100 m from the section measured by El-Azabi and El-Araby (2000), in order to maximize the biodiversity of the assemblage that is associated with the deeper marine facies. A total of 577 rock samples were examined for microfossil content; of these 217 samples were prepared from the seven newly measured sections. Samples for foraminiferal studies were treated using the standard methods of Keller (2002). Foraminifera were counted to achieve the planktic/benthic (P/B) ratio. The paleoenvironments of the studied sediments are interpreted relying on the lithological aspects, microfacies analysis, faunal types, faunal diversity/abundance and P/B ratio. The sequence stratigraphy is interpreted by defining the stratigraphic surfaces, stacking patterns and variations in facies and environments.

4 Results

4.1 Characteristics of Facies Associations

The laterally equivalent Garra El-Arbain, Nile Valley and Farafra facies associations of the Western Desert display distinctive depositional facies and environments (Table 1).

4.1.1 Garra El-Arbain Facies Association

This association marks shallow to partially deep marine sediments that occur in the Abu Tartur Plateau, southeast Kharga and south of Beris (Fig. 1, Sites 1–2). It forms the Kurkur and Garra formations (Fig. 4, Sects. 1 and 2). Oyster rudstone, bioclastic packstone and shale comprise the Kurkur Formation. The limestone facies contain abundant small- and large-sized bivalves, in complete and broken forms, with some echinoids (Fig. 5a). The intervening shale yields a dominance of low diversity benthics. Foraminiferal wackestone and packstone are the dominant facies in the Garra Formation (Fig. 4, Sects. 1 and 2). They hold abundant, highly diversified planktic species and thin-walled shell debris (Fig. 5b). The faunal content decreases in abundance in the upper part of the Garra Formation.

4.1.2 Nile Valley Facies Association

This association represents quite variable shallow and deep marine sediments that crops out in the northeast Kharga, Dakhla and Abu Minqar areas (Fig. 1, Sites 3–5). It defines the Dakhla, Tarawan, Esna and Thebes formations, from base upward (Fig. 4, Sects. 3, 4 and 5). The Dakhla Formation consists of calcareous shale containing low to moderate diversity benthic foraminifera, sometimes, with skeletal wackestone and oyster rudstone. It holds high planktic foraminiferal-species abundance in its upper Kharga Shale unit. Foraminiferal packstone and shale typify the Tarawan Formation and the lower part of the Esna Formation,

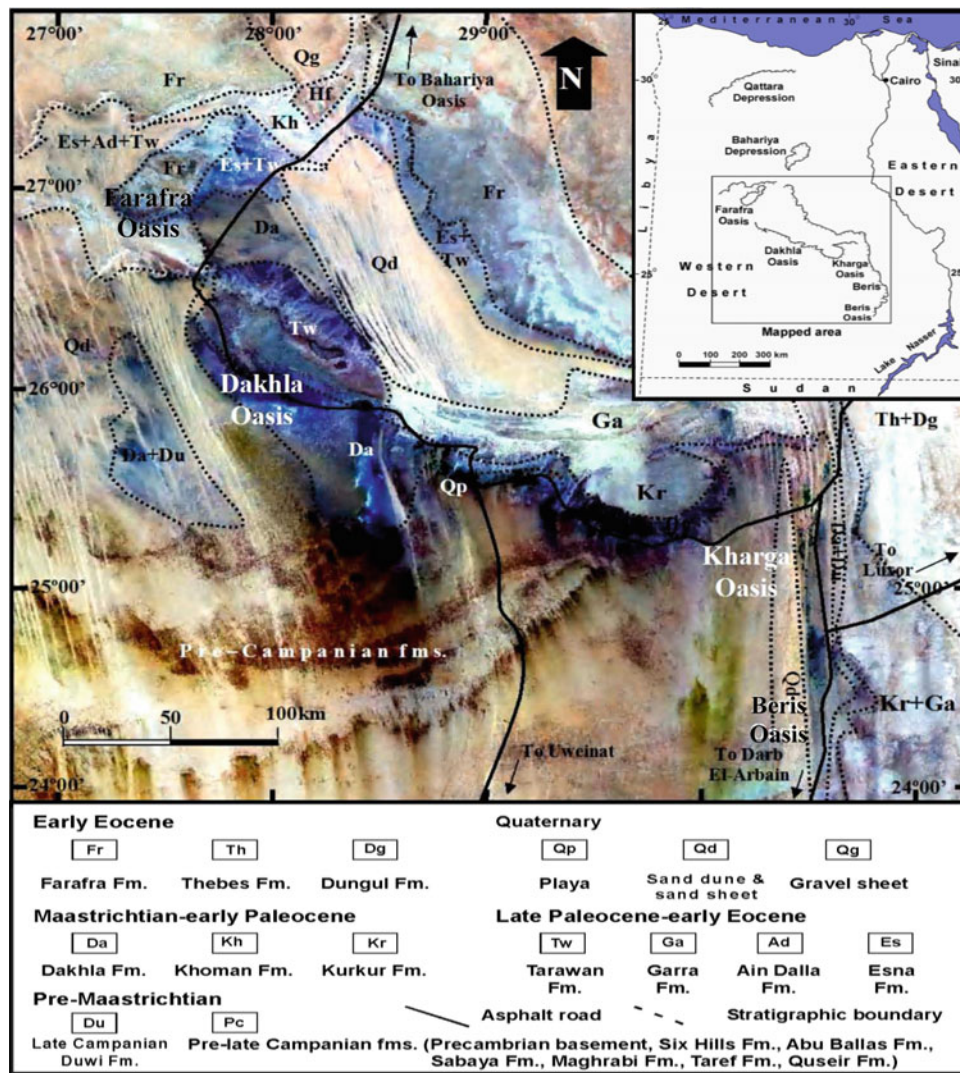


Fig. 2 Landsat image shows the distribution of the exposed stratigraphic units in the southern and central Western Desert

respectively (Fig. 4, Sects. 3–5). These facies comprise abundant and diverse planktic species and common benthics (Fig. 5c). Calcareous shale characterizes the upper part of the Esna Formation, while nummulitic bioclastic wacke-/packstone, nummulitic wackestone and shale characterize the Thebes Formation (Fig. 4, Sects. 3 and 4). The Eocene facies consist of complete and fragmented *Nummulites* and *Alveolina*, along with miliolids and echinoids (Fig. 5d).

4.1.3 Farafra Facies Association

This association typifies the deep and shallow marine sediments widely prevalent in the Farafra Oasis (Fig. 1, Sites 6–10). The Khoman, Dakhla, Tarawan, Esna or its coeval Ain Dalla, and Farafra formations, comprise the Farafra facies association (Fig. 6). Wackestone with loosely packed planktic foraminifera is the dominant facies in the Khoman Formation (Fig. 5e), with pectenid lime-mudstone and dolostone at the top. Richly fossiliferous wackestone and shale with

well-preserved planktic species characterize the exposed part of the Dakhla Formation (Fig. 6). Similar facies of packstone and shale signify the Tarawan Formation (Fig. 6). Pelagic shale and intercalating shale and packstone mark the lower and upper parts of the Esna Formation, respectively. The packstone holds abundant larger benthics of *Nummulites*, *Alveolina* and micritized bioclasts (Fig. 5f). The Esna shale is replaced by a carbonate facies of wackestone, lime-mudstone and dolostone in the NW Farafra Oasis (Ain Dalla Formation, Fig. 6, Sects. 9–10). Alveolinid wackestone, nummulitic alveolinid packstone and lime-mudstone are evident in the overlying Farafra Limestone.

4.2 Depositional Facies and Environments

Shallow and deep marine facies mark the Maastrichtian-Ypresian sediments of the studied areas. The facies

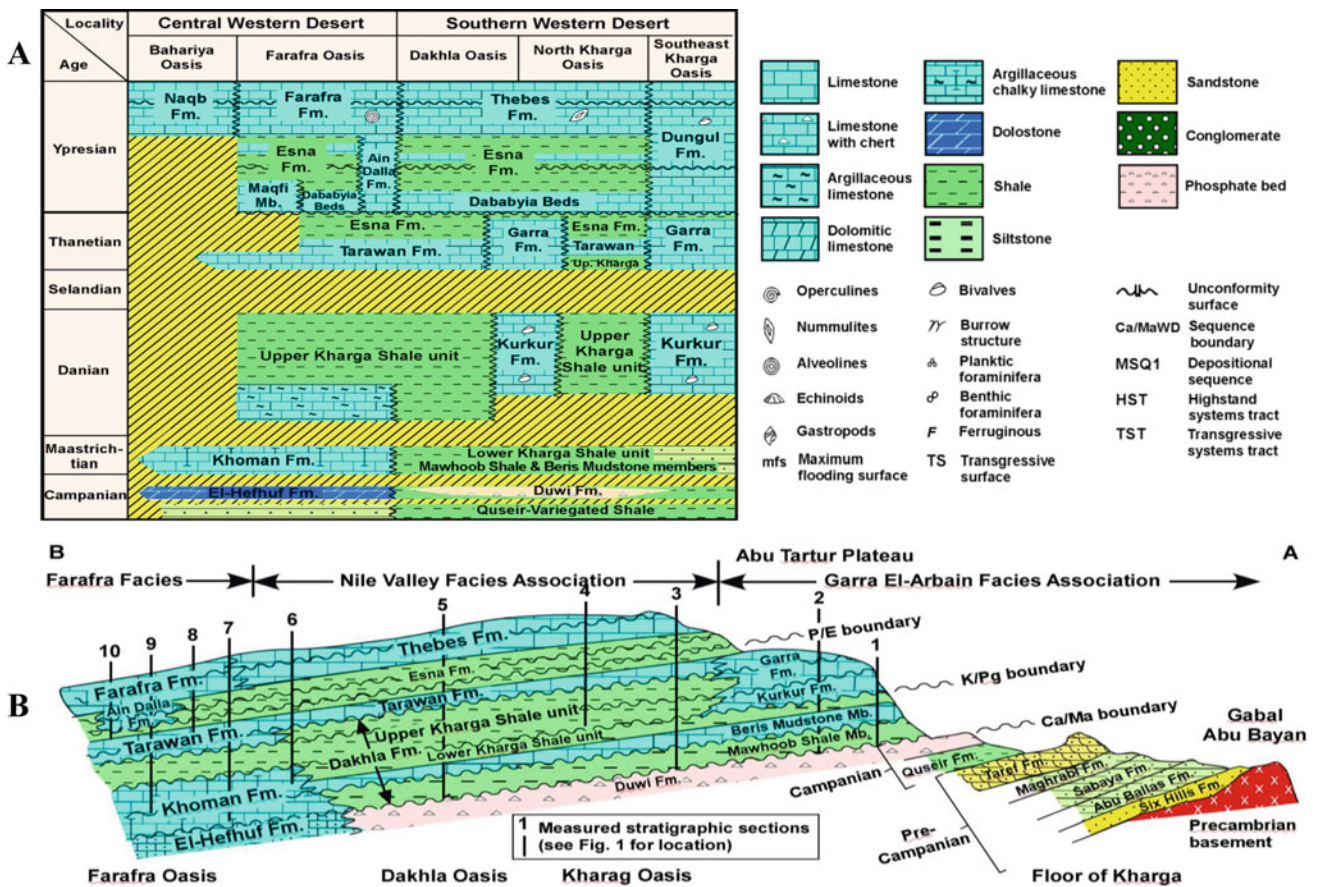


Fig. 3 a Time-facies correlation scheme of the different rock units exposed in the southern and central Western Desert. b Panoramic stratigraphic sketch shows the distribution of the laterally equivalent Garra El-Arbain, Nile Valley and Farafra facies associations in the studied areas (not to scale). Location of the line of section is given in Fig. 1

distribution is largely affected by the paleo-relief irregularity of the Dakhla Basin (Fig. 7). The shallow marine facies is restricted to the submerged, paleo-structural highs (Abu Tartur Plateau, Beris Oasis, Abu Bayan area). It typifies the Garra El-Arbain facies association and in parts the Nile Valley and Farafra facies associations. It consists of shale and limestone with benthic foraminifera and bivalves. The shale holds rare to high dominance-low diversity benthic species (Mawhoob Shale Member, lower Kharga Shale unit, Fig. 4) that indicate accumulation in a shallow to slightly deep subtidal flat, under restricted conditions. The limestone facies (bioclastic wackestone to packstone, oyster rudstone to floatstone) of the Mawhoob Shale Member and Kurkur Formation (Figs. 4 and 5a) are interpreted as representing a shallow subtidal setting with submerged shoals formed during periods of warm, arid climate and high carbonate productivity. The dominance of low species diversity points to deposition under increasingly restricted conditions. In contrast, the shallow marine setting with normal salinity and high organic detritus characterizes the deposits of the Thebes, Farafra and upper Ain Dallah formations (Nile Valley

and Farafra facies associations, Figs. 4, 5d and 6), which provide favorable conditions for the growth of larger benthics. The resultant limestone facies contain abundant, low diversity *Nummulites*, *Alveolina* and *Orbitolites* that are ubiquitous in the shallow water habitats (Jorry et al., 2006). The wackestone and packstone reflect deposition in lower and upper shallow subtidal flats, respectively, while the lime-mudstone is interpreted as representing restricted lower intertidal deposition, as evidenced by the scarcity of faunal content.

The deep marine facies, on the other hand, marks the paleo-structural lows (Kharga, Dakhla and Farafra sub-basins, Fig. 7) of the Dakhla Basin. It typifies the Nile Valley and Farafra facies associations. This facies yields abundant and diverse planktic foraminifera with common deep-water benthics indicating deposition in an open marine environment (Khoman Formation, upper Kharga Shale unit, Tarawan Formation, Fig. 6). Deposition oscillates from deep inner to outer shelf setting depending on the recorded planktic/benthic ratio (Gibson, 1989; Murray, 1976). Foraminiferal shale, wackestone and packstone, the dominant

Table 1 Lithological and paleontological aspects of the Maastrichtian-Ypresian formations in the southern and central Western Desert with their depositional facies and environments

Formations	Lithological characteristics	Faunal types, diversity and abundance	Major taxa	Depositional facies	Paleo-environments
<i>1. Garra El-Arbain Facies Association (Abu Tartur Plateau, southeast Kharga Oasis and south of Beris Oasis)</i>					
Kurkur (6–12 m thick)	Massive, highly fractured coquinal limestone with shale interbeds	Abundant bivalves and echinoids of low diversity with few gastropods	<i>Ostrea orientalis</i> and <i>Nemocardium fecundum</i>	Oyster rudstone, bioclastic packstone and shale	Shallow to deep subtidal flat
Garra (27 m thick)	Massive bedded limestone, hard to moderately hard, partly chalky and argillaceous	Low to moderately abundant and diversified planktic and benthic foraminifera	<i>Morozovella</i> and <i>Acarinina</i>	Foraminiferal wackestone and packstone	Shallow subtidal flat and shallow middle shelf
<i>2. Nile Valley Facies Association (northeast Kharga Oasis, Dakhla Oasis and Abu Minqar area)</i>					
Dakhla (58–76 m thick)	Fissile shale, grey, slope-forming, calcareous, with a varying amount of fossils, intercalated with massive argillaceous limestone and mudstone	Rare to common agglutinated benthic foraminifera with some planktic-rich intervals in lower part, large oysters in middle part and common highly diversified planktic foraminifera in upper part	<i>Ammobaculites khargensis</i> at base, <i>Exogyra overwegi</i> at middle, <i>Acarinina</i> <i>Praemurica</i> at top	Calcareous and pelagic shale, bioclastic wackestone, oyster floatstone to rudstone and lime-mudstone	Shallow to deep subtidal flat, and middle to outer shelf in the upper part
Tarawan (7–25 m thick)	Thick-bedded, snow white chalky limestone, highly fossiliferous	Abundant and highly diversified planktic foraminifera, common benthics, few echinoids, gastropods	<i>Acarinina</i> and <i>Morozovella</i>	Foraminiferal packstone	Shallow middle to outer shelf
Esna (45–48 m thick)	Fissile shale, slope-forming, intercalated with ledge-forming argillaceous limestone in lower part	Moderate to abundant and highly diversified planktics and benthics in lower part and common, moderately diversified benthics in upper part	<i>Morozovella</i> and <i>Acarinina</i> ,	Pelagic shale, calcareous shale and lime-mudstone	Shallow middle to outer shelf, deep subtidal flat at top part
Thebes (50–55 m thick)	Thick-bedded, cliff-forming limestone with chert bands and nodules as well as intercalations of shale in lower part	Abundant, low diversity larger benthics and macrofossils (bivalves, gastropods and echinoids) which decrease in abundance in upper part	<i>Nummulites</i> , <i>Operculina</i> , <i>Alveolina</i> and <i>Assilina</i>	Nummulitic bioclastic wackestone and packstone, nummulitic wackestone and calcareous shale	Shallow subtidal flat, deep subtidal flat in lower part
<i>3. Farafra Facies Association (Farafra Oasis and its northern vicinity)</i>					
Khoman (5–55 m thick)	Massive to bedded, snow white chalk, partly with limestone	Abundant and highly diversified planktic and benthic foraminifera, barely fossiliferous at top part	<i>Globotruncana</i> , <i>Heterohelix</i> and <i>Pecten farafrensis</i>	Foraminiferal wackestone, bioclastic wackestone and lime-mudstone	Middle/outer shelf, deep subtidal and lower intertidal
Dakhla (1–10 m thick)	Massive argillaceous limestone in lower part and calcareous shale in upper part	Moderately to highly abundant and diversified planktic and benthic foraminifera	<i>Parasubbotina</i> , <i>Praemurica</i> and <i>Morozovella</i>	Foraminiferal wackestone and pelagic shale	Shallow to deep middle shelf and outer shelf
Tarawan (1–23 m thick)	Massive to thick-bedded, snow white chalky limestone with shale interbeds	Abundant and highly diversified planktic foraminifera which decrease in abundance in upper part	<i>Acarinina</i> and <i>Morozovella</i>	Foraminiferal packstone, pelagic shale, calcareous shale and lime-mudstone	Middle/outer shelf, deep subtidal and lower intertidal
Esna (20–100 m thick)	Fissile shale with massive argillaceous limestone interbeds	Abundant and highly diversified planktic and benthic foraminifera with larger benthic foraminifera,	<i>Morozovella</i> , <i>Acarinina</i> , <i>Nummulites</i> and <i>Operculina</i>	Pelagic shale, calcareous shale and foraminiferal wackestone and packstone	Middle/outer shelf in lower part, deep to shallow subtidal in upper part

(continued)

Table 1 (continued)

Formations	Lithological characteristics	Faunal types, diversity and abundance	Major taxa	Depositional facies	Paleo-environments
		bivalves and echinoids in upper part			
Ain Dalla (70–80 m thick)	Well-bedded, hard, massive chalky limestone with some dolostone and shale interbeds	Abundant and moderately diversified planktic foraminifera with larger benthics, bivalves and echinoids in the upper part	Morozovella, Acarinina, Alveolina	Foraminiferal wackestone, alveolinid wackestone, calcareous shale, lime- mudstone and dolostone	Middle to outer shelf, shallow to deep subtidal and lower intertidal
Farafra Limestone (13–50 m thick)	Thick-bedded limestone with dolostone and shale interbeds	Abundant, low diversity larger benthic foraminifera and macrofossils that decrease in abundance in upper part	Alveolina, Orbitolina, Assilina, Nummulites and miliolids	Alveolinid wackestone, nummulitic alveolinid packstone, lime-mudstone, dolostone and shale	Shallow to deep subtidal and lower intertidal

facies, are interpreted as having deposited during rapid sea-level rise under conditions of warm water, high nutrient supply and fair circulation to the open sea.

4.3 Planktic Foraminiferal Biostratigraphy

Planktic foraminiferal analysis enables the establishment of a robust biostratigraphic framework for the Maastrichtian-Ypresian successions. In this study, the biozonation schemes of Li and Keller (1998a, 1998b) and Li et al. (1999) were followed in the Maastrichtian record, while the schemes of Berggren and Pearson (2005) and Wade et al. (2011) were applied to the Paleocene-early Eocene record. The numerical ages of the zonal boundaries are consistent with the time scales of Li et al. (1999) and Wade et al. (2011) for the Maastrichtian and Paleocene-Eocene intervals, respectively. Ninety-one planktic foraminiferal species assigned to thirteen zones were recorded in the Maastrichtian-Ypresian deposits. The characteristic planktic foraminiferal zonal species of the studied successions are shown (Fig. 8).

4.3.1 Maastrichtian

The Lower Maastrichtian deposits mark the Mawhoob Shale Member in the southern oases and the lower part of the Khoman Formation at the Farafra Oasis (Figs. 4 and 6). The Mawhoob Shale Member yields rare to high dominance-low diversity agglutinated benthic species (e.g., *Ammobaculites khargensis* and *Haplophragmoides*, Table 2). It holds few intervals in the lower part rich in planktic foraminifera such as *Rugoglobigerina hexacamerata*, *Gansserina gansseri*, *Globotruncana aegyptiaca* and others, which are related to zones CF8b and CF7 (Fig. 9, Table 2). Similar planktic

species were recorded in the Kharga and Dakhla areas (Tantawy et al., 2001). The upper part of the Mawhoob Member is a barren interval. The topmost part of this interval represents the contact between the early and late Maastrichtian (Fig. 9). In the Farafra Oasis, the Khoman Formation yields abundant and high diversity planktic foraminifera in its lower part which attest to zones CF8b, CF7 and undifferentiated CF6–CF5 (Fig. 10). The dominant species are *Gansserina gansseri*, *Globotruncana aegyptiaca* and *Heterohelix globulosa* among others (Table 2).

The Upper Maastrichtian deposits signify the Beris Mudstone Member and the lower Kharga Shale unit in the southern oases and the upper part of the Khoman Formation in the Farafra Oasis (Figs. 4 and 6). In the southern oases, these sediments are marked by the occurrence of agglutinated benthic species of *Trochammina globigeriniformi*, *Ammobaculites khargensis* and *Haplophragmoides glabra* (Table 2). These species show low diversity and high dominance value suggesting development in a high-stress environment. In the Dakhla Oasis, the lower Kharga Shale unit contains planktic foraminifera belonging to Zone CF3 (Fig. 4, Sect. 5, Table 2). In the Farafra Oasis, the upper part of the Khoman Formation yields planktic species ascribed to zones CF4 and CF3 (Hewaidy et al., 2006). The lower Kharga Shale unit and the top part of the Khoman Formation are characterized by a sharp drop in faunal diversity (Figs. 9 and 10), which is likely related to the global climatic cooling and the sea-level fall that occurred at about 65.5 Ma (Zone CF3 'top', Li et al., 2000). The latest Maastrichtian zones CF2 and CF1 appear to be missing in the Western Desert. The top of the lower Kharga Shale and the Khoman Formation (i.e., top of zones CF4 and CF3) is represented by an erosion surface (Figs. 9 and 10), which corresponds to the K/Pg boundary

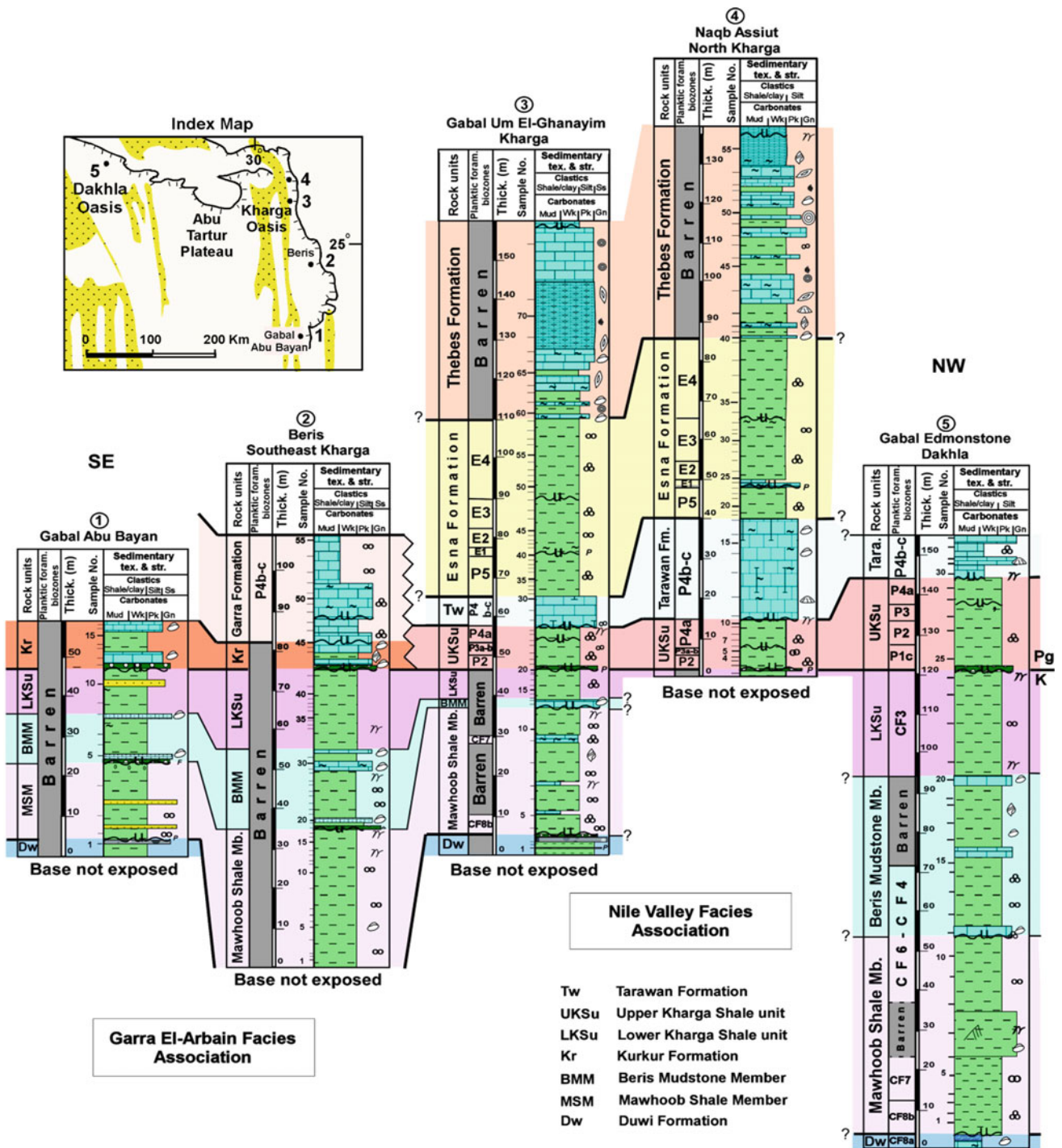


Fig. 4 Correlation chart of the Maastrichtian-Ypresian sediments in the southern Western Desert shows the Garra El-Arbain and Nile Valley facies associations, and their lithological and paleontological aspects (horizontal distance not to scale). Stratigraphic Sects. 2–4 modified after El-Azabi and Farouk (2011). For symbols and keys see Fig. 3

(e.g., Abdel-Kirrem and Samir, 1995; Hewaidy et al., 2006, 2017; Tantawy et al., 2001). The first Danian planktic foraminifera, found in the overlying upper Kharga Shale unit, are characterized by the presence of planktic species denoting Subzone P1c in the Dakhla and Fara

oases (Figs. 4, 6 and 10) and Zone P2 in the Kharga area (Fig. 9). This indicates a significant gap with the absence of the early Danian subzones P0, P α , P1a, P1b and the mid-late Danian Subzone P1c (Kharga Oasis) in addition to the latest Maastrichtian zones CF2 and CF1.

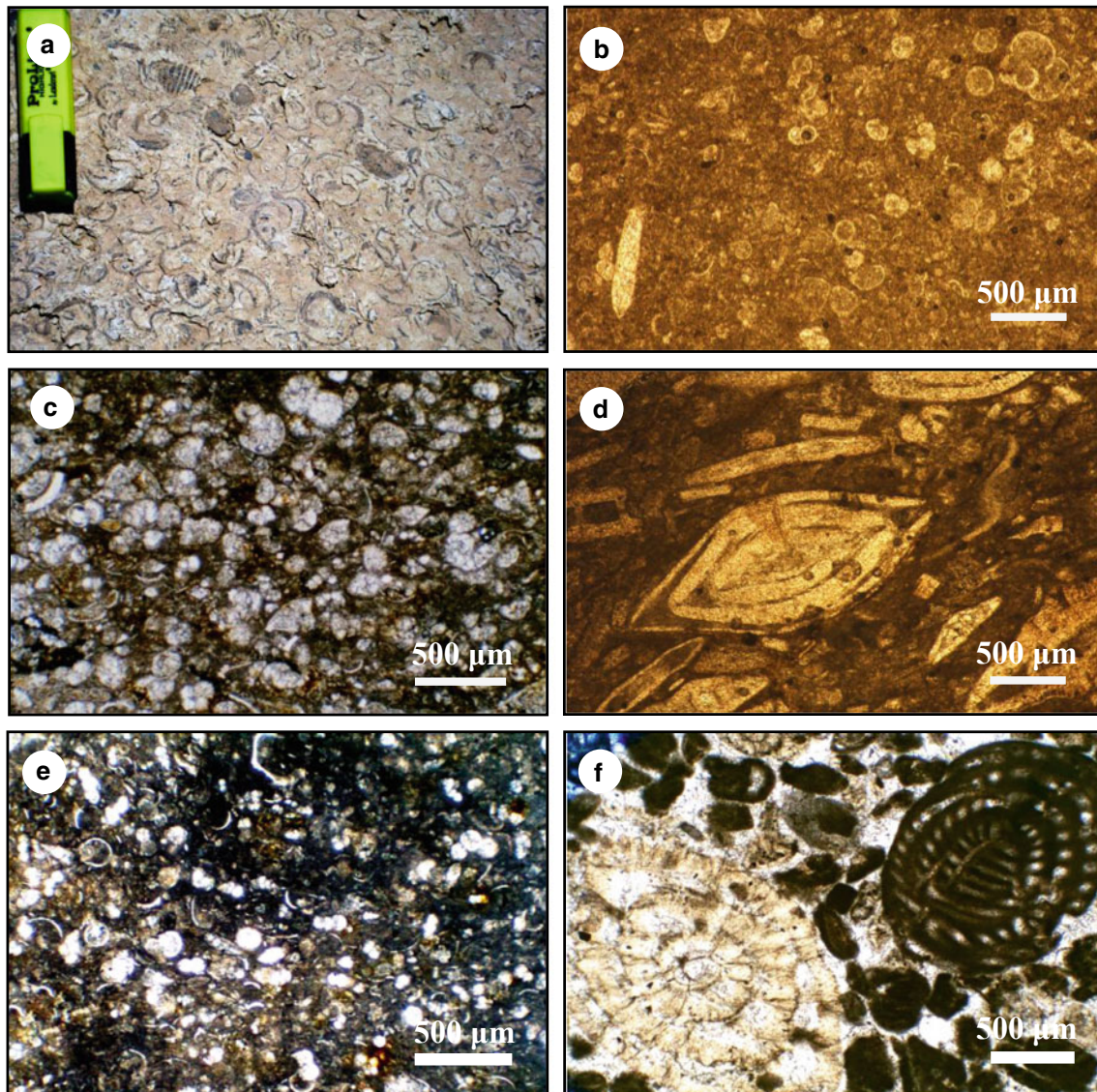


Fig. 5 **a** Complete bivalve shells and fragments densely packed in a lime mud matrix, oyster rudstone, Kurkur Formation, Gabal Abu Bayan, Sect. 1, bed 12. **b** Randomly scattered planktic species in a dense lime mud matrix, foraminiferal wackestone, Garra Formation, Beris, Sect. 2, bed 50, Fig. 4, P.P.L. **c** Abundant planktic tests tightly packed in a dark lime mud matrix, foraminiferal packstone, Tarawan Formation, Naqb Assiut, Sect. 4, bed 13, Fig. 4, P.P.L. **d** Nummulites and shell debris disseminated in a dark lime mud matrix, Nummulitic bioclastic packstone, Thebes Formation, Naqb Assiut, Sect. 4, bed 44, Fig. 4, P.P.L. **e** Randomly dispersed planktic species in a dense lime mud matrix, foraminiferal wackestone, Khoman Formation, NW Ain Maqfi, Farafra Oasis, Sect. 7, bed 19, Fig. 6, P.P.L. **f** Nummulites, alveolina and dense micritized bioclasts cemented by equant spar, alveolinid nummulitic bioclastic packstone, Maqfi Member, Esna Formation, NW Ain Maqfi, Sect. 7, bed 76, Fig. 6, P.P.L.

4.3.2 Paleocene

The Paleocene planktic foraminifera are abundant and diverse. They are marked by six biozones (P1c, P2, P3a, P3b 'base', P4c, P5; Fig. 8). The Danian planktic species are found in the lower and middle parts of the upper Kharga Shale unit (Fig. 4, Sects. 3–5). At the base, this interval yields assemblages, such as *Parasubbotina pseudobulloides*, *Praemurica inconstans* and *Globanomalina compressa* that are ascribed to the mid-late Danian Subzone P1c in the

Dakhla and Farafra oases (Table 2). These assemblages belong to the Subzone P1c(2) of Keller (2002). They are followed by highly diverse planktic species such as *Praemurica uncinata*, *Pr. trinidadensis* and others attributed to the late Danian Zone P2 (Figs. 4, 6 and 9). The abundance of these species reaches its maximum in Zone P2, but decreases at the base of Zone P3. The planktic percentage decreases from as much as 90% in Zone P2 to 30% in Subzone P3a. The latter contains *Morozovella angulata*, *M. praecursoria*,

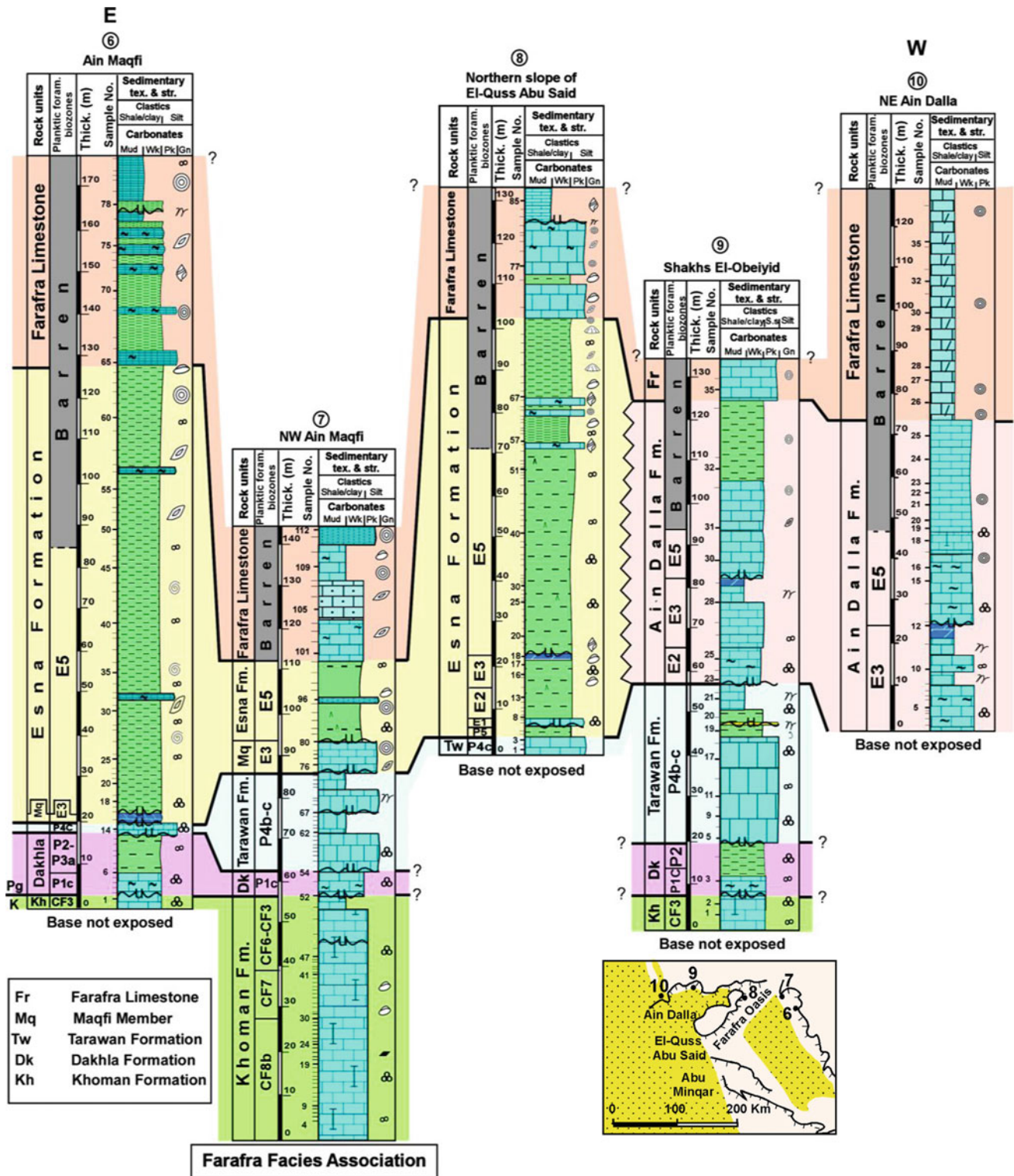


Fig. 6 Correlation chart of the Maastrichtian-Ypresian sediments in the Farafra Oasis shows the Farafra facies association and its lithological and paleontological aspects (horizontal distance not to scale). For symbols and keys see Fig. 3

Igorina pusilla and others (Fig. 9, Table 2). These assemblages are followed by species such as *Igorina albeari*, *Parasubbotina varianta* and *P. variospira* ascribed to the

Subzone P3b 'base' in the Dakhla Oasis. The Danian/Selandian (D/S) boundary lies within Subzone P3b, which dates back to 61.66 Ma (Arenillas, 2012).

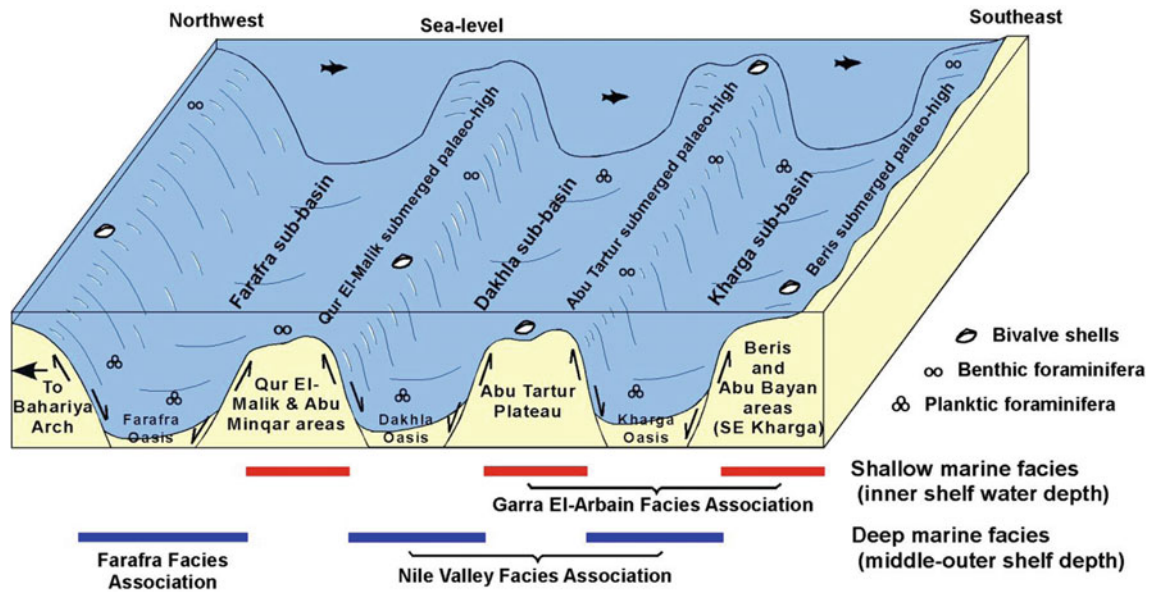


Fig. 7 A simplified northwest-southeast trending block diagram shows the submerged paleo-structural highs and lows of the Dakhla intra-shelf Basin and the distribution of its facies associations and paleoenvironments (Not scaled)

Re-sampling of this interval in Naqb Assiut and Gabal Um El-Ghanayim, previously studied by El-Azabi and Farouk (2011), proves the absence of the top part of Subzone P3b. The lack of subzonal interval P3b 'top' in the studied sections points to the finding of another major hiatus causing the absence of the lower part of the Selandian stage. The uppermost part of the calcareous nannofossil NP4 Zone is also lacking due to the absence of Varol's (1989) NTp8A-B Subzones (Abu Shama et al., 2019).

The Upper Thanetian sediments span the upper Kharga Shale unit 'top part', the Tarawan Formation and the Esna Formation 'basal part' (Figs. 4 and 6). They contain very rich and diverse planktic species indicative of Subzone P4c and Zone P5 of the late Thanetian and latest Thanetian ages, respectively. The dominant species attributed to Subzone P4c are *Morozovella acuta*, *Acarinina soldadoensis*, *Globanomalina pseudomenardii* and others (upper Kharga Shale and Tarawan Formation, Figs. 9 and 10, Table 2). Thus, the Dakhla/Tarawan contact is located within Subzone P4c. The planktic species of Subzone P4c are also identified at Beris (Garra Formation) with moderate diversity and abundance (Fig. 4). The common species found in Zone P5 are *Acarinina soldadoensis*, *Morozovella subbotinae* and many others (Esna Formation, basal part, Figs. 9 and 10, Table 2).

4.3.3 Ypresian

The Ypresian planktic species denote the middle-upper part of the Esna Formation, or its correlative the Ain Dalla Formation, and the Thebes Formation or its coeval the

Farafra Limestone (Figs. 4 and 6). The studied sections show a major biotic anomaly at the P/E contact, where the Paleocene benthic species experienced a pronounced extinction. A number of events known as the Paleocene/Eocene Thermal Maximum, a transient period of global warmth at 55.5 Ma, mark the P/E transition (Zachos et al., 1993). This globally rising temperature caused a major extinction among benthic species (Thomas et al., 2000). In the Kharga Oasis, the P/E contact defines the base of the Dababiya Quarry Beds (DQB, Dupuis et al., 2003). The planktic species disappear and start to recover at ~ 20 cm above this boundary, where excursion fauna of *Acarinina sibaiyaensis* and *Ac. africana* and rare *Morozovella allisonensis* are traced, indicative of Zone E1. The abundance and diversity of planktic species gradually increase upwards in the Esna Formation (Figs. 8 and 10). In the Farafra Oasis, a record of the DQB was revealed on the northern part of El-Quss Abu Said (Fig. 6, Sect. 8) and in the northwest of Bir Bidni, along the Farafra-Ain Dalla road. It consists of a 0.5 m thick limestone, barren of foraminifera. The middle part of the Esna Formation holds abundant planktic species such as *Pseudohastigerina wilcoxensis*, *Acarinina sibaiyaensis*, *Morozovella velascoensis*, *M. formosa* and *M. marginodentata* (Figs. 9 and 10), which are ascribed to zones E1 to E4 in the Kharga Oasis (Fig. 4, Sects. 3–4) and zones E1 to E3 and E5 'base' in the Farafra Oasis (Fig. 6, Sects. 6–8). The recorded species in the Ain Dalla Formation is attributed to zones E2, E3 and E5 'base' (Fig. 6). The upper part of the Esna and Ain Dalla formations show a marked decrease in the abundance and diversity of planktic species. This interval

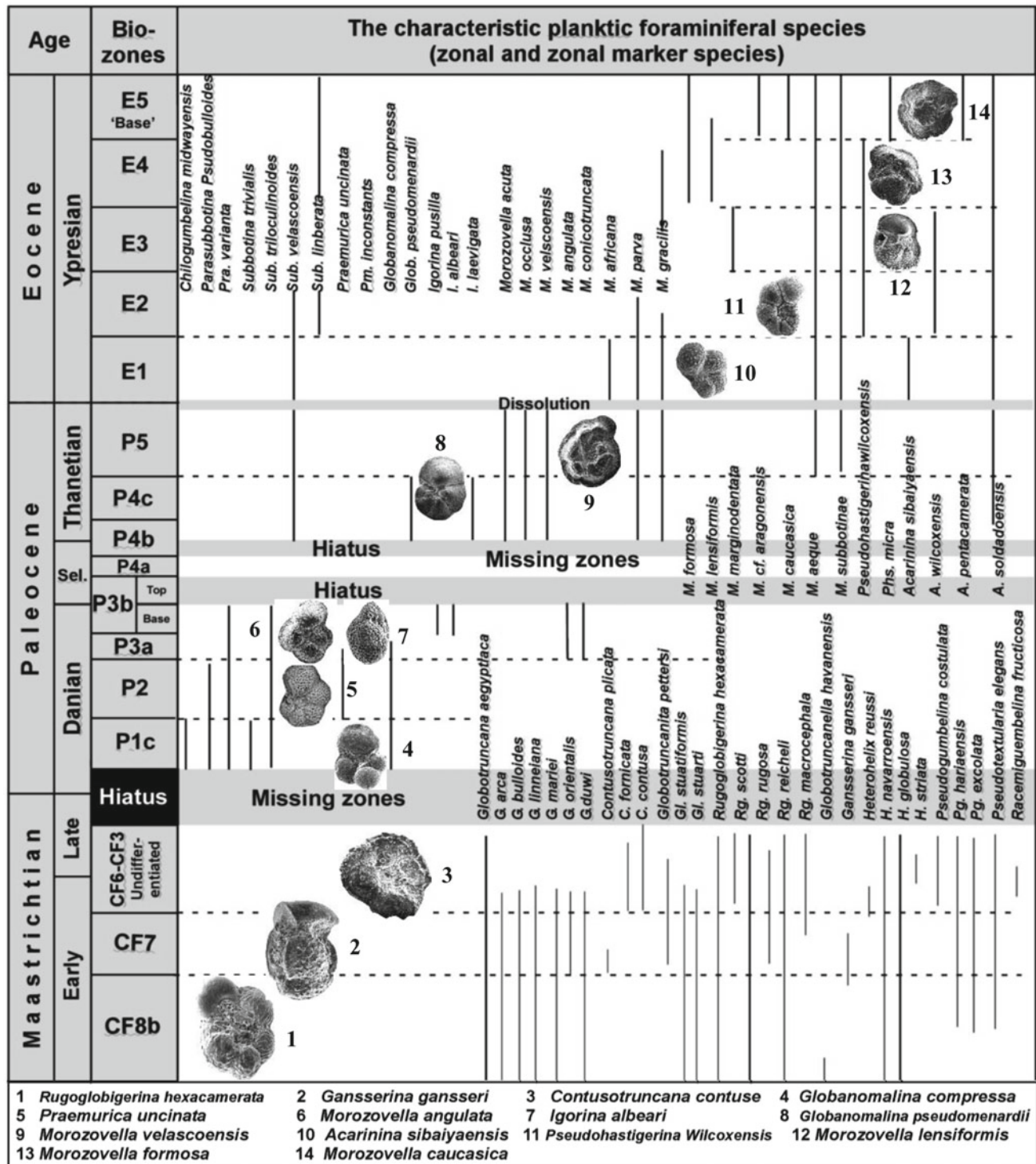


Table 2 Dominant planktic and benthic foraminiferal assemblages recorded in the rock units of the southern and central Western Desert and their related planktic foraminiferal biozones as well as the planktic and benthic percentages. Late Cretaceous biozones are after Li and Keller (1998a, 1998b) and Li et al. (1999), and Paleocene-early Eocene biozones after Berggren and Pearson (2005) and Wade et al. (2011)

Age		Rock units		Planktic biozones	Dominant planktic assemblages	Characteristic benthic assemblages	P/B ratio	Benthic type (%)
Eocene	Ypresian	Thebes Fm	Farafra Limestone	Barren	-	Abundant, low diversity larger foraminifera such as nummulites, operculines, alveolines and discocyclines	-	100%C
		Esna Formation	Unit Esna 2 and 3	E2-E4 Southern oases E2-E3 and E5 'base' Farafra	<i>Pseudohastigerina wilcoxensis</i> , <i>Morozovella formosa</i> , <i>M. velascoensis</i> , <i>M. subbotinae</i> , <i>M. marginodentata</i> , <i>M. aragonensis</i> , <i>M. gracilis</i> , <i>M. allisonensis</i> , <i>Subbotina triangularis</i> , <i>S. linaperta</i> , <i>Acarinina pseudotopilensis</i> and <i>Ac. soldadoensis</i> which decrease in abundance & diversity upward	<i>Margulinina wetherellii</i> , <i>Loxostomoides applinae</i> , <i>Epontides mairiei</i> , <i>E. lotus</i> , <i>Fronducularia wanneri</i> , <i>Bulimina farafraensis</i> , <i>B. quadrata</i> , <i>B. pupoides</i> , <i>Pseudonodosaria manifestata</i> , <i>Uvigerina maqfensis</i> <i>Dentalina gracilis</i> , <i>Cibicides rigidus</i> , <i>Nonionela cretacea</i>	Variable from 20-90% P, rarely barren	> 85%C
			Dababiya Quarry Beds	E1 Kharga and locally in Farafra	<i>Acarinina sibiyaensis</i> , <i>A. africana</i> and <i>Morozovella allisonensis</i>	and <i>Bulimina midwayensis</i> . Abundant, low-diversity larger benthics such as nummulites, alveolines and operculines are present in upper part of Esna and Ain Dalla formations	0 'basal part' -90% P	> 95%C
Paleocene	Thanetian	Unit Esna 1		P5 Kharga and Farafra	<i>Acarinina angulosa</i> , <i>Ac. interposita</i> , <i>Ac. esnaensis</i> , <i>Ac. soldadoensis</i> , <i>Morozovella oclusa</i> , <i>M. parva</i> , <i>M. Acuta</i> , <i>M. velascoensis</i> , <i>M. subbotinae</i> and <i>M. gracilis</i> , <i>M. edgari</i> . In Farafra, this zone is totally absent or contain a very few specimens	<i>Dentalina gracilis</i> , <i>D. basiplanata</i> , <i>Oolina globosa</i> , <i>Gyroidinoides giradani</i> , <i>Alabamina midwayensis</i> , <i>Marginulinopsis tuberculata</i> , <i>Valvulina colei</i> , <i>Textularia farafraensis</i> and <i>Bulimina midwayensis</i>	45-90% P	> 90%C
		Tarawan Fm.	Garra Fm.	P4c	<i>Globanomalina pseudomenardii</i> , <i>M. velascoensis</i> , <i>M. acuta</i> , <i>M. aequa</i> , <i>M. oclusa</i> , <i>Acarinina soldadoensis</i> , <i>Ac. Mckannai</i> , <i>Ac. primitive</i> , <i>Ac. nitida</i> and <i>Subbotina velascoensis</i>	<i>Fronducularia phosphatica</i> , <i>Margulinopsis tuberculata</i> , <i>Spiroloculina proboscidea</i> and <i>Bulimina cushmani</i>	20-90% P, rarely barren	> 95%C
		Upper Kharga Shale unit (Dakhla Fm.)	KurKur Fm.	P3a-b 'base' P2	<i>Morozovella conicotruncata</i> , <i>M. praecursoria</i> , <i>M. angulata</i> , <i>Igorina pusilla</i> and <i>I. albeiri</i>	Low diversity of genera such as <i>Lenticulina</i> , <i>Cibicides</i> and <i>Cibicides</i>	30% P	> 90%C
	Daimian							> 90%C
								> 90%C

(continued)

Table 2 (continued)

Age	Rock units	Planktic biozones	Dominant planktic assemblages	Characteristic benthic assemblages	P/B ratio	Benthic type (%)
Maastrichtian	Early-Late	Khoman Formation	<p><i>Globotruncana arca</i>, <i>G. aegyptiaca</i>, <i>G. orientalis</i>, <i>G. dwi</i>, <i>G. bulloides</i>, <i>G. limneiana</i>, <i>G. conica</i>, <i>G. formicata</i>, <i>Globotruncanella stuartiformis</i>, <i>Gl. stuarti</i>, <i>Contusotruncana formicata</i>, <i>Contusotruncana contusa</i>, <i>Rugoglobigerina rugosa</i>, <i>R. macrocephala</i>, <i>Gansserina gansseri</i>, <i>Heterohelix globulosa</i>, <i>H. navaroensis</i>, <i>H. reussi</i> and <i>H. striata</i></p>	<p><i>Bolivinoidea draco</i>, <i>B. decoratus</i>, <i>Nodosaria semispinosa</i>, <i>Pseudoclavulina magfiensis</i>, <i>Gaudryina pyramidata</i>, <i>Bolivinospis minuta</i>, <i>Præbulimina carseyae</i>, <i>Sitella cushmani</i> <i>Neoflabellina rugosa</i>, <i>Saracenaria triangularis</i>, <i>Lagena sulcata</i>, <i>Anomalinoidea sinaensis</i>, <i>A. grandis</i>, <i>Neoflabellina jarvisi</i>, <i>Clavulinoidea trilaterus</i> and <i>Tritaxia barakai</i></p>	25–80% P	> 95% C
	Late					
Early	Dakhla Formation	Barren in Kharga	<p><i>Rugoglobigerina rugosa</i>, <i>R. hexacamerata</i>, <i>R. scotti</i>, <i>Pseudogumbelina hariensis</i>, <i>Racemiguembelina fructicosa</i>, <i>Globotruncana aegyptiaca</i>, <i>G. arca</i></p>	<p><i>Neoflabellina jarvisi</i>, <i>Lenticulina girardanus</i>, <i>Gyroidinoidea girardanus</i>, <i>Anomalinoidea pseudoacutus</i> and <i>A. rubiginosus</i></p>	0–20% P in Dakhla	> 60% C
Early	Mawhoob Shale Member	CF8b–CF7	<p><i>Rugoglobigerina hexacamerata</i>, <i>R. macrocephala</i>, <i>R. rugosa</i>, <i>Globotruncana arca</i>, <i>G. aegyptiaca</i>, <i>G. orientalis</i>, <i>G. bulloides</i>, <i>Globotruncanella stuarti</i>, <i>Gl. stuartiformis</i>, <i>Heterohelix reussi</i>, <i>H. navaroensis</i>, <i>H. globulosa</i>, <i>H. striata</i>, <i>Contusotruncana formicata</i>, <i>Rugotruncana subcircummodijer</i> and <i>Gansserina gansseri</i> in planktic-rich intervals</p>	<p>Rare to common agglutinated benthics of low species diversity such as <i>Ammobaculites khargensis</i>, <i>Trochammina</i>, <i>Haplophragmoides</i> and <i>Reophax</i>. Calcareous benthics in planktic-rich intervals are <i>Orthokarstenis oveyi</i>, <i>Nodosaria zippei</i>, <i>Neoflabellina reticulata</i>, <i>Vaginulina cretacea</i>, <i>Cibicides zitteli</i>, <i>Bulinina kickapoensis</i>, <i>Gaudryina africana</i>, <i>Cibicides libycus</i> and <i>Pseudonodosaria manifestata</i></p>	Barren, some intervals hold 30% P and 25% P in Dakhla	90–100% A in barren intervals

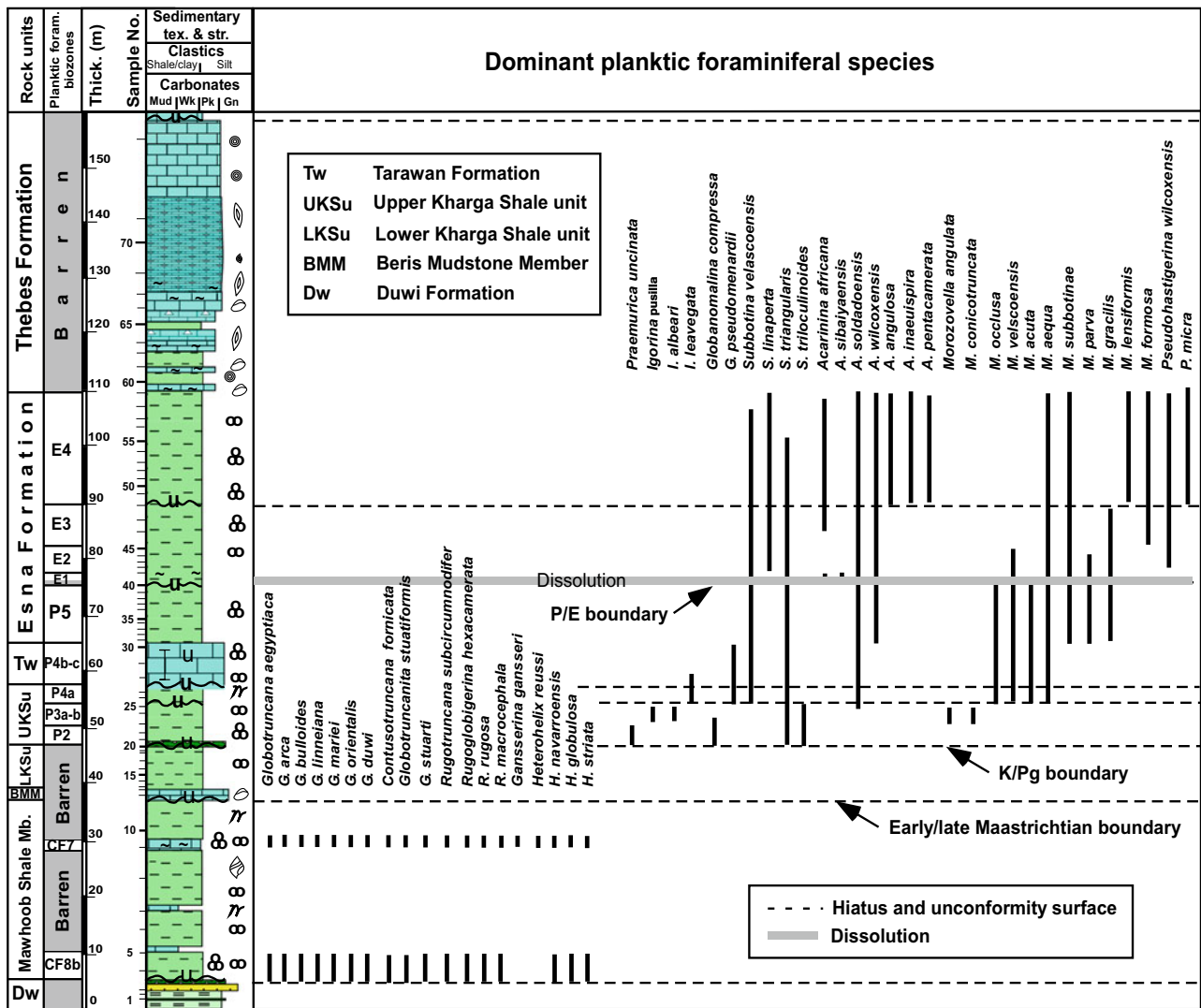


Fig. 9 Frequency distribution of the Maastrichtian-Ypresian planktic foraminiferal species present in Gabal Um El-Ghanayim, Kharga Oasis. For location see Fig. 1 and for symbols and keys see Fig. 3

contains an abundance of *Alveolines* and *Nummulites* of low diversity. These forms extend into the Thebes Formation and its time correlative the Farafra Limestone.

4.4 Maastrichtian-Ypresian Sequence Stratigraphy

A number of sequence boundaries truncate the Maastrichtian-Ypresian sediments of the southern and central Western Desert. They defined eight depositional sequences that are attributed to early Maastrichtian, late Maastrichtian, mid-late Danian, late Selandian, late Thanetian, late-latest Thanetian, early Ypresian and early-late Ypresian. A high-resolution planktic foraminiferal biostratigraphy helped to determine the

time framework of these sequences and the time span of the outlined hiatuses.

4.4.1 Sequence Boundaries

Nine sequence boundaries representing either short- or long-term hiatuses are present in the studied sediments. They are delineated by faunal and sedimentation breaks such as erosional/indurated contacts, dolomitization, biozonal lack, hardgrounds and reworking. These boundaries are mostly associated with sudden changes in facies and in P/B ratios across sharp surfaces.

The Campanian/Maastrichtian boundary defines the top of the Duwi Formation. This boundary is consistent with a faunal break at the CF8a/CF8b zonal boundary, which was assigned at 71 Ma by Li et al. (1999). It typifies a sharp

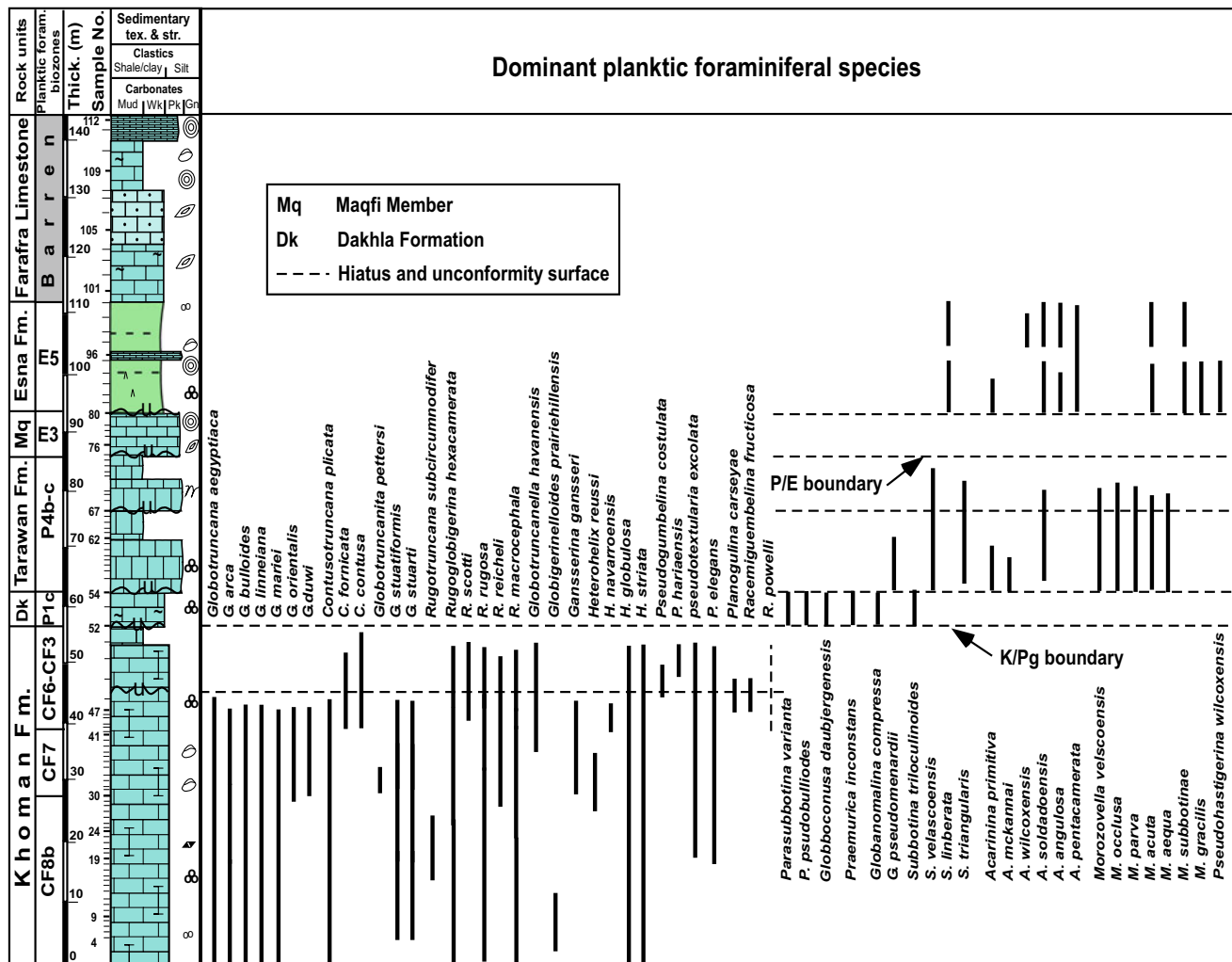


Fig. 10 Frequency distribution of the Maastrichtian-Ypresian planktic foraminiferal species present in NW Ain Maqfi, Farafra Oasis. For location see Fig. 1 and for symbols and keys see Fig. 3

erosional surface with reworked pebbles at Abu Bayan and the Kharga Oasis (Ca/MaWD, Fig. 11, Sects. 1 and 3, Fig. 12a). It marks the top of a 2 m thick, dolostone at the Dakhla area (Fig. 11, Sect. 5). The Lower/Upper Maastrichtian boundary forms the top of the Mawhoob Shale Member. It matches a time lapse at the CF5/CF4 zonal boundary dating to 68.3 Ma (Li et al., 1999). This boundary defines a thin, iron-stained conglomerate at Abu Bayan and a 5 cm thick, highly oxidized and bioturbated hardground with abraded shell debris and iron-rich clasts at the Kharga and Dakhla oases (L/UMaWD, Fig. 11). At the Farafra Oasis, it is identified tentatively within the Khoman Chalk, due to biostratigraphic limitation and the lack of clear evidence of erosion (Fig. 13, Sect. 7).

The Maastrichtian/Danian boundary occurs at the top of the lower Kharga Shale and the Khoman Formation. It forms the K/Pg hiatus that occurred at 65.5 Ma (top of Zone CF3). At the Kharga Oasis, this boundary records the absence of

zonal interval CF2-P1c (Ma/Da WD, Fig. 11, Sects. 3–4). It is defined by a 20–30 cm thick, conglomerate with crushed late Maastrichtian foraminifera (Fig. 12b). This bed reaches 1 m in thickness at Beris. At the Dakhla and Farafra oases, the erosional surface of this hiatus denotes the absence of zones CF2-P1b (Fig. 11, Sect. 5, Fig. 13, Sects. 7 and 9). The Danian/Selandian hiatus is present within the upper Kharga Shale unit in Dakhla and Kharga oases and within its coeval the Kurkur Formation at Beris (Da/SelWD, Fig. 11). It typifies a sharp contact associated with a faunal change from benthic species of low diversity to planktic species of high diversity. At the Farafra Oasis, this boundary displays a faunal break at the contact between the Dakhla and Tarawan formations (Fig. 12c), where the Tarawan Formation begins early within the Selandian Subzone P4a because of a lateral change in facies. The Selandian/Thanetian boundary displays a faunal break, where Subzone P4b is missing. At the Dakhla and Kharga oases, the S/Th hiatus occurs at the

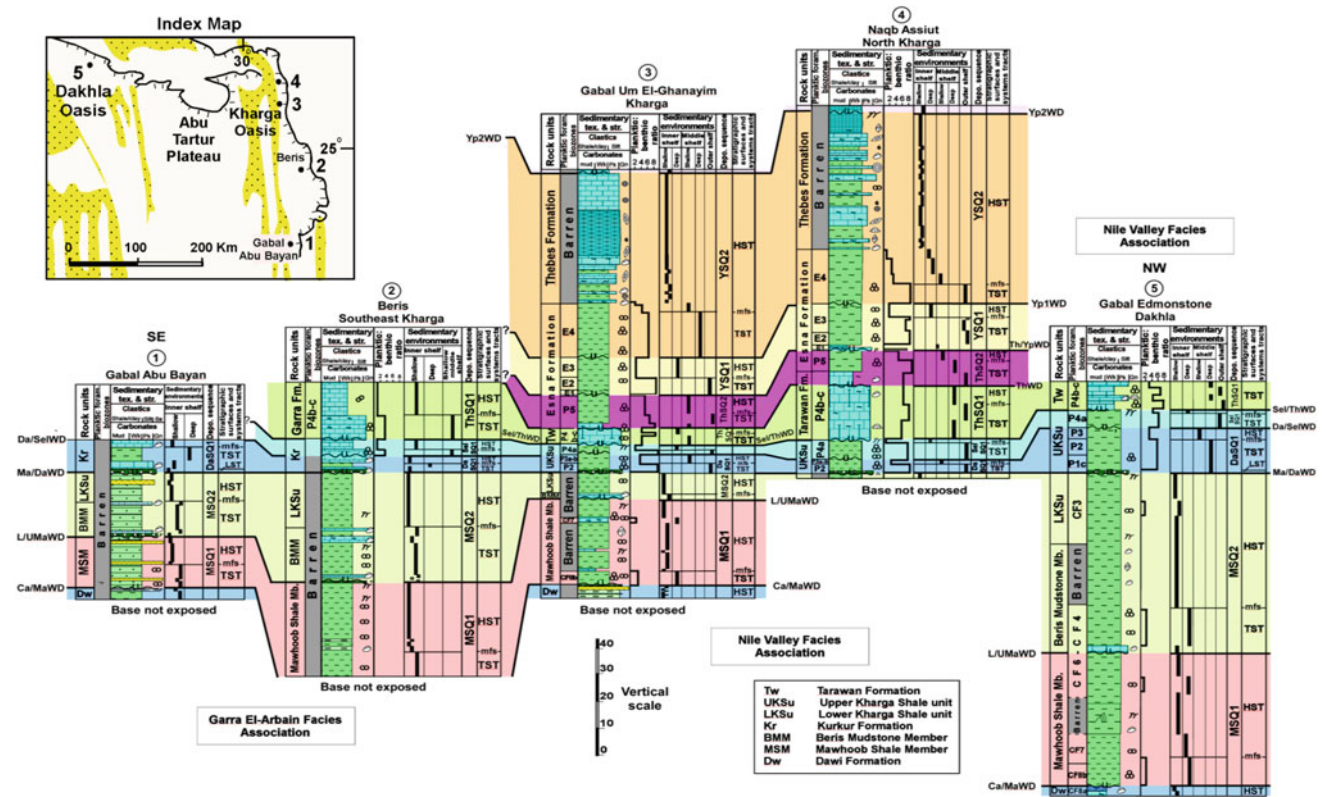


Fig. 11 Correlation chart of the Maastrichtian-Ypresian sequences in the southern Western Desert shows their lithofacies, P/B ratio, paleoenvironments and sequence stratigraphic interpretation (horizontal distance not to scale). For symbols and keys see Fig. 3

Dakhla/Tarawan contact (Sel/ThWD, Fig. 11) while it occurs in the Farafra Oasis within the Tarawan Formation due to a lateral change in facies (Sel/ThWD, Fig. 13). The lack of zones P3b-P4b at Ain Maqfi, zones P2-P4b at NW Ain Maqfi and zones P3-P4b at Shakhs El-Obeiyid refer to the D/S and S/Th hiatuses, which merged due to tectonic uplift (Fig. 13, Sects. 6–7). At Beris, this boundary typifies a sharp surface between the Kurkur/Garra formations linked with a faunal change from benthics of low diversity to planktics of high diversity.

The intra-Thanetian boundary outlines the top part of the upper Kharga Shale unit and its coeval the lower part of the Garra Formation (ThWD, Fig. 11). It is located in the late Thanetian Subzone P4c and represents a bioturbated hard-ground with *Thalassinoides* at the Dakhla/Tarawan contact. A thin conglomerate or a hardground defines this boundary in west Dakhla area (El-Azabi & El-Araby, 2000). At Qur El Malik, a thin pebbly mudstone with an irregular base marks the boundary ThWD (Fig. 12d). At the Farafra area, this boundary is traced within the Tarawan Formation (Fig. 13, Sects. 7 and 9) since the lower part of this formation becomes older as one proceeds from the Kharga to the Farafra areas. The Thanetian/Ypresian boundary is located within the lower part of the Esna Formation (Th/YpWD, Fig. 11). It signifies a faunal break at the P5/E1 zonal

boundary, dated at 55.5 Ma. This boundary is evident by a bioturbated bed with reworked pebbles in the Kharga area. At Gabal Um El-Ghanayim and on the northern slope of El-Quss Abu Said, the boundary Th/YpWD is a concordant surface with no zonal break since the planktic species confirm a complete P/E transition interval. This contact is akin to that of the Dababiya Quarry section, which hosts the Global Standard Stratotype-section and Point of the P/E contact (Dupuis et al., 2003). At the Farafra Oasis, this boundary marks the base of a 15–20 cm thick, limestone with gravels at NW Bir Bidni (Fig. 12e and f). In other sections, it shows a long hiatus in the upper part of the Tarawan Formation because of the lack of all or parts of zones P5-E2 (Figs. 12g, h and 13).

The Lower Ypresian boundary occurs in the middle of the Esna Formation. It defines the upper limit of Zone E3, dated at 54 Ma (Yp1WD, Fig. 11). A thin conglomerate or a cemented marl bed demarcates the boundary Yp1WD in the Kharga area (El-Azabi & Farouk, 2011). In the Farafra area, this boundary denotes the absence of Zone E4. It designates the top of a dolostone bed present at Ain Maqfi, on the northern slope of El-Quss Abu Said and at NE Ain Dalla (Fig. 13). The Upper Ypresian boundary is outlined in the upper part of the Thebes Formation and the Farafra Limestone (Yp2WD, Figs. 11 and 13). It is most likely located

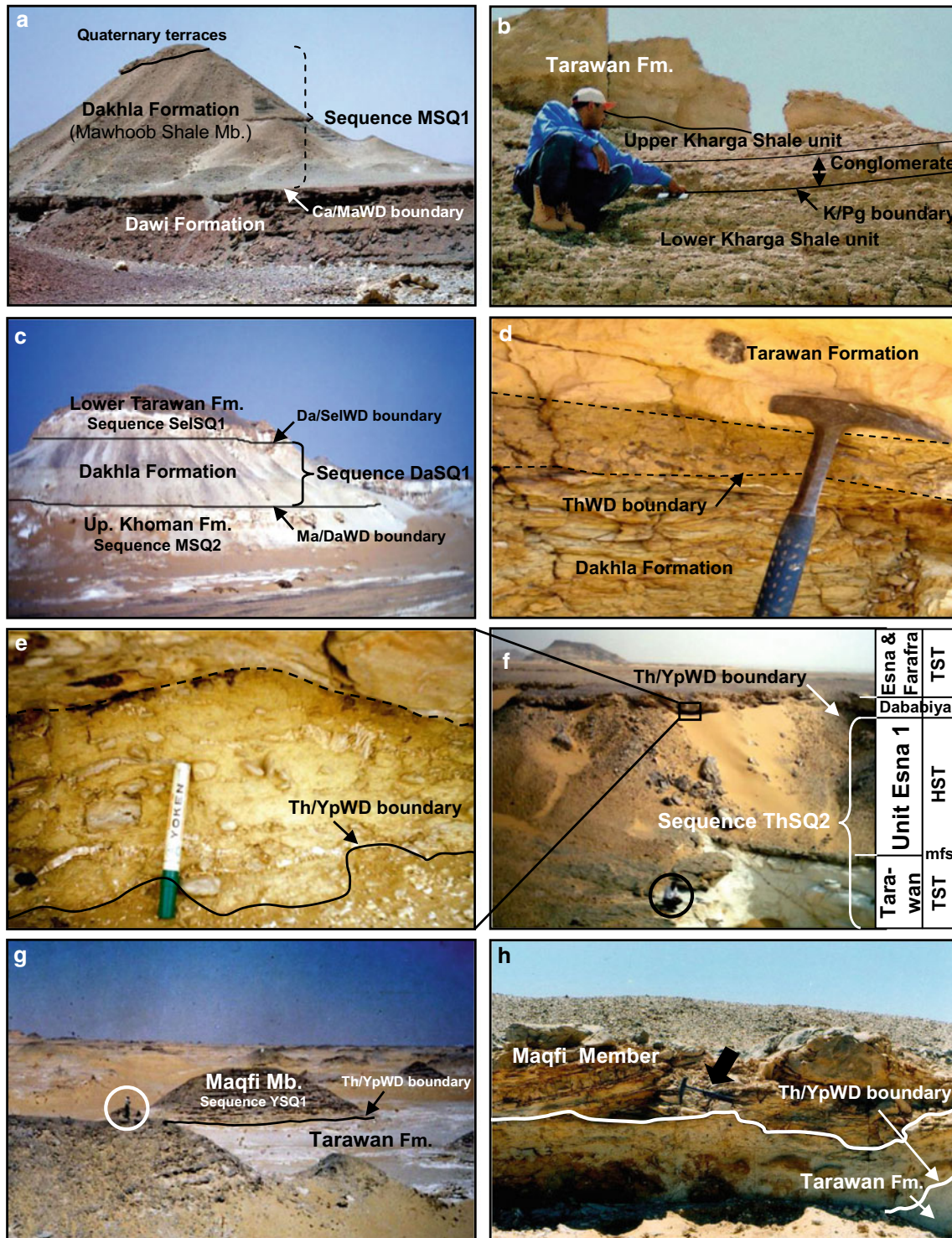


Fig. 12 **a** A sharp erosional surface with chert and phosphate pebbles at the top of a 1 m thick, phosphatic bed marks the boundary Ca/MaWD at the Duwi/Dakhla contact, Tenida area, Kharga Oasis. Outcrop is about 20 m in height. Photograph is looking NW. **b** A 20–30 cm thick, phosphatic conglomerate denotes the boundary Ma/DaWD (K/Pg hiatus) in Gabal Um El-Ghanayim, Fig. 11, Sect. 3. **c** Sequence boundaries Ma/DaWD and Da/ThWD that designate the Khoman/Dakhla and Dakhla/Tarawan contacts, respectively in NW Bir Bidni, 30 km along the Farafra-Ain Dalla road. Succession is about 35 m thick. Photograph is looking north. **d** A 10 cm thick, pebbly mudstone with an irregular basal surface marks the boundary ThWD at the Dakhla/Tarawan contact in Qur El Malik, Dakhla-Farafra asphalt road. **e** A thin gravelly lime-mudstone denotes the unconformable contact at the P/E boundary (Th/YpWD) in NW Bir Bidni, NE Farafra Oasis. **f** Sequence stratigraphy of the latest Paleocene-earliest Eocene sediments of NW Bir Bidni, NE Farafra. Note the Dababiya Quarry Beds that signify the base of the Eocene. Person for scale is about 1.7 m tall. Photograph is looking north. **g** The P/E unconformable contact (boundary Th/YpWD) between the Tarawan Formation and the Maqfi Member of the Esna Formation at NW Ain Maqfi, Fig. 13, Sect. 7. Standing man for scale is about 1.8 m tall. Photograph is looking NE. **h** Close up view shows a gravel-rich band defining the boundary Th/YpWD at the top of the Tarawan Formation at NW Ain Maqfi. Hammer for scale is 35 cm long

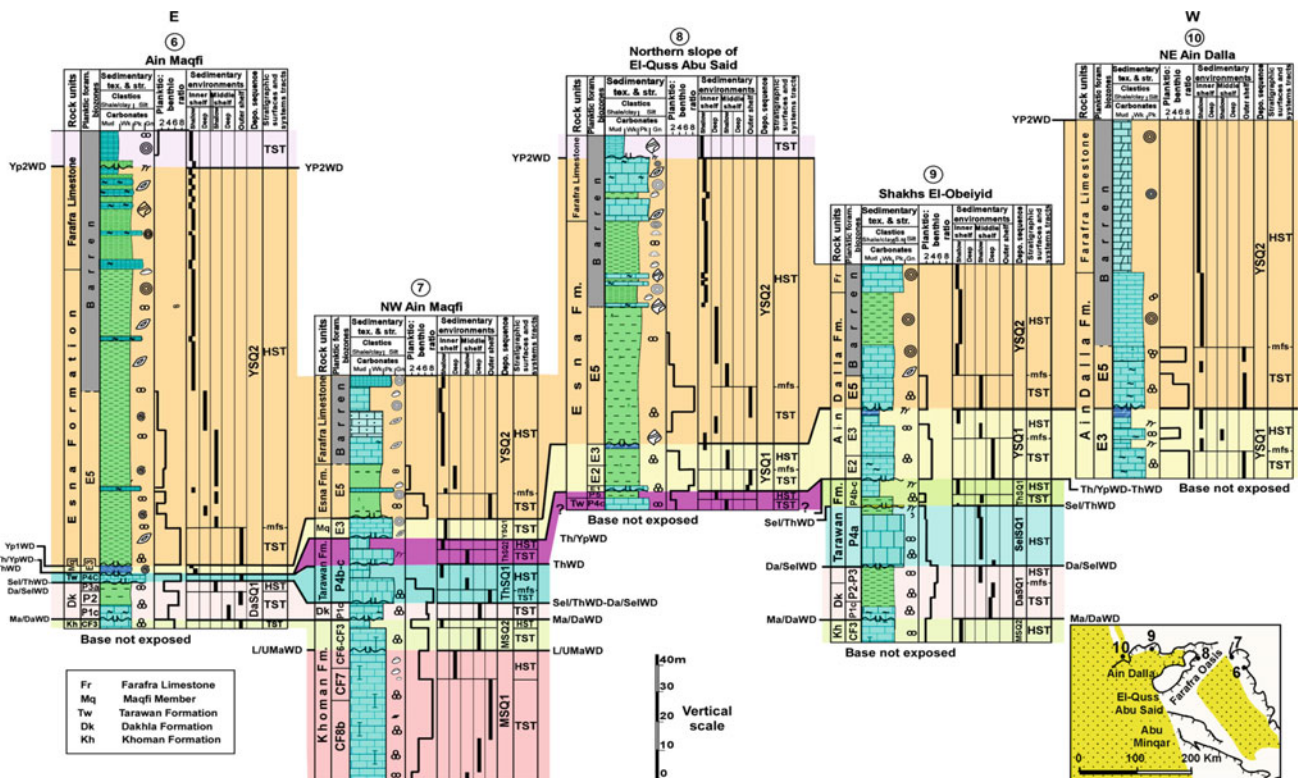


Fig. 13 Correlation chart of the Maastrichtian-Ypresian sequences of the Farafra Oasis shows their lithofacies, P/B ratio, paleoenvironments and sequence stratigraphic interpretation (horizontal distance not to scale). For symbols and keys see Fig. 3

close to the Ypresian/Lutetian boundary since the early/middle Eocene zonal boundary is hard to detect using the larger foraminifera. This boundary is indicated by a micro-karst surface stained with iron oxide in the Kharga Oasis, and by a 1 m thick, *Thalassinoides* burrowing in El-Quss Abu Said. It denotes the top part of an intensively dolomitized limestone at Ain Dalla.

4.4.2 Depositional Sequences

The inferred sequence boundaries in the studied successions evidence the occurrence of eight third-order depositional sequences (Table 3). These sequences vary in duration from 0.4 to 2.9 Ma and in thickness from a few meters to several tens of meters.

The Lower Maastrichtian sequence (MSQ1) comprises the Mawhoob Shale Member in the southern oases and the lower part of the Khoman Formation at the Farafra Oasis (Fig. 12a). The thickness of this sequence is in the range from 18 to 38 m. Sequence MSQ1 belongs to planktic zones CF8b and CF7, which span 1.4 m.y. (71.0–69.6 Ma, Fig. 14). However, the time span is not complete because the upper part of this sequence is a barren interval (Kharga Oasis) or lies within undifferentiated zones (Dakhla and Farafra oases). The poorly dated interval could be ascribed to the early Maastrichtian zones CF6 and CF5. Sequence

MSQ1 starts with shallow to deep subtidal shale in the southern oases, and middle to outer shelf foraminiferal wackestone at the Farafra Oasis. This denotes the transgressive systems tract (TST), which indicates a deepening of the depositional environment and the setting of a retrogradational pattern (MSQ1, Figs. 11 and 13). The TST is followed upwards by a progradational facies of shallow subtidal shale in the southern areas and deep subtidal wackestone at the Farafra area. These regressive facies assigned to the highstand systems tract (HST, MSQ1, Figs. 11 and 13). The changes in environment and stacking pattern at the top of the transgressive facies mark the maximum flooding surface (MFS), evidenced by the planktic foraminiferal abundance maxima.

The Upper Maastrichtian sequence (MSQ2) includes both the Beris Mudstone Member and the lower Kharga Shale in the southern oases, and the upper part of the Khoman Formation at the Farafra Oasis (Fig. 12c). The thickness of this sequence ranges from 3 to 57 m. It is difficult to determine the exact age of sequence MSQ2 because most of the facies lies either in a barren interval or in undifferentiated zones. The upper part of this sequence belongs to Zone CF3 in the Dakhla area (Fig. 11). However, sequence MSQ2 can be linked to the late Maastrichtian zones CF4 and CF3 (68.3–65.5 Ma) which correspond to a similar interval in the

Table 3 Summary of the depositional sequences of the southern and central Western Desert shows their stratigraphic levels, planktic foraminiferal zones, age estimates, P/B ratio, parasequence stacking patterns and systems tracts

Age	Depositional sequences	Stratigraphic intervals		Planktic biozones	Time (m.y.)	P/B ratio	Parasequence stacking patterns; their lithological and environmental characteristics	Systems tracts
Eocene	Lower-Upper Ypresian sequence YSQ2 (50–142 m thick)	Thebes Fm	Farafra Limestone	E4 'Kharga' E5 'base' 'Farafra' and long barren interval	> 1.7	10–35% P basal part, barren middle- upper part	Aggradational parasequences of shallow/deep subtidal limestone/ shale, and lower intertidal lime- mudstone with shallow middle/ deep inner shelf shale at the base	HST
		Upper Esna	Up Ain Dalla					
Paleocene	Lower Ypresian sequence YSQ1 (4–33 m thick)	Middle Esna Fm	L. Ain Dalla Fm	E1–E3 Kharga E3 , locally E2 Farafra	0.5 - 1.5	10–25% P , barren in Farafra	Progradational parasequences of shallow/deep subtidal shale and lower intertidal lime-mudstone	HST
		Lower Esna Fm	Lower Esna Fm					
	Up. Garra Fm	Tarawan Fm	P4c 'lower part'	Hard to assign	20–90% P	Retrogradational parasequences of middle/outer shelf wacke- stone, packstone and shale	TST	
	Lower Garra Fm	Tarawan Fm						P4a
	Kurkur Fm	Upper Kharga Shale unit (upper part)	P3a–b 'base'	1.4 - 2.9	25–35% P	Retrogradational parasequences of shallow middle to outer shelf shale and packstone	TST	
	Upper Selandian sequence SeSQ1 (3–7 m thick)	Upper Kharga Shale unit (lower-middle part)						P2 Kharga P1c–P2 Dakhla and Farafra
Upper Danian sequence DaSQ1 (5–10 m thick)	Upper Kharga Shale unit (lower-middle part)	P2 Kharga P1c–P2 Dakhla and Farafra	Hard to assign	40–90% P	Retrogradational parasequences of shallow middle to outer shelf shale and packstone	TST		
	Upper Kharga Shale unit (lower-middle part)						P2 Kharga P1c–P2 Dakhla and Farafra	Hard to assign
	Upper Kharga Shale unit (lower-middle part)	P2 Kharga P1c–P2 Dakhla and Farafra	Hard to assign	30–80% P	Retrogradational parasequences of middle/outer shelf shale. Deep middle/outer shelf wackestone and shale at Farafra, shallow/deep subtidal limestone and shale at Beris	TST		

(continued)

Table 3 (continued)

Age	Depositional sequences	Stratigraphic intervals		Planktic biozones		Time (m.y.)	P/B ratio	Parasequence stacking patterns; their lithological and environmental characteristics	Systems tracts
Maastrichtian	Upper Maastrichtian sequence MSQ2 (3–57 m thick)	Lower Kharga Shale unit	Upper Khoman Fm	CF3 Dakhla Barren Kharga	Undifferentiated CF6–CF3	> 1.3	0–20% P Dakhla and Farafra	Progradational parasequences of shallow subtidal shale. Deep subtidal wackestone and lower inter-tidal lime-mudstone at Farafra	HST
		Beris Mudstone Mb		Barren Abu Bayan, Beris and Kharga, undiffer. Dakhla					
	Lower Maastrichtian sequence MSQ1 (18–38 m thick)	Mawhoob Shale Mb	Lower Khoman Fm	CF8b–CF7 Barren at Beris and Abu Bayan areas		> 1.4	0–40% P Farafra and Dakhla	Progradational parasequence of shallow subtidal shale. Deep sub-tidal wackestone at the Farafra	HST
							25–80% P Farafra, 25% P Dakhla 0–30% P Kharga	Retrogradational parasequence set of shallow to deep inner shelf shale in the southern oases and middle to outer shelf foramini-feral wackestone at the Farafra	TST

deeper parts of the Dakhla Basin (Tantawy et al., 2001). Sequence MSQ2 consists of retrogradationally stacked deep subtidal shale with wackestone and floatstone in the southern oases and deep middle shelf wackestone at the Farafra area (MSQ2, TST, Figs. 11 and 13). The TST is followed by progradationally stacked shallow subtidal shale in the southern oases, and deep subtidal wackestone and intertidal lime-mudstone at the Farafra area (MSQ2, HST; Figs. 11 and 13). The MFS at the base of the HST corresponds to the boundary between the Beris Mudstone and Lower Kharga Shale, as indicated by the faunal dominance that shows distinct maxima.

The Upper Danian sequence (DaSQ1) embraces the lower and middle parts of the upper Kharga Shale unit or the Kurkur Formation in the southern oases. It represents the reduced part of the Dakhla Formation in the Farafra area (Fig. 12c). The thickness of this sequence varies from 6 to 12 m. It spans zones P2 to P3b 'base' in the Kharga, and zones Plc to P3b 'base' in the Dakhla (Fig. 11), with a duration ranging from 1.4 to 2.9 m.y. At the Farafra Oasis, sequence DaSQ1 covers Zone P1c at NW Ain Maqfi, zones Plc to P2 at Shakhs El-Obeiyid, and zones Plc to P3a at Ain Maqfi (Fig. 13). It begins with back-stepping middle/outer shelf shale in the Kharga and Dakhla areas, and deep middle/outer shelf wackestone and shale at the Farafra area (DaSQ1, TST; Figs. 11 and 13). This sequence is marked at the base by the presence of conglomerate in the southern areas that is interpreted as a lowstand systems tract (LST, Fig. 11). It terminates with a progradational shallow middle shelf shale (DaSQ1, Figs. 11 and 13). At Beris, transgressive deep subtidal limestone and shale, and regressive shallow subtidal packstone and rudstone characterize the lower and upper parts of sequence DaSQ1.

The Upper Selandian sequence (SelSQ1) spans Subzone P4a and encompasses the upper part of the upper Kharga Shale unit or the Kurkur Formation in the southern oases. It covers the lower part of the Tarawan Formation at the Farafra Oasis (Fig. 12c). Sequence SelSQ1 begins with back-stepping middle/outer shelf shale in the Kharga and Dakhla oases, and deep middle/outer shelf wackestone and shale at the Farafra area (SelSQ1, TST; Figs. 11 and 13). It is marked at the base by the presence of *Thalasinoides* in the southern areas that is interpreted as a transgressive surface (TS, Fig. 11). This sequence is terminates with progradational shallow middle shelf shale (SelSQ1, Figs. 11 and 13).

The Upper Thanetian sequence (ThSQ1) includes the top part of the upper Kharga Shale unit in the Kharga and Dakhla oases, and the lower part of the Garra Formation at Beris. At the Farafra Oasis, sequence ThSQ1 comprises the lower part of the Tarawan Formation where deposition of this formation started earlier in that area (Fig. 12c). The thickness of this sequence ranges from 3 to 25 m. It belongs to the lower part of Subzone P4c. The age designation of sequence ThSQ1 is

less certain, since its top hiatus is located within Subzone P4c. This sequence starts with retrogradational facies of outer shelf shale in the Kharga and Dakhla areas, and shallow middle shelf packstone at Beris (ThSQ1, TST, Fig. 11). These planktic-rich facies are followed by progradational facies of deep subtidal shale in the Kharga and Dakhla areas, and shallow subtidal wackestone at Beris. At the Farafra area, sequence ThSQ1 is formed of two stacked parasequence sets; retrogradational outer shelf packstone and shale in the lower part, and shallow middle shelf shale/packstone, and lower intertidal lime-mudstone in the upper part, stacked in a progradational pattern (ThSQ1, Fig. 13).

The Upper-uppermost Thanetian sequence (ThSQ2) forms the Tarawan Formation and the lower part of the Esna Formation in the Kharga and Dakhla areas, and the upper part of the Garra Formation at Beris. The thickness of the sequence varies from 8 to 31 m. This sequence is ascribed to zones P4c 'top' and P5. It begins with a transgressive middle to outer shelf foraminiferal shale, wackestone and packstone parasequence set, which is followed by progradational middle shelf shale in the Kharga and Dakhla areas, and shallow subtidal wackestone at Beris (ThSQ2, Fig. 11). At the Farafra Oasis, sequence ThSQ2 marks the upper part of the Tarawan Formation (Fig. 12f), locally the Esna Formation (lower part). It starts with retrogradational shallow middle shelf shale and packstone, which are succeeded by highstand deep subtidal shale and intertidal lime-mudstone (ThSQ2, Fig. 13).

The Lower Ypresian sequence (YSQ1) involves the middle of the Esna Formation. This sequence is dated fairly well and includes zones E1 to E3 with duration of 1.5 m.y. (55.5–54.0 Ma, Fig. 14). It consists of a transgressive outer shelf shale parasequence set in the lower part and a progradational deep subtidal shale parasequence set in the upper part (YSQ1, Fig. 11). At the Farafra Oasis, this sequence typifies the middle of the Esna Formation or its coeval lower part of the Ain Dalla Formation. In most cases, the lower part of sequence YSQ1 is eroded (zones E1 and E2), and hence most of the sequence is dated to early Ypresian Zone E3, locally E2 (Fig. 13). It begins with retrogradational wackestone and shale of middle to outer shelf setting, which grade upwards into progradationally stacked middle shelf wackestone/shale, shallow subtidal shale and lower intertidal lime-mudstone (YSQ1, Fig. 13). The latter, which marks the top of the progradational set, is dolomitized due to subaerial exposure linked with an early diagenetic dolomitization.

The Lower–Upper Ypresian sequence (YSQ2) covers the upper part of the Esna Formation and most parts of the Thebes Formation. In the Farafra area, this sequence includes the Esna Formation 'upper part', or its lateral coeval, the Ain Dalla Formation 'upper part', and most of the Farafra Limestone. The thickness of the sequence grades from 50 to

142 m. In the Kharga Oasis, sequence YSQ2 is attributed to the early Ypresian Zone E4 with a long, barren interval of planktic species corresponding to the Thebes Formation. The early to latest Ypresian zones E5–E7 define this interval in adjacent areas (e.g., Berggren & Ouda, 2003). At the Farafra area, it spans Zone E5 'base' and a long barren interval, which is assigned to late-latest Ypresian zones E6–E7a (zones P8 and P9 of Ouda, 2003). Sequence YSQ2 is built up of retrogradational facies of middle to outer shelf shale in the southern oases, and middle to outer shelf shale and wackestone at the Farafra area. The pelagic facies grade upwards into shallow middle/deep inner shelf shale, and then by an aggradational set of intervening shallow subtidal wackestone/packstone and deep subtidal shale (YSQ2, Fig. 11). Similar progradational to aggradational facies of deep subtidal shale, shallow subtidal alveolinid wackestone and nummulitic packstone, and lower intertidal lime-mudstone are found at the Farafra area (YSQ2, HST, Fig. 13).

5 Discussion

5.1 Biostratigraphic Resolution

The biostratigraphic resolution of the Maastrichtian–Ypresian sediments of the studied areas is highly variable in terms of age assignment. The foraminiferal content is valuable in the late Danian–early Ypresian sediments (zones PIC to E5 'base') owing to deposition in a chiefly deep marine setting. The sediments hold highly abundant and diverse planktic species with a high preservation potential that enables the attainment of high-resolution biostratigraphy. A drop in planktic percentage and diversity and in P/B ratio is traced at several levels in these sediments when sea-level falls. The biostratigraphic resolution is less reliable in the Maastrichtian and late Ypresian sediments due to the lack of marker fauna in their shallow marine facies. Nevertheless, a correlation with the adjacent areas contributes greatly to the insufficient biostratigraphic control of these sediments (e.g., Beris Mudstone Member, Thebes Formation).

5.2 Depositional Systems Tracts

Two types of stacked systems tracts, TST and HST, are defined in the Maastrichtian–Ypresian sequences (Figs. 11 and 13, Table 3). LST is hardly developed in the studied sequences due to deposition in a shelf basin marked by submerged highs and lows (Fig. 7). In most cases, the LST spans the erosional time associated with the sea-level drop and marks the sequence boundary. However, it may include a thin conglomerate of incised valley fills, if present

(boundary Ma/DaWD, Figs. 11 and 12b). This channel fill was accumulated during a slow sea-level rise. The TST is generally thin and consists of retrogradational deposits bounded above by the MFS, which is overlain by progradational deposits of the HST. The MFS typically represents the level of maximum P/B value associated with the change in the stacking pattern. The sedimentation patterns of the TSTs and HSTs vary from mixed siliciclastic/carbonate to pure carbonate. The stacking patterns within the systems tracts show upward deepening (TSTs) and upward shallowing (HSTs) in faunal assemblages, associated with variations in the diversity, frequency and type of foraminifera and/or in P/B value. A rapid sea-level rise produces highly diverse planktic species with high P/B value (deep marine facies), while a lowering of sea level shows signs of abundance of benthic species supplemented by a marked decrease in the P/B value (shallow marine facies). The interpretation of these systems tracts permits the generation of relative sea-level curves for the Maastrichtian-Ypresian sediments (Figs. 11 and 13).

5.3 Comparison of Sea-Level Falls

The southern Western Desert was situated in a quiescent tectonic regime during the Maastrichtian-Ypresian time. In contrast, the central Western Desert was located near a tectonically active region influenced by the compressional effect of the Syrian Arc system in Northern Egypt (Moustafa et al., 2003). This tectonic effect, however, cannot be completely ruled out in the southern Western Desert. In order to assess whether the defined depositional sequences are due to eustatic sea-level changes or regional tectonics, a comparison is made with sea-level curves documented in Egypt (El-Azabi & Farouk, 2011; Hewaidy et al., 2006; Lüning et al., 1998a), Libya (Jorry, 2004; Mresah, 1993), Tunisia (Kouwenhoven et al., 1997; Li et al., 1999; and references therein) and in the Arabian Platform (Haq & Al-Qahtani, 2005). In addition, a correlation is carried out with the global sea-level curves of Haq et al. (1987) and Haq (2014), the Western European sea-level curve of Hardenbol et al. (1998), and the New Jersey sea-level curve of Miller et al. (2005).

5.3.1 Local and Regional Comparison

The first sequence boundary detected in the studied areas refers to a marked sea-level lowstand at the Campanian/Maastrichtian contact (Ca/MaWD, Fig. 14). This sea-level fall has been witnessed by some authors in the Western Desert (e.g., El-Azabi & El-Araby, 2000; El-Azabi & Farouk, 2011; Farouk et al., 2019b; Hermina, 1990; Hewaidy et al., 2006; Tantawy et al., 2001). The boundary Ca/MaWD is coeval with the boundaries Ca/MaSin in

central Sinai (Lüning et al., 1998a, 1998b) and CaGal2 on the Galala plateaus (Scheibner et al., 2001). It is also isochronous with the boundary SB2 of Hewaidy et al. (2006) in the Farafra area and the boundary Ca/MaKh1 of El-Azabi and Farouk (2011) in the Kharga area (Fig. 14). The sequence boundary L/UMaWD, which typifies a sea-level fall dated at 68.3 Ma and marks the Lower/Upper Maastrichtian contact (Fig. 14), is equivalent to the boundary MaGal1 in the Galala plateaus (Kuss et al., 2000; Scheibner et al., 2001). It is compatible with the boundaries SB2 and MaKh2 of El-Azabi and El-Araby (2000), and El-Azabi and Farouk (2011) in the Dakhla and Kharga areas, respectively.

The sequence boundary Ma/DaWD defines a major hiatus associated with a sea-level drop at 65.5 Ma. This hiatus represents one of the long-lived hiatuses found in the Western Desert and is attributed to the K/Pg contact. The boundary Ma/DaWD is an amalgamation of many boundaries recorded by some authors in the Nile Valley, Eastern Desert and Sinai (e.g., Farouk, 2016; Farouk et al., 2019a). It makes up a combination of short hiatuses recorded at the CF3/CF1, CF1/P0, P0/P1a, P1a/P1b and P1b/P1c zonal boundaries at Gabal Qreiya, central Egypt (Keller et al., 2002). This boundary also constitutes a merger of the boundaries MaSin-Z, DaSin-1, DaSin-2 and DaSin-3 defined in central Sinai (Lüning et al., 1998a, Fig. 14). It is equivalent to the boundaries SB3 of Hewaidy et al. (2006), Ma/DaKh3 of El-Azabi and Farouk (2011), and Eg.Da-1 of Farouk (2016). The boundary Da/SelWD, defined at the top of the Danian sediments, has been detected in the Kharga and Dakhla areas (Faris et al., 1999; Tantawy et al., 2001). This boundary equates to the boundary SelGal2 of Kuss et al. (2000), which is a composite hiatus comprising the boundaries ThSin2 to ThSin4 of Lüning et al. (1998a). It also correlates with the boundary SB4 of Hewaidy et al. (2006) and the boundary Se/ThKh4 of El-Azabi and Farouk (2011).

The sequence boundary Sel/ThWD is a remarkable hiatus at the base of the Thanetian. It is related to a global sea-level fall and subaerial exposure, which caused the absence of the calcareous nannofossil Zone NP6 (Faris & Farouk, 2012). This boundary coincides with the emergence and erosion of many positive structures associated with increased subsidence in the basal areas. It belongs to the so-called Velascoensis Event of Strougo (1986).

The boundary ThWD, identified at the topmost part of the Upper Thanetian sequence (ThSQ1, Fig. 14), has been described in the Kharga (Bassiouni and Luger, 1990), Dakhla (Barthel & Herrmann-Degen, 1981) and Kom Ombo-Qena areas (Hendriks et al., 1987). It seems to be synchronous with the boundary ThSin-5 of Lüning et al. (1998a) and the boundary ThGal1 of Scheibner et al. (2000). This sequence boundary is comparable with the boundary SB5 of El-Azabi and El-Araby (2000) and the boundary

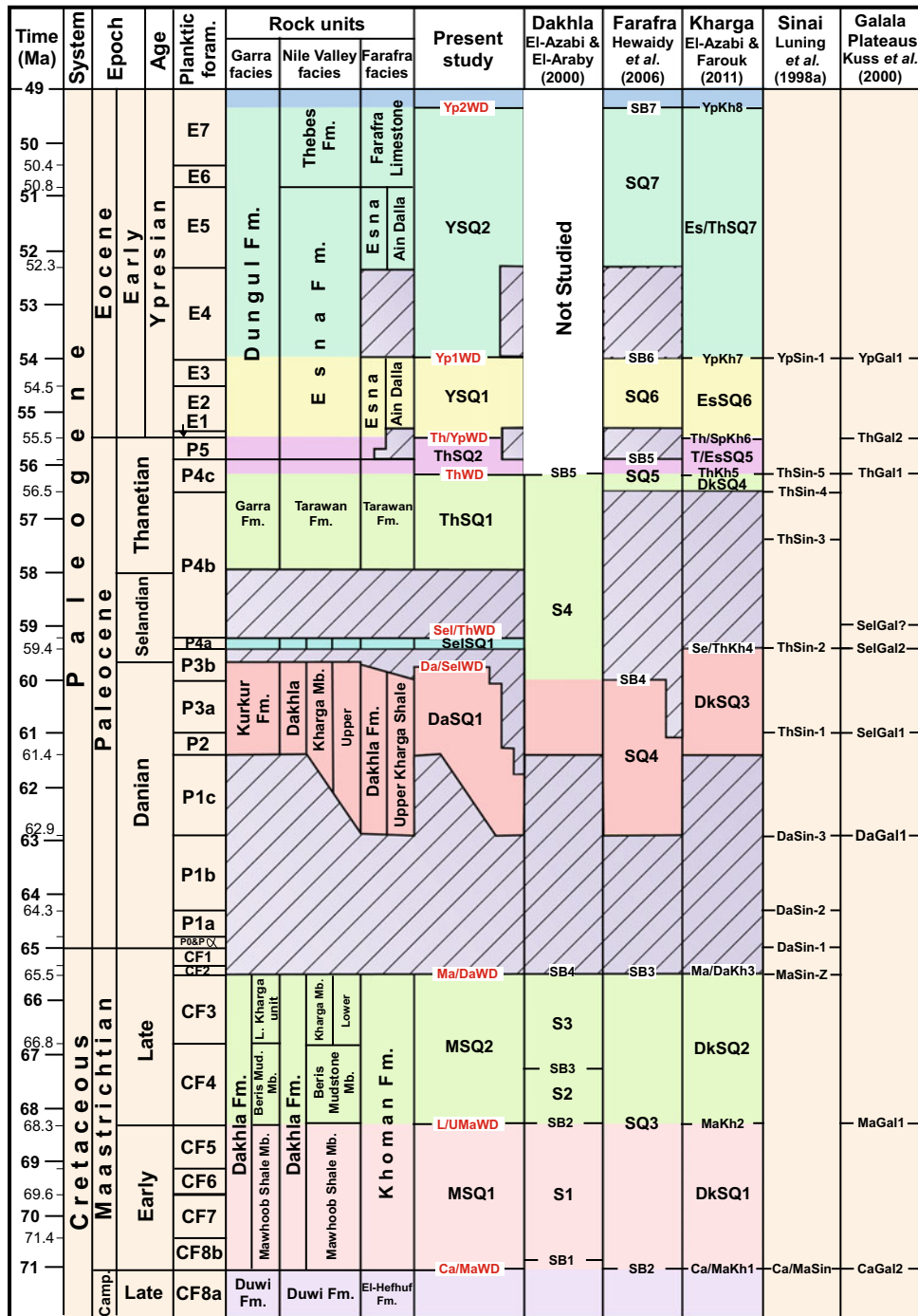


Fig. 14 Integrated summary of the planktic foraminiferal zonation, age estimates of the biozones/hiatuses and sequence stratigraphic interpretation of the Maastrichtian-Ypresian sediments in the southern and central Western Desert as well as the correlation of the inferred sequences and boundaries with the previous studies in and outside the studied areas. Age estimates and planktic zonation are based on the work of Li and Keller (1998a, 1998b) and Li et al. (1999) for the Maastrichtian and of Berggren and Pearson (2005) and Wade et al. (2011) for the Paleogene. Cross-hatched pattern indicates long-term hiatuses

ThKh5 of El-Azabi and Farouk (2011). The sequence boundary Th/YpWD, which represents the P/E contact, is delineated in the latest Paleocene-earliest Eocene sea-level record of Speijer and Wagner (2002). It was defined in the Dababiya Quarry section, Luxor (Ernst et al., 2006). This

boundary may be related to the sequence boundary ThGal2 of Kuss et al. (2000), which occurs within the undifferentiated Zone P5. It is synonymous with the boundary SB5 of Hewaidy et al. (2006) and the boundary Th/SpKh6 of El-Azabi and Farouk (2011).

The sequence boundary Yp1WD, found at the top of the Lower Ypresian sequence YSQ1, denotes a hiatus associated with a sea-level drop described in the Farafra Oasis (Abdel-Kireem & Samir, 1995; Farouk et al., 2019b; Ouda, 2003), central Sinai (Lüning et al., 1998a) and the Galala plateaus (Kuss et al., 2000). It is comparable with the boundary SB6 of Hewaidy et al. (2006) and the boundary YpKh7 of El-Azabi and Farouk (2011), whereas the sequence boundary Yp2WD, located close to the contact between Ypresian and Lutetian, correlates with the boundary SB7 of Hewaidy et al. (2006) and the boundary YpKh8 of El-Azabi and Farouk (2011).

The current work verifies the occurrence of eight depositional sequences outlined by nine basin-wide boundaries. These boundaries are relatively consistent with those defined by El-Azabi and Farouk (2011) in the Kharga area, which assert the legality of their boundaries in the whole of southern Egypt. Despite that, some differences exist regarding the time lapse of the hiatuses associated with these boundaries, especially in the Farafra Oasis. Of interest is the time gap of the boundaries Ma/DaWD, Sel/ThWD, Th/YpWD and Yp1WD (Fig. 14). The present work maintains the absence of the top part of Subzone P3b in the Kharga and Dakhla oases and the existence of the boundary Da/SelWD, in contrast to the study of El-Azabi and Farouk (op. cit.) which identified a similar boundary at the top of Zone P3. It also shows that the Danian sea-level rise started earlier in the Farafra Oasis than that indicated in the Kharga area by El-Azabi and Farouk (2011, Fig. 14).

Although the inferred sequences in the current work are slightly similar in number to those of El-Azabi and Farouk (2011), many differences exist. These sequences are not similarly developed in the studied areas, showing differences in thickness and in time span. The thickness variation is attributed to paleo-relief irregularity of the Dakhla Basin, the different rate of clastic supply, and the strength of erosion associated with the hiatus. The time span of the defined sequences is normally reduced in the Farafra Oasis due to the regional tectonic impact. The recent demarcation of the D/S boundary within Subzone P3b (e.g., Arenillas, 2012) and the absence of the top part of Subzone P3b in the Kharga area re-interpret the late Danian-Selandian age of sequence DkSQ3 given by El-Azabi and Farouk (2011) to the late Danian. In fact, the present work has improved the planktic foraminiferal framework of the studied sequences. It proves the presence of Zone CF3 in the lower Kharga Shale unit (Dakhla Oasis), Subzone P1c in the upper Kharga Shale unit (Dakhla and Farafra oases), and Zone E5 'base' in the Esna and Ain Dalla formations (Farafra Oasis). These biozones, not found in the Kharga area, were allowed to review the boundary time gaps defining sequences in the different areas.

5.3.2 Comparison with Tunisia and Libya

The Maastrichtian-Ypresian sediments in Tunisia have shown significant changes in sea level (Kouwenhoven et al., 1997; Li et al., 1999, 2000), with several cases of sea-level falls similar to those in the Western Desert. The eustatic sea-level falls, which occurred at 71 Ma, 68.3 Ma and 65.5 Ma in the Maastrichtian sections of Tunisia, are associated with the sequence boundaries of Ca/Ma WD, L/UMaWD and Ma/DaWD in the Western Desert, respectively. These sea-level falls have been documented in El Kef, northwest Tunisia (Li et al., 1999; Molina et al., 2006), and Halk el Menzel, northeast Tunisia (Sebei et al., 2007). Similar global sea-level falls dated at 71 Ma and at 65.5 Ma have been documented in Elles, central Tunisia (Li et al., 2000) and Ain Settara, north-central Tunisia (Luciani, 2002), respectively. Indeed, the K/Pg boundary of the Western Desert (Ma/DaWD) represents a significant time span in contrast to corresponding boundary in the Tunisian sections. This indicates that the Western Desert was affected by regional tectonics coupled with the latest Maastrichtian sea-level fall resulting in a long-lived subaerial exposure. The boundary Da/SelWD in the Western Desert can be linked to a short-term, sea-level fall found in the upper part of Zone P3 in the Paleocene succession of El Kef (Guasti et al., 2005). By contrast, this boundary marks a major hiatus lasting about 3 m.y. in the Kharga and 3.5–5 m.y. in the Farafra (Fig. 14), suggesting regional tectonic control accompanying the late Paleocene sea-level fall. Lüning et al. (1998a) concluded that there is a good relationship between the Paleocene sea-level changes in El Kef and those occurred in the central east Sinai. The boundaries Th/YpWD and Yp2 WD, on the other hand, seem to fit with the boundaries SB7 and SB8 of Sebei et al. (2007).

The correlation between the proposed sea-level changes for the Western Desert and those constructed for Libya displays good agreement. The only exception to this agreement is the K/Pg hiatus (boundary Ma/DaWD), which has an extended span lasting 19 m.y. in Cyrenaica, northeast Libya (Jorry, 2004). The boundary Da/SelWD is synchronous with an age-equivalent sea-level drop observed in zones P3b-P4 in the Sirt Basin (Berggren, 1974). The Paleocene sea-level curve given by Mresah (1993) for the northeast Sirt Basin seems to correspond well with that of the present study, but the absence of biostratigraphic time control for his shallowing-upward cycles and their sequence boundaries precludes an adequate correlation. The sequence boundary Th/YpWD is identified in Jabal al Akhdar, northeast Libya (Tmalla et al., 2007). The boundary Yp2WD is linked well with the boundary CSB-1 of El Hawat et al. (2008) at Ra's al Hilal, Cyrenaica. It could also be linked to the boundary SB1 at the top of Zone E7 in Cyrenaica (Jorry, 2004) and with a major unconformity at the top of the Ypresian in al Jabal al Akhdar (Abdulsamad et al., 2009).

5.3.3 Comparison with Arabian Platform

The Arabian Platform has been widely influenced by eustatic sea-level changes associated with a complex history of tectonics (Haq & Al-Qahtani, 2005). It contains two megasequences named AP9 of Late Cretaceous-Early Paleogene (92–63 Ma) and AP10 of Early Paleogene-Latest Eocene (63–34 Ma) (Sharland et al., 2001, 2004; Haq & Al-Qahtani, 2005). In comparison with the cycle chart of Sharland et al. (2001), which identified eleven Arabian Plate megasequences (AP1–AP11), the MFSs studied in the Western Desert are collectively attributed to the MFSs K180 and Pg10 sequences of the upper and lower parts of the megasequences AP9 and AP10, respectively. Most of the sequence boundaries identified in southern and central Western Desert have no counterpart in the Arabian Platform-wide cycle charts (Haq & Al-Qahtani, 2005).

5.3.4 Comparison with Global and Western European Sea-Level Curves

Are the sea-level changes of the southern and central Western Desert due to eustatic sea-level variations or regional tectonics? To answer this question, changes in sea level of

the studied areas are related to the eustatic ones. The commonly used record of the past sea-level changes was given by Exxon Production Research Company, ‘EPR’ (Haq et al., 1987). Hardenbol et al. (1998) and Haq (2014) have refined these curves. The sequence boundary Ca/MaWD coincides with a significant global cooling and eustatic sea-level drop at 71 Ma (Haq et al., 1987; Li & Keller, 1998a), which marks the base of the UZA4.5 cycle of Haq et al. (1987). It also matches the boundary Ma2 of the Western European sea-level curve (Hardenbol et al., 1998, Fig. 15). The boundary L/UMaWD corresponds to a global sea-level fall at 68 Ma, which lies at the base of the TA1.1 cycle of Haq et al., (1987; Fig. 15). It is also comparable to the sequence boundary Ma4 given by Hardenbol et al. (1998). The boundary Ma/DaWD is isochronous with a well-defined global cooling at 65.5 Ma (Li et al., 2000). This sea-level fall is not documented on the global sea-level curve of Haq et al. (1987). In fact, the boundary Ma/DaWD typifies a long time of uplift in the Western Desert that followed a global fall in relative sea level during the latest Maastrichtian (Li et al., 2000). The boundary Da/SelWD is concurrent with a significant sea-level drop at the base of the TA2.1 cycle of

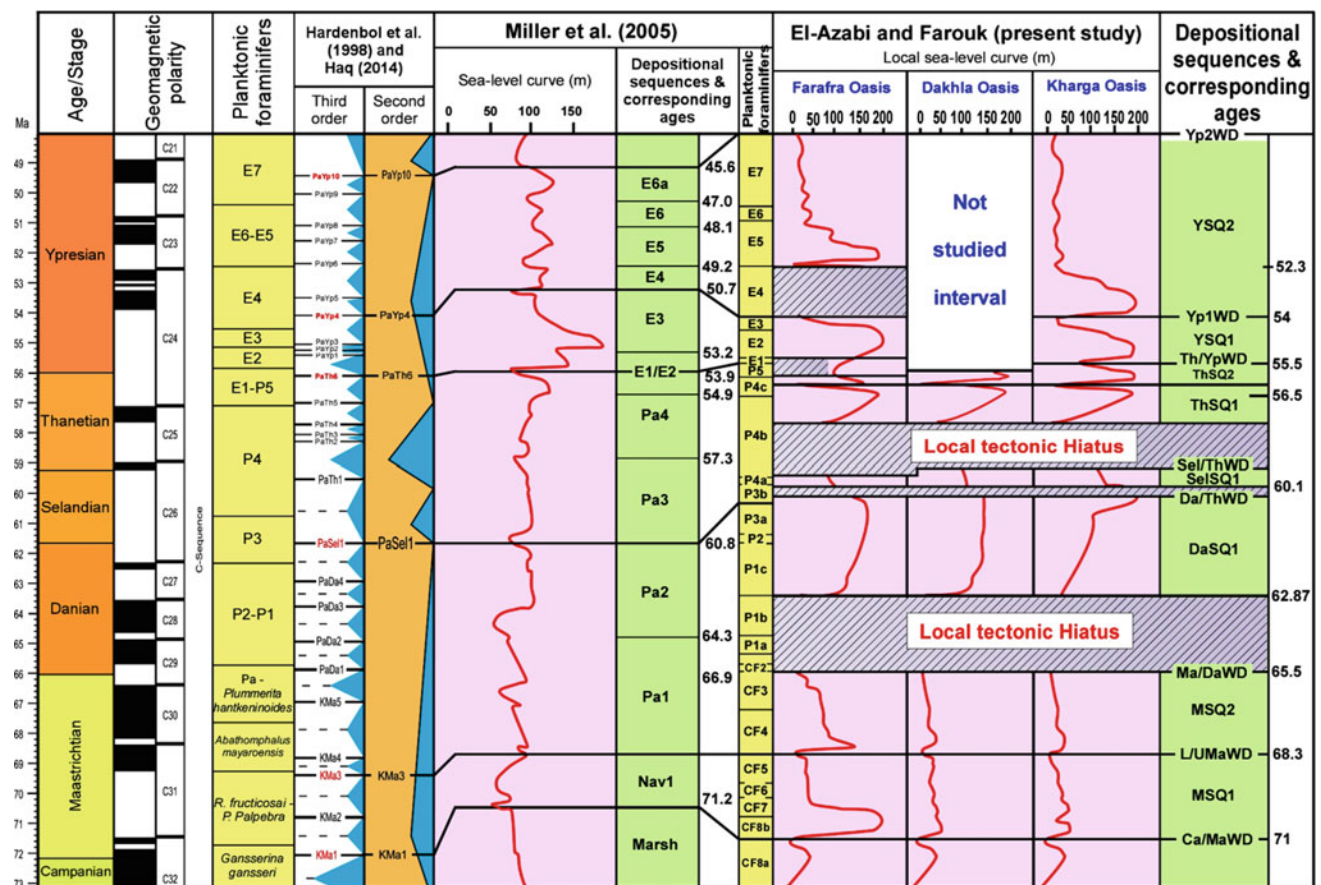


Fig. 15 Comparison of the inferred Maastrichtian-Ypresian sea-level curves in the southern and central Western Desert with the eustatic records of Hardenbol et al. (1998), Miller et al. (2005) and Haq (2014). Cross-hatched pattern indicates long-term hiatuses

Haq et al. (1987). It is comparable to the boundary PaSel1 of Hardenbol et al. (1998, Fig. 15). This boundary also has a long duration in the studied areas, indicating its attribution to regional tectonics along with a global sea-level fall during the latest Danian. The boundary ThWD has no equivalent in the eustatic sea-level charts of Haq et al. (1987). It matches well the boundary Th4 of Hardenbol et al. (1998, Fig. 15). The boundary Th/Yp WD coincides with a global, short-term sea-level drop that forms the base of the TA2.2 cycle (Haq et al., 1987). It may be equated with the boundary Th7/Yp1 of Hardenbol et al. (1998). In the Farafra Oasis, the boundary Th/YpWD marks a major hiatus associated with the absence of all or parts of zones P5 to E2, which implies that local tectonic uplift accompanied the global P/E sea-level fall. An equivalent hiatus to boundary Yp1WD occurs at the base of the TA2.4 cycle in the eustatic sea-level charts of Haq et al. (1987). The boundary Yp3 of Hardenbol et al. (1998) matches that of Yp1WD. In the Farafra Oasis, the hiatus caused the boundary Yp1WD, which has also a much longer time lapse, asserting that the area was affected by tectonic uplift coincident with the eustatic sea-level fall in early Ypresian. Lastly, as the age dating of the boundary Yp2WD is hard to define accurately because of biostratigraphic limitation, it is likely to be comparable to a significant eustatic sea-level drop documented close to the Ypresian/Lutetian contact, at the base of the TA3.1 cycle of Haq et al. (1987). The boundary Yp2WD correlates with the boundary Yp10 of Hardenbol et al. (1998) that occurred at 50.02 Ma.

5.3.5 Comparison with the New Jersey Passive Continental Margin

The Ocean Drilling Program on the New Jersey passive continental margin has set a new global sea-level record for the past 100 M.y. with implications for causal mechanisms for 10⁶-year changes (Miller et al., 2005). Fourteen late Cretaceous sequences and thirty-three Paleocene to Miocene sequences were identified and dated by integrating biostratigraphy, Sr-isotopic stratigraphy and magnetostratigraphy to establish a chronology with an age resolution of better than ± 1.0 M.y. for the Cretaceous and ± 0.5 M.y. for the Cenozoic (Miller et al., 2004). The sequence boundaries Ca/MaWD, L/UMaWD, Da/SelWD, Th/YpWD, Yp1WD and Yp2WD can be firmly linked with the hiatuses at the tops of the sequences Marsh, Nav1, Pa2, E1, E3 and E6a of the Miller et al. (2005) record, respectively (Fig. 15). In the Farafra Oasis, the hiatuses associated with the boundaries Th/YpWD and Yp1WD are of long duration relative to their counterparts on the sea-level curve of Miller et al. (op. cit.), whereas the boundaries Ma/DaWD, Sel/ThWD and ThWD have no equivalents denoting that the regional tectonics were responsible for their initiation.

5.4 Remarks on Inferred Sea-Level Falls

The relative changes in sea level have left their mark on the Maastrichtian-Ypresian sediments of the southern and central Western Desert. This has resulted in the formation of sequence boundaries, which typify either eustatic or regional sea-level falls. High biostratigraphic resolution allows correlation of these boundaries within and outside of Egypt. Most of the inferred boundaries are closely related to those recorded in the Eastern Desert, the Sinai Peninsula, Libya, Tunisia, the Arabian Platform, Western Europe and the New Jersey continental margin in addition to those given by EPR, denoting that they are mostly global in origin and formed in response to eustatic sea-level falls. Some boundaries, especially in the Farafra Oasis, were developed in relation to tectonic activity. The studied sequence boundaries are nearly similar to those previously described by Hewaidy et al. (2006), and El-Azabi and Farouk (2011). Only the boundaries L/UMaWD and Sel/ThWD are not evident in the work of Hewaidy et al. (2006).

Correlation with the sea-level records of Tunisia reflects mostly simultaneous changes in sea level, but the agreement is not close to Libya since no informative data are available. The boundaries Ma/DaWD, Da/SelWD and Sel/ThWD that are attributed to regional tectonics reveal longer-term hiatuses than their coevals in the sea-level records of Tunisia. This asserts that they were initiated because of tectonic activity with a little influence from eustatic changes. Also, the sea-level fall marking the P3a/P3b subzonal boundary in many Tunisian sections cannot be proved in the Western Desert. Comparison with the sea-level changes of the Arabian Plate shows that most the studied boundaries are regional in nature. Others boundaries that have no correspondence in the Arabian Plate imply an overriding control by local tectonics.

Correlation with the eustatic sea-level curves of Haq et al. (1987), Haq (2014) and Miller et al. (2005) highlights many similarities. Of nine sea-level falls recorded in the southern oases, six display eustatic origin (Ca/MaWD, L/UMaWD, Da/SelWD, Th/YpWD, Yp1WD, Yp2WD, Fig. 15). The boundaries Ma/DaWD, Sel/ThWD and ThWD have no equivalents in the eustatic cyclic charts of Haq et al. (1987), affirming that the tectonics cannot be completely ruled out in the southern Western Desert. The boundary Da/SelWD, which is considered to be of regional significance, attended the latest Danian sea-level fall on the eustatic sea-level curves of Haq et al. (op. cit., top Zone P3b). The three boundaries Ma/DaWD, Sel/ThWD and ThWD have also no correspondences on the sea-level curve of Miller et al. (2005). Most of the sea-level falls defined in the Farafra Oasis do not coincide with the eustatic charts. The boundaries Ma/DaWD, Sel/ThWD and ThWD have also no

apparent correlations with these global sea-level charts. The boundaries Sel/ThWD, Th/YpWD and Yp1WD have a much longer time gap relative to their coevals on the eustatic sea-level charts (Fig. 15). This confirms that regional tectonics played a major role in the generation of depositional sequences in the Farafra Oasis along with minor eustatic controls.

Regarding the cyclic charts of Hardenbol et al. (1998), similarities in sea-level falls are remarkable. Most (6 of 9) of the studied boundaries are detected. Good correlations exist for the boundaries Ca/MaWD, L/UMaWD, Da/SelWD, Th/YpWD, Yp1WD and Yp2WD, indicating a global cause (Fig. 15). However, the hiatuses related to the boundaries Da/SelWD, Th/YpWD and Yp1WD have a long duration in the Farafra Oasis. The long-term hiatus across the Selandian/Thanetian transition was responsible for the elimination of PaTh1, PaTh2, PaTh3, PaTh4 and PaTh5 sequence boundaries on the cyclic charts of Hardenbol et al. (op. cit.).

5.5 Evolution of the Maastrichtian-Ypresian Sequences

The interaction of global eustatic sea-level changes and regional tectonics, besides the changes in clastic supply and climate, has greatly influenced the facies, paleoenvironments

and spatial distribution of the Maastrichtian-Ypresian sediments. The current multi-disciplinary sequence stratigraphy contributes significantly in revealing the way in which the depositional sequences were developed and changed throughout the Maastrichtian-Ypresian time. The Dakhla Basin is a NW–SE trending intra-shelf basin located in central Egypt. It was bounded to the northeast by the Assiut Basin, to the southeast by the Aswan uplift and to the southwest by the Gilf El-Kebir-Uweinat uplift (Fig. 16). The bottom of the Dakhla Basin was affected by deep-seated basement faults that have repeatedly been rejuvenated during the Phanerozoic (Schandelmeier et al., 1987). This led to the initiation of several paleo-structural highs and lows striking in an ENE-WSW direction during the late Carboniferous-early Jurassic (Klitzsch, 1986). These submerged highs and lows along with frequent sea-level changes governed the paleoenvironments and resultant facies in the studied sequences.

The Dakhla Basin was bathed at inner to outer shelf depths that were interrupted at times by sea-level falls and subaerial exposures throughout the Maastrichtian-Ypresian time. The first marine invasion, which started during the early Maastrichtian zones CF8b to CF7, initiated a deep marine setting in the Farafra Oasis and extended to a shallow sea in the southern oases. Because of the relative sea-level rise, a retrogradational shallow to deep subtidal shale was deposited under a tropical to sub-tropical climate (lower Mawhoob Shale Member, MSQ1, Fig. 11). In the Farafra

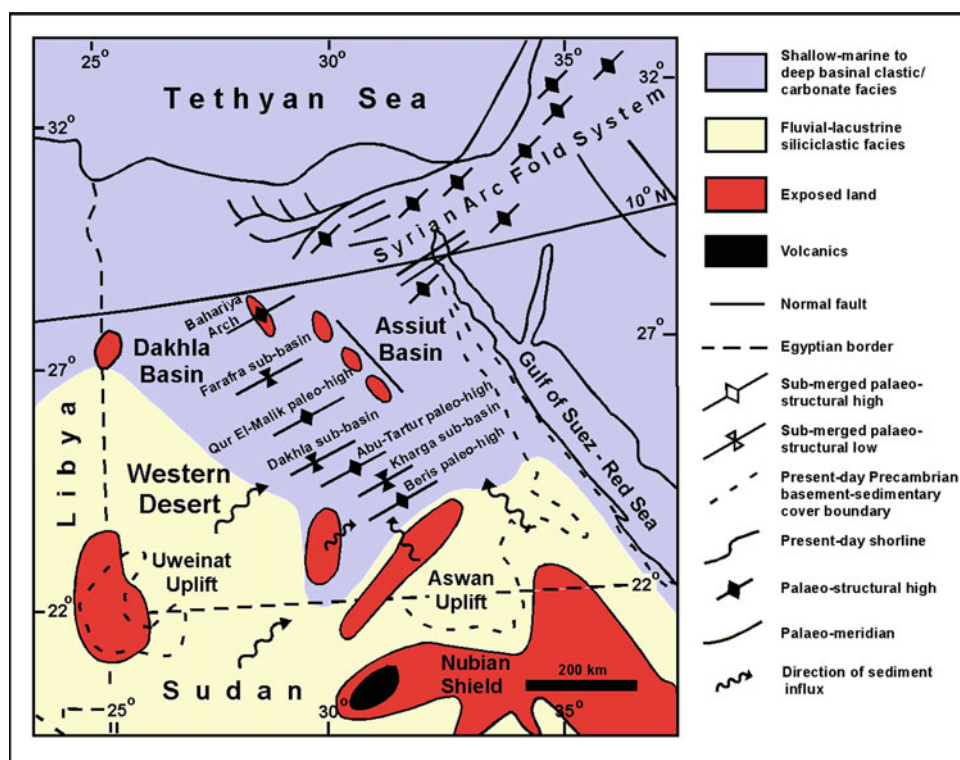


Fig. 16 Late Maastrichtian paleogeographic/paleotectonic map shows the depositional setting of the Dakhla Basin (modified after El-Azabi & Farouk, 2011)

area, a retrogradational foraminiferal wackestone was deposited indicating deposition in the middle to outer shelf setting beyond the reach of the clastic influx (lower Khoman Formation, MSQ1, Fig. 13). Later, when the rate of accommodation increase began to fall, during zones CF6 to CF5, a progradational shallow subtidal shale with low diversity benthics was deposited (upper Mawhoob Shale Member, MSQ1, HST, Fig. 11). At the same time, a progradational deep subtidal wackestone was deposited in the Farafra area (MSQ1, HST, Fig. 13). A minor drop in global sea level that occurred in the late early Maastrichtian terminated these regressive deposits (sequence boundary L/UMaWD).

During the late Maastrichtian Zone CF4, the increasing rate of relative sea-level rise caused deposition of retrogradational subtidal wackestone, floatstone and shale with dominant, low diversity benthic species and oysters in the southern areas, and deep middle shelf wackestone in the Farafra area (Beris Mudstone Member, upper Khoman Formation, MSQ2, TST, Figs. 11 and 13). Later, as the rate of sea-level rise declined, during Zone CF3, a progradational shallow subtidal shale was deposited (lower Kharga Shale, MSQ2, HST, Fig. 11). In the Farafra area, the HST is characterized by progradational wackestone and lime-mudstone that denote deposition in deep subtidal and lower intertidal settings, respectively. Deposition of the HST matches the onset of a prolonged regional uplift due to emersion of the Bahariya Arch that is linked with the K/Pg event. The cooling of the global climate and the lowering of sea level (Keller, 2004) accentuate this event. The global cooling reached its maximum at 65.5 Ma (Li et al., 2000). The studied areas were subaerially exposed during the latest Maastrichtian zones CF2 and CF1 through early/late Danian zones P0 to P1b and c (boundary Ma/DaWD). This caused severe erosion and accumulation of thin channel fill conglomerate during the sea-level drop (DaSQ1, LST, Fig. 11).

The long-lived latest Maastrichtian uplift was followed by the initiation of open shelf conditions during the mid-late Danian. This sea-level rise took place during Zone P1c in the Dakhla and Farafra areas, and Zone P2 in the Kharga area. It began with deposition of a back-stepping middle to outer shelf shale in the southern areas (DaSQ1, TST, Fig. 11). In the Farafra, deposition started with wackestone and shale of deep middle to outer shelf setting (zones P1c to P2, Fig. 13). This was followed by deposition of shallow middle shelf shale at Ain Maqfi (Zone P3a, HST, Fig. 13). The HST is missing in other sections, likely due to erosion during the subsequent sea-level fall and subaerial exposure. These deposits, in the southern oases, are dominated by a progradational shallow middle shelf shale (Zone P3, HST, Fig. 11). The MFS coincides with the P2/P3 zonal boundary. During zones P2 to P3, the Beris area was submerged at inner shelf depths. Retrogradational limestone and shale were

developed in a shallow to deep subtidal setting. This was succeeded by progradational, shallow subtidal packstone and rudstone due to relative sea-level fall (Kurkur Formation, DaSQ1, Fig. 11). A subsequent long-term fall in relative sea level combined with regional uplift caused subaerial exposure and the initiation of boundary Da/SelWD.

During the Selandian Subzone P4a and Thanetian Subzones P4b-c 'base', the studied areas were inundated again due to a short-lived, rapid sea-level rise. The increasing accommodation space caused a deepening of the environment and deposition of outer shelf shale in the Kharga and Dakhla areas (SelSQ1, ThSQ1, TST, Fig. 11) that displays a high dominance of planktic species. Later, the increasing accommodation space slowed down, allowing progradation of deep subtidal shale with sharply reduced P/B ratios (SelSQ1, ThSQ1, HST, Fig. 11). Concurrently, a transgressive shallow middle shelf packstone followed by a regressive shallow subtidal wackestone was formed on the Beris submerged paleo-high (SelSQ1, ThSQ1, Fig. 11). In the Farafra area, a rapid relative rise of sea level led to deposition of retrogradational outer shelf packstone and shale (SelSQ1, ThSQ1, TST, Fig. 13), which was followed by the laying down of shallow middle shelf shale/packstone, and lower intertidal lime-mudstone (SelSQ1, ThSQ1, HST, Fig. 13). Sequence ThSQ1 ended with a minor sea-level fall at the top of the late Thanetian Subzone P4c 'base'.

Marine incursion soon followed during the late Thanetian Zone P4c 'top'. It began with deposition of retrogradational foraminiferal wackestone, packstone and shale of middle to outer shelf setting (ThSQ2, TST, Fig. 11). These planktic-rich sediments were followed by accumulation of progradational shallow middle shelf shale. Time-correlative facies, consisting of a transgressive shallow middle shelf packstone followed by a regressive shallow subtidal wackestone, were accumulated over the Beris paleo-high (ThSQ2, Fig. 11). Meanwhile, deposition started in the Farafra area with shallow middle shelf shale and packstone, succeeded by deep subtidal shale and intertidal lime-mudstone (ThSQ2, Fig. 13). The reduced thickness of sequence ThSQ2 is due to the near absence of Zone P5 at the bottom of the Esna Formation. A minor hiatus terminated sequence ThSQ2 at the P5/E1 zonal boundary, which is attributed to a brief global warming. This hiatus led to the modification of the local tectonic uplift that developed at the top of Zone P4c in the Farafra area.

The worldwide-elevated temperatures at the P/E boundary have caused the initiation of warm, low-oxygen bottom waters, carbonate dissolution and a major extinction of benthic species (Berggren & Aubry, 1998). This resulted in the disappearance of the planktic foraminifera. Subsequently, a progressive return to normal marine conditions led to a gradual increase in abundance and diversity of foraminifera. Thus, outer shelf shale was laid down during the

transgressive event (YSQ1, zones E1 to E3 'lower part', TST, Fig. 11). The high clastic input from the south gave rise to widespread shale deposition. Locally in Shakhs El-Obeiyid and NE Ain Dalla, a switch to carbonate sedimentation, represented by middle to outer shelf wackestone, took place (YSQ1, Fig. 13). In the southern areas, the TST was followed by accumulation of a progradational deep subtidal shale during the regressive event (YSQ1, Zone E3 'upper part', HST, Fig. 11). Meantime, shallow middle shelf wackestone/shale, shallow subtidal shale and intertidal lime-mudstone prevailed in the Farafra area (YSQ1, HST, Fig. 13). Sequence YSQ1 was terminated by a minor fall in relative sea level with the initiation of boundary Yp1WD. In the Farafra area, this boundary is linked with a long-lived hiatus and subaerial exposure with dolomite formation during the early Ypresian Zone E4.

During Zone E4, another marine invasion took place, most likely assisted by rising eustatic sea level. It started later in the Farafra area during Zone E5. The marine invasion caused deposition of transgressive middle to outer shelf shale in the southern oases and middle to outer shelf shale and wackestone in the Farafra area (YSQ2, TST, Figs. 11 and 13). These deposits were succeeded by deposition of a progradational middle to deep inner shelf shale and then by thick aggradational shallow subtidal wackestone to packstone and deep subtidal shale (YSQ2, HST, Fig. 11). In the Farafra area, progradational to aggradational inner shelf shale, shallow subtidal alveolinid wackestone and nummulitic packstone, and lower intertidal lime-mudstone prevailed as the relative sea-level rise progressively slowed (YSQ2, HST, Fig. 13). Deposition of the highstand deposits denotes the onset of regional tectonic uplift during the latest Ypresian with the initiation of sequence boundary Yp2WD.

6 Conclusions

Three coeval facies associations, namely Garra El-Arbain, Nile Valley and Farafra, typify the depositional sequences of the southern and central Western Desert. These facies provide an excellent model for understanding the interaction between eustasy, tectonics and sediment supply. They are truncated by eight sequence boundaries; their correlation regionally, interregionally and with those of Western Europe, the New Jersey continental margin and the EPR data indicates that they are developed as a result of eustatic sea-level changes associated with regional tectonics, as evidenced by the global recognition of at least five of the eight inferred sea-level falls. The tectonics was significant in generating sequence boundaries with long-term hiatuses in the Farafra Oasis. The studied sequences show vertically stacked transgressive and regressive deposits. They remain

incomplete due to the lack of lowstand deposits. The evolution of these sequences was managed primarily by global changes in sea level, and partly by tectonics. The type, thickness and facies change of these eustatically and tectonically induced sequences were also influenced by the paleo-relief irregularities of the Dakhla Basin, variable sediment influx and differential sedimentation rate. Such sequence stratigraphic framework provides a template for future progress to a unified sequence stratigraphic scheme for the whole of Egypt.

References

- Abdel-Kireem, M. R., & Samir, A. M. (1995). Biostratigraphic implications of the Maastrichtian-Lower Eocene sequence at the North Gunna section, Farafra Oasis, Western Desert, Egypt. *Marine Micropaleontology*, 26, 329–340.
- Abdulsamad, E. O., Bu-Argoub, F. M., & Tmalla, A. F. A. (2009). A stratigraphic review of the Eocene to Miocene rock units in the al Jabal al Akhdar, NE Libya. *Marine and Petroleum Geology*, 26, 1228–1239.
- Abu Shama, A. M., Wanas, H. A., & El-Nahrawy, S. A. (2019). Calcareous nannofossil biostratigraphy of the Paleocene-Lower Eocene successions in the Farafra Oasis, Western Desert, Egypt. *Journal African Earth Sciences*, 150, 466–484.
- Arenillas, I. (2012). Patterns of spatio-temporal distribution as criteria for the separation of planktic foraminiferal species across the Danian-Selandian transition in Spain. *Acta Palaeontologica Polonica*, 57(2), 401–422.
- Awad, G. H., & Ghobrial, M. G. (1965). Zonal stratigraphy of the Kharga Oasis. *Geology Survey Egypt, Cairo, Paper No. 34*, 77.
- Barthel, K. W., & Herrmann-Degen, W. (1981). Late Cretaceous and Early Tertiary stratigraphy in the Great Sand Sea and its SE Margins (Farafra and Dakhla Oases), SW Desert, Egypt. *Mitteilungen der Bayerischen Staatssammlung für Paläontologie und Histor. Geologie*, 21, 141–182.
- Bassiouni, M. A. A. & Luger, P. (1990). Maastrichtian to Early Eocene ostracoda from southern Egypt; palaeontology, palaeoecology, paleobiogeography and biostratigraphy. *Berliner geowiss. Abh., (A)*, Berlin, 120, 755–877.
- Berggren, W. A. (1974). Paleocene benthonic foraminiferal biostratigraphy, biogeography and paleoecology of Libya and Mali. *Micropaleontology*, 20, 449–465.
- Berggren, W. A., & Aubry, M.-P. (1998). The Paleocene/Eocene Epoch/Series boundary: Chronostratigraphic framework and estimated geochronology. In M.-P. Aubry, S. Lucas, & W. A. Berggren (Eds.), *Late Paleocene-Early Eocene Climatic and Biotic Events in the Marine and Terrestrial Records* (pp. 18–36). Columbia University Press.
- Berggren, W. A., & Ouda, K. (2003). Upper Paleocene-lower Eocene planktonic foraminiferal biostratigraphy of the Dababiya section, Upper Nile Valley (Egypt). In K. Ouda & M.-P. Aubry (Eds.), *The Upper Paleocene-Lower Eocene of the Upper Nile Valley: Part 1, stratigraphy*. *Micropaleontology* (Vol. 49 (1), pp. 61–92).
- Berggren, W. A., & Pearson, P. N. (2005). A revised tropical to subtropical Paleogene planktonic foraminiferal zonation. *Journal Foraminiferal Research*, 35(4), 279–298.
- Bernaola, G., Martin-Rubio, M., & Baceta, J. I. (2009). New high resolution calcareous nannofossil analysis across the Danian/Selandian transition at the Zumaia section: Comparison with South Tethys and Danish sections. *Geologica Acta*, 7(1–2), 79–92.

- Brookes, I. A. (2003). Palaeofluvial estimates from exhumed meander scrolls, Taref Formation (Turonian) Dakhla Region, Western Desert, Egypt. *Cretaceous Research*, 24, 97–104.
- Dercourt, J., Ricou, L. E., & Vrielynck, B. (1993). Atlas Tethys Palaeoenvironmental maps, Explanatory notes, Gauthier-Villars, 307 p.
- Dupuis, Ch., Aubry, M. -P., Steurbaut, E., Berggren, W. A., Ouda, K., Magioncalda, R., Cramer, B. S., Kent, D. V., Speijer, R. P., & Heilmann-Clausen, C. (2003). The Dababiya Quarry Section: Lithostratigraphy, clay mineralogy, geochemistry and paleontology. In K. Ouda & M. -P. Aubry (Eds.), *The Upper Paleocene-Lower Eocene of the Upper Nile Valley: Part 1, stratigraphy. Micropaleontology* (Vol. 49(1), pp. 41–59).
- El-Azabi, M. H., & El-Araby, A. (2000). Depositional cycles, an approach to the sequence stratigraphy of the Dakhla Formation, west Dakhla-Farafra stretch, Western Desert, Egypt. *Journal African Earth Sciences*, 30(4), 971–996.
- El-Azabi, M. H., & Farouk, S. H. (2011). High-resolution sequence stratigraphy of the Maastrichtian-Ypresian succession along the eastern scarp face of the Kharga Oasis, south Western Desert, Egypt. *Sedimentology*, 58, 579–617.
- El Hawat, A. S., Jorry, S., Caline, B., Davaud, E., & Masse, P. (2008). The Ypresian-Early Lutetian facies, sequences, and unconformities of Cyrenaica: Their correlation and implications in North Africa. *Geology of East Libya*, 1, 85–120.
- Ernst, S. R., Guasti, E., Dupuis, C., & Speijer, R. P. (2006). Environmental perturbation in the southern Tethys across the Paleocene/Eocene boundary (Dababiya, Egypt): Foraminiferal and clay mineral records. *Marine Micropaleontology*, 60, 89–111.
- Faris, M., & Farouk, S. H. (2012). Integrated biostratigraphy of two Upper Maastrichtian-Paleocene successions in north-central Sinai, Egypt. *Geologia Croatica*, 65(2), 139–160.
- Faris, M., Abd El-Hameed, A.T., Marzouk, A.M., & Ghandour, I.M., (1999). Early Paleogene calcareous nannofossil and planktonic foraminiferal biostratigraphy in central, Egypt. *Neues Jahrbuch für Geologie und Paläontologie, Abhandlungen*, 213 (2), 261–288.
- Farouk, S. (2016). Paleocene stratigraphy in Egypt. *Journal African Earth Sciences*, 113, 126–152.
- Farouk, S., & Jain, S. (2018). Benthic foraminiferal response to relative sea-level changes in the Maastrichtian-Danian succession at the Dakhla Oasis, Western Desert, Egypt. *Geological Magazine*, 155 (3), 729–746.
- Farouk, S., Askalany, M., Ahmad, F., El-Sorogy, A., Youssef, M., & Taha, S. (2019a). Maastrichtian-early Paleocene foraminiferal palaeobathymetry and depositional sequences at Gebel El Sharawna, south Luxor, Egypt. *Lethaia*, 53, 316–331.
- Farouk, S., Khalifa, M., Abu El-Hassan, M., Papazzoni, C., Fabrizio, F., Coccioni, R., & Zaky, A. (2019b). Upper Paleocene to lower Eocene microfacies, biostratigraphy, and paleoenvironmental reconstruction in the northern Farafra Oasis, Western Desert (Egypt). *Micropaleontology*, 65, 5381–5406.
- Flexer, A., & Reyment, R. A. (1989). Note on Cretaceous transgressive peaks and their relation to geodynamic events for the Arabo-Nubian and the northern African shields. *Journal African Earth Sciences*, 8 (1), 65–73.
- Gibson, T. G. (1989). Planktonic benthonic foraminiferal ratios: Modern patterns and Tertiary applicability. *Marine Micropaleontology*, 15, 29–52.
- Guasti, E., Kouwenhoven, T. J., Brinkhuis, H., & Speijer, R. P. (2005). Paleocene sea-level and productivity changes at the southern Tethyan margin (El Kef, Tunisia). *Marine Micropaleontology*, 55, 1–17.
- Haq, B. U. (2014). Cretaceous eustasy revisited. *Global and Planetary Change*, 113, 44–58.
- Haq, B. U., & Al-Qahtani, A. M. (2005). Phanerozoic cycles of sea-level change on the Arabian Platform. *GeoArabia*, 10(2), 127–160.
- Haq, B. U., Hardenbol, J., & Vail, P. R. (1987). Chronology of fluctuating sea levels since the Triassic (250 million years ago to present). *Science*, 235, 1156–1167.
- Hardenbol, J., Thierry, J., Farley, M. B., Jacquin, T., de Graciansky, P. -C., & Vail, P. R. (1998). Mesozoic-Cenozoic sequence chronostratigraphy framework of European basins. In P. -C. de Graciansky; J. Hardenbol; T. Jacquin & P. R. Vail (Eds.), *Sequence stratigraphy of European basins* (No. 60, pp. 3–14) SEPM Special Publication.
- Hendriks, F., Luger, P., Kallenbach, H., & Schroeder, J. H. (1984). Stratigraphical and sedimentological framework of the Kharga-Sinn El-Kaddab stretch (western and southern part of the Upper Nile Basin), Western Desert, Egypt. *Berliner geowiss. Abh., (A), Berlin*, 50, 117–151.
- Hendriks, F., Luger, P., Bowitz, J., & Kallenbach, H. (1987). Evolution of the depositional environments of the SE-Egypt during the Cretaceous and Lower Tertiary. *Subproject A3 Sedimentary Basin of Southern Egypt. Berliner geowiss. Abh., (A), Berlin*, 75 49–82.
- Hermina, M. H. (1990). The surroundings of Kharga, Dakhla and Farafra oases. In R. Said (Ed.), *The Geology of Egypt* (pp. 259–292) Balkema, Rotterdam, Chap. 14.
- Hewaidy, A. G., El-Azabi, M. H., & Farouk, Sh. (2006). Facies associations and sequence stratigraphy of the Upper Cretaceous-Lower Eocene succession in the Farafra Oasis, Western Desert, Egypt. In *8th International Conference on the Geology of the Arab World (GAW 8)* (Vol. 2, pp. 569–599) Cairo University.
- Hewaidy, A. G., Farouk, S., & Bazeen, Y. S. (2017). Sequence stratigraphy of the Maastrichtian-Paleocene succession at the Dakhla Oasis, Western Desert, Egypt. *Journal African Earth Science*, 136, 22–43.
- Hewaidy, A. G., Farouk, S., & Bazeen, Y. (2019a). Foraminiferal biostratigraphy and paleoenvironments of the Danian-Selandian succession at the Kharga Oasis, Western Desert, Egypt. *Arabian Journal of Geosciences*, 12, 1–17.
- Hewaidy, A. G., Farouk, S., & Bazeen, Y. (2019b). The Selandian/Thanetian transition of the Naqb El-Rufuf section, Kharga Oasis, Western Desert, Egypt: Foraminiferal biostratigraphy and sequence stratigraphy implications. *Journal African Earth Science*, 150, 499–510.
- Hewaidy, A. G., Farouk, S., & Bazeen, Y. (2019c). Upper Palaeocene-lower Eocene succession of the Kharga Oasis, Western Desert, Egypt: Foraminiferal biostratigraphy and sequence stratigraphy. *Geological Journal*, 55, 4375–4397. <https://doi.org/10.1002/gj.3674>
- Ibrahim, M. I. A., & Abdel-Kireem, M. R. (1997). Late Cretaceous palynofloras and foraminifera from Ain El-Wadi area, Farafra Oasis, Egypt. *Cretaceous Research*, 18, 633–660.
- Issawi, B. (1972). Review of Upper Cretaceous-Lower Tertiary stratigraphy in central and southern Egypt. *American Association Petroleum Geologists Bulletin*, 56(8), 1448–1463.
- Jorry, S. (2004). The Eocene Nummulite carbonates (Central Tunisia and NE Libya): sedimentology, depositional environments, and application to oil reservoirs. Ph.D. Thesis, Terre & Environment, (Vol. 48, p. 206) University of Geneva.
- Jorry, S. J., Haster, C.-A., & Davaud, E. (2006). Hydrodynamic behaviour of Nummulites: Implications for depositional models. *Facies*, 52, 221–235.
- Keller, G. (2002). *Guembelitra* dominated late Maastrichtian planktic foraminiferal assemblages mimic early Danian in Central Egypt. *Marine Micropaleontology*, 47, 71–99.
- Keller, G. (2004). Low-diversity, Late Maastrichtian and Early Danian planktic foraminiferal assemblages of the Eastern Tethys. *Journal Foraminiferal Research*, 34(1), 49–73.

- Keller, G., Adatte, T., Burns, S. J., & Tantawy, A. A. (2002). High-stress paleoenvironment during the late Maastrichtian to early Paleocene in central Egypt. *Palaeogeography, Palaeoclimatology, Palaeoecology*, 187, 35–60.
- Keller, G., Mateo, P., Monkenbusch, J., Thibault, N., Punekar, J., Spangenberg, J. E., Abramovich, S., Ashckenazi-Polivoda, S., Schoene, B., Eddy, M. P., Samperton, K. M., & Adatte, T. (2020). Mercury linked to Deccan Traps volcanism, climate change and the end-Cretaceous mass extinction. *Global and Planetary Change*, 194, 103312.
- Klitzsch, E. (1986). Plate tectonics and cratonal geology in northeast Africa (Egypt, Sudan). *Geologische Rundschau*, 75(3), 755–768.
- Kouwenhoven, T. J., Speijer, R. P., Van Oosterhout, C. W. M., & Van der Zwaan, G. J. (1997). Benthic foraminiferal assemblages between two extinction events: The Paleocene El Kef section, Tunisia. *Marine Micropaleontology*, 29, 105–127.
- Kuss, J., Scheibner, C., & Gietl, R. (2000). Carbonate platform to basin transition along an Upper Cretaceous to Lower Tertiary Syrian Arc uplift, Galala Plateaus, Eastern Desert, Egypt. *GeoArabia*, 5(3), 405–424.
- Li, L., & Keller, G. (1998a). Maastrichtian climate, productivity and faunal turnovers in planktic foraminifera in South Atlantic DSDP sites 525 and 21. *Marine Micropaleontology*, 33, 55–86.
- Li, L., & Keller, G. (1998b). Diversification and extinction in Campanian-Maastrichtian planktic foraminifera of northwest Tunisia. *Eclogae Geologicae Helveticae*, 91, 75–102.
- Li, L., Keller, G., & Stinnesbeck, W. (1999). The Late Campanian and Maastrichtian in northwestern Tunisia: Paleoenvironmental inferences from lithology, macrofauna and benthic foraminifera. *Cretaceous Research*, 20, 231–252.
- Li, L., Keller, G., Adatte, T., & Stinnesbeck, W. (2000). Late Cretaceous sea level changes in Tunisia: A multi-disciplinary approach. *Journal of the Geological Society (London)*, 157, 447–458.
- Luciani, V. (2002). High-resolution planktonic foraminiferal analysis from the Cretaceous-Tertiary boundary at Ain Settara (Tunisia): Evidence of an extended mass extinction. *Palaeogeography, Palaeoclimatology, Palaeoecology*, 178, 299–319.
- Luger, P. (1985). Stratigraphie der marinen Oberkreide und des Alttertiars im Südwestlichen Oberrhin-Becken (SW-Aegypten) unter besonderer Berücksichtigung der mikropaläontologie, paläoökologie und paläogeographie. *Berliner geowiss. Abh., (A), Berlin*, 63, 1–150.
- Luger, P., & Schrank, E. (1987). Mesozoic to Paleogene transgressions in middle and southern Egypt - Summary of paleontological evidence. In G. Matheis & H. Schandelmeier (Eds.), *Current research in African earth sciences* (pp. 199–202). Balkema.
- Lüning, S., Marzouk, A., & Kuss, J. (1998a). The Paleocene of central east Sinai, Egypt: “sequence stratigraphy” in monotonous hemipelagites. *Journal Foraminiferal Research*, 28(1), 19–39.
- Lüning, S., Marzouk, A. M., Morsi, A. M., & Kuss, J. (1998b). Sequence stratigraphy of the Upper Cretaceous of central-east Sinai, Egypt. *Cretaceous Research*, 19, 153–196.
- Miller, K. G., Sugarman, P. J., Browning, J. V., Kominz, M. A., Olsson, R. K., Feigenson, M. D., & Hernández, J. C. (2004). Upper Cretaceous sequences and sea-level history, New Jersey coastal plain. *Geological Society of America*, 116(3/4), 368–393.
- Miller, K. G., Kominz, M. A., Browning, J. V., Wright, J. D., Mountain, G. S., Katz, M. E., Sugarman, P. J., Cramer, B. S., Christie-Blick, N., & Pekar, S. F. (2005). The Phanerozoic record of global sea-level change. *Science*, 310, 1293–1298.
- Molina, E., Alegret, L., Arenillas, I., Arz, J. A., Gallala, N., Hardenbol, J., van Salis, K., Steurbaut, Vandenberghe, N., & Zaghbib-Turki, D. (2006). The Global Boundary Stratotype Section and Point for the base of the Danian Stage (Paleocene, Paleogene, Tertiary, Cenozoic) at El Kef, Tunisia—Original definition and revision. *Episodes*, 29(4), 263–273.
- Moustafa, A. R., Saoudi, A., Moubasher, A., Ibrahim, I. M., Molokhia, H., & Schwartz, B. (2003). Structural setting and tectonic evolution of the Bahariya Depression, Western Desert, Egypt. *GeoArabia, Bahrain*, 8(1), 91–124.
- Mresah, M. H. (1993). facies patterns and stratal geometries: Clues to the nature of the platform margin during the Paleocene, northeast Sirte Basin, Libya. *Sedimentary Geology*, 84, 149–167.
- Murray, J. W. (1976). A method of determining proximity of marginal seas to an ocean. *Marine Geology*, 22, 103–119.
- Ouda, K. (2003). The Paleocene/Eocene boundary in Egypt: An overview. *Micropaleontology*, 49(1), 15–40.
- Schandelmeier, H., Klitzsch, E., Hendriks, F., & Wycisk, P. (1987). Structural development of north-east Africa since Precambrian times. *Berliner geowiss. Abh., (A), Berlin*, 75, 5–24.
- Scheibner, C., Kuss, J., & Marzouk, A. M. (2000). Slope sediments of a Paleocene ramp-to-basin transition in NE Egypt. *International Journal of Earth Sciences*, 88, 708–724.
- Scheibner, C., Marzouk, A. M., & Kuss, J. (2001). Shelf architectures of an isolated Late Cretaceous carbonate platform margin, Galala Mountains (Eastern Desert, Egypt). *Sedimentary Geology*, 145, 23–43.
- Schnack, K., & Luger, P. (1998). Facies and structural evolution during the Maastrichtian and Paleocene in the Kharga uplift area and adjacent areas (Western Desert, SW-Egypt). *Zbl. Geol. Palaeontol. Teil, I*, 311–351.
- Sebei, K., Inoubli, M. H., Boussiga, H., Tlig, S., Alouani, R., & Boujamaoui, M. (2007). Seismic Stratigraphy, tectonics and depositional history in the Halk el Menzel region, NE Tunisia. *Journal African Earth Sciences*, 47, 9–29.
- Sharland, P. R., Archer, R., Casey, D. M., Davies, R. B., Hall, S. H., Heward, A. P., Horbury, A. D., & Simmons, M. D. (2001). Arabian Plate Sequence Stratigraphy. *GeoArabia Special Publication No. 2*, 371p and 3 enclosures.
- Sharland, P. R., Casey, D. M., Davies, R. B., Simmons, M. D., & Sutcliffe, O. E. (2004). Arabian Plate sequence stratigraphy. *GeoArabia*, 9(1), 199–214.
- Speijer, R. P., & Wagner, T. (2002). Sea-level changes and black shales associated with the late Paleocene thermal maximum: Organic-geochemical and micropaleontologic evidence from the southern Tethyan margin (Egypt-Israel). In C. Koeberl & K. G. MacLeod (Eds.), *Catastrophic events and mass extinction: Impacts and Beyond: Boulder* (Vol. 356, pp. 533–549) Colorado, Geol. Soc. Amer. Paper.
- Sprong, J., Speijer, R. P., & Steurbaut, E. (2009). Biostratigraphy of the Danian/Selandian transition in the southern Tethys. Special reference to the Lowest Occurrence of planktic foraminifera Igorina albeari. *Geologica Acta*, 7(1–2), 63–77.
- Stokke, E. W., Liu, E., & Jones, M. T. (2020). Evidence of explosive hydromagmatic eruptions during the emplacement of the North Atlantic Igneous Province. *Volcanica*, 3(2), 227–250.
- Strougo, A. (1986). The *velascoensis* event: A significant episode of tectonic activity in the Egyptian Paleogene. *Neues Jahrbuch für Geologie und Paläontologie, Abhandlungen*, 173, 253–269.

- Tantawy, A. A., Keller, G., Adatte, T., Stinnesbeck, W., Kassab, A., & Schulte, P. (2001). Maastrichtian to Paleocene depositional environment of the Dakhla Formation, Western Desert, Egypt: Sedimentology, mineralogy, and integrated micro- and macrofossil biostratigraphies. *Cretaceous Research*, 22, 795–827.
- Thomas, D. J., & Bralower, T. J. (2005). Sedimentary trace element constraints on the role of North Atlantic Igneous Province volcanism in late Paleocene–early Eocene environmental change. *Marine Geology*, 217(3–4), 233–254.
- Thomas, E., Zachos, J. C., & Bralower, T. J. (2000). Deep-sea environments on a warm earth: Latest Paleocene–early Eocene. In B. T. Huber, K. G. Macleod, & S. L. Wing (Eds.), *Warm climates in the earth history* (pp. 132–160). Cambridge University Press.
- Tmalla, A. F. A. (2007). The stratigraphic positions of Wadi Dukhan and Al Uwayliah formations, northeast Libya—A review. *Scripta Geologica*, 134, 119–130.
- Varol, O. (1989). Palaeocene calcareous nannofossil biostratigraphy. In J. A. Crux & S. E. Van Heck (Eds.), *Nannofossils and their applications*. (Vol. 12, pp. 267–310) British Micropaleontologica Society Publication.
- Wade, B. S., Pearson, P. N., Berggren, W. A., & Pälike, H. (2011). Review and revision of Cenozoic tropical planktonic foraminiferal biostratigraphy and calibration to the Geomagnetic Polarity and Astronomical Time Scale. *Earth Science Reviews*, 104, 111–142.
- Zachos, J. C., Lohmann, K. C., Walker, J. C. G., & Wise, S. W. (1993). Abrupt climate change and transient climates during the Paleogene: A marine perspective. *The Journal of Geology*, 101, 191–213.
- Zaky, A., Coccioni, R., Farouk, S., Khalifa, M., Abu El-Hassan, M., Papazzoni, C., Fabrizio, F. (2020). The Maastrichtian-Danian transition in the northern Farafra Oasis, Western Desert (Egypt): Implications from foraminiferal paleobathymetry and paleoenvironmental reconstructions. *Journal African Earth Sciences*, 103853.



Mounir El-Azabi is a professor of sedimentology and sequence stratigraphy at the Department of Geology, Faculty of Science, Cairo University (Egypt) from where he received an M.Sc degree in geology (1986). He also obtained a Ph.D in geology in 1992 from Cairo University. His field of specialization includes facies analysis, paleoenvironment, basin architecture, modeling, facies evolution, and sequence stratigraphy of clastic/carbonate deposits in different regions, and stratigraphic records (Middle Triassic-Miocene).



Sherif Farouk is a professor in the Exploration Department of the Egyptian Petroleum Research Institute, Cairo. He obtained a Ph.D degree from Al-Azhar University (Egypt). He worked for the Geological Survey of Egypt from 1996 until 2007. He is a specialist in high-resolution stratigraphy, paleoenvironmental analysis, sequence stratigraphic studies, and paleontological applications. He has published about 101 scientific articles in several international journals on Phanerozoic stratigraphy, especially of Egypt, Jordan, Saudi Arabia, Iraq, United Arab Emirates, and Tunisia



The Eocene–Oligocene Vertebrate Assemblages of the Fayum Depression, Egypt

Panagiotis Kampouridis, Josephina Hartung, and Felix J. Augustin

Abstract

The Fayum has yielded one of the oldest and richest records of fossil mammals from Africa. Today, the Fayum Depression represents an oasis in the Western Desert of Egypt, south of Cairo, and contains several localities that are world renowned for their diverse Eocene to Oligocene vertebrate assemblages. The fossil sites of the Fayum area have provided numerous extraordinarily well-preserved vertebrate remains including complete skulls and partial skeletons of turtles, crocodiles, birds, and mammals. Thus, the Fayum Depression has shed light onto the evolution and biogeography of vertebrates during the Paleogene leading to the establishment of two new orders, several new families and subfamilies, and numerous new species of mammals. In recent years, these fossils have provided clues about ecological aspects of some groups using new methods such as stable isotope analysis and μ CT scanning. Despite the fact that the Fayum Depression represents a historical excavation site that has been excavated and studied by numerous famous palaeontologists since the nineteenth century, the area continues to provide new insights into the evolution of mammals during the Eocene to Oligocene, greatly improving our understanding of early Cenozoic vertebrate evolution. This chapter presents a historical review of the excavations in the Fayum Depression and a taxonomic overview of its fossil fauna. Special focus was placed on the taxonomy and, where applicable, ecology of terrestrial mammals from the historical Paleogene Fayum localities.

Keywords

Egypt • Fayum Depression • Cenozoic • Paleogene • Mammalia • Vertebrate assemblages • Fossil fauna

Abbreviations

AMNH	American Museum of Natural History, New York City, USA
BSPG	Bayerische Staatssammlung für Paläontologie und Geologie in München, Germany
DPC	Duke Lemur Center, Division of Fossil Primates, Durham, North Carolina, USA
GPIT	Palaeontological Collection of the University of Tübingen, Germany
MNHN	Muséum national d'Histoire naturelle, Paris, France
NHMUK	Natural History Museum of the United Kingdom London, UK
NHMW	Naturhistorisches Museum in Wien, Austria
SMNS	Staatliches Museum für Naturkunde Stuttgart, Germany

1 Introduction

The Fayum Depression (Fig. 1) represents today an oasis approximately 80 km southwest of Cairo, in the Western Desert of Egypt (El-Shabrawy & Dumont, 2009). The region is renowned for its plethora of fossiliferous localities, which demonstrate extremely rich and diverse Eocene to Oligocene vertebrate assemblages (Andrews, 1906a; Seiffert et al., 2008; Simons & Rasmussen, 1990). These vertebrate localities of the Fayum Depression have been excavated and studied extensively by numerous famous palaeontologists since the nineteenth century, including Charles W. Andrews, Eberhard Fraas, Ernst Stromer von Reichenbach, and Henry F. Osborn. These palaeontologists, along with many others after them, provided detailed studies about the Fayum fossils and revealed new information about the Eocene to Oligocene mammal communities of Africa, thereby elucidating the origin and early evolution of many mammal groups (e.g. de

P. Kampouridis (✉) · J. Hartung · F. J. Augustin
Department of Geoscience, Eberhard Karls University of Tübingen, Hölderlinstraße 12, 72074 Tübingen, Germany
e-mail: pkampouridis94@gmail.com

Vries et al., 2021; Simons, 2008; Simons & Rasmussen, 1990). Some of the most extensively studied mammal groups include the Proboscidea, Cetacea, and Primates, which significantly advanced our knowledge on these groups.

The aim of this chapter is mainly twofold: first, we present a historical review of the excavations that were carried out in the Fayum Depression, and second, we provide a taxonomic overview of its fossil vertebrate fauna. For this, we almost exclusively focused on the terrestrial vertebrates, but also refer to aquatic mammals, cetaceans, and sirenians, while other aquatic taxa such as fishes were excluded. As the majority of studies dealing with the palaeontology of the Fayum Depression focused on terrestrial mammals and cetaceans, this is also reflected herein and accordingly, these groups received the most attention, seconded by reptiles and birds. Moreover, a short introduction to the geology of the Fayum Depression and the three different terrestrial vertebrate-bearing formations is given at the beginning. Finally, as a conclusion, we discuss the importance of the Fayum Depression for our understanding of mammalian evolution.

2 Historical Overview

The first fossils from the Fayum Depression were discovered by Orlebar (1845), who studied the geology of the Egyptian deserts. He described many fossils, including several invertebrates, as well as plant remains, comprising up to 20-m-long tree trunks. Orlebar (1845) even reported some mammalian remains, without any description of the specimens though.

The German botanist Georg August Schweinfurth was the first to conduct a detailed geological survey in the area of the Fayum Depression in 1877. In 1879, he collected several shark teeth and cetacean bones from Gezirit El Qarn, a small island within the Birket Qarun Lake. Shortly after, this material was studied by Dames (1883a). Schweinfurth continued his work in the Fayum Depression, uncovering more vertebrate fossils (Schweinfurth, 1886). After receiving further material from Schweinfurth, Dames (1894) described the first fossil whale species from Egypt, *Zeuglodon osiris* (today known as *Saghacetus osiris*).

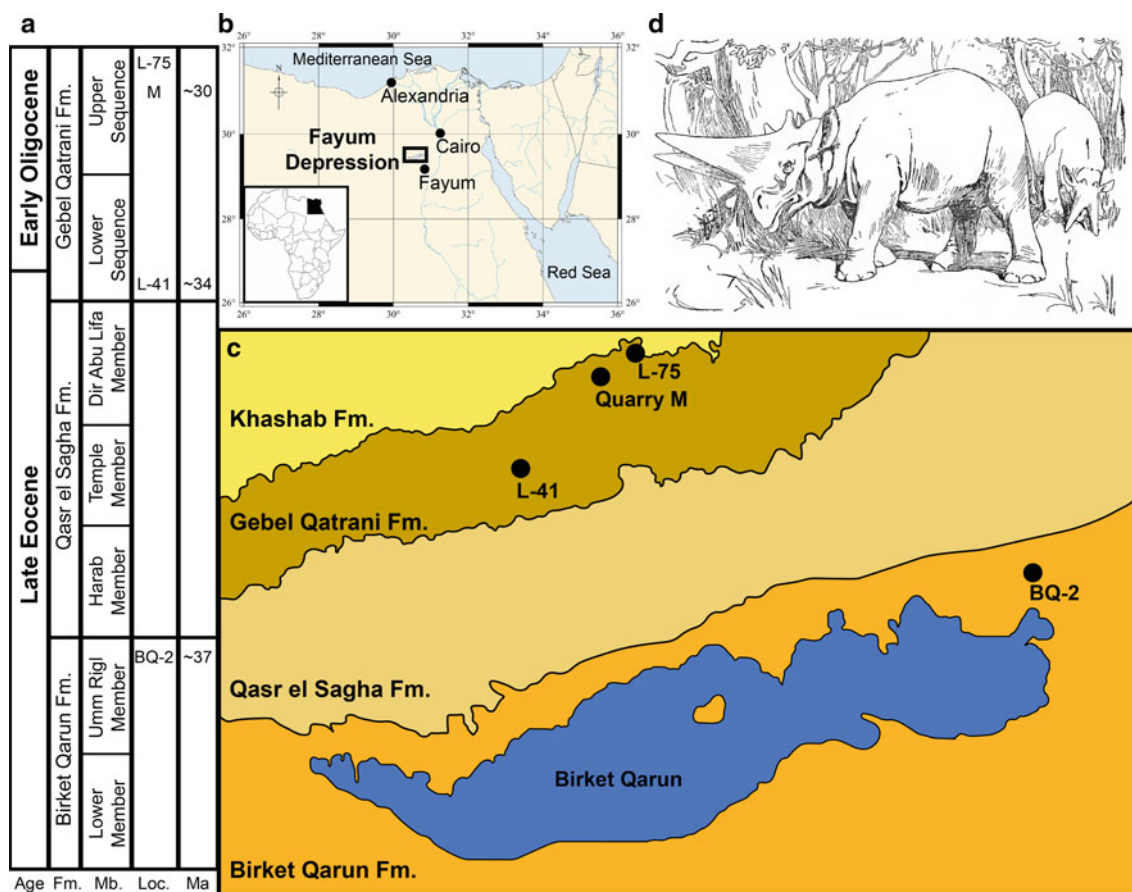


Fig. 1 Geographical and stratigraphical setting of the Fayum Depression (Egypt): **a** stratigraphical context of the Upper Eocene to Lower Oligocene Fayum deposits. **b** Geographical map of Egypt showing the position of the Fayum Depression, created with GMT6 (Wessel et al., 2013). **c** Geological map of the northern part of the Fayum Depression (modified after Sallam et al., 2011). **d** Reconstruction of the iconic *Arsinoitherium* in the Early Oligocene Fayum forest (Andrews, 1906a)

Later, in 1898, the British geologist Hugh John Llewellyn Beadnell was employed by the Egyptian Geological Survey to conduct a geological expedition to the Fayum Depression. Beadnell published his findings initially as a preliminary report on the Fayum Depression and its Paleogene fauna (Beadnell, 1901) and later in a monograph about the geology of the region (Beadnell, 1905). During his fieldwork in the marine sediments north of Birket Qarun, Beadnell and his team found numerous vertebrate fossils, which he sent to the Natural History Museum of the UK in London. There they were studied by British palaeontologist Andrews (1899), who was intrigued by the material and subsequently travelled several times to the Fayum Depression himself to collect fossils. In April 1901, Beadnell was accompanied by Andrews in his fieldwork in the Fayum Depression. Andrews returned to Egypt in the spring of 1902 and 1903, collecting a considerable number of specimens, which he included in his monumental monograph on the vertebrates from the Fayum fauna (Andrews, 1906a). This work represents, to this day, the most important and extensive study on the macrovertebrate fossils from Egypt.

Between 1897 and 1899, the German geologist Max Blanckenhorn was employed by the Geological Survey of Egypt to study the geology and collect fossils from Egypt. He published his findings in 1900, including an examination of the stratigraphy of the Fayum Depression (Blanckenhorn, 1900). In 1902, he returned to Egypt together with the German palaeontologist Ernst Freiherr Stromer von Reichenbach to collect fossils, including a large collection of mammal remains, which were sent to the palaeontological collection in Munich (Stromer, 1902). In November 1903, Stromer returned to Egypt for three months, mainly for the collection of Tertiary mammals, from the Fayum Depression (Stromer, 1904).

There, he met Richard Markgraf, an Austro-German fossil collector who was among the most important people who excavated fossils in the Paleogene as well as in the Cretaceous (see Augustin et al., 2023) of Egypt. In 1897, Markgraf joined the team of German palaeontologist Eberhard Fraas from Stuttgart, in a palaeontological expedition to the Fayum. Fraas taught Markgraf how to excavate fossils, and later, after recognising his skills, he hired him to continue collecting fossils for the Staatliches Museum für Naturkunde Stuttgart in Germany (SMNS) for many years. During his second expedition to the Fayum Depression, in 1903, Stromer was accompanied by Markgraf who was extremely helpful and remained there collecting many more fossils, which he sent to Munich for Stromer to study them (e.g. Stromer, 1903, 1904, 1908). In 1906, Fraas planned another expedition to the Fayum, which was organised and carried out thanks to Markgraf. They uncovered many important specimens that were sent to Stuttgart. Markgraf continued collecting fossils from the Paleogene of the Fayum Depression and the Cretaceous of the Bahariya Oasis

(Augustin et al., 2023) until the First World War. He brought to light some of the most important finds from the Fayum area, such as a number of primate fossils. Because of his astonishing achievements in the collection of fossils in Egypt, Markgraf received the silver medal of Bene Merenti from the Bavarian Academy of Sciences in 1902 and the Medal of Merit of the Royal Württemberg Crown Order in 1904. Furthermore, several species were named in his honour, including the primates *Propliopithecus markgrafi* from the Fayum Depression (Schlosser, 1910) and *Libypithecus markgrafi* from the Miocene Wadi el Natrun (Stromer, 1913). Nonetheless, he did not receive any real fame or fortune for his services and lived a very simple life. Unfortunately, nowadays his name has fallen into oblivion, despite his incredible impact on the knowledge of the fossil vertebrate faunas of Africa and their significance for our understanding of vertebrate evolution during the Paleogene.

Another palaeontological expedition to the Fayum Depression was organised by Marcellin Boule and Jean Albert Gaudry from the Muséum national d'Histoire naturelle (MNHN) in Paris and carried out in 1904 by René Fourtau. He was a French civil engineer who worked for the Geological Survey of Egypt and studied invertebrates, mainly echinoderms. During their two-week expedition they were able to collect about 30 mammalian fossils that were transferred to the MNHN (Tabuce, 2016).

Henry Fairfield Osborn, an American palaeontologist who worked intensively on the evolution of Proboscidea at the American Museum of Natural History (AMNH), decided to organise an expedition to the Fayum Depression, in 1907, after reading the findings of Andrews (1906a), that had a significant impact on the understanding of proboscideans. Osborn's team was joined by Walter Granger and George Olsen, who oversaw the expedition that represented America's first palaeontological expedition in the Old World and was supported by President Roosevelt (Morgan & Lucas, 2002). Osborn left the group after a short time and hired Markgraf to assist the expedition. This expedition collected about 550 fossils that were later studied by Osborn (1908), who erected, among others, the new family of Ptolemaiidae, a peculiar group of mammals, which today is placed in its own order, the Ptolemaiida.

The material collected by these first expeditions was later studied by many renowned palaeontologists and gave significant insights into the evolution of several vertebrate groups, such as Primates, Proboscidea, Sirenia, and Cetacea (Andrews, 1899, 1906a; Osborn, 1908; Schlosser, 1911; Stromer, 1916). Nevertheless, the Fayum fossil localities remained forgotten for almost five decades, mainly due to the two world wars, with the only expedition in the area carried out in 1947 by a team led by American archaeologist Wendell Phillips, from the University of California at Berkeley. Then, a renewed period of extensive excavations in the Fayum

Depression began with Elwyn LaVerne Simons. After describing a skull fragment of an anthropoid, Simons (1959) initiated a new series of excavations in the area that lasted from 1961 until 1967. The main purpose of these expeditions was the search for further primate remains and small mammals, which were under-represented in the old Fayum collections (Simons & Rasmussen, 1990). In 1971, the exploration for the Fayum fossils continued under the leadership of Simons. This time the fieldwork and studies carried out in the Fayum area were marked by the interdisciplinary approach of the researchers, with the inclusion of specialists from different fields that also led to the first precise dating of the sedimentary rocks in the Fayum Depression (Bown & Kraus, 1988; Kappelman, 1992; Kappelman et al., 1992; Seiffert, 2006; Seiffert et al., 2008; Van Couvering & Harris, 1991). The efforts of Simons and his team shed new light on the classical vertebrate assemblages of the Fayum Depression, revealing previously unknown details about the locality and many new extraordinary fossils. Palaeontological excavations in the area and the study of the new, but also the re-evaluation of old material continue to this day, producing consistently new research about the Paleogene fauna of Egypt (e.g. Al-Ashqar et al., 2021; El-Sayed et al., 2020; Gohar et al., 2021; Sallam & Seiffert, 2019).

3 Geology of the Fayum Depression

The geology of the Fayum Depression has been studied by numerous researchers over the last two centuries. The most important studies on the geology of the Fayum area include Beadnell (1905), Bown and Kraus (1988), and Gingerich (1992). The Fayum Depression represents a 120-km-wide Graben structure filled with Eocene–Oligocene sediments that have been deposited unconformably on top of Upper Cretaceous sediments (Salem, 1976). The terrestrial vertebrate-yielding sediments in the northern part of the Fayum Depression (Fig. 1) belong to three different formations, which range in age from the Late Eocene to the Early Oligocene and are overlain by the Widan el Faras Basalt. The thickness of this basalt varies from 2 to 25 m, and it has been radio-isotopically ($^{40}\text{Ar}/^{39}\text{Ar}$) dated to 23.64 ± 0.035 Ma (Kappelman et al., 1992). Both the Paleogene sediments and the Widan el Faras Basalt are overlain by Neogene sediments of the Khashab Formation.

3.1 Birket Qarun Formation

The stratigraphically lowest formation that includes terrestrial fossils is the Birket Qarun Formation (Birket el Qarun Series after Beadnell, 1905). The thickness of the Birket Qarun Formation ranges from 20 to 85 m and includes mainly clays,

shales, thick fine-grained sandstones, but also ferruginous bioclasts and calcareous grits (Anan & El Shahat, 2014; Zalmout & Gingerich, 2012). One of its most characteristic layers is the Camp White Layer, which can be up to 2 m thick. It is known for its richness in marine mammals (Gingerich, 1992) and for the existence of vertical, rod-like structures which had been interpreted as “mangrove pneumatophores”, but were most recently re-evaluated and described as burrows of different invertebrates (Gee et al., 2019).

The Birket Qarun Formation comprises an unnamed lower member and the Umm Rigl Member. The assignment of the Umm Rigl Member to the Birket Qarun Formation has been questioned in the past (see King et al., 2014) and its attribution to the overlying Qasr el Sagha Formation has been proposed instead (Gingerich, 1992). Seiffert et al. (2008) discussed the history of the Birket Qarun Formation, including the Umm Rigl Member, and supported the original position of the latter in the Birket Qarun Formation, because it is consistent with previous works and because of the lack of any distinctive features that would allow its association with the Qasr el Sagha Formation. Herein we follow Seiffert et al. (2008) in regarding the Umm Rigl Member as part of the Birket Qarun Formation.

The Birket Qarun Formation contains in total nine fossiliferous localities (Rasmussen et al., 1992; Sileem et al., 2015), whereas the Umm Rigl Member specifically includes one of the richest fossil sites, called Birket Qarun Locality-2 (BQ-2, see Fig. 1a and c). It was discovered in 2000 and has yielded a very rich fauna with an age of ~ 37 Ma, representing one of the most diverse vertebrate localities in the Paleogene of Afro-Arabia (Seiffert et al., 2008). BQ-2 represents the oldest primate-bearing locality in Egypt, with the coexistence of five primate taxa: *Karanisia clarki* and *Saharagalago misrensis* (Seiffert et al., 2003), *Biretia fayumensis* and *Biretia megalopsis* (Seiffert et al., 2005), and *Masradapis tahai* (Seiffert et al., 2018). The fauna also contains several fish taxa (El-Sayed et al., 2020; Murray et al., 2010), snakes (McCartney & Seiffert, 2016), and a very rich mammalian assemblage, including proboscideans, hyracoids, herodotiines, ptolemaiids, creodonts, anomaluroid and hystricognathous rodents, chiropterans, and insectivores (Seiffert et al., 2005, 2008; Simmons et al., 2016).

The palaeoenvironment of the Birket Qarun Formation, including BQ-2, has traditionally been regarded as marine (Anan & El Shahat, 2014; Beadnell, 1905; Gingerich, 1992; Kappelman et al., 1992; Van Couvering & Harris, 1991; Wanas, 2008). Gingerich (1992) suggested that the Birket Qarun Formation represents an offshore barrier bar complex parallel to the Tethys shoreline. However, Seiffert et al. (2005, 2008) suggested that BQ-2 represents a fluvial environment. The ichthyofauna from BQ-2 has recently been studied in detail and suggests a freshwater environment, with some nearshore marine influences (El-Sayed et al., 2020; Murray et al., 2010).

3.2 Qasr el Sagha Formation

The Qasr el Sagha Formation was initially described as the “Qasr el Sagha Series” by Beadnell (1905) and later also used by Said (1962). It includes Late Eocene sediments that can be up to 200 m thick and can be divided into two to four members, depending on the authors (El-Younsy & Salman, 2021; Gingerich, 1992, 1993). As already mentioned above, herein the Umm Rigl Member will be considered as part of the Birket Qarun Formation (following Seiffert et al., 2008). Therefore, the lowermost part of the Qasr el Sagha Formation is the Harab Member, which consists of 30–40 m of brown shales (Gingerich, 1992). It is overlain by the Temple Member, which can be up to 80 m thick. It consists of thin layers of highly fossiliferous, glauconitic and limonitic arenaceous limestones, fine rippled, cross-laminated and highly bioturbated siliceous sandstones interbedded with thick laminated siltstones and gypsiferous sandy mudstones (El-Younsy & Salman, 2021). The upper part of the Qasr el Sagha Formation is composed of the Dir Abu Lifa Member, which can be up to 80 m thick. It comprises colourful, cross-stratified sandstones, alternating with siltstone, silty claystone and shale, topped by a yellow, fine-to-coarse sandy limestone, with many gradational to erosional surfaces in between (El-Younsy & Salman, 2021). The Dir Abu Lifa Member is overlain by the Gebel Qatrani Formation with an erosional contact.

The Upper Eocene Qasr el Sagha Formation contains eight fossiliferous localities (Rasmussen et al., 1992; Sileem et al., 2015). The Temple Member has yielded only few, and mostly marine, mammals (Bown & Kraus, 1988; Holroyd et al., 1996). Most vertebrate fossils have been recovered from the Dir Abu Lifa Member (Bown & Kraus, 1988), including fishes, crocodylians, turtles, snakes, and some mammalian representatives, including sirenians, cetaceans, and proboscideans. Recent re-evaluation of the sequence stratigraphy of the Qasr el Sagha Formation shows that it was deposited in a range of depositional environments, from shallow marine to fluvial environments (El-Younsy & Salman, 2021).

3.3 Gebel Qatrani Formation

The Gebel Qatrani Formation (also referred to as Jebel Qatrani, Gabal Qatrani, and Djebel Qatrani Formation) was initially named “Fluvio-Marine Series” by Beadnell (1905), but was later re-described by Said (1962). It lies unconformably on the Qasr el Sagha Formation and is topped by the Widan el Faras Basalt. The Gebel Qatrani Formation is of Late Eocene to Early Oligocene age (Beadnell, 1905; Bown et al., 1982; Kappelman et al., 1992; Murray, 2004) and can be up to 300 m thick. The Gebel Qatrani Formation contains variegated sandstones and mudstones with minor carbonates and chert pebble conglomerates and pebbly mudstones (Bown

et al., 1982). It has been suggested that it can be subdivided into three members (see El-Younsy & Salman, 2021).

The Gebel Qatrani Formation has been divided into two sequences, the “Lower Fossil Wood Zone” and the “Upper Fossil Wood Zone” (Simons & Wood, 1968). These two zones are separated by a marker bed, consisting of cliff-forming baryte sandstones. The formation consists mainly of alluvial sediments of meandering rivers deposited during the Oligocene (Bown et al., 1982). Remarkably, it represents the first major terrestrial sedimentation in Egypt since the Cretaceous (Bown & Kraus, 1988). Some minor developments of shorelines and shallow marine facies continuing for short periods of time are also present however, as indicated by thin sandstones bearing marine molluscs (Bown & Kraus, 1988; Salem, 1976). Bown et al. (1982) proposed that the environment of the Gebel Qatrani Formation, in which several primate taxa coexisted, represented a sub-tropical to tropical lowland plain, with several large meandering streams and extensive ponds (contra Kortlandt, 1980). Murray (2004) studied the fish assemblage from the Gebel Qatrani Formation, which supports the existence of swampy rivers with overgrown banks, along with abundant vegetation, as also proposed by previous studies (Rasmussen et al., 1987; Wing & Tiffney, 1982). Fossil flora evidence outlined that during the Paleogene, a belt of tropical forests stretched along the coast of the Tethys Ocean, surrounding the Fayum area and its vicinity, whereas some distance further inland a belt of open wood land or even a steppe-like vegetation existed during large parts of the Paleogene (e.g., El Atfy et al., 2021).

The vast majority of the over 100 vertebrate localities of the Fayum Depression are distributed throughout the Gebel Qatrani Formation (Rasmussen et al., 1992). Of these, eight have produced almost 90% of the total mammalian remains (Rasmussen et al., 1992; Sileem et al., 2015); these sites are the quarries A, B, E, G, I, M, V, and Locality 41 (L-41). The site L-41 represents, with an age of about 34 Ma, the oldest and richest fossiliferous locality in the Gebel Qatrani Formation (Sallam et al., 2011; Simons, 2008) and has brought to light a very diverse fauna, comprising fishes (Murray, 2004), birds (Miller et al., 1997; Rasmussen et al., 2001), and a very rich mammalian fauna. It consists mainly of hyracoids, as well as rodents, primates, creodonts, macroscelideans, and anthracotheres, indicating a forested environment (Gagnon, 1997).

4 Fauna Overview

4.1 Reptilia

4.1.1 Serpentes

The fossil record of snakes in the Fayum Depression is rather limited. Andrews (1901a) described the very large

Gigantophis garstini, based on a series of 20 associated vertebrae from the Qasr el Sagha Formation. He originally compared it to the extant genus *Python*, while assigning it to the Boidae (Andrews, 1906a). Recently, however, this taxon was placed in the Madtsoiidae (McCartney & Seiffert, 2016). One year later, a revision of this taxon suggested an estimated length of about 7 m, a sister-taxon relationship to the latest Cretaceous Indian snake *Madtsoia pisdurensis* and discussed potential biogeographical implications for the group (Rio & Mannion, 2017).

Andrews (1901a) described another somewhat smaller, but still relatively large, snake species, *Moeriophis schweinfurthi*, based on vertebrae from the Qasr el Sagha Formation. A few years later, Andrews (1906a) assigned this species to the palaeophiid genus *Pterosphenus*, erected by Lucas (1898). Andrews (1906a) also suggested that *Pterosphenus schweinfurthi* was aquatic, as indicated by the high frequency of its remains in the Qasr el Sagha Formation along with fully aquatic vertebrates like fishes, sirenians, and whales; this notion was also supported by a more recent study (McCartney & Seiffert, 2016).

Recently, the new excavations at BQ-2 in the Birket Qarun Formation brought to light a large collection of snake material (McCartney & Seiffert, 2016). McCartney and Seiffert (2016) recognised the two previously described Fayum snakes together with a variety of other snake taxa, including two distinct booids, a tropidophiid, a probable russellophiid, and a new colubroid, *Renenutet enmerwer*. The authors also suggested a niche partitioning between the smaller snakes, where small mammals, including rodents, small hyracoids, and primates, as well as small fishes and lizards would be potential prey items for these species (McCartney & Seiffert, 2016).

4.1.2 Varanidae

Since the first discovery of vertebrate fossils in the Fayum Depression, in the nineteenth century, no lizards had been found in its Paleogene deposits until recently. Smith et al. (2008) reported a single posterior presacral vertebra of a varanid, from the Early Oligocene Quarry I of the Gebel Qatrani Formation. This vertebra was considered the oldest African record of a stem *Varanus* (Smith et al., 2008). Soon after, Holmes et al. (2010) studied a large collection of vertebrae, from the Late Eocene BQ-2 of the Birket Qarun Formation and from the Oligocene Quarries I and M of the Gebel Qatrani Formation, which they assigned to the genus *Varanus*. Based on this material, the authors argued for a potential African origin for the genus and discussed its dispersal to the Eurasian and Australian continents (Holmes et al., 2010). Holmes et al. (2010) pointed out some morphological differences between their material and the vertebra described by Smith et al. (2008), the latter of which they considered as an indeterminate varanid.

4.1.3 Testudines

Turtles are a well-represented group in the Paleogene sediments of the Fayum Depression. The first chelonian remains were reported by Andrews (1901a) who erected three new species, *Psephophorus eocaenus*, represented by some isolated fragmentary postcranial elements, *Thalassochelys libyca*, represented by several skulls, and the pleurodiran *Stereogenys cromeri*, also represented by several well-preserved skulls, all from the Qasr el Sagha Formation. Two years later, the same author described three new pleurodiran species *Stereogenys libyca*, founded on an almost complete carapace from the Gebel Qatrani Formation, *Podocnemis antiqua* from the Qasr el Sagha Formation, and *Podocnemis fajumensis* from the Gebel Qatrani Formation (Andrews, 1903a).

In the same year, a new large tortoise, *Testudo ammon*, was described from a complete carapace from the Gebel Qatrani Formation (Andrews, 1903b, 1904a, 1906a). In his monograph about the Fayum fauna, Andrews (1906a) studied a large collection of new turtle material from the Fayum Depression, re-examining the previously described species and erected two new species of tortoises, *Testudo beadnelli* and *Testudo isis*. Later, all Fayum tortoises were synonymised and placed under a different generic name, as *Gigantochersina ammon* (Holroyd & Parham, 2003; Laparent de Broin, 2000).

Half a century after the description of the first pleurodirans from the Fayum Depression, Williams (1954) described the new pleurodiran genus and species *Dacquemys paleomorphia* from its Upper Eocene strata. More recently, Gaffney et al. (2011), in their revision of the pleurodiran family Podocnemididae, described the new pleurodiran genus and species *Albertwoodemys testudinum* based on a shell from the Early Oligocene Fayum deposits, placed "*Podocnemis*" *fajumensis* in the genus *Neochelys*, and erected the new genus *Cordichelys*, for *Cordichelys antiqua* (originally *P. antiqua*; Andrews, 1903a). Cherney et al. (2020) studied new pleurodiran material, which they referred to *C. antiqua*, including a skull and a shell from the Late Eocene Birket Qarun Formation, thus, extending the stratigraphical distribution of this taxon and adding insights about its ecology, as it was probably inhabiting marine waters.

4.1.4 Crocodyliformes

Crocodyliformes are important representatives of the Fayum faunal assemblages. Overall, eight new species of crocodylians have been described based on material from the Fayum Depression (Andrews, 1901a, 1905a; Brochu & Gingerich, 2000; Müller, 1927). Although, many of these were later synonymised; at least five distinct Crocodyliformes seem to have occurred in the Eocene to Oligocene deposits of the Fayum Depression (Brochu & Gingerich, 2000; Stefanic et al., 2019). Andrews (1901a) described the new species

Tomistoma africanum (now referred as *Eogavialis africanum*; Stefanic et al., 2019) from the Qasr el Sagha Formation and mentioned that crocodylian remains are very common in this formation. Later, Andrews (1905a) erected four new species of crocodylians from the Fayum area. He assigned two of them to the genus *Crocodylus*, the “narrow-snouted” *Crocodylus articeps* and the “broad-snouted” *Crocodylus megarhinus*, based on well-preserved skulls from the Gebel Qatrani Formation (Andrews, 1905a). The other two new species were referred to *Tomistoma* by him (Andrews, 1905a). *Tomistoma gavialoides* is very common in the Gebel Qatrani Formation, and *Tomistoma kerunense* is present in the Birket Qarun Formation (Andrews, 1905a), though both of them are now attributed to *Eogavialis* (see Brochu & Gingerich, 2000). Andrews (1906a) offered a detailed description of crocodylian material from the Fayum, referring to all five previously described species, and to one indeterminate crocodylian from the Qasr el Sagha Formation, referred to as *Crocodylus* sp.

Müller (1927) studied the crocodylian material from the Paleogene of Egypt, collected by Markgraf for Fraas and Stromer. This work represents the most detailed study that is dedicated solely to the Paleogene crocodylians of Egypt. He described two new species. The first is *Tomistoma cairense*, based on a skull from the Middle Eocene marine deposits of the Mokattam Formation (Müller, 1927). The second is *Tomistoma tenuirostre*, which he erected based on two mandibular symphyses from the Gebel Qatrani Formation in the Fayum Depression (Müller, 1927). The latter species was afterwards assigned to the genus *Eogavialis* (Brochu & Gingerich, 2000).

Brochu and Gingerich (2000) offered a short review of the Fayum crocodylians and described the new genus and species *Paratomistoma courti*, based on a partial skull and

mandible from the Middle Eocene Gehennam Formation in Wadi al Hitan. They also discussed the taxonomic and phylogenetic status of the Fayum gavialoids and proposed that *Eogavialis gavialoides*, *Eogavialis kerunense*, and *Eogavialis tenuirostre* represent junior synonyms of *E. africanum*. The four previously suggested distinct species are morphologically indistinguishable and only differ in their stratigraphical position, ranging from the Late Eocene Qasr el Sagha Formation to the Early Oligocene Gebel Qatrani Formation (Brochu & Gingerich, 2000). Furthermore, Brochu and Gingerich (2000) suggested that *C. articeps* represents a juvenile *C. megarhinus*.

Stefanic et al. (2019) studied the new crocodyliform material from BQ-2, of the Birket Qarun Formation. They described some material assignable to Crocodylia, as well as a non-crocodylian mesoeucrocodylian partial right dentary, which they referred to the extinct crocodyliform clade of Sebecosuchia. This is the first report of Sebecosuchia from the Fayum Depression and one of its youngest records in Africa (Stefanic et al., 2019).

4.2 Aves

The Fayum Depression has yielded the oldest diverse avifauna from Africa, including at least seven orders of birds (Rasmussen et al., 1987). However, its avifauna remained rather poorly known until the study of Rasmussen et al. (1987), in which they offered a detailed overview of the Fayum birds. Until then, only four species of birds had been known from the Fayum fauna (Andrews, 1904b; Lambrecht, 1929, 1930).

One of the most interesting features of the Fayum avifauna is certainly the existence of a large flightless bird. Andrews (1904b) described the new ratite *Eremopezus eocaenus*, based on a distal end of a large left tibiotarsus from the Gebel Qatrani Formation. Later, Lambrecht (1929) described the new species *Stromeria fajumensis*, based on a distal end of a right tarsometatarsus from the Gebel Qatrani Formation, which he assigned to the Aepyornithidae. Later, it was noted that these two species might in fact be synonymous (Moustafa, 1974; Rasmussen et al., 1987, 2001). Rasmussen et al. (2001) studied several newly found specimens of a large bird from the Late Eocene site L-41 of the Gebel Qatrani Formation and, based on this material, they revised the flightless, cursorial bird from the Fayum fauna, concluding that *S. fajumensis* does in fact represent a junior synonym of *E. eocaenus*. In addition, they suggested that *Eremopezus* belongs to its own family, Eremopezidae, which is not closer related to any ratite lineage or any other large bird (Rasmussen et al., 2001).

In their review of the Fayum avifauna, Rasmussen et al. (1987) also described four new species, *Nupharanassa*



Fig. 2 Skull (GPIT-PV-41686) of *Eogavialis africanum* (sensu Brochu & Gingerich, 2000) from the Late Eocene to Early Oligocene Gebel Qatrani Formation of the Fayum Depression (Egypt) collected by Richard Markgraf in 1905 (originally described as *Eogavialis gavialoides* by Müller, 1927). Scale bar is 10 cm

bulotorum, *Nupharanassa tolutaria*, *Janipes nymphaeobates*, and *Xenerodiops mycter* and erected the new family Xenerodiopidae for the latter one. In total, they reported the presence of at least 17 different species, belonging to 13 families. Remains of another relatively large, potentially flightless, bird were uncovered in the Early Oligocene Quarry E of the Gebel Qatrani Formation, which they tentatively attributed to Ameghinornithidae (Stidham & Smith, 2015). More recently, Smith et al. (2020) described the oldest fossil owl from Africa, based on a distal end of a left tibiotarsus from the Early Oligocene Quarry I of the Gebel Qatrani Formation, whereas one year later El Adli et al. (2021) described the oldest remains of a pelican from the Birket Qarun Formation in Wadi el Hitan, based on which they founded the new genus and species *Eopelecanus aegyptiacus*.

4.3 Mammalia

4.3.1 Marsupialia

The most basal mammalian group in the Fayum Depression is represented by the marsupials. Only few fragmentary specimens have been discovered, but have led to the description of two distinct new marsupial taxa, which represent the first record of marsupials in Africa (Bown & Simons, 1984; Gunnell, 2010). The first specimens comprise three fragmentary mandibles, which come from the Early Oligocene of Quarry M (Gebel Qatrani Formation) and were initially published by Bown and Simons (1984). Later that same year, they were described as the new species *Peratherium africanum* (Simons & Bown, 1984). Crochet et al. (1992) erected the new genus *Qatranitherium* for this species. Subsequently, Hooker et al. (2008) described some new material of *Peratherium africanum*, including the first maxilla, from the same fossil site where the holotype came from. They concluded that *Qatranitherium* represents a junior synonym of *Peratherium* and provided information about the phylogenetic position of this species, indicating a European origin for this “didelphimorph” species.

Sánchez-Villagra et al. (2007) described the new potential “didelphimorphian” marsupial *Ghamidtherium dimaiensis*, based on a fragmentary right mandible from the Late Eocene of BQ-2 (Birket Qarun Formation), which weighed about 300–500 g. The same authors also reported an isolated lower tooth that might belong to the same species or could represent a close relative, and two isolated upper molars, which can be referred to another potential marsupialian taxon, from the same locality. However, the exact systematic position of the BQ-2 specimens could not be assessed and an association to a marsupial-like chiropteran cannot be excluded (Sánchez-Villagra et al., 2007).

4.3.2 Ptolemaiida

The Ptolemaiida is an enigmatic group of medium- to small-sized mammals, potentially assignable to Afrotheria, comprising three genera and five species, almost exclusively known from the Early Oligocene deposits of the Gebel Qatrani Formation in the Fayum Depression. Over a century ago, Osborn (1908) described the first taxon of this group, *Ptolemaia lyonsi*, based on a dog-sized left mandible, only missing the p4 and the front teeth (Fig. 3A). He erected the new family Ptolemaiidae for this peculiar animal. He also noted that it might represent a new order and that it is evidently very different from any primate or ungulate (Osborn, 1908). Due to the fragmentary state of the specimen, Osborn (1908) was not able to make any suggestions about the animal’s ecology. Schlosser (1911) described new material, including two mandibles, several isolated teeth and possibly a radius, which he attributed to the same species. Based on these new specimens he concluded that *P. lyonsi* must belong to the carnivorous “creodont” family of Hyaenodontidae (Schlosser, 1911). Matthew (1918) noted that this

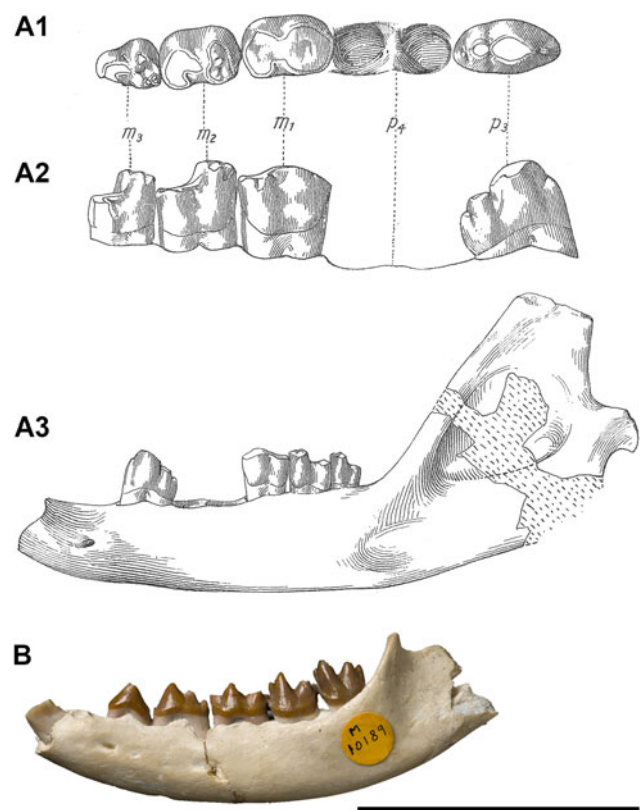


Fig. 3 Ptolemaiida material from the Late Eocene to Early Oligocene Gebel Qatrani Formation of the Fayum Depression (Egypt): **A** left mandible (holotype) of *Ptolemaia lyonsi* (Amer. Mus. No. 13269; Osborn, 1908, figs. 1 and 2). 1, occlusal view of the dentition; 2, lingual view of the dentition; and 3, buccal view of the mandible. **B** left mandible (holotype) of *Qarunavus meyeri* (NHMUK PV M 10189; Simons & Gingerich, 1974), originally referred to *Ptolemaia lyonsi* (Schlosser, 1911). Scale bar is 10 cm for **A1–2** and 5 cm for **A3** and **B**

new material, described by Schlosser (1911), did not belong to the genus *Ptolemaia*. Subsequently, Simons and Gingerich (1974) included this material in their new genus and species *Qarunavus meyeri*, which they referred to the Ptolemaiidae, order incertae sedis, along with *Ptolemaia lyonsi*. Bown and Simons (1987) erected the new species *Ptolemaia grangeri*, based on a left m3 from Quarry V (Gebel Qatrani Formation), and the new genus *Cleopatrodon*, comprising two new species *Cleopatrodon ayeshae*, from Quarry V (Gebel Qatrani Formation) and *Cleopatrodon robusta*, from Quarry I (Gebel Qatrani Formation), which were described based on relatively well-preserved mandibles. The same authors argued about a close phylogenetic relationship between the genera *Qarunavus* and *Cleopatrodon*, to the exclusion of *Ptolemaia*.

The origin and systematic position of the ptolemaiids has been a matter of considerable debate, and the family has been assigned to various groups, including creodonts, pantolestids, tubulidentates, and chiropterans (Gunnell et al., 2010; Van Valen, 1966). Simons and Bown (1995) described new material of ptolemaiids from the Quarry V (Gebel Qatrani Formation), including an almost complete, but distorted, skull of *Ptolemaia grangeri*. Based on this new material, they revised the previously described ptolemaiid material and erected the new order Ptolemaiida for the genera *Ptolemaia*, *Qarunavus*, and *Cleopatrodon*. Later, the group Ptolemaiida was included in Afrotheria (Cote et al., 2007; Nishihara et al., 2005). Seiffert (2007) also placed the ptolemaiids within the Afrotheria and supported the previous suggestions that they might be allied with aardvarks (Cote et al., 2007; Simons & Gingerich, 1974). A revision of the two mandibles of *Qarunavus meyeri* supports the notion of Bown and Simons (1987) that it shares a closer phylogenetic relationship with *Cleopatrodon* than with *Ptolemaia* and further supports an inclusion into the Afrotheria (Kampouridis et al. In prep).

The ecology of the ptolemaiids has remained elusive ever since their first discovery, because the fragmentary nature of the material does not allow for any decisive conclusions about their preferred environment, feeding habits or any other aspect of their ecology (Osborn, 1908; Schlosser, 1911; Simons & Bown, 1995). Simons and Rasmussen (1990) suggested that *Q. meyeri* may have been a racoon-like, omnivorous animal, which preferred small riverside prey.

Overall, the Fayum ptolemaiids are known from only few and mostly fragmentary specimens that record three genera and five species (Simons & Bown, 1995). Until recently, ptolemaiids were known exclusively from the Oligocene deposits of the Gebel Qatrani Formation, in the Fayum Depression. However, material assigned to *Ptolemaia* has recently been reported from the Late Oligocene of Western Turkana, in Kenya (Miller et al., 2015). Lastly, the genus *Kelba*, which is known from several Miocene localities in East Africa (Cote et al., 2007), has also been suggested to

belong to the Ptolemaiida, thus, potentially expanding the temporal distribution of the group significantly.

4.3.3 Macroscelidea

This group was long regarded as closely related to the Eulipotyphla, due to their overall similar appearance. Their fossil record is extremely scanty, which has made the investigation of their origin and phylogenetic position very difficult (e.g. Senut & Pickford, 2021; Stevens et al., 2021). Schlosser (1910) described the first macroscelidean from the Fayum Depression, which he named *Metoldobotes stromeri* in honour of Ernst Stromer von Reichenbach, based on a mandible, though he initially regarded it as an insectivoran (Schlosser, 1911). More recently, Simons et al. (1991) studied new macroscelidean material from the Gebel Qatrani Formation. They assigned part of this material to *Metoldobotes stromeri*, while the rest of the material was used to describe the new genus and species *Herodotius pattersoni*. The genus was named after the ancient Greek historian Herodotus who had travelled to and written about the Fayum, while the species was named in honour of Harvard Professor Bryan Patterson, who extensively studied the clade Macroscelidea. Subsequently, Simons et al. (1991) erected two new subfamilies for these species, Metoldobotinae and Herodotinae. The Fayum macroscelideans seem to be relatively primitive representatives of this group and their morphological affinities support their inclusion in the afrotheres (Simons et al., 1991). Later, Holroyd (2010) included in the Herodotinae also the genera *Nementchatherium*, from the Eocene of Algeria and *Chambius*, from the Eocene of Tunisia and Algeria.

4.3.4 Afrosoricida

Today, this enigmatic group includes the tenrecs (Tenrecoidea) and golden moles (Chrysochloridea). In the past, these animals were associated with the Eulipotyphla. They have a very poor fossil record and thus much about their systematic position and origin had remained ambiguous. Relatively recently, the first remains of these animals were uncovered from the Paleogene sediments of the Fayum Depression (Seiffert, 2010; Seiffert & Simons, 2000; Seiffert et al., 2007). Seiffert and Simons (2000) described the new genus *Widanelfarasia*, which included the two new species *Widanelfarasia bowni* and *Widanelfarasia rasmusseni*, based on partial mandibles from the Late Eocene site L-41 of the Gebel Qatrani Formation. In the initial description, their systematic position was not completely clear; they were regarded as potential relatives of either the Afrosoricida or the Eulipotyphla, though the former hypothesis was regarded as more likely by Seiffert and Simons (2000). Seiffert et al. (2007) described additional material of *W. bowni*, which they regarded as a tenrecomorph and also erected the new tenrecomorph afrosoricid *Jawharia tenrecoides*, as well as the new purported chrysochlorid afrosoricid *Eochrysochloris*

tribosphenus. Both new taxa were found in the Early Oligocene site Quarry E of the Gebel Qatrani Formation (Seiffert et al., 2007). Seiffert (2010) studied further afrosoricid material from the Fayum Depression and described two additional new species. The first was named *Dilambdogale gheerbranti*, based on dental material from the Late Eocene locality BQ-2 of the Birket Qarun Formation, representing the oldest record of an afrosoricid from the Fayum succession. The second species was named *Qatranilestes oligocaenus*, based on a right mandibular fragment from the Early Oligocene site Quarry I of the Gebel Qatrani Formation and represents the youngest find of an afrosoricid from the Fayum. In his phylogenetic analysis, *Dilambdogale* and *Widanelfarasia* are placed as sister taxa of crown afrosoricids, though it could not be excluded that they actually represent stem tenrecoids (Seiffert, 2010). Furthermore, it has been argued that *Eochrysochloris* might be a member of the tenrecs rather than a golden mole (Pickford, 2015a).

4.3.5 Embrithopoda

The Embrithopoda is a group of impressive large-sized, but poorly known, afrotherians that lived during the Paleogene. The most emblematic representative of the clade is *Arsinoitherium*. This taxon is characterised by the presence of two huge anterior horns formed by the nasal bones and two smaller, posterior horns formed by the frontal bones, as well as peculiar hypsodont teeth (Court, 1992a; Sanders et al., 2010a). Two species of *Arsinoitherium* have been erected based on material from the Gebel Qatrani Formation of the Fayum Depression. The first is *Arsinoitherium zitteli* (Fig. 4), which was erected by Beadnell (1902) and represents the type species of the order. Lankester (1903) erected a second species, *Arsinoitherium andrewsi*, based on a mandible from the Fayum (Fig. 5c), that is about one-third larger than the previously described arsinotherium material,

and also reported an almost complete skull of *Arsinoitherium zitteli*. Andrews (1906a) studied a large amount of *Arsinoitherium* material from the Fayum area, recognising both previously described species, with *Arsinoitherium zitteli* representing the more abundant one. Later, Osborn (1907, 1908) reported the presence of *Arsinoitherium* sp. in their material from the Gebel Qatrani Formation, without any detailed description. Sanders et al. (2004) suggested that *Arsinoitherium andrewsi* in fact represents a junior synonym of *Arsinoitherium zitteli* and that the metric variation between those two suggested species is within the expected range of a sexually dimorphic species, with the “*Arsinoitherium andrewsi*” holotype representing the largest known individual of *Arsinoitherium* from the Fayum. However, Pickford (2015b) suggested that there is significant variability within the *Arsinoitherium* material from the Fayum Depression and considered *Arsinoitherium andrewsi* as a valid species, based on some variable dental features and their postcranial size difference. The genus *Arsinoitherium* is present throughout the Gebel Qatrani Formation in the Fayum Depression (Sanders et al., 2010a), from L-41 at the base to Quarry M at the top of the formation (Fig. 1a), spanning a range of approximately 34 to 30 Ma (Kappelman, 1992; Seiffert, 2006).

The Embrithopoda was known only from the Fayum deposits for many decades, until some discoveries of fragmentary remains in other Oligocene localities in Africa (Pickford, 1986, 2017; Thomas et al., 1989; Vialle et al., 2013; Wight, 1980). Further, material associated with *Arsinoitherium* has also been found on the Arabian Peninsula, in the Early Oligocene of Oman (Al-Sayigh et al., 2008; Pickford, 2015b; Thomas et al., 1989, 1999) and Saudi Arabia (Zalmout et al., 2010). Sanders et al. (2004) described numerous fragmentary embrithopod remains from the Late Oligocene of Chilga (Ethiopia) (Kappelman et al.,

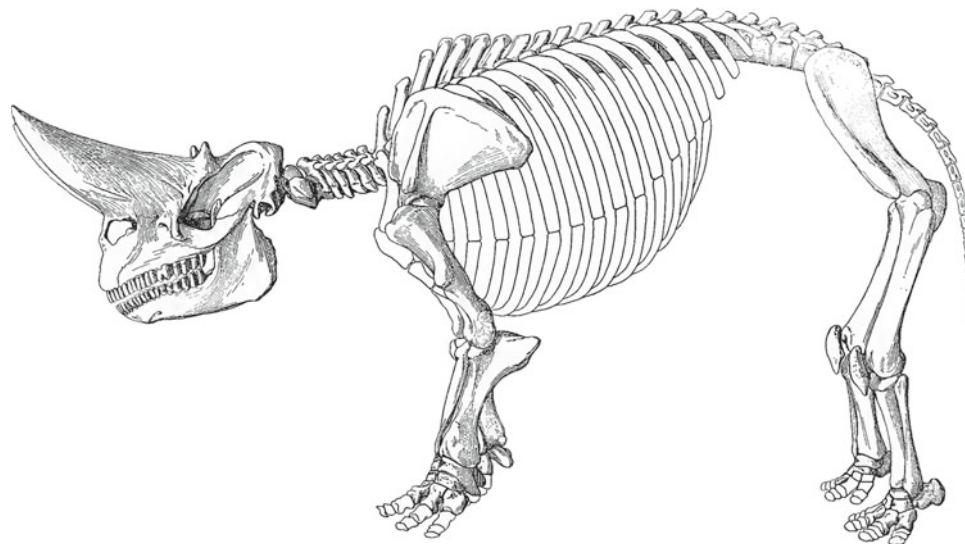


Fig. 4 *Arsinoitherium zitteli* skeleton reconstruction (Andrews, 1906a, text—fig. 36)

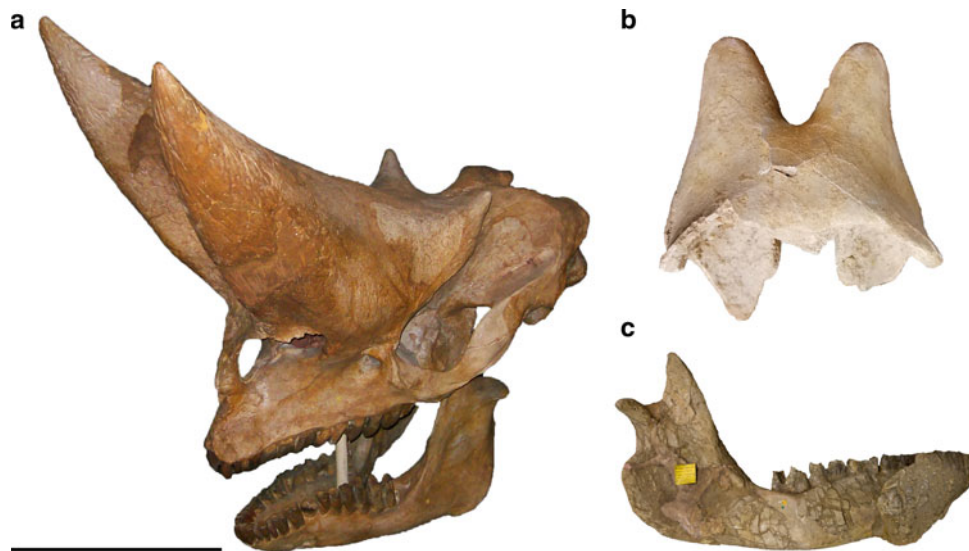


Fig. 5 Embrithopoda material from the Late Eocene to Early Oligocene Gebel Qatrani Formation of the Fayum Depression (Egypt): **a** complete skull and mandible of *Arsinoitherium zitteli* (NHMUK PV M 8463; Andrews, 1906a); **b** nasal horns of a juvenile *Arsinoitherium zitteli* (SMNS-P-12611); and **c** mandible of *Arsinoitherium zitteli* (NHMUK PV M 8461b) (holotype of *Arsinoitherium andrewsi* Lankester, 1903). Scale bar 40 cm for **a** and **c** and 10 cm for **b**

2003), which he referred to their new species *Arsinoitherium giganteum*. This species differs from *Arsinoitherium zitteli* in having larger dental dimensions, with the M2 of the holotype of *Arsinoitherium giganteum* exceeding even the large “*Arsinoitherium andrewsi*” from the Fayum in size (Sanders et al., 2004). Pickford et al. (2008) described the embrithopod *Namatherium blackcrowense* from the Middle Eocene of Namibia, which is characterised by its very wide zygomatic arches. Recently, Gheerbrant et al. (2021) described the oldest and basal-most embrithopod from the Eocene of Morocco, erecting the new family Stylolophidae, which includes the two species *Stylolophus major* and *Stylolophus minor* (Gheerbrant et al., 2018, 2021). Thus, a total of three genera and five species of Embrithopoda have been suggested to be present in the Eocene to Oligocene of Africa (Andrews, 1906a; Beadnell, 1902; Gheerbrant et al., 2018, 2021; Pickford et al., 2008; Sanders et al., 2004).

For many years, the Embrithopoda was considered endemic to Africa (Sen, 2013). Matthew and Granger (1925) studied the Paleogene fauna of the Gashato Formation (Mongolia) and described the new genus and species *Phenacolophus fallax*, which they did compare, but not attribute, to arsinotheres. More than 50 years later, McKenna and Manning (1977) described further material of this taxon and suggested that it represents a primitive arsinotheres. Some new studies support the position of *Phenacolophus* as a potential stem-group member of Embrithopoda (Erdal et al., 2016; Sen, 2013), although other recent studies have argued against its inclusion in this order (Gheerbrant et al., 2021; von Koenigswald, 2013).

Almost half a century ago, Radulescu et al. (1976) studied the geology of the Hațeg Basin (Romania) and founded the new taxon *Crivadiatherium mackennai*, based on three lower teeth from Lower Oligocene freshwater limestones in Crivadia (Romania). Radulescu and Sudre (1985) described some teeth from the same locality, which they referred to the new species *Crivadiatherium iliescui*, characterised by its larger size, compared to *Crivadiatherium mackennai*. In general, *Crivadiatherium* from the Oligocene of Romania seems to be smaller, and exhibit more primitive features than *Arsinoitherium* (Radulescu & Sudre, 1985; Radulescu et al., 1976).

Rich embrithopod material has been also described from Paleogene coal deposits of Anatolia, which was mainly attributed to *Palaeoamasias kansui*, initially regarded as a chalicotheriid perissodactyl (Ozansoy, 1966). Later, Sen and Heintz (1979) revised this taxon, included it in the Embrithopoda, and erected the new subfamily Palaeoamasiinae for this species, including also *Crivadiatherium* from Romania. Some of the oldest embrithopods, from the Late Palaeocene to Early Eocene of Turkey (Uzunçarşidere Formation), were used to establish the new embrithopod *Hypsamasias seni* (Maas et al., 1998). Moreover, the youngest specimens from Turkey (Cemalettin Formation) were suggested to belong to a new species of *Palaeoamasias* (referred to as “*Palaeoamasias* sp. nov.”), without any formal description of the species (Sanders et al., 2014).

In his initial description of *Arsinoitherium*, Beadnell (1902) suggested that the genus may be an ancestor of today’s rhinoceroses, based on the dentition, though noting

some similarities to the strange, horned Dinocerata. Soon after its first description, *Arsinoitherium* was included by Andrews (1904c) in the order Amblypoda, which also included the Dinocerata. In another contribution in the same volume, Andrews (1904d) argued against this assignment and in fact erected the new order Barypoda for the genus *Arsinoitherium*. However, the name Barypoda had already been used earlier by Haeckel (1866) for a group of marsupials. Therefore, two years after its creation, Andrews (1906b) published a note discussing this issue and proposing the new name Embrithopoda for the order that includes *Arsinoitherium*. In his monograph on the vertebrate assemblages of the Fayum Depression, Andrews (1906a) still uses the term Barypoda, but added a footnote mentioning the aforementioned issues with this name and that the alternative Embrithopoda has been proposed (Andrews, 1906a, p. xiv).

The exact phylogenetic position of embrithopods has long been debated (e.g. Andrews, 1904d, 1906a; Court, 1992a; Gheerbrant et al., 2014; Pickford et al., 2008; Tabuce et al., 2007). In the afrotherian phylogenetic analysis performed by Seiffert (2007), *Arsinoitherium zitteli* was recovered as the sister taxon to the Sirenia. More recently, comprehensive phylogenetic analyses performed to recover the systematic affinities of the Embrithopoda (Erdal et al., 2016; Gheerbrant et al., 2018, 2021) confirmed their placement in the Paenungulata, within the Afrotheria, and suggest a close relationship to Proboscidea, Sirenia, and Hyracoidea.

The phylogenetic relationships within the Embrithopoda have been the focus of many studies (e.g. Erdal et al., 2016; Gheerbrant et al., 2021; Sen & Heintz, 1979) but still remain somewhat controversial. The phylogenetic analysis of Erdal et al. (2016) supports the separation of Embrithopoda into *Arsinoitheriinae* (*Arsinoitherium*) and *Palaeoamasiinae* (*Palaeoamasiasia*, *Hypsamasiasia* and *Crivadiatherium*), as previously proposed by Sen and Heintz (1979), and implies *Namatherium* as the sister group to all other embrithopods. The phylogenetic analysis performed by Gheerbrant et al. (2021) offers different results, with *Palaeoamasiasia* being distinct from all other embrithopods and *Stylolophus* being placed as the most basal embrithopod. It has to be noted that in both analyses most embrithopods were recovered to form a polytomy (Erdal et al., 2016; Gheerbrant et al., 2021).

The iconic massive horns of *Arsinoitherium* are formed mainly by the nasals which are fused even in juvenile individuals (Fig. 5b; Andrews, 1906a, pl. III, fig. 2). The base of the horns is composed by the frontals, which also form a smaller, posterior pair of horns (Andrews, 1906a). There, numerous grooves, probably representing impressions of blood vessels, run across the surface of the horns, on the nasals and frontals. Based on this feature, Andrews (1906a, p. 7) suggested that the horns were covered by keratin, similar to modern-day bovids (Sanders et al., 2010a; Simons & Rasmussen, 1990; Tanner, 1978). Other authors

suggested that the horns were covered only by skin (Pickford et al., 2008; Prothero & Schoch, 2002; Rose, 2006). Despite their massive appearance, at the centrum of the horns, the bone is at some places as thin as 1 cm (Andrews, 1906a, p. 7), bearing a large sinus. Pickford et al. (2008) discussed the possible functions of the horns, supporting the hypothesis of the sinus within the horns acting as a resonance chamber, implying that vocalisation played an important role in the animal's ecology. Subsequently, Benoit et al. (2013) studied the inner ear of *Arsinoitherium*, leading them to conclude that the animals might have been able to hear very low frequencies, and proposed that *Arsinoitherium* was most probably able to communicate through seismic vibrations similar to extant elephants. Pickford et al. (2008) suggested that the horns were covered by skin and were used secondarily for visual signals and not for intraspecific combat purposes. Furthermore, a visible sexual dimorphism in the horns has been suggested by many authors, with males bearing larger, pointed horn and females smaller, rounded ones (e.g. Andrews, 1906a; Prothero & Schoch, 2002).

The dentition is another peculiar feature, characteristic for *Arsinoitherium*. This and its mandibular morphology are probably associated with a specialised masticatory apparatus, and it has been proposed that it represents a highly selective browser (Court, 1992b). This would also be consistent with the high $\delta^{13}\text{C}$ values measured in the enamel of *Arsinoitherium* by Clementz et al. (2008). Regarding the ecology of *Arsinoitherium*, also a semi-aquatic lifestyle has been proposed based on the reconstructed palaeoenvironmental context and the postcranial morphology (Carroll, 1988; Court, 1993; Moustapha, 1955; Sen & Heintz, 1979). However, Clementz et al. (2008) argued that the $\delta^{18}\text{O}$ values obtained for *Arsinoitherium* point to a terrestrial lifestyle, as also supported by Sanders et al. (2010a), who based their interpretation on the graviportal features exhibited by *Arsinoitherium*.

In total, only eight rather complete *Arsinoitherium* skulls have been uncovered, including three adult, four sub-adult, and one juvenile skull (Court, 1992a; Osborn, 1907). An additional complete skull, allegedly representing the largest of the species was unfortunately destroyed during its transport (Osborn, 1907). The detailed study of this limited cranial material, along with the rich postcranial elements found in the Fayum area, also with new and innovative methods has significantly added to our understanding about this peculiar animal (e.g. Benoit et al., 2013; Clementz et al., 2008; Court, 1992a, 1992b, 1993).

4.3.6 Proboscidea

Proboscidea is one of the most fascinating mammal groups from the Fayum Depression and indeed, it was this group that primarily sparked the interest of American palaeontologist Henry F. Osborn to start excavations in the Fayum

Depression (Osborn, 1907). The first proboscideans were described by Andrews (1901b). He erected three new genera and species of proboscideans, *Palaeomastodon beadnelli*, *Moeritherium lyonsi*, and *Barytherium grave* (Andrews, 1901b). A more detailed description of these species was provided later in the same year (Andrews, 1901c).

Andrews (1901c) described the type mandible of *Palaeomastodon beadnelli* from the Gebel Qatrani Formation and noted the similarities to some Miocene proboscideans. Later, Andrews (1904e) reported a right mandibular ramus from the same formation, differing from *Palaeomastodon beadnelli* and established for it the new species *Palaeomastodon minor*, due to its smaller size. In the next year, Andrews (1905b) described two additional species of *Palaeomastodon*. The first was named *Palaeomastodon parvus*, because of its smaller size in comparison to the type species. The second species, named *Palaeomastodon wintoni*, is morphologically more similar to *Palaeomastodon minor*, but much larger, though smaller than the type species. Andrews (1905b) also noted that this last species is the most common one in the Gebel Qatrani Formation, from which almost all *Palaeomastodon* material was derived. Andrews (1906a) erected the new family Palaeomastodontidae to include originally the genera *Palaeomastodon*, *Tetrabelodon*, and potentially *Phiomia*. Nowadays, the family includes only the genera *Palaeomastodon* and *Phiomia*, which can be regarded as the most primitive elephantiforms (e.g. Hautier et al., 2021; Sanders et al., 2010b; Seiffert, 2006; Tobien, 1978). Though, the validity of the species within *Palaeomastodon* remains a complex issue that has been discussed repeatedly (e.g. Sanders et al., 2004, 2010b). Recently, Sanders et al. (2004) discussed the presence of two new *Palaeomastodon* species from the Late Oligocene of Chilga in Ethiopia, without naming them.

Andrews (1901b) suggested *Moeritherium lyonsi* as an ancestor of proboscideans. He also mentioned that *Moeritherium* is quite common in the Qasr el Sagha Formation and that it has the size of a large tapir and is known from cranial and postcranial elements, though only describing the cranial and dental features (Andrews, 1901c). In the following year, Andrews (1902) described the new species *Moeritherium gracile* from the Qasr el Sagha Formation, which he regarded as smaller than the type species *Moeritherium lyonsi*. Two years later, Andrews (1904e) described a third species for this genus, *Moeritherium trigodon* (later referred to as *Moeritherium trigonodon* by Andrews (1906a) and *Moeritherium trigonodum* by Schlosser, 1911), based on a right mandibular ramus from the Gebel Qatrani Formation. He noted that the dental morphology of this latter species seems to differ considerably from other material of *Moeritherium* and that it might in fact represent a distinct genus (Andrews, 1904e). Andrews (1906a) proposed that the genus *Moeritherium* constitutes a distinct family, called

Moeritheriidae, in the Proboscidea. Half a decade later, Schlosser (1911) studied a large collection of *Moeritherium* material and decided to erect the new species *Moeritherium andrewsi* for material from the Gebel Qatrani Formation. Later, Matsumoto (1922, 1923) suggested that all four species were valid and that *M. lyonsi* and *M. gracile* might represent potential ancestors of *M. andrewsi* and *M. trigodon*, respectively. Petronievics (1923) described the new species, *Moeritherium ancestrale*, based on a well-preserved skull from the Qasr el Sagha Formation found by Baron Franz Nopcsa, during a short trip to the Fayum Depression in 1905. Over half a century after the initial description of the genus *Moeritherium*, Deraniyagala (1955) described the two new species *Moeritherium latidens* and *Moeritherium pharaonensis*, based on two partial mandibles collected by the African Expedition of the University of California. Later, Holroyd et al. (1996) reported the presence of *M. lyonsi* at the base of the Qasr el Sagha Formation. More recently, Delmer et al. (2006) described the new species *Moeritherium chehbeurameuri* from the Eocene of Algeria. Since the first description of the various species of *Moeritherium*, many authors have discussed their validity and potential synonymy. Most *Moeritherium* species have been synonymised and probably only *M. lyonsi* and *M. trigodon* can be regarded as valid (for an overview see Delmer et al., 2006; Sanders et al., 2010b).

In addition to his extensive work on *Palaeomastodon* and *Moeritherium*, Andrews (1901c) described a peculiar mandible that he referred to as “*Bradytherium*” *grave*. However, in the same year Andrews (1901d) noted that the genus name *Bradytherium* was already preoccupied for the Madagascan purported edentate *Bradytherium madagascariense*, which is now synonymised with the primate *Palaeopropithecus ingens* (MacPhee & Raholimavo, 1988). Andrews (1901d) accordingly proposed the name *Barytherium* to replace it. Andrews (1904d) discussed the controversial systematic position of this genus and proposed the name Barytheria for the clade that at the time only included *Barytherium grave*. He also suggested that Barytheria can be included in the Amblypoda and are of the same rank as Dinocerata (Andrews, 1904d). In his extensive description of the Fayum fauna, Andrews (1906a) erected also the new family Barytheriidae for *Barytherium grave*, but did not assign it to any definite order or suborder. Later, it was suggested that Barytheriidae, including only *Barytherium*, was closely related to the proboscidean Numidotheriidae, including several species of *Numidotherium*, and together constituted the Barytherioidea (for an overview, see Sanders et al., 2010b). Recently, Seiffert et al. (2012) described the new proboscidean genus and species *Omanitherium dhofarensis*, based on a partial mandible from the Oligocene of Oman and regarded it as the sister taxon of *Barytherium*.

The last proboscidean genus to date that was named from the Fayum area is *Phiomia*. Andrews and Beadnell (1902) described the new genus and species *Phiomia serridens* based on a partial left mandible from the Gebel Qatrani Formation. The authors initially thought that this animal might have been a specialised creodont (Andrews & Beadnell, 1902). Andrews (1906a) later re-examined the type mandible of *Phiomia serridens* and compared it to *Palaeomastodon*, suggesting a close relationship, following Schlosser (1905). Matsumoto (1922) described the new species *Phiomia osborni* based on a complete mandible from the Gebel Qatrani Formation (Fig. 6a) and referred some *Palaeomastodon* species to the genus *Phiomia*, “*Phiomia (minus) minor*” and “*Phiomia wintoni*”. Subsequently, Sanders et al. (2004) described the new species *Phiomia major* based on several dental remains from the Late Oligocene of Chilga in Ethiopia, which are considerably larger than *Phiomia serridens*. Today, only the last described species, *Phiomia major*, and the type species, *Phiomia serridens* are regarded as valid (Sanders et al., 2004, 2010b).

Concerning the ecology of these early proboscideans, some interesting points as to their preferred habitat have been discussed. The primitive proboscidean *Moeritherium*, whose remains were very abundant in the Qasr el Sagha Formation and also present in the marine Birket Qarun Formation, was relatively small and had a relatively stout body plan, remarkably similar to extant hippos. Based on this, Andrews (1906a) regarded it as a swamp inhabitant. Matsumoto (1923) discussed the features of *Moeritherium* that point to either aquatic or non-aquatic lifestyle, concluding that although it might not have been as adapted to an aquatic lifestyle as extant hippos; it probably preferred environments close to water bodies. *Palaeomastodon* and *Phiomia*, on the other hand, seem more similar to the more derived elephantiforms and are usually regarded as

terrestrial. In more recent studies, the isotopic signature of these species was compared, leading to the conclusion that *Moeritherium* and *Barytherium* were at least semi-aquatic, whereas the other Fayum proboscideans were fully terrestrial (Clementz et al., 2008; Liu et al., 2008).

4.3.7 Hyracoidea

The hyracoids represent one of the most diverse groups in the Fayum (Matsumoto, 1926; Rasmussen & Gutiérrez, 2010; Rasmussen & Simons, 1988a; Tabuce et al., 2021), including both small taxa such as *Sagatherium* and *Thyrohyrax* (Barrow et al., 2010; Rasmussen & Simons, 1991), comparable in size to modern-day hyraxes, and very large ones such as *Titanohyrax* that may have weighed up to a ton (Schwartz et al., 1995; Tabuce, 2016).

The first remains of hyracoids were reported by Andrews and Beadnell (1902), for which they erected the new small-sized hyracoid genus *Sagatherium*, including the two new species *Sagatherium antiquum* and *Sagatherium minus* from the Gebel Qatrani Formation. Subsequently, however, these two taxa have been synonymised (Tabuce, 2016). Thus, *Sagatherium* represented the oldest hyracoid finds at the time and the second hyracoid fossil taxon ever described, after *Pliohyrax graecus* from the famous Greek Late Miocene locality Pikermi (Gaudry, 1862; Roussiakis et al., 2019). One year after the initial description of *Sagatherium*, Andrews (1903c) described a new genus and species of a large-sized hyracoid, *Megalohyrax eocaenus*. In the following year, Andrews (1904c) described the new genus *Geniohyus*, with two new species, *Geniohyus mirus* and *Geniohyus fajumensis*, which he originally considered as “pig-like” and later even referred to the Suidae (Andrews, 1906a). Andrews (1904f) founded three further new species for previously described genera, *Geniohyus major*, *Megalohyrax minor*, and *Sagatherium magnum*, based on dental



Fig. 6 Proboscidea material from the Late Eocene to Early Oligocene of the Fayum Depression (Egypt): **a** complete mandible of *Phiomia serridens* (NHMUK PV M 9449, holotype of *Phiomia osborni*); **b** skull of *Moeritherium lyonsi* (SMNS-P-12617); and **c** skull and mandible of *Palaeomastodon beadnelli* (NHMUK PV M 8464; Andrews, 1906a, pl. XII, fig. 1). Not to scale

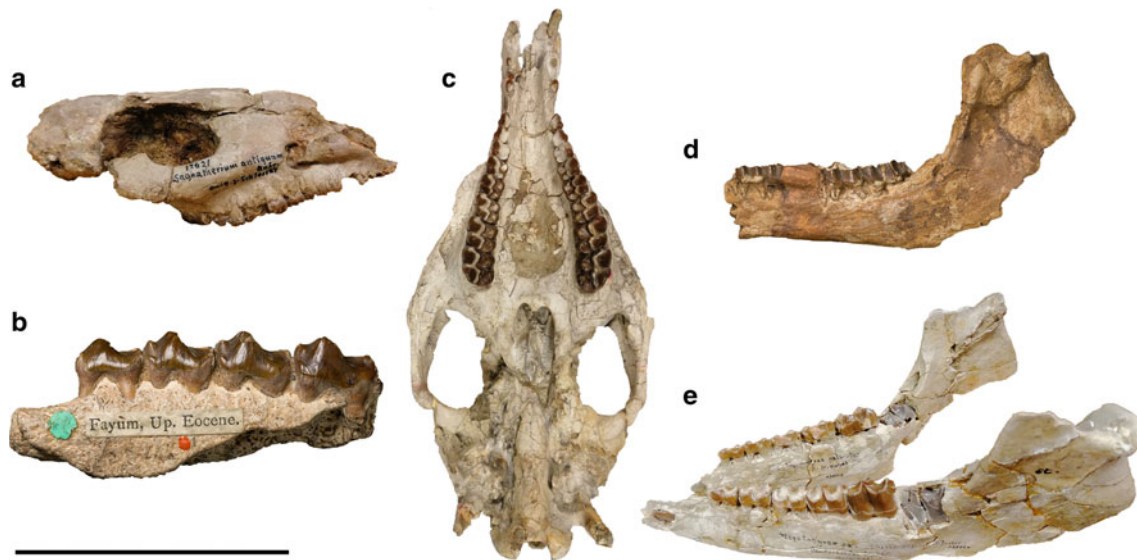


Fig. 7 Hyracoida material from the Late Eocene to Early Oligocene Gebel Qatrani Formation of the Fayum Depression (Egypt): **a** skull of *Saghatherium antiquum* (SMNS-P-12621; Schlosser, 1911, taf. II, fig. 12), in right lateral view; **b** fragment of a mandibular ramus of *Bunohyrax fajumensis* (NHMUK PV M 8435), originally described as *Geniohyus fajumensis* (Andrews, 1904c), in lateral view; **c**, type skull of *Megalohyrax niloticus* (SMNS-P-12624), originally referred to as *Mixohyrax niloticus* (Schlosser, 1910, 1911, taf. VII, figs. 1 and 8), in ventral view; **d** mandible of *Titanohyrax andrewsi* (NHMUK PV M 9220), in lateral view; and **e** mandible of *Titanohyrax palaeotherioides* (SMNS-P-43922) originally referred as *Megalohyrax palaeotherioides* (Schlosser, 1911, taf. IV, fig. 1), in right lateral view. Scale bar is 10 cm for **a**, 5 cm for **b**, 20 cm for **c**, and 15 cm for **d** and **e**

remains from the Gebel Qatrani Formation. Two years later, Andrews (1906a) erected the medium-sized species *Saghatherium majus* and introduced the family Saghatheriidae for the Fayum hyracoids. Schlosser (1910) proposed the name Palaeohyracidae to include these primitive hyracoids and the subfamily Saghatheriinae for the selenodont representatives of this group. He also included *Geniohyus* in the Hyracoida and described several new species of this group, including *Geniohyus minutus* and *Megalohyrax palaeotherioides*, as well as the new genera *Pachyhyrax*, with the relatively rare *Pachyhyrax crassidentatus*, *Mixohyrax*, with the three species *Mixohyrax andrewsi*, *Mixohyrax niloticus* (Fig. 7c), *Mixohyrax suillus*, and *Bunohyrax*, in which he included the previously described species *Bunohyrax* (= *Geniohyus*) *fajumensis*. One year later, Schlosser (1911) offered detailed descriptions of the rich hyracoid material from the Fayum Depression, including all species he previously erected and also described the new species *Geniohyus macrognathus*, which he referred tentatively to the genus *Geniohyus*. Matsumoto (1921) revised the hyracoid genus *Megalohyrax* in which he included the species *Megalohyrax eocaenus*, *Megalohyrax minor*, *Megalohyrax niloticus* (originally *Mixohyrax niloticus*), *Megalohyrax suillus* (originally *Mixohyrax suillus*), and the new species *Megalohyrax pygmaeus*. He also erected the new genus *Titanohyrax* for very large-sized hyracoids, in which he included the new species *Titanohyrax ultimus*, *Titanohyrax schlosseri*, *Titanohyrax andrewsi*, and *Titanohyrax palaeotherioides* as the type

species (originally *Megalohyrax palaeotherioides*). Five years later, Matsumoto (1926) revised all Fayum hyracoids, erecting three new families. He named the first Geniohyidae, and included in this the three bunodont genera *Geniohyus*, with the new species *Geniohyus gigas*, *Geniohyus subgigas* and *Geniohyus diphycus*, *Bunohyrax*, for which he described the new species *Bunohyrax affinis*, and *Megalohyrax*. The second family is Titanohyracidae, which includes only the genus *Titanohyrax*. The third family is Pliohyracidae, a family that actually had already been established by Osborn (1899) for the Miocene genus *Pliohyrax* (Pickford et al., 2021). In this family, Matsumoto (1926) included the monospecific genus *Pachyhyrax* and the genus *Saghatherium*, for which he described four new species, *Saghatherium macrodon*, *Saghatherium euryodon*, *Saghatherium annectens*, and *Saghatherium sobrina*. Almost half a century later, Meyer (1973) described a new genus and species of saghatheriine hyracoid, *Thyrohyrax domorictus*, known from several Early Oligocene fossil sites (Quarries M, G, I) of the Gebel Qatrani Formation. Rasmussen and Simons (1988a) studied new hyracoid material from the Fayum Depression and erected the new large hyracoid species *Titanohyrax angustidens*, the small *Saghatherium humarum*, and the new genus and species *Selenohyrax chatrathi*, all from the Oligocene of the Gebel Qatrani Formation. Shortly after, Rasmussen and Simons (1991) studied the hyracoid material from the Late Eocene site L-41 of the Gebel Qatrani Formation and described three new species. The first one is *Saghatherium bowni*, which is fairly

common in L-41 and exhibits a considerable size-related sexual dimorphism (Rasmussen & Simons, 1991). The other two species are *Thyrohyrax meyeri* and *Thyrohyrax litholagus*, representing more primitive relatives to the somewhat bigger and more derived *Thyrohyrax domoricetus* and *Thyrohyrax pygmaeus*, respectively (Rasmussen & Simons, 1991). Almost a decade later, the same authors (Rasmussen & Simons, 2000) described a new titanohyracine species, *Antilohyrax pectidens*, from the Late Eocene site L-41 of the Gebel Qatrani Formation, based on its comb-like first incisor. This new species is of medium size and seems to be related to the huge *Titanohyrax* based on their similarly selenodont cheek teeth and broad incisors, among other features (Rasmussen & Simons, 2000). Barrow et al. (2010) described the new small species *Dimatherium patnaiki*, based on a partial left mandible as the holotype and numerous isolated dental elements from the Late Eocene locality BQ-2, all from the Birket Qarun Formation. A partial cranium from the Late Eocene locality BQ-7 can also be referred to this species. Thus, *Dimatherium patnaiki* represents the oldest and most primitive hyracoid taxon from the Fayum Depression and seems to be most closely related to the genus *Thyrohyrax* (Barrow et al., 2010).

Hyracoids are extremely diverse and well represented in the Fayum fauna, but almost all finds come from the Late Eocene to Early Oligocene Gebel Qatrani Formation (e.g. Andrews, 1906a; Rasmussen & Simons, 1988a). The Late Eocene fossil site L-41 of this formation preserves the highest diversity of hyracoids in the Fayum succession, including eight genera and nine species (Barrow et al., 2010; Rasmussen & Simons, 1988a, 1991). Only a single fragmentary hyracoid specimen has been described from the underlying Qasr el Sagha Formation (Holroyd et al., 1996), and one primitive taxon, *Dimatherium patnaiki*, is exclusively found in the Birket Qarun Formation (Umm Rigl Member) (Barrow et al., 2010).

Over the last century, more than 30 hyracoid species have been described from Fayum material. Many of these species have been synonymised and/or referred to different genera afterwards. Beside the taxonomic diversity in the Fayum hyracoids, the representatives of this group seem to cover a wide array of ecological niches. This is indicated by the different dental morphologies including the more generalised *Sagatherium* and *Thyrohyrax* and the bunodont, probably omnivorous *Geniohyus* (Barrow et al., 2010). One of the most peculiar hyracoids of the Fayum fauna is certainly the gazelle-sized *Antilohyrax pectidens* (Rasmussen & Simons, 2000). It exhibits hyper-pectinate lower incisors, but no upper incisors (de Blieux & Simons, 2002). The dentition is sharp-edged selenodont, pointing to a folivorous diet and its postcranial morphology suggests that it was cursorial browser, representing an Eocene analogue to modern bovids (Rasmussen & Simons, 2000).

4.3.8 Sirenia

The sirenians or sea-cows are among the first vertebrate fossils that have been described from Egypt. Owen (1875) described the new species *Eotherium aegyptiacum* from the Eocene of the “Mokattam cliffs” near Cairo, representing the first sirenian species to be described from Egypt. From Middle to Upper Eocene strata of the same area, close to Cairo, four further species have been described, *Manatus coulombi* Filhol, 1878, *Protosiren fraasi* Abel, 1907, *Eosiren abeli* Sickenberg, 1934, and *Eotherium majus* Zdankys, 1938, of which the holotype is now considered lost (Zalmout & Gingerich, 2012). It is important to note that the genus name *Eotherium* was actually preoccupied, and thus, Palmer (1899) proposed the new name *Eotheroides* for this genus, which is still in use today.

Andrews (1902) described the first sirenian remains from the Fayum Depression. This material comes from the Qasr el Sagha Formation and includes an almost complete skull and associated mandible, for which Andrews (1902) erected the genus and species *Eosiren libyca*. Three decades later, Sickenberg (1934) described the new species *Eosiren stromeri*, in honour of Ernst Stromer von Reichenbach, from the Qasr el Sagha Formation of the Fayum. More than half a century later, Domning et al. (1994) described the new species *Eosiren imenti* based on a cranium from the Early Oligocene of the Gebel Qatrani Formation in the Fayum. Based on the fluvial environment of the Gebel Qatrani Formation, it is possible that *Eosiren imenti* had a wide salinity tolerance (Domning et al., 1994). In the same year, Domning and Gingerich (1994) described the new species *Protosiren smithae*, based on a partial skeleton that comprises a fairly well-preserved skull, its mandible, and several postcranial elements, from the Gehannam Formation in Wadi al Hitán. More recently, Zalmout and Gingerich (2012) described two additional species of sea-cows, from the Birket Qarun Formation of Wadi al Hitán. The first species is *Eotheroides clavigerum* and was based on a partial skeleton of an adult individual. The second species, *Eotheroides sandersi*, was based on more fragmentary cranial and postcranial elements that were found in association (Zalmout & Gingerich, 2012, fig. 8).

4.3.9 Primates

The Fayum Depression has offered significant insight into the early evolution of primates during the Eocene and Oligocene. When the locality was first discovered in the late nineteenth and early twentieth century, it provided the oldest fossil primates known at that time. More specifically, Osborn (1908) described the small *Apidium phiomense* (originally mentioned as *Apidium phiomensis*) based on a partial left mandibular ramus from the Gebel Qatrani Formation, which he initially compared to bunodont artiodactyls and primates, but was unable to assign it to any of them. It was soon after

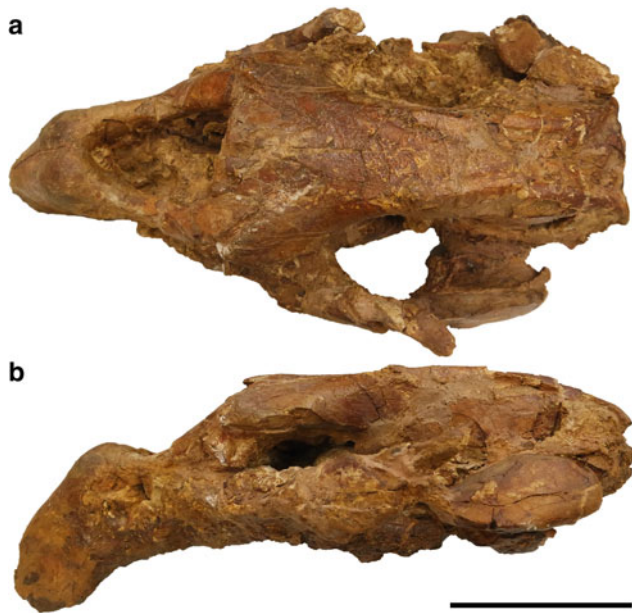


Fig. 8 Skull of *Eosiren libyca* (GPIT-PV-41670) from the Fayum Depression (Egypt), collected by Richard Markgraf, in **a** dorsal and **b** left lateral view. Scale bar is 10 cm

referred to a primate (Schlosser, 1911), though the discussion about its systematic position was far from over (Simons, 1960). Fleagle and Simons (1995) studied the limb skeleton of *Apidium phiomense* and compared it to other primates, concluding that it was a very primitive arboreal quadrupedal primate, weighing about 1.6 kg. Today, *Apidium* is well recognised as a primate that belongs to the family of Parapithecidae (Beard et al., 2016; Fleagle & Simons, 1995; Simons, 1995a) and is very common in the Gebel Qatrani Formation (Simons & Rasmussen, 1990). The genus includes three species along with *Apidium phiomense*, *Apidium moustafai* from Quarry G of the Gebel Qatrani Formation (Simons, 1962), *Apidium bowni* from Quarry V of the Gebel Qatrani Formation (Simons, 1995a), and *Apidium zuetina* from the Early Oligocene of the Sirt Basin in central Libya (Beard et al., 2016).

Soon after the description of the first primate material from the Fayum deposits (Osborn, 1908), Schlosser (1910) published a preliminary report on the Fayum fossils collected by Markgraf from the Gebel Qatrani Formation and described three new primate taxa: *Moeripithecus markgrafi*, *Parapithecus fraasi*, and *Propliopithecus haeckeli*. Schlosser (1910) even suggested that *Propliopithecus haeckeli* represents an ancestor of hominids. *Moeripithecus markgrafi* was based on a mandibular ramus fragment with two preserved molars (Schlosser, 1910, 1911). It was later suggested to be a juvenile *Propliopithecus* (Simons, 1967; Szalay & Delson, 1979). Nowadays, the synonymy of *Moeripithecus* and *Propliopithecus* is well established, and the name *Propliopithecus* is used (e.g. Simons & Rasmussen, 1990; Simons

et al., 1987). Simons (1965) described the new taxa *Aegyptopithecus zeuxis*, based on two mandibular fragments, and *Aeolopithecus chirobates*, based on a nearly complete mandibular corpus, from Quarry I of the Gebel Qatrani Formation. Since its first description, much more material of *Aegyptopithecus zeuxis* has been found, including several more or less complete skulls (Fig. 9a and b), of both male and female individuals (e.g. Fleagle et al., 1980; Kay et al., 1981; Simons, 1987; Simons et al., 2007). Subsequently, however, the validity of *Aeolopithecus chirobates* has been questioned after its initial description by Gingerich and Arbor (1978), who argued for a potential synonymy with *Propliopithecus haeckeli*. Szalay and Delson (1979) later supported the notion that *Aeolopithecus chirobates* might in fact be assignable to the genus *Propliopithecus*. This was also followed by Kay et al. (1981), who also discussed some ecological aspects of these animals, such as the existence of sexual dimorphism. Furthermore, Simons et al. (1987) erected the new species *Propliopithecus ankei* based on dental material from Quarry V of the Gebel Qatrani Formation. The genera *Propliopithecus* (including *Aeolopithecus* and *Moeripithecus*) and *Aegyptopithecus* are regarded as members of the Propliopithecidae (Ducrocq, 2001).

Parapithecus fraasi is based on a complete mandible (Fig. 9d), only lacking the right p2 (Schlosser, 1910, 1911). Schlosser (1911) established the new family Parapithecidae for this taxon. Later, Simons (1974) described the new species *Parapithecus grangeri*, based on a mandibular fragment with five teeth preserved, from Quarry I of the Gebel Qatrani Formation that is somewhat larger and presumably stratigraphically younger than the type mandible of *Parapithecus fraasi*. Few years later, Gingerich and Arbor (1978) proposed the synonymy of *Parapithecus fraasi* and *Apidium phiomense* and erected the new genus *Simonsius* for *Parapithecus grangeri*. Although this view was not supported by most authors in the following years (e.g. Kay et al., 1981; Seiffert et al., 2020; Simons & Rasmussen, 1991; Simons, 1986, 1992, 1995b, 2001), it was nevertheless adopted by some and is used even in more recent studies (e.g. Fleagle & Kay, 1985; Harrison, 1987; Mattingly et al., 2021). Mattingly et al. (2021) considered *Simonsius* as a valid genus and described the new species *Simonsius harujensis*, a small (1–1.5 kg) parapithecine from the Early Oligocene of Libya.

Simons and Kay (1983) erected the genus *Qatrania*, with the sole species *Qatrania wingi*, based on some fragmentary dental elements from Quarry E of the Gebel Qatrani Formation. *Qatrania* represents a parapithecine of very small size, ~ 300 g (Mattingly et al., 2021; Simons & Kay, 1983). Five years later, the same authors described the new species *Qatrania fleaglei* based on a fragmentary right hemimandible from Quarry M of the Gebel Qatrani Formation (Simons & Kay, 1988), which constitutes the youngest representative of the genus (Beard & Coster,

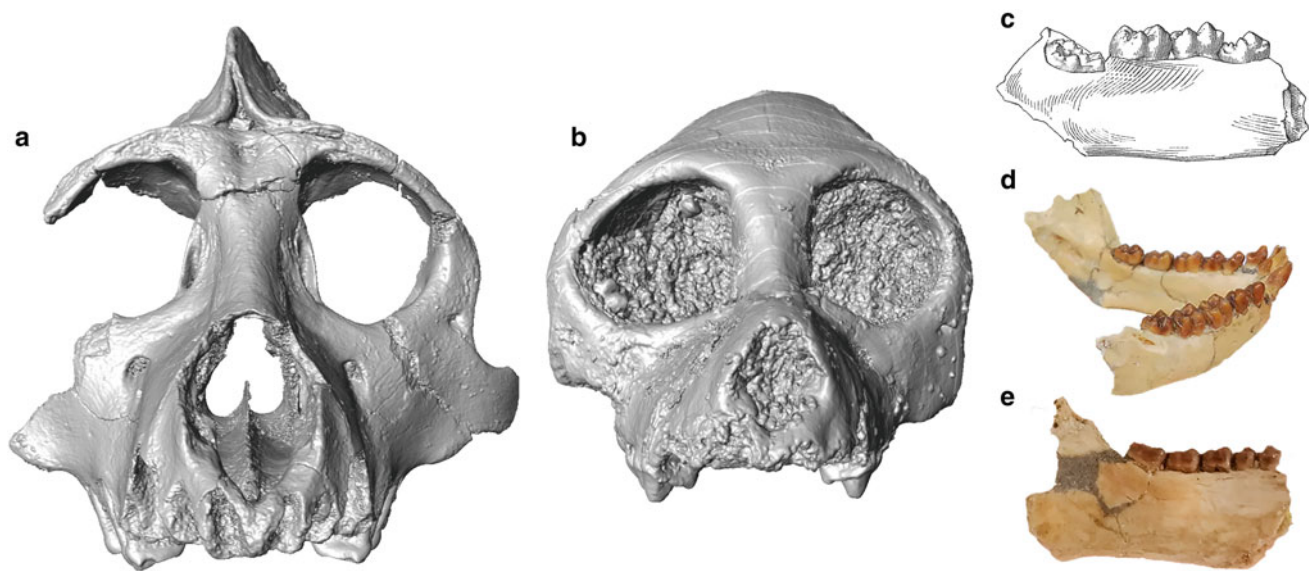


Fig. 9 Primate material from the Late Eocene to Early Oligocene Gebel Qatrani Formation of the Fayum Depression (Egypt): **a** μ CT-scan of a male skull of *Aegyptopithecus zeuxis* (DPC 2803), provided by the DPC; **b** μ CT-scan of a female skull of *Aegyptopithecus zeuxis* (CGM 85785), provided by the DPC; **c** type mandible of *Apidium phiomense* in medial view (taken from Osborn, 1908, fig. 6A2); **d** type mandible of *Parapithecus fraasi* (SMNS-P-43461) in right lateral view (Schlosser, 1911, taf. I, fig. 3); and **e** type mandible of *Propithecus haeckeli* (SMNS-P-12638) in medial view (Schlosser, 1911, taf. I, fig. 1). Not to scale

2016). Simons et al. (2001) erected a new genus and species of Parapithecidae, *Abuqatrania basiodontos*, based on a small mandible from the Late Eocene site L-41 of the Gebel Qatrani Formation. This species was later attributed to the genus *Qatrania* (Beard, 2013; Beard & Coster, 2016; Mattingly et al., 2021).

Simons and Bown (1985) erected the small, peculiar primate *Afrotarsius chatrathi* based on a mandible from the Oligocene site Quarry M, of the Gebel Qatrani Formation. It was initially regarded as a relative of the tarsier (Simons & Bown, 1985). More recently, Jaeger et al. (2010) described a second species for the genus, *Afrotarsius libycus*, from the late Middle Eocene of Libya, whereas Chaimanee et al. (2012) erected a new primate species, *Afrasia djijidae*, from the late Middle Eocene of Myanmar and proposed that it belongs, along with *Afrotarsius libycus*, to the Afrotarsiidae, within the Eosimiiformes.

De Bonis et al. (1988) erected the genus *Biretia* for a potential primitive Catarrhini from the Eocene of Algeria. This genus was later included in the Parapithecidae (e.g. Mattingly et al., 2021; Seiffert et al., 2005, 2020). Later, two species of *Biretia* were described based on the material from the Fayum Depression: *Biretia fayumensis* and *Biretia megalopsis*, both based on mandibular fragments preserving the m2 and m3 from the Late Oligocene locality BQ-2 of the Birket Qarun Formation (Seiffert et al., 2005).

Simons (1962) described, alongside *Apidium moustafai*, also the new genus and species *Oligopithecus savagei* from Quarry F of the Gebel Qatrani Formation. Later, Rasmussen

and Simons (1988b) described further material of *Oligopithecus savagei*, supporting a close relationship to the Propithecidae. Simons (1989) described two new small primate taxa, *Catopithecus browni* and *Proteopithecus sylviae*, from the Late Eocene site L-41 of the Gebel Qatrani Formation. The same author erected the Oligopithecinae to include *Oligopithecus*, *Catopithecus* and possibly *Proteopithecus*, though the lower dentition of the latter was still unknown (Simons, 1989). Some years later, a large collection of additional material of *Proteopithecus sylviae* was published, including even a partial skull (Miller & Simons, 1997), which led Simons (1997a) to erect the family Proteopithecidae, with the sole representative being *Proteopithecus sylviae*.

Simons (1992) described three new genera and species of primates, *Serapia eocaena*, *Plesiopithecus teras*, and *Arsinoea kallimos*, based on three partial mandibles from L-41 in the Upper Eocene strata of the Gebel Qatrani Formation. Simons (1992) suggested that *Serapia* belonged to the Parapithecidae, while not being able to attribute the other two new taxa to any family. A new phylogenetic analysis placed *Serapia* as the sister taxon of *Proteopithecus*, forming together the Proteopithecidae, whereas *Arsinoea* seems to represent a basal stem-group member of the Parapithecidae (Seiffert et al., 2020). Seiffert et al. (2020) suggested that the Proteopithecidae and the Parapithecidae belong to the Parapithecidae, an autochthonous group of Afro-Arabia, with a single representative from the Oligocene of South America, *Ucayalipithecus perdita* (Seiffert et al., 2020).

A new superfamily, the Plesioptithecoidae, and family, the Plesioptithecidae, were erected by Simons and Rasmussen (1991) for the small primate *Plesioptithecus teras*. Simons (1997b) described two new extremely small prosimians (Kirk & Simons, 2001), the new genus and species *Wadilemur elegans* and the new species *Anchomomys milleri*, from the Late Eocene site L-41, of the Gebel Qatrani Formation. In their phylogenetic analysis, Seiffert et al. (2003) placed *Plesioptithecus* as a stem Strepsirrhini. Gunnell et al. (2018) recovered *Plesioptithecus* as a basal Chiromyiformes and a relative to both the extant Madagascan aye-aye (*Daubentonia*) and the Early Miocene *Propotto* from Kenya. Although, *Propotto* has been suggested to belong to the Megachiroptera (Pickford, 2018).

Seiffert et al. (2003) also erected the loriform primates *Karanisia clarki* and *Saharagalago misrensis*, based on a partial mandible and a single lower tooth from BQ-2, respectively, both from the Late Eocene Birket Qarun Formation (Seiffert et al., 2003). A second species was added to *Karanisia*, when Jaeger et al. (2010) described the new *Karanisia arenula* based on an m2 from the late Middle Eocene of Libya. Gunnell et al. (2018) included *Wadilemur*, *Saharagalago*, and *Karanisia* in their phylogenetic analysis, which placed them as relative basal loriforms (Gunnell et al., 2018).

Simons et al. (1995) described the new adapid primate *Aframomius dieides*, based on three partial mandibles from the Late Eocene L-41 of the Gebel Qatrani Formation. Seiffert et al. (2009) described a new large adapiform, *Afradapis longicristatus*. Soon after, the description of an astragalus assigned to this species further supported its phylogenetic position (Boyer et al., 2010). More recently, Seiffert et al. (2018) assigned a plethora of isolated dental remains and some partial mandibles to the new adapiform *Masradapis tahai*, which seems to represent a sister taxon to *Aframomius dieides* (Seiffert et al., 2018).

Seiffert et al. (2010) described a puzzling new primate, *Nosmips aenigmaticus*, named after George Gaylord Simpson, based on some isolated teeth from the Late Eocene site BQ-2 of the Birket Qarun Formation. The phylogenetic position of this taxon and its affinities remain uncertain (e.g. Gunnell et al., 2018; Seiffert, 2012; Seiffert et al., 2010). Seiffert et al. (2010) suggested that it might represent a highly specialised representative of an unknown primate lineage, endemic to Africa.

4.3.10 Rodentia

The rodents are well known from the Fayum Depression, especially from the Oligocene of the Gebel Qatrani Formation (Wood, 1968). The most frequent representatives of this group are the hystricomorphs and the anomaluroids (Al Ashgar et al., 2019). Most of the material of this group from the Fayum area was collected during the second half of the

twentieth century; before, most collecting efforts aimed principally at large mammals (Simons, 1968).

Nonetheless, the first micromammals were described by Osborn (1908) who erected *Phiomys andrewsi*, named after Charles W. Andrews, for two partial right mandibles, and *Metaphiomys beadnelli*, named after Hugh J. L. Beadnell, for a partial left mandible, both species occurring in the Gebel Qatrani Formation. Wood (1968) presented the first comprehensive study of rodents from the Fayum deposits. He described two new species of *Phiomys*, *Phiomys paraphiomysoides* and *Phiomys lavocati*, the new species *Metaphiomys schaubi* and *Paraphiomys simonsi* and introduced two new genera, *Gaudeamus* and *Phiocricetomys*, from the Oligocene of the Gebel Qatrani Formation (Wood, 1968). Sallam et al. (2009) studied the rodent material from BQ-2, erecting the new species *Protophiomys aegyptensis* and the new genus and species *Waslamys attiai*. They performed a phylogenetic analysis, which recovered both taxa as stem-group members of Hystricognathi, to draw conclusions on the biogeographic history of the hystricognathous evolution and their dispersal from Africa to South America (Sallam et al., 2009). Sallam et al. (2010a, 2010b) studied the anomaluroid rodent material from BQ-2 of the Birket Qarun Formation and described two new species *Shazurus minutus* and *Kabirmys qarunensis*. Both were suggested to be members of the Anomaluridae (Sallam et al., 2010a, 2010b). Sallam et al. (2011) described two new species, *Gaudeamus aslius* and *Gaudeamus hylaeus* from the Late Eocene site L-41 of the Gebel Qatrani Formation. This genus also includes *Gaudeamus aegyptius* as the type species, also known from the Gebel Qatrani Formation, *Gaudeamus lavocati*, and potentially a third species from the Fayum succession, which they referred to as *Gaudeamus* aff. *aslius*. For these taxa, they erected the new hystricognathous family Gaudeamuridae, which they regarded as autochthonous for Afro-Arabia and as potentially being closely related to the hystricids (Sallam et al., 2011, figs. 20 and 21).

A new species of phiomyid, *Acritophiomys boweni*, was described by Sallam et al. (2012) from the Late Eocene site L-41 of the Gebel Qatrani Formation in the Fayum succession. In their phylogenetic analysis, this species was recovered as a basal member of the Phiomorpha (Sallam et al., 2012). Sallam and Seiffert (2016) described two new phiomorphs, *Birkamys korai* and *Mubhammys vadumensis*, from the Late Eocene site L-41 of the Gebel Qatrani Formation, which seem to form a monophyletic group. Later, the same authors (Sallam & Seiffert, 2019) erected the new genus *Monamys* for the previously described species *Monamys simonsi* (originally named *Paraphiomys simonsi* by Wood, 1968), which they regarded as a stem thryonomyoid. Most recently, Al-Ashgar et al. (2021) studied new material of the Phiocricetomyinae and erected a new genus and species,

Qatranimys safroustus, from the Late Eocene site L-41, from the base of the Gebel Qatrani Formation.

4.3.11 Pholidota

The potential existence of pangolins in the Paleogene of the Fayum Depression was unknown for almost a century. Until Gebo and Rasmussen (1985) reported two distal phalanges, which resemble those of an extant pangolin (i.e. *Manis pentadactyla*). The specimens come from the Early Oligocene deposits of Quarry M and Locality 12 (L-12), of the Gebel Qatrani Formation. Furthermore, numerous termite- and ant-nests have been reported from the Gebel Qatrani Formation, some of which exhibit potential vertebrate excavation marks (Bown, 1982). Thus, despite the ambiguous taxonomy of the two phalanges, it has been suggested that the Fayum pangolin dug and fed on termites, similar to some modern-day pangolins (Gebo & Rasmussen, 1985). Due to the fragmentary nature of the fossils and the absence of any teeth or cranial material from the Fayum Depression, the attribution of these specimens to pangolins has been questioned (Gaudin et al., 2009).

4.3.12 Cetacea

Cetaceans are one of the most extensively studied and best-known fossil vertebrate groups from the Paleogene of Egypt. Complete skeletons have been recovered from the Gehannam Formation and Birket Qarun Formation (from the Wadi al Hitan or Valley of Whales); however, they occur only sparsely in the Qasr el Sagha Formation (Gameil et al., 2016; Gingerich, 1992, 2010). The first fossil whales from Africa were found by Georg Schweinfurth in 1879, representing the first archaeocete cetaceans known from the eastern hemisphere. The remains were found in the Birket Qarun Formation on the island of Geziret el Qarn in the centre of lake Birket Qarun (Dames, 1883a; Gingerich, 2010). These fossils include vertebrae (Dames, 1883a, 1894) and skull fragments (Dames, 1883b) of “*Zeuglodon*” sp. as well as the holotype of “*Zeuglodon*” *osiris* (now *Saghacetus osiris*), an almost complete dentary (Dames, 1894, pl. I; fig. 10).

At the beginning of the twentieth century, Beadnell collected a considerable amount of archaeocete remains from the Birket Qarun Formation, which were briefly described by Andrews (1901c, 1904f). Andrews (1904f) established the species “*Zeuglodon*” *isis* (now *Basilosaurus isis*). The name

of this species was originally proposed by Beadnell in a memoire about the geology of the Fayum Province (Beadnell, 1905) that was, however, published after Andrews (1904f). The holotype is a complete mandible containing the entire dentition. Beadnell also collected fossil archaeocetes from an area west of Garet Gehannam. The fossils were so abundant there that he called this area “*Zeuglodon* Valley” (Beadnell, 1905), which was later named Wadi al Hitan or Valley of Whales. During this phase, he collected a complete skull of an archaeocete that was later described as the holotype of “*Prozeuglodon*” *atrox* (now *Dorudon atrox*), by Andrews (1906a). All fossil archaeocetes collected by Beadnell and Andrews at the beginning of the twentieth century were described in detail by Andrews (1906a) in his monograph about the vertebrate fauna of the Fayum.

Andrews (1906a) described the holotype skull of “*Prozeuglodon*” as intermediate between *Protocetus* and “*Zeuglodon*”, but in 1908 he revised the specimen, concluding that it instead represented a juvenile with deciduous teeth. Therefore, “*Prozeuglodon*” *atrox* was long thought to be the juvenile form of “*Zeuglodon*” *isis* (e.g. Barnes & Mitchell, 1978; Kellogg, 1936). However, Gingerich et al. (1990) studied complete skeletons of both species and showed that “*Prozeuglodon*” *atrox* is not a juvenile of “*Zeuglodon*” *isis* and thus belongs to a separate genus and species. The archaeocete fossil collected by Andrews and Beadnell were furthermore studied by Dart (1923), who established three new species of “*Zeuglodon*” (*Zeuglodon sensitives*, *Zeuglodon elliotsmithii*, and *Zeuglodon intermedius*) based on natural endocasts of the brain cavity (Fig. 11).

Besides Beadnell and Andrews, Stromer and Fraas also collected archaeocete remains from the Fayum region, north of Birket Qarun. They discovered a new skull and lower jaw of “*Zeuglodon*” *osiris* from the Qasr el Sagha Formation (Stromer, 1902) and, furthermore, established the species “*Zeuglodon*” *zitteli* based on a natural endocast of the nasal region, skull remains, as well as vertebrae (Stromer, 1903, pl. 10–11). More recently, Gingerich (2007) established a new species of archaeocete whale from that region based on the vertebrae collected by Stromer and additional vertebrae from Garet el Esh, which he named in honour to Stromer, *Stromerius nidensis*.

During the same period, Fraas and Markgraf collected a cranium and associated postcranial remains of a small

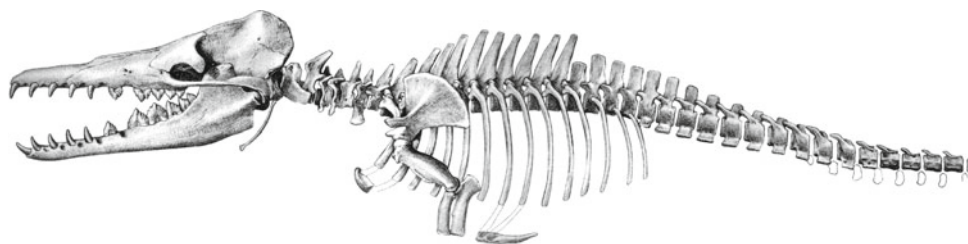


Fig. 10 *Saghacetus osiris* skeleton reconstruction (Stromer, 1908, taf. I, fig. 1)



Fig. 11 Cetacea material from the Eocene of the Fayum Depression (Egypt): **a** skull of *Saghacetus osiris* (NHMUK M 10228) in right lateral view; and **b** “*Zeuglodon intermedius*” (NHMUK M 10173, now *Dorudon atrox*) in left lateral view. Scale bar is 20 cm

archaeocete from Gebel Mokattam. The specimen was described by Fraas (1904) as *Protocetus atavus* a new genus and species, which became the type genus of the new family Protocetidae (Stromer, 1908). Another skull from the same formation was named by Fraas (1904, 1906) as “*Mesocetus*” *schweinfurthi* (now known as *Eocetus schweinfurthi*). In 1906, Fraas and Markgraf excavated a large skeleton of “*Zeuglodon*” *isis* west of Birket Qarun comprising a skull with a length of 1.3 m and a sequence of vertebrae and ribs about 10 m in length (Fraas, 1906; Gingerich, 2010). This skull was described by Stromer (1908) and Slijper (1936) and was later depicted by Heizmann (1991). After the excavations of Fraas and Markgraf, Stromer together with Markgraf went to the Fayum Depression in order to collect fossil whales (Gingerich, 2010). They recovered two large archaeocete vertebrae from Gebel Mokattam, an archaeocete skull with jaws, and some vertebrae from the Birket Qarun Formation (Stromer, 1904).

After the expeditions of Fraas and Stromer, several scientists and fossil collectors from the USA, such as Henry F. Osborn and Walter Granger (in 1907), as well as Robert H. Denison and Paules E. P. Deraniyagala (in 1947) visited the areas around Qasr el Sagha, Birket Qarun, and Wadi al Hitan (Gingerich, 2010). They collected many large zeuglodonts from Wadi al Hitan (Deraniyagala, 1948; Kellogg, 1936; Osborn, 1907) and partial skulls of “*Zeuglodon*” *isis*, as well as endocranial casts of “*Prozeuglodon*” *atrox* (Pilleri, 1991). Kellogg (1936) was the first to mention the use of *Basilosaurus* over *Zeuglodon*, as he regarded them as synonyms. Later, Gingerich et al. (1990) and Uhen (2004) supported this taxonomic assignment. Furthermore, Kellogg (1936) placed “*Zeuglodon*” *osiris* in *Dorudon*, and later Uhen

(2004) included “*Prozeuglodon*” *atrox* in *Dorudon* as well. The species “*Zeuglodon*” *osiris* was later placed into *Saghacetus* by Gingerich (1992).

Moustafa (1954) described a partial skull of a subadult “*Zeuglodon*” *isis* in the Birket Qarun Formation that was collected by him in 1950. In the following two decades, the palaeontologists Simons and Meyer visited the area around Birket Qarun, Qasr el Sagha, and Wadi al Hitan (Gingerich, 2010). They found skulls of “*Zeuglodon*” *isis* in the Birket Qarun Formation and some archaeocete remains in the Qasr el Sagha Formation (Simons & Wood, 1968). Barnes and Mitchell (1978) provided a review of African cetaceans, in which they included *Prozeuglodon atavus*, *Eocetus schweinfurthi*, and *Pappocetus lugardi* in Protocetidae. They also placed among others “*Zeuglodon*” *osiris* and “*Zeuglodon*” *isis* into Basilosauridae.

Shortly after, Gingerich and Simons excavated in the Fayum region, uncovering new archaeocete remains from the Birket Qarun Formation (Wadi al Hitan) and Qasr el Sagha Formation in 1983 (Gingerich, 2010). They found many well-preserved skeletons of archaeocete whales. The most common taxa in Wadi al Hitan were *Basilosaurus isis* and *Dorudon atrox*, both represented by equal numbers of individuals (Gingerich, 2010). Both species are described to be morphologically quite similar with slight osteological differences (Gingerich & Smith, 1990; Gingerich et al., 1990; Luo & Gingerich, 1999). Furthermore, recent studies using stable isotopes confirmed that both, *Basilosaurus* and *Dorudon*, were fully aquatic (Clementz et al., 2006). Moreover, Gingerich et al. (1990) focused on the development of the hindlimbs in archaeocetes based on fossils from Wadi al Hitan ultimately providing insights into archaeocete

evolution. In addition to *Basilosaurus isis* and *Dorudon atrox*, further archaeocete whales are known from Wadi al Hitan such as *Ancalocetus simonsi* (Gingerich & Uhen, 1996) and *Masracetus markgrafi* (Gingerich, 2007). From the Qasr el Sagha Formation, *Saghacetus osiris* and *Stromerius nidensis* are known (Gingerich, 2007).

Most recently, Gohar et al. (2021) described a new medium-sized protocetid, *Phiomicetus anubis*, from the Middle Eocene Midawara Formation in the south-western part of the Fayum Depression. A partial skeleton, including a fragmentary skull, was reported. The material enabled the authors to establish *Phiomicetus* as the most basal African protocetid and as a highly efficient hunter of elusive prey (Gohar et al., 2021).

4.3.13 Anthracotheriidae

Anthracotheres are among the most abundant fossils recovered from the Fayum Depression (Sileem et al., 2016). They were the first artiodactyls that reached the African continent (Sileem et al., 2016; Simons, 2008; Simons & Rasmussen, 1990); however, the origin of African anthracotheres is still largely unknown. According to Lihoreau and Ducrocq (2007), anthracotheres likely originated in North America or Eurasia with the oldest known fossils from North America (42 Ma) and Myanmar (~ 40 Ma; Zaw et al., 2014). Anthracotheres then spread and diversified throughout Laurasia and Africa. However, Simons and Rasmussen (1990) mentioned that Anthracotheriidae are not related to African Paenungulata, but instead originated from the Eurasian forms (Black, 1978; Schmidt, 1913).

Andrews and Beadnell (1902) reported the first anthracothere material from the Fayum area and described the new species *Ancodus gorringei* from the Gebel Qatrani Formation based on a nearly complete mandible. This species was described in detail by Andrews (1906a) as *Ancodon gorringei*. Andrews (1906a) furthermore established the new species *Ancodon parvus*, in addition to unassigned material of *Ancodon* sp. Specimens of *Ancodon gorringei* and *Ancodon parvus* comprise mainly mandible remains including teeth and provisionally referred postcranial material. Together with the remains of *Ancodon*, Andrews (1906a) also established the species *Rhagatherium aegyptiacum* based on an upper left molar. All fossils described by him in 1906 were recovered from the Gebel Qatrani Formation. Depéret (1908) assigned *Ancodon gorringei* and *Ancodon parvus* to the bunodont anthracothere genus *Brachyodus*, and later Schmidt (1913) mentioned that the unassigned material of *Ancodon* sp. (Andrews, 1906a, p. 191) belonged to *Brachyodus parvus*. Schmidt (1913) reported the presence of the two already known species of *Brachyodus* and erected three new species, *Brachyodus andrewsi*, *Brachyodus fraasi*, and *Brachyodus rugulosus*. He also erected the new subgenus *Bothriogenys* (Schmidt,



Fig. 12 Anthracotheriidae material from the Late Eocene to Early Oligocene Gebel Qatrani Formation of the Fayum Depression (Egypt): **a** complete skull of *Bothriogenys fraasi* (NHMUK PV M 10186; Schmidt, 1913, taf. II, fig. 1) in ventral view; and **b** right mandibular ramus of *Bothriogenys gorringei* (SMNS-P-44080; Schmidt, 1913, taf. IV, fig. 9) in lateral view. Scale bar is 10 cm

1913), which was later raised by Black (1978) to genus rank and since then retained this status (e.g. Black, 1978; Dineur, 1982; Sileem et al., 2015, 2016). In 1997, Ducrocq (1997) erected the genus *Qatraniodon* to which he referred the previously described species *Bothriogenys parvus*.

At present, the existence of three genera of Anthracotheriidae in the Fayum succession is accepted: *Bothriogenys*—including the four species *Bothriogenys gorringei*, *Bothriogenys rugulosus*, *Bothriogenys fraasi*, and *Bothriogenys andrewsi*; *Qatraniodon*—comprising one species, *Qatraniodon parvus*; and *Nabotherium*—replacing *Rhagatherium*, thus including *Nabotherium aegyptiacum*

(Sileem et al., 2015, 2016). These species differ from one another primarily in size, specializations of the anterior dentition, and degree of brachydonty versus selenodonty (Holroyd et al., 2010, fig. 12).

Anthracotheres are absent in the Birket Qarun Formation. They first appear in the Dir Abu Lifa Member of the Qasr el Sagha Formation as Anthracotheriidae indet. Above the Eocene–Oligocene boundary; *Nabotherium*, *Qatraniodon*, and *Bothriogenys* are present in the Gebel Qatrani Formation (Sileem et al., 2015, 2016).

Anthracotheres were large, stout-bodied animals that might have been semi-aquatic (Pickford et al., 2008; Sileem et al., 2016; Simons, 2008). Boissier et al. (2005) even reaffirmed a distant relationship to hippopotamuses. Simons and Rasmussen (1990) assumed that anthracotheres partially replaced hyracoids, when they arrived in Africa, because hyracoids were the dominant terrestrial plant eating group at that time that had radiated into several species and their number decreased after the arrival of anthracotheres (Simons, 2008).

Schmidt (1913) already implied that the Fayum anthracotheres consisted of two different lineages and later, Sileem et al. (2016) classified *Nabotherium* as bunodont and *Bothriogenys*, as well as *Qatraniodon* as bunoselenodont representatives. He also concluded that the abundant *Bothriogenys* probably had a browsing/grazing adaptation and was eating foliage based on the morphology of its dentition. Due to their hydrophilic nature, it is possible that they also fed on water plants (Pickford et al., 2008; Simons, 2008). In contrast, the bunodont *Nabotherium* was according to Sileem et al. (2016) probably a selective frugivore/herbivore.

4.3.14 Chiroptera

Bats are a quite rare and under-represented group in the Fayum deposits. The first remains were described well over a century ago, when Schlosser (1910) erected the new genus and species *Vampyravus orientalis* for a relatively big humerus from the Gebel Qatrani Formation. This species represents the first fossil bat described from Africa. In his extensive work about the Fayum fauna, Schlosser (1911) actually coined a new genus name for this specimen, *Provampyrus orientalis*, without explaining the reasons behind this change. Of course, the genus name *Vampyravus* has priority over *Provampyrus*, a fact that has been mentioned repeatedly in the literature (e.g. Gunnell et al., 2008; Rosina & Pickford, 2019; Sigé, 1985). The humerus housed in the SMNS that was described by Schlosser (1910, 1911) remains the only known specimen assignable to this species (Gunnell et al., 2008, 2009). Gunnell et al. (2009) studied the holotype of the species and compared it to the other bats that were described later from the Fayum Depression. He concluded that *Vampyravus orientalis* was the largest bat in the Fayum fauna, weighing about 120 g, distinct from any other taxon from the Fayum and probably belonged

to a derived bat family, such as the emballonurids or rhinopomatids (Gunnell et al., 2009).

Gunnell et al. (2008) studied new chiropteran material from different localities from the Birket Qarun Formation and the Gebel Qatrani Formation of the Fayum region. They recognised two previously described species and also founded four new genera, *Witwatia*, *Qarunycteris*, *Saharaderma*, and *Khonsunycteris*, and six new species of bats, *Witwatia schlosseri*, *Witwatia eremicus*, *Dhofarella sigei*, *Qarunycteris moerisae*, *Saharaderma pseudovampyrus*, and *Khonsunycteris aegypticus* (Gunnell et al., 2008). Gunnell et al. (2014) erected a new genus of myzopodid bat, *Phasmatonycteris*, to which he referred two new species *Phasmatonycteris phiomensis*, from the Early Oligocene site Quarry I of the Gebel Qatrani Formation, and *Phasmatonycteris butleri*, from the Late Eocene site BQ-2 of the Birket Qarun Formation. Simmons et al. (2016) described the new genus and species *Aegyptonycteris knightae*, based on a partial right maxilla from the Late Eocene site BQ-2. This large bat differed considerably from any existing bat family, leading the authors to erect the new family Aegyptonycteridae (Simmons et al., 2016).

4.3.15 Hyaenodonta

Large terrestrial carnivores of the Fayum fauna are represented by the hyaenodonts. The first remains of this extinct group in the Fayum deposits were described by Andrews (1903c), who erected the new “creodont” species *Pterodon africanus* for a partial right mandible. One year later, Andrews (1904f) described another new “creodont” species, *Pterodon macrognathus*, based on a partial left mandible from the Gebel Qatrani Formation. In his monograph about the Fayum fauna, Andrews (1906a) offered detailed descriptions of both previously described carnivorous species, re-examining the generic assignment of the second species and referring to it as *Apterodon macrognathus*. He reported the presence of the genus *Hyaenodon*, based on a partial mandible, and described a new small “creodont” species, *Sinopa ethiopica*, based on a partial left fragment of a mandible (Andrews, 1906a). Shortly after, Osborn (1909) described two complete skulls of *Apterodon macrognathus*, one possibly belonging to a female and the other to a male, two mandibles of *Pterodon africanus*, a slender mandible, which he assigned to a new species, *Pterodon leptognathus*, and a somewhat smaller mandible, on the basis of which he founded the new species *Pterodon phiomensis*. Osborn (1909) also erected the new genus and species *Metasinopa fraasi* and the new species *Hyaenodon brachycephalus*, both based on almost complete mandibles from the Gebel Qatrani Formation. Schlosser (1910) described two new species, *Apterodon altidens* and *Apterodon minutus*, and suggested that a giant “creodont”, like *Palaeonictis* or *Pachyaena*, existed in the Fayum fauna, based on a very large carpal

bone. Schlosser (1911) offered extensive descriptions and comparisons of his new carnivore material from the Fayum Depression. More than half a century later, Simons and Gingerich (1974) founded the new genus and species *Masrasetor aegypticum* on the basis of dental remains from the Gebel Qatrani Formation. Two years later, the same authors (Simons & Gingerich, 1976) described the new carnivore *Apterodon saghensis*, based on a left mandible from the Late Eocene of the Qasr el Sagha Formation. Holroyd (1999) studied the “creodont” assemblage of the Fayum succession and described the new species and included the two species *Metapterodon schlosseri*, and *Metapterodon markgrafi*, both from the Gebel Qatrani Formation, in the genus *Metapterodon*. More recently, Borths et al. (2016) offered a revision of the Fayum hyaenodonts and erected the new genus and species *Brychotherium ephalmos* and the new species *Akhnatnavus nefertiticyon*. One year later, Borths and Seiffert (2017) described the new species *Masrasetor nananubis*, of which complete skulls are known from the Late Eocene site L-41 of the Gebel Qatrani Formation.

Other taxa which had been previously associated with the “creodonts” are the ptolemaiids, which have already been discussed above (e.g. Schlosser, 1911; Simons & Gingerich, 1974). The generic status of the carnivore species has been debated by many authors over the past century and many have been reassigned to new genera, adding to the confusion about the Fayum carnivores (e.g. Holroyd, 1999; Lewis & Morlo, 2010; Morales & Pickford, 2017).

5 Importance of the Fayum Depression for Mammalian Evolution

The Fayum Depression represents the first Paleogene locality that was discovered in Africa. In the early years, the remarkable richness and diversity of the Fayum faunal assemblages sparked the interest of many important vertebrate palaeontologists, who were then involved in the collection and description of the Fayum fossils. These palaeontologists include the British Charles W. Andrews, the Germans Eberhard Fraas, Ernst Stromer von Reichenbach, and Max Schlosser, as well as the American Henry F. Osborn.

These Paleogene deposits in the Fayum Depression yielded the oldest well-documented record of fossil vertebrates from Africa at the time and provided important information on many mammalian groups. The Fayum fossils even led to the establishment of two new orders of mammals: the huge horned Embrithopoda, the ecological affinities of which are not entirely clear, and the small enigmatic Ptolemaiida, whose systematic position is still debated. In addition, numerous new families (e.g. Eremopezidae, Moeritheriidae, Saghatheriidae, Parapithecidae, Propliopithecidae, and Aegyptoncyteridae) and subfamilies (e.g.

Oligopithecinae, Geniohyinae, Titanohyracinae, and Metoldobotinae) were erected for different Fayum taxa. Extremely rich fossil material of clades, such as the proboscideans and cetaceans, helped unravel the origins and early evolutionary histories of these groups. Eocene–Oligocene members of Proboscidea demonstrate the diversity of this group and point to a semi-aquatic lifestyle for some basal representatives such as *Moeritherium*, whereas the cetaceans from the Eocene of the Fayum Depression show how morphologically advanced and diverse their early representatives from this time were. Wadi al Hiton has provided evidence for at least four distinct whale species, *Basilosaurus isis*, *Dorudon atrox*, *Ancalecetus simonsi*, and *Masrasetus markgrafi*. Moreover, the Fayum deposits yielded a remarkable diversity of hyracoids and primates, for which over 30 different species have been named, respectively. Regarding the hyracoids, 10 distinct genera have been erected, to include 37 species (some of which have been synonymised over the years). This high number of taxa likely covered a wide array of ecological niches, from the small-sized *Saghatherium*, weighing below 10 kg, to the large-sized *Titanohyrax*, potentially weighing up to a ton, and from the probably climbing *Dimatherium* to the cursorial, gazelle-sized *Antilohyrax*. The primates from the Fayum Depression have revealed a similar diversity, with about 20 genera, including about 30 species, most of which are still considered valid, representing several different clades. The most common primate group in the Fayum fauna is the Parapithecoidea, which is regarded as a basal group of Anthropoidea and can be divided into the Parapithecidae and Proteopithecidae. This superfamily also includes the first ever described primate from the Fayum Depression, *Apidium phiomense*. Another common family of primates is the Propliopithecidae, known from many species from the Gebel Qatrani Formation. Other primate groups include the Afrotarsiidae, which in the past was regarded as closely related to the extant *Tarsius*, the Lorisiformes, and the Adapidae.

Fossils from the Fayum Depression that were collected at the end of the nineteenth and the beginning of the twentieth century have been distributed throughout many different collections, including some of the largest natural history museums, such as the AMNH, BSPG, MNHN, NHMUK, NHMW, and SMNS. Important collections of Fayum fossils are also housed at the DPC, the Egyptian Geological Museum in Cairo (Egypt) and the Mansoura University Vertebrate Paleontology Center (Egypt). Even in recent years, over one century after the first discovery of fossils in the Fayum Depression, the region continues to yield rich fossil material that keeps providing new insight into vertebrate evolution during the Paleogene. Especially the discovery of rich fossil localities such as L-41 in the Gebel Qatrani Formation and BQ-2 in the Birket Qarun Formation have provided a wealth of information on the faunal

diversity of the Fayum succession and the Paleogene of Africa in general. New cranial material of primates such as *Aegyptopithecus zeuxis* has helped to resolve its phylogenetic relationship to other primates and revealed a pronounced sexual dimorphism. Recently, also the use of new methods such as CT scanning and stable isotope analysis of vertebrate remains has significantly enhanced our understanding of many mammals from the Fayum Depression, including the potential ecology of animals such as *Arsinoitherium*, the anthracotheres, and the hyracoids. As the excavations in the area and the study of old and new fossils from the Fayum with new methods continue, many new and exciting studies are to be expected. The Fayum Depression may continue to shed light on the origin and evolution of many mammalian groups during the Eocene–Oligocene.

Acknowledgements We would like to express our gratitude to H. El Atfy University of Tübingen for his invitation to contribute to this book and his helpful comments. We would like to thank S. Heritage and the Division of Fossil Primates (DPC) for access to the scans of *Aegyptopithecus zeuxis*, I. Werneburg (GPIT) for access to the Fayum material in the GPIT, P. Brewer (NHMUK) for photographs of material housed in the NHMUK, U. Göhlich (NHMW) for access to the Fayum collection of the NHMW, and E. Amson (SMNS) for access to the Fayum collection of the SMNS. This research received support from the SYNTHESYS+ project <http://www.synthesys.info/> which is financed by European Community Research Infrastructure Action under the H2020 Integrating Activities Programme, Project number 823827 (AT-TAF-TA3-9 to PK). We would like to thank Editor Z. Hamimi (Benha University) and the reviewers M. Pickford (MNHN) and S. Sen (MNHN) for helpful comments and suggestions, which greatly improved this chapter.

References

- Abel, O. (1907). Die Stammesgeschichte der Meeressäugetiere. *Meereskunde*, 1, 1–36.
- Al Ashgar, S. F., Sallam, H. M., El-Sayed, S., Antar, M. S. M., & Seiffert, E. R. (2019). A review of Fayum Rodentia. In *The 57th Annual Conference of the Geological Society of Egypt* (p. 20).
- Al-Ashqar, S. F., Seiffert, E. R., de Vries, D., El-Sayed, S., Antar, M. S., & Sallam, H. M. (2021). New phiocricetomyine rodents (*Hystricognathi*) from the Jebel Qatrani Formation, Fayum Depression, Egypt. *PeerJ*, 9, e12074.
- Al-Sayigh, A. R., Nasir, S., Schulp, A. S., & Stevens, N. J. (2008). The first described *Arsinoitherium* from the upper Eocene Aydim Formation of Oman: Biogeographic implications. *Palaeoworld*, 17, 41–46.
- Anan, T., & El Shahat, A. (2014). Provenance and sequence architecture of the Middle-Late Eocene Gehannam and Birket Qarun formations at Wadi Al Hitan, Fayum Province, Egypt. *Journal of African Earth Sciences*, 100, 614–625.
- Andrews, C. W. (1899). Fossil Mammalia from Egypt. *Geological Magazine*, 4, 481–484.
- Andrews, C. W. (1901a). Preliminary note on some recently discovered extinct vertebrates from Egypt. (Part II.). *Geological Magazine*, 4, 436–444.
- Andrews, C. W. (1901b). Über das Vorkommen von Proboscidiern in untertertiären Ablagerungen Aegyptens. *Tageblatt Des V Internationalen Zoologischen-Kongresses, Berlin*, 6, 4–5.
- Andrews, C. W. (1901c). Preliminary note on some recently discovered extinct vertebrates from Egypt. (Part I.). *Geological Magazine*, 4, 400–409.
- Andrews, C. W. (1901d). A new name for an ungulate. *Nature*, 64, 577.
- Andrews, C. W. (1902). Preliminary note on some recently discovered extinct vertebrates from Egypt (Part III.). *Geological Magazine*, 4, 291–295.
- Andrews, C. W. (1903a). On some pleurodiran chelonians from the Eocene of the Fayum, Egypt. *Annals and Magazine of Natural History*, 11, 115–122.
- Andrews, C. W. (1903b). A preliminary notice of a land-tortoise from the Upper Eocene of the Fayûm (11 pp.). National Printing Department.
- Andrews, C. W. (1903c). Notes on an expedition to the Fayûm, Egypt, with descriptions of some new mammals. *Geological Magazine*, 4, 337–343.
- Andrews, C. W. (1904a). Note on the gigantic land tortoise (*Testudo ammon*, Andrews), from the Upper Eocene of Egypt. *Geological Magazine*, 5, 527–530.
- Andrews, C. W. (1904b). On the pelvis and hind-limb of *Mullerornis betsilei* M.-Edw. and Grand.; with a note on the occurrence of a ratite bird in the Upper Eocene Beds of the Fayum, Egypt. *Proceedings of the Zoological Society of London, 1904*, 163–171.
- Andrews, C. W. (1904c). Further notes on the mammals of the Eocene of Egypt. Part II. *Geological Magazine*, 5, 157–162.
- Andrews, C. W. (1904d). Note on the Barypoda, a new order of ungulate mammals. *Geological Magazine*, 5, 481–482.
- Andrews, C. W. (1904e). Further notes on the mammals of the Eocene of Egypt. Part I. *Geological Magazine*, 5, 109–115.
- Andrews, C. W. (1904f). Further notes on the mammals of the Eocene of Egypt. Part III. *Geological Magazine*, 5, 211–215.
- Andrews, C. W. (1905a). Notes on some new Crocodylia from the Eocene of Egypt. *Geological Magazine*, 5, 481–484.
- Andrews, C. W. (1905b). Note on the species of *Palaeomastodon*. *Geological Magazine*, 5, 562–563.
- Andrews, C. W. (1906a). A descriptive catalogue of the Tertiary Vertebrata of the Fayum, Egypt. Order of the Trustees of the British Museum (324 pp.).
- Andrews, C. W. (1906b). A suggested change in nomenclature. *Nature*, 73, 224–224.
- Andrews, C. W., & Beadnell, H. J. L. (1902). A preliminary note on some new mammals from the Upper Eocene of Egypt (9 pp.). Survey Department Egypt.
- Augustin, F. J., Hartung, J., & Kampouridis, P. (2023). Dinosaur faunas of Egypt—the terrestrial late cretaceous vertebrate record. In: Hamimi, Z., Khozyem, H., Adatte, T., Nader, F. H., Obloh-Ikuenobe, F., Zobaa, M. K., & El Atfy, H. (Eds.), *The phanerozoic geology and natural resources of Egypt* (pp. 255–286). Springer. https://doi.org/10.1007/978-3-030-95637-0_9.
- Barnes, L. G., & Mitchell, E. D. (1978). Cetacea. In V. J. Maglio & H. B. S. Cooke (Eds.), *Evolution of African mammals* (pp. 582–602). Harvard University Press.
- Barrow, E., Seiffert, E. R., & Simons, E. L. (2010). A primitive hyracoid (Mammalia, Paenungulata) from the early Priabonian (Late Eocene) of Egypt. *Journal of Systematic Palaeontology*, 8, 213–244.
- Beadnell, H. J. L. (1901). The Fayum depression: A preliminary notice of the geology of a district in Egypt containing a new Palaeogene vertebrate fauna. *Geological Magazine*, 4, 540–546.
- Beadnell, H. J. L. (1902). A preliminary note on *Arsinoitherium Zitteli* Beadnell, from the Upper Eocene Strata of Egypt (4 pp.). Egyptian Survey Department, Public Works Ministry.

- Beadnell, H. J. L. (1905). *The topography and geology of the Fayum Province of Egypt* (101 pp.). Survey Department Egypt.
- Beard, K. C. (2013). Anthropoid origins. In *A companion to paleoanthropology* (pp. 358–375). Wiley.
- Beard, K. C., & Coster, P. M. C. (2016). Upper molar morphology of the Early Oligocene Egyptian anthropoid *Qatrania wingi*. *American Journal of Physical Anthropology*, *159*, 714–721.
- Beard, K. C., Coster, P. M. C., Salem, M. J., Chaimanee, Y., & Jaeger, J.-J. (2016). A new species of *Apidium* (Anthropoidea, Parapitheciidae) from the Sirt Basin, central Libya: First record of Oligocene primates from Libya. *Journal of Human Evolution*, *90*, 29–37.
- Benoit, J., Merigeaud, S., & Tabuce, R. (2013). Homoplasy in the ear region of Tethytheria and the systematic position of Embrithopoda (Mammalia, Afrotheria). *Geobios*, *46*, 357–370.
- Black, C. C. (1978). Anthracotheriidae. In V. J. Maglio & H. B. S. Cooke (Eds.), *Evolution of African mammals* (pp. 423–434). Harvard University Press.
- Blanckenhorn, M. (1900). Neues zur Geologie und Paläontologie Aegyptens II. Das Palaeogen. *Zeitschrift Der Deutschen Geologischen Gesellschaft*, *52*, 403–479.
- Boisserie, J.-R., Lihoreau, F., & Michel, B. (2005). The position of Hippopotamidae within Cetartiodactyla. *Proceedings of the National Academy of Sciences*, *102*, 1537–1541.
- Borths, M. R., Holroyd, P. A., & Seiffert, E. R. (2016). Hyainailourine and teratodontine cranial material from the late Eocene of Egypt and the application of parsimony and Bayesian methods to the phylogeny and biogeography of Hyaenodonta (Placentalia, Mammalia). *PeerJ*, *4*, e2639.
- Borths, M. R., & Seiffert, E. R. (2017). Craniodental and humeral morphology of a new species of *Masrasetor* (Teratodontinae, Hyaenodonta, Placentalia) from the late Eocene of Egypt and locomotor diversity in hyaenodonts. *PLoS ONE*, *12*, e0173527.
- Bown, T. M. (1982). Ichnofossils and rhizoliths of the nearshore fluvial Jebel Qatrani Formation (Oligocene), Fayum Province, Egypt. *Palaeogeography, Palaeoclimatology, Palaeoecology*, *40*, 255–309.
- Bown, T. M., & Kraus, M. D. (1988). *Geology and paleoenvironment of the Oligocene Jebel Qatrani Formation and Adjacent Rocks, Fayum Depression, Egypt* (60 pp.). U.S. Geological Survey.
- Bown, T. M., Kraus, M. J., Wing, S. L., Fleagle, J. G., Tiffney, B. H., Simons, E. L., & Vondra, C. F. (1982). The Fayum primate forest revisited. *Journal of Human Evolution*, *11*, 603–632.
- Bown, T. M., & Simons, E. L. (1984). First record of marsupials (Metatheria: Polyprotodontia) from the Oligocene in Africa. *Nature*, *308*, 447–449.
- Bown, T. M., & Simons, E. L. (1987). New Oligocene Ptolemaïidae (Mammalia: ?Pantolestia) from the Jebel Qatrani Formation, Fayum Depression, Egypt. *Journal of Vertebrate Paleontology*, *7*, 311–324.
- Boyer, D. M., Seiffert, E. R., & Simons, E. L. (2010). Astragalar morphology of *Afradapis*, a large adapiform primate from the earliest late Eocene of Egypt. *American Journal of Physical Anthropology*, *143*, 383–402.
- Brochu, C. A., & Gingerich, P. D. (2000). New tomistomine crocodylian from the Middle Eocene (Bartonian) of Wadi Hitán, Fayum Province, Egypt. *Contributions from the Museum of Paleontology, the University of Michigan*, *30*, 261–268.
- Carroll, R. L. 1988. *Vertebrate paleontology and evolution* (698 pp.). W.H. Freeman.
- Chaimanee, Y., Chavasseau, O., Beard, K. C., Kyaw, A. A., Soe, A. N., Sein, C., Lazzari, V., Marivaux, L., Marandat, B., Swe, M., Rugbumrung, M., Lwin, T., Valentin, X., Zin-Maung-Maung-Thein, & Jaeger, J.-J. (2012). Late Middle Eocene primate from Myanmar and the initial anthropoid colonization of Africa. *Proceedings of the National Academy of Sciences*, *109*, 10293–10297.
- Cherney, M. D., Mantilla, J. A. W., Zalmout, I., Antar, M. S. M., & Gingerich, P. D. (2020). New specimens of the Late Eocene turtle *Cordichelys* (Pleurodira: Podocnemididae) from Wadi Al Hitán and Qasr El-Sagha in the Fayum province of Egypt. *Contributions from the Museum of Paleontology, the University of Michigan*, *33*, 29–64.
- Clementz, M. T., Goswami, A., Gingerich, P. D., & Koch, P. L. (2006). Isotopic records from early whales and sea cows: Contrasting patterns of ecological transition. *Journal of Vertebrate Paleontology*, *26*, 355–370.
- Clementz, M. T., Holroyd, P. A., & Koch, P. L. (2008). Identifying aquatic habits of herbivorous mammals through stable isotope analysis. *Palaios*, *23*, 574–585.
- Cote, S., Werdelin, L., Seiffert, E. R., & Barry, J. C. (2007). Additional material of the enigmatic Early Miocene mammal *Kelba* and its relationship to the order Ptolemaïida. *Proceedings of the National Academy of Sciences*, *104*, 5510–5515.
- Court, N. (1992a). The skull of *Arsinoitherium* (Mammalia, Embrithopoda) and the higher order interrelationships of ungulates. *Palaeovertebrata*, *22*, 1–43.
- Court, N. (1992b). A unique form of dental bilophodonty and a functional interpretation of peculiarities in the masticatory system of *Arsinoitherium* (Mammalia, Embrithopoda). *Historical Biology*, *6*, 91–111.
- Court, N. (1993). Morphology and functional anatomy of the postcranial skeleton in *Arsinoitherium* (Mammalia, Embrithopoda). *Palaeontographica Abteilung A*, *226*, 125–169.
- Crochet, J.-Y., Thomas, H., Sen, S., Rogers, J., Gheerbrant, E., & Al-Sulaimani, Z. (1992). Découverte d'un Péradectidé (Marsupialia) dans l'Oligocène inférieur du Sultanat d'Oman: Nouvelles données sur la paléobiogéographie des Marsupiaux de la plaque arabo-africaine. *Comptes Rendus Hombomadaires Des Séances De L'académie Des Sciences, Paris*, *2*(314), 539–545.
- Dames, W. B. (1883a). Über eine tertiäre Wiberlthierfauna von der westlichen Insel des Birket el Qarun im Fajum (Aegypten). *Sitzungsberichte Der Königlich Preussischen Akademie Der Wissenschaften Zu Berlin*, *1883*, 129–153.
- Dames, W. B. (1883b). Ein Epistropheus von *Zeuglodon* sp. *Sitzungsberichte Der Gesellschaft Naturforschender Freunde*, *1883*, 3.
- Dames, W. B. (1894). Ueber Zeuglodonten aus Aegypten und die Beziehungen der Archeoceten zu den übrigen Cetaceen. *Paläontologische Abhandlungen*, *1*, 189–221.
- Dart, R. A. (1923). The brain of the Zeuglodontinae (Cetacea). *Proceedings of the Zoological Society of London*, *1923*, 615–648.
- de Blieux, D. D., & Simons, E. L. (2002). Cranial and dental anatomy of *Antilohyrax pectidens*: A Late Eocene hyracoid (Mammalia) from the Fayum, Egypt. *Journal of Vertebrate Paleontology*, *22*, 122–136.
- de Bonis, L., Jaeger, J.-J., Coiffat, B., & Coiffat, P. E. (1988). Découverte du plus ancien primate catarrhinien connu dans l'Éocène supérieur d'Afrique du Nord. *Comptes Rendus De L'académie Des Sciences, Séries 2, Paris*, *306*, 929–934.
- de Vries, D., Heritage, S., Borths, M. R., Sallam, H. M., & Seiffert, E. R. (2021). Widespread loss of mammalian lineage and dietary diversity in the early Oligocene of Afro-Arabia. *Communications Biology*, *4*, 1172.
- Delmer, C., Mahboubi, M., Tabuce, R., & Tassy, P. (2006). A new species of *Moeritherium* (Proboscidea, Mammalia) from the Eocene of Algeria: New perspectives on the ancestral morphotype of the genus. *Palaeontology*, *49*, 421–434.
- Depéret, G. (1908). L'histoire géologique et la phylogénie des Anthracothéridés. *Comptes Rendus Hebdomadaires Des Seances De L'académie Des Sciences*, *146*, 158–162.
- Deraniyagala, P. E. P. (1948). Some scientific results of two visits to Africa. *Spolia Zeylanica*, *25*, 1–42.
- Deraniyagala, P. E. P. (1955). *Some extinct elephants* (p. 161). Ceylon National Publications.

- Dineur, H. (1982). Le genre *Brachyodus*, *Anthracotheriidae* (*Artiodactyla*, *Mammalia*) du Miocène inférieur d'Europe et d'Afrique (Ph.D. Dissertation). Université Pierre et Marie Curie, Paris, 180 pp.
- Domning, D. P., & Gingerich, P. D. (1994). *Protosiren smithae*, new species (Mammalia, Sirenia), from the late Middle Eocene of Wadi Hitan, Egypt. *Contributions from the Museum of Paleontology, the University of Michigan*, 29, 69–87.
- Domning, D. P., Gingerich, P. D., Simons, E. L., & Ankel-Simons, F. A. (1994). A new early Oligocene dugongid (Mammalia, Sirenia) from Fayum province, Egypt. *Contributions from the Museum of Paleontology, the University of Michigan*, 29, 89–108.
- Ducrocq, S. (1997). The anthracotherid genus *Bothriogenys* (Mammalia, Artiodactyla) in Africa and Asia during the Paleogene: Phylogenetical and paleobiographical relationship. *Stuttgarter Beiträge Zur Naturkunde, Serie B*, 250, 1–44.
- Ducrocq, S. (2001). Palaeogene anthropoid primates from Africa and Asia: New phylogenetical evidences. *Comptes Rendus De L'académie Des Sciences—Series IIA—Earth and Planetary Science*, 332, 351–356.
- El Adli, J. J., Wilson Mantilla, J. A., Antar, M. S. M., & Gingerich, P. D. (2021). The earliest recorded fossil pelican, recovered from the late Eocene of Wadi Al-Hitan, Egypt. *Journal of Vertebrate Paleontology*, e1903910.
- El Atfy, H., El Beialy, S. Y., El Khoriby, E. M., Uhl, D. (2021). Continental palynomorphs from the Dabaa Formation, North-Western Desert, Egypt: A contribution to the reconstruction of the vegetation on the southern shores of the Tethys Ocean during the Early Oligocene. *Botanical Journal of the Linnean Society*, 197, 291–321.
- El-Sayed, S., Murray, A. M., Kora, M. A., Abu El-Kheir, G. A., Antar, M. S., Seiffert, E. R., & Sallam, H. M. (2020). Oldest Record of African Bagridae and evidence from catfishes for a marine influence in the Late Eocene Birket Qarun Locality 2 (BQ-2), Fayum Depression, Egypt. *Journal of Vertebrate Paleontology*, 40, e1780248.
- El-Shabrawy, G. M., & Dumont, H. J. (2009). The Fayum Depression and its lakes. In H. J. Dumont (Ed.), *The Nile*. Monographiae Biologicae (Vol. 89, pp. 95–124). Springer.
- El-Younsi, A.-R.M., & Salman, A. M. (2021). Sequence stratigraphic framework of the Upper Eocene-Oligocene succession, northwest Birket Qarun. *Fayum-Egypt. Environmental Earth Sciences*, 80, 350.
- Erdal, O., Antoine, P.-O., & Sen, S. (2016). New material of *Palaeoamasia kansui* (Embrithopoda, Mammalia) from the Eocene of Turkey and a phylogenetic analysis of Embrithopoda at the species level. *Palaeontology*, 59, 631–655.
- Filhol, H. (1878). Note sur la découverte d'un nouveau Mammifère marin (*Manatus coulombi*) en Afrique dans les carrières de Mokattam près du Caire. *Bulletin De La Société Philomathique De Paris*, 7, 124–125.
- Fleagle, J. G., & Kay, R. F. (1985). The paleobiology of Catarrhines. In E. Delson (Ed.), *Ancestors: The hard evidence* (pp. 23–36). Alan R. Liss.
- Fleagle, J. G., Kay, R. F., & Simons, E. L. (1980). Sexual dimorphism in early anthropoids. *Nature*, 287, 328–330.
- Fleagle, J. G., & Simons, E. L. (1995). Limb skeleton and locomotor adaptations of *Apidium phiomense*, an Oligocene anthropoid from Egypt. *American Journal of Physical Anthropology*, 97, 235–289.
- Fraas, E. (1904). Neue Zeuglodonten aus dem unteren Mitteleocän vom Mokattam bei Cairo. *Geologisches Centralblatt*, 5, 374.
- Fraas, E. (1906). Wüstenreise eines Geologen in Ägypten. *Kosmos, Handweiser Für Naturfreunde, Stuttgart*, 3, 263–269.
- Gaffney, E. S., Meylan, P. A., Wood, R. C., Simons, E., & De Almeida Campos, D. (2011). Evolution of the side-necked turtles: The family Podocnemididae. *Bulletin of the American Museum of Natural History*, 350, 1–237.
- Gagnon, M. (1997). Ecological diversity and community ecology in the Fayum sequence (Egypt). *Journal of Human Evolution*, 32, 133–160.
- Gameil, M., Al Anbaawy, M., Abdel Fattah, M., & Abu El-Kheir, G. (2016). Lithofacies and biofacies characteristics and whale skeletons distribution in the Eocene rock units of Fayoum Area, Egypt. *Journal of African Earth Sciences*, 116, 42–55.
- Gaudin, T. J., Emry, R. J., & Wible, J. R. (2009). The phylogeny of living and extinct pangolins (Mammalia, Pholidota) and associated taxa: A morphology based analysis. *Journal of Mammalian Evolution*, 16, 235–305.
- Gaudry, A. (1862). *Animaux fossiles et géologie de l'Attique* (472 pp.). F. Savy.
- Gebo, D. L., & Rasmussen, D. T. (1985). The earliest fossil pangolin (Pholidota: Manidae) from Africa. *Journal of Mammalogy*, 66, 538–541.
- Gee, C. T., Sander, P. M., Peters, S. E., El-Hennawy, M. T., Antar, M. S. M., Zalmout, I. S., & Gingerich, P. D. (2019). Fossil burrow assemblage, not mangrove roots: Reinterpretation of the main whale-bearing layer in the late Eocene of Wadi Al-Hitan, Egypt. *Palaeobiodiversity and Palaeoenvironments*, 99, 143–158.
- Gheerbrant, E., Amaghaz, M., Bouya, B., Goussard, F., & Letenneur, C. (2014). *Ocepeia* (Middle Paleocene of Morocco): The oldest skull of an afrotherian mammal. *PLoS ONE*, 9, e89739.
- Gheerbrant, E., Khaldoune, F., Schmitt, A., & Tabuce, R. (2021). Earliest embrithopod mammals (Afrotheria, Tethytheria) from the early Eocene of Morocco: Anatomy, systematics and phylogenetic significance. *Journal of Mammalian Evolution*, 28, 245–283.
- Gheerbrant, E., Schmitt, A., & Kocsis, L. (2018). Early African fossils elucidate the origin of embrithopod mammals. *Current Biology*, 28, 2167–2173.e2.
- Gingerich, P. D. (1992). Marine mammals (Cetacea and Sirenia) from the Eocene of Gebel Mokattam and Fayum, Egypt: Stratigraphy, age, and paleoenvironments. *Papers on Paleontology*, 30, 1–84.
- Gingerich, P. D. (1993). Oligocene age of the Gebel Qatrani Formation, Fayum, Egypt. *Journal of Human Evolution*, 24, 207–218.
- Gingerich, P. D. (2007). *Stromerius nidensis*, new archaeocete (Mammalia, Cetacea) from the Upper Eocene Qasr el-Sagha Formation, Fayum, Egypt. *Contributions from the Museum of Paleontology, the University of Michigan*, 31, 363–378.
- Gingerich, P. D. (2010). Cetacea; pp. In L. Werdelin & W. J. Sanders (Eds.), *Cenozoic mammals of Africa* (pp. 881–908). University of California Press.
- Gingerich, P. D., & Arbor, A. (1978). The Stuttgart collection of Oligocene primates from the Fayum Province of Egypt. *Paläontologische Zeitschrift*, 52, 82–92.
- Gingerich, P. D., & Smith, B. H. (1990). Forelimb and hand of *Basilosaurus isis* (Mammalia, Cetacea) from the middle Eocene of Egypt. *Journal of Vertebrate Paleontology*, 10, 24.
- Gingerich, P. D., Smith, B. H., & Simons, E. L. (1990). Hind limbs of Eocene *Basilosaurus*: Evidence of feet in whales. *Science*, 249, 154–157.
- Gingerich, P. D., & Uhen, M. D. (1996). *Ancalecetus simonsi*, a new dorudontine archaeocete (Mammalia, Cetacea) from the early late Eocene of Wadi Hitan, Egypt. *Contributions from the Museum of Paleontology, the University of Michigan*, 29, 359–401.
- Gohar, A. S., Antar, M. S., Boessenecker, R. W., Sabry, D. A., El-Sayed, S., Seiffert, E. R., Zalmout, I. S., & Sallam, H. M. (2021). A new protocetid whale offers clues to biogeography and feeding ecology in early cetacean evolution. *Proceedings of the Royal Society b: Biological Sciences*, 288, 20211368.
- Gunnell, G. F. (2010). Marsupialia. In L. Werdelin & W. J. Sanders (Eds.), *Cenozoic mammals of Africa* (pp. 77–79). University of California Press.
- Gunnell, G. F., Boyer, D. M., Friscia, A. R., Heritage, S., Manthi, F. K., Miller, E. R., Sallam, H. M., Simmons, N. B., Stevens, N. J., &

- Seiffert, E. R. (2018). Fossil lemurs from Egypt and Kenya suggest an African origin for Madagascar's Aye-aye. *Nature Communications*, 9, 3193.
- Gunnell, G. F., Gingerich, P. D., & Holroyd, P. A. (2010). Ptolemaiida. In L. Werdelin & W. J. Sanders (Eds.), *Cenozoic mammals of Africa* (pp. 83–87). University of California Press.
- Gunnell, G. F., Simons, E. L., & Seiffert, E. R. (2008). New bats (Mammalia: Chiroptera) from the late Eocene and early Oligocene, Fayum Depression, Egypt. *Journal of Vertebrate Paleontology*, 28, 1–11.
- Gunnell, G. F., Simmons, N. B., & Seiffert, E. R. (2014). New Myzopodidae (Chiroptera) from the Late Paleogene of Egypt: Emended Family diagnosis and biogeographic origins of Noctilionoidea. *PLoS ONE*, 9, e86712.
- Gunnell, G. F., Worsham, S. R., Seiffert, E. R., & Simons, E. L. (2009). *Vampyravus orientalis* Schlosser (Chiroptera) from the Early Oligocene (Rupelian), Fayum, Egypt —Body mass, humeral morphology and affinities. *Acta Chiropterologica*, 11, 271–278.
- Haeckel, E. (1866). *Generelle Morphologie Der Organismen*. Verlag von Georg Reimer.
- Harrison, T. (1987). The phylogenetic relationships of the early catarrhine primates: A review of the current evidence. *Journal of Human Evolution*, 16, 41–80.
- Hautier, L., Tabuce, R., Mourlam, M. J., Kassegne, K. E., Amoudji, Y. Z., Orliac, M., Quillévéré, F., Charruault, A.-L., Johnson, A. K. C., & Guinot, G. (2021). New Middle Eocene proboscidean from Togo illuminates the early evolution of the elephantiform-like dental pattern. *Proceedings of the Royal Society b: Biological Sciences*, 288, 20211439.
- Heizmann, E. P. J. (1991). Durch die Wüste. Die Fayum-Expedition von Eberhard Fraas im Jahre 1906. Stuttgarter Beiträge Zur Naturkunde. *Serie C (populärwissenschaftlich)*, 30, 65–70.
- Holmes, R. B., Murray, A. M., Attia, Y. S., Simons, E. L., & Chatrath, P. (2010). Oldest known *Varanus* (Squamata: Varanidae) from the Upper Eocene and Lower Oligocene of Egypt: Support for an African origin of the genus. *Palaeontology*, 53, 1099–1110.
- Holroyd, P. A. (1999). New Pterodontinae (Creodonta: Hyaeodontidae) from the late Eocene–early Oligocene Jebel Qatrani Formation, Fayum Province, Egypt. *PaleoBios*, 19, 1–18.
- Holroyd, P. A. (2010). Macroscelidea. In L. Werdelin & W. J. Sanders (Eds.), *Cenozoic mammals of Africa* (pp. 89–98). University of California Press.
- Holroyd, P. A., Lihoreau, F., Gunnell, G. F., & Miller, E. (2010). Anthracotheriidae. In L. Werdelin & W. J. Sanders (Eds.), *Cenozoic mammals of Africa* (pp. 851–860). University of California Press.
- Holroyd, P. A., & Parham, J. F. (2003). The antiquity of African tortoises. *Journal of Vertebrate Paleontology*, 23, 688–690.
- Holroyd, P. A., Simons, E. L., Bown, T. M., Polly, P. D., & Kraus, M. D. (1996). New record of terrestrial mammals from the Upper Eocene Qasr el Sagha Formation, Fayum Depression, Egypt. *Palaeovertebrata*, 25, 175–192.
- Hooker, J. J., Sánchez-Villagra, M. R., Goin, F. J., Simons, E. L., Attia, Y., & Seiffert, E. R. (2008). The origin of Afro-Arabian “didelphimorph” marsupials. *Palaeontology*, 51, 635–648.
- Jaeger, J.-J., Beard, K. C., Chaimanee, Y., Salem, M., Benammi, M., Hlal, O., Coster, P., Bilal, A. A., Düringer, P., Schuster, M., Valentin, X., Marandat, B., Marivaux, L., Métais, E., Hammuda, O., & Brunet, M. (2010). Late middle Eocene epoch of Libya yields earliest known radiation of African anthropoids. *Nature*, 467, 1095–1098.
- Kappelman, J. (1992). The age of the Fayum primates as determined by paleomagnetic reversal stratigraphy. *Journal of Human Evolution*, 22, 495–503.
- Kappelman, J., Rasmussen, D. T., Sanders, W. J., Feseha, M., Bown, T., Copeland, P., Crabaugh, J., Fleagle, J., Glantz, M., Gordon, A., Jacobs, B., Maga, M., Muldoon, K., Pan, A., Pyne, L., Richmond, B., Ryan, T., Seiffert, E. R., Sen, S., ... Winkler, A. (2003). Oligocene mammals from Ethiopia and faunal exchange between Afro-Arabia and Eurasia. *Nature*, 426, 549–552.
- Kappelman, J., Simons, E. L., & Swisher, C. C. (1992). New age determinations for the Eocene-Oligocene boundary sediments in the Fayum Depression, Northern Egypt. *The Journal of Geology*, 100, 647–667.
- Kay, R. F., Fleagle, J. G., & Simons, E. L. (1981). A revision of the Oligocene apes of the Fayum Province, Egypt. *American Journal of Physical Anthropology*, 55, 293–322.
- Kellogg, R. (1936). A review of the Archaeoceti. *Carnegie Institution of Washington Publications*, 482, 1–366.
- King, C., Underwood, C., & Steurbaut, E. (2014). Eocene stratigraphy of the Wadi Al-Hitan World Heritage Site and adjacent areas (Fayum, Egypt). *Stratigraphy*, 11, 185–234.
- Kirk, E. C., & Simons, E. L. (2001). Diets of fossil primates from the Fayum Depression of Egypt: A quantitative analysis of molar shearing. *Journal of Human Evolution*, 40, 203–229.
- von Koenigswald, W. (2013). Unique differentiation of radial enamel in *Arsinoitherium* (Embrithopoda, Tethytheria). *Historical Biology*, 25, 183–192.
- Kortlandt, A. (1980). The Fayum primate forest: Did it exist? *Journal of Human Evolution*, 9, 277–297.
- Lambrecht, K. (1929). Ergebnisse der Forschungsreisen Prof. E. Stromers in den Wüsten Ägyptens. V. Tertiäre Wirbeltiere. 4. *Stromeria fajumensis* n.g., n.sp. die kontinentale Stammform der Aepyornithidae, mit einer Übersicht über die fossilen Vögel Madagaskars und Afrikas. *Abhandlungen Der Bayerischen Akademie Der Wissenschaften*, 4, 1–18.
- Lambrecht, K. (1930). Studien über fossile Riesenvogel. *Geologica Hungarica, Series Palaeontologica*, 7, 1–37.
- Lankester, E. R. (1903). *A new extinct monster* (238 pp.). Sphere.
- Lapparent de Broin, F. (2000). African chelonians from the Jurassic to the present: Phases of development and preliminary catalogue of the fossil record. *Palaeontologia Africana*, 36, 43–82.
- Lewis, M. E., & Morlo, M. (2010). Creodonta: pp. In L. Werdelin & W. J. Sanders (Eds.), *Cenozoic mammals of Africa* (pp. 549–566). University of California Press.
- Lihoreau, F., & Ducrocq, S. (2007). Family Anthracotheriidae. In *The evolution of artiodactyls* (pp. 89–105). The Johns Hopkins University Press.
- Liu, A. G. S. C., Seiffert, E. R., & Simons, E. L. (2008). Stable isotope evidence for an amphibious phase in early proboscidean evolution. *Proceedings of the National Academy of Sciences*, 105, 5786–5791.
- Lucas, F. A. (1898). A new snake from the Eocene of Alabama. *Proceedings of the United States National Museum*, 21, 637–638.
- Luo, Z., & Gingerich, P. D. (1999). Terrestrial Mesonychia to aquatic Cetacea: Transformation of the basicranium and evolution of hearing in whales. *University of Michigan Papers on Paleontology*, 31, 1–98.
- Maas, M. C., Thewissen, J. G. M., & Kappelman, J. (1998). *Hypsamasia seni* (Mammalia: Embrithopoda) and other mammals from the Eocene Kartal Formation of Turkey. *Bulletin of Carnegie Museum of Natural History*, 34, 286–297.
- MacPhee, R. D. E., & Raholimavo, E. M. (1988). Modified subfossil aye-aye incisors from outwestern Madagascar: Species allocation and paleoecological significance. *Folia Primatologica*, 51, 126–142.
- Matsumoto, H. (1921). *Megalohyrax* Andrews and *Titanohyrax* g. n.—A revision of the genera of hyracoids from the Fayum, Egypt. *Proceedings of the Zoological Society of London*, 1921, 839–850.
- Matsumoto, H. (1922). Revision of *Palaeomastodon* and *Moeritherium*. *Palaeomastodon intermedius*, and *Phiomia osborni*. *American Museum Novitates*, 51, 1–6.

- Matsumoto, H. (1923). A contribution to the knowledge of *Moeritherium*. *Bulletin of the American Museum of Natural History*, 48, 97–139.
- Matsumoto, H. (1926). Contribution to the knowledge of the fossil Hyracoidea of the Fayum, Egypt, with description of several new species. *Bulletin of the American Museum of Natural History*, 56, 253–350.
- Matthew, W. D. (1918). A revision of the Lower Eocene Wasatch and Wind River faunas. Part V. Insectivora (continued), Glires, Edentata. *Bulletin of the American Museum of Natural History*, 38, 565–657.
- Matthew, W. D., & Granger, W. (1925). Fauna and correlation of the Gashato Formation of Mongolia. *American Museum Novitates*, 189, 1–12.
- Mattingly, S. G., Beard, K. C., Coster, P. M. C., Salem, M. J., Chaimanee, Y., & Jaeger, J.-J. (2021). A new parapithecine (Primates: Anthropeidea) from the early Oligocene of Libya supports parallel evolution of large body size among parapithecids. *Journal of Human Evolution*, 153, 102957.
- McCartney, J. A., & Seiffert, E. R. (2016). A late Eocene snake fauna from the Fayum Depression, Egypt. *Journal of Vertebrate Paleontology*, 36, e1029580.
- McKenna, M. C., & Manning, E. (1977). Affinities and palaeobiogeographic significance of the Mongolian Paleogene genus *Phenaccolophus*. *Geobios*, 10, 61–85.
- Meyer, G. E. (1973). A new Oligocene hyrax from the Jebel el Qatrani Formation Fayum Egypt. *Postilla*, 163, 1–11.
- Miller, E. R., Rasmussen, D. T., Kappelman, J., Friscia, A. R., Muteti, S. N., & Gutierrez, M. (2015). *Ptolemaia* from West Turkana, Kenya. *Bulletin of the Peabody Museum of Natural History*, 56, 81–88.
- Miller, E. R., Rasmussen, D. T., & Simons, E. L. (1997). Fossil Storks (Ciconiidae) from the Late Eocene and Early Miocene of Egypt. *Ostrich*, 68, 23–26.
- Miller, E. R., & Simons, E. L. (1997). Dentition of *Proteopithecus sylviae*, an archaic anthropoid from the Fayum, Egypt. *Proceedings of the National Academy of Sciences*, 94, 13760–13764.
- Morales, J., & Pickford, M. (2017). New hyaenodonts (Ferae, Mammalia) from the Early Miocene of Napak (Uganda), Koru (Kenya) and Grillentale (Namibia). *Fossil Imprint*, 73, 332–359.
- Morgan, V. L., & Lucas, S. G. (2002). Notes From Diary-Fayum Trip, 1907. *Bulletin of the New Mexico Museum of Natural History and Science*, 22, 1–148.
- Moustafa, Y. S. (1954). Additional information on the skull of *Prozeuglodon isis* and the morphological history of the Archaeoceti. *Proceedings of the Egyptian Academy of Sciences*, 9, 80–88.
- Moustafa, Y. S. (1974). Studies on the palaeopathology and taxonomic problems of some Fayum fossil vertebrates, Part II: Palaeornithological taxonomy and the first Fayum fossil egg shells. *Annals of the Geological Survey of Egypt*, 4, 142–145.
- Moustapha, W. (1955). An interpretation of *Arsinoitherium*. *Bulletin, Institut D'egypte*, 36, 111–118.
- Müller, L. (1927). Ergebnisse der Forschungsreisen Prof. E. Stromers in den Wüsten Ägyptens. V. Tertiäre Wirbeltiere. I. Beiträge zur Kenntnis der Krokodilier des ägyptischen Tertiärs. *Abhandlungen Der Bayerischen Akademie Der Wissenschaften*, 31, 1–96.
- Murray, A. M. (2004). Late Eocene and early Oligocene teleost and associated ichthyofauna of the Jebel Qatrani Formation, Fayum, Egypt. *Palaeontology*, 47, 711–724.
- Murray, A. M., Cook, T. D., Attia, Y. S., Chatrath, P., & Simons, E. L. (2010). A freshwater ichthyofauna from the late Eocene Birket Qarun Formation, Fayum, Egypt. *Journal of Vertebrate Paleontology*, 30, 665–680.
- Nishihara, H., Satta, Y., Nikaido, M., Thewissen, J. G. M., & Stanhope, M. J. (2005). A retroposon analysis of afrotherian phylogeny. *Molecular Biology and Evolution*, 22, 1823–1833.
- Orlebar, A. B. (1845). Some observations on the geology of the Egyptian desert. *Journal of the Bombay Branch of the Royal Society*, 2, 229–250.
- Osborn, H. F. (1899). On *Pliohyrax kruppi* Osborn, a fossil hyracoid from Samos, Lower Pliocene in the Stuttgart collection. A new type and first known Tertiary hyracoid. In *Proceedings of the 4th International Congress of Zoology* (pp. 172–173).
- Osborn, H. F. (1907). The Fayûm expedition of the American Museum. *Science*, 25, 513–516.
- Osborn, H. F. (1908). New fossil mammals from the Fayûm Oligocene, Egypt. *Bulletin of the American Museum of Natural History*, 24, 265–272.
- Osborn, H. F. (1909). New carnivorous mammals from the Fayûm Oligocene, Egypt. *Bulletin of the American Museum of Natural History*, 26, 415–424.
- Owen, R. (1875). On fossil evidences of a sirenian mammal (*Eotherium aegypticum*, Owen) from the nummulitic Eocene of the Mokattam cliffs, near Cairo. *Quarterly Journal of the Geological Society of London*, 31, 100–105.
- Ozansoy, F. (1966). Türkiye Senozoik çağlarında fosil insan formu problemi ve biostratigrafi dayanakları. *Ankara Üniversitesi D.t.c.f. Yayınları*, 172, 1–104.
- Palmer, T. S. (1899). Catalogus Mammalium tam viventium quam fossilium. *Science*, 10, 491–495.
- Petronievics, B. (1923). II—Remarks upon the skulls of *Moeritherium* and *Palaeomastodon*. *Annals and Magazine of Natural History*, 12, 55–61.
- Pickford, M. (1986). Première découverte d'une faune mammalienne terrestre paléogène d'Afrique sub-saharienne. *Comptes Rendus De L'académie Des Sciences, Série 2, Paris*, 302, 1205–1210.
- Pickford, M. (2015a). Cenozoic geology of the Northern Sperrgebiet, Namibia, accenting the Palaeogene. *Communications of the Geological Survey of Namibia*, 16, 10–104.
- Pickford, M. (2015b). Large ungulates from the basal Oligocene of Oman: 1—Embrithopoda. *Spanish Journal of Palaeontology*, 30, 33.
- Pickford, M. (2017). *Arsinoitherium* (Embrithopoda) and other large mammals and plants from the Oligocene of Tunisia. *Fossil Imprint*, 73, 172–181.
- Pickford, M. (2018). Fossil fruit bat from the Ypresian/Lutetian of Black Crow, Namibia. *Communications of the Geological Survey of Namibia*, 18, 64–71.
- Pickford, M., Kaya, T., Mayda, S., & Yilmaz Usta, N. D. (2021). A new look at Eurasian Neogene Pliohyracidae (Afrotheria, Hyracoidea). *Münchner Geowissenschaftliche Abhandlungen A*, 52, 1–47.
- Pickford, M., Senut, B., Morales, J., Mein, P., & Sanchez, I. M. (2008). Mammalia from the Lutetian of Namibia. *Memoir Geological Survey of Namibia*, 20, 465–514.
- Pilleri, G. E. (1991). Betrachtungen über das Gehirn der Archaeoceti (Mammalia, Cetacea) aus dem Fayûm Ägyptens. *Investigations on Cetacea, Paciano*, 23, 193–211.
- Prothero, D. R., & Schoch, R. M. (2002). *Horns, tusks, and flippers: The evolution of hoofed mammals* (327 pp.). The Johns Hopkins University Press.
- Radulescu, C., Iliescu, G., & Iliescu, M. (1976). Un Embrithopode nouveau (Mammalia) dans le Paléogène de la Dépression de Hateg (Roumanie) et la géologie de la région. *Neues Jahrbuch für Geologie und Paläontologie, Monatshefte*, 11, 690–698.
- Radulescu, C., & Sudre, J. (1985). *Crivadiatherium iliescui* n. sp., nouvel embrithopode (Mammalia) dans le Paléogène ancien de la Dépression de Hateg (Roumanie). *Palaeovertebrata*, 15, 139–157.
- Rasmussen, D. T., Bown, T. M., & Simons, E. L. (1992). 28. The Eocene-Oligocene transition in continental Africa. In D. R. Prothero, & W. A. Berggren (Eds.), *Eocene-Oligocene climatic and biotic evolution* (pp. 548–566). Princeton University Press.

- Rasmussen, D. T., & Gutiérrez, G. (2010). Hyracoidea. In L. Werdelin & W. J. Sanders (Eds.), *Cenozoic mammals of Africa* (pp. 123–145). University of California Press.
- Rasmussen, D. T., Olson, S. L., & Simons, E. L. (1987). Fossil birds from the Oligocene Jebel Qatrani Formation Fayum Province, Egypt. *Smithsonian Contributions to Paleobiology*, 1–20.
- Rasmussen, D. T., & Simons, E. L. (1988a). New Oligocene hyracoids from Egypt. *Journal of Vertebrate Paleontology*, 8, 67–83.
- Rasmussen, D. T., & Simons, E. L. (1988b). New specimens of *Oligopithecus savagei*, Early Oligocene primate from the Fayum, Egypt. *Folia Primatologica*, 51, 182–208.
- Rasmussen, D. T., & Simons, E. L. (1991). The oldest Egyptian hyracoids (Mammalia: Pliohyracidae): New species of *Saghatarium* and *Thyrohyrax* from the Fayum. *Neues Jahrbuch für Geologie und Paläontologie, Abhandlungen*, 182, 187–209.
- Rasmussen, D. T., & Simons, E. L. (2000). Ecomorphological diversity among Paleogene hyracoids (Mammalia): A new cursorial browser from the Fayum, Egypt. *Journal of Vertebrate Paleontology*, 20, 167–176.
- Rasmussen, D. T., Simons, E. L., Hertel, F., & Judd, A. (2001). Hindlimb of a giant terrestrial bird from the upper Eocene, Fayum, Egypt. *Palaeontology*, 44, 325–337.
- Rio, J. P., & Mannion, P. D. (2017). The osteology of the giant snake *Gigantophis garstini* from the upper Eocene of North Africa and its bearing on the phylogenetic relationships and biogeography of Madtsoiidae. *Journal of Vertebrate Paleontology*, 37, e1347179.
- Rose, K. D. (2006). *The beginning of the age of mammals* (428 pp.). Johns Hopkins Univ. Press.
- Rosina, V. V., & Pickford, M. (2019). Preliminary overview of the fossil record of bats (Chiroptera, Mammalia) from the Miocene sites of Otavi Mountainland (Northern Namibia). *Communications of the Geological Survey of Namibia*, 21, 48–58.
- Roussiakis, S., Filis, P., Sklavounou, S., Giaourtsakis, I. X., Kargopoulos, N., & Theodorou, G. (2019). Pikermi: A classical European fossil mammal geotope in the spotlight. *European Geologist*, 48, 28–32.
- Said, R. (1962). *The geology of Egypt* (377 pp.). Elsevier Pub. Co.
- Salem, R. (1976). Evolution of Eocene-Miocene sedimentation patterns in parts of Northern Egypt. *AAPG Bulletin*, 60, 34–64.
- Sallam, H. M., & Seiffert, E. R. (2016). New phiomorph rodents from the latest Eocene of Egypt, and the impact of Bayesian “clock”-based phylogenetic methods on estimates of basal hystricognath relationships and biochronology. *PeerJ*, 4, e1717.
- Sallam, H. M., & Seiffert, E. R. (2019). Revision of Oligocene ‘*Paraphiomys*’ and an origin for crown Thryonomyoidea (Rodentia: Hystricognathi: Phiomorpha) near the Oligocene–Miocene boundary in Africa. *Zoological Journal of the Linnean Society*, 20.
- Sallam, H. M., Seiffert, E. R., & Simons, E. L. (2010a). A highly derived anomalurid rodent (Mammalia) from the earliest Late Eocene of Egypt. *Palaeontology*, 53, 803–813.
- Sallam, H. M., Seiffert, E. R., & Simons, E. L. (2010b). A large-bodied anomaluroid rodent from the earliest late Eocene of Egypt: Phylogenetic and biogeographic implications. *Journal of Vertebrate Paleontology*, 30, 16.
- Sallam, H. M., Seiffert, E. R., & Simons, E. L. (2011). Craniodental morphology and systematics of a new family of hystricognathous rodents (Gaudeamuridae) from the Late Eocene and Early Oligocene of Egypt. *PLoS ONE*, 6, e16525.
- Sallam, H. M., Seiffert, E. R., & Simons, E. L. (2012). A basal phiomorph (Rodentia, Hystricognathi) from the late Eocene of the Fayum Depression. *Egypt. Swiss Journal of Palaeontology*, 131, 283–301.
- Sallam, H. M., Seiffert, E. R., Steiper, M. E., & Simons, E. L. (2009). Fossil and molecular evidence constrain scenarios for the early evolutionary and biogeographic history of hystricognathous rodents. *Proceedings of the National Academy of Sciences*, 106, 16722–16727.
- Sánchez-Villagra, M. R., Seiffert, E. R., Martin, T., Simons, E. L., Gunnell, G. F., & Attia, Y. (2007). Enigmatic new mammals from the late Eocene of Egypt. *Paläontologische Zeitschrift*, 81, 406–415.
- Sanders, W. J., Gheerbrant, E., Harris, J. M., Saegusa, H., & Delmer, C. (2010b). Proboscidea. In L. Werdelin & W. J. Sanders (Eds.), *Cenozoic mammals of Africa* (pp. 161–251). University of California Press.
- Sanders, W. J., Kappelman, J., & Rasmussen, D. T. (2004). New large-bodied mammals from the late Oligocene site of Chilga, Ethiopia. *Acta Palaeontologica Polonica*, 49, 365–392.
- Sanders, W. J., Nemeč, W., Aldinucci, M., Janbu, N. E., & Ghinassi, M. (2014). Latest evidence of *Palaeoamasia* (Mammalia, Embrithopoda) in Turkish Anatolia. *Journal of Vertebrate Paleontology*, 34, 1155–1164.
- Sanders, W. J., Rasmussen, D. T., & Kappelman, J. (2010a). Embrithopoda. In L. Werdelin & W. J. Sanders (Eds.), *Cenozoic mammals of Africa* (pp. 115–122). University of California Press.
- Schlosser, M. (1905). Review of “C. W. Andrews: Notes on an Expedition to the Fayum, Egypt, with descriptions of some new mammals. (The Geol. Mag. Decade IV. 10. 1903. 337–343, 3 Fig.)” *Neues Jahrbuch für Mineralogie, Geognosie, Geologie und Petrefaktenkunde*, 1, 156–157.
- Schlosser, M. (1910). Über einige fossile Säugetiere aus dem Oligocän von Ägypten. *Zoologischer Anzeiger*, 34, 500–508.
- Schlosser, M. (1911). Beiträge zur Kenntnis der Oligozänen Land-Säugetiere aus dem Fayum: Ägypten. *Beiträge Zur Paläontologie Und Geologie Österreich-Ungarns Und Des Orients*, 24, 51–167.
- Schmidt, M. (1913). Über Paarhufer der fluviomarinen Schichten des Fayum. *Geologische Paläontologische Abhandlungen*, 15, 1–112.
- Schwartz, G. T., Rasmussen, D. T., & Smith, R. J. (1995). Body-size diversity and community structure of fossil hyracoids. *Journal of Mammalogy*, 76, 1088–1099.
- Schweinfurth, G. (1886). Reise in das Depressionsgebiet im Umkreise des Fayum. *Zeitschrift Der Gesellschaft Für Erdkunde Berlin*, 21, 96–149.
- Seiffert, E. R. (2006). Revised age estimates for the later Paleogene mammal faunas of Egypt and Oman. *Proceedings of the National Academy of Sciences*, 103, 5000–5005.
- Seiffert, E. R. (2007). A new estimate of afrotherian phylogeny based on simultaneous analysis of genomic, morphological, and fossil evidence. *BMC Evolutionary Biology*, 7, 224.
- Seiffert, E. R. (2010). The oldest and youngest records of afrotheric placentals from the Fayum Depression of northern Egypt. *Acta Palaeontologica Polonica*, 55, 599–616.
- Seiffert, E. R. (2012). Early primate evolution in Afro-Arabia. *Evolutionary Anthropology: Issues, News, and Reviews*, 21, 239–253.
- Seiffert, E. R., Bown, T. M., Clyde, W. C., & Simons, E. (2008). Geology, paleoenvironment, and age of Birket Qarun locality 2 (BQ-2), Fayum Depression, Egypt. In *Elwyn Simons: A search for origins. Developments in primatology: Progress and prospects* (pp. 71–86). Springer.
- Seiffert, E. R., Boyer, D. M., Fleagle, J. G., Gunnell, G. F., Heesy, C. P., Perry, J. M. G., & Sallam, H. M. (2018). New adapiform primate fossils from the late Eocene of Egypt. *Historical Biology*, 30, 204–226.
- Seiffert, E. R., Nasir, S., Al-Harthy, A., Groenke, J. R., Kraatz, B. P., Stevens, N. J., & Al-Sayigh, A. R. (2012). Diversity in the later Paleogene proboscidean radiation: A small barytheriid from the Oligocene of Dhofar Governorate, Sultanate of Oman. *Naturwissenschaften*, 99, 133–141.

- Seiffert, E. R., Perry, J. M. G., Simons, E. L., & Boyer, D. M. (2009). Convergent evolution of anthropoid-like adaptations in Eocene adapiform primates. *Nature*, *461*, 1118–1121.
- Seiffert, E. R., & Simons, E. L. (2000). *Widanelfarasia*, a diminutive placental from the late Eocene of Egypt. *Proceedings of the National Academy of Sciences*, *97*, 2646–2651.
- Seiffert, E. R., Simons, E. L., & Attia, Y. (2003). Fossil evidence for an ancient divergence of lorises and galagos. *Nature*, *422*, 421–424.
- Seiffert, E. R., Simons, E. L., Boyer, D. M., Perry, J. M. G., Ryan, T. M., & Sallam, H. M. (2010). A fossil primate of uncertain affinities from the earliest late Eocene of Egypt. *Proceedings of the National Academy of Sciences*, *107*, 9712–9717.
- Seiffert, E. R., Simons, E. L., Clyde, W. C., Rossie, J. B., Attia, Y. S., Bown, T. M., Chatrath, P., & Mathison, M. E. (2005). Basal anthropoids from Egypt and the antiquity of Africa's higher primate radiation. *Science*, *310*, 300–304.
- Seiffert, E. R., Simons, E. L., Ryan, T. M., Bown, T. M., & Attia, Y. (2007). New remains of Eocene and Oligocene Afrosoricida (Afrotheria) from Egypt, with implications for the origin(s) of afrosoricid zalambdodonty. *Journal of Vertebrate Paleontology*, *27*, 963–972.
- Seiffert, E. R., Tejedor, M. F., Fleagle, J. G., Novo, N. M., Cornejo, F. M., Bond, M., de Vries, D., & Campbell, K. E. (2020). A parapihithicid stem anthropoid of African origin in the Paleogene of South America. *Science*, *368*, 194–197.
- Sen, S. (2013). Dispersal of African mammals in Eurasia during the Cenozoic: Ways and whys. *Geobios*, *46*, 159–172.
- Sen, S., & Heintz, E. (1979). *Palaeoamasia kansui* Ozansoy 1966, Embrithopode (Mammalia) de l'Éocène d'Anatolie. *Annales De Paléontologie (vertébrés)*, *65*, 73–91.
- Senut, B., & Pickford, M. (2021). Micro-cursorial mammals from the late Eocene tufas at Eocliff, Namibia. *Communications of the Geological Survey of Namibia*, *23*, 90–160.
- Sickenberg, O. (1934). Beiträge zur Kenntnis Tertiärer Sirenen. I. Die Eozänen Sirenen des Mittelmeergebietes; II. Die Sirenen des Belgischen Tertiärs. *Mémoires Du Musée Royal d'Histoire Naturelle de Belgique*, *63*, 1–352.
- Sigé, B. (1985). Les chiroptères oligocènes du Fayum, Egypte. *Geologica et Palaeontologica*, *161*–189.
- Sileem, A. H., Sallam, H. M., Hewaidy, A. G. A., & Miller, E. R. (2015). Anthracotheres (Mammalia, Artiodactyla) from the upper-most horizon of the Jebel Qatrani Formation, latest Early Oligocene, Fayum Depression, Egypt. *Egyptian Journal of Paleontology*, *15*, 1–11.
- Sileem, A. H., Sallam, H. M., Hewaidy, A. G. A., Miller, R., & Gunnell, G. F. (2016). A new anthracothere (Artiodactyla) from the early Oligocene, Fayum, Egypt, and the mystery of African 'Rhagatherium' solved. *Journal of Paleontology*, *90*, 170–181.
- Simons, E. L. (1959). An anthropoid frontal bone from the Fayum Oligocene of Egypt: The oldest skull fragment of a higher primate. *American Museum Novitates*, *1976*, 1–16.
- Simons, E. L. (1960). *Apidium* and *Oreopithecus*. *Nature*, *186*, 824–826.
- Simons, E. L. (1962). Two new primate species from the African Oligocene. *Postilla*, *64*, 1–12.
- Simons, E. L. (1965). New fossil apes from Egypt and the initial differentiation of Hominoidea. *Nature*, *205*, 135–139.
- Simons, E. L. (1967). Review of the phyletic interrelationships of Oligocene and Miocene Old World Anthropoidea. *Colloques Internationaux Du CNRS*, *163*, 597–602.
- Simons, E. L. (1968). Early Cenozoic mammalian faunas, Fayum Province, Egypt, Part I. African Oligocene Mammals. Introduction history of study and faunal succession. *Bulletin of the Peabody Museum of Natural History*, *28*, 1–21.
- Simons, E. L. (1974). *Parapithecus grangeri* (Parapithecidae, Old World higher primates) new species from the Oligocene of Egypt and the initial differentiation of Cercopithecoidea. *Postilla*, *166*, 1–12.
- Simons, E. L. (1986). *Parapithecus grangeri* of the African Oligocene: An archaic catarrhine without lower incisors. *Journal of Human Evolution*, *15*, 205–213.
- Simons, E. L. (1987). New faces of *Aegyptopithecus* from the Oligocene of Egypt. *Journal of Human Evolution*, *16*, 273–289.
- Simons, E. L. (1989). Description of two genera and species of late Eocene Anthropoidea from Egypt. *Proceedings of the National Academy of Sciences*, *86*, 9956–9960.
- Simons, E. L. (1992). Diversity in the early Tertiary anthropoidean radiation in Africa. *Proceedings of the National Academy of Sciences*, *89*, 10743–10747.
- Simons, E. L. (1995a). Crania of *Apidium*: Primitive anthropoidean (Primates, Parapithecidae) from the Egyptian Oligocene. *American Museum Novitates*, *3124*, 1–10.
- Simons, E. L. (1995b). Egyptian Oligocene primates: A review. *American Journal of Physical Anthropology*, *38*, 199–238.
- Simons, E. L. (1997a). Preliminary description of the cranium of *Proteopithecus sylviae*, an Egyptian late Eocene anthropoidean primate. *Proceedings of the National Academy of Sciences*, *94*, 14970–14975.
- Simons, E. L. (1997b). Discovery of the smallest Fayum Egyptian primates (Anchomomyini, Adapidae). *Proceedings of the National Academy of Sciences*, *94*, 180–184.
- Simons, E. L. (2001). The cranium of *Parapithecus grangeri*, an Egyptian Oligocene anthropoidean primate. *Proceedings of the National Academy of Sciences*, *98*, 7892–7897.
- Simons, E. L. (2008). Eocene and Oligocene mammals of the Fayum, Egypt. In J. G. Fleagle, & C. C. Gilbert (Eds.), *Elwyn Simons: A search for origins. Developments in primatology: Progress and prospects* (pp. 87–105). Springer.
- Simons, E. L., & Bown, T. M. (1984). A new species of *Peratherium* (Didelphidae; Polyprotodonta): The first African marsupial. *Journal of Mammalogy*, *65*, 539–548.
- Simons, E. L., & Bown, T. M. (1985). *Afrotarsius chatrathi*, first tarsiiform primate (? Tarsiidae) from Africa. *Nature*, *313*, 475–477.
- Simons, E. L., & Bown, T. M. (1995). *Ptolemaiida*, a new order of Mammalia—With description of the cranium of *Ptolemaiia grangeri*. *Proceedings of the National Academy of Sciences*, *92*, 3269–3273.
- Simons, E. L., Holroyd, P. A., & Bown, T. M. (1991). Early Tertiary elephant-shrews from Egypt and the origin of the Macroscelideae. *Proceedings of the National Academy of Sciences*, *88*, 9734–9737.
- Simons, E. L., & Gingerich, P. D. (1974). New carnivorous mammals from the Oligocene of Egypt. *Annals of the Geological Survey of Egypt*, *4*, 157–166.
- Simons, E. L., & Gingerich, P. D. (1976). A new species of *Apterodon* (Mammalia, Creodonta) from the Upper Eocene Qasr el-Sagha Formation of Egypt. *Postilla*, *168*, 1–9.
- Simons, E. L., & Kay, R. F. (1983). *Qatrania*, new basal anthropoid primate from the Fayum, Oligocene of Egypt. *Nature*, *304*, 624–626.
- Simons, E. L., & Kay, R. F. (1988). New material of *Qatrania* from Egypt with comments on the phylogenetic position of the Parapithecidae (Primates, Anthropoidea). *American Journal of Primatology*, *15*, 337–347.
- Simons, E. L., & Rasmussen, D. T. (1990). Vertebrate paleontology of Fayum: History of research, faunal review and future prospects. In *The geology of Egypt* (pp. 627–638). A. A. Balkema.
- Simons, E. L., & Rasmussen, D. T. (1991). The generic classification of Fayum Anthropoidea. *International Journal of Primatology*, *12*, 163–178.

- Simons, E. L., Rasmussen, D. T., & Gebro, D. L. (1987). A new species of *Propliopithecus* from the Fayum, Egypt. *American Journal of Physical Anthropology*, 73, 139–147.
- Simons, E. L., Rasmussen, D. T., & Gingerich, P. D. (1995). New cercamoniine adapid from Fayum, Egypt. *Journal of Human Evolution*, 29, 577–589.
- Simons, E. L., Seiffert, E. R., Chatrath, P. S., & Attia, Y. (2001). Earliest record of a parapithecoid anthropoid from the Jebel Qatrani Formation, northern Egypt. *Folia Primatologica*, 72, 316–331.
- Simmons, N. B., Seiffert, E. R., & Gunnell, G. F. (2016). A new family of large omnivorous bats (Mammalia, Chiroptera) from the late Eocene of the Fayum Depression, Egypt, with comments on use of the name “Eochiroptera.” *American Museum Novitates*, 1–44.
- Simons, E. L., Seiffert, E. R., Ryan, T. M., & Attia, Y. (2007). A remarkable female cranium of the early Oligocene anthropoid *Aegyptopithecus zeuxis* (Catarrhini, Propliopithecidae). *Proceedings of the National Academy of Sciences*, 104, 8731–8736.
- Simons, E. L., & Wood, A. E. (1968). Early Cenozoic mammalian faunas, Fayum Province, Egypt. *Bulletin of the Peabody Museum of Natural History*, 28, 1–105.
- Slijper, E. J. (1936). Die Cetaceen, Vergleichend-Anatomisch und Systematisch. *Capita Zoologica*, 6–7, 1–590.
- Smith, K. T., Bhullar, B.-A.S., & Holroyd, P. A. (2008). Earliest African record of the *Varanus* stem-clade (Squamata: Varanidae) from the early Oligocene of Egypt. *Journal of Vertebrate Paleontology*, 28, 909–913.
- Smith, N. A., Stidham, T. A., & Mitchell, J. S. (2020). The first fossil owl (Aves, Strigiformes) from the Paleogene of Africa. *Diversity*, 12, 163.
- Stefanic, C. M., Nestler, J. H., Seiffert, E. R., & Turner, A. H. (2019). New crocodylomorph material from the Fayum Depression, Egypt, including the first occurrence of a sebecosuchian in African Late Eocene deposits. *Journal of Vertebrate Paleontology*, 39, e1729781.
- Stevens, N. J., O'Connor, P. M., Mtelega, C., & Roberts, E. M. (2021). Macroscelideans (Myohyracinae and Rhynchocyoninae) from the late Oligocene Nsungwe formation of the Rukwa Rift Basin, southwestern Tanzania. *Historical Biology*, 1–7.
- Stidham, T., & Smith, N. (2015). An ameghinornithid-like bird (Aves, Cariamae, ?Ameghinornithidae) from the early Oligocene of Egypt. *Palaeontologia Electronica* 18.1.5A, 1–8.
- Stromer, E. (1902). Bericht über eine von den Privatdozenten Dr. Max Blanckenhorn und Dr. Ernst Stromer von Reichenbach ausgeführte Reise nach Aegypten. *Sitzungsberichte Der Mathematisch-Physikalischen Classe Der Königlichen Bayerischen Akademie Der Wissenschaften München*, 32, 341–352.
- Stromer, E. (1903). *Zeuglodon*-Reste aus dem oberen Mitteleocän des Fajûm. *Beiträge Zur Paläontologie Und Geologie Österreich-Ungarns Und Des Orients*, 15, 65–99.
- Stromer, E. (1904). Bericht über die Sammlungsergebnisse einer paläontologisch-geologischen Forschungsreise nach Ägypten. *Bericht Der Senckenbergischen Naturforschenden Gesellschaft in Frankfurt a. M.*, 1904, 111–113.
- Stromer, E. (1908). Die Archaeoceti des Ägyptischen Eozäns. *Beiträge Zur Paläontologie Und Geologie Österreich-Ungarns Und Des Orients*, 21, 106–177.
- Stromer, E. (1913). Mitteilungen über Wirbeltierreste aus dem Mittelpliocän des Natrontales (Ägypten)—1. Affen. *Zeitschrift Der Deutschen Geologischen Gesellschaft*, 65, 350–372.
- Stromer, E. (1916). Die Entdeckung und die Bedeutung der Land und Süßwasser bewohnenden Wirbeltiere im Tertiär und in der Kreide Ägyptens. *Zeitschrift Der Deutschen Geologischen Gesellschaft*, 68, 397–425.
- Szalay, F. S., & Delson, E. (1979). *Evolutionary history of the primates* (580 pp.). Academic.
- Tabuce, R. (2016). A mandible of the hyracoid mammal *Titanohyrax andrewsi* in the collections of the Muséum National d'Histoire Naturelle, Paris (France) with a reassessment of the species. *Palaeovertebrata*, 40, 1–14.
- Tabuce, R., Lihoreau, F., Mees, F., Orliac, M. J., De Putter, T., & Smith, T. (2021). A reassessment of the Oligocene hyracoid mammals from Malembo, Cabinda, Angola. *Geobios*, 66–67, 207–215.
- Tabuce, R., Marivaux, L., Adaci, M., Bensalah, M., Hartenberger, J.-L., Mahboubi, M., Mebrouk, F., Tafforeau, P., & Jaeger, J.-J. (2007). Early Tertiary mammals from North Africa reinforce the molecular Afrotheria clade. *Proceedings of the Royal Society b: Biological Sciences*, 274, 1159–1166.
- Tanner, L. G. (1978). Embrithopoda. In V. J. Maglio, & H. B. S. Cooke (Eds.), *Evolution of African mammals* (p. 641). Harvard University Press.
- Thomas, H., Roger, J., Sen, S., Bourdillon-De-Grissac, C., & Al-Sulaimani, Z. (1989). Découverte de Vertébrés fossiles dans l'Oligocène inférieur du Dhofar (Sultanat d'Oman). *Geobios*, 22, 101–120.
- Thomas, H., Sen, S., Roger, J., Pickford, M., Gheerbrant, E., Al-Sulaimani, Z., & Al-Busaidi, S. (1999). Oligocene and Miocene terrestrial vertebrates in the Southern Arabian Peninsula (Sultanate of Oman) and their geodynamic and palaeogeographic settings. In *Fossil vertebrates of Arabia: With emphasis on the Late Miocene Faunas, Geology & Palaeoenvironments of the Emirate of Abu Dhabi* (pp. 430–442). Yale University Press.
- Tobien, H. (1978). The structure of the mastodont molar (Proboscidea, Mammalia). Part 3: The Oligocene mastodont genera *Palaeomastodon*, *Phiomia* and the Eo/Oligocene paenungulate *Moeritherium*. *Mainzer Geowissenschaftliche Mitteilungen*, 6, 177–208.
- Uhen, M. D. (2004). Form, function, and anatomy of *Dorudon atrox* (Mammalia, Cetacea): An archaeocete from the middle to late Eocene of Egypt. *University of Michigan Papers on Paleontology*, 34, 1–222.
- Van Couvering, J. A., & Harris, J. A. (1991). Late Eocene age of Fayum mammal faunas. *Journal of Human Evolution*, 21, 241–260.
- Van Valen, L. (1966). Deltatheriidae, a new order of mammals. *Bulletin of the American Museum of Natural History*, 132, 1–126.
- Vialle, N., Merzeraud, G., Delmer, C., Feist, M., Jiquel, S., Marivaux, L., Ramdarshan, A., Vianey-Liaud, M., Essid, E. M., Marzougui, W., Ammar, H. K., & Tabuce, R. (2013). Discovery of an embrithopod mammal (*Arsinoitherium?*) in the late Eocene of Tunisia. *Journal of African Earth Sciences*, 87, 86–92.
- Wanas, H. A. (2008). Calcite-cemented concretions in shallow marine and fluvial sandstones of the Birket Qarun Formation (Late Eocene), El-Faiyum depression, Egypt: Field, petrographic and geochemical studies: Implications for formation conditions. *Sedimentary Geology*, 212, 40–48.
- Wessel, P., Smith, W. H. F., Scharroo, R., Luis, J., & Wobbe, F. (2013). Generic mapping tools: Improved version released. *Eos*, 94, 409–410.
- Wight, A. W. R. (1980). Palaeogene vertebrate fauna and regressive sediments of Dur at Talhah, southern Sirt Basin, Libya. In *Geology of Libya* (Vol. 1, pp. 309–325). Academic.
- Williams, E. (1954). New or redescribed pelomedusid skulls from the Tertiary of Africa and Asia (Testudines, Pelomedusidae) 1. *Dacquemys paleomorpha*, new genus, new species from the Lower Oligocene of the Fayum, Egypt. *Breviora*, 35, 1–8.
- Wing, S. L., & Tiffney, B. H. (1982). A paleotropical flora from the Oligocene Jebel Qatrani Formation of northern Egypt: A preliminary report. *Botanical Society of America, Miscellaneous Series Publication*, 162, 67.
- Wood, A. E. (1968). Early Cenozoic mammalian faunas, Fayum Province, Egypt, Part II: The African Oligocene Rodentia. *Bulletin of the Peabody Museum of Natural History*, 28, 23–105.

- Zalmout, I., & Gingerich, P. D. (2012). Late Eocene sea cows (Mammalia Sirenia) from Wadi Al Hitán in the western Desert of Fayum (Egypt). *Papers on Paleontology*, 37, 1–158.
- Zalmout, I. S., Sanders, W. J., MacLatchy, L. M., Gunnell, G. F., Al-Mufarreah, Y. A., Ali, M. A., Nasser, A.-A.H., Al-Masari, A. M., Al-Sobhi, S. A., Nadhra, A. O., Matari, A. H., Wilson, J. A., & Gingerich, P. D. (2010). New Oligocene primate from Saudi Arabia and the divergence of apes and Old World monkeys. *Nature*, 466, 360–364.
- Zaw, K., Meffre, S., Takai, M., Suzuki, H., Burrett, C., Thaug, H., Zin, M., Maung, T., Tsubamoto, T., Egi, N., & Maung, M. (2014). The oldest anthropoid primates in SE Asia: Evidence from LA-ICP-MSUPb zircon age in the late middle Eocene Pondaung Formation, Myanmar. *Gondwana Research*, 26, 122–131.
- Zdankys, O. (1938). *Eotherium majus* sp.n., eine neue Sirene aus dem Mitteleozän von Aegypten. *Palaeobiologica*, 6, 429–434.



Josephina Hartung is a vertebrate paleontologist focusing on Cenozoic mammals and Mesozoic sarcopterygians. Her study on mammals focuses on artiodactyls from the Miocene of Europe. She completed her BSc studies at the Freie Universität Berlin and her MSc at the Rheinische Friedrich Wilhelms Universität Bonn, both in Germany. During her MSc degree, she studied the bovids from the Late Miocene hominid locality of Hammerschmiede (Germany) and continued her research on ruminants from this locality as her Ph.D. project at the University of Tübingen. Together with the University of Bonn, she works on the evolution of Late Triassic coelacanths from Europe and South America.



Panagiotis Kampouridis is a vertebrate paleontologist with his main focus on the study of Old-World mammals. He completed a BSc degree at the National and Kapodistrian University of Athens (Greece) where he focused on the Neogene and Quaternary terrestrial faunas of Greece and the adjacent region, including the world-renowned Late Miocene localities of Pikermi and Samos (Greece). During his MSc studies at the University of Tübingen (Germany) he expanded on the study of non-mammalian vertebrates, while



working on the Late Miocene hominid locality of Hammerschmiede (Germany). His Ph.D. dissertation focuses on the evolution of the Eurasian rhinocerotid genus *Chilotherium*. During this time, he has also expanded his studies on the Paleogene mammals of the Old World, including the Eocene–Oligocene fauna of the Fayum (Egypt).



Felix J. Augustin is a paleontologist from Germany who focuses on terrestrial Mesozoic ecosystems. He graduated from the Technical University Freiberg (Germany) in 2016 with a BSc degree and earned an MSc degree from the University of Tübingen (Germany), where he is currently writing his Ph.D. His research interests focus on terrestrial Mesozoic vertebrates, ranging from taxonomy to paleoecology and taphonomy. His research interests span all aspects of vertebrate taxonomy, paleoecology and taphonomy of the Late Jurassic of Germany, the Late Jurassic and Early Cretaceous of northwestern China and the Late Cretaceous of Romania. He has participated in field trips to and excavations in Germany, Romania, Bulgaria and the United States. The Late Cretaceous vertebrates from Egypt have fascinated him for long, especially the peculiar dinosaur faunas.



The Oligocene Palynology and Palaeoclimates of Northern Egypt as Recorded in the Dabaa Formation

Salah Y. El Beialy , Ahmed Mohamed, Mohamed K. Zobaa, Asmaa A. Taha, Dieter Uhl, and Haytham El Atfy 

Abstract

In this chapter, we present the story of the Oligocene palynostratigraphy and floral composition in Egypt as told by the preserved palynomorphs in the Dabaa Formation. It is a step in establishing a regional biostratigraphic and vegetational framework for the Oligocene, thus making future integration of regional and global schemes possible, especially when more independent biostratigraphic information becomes available. Synthesis of published materials from surface and subsurface sections points to significant floral changes during the Oligocene time leading to the development of a number of different vegetation belts in this part of North Africa. These include coastal mangrove forests, back-mangrove wetland ecosystems such as freshwater marshes, lakes, and swamps, as well as inland forests and open woodland-savannah habitats. The prevailing climate is interpreted to have been warm and humid with local or seasonal dry conditions.

Keywords

Oligocene Palynology • Palynostratigraphy • Biostratigraphy • Dabaa Formation • Egypt • North Africa

S. Y. El Beialy (✉) · A. Mohamed · A. A. Taha · H. El Atfy
Geology Department, Faculty of Science, Mansoura University,
Mansoura, 35516, Egypt
e-mail: salsolabeialy@gmail.com

M. K. Zobaa
Department of Geosciences, University of Texas Permian Basin,
Odessa, TX 79762, USA

D. Uhl
Senckenberg Forschungsinstitut und Naturmuseum Frankfurt,
Frankfurt, 60325, Germany

H. El Atfy
Department of Geosciences, University of Tübingen,
Tübingen, 72076, Germany
e-mail: El-Atfy@daad-alumni.de

1 Introduction

The Paleogene palynology of Egypt, especially the Oligocene, is less studied than other periods. Only a small number of contributions have been carried out on Cenozoic strata in general (Kedves, 1971, 1985; El-Sabrouty, 1984; El-Bassiouni et al., 1988; Takahashi & Jux, 1989a) and on the Oligocene particularly (e.g. El Beialy et al., 2019). Most of these previous studies have primarily focused on taxonomy, palynostratigraphy, and palaeoenvironmental interpretations in addition to palynofacies (El Beialy et al., 2016). Only recently studies that tackled vegetation analysis have emerged (El Atfy et al., 2021, 2022). Previous palynological investigations on the Oligocene sedimentary successions of the north Western Desert of Egypt include Kedves (1971, 1984, 1985), El-Sabrouty (1984), El-Bassiouni et al. (1988), Takahashi and Jux (1989a), El Beialy et al. (2019), Mohamed et al. (2020). Those targeting the Nile Delta include exclusively El-Beialy (1988a, 1990a, b), despite dealing with the Oligocene as part of their studied successions with no detailed data. To the best of the authors' knowledge, no other palynological data exist for the Oligocene from any other location in Egypt (Fig. 1). The goal of this chapter is to review the previous contributions and shed more light on the palynostratigraphy, vegetation, and palaeoclimate of the Oligocene deposits in Egypt with a special emphasis on the Dabaa Formation.

2 Oligocene in Egypt: Geology and Facies Distribution

Fluvio-deltaic and shelf progradation were the dominant depositional schemes in the Oligocene in northern Egypt (Fig. 2). The innermost (southern) basins were completely filled by the end of the Eocene. Oligocene thickness variations show an irregular bottom topography in the north's remnant basin, which was continuous and open. In the

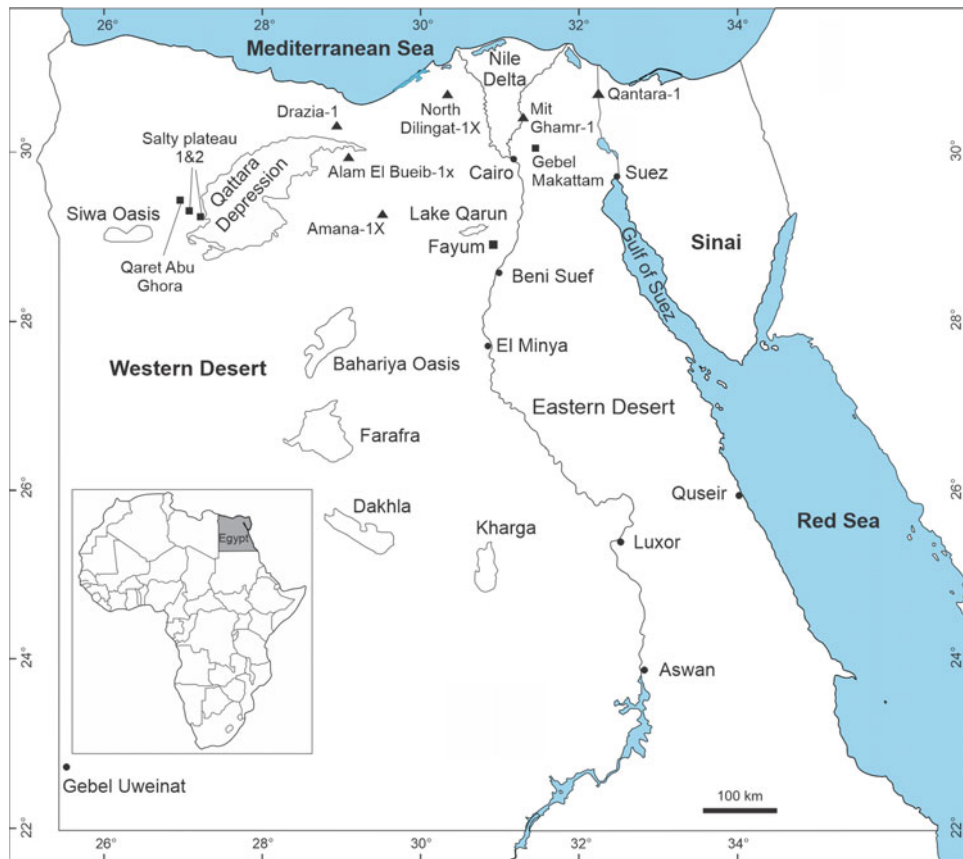


Fig. 1 Location map of Egypt showing the previously studied Oligocene locations and boreholes; triangles represent subsurface occurrences while quadrangles denote surface exposures

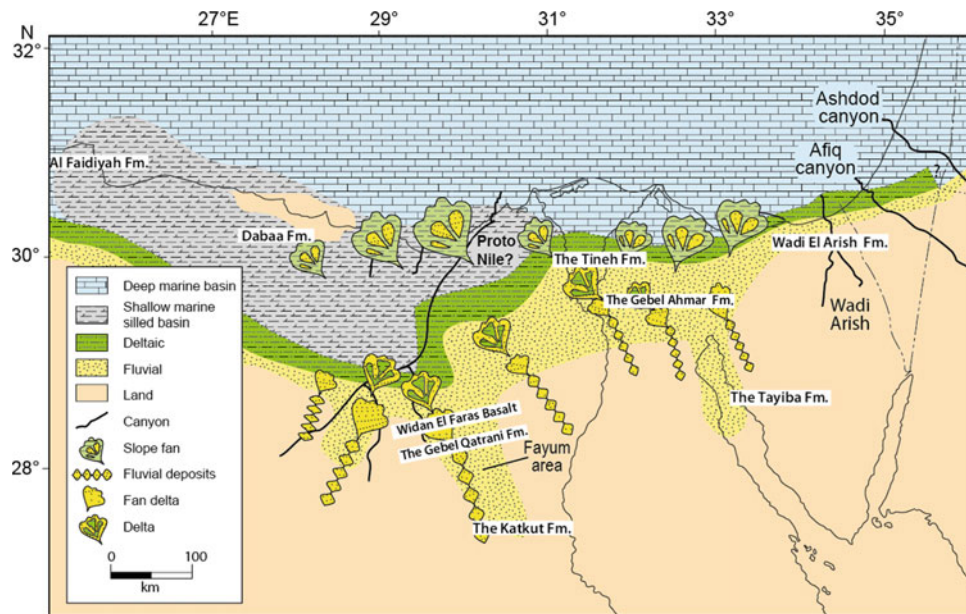


Fig. 2 Egypt during the Oligocene time, simplified and redrawn after Salem (1976) and Kuss and Boukhary (2008)

Oligocene basin, these morphologic irregularities were acquired from the preceding structures and/or compaction of the underlying sediments. Terrigenous clastic deposits from the Oligocene continued to prograde north-westward over an immature shelf with passive ridges extending northeast–southwest (Salem, 1976). Irregular bathymetry is an “immature shelf”, regardless of where it originated (Emery, 1968). The shelf was prograded by Oligocene sedimentation filling the inner lows first. The northern flank of the next ridge became the shelf’s outer slope when the shelf edge had prograded distant enough northwest to reach it. Submarine highs were also seen in the northwest during the same period. This is corresponding to a shelf with structural dams, as outlined by Curry (1965). It is difficult to determine the features and types of depositional processes that operate in the region because of the immature Oligocene shelf as well as lack of data. Salem (1976) assumed that high constructive delta systems dominated the scene due to the high content of mud. Many slope cones (turbidites) are likely to be present in the Oligocene sedimentary section. Oligocene slope fans are most likely to be found in the area directly south of the existing coastline (Fig. 2).

The Oligocene sedimentary facies comprise sandstones, siltstones, and clays of the deltaic Gebel Qatrani, the fluvial Gebel Ahmar, and the lacustrine Nakheil formations as the most significant Oligocene outcrops in the Fayum area and its surroundings (Fig. 2). Osman (2003) proposed that the Oligocene shoreline passed north of the Fayum Depression, skirted the southern slope of the El Arag, and continued into the Siwa Oasis in his study of the El Arag area in the north Western Desert. Moreover, El Heiny and Enani (1996) termed the Oligocene (Chattian) section north of the Nile Delta and offshore to the northwest of the Sinai Peninsula the Tineh Formation. The latter is made up of prodeltaic sediments that interfinger with open-marine basinal deposits further offshore (Dolson et al., 2002). As ancient river systems developed in the Red Sea and Uweinat regions, they drained ancient uplifted areas where these facies were distributed regionally throughout the early Oligocene. Issawi and McCauley (1993) proposed that these palaeo-drainage systems shifted position during the Oligocene–Miocene interval. Even though the exact pathways, timing, and position of several valleys and canyons are still being debated (Dolson et al., 2002), it is undeniable that these features are critical to the far-piece transport of clastics as well as several shelf dissections and incision processes.

Many episodes of volcanic activity occurred in Egypt during the Cenozoic. The most widespread volcanic activity was during the Paleogene. Isotopic age determinations indicate that several successive volcanic pulses occurred in the late Eocene with subsequent extensional phases ranging from late Oligocene to middle Miocene (Ibrahim, 2008). The

Red sea opening was immediately conjugated with this volcanic activity. It is strongly believed that the Red Sea gained its physiognomies and isolation from the Tethys as a result of the Cenozoic tectonics, starting with the late Eocene–Oligocene-early Miocene uplift and expansion of a major fault system (Ibrahim, 2008). These faults trending NW–SE show a substantial displacement along fault planes dipping away from the Red Sea. The basaltic volcanic rocks are extensively distributed in the northern part of Egypt underneath the Nile Delta and the Western Desert (Said, 1981; Williams & Small, 1984). Also, some isolated outcrops along the Fayum-Abu Rowash, Cairo-Suez, and Tihna-El Bahnasa stretch. The volcanic rocks of the Western Desert vary in composition and belong to more than one phase of volcanic activity (Meneisy & Abdel-Aal, 1984).

During the Oligo-Miocene, normal faults of a northwest trend echoed the opening of the Red Sea and Gulf of Suez (Meshref, 1990). The main trend affecting the area is a roughly east northeast–west southwest and is represented by a normal fault. This trend is reflected in the elongation of the scarp, and of Lake Qarun, to the south. This trend, called the “Tethyan” trend, has affected most of the African continent since earlier Mesozoic times (Pavoni, 1993). It could be the echo of the opening of the South Atlantic Ocean.

The major faults affecting the area are mostly of the normal type and have different trends, such as a roughly north–south or north northwest–south southeast trend, especially east of the Qatrani scarp. The intersection of the latter with the east northeast–west southwest master fault gives rise to the sudden change of the scarp direction and the drainage pattern. A group of northwest–southeast trending faults affects the basaltic rocks west and east of Widan El Faras. These synbasaltic trends could be due to the opening of the Red Sea and the Gulf of Suez. A northeast–southwest right-lateral strike-slip fault west of the Gebel Qatrani scarp brings the Gebel Qatrani Formation side by side with the basaltic rocks (Ibrahim, 2008).

3 Lithostratigraphic Framework of the Oligocene in Egypt

The Oligocene deposits overlie disconformably late Eocene sediments and they are only recorded in the northern part of Egypt. They were classified into two well-defined facies: fluvial facies of sands and gravels with minor deltaic facies and marine facies of shales and negligible limestone interbeds in the subsurface of northern Egypt. The volcanic, geyser activity and tectonism affected the Red Sea region and the belt of highs amid the stable and unstable shelves during the Oligocene. This governed the distribution of these sediments to a large extent (Said, 1962). Oligocene fluvial

sediments crop out along a narrow belt extending from Suez to Fayum via Cairo and onward into the Western Desert (Fig. 2). Small and isolated outcrops of this facies are also known from west of Beni Suef and the Bahariya Oasis. Generally, these deposits are difficult to date and they are classified as Oligocene based on stratigraphic correlation, and most lack reliable biostratigraphic data (Ibrahim, 2008).

3.1 The Gebel Qatrani Formation

Considerably, thick deposits of Oligocene sands occur along the northern and western scarps of the Fayum depression. The Gebel Qatrani Formation is the subject of the classical work of Beadnell (1905), Said (1962), Bowen and Vondra (1974), and Bown et al. (1982). It is mainly controlled by the presence or absence of the Widan El Fars basalt and by the development of large east–west trending normal faults. Beadnell (1905) used the term “Fluvio-marine series” however, Said (1962) favours the term Gebel Qatrani Formation or “Qatrani Formation” for the variegated sandstones, gravelly sandstone, sandy mudstones, limestones, and shales that form Gebel Qatrani and extended northeast to greater Cairo area.

In its type section, the Gebel Qatrani Formation is about 340 m thick; however, it thins considerably to the west. It is readily distinguished from the underlying dark green and grey Dir Abu Lifa Member of the Qasr El Sagha Formation by the dominance of brightly coloured-variegated sandy mudstones, sandstones, and gravelly sandstones. The overlying alluvial Miocene Khashab Formation, the Gebel Qatrani is separated by an erosional unconformity, followed in places by up to 25 m of Widan El Faras Basalt (Bowen & Vondra, 1974), a dense, iron-rich, cliff-forming unit capping the Gebel Qatrani. In areas where the Widan El Faras Basalt is absent, the Gebel Qatrani Formation is overlain by the Khashab Formation with an erosional unconformity (Ibrahim, 2008).

3.2 Widan El Faras Basalt

The Widan El Faras Basalt is a dark, generally densely aphanitic iron-rich extrusive basalt. It seems to be composed of a single flow in areas where it is thinnest; however, weathered and sometimes charred contacts within the basalt, as well as thin coarse sandstone interbeds (some containing mixed quartz sand and basaltic debris), demonstrate the existence of no less than two or three distinct flows over a great area of exposure of the basalt. These shallow scours show that unconformities of unknown magnitude are contained in the Widan El Faras Basalt. The basalt’s upper contact with the overlying Khashab Formation is also

erosional and, in the area between Widan El Faras and Tel Homar, is marked by at least 9 m of relief (Bowen & Kraus, 1988).

3.3 The Gebel Ahmar Formation

A typical example of the sands and gravels of the Cairo-Suez district is exposed in Gebel Ahmar, east of Cairo (Barron, 1907; Shukri, 1954). Lateritic soils cap the deposit in places, inducing red colouration to the underlying sediments. Shukri (1954) assumes that fluids ascended along faults caused the colouration and silicification of the Oligocene sands and gravels of Cairo-Suez district. The Oligocene Gebel Ahmar Formation detours Gebel Mokattam to the north, where it blankets the desert between Cairo and Suez. The E–W faults also displaced the continental Miocene sediments in the north counter to the Oligocene Gebel Ahmar Formation to the south. Within this huge surface area, prominent hills rise 60–70 m above the desert plain. The Gebel Yahmoum El Asmar, Gebel El Khashab (Petrified Forest), and Gebel Ahmar overlook Nasr City to the northeast of Cairo (Issawi et al., 2009).

The Gebel Ahmar Formation (at its type section) is composed of 40–100 m thick, coarse-grained, cross-bedded, vividly coloured, frequently friable sands, with a hard quartzitic dark brown bed at the top. At Gebel Ahmar, geyser action is well seen in the dark red and dark brown silicified tubes which cut erratically through the sands rising several metres in castle-like forms. Regrettably, this national park—as it should be—was damaged under the construction of the Arab Contractors Medical Centre and Elmokawelon Arena; even the designation transformed into Gebel Akhdar (Issawi et al., 2009).

3.4 The Nakheil Formation

The Nakheil Formation is recorded from the synclinal troughs of the coastal areas of the Red Sea south of Quseir city. Lithologically, the Nakheil Formation is 60 m thick of very coarse breccia and angular blocks of limestone and chert concretions that originated from the underlying Thebes Formation. Fine lacustrine sediments made of fine carbonates, clays, and sandstones alternate with the coarse breccia. No in-situ fossils were recorded except those reworked from the older beds (El Akkad & Dardir, 1966).

3.5 The Katkut Formation (Serir Deposits)

The Katkut Formation or Katkut Gravels was first presented to represent the post-Eocene strata west of the Nile Valley by some authors (e.g. El Hinnawi et al., 1978; Issawi & Osman,

2008; Issawi et al., 2009), encompassing all the reddish-brown coarse clastics that unconformably overlie the early Eocene limestone beds. These are allocated to late Oligocene to early Miocene age (Abu Seif, 2015; Mahran et al., 2013). These fluvial sediments resemble the undistinguishable gravel unit west of Nagh Hammadi (Klitzsch et al., 1987), to Higaza Formation east of Qena (Philobos & Abdel Rahman, 1990), and to pre-Eonile gravels in the extent between Aswan and Nagh Hammadi, west of the Nile (Lansbery, 2011). Mahran et al. (2013) and Abo Seif (2015) documented three informal lithologic subdivisions of the Katkut Formation; gravel, sands and silts, gravel, and sands.

The Katkut Gravels are developed on the plateau surface to the southwest of Sohag opposite El Minshah village with a greater thickness ca. 50 m. The gravels are embedded in a highly ferruginous red matrix, stretching for 30 km on the western Limestone Plateau and also on its eastern slope (Issawi et al., 2009).

3.6 The Tayiba Formation/Red Beds

The Tayiba (also referred to as the Abu Zeneima Formation in some works) overlies unconformably the late middle Eocene Tanka Formation in the Abu Zeneima-Feiran area in Sinai and the Gulf of Suez. It comprises a 5-m-thick basal conglomerate, a 15-m-thick sequence, and an upper 15-m-thick porcelaneous limestone bed, coarsening-upward siltstone beds (Ibrahim, 2008).

3.7 The Tineh Formation

The Tineh Formation represents the early Oligocene-lower Miocene sediments in the central and eastern Nile Delta regions. The Qantara-1 well penetrated a thickness of 1086 m of the Tineh Formation, which consists of dark grey shales interbedded with sandstone bands representing pro-deltaic sediments, interfingering with open-marine basinal facies further offshore (Dolson et al., 2002). The penetrated late Oligocene-early Miocene section in this well includes planktonic foraminifera deposited under outer neritic to upper bathyal conditions (El Heiny & Morsi, 1992). The Tineh Formation was deposited on a submarine high during the late Oligocene time as evidenced by the absence of its lower part and the relatively thin units encountered in this formation (El Heiny & Enani, 1996).

3.8 Wadi El Arish Formation

The Wadi Arish Formation was so-called after Wadi Arish, a large valley that drains the Central Sinai Peninsula in the

south and laid-off into the Mediterranean Sea to the east of El Arish town, it was divided into three members (Kuss & Boukhary, 2008). The lower member is best detected at the eastern part of Gebel Risan Eneiza, 20 km south of El Arish. The member unconformably overlies the karstified Albian limestones of the Risan Eneiza Formation. The Lower member of the Wadi El Arish Formation is 42-m-thick, coarse-grained sandstone intercalated with gypsum layers, including larger foraminifera and coralline algae (Kuss & Boukhary, 2008).

The middle member is 8 m thick consisting of clay and marls with thin intercalations of nodular limestones or rhodoliths. The upper member is 26.5 m thick, well-bedded, or massive limestones, including larger foraminifera and algal rhodoliths. The foraminiferal assemblage, identified by Kuss and Boukhary (2008) from the Wadi El Arish Formation includes *Nephrolepidina*., *Lithothamnium* sp., *Lithoporella melobesoides* (Foslie), *Sporolithon* sp. and *Neogoniolithon* sp.

3.9 Dabaa Formation

The Dabaa Formation is defined by Norton (1967) as a subsurface rock unit in the north Western Desert. The name was also used by Abdallah (1967) to designate Pliocene pink limestone of the Mediterranean littoral zone, but this is a homonym (Hantar, 1990). In this chapter, we employ the term Dabaa Formation in the sense of Norton (1967). It consists mainly of grey shale and thin limestone interbeds and has a uniform thickness in the north Western Desert (Norton, 1967). The Dabaa Formation has a thickness of 442 m at its type section (Dabaa-1 well) and its depositional environment is mainly inner shelf to littoral that changes to estuarine near its top (Issawi et al., 2009).

The Dabaa Formation has been dated to the Oligocene (Issawi et al., 2009), though oil geologists account it to be late Eocene–Oligocene. Alike was anticipated by Hantar (1990) who measured the lower 33 m of the Dabaa Formation, in its type section, to reveal upper Eocene, and the upper 209 m to be Oligocene. Palynologically, it was dated as Rupelian (early Oligocene) or late Eocene–Oligocene, based on dinocyst evidence from surface material in the vicinity of the Qattara Depression (El Beialy et al., 2019).

3.10 Al Faidiyah Formation

In Libya across the borders from Egypt, El Deftar and Issawi (1977) mapped a 55 m section of alternating limestone, marly limestone and clay which they named the Al Faidiyah Formation. Its faunal content included both macro- and microfossil assemblages including *Brisopsis frassi* Fuchs,

Tellina lacunosa Chemnitz, *Cardium gallicum* Mayer, *Lepidocyclines*, and *Operculines* that suggest Chattian to Aquitanian age. It makes the basal cliffs overlooking the Mediterranean near Tobruk, hence there is a great possibility that the section extends into Egypt. The vertical cliffs of the Sallum area have to be checked for the Al Faidiyah Formation especially when the unit is overlain by Al Jaghbub in Libya, a unit also known in west Egypt (Ibrahim, 2008).

It is worth mentioning that palynological dating based mainly on dinocyst evidence on the Al Faidiyah Formation has been introduced by El-Mehdawi and El Beialy (2008) from surface samples from Al Jabal Al Akhdar, NE Libya. They established a late Oligocene to early Miocene age, rather than early Miocene which could reveal that Al Faidiyah Formation is younger than the Dabaa Formation and other Oligocene equivalent rock units in Egypt.

4 Terrestrial Megaf flora

The Oligocene plant-bearing strata in North Africa are generally rare. They produce mostly petrified wood indicative of a diverse terrestrial floral community (e.g. Dupéron-Laudoueneix & Dupéron, 1995; Jacobs et al., 2010; El-Saadawi et al., 2020). Based on the spatial variation within such community, the Oligocene vegetation in North Africa is believed to have been tropical forests along the Tethys coastal line, transitioning to an inland zone of mixed woodland and grassland (Boureau et al., 1983; Louvet, 1971).

In Fayum, Egypt, an area well-known for its palaeobiodiversity, a plethora of vertebrate fossils as well as a diverse early Oligocene macrofloral community are preserved within the Gebel Qatrani Formation. Floral remains include wood, fruits, seeds, and leaves (Blanckenhorn, 1921; Kräusel & Stromer, 1924; Kräusel, 1939; Bown et al., 1982; El-Saadawi et al., 2014, 2020; Stull et al., 2020). Louvet (1971) interpreted the floral community of the Gebel Qatrani Formation to represent a portion of a tropical forest formed on the northern coast of Africa. However, to the authors' knowledge, no more data are available outside Fayum detailing the megaf floral assemblages of Egypt.

5 Floristic Composition, Vegetation, and Palaeoclimatic Inferences

In Egypt, Oligocene spores and pollen were initially reported from the regions of Abu Rauwash and Moquattam (Kedves, 1971, 1985). This was followed by studying the spores and pollen of the late Eocene-early Oligocene Qasr El Sagha Formation in the Fayum area (Takahashi & Jux, 1989a). Recently, El Atfy et al., (2021, 2022) studied the Dabaa

Formation sporomorphs from surface exposures near the Qattara depression and from the Amana-IX well, respectively, both located in the north Western Desert (Fig. 1).

The palynofloral elements known from the Dabaa Formation in the north Western Desert of Egypt display taxonomic resemblances to the hitherto-described Oligocene macroflora, and palynoflora from the Oligocene of Egypt (e.g., Kedves, 1985; El Atfy et al., 2021, 2022 and discussion therein). These elements include, for example, fern and lycopsid spores such as *Crassoretitriletes vanraadshooveni*, *Magnastriatites howardi*, and *Verrucatosporites usmensis*, gymnosperm pollen like *Ephedripites* in addition to diverse angiosperm pollen species such as *Aceripollenites striatus*, *Bombacacidites nacimientoensis*, *Chenopodipollis multiplex*, *Echiperiporites estelae*, *Monoporopollenites annulatus*, and *Peregrinipollis nigericus*. The presence of these and other species (Fig. 3) within the Dabaa Formation indicates mixed tropical habitats including coastal mangroves with back swamps, ever-wet inland forests, and open woodland-savannah ecosystems. Temperate indicative species may have also been present (El Atfy et al., 2021, 2022). A distinct vegetational pattern could be outlined during the deposition of the Dabaa Formation in the north Western Desert as shown in Fig. 4. This vegetational pattern has been described so far from only the Dabaa Formation based on palynomorphs. Therefore, further palynological investigations are required to confirm its extent, although macro-palaeobotanical data point to an extension of this pattern across all of northern Africa during this period.

In terms of palaeoclimate, the Dabaa Formation preserves a terrestrial palynomorph assemblage indicative of predominantly warm and humid conditions (El Atfy et al., 2021, 2022). This is evident by the abundance of angiosperm pollen species of the families Areaceae, Malvaceae (subfamily Bombacoideae), Dipterocarpaceae, and Ctenolophonaceae. The abundance of precipitation and humidity are also inferred from the presence of fern and lycopsid spores which are known to be water-loving and thrive under wet conditions. Local or seasonal dry and arid conditions may have existed based on the reported species of *Chenopodipollis*, *Monoporopollenites*, and *Ephedripites* (El Atfy et al., 2021) from surface samples collected from the vicinity of the Qattara Depression.

6 Marine Palynomorphs, Primarily Dinoflagellates

The analysed samples from the Dabaa Formation in the north Western Desert (namely from the Qattara profiles and the Amana-IX well) have high to moderate recovery of well-preserved dinoflagellate cyst assemblages (Fig. 5) besides sporomorphs (Fig. 3) and palynofacies particles as

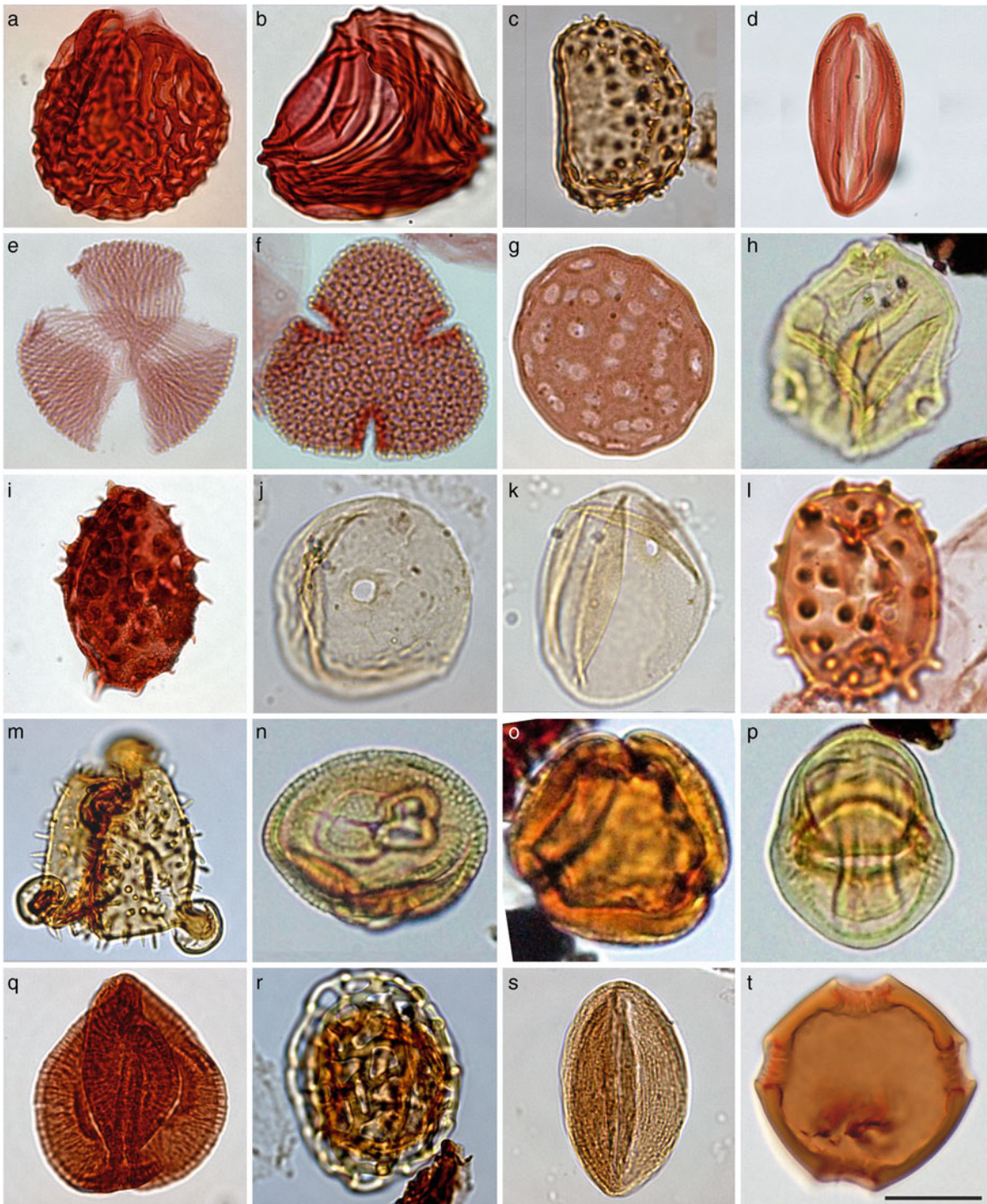


Fig. 3 The most significant Oligocene spores and pollen assemblage from the Dabaa Formation, Qattara area, north-Western Desert, Egypt. All photomicrographs are in bright field illumination. An England Finder reference follows the sample number for each specimen. **a–c**; fern and lycopsid spores **a** *Crassoretitrites vanraadshooveni* Hopping & Muller; P1-2_X37. **b** *Magnastriatites howardi* Germeraad, Hopping & Muller; P1-1_O35. **c** *Verrucatosporites usmensis* (van der Hammen) Germeraad, Hopping & Muller; P1-1_U39. **d** Gymnosperm; *Ephedripites* sp.; P1-2_O31. **e–t**, angiosperms; **e** *Aceripollenites striatus* (Pflug) Thiele-Pfeiffer; P1-2_L30. **f** *Bombacacidites nacimientoensis* (Anderson) Elsik; P1-1_O35. **g** *Chenopodipollis multiplex* (Weyland & Pflug) Krutzsch; P1-2_L34. **h** *Corsinipollenites* sp.; Am-09. **i** *Echiperiporites estelae* Germeraad, Hopping & Muller; P1-2_K38. **j** *Graminidites* sp.; P2-1_H35. **k** *Monoporopollenites annulatus* Jaramillo & Dilcher; P1-1_T37. **l** *Mauritiidites crassixinus* van Hoeken-Klinkenberg; P2-1. **m** *Auriculopollenites echinatus* Salard-Cheboldaef; Am-15_K21. **n** *Retibrevitricolporites ibadanensis* Jan du Chêne et al.; Am-07. **o** *Psilatricolporites crassus* van der Hammen & Wymstra; Am-10. **p** *Zonocostites ramonae* Germeraad, Hopping & Muller; Am-13. **q** *Perforitricolpites digitatus* González; P1-2_N38. **r** *Peregrinipollis nigericus* Clarke; Am-07_P22. **s** *Striatopollis catatumbus* (González) Ward; P1-1_E26. **t** *Pachydermites diderixi* Germeraad, Hopping & Muller; Am-01_J22. Scale bar = 20 µm

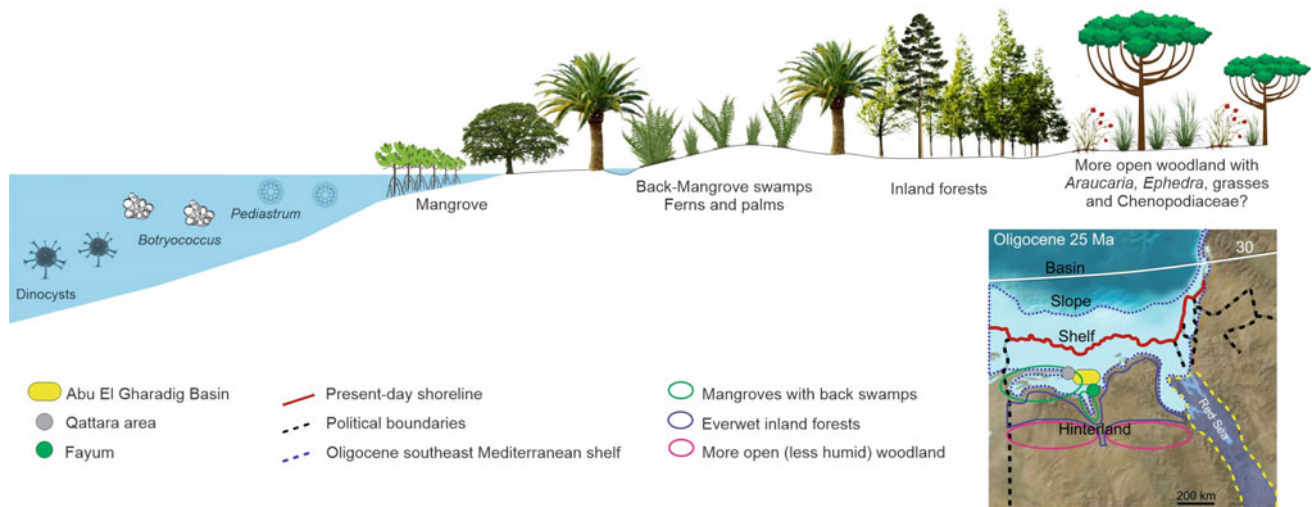


Fig. 4 Tentative reconstruction of the probable vegetation belts during the deposition of the Dabaa Formation, Amana-IX well, north–Western Desert, Egypt (modified after El Atfy et al., 2021). The palaeogeographic base map is after Ron Blakey, Colorado Plateau Geosystems, Arizona, USA (<http://cpgeosystems.com>)

well as a few numbers of acritarchs, dispersed fungal remains, algae, and foraminiferal test linings.

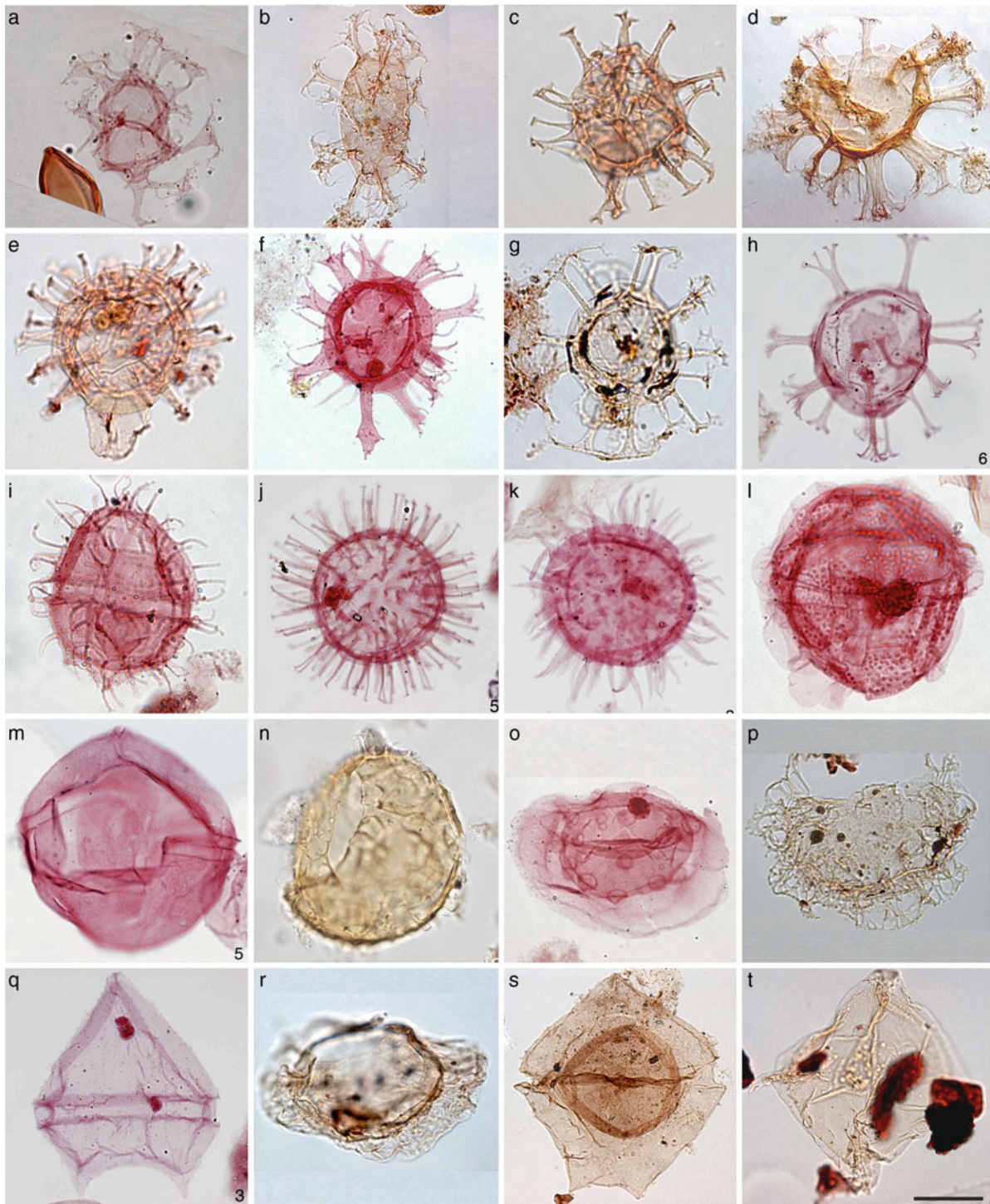
The Dabaa Formation contains diverse assemblages of dinoflagellate cysts, some of which are sufficiently restricted as to be useful in age determination. The dinocyst *Thalassiphora pelagica* (Fig. 5r) is not usually recorded above the lowermost Miocene (e.g. Fensome et al., 2009 for offshore Canada). However, it has a known range of Late Cretaceous to late Oligocene in Italy, Turkey and Tunisia (Wilson, 1971; Powell, 1986; Erkmén & Sadek, 1981; Torricelli & Biffi, 2001). In Egypt, *T. pelagica* was previously recorded from the late Oligocene of the Nile Delta, (El-Beialy, 1990b), the early Miocene of North Sinai (El-Beialy & Gheith, 1989), the Gulf of Suez (El Atfy et al., 2017), and the early Oligocene of the north Western Desert (El Beialy et al., 2019).

Diphyes colligerum (Fig. 5e) shows a reliable end Luteitan (Chron C19n) highest occurrence (HO) in the North Sea

and the Norwegian–Greenland Sea (Eldrett et al., 2004), but exhibits a range of mid-Lutetian to lower Oligocene highest occurrences in places like Italy, Denmark, Germany, and the Labrador Sea (Brinkhuis & Biffi, 1993; Heilmann-Clausen & van Simaëys, 2005; Köthe & Piesker, 2008; Firth et al., 2012). In Egypt, this species was recorded from the upper Eocene to lower Oligocene of the north Western Desert and the Nile Delta (El-Bassiouni et al., 1988; El Beialy, 1988b; El-Beialy, 1990a; El Beialy et al., 2019).

Dinopterygium cladoides (Fig. 5l) has an early Oligocene to middle Miocene HO in Africa. It was previously reported from the early Oligocene of Tunisia (Torricelli & Biffi, 2001), the late Oligocene of Morocco (Chekar et al., 2018), the Oligocene of the north Western Desert, Egypt (El Beialy et al., 2019), and the middle Miocene of the Gulf of Suez, Egypt (El Beialy & Ali, 2002; Soliman et al., 2012).

Fig. 5 Most significant Oligocene dinocyst assemblage from the Dabaa Formation, Qattara area, north-Western Desert, Egypt. All photomicrographs are in bright field illumination. An England Finder reference follows the sample number for each specimen. **a** *Distatodinium craterum* Eaton; P1-2_N36. **b** *Distatodinium paradoxum* Brosius; Am23B_E24.3.4_5.6 m.; central body length 43 µm. **c** *Melitasphaeridium pseudorecurvatum* (Morgenroth) Bujak et al.; Am24B_D36_515.1 m.; central body maximum diameter 30 µm. **d** *Cordosphaeridium inodes* (Klump) Eisenack; Am22B_T14_496.8 m; central body maximum diameter 45 µm. **e** *Diphyes colligerum* (Deflandre & Cookson) Cookson, emend. Goodman & Witmer; Am5A_O17.1.3_341.4 m. **f** *Hystriocholpoma rigaudiae* Deflandre & Cookson; P1-2_W36; central body length 41 µm. **g** *Enneadocysta multicornuta* (Eaton) Stover & Williams, emend. Stover & Williams; Am1A_K13.1.3_304.8 m; central body maximum diameter 36 µm. **h** *Homotryblium floripes* subsp. *floripes* (Deflandre & Cookson) Stover; P1-1_U40; central body maximum diameter 45 µm. **i** *Phthanoperidinium comatum* (Morgenroth) Eisenack & Kjellström; P1-2_K41; central body length 44 µm. **j** *Polysphaeridium?* sp. 2; P1-2_C31; central body maximum diameter 39 µm. **k** *Lingulodinium machaerophorum* (Deflandre & Cookson) Wall; P1-2_C37; central body maximum diameter 40 µm. **l** *Dinopterygium cladoides* sensu Morgenroth; P1-2_C44; central body length 49 µm. **m** *Cribooperidinium tenuitabulatum* (Gerlach) Helenes; P1-2_B43; cyst length 67 µm. **n** *Samlandia?* sp.; Q1_Q15; central body length 52 µm. **o** *Tuberculodinium vancampoeae* (Rossignol) Wall 1967; P1-2_W38; central body maximum diameter 50 µm. **p** *Polysphaeridium zoharyi* (Rossignol) Bujak et al.; P1-2_K42; central body maximum diameter 54 µm. **q** *Glaphyrocysta intricata* (Eaton) Stover & Evitt; Am2A_G21. **r** *Lentinia serrata* Bujak in Bujak et al.; P1-1_W39; cyst length 56 µm. **s** *Thalassiphora pelagica* (Eisenack) Eisenack & Gocht, emend. Benedek & Gocht; Am2A_O17. **t** *Deflandrea phosphoritica* Eisenack; Am11A_U44; central body maximum length 40 µm. **u** *Rhombodinium draco* Gocht; Am16A_T26; central body length 54 µm. Scale bar = 20 µm



Phthanoperidinium comatum (Fig. 5i) has a consistent record of lower Rupelian highest occurrences from the western North Atlantic (Stover, 1977, the Labrador Sea Head & Norris 1989, the North Sea (van Simaey et al., 2005), Italy (van Mourik & Brinkhuis, 2005), Germany (Köthe & Piesker 2008), Denmark (Śliwińska et al., 2012). In North Africa, *P. comatum* has been documented from the

lower Oligocene of the Nile Delta and Qattara Depression of Egypt as well as the Lutetian–Chattian of Morocco (El Beialy, 1988b; El Beialy et al., 2019; Chekar et al., 2018).

Glaphyrocysta intricata (Fig. 5p) has its HO in the lower Miocene of western Tasmania in the Indian Ocean (Brinkhuis et al., 2003) and Germany (Strauss, 1993). The HO of this taxon is also documented from the upper Oligocene of west

Germany (Weiler, 1982; Sonne & Weiler, 1984) and the Nile Delta, Egypt (El-Beialy, 1990b), lower Oligocene of Italy and Tunisia (Brinkhuis & Biffi, 1993; Brinkhuis, 1994; van Mourik & Brinkhuis, 2005; Torricelli & Biffi, 2001). The lowest occurrence of this species has been recorded in the upper Paleocene (Thanetian) of England (Powell et al., 1996).

The genus *Rhombodinium* has a Bartonian–Rupelian stratigraphic range (Fensome et al., 2009). Its top range, Rupelian, is based on the HO *R. draco* (Fig. 5t) by Powell and Brinkhuis in Gradstein et al. (2004) as well as Williams et al. (2004) from the mid-latitudes of the Northern Hemisphere. In Egypt, *R. draco* was recorded from the early Oligocene of the Nile Delta by El Beialy (1988b). Reported anomalous Miocene records of *R. draco* from Russia and East Germany by Zosimovich (1991) and Strauss (1993) are assumed to be reworked.

Enneadocysta multicornuta (Fig. 5g) was recorded in deposits ranging in age from the late Paleocene of India (Khanna, 1979) to early Miocene of Europe (Hochuli, 1978). Elsewhere, this species has the HO in the early Oligocene of Italy (Gruas-Cavagnetto & Barbin, 1988), Mississippi, Alabama (Jaramillo & Oboh-Ikuenobe, 1999, 2001), Poland (Gedl & Leszczynski, 2005), and Azerbaijan (Bati, 2015).

Williams et al. (2004) recorded the first occurrence of *Melitasphaeridium pseudorecurvatum* (Fig. 5c) from the early Eocene (Ypresian) in northern Hemisphere mid-latitudes, southern Hemisphere high latitudes and equator. The high occurrence of this species is recorded from the early Eocene in the southern Hemisphere high latitude (51.4 Ma), the late Eocene (Priabonian) in the equator (35 Ma), and the early Oligocene (Rupelian) in northern Hemisphere mid-latitude (33.07 Ma) (Williams et al., 2004). Elsewhere, the highest occurrence of this species was recorded from the lower Oligocene of Belgium (De Coninck, 1999), Poland (Gedl & Leszczynski, 2005), Italy (van Mourik & Brinkhuis, 2005), and Azerbaijan (Bati, 2015). In Egypt, *M. pseudorecurvatum* was firstly recorded from the lower Oligocene Dabaa Formation in the Qattara Depression, Western Desert (El Beialy et al., 2019).

Lentinia serrata (Fig. 5q) has been previously recorded from the Lutetian to lower Rupelian strata of multiple European countries including England, Belgium, and Italy (Aubry, 1986; De Coninck, 2001; Pross et al., 2010) as well as from the offshore of eastern Canada (Fensome et al., 2008). In North Africa, it was recorded from the middle Eocene of Morocco (Chekar et al., 2018) and from the lower Oligocene of the Qattara Depression, Egypt (El Beialy et al., 2019).

According to Brinkhuis et al. (2009), *Deflandrea phosphoritica* (Fig. 5s) has a mid-Aquitainian highest occurrence in low- and mid-latitudes of the Northern Hemisphere. In North Africa, *D. phosphoritica* was reported from the Eocene of Morocco (Chekar et al., 2018), the early Miocene

of Tunisia (Torricelli & Biffi, 2001) and Libya (El-Mehdawi & El Beialy, 2008), and the late Oligocene of the Nile Delta, Egypt (El Beialy, 1990b).

Distatodinium paradoxum (Fig. 5b) has middle Miocene highest occurrences in many parts of the world including the USA (de Verteuil & Norris, 1996), the Canadian Scotian shelf (Fensome et al., 2008), Germany (Köthe & Piesker, 2007), Belgium (Louwye et al., 2000), Norwegian–Greenland Sea (Poulsen et al., 1996), and Italy (Zevenboom, 1995). In Egypt, *D. paradoxum* has its HO in the early Miocene (e.g., El Beialy & Ali, 2002; El Atfy et al., 2017).

Distatodinium craterum (Fig. 5a) has relatively a long stratigraphic range (lower Eocene to middle Miocene, collectively) in Egypt as reported from multiple localities including the Gulf of Suez and the north Western Desert (Ahmed & Pocknall, 1994; El Beialy et al., 2019).

7 Oligocene Palynostratigraphical Framework in Egypt

The excellent state of preservation of dinoflagellate cysts, as well as sporomorphs encountered in the studied materials of the Dabaa Formation by El Beialy et al. (2019) and El Atfy et al. (2021, 2022) promises considerable future advances to the Oligocene palynology of Egypt. This will provide a sound basis for surface and subsurface correlations in the region. This palynostratigraphical correlation (Figs. 6 and 7) is still seriously hampered by the limited extent of published data. This chapter is intended in part to highlight such a gap, as further sample coverage is needed to allow for a more complete regional picture to emerge.

The biostratigraphy of the late Paleogene subsurface sequences in the Western Desert, Egypt, based initially on calcareous microfossils mainly foraminifera and nannoplankton, was discussed by several authors (e.g., Ouda, 1998). So far, there is no standard zonation established for dinocysts or sporomorphs of the Paleogene rocks in Egypt, where published records are existing only from the Western Desert (El Beialy & Kora, 1987; Mahmoud, 1998; El Beialy et al., 2019; El Atfy et al., 2021) and Nile Delta (El Beialy, 1988a, b; El Beialy, 1990a, b).

From a palynostratigraphical perspective, it is still not tenable to provide accurate Paleogene dating and biozonation based on terrestrial evidence in Egypt. However, some sporomorph taxa retrieved in the Egyptian strata (especially from the Dabaa Formation) display biostratigraphic potential, especially when they are correlated with regional counterparts in Africa and the Tethyan realm, as follows:

Cicatricosisporites dorogensis has been recorded from Eocene to early Miocene strata of Nigeria (Legoux, 1978), Tunisia (Torricelli & Biffi, 2001), Cameroon (Salard-Cheboldaeff, 1979), and Sudan (Stead & Awad, 2005;

System / Period / Series / Epoch	Numerical age (Ma)	Tropical areas Germeraad et al. 1968			North South America	Cameroon & Nigeria	Cameroon	Sudan				North Western Desert, Egypt (El Atfy et al. 2021, 2022)	
		Caribbean Zone	Atlantic Zone	Pantropical Zone	Muller et al. 1987	Legoux, 1978	Salard-Cheboldaëff, 1979	Zone	Kaska, 1989	Zone	Stead & Awad, 2005		Zone
Paleogene Oligocene Eocene Early Middle Late Paleocene	23.03		<i>C. dorogensis</i>	<i>M. howardi</i>	<i>Magnastriatites - C. dorogensis</i>	B3 B2-1 A	<i>Verrucatosporites usmensis</i> <i>Cicatricosisporites dorogensis</i> <i>Magnastriatites howardi</i>	E	<i>Praedapollis africanus</i> <i>Retibrevitricolpites ibadanensis</i> <i>Pereregripollis nigericus</i> <i>Verrucatosporites usmensis</i> <i>Magnastriatites howardi</i> <i>Striatopollis catatumbus</i> <i>Peritricolpites digitatus</i>	3	Abundant <i>Cyathidites minor</i> <i>Peritricolpites digitatus</i>	VI	<i>Cricotriporites camerounensis</i> , <i>Brevicopites gunetti</i> , <i>Bomacacidites namientoensis</i> , <i>Palastephanoecolpites perforatus</i> , <i>Claviperforatus cl. clavatus</i> , <i>Palastephanoecolpites operculatus</i>
	33.9			<i>V. usmensis</i>	<i>E. estelae</i>	T II G2-3 G1	<i>Psilatricolpites crassus</i> <i>Monoporites annulatus</i> <i>Retibrevitricolpites triangulatus</i>	D	<i>Auriculidites reticulatus</i> <i>Proxapertites operculatus</i> <i>Longapertites vaneendenburgi</i> <i>Periretisyncolpites giganteus</i> <i>Monosulcites perispinosus</i> <i>Auriculipollentes echinatus</i> <i>Grimsdalea magnaclavata</i> <i>Ariadnaesporites</i>	4	<i>Striatopollis</i> spp.	V	<i>Retistephanoecolpites williamsii</i> , <i>Muritidites crassixinus</i> , <i>Gemmatricolpites cf. pergemmatus</i> , <i>Proxapertites operculatus</i> , <i>Bacutriporites oriensis</i> , <i>Corsipollentes jussiaeensis</i> sensu Stead & Awad 2005.
		<i>R. guianensis</i> <i>P. operculatus</i> <i>P. crassus</i>		<i>M. annulatus</i>	Zone 23 Zone 18								
			<i>R. triangulatus</i>	<i>Proxapertites operculatus</i>	<i>Rugulicopites felix</i>								
		56.0	<i>F. perforatus</i> <i>C. isamae</i> <i>R. margaritae</i> <i>Retibrevitricolpites megralensis</i>		<i>Foveitricolpites perforatus</i>			<i>Proxapertites operculatus</i>					
	66.0			<i>G. gemmatus</i> <i>S. baculatus</i>									
										5	<i>Mauritidites crassiximus</i>	IV	<i>Periretisyncolpites giganteus</i> , <i>Monocolpites marginatus</i> , <i>Muritidites crassibaculatus</i> , <i>Foveomonocolpites bauchiensis</i> , <i>Gemmanonocolpites macrogemmatus</i> , <i>Longapertites marginatus</i>

Fig. 6 Correlation of the sporomorph assemblage identified in this study with other zonations elsewhere, mainly from Sudan, West Africa, and North-South America

System / Period / Series / Epoch	Numerical age (Ma)	Italy			Tunisia	Egypt				
		Brinkhuis et al. 1992	Brinkhuis & Biffi, 1993	Biffi & Manum, 1988	Toricelli & Biffi, 2001	Nile Delta			North Western Desert	
Paleogene Oligocene Eocene Early Middle Late Paleocene	23.03	Ebu Dbi	Def Chi Hob	DO 3 DO 3b DO 3a	Edu Dbi	B				
	27.8			DO 2	Clo	B				
				DO 1	Hpu Cin Rac Zs	A	<i>Deflandrea heterophlycta</i>		<i>Deflandrea heterophlycta</i>	Dabaa Assemblage
	33.9			DE	Aal Cfu Ssp Mps		<i>Diphyes colligerum</i> <i>Kisselovia coleothrypta</i>	<i>Diphyes colligerum</i>	<i>Diphyes colligerum</i>	
	56.0									
	66.0									

Fig. 7 Dinocyst zonation scheme for the studied Oligocene succession, Western Desert, Egypt. Correlation with previously published local and regional dinocyst zonations is shown

Eisawi & Schrank, 2008). In Egypt, *C. dorogensis* has been reported from the Rupelian of the Western Desert (El Atfy et al., 2022) and the early Miocene of the Gulf of Suez (El Atfy et al., 2017).

Magnastriatites howardi (Fig. 3b) is generally found in Eocene to Oligocene rocks in many African countries including Tunisia (Toricelli & Biffi, 2001), Sudan (Kaska, 1989; Stead & Awad, 2005), and Cameroon (Salard-Cheboldaëff, 1979), despite the early Miocene record by Eisawi and Schrank (2008) from Sudan. In Egypt, *M. howardi* has been reported from the late Eocene of the Saccara area (Kedves, 1986; as *Cicatricosisporites grandiosus*), the Rupelian of the Western Desert (El Atfy

et al., 2021, 2022) as well as the early Miocene of the Gulf of Suez (Ahmed & Pocknall, 1994; El Atfy et al., 2013) and Sinai (Wescott et al., 2000).

Verrucatosporites usmensis (Fig. 3c) is generally a long ranging (Eocene–Pliocene) species in Africa (e.g., Salard-Cheboldaëff, 1979, 1990; Kaska, 1989; Stead & Awad, 2005; Eisawi & Schrank, 2008). In Egypt, however, it was recorded from the Burdigalian of Sinai (Wescott et al., 2000), early Miocene of the Gulf of Suez (El Atfy et al., 2013), and the Rupelian of the Western Desert (El Atfy et al., 2021, 2022).

Mauritidites crassixinus (Fig. 31) was previously recorded from Paleocene to Eocene strata of Nigeria and

Sudan (Jan du Chêne et al., 1978; Adegoke et al., 1978; Stead & Awad, 2005; Eisawi & Schrank, 2008). In Egypt, it was reported by El Atfy et al. (2021) from the Rupelian of the Qattara area.

Echiperiporites estelae (Fig. 3i) was recovered from Oligocene to Miocene rocks from Tunisia (Torricelli & Biffi, 2001), Sudan (Eisawi & Schrank, 2008), and Cameroon (Salard-Cheboldaeff, 1979). In Egypt, *E. estelae* has a rather longer age range (Eocene–Miocene) as reported by El-Beialy and Shahin (1990), El Beialy et al. (2005) and El Atfy et al. (2021).

The first record of *Magnaperiporites spinosus* from Egypt was reported by El Atfy et al. (2022) from the Rupelian of the Dabaa Formation. Its actual age range in Egypt is yet to be determined through further investigation.

Perfotricolpites digitatus (Fig. 3q) was previously reported from the upper Eocene to Miocene strata from Nigeria and Sudan (Germaraad et al., 1968; Kaska, 1989; Stead & Awad, 2005). In Egypt, it was recorded from the Burdigalian of Sinai, (Wescott et al., 2000), early Miocene of the Gulf of Suez (El Atfy et al., 2017), as well as the Rupelian of the Western Desert (El Atfy et al., 2021, 2022).

Praedapollis africanus has been repeatedly documented from the late Oligocene to early Miocene of Cameroon, (Salard-Cheboldaeff, 1978), Tunisia, (Torricelli & Biffi, 2001) and the Sudan (Eisawi & Schrank, 2008). In Egypt, it was recorded from the early Miocene of the Gulf of Suez (El Atfy et al., 2013) and the Rupelian of the Western Desert (El Atfy et al., 2021, 2022).

Striatopollis catatumbus (Fig. 3s) was previously recorded from the upper Eocene to Oligocene of Sudan (Kaska, 1989; Stead & Awad, 2005) as well as the lower Eocene of Nigeria (Takahashi & Jux, 1989b). In Egypt, it was recorded from the Rupelian of the Western Desert as well as the Burdigalian of the Gulf of Suez (El Atfy et al., 2021, 2022; El Beialy et al., 2005).

Zonocostites ramonae (Fig. 3p) was recorded in Egypt by El Atfy et al. (2022) from the Rupelian of the north Western Desert.

It is worth noting that *Cicatricosisporites dorogensis*, *Magnaperiporites spinosus*, *Magnastriatites howardi*, *Peregrinipollis nigericus* (Fig. 3r), *Perfotricolpites digitatus*, *Praedapollis africanus*, *Retibrevitricolporites ibadanensis* (Fig. 3n), *Striatopollis catatumbus*, and *Verrucatosporites usmensis* have an Eocene first occurrence that extended to the Oligocene in West Africa (Salard-Cheboldaeff, 1979, 1990). These taxa correlate (Fig. 6) well with the late Eocene to Oligocene Zone E of Kaska (1989) and the Oligocene-early Miocene Zone VI–VII of Eisawi and Schrank (2008) from Sudan. The stratigraphic ranges of the concurrent species *Cicatricosisporites dorogensis* (Zones 22–25, middle Eocene to Oligocene), indicate that the spore/pollen assemblage from the Dabaa Formation within the Western Desert can be

allocated to the *Magnastriatites-Cicatricosisporites dorogensis* Zone (Zone 25, Oligocene) of Muller et al. (1987). Alike postulation was established for material from Venezuela (Helenes & Cabrera, 2003) and Zone F (Oligocene-early Miocene) *Verrucatosporites usmensis-Magnastriatites howardi* (Ikegwuonu et al., 2020) from Nigeria. On the other hand, the dinocyst evidence from the exposed Dabaa Formation in the Qattara Depression, north Western Desert (El Beialy et al., 2019) assigns it to Rupelian.

From the above discussion, one can conclude that the age of the Dabaa Formation is postulated to be late Eocene to early Oligocene based on combined dinoflagellate and miospore evidence from different locations within the Qattara Depression (El Beialy et al., 2019; El Atfy et al., 2021).

8 Conclusions

A review of the palynology of the Oligocene Dabaa Formation in the north Western Desert, based on data gathered from the Qattara surface sections and the Amana-1X well (Abu El Gharadig Basin), shows the existence of diverse palynomorph assemblages including dinoflagellate cysts, spores, pollen, acritarchs, fungal spores, and foraminiferal test linings. The palynostratigraphic and palaeofloristic significance of these assemblages have been discussed highlighting the following points as especially important:

1. The early Oligocene vegetation was composed of several zones that extended approximately parallel to the Tethys' coastline (Fig. 4). These include the mangroves which expanded greatly, in addition to marshes, lakes, swamps, streams, and rivers. Tropical forests probably developed in mountainous areas.
2. The Oligocene was marked by predominantly wet climatic conditions with fluctuating moisture regimes. A tropical coastal plain with wet soil and seasonal rainfall developed in the northern Western Desert which led to considerable floral abundance and diversity.
3. The dating of the Dabaa Formation is based mainly on diagnostic dinoflagellate cysts including *Phthanoperidinium comatum*, *Rhombodinium draco*, *Lentinia serrata*, *Diphyes colligerum*, *Deflandrea phosphoritica*, *Distatodinium paradoxum*, *D. craterum*, and *Melitasphaeridium pseudorecurvatum*, which is also supplemented with some age-diagnostic sporomorphs.
4. Dinoflagellate cysts and sporomorphs are numerous, morphologically diverse, and well preserved in most of the preparations retrieved from the Oligocene Dabaa Formation in the north Western Desert. The general aspect of the preparations is consistent with late Eocene to early Oligocene age. Good analogies exist with associations described from the Oligocene of the Sudan,

Tunisia, and Libya demonstrating common sedimentation environments on the northern margin of Gondwana. These conclusions need further verification based on materials from other localities.

Acknowledgements S.Y.E. is indebted to the Arab Fund Fellowships Programme, Kuwait, for financial support through a Distinguished Scholar Award that allowed one-year research stay hosted by Martin Head (Brock University), their support and generosity are highly appreciated. H.E. acknowledges the financial support from the Alexander von Humboldt Foundation, Germany (EGY-1190326-GF-P). The authors wish to thank Dimiter Ivanov, for his insightful comments and constructive criticism that improved the manuscript.

References

- Abdallah, A. M. (1967). Geology of some gypsum deposits in the north Western Desert of Egypt. *Geological Survey of Egypt, paper no. 41*, 11.
- Abu Seif, E. S. (2015). Geological evolution of Nile Valley, west Sohag, Upper Egypt: A geotechnical perception. *Arabian Journal of Geosciences*, 8, 11049–11072.
- Adegoke, O. S., Jan du Chêne, R. E., Agumanu, A. E., & Ajayi, P. O. (1978). Palynology and the age of the Kerri-Kerri Formation, Nigeria. *Revista Española de Micropaleontología*, 10, 267–283.
- Ahmed, A. B. A., Pocknall, D. T. (1994). The application of palynology to exploration in the Miocene-Pliocene sequence in the Gulf of Suez, Egypt. In *Proceedings of 12th Petroleum Exploration and Production Conference. The Egyptian General Petroleum Corporation*, (pp. 468–481). EGPC, Cairo.
- Aubry, M.-P. (1986). Paleogene calcareous nannoplankton biostratigraphy of northwestern Europe. *Palaeogeography, Palaeoclimatology, Palaeoecology*, 55, 267–334.
- Barron, T. 1907. The topography and geology of the district between Cairo and Suez. *Cairo*, (p. 133). Survey Department of Egypt.
- Bati, Z. (2015). Dinoflagellate cyst biostratigraphy of the upper Eocene and lower Oligocene of the Kirmizitepe Section, Azerbaijan, south Caspian Basin. *Review of Palaeobotany and Palynology*, 217, 9–38.
- Beadnell, H. J. L. (1905). The topography and geology of the Fayum Province of Egypt. *Cairo*, (p. 101). Egypt. Survey Department.
- Blanckenhorn, M. (1921). Ägypten. Handb. Region. *Geol. Bd. I, Hft. 9*. Heidelberg.
- Boureau, E., Cheboldaëff-Salard, M., Koeniguer, J.-C., & Louvet, P. (1983). Evolution des flores et de la vegetation Tertiaires en Afrique, au nord de l'Equateur. *Bothalia*, 14, 355–367.
- Bowen, B. E., & Vondra, C. F. (1974). Paleoenvironmental interpretations of the Oligocene Gabal El Qatrani Formation, Faiyum Depression. *Egypt. Annals of the Geological Survey of Egypt*, 4, 115–138.
- Bown, T. M., & Kraus, M. J. (1988). Geology and paleoenvironment of the Oligocene Jebel El Qatrani Formation and adjacent rocks, Fayum Depression. *Geological Survey. Professional Paper 1452*, 60.
- Bown, T. M., Kraus, M., Wing, S., Fleagle, J., Tiffney, B. H., Simons, E., & Vondra, C. F. (1982). The Fayum primate forest revisited. *Journal of Human Evolution*, 11, 603–632.
- Brinkhuis, H. (1994). Late Eocene to Early Oligocene dinoflagellate cysts from the Priabonian type-area (Northeast Italy): Biostratigraphy and paleoenvironmental interpretation. *Palaeogeography, Palaeoclimatology, Palaeoecology*, 107, 121–163.
- Brinkhuis, H., & Biffi, U. (1993). Dinoflagellate cyst stratigraphy of the Eocene/Oligocene transition in central Italy. *Marine Micropaleontology*, 22, 131–183.
- Brinkhuis, H., Head, M.J., Pross, J., Riding, J.B., Schiøler, P., Sluijs, A., with contributions by Pearce M. A., Weegink J. W., Fensome R., Williams G. L. (2009). Advanced course in Jurassic–Cretaceous–Cenozoic organic-walled dinoflagellate cysts: morphology, paleoecology and stratigraphy. *Urbino, Course Manual, plus two CD*, 246. July 17–21
- Brinkhuis, H., Sengers, S., Sluijs, A., Warnaar, J., Williams, G. L. (2003). Latest Cretaceous to earliest Oligocene, and Quaternary dinoflagellate cysts from ODP Site 1172, East Tasman Plateau. In Exon, N. F., Kennett, J. P., Malone, M. J. (Eds). *Proceedings of the Ocean Drilling Program*, (Vol. 189, pp. 1–48). Scientific Results.
- Chekar, M., Slimani, H., Jbari, H., Guédé, K. E., Mahbou, I., Asebriy, L., & Aassoumi, H. (2018). Eocene to Oligocene dinoflagellate cysts from the Tattofte section, western External Rif, northwestern Morocco: Biostratigraphy, paleoenvironments and paleoclimate. *Palaeogeography, Palaeoclimatology, Palaeoecology*, 507, 97–114.
- Curray, J. R. (1965). Late Quaternary history, continental shelves of the United States, In *The Quaternary of the United States: Princeton*, (pp. 723–735). Princeton University Press.
- De Coninck, J. (1999). Organic-walled phytoplankton biostratigraphy of the Eocene-Oligocene transition in the Kallo borehole and the Rupelian stratotype area (northwestern Belgium). *Bulletin De Société Belge De Géologie*, 105(3–4), 171–209.
- De Coninck, J. (2001). Organic-walled microfossils in the Oligocene Grimmeringen and Neerrep Sand Members from the Grimmeringen type locality. *Geological Survey of Belgium, Professional Paper 2001/2*, 294, 1–57.
- de Verteuil, L., & Norris, G. (1996). Miocene dinoflagellate stratigraphy and systematics of Maryland and Virginia. *Micropaleontology*, 42(Supplement), 1–172.
- Dolson, J., El Barkooky, A., Wehr, F., Gingerich, P.D., Prochazka, N., & Shann, M. (2002). The Eocene and Oligocene Paleo-ecology and Paleo-geography of Whale Valley and the Fayoum Basins. *Implications for Hydrocarbon Exploration in the Nile Delta and Eco-Tourism in the Greater Fayoum Basin* (pp. 1–79). Cairo 2002, AAPG/EPEX/SEG/EGS/EAGE Fieldtrip Guidebook (Nr.).
- Dupéron-Laudoueneix, M., & Dupéron, J. (1995). Inventory of Mesozoic and Cenozoic woods from Equatorial and North Equatorial Africa. *Review of Palaeobotany and Palynology*, 84, 439–480.
- Eisawi, A., & Schrank, E. (2008). Upper Cretaceous to Neogene palynology of the Melut Basin, Southeast Sudan. *Palynology*, 32, 101–129.
- El Akkad, S., & Dardir, A. A. (1966). Geology of Red Sea coast between Ras Shagra and Mersa Alam with Short Note on Results of Exploratory Work at Gebel El-Rusas Lead-Zinc Deposits. *Geological Survey of Egypt*, 35, 67.
- El Atfy, H., Brocke, R., & Uhl, D. (2013). Age and paleoenvironment of the Nukhul Formation, Gulf of Suez, Egypt: Insights from palynology, palynofacies and organic geochemistry. *GeoArabia*, 18 (4), 137–174.
- El Atfy, H., Brocke, R., & Uhl, D. (2017). Miocene palynology of the Rudeis and Kareem formations (Gharandal Group), GH 404–2A Well, Gulf of Suez. *Egypt. Abhandlungen Der Senckenberg Gesellschaft Für Naturforschung*, 573, 1–134.
- El Atfy, H., El Beialy, S. Y., El Khoriby, E. M., & Uhl, D. (2021). Continental palynomorphs from the Dabaa Formation, North-Western Desert, Egypt: A contribution to the reconstruction of the vegetation on the southern shores of the Tethys during the Early Oligocene. *Botanical Journal of the Linnean Society*, 197, 291–321.

- El Atfy, H., El Beialy, S. Y., Zobaa, M. K., Taha, A. A., & Uhl, D. (2022). A snapshot into the Oligocene vegetation of the Tethyan southern shores: new fossil pollen evidence from North Africa (Egypt). *Palynology*. <https://doi.org/10.1080/01916122.2021.2023057>.
- El-Bassiouni, A. E., Ayyad, S. N., & El-Beialy, S. Y. (1988). On the Eocene/Oligocene boundary in the Alam El-Bueib-IX, Western Desert. *Egypt. Revista Española De Micropaleontología*, 20, 59–70.
- El-Beialy, S. Y. (1988a). The dinocyst biostratigraphy of the Upper Eocene subsurface sediments, west Nile Delta. *Egypt. Newsletters on Stratigraphy*, 19, 131–141.
- El Beialy, S. Y. (1988b). Palynostratigraphy of Late Tertiary sediments in Kafr El- Dawar well No. 1, Nile Delta. *Egypt. Revue De Micropaléontologie*, 30, 249–260.
- El-Beialy, S. Y. (1990a). Tertiary dinoflagellate cysts from the Mit Ghamr-1 well, Nile Delta. *Egypt. Review of Palaeobotany and Palynology*, 63, 259–267.
- El-Beialy, S. Y. (1990b). Palynology, palaeoecology, and dinocyst stratigraphy of the Oligocene through Pliocene succession in the Qantara-1 well, Eastern Nile Delta. *Egypt. Journal of African Earth Sciences*, 11, 291–307.
- El Beialy, S. Y., & Ali, A. S. (2002). Dinoflagellates from the Miocene Rudeis and Kareem formations borehole GS-78-1, Gulf of Suez. *Egypt. Journal of African Earth Sciences*, 35, 235–245.
- El-Beialy, S. Y., & Gheith, A. M. (1989). Dinocyst biostratigraphy and depositional environments of the subsurface Miocene sequence, north Sinai. In Morsi, A. M. (Ed.). *Proceedings of the 2nd Conference on the Geology of Sinai for Development* (pp.73–85). Ismailia, Egypt.
- El Beialy, S. Y., Head, M. J., El Atfy, H., & El Khoriby, E. M. (2019). Dinoflagellate cyst evidence for the age and palaeoenvironments of the Upper Eocene-Oligocene Dabaa Formation, Qattara Depression, north Western Desert. *Egypt. Palynology*, 43, 268–291.
- El-Beialy, S., & Kora, M. (1987). Late Cretaceous-Early Tertiary palynomorphs from Darb El Arbain, southern Egypt. *Bulletin of the Faculty of Science, Mansoura University*, 14, 343–358.
- El Beialy, S. Y., Mahmoud, M. S., & Ali, A. S. (2005). Insights on the age, climate and depositional environments of the Rudies and Kareem formations, GS-78-1 Well, Gulf of Suez, Egypt: A palynological approach. *Revista Española De Micropaleontología*, 37, 273–289.
- El-Beialy, S. Y., & Shahin, A. M. (1990). Planktonic foraminifera and dinoflagellate cysts across the Cretaceous/Tertiary boundary in the Nile Delta area. *Egypt. Neues Jahrbuch für Geologie und Paläontologie, Abhandlungen*, 180, 117–137.
- El Beialy, S. Y., Zobaa, M. K., & Taha, A. A. (2016). Depositional paleoenvironment and hydrocarbon source potential of the Oligocene Dabaa Formation, north Western Desert, Egypt: A palynofacies approach. *Geosphere*, 12, 346–353.
- El Deftar, T., & Issawi, B. (1977). *Geological map of Libya; 1: 250,000. Sheet: Al Bardia NH 35-1* (p. 93). Explanatory Booklet. Industrial Research Centre.
- El Heiny, I., & Enani, N. (1996). Regional stratigraphic interpretation pattern of Neogene sediments, northern Nile Delta, Egypt. *Proceedings of 13th Petroleum Exploration and Production Conference, The Egyptian General Petroleum Corporation, EGPC, Cairo*, pp. 270–290.
- El Heiny, I., Morsi, S. (1992). Stratigraphic correlation of Neogene sediments in the eastern Nile Delta and Gulf of Suez, Egypt. *Proceedings of 11th Petroleum Exploration and Production Conference, The Egyptian General Petroleum Corporation, EGPC, Cairo*, pp. 166–193.
- El Hinnawi, M., Abdallah, A. M., & Issawi, B. (1978). Geology of Abu Bayan - Bolaq stretch, Western Desert. *Egypt. Annals of the Geological Survey of Egypt*, 8, 19–50.
- Eldrett, J. S., Harding, I. C., Firth, J. V., & Roberts, A. P. (2004). Magnetostratigraphic calibration of Eocene-Oligocene dinoflagellate cyst biostratigraphy from the Norwegian-Greenland Sea. *Marine Geology*, 204, 91–127.
- El-Mehdawi, A. D., & El Beialy, S. Y. (2008). Palynological contribution to the stratigraphy of the Al Faidiyah Formation, Al Jabal Al Akhdar, NE Libya. In M. J. Salem (Ed.), *The Geology of East Libya: Third symposium on the sedimentary basins of Libya* (pp. 171–186). Earth Science Society of Libya.
- El-Saadawi, W., Kamal-El-Din, M., Wheeler, E., Osman, R., El-Faramawi, M., & El-Noamani, Z. M. (2014). Early Miocene woods of Egypt. *IAWA Journal*, 35(1), 35–50.
- El-Saadawi, W.E., Nour-El-Deen, S., El-Noamani, Z.M., Darwish, M. H., Kamal El-Din, M.M. (2020). Fossil Flora of Egypt. In: Hamimi, Z. et al. (Eds). *The Geology of Egypt. Regional Geology Reviews*. (pp. 495–520), Cham: Springer.
- El-Sabrouty, M. N. (1984). Palynological studies of some Tertiary sedimentary rocks from the north Western Desert of Egypt. Unpublished Ph.D. thesis, (p. 123). Assiut, Egypt, Assiut University.
- Emery, K. O. (1968). Relict sediments on continental shelves of world. *AAPG Bulletin*, 52, 445–464.
- Erkmen, U., & Sadek, A. (1981). Contribution to the stratigraphy of the Germav Formation, (Late Cretaceous-Early Tertiary), in southeast Turkey by means of dinoflagellates and nannoplankton. *Neues Jahrbuch Für Geologie Und Paläontologie Monatshefte*, 3, 129–140.
- Fensome, R. A., Crux, J. A., Gard, I. G., MacRae, R. A., Williams, G. L., Thomas, F. C., Fiorini, F., & Wach, G. (2008). The last 100 million years on the Scotian Margin, offshore eastern Canada: An event-stratigraphic scheme emphasizing biostratigraphic data. *Atlantic Geology*, 44, 93–126.
- Fensome, R. A., Williams, G. L., & MacRae, R. A. (2009). Late Cretaceous and Cenozoic fossil dinoflagellates and other palynomorphs from the Scotian Margin, offshore eastern Canada. *Journal of Systematic Palaeontology*, 7, 1–79.
- Firth, J. V., Eldrett, J. S., Harding, I. C., Coxall, H. K., & Wade, B. S. (2012). Integrated biomagnetostratigraphy for the Palaeogene of ODP Hole 647A: implications for correlating palaeoceanographic events from high to low latitudes. In Jovane, L., Herrero-Bervera, E., Hinnov, L. A., Housen, B. A. (Eds). *Magnetic methods and the timing of geological processes* (Vol. 373, pp. 29–78). Geological Society, Special Publications.
- Gedl, P., & Leszczynski, S. (2005). Palynology of the Eocene-Oligocene Transition in the Marginal Zone of the Magura Nappe at Folsz (Western Carpathians, Poland). *Geologica Carpathica (geologicky Zbornik)*, 56, 155–167.
- Germeraad, J. H., Hopping, C. A., & Muller, J. (1968). Palynology of Tertiary sediments from tropical areas. *Review of Palaeobotany and Palynology*, 6, 189–348.
- Gradstein, F. M., Ogg, J. G., Smith, A. G., Agterberg, F. P., Bleeker, W., Cooper, R. A., Davydov, V., Gibbard, P., Hinnov, L. A., House, M. R. (†), Lourens, L., Luterbacher, H-P., McArthur, J., Melchin, M. J., Robb, L. J., Shergold, J., Villeneuve, M., Wardlaw, B. R., Ali, J., Brinkhuis, H., Hilgen, F. J., Hooker, J., Howarth, R. J., Knoll, A. H., Laskar, J., Monechi, S., Powell, J., Plumb, K. A., Raffi, I., Röhl, U., Sanfilippo, A., Schmitz, B., Shackleton, N. J., Shields, G. A., Strauss, H., Van Dam, J., Veizer, J., van Kolfshoten, Th., Wilson, D. (2004). *A Geologic Time Scale 2004*. Cambridge University Press, 589 p.

- Gruas-Cavagnetto, C., & Barbin, V. (1988). Les dinoflagellates du Priabonien stratotypique (Vicentin, Italy); mise en évidence du passage Eocene/Oligocene. *Revue De Paléobiologie*, 7, 163–198.
- Hantar, G. (1990). North Western Desert. In R. Said (Ed.), *The Geology of Egypt* (pp. 293–319). Elsevier.
- Head, M. J., Norris, G. (1989). Palynology and dinocyst stratigraphy of the Eocene and Oligocene in ODP Leg 105 Hole 647A, Labrador Sea. In Srivastava, S. P., Arthur, M., Clement, B., et al. (Eds). *Proceedings, Ocean Drilling Program, Scientific Results 105; College Station (TX): Ocean Drilling Program* (pp. 515–550), 3 tables (one as back-pocket foldout).
- Heilmann-Clausen, C., & van Simaëys, S. (2005). Dinoflagellate cysts from the middle Eocene to ?lowermost Oligocene succession in the Kysing Research Borehole, central Danish Basin. *Palynology*, 29, 143–204.
- Helenes, J., & Cabrera, D. (2003). Oligocene-Miocene palynomorph assemblages from Eastern Venezuela. *Palynology*, 27, 5–25.
- Hochuli, P. A. (1978). Palynologische Untersuchungen im Oligozän und Untermiozän der Zentralen und Westlichen Paratethys. *Beiträge Zur Paläontologie Von Österreich*, 4, 1–132.
- Ibrahim, S. M. (2008). *Stratigraphic, sedimentologic and mineralogic studies on the Oligocene red beds and the associated volcanics of El Fayoum and greater Cairo district* (p. 150). Egypt. Unpublished MSc.
- Ikegwuonu, O. N., Umeji, O. P., Chiaghanam, O. I., Nwozor, K. K., Ndukwe, O. S., & Chiadikobi, K. C. (2020). Palynomorph assemblage biozonation of Paleogene strata in Bende-Umuahia Area, Niger Delta Basin, southeastern Nigeria. *Journal of Palaeogeography*, 9, 13.
- Issawi, B., Francis, M. H., Youssef, E. A. A., Osman, R. A. (2009). The Phanerozoic geology of Egypt. A Geodynamic Approach. In *2nd edition. Cairo: Ministry of Petroleum* (Vol. 81, p. 589). The Egyptian Mineral Resources Authority, Special Publication.
- Issawi, B., & McCauley, J.F. (1993). The Cenozoic landscape of Egypt and its river systems. *Annals of the Geological Survey of Egypt XIX*, 357–384.
- Issawi, B., & Osman, R. (2008). Egypt during the Cenozoic: Geological history of the Nile River. *Bulletin of the Tethys Geological Society 3. Cairo*, 3, 43–62.
- Jacobs, B. F., Pan, A. D., & Scotese, C. R. (2010). A review of the Cenozoic vegetation history of Africa. In L. Werdelin & W. J. Sanders (Eds.), *Cenozoic mammals of Africa* (pp. 57–72). University of California Press.
- Jan du Chêne, R. E., Onyike, M. S., & Sowunmi, M. A. (1978). Some new Eocene pollen of the Ogwashi-Asaba Formation, Southeastern Nigeria. *Revista Española De Micropaleontología*, 10, 285–322.
- Jaramillo, C. A., & Oboh-Ikuenobe, F. E. (1999). Sequence stratigraphic interpretations from palynofacies, dinocyst and lithological data of Upper Eocene—Lower Oligocene strata in Southern Mississippi and Alabama, U.S. Gulf Coast. *Palaeogeography, Palaeoclimatology, Palaeoecology*, 145, 259–302.
- Jaramillo, C. A., & Oboh-Ikuenobe, F. E. (2001). Sequence stratigraphy of the Pachuta-Marianna interval (Upper Eocene-Lower Oligocene) in the U.S. Gulf Coast. In: Goodman, D. K., & Clarke, R. T. (Eds.). *Proceedings of the IX International Palynological Congress* (pp. 263–276). AASP Foundation, Houston (TX).
- Kaska, H. V. (1989). A spore and pollen zonation of Early Cretaceous to Cenozoic nonmarine sediments in central Sudan. *Palynology*, 13, 79–90.
- Kedves, M. (1971). Présence de types sporomorphes importantes dans les sédiments préquaternaires Egyptiens. *Acta Botanica Academiae Scientiarum Hungaricae, Tomus*, 17, 371–378.
- Kedves, M. (1984). Études Palynologiques sur les sédiments préquaternaires de l'Égypte. *Danien. Revista Española De Micropaleontología*, 16, 43–50.
- Kedves, M. (1985). Études palynologiques sur les sédiments préquaternaires de l'Égypte. *Oligocene. Revista Española De Micropaleontología*, 17, 333–346.
- Kedves, M. (1986). Études palynologiques sur les sédiments préquaternaires de l'Égypte. *Eocene. Revista Española De Micropaleontología*, 18, 5–26.
- Khanna, A. K. (1979). Subathus: Stratigraphic status and nomenclature. *Himalayan Geology*, 8(1), 209–223.
- Klitzsch, E., List, F. K., & Pohlmann, G. (1987). Geological Map of Egypt. Conoco Coral and Egyptian General Petroleum Company, Cairo, Egypt, 24 Sheets, scale 1:500,000.
- Köthe, A., & Piesker, B. (2007). Stratigraphic distribution of Paleogene and Miocene dinocysts in Germany. *Revue De Paléobiologie*, 26(1), 1–39.
- Köthe, A., Piesker, B. (2008). Stratigraphic distribution of Paleogene and Miocene dinocysts in Germany. *Bundesanstalt für Geowissenschaften und Rohstoffe*, 1–36.
- Kräusel, R. (1939). Ergebnisse der Forschungsreisen Prof. E. Stromers in den Wüsten Ägyptens, IV. Die fossilen Floren Ägyptens 3. Die fossilen Pflanzen Ägyptens, *E-1: Abhandlungen der Bayerischen Akademie der Wissenschaften*, 47, 1–140.
- Kräusel, R., Stromer E. (1924). Ergebnisse der Forschungsreisen Prof. E. Stromers in den Wüsten Ägyptens, IV. Die fossilen Floren Ägyptens 1–3. *A–C. Abhandlungen der Bayerischen Akademie der Wissenschaften*, 30(2), 1–48.
- Kuss, J., & Boukhary, M. A. (2008). A new upper Oligocene marine record from northern Sinai (Egypt) and its paleogeographic context. *GeoArabia*, 13(1), 59–84.
- Lansbery, L. (2011). Geological and geomorphological evolution of the Egyptian Nile between Aswan and Kom Ombo. In *A remote sensing and field study approach* (p. 83). MS Thesis. Missouri University of Science and Technology, Rolla, MO.
- Legoux, O. (1978). Quelques espèces de pollen caractéristiques du Néogène du Nigéria. *Bulletin Des Centres De Recherche Exploration-Production Elf-Aquitaine.*, 2, 265–317.
- Louvet, P. (1971). Sur l'évolution des flores tertiaires de l'Afrique nord-équatoriale. Thèse de Doctorat, (5613, p. 497). Paris CNRS n AO.
- Louwey, S., De Coninck, J., & Verniers, J. (2000). Shallow marine Lower and Middle Miocene deposits at the southern margin of the North Sea Basin (northern Belgium): Dinoflagellate cyst bio-stratigraphy and depositional history. *Geological Magazine*, 137, 381–394.
- Mahmoud, M. S. (1998). Palynology of Middle Cretaceous-Tertiary sequence of Mersa Matruh-1 well, northern Western Desert. *Egypt. Neues Jahrbuch für Geologie und Paläontologie, Abhandlungen*, 209, 79–104.
- Mahran, T., El Shater, A., Youssef, A., El Haddad, B. (2013). Facies analysis and tectonic-climatic controls on development of Pre-Eonile sediments of the Egyptian Nile west Sohag. In *7th International Conference on the Geology of Africa*, Assiut, Egypt (abstract).
- Meneisy, M. Y., & Abdel-Aal, A. Y. (1984). Geochronology of Phanerozoic volcanic activity. *Egypt. Bulletin of the Faculty of Science, Ain Shams University Bulletin, Faculty of Science, Ain Shams University, Cairo, Egypt*, 24, 163–176.
- Meshref, W. M. (1990). Tectonic Framework. In R. Said (Ed.), *The Geology of Egypt* (pp. 113–155). Balkema.
- Mohamed, O., Mahdy, F., & Tahoun, S. S. (2020). Palynofacies analysis and source rock evaluation of the Upper Cretaceous-Oligocene succession in the Drazia-1 well, Alamein Basin. *Egypt. Arabian Journal of Geosciences*, 13, 1192.

- Muller, J., Di Giacomo, E., & van Erve, A. W. (1987). A palynological zonation for the Cretaceous, Tertiary and Quaternary of northern South America. *AASP Contribution Series*, 19, 7–76.
- Norton, P. (1967). Rock stratigraphic nomenclature of the Western Desert. *Cairo, Egypt* (p. 557). Pan-American Oil Company. Internal Report.
- Osman, R. (2003). New findings in the Eocene stratigraphy of Gebel Ataq-Northern Galala. *North Eastern Desert, Egyptian Journal of Sedimentology*, 11, 95–109.
- Ouda, K. (1998). Biostratigraphy, paleoecology and paleogeography of the middle and late Tertiary deposits of the northern Western Desert. *Egypt. Neues Jahrbuch für Geologie und Paläontologie, Abhandlungen*, 207, 311–394.
- Pavoni, N. (1993). Pattern of mantle convection and Pangea breakup, as revealed by the evolution of the African Plate. *Journal of the Geological Society*, 150, 927–964.
- Philobos, E. R., & Abdel Rahman, M. A. (1990). Remarks on lithostratigraphy and sedimentological history of the Pliocene (?) sediments of the Qena area: Bulletin of the Faculty of Science. *Assiut University*, 19, 15–33.
- Poulsen, N. E., Manum, S. B., Williams, G. L., & Ellegaard, M. (1996). Tertiary dinoflagellate biostratigraphy of Sites 907, 908, and 909 in the Norwegian-Greenland Sea. In Thiede, J., Myhre, A. M., Firth, J. V., Johnson, G. L., Ruddiman, W. F. (Eds) *Proceedings of the Ocean Drilling Program* (pp. 255–287). Scientific Results 151. Ocean Drilling Program, College Station.
- Powell, A. J. (1986). A dinoflagellate cyst biozonation for the Late Oligocene to Middle Miocene succession of the Langhe Region, Northwest Italy. In Wrenn, J. H., Duffield, S. L., & Stein, J. A. (Eds) *Papers from the First Symposium on Neogene Dinoflagellate Cyst Biostratigraphy* (pp. 105–128) AASP Contributions Series 17. Dallas (TX): AASP Foundation.
- Powell, A. J., Brinkhuis, H., & Bujak, J. P. (1996). Upper Paleocene-Lower Eocene dinoflagellate cyst sequence biostratigraphy of Southeast England. In Knox, R. W. O et al. (Eds) *Correlation of the Early Paleogene in Northwest Europe* (Vol. 101, pp. 145–183). Geological Society Special Publication.
- Pross, J., Houben, A. J. P., van Simaey, S., Williams, G. L., Kotthoff, U., Coccioni, R., Wilpshaar, M., & Brinkhuis, H. (2010). Umbria-Marche revisited: A refined magnetostratigraphic calibration of dinoflagellate cyst events for the Oligocene of the Western Tethys. *Review of Palaeobotany and Palynology*, 158, 213–235.
- Said, R. (1962). The geology of Egypt (p. 377). Elsevier.
- Said, R. (1981). The geological evolution of the River Nile (p. 151). Springer Verlag, viii +.
- Salard-Chebouldaëff, M. (1978). Sur la palynoflore Maestrichtienne et Tertiaire du Bassin Sédimentaire littoral du Cameroun. *Pollen Et Spores*, 20, 215–260.
- Salard-Chebouldaëff, M. (1979). Palynologie Maestrichtienne et Tertiaire du Cameroun. Etude qualitative et répartition verticales des principales espèces. *Review of Palaeobotany and Palynology*, 28, 365–388.
- Salard-Chebouldaëff, M. (1990). Intertropical African palynostratigraphy from Cretaceous to Late Quaternary times. *Journal of African Earth Sciences*, 11, 1–24.
- Salem, R. (1976). Evolution of Eocene-Miocene sedimentation patterns in parts of northern Egypt. *American Association of Petroleum Geologists Bulletin*, 60, 34–64.
- Shukri, N. M. (1954). Remarks on geological structure of Egypt. *Bulletin de la Societe de Geographie d'Egypte*, 27, 65–82.
- Śliwińska, K. K., Abrahamsen, N., Beyer, C., Brünings-Hansen, T., Thomsen, E., Ulleberg, K., & Heilmann-Clausen, C. (2012). Bio- and magnetostratigraphy of Rupelian–mid Chattian deposits from the Danish land area. *Review of Palaeobotany and Palynology*, 172, 48–69.
- Soliman, A., Ćorić, S., Head, M. J., Piller, W. E., & El Beialy, S. Y. (2012). Lower and Middle Miocene biostratigraphy, Gulf of Suez, Egypt based on dinoflagellate cysts and calcareous nannofossils. *Palynology*, 36, 38–79.
- Sonne, V., & Weiler, H. (1984). The Lower Tertiary, (Oligocene), detritic fauna and flora elements in the sediments of the Meerfelder Maar. *Courier Forschungsinstitut Senckenberg*, 65, 87–95.
- Stead, D. T., & Awad, M. Z. (2005). Palynological zonation of Cenozoic non-marine sediments, Muglad Basin, Sudan. In Powell, A. J., & Riding, J. B. (Eds) *Recent Development in Applied Biostratigraphy* (pp. 161–178). The Micropalaeontological Society, Special Publications.
- Stover, L. E. (1977). Oligocene and early Miocene dinoflagellates from Atlantic Corehole 5/5B, Blake Plateau. In Sullivan, H. J., Brideaux, W. W., & Elsik, W.C. (Eds) *Contributions of stratigraphic palynology (with emphasis on North America)* (Vol. 1, pp. 66–89). Cenozoic Palynology. AASP Contributions Series 5A. Dallas (TX): AASP Foundation.
- Strauss, C. (1993). Taxonomy and biostratigraphy of marine microplankton within the Oligocene-Middle Miocene of East Germany. *Disseration Bergakademie Freiberg* (p. 110).
- Stull, G. W., Tiffney, B. H., Manchester, S. R., Del Rio, C., & Wing, S. L. (2020). Endocarps of *Pyrenacantha* (Icacinaeae) from the early Oligocene of Egypt. *International Journal of Plant Sciences*, 181, 432–442.
- Takahashi, J., & Jux, U. (1989a). Palynologic investigation of Late Eocene to Early Oligocene lignites from Fayum Oasis. *Egypt. Bulletin of the Faculty of Liberal Arts, Nagasaki University, Natural Science*, 29, 369–463.
- Takahashi, J., & Jux, U. (1989b). Palynology of Middle Cenozoic lacustrine deposits from the Jos Plateau, Nigeria. *Bulletin of the Faculty of Liberal Arts, Nagasaki University, Natural Science*, 29, 181–367.
- Toricelli, S., & Biffi, U. (2001). Palynostratigraphy of the Numidian Flysch of Northern Tunisia (Oligocene–Early Miocene). *Palynology*, 25, 29–55.
- van Mourik, C. A., & Brinkhuis, H. (2005). The Massignano Eocene-Oligocene golden spike section revisited. *Stratigraphy*, 2, 13–30.
- van Simaey, S., Munsterman, D., & Brinkhuis, H. (2005). Oligocene dinoflagellate cyst biostratigraphy of the southern North Sea Basin. *Review of Palaeobotany and Palynology*, 134, 105–128.
- Weiler, H. (1982). Inventory of the phytoplankton (dinoflagellate cysts, Prasinophyceae and Calciodinelloideae) in the Pre-Aquitania Tertiary of the Mainz Basin. *Mainzer Geowissenschaftliche Mitteilungen*, 10, 13–17.
- Wescott, W. A., Krebs, W. N., Bentham, P. A., & Pocknall, D. T. (2000). Miocene brackish water and lacustrine deposition in the Suez Rift, Sinai. *Egypt. PALAIOS*, 15, 65–72.
- Williams, G., & Small, J. (1984). A study of the Oligo-Miocene basalts in the Western Desert. In: *Proceedings of the 7th Petroleum Exploration and Production Conference, The Egyptian General Petroleum Corporation, Cairo* (pp. 252–268), EGPC.
- Williams, G. L., Brinkhuis, H., Pearce, M. A., Fensome, R. A., & Weegink, J. W. (2004). Southern Ocean and global dinoflagellate

cyst events compared: index events for the Late Cretaceous–Neogene. In: Exon, N. F., Kennett, J. P., & Malone, M. J. (Eds), *Proceedings of the Ocean Drilling Program, Scientific Result* (Vol. 189, pp. 1–98). College Station (TX): Ocean Drilling Program.

- Wilson, G. J. (1971). Observations on European Late Cretaceous dinoflagellate cysts. Part 1. In *Proceedings of the 2nd Planktonic Conference, 1970*, (Vol. 2, pp. 1259–1275) Edizioni Tecnoscienza.
- Zevenboom, D. (1995). Dinoflagellate cysts from the Mediterranean Late Oligocene and Miocene. PhD thesis. Den Haag: State University of Utrecht and CIP-Gegevens Koninklijke Bibliotheek (p 221)
- Zosimovich, V. Y. (1991). A boundary of Oligocene and Miocene in the Boreal Province of the East-European Platform. *Geologicheskii Zhurnal*, 3, 89–98.



Salah Y. El Beialy is an emeritus professor of palynology at Mansoura University (Egypt), and was Head of its Geology Department in 2011–2013. He has long been involved in stratigraphical palynology. He received an M.Sc degree in 1980 from Mansoura University and a Ph.D in 1985 from the University of Sheffield (UK) and acquired experience in industrial palynology through work with Paleoservices Ltd., Shell, BP and GUPCO, Egypt. In 2006, he spent a year as a Visiting International Scholar at Brock University

(Canada). His main interests are in the application of palynology in dating, paleoenvironmental interpretation, spore-colour maturity determination, and hydrocarbon exploration in the surface and subsurface Palaeozoic–Cenozoic of North Africa and the Middle East. He received the Mansoura University Prize for Scientific Excellence in 2009.



Ahmed Mohamed is an assistant professor at Mansoura University (Egypt), from which he received an M.Sc degree in applied sedimentology, and a Ph.D in geology (sedimentary rocks and sedimentation) in 2018. His research interests cover most aspects of sedimentology and its applications in industry, and is a joint author of several publications in this subject. He has 13 years of research and field experience studying the stratigraphy and sedimentary rocks of some of Egypt's outcrops (e.g. Cretaceous and Eocene of the Bahariya Oasis, Eocene of the

Minya Governorate, and Cretaceous–Paleogene successions at the Dakhla Oasis and the Red Sea). He has more recently become involved in the reservoir characterization of the Nile Delta province.



Mohamed K. Zobaa is an assistant professor at the University of Texas Permian Basin (USA). He received a Ph.D degree in geology and geophysics from Missouri University of Science and Technology (USA). He leads the palynology and sedimentary organic matter research group at his institution, focusing primarily on the accumulation, distribution, and diagenesis of organic matter in time and space, and how they can be used to characterize petroleum systems through the interpretation

of depositional paleoenvironments, kerogen type, and organic thermal maturity. He has over 20 years of research experience studying the stratigraphy, palynology, and sedimentary organic matter content of some of the world's most important hydrocarbon-generating provinces (e.g., Gulf of Mexico, the Permian Basin in Texas, the San Juan Basin in New Mexico, the Williston Basin in North Dakota, and the North Western Desert of Egypt). He is the recipient of the prestigious University of Texas System's Rising STARS Award (\$500,000) which he used to establish his Sedimentary Organic Matter and Hydrocarbon Source-Rock Research Laboratory, the first of its kind in the Permian Basin area that provides comprehensive research and development support to the local hydrocarbon exploration and production operators.



Asmaa A. Taha has been an assistant lecturer in the Department of Geology, Faculty of Science, Mansoura University (Egypt) since 2019, from where she received B. Sc (2011) and M.Sc (2019) degrees in geology. Her main interests are in Paleogene palynology and its applications in age dating, paleoenvironmental interpretation, palaeoecology, palaeoclimatology, and palynofacies and its uses in hydrocarbon exploration. She is a joint author on a number of publications dealing with the Paleogene palynology and palynofacies of the north Western Desert, Egypt.



Dieter Uhl is the head of the Department of Palaeontology at the Senckenberg Research Institute and Natural History Museum in Frankfurt am Main (Germany) and also adjunct professor at Tübingen University (Germany). He was awarded his Diploma in biology in 1994 from the Technical University of Kaiserslautern (Germany) and his Ph.D (Dr. rer. nat.) in paleontology in 1999 from the University of Tübingen. After doing research at Münster University (Germany), Utrecht University (The Netherlands)

and Tübingen University (Germany), he joined the Senckenberg Research Institute and Natural History Museum in Frankfurt am Main (Germany) in 2007. He is a member of the International Organisation of Paleobotany, Paläontologische Gesellschaft, and a fellow of the Linnean Society of London. His main research interest is on the use of fossil plants (macroremains and palynomorphs) as paleoenvironmental proxies. So far he has published more than 200, mostly peer reviewed, scientific papers and book chapters. His works span a wide variety of topics, stratigraphically ranging from the Carboniferous up to the Pliocene, with a focus on the former supercontinent Gondwana.



Haytham El Atfy is an associate professor at Mansoura University (Egypt) from where he received a B.Sc degree in geology and an M.Sc in palynology. He received a Ph.D in geosciences (palynology and organic geochemistry) from Goethe University, Frankfurt (Germany) in 2014, and PD (Habilitation) from the University of Tübingen (Germany) in 2022. He acquired experience in industrial palynology through work with GUPCO (BP), Egypt. Haytham has been a Research Fellow of the

Alexander von Humboldt Foundation at the University of Tübingen (Germany) since 2019. He was recently a visiting scientist at the Senckenberg Research Institute, Germany. His research interests span all aspects of palynology and its applications in dating, palaeoenvironmental and palaeoclimatical reconstructions, and hydrocarbon exploration, particularly of the Mesozoic and Cenozoic and, to a lesser extent, the Palaeozoic. He has more recently become involved in organic geochemistry. He is a member of the AASP—The Palynological Society, the Micropalaeontological Society (TMS), Arbeitskreis für Paläobotanik und Palynologie (APP), and the Paleontological Society of Egypt (PSE). He is a recipient of many awards, including the Bernd Rendel Prize from the German Science Foundation (DFG), Egyptian State Incentive Award, and the First-Class Excellence Concession that is provided by the Egyptian president.



Quaternary Environmental and Climatic Changes in Egypt: Proxies from Sedimentary Records

Hesham M. El-Asmar

Abstract

The Quaternary sediments in Egypt record the interplay of several factors, the most important of which are marine, fluvial, terrestrial and climatic factors. According to the strength of each factor, the Egyptian territories are subdivided into several basins reflecting the potential depositional environments. The present review promotes the Quaternary sediments of the Nile Delta, the North Western coast, the Western Desert and the Red Sea and Gulf of Aqaba coasts as proxies for Quaternary paleoclimate. The Quaternary Nile Delta sediments clearly reflect the African monsoons and the associated Nile floods correlated with the Eastern Mediterranean and global marine isotope stratigraphy. The fossil records of both planktonic and benthonic foraminifera (Pl/Be) and their $\delta^{18}\text{O}$ represent potential references to Marine Isotope Stages (MIS) and sea level changes. Pollen and spores, $\delta^{13}\text{C}$, C_3 and C_4 plants record paleovegetation cover, and thus paleoenvironments and paleoclimate. It has been globally agreed that the primary control of climate changes and the region's hydrological cycle are the insolation-driven changes in the strength and shifting of the Intertropical Convergence Zone (ITCZ), and therefore the intensity and northward extent of the African Humid Period (AHP), non-excluding the Atlantic westerlies (NAO). Such conditions induced intervals of heavy rainfall in Egypt as well as the Nile Headwaters. In Egyptian Sahara, such heavy rains charged the groundwater and dissolved the Paleocene–Eocene carbonate leaving deposits of lacustrine and freshwater carbonate and other karstic landforms. These terrestrial deposits supported with the calibrated age dating are used as proxies for paleoclimate along the Sahara. At the Red Sea coast, the growth of coral reefs and deposition of thick

fluvial gravels are used as proxies for climate and sea level changes, while the aeolianites and paleosols are the available proxies at the NW Mediterranean coast of Egypt. On the other hand, the increase in outflow of the River Nile led to stagnation of freshwater over the marine water and formation of sapropel layers in Eastern Mediterranean. The oxygen isotopes and age determination of the above-mentioned materials allow correlation with global climate conditions; however, such correlation is not always isochronic. The offsets are explained by the presence of regional driving forces overriding the global influences.

Keywords

Quaternary geology • Nile Delta sediments • NW calcarenite ridges • Red sea coast • Egyptian Sahara • Isotope stratigraphy • Paleoclimate

1 Introduction

Since the nineteenth century, the distribution and spread of glacial materials in the landscape, particularly tills, erratic rocks and associated meltwater deposits connected to various eras in the past with more widespread glaciation, have served as the foundation for Quaternary history. In order to categorize these climate changes, James Geikie from the University of Edinburgh (1839–1915), among others, used the words “glacial” and “interglacial”. The existence of intercalated fossil-bearing layers gave evidence that temperate climatic episodes interposed. Following that, a climate stratigraphy was created using these terms for subdividing the Quaternary. The Alpine successions (Penck & Brückner, 1911), sea level changes chronology (Evans, 1971; Zeuner, 1959) and more recent marine oxygen isotope and polar ice-core stratigraphies all of which represent new insights into understanding the climatic drivers of these

H. M. El-Asmar (✉)
Geology Department, Faculty of Science, Damietta University,
New Damietta 34517, Egypt
e-mail: hmelasmr@yahoo.com

alternating sediments. Terrestrial evidences served as the basis for the division of Quaternary time until the late 1960s and early 1970s, when the implications of the marine isotope succession were recognized (Berger, 1992; Broecker & Van Donk, 1970; Hays et al., 1976; Shackleton, 1967; Shackleton & Opdyke, 1973). Today, the differences between marine and terrestrial-based classification could not be great, with many abandoning of the terrestrial chronostratigraphic classification in favour of the ocean-floor isotope and ice-core stratigraphies. The timescale to which both the marine isotope and ice-core records are tuned has been predicated on the hypothesis that orbital forcing is the principal cause of the cyclic oscillations in marine oxygen isotopes (Dansgaard et al., 1985; Hays et al., 1976; Imbrie & Imbrie, 1980; Imbrie et al., 1984; Lisiecki & Raymo, 2005; Ruddiman et al., 1989). Marine isotope on ice-core sequences provide a solid framework, but it is important to keep in mind that these sequences, particularly those found in sediments at the ocean's bottom, record changes on a global scale, which is not always the case with terrestrial sequences that reflect both global and regional changes. This is why it is important to carefully consider any direct association between sedimentary sequences on land and those in the oceans and ice cores, and the simple mechanical correlation is often inappropriate (Gibbard & Hughes, 2021). For example, wet intervals in arid regions may correlate with glacial rather than interglacial stages due to local or regional conditions (Jimenez, 2014; Revel et al., 2010; Szabo et al., 1995). Nonetheless, terrestrial Quaternary sediments still contain potential paleoclimate signatures. This chapter reviews some examples of Quaternary sediments that provide a record of the paleoclimatic history of Egypt.

Egypt lies between two sedimentary basins, the Eastern Mediterranean basin with its characteristic sapropel layers and the East Africa basin, which record the monsoonal cycles. The terrestrial sequences are driven by the interplay of forcing factors from these two basins. River Nile is the critical artery, which connects the two basins and helps in recording the response of changes from one basin to the other. Accordingly, the present chapter will focus on four areas that reflect the interrelationship between the two basins (Fig. 1a). The Nile Delta area (Fig. 1a; area 1; Fig. 1b) is the first where several studies on the Quaternary stratigraphy had been carried out by the Department of Geology at Mansoura University over the last 50 years. Also, the Mediterranean Basin (MEDIBA) team at the Smithsonian Institution, Washington, USA, have authored substantial numbers of Late Quaternary research articles. A second important area is the northwestern coast of Egypt (Fig. 1a; area 2), where a belt of successive calcarenite ridges are oriented parallel to the coast. The construction of roads and resort facilities have allowed for several cross cuts along these ridges that offer an interesting record of Quaternary

sedimentation in relation to paleoclimate and sea level changes. A third area is the area of the uplifted coral reefs alternated with gravel terraces at the Red Sea (Fig. 1a; area 3) and Gulf of Aqaba (Fig. 1a; area 3-1), which provide both $\delta^{18}\text{O}$ data and age determinations. The fourth area described (Fig. 1a; area 4) is the Western Desert or the Green Sahara, where substantial geo-archaeological works have been carried out on tufa and other lacustrine carbonates.

2 Quaternary Sedimentation and Stratigraphy Along the Nile Delta and Valley

The Quaternary sedimentation and stratigraphy along the Nile Delta (location, Fig. 1b) and its relation to paleoclimate fall naturally into two parts: the Plio-Pleistocene Nile Delta and the Holocene Nile Delta (Fig. 2).

2.1 The Plio-Pleistocene Nile Delta Stratigraphy as a Proxy of Paleoclimate

Since the late 1970s, much attention has been paid to the Plio-Pleistocene stratigraphy of the Nile Delta and its depositional environments (e.g. Ayyad et al., 1987; El-Asmar, 1998; El-Asmar & Gheith, 1995; El-Bassiouni & Ayyad, 1986; El-Shahat & Kora, 1986; Gheith, 1985; Rizzini et al., 1978; Sestini, 1989; Summerhayes et al., 1978; Zaghoul et al., 1977, 1979, 1989). This was followed by investigation of Nile Delta subsidence (Aly et al., 2012; Becker & Sultan, 2009; El-Bastawesy et al., 2017; Stanley, 1988, 1990, 2005; Stanley & Corwin, 2013; Stanley & Toscano, 2009; Stanley & Warne, 1998). Then, focus has been conducted on the Late Quaternary stratigraphy and sedimentation in response to paleoenvironment and paleoclimatic, with geoarchaeological implications (Bernhardt et al., 2012; El-Asmar et al., 2015; Marriner et al., 2012; Stanley & Clemente, 2014, 2017; Pennington et al., 2016, 2019; Stanley, 2005; Stanley & Warne, 1997, 1998; Stanley & Wedl, 2021; Stanley et al., 2004).

Generally, the study of the stratigraphy and sedimentation of the Neogene–Quaternary succession from the subsurface of the Nile Delta (Rizzini et al., 1978) identified three cycles of sedimentation related to the transgression/regression of the sea. These cycles are: the Miocene cycle (Sidi Salim and Qwasim Formations), the Plio-Pleistocene cycle (Abu Madi, Kafr El-Sheikh, El-Wastani and Mit Ghamr Formations) and the Holocene cycle (Bilqas Formation; Fig. 2). On the other hand, Zaghoul et al. (1977) classified the Neogene–Quaternary Nile Delta to four cycles (Fig. 2): the Neogene (split into Miocene and Pliocene cycles) and the Quaternary (split into Pleistocene and Holocene cycles equivalent to the Mit

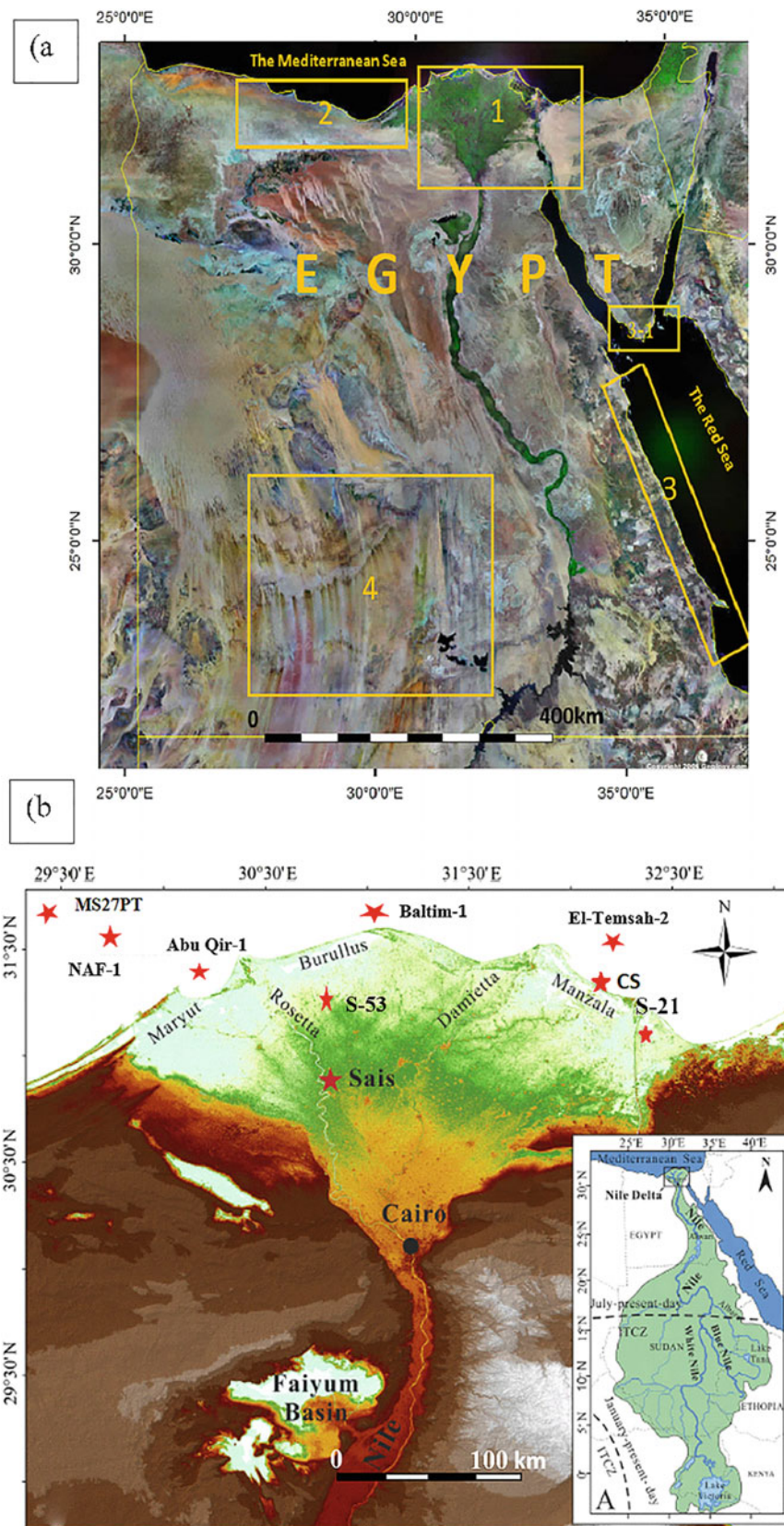


Fig. 1 Satellite image of Egypt, showing location of the subdivided sedimentary areas, the Nile Delta, (1), the Red Sea coast (3) and the Gulf of Aqaba 3-1, and the northwestern coast of Egypt (2), the southwestern Desert (4) (a). Location of the drilled inland and offshore wells of the Nile Delta Abu Qir-1 (Saad et al., 1987), NAF-1, Baltim-1, and El-Temsah-2 (El-Asmar, 1998), MS27PT (Revel et al., 2010), S-53 (Arbouille & Stanley, 1991; Bernhardt et al., 2012), S-21 (Stanley et al., 2003), CS (Kholeif, 2010), and Sais (Zhao et al., 2020) (b)

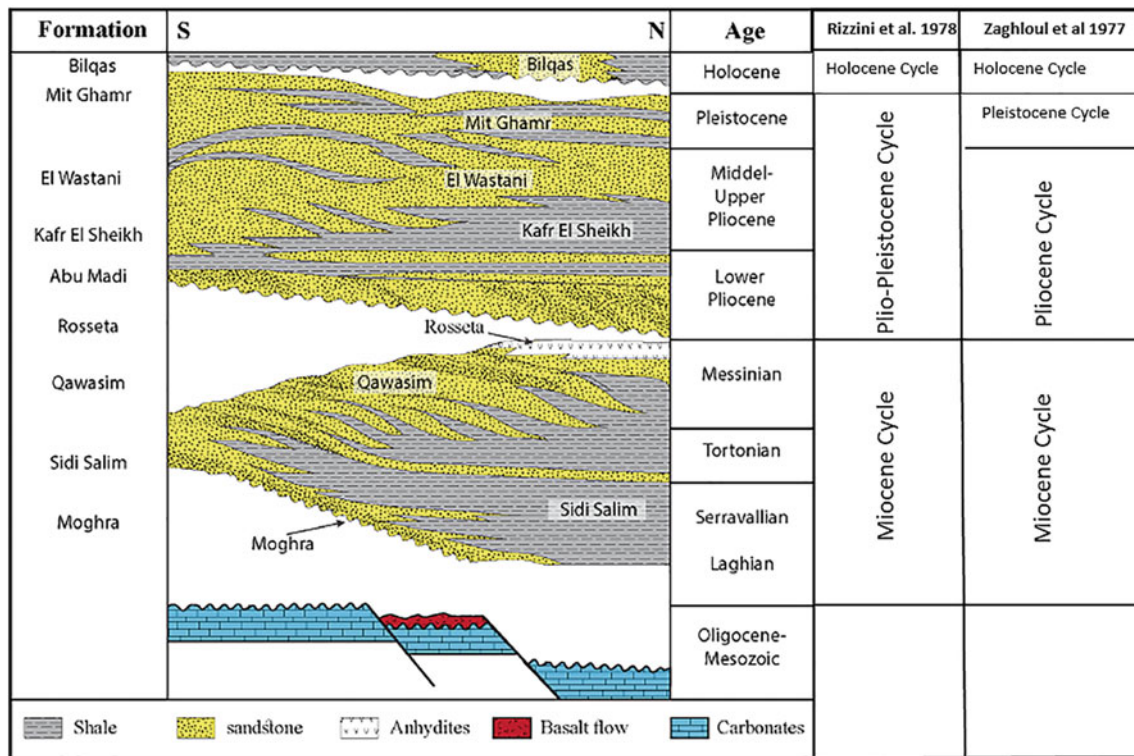


Fig. 2 Stratigraphic model of the Neogene–Quaternary subsurface of the Nile Delta showing the successive cyclic sedimentation with major unconformities. Sources Rizzini et al. (1978) and Zaghloul et al. (1977)

Ghamr and Bilqas Formations). The boundary between the Pliocene and the Quaternary was placed tentatively at the last appearance of *Globigerinoides obliquus* (Bolli) at the top of the El-Wastani Formation (El-Bassiouni & Ayyad, 1986) and the first appearance of the planktonic foraminifera *Globigerina calida* (*calida*) at the bottom of Mit Ghamr Formation (El-Bassiouni & Ayyad, 1986). Zaghloul et al. (1977) interpreted the Mit Ghamr Formation as a coastal and/or distributary mouth bar sand, while the Bilqas Formation deposited in a lagoonal to beach environment.

The patterns of sedimentation of the Quaternary Nile Delta deduced from both the subaerial and the subaqueous profiles (Figs. 3 and 4) reflect the interplay of marine, terrestrial, Nile flux and regional climatic conditions (Zaghloul et al., 1989). The subaerial Quaternary is relatively thinner (Fig. 3, profiles 1, 2 and 3) and composed mainly of sand and gravels derived from the Nile or regional sources. It is interpreted as deposited in shallow distributary mouth bar subenvironment. The subaqueous Quaternary is thicker and shows rhythmic pattern (Fig. 3 profile 4; and Fig. 4 northward) in which alternations of sand and mud of Nile sources mix with marine sediments (El-Asmar, 1986; Zaghloul et al., 1989). It was formed in delta front and prodelta subenvironments characterized by sand and mud, respectively (Zaghloul et al., 1979, 1989). These patterns are interpreted as reflecting three phases of a prograding delta in a subsiding basin with a generally regressive sea (Fig. 5; Coleman &

Gagliano, 1964). However, the grain size and mineralogical content in the Nile Delta Quaternary reveal only two sequences (El-Asmar, 1986; Gheith, 1985). The lower one is a coarsening-upward sequence enriched with epidote and amphiboles suggesting White Nile source of sediments. The upper one is a fining-upward sequence enriched with pyroxenes, which indicate flooding from the Blue Nile derived from the Ethiopian plateau (the Prenile of Hegab, 1989; Said, 1981). This is not conflicted with the conclusions approved the Blue Nile connection with the lower Nile at Late Messinian and White Nile until 0.5 Ma (Fielding et al., 2014). The U/Pb rutile and Lu/Hf zircon age dating indicates that the Blue Nile and/or Red Sea Hills input to the Nile Delta since at least the Oligocene with very little input from the White Nile (Fielding et al., 2017). The pre-Messinian Nile Delta sediments are locally derived from the Red Sea Hills and the Blue Nile has been connected to the lower Nile since the Oligocene (Issawi & McCauley, 1992). The presence of Ethiopian Cenozoic Continental Flood Basalts detritus in the Nile Delta recorded (c. 31 Ma) supports the Blue Nile connection to the lower Nile (Fielding et al., 2018). Such connection does not conflict with the fact of capturing of the Blue Nile is resulted due to the strength of African monsoons (Hamdan et al., 2019; Revel et al., 2010), and during the low monsoons, the contribution of the White Nile is evident (see Fig. 43). The isotope composition of core MS27PT (location; Fig. 1b) of the

terrigenous fraction and the major element distribution revealed large and abrupt changes in source, oscillating between a dominant aeolian Saharan contribution during arid intervals and a dominant Nile River contribution during pluvial interval (see Fig. 43; Revel et al., 2010).

In order to study the paleoenvironment of the Quaternary Nile Delta sediments in response to climate and sea level changes, several paleontological studies have examined the fossil biozonation of sediments (e.g. El-Bassiouni & Ayyad, 1986). Based on CaCO₃% and the lithologic composition of

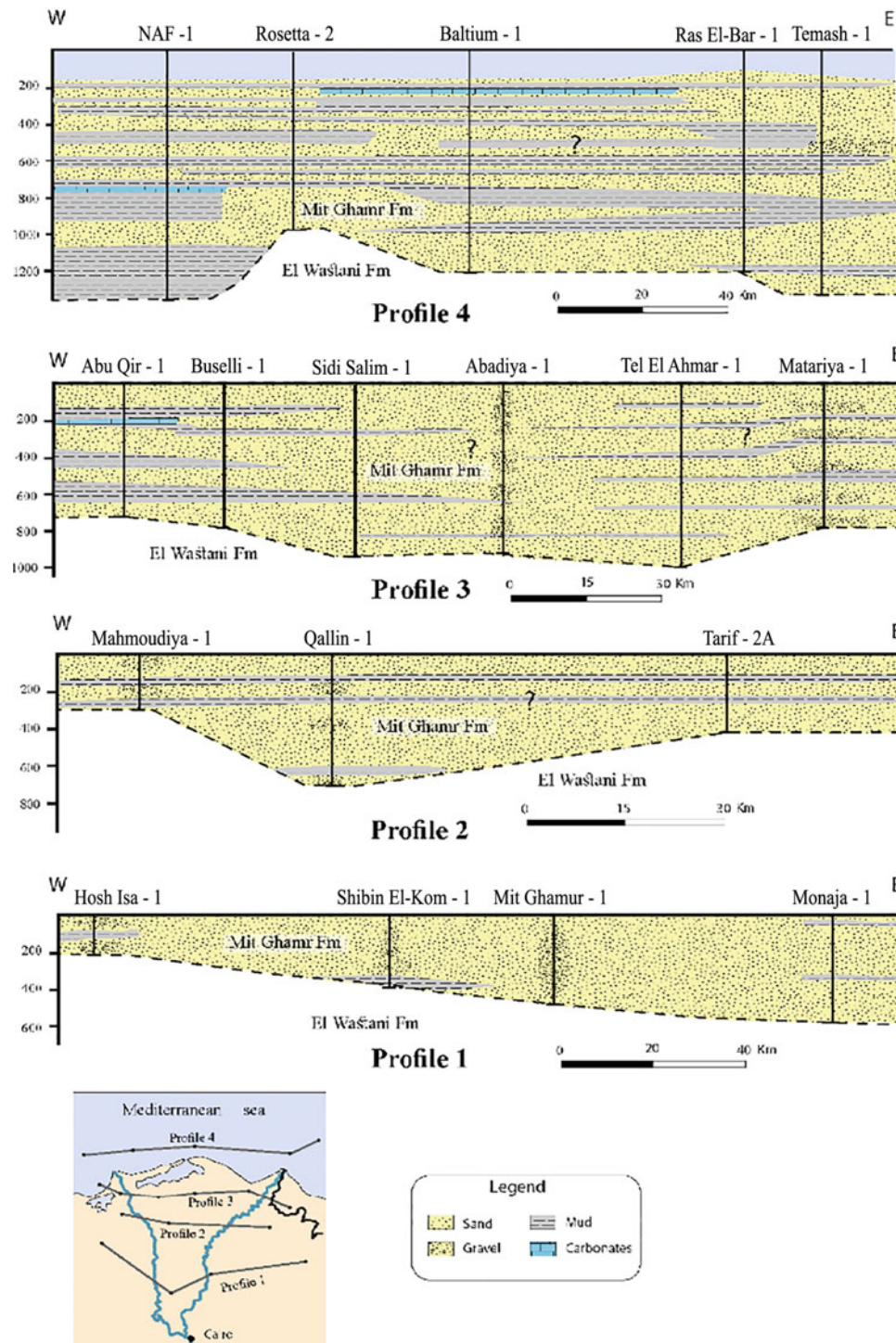


Fig. 3 Latitudinal profiles showing cross-section along the Quaternary subsurface succession, Nile Delta. Profiles (1–3) composed mainly of yellow sand and gravel in thin bedding of distributary mouth bar subenvironment. The subaqueous Quaternary profile 4 is thicker and composed of alternations of sand and mud of delta front and prodelta subenvironments. *Source* Zaghloul et al. (1989)

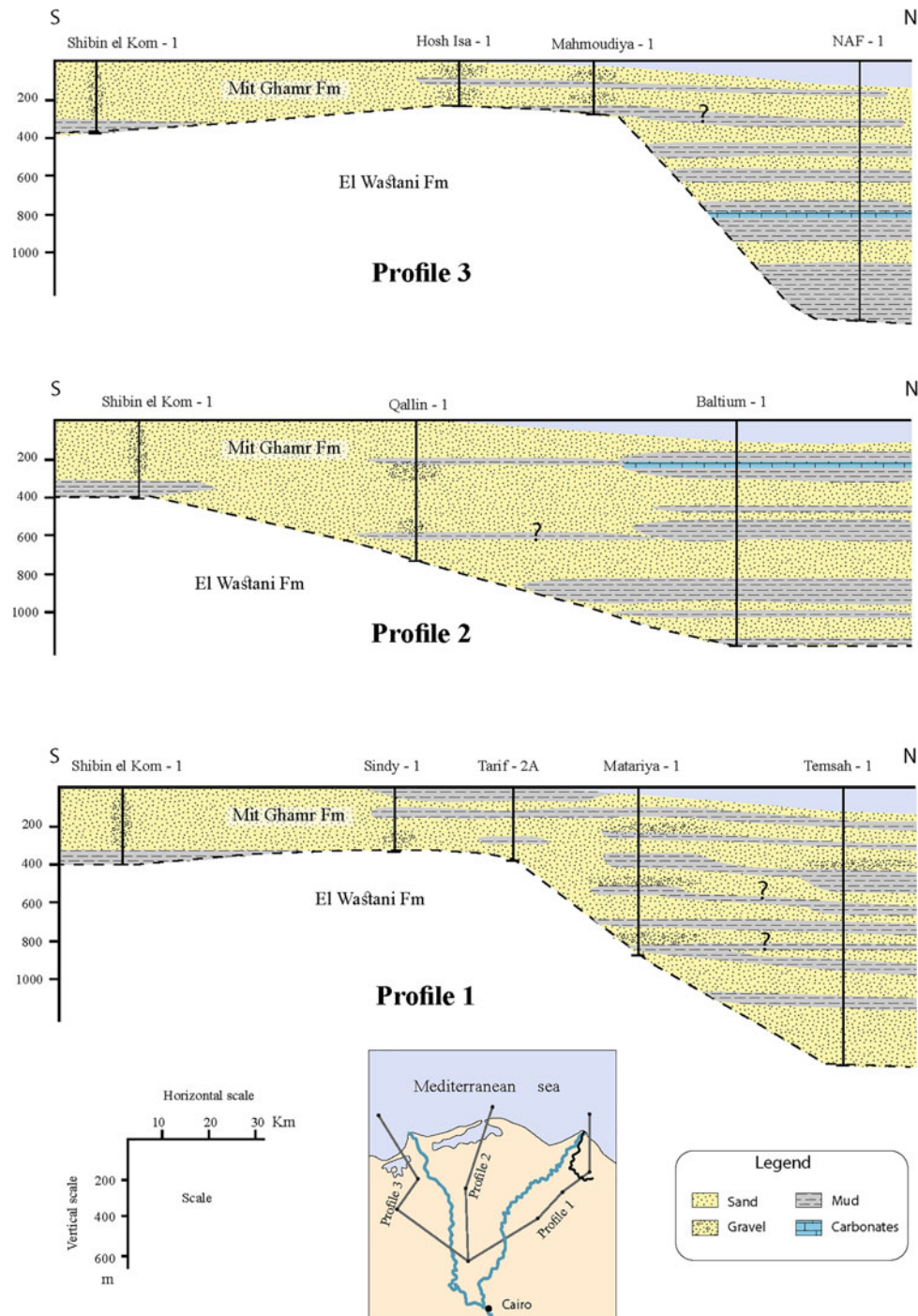


Fig. 4 Longitudinal profiles showing cross-section along the Quaternary subsurfaces succession, Nile Delta. The sediments are thicker northward rather than the southward indicating deposition of prograding delta in an active marine basin. *Source* Zaghloul et al. (1989)

NW Rosetta offshore well-1, the Pleistocene section exhibits intervals enabled the subdivision of the Pleistocene sequences into three zones (Fig. 6a) correlated with that of El-Temsah well-2 (Fig. 6b). The later (Location; Fig. 1b) is classified according to the paleosalinities and planktonic/benthonic foraminifera (PI/Be) (Fig. 6b) into three zones (El-Bassiouni & Ayyad, 1986). The lower zone (zone I,

Fig. 6b) is characterized by presence of marine to brackish planktonic, with rare *Miliolides*, and *Ammonia beccarii*. This zone ends with low (PI/Be) ratio with abundant benthonic and molluscan shells. The middle zone (zone II, Fig. 6b) is brackish water to shallow marine environment characterizes with a relatively high (PI/Be), and diversity of planktonic foraminifera and scarcity of arenaceous forams.

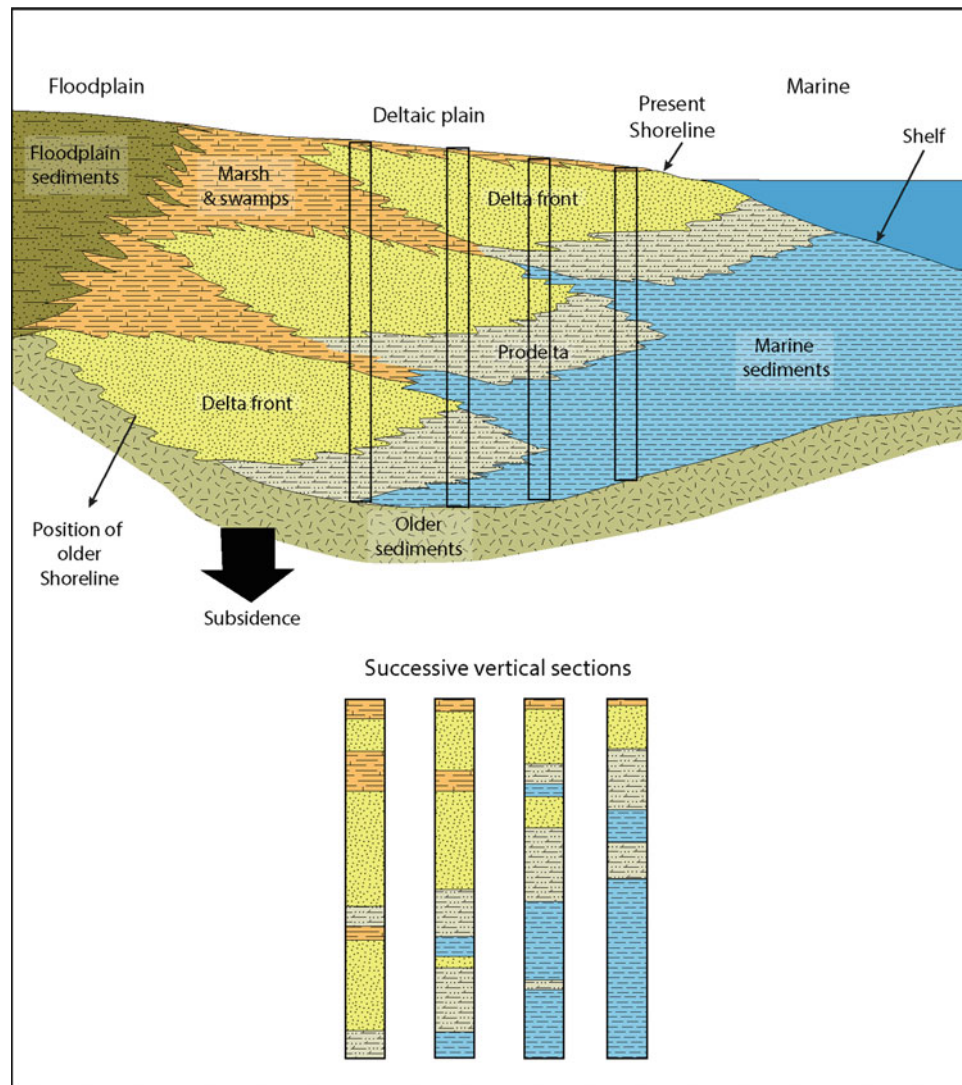


Fig. 5 Model of delta prograding and formation of successive clinoforms composed of distributary mouth bar sands and gravels, delta front sand and silt, and prodelta mud (modified after Coleman & Gagliano, 1964)

The upper zone (zone III, Fig. 6b) is characterized by low (P/Be) with abundant *Amonia beccarii* and porcellaneous *Miliolida* and *Rotalida* indicating a high to hyper saline photic shallow marine water. These zones composed of six intervals (II–VII) related to water depths (Fig. 6c) (intervals II to VII; Ayyad et al., 1987). These zones comprise regression/transgression intervals represented by Mit Ghamr Formation (Fig. 6c; cycles II–III; IV–V; VI–VII; Ayyad et al., 1987). The lower most (interval I) represents a regressive phase that prevailed during the deposition of the uppermost Pliocene El-Wastani Formation, which deposited under a continental (coastal) environment. This sea regression is evidenced by the absence of foraminiferal and bryozoan content (barren interval; Fig. 6), not to mention the dominantly sandy nature of this interval (Fig. 6a). Such a retreat of the sea towards the north took place in Egypt in the

Late Pliocene (El-Shahat & Kora, 1986; Rizzini et al., 1978; Zaghloul et al., 1977).

Some elements have environmental implications in sediments, such as benthonic percentage, mollusc percentage, Ca CO₃ percentage and organic carbon percentage (El-Asmar, 1998). Such elements have been examined for samples collected from NAF-1 and El-Temsah-2 offshore wells (Location; Fig. 1b). The vertical variations of benthonic forams, mollusc, and organic carbon percentages are correlated with the variations of $\delta^{18}\text{O}$ and $\delta^{13}\text{C}$ for foraminifera samples from NAF-1 (Fig. 7) and El-Temsah-2 (Fig. 8) offshore wells, north of the Nile Delta (El-Asmar & Gheith, 1995). The $\delta^{18}\text{O}$ of foraminifera tests is used to estimate the sea surface temperature. The intervals of increase in $\delta^{18}\text{O}$ indicate high temperature where light ^{16}O is preferentially depleted during evaporation, and salinity increases. On the

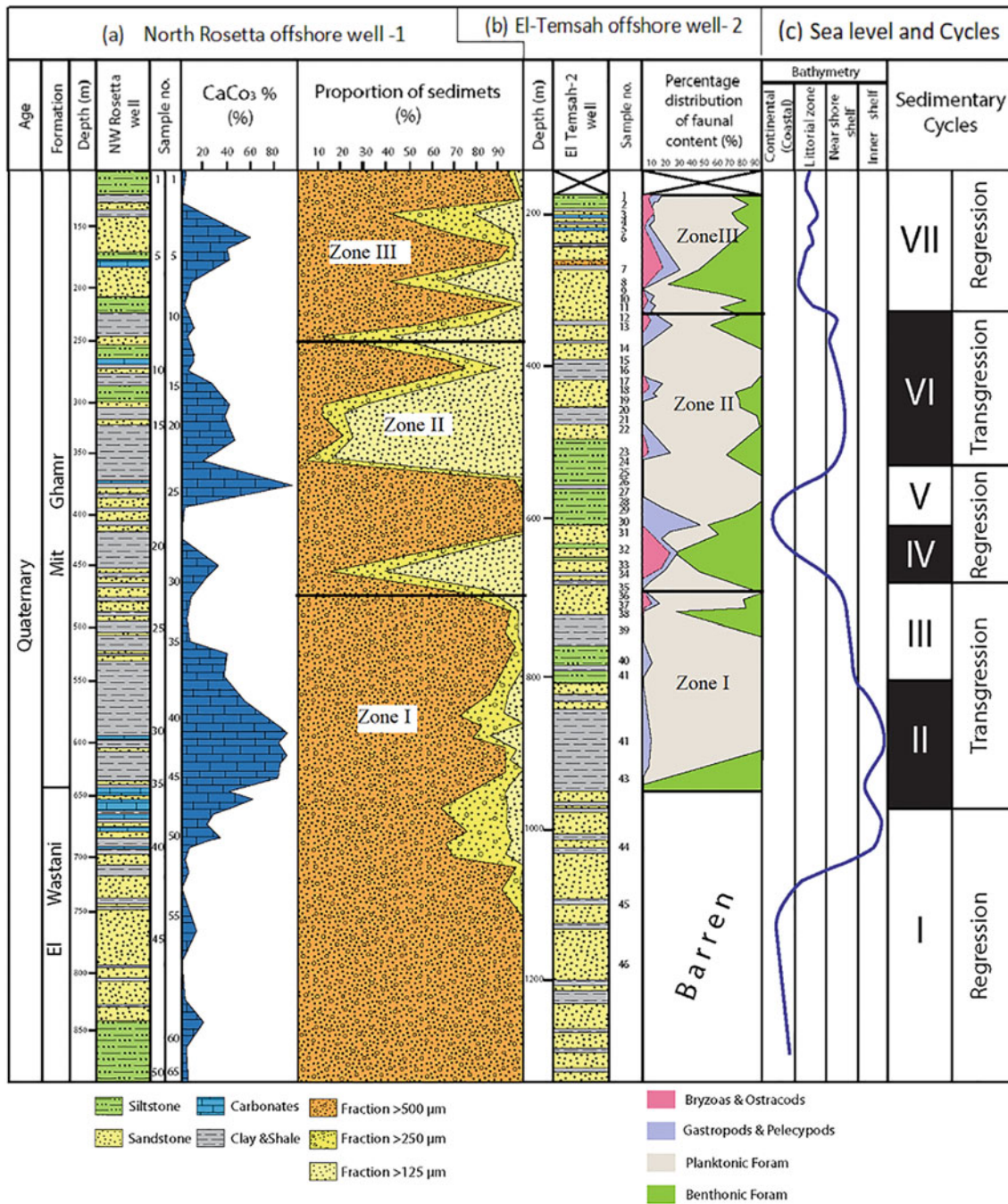


Fig. 6 Correlation of the vertical distribution of carbonate %, grain size along north Rosetta well-1 (a) and the vertical distribution of benthonic and planktonic foraminifera, mollusc and bryozoan of Quaternary offshore succession along El-Temsah-2 (b). This correlation demonstrated three cycles of transgression-regression representing at least 6 intervals in correlation with sea level changes (c). Sources El-Bassiouni and Ayyad (1986) and Ayyad et al. (1987)

other hand, the intervals of decrease in $\delta^{18}\text{O}$ indicate a preferential increase in the light ^{16}O , reflecting a warm wet climate and freshwater influx. Negative values of $\delta^{13}\text{C}$ indicate an increase in the light ^{12}C organic carbon due to organic activities associated with warm and wet climate, whereas the increase in $\delta^{13}\text{C}$ indicates an increase in organic heavy ^{13}C in marine CaCO_3 , coinciding with high mollusc

and benthonic variations. The vertical distribution of these factors (Figs. 7 and 8) show nine alternations of wet and dry intervals grouped into four cycles in relation with sea level changes, of which three cycles (II, III, I) of regression/transgression are tentatively correlated with the Pleistocene Mit Ghamr Formation (Fig. 6; Ayyad et al., 1987; El-Asmar & Gheith, 1995).

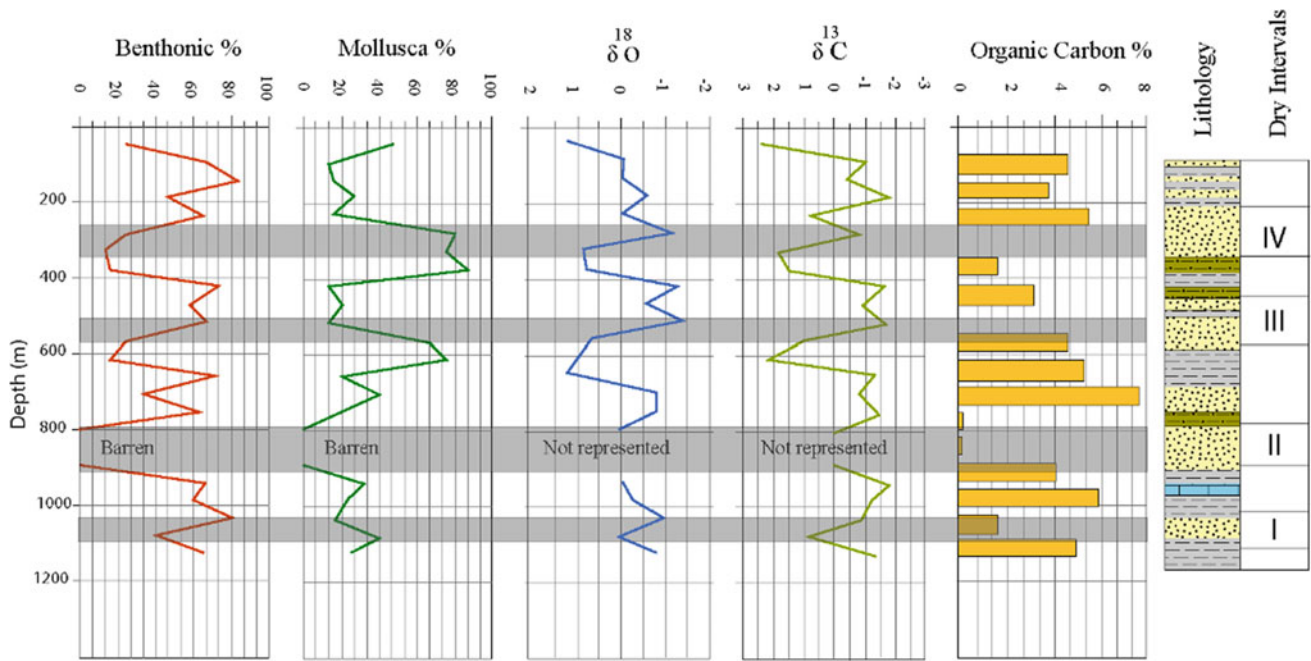


Fig. 7 Vertical distributions of benthonic foraminifera %, mollusc %, $\delta^{18}\text{O}$, $\delta^{13}\text{C}$ and organic carbon % for NAF-1, offshore Nile Delta. Grey related to barren or dry intervals. *Source* El-Asmar (1998)

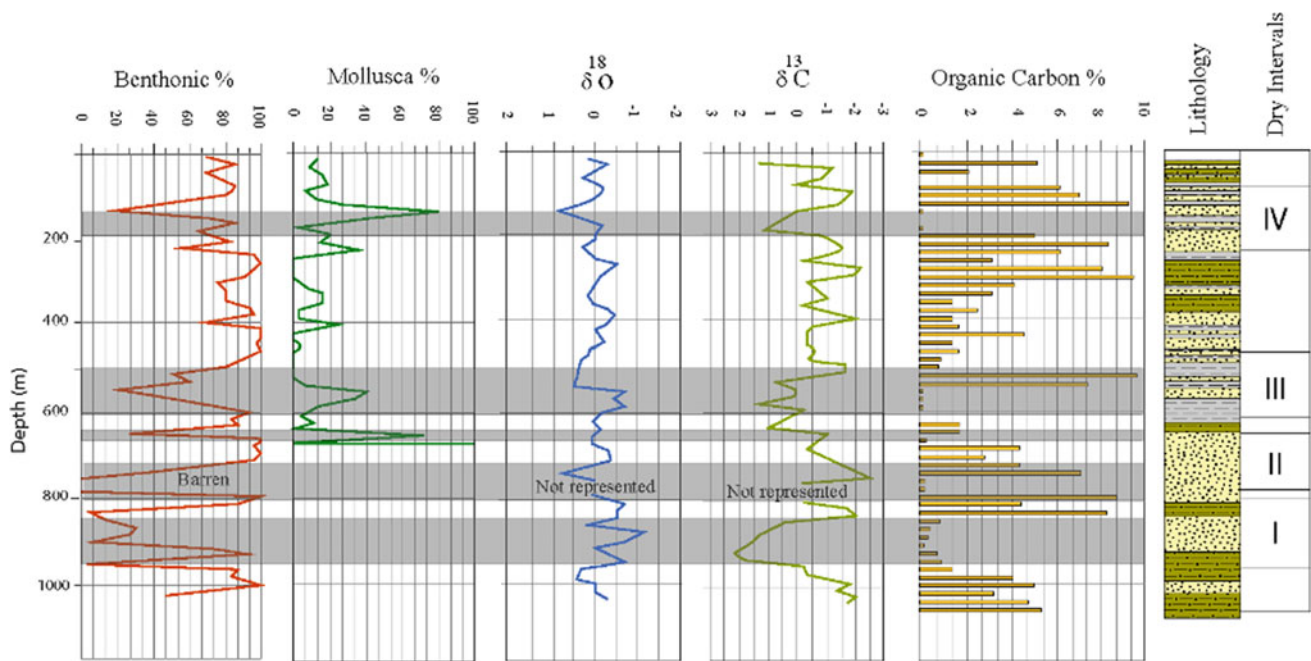


Fig. 8 Vertical distributions of benthonic foraminifera %, mollusc %, $\delta^{18}\text{O}$, $\delta^{13}\text{C}$ and organic carbon % for El-Temshah-2, offshore Nile Delta. Grey related to barren or dry intervals. *Source* El-Asmar (1998)

2.2 The Late Quaternary Nile Delta Sediments as a Proxy of Paleoclimate

To identify the Late Pleistocene and Holocene sediment (Mit Ghamr and Bilqas Formations, Fig. 2) in the Nile Delta, the

whole set of petrologic properties, including sedimentary structures, colour, hardness, texture, mineralogy, faunal and floral content, and radiocarbon dates, is used. An age of about 10,000 BP was assigned to the boundary between the Pleistocene and Holocene (Coutellier & Stanley, 1987)

although now a value of cal. 11,700 BP would be deemed more appropriate (Walker et al., 2009, 2018). Figure 9 shows a generalized lithological succession starting with Late Pleistocene non-marine fluvial iron-stained coarse sand, with gypsum and carbonate (Fig. 9; bed 1), deposited while sea level was low between cal. > 11,000 BP (Fig. 10c; Coutellier & Stanley, 1987). The sequence shows the delta prograding during the Holocene with prodelta (Fig. 9; bed 5) to delta front (Fig. 9; beds 6, 7) overlain by the distributary mouth bar or subaerial (Fig. 9; beds 8–10). Three distinctive Late Pleistocene–Holocene sequences were identified (Stanley & Warne, 1993). Sequence I is of Late Pleistocene Mit Ghamr Formation, which subdivided into two members the Zagazig and Minuf Members from older to younger, respectively (Fig. 10a and b; Pennington et al., 2017). The Zagazig Mbr. is generally coarse massive to laminated or cross-stratified; yellow fine to medium-grained sands with scattered coarse clasts. The grains have very thin coatings of iron oxide (magnetite, hematite and ilmenite), sometimes carbonate, hornblende, augite and epidote, and correlated within the Prenile at Qena (El-Asmar, 1986; Gheith, 1985; Hamdan, 2003a; Hegab, 1989; Pennington et al., 2017; Said, 1981). Minuf Mb. unconformably the Zagazig Mb. consists of fine-grained micaceous sand with stiff compacted clayey lenses that originated as fragmented Late Pleistocene flood basins, especially near the modern-day coastline (Chen & Stanley, 1993). Minuf Mbr. expands over long time of Late Pleistocene and deposited under an earlier, braided Nilotic regime with humid climate (Fig. 10d; Adamson et al., 1980; Said, 1981).

The onset of the Holocene sequence started with transgressive olive-grey of medium-grained sand with a shallow marine fauna (Fig. 10a). It is deposited when sea started transgressing, with a suggested age between cal. 11,000 and 7000 BP (Fig. 10c). These beds described as Gezira cover Formation (Fig. 10b) of mixed coastal and aeolian sands and related to sequence II of transgressive sea with decelerating of sea level rise (Fig. 10c; Pennington et al., 2017). These also correlated with sediments from bed 1 to bed 4 (Fig. 9) of 2–20 m thick, and rich in heavy minerals, notably hornblende, and contain orthoclase feldspar grains and iron-stained sands all consistent with a Nile provenance in a relatively dry climate (Fig. 10d; Chen et al., 1992; Coutellier & Stanley, 1987). The onset of Bilqas Formation and the inception of the Holocene alluvial delta plain first occurred around cal. 8–7 ka BP in northern Nile Delta associated with intermittent humid and dry climate (Fig. 10d), sequence III (Fig. 10a; Pennington et al., 2017). It began with Holocene marine muds of prodelta (III a or Bilqas 2, Fig. 10b; Pennington et al., 2017), with cal. 7–3 ka BP (Fig. 9, bed 5; Fig. 10b). A period of marked decrease in sea level rise was detected at cal. 7–6 ka BP (Fig. 10c and d; Pennington et al., 2016). A coarser olive-grey delta front sand occurs overlying

the IIIa; it is IIIb or Bilqas 1 (Pennington et al., 2017) with cal. 3–1 ka BP (Fig. 9, bed 7 or Fig. 10b). A progressive development of hyperaridity with increase results from elevated flux of aeolian material entering the Nile River system from calcareous source rock in the dryer Egyptian Sahara. The major increase in hyperaridity occurs around cal. 4.2 ka BP (Pennington et al., 2019; Welc & Marks, 2014). 300–200 yrs around 4.2-ka BP of reduced Nile flow is recognized associated with arid climate (Hamdan et al., 2019; Stanley, 2019; Stanley & Wedl, 2021). Most Egyptologists consider the 4200 major event of aridity during which major changes in annual flooding and base flow of the River Nile marked the collapse of the Old Kingdom (Bárta & Bezdek, 2008; Hassan, 1981, 2010; Marriner et al., 2012; Pennington et al., 2019; Stanley et al., 2003). The top of the sequence is represented by a variety of lithologies of marine, semi-terrestrial, coastal sands, estuarine, lagoonal and in some cases fluvial deltaic environments. The age of this sequence ranges between cal. 1.5 and < 1 ka BP (Fig. 9, beds from 8 to 10; Fig. 10a and b) and equal to sequence IIIb or Bilqas 2 (Pennington et al., 2017). This sand formed as an extensive accreted beach ridges system at the headland of a cusped-shaped, river-dominated delta (El-Asmar et al., 2015). The subaerial Holocene lithofacies (sand ridges, coastal dunes, lagoonal and marshes; Fig. 9, beds 8–10; subaerial Bilqas Fm., Fig. 10b) formed at about the time of sea level reaching its approximate present level and the climate became markedly arid at about cal. 1–1.5 ka BP (Smith & Ross, 2008; Fig. 10c and d). Depressions behind the ridges received incursions of freshwater during flood stages of ancient distributaries and also of salt water as a result of storms and the formation of sabkhas and the presence of anoxic organic matter, indicate changes towards an arid climate (Fig. 10c and d; Butzer, 1959).

Strontium isotopes of the Nile River sediments can be used as a proxy for paleoclimatic changes in East Africa. It has been shown that the Late Holocene major changes in a given Nile subcatchment have been controlled by climatic conditions (Stanley et al., 2003). It has been demonstrated that climatic factors have influenced the significant Late Holocene alterations in a particular Nile subcatchment (Stanley et al., 2003). Paleoclimatic and paleoenvironmental changes in the upstream catchments can be defined with the use of information on the origin of suspended sediment conveyed by the main river. The White Nile catchment is dominated by crystalline basement rocks with high $^{87}\text{Sr}/^{86}\text{Sr}$ ratios, whereas the Blue Nile–Atbara drains the Ethiopian highlands, which are dominated by Cenozoic volcanic rocks with characteristically low $^{87}\text{Sr}/^{86}\text{Sr}$ ratios (Fig. 11, Krom et al., 2002). The $^{87}\text{Sr}/^{86}\text{Sr}$ ratio has been effectively employed for provenance studies of water and sediment in the Nile system, and it is an isotopic ratio indicative of the source of both the suspended sediment and the river water in

Sequences	Bed No	Thickness (m) and Lithology		Age cal. BP	
Marine and Non- Marine Holocene Nile Delta Sequence	10	1-6		Lagoonal or Marsh	<1000
	9	1-2			
	8	0-10		Coastal Sand Ridges	
	7	1-6		Delta-Front	3000- 1000
	6	4-10			
5	1-25		Prodelta	7000-3000	
Ancient Alluvial Nile Sediments (Pleistocene)	4	0-1		Marsh and Swamp	11000 - 7000
	3	2-10		Littoral (North) or Fluvial (south)	
	2	0-8		Swamp ?	
	1	> 10		Fluvial	> 110000

Fig. 9 A general composite lithostratigraphic sequence depicting the major Late Pleistocene and Holocene facies their thickness, subenvironments and age reflecting the interplay of marine, fluvial and terrestrial subenvironments. *Source* Coutellier and Stanley (1987)

these catchments (Fig. 11; Krom et al., 2002; Stanley et al., 2003). A high-resolution profile of $^{87}\text{Sr}/^{86}\text{Sr}$ ratio recovered from a well-dated S-21 core (Location, Fig. 1b) shows a close correspondence with the changes in Nile flow over the past 7000 yrs (Krom et al., 2002). The times of higher riverflow are associated with northward movement of the ITCZ. The depth profile of $^{87}\text{Sr}/^{86}\text{Sr}$ (Fig. 11) in the Nile Delta shows high values (0.7088) for samples older than cal. 6000 BP (Fig. 11a). At cal. 4670 BP, the $^{87}\text{Sr}/^{86}\text{Sr}$ ratio

rapidly drops to a minimum of 0.7078 (Fig. 11b). Then, over the time between cal. 4000 and 2350 BP, the $^{87}\text{Sr}/^{86}\text{Sr}$ ratio rises to varying values between 0.7080 and 0.7082 (Fig. 11c). Between cal. 2200 and 950 BP, the $^{87}\text{Sr}/^{86}\text{Sr}$ ratio underwent a second, fast drop, reaching a rather stable value of 0.7075 (Fig. 11d, Krom et al., 2002). Measurements of concurrent paleontological and Sr isotope analyses from samples collected from Alexandria nearshore indicated an increase in salinity at the Mid-Holocene around cal. 4300 BP

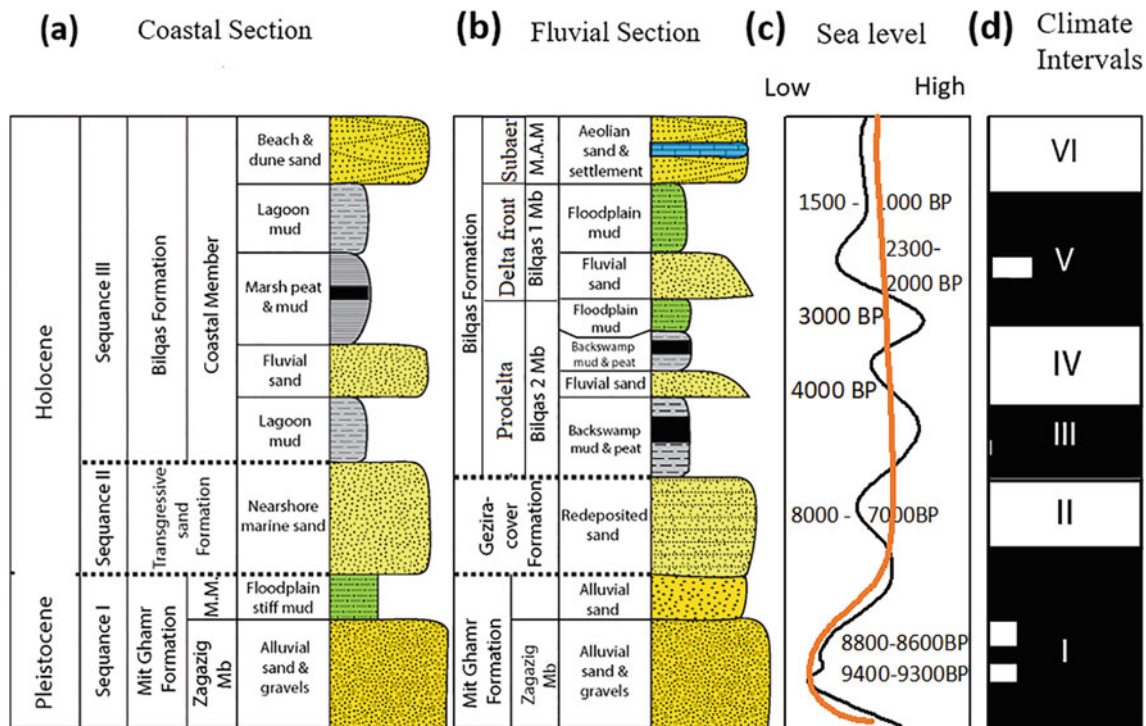


Fig. 10 Holocene sedimentary sequence and depositional environments through the coastal (a) and fluvial (b) zones of the Nile Delta correlated with Late Pleistocene–Holocene sea level (c), and deduced climatic intervals (d). M.A.M = Modern Aeolian Member; M.M. = Minuf Member. Black quadrant related to possible wet intervals while the white ones related to dry intervals, unconformities. Sources Chen et al. (1992), Stanley and Warne (1993, 1998), Bárta and Bezdek (2008), and Pennington et al. (2017)

(Bernasconi et al., 2006), which confirms a reduction of the Nile freshwater flow to the coast (Stanley, 2019). The Ti/Al ratio shows a reverse behaviour of $^{87}\text{Sr}/^{86}\text{Sr}$. When $^{87}\text{Sr}/^{86}\text{Sr}$ ratio increases, the Ti/Al decreases (Krom et al., 2002). The records of Fe and Ti determined from the analyses of core MS27PT (Location; Fig. 1b) are consistent with subtropical African records of well-dated lake level fluctuations and thus, constitute a continuous high-resolution record of the East African monsoon regime intensity over Ethiopia. They record two main known pluvial intervals attributed to the strengthening of the African monsoon over Ethiopia (The Blue Nile source). These are the (Nabtian pluvial) or AHP from 14 to 8 ka and the Saharan pluvial from 98 to 72 ka (see Fig. 43). The last glacial period (MIS 2, 3 and 4) shows a continuous record with large oscillations between high and low East African monsoon regimes (Revel et al., 2010). Ca/Ti ratio of sediments from Kom al-Ahmer and Kom Wasit of age between cal. 5000 and 4000 BP shows an increase with a progressive development of hyperaridity. The higher flux of aeolian material into the Nile River system from calcareous source rock obtained from the Egyptian Sahara was the cause of this rise (Pennington et al., 2019). Such a viewpoint implies a locally sudden, temporally retrogressive beginning of hyperaridity at the conclusion of the AHP. Less Saharan-derived aeolian material began to reach the Nile Valley at this point, and the contribution of aeolian

material to the Nile's sedimentary signal was greatly outweighed by an increase in Blue Nile sedimentary flux (Pennington et al., 2019).

2.2.1 The Quaternary Nile Sediments; the Monsoons and the Pluvial Intervals

During the Quaternary, the River Nile's geologic development was influenced by significant tectonic processes, such as the rifting of East Africa, climate changes and other reasons (Said, 1981). The Nile Basin is divided into five main areas, each of which has a unique structure and geological history (Said, 1981). The first one is the Equatorial Lake Plateau, the second is the Sudd area and central Sudan, the third is the Ethiopian Highlands, the fourth is the major bends and waterfalls of the desert's Nile, and the fifth is the Egyptian region, which includes the low gradient delta complex (Woodward et al., 2007). Five successive Nile systems were recognized (Said, 1981), and numerous publications discussed the evidences and timing of the flow of these rivers (Fig. 12), their sedimentary characteristics and hydrogeology (e.g. Abu Seif, 2015; Ghilradi et al., 2012; Hamdan, 2013; Hassan, 1981, 2010; Hegab, 1989; Said, 1981, 1990, 1993; Wysocka et al., 2016). In addition, their correlation with global climate and African monsoons (Fig. 12; e.g. Ducassou et al., 2009; Hamdan & Hassan, 2020; Hassan et al., 2017; Murat & Got, 1987). Each of these

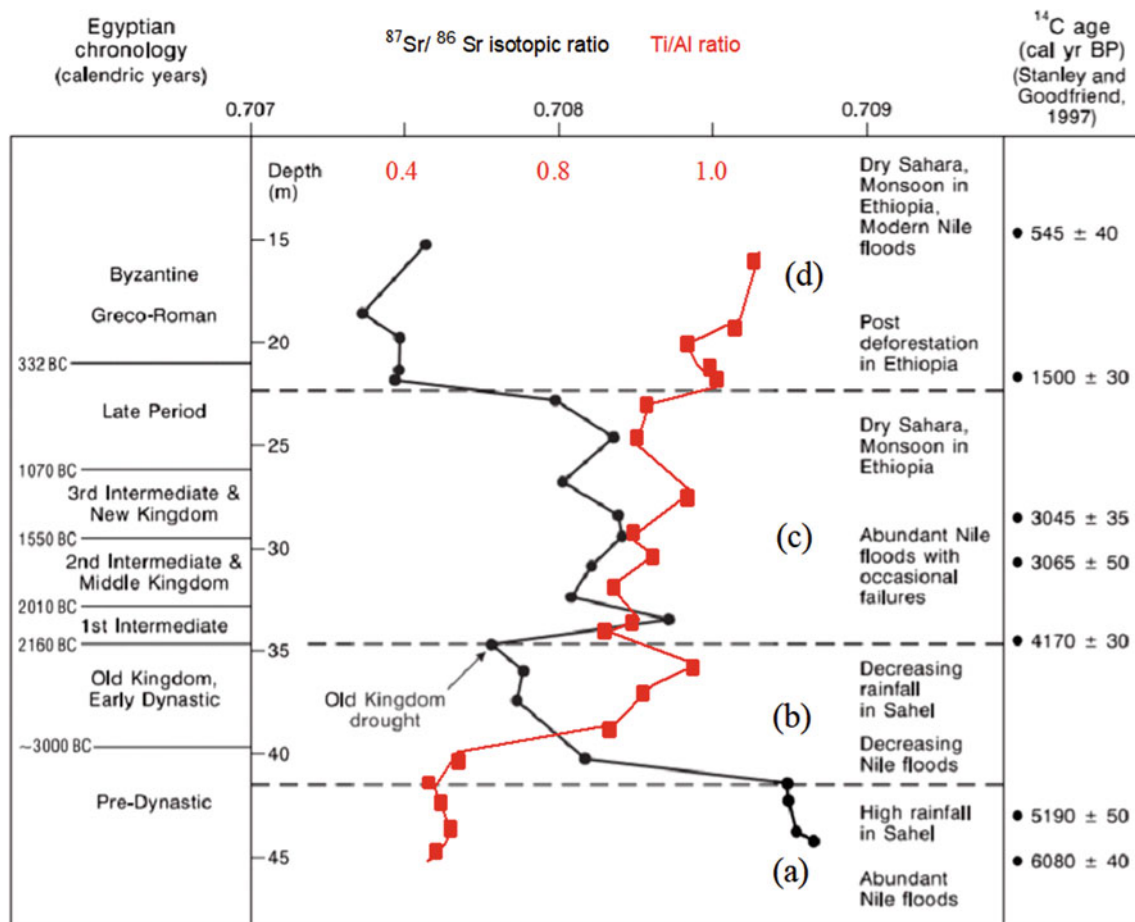


Fig. 11 Depth profile of $^{87}\text{Sr}/^{86}\text{Sr}$ and Ti/Al ratios from core S-21 (Location; Fig. 1b) in the Nile delta (at coast, east of Suez Canal; together with interpretation of changes in paleoclimate in the catchment and the state of the Nile flood as given in Krom et al. (2002)). The Egyptian chronology in calendric years, from Kitchen (1991), is given in the left-hand column. The ^{14}C calibrated age of the core, calculated by linear regression, together with the individual points from which the timescale was derived (Stanley & Goodfriend, 1997; Stanley et al., 2003), corrected for a 400 year initial age, is presented in the right-hand column. For details of sample treatment and geochemical analysis of the $^{87}\text{Sr}/^{86}\text{Sr}$ isotopic ratio, see Krom et al. (2002). Source Stanley et al. (2003)

rivers has the characteristic sedimentary deposits referring to the provenance, physical conditions and paleoclimate. These are from oldest to youngest: Eonile, Paleonile, Protonile, Prenile and Neonile, of which the last three river systems are recorded in Egypt and dated to the Quaternary (Fig. 12).

The term pluvial was introduced to refer to the wet or humid climate associated or designate episodes of wetness in arid regions (e.g. Hamdan & Brook, 2015; Osmond & Dabous, 2004; Said, 1981, 1990; Schild & Wendorf, 2013; Wendorf et al., 1976). Interpluvial, on the other hand, refers to the interval of dry climate (Hamdan & Brook, 2015; Said, 1981, 1990). At present, it is accepted that there are seven pluvial episodes occurred during the Nile River Quaternary history, corresponding to global eustatic events and warm humid phases. Such pluvials are controlled by the monsoons and the headwater climate, which is associated with ITCZ shifting and AHP (e.g. Hamdan & Hassan, 2020; Said, 1990, Fig. 12). The Quaternary Nile system is subdivided as follows:

The Protonile (Q1): It was a competent braided stream with a well-developed flood, flowed during a general aridity prevailed at Early Pleistocene ~ 2.8 Ma to ~ 800 – 700 ka (Fig. 12). However, there were two short humid episodes, during which the Idfu and Armant Formations were deposited; these are the Idfu Pluvial and the Armant Pluvial (Said, 1981). Idfu Formation is composed of complex gravel, coarse sand and loamy sediments (Fig. 13d), best developed and exposed at the western Nile at Kom Ombo. The Armant Formation is made up of alluvial fans that form around the wadi mouths that drain Egypt's highlands into the Nile (Said, 1993). It is composed of travertine reeds that are horizontally bedded on top of subangular and poorly sorted pebbles, fine-grained calcareous sands and marls that may be of Eocene limestone and are locally generated (Said, 1981). The sand is devoid of augite, rich in epidote, and has a completely different composition from Qena sands. The gravels are bonded by tuffaceous material (Hassan, 1976).

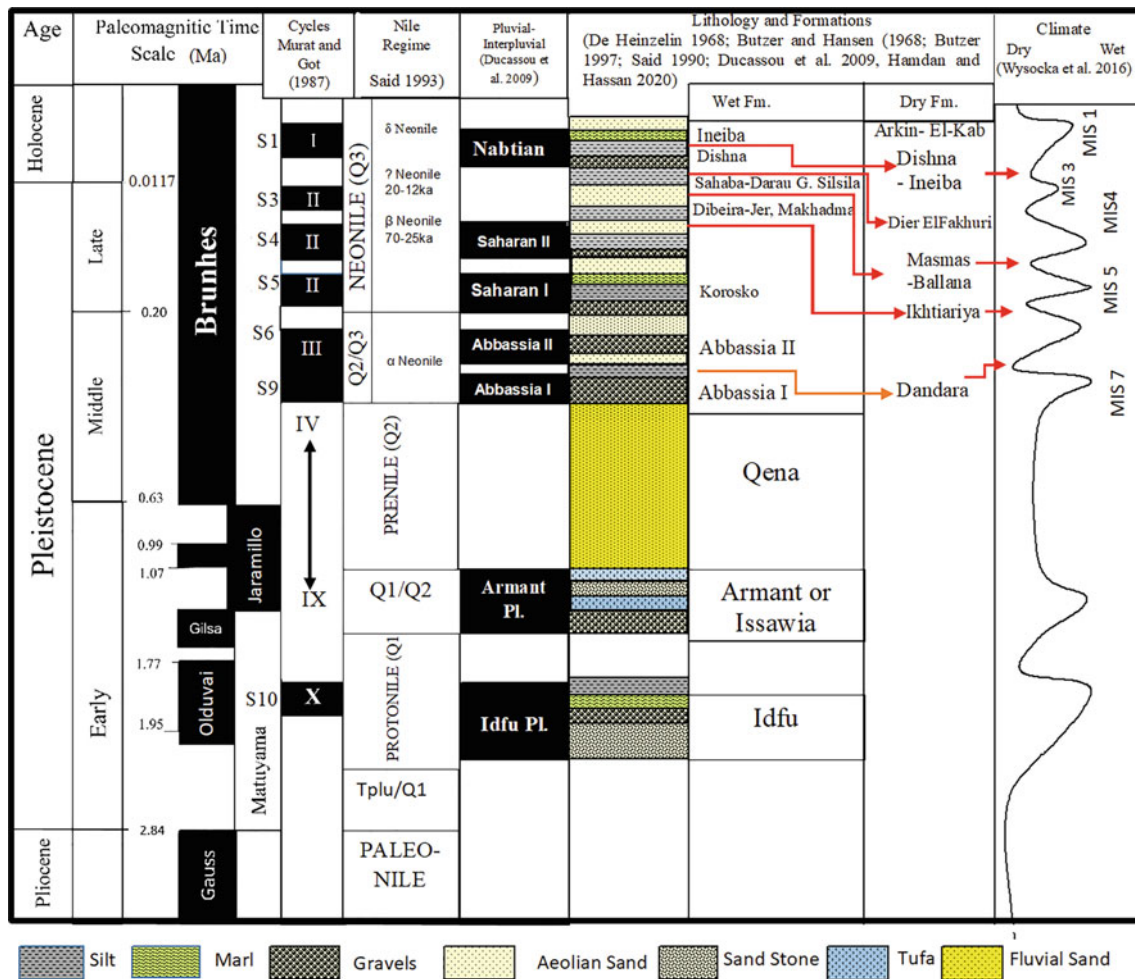


Fig. 12 Pliocene–Quaternary Paleomagnetic scale correlated with sapropel layers (S1–S10) and the I–X cycles of 650 ka (Murat & Got, 1987), the Nile regime (Said, 1981), formations and lithology (Said, 1990), the pluvial intervals as discussed in Ducassou et al. (2009) all correlated with climatic periods and marine isotopic stages (Wysocka et al., 2016)

The provenance investigations confirmed different sources for the gravels on the two sides of the Nile at Idfu to the west and Kom Ombo to the east. The western Idfu gravels made up of quartz, while the eastern Kom Ombo gravels are of polygenetic origin including a large variety of igneous and metamorphic pebbles (Said, 1993). The Idfu gravels are noticeably different from those of the Armant formation because they contain pebbles that transported from a distant source rather than being derived from a local source. These pebbles are noticeably smaller than the boulders of the Armant formation, which derived from local sources (Said, 1981; Wysocka et al., 2016). A mineral assemblage characterizes that the Idfu Protonile sediments are mainly amphiboles, epidote, garnet, staurolite, tourmaline, zircon, pyroxenes and other minor accessories. This assemblage is different from that of the Modern River and points to a derivation from outside origin (Said, 1981). The Protonile was dependent upon discharge from equatorial and sub-equatorial tributaries in East Africa and from

Sudano-Egyptian affluents (Hassan, 1976). There is still strong debate regarding the age of both the Armant and Idfu pluvials, because of the lack of reliable dating and the absence of interpluvial sediments (Wysocka et al., 2016). However, possible ages of 650 ka and 1.86 Ma were inferred and correlated with Jaramillo and Olduvai normal magnetic polarity, respectively (Fig. 12, Said, 1990).

The Prenile (Q2): A long period had passed before the connection of the first river with sub-Saharan African came to Egypt. It represents a significant development in the history of the Nile that took place between 800 and 700 years ago. The river, known as the Prenile, was resulted due to the new drainage pattern that emerged after Ethiopian's tectonic relief and the lake plateau's shape had resembled one another due to the major earth movements of that era (Said, 1993). It is of Middle Pleistocene age, extends for about ~ 400 ka (Fig. 12) and derived its water from Ethiopian heights through the Blue Nile and the Atbara,

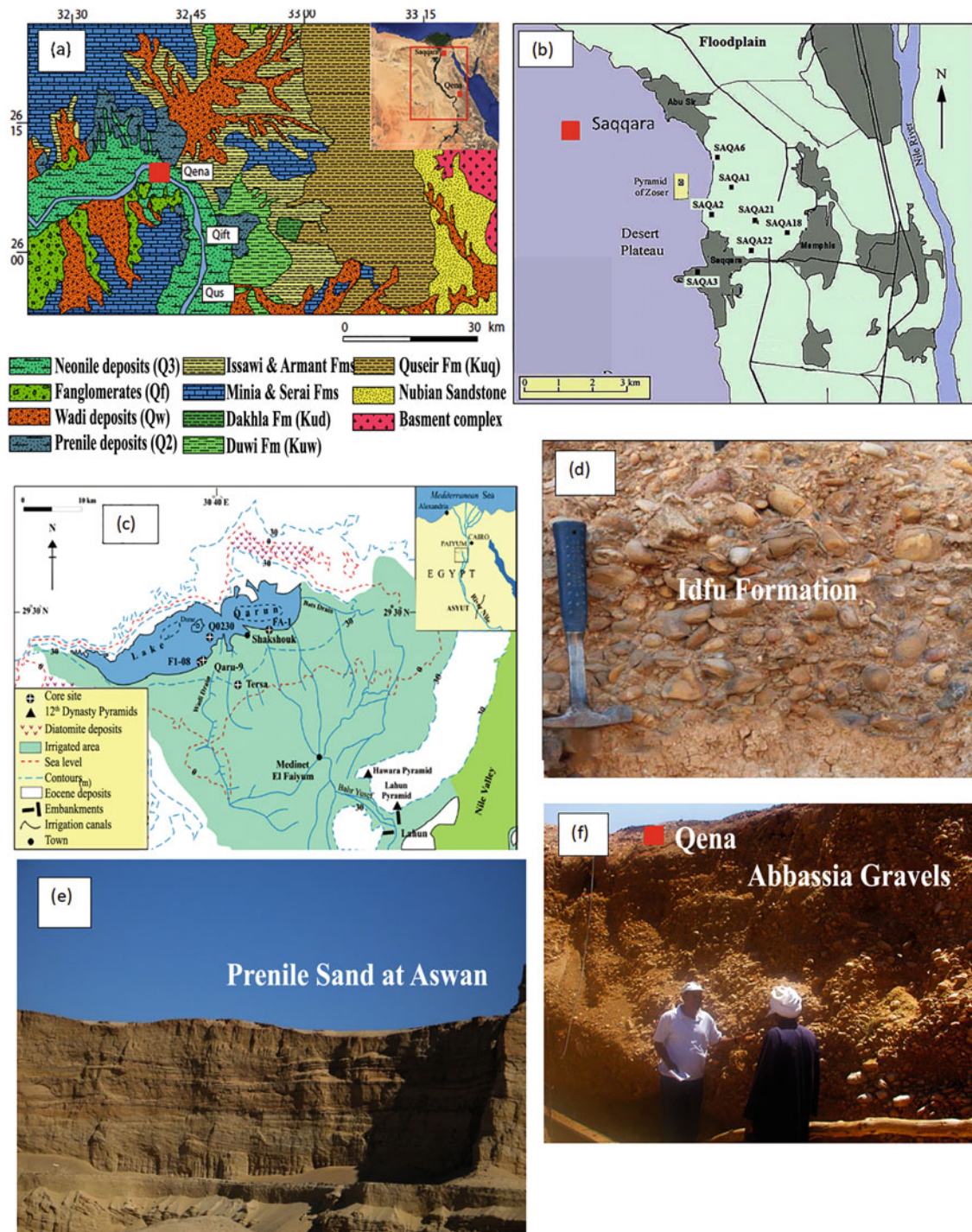


Fig. 13 Location map for the Prenile sediments at Wadi Qena (a) (Hamdan, 2013). Location map for Neonile Holocene sediments at Saqqara (b) (Hassan et al., 2017). Location map for the drilled boreholes at the Faiyum Depression (c) (Hamdan et al., 2020). The Idfu Formation composed of gravels of outside source (d) (Wysocka et al., 2016). The Prenile sediments at Aswan (e) (courtesy of Prof. Dr. Mohamed Hamdan). The Abbassia gravel at Wadi Qena (f) (Hamdan, 2013)

profound their course through the Nubia (Said, 1981, 1993). The Prenile (Qena Formation; Figs. 12 and 13a, e) in its type locality attains 32 m thick (Hegab, 1989). The Prenile sediments reach great thicknesses averaging between 70 m in the valley and between 300 and 400 m in the delta (Said,

1993). It is composed of cross-bedded, cyclic fining-upward sequence of gravel and coarse sands (Fig. 13e) with no mud reflecting a transitional of meander to Braided stream (Hegab, 1989). The Prenile delta extended well into the Mediterranean and had an area at least three times as large as

the modern delta. The extent and thickness of the deposits of the Prenile make it certain that this was a vigorous and very competent river, developed in arid climate and high sea level (Said, 1993). The Prenile deposits are estimated as one hundred million cubic metres of sediment every year for the duration of its life, which is more than double the quantity of sediment carried by the modern Nile (Said, 1993). This can be attributed, in part, to the great erosive power, swift and steep sloping of the river both in Ethiopia and in Nubia. The river left no deposits except rock cut platforms indicating that it was incising its course and transporting the eroded materials from both Ethiopia and Nubia into Egypt. A good portion of the sand of the Prenile deposits seems to have come from Nubia, which is covered by the friable sandstones of the famous Nubian Sandstone Formation. The accumulation of layer upon layer of the thick column of sediments of the Prenile must have taken place during a period of rising sea level when the river, in response to this rising level of the sea, aggraded and built up its bed (Said, 1993).

The Neonile (Q3): It is the third Quaternary regime extends from 400 ka ago, of Middle–Late Pleistocene (Early Paleolithic). It is a considerably less competent river, broke into Egypt, following the cessation of the Prenile River's connection with the Ethiopian Highlands. The African sources became tenuous and sporadic with great climatic fluctuations, which affected the Nile headwaters and the climate of Egypt (Said, 1993). Three sets of events can be distinguished in the evolution of the Neonile (Fig. 12). The oldest of these is the Nile aggregation (Said, 1993) that associated with the Early Paleolithic wet interval. It consists of two gravel formations (the Abbassia I and Abbassia II; Figs. 12 and 13f). Massive, weakly cemented gravels with a polygenetic origin make up the Abbassia Formation (Fig. 13f; Said, 1990). The pebbles are subround and come from the Eastern Desert's exposed basement (Hamdan, 2013). Between a brief dry event (Dandara Formation or α -Neonile; Fig. 12) and two pluvials (Abbassia I and Abbassia II Pluvials), the Abbassia Formation is connected with these two deposits (Said, 1993). The Dandara assumed the resumed connection of the Egyptian Nile with Ethiopia (Said, 1993). The Dandara Formation is about 15 m thick and is made up of a base of grey, loose and fine-grained sandstone, then brown silts with thin carbonate interbeds and sporadic lenses of gravel, and finally, a characteristic red soil (Hamdan & Hassan, 2020; Said, 1993). It was dated more than 40–39 ka (Wendorf & Schild, 1976). However, age of 117–105 ka was inferred (Ducassou et al., 2009), and Late Acheulean > 200 kyr BP (Deino et al., 2018; Hamdan & Hassan, 2020). The Abbassia pluvials are correlated with MIS 7 (Fig. 12). The Abbassia I gravels are archaeologically barren, but the Abbassia II gravels are abundant in Early Paleolithic (Late Acheulean) tradition archaeological material (Hamdan & Hassan, 2020).

The second set of events was associated with the succeeding pluvial (200–70 ka BP), the Saharan I and Saharan II Pluvials (Korosko, Ducassou et al., 2009; Said, 1990; Fig. 12). During this wet interval, local winter rains supplemented a low and erratic river with an African connection. This interval showed the appearance and spread of Middle Paleolithic man in Egypt (Said, 1993). The Saharan I pluvial is related to MIS 5 indicating the interglacial (MIS5), while the Saharan II Pluvial was lasted at 70 ka and is correlated with MIS4 (Fig. 12). The third set of events was linked to the glacial period, with two successive rivers: one is related to beta β -Neonile (70–25 ka BP; Middle to Late Paleolithic), and the second river is the gamma γ -Neonile (20–12 ka BP; Late Paleolithic, Fig. 12). In relation to β -Neonile, three formations were identified: the Dibeira-Jer Formation of Middle Paleolithic silt (De Heinzelin, 1968); Makhadma, which is composed of sheets, wash gravels, pebbles and boulders (Wendorf & Schild, 1976); and Ikhtiariya Formation of Middle Paleolithic artefacts (Fig. 12), which is composed of huge, well-sorted, dune sands with a thickness of 4–6 m. They are resting unconformably on top of the Prenile or Dandara Sands (Said, 1993), which are covered by layers containing fresh Late Paleolithic items (e.g. Masmal-Ballana Formation and fluvial sands). Two over-bank silts are interspersed with dune sands in Wadi Kubaniya (west Aswan); the lowest and oldest sections of the silts fall beyond the limit of radiocarbon dating; they may be as ancient as 70 ka BP (Butzer, 1997). On the other hand, the uppermost portions were finished long before 30 ka BP (Wendorf et al., 1989). The second river is the gamma γ -Neonile which shows the connection of the two rivers arrived to Egypt. They drew their water from the Ethiopian Highlands, with little contribution from the equatorial lake Plateau, and the climate over Egypt was arid (Said, 1993). Masmal-Ballana Formation is composed of dune sands intercalated with silts and covered by soil (Said, 1981). There are several Late Paleolithic artefacts in the sediments near the top of the dunes. L. While De Heinzelin (1968) gave the name Ballana Formation to dune sands that interfinger the upper portion of the Dibeira-Jer silts in the Egyptian Nubia, Butzer and Hansen (1968) gave the name Masmal Formation to silts and channel beds in the Kom Ombo. The majority of the Sahaba-Darau Formation (Said, 1981) is made up of silts from floodplains. It is more than 6 m thick. The formation lies above the Deir El-Fakhuri Formation's recessional pond deposits (Fig. 12). The Gebel Silsila Formation described by Butzer and Hansen (1968) in the Kom Ombo region is comparable to the Sahaba-Darau Formation. According to De Heinzelin's, 1968 account of the Sahaba Formation, it is subdivided into two aggradational units, separated from one another by a down-cutting occurrence (Deir El-Fakhuri Formation).

The Holocene Nile: It is represented by δ -Neonile aggradation (Said, 1993), which started about 10 ka BP after the last glacial period's ice had retreated and a river had emerged. The Holocene (Nabtian) or AHP was a wet period during which the modern river was created. This phase allowed the river to flow year-round by increasing the river's flow and expanding its catchment area. This river's sediments are divided into the Dishna-Ineiba, Arkin and El-Kab Formations (Fig. 12). A series of playa deposits and Nile silt with interbeds of gravels and pebble sheets make up the 10–9 ka BP Dishna Formation (Hamdan & Hassan, 2020). The Sahaba Formation is situated below this Formation, which is followed by the Arkin Formation. The Ineiba Formation, on the other hand, is a broad wadi deposit that dates to 9–7 ka BP (Butzer & Hansen, 1968), of brown clays on the top section (Sinqari Member), and a lower conglomeratic bed (Malki Member) (Hamdan & Hassan, 2020). Such sediments represent wet with increasing flow of the Nile, during which the silts were carried from the Nile Headwater and were deposited on the flood plain of Egypt (Said, 1981). The recession that followed the Sahaba-Darau aggradation gave rise to the Dishna-Ineiba Formation, a period of aridity. The playa deposits built up behind the Sahaba-Darau aggradation's natural levees and abandoned channels. 6 m of silts and fine-grained micaceous sands make up the Arkin Formation, which overlies the Dishna Formation, of estimated date 9.2–7.2 ka BP (Said, 1981).

The Faiyum Depression (Fig. 13c) is bound from the north by several escarpments. Historically, the depression was occupied with large lake (Lake Moeris); the current Lake Qarun is a relic from the earlier Lake Moeris, which was supplied with water from the Nile runoff through the Bar Yussef. The presence of lake-beaches and lacustrine sediments at different levels indicates fluctuations in the connection of Nile and interruption in the source of water since the Middle Pleistocene (Butzer, 1997; Hassan, 1986). The level of the lake was directly influenced by variations in Nile flooding, which in turn had an impact on the ancient settlement patterns in the Faiyum (Hassan, 1986). Paleoshorelines are defined by a succession of ridges along the depression's western side at elevations of 44–42, 34–39, 28–32 and 23–24 m, which are equal to heights of 71, 61–66, 55–59 and 50–51 m in the floodplain at Beni Suef in the Nile Valley (Hamdan, 1993). From the Early Holocene to the Greece-Roman era, the Blue Nile flow from monsoonal rainfall in Ethiopia and, to a lesser extent, the White Nile flow from central East African rainfall to the basin's lakes fluctuated in accordance with the flow of Nile water, which was primarily controlled by climate (Williams et al., 2000). Since the Middle Kingdom, hydrological changes have controlled Nile flow (Hamdan & Hassan, 2020). Instead of the fluvial sediments in the Nile Valley, where some records are absent owing to erosion during low Nile floods, the

Faiyum Depression may give sedimentary records of Nile floods (Hamdan et al., 2019). The lacustrine sedimentary sequences in Faiyum Lake therefore likely include the most comprehensive paleoenvironmental records during the Holocene in the area (Flower et al., 2012; Hamdan et al., 2016; Marks et al., 2018). The Holocene paleoclimate deduced from sediments recovered from two lake cores in order to reveal the ambiguity about the Faiyum Depression Holocene history. The following units were recorded (Hamdan et al., 2020):

Late Pleistocene sediments (Unit I; Fig. 14): The whole depression was dry and home to sand dunes until the Early Holocene began. The sedimentological features of the Unit I sands and those of contemporary dunes are comparable. However, a sample of modern sand dunes had neither microfossils nor glauconite grains (Flower et al., 2018). This suggests that there may have been some sorting by aeolian processes and that the core locations were near ancient sea deposits. Additionally, low Fe/Al and Ti/Al ratios and high Zr/Al ratios (Fig. 14) confirm the aeolian origin of sands from Unit I. In Egypt, dune sand deposition predominated during the Late Pleistocene dry periods (Late Glacial Maximum or Younger Drays; Hamdan et al., 2020).

Early Holocene sediments (Unit II; cal. 9.9–8 ka BP, Fig. 14): It occurs on top of the Late Pleistocene aeolian sands (Unit I), and it is made up of sub-mm laminations of white diatomite and calcite, which are non-glacial varves, interspersed with layers of yellowish-green mineralogenic beds, which indicate a deep freshwater lake phase (Hamdan et al., 2020). In summer, the Nile floods controlled the sedimentation of Nile silts and clays through the Howara channel. In winter, the controlling factor was the local rain responsible on the carbonate lamina in undisturbed varved units deposited in the deep lake that was quickly filling up (Flower et al., 2012). The Early Holocene sediment's predominance of silt and clay-sized particles, low magnetic susceptibility, and slow pace of sedimentation can also be partly attributable to an increase in the amount of Nile water entering the lake at that time. Additionally, the sediments show noticeably high Ti/Al and Fe/Al ratios, which point to Ethiopian origins (Krom et al., 2002). Lower diatom abundance and larger grain size due to altering Zr/Al ratios, as well as additional increases in magnetic minerals, together with a significant fall in Fe/Al and Ti/Al, were all signs that this Early Holocene wet phase had come to an end (Hamdan et al., 2020).

The Early-Middle Holocene sediments (Unit III, cal. 8–6 ka BP, Fig. 14): This unit is made up of pockets of non-glacial varved laminae intercalated with turbidites and thickening silty clay layers, indicating a period of shallow

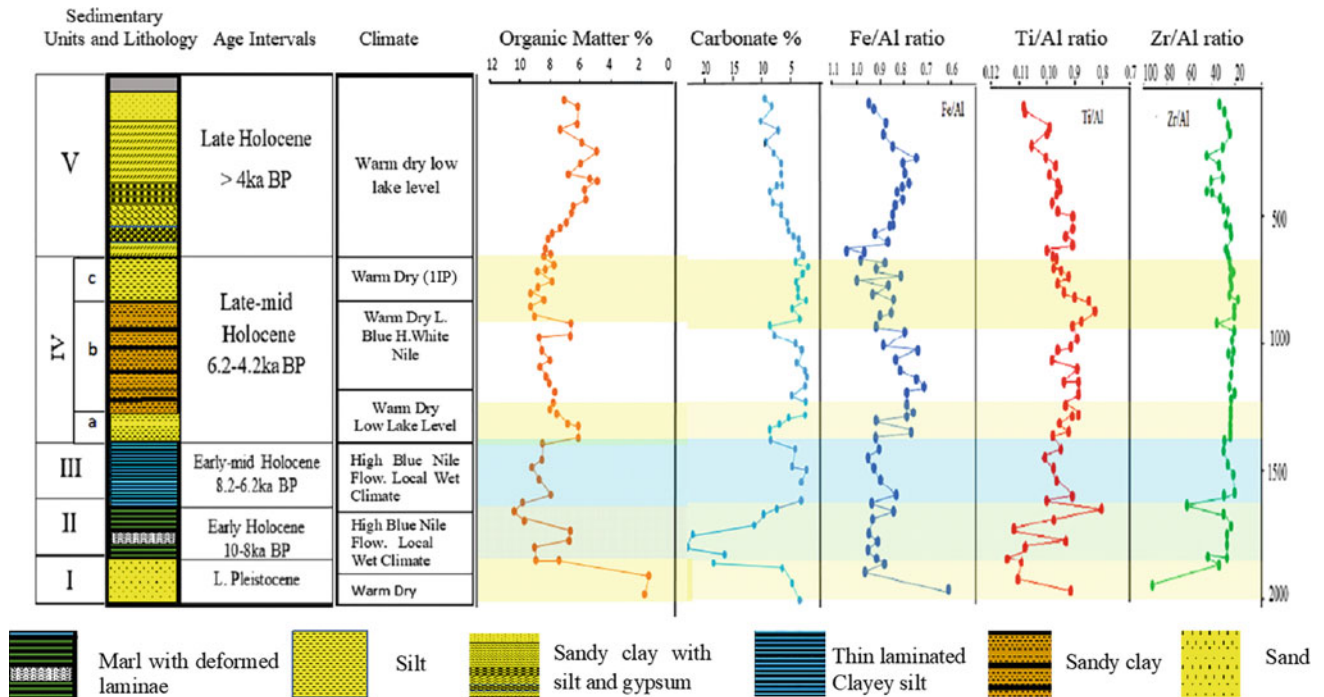


Fig. 14 Holocene sedimentary units at Fayum Depression, with deduced paleoclimate based on the vertical distribution of organic matter and carbonate percentages, as well as Fe/Al, Ti/Al and Zr/Al ratios. The climate shows regional wet and warm correlated with the Blue Nile flow until 6 ka BP and then changed to dry with low Blue Nile and relatively high White Nile contribution from 6 ka BP to reach the drought at 4 ka BP during which a collapse of the Old Kingdom was occurred. *Source* Hamdan et al. (2020)

freshwater lakes with rising nutrient levels (Hamdan et al., 2020). This unit describes a humid environment with proof that the lake level started to rise and the Nile floods reached a level of 25 m a.s.l. about 7 ka BP (Hassan, 1986; Wendorf & Schild, 1976). During that time, the lake was not adapting to local sources; instead, it was likely responding to climate change factors brought on by increased Nile flooding. This unit's sediment features include layers of abundant turbidity in varied thickness and additional thickening of the darker clastic laminae by terrigenous silty clays. The input of Blue Nile silt seems to have significantly diminished towards the end of that time, as shown by a slight rise in magnetic susceptibility and varied Ti/Al and Fe/Al geochemical ratios (Fig. 14; Unit III compared to Unit II). According to Said (1993), the peak Nile flow occurred at around 6 ka BP, during the Nabtian pluvial epoch (Butzer, 1997; Williams & Adamson, 1980). However, Blanchet et al. (2013) hypothesized that after 8.5 ka cal BP, the Blue Nile contributed less water to the main Nile.

The Late-Middle-Holocene lake phase, Unit IV (cal. 6–4 ka BP, Fig. 14): This unit lacks any documented varve structure indicating more significant hydrological changes and is mostly made up of sediments that are silty clay-dominated (Hamdan et al., 2020). Despite the thin laminated silty clay's presence, there has not been a

consistent inflow of water from the Nile, which is thought to have caused the lake to further shallowing approximately 6 ka BP. These clues point to significant climatic shifts in the Nile headwaters, which will lead to a decline in Nile floods. The three sub-units IV-a, IV-b and IV-c make up this unit.

The sub-unit IV-a (Fig. 14): Grey massive mud makes up the majority of the material, with sporadic thick (> 1 cm) diatomite-carbonate layers and thin gypsum and iron-hydroxide layers indicating a lake-shrinking phase as well as a sand-evaporation period when freshwater input was at its lowest. The predominant sediment type throughout this time was silty clay, and there was no proven varve structure showing additional significant hydrological changes. According to Hamdan et al. (2020), these signs point to significant climate changes in the Nile headwaters, which would reduce the lake. In the Late-Middle Holocene, there was an increase in aeolian activity due to the abundance of carbonate laminae, low organic matter content and high Zr/Al ratios (Fig. 14). The beginning of the Late-Middle Holocene lake appears to be contemporaneous with the end of the African Humid Period (AHP) in NE Africa, a period during which the intensity of Nile floods sharply dropped and became more erratic (Williams et al., 2010). An Old Kingdom or Neolithic lowstand lake might be represented by this sub-unit IV-a (Hassan, 1986).

The sub-unit IV-b (Fig. 14): It is made up of layers of rich iron and manganese hydroxide with white carbonate laminae. Iron and manganese hydroxides may associate with postdepositional water losses due to burial diagenesis and formation of oxidized mineral crusts on the surface of sediments (Hamdan et al., 2020). This indicates a deposition in a hot arid climate with low lake levels with little input of the Nile water. The Late-Middle Holocene Ti/Al and Fe/Al ratios are significantly low, which indicate a lower contribution from the Blue Nile to the main Nile and a larger flow from the White Nile. The latter represents the humid conditions that prevailed in central Africa during the Mid-Holocene, when the Wadi Howara was active and supplied sediments that had similarities to the White Nile (Woodward et al., 2007).

The sub-unit IV-c (cal. 4.2 ka BP; First Intermediate Period IIP; Fig. 14): Because of the catastrophically low Nile flood, the lake experienced a significant drop (Hassan, 1986). Sand carbonate intercalation facies with significant iron and manganese oxide material and a relatively high Zr/Al ratio signify the sediment transition at the end of sub-unit IV-c. The lower lake level and sediment reworking caused by the arid climate and strong aeolian activity are clearly shown by these sedimentological and geochemical properties. This change roughly corresponds to the catastrophic drought (IIP), which is indicated by an erosional pause in an Ain Seleen core (a terrestrial site within the ancient Faiyum delta, Hassan et al., 2017).

The Late Holocene lake phase (Unit V, cal. 4.0 ka BP to present, Fig. 14): Massive sedimentary structure and an increase in sand content characterize this unit, which indicates strong disturbance, low lake levels and sediment reworking. In this unit, low microfossil abundance of broken mollusc shells, potsherd organic matter and Ti/Al and Fe/Al ratios is noticeably low, with a relative increase in Zr/Al ratio (Fig. 14). These correspond to reduced Nile water influx and aeolian activities and are more or less indicators of dramatic declines in lake level (Hamdan et al., 2020).

The geochemistry and mineralogy of the Holocene sediments recovered from two shallow drilled cores at Saqqara (SAQA 21 and 22; Fig. 13b) were investigated (Hamdan et al., 2019). This study offers new insights into understanding the provenance, local paleoclimate as well as paleoclimatic variations at the Nile headwaters. Six Holocene units (II-VII) were recognized; another two units (I and VIII) were belonged to the Late Pleistocene and Recent, respectively (Fig. 15a). These are described as following:

Unit I (Late Pleistocene cal. 11–8.2 ka BP; Fig. 15): This unit, which dates to the Late Pleistocene, is made up of the basal fluvial sands found below the Holocene floodplain

deposits of the Nile Valley and Delta (e.g. Coutellier & Stanley, 1987). Pebbly, medium to coarse-grained quartzose sand with upward fining sequences from pebbly sand to fine-grained sands is seen in this unit. The lithological features of unit I show lateral river migration over the alluvial plain during deposition in a high-energy braided river (Hassan et al., 2017). According to Wendorf and Schild's (1976) hypothesis, the wet seasons in the Nile headwaters were shorter but more intense over the majority of the Late Pleistocene, resulting in a substantially lower total flow of the River Nile than they are now. The Nile Valley was occupied with many braided channels as a result of decreased stream competency and an increase in sediment load. Additionally, according to Stanley and Warne (1993), the whole Nile Valley was covered by braided-river systems during the Late Pleistocene, when the sea level was at least 120 m b.s.l. and the river gradient was much larger than it is now.

Unit II (Neolithic-Predynastic, cal. 7.5–5 ka BP; Fig. 15): This unit is made up of thin streaks of calcareous silt and fine to very fine-grained, micaceous and quartzose sand with dispersed limestone particles. This unit was deposited during a strong Nile flow, fast sea level rise and locally wet conditions. Swamps and anastomosing channels consequently covered the floodplain (Hassan et al., 2017). Unit II sediments are distinguished by a high IAmph index, high Fe/Al, Ti/Al ratios, high silica and alumina (Fig. 15a), and a low K/Al, K/Rb, Cr/Al and Mn/Al ratio that supports White Nile origins (i.e. Central African; Hamdan et al., 2019).

Unit III (Old Kingdom, cal. 5–4.2 ka BP; Fig. 15): The sediments of unit III show moderate to low Fe/Al, Ti/Al (Fig. 15a), Cr/Al and Mn/Al ratios, as well as comparatively high IAmph over IPyrox. This indicates a mixture of contributions from the White Nile and Blue Nile due to flocculation, reduced flow and increased contribution of silt from the Ethiopian Highlands (Hamdan et al., 2019). The top of unit III is distinguished by a high concentration of heavy zircon minerals, a lack of clay minerals and a high Zr/Al ratio, all of which point to intensive aeolian activity. In this context, a meandering channel system with strong levees and flood basins is referred to as being more stable (Hassan et al., 2017). This unit coincides with severe drought 1st Intermediate Period (FIP) resulted due to a southward shift of the summer ITCZ and intensive rainfalls resulted in widespread sheet-flood accumulations in northern triggered by variation of the North Atlantic Oscillation (NAO); these were led to collapse of Old Kingdom (4.2 ka BP; Hamdan et al., 2019; Welc & Marks, 2014).

Unit IV (Middle Kingdom-New Kingdom; cal. 4.055–3.070 ka BP; Fig. 15): It is a massive unit of sandy silt, silt and clayey silt, enriched with carbonate and manganese

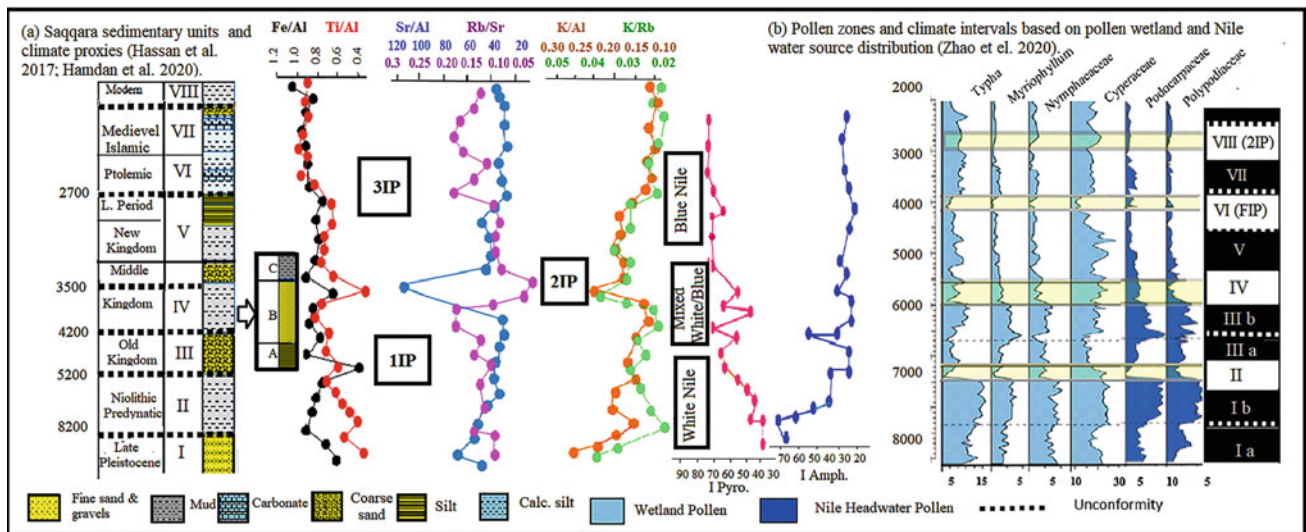


Fig. 15 Holocene sedimentary units in relation to paleoclimate deduced from Saqqara, Egypt. The subdivision based on the vertical distribution Fe/Al, Ti/Al, Sr/Al, Rb/Sr, K/Al and K/Rb ratios as well as the distribution of *I Amph* and *I Pyro* (a) and smectite, kaolinite and Illite clay minerals (Hamdan et al., 2019). These are correlated with the vertical distribution of wetland and Nile Headwater pollen (b) (Zhao et al., 2020) and the Intermediate Periods (1IP to 3IP) of aridity crisis (Hamdan et al., 2020). The deduced climatic intervals clue the sources of Blue Nile and White Nile discharges. Sources Welc and Marks (2014), Hassan et al. (2017), and Hamdan et al. (2019)

concretions, with abundant potsherds and freshwater shells, indicating extremely Nile floods that correspond with historical records of exceptionally high floods during the Middle Kingdom (Hassan et al., 2017). This unit is clearly divided into three sub-units: (a) a thick sub-unit of massive quartzose sand; (b) a thick, massive clayey silt sub-unit; and (c) a thick, massive clayey silt sub-unit with New Kingdom potsherds in the upper part. The red potsherds and reworked limestone pebbles from the Middle Kingdom are found at the base of the sandy silt sub-unit. The Faiyum Depression is linked with these components (Figs. 14 and 15a).

Unit V (Late Period; cal. 3.070–2.343 ka BP; Fig. 15): This unit comprises Late Period potsherds and dates to between cal. 2.71 and 2.35 ka BP (Hamdan et al., 2019). It is characterized by clayey sandy silt and sandy silt with carbonate and manganese concretions, as well as freshwater shells and pottery. It is also rich in freshwater mollusc shells and cemented root casts. Sharp erosive contact between unit V and unit VI is visible (Hamdan et al., 2019). The Fe/Al and Ti/Al ratios of the two units are varied (Fig. 15a) and the pyroxene index is greater, indicating a larger Nile flow and an increase in contributions from Ethiopian sources (Fig. 15a).

Unit VI (Ptolemaic and Roman, cal. 2.332–1.360 kyr BP; Fig. 15): This unit is primarily characterized by clayey silt, sandy silt and micaceous silty quartzose sand. Ptolemaic and Roman pottery fragments, freshwater mollusc shells, ash and mud-brick are also prevalent in these lithologies (Hassan et al., 2017).

Unit VII (Fig. 15): This unit is made up of clayey silt with intercalations of silty sand and sandy silt, as well as calcareous gravelly sandy silt, which is frequently replete with calcified root casts, freshwater shells and pottery fragments (Hamdan et al., 2019). This unit's upper portion is made up of freshly disturbed, farmed soil with sporadic examples of contemporary artefacts and live plant root casts. Units VI to VII cover the majority of the time from the Ptolemaic to the Early-Middle Islamic periods. Several extremely low and extremely high floods happened, leading to numerous famines and terrible disasters, particularly during the Medieval Islamic Period (Hassan, 2007).

Unit VIII: This unit is represented by modern cultivation soil with living plant roots.

Investigations on the Saqqara-Memphis floodplain cores have shown that the studied area was subjected to wet regional conditions for the majority of the Middle Holocene (i.e. unit II), wet in the Middle Kingdom and in the Late Old Kingdom. With frequently dry during the New Kingdom to Late Period. After cal. 2.7 ka BP, dry climatic conditions were in place (Figs. 14 and 15a). The proxies for the Holocene paleoclimate of the local wetland and Nile Headwater show that the Blue Nile delivers more than half of the main Nile discharge and over three-quarters of the sediment load. Given that it passes through Cenozoic volcanic areas of the Ethiopian Highlands, the high amount of pyroxene in comparison with amphiboles is a great indicator of the Blue Nile's contribution (Williams & Adamson, 1980). Fe/Al and Ti/Al ratios rise in the Blue Nile region due

to erosion during drier times, as is the case at the moment (Figs. 14 and 15a; Krom et al., 2002). As a result, changes in these ratios might be used to monitor historical changes in rainfall in the Nile River catchment region (Figs. 14 and 15a). The distribution of the main and trace elements in the sediments from the Fayum Depression (Fig. 14) and Saqqara (Fig. 15) reveals a very straight forward mixing connection between the end members of the White Nile and the Blue Nile. The Blue Nile and Atbara rivers, on the other hand, have larger levels of smectite, which is produced in enormous amounts by the chemical weathering of basaltic rocks (Maldonado & Stanley, 1981). Egyptian wadis, lateritic soils, erosion of Eocene and Mesozoic strata, and wind-borne supplies are the principal sources of kaolinite (Stanley & Wingerath, 1996). Illite is derived from the Red Sea Hill's surrounding Cenozoic and Mesozoic deposits, as well as some Proterozoic rocks (Stanley & Wingerath, 1996). These demonstrate the White Nile's significant contribution throughout the Middle Holocene (unit II) and the Blue Nile's supremacy during the Late Holocene (Hamdan et al., 2019). Up to 6 ka cal BP, or the Nabtian Pluvial time, which was brought on by a northward shift in the ITCZ, the Nile flows were high (Butzer, 1997; Krom et al., 2002; Williams et al., 2000). More recently, Blanchet et al. (2013) highlighted that the White Nile maintained the main Nile flow until cal. 4 ka BP and that the Blue Nile provided less water to the River Nile after cal. 8.5 ka BP. (i.e. units II and III; Fig. 15a). According to Williams et al. (2015), the rain belt began moving southward around 8 ka BP, which decreased precipitation over the Ethiopian Highlands and caused the flow of the Blue Nile to fall and the flow of the White Nile to increase. Warmer and more humid climate was seen in the Nile headwaters together with low Blue Nile sediment flows and greater White Nile fluxes. Due to the Ethiopian Highland's extensive forest cover, the Blue Nile's contribution was diminished (Krom et al., 2002). During the Early to Mid-Holocene humid climate (or African Humid Period "AHP"), there was a widespread dense vegetation cover, which stabilized slopes and reduced the amount of soil erosion. Several breaks in sedimentation were detected at 8.2, 5.2, 4.2, 3.5 and 2.7 ka BP. These are located at the boundaries between (units I and II), (units II and III), (units III and IV) 1IP Old Kingdom, (within unit IV) 2IP and (units V and VI) 3IP (Fig. 15a), respectively. These dry events indicate low Nile floods that were well correlated with low African lake levels in the Nile headwaters and generally colder global conditions (Hamdan et al., 2019). The results of Hassan et al. (2017) and Hamdan et al. (2019) show correlation with the pollen zones of local wetland intervals and Nile headwater during the Holocene (Fig. 15b, Zhao et al., 2020).

2.2.2 The Quaternary Nile Delta Sediments and Eastern Mediterranean Sapropels

To provide the context, this section discusses the formation of sapropel layers, their role in the stratigraphy of Eastern Mediterranean basin. This basin is susceptible to variations in the African monsoon and fluctuations in global sea level. Both of these processes are contributed significantly to the deposition of organic-rich sediment layers, or "sapropels", correlated with $\delta^{18}\text{O}$ and the African monsoon, which affects the flow of the Nile and pluvial intervals in Egypt. In marine geology, the name "sapropel" refers to deposits of dark-coloured mud that typically range in thickness from 1 to 60 cm and contain up to 25% organic carbon (Emeis et al., 2000; Hilgen, 1991; Kidd et al., 1978; Lourens et al., 1996; Rohling & Hilgen, 1991). The sapropels in the Eastern Mediterranean comprise layers of coccolith-foraminiferal marl that oozed from the Late Neogene to the Holocene, since the closure of the Eastern Tethys Ocean, 13.5 million years ago (Kroon et al., 1998; Lourens et al., 1996; Rohling, 1994). Most publications agree that the sapropel formation via increased organic carbon preservation under deep-water anoxia in the Eastern Mediterranean Sea is linked to climate optima of temperature (e.g. Emeis et al., 2000; Rossignol-Strick, 1985; Rossignol-Strick et al., 1982). The sapropels formed during intervals of increased freshwater influx into the Eastern Mediterranean basin closely match insolation cycles. Sapropels are important because they mark the effect of orbital forcing, exceptionally amplified due to the semi-enclosed nature of the Eastern Mediterranean (Mangini & Schlosser, 1986; Rossignol-Strick et al., 1982). The formation of sapropels occurs approximately every 21 ka due to periodic precessional changes for solar energy received in the northern low- and mid-latitudes during boreal summer insolation maxima (Emeis et al., 2000; Hilgen, 1991; Lourens et al., 1996). When insolation-driven strengthening of the monsoon led to the increase of precipitation and runoff through the Nile River (Calvert & Fontugne, 2001; De Menocal & Tierney, 2012; Revel et al., 2010). However, the response of Mediterranean climate to orbital forcing is a heavily debated topic in paleoclimatology. A large body of data has shown that at times of enhanced insolation seasonality, i.e. minimum precession and maximum obliquity, the Mediterranean area was wetter and the Mediterranean Sea surface freshwater budget increased precipitation is important in winter for both precession and obliquity (Bosmans et al., 2015; Kutzbach et al., 2013; Larrasoana et al., 2013). The obliquity appears responsible on winter precipitation on the Mediterranean basin itself and increased the winter rain seasons (Bosmans et al., 2015). The freshwater flow caused profound changes in the surface and deep-water circulation, productivity,

bottom water oxygenation and sediment supply in the Eastern Mediterranean basin (Calvert & Fontugne, 2001). Basin stagnation and sapropel formation then occur due to the preservation of organic matter inputted into the basin from a greatly increased runoff and hydrogen sulphide accumulated in the bottom of the water column (Emeis et al., 2000; Rossignol-Strick et al., 1982).

A synthesized standard Quaternary succession of the Eastern Mediterranean for about 650 ka deduced from the calculated rate of sedimentation of $1.7 \text{ mm } 1000 \text{ yr}^{-1}$ is proposed (Murat & Got, 1987). This succession appears to be modulated by cyclic events: large-scale periods (200 ka) of reduced and oxidized sequences (Figs. 12 and 16) driven by the heaviest monsoons and short-scale fluctuations (20–50 ka) driven with global climatic changes (Eurasian ice sheet meltwater; Ducassou et al., 2009; Revel et al., 2010; Said, 1990, 1993). These two factors act synchronously or independently along the studied time-span. Accordingly, ten periods (I–X) of climatic changes from dry oxidation intervals to wet reduction intervals were recorded along the Eastern Mediterranean (Murat & Got, 1987). During the reduced sequence, several sapropel layers (sapropels S1–S10) (Figs. 12 and 16) were formed (Hallberg, 2004; Rohling, 1994). These layers correlated with isotope terminations (Fig. 12); (Shackleton and Opdyke, 1973) and with the major glacial/interglacial periods (MIS 1, 5, 7, 9 (Figs. 12 and 16)). Accordingly, Murat and Got (1987) introduced their cycles. Cycle I is related to Nabtian pluvial (AHP), while cycle II is related to the Saharan pluvial (Fig. 12; Sapropels S3, S4 and S5 or termination II). Furthermore, cycle III is related to the Abbassia pluvial (Fig. 12; Sapropel S6–S9, and termination III or MIS 7), and cycle (X) is related to Idfu pluvial (sapropel S10) (Cita et al., 1977; Murat & Got, 1987; Thunell & Williams, 1998; Vergnaud-Grazzini et al., 1977; Williams & Thunell, 1979). The oxidized interval (sequences IV to IX; Murat & Got, 1987) occurred during the Pre Nile arid episode (Figs. 12 and 16). Correlation of the offshore Quaternary Nile Delta sediments collected from (NAF-1, Balim-1, and El-Temsah-2 well; Location; Fig. 1b), with cycles of Murat and Got (1987) at Eastern Mediterranean basin (Fig. 16), reveals 7 intervals of climate in relationship with sea level changes (Fig. 16), which had seen in many other areas (e.g. Fleitmann et al., 2011; Revel et al., 2010). The Quaternary Nile Delta sediments seem responding to both Eastern Mediterranean climate and African monsoons (i.e. the global climate and sea level changes) rather than other proxies in Egypt.

There is still something worth discussing and arguing that some monsoonal intervals are devoid of any sapropels or with poorly ghosts. These intervals are during the last glacial MIS 2, 3 and 4 (Revel et al., 2010) and MIS 9 to 13 from 300 to 600 ka (Konijnendijk et al., 2014) and MIS 17–19 from 700 to 900 ka (Kroon et al., 1998). During MIS 2, a

humid interval was recorded between 17 and 25 ka, and two other humid intervals recorded at 30–38 and 50–60 ka. The first related to Kubbanian pluvial of Wendorf et al. (1989), later dated as $38 \pm 5 \text{ ka}$ and related to MIS 3 (Dawood, 2001), and the second related to 67–70 ka (MIS 4) during which poorly S2 was developed (Revel et al., 2010). Another interesting issue is the time lag of the sapropel ages with the astronomical isolation (Grant et al., 2016). The end of the Saharan II pluvial corresponds to the deposition of sapropel 4 and 3, which related to MIS 5 (Fig. 12). It is agreed that the onset of the Nabtian pluvial was at 12 ka based on the East African lakes (Marshall et al., 2011), and offset occurs around 8 ka, corresponding to the deposition of sapropel S1, MIS 1, which is much earlier than the East African Equatorial region where it is at around 5.5 ka (Beck et al., 2019; Casanova & Hillaire-Marcel, 1991). This offset reveals that the southward shift of the rain belt occurred 3000 years earlier over the Eastern Ethiopian Highlands (Collins et al., 2017; Shanahan et al., 2015). It is also trace the gradual southward migration of the rain belt with probably highly variable precipitation intensity and/or longer rainy seasons between 8 and 5 ka BP (Jaeschke et al., 2020; Revel et al., 2010). Assuming a 3000 years BP lag between precession minima and sapropel mid-points, this shift was also discovered in the sapropel formation and was linked to the commonly recognized astronomically calibrated time-frame for Mediterranean sediments (Grant et al., 2016; Hilgen et al., 1993; Lourens et al., 1996; Ziegler et al., 2010). The tuning process used a 3000-year precession lag since radiocarbon dating showed that the youngest sapropel S1's midpoint happened at 8.5 ka, while the insolation maximum occurred at 11.5 ka (Lourens et al., 1996). In-depth radiocarbon tests on sediment cores from the Eastern Mediterranean have verified the simultaneous production of sapropel S1 over the whole basin (De Lange et al., 2008), resulting in an age range for S1 of around 10.8–6.1 ka BP.

2.2.3 The Quaternary Nile Delta Sediments and Pollen Zones

Pollen grains are significant for determining the paleovegetation and hence paleoenvironments in regions like the Eastern Mediterranean and Near East where few onshore sites provide long pollen records (Mudie et al., 2002). The Quaternary vegetation and climate of the Eastern Mediterranean borderland have long investigated and documented in many countries around the Mediterranean (Rossignol-Strick, 1985, 1995; Saad & Sami, 1967; Saad et al., 1987; Van Zeist & Bottema, 1982).

During interglacials, the abundance of tree pollen is maximal and points to an optimum Mediterranean climate with greatest humidity and with some summer rainfall. Such conditions favour C3 plants with Calvin-Benson

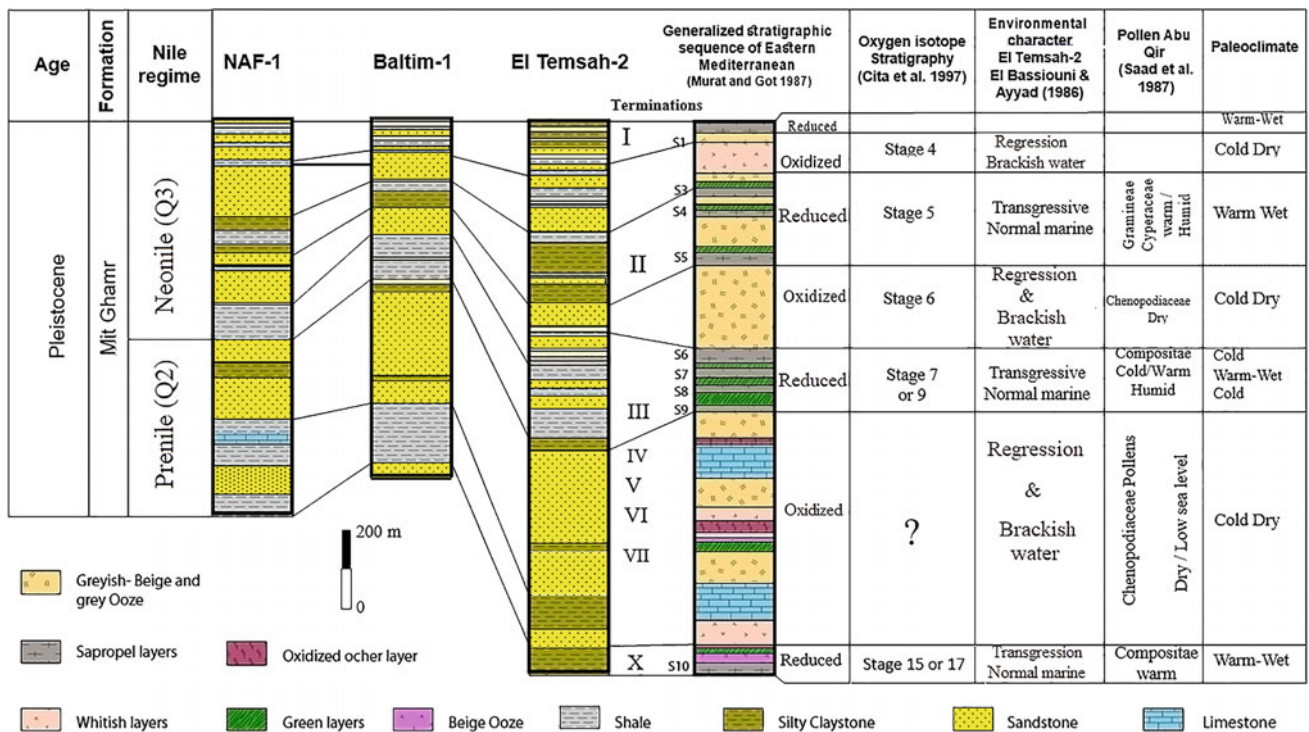


Fig. 16 Subsurface Quaternary sediments collected from offshore wells NAF-1, Baltim-1, El-Temsah-2 (Location; Fig. 1b), north of the Nile Delta correlated with Sapropel layers, the reduced–oxidized cycles of Eastern Mediterranean (Murat & Got, 1987), marine isotope stages (El-Asmar & Gheith, 1995) and pollen zones (Saad et al., 1987). The correlation reflects dry and wet intervals possibly correlated with sea level changes. *Source* El-Asmar (1998)

photosynthesis (Cerling, 1984; Cerling & Harris, 1999; Cerling et al., 1997; Ehleringer, 2005; Lattanzi, 2010). In contrast, steppe and semi-desert are abundant, but tree pollen is low, indicating a more arid, terrestrial and probably colder climate (Cheddadi & Rossignol-Strick, 1995) with abundance of grasses of C4 Hatch-Slack photosynthesis (Cerling, 1984; Lattanzi, 2010; Zhou et al., 2018). Thus, the isotope results on paleosols can help in understanding the paleovegetation cover and, hence, the paleoenvironments (El-Asmar, 1991).

The pollen data emerged from the study of Quaternary sediments from Abu Qir offshore well-1 (Location; Fig. 1b) are scheduled in Fig. 16. It shows the pollen distribution in response to climate change that is based on the assumption that Cyperaceae pollen is a sensitive marker of freshwater input into and around the Nile Delta (Figs. 16 and 17, Bernhardt et al., 2012; Saad et al., 1987; Zaky et al., 2020). Cyperaceae pollen abundance, therefore, indicates increase in precipitation over the Nile headwaters and in the Nile flow (Revel et al., 2015; Williams, 2009). Contrary is the sensitivity of Gramineae to dry climate and the increase in Gramineae/Cyperaceae ratio refers to aridity, while its decrease is related to more humidity with a possible sea level rise (Kholeif, 2004; Saad et al., 1987). On the other hand, Chenopodiaceae or Poaceae pollen described as salt tolerant

and abundant in dry and warm intervals flourished in marginal lagoons and was associated with low sea level (González & Dupont, 2009; Kholeif, 2004; Shaltout & Azzazi, 2014; Zaky et al., 2020). Asteraceae, Compositae and Amaranthaceae are predominantly tropical, indicating warm and wet climate. The Artemisia/Chenopodiaceae (A/C) ratio is higher than 1.2 in steppe vegetation and lower than 1.2 in the desert; it can discriminate between plant types (Herzschuh, 2007; Wang et al., 2020). Pollen spectra show that the climate was dry and possibly cool when the steppe pollen was abundant. On the other hand, when the environment grew warm and humid, there was a lot of tree forest. When the environment was mild between arid and humid periods, the quantities of steppe and tree pollen were comparable or about equal (Kholeif, 2004). Investigation of core samples collected from borehole S-53 (Location; Fig. 1b) drilled southwest of the Burullus lagoon showed the vertical distribution of Cyperaceae pollen correlated with other proxies of regional climate (Fig. 17). Decreases in Cyperaceae (including Cladium) pollen with increase in relative abundance of microscopic charcoal are interpreted as markers for diminished Nile flow (Bernhardt et al., 2012; Zhao et al., 2020). These are correlated with Kilimanjaro $\delta^{18}\text{O}$ ice-core record (Thompson et al., 2002; Fig. 17b) and detrital dolomite aeolian dust (Cullen et al., 2000; Fig. 17c). Other

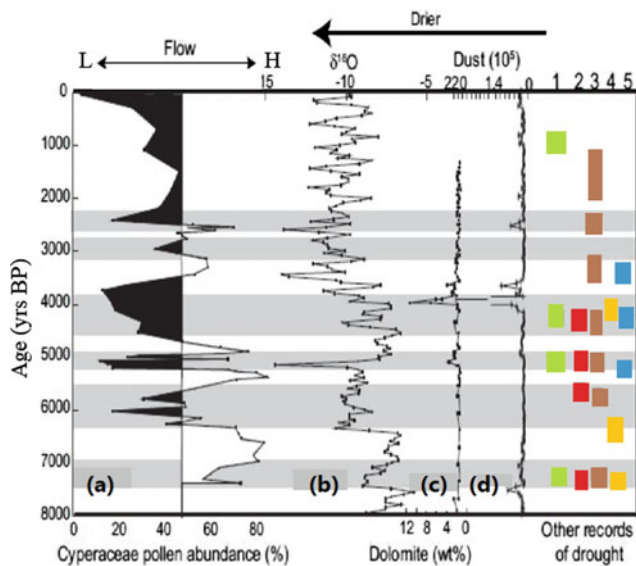


Fig. 17 Vertical distribution of Cyperaceae pollen collected from borehole S-53 (Location; Fig. 1b) correlated with other proxies of regional climate. Decrease in Cyperaceae (including Cladium) pollen is interpreted as a decrease in Nile flow and regional precipitation (a). Changes in proxies presented for comparison are thought to be influenced by changes in regional precipitation. Kilimanjaro $\delta^{18}\text{O}$ ice-core record; depletion indicates cooling (Thompson et al., 2002) (b). Detrital dolomite aeolian dust (Cullen et al., 2000) (c). Kilimanjaro ice-core dust deposited during extreme dry conditions or ice field retreat (Thompson et al., 2002) (d). Other proxy records of drought are numbered 1–5. Green increased heavy minerals (Stanley et al., 1996) (1) and red boxes indicate peaks in microscopic charcoal (Bernhardt et al., 2012) (2). The brown boxes indicate decrease in Nile flow (Krom et al., 2002) (3); the orange boxes show lowered East African lake levels (Gasse, 2000) (4), and the blue boxes indicate cultural change in the Mediterranean (Kaniewski et al., 2008; Staubwasser & Weiss, 2006; Weiss, 2000) (5). The horizontal shaded bars show intervals of regional drought that are also observed in the pollen record of this study. Source Bernhardt et al. (2012)

proxies of drought (Fig. 17d, 1–5) indicated changes in heavy minerals, microscopic charcoal with Nile flow, lowered East African lake levels and the cultural change in the Mediterranean (Gasse, 2000; Kaniewski et al., 2008; Stanley et al., 1996; Staubwasser & Weiss, 2006; Weiss, 2000).

The palynology of marine sediments from CS Core (Location; Fig. 1b) along the Manzala lagoon obtained on the inner continental shelf offshore Nile Delta has been used to reconstruct the regional paleoenvironment during the last 5380 yrs BP (Kholeif, 2010). There are number of dinoflagellates that have been identified, including *Lingulodinium machaerophorum*, *Operculodinium centrocarpum*, *Operculodinium israelianum*, *Polysphaeridium zoharyi*, *Spiniferites ramosus*, *Spiniferites mirabilis*, *Echinidinium transparantum* and *Protoperidinium nudum*. With more protoperidinioid cysts, these were comparable to those on the Tunisian Shelf. These point to shelf sediments and deposition in suboxic bottom waters during the transition

from the last glacial period (14.6–9.4 ka BP) to the present (Kholeif & Mudie, 2009). Variations in these taxa and the overall Impagidinium species point to a warming trend that was broken by a pre-Holocene cool period about 11 ka BP. Early Holocene pollen evidence of a relatively high Nile flow and the organic-rich S1 sapropel are consistent with the AHP (Filippidi & De Lange, 2019). The episode that dated around 9.5–6.27 ka BP, the mild Nile flooding, increased dinoflagellate cyst production and oxygen-deficient or anoxic bottom water on the upper Nile cone all served to support the enhanced production in carbon import theory for the establishment of the Eastern Mediterranean S1 sapropel (Kholeif & Mudie, 2009).

24 pollen and spore species were identified in core SH-1 at the archaeological site of Sais on the Nile Delta (Location; Fig. 1b). The subdivision of climatic intervals was based on the pollen and spore clusters, and seven groups of vegetation (Table 1; Fig. 18) were identified (Zhao et al., 2020). According to the vertical distribution of these groups, seven (I–VII) pollen-spore zones were identified (Fig. 18), of which four interpreted as representing dry intervals (Zhao et al., 2020). Such zones recorded at 7–6.7 ka BP (zone II), 5.8–5.5 ka BP (Zone IV), 4.2–4 ka BP (zone VI) and 3.4–3.05 ka BP (within zone VII). These dry intervals characterized by presence of increasing proportions of Xerophytic Indicators, Mediterranean Indicators, Cereal pollen, Weeds and Minor Cultivars and a higher charcoal percentage. The wet zones are distinguished by increasing proportions of Nile Headwater Indicators, Wetland Indicators and Mesophytic Indicators (Zhao et al., 2020). These zones roughly correlated with most Holocene climate subdivisions (see Figs. 10, 12 and 18, Bernhardt et al., 2012; Hamdan et al., 2016, 2019). The timing also strengthens the evidence for the importance of the AHP on Nile flow during the Holocene and on the relationship of these drought intervals with Egyptian civilizations (e.g. collapse of the Old Kingdom, Bárta & Bezdek, 2008; Marriner et al., 2012; Stanley et al., 2003; Zaky et al., 2020). Accordingly, several zones of aridity can be roughly grouped into four zones (Figs. 16 and 18), were detected in the Holocene sediments of the Nile Delta and occurred at 7.5–7, 6–5, 4.2–3.8 and 3–2 ka BP (Bernhardt et al., 2012; Zhao et al., 2020). These zones correlated with the intervals of non-deposition detected by Hamdan et al. (2019). These correspond to extreme regional and global aridity events associated with a more southerly mean position of the ITCZ (Bernhardt et al., 2012). The timing of three (5, 4.2 and 3 ka BP) of the four low Cyperaceae pollen events in (Figs. 17 and 18) coincides with documented intervals of extreme regional droughts that also affected the Egyptian civilizations (see Fig. 15). Strontium and neodymium isotopes and preliminary palynological analyses reveal large changes in provenances from a dominant aeolian Saharan contribution during the Last Glacial Maximum (LGM) and the Late

Table 1 Cluster groups of pollen zones used for subdivision of the Holocene sequence identified in core SH-1 at the archaeological site of Sais on the Nile Delta (after Zhao et al., 2020)

Group No.	Cluster indicators	Pollen indicators	Climate	References
1	Mediterranean	Betulaceae, Cupressaceae, Juglandaceae, Moraceae, Querus, Salix and Ulmaceae	Dry	Carrión & Van Geel, 1999; Sadori et al., 2011
2	Wetland	Typha, Nymphaeaceae, Myriophyllum and Cyperaceae	Wet	Tiner, 2016
3	Nile headwater	Podocarpaceae and Polypodiaceae	Wet	Rosignol-Strick, 1972
4	Mesophytic	Urticaceae and Restionaceae	Wet	Schalke, 1973
5	Xerophytic	Poaceae (< 35 µm), Asteraceae, Artemisia, Chenopodiaceae/Amaranthaceae	Dry	Cheddadi & Rosignol-Strick, 1995; Messenger et al., 2011
6	Weeds, minor cultivars and high charcoal percentages	Rumex, Silene, Ranunculaceae and Azolla	Dry	Behre, 1981; Leroy, 1992; Li et al., 2008
7	Cereal pollen	Poaceae (> 35 µm)	Dry	Andersen, 1979; Tweddle et al., 2005

Holocene (4000–2000 years). This is resulted due to a northward migration of the ITCZ that strengthened Blue Nile monsoons over the White Nile and increased the Nile flow (Adkins et al., 2006; Krom et al., 2002; Rosignol-Strick, 1985). Thus the Nile delta sedimentation constitutes a continuous high-resolution record of the Ethiopian African monsoon, the Saharan aeolian dust and the Blue/White Nile River suspended matter frequency fluctuated during the last 21,000 years (Revel et al., 2014).

3 The Quaternary Sedimentation and Stratigraphy of the Northwestern Coast of Egypt

One of the most reliable areas for studying the Quaternary sediments in relation to paleoclimate and paleoenvironment is the Northwestern coast of Egypt (Location; Fig. 1a; area 2). The coastal strip between Burg El-Arab and El-Hammam characterized by a retrogradational embayment (Fig. 19a) offers the conditions suitable for the formation of successive ridges parallel to the coastline (El-Asmar, 1991). Due to this embayment, most of the waves reaching the coast are divergent (Fig. 19b) with relatively low energy. These led to the formation of calcarenite (later called aeolianites; El-Asmar, 1994; Hegab & El-Asmar, 1995) along the coastline, forming successive ridges (R1–R4) parallel to the coastline (Fig. 19c) and recording the Quaternary sea level history (El-Asmar et al., 2012). The white oolitic limestones that make up the ridges are part of the Alexandria Formation (Attia & El-Ghazawy, 1984). Topographic low depressions (Fig. 19c) divide the ridges; El-Dekheila separates R1 and

R2. It is a sabkha depression that is 100 km long and 0.5 km broad. Another depression is the Lake Mariyut, which is home to gypsiferous sabkhas, and divides R2 from R3 (Fig. 19c). In contrast, the extensive Pleistocene gypsum deposits, which are quarried at numerous locations, are what distinguish the third depression Burg El-Arab (Fig. 19c). These gypsum deposits were thought to be saline lagoonal deposits (Ali & West, 1983; Wali et al., 1994). Two ridges were originated as coastal calcarenite dunes (El-Asmar, 1994) where the alternation of aeolianites with red paleosols reflects climatic changes (the Coastal “R1” and El-Max–Abu Sir “R2” ridges; Figs. 19c and 20a, b). In contrast to the situation at Gebel Mariyut ridge “R3” (Figs. 19c and 20c), the bottom of the ridge is composed of marine reworked beach boulder that deposited wedging the aeolianites (Fig. 21a). The age of these ridges is tentatively based on the stratigraphic positions of the ridges in relation to other marine episodes along the other side of the Mediterranean (Butzer, 1959; Zeuner, 1972). More recently, the Quaternary age has been calibrated by correlation with stable-isotope stratigraphy and sea level fluctuations (Assal et al., 2020; El-Asmar, 1991, 1994; Hegab & El-Asmar, 1995).

Summarizing the results of age determination along the coastal ridges (Fig. 22), including amino-acid geochronology (AAG) calibrated with ^{14}C and $^{230}\text{Th}/^{234}\text{U}$ (El-Asmar, 1991, 1994), in addition to new samples dated by ESR (electron spin resonance) (El-Asmar & Wood, 2000) and optically stimulated luminescence (OSL) (El-Asmar, 2000) provides significant ages. R1 the aeolianites seems to have accumulated due to an active arid climate between 7000 and 4000 BP with paleosols recording intermittent short wet intervals \sim 3680–4100 BP (Aminozone A). R2 is the

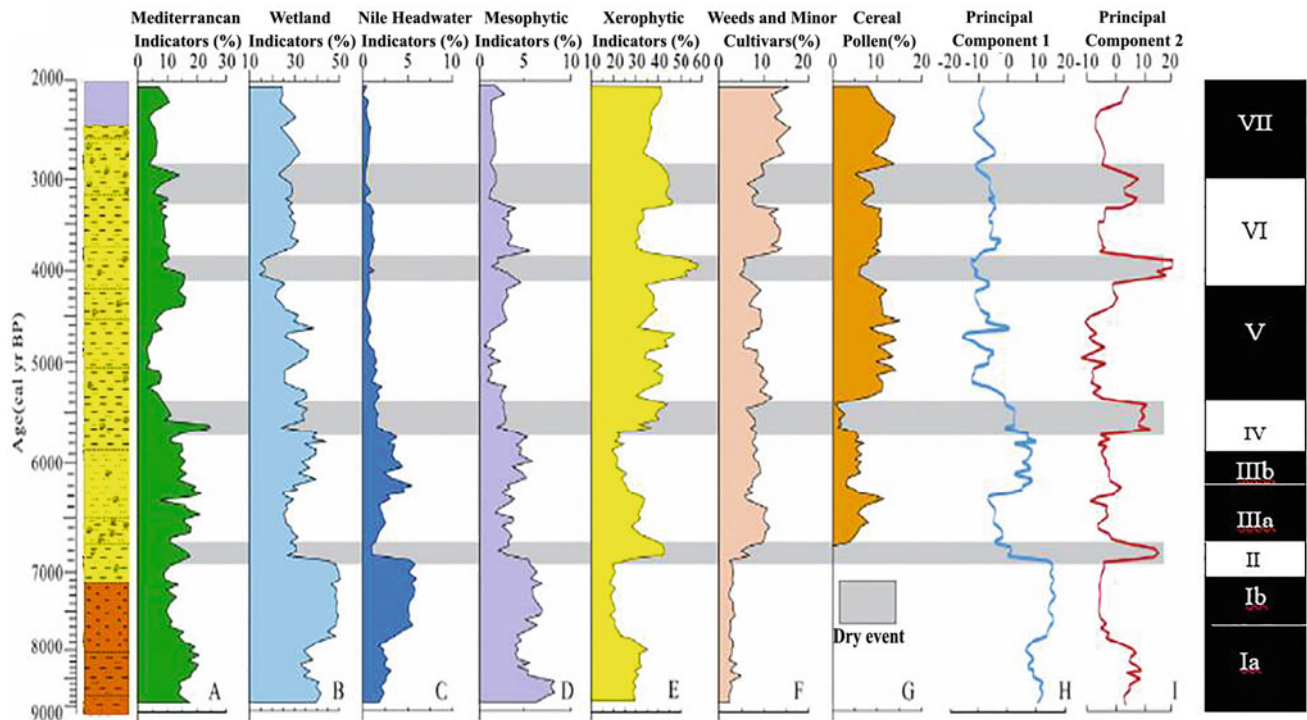


Fig. 18 Seven groups of cluster indicators of pollens collected from sediments raised from the archaeological site at Sais (Ib) to cover the last 9000 yrs. These clusters correlated together and with the main two principle components (PC1 and PC2) in order to deduce the climatic intervals. The correlation reflects subdivision of the section to seven intervals of which four are dry having white intervals, while the wet ones have the black intervals. *Source* Zhao et al. (2020)

coastal dune associated with a sea level highstand at age 100–80 ka (Aminozone C) relating to MIS 5c and 5a. R3 is dated as 121 ka (Aminozone E), relating to MIS 5e. It is intriguing to refer here to the marine beach boulders at the bottom of Gebel Mariyut ridge (R3) (Fig. 20c and for close-up see Fig. 21), dated as MIS 5e. Such sedimentary structure (Fig. 21) is observed along several coasts of the world (e.g. Hearty, 1997) and assigned to the Last Interglacial episode (El-Asmar, 1991, 1994; El-Asmar & Wood, 2000; Hegab & El-Asmar, 1995). These boulders were deposited during a Tsunami, when huge blocks of sediments were broken from the platform, dislocated and reworked. The small pieces of less than 75 cm rolled along the beach and imbricated in two phases (Fig. 21a) at altitudes of 3 m and at 6 m a.s.l. (Fig. 21b and c). This episode was described as the bipartite or double peaked famous last interglacial (MIS 5e) that was recorded in many parts of the coast around the Mediterranean and East Atlantic (Hearty, 1986, 1987, 2002; Hearty & Neumann, 2001; Hearty et al., 2007). Such boulders are the unique marine marker horizon or hypostatotype discovered along the NW coast of Egypt (El-Asmar, 1991) Study of the three ridges (R1–R3), and the top soil at Khashm El-Ish ridge (R4), reflects nine genetically related aeolianite units separated by eight aeolianite-bounding surfaces and paleosol/protosol horizons

(Fig. 22). The microfacies reflect the deposition of twelve depositional facies belonging to three main facies associations. The aeolianite facies association comprises cross-stratified oolitic and bioclastic grainstones. The inter-aeolianite facies association includes paleosols, protosols and calcretes. The intra-aeolianite facies association is represented by grainstone and rudstone in the coastal ridge (R1) and Gebel Mariyut aeolianite (R3) (Assal et al., 2020).

Assal et al. (2020) proposed a depositional model interpreting the sedimentary paleoclimate interrelationship (Fig. 23), in which the aeolianite units were mostly deposited on shallow agitated intertidal to shallow subtidal carbonate ramp during highstand periods under warm and arid climate (Fig. 23a and c). This climate favours effective carbonate pumping and the accumulation of ooids on the beach, forming dunes lining the shoreline, contemporaneous with the accumulation of Sahara dust deposition. The carbonate sediments later transported to the beach and migrated to backshore zone during arid periods (El-Asmar, 1994). With sea regression and the low stand of sea level, the climate tends to be wet and cold under the forces of Atlantic westerlies (NAO). These conditions are highly poor for carbonate pumping, while they are more appropriate for soil formation on the expense of the accumulated dust (Fig. 23b and d). The studied aeolianite units are attributed herein to

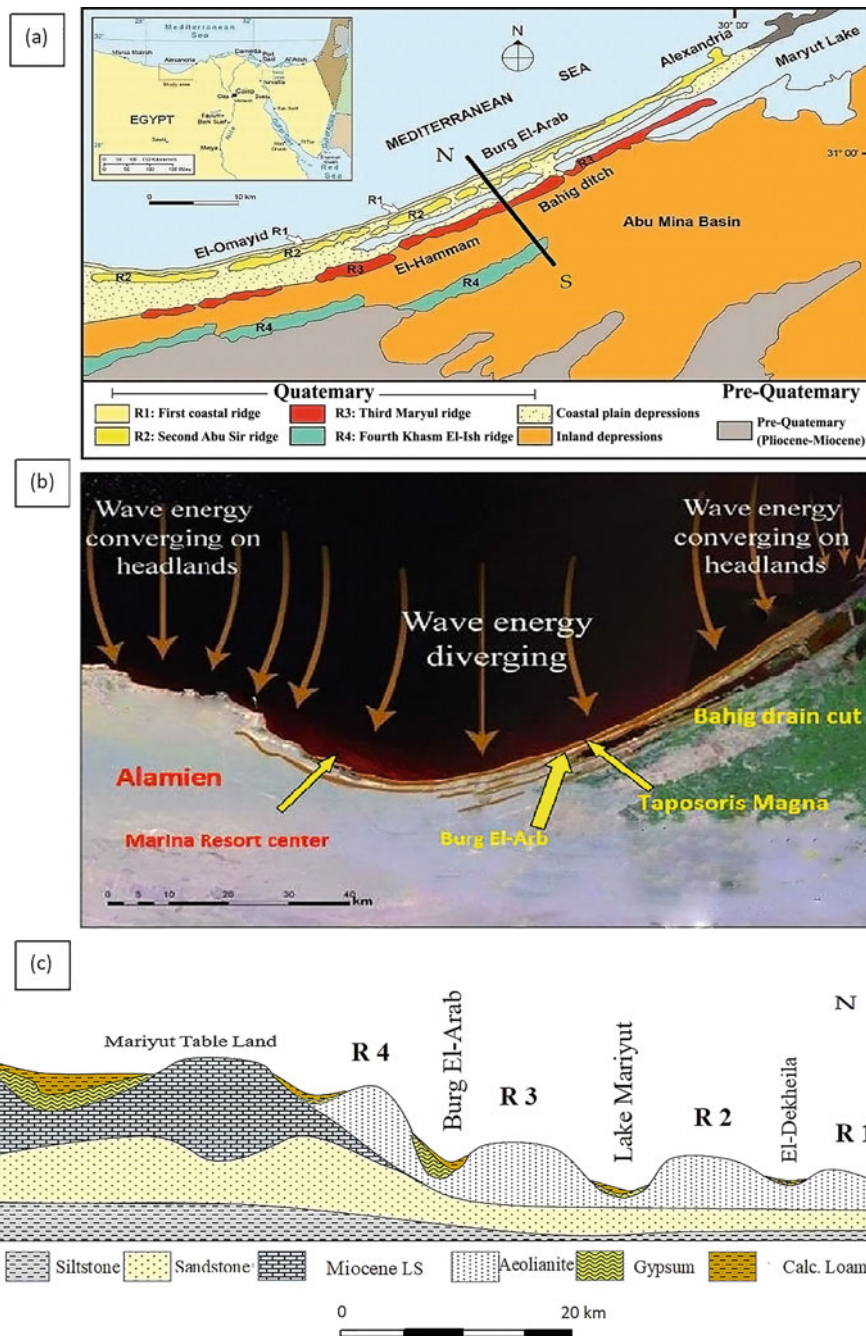


Fig. 19 Location map of the study sections near Burg El-Arab NW coast of Egypt showing the coastal ridges parallel to the shoreline and location of Bahig drain cut (a) (Assal et al., 2020). The retrogradational embayment at Burg El-Arab shows the wave orthogonals, with strong wave convergence at the headlands and weak wave divergence at the embayment. b Such waves allow sand accumulation as a coastal dune lining the shoreline (El-Asmar et al., 2012). Cross-section along N-S (a) is illustrated showing the stratigraphy and the sedimentary architecture of the calcarenite ridge with the intercalated depressions (c)

periods of highstand and stillstand, which can be correlated with the Marine Isotope Stages (MIS) of the Middle Pleistocene (R4 during MIS 9 to 7), the Late Pleistocene (R3 during MIS 5e and R2 during MIS 5c-5a) and finally, the Holocene, R1, during MIS 1 (Fig. 22). The aeolianites at R3 and R4 show controversial with large errors age estimates

between 300 and 500 ka, which are interpreted as relating to low percentages of detrital quartz grains or possibly due to reworking and deposition from older sediments (El-Asmar & Wood, 2000). Thus, the Quaternary sediments along the northwestern coast of Egypt supported with age dating can be used as a proxy of climate changes.

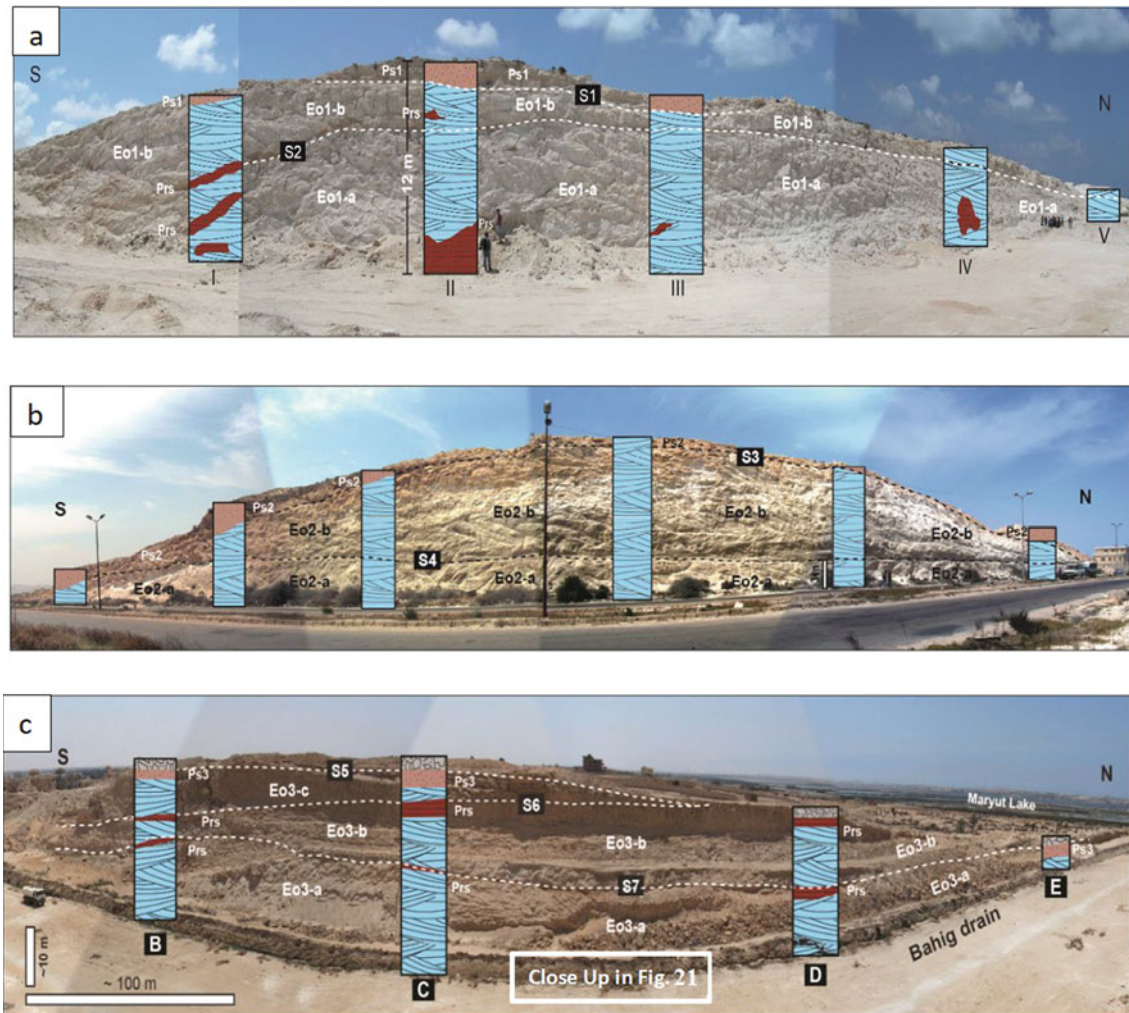


Fig. 20 Field relation, stratigraphy, sedimentary structure and alternations of aeolianites (Eo) with cross stratification, paleosols (Ps) and protosols (Prs), with surface boundaries (s) across the coastal ridge (R1) (a), El-Mxa Abu Sir ridge (R2) (b) and Gebel Maryiut ridge (R3) (c). The white quadrant shows the area of beach boulders at Bahig drain cut. *Source* Assal et al. (2020)

4 The Coral Reef Terraces Along the Red Sea Coast as a Proxy for Paleoclimate

Corals form skeletons by extracting calcium carbonate from the ocean waters, and the calcium carbonate densities in the skeletons change when the seawater temperature changes. The coral formed in the summer has a different density than that formed in the winter. This creates seasonal growth rings on the coral like those on a tree (Fig. 24a, Flannery & Poore, 2013). Such growth bands and reef accretion have been sensitive to the signals provided by the environment in the form of changes in water depth, temperature, salinity, nutrient supply, turbidity, pollution, runoff and changes in the pH of seawater which decreases as more carbon dioxide enters the ocean, a trend known as ocean acidification (Braithwaite, 2016; Felis & Patzold, 2004). Scientists can therefore study these bands, their isotopic and geochemical

compositions to determine the season in which the coral grew and the temperature of the water (Suzuki, 2018). It is possible to get the samples using a path drill of continuous sampling along the growth axis of a coral, resulting in sub-annual sampling with 10–20 samples/year, depending on the coral linear extension rate (Flannery & Poore, 2013). Different investigations can be performed to construct the paleoclimatic and paleoceanographic conditions on interannual-to-centennial timescale (Fig. 24a). Living colonies can provide several centuries of continuous paleo-recordings and have been combined with fossil corals to reveal conditions over recent millennia and earlier periods (Eakin & Grottole, 2006). Accordingly, the samples can be analysed for $\delta^{18}\text{O}$ and Sr/Ca and other elemental ratios (Fig. 24b) from long-lived coral species (Flannery & Poore, 2013). Sr/Ca ratio of the coral aragonite is sensitive to water temperature growth, colonies and species (Felis & Patzold, 2004). Similar is the $\delta^{18}\text{O}$ of coral aragonite, it is sensitive to

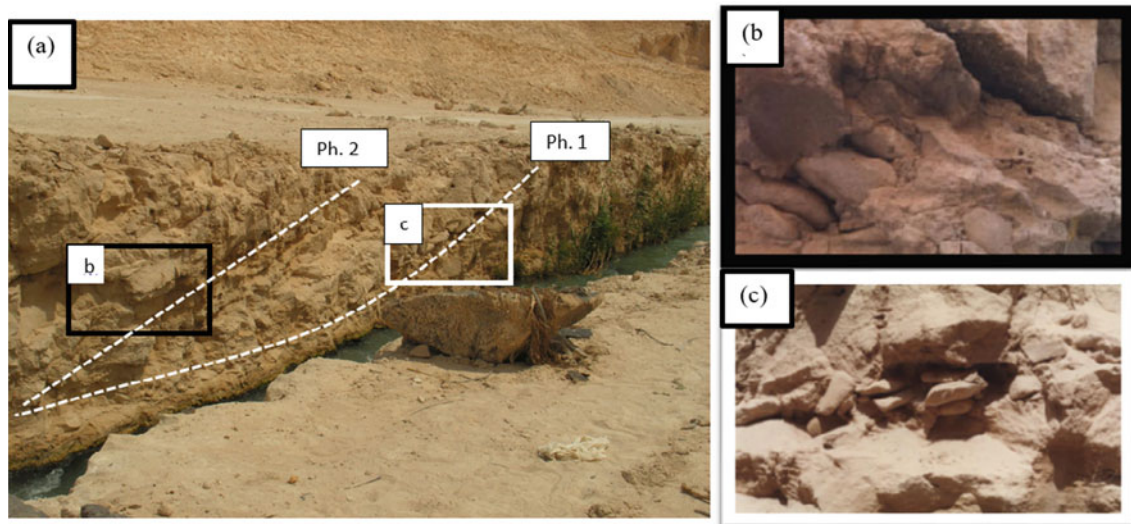


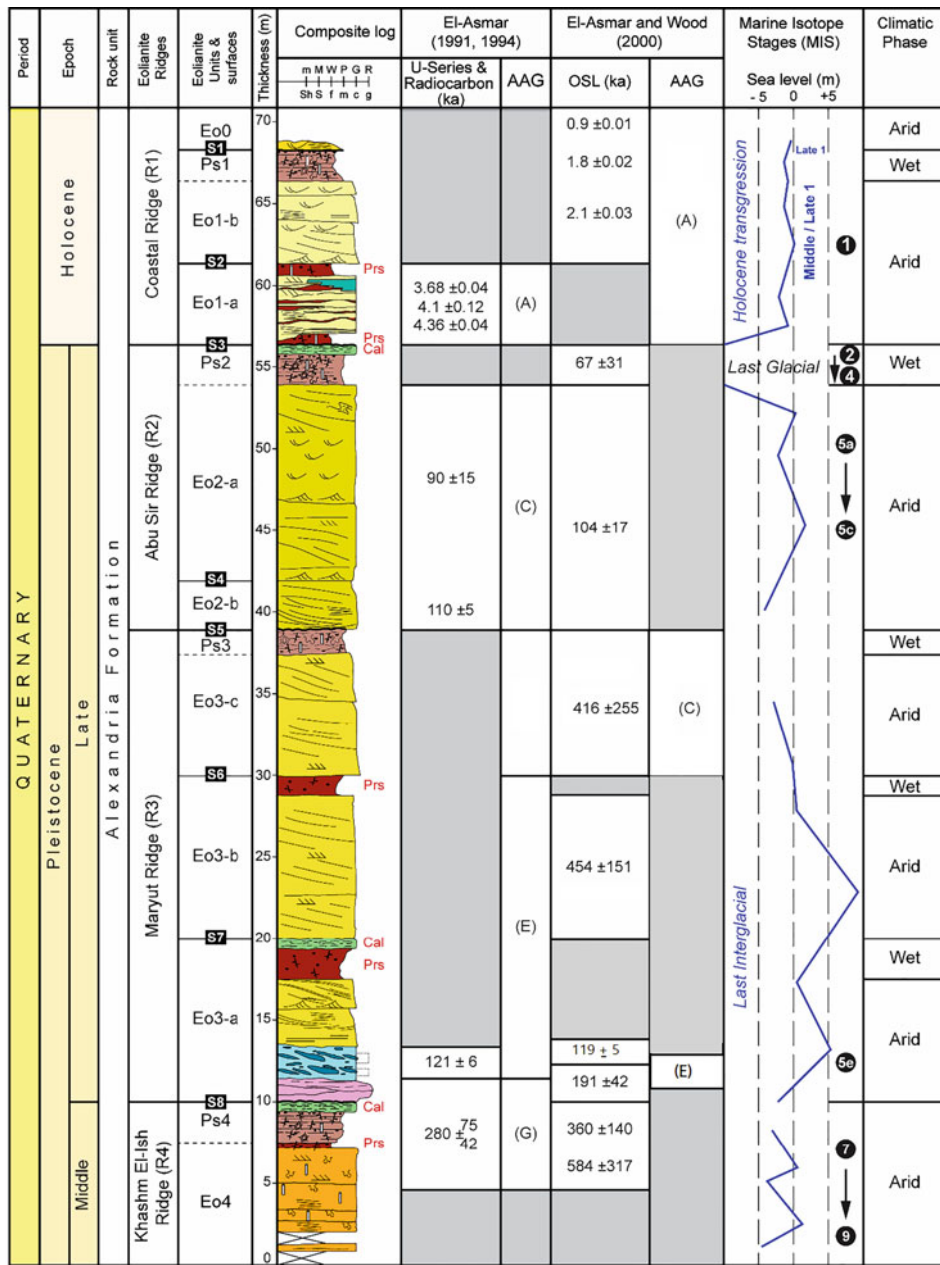
Fig. 21 Close-up for the quadrant area at (Fig. 20c) showing the imbricated beach boulders in two phases (Ph. 1, and Ph. 2) deposited wedging the aeolianites (a) at two episodes dated as record the last interglacial (LIG) episode MIS 5e (El-Asmar, 1991; Hegab & El-Asmar, 1995). The two quadrants show close-up for the 2nd phase (b) and the 1st phase (c) of the beach boulders (El-Asmar & Wood, 2000). Source El-Asmar under publication

temperature and salinity of seawater. Both Sr/Ca and $\delta^{18}\text{O}$ measurements in corals are used to make inferences about past changes in temperature and salinity. Other additional geochemical proxies in corals (e.g. B/Ca, $\delta^{11}\text{B}$, Li/Ca) may tell us more about water nutrients, pH, salinity and temperature (Flannery & Poore, 2013).

Data from corals on tropical reefs may offer fresh indicators of sea surface temperatures at low latitudes (Lauchstedt et al., 2017). A regionally explicit model of sea surface temperatures was built using the distributions of contemporary reef corals. The Last Interglacial (LIG) coral occurrence data can be used to apply this model, and the results show a latitudinal U-shaped pattern of temperature anomalies (Lauchstedt et al., 2017). In the northern hemisphere for the most of the LIG, the temperature should have been greater than it is now if the seasonality of temperature is accepted. In the mid-LIG, seasonal anomalies may have been as high as 4–5 °C at 12° N and 8.4 °C at 30° N. In the older LIG (127 ka), there was likely more seasonality as a result of winter chilling and some summer warming. Coral reefs provide significant evidence for former sea level positions because of their geological preservation and suitability for dating (Woodroffe & Webster, 2014). Whilst coral reefs are hard to use as reliable frameworks for long-term climatic and sea level changes if compared with ice cores and deep-sea sediments (Braithwaite, 2016). They still provide significant evidences for major climatic events and former sea level positions if supported with reliable age dating and in the absence of tectonic activities (Woodroffe & Webster, 2014). The interpretation of these evidences presumes an understanding of reef geomorphology, modern reef

organism distributions and the controlled environmental factors (Woodroffe & Webster, 2014). Recent coral reefs and elevated Pleistocene reef terraces are well developed along several parts of the Red Sea coast of Egypt (Location; Fig. 1a; area 3) and the Gulf of Aqaba at Sharm El-Sheikh-Ras Mohamed coast (Location; Fig. 1a; area 3-1, El-Asmar, 1997; Gvirtzman et al., 1992; Plaziat et al., 1995, 1998). The dominant reef type is the fringing reef because the Red Sea is devoid of a true continental shelf and the offshore profile is very steep (Gvirtzman & Buchbinder, 1978). During several field trips to the Red Sea and Gulf of Aqaba coasts, the architecture build-up of the raised coral reef terraces and their relation to paleo-sea level have been attracted the attention of several Quaternary geologists (El-Asmar, 1997; El-Asmar & Abdel-Fattah, 2000; Gvirtzman et al., 1992; Kora et al., 2013; Yehudai et al., 2017).

Along the Red Sea, several locations of reef terraces (Fig. 25) have been investigated. Among such locations are Sharm El-Bahari, Marsa Wizr, Marsa Abu Dabab, Ras Shagara, Assalyia, Ras Samadai, Marsa Tundebai and Ras Ambaut, Sharm El-Fuquiri and Sharm El-Luli (locations 1, 2, 3, 4, 5, 6, 7, 8, 9 and 10) which have been extensively examined (El-Asmar & Abdel-Fattah, 2000; Kora et al., 2013; Plaziat et al., 1995, 1998). Five sections of well-developed coral reef terraces were studied (Fig. 25 locations 3, 5, 6, 9 and 10) along the Pleistocene Red Sea coast (Kora et al., 2013), comprise alternating of siliciclastic-carbonate successions (Fig. 26) and attributed to the Samadai Formation (Fig. 26a and b) of Pleistocene age (Khalil & McClay, 2009). The Samadai Formation was described and interpreted as related to the upper part of the *Laganum*



LEGEND

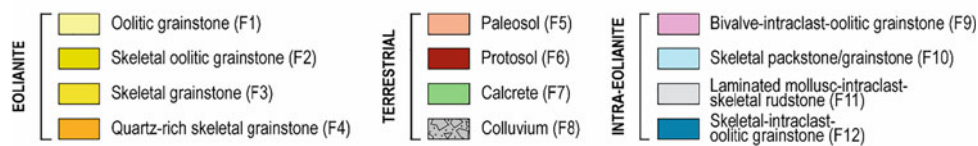


Fig. 22 Composite stratigraphic correlation chart showing different rock unites and related chronologies in relation to the marine isotope stages (MIS), sea level fluctuations and climatic changes (Assal et al., 2020). Some OSL dates show large errors in age estimates due to the lower content of detrital quartz grains possibly reworked from older sediments (El-Asmar & Wood, 2000)

depressum-Clypeaster scutiformis Series (Beadnell, 1924), the older organic reefs (El-Akkad & Dardir, 1966), the Wizr Formation and the older raised reefs of Al-Rifaiy and Cherif (1989), and to the upper part of the upper member of the Shagra Formation (Issawi et al., 2009). The lithology and the

fossil association in this rock unit suggest a littoral to beach environment with alternations of coral reefs with conglomerate and gravelly sandstones (Fig. 26) of fining-upward sequence (Kora et al., 2013). Tucker (2003) interpreted the coral reefs as relating to highstands of sea level with evidence

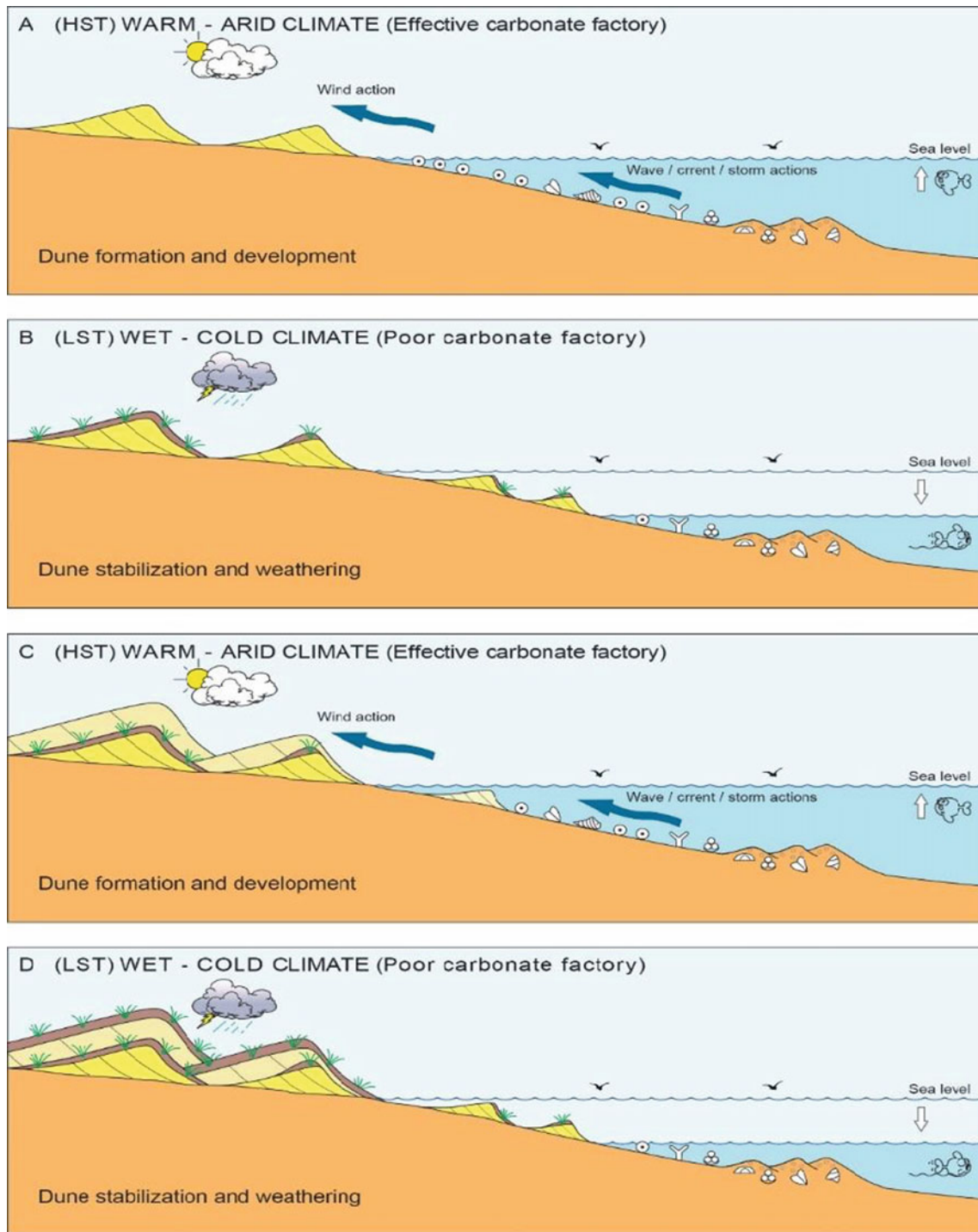


Fig. 23 Schematic model of formation of the coastal ridges NW coast of Egypt where deposition of aeolianites (a, c) associated with warm dry conditions in a HST to SST favour pumping carbonates contemporaneous to deposition of Saharan dust. At LST and wet cold climate derived-Atlantic circulation, the dust transformed to soil with growth of vegetations (b, d). Source Assal et al. (2020)

of warm climate suitable for carbonate deposition. With low stands of sea level, the climate seems cold but humid enough to transport gravels within other detrital sediments across the Eastern Desert wadis seaward forming conglomerate deposits alternating with the coral reef terraces (Fig. 26).

At the Gulf of Aqaba at Sharm El-Sheikh-Ras Mohamed, two sections (Fig. 27a) have been studied regarding to the field relations, sedimentology, microfacies, diagenesis and age dating (El-Asmar, 1997; El-Asmar & Attia, 1996; Gvirtzman et al., 1992; Yehudai et al., 2017). At Sharm

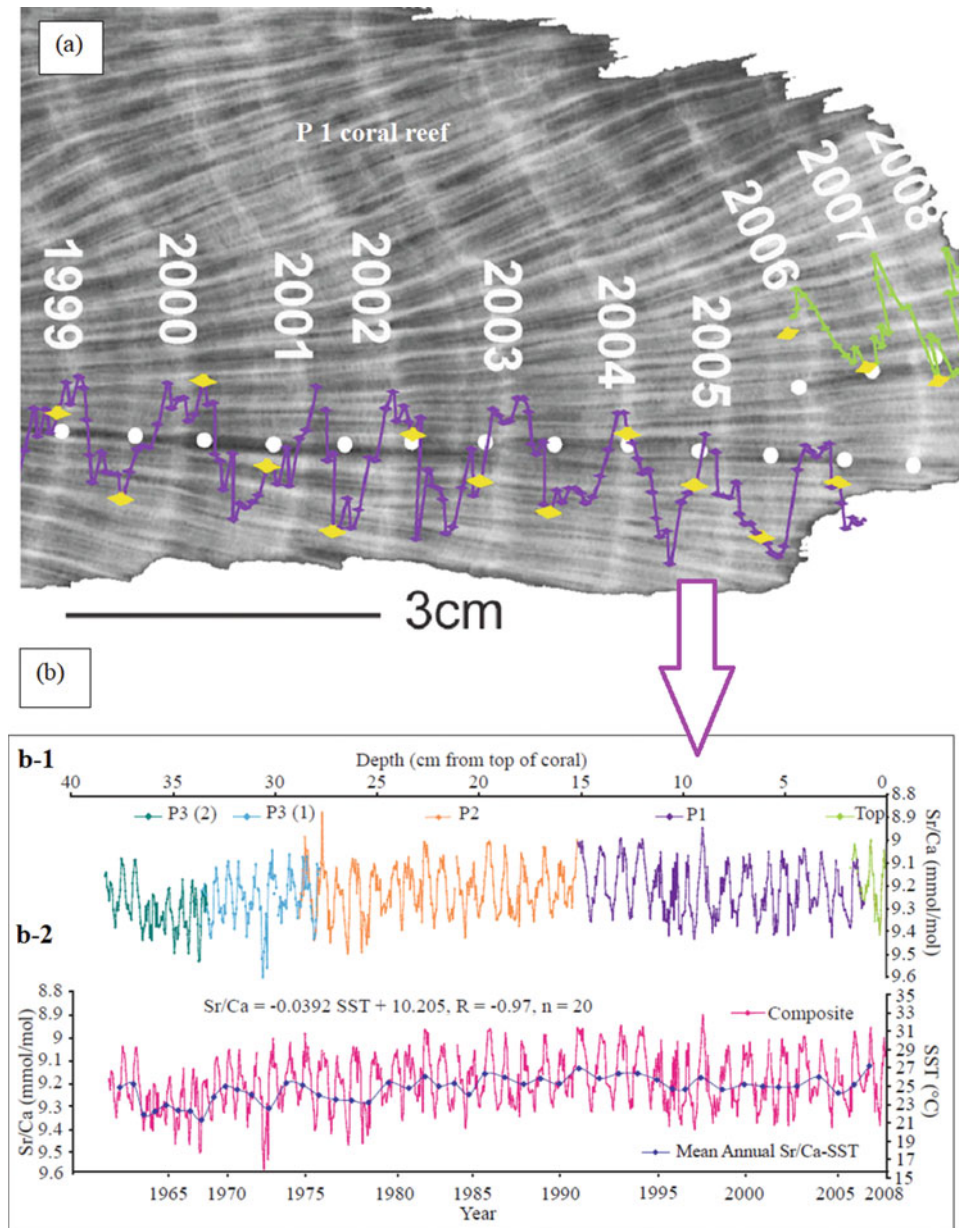


Fig. 24 Enlarged X-radiograph of modern coral overlaid with the raw Sr/Ca record (in navy blue) in depth and time space. Time series of Sr/Ca data are overlain on the X-radiograph to verify that annual bands have been counted correctly. Each Sr/Ca maximum (winter) to the next maximum (winter) represents an annual temperature cycle (a). A raw plot of coral Sr/Ca with depth in centimetres from the top of the core. Sr/Ca values are plotted with reversed y-axis (b-1). Raw data are converted to coral-derived modern SST values from the equation $Sr/Ca = -0.0392 * SST + 10.205$ for *Montastraea faveolata* reef with mean annual values shown as navy blue curve points and line. Sr/Ca values are plotted with reversed y-axis so that warmer values are up (b-2). Sources Flannery and Poore (2013)

El-Sheikh, four Pleistocene coral reef terraces have been recognized at Um Seed (Fig. 27b and c, I–IV) terraces forming a well-developed staircase, at altitudes of 3, 6, 10–12 and 15–20 m a.s.l., respectively. At Ras Mohamed, three terrace levels were distinguished (Fig. 27d and e).

$^{230}\text{Th}/^{234}\text{U}$ dating for the studied terraces at the Red Sea coast revealed four uplifted terraces at Zabargad island (Location; Fig. 1a; area 3; Hoang & Taviani, 1988). The oldest terrace (> 290 and 300 ka) is found at + 10 to + 15

m. Another terrace relict at + 17 m on peridotite bedrock recorded a 200 ka high sea stand, and the youngest one (125–138 ka) is very well represented around the island, with double terraces at about + 6 to + 8 m (Fig. 28a). These suggest a correlation with MIS 9, 7 and 5e and indicate the tectonic stability of these islands since at least 125 ka (Fig. 28a, Hoang & Taviani, 1991). Three cycles of reef formation were recognized along the Red Sea coastal plain of Egypt (El-Moursi et al., 1994). The first two cycles were

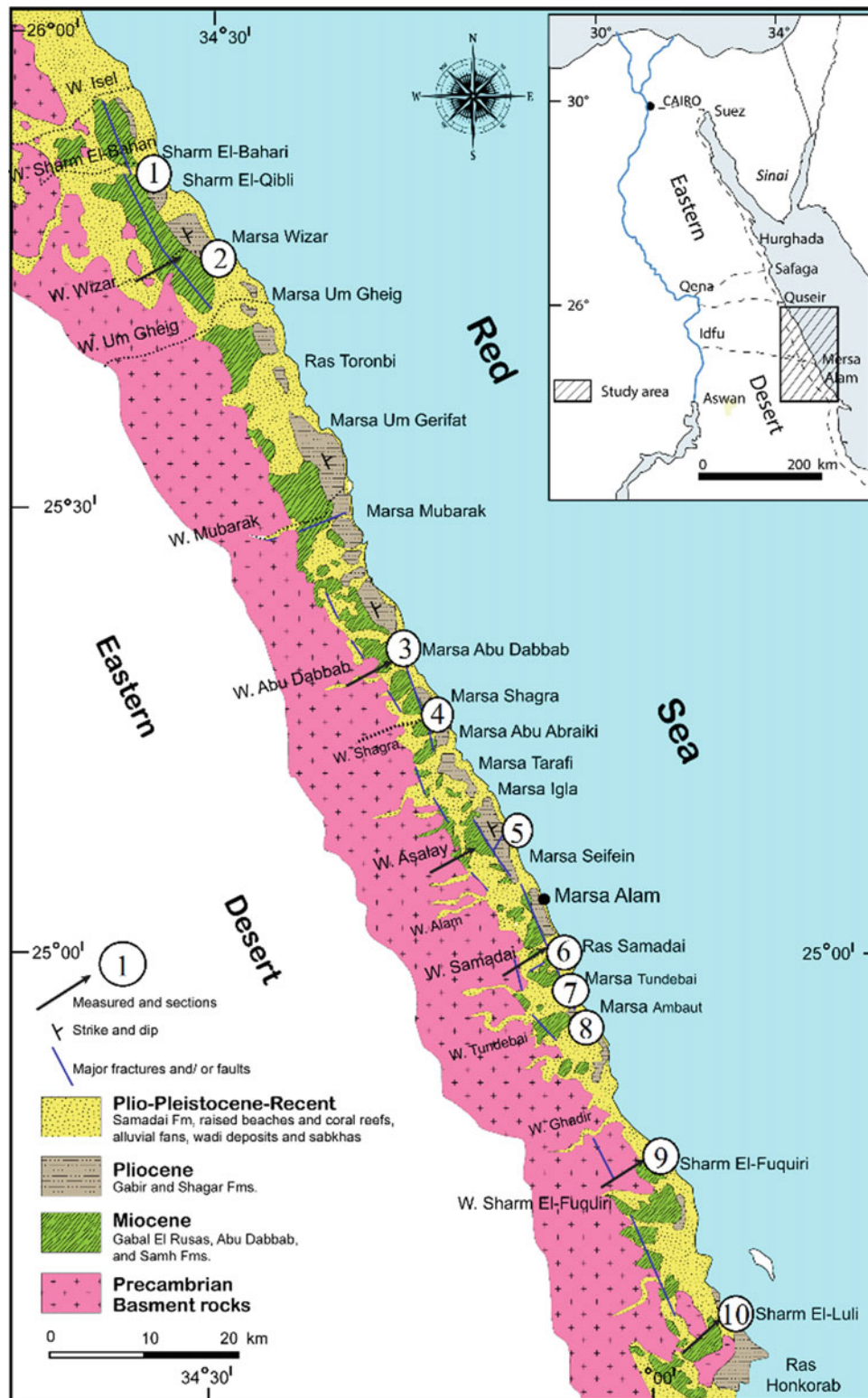


Fig. 25 Geologic map of the Red Sea coast showing rock units and location (Location; Fig. 1a; area 3) of the measured Quaternary sections from 1 to 10. The measured sections are Sharm El-Bahari 1, Marsa Wizar 2, Marsa Abu Dabbab 3, Marsa Shagra 4, Wadi Asalaya 5, Ras Samada 6, Marsa Tundebai 7, Marsa Ambaut 8 and Sharm El-Luli 10. *Source* El-Asmar and Abdel-Fattah (2000)

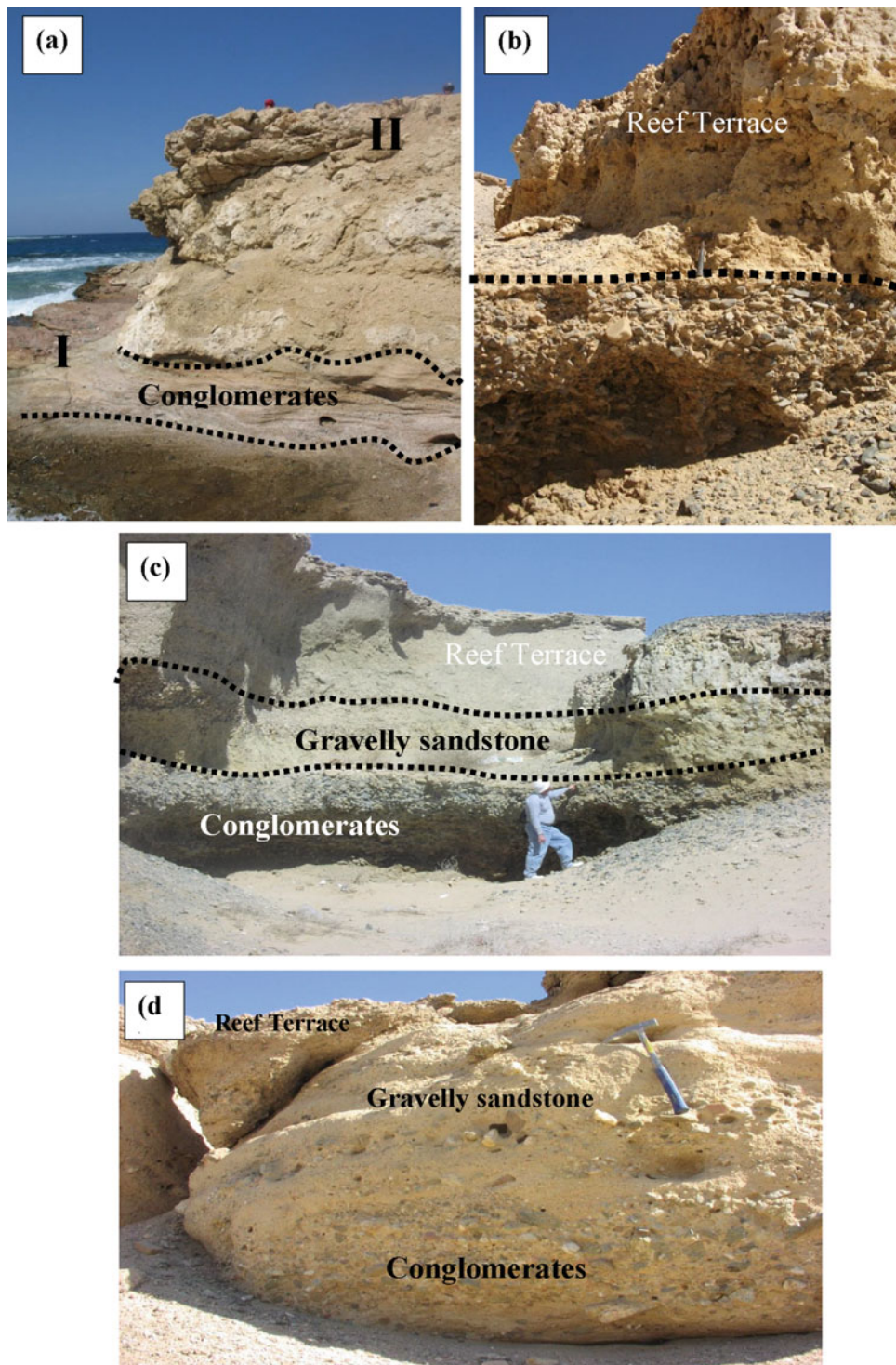
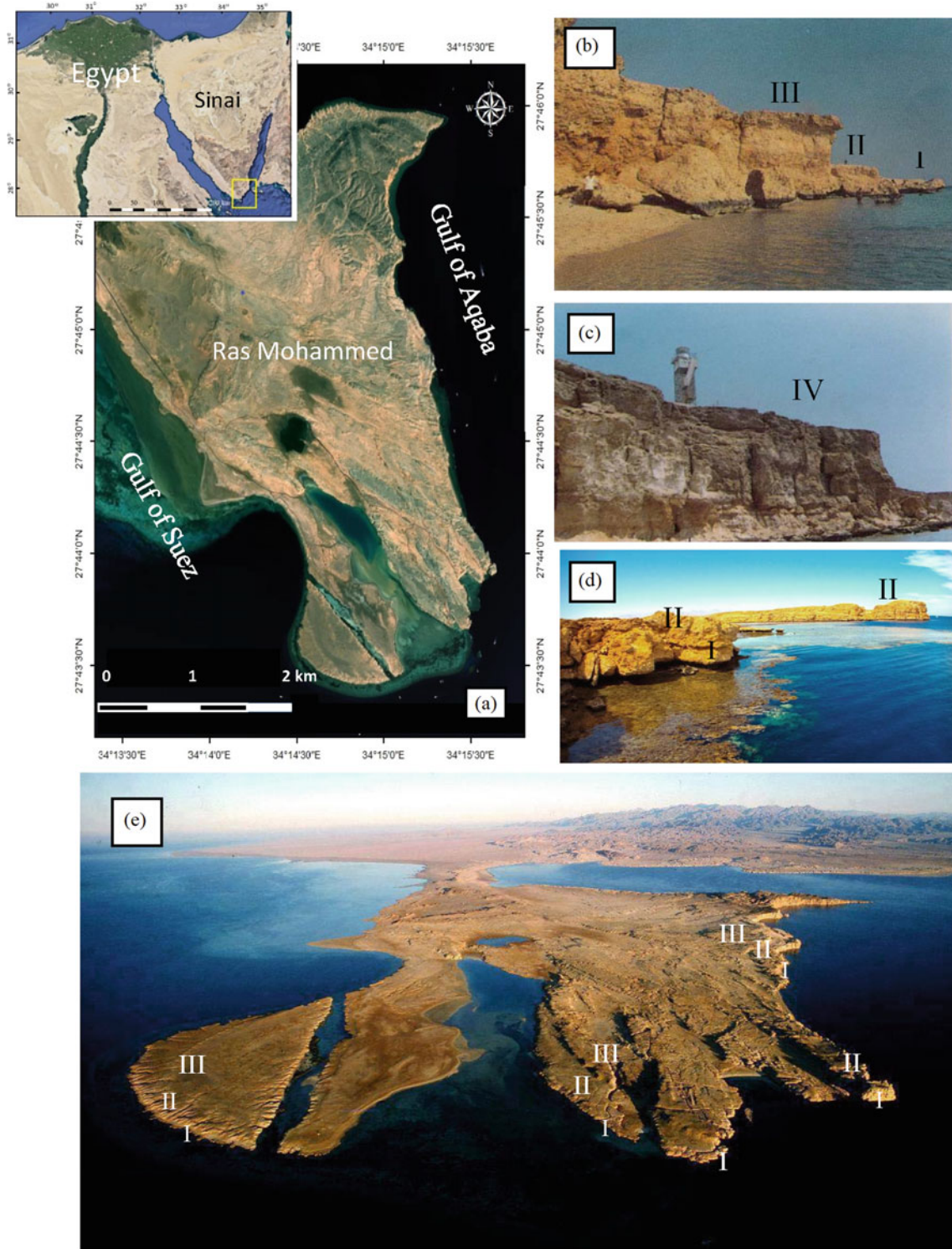


Fig. 26 Several field sections at Ras Samadai (a, b), Marsa Abu Dabab (c) and Sharm El-Luli (d) showing the alternations of coral reef terraces with conglomerate and gravelly sandstone in fining-upward sequence of littoral environment (courtesy from Prof. Dr. Mahmoud Kora)

out of the limit of radiometric dating and highly subjected to diagenesis. The youngest cycle belong to the Middle and Late Quaternary, and represented by four terraces IV-I at altitudes of + 9, + 6, + 3 and + 2 m, respectively (Fig. 28 b). The $^{230}\text{Th}/^{234}\text{U}$ dates of representative samples range at

72.1 ± 2.5 ka, 112.1 ± 3.3 ka to 131.2 ± 4.4 ka, and related to MIS 5a, c, e, MIS 7 (170–230 ka) and MIS 9 (300–330 ka, Fig. 28a, El-Moursi et al., 1994). On the other hand, the $^{230}\text{Th}/^{234}\text{U}$ dates of the samples representing terraces at Sharm El-Sheikh-Ras Mohamed show ages



<https://www.reefoasisdiveclub.com/diving-sharm-el-sheikh/dive-sites/>

Fig. 27 Location for area 3-1 (Fig. 1b) at Sharm El-Sheikh-Ras Mohammed, the Gulf of Aqaba (a), the uplifted terrace at Um El-Seed showing four terraces I, II, and III (b) and terrace IV at the light house, Um Seed (c) (El-Asmar, 1997). Three terraces at Ras Mohammed (d) and aerial view for three terraces lining the shoreline at Ras Mohammed National Park (e). Source <https://www.reefoasisdiveclub.com/diving-sharm-el-sheikh/dive-sites/>

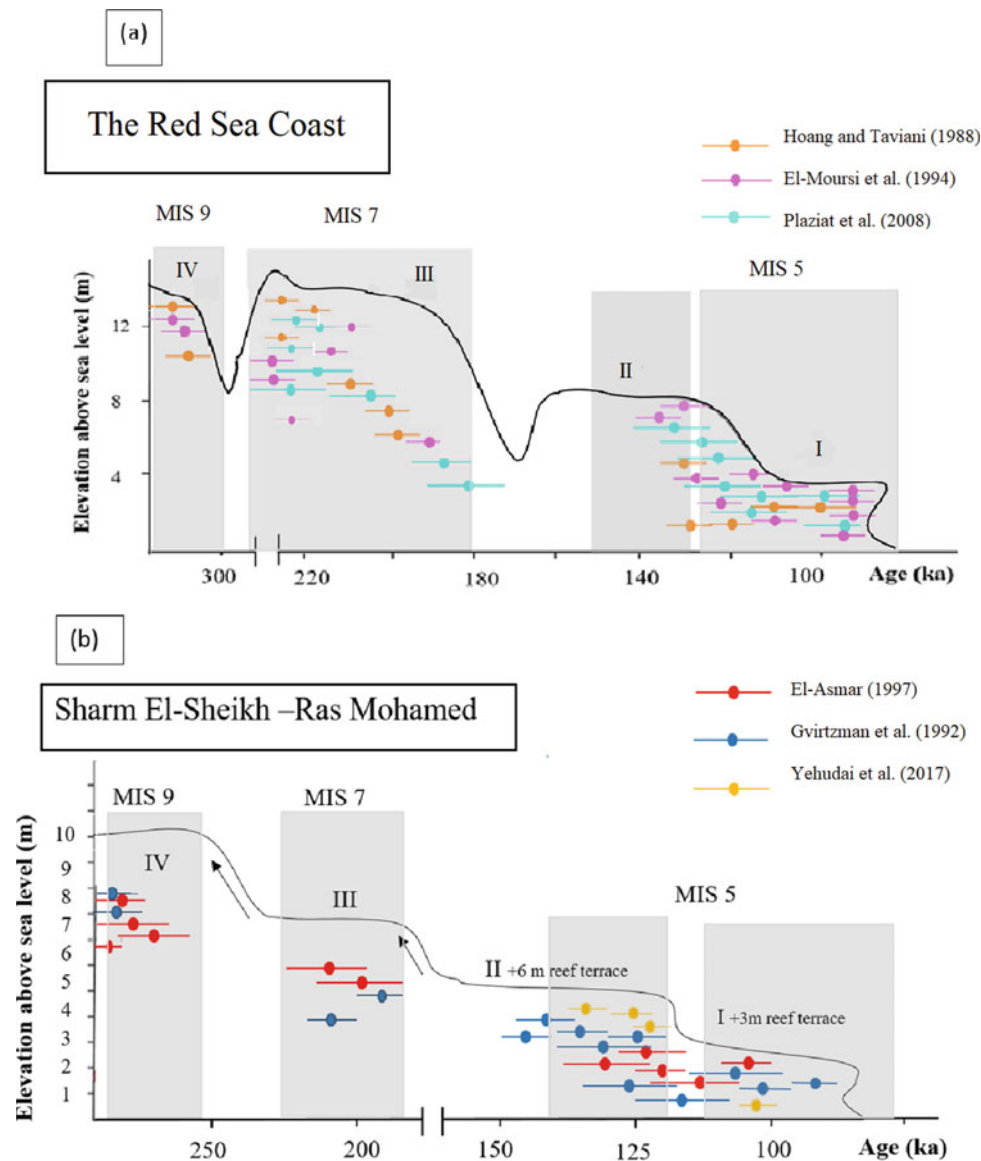


Fig. 28 Age data collected from several studies for samples representing different coral reef terraces at the Red Sea (a) and at Sharm El-Sheikh-Ras Mohamed (b) showing age dating correlation with MIS 5, 7 and 9. The data confirm the stability of the coast since the MIS 5. Sources Hoang and Taviani (1988), Gvirtzman et al. (1992), El-Moursi et al. (1994), Plaziat et al. (1995), El-Asmar (1997), and Yehudai et al. (2017)

clustered as 100–128 ka, 200 ka, 280–300 ka and older than 300 ka, which is related to isotope stages 5e, 7 and 9, respectively (Fig. 28b), and closely related to paleoclimate and sea level during the Middle to Late Quaternary (El-Asmar, 1997).

Plaziat et al. (1995, 1998, 2008) studied the relations between continental and marine deposits along the 800 km of northern most coast of the Red Sea. $^{230}\text{Th}/^{234}\text{U}$ dates of the marine units (coral reefs, molluscs, echinoids and gypsum) together with 20 site descriptions with age dating and tectonic relationship enabled interpretation of paleoclimatic and glacio-eustatic sea level changes. The double-peaked MIS 5e is particularly studied in detail, at the Gulf of Suez

(Location; Fig. 1; area 3) and at Sharm El-Sheikh (El-Asmar, 1997). The recorded ages range from 117 to 129 ka at an elevation of 12–17 m a.s.l. (Figs. 28 and 29). This stage was also dated as 121–131 ka at an elevation of 8–17 m a.s.l. at Gebel El-Zeit, the Gulf of Suez (Plaziat et al., 2008). Southward at the Red Sea coast, several sections were studied focusing on the MIS 5e. These show double (Fig. 29) terraces separated by conglomerate beds and reef rubbles: the two peaks dated to 90–130 ka and detected at elevations between 1 and 6 m a.s.l. (Fig. 29). Plaziat et al. (2008) in calibrating the dates of the terraces at Sharm El-Bahari, Sharm El-Qibli, Ras Shagra, Ras Samadai, Ras Tundeaba and Ras Ambaut emphasized the records for

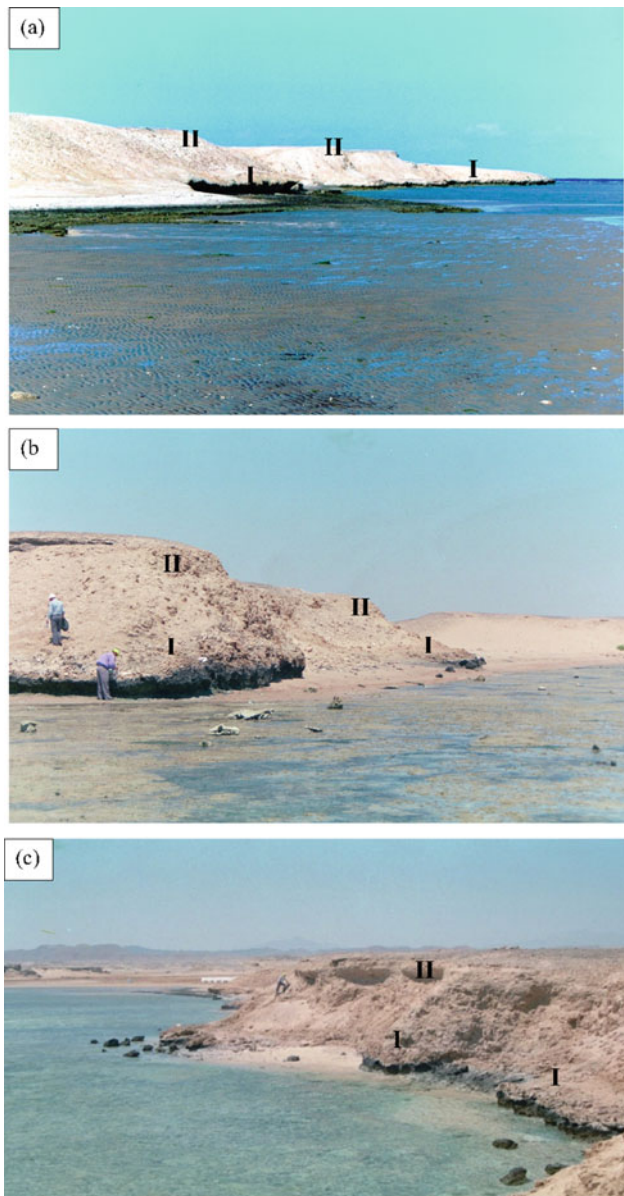


Fig. 29 Field photos for the double-peaked (I and II) terrace of MIS 5e showing two coral reefs separated by gravels and reef rubbles at Marsa Wizr (a), Marsa Tundebai (b) and Marsa Ambaut (c). *Source* Prof. Dr. Hesham El-Asmr

the MIS 5e at the range of 3–6 m a.s.l. (Fig. 29) and supported the concept of coastal stability since the LIG (Hoang & Taviani, 1991).

A synthesized composite succession (Fig. 30) deduced from the correlation of different sections along the Red Sea coast reflects deposition of cycles of coral reefs developed at times with sea level highstand and warm water favourable for carbonate deposition. With lowstands, the climate became colder with heavy rains able to transport gravels within other detrital sediments across Eastern Desert wadis seaward forming conglomerate deposits alternating with the coral reef terraces (Fig. 26). These sequences preserve four

deduced paleoclimatic cycles where the coral reef terraces are associated with MIS 5, 7 and 9 (Figs. 26 and 28) and sea level changes, while the conglomerate beds related to humid climate (El-Asmar, under publication).

5 The Quaternary Sedimentation Along the Western Desert of Egypt

5.1 The Geology of the Southwestern Desert of Egypt

The Southwestern Desert of Egypt (location; Fig. 1a; area 4) is structurally controlled basin confined to the Libyan plateau, and the Nubian group excavated by several episodes among is the deflation (Issawi, 1968). There are several major depressions in the Western Desert that hosted large-scale paleoclimatic proxies among are Farafra, Dakhla, Kharga and Kurkur (Fig. 31a) though no active deposition occurs at present time. Before describing the terrestrial sediments in this region, the geology of the basin with the associated sediments will be outlined, along with the conditions favouring formation of these proxies.

Geomorphic landforms in the Dakhla Depression (Fig. 31b) include the Libyan or Egyptian Plateau, the Dakhla Scarp and Piedmont, the Dakhla Lowland, the Southern Cuesta and the Plain (Fig. 32). The Palaeocene limestones of the Tarawan, Kurkur and Garra Formations make up the 450–500 m above sea level Libyan Plateau, which is situated above Dakhla (Fig. 32; Brookes, 1993). Eight sedimentary strata were produced during the Quaternary period's history (Table 2) and were spaced apart by erosion during periods of extreme aridity. The three generations of Piedmont Bajada (P/B) colluvial/fluvial conglomerates that record three episodes of erosion and deposition of superposed bajada gravels make up the sediments (P/B I, II, and III; Fig. 32). Additionally, there are two generations of mound springs and basinal sediments (Pleistocene and Early Holocene wetland and spring mounds, Fig. 32) of fluvio-lacustrine, as well as two generations of tabular spring-laid clastic and chemical sediments (Calcareous Spring Sediments—CSS and Ferruginous Spring Sediments—FSS) (Fig. 32).

Large Pleistocene lacustrine deposits are located in the Dakhla piedmont and plain and are seen in two facies (Table 2). **Facies A** is composed of stratified turbidite beds that fork upward, being sandy at the bottom and muddy at the top and formed from Dakhla shale. **Facies B** has two sub-facies: sub-Facies B1 has 10–20 cm strata of biogenic lacustrine marl that were likely deposited in a salty lake and thin couplets of large-crystal gypsum and clastics. Massive, light-brown muddy sand that was deposited as pluvio-aolian loess makes up sub-Facies B2 (Brookes, 1993). Another two stratigraphically equivalent non-lacustrine

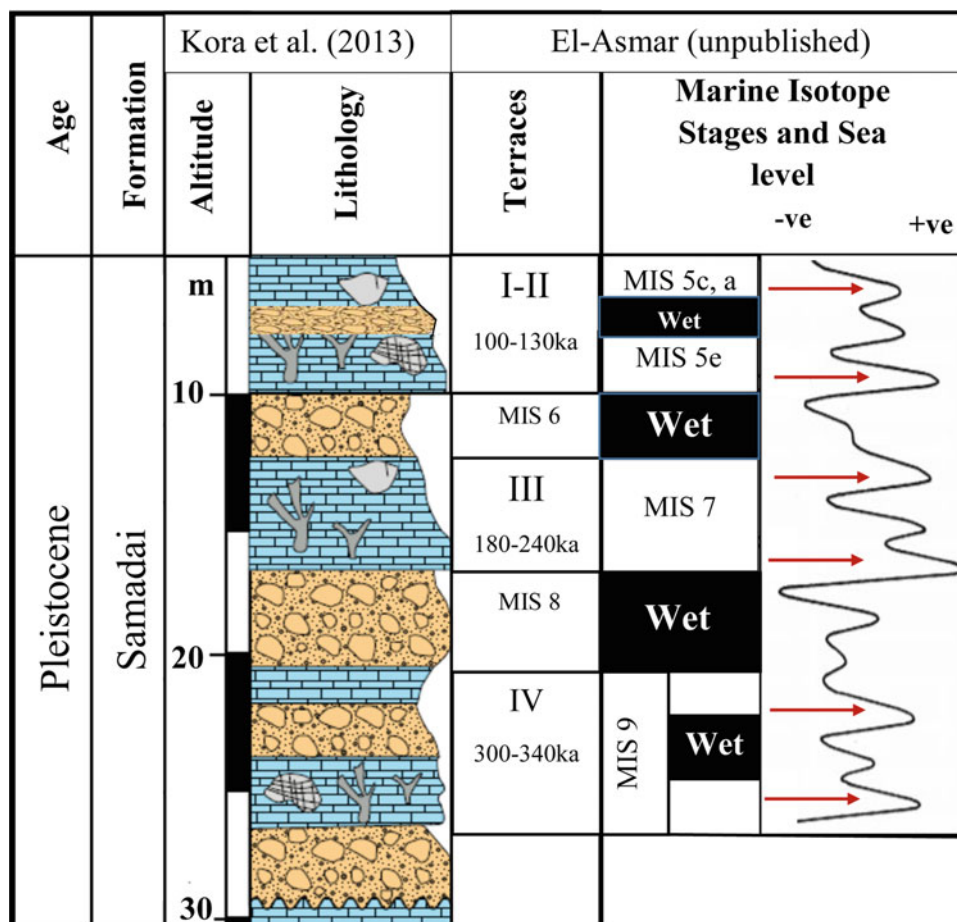


Fig. 30 A synthesized composite succession deduced from the correlation of different sections along the Red Sea coast. It reflects deposition of cycles of coral reefs developed through a condition of sea level highstand and warm water favourable carbonate deposition. With lowstands, the climate became colder with rains able to transport gravels within other detrital sediments across the Eastern Desert wadies seaward forming conglomerate deposits alternating with the coral reef terraces. These dated and correlated with sea level and paleoclimate changes. *Source* Prof. Dr. Hesham El-Asmar

Facies, C and D (Table 2), occupy basins between Dakhla and the facies B at Zayat. Southeast of the Dakhla, between digitate sandstone pediment terraces and broad level plains, **Facies C** is composed of vast pale-brown muddy sands that are similar to B2. These plains are covered in limestone fan gravels that are part of P/B II. A thin lamina of extremely fine sand and silt covers each layer of horizontally stratified, 1–2 cm thick, angular, medium to fine quartz sand that makes up **Facies D**. These beds show the aggradation of sand sheets from a source in the sandstone upwind. The genesis of these sand beds is compared to Facies B.2 and C of pluvio-aeolian fall-out. The unbroken buried beds make it possible to see signs of recent shrubby flora (Brookes, 1993). Unique Quaternary event in Dakhla is the silicate glass resulted due to catastrophic meteoritic impact event at mid-Pleistocene ~ 200–100 ka over an area of ~ 400 km². The glass, locally referred to as “Dakhla Glass” (DG), was created by the shock melting of several unconsolidated

sediments that were covered by lithologies rich in phosphate and carbonates (Fig. 39f). The abundance of large DG specimens of up to 50 cm across, which form at temperatures of 1700 °C, and the chemistry (e.g. CaO and Al₂O₃ contents up to ~ 25 and ~ 18 wt%). In addition to the presence of burnt sediments, the inclusion of clasts and spherules, and the presence of impact meltbearing rock (lechatelierite) are incompatible with known processes of terrestrial glass formation (Osinski et al., 2007, 2008). Given the lack of a proven crater and the hypervelocity impact into a volatile-rich target, it was determined that the best explanation for the characteristics of Dakhla glass was the melting of surface sediments brought on by a significant airburst event (Osinski et al., 2008). The Middle Stone Age period of habitation was when the DG-forming impact event took place. Based on a ⁴⁰Ar/³⁹Ar isochron age of 145 ± 19 ka, the age of the impact event was established (Renne et al., 2010; Smith et al., 2009).

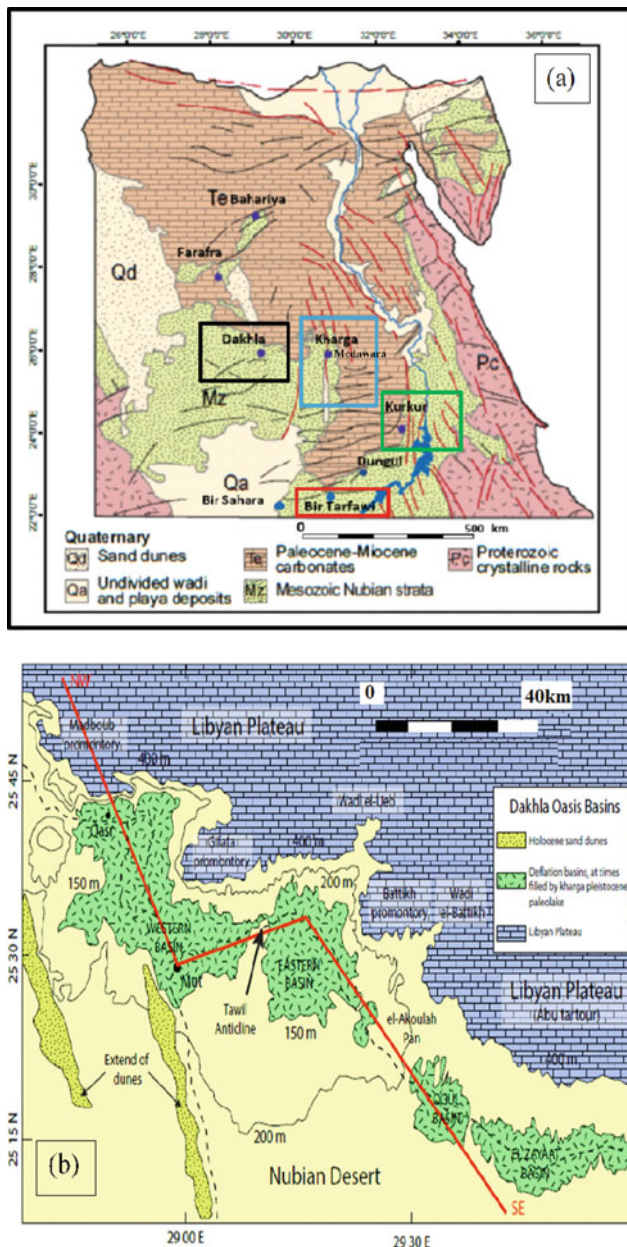


Fig. 31 Location map showing general geology of the Western Desert of Egypt and different depressions (a) (Jimenez, 2014). The geology of the Dakhla Depression (b) with the Libyan Plateau and the Tawil Anticline, a sandstone ridge, splits the two large eastern and western basins in the bottom of the Dakhla Depression. In the mid-Pleistocene, a paleolake, Lake Balat, occupied as much as 1735 km² in the depression, with its surface reaching at least 160 m a.s.l. Northwestern prevailing winds drive sand dunes across the western depression, the red line tracing the section of Fig. 32 (b). Sources Kleindienst et al. (2016) and Blackwell et al. (2017)

Like Dakhla, the Kharga Depression (Figs. 31a, 33 and 34) occurs in the hyperarid desert, where artesian wells drawing water from the Nubian Sandstone Aquifer. The Kharga Depression excavated by several episodes of deflation on the Libyan Plateau (local name in Kharga is Sinn

El-Kaddab), which bounds the Kharga Depression from the north (Fig. 33a and b). The scarp, the piedmont and a low land deflated depression elongated NS between 29° 58' N and 24° 21' 30" N, lie west of, and ~ 350 m below, the Sinn El-Kaddab Plateau (Blackwell et al., 2017). Lacustrine and palustrine sediments, artesian springs and tufa units (Fig. 39) are deposited just below the Escarpment rim (Fig. 33b), all demonstrating that areas in, and near, Kharga Depression had frequent surface water during the Pleistocene (Abotalib et al., 2016; Blackwell et al., 2017). At the Kharga Depression, several sections of tufa deposits were studied at Medawara (Fig. 33), Bulaq and Matana among the large escarpment east and north of the basin hosts several distinct tufa deposits (Figs. 33 and 34) including the massive mesa at Medawara (Fig. 33). In the Medawara Embayment near the Medawara tufa deposit, the El Refûf (Fig. 34) has formed at or just below the Escarpment edge (Fig. 34a and b). Most of these deposits were dated (Figs. 33c and 34c) and will discuss later in Sect. 5.2.

The Quaternary geology of the north-central Bir Tarfawi (Fig. 35a and b) records the presence of Pleistocene basin-fill deposits (Issawi, 1978). During arid climate, a decline in the local groundwater level led to the formation of three deflationary topographic basins (the Acheulian basin, the White lake basin and the Grey-Green lake basin (Fig. 36a). These were later filled with aggradational sediments (Fig. 36a) when the groundwater table rose and the climate changed from dry to wet (Hill & Schild, 2017). Pleistocene silt in the Bir Tarfawi deflationary depressions preserve substantial climatic and environmental changes over the last 500,000 years (Wendorf et al., 1993). In the White lake sequence (Fig. 36a), a sedimentary relic that rises 1–3 m above the surrounding terrain with a surface elevation of about ~ 246 m a.s.l. is located in the depression's north-central region on an extended, low mesa (Hill & Schild, 2017). The Late Pleistocene deposits of the Grey-Green lake basin sequences are located about 4 km to the southwest of the White lake remnant (Fig. 36a; Hill, 1993; Hill & Schild, 2017). Freshwater molluscs that can only survive in fresh or brackish water, neither saline nor hypersaline, can be found in the sediment at both sites, most notably *Melanoides tuberculata* (cf. Wingard et al., 2008). Comparison of three sections across the Bir Tarfawi Grey-Green lake basin-fill sequence shows six sand-dominated units related to four episodes of high lake level (Fig. 36b of Wendorf, 1977; Wendorf et al., 1993, Fig. 37a, of Hill & Schild, 2017, Fig. 37b, of Blackwell et al., 2017). The recorded strata from the bottom to top are the basal sandy gravels, dark fine-grained sand and silt, calcareous coarse sands, calc. muddy sands and gravelly muddy sands (Figs. 36b and 37a, b). The sands reflecting transgressive lake level (Fig. 36b) and the deflation at the boundaries of the strata are related to arid climatic intervals (Hill, 1993).

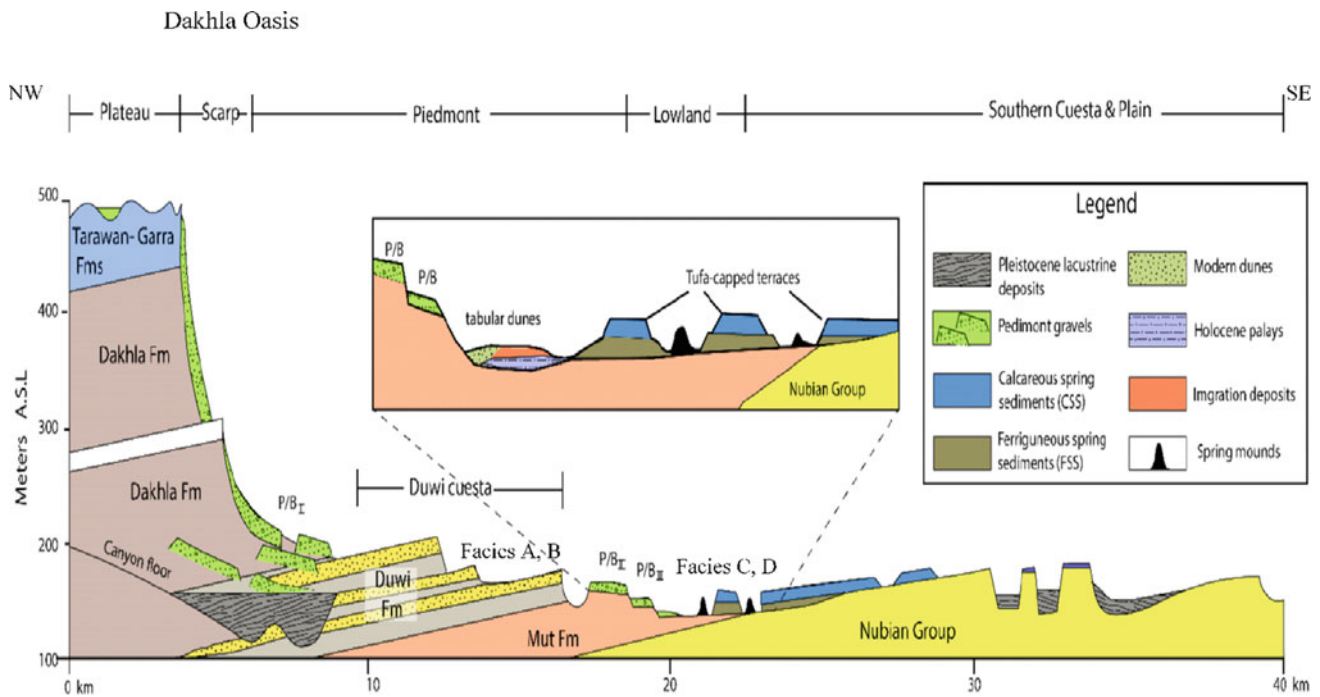


Fig. 32 Schematic cross-section along NW–SE of the Dakhla Depression (Fig. 31b), the section shows the main geomorphologic and geologic elements along the Dakhla Depression from the plateau, the scarp, the piedmont and the low land with the characteristic Quaternary sediments. Source Brookes (1993)

Shells and animal teeth collected from these strata in addition to tufa and travertine deposits were dated (Blackwell et al., 2017; Hill & Schild, 2017; Miller et al., 1991; Szabo et al., 1995) as will be later seen in Sect. 5.2.

The Kurkur–Dungul region is part of Sinn El-Kaddab Plateau (Fig. 38a). A thick sedimentary section comprising parts of the Nubian plain and basement rocks is exposed at Kurkur–Dungul area (Fig. 38b–d, Issawi, 1968). This section ranges from the Late Cretaceous to the Quaternary. The Quaternary succession (Fig. 38b, c, d) comprises the following: (1) conglomerate sheets, (2) freshwater carbonates (tufa and travertine), (3) freshwater limestone mapped from Gebel El-Digm (Fig. 38d). In addition to (4) calcareous deposits covering some wadi channel banks in-between Gebel Kalabsha and Gebel El-Digm, (5) mud pans covering the Pedi-plain between the Nile and the Sinn El-Kaddab scarp, and (6) sand dunes developed in arid intervals during the Late Quaternary (Issawi, 1968). At least three episodes of travertine formation were observed. The oldest deposits were the most extensive and were deposited on the Garra Formation (Kele et al., 2021, Fig. 38b and c). The intermediate age deposits correspond to the spring mounds sitting on the Kurkur Formation (Fig. 38b and d). The youngest deposits were found in association with the terraces in modern Wadi Kurkur (Fig. 38b, Crombie et al., 1997). During wet periods when the water table was noticeably higher, the tufa deposits in the Kurkur–Dungul region precipitated from springs as perched aquifers above this major Nubian Aquifer System

(Crombie et al., 1997; Hamdan, 2003b; Nicoll & Sallam, 2017). The Nubian Aquifer in the southern regions was refilled in this scenario by previous pluvial occurrences, which caused deep groundwater to migrate northwestwards. The isotopic analyses of hydrogen and oxygen for fossil ground water and the recent water together with the results from tufa and travertines suggest water recharge associated with monsoonal periods and enhanced by Atlantic westerlies (NAO) where the water came across North Africa source of pluvial water (Crombie et al., 1997; Sultan et al., 1997). According to Jimenez (2014), who compared tufa geochemistry ($^{87}\text{Sr}/^{86}\text{Sr}$, stable isotopes) with contemporary groundwater chemistry, a persistent Nubian groundwater source with some deeply derived components has existed in the Western Desert for the past 500 ka.

5.2 The Freshwater Carbonates and Lacustrine Sediments as Proxies for Green Sahara

The Quaternary sediments at the Western Desert, supported by archaeological evidence, tells us that 11,000–5000 years ago and at earlier times in the Pleistocene, the Earth's slow orbital “wobble” transformed today's Sahara desert to a land covered with vegetation and lakes, the so-called Green Sahara (De Menocal & Tierney, 2012; De Menocal et al., 2000; Tierney et al., 2017). The “Green Sahara” pluvial phases that overprinted North African aridity during the

Table 2 Summary of the Quaternary sedimentary geology and geomorphology along the Dakhla Depression (after Brookes, 1993)

Quaternary sediments	Relative age	Sedimentomorph evolution
8. Irrigation deposits	2200–2000 BP	a. The youngest sedimentary formation in the Dakhla sequence is anthropogenic or irrigation playa. It manifests largely purposeful accretion of stratified muddy sands of variable structure under a system of arable farming, irrigated from wells, with or without mechanical lift by the animal-powered water wheel (Brookes, 1993)
7. Playas, spring mounds	9000–4500 BP	a. Playa sediments were deposited in basins on the Libyan Plateau, the sandstone cuesta, and on northern and southern cuesta margins b. On the cuesta's north eastern margin, small spring mounds were constructed. Both playas and spring mounds reflect an Early Holocene semiarid pluvial interval from 9.0 to 4.5 ka BP, which is widely recognized (Brookes, 1993) c. Desiccation to the modern hyper-arid condition ensued. This is marked by (i) partial deflation of Early Holocene playa sediments; (ii) complete or partial deflation of mud-brick architecture of Old Kingdom (ca. 2200 B.C.), and younger date; and (iii) mobile dunes of far-travelled quartz sand (suddenly invading long-established settlements in several cases) across the Sahara
6a. P/B III glaciais and bajada	65–60 ka	a. Termination of Facies A (and, by extension, Facies B and C) merged abruptly with deposition of fluvial gravels of P/B m over it in partially filled piedmont deflation basins. Basins occupied by Facies D were too distant and topographically isolated from floodwaters generated on the Dakhla Scarp to receive P/BIII gravels b. An interval of aeolian erosion ensued. This was sufficiently intense and/or long to remove P/B III gravels from most piedmont repositories of Facies A and C. Yardangs up to 10 m high were formed in Facies A and B, and up to 6 m of Facies C were deflated
6b. Pleistocene lacustrine sediments	150–130 ka	a. The Pleistocene Lacustrine Sediments deposited in four facies. Facies A were deposited in piedmont deflation basins across Dakhla. Interstratified lacustrine evaporates and pluvio-aeolians (Facies B) were deposited in piedmont basins southeast of Dakhla. Pluvio-aeolian (Facies C), and interstratified aeolian sand-sheet and pluvio-aeolian (Facies D) were deposited in cuesta deflation basins
5. Spring mounds		a. Disordered spring mounds and Pleistocene Lacustrine Sediments were deposited. It remains, therefore, only hypothetical that the spring mounds were first erupted through the floors of newly deepened lowlands and basins b. Spring mounds were superficially ferruginized and indurated. The Dakhla spring sediments represent peri-lacustrine or lake independent features, and can be differentiated from fully lacustrine deposits on the basis of their sedimentary characteristics as well as the presence of goethite and jarosite in a region where authigenic deposition during Pleistocene pluvial activity principally resulted in tufas and lacustrine marls. The spring mounds record a unique groundwater controlled paleoenvironment, providing the first evidence of a bog iron in Egypt and one of the few occurrences of iron-rich wetland remnants in the modern Sahara (Adelsberger & Smith, 2010) c. An interval of erosion in which some mounds were reduced
4b. P/B II glaciais and bajada	190–160 ka	a. P/BII colluvial and fluvial gravels were shed from Dakhla Scarp and deposited in broad bajadas below P/B I remnants. In eastern Dakhla, P/BII extended a little onto the cuesta, from which P/B I and CSS had been removed
4a. Scarp travertine		b. P/BII were fluvially incised by convergent escarpment streams, leaving relatively narrow, digitate terraces extending into Dakhla lowland c. An interval of aeolian erosion ensued. Erosion was either very intense or relatively extended in time, or both. On the plateau, one basin was deflated down to Dakhla Formation shales, through thick Palaeocene limestone. On the piedmont, basins were eroded below fluvial valley floors. Basins were also eroded through the CSS-capped sandstone cuesta, and the piedmont escarpment on the Duwi Formation was eroded into yardangs
3. Calcareous spring sediments (CSS)		a. Calcareous Spring Sediments (CSS) were deposited over the southern Cuesta, over the terrace of FSS, and in embayments flanking the dividing ridge. Groundwater discharged diffusely and copiously over an intact cuesta and converged on the embayments. In embayments, early sheet floods laid down stratified gravelly and/or muddy sand beds, incorporating residual chert clasts from P/B ~ . The surface was then converted to a vegetated wetland, over which copious amounts of northerly derived carbonate dust were deposited, dissolved and reprecipitated as laminar, massive, or tufaceous marl. Aeolian sand was incorporated diffusely, while, locally, quartzose calcarenite dunes accumulated b. CSS were calcified c. CSS were eroded from distal areas bordering Dakhla lowland, leaving a few buttes there, but probably remained more intact over the cuesta
2. P/B I glaciais and bajada		a. P/BI colluvial and fluvial gravels were shed from the northern scarp, forming a mantle over it, and extending southward across the Dakhla lowland onto the dividing ridge and the embayment east of it. All that remains today of this cover in its distal part is a lag of varnished chert b. P/B I was fluvially incised, removed distally and left only as small remnants, mostly on or close to the scarp
1. Ferruginous spring sediments (FSS)		a. Ferruginous spring sediments (FSS) were deposited from vigorous overland flows fed from copious springs, which discharged both from a bluff bordering the dividing sandstone ridge and from beneath the mudstone-floored embayment to the west b. FSS were lateralized c. Most of FSS were eroded from the embayment, leaving only a broad terrace on the east side

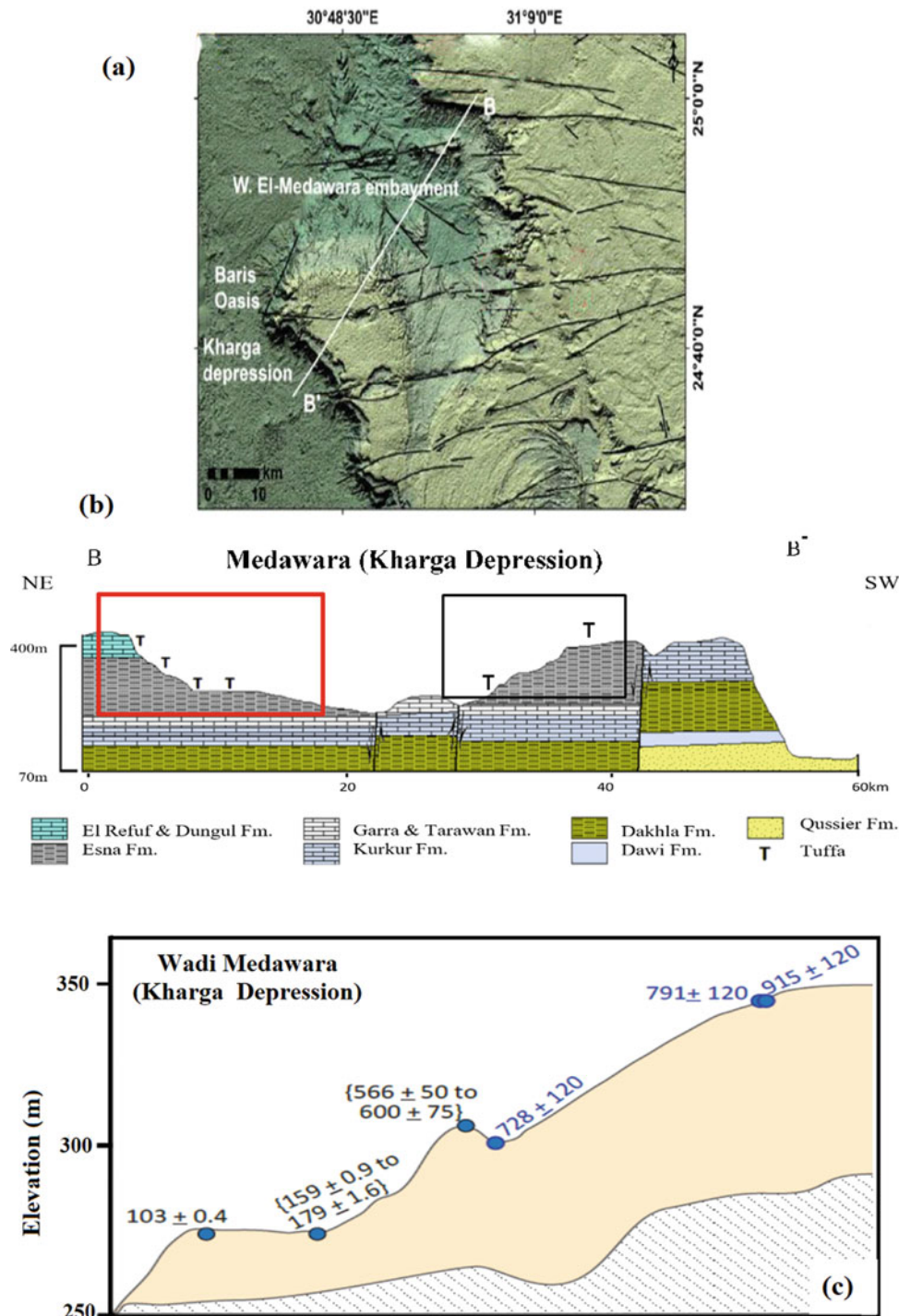


Fig. 33 Satellite image showing geology and structure of Kharga Depression, and cross-section B B' at Medawara (a) (Abotalib et al., 2016). The cross-section BB' shows the main rock units; (b) the black rectangle shows the tuffa dated terraces at Wadi Medawara (c). The red rectangle at El-Rufuf showing tuffa terraces (Fig. 34c) (Jimenez, 2014)

Pleistocene are well recognized in tropical and Mediterranean records (De Menocal, 2004; Larrasoana et al., 2003; Trauth et al., 2009; Tzedakis, 2007). The high-insolation/high-monsoon intervals have been linked to the orbital precession index (Larrasoana et al., 2003; Lourens et al., 2001;

Trauth et al., 2009). Indeed, there is evidence that precessional forcing of North African climate has been pervasive for at least the last 1.2 Ma, and that the climate of the Egyptian Sahara experienced wet episodes during the AHP associated with strength of the ITCZ (Blome et al., 2012; Rohling et al.,

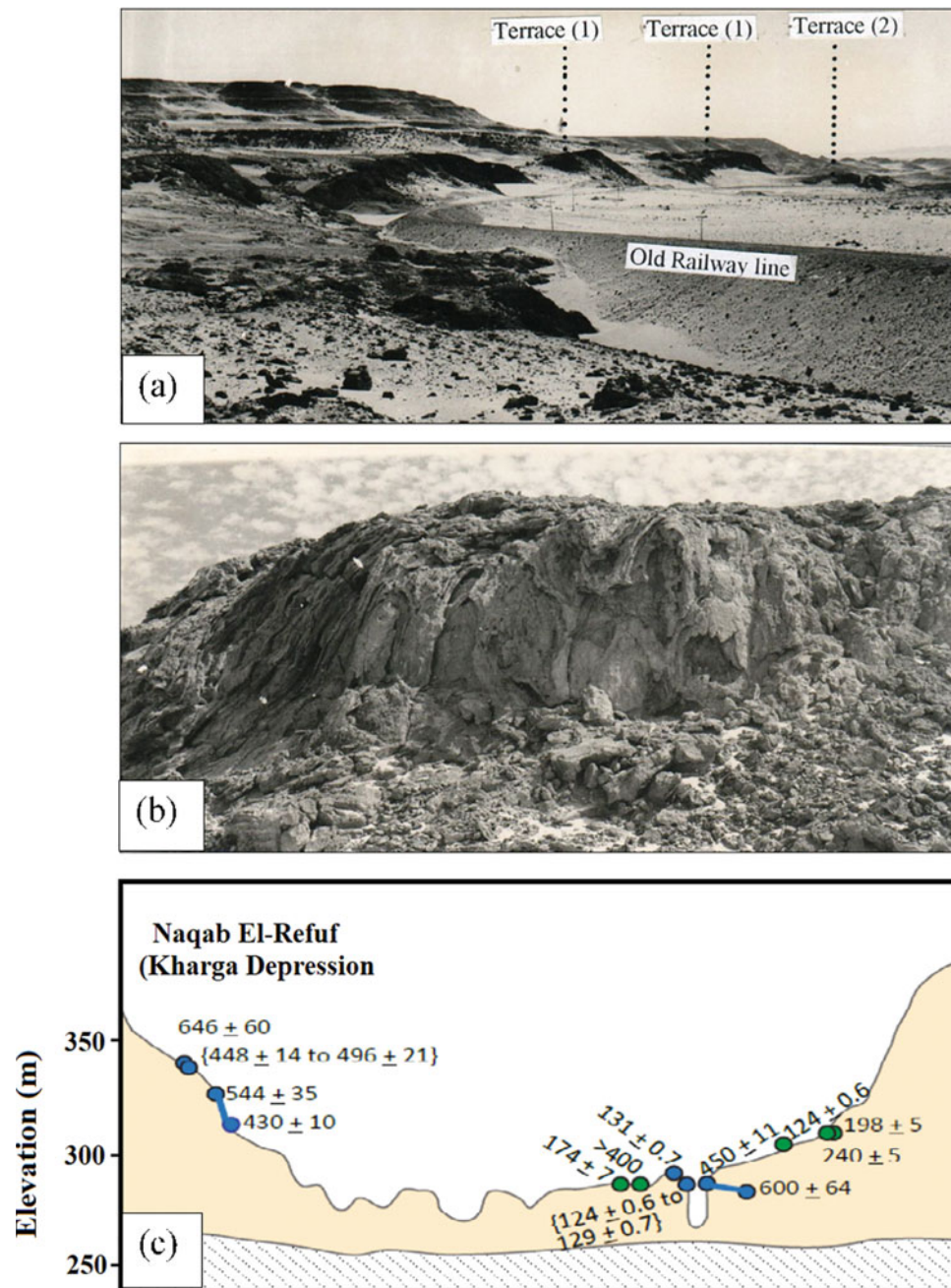


Fig. 34 Field photo at Naqab El-Refuf showing tufa terraces (a) and close-up showing the tufa deposits at the lower terrace (b) (courtesy from Prof. Dr. Nabil Embabi), and age dates of the tufa terrace (c) (Jimenez, 2014)

2002; Rossignol-Strick, 1985; Trauth et al., 2009; Tuenter et al., 2003). Such climate is well documented by both archaeological and geomorphological investigations (De Menocal, 2004). In the Sahara, geological evidence for former lake basins is frequently discovered close to interdune depressions and other low-lying areas, where ancient lake bed sediment crops out and shoreline deposits are exposed (Embabi, 1999). The majority of Early Holocene paleolakes were tiny, but they were numerous and widely dispersed.

These must have been permanent, open-basin lakes because of their stratigraphic records, which show that annual water supply far exceeded evaporation for many centuries even in the driest parts of the present Sahara (De Menocal & Tierney, 2012; Donner et al., 2015; Embabi, 2018). Before discussing the results of age determination of the terrestrial proxies, it is very important to answer the key questions about the nature of the Green Sahara pluvial, which have remained unanswered: (1) What was the spatial extent of monsoonal rains across the

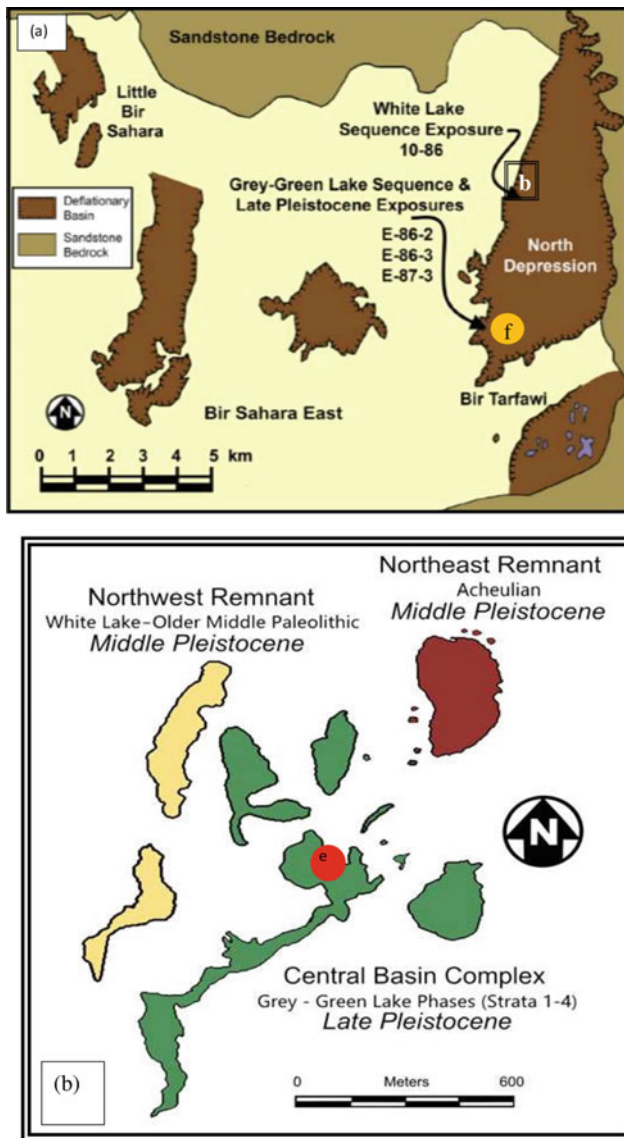


Fig. 35 Location map of Bir Tarfawi Depression (a) showing the northern depression with the white lake deposits “quadrant b” at the central depression and the southern Grey-Green deposits of Late Pleistocene age “yellow circle f” and three drilled trenches E-86-2, E-86-3 and E-87-3 (a) (Blackwell et al., 2017). Close-up map (b) of the area in “quadrant b” at a showing the major sedimentary remnants. The northeast remnant is associated with Acheulian artefacts (brown on map b). The northwest “white lake” remnant sequence contains middle Paleolithic artefacts (yellow-tan on the map b). The central basin deposits are associated with the Grey-Green lake basin-fill sequence and contain Middle Paleolithic artefacts and fossils (green on the map b). Sources Hill and Schild (2017) and Blackwell et al. (2017)

North Africa? (2) What are the sources that fed monsoonal rains? (3) Are these consistent across the North Africa? Finally, (4) What was the response of the terrestrial evidence to such climate compared with marine evidences? It is interesting to say that marine records integrating large regional signals have not been able to address these questions, while terrestrial records offer tantalizing evidence for the effects of

past humid intervals on local paleohydrology (Jimenez, 2014). However, the investigations show abundant evidence for profoundly altered hydroclimate over the past 300 ka (Szabo et al., 1995) and 650 ka (Jimenez, 2014). These have been dated by U-series methods through proxies derived from several depressions at the Western Desert (Fig. 31a) such as those previously described at Dakhla (Fig. 32), Kharga (Figs. 33 and 34), Bir Tarfaw (Figs. 36 and 37), Kurkur and Dungul (Fig. 38). These proxies (Fig. 39) include tufa proxies (Brook et al., 2003; Hamdan & Brook, 2015; Kele et al., 2021; Nicoll & Sallam, 2017; Smith et al., 2004; Sultan et al., 1997; Szabo et al., 1995), travertine proxies (Crombie et al., 1997; Hamdan, 2000; Jimenez, 2014), ground water, secondary ore precipitates and yarding proxies (Bravard et al., 2016; Donner et al., 2015; Osmond & Dabous, 2004; Sultan et al., 1997). These are supported with the results of speleothems (Brook et al., 2002; Dabous & Osmond, 2000). All are used as paleoclimatic proxies derived from the precipitation of water-dissolved carbonate either from the direct rains or from groundwater discharge (Fig. 39).

In the Grey-Green lake basin-fill sequence (Fig. 36), Miller et al. (1991) successfully employed the isoleucine epimerization (alle/Ile ratio) in the ostrich eggshell calibrated with uranium dating at Bir Tarfawi and Bir Sahara East. They showed that major wet interval occurred at ages ranging at 115–130 ka, while $^{230}\text{Th}/^{234}\text{U}$ dates ranged from 122 ± 3 to 136 ± 6 ka in addition to two older intervals: one at about 200 ka, and another occurred prior to 250 ka, which are correlated with MIS 5e and 7 (Fig. 40). The other ostrich egg shell AAR dates match better with MIS 5c–5e, with the exception of one at 141 ka that correlates with MIS 6a/6b. The findings highlighted the wet phase’s persistence over the majority of MIS 5, presumably because the four phases in the Grey-Green lake basin-fill sequence correspond to the different substages within MIS 5 (Miller et al., 1991). In addition, small lakes support freshwater snails, large herbivores and hominins associated with MIS 5, 7 and 13 (Fig. 40). $^{230}\text{Th}/^{234}\text{U}$ of the White Lake marl and limestone sequence (Figs. 36 and 37) dated as 220 ± 60 ka and $233 \text{ ka} \pm \begin{matrix} 17 \\ 14 \end{matrix}$ respectively (Schwarcz & Morawska, 1993). While $^{230}\text{Th}/^{234}\text{U}$ dating of the Acheulean lake sequence in north Bir Tarfawi near the White Lake, which is linked with Acheulean tools as 495 ± 52 ka (Fig. 36b), coincides with MIS 13. As a result, MIS 5, 7 and 13 have dated evidence for water at Bir Tarfawi (Schwarcz & Morawska, 1993). The data collected from lacustrine carbonates from Bir Tarfawi, Sahara East and the Great Selima Sand Sheet localities indicate five paleolake forming episodes that occurred at about 10–5, 65–90, 120–155, 190–240, 250–330 and > 350 ka (Szabo et al., 1995). Four of the pluvial episodes are correlated with major interglacial stages 1, 5e, 7, 9 and 11, respectively (Fig. 40). The fifth episode at 65–90 ka

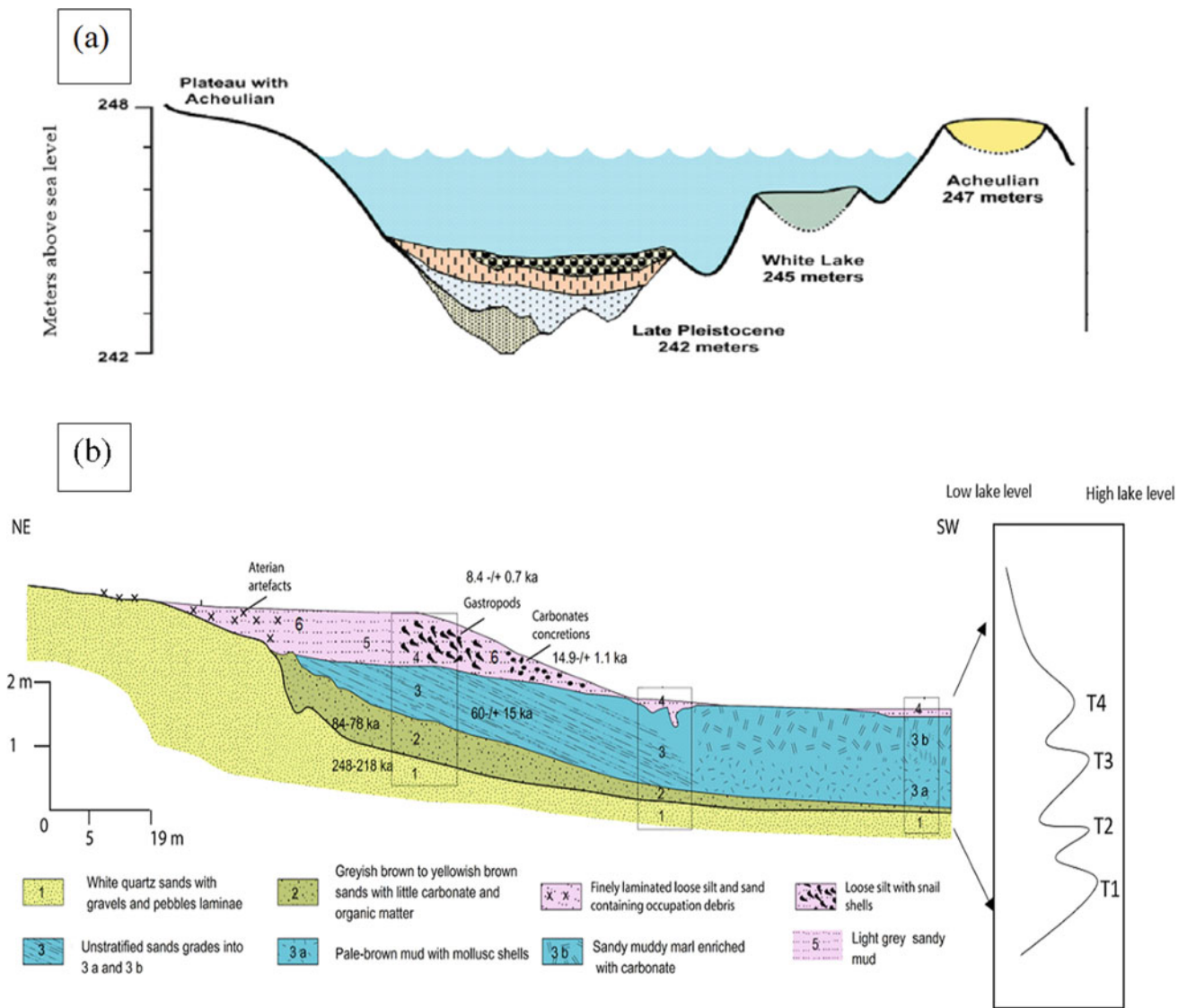


Fig. 36 Stratigraphy of Bir Tarfawi refers to three sets of lacustrine deposits occur at slightly different elevations. The oldest deposits are associated with Acheulian artefacts found at elevations near 247–248 m a.s.l. The Middle occurs at 245–246 m a.s.l. dated as Late Pleistocene, and the youngest deposits occur at 242–244 m a.s.l. during the Late Pleistocene red circle “e” of Fig. 35 (a) (Hill & Schild, 2017). Another section located within the yellow circle “P” of Fig. 35 at central Bir Tarfawi shows six stratigraphic units or stratum of four transgressions (b). Sources Wendorf (1977), Wendorf et al. (1993), and Hill (1993)

possibly correlated with MIS 5c or 5a (Szabo et al., 1995). However, still pluvial episode recorded at 20–50 ka and related to last glacial MIS 2 and/or 3 (Fig. 40, Szabo et al., 1995). Two pluvials were detected to be related to isotope stages 5 (70–160 ka) and 7 (191–220 ka) which were recorded due to uranium dating of two travertine terraces found in wadi Kurkur (Crombie et al., 1997). In Kharga, $^{230}\text{Th}/^{234}\text{U}$ dates for Wadi Tufa and cave-filling deposits collected from oases from Bahariya to Kharga gave ages of 45 ka, 150–200 ka, 250–280 ka, 300–350 ka and > 400 ka (Sultan et al., 1997), related to MIS 1, 6c, e, 7d, 8/9a, 9e/10 and 11, respectively (Fig. 40). At Dakhla, based on radiocarbon and $^{230}\text{Th}/^{234}\text{U}$ age dating, the presence of permanent

lakes was confirmed between 8–1 ka, 30–50 ka, 120–130 ka, 220–230 ka and > 300 ka (Fig. 40) related to MIS 1, 3, 5, 7 and 9, respectively (Churcher et al., 1997, 1999; Kieniewicz & Smith, 2007, 2009; Smith, 2012). Osmond and Dabous (2004) showed that the times of enhanced groundwater movement can also be determined by $^{230}\text{Th}/^{234}\text{U}$ dating of secondary U in ores of uranium, iron and phosphate. Several age dates use $^{230}\text{Th}/^{234}\text{U}$ on samples collected from Bahariya oases iron ore. These presented evidences of pluvial intervals associated with MIS 3, 4, 5, 6 and 7 (Fig. 40). They are consistent with the view that the wet episodes are the results of migration of the tropical monsoonal belt driven primarily by the 23 ka precession

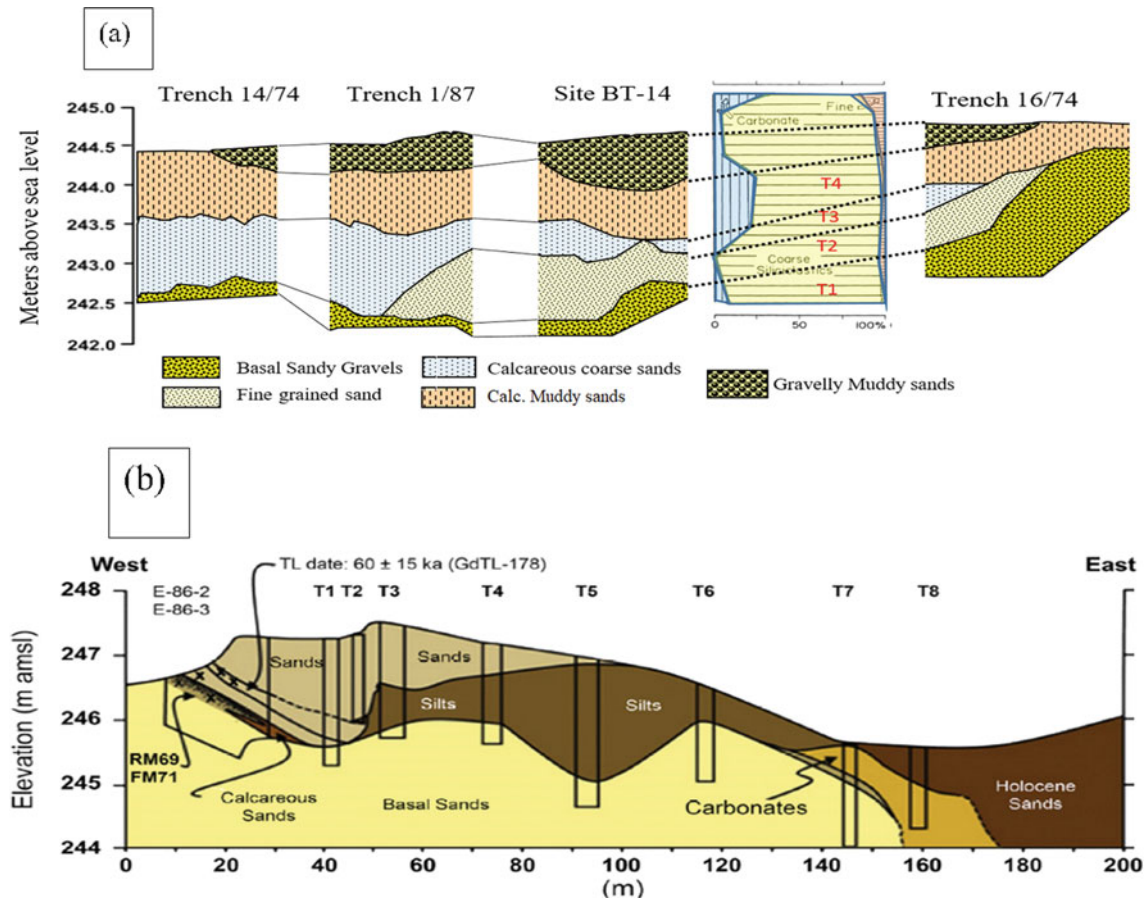


Fig. 37 Two sections at the southern Bir Tarfawi (for location see Fig. 35a) where silts and carbonates deposits in the E-86-2/E-87-3 area correlate with the Grey-Green lake basin-fill sequence to the northeast (a). The deposits likely formed in a lake during rise in water tables, possibly added by local precipitation that filled the depression. The section is composed of basal yellow sands in alternation with dark silt and sands. TL analyses on the sand overlying the lake deposits produced an age of 60 ± 15 ka BP (b). *Source* Blackwell et al. (2017)

cycle of the Milankovich curve, modulated by the 100 ka eccentricity cycle (Osmond & Dabous, 2004). At Wadi, Tufa U/Th dates of 49.8 ka, 103–126 ka, 136–150 ka and 359 ka (Fig. 40) were detected to be related to MIS 3b–c, 5c–e, 6a–c, 10, respectively (Smith et al., 2004). Further, U/Th dates from Kharga (Matana and Bulaq Wadi) gave ages of 118–130 ka and 130–150 ka were recorded and related to MIS 5e, and 6a, b, respectively (Smith et al., 2007).

Electron spin resonance (ESR) dating can provide absolute dates over a substantial time range, from as young as 0.5 ka to about 5–10 Ma, with 2–10% precision (Blackwell, 1995). Many materials that are frequently found at limnological locations can be dated using ESR. In archaeological contexts, ESR's significance in dating Quaternary and Pliocene sites have been proved, substantially altering our understanding of human origins and societies (Blackwell, 2001). Many materials, including hydroxyapatite in fish scales, bone and travertine, aragonite and calcite in calcrete, and quartz from ash, have been developed for ESR dating (Blackwell, 2006).

At Dakhla Depression, another ESR age of molluscs and tooth fragments of Middle Pleistocene paleolake covered > 1700 km² shows ages of 8, 14, 48, 84–129, 154–185, 201–229, 270, 307–334, 342, 365 and 458 ka, correlated with MIS 1, 2, 3, 5, 6, 7, 8, 9, 10 and 11 (Fig. 40, Kleindienst et al., 2016). Ponds formed during MIS 1 and 2, according to molluscs from Romano-Byzantine back soil found in a breached artesian vent with an $8\text{--}15 \pm 1$ ka age. According to ESR frequency data, the oasis was inhabited by herbivores for at least twelve stages during the Mid-Late Quaternary, making it likely that people also lived there (Kleindienst et al., 2016). According to Blackwell et al. (2017), the Dakhla Depression was home to a sizable lake in MIS 6 that offered a deep, dependable water supply for many centuries. Lacustrine and terrestrial ecosystems were thriving at Dakhla during MIS 5, 7, 9, 11 and 17, as well as in shorter episodes in MIS 1, 2, 3 and 6 (Blackwell et al., 2017). Although no molluscs associated with MIS 10 have yet been found (Abdel-Monem et al., 2006), ESR ages for tufa in Kharga Depression suggest that tufa occurred when

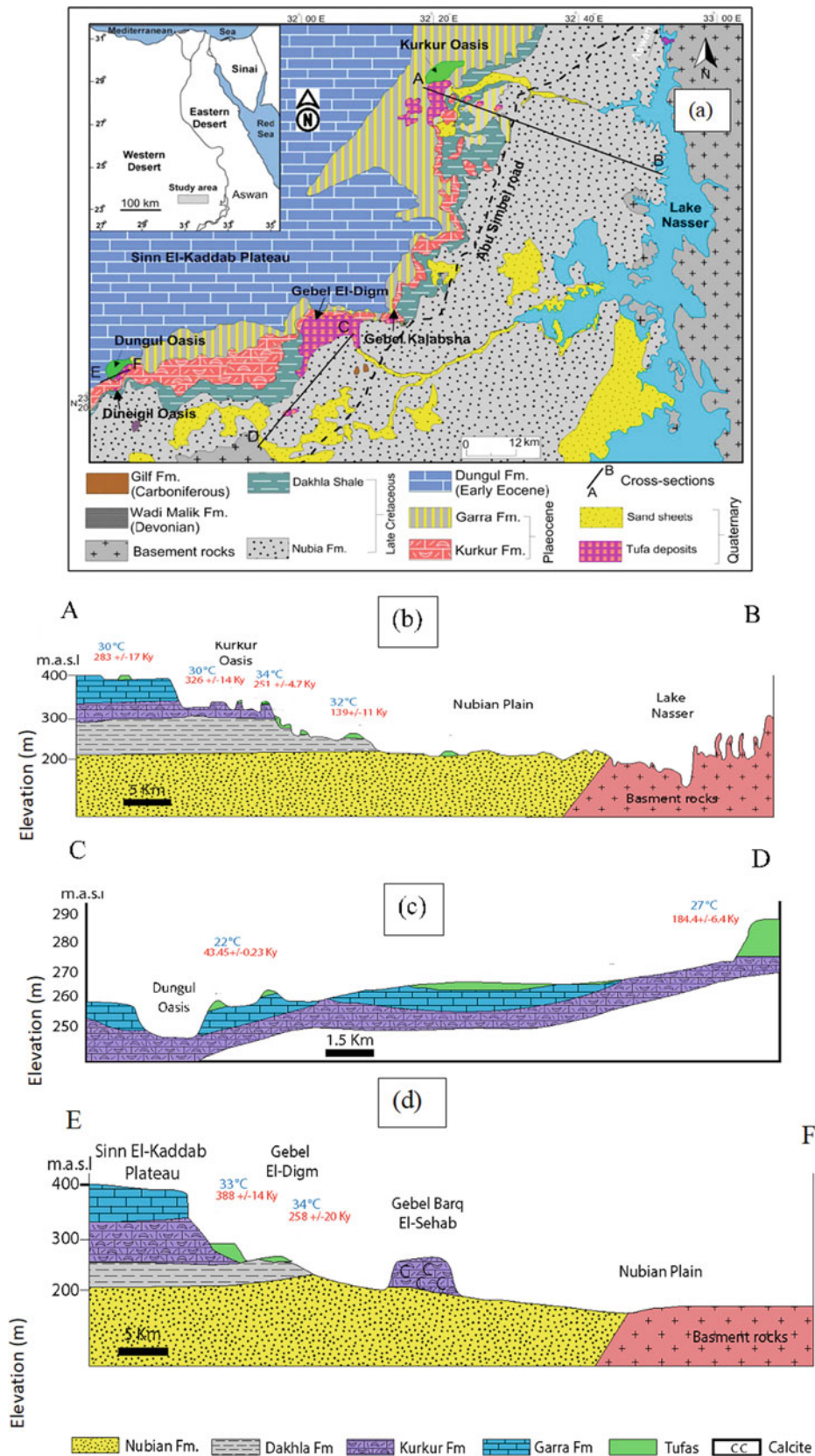


Fig. 38 The Geologic map of the Kurkur–Dungul Oases shows the exposed rock units (a) (Issawi, 1968). Three sections are detected; these are AB at Kurkur Oasis (b), CD at Dungul Oasis (c) and EF at Gebel El-Digm area (d). The sections show the altitude of the studied sites, the $^{230}\text{Th}/^{234}\text{U}$ age data (in red) and temperature data (in blue). Source Kele et al. (2021)



Fig. 39 Quaternary sedimentary carbonate spring and lacustrine deposits used as climate proxies. Phytothermal tufa deposits from Kurkur Oasis (a). The tufas are rich in plant casts, stems, reeds, grasses and mosses (b). Tufa sheets of concentric spherical-shaped laminar accretions, stromatolitic and banded (> 10 cm thick) (c) from Medawara at Kharga Depression (Jimenez, 2014), fractured, crystalline with alternating laminations of successive generations of epiphyte generations creating light- and dark-coloured layers (d) (Nicoll & Sallam, 2017). Tufa from Kharga (courtesy from Prof. Dr. Mohamed Hamdan) (e) the crystal mountain at DG with close-up showing travertine and crystal glacia (f) at Dakhla (Jimenez, 2014) and erosional yardangs in old playa (Lacustrine deposits) (g) (courtesy from Dr. Emad Sallam)

surface water was present during the generally cooler mid-Pleistocene period. Tufa formed between 340 and 360 ka (Abdel-Monem et al., 2006). Several $^{230}\text{Th}/^{234}\text{U}$ dates on tufa and carbonates correlated with MIS 6, another

very cold period (Osmond & Dabous, 2004; Smith et al., 2004; Sultan et al., 1997). At Matana and Medawara ESR dates on freshwater gastropods yielded ages of between 20–27 ka, 30–60 ka, 60–70 ka and 75–100 ka that are

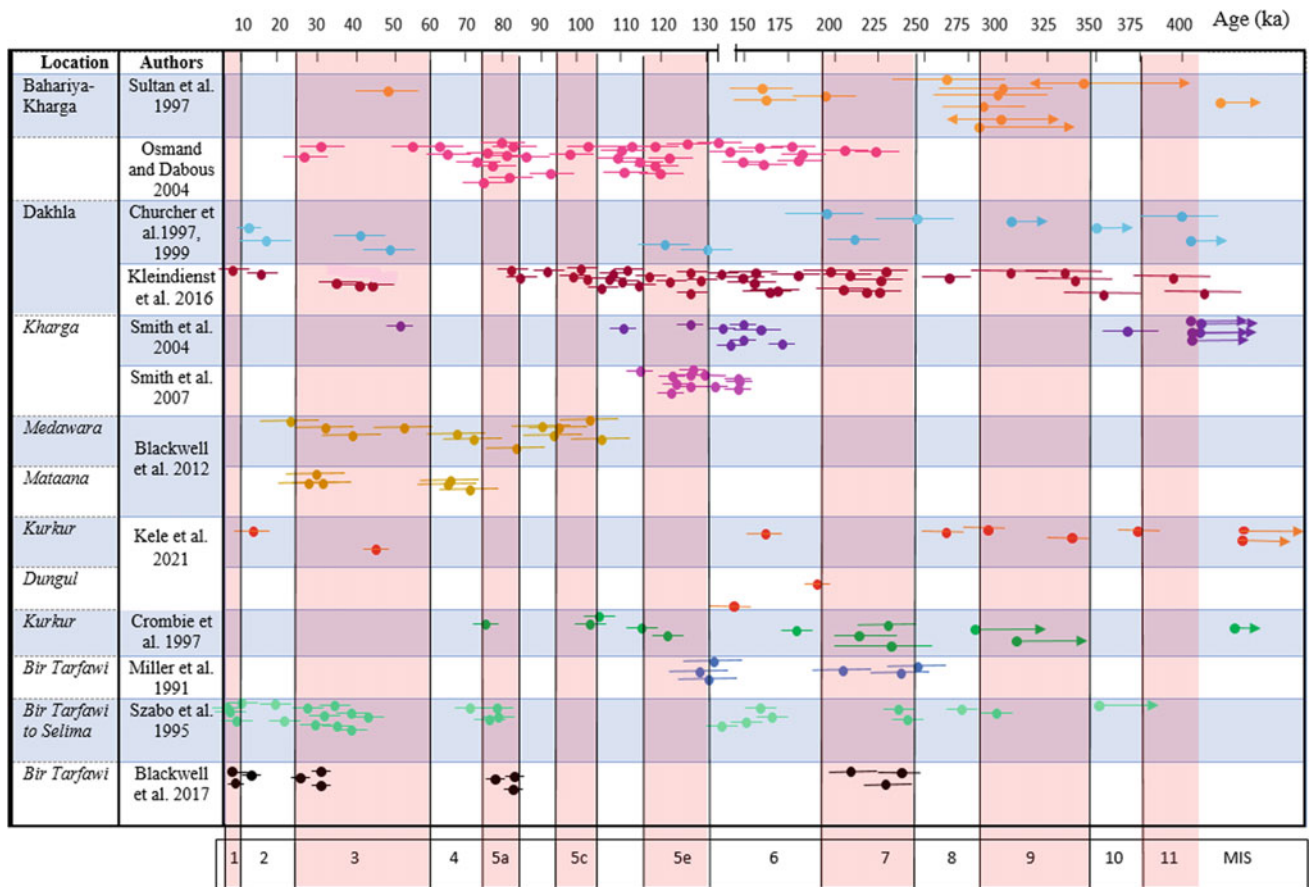


Fig. 40 Summary of the most reliable age dating from lacustrine and spring samples collected from different oases at the Western Desert of Egypt and correlated with $\delta^{18}O$ stratigraphy. The results show coincidence with most interglacial MIS 1, 3, 5, 7 and 9 (red cells or areas), while others show considerable ages corresponding to glacial MIS 2, 4, and 6. These results give a way to the concept that supports the presence of regional pluvial or wet conditions interpreted due to the Atlantic westerlies (NAO) or rise in water table or possible shifting in ITCZ (Hoffmann et al., 2016; Revel et al., 2010)

correlated with MIS 2, 3, 4, 5a, c and 6, respectively (Fig. 40, Blackwell et al., 2012). Along the Libyan Escarpment’s edge, springs also drained at Kharga Depression, but the water was ponded in little basins that had been blocked by tufa deposits. These dated fossils and sediments confirm the presence of water there in MIS 2–11. While another two ages averaged 28.2 ka, which fits with the MIS 3/2 border, two independent ESR ages averaged 65.4 ka (mid MIS 4). With an ESR age of 24.3 ka on *Melanoides tuberculata* shells from a thin pond deposit snails inside the tufa at Bulaq, another tufa that is much thinner and less extensive than Midauwara, this tufa correlates with a cooler phase during MIS 2 but not the glacial maximum. Therefore, it is possible that the Bulaq and Matana shells are related in time (Blackwell et al., 2017).

ESR for *Melanoides tuberculata* and carbonate sand samples collected from Bir Tarfawi White lake sequence (Fig. 31a and c) show ages of 19.3, 26.8, 27.5, 217.6, 234.5 and 248.1 ka (Fig. 40) and related to MIS 2, 7 (Blackwell et al., 2017). The samples from the Grey-Green lake

sequence (Fig. 31a and c) show ages 4.8, 6.4, 7.3, 78.4, 81.8 and 84 ka (Fig. 40) and related to MIS 1, 5a (Blackwell et al., 2017). Tufa from Kurkur and Dungul oases (Fig. 40) have dated back to 11 ± 1.2 ka, 43.52 ± 0.23 ka, 139 ± 11 ka, 184 ± 5.4 ka, 258 ± 20 ka, 326 ± 14 ka and 368 ± 14 ka (Kele et al., 2021). These dates are grouped according to the correlated MIS into stages 2, 3c, 4, 5e, 6, 8, 9 and 11 in non-isochronism with the interglacial stages.

Although the high-resolution marine records from the deep sea or ice cores reflect the global climate, and the MIS 1, 3, 5, 7, 9 (Fig. 40) correlated with sapropels in the Eastern Mediterranean enforced with African monsoons, the terrestrial records offer detailed integrating evidences for several regional paleoclimatic events that did not recorded globally. It is also interesting to confirm the potential terrestrial climatic proxies (Fig. 35) in improving our understanding regarding the Green Sahara episodes, however, emphasizing the non-isochronism of the Quaternary climate in North Africa boundaries. There are, however, lacustrine sediments that contradict this, associated with glacial MIS 2, 4, 6

(Fig. 40, Hoffmann et al., 2016). This suggests that other regional forces played a potential role in determining the regional climate and strengthening the role of North Atlantic (NAO) sea surface temperatures (SSTs) (Blome et al., 2012; Jimenez, 2014; Kele et al., 2021). Similar was the study of speleothem-derived central North Africa rainfall records for the last glacial period that revealed three main wet intervals at 65–61, 52.5–50.5 and 37.5–33 ka, and related to obliquity maxima and precession minima (Bosmans et al., 2015). In addition, North Atlantic (NAO) humid sources may explain the presence of several recorded pluvial intervals that belong to the glacial stages 2, 4, 6 and 8 (Hoffmann et al., 2016). In this concern, in order to understand Saharan paleoclimates and patterns of modern human migration, Abotalib et al. (2019) used $^{230}\text{Th}/^{234}\text{U}$ in dating to determine the age of thick accumulations of scarp and scarp-foot depression sediments. They confirmed that there was little or no deposition during the warm interglacial periods of MIS 5, 7 and 13, and that deposition was most common during the lengthy cool glacial periods of MIS 6, 8 and 10. In contrast, Quaternary sediments connected to hydrologic systems with short residence times produced MIS 2 OSL ages ranging from 27.7 to 10.2 ka. It is believed that age misinterpretation, which reflects the timing of groundwater discharge rather than the ages of the wet periods during which recharge occurred, is to blame for the lack of scarp and scarp-foot depression sediments of MIS 2 ages and the wide range of warm and cool stages in Eastern Sahara.

5.3 The Aeolian Sediments as a Proxy to Arid Climate

The dominance of arid environments in several regions make the study of these regions of critical importance for the development and global models of environmental change (Chase, 2009). The Quaternary geology of Egypt includes substantial amounts of aeolian sands, which are indicative of arid climate. About 283,836 km² of the Egyptian landmass, or about 16% of the total area of the state, are covered with aeolian deposits. Six sand seas, including the Great Sand Sea, Abu Moharik and North Sinai, span more than 5000 km², accounting for at least 50% of the total dune coverage, while the remaining 10 dune fields have less than 50% of the total dune coverage, including the West Delta and South Rayan (Bubenzer et al., 2020; Embabi, 2018). All other Egyptian sand seas, with the exception of the North Sinai Sand Sea, are found in the Western Desert, whereas the Eastern Desert's dune fields are concentrated in the extreme Southeast (El-Hebal Dune Fields) and Northeast (El-Khanka Dune Field). The Great Sand Sea, along with all other dune fields and sand seas, is produced in the Western Desert. The Great Sand covers more than 100,000 km² in size (Besler,

2008). It is not limited to Egypt; it spans a distance of roughly 600 km from the southern borders of the Siwa depression in the north to the northern scarps of the Gilf Kebir and Abu Ras plateaus in the south. Its width from east to west varies between 60 and 200 km (Embabi, 2018). The sand sea is not in a clearly defined depression; rather, it is a weakly sculpted area of ground that slopes from more than 500 m a.s.l in the south to less than 100 m a.s.l towards the Siwa Depression in the north (Besler, 2008). The Great Sand Sea contains three distinct forms of dunes. The first is the linear/longitudinal forms (Fig. 41a), followed by the transverse, barchans and barchanoid forms (Fig. 41b and c), and finally, the star dunes (Embabi, 2018). The most prevalent dunes are linear dunes, which come in two different varieties: broad-crested megadunes and sharp-crested recent linear (seif) ridges or Silk (Besler, 2000; whalebacks of Bagnold, 1941, 1953 or draa of Besler, 2000). The Silk dunes (Fig. 41d) are active right now as the draa settle. From the end of the Middle Paleolithic pluvial to the start of the (AHP) ~ 10 ka BP, the draa were active dunes (Haynes, 1982) and later were fixed ~ cal. 6.5 ka BP by the combined action of bioturbation, human occupation, pedogenesis and slope wash vegetation (Hamdan & Hassan, 2020). M24 cross-sections along 450 km of a chosen dune ridge showed changes in paleoclimate (Besler, 2000). In the Late Pleistocene (> 20 ka BP), stronger trade winds helped to create the southern longitudinal draa megadunes. In a wet Late Glacial to Early Holocene epoch when the southern draa were fixed by vegetation and their sands turned red, there were signs of prehistoric man on their flanks ~ 7–9 ka BP (Besler, 2000). The distinctive northern megadunes were likely patterned by dry extra-tropical westerlies in an arid time at 20–11 ka BP. They are transverse draa of the northern sand sea (Embabi, 2018). Aeolian sands likely took the shape of barchan dunes and moved several tens of kilometres farther south after this aridity. Strong, dry westerlies pushed sands farther south and dumped them on the eastern slopes of the draa during the end of the Pleistocene (~ 12–10 ka BP). As a result, sand accumulation near the surface on the western flanks of the draa is older than that on the eastern flanks. Runoff following annual precipitation quantities of 50–100 mm and intermediate short deflation phases during the Holocene humid phase or Holocene humid optimum (10,600–7300 BP) transformed the draa into the current whalebacks (Bagnold, 1941). Seasonal ponds and lakes were hydrated by runoff from the condensed draa surfaces and seepage at their bases in shallow depressions of the inter-draa corridors. Because of these circumstances, people were able to live there as hunters and gatherers. These “playa sediments” in the southern Great Sand Sea have redder colours and more silt than draa and dune sediments because of weathering during the Holocene wet period (Embabi, 2018). The available data were related to the

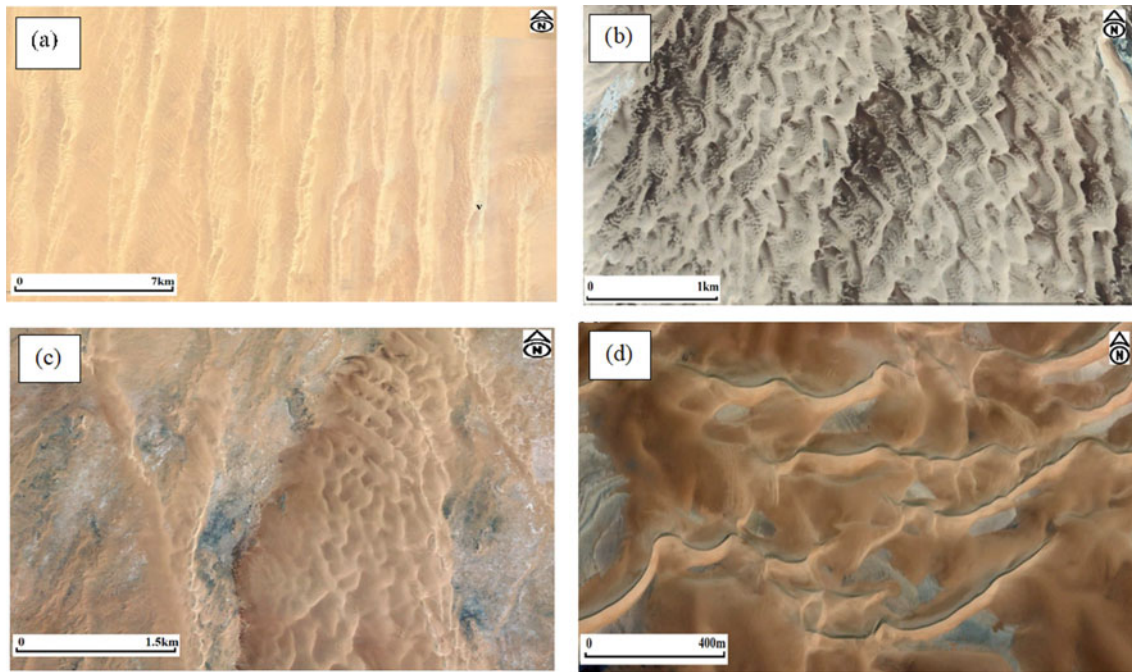


Fig. 41 Selected Google images for some dune forms, the Great Sand Sea. The longitudinal (a) the barchan (b), the complex barchan (c) and the travers or silk (d) dune forms

geology, geomorphology and archaeology; three cycles of dunes were distinguished (Embabi, 2018):

The first cycle 700–200 ka: It is the oldest dune cycle occurred during Middle Pleistocene, aridity, which started 700 ka years ago and ended 200–300 ka. This estimation is supported by archaeological data discovered in the Great Sand Sea's inter-draa corridors. On the surfaces of the interdune zones, there were also scattered artefacts of the Acheulean type (Haynes, 1982).

The second cycle 60–10 ka: It is the middle dune cycle associated with Late Pleistocene aridity extended from 35 ka or earlier to 10 ka BP. While there is little trace of human habitation during that time, there is a great deal of evidence of aeolian activity (Haynes, 1982). According to Wendorf et al. (1993), the beginning of this aridity was 60 ka BP. The draa dunes were active dune ridges during this dry time between the end of the Middle Paleolithic pluvial period and the start of the Neolithic period (Haynes, 1982).

The third cycle 7 ka to present: It represents the last cycle of dune growth in the Great Sand Sea. It extends from the Middle Holocene to the present time. Field observations and the dating of several samples led researchers to conclude that draa reactivation took place during the Middle and Late Holocene (Besler, 2000). The result of recent wind activity on dunes in the Great Sand Sea are active silks

(sharp-crested seif ridges) on the draa (whalebacks) (Besler, 2000). The southern draa were reactivated at least 3 ka ago as a result of rising aridity. Since then, blown sands and barchan dunes have moved around 60 km further south. Later, lighter sands from the northern draa covered the reddish southern draa. Due to the strong westerly component of the bimodal wind system, the secondary Holocene and current dunes were primarily developed in the lee east of the northern draa, but on the southern draa due to the stronger northern wind component (Besler, 2000).

Besler (2008) performed three transections in which samples for optical simulated luminescences (OSL) representing the transverse draa (I), longitudinal draa western flank (II) and eastern flank (III) were obtained (Table 3). According to the findings, the draa's western flanks have accumulated more sand near the surface over time than its eastern flanks. The findings also demonstrate that age generally increases with depth; the oldest sample, which was obtained at a maximum depth of 5 m, is 22.8 ± 3.8 ka, while the youngest sample, which was taken at a depth of 1.0 m, is 240 ± 50 (Embabi, 2018). This makes it very evident that depth has a significant role in estimating age and, by extension, the paleoclimate and depositional environment.

The southern increase in the reddened sands is interpreted as the presence of kaolinite and hematite coating (El-Baz & Prestel, 1982) together with sand size, which is a factor equivalent to high wind velocities, may reinforce the

Table 3 Spatial distribution of OSL data along the transections (Besler, 2008)

Draa type	West transection			Middle transection			East transection		
	Position	Depth (m)	Age (ka)	Position	Depth (m)	Age (ka)	Position	Depth (m)	Age (ka)
I	N 26° 51' E 25° 36'	2	17.1 ± 2.7	N 27° 12' E 26° 02'	2	11.8 ± 1.8	N 27° 19' E 26° 32'		
		3	18.1 ± 1.6		3	12.7 ± 1.8			
		4	20.4 ± 3.1		4	15.9 ± 2.1		4.0	12.5 ± 3.0
II	N 25° 42' E 25° 40'	2	20.4 ± 3.8	N 25° 24' E 26° 36'	2	21.3 ± 3.0			
		3	21.3 ± 2.9						
		4	21.9 ± 4.5						
		5	22.8 ± 3.8						
III	N 25° 07' E 25° 37'	2	11.8 ± 3.0	N 25° 25' E 26° 36'	3.5	9.8 ± 1.6	N 25° 25' E 27° 05'	1.0	0.24 ± 0.05
		3	11.5 ± 2.1					1.4	0.28 ± 0.06
								1.5	0.25 ± 0.07
								1.8	0.24 ± 0.06
								2.0	5.0 ± 1.05

climatic aridity. However, from my opinion, the wide range of the suggested age may require further dating and deep core sampling due to the cumulative nature of dune formation. The sand dunes then can be tentatively used as a paleoclimatic proxy. With the aid of the OSL dating method, Chase (2009) determined the ages of three dune relics in South Africa and established that there were three main periods of activity at $\sim 60\text{--}40$, $\sim 35\text{--}20$ and $\sim 17\text{--}4$ ka. The frequent disagreements with other terrestrial records that show concurrent increases in humidity and the close relationships between these phases and wind strength proxies suggest that aridity is unlikely to be the only forcing mechanism for aeolian activity (Chase, 2009).

Another proxy for paleoclimate is the Saharan dust, which refers to dry intervals. The glacial–interglacial (100 ka eccentricity cycle; Fig. 42a) pointing to the presence of coarser terrigenous (Fig. 43f) rather than Saharan dust particles, and high wind strengths during the last three glacial terminations II, IV, and VI related to MIS 2, 4 and 6 (Fig. 42a). The precession isolation (21 ka cycle) (Fig. 42c) controls the dust input (Guieu & Thomas, 1996; Fig. 42d and e, Moreno, 2012). Remanent magnetism resulting from short-term exposure to strong magnetizing fields at constant temperature is referred to as *isothermal remanent magnetism* (IRM). The IRM@AF parameter is the measure of the intensity of the laboratory-induced magnetization (Larrasoña, 2012). The high-resolution measurements of IRM@AF for dust recorded in the Eastern Mediterranean (Fig. 42d) have been found to be proportional to the content of hematite. The later constitutes about 6.5% (in weight) of the Saharan dust transported (dust flux, Fig. 42e) into the Eastern Mediterranean (Emeis et al., 2000; Kroon et al., 1998; Larrasoña, 2012; Lourens et al., 2001; Tomadini

et al., 1984). Fe content thus is used as a proxy for aeolian particles coming from the Sahel area within Sahara dust (Balsam et al., 1995). The IRM@AF parameter of the Sahara dust is very interesting proxy for climatic changes as it is inversely proportional with the light $\delta^{18}\text{O}$ values (Fig. 42b and d), high-insolation (Fig. 42c) and the high-monsoon runoff (Fig. 42e). The IRM@AF parameter also shows a non-isochronism with grain size, the Si/Al ratio (Fig. 43e). The latter is used as a proxy for wind strength and indicates an increase in terrigenous quartz rather than in dust (Fig. 43f, Guieu & Thomas, 1996). Al percentage decreases in the dry intervals (Fig. 43b and e); consequently, Si/Al ratio increases within the sediments intercalated sapropel layers (Revel et al., 2010), while decreases in sapropel layers themselves (Fig. 43e). However, Al is related to both aeolian (e.g. kaolinite; Foucault & Mélières, 2000) and fluvial (e.g. smectite; Lourens et al., 2001) sources. Variations in Ti/Al, therefore, can be interpreted in terms of the relative contributions of aeolian (Saharan dust) and fluvial (Nile) sources whether Blue or White Nile (Fig. 43; Larrasoña, 2012; Scheuven et al., 2013). The Fe and Ti usually have parallel behaviour (Fig. 43b and c) referring to aeolian Sahel particles (Balsam et al., 1995; Bergametti et al., 1989; Moreno, 2012; Moreno et al., 2001, 2002; Figs. 42 and 43). A distinctive cyclic pattern of correspondence of Fe and Ti percentages is evident (Fig. 43), with highest values in the sapropels and lowest values in the intercalated marls in contrast to Al (Fig. 43e; Foucault & Mélières, 2000; Lourens et al., 2001).

The high-resolution record of fine-grained eastern Saharan dust from the Eastern Mediterranean Sea spans the last 180 ka, which is based on the clay mineral composition of the marine sediments collected from core M40/4_SL71 in

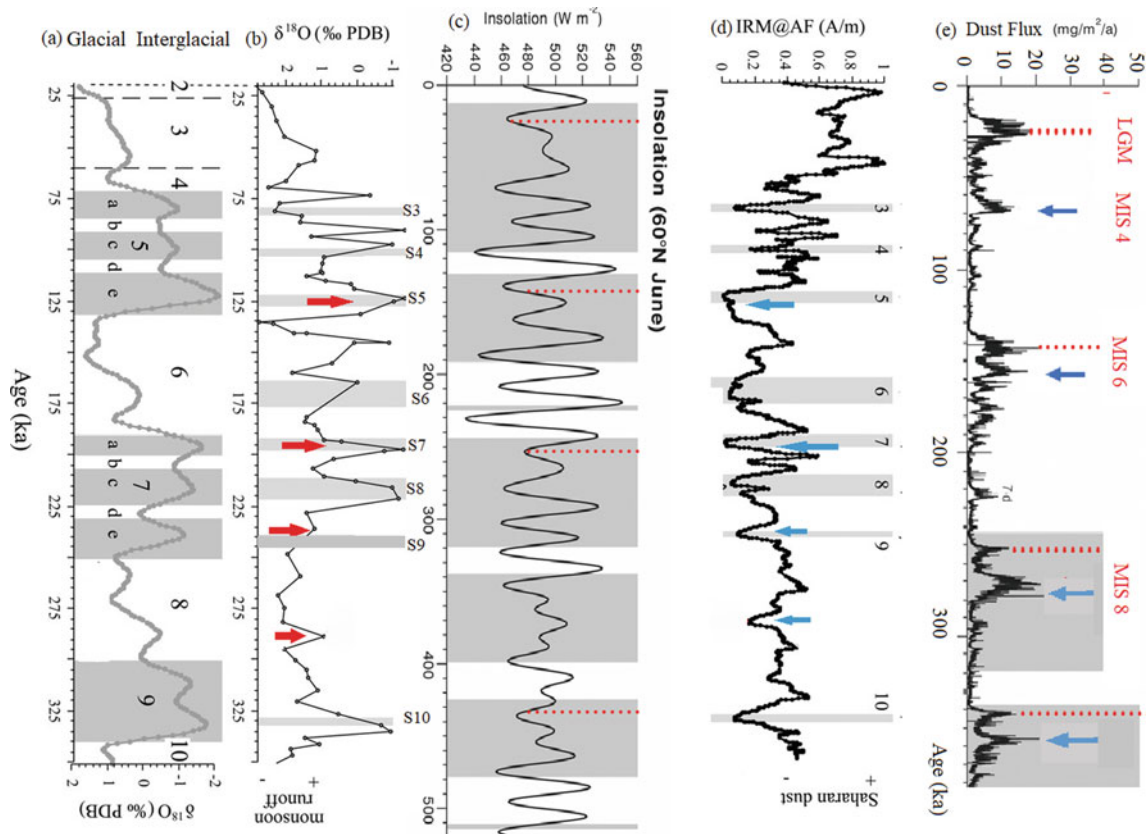


Fig. 42 Glacial-interglacial cycles (a) with corresponding $\delta^{18}\text{O}$ stratigraphy grey-shaded bars represent sapropel layers (b) of high monsoons (Imbrie et al., 1984; Kroon et al., 1998), correlated with the precession insolation curve with dashed red line eccentricity (c) (Laskar et al., 2004). All plotted against IRM@AF (d) (Larrasoña et al., 2003) and the Dust Flux (e) (Lambert et al., 2012). The red arrow indicates correspondence of $\delta^{18}\text{O}$ with insolation and monsoons, while the blue arrow shows decrease in intervals of IRM@AF and dust storm flux. 2021 Source Gibbard and Hughes (2021)

the Eastern Mediterranean Sea, especially the kaolinite/chlorite ratio (Fig. 44a–e; Ehrmann et al., 2017). The concept assumes that there was very little aeolian kaolinite movement during the AHP because kaolinite deflation was inhibited by increased humidity and vegetation cover. As an alternative, soil, lake basins and riverbeds were used to retain kaolinite that weathered from kaolinite-containing Cenozoic rocks. Maximum aeolian uptake and transport of kaolinite was achieved during the succeeding dry phases as fine-grained dust was mobilized from the dried lakes, rivers and soils (Fig. 44b; Bullard et al., 2011; Tegen et al., 2002). When these sediment supplies ran out, kaolinite transport dropped once more. The amount of clay-sized dust that is blown out of the Sahara into the Eastern Mediterranean Sea and North Africa is inversely correlated with the amount of kaolinite weathering and accumulation in soils and lake sediments, and hence with the strength of the previous humid interval. An example is the strongest humid interval occurred during MIS 5e, c, a (Fig. 44), which was followed by weaker phases that centred at 118, 100, 90 and 75 ka with

characteristic high kaolinite percentages (Fig. 44b and d, black arrows). It is well established that these dust fluxes are predominantly controlled by wind and topography, rather than by aridity (e.g. Crouvi et al., 2012; Engelstaedter et al., 2006; Kohfeld & Harrison, 2001). Along with kaolinite, palygorskite is a common wind-blown mineral in the sediments of the Eastern Mediterranean Sea and a superb Saharan dust tracer (Fig. 44c). It primarily comes from deposits found in Palaeogene North African countries like Morocco, Tunisia, Libya and Egypt (Goudie & Middleton, 2001; Larrasoña et al., 2003). Similar to kaolinite, palygorskite sources undergo severe erosion when it is humid, and the weathering by-products are then retained in soils, lake and river sediments, and depressions. High wind speeds and dry periods during which the percentage of dust components rose can be seen in the coincidence of high kaolinite percentages (Fig. 44b), high palygorskite percentages (Fig. 44c) and high kaolinite/chlorite ratios (Fig. 44d). In contrast, these elements diminished along with the increase in light $\delta^{18}\text{O}$ values (Fig. 44e), indicating humid climate

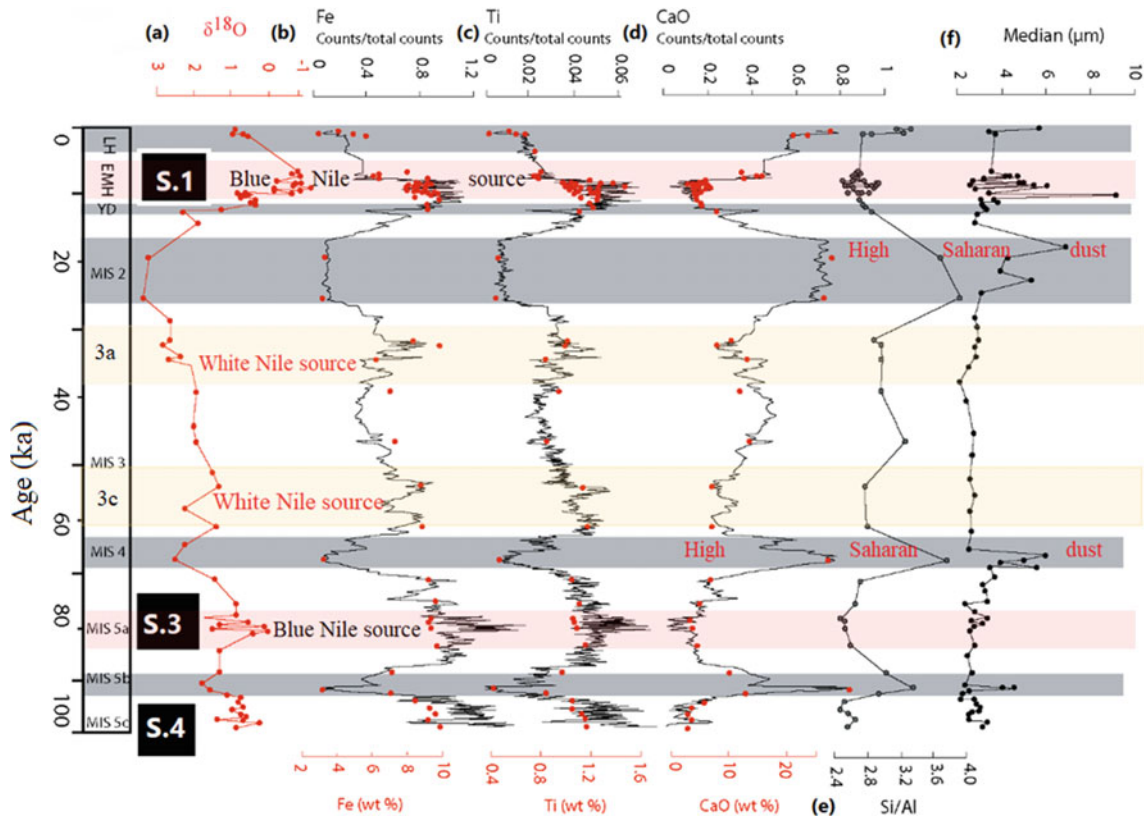


Fig. 43 $\delta^{18}\text{O}$ stratigraphy with sapropel layers S1 to S4 (a) positively corresponding with increasing of the Fe% (b) and Ti% (c) by weight during interglacial MIS and retreat during glacial intervals. The grey areas refer to the dry intervals with high CaO (d), Si/Al ratio (e) and grain size (f). The results distinguish the Nile discharge, the red-shaded bars indicate Blue Nile while the orange bars refer to the White Nile source. Source Revel et al. (2010)

intervals, correlated with the development of sapropels (S1, S3, S4, S5 and S6) at the Eastern Mediterranean (Fig. 44a, Ehrmann et al., 2017), the Blue Nile regime, while conflicting with dust storms (Fig. 42e, Lambert et al., 2012).

6 Conclusions

The Quaternary sediments and stratigraphy in Egypt including benthonic and planktonic foraminiferal distributions, pollen and spore zonation, distribution of minerals, major and trace elements, and isotopic composition have been implemented on the Quaternary sediments as proxies of paleoclimate. The Quaternary Nile Delta sediments are subdivided into several intervals of humid and arid associated with African monsoons and controlled with the Nile flow. The distribution of pyroxenes, amphiboles, Fe, Al, Ti, Si, Ca, Sr, Mn and Cr Zr enabled provenance identification of either regional or Nile Headwater. These intervals can be correlated with sapropel layers at the Eastern Mediterranean and global climatic and sea level changes. Deposition of lacustrine and spring sediments supported with calibrated age determinations, and analysis of Sahara dust, its

mineralogical and elemental distribution allow classification into humid and arid intervals that correlated globally with $\delta^{18}\text{O}$ stratigraphy. Debates regarding such correlations are ongoing. While correlation was possible along the Nile Delta with precessional insolation and monsoonal runoff and the Eastern Mediterranean sapropels, such correlation is harder for the coral reefs and aeolianites along the Red Sea and the Mediterranean Sea, respectively, as well as the other terrestrial sediments along the Sahara. While the coral reefs and aeolianites refer to highstand of sea level, they do not directly correspond to climatic wet episodes. The presence of paleosols intercalated with aeolianites on the northwestern Mediterranean coast, and coral reef terraces in alternation with conglomerates at the Red Sea coast offer strong evidence that the humid climates postdated the sea level highstands. Although warm climates are very important for carbonate pumping and deposition as corals or ooids, it is not necessary to have contemporaneous wet conditions. In addition, the presence of lacustrine and spring deposits associated with MIS 2, 4 and 6 supports the presence of wet climate during glacial episodes. Such offsets offer a role to the obliquity beside both eccentricity and precession. It gives a way to the concept that during interglacials it is not always wet

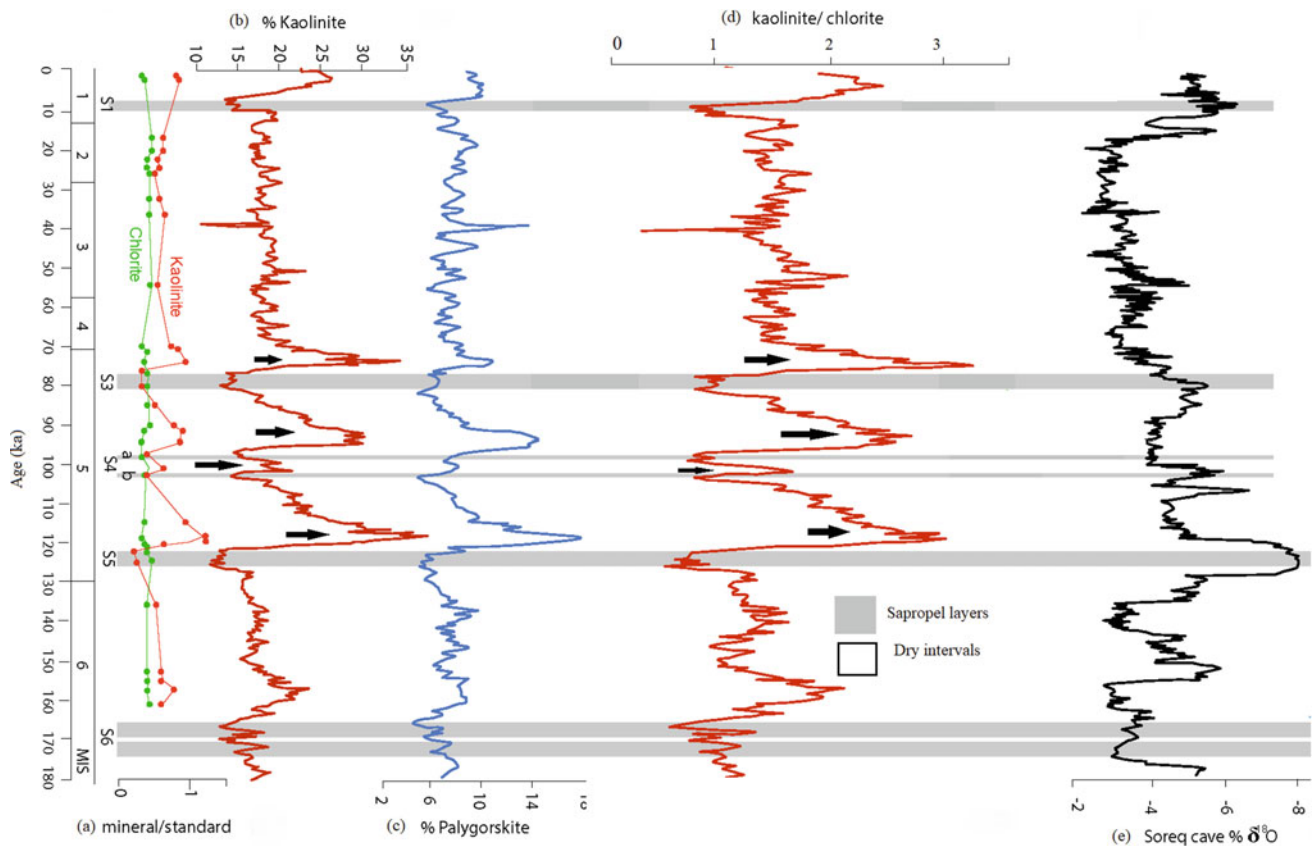


Fig. 44 Correlation of kaolinite and chlorite standard as proxies of paleoclimate (a) with detected contents of kaolinite % (b), palygorskite % (c) and kaolinite/chlorite ratio (d) (Ehrmann et al., 2013), correlated with Speleothem $\delta^{18}\text{O}$ record of Soreq Cave, Israel (Bar-Matthews et al., 2003) (e). The grey areas refer to the sapropels (S1, S3, S4, S5 and S6) at the Eastern Mediterranean, while the black arrows refer to high kaolinite/Chlorite ratio. Source Ehrmann et al. (2013)

everywhere, which interpreted in the frame of a time transgressive climate change and a 3000 yrs shifting in the ITCZ and AHP or possibly attributed to regional conditions such as Atlantic (NAO) westerlies and the associated low SSTs.

Acknowledgements I would like to thank God, who helped me to complete this work during a short time and critical circumstances. I am certain that this work is not a Holy Book, and it may contain several errors or disputed concepts; therefore, please forgive any discrepancies; it is a human work. I especially thank great scholars who reviewed this work. Professor Dr. James Rose Professor Emeritus, Department of Geography at Royal Holloway, University of London, UK. Professor Dr. Daniel J. Stanley, Senior Scientist Emeritus, Department of Paleobiology, National Museum of Natural History, Smithsonian Institution, Washington, D.C., USA, and Dr. Becky Briant, Department of Geography, Birkbeck, University of London, UK. Their critical reviewing, discussions and comments are highly appreciated. I am very grateful of Professor Dr. Nabil Sayd Embabi, Professor Emeritus, Department of Geography, Ain Shams University, Professor Dr. Mahmoud Ahmed Kora, Professor Emeritus, Department of Geology, Mansoura University, and Professor Dr. Mohamed Abdel-Rahman Hamdan Department of Geology, Cairo University, for their discussions and supports with several field experiences.

References

- Abdel-Monem, A. A., Hassan, G. M., Eissa, H. M., El-Sankary, M. M., Abdel-Razek, Y. A., Rasheed, N. M., & El-Morsy, M. (2006). ESR studies and dating of natural carbonates (tufas) from Egypt. *Egyptian Journal of Biophysics*, 12, 59–76.
- Abotalib, A. Z., Sultan, M., & Elkadiri, R. (2016). Groundwater processes in Saharan Africa: Implications for landscape evolution in arid environments. *Earth Science Reviews*, 156, 108–136.
- Abotalib, A. Z., Sultan, M., Jimenez, G., Crossey, L., Karlstrom, K., Forman, S., Krishnamurthy, R. V., Elkadiri, R., & Polyak, V. (2019). Complexity of Saharan paleoclimate reconstruction and implications for modern human migration. *Earth and Planetary Science Letters*, 508, 74–84.
- Abu Seif, E. S. (2015). Geological evolution of Nile Valley, west Sohag, Upper Egypt: A geotechnical perception. *Arab Journal of Geosciences*, 8, 11049–11072. <https://doi.org/10.1007/s12517-015-1966-5>
- Adamson, D. A., Gasse, F., Street, F. A., & Williams, M. A. J. (1980). Late Quaternary history of the Nile. *Nature*, 88, 50–55.
- Adelsberger, K. A., & Smith, J. R. (2010). Paleolandscape and paleoenvironmental interpretations of spring deposited sediments (sic) in Dakhleh Oasis, Western Desert, Egypt. *CATENA*, 83 (1), 7–22.

- Adkins, J., De Menocal, P., & Eshel, G. (2006). The "African humid period" and the record of marine upwelling from excess ^{230}Th in Ocean Drilling Program Hole 658C. *Paleoceanography*, 21, PA4203. <https://doi.org/10.1029/2005PA001200>
- Ali, Y. A., & West, I. (1983). Relationship of modern gypsum nodules in sabkhas of loess to compositions of brines and sediments in northern Egypt. *Journal of Sediment Petrology*, 53, 1151–1168.
- Al-Rifaiy, I. A., & Cherif, O. H. (1989). Paleogeographic significance of Pliocene and Pleistocene mega-invertebrates of the Red Sea and the Gulf of Aqaba. *Journal of the University of Kuwait (Science)*, 16(2), 367–399.
- Aly, M. H., Klein, A. G., Zebker, H. A., & Giardino, J. R. (2012). Land subsidence in the Nile Delta of Egypt observed by persistent scattered interferometry. *Remote Sensing Letters*, 3(7), 621–630.
- Andersen, S. T. (1979). Identification of wild grass and cereal pollen. *Danmarks Geol Undersøgelse Aarbog*, 69–92.
- Arbouille, D., & Stanley, D. J. (1991). Late Quaternary evolution of the Burullus lagoon region, north-central Nile delta, Egypt. *Marine Geology*, 99, 45–66.
- Assal, E. M., Abdel-Fattah, Z., & El-Asmar, H. M. (2020). Facies architecture and controlling factors induced depositional model of the Quaternary carbonate aeolianites in the northwestern Mediterranean coast of Egypt. *International Journal of Earth Sciences*, 109, 1659–1682. <https://doi.org/10.1007/s00531-020-01863-3>
- Attia, S. H., & El-Ghazawy, M. (1984). Microfacies studies on some Tertiary and Quaternary deposits east of El-Hammam NW Desert, Egypt. *Middle East Research Centre, Ain Shams University*, 4, 239–273.
- Ayyad, S., El-Bassiouni, A. E., & Ziko, A. (1987). Benthonic foraminifera, Bryozoa and the paleoenvironments of the Quaternary succession in north west Rosetta of shore well No.1, Nile Delta, Egypt. In *6th Symposium on Quaternary and Development*, Mansoura University, Egypt.
- Bagnold, R. A. (1941). *The physics of blown sand and desert dunes* (265 pp.). Methuen.
- Bagnold, R. A. (1953). The surface movement of blown sand in relation to meteorology. *Research Council of Israel Special Publication*, 2, 89–93.
- Balsam, W. L., Otto-Bliesner, B. L., & Deaton, B. C. (1995). Modern and last glacial maximum aeolian sedimentation patterns in the Atlantic Ocean interpreted from sediment iron oxide content. *Paleoceanography*, 10(3), 493–507.
- Bar-Matthews, M., Ayalon, A., Gilmour, M., Matthews, A., & Hawkesworth, C. J. (2003). Sea-land oxygen isotopic relationships from planktonic foraminifera and speleothems in the Eastern Mediterranean region and their implication for paleorainfall during interglacial intervals. *Geochimica et Cosmochimica Acta*, 67, 3181–3199.
- Bárta, M., & Bezdek, A. (2008). Beetles and the decline of the old kingdom: Climate change in ancient Egypt. In H. Vymazalová, & B. Bárta (Eds.), *Chronology and archaeology in ancient Egypt (The Third Millennium B.C.)* (pp. 214–222).
- Beadnell, H. J. L. (1924). Report on the geology of the Red Sea coast between Qoseir and Wadi Ranga. *Petroleum Research Bulletin*, 13, 1–37.
- Beck, C. C., Feibel, C. S., Wright, J. D., & Mortlock, R. A. (2019). Onset of the African humid period by 13.9 kyr BP at Kabua Gorge, Turkana Basin, Kenya. *The Holocene*, 29(6), 1011–1019. <https://doi.org/10.1177/0959683619831415>
- Becker, R. H., & Sultan, M. (2009). Land subsidence in the Nile Delta: Inferences from radar interferometry. *The Holocene*, 19(6), 949–954.
- Behre, K. E. (1981). The interpretation of anthropogenic indicators in pollen diagrams. *Pollen Et Spores*, 23, 225–245.
- Bergametti, G., Gomes, L., Coude-Gaussen, G., Rognon, P., & Lecoustumer, M. N. (1989). African dust observed over Canary Islands β source-regions identification and transport pattern for some summer situations. *Journal of Geophysical Research: Atmospheres*, American Geophysical Union, 94(D12), 855–869.
- Berger, A. (1992). Orbital variations and insolation database. IGBP PAGES/World Data Center for Paleoclimatology Data Contribution Series # 92-007. NOAA/NGDC Paleoclimatology Program.
- Bernasconi, M. P., Melis, R., & Stanley, D. J. (2006). Benthic biofacies to interpret Holocene environmental changes and human impact in Alexandria's Eastern Harbour, Egypt. *The Holocene*, 16(8), 1163–1176.
- Bernhardt, C., Horton, B. P., & Stanley, D. J. (2012). Nile Delta vegetation response to Holocene climate variability. *Geology*, 40(7), 615–618.
- Besler, H. (2000). Modern and palaeo-modelling in the Great Sand Sea of Egypt initial results from the Cologne Cooperative Research Project 389. *Global and Planetary Change*, 26, 13–24.
- Besler, H. (2008). *The great sand sea in Egypt: Formation, dynamics and environmental change—A sediment analytical approach*. Elsevier.
- Blackwell, B. A. (1995). Electron spin resonance dating. In N. W. Rutter, & N. R. Catto (Eds.), *Dating methods for quaternary deposits*. Geological Association of Canada, St. John's. Geotext (Vol. 2, pp. 209–251).
- Blackwell, B. A. (2001). Electron spin resonance (ESR) dating in lacustrine environments. In W. M. Last, & J. P. Smol (Eds.), *Tracking environmental change using lake sediments, basin analysis, coring, and chronological techniques* (Vol. 1, pp. 283–369).
- Blackwell, B. A. (2006). Electron spin resonance (ESR) dating in karst environments. *Acta Carsologica*, 35, 123–153.
- Blackwell, B. A., Skinner, A. R., Mashriqi, F., Deely, A. E., Long, R. A., Gong, J. J. J., Kleindienst, M. R., & Smith, J. R. (2012). Challenges in constraining pluvial events and hominin activity: Examples of ESR dating molluscs from the Western Desert, Egypt. *Quaternary Geochronology*, 10, 430–435.
- Blackwell, B. A., Skinner, A. R., Smith, J. R., Hill, C. L., Churcher, C. S., Kieniewicz, J. M., Adelsberger, K. S., Blickstein, J. I. B., Florentin, J. A., Deely, A. E., & Spillar, K. V. (2017). ESR analyses for herbivore teeth and molluscs from Kharga, Dakhleh, and Bir Tarfawi Oases: Constraining water availability and hominin Paleolithic activity in the Western Desert, Egypt. *Journal of African Earth Sciences*, 136, 216–238.
- Blanchet, C. L., Tjallingii, R., Frank, M., Lorenzen, J., Reitz, A., Brown, K., Feseker, T., & Brueckmann, W. (2013). High- and low-latitude forcing of the Nile River regime during the Holocene inferred from laminated sediments of the Nile deep-sea fan. *Earth and Planetary Science Letters*, 364, 98–110.
- Blome, M. W., Cohen, A. S., Tryon, C. A., Brooks, A. S., & Russell, J. (2012). The environmental context for the origins of modern human diversity: A synthesis of regional variability in African climate 150,000–30,000 years ago. *Journal of Human Evolution*, 62(5), 563–592. <https://doi.org/10.1016/j.jhevol.2012.01.011>
- Bosmans, J. H. C., Drijfhout, S. S., Tuenter, E., Hilgen, F. J., & Lourens, L. J. (2015). Response of the North African summer monsoon to precession and obliquity forcings in the EC-Earth GCM. *Climate Dynamics*, 44, 279–297. <https://doi.org/10.1007/s00382-014-2260-z>
- Braithwaite, C. J. R. (2016). Coral-reef records of Quaternary changes in climate and sea-level. *Earth-Science Reviews*, 156, 137–154.
- Bravard, J.-P., Mostafa, A., Davoli, P., Adelsberge, K. A., Ballet, P., Garcier, R., Calcagnile, L., & Quarta, G. (2016). Construction and deflation of irrigation soils from the Pharaonic to the Roman period at Amheida (*Trimithis*), Dakhla Depression, Egyptian Western Desert. *Geomorphologie: Relief, Processus, Environment*, 22(3), 305–324. <https://doi.org/10.4000/geomorphologie.11479>

- Broecker, W. S., & Van Donk, J. (1970). Insolation changes, ice volumes, and the O¹⁸ record in deep-sea cores. *Reviews of Geophysics*, 8, 169–198. <https://doi.org/10.1029/RG008i001p00169>
- Brook, G. A., Embabi, N. S., Ashour, M. M., Edwards, R. L., Cheng, H., Cowart, J. B., & Dabous, A. A. (2002). Djara cave in the Western desert of Egypt: Morphology and evidence of Quaternary climatic change. *Cave and Karst Science*, 29, 57–66.
- Brook, G., Embabi, N. S., Ashour, M. M., Edwards, R. L., Cheng, H., Cowart, J. B., & Dabous, A. A. (2003). Quaternary environmental change in the Western Desert of Egypt: Evidence from cave speleothems, spring tufas and playa sediments. *Zeitschrift Fur Geomorphologie N.f. Suppl.*, 131, 59–87.
- Bubbenzer, O., Embabi, N. S., & Ashour, M. M. (2020). Sand seas and dune fields of Egypt. *Geosciences*, 10, 101. <https://doi.org/10.3390/geosciences10030101>
- Bullard, J. E., Harrison, S. P., Baddock, M. C., Drake, N., Gill, T. E., McTainsh, G., & Sun, Y. (2011). Preferential dust sources: A geomorphological classification designed for use in global dust-cycle models. *Journal of Geophysical Research*, 116(4), F04034.
- Brookes, I. (1993). Geomorphology and Quaternary geology of the Dakhla oasis region, Egypt. *Quaternary Science Reviews*, 12, 529–553.
- Butzer, K. W. (1959). Environment and human ecology in Egypt during Predynastic and Early Dynastic times. *Bulletin De La Société De Géographie D'égypte*, 32, 43–87.
- Butzer, K. W. (1997). Late Quaternary problems of the Egyptian Nile: Stratigraphy, environments, prehistory. *Paléorient*, 23(2), 151–173.
- Butzer, K. W., & Hansen, C. L. (1968). *Desert and river in Nubia* (p. 256). University of Wisconsin Press.
- Calvert, S. E., & Fontugne, M. R. (2001). On the Late Pleistocene-Holocene sapropel record of climatic and oceanographic variability in the eastern Mediterranean. *Paleoceanography*, 16(1), 78–94.
- Carrion, J. S., & Van Geel, B. (1999). Fine resolution Upper Weichselian and Holocene Palynological record from Navarrés (Valencia, Spain) and a discussion about factors of Mediterranean forest succession. *Review of Palaeobotany and Palynology*, 106, 209–236.
- Casanova, J., & Hillaire-Marcel, C. (1991). Late Holocene hydrological history of Lake Tanganyika, East Africa, from isotopic data on fossil stromatolites. *Palaeogeography, Palaeoclimatology, Palaeoecology*, 91, 35–42
- Cerling, T. E. (1984). The stable isotopic composition of soil carbonate and its relation to climate. *Earth Planetary Science Letters*, 71, 229–240.
- Cerling, T. E., & Harris, J. M. (1999). Carbon isotope fractionation between diet and bioapatite in ungulate mammals and implications for ecological and paleoecological studies. *Oecologia*, 120, 347–363.
- Cerling, T. E., Harris, J. M., MacFadden, B. J., Leakey, M. G., Quade, J., Eisenmann, V., & Ehleringer, J. R. (1997). Global vegetation change through the Miocene-Pliocene boundary. *Nature*, 389, 153–158.
- Chase, B. (2009). Evaluating the use of dune sediments as a proxy for palaeo-aridity: A southern African case study. *Earth-Science Reviews*, 93, 31–45.
- Cheddadi, R., & Rossignol-Strick, M. (1995). Improved preservation of organic matter and pollen in eastern Mediterranean sapropels. *Paleoceanography*, 10, 301–309.
- Chen, Z., & Stanley, D. J. (1993). Alluvial stiff muds (Late Pleistocene) underlying the lower Nile Delta plain: Petrology, stratigraphy and origin. *Journal of Coastal Research*, 9(2), 539–576.
- Chen, Z., Warne, A. G., & Stanley, D. J. (1992). Late Quaternary evolution of the North western Nile Delta between the Rosetta Promontory and Alexandria, Egypt. *Journal of Coastal Research*, 18(3), 527–561.
- Churcher, C. S., Kleindienst, M. R., & Schwarcz, H. P. (1999). Faunal remains from a Middle Pleistocene lacustrine marl in Dakhleh Oasis, Egypt: Palaeoenvironmental reconstructions. *Palaeogeography, Palaeoclimatology, Palaeoecology*, 154, 301–312.
- Churcher, C. S., Kleindienst, M. R., Wiseman, M. F., & McDonald, M. M. A. (1997). Quaternary faunas of Dakhla Oasis, Western Desert of Egypt. Abstracts of the Second Dakhleh Oasis Project Research Seminar, June 16–20, Royal Ontario Museum and University of Toronto, Toronto.
- Cita, M. B., Vergnaud-Grazzini, C., Robert, C., Chamley, H., Ciaranfi, N., & d'Onofrio, S. (1977). Palaeoclimatic record of a long deep-sea core from the eastern Mediterranean. *Quaternary Research*, 8, 205–235.
- Coleman, J. M., & Gagliano, S. M. (1964). Cyclic sedimentation in the Mississippi River Deltaic Plain. *Transactions. Gulf Coast Association of Geological Societies*, 14, 67–80.
- Collins, J. A., Prange, M., Caley, T., Gimeno, L., Beckmann, B., Mulitza, S., Skonieczny, Ch., Roche, D., & Schefuß, E. (2017). Rapid termination of the African Humid Period triggered by northern high-latitude cooling. *Nature Communications*, 8, 1372. <https://doi.org/10.1038/s41467-017-01454-y>
- Coutellier, V., & Stanley, D. J. (1987). Late Quaternary stratigraphy and paleogeography of the eastern Nile Delta shelf. *Marine Geology*, 77, 257–275.
- Crombie, M. K., Arvidson, R. E., Sturchio, N. C., El Alfy, Z. E., & Abu Zeid, K. (1997). Age and isotopic constraints on Pleistocene pluvial episodes in the Western Desert, Egypt. *Palaeogeography, Palaeoclimatology, Palaeoecology*, 130, 337–355.
- Crouvi, O., Schepanski, K., Amit, R., Gillespie, A. R., & Enzel, Y. (2012). Multiple dust sources in the Sahara Desert: The importance of sand dunes. *Geophysical Research Letters*, 39, L13401.
- Cullen, H. M., De Menocal, P. B., Hemming, S., Hemming, G., Brown, F. H., Guilderson, T., & Sirocko, F. (2000). Climate change and the collapse of the Akkadian empire: Evidence from the deep sea. *Geology*, 28, 379–382. [https://doi.org/10.1130/0091-7613\(2000\)28%3c379:CCATCO%3e2.0.CO;2](https://doi.org/10.1130/0091-7613(2000)28%3c379:CCATCO%3e2.0.CO;2)
- Dabous, A. A., & Osmond, J. K. (2000). U/Th isotopic study of speleothems from the Wadi Sannur Cavern, Eastern Desert of Egypt. *Carbonates and Evaporites*, 15, 1–6.
- Dansgaard, W., Clausen, H., Gundestrup, N., Johnsen, S., & Rygner, C. (1985). Dating and climatic interpretation of two deep Greenland ice cores. In C. C. J. Langway (Ed.), *Greenland ice core: Geophysics, geochemistry, and the environment*. American Geophysical Union.
- Dawood, Y. (2001). Uranium-series disequilibrium dating of secondary uranium ore from the south Eastern Desert of Egypt. *Applied Radiation and Isotopes*, 55, 881–887.
- De Heinzelin, J. (1968). Geological history of the Nile Valley in Nubia. In I. F. Wendorf (Ed.), *The Prehistory of Nubia* (pp. 19–55). Southern Methodist University, Dallas.
- Deino, A. L., Behrensmeier, A. K., Brooks, A. S., Yellen, J. E., Sharp, W. D., & Potts, R. (2018). Chronology of the Acheulean to Middle stone age transition in eastern Africa. *Science*, 360(6384), 95–98.
- De Lange, G. J., Thomson, J., Reitz, A., Slomp, C. P., Speranza Principato, M., Erba, E., & Corselli, C. (2008). Synchronous basin-wide formation and redox-controlled preservation of a Mediterranean sapropel. *Nature Geoscience*, 1(9), 606–610.
- De Menocal, P. B. (2004). African climate change and faunal evolution during the Pliocene-Pleistocene. *Earth and Planetary Science Letters*, 220, 3–24.
- De Menocal, P. B., Ortiz, J., Guilderson, T., & Sarnthein, M. (2000). Coherent high- and low-latitude climate variability during the Holocene warm period. *Science*, 288, 2198–2202.

- De Menocal, P. B., & Tierney, J. E. (2012). Green Sahara: African humid periods paced by Earth's orbital changes. *Nature Education Knowledge*, 3(10), 12.
- Donner, J., Ashour, M. M., Brook, G. A., & Embabi, N. S. (2015). The quaternary history of the Western Desert of Egypt as recorded in the Abu El-Egl playa. *Bulletin De La Société De Géographie d Egypte*, 88, 1–18.
- Ducassou, E., Migeon, B., Mulder, T., Murat, A., Capotondi, L., Bernasconi, S. M., & Mdscl, J. (2009). Evolution of the Nile deep-sea turbidite system during the Late Quaternary: Influence of climate change on fan sedimentation. *Sedimentology*, 56, 2061–2090. <https://doi.org/10.1111/j.1365-3091.2009.01070.x>
- Eakin, M., & Grottoli, A. (2006). Coral reef records of past climatic change. In *Coral reefs and climate change: Science and management*. Coastal and Estuarine Studies. The American Geophysical Union (Vol. 61, pp. 33–54). <https://doi.org/10.1029/61CE04>
- Ehleringer, J. R. (2005). The influence of atmospheric CO₂, temperature, and water on the abundance of C3/C4 taxa. In I. Baldwin et al. (Eds.), *A history of atmospheric CO₂ and its effects on plants, animals, and ecosystems*. Ecological Studies (Analysis and Synthesis) (Vol. 177). Springer. https://doi.org/10.1007/0-387-27048-5_10
- Ehrmann, W., Schmied, G., Beuscher, G., Beuscher, S., & Kruger, S. (2017a). Intensity of African humid periods estimated from Saharan dust fluxes. *PLoS ONE*, 12(1), e0170989. <https://doi.org/10.1371/journal.pone.0170989>
- Ehrmann, W., Seidel, M., & Schmiedl, G. (2013). Dynamics of Late Quaternary North African humid periods documented in the clay mineral record of central Aegean Sea sediments. *Global and Planetary Change*, 107, 186–195.
- El-Akkad, S., & Dardir, A. (1966). Geology of the Red Sea coast between Ras Shagra and Marsa Alam with short notes on the exploratory work at Gebel El-Rusas lead-zinc deposits. *Geologic Survey Egypt*, 35, 1–67.
- El-Asmar, H. M. (1986). *Lithological and mineralogical investigation of the subsurface Quaternary succession in the Nile Delta region, Egypt* (M.Sc. Thesis). Faculty of Science, El Mansoura University Egypt.
- El-Asmar, H. M. (1991). *Old shorelines of the Mediterranean coastal zone of Egypt in relation with sea level changes* (Ph.D. thesis). Faculty of Science, El Mansoura University, Egypt.
- El-Asmar, H. M. (1994). Aeolianite sedimentation along the north-western coast of Egypt: Evidence for Middle to Late Quaternary aridity. *Quaternary Science Reviews*, 13, 699–708.
- El-Asmar, H. M. (1997). Quaternary isotope stratigraphy and paleoclimate of coral reef terraces, Gulf of Aqaba, south Sinai, Egypt. *Quaternary Science Reviews*, 16, 911–924.
- El-Asmar, H. M. (1998). Middle and Late Quaternary palaeoclimatic evolution, northern Mediterranean coast of Egypt. In A. S. Al-Shrhan, K. W. Glennie, G. L. Whittle, & C. G. S. C. Kendall (Eds.), *Quaternary deserts and climatic changes* (pp. 261–271). Balkema.
- El-Asmar, H. M. (2000). Optical stimulated luminescence age estimates of Quaternary aeolianites and paleosols, NW coast, Egypt. *Sedimentology of Egypt*, 8, 255–264.
- El-Asmar, H. M., & Abdel-Fattah, Z. A. (2000). Lithostratigraphy and facies development of the Neogene-Quaternary succession in the Mersa Alam area Red Sea coastal plain, Egypt. *Neues Jahrbuch für Geologie und Paläontologie, Abhandlungen*, 217(3), 397–431.
- El-Asmar, H. M., Ahmed, M. H., Taha, M. M. N., & Assal, E. M. (2012). Human impacts on geological and cultural heritage in the coastal zone west of Alexandria to Al-Alamein, Egypt. *Geoheritage*, 4, 263–274. <https://doi.org/10.1007/s12371-012-0066-0>
- El-Asmar, H. M., & Attia, G. (1996). Diagenetic trends in Quaternary coral reef terraces, Ras Mohamed-Sharm El-Sheikh coast, southern Sinai, Egypt. *Sedimentology of Egypt*, 4, 19–31.
- El-Asmar, H. M., & Gheith, A. M. (1995). Stable isotope stratigraphy and paleoclimatology of the offshore subsurface Quaternary sediments, Nile Delta, Egypt. *Sedimentology of Egypt*, 3, 39–49.
- El-Asmar, H. M., Taha, M. M. N., El-Kafrawy, S. B., & El-Sorogy, A. S. (2015). Control of Late Holocene Geo-processes on the sustainable development plans of the Tineh Plain, NW Sinai coast, Egypt. *Journal of Coastal Conservations*, 19, 141–156. <https://doi.org/10.1007/s11852-015-0377-9>
- El-Asmar, H. M., & Wood, P. (2000). Quaternary shoreline development: The Northwestern coast of Egypt. *Quaternary Science Review*, 19, 1137–1149.
- El-Bassiouni, A. E., & Ayyad, S. N. (1986). Quaternary Foraminifera of El-Temsah well-2, offshore Nile Delta, Egypt. *El Mansoura Science Bulletin*, 13(1), 133–188.
- El-Bastawesy, M., Cherif, O. H., & Sultan, M. (2017). The geomorphological evidences of subsidence in the Nile Delta: Analysis of high resolution topographic DEM and multi-temporal satellite images. *Journal of African Earth Sciences*, 136, 252–261.
- El-Baz, F., & Prestel, D. (1982). Coatings on sand grains from Southwestern Egypt. In F. el Baz & T. Maxwell (Eds.), *Desert landforms of Southwest Egypt: A basis for comparison with Mars* (pp. 175–188). NASA.
- El-Moursi, M., Hoang, C. T., El Fayoumi, I. F., Hegab, O., & Faure, M. (1994). Pleistocene evolution of the Red Sea coastal plain, Egypt: Evidence from uranium-series dating of emerged reef terraces. *Quaternary Science Reviews*, 13, 345–359.
- El-Shahat, A., & Kora, M. A. (1986). Size analysis and paleoenvironments of the subsurface sediments, west of Nile Delta. *El Mansoura Science Bulletin*, 13(2), 185–207.
- Embabi, N. S. (1999). Playas of the Western Desert, Egypt. *Annales Academiae Scientiarum Fennicae, Geologica-Geographica*, 160, 5–47.
- Embabi, N. S. (2018). Landscapes and landforms of Egypt: Landforms and evolution. *World Geomorphological Landscapes*, 336. <https://doi.org/10.1007/978-3-319-65661-8>
- Emeis, K. C., Sakamoto, T., Wehausen, R., & Brumsack, H. J. (2000). The sapropel record of the eastern Mediterranean Sea results of ocean drilling program Leg 160. *Palaeogeography, Palaeoclimatology, Palaeoecology*, 158, 371–395.
- Engelstaedter, S., Tegen, I., & Washington, R. (2006). North African dust emissions and transport. *Earth Science Reviews*, 79, 73–100.
- Evans, P. (1971). Towards a Pleistocene time-scale. In: W. B. Harland, H. Francis, & P. Evans (Eds.), *The Phanerozoic time-scale, a supplement. Part 2* (pp. 123–356). Geological Society of London.
- Felis, T., & Patzold, J. (2004). Climate reconstructions from annually banded corals. In M. Shiyomi, et al. (Eds.), *Global environmental change in the ocean and on land* (pp. 205–227). TERRAPUB.
- Fielding, L., Najman, Y., Millar, I., Butterworth, P., Ando, S., Padoan, M., Barfod, D., & Kneller, B. C. (2017). A detrital record of the Nile River and its catchment. *Journal of Geological Society*, 174, 301–317.
- Fielding, L., Najman, Y., Millar, I., Butterworth, P., Garzanti, E., & Kneller, B. C. (2014). Determining the paleodrainage of the Nile River from a provenance study of the Nile Delta cone sediments. American Geophysical Union, Fall Meeting 2014, abstract id. EP21D-3556.
- Fielding, L., Najman, Y., Millar, I., Butterworth, P., Garzanti, E., Vezzolid, G., Barfod, D., & Kneller, B. C. (2018). The initiation and evolution of the River Nile. *Earth and Planetary Science Letters*, 489, 166–178.
- Filippidi, A., & De Lange, G. J. (2019). Eastern Mediterranean deep water formation during Sapropel S1: A reconstruction using geochemical records along a bathymetric transect in the Adriatic outflow region. *Paleoceanography and Paleoclimatology*, 34, 409–429. <https://doi.org/10.1029/2018PA003459>

- Flannery, J. A., & Poore, R. Z. (2013). Sr/Ca proxy sea-surface temperature reconstructions from modern and Holocene *Montastraea faveolata* specimens from the dry Tortugas National Park, Florida, U.S.A. *Journal of Coastal Research SI*, 63, 20–31.
- Fleitmann, D., Burns, S. J., Pekala, M., Mangini, A., Al-Subbary, A., Al-Aowah, M., Kramers, J., & Matter, A. (2011). Holocene and Pleistocene pluvial periods in Yemen, southern Arabia. *Quaternary Science Reviews*, 30, 783–787.
- Flower, R. J., Keatings, K., Hamdan, M., Hassan, F. A., Boyle, J. F., Yamada, K., & Yasuda, Y. (2012). The structure and significance of Early Holocene laminated sediments in the Faiyum Depression (Egypt) with special reference to diatoms. *Diatom Research*, 27, 127–140.
- Flower, R. J., Keatings, K., Hamdan, M. A., Yamada, N., & Yasuda, Y. (2018). Palaeolimnological evidence for the development of an early Holocene lake in the Faiyum Depression, Egypt. In G. Trafford, J. Tassie, J. van Wetering, & O. El Daly (Eds.), *A river runs through it: Studies in honour of Prof. Fekri A. Hassan* (pp. 8–54). Golden House Publications.
- Foucault, A., & Mélières, F. (2000). Palaeoclimatic cyclicity in central Mediterranean Pliocene sediments: The mineralogical signal. *Palaeogeography, Palaeoclimatology, Palaeoecology*, 158, 311–323.
- Gasse, F. (2000). Hydrological changes in the African tropics since the Last Glacial Maximum. *Quaternary Science Reviews*, 19, 189–211. [https://doi.org/10.1016/S0277-3791\(99\)00061-X](https://doi.org/10.1016/S0277-3791(99)00061-X)
- Gheith, A. M. (1985). Sedimentological and mineralogical investigations of the subsurface Quaternary succession of Tamsah offshore well-2, Nile Delta Coast. *Egyptian Journal of Geology*, 29(1–2), 20–50.
- Ghilrardi, M., Tristant, Y., & Boraik, M. (2012). Nile River evolution in Upper Egypt during the Holocene: Palaeoenvironmental implications for the Pharaonic sites of Karnak and Coptos. *Geomorphologie: Relief, Processus, Environment*, 18(1), 7–22. <https://doi.org/10.4000/geomorphologie.9685>
- Gibbard, P. L., & Hughes, P. D. (2021). Terrestrial stratigraphical division in the Quaternary and its correlation. *Journal of the Geological Society*, 178. <https://doi.org/10.1144/jgs2020-134>
- González, C., & Dupont, L. M. (2009). Coastal vegetation evidence for sea level changes associated with Heinrich Events. *PAGES News*, 17(2).
- Goudie, A. S., & Middleton, N. J. (2001). Saharan dust storms: Nature and consequences. *Earth Science Reviews*, 56, 179–204.
- Grant, K. M., Grimm, R., Mikolajewicz, U., Matino, G., Ziegler, M., & Rohling, E. J. (2016). The timing of Mediterranean sapropel deposition relative to insolation, sea-level and African monsoon changes. *Quaternary Science Reviews*, 140, 125–141.
- Guiou, C., & Thomas, A. J. (1996). Saharan aerosols: From the soil to the ocean. In S. Guerzoni, & R. Chester (Eds.), *The Impact of desert dust across the Mediterranean* (pp. 207–216). Kluwer Academy.
- Gvirtzman, G., & Buchbinder, B. (1978). Recent and Pleistocene coral reefs and coastal sediments of the Gulf of Aqaba. In *10th International Sedimentological Congress*, Jerusalem, Post Congress Excursion, Y4 (pp. 163–191).
- Gvirtzman, G., Kronfeld, J., & Buchbinder, B. (1992). Dated coral reefs of southern Sinai (Red Sea) and their implication to Late Quaternary sea levels. *Marine Geology*, 108, 29–37.
- Hallberg, R. (2004). Formation of Eastern Mediterranean sapropels—What can be learnt from Baltic Sea sapropels? In *Geochemical investigations in earth and space science: A tribute to Isaac R. Kaplan*. The Geochemical Society (Vol. 9, pp. 425–439).
- Hamdan, A. M. (2013). Hydrogeological and hydrochemical assessment of the Quaternary aquifer south Qena City, Upper Egypt. *Earth Science Research*, 2(2). <https://doi.org/10.5539/esr.v2n2p11>
- Hamdan, M. A. (1993). *Pliocene and quaternary sediments and their relationship to the geological evolution of River Nile at lower Egypt* (PhD thesis). Cairo University.
- Hamdan, M. A. (2000). Quaternary travertines of Wadis Abu Had-dib area Eastern Desert, Egypt: Paleoenvironment through field, sedimentology, age, and isotopic study. *Sedimentology of Egypt*, 8, 49–62.
- Hamdan, M. A. (2003a). Late Quaternary geology and geoarchaeology of Kafr Hassan Dawood, East Delta. In Z. Hawass, & L. Pinch Brock (Eds.), *Egyptology at the Dawn of the Twenty-first Century: Proceedings of the Eighth International Congress of Egyptologist* (Vol. 1, pp. 221–228). The American University in Cairo Press.
- Hamdan, M. A. (2003b). Stable isotope and geochemistry of some travertine deposits of southern Egypt and their paleoclimatic and paleoenvironmental implications. *Sedimentology of Egypt*, 11, 43–61.
- Hamdan, M. A., & Brook, G. A. (2015). Timing and characteristics of Late Pleistocene and Holocene wetter periods in the Eastern Desert and Sinai of Egypt, based on 14C dating and stable isotope analysis of spring tufa deposits. *Quaternary Science Reviews*, 130, 168–188.
- Hamdan, M. A., Flower, R. J., Hassan, F. A., & Hassan, S. M. (2020). The Holocene history of the Faiyum Lake (Egypt) based on sediment characteristics, diatoms and ostracods contents. *Journal of Great Lakes Research*, 46, 456–475.
- Hamdan, M. A., & Hassan, F. A. (2020). Quaternary of Egypt. In Z. Hamimi, A. El-Barkooky, J. M. Frías, H. Fritz, & Y. Abd El-Rahman (Eds.), *The geology of Egypt* (pp. 445–493).
- Hamdan, M. A., Hassan, F. A., Flower, R. J., Leroy, S. A. G., Shallaly, N. A., & Flynn, A. (2019). Source of Nile sediments in the floodplain at Saqqara inferred from mineralogical, geochemical, and pollen data, and their palaeoclimatic and geoarchaeological significance. *Quaternary International*, 50, 272–288.
- Hamdan, M. A., Ibrahim, M. I. A., Shiha, M. A., Flower, R. J., Hassan, F. A., & Eltelet, S. A. M. (2016). An exploratory Early and Middle Holocene sedimentary record with palynofossils and diatoms from Faiyum Lake, Egypt. *Quaternary International*, 410, 30–42.
- Hassan, F. A. (1976). Heavy minerals and the evolution of the modern Nile. *Quaternary Research*, 6, 425–444.
- Hassan, F. A. (1981). Historical Nile floods and their implications for climatic change. *Science*, 212, 1142–1144.
- Hassan, F. A. (1986). Holocene lakes and prehistoric settlements of the Western Faiyum, Egypt. *Journal of Archaeological Science*, 13, 483–501.
- Hassan, F. A. (2007). Extreme Nile floods and famines in Medieval Egypt (AD 930–1500) and their climatic implications. *Quaternary International*, 173(174), 101–112.
- Hassan, F. A. (2010). Climate change, Nile floods and riparia. In: Hermon, Ella (Ed.), *Riparia dans l'empire romain pour la définition du concept* (pp. 131–152). BAR International S2066.
- Hassan, F. A., Hamdan, M. A., Flower, R. J., Shallaly, N. A., & Ebrahem, E. (2017). Holocene alluvial history and archaeological significance of the Nile floodplain in the Saqqara-Memphis region. *Egypt. Quaternary Science Reviews*, 176, 51–70.
- Haynes, C. V. (1982). Great Sand Sea and Selima sand sheet. *Geomorphology and desertification. Science*, 217, 629–632.
- Hays, J. D., Imbrie, J., & Shackleton, N. J. (1976). Variations in the Earth's orbit: Pacemaker of the ice ages. *Science*, 194, 1121–1132. <https://doi.org/10.1126/science.194.4270.1121>
- Hearty, P. J. (1986). An inventory of Last Interglacial age deposits from the Mediterranean basin: A study in isoleucine epimerization and U/Th dating. *Zeitschrift Fur Geomorphologie*, 62, 51–69.
- Hearty, P. J. (1987). New data on the Pleistocene of Mallorca. *Quaternary Science Reviews*, 6, 245–257.

- Hearty, P. J. (1997). Boulder deposits from large waves during the Last Interglaciation on North Eleuthera, Bahamas. *Quaternary Research*, 48, 326–338.
- Hearty, P. J. (2002). Revision of the Late Pleistocene stratigraphy of Bermuda. *Sedimentary Geology*, 153, 1–21.
- Hearty, P. J., Hollin, J. T., Neumann, A. C., O'Leary, M. J., Mc, M., & Culloch, M. (2007). Global sea-level fluctuations during the Last Interglaciation (MIS 5e). *Quaternary Science Reviews*, 26, 2090–2112.
- Hearty, P. J., & Neumann, A. C. (2001). Rapid sea level and climate change at the close of the Last Interglaciation (MIS 5e): Evidence from the Bahama Islands. *Quaternary Science Reviews*, 20, 1881–1895.
- Hegab, O. A. (1989). The Nile alluvium at Qena, upper Egypt. *Faculty of Science, Bulletin Mansoura University*, 16(1), 73–94.
- Hegab, O. A., & El-Asmar, H. M. (1995). Last interglacial stratigraphy in the Burg El-Arab region northwestern coast of Egypt. *Quaternary International*, 29(30), 23–30.
- Herzschuh, U. (2007). Reliability of pollen ratios for environmental reconstructions in the Tibetan Plateau. *Journal of Biogeography*, 34, 1265–1273.
- Hilgen, F. J. (1991). Astronomical calibration of Gauss to Matuyama sapropels in the Mediterranean and implications for the geomagnetic polarity timescale. *Earth Planetary Science Letters*, 104, 226–244.
- Hilgen, F. J., Lourens, L. J., Berger, A., & Loutre, M. F. (1993). Evaluation of the astronomically calibrated time scale for the Late Pliocene and earliest Pleistocene. *Paleoceanography*, 8, 549–565.
- Hill, C. L. (1993). Sedimentology of Pleistocene deposits associated with Middle Paleolithic sites in Bir Tarfawi and Bir Sahara east. In F. Wendorf, R. Schild, & A. Close (Eds.), *Egypt during the late interglacial* (pp. 66–105). Plenum.
- Hill, C. L., & Schild, R. (2017). Pleistocene deposits in southern Egyptian Sahara: Lithostratigraphic relationships of sediments and landscape dynamics at Bir Tarfawi. *Studia Quaternaria*, 34(1), 23–38. <https://doi.org/10.1515/squa-2017-0002>
- Hoang, C. T., & Taviani, M. (1988). $^{230}\text{Th}/^{234}\text{U}$ ages of raised coral reefs from tectonically uplifted Red Sea islands. *Tectonophysics*, 150(1), 251. [https://doi.org/10.1016/0040-1951\(88\)90306-X](https://doi.org/10.1016/0040-1951(88)90306-X)
- Hoang, C. T., & Taviani, M. (1991). Stratigraphic and tectonic implications of uranium-series-dated coral reefs from uplifted Red Sea islands. *Quaternary Research*, 35, 264–273.
- Hoffmann, D. L., Rogerson, M., Spötl, C., Luetscher, M., Vance, D., Osborne, A. H., Fello, N. M., & Moseley, G. E. (2016). Timing and causes of North African wet phases during the last glacial period and implications for modern human migration. *Scientific Reports*, 6, 36367. <https://doi.org/10.1038/srep36367>
- Imbrie, J., Hays, J. D., Martinson, D. G., McIntyr, A., Mix, A. C., Morley, J. J., Pisias, N. G., Prell, W. L., & Shackleton, N. J. (1984). The orbital theory of Pleistocene climate: Support from a revised chronology of the marine $\delta^{18}\text{O}$ record. In A. Berger, J. Imbrie, G. Hays, G. Kukla, & B. Saltzman (Eds.), *Milankovitch and climate* (pp. 269–306). Reidel.
- Imbrie, J., & Imbrie, J. Z. (1980). Modeling the climatic response to orbital variations. *Nature*, 4434, 943–953.
- Issawi, B. (1968). The geology of Kurkur Dungul area. General Egyptian organization for geological research and mining. *Geological Survey Paper*, 46, 1–102.
- Issawi, B. (1978). Quaternary geology of Bir Sahara, western desert, Egypt. *Annals Geological Survey Egypt*, 8, 29–304.
- Issawi, B., Francis, M. H., Youssef, E. A. A., & Osman, R. A. (2009). *The Phanerozoic geology of Egypt, a geodynamic approach* (2nd ed., p. 589). The Egyptian Mineral Resources Authority, Spec. Publ. No. 81.
- Issawi, B., & McCauley, J. F. (1992). The Cenozoic rivers of Egypt: The Nile problem. In B. Adams & R. Friedman (Eds.), *The followers of Horus* (pp. 1–18). Oxbow Press.
- Jaeschke, A., Thienemann, M., Schefuß, E., Urban, J., Schäbitz, F., Wagner, B., & Rethemeyer, J. (2020). Holocene hydroclimate variability and vegetation response in the Ethiopian highlands (Lake Dendi). *Frontiers in Earth Science*, 8, 585770. <https://doi.org/10.3389/feart.2020.585770>
- Jimenez, G. (2014). *Travertine from Egypt's Western Desert: A terrestrial record of North African paleohydrology and paleoclimate during the Late Pleistocene* [Master's thesis, University of New Mexico] (p. 95).
- Kaniewski, D., Paulissen, E., Van Campo, E., Al- Maqdissi, M., Bretschneider, J., & Van Lerberghe, K. (2008). Middle East coastal ecosystem response to Middle-to-Late Holocene abrupt climate changes. *Proceedings of the National Academy of Sciences of the United States of America*, 105, 13941–13946. <https://doi.org/10.1073/pnas.0803533105>
- Kele, S., Sallam, E., Capezzuoli, E., Rogerson, M., Wanas, H., Shen, C. C., Mahjoor, A. L., Yu, T. L., Andrew Schauer, A., & Huntington, K. W. (2021). Were springline carbonates in the Kurkur-Dungul area (Southern Egypt) deposited during glacial periods? *Journal of the Geological Society*, 178(3), 147. <https://doi.org/10.1144/jgs2020-147>
- Khalil, S. M., & McClay, K. R. (2009). Structural control on syn-rift sedimentation northwestern Red Sea margin, Egypt. *Marine and Petroleum Geology*, 26, 1018–1034.
- Kholeif, S. E. A. (2004). Palynology and palaeovegetation reconstruction in Late Quaternary sediments of the southern Suez Isthmus, Egypt. *Journal of African Earth Sciences*, 40, 31–47.
- Kholeif, S. E. A. (2010). Holocene paleoenvironmental change in inner continental shelf sediments, Southeastern Mediterranean, Egypt. *Journal of African Earth Sciences*, 57, 143–153.
- Kholeif, S. E. A., & Mudie, P. J. (2009). Palynological records of climate and oceanic conditions in the Late Pleistocene and Holocene of the Nile cone, southeastern Mediterranean, Egypt. *Palynology*, 33(1), 1–24. <https://doi.org/10.1080/01916122.2009.9989664>
- Kidd, R. B., Cita, M. B., William, B., & Ryan, F. (1978). Stratigraphy of Eastern Mediterranean sapropel sequences recovered during DSDP LEG 42A and their paleo environmental signature. In *Initial reports of the Deep Sea Drilling Project* (Vol. 42, No. 1). <https://doi.org/10.2973/dsdp.proc.42-1.113-1>
- Kieniewicz, J. M., & Smith, J. R. (2007). Hydrologic and climatic implications of stable isotope and minor element analyses of authigenic calcite silts and gastropod shells from a mid-Pleistocene pluvial lake, Western Desert, Egypt. *Quaternary Research*, 68, 341–344.
- Kieniewicz, J. M., & Smith, J. R. (2009). Paleoenvironmental reconstruction and water balance of a mid-Pleistocene pluvial lake, Dakhleh Oasis, Egypt. *Bulletin Geological Society of America*, 121, 1154–1171.
- Kitchen, K. A. (1991). The chronology of ancient Egypt. *World Archaeology*, 23, 201–208.
- Kleindienst, M. R., Blackwell, B. A. B., Skinner, A. R., Churcher, C. S., Kieniewicz, J. M., Smith, J. R., Wise, N. L., Long, R. A., Deely, A. E., Blickstein, J. I. B., Chen, K. K. L., Huang, A., & Kim, M. K. D. (2016). Assessing long-term habitability at an eastern Sahara oasis: ESR dating of molluscs and herbivore teeth at Dakhleh Oasis, Egypt. *Quaternary International*, 408, 106–120.
- Kohfeld, K. E., & Harrison, S. P. (2001). DIRTMAP: The geological record of dust. *Earth Science Reviews*, 54(1–3), 81–114.
- Konijnendijk, T. Y. M., Ziegler, M., & Lourens, L. J. (2014). Chronological constraints on Pleistocene sapropel depositions from

- high-resolution geochemical records of ODP Sites 967 and 968. *Newsletters on Stratigraphy*, 47(3), 263–282.
- Kora, M. A., Ayyad, S. N., & El-Desouky, H. (2013). Microfacies and environmental interpretation of the of the Pliocene-Pleistocene carbonates in the Marsa Alam Area, Red Sea coastal plain, Egypt. *Journal of Environmental Sciences*, 42(1), 155–182.
- Krom, M. D., Stanley, D. J., Cliff, R. A., & Woodward, J. C. (2002). Nile River sediment fluctuations over the past 7000 yr and their key role in sapropel development. *Geology*, 30, 71–74.
- Kroon, D., Alexander, I., Little, M., Lourens, L. J., Matthewson, A., Robertson, A. H. F., & Sakamoto, T. (1998). Oxygen isotope and sapropel stratigraphy in the Eastern Mediterranean during the last 3.2 million years. In A. H. F. Robertson, K.-C. Emeis, C. Richter, & A. Camerlenghi (Eds.), *Proceedings of the Ocean Drilling Program. Scientific results* (Vol. 160, pp. 181–189).
- Kutzbach, J. E., Chen, G., Cheng, H., Edwards, R., & Liu, Z. (2013). Potential role of winter rainfall in explaining increased moisture in the Mediterranean and Middle East during periods of maximum orbitally-forced insolation seasonality. *Climate Dynamics*. <https://doi.org/10.1007/s00382-013-1692-1>
- Lambert, F., Bigler, M., Steffensen, J. P., Hutterli, M., & Fischer, H. (2012). Centennial mineral dust variability in high-resolution ice-core data from Dome C, Antarctica. *Climate of the past*, 8, 609–623. <https://doi.org/10.5194/cp-8-609-2012>
- Larrasoana, J. C. (2012). A northeast Saharan perspective on environmental variability in North Africa and its implications for modern human origins. In J. J. Hublin, & S. P. McPherron (Eds.), *Modern origins: A North African perspective*. Vertebrate paleobiology and paleoanthropology (pp. 17–34). Springer.
- Larrasoana, J. C., Roberts, A. P., & Rohling, E. J. (2013). Dynamics of Green Sahara periods and their role in Hominin evolution. *PLoS ONE*, 8(10), 76514. <https://doi.org/10.1371/journal.pone.0076514>
- Larrasoana, J. C., Roberts, A. P., Rohling, E. J., Winkhofer, M., & Wehausen, R. (2003). Three million years of monsoon variability over the northern Sahara. *Climate Dynamics*, 21, 689–698.
- Laskar, J., Robutel, P., Joutel, F., Gastineau, M., Correia, A. C. M., & Levrard, B. (2004). A long term numerical solution for the insolation quantities of the Earth. *Astronomy and Astrophysics*, 428, 261–285.
- Lattanzi, F. A. (2010). C3/C4 grasslands and climate change. In H. Schnyder, J. Isselstein, F. Taube, et al. (Eds.), *Grassland in a changing world*. Grassland science in Europe (Vol. 15, pp. 3–15).
- Lauchstedt, A., John, M., Pandolfi, J. M., & Kiessling, W. (2017). Towards a new paleotemperature proxy from reef coral occurrences. *Nature Scientific Reports*, 7, 10461. <https://doi.org/10.1038/s41598-017-10961-3>
- Leroy, S. A. (1992). Palynological evidence of *Azolla nilotica* Dec. in recent Holocene of the eastern Nile Delta and palaeoenvironment. *Vegetation History and Archaeobotany*, 1, 43–52.
- Li, Y., Zhou, L., & Cui, H. (2008). Pollen indicators of human activity. *Chinese Science Bulletin*, 53, 1281.
- Lisiecki, L., & Raymo, M. R. (2005). A Pliocene-Pleistocene stack of 57 globally distributed benthic $\delta^{18}\text{O}$ records. *Paleoceanography*, 20, PA1003. <https://doi.org/10.1029/2004PA001071>
- Lourens, L. J., Antonarakou, A., Hilgen, F. J., Van Hoof, A. A. M., Vergnaud-Grazzini, C., & Zachariasse, W. J. (1996). Evaluation of the Plio-Pleistocene astronomical timescale. *Paleoceanography*, 11, 391–413.
- Lourens, L. J., Wehausen, R., & Brumsack, H. J. (2001). Geological constraints on tidal dissipation and dynamical ellipticity of the Earth over the past three million years. *Nature*, 409, 1029–1033.
- Maldonado, A., & Stanley, D. J. (1981). Clay mineral distribution patterns as influenced by depositional processes in the South eastern Levantine Sea. *Sedimentology*, 28, 21–32.
- Mangini, A., & Schlosser, P. (1986). The formation of Eastern Mediterranean sapropels. *Marine Geology*, 72, 115–124.
- Marks, L., Salem, A., Welc, F., Nitychoruk, J., Chen, Z., Blaauw, M., Zalat, A., Majecka, A., Szymanek, M., Chodyka, M., Tofczko-Pasek, A., Sun, Q., Zhao, X., & Jiang, J. (2018). Holocene lake sediments from the Faiyum Oasis in Egypt: A record of environmental and climate change. *Boreas*, 47, 62–79.
- Marriner, N., Flaux, C., Morhangem, C., & Kaniewski, D. (2012). Nile Delta's sinking past: Quantifiable links with Holocene compaction and climate-driven changes in sediment supply? *Geology*, 40(12), 1083–1086. <https://doi.org/10.1130/G33209.1>
- Marshall, M. H., Lamb, H. F., Huws, D., Davies, S., Bates, R., Bloemendal, J., Boyle, J., Leng, M. J., Umer, M., & Bryant, Ch. (2011). Late Pleistocene and Holocene drought events at Lake Tana, the source of the Blue Nile. *Global and Planetary Change*, 78, 147–16.
- Message, E., Lebreton, V., Marquer, L., Ermolli, R. E., Orain, R., Miskovsky, R. J., Lordkipanidze, D., Despriée, J., Peretto, C., & Arzarello, M. (2011). Palaeoenvironments of early hominins in temperate and Mediterranean Eurasia: New palaeobotanical data from Palaeolithic key-sites and synchronous natural sequences. *Quaternary Science Reviews*, 30, 1439–1447.
- Miller, G. H., Wendorf, F., Ernst, R., Schild, R., Close, A. E., Friedman, I., & Schwarcz, H. P. (1991). Dating lacustrine episodes in the eastern Sahara by the epimerization of isoleucine in ostrich eggshells. *Palaeogeography, Palaeoclimatology, Palaeoecology*, 84, 175–189.
- Moreno, A. (2012). A multiproxy paleoclimate reconstruction over the last 250 kyr from marine sediments: the northwest African margin and the western Mediterranean sea. In J.-J. Hublin, & S. P. McPherron (Eds.), *Modern origins: A North African perspective*. Vertebrate paleobiology and paleoanthropology (pp. 3–17). Springer.
- Moreno, A., Cacho, I., Canals, M., Prins, M. A., Sánchez-Goñi, M. F., Grimalt, J. O., & Weltje, G. J. (2002). Saharan dust transport and high-latitude glacial climatic variability: The Alboran Sea record. *Quaternary Research*, 58, 318–328.
- Moreno, A., Targarona, J., Henderiks, J., Miquel Canals, M., Freudenthal, T., & Meggers, H. (2001). Orbital forcing of dust supply to the North Canary Basin over the last 250 kyr. *Quaternary Science Reviews*, 20, 1327–1339.
- Mudie, P. J., Rochon, A., & Aksu, A. E. (2002). Pollen stratigraphy of Late Quaternary cores from Marmara Sea: Land-sea correlation and paleoclimatic history. *Marine Geology*, 190, 233–260.
- Murat, A., & Got, H. (1987). Middle and Late Quaternary depositional sequence and cycles in the Eastern Mediterranean. *Sedimentology*, 39, 885–899.
- Nicoll, K., & Sallam, E. S. (2017). Paleospring tufa deposition in the Kurkur Oasis region and implications for tributary integration with the River Nile in southern Egypt. *Journal of African Earth Sciences*, 136, 239–251.
- Osinski, G. R., Kieniewicz, J., Smith, J. R., Boslough, M. B., Eccleston, M., Schwarcz, H. P., Kleindienst, M. R., Haldeman, A. F. C., & Churcher, C. S. (2008). The Dakhleh glass: Product of an impact airburst or cratering event in the western desert of Egypt. *Meteoritics and Planetary Science*, 43(12), 2089–2107.
- Osinski, G. R., Schwarcz, H. P., Smith, J. R., Kleindienst, M. R., Haldemann, A. F. C., & Churcher, C. S. (2007). Evidence for a 200–100 ka meteorite impact in the Western Desert of Egypt. *Earth and Planetary Science Letters*, 253, 378–388.

- Osmond, J. K., & Dabous, A. A. (2004). Timing and intensity of groundwater movement during Egyptian Sahara pluvial periods by U-series analysis of secondary U in ores and carbonates. *Quaternary Research*, *61*, 85–94.
- Penck, A., & Brückner, E. (1911). *Die Alpen im Eiszeitalter* (p. 1199). Taunitz.
- Pennington, B. T., Bunbury, J., & Hovius, N. (2016). Emergence of civilization, changes in fluvio-deltaic style, and nutrient redistribution forced by Holocene Sea-Level rise. *Geoarchaeology: An International Journal*, *31*, 194–210.
- Pennington, B. T., Hamdan, M., Pearsa, B. R., & Sameh, H. I. (2019). Aridification of the Egyptian Sahara 5000–4000 cal BP revealed from X-ray fluorescence analysis of Nile Delta sediments at Kom Al-Ahmer/Kom Wasit. *Quaternary International*, *30*, 108–118.
- Pennington, B. T., Sturt, F., Wilson, P., Rowland, J., & Brown, A. G. (2017). The fluvial evolution of the Holocene Nile Delta. *Quaternary Science Reviews*, *170*, 212–231.
- Plaziat, J. C., Baltzer, F., Choukri, A., Conchon, O., Freyret, P., Orszag-Sperber, F., Purser, B., Raguideau, A., & Reyss, J. L. (1995). Quaternary changes in the Egyptian shoreline of the north-western Red Sea and Gulf of Suez. *Quaternary International*, *29*(30), 11–22.
- Plaziat, J. C., Baltzer, F., Choukri, A., Conchon, O., Freyret, P., Orszag-Sperber, F., Raguideau, A., & Reyss, J. L. (1998). Quaternary marine and continental sedimentation in the northern Red Sea and Gulf of Suez (Egyptian coast): Influences of rift tectonics, climatic changes and sealevel fluctuations. In B. H. Purser & D. W. J. Bosence (Eds.), *Sedimentation and tectonics of Rift Basins: Red Sea-Gulf of Aden* (pp. 537–573). Chapman and Hall.
- Plaziat, J. C., Reyss, J. L., Choukri, A., & Cazala, C. (2008). Diagenetic rejuvenation of raised coral reefs and precision of dating. The contribution of the Red Sea reefs to the question of reliability of the Uranium-series datings of Middle to Late Pleistocene key reef-terraces of the world. *Carnets de Geologie/Note books on geology, Brest*, Article/04.
- Renne, P. R., Schwarcz, H. P., Kleindienst, M. R., Osinski, G. R., & Donovan, J. J. (2010). Age of the Dakhleh impact event and implications for Middle stone age archeology in the western desert of Egypt. *Earth and Planetary Science Letters*, *291*, 201–206.
- Revel, M., Colin, C., Bernasconi, S., Combourieu-Nebout, N., Ducassou, E., Grousset, F. E., Rolland, Y., Migeon, S., Bosch, D., Brunet, P., Zhao, Y., & Masclé, J. (2014). 21,000 Years of Ethiopian African monsoon variability recorded in sediments of the western Nile deep-sea fan. *Regional Environmental Change*, *14*, 1685–1696. <https://doi.org/10.1007/s10113-014-0588-x>
- Revel, M., Ducassou, E., Grousset, F. E., Bernasconi, S., Migeon, S., Revillon, S., Masclé, J., Murat, A., Zaragosi, S., & Bosch, D. (2010). 100,000 years of African monsoon variability recorded in sediments of the Nile margin. *Quaternary Science Reviews*, *29*, 1342–1362.
- Revel, M., Ducassou, E., Skonieczny, C., Colin, C., Bastian, L., Bosch, D., Migeon, S., & Masclé, J. (2015). 20,000 years of Nile River dynamics and environmental changes in the Nile catchment area as inferred from Nile upper continental slope sediments. *Quaternary Science Reviews*, *130*, 200–221.
- Rizzini, A., Vezzani, F., Cococchetta, V., & Milod, G. (1978). Stratigraphy and sedimentation of the Neogene-Quaternary section in the Nile Delta area. *Marine Geology*, *27*, 327–348.
- Rohling, E. J. (1994). Review and new aspects concerning the formation of eastern Mediterranean sapropels. *Marine Geology*, *122*, 1–28.
- Rohling, E. J., Cane, T. R., Cooke, S., Sprovieri, M., Bouloubassi, I., Emeis, K. C., Schiebel, R., Kroon, D., Jorissen, F. J., & Lorre, A. (2002). African monsoon variability during the previous interglacial maximum. *Earth and Planetary Science Letters*, *202*(1), 61–75.
- Rohling, E. J., & Hilgen, F. J. (1991). The eastern Mediterranean climate at times of sapropel formation: A review. *Geologie En Mijnbouw*, *70*, 253–264.
- Rosignol-Strick, M. (1972). Pollen analysis of some sapropel layers from the deep-sea floor of the Eastern Mediterranean. *Initial Reports of the Deep Sea Drilling Project, XIII* (pp. 971–991). US Government Printing Office.
- Rosignol-Strick, M. (1985). Mediterranean Quaternary sapropels, an immediate response of the African monsoons to the variation of insolation. *Palaeogeography, Palaeoclimatology, Palaeoecology*, *49*, 237–263.
- Rosignol-Strick, M. (1995). Sea-land correlation of pollen records in the Eastern Mediterranean for the glacial-interglacial transition: Biostratigraphy versus radiometric timescale. *Quaternary Science Reviews*, *14*, 893–915.
- Rosignol-Strick, M., Nesterof, W., Olive, P., & Vergnaud-Grazzini, C. (1982). After the deluge: Mediterranean stagnation and sapropel formation. *Nature*, *295*, 105–110.
- Ruddiman, W. F., Raymo, M. E., Martinson, D. G., Clement, B. M., & Backman, J. (1989). Pleistocene evolution of Northern Hemisphere climate. *Paleoceanography*, *4*, 353–412. <https://doi.org/10.1029/PA004i004p00353>
- Saad, S. I., & Sami, S. (1967). Studies of pollen and spores content of Nile Delta deposits (Berenbal region). *Pollen et Spores*, *9*, 467–502.
- Saad, S., Zaghoul, Z., & El-Beialy, S. (1987). Late Tertiary-Quaternary palynomorphs from the northern coast of the Nile Delta, Egypt. *Neues Jahrbuch für Geologie und Paläontologie, Monatshefte*, *5*, 314–320.
- Sadori, L., Jahns, S., & Peyron, O. (2011). Mid-Holocene vegetation history of the central Mediterranean. *The Holocene*, *21*, 117–129.
- Said, R. (1981). *The geological evolution of the River Nile* (p. 151). Springer.
- Said, R. (1990). *The Geology of Egypt* (p. 717). Balkema.
- Said, R. (1993). *The River Nile: Geology, hydrology and utilization* (p. 320). Pergamon Press.
- Schalke, H. (1973). The Upper Quaternary of the Cape Flats Area (Cape Province, South Africa). *Scripta Geologica*, *15*, 1–57.
- Scheuven, D., Schutz, L., Kandler, K., Ebert, M., & Weinbruch, S. (2013). Bulk composition of northern African dust and its source sediments—A compilation. *Earth-Science Reviews*, *116*, 170–194.
- Schild, R., & Wendorf, F. (2013). Early and Middle Holocene paleoclimates in the South Western Desert of Egypt—The World before unification. *Studia Quaternaria*, *30*(2), 125–133.
- Schwarcz, H. P., & Morawska, L. (1993). Uranium-series dating of carbonates from Bir Tarfawi and Bir Sahara east. In F. Wendorf, R. Schild, & A. Close (Eds.), *Egypt during the Late Interglacial* (pp. 205–217). Plenum.
- Sestini, G. (1989). Nile Delta: A review of depositional environments and geological history. In M. K. G. Whateley & K. T. Picering (Eds.), *Deltas: Sites and traps for fossil fuels*. Geological Society Special Publication 1, 99–127.
- Shackleton, N. J. (1967). Oxygen isotope analysis and Pleistocene temperatures reassessed. *Nature*, *215*, 15–17. <https://doi.org/10.1038/215015a0>
- Shackleton, N. J., & Opdyke, N. (1973). Oxygen isotope and palaeomagnetic stratigraphy of the equatorial Pacific core V28–238: Oxygen isotope temperatures and ice volumes on a 105 and 106 year scale. *Quaternary Research*, *3*, 39–55. <https://doi.org/10.1016/0033-5894>

- Shanahan, T. M., McKay, N. P., Hughen, K. A., Overpeck, J. T., Otto-Bliesner, B., Heil, C. W., King, J., Scholz, C. A., & Peck, J. (2015). The time-transgressive termination of the African humid period. *Nature Geoscience*, 8, 140–144.
- Shaltout, M., & Azzazi, M. (2014). Climate change in the Nile Delta from Prehistoric to the Modern Era and their impact on soil and vegetation in some Archaeological sites. *Journal of Earth Science and Engineering*, 4, 632–642. <https://doi.org/10.17265/2159-581X/2014.10.006>
- Smith, J. R. (2012). Spatial and temporal variation in the nature of Pleistocene pluvial phase environments across North Africa. In J. J. Hublin, & S. P. McPherron (Eds.), *Modern origins: A North African perspective. Vertebrate Paleobiology and Paleoanthropology* (pp. 35–47). Springer.
- Smith, J. R., Giegengack, R., Schwarcz, H. P., McDonald, M. M. A., Kleindienst, M. R. K., Hawkins, A. L., & Churcher, C. S. (2004). A reconstruction of Quaternary pluvial environments and human occupations using stratigraphy and geochronology of fossil-spring Tufas, Kharga Oasis, Egypt. *Geoarchaeology*, 5, 407–439.
- Smith, J. R., Hawkins, A. L., Asmerom, Y., Polyak, V., & Giegengack, R. (2007). New age constraints on the Middle Stone age occupations of Kharga Oasis, Western Desert, Egypt. *Journal of Human Evolution*, 52(6), 690–701. <https://doi.org/10.1016/j.jhevol.2007.01.004>
- Smith, J. R., Kleindienst, M. R., Schwarcz, H. P., Churcher, C. S., Kieniewicz, J. M., Osinski, G. R., & Haldemann, A. F. C. (2009). Potential consequences of a mid Pleistocene impact event for the Middle stone age occupants of Dakhleh oasis, western desert, Egypt. *Quaternary International*, 195(1–2), 138–149.
- Smith, M. A., & Ross, J. (2008). What happened at 1500–1000 cal. BP in Central Australia? Timing, impact and archaeological signatures. *The Holocene*, 18(3), 379–388.
- Stanley, D. J. (1988). Subsidence in the northeastern Nile delta: Rapid rates, possible causes and consequences. *Science*, 240(497), 500.
- Stanley, D. J. (1990). Recent subsidence and northeast tilting of the Nile delta, Egypt. *Marine Geology*, 94, 147–154.
- Stanley, D. J. (2005). Submergence and burial of ancient coastal sites on the subsiding Nile delta margin, Egypt. *Méditerranée*, 1(2), 65–73.
- Stanley, D. J. (2019). Egypt's Nile Delta in late 4000 years BP: Altered flood levels and sedimentation, with archaeological implications. *Journal of Coastal Research*, 35(5), 1036–1050.
- Stanley, D. J., & Clemente, P. L. (2014). Clay distributions, grain sizes, sediment thicknesses, and compaction rates to interpret subsidence in Egypt's Northern Nile Delta. *Journal of Coastal Research*, 30(1), 88–101.
- Stanley, D. J., & Clemente, P. L. (2017). Increased land subsidence and sea-level rise are submerging Egypt's Nile Delta coastal margin. *Geological Society of America Today*, 27(5), 411–464.
- Stanley, D. J., & Corwin, K. A. (2013). Measuring strata thicknesses in cores to assess recent sediment compaction and subsidence of Egypt's Nile Delta coastal margin. *Journal of Coastal Research*, 29(3), 657–670.
- Stanley, D. J., Goddio, F., Jorstad, T. F., & Schnepf, G. (2004). Submergence of ancient Greek cities off Egypt's Nile delta—A cautionary tale. *GSA Today* 14(1), 4–10. [https://doi.org/10.1130/1052-5173\(2004\)0142.0.CO:2](https://doi.org/10.1130/1052-5173(2004)0142.0.CO:2)
- Stanley, D. J., & Goodfriend, G. A. (1997). Recent subsidence of the northern Suez canal. *Nature*, 388, 335–336.
- Stanley, D. J., Krom, M. D., Cliff, R. A., & Woodward, J. C. (2003). Short contribution: Nile flow failure at the end of the old kingdom, Egypt: Strontium isotopic and petrologic evidence. *Geoarchaeology: An International Journal*, 18(3), 395–402.
- Stanley, D. J., McRea, J. E., Jr., & Waldron, J. C. (1996). Nile Delta drill core and sample database for 1985–1994: Mediterranean Basin (MEDIBA) Program. Smithsonian Contributions to the Marine Sciences, No. 37. National Museum of Natural History, 428.
- Stanley, D. J., & Toscano, M. A. (2009). Ancient archaeological sites Buried and submerged along Egypt's Nile Delta coast: Gauges of Holocene Delta margin subsidence. *Journal of Coastal Research*, 25(1), 158–170.
- Stanley, D. J., & Warne, A. G. (1997). Holocene sea-level change and early human utilization of deltas GSA. *Geological Society America: Gas Today*, 7(12), 1–7.
- Stanley, D. J., & Warne, A. G. (1993). Nile Delta: Recent geological evolution and human impact. *Science*, 260, 628–634. <https://doi.org/10.1126/science.260.5108.628>
- Stanley, D. J., & Warne, A. G. (1998). Nile Delta in its destruction phase. *Journal of Coastal Research*, 14(3), 794–825.
- Stanley, D. J., & Wedl, S. E. (2021). Significant depositional changes offshore the Nile Delta in late third millennium BCE: Relevance for Egyptology. *E&G Quaternary Science Journal*, 70, 83–92. <https://doi.org/10.5194/egqsj-70-83-2021>
- Stanley, D. J., & Wingerath, J. G. (1996). Clay mineral distributions to interpret Nile Cell provenance and dispersal: I. Lower River Nile to Delta sector. *Journal of Coastal Research*, 12, 911–929.
- Staubwasser, M., & Weiss, H. (2006). Holocene climate and cultural evolution in late prehistoric–early historic West Asia. *Quaternary Research*, 66, 372–387. <https://doi.org/10.1016/j.yqres.2006.09.001>
- Sultan, M., Sturchio, N., Hassan, F. A., Hamdan, M. A., Mahmood, A. M., Alfay, Z. E., & Stein, T. (1997). Precipitation source inferred from stable isotopic composition of Pleistocene groundwater and carbonate deposits in the Western desert of Egypt. *Quaternary Research*, 48(1), 29–37.
- Summerhayes, C. P., Sestini, G., Misdorp, R., & Marks, N. (1978). Nile Delta: Nature and evolution of the continental shelf sediments. *Marine Geology*, 27(1–2), 43–65.
- Suzuki, A. (2018). Coral-based approaches to paleoclimate studies, future ocean environment assessment, and disaster research. In K. Endo, T. Kogure, & H. Nagasawa (Eds.), *Biominalization*. Springer. https://doi.org/10.1007/978-981-13-1002-7_29
- Szabo, B. J., Haynes, J. C. V., & Maxwell, T. A. (1995). Ages of Quaternary pluvial episodes determined by uranium-series and radiocarbon dating of lacustrine deposits of Eastern Sahara. *Palaeogeography, Palaeoclimatology, Palaeoecology*, 113, 227–242.
- Tegen, I., Harrison, S. P., Kohfeld, K., Prentice, I. C., & Heimann, C. M. (2002). Impact of vegetation and preferential source areas on global dust aerosol: Results from a model study. *Journal of Geophysical Research*, 107(21), 4576.
- Thompson, L. G., Thompson, M. E., Davis, M. E., Henderson, K. A., Brecher, H. H., Zagorodnov, V. S., Mashiotto, T. A., Lin, P., Mikhalenko, V. N., Hardy, D. R., & Beer, J. (2002). Kilimanjaro ice core records: Evidence of Holocene climate change in tropical Africa. *Science*, 298, 589–593. <https://doi.org/10.1126/science.1073198>
- Thunell, C. R., & Williams, D. F. (1998). Glacial-Holocene salinity changes in the Mediterranean Sea: Hydrographic and depositional effects. *Nature*, 338, 493–496.
- Tierney, J. E., Pausata, F. S. R., & De Menocal, P. B. (2017). Rainfall regimes of the Green Sahara. *Science Advances*, 3(1), e1601503.
- Tiner, R. W. (2016). *Wetland indicators: A guide to wetland formation, identification, delineation, classification, and mapping*. CRC Press.

- Tomadini, L., Lenaz, R., Landuzzi, V., Mazzucotelli, A., & Vannucci, R. (1984). Wind-blown dust over the Central Mediterranean. *Oceanologica Acta*, 7, 13–23.
- Trauth, M. H., Larrasoana, J. C., & Mudelsee, M. (2009). Trends, rhythms and events in Plio-Pleistocene African climate. *Quaternary Science Reviews*, 28(5–6), 399–411. <https://doi.org/10.1016/j.quascirev.2008.11.003>
- Tucker, M. E. (2003). Mixed clastic-carbonate cycles and sequences: Quaternary of Egypt and carboniferous of England. *Geologica Croatica*, 56(1), 19–37.
- Tuenter, E., Weber, S. L., Hilgen, F. J., & Lourens, L. J. (2003). The response of the African summer monsoon to remote and local forcing due to precession and obliquity. *Global and Planetary Change*, 36(4), 219–235. [https://doi.org/10.1016/S0921-8181\(02\)00196-0](https://doi.org/10.1016/S0921-8181(02)00196-0)
- Tweddle, J. C., Edwards, K. J., & Fieller, N. R. (2005). Multivariate statistical and other approaches for the separation of cereal from wild Poaceae pollen using a large Holocene dataset. *Vegetation History and Archaeobotany*, 14, 15–30.
- Tzedakis, P. C. (2007). Seven ambiguities in the Mediterranean palaeoenvironmental narrative. *Quaternary Science Reviews*, 26 (17–18), 2042–2066.
- Van Zeist, W., & Bottema, S. (1982). Vegetational history of the Eastern Mediterranean and the near East during the last 20,000 years. In J. L. Bintliff, & W. van Zeist (Eds.), *Paleoclimates, paleoenvironments and human communities in the Eastern Mediterranean region in later prehistory*. Br. Archaeol. Rep. (BAR), International Series (Vol. 133, No. 2, pp. 277–321).
- Vergnaud-Grazzini, C., Ryan, W. B. F., & Cite, M. B. (1977). Stable isotopic fractionation, climate change and episodic stagnation in the eastern Mediterranean during the Late Quaternary. *Marine Micropaleontology*, 2, 353–370.
- Wali, A. M. A., Brookfield, M. E., & Schreiber, B. C. C. (1994). The depositional and diagenetic evolution of the coastal ridges of north western Egypt. *Sedimentary Geology*, 90, 113–136.
- Walker, M., Head, M., Berkelhammer, M., Björck, S., Cheng, H., Cwynar, L., Fisher, D., Gkinis, V., Long, A., Lowe, J., Newnham, R., Rasmussen, S. O., & Weiss, H. (2018). Formal ratification of the subdivision of the Holocene Series/Epoch (Quaternary System/Period): Two new Global Boundary Stratotype Sections and Points (GSSPs) and three new stages subseries. *Episodes*. <https://doi.org/10.18814/epiugs/2018/018016>
- Walker, M., Johnsen, S., Rasmussen, S. O., Popp, T., Steffensen, J. P., Gibbard, P., Hoek, W., Lowe, J., Andrews, J., Björck, S., Cwynar, L. C., Hughen, K., Kershaw, P., Kromer, B., Litt, T., Lowe, J., Nakagawa, T., Newnham, R., & Schwander, J. (2009). Formal definition and dating of the GSSP (Global Stratotype Section and Point) for the base of the Holocene using the Greenland NGRIP ice core, and selected auxiliary records. *Journal of Quaternary Science*, 24(1), 3–17. <https://doi.org/10.1002/jqs.1227>
- Wang, Y., Wang, W., Liu, L., Jiang, Y., N. Z., Yuzhen, M., Jiang, H., & Mensing, S. A. (2020). Reliability of the Artemisia/Chenopodiaceae pollen ratio in differentiating vegetation and reflecting moisture in arid and semi-arid China. *The Holocene*, 30(6), 858–864. <https://doi.org/10.1177/0959683620902219>
- Weiss, H. (2000). Beyond the Younger Dryas: Collapse as adaptation to abrupt climate change in ancient West Asia and the Eastern Mediterranean. In G. Bawden, & R. E. Reyrcraft (Eds.), *Environmental disaster and the archaeology of human response*. Maxwell Museum of Anthropology Anthropological Paper No. 7 (pp. 75–98).
- Welch, F., & Marks, L. (2014). Climate change at the end of the old kingdom in Egypt around 4200 BP: New geoarchaeological evidence. *Quaternary International* 324, 124–133.
- Wendorf, F., & Schild, R. (1976). *Prehistory of the Nile Valley*. Academic.
- Wendorf, F., Schild, R., & Close, A. E. (Eds.). (1989). *Prehistory of Wadi Kubbania III*. Southern Methodist University Press.
- Wendorf, F., Schild, R., & Close, A. (1993). *Egypt during the last interglacial: The Middle Palaeolithic of Bir Tarfawi and Bir Sahara East* (p. 596). Plenum Press.
- Wendorf, F., Schild, R., Said, R., Haynes, C. V., Gautier, A., & Koubisiewicz. (1976). The prehistory of the Egyptian Sahara. *Science*, 193, 103–114.
- Wendorf, F., & The Members of the Combined Prehistoric Expedition. (1977). Late Pleistocene and recent climatic changes in the Egyptian Sahara. *The Geographical Journal*, 143(2), 211–234.
- Williams, D. F., & Thunell, R. C. (1979). Faunal and oxygen isotopic evidence for surface water salinity changes during sapropel formation in the Eastern Mediterranean. *Sedimentary Geology*, 23, 81–93.
- Williams, M. A. J. (2009). Late Pleistocene and Holocene environments in the Nile basin. *Global and Planetary Change*, 69, 1–15. <https://doi.org/10.1016/j.gloplacha.2009.07.005>
- Williams, M. A. J., Adamson, D. A. (1980). Late quaternary depositional history of the Blue and white Nile rivers in central Sudan. In: Williams, M. A. J., Faure, H. (Eds.), *The Sahara and the Nile* (pp. 281–304). A. A. Balkema, Rotterdam.
- Williams, M. A. J., Adamson, D., Cock, B., & Evedy, R. (2000). Later Quaternary environments in the White Nile region, Sudan. *Global and Planetary Change*, 26, 305–316.
- Williams, M. A. J., Duller, G. A. T., Williams, F. M., Woodward, J. C., Macklin, M. G., El Tom, O. A. M., Munro, R. N., El Hajaz, Y., & Barrows, T. T. (2015). Causal links between Nile floods and eastern Mediterranean sapropel formation during the past 250 kyr confirmed by OSL and radiocarbon dating of Blue and White Nile sediments. *Quaternary Science Reviews*, 130, 89–108.
- Williams, M. A. J., Williams, F. M., Duller, G. A. T., Munro, R. N., El Tom, O. A. M., Barrows, T. T., Macklin, M., Woodward, J., Talbot, M. R., Haberlah, D., & Fluin, J. (2010). Late Quaternary floods and droughts in the Nile valley, Sudan: New evidence from optically stimulated luminescence and AMS radiocarbon dating. *Quaternary Science Reviews*, 29, 1116–1137.
- Wingard, G. L., Murray, J. B., Schill, W. B., & Phillips, E. C. (2008). The red-rimmed melania (*Melanoides tuberculata*), a snail in Biscayne National Park, Florida: Harmful invader or just a nuisance? USGS Fact Sheet 2008-3006. U. S. Geol. Surv. 6. <http://pubs.usgs.gov/fs/2008/3006>.
- Woodroffe, C. D., & Webster, J. M. (2014). Coral reefs and sea-level change. *Marine Geology*, 352, 248–267.
- Woodward, J. C., Macklin, M. G., Krom, M. D., & Williams, M. A. J. (2007). The Nile: Evolution, quaternary river environments and material fluxes. In A. Gupta (Ed.), *Large rivers: Geomorphology and management*. Wiley.
- Wysocka, A., Welch, F., & Czarniecka, U. (2016). Sedimentary environment of the Early Pleistocene gravels of the Edfu Formation from the Saqqara archaeological site (Egypt)—Preliminary results. *Studia Quaternaria*, 33(1), 69–78. <https://doi.org/10.1515/squa-2016-0007>
- Yehudai, M., Lazar, B., Bar, N., Kiro, Y., Agnon, A., Shaked, Y., & Stein, M. (2017). U-Th dating of calcite corals from the Gulf of Aqaba. *Geochimica Et Cosmochimica Acta*, 198, 285–298.
- Zaky, A., Kashima, K., Frontalini, F., Ibrahim, M. I. A., Khalifa, M. M., Fukumoto, Y., Gad, D., & Behling, H. (2020). Mid-to Late Holocene paleoclimatic changes and paleoenvironmental shifts inferred from pollen and diatom assemblages at Lake Hamra, Wadi El Natrun (Western Nile Delta, North Western Desert, Egypt). *Quaternary International*, 542, 109–120.

- Zaghloul, Z. M., Gheith, A. M., Abdel-Daiem, A. A., & El Asmar, H. M. (1989). The pattern of sedimentation of the Quaternary Nile Delta, Egypt. *El Mansoura Science Bulletin*, 16(2), 393–413.
- Zaghloul, Z. M., Taha, A. A., Hegab, O., & El-Fawal, F. (1977). The Neogene-Quaternary sedimentary basins of the Nile delta, Egypt. *Journal of Geology*, 21, 1–19.
- Zaghloul, Z. M., Taha, A. A., Hegab, O., & El-Fawal, F. (1979). The Plio-Pleistocene Nile subenvironments stratigraphic section and genetic class. In *The Fifth Conference on African Geology*, Geological Survey, Egypt, Cairo.
- Zeuner, F. E. (1959). *The Pleistocene period* (p. 447). Hutchinson.
- Zeuner, F. E. (1972). *Dating the past* (4th ed.). Methuen.
- Zhao, X., Thomasb, I., Salem, A., Alassal, S. E., Liu, Y., Sun, Q., Chen, J., Maa, F., Finlayson, B., & Chen, Z. (2020). Holocene climate change and its influence on early agriculture in the Nile Delta, Egypt. *Palaeogeography, Palaeoclimatology, Palaeoecology*, 547, 109702.
- Zhou, H., Helliker, B. R., Huber, M., Dicks, A., & Akçay, E. (2018). C4 photosynthesis and climate through the lens of optimality. *PNAS*, 115(47), 12057–12062.
- Ziegler, M., Tuenter, E., & Lourens, L. J. (2010). The precession phase of the boreal summer monsoon as viewed from the eastern Mediterranean (ODP Site 968). *Quaternary Science Reviews*, 2, 1481–1490.



Hesham M. El-Asmar is a professor of Quaternary geology at Damietta University (Egypt). He received an MSc degree from Mansoura University (1986), and Ph.D. (1991) in collaboration with the IFAQ-UNESCO program, Free University of Brussels, Belgium. Later, he obtained a fellowship from the Royal Society of London to the University of Reading and Royal Holloway College (University of London, UK). He served as an expert at the Egyptian Technical Cooperation Fund for Africa in Uganda, and was also appointed as a Cultural Attaché and the director of the Egyptian Culture Center at the Egyptian Embassy in Athens, Greece. He was a former advisor to the Minister of Higher Education for cultural and scientific strategic reform, and advisor to the Vice Rector, King Saud University (Saudi Arabia) for knowledge exchange and technology transfer. He is a specialist in the field of Quaternary geology in Mediterranean and Red Sea coastal areas in Egypt.



Evolution of the Nile River Through Time

Bahay Issawi and Sherif Farouk

Abstract

The Nile River, which receives its water from the Ethiopian Highlands and the Central African lakes, is often considered as the world's longest South-North river. The purpose of this chapter is to produce an updated overview of the stages of the formation of the Nile drainage system. It is based on bringing together all of the available data concerning the stratigraphy and paleoenvironments which prevailed during the evolution of the Nile River from the Ethiopian Highlands to the Mediterranean Sea. During the Messinian Salinity Crisis (MSC) in the whole Mediterranean, river systems were deeply down-cut and extended throughout most of North Africa and South Europe. The Qena River, which had its catchment area in the Southern Galala Plateau and the surrounding desert before the Nile, was Egypt's master stream before the Nile, a south-west ward drainage. It has been proposed that waters from the Qena River continue to flow to the Atlantic Ocean, which is known as the Trans African Drainage System (TADS). The earliest Nile sediment deposited by a river flowing into Egypt from Ethiopia on its way to the Mediterranean is considered to be the Dandara Formation. The presence of an Ethiopian heavy mineral suite within the Middle Pleistocene Dandara Formation, which has been extensively documented on both banks of the Nile River in Upper Egypt, distinguishes Nile sediments from those found in other riverine systems.

Keywords

Nile River • White Nile • Blue Nile • Nile evolution • Africa • Egypt

B. Issawi (✉)
Egyptian Geological Survey, Cairo, Egypt
e-mail: bahyalesawy@gmail.com

S. Farouk
Exploration Department, Egyptian Petroleum Research Institute,
Nasr City, 11727, Egypt

1 Introduction

The Nile is generally regarded as the world's longest river with a total length of about 6800 km and one of the most notable geomorphological characteristics in Africa. Its drainage basin is shared by eleven countries (Fig. 1): Tanzania, Rwanda, Uganda, Burundi, Kenya, the Democratic Republic of the Congo, Eritrea, Ethiopia, South Sudan, the Republic of Sudan, and Egypt (Liu et al., 2009). By measure of the volume of water flowing annually, the Nile is one of the smallest of the main world rivers. It has two main tributaries that meet at Khartoum: the White Nile, which starts from the Lake Victoria basin, and the Blue Nile, which starts from the Ethiopian Plateau. The Nile River is the primary source of water supply for Egypt and Sudan, besides both renewable and non-renewable groundwater. The Holocene Nile is regarded to be of significant archaeological importance, since ancient communities in Egypt were largely dependent on it for drinking water and irrigation. Most Egyptians lived along the Nile banks, and the Nile has played an important role in establishing one of the planet's earliest civilizations. Today, the most important problems facing many African countries north of the equator in achieving sustainable development are the scarcity of fresh and clean water, which is combined with a rapid increase in the population, and extreme climate change (Issawi et al., 2016). Egypt is one of the most drought-stricken countries in the world due to its location in the arid belt of North Africa. The previous evolution of the Nile River and the shifting tectonic and climate factors over time are not well understood until now (e.g., Fielding et al., 2018; Macgregor, 2012; Woodward et al., 2015).

Our knowledge of the geological and geomorphological evolution of the integrated drainage system of the Nile come from the early and pioneering contributions of Issawi (1976), Said (1981, 1993), and McCauley et al. (1982, 1986) which dealt with the physiography of the Nile in modern times. These studies were followed by more detailed reviews which

images started a long-lasting debate on whether a north-flowing pre-Messinian 'Blue Nile' with connecting tributaries from southern Egypt reached the Mediterranean or Egypt was drained by a significant drainage system prior to the Nile.

In investigating the relation between the Messinian Nile canyon east of the Nile Delta and the Quaternary Nile channels, Egypt, Said (1981) stated that it was one river with different names which flew from south to north across Egypt heading to the Mediterranean Sea and there were five river phases that succeeded each other: Eonile (Late Miocene), Paleonile (Late Pliocene), and the Pleistocene Proto-, Pre-, and Neo-Niles. These river phases are separated from one another by long periods of recession and great unconformities. However, Issawi et al. (2009) disagreed with this theory and suggested that the term "Nile" should be applied only to the south-north-flowing river which gets its water from the Ethiopian Plateau and Central African lakes. He also advocated that the previous rivers that were running during the Oligo-Miocene and the Late Miocene should be considered independent systems. Those rivers that antedated the modern Nile are generally of east–west slope that flew from the eastern part of the Egypt including most of the Eastern Desert to the present-day Western Desert.

During the Late Mesozoic, the maximum north–south transgression of the Tethys took place, covering most of Egypt's surface. This was followed by a retreat of the shoreline during the Early Eocene up until the Oligocene north of Fayoum depression (Issawi et al., 2009). The opening of the Red Sea and the uplift of the Red Sea Mountains in the Eastern Desert started with the retreat of the Tethys shorelines during the Late Eocene (Priabonian) and terminated in the final pulse at about 21 Ma, the boundary between the Aquitanian and the Burdigalian (Early Miocene) (Omar & Steckler, 1995). The initiation and evolution of the Nile River is the result of contribution of several events: regional tectonics (the opening of the Red Sea and East African Rift System accompanying with uplifting of the Red Sea Hills) (Issawi & Osman, 2008), local structures (the presence of Cretaceous and younger faulting), and climate change (the MSC, the emergence of the Sahara and the alternation of wet and dry climate) (Butzer & Hansen, 1968; Said, 1993).

2 Stages of the Nile Evolution

The rise of African swells and Ethiopian Plateau have had an impact on shaping of the Nile Basin which result to change in river patterns and caused the drainage systems to switch northward to initiate the current Nile system and form the modern catchment. This must have caused climatic changes accompanied by increased precipitation and runoff. It is

questionable whether this increase of runoff was sufficient to provide permanent integrated river system or each river ended in a separate delta. To answer this question much work has been done on the source to sink relationships to determine the nature and timing of the connection between the Egyptian Nile and the Blue Nile. There is no agreement on when the river first initiated; periods ranging from the Oligocene (Fielding et al., 2018; Gani et al., 2007; MacGregor, 2012; Said, 1981; Steinberg et al., 2011) to the Pleistocene (Issawi et al., 2009; Shukri, 1950) have been proposed for when the Nile trunk river first drained as far south as the Ethiopian Highlands.

2.1 Early Origins of the Oligocene to Late Miocene Nile (North-Flowing Pre-Messinian Nile)

Evidence collected by Issawi and Osman (2008) suggested that there was no Nile till the end of the Miocene but there were many major rivers flowing over Egypt (Fig. 2). The uplift of the southern Galala Bridge led to the formation of north-flowing rivers to the Mediterranean (Ur-Nil River and Bown-Kraus River) and the south-flowing main master stream which had a N-SW direction forming the beginning of the Qena system and the Gilf river, which ran from south to north and during an earlier history (Late Eocene–Oligocene) formed a westerly channel of the rivers which dominated Egypt's surface.

2.2 The Late Miocene Nile (the Messinian Nile Canyon)

The Messinian breaking near the end of the Miocene (~ 5.8 Ma) of the connection between the Atlantic Ocean and the Mediterranean Sea led to the desiccation of the sea into a number of isolated lakes (Hsü et al., 1973). The dramatic sea-level fall during the Messinian salinity crisis and the nearly empty Mediterranean Sea caused a phase of acute degradation and produced canyons along the course when the rivers were emptying their waters into the sea as they carved their channels at least 2–3 km deep to reach the new base level, the floor of the Mediterranean Sea. The Nile carved a deep bedrock canyon (Fig. 3), which extended for 1200 km from the Mediterranean Sea to just north of Aswan (Chumakov, 1967). This canyon was deeper and longer than the Grand Canyon of the Colorado River. Approximately 80,000 km² of rock and sediment were eroded from the canyon during the Messinian and replaced by Pliocene deposits. The Late Miocene Nile generated a number of fans further downstream in the area of the North Delta Embayment.

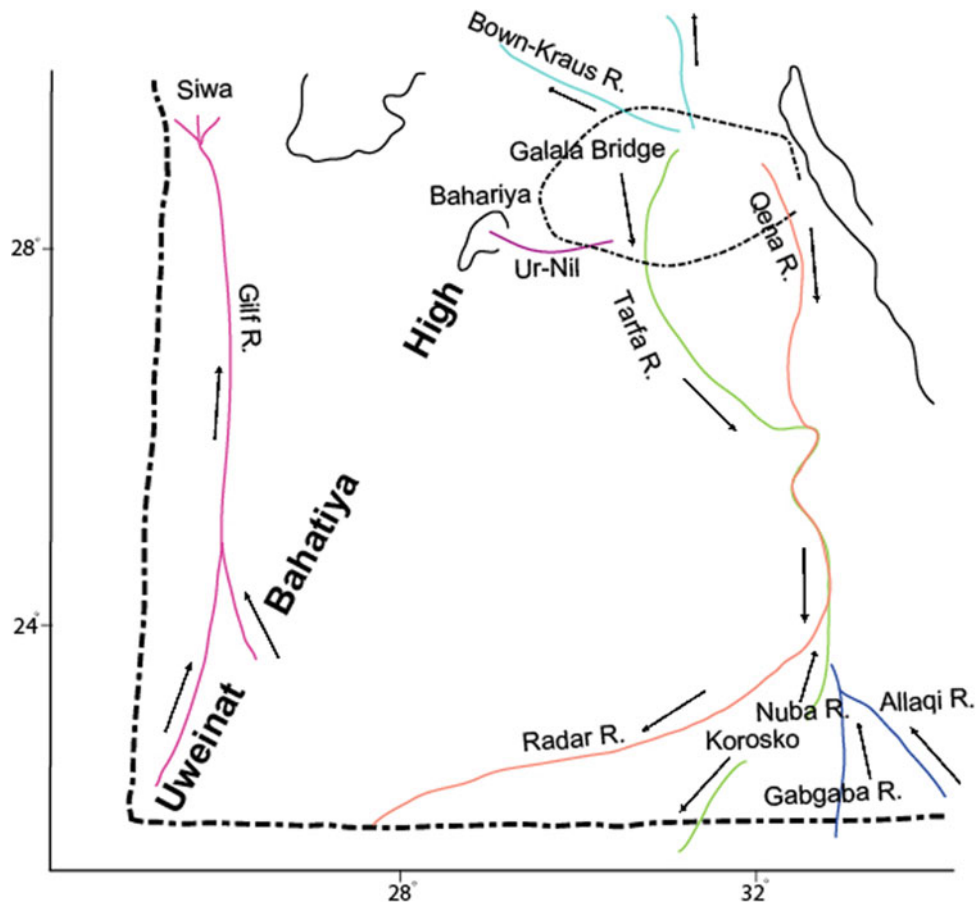


Fig. 2 Egypt during the Late Oligocene–Miocene (after Issawi & Osman, 2008)

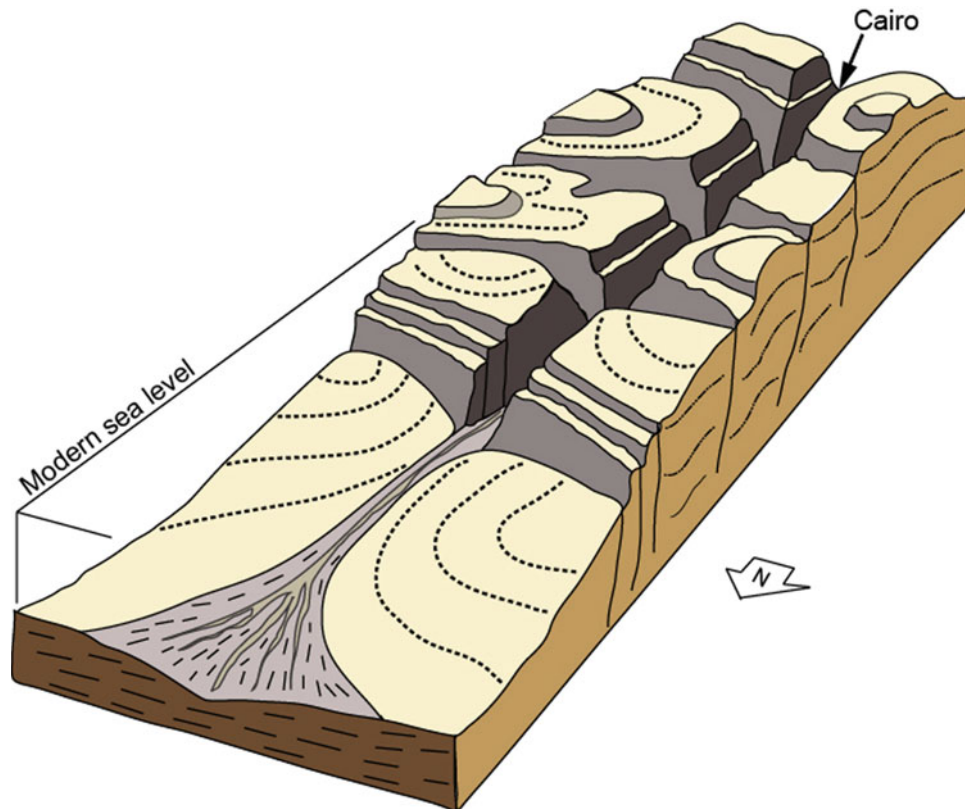


Fig. 3 Block diagram of the Nile Canyon (after Said, 1981)

2.3 The Pliocene and Quaternary Niles

By the end of the Miocene and the start of the Pliocene, the Mediterranean Sea and the Atlantic Ocean were connected again. Higher Pliocene sea-levels flooded the canyon, turning it into a narrow, long gulf that reaches Aswan in the south and filling about one-third of the depth with marine sediments (Chumakov, 1967). The sea water penetrated the Egyptian land, filling a wide area estimated to be 60 km wide (Issawi et al., 2001). During the Late Pliocene, the transgressive water changed into regressive water, resulting in a changed in lithofacies from marine to brackish deposited with a sediment load derived from local wadis of fine-grained clastics as the fluvial freshwater zone shifted progressively northwards toward the modern Mediterranean coastline. The deeper part of the gulf in the north contains a huge thickness of clay deposits, 1854 m in the subsurface Kafr El Sheikh Formation of the Delta (Issawi et al., 2005). Only drilling in the Aswan area has revealed the deep buried Pliocene marine facies. The filling of the gulf area continued through the whole Early Pliocene. During the Middle and Late Pliocene, the nearly empty gulf became a good burial place for the sediments brought by the Nile River. By the end of the Pliocene and the beginning of the Quaternary, the shoreline of the Mediterranean Sea nearly coincided with its present line. The drop of water level in the Mediterranean was a result of the building of thick ice sheets on both poles of the earth. In the upper Nile Basin, Late Quaternary climates have fluctuated between cold-dry and warm-wet conditions. Fluctuations in the climate in Africa during the Quaternary holds a great impact on the behavior of the Nile sediment system (Cockerton et al., 2015). El Mahmoudi and Gaber (2009) carried out geoelectric resistivity surveys in the eastern part of the Nile Delta and correlated between the Messinian canyons (wadis) and the Late Quaternary channels. It was revealed that above the Messinian canyons remained a negative geomorphic characteristic until the time of the channeling of the Nile historical branches into the Nile Delta.

The Nile today flows through a variety of strata, including the volcanic Ethiopian Highlands in the south, Precambrian foundation rocks of the Saharan Metacraton and Arabian–Nubian Shield, and a Phanerozoic successions cover that extends over much of its drainage area (Fig. 4). The Qena Sand (Said et al., 1970) is the oldest Quaternary deposit in the Nile Valley. It unconformably overlies, perhaps, the Pliocene (?) Muneiha or the Issawia formations. Both of these units represent the Late Pliocene's regressive phase; the Muneiha is a 14.5-m-thick clastic layer, while the Issawia is a 22-m-thick brecciated limestone. The Qena Formation at east Kom Ombo covers the plain of Burg El Makhazin between the embouchures of Wadi Kharit and

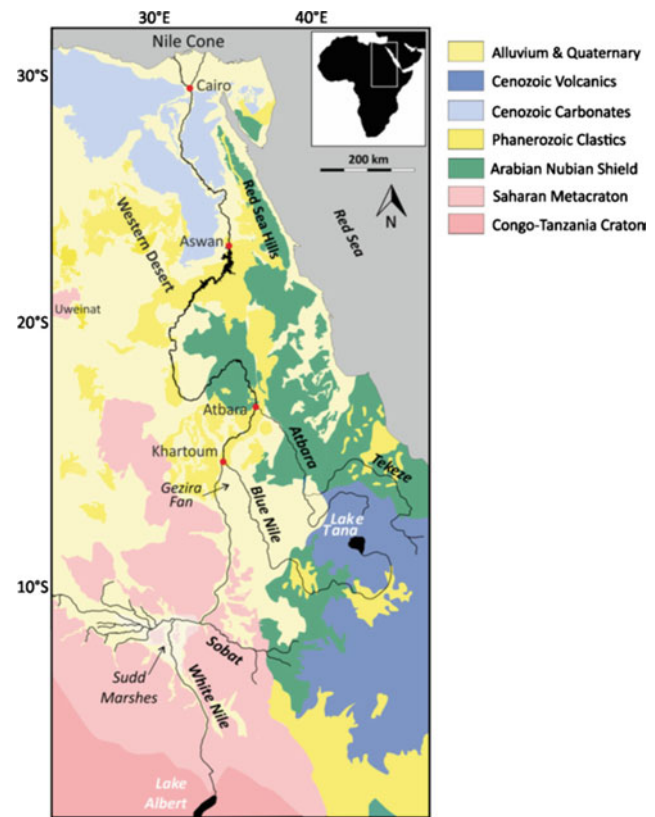


Fig. 4 Geological map of the Nile drainage (Fielding et al., 2018)

Wadi Shait. The very interesting observation about the Qena Formation is that it stretches to the other west side of the river in a sloping sheet-like feature which is now cut by the Nile water. The sheet was deposited by a river running from east to west before the onset of the Nile. The Qena Formation represents the resumption of the E–W drainage system above the buried gulf channel after the regressive phase of the Late Pliocene. The chocking of the channel was very uneven, resulting (later when the current Nile used this channel) in an irregular floor of the river which obstructs the navigation routes at present.

The important diagnostic characteristic distinguishing Nile sediments from other riverine systems is the inclusion of an Ethiopian heavy mineral suite. The sediments are rich in pyroxenes (mainly augite) and amphiboles, with an intermediate epidote content and strongly dwindled zircon and ZTR values; certainly indicating Ethiopian derivation. This suite is found in the silt of the Dandara Formation, which is well exposed in Upper Egypt on both banks of the Nile. It is believed that the Dandara is the first sediment deposited by a river coming into Egypt from Ethiopia heading toward the Mediterranean.

The silt beds below the Dandara Formation are known as the Ghawanim Formation (Omar, 1996), and include both

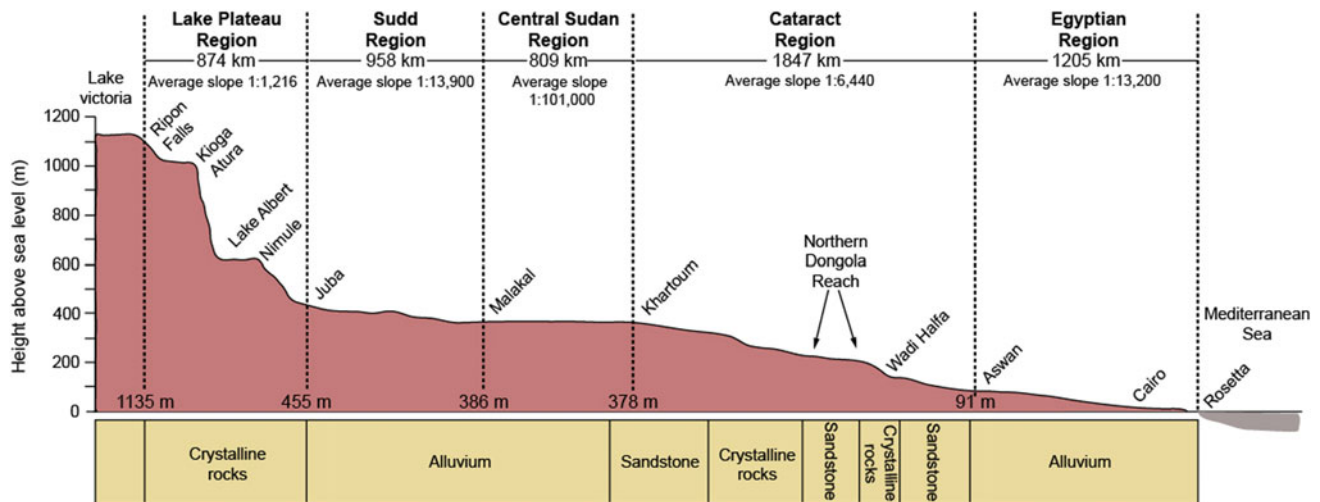


Fig. 5 Long profile of the Nile from the White Nile headwaters to the Mediterranean Sea (after Said, 1981)

Egyptian and, to a lesser extent, Ethiopian minerals. Thus, it seems that the beginning of the Nile in Egypt was a weak flowing drainage while the Qena System was still active, hence the mixture of the two suites of minerals. Since the Dandara Formations includes only Ethiopian minerals, a cessation of Egyptian waters into the old river systems is indicated. Radiocarbon dating of the upper Dandara Formation gives an age of 213 ± 14 ka (Issawi & McCauley, 1992), which indicates even an older age for the lower part of the Dandara and the Ghawanim formations. The presence of seventy species of nilotic fishes and crocodile remains in the Tarfawi–Sahara area, 300 km west of the Nile, demonstrates a link between the Nile and the faunal location (Wendorf & Schild, 2014). The fauna is 174 ka at elevation of about 247 m above sea-level. The various and extensive playas south of Sin El Kaddab, as well as the Bir Tarfawi–Bir Sahara stretch as well as the playas along the Darb El Arbain, Kharga, and Dakhla scarps are all less than 200 m above sea-level, meaning that during the Late Pleistocene, Nile waters flowed into these depressions.

2.4 The Modern Nile

The White Nile supplies only about 30% of the water and 3% of the sediments to the Nile System because most of the sediment load is trapped in the Sudd marshes. The Blue Nile, which flows in a northwest direction and joins the White Nile at Khartoum, supplies the Nile System with about 57% of its water and about 60% of its sediment load. The Tekeze–Atbara River contributes an additional $\sim 22\%$ of water and $\sim 25\%$ of sediments to the Nile System (Garzanti et al., 2015). The Nile flows through six discrete regions which display differences in their geologic history,

geomorphological features, and environment. These regions were described by Said (1981) (Fig. 5) as:

1. The Lake Plateau at the southern headwaters of the White Nile in equatorial Africa.
2. The Sudd swampy areas and Central Sudan regions with larger channel belts and low-gradient floodplains.
3. The Highlands of Ethiopia form the headwaters of the Blue Nile and the Atbara River.
4. The Cataracts region extends from northern Egypt to Cairo to Sudan at Khartoum.
5. The Egyptian Nile delta is a low-gradient complex in the Mediterranean Sea.

3 The Nile's Water and Resources

The most significant concern facing many African countries north of the equator is the scarcity of freshwater, which when paired with rapid population increase, might lead to a shortage of water for irrigation and economic necessities. In comparison to the United States, which has a freshwater potential of about $10,000 \text{ m}^3$ per person per year, Egypt, west Sudan, east Libya, and east Chad have freshwater potentials of less than 700 m^3 per person per year, with Somalia having even less. Such scarcity of water inevitably leads to conflicts such as the Darfur tribal war and the Sudan–Chad confrontation, not to mention the dispute between Ethiopia and Sudan and Egypt over the construction of a massive dam on the Blue Nile just upstream from the Sudan border, in a seismically active region near the Ethiopian Rift. It is surprising, therefore, to realize that large amounts of water originating in central Africa and the Congo

are lost in the wetlands of the Bahar El Gebeland and Bahar El Zaraf depressions in western South Sudan. This leads to the suggestion that the ancient Cenozoic river system, which flowed naturally from the south over what is now the Sahara Desert, may be exploited to bring freshwater to the populous areas of northern Africa at a comparatively modest cost. Some of the Congo River's northern feeders, such as those around Buta or Ueley further north, have modest gradients that might be reversed to allow water to flow into these natural collectors. Satellite imagery reveal river channels that could convey water from the sand-filled Gilf river channel or further west into the ancient Chad–Libya mega system. The main trunk of the rejuvenated channel would run from the swampy areas in western South Sudan to Darfur at El Fasher, then to the Wadi Magrur and Wadi Howar. A reservoir could be built at Merga, 100 km north, to supply two primary systems: the Paleo Gilf, which flows into Egypt across the Sudanese border east of Gebel Kamel, and the Paleo Kufra, which flows into north Chad and south Libya west of Gebel Uweinat. The proposed new canals would use the existing excavations made by the paleo river systems to establish new life in dead deserts. Gradient reversal can be done in recent streams, such as Uere and Uele, as well as in some of the underground channels and Wadi Howar, by elevating the water level through dams on the channels' courses. The dams would serve a variety of purposes including generating electricity, creating farmlands in currently desert areas, and generally increasing the amount of water available to residents in these thirsty places.

4 Conclusions

The evolution of the Nile drainage system remains poorly understood. Since the acquisition of the Shuttle Radar Topography Mission (SRTM) images, which has the capability of mapping paleodrainage systems, a debate has erupted concerning the nature and timing of the connection between the Blue Nile and the Egyptian Nile. We presented the geological arguments based on source to sink evidence supporting the idea that the Nile River was established as a main drainage system reaching from the Ethiopian Highland to the Mediterranean Sea around 30 Ma ago (Oligocene). The oldest Quaternary deposits in the Nile Valley are the Qena Sand, which has a suite of minerals specific to Egypt's Eastern Desert. The Ethiopian mineral suite is different and only recognized in the Ghawanim Formation and the overlying Dandara Formation. The Ghawanim Formation includes both Egyptian and Ethiopian suites, indicating that the Qena System was still partially active when the Ethiopian water reached Egypt. The top third of the Dandara is about 213 ± 14 ka, which gives an approximate age for the

Ethiopian water with its special mineral suite of at least 1/2 million years; the age of the present Nile.

Within the population growth and water scarcity, we have no other source for water increase except to obtain water from the White Nile or the Congo River by digging a canal in the Sudan's Western Desert and through rejuvenating the old dry rivers in west Egypt (Gilf River) and in east Libya (Kufra River). Prosperous settings for people in south and west Sudan, east Chad, west Egypt, and east Libya will be possible.

References

- Abdelkareem, M., Ghoneim, E., El-Baz, F., & Askalany, M. (2012). New insight on paleoriver development in the Nile basin of the eastern Sahara. *Journal of African Earth Sciences*, 62(1), 35–40.
- Abdelsalam, M. G. (2018). The Nile's journey through space and time: A geological perspective. *Earth-Science Reviews*, 177, 742–773.
- Butzer, K. W., & Hansen, C. L. (1968). *Desert and river in Nubia: Geomorphology and prehistory environments at the Aswan reservoir* (p. 562). University of Wisconsin Press.
- Chumakov, I. S. (1967). Pliocene and Pleistocene deposits of the Nile Valley in Nubia and Upper Egypt (in Russian). *Transactions of the Geological Institute of the Academy of Sciences (USSR)*, 170, 1–11.
- Cockerton, H. E., Street-Perrott, F. A., Barker, P. A., Leng, M. J., Sloane, H. J., & Ficken, K. J. (2015). Orbital forcing of glacial/interglacial variations in chemical weathering and silicon cycling within the upper White Nile basin, East Africa: Stable-isotope and biomarker evidence from Lakes Victoria and Edward. *Quaternary Science Reviews*, 130, 57–71.
- El Mahmoudi, A. S., & Gaber, A. (2009). Geophysical surveys to investigate the relation between the Quaternary Nile channels and the Messinian Nile canyon at East Nile Delta, Egypt. *Arabian Journal of Geoscience*, 2, 53–67.
- Faccenna, C., Glišović, P., Forte, A., Becker, T., Garzanti, E., Sembroni, A., & Zohar Gvirtzman, Z. (2019). Role of dynamic topography in sustaining the Nile River over 30 million years. *Nature Geoscience*, 12, 1012–1017.
- Fielding, L., Najman, Y., Millar, I., Butterworth, P., Ando, S., Padoan, M., Barfod, D., & Kneller, B. (2017). A detrital record of the Nile River and its catchment. *Journal of the Geological Society*, 174, 301–317.
- Fielding, L., Najman, Y., Millar, I., Butterworth, P., Garzanti, E., Vezzoli, G., Barfod, D., & Kneller, B. (2018). The initiation and evolution of the River Nile. *Earth and Planetary Science Letters*, 489, 166–178.
- Garzanti, E., Andò, S., Padoan, M., Vezzoli, G., & El Kammar, A. (2015). The modern Nile sediment system: Processes and products. *Quaternary Science Reviews*, 130, 9–56.
- Hsü, K. J., Ryan, W. B. F., & Cita, M. B. (1973). Late Miocene desiccation of the Mediterranean. *Nature*, 242, 239–243.
- Issawi, B. (1976). An introduction to the physiography of the Nile Valley. In F. Wendorf & R. Schild (Eds.), *Prehistory of the Nile Valley* (pp. 3–22). Academic.
- Issawi, B., Ahmed, S. M., Osman, R., & Sallam, E. S. (2005). Studies on the Pliocene—Quaternary sediments in the western fringes of the Nile Delta—Lower Nile Valley stretch, Egypt. *Journal of Sedimentology, Egypt*, 13, 277–296.
- Issawi, B., Francis, M. H., Youssef, E. S., Osman, A. A., & Rifaat, A. (2009). The Phanerozoic geology of Egypt: A geodynamic

- approach (Vol. 81, p. 571). Ministry of Petroleum and the Egyptian Mineral Resources Authority Special Publication.
- Issawi, B., & McCauley, J. F. (1992). The Cenozoic rivers of Egypt: The Nile problem. In R. Friedman, & B. Adams (Eds.), *The followers of Horus: Studies in memory of MA Hoffman*. Egyptian Studies Association Publication no. 2, Oxbow Monograph 20.
- Issawi, B., & Osman, R. (2008). Egypt during the Cenozoic: Geological history of the Nile River. In E. A. A. Yousef (Ed.), *Bulletin of the Tethys Geological Society* (Vol. 3, pp. 43–62). Cairo University.
- Issawi, B., Osman, R., & Meibed, A. (2001). The Faiyum Depression—Qarun Lake, a geologic study. In *Assiut Univ., 2nd Conf. Africa* (Vol. 1, pp. 307–322).
- Issawi, B., Youssef, E. S. A., & Maxwell, T. (2016). Cenozoic rivers of northeast Africa: Evidence of trans-Saharan drainage. *Stratigraphy*, 13(1), 49–66.
- Liu, S., Lu, P., Liu, D., Jin, P., & Wang, W. (2009). Pinpointing the sources and measuring the lengths of the principal rivers of the world. *International Journal of Digital Earth*, 2(1), 80–87.
- Macgregor, D. S. (2012). The development of the Nile drainage system: Integration of onshore and offshore evidence. *Petroleum Geoscience*, 18, 417–431.
- McCauley, J. F., Breed, C. S., Schaber, G. G., McHugh, W. P., Issawi, B., Haynes, C. V., & El Kilani, A. (1986). Paleodrainages of the eastern Sahara—The radar rivers revisited (Sir-A/B implications for a Mid-Tertiary Trans-African Drainage System). *IEEE Transactions on Geoscience and Remote Sensing*, 4, 624–648.
- McCauley, J. F., Schaber, G. G., Breed, C. S., Grolier, M. J., Haynes, C. V., Issawi, B., & Blom, R. (1982). Subsurface valleys and geoarcheology of the eastern Sahara revealed by shuttle radar. *Science*, 218(4576), 1004–1020.
- Omar, A. (1996). *Geological, mineralogical and geochemical studies on the Neogene and Quaternary Nile Basin deposits, Qena-Assiut stretch, Egypt* [Ph.D. Thesis] (p. 324). South Valley University.
- Omar, G. I., & Steckler, M. S. (1995). Fission track evidence on the initial rifting of the Red Sea: Two pulses, no propagation. *Sciences*, 270, 1341–1344.
- Said, R. (1981). *The geological evolution of the River Nile* (151 pp.). Springer.
- Said, R. (1993). *The river Nile, geology, hydrology and utilization* (320 pp.). Pergamon Press.
- Shukri, N. M. (1950). The mineralogy of some Nile sediments. *Quarterly Journal of the Geological Society of London*, 106, 466–467.
- Steinberg, J., Gvirtzman, Z., Folkman, Y., & Garfunkel, Z. (2011). Origin and nature of the Tertiary infilling of the Levant Basin. *Geology*, 39, 355–358.
- Talbot, M. R., & Williams, M. A. J. (2009). Cenozoic evolution of the Nile basin. In: H. J. Dumont (Ed.), *The Nile*. Monographiae Biologicae (Vol. 89, pp. 37–60). Springer.
- The World Bank. (2000). Available from <https://www.worldbank.org/689>.
- Wendorf, F., & Schild, R. (2014). *Prehistory of the Nile valley*. Academic.
- Woodward, J. C., Macklin, M. G., Fielding, L., Millar, I., Spencer, N., Welsby, D., & Williams, M. (2015). Shifting sediment sources in the world's longest river: A strontium isotope record for the Holocene Nile. *Quaternary Science Reviews*, 130, 124–140.



Bahay Issawi graduated his BSc (1955) and MSc (1964) degrees from Cairo University, and also holds a Ph.D. in Stratigraphy and Structures (1968) from the same institution. His work in the Western Desert is extensive where he conducted extensive field work and aerial-photo mapping over many years. He discovered the Abu Tartur phosphate deposits, iron ore deposits of the Bahariya Oasis, and the Kalabsha kaolin deposits south of Aswan. He has authored many carefully documented papers that are

still cited today. He contributed many articles and books on the Phanerozoic geology of Egypt.



Sherif Farouk is a professor in the Exploration Department of the Egyptian Petroleum Research Institute, Cairo. He obtained a Ph.D. degree from Al-Azhar University (Egypt). He worked for the Geological Survey of Egypt from 1996 until 2007. He is a specialist in high-resolution stratigraphy, paleoenvironmental analysis, sequence stratigraphic studies, and paleontological applications. He has published about 101 scientific articles in several international journals on Phanerozoic stratigraphy, especially of Egypt, Jordan, Saudi Arabia, Iraq, United Arab Emirates, and Tunisia.

Natural Resources in Egypt



The Phanerozoic Stratabound/Stratiform Ore Deposits of Egypt: Their Mode of Occurrence and Formation in Accordance with the Phanerozoic Geological Evolution

Mortada Mourad Taha El Aref

Abstract

The present work provides an integral and comprehensive view on the mode of occurrence and the mode formation of the ores hosted in outcropped Egyptian Phanerozoic rock sequences. The main goal of this work is to discuss the time/space problem of the formation of these deposits and to clarify the regional and local geological factors controlled their formation, in order to be fundamental guides for future exploration and investment plans. Also focusing has been bayed to clarify the sedimentary environments, parageneses, geochemical characteristics, possible source, and economic potentiality of each ore type as well as detailed explanation of the depositional, digenic, and post-diagenetic (supergenic) processes involved during the ore formation. The work shed some light on the mining advantages and investment opportunities of some of these ore deposits, as well as the challenges facing the development of their economic return. The ore deposits under consideration are of stratabound/stratiform types, being confined within certain stratigraphic horizons of different ages and paleo-geographic settings which concurrent well with the Phanerozoic geologic history of North Africa and the associated paleo-geographic evolution patterns of the paleo-shorelines and the simultaneous paleo-topographic configurations. The stratiform deposits show conspicuous depositional and diagenetic features of shallow near-shore environments and are hosted within certain marginal stratigraphic units of regional or local magnitudes. The

stratabound deposits are genetically related to paleo-erosion surfaces (sequence boundaries) and the related supergenesis as they constitute the main product of deep weathering processes. The concluded basic factors which controlled the formation of these ores at the time(s) and in the place(s) of their formation, can be summed up as follows: (a) the paleo-geography of the paleo-shorelines, (b) the paleo-topographic configurations and distribution of paleo-highs and paleo-lows, (c) the prevailed paleo-climates, (d) the simultaneous availability of the ore components, either from the local medium or from the adjacent hinterlands (d) the availability of a suitable paleo-environments with the related facies hierarchy and possible lateral facies changes, and (e) the prevailed sedimentary dynamics and sedimentation and post-sedimentation processes.

Keywords

Stratabound deposits • Digenetic processes • Paleo-Tethys • Neo-Tethys • Sedimentary dynamics • Egypt

1 Introduction

Egypt is located in the northeastern part of the African continent and consists of Precambrian igneous and metamorphic rock association followed by Phanerozoic sedimentary successions. The Precambrian rocks have been affected by various deformational episodes, ended by the Proterozoic Pan-African tectonothermal deformation. According to Schandelmair et al. (1987), the erosion and deposition of the Phanerozoic rock successions are generally controlled by reactivated faults and global sea level changes. The Phanerozoic history of Egypt is a part of the Phanerozoic evolution of the African continent which reflect the assembly of Pangea and the poly-phase breakup and the

The original version of this chapter has been revised. The chapter was published with incorrect words [paleo–karst] that have been corrected. The correction to this chapter can be found at https://doi.org/10.1007/978-3-030-95637-0_27.

Present Address:

M. M. T. El Aref (✉)

Department of Geology, Faculty of Science, Cairo University,
Giza, Egypt

e-mail: elaref@sci.cu.edu.eg

related tectonic phases of the Gondwana supercontinent. The details of the Phanerozoic geological history of North Africa have carefully studied and reviewed by distinguished scientists, among them are: Klitzsch and Wycisk (1987), Klitzsch (1984), Morgan (1990), Meshref (1990), Said (1990a, 1990b, 1990c), Stern (1994), Wilson and Guiraud (1998), Bosworth et al. (1999), Guiraud and Bosworth (1999), Guiraud et al. (2001, 2005), Issawi (2002) and Issawi et al. (1999, 2009). During the Phanerozoic time, North Africa including Egypt comprises an essential part of the southern boundary of the paleo- and new-Tethian seas. Accordingly, its Phanerozoic geological history was based mainly on the following dominating factors: (a) the effect of many structural events and successive periods of rifting phases accompanied by basaltic magmatic activities, (b) the domination of the paleo-Tethys and neo-Tethys shorelines along the northeast African margin, (c) sea level fluctuation, and southward transgression and northward regression of the seas, and (d) the geographic distribution and diversity of sedimentary environments and the related rock facies associations. With the context of the identification of the geology of the Egyptian Phanerozoic time span, it is necessary to clarify the geological setting and genesis of the ore deposits hosted in the Phanerozoic rock sequences.

This chapter aims to update the previously published contribution of El Aref (1996) on the origin of The Egyptian Phanerozoic stratabound and/or stratiform ore deposits. The inevitability, re-revision, updating, and republication of this version are due to the following objective reasons: (a) the original version is available only in the limited version and locally distributed proceeding of the second International Conference on the Geology of the Arab World (GAW II, Cairo, 1994, published in 1996), (b) there are many consequent scientific additions published after 1996 by the author and his colleagues, containing more explanations and detailed discussions on the nature and mode of formation of the ores involved, and (c) the dealt stratabound ore deposits constitute integral parts of the Egyptian Phanerozoic successions and coincided well with the geological history of this Epoch. The current comprehensive view, which is enhanced by new additional and redirected illustrations, throws more light on the main geological factors that controlled the development of the Phanerozoic stratabound/stratiform deposits of Pb, Zn, Cu, Fe, Mn, Sr, Ba, Al, P, and carbonate ore (the so-called Egyptian Alabaster) in their spaces and times of formation (Fig. 1; Table 1). The paleo-environments of these ores and the processes involved during their formation are clarified and discussed in detail. The other Phanerozoic geological resources such as the varieties of building stones, industrial non-metallic mineral resources, salts and evaporites, mineral fuels and fluvial and heavy mineral concentrates are not intended in this work. The chapter provides a compiled and an integrated genetic scheme, exhibiting the intimate genetic

relation between the ore formation and multiple regional and local geological processes (i.e. tectonic events, sedimentary environments, paleo-drainage, and volcanic activities), and also the general directions of the paleo-shorelines (transgression and regression trends), which all or some of them gathered at certain time(s) in a certain geological and geographic site(s) during the Phanerozoic history of Egypt (Table 1). The stratiform deposits show conspicuous depositional and diagenetic features of shallow near-shore environments and are hosted within certain stratigraphic units of regional or local magnitudes. The stratabound deposits are genetically related to paleo-erosion surfaces (sequence boundaries) and the related supergenesis as they constitute the main product of the related deep weathering processes. Besides the concerned ore deposits, wide varieties of the stratigraphic rock sequences and environments in which the deposits were accumulated were carefully studied. For clarification, the formal lithostratigraphic nomenclature is used for the viewed rock units, while the term time rock unit (sequence) is applied to those sandwiched between major unconformities or stratigraphic gaps.

The achievement of this work is based mainly on a very systematic way of deep observations and interpretations (i.e. inductive reasoning, “bottom-up approach”), moving from regional and local field investigations and mapping of the mine areas with stratigraphic correlations and verification of breaks of sedimentation and sequence boundaries to more detailed megascopic and microscopic examinations of representative and oriented polished slabs and thin and polished sections as well as much-sophisticated “nono-scopic” inspections of representative textures and spots, major and trace chemical analyses and isotope measurements. The fine (high resolution) stratigraphy of the ore intervals and the ore architecture, ore geometry, and the degree of congruency (fabric characteristics, fabric relations, and evolution), in all scales, are essentially considered. Considerable attention is attributed to the main characteristic features of the different ore types, their regional or local paleo-geographic concordances with the host rocks as well as the processes involved during their formation. This is accompanied by the interpretation of the several geological aspects that controlled the structural, sedimentological, and paleo-topographical setting of the host rocks and the associated deposits and the accompanied distribution of paleo-highs and paleo-lows that fairly settled at certain times and in certain places during the Phanerozoic history of Egypt.

As a general main outcome, the concluded integral scheme clarifies the situation (space and time) of the ore formation which may hopefully assist further exploration programs for new economic ore sites. It is important to clarify that the present work did not neglect attention to the geological setting, characteristics, and mode of the formation of many small-scale mineral occurrences or shows, in order for

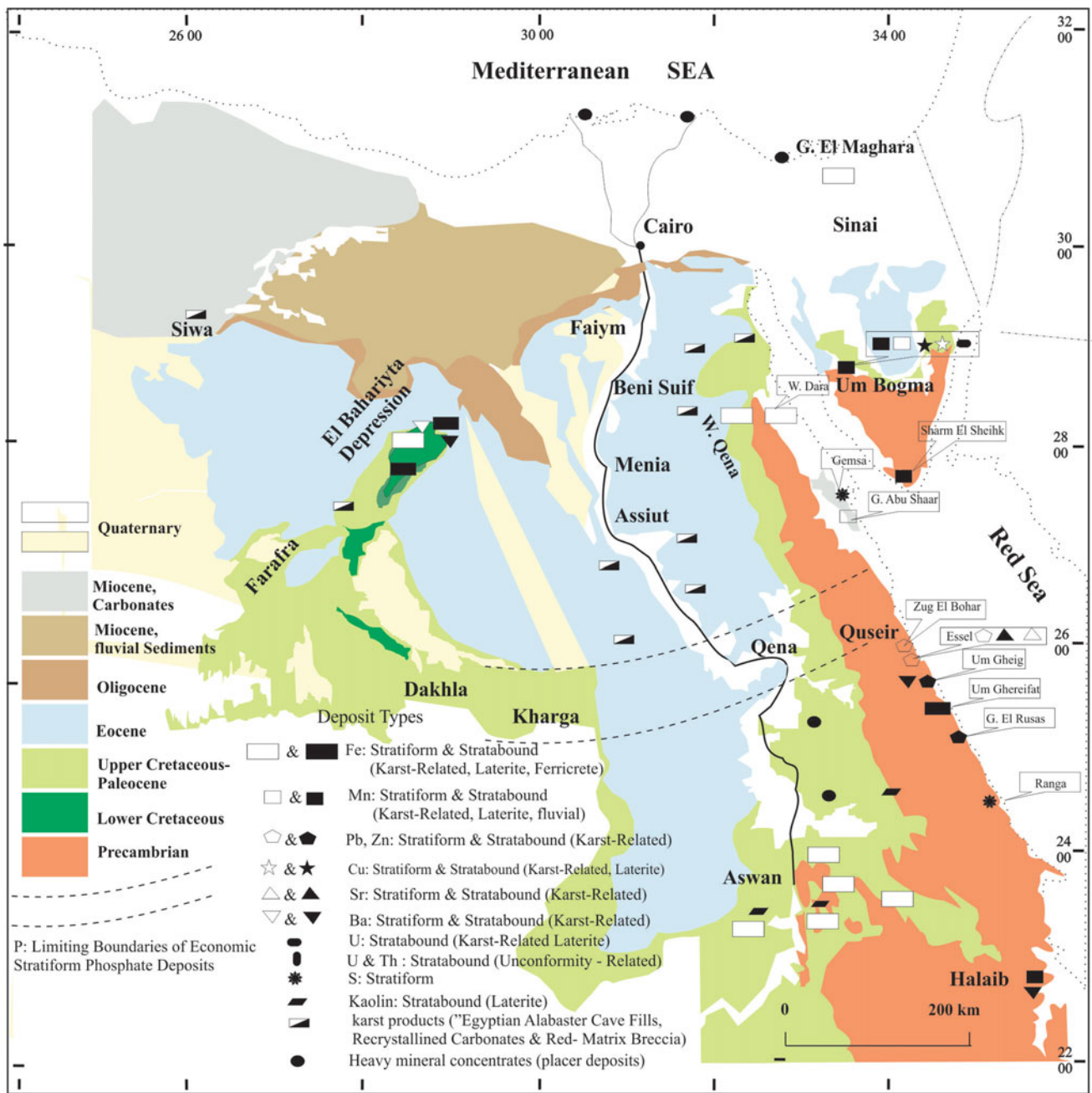


Fig. 1 Simplified geological map of Egypt and distribution of the Phanerozoic stratabound/stratiform ore deposits (modified after El Aref, 1996)

these occurrences to be fundamental necessities to future evaluation or exploration plans for similar new more economic places of the same geological setting or even to encourage their investment as small or very small enterprises.

The different genetic classifications of the Egyptian ore deposits including those confined within Phanerozoic rock units are reviewed and discussed by El Shazly (1957) and Hussein and El Sharkawi (1990). Hussein and El Sharkawi (op. cit.) presented a modified classification which follows the general scheme outlined by Hilmy and Hussein (1978).

El Aref (2001) has outlined the geologic setting of the Phanerozoic sedimentary hosted deposits within the chronologic framework of the Egyptian geological column of the metallurgical map of Egypt. Most if not all of the Egyptian ore deposits under consideration, occurred within the Phanerozoic sediments, has previously been attributed by the pioneer Egyptian epigenetists to epigenetic replacement processes by hydrothermal solutions of the Oligocene volcanisms or of unknown sources. Meneisy (1990) in his study of the Phanerozoic volcanic activities of Egypt related

deposits and the role of diagenesis and/or supergenesis in their formation. More recently, El Aref (2020a, 2020b) has provided a compiled synopsis on the Egyptian Fe and Mn deposits. However, the present chapter includes more information than those revised in El Aref (1996) and much genetic details and illustrations than what has been inspected in El Aref (2020a, 2020b). Table 2 shows the chronological arrangement of the Phanerozoic ore deposits.

2 Paleozoic Framework and Related Ore Deposits

During the Early Paleozoic, Egypt as a part of Gondwana was drifting toward the south reaching a paleo-latitude 70° S during the Ordovician and subsequently moved northwards rotating 180° (Smith, 1981). The Phanerozoic history of the northern margin of North Africa including Egypt started after the culmination of the Pre-Cambrian tectonic deformations. The surface of the northern Africa generally slope toward the paleo-Tethys and became very irregular, being dominated by paleo-highs and paleo-lows. Throughout the Paleozoic Era, the northern margin of North Africa, including Egypt, exposed to significant tectonic activities of regional or local magnitudes accompanied by alternating episodes of sea transgression and regression (Guiraud et al., 2001; Issawi et al., 2009). The early sea transgression over Egypt is expressed by the deposition of the Infra-Cambrian (earliest Cambrian) terrigenous sediments in Sinai (Taba Formation). During the Late Early Cambrian, mixed platform (varied facies) of the Araba Formation deposited on irregular Pre-Cambrian topography and well exposed in central Sinai and north Wadi Qena (Fig. 2a). Marine regression took place during Mid-Late Cambrian, most probably related to the latest Cambrian-Ordovician tectonic event. Fluvio-glacial clastics of the Ordovician Naqus Formation deposited on the Early Cambrian Araba Formation (Fig. 2b). The Silurian and Devonian seas have advanced only up to the northwestern corner of Egypt, against high positive lands in most of Egypt (Fig. 2b). During Early Carboniferous, marine transgression invaded east central Sinai, depositing the Visean carbonate rock successions (Um Bogma Formation) in the Um Bogma Region (Fig. 2c, d), directly over the Cambrian-Ordovician sediments, while the southeastern sector remained positive land under erosion. Tensional tectonic activity prevailed during the Late Permian (Guiraud et al., 2001) followed the opening of the neo-Tethys. As a consequence of plate collision and construction of the supercontinent Pangaea (Late Paleozoic-Early Mesozoic tectonic event Klitzsch, 1986), Upper Egypt was uplifted along rejuvenated ENE trending faults (Schandelmeier et al., 1987) and volcanic activities predominate (Meneisy, 1990).

The end results of the Cambrian-Carboniferous paleotopographic evolution patterns together with the configurations of the paleo-shorelines during the Cambrian and Carboniferous times are well expressed in the Um Bogma region (Fig. 2c). The lithostratigraphic rock sequences and their environments of this region are shown in Table 3. As it is evident, the Early Cambrian (Araba), and the Ordovician (Naqus) sequences rest on irregular relief of the Pre-Cambrian rocks and are followed unconformably by Mn bearing carbonate unite of the well-known Um Bogma Formation (Visean) which is punctuated by intra-Um Bogma paleo-karst surface, separating this unite into two easily identifiable sequences, a lower Mn bearing sequence and an upper carbonate sequence. The Cambrian-Carboniferous stratigraphic sequences of this region include varieties of stratabound deposits (Table 1; Figs. 3, 4, 5, 6, 7 and 8), among which are: (a) Thorium-Uranium bearing heavy mineral concentrates, building up the basal polymictic conglomerates of the Cambrian sequence, (b) Cambrian stratiform malachite, and (c) Early Carboniferous stratabound/stratiform manganese deposits with copper and uranium enrichment.

2.1 Cambrian Stratabound Th–U and Cu Occurrences

In Um Bogma region, the Cambrian strata comprise the shore face clastic sediments of the Araba sequence (Araba “Formation”) with its trilobites and bilobites tracks as well as detectable Th, U, and Cu occurrences.

2.1.1 Cambrian Th–U Occurrence

Cambrian radioactive conglomerates (up to 410–600 ppm Th and 170–238 ppm U) build up the basal polymictic conglomerate unit of the proximal fluvial clastics of the Cambrian sequence (Aita, 1996; Hussein et al., 1998). The radioactivity of these conglomerates is related to the concentration of detrital radioactive mineral grains including uranorthorite, thorite, and xenotime and metamict zircon, probably derived from the nearby paleo-highs of the Pre-cambrian igneous and metamorphic rocks, and shortly transported together with other components into the upper reaches of braided streams. Decomposition of the radioactive heavy grains during transportation, deposition, and diagenesis is responsible for the redistribution of Th and U in the Fe oxyhydroxides’ matrix and hematite cement of the host rocks. The host conglomerates of this type could be more uraniferous and of economic interest if they are traced far from the weathering and oxidation zones, meaning secondary uranium, could be found on the surface.

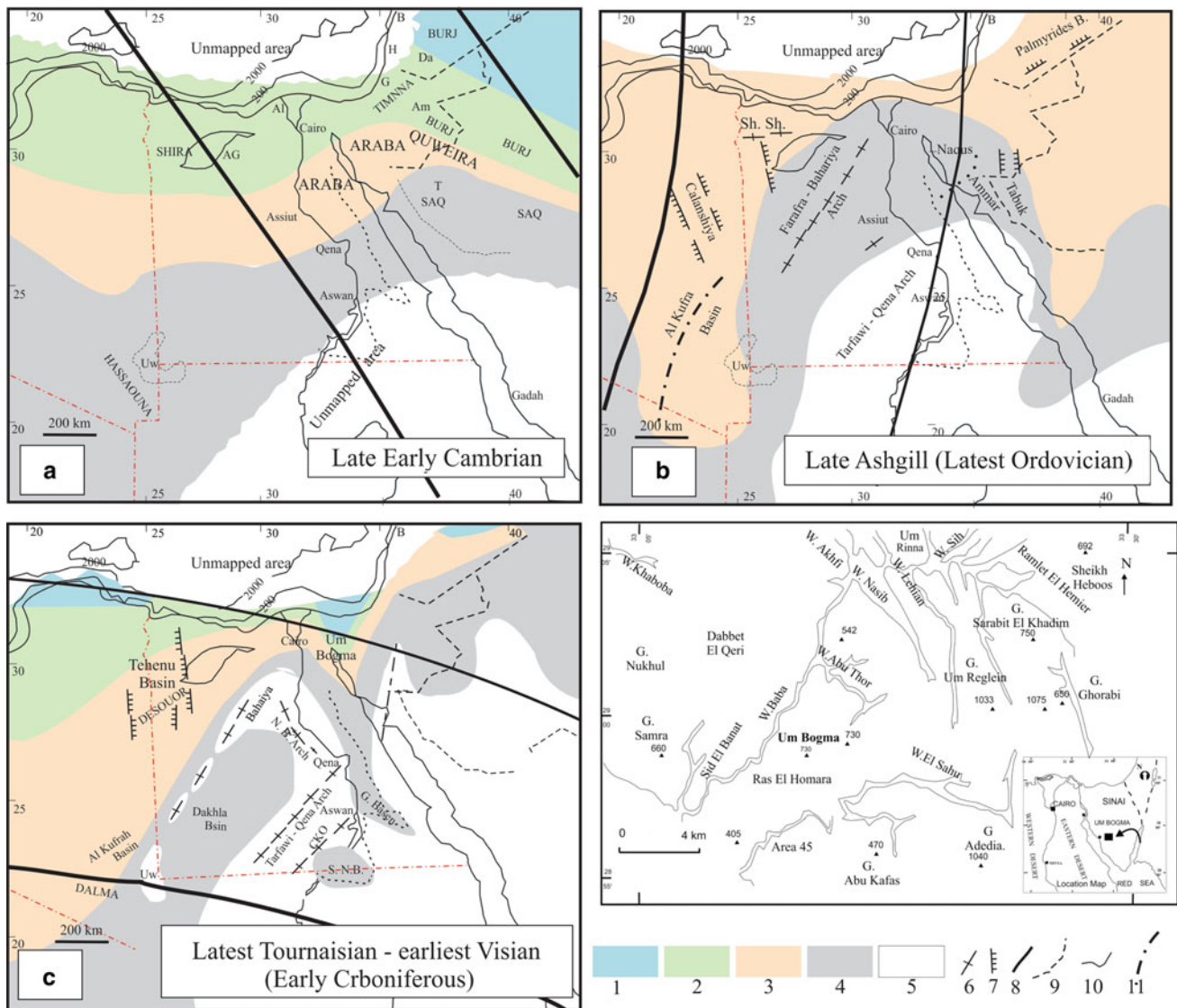


Fig. 2 (a–c): Late Early Cambrian, Latest Ordovician, and Latest Tournaisian-earliest Visian (Early Carboniferous) paleo-geographic/paleo-tectonic map (simplified after Guiraud et al., 2001). 1 = carbonate platform, 2 = mixed platform (varied facies), 3 = terrigenous platform, 4 = fluvial–lacustrine environment, 5 = exposed land, 6 = uplifted arch, 7 = active normal fault, 8 = unspecified active fault, 9 = present-day Precambrian basement–sedimentary cover limit, 10 = present-day shoreline, 11 = depocenter. Figure (d): Location map of the Um Bogma Region and the study sites and measured stratigraphic sections

2.1.2 Cambrian Stratiform Malachite

Stratiform malachite is found within the upper part of the shore face clastics of the Cambrian Araba sequence which is correlated with the Cambrian cupriferous sediments of Timna, Israel and Wadi Dana, Jordan. The malachite is mostly confined to the middle green variegated part of the host rocks (Figs. 3 and 4). In the overlying and underlying parts, no malachite or other copper minerals are detected. The Malachite of this type occurs as interstitial material in the host sandstone, siltstone, and shale interbeds and is often associated with kaolinite, illite, chlorite, and calcite (El Sharkawi et al., 1990a).

The megascopic and microscopic geometric patterns of the malachite and the associated minerals are almost conformable with or even form the syn-sedimentary (syn-depositional, syn-deformational, and biogenic) structures of the host rocks, e.g. horizontal, adulatory, and cross-laminations; ripple marks, flasers, biogenic (burrowing), scour and fill structures and desiccation cracks (Fig. 3, sections A*– C** and Fig. 5). The close congruence of the geometric patterns of the malachite with the syn-sedimentary structures suggests that Cu has been leached from nearby copper bearing paleo-highs and transported with other land-derived clays into the basin of deposition as copper

Table 2 Chronological classification of the Phanerozoic stratabound ore deposits

Paleozoic		• Cambrian Th–U occurrence
		• Cambrian stratiform Malachite
		• Intra-Carboniferous stratabound/stratiform
		• Mn ores with Cu and U enrichment
Mesozoic		• Jurassic-lower Cretaceous ironstones
		• Upper Cretaceous ironstones, laterites, and phosphorite deposits
		• Cenomanian ironstones
		• Turonian laterites
		• Coniacian-Santonian oolitic ironstones
		• Campanian-Maastrichtian stratiform phosphorite deposit
Cenozoic	Paleogene	• Lutetian-Bartonian stratabound oolitic-oncolitic iron ores
		• Fe-rich lateritic blankets (surficial ferricrete duricrust)
		• Pre-rift fossilized aluminous ferruginous latosol
		• Karst economic carbonate stones (karst cave fills, “Egyptian Alabaeter”) Paleogene-Quaternary (?)
	Neogene (rift-related ore deposits)	• Oligo-Miocene (?) flinty conglomeritic Mn ore
		• Middle Miocene stratiform to stratabound galena of beach environment
		• Middle Miocene stratiform oolitic-oncolitic Mn ore
		• Middle Miocene stratiform and post-Middle Miocene stratabound celestite
		• Middle to Late Miocene stratiform and stratabound barite
		• Middle to Late Miocene stratiform and stratabound biogenic sulfur deposit
		• Post-Late Miocene stratabound Pb, Zn sulfides, and calamine ore
		• Post-Miocene surficial Mn deposits
		• Post-Miocene-Quaternary (?) surficial conglomeritic Mn deposits

bicarbonate or microbial complex, where it was diagenetically crystallized into malachite during the drying-out of the host sediments (El Sharkawi et al., 1990a). The occurrence of this malachite type in Um Bogma environ may be attributed to the availability and proximity of copper bearing Pre-Cambrian or Cambrian hinterlands.

2.2 Intra-Carboniferous Stratabound/Stratiform Mn Ores with Cu and U Enrichment

• Geologic and stratigraphic setting

During the Carboniferous (Visean) time, the northeastern corner of Egypt, particularly the entire Um Bogma region, was transgressed by shallow Carboniferous sea, where carbonate sequences hosting Mn deposits (Um Bogma sequences) were laid down (Fig. 2).

The Carboniferous carbonates are of limited distribution and restricted only to the Um Bogma region. Meanwhile, the southern and eastern hinterlands remained positive land under erosion (Klitzsch & Wycisk, 1987). The Early Carboniferous Um Bogma carbonates rests unconformably

above the Pre-Cambrian rocks and/or above different clastic horizons of the Cambrian Araba and Ordovician Naqus sequences (Figs. 6, 7 and 8). Toward east and south, the carbonate successions are highly attenuated and being divided into two distinguished sequences separated by intra-Um Bogma paleo-karst surface (Figs. 6, 7 and 8; Tables 3 and 4). The lower sequence is formed by laterally changed and intertongued stratabound/stratiform Mn facies associations (Fig. 7), sandwiched between two sequence boundaries, i.e. the Cambrian/Ordovician-Carboniferous sequence boundary and the intra-Um Bogma paleo-karst surface (Figs. 6 and 7). The lower Mn bearing sequence is covered by overstepped rhythmic alternations of dolostones and mudstones of the Upper Um Bogma sequence (Figs. 6 and 7). The lithofacies associations of the Mn deposits and the equivalent and overlying carbonates are summarized in Table 3.

The fluvial and near-surface sedimentations of the Late Visean–Early Namurian Abu Thora (Weissbrod, 1969) or Ataq (Issawi et al., 2009) Formation (sequence) rests on different carbonate horizons of the upper carbonate sequence and/or directly on different horizons of the Mn facies of the lower Mn bearing sequence (Figs. 7 and 8). As clarified by Klitzsch (1990), El Aref (1996), and El Aref and Adel

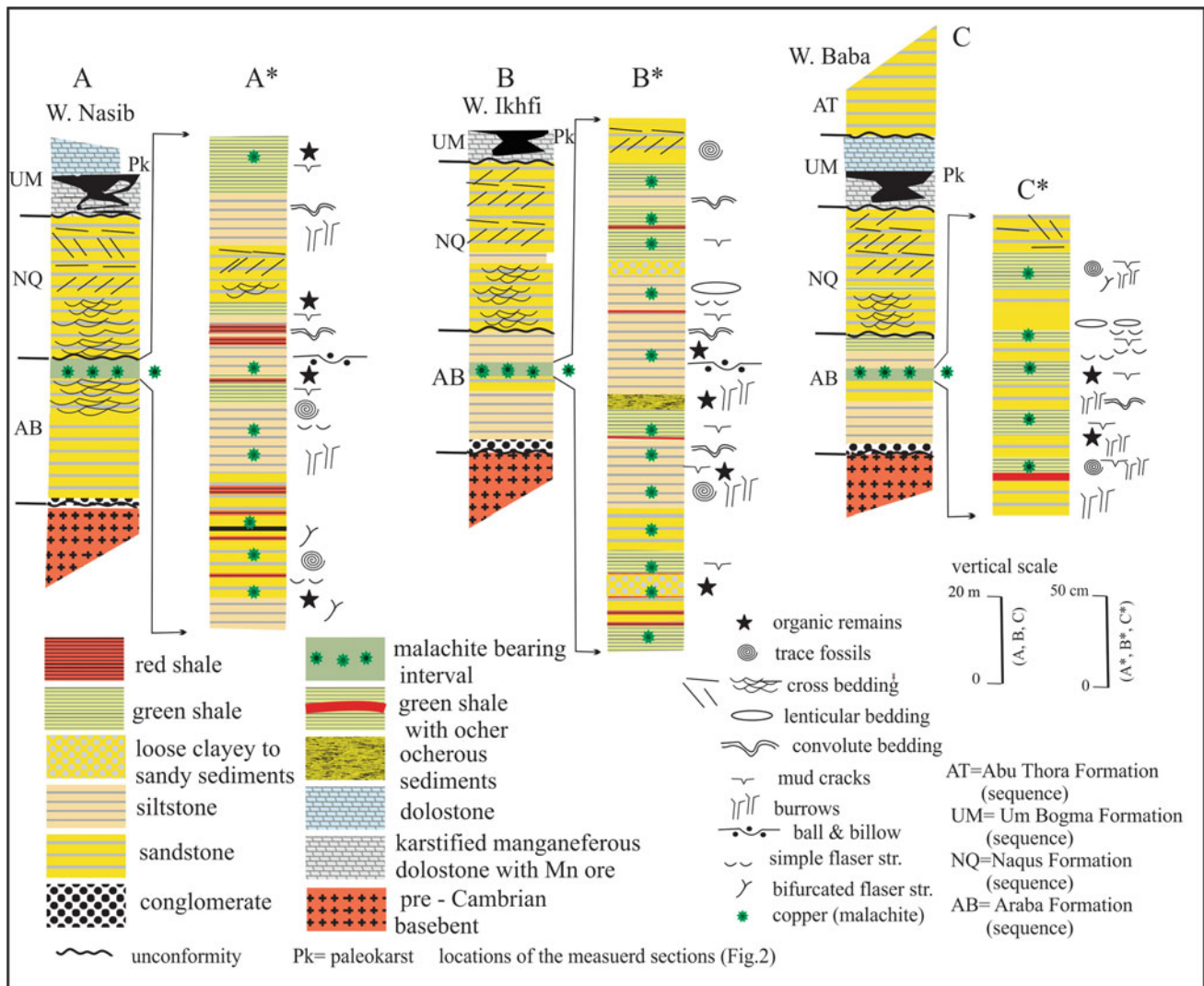


Fig. 3 General lithostratigraphic sections (A, B, and C) and fine (high resolution) stratigraphy (A*, B*, and C*) showing the stratigraphic setting of the stratiform malachite interval of the Cambrian Araba Formation (sequence), Um Bogma region (El Sharkawi et al., 1990a)

Motilib (2001), the Um Bogma sequences are completely missing south of the Um Bogma environ. At northern Wadi Qena in the Eastern Desert, Abu Thora fluvial sequence unconformably deposited on the Cambrian clastics (Abdallah et al., 1992).

• Mn ore facies (types) association

The Lower Um Bogma sequence is composed of the following continental and marine Mn ore facies (Table 4; Figs. 6, 7 and 8 zones A–D):

1. Stratiform continental Mn ore type (facies),
2. Stratiform Lagoonal to swampy Mn ore type (facies), superimposed by Stratabound karst Mn ore type, and

3. Stratiform near-shore oncolitic Mn ore type (facies).

These Mn ore facies or types intertongue from east to west and change westward into up 0–45 m thick of continuous section of marine fossiliferous (oolitic) carbonates and shales (the type section of Um Bogma “Formation” at Gabal Khabuba), (Figs. 6, 7 and 8). The intra-Um Bogma paleo-karstification led to the destruction, dissolution, and decomposition of the manganese dolostones and mudstones of the lower sequence and re-concentration of the fourth enriched karst ore type.

The composition and main characteristics of the recognized ore facies (types) and the superimposed paleo-karst horizons are compiled and summarized by El Aref (2020b; Table 5).



Fig. 4 Field photograph showing the Paleozoic sequences of Wadi Nasib, Um Bogma region, and the stratigraphic position of the stratiform malachite (red arrow) that is confined within the middle green shale of the upper part of the Araba sequence (2). 1 = the lower part of the Araba sequence

A. Stratiform continental Mn facies

This ore type is well-displayed in the extreme eastern zone of the Um Bogma region (Figs. 6, 7 and 8 zone D, Table 4). It consists of successive cyclic bodies (30–80 cm thick) being lenticular in shape and of fining-upward pattern, often interrupted by reactivation surfaces. The lower part is formed by Mn conglomerates followed upward by Mn sandstones and mudstones. The Mn-rich framework components (up to boulder, gravel, and sand sizes) are usually elongated parallel to the current direction and are flanked by cross-laminated sandstones or as lags along troughs of cross-sets. This ore type reflects deposition in braided streams by land-derived lateritic Mn-rich clastic and muddy materials, probably derived from nearby contiguous source (paleo-highs).

B. Stratiform manganiferous mudstones and dolostones (lagoonal to swampy facies)

This ore type is well-developed in the central zone of the Um Bogma region (Figs. 6, 7, and 8 zone C; Table 4). It forms stratified meter-scale sequences, each of which begins with manganiferous and ferruginous mudstones at the base, terminating upward by cyclic rhythmically alternating beds of karstified and rotten manganiferous dolostones and mudstones, earthy or sooty in part, and rich in evaporite nodules. It represents deposition in shallow shelf-restricted lagoonal environment enriched by land-derived Mn and Fe oxyhydroxides in association with marine influx. The depositional and marine diagenetic processes and textures of the Mn dolostones are simply illustrated in Fig 9.

Karst Ore

As a result of the uplifting and exposing of the lower Mn bearing sequence, the genuine lagoonal manganiferous dolostones were highly subjected to intensive post-digenetic processes (Fig. 10). These processes resulted in the formation of enriched karst ore (Figs. 6, 10, and 11; Tables 4, 5 and 6). The paleo-karst profile comprises three transitional horizons, including (a) a lower horizon of karstified manganiferous dolostones, (b) a middle subsoil (enrichment) breccia horizon, and (c) an upper variegated topsoil (lateritic) horizon (Figs. 10 and 11).

Along the paleo-karst surface, the karstified country rocks show varieties of vadose and vadose to phreatic solution features accompanied by telogenetic wall rock alteration processes and pyrogenesis (Figs. 9 and 10). Among which are: dissolution, dedolomitization, pulverization, collapsing, and accumulation of lateritic earthy Mn and Fe products, vadose geopetal fillings, formation of coarse-grained Mn and Fe-rich dolomite, Ferron calcite, late orthosparite, and barite cementation (Fig. 9). The overlying gradational subsoil (enrichment, illuvial) horizon (2–8 m thick) is dominated by morphogenetic filled solution features of various shapes and diameters, ranging from small passages of network pattern, trough to V-shaped depressions as well as infilled solution cavities, that developed along cross-cutting cracks or/and bedding planes (Fig. 10). Predominant large scale infilled cavities connected through solution passages and small-scale sinkholes and collapse dolines, form detectable surface of cusped form. The solution features are often bordered by crackled rocks and commonly filled with re-deposited crustified colloform layers of Mn oxides and hydroxides, mantling the cavities walls and ceils or surrounding collapse

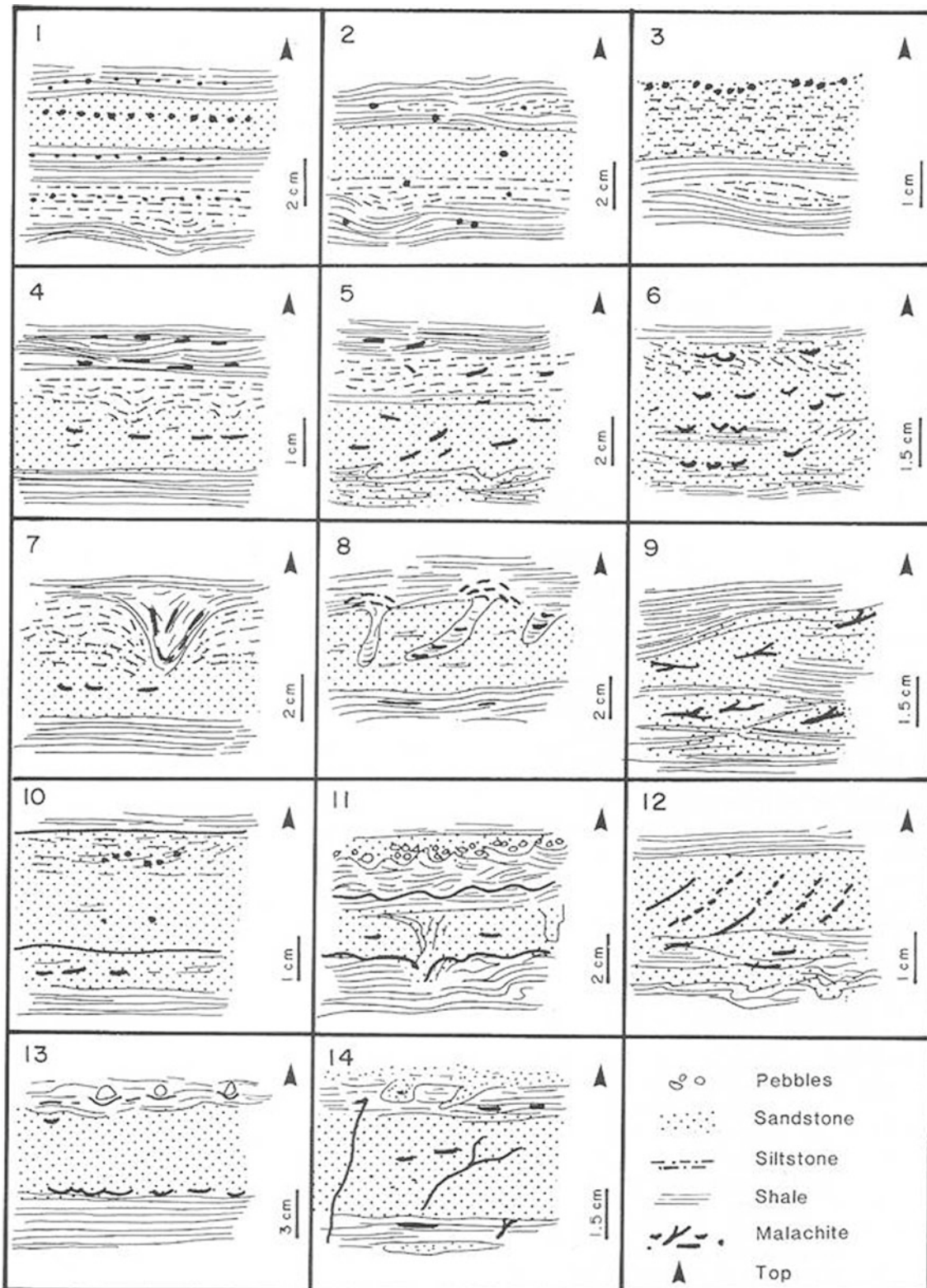


Fig. 5 Geometric distribution patterns of the Cambrian malachite (after El Sharkawi et al., 1990a). 1–3 = stratabound to stratiform malachite disseminations, 1 = dissected lamina, 2 = stratabound randomly distributed spots, 3 = spotty ripple marks. 4–6 = stratabound to stratiform streaks, 4 = stratified discontinuous streaks, 5 = planer non-parallel flasers, 6 = concave-convex oscillation ripples, 7 = filling scour and fill structure, 8 = filling shallow burrow pipes, 9 = bifurcated flasers, 10 = stratified lamination, 11 = undulated lamination, 12 = spotted cross-lamination, 13 = buried mud cracks, 14 = stratabound veinlet's

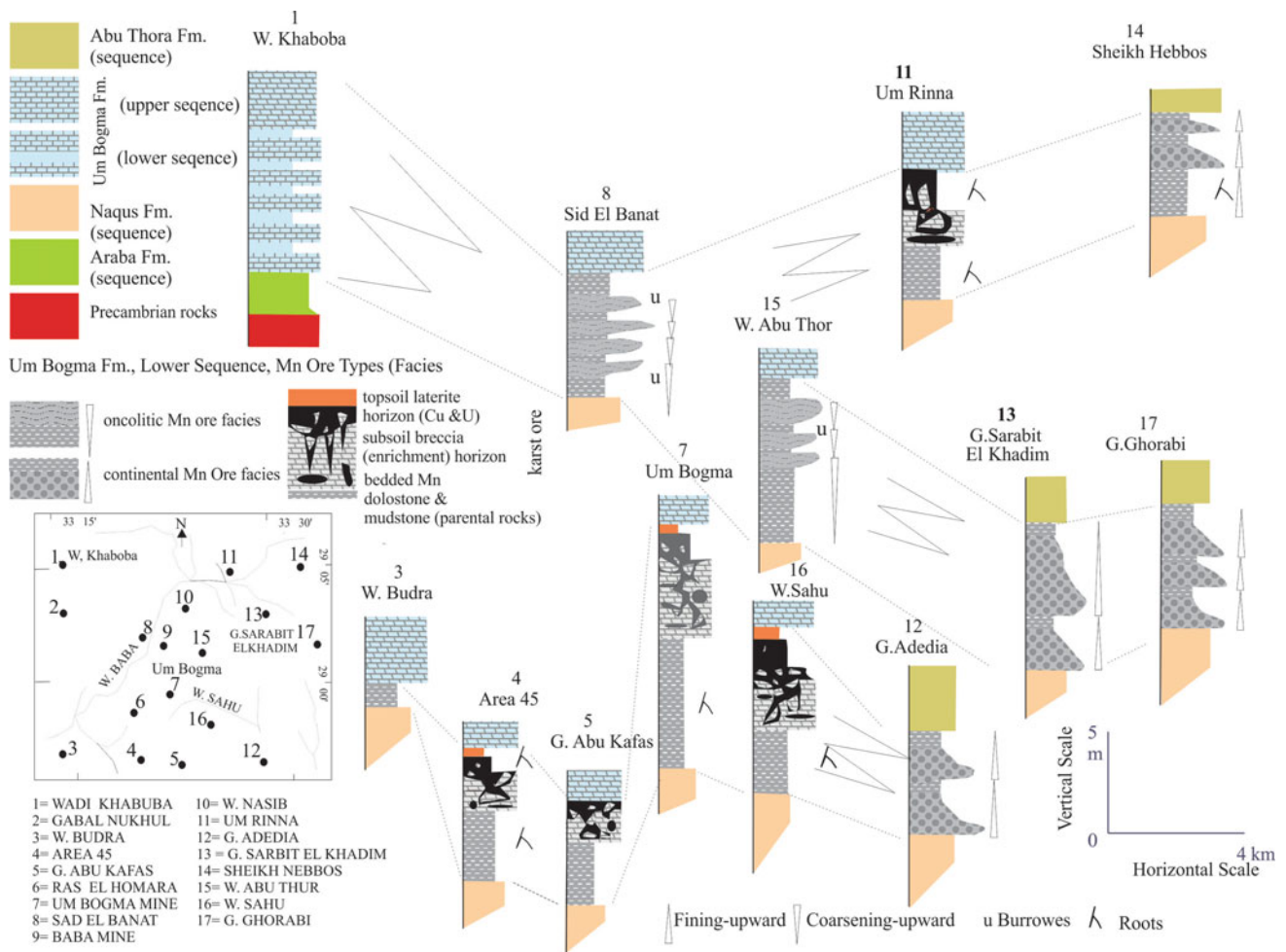


Fig. 6 Fine stratigraphy and lateral facies changes of the Carboniferous Um Bogma sequences (modified after El Aref & Abdel Motelib, 2001)

breccia fragments forming cockade textures, or may form isolated or grouped, nodules and concretions of variable diameters setting in earthy matrix. The topsoil horizon (20–60 cm, Figs. 10 and 11; Tables 5–7) is a leaching (eluvial) horizon being composed of multi-colored lenticular and patchy segregations of nodular kaolinite, gibbsite, and jarosite mixed with red and yellow ochers, black earthy manganese materials, alunite nodules, bituminous plant remains (woody particles and organic detritus) and land-derived palynomorphs. Barite and gypsum veinlets, nodules and rosette forms, circular pores, tubules, root molds and alveolar textures and desiccations are very common within these lateritic products. Mn, Cu, and U bearing carbonate, chloride, sulfate, silicate, phosphate, and vanadate minerals are frequently distributed within the topsoil horizon (Table 6) filling shrinkage cracks or may migrate downward through solution passages into the Mn-rich subsoil horizon. The Egyptian Nuclear Materials Authority (NMA)

undertakes the study and evaluation of the radioactive elements concentrated in the intra-Um Bogma paleo-karst soil sediments. According to Abdel Motelib (1987), the subsequent erosion of the exposed Mn bearing carbonates in some sites led to gradual destruction and decomposition of the paleo-karst horizons and the Mn deposits and the associated Cu and U mineral associations.

C. Stratiform oncolitic Mn ore (Figs. 6 and 8 zone B; Table 4)

This ore type represents the northwest lateral facies change of the lagoonal Mn facies association. It is fairly bedded and consists of small-scale (30–80 cm) coarsening-upward sequences. Each sequence starts at the base by bioturbated manganese to ferruginous mudstones rich in organic matter, grading upward into manganese oncolitic

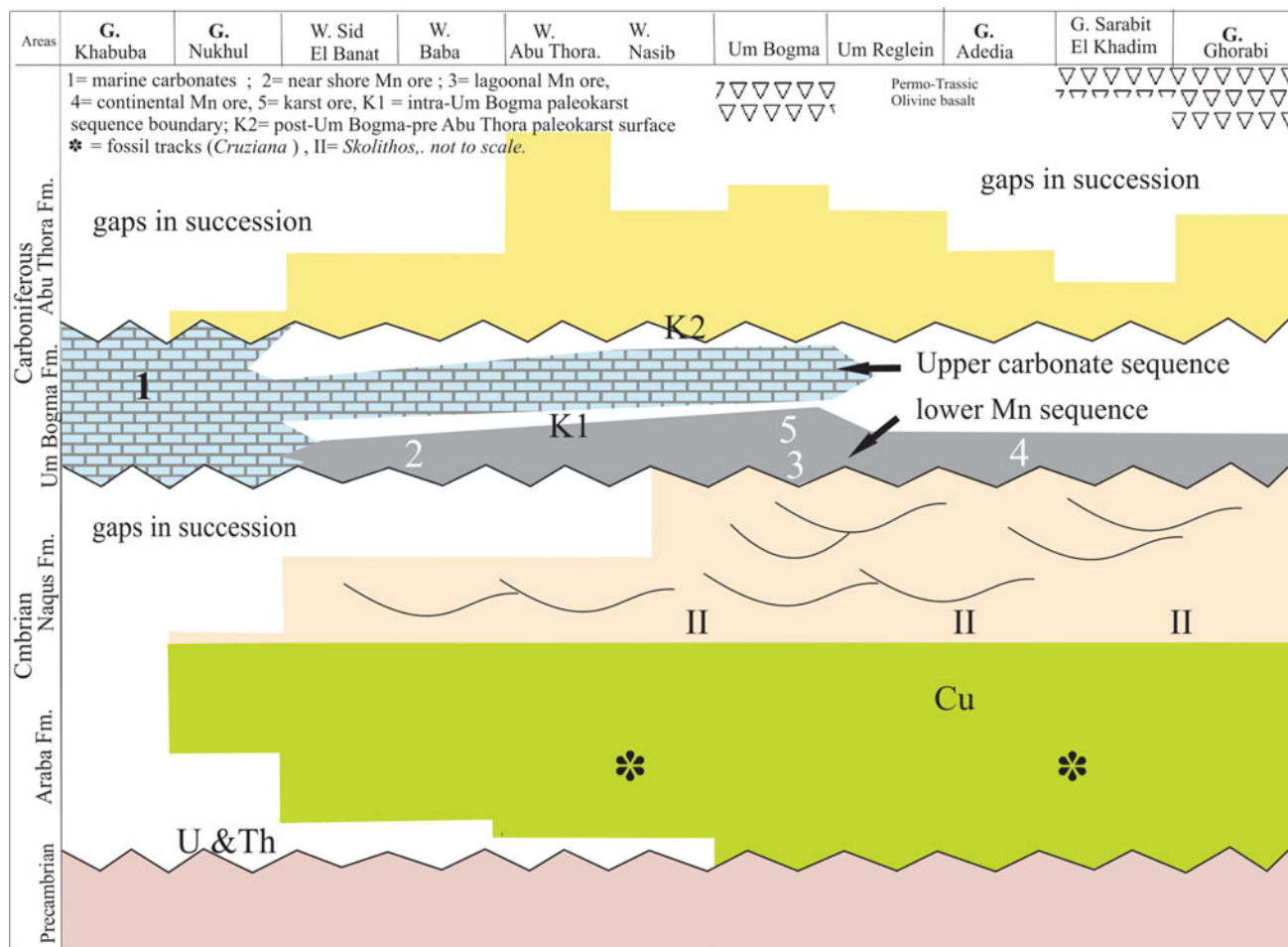


Fig. 7 Different gaps intervene of the Paleozoic sequences of Um Bogma Region and the stratigraphic setting of the associated stratabound ore types (El Aref & Adel Motelib, 2001). 1 = carbonate facies; 2 = oncolytic Mn facies; 3 = lagoonal Mn facies; 4 = continental Mn facies; 5 = karst ore

storm-generated beds or coarse lags consisting of manganeseiferous oncolites, goethitic in part, coarse skeletal fragments, and fossil molds. The framework components set in a Mn-rich clayey matrix. The sedimentological characters of this ore type reflect formation under marginal marine conditions with the deposition of land-derived manganeseiferous materials from suspension in a calm environment followed by storm-generated deposition responsible for the accumulation of the oncolite and skeletal components.

• Genetic considerations

1. The intra-Carboniferous Um Bogma Mn ore is confined within the lower Um Bogma sequence and consists of laterally changed stratiform continental and shallow marine Mn facies. The paleo-geography, stratigraphic setting, composition, and paleo-environments of the different recognized Mn ore facies indicate the following:

- The Um Bogma Mn ore is of sedimentary origin developed along the Visean paleo-shoreline.
 - Land-derived lateritic Mn-rich lateritic clasts and/or suspensions were transported from the adjacent lateritized hinterlands and deposited as fluvial Mn facies in the eastern zone.
 - The land-derived lateritic products moved into the Visean shoreline, depositing lagoon to shallow marine Mn ore type in the central zone, contemporaneous with the deposition of the equivalent oolitic marine carbonates further west.
 - The different Mn facies exhibits varieties of syn-depositional textures and subjected to a series of diagenetic processes. The central Mn carbonates undergone subaerial dissolution and enrichment as a result of paleo-karstification processes of humid paleo-climatic condition.
2. The detailed field, megascopic, and microscopic investigations, chemical analyses and radioactive

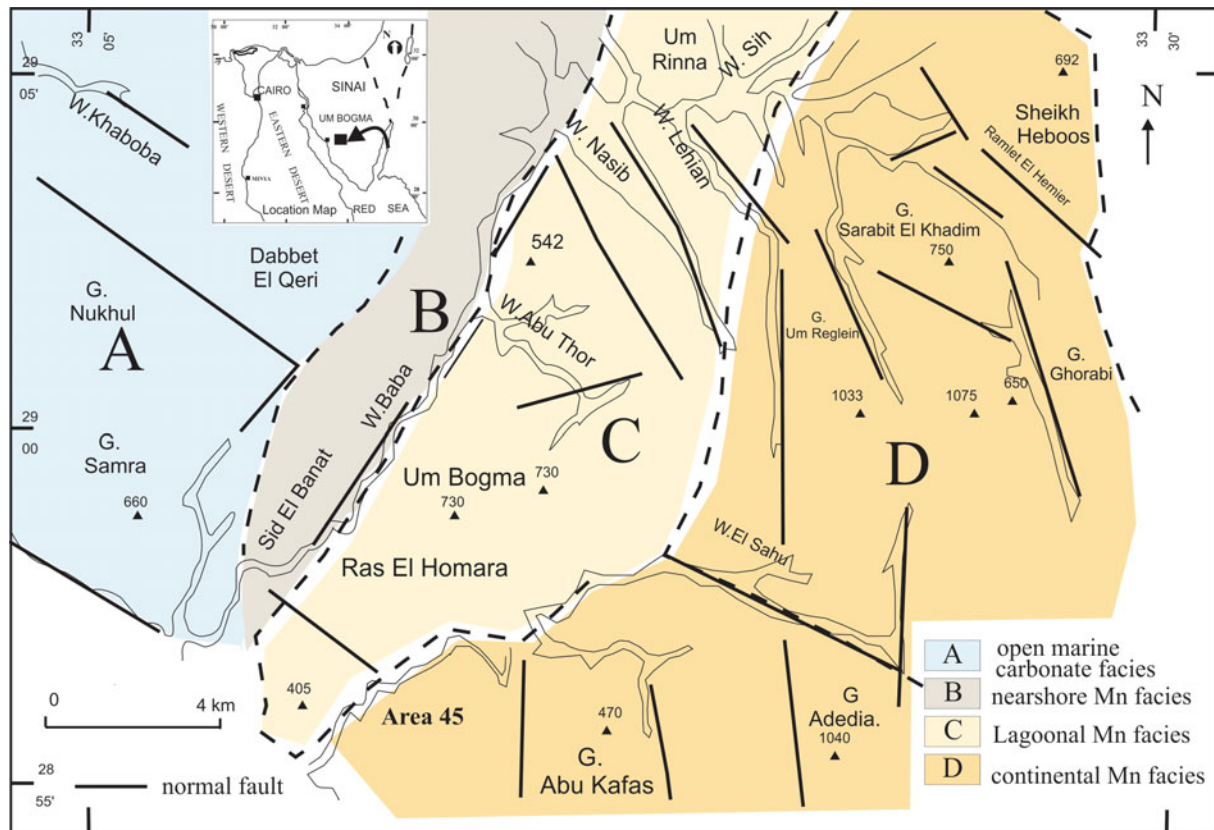


Fig. 8 Simplified structural map of Um Bogma region showing the geographic distribution of the recognized Mn facies and the equivalent carbonates of the lower Um Bogma sequence (El Aref & Abdel Motelib, 2001)

measurements of the karst Mn products, carried out by: Hilmy and Mohsen (1965), Hilmy et al. (1958), El Sharkawi et al. (1990a, 1990b), El Aref (1996), Abdel Motelib (1987, 1996), Aita (1996), El Aref et al., 1998; Hussein et al. (1998), El Aref and Abdel Motelib (2001), and El Aref (2000) enable the recognition of the detailed genetic processes prevailed during the intra-Carboniferous paleo-karstification and the formation of the different mineral assemblages throughout the karst profile, as has been briefly reviewed below: Three main progressive processes have been taken place during the periods of active weathering under humid condition, including

- a. Carbonate dissolution with desilication, hydrolysis, enrichment of Fe and Al and formation of kaolinitic latosol along the surface of the weathered carbonates, forming the upper soil horizon, accompanied by Mn separation and concentration in the subsoil horizon.
- b. Secondary bauxitization through continuous desilication and hydrolysis together with Mn–Si–Al–Fe dissociation and gibbsite formation, and
- c. Subsequent alunization and formation of alunite and evaporitic Cu and U minerals during the

general desiccation of the lateritic products under arid to semiarid paleo-climate.

3. During the humid periods, the dissolution of the exposed manganiferous dolostones is favored during the increase in the pH and CO₂ content of the soil water, resulting from the plant and organic matter decomposition. During the carbonate dissolution, the mobile cations and anions (e.g. Ca²⁺, Mg²⁺, Na⁺, K⁺, Sr²⁺, Ni²⁺, CO₃²⁻, Pb²⁺, Zn²⁺, Cu²⁺, Ba⁺, V³⁺, U⁴⁺, Th⁴⁺, CO₃²⁻, SO₄²⁻, OH⁻, CO₃ H⁻, Cl⁻, PO₄³⁻, NO₃⁻, and H²⁺VO₄⁻) moved in the soil water. The less mobile elements Fe³⁺, Mn²⁺, Si²⁺, and Al³ left as residual products, i.e. formation of kaolinite and Fe oxides and hydroxides under fairly acidic condition.
4. The concentration of the Mn oxides and hydroxides in the subsoil solution openings as infilling crustified (colloform) layers indicate the differential leaching of the less mobile elements (i.e. Si, Al, Fe, Mn) from the uppermost acidic topsoil (leaching horizon) during the soilification processes with changing pH and Eh values. The leached Mn migrated downward toward the subsoil horizon (enrichment horizon) and deposited under more suitable pH-Eh conditions, leaving behind the more resistant Si, Al, and Fe bearing minerals.

Table 3 Lithostratigraphic sequences and their depositional environments of Um Bogma Region (modified after Abdel Motelib, 1996)

Age	Thick	Sequences ("formations")	Lithology	Environment
Permo-Triassic	20 m	Volcanics	Olivine basalt	
Paleozoic	200 m	Abu Thora	Conglomerate, sandstone, mudstone, coal	Shallow marine to fluvial paralic sedimentation
		Um Bogma sequences	<i>Intra-Carboniferous paleo-karst surface (sequence boundary)</i>	
	0-45 m	Upper dolostone sequence (0-25 m)	Dolostone and shale intercalations	Marine transgression, tidal flat to open marine
			<i>Intra-Um Bogma paleo-karst surface (sequence boundary)</i>	
Unconformity		Lower dolostone sequence (0-20 m)	Western part	Eastern part
			Dolostone and shale intercalation	Karst Mn ore karstified Mn dolostone and mudstone
Late Ordovician-Early Silurian		Naqus sequence	Gravely cross-bedded sandstones and conglomerates	
		Unconformity		
Early Cambrian	130 m	Araba sequence	Upper part	Variegated coarsening-upward successions of sandstones and mudstones with <i>Cruziana</i> Sp.
			Lower part	Fining-upward successions of conglomerate, gravely sandstone and sandstone and mudstone
Precambrian-Cambrian unconformity				
Precambrian granites, granodiorites, schists, gneisses and migmatites				

Table 4 Mn ore Facies and the equivalent carbonate Facies of the early Carboniferous Um Bogma sequences (Abdel Motelib, 1996; El Aref & Abdel Motelib, 2001; El Sharkawi et al., 1990b)

		Western facies	Central facies		Eastern facies
		Carboniferous Um Bogma sequences	Locations in Fig. 2	W. Khaboba, G. Nukhul	Sid El Banat, W. Kharig
Upper Um Bogma sequence (rock unit facies)	Oolitic Grst				Sandy dolomitic Grst
	Fossiliferous shale				
	Argillaceous Echainoidal Wkst–Pkst				
	Brachipod Pkst				
m Intraformational paleo-karst + paleosol unconformity					
Lower Um Bogma sequence (Mn ore and carbonate facies)	Fossiliferous shale–Grst–sandy oolitic Grst	Oncolitic Mn facies	Karst ore bedded Mn dolostone and mudstone	Mn conglomerate, sandstone and mudstone	
Grst = grainstone; Pkst= packstone; Wkst= wackestone					
Grst = grainstone, Pkst = packstone, Wkst = wackestone, Mdst = mudstone					

- Cu and U minerals were deposited from pore soil solution containing Cu^{2+} , Cl^- , SO_4^{2-} , CO_3^{2-} , PO_4^{3-} , SiO_3^{2-} , V^{3+} , and Al^{3+} ions and entrapped within the topsoil products. The geochemical behavior of U during the soilification and its concentration in the topsoil products is mostly controlled by the Eh and the amount of CO_2 in the system and the concentration of vanadium and phosphorous and other soluble cations and anions. The humic constituents of the soil products are very effective trapping material and the Fe, Al, and Mn hydroxides. Clays can also adsorb uranium. The formation of copper minerals was prevailed during low moister regimes or periods of evaporation and under neutral to alkaline conditions. Veinlet's of copper minerals cutting through certain karst ore or karst alteration products indicate the mobilization of the above-mentioned ions during the subsequent acidic leaching and their re-deposition during the drying out of the soil moister.
- The late cements and dripstones of carbonate and sulfate minerals reflect crystallization during the arid periods, as a result of ultimate evapotranspiration of the soil moister and decrease in the biological activity and CO_2 content.
- More details on the mechanism and geochemical behaviors of the constituent elements and minerals during their formation appear in the mentioned relevant publications.

3 Mesozoic Framework and Related Ore Deposits

The Late Paleozoic “Hercynian” tectonic event was followed by Triassic sea transgression depositing marine rock association in the structurally low area of Arif El Naqa, northeast Sinai. Southwards, along the Gulf of Suez, Permo-Triassic paracontinental sediments (Quseib Formation) were accumulated. In general, during Jurassic-Early Tertiary, coastal plains and shallow shelves of low relief prevailed in the northern and central parts of Egypt, separating erosive paleo-highs and continental sediments toward the south from the marine Tethian Sea to the north, as shown in Table 1 and Fig. 12 and as has been discussed and explained in detail by Bosworth et al. (1996, 1999), Derocourt et al. (1993), Guiraud and Bosworth (1999), Guiraud et al. (2001, 2005), and Issawi et al. (1999, 2009). The marginal shorelines of North Africa continued transgression southward until reaching north Sudan at the Early Eocene time (Derocourt et al., 1993) depositing the Thebes Formation (Fig. 16).

Stratiform oolitic and non-oolitic ironstones are mostly congruent with the marginal paralic facies of the Jurassic to Santonian Tethyan paleo-shorelines (Figs. 12, 13 and 14). During the Campanian–Maastrichtian time duration, stratiform phosphorite deposits accumulated along the relatively stable epicontinental marginal facies of the Tethys. Mesozoic oolitic and non-oolitic ironstones of considerable Fe content are recorded in:

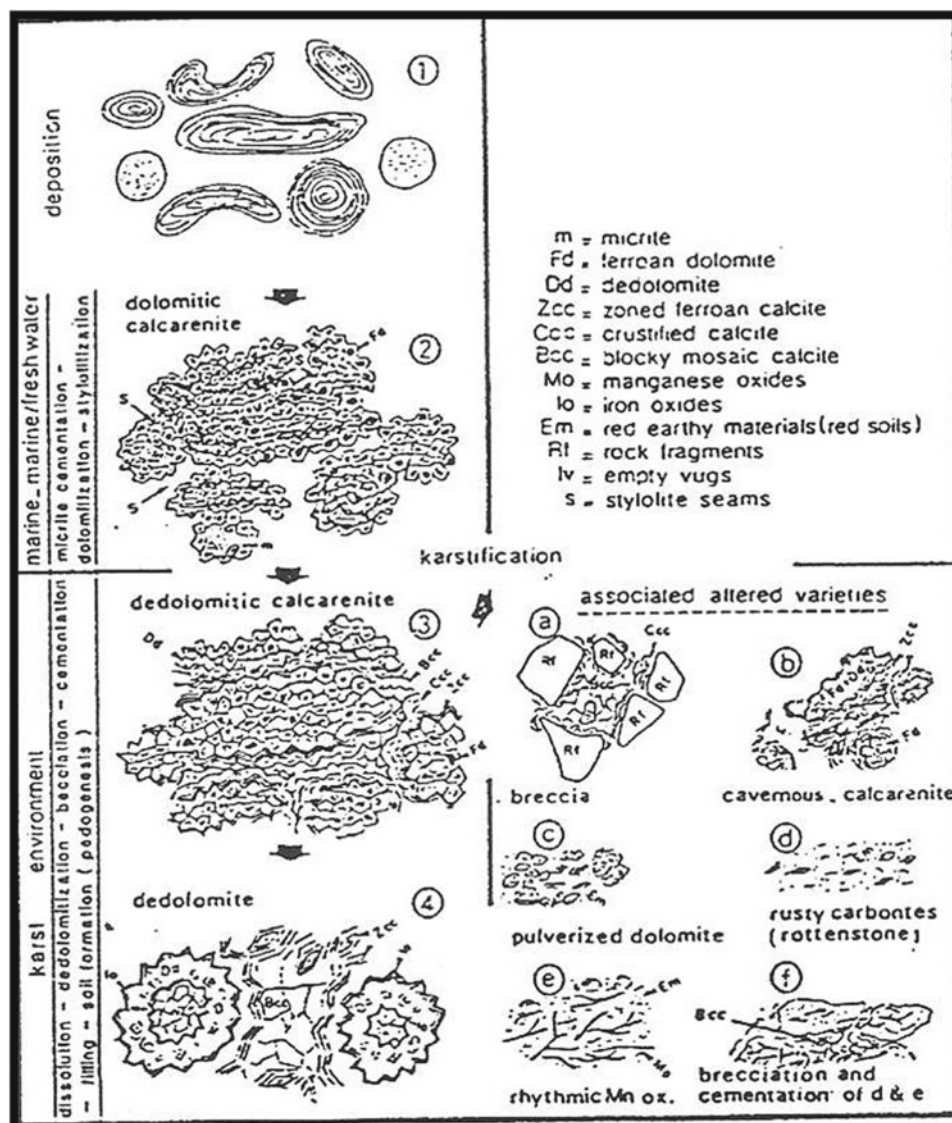


Fig. 9 Diagenetic and wall rock alteration processes of the karstified manganiferous carbonates in the lower Um Bogma sequence (Abdel Motelib, 1987)

- (a) North Sinai (El Maghara environ)
- (b) North Eastern Desert (Wadi Qena)
- (c) Gulf of Sues (W. Dara)
- (d) Aswan region
- (e) Central Western Desert.

The paleo-topographic and stratigraphic settings and paleo-facies of the ironstones of these sites clearly demonstrate their development along the paralic marginal facies of the southward migrating Tethyan paleo-shorelines (Figs. 12, 13 and 14), which support their formation simultaneously with lateritization (in situ or transported laterite) and continental sedimentation on the adjacent hinterlands. Although the well-known Mesozoic oolitic ironstone of Egypt is encountered within the Coniacian-Santonian sequence of east and eastwest Aswan, however the other equivalent and

older occurrences were carefully studied in order to clarify the mode of formation of this ore type in accordance with the regional and local geological parameters which controlled their formation and also to shed light on the geology and geographic distributions of the host rocks, as a fundamental data required for further geological exploration and ore evaluation. Figures 13 and 14 show the geology of each site and the detailed stratigraphy of the encountered non-oolitic and oolitic ironstone intervals. The age, mode of occurrence, the average Fe content of these ironstones and their economic potentiality as well as their detailed sedimentological and mineralogical aspects are compiled and summarized in Table 8. The youngest rather most economic Phanerozoic (Tertiary) oolitic-oncolitic ironstone of Egypt is the Middle Eocene iron ore of El Bahariya Depression, Western Desert (Section 4).

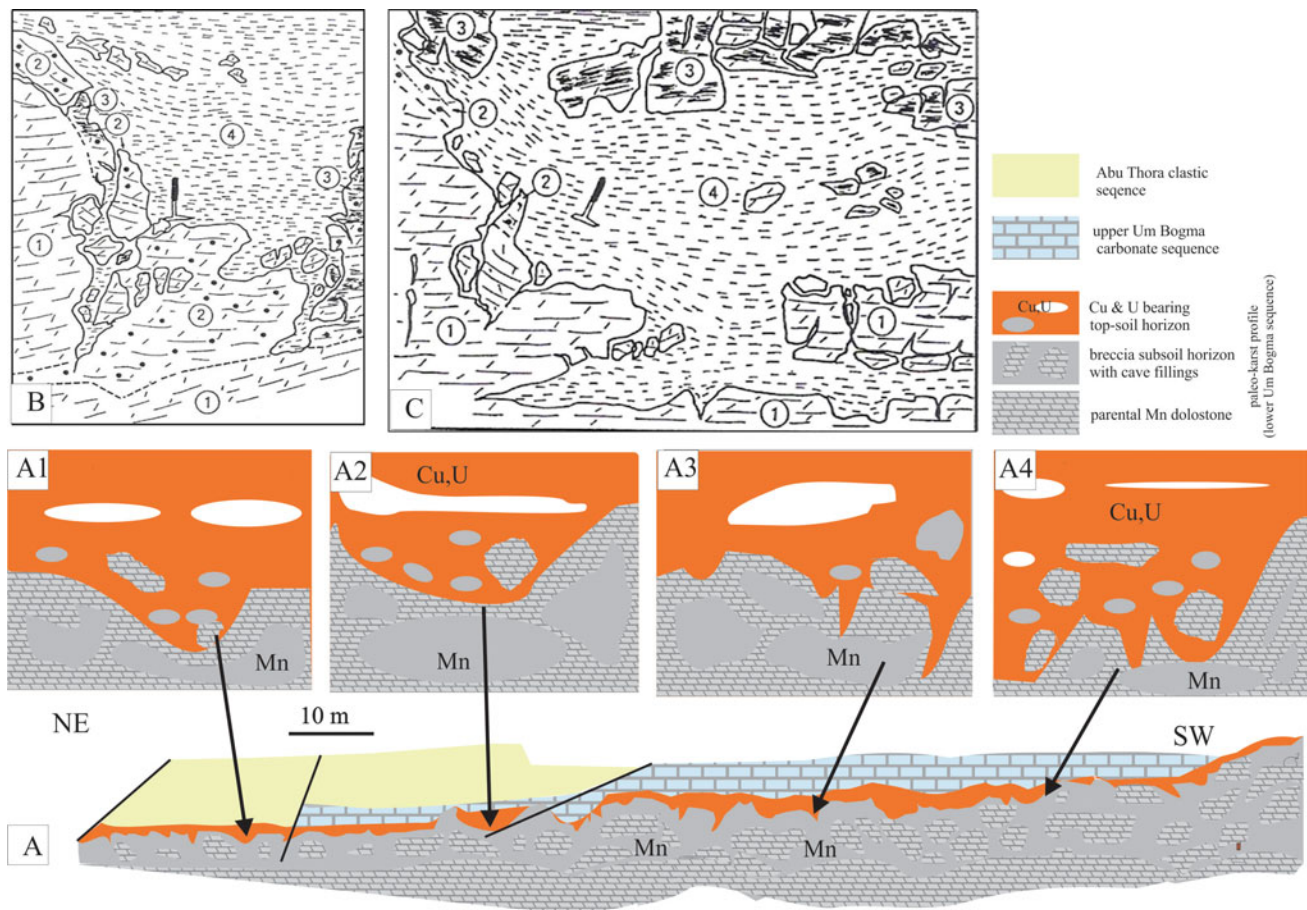


Fig. 10 A = representative drawing of the intra-Carboniferous fossilized paleo-karst profile and the related Mn ore and Cu and U concentration. A1–A4 = enlargement of solution features (A1 and A2 = trough-like depressions, A3 and A4 = V-shaped depressions) filled with collapse breccia and soil materials. B and C = representative drawings of solution hole (B) and subsurface solution cavity (C) showing the alteration varieties developed along the walls and roofs of the solution features, 1 = intact bed rock, 2 = pulverized dolomite, 3 = rusty carbonate, 4 = residual and infiltrated red soily materials (modified and simplified after Abdel Motelib, 1987)

3.1 Jurassic—Lower Cretaceous Ironstones

The Jurassic sea covered northern Egypt (Fig. 12). The thickest Jurassic succession crop out in northern Sinai at Gabal El Maghara (Fig. 13) and comprises an alternation of transgressive marine and regressive paralic sequences. The paralic facies association includes seams and ironstone bands (Fig. 14). Albian-Aptian carbonates including ironstone bands are also exposed in Gabal Manzur, east of Gabal El Maghara (Fig. 14). During the Jurassic–Early Cretaceous transgressive–regressive cycles on northern Sinai, the hinterlands were under erosion with the deposition of the continental clastics and the associated currently quarried kaolinite-rich laterites and paleosols of the Ragqaba, Temmariya, and Malha formations in Sinai and the continental clastics of Gilf Kebir, Six Hill, and Sabaya formations in the Western Desert. The Jurassic and Early Cretaceous ironstone intervals of north Sinai are of variable thicknesses and Fe content. The ironstone bands comprise two, rather distinct

types including (a) non-oolitic ironstone horizons formed by concretionary, massive, clayey ochreous, and rhythmic laminated varieties. They represent either paleosols and/or ferruginous mud flat intervals interrupting the cyclic clastic sequences of the host Jurassic deltaic sediments, and (b) oolitic ironstone bands often terminating an intermitted short-lived small-scale shoaling cycles of intertidal regressive falling sea level.

3.2 Upper Cretaceous Ironstones, Laterites and Phosphorite Deposit

The Tethys initiated in Early Cenomanian by high stand sea level, started to close with the development of widespread Cenomanian–Turonian successions (Darwish, 1994; Issawi et al., 1999). This led to the deposition of marine carbonates, marls, and shales toward the north (Halal and Raha formations) and the equivalent paralic sediments of the Galala

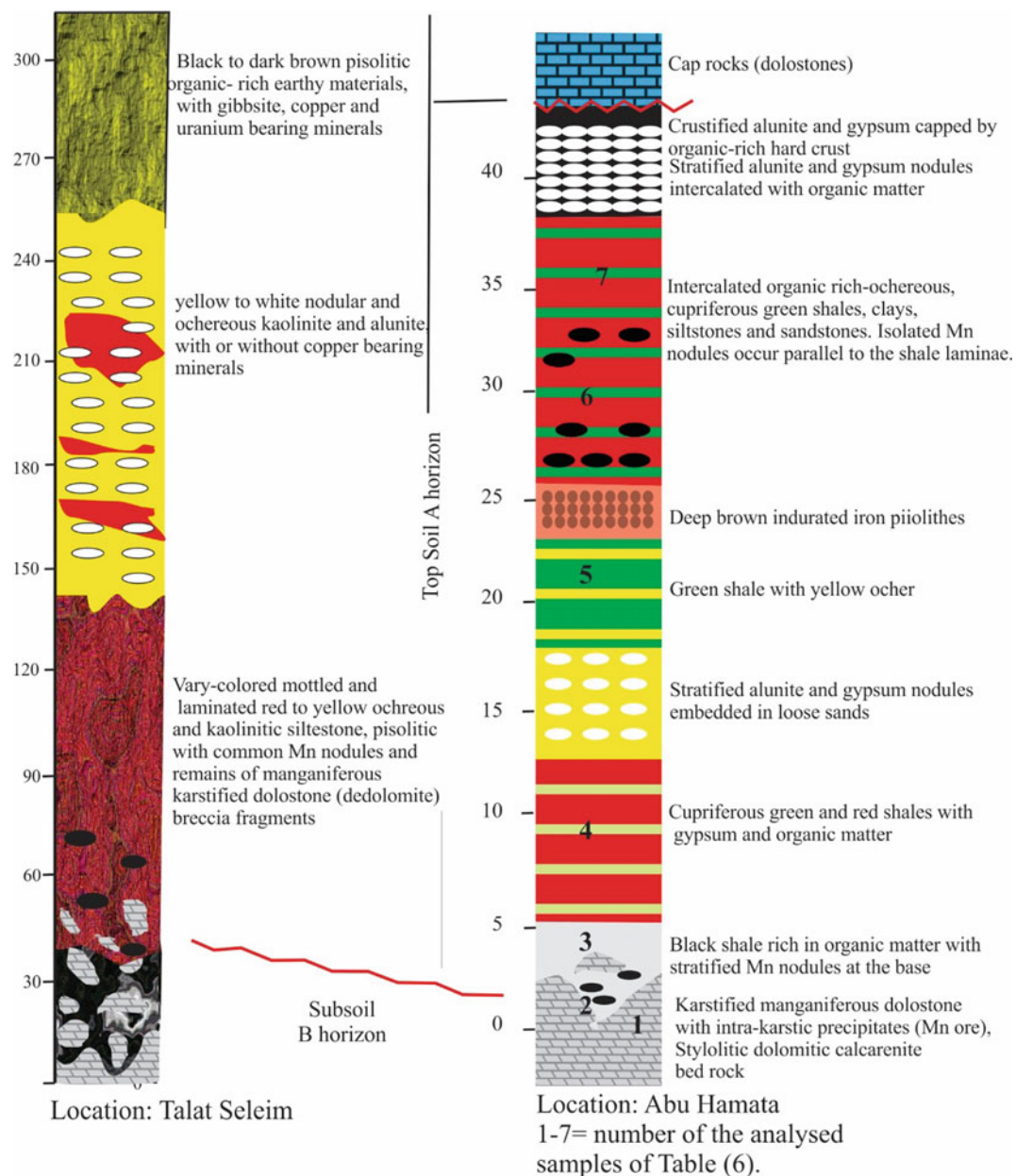


Fig. 11 Fine stratigraphy of the intra-Carboniferous paleo-karst profile and the topsoil sediments of two representative locations, including Talat Salem (after Aita, 1996) and Abu Hamata (after El Sharkawi et al., 1990a)

Formation as well as the Bahariya and El Heiz formations in the central Western Desert (Fig. 12). Further south, the comparable clastics of the Maghrabi Formation (Kharga-Dakhla district) show lesser marine influence. The entrance of Wadi Dara, Gulf of Suez is occupied by late Cenomanian siliciclastics and carbonate rocks, para-conformably overlain by reduced Turonian succession and Miocene evaporites (El Manawi, 2006, personal communication). In this site, the Late Cenomanian rocks of the Galala Formation contain, within its shallow marine middle part, an oolitic ironstone interval of about 18 m thick and 21–46% Fe (Figs. 13 and

14; Table 8). This interval is divided into a series of small-scale prograding parasequence sets of coarsening up pattern, mostly restricted to tidal flat facies. The Cenomanian paralic Bahariya Formation of the Western Desert includes within its lower and upper members ironstone bands and lenses, up to 15–150 cm in thickness, well exposed in El Bahariya Depression or along its surrounding scarps as a result of repeated tectonic pulses of the Late Cretaceous-Early Tertiary “Laramide” tectonic event (Figs. 2 and 14; Table 1). Economic ironstone bands are reported in El Harra mine area. Estuarine Cenomanian clastics of the

Table 5 Manganese ore facies types, environments, sedimentary structures, lithologies, and paragenesis (compiled by El Aref, 2020b and references therein)

Ore types (facies) and environment		Sedimentary structures	Ore lithologies	Ore fabrics	Paragenesis
Karstified manganese dolostone and mudstone (Drowned karst profile), Fig.9, Zone C	Soil horizons (Lower horizon) parental (intact) rocks, (up to 9 m thick)	<ul style="list-style-type: none"> • Stratified stvolutic manganese dolostones • Cyclic alternating beds with ooids and peloids, abundant marine fossils and bioclasts • Thin lamination and desiccation cracks, stratified gypsum and barite nodules, crackle breccia, in-situ brecciation, abundant in-filled solution openings (variable diameters) with collapse breccia and Mn-rich encrustation along cave walls, ceiling and floors, pulverization, mottling, intensive karstification and brecciation toward the overlying horizon 	<ul style="list-style-type: none"> • Mn para-conglomerate • Mn sandstone • Mn mudstone • Red ochers 	<ul style="list-style-type: none"> • Bedding, lamination and desiccation, stylolization • In place brecciation and fracturing strata • Mn concretions, pisoliths and glaebules • Reddening • Encrustation, filling cavities and solution opening • Collapsing, cockade structure, boxwork and alveolar structures • Dedolomitization • Leaching and accumulation of Mn-rich earthy materials (soils) • Filamentous algal fabrics 	Pyrolusite, manganese, romanechite, fear on dolomite, dedolomite goethite, hematite, Fe sesquioxides, calcite barite, gypsum, kaolinite
	Topsoil (eluvial) horizon Subsoil (illuvial) horizon				
Stratiform continental (channel fill) Mn conglomerate, sandstone and mudstone (Fig. 9, Zone D)	Fining-upward cyclic sequences with erosive bases, lamination and cross-lamination, desiccations, lenticular bedding, scouring and erosive soils	Alternating multicolored layers of organic-rich aluminic, kaolinitic, gibbsitic, cuprefeous and ochreous shales, siltstones and sandstones with abundant Cu, U and V minerals and organic and plant remains (polymorphs), shrinkage cracks, nodular forms, rhizoliths and rhyzocions	Mn boulders, gravels, sands and silts: Mn-rich matrix, colloform encrustation and cockade structure, filamentous algae, dendritic leaf-like and cellular patterns	Pyrolusite, romanechite, goethite, hematite, kaolinite, quartz, organic remains	
Surface slope deposits accumulated through mud flow of braided tributaries with derivation of framework components from nearby contiguous sources	• Karst lateritization and bouxitzation involving eluviation and illuviation processes (pedogenesis) and development of subsoil and topsoil horizons	• Laminated and crustified manganese dolostone • Mottled ferruginous and manganese dolostone • Manganiferous dolostone	• Mn para-conglomerate • Mn sandstone • Mn mudstone • Red ochers	• Bedding, lamination and desiccation, stylolization • In place brecciation and fracturing strata • Mn concretions, pisoliths and glaebules • Reddening • Encrustation, filling cavities and solution opening • Collapsing, cockade structure, boxwork and alveolar structures • Dedolomitization • Leaching and accumulation of Mn-rich earthy materials (soils) • Filamentous algal fabrics	Mn and Fe oxides and hydroxides; Cu, U, V, carbonates, chlorides, silicates, sulfates, phosphates and vanadates; kaolinite, gibbsite, calcite, quartz, jarosite, dolomite, ankarite, Illite, montmorillonite
Karstified manganese dolostone and mudstone (Drowned karst profile), Fig.9, Zone C	• Lagoonal to swampy manganese dolostones and dolostones • Deposition in coastal low energy shallow lagoons, charged with Mn continental sediments • Prevalence of splash meteoric water with continuous uplifting and subsequent karstification	• Fairly bedded showing small-scale coarsening-upward arrangement, bioturbation, abundant organic matter, pisoliths (oncoids), shrinkage fractures, ripple marks, flaser structure, matrix to grain-supported fabrics, skeletal fragments, fossil molds, isolated Mn-rich spherules and concretions, evaporite nodules	• Organic-rich bioturbated manganiferous and ferruginous mudstones	Pyrolusite, goethite, calcite, barite, gypsum, anhydrite, Fe and Mn sesquioxides	
Stratiform pisolitic (oncolitic) ore type (0–5 m thick), (Fig. 9, Zone B)	• Near-shore (marginal marine environment, under shoaling storm-generated conditions	• Fairly bedded showing small-scale coarsening-upward arrangement, bioturbation, abundant organic matter, pisoliths (oncoids), shrinkage fractures, ripple marks, flaser structure, matrix to grain-supported fabrics, skeletal fragments, fossil molds, isolated Mn-rich spherules and concretions, evaporite nodules	• Organic-rich bioturbated manganiferous and ferruginous mudstones	Pyrolusite, goethite, calcite, barite, gypsum, anhydrite, Fe and Mn sesquioxides	

Table 6 Identified Cu, U, and rock-forming minerals of the intra-Carboniferous paleo-karst profile (compiled from Abdel Motelib, 1987, 1996; Aita, 1996; El Aref & Abdel Motelib, 2001; El Sharkawi et al., 1990a)

Sulfates	Phosphates	Carbonates	Oxides	Silicates
Jarosite $KFe_3(SiO_4)(OH)_6$, Alumite $KAl_3(SiO_4)_2(OH)_6$, Gypsum $GaSiO_4 \cdot 2H_2O$, Anhydrite $GaSiO_4$ Zippelite, $(UO_2)_2(SO_4)(OH)_2 \cdot 4H_2O$ Chalcanthite $CuSO_4 \cdot 5H_2O$ Antlerite $Cu_3(SO_4)(OH)_4$ Barite $BaSiO_4$	Phosphosiderite $FePO_4 \cdot 2H_2O$, Bassetite $Fe(UO_2)_2(PO_4)_2 \cdot 8H_2O$, Pseudomalachite $Cu_5(PO_4)_2(OH)_4 \cdot H_2O$ Turquoise $CuAl_6(PO_4)_4(OH)_8 \cdot 5H_2O$	Calcite $CaCO_3$, Dolomite $CaMg(CO_3)_2$, Aukerite $Ca(FeMgMn)(CO_3)_2$, Malachite $Cu_2CO_3(OH)_2$ Liebigite $Ca_2U(CO_3)_4 \cdot 10H_2O$	Hematite, Quartz, Hausmanite Mn_3O_4	Chrysocolla $Cu_2H_2(Si_2O_5)(OH)_4$ Lungite $Cu_4(SO_4)(OH)_6 \cdot H_2O$ Spangolite $Cu_6Al(SO_4)(OH)_{12}$ $Cl \cdot H_2O$ Kaolinite, Illite, Montmorillonite
Hydroxides	Vanadates	Halides	Nitrates	
Gibbsite $Al(OH)_3$, Goethite	Metatyuyamunite $Ca(UO_2)_2(VO_4)_2 \cdot 35H_2O$	Atacamite $Cu_2Cl(OH)_3$ Paratacamite $Cu_2(OH)_3Cl$ Connelite $Cu_{19}Cl_4(SO)(OH)_{32} \cdot 3H_2O$	Bultgenbachite $Cu_{10}(NO_3)(OH)_{32}Cl_4 \cdot 3H_2O$	

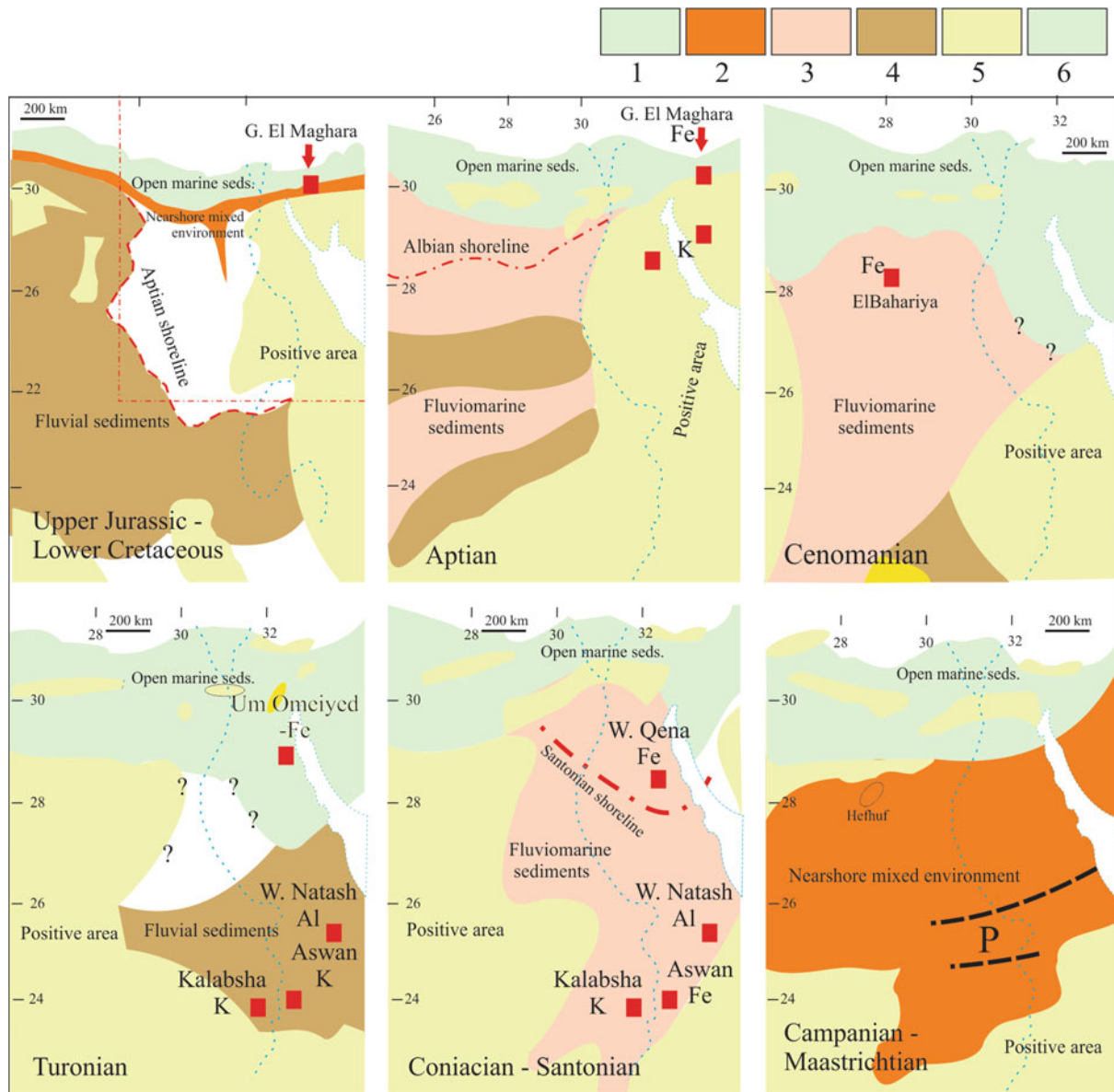


Fig. 12 Paleogeography of the Mesozoic stages and distribution of the related stratabound and stratiform deposits (compiled and simplified after Klitzsch & Wycisk, 1987; Said, 1990a). 1 = open marine sediments, 2 = near-shore mixed sediments, 3 = fluviomarine sediments, 4 = fluvial sediments, 5 = positive land, Fe = ironstone, K = kaolin laterite, Al = laterite

Bahariya Formation including ironstone bands of up to 1 m thick are recorded to the west of Lake Naser at Gabal Saad (Issawi & Osman, 1993).

3.2.1 Turonian Laterites

A major regressive phase has been established during the Middle Turonian accompanying an important pulse of the “Laramide” movement which was responsible for the elevation for southern Egypt, El Bahariya arc and numerous structures across northern Egypt and Sinai (Fig. 12). Thick marine carbonates related to the Wata Formation were deposited over the structural lows of northern Egypt, while

the coeval paralic sediments of the Um Umeiyed Formation were deposited southwards and crop out in central Wadi Qena. Meanwhile, the extreme southern hinterlands were subjected to deep weathering processes inducing lateritization and bauxitization and received simultaneous fluvial deposits. Exposed outcrops of lateritized Pre-Cambrian metamorphic and igneous rocks are widespread east and south of Aswan and in the western part of Kalabsha area near Sinn El Kadabb, southwest Aswan area (Fig. 12). The continental Abu Agag Formation (~ 5–40 m thick) overlies an irregular relief of the extensively lateritized Precambrian rocks. It consists of fining-upward sequences of breaded

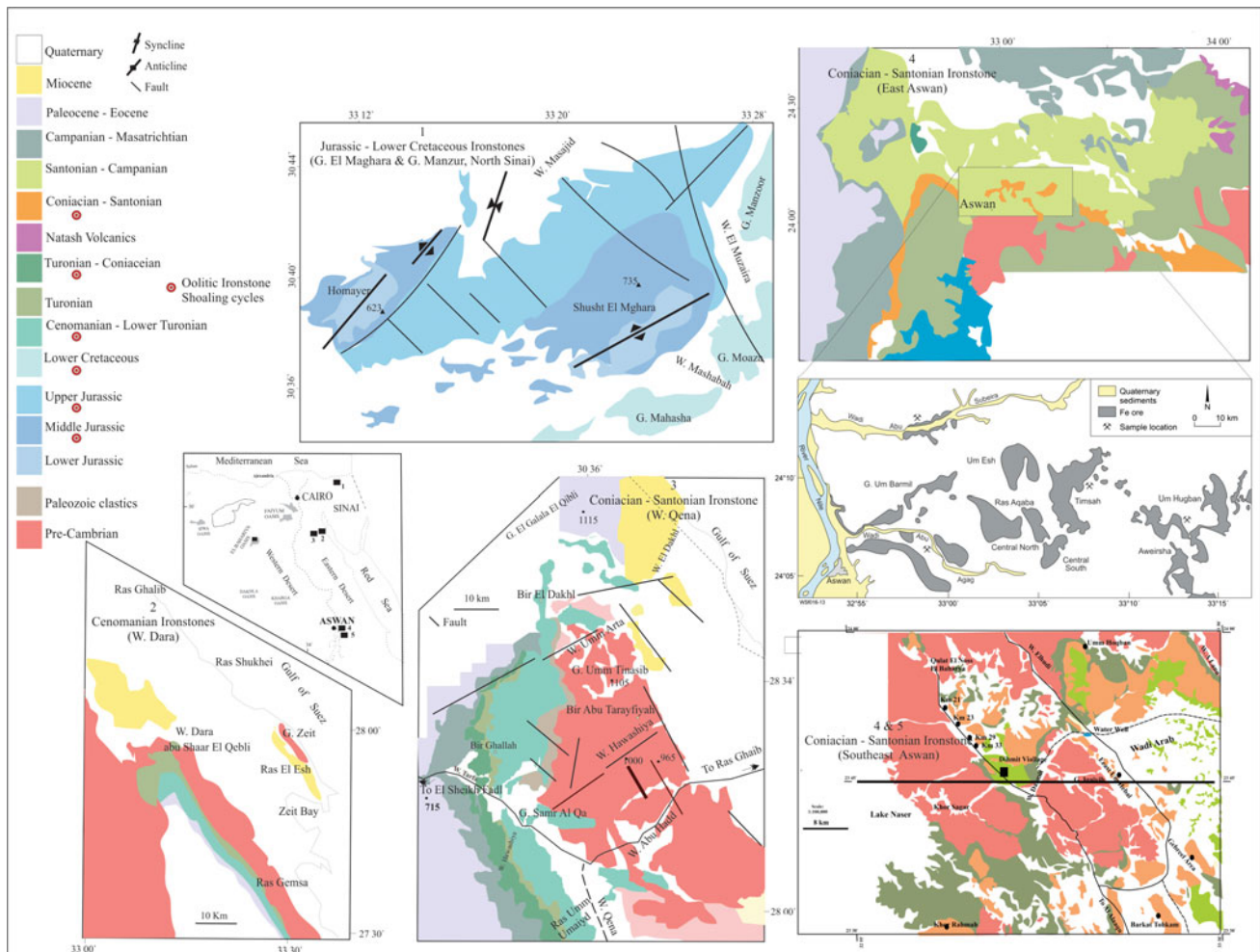


Fig. 13 Simplified geological maps showing the stratigraphic settings and areal distributions of the ironstone hosting sequences (G. El Maghara, W. Dara, W. Qena, and Aswan occurrences), compiled from El Sharkawi et al. (1989); Helba et al. (2003); El Manawi (2006) and IEP (1993–1997)

river environment, including trough cross-bedded conglomerates and sandstones, kaolinite-rich laterite and in situ latosols. Southwest Aswan at Wadi Kalabsha, the probably correlative Kaolin Member of Said and Mansour (1971) is overlain and underlain by the Abu Agag fluvial conglomerates and sandstones. Eastward of Aswan at Wadi Natash (Fig. 13), Abu Agag Formation is intercalated with the Natash volcanic sheets and their lateritic cap. The Turonian Laterite deposits of southern Egypt could be classified into two types according to their relation with the country rocks within which they are found. These types are:

- (a) Stratabound autochthonous bauxitic laterites (fossil latosols) of two different stratigraphic positions, including latosol capping Pre-Cambrian granites, schist's and migmatites and truncated by Abu Agag fluvial clastics, and laterites capping Cretaceous
- (b) Stratiform allochthonous kaolin-rich laterites, locally bauxitic, intercalated within the Abu Agag fluvial sediments in the form of either thick (up to 9 m) succession as in W. Kalabsha or accumulated within the troughs of the cross-bedded fluvial clastics. Ferruginous kolinitic

paleosol intervals often terminate the fining-upward sequences of the host Abu Agag sediments. In situ second bauxitization of some of the laterite intervals resulted into the formation of bauxite bearing latosol of different thicknesses (Germann et al., 1987).

3.2.2 Coniacian-Santonian Oolitic Ironstones

The paleo-geographic patterns of the Coniacian-Santonian shorelines were obviously controlled by two main factors: (a) the continuation of the Late Cretaceous-Early Tertiary “Laramide” tectonic movement and (b) the southward transgression of the shallow Coniacian-Santonian Sea which extended until northern Sudan. Genuine marine sediments laid down in the structural lows of northern Egypt and the Gulf of Suez (Fig. 12). Meanwhile, near-shore paralic sediments including stratiform ironstone bands dominated within the restricted Coniacian-Santonian basin. These sediments crop out at central Wadi Qena (Hawashiya Formation, Figs. 13 and 14; Table 8) and at the vicinity of Aswan

(Timsah Formation, Figs. 13 and 14). In north Wadi Qena, microglabular ooidal ironstones occur within the Coniacian transgressive succession of the Hawashiya Formation, delineating basal transgressive facies and terminating shallower regressive assemblages (Figs. 13 and 14; Table 8). According to Helba et al. (2003), the ironstone development is intimately related to the duration of specific sedimentary dynamics, which reflect interaction between sediment supply and hydrodynamic regime. The majority of the welded feriferous framework components are related to in situ growth from glauconite in sands and muds that are exposed to lateritic weathering during periods of sea level fall (Helba et al., 2003).

The Coniacian-Santonian Aswan ironstones constitute the third shallowing-upward cycle of the Timsah Formation (Figs. 12, 13 and 14; Table 8). The shallowing cycle, 1–3 m in thickness, starts in the base with muddy ironstone followed upwardly by Fe-rich oolitic ironstone band, representing gradual migration of tidal Fe ooid bar on basal

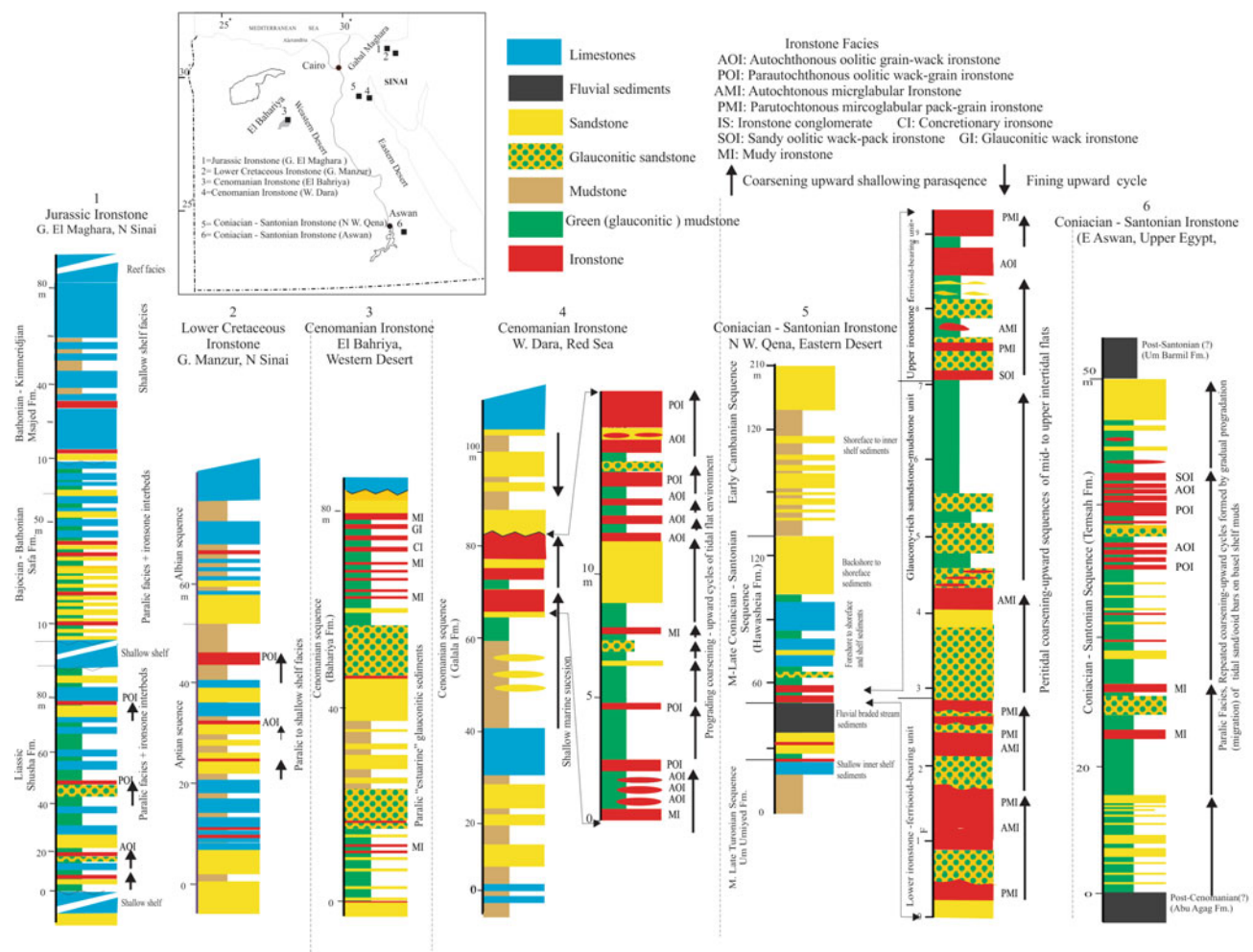


Fig. 14 Stratigraphic settings, facies, and environments of the Egyptian oolitic Mesozoic ironstones. 1 and 2 (El Sharkawi et al., 1989), 3 (IEP, 1993–1997), 4 (El Manawi, 2006), 5 (Helba et al., 2003), 6 (El Sharkawi et al., 1999)

Table 7 Major and trace element content of Abu Hamata paleo-karst profile of Fig. 11, after El Sharkawi et al. (1990a)

	SiO ₂	TiO ₂	Al ₂ O ₃	Fe ₂ O ₃	MnO	MgO	CaO	K ₂ O	Na ₂ O	P ₂ O ₅	LoI	Total
7	57.44	1.18	15.00	6.99	0.02	0.79	0.25	3.17	0.10	0.09	14.21	99.24
6	49.96	0.82	12.82	12.04	2.63	8.63	0.82	2.64	0.42	0.17	6.76	97.76
5	50.27	0.90	13.38	23.34	0.07	1.70	0.10	2.78	0.35	0.10	3.81	96.80
4	47.37	1.48	19.76	8.87	0.45	4.38	0.45	5.43	1.01	0.09	7.30	96.59
3	55.69	1.09	18.19	11.93	0.05	2.31	0.58	3.96	0.45	0.42	5.08	99.75
2	7.34	0.17	0.36	2.93	2.19	14.05	31.81	0.35	0.01	0.01	40.35	99.59
1	2.77	0.08	0.24	1.31	0.14	19.75	29.92	0.19	0.01	0.01	45.06	99.48
	Rb	Ba	Pb	Sr	La	Ce	Nd	Y	Th	Zr	Nb	Zn
7	49	74	135	143	92	155	66	68	29	524	72	58
6	83	1282	69	192	84	176	75	72	16	412	50	423
5	89	76	146	200	108	220	102	69	12	431	50	498
4	171	105	221	126	155	241	133	82	27	715	84	1020
3	128	93	31	179	127	242	162	115	21	524	69	446
2	22	1610	172	88	259	207	342	231	1	110	15	567
1	-	125	101	35	-	-	-	-	-	-	-	61
	Cu	Co	Ni	Sc	V	Cr	Ga	Code (sample locations in Fig. 11)				
7	151	7	17	15	350	346	26	7 = green shale				
6	476	35	97	13	555	614	20	6 = cupriferous green shale				
5	438	44	58	16	1480	1310	19	5 = ferruginous shale				
4	178	42	328	16	1430	1140	29	4 = green shale				
3	470	23	93	17	193	625	28	3 = black shale				
2	74	61	291	14	286	544	9	2 = dedolomite (subsoil)				
1	110	-	-	-	10	9	-	1 = bed rock				

shallow shelf mud (Fig. 14, El Sharkawi et al., 1999). The framework component of the oolitic ironstone bands are represented mainly by mechanically accreted Fe ooids, with or without sand grains. The ooids are formed by well or ill-defined concentric laminae of hematite, chamosite, goethite and Fe oxyhydroxides, kaolinite, calcite and ultra-fine

fluorapatite having variable Fe content (Fig. 15). According to, the high phosphorous content of Aswan ironstone (up to 3 wt%) is related to the presence of disseminated aluminum phosphate-sulfate (APS) minerals within the ferriferous ooids and the matrix (Salama, 2014). However, Omran (2015) and Omran et al. (2014, 2015) succeeded in removing

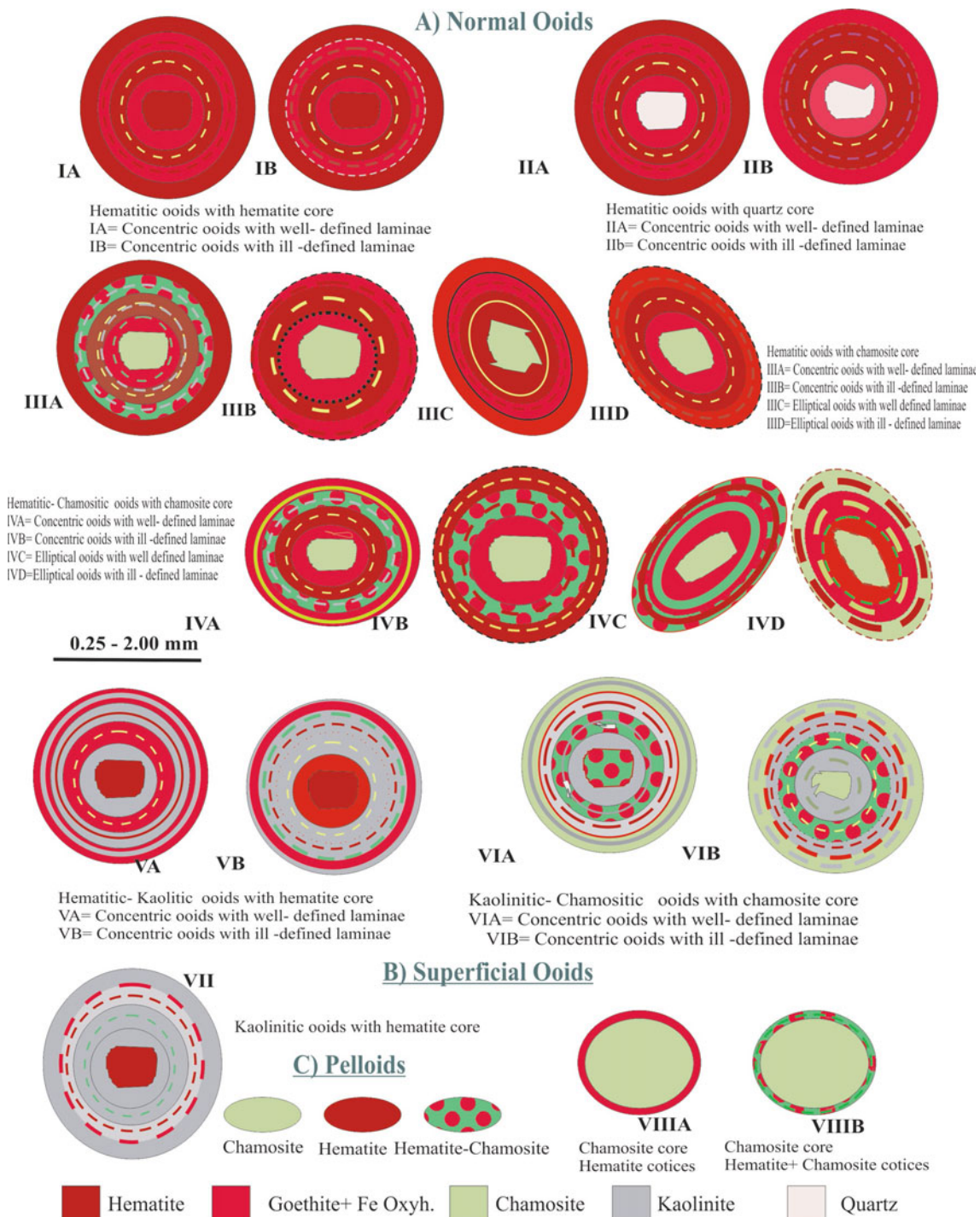


Fig. 15 Internal geometry and ooids and peloids composition Aswan Ironstone (CMRDI, 1998)

phosphorous from this ore type by combined microwave and ultrasound treatments. In addition to that, promising upgrading results are concluded by Yahiya (2007). The probable regional southward and south-eastward extensions of Aswan oolitic ironstones, particularly along Wadi Garrara-Gabal Abraq graben and Aswan-Allaqi sector, (until lat. 22°), are considered as a good target for further ore exploration (IEP Iron Exploration Project, 1993–1997; El Aref, 1999b).

3.2.3 Campanian–Maastrichtian Stratiform Phosphorite Deposit

The early Campanian–Maastrichtian sea transgression led to the deposition of wide carbonate/clastic facies, containing great reserves of phosphorite deposits (Fig. 12). The economic phosphate strata are confined to the Campanian–Maastrichtian phosphate bearing Duwi Group of Glenn and Arthur (1990). The Duwi Group, up to 145 m thick, is best exposed in a generally E-W trending belt extending along the middle latitude of Egypt (Figs. 1 and 12). It overlies non-marine, varicolored shales (Quseir Formation) and is conformably overlain by gray, laminated, foraminiferal-rich marine shales (Dakhla Formation). Within the Duwi Group, two main depositional realms are identified by Glenn and Arthur (1990): (a) a shallow hemi-pelagic environment responsible for the formation of organic-rich shales, bio-siliceous sediments and phosphorites and (b) a relatively high energy depositional regime. The formation of the phosphorites is attributed to current winnowing and concentration in reducing environment, associated with the deposition of shales and biosilicious sediments (Glenn & Arthur, 1990). In some sites, the phosphate ore shows abnormal concentration of trace elements, REEs, and uranium. The U content ranges between 20 and 180 ppm, averaging 58 ppm (El Kammar, 2020). El Kammar (2020) directed to utilize the rare earth elements (REE) as additional products from the phosphoric acid industry.

4 Cenozoic Stratabound Ore Deposits

4.1 Cenozoic Framework and Related Ore Deposits

The Cenozoic evolution witnessed global sea level changes and crustal deformations (Table 1), involving: (a) the culmination of the Early Tertiary “Syrian Arc” or “Laramide” movement, (b) Oligo-Miocene volcanic activity, and (c) the initiation and development of the Red Sea rift system. Humid and warm conditions dominated most of the Tertiary, while arid episodes were of short durations. A relatively long interval of aridity was exclusively a Late Pleistocene feature (McCauley et al., 1982; Said, 1990a). Late

Cretaceous–Early Tertiary worldwide rising of sea level resulted in the submergence of most of Egypt by the Tethyan Epicontinental Sea, depositing the Dakhla shales, chalk formations, and the Esna shales. The southward migration of the Early Eocene paleo-shoreline continued until north Sudan. According to Issawi et al (1999), emergence of the Egyptian land took place from south to north at the close of the Late Eocene, accompanied by a major northward regressive phase of the paleo-shorelines (Table 1; Fig. 16). During the Middle and Late Eocene time span, further northward retreat of the shoreline took place (Table 1; Fig. 16). The Middle Eocene shoreline was approximately along south Minea-El Bahariya latitudes (Table 1; Fig. 16). The Early Cenozoic consequent streams (Gilf system of Issawi & McCauley, 1992) followed this phase of sea retreat and resulted in the initial stripping of the emerged Lower Tertiary, Mesozoic, and Paleozoic rock successions to the south. The denudation of these rocks was accelerated by karst processes (El Aref et al., 1987; Issawi & McCauley, 1993). A late Eocene delta was developed in Fayum basin, where the deltaic sediments of Qasr El Sagha Formation were laid down. The Oligocene shoreline was confined to the north, shelf marine sediments dominated in north Egypt, while fluvial sediments were deposited in the Suez-Cairo-north Fayum land stretch and El Bahr area (northeast El Bahariya Depression). During the Neogene, two main depositional regimes prevailed (Table 1), involving: (a) continental and shallow marine environments covering the extreme northern part of Egypt, accompanying advanced northward sea retreats, and (b) rift-related continental and coastal environments corresponding to the Red Sea rift dynamic (Table 1). The northward retreat of the Tethyan paleo-shorelines and syn-rift uplifting phases left behind vast areas of exposed carbonates of older ages, that continued to be exposed to subsequent phases of paleo-karstification processes during post-Eocene-Quaternary humid rainy periods. This is what led to the gradual lowering of the carbonate relief, ultimately into the exposing and denudation of older fossilized paleo-karst surfaces and the related cave systems and formation of the present-day karst morphogenetic carbonate landscape.

Two groups of Cenozoic stratabound and stratiform ore deposits of different paleo-geographic positions, stratigraphic setups, and paleo-environments are distinguished and deeply examined. These are: (a) Paleogene stratabound deposits and (b) Neogene rift-related deposits.

4.2 Paleogene Stratabound Deposits

These deposits encompass varieties of unconformity bounded fossilized oolitic-oncolitic ironstones and iron laterite, iron-rich lateritic blankets (surficial ferricrete duricrust) as

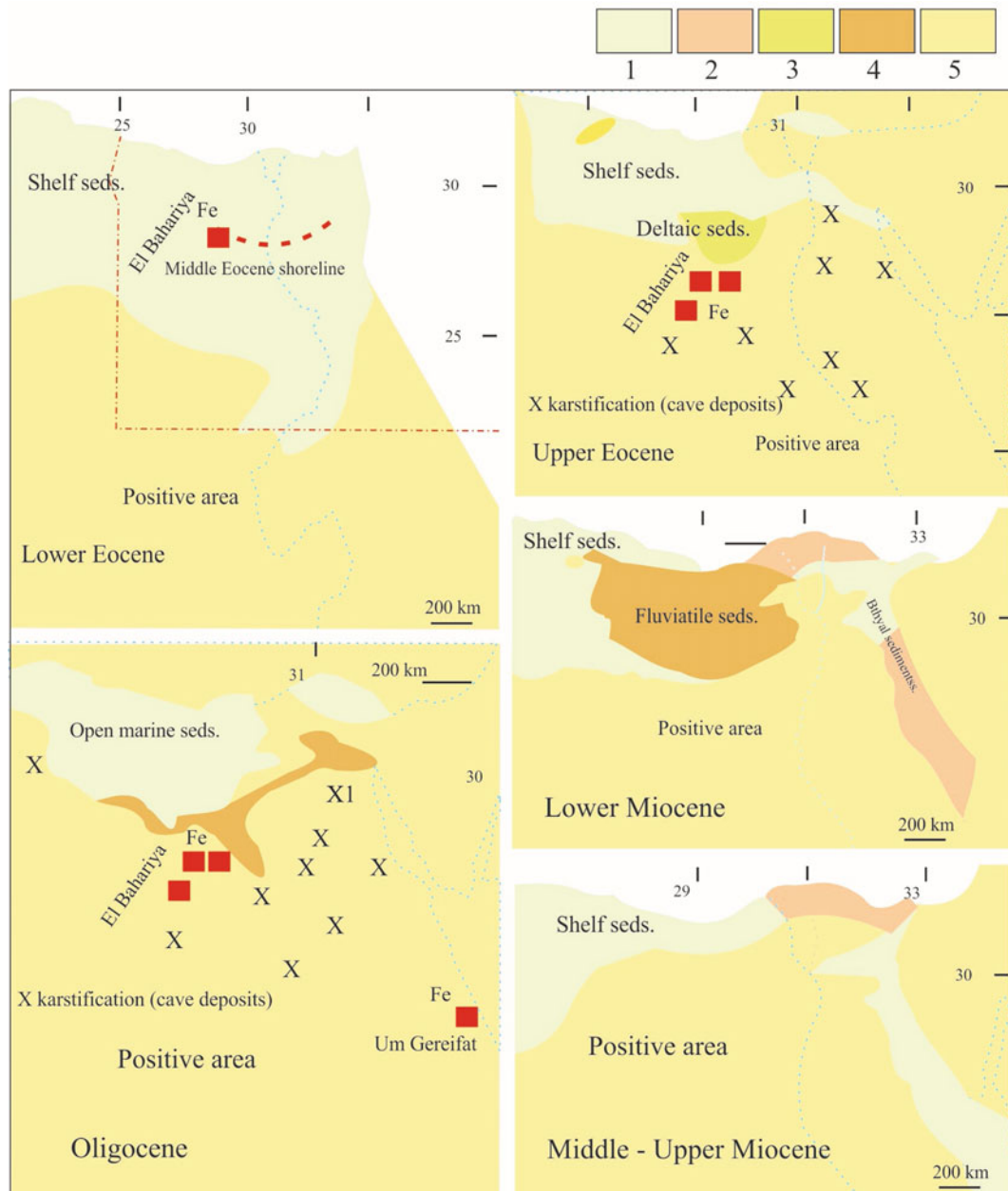


Fig. 16 Paleogeography of the Cenozoic series (compiled from Klitzsch & Wycisk, 1987; Said, 1990b and simplified by El Aref, 1996). 1 = marine sediments, 2 = bathetic sediments, 3 = deltaic sediments, 4 = fluvial sediments, 5 = positive land, Fe = iron deposits

well as karst precipitates and recrystallized carbonates (“Egyptian Alabaster” and the associated red-matrix breccia).

4.2.1 Lutetian-Bartonian Stratabound Oolitic-Oncolitic Iron Ore (El Bahariya Depression, Western Desert)

El Bahariya district (Fig. 17) is of special interest because it contains exploitable large reserves of middle Eocene iron ores (Table 9. This district represents one of the main

outcrops of Cretaceous rocks in North Western Desert, the other outcrop is at Gabal Abu Roash west of Cairo. These two localities display the highest push-up structural domains aligned along a giant tectonic Line trending in ENE direction of the Syrian Arc System or “Laramide” movement. The associated structural elements are related to a wrenching stress type of regime as concluded by Sehim (1993) and Moustafa et al. (2003). In the Early Lutetian, sea drowns the Bahariya paleo-high, which was subjected to denudation since Late Cretaceous time. A general N to NE gentle

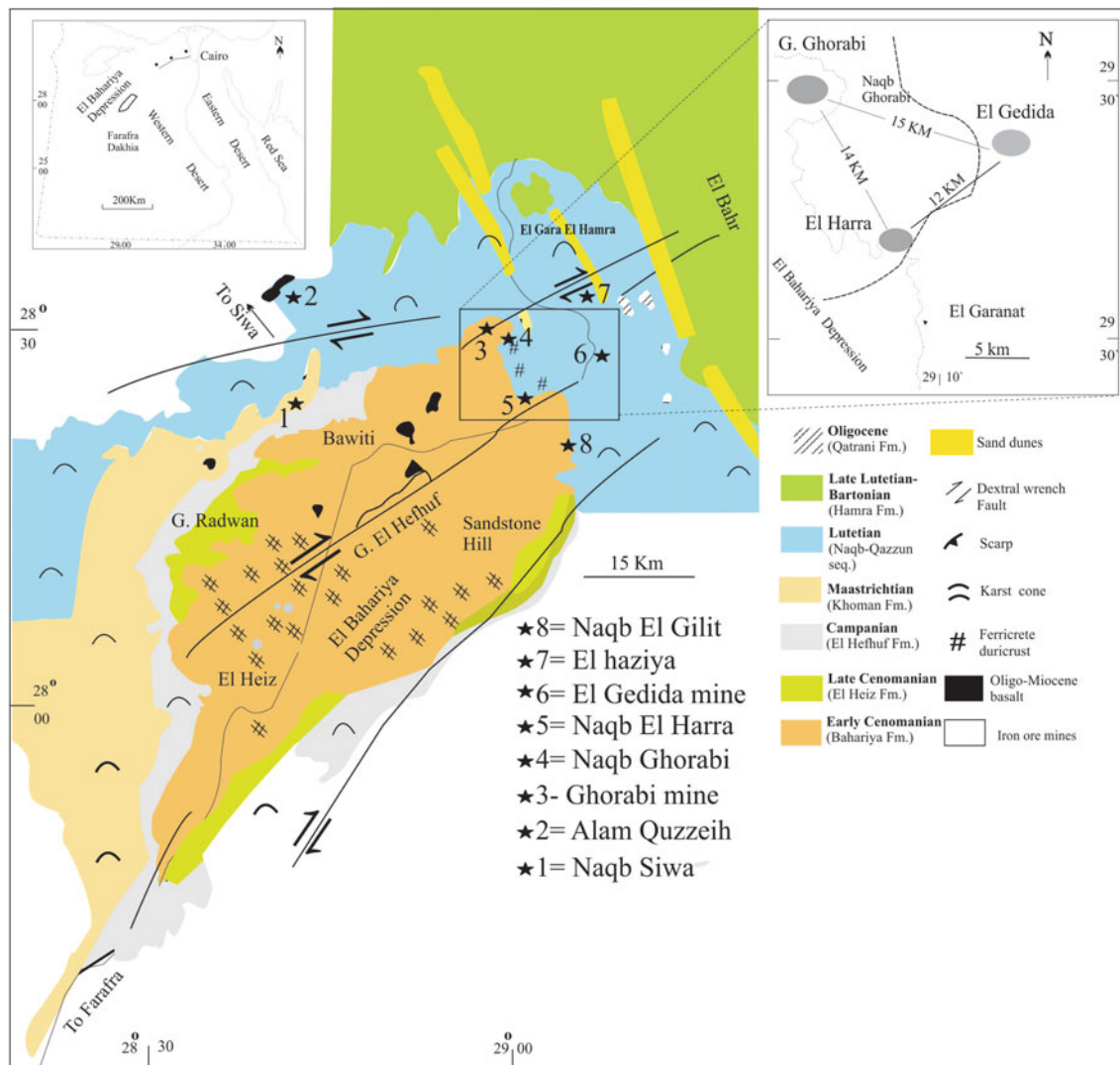


Fig. 17 Simplified geological and geomorphological map of El Bahariya Depression and locations of El Bahariye Fe mine areas and El Heiz duricrusted hills (modified by El Aref et al., 1999a after Hermina et al., 1989, detailed structural elements are shown in Sehim, 1993)

sloping ramp was developed, containing isolated submarine swells and islands in the northeastern plateau of the depression, namely El Gedida (6.5 km²), El Harra (2.9 km²), and Ghorabi (3.5 km²) submarine swells (El Aref et al., 2001, 2006a, Fig. 17). The Cenomanian Bahariya Formation constitutes the floor of the depression and most of the scarp faces, and locally crops out on the northeastern plateau surface as minor fault blocks (e.g. El Gedida, El Harra and Ghorabi mine areas, Table 9). Along the ramp, Lutetian fossiliferous carbonates (Naqb and Qazun formations) cover different Cretaceous rock units. The northward retreat of the Tethyan paleo-shoreline which was accompanied by the culmination of the Syrian arc system led to the uplifting of the Cretaceous strata in El Bahariya region. This is evidenced by the development of lateritic iron deposits demarcating the Cenomanian-Eocene unconformity surface

(e.g. the basal part of El Harra ore section, ore type 2 of Table 10). The Facies assemblages of the Lutetian ramp carbonate succession are accreted in three distinct depositional belts, comprising: (a) back-bank/pritiadal belt, (b) bank/shoal belt, and (c) fore-bank/open marine belt (El Aref et al., 2001), often disrupted by several depositional breaks augmented by paleo-karstification processes. Upon the submarine swells (mine areas), the Eocene carbonate succession entirely changes into a very condensed section of oncolitic-oolitic and nummulitic ironstone facies of shallowing-upward pattern (Table 10; Figs. 18, 19 and 20).

As shown in Table 10, the condensed iron ore succession is bounded between two unconformities (sequence boundaries), namely the Lower Cretaceous–Middle Eocene boundary and the upper Eocene–Oligocene boundary. The

Table 8 Main geological, stratigraphic, geometric, mineralogical, and chemical characteristics of the Egyptian Mesozoic ironstones (IS) and their economic potentialities (compiled and simplified from El Aref et al., 1999b; El Manawi, 2006; El Sharkawi et al., 1989, 1999; Helba et al., 2003)

Age	Jurassic—Early Cretaceous G. El Maghara environ, N. Sinai			Late Cretaceous	
Location	G. El Maghara Jurassic	G. Manzur Early Cretaceous	W. Dara cenomanian	W. Qena Coniacian	Aswan Coniacian-Santonian
References	El Sharkawi et al. (1989)		El Manawi (2006)	Helba et al. (2003)	El Sharkawi et al. (1999) El Aref et al. (1999b)
Host rock units	Shallow marine marginal facies of the Tethyan paleo-shore lines represented by of the following transgressive units				
	Jurassic Shusha (Late Triassic), Safa (Bathonian) and Masajid (Bathonian-Kemmeridjin) formations	Aptian-Albian G. Manzur formation	Late Cenomanian Galala formation (~ 100 m thick)	Coniacian Hawshiya formation (~ 178 m)	Coniacian-Santonian Tensah formation (~ 40 m thick)
Host rock environment	Shallow marine tidal flat marginal facies				
IS bearing interval (succession)	Up to 5 m thick		Up to 18 m thick	Up to 10 m thick	6–8 m thick
Fe % content	17–42% Fe		21–46% Fe		25–75 % Fe (exploitable, ~ 43% Fe)
Congruence: (stratified bands)	Up to 4 m thick of concretionary IS, massive IS, clayey IS, banded IS, laminated IS, oolitic IS		5 cm–2 m thick	5–40 cm thick	0.5–2 m thick
Geometrical arrangement	Non-oolitic IS (muddy ISs, sandy ISs), oolitic IS, IS conglomerates Small-scale (short-lived) shoaling-upward cycles				
Framework components	Variable proportions of welded ferriferous allochems of micro-nodules, coated grains, ooids, micro-glaebules skeletal particles, rock fragments, quartz and glauconitic grains, pyrite				

Table 9 Summary of the estimated ore reserves of El Gedida, Ghorabi, Nasser, and El Harra mine areas (Technical and internal reports of EGSMA (1969–1971), ISCo Annual Internal Reports (1987–1977), IEP (1993–1997), El Aref, 1999)

Area	Area (km ²)	Overb. thickness (av., m)	Iron ore thickness (av., m)	Cutoff grade Fe %	Reserves (m.t.)-by			
					EGSMA (1969–1971)	UEC (1976)	ISCo (1987–1977)	IEP (1993–1997)
Ghorabi	2.308	0.1–2.0	11.1	40%	55,528,840	56,971,689		
Nasser	1.203	0.1–20.0	12.68	30% (25%)	28,990,760	26,023,281		
Nasser (2) (new discovery by ISCo. 1989)				30% 40%			10,044,356 7,856,000	
El Harra	2.9	5.90	8.0	30%	53,744,291	61,226,230		
NE-El Harra (new discovery by IEP 1997)	2.4			40%				16,302,809 (40% Fe) 22,937,730 (Fe%?)
El Gedida	6.464	7.20	10.52	40%	117,000,000	123,718,000	148,640,358 (re-evaluation)	
South El Gedida (new discovery by IEP 1995)	0.5							12,650,497 (geological reserve)
Additional reserves							34,926,714 (Nasser 2 + re-evaluation of El Gedida)	35,588,227 (NE-El Harra+ S. El Gedida)

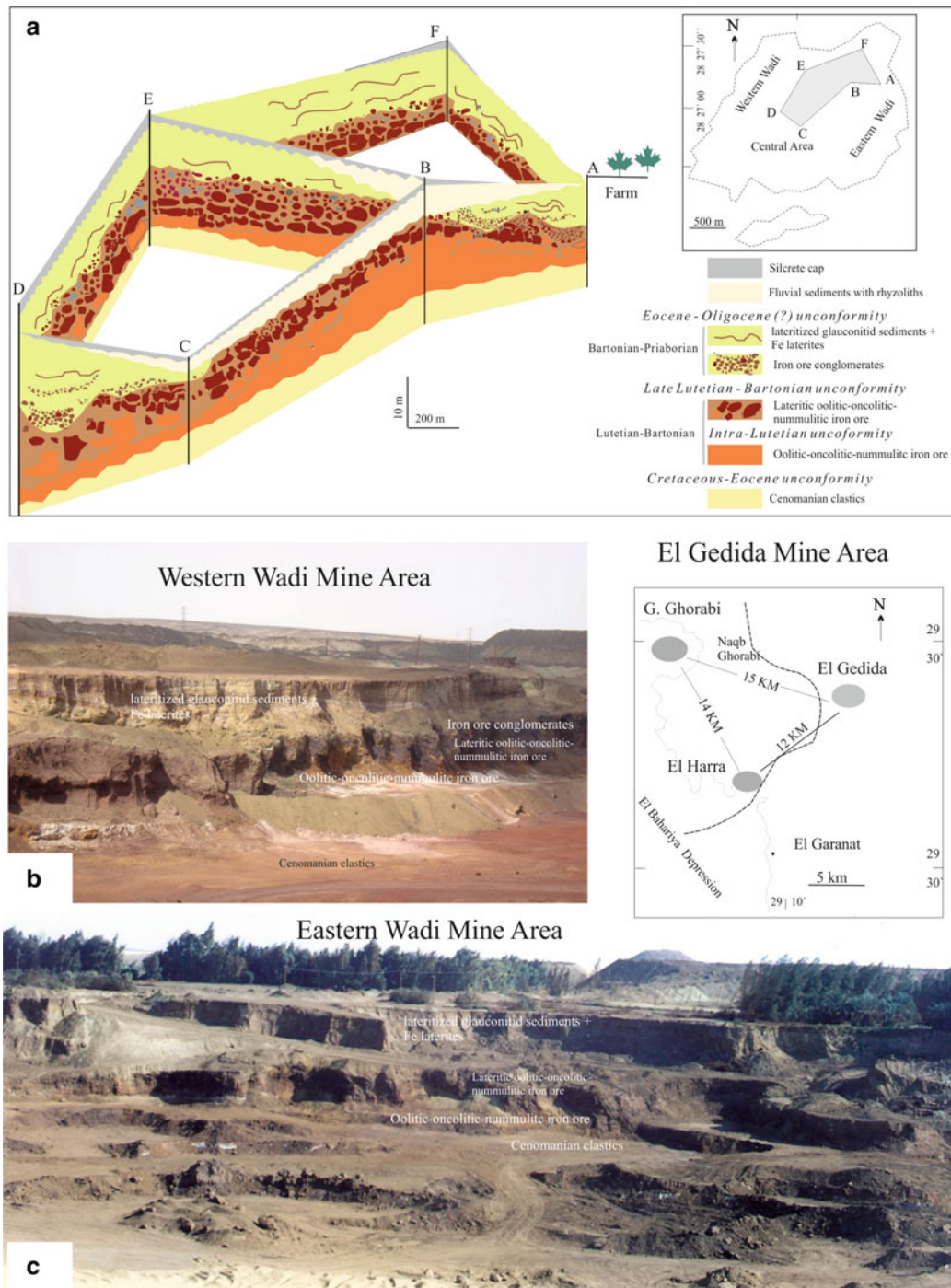


Fig. 18 a = Panel diagram showing the stratigraphic setting, lateral extension, and thickness variation of the different ironstone types of El Gedida mine area (IEP, 1993–1997). b and c = Panoramic field photographs showing the stratigraphic settings of the different ironstone types of the Eastern and Western Wadi sectors of El Gedida mine

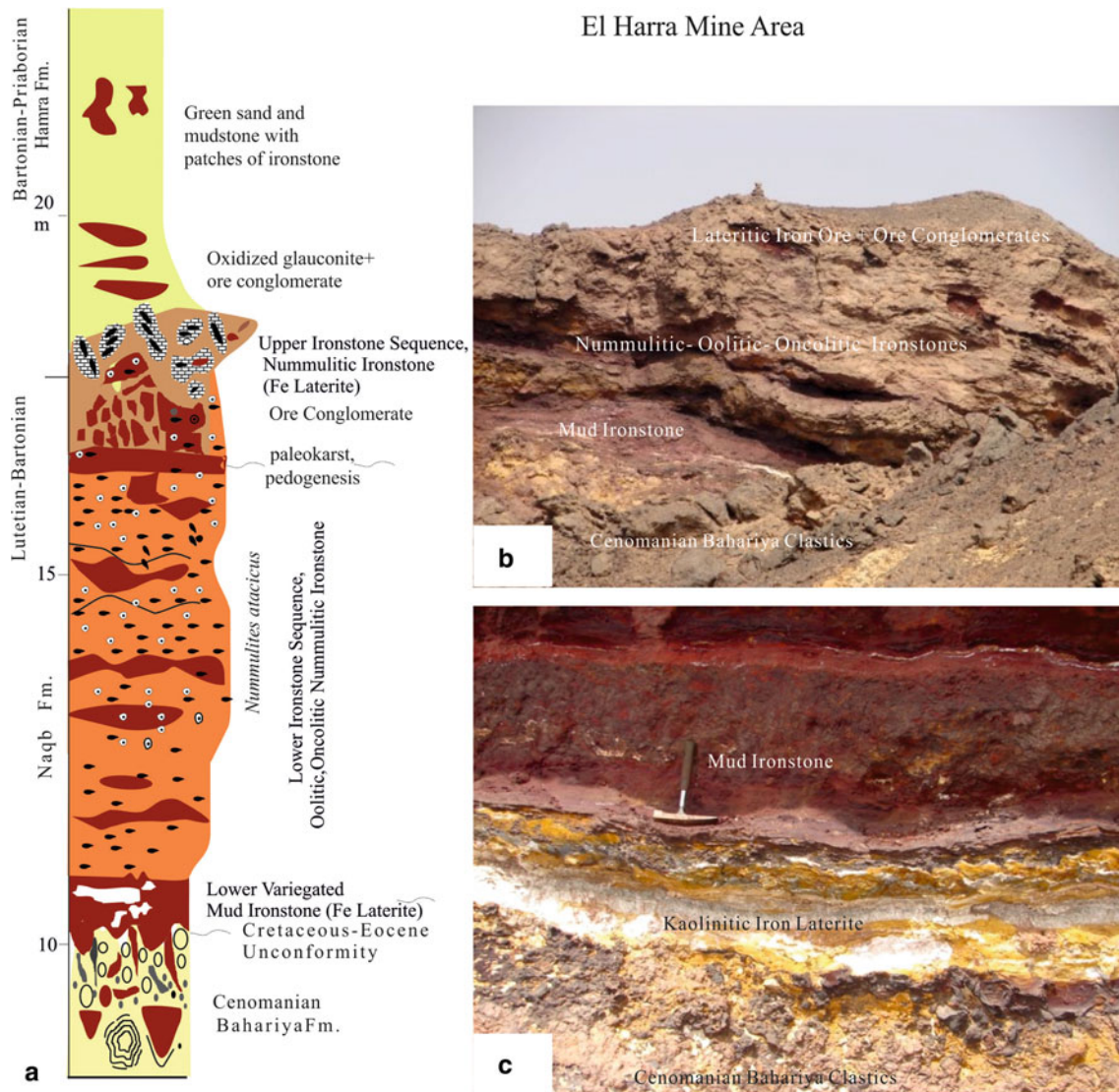


Fig. 19 a = Fine lithostratigraphy of the Lutetian ironstones at the upstream of Wadi El Harra mine area (Helba et al., 2001). b = Close-up view of the kaolinitic iron laterite developed along the Cenomanian-Lutetian contact, El Harra mine area. c = Field photograph showing the ironstone succession of El Harra mine area and the related main ironstone facies

ore succession includes the following vertically stacked ore facies types, arranged chronologically as follows:

- (1) Stratiform ironstone bands and concretions encountered within the upper storm-influenced shallow shelf sediments of the Cenomanian sequence (ore type 1, Table 10). Most of these bands contain relics of oxidized glauconite and quartz grains floating in earthy goethite and hematite matrix mixed with amorphous oxyhydroxids. Such bands and concretions reach
- (2) Stratabound iron and manganese-rich laterite hosting kaolinite, alunite, and gibbsite nodules, developed along the Cenomanian–Lutetian boundary in El Harra and El Gedida mine areas (ore type 2, Table 10).
- (3) Stratiform lateritized oolitic-oncolitic and nummulitic ironstone sequences of shallow marine environment superimposed by lateralization processes (ore type 3, Table 10).

workable dimension and thickness in Nasser (north Ghorabi) and El Harra mine areas.

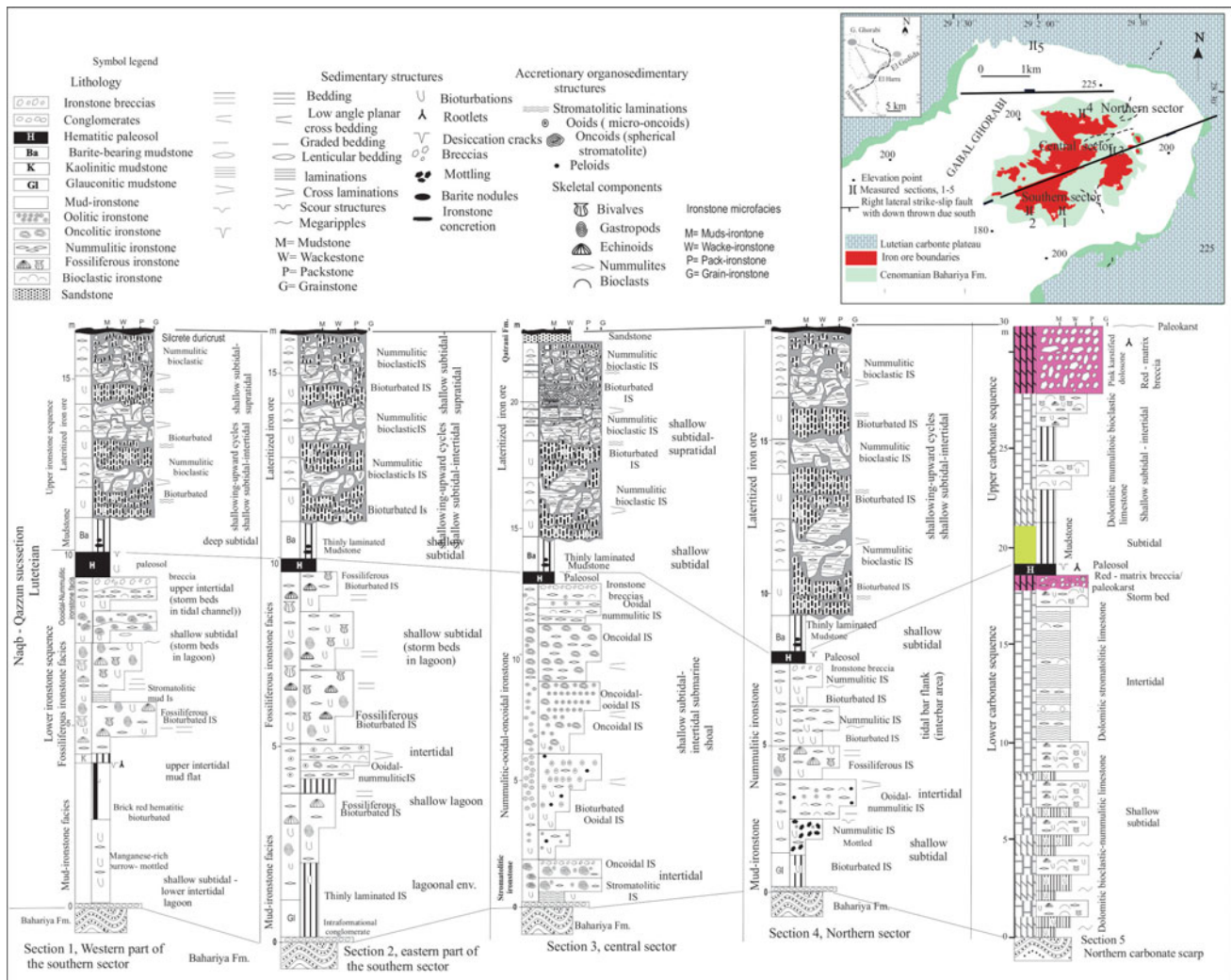


Fig. 20 Stratigraphic sections showing the distribution of the different ironstone units and the related facies of the different sectors of Gabal Ghorabi area (after El Aref et al., 2006a)

- (4) Stratiform channel fill ore conglomerates with abundant melon-shaped concretions of silicified limestone and chert enclosing abundant molds of *Nummulites gizehensis*, truncating the Lutetian lateritized oolitic-oncolitic-nummulitic ironstones (ore type 4, Table 10).
- (5) Bartonian iron laterite developed during intermitted lateritization of the Bartonian glauconitic sediments (ore type 5, Table 10) well-represented in El Gedida mine area (El Sharkawi & Khalil, 1977).

Stratigraphic Architecture and Facies Hierarchy of the Oolitic–Oncolytic–Nummulitic Ironstone

The encompassed Lutetian oolitic-oncolitic-nummulitic ironstone succession is underlain by the Cenomanian paleo-highs and or the Cretaceous-Eocene laterite deposits and overlain by channel fill iron conglomerates, Bartonian

glauconitic succession, fluvial sediments, and/or silcrete hard cap (Figs. 18, 19 and 20). The main ironstone facies assemblage comprises two main sequences separated by thin red veneer of lateritic paleosol (Figs. 18, 19 and 20; Table 11). The lower sequence starts with tidal flat/lagoonal mud-ironstones with minor siliciclastic mudstones, representing deposition from suspension in low energy depositional environment (Figs. 19 and 20). These pass upward to shoals/mega-rippled yellow oncolytic-oolitic-nummulitic, grain-to pack-ironstone peritidal facies association, and indicating deposition under tidal and/or storm-generated shoaling-upward conditions during periods of sea level fall. The oncolitic-oolitic-nummulitic ore type constitutes the thickest ore type in El Gedida mine (up to 22 m thick, Fig. 18). In Ghorabi mine area (Fig. 20), the upper ironstone sequence begins with the deposition of shallow subtidal

Table 10 Upper Cretaceous and Tertiary stratigraphic units of the northern part of El Bahariya Depression and the related stratigraphic gaps and ironstone types (after El Aref et al., 1999a, 1999b)

Location Age	Alam Quzzeh	Naqb Siwa	G. Ghorabi	Naqb Ghorabi	Naqb El Harra	El Cealida mine	Naqb El Gilit	El Ghaziyah	Deformational phases
Oligocene	Qatrani Fm.	Not preserved	Eocene - preserved	Not preserved	Not preserved	Unconformity	Not preserved	Unconformity	Extensional Deformation (faulting)
Bartonian	Hamra Fm.	Not	Lutitian - Bartonian	Not	Bartonian	5	Paleokarst		
Lutetian - Partionian	Naqb - Qazun Succession	Carbonates	4 Ore 3 Intra- Lutecian	Carbonates	4 Ore 3 Lutecian	4 Ore 3 Unconformity	Carbonates Rayan Fm. Minia Fm.	Carbonates	Deformation (Faulting & folding)
Early Eocene	unexposed		Cretaceous - Eocene		Eocene	Unconformity			
Paleocene	unexposed								Wrenching (Faulting & folding)
Maastrichtian	Base	Khoman Fm.					Base	unexposed	
Campanian	Base	El Hehnaif Fm.							
Turonian- Santonian									
Cenomanian		El Heiz Fm.							
		Bahariya Fm.	1	Bahariya Fm.	1	Bahariya Fm.	Bahariya Fm.	Bahariya Fm.	
		Bahariya Fm.	1	Bahariya Fm.	1	Bahariya Fm.	Bahariya Fm.	Bahariya Fm.	

Ironstone types: 1 = Cenomanian ironstone, 2 = Cretaceous-Eocene ferruginous latosol, 3 = Lutetian oolitic-oncolitic ironstone, 4 = ore conglomerates, 5 = Bartonian glauconitic Fe laterite

green mudstone facies of new marine transgression followed by peritidal shallowing-upward cycles of ironstones terminated by supratidal stratiform barite (Fig. 20). Each cycle begins by shallow subtidal mud-ironstones grading upward into shallow subtidal-intertidal nummulitic-bioclastic ironstones. The facies hierarchy of these ironstone sequences, their vertical arrangement and lateral variation changes into the coeval shallow subtidal-intertidal carbonate facies are well recognized and identified in Ghorabi mine area (Fig. 20; Table 11). The upper ironstone sequence is intensively lateritized forming iron ore laterite. The superimposed subaerial weathering complicated the diagenetic history and in many cases may partially to completely obliterate the original marine fabrics and textures of the upper ironstone sequence (Figs. 18, 19 and 20; Table 11).

Petrographically, the Lutetian oolitic-oncolitic-nummulitic ironstones comprise varieties of grain- and mud-supported microfacies, which are defined relying on the type and content of ferriferous allochems as well as depositional fabrics and structures. The matrix of these facies consists mainly of earthy iron oxides and hydroxides, ferrihydrite, amorphous

iron oxyhydroxide, sooty manganese-rich materials, phosphoric clays, ultra-fine kaolinite particles as well as sandy to silty sized quartz and glauconite grains. The cement is formed mainly of iron oxides and hydroxides and less abundant manganese oxides and hydroxides, barite, dolomite, calcite, siderite, quartz, gypsum, and halite. The recorded ferriferous allochems are classified into three main categories, including (a) ferruginized skeletal particles (tests and molds of nummulites, alveolinids, with body fossils of gastropods, bivalves, echinoderms, and benthic algae as well as microbial remains), (b) ferruginous coated grains and ooids (biogenically encrusted or microbial-mediated grains such as ferriferous oncoids and ooids, ferriferous cortoids and ferriferous concretionary glaeubles, and (c) ferriferous peloids and intraclasts. The development of the various microbial-mediated structures (stromatolites, oncoids, and ooids) is attributed to biogenic accretion mechanism (El Aref et al. 1999b, 1999b, 2006b and Helba et al. (2001). The biogenic accretion was responsible for the accumulation and early cementation of the original precipitates, i.e. amorphous Fe oxyhydroxides. The ferruginous microbialite morpho-structures are classified into three main morpho-types (Fig. 21), including (1) Ferruginous

Table 11 Distribution of ironstone facies and microfacies of the ironstone sequences of Gabal Ghorabi mine area and their lateral variation into the equivalent Lutetian carbonate facies (Salama, 2006)

	Southern sector	Central sector	Northern sector	Eastern scarp	Northern scarp		
Upper ironstone sequence	Stratabound karst (lateritized) iron ore, karst-related barite deposits Stratiform barite layers Nummulitic-bioclastic wacke-/pack-ironstone Bioturbated mud-ironstone Stratiform barite layers Nummulitic-bioclastic wacke-/pack-ironstone Bioturbated mud-ironstone Nummulitic-bioclastic wacke-/pack-ironstone Bioturbated mud-ironstone	Stratabound karst (lateritized) iron ore, karst-related barite deposits and terra rossa sediments Stratiform barite layers Nummulitic-bioclastic wacke-/pack-ironstone Bioturbated mud-ironstone Stratiform barite layers Nummulitic-bioclastic wacke-/pack-ironstone Bioturbated mud-ironstone Nummulitic-bioclastic wacke-/pack-ironstone Bioturbated mud-ironstone		Nummulitic-bioclastic wackestone/packstone Lime mudstone Nummulitic-bioclastic wackestone/packstone Lime mudstone Nummulitic-bioclastic wackestone/packstone Stromatolitic wackestone Lime mudstone			
Green mudstone facies containing barite nodules							
Lower ironstone sequence		Red hematitic paleosol and collapse ironstone breccias				Terra rossa sediments	
		Ooidal-nummulitic grain-ironstone		Ooidal-nummulitic	Nummulitic wacke-ironstone	Glauconitic mud-ironstones	
		Mud-ironstone		Oncoidal	Mud-ironstone		
		Oncoidal/float-/rud-ironstone		Oncoidal	Pack-ironstone	Stromatolitic limestone (wackestone)	
		Mud-ironstone		Oncoidal-ooidal	Pack-ironstone		
		Wacke-/pack-ironstone		Oncoidal	Wacke-ironstone		
		Stromatolitic mud-ironstone					
		Float-/rud-ironstone					
		Mud-ironstone					
		Mudstone		Ooidal	Rud-ironstone	Wacke-ironstone	Five repeated shallowing-upward cycles: each of which begins by bioturbated nummulitic mud-/wacke stones and terminated by bioclastic-nummulitic packstones
					Float-ironstone	Wacke-/pack-fossiliferous ironstone	
					Pack-/grain-ironstone	Fossiliferous mud-ironstone	
		Mud-ironstone		Ooidal	Mud-/wacke-ironstone	Ooidal pack-/grain-ironstone	
					Stromatolitic ironstone	Wacke-ironstone	
		Mud-ironstone		Stromatolitic ironstone	Oncoidalrud-ironstone	Wacke-ironstone	
Stromatolitic mud-ironstone	Mud-ironstone						

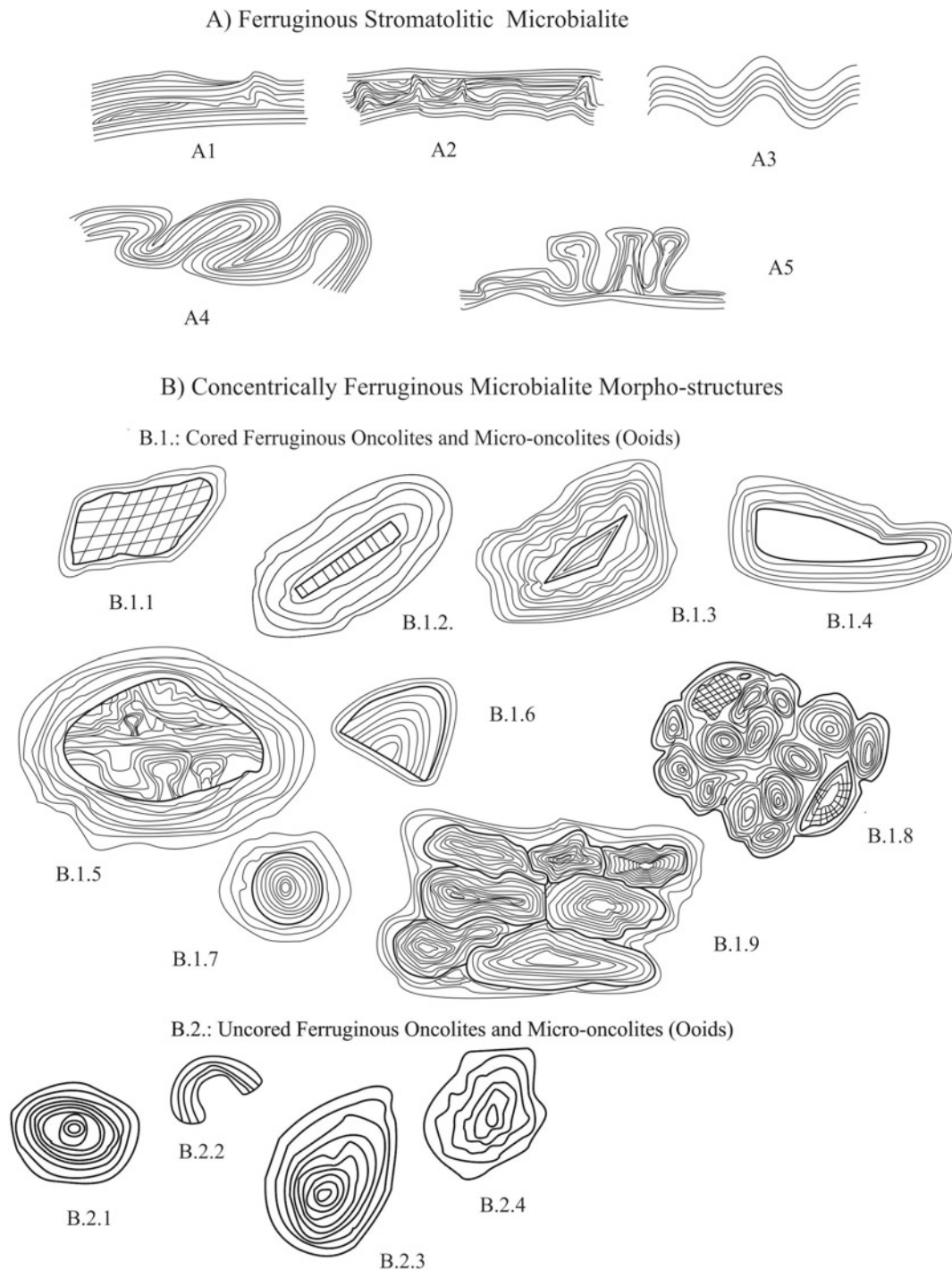


Fig. 21 Schematic illustrations of the recognized ferruginous microbialite morpho-structures of the Lutetian ironstones, not to scale (El Aref et al., 2006b). Types (A1–A4): biostromal (stratiform) stromatolitic buildups, Type A5: digitate stromatolites, Types (B1.1–B1.9): cored oncolites and micro-oncolites (ooids) with cores of: nonskeletal particles (Types B1.1–B1.3); mud ironstone clasts (Type B1.4); stromatolitic mat chips and fragments (Type B1.5); intact and/or segments of ferruginous ooids and peloids (Types B1.6 and B1.7); and groups of ferruginous ooids and oncolites Types (B1.8 and B1.9). Types (B2.1–B2.4): uncored ferriferous oncolites and micro-oncolites. Types (B2.1 and B2.2) are oncolites of spherical to ellipsoidal shapes having plastically deformed or spastolitic forms (Type B2.2); Types B2.3 and B2.4 are oncolites with internal convex outward discontinuous, wavy to slightly crenulated laminae

stromatolitic microbialites (Fig. 22a, b), (2) ferruginous concentrically laminated microbialites (ferruginous oncoids, micro-oncoids and ooids, and (3) ferruginous peloids. The internal structure of the ferruginous stromatolites and microbially coated grains consists of cyclic microbial and Fe oxyhydroxide laminae. The microbial laminae consist of fossilized neutrophilic filamentous iron-oxidizing bacteria (Salama et al., 2013, Fig. 22c).

The lateritization processes acted upon the upper ironstone sequence led to the development of solution openings, passages and cavities and angular rubble to boulder-sized collapse breccia's of ooidal and nummulitic ironstones (Figs. 18, 19, 20 and 22d–f). The solution features are mostly filled by chemical and biogenic products. Their internal walls are often lined by crustified banded yellow amorphous iron oxyhydroxides and brown radial goethite

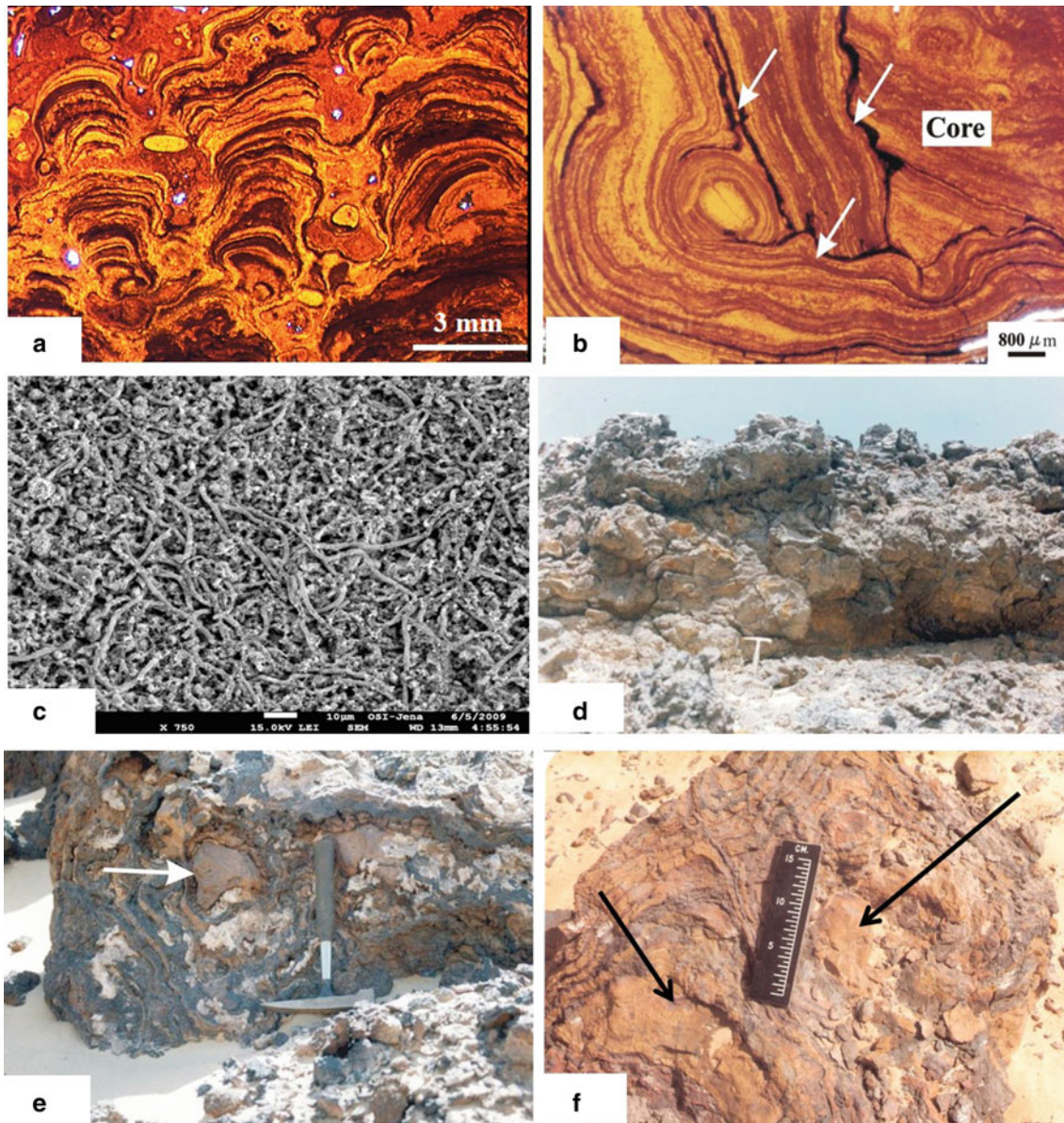


Fig. 22 **a** = Transmitted light photomicrograph of micro-columnar and micro-domal ferruginous stromatolites. **b** = Transmitted light photograph of Large ferriferous oncoids with inner core made up of stromatolitic fragment and outer multiphase encrustations separated by micro-erosional surfaces (arrows). **c** = SEM photomicrograph shows microbial ferruginous laminae consisting entirely of leptothrix-like bacteria (Salama et al., 2012). **d** = An outcrop of the upper lateritic Fe sequence dominated by collapsed ironstone boulders setting in soily matrix. **e** and **f** = Cockade structures of the upper Fe laterite sequence showing crustified colloform goethite cementing omcolitic ironstone fragments (arrows)

crystals of colloform outlines. Cockade structure of crustified colloform goethite enveloping ironstone breccia fragments is very common.

The mineralogy and geochemical characteristics of the different marine ironstones and the related lateritic products are intensively investigated by Salama et al. (2012, 2013, 2014, 2015) and Valerian Ciobotă et al. (2011), using a Jeol JSM-7001 field emission scanning electron microscope, applied Mössbauer spectroscopy, SEM, XPS, XRD, FTIR and ICP-OES methods, thermoanalyses (DTA-TGA) and isotope measurements. The lagoonal ironstone facies association consists mainly of goethite, hematite, todorokite, psilomelane, pyrolusite, birnessite, aurorite and manjiroite, and authigenic kaolinite and illite together with detrital minerals (quartz, rutile, and feldspars). The peritidal microbially mediated ironstone facies association consists mainly of goethite, psilomelane, pyrolusite, apatite, quartz, and jarosite with organic materials such as proteinaceous compounds, lipids, cellulose, and carotenoids are detected in the cortices of the ferruginous ooids and oncoids. The iron laterite consists mainly of crustified colloform goethite, hematite and psilomelane, alunite, kaolinite, gibbsite, palygorskite, and halloysite.

Sedimentary Processes, Diagenesis, and Supergene

As it has been concluded by the above-mentioned publications, the original precursor materials include iron-rich kaolinitic clays and amorphous iron oxyhydroxides (ferrihydrite) with less frequent oxidized glauconite peloids and sandstone rock fragments. The iron compounds were transported as an organic-rich colloidal suspension from the Cenomanian paleo-highs by rivers to the depositional system. The depositional processes include:

- (a) Deposition of detrital Fe-rich glauconitic and kaolinitic clays and yellow amorphous Fe oxyhydroxides in areas of variable water depths, Eh, pH, and organic matter content with or without manganese enrichment in some horizons depends on the behavior of the manganese and iron in the solution during the depositional and diagenetic processes,
- (b) Growth of stromatolitic (microbial) buildup and formation of in situ Fe oncoids and ooids (Fig. 22a–c) in a quiet water condition intermittent with short agitated periods of storm waves. The detailed composition of the accreted microbialites, the precipitation, and accretion mechanism of the different various microbial forms as well as the ferruginization processes of the associated skeletal particles during the marine deposition, subsequent diagenesis, and subaerial processes are discussed in detail by

Mesaed et al (2005), Helba et al. (2001), Salama (2006, 2010) and Salama et al., (2012, 2013, 2014, 2015). According to Salama et al. (2013), the microbialites consist of cyclic alternations of microbial and iron oxyhydroxide laminae formed by neutrophilic iron-oxidizing bacteria at the interface between ascending acidic Fe (II)-rich groundwater and marine water. The microbial laminae consist mainly of fossilized filamentous iron-oxidizing bacteria, most similar to the modern *Leptothrix* species, which indicate microbial precipitation of amorphous iron oxyhydroxides around the bacterial surfaces, crystallized during early diagenesis into nano-crystalline goethite. Acidic groundwater may have induced syn- and post-depositional alteration by oxidation of sulfides (primarily pyrite) hosted in the underlying Cenomanian Bahariya Formation. Iron sulfates and oxides were precipitated by another generation of acidophilic iron-oxidizing bacteria (Salama et al., 2013), and

- (c) Reworking and distribution of shells and shell fragments and their admixing with the other biogenic Fe components in storm-dominated condition during shallowing regimes.

• Early diagenesis

The early diagenetic processes include:

- (a) Organic matter degradation by benthic microbes mainly cyanobacteria, which create a weakly reducing (post-oxic) diagenetic environment of low pH and Eh,
- (b) releasing of Fe, Mn, silica, and other residual elements and their re-concentration in the interstitial pore water as a result of lowering in pH and Eh,
- (c) Matrix pelletization and growing of in situ peloids and ooids. In situ ferriferous peloids and ooids are formed as organic-rich windows within the matrix components due to the inhomogeneous distribution of the organic matter with the precursor materials,
- (d) Dissolution and replacement of the original calcareous wall structures of the skeletal particles and the formation of intra- and inter-skeletal porosities. The calcareous skeletal particles and bioclastic debris are also subjected to early weakly reducing diagenetic changes within the semi-confined micro-cavities of the foraminiferal tests and bioclastic debris. This may facilitate dissolution of the original calcareous wall structures leaving ferruginized fossil molds and casts, and
- (e) Growing of barite nodules.

- **Late diagenesis**

During the late diagenetic stage, the amorphous to poorly crystalline iron oxyhydroxides (ferrihydrites) together with the in situ formed early diagenetic ferriferous ooids and peloids as well as the ferruginized skeletal particles undergo diagenetic dehydration and recrystallization. During these processes, the unstable yellow to reddish brown ferrihydrite phase is directly transformed into varicolored stable phases of well crystalline goethite and/or hematite of different morphological forms. The recrystallization processes begin within the interstitial iron oxyhydroxides matrix and extend outwards into the enclosing ferriferous grains consequently until the hematitization of the original components. Silicic acids are released into the interstitial pore solution during the early post-oxic diagenetic stage as a silica-like gel phase. During the subsequent stages of dehydration, the silica gel phase recrystallized into cryptocrystalline and microcrystalline quartz, this was followed by late siderite, calcite, barite, and halite cements.

- **Subaerial lateritization (supergeneses or telogeneses)**

The superimposed subaerial lateritization complicates the diagenetic history of the ironstones and partially to completely obliterates their original marine fabrics and textures (Fig. 22d). Crustified colloform layers of goethite, hematite, and pyrolusite form megascopic reniform textures, spherules, and/or bundle-like or flower-like textures. The collapsed ironstone breccia fragments are embedded in illuviated iron oxyhydroxides and often cemented by layers of colloform goethite, forming cockade structures (Fig. 22e, f). The ferriferous ooids and ferruginized skeletal particles are cemented by meniscus goethite vadose cement. Other pedogenic features are also displayed by coating of ferriferous ooids and peloids by amorphous iron oxyhydroxides and goethite cutans, the presence of well-developed grain bridges and sinuous fenestrae forming alveolar textures, as well as the presence of root mold porosities. The formation of sulfate, nitrate, carbonate, and silicate minerals in solution openings may indicate more recent alteration under arid climatic conditions.

Genetic Considerations and Recommendations

Summing up, the original Lutetian ironstones (iron ores) had been accumulated on submarine swells (the wrench-related Cenomanian swells) under well-aerated and intermittent agitated and quiet water conditions. Hence, the paleo-topographic evolution during the post-Cenomanian and Eocene time span resulted in the drastic variations in both facies and thickness of these ironstones. The humid paleo-climate during the Cretaceous-Eocene time and the

paleo-geographic distribution pattern of the paleo-Tethyan shoreline are other essential genetic parameters in the formation of these ironstones. The main genetic parameters responsible of the formation of these iron ores can be summarized as follows:

1. paleo-topography of the glauconitic Cenomanian paleo-highs,
2. paleo-climatic evolution,
3. paleo-geographic distribution pattern of the Tethyan shoreline,
4. paleo-environments of the ramp carbonates and the equivalent ironstone facies
5. syn-sedimentary supply of amorphous iron,
6. sedimentation and biogenic microbialite accretion of iron oxide, in situ reworking and local transportation, via mega ripple migration,
7. shallow marine and subaerial paleo-environments with marine diagenetic modifications,
8. intermittent phase of uplifting and lateritization responsible for the modification of the original marine ironstone facies association and redistribution of iron as cavity filling or laterite products,
9. authigenesis of iron and manganese oxides, silica, and sulfates.

4.2.2 Fe-Rich Lateritic Blankets (Surficial Ferricrete Duricrust)

In order to complete the perception of the geomorphological history of El Bahariya region, special importance must be focused on the developed El Heiz ferricrete high-laying duricrust of El Bahariya Depression (Figs. 17 and 23a-d, El Aref & Lotfy, 1989; Sokker, 1991; El Aref et al., 1991, 1992), touristically known as El Heiz black desert natural protected area. It shows the extent of the lateritization and karstification of the uplifted hinterlands of El Bahariya, since the regression of the Eocene sea. The high-lying ferricrete duricrust forms a clear black morphologic marker of fairly constant altitude, ranging from extensive sheet as in Gabal Radwan and Sandstone hills until discrete lenticular or rounded masses within the depression, capping the summits of isolated cone hills, inselbergs, and flat-topped tablelands of different clastic and carbonate stratigraphic units (Fig. 23). It represents remnants of an old erosion surface of old erosion cycle and was formed by general lowering of the landscape over long period of humid paleo-climate. The ferricrete profile, 6–16 m thick, consists of three main gradational horizons corresponding to the typical laterite profile (Fig. 23), including (a) an upper hard cap, (b) a middle varicolored (illuvial) horizon, and (c) a lower horizon of

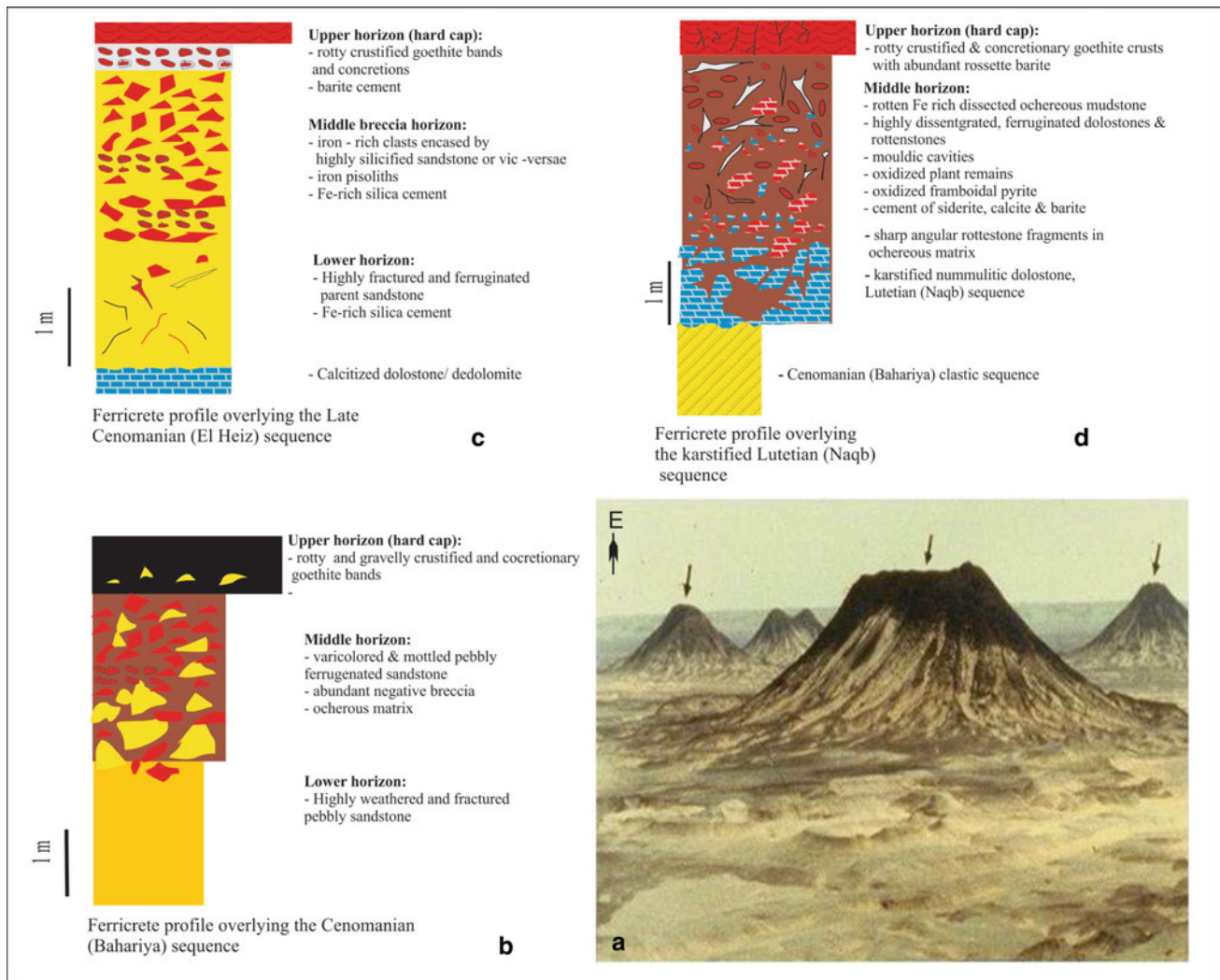


Fig. 23 El Heiz high-lying ferricrete duricrust, El Heiz black desert Protected area, El Bahariya depression, Western Desert. **a** = field view showing the high-lying ferricrete duricrust (arrows) capping isolated cone hills, **b** = ferricrete profile overlying Cenomanian clastics, **c** = ferricrete profile overlying Cenomanian dolostone, **d** = ferricrete profile overlying Lutetian dolostone. Simplified after El Aref et al., (1991, 1992)

weathered rocks. Subsequent weathering and paleo-karstification cycles with etchplanation and pedimentation processes, (post-Eocene-Quaternary) affected the high-lying paleo-peneplained surface and the surrounding carbonate plateau. These processes led to continuous stripping of regolith's, incision and deepening of rivers, gradual consumption of the interfluves, gradual slope, and scarp retreat until the complete excavation of the depression and development of remnants of duricrusted cone hills of black appearance (Fig. 23c). Hence, the landform evolution of El Bahariya region and the related development of lateritic deposits indicate that the whole region was subjected to multiple erosion cycles under humid conditions (lateritization and karstification) affected the exposed carbonates and

clastics of the hinterlands, since the Middle Eocene northward sea retreat.

4.2.3 Fossil Pre-rift (Post-Eocene-Pre-early Oligocene?) Alumino-Ferruginous Latosol

Another proof of continuous weathering of the hinterlands is manifested by well-developed alumino-ferruginous latosol of Um Gerefat mine, Red Sea coast (El Aref, 1993a, 2020a). It demarcates a pre-rift paleo-erosion surface acted upon Pre-Cambrian granite and was later truncated by the proto-rift Late Oligocene-Early Miocene fanglomerates of the Ranga Formation (Fig. 24a). The latosol profile comprises three main horizons representing a series of weathering degrees grading from slightly weathered Pre-Cambrian

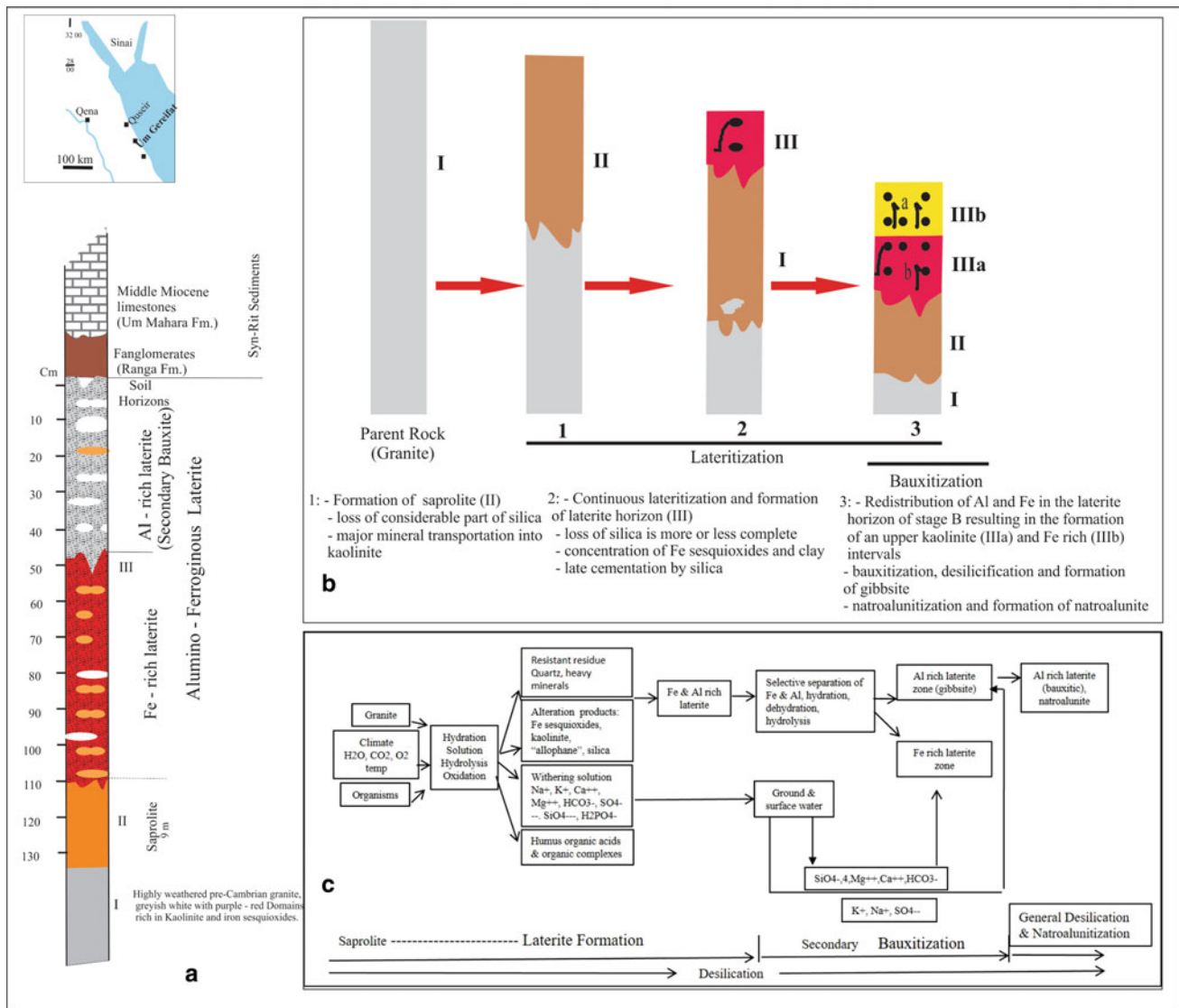


Fig. 24 a = Vertical lithostratigraphic profile of Um Gherifat alumino-ferruginous latosol, Red Sea Zone. b and c = Schematic illustrations of the concluded stages of lateritization, secondary bauxitization and natroalunitization processes and formation of Um Gherifat lateritic iron deposits, Red Sea Zone (after El Aref, 1993a)

granite into saprolite and Al and Fe-rich laterite (Fig. 24a). The saprolite horizon is composed of thoroughly decomposed and disintegrated granitic minerals being enriched in kaolinite mixed with Fe sesquioxides. The top laterite horizon (up to 1.4 m thick) is obviously divided into a lower Fe-rich ochreous zone and an upper Al-rich argillite (bauxitic) zone (Fig. 24a). The lower zone (up to 60 cm thick and of about 35% Fe) is formed of alternating continuous and discontinuous nodular layers and laminae of reddish to yellow ochres and brick red mudstones, showing abundant pelitomorphous to microgranular textures, lenticular to patchy segregations of earthy goethite and kaolinite, massive glaebules, clay aggregates, intra-formational contortions, desiccations, spastoids, circum granular cracks,

vertically arranged goethite concretions, goethite coatings and diffuse concentric layers of earthy goethite together with root molds and root hairs, and microcellular and alveolar textures. The uppermost yellowish to yellowish brown Al-rich zone (15–21% Al) is bauxitic in nature being composed entirely of nodular kaolinite and gibbsite with less abundant amorphous “allophane,” natroalunite, goethite, and hematite. Worm burrows, tubular voids, shrinkage cracks, and load casts are very common in this zone. The extensive petrographic and geochemical investigations conducted by El Aref (1993a) led to recognition of the processes involved during the lateritization, bauxitization, natural unitization, and development of this laterite ore (Fig. 24b, c). The geologic setting of this latosol type encourages more intensive

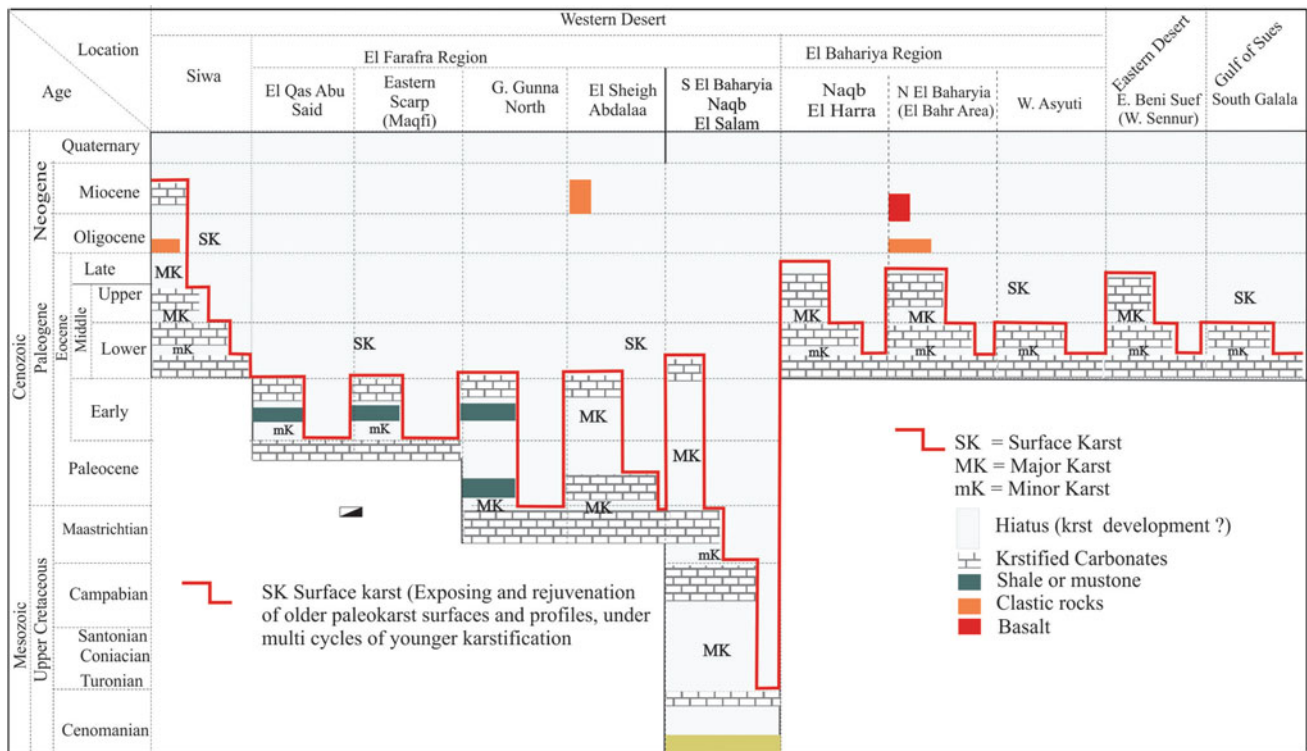


Fig. 26 Intra-, inter-formational, and surface paleo-karst surfaces of the Western and Eastern Deserts and Gulf of Suez (modified after El Aref et al. 2017a, 2017b)

paleo-karst profiles (e.g. Fig. 27) that formed along paleo-karst processes acted upon Cretaceous-Neogene carbonates, since Upper Cretaceous and until the last rainy periods of the Quaternary (Figs. 26, 27, 28, 29 and 30) and completely or partially fill solution openings and caves of variable scales. The re-precipitated cave calcite (flowstones) form crustified rhythmic botryoidal layers and stomatolitic laminae depositing on the internal walls and ceilings of caves and solution passages (Fig. 28a and b) or all around collapse breccia fragments forming cockade structure (Fig. 28c and d). The re-precipitated crustified calcite layers together with the collapse breccia fragments and red soils also form wide decorative textures such as crackle breccia, mosaic breccia, clast, and red matrix-supported chaotic breccia. Calcite crystals also form stalactites and stalagmites, spheriolites, geoids, cave pearls, and hopper structure. Unroofed karst carbonate fills and the associated red soil products hosted in different carbonate sequences of different ages (Upper Cretaceous-Miocene) are widespread as remarkable small exposures all over the Western and Eastern Desert (Figs. 25 and 28e, f). This confirms the findings of Halliday (2003) proving that potentially karstified rocks form the surface of much of Egypt and northern Libya.

The intensive field investigations on the Egyptian carbonate outcrops enable the recognition of the following types of paleo-karst surfaces (El Aref, 2000, El Aref et al. 2017a, 2017b and Fig. 26):

1. Drowned (fossilized or buried) paleo-karst surfaces, including
 - (a) Inter-formational fossilized paleo-karst surfaces displaying break in sedimentation or great hiatus developed during periods of relatively long-lived exposure of carbonate sequences (paleo-highs) subjected to intensive karstifications.
 - (b) Inter-formational and Intra-formational fossilized paleo-karst intervals displaying break of sedimentation and karstification during relatively short periods of exposure.
 - (c) Fossilized depositional paleo-karst surfaces terminating meter-scale shoaling cycles.
2. Surface karst, responsible for the development of the present-day geomorphological karst landscape, characterizing the carbonate rock sequences all over the Egyptian Sahara, as well as progressive destruction and denudation of the outcropped fossilized paleo-karst features and the related deposits.

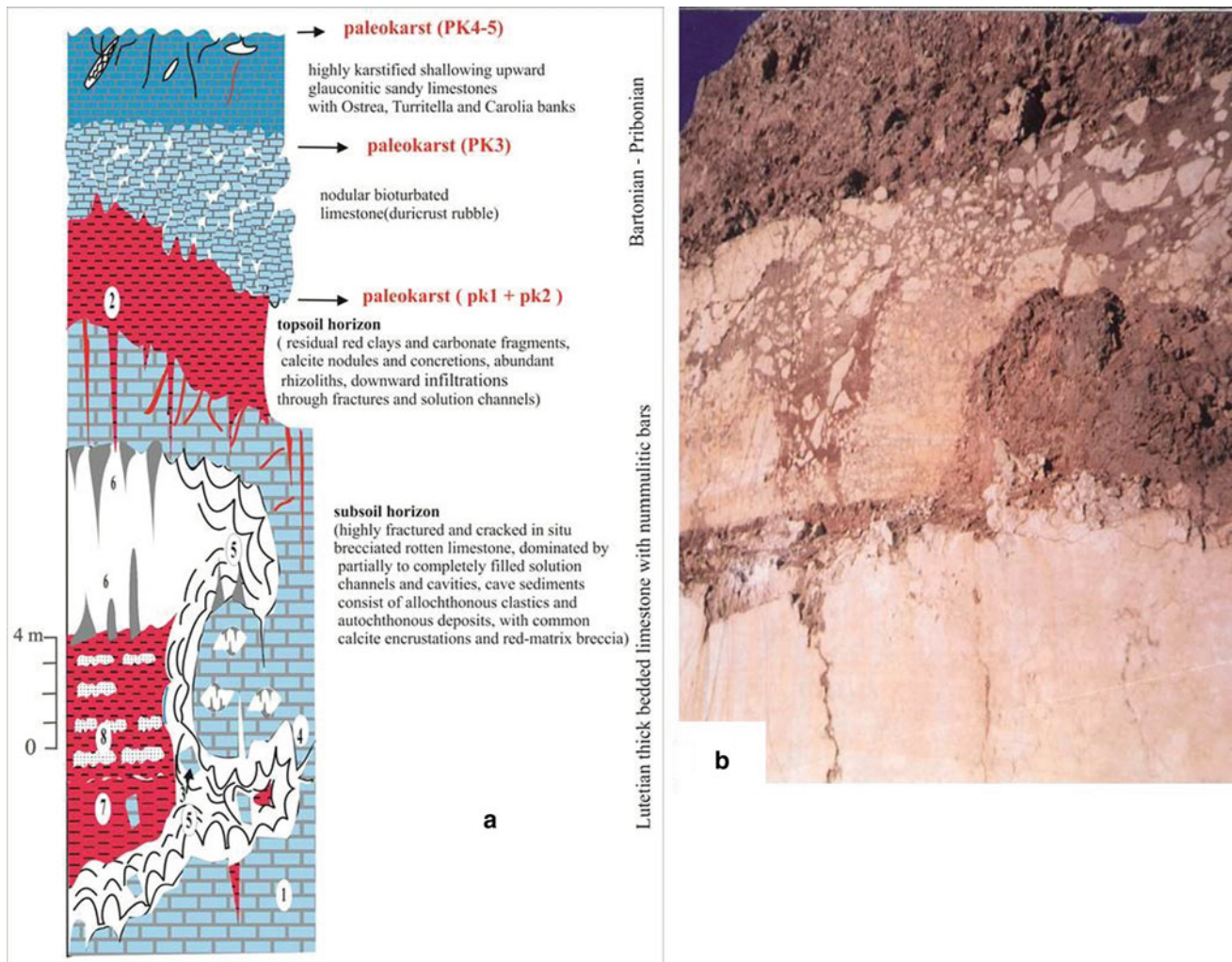


Fig. 27 **a** = Fossilized paleo-karst surfaces and related facies of Wadi Sannur karst region (Gharieb, 1998). 1 = host rocks, karstified limestone, 2 = fossilized sinkholes, 3 = collapse breccia, 4 = crackle breccia, 5 = crustified calcite, 6 = stalactites and stalagmites, 7 = laminated red soil, 8 = concretionary soil. **b** = An outcrop of representative intra-Eocene paleo-karst profile of south Galala, Gulf of Suez, showing the upper red soil, the middle breccia, and the lower karstified rock horizons

The recognized paleo-karst surfaces of the exposed Upper Cretaceous-Miocene carbonate sequences are shown in Fig. 26 and include:

- I. Inter-formational fossilized major sequence boundaries (MK, Fig. 26), among which are:
 - i. Cretaceous-paleocene (K/P) paleo-karst boundary,
 - ii. Cenomanian-Middle Eocene unconformity,
 - iii. Intra-Middle Eocene paleo-karst boundary,
 - iv. Middle to late Eocene-Oligocene paleo-karst boundary.
- II. Inter- and Intra-formational minor paleo-karst intervals (mK, Fig. 26).

- III. Intra-formational fossilized (depositional) micropaleo-karst surfaces (mk, Fig. 26), and
- IV. Surface paleo-karst (SK, Fig. 26).

Post-Eocene-Quaternary (?) karstification processes are clearly manifested by the continuous lowering and back wearing of the landscape of the exposed Cretaceous- Miocene carbonates through successive processes of karstification, and gradual unroofing, destruction and rejuvenation of the naked paleo-features and related karst products, including the “Egyptian Alabaster” (Fig. 28e and f). Intra- and post-Miocene karst events are reviewed in section (5). The karst-related red soils contain small vertebrate fossils of Late Miocene age (Gunnell et al., 2016; Mein & Pickford, 2010;

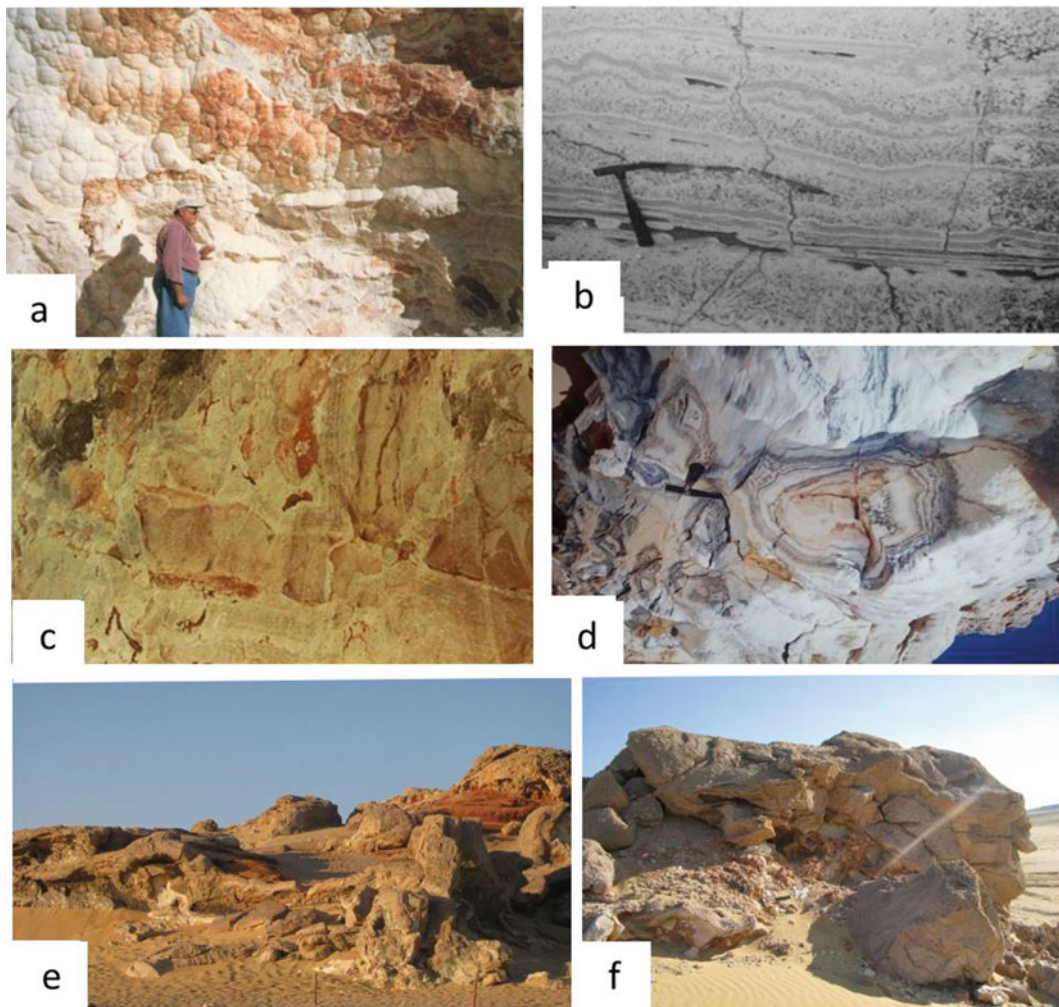


Fig. 28 **a** = Cave deposits entirely formed by crustified colloform calcite (“Egyptian Alabaster”). **b** = Polished slab of the “Egyptian Alabaster” consisting of successive stromatolitic calcite laminae. **c** and **d** = Cockade structures formed of crustified calcite layers deposited all around collapse breccia fragments (cave fill, “Egyptian Alabaster”). **e** = Partially unroofed elliptical cave filled by alternating layers of crustified calcite and red soil precipitates, El Sheigh Ab Dallah denuded paleo-karst, White Desert Protected Area, Western Desert. **f** = Residual mound of unroofed cave deposits being composed of red-matrix breccia enveloped by crustified calcite layers, El Bahariya-Farafra karst Territory

Pickford et al., 2006). Younger karstification processes are recorded along the Mediterranean coast (Halliday, 2003). The exposed karstified carbonates (e.g. Figs. 26 and 29a and b) are dominated by input, output, and residual polygonal karst landforms of allogenic and autogenic recharge areas, expressed by karst depressions (poljes, uvalas, sinkholes, dolines), Karren, tower, pinnacle, cone and cockpits, allogenic and blind rivers, sinking streams and degraded and rejuvenated karst systems, leaving behind remnants of cave fill precipitates (e.g. Figure 28e and f). The gradual lowering and back wearing of the present karst landscape could be reached by determining the paleo-erosion (paleo-karst) surfaces and related. Each of which is of consistent altitude range and demarcate certain paleo-erosion level resulted from an old erosion cycle (e.g. S1–S4 paleo-surfaces of

Fig. 29c). The relatively old surfaces are topographically inverted through subsequent etchplanation and pedimentation processes involving destruction and stripping of the high-lying duricrusts, lateritic deposits and karst regolith’s and the exposure of the bedrock forms; incision of valleys; slope and scarp retreat; gradual consuming of the residual hills, pedimentation and pavementation and development of younger exposed karst surface (S1–S4, Fig. 29c). East of the River Nile, The karst products including the “Egyptian Alabaster” are usually confined within vertical staked (amalgamated) paleo-karst surfaces and often truncated by younger post-Eocene karst event as well-expressed in Wadi Sannur area (Fig. 30). The detected main hiatus displayed by intra-Eocene fossilized paleo-karst surfaces, most probably coeval to those of the Western Desert. These are: (a) top

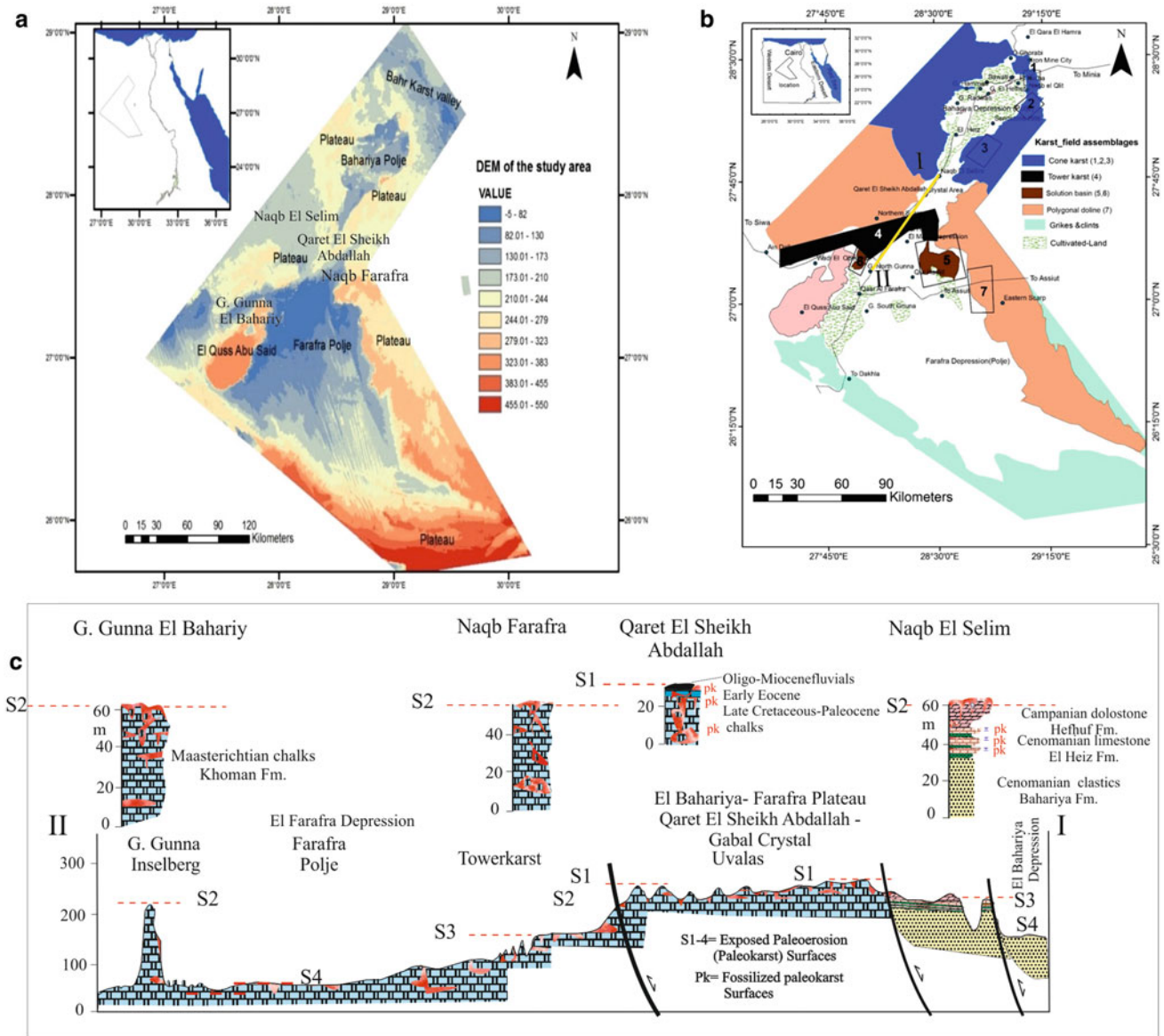


Fig. 29 a = GIS layer of the DEM and topographical features of El Bahariya-Farafra karst Territory showing the main karst depressions (El Aref, 2017a), b = karst map of El Bahariya-Farafra karst Territory showing the karst landforms zonation's (El Aref, 2017a), c = Sketch profile of the exposed paleo-karst surfaces (S1–S4) of El Bahariya-Farafra karst Territory, compiled and modified after Sokker (1991), Abu Khadra et al. (1987), El Aref et al. (2000, 2017a, 2020a, 2020b)

Lutetian-Bartonian paleo-karst, and (b) top Bartonian-Pribonian paleo-karst. The karstified carbonate sequences of this area and the interrupted paleo-karst surfaces were also subjected to post-dated intensive karstification in younger time.

General Comments and Recommendations

(1) The study results emphasize the importance of all types of unconformities especially paleo-karst sequence boundaries as potential sites for ore exploration. It is highly recommended to intensively examine such

paleo-karst surfaces and the related soil products (in situ or transported) as a good environment for concentration of varieties of trace or major elements. Furthermore, Karst features are of high economic values for underground storage of water and certain oil and gas products.

(2) The surface landscape and the related features are now considered as a valuable and most significant geo-morphosites showing amazing complex paleo-karst landforms side by side with the present-day arid morphologies, which are very much attractive for geo-tourism and research activities. Therefore, the karst

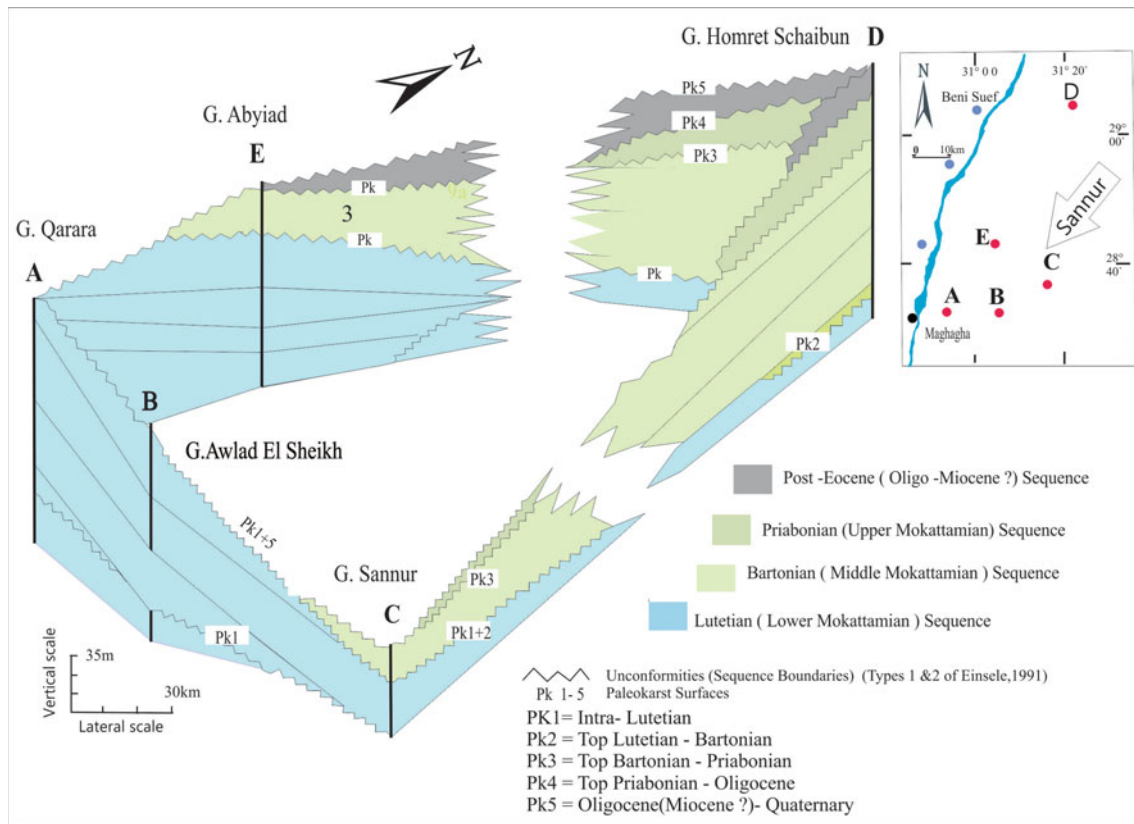


Fig. 30 Isometric panel diagram of Wadi Sannur karst region and the stratigraphic settings of the different time rock units and the associated facies and paleo-karst surfaces. A–E = measured sections (simplified after Ghariieb, 1998, 2003; Philip et al., 1991a)

territories of Siwa Oasis, El Bahariya-Farafra, and Wadi Sannure are declared by Ministerial Decrees as Protected National Geological Parks.

- (3) Also, and in order to enhance the economic potentiality of Karst, karst features must be included in every land use planning and urban development.
- (4) For accurate determination of the ages of the successive karst events, an extended range of isotope measurements are required, taking into consideration the successive generations of the calcic crystals, as well as intensive paleontological studies on the karst sediments.
- (5) Detailed information about the Egyptian karst morphology and karst products are extensively studied and discussed in an ample of publications and M.Sc. and Ph.D. projects, among which are: El Aref (1984, 1993b; 1996, 2000, 2005–2006), El Aref and Amstutz (1983), Ahmed (1986), Abdel Motelib (1987,1996), Lotfy (1989); El Aref and Ahmed (1986), El Aref and Refai (1987), El Aref and Lotfy (1989), El Aref et al. (1985, 1986, 1987, 1991, 1992, 1999a, 2001, 2006a, 2006b, 2017a, 2017b, 2021), Ghariieb (1990, 1998, 2003), Sokker (1991), Philip et al. (1991a, 1991b), Halliday (2003), Salama (2006, 2010), Pickford et al. (2006), Mein and Pickford (2010), Hamdan and Lucarini

(2013), Salama et al. (2014), Gunnell et al. (2016), Embabi (2004, 2018), Soliman (2018) and Hamdan and Hassan (2020).

5 Cenozoic Stratabound Ore Deposits

5.1 Neogene Rift-Related Ore Deposits

Neogene stratabound/stratiform ore deposits are intimately related to syn-rift facies and syn-rift paleo-karst surfaces (Figs. 1, 31, and 32; Table 1). The Neogene deposition under the Red Sea rifting dynamics led to the formation of a series of faulted clastic, carbonate, and evaporite facies association of variable stratigraphic setup and lateral distributions (El Aref, 1993b; Monetant et al., 1988; Philobos et al., 1988). The main faulted rock association is classified into four main stratigraphic sequences punctuated by regional unconformities (Fig. 32). The basal Late Oligocene-Early Miocene proto-rift sequence is represented by the of continental clastics, paleosols, and basalt flows of the Ranga Formation in the Red Sea and the Abu Gerfan Formation in the Gulf of Suez. The succeeding Middle Eocene sequence (Um Mahara

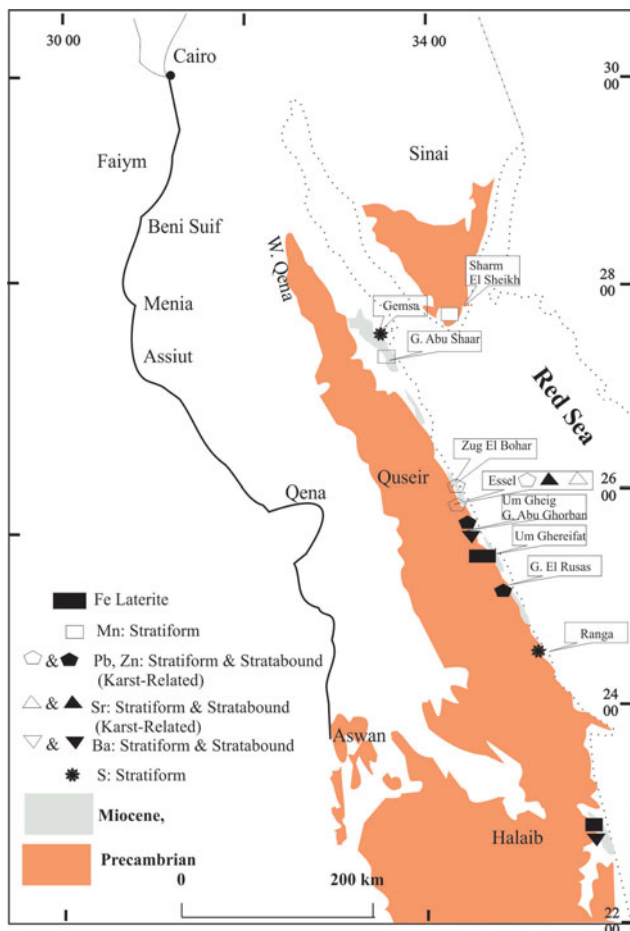


Fig. 31 Location map of the Red Sea Neogene rift-related stratabound and stratiform deposits

Sequence) overlies irregular relief of pre- and syn-rift units and consists of mixed clastics and carbonates of reefal, beach, lagoonal, tidal flat, subtidal-intertidal, and supratidal environments. The upper carbonates of the Um Mahara Formation (sequence) are truncated by a regional paleo-karst surface related to the main phase of rift faulting, postdating the development of this unit. Following this, paleo-karst event is the deposition of subaqueous and sabkha evaporites of the Middle to Late Miocene Abu Dabab sequence. South of Quseir, supratidal-intertidal dolostones of the Upper Miocene-Paleocene? Um Gheig Sequence terminates the Neogene successions. It either overlies the Abu Dabbab evaporates or in some places (e.g. Um Gheig and Essel mine areas) rests directly on Um Mahara rock association. Almost all the exposed evaporites and carbonate sequences show remarkable solution karst features and karst sediments, such as allogenic dray rivers, conekarst and directed cockpits, karst linear ridges, surface depressions, and subsurface solution openings and cavities. The hill summits and hillside slopes are often mantled by relatively thick calcrete crusts or talus sediments derived from the karstified rocks, whereas,

the solution openings and cavities are commonly filled by collapse breccia's with or without concentration of some mineral deposits mixed with autochthonous and allochthonous cave sediments. The development of the syn-rift intra-formational and surface karst features is most probably coincided with the evolution of the syn-rift river system of Issawi and McCauley (1992, 1993) and Guiraud et al. (2001) and the post-Late Miocene-Plio-Pliocene heavy rainy periods (El Aref et al., 1985, 1986, 1987).

5.2 Oligo-Miocene (?) Mn Conglomerates

This stratabound Mn ore is recorded in Sharm El Sheikh, Sinai (Fig. 31) and previously described as post-Oligocene/pre-Pleistocene fault-related mineralized breccia ore type (Omara, 1959). However, El Aref (2020b) has clarified that this ore type represents the basal conglomerates of the syn-rift Miocene clastics of Abu Gerfan Formation of El Azabi and Eweda (1996). It needs more study and evaluation of its economic return.

5.3 Middle Miocene Stratiform Galena of Beach Environment

At Essel and Zug El Bohar mine areas (Figs. 31, 32, and 33), stratiform galena deposit is confined within the basal beach sandstones of the Middle Miocene Um Mahara sequence (Formation), overlaying the Pre-Cambrian rocks. The clastic galena bearing succession consists mainly of mature cross-bedded sandstones including abundant heavy minerals of beach environment. The galena shows typical stratiform and stratabound geometrical patterns forming layers or bedding structures closely symmetrical and concordant with the primary structures of the enclosing sandstones. Galena with or without cerussite constitutes the main cementing materials of the sandstones as they fill the pores or spaces left after diagenetic quartz overgrowths. Galena pore filling is undergrown with a microcrystalline quartz, forming network intergrowth patterns, and with cerussite forming zoning textures. In comparison with the well-led belts of the world, the geologic setting, the nature of the host rocks, the geometric distribution, and sedimentological features of this galena ore, are almost identical with the situation in the Cambrian sandstone around the (partly) buried Pre-Cambrian hills of mine Lamotte of the old Lead Belt, or even at Viburnum in the new Lead Belt of Missouri (USA), Lisvall (Sweden), Maubach-Michernich (Germany), Morocco, etc. (El Aref & Amstutz, 1983). The Egyptian Pb occurrences may represent the most recent stratiform-stratabound lead deposits of this type in the world known today.

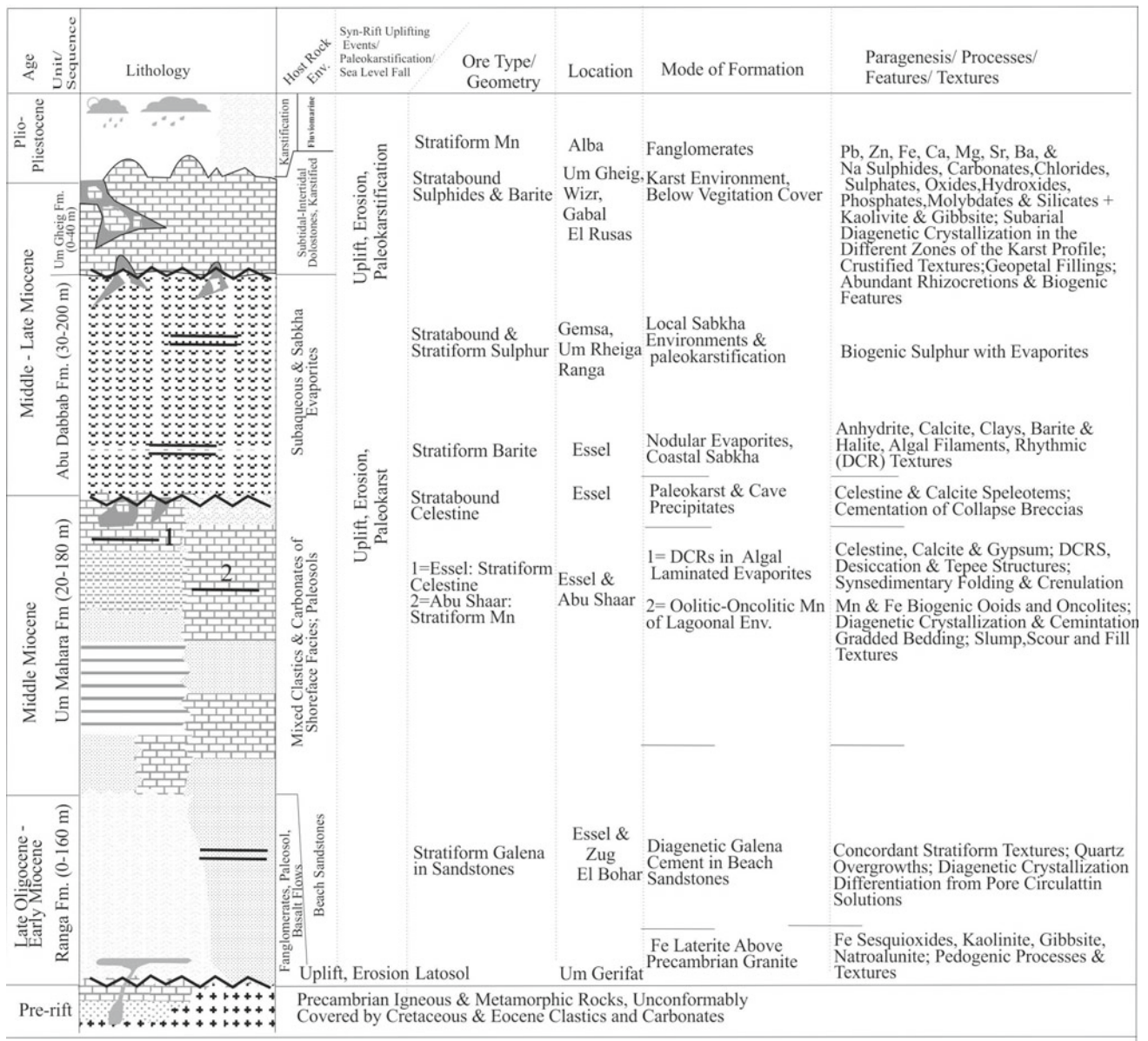


Fig. 32 Syn-rift sedimentation, uplifts, erosion, and related ore deposits in the Red Sea Coastal Zone between latitudes 24° and 28° N (El Aref, 1993b, 1996)

5.4 Middle Miocene Stratiform Oolitic-Oncolitic Mn Ore

This ore type forms a stratified oolitic-oncolitic Mn bed, up to 80 cm thick and of 35.8–45.14 MnO%, encountered within syn-rift Middle Miocene carbonates of reef, shoal, and lagoonal environments (Figs. 1, 34 and 35). The Mn-rich bed is formed by small-scale coarsening-upward cycles of Mn and Fe ooids and oncolites setting in a

matrix of earthy manganese and carbonate mud (Fig. 35a and b). The zonation, mineral composition, and geochemical characteristics of this ore type are studied and discussed in detail by Abdel Motelib (1996). The Mn source and the depositional and diagenetic conditions prevailed during the ore formation are also concluded. El Aref (2020b) recommended further exploration survey in order to evaluate the economic potentiality of this ore type.

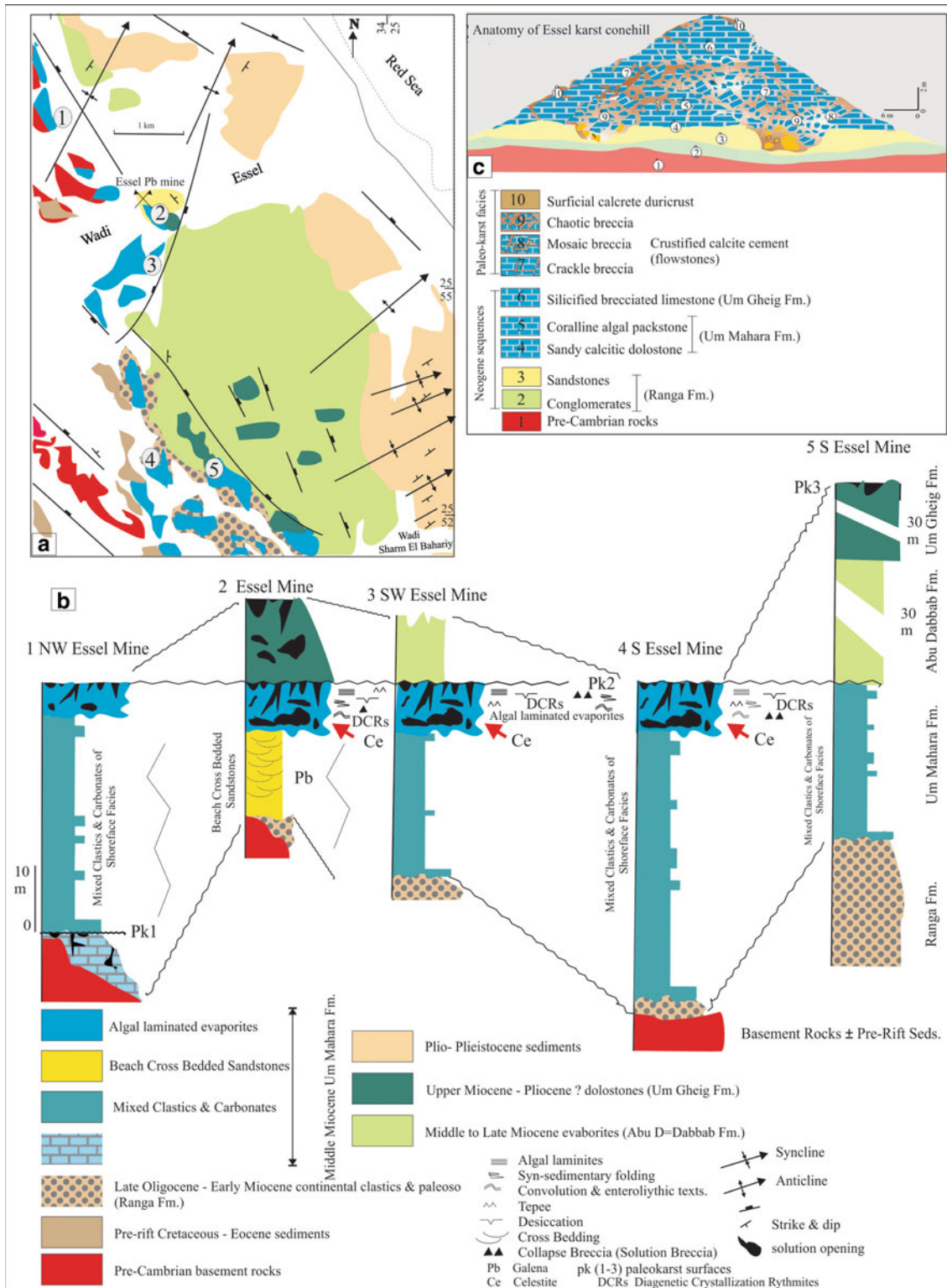


Fig. 33 a = Geological map of Essel-Wadi Sharm El Bahary area. b = Stratigraphic columns showing the stratigraphic settings of the recognized paleo-karst surfaces and the stratiform and stratabound Pb and Ce deposits, c = Schematic representation of isolated cone karst of the Miocene carbonates of Essel mine area, showing the internal cave fills (El Aref, 1993b)

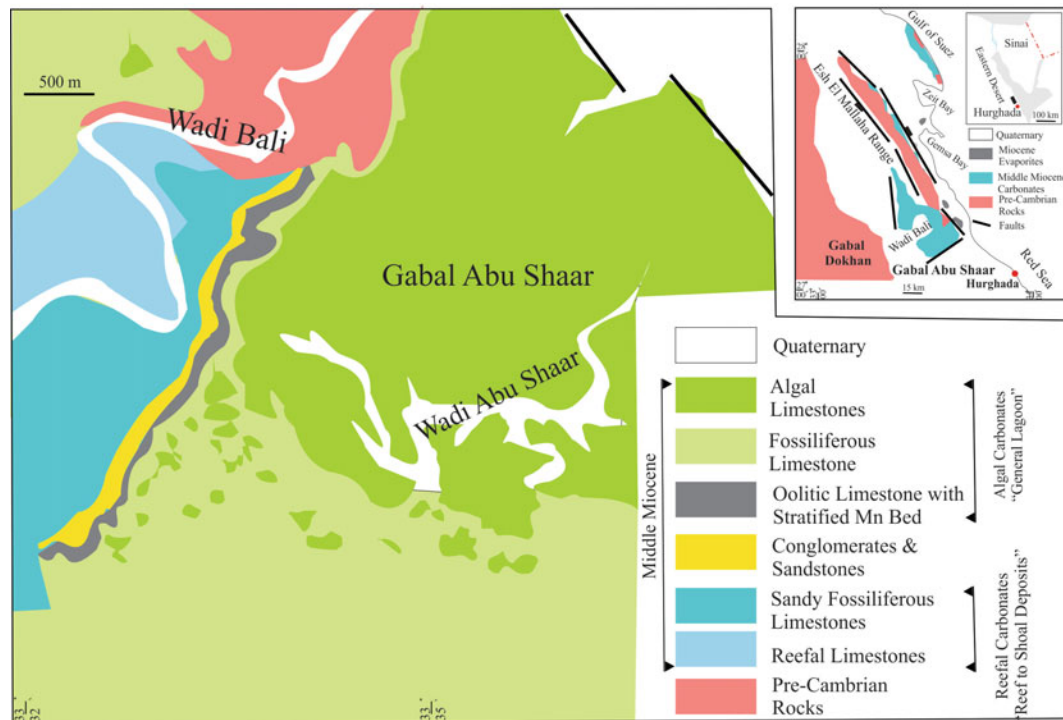


Fig. 34 Simplified geological map of Gabal Abu Shaar El Qebli (after Abdel Motelib, 1996), showing the stratigraphic setting of the oolitic limestone hosting the Mn bed

5.5 Middle Miocene Stratiform and Post-middle Miocene Stratabound Celestite, Essel Mine and South Essel Areas (Stratigraphic Sections 2–5, Fig. 33)

Resting on the tidal flat and galena bearing beach facies of Essel mine area, is a 6–10 m thick celestite bearing supratidal-intertidal facies, representing deposition in a near-shore restricted basin during a period of tectonic stability and constant sea level. This facies comprises alternated beds, 10–50 cm thick, of algal laminated and evaporitic limestones and thin massive calcareous mudstones, dolomitic in part. This succession is topped by paleo-karst surface (pk₂, sections 2 and 3, Fig. 33), where this surface is buried under either mudstones and evaporates of the Abu Dabbab sequence or the karstified bedded dolostones of the Um Gheig sequence. Some tectonic blocks of this facies remained exposed during the deposition of the succeeded Abu Dabbab and Um Gheig sequences and have clearly undergone later intensive weathering during a third karst event postdating the uplifting of Um Gheig sequence (pk₃, Fig. 33). Two interesting types of celestite are recognized within this facies, namely (a) stratiform celestite of rhythmic pattern (assigned here as generation I celestite (Fig. 36a and b), and (b) stratabound intra-karstic celestite related to the post-Um Mhara paleo-karst event (generation 2 celestite, Figs. 36c and d). It is recommended to intensify the

examination along the unconformity surface between Um Mahara and Abu Dabbab syn-rift sequences for the high probability of discovering new reserves of this ore type.

5.5.1 Middle Miocene Stratiform Celestite (Generation I Celestite, Diagenetic Crystallization Rhythmites, DCRs)

The primary lamination of this bedded facies is formed of 1 mm–3 cm couplets of alternating brownish stromatolitic laminae and celestite-rich laminae, giving rise to characteristic syn-sedimentary rhythmic patterns (Fig. 36a and b), similar to the diagenetic rhythmic texture of Fontboté and Amstutz (1980). This type of rhythmic lamination often forms connected or disconnected domes, up to 40 cm high, encountered within evenly laminated beds. Laminated fenestrae, desiccation cracks, tepee and enterolithic textures, convolute lamination and syn-sedimentary slump folds and faults are frequently observed within evenly laminated beds. Progressive desiccation forms aligned polygonal plates. Slump movement may affect several beds forming small-scale recumbent and tight overturned folds, up to 40 cm in thickness, most of them are flat-based with convex upper surface and usually arranged parallel to the strike of the host strata) Figs. 36 and 37). Some isolated wedge-shaped bodies become highly crumpled, over folded forming disharmonic patterns. The rhythmic characteristic of this celestite type is expressed by parallel algal mats and

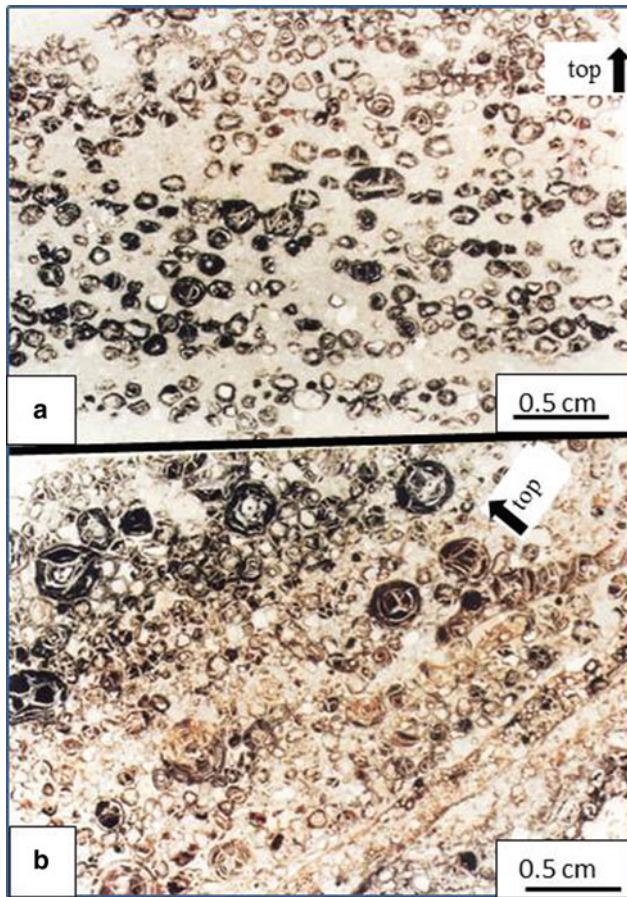


Fig. 35 (a and b) Thin microphotographs of fairly stratified oolitic-oncolitic Mn (a) and Fe (b) grainstones, with local grading in the framework components (Abdel Motelib, 1996)

spots rich in ultra-fine-grained celestite mixed with micrite, acting as starting sheets for further crystallization, as well as alternating rosettes or spherules, flat lens-like, fibroradiating coarse-grained celestite and gypsum crystals, growing all around the celestite rich spots or above and below the starting algal mats with idiomorphic termination toward the remaining pore spaces. The remaining pore spaces are usually filled by late coarse-grained celestite, blocky calcite, and gypsum crystals. The paleo-environment and syn-sedimentary fabrics of this Middle Miocene celestite type can be correlated with the syn-genetic celestite deposits elsewhere, e.g. Permian of Greenland (Scholle et al., 1990); Triassic of Bristol area, England (Nickless et al., 1976); Jurassic Hammelete West deposit, Germany (Brodkorb et al., 1982), Late Miocene celestite of Granada basin, Spain (Martin et al., 1984), and the celestite of Wenlock Oslo Region, Norway (Olausson, 1981).

5.5.2 Post-middle Miocene Stratabound Celestite (Generation II Celestite, Karst-Related Cavity Filling)

The post-Um Mahara paleo-karst surface, hosting the second celestite ore type, is generally of cusped form being pitted and rubbly in some places. Near-surface solution joints and channels are often connected with solution cavities of variable diameters (Figs. 36c, d and 37a–c). The solution features show successive stages of widening as a result of dissolution under vadose or transitional vadose-phreatic conditions possibly under progressive lowering of the paleo-water table. Karst effects may extend down to the contact between the hosts karstified celestite-bearing facies and the underlying subtidal-intertidal facies association. Re-precipitation of coarse-grained calcite and celestite (generation II celestite) together with internal geopetal sediments caused partial to complete filling of the intergranular spaces between solution and collapse breccia fragments and the megascopic and microscopic solution openings or may form asymmetrical fringe growing preferentially downwards into open spaces (Figs. 36c, d and 37a–c).

The karst-related calcite and celestite constitute stalactites, stalagmites and flowstones composed of radial fibrous mosaic, bladed and wedge-shaped crystal growing perpendicular to the roofs and floors of the solution features (Fig. 36c–d). These crystals often show increase in size and pyramidal or comb structure against the internal geopetal sediments (mainly a mixture of silt-sized calcite and celestite particles and red-stained calcareous mud), and/or late coarse-grained blocky calcite crystals.

5.6 Middle to Late Miocene Stratiform and Stratabound Barite

The Middle to Late Miocene evaporite sequence includes small-scale occurrences of stratiform barite layers and stratabound barite buckets widely distributed within the intercalated thin dolostone layers. The stratiform barite layers are confined to restricted sabkha facies (Abdel Wahab and Ahmed, 1987), while the stratabound barite fills solution features as well represented in Gabal Abu Ghorban, south Um Gheig mine area (Fig. 38). In this site, barite exhibit well-defined geometrical rhythmic patterns, being composed of rhythmic alternations of dark and light bands and streaks (Fig. 38). The rhythmic characteristics of this barite type are due to repetition of three subsequent generations of crystallization. Generation I (corresponding to the starting sheets of Fontboté and Amstutz, 1980) is represented by dark

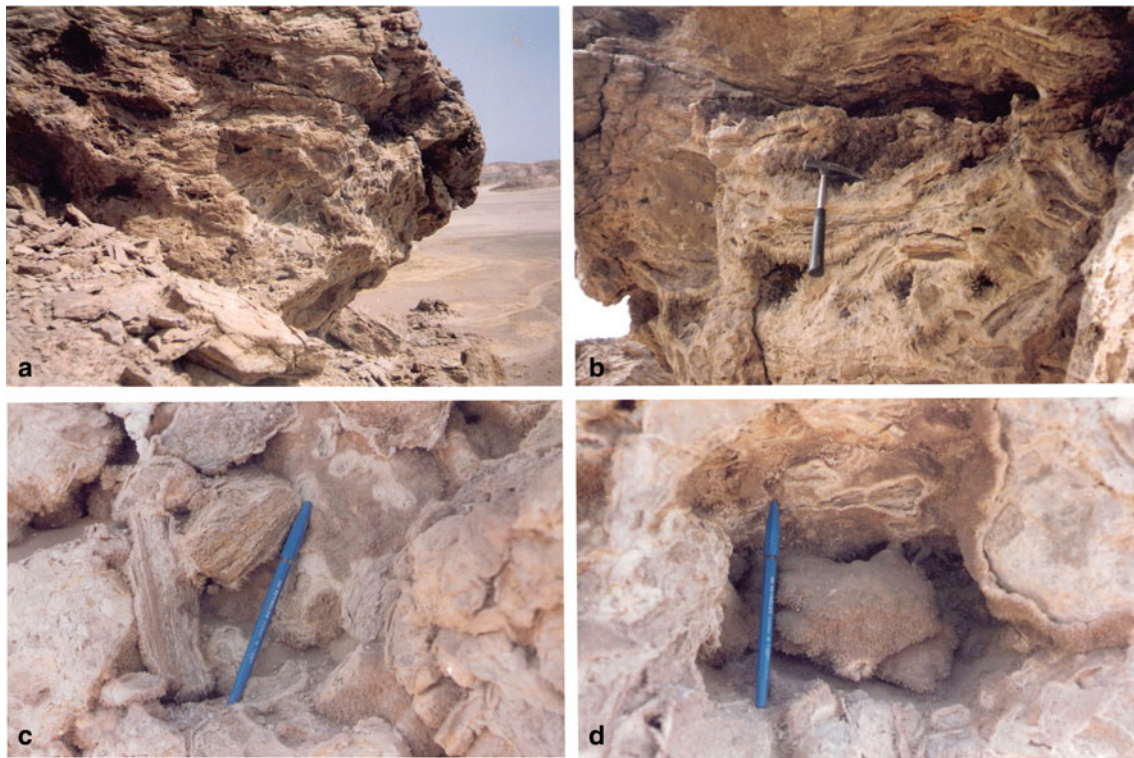


Fig. 36 (a–d): Field photographs of the stratiform rhythmic celestite (a, b) showing enlarged solution openings features with precipitated calcite and celestite. c = collapse breccia of laminated rhythmic celestite cemented by large celestite and calcite crystals. d = solution cavity coated by celestite and calcite

bands, streaks, or spots being composed of cloudy aggregates of fine-grained dolomite together with algal filaments and cellular organic materials. Generation II forms the major parts of the rhythmic light bands consisting of barite crystals symmetrically arranged in bipolar patterns with idiomorphic terminations growing on both sides of generation I. Generation III is displayed by the remaining empty spaces left by generation I which are partially lined or completely filled with celestite, calcite, and/or felty anhydrite. The geologic setting and geometry of this barite type indicate development during “syn-diagenetic” or syn-supergene crystallization generations in restricted karst environment. The record of these barite types within the Middle to Late Middle Miocene evaporates of the Abu Dabbab sequence may encourage further and intensive exploration for similar and more promising barite occurrences in this stratigraphic and lithologic evaporitic interval, widely cropping out along the whole Red Sea Coastal Zone.

5.7 Middle to Late Miocene Stratiform and Stratabound Biogenic Sulfur Deposits

Sulfur deposits associated with bituminous materials and/or surface oil seepages are confined to sabkha stromatolitic carbonates and evaporites of the Abu Babbab sequence (e.g.

Ranga and Um Reiga occurrences (El Aref, 1984 and Abdel Wahab and Ahmed, 1987) or the coeval Gemsa and Gabal El Zeit occurrences (Shukri & Nakhla, 1955; Wali et al., 1989 and Youssef, 1989). Sulfur has been long extracted from the range occurrence, where it forms as yellow stratiform layers confined to the middle unit of the Middle to Early evaporate section of this location (Fig. 39a and b), overlaying thick biogenic framboidal pyrite layer and overlain by brecciated limestone. Sulfur, anhydrite, calcite, and bituminous materials are rhythmically arranged, showing well-defined syn-sedimentary and syn-diagenetic textures. The congruent arrangement and the sedimentary textures of these components (Fig. 39c) suggest deposition in a partially closed evaporitic system, under biogenic processes (bacterial metabolisms) and rhythmic crystallization differentiation during the diagenesis (El Aref, 1984).

5.8 Post-late Miocene Stratabound Pb, Zn Sulfides, and Calamine Ore

The stratabound Pb–Zn sulfide deposits of Um Gheig mine (Fig. 40) were extracted since the ancient Pharaoh Time as a main source for lead and zinc. Unfortunately, the mine is now closed and not declared for investment because of the sulfide depletion. The hole mineral assemblage of this mine

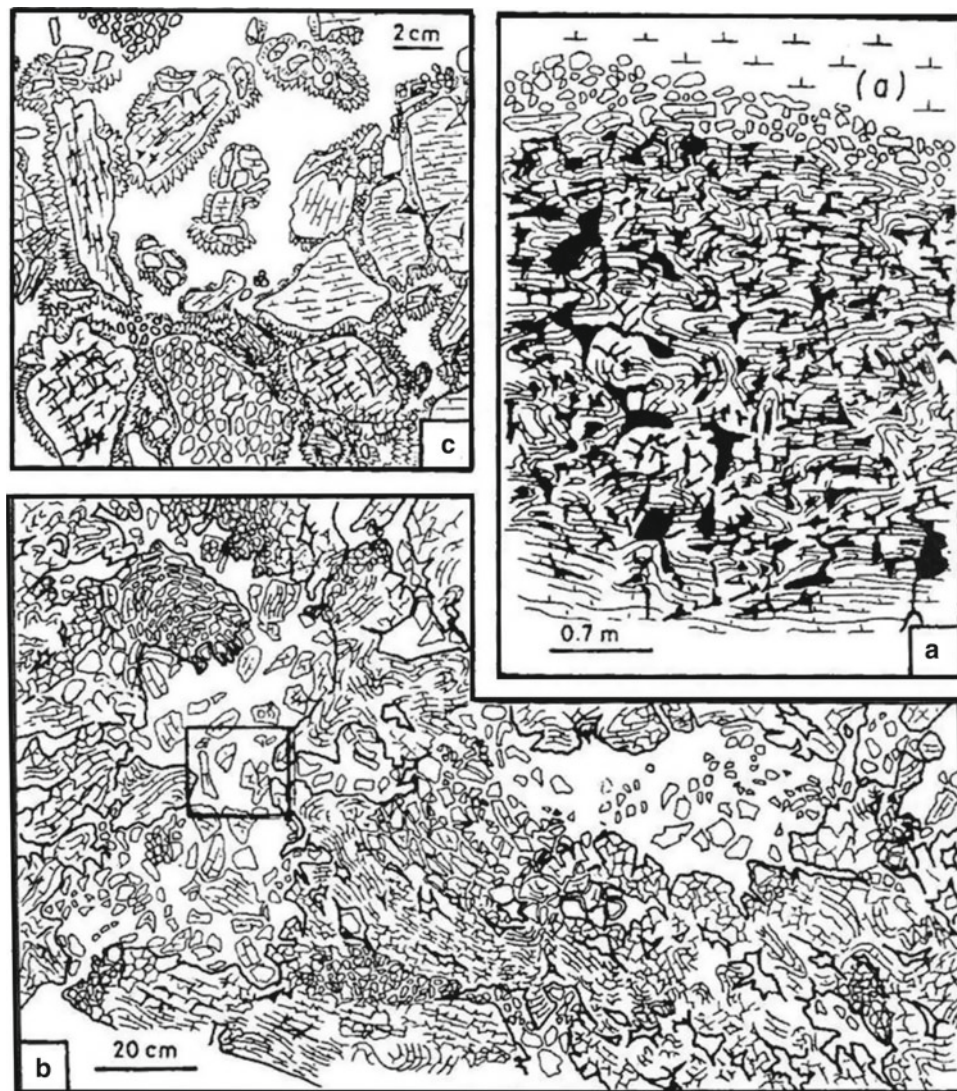


Fig. 37 (a–c): **a** = Representative cross-sectional drawing of the K2 karst surface beneath Abu Dabbab Fm., notice, the rubbly upper portion and the distribution of solution passages and cavities (in black). **b** = solution cavities and channels with intra-karstic celestite crystals. **c** = enlargement of the channel fill sediments squared in figure **b** showing in situ brecciating of large celestite bearing clasts and encrustation by new generations of calcite and celestite speleothems (from El Aref, 1993b)

is hosted in a fill mass developed along a major NW–SE post-Late Middle Miocene rift fault by water and gravity as a response of Plio-Pleistocene (?) paleo-karst event (El Aref & Amstutz, 1983). This ore type can be correlated to the upper karst-related sulfides of the Mississippi Valley Pb–Zn–Cu deposits (USA) and probably, representing the youngest Mississippi Valley ore type in the world. Among this deposit type are the karst-hosted sulfides of W. Wizr, Gabal El Rusas, Anz and Ranga occurrences. The fill mass of Um Gheig mine consists of chaotic breccia fragments derived from the Middle and Late Middle Miocene carbonates and evaporites (Fig. 40), embedded in soily clayey matrix, that mixed with chemical materials of lead and zinc sulfides, sulfates, carbonates, chlorides, phosphates, molybdates, and silicates as well as Fe oxides and hydroxides, silica, Ca, Mg

and Fe carbonates and kaolinite. Three zones are recognized in this ore type (Fig. 40). Based on the Zn content and mineral assemblage, the oxidation (calamine) zone is differentiated into two horizons: (a) an upper varicolored ferrous Zn-poor horizon (1.01–3.7% PbO and 1.88–3.22% ZnO) being composed mainly of red and yellow earthy ochreous sediments including quartz, hematite, goethite, alunite, jarosite, calcite, gypsum, kaolinite, illite, and montmorillonite, with variable proportion of lead and zinc oxides and (b) a lower white to gray zinc-rich horizon (43–58% Zn% and 2.0–6% PbO%) composed mainly of smithsonite, hydrozincite, and hemimorphite with variable contents of goethite, calcite, quartz, and lead bearing minerals (mainly cerussite). The recent development of worldwide beneficiation techniques for the treatment of the non-sulfide

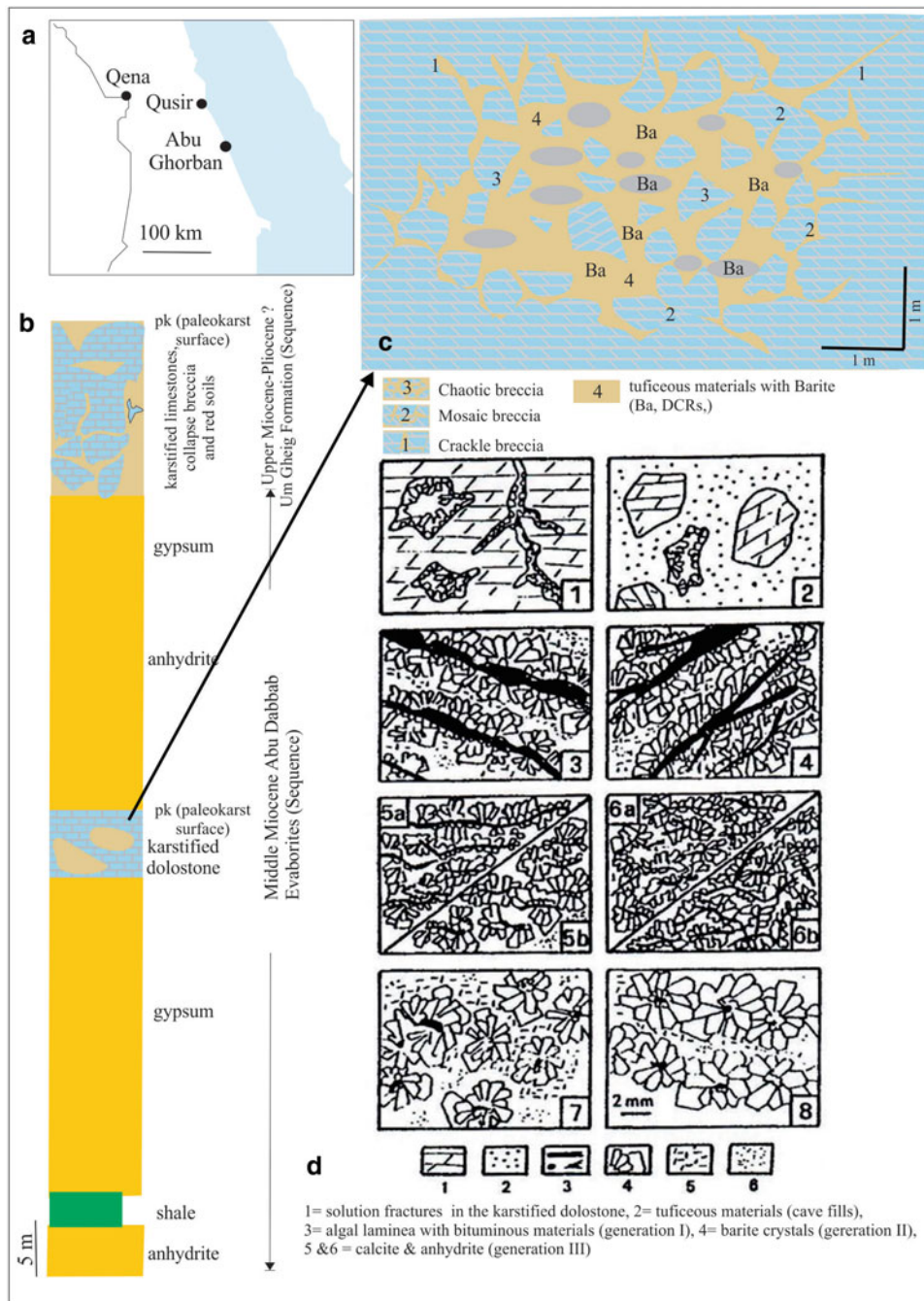


Fig. 38 **a, b** = Location and generalized lithostratigraphic section of Abu Dabbab Formation of Gabal Abu Ghorban. **c** = schematic drawing of the karst filling cavity. **d** = geometric distribution patterns of the barite: Type 1 = symmetrical filling of fractures within the host karstified dolostone. Type 2 = drusy filling of geodes, vugs, and grooves within the tuffaceous matrix of the cave. Types 3–8 = internal fabrics of the barite nodules, 3 and 4 = rhythmic alternations of dark (organic-rich) and light (barite) even (3) or branched (4) bands or streaks. Types 5 a and b = parallel undulated thin rhythmic laminae of wavy appearance or flaser-like structure (5b). Types 6 a and b = branched interrupted streaks (6a) and interconnected network pattern (6b). Types 7 and 8 = irregularly distributed (7) or connected spherulitic or orbicular patterns. Notice, the possible transitional evolutions of the rhythmic growing from type to type (after El Aref & Ahmed, 1986)

zinc ores through light into the commercial importance of this calamine ore type, which becomes a major source of zinc metal in this century (Large, 2001). Recent detailed investigations on the oxidation zone (calamine bearing zone)

by Farag (2011) and Farag et al. (2011, 2012) confirmed the shearing of the calamine deposits of Um Gheig mine in many characteristics with the typical carbonate-hosted non-sulfide Zn ore (calamine ore type) all over the world.

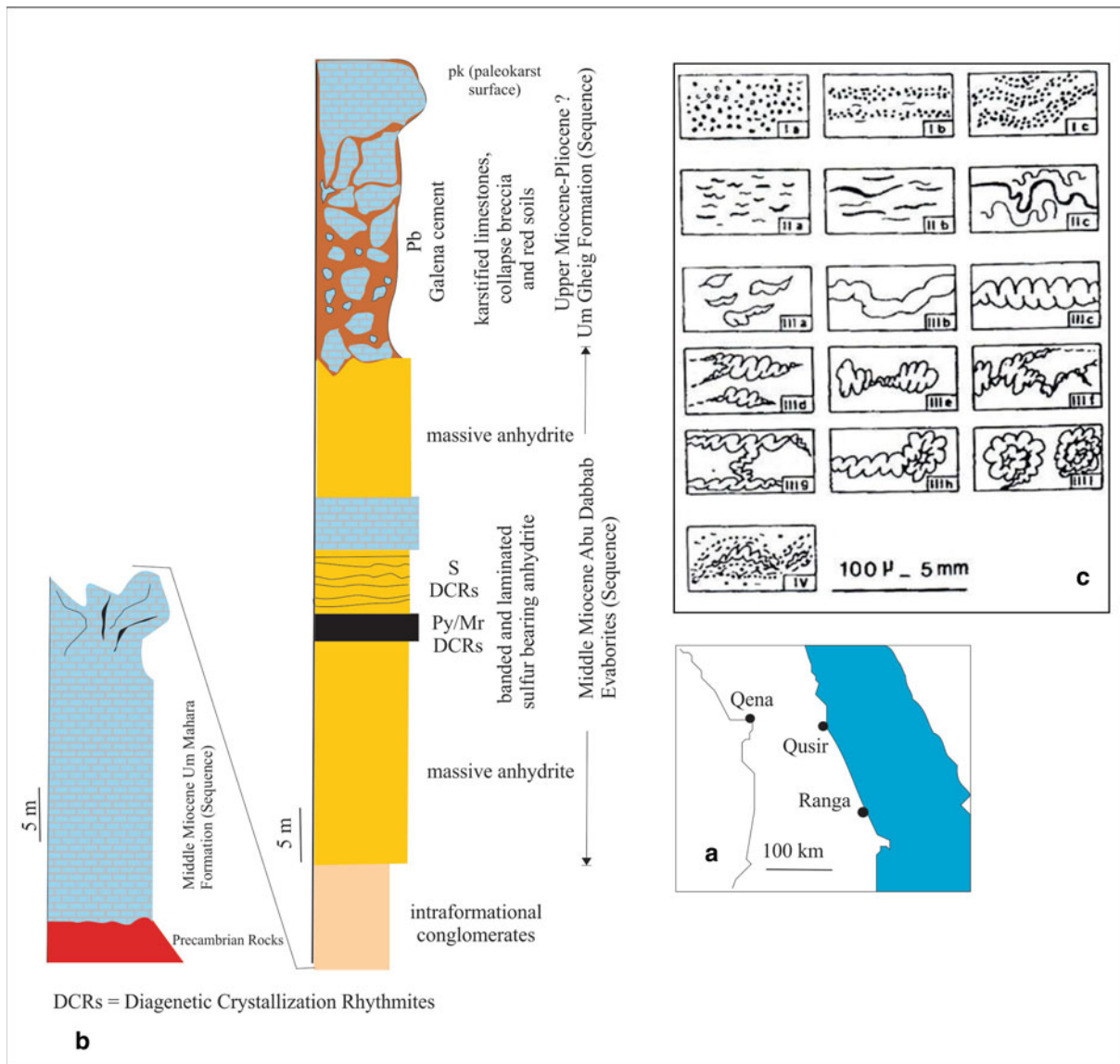


Fig. 39 Location map (a) and a composite lithostratigraphic section of the Miocene sequences of the Ranga occurrence (b), showing the position of the different ore minerals. c = the basic megascopic and microscopic geometric patterns of the sulfur with bitumen. Patterns I a-c = stratified sulfur dust of isotropic appearance (I a), stratified layered pattern (I b) or openly folded pattern (I c). Patterns II a-c = stratiform lenticels gently folded (II a, b) or disharmonically folded (II c). Types III a-i = show examples of derivations of deformed banded segregations as isolated nebulitic-like texture (IIIa) with lateral gradation to stratified complicated and folded bands drawn out in the center and outwards (III b-i). Type IV displays an example of an assemblage of different types in a gently folded arrangement (After El Aref, 1984)

The liberation and mineralogical investigations and mineral evaluation of representative samples of the Zn-rich lower horizon proved that higher degree of liberation (over 90%) between the valuable zinc bearing minerals and their gangues can be achieved below size 0.106 mm at inclination angle (25 1 min (Farak et al., 2012). At these optimum conditions, a concentrate assaying 63.4% ZnO was obtained with a recovery of ~ 93%.

Although the sulfides of Um Gheig mine are highly depleted, the mine should be re-considered as a non-sulfide zinc ore of high potentiality, highly recommended for

investment as a calamine ore for the production of Zn metals. The geological setting of Um Gheig mine either as sulfide or non-sulfide ore types can be used as a guide for further exploration for similar deposits.

5.9 Post-Miocene Surficial Mn Deposits

Post-Miocene Mn and Ba deposits (up to 45% Mn) cover the eroded surfaces of Pre-Cambrian and Miocene rocks in Halaib-Elba-Abu Ramad land stretch (Figs. 1 and 31). The

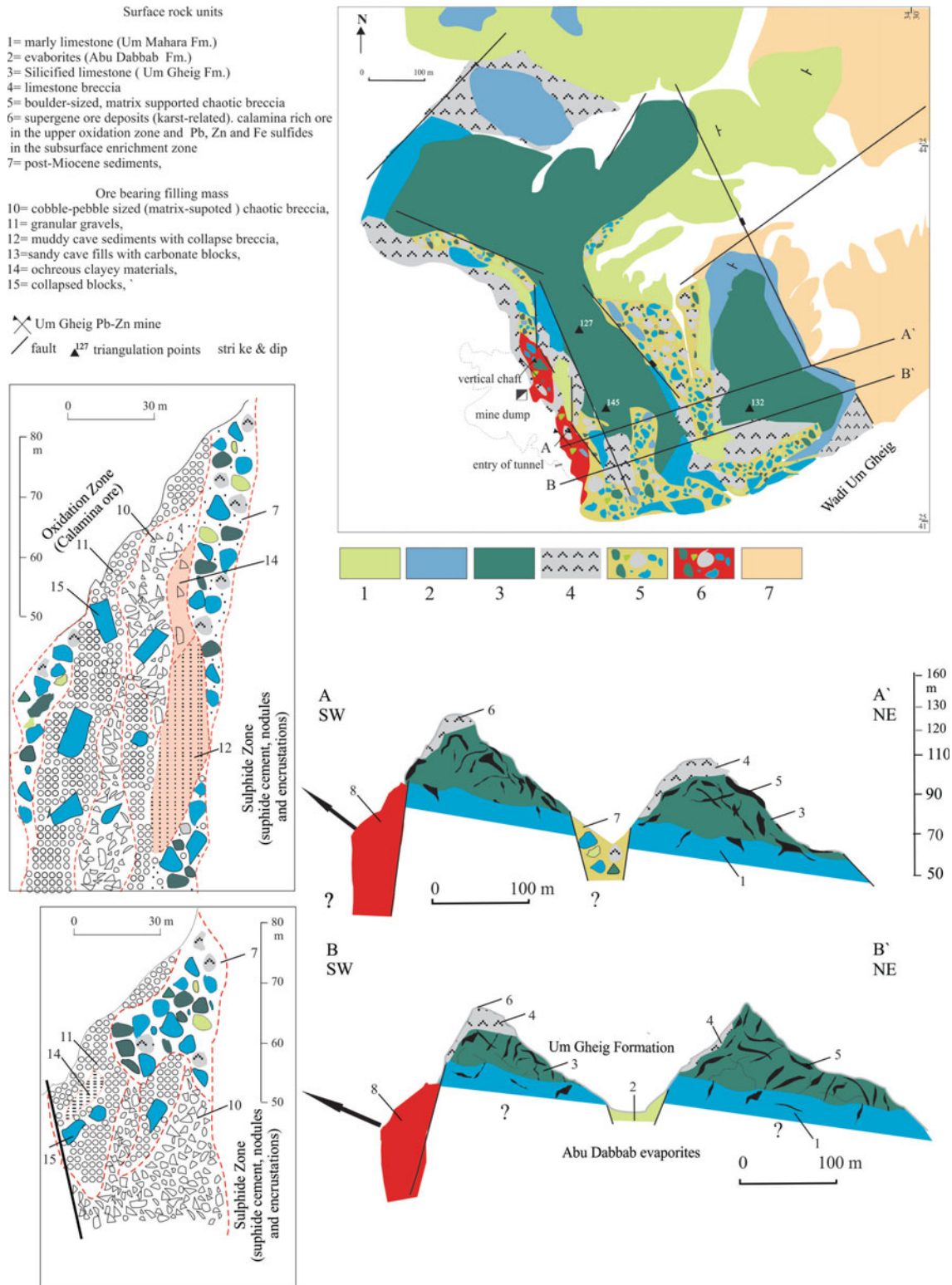


Fig. 40 Simplified geological map of Um Gheig mine area and A–A' and B–B' sketch profiles illustrating the grain size distribution, composition, and vertical zonation of the ore-bearing channel fill materials, (updated and modified after El Aref & Amstutz, 1983)

origin of these deposits is attributed to: (a) weathering of the Pre-Cambrian rocks and supergene deposition (El Shazly, 1957 and El Shazly & Saleeb, 1959), (b) epigenetic low-temperature replacement processes (Basta & Saleeb, 1971), and (c) deposition from deep-seated trans-magmatic ore-bearing solutions (Balkhanov & Razvalyayev, 1981). The surficial setting, mineral paragenesis, and textural characteristics of these deposits described by El Shazly and Saleeb (1959) and Basta and Saleeb (1971) led El Aref (1996, 2020b) to classify this ore type as a Neogene surficial deposits related to Plio-Pleistocene uplifting phase and weathering processes.

5.10 Post-Miocene-Quaternary (?) Surficial Conglomeritic Mn Deposits

This ore type is represented by small occurrences of Mn–Fe bearing rocks recorded in Wadi Araba, Gulf of Suez (Figs. 1 and 31) and suggested to be formed by Mn–Fe solutions of volcanic origin (Abdallah, 1961). The total estimated reserves of these deposits are ~ 4000 tons with 20–65 MnO% (Mineral Map of Egypt, EGSMA, 1979). These deposits form morphogenetic hard cap (surficial crust) of conglomeritic nature forming the summits of isolated small residual hills of Cretaceous clastics and/or Eocene carbonates and represent Post-Miocene to Recent surficial fluvial accumulation during the senile stage of Wadi Araba (El Aref, 1996, 2020b).

Acknowledgements This work is credited to the fruitful scientific cooperation with my colleagues and students at Cairo University, and from local and international universities, institutions, and scientific centers, where we formed together distinguished research teams. I offer them all my sincere thanks and gratitude as much I benefit from them and enjoy their company and cooperation. I must mention the extent to which we enjoy together scientific discussions and exchanges of ideas and knowledge procession to continue to address the difficulties and challenges. I am proud of them as co-researchers and co-authors in my publications or as I am co-author in their published contributions. Difficult here to mention them all and I invite to know them from the attached list of references.

References

- Abdallah, A. M. (1961). Note on the manganese-iron deposit in Wadi Araba, Gulf of Suez. *Journal of Geology of the United Arab Republic*, 5(1), 77–79.
- Abdallah, A. M. (1992). Paleozoic rocks in Egypt. *Technika Geologicznych Geosynoptyka, Geotermia*, 3, 1–12.
- Abdallah, A. M., El Darwish, M. Aref, M. M., & Helba, A. A. (1992). Lithostratigraphy of the pre-cenomanian clastics of North Wadi Qena, Eastern Desert, Egypt. In A. Sadek (Ed.), *Proceedings of the First International Conference on Geology of the Arab World (1992)*. *Geology of the Arab world* (pp. 255–282).
- Abdel Motelib, A. (1987). *The cupriferous sediments in West Central Sinai, Egypt* [M.Sc. thesis]. Cairo University, Faculty of Science, Egypt (p. 194).
- Abdel Motelib, A. (1996). *Geological and mineralogical studies of some manganese occurrences of Egypt* [Ph.D thesis]. Department of Geology, Faculty of Science, Cairo University (p. 304).
- Abdel Wahab, S., & Ahmed, S. M. (1987). Evaporite facies and depositional environment of the Abu Dabbab Formation, Red Sea Coast, Egypt. *Geologie en, Mijnbouw*, 66, 121–138.
- Abu Khadra, A., El Aref, M. M., & Sokar, A. (1987). Karst evolution and pedological processes along El Bahariya-El Farafra Road, Western Desert, Egypt. Presented by El Aref in the 25th Annual Meeting of the Geological Society of Egypt (Abstract).
- Afify, A. M. (2017). *Ironstone occurrences in the northern part of the Bahariya Depression, Western Desert, Egypt: Geology, mineralogy, geochemistry and origin* [Ph.D. thesis]. Universidad Complutense De Madrid, Facultad De Ciencias Geológicas (p. 166).
- Afify, A. M., Sanz-Montero, M. E., & Calvo, J. P. (2015a). Ironstone deposits hosted in Eocene carbonates from Bahariya(Egypt)—New perspective on cherty ironstone occurrences. *Sedimentary Geology*, 329, 81–97.
- Afify, A. M., Serra-Kielc, J., Sanz-Montero, J. M. E., Calvo, P., & Sallamb, E. S. (2015b). Nummulite biostratigraphy of the Eocene succession in the Bahariya Depression, Egypt: Implications for timing of iron mineralization. *Journal of African Earth Sciences*, 120, 44–55.
- Ahmed, S. M. (1986). *Geological, stratigraphical and mineralogical studies on the Miocene sediments of the Red Sea Coast between Quseir and Marsa Alam, Egypt* [Ph.D. thesis]. Department of Geology, Faculty of Science, Cairo University (p 230).
- Aita, S. K. (1996). *Geological, mineralogical and geochemical studies on some radioactive anomalies of the Paleozoic sediments of Um Bogma area, West Central Sinai, Egypt* [M.Sc. thesis]. Geology Department, Faculty of Science, Cairo University, Egypt (p. 262).
- Baoumya, H. M., Ahmed, A. H., & Khedr, M. Z. (2014). A mixed hydrogenous and hydrothermal origin of the Bahariya iron ores, Egypt: Evidences from the trace and rare earth element geochemistry. *Journal of Geochemical Exploration*, 146, 149–162.
- Balkhanov, V. V., & Razvalyayev, A. V. (1981). The origin of the manganese deposits of the western shore of the Red Sea (in association with rifting). *International Geology Review*, 23(2), 162–166. <https://doi.org/10.1080/00206818209467226>
- Basta, E. Z., & Saleeb, G. R. (1971). Elba manganese ores and their origin, South Eastern Desert, UAR. *Mineralogical Magazine*, 38, 235–244.
- Bosworth, W., Darwish, M., Crevello, P., Taviani, M., & Marshak, S. (1996). Stratigraphic and structural evolution of Zabargad Island (Red Sea Egypt) since the Early Cretaceous. In A. Y. Sayed (Ed.), *The third International Conference on Geology of the Arab World* (pp. 161–190). Cairo University, Cairo.
- Bosworth, W., Guiraud, R., & Kessler, L. G. (1999). Late Cretaceous (ca. 84 Ma) compressive deformation of the stable platform of NE Africa (Egypt): Far field stress effects of the “Santonian event” and origin of the Syrian arc deformation belt. *Geology*, 27(7), 633–636.
- Brodkorb, M. K., Ramos, V., Barbieri, M., & Ametrano, S. (1982). The evaporate celestite-barite deposits of Neuquen, Argentina. *Mineral Deposita*, 17, 423–436.
- Ciobotă, V., Salama, W., Tarcea, N., Rösch, P., El Aref, M., Gaupp, R., & Popp, J. (2011). Identification of minerals and organic materials of Middle Eocene ironstones, the Bahariya Depression, Western Desert, Egypt, by means of micro-Raman spectroscopy. *Journal of Raman Spectroscopy*, 43, 405–410.
- CMRDI “Central Metallurgical Research and Development Institute, Helwan, Cairo, Egypt”. (1998). Evaluation and beneficiation studies of Um-Hebal iron ore deposit, south Aswan, for blast furnace purposes. *Internal Progress Report*, 1, 92.
- Darwish, M. (1994). Cenomanian-Turonian sequence stratigraphy, basin evolution and hydrocarbon potentialities of Northern Egypt. In A. Sadek (Ed.), *Proceedings of the 2nd International Conference on Geology of the Arab World*, GAW (Vol. 1, pp. 261–303).

- Derocourt, J., Raicu, L. E., & Vrielynck, B. (Eds.). (1993). *Atlas Tethys, Pleo-environmental maps*. Gauthier-Villars (1307, 14 maps, 1 pl).
- EGSMA "Egyptian Geological Survey and Mining Authority". (1969–1971). *Reserve calculation plan, El Bahariya Oasis, internal reports*.
- El Aref, M. M. (1984). Strata-bound and stratiform iron sulfides, sulfur and galena in the Miocene evaporites, Ranga, Red Sea, Egypt (with special emphasis on their diagenetic crystallization rhythmites). In A. Wauschkuhn (Ed.), *Syngeneses and epigenesis in the formation of mineral deposits* (pp. 457–467). Springer.
- El Aref, M. M. (1993a). Pedogenesis and related gibbsite and natroalunite formation in Um Gereifat area, Red Sea Coastal Zone, Egypt. *Egyptian Journal of Geology*, 37(1), 307–333.
- El Aref, M. M. (1993b). Paleo-karst surfaces in the Neogene succession of Wadi Essel-Wadi Sharm El Bahari area, Egyptian Red Sea Coast, as indication of uplifting and exposure. In B. H. Purser & E. R. Philobos (Eds.), *Proceedings of the International Conference on Geodynamics and Sedimentations of the Red Sea-Gulf of Aden Rift System, Cairo, 1993*. *Egyptian Journal of Geology* (Vol. 1, pp. 205–231).
- El Aref, M. M. (1996). Phanerozoic stratiform and stratabound deposits of Egypt; their stratigraphic, paleo-geographic, -topographic and -environmental controls. In A. Sadek (Ed.), *Proceedings of the 2nd International Conference on Geology of the Arab World, GAW (1994)* (pp. 97–124). Cairo University, Egypt.
- El Aref, M. M. (1999). Achievements of the Egyptian iron exploration project (IEP, 1993–1997). In Hafez et al. (Eds.), *Proceedings of the 4th International Conference on Geology of the Arab World, GAW (1998)* (pp. 10–22). Cairo University, Egypt.
- El Aref, M. M. (2000). Paleo-karst surfaces and Karst morphology of the Western Desert of Egypt, history and economic potentialities. Presented in the *International Conference on the Western Desert of Egypt: Geological Environment and Development Potentials, NARSS, EGSM, BOSTON UNIVERSITY, UNDP, UNESCO* (pp. 17–20).
- El Aref, M. M. (2001). Phanerozoic stratabound ore deposits. In *The metallogenic map of Egypt, scale 1:1000,000 (Dardir et al., 2001), Part Three* (pp. 26–43).
- El Aref, M. M. (2006). Egyptian Karst morphology and processes, its economic potentiality and environmental impacts. In *Invited lectures, presented in the Annual Meeting of the Sedimentary Society of Egypt (2005) and the Annual Meeting of the Geological Society of Egypt (2006)*.
- El Aref, M. M. (2020a). Iron ores in Egypt. In Z. Hamimi et al. (Eds.), *The geology of Egypt* (pp. 522–529). Springer Nature Switzerland, AG 2020 (Chapter 14.1). ISSN 2364-6438, ISSN 2364-6446 (electronic), Regional Geology Reviews, ISBN 978-3-030-15264-2, ISBN 978-3-030-15265-9 (eBook).
- El Aref, M. M. (2020b). Egyptian manganese deposits. In Z. Hamimi et al. (Eds.), *The geology of Egypt* (pp. 570–578). Springer Nature Switzerland, AG 2020 (Chapter 14.9). ISSN 2364-6438, ISSN 2364-6446 (electronic), Regional Geology Reviews, ISBN 978-3-030-15264-2, ISBN 978-3-030-15265-9 (eBook).
- El Aref, M. M., Abdel, W. S., & Ahmed, S. (1985). Surficial calcareous crust of caliche type along the Red Sea Coast, Egypt. *Geologische Rundschau, Sonderdruck, Geologische Vereinigung, Mending*, 74 (1), 155–163.
- El Aref, M. M., & Abdel Motelib, A. (2001). Geology, facies distribution and environments of the Carboniferous stratabound Mn deposits of Um Bogma region, Sinai, Egypt. In *Proceedings of the 2nd Conference on the Geology of Africa* (pp. 61–77). Assiut University, IA.
- El Aref, M. M., Abu Khadra, A. M., & Lotfy, Z. H. (1987). Karst topography and karstification processes in the Eocene limestone plateau of El Bahariya Oasis, Western Desert, Egypt. *Zeitschrift für Geomorphologie. N.F. Gebrüder Borntraeger, Berlin-Stuttgart*, 31 (1), 45–64.
- El Aref, M. M., & Ahmed, S. (1986). Diagenetic crystallization rhythmites (DCRs) of dolomite—barite—calcite in karst environment, Gabal Abu Ghorban, Red Sea Coastal Zone, Egypt. In R. Rodriguez-Clemente, Y. Tardy (Eds.), *Proceedings of the International Meeting "Geochemistry of the Earth Surface and Processes of Mineral Formation" held in Granada (Spain), March 16–22, 1986* (pp. 611–622).
- El Aref, M. M., & Amstutz, G. C. (1983). Lead-zinc deposits along the Red Sea Coast of Egypt. In *New observations and genetic models on the occurrences of Um Gheig, Wizr, Essel and Zug El Bohar. Monograph series on mineral deposits* (Vol. 21, p. 103). Gebrüder Borntraeger.
- El Aref, M. M., Awadallah, F., & Ahmed, S. (1986). Karst landform development and related sediments in the Miocene rocks of the Red Sea Coastal Zone, Egypt. *Geologische Rundschau, Sonderdruck, Geologische Vereinigung, Mending*, 75(3), 781–790.
- El Aref, M. M., El Dougdog, A. A., & Mesaed, A. A. (1991). Landform evolution and formation of ferricrete duricrusts, El Heiz area, El Bahariya Depression, Western Desert, Egypt. *Egyptian Journal of Geology*, 34(1 and 2), 1–39.
- El Aref, M. M., El Dougdog, A. A., & Mesaed, A. (1992). Petrography and diagenesis of the high-laying ferricrete of El Bahariya depression, Western Desert, Egypt. *Egyptian Mineralogist*, 4, 23–53.
- El Aref, M. M., El Sharkawi, M. A., & Khalil, M. (1999a). Geology and genesis of the stratabound and stratiform Cretaceous-Eocene iron ore deposits of El Bahariya region, Western Desert, Egypt. In Hafez et al. (Eds.), *Proceedings of the 4th International Conference on Geology of the Arab World, Cairo University, Egypt. 1998. Geology of the Arab World* (pp. 450–475).
- El Aref, M. M., El Sharkawi, M. A., & Mesaed, A. (1999b). Depositional and diagenetic microfabric evolution of the Cretaceous oolitic ironstone of Aswan, Egypt. Research Studies on Some Cretaceous Sequences of Egypt. *Geological Society of Egypt Special Publications*, 2, 280–312.
- El Aref, M. M., Helba, A. A., & Saad, F. (2001). Lutetian ramp carbonate facies, hierarchy and environments, northeast El Bahariya depression. In *Proceedings of the 2nd International Conference on the Geology of Africa* (pp. 385–403). Assiut University, IB.
- El Aref, M. M., Hussein, H. A., El Aassy, I. E. and Aita S. K. (1998). Mineralogy and Geochemistry of the Carboniferous stratabound U karst Latosol of Um Bogma Region, West Central Sinai, Egypt. In Hafez et al. (Eds.), *Presented by El Aref in the 4th International Conference on Geology of the Arab World, GAW4*. Cairo University (Abstract).
- El Aref, M. M., & Lotfy, Z. H. (1989). Genetic karst significance of the iron ore deposits of El Bahariya Oasis, Western Desert, Egypt. *Annals of the Geological Survey of Egypt*, XV, 1–3.
- El Aref, M. M., Mesaed, A. A., Khalil, M. A., & Salama, W. S. (2006a). Stratigraphic setting, facies analyses and depositional environments of the Lutetian Ironstones of Gabal Ghorabi mine area, El Bahariya Depression, Western Desert, Egypt. *Egyptian Journal of Geology*, 50, 29–57.
- El Aref, M. M., Mesaed, A. A., & Salama, W. S. (2006b). Microbialite morpho-structures and biogenic accretion mechanism of the Lutetian Ironstones of Gabal Ghorabi mine area, El Bahariya Depression, Western Desert, Egypt. *Egyptian Journal of Geology*, 50, 59–81.
- El Aref, M. M., & Refai, E. (1987). Paleo-karst processes in the Eocene limestones of the Pyramids Plateau, Giza, Egypt. *Journal of African Earth Sciences, Great Britain*, 6(3), 367–377.
- El Aref, M., Salama, A., & Hamed, M. (2021). Morphotectonic evolution of Qaret El Sheikh Abdallah depressions and Denuded

- paleo-karst in the White Desert, El Bahariya-Farafra Karst Territory, Egypt. *Egyptian Journal of Geology*, 65, 27–53.
- El Aref, M. M., Saleh, M. H., & Salama, A. (2017a). Geomorphological classification and zonation of the exposed karst landforms in Bahariya-Farafra region, Western Desert Egypt. *International Journal of Science and Research (IJSR)*, 6(5), 956–965.
- El Aref, M. M., Saleh, M. H., & Salama, A. (2017b). Inventory and assessment of the geomorphosites of Bahariya-Farafra Territory, Western Desert, Egypt. *International Journal of Sciences: Basic and Applied Research (IJSBAR)*, 33(2), 128–143.
- El Azabi, M., & Eweda, S. (1996). Clastic-carbonate sequence of Gabal El Sara, Sharm El Sheikh Area, southern Sinai, Egypt. *Egyptian Journal of Geology*, 40–2(1996), 805–844.
- El Kammar, A. (2020). Phosphate deposits of Egypt: Composition, origin and utilization. In Z. Hamimi et al. (Eds.), *The geology of Egypt* (pp. 590–563). Springer Nature Switzerland, AG 2020 (Chapter 15.1). ISSN 2364-6438 ISSN 2364-6446 (electronic), Regional Geology Reviews, ISBN 978-3-030-15264-2, ISBN 978-3-030-15265-9 (eBook).
- El Manawi, A. W. (2006). Geologic setting and mineralogical investigations of Cenomanian ironstones, Wadi Dara, north Eastern Desert, Egypt. *Egyptian Journal of Geology* (Abstract and Prof. El Manawi personal communication).
- El Miligy, A., & El Aref, M. M. (2004–2006). *The Guide (investment) map for limestone ore in Egypt* (Progress and final reports 1–6). The Egyptian Academy of Scientific Research and Technology, Cairo, Egypt.
- El Sharkawi, M. A., El Aref, M. M., & Abdel Motelib, A. (1990a). Syngeneic and paleo-karstic copper mineralization in the Paleozoic platform sediments of West Central Sinai, Egypt. In J. Parnell et al (Eds.), *Sediment-hosted mineral deposits. Special publication, The international association of sedimentologists* (Vol. 11). Black Well Scientific Publications (pp. 159–172).
- El Sharkawi, M. A., El Aref, M. M., & Abdel Motelib, A. (1990b). Manganese deposits in Carboniferous paleo-karst profile, Um Bogma region, West Central Sinai, Egypt. *Mineralium Deposita*, 25, 34–43.
- El Sharkawi, M., El Aref, M. M., & El Manawi, A. W. (1989). Paleoenvironments, classification and diagenetic aspects of ironstones in the Mesozoic sediments of El Maghara Area, Egypt. *Mineralogist*, 1, 1–25.
- El Sharkawi, M. A., El Aref, M. M., & Mesaed, A. (1999). Stratigraphic setting and paleo-environment of the Coniacian-Santonian Ironstones of Aswan, South Egypt. *Geological Society of Egypt Special Publications*, 2, 243–278.
- El Sharkawi, M. A., & Khalil, M. A. (1977). Glauconite, a possible source of iron for El Gedida iron ore deposits, Bahariya Oases, Egypt. *Egyptian Journal of Geology*, 21, 109–116.
- El Shazly, E. M. (1957). Classification of Egyptian mineral deposits. *The Egyptian Journal of Egypt*, 1(1), 1–21.
- El Shazly, E. M., & Saleeb, G. R. (1959). Contribution to the mineralogy of Egyptian manganese deposits. *Economic Geology*, 54, 59–71.
- Embabi N. S. (2004) *The geomorphology of Egypt, landforms and evolution. Volume I: The Nile Valley and the Western Desert. The Egyptian Geographical Society, Special Publication* (p. 447).
- Embabi, N. S. (2018). Landscapes and landforms of Egypt: Landforms and evolution. In *World geomorphological landscapes* (p. 336).
- Farag, M. Z. (2011). *Mineral evaluation and beneficiation of the oxidation zone Um Gheig Pb–Zn deposits, Red Sea Coast, Egypt* [MSc. Thesis]. Faculty of Science, Cairo University (p. 163).
- Farag, M. Z., Abdel Khalek, N. A., El Aref, M. M., Hassan, M. S., & El Manawi, M. A. (2011). Characterization and gravity separation of non-sulfide Zn deposit from Um Gheig Mine, Red Sea Coast, Egypt. *Journal of Engineering Sciences (JES), Faculty of Engineering, Assiut University*, 39(1).
- Farag, M. Z., Abdel Khalek, N. A., Hassan, M. S., El Aref, M. M., & El Manawi, A. W. (2012). Upgrading of Egyptian non-sulfide zinc ore by gravity separation techniques. *Journal of Metallurgical Engineering (ME)*, 1(1), 6–13.
- Fontboté, L., & Amstutz, G. C. (1980). New observations on diagenetic crystallization rhythmites in the carbonate facies of the Triassic of the Alpujarrides (Betic Cordillera, Southern Spain). Comparison with other diagenetic rhythmites. I. sym. diagenesis, Barcelona, 1980. *Revista del Instituto de Investigaciones Geológicas de la Diputación de Barcelona*, 34, 293–310
- GAW. (1994). In A. Sadik (Ed.), *2nd International Conference on the Geology of the Arab World (GAW) Conference Proceedings, Cairo* (p 553).
- Germann, K., Mocke, A., Doering, T., & Fisher, K. (1987). Late Cretaceous laterite-derived sedimentary deposits (oolitic ironstones, kaolins, bauxites) in Upper Egypt. *Berliner Geowissenschaftliche Abhandlungen*, 73(3), 727–758.
- Gharieb, S. E. M. (1990). *Geological and geomorphological studies on limestones, East of the Nile* [M.Sc. thesis]. Department of Geology, Faculty of Science, Cairo University (p. 168).
- Gharieb, S. E. M. (1998). *Geological studies on the Eocene rocks and the associated karst features and facies in the east Bei Suief area, North Eastern Desert, Egypt* [Ph.D. thesis]. Department of Geology, Faculty of Science, Cairo University (p. 226).
- Gharieb, S. E. M. (2003). Eocene rocks and associated karst features in the East Beni Suef area, North Eastern Desert, Egypt. *Göttinger Arbeiten zur Geologie und Paläontologie Sb*, 5, 7–22, Göttingen, 7–21.
- Glenn, C. R., & Arthur, M. A. (1990). Anatomy and origin of a Cretaceous phosphorite-greenand giant, Egypt. *Sedimentology*, 37, 123–154.
- Guiraud, R., & Bosworth, W. (1999). Phanerozoic geodynamic evolution of the northeastern Africa and the northeastern Arabian platform. *Tectonophysics*, 315(1999), 73–108.
- Guiraud, R., Bosworth, W., Thierry, J., & Delplanque, A. (2005). Phanerozoic geological evolution of Northern and Central Africa. *Journal of African Earth Sciences*, 43(2005), 83–143.
- Guiraud, R., Issawi, B., & Bosworth, W. (2001). Phanerozoic history of Egypt and surrounding areas. In P. A. Ziegler, W. Cavazza, A. H. F. Robertson, & S. Crasquin-Soleau (Eds.), *Peri-Tethys Memoir 6: Peri-Tethyan/Rift/Wrench Basins and Passive Margins. Mémoires du Muséum national d'histoire naturelle* (Vol. 186, pp. 469–509). Paris. ISBN: 2-85653-528-3.
- Gunnell, G. F., Winkler, A. J., Miller, E. R., Head, J. J., El-Barkooky, A. N., Abdel, G. M., Sanders, W. J., & Gingerich, P. D. (2016). Small vertebrates from Khashm El-Raqaba, late middle Miocene, Eastern Desert, Egypt. *Historical Biology*, 28(1–2), 159–171.
- Halliday, W. R. (2003). Caves and karsts of Northeast Africa. *International Journal of Speleology*, 32(1/4), 19–32.
- Hamdan, M. A., & Hassan, F. A. (2020). *Quaternary of Egypt. In the Geology of Egypt (Hamami et al., 2020), Regional Geology Reviews*. ISSN 2364-6438 ISSN 2364-6446 (electronic), ISBN 978-3-030-15264-2 ISBN 978-3-030-15265-9 (eBook), © Springer Nature Switzerland AG 2020. <https://doi.org/10.1007/978-3-030-15265-9>
- Hamdan, M. A., & Lucarini, G. (2013). Holocene paleo-environmental, paleo-climatic and geoarchaeological significance of the Sheikh El-Obeiyid area (Farafra Oasis, Egypt). *Quaternary International*, 320, 154–168.
- Hassan, M. M. (1990). Studies on lead-zinc sulphide mineralization in the Red Sea Coastal zone, Egypt. In *Proceedings of Eighth Quadrennial IAGOD Symp. Schweitzer Bartsche-Verlags bunch handlung*.
- Hassan, M. M. (2002). Genesis of miocene polymetals mineralization, Western coastal zone, Egypt. *Journal of Sedimentology, Egypt*, 10.
- Hassan, M. M. (2016). Phanerozoic rifting phases and mineral deposits. *EGU*, 18, 2016–3304.

- Hassan, M. M. (2018). The Red Sea polymetallogenic province: the newest of the world. In *The Annual 56th Meeting of the Geological Society of Egypt, November, 2018, Invited Talk, Abstract* (pp. 1–4).
- Hassan, M. M., Awed, M. H., El Sweifi, B., & El Nadeem, G. A. (2004). The South East Aswan iron ore deposits: An approach for qualitative evaluation. In *14th Symposium Planer and Development, Egypt* (pp. 99–120). May 2004.
- Hassan, M., El-Afandy, H., El-Desoky, A., Hatem, A. M., Hassan, A., & Soliman, O. A. (2006). Studies on ferrugination in Gabal Agib Ring Complex, South Eastern Desert, Egypt. *Nuclear Sciences Scientific Journal*, 4, 1–18.
- Hassan, M. M., El Dosoky, H., Salem, S., El Afendy, A., & Soliman, O. A. (2018). Genesis of iron deposits in Bir Um Hebal area, Southeast Aswan, Egypt: Remote sensing-structural-lithological-ore mineralogical contributions. *Middle East Journal of Applied Sciences*, 8(1), 19–36.
- Helba, A. A., El Aref, M. M., & Saad, F. (2001). Lutetian oncoidal and ooidal ironstone sequences; Depositional setting and origin, north-east El Bahariya depression, Western Desert, Egypt. *Journal of Geological Society of Egypt*, 45(1A), 325–351.
- Helba, A., El Manawy, A. W., & El Aref, M. M. (2003). Syn-depositional lateritic alteration and clastics starvation as pathways in the formation of the oolitic ironstones of North Wadi Qena, Eastern Desert, Egypt. *Egyptian Journal of Geology*, 47(1), 255–274.
- Hermima, M., Klitzsch, E., & List, F. K. (1989). *Stratigraphic Lexicon and explanatory notes to the geological map of Egypt 1; 500000* (p. 251). Conoco Co. Inc.
- Hilmy, M. E., Ghazlan, A. E., & Sleem, Y. S. (1958). Uranium in some manganese ores, Um Bogma, Sinai. In *3rd Scientific Arab Conference, Beirut* (pp. 350–355).
- Hilmy, M. A., & Hussein, A. (1978). A proposed classification for mineral deposits and occurrences in Egypt. *Precambrian Research*, 6 (Abstract).
- Hilmy, M. E., & Mohsen, L. (1965). Secondary copper minerals from West Central Sinai. *Journal of Geology UAR*, 9, 1–2. <https://doi.org/10.1007/978-3-030-15265-9>
- Hussein, H. A., El Assy, I. E., El Aref, M. M., & Aita, S. K. (1998). Paleozoic stratabound Th and U lathosol type of Um Bogma Region, Egypt, their geological setting and mode of formation. In A. Hafez et al. (Eds.), *4th International Conference, Geology of the Arab World (GAW)* (p. 117). Geology Department, Faculty of Science, Cairo University (Abstract).
- Hussein, H. A., & El Sharkawi, M. (1990). Mineral deposits. In R. Said (Ed.), *The geology of Egypt* (pp. 511–566). A. A. Balkema, Brookfield (Chapter 26).
- IEP “Iron Exploration Project”. (1993–1997). *Iron exploration project, reports of phases 1–3, El Bahariya and Aswan Regions (Geol. Naim N (leader of the consortium), El Sharkawi M. and El Aref M. M. (Principle Investigators)*. Geology Department, Cairo University and Geological Survey of Egypt (EGSMA). Phase I Report (1994, 147p), Phase II Report (1995, 162p), Phase III Report (1997, 287p).
- ISCO, Iron Steel Company. (1987–1977, 2010). Exploration and re-evaluation of the iron ores of El Bahariya Oasis Ghorabi, Naser, El Harra, El Gedida. In *Annual internal technical reports*.
- Issawi, B. (2002). Egypt during the phanerozoic. In Sadik et al. (Ed.), *5th International Conference on the Geology of the Arab World (GAW VI)*, Cairo (pp. 401–440).
- Issawi, B., El Hinawi, M., Francis, M., & Mazhar, A. (1999). *The phanerozoic geology of Egypt; geodynamic approach. Special publication* (Vol. 76, p. 462). Egyptian Geological Survey.
- Issawi, B., Francis, M., Youssef, E. A., & Osman, R. I. (2009). The phanerozoic geology of Egypt, a geodynamic approach. In *Ministry of petroleum, the Egyptian mineral resources authority, Special publication* (Vol. 81, 2nd ed., p. 589).
- Issawi, B., & McCauley, J. (1992). The Cenozoic rivers of Egypt: the Nile problem. In R. Hriedman & B. Adams (Eds.), *The flowers of horus, Egyptian studies association publication 2, Oxbow monograph* (Vol. 20, pp. 121–145).
- Issawi, B., & McCauley, J. (1993). The Cenozoic landscape of Egypt and its river systems. *Annals of the Geological Survey of Egypt*, 19, 357–384.
- Issawi, B., & Osman, R. (1993). Tectono-sedimentary synthesis of the Paleozoic-Cretaceous clastics, southwest Aswan, Egypt. *Journal of Sedimentary*, 1, 11–21.
- Klitzsch, E. (1984). Northwestern Sudan and bordering areas: Geological development since Cambrian time. *Berliner Geowissenschaftliche Abhandlungen*, 50, 23–45.
- Klitzsch, E. (1986). Plate tectonics and cratonic geology in Northeast Africa (Egypt and Sudan). *Geologische Rundschau*, 75(3), 753–768.
- Klitzsch, E. (1990). Paleozoic. In R. Said (Ed.), *The geology of Egypt* (pp. 393–406). A. A. Balkema, Brookfield (Chapter 21).
- Klitzsch, E., & Wycisk, P. (1987). Geology of the sedimentary basins of northern Sudan and bordering areas. *Berliner Geowissenschaftliche Abhandlungen*, 75(1), 97–136.
- Large, D. (2001). The geology of non-sulphide Zn deposits—An overview. *Eazmetall*, 54, 264–276.
- Lotfy, Z. H. (1989). *Geological, sedimentological and mineralogical study of the Northeastern Plateau, Bahariya Oasis* [Ph.D. thesis]. Department of Geology, Faculty of Science, Cairo University (p. 290).
- Martin, J. M., Ortega, H. M., & Torres-Ruiz, J. (1984). Genesis and evolution of strontium deposits of the Granada Basin (Southeastern Spain): Evidence of diagenetic replacement of stromatolite belt. *Sedimentary Geology*, 39, 281–298.
- McCauley, J. E., Schaber, G. G., Breed, C. S., Grolier, M. J., Haynes, C. V., Issawi, B., Elchi, C., & Blom, R. (1982). Subsurface Valleys and geochronology of the Eastern Sahara revealed by shuttle Radar. *Science*, 218(4516), 1004–1020.
- Mein, P., & Pickford, M. (2010). Vallesian rodents from Sheikh Abdallah, Western Desert, Egypt. *Historical Biology*, 22(1–3), 224–259.
- Meneisy, M. S. (1990). Vulcanicity. In R. Said (Ed.), *The geology of Egypt* (pp. 157–172). A. A. Balkema, Brookfield (Chapter 9).
- Mesaed, A. A., Khalil, M. A., Salama, W. S., & El Aref, M. M. (2005). Diagenetic history and mineral evolution of the Lutetian ironstones of Gabal Ghorabi mine area, El Bahariya Depression, Western Desert, Egypt. In *Annual Meeting of the Egyptian Geological Society* (Abstract).
- Meshref, W. M. (1990). Tectonic framework. In R. Said (Ed.), *The geology of Egypt* (pp. 113–156). A. A. Balkema, Brookfield (Chapter 8).
- Mineral Map of Egypt, EGSM. (1979). In M. S. Afia & I. Imam (Ed.), *Mining authority* (p. 44).
- Monetant, C., Ott D’Esteveu, P. O., Purser, B. H., Buroller, P. T., Jarrige, J. J., Orszag-Sperber, F., Philobos, E. R., Plaziat, J.-C., Part, P., Richert, J. P., Roussel, N., & Thiriet, J. P. (1988). Tectonic and sedimentary evolution of the Gulf of Suez and the northwestern Red Sea. *Tectonophysics (Amsterdam)*, 153, 161–177.
- Morgan, P. (1990). Egypt in the framework of global tectonics. In R. Said (Ed.), *The geology of Egypt* (pp. 91–111). A. A. Balkema, Brookfield (Chapter 7).
- Moustafa, A. R., Saoudi, A., Moubasher, A., Ibrahim, I. M., Molokhia, H., & Schwartz, B. (2003). Structural setting and tectonic evolution of the Bahariya Depression, Western Desert, Egypt. *GeoArabia. Gulf Petrolink, Bahrain*, 8(1).
- Nickless, E. F. P., Booth, S. J., & Mosley, P. N. (1976). The celestite resources of the area northeast of Bristol. *Institute of Geological Science, Mineral Assessment Report*, 25, 83p.

- Olausson, S. (1981). Formation of celestite in the Wenlock, Oslo Region, Norway, evidence of evaporitic deposition environments. *Journal of Sedimentary Research*, 51, 37–46.
- Omara, S. (1959). The geology of Sharm El Sheikh Sandstone, Sinai. *Egyptian Journal of Geology*, III(1), 107–120.
- Omran, M. (2015). *Microwave dephosphorisation of high phosphorus iron ores of the Aswan region* (p. 427). University of Oulu Graduate School, University of Oulu, Faculty of Technology.
- Omran, M., Fabritius, T., Abdel-Khalek, A., El-Aref, M., Elmanawi, A., Nasr, M., & Elmahdy, A. (2014). Microwave assisted liberation of high phosphorus oolitic iron ore. *Journal of Minerals and Materials Characterization and Engineering*, 2, 414–427.
- Omran, M., Fabritius, T., Elmahdy, A., Abdel-Khalek, A., El-Aref, M., & Elmanawi, A. (2015). XPS and FTIR spectroscopic study on microwave treated high phosphorus iron ore. *Applied Surface Science*, 345(2015), 127–140.
- Philip, G., El Aref, M. M., Darwish, M., & Ewais, S. (1991a). Paleo-erosion surfaces and karst manifestations including “Egyptian Alabaster”. In *Gabal Homret Schaibun—Gabal Sannur Area, East of the Nile Valley, Egypt*. *Egyptian Journal of Geology*, 34(1 and 2), 41–79.
- Philip, G., El Aref, M. M., Darwish, M., & Ewais, S. (1991b). Organic and inorganic fabrics of paleo-karst sediments, east of Bani Suef, Nile Valley, Egypt. In *Twenty Ninth Annual Meeting, Abstract*. *Egyptian Journal of Geology*.
- Philobos, E. R., Plaziat, J.-C., Part, P., Richert, J. P., Roussel, N., & Thiriet, J. P. (1988). Tectonic and sedimentary evolution of the Gulf of Suez and northwestern Red Sea. *Tectonophysics (Amsterdam)*, 153, 161–177.
- Pickford, M., Wanas, H., & Soliman, H. (2006). Indications for a humid climate in the Western Desert of Egypt, 1–10 Myr ago: Evidence from Galagidae (Primates, Mammalia). *Paleo-ecology*, 5, 935–943.
- Said, R. (1990a). Cretaceous paleo-geographic maps. In R. Said (Ed.), *The geology of Egypt* (pp. 439–450). A. A. Balkema, Brookfield (Chapter 23).
- Said, R. (1990b). Cenozoic. In R. Said (Ed.), *The geology of Egypt* (pp. 451–486). A. A. Balkema, Brookfield (Chapter 24).
- Said, R. (1990c). In R. Said (Ed.), *The geology of Egypt* (p. 734). A. A. Balkema.
- Said, R., & Mansour, A. (1971). The discovery of new kaolin deposits in Wadi Kalabsha, Western Desert, Egypt. *Geological Survey of Egypt*, 54, 138.
- Said, R., Sabet, A., Zalata, A., Teniakov, V., & Porkyshkin, V. (1967). A review of theories on the geological distribution of bauxite and their application for bauxitic prospecting in Egypt. *Annals of the Geological Survey of Egypt*, 6, 6–32.
- Salama, W. S. (2006). *Geology and genesis of Ghorabi iron ore and associated barite and manganese rich deposits, El Bahariya Depression, Western Desert, Egypt* [M.Sc. thesis]. Faculty of Science, Cairo University (p. 201).
- Salama, W. S. (2010). *Geological and mineralogical studies on the microbially mediated Ironstone Facies, El Bahariya Depression, Western Desert, Egypt* [Ph.D. thesis]. Faculty of Science, Cairo University (p. 245).
- Salama, W. S. (2014). Paleo-environmental significance of aluminum phosphate-sulfate minerals in the upper Cretaceous ooidal ironstones, E-NE Aswan area, southern Egypt. *International Journal of Earth Sciences (geologische Rundschau)*, 103, 1621–1639.
- Salama, W. S., El Aaref, M. M., & Gaupp, R. (2012). Mineralogical and geochemical investigations of the Middle Eocene ironstones, El Bahariya Depression, Western Desert, Egypt. *Gondwana Research*, 22, 717–736.
- Salama, W. S., El Aaref, M. M., & Gaupp, R. (2013). Mineral evolution and processes of ferruginous microbialite accretion—An example from the Middle Eocene stromatolitic and ooidal ironstones of the Bahariya Depression, Western Desert, Egypt. *Geology*, 11, 15–28.
- Salama, W. S., El Aaref, M. M., & Gaupp, R. (2014). Facies analysis and palaeo-climatic significance of ironstones formed during the Eocene greenhouse. In *Sedimentology 2014, International Association of Sedimentologists* (pp. 1–31).
- Salama, W. S., El Aaref, M. M., & Gaupp, R. (2015). Spectroscopic characterization of iron ores formed in different geological environments using FTIR, XPS, Mossbauer spectroscopy and thermoanalyses. *Spectrochimica Acta Part A: Molecular and Biomolecular Spectroscopy*, 136, 1816–1826.
- Schandelmeier, A., Klitzsch, E., Hendrix, F., & Wycisk, P. (1987). Structural development of northeast Africa since Pre-Cambrian times. *Berliner Geowissenschaftliche Abhandlungen*, 75(1), 5–25.
- Scholle, P. A., Stemmerik, I., & Harpoth, O. (1990). Origin of karst-associated celestite mineralization in Karstryggen, Central East Greenland. *Journal of Sedimentary Research*, 60, 397–410.
- Sehim, A. A. (1993). Cretaceous tectonics in Egypt. *Egyptian Journal of Geology*, 37(1), 335–372.
- Shukri, N. M., & Nakhla, F. M. (1955). The sulfur deposits of Ras Gemsa coast. In *Symposium on Applied Geology in the Near East* (pp. 114–123). UNESCO, Ankara.
- Smith, A. G. (1981). Phanerozoic equal area maps. *Geologische Rundschau*, 1, 91–127.
- Sokker, A. M. (1991). *Geomorphological, petrological and mineralogical studies on the carbonate sediments between Bahariya-Farafra, Western Desert, Egypt* [M.Sc. thesis]. Faculty of Science, Cairo University (p. 256).
- Soliman, A. S. M. (2018). *Geology, genetic classifications and inventory of paleo-karst related landforms of the Cretaceous-Tertiary carbonate sequences, Bahariya-Farafra Territory, Western Desert, Egypt* [Ph.D. thesis]. Department of Geology, Faculty of Science, Cairo University (p. 249).
- Stern, R. F. (1994). Arc assembly and continental collision in the Neoproterozoic East African orogeny; implication for the consolidation of Gondwanaland. *Annual Reviews of Earth and Planetary Sciences*, 22, 319–351.
- UEC “United Engineering Consultant”. (1976). *Development of iron ore deposits, Bahariya Oasis* (Project 4741, report). USS “United State Steel Engineering and Consultants INC.
- Wali, A. M., El Dougdoug, A. A., & Aref M. A. (1989). Geology, isotope geochemistry and the role of salt spines sulfur genesis, Gemsa area, Red Sea, Egypt. *Annals of the Geological Survey of Egypt*, XVI (1986–1989).
- Weissbrod, T. (1969). The Paleozoic of Israel and adjacent countries. Part I, the subsurface Paleozoic stratigraphy of S Israel. In *Bulletin—geological survey of Israel, 1–25; Part II, the Paleozoic outcrops in SW00 Israel and their correlation with those of S Israel* (Vol. 48, pp. 1–32).
- Wilson, M., & Guiraud, R. (1998). Late permian to recent magmatic activity of the Africa-Arabian Margin of the Tethys. In D. S. MacGregor, T. J. Moody, & D. D. Clark-Lowes (Eds.), *Hydrocarbon geology of North Africa. Special publication, Geological society of London* (Vol. 132, pp. 231–263).
- Yahiya A. (2007). Beneficiation of Aswan iron ores. In *Iron Symposium*. Central Metallurgical Research and Development Institute, Cairo, Egypt.
- Youssef, E. A. (1989). Geology and genesis of sulfur deposits at Ras Gemsa area, Red Sea coast, Egypt. *Geology*, 17, 797–801.



Mortada Mourad Taha El Aref is a professor of ore geology in the Geology Department, Faculty of Science, Cairo University, Egypt. Prof. El Aref has worked on and deeply investigated different types of metallic and non-metallic stratabound ore deposits of the Eastern and Western Deserts of Egypt and Sinai. He has led several regional projects in the field of ore exploration and beneficiation. He was the Director of the Regional Centre for Training and Technology Transfer for Arab States (Cairo-BCRC), Basel Convention on

the Control of Transboundary Movements of Hazardous Wastes and their Disposal, UNEP, (2003–2008). He became interested in environmental sciences and management since his election as a director of the Cairo University Centre for Environmental Hazard Mitigation (CEHM) from 2003 to 2008. He has supervised numerous environmental protection mega projects, including air pollution, noise, environmental impact assessment (EIA) studies, hazard mitigation studies, and urban land use planning. Currently, Prof. El Aref holds the position of Chairman of the Board of Directors of the Iron and Steel Company for Mines and Quarries (ISMQ).



Potential Exploitation of the Phanerozoic Glauconites in Egypt

Galal El-Habaak and Mahmoud Abdel-Hakeem

Abstract

Glauconite deposits are considered as one of the most important sources of K commodity. More attention has been paid to these deposits as being an alternative potash fertilizer for the ever-increasing global K demand. Egypt has considerable accumulations of glauconite deposits, with an average 6 wt% K_2O after adequate magnetic separation. These accumulations are reported at many localities in the Western Desert of Egypt: (a) Ghorabi iron mine and on the eastern and western sides of El-Gedida iron mine of El-Bahariya Oasis, (b) through the northern plateau of the Kharga Oasis, (c) the mining sectors of Abu-Tartur Plateau, and (d) at the Fayum Depression and Wadi Al-Hitan, with total thickness varying between 6 and 25 m. Other limited occurrences are distributed through the Upper Nile Valley and the west central Sinai. The Egyptian glauconites are marine Phanerozoic deposits assigned to four different geological ages, including Cenomanian, Lower-Middle Campanian, Upper Campanian, Upper Eocene, and Oligocene. Also, glauconite deposits impart their distinctive green color to some parts of eight rock formations, namely Bahariya, Raha, Quseir variegated shale, Duwi, Hamra, Qasr el Sagha, Ghannam, and Qatrani Formations, and considered useful indications for the sea level changes in Egypt and the world. These Phanerozoic glauconites occur as an overburden above the commercial iron deposits of the El-Bahariya Oasis and the mineable phosphorites of the Abu-Tartur Plateau, a constitutional part of sandstone-dominated

formations in the northern Western Desert. This mode of occurrence may be the main reason behind the little attention for the commercial value of such deposits in Egypt. Like the other developing countries, Egypt has limited potash resources and depends mainly on the imported fertilizers to increase the arable areas and crops production for the ever-increasing population. At this point, the present chapter discusses the characterization of the Phanerozoic glauconites in Egypt as a direct K fertilizer and sheds more light on the economic potential of these deposits as one of the key corners of the future potash industry.

Keywords

Phanerozoic glauconites • Fayum depression • Wadi Al-Hitan • Qatrani formation • Abu-Tartur Plateau • Fertilizers

1 Introduction





According to the pioneer works (Burst, 1958a, 1958b; Hower, 1961; McRae, 1972; Odin & Fullagar, 1988; Odin & Matter, 1981; Odom, 1984), glauconite is defined as a green-colored phyllosilicate mineral rich in Fe and K ions, which are trapped within the 2:1 dioctahedral illite-like structure consisting of nonexpandable micaceous layers “10 Å” alternating with expandable smectite layers. Glauconite contains variable Fe content as Fe^{+2} and Fe^{+3} ions, which substitute for Al^{+3} sites in the octahedral sheets. On the other hand, K_2O content is increased from 2 wt% to more than 8 wt% with the progression of glauconite maturation starting from the yellow nascent smectitic glauconite to the deep green micaceous glauconite (Table 1). Apart from the chemical weathering, color variation of glauconite grains is thought to be a function of the Fe^{+2}/Fe^{+3} ratio in the octahedral sheets rather than K content. The deficiency in

G. El-Habaak (✉)
Department of Geology, Faculty of Science, Assiut University,
Asyut, Egypt
e-mail: habaak@aun.edu.eg

M. Abdel-Hakeem
Department of Geology, Faculty of Science, South Valley
University, Qena, Egypt

Remote Sensing and Applied Geology Lab, South Valley
University, Qena, Egypt

Table 1 Glauconite maturation and structure in relative to potassium content (after Odin & Matter, 1981)

Evolution stages	Maturation stages	Mineralogical structure	Grain color	K ₂ O wt%	
Nascent	Low	Smectitic glauconite	Yellowish green 	2–4	
Slightly evolved	Moderate	↓	Light green 	4–6	
Evolved	High		Green 	6–8	
Highly evolved	Very high		Micaeous glauconite	Dark green 	> 8

Fe⁺²/Fe⁺³ ratio, taking place during glauconitization as a result of the microbial reduction of the octahedral Fe⁺³, is the main reason behind the gradual absorption of K to compensate the octahedral layer charge (López-Quirós et al., 2020).

Glauconite deposits are mostly recorded in rock successions assigned to the Cambrian-Recent in age and associated with the global sea level changes (Amorosi, 1995, 2012; Baioumy & Boulis, 2012a, 2012b; El-Habaak et al., 2016a; López-Quirós et al., 2019; Van Houten & Purucker, 1984). These deposits are distributed in various geographic zones (e.g., North American continental margin, Palaeo-Tethys, Palaeo-North Sea, and the high southern latitudes) and several countries (e.g., USA, UK, Brazil, Australia, India, and Egypt) (Fig. 1) and exploited for more than 100 years for agricultural purposes due to their K enrichment. However, the exploitation of these deposits as K fertilizers was excluded after the World War I when the manufacturing of K-salt fertilizers (e.g., KCl, K₂SO₄, and KNO₃) was initiated. This can be attributed to the lower water solubility of glauconite compared with the commonly used chemical fertilizers (Dooley, 2006).

K is considered as a critical macronutrient without which plants cannot survive. It is confined to many physiological processes that are necessary for plant growth such as the protein synthesis, enzymes activation, photosynthesis, water relations, and transportations (Lidon & Cebola, 2012; Mengel, 2007; Pettigrew, 2008). The most common K sources applied to plants are mined from brines and salts (e.g., sylvite and carnallite), with about 39 million tons of K₂O mostly come from ten companies in the northern hemisphere, in particular, Russia, Belarus, Germany, UK, and North America, where about 92% of the global potash reserve occurs (Manning, 2017; Sheldrick et al., 2002). On contrast, the developing countries of the southern

hemisphere are in a critical need to secure the food supplies and increase the crop production to face the continuously growing population. For example, potash consumption of Africa is expected to be more than 1.6% of the world's potash fertilizers between 2015 and 2050 (Manning, 2015).

In general, the developing countries have limited potash reserves and mainly rely on the imported K fertilizers, which are transported over vast distances, resulting in a high sale price of potash and probable limited access to the conventional markets. This in turn attracted the attention of many researchers to focus and shed more light on the reconsideration and exploitation of the alternative indigenous K sources such as glauconite deposits.

Most literature concerned with evaluation and roast leaching of glauconite as an alternative K fertilizer and soil conditioner. Through this context, glauconite deposits from different regions, including Iran, New Zealand, New Jersey, Southwest Argentina, and India, have been subjected to chemical characterization and lixiviation in water and different acid solutions (e.g., Mazumder et al., 1993; Karimi et al., 2011; Merchant, 2012; Franzosi et al., 2014; Smaill, 2015; Shirale et al., 2019; Shekhar et al., 2020). The results indicated that glauconite grains release lower K⁺ levels in water (23 mg K⁺/kg) compared to acid solutions (2200 mg K⁺/kg). So, glauconite is favored to be used for acidic soils, where K release rate can be accelerated to reach sufficient levels needed by crops.

The agronomic experiments (e.g., McRae, 1972; Bambilov & Sokolov, 1998; Heckman & Tedrow, 2004; Karimi et al., 2011; Franzosi et al., 2014; Rudmin et al., 2020) also proven the efficient contribution of glauconite fertilizers, even those of lower maturity “2.24 wt% K₂O,” to enhance the growth rate and production of some crops (e.g., olive plants, wheat, potatoes, and oats) in a similar effect to the application of the commonly used KCl. However, the

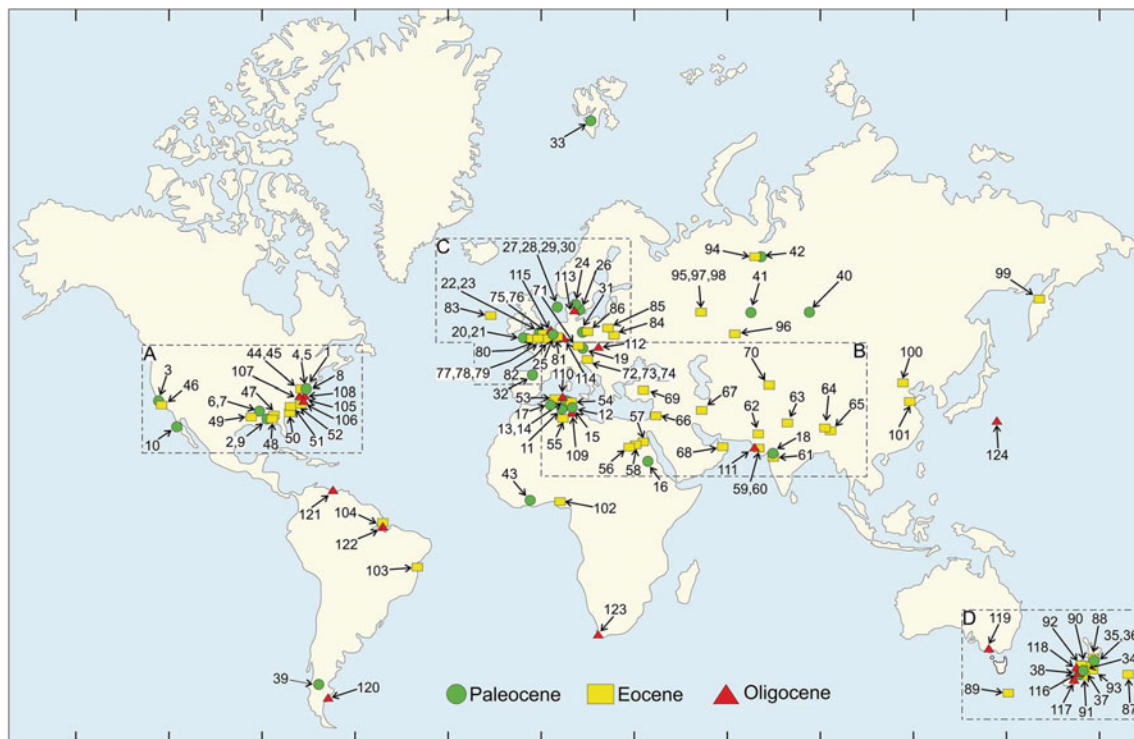


Fig. 1 Palaeogeographic distribution of the Paleogene glauconite deposits mainly at four zones: **a** North American continental margin (1–9, 44–48, and 105–108), **b** Palaeo-Tethys (11–19, 54–74, and 109–111), **c** Palaeo-North Sea deposits (21–32, 76–86, and 113), and **d** High southern latitudes (34–36, 88–93, and 119) (after, Banerjee et al., 2020)

chemical K fertilizers still attracted more farmer attention due to their high water solubility, resulting in immediate nutrient supply for plants. This pushed many researchers to find out a suitable technique to accelerate the K release rate from glauconite grains. Some studies dealt with increasing the water solubility of glauconite via adequate roasting with a fluxing agent (e.g., $\text{CaCl}_2 \cdot \text{H}_2\text{O}$ and LiCl) followed by water leaching. About 96–100 wt% K_2O can be obtained from this route (Mazumder et al., 1993; Santos et al., 2017). The other trend highlighted the production amenability of liquid K fertilizers (e.g., KCl and K_2SO_4) from glauconite through acid roasting followed by water leaching (e.g., Shekhar et al., 2017, 2020).

As aforementioned, glauconite deposits have been and still a matter of several discussions in the field of agriculture and soil fertility. The cultivation activities in Egypt are highly limited to fertile soils distributed along the Nile Valley provenance, with little attention paid to the other sandy soils that occupy vast areas through the Western and Eastern Deserts. Reclamation and mediation strategies of such sandy soils are indispensable demand to secure sufficient food supplies for the ever-increasing populations. Generally, systematic plans are required to exploit the indigenous Egyptian mineral resources for agricultural purposes, leading to sufficient crops production and great

progression in the sustainable agricultural development. Egypt has considerable quantities of glauconite deposits and limited potash resources, which makes a continuous demand for the imported potash fertilizers. From this perspective, the current review will discuss all the previous studies conducted on the Egyptian glauconite in terms of the occurrence, characterization, and beneficiation along with the agronomic experiments to highlight the economic potential of the Phanerozoic glauconites in Egypt as an alternative potash fertilizer and soil conditioner.

2 Glauconite Occurrence and Stratigraphy in Egypt

Occurrences and stratigraphy of the Egyptian glauconite deposits are discussed by many works (Said, 1971; El-Sharkawi & Khalil, 1977; Khalifa, 1983; Soliman & Khalifa, 1993; El Aref et al., 1999; Masaed and Suror, 1999; Hassan & El-Shall, 2004; Mesaed, 2006; El Aref et al., 2006; Pestitschek et al., 2012; Baioumy et al., 2011; Baioumy & Boulis, 2012a, 2012b; El-Habaak et al., 2016a, 2016b; Hegab & Abd El-Wahed, 2016; Ibrahim et al., 2017; Banerjee et al., 2019; El-Habaak et al., 2019). Glauconite deposits, as a pelletal type, are mainly recorded in detail

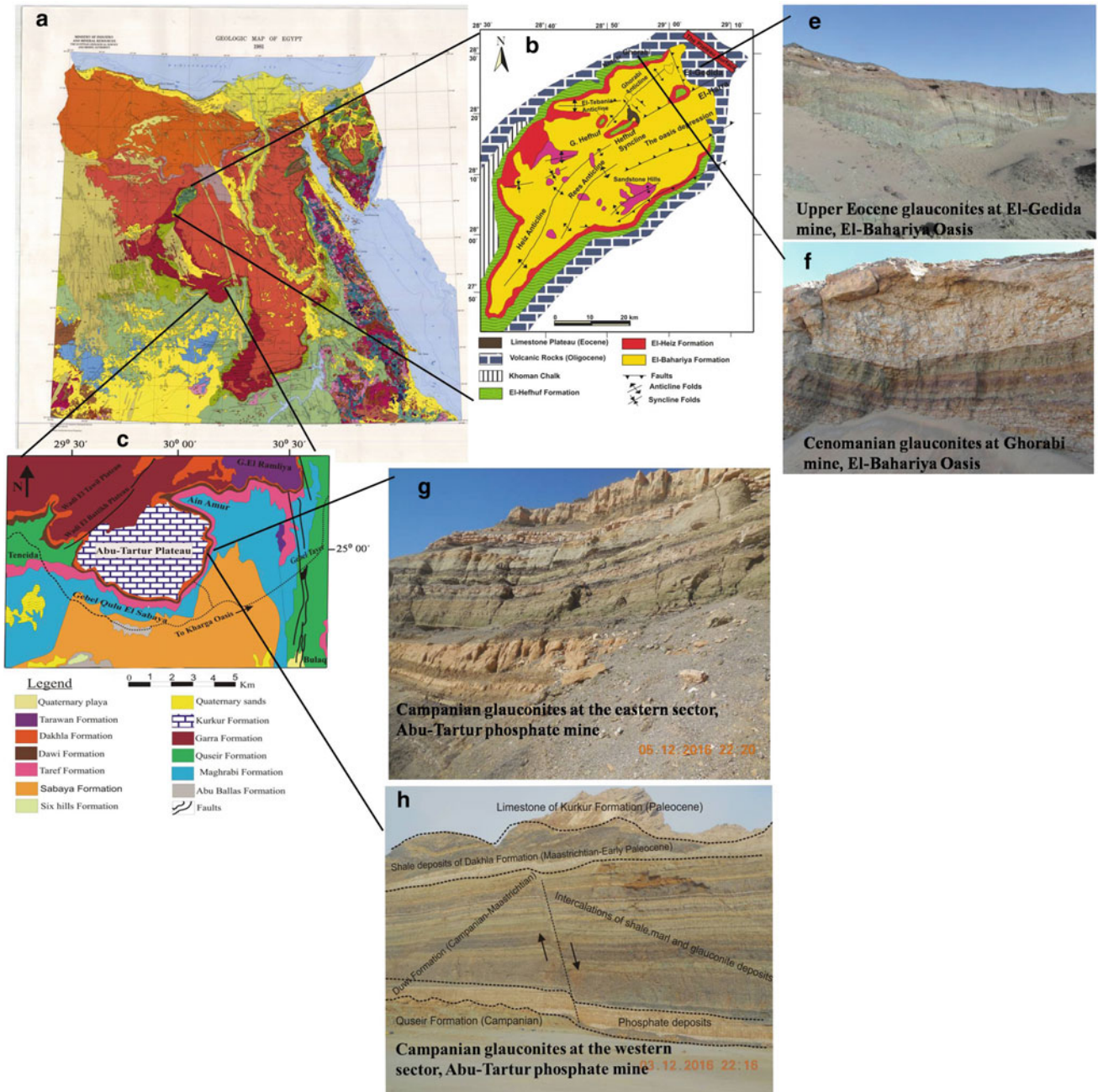


Fig. 2 Geological map of Egypt **a** with a close-up showing the different rock units at El-Bahariya Oasis **b** and Abu-Tartur Plateau **c** as well as field views of the Cenomanian and Upper Eocene glauconites at El-Bahariya Oasis (**e** and **f**, respectively) and the Campanian counterparts at Abu-Tartur Plateau (**g** and **h**)

through two localities in the Western Desert of Egypt, namely El-Bahariya Oasis and the Abu-Tartur Plateau (Fig. 2).

El-Bahariya Oasis is an oval-shaped depression that can be encountered toward the northern part of the Western Desert between coordinates of $27^{\circ} 48' - 28^{\circ} 30' N$ and $28^{\circ} 35' - 29^{\circ} 10' E$. It is built up of the Upper Cretaceous succession, including the Bahariya, El-Heiz, El-Hefuf, and

Khoman Formations, unconformably covered by the Upper-Middle Eocene Naqb, Qazzun, and Hamra Formations. El-Bahariya Oasis is well-known for its considerable reserves of iron deposits located in the northeastern part of the depression at four sites: El-Gedida, Ghorabi, Nasser, and El Harra. Glauconite deposits are mainly reported in El-Gedida and Ghorabi mining areas and confined to the Cenomanian Bahariya Formation and the Upper Eocene

Hamra Formation. The Cenomanian glauconites represent the upper part of the Bahariya Formation and are exposed as 4 m thick brownish-green to yellowish-green, moderately hard-friable, fine-medium-grained deposits with 50 cm thick concretions of glauconitic ironstone. These deposits are overlain by the Middle Eocene iron deposits of the Naqb-Qazzun sequence and considered as an indication for the Cenomanian sea level rise in Egypt. Moreover, some restricted occurrences of the Cenomanian glauconites are reported from the lower beds of the Raha Formation located at Wadi Feiran and Wadi El Gheib, west central Sinai (Gertsch et al., 2010; Kora et al., 1994). The Upper Eocene glauconites occur at the eastern wadi of El-Gedida mine as an overburden above the Middle Eocene iron deposits and appear as 6–25 m thick green, moderately hard, moderately sorted deposits with spots of iron oxyhydroxides and veinlets of calcite and alunite. On the western wadi of El-Gedida mine, glauconites are affected by minor postdepositional folding and faulting. Likewise the Cenomanian counterpart, the Upper Eocene glauconites are related to the Upper Eocene marine regression in Egypt.

On the other side, another accumulation of glauconite is outcropped at the Abu-Tartur Plateau in the central part of the Western Desert between latitude 25° 25' 23.78" N and longitude 30° 05' 15.6" E. Abu-Tartur Plateau is a limestone plateau that contains one of the most important phosphorite deposits in North Africa. Lithologically, the plateau escarpment is started, from base to top, by the Upper Cretaceous Nubia plains covered by the Campanian Quseir and Duwi Formations, Maastrichtian Dakhla Formation, and Early Paleocene Kurkur Formation. Abu-Tartur glauconite is enclosed within the Campanian Duwi Formation-hosted phosphorites. At the western mining sector, it is restricted to the middle part of the Duwi Formation as 5 m thick green to yellowish-green, moderately hard, sandy deposits with gray clay intercalations. Occasionally, these glauconite deposits undergone postdepositional faulting and enclosed ferruginous concretions of glauconitic ironstone along with evaporites interlayers: Veinlets are perceived within the upper part of glauconite deposits. Glauconite deposits cover 3.5 m intercalations of black shale and marl. Toward the uppermost part of the succession, 2 m thick greenish to brownish shale deposits belonging to the Dakhla Formation overlay glauconite deposits. At the eastern mining sector, glauconite deposits are reported in a greater thickness compared to the western sector succession. They attain about 8 m thick beds alternating with 10.5 m thick gray to brown shale to form a total of 18.5 m thick section that covers the mineable phosphate bed and underlain by the Maastrichtian Dakhla Formation and the Early Paleocene Kurkur Formation. Moreover, restricted occurrences are perceived from the Beris member of the Maastrichtian Dakhla Formation at Gabal Um

El-Ghanayem, 19 km to the northeastern part of El Kharga Oasis (Orabi & Khalil, 2014).

The northern part of the Western Desert, in particular the northern escarpment of the Fayum Depression, is also endowed with considerable accumulations of pelletal glauconite deposits that are assigned to the Upper Eocene Qasr el Sagha Formation (Dir Abu-Lifa Member) and the overlying Oligocene Qatrani Formation. Glauconite deposits of Dir Abu-Lifa Member are made up of 7.5 m fine-medium-grained glauconitic sandstone characterized by bioturbation and nodules of barite and siderite. These deposits are considered as a part of 77 m thick accumulation of gypsiferous, muddy, and cross-bedded sandstone whose uppermost part is marked by unconformity surface separating between the Dir Abu-Lifa Member and the Oligocene Qatrani Formation. The latter contains about 10–13 m thick glauconitic sandstone that represents the lower part of the Qatrani Formation and contains mud clasts, reworked nodules of limonite, interbeds of gypsiferous sandstone, and sometimes rhizolith masses cemented by calcite. It is worthy to mention that the two glauconite types here are confined to the gradual Late Eocene marine regression in Egypt, which results in the deposition of nearshore marine and alluvial deposits dominated by variegated, cross-bedded sandstone (Bown & Kraus, 1988; Gingerich, 1992). Furthermore, minor occurrences of glauconitic clays intercalated with sandy mudstone, marls, and calcareous sandstone were documented from the Upper Eocene Gehannam Formation in the Wadi Al-Hitan area, about 80 km west of the Fayum Depression (Gingerich et al., 2019) (Fig. 3).

By comparing with the Western Desert, occurrences of glauconite through the Nile Valley provenance are only

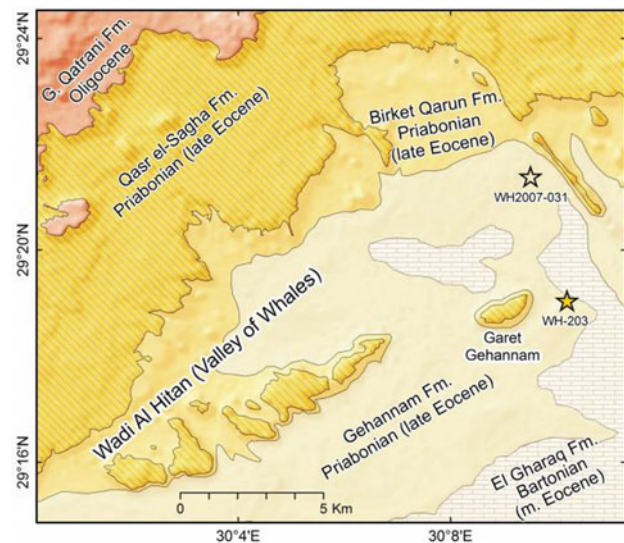


Fig. 3 Location map of the Wadi Al-Hitan in the northern Western Desert showing the distribution of the glauconite-bearing rock units (Qatrani Fm., Qasr el Sagha Fm., and Gehannam Fm.) (after Gingerich et al., 2019)

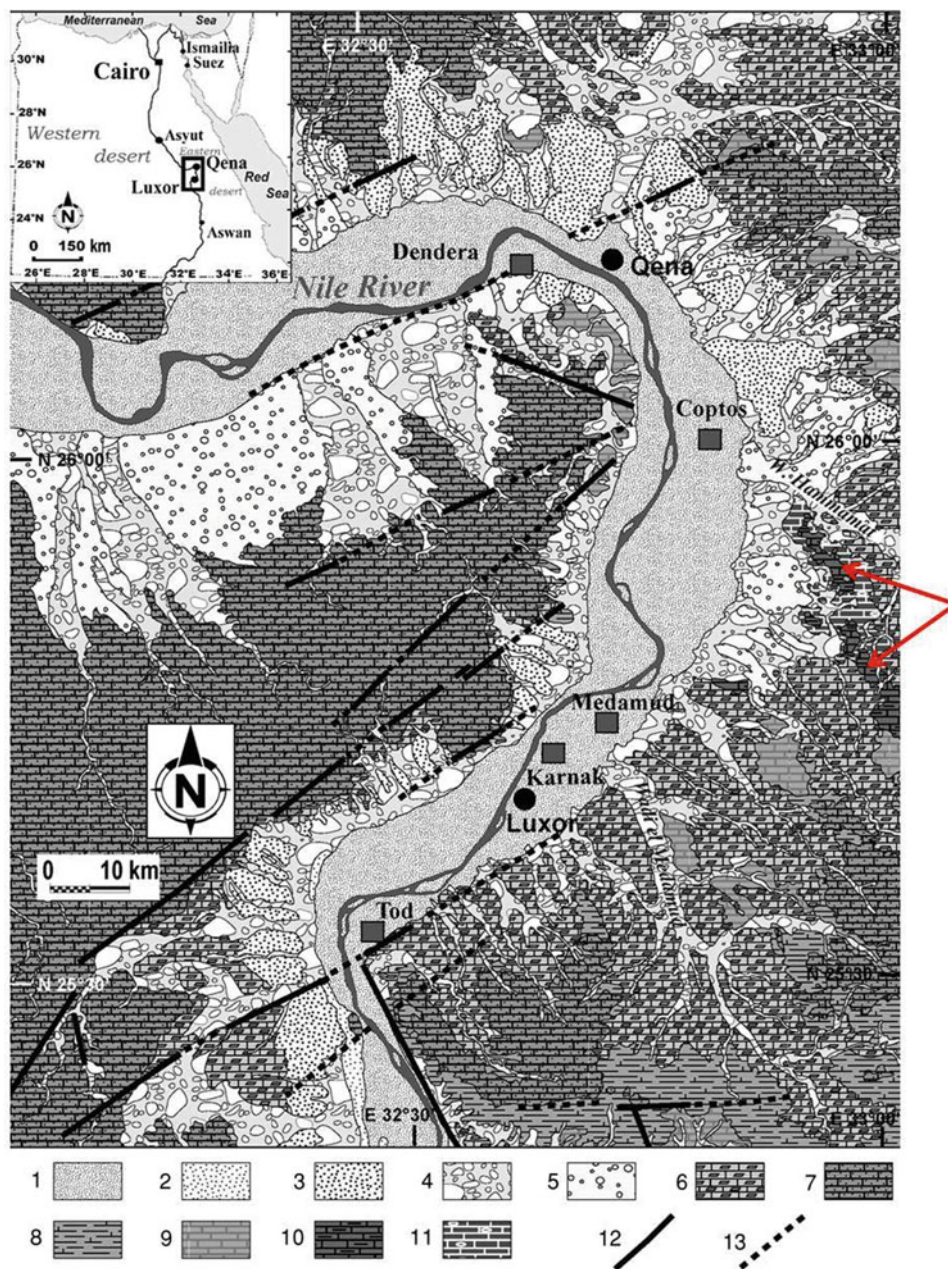


Fig. 4 Geological map of the Theban Plateau, Upper Egypt, showing the Upper Cretaceous-Lower Tertiary succession among which the glauconite-bearing Duwi Formation exists (look at red arrow) (after Ghilardi et al., 2012). The illustrated rock units include: (1 and 2) Holocene Nile alluvial sediments; (3) Pleistocene Prenile sediments; (4) Wadi deposits; (5) Fanglomerate; (6) Pliocene intercalations of sandstone, siltstone, and claystone; (7) Thebes formation (Eocene); (8) Esna formation (Paleocene-Eocene); (9) Dakhla formation (Campanian-Maastrichtian); (10) Duwi formation (Upper Campanian), consisting of phosphorites overlain by intercalations of glauconitic sandstone, gray shale, and oyster limestone; (11) Quseir variegated shale (Lower-Middle Campanian); (12) Main fault line; (13) Hidden fault lines

documented in the geological map of Qena (Fig. 4). It is confined to the Campanian Duwi Formation intercalated with gray shale and oyster limestone (Ghilardi et al., 2012). These lithological associations are laterally changed toward the Eastern Desert, where the Duwi Formation is expressed as a considerable thick succession of phosphorites overlain by gray shale, marl, and oyster limestone (Baoumy & Tada,

2005). Until the present day, there is no published information about any accumulation of mineable pelletal glauconite deposits through the Upper Cretaceous-Lower Tertiary succession in the Eastern Desert of Egypt. On contrast, the nonpelletal glauconite, occurring as clayey layers and as argillaceous matrix under the optical microscope, is widely distributed through the Western Desert, Nile

Valley, and Eastern Desert. It is reported from the Lower-Middle Campanian Quseir variegated shale whose greenish color is imparted from glauconite (Baoumy & Boulis, 2012a, 2012b). Moreover, some restricted occurrences of the Cenomanian glauconites are reported from the lower beds of the Raha Formation located at Wadi Feiran and Wadi El Gheib, west central Sinai (Gertsch et al., 2010; Kora et al., 1994).

3 Glauconite Genesis

Glauconite deposits are mainly deposited under marine conditions from a wide variety of substrates, including Fe-smectite, mica, Al-illite, bioclasts, fecal pellets, and feldspar. Two main hypotheses were suggested for glauconite formation (Burst, 1958a, 1958b; Hower, 1961; Odin & Matter, 1981). They are degraded lattice theory and

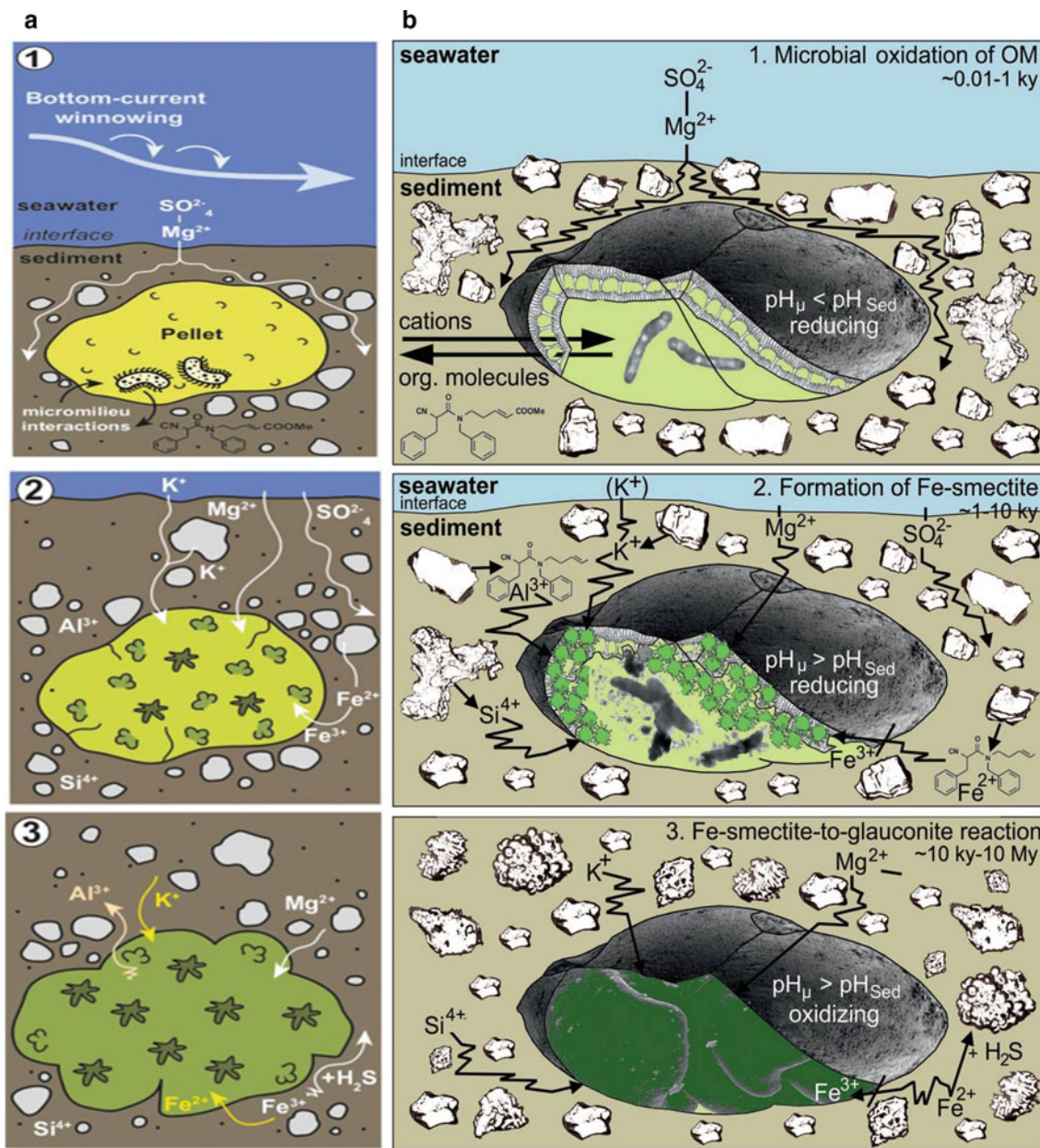


Fig. 5 Glauconitization mechanisms of argillaceous pellet (a) and foraminifera test precursors (b) by the degraded lattice and neoformation theories, respectively (after Baldermann et al., 2013; López-Quirós et al., 2020)

neof ormation theory (Fig. 5). The first hypothesis involves simultaneous absorption of K^+ and Fe^{+2} ions from the ambient seawater into degraded crystal lattice of clay particles. For more explanation, clay particles may be enclosed within fecal pellets, which undergo microbial oxidation at the sediment–water interface, resulting in partial/complete degradation of the contained clay minerals and also the surrounding sediment particles due to the surrounding metabolic activities. The degraded clay lattice gradually uptakes K^+ and Fe^{+2} from the surrounding microenvironment and is converted from nascent glauconitic smectite into evolved/highly evolved glauconite. The latter theory proposes that glauconite starts as a glauconitic smectite directly precipitated from seawater within the micropores of substrate (e.g., foraminifera tests) and its micaceous nonexpandable layers are then increased by the gradual incorporation of K^+ from the surrounding pore water. Banerjee et al. (2012) added that the co-incorporation of K^+ and Fe^{+2} into the interlayer sites and octahedral sites, respectively, is associated with the release of Al^{3+} from glauconite crystal structure. This can be undertaken as the main difference between glauconite and its analogue high Al-illite. According to these theories, the Phanerozoic glauconites in Egypt were interpreted as a result of the successive formation of nonexpandable, K^+ and Fe^{+2} -enriched layers at the expense of degraded smectite lattice (e.g., the Cenomanian glauconite deposits) (Baioumy & Boulis, 2012a, 2012b), the direct precipitation from seawater, starting as Fe-smectite from gel precursor rich in K, Fe, Mg, Al, and Si, within the micropores of argillaceous pellets (e.g., the Upper Eocene glauconite deposits) (Masaed & Suror 2000; El-Habaak et al., 2016a), and the degraded layer and neof ormation mechanisms together (e.g., the Campanian glauconite deposits) (Banerjee et al., 2019).

4 Glauconite Alteration Products

Numerous white-pinkish pockets of alunite, halloysite, and kaolinite are randomly distributed through glauconite successions at El-Gedida mine and recorded by Hassan and Baioumy (2007). They interpreted the formation of these pockets as alteration products of glauconite under oxidizing, acid sulfate environment, where glauconite is gradually dissociated into mobilized Fe, K, Al, and Si. Fe species may form amorphous grains of iron oxyhydroxides associated with glauconite grains or may percolate downward forming at least part of El-Gedida iron ores. K may combine with Al, Si, and sulfate ions, resulting in alunite, halloysite, and kaolinite. These alteration products are absent in the case of Abu-Tartur counterpart, but instead evidences on the destabilization of glauconite into Fe-rich smectite along with color zonation of glauconite grains are documented by

Pestitschek et al. (2012). They suggested that glauconite grains release differential amounts of K and Fe under acidic oxidizing conditions, causing fuzzy grain boundaries and gradual transformation into argillaceous matrix of reddish-brown Fe-rich smectite. The acidic environment may be driven by the chemical oxidation of pyrite, resulting in free sulfate ions. The latter reacted with Ca ions in the percolating surface water to form gypsum and anhydrite, while the interaction with K ions enabled jarosite to precipitate.

5 Glauconite Characterization as K Fertilizers

In order to directly exploit glauconites as K fertilizer and soil conditioner, some physical and chemical requirements have to be assessed such as grain-size range “–250 μm + 88 μm ,” the proportions of clay matrix “2–3%” and glauconite pellets “90%,” and the contained K level “at least 6%” (Dooley, 2006). Accordingly, the following lines highlight the physical and chemical properties of the glauconite in Egypt and the optimum conditions by which we can achieve the ideal exploitation of such deposits.

5.1 Physical Characterization

Glauconite appears in different shades of green color as oval, suboval, rounded, moderately sorted grains set in glauconitic argillaceous and iron oxides-rich cement (Fig. 6). Three main size fractions, including 100–200 μm , 125–400 μm , and 100–500 μm , were reported for the Cenomanian, Campanian, and Upper Eocene glauconites, respectively (Baioumy & Boulis, 2012a, 2012b; Baioumy et al., 2011; Banerjee et al., 2019; El-Habaak et al., 2016b; Ibrahim et al., 2017). They all fall within the sand size and can be reached the optimum size fraction of glauconite fertilizers (–250 μm + 88 μm) by means of crushing and grinding. As such example, El-Habaak et al. (2016b) found that about 73.94–81.74 wt% of the Upper Eocene glauconite grains are concentrated at grain fraction –250 μm + 125 μm after adequate crushing and grinding up to –1 mm using jaw crusher and rod mill in a closed circuit (Fig. 7). This uniform size of glauconite causes a great enhancement in soil texture, porosity, and permeability, and considered valuable character stands behind the application of glauconite as a soil conditioner (Heckman & Tedrow 2004; Indian Minerals Yearbook, 2011, 2012). Further, the dry sieve analysis of the Egyptian glauconite revealed that the finer size fraction –75 μm , where clay matrix is concentrated, does not exceed the range 2.2–2.5 wt% (El-Habaak et al., 2016b; Ibrahim et al., 2017). The increased proportion of clay matrix can be

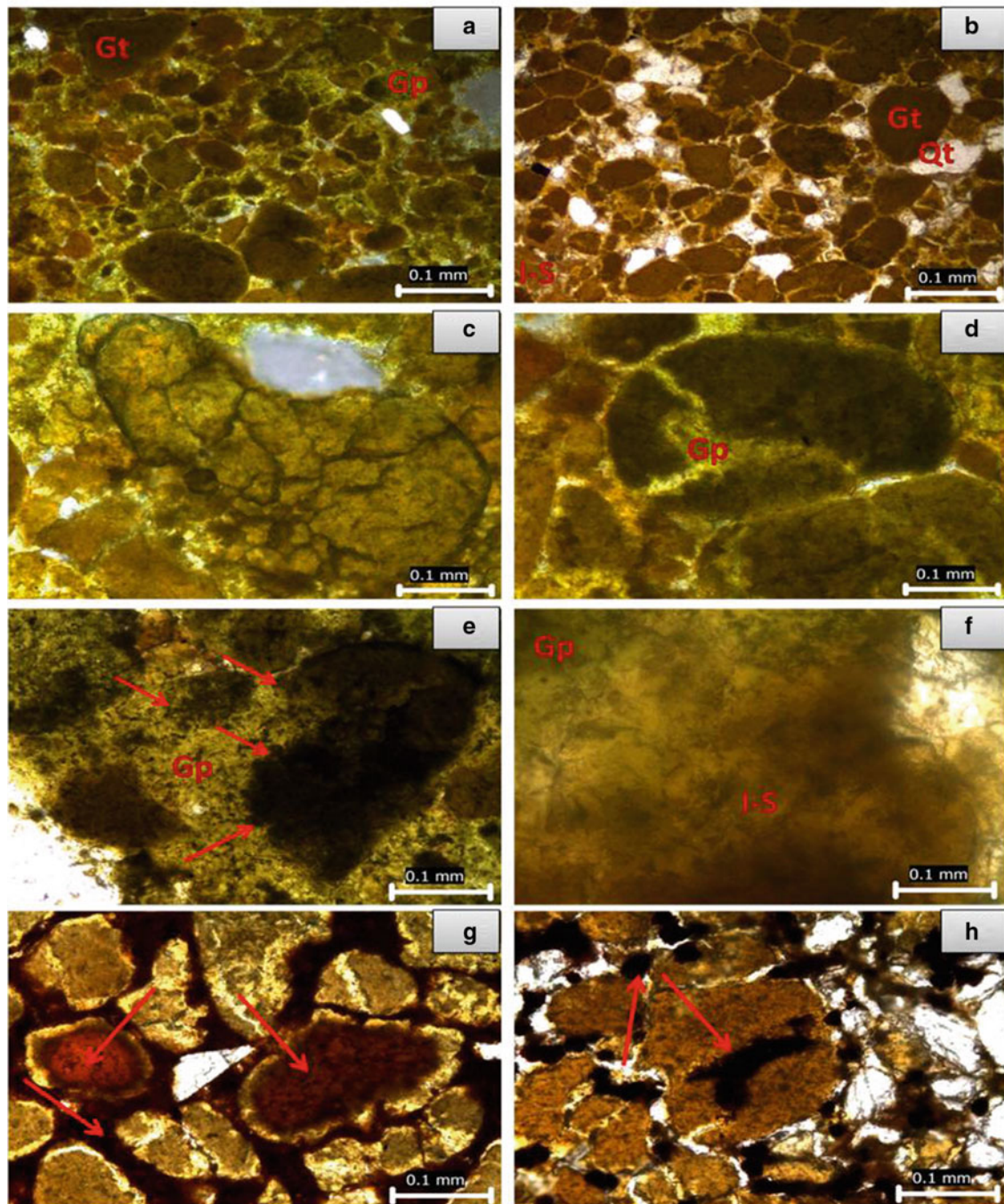


Fig. 6 Photomicrographs showing green-yellowish green, oval, suboval, rounded, fine to medium-grained glauconite pellets (Gt) along with quartz grains (Qt) set in argillaceous matrix of greenish glauconitic plasma (Gp) and reddish-brown illite-smectite mixed layer (I-S) (a and b); glauconite pellets with deeply invading fractures within the entire grain (c) and interior as triangular cracks (d) filled by the glauconitic plasma; alteration of glauconite pellets manifested by the fuzzy grain peripheries and formation of the glauconitic plasma (e) that gradually converted to the reddish-brown illite-smectite mixed layer (f); the liberation of Fe from altered glauconite grains cementing the pellets (g) or as individual grains (h) (look at arrows)

an indication for the imposed chemical weathering conditions, which lead the external boundaries of glauconite pellets to be fuzzy as well as a greenish alteroplasma forms. The latter becomes reddish brown (iron-rich illite/smectite-mixed layer) due to the gradual decrease in Fe and K-contents

(Meunier, 2004). As a result, the economic value of glauconite is expected to dropdown.

Regarding glauconite grains' percentage, the Upper Eocene glauconite contains about 75%, while the Campanian counterpart comprises about 65–75% compared to the

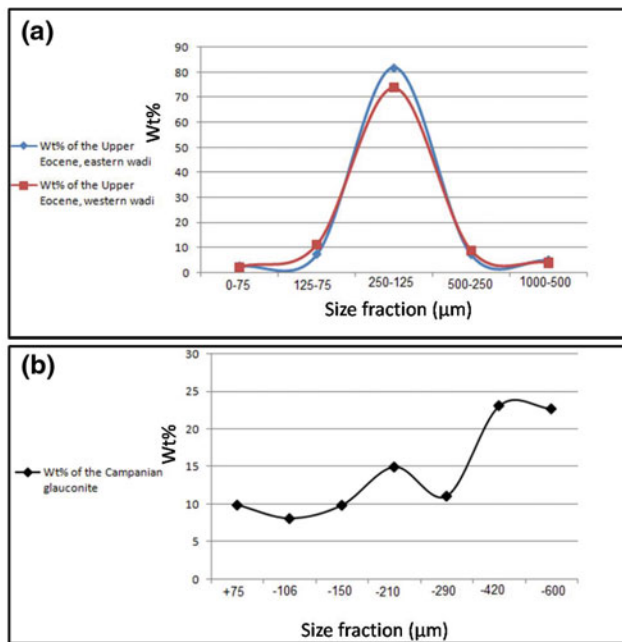


Fig. 7 Distributions of wt% of the Egyptian glauconite showing that the majority of the Upper Eocene glauconite is concentrated at + 250–125 μm fraction (a), while that of the Campanian counterpart is met at the coarser fractions (b)

associated impurities including quartz, calcite, gypsum, and goethite. These percentages were upgraded to about 94–97% using Frantz isodynamic magnetic separator, and the results were supported by conducting XRD analysis on the head samples along with the magnetic and nonmagnetic fractions (El-Habaak et al., 2016b; Ibrahim et al., 2017). The magnetic susceptibility of glauconite is ascribed to the contained Fe^{+2} in the octahedral sheets. Glauconite with high $\text{Fe}^{+2}/\text{Fe}^{+3}$ ratio is characterized by highly magnetic, dark green grains (Baldermann et al., 2015, 2017; Bentor & Kastner, 1965). The high recovery of glauconite grains can be interpreted here depending on the discussions of Amstutz and Giger (1972) and Petruk (2000) regarding the critical influence of the interlocking nature between valuables and gangues. For example, the straight, rectilinear, curved grain boundaries are regarded as indications for the high liberation degree during comminution and concentration processes due to the simple locking between the mineral grains. This example was manifested by El-Habaak et al. (2016b) who expected high glauconite recovery from the Upper Eocene deposits as a result of the simple locking between glauconite grains and quartz, the main gangue mineral. According to the previously mentioned physical characters, the Egyptian glauconite deposits are suitable to be exploited as a direct K fertilizer and soil conditioner. Also, the Cenomanian glauconite needs further studies and investigations through the northern and central parts of the Western Desert, where the host Bahariya Formation is 90–100 m thick (Said, 1971).

5.2 Chemical Characterization

For considering a given deposit as a potential fertilizer, there are specific chemical aspects that have to be considered including the valuable nutrient concentration, the contained levels of heavy metals to avoid the toxicity of plants and animals, the values of pH and salinity to protect the cultivated soil from long-term acidification and salinization, and the solubility in water. At this point, the current review discusses the economic value of the Egyptian glauconites as a potential potash resource.

5.2.1 Macronutrients Content

K is one of the most important macronutrients needed by plants, for which glauconite deposits are considered the future potash resource. As listed in Table 2, there is a similarity in the content of most nutrients between the Upper Eocene glauconite of Egypt and the exploited deposits of New Jersey, USA. It can be also classified as evolved glauconites with higher K-contents (6.75–7.3 wt% K_2O) than the other nascent-moderately evolved Campanian (3.12–5.3 wt% K_2O) and Cenomanian glauconite types (4.84–6.11 wt% K_2O). According to Dooley (2006), the Upper Eocene glauconites can be undertaken for direct fertilizing applications, while the other types need to be benefited by a suitable procedure. This was done by Ibrahim et al. (2017), as mentioned before, depending on the magnetic susceptibility of glauconite. They obtained magnetic fraction assaying 6.14 wt% K_2O from head glauconite sample containing 4.41 wt% K_2O . Besides K commodity, the present glauconites contain 50.89–59.12 wt% SiO_2 . Silicon is considered to be another commodity and a beneficial element for different crops due to its ability to enhance the maintenance of nutrients for plants in available forms and increases the tolerance level of plants to diseases and insect attacks (Meena et al., 2013). Al_2O_3 content varies between 5.88 and 13.84 wt%. The increased alumina content is related to glauconite maturity. The gradual absorption of K^+ and Fe^{+2} from the surrounding seawater is associated with the liberation of Al^{+3} from the octahedral sites during the glauconitization process (Banerjee et al., 2012). So, it is expected that the high Al-glauconite is enriched in smectite as a product of the deglauconitization process, as revealed during the mineralogical studies performed by Pestitschek et al. (2012), Baioumy and Boulis (2012a, 2012b), El-Habaak et al. (2016b), Banerjee et al. (2019). In all cases, high alumina concentration is not favorable for most crops due to the toxic effects of aluminum on plant growth represented by the disturbance of the uptake and transport of water and essential nutrients (Ca, K, and P) by plant roots, leading to increase the sensitivity to drought stress. However, the toxic effects of aluminum can be mitigated by

Table 2 Comparison between the chemical composition of glauconites in Egypt and the exploited New Jersey glauconite (USA) (after Baioumy & Boulis, 2012a, 2012b; Banerjee et al., 2019; El-Habaak et al., 2016b)

Oxides (100%)	Upper Eocene glauconite		Cenomanian glauconite	Campanian glauconite	New Jersey glauconite
	El-Bahariya Oasis			Abu-Tartur Plateau	
	El-Gedida mine		Ghorabi mine		
	Eastern wadi	Western wadi			
SiO ₂	52.10	50.89	58.19	54.74	51.83
TiO ₂	0.13	0.04	0.40	0.02	nd
Al ₂ O ₃	5.99	5.88	7.74	13.84	6.23
Fe ₂ O ₃	22.23	22.99	17.64	25.56	20.08
MgO	3.75	4.34	2.49	4.01	3.66
CaO	0.31	0.20	0.58	0.18	0.52
Na ₂ O	0.10	0.05	0.30	0.02	0.76
K ₂ O	6.75	7.30	5.41	3.12–5.30	6.60
MnO	0.02	0.08	0.02	0.04	nd
P ₂ O ₅	0.14	0.07	0.29	0.45	0.31
SO ₃	0.21	nd	nd	nd	nd

nd not determined

silicon, which promotes higher accumulation of biomass by increasing the supplement of nitrate and iron and stimulating the photosynthesis process (Ma, 2005). The soluble forms of iron (Fe⁺²) have a vital role in the building up of chlorophyll and facilitating the transport of oxygen through the roots and leaves of plants. Under acidic soil conditions, the iron concentration will increase in the soil solution. This can cause harmful effects for plants such as the root flaccidity and leaves mottling (Rout et al., 2014). The present glauconites have noticeable iron content varying between 19.54 and 25.56 wt% as Fe₂O₃, which must be considered for the cultivation-based glauconite in acidic soils.

5.2.2 Heavy Metals Content

The high levels of heavy metals have toxic effects on soils, plants, animals, and human health. For instance, heavy metal contamination of the soil is caused by various metals among which Cr, Mo, Pb, and Cd, leading to decrease the diversity

and activity of soil microorganisms responsible for the supplement of plant nutrients through degradation of organic matter. Also, accumulation of plentiful amounts of heavy metals in plants can prevent them from absorbing water and photosynthesis, resulting in reducing the growth rates of roots and seedlings (Hinojosa et al., 2004). Human health can also be subjected to the heavy metal toxicity through the food chain, which starts with plants and animals. As, Cd, Hg, Cr, and Pb are considered as the most toxic metals and classified as human carcinogens (Tchounwou et al., 2012). Accordingly, the heavy metal content of the present glauconite was compared with the tolerant levels issued by the Canadian Inspection Food Agency “CIFA” (2020) and Kenya Bureau of Standards for fertilizers (2018), as listed in Table 3. It is clear that glauconite deposits in Egypt have allowable content of the harmful heavy metals, and their exploitation as natural fertilizers does not pose critical environmental thrives.

Table 3 Comparison between heavy metal contents of the Upper Eocene glauconite in Egypt and that reported by the Canadian Food Inspection Agency (CFIA, 2020) and Kenya Standards (2018)

Heavy metal content (ppm)		Mo	Cu	Pb	Zn	Ni	As	Cd	Co	Cr
Upper Eocene glauconite	Eastern wadi glauconite, El-Gedida mine	< 0.1	3.7	2.0	86	15.4	2.4	< 0.1	25.8	110
	Western wadi glauconite, El-Gedida mine	< 0.1	2.4	0.3	208	30.7	2.2	< 0.1	28.0	130
CFIA		5	400	150	700	62	13	3	34	210
Kenya Standards		–	–	30	–	–	20	15	–	500

5.2.3 PH and Salinity

Measurement of pH values and salinity levels for a given rock-based fertilizer is an important procedure for two reasons. The first one is that the continuous and intensive application of fertilizers contributes mainly to change the soil pH value to become more acidic or highly basic state. For most plants, the appropriate pH values range between 5.5 and 7 (Kidd & Proctor, 2001). Under highly acidic conditions ($\text{pH} \leq 4.5$), some harmful elements (e.g., Al) can be released into the soil solution and affect the availability of macronutrients such as phosphorous, which easily reacts with aluminum to form insoluble aluminum phosphate (Matsumoto, 2000). Further, pH values > 8 lead to increase the adsorption of nutrients on the particles of clay minerals and organic matter, which makes them unavailable for plants (Neina, 2019). The second reason is owing to the detrimental effects stem from the annual consumption of the fertilizers. For example, the salt stress can lead to several disorders for plants including osmotic imbalance, nutrient imbalance, reduction in leaves number and roots length as well as low photosynthesis activity due to the competitive process between nutrients and salt ion species, in particular Na^+ and Cl^- (Munns & Tester, 2008). Literature (El-Habaak et al., 2016b; Morsy et al., 2016) has showed that the glauconite deposits in Egypt are characterized by mild pH values (19.10–7.59) and lower salinity levels (0.1–2.83 dS/m), which are consistent with the other studies carried out in other countries, e.g., Argentina and India, on the low pH and salinity effects of glauconite on arable soils (Franzosi et al., 2014; Rudmin et al., 2020).

5.2.4 Glauconite Solubility

Glauconite is well-known for its low water solubility along with its behavior as a slow-acting K source. This character can be attributed to the low hydration energy of K^+ ions occurring in the crystal structure of glauconite as nonexchangeable interlayer cations tightly bonded to the negatively charged tetrahedral layers (McRae, 1972, 1975). Water solubility rate of K from glauconite crystal lattice is measured between 6.94 and 23 mg K^+ /kg of glauconite (Rao & Rao, 2008; Karimi et al., 2012; Smaill, 2015). From an environmental perspective, the slow-release nature of glauconite is favored to make a sustainable supplement of nutrients needed by plants and to avoid the detrimental accumulation of heavy metals in soil resulted from the continuous application of the fast-release salt fertilizers (Rudmin et al., 2019). Also, glauconite can remediate the soil deficiency in K, which results from the downward percolation of K-bearing soil solution, crop harvest, and K-fixation in the interlayer sites of the weathered clay minerals (e.g., vermiculite and smectite) (Meena et al.,

2016). However, the direct application of glauconite is not preferred for the short-season crops, which need an immediate supplement of K. At this point, the chemical K fertilizers outperform glauconite due to their high water solubility and the quick nutrient supplement for plants. Consequently, the research work was directed to investigate all possible methods by which the water solubility of glauconite can be accelerated. It was found that about 96–100% of the interlayer K can be lixiviated either after adequate roasting at 900 °C in the presence of the chloridizing agent, in particular $\text{CaCl}_2 \cdot \text{H}_2\text{O}$ and LiCl, followed by water leaching or through acid roasting to obtain liquor rich in KCl or K_2SO_4 (Mazumder et al., 1993; Santos et al., 2017; Shekhar et al., 2017, 2020). Also, the liberation of K can be promoted by mixing glauconite with composts or inoculation with K-solubilizing bacteria (e.g., *Thiobacillus*, *Bacillus*, and *Clostridium*), resulting in a gradual destruction and collapse of glauconite crystal lattice due to the metabolic microbial products (e.g., organic and inorganic acids, extracellular polysaccharides, enzymes, and hydroxyl anions) (Ullman et al., 1996). In Egypt, the only published work on K extraction from glauconite is that of Amer and Sediek (2003). They recovered about 90% of the interlayer K from the Campanian Abu-Tartur glauconite by the direct acid leaching for 2 h at 20 wt% HCl and 225 °C. So, this point needs more consideration to perform a detailed study on the possible response of the Cenomanian, Campanian, and Upper Eocene glauconites to the thermal, chemical, and biological treatments. This is considered the second important step after glauconite evaluation for building up the future potash industry in Egypt.

6 Glauconite as a Soil Conditioner

Glauconite grains are characterized by high cation exchange capacity, up to 30 cmol/kg, and numerous micropores. Consequently, the application of glauconite to agricultural soils can contribute to enhance the ability of soil to hold water and store substantial amounts of plant nutrients (e.g., K, Ca, and Mg) (Heckman & Tedrow, 2004). Also, the uniform sand size of glauconite grains makes a noticeable improvement in soil porosity, permeability, and texture (Indian Minerals Yearbook, 2011, 2012). Accordingly, glauconite deposits are considered as a good soil conditioner. Moreover, glauconite is commonly found in association with gypsum, anhydrite, and calcite minerals, which behave as amendments to strength the erosion resistivity of soil and increase the pH value of soil solution. The latter reduces the movement of toxic metals (e.g., Al) and inhibits their reaction with the essential macronutrients (Roy et al., 2006).

Table 4 Comparison between the efficiency of glauconite application on some vegetation parameters in Egypt and the Western Siberia (after, Morsy et al., 2016; Rudmin et al., 2019)

Fertilizing rate (ton/feddan)	Upper Eocene glauconites of Egypt						Meso-Cenozoic glauconites of Western Siberia			
	Plant height		Fresh weight		Dry weight		Plant height		Grain yield	
	cm	R. C.	g/pot	R. C.	g/pot	R. C.	cm	R. C.	Kg/ha	R. C.
0	66.6	100	24.6	100	2.32	100	69.6	132	1613	118
2	74.0	111	26.3	106	2.78	119				
4	75.8	113	29.0	117	2.92	125				
6	77.8	116	30.2	122	2.94	126				
8	77.6	116	30.5	123	3.03	130				
10	78.6	118	32.5	132	3.12	134				

Note R.C.— Relative to control

7 Cultivation with Glauconite

Glauconite deposits were investigated in different regions as a direct K fertilizer applied to various crop types such as olive trees, coffee, oats, and sunflowers. The field experiments were monitored during the first and second cultivation seasons, and all results indicated the effective role of glauconite-based fertilizers in enhancing the plant height and the total yield of crops (Karimi et al., 2012; Franzosi et al., 2014; Rudmin et al., 2019, 2020). In addition, the glauconite-amended soils are characterized by increasing the concentrations of organic carbon, exchangeable ammonium, K, P, Ca, and Mg as well as a noticeable improvement of the soil physical characters (e.g., moisture retention capacity, porosity, and permeability) due to the uniform size of glauconite grains and their surface micropores. Field experiments were also conducted on the sandy soils of El-Minia Governorate, Egypt, using the Campanian and Upper Eocene glauconites collected from El-Bahariya Oasis and the Abu-Tartur Plateau (Morsy et al., 2016). Six treatment rates of glauconite deposits (0, 2, 4, 6, 8, and 10 ton/feddan) were applied to the sandy soil cultivated with peas plants. The obtained results indicate the efficiency of glauconite in enhancing some vegetation parameters (e.g., plant height and fresh and dry weight of plant shoots) as well as increasing the water efficiency use by plants at application rate of 10 ton/feddan (Table 4).

8 Conclusions and Recommendations

Egypt has considerable accumulations of the Phanerozoic glauconites reported mainly in El-Bahariya Oasis, the Abu-Tartur Plateau, west central Sinai, and Fayum Depression. They are assigned to the Cenomanian, Campanian, Upper Eocene, and Oligocene ages. The Egyptian glauconites are associated with the Tethys sea level changes in

terms of transgression (Cenomanian) and regression (Upper Eocene and Oligocene). The reported glauconites are condensed sections of variable thickness between 7.5 and 25 m. The present glauconite deposits were subjected to more detailed geochemical, mineralogical, and beneficiation studies to reveal their economic potential as alternative potassium fertilizers. At El-Bahariya Oasis and the Abu-Tartur Plateau, glauconites form green-yellowish green, friable-moderately hard, moderately sorted deposits and can be classified as low-high mature deposits, with K-content varying between 3.12 and 7.3 wt% K₂O. Mineralogically, glauconite deposits comprise 65–75% glauconite pellets together with quartz, calcite, goethite, gypsum as the main gangues. Although the Egyptian glauconite deposits are in accordance with the physical and chemical specifications as an alternative potash fertilizer, they attract little attention. This is ascribed to the occurrence of such deposits as overburden covering the commercial iron deposits in El-Bahariya Oasis and the mineable phosphorites in the Abu-Tartur Plateau. Egypt has limited potash resources and depends mainly on the imported fertilizers to increase the arable areas and secure the food supplies for the ever-increasing population. Any probable future control on the imported potash (e.g., the German control on potash exports in the early twentieth century) will negatively affect the agricultural activities and crops production in Egypt. So, it is the time to investigate and exploit the alternative K resource for the future potash industry in Egypt. Glauconites are one of these resources and greatly eligible for the production of potash fertilizer after the following recommendations:

- First of all, the present glauconite deposits need a systematic plan to explore and estimate the possible occurrences and reserves in other areas of the Western Desert, Nile Valley, and Eastern Desert.
- Microscopical, mineralogical, and chemical characterizations have to be carefully performed for the discovered deposits to evaluate the interlocking nature between

glaucinite grains and the associated gangues as well as to determine the extent to which such deposits are suitable for potash production.

- A combination of size reduction (–1 mm in diameter) and high-intensity dry magnetic separation is recommended for upgrading K-content. Hence, the obtained glauconite concentrate can be used as a slow-release K fertilizer.
- From another perspective, the concentrated glauconite can undergo procedures of roast leaching or direct acid leaching to produce potash fertilizers in the form of water-soluble K salts (e.g., KCl and K₂SO₄).

References

- Amer, A. M., & Sediek, K. N. (2003). Compositional and technological characteristics of selected glauconite deposits of North Africa. *Physicochemical Problems of Mineral Processing*, 37, 159–168.
- Amorosi, A. (1995). Glaucony and sequence stratigraphy: A conceptual framework of distribution in siliciclastic sequence. *Journal Sedimentary Research*, 65, 419–425.
- Amorosi, A. (2012). The occurrence of glaucony in the stratigraphic record: distribution patterns and sequence-stratigraphic significance. In S. Morad, J. M. Ketzer, & L. F. De Ros (Eds.), *Linking diagenesis to sequence stratigraphy* (Vol. 45, pp. 37–54). Special Publication of the International Association of Sedimentology, Wiley-Blackwell.
- Amstutz, G. C., & Giger, H. (1972). Stereological methods applied to mineralogy, petrology, mineral deposits and ceramics. *Journal of Microscopy*, 95, 145–157.
- Baioumy, H. M., Boulis, S. N., & Hassan, M. S. (2011). Occurrences and petrographical variations among the glauconite deposits from Egypt. In M. Broekmans (Ed.), *Proceedings of the 10th international congress for applied mineralogy (ICAM)* (pp. 39–47).
- Baioumy, H., & Boulis, S. (2012a). Non-pelletal glauconite from the Campanian Qusseir formation, Egypt: Implication for glauconitization. *Sedimentary Geology*, 249–250, 1–9.
- Baioumy, H. M., & Boulis, S. N. (2012b). Glauconites from the Bahariya Oasis: An evidence for Cenomanian marine transgression in Egypt. *Journal of African Earth Sciences*, 70, 1–7.
- Baioumy, H. M., & Tada, R. (2005). Origin of Upper Cretaceous phosphorites in Egypt. *Cretaceous Research*, 26, 261–275.
- Baldermann, A., Dietzel, M., Mavromatis, V., Mittermayr, F., Warr, L., & Wemmer, K. (2017). The role of Fe on the formation and diagenesis of interstratified glauconite-smectite and illite-smectite: A case study of Upper Cretaceous shallow-water carbonates. *Chemical Geology*, 453, 21–34.
- Baldermann, A., Warr, L. N., Grathoff, G. H., & Dietzel, M. (2013). The rate and mechanism of deep-sea glauconite formation at the Ivory Coast-Ghana marginal ridge. *Clays and Clay Minerals*, 61, 258–276.
- Baldermann, A., Warr, L., Letofsky-Papst, I., & Mavromatis, V. (2015). Substantial iron sequestration during green clay authigenesis in modern deep-sea sediments. *Nature Geoscience*, 8, 885–889.
- Bambalov, N., & Sokolov, G. (1998). New soil improving agents for accelerated cultivation of soils with low fertility or damaged. *International Agrophysics*, 12, 357–360.
- Banerjee, S., Chatteraj, S. L., Saraswati, P. K., Dasgputa, S., Sarkar, U., & Bumby, A. (2012). The origin and maturation of lagoonal glauconites: A case study from the Oligocene Maniyara Fort formation, western Kutch, India. *Geological Journal*, 47, 357–371.
- Banerjee, S., Choudhury, T. R., Saraswati, P. K., & Khanolkar, S. (2020). The formation of authigenic deposits during Paleogene warm climatic intervals: A review. *Journal of Palaeogeography*, 9, 1–27.
- Banerjee, S., Farouk, S., Nagm, E., Choudhury, T. R., & Meena, S. S. (2019). High Mg-glaucinite in the Campanian Duwi formation of Abu Tartur Plateau, Egypt and its implications. *Journal of African Earth Sciences*, 156, 12–25.
- Bentor, Y. K., & Kastner, M. (1965). Notes on the mineralogy and origin of glauconite. *Journal of Sedimentary Petrology*, 35, 155–166.
- Bown, T. M., & Kraus, M. J. (1988). Geology and Paleoenvironment of the Oligocene Jebel Qatrani formation and adjacent rocks, Fayum depression, Egypt. U.S. *Geological Survey Professional Paper*, 1452, 1–60.
- Burst, J. F. (1958a). “Glaucinite” pellets: Their mineral nature and applications to stratigraphic interpretations. *Bulletin-American Association of Petroleum Geologists*, 42, 310–327.
- Burst, J. F. (1958b). Mineral heterogeneity in glauconite pellets. *American Mineralogist*, 43, 481–497.
- Canadian Food Inspection Agency Standards for Metals in Fertilizers and Supplements. (2020). Trade Memorandum T-4-93. (February 22 2021).
- Dooley, J. H. (2006). Glauconite. In J. Koger, N. Trivedi, J. Barrer, & N. Krukowsky (Eds.), *Industrial minerals and rocks: Commodities market and uses* (pp. 493–495). Society for Mining.
- El Aref, M. M., El-Sharkawi, M. A., & Khalil, M. A. (1999). Geology and genesis of the stratabound to strataform Cretaceous, Eocene iron ore deposits of El-Bahariya region, Western Desert, Egypt. In *The 4th international conference on geology of the Arab world* (pp. 450–475).
- El Aref, M. M., Mesaed, A. A., Khalil, M. A., & Salama, W. S. (2006). Stratigraphic setting, facies analyses and depositional environments of the Eocene ironstones of Gabal Ghorabi mine area, El Bahariya depression, Western Desert, Egypt. *Egyptian Journal of Geology*, 50, 29–57.
- El-Habaak, G., Askalany, M., & Abdel-Hakeem, M. (2019). Possibility of mixed origin of rare earth elements in sedimentary marine apatites: A case study from phosphorites in the Cretaceous (Campanian-Maastrichtian) Duwi formation, Abu-Tartur Plateau, Egypt. *The Journal of Geology*, 127, 643–663.
- El-Habaak, G., Askalany, M., Farghaly, M., & Abdel-Hakeem, M. (2016a). The economic potential of El-Gedida glauconite deposits, El-Bahariya Oasis, Western Desert, Egypt. *Journal of African Earth Sciences*, 120, 186–197.
- El-Habaak, G., Askalany, M., Galal, M., & Abdel-Hakeem, M. (2016b). Upper Eocene glauconites from the Bahariya depression: An evidence for the marine regression in Egypt. *Journal of African Earth Sciences*, 117, 1–11.
- El-Sharkawi, M. A., & Khalil, M. A. (1977). Glauconite, a possible source of iron for El-Gedida iron ore deposits, Bahariya Oasis, Egypt. *Egyptian Journal of Geology*, 21, 109–116.
- Franzosi, C., Castro, L. N., & Celeda, A. M. (2014). Technical evaluation of glauconites as alternative potassium fertilizer from the Salamanca formation, Patagonia, Southwest Argentina. *Natural Resources Research*, 23, 311–320.
- Gertsch, B., Keller, G., Adatte, T., Berner, Z., Kassab, A. S., & Tantawy, A. A. A. (2010). Cenomanian-Turonian transition in a shallow water sequence of the Sinai, Egypt. *International Journal of Earth Sciences*, 99, 165–182.
- Ghilardi, M., Tristant, Y., & Boraik, M. (2012). Nile River evolution in Upper Egypt during the Holocene: Palaeoenvironmental implications for the Pharaonic sites of Karnak and Coptos. *Géomorphologie*, 18(1), 1–26.
- Gingerich, P. D. (1992). *Marine mammals (Cetacea and Sirenia) from the Eocene of Gebel Mokattam and Fayum, Egypt: Stratigraphy, age, and Paleoenvironments*. University of Michigan, Papers on Paleontology, No. 30, pp. 1–98.

- Gingerich, P. D., Antar, M. S. M., & Zalmout, I. S. (2019). *Aegicetusgehennae*, a new late Eocene protocetid (Cetacea, Archaeoceti) from Wadi Al Hitan, Egypt, and the transition to tail-powered swimming in whales. *PLoS ONE*, *14*(12), 1–55.
- Hassan, M., & Baioumy, H. (2007). Characterization and origin of alunite in El-Gedida iron mine (Egypt). *Periodico Di Mineralogia*, *76*, 11–24.
- Hassan, M., & El-Shall, H. (2004). Glauconitic clay of El-Gedida, Egypt: Evaluation and surface modification. *Applied Clay Science*, *27*, 219–222.
- Heckman, J. R., & Tedrow, J. C. F. (2004). Green sand as a soil amendment. *Better Crops*, *88*, 1–17.
- Hegab, O. A., & Abd El-Wahed, A. G. (2016). Origin of the glauconite from the Middle Eocene, Qarara formation, Egypt. *Journal of African Earth Sciences*, *123*, 21–28.
- Hinojosa, M. B., Carreira, J. A., Ruiz, R. G., & Dick, R. P. (2004). Soil moisture pre-treatment effects on enzyme activities as indicators of heavy metal contaminated and reclaimed soils. *Soil Biology & Biochemistry*, *36*, 1559–1568.
- Hower, J. (1961). Some factors concerning the nature and origin of glauconite. *American Mineralogist*, *46*, 313–334.
- Ibrahim, S. S., El Kammar, A. M., Guda, A. M., Boulos, T. R., & Saleh, A. (2017). Characterization and mineral beneficiation of Egyptian glauconite for possible industrial use. *Particulate Science and Technology*, 1–11.
- Indian Minerals Yearbook 2011. (2012). *Potash (Advance Release)*. Government of India, Ministry of Mines, Indian Bureau of Mines, pp. 2–5.
- Karimi E, Abdolzadeh A, Sadeghipour H.R., & Aminei A. (2012). The potential of glauconitic sandstone as a potassium fertilizer for olive plants. *Archives of Agronomy and Soil Science* *58* (9), 983–993.
- Karimi, E., Abdolzadeh, A., Sadeghipour, H. R., & Aminei, A. (2011). The potential of glauconitic sandstone as a potassium fertilizer for olive plants. *Archives of Agronomy and Soil Science*, *1*, 1–11.
- Kenya Standard. (2018). *Soluble compound fertilizer, specification*. Kenya Bureau of Standards, pp. 1–8.
- Khalifa, M. A. (1983). Origin and occurrence of glauconite in the green sandstone associated with unconformity, Bahariya Oases, Western Desert, Egypt. *Journal of African Earth Sciences*, *1*, 321–325.
- Kidd, P. S., & Proctor, J. (2001). Why plants grow poorly on very acid soils: Are ecologists missing the obvious? *Journal of Experimental Botany*, *52*, 791–799.
- Kora, M., Shahin, A., & Semiet, A. (1994). Biostratigraphy and paleoecology of some Cenomanian successions in the west central Sinai, Egypt. *Neues Jahrbuch für Geologie und Paläontologie, Monatshefte* *10*, 597–617.
- Lidon, Z. Z., & Cebola, F. (2012). An overview on drought induced changes in plant growth, water relations and photosynthesis. *Emirates Journal of Food and Agriculture*, *24*, 57–72.
- López-Quirós, A., Escutia, C., Sánchez-Navas, A., Nieto, F., García-Casco, A., Martín-Algarra, A., Evangelinos, D., & Salabarnada, A. (2019). Glaucony authigenesis, maturity and alteration in the Weddell Sea: An indicator of paleoenvironmental conditions before the onset of Antarctic glaciations. *Scientific Reports*, *9*, 13580.
- López-Quirós, A., Sánchez-Navas, A., Nieto, F., & Escutia, C. (2020). New insights into the nature of glauconite. *American Mineralogist*, *105*, 674–686.
- Ma, J. F. (2005). Physiological mechanisms of Al resistance in higher plants. *Soil Science and Plant Nutrition*, *61*, 609–612.
- Manning, D. A. C. (2015). How minerals will feed the world in 2050. *Proceedings of the Geologist's Association*, *126*, 14–17.
- Manning, D. A. C. (2017). Innovation in resourcing geological materials as crop nutrients. *Natural Resources Research*, 1–11.
- Masaed, A. A., & Suror, A. A. (1999). Mineralogy and geochemistry of the Bartonian stratabound diagenetic and lateritic glauconitic ironstones of El-Gedida mine, Bahariya Oasis, Egypt. In *Second international conference on the geology of the Arab world* (Vol. 1, pp. 509–540) Cairo Univ., Egypt.
- Mesaed A. A., & Suror A. A. (2000). Mineral chemistry and mechanism of formation of the bartonian glaucony of el-gedida mine, El Bahariya Oases, Egypt. *Egyptian Mineralogist* *12*, 1–28.
- Matsumoto, H. (2000). Plant responses to aluminium stress in acid soil: molecular mechanism of aluminium injury and tolerance. *Kagaku to Seibutsu*, *38*, 425–458.
- Mazumder, A. K., Sharma, T., & Rao, T. C. (1993). Extraction of potassium from glauconitic sandstone by the roast-leach method. *International Journal of Mineral Processing*, *38*, 111–123.
- McRae, S. G. (1972). Glauconite. *Earth-Science Reviews*, *8*, 397–440.
- McRae, S. G. (1975). The presence of indigenous glauconite in soils and its effect on soil fertility. *The Journal of Agricultural Science*, *84*, 137–141.
- Meena, V. S., Maurya, B. R., Verma, J. P., & Meena, R. S. (2016). *Potassium solubilizing microorganisms for sustainable agriculture* (pp. 5–7). Springer.
- Meena, V. D., Dotaniya, M. L., Coumar, V., Rajendiran, S., Ajay, K. S., & Rao, A. S. (2013). A Case for silicon fertilization to improve crop yields in tropical soils. *Proceedings of the National Academy of Sciences, India Section B: Biological Sciences*, *84*, 505–518.
- Mengel, K. (2007). Potassium. In A. V. Barker, & D. J. Pilbeam (Eds.), *Handbook of plant nutrition* (pp. 91–102). Taylor & Francis Group (CRC).
- Merchant, R. J. (2012). Glauconite-the future potash for fertilizers in New Zealand. *AusIMM Bulletin*, *1*, 78–81.
- Mesaed, A. A. (2006). Mechanism of formation of the Cenomanian glauconitic ironstones of the Bahariya formation, Gabal el Dist, Bahariya Oases, Western Desert, Egypt. *Bulletin of the Tethys Geological Society, Cairo*, *1*, 17–36.
- Meunier, A. (2004). *Clays* (pp. 83–327). Springer.
- Morsy, M. A., Darwish, O. H., & Eldawwy, N. G. (2016). Evaluation of glauconite deposits as an amendment for sandy soil: 1-preliminary studies. *El-Minia Journal of Agricultural Research and Development*, *36*, 343–355.
- Munns, R., & Tester, M. (2008). Mechanisms of salinity tolerance. *Annual Review of Plant Biology*, *59*, 651–681.
- Neina, D. (2019). The role of soil pH in plant nutrition and soil remediation. *Applied and Environmental Soil Science*, *19*, 1–9.
- Odin, G. S., & Fullagar, P. D. (1988). Geological significance of glaucony facies. In G. S. Odin (Ed.), *Green Marine clays: Oolitic ironstone facies—A comparative study* (pp. 295–332). Elsevier.
- Odin, G. S., & Matter, A. (1981). De glauconiarum origine. *Sedimentology*, *28*, 611–641.
- Odom, E. (1984). Glauconite and celadonite minerals. *Reviews in Mineralogy*, *13*, 545–572.
- Orabi, H. O., & Khalil, H. M. (2014). Calcareous benthonic foraminifera across the Cretaceous/Paleocene transition of Gebel Um El-Ghanayem, Kharga Oasis, Egypt. *Journal of African Earth Sciences*, *96*, 110–121.
- Pestitschek, B., Gier, S., Essa, M., & Kurzweil, H. (2012). Effects of weathering on glauconite: Evidence from the Abu Tartur plateau. *Egypt. Clays and Clay Minerals*, *60*, 76–88.
- Petruk, W. (2000). *Applied mineralogy in the mining industry* (pp. 83–94). Elsevier Science BV.
- Pettigrew, W. T. (2008). Potassium influences on yield and quality production for maize, wheat, soybean and cotton. *Physiologia Plantarum*, *133*, 670–681.
- Rao, C. S., & Rao, A. S. (2008). Characterization of indigenous glauconitic sandstone for its potassium supplying potential by

- chemical, biological, and electroultrafiltration methods. *Communications in Soil Science and Plant Analysis*, 30, 1105–1117.
- Rout, G. R., Sahoo, S., Das, A. B., & Das, S. R. (2014). Screening of iron toxicity in rice genotypes on the basis of morphological, physiological and biochemical analysis. *Journal of Experimental Biology and Agriculture Sciences*, 2, 567–582.
- Roy, R. N., Finck, A., Blair, G. J., & Tandon, H. I. S. (2006). Plant nutrition for food security: A guide for integrated nutrient management. *FAO Fertilizer and Plant Nutrition Bulletin*, 16, 135–139.
- Rudmin, M., Banerjee, S., & Makarov, B. (2020). Evaluation of the Effects of the application of glauconitic fertilizer on oat development: A two-year field-based investigation. *Agronomy*, 10, 872.
- Rudmin, M., Banerjee, S., Makarov, B., Mazurov, A., Ruban, A., Oskina, Y., Tolkachev, O., Buyakov, A., & Shaldybin, M. (2019). An investigation of plant growth by the addition of glauconitic fertilizer. *Applied Clay Science*, 180, 105178.
- Said, R. (1971). Explanatory notes to accompany geological map of Egypt. *Geological Survey of Egypt*, 56, 120–123.
- Santos, W. O., Mattiello, E. M., Pacheco, A. A., Vergutz, L., Souza-Filho, L. F. S., & Abdala, D. B. (2017). Thermal treatment of a potassium-rich metamorphic rock in formation of soluble K forms. *International Journal of Mineral Processing*, 159, 16–21.
- Shekhar, S., Mishra, D., Agrawal, A., & Sahu, K. K. (2017). Physical and chemical characterization and recovery of potash fertilizer from glauconitic clay for agricultural application. *Applied Clay Science*, 143, 50–56.
- Shekhar, S., Sinha, S., Mishra, D., Agrawal, A., & Sahu, K. K. (2020). A sustainable process for recovery of potash fertilizer from glauconite through simultaneous production of pigment grade red oxide. *Sustainable Materials and Technologies*, 23, 1–8.
- Sheldrick, W. F., Syers, J. K., & Lingard, J. (2002). A conceptual model for conducting nutrient audits at national, regional and global scales. *Nutrient Cycling in Agroecosystems*, 62, 61–67.
- Shirale, A. O., Meena, B. P., Gurav, P. P., Srivastava, S., Biswas, A. K., Thakur, J. K., Somasundaram, J., Patra, A. K., & Rao, A. S. (2019). Prospects and challenges in utilization of indigenous rocks and minerals as source of potassium in farming rocks and minerals as source of potassium. *Journal of Plant Nutrition*, 1–22.
- Smaill, J. B. (2015). *Geochemical variations in glauconitic minerals: Applications as a potassium fertilizer resource*. MSc Thesis, Department of Geological Science, University of Canterbury.
- Soliman, H. E., & Khalifa, M. A. (1993). Stratigraphy, facies and depositional environments of the lower Cenomanian Bahariya formation, Bahariya Oasis, Western Desert. *Egypt. Egyptian Journal of Geology*, 37, 193–209.
- Tchounwou, P. B., Yedjou, C. G., Patololla, A. K., & Sutton, D. J. (2012). Heavy metals toxicity and the environment. *Experiential Supplementum*, 101, 133–164.
- Ullman, W. J., Kirchman, D. L., & Welch, W. A. (1996). Laboratory evidence by microbially mediated silicate mineral dissolution in nature. *Chemical Geology*, 132, 11–17.
- Van Houten, F. B., & Purucker, M. E. (1984). Glauconite peloids and chamositic ooides-favorable factors, constraints, and problems. *Earth Science Reviews*, 20, 211–243.



Galal El-Habaak is a professor of economic geology at the Department of Geology, Faculty of Science, Assiut University (Egypt). He obtained MSc and Ph.D. degrees in economic geology from Assiut University in 1986 and 1992, respectively. He is a specialist in the geology and potential exploitation of varied metallic and non-metallic mineral deposits (e.g. volcanogenic massive sulphides, Fe- and Mn-ores, barites, glauconites, black shale, and phosphorites), as well as characterization and valorization of mining wastes, geopolymer synthesis, and biogas production from black shale.



Mahmoud Abdel-Hakeem is an assistant professor of economic geology in the Department of Geology, Faculty of Science, South Valley University (Egypt). He obtained MSc (2016) and Ph.D. (2020) degrees in economic geology from South Valley University. He is a specialist in the geology and the economic potential of some non-metallic mineral deposits, along with the mining wastes.



Phanerozoic Rare Earth Element Resources of Egypt: Metallogenic and Mineral Exploration Constraints

Hamdy Mahmoud Abdalla, Hiroharu Matsueda, Gehad M. Saleh, and Shunso Ishihara

Abstract

The rare earth element (REE) Phanerozoic rocks in the Egyptian Arab Republic can be categorized into four classes as follows: (1) Mesozoic, anorogenic nepheline syenite ring complexes with LREE amounting up to 0.5%, particularly in fenitized and carbonatized parts (Abu Khruq, Naga, and El Gezira), (2) Anorogenic post-Cretaceous Y, Th, HREE, and P-enriched, peralkaline complexes that intrude the Phanerozoic rocks of the Southwestern Desert with HREE amounting up to 2% (Gara El Hamra and Nusab El Balghoum), (3) Carboniferous sandstones of Southwest Sinai with conspicuous xenotime contents attributing up to 0.8% of HREE (Ramlet Hemyir, Um Hamad, El Adidiya), and (4) Quaternary Littoral black sand deposits at the junctures of the Nile branches with the Mediterranean Sea. Special attention will be given for Abu Khruq, Gabal El Gara El Hamra, Ramlet Hemyir, Um Hamad, and Rosetta. Gabal El Gara El Hamra (GH) complex is an elliptical stock of 0.4×0.8 km made up of peralkaline granite-syenite. Considerably anomalous radioactivity (U and Th reach up to 2800 and 16,500 ppm, respectively) in addition to the rare: Y (up to 62,500 ppm), HREE (31,580 ppm), Zr (7200 ppm), Nb (710 ppm), Be (48 ppm), match with these hydrothermally altered zones. Besides, P and Ba reach up to 67,600 and 16,000 ppm, respectively. The core of Abu Khruq ring complex (AK) comprises a crescent-shaped body of nepheline syenite which has experienced subsolidus metasomatic reworking. Metasomatic reactions result in sizeable linear

zones of Na-feldasphized (i.e. albitized), carbonatized (i.e. development of cancrinite + calcite \pm analcite \pm sodalite \pm natrolite) and reddish, hematized nepheline syenite. Anomalous radioactivity as well as pronounced contents of the rare elements: Zr (up to 4230 ppm), Nb (6130 ppm), U (258 ppm), Th (2060 ppm), Y (195 ppm), Be (59 ppm), and LREE (4900 ppm) coincide with these hydrothermally altered zones. Concomitant enrichment of Na, Ca, S, Cl, CO₂, and Sr at early stage was accompanied by a strong depletion in Al, Mg, K, Ba, and Rb in these zones at late hematization stage. This alteration sequence can be equated with the waning stage of the alkali metasomatism or “fenitization” typically associating many carbonatite centres. A striking feature for the mineralized alkaline ring complexes is the emplacement of the nepheline syenite at late stage at their interiors. These complexes themselves are arranged along tectonic zones trending ENE-WSW and exhibit a migrating age trend at specified time intervals. In addition, mineralized nepheline syenite complexes are highly differentiated, possessing a specialized geochemical signature. The REEs content of Ramlet Hemyir (RH) and Um Hamad (UH) areas, Southwestern Sinai, Egypt, bear signatures of paleoplacer xenotime concentrations with significant REEs contribution due to adsorption on clays or scavenging by ferromanganese materials. Xenotime occurs mostly in clay to silty size fractions. Close attention should be paid to the Paleozoic rocks in the Sinai Peninsula, e.g. Um Bogma and Abu Durba in Southwestern Sinai, and in eastern Sinai at the Katherine-Nubie Road. The black sand placer deposits at the outpouring of the River Nile into the Mediterranean Sea coast contain monazite (up to 0.6%) and other economic heavy minerals. The distribution of monazite was found to be largely governed by the accretion/erosion pattern affecting shore lines. Thus, monazite as do other dense opaque minerals is largely accumulated as a lag deposit within erosion areas.

H. M. Abdalla · G. M. Saleh (✉)
Nuclear Materials Authority, Box: 530 El Maadi, Cairo, Egypt
e-mail: drgehad_m@yahoo.com

H. Matsueda · S. Ishihara
Hokkaido University, Sapporo, Japan

Keywords

Phanerozoic REE resources • Ring complexes • Peralkaline granites • Xenotime-enriched sandstones • Sinai Peninsula • Black sands • Egypt

1 Introduction

The demands for REEs are increasing in importance due to new technologies and clean energy production. REE's consumers became aware of possible supply shortages and are looking for new resources (Takilharal et al., 2016). The four classes of REE-mineralized Phanerozoic rocks in Egypt are, namely (1) LREE-enriched, anorogenic Mesozoic nepheline syenite ring complexes with LREE amounting up to 0.5%, particularly in their fenitized and carbonatized parts (Abu Khruq, Naga, and El Gezira), (2) Y, Th, HREE, and P-enriched post-Cretaceous anorogenic, peralkaline complexes that intrude the Phanerozoic sedimentary rocks of the Southwestern Desert with HREE amounting to 2% (Gabal El Gara El Hamra and Nusb El Balghoum), (3) Carboniferous sandstones of Southwest Sinai with conspicuous xenotime contents attributing to up to 0.8% of HREE (Ramlet Hemyir and Um Hamad), and (4) Black sand placers deposits at the junctures of the Nile branches with the Mediterranean Sea (Rosetta). The locations of the investigated resources in relation to the Pan-African basement complex and the Phanerozoic cover of Egypt are shown in Figs. 1a and 21.

Focussing on the available information regarding the tectonic, geological, geochemical, and mineralogical features of the known REEs localities in Egypt, the present article attempts to deduce an up-to-date review of Phanerozoic REE resources in Egypt.

Large arrays of granite-syenite complexes are recorded in both the Southeastern and Southwestern Deserts of Egypt (Fig. 1b). At the Southeastern Desert, they are intruded into the Pan-African basement rocks, whereas in the Southwestern Desert, they are either unconformably overlain or frequently intruding the Phanerozoic sediments. The complexes occur as stocks and plugs of alkaline granite and syenites, some of which exhibit ring structure, whereas the others are isometric stock-like masses (Abdel-Karim et al., 2020; Saleh et al., 2021). This is confirmed by spatial and genetic relationships with the ring complexes and confinement to the same tectonic lineaments.

Some of these alkaline complexes are either LREE mineralized, particularly those exhibiting ring structures with nepheline syenite cores, whereas those occurring in stock-like masses are typically peralkaline granites and syenites with HREE-enriched signature.

In the following sections, detailed geological and geochemical overview will be given to the aforementioned four REE-enriched Phanerozoic rock associations (Gabal El Gara El Hamra (GH), Abu Khruq ring complex (AK), Ramlet Hemyir (RH) and Um Hamad (UH), and Rosetta black sands on the Mediterranean shoreline of Egypt (Figs. 1a and 21).

2 HREE-Mineralized Alkaline Rocks (Gabal El Gara El Hamra Complex) (GH) of Southwestern Desert, Egypt

The Phanerozoic alkaline complexes in Southern Egypt are typically occurring in a definable linear groups or arrays. These arrays are observed and aligned along major tectonic lineaments. Obviously, there are two sets of major structural lineaments. One represents a series of onshore extensions of transform faults, trending N60°E (Garson & Krs, 1976). Many of the alkaline complexes are located either along one of these two trends or at their intersections (GH and Nusb El Balghoum, NB, Fig. 1c). GH complex is characterized by development of HREE mineralization (El Agami & Abdalla, 2003; Abdalla, 2006), whereas little enhancement of REE is recorded associating NB complex (Ibrahim et al., 2015) and Wadi Natash alkaline volcanics (Ibrahim, 2010). Hence, GH was selected to throw light on such paragenetic type of REE mineralization (Fig. 1c).

2.1 Geologic Setting of Gabal El Gara El Hamra Complex

A TM image of band ratios includes the investigated area (Fig. 2a) which was used in the regional evaluation for identification and association of general rock types. A rare metal-mineralized stock (GH) was discovered at Gabal Gara El Hamra area during a ground radiometric survey (El Shazly et al., 1969; Abdalla, 2006).

GH complex is located along an ENE-WSW trending, right strike-slip fault (Figs. 1c and 2b). The complex is elongated (stretched) and teared horizontally into two parts, northwestern and southeastern. The two parts are slipped against each other for 600 m in the ENE-WSW direction with a considerable brecciation zone. Moreover, this tectonic zone seemed to be the WSW extension of the tectonic zone that encompasses the Um Hibal (223 Ma, Hashad & El Reedy, 1979) and Trabite North (351 Ma, Serencsits et al., 1981) alkaline complexes (Abdalla, 2006; Abdalla & El Afandy, 2003; El Afandi & Abdalla, 2002). According to Black et al. (1985), Bowden (1985), the occurrence of alkaline provinces in North Africa is controlled by major lithospheric weaknesses represented by two major

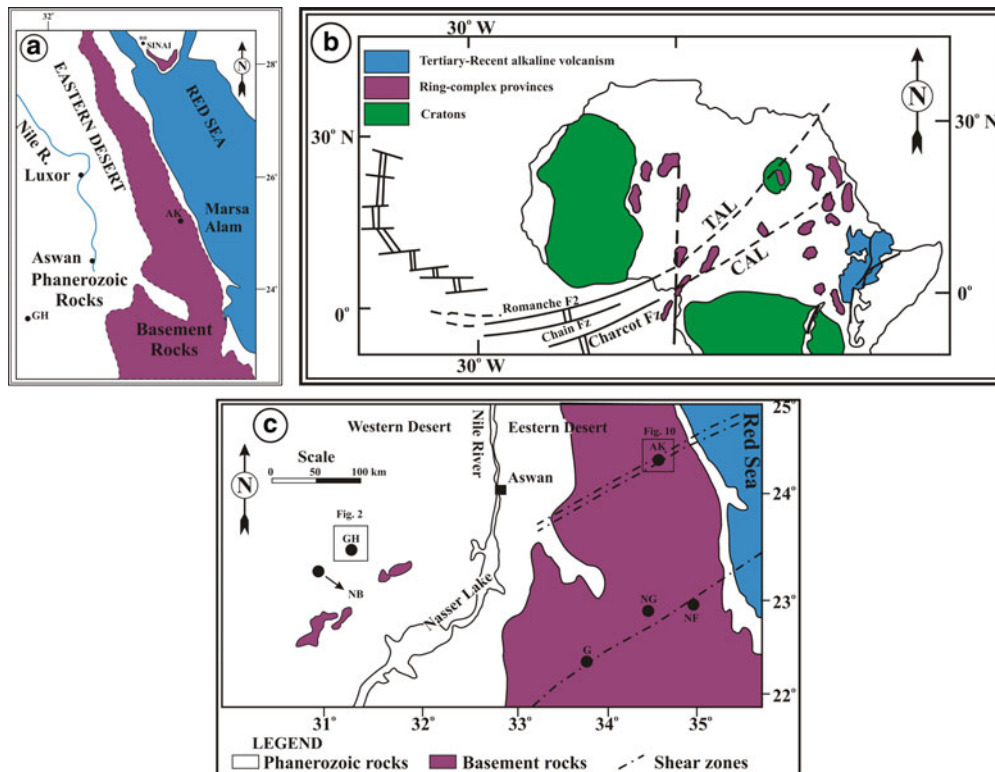


Fig. 1 a Location map of Gabal El Gara Hamra (GH), Abu Khruq ring complex (AK), and Ramlet Hemyir (RH) (by Hamdy M. Abdalla and Gehad M. Saleh). b Distribution of Precambrian craton, alkaline provinces and Trans-African lineaments in the Northern Africa. Figure 1c is outlined. Also shown the Central Africa Lineament (CAL) and the Trans-African Lineament (TAL) and their relation to the transform faults of the equatorial Atlantic Ocean (Schandelmeier & Pudolo, 1990), and c Location of Gabal El Gara El Hamra, (GH), Nasub El Balghoum (NB), peralkaline granite-syenite masses, and Abu Khruq ring complex (AK), in relation to the alkaline province of southern Egypt (by Hamdy M. Abdalla and Gehad M. Saleh). Locations of other specialized and/or mineralized nepheline syenite complexes, e. g. Nigrub El Fogani (NF), Naga (NG), and El Gezira (G), are also shown. The areas of Figs. 2 and 10 are also outlined. Structural elements are from Garson and Krs (1976), Conoco Coral (1987)

megashears and rift zones that transect the African continent. These megashear zones are the Trans-African Lineament (TAL, Nagy et al., 1976) which extends from the Niger delta in Nigeria to the Nile delta in Egypt and the Central African Lineament (CAL, Brown & Fairhead, 1983) which extends from the Cameroon volcanic line to the Red Sea Hills in NE Sudan (Schandelmeier and Pudolo, 1990).

GH complex is an elliptical, S-shaped, subvolcanic intrusion of 400×800 m (Fig. 2c). Field relations indicate that the evolutionary history of Gabal El Gara El Hamra complex started with the early extrusion of volcanic pile (mainly alkaline trachyte and rhyolite porphyry and their breccia) occurring at the inner parts of the massif. This is followed by successive intrusion of peralkaline syenites and subordinate granites. The volcanic pile could represent domes over small conduits since there are no conspicuous indications of any unified volcanic structure. Thus, the extrusion of volcanics may happen from dispersed conduits. Cross-cutting dykes and apophyses of peralkaline granites are frequently recorded intruding the syenites. The peripheral parts of Gabal El Gara El Hamra complex contain

xenoliths and fragments of the overlying Cretaceous Nubian sandstone. So, the emplacement of Gabal El Gara El Hamra complex can be constrained as post-Cretaceous as suggested by Kamal (2004). Moreover, the forcible effect of intrusion of Gabal El Gara El Hamra complex resulted into the formation of domal to doubly plunging anticlinal form in the overlying Cretaceous Nubian sandstone.

2.2 Petrography

GH peralkaline granite-syenite rocks are characterized by complex textural features of both magmatic and subsolidus reworking.

GH peralkaline granite is leucocratic, pink, equigranular, medium- to coarse-grained. It is mainly made up of perthitic K-feldspar, quartz, aegirine, and riebeckite. Zircon, apatite, pyrochlore, and Fe-Ti oxides represent accessory minerals. Alkali feldspar constitutes 60–70 modal% of the rock. String, ribbon, and patchy exsolved perthites are the dominant perthite texture. Aegirine forms ragged prisms,

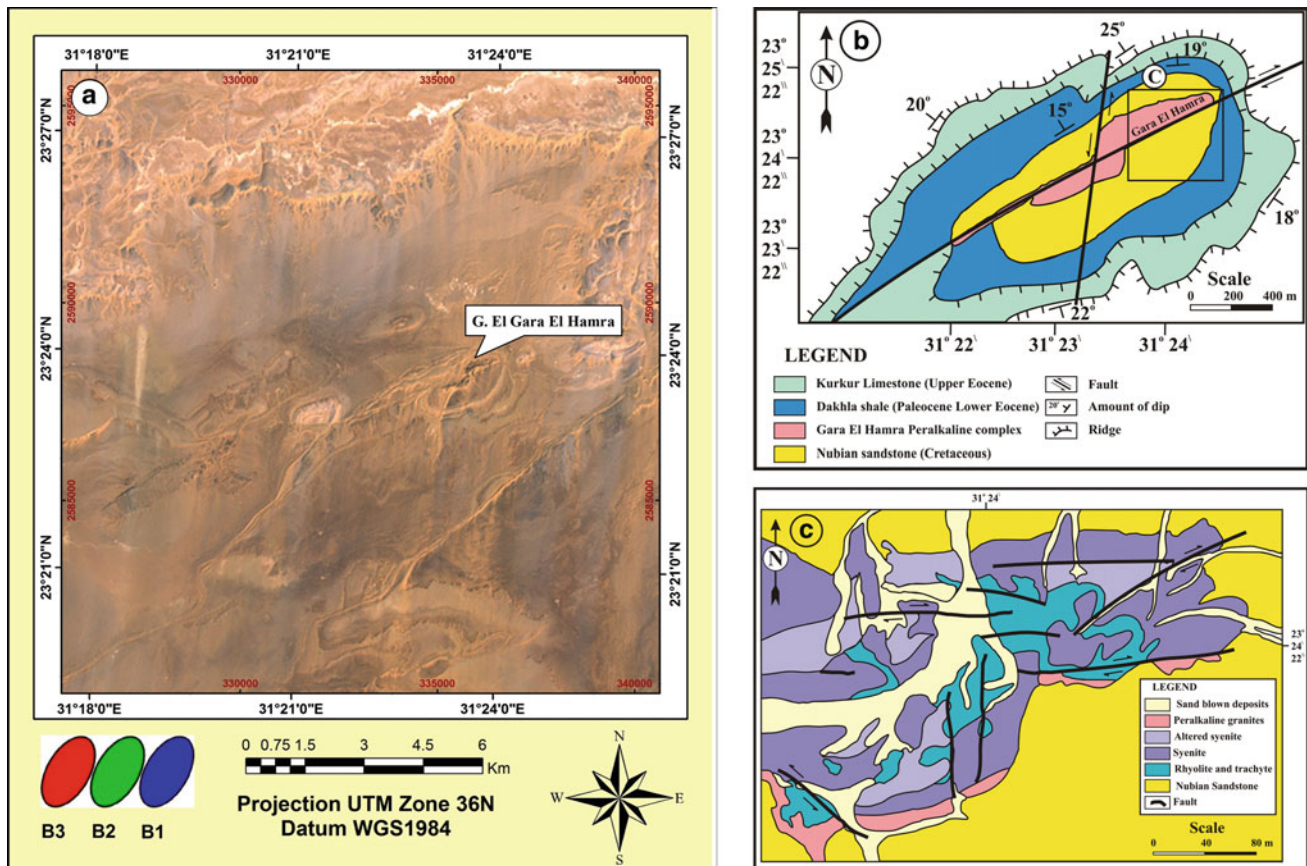


Fig. 2 a Landsat image with the S-shaped Gabal El Gara El Hamra complex (by Hamdy M. Abdalla and Gehad M. Saleh) occupying the central part of the image (See the text for further explanation). b General geological map of Gabal El Gara El Hamra complex with the area of (Fig. 2c) is also outlined and c Detailed geological map of the hydrothermally altered, northern part of Gabal El Gara El Hamra peralkaline granite-syenite complex, Egypt

pleochroic in shades of yellowish-green to deep grass-green (Fig. 3a). Fe-Ti oxides and apatite inclusions are common within aegirine crystals.

GH syenite is medium- to coarse-grained and pink to red in colour with hypidiomorphic texture. It is composed of alkali feldspar, alkali pyroxene, and quartz. Alkali feldspar is highly turbid and perthitic with exsolved albite phase (An_{0-5}) exhibiting the ribbon and patchy forms. Flow textures are frequently remarked and typically trend ENE-WSW. They are manifested by alignment of feldspar laths and segregations of aegirine crystals and by interdigitations of the peralkaline syenite and granite. Such phenomena indicate that the two rock types represent synchronous phases of magma that were controlled by regional structure during their emplacement. In places, melanocratic patches or clots, 5–10 cm wide, of radiating acicular aegirine crystals exhibiting the form of brushes and rosettes, are developed. These features are typical vapour phase phenomena.

Aegirine of Gabal El Gara El Hamra granite-syenite complex is commonly displaying four styles of zoning, namely normal, concentric, reverse, and sector (El Agami &

Abdalla, 2003; Abdalla, 2006). In the normally zoned crystals, the deep-green aegirine core is followed by a yellowish-green rim. This corresponds to rim-wards increasing content of Zr and Ti concurrent with depletion of Fe^{3+} . Some crystals exhibit a concentric pattern of zoning with a homogeneous grass-green to bluish green core followed by successive rims of yellowish-green zoned aegirine (Ferguson, 1977). In some samples, aegirine crystals turn black to nearly opaque due to oxidation and hence the increase of Fe^{3+} content. Such oxidized aegirine is commonly degraded into or replaced by fine-grained zircon, quartz, and Fe-Ti oxides pseudomorphs.

Late- to post-magmatic development included the formation of carbonate-fluorite-barite veins as well as deuteric and hydrothermal reworking of syenite rock particularly at its apical parts. The contact between fresh and altered syenite is always gradational. In places, particularly along the ENE-WSW right strike-slip fault, the altered syenite has sheared and brecciated contacts against the unaltered variant.

Field observation and microscopic examination revealed that alteration phenomena are overwhelmed by

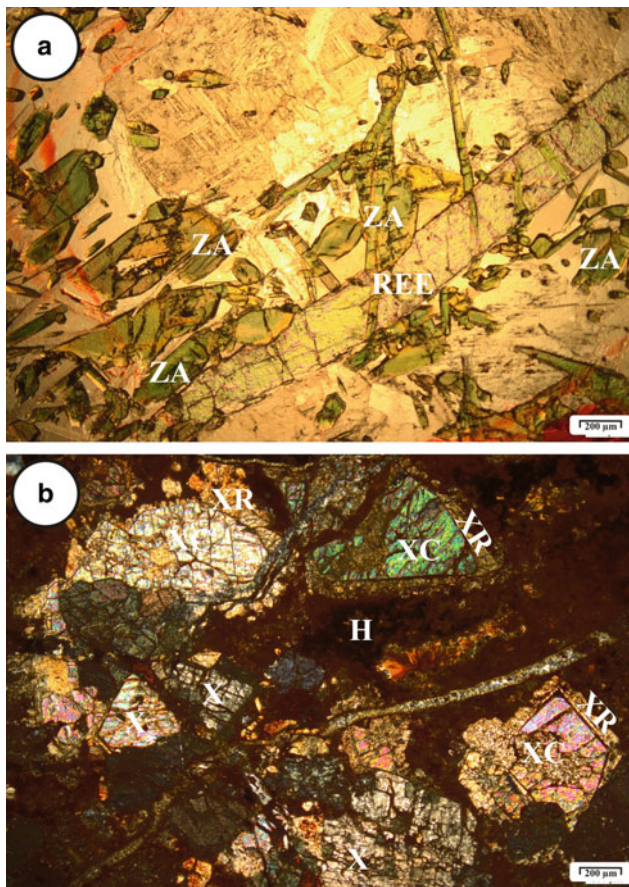


Fig. 3 Textural and mineralogical characteristics of Gabal El Gara El Hamra mineralization. **a** Photomicrograph showing aggregates of acicular to prismatic pleochroic aegirine crystals clustered in feldspathic matrix, fresh syenite of Gabal El Gara El Hamra (Polarized light). Zoned aegirine (ZA) crystals are also shown. Notice the long unidentified REE mineral (REE) is also shown (by Hamdy M. Abdalla and Gehad M. Saleh) and **b** photomicrograph of pervasively deep brown, hematitized, and mineralized syenite with hydrated ferric oxides (H) filling voids and exhibiting the colloform texture (crossed polars) (by Hamdy M. Abdalla and Gehad M. Saleh). Ferric oxides occur as coatings on the other minerals and cleavage planes of xenotime mineral (X). Xenotime reaches 50 modal% of the rock with crystals exhibiting zonal growth with core (XC) and rim (XR); see the text for further discussion

hematitization which is manifested by reddish-brown coloration due to deposition of hydrous ferric oxides. These oxides occur as coatings on the other minerals and planar zones of feldspar and alkali pyroxene, microfracture-fillings, and impregnations (Fig. 3b). Hydrous ferric oxides occur as amorphous to colloform aggregates. At incipient stage, the rock is stained red by dust-sized hematite and hydrous ferric oxides. When the process becomes pervasive, the rock turns brick-red to orange in colour where the rock-forming minerals are strongly leached and replaced by hydrated ferric oxides. Even pyroxene crystals turn black to nearly opaque due to the increasing contents of the invading Fe^{3+} -rich fluids. Hematitization of Gabal El Gara El Hamra alkali

syenite is similar to the alteration phenomena described in alkali rock associations elsewhere (Le Bas, 1977 “Rodberg rock”; Andersen, 1984; and Abu Khruq, El Afandi & Abdalla, 2002; Abdalla, 2006; Saleh et al., 2021).

2.3 Mode of Occurrence of Y, HREE, and Th Mineralization

Rare metals mineralization recorded in Gabal El Gara El Hamra altered syenite consists of a variety of exotic, rare metal-bearing minerals. The degree of alteration directly affects the content of ore minerals that ranges from 2 to 50% of the rock volume (Fig. 3b). Generally, the higher the degree of alteration, the greater potential abundance of rare metal ore minerals. The principal ore minerals are arranged according to their abundances as follows: xenotime, thorite, zircon, parisite, bastnasite, and pyrochlore. Scarce grains of gittinsite, gadolinite, and gaggarrinite were also recorded.

Xenotime (YPO_4) occurs as greyish to yellowish brown, stubby bipyramidal crystals with short prisms (Fig. 3b). The perfect [010] cleavage intersects giving rise to elongated fractures. Commonly, xenotime occurs as compositionally homogeneous crystals; with variable optical and chemical compositions from core towards outer zones are also recorded (Fig. 3b).

Thorite ($ThSiO_4$) occurs as light brown to black, tetragonal prismatic crystals with pinacoid and pyramid forms. Under crossed nicols, some crystals exhibit a mottled appearance with both amorphous, isotropic domains interfering with anisotropic and microcrystalline areas. Corroded and resorbed xenotime crystals are commonly mantled by thorite overgrowths. This thorite overgrowth, which is presumably epitaxial, occurs as irregular zones reaching a maximum width of 50 μm . Heterogeneous thorite exhibits variable optical characteristics due to the inclusion of variable contents of Zr, Y, U, and HREE.

Zircon occurs as brownish crystals, optically anomalous, possessing a zonal structure with almost translucent to isotropic zones.

Parisite occurs as yellowish to reddish pseudo-hexagonal crystals with good [0001] cleavage. The crystal exhibits the doliform habit due to the extreme development of steep dihedral pyramids of prismatic appearance. Bastnasite ($Ce, La, NdCO_3F$) occurs as orange to reddish-brown, hexagonal plates (dimensions are thin in one direction). Bastnasite, parisite, and fluorite occur essentially as microscopic veinlets.

Pyrochlore occurs as small (< 100 μm) yellowish brown, rounded to octahedral crystals. Some grains exhibit a radial fracture pattern manifesting the existence of radioelements within the pyrochlore of GH altered syenite.

2.4 Mineral Chemistry

2.4.1 Essential Minerals

(i) Feldspars

The alkali feldspars were detected to possess a restricted compositional range in both GH peralkaline granites and syenites, i.e. between $Or_{74}Ab_{25}An_1$ and $Or_{79}Ab_{20}An_1$.

(ii) Alkali pyroxene

The general pyroxene formula is $X Y Z_2 O_6$ in which X position is occupied by Ca, Na, and little Mg, Fe^{2+} , Mn; Y = Mg, Fe^{2+} , Fe^{3+} , Al, little Ti and Zr; and Z = Si and little Al, as GH peralkaline granite-syenite complex contains Na-enriched pyroxenes with appreciable amount of Fe as Fe^{3+} . Following Bonin and Giret's (1985; 1990) ternary Ac-Hd-Di end members scheme, aegirine of GH syenite ranges between $Di1Hd16Ac83$ and $Di0Hd5Ac95$, where Di, Hd, and Ac refer to the diopside, hedenbergite, and acmite end members, respectively. Worthy to note that aegirine of Gabal El Gara El Hamra syenite contains enhanced contents of Ti and Zr. The TiO_2 and ZrO_2 contents may reach 0.9 and 0.31%, respectively. The optically detected zoning in aegirine of GH complex was ascertained by electron probe micro-analyser (EPMA) analysis (Table 1).

2.4.2 Ore Minerals

(i) Thorite

The average composition of thorite of GH altered syenite is given in Table 1 and Fig. 4. The data points for selected thorite analyses depict the existence of two solid solution phases of thorite-xenotime and thorite-zircon due to the inclusion of variable contents of HREE, Y, P, and Zr.

(ii) Xenotime

However, some xenotime contain appreciable contents of U and Th through minor substitution with other end members, e.g. thorite and coffinite (Forster, 1998). The HREEPO₄ component of xenotime of the GH altered syenite ranges between 22 and 43 mol%. Moreover, the proportion of YPO₄ correlates inversely with the HREE component. High HREE content in GH xenotime is closely similar to those of A-type granitoids (Forster, 1998). This heterogeneity constitutes either concentric core-rim zonation or irregular domains distributed within host crystals. The rim is

frequently enriched in HREEPO₄ component relative to the core (Table 1 and Figs. 4 and 5).

(iii) Zircon

Zircon of Gabal El Gara El Hamra altered syenite is characterized by moderate contents of Y, U, and Hf. However, Th and HREE occur in appreciable contents (Table 1 and Fig. 4) reflecting the probable formation of solid solution phases of zircon-thorite series.

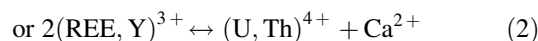
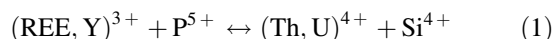
(iv) Pyrochlore

Pyrochlore is a group of minerals possessing the general formula of $A_{2-m} M_2 O_6 (O, OH, F)_n \cdot p H_2 O$, where A = Na, Ca, Sr, Ba, Fe^{2+} , U, Th, and REE; M = Nb, Ti, Ta, and Zr, with the current limits of $m = 0-2$; $n = 0-1$ and $p = 0-?$ (Foord, 1982; Hoggarth, 1977, 1989). GH pyrochlore is typically enriched in LREE (Table 1).

(v) Bastnasite and Parisite

Bastnasite and parisite belong to the same group of REE-fluorocarbonate minerals. They are intimately associating each other, even in syntactic intergrowth, in most REE paragenetic assemblage. According to Ni et al. (1993), these minerals consist of layers of REEF, CO₃, and CaCO₃ in the ratio of 1:1:0 (bastnasite) and 2:2:1 (parisite). Characteristically, GH parisite and bastnasite are enriched in middle REE (e.g. Sm and Nd), Y, and to some extent in HREE (Table 1).

The minerals of zircon, thorite, and xenotime possess the ABO₄ structure type. Thus, the kind of association of thorite and xenotime is presumably possible because of the similar cell dimensions and isostructural relationship between these groups of minerals (Speer, 1982a and b). Worth to note that thorite of Gabal El Gara El Hamra altered syenite is strongly depleted in U (average UO₂ wt.% is 2.14), although this mineral is structurally tolerant towards cationic substitution of U. This may indicate that different behaviours for Th and U were exhibited during the late evolution of El Gara El Hamra peralkaline magma. Pronounced substitution of Th and U was detected in the GH xenotime. According to (Van Enden et al., 1997), two solid solution substitution mechanisms could be involved:



Clustering of data point of Gabal El Gara El Hamra xenotime along the vector (Th, U) SiREE₋₁P₋₁, Fig. 4, confirms the dominant role of the first substitution scheme

Table 1 Average chemical compositions of aegirine and ore minerals recorded in Gabal El Gara El Hamra altered syenite, Egypt (El Agami & Abdalla, 2003; Abdalla, 2006)

No.*	1	2	3	4	5	6	7	8	9	10	11			
Nb ₂ O ₅	–	–	–	–	–	–	–	57.50						
Ta ₂ O ₅	–	–	–	–	–	–	–	3.50						
P ₂ O ₅	32.57	34.95	32.15	2.24	0.65	–	0.01	0.20						
SiO ₂	1.99	2.96	1.91	13.12	30.05	0.52	0.33	–	52.80	52.32	52.95			
ZrO ₂	0.01	0.01	0.02	3.92	60.03	–	0.01	–	0.21	0.16	0.31			
HfO ₂	–	–	–	0.40	1.60	–	–	–						
TiO ₂	–	–	–	0.03	0.02	–	0.02	3.20	0.53	0.34	0.91			
ThO ₂	1.88	3.90	1.90	70.90	3.50	0.53	0.40	1.51						
UO ₂	0.54	0.80	0.50	2.14	0.50	0.46	0.52	5.22						
Y ₂ O ₃	33.86	30.41	27.53	3.68	1.40	2.42	6.51	2.82						
La ₂ O ₃	0.01	–	–	0.01	0.01	18.10	17.31	3.21						
Ce ₂ O ₃	0.01	–	–	0.01	0.02	32.51	32.74	7.43						
Nd ₂ O ₃	0.02	0.01	0.01	0.01	0.02	9.54	8.92	3.50						
Sm ₂ O ₃	0.02	0.02	0.04	0.03	0.03	1.11	1.30	0.54						
Gd ₂ O ₃	4.16	4.11	4.90	0.78	0.06	0.28	0.85	0.53						
Tb ₂ O ₃	0.92	0.95	1.10	0.20	0.12	0.25	0.31	0.20						
Dy ₂ O ₃	5.84	5.10	6.50	0.90	0.25	0.62	0.91	0.40						
Ho ₂ O ₃	1.26	1.03	2.10	0.15	0.11	0.20	0.31	0.12						
Er ₂ O ₃	5.74	5.90	6.53	1.02	0.30	0.43	0.82	0.20						
Tm ₂ O ₃	1.00	1.10	1.20	0.17	0.18	0.25	0.42	0.15						
Yb ₂ O ₃	7.29	7.90	9.50	0.40	0.25	0.46	0.51	0.40						
Lu ₂ O ₃	1.31	1.90	2.10	0.12	0.18	0.18	0.21	0.20						
Al ₂ O ₃	–	–	–	0.01	0.01	–	–	–	0.18	0.15	0.15			
FeO**	0.02	0.02	0.01	0.40	0.81	0.12	0.41	1.31	31.01	32.00	30.91			
MnO	0.01	–	0.01	–	0.01	–	–	0.01	0.25	0.18	0.20			
MgO	–	–	–	–	–	–	–	–	0.28	0.26	0.22			
CaO	0.30	0.38	0.25	0.80	0.40	7.16	0.82	3.51	0.50	0.42	0.31			
Na ₂ O	–	–	–	–	–	–	–	1.22	12.54	12.41	12.61			
CO ₂ ***						21.22	22.57							
F						6.41	6.53	4.63						
_F = O						2.69	2.74	1.94						
Total	98.76	101.46	98.26	101.44	100.51	100.00	100.00	99.57	98.31	98.24	96.57			
No. of cations****														
P	3.855	4.024	3.835	0.102	0.017	P	0.000	0.002	Si	0.000	Z Si	2.148	2.165	2.174
Si	0.278	0.403	0.269	0.704	0.957	Si	0.050	0.092	Th	0.023	Al-iv	0.000	0.000	0.000
∑B	4.133	4.427	4.104	0.806	0.974				U	0.079	Al-vi	0.009	0.007	0.007
Zr	0.001	0.001	0.002	0.102	0.935	Zr	0.000	0.001	Y	0.102	Zr	0.004	0.003	0.007
Hf	0.000	0.000	0.000	0.006	0.014	Hf	0.000	0.000	La	0.080	Y Ti	0.017	0.011	0.029
Th	0.060	0.121	0.061	0.877	0.024	Th	0.011	0.025	Ce	0.185	Fe*	1.056	1.055	1.077
U	0.017	0.024	0.016	0.026	0.003	U	0.010	0.032	Nd	0.085	Mn	0.009	0.006	0.007
Y	2.519	2.280	1.992	0.105	0.023	Y	0.124	0.968	Sm	0.012	Mg	0.005	0.004	0.004
La	0.001	0.000	0.000	0.000	0.000	La	0.644	1.783	Gd	0.012	Mg	0.000	0.000	0.000
Ce	0.001	0.000	0.000	0.000	0.000	Ce	1.147	3.348	Dy	0.009	Ca	0.023	0.019	0.014

(continued)

Table 1 (continued)

No.*	1	2	3	4	5		6	7		8		9	10	11
Nd	0.002	0.001	0.001	0.000	0.000	Nd	0.329	0.900	Er	0.004	X Na	0.982	1.015	1.009
Sm	0.001	0.001	0.002	0.000	0.000	Sm	0.036	0.125	Yb	0.008				
Gd	0.193	0.185	0.229	0.014	0.001	Gd	0.009	0.079	Lu	0.004				
Tb	0.042	0.042	0.051	0.004	0.001	Tb	0.008	0.028	Fe*	0.074				
Dy	0.263	0.223	0.295	0.016	0.003	Dy	0.019	0.082	Ca	0.256				
Ho	0.056	0.045	0.094	0.003	0.001	Ho	0.006	0.028	Na	0.159				
Er	0.252	0.252	0.288	0.017	0.003	Er	0.013	0.072	∑A	1.092				
Tm	0.044	0.047	0.053	0.003	0.002	Tm	0.007	0.037	Nb	1.772				
Yb	0.311	0.328	0.408	0.007	0.002	Yb	0.013	0.043	Ta	0.065				
Lu	0.055	0.078	0.089	0.002	0.002	Lu	0.005	0.018	Ti	0.164				
Fe*	0.002	0.001	0.001	0.013	0.021	Fe*	0.010	0.096	∑M	2.000				
Ca	0.045	0.055	0.400	0.043	0.013	Ca	0.740	0.245	O	5.832				
∑A	3.865	3.684	3.982	1.238	1.048	C	2.794	8.608	F	0.998				
						F	1.954	5.768	∑O + F	6.830				

*Column nos. are average analyses of: 1 = xenotime; 4 = thorite; 5 = zircon; 6 = parisite; 7 = bastnasite; 8 = pyrochlore, and 9 = aegirine. However, column nos. 2 and 3 refer to the core and rim of xenotime crystal; 10 and 11 refer to the core and rim of aegirine crystal, respectively

**Total Fe is determined as FeO

***CO₂ is calculated to sum of 100%

****No. of cations are based on ⁴O for both of zircon and thorite; ¹⁶O for xenotime; 11(O + F) for parisite; 32(O + F) for bastnasite; ⁶O for aegirine; and based on M = 2 for pyrochlore

The blank sites mean no determination, whereas (–) means below detection limit

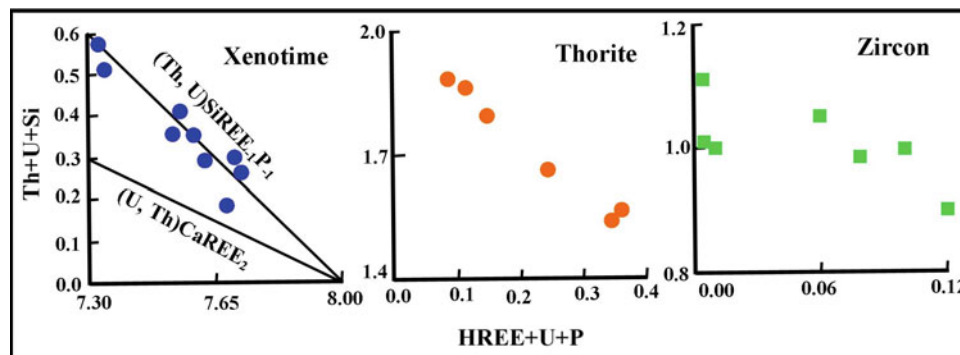


Fig. 4 Distribution of formula proportions (U + Th + Si) versus (HREE + Y + P) in xenotime, thorite, and zircon of Gabal Gara El Hamra altered syenite. Cation proportions calculated on basis of 4 oxygen for both of zircon and thorite and 16 O for xenotime

which reflects the existence of solid solution between xenotime and thorite-coffinite (Van Enden et al., 1997). However, only one point is shifted towards the vector (U, Th)CaREE₋₂ indicating the minor role of the second substitution scheme which reflect the probable existence of limited solid solution between xenotime-barbantite and its uranium equivalent.

It is distinguished that GH pyrochlore is enriched in U, Th, Y, and to some extent HREE (Table 1). Moreover, parisite and bastnasite are also characteristically enriched in middle REE (e.g. Sm and Nd), Y, and to some extent in HREE, U, and Th (Table 1).

2.5 Rock Geochemistry

Average major and trace element contents for GH granite, syenite, and related alteration facies are given in Tables 2 and 3. The investigated rocks are typically peralkaline (with alumina saturation and peralkalinity molar indices, ASI = Al/(Na + K + Ca) < 1 and AI = Al/(Na + K) < 1, Fig. 6). High normative quartz, albite, and K-feldspars (the three components sum 80–90%) of the investigated rocks coupled with the characteristically low abundance of anorthite (< 3 norm%) justify using the quartz-orthoclase-albite eutectic granite system for estimating their crystallization paths. On

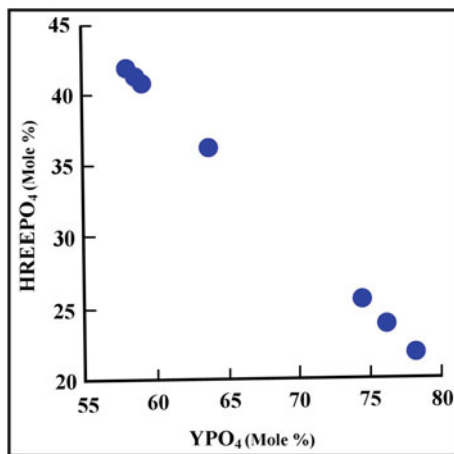


Fig. 5 Compositional range of xenotime of Gabal El Gara El Hamra altered syenite in terms of mole % HREEPO₄ versus YPO₄

the Qz–Ab–Or haplogranite system, Fig. 7, the plot of Gabal El Gara El Hamra granite-syenite rocks defines a continuous linear trend close to the thermal valley and down the granite minima, i.e. parallel to the general trend of feldspar cotectics from c. 35% or on the Ab–Or join towards Qz apex. The bulk compositions of GH complex follow the trend expected of magmatic evolution of a syenitic parental melt on the Ab–Or side towards the H₂O-saturated minima at confining pressure. However, the altered samples are largely shifted away from the melt minima (largely towards the Ab–Qz side) manifesting the role of subsolidus reactions that affect the feldspar assemblage. The field of Um Hibal Zr-, Nb-mineralized peralkaline pegmatites (Abdalla & El Afandy, 2003) lies in the Southeastern Desert (~ 70 km SW of Aswan city) on the extension of GH fracture zone.

Both of GH granite and syenite are characterized by the enrichment of many large ion lithophile elements (LILE), e.g. Ba, Rb, and high field strength elements (HFSE), e.g. Zr, Hf, Nb, Ta, and REE clearly reflecting their alkaline character (Tables 2 and 3). The alkaline nature is also ascertained by low Ca, Mg, and Sr contents.

GH peralkaline granite and syenite show closely similar chondrite-normalized REE patterns (Fig. 8), but syenite is considerably more enriched in total REE content. This manifests that these rocks are genetically related and evolved from the same magma source. The LREE/HREE ratio averages 0.06, 0.06, and 0.27 in the granite, fresh syenite, and altered syenite facies, respectively, manifesting preferential enrichment of HREE (Gd, Tb, Tm, Er, Ho, Yb, and Lu which constitute between 60 and 90% of the total REE). However, a moderate Eu anomaly (0.46) is observed in the altered syenite facies.

Moreover, the intensity of the tetrad effect for REE patterns was calculated for either fresh granite-syenite complex or the hydrothermally altered syenite facies (Table 3). Both

the granite and fresh syenite display a non-significant to moderate tetrad effect; meanwhile, the altered syenite exhibits a pronounced significant tetrad effect ($TE_{1,3} = 1.24$).

Comparison of the REE normalized pattern of GH peralkaline syenite and granite with that of Um Hibal mineralized peralkaline granite-pegmatites reveals contrasting types (Fig. 8). GH complex exhibits a pronounced HREE-enriched pattern, whereas Um Hibal rock (Nb, Zr-enriched)-association displays a positive distribution pattern with marked LREE-enriched signature.

Ratios of geochemically coherent and antipathetic element pairs such as Zr/Hf, Nb/Ta, and Th/U can be used as indicators for the evolution of felsic rocks and related rare metal mineralization. Because of the marked incompatibility of Ta, Hf, and U, the aforementioned ratios tend to decrease in crustal phases crystallizing at late stage. Thus, the higher and nearly constant of Zr/Hf, Nb/Ta, and Th/U ratios in GH fresh syenite and granite, Tables 2 and 3, reflects a primitive fractionation level of the elements Ta, Hf, and U which is a characteristic feature for the mantle-derived rocks (Cerny et al., 1985; Batchelor and Bowden, 1985) (Fig. 9).

Among all petrotextonic associations, alkaline igneous rocks (including those of carbonatites) are the most enriched in HFSE and are frequently potential repositories of deposits of these metals (e.g. Lovozero massif, Russia (Kogarko, 1980); Ilimaussaq and Narsarsuk, Greenland (Karup-Moller, 1978), Arabian Shield, (Drysdall et al., 1984; Jackson & Douch, 1986; Hackett, 1986; Harris et al., 1986)). This can be attributed to the increasing of depolymerization degree of alkaline melt as the result of existence of elevated contents of alkalis and anhydrous volatile phases (e.g. CO₂, F⁻, and Cl⁻). These components increase the solubility of HFSE via complexing them with alkali-silicate complexes and/or alkali-fluoride complexes (Watson, 1979). The effects of late-stage fluids in some alkaline rocks have been described elsewhere (Gardar province, Greenland, Markl, 2001; Marks et al., 2003).

Many studies on the mineralized alkaline rocks revealed that F-rich aqueous solutions have the capacity to remobilize and redistribute the HFSE and REE's (Boily & Williams-Jones, 1994; Ngwenya, 1994; Salvi et al., 2000) and hence resulted into rare metal concentration during post-magmatic alteration. The stability of F-complexes increases from the LREE towards the HREE (Wood, 1990). The conspicuously low LREE/HREE ratio in GH altered syenite coupled with the high F contents in the fresh and altered syenite (Table 2) manifests the dominant role of F in mobilization of HREE via hydrothermal fluids.

According to the experimental data of (Wood, 1990; Giere & Williams, 1992), F⁻ and CO₃²⁻ form the strongest complexes with REE. Yttrium behaves like HREE in F-dominated solutions, whereas in carbonate-rich solutions, it behaves more like the LREE (Bau and Dulski, 1995).

Table 2 Averages and ranges of major and trace element contents of Gabal El Gara El Hamra peralkaline complex, Egypt (El Agami & Abdalla, 2003; Abdalla, 2006)

Major oxides (Wt.%)	Fresh	Altered	Peralkaline
	Syenite	Syenite	Granite
SiO ₂	65.08	60.88	73.15
	62.81–66.22	60.31–62.72	72.13–74.20
TiO ₂	0.40	0.17	0.21
	0.31–0.52	0.12–0.22	0.18–0.25
Al ₂ O ₃	13.98	6.75	11.17
	13.61–14.35	5.91–7.55	10.96–11.42
Fe ₂ O ₃ *	4.84	10.55	3.80
	3.80–5.41	9.12–12.73	3.10–4.60
MnO	0.07	0.11	0.09
	0.03–0.10	0.01–0.22	0.06–0.10
MgO	0.11	0.19	0.05
	0.03–0.21	0.15–0.23	0.02–0.08
CaO	0.79	1.20	0.48
	0.49–0.95	0.49–1.83	0.39–0.54
Na ₂ O	5.34	3.15	4.30
	4.10–5.95	2.71–3.34	3.85–4.65
K ₂ O	5.92	2.98	4.95
	4.90–6.91	1.86–5.25	4.80–5.35
P ₂ O ₅	0.20	3.06	0.15
	0.10–0.25	0.92–6.76	0.12–0.18
H ₂ O	0.62	4.18	0.70
	0.42–0.91	2.23–5.31	0.51–0.83
CO ₂	0.18	0.31	0.20
	0.12–0.26	0.22–0.43	0.14–0.28
Total	97.53	93.53	99.25
F	2460.0	8530.0	2080.0
	2050.0–2600.0	5350.0–11,300.0	1650.0–2400.0
Trace elements (ppm)	50.0	60.0	43.0
Li	40.0–57.0	45.0–80.0	38.0–50.0
Be	6.0	38.0	4
	4.0–10.0	27.0–48.0	3.0–5.0
Rb	125.0	161.0	140.0
	90.0–160.0	110.0–260.0	110.0–195.0
Ba	120.0	11,250.0	160.0
	78.0–180.0	7400–16,000	89.0–220.0
Sr	42.0	119.0	50.0
	38.0–45.0	78.0–200.0	45.0–59.0
Zr	580.0	3400.0	515.0
	390.0–700.0	900.0–7200.0	380.0–620.0
Hf	15.7	89.5	13.7
	10.5–19.0	24.0–185.0	10.2–16.5

(continued)

Table 2 (continued)

Major oxides (Wt.%)	Fresh	Altered	Peralkaline
	Syenite	Syenite	Granite
Y	180.0	28,937.0	142.0
	125.0–240.0	8730.0–62,500.0	115.0–162.0
Nb	198.0	470.0	150.0
	144.0–295.0	290.0–710.0	130.0–184.0
Ta	13.7	32.5	10.2
	9.6–26.0	19.8–48.0	8.7–12.1
Ga	31.0	35.0	34.0
	24.0–38.0	27.0–40.0	28.0–40.0
U	9.0	1278.0	5.0
	3.0–15.0	330.0–2800.0	4.0–9.0
Th	43.0	10,725.0	21.0
	15.0–75.0	4900.0–16,500.0	16.0–33.0
Th/U	4.6	10.8	4.3
	3.8–5.4	5.1–14.9	3.3–5.0
Zr/Hf	37.0	37.5	37.5
	36.8–37.1	36.8–38.9	37.3–37.6
Nb/Ta	14.5	14.6	14.9
	14.1–15.0	13.6–15.8	14.7–15.2

Number of samples analysed is 4 for each rock type

Major oxides are in wt.%, and trace elements are in ppm

*Fe₂O₃: Total iron as Fe₂O₃

Thus, the abundantly developed xenotime (up to 50% by mode of the rock) and its accumulation in the form of clots (1–3 cm wide, Fig. 3b) confirm the speciation of Y and HREE to an orthomagmatic F⁻ and P-rich fluid in which the HREE fluoro complexes are most stable (Haas et al., 1995). Besides, an increase in the stability of REE₂H₂PO₄²⁺ complexes with increasing temperature is predicted, above approximately 150 °C, (Haas et al., 1995).

The late-stage formed bastnasite and parisite veinlets also confirm the preferential removal of LREE in a carbonate-dominated fluid. The similarity of REE patterns of both fresh and hydrothermally altered syenite (Fig. 8a–c) may indicate that the hydrothermal fluid originated as a residual aqueous phase from evolved alkali syenite crystallization. Moreover, the tetrad effect detected in GH altered syenite (Table 3) has been recognized in granitic rocks which have undergone high degree of fractional crystallization, hydrothermal alteration, and mineralization (Bau, 1996; Irber, 1999; Jahn et al., 2001; Monecke et al., 2002). The detected cerium anomaly (i.e. Ce/Ce* = 1.27, Table 3) in the altered syenite may confirm the higher fO₂ under which the alteration process had undertaken. Besides, the relative Eu enrichment in the altered syenite, as manifested by the weakness of Eu anomaly, can be also reasoned due to

desorption of Eu released from feldspar alteration in the oxidized mineralizing fluids (Bau & Moller, 1992).

Moreover, rapid focussed release of such fluids brought about brecciation of the solidifying peralkaline granite-syenite magma which provided additional sites for localizing the mineralization.

2.6 Petrotectonic Setting, Mineralization Type, and Metallogenesis

The confining of alkaline rocks of anorogenic setting to lines of weakness and tectonic zones together with its repeated implies a tectonic control by the underlying lithosphere for their magma production. Figure 1c shows that Gara El Hamra complex (post-Cretaceous) and Um Hibal peralkaline granite-pegmatite complex (223 Ma; Hashad & El Reedy, 1979) are all located along an ENE-WSW trending zone. According to (Garson & Krs, 1976), the age of the ENE-WNW block faulting is not constrained, but it was probably initiated in the Precambrian and rejuvenated during the intrusion of the alkaline ring complexes during the time of Permian-early to late Cretaceous and Cenozoic.

Table 3 Average, range, and ratios of rare earth element contents in Gabal El Gara El Hamra peralkaline complex, Egypt (Abdalla, 2006)

Rare earth elements (ppm)	Fresh	Altered	Peralkaline
	Syenite	Syenite	Granite
La	18.2	427.8	13.8
	15.0–20.4	146.0–688.0	12.0–16.0
Ce	46.0	1592.5	25.8
	38.0–51.0	520.0–2600.0	24.0–28.0
Pr	8.2	232.5	2.8
	6.9–8.1	70.0–360.0	2.6–3.1
Nd	39.3	1170.0	18.9
	37.0–45.0	330.0–1900.0	16.6–25.2
Sm	44.2	637.5	17.8
	25.3–57.0	180.0–1200.0	14.0–28.0
Eu	2.2	166.0	1.7
	1.9–2.8	47.0–330.0	1.6–1.8
Gd	127.0	1860.0	81.9
	112.0–140.0	560.0–3800.0	74.5–92.0
Tb	50.1	602.5	17.9
	37.2–60.0	170.0–1200.0	13.5–27.0
Dy	662.5	4875.0	238.0
	420.0–980.0	1400.0–10,000.0	162.0–430.0
Ho	202.3	1157.5	119.5
	165.0–271.0	360.0–2400.0	96.0–165.0
Er	676.3	3525.0	323.0
	560.0–945.0	1000.0–7300.0	281.0–412.0
Tm	82.0	540.0	45.7
	78.1–85.0	160.0–1100.0	42.3–47.1
Yb	710.5	2591.0	384.5
	680.0–750.0	704.0–5130.0	335.0–520.0
Lu	126.8	342.8	94.0
	111.2–140.0	96.0–650.0	75.0–130.0
\sum REE	2796	19,720	1420
	2332–3439	5743–38,217	1144–1921
\sum LREE	157	4226	82
	128.6–181.3	1293–6637	74.6–98.0
\sum HREE	2616	15,494	1323
	2203–3288	4450–31,580	1069–1823
\sum LREE/ \sum HREE	0.06	0.27	0.06
	0.04–0.07	0.21–0.35	0.05–0.06
(La/Yb) _N	0.02	0.11	0.03
	0.02	0.07–0.18	0.02–0.03
Eu/Eu*	0.09	0.46	0.14
	0.07–0.11	0.44–0.47	0.1–0.2
Ce/Ce*	0.94	1.27	0.81
	0.66–1.07	0.97–1.4	0.71–0.87
TE _{1,3}	1.13	1.24	0.73
	0.88–1.4	1.2–1.33	0.4–0.85

TE_{1,3} = degree of tetrad effect calculated according to (Irber, 1999)

The Eu and Ce anomalies are calculated as $Eu/Eu^* = Eu/Eu_{ch.}/(Sm/Sm_{ch.} \times Gd/Gd_{ch.})^{0.5}$ and $Ce/Ce^* = Ce/Ce_{ch.}/(La/La_{ch.})^{2/3} (Nd/Nd_{ch.})^{1/3}$, respectively

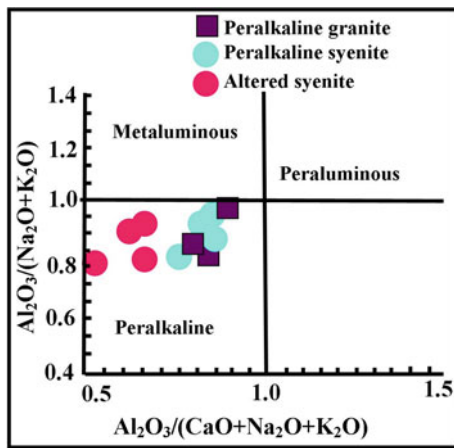


Fig. 6 Plot of agpacity versus peraluminosity indices (molar ratios) for Gabal El Gara El Hamra. Discrimination fields for different rock types are from (Manair & Piccoli, 1989)

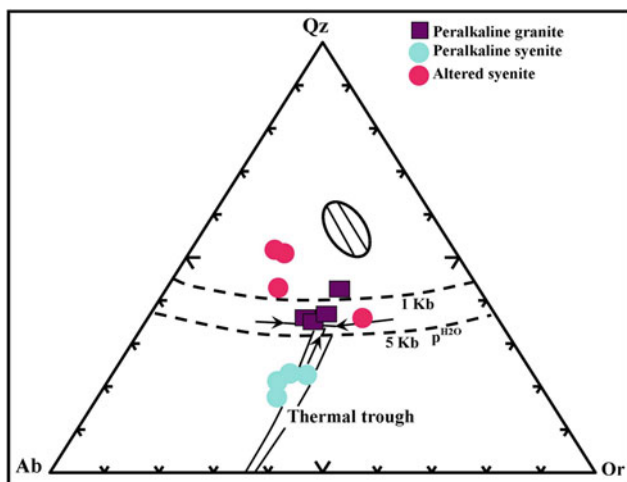


Fig. 7 Qz–Ab–Or plot showing the normative compositions of Gabal El Gara El Hamra peralkaline syenite-granite complexes. The stippled area encompasses the field of mineralized peralkaline pegmatites from Um Hibal area (Abdalla & El Afandy, 2003). The 1 and 5 kb cotectic surfaces (Tuttle & Bowen, 1958); the feldspar cotectic for An₃ (shown as arrows indicating the downward slope of the liquids surface, and the location of thermal trough (Carmichael & Mackenzie, 1963))

Bonin (1986) reported three possibilities to account for the distribution of alkaline complexes, namely distension and formation of a rift; hot spot above plume and lithospheric shearing. In the third setting, major shear zones exist which affect the whole extent of lithosphere, and the anorogenic alkaline magmas collect together at the level of pre-existing fractures which are conjugately linked to the direction of shear zones. This is most probably the setting for emplacement of Um Hibal- Gabal El Gara El Hamra complexes along the ENE shear zone with WSW age migration. Serencsits

et al. (1979, 1981) were the first to recognize the periodicity of intrusion of alkaline complexes in Egypt through specified time span (every 52 Ma). They added that some of these cycles are either not represented by intrusives or such intrusives were formed but do not crop out on the present-day surface of erosion. The periodicity of alkaline rocks is most probably compared with the reverse of motion along this shear system particularly in the early and late Cretaceous (Schandelmeier and Pudolo, 1990). Such reversal movement could trigger off partial melting in the mantle (Black et al., 1985; De Gruyter & Vogel, 1981).

Worthy to note that the ages of Um Hibal (223 Ma) and Gabal El Gara El Hamra (post-Cretaceous) are corresponding to Cretaceous and early Cenozoic time span, coinciding with late Paleozoic-late Mesozoic ring complexes of Nigeria and Niger. According to El Afandi and Abdalla (2002) and Abdalla and El Afandy (2003), the ENE-WSW trending tectonic zone appears to have much control on the localizing of the mineralized alkaline centres. Worth noting that the mineralized alkaline granites province of Nigeria exhibits a migrating ages from north to south at more or less fixed time intervals (Bowden et al., 1984). Hence, it is suggested that more attention should be paid for detailed exploration for the alkaline complexes lying along the ENE-WSW trending shear zones, e.g. those comprising Gabal El Gara El Hamra and Um Hibal (Fig. 1c). So, an important exploration parameter for recognizing such mineralized alkaline complexes is to record the progressive uplift ages over Phanerozoic time.

Close look at Figs. 7 and 8 indicates that the specialized and/or mineralized A1-alkaline rock associations could be possibly discriminated into two types.

(a) **Um Hibal type**

This type includes the peralkaline, A₁-type granite-syenite associations and distinguished by the specialized geochemical signature of Zr, Nb, Th, and LREE. This type is also characterized by the presence of the zircon and pyrochlore mineralization. According to Abdalla and El Afandy (2003), the alkaline granites of Zarget Naam, Tarbite North and South, and Um Hibal possess the characteristics fitting to this specialized type.

(b) **Gabal El Gara El Hamra type**

This type is also included in the peralkaline, A₁-type and can be distinguished by the specialized geochemical signature of Y, Th, HREE, and P. It appears that GH and the post-cretaceous peralkaline complexes that intrude the Southwestern Desert (Fig. 1c) are all belonging to this class.

The high F contents of Gabal Gara El Hamra complex manifest the F-enriched nature of the syenitic magma in

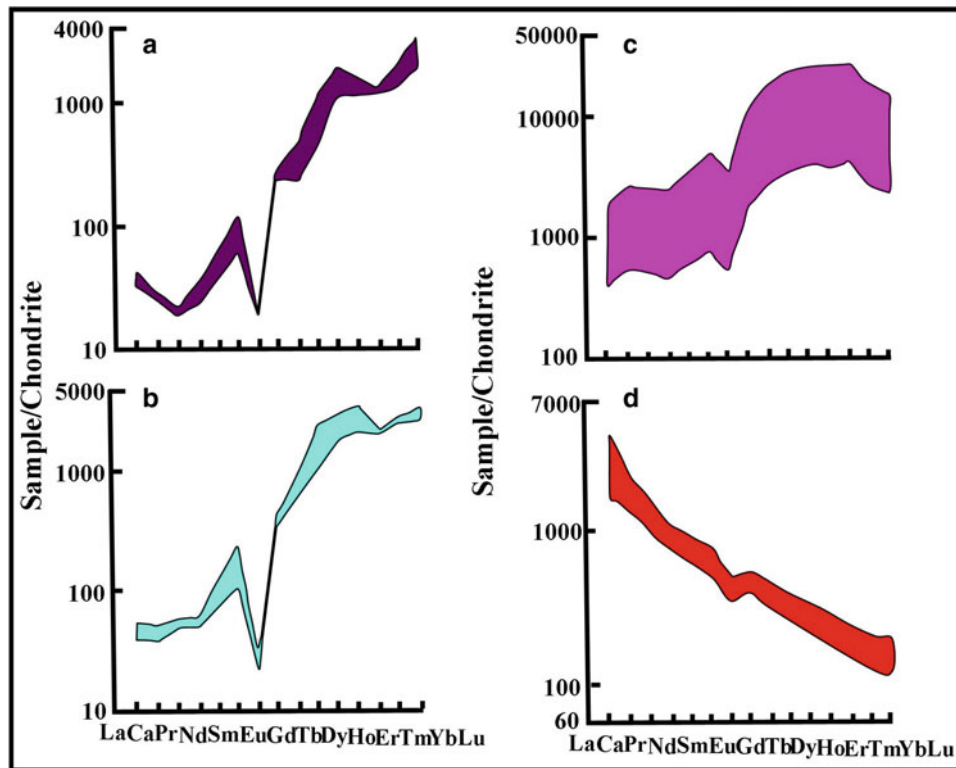


Fig. 8 REE distribution patterns of Gabal El Gara El Hamra peralkaline granite (a), syenite (b), and altered syenite facies (c) and (d). Notice that the pattern of Um Hibal peralkaline, Zr–Nb-mineralized granitic pegmatite association, (Abdalla & El Afandy, 2003) is shown for comparison

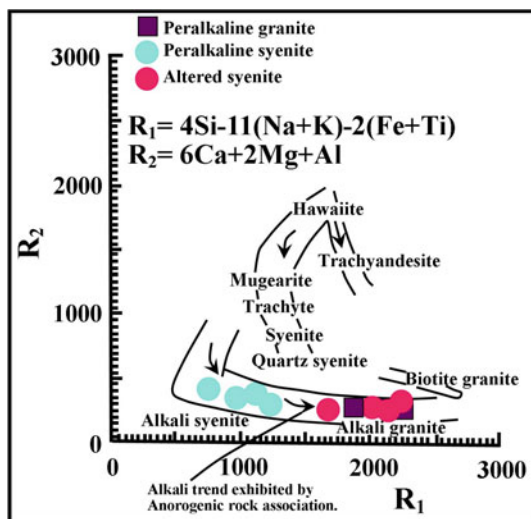


Fig. 9 R1-R2 diagram (in millications), illustrating the fractionation trend exhibited by Gabal El Gara El Hamra peralkaline syenite-granite complex. The diagram is adapted from Bowden et al. (1984), Batchelor and Bowden (1985) for volcanic and high-level intrusive alkaline rock series. The arrows indicate fractionation trends in different alkaline rock associations

this element. The experimental work of (Flynn & Burnham, 1978) has demonstrated that LREE is fractionated into Cl^- -bearing fluids, whereas HREE is stabilized by

F^- - or CO_3^{2-} -rich fluids. Thus, the aforementioned two peralkaline rock associations (i.e. Um Hibal and Gabal El Gara El Hamra types) are products of volatile system dominated by Cl^- and F^-/CO_3^{2-} , respectively. Although the role of both F^- and Cl^- in deriving Um Hibal peralkaline mineralized granite-pegmatite system was discussed by Abdalla and El Afandy (2003), yet, it seems that both F^- and CO_3^{2-} were the major components of the volatile system prevailed during the petrogenesis of Gabal Gara El Hamra type.

3 LREE-Mineralized Nepheline Syenites (Abu Khruq) (AK) Ring Complexes, Egypt

The Abu Khruq ring complex (AK) is a member of a group of complexes that display typical rings, conical or stock-like bodies, a prominent, clearly defined ring structure, and intrusions of nepheline syenite at their centres. Along with Abu Khruq, Nigrub Fogani, El Gezira, and El Naga are also members of this group (Figs. 1c, 15a and b). These complexes have comparable levels of magmatic differentiation, which is evident in the different types of rocks that they contain. With a 7 km diameter, Abu Khruq's centre is shaped like a circle. Alkaline volcanic and plutonic rocks make up its suite (mainly alkali gabbro, syenite, and nepheline

syenites). Numerous petrographic indicators show that hydrothermal alteration processes affected nepheline syenite, resulting in high concentrations of rare metals, including Nb, Ta, Zr, Hf, Y, Be, LREE, and the radioelements: U and Th (El Afandi & Abdalla, 2002; Hussein, 1990).

3.1 Geological Setting of Abu Khruq Ring Complex

The locations of the alkaline ring complexes in the South-eastern Desert province of Egypt are controlled by two sets of major structural lineaments trending ENE-WSW and NW-SE (Garson & Krs, 1976; Vail, 1985; Saleh et al., 2021).

The TM image of band ratios covers a major part of Abu Khruq area as shown in Fig. 10a. Field relations indicate that the evolutionary history of Abu Khruq started (Fig. 10b) with major early volcanic activity (mainly alkaline trachyte and

rhyolite porphyry and their breccia) occurring at the centre of the ring. This is followed by cauldron subsidence associated with the successive intrusion of alkali gabbro, quartz syenite (oversaturated), alkaline syenites (saturated), and nepheline syenite (undersaturated). Alkali and nepheline syenites, which occupy the core of Abu Khruq ring, are separated from quartz syenite, which lies on the circumference (outer ring) of the massif, by a large annular wadi. The quartz syenites form incomplete circle along the country rock contact of the massif (small part of which is shown in (Fig. 10c).

K–Ar age of Abu Khruq is established by (Serencsits et al., 1981) at 90 ± 2 and 89 ± 2 Ma (late Cretaceous) for biotite from alkali gabbro and nepheline syenite, respectively. This age is consistent with Rb/Sr dating obtained by Lutz et al. (1988). The indistinguishable ages of the different units of Abu Khruq indicate that various lithologies are cogenetic and that the nepheline syenite is likely representing the product of fractionation of mildly alkaline mafic magma.

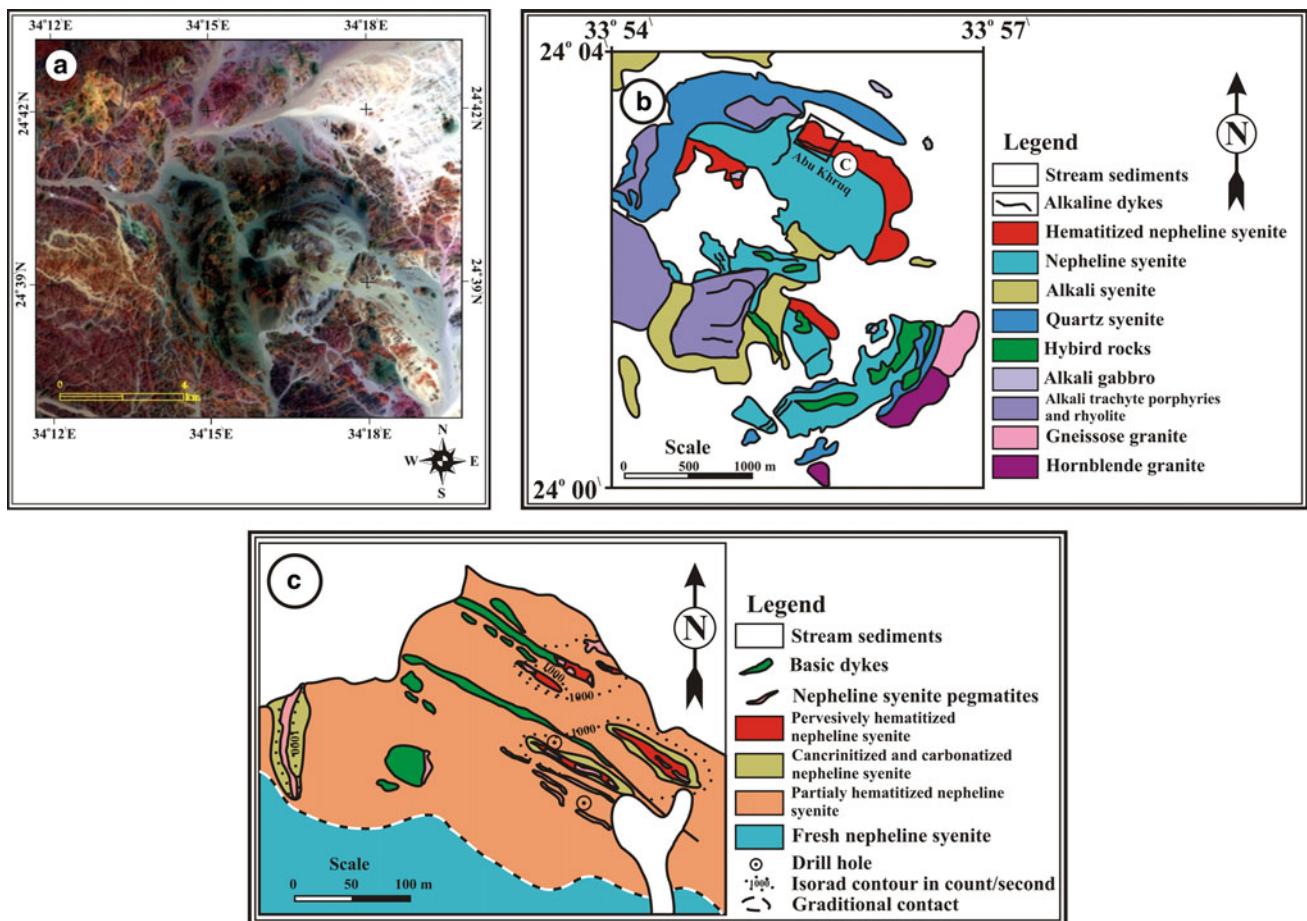


Fig. 10 a Landsat image with the Abu Khruq (AK) ring complex (by Hamdy M. Abdalla and Gehad M. Saleh). The annular structure with nepheline syenites core is conspicuous. b Geological map of central part of Abu Khruq complex (modified from El Ramly et al., 1969) with the area of Fig. 10c outlined, and c Detailed geological map of the LREE-enriched and hydrothermally altered northern zone of Abu Khruq (Without latitudes and longitudes) (Modified from Bugrov, 1972)

3.2 Petrography of Abu Khruq Ring Complex

Detailed petrographical description of various rock types building the Abu Khruq was given in El Ramly et al. (1969; 1971). Here the article will focus on the textural characteristics of the nepheline syenite and its altered facies in particular that are associated with anomalous radioactivity and high concentrations of the rare metals and LREEs.

In the second type, the rock is less undersaturated (< 10% nepheline), typically fine-grained, isotropically structured, and idiomorphically textured. These two varieties were distinguished by El Ramly et al. (1969), De Gruyter (1983) as foyaite and ditroite, respectively.

The main petrographical features of the nepheline syenites are displayed by nepheline, alkali feldspar, and alkali pyroxenes. Nepheline commonly forms sub- to euhedral quadrangular tabular to bladed and hexagonal crystals of sizes 3–5 × 5–8 mm. Feldspar crystals are commonly cloudy due to the incorporation of dust-sized hematite. The turbidity, the degree of exsolution of alkali feldspar increased as a result of interaction with peralkaline fluids (Charmichael & Mackenzie, 1963; Martin, 1969). Aegirine-augite forms sub- to euhedral prismatic crystals of size 2–4 × 5–8 mm. The crystals are commonly exhibiting marked inhomogeneity in optical properties (e.g. colour and pleochroism) which corresponds to variation in chemical composition (zoning). Four styles of zoning were recorded: normal, concentric, reverse, and sector. In the normally zoned crystals, the Na-augitic, lighter-coloured, and less pleochroic core followed by a strongly pleochroic and deep-green rim. This corresponds to an increasing content of the aegirine (acmite) molecule rim-wards. The reverse type of zoning with Na-depleted rim is commonly encountered in subsolidus clots of alkali pyroxene crystals.

In incipiently altered nepheline syenite, fine-grained subsolidus albite clots are developed on the expense of K-feldspar, manifesting early albitization process resulted from the Na-rich fluids which emerged at late stage of crystallizing nepheline syenite magma. In addition, the albite domains in perthitic K-feldspar crystals are enlarged during the process of alkali exchange till the perthite crystal is completely replaced by them. This stage is subsequently followed by turning the nepheline syenite into pale pinkish to buff-coloured rock due to partial hematitization and concomitant development of some deuteric minerals, e.g. cancrinite ((Na, Ca, K)_{6–8}(Al₆Si₆O₂₄)(CO₃, SO₄, Cl)_{1–2} 1–5 H₂O, 1–5 modal%), calcite (1–12%) ± sodalite (Na₈(Al₆Si₆O₂₄)Cl₂, 1–3%) ± analcite (Na(AlSi₂)O₆ 1–5%), and natrolite (Na₂Al₂Si₃O₁₀.2H₂O, 1–7%) in addition to acicular aegirine. These neoformed minerals are selectively replacing the early formed nepheline crystals. The nepheline crystals are commonly altered into cancrinite and fine-grained

micaceous and fibrous product (i.e. libenerite or hydro-nepheline composed largely of secondary micas, probably paragonite) and finally into fibrous natrolite. The alteration proceeds along the grains peripheries and microfractures until the whole grains becomes pseudomorphed by the neoformed minerals. The close association of cancrinite and calcite may indicate that cancrinite can pseudomorphs nepheline in high P_{CO2} environment.

Superimposing and widespread hematitization is manifested as a reddish-brown coloration due to deposition of hydrous ferric oxides. Ferrihydrite and hematite, as detected by X-ray diffraction technique, are the essential minerals in the hematitized nepheline syenite. They occur as coatings on the other minerals and planar zones in the feldspars, microfracture-fillings, and impregnations. At incipient stage, the rock is stained red by dust-sized hematite. When the process becomes overwhelming (pervasive), the rock turns brick-red in colour where the rock-forming minerals, except alkali pyroxene, are strongly leached and replaced by hematite.

3.3 Mineral Chemistry

3.3.1 Feldspars

Alkali feldspars of Abu Khruq nepheline syenites commonly occur as sub- to euhedral laths exhibiting fine to coarse perthitic exsolution lamellae. The laths have composition of the host orthoclase component ranging from Or₇₀Ab₃₀ to Or₇₉Ab₂₁, and the exsolved albite component is of nearly constant composition, Ab₉₇An₂Or₁. Like many hypersolvus rocks, the composition of alkali feldspars is rather restricted (Parson, 1978).

3.3.2 Alkali Pyroxene

Following Bonin and Giret's (1985) ternary diagram, the alkali pyroxene of the fresh nepheline syenite ranges between Di₇Hd₅₅Ac₃₈ and Di₁₆Hd₃₅Ac₄₉. Those of subsolidus and acicular variety are aegirine rich, ranging between Di₃Hd₁₇Ac₈₀ and Hd₁₀Ac₉₀, respectively. The optically detected zoning in alkali pyroxenes of Abu Khruq nepheline syenite was ascertained by the electron probe micro-analyzer (EPMA) analysis (El Afandi & Abdalla, 2002). The normally zoned crystals range from aegirine augite with Di₈Hd₃₈Ac₅₄ in core to aegirine with Di₆Hd₂₁Ac₇₃ in their rims.

3.4 Rock Geochemistry

Averages and ranges of major oxides and trace elements (El Afandi & Abdalla, 2002) of Abu Khruq nepheline syenites and its altered facies are given in Table 4. The moderately

elevated $\text{Na}_2\text{O}/(\text{Na}_2\text{O} + \text{K}_2\text{O})$ ratio values (averages 0.62, Table 5) in the fresh nepheline syenite samples indicate the sodic nature of these rocks and their parental magma. The calculated alumina saturation and peralkalinity molar indices are given in Table 5. Also, a very close discrimination scheme (Hess, 1989) based on the atomic per cent of alkalis, alumina, and calcium shown in Fig. 11a has the advantage of calcium display and allowing comparison with other elements (e.g. Fe in Fig. 11b). Figure 11a shows that nepheline syenite and related pegmatites of Abu Khruq ring complex range from metaluminous to peralkaline due to the petrographic characteristics (e.g. varying proportions of nepheline, alkali feldspars, and alkali pyroxene) of the studied samples. However, the hematitized facies exhibits a distinctive peralkaline character.

Figure 11a and b show that fresh samples plot midway along the alkali-Al join. Meanwhile, two concurrent trends towards Fe and Ca enrichment are observed among the altered nepheline syenites facies. These trends reflect the overwhelming increase of Fe content and the concurrent decrease of alumina and alkalis from fresh nepheline syenite towards the hematitized facies.

High contents of high field strength elements, i.e. Nb, Y, Zr coupled with low contents of the compatible elements of Ba and Sr, impart the fresh nepheline syenite an evolved geochemical signature. A gradual and gross enrichment of Nb, Ta, Zr, Hf, Y, U, Th, Ga, Sc, and Sr occurs from the fresh nepheline syenite to the hematitized facies (Table 4). The REE distribution patterns for the averaged fresh and altered nepheline syenites facies are displayed in Fig. 12. All of variants are steeply LREE enriched with high positive values of $(\text{La}/\text{Yb})_N$ ratios ranging from 12.5 in fresh nepheline syenites to 42 in the hematitized facies. The hydrothermal alteration appears to have enhanced La and Ce compared to the unaltered rocks as indicated by the increasing of $(\text{La}/\text{Yb})_N$ ratio (Table 4). Meanwhile, the amount of Eu anomaly diminishes in the albitized facies and nearly disappears in the carbonatized and hematitized nepheline syenites (Fig. 12). The pronounced negative Eu anomaly in Abu Khruq nepheline syenites and related pegmatites (Fig. 12) manifests their derivation as late-stage products of protracted fractionation.

3.5 Genesis of the Alteration Phenomena

The question arises now how such evolved nepheline syenites can be a progenitor to specialized mineralized system. Mineralogical similarity between nepheline syenite and its related pegmatites indicates that crystallization of nepheline syenite had progressed to the stage where pockets and miaroles of residual Na, Cl, F, CO_2 , and SO_4 -rich fluids

were separated from melt and trapped along the NW–SE trending shear zone. This fluid reacts with the primary minerals, and pneumatolytic assemblage of acicular aegirine, sodalite, and natrolite was deposited as replacement, pegmatite-forming, and vugs-fillings. Crystallization of acicular aegirine and carbonate rather than alkali amphibole indicates an Na-rich environment and high $f\text{O}_2$, above the fayalite-magnetite-quartz (FMQ) buffer (Stephenson & Upton, 1982) and low $a_{\text{H}_2\text{O}}$.

Hussein (1990) attributed the origin of the hematitized zones at Abu Khruq to the action of the meteoric water which leached the ore constituents from the alkaline rocks and re-depositing them in the surface fractures. However, field, petrographical, and geochemical data support the idea that the recorded alteration phenomena, which brought about by lately emerged oxidized fluids, were related to mineralizing source similar to that can give rise carbonatite bodies as it will be verified:

- (i) **Field observations**, textural characteristics, and geochemical evidences all are pointing to that the recorded alteration zones at Abu Khruq are closely similar to late-stage alkali metasomatic features referred to as “fentization” typically associating many carbonatite centres (Bowden, 1985). Fentization is an alkali element's enrichment apparently induced by solution or fluid activities.
- (ii) **Hematitization of Abu Khruq** is equivocal with that responsible for the formation of the “Rodberg rock” (Andersen, 1984; Le Bas, 1977). Rodberg is a late-stage secondary hematite-calcite carbonatite most commonly associated with alkaline complexes elsewhere. Field evidence includes the occurrence of large intrusion of undersaturated rocks, e.g. nepheline syenites, which are typical associates for carbonatite (Le Bas, 1981, 1987).
- (iii) **Confining of nepheline syenites** (as the youngest rock type) and its alteration facies to the central part of Abu Khruq ring is a typical petrologic and structural feature for the nepheline syenites commonly hosting carbonatites as described (Kapustin, 1980; Le Bas, 1977) for the African, European, and Brazilian carbonatites.
- (iv) **Geochemical evidence** includes the concomitant of the light REE enrichment and steeply decreasing concentration gradients in the interval Nd-Eu (Fig. 12) in the cancrinitized and hematitized nepheline syenites. Anomalously high REE (particularly, the LREE) is a distinctive feature of carbonatite. Gradual diminution in Eu anomaly from carbonatized to hematitized facies is consistent with Eby (1975) about the addition of Eu during fentization. This

Table 4 Averages and ranges of major and trace element contents of Abu Khruq nepheline syenites and its altered facies, Egypt (El Afandi & Abdalla, 2002)

N* Major oxides (Wt.%)	Fresh	Nepheline	Albitized	Carbonatized	Moderately	Strongly
	Nepheline	Syenite	Nepheline	Nepheline	Hematitized	Hematitized
	Syenite	Pegmatite	Syenite	Syenite	Nepheline	Nepheline
	5	4	2	3	Syenite 3	Syenite 2
SiO ₂	57.77	57.66	58.16	56.66	51.13	37.20
	55.90–60.58	56.10–59.85	57.21–59.10	54.10–59.20	46.10–55.20	36.30–38.10
TiO ₂	0.21	0.16	0.11	0.20	0.13	0.11
	0.14–0.25	0.09–0.25	0.09–0.12	0.14–0.27	0.11–0.16	0.10–0.11
Al ₂ O ₃	20.48	19.34	22.21	16.51	9.09	4.16
	17.81–23.76	18.10–21.50	21.40–23.01	15.95–17.40	6.50–11.61	4.01–4.30
Fe ₂ O ₃ *	5.94	5.82	4.12	7.64	15.53	34.10
	5.33–6.83	4.91–6.82	3.43–4.81	6.38–9.35	9.53–21.30	31.50–36.70
MnO	0.13	0.16	0.19	0.10	0.84	0.97
	0.08–0.18	0.14–0.18	0.18–0.20	0.07–0.13	0.71–0.99	0.82–1.12
MgO	0.27	0.19	0.08	0.19	0.03	0.01
	0.06–0.51	0.12–0.23	0.08	0.10–0.33	0.02–0.04	0.01
CaO	0.76	0.91	0.37	1.63	2.87	1.17
	0.65–0.88	0.70–1.20	0.31–0.43	1.37–2.01	2.31–3.95	0.83–1.51
Na ₂ O	8.67	8.79	10.51	7.80	5.69	3.02
	7.71–9.79	7.70–10.20	10.21–10.81	7.29–8.12	5.51–6.04	2.81–3.23
K ₂ O	5.37	5.14	4.02	3.18	0.58	0.09
	4.91–6.27	4.61–5.57	3.93–4.11	1.30–5.82	0.09–1.50	0.08–0.10
P ₂ O ₅	0.14	0.05	0.13	0.20	0.24	0.13
	0.11–0.21	0.02–0.07	0.12–0.13	0.16–0.28	0.11–0.30	0.12–0.14
H ₂ O +	0.43	0.99	0.48	2.77	9.83	17.30
	0.3–0.48	0.88–1.20	0.41–0.54	1.21–4.40	6.80–12.60	16.10–18.50
CO ₂	0.40	0.65	0.50	1.48	2.28	0.90
	0.2–0.5	0.45–0.84	0.45–0.54	1.25–1.80	1.75–3.01	0.60–1.20
S	< 0.01	0.06	< 0.01	0.09	0.12	0.08
	< 0.01–0.03	0.05–0.08	< 0.01	0.07–0.12	0.05–0.16	0.07–0.08
Total	100.57	99.92	100.88	98.45	98.36	99.24
F	440.0	1250.0	565.0	920.0	620.0	340.0
	300.0–600.0	840.0–1700.0	400.0–730.0	625.0–1320.0	400.0–710.0	230.0–450
Trace elements (ppm)	36.0	40.0	32.0	25.0	15.0	9.0
Li	23.0–48.0	28.0–50.0	25.0–39.0	21.0–30.0	10.0–22.0	6.0–12.0
	5.0	3.8	8.0	12.0	49.0	22.0
Be	3.0–8.0	3.0–5.0	4.0–12.0	8.0–15.0	41.0–59.0	18.0–25.0
	122.0	148.0	89.0	84.0	28.0	11.5
Rb	92.0–160.0	112.0–198.0	80.0–98.0	60.0–112.0	10.0–61.0	11.0–12.0
	43.0	256.0	19.0	28.0	37.0	23.5
Ba	34.0–60.0	210.0–312.0	18.0–20.0	18.0–39.0	32.0–41.0	22.0–25.0
	13.0	12.0	15.0	64.0	151.0	184.0
Sr	7.0–18.0	9.0–15.0	14.0–15.0	44.0–83.0	92.0–220.0	172.0–195.0

(continued)

Table 4 (continued)

<i>N</i> * Major oxides (Wt.%)	Fresh	Nepheline	Albitized	Carbonatized	Moderately	Strongly
	Nepheline	Syenite	Nepheline	Nepheline	Hematitized	Hematitized
	Syenite	Pegmatite	Syenite	Syenite	Nepheline	Nepheline
	5	4	2	3	Syenite	Syenite
				3	2	
Zr	648.0	767.0	648.0	779.0	3144.0	1565.0
	518.0–750.0	586.0–925.0	530.0–765.0	587.0–940.0	2130.0–4230.0	1480.0–1650.0
Hf	17.0	20.0	17.0	20.0	81.0	40.5
	14.0–19.0	15.0–24.0	13.8–20.0	15.0–24.0	55.0–110.0	38.0–43.0
Nb	157.0	185.0	208.0	263.0	5283.0	1600.0
	122.0–180.0	158.0–220.0	195.0–220.0	145.0–385.0	3855.0–6130.0	1400.0–1800.0
Ta	10.5	12.0	17.0	17.1	340.0	107.0
	8.1–12.1	10.1–14.3	13.0–21.0	9.2–25.0	250.0–393.0	93.0–120.0
Sc	1.2	1.8	1.3	3.9	33.0	15.3
	1.0–1.4	1.1–3.5	1.0–1.6	1.4–6.8	25.0–40.0	12.5–18.0
Ga	23.0	30.0	37.0	41.0	35.0	21.5
	19.0–29.0	28.0–32.0	36.0–38.0	38.0–44.0	32.0–38.0	18.0–25.0
Y	37.0	35.0	42.0	39.0	170.0	78.0
	24.0–50.0	18.0–48.0	36.0–48.0	22.0–53.0	125.0–195.0	75.0–81.0
Pb	9.0	7.5	9.0	62.0	257.0	133.0
	7.0–12.0	5.0–10.0	7.0–12.0	40.0–90.0	150.0–397.0	105.0–160.0
Zn	156.0	141.0	170.0	566.0	1487.0	965.0
	106.0–190.0	93.0–195.0	160.0–180.0	420.0–690.0	960.0–1830.0	910.0–1020.0
U	3.3	6.4	4.5	6.8	203.0	64.0
	2.9–3.7	3.9–9.0	4.0–5.0	4.3–9.0	132.0–258.0	58.0–70.0
Th	14.3	20.0	18.0	27.0	1104.0	352.0
	13.0–16.0	11.7–32.0	13.0–22.0	19.0–34.0	480.0–2060.0	350.0–354.0
La	101.0	107.0	141.0	171.0	1567.0	328.0
	82.3–120.0	75.8–140	133.0–149.0	94.4–280.0	1200.0–1900.0	320.0–335.0
Ce	209.0	202.0	308.0	283.0	2250.0	455.0
	155.0–285.0	123.0–310.0	295.0–320.0	160.0–370.0	1710.0–2740.0	450.0–460.0
Nd	60.0	59.0	101.0	83.0	573.0	118.0
	45.0–71.0	43.0–80.0	95.0–107.0	47.0–112.0	450.0–690.0	115.0–120.0
Sm	13.0	11.4	13.5	17.0	109.0	26.0
	10.8–16.5	8.4–15.0	13.0–14.0	11.0–22.0	83.0–138.0	24.0–27.0
Eu	1.7	1.4	2.1	4.0	20.1	8.0
	1.0–2.8	1.0–1.6	2.0–2.1	1.5–6.5	9.3–27.0	7.4–8.0
Gd	15.1	14.1	12.5	17.3	47.0	26.0
	13.0–17.0	12.0–16.0	11.0–14.0	10.0–22.0	28.0–60.0	25.0–26.0
Tb	1.5	1.2	2.3	3.9	7.0	4.5
	1.3–1.6	0.5–2.0	2.1–2.4	1.7–5.1	6.3–7.5	4.3–4.5
Yb	3.9	4.1	7.8	7.4	26.2	14.5
	3.3–4.2	3.3–4.6	7.5–8.0	5.7–8.5	16.1–34.0	14.0–15.0
Lu	0.7	0.6	1.5	1.4	4.0	2.3
	0.6–0.8	0.5–0.7	1.4–1.5	1.0–2.2	2.5–5.2	2.1–2.5

**N*: number of samples analysed and ** Total iron was determined as Fe₂O₃

Table 5 Characterization of rare metal potentiality of Abu Khruq nepheline syenites and its altered facies using different metallogenic indices, Egypt (El Afandi & Abdalla, 2002)

Element	Fresh	Nepheline	Albitized	Carbonatized	Hematized
Ratio	Nepheline	Syenites	Nepheline	Nepheline	Nepheline
	Syenites	Pegmatite	Syenites	Syenites	Syenites
Na ₂ O/K ₂ O	0.62	0.63	0.72	0.73	0.94
	0.58–0.66	0.58–0.69	0.71–0.73	0.56–0.86	0.79–0.98
(Na + K)/Al	0.93	0.99	0.98	0.98	1.18
	0.79–1.04	0.93–1.02	0.92–1.03	0.92–1.10	0.92–1.41
Al/(Na + K + Ca)	0.96	0.93	1.00	0.87	0.60
	0.89–1.07	0.91–0.95	0.94–1.05	0.81–0.93	0.4–0.78
Rb/Sr	10.00	12.70	6.20	1.50	0.19
	7.30–16.70	10.20–15.30	5.30–7.00	0.90–2.50	0.06–0.70
K/Rb	380.00	300.00	380.00	300.00	101.00
	255–458	202–342	333–426	133–431	55–204
10,000 * Ga/Al	2.10	3.00	3.20	4.70	8.60
	1.80–2.30	2.50–3.20	3.00–3.40	4.40–5.20	5.20–11.70
Zr/Hf	38.61	38.58	38.33	38.96	38.68
	37.00–39.10	37.84–39.00	38.25–38.41	38.57–39.17	38.37–38.95
Nb/Ta	14.97	15.41	14.84	15.48	15.33
	14.88–15.06	15.24–15.64	14.67–15.00	15.29–15.76	15.00–15.60
Th/U	4.37	3.03	3.83	4.07	5.25
	4.14–4.69	2.71–3.55	3.25–4.40	3.78–4.42	3.54–7.98
Zn/Pb	16.60	20.40	19.00	9.60	6.80
	15.10–17.80	16.00–23.30	15.00–22.90	7.70–10.70	4.20–8.70
(La/Yb)N	14.60	14.90	12.30	13.00	28.30
	12.50–16.00	12.80–15.40	12.01–12.70	9.50–19.90	12.70–42.00
(Eu/Eu*)N	0.38	0.34	0.50	0.66	0.87
	0.25–0.54	0.23–0.45	0.48–0.52	0.42–0.90	0.60–1.00

The element ratios are cited as average and ranges. The agpacity (Na + K)/Al and peraluminicity (Al/(Na + K + Ca)) indices are expressed as molar ratios of oxides. The subscription N in the REE ratios indicates the chondrite normalized values

phenomenon is again ascertained by the interesting relationship between the Eu anomaly and Sr, one of typomorphic elements characterizing carbonatites, contents in the investigated altered nepheline syenite samples (Fig. 13). The $Eu/Eu^* < 1$, i.e. negative anomaly in Sr-poor, fresh, and highly fractionated nepheline syenite is increased to the unit value in Sr-rich carbonatitized and hematitized facies. Thus, the REE distribution in metasomatized nepheline syenites at Abu Khruq is most probably ascribed to extreme mobility of REE in CO₂-rich fluid derived from underlying carbonatite bodies. In such fluids, the REE-carbonate complexes are stably formed (Wendlandt & Harrison, 1979).

(v) **Worth noting that in the altered nepheline syenites samples**, averages of H₂O, CO₂, S, and F range

between 4.4 and 15.4%, related predominantly to increasing amount of hydronepheline (libenerite) cancrinite, zeolite, carbonate, and ferrihydrite. The broadly sympathetic REE patterns of nepheline syenites and its altered variants, e.g. enrichment in LREE and the exhibition of steep slopes from La to Yb (Fig. 12). Such a source is an alkalic silicate melt most probably saturated with respect to carbonates.

(vi) **The last geochemical evidence supporting** the carbonatitic rather meteoric source for the emerged fluids is the very close ages of the nepheline syenites and hematitization as reported by Lutz et al. (1988) at 90 ± 2 Ma. This is consistent with dominant magmatic source rather than derivation from later meteoric water contribution.

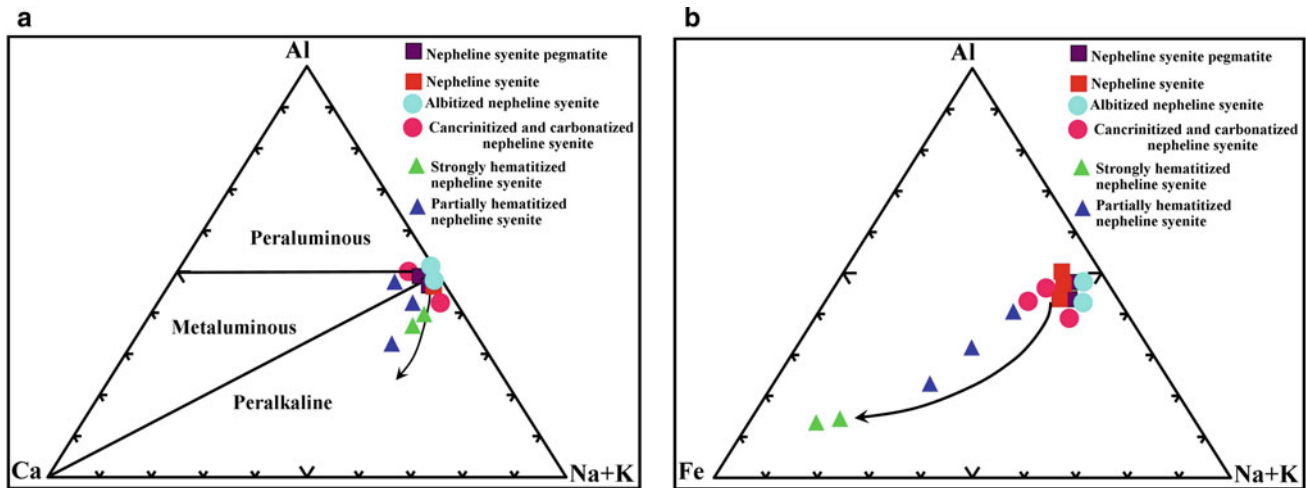


Fig. 11 Al–Ca–(Na + K) and Al–Fe–(Na + k) ternary diagrams (atomic proportions) of Abu Khruq nepheline syenites and its alteration facies showing: **a** Degree of peralkalinity using the classification of Shand (1951) and **b** Migration of composition away from the alumina-alkalies joins towards the Fe apex with increasing the intensity of hematization. The arrows indicate the concomitant enrichment in Fe and Ca during the progress of alteration from albitized to hematitized rock

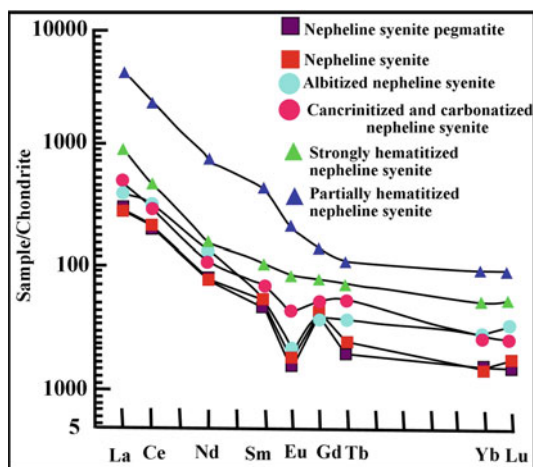


Fig. 12 REE distribution patterns of Abu Khruq nepheline syenites and its alteration facies

The nepheline syenites complexes and related carbonatites can be plotted on the R1-R2 cationic diagram showing the evolution trends of the various rock types as well as illustrating the trend of fenitization at carbonatite centres (trend F, Fig. 14). This figure shows that the alteration facies (fenitized wall rock) of AK exhibit a trend of increasing of Fe (lesser R2 factor) and Ca (more positive R1 factor) at nearly constant silica content (trend H). This trend is inconsistent with that described for the carbonatite rocks and their genetically related fenitized aureoles elsewhere (Kampunzu & Lubala, 1991). The inconsistency can be understood by realizing the typical assemblage of fenites that is formed at higher-temperature conditions. This assemblage includes both K-metasomatized (i.e. microclinization and development of biotite-phlogopite) and Na-metasomatized

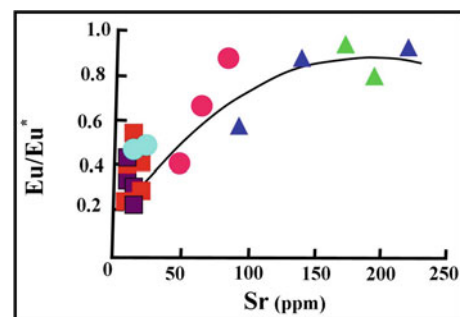


Fig. 13 Eu/Eu* versus Sr in the Abu Khruq nepheline syenites and its alteration facies. The shown trend demarcates the diminution of europium anomalies as the alteration processes progressed towards carbonatization and hematization

(i.e. overwhelming albitization and development of magnesio-arfvedsonite to eckermannite) country rocks (Bowden, 1985; Trueman et al., 1988). However, the recorded alteration phenomena at AK are small and erratic occurrences of albitized facies, restricted zones of cancrinitized and carbonatized facies, and widespread hematitized facies. Thus, it is reasonable to akin the alteration facies of Abu Khruq ring complex to trend H rather following trend F (Fig. 14). In the high-level intrusion setting, as the case of Abu Khruq, where the late-stage evolution of the system is proceeding at variable scale of disequilibrium effects, it is difficult to estimate the physico-chemical conditions (i.e. pressure, temperature, volatile fugacities, and component activities). The temperature and pressure of the emerged fluids, based on the mineral equilibria of the pegmatitic K-feldspar and aegirine, can be defined at nearly 500 °C and 1300 bars, respectively (Prins, 1981; Naldrett & Watkinson, 1981).

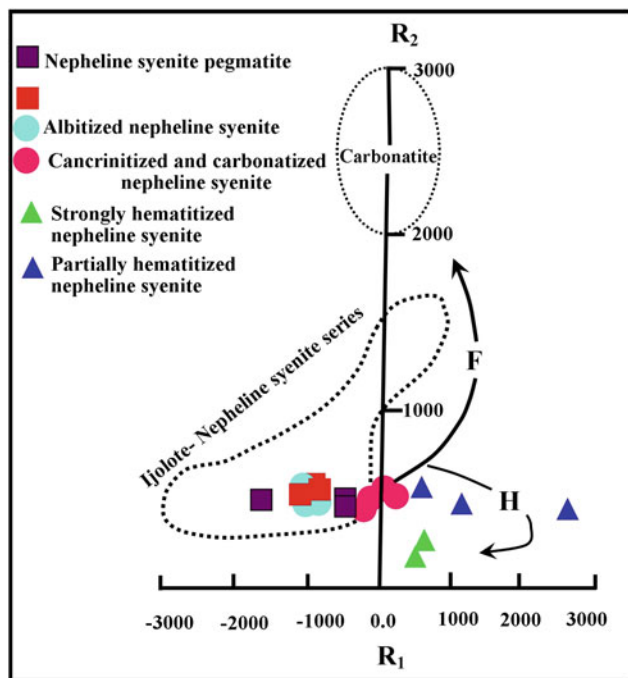


Fig. 14 Cationic diagram R1-R2 for Abu Khruq nepheline syenites and its alteration facies. The dominant compositional trend in undersaturated rock series and the related carbonatites are from (Kampunzu & Lubala, 1991). The trend F indicates the evolution path of typical fenitization process associating carbonatite centres, whereas the trend H demarcates the evolution of low-temperature hematitization process recorded at Abu Khruq ring complex

It is worthy to note that the markedly increased peralkalinity in the carbonatized and hematitized facies can be attributed to the fact that the alkali feldspars and nepheline are gradually destabilized during the hydrothermal reworking, whereas the alkali pyroxene is the only phase persisting the fluid action even in the strongly hematitized nepheline syenites rock as petrographically detected.

Weak depletion in silica of the albitized, carbonatized, and moderately hematitized nepheline syenite is contradicting with the usual desilication observed in the fenitized rocks. Prins (1981) attributed such phenomenon to the degree of saturation in Si of the infiltrating fluid relative to the invaded wall rock. Thus, it is reasoned that, if the fluids percolate, a Si-undersaturated wall rock such as the case of Abu Khruq, desilication will not occur to establish equilibrium with the metasomatizing fluids, whereas the opposite will occur if the wall rocks are Si oversaturated.

Ratios of geochemically coherent and antipathetic elements such as K/Rb, Rb/Sr, Nb/Ta, Zr/Hf, Ga/Al, and Pb/Zn (Table 5) can be used as indicators for the evolution and specialization of the alkaline rocks and their alteration zones and hence their potentialities as a sources for rare metals and REE mineralization.

3.6 Pyroxene as Petrogenetic Tracer

Pyroxenes of the fresh nepheline syenites being sodic-calcic (Ac 38–49) to sodic (Ac73) especially along the outer rims and Fe-rich ($\text{Fe}/(\text{Fe} + \text{Mg})_{\text{atom}}$ range between 0.83 and 0.93). Thus, pyroxene mineral of the nepheline syenites is very sensitive to oxidation–reduction conditions during the crystallization of the nepheline syenite and related pegmatite rocks. They are considered as good mineralogical tracers of the chemical evolution of the magma, e.g. aegirine content in the pyroxene with the progression of crystallization as manifested in either the rim zones, pyroxene from pegmatites, or subsolidus acicular pyroxenes may indicate the increasing of $f\text{O}_2$ of the evolved magma till the emergence of highly oxidized fluids at late to post-magmatic stage. Oxygen is provided by the thermal decomposition of water. The trend exhibited by alkali pyroxenes of Abu Khruq nepheline syenite is consistent with miaskitic under saturated rock series (Bonin & Giret, 1985). This trend is confined by two substitution schemes. The first is the acmitic-hedenbergite type of substitution (i.e. $\text{Ca}, \text{Mg} \leftrightarrow \text{Na}, \text{Fe}^{3+}$) which is characteristic for silico-carbonatite and related nepheline syenites. The second is the diopside-acmite type of substitution (i.e. $\text{Ca}, \text{Fe} \leftrightarrow \text{Na}, \text{Fe}^{3+}$) which is found in urtite and related carbonatite. The evolution path exhibited by alkali pyroxenes of Abu Khruq nepheline syenites and pegmatites depicts well its crystallization from a relatively Mg-poor syenite magma.

3.7 Metallogenetic and Exploration Constraints

There are three ring complexes that share Abu Khruq with many common features. These are the Nigrub Fogani (NF), Naga (NG), and El Gezira (G) (Figs. 15a and b). Abu Khruq (92 Ma) lies on a NW–SE tectonic zone, implying a tectonic control for its intrusion. The three ring complexes are of late Jurassic-early Cretaceous magmatism (140 ± 4 Ma), which includes Nigrub Fogani-Naga-Gezira. These rings are confined to $\text{S}60^\circ\text{W}$ tectonic zone. A progression in ages is shown by these complexes. They increase in ages south-westward along the tectonic zone. The identification of linear age trends indicates a possible tectonic control, contemporaneous or shortly earlier activity commenced with Red Sea rifting, for the distribution of alkaline magmatism along the NE–SW tectonic zones.

According to Garson and Krs (1976), the age of the $\text{N}60^\circ\text{E}$ block faulting is not constrained, but it was probably initiated in the Precambrian and rejuvenated during the intrusion of the alkaline ring complexes in the early and late Cretaceous.

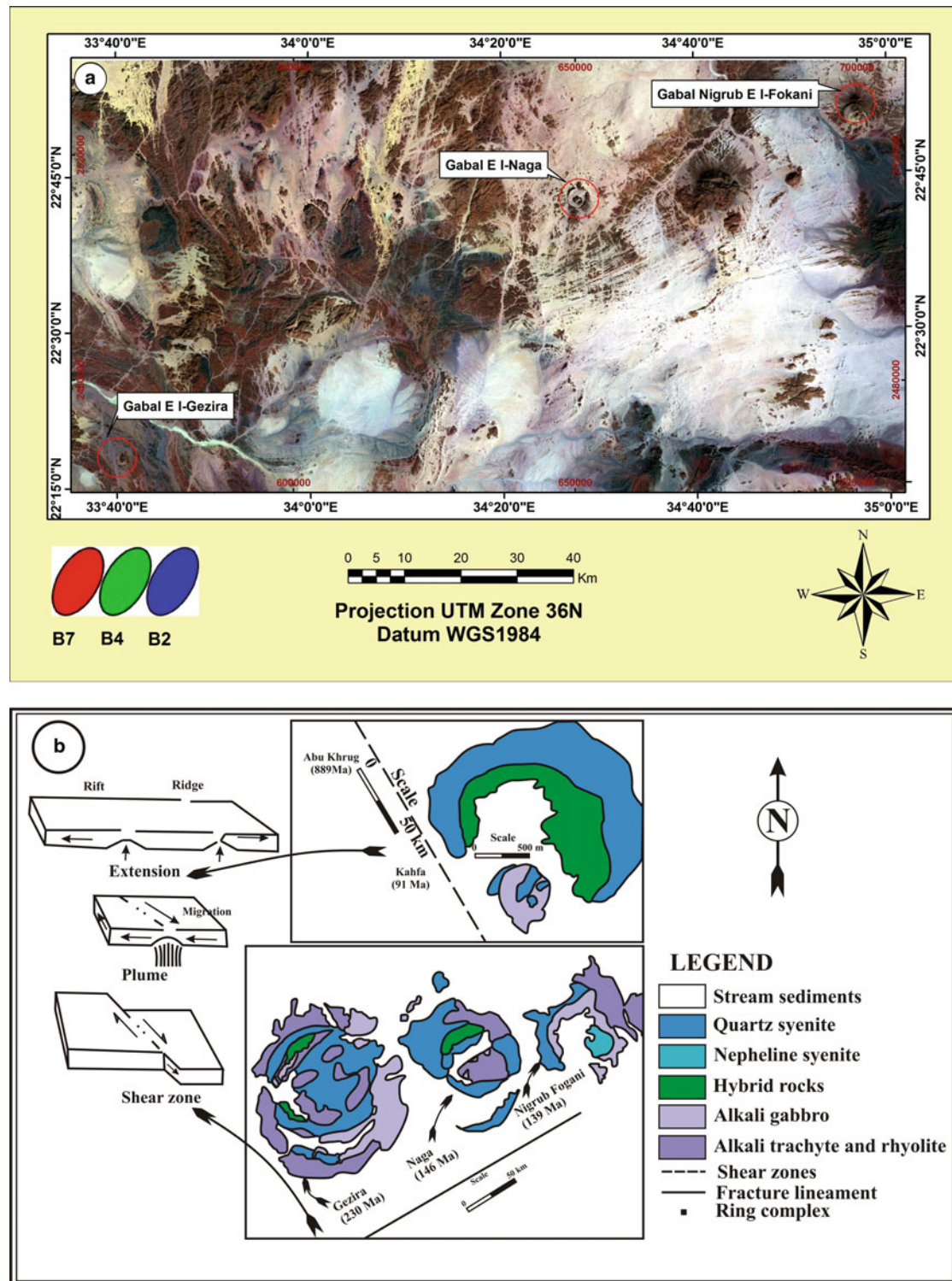


Fig. 15 a Landsat image showing the alignment of some mineralized/and or specialized ring complexes (e.g. Abu Khruq, Nigrub Fogani, Naga, and El Gezira) along ENE shear zone (by Hamdy M. Abdalla and Gehad M. Saleh) and b Generalized geological maps showing geology and ages of those with high potentialities (e.g. Abu Khruq, Nigrub Fogani, Naga, and Gezira). The cited ages in practices are compiled from (Hashad & El Reedy, 1979; Serencsits et al., 1981). The geology of the rings is compiled from El Ramly et al. (1971). To the left side of Fig. 15b, the schematics controls of alkaline magmatism (Bonin, 1983). 1. Effects of extensional setting, causing linear doming expresses as a ridge and ultimately as rift, which is the case of Abu Khruq ring complex-Kahfa zone; 2. Hot spot model generated by upwelling mantle plume; 3. Alkaline complexes located along shear zone which is the case ascribed for the ring complexes located along the ENE tectonic zones, e.g. Nigrub Fogani, Naga, and El Gezira, Egypt

Bonin (1986) reported three possibilities to account for the distribution of alkaline complexes, namely distension and formation of a rift; hot spot above plume and lithospheric shearing (i.e. Harpoon effect of Black et al. (1985)). In the distension or extensional setting, the alkaline melt collects together at the level of fracture system and emplaced along the length of pre-existing lineament, e.g. transform fault. In this case, ring complexes will be aligned parallel to the structural lineament and will not show difference in age as in the case of Kahfa-Abu Khruq along the NW-SE rift zone which is parallel to the axis of Red Sea rift. In the plume setting, the asthenosphere swells up as a magmatic balloon-like rising structure causing the distension of the overlying lithosphere. The cause of updoming and swells of the crust is related to intraplate mantle hot spots (Wright, 1973), where parts of the plate overlying positive thermal anomalies are heated by the upwelling convection columns in the mantle (Briden & Gass, 1974). In the plume setting, the alignment of alkaline magma is parallel to the directions of plate motion and will reveal a well-defined trend of ages migration. In the third setting, major shear zones exist which affect the whole extent of lithosphere and the alkaline magmas collect together at the level of pre-existing fractures which are conjugately linked to the direction of shear zones. In such situation, the alkaline complexes will be aligned along the shear zones and will show migration of their ages at specified time intervals corresponding to the time at which these zones are reactivated. This is the typical case for the complexes aligned along the ENE-WSW shear zones, which comprises the mineralized complexes of Nigrub Fogani, Naga, and El Gezira with WSW-ENE intermittent age migration through specified time span. Serencsits et al. (1979, 1981; Saleh et al., 2021) recognized the periodicity of intrusion of alkaline ring complexes in Egypt, every 52 Ma, spanning the time interval from Cambrian through the Cretaceous. Worth noting that the mineralized alkaline granites province of Nigeria exhibits a migrating ages from north to south at more or less fixed time intervals (Bowden et al., 1984). Hence, it is suggested that more attention should be paid for detailed exploration for the ring complexes lying along the ENE trending shear zones, e.g. those comprising Abu Khruq; Nigrub Fogani-Naga-El Gezira; and the southernmost Mansoury ring complex.

4 HREE-Mineralized Carboniferous Sandstones (Ramlet Hemyir and Um Hamad) of Southwestern Sinai, Egypt

The Landsat thematic map image (TM) of Um Bogma area (Fig. 16a) shows the Phanerozoic (Lower Carboniferous) sedimentary cover exposed in the region and discriminated in the geological map of Fig. 16b. Three main subdivisions

of Lower Carboniferous: the lower sandstone, middle carbonate, and the upper sandstone units (Baron, 1907). The base of the middle carbonate and the upper layers of the lower sandstone units contain possible resources of anomalously radioactive xenotime (YPO₄), e.g. those recorded at Um Hamad and Ramlet Hemyir (El Kammar et al., 1997).

The areas of potential xenotime, known locally as Ramlet Hemyir and Um Hamad, are located at the environs of Um Bogma to the northeast of Abu Zeneima town (Fig. 16b). The middle carbonate unit is considered as promising unit with respect to economic ores, e.g. manganese, uranium, and rare earth elements. Ferruginous cement imparts the sediments the characteristic reddish to brownish coloration (Fig. 17).

Chemical analysis, supported with X-ray diffraction data, indicates that the xenotime-bearing sediments of Ramlet Hemyir and Um Hamad are highly ferruginous (FeO_{Total} + MnO may reach up to 75%) and argillaceous (El Kammar et al., 1997). The sediments of Um Hamad are more argillaceous than those of Ramlet Hemyir which are more arenaceous. In Ramlet Hemyir, the molecular ratio of Si:Al ranges between 8:1 and 32:1, due to increasing content of free silica (e.g. detrital quartz) on the expense of the argillaceous material. Data of xenotime-concentrates and pure xenotime fractions separated from the investigated potential sandstone (El Kammar et al., 1997) are represented through Figs. 18 and 20.

The chondrite-normalized patterns of representative bulk sandstone samples from Ramlet Hemyir and Um Hamad are graphically constructed in (Figs. 18a and b). Besides, the chondrite-normalized patterns of xenotime mineral and xenotime-rich concentrates are also displayed in Fig. 19. The patterns bear clear and easily distinguishable “finger prints” of xenotime mineral with sharp enrichments of the HREEs (Gd, Tb, Er, Yb, and Lu) over the LREEs (La, Ce, Nd, and Sm). According to Shata (2013), xenotime is among other detrital heavy minerals (ilmenite, rutile, zircon, and ilmenorutile) that were recorded in the basal conglomerate and the black sand lenses encountered within the ferruginous sandstones in Um Bogma environs. Shinkawa (2013) stated that, in Lower Carboniferous Um Bogma Formation, Fe-Mn sediments were deposited undersea from hydrothermal plume. The REE from hydrothermal fluid coprecipitated with MnO and/or FeO and was mainly absorbed into FeO. Besides, Ce in seawater was deposited on the Fe-Mn sediments. Then, terrigenous sediments were deposited on the Fe-Mn sediments. The REE in terrigenous sediments exists in hardly soluble mineral like zircon. Um Bogma Formation (Fe-Mn sediments and terrigenous sediments) came ashore by diastrophism and was covered by upper sandstone unit between Upper Carboniferous and Permian. The REEs in Um Bogma Formation were concentrated in Fe-bearing mineral due to chemical weathering.

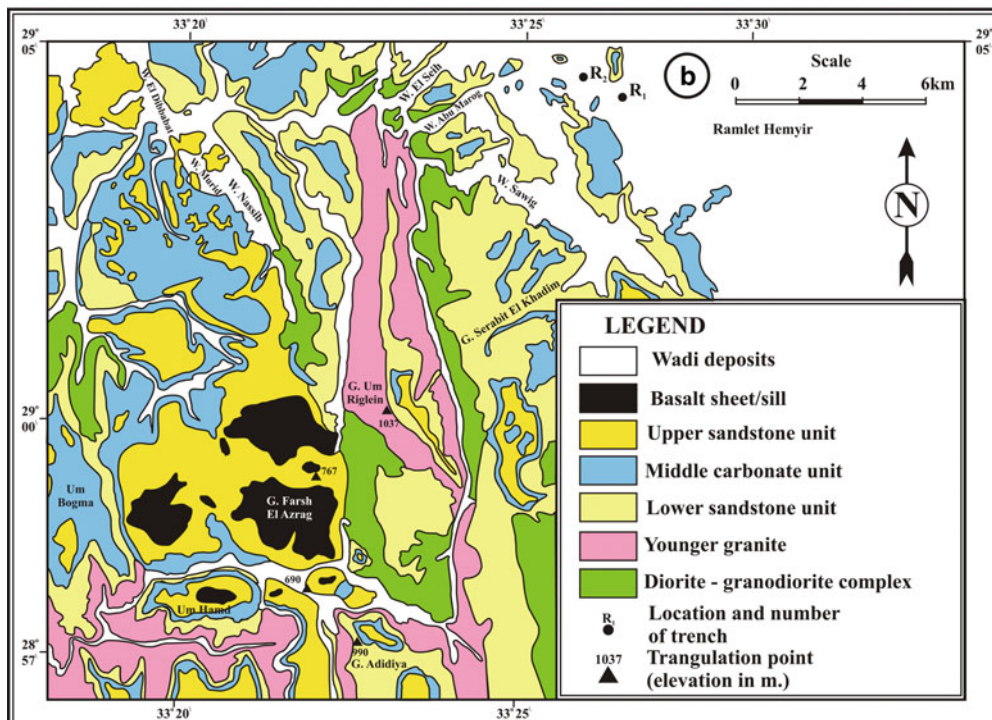
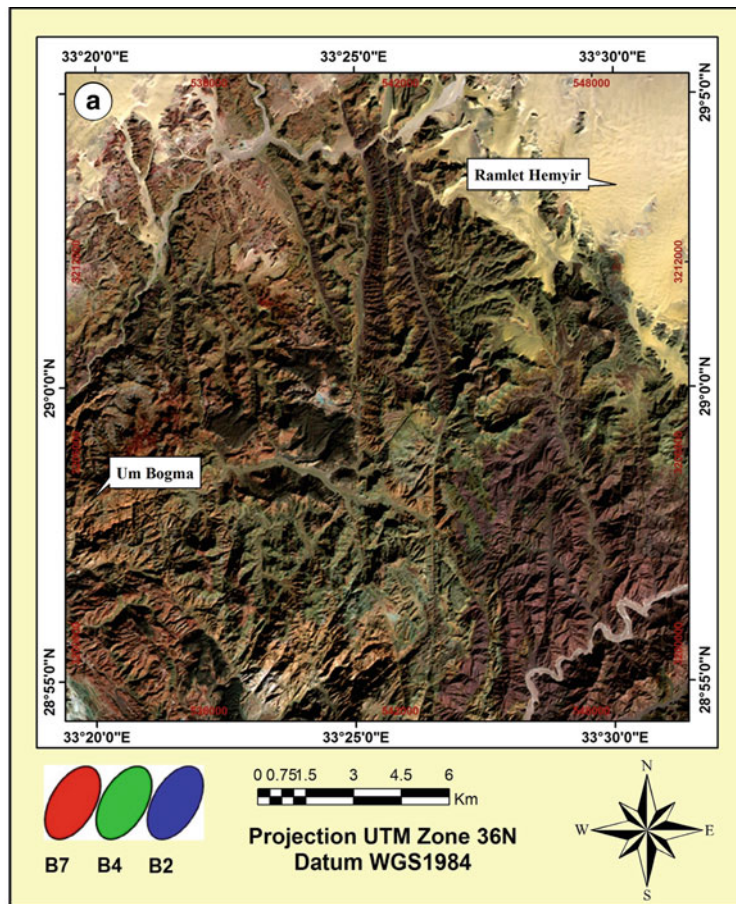


Fig. 16 **a** Landsat image with the Ramlet Hemyir, Sinai, Egypt and **b** Geological map of the Ramlet Hemyir (modified from El Sokkary, 1971), Sinai, Egypt



Fig. 17 Photograph showing the ferruginated radioactive, xenotime-bearing sandstone, Ramlet Hemyir area, Sinai, Egypt (Photo by Gehad M. Saleh)

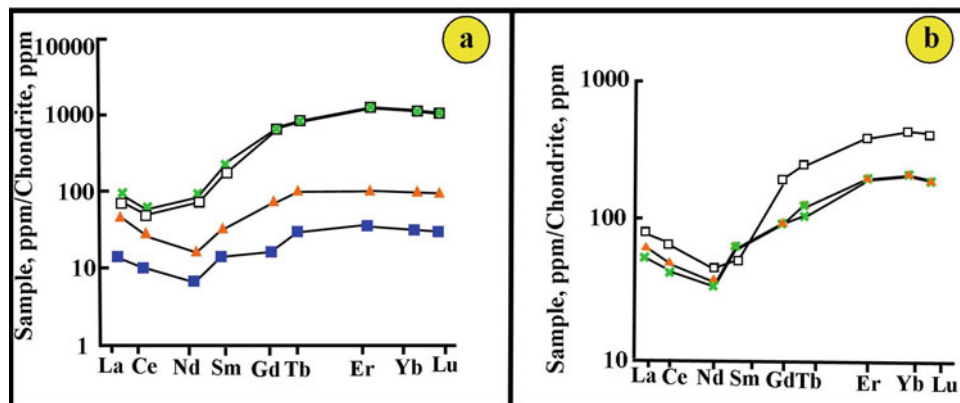


Fig. 18 (a) and (b) Chondrite-normalized REE patterns of some representative samples of **a** Um Hamad (UH) and **b** Ramlet Hemyir (RH) areas, Sinai, Egypt

The frequency distribution of the HREEs and LREEs in the various size fractions (Fig. 20) implies the following significant inferences:

1. Both light and heavy REEs display almost identical frequency confirming their incorporation within the same mineral (i.e. xenotime).
2. The frequency distributions are in each case bimodal with (+2.0– +1.0 mm) and (+0.125 mm) size fractions exhibiting the highest REEs contents.
3. Generally speaking, the LREE/HREE ratio increases with decreasing grain sizes. This phenomenon can be

attributed to the selective adsorption of LREE on clays or scavenged on ferromanganese cementing materials.

4. In spite of the obvious HREE-enriched signature of the analysed bulk samples, still bulk rock samples and size fractions contain high Ce and La, which cannot be contributed from xenotime.

In summary, it can be concluded that the REEs content of the Ramlet Hemyir and Um Hamad areas, Southwestern Sinai, Egypt, bears signatures of xenotime with significant REEs contribution due to adsorption on clays or scavenging by the ferromanganese material. Xenotime occurs mostly in

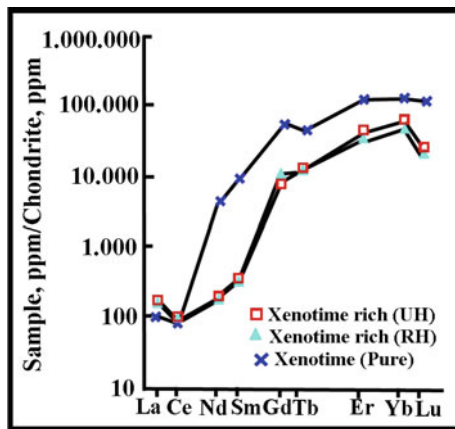


Fig. 19 Chondrite-normalized patterns of xenotime mineral and xenotime-rich concentrates, Ramlet Hemyir (RH) and Um Hamad (UH) areas, Southwest Sinai, Egypt

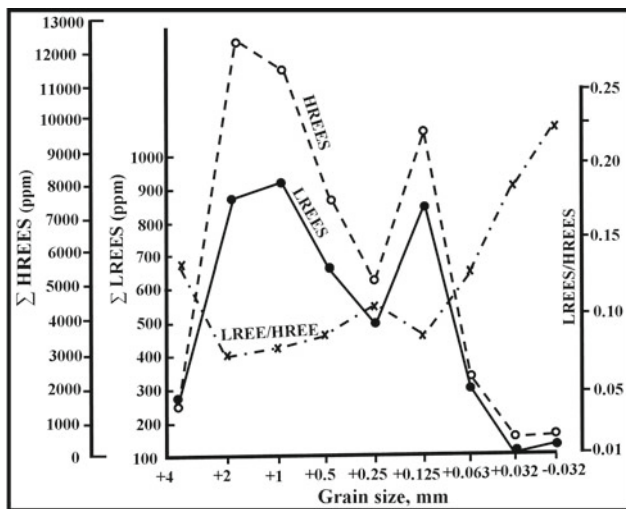


Fig. 20 Abundance distribution of light and heavy rare earths in the various grain sizes of representative sample from Um Hamad xenotime-bearing sediment, Southwest Sinai, Egypt

clay to silty size fractions; therefore, it dominates in the more argillaceous sediments of Ramlet Hemyir. Aero radiometric exploration survey is a priority to delineate the promising xenotime paleoplacers potential sandstone beds.

5 REE Resources in Black Sand Deposits of Egypt

Black sands, which are found as a component of placer deposits, are a heavy, partially magnetic mixture of typically fine sands. On beaches, heavy minerals that are resistant to mechanical concentration mostly occur under high-energy conditions. Along its course from central and eastern Africa in the south to the Mediterranean Sea in the north, the River Nile and its tributaries draw minerals from various sources.

The amount of trace elements in the heavy minerals fraction of the Nile sediments reflects the make-up of the minerals and the origins of the sediments (El Kammar et al., 1992).

The Egyptian placer black sand comprises huge reserves of economic metals-rich heavy minerals that include ilmenite, magnetite, garnet, zircon, rutile, and monazite in addition to the industrial green silicates at the outpouring of the whether today active Rosetta and Damietta branches or the old extinct branches of the River Nile into the Mediterranean Sea coast. Of considerable potentiality is the coastal deposit extending for 17 and 36 km to the west and east of Rosetta promontory (Fig. 21). Monazite with concentrations up to 0.6 wt.% (Moustafa & Abdelfattah, 2011) is considered as an important source for REEs.

Rosetta promontory is surrounded by two embayments to the west and east separated by protruding headland, Rosetta mouth, in the sea formed during the growth of delta. The area west is characterized by narrow to moderately beach face and wide backshore zone (coastal flat). Meanwhile, the area east exhibits moderately beach face and relatively wide backshore zone. The coastal plain is generally flat. The surficial sediments of the backshore flat are composed of well sorted fine to very fine sand.

The Egyptian black sand deposits are present either as beach sediments or in the form of coastal sand dunes. Monazite is one of the economic minerals among the Rosetta beach sands. The assessment of black sand is now being explored by Nuclear Materials Authority of Egypt. The content of monazite in beach sands and coastal sand dunes along the Egyptian Mediterranean coast is normally below 0.01 wt.%. However, monazite concentrations reach to 0.6 wt.% in the eroded beach zones as discontinuous patches or as thin (10-30 cm) layers of surficially highly concentrated black sands near and parallel to the shoreline (Moustafa & Abdelfattah, 2011).

Distribution of Monazite in west Rosetta area grades relatively increases from 0.01 to 0.166% near the promontory to 7.0 km with an average of 0.066% and then decreases westward. Meanwhile, in the east Rosetta area, two sites of monazite accumulations can be recorded. The higher one near the promontory, 3 km from the Rosetta branch eastern bank, after dried lagoonal locality and extend for 10 km. Another site is rather lower, occurring at 24 km to the east from Rosetta mouth. Monazite grades vary between 0.03 and 0.6 wt.% with an average of 0.2 wt.% in the Rosetta east area (Hammoud, 1966). Areas of low and high grades of monazite (and other heavy minerals) are coinciding with the accretion and erosion zones delineated by (Frihy & Komar, 1991; Frihy & Lotfy, 1994).

Two monazite varieties, in the Egyptian black sands, are distinguished, namely Ce-monazite and Th-monazite, however, the extreme Eu deficiency ($\Delta Eu = < 0.1$) (El Kammar et al., 2011, Table 6). Deposits of suitable grades for future

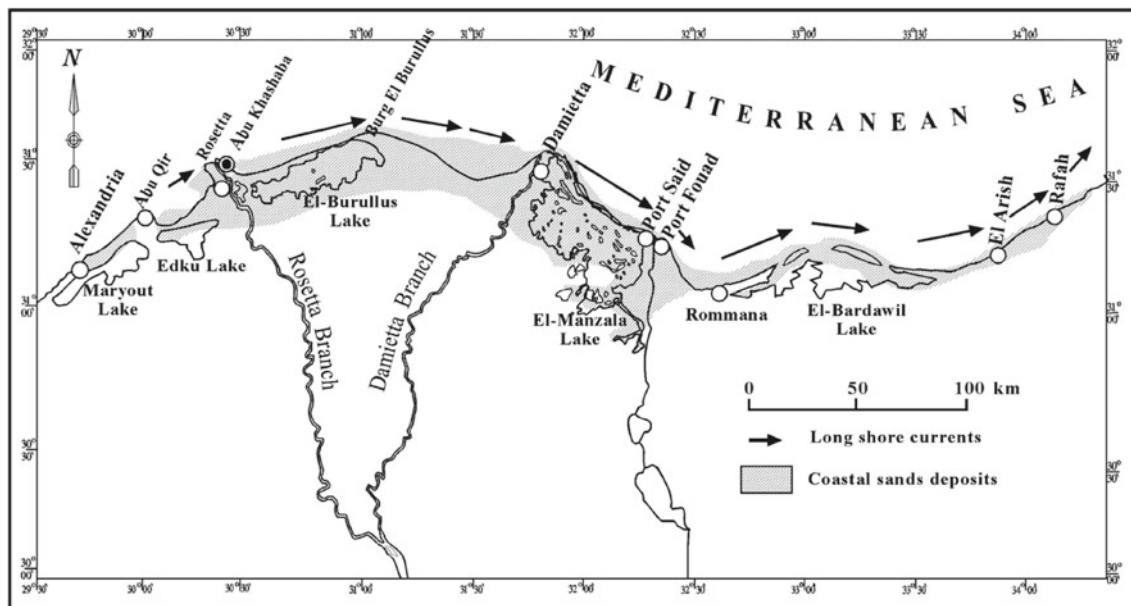


Fig. 21 Location of the coastal placer black sand deposits of Egypt (The stippled belt)

Table 6 Mean data of probe microanalysis for Rosetta monazite, Egypt (El Kammar et al., 2011)

Major oxides (Wt.%)	Monazite (N = 219)
P ₂ O ₅	29.84
SiO ₂	0.79
ZrO ₂	0.01
HfO ₂	< 0.01
ThO ₂	6.05
UO ₂	0.06
Y ₂ O ₃	1.99
La ₂ O ₃	12.52
Ce ₂ O	27.32
Pr ₂ O ₃	3.10
Nd ₂ O ₃	11.10

exploitation (Fig. 21) mainly occur in four localities: the coastal area to the east and to the west of Rosetta, the coastal sand dunes of El Burullus-Baltim, the coastal area of Damietta, and the north Sinai coastal area (Dawood & Abd El-Nabi, 2007).

Acknowledgements The authors would like to express their gratitude to Prof. Dr. Hamed I. Mira, chairman of the Nuclear Materials Authority, for kind facilities during the present work. The authors would like to thank Prof. Dr. Zakaria Hamimi for his kind invitation to contribute the Springer's book "The Phanerozoic Geology and Natural Resources of Egypt". Thanks are also due to Prof. Mahmoud H. Shalaby and Prof. Mohamed A. Obeid for their critical and valuable comments. Thanks are due to Dr. Baaha M. Emad, Nuclear Materials Authority, for helping me in drawing geochemical figures.

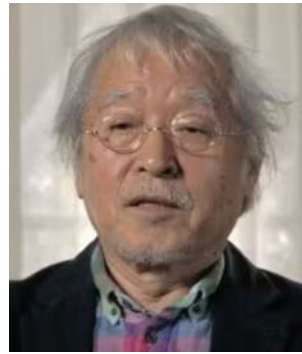
References

- Abdalla, H. M. (2006). An overview on the REE-mineralized alkaline granites in Egypt, with special reference to the Abu Khruq and Gara El Hamra bodies. *Resource Geology*, 56, 365–370.
- Abdalla, H. M., & El Afandy, A. H. (2003). Contrasting mineralogical and geochemical characteristics of two A-type pegmatite fields, Eastern Desert, Egypt. *Egypt Mineral*, 12, 298–328.
- Abdel-Karim, A.-A. M., Azer, M., & Sami, M. (2020). Petrogenesis and tectonic implications of the Maladob ring complex in the South Eastern Desert, Egypt: New insights from mineral chemistry and whole-rock geochemistry. *International Journal of Earth Sciences*. <https://doi.org/10.1007/s00531-020-01937-2>
- Andersen, T. (1984). Secondary processes in carbonatites: Petrology of of "rodberg" (hematite-calcite-dolomite carbonatite) in the Fen central complex, Telemark (South Norway). *Lithos*, 17, 227–245.
- Bachelor, R. A., & Bowden, P. (1985). Petrogenetic interpretation of granitoid rock series using multicationic parameters. *Chemical Geology*, 46.
- Baron, T. (1907). *The topography and geology of the Peninsula of Sinai (western portion)* (Vol. 241). Surv. Dept., Cairo.
- Bau, M. (1996). Controls on the fractionation of isoivalent trace elements in magmatic and aqueous systems: Evidence from Y/Ho, Zr/Hf, and lanthanide tetrad effect. *Contributions to Mineralogy and Petrology*, 123, 323–333.
- Bau, M., & Moller, P. (1992). Rare earth element fractionation in metamorphogenic hydrothermal calcite, magnesite and siderite. *Mineralogy and Petrology*, 45, 231–246.
- Bau, M., & Dulski, P. (1995). Comparative study of yttrium and rare-earth element behaviour in fluooorinerich hydrothermal fluids. *Contributions to Mineralogy and Petrology*, 119, 213–223.
- Black, R., Lameyre, J., & Bonin, B. (1985). The astructural setting of alkaline complexes. *Journal of African Earth Sciences*, 3, 5–16.
- Boily, M., & Williams-Jones, A. E. (1994). The role of magmatic and hydrothermal processes in the chemical evolution of the Strange Lake Plutonic complex, Quebec-Labrador. *Contributions to Mineralogy and Petrology*, 118, 33–47.

- Bonin, B. (1983). *Les granites des complexes annulaires* (Vol. 4). Bureau de Recherches Geologiques et Minières, Manuels et Methodes.
- Bonin, B. (1986). *Ring complex granites and anorogenic magmatism* (Vol. 187). Elsevier.
- Bonin, B., & Giret, A. (1985). Clinopyroxene compositional trends in oversaturated and under saturated alkaline ring complexes. *Journal of African Earth Sciences*, 3, 175–183.
- Bonin, B., & Giret, A. (1990). Plutonic alkali series: Daly gap and intermediate compositions for liquids filling up crustal magma chambers. *Schweizerische Mineralogische Und Petrographische Mitteilungen*, 70, 173–185.
- Bowden, P. (1985). The geochemistry and mineralization of alkaline ring complexes in Africa (a review). *Journal of African Earth Sciences*, 3, 17–39.
- Bowden, P., Kinnaird, J. A., Abaa, S. I., Ike, E. C., & Turki, U. M. (1984). Geology and mineralization of Nigerian anorogenic ring complexes. *Geologisches Jahrbuch Reihe B*, 56, 1–65.
- Briden, J. C., & Gass, I. G. (1974). Plate movement and continental magmatism. *Nature*, 248, 650–653.
- Brown, S. E., & Fairhead, J. D. (1983). Gravity study of Central African rift system: A model of continental disruption. 1-The Ngaoundere and Abu Gabra Rifts. *Tectonophysics*, 94, 187–203.
- Bugrov, V. (1972). *Technical report on follow-up geochemical operations in the period 1968–1972* (Vol. 155). Aswan Mineral survey project, Geol. Surv. Egypt.
- Cerny, P., Meintzer, R. E., & Anderson, A. J. (1985). Extreme fractionation in rare-element granitic pegmatites: Selected examples of data and mechanisms. *The Canadian Mineralogist*, 23, 381–421.
- Charmichael, I. S., & Mackenzie, W. S. (1963). Feldspar-liquid equilibria in pantellerites: An experimental study. *American Journal of Science*, 261, 382–396.
- Conoco Coral (1987). Geological map of Egypt, scale 1:500,000.
- Dawood, Y., & Abd El-Nabi, H. H. (2007). Mineral chemistry of Monazite from the black sand deposits, Northern Sinai, Egypt. *Mineralogical Magazine*, 71, 389–406.
- De Gruyter, P. C. (1983). *The petrogenesis and tectonic setting of the Egyptian alkaline complexes* (Vol. 175). M. Sc. Thesis. Michigan State University.
- De Gruyter, P., & Vogel, T. A. (1981). A model for the origin of the alkaline complexes of Egypt. *Nature*, 291, 571–574.
- Drysdall, A. R., Jackson, N. J., Ramsay, C. R., Douch, C. J., & Hackett, D. (1984). Rare element mineralization related to Precambrian alkali granites in the Arabian shield. *Economic Geology*, 79, 1366–1377.
- Eby, G. N. (1975). Abundance and distribution of the rare-earth elements and yttrium in the rocks and minerals of the Oka carbonatite complex, Quebec. *Geochimica Et Cosmochimica Acta*, 39, 597–620.
- El Kammar, A. A., Philip, G., & Arafa, I. (1992). Geochemistry of recent Nile sediment from the main Nile course in Egypt and the principle tributaries in Ethiopia and Sudan. In *Proceeding of the 1st international conference on the geology of the Arab World* (pp. 527–541), Cairo Univ.
- El Kammar, A. A., Ragab, A., & Moustafa, M. I. (2011). Geochemistry of economic heavy minerals from Rosetta black sand of Egypt. *Journal of Kuwait University: Earth Science*, 22(2), 69–97.
- El Afandi, A. H., & Abdalla, H. M. (2002). Geochemistry of radioactive mineralization at Abu Khruq ring Complex, Southeastern Desert, Egypt: Metallogenetic constraints. *Egypt Mineral*, 11, 329–355.
- El Agami, N. L., & Abdalla, H. M. (2003). Geochemistry of Gara El Hamra Y, Th, REE-mineralized peralkaline granite-syenite complex, Southwestern Desert, Egypt: Metallogenetic constraint. *Egypt Mineral*, 15, 43–77.
- El Kammar, A. M., El-Assy, I. E., & Abram, F. B. (1997). Rare earth elements and crystal chemistry of xenotime bearing sediments of Um Bogma area, Southwestern Sinai, Egypt. *Chemie Der Erde*, 57, 91–101.
- El Ramly, M. F., Budanov, V. I., & Hussein, A. A. (1971). *The alkaline rocks of Southeastern Desert, Egypt*. Egypt Geol. Surv., Paper No. 53.
- El Ramly, M. F., Dereniuk, N. E., Budanov, V. I., Armanious, L. K., & Hayek, G. G. (1969). *Apetrological study on the central part of the Gabal Abu Khruq ring complex*. Geol. Surv. Egypt, Paper No. 52.
- El Shazly, E. M., Assaf, H. S., & El Kassas, I. A. (1969). *The radioactive mineralization of south west Aswan* (Vol. 35). Int. Rep. Geol. And Nuclear Raw Mat. Dept. Atom. Energy Establishment, Cairo.
- El Sökkary, A. A. (1971). Radio-geologic studies of some Carboniferous rocks of West-central Sinai. *Journal of Geology, U. A. R.*, 15 (2), 119–127.
- Ferguson, A. K. (1977). The natural occurrence of aegirine-neptunite solid solution. *Contributions to Mineralogy and Petrology*, 60, 247–253.
- Flynn, R. T., & Burnham, C. W. (1978). An experimental determination of rare earth partition coefficients between chloride-containing vapour phase and silicate melts. *Geochimica Et Cosmochimica Acta*, 42, 679–684.
- Food, E. E. (1982). Minerals of tin, titanium, niobium and tantalum in granitic pegmatites. In P. Cerny (Ed.), *Granitic pegmatites in research and industry. Short course handbook* (Vol. 8, pp. 187–238). Mineralogical Association of Canada.
- Forster, H. J. (1998). The chemical composition of REE-Y-Th-U-rich accessory minerals in peraluminous granites of the Erzgebirge-Fichtelgebirge region, Germany Part II-Xenotime. *American Mineralogist*, 83, 1302–1315.
- Frihy, O. E., & Komar, P. D. (1991). Patterns of beach-sand sorting and shoreline erosion on the Nile Delta. *Journal of Sedimentary Petrology*, 61, 544–550.
- Frihy, O. E., & Lotfy, M. F. (1994). Mineralogy and texture of beach sand in relation to erosion and accretion along the Rosetta Promontory of the Nile Delta, Egypt. *Journal of Coastal Research*, 10, 588–599.
- Garson, M., & Krs, M. (1976). Geophysical and geological evidence of the relationship of Red Sea transverse tectonic to ancient features. *Bulletin Geological Society of America*, 87, 169–181.
- Giere, R., & Williams, C. T. (1992). REE-bearing minerals in a Ti-rich vein from the Adamello contact aureole (Italy). *Contributions to Mineralogy and Petrology*, 112, 83–100.
- Haas, J. R., Shock, E. L., & Sassani, D. (1995). Rare earth elements in hydrothermal systems: Estimates of standard partial molal thermodynamic properties of aqueous complexes of the rare earth elements at high pressures and temperatures. *Geochimica Et Cosmochimica Acta*, 59, 4329–4350.
- Hackett, D. (1986). Mineralized aplite-pegmatite at Jabal Said, Hijaz region, Kingdom of Saudi Arabia. *Journal of African Earth Sciences*, 4, 257–268.
- Hammoud, N. M. S. (1966). *Concentrations of monazite from Egyptian black sands employing industrial techniques* (Vol. 45). Dissertation, Cairo University.
- Harris, N. B. W., Marzuki, F. M. H., & Ali, S. (1986). The Jabel Sayid complex, Arabian Shield: Geochemical constraints on the origin of peralkaline and related granites. *Journal of the Geological Society of London*, 143, 287–295.

- Hashad, A. H., & El Reedy, M. W. (1979). Geochronology of the anorogenic alkalic rocks South Eastern Desert, Egypt. *Annals of the Geological Survey of Egypt*, 9, 81–101.
- Hess, P. C. (1989). *Origins of igneous rocks* (Vol. 336). Harvard University Press.
- Hoggarth, D. D. (1977). Classification and nomenclature of the pyrochlore group. *American Mineralogist*, 63, 403–410.
- Hoggarth, D. D. (1989). Pyrochlore, apatite and amphibole: Distinctive minerals in carbonatite. In K. Bell (Ed.), *Carbonatites: Genesis and evolution* (pp. 105–148). Unwin Hyman.
- Hussein, A. A. (1990). *Mineral deposits*. In R. Said (Ed.), *The geology of Egypt* (pp. 511–566). A. A. Balkema.
- Ibrahim, M. A. (2010). Laterites-bearing REEs, Wadi Natash, South-eastern Desert, Egypt. *Journal of Rare Earths*, 28(3), 471–482.
- Ibrahim, M. A., El-Kalioby, B. A., Aly, G. M., El-Tohamy, A. M., & Watanabe, K. (2015). Altered granitic rocks, Nusab El Balghum area, Southwestern Desert, Egypt: Mineralogical and geochemical aspects of REEs. *Ore Geology Reviews*, 70, 252–261.
- Irber, W. (1999). The lanthanide tetrad effect and its correlation with K/Rb, Eu/Eu*, Sr/Eu, Y/Ho, and Zr/Hf of evolving peraluminous granite suites. *Geochimica Et Cosmochimica Acta*, 63, 489–508.
- Jackson, N., & Douch, C. (1986). Jabal Hamra REE-mineralized silexite, Hijaz region, Kingdom of Saudi Arabia. *Journal of African Earth Sciences*, 4, 269–274.
- Jahn, B., Fuyuan, W. U., Capdevila, R., Martineau, F., Zhao, Z., & Wang, Y. (2001). Highly evolved juvenile granites with tetrad REE patterns: The Woduhe and Baerzhe granites from the Great Xing'an Mountains in NE China. *Lithos*, 59, 171–198.
- Kamal, H. M. (2004). *Mineralogy, geochemistry and extraction of U, Th, and REE from their bearing igneous rocks at southwest Aswan area, Western Desert, Egypt* (Vol. 210). Ph. D. Thesis, Faculty of Sci., Cairo Univ.
- Kampunzu, A. B., & Lubala, R. T. (1991). *Magmatism in extensional structural setting* (Vol. 637). Springer.
- Kapustin, Y. U. L. (1980). *Mineralogy of carbonatites* (Vol. 55). Amerind Publishing Company.
- Karup-Moller, S. (1978). The ore minerals in Ilmaussaq intrusion: Their mode of occurrence and their conditions of formation. *Gronlands Geologiske Undersogelse*, 127, 1–51.
- Kogarko, L. N. (1980). Ore-forming potential of alkaline magmas. *Lithos*, 26, 167–175.
- Le Bas M. J. (1977). *Carbonatite-nephelinite volcanism* (Vol. 347). Wiley.
- Le Bas, M. J. (1981). Carbonatite magmas. *Mineralogical Magazine*, 44, 133–140.
- Le Bas, M. J. (1987). Nephelinite and carbonatites. In J. G. Fitton, & B. G. Upton (Eds.), *Alkaline igneous rocks* (Vol. 30, pp. 53–83). Geological Society of London, Spec. Publ.
- Lutz, T. M., Foland, K. A., Faul, H., & Srogi, L. A. (1988). The strontium and oxygen isotopic record of hydrothermal alteration of syenites from the Abu Khruq complex, Egypt. *Contributions to Mineralogy and Petrology*, 98, 212–223.
- Maniar, P. D., & Piccoli, P. M. (1989). Tectonic discrimination of granitoids. *Geological Society of America Bulletin*, 101, 635–643.
- Markl, G. (2001). Stability of Na-Be minerals in late-magmatic fluids of the Ilmaussaq alkaline complex, South Greenland. *Geology of Greenland Survey Bulletin*, 190, 145–198.
- Marks, W., Vennemann, T., Siebel, W., & Markl, G. (2003). Quantification of magmatic and hydrothermal processes in a peralkaline syenite-alkali granite complex based on textures, phase equilibria, and stable and radiogenic isotopes. *Journal of Petrology*, 44, 1247–1280.
- Martin, R. F. (1969). The hydrothermal synthesis of low albite. *Contributions to Mineralogy and Petrology*, 23, 323–329.
- Monecke, T., Kempe, U., Monecke, J., Sala, M., & Wolf, D. (2002). Tetrad effect in rare earth element distribution patterns. A method of quantification with application to rock and mineral samples from granite-related rare mineral deposits. *Geochimica Et Cosmochimica Acta*, 66, 1158–1196.
- Moustafa, M. I., & Abdelfattah, N. A. (2011). Physical and chemical beneficiation of the Egyptian beach monazite. *Resource Geology*, 60(3), 288–299.
- Naldrett, A. J., & Watkinson, D. H. (1981). Ore formation within magmas. In P. B. Barton (Ed.), *Mineral resources: Genetic understanding for practical applications* (Vol. 165). Natl. Acad., Washington.
- Nagy, R. M., Ghuma, M. A., & Rogers, J. W. (1976). A crustal suture and lineament in North Africa. *Tectonophysics* 31, Issues 3–4, 67–72.
- Ngwenya, B. T. (1994). Hydrothermal rare earth mineralization in carbonatites of the Tundulu complex, Malawi: Processes at the fluid/rock interface. *Geochimica Et Cosmochimica Acta*, 58, 2061–2072.
- Ni, Y., Hughes, J. M., & Mariano, A. N. (1993). The atomic arrangement of bastnasite-(Ce), Ce(CO₃)F, and structural elements of synchysite-(Ce), rotegenite-(Ce), and parisite-(Ce). *American Mineralogist*, 78, 415–418.
- Parson, I. (1978). Feldspar and fluids in cooling plutons. *Mineralogical Magazine*, 42, 1–17.
- Prins, P. (1981). *The geochemical evolution of the alkaline and carbonatite complexes of the Damaraland igneous province, South West Africa* (Vol. 3, pp. 145–178). Ann. Univ. Stellenbosch Ser. A1 (Geol.).
- Saleh, G. M., Kamar, M. S., & Mira, H. I. (2021). Phanerozoic minor volcanics and intrusives of the Arabian-Nubian shield. In Z. Hamimi et al. (Eds.), *The geology of the Arabian-Nubian shield, regional geology reviews*. https://doi.org/10.1007/978-3-030-72995-0_26
- Salvi, S., Fontan, F., Monchoux, P., Williams-Jones, A. E., & Moine, B. (2000). Hydrothermal mobilization of high field strength elements in alkaline igneous systems: Evidence from the Tamazeght complex (Morocco). *Economic Geology*, 95, 559–576.
- Schandelmeier, H., & Pudolo, D. (1990). The Central-African fault zone in Sudan- a possible continental transform fault. *Berliner Geowiss. Abh.*, 120-A, 31–44.
- Serencsits, C., Faul, H., Foland, K. A., El Ramly, M. F., & Hussein, A. A. (1979). Alkaline ring complexes in Egypt: Their ages and relationship to tectonic development of the Red Sea. *Annals of the Geological Survey of Egypt*, 9, 102–116.
- Serencsits, C., Faul, H., Foland, K. A., Hussein, A. A., & Lutz, T. M. (1981). Alkaline ring complexes in Egypt: Their ages and relationship in time. *Journal of Geophysical Research*, 86, 3009–3013.
- Shand, S. J. (1951). *Eruptive rocks* (Vol. 145). Murby, London.
- Shata, A. E. A. (2013). Uranium mineralization hosted by the Paleozoic sandstones at Southwest Sinai, Egypt. *Nuclear Sciences Scientific Journal*, 2, 99–122.
- Shinkawa, (2013). *Characteristic of REE-bearing Um Bogma formation in Southwestern Sinai Peninsula and REE-bearing volcanic rocks in Wadi Natash of Eastern Desert, Egypt* (Vol. 145). Economic Geology Laboratory Department of Earth Resources Engineering, Faculty of Engineering, Kyushu University, M.Sc. Thesis.
- Speer, J. A. (1982a). Zircon. In P. H. Ribbe (Ed.), *Orthosilicates* (Vol. 5, pp. 67–112). Rev. Mineral.
- Speer, J. A. (1982b). The actinides orthosilicates. In P. H. Ribbe (Ed.), *Orthosilicates* (Vol. 5, pp. 113–135). Rev. Mineral.
- Stephenson, D., & Upton, B. G. J. (1982). Ferromagnesian silicates in differentiated alkaline complex: Kungnat Field, South Greenland. *Mineralogical Magazine*, 46, 283–300.

- Takelharal, L., Silveira, F., & Santos, R. V. (2016). Potentiality of rare earth elements in Brazil. In *Rare Earths industry* (pp. 57–71).
- Trueman, D. L., Pedersen, J. C., DE, S. T., Jorre, L., & Smith, D. G. W. (1988). The Thor Lake rare-metal deposits, Northwest Territories. In R. P. Taylor & D. F. Strong (Eds.), *Recent advances in the geology of granite-related mineral deposits* (Vol. 39, pp. 280–290). Can. Inst. Min. Metall., Spec.
- Tuttle, O. F., & Bowen, N. L. (1958). Origin of granite in the light of experimental studies in the system $\text{NaAlSi}_3\text{O}_8\text{-KAlSi}_3\text{O}_8\text{-SiO}_2\text{-H}_2\text{O}$. In *GSA Memoirs* (Vol. 74, p. 153). The Geological Society of America.
- Vail, J. R. (1985). Alkaline ring complexes in the Sudan. *Journal of African Earth Sciences*, 3, 51–59.
- Van Enden, B., Thornber, M. R., Graham, J., & Lincoln, F. J. (1997). The incorporation of actinides in monazite and xenotime from placer deposits in western Australia. *The Canadian Mineralogist*, 35, 95–104.
- Watson, B. (1979). Zircon saturation in felsic liquids. Experimental results and applications to trace elements geochemistry. *Contributions to Mineralogy and Petrology*, 70, 407–419.
- Wendlandt, R. F., & Harrison, W. J. (1979). Rare earth partitioning between immiscible carbonate and silicate liquids and CO_2 vapor: Results and implications for the formation of light rare earth-enriched rocks. *Contributions to Mineralogy and Petrology*, 69, 409–419.
- Wood, S. A. (1990). The aqueous geochemistry of the rare-earth elements. Theoretical predictions of speciation in hydrothermal solutions to 350C at saturation vapor pressure. *Chemical Geology*, 88, 99–125.
- Wright, J. B. (1973). Continental drift, magmatic provinces and mantle plumes. *Nature*, 244, 565–567.



Hiroharu Matsueda is a former professor of economic geology at Hokkaido University (Japan). His mineralogical research on the hydrothermal Japanese systems, especially on gold and the associated alteration phenomena, is well known. Skills and expertise, ore geology, mineral exploration and ore microscopy.



Gehad Mohamed Saleh is a professor of geology and Vice Chairman of Nuclear Materials Authority in Cairo, Egypt. He received MSc (1993) and Ph.D. (1997) degrees from Mansoura University (Egypt), and obtained a postdoctoral fellowship (2005) from the Department of Earth Sciences, Faculty of Engineering at Kyushu University, Fukuoka, Japan. He was affiliated professor in the Geology Department, Faculty of Science, Damietta University (Egypt). His area of interest deals with radioactive minerals in igneous and metamorphic rocks and he supervises several projects in the same domain.



Hamdy Mahmoud Abdalla is an exploration geochemist at Nuclear Materials Authority, Cairo, Egypt. He received BSc and MSc degrees from Alexandria University, Egypt. In 1996, he received a Ph.D. degree from Hokkaido University, Japan. His research interests focus on the rare metals and radio-elements in the specialized granitic rocks of the Nubian Shield from the exploration and genetic points of view.



Shunso Ishihara was a renowned Japanese geologist in the field of the mineralized granite systems. He received an MSc degree in 1963 from Columbia University (USA). He was known for his expertise on ilmenite- and magnetite- mineralized granitoid rocks which he began studying in 1977. His works on Japanese, Thai, Mongolian, Chinese, Australian, and Egyptian granitic rocks were published in more than 120 research papers worldwide. Sadly, Prof. Ishihara passed away on October 3, 2020.



Major Groundwater Reservoirs of Egypt

Mohamed H. Geriesh, Abdou Abouelmagd, and Basma M. H. Mansour

Abstract

Egypt is known as the Nile's gift because it relies on the Nile River for around 94% of its freshwater resources. As a result, Egypt's national security is clearly dependent on the Nile River, where over a hundred million people are now concentrated in a narrow swath of the Nile Valley, which stretches from Aswan in the south to Cairo in the north. The Nile Valley and Delta are home to more than 97% of Egypt's population. The Nile River supplies Egypt with 55.5 billion m³/year reflecting that the average available fresh water resources stand at 600 m³/year/capita in 2020 but considering population growth is expected to drop below the 500 m³/year/capita threshold of absolute water scarcity by 2030. The strategy of the Egyptian Government indicates that the agriculture sector holds 85%, industry 9.5%, and drinking 5.5%. Egypt anticipates a severe water shortage because of the Grand Ethiopian Renaissance Dam (GERD) building upstream of the Blue Nile. Great water demands due to increasing population rate and fixing water resource budget along with great water losses due to evaporation damming of water flow and supply are expected. Therefore, a promising strategic plan to develop water resources in Egypt that depends on developing traditional and non-traditional water resource supplies is recommended. Additionally, the deep groundwater beneath the vast deserts of the western, eastern, and Sinai Peninsula along with limited quantities of rainwater and flooding are considered non-renewable resources and can be exploited according to the development conditions and the water needs. Non-traditional water resources include the reuse of exhaust uses from agriculture, industry, sanitary, industrial sewage, and desalination. This chapter sheds the light on Egypt's major groundwater reservoirs as a potential and strategic solution for water shortage for

expanding agricultural and economic activities until 2030. Egypt's primary groundwater reservoirs are comprised of six aquifers, namely: (1) the aquifers of the Nile Valley and Delta, which are recognized as Egypt's primary source of groundwater supplies and they both provide about 85% of all groundwater abstractions. Annual aquifer withdrawals are estimated at 6.1 Bm³/year, which is mostly replenished by excess irrigation water infiltration or through the irrigation network and Nile distributaries (2) The Nubian Sandstone Aquifer System (NSAS) is Africa's largest fossil aquifer system, with estimated reserves of 150.000 Bm³. Around 2.2 million km² of the NSAS are shared by Egypt, Libya, Sudan, and Chad, with Egypt contributing 828,000 km² (38%). The thickness of the fresh water-bearing layer ranges from 200 meters in East Uwinat to 3,500 meters in the northwestern of El-Farafra Oasis. Between East Uweinat and El-Farafra Oasis, the fresh water layer's thickness ranges from 200 to 3500 m. Recent studies have revealed that the NSAS receives transboundary recharge from Egypt's, Sudan's, and Chad's southern and southwestern borders, as well as local recharge through major fractures and joints along its southern outcrops; (3) the Fissured Carbonate Rock Aquifer, which occupies more than half of Egypt's land area and stretches from the Sinai Peninsula to Libya. . It serves as a confining layer on top of the Nubian Sandstone Aquifer System and features numerous natural springs.; (4) the Fissured Basement Aquifer System, which is located in the Eastern Desert and the southern Sinai Peninsula and is often recharged by modern rainfall ; (5) the Moghra aquifer, which is located in the northwestern Desert of Egypt and the groundwater is flowing towards the Qattara Depression; (6) the Coastal Aquifers that are located along the coastal areas on the Mediterranean and Red seas. The groundwater abstractions are limited due to the risk of saltwater upconing . The groundwater reserve storage in these six aquifers has been estimated to be roughly 1200 Bm³ with variable recharge

M. H. Geriesh (✉) · A. Abouelmagd · B. M. H. Mansour
Geology Department, Faculty of Science, Suez Canal University,
Ismailia, Egypt
e-mail: mohamed_geriesh@science.suez.edu.eg

rates. The long-term sustainability of these aquifers depends on corrective actions including lowering the number of pumping wells, decreasing start-up and operating times, and setting up a drip irrigation system. It is strongly advised to monitor the quantity and quality of groundwater resources.

Keywords

Groundwater reservoirs • Moghra Aquifer • Nile Valley Aquifer • Nile Delta aquifer • Aquifer of Nubian Sandstone Aquifer System • El-Farafra Oasis • Egypt

1 Introduction

Egypt is the Nile's gift (Herodotus, c. 425 BC) as it is dependent on the Nile River in providing approximately 94% of its freshwater resources. As a result, Egypt's national security is clearly dependent on the Nile River, where more than 100 million people are now confined to a small area of the Nile Valley that stretches from Cairo in the north to Aswan in the south. Further, Northern Egypt's Nile Delta population, is quite dependent on the Nile River, whether for drinking, agriculture, industry, or other economic activities. The Nile basin includes a significant mass of Egypt, with the exception of numerous ephemeral drainage networks that drain the Red Sea Hills in the Eastern Desert toward the Red Sea and to the Western Desert in the west. The longest river in the world is the Nile River and the only perennial river that crosses the Sahara Desert, with an estimated length of 6800 km (Said, 1981). The basin course of this significant river is remarkable in that it nearly totally flows from south to north before emptying into the Mediterranean Sea at a latitude of 31° N (Fig. 1). Its basin is relatively narrow and modest in contrast to most other prominent rivers around the world. The Nile Valley and its Delta stretch from south of the Nile valley to the Mediterranean Sea extending from Aswan to the south of Cairo to the Mediterranean Sea north of Cairo. The Nile Valley and Delta are home to about 97% of Egypt's population (Frenken, 2005). The Nile River supplies Egypt with 55.5 billion m³/year reflecting that the average available fresh water resources stand at 600 m³/year/capita in 2020 but considering population growth is expected to drop below the 500 m³/year/capita threshold of absolute water scarcity by 2030 (FAO, 2016). Further water shortage is expected due to building dams on upstream areas of the Nile River. Significant water losses due to evaporation and damming of water flow and supply are expected, as well as the risk of destructive flooding if such dams have weak structural integrity after its complete filling with water is another scenario (Mohamed & El-Mahdy, 2017). The water losses are

usually caused by either poor land-use practices, including the building of canals and drains in poorly suited areas, or flood irrigation techniques (Geriessh et al., 2015; Mansour, 2015). In 1987, the Egyptian government developed a water master plan. This was the first organized attempt to envision the future of the country's water resources and its use. To follow up with that plan, the Ministry of Water Resources and Irrigation (MWRI) established a multidisciplinary group in 2017 to picture the future of water resources and their applications. Egypt's water resources development strategy is based primarily on the development of traditional and non-traditional water resource supplies. It has been common to distinguish between two types of supply:

1. Natural or physical resources: means the volume of water available, whether visible or underground, salty, or fresh.
2. Available resources: The actual available water supply from various water sources is difficult for humans to exploit economically.

According to the Nile Waters Agreement, which Sudan and Egypt signed in 1959 to give themselves full authority over the use of the Nile waters, the Nile River's water resources offer a sizable supply, amounting to 55.5 billion cubic meters annually. Furthermore, deep groundwater beneath enormous deserts in the western, eastern, and Sinai Peninsula, in addition limited amounts of rains and flooding, are considered non-renewable resources that can be utilized based on development conditions and water needs. Non-traditional water resources include the reuse of exhaust uses from agriculture, industry, sanitary, and industrial sewage.

Another unconventional source is the exploitation of shallow underground aquifers in the Nile Delta and valley whose water comes from Nile water leakage or canals, banks, and agricultural water. Finally, desalination as a potential water resource can be exploited, especially on coastal areas on the northern and eastern borders, and some local aquifers with very high-water salinity. The strategy also indicates that the agriculture sector uses 85%, industry 9.5%, and drinking 5.5% of the available water. The water resource development strategy is divided into various stages, the most important of which are:

- Developing additional water resources by expanding the uses of the desalinated saltwater plants to reach 11 billion m³ and exploitation of the deep groundwater to reach 5 billion m³.
- Establishing joint projects with countries of the Nile River basin.
- Applying best management practices that maximize water uses to reconcile the different needs of providing drinking, domestic, agriculture, river navigation, and demands for power production.

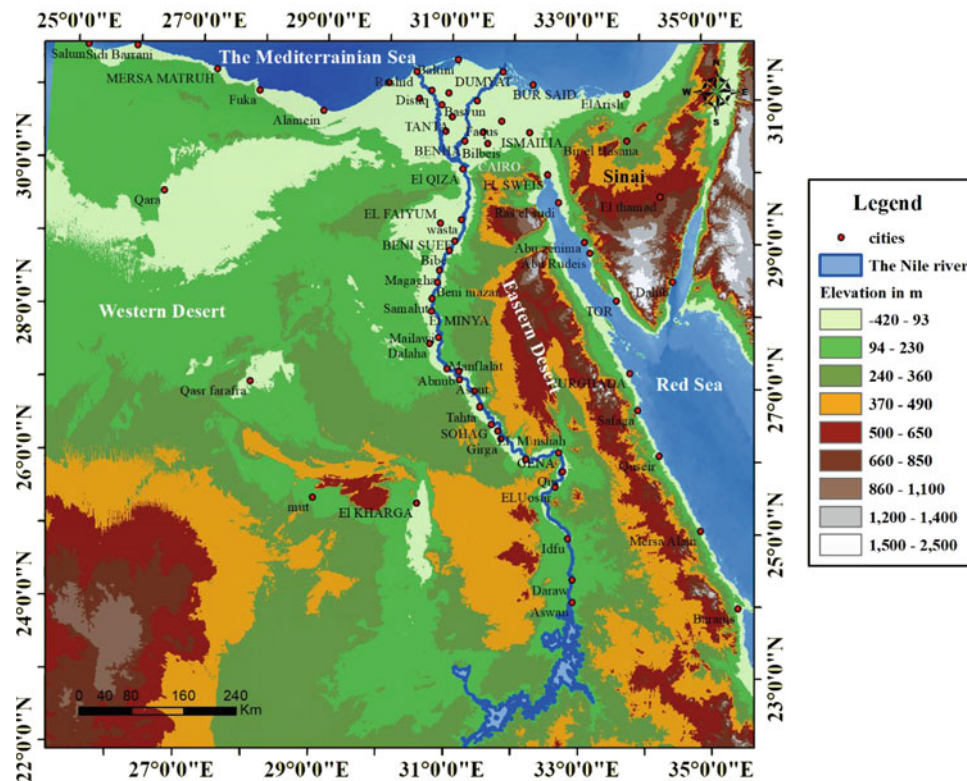


Fig. 1 Nile River location and physiographic map of Egypt

- Maintaining the flow of the Nile River and waterways at a cost of 255 million EGP through the implementation of maintenance and periodic disinfection of irrigation and drainage networks, as well as covering canals and banks that infiltrate residential areas at a cost of 1.4 billion EGP.
- Maintaining a high standard of water quality through cooperation with relevant ministries in the treatment of wastes from industrial and sewage.
- Daily coordination with various ministries and agencies (the ministries of agriculture, electricity, tourism, transport, housing, health, and interior).

This chapter sheds light on Egypt's major groundwater reservoirs (i.e., aquifers) as a potential and strategic solution for water shortage, thus expanding agricultural and economic activities according to the 2030 national plan.

Egypt's primary groundwater reservoirs are made up of six primary aquifers, which are listed below (Fig. 2):

- The Nile Valley and Nile Delta Aquifer (NVNDA).
- The Nubian Sandstone Aquifer System (NSAS).
- The Fissured Carbonate Rock Aquifer (FCRA).
- The Fissured Hard Rock Aquifer (FHRA).
- The Moghra Aquifer.
- The Coastal Aquifer.

2 Nile Valley and Nile Delta Aquifer (NVNDA)

The NVNDA aquifer is of Quaternary and Late Tertiary age, and is overlain by the Nile flood plain, Nile Delta, and its desert fringes. In its majority, it consists of a thick layer of graded sand and gravel that is covered by a clay layer. .

2.1 Geologic and Hydrogeologic Settings

The geologic succession of the Nile Valley ranges in age from Precambrian to Quaternary. Precambrian rocks are mostly igneous and metamorphic in nature. The basement complex's sedimentary strata date from the Paleozoic to the Recent. The NVNDA is mostly made up of Quaternary fluvial sediments. Figure 3 illustrates how its thickness ranges from 300 m in the Middle of Egypt (Sohag Governorate) to just a few meters in the north towards Cairo and south towards Aswan. (Fig. 3). There is no hydraulic linkage between the NVNDA and the underlying Nubian Sandstone Aquifer due to the presence of impermeable Pliocene clayey layers underneath the NVNDA aquifer. However, there could be a linkage between the Quaternary deposits of the

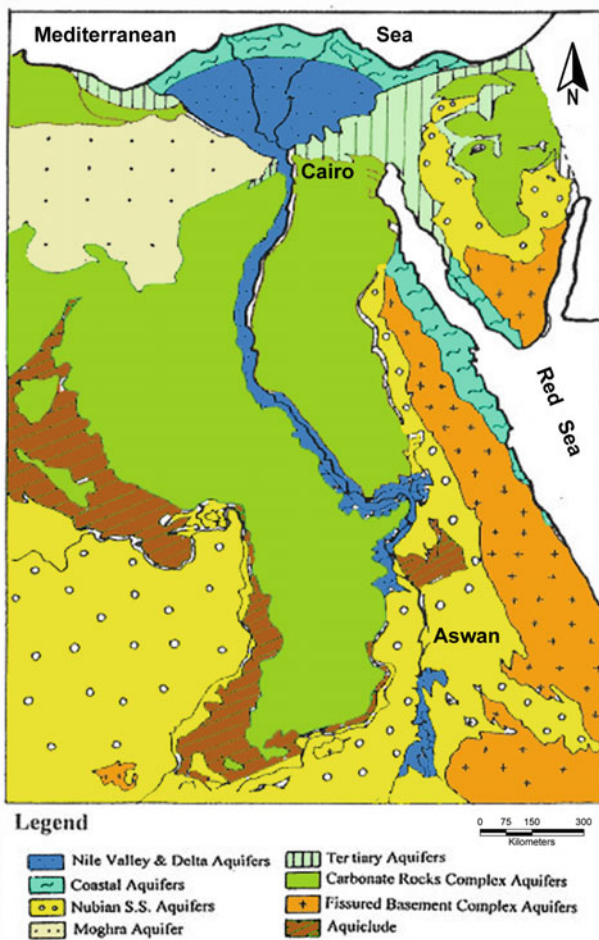


Fig. 2 Hydrogeologic map showing the major groundwater aquifers in Egypt (modified after RIGW/IWACO, 1988)

NVNDA aquifer and the surrounding limestone rocks (Geriesh, 1998). The entire Egyptian Nile Valley is governed by wrench faults that run parallel to both Gulfs of Suez and Aqaba (Geriesh et al., 2020; Youssef, 1968).

Because its salinity is less than 1500 parts per million, the water in the NVNDA is mostly used for domestic uses and irrigation. The NVNDA is a renewable resource, with key recharge sources being infiltration from surplus agricultural water application and leakage from the irrigation canals (El Tahlawi et al., 2008; Geriesh, 1998; Geriesh et al., 2015). The NVNDA’s saturated thickness ranges from 10 to 200 m and its hydraulic conductivity, on the other hand, ranges from 50 to 70 m/day. The Fluvial Pleistocene aquifer (*MitGhamr Formation*) is the Nile Delta’s principal groundwater-bearing layer. It is mostly composed of gravely sand with interbedded and low-extendable clay lenses in the north. The Nile Delta Aquifer is classified as a semi-confined aquifer because it is overlain by Holocene silt, clay, and fine sand in the Nile floodplain (Fig. 4). In the Delta’s northwestern part, a calcareous loamy layer with a thickness varying from 0 to 20 m acts as a confining layer beyond the floodplain. However, there is a hydraulic connection between the Quaternary aquifer and the Moghra aquifer to the west (Fig. 2). Such connection can be confirmed by observing the westward continuation of the piezometric gradient. At the desert’s fringes, the semi-confined layer is vanished, and phreatic conditions prevail (El Tahlawi et al., 2008; Geriesh et al., 2015). The thickness of the groundwater storage strata varies depending on location; nevertheless, 190 m is the average thickness. It progressively rises to the north, reaching 350 m in Tanta City. The water layer thickness ranges between 120 and

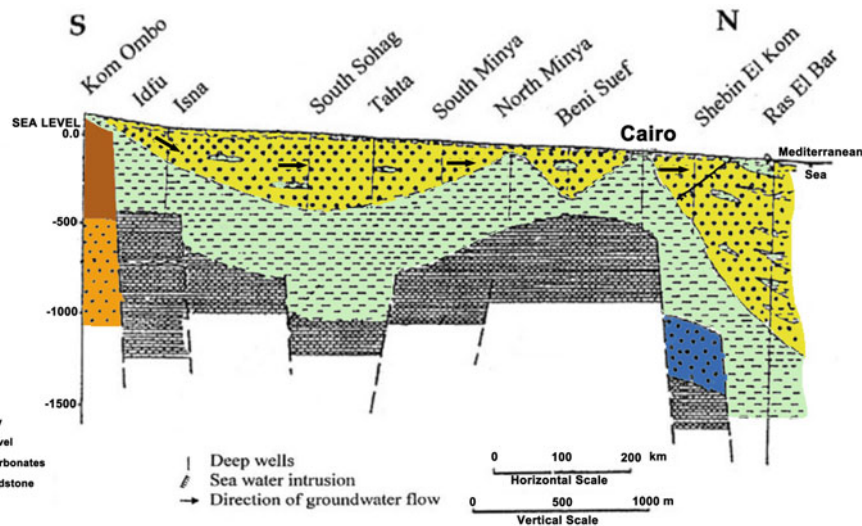


Fig. 3 Hydrogeologic profile through the Nile Valley and Delta basins (modified after Hefny & Shata, 2004)

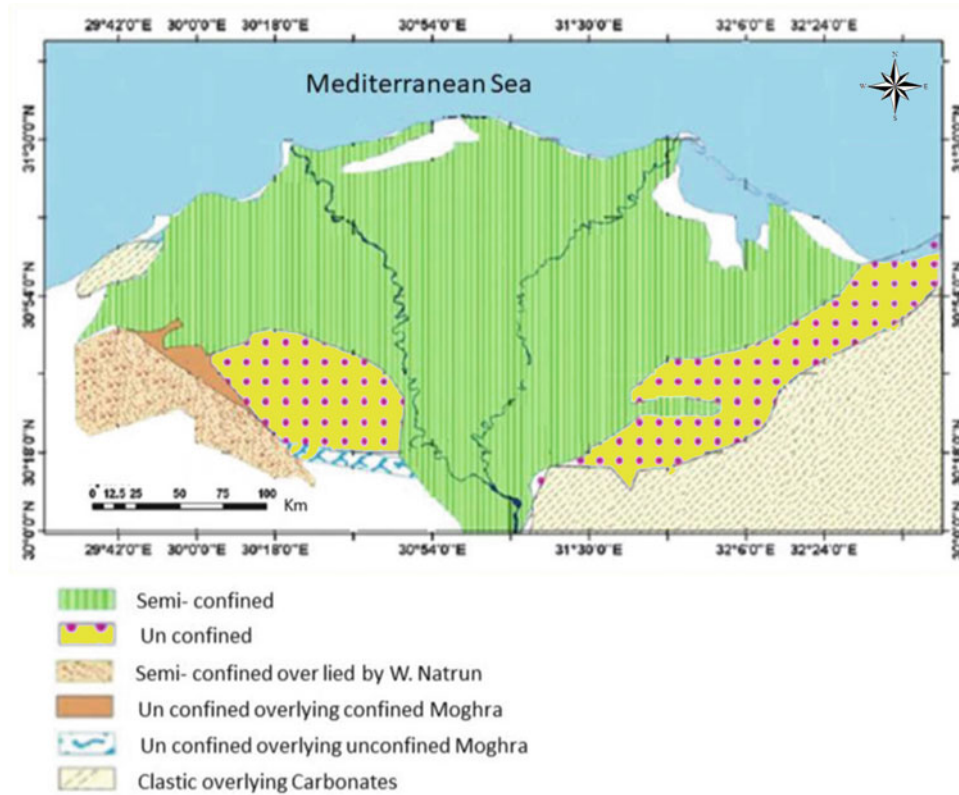


Fig. 4 Groundwater aquifers in the Nile Delta (modified after El Tahlawi et al., 2008)

220 m in the western section of the Nile Delta, and gradually decreasing toward the east. The entire thickness of the aquifer grows from Cairo northward to reach about 1000 m toward the Mediterranean coast (Idris & Nour, 1990). The depth of the groundwater level in the Nile Delta Aquifer increases from north to south. It ranges from one to two meters in the north to three to four meters in the center and five meters in the south (Armanious et al., 1988).

Because the salinity does not exceed 1000 ppm, the southern part of the aquifer has better quality and quantity than the northern part as the irrigation water infiltration always recharges the aquifer (Geriesh et al., 2015; Idris & Nour, 1990). In the Quaternary Nile Delta aquifer, the horizontal hydraulic conductivity ranges between 0.05 and 0.5 m/day. The storage coefficient ranges between 10^{-4} and 10^{-3} , with 0.3 indicating the porosity of the aquifer medium. The transmissivity ranges from 500 m²/day at the desert's edge to 25,000 m²/day in the Nile Delta's apex. The northern regions of the aquifer have quite distinct conditions as the aquifer becomes less productive, higher salinity due to saltwater upconing, high evaporation, and rising groundwater levels, Figure 5 depicts the vertical distribution of the water-bearing layers in the Nile Delta (5). The Holocene silty sand and mud (*Belqas Formation*) overlay the Pleistocene aquifer along the main southern flood plain but with an extremely variable thickness ranging from the south to north

between 4 and 50 m, respectively. This aquifer is also confined along the northern boundaries, especially along the coastal zone. While the majority of the other parts of the desert fringes are considered unconfined, the Pleistocene aquifer is generally under phreatic conditions. Several perched aquifers are formed together with the northern coastal plain's lowlands and the Delta of Wadi El-Tumilat branched to the east, particularly within dune accumulations. Most of these parts are suffering from water logging and soil salinization due to the high prevailing evaporation rate (El-Fawal & Shendi, 1991; Geriesh, 2000). Global glacial-eustatic sea-level changes were the most powerful paleoenvironmental impacts the Nile Delta's groundwater flow regimes, particularly throughout the Quaternary period (Diab et al., 1997; Fairbanks, 1989; Geirnaert & Laeven, 1992; Geriesh, 2000; Geriesh et al., 2015; Perissorateis & Conispoliatis, 2003; Zaghoul et al., 1979).

2.2 Palaeohydrogeologic History

The Nile Delta's principal fluvial Pleistocene aquifer is the most potential water-bearing layer. It is made of porous sand and gravel with clay lenses and has a maximum thickness of around 975 m (Zaghoul et al., 1979). At the central Nile Delta, the Holocene silt and clays overlay the Pleistocene

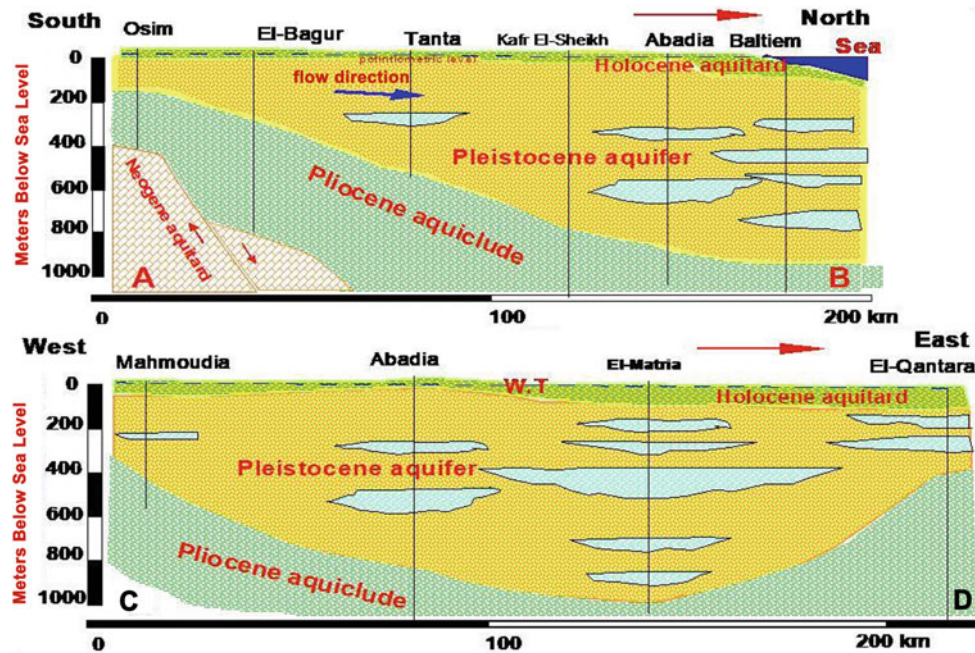


Fig. 5 Hydrogeologic cross-sections in the Nile Delta (modified after Geriesh et al., 2015)

aquifer. While along the western and eastern flanks, it is unconformably overlain by a thin reddish pebbly gravel layer, most probably El Abbassia gravel, which was deposited by the Late Pre Nile-early New Nile system (Said, 1981). In most areas, the Miocene and Pliocene successions underlain the Quaternary sediments in the Nile delta, functioning as an impermeable layer for the main Quaternary aquifers. From bottom to top, the Nile Delta's Neogene-Quaternary subsurface is divided into eight formations: *Sidi Salim*, *Qawasim*, *Rosetta*, *Abu Madi*, *Kafr El-Sheikh*, *El-Wastani*, *Mit Ghamr*, and *Bilqas*. Three cycles are represented by these formations (Rizzini et al., 1978) or four cycles (Zaghloul et al., 1979) and can be distinguished based on the environmental conditions of deposition (Fig. 3). The Neogene-Quaternary succession is mainly represented by shale, with interbedded layers of dolomitic marl in the bottom section and sandstone and siltstone at the top. According to Zaghloul et al. (1979), the shale has a foreshore to nearly deep marine character and was formed in a transgressive sea, whereas the top sandstone appears to have been deposited in a somewhat regressive sea. The *Mit Ghamr Formation*, on the other hand, is the most important hydrogeological unit in the aforementioned successions. Its thickness increases gradually northwards and is open into the sea to form the Nile cone deposit (Fig. 5). This unit's basin mostly covered the area of the present Delta, and its fringes with a shoreline formed nearly at the present coast but extended further southeast and southwest (Attia, 1954). The Pleistocene water-bearing layers appear to have been deposited under lagoon fluvial and beach environments,

according to Zaghloul et al. (1979). These sediments reflect the start of the third Holocene Sea transgression phase, advancing primarily from the north and northeast. The Plio-Pleistocene aquifer's deposition regime is more influenced by Europe's glacial periods. During that time, the coastline was near the continental shelf's edge, and the Nile River created new channel deposits of sands and gravels with minor clay. The entire delta surface was thus sub-aerially exposed, resulting in clay oxidation and the production of gypsum and salt crusts during arid phases (Geirnaert & Laeven, 1992). The sea level rose rapidly between 18,000 and 7500 years B.P., and the marine clays can be found up to 50 km inland. The sea reached its greatest extent at 5000 years B.P., after which it receded to its current shoreline. During the Holocene, regular flooding resulted in the deposition of thick layers of clay and silt until the High Dam construction in 1970, which eliminated the Nile's seasonal floods. The necessary information about this subject was collected from different sources such as (Butzer, 1967; El-Fayoumi, 1987; Fairbridge, 1967; Geriesh et al., 2015; Sestini, 1989; Shackleton & Opdyke, 1977; Shepard, 1963; Zaghloul et al., 1979). The Nile Delta witnessed significant changes during the Late Pleistocene due to major changes in sea level and climate conditions. The interglacial periods that separated the Middle Pleistocene from the Late Pleistocene caused a sea-level rise of roughly 13 m above its current level (Fairbridge, 1967), undulating the sub-aerial delta plain and aggravating the distributaries on the lowlands. The last Pleistocene maximum transgression invaded most central lowlands at the period from 13,000 to

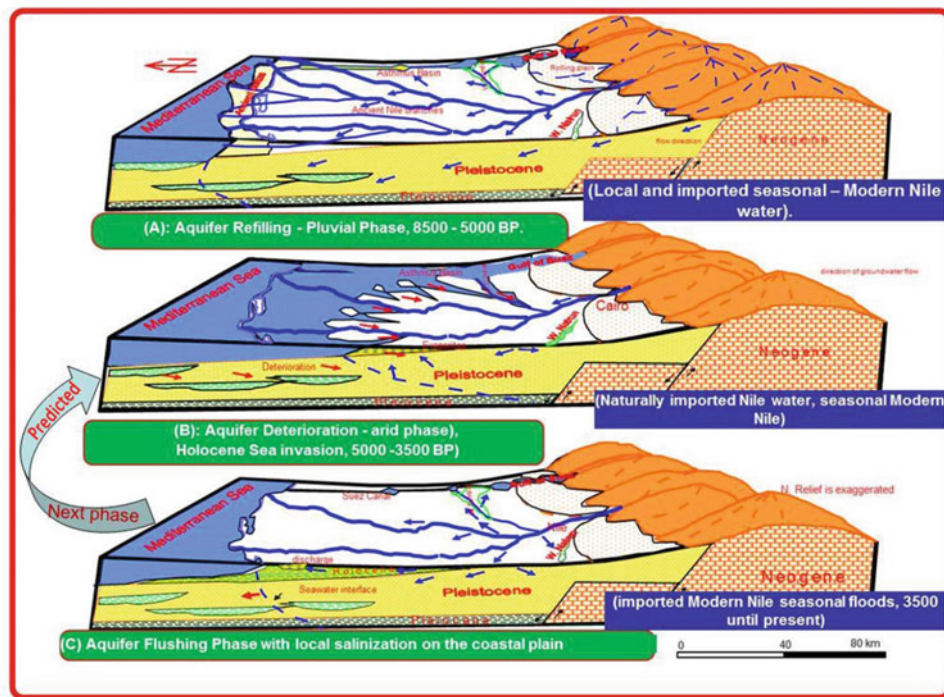


Fig. 6 3D model shows the paleo-hydrogeological history of groundwater recharge of the Nile Delta during the Holocene episode. Model (A) shows the aquifer refilling phase during the pluvial phase (8500–5000 B.P.), model (B) shows the aquifer deterioration phase during Holocene (5000–3500 B.P.), and model (C) shows the aquifer flushing phase from 3500 BP until the present. The blue curved arrow indicates that model (B) is expected to prevail as the next phase (modified after Geriessh et al., 2015)

6000 years B.P. It rose to a level varying between 9–15 m above the present sea level. Continuous Sea level fluctuation but within the range of its present Sea level characterized the latest Pleistocene period (Geriessh et al., 2015). The statistical analysis of radiocarbon dates for Saharan groundwater has supported the Holocene recharging period (Geyh & Jakel, 1974). Two or three different distinct short and humid phases have been discussed in the literature, with rainfall maximums ranging between 8500 and 5500 years B.P. (Rognon & Williams, 1977). There is also general agreement that one intermediate arid phase occurred approximately 7000 years B.P. and that no major humid period has occurred since 3500 years B.P. Inspection of the above-discussed paleo-hydrogeological history suggests that the most critical events to evaluate the existing groundwater aquifers are those that prevailed during the Holocene (Fig. 6). The Holocene time is characterized by two major climatic phases (El-Asmar, 1991; Geriessh, 2000; Geriessh et al., 2015). The older phase, which corresponded to the early Holocene, was distinguished by a warm-wet climate. Whereas, the younger one, 5000 to 3000 years B.P., was distinguished by arid climatic conditions associated with the Atlantic-sub-boreal phases. These two major climatic changes were also mentioned by Wendorf et al. (1977), Stanely and Maldonado (1977), Paulissen and Vermeersch (1987), Paepe and Mariolokos (1984), Van Overlop (1984) and were deduced from

the post-glacial climatic curve of the Levant who pointed out the two climatic phases related to the Holocene. The older one (10,000–7500 B.P.) was humid, and the younger one was dry and related to the Atlantic stage. According to Rognon (1987) and Geriessh et al. (2015), there was a wet phase during the Holocene dated up to 6000 years B.P., followed by an arid phase during which gypsiferous deposits occurred formed at low land areas. It should be noted that groundwater age of the Pleistocene aquifer of the Nile Delta spans between 3000 and 8000 years B.P. (Geirnaert & Laeven, 1992; Geriessh et al., 2015).

2.3 Groundwater Recharge

Many authors have discussed the Nile Delta's hydrogeology and groundwater movement, including Shata and El-Fayoumy (1970), Geirnaert and Laeven (1992), Dahab (1994), Diab et al. (1997), Geriessh (2000), and Geriessh et al. (2015). Groundwater recharge (Fig. 7) to the Pleistocene aquifer occurred via downward seepage from surface water (Nile branches and surface irrigation system) and by excessive irrigation in the traditionally cultivated lowlands and reclaimed desert fringes, (Geriessh et al., 2015). Rainstorms may also contribute in recharging, particularly in the unconfined aquifers of the southeast and southwest rolling plains.

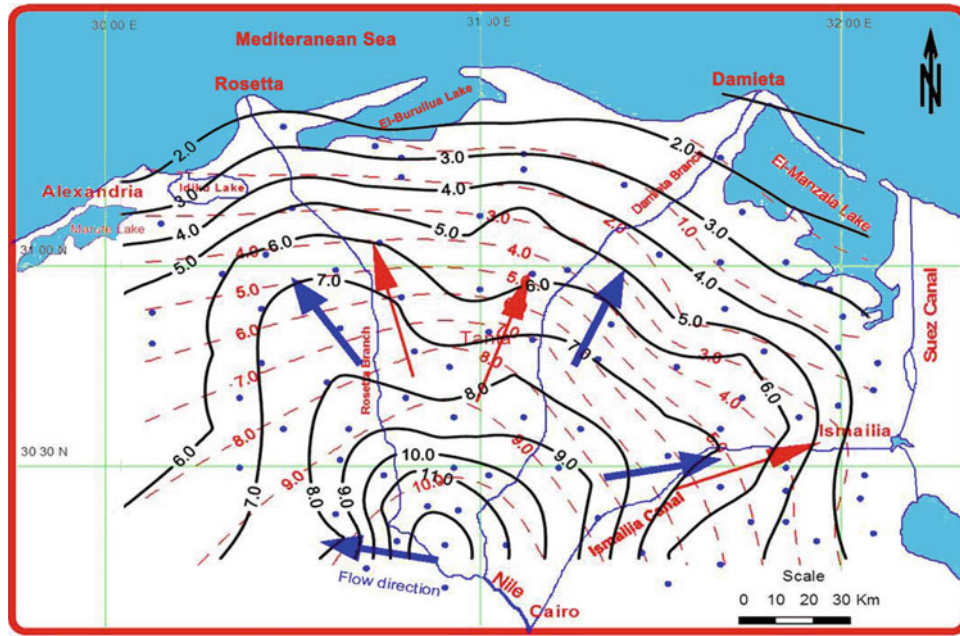


Fig. 7 Groundwater table map of both Pleistocene aquifer (black) and Holocene aquifer (red) of the Nile Delta (modified after Geriesh et al., 2015)

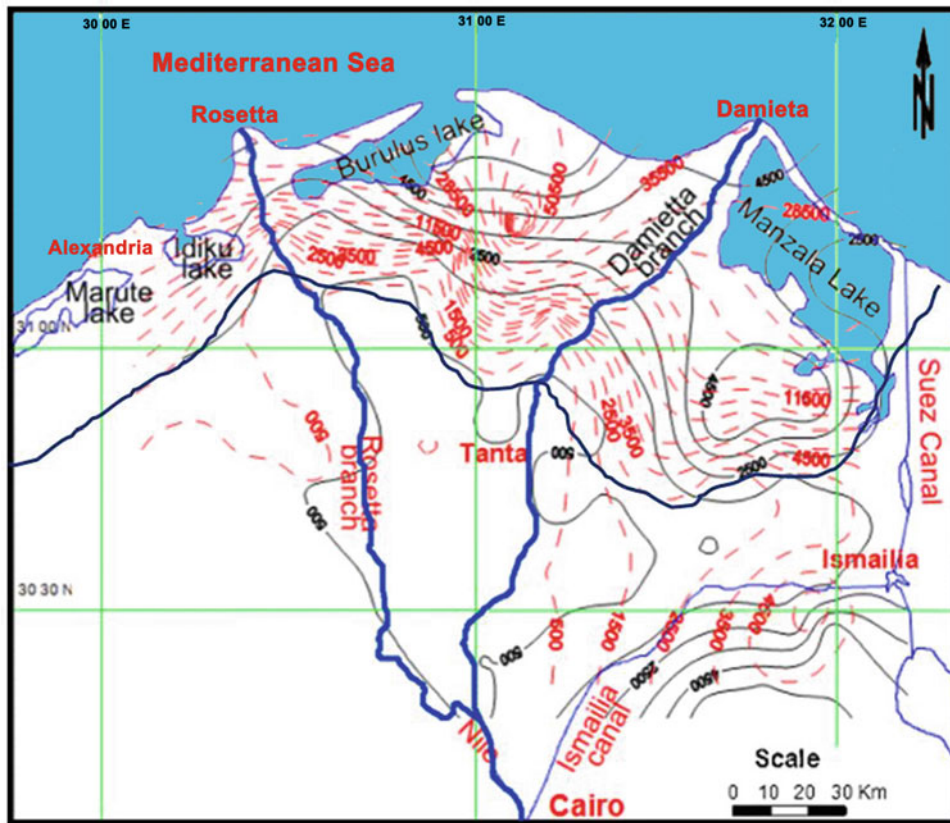


Fig. 8 Groundwater salinity in ppm of both Pleistocene aquifer (black) and Holocene aquifer (red) of the Nile Delta (modified after Geriesh et al., 2015)

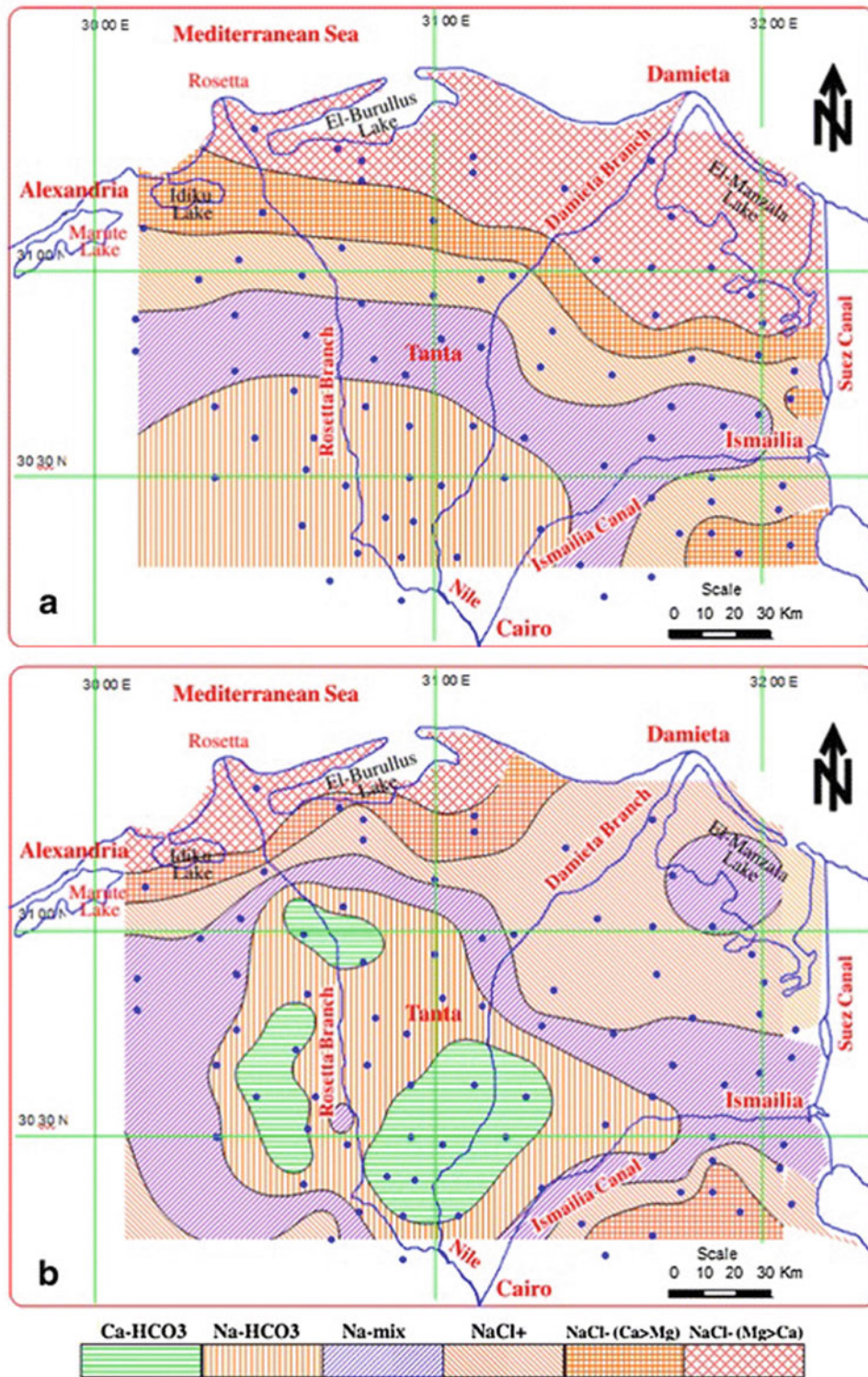


Fig. 9 Hydrochemical facies of both Holocene (a) and Pleistocene (b) aquifers of the Nile Delta (modified after Geriesh et al., 2015)

The general groundwater flow is from south to north, eventually reaching the Mediterranean Sea and coastal lakes. Local groundwater flows from the Nile branches eastward to the Suez Canal and northern lakes (El-Manzala

and El-Balah lakes), and westward to Wadi El Natrun (Fig. 7). The hydraulic gradient is quite low throughout the area, ranging between 0.1 and 0.3 m/km (Geriesh et al., 2015).

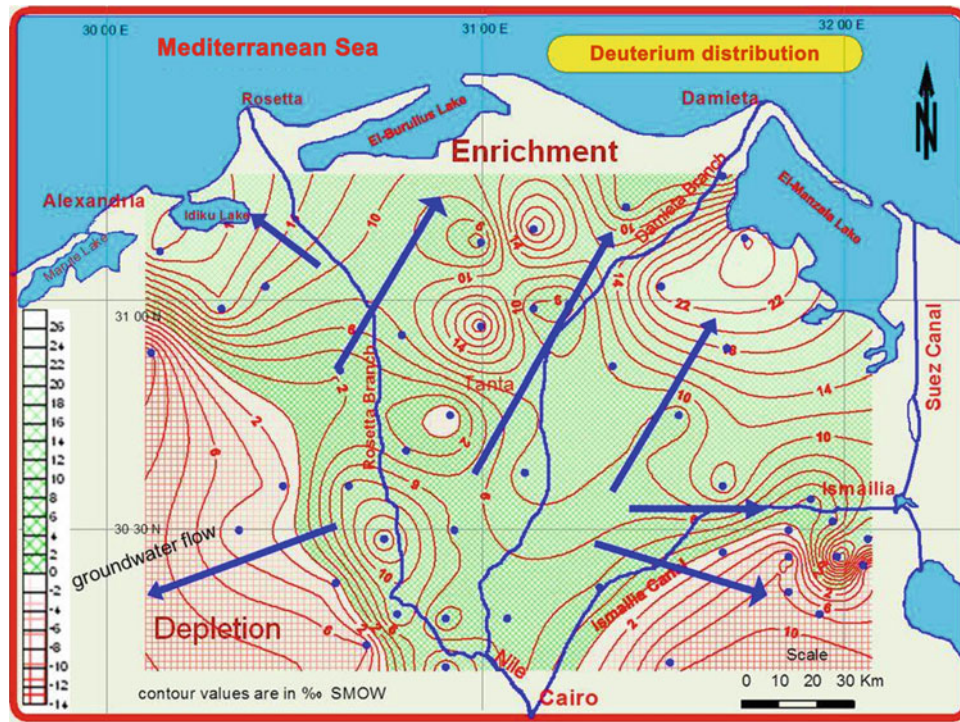


Fig. 10 Deuterium distribution map of Nile Delta aquifer (modified after Geriesh et al., 2015)

2.4 Hydrogeochemistry and Groundwater Quality

Many studies have been carried out about the hydrochemistry of the Nile Delta's groundwater aquifers including Shata and El-Fayoumy (1970), Abdel Mogheeth (1975), Diab et al. (1997), Geirnaert and Laeven (1992), Mansour (2015), and Geriesh et al. (2015). According to these investigations, Nile Delta groundwater varies greatly in composition and salinity (Fig. 8). Salinity maps show two distinct zones, low salinity (TDS < 1000 ppm) nearby the flood plain and the Rosetta branch and high salinity (TDS > 10,000 ppm) along the coastal plain to the north and nearby the Suez Canal to the east (Fig. 8) are separated by a distinct interface as shown in Fig. 8, which could be attributed to the change in lithologic facies from alluvial to fluvio-marine salty facies and the impact of evaporation on the shallow water of the lowland areas to the north. The salinity contour lines around the Suez Canal and the attached lakes indicate discharge boundaries. Groundwater facies (Fig. 9) vary gradually from Ca-HCO₃ and Mg-HCO₃ close to the flood plain and Rosetta branch to Na-HCO₃ and Na-Mix to the west and the north and finally to Na-Cl and Ca-Cl toward the desert fringes and Na-Cl and Mg-Cl toward the coastal plain (Fig. 9). In the Na-Mix zone, Na exists as a surplus ion (Na > Cl), which may be attributed to the leaching process to a former brackish or saline water in this zone. Stable isotope analyses of the western Nile Delta flank indicated that most analyzed samples are arranged in a

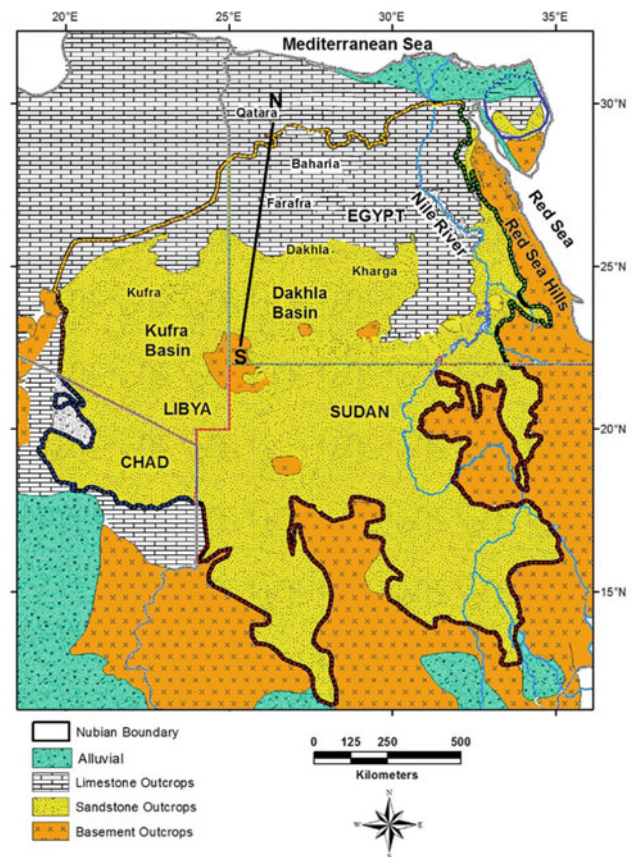


Fig. 11 Geographic distribution and regional geology of the Nubian sandstone aquifer system (NSAS) with delineating recharge areas (modified after Sultan et al., 2013; Thorweihe, 1982)

Table 1 Average aquifer thickness, transmissivity, and hydraulic conductivity of the NSAS in the Oases of the Western Desert (Hesse et al., 1987; Sefelnasr, 2002)

Area	Thickness (m)	Transmissivity (m ² /s)	Conductivity (m/s)
Kharga	1250	$3.2 * 10^{-2}$	$2.5 * 10^{-5}$
Dakhla	1750	$7.5 * 10^{-2}$	$4.8 * 10^{-5}$
Farafra	2600	$1.2 * 10^{-2}$	$4.2 * 10^{-5}$
Bahariya	1880	$8.8 * 10^{-3}$	$4.5 * 10^{-5}$
East Uweinat	430	$1.3 * 10^{-2}$	$2.3 * 10^{-5}$
Kufra	2850	$1.1 * 10^{-2}$	$5.9 * 10^{-5}$
Selima	260	$2.6 * 10^{-2}$	$1.3 * 10^{-5}$

Adapted from Hesse et al. (1987) and Sefelnasr (2002)

linear relationship between precipitation and Nile water (Awad & Nada, 1992; Geirnaert & Laeven, 1992; Geriessh et al., 2015). This might imply that the Nile is constantly releasing groundwater from the southern flood plain and Rosetta branch into the lowlands of Wadi El-Natrun (Fig. 10). This association shows that mixing of Nile water and fossil groundwater occurs where groundwater becomes more depleted in heavy isotopes as it moves toward the desert fringes, yet samples near Nile branches are enriched in heavy isotopes.

3 The Nubian Sandstone Aquifer System (NSAS)

The NSAS is Africa's most widespread fossil aquifer system, with a groundwater capacity estimated to be 150,000 Bm³, equivalent to about 500 years of Nile River discharge (CEDARE, 2002; Salem & Pallas, 2002; Thorweihe, 1990; Thorweihe & Heintl, 2002). The NSAS is one of the world's largest transboundary aquifers, shared by Egypt, Libya, Sudan, and Chad (Fig. 11). It covers an area around 2.2 million km², including 828,000 km² in Egypt (38%), 760,000 km² in Libya (34%), 376,000 km² in Sudan (17%), and 235,000 km² in Chad (11%). The majority of the aquifer's water resources are located in Egypt and Libya, with Chad and Sudan having a lesser fraction (CEDARE, 2002; Thorweihe & Heintl, 2002). The NSAS has a maximum depth of 4500 m and a hydraulic head varying from 570 m above mean sea level west of Darfur in Sudan to -78 m below mean

sea level in Egypt's Qattara Depression (Sefelnasr et al., 2015). The freshwater layer's thickness ranges from 200 m east of Uweinat to 3500 m northwest of El-Farafra Oasis (RIGW, 1990), with medium to good hydraulic properties, as shown in Table 1. The following are the actual withdrawal rates from the NSAS as of 2012: Egypt: 1029 Mm³/yr; Libya: 851 Mm³/yr; Sudan: 406 Mm³/yr; and Chad: 1 Mm³/yr (Ahmed, 2013). The NSAS water storage in Egypt is believed to be roughly 40,000 Bm³, but unfortunately this is not renewable due to the low recharge of groundwater in the Western Desert (El-Rawy et al., 2020; Heintl & Thorweihe, 1993). The NSAS was initially used on a wide scale in Egypt in 1960, in the main Oases of the Western Desert, with total groundwater extraction projected to be in the billions of cubic meters (CEDARE, 2014).

3.1 Geologic and Hydrogeologic Settings

The Nubian Aquifer System (NSAS) is made up of Paleozoic and Mesozoic deposits that overlying the Precambrian basement complex that underlies the entire NSAS basin. The NSAS is composed of medium to coarse sandstone formation (Fig. 12). Because of different water-bearing strata, the NSAS contains two distinct groundwater systems: (1) the Lower Nubian Aquifer System (LNAS), which is over 400 m thick and is under unconfined condition below the 25th latitude, but confined in the north; and (2) the Post Nubian Aquifer System (PNAS), which often occurs north of the 25th latitude and overlies the (LNAS) in Egypt's Western Desert and northeastern Libya.

The NSAS is divided into three major sub-basins:

- Kufra sub-basin in northeastern Chad, northwestern Sudan, and Libya.
- Dakhla sub-basin in Egypt.
- Northern Sudan Platform sub-basin in northern Sudan.

At the western desert, the aquifer is mostly made of hard ferruginous sandstone with thick shale and clay intercalation and ranges in thickness from 140 to 230 m (Sefelnasr et al., 2015).

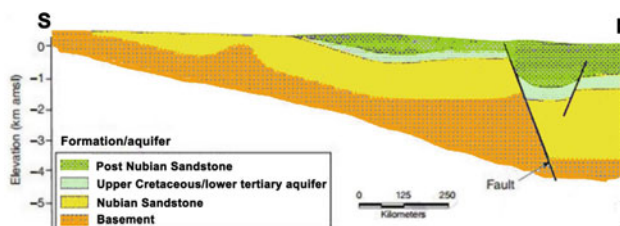


Fig. 12 Geologic cross-section of the Nubian sandstone aquifer system from S to N along the western desert of Egypt (modified after Thorweihe, 1990)

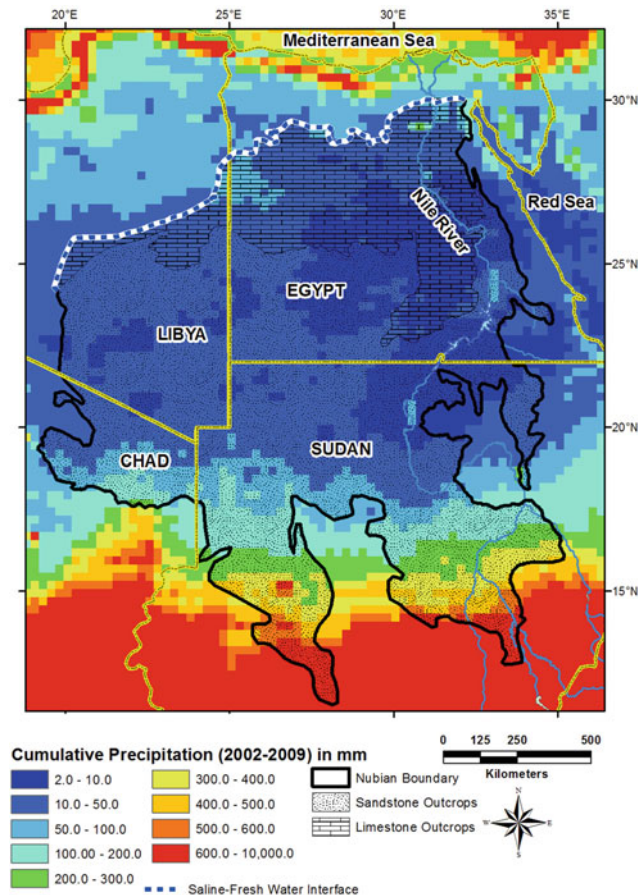


Fig. 13 Cumulative average precipitation rate derived from three-hourly Tropical rainfall measuring mission (TRMM) data over NSAS during the period from 2002 to 2009 (Sultan et al., 2013)

The Upper Cretaceous Nubian Sandstone Aquifer, which lies near the land surface in some regions, is the major aquifer in the Western Desert. The Late Paleocene and Early Eocene Esna Shale cover most of it, followed by a highly broken Eocene limestone (Geriesh et al., 2020). In West of Aswan, an erosional unconformity can be detected, and thick fluvial deposits from various origins and ages cover the Nubian Sandstone Aquifer. Despite its enormous size, the NSAS is regarded a closed system since it is naturally bounded to the west and south by mountainous outcrops of the Kordofan Block, Ennedi, and Tibesti, and to the east and southeast by Nubian Shield mountain ranges (Fig. 11). The Saline-Freshwater Interface is the natural northern boundary of the Nubian Sandstone Aquifer System, and its location is assumed to remain spatially constant (Fig. 12). Most groundwater in the NSAS is meteoric in origin (i.e., atmospheric), while minor part is derived from magma (Juvenile water). Low irregular rainfall, constant drought, land degradation, and desertification characterize the region's climate. Rainfall occurs most frequently between June and October, with an annual average of less than 25 mm in the

far north. It usually increases to the south, with an average of 200 mm near Khartoum, although its distribution is highly varied (Fig. 13).

3.2 Aquifer Recharge and Hydrogeochemistry

Several studies relate the recharge of the NSAS to Nile River along its eastern borders, groundwater flow from the Blue Nile, and local rainfall on ephemeral watersheds in the mountainous terrains. Due to groundwater discharge into depressions, evaporation potential in regions with shallow groundwater table, and upward leakage into confining beds, low values of infiltration rate were obtained when compared to natural groundwater flow. As a result, under current climate conditions, the NSAS is considered as a non-renewable groundwater resource (Mirghani, 2012). It is also believed that the NSAS receives current recharge regionally from southern borders (Sudan and Chad) and locally (west of Nasser Lake and Aswan) through significant fractures and joints, as well as in the northern regions of Sinai Peninsula where exposed aquifer rocks receive high amounts of rainfall (e.g., Geriesh et al., 2020; Robinson et al., 2007; Sultan et al., 2013). The NSAS has an isotopic signature that is depleted, with ^{18}O levels ranging from -9.8 to -10.99 ‰ and ^2H values ranging from -77.6 to -87.8 ‰ (Abouelmagd et al., 2012, 2014; Aly et al., 1989; Geriesh et al., 2020; Hamza et al., 1982; Swailem et al., 1983). Further studies on fossil groundwater from the Nubian Aquifer in the Sinai Peninsula revealed that their radiocarbon ages ranged from ~ 24,000 to ~ 31,000 years B.P., indicating recharge during and/or before the Last Glacial Maximum (Abouelmagd et al., 2014). These isotope signatures may have indicated paleo-water replenishment during the Late Pleistocene (Geriesh et al., 2015). Nile water seepage; local rainfall on aquifer outcrops, and local infiltration from precipitation during previous wet periods are also sources of recharge. Groundwater varies from fresh to somewhat saline (salinity ranges between 240 and 1300 ppm). Low salinity and, in some cases, super-fresh groundwater characterize the majority of the water-bearing Nubian sandstone layers. In many areas such as the Farafra Oases and deep layers in the Siwa Oasis. The Na-Cl and Na-Cl- HCO_3 groundwater types represent the Nubian Sandstone aquifer's old meteoric water (Geriesh et al., 2020)

3.3 Groundwater Flow and Aquifer Characteristics

Groundwater flow in the NSAS is generally from South to North at Dakhla Basin in the Western Desert (Sefelnasr et al., 2015) and Sinai Peninsula (Abouelmagd, 2014). However,

because the Uweinat-Aswan uplift impedes groundwater flow from south to north, the flow in the Kufra basin is from southwest to north and northeast (Sultan et al., 2013). The groundwater ages range from less than 30,000 years in the south to one million years in the north (Sturchio et al., 2004). The age increases to the north, and there is local groundwater recharge west of Lake Nasser and the Toshka plain to the Nubian sandstone aquifer that extends for less than 5 km in length (Geriesh et al., 2020; Masoud et al., 2013). Findings indicate strong correlation between low-salinity groundwater and the spatial distribution of fluvial and structural features. Low-salinity water can be found near alluvial fans especially in the southwest reaches of structurally enclosed streams. The presence of low-salinity water in wells near structures emphasizes the need of structural knowledge in understanding groundwater flow patterns (Geriesh et al., 2020; Koch et al., 2012; Robinson et al., 2007). Between the late 1950s and the early 2010s, when the New Valley project was initiated, there was an urgent need to examine the underground reserves of the land reclamation areas. The following groundwater extraction results were obtained from all models in the region:

1. El-Bahariya Oases drawing areas were in the range of 30 Mm³/yr (1990) and could be increased to 143 Mm³/yr (2000).
2. Areas of the Farafra Oasis: The current pumpage is in the range of 131 Mm³/yr in 1996 and can be increased to about 469 Mm³/yr.
3. El-Dakhla Oases: The current abstraction is 185 Mm³/yr and can be increased by 217 Mm³/yr, while reports from the Ministry of Irrigation indicate that a potential for an increase of 76 Mm³/yr could be added.
4. El-Kharga Oases: The current figure is estimated at 110.3 Mm³/yr, and the report of the University of Berlin advises against increasing.
5. South of Baris Oasis, there are no studies of the possibility of land reclamation, and it is recommended to develop a hydrogeological model to include this area using data and information that can be obtained from existing wells, wells being drilled, and future wells in this area.
6. East Uweinat: Based on numerical modeling for the Eastern Uweinat region, three scenarios were simulated for the exploitation of the NSAS water. These scenarios build up based on keeping the potentiometric water level do not complete the model area's aquifer's complete depletion. A realistic plan would be based on lowering the water level at a maximum drop to a depth of fewer than 100 m. Egypt's total storage capacity is estimated to be 40,000 Bm³/yr; however, usage of this resource is dependent on pumping costs and economic returns over a short time. In the Western Desert (East Uweinat, Farafra,

and Dakhla Oases), the total potential groundwater withdrawal is roughly 3.5 Bm³/y (El Alfy, 2014). In central Sinai, the NSAS aquifer has potential for further development (200–300 Mm³/y, JICA, 1992), while, in the Eastern Desert, the aquifer potential ranges between 50–100 Mm³/y.

If large-scale depletion continues in the Western Desert, the aquifer will be stressed and the water level will fall to the point of being depleted. Superior quality water with relatively high iron and manganese concentrations is pumped from the Nubian Aquifer in several regions across the Western Desert and the Sinai Peninsula. The salinity of groundwater varies vertically and horizontally. Groundwater abounds with high potentiality in four water-bearing strata separated by interbedded shale and clay beds in the El-Bahariya Oasis, with its flow patterns varying from SW to NE (Khaled & Abdalla, 2013). In Kharga and Dakhla Oases, salinity drops with depth from more than 1000 mg/l in the top water-bearing layer to 200 mg/l in the lowest water-bearing layer. The top water-bearing layer near the saltwater boundary in the Siwa region includes freshwater (200–400 mg/l), but the deeper water-bearing layer contains hypersaline water (up to 100,000 mg/l). Because of the high quantities of free CO₂ and H₂S, as well as the low redox potential, this groundwater is particularly corrosive. The high iron and manganese concentrations (2–20 mg/l) found in Farafra, Bahariya, and other locations cause well-screen clogging (Korany, 1995). Furthermore, groundwater radium pollution beyond the maximum contaminant limit (MCL) of drinking water has been recorded in the Nubian Aquifer in the Western Desert (Sherif & Sturchio, 2021) and the Sinai Peninsula (Sherif et al., 2018).

4 The Fissured Carbonate Rock Aquifer (FCRA)

Over half of Egypt's land area is covered by the FCRA, which stretches from the Sinai to Libya (see Fig. 2). It has several natural springs because it functions as a confining layer on top of the NSAS. Uncertainty surrounds the aquifer's recharge, and its potential is not well understood (MWRI, 2013). Despite accounting for at least half of Egypt's entire surface area, the FCRA is the least studied and utilized. It is mostly found in Egypt's Western Desert's northern and central sections. The aquifer's recharge is dependent on upward seepage from the deeper Nubian Sandstone aquifer and, occasionally, local precipitation. Its thickness extends from 200 to 1000 m, with an estimated 5 billion m³ of exploitable brackish water in the fissured carbonates (MWRI, 2013).

4.1 Geologic and Hydrogeologic Settings

Three formations may be distinguished within the carbonate complex:

- Lower Formation: Upper Cretaceous,
- Middle Formation: Lower and Middle Eocene,
- Upper Formation: Middle Miocene.

An upper fractured limestone complex with a thickness varying around 650 meters (Upper Cretaceous to Middle Miocene) and lying irregularly on the NSAS is discovered in wells dug in the Siwa Oasis. There are 200 or more natural springs scattered around the top of the Middle Miocene fissured limestone outcrop, with a daily flow of about 200,000 m³ and salinities varying from 1500 to 7000 ppm. At Gebel Anguilla and the El-Farafra Oasis, the aquifer's water levels range from 62 to 80 m above mean sea level, and various wells tapping it (Khalifa, 2014). With extremely few exceptions, direct rainfall, and surface runoff, the FCRA is mostly recharged by upward groundwater leakage from the underlying Nubian Sandstone Aquifer via existing deep faults (El-Ramly, 1967; II Nouva Castoro, 1986). The Upper Cretaceous aquifer in central Sinai is distinguished by a thick section that rises over 800–1000 m and is mostly made of chalk, chalky limestone, marl, dolomite, dolomitic limestone, and shale (Abdalla & Scheytt, 2012). Numerous limestone, marl limestone, and marl layers make up the Eocene rock. Near the outcrops of the El Egma and El Tih Plateaus, the thickness of these strata progressively reduces southward to about 200 m. Salinity levels in groundwater climb northward and range from 3800 to 5000 mg/l (JICA, 1992). The yearly recharge for the Sinai Peninsula is anticipated to reach 76 Mm³ (JICA, 1992). The Upper Cretaceous aquifer is contained by a down-faulted tertiary-age rock that stretches from the district's central region to the north of Gabal Maghara and Gabal El-Halal districts. The free to semi-confined properties of this aquifer system in the center of Sinai are accompanied by modest discharge rates through several shallow wells and natural contact springs. The groundwater flows from the southern terrains towards the northern lowlands. A typical SE-NW flow with a hydraulic gradient of 0.0035 is present. In southern Sinai, intercalation of Cenomanian, marly limestone, and shale occurs downstream of Wadi Feiran, forming a confining unit (aquitarde) for the underlying NSAS. The aquifer thickness and top confining unit vary from 100 m near its outcropping sections along the eastern portions to approximately 450 m westwards with the Wadi exit to the Gulf of Suez (Geriesh & El-Rayes, 2000). The aquifer is discharged westward into the Gulf of Suez through natural springs near the coastline (e.g., Hammam

Pharaon and Ayoun Moussa). Marine Miocene carbonate rocks, which may influence water quality due to their high evaporite concentration, underlie the aquifer's furthest downstream reaches. Hydraulic conductivity in central Sinai is 18.4 m/day, while transmissivity is 663.7 m²/day (Abdalla & Scheytt, 2012). Karstified sedimentary formations are the only places where groundwater occurs and flows freely. The aquifer's groundwater potential is growing due to fault and fissure systems. The transmissivity of Helwan, south of Cairo, ranges from 4.6 10⁻³ m/s to 9.3 10⁻³ m/s. The degree and continuity of fractures affect well productivity, which varies by geography (Abdalla & Scheytt, 2012). The fissured limestone possesses karstic properties due to groundwater circulation through many warm springs, and salt concentrations can reach > 5000 ppm (Abdalla & Scheytt, 2012). Well discharge rates in the Siwa Oasis, Western Desert, range from 5 to > 300 m³/h. Salinity varies according to the recharge area's location and the kind of rock found in the water-bearing strata. Freshwater only appears if the aquifer is significantly recharged with freshwater from wadi infiltration or upward leaking from the Nubian Aquifer into overlying carbonate aquifers. Groundwater in the western desert's Farafra Oasis is extremely fresh and has a salinity of less than 1000 ppm. Salinity ranges from 2000 to 5000 ppm in the southern part of the northern plateau, and it rises to more than 10,000 ppm in the north, where the Dabaa Shales cover the aquifer (Joint Venture Qattara, 1979). The Middle Eocene through the Pleistocene and Holocene are covered by the El Minia Governorate's FCRA. Eocene rocks provide a wide variety of limestone formations (fissured, chalky, and silicified). An Eocene (limestone) aquifer known as the Samalut Formation is made up of hard, white, and abundantly fossiliferous limestone that is intercalated with shale and marl. A fault network that affects the Eocene aquifer could have an impact on how the aquifer recharges. Under porous alluvium layers, groundwater is present under unconfined condition. The Eocene aquifer's water depth varies between 25 and 120 m west of the Nile and 6 and 153 m east of the Nile. The eastern bank of the Nile is where you will most observe an increase in water depth from north to south. Recharge sources for the Eocene aquifer include current precipitation percolation, periodic flash floods, downward leakage from the upper Quaternary aquifer, and perhaps upward leaking from the Nubian sandstone aquifer. In the northern part of the Eastern Desert, thick wide multi-horizon successions of carbonate rock facies, sandstones, shale, and clay constitute the main representation of the fractured limestone and sandstone aquifers. The Middle Miocene aquifers have hydraulic conductivity, storativity, and transmissivity values of 4.31 m/d, 1.2 × 10⁻³, and 70 m²/d, respectively (El-Ghazawi and Abdel Baki 1991).

5 The Fissured Hard Rock Aquifer (FHRA)

Non-volcanic (plutonic) igneous and metamorphic rocks are usually referred to as crystalline rocks according to their origin from the crystallization of magmas and re-crystallization of other rocks. They occur as intrusive amidst other rocks, as extrusive on the surface, or as large bodies or plutons, crystallized at considerable depths. The aquifer runs through the Red Sea hills and the southern Sinai Peninsula, where exposed schist, gneiss, and granite rocks (see Fig. 2).

5.1 Aquifer Geology and Hydraulic Characteristics

The FHRA is primarily made of granite, granodiorite, and gabbros. Rhyolite and andesite dikes are abundantly distributed throughout the Red Sea and southern Sinai (Fig. 14). The composition of crystalline rocks varies from acidic to basic depending on the silica amount and composition of feldspars and ferromagnesian minerals. The Precambrian basement aquifers are outcropped along most of the investigated watershed area, as well as in southern Sinai (Fig. 14). The fractured and worn crown (up to 5 m depth) of these rocks serves as the primary recharging location for the basement wadi filling aquifers and is regarded as a water collector from a hydrogeological standpoint, with groundwater occurring largely in the joints and cracks within these rocks (Geriesh & El-Rayes, 2000). The joint density, the number of tapped fault zones, and the terrain of the

immediate area around the well site all affect the wells' output (El-Rayes, 1992). Southern Sinai's Precambrian and Cambrian rocks get an estimated 52,000 m³/d of recharge (Dames & Moore, 1985). Fresh, solid, unaltered, and unfractured specimens of crystalline igneous and most metamorphic rocks have primary porosities that rarely exceed 2%. Many rock types are, therefore, impervious and impermeable. Secondary porosity and permeability are imparted to these rocks by weathering and fracturing. The permeability of crystalline rocks varies greatly depending on the degree of weathering, the composition of the weathered components, and the intensity of fracturing and open spaces in the cracks. The hydraulic conductivity of the upstream sediments (3–6.8 m/d) increases in tandem with the wadi filling deposits in the basement terrains. The hydraulic conductivity of downstream sediments, on the other hand, is the lowest (< 0.5 m/d), which can be related to the abundance of carbonate rocks and large mud proportions in most downstream streams. Also, hydraulic conductivities of the trough areas (i.e., basins) are much lower than those areas of the steeply sloped stream gradients (Geriesh & El-Rayes, 2000). The depth of the water table fluctuates significantly throughout the FHRA due to its undulating topography. In the Wadi Feiran basin in the southern Sinai, the fractured basement rocks aquifer has an estimated average transmissivity of 57.3 m²/day and a specific yield of 0.017. (Abouelmagd, 2003). The FHRA may be divided into the following three units based on the hydrogeological significance and areal distribution:

1. Pre-Cambrian fractured basement rocks.
2. Quaternary alluvial deposits.
3. Volcanic dykes and sills.

Because of the decrease in the porosity and specific yield with depth, water held in storage and water potential for extraction from a unit volume of basement rock decrease with increasing depth. Although the worn and interconnected fracture zones form a continuous aquifer with hydraulic continuity, the heads in individual zones might vary, lowering in recharge areas and increasing in discharge areas. The crystalline aquifers are affected by lithologic and structural control. Depth to water levels broadly follows the topography. Where the rocks are highly permeable and where the local base level of erosion lies deep, the water level may also be deep due to quick water drainage. If there are several flows, perched aquifers may be formed above the impermeable horizons of different flows. The alternating succession of permeable and dense horizons in volcanic rocks form a multi-aquifer system. Wadi filling deposits in most basement hydrographic basins act as good collectors for rainfall and flash floods that occur in the basement terrains' watershed zones.

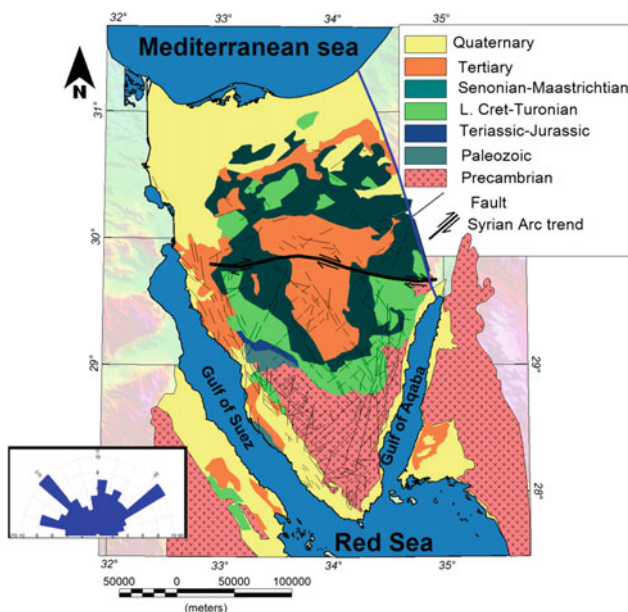


Fig. 14 Geology of the crystalline province of Southern Sinai (after Ginzburg et al., 1979; Neev, 1975)

Aquifer storage and depths of these wadi filling deposits depend mainly on the underlying basement topography and wadi crossing dykes (Geriesh et al., 2004; Shendi & Abouelmagd, 2004). The topmost weathered, jointed, volcanic dykes, and the vesicular layer form phreatic aquifers. The inter-flow permeable horizons occurring below the massive zone comprise confined aquifers, with interconnections to a varying degree, depending on the nature of layers in between. Small, thin, intrusive bodies like sills and dykes emplaced far away from the volcanic vents may have congealed rapidly and developed joints within the intrusive body as well as in the host rocks. When bordered by less permeable host rock, weathered dykes can operate as preferred flow conduits, but impermeable dykes can significantly contribute to impounding groundwater flow, acting as barriers, and causing local aquifer compartmentalization (Houben et al., 2018; Mohamed et al., 2015).

5.2 Groundwater Recharge and Quality

Precipitation is considered as the main source of groundwater recharge in the FHRA. Massive runoff along the main wadis toward the Red Sea may be the result of heavy rainfall in the Eastern Desert. However, a significant amount of rainfall can percolate downward and be stored in the cracked basement rocks via open areas and fracture systems. Groundwater flows downward through the cracks because of the hydraulic gradient and gravity force to replenish both the Phanerozoic sedimentary aquifers and the Quaternary alluvial deposits that fill the hydrographic basins and plains (e.g., El-Qaa Plain in southern Sinai). In southern Sinai, the FHRA is also recharged by small infiltrating rainwater quantities (El-Rayes, 1992), so water flows through fractures, joints, and voids. Hand-dug wells provide a limited quantity of water with good salinity along with the wadi filling deposits in most southern Sinai and Eastern Desert areas. Deep wells, such as the El-Baramya Well in the Eastern Desert, provide a plentiful supply of water. The water quality ranges between 300 and 800 ppm in the watershed areas and between 1800 and 2500 ppm in the downstream areas (Geriesh & El-Rayes, 2000; Geriesh et al., 2004). The groundwater quality of the Pre-Cambrian basement aquifer is significantly influenced by the geochemistry of the host rock and the surrounding area. In the northern region of the Eastern Desert, the quality of the water ranges from fresh to brackish. Salinity levels vary between 600 and 3500 ppm. The most dominant ion orders in the headwaters are $\text{Ca} > \text{Na} > \text{Mg}$ and $\text{HCO}_3 > \text{Cl} > \text{SO}_4$. Because of a possible ion exchange mechanism, Na replaces Ca and Cl, and SO_4 replaces HCO_3 . The arrangement of ion dominance changes downstream to $\text{Na} > \text{Ca} > \text{Mg}$ and $\text{Cl} > \text{HCO}_3 > \text{SO}_4$. The fractured basement aquifer is characterized by the Ca-bicarbonate facies, while the Quaternary aquifer of the

wadi filling deposits is characterized by the Na-mix facies (Geriesh & El-Rayes, 2000). The biochemical interferences could change water facies in the shallow dug wells found in hard rock (Geriesh et al., 2004). The presence of algae in the shallow dug wells water indicates an environment rich in nutrients and organic matters that help grow these algae. Algae create an oxidizing environment as a result of the photosynthetic process during which oxygen increases. Moreover, the alkalinity of water also increases, consequently reacting with Ca ions to form calcite that precipitates once the water reaches the saturation state. On the other hand, the presence of bacteria and organic matter in some of these wells reduces SO_4 ions and, consequently, increases HCO_3 content. This biochemical interference may explain the enrichment in HCO_3 ions and the decline in Ca/Na ratio along the upstream reaches in basement terrains, characterized by low salt contents.

6 The Moghra Aquifer

In Moghra aquifer, groundwater flows westward from the northwestern desert to the Qattara Depression (Fig. 2). Rainfall and lateral inflow from the Nile Delta aquifer recharge the Moghra aquifer. Only freshwater is present, and salinity increases in the north and west (Khalifa, 2014). The Nile Delta aquifer is thought to recharge the Moghra aquifer at a rate of 50–100 Mm^3/yr . Evapotranspiration from the Qattara Depression in the southwest and Wadi El-Natron in the west leads to natural discharges.

6.1 Aquifer Geology and Hydrogeologic Settings

The Moghra aquifer is made up of Lower Miocene sandstone with claystone and siltstone intercalations that shift to shale as you get closer to the Mediterranean (Fig. 15). The aquifer's base is Oligocene basalt and Dabaa shale. The aquifer slopes from ground surface level at Cairo to 1000 m below mean sea level west of Alexandria. (Khalifa, 2014). Its thickness is thinned in the north and west to overlap with the Marmarica Limestone and ranges from 200 m in Wadi El-Farigh to 800 m in the Abu El-Gharadig basin east of the Qattara Depression. Both fossil and renewable water can be found in the Moghra aquifer. The Moghra aquifer exists under phreatic condition, with groundwater table varying from 60 m below MSL in the west in the Qattara Depression to 10 m above MSL near the Nile Delta aquifer boundary. With an average gradient of less than 0.2 m/km, the hydraulic gradients are quite gentle. The permeability of the aquifer varies from less than 1.0 m/day in the Qattara area and along the coast to 25 m/day east of Wadi El-Farigh. In m^2/day , the transmissivity ranges from 500 to 5000. Groundwater is

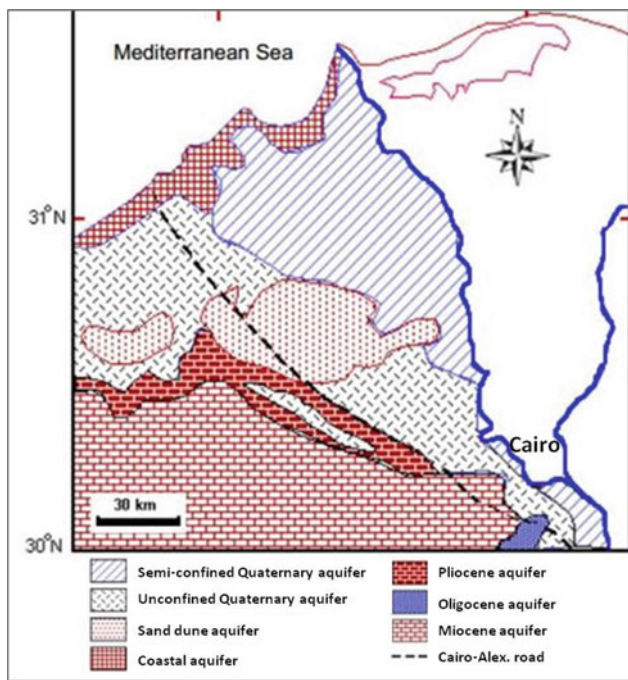


Fig. 15 Geology of El-Moghra aquifer (modified after RIGW, 1991)

utilized to irrigate more than 60,000 Feddans (252 Mm^2) in Wadi El-Farigh, and irrigation wells yield outputs of more than $200 \text{ Mm}^3/\text{y}$ at the water-table/ground-surface junction (Youssef, 2012). The Qattara and Wadi El Natrun depressions, where multiple springs discharge $706 \text{ Mm}^3/\text{y}$, are the sites of substantial evaporation. Aquifer discharge occurs by lateral seepage into carbonate rocks west of the Qattara Depression (El-Rawyet et al., 2020).

6.2 Aquifer Recharge and Groundwater Quality

The Nile Delta Aquifer, the Marmarica Limestone Aquifer, the direct rainfall on the aquifer's outcrops, and the upward seeping from the underlying Nubian Sandstone Aquifer are the four sources of recharge for the aquifer (El-Sayed & Morsy, 2018; Geriesh et al., 2015; Salah & Samah, 2018). Groundwater predominantly flows west from the Nile Delta aquifer to Wadi El-Natron and the northern parts of the El-Moghra aquifer with a gentle hydraulic gradient of around 0.003 (Gerish et al., 2015). The water salinity in the El-Qattara depression varies from less than 1000 (ppm) in the east (next to the primary recharge area) to more than 5000 ppm in the west (near the main discharging area). The water type exhibits mixed facies of renewable and fossil water recharge from the Nile in the east (Geriesh et al., 2015). The saturated thickness varies from 70 to 700 m (RIGW, 1991). While conditions are unconfined in the south, they are confined as you move north. While the

present yearly discharge is anticipated to be 200 million m^3 , the annual production surpasses one billion cubic meters. A hydraulic gradient of 0.2 m/km directs groundwater flow farther westward into the El-Qattara Depression. Permeability drops from 25 m/day in Wadi El-Farigh to 1 m/day on the Mediterranean coast in the north. The transmissivity ranges from 500 to 5000 m^2/day , (Salah & Samah, 2018). The anticipated yearly lateral leakage from the Nile Delta aquifer to the Moghra aquifer is about $50\text{--}100 \text{ Mm}^3$

Only in Wadi El-Farigh, on the aquifer's eastern boundary, can fresh groundwater exist (500–1000 ppm), and salinity rises north and westward until it reaches > 5000 ppm (Salah & Samah, 2018). As water levels drop, salinization and nitrate contamination caused by over-pumping along the aquifer basin impair water quality and its viability for drinking, residential, and agricultural uses. The hydraulic head falls off in the Wadi El-Natron region by around 0.5 m/y due to over pumping from wells. To maintain this aquifer, corrective actions must be taken, including decreasing the number of pumping wells, decreasing initial and operational well time, and installing drip irrigation systems (Youssef, 2012). According to isotopic fingerprints, the west of the site had a major depletion, while there is a gradual enrichment towards the northern and eastern Nile Delta reaches (Geriesh et al., 2015).

7 The Coastal Aquifer

Direct rainfall recharges the coastal aquifer, but the presence of saline water under the freshwater lenses restricts abstractions (MWRI, 2013). Quaternary sediments are the major unit of the coastal aquifer. Its thickness ranges from 30 to 90 m, and the groundwater along the eastern Mediterranean coast is generally brackish ($> 3,000$ ppm).

7.1 Aquifer Geology and Hydraulic Properties

The hydrogeology of the northern Mediterranean coast has been studied by RIWR (1995), Ghodeif and Geriesh (2003), Geriesh et al. (2004), Geriesh et al. (2015a), and Arnous et al. (2015, 2017). They described the physical and chemical parameters of the northern coastal aquifers and further discussed the problem of seawater intrusion. According to these studies, the groundwater exists in three rock units: (1) the sand dune unit; (2) the old beach sand unit, and (3) the calcareous sandstone (*Kurkar Formation*) unit to the east and the calcareous sandstone aquifer to the west of the Mediterranean shore line (Fig. 16). Most of the water well fields tap the last two aquifer units. The sand dune aquifer consists of well-sorted sands attaining 5–15 m in thickness and extends horizontally to cover most of the eastern parts of

Fig. 16 Geology of the Mediterranean coastal aquifer (modified after CONOCO, 1987)

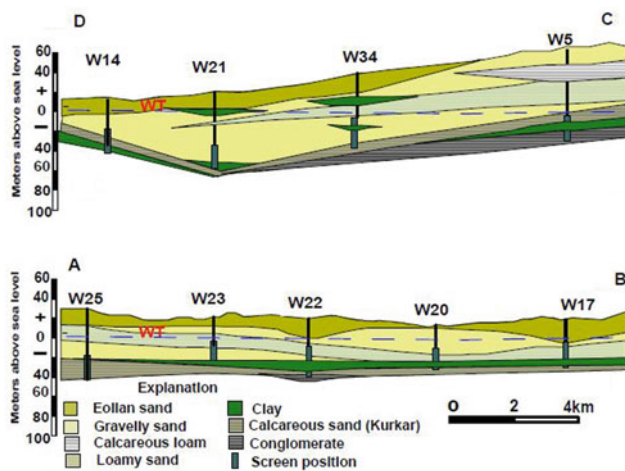
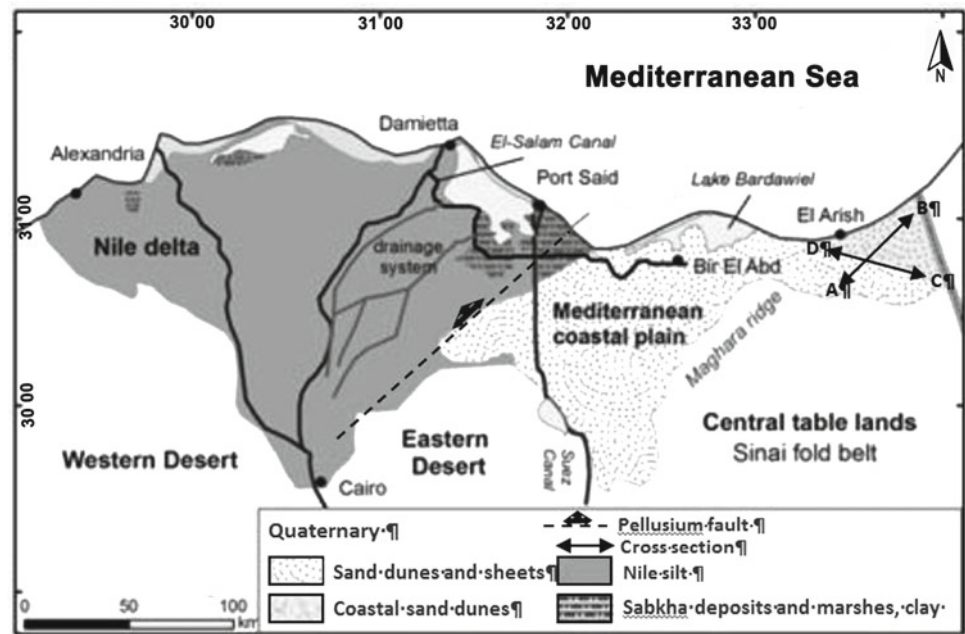


Fig. 17 Hydrogeologic cross-sections along the Mediterranean coastal aquifer, northern Sinai, A-B and D-C of Fig. 16 (modified after Geriesh et al., 2004)

the northern Sinai Mediterranean coast (Fig. 17). They vary in thickness between 30 and 90 m. The good hydraulic conductivity and high porosity of the sand dunes characterize its good potentiality. The calcareous sandstone aquifer is divided into two layers: upper alluvial and lower old beach sands. Groundwater capacities in the northwestern Sinai are more restrained than in the northeastern area. The latter is covered in sand dunes, which make up the principal aquifer. Water is found there between 1 and 7 m below the surface, where it is present as a thin layer on top of the main saline water (El-Shazly et al., 1975). As a result, pollution poses a serious threat to this valuable water supply. Two transverse zones might be created from the western coastal area. The

groundwater potentiometric surface is greater than the ground surface of the northern El-Tina plain, a part of the Nile flood plain coastal aquifer made of silty clay intercalated with salts, evaporites, and sands. The groundwater is primarily salty and unsuitable for irrigation (Fig. 16). Eastward, the aquifer's composition transforms into silty clay and clayey silt that is covered in a salt crust (Arnous et al., 2017; El-Rayes et al., 2017; Geriesh et al., 2015a). The Pelusium line and the coastal hinge fault are tectonic features that control the Sinai Mediterranean coast. A section of the Egyptian Mediterranean coast zone to the east of Port Said occupies El-Tina plain and its environs. The Mediterranean coast's dynamic processes include sea components (waves, currents, and tides), wind, and sometimes rainfall. Quaternary sediments cover the southern area and control the land sculpturing rate (degradation and aggradations processes). The hydraulic properties of the Quaternary aquifers vary from north to south, where the hydraulic conductivity varies between 1.25 and 12 m/d along the southern zones to 38 and 64 m/d along the sand dune belt to the north. The transmissivity varies between 86 and 690 m²/d at the south to 700 and 1910 m²/d in the north, whereas storativity (S) varies between 0.01 and 0.05 at the south to 0.15 at the northern sand dunes zones (RIWR, 1995).

From these hydraulic characteristics, it could be concluded that the sand dune and old beach aquifers in the north are highly productive and highly vulnerable to contamination relative to the Kurkar aquifer in the southeast. The three Quaternary aquifer units are hydraulically connected. Along El-Tina plain, the coastal aquifer is composed mainly of fluviomarine sediments, and therefore, its water quality is highly saline (Geriesh et al., 2015a).

The Miocene (Rudies Formation) and Nubian Sands comprised groundwater wells excavated in the coastal aquifer along the Red Sea Coast in Wadi Dara, Ras Ghareb, and Ras Shoqeir. Depth of groundwater formations reaches 600 to 900 m from the land surface. The Aquifer's thickness ranges from 90 to 140 m. Water depths vary from 30 to 50 m.

7.2 Groundwater Recharge and Quality

The main source of groundwater recharge in the coastal aquifer is rainfall. It can reach 300 mm per year near the Sinai Shore and 170–200 mm per year along the Nile Delta and western coast. About 10% of the rainwater feeds the Quaternary aquifers in the coastal area (RIWR, 1995). Sewage effluent and irrigation return flow from cultivated fields serve as supplementary recharge supplies for the shallow, highly vulnerable aquifers in the central and northern sand dunes belts, as well as the scattered agricultural lands along the Mediterranean coast zone (Geriesh et al., 2004). The existing water wells yielded about 27,000 m³ of water per day. Water salinity shows high variability from west to east. It varies between 600 ppm along the northeastern sand dune zone and more than 6000 ppm along the northwestern coastal zone. Water composition varies between Na/Ca–HCO₃ along the fresh water zone to Na-Cl facies along the salty water zone reflecting interferences of seawater intrusion.

Rainfall along the Red Sea coast is less than 100 mm/year. However, thunderstorms of high precipitation rates could form intermittent flash floods causing catastrophic problems. Harvesting flood water could increase the recharge of groundwater resources of the coastal aquifer. Basins of Wadi Hodeen and Kerafon at the Red Sea coast have high groundwater potential as they have fair water quality (1000–1500 ppm). In the Ras Banas—Halayib Sector, where water is found in Quaternary sediments along the coastal zone's limited coastal strip, groundwater is the main source of fresh water. The salinity range for groundwater in these areas is between 1700 and 3400 ppm.

8 Conclusions

The construction of the Grand Ethiopian Renaissance Dam (GERD) on the upstream sections of the Blue Nile is expected to cause a significant water scarcity in Egypt. Great water demands due to increasing population rate and fixing water resource budget along with great water losses due to evaporation, damming of water flow, and supply are expected. As a result, it is advised that Egypt design a potential strategic plan for growing water resources that is based on developing traditional and non-traditional water resource supplies. The Nile water resources, which total 55.5 billion m³ per year, are a

significant supply of water in Egypt. Additionally, rainfall, flooding, and deep groundwater are scarce in the Sinai Peninsula, Western Desert, and Eastern Desert. Desalination is a water resource that can be explored and used, particularly in coastal areas that stretch east and north, as well as in some high-water salinity aquifers. The strategy also indicates that the agriculture sector uses 85%, industry 9.5%, and drinking 5.5% of the water supply. The plan gives Egypt's major groundwater reservoirs great attention as an alternative solution for water shortages for expanding agricultural and economic activities until 2030.

The major groundwater reservoirs of Egypt consist of several aquifers, summarized as: (1) The Nile Valley and Delta Aquifers, which are acknowledged as Egypt's main source of groundwater supplies, are among the most prominent of the many aquifers that make up the country's main groundwater reserves. It has a thick layer of sand and gravel on top of which is a clay cap that ranges in depth from 1 to 50 meters. 85% of Egypt's total groundwater abstractions are provided by it; (2) The Nubian Sandstone Aquifer System (NSAS) is Africa's most extensive fossil aquifer system, with reserves estimated at 150,000 Bm³. Around 2.2 million km² of the NSAS are shared by Egypt, Libya, Sudan, and Chad, with Egypt contributing 828,000 km² (38%). With a hydraulic head that varies from 570 m above sea level west of Darfur to 78 m below sea level in the Qattara Depression, the NSAS has a maximum depth of 4500 m. From 200 m in East Uweinat to 3500 m northwest of El-Farafra Oasis, the fresh layer's thickness varies. Recent research has shown that the NSAS receives local recharge through significant fractures and joints along its southern outcrops as well as transboundary recharge from Egypt's, Sudan's, and Chad's southern and southwestern borders; (3) The Fissured Carbonate Rock Aquifer stretches from Sinai to Libya and makes up more than half of Egypt's land area. It serves as a confining cap to the Nubian Sandstone Aquifer System and features several natural springs. Recharge potential of the aquifer remains uncertain. (4) The Fissured Hard Rock Aquifer is commonly recharged by moderate quantities of infiltrating precipitation along the Eastern Desert and the Southern Sinai Peninsula. (5) The Moghra aquifer is located southwest of the Nile Delta, and groundwater is diverted into the Qattara Depression. It is replenished by rainfall and Nile aquifer recharge. (6) The Coastal Aquifer is recharged by local precipitation, and the abstraction rates are limited avoid saltwater upconing and seawater intrusion. The total reserved storage of the significant groundwater reservoirs of Egypt is expected to have a round figure of 1200 Bm³ of variable recharge rates from high along the Nile Delta and Valley, moderate along the Coastal aquifer system to low along the Moghra Aquifer, and very low to non-renewable along the main Nubian Sandstone Aquifer m³.

As water levels decrease across the majority of the Western and Eastern Deserts, as well as Sinai, the quality and sustainability of groundwater are in jeopardy. Over-pumping in the Nile Delta and in the Valley and El-Moghra aquifer areas to the west of the Nile Delta negatively impacts water quality by causing salinization and nitrate pollution. Therefore, the strategic approach should take these risk priorities into account. The hydraulic head decreases by around 0.5 m/y in arid conditions. For the long-term extension of these aquifers, recovery actions including reducing the number of pumping wells, cutting start-up and running periods, and switching to drip irrigation are crucial. It is highly advised to keep track on the quantity and quality of groundwater. On the other hand, careful extraction rates should be used and monitored in conjunction with the Nile Delta and Coastal regions, which are very sensitive aquifers, to minimize saltwater intrusion and deterioration of water quality.

The deep groundwater beneath the vast deserts of the western, eastern, and Sinai Peninsula along with limited quantities of rainwater and flooding are considered non-renewable resources and can be exploited according to the development conditions and the water needs. Non-traditional water resources, such as the reuse of exhaust uses from agriculture, industry, sanitary, and industrial effluent, are strongly suggested to meet Egypt's anticipated shortfalls in available water resources in the next years.

References

- Abdalla, F. A., & Scheytt, T. (2012). Hydrochemistry of surface water and groundwater from a fractured carbonate aquifer in the Helwan area, Egypt. *Journal of Earth System Science*, 121(1), 109–124.
- Abdel Mogheeth, S. M. (1975). *Hydrogeochemical studies of some water-bearing formation in ARE with special reference to the area west of the Nile Delta*. Ph.D. Dissertation, Alexandria University, Egypt.
- Abouelmagd, A., Sultan, M., Milewski, A., Kehew, A. E., Sturchio, N. C., Soliman, F., Krishnamurthy, R. V., & Cutrim, E. (2012). Toward a better understanding of palaeoclimatic regimes that recharged the fossil aquifers in North Africa: Inferences from stable isotope and remote sensing data. *Palaeogeography, Palaeoclimatology, Palaeoecology*, 329–330, 137–149.
- Abouelmagd, A., Sultan, M., Sturchio, N. C., Soliman, F., Rashed, M., Ahmed, M., Kehew, A. E., Milewski, A., & Chouinard, K. (2014). Paleoclimate record in the Nubian sandstone aquifer, Sinai Peninsula, Egypt. *Journal of Quaternary Research*, 81(1), 158–167.
- Abouelmagd, A. A. (2003). *Quantitative hydrogeological studies on WadiFeiran basin, south Sinai, with emphasis on the prevailing environmental conditions*. M.Sc. thesis, Fac. Sci. Suez Canal Univ., Ismailia, p. 353.
- Ahmed, E. H. M. (2013). Nubian sandstone aquifer system. *Journal of Environmental Science and Toxicology*, 1(6), 114–118.
- Aly, A. I. M., Nada, A., Awad, M., Hamza, M. S., & Salman, A. B. (1989). Isotope hydrological investigation on Qattara depression, Egypt. *Isotopenpraxis*, 25(1), 22–24.
- Armanious, S. D., Khalil, J. B., & Atta, S. A. (1988). Groundwater hydrology, geological and hydrogeological features of the Nile Delta Quaternary aquifer, Egypt. *Journal of Civil Engineering*, 1(23), 50–65.
- Arnous, M. O., El-Rayes, A. E., & Helmy, A. M. (2017). Land-use/land-cover change: A key to understanding land degradation and relating environmental impacts in Northwestern Sinai, Egypt. *Environmental Earth Sciences*, 76, 263.
- Attia, M. L. (1954). *Deposits in the Nile Valley and the Delta*. Geological Survey, Egypt, Cairo, p. 356.
- Awad, M. A., & Nada, A. A. (1992). Tritium content of groundwater aquifer in western Nile Delta. *Journal of Isotopen Prates USA*, 28, 167–173.
- Butzer, K. W. (1967). Late Pleistocene deposits of the Kom Ombo Plain, Upper Egypt. In: Gripp, Schwabedissen (Eds.), *Frühe Menschheit und Umwelt. Teil II: Naturwissenschaftliche Beiträge* (pp. 213–227). BöhlauVerlag.
- CEDARE. (2002). *Regional strategy for the utilization of the Nubian sandstone aquifer system*. Center for the Environment and Development for the Arab Region and Europe, Cairo, Egypt, pp. 22–82.
- CEDARE. (2014). *Nubian sandstone aquifer system (NSAS) M&E rapid assessment report; Monitoring & evaluation for water in North Africa (MEWINA) project, water RESOURCES management program*. CEDARE, Cairo Governorate, Egypt, p. 95.
- CONOCO. (1987). *Geological map of Egypt. Scale 1:500,000*. Egyptian General Petroleum Corporation.
- Dahab, K. (1994). *Hydrogeological evolution of the Nile Delta aquifer after construction of Aswan High Dam, Egypt*. Ph.D. thesis, Geol. Depart. Menoufia University, Egypt, p. 194.
- Dames & Moore. (1985). *Sinai development study phase I final report* (Vol. V). Cairo, Egypt: Water supplies and coasts, Ministry of Development.
- Diab, M. S., Dahab, K. A., & El-Fakharany, M. A. (1997). Impact of paleo-hydrogeological conditions on the groundwater quality in the northern part of the Nile Delta, Egypt. *Egyptian Journal of Geology*, 41(2B), 779–796.
- El-Asmar, H. M. (1991). *Old shorelines of the Mediterranean coastal zone of Egypt in relation with sea-level changes*. Ph.D. thesis, Faculty of Science, El Mansoura University, Egypt, p. 219.
- El-Ramly, I. (1967). Contribution to the hydrogeological study of limestone terrains in UAR. In *Actes du Colloques de Dubrovnik, Octobre 1965, Hydrologie des Roches Fissures* (Vol 1, Publ. No. 73), AIRS—UNESCO.
- El Alfy, M. (2014). Numerical groundwater modeling as an effective tool for management of water resources in arid areas. *Hydrological Sciences Journal*, 59(6), 1259–1274. <https://doi.org/10.1080/02626667.2013.836278>
- El Tahlawi, M., Farrag, A., & Ahmed, S. (2008). Groundwater of Egypt: “An environmental overview”. *Environmental Geology*, 55 (3), 639–652.
- El-Fayoumi, I. F. (1987). Geology of the quaternary succession and its impact on the groundwater reservoir in the Nile Delta region. *Bulletin of the Faculty of Science*, Mansoura University, Egypt.
- El-Rawy, M., Abdalla, F., & El Alfy, M. (2020). Water resources in Egypt. In Z. Hamimi, A. El-Barkooky, J. MartínezFrias, H. Fritz, & Y. Abd El-Rahman (Eds.), *The geology of Egypt. Regional geology reviews* (pp. 687–711). Springer Nature.
- El-Rayes, A. E., Arnous, M. O., & Aziz, A. M. (2017). Morphotectonic controls of groundwater flow regime and relating environmental impacts in Northwest Sinai, Egypt. *Arabian Journal of Geosciences*, 10, 401. <https://doi.org/10.1007/s12517-017-3188-5>
- El-Rayes, A. E. (1992). *Hydrogeological studies of Saint Katherine Area, South Sinai, Egypt* (Master's thesis, Suez Canal University, Ismailia, Egypt), p. 95.
- El-Sayed, S. A., & Morsy, S. M. (2018). Hydrogeological assessment of Moghra aquifer, North Western Desert, Egypt. *Annals of the Geological Survey of Egypt*, XXXV, 110–130.

- Fairbanks, R. O. (1989). A 17000-year glacioeustatic sea-level record: Influence of glacial melting rates on the Younger Dryas event and deep-ocean circulation. *Nature*, 342, 637–642.
- Fairbridge, R. W. (1967). Global climate change during the 13,500 B. P. Gothenburg geomagnetic excursion. *Nature*, 265, 430–431.
- FAO. (2016). *Egypt, regional report*. AQUASTAT website, Food and Agricultural Organization of the United Nations.
- El Fawal, F. M., & Shendi, E. H. (1991). Sedimentology and groundwater of the quaternary Sandy layer North of Wadi El Tumilat, Ismailia, Egypt. *Annals of the Geological Survey of Egypt*, XVII, 305–314.
- El Ghazawi, A., Abdel Baki, A. (1991) Groundwater in Wadi Asel Basin, Eastern Desert, Egypt. *Bull of Meneufia Uni* V:25–44
- Frenken, K. E. (2005). *Irrigation in Africa in figures: AQUASTAT Survey*. p. 29.
- Geirnaert, W., & Laeven, M. P. (1992). Composition and history of groundwater in the western Nile Delta. *Journal of Hydrology*, 138, 169–189.
- Geriesh, M. H. (1998). Hydrogeological assessment of the groundwater resources around the Nile Valley between Qift and Nag-Hammady, Upper Egypt. *Al-Azhar Bulletin of Science*, 9(1), 307–325.
- Geriesh, M. H., El-Rayes, A. E., Gom'aa, R. M., Kaiser, M. F., & Mohamed, M. A. (2015a). Geoenvironmental impact assessment of El-salam Canal on the surrounding soil and groundwater flow regime, Northwestern Sinai, Egypt. *Catrina*, 11(1), 103–115.
- Geriesh, M. H., Mansour, B. M. H., Gaber, A., & Mamoun, K. (2020). Exploring groundwater resources and recharge potentialities at El-Gallaba Plain area, Western Desert, Egypt. *Groundwater*, 58(5), 842–855.
- Geriesh, M. H., & El-Rayes, A. E. (2000). Water quality assessment of Wadi Feiran catchment area, South Sinai, Egypt. In *Proceedings of the 5th international water technology conference, Alexandria, Egypt* (pp. 139–153).
- Geriesh, M. H., El-Rayes, A. E., & Ghodeif, K. (2004). Potential sources of groundwater contamination in Rafah environs, North Sinai, Egypt. In *Proceedings of the 7th conference of the geology of Sinai for Development, Ismailia* (pp. 41–52).
- Geriesh, M. H., D-Klaus, B., El-Rayes, A., & Mansour, B. (2015). Implications of climate change on the groundwater flow regime and geochemistry of the Nile Delta, Egypt. *Journal of Coastal Conservation*, 19(4), 589–608.
- Geriesh, M. H. (2000). Paleohydrogeological regime of groundwater flow in the eastern Nile Delta Region, Egypt. In *Proceedings of the 4th international conference on water supply and water quality, Krakow, Poland* (pp. 229–241).
- Geyh, M. A., & Jäkel, D. (1974). Late Glacial and Holocene climatic history of the Sahara Desert derived from a statistical assay of 14C dates. *Palaeogeography, Palaeoclimatology, Palaeoecology*, 15, 205–208.
- Ghodeif, K., & Geriessh, M. H. (2003). Contamination of domestic groundwater supplies at El Arish city, North Sinai, Egypt. In *3rd International conference of geology of Africa*, Assuit University, Egypt. December 2003.
- Ginzburg, A., Makris, J., Fuches, K., Prodehl, C., Kaminsky, W., & Amitai, U. (1979). A seismic study of the crust and upper mantle of the Jordan-Dead Sea rift and their transition toward the Mediterranean Sea. *Journal of Geophysical Research*, 84, 1569–1582.
- Hamza, M. S., Swallem, F., & Abdel-Monem, A. (1982). Groundwater hydrology of Wadi El-Natron. III. Distribution of radium and deuterium contents. *Applied Radiation and Isotopes*, 14, 9.
- Hefny, K., & Shata, A. (2004). *Underground water in Egypt*. Ministry of water supplies and irrigation, Cairo, Egypt, p. 295 (in Arabic).
- Heinl, M., & Thorweihe, U. (1993). Groundwater resources and management in SW Egypt. In B. Meissner, P. Wycisk (Eds.), *Geopotential and ecology: Analysis of a desert region* (pp. 99–122) Catena Suppl. 26.
- Hesse, K. H., Hissene, A., Kheir, O., Schnaecker, E., Schneider, M., & Thorweihe, U. (1987). Hydrogeological investigations of the Nubian aquifer system. *Eastern Sahara. Berliner Geowiss. Abh. (a)*, 75, 397–464.
- Houben, G. J., Stoeckl, L., Mariner, K. E., & Choudhury, A. S. (2018). The influence of heterogeneity on coastal groundwater flow—Physical and numerical modeling of fringing reefs, dykes, and structured conductivity fields. *Advances in Water Resources*, 113, 155–166.
- Idris, H., & Nour, S. (1990). Present groundwater status in Egypt and the environmental impacts. *Environmental Geology and Water Sciences*, 16, 171–177.
- Il Nouva Castoro Co. (1986). *Techno-economical feasibility study for the reclamation of 50,000 feddans in Farafra Oasis, Part 1—Geohydrology: Unpublished report to the General Authority for Land Reclamation*, Cairo.
- JICA. (1992). *Basic study on North Sinai groundwater resources development study*. Cairo University.
- Joint Venture Qattara. (1979). *Study Qattara depression* (Vol. III), Part 1 *Topography, regional geology, and hydrogeology*. Lahmeyer International, Salzgitter Consult and Deutsche Project, Union GmbH, German Federal Republic.
- Khaled, M., & Abdalla, F. (2013). Hydrogeophysical study for additional groundwater supplies in El Heiz Area, Southern part of El Bahariya Oasis, Western Desert, Egypt. *Arabian Journal of Geosciences*, 6, 761–774.
- Khalifa, E. A. (2014). Sustainable groundwater management in El-Moghra aquifer. *International Journal of Engineering Research and Technology*, 7(2), 131–144.
- Koch, M., Gaber, A., Burkholder, B., & Geriessh, M. H. (2012). Development of new water resources in Egypt with earth observation data: Opportunities and challenges. *International Journal of Environment and Sustainability*, 1(3), 1–11.
- Korany, E. (1995). Hydrogeologic evaluation of the deeper aquifer in Bahariya mines area, Egypt. In *Symposium of Nubia sandstone rocks* (pp. 1–38). Benghazi, Libya.
- Mansour, B. M. H. (2015). *Climatic and human impacts on the hydrogeological regime of East Nile Delta, Egypt*. Ph.D. Dissertation, Suez Canal University.
- Masoud, M. H., Schneider, M., & El Osta, M. M. (2013). Recharge flux to the Nubian sandstone aquifer and its impact on the present development in Southwest Egypt. *Journal of African Earth Sciences*, 85(1), 115–124.
- Mirghani, M. (2012). *Groundwater need assessment: Nubian sandstone Basin*. Rio de Janeiro, Brazil: WATERTRAC—Nile IWRM-NET.
- Mohamed, M. M., & El-Mahdy, S. I. (2017). Remote sensing of the grand Ethiopian Renaissance Dam: A hazard and environmental impacts assessment. *Geomatics, Natural Hazards, and Risk*, 8(2), 1225–1240. <https://doi.org/10.1080/19475705.2017.1309463>
- Mohamed, L., Sultan, M., Ahmed, M., Zaki, A., Sauck, W., Soliman, F., Yan, E., Elkadiri, R., & Abouelmagd, A. (2015). Structural controls on groundwater flow in basement terrains: Geophysical, remote sensing, and field investigations in Sinai. *Surveys in Geophysics*. <https://doi.org/10.1007/s10712-015-9331-5>

- MWRI. (2013). *NWRP measures. National water resources plan, coordination project* (NWRP-CP). Technical Report 44. Ministry of Water Resources and Irrigation—Planning Sector.
- Neev, D. (1975). Tectonic evolution of the Middle East and Levantine basin (easternmost Mediterranean). *Geology*, 3, 683–686.
- Paepe, R., & Mariolakis, I. (1984). Paleoclimatic reconstruction in Belgium and Greece based on quaternary lithostratigraphic sequences. In *Proceedings of E. C. climatology Sophia Antipolis, France* (pp. 1–18).
- Paulissen, E., & Vermeersch, P. M. (1987). Earth, man and climate in the Egyptian Nile Valley during the Pleistocene. In A. E. Close (Ed.), *Prehistory of Arid North Africa* (pp. 29–67). Southern Methodist University Press.
- Perissoratis, C., & Conispoliatis, N. (2003). The impacts of sea-level changes during the latest Pleistocene and Holocene times on the morphology of the Ionian and Aegean seas (SE Alpine Europe). *International Journal of Marine Geology*, 196, 145–156.
- RIGW. (1990). *Hydrogeological inventory and groundwater development plan, western Nile Delta region* (Vol. 1). Research Institute for Groundwater, Main report, TN 70–130–90–02, RIGW, Cairo.
- RIGW. (1991). *Hydrogeological map of Egypt-Burg El-Arab, scale 1:100,000*. Research Institute for Groundwater, Cairo, Egypt.
- RIGW/IWACO. (1988). *Hydrogeological mapping of Egypt; scale 1:2,000,000*.
- RIWR. (1995). *Sinai water resources study*. Final report, A.R.E., Research Institute of Water Resources, Ministry of Public Works and Water Resources.
- Rizzini, A., Vezzani, F., Cococetta, V., & Milad, G. (1978). Stratigraphy and sedimentation of a Neogene-quaternary section in the Nile Delta area. *Marine Geology*, 27(3–4), 327–348.
- Robinson, C. A., Werwer, A., El-Baz, F., El-Shazly, M., Fritch, T., & Kusky, T. (2007). The Nubian aquifer in Southwest Egypt. *Hydrogeology Journal*, 15, 33–45.
- Rognon, P. (1987). Late quaternary climatic reconstruction for the Maghreb (North Africa). *Palaeogeography, Palaeoclimatology, Palaeoecology*, 58, 11–34.
- Rognon, P., & Williams, M. A. J. (1977). Late quaternary climatic changes in Australia and North Africa: A preliminary interpretation. *Palaeogeography, Palaeoclimatology, Palaeoecology*, 21, 285–327.
- Said, R. (1981). *The geological evolution of the river Nile* (p. 151). Springer.
- Salah, A. E., & Samah, M. M. (2018). Hydrogeological assessment of Moghra aquifer, North Western Desert, Egypt. *Annals of the Geological Survey of Egypt*, V. XXXV, 110–130.
- Salem, O. M., & Pallas, P. (2002). The Nubian Sandstone aquifer system. In B. Appelgren (Ed.), (2004). *Managing shared aquifer resources in Africa*. ISARM-AFRICA. *Proceedings of the international workshop*, Tripoli, Libya, 2–4 June 2002. IHP-VI, Series on Groundwater No. 8. UNESCO, Paris.
- Sefelnasr, A., Gossel, W., & Wycisk, P. (2015). Groundwater management options in an arid environment: The Nubian Sandstone aquifer system, Eastern Sahara. *Journal of Arid Environments*, 122, 46–58.
- Sefelnasr, A. M. (2002). *Hydrogeological studies on some areas on the new Valley governorate*, Western Desert, Egypt. MSc thesis, Assiut University.
- Sestini, G. (1989). Nile Delta: A review of depositional environments and geological history. *Geological Society*, 41, 99–127 (Special Publications). <https://doi.org/10.1144/GSL.SP.1989.041.01.09>
- Shackleton, N., & Opdyke, N. (1977). Oxygen isotope and palaeomagnetic evidence for early Northern Hemisphere glaciation. *Nature*, 270, 216–219.
- Shata, A., & El Fayoumy, I. F. (1970). Remarks on the hydrogeology of the Nile Delta. In *Proceedings of the symposium on hydrogeology of Deltas*. UNESCO v. II.
- El Shazly, E. M., Abd El Hady, M. A., El Shazly, M. M., El Kassas, I. A., El Ghawaby, M. A., Salman, A. B., Morsi, M. A. (1975). *Geology and groundwater potential studies of El Ismailia master plan study area*. Remote Sensing Research Project, Academy of Scientific Research and Technology, Cairo, Egypt.
- Shendi, E., & Abouelmagd, A. (2004). New approach for ground geophysics in the development of groundwater in the basement terrains (A case study from South Sinai, Egypt). In *Proceedings of the 7th conference geology of Sinai for development*, Ismailia, Egypt (pp 129–140).
- Shepard, F. P. (1963). *Submarine geology* (p. 557). Harper & Row.
- Sherif, M. I., & Sturchio, N. C. (2021). Elevated radium levels in Nubian Aquifer groundwater of Northeastern Africa. *Science and Reports*, 11, 1–12. <https://doi.org/10.1038/s41598-020-80160-0>
- Sherif, M. I., Lin, J., Poghosyan, A., Abouelmagd, A., Sultan, M. I., & Sturchio, N. C. (2018). Geological and hydrogeochemical controls on radium isotopes in groundwater of the Sinai Peninsula, Egypt. *Science of the Total Environment*, 613–614, 877–885.
- Stanley, D., & Maldonado, A. (1977). Nile Cone: Late quaternary stratigraphy and sediment dispersal. *Nature*, 266, 129–135.
- Stanley, D., & Warne, A. (1998). Nile Delta in its destruction phase. *Journal of Coastal Research*, 14(3), 795–825.
- Sturchio, N. C., Du, X., Purtschert, R., Lehmann, B. E., Sultan, M., Patterson, L. J., Lu, Z. T., Müller, P., Bigler, T., Bailey, K., O'Connor, T. P., Young, L., Lorenzo, R., Becker, R., El Alfy, Z., El Kaliouby, B., Dawood, Y., & Abdallah, A. M. A. (2004). One million-year-old groundwater in the Sahara revealed by krypton-81 and chlorine-36. *Geophysical Research Letters*, 31, 2–5.
- Sultan, M., Ahmed, M., Sturchio, N., Eugene, Y., Milewski, A., Becker, R., Wahr, J., Becker, D., & Chouinard, K. (2013). Assessment of the vulnerabilities of the Nubian sandstone fossil aquifer, North Africa. In R. A. Pielke (Ed.), *Climate vulnerability: Understanding and addressing threats to essential resources* (pp. 311–333). Elsevier Inc.
- Swaiem, F. M., Hamza, M. S., & Aly, A. I. M. (1983). Isotopic composition of groundwater in Kufra, Libya. *Water Resources Development*, 1, 331–341.
- Thorweihe, U., & Heintz, M. (2002). *Groundwater resources of the Nubian aquifer system, NE-Africa*. Modified synthesis submitted to Observatoire du Sahara et du Sahel. OSS, Paris, p. 23.
- Thorweihe, U. (1982). *Hydrogeologie des Dakhla Beckens (Ägypten)* (Vol. 38, pp. 1–58). Berliner geowiss. Abh.
- Thorweihe, U. (1990). Nubian aquifer system. In: R. Said (Ed.), *Geology of Egypt* (pp. 601–611). Balkema.
- Van Overlop. (1984). Desertification cycles in historical Greece. In *Symposium on interactions between climate and biosphere*, March 21–23, 1983, Osnabruck, West Germany.
- Wendorf, F., & Expedition, T.M. of the C.P. (1977). Late Pleistocene and recent climatic changes in the Egyptian Sahara. *Geographical Journal*, 143, 211–234.
- Youssef, M. I. (1968). Structural pattern of Egypt and its interpretation. *AAPG Bulletin*, 52, 601–614.
- Youssef, T. (2012). Assessment of groundwater resources management in WadiEl-Farigh area using MODFLOW. *IOSR Journal of Engineering*, 02, 69–78. <https://doi.org/10.9790/3021-021016978>
- Zaghloul, Z. M., Taha, H. H., Hegab, O. A., & El Fawal, F. M. (1979). *The Plio-Pliostocene Nile Delta sub-environments; stratigraphic section and genetic class* (Vol. 1X). Geological Society, Cairo.



Mohamed Helmi Geriesh is a professor of hydrogeology in the Geology Department, Faculty of Science, Suez Canal University (Egypt). He received a Ph.D. degree (1995) in groundwater evaluation and management through a channel system program between Suez Canal University and the University of Tübingen (Germany). His research interests focus on hydrogeology, water resources management, groundwater modelling, hydrogeochemistry, paleohydrology, climate change, and environmental pollution. He has

worked as a consultant for the Suez Canal and Sinai governorates and several companies, among which are Arab contactors, Misrcom, Water Technology Center, Scientific Society of Desert Reclamation, and Natural Protectorate Heritages of Egypt. He worked as Head and Secretary General of the Scientific Professions Syndicate, representing Ismailia Governorate, Egypt, and as Chairman of the Geology Department Council (2008–2017). He has received several national and international awards of excellence and participated as a visiting professor for short periods at the University of Tübingen (1999, 2007 and 2013), Karlsruhe University, Germany (2003), Poznan University, Poland (2000), Western Michigan University, USA (2003), Zhejiang University, Hangzhou, China (2007), and Boston University, USA (2013).



Basma M. H. Mansour is an assistant professor of hydrogeology in the Geology Department, Faculty of Science, Suez Canal University (Egyp). She earned MSc (2012) and Ph.D. (2015) degrees in groundwater management from Suez Canal University. Her research interests focus on hydrogeology, water resources management, groundwater modeling, environmental pollution, climate change, and related fields. She was awarded a prize for the best applied research in Sinai International Conference for Geology and Development in 2010. She has also received

several national and international awards of excellence. She was an exchange student at Western Michigan University (USA) from September–October 2008 and a Ph.D. candidate at the University of Tübingen (Germany) in 2013. She was recently awarded a postdoctoral grant at Utrecht University, Netherlands (2021–2023).



Abdou Abouelmagd is an associate professor of hydrogeology in the Geology Department, Suez Canal University (Egypt). In 2013, he received a two-year postdoctoral fellowship at the Water Desalination and Reuse Center, King Abdullah University of Science and Technology (KAUST, Saudi Arabia). Prior to this, he was a postdoctoral fellow in the Earth Sciences Remote Sensing Lab. (ESRS) at Western Michigan University, USA where he also received a Ph.D. degree in Geosciences in 2012. He was awarded the Michigan Section of the American Water Works Association (MI

AWWA) Fellowship for water quality and treatment in 2010. Other awards include the Excellent Academics Award from the National Association of Black Geologists and Geophysicists (NABGG, USA) in 2011, First Prize Award in the postdoctoral research poster competition in the Winter Enrichment Program (WEP) at KAUST in 2015, and the Late Prof. Ahmed Askar university-wide award for the best applied research paper, Suez Canal University in 2018. His research covers interdisciplinary approaches utilizing hydrogeology, hydrogeochemistry, geophysics, groundwater modeling, remote sensing, and GIS.



Geothermal Potentiality of Egypt: Review and Updated Status

Mohamed Abdel Zaher, Gad El-Qady, and Samah Elbarbary

Abstract

Egypt seeks to diversify in exploiting new energy resources that can be obtained at competitive rates in order to continue sustainable development processes. Whereas due to limited water and fossil fuel supplies, as well as growing environmental concerns, Egypt's demand for clean and renewable alternative energy is increasing. Unexploited geothermal resources may contribute with additional forms of renewable energy to meet domestic energy requirements while also allowing electricity exports to increase. In this chapter, we review the state-of-the-art geothermal potentialities and resources in Egypt as well as current geothermal energy uses and future developments. Generally, almost all prior studies agree that the highest geothermal prospective sites are located in the eastern part of Egypt near the Red Sea, the Gulfs of Suez and Aqaba. However, some areas in the Nile Delta and Western Desert have normal to low-temperature geothermal resources that can be utilized in many direct applications.

Keywords

Renewable energy • Geothermal potentiality • Geothermal resources • Red Sea • Gulf of Suez

1 Introduction

Fossil fuels (oil and gas) are the essential resources for Egypt's energy needs, accounting for 95% of the country's overall energy consumption in 2020 (BP, 2021; Enerdata, 2021). In January 2021, Egypt's electricity consumption was estimated to be 11,878.000 kWh mn. The data is updated

monthly, with 289 observations averaging 9382.000 kWh mn from January 1997 to January 2021 (Ceicdata, 2021). Subsequently, Egypt's energy is primarily derived from petroleum products, however Egypt's Supreme Energy Council has set an ambitious plan to rise the share of renewable energy to 20% of total energy demand by 2030. Whereas a huge shift away from fossil fuel-based energy production and toward renewable energy sources is taking place throughout the world. Geothermal energy is a valuable renewable and clean energy source that can help with carbon emission reduction and the global energy transition. Hence, geothermal is a promising source of renewable energy for generating power and contributing to addressing Egypt's energy needs in a clean and efficient manner.

The most common categorization for geothermal resources is based on the temperature of the fluid in the geothermal reservoir. Temperatures above 150 °C are found in high enthalpy resources, which are good for power generation, whereas temperatures below this are found in low-enthalpy sources (Martín-Gamboa et al., 2015). The recognized geothermal resources of Egypt are mostly low to medium enthalpy, however there are some high enthalpy locations in deep water along the Red Sea rift (Lashin, 2020). The geothermal systems are expected to develop in a variety of structurally geological sediments in Egypt. They can be originated from deep fluid circulation through faults or folded permeable strata, tectonic uplift of hotter rocks, and residual heat from intruded plutons. Whereas the geothermal energy is found all over the world and the only concern is the depth of drilling necessary to reach the required amount of heat for energy production.

The rift zones are a good example of geothermal fields that are tectonically delimited (Latin et al., 1993; Nyblade et al., 2000). One of the world's largest rift systems is the East African Rift System (EARS), it is structurally active zone, which is portrayed by a spreading crust, covers 6400 km long and up to 64 km in width, and reaches out across various countries in Eastern Africa including eastern part of Egypt

M. Abdel Zaher · G. El-Qady (✉) · S. Elbarbary
National Research Institute of Astronomy and Geophysics
(NRIAG), Helwan, Cairo, 11421, Egypt
e-mail: gadosan@nriag.sci.eg

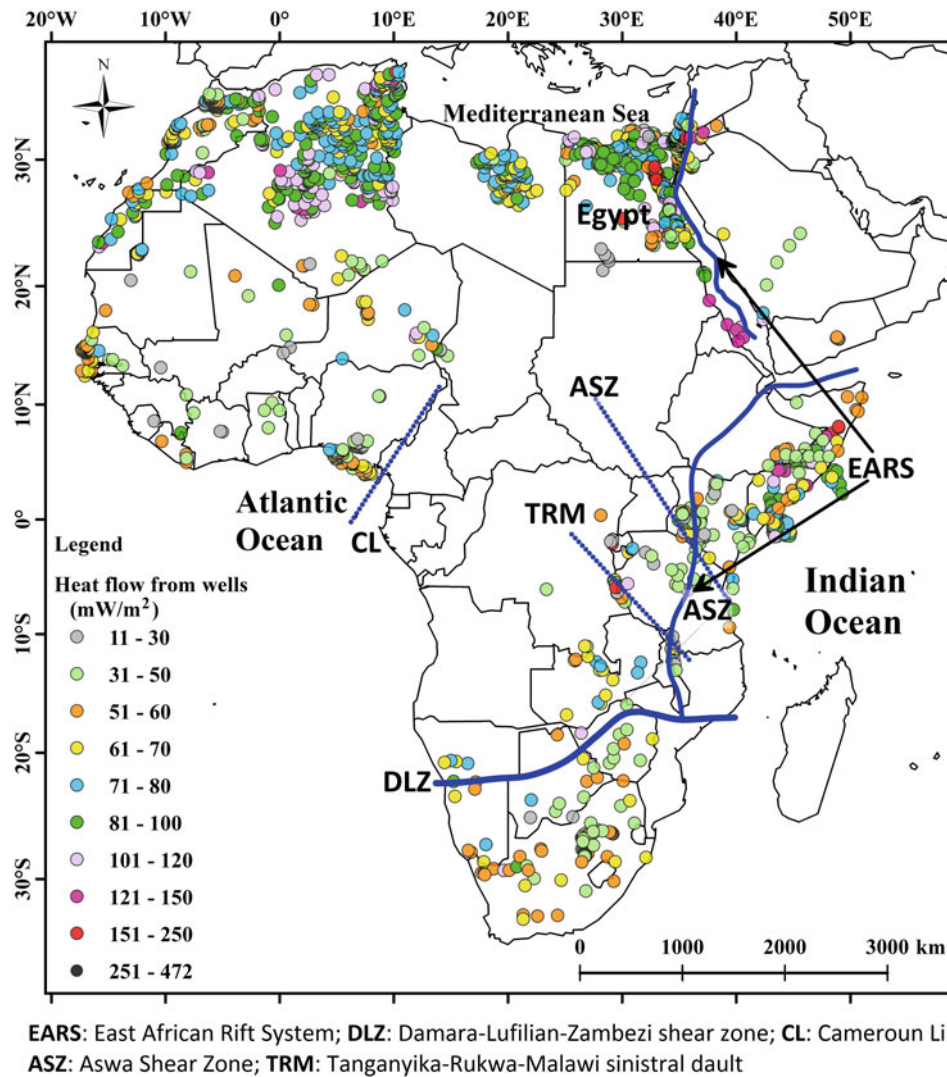


Fig. 1 The location of Egypt on the map of Africa continent showing the distribution of heat flow from wells in different countries, modified after Macgregor (2020). The map depicts the eastern part of Egypt with a significant heat flow

(Fig. 1). The EARS' geological features rich in geothermal energy resources that, can provide a reliable, economical, and indigenous source of renewable energy. Hence, the eastern side of Egypt which is limited by a middle spreading center in the Gulf of Suez and Red Sea indicate the significance of these regions for geothermal development.

2 Geothermal Surface Manifestations in Egypt

Geologically, Egypt's geothermal resources can be classified into two main systems: one is tectonically controlled, which is found in the rift of the Red Sea and the Gulf of Suez, where there are a number of hot springs. The other resources are governed by the sedimentological system of the many

stratigraphic units of Egypt's Western Desert, which is home to several flowing hot springs. Egypt's geothermal manifestations can be found in many places, including hot springs near the surface and thermal deep wells (Lashin, 2020) (Fig. 2).

The hottest springs in Egypt are often found near the Gulf of Suez's coasts, including Ain Sokhna on the western shore of the Gulf and Ayun Musa, Ain Hammam Faraun, and Hammam Musa on the eastern shore (the location of these hot springs are shown in Fig. 2). The rift of the Gulf of Suez is thought to have resulted in the formation of these springs, which are tectonic or non-volcanic in origin (Boulos, 1990). The Helwan sulfur spring, 25 km south of Cairo, is another probable thermal spring, with temperatures ranging from 23 to 32 °C (El-Ramly, 1969). In the Western Desert, all thermal water comes from deep wells, which many of them are artesian (Lashin, 2013).

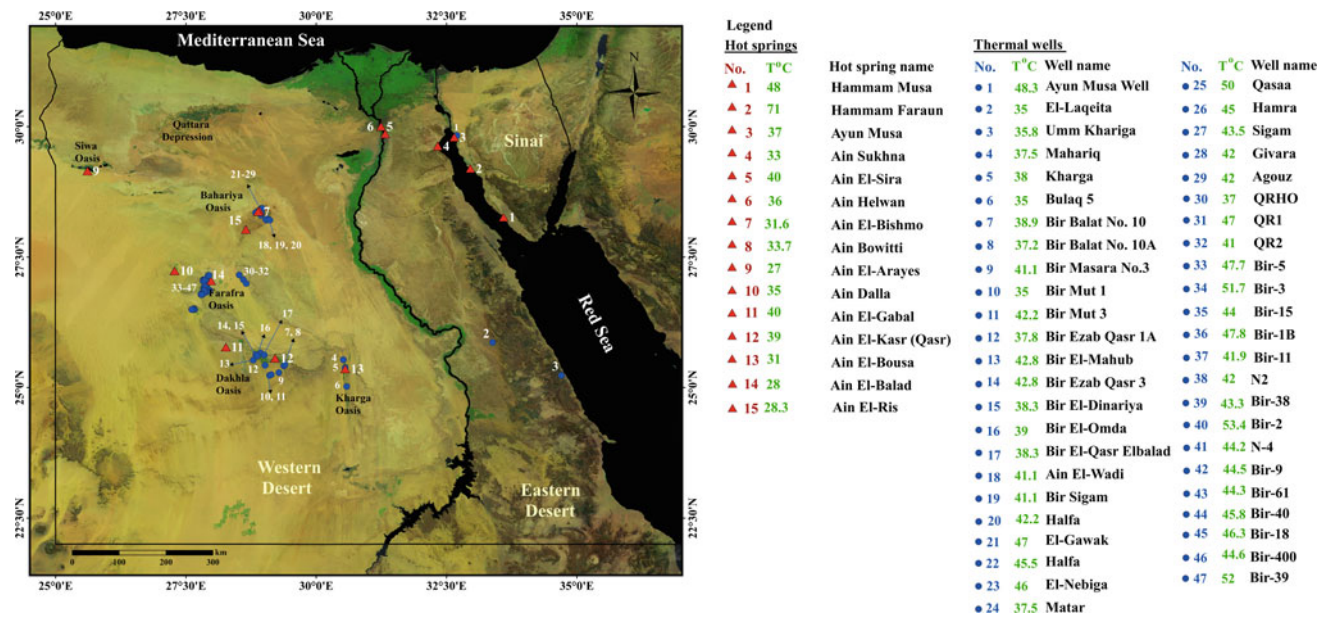


Fig. 2 Landsat image of Egypt showing the distributions of hot spring and thermal well and their temperatures (modified after Abdel Zaher et al., 2018)

3 Geology and Structural Setting of Egypt

Egypt’s geology contains rocks dating from the Archaean through the early Proterozoic periods (Said, 1962). These oldest rocks can be found as inliers, older rocks encircled by younger rocks, in the Egypt’s Western Desert. While, the rocks of the Eastern Desert are mostly late Proterozoic in age (Hamimi et al., 2020). The older basement is covered by Paleozoic sedimentary rocks all around the country. The majority of Egypt’s surface is covered with limestone, which sits atop a layer of sandstone that represents the surface rocks of Nubia and southern Egypt. Tectonism governs the surface outcroppings of Egypt’s Basement rocks, with about 90% of these rocks buried beneath the Phanerozoic sedimentary layer (El-Shazly, 1977). Basement exposures are set up in the most rugged mountainous sections of the Eastern Desert and the southern Sinai Peninsula, as well as isolated areas of southern Egypt, such as those near Aswan and Gebal El-Uweinat in Egypt’s southwest corner (Fig. 3).

The unstable shelf, the stable shelf and the Arabian-Nubian massif make up Egypt’s overall tectonic framework, which has shaped the country’s sedimentological and structural history (Bosworth et al., 2015; Hussein & Abd-Allah, 2001; Youssef, 2003). The stable shelf, which surrounds the Arabian-Nubian massif, represents relative tectonic stability in southern Egypt and covers a large portion of Egypt. It is protected by a pre-Cretaceous rock base (Said, 1962). On the other hand, northern Egypt is part of the unstable shelf, which has seen extensive rock deformation, basin subsidence, and the creation of steep northeast-trending anticlines and

cross-cutting faults (i.e., the Syrian Arc). Eastward, the northern extension of the East African Rift System (EARS) is encompass of the Red Sea and its two branches; the Gulf of Suez and the Gulf of Aqaba linked with the divergence of the Arabian and African plates (Dahy, 2012).

4 Heat Flow of Egypt

Regional heat flow studies can help in preliminary assessment of the prospective areas of geothermal potential. Areas with high heat flow and hydrological media to transfer the heat to the near surface or even to the surface enable geothermal energy to be utilized for producing electricity, space heating, local industry and agriculture. Based on data from 596 deep wells with bottom-hole temperatures (BHT), Abdel Zaher et al. 2018 estimated the heat flow map of Egypt and temperature distribution at various depths (Fig. 4). Heat flow values of Egypt range from 27 to around 180 mW/m², with an average of about 78 mW/m². They came to the conclusion that the most encouraging locales for geothermal potential in Egypt are around the Red Sea and Gulf of Suez coasts. El-Gouna region, found south of the Gulf of Suez, has a more noteworthy geothermal chance, which may be connected to the Sinai triple intersection of Africa, Arabia, and Sinai.

In addition to the oil wells, there are minor boreholes devoted primarily to heat flow studies, where the heat flow patterns of Sinai are assessed. The eastern edge of the crystalline Sinai massif, on the other hand, has the highest heat flow values, exceeding 90 mW/m² (Fig. 5). The heat

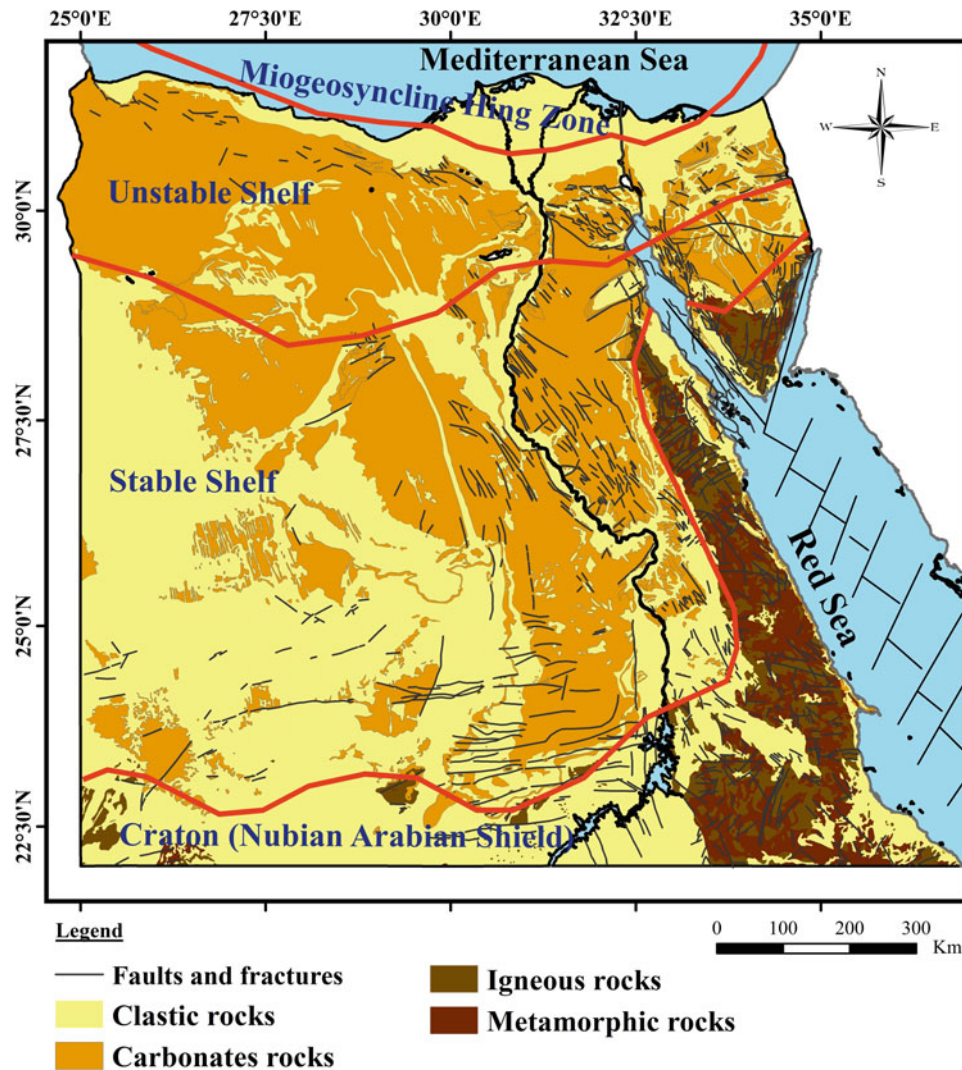


Fig. 3 Simplified geological map of Egypt, map in scale 1:2 million @Geological Survey of Egypt (GSE, 1981). The Nubian-Arabian Shield margin's structural elements are based on Said (1962). Surface structural lines are denoted by black lines

flow along the western margin of the Gulf of Suez was predicted to be 60–80 mW/m² and may reach to 100 mW/m², assuming a thermal conductivity of 2.3 W/mK as a minimum value (Morgan et al., 1985; Boulos, 1990). These values must be doubled due to the presence of a thick evaporates layer with high conductivity in the Gulf of Suez portion. The thermo-mechanics process that governs the tectonic development of the Gulf of Suez remains a mystery. However, the rift flank's very enormous magnitude given the amount of extension in the Gulf of Suez points to a thermal uplift component (Feinstein et al., 1996). According to geothermometer data, the Hammam Faraun area has a subsurface reservoir temperature of 94.5 °C and a heat flow of roughly 122 mW/m². (Lashin & Al-Arifi, 2010, El-Qady et al., 2005).

At a depth of 1720 m, the estimated formation temperature in the Hammam Faraun-Sudr region reaches 128 °C,

which is considered high when compared to other equivalent depths in other regions (Lashin, 2013). In front of the Upper Eocene rocks, both thermal conductivity (2.8–3 W/m/K) and heat flow (105–120 mW/m²) increase, implying that these rocks could be the future geothermal hot water reservoir. The temperature gradient in the Hammam faraun area was measured as 42.9 °C/km (Lashin, 2013) (Fig. 6).

Morgan et al., 1983 reported subsurface temperature data from oil wells in northern Egypt, the Nile Delta, and the Gulf of Suez. A thermistor, a gadget whose electrical resistance varies with temperature, was used to measure the temperatures in the boreholes at 5 m intervals with a precision of 0.01 °C. Figure 7 shows the locations of existing boreholes in which temperatures were measured and temperature gradients were calculated. The findings from the Western Desert show modest temperature gradients of between 15 and 19 mK m⁻¹, which were calculated in sediments with low

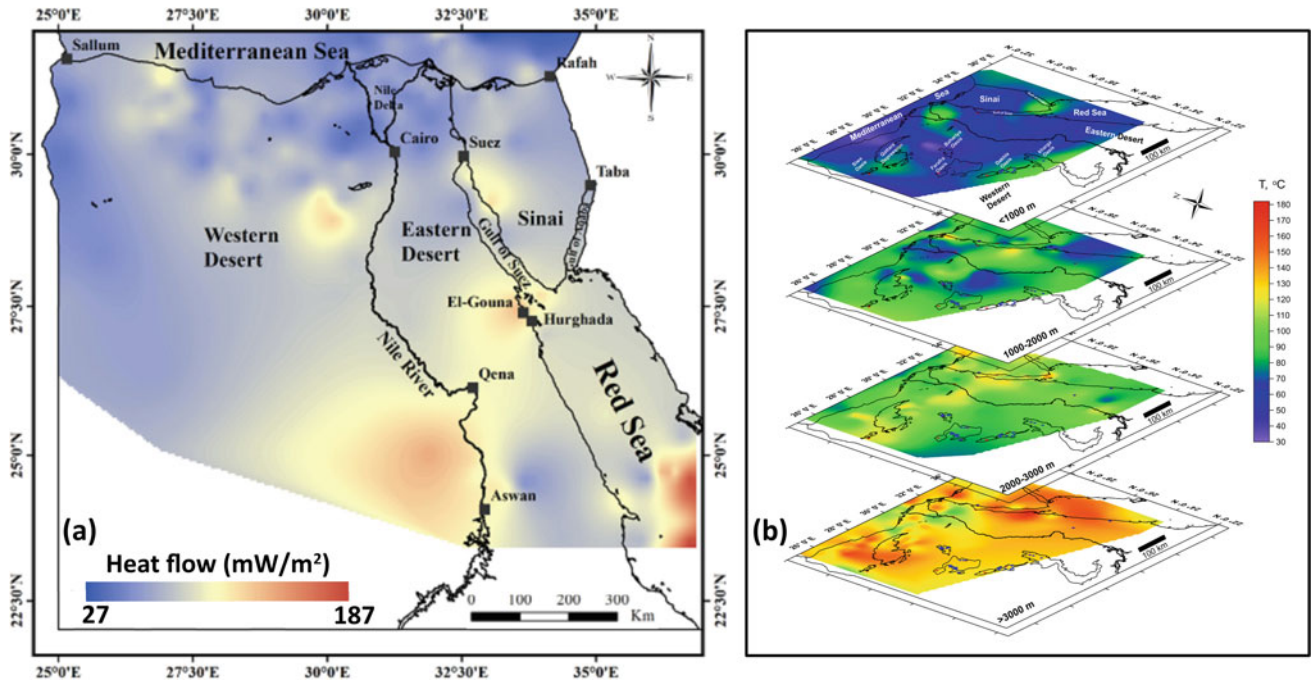


Fig. 4 a Heat flow map of Egypt based on temperature data from deep onshore and off shore wells, b the distribution of temperatures at various depths (modified after Abdel Zaher et al., 2018)

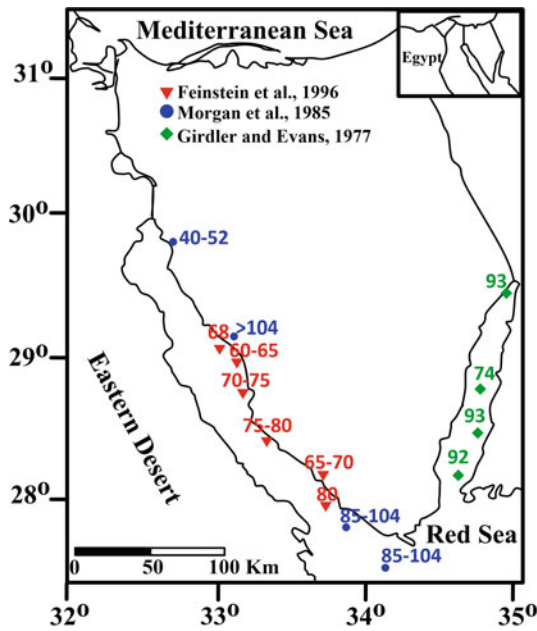


Fig. 5 Heat flow values in mW/m^2 in Sinai Peninsula and vicinity (modified after El-Qady et al., 2005)

thermal conductivity, implying minimal heat flow. The oxidative heating of pyrite in the phosphate deposit at a depth of around 80–150 m causes the significant temperature gradients in the Abu Tarture region (74 mKkm^{-1}). On the other hand, temperatures were taken in Precambrian basement outcrops in the Eastern desert, which have a

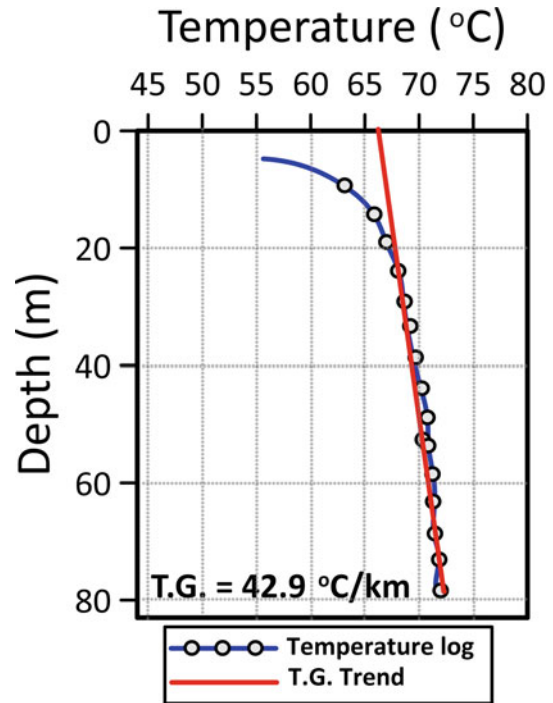


Fig. 6 A borehole's temperature profile and average geothermal gradient in the Hammam Faraun region of the Gulf of Suez (Lashin, 2013)

greater heat conductivity than the sediments in western Egypt. In the Hammam Faraun hot spring, a large temperature gradient was observed (48 mKkm^{-1}).

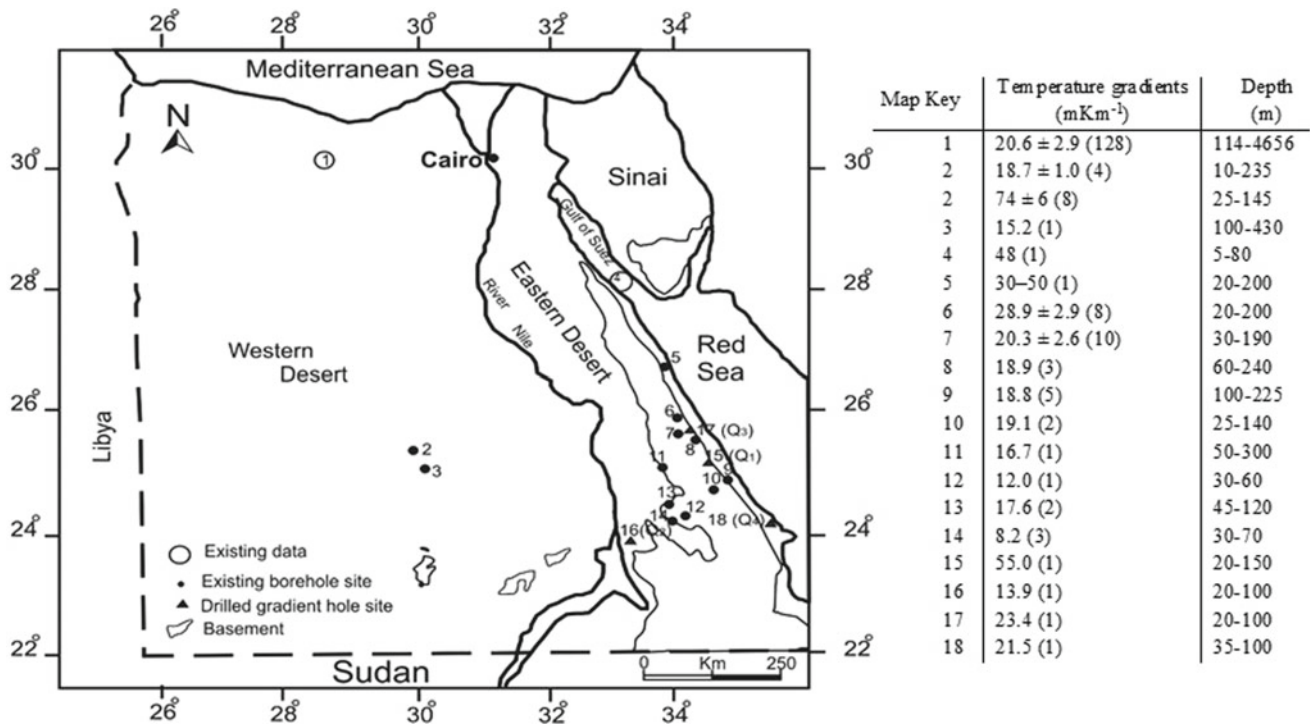


Fig. 7 Locations of the boreholes where temperature logs were measured by Morgan et al. (1985). The table on the right refers to the depth and temperature gradient for each well

High heat flow values of up to 175 mW/m^2 , roughly three times average, have been reported in eastern Egypt, according to Morgan and Swanberg (1979), and the heat flow appears to increase toward the Red Sea coast. Furthermore, the heat flow values in the northern part of the Nile Delta were calculated by Riad et al. (1989) using 228 temperature observations from 48 wells, with thermal conductivity values for the rocks composing the stratigraphic section in the Nile Delta ranging between 2 and $2.3 \text{ w/m}^2\text{C}$. The heat flow values were found to range between 39 and 56 mW/m^2 , showing that due to lithological changes, the Nile Delta is a geothermally anomalous area. Mohamed et al. (2015) calculated the heat flow in the northern Western Desert using bottom-hole temperature (BHT) data from 116 deep oil wells. The heat flow is generally $40\text{--}70 \text{ mW/m}^2$, although a few locally moderate heat flow (100 mW/m^2) are observed and are explained by potential local geothermal fields.

5 Exploration of Geothermal Resources in Egypt

Several studies have been published on the exploration and evaluation of geothermal resources in Egypt's regions (such as, Abdel Zaher et al., 2011a, 2011b, 2012; Chandrasekharan et al., 2016; El-Qady, 2006; El-Qady et al., 2000, 2005, 2020; Feinstein et al., 1996; Lashin, 2007,

2013; Morgan et al., 1983). Recently, Abdel Zaher et al. (2018) used digital data layers and maps in a GIS model to develop a geothermal favorability map of Egypt that focuses on the most promising geothermal locations (Fig. 8). Temperatures at various depths, heat flow, Curie Point Depth (CPD), distance to seismic activity, Bouguer gravity anomaly and distance to faults, are the evidence thematic layers. In general, between the Red Sea and the Gulf of Suez coastlines, Egypt has the most promising geothermal potential.

Fahil et al. (2020) adjusted temperature data from 197 onshore and offshore oil wells in the Gulf of Suez region. According to the findings, the research region has an amplitude temperature of $49.48\text{--}157.8 \text{ }^\circ\text{C}$, a geothermal gradient of $24.9\text{--}86.66 \text{ }^\circ\text{C/km}$, a thermal conductivity of $2.6\text{--}3.2 \text{ Wm}^{-1} \text{ K}^{-1}$, and a heat flow of $31\text{--}127.2 \text{ mWk}^{-1}$. Nine raster layers were interpolated over the research region to produce continuous raster layers for inclusion in the GIS-based geothermal potential model, including geothermal gradient, heat flow, thermal conductivity, and depth to crystalline basement, elevation, lineaments density, land surface temperature, drainage density, and major lithological units (Fig. 9a). Additionally, Abuzied et al. (2020) combined several evidence layers to create a geothermal potential map in the Gulf of Suez region showing the locations of the most promising geothermal reservoirs. The ideal sites are found in places with highly structured and porous surficial

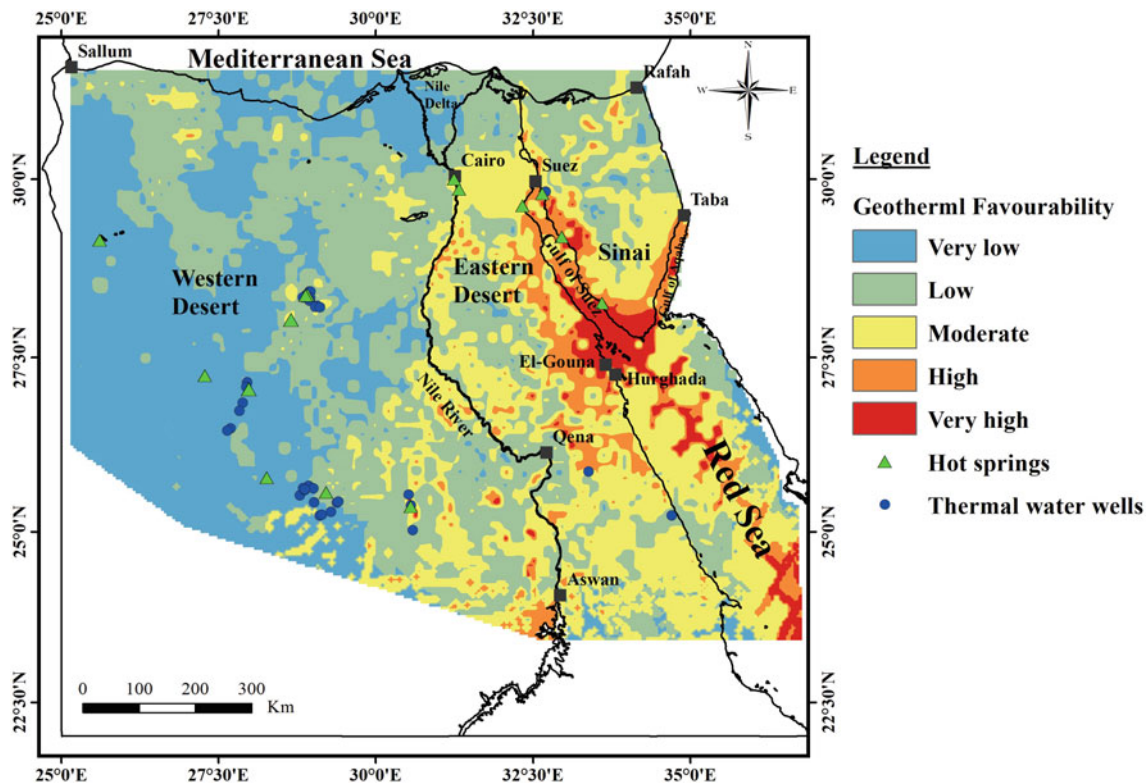


Fig. 8 Egypt's geothermal favorability map, based on weight overlay assessments of many thematic layers (Abdel Zaher et al., 2018)

outcropped lithologies. El-Tur, Abu Durba, Belayim, Abu Rudies, Ras Badran, Ras Matarma, and several sites on the southwestern shore of the Gulf of Suez are expected to prove fruitful (Fig. 9b).

Using power spectrum analysis, an aeromagnetic map of Egypt was utilized by Elbarbary et al. (2018) to predict the Curie point depth (CPD), temperature gradient, and heat flow (Fig. 10). The deduced heat flow values range between 47 and 195 mW/m², with the largest temperature gradient and heat flow found in the Red Sea and the Gulf of Suez, due to tectonic processes in the region linked with the Eastern African Rift System (EARS).

Aboulela et al. (2021) used chemical geothermometers to determine the subsurface conditions in terms of reservoir temperature and heat flow in hot springs that are located around the Gulf of Suez. The calculated reservoir temperatures are around 96, 82, and 86 °C while the heat flows range around 124, 102, and 108 mW/m² for Hammam Faroun, Hammam Musa, and Ain Sukhna hot springs, respectively. In the western side of Egypt, the Artificial Neural Network (ANN) approach was used to link geothermal gradients from 116 deep oil well BHT logs with gravity data in order to develop geothermal gradient maps of

the northern Western Desert (Mohamed et al., 2015). They concluded that despite the modest regional temperature gradients (30 °C/km) in Egypt's northern Western Desert, numerous possible local geothermal fields (> 40 °C/km) were discovered (Fig. 11).

6 Geothermal Present Utilizations and Future Developments

No real assessment is made for the whole geothermal probability in Egypt. However, a geothermal asset appraisal was made in Gulf of Suez region because of its extraordinary geothermal attributes. As indicated by Lashin (2007, 2013), a 12.4 MWt geothermal energy potential is given for Hammam Faraun region, accepting geothermal supply temperature of 95 °C. The planned geothermal plant has a turbine transformation proficiency factor of 0.26, 50 years of work, and a recovery factor of 0.20. On the other side, based on a numerical calculation, Abdel Zaher et al. (2012) found that the Hammam Faraun hot spring area has a slightly higher geothermal potential of 19.8 MWt, suggesting a reservoir thickness of 500 m, an initial temperature of 130 °C,

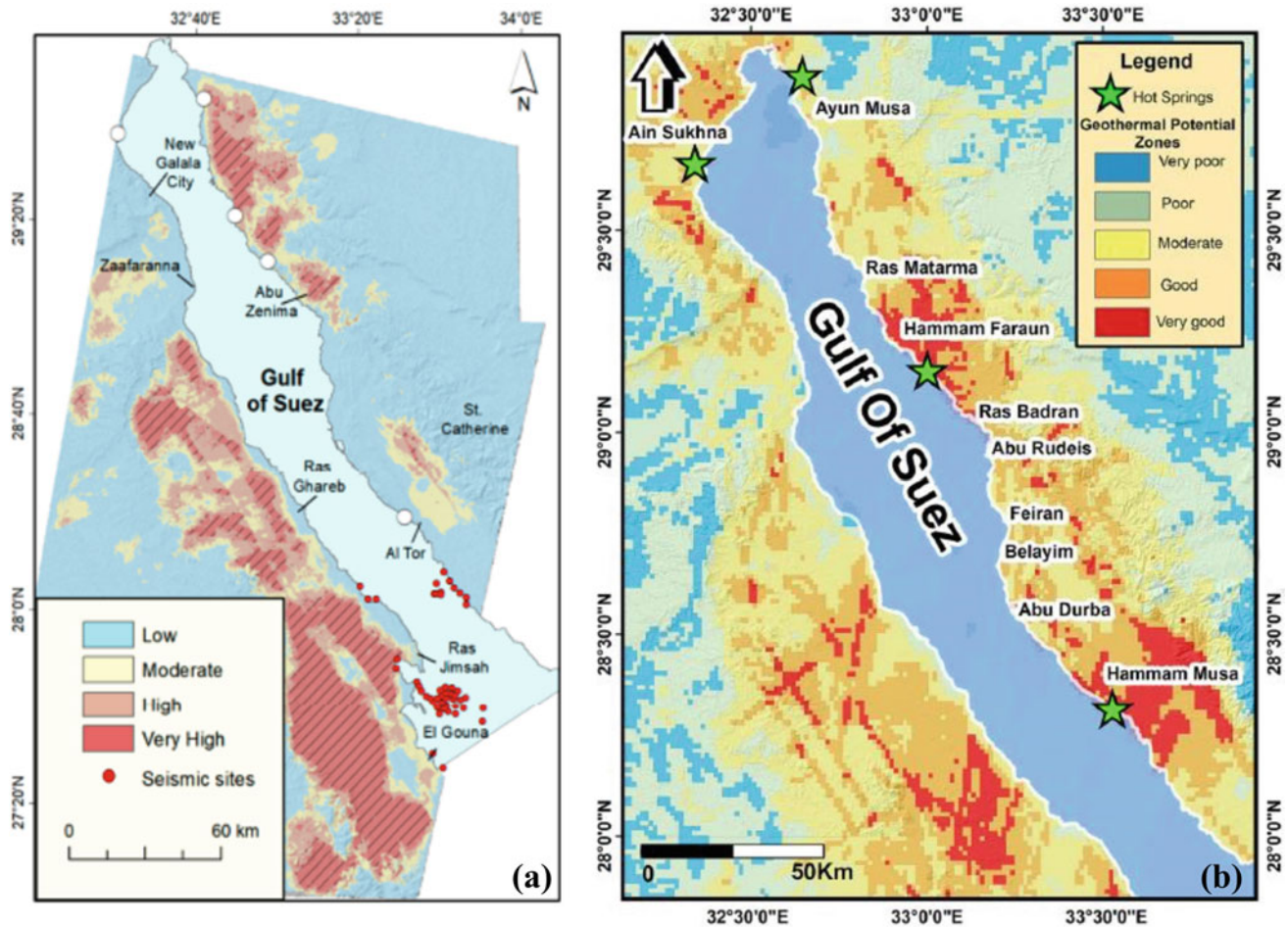


Fig. 9 Gulf of Suez geothermal potential maps based on: **a** simple additive weight (SAW) procedure (Fahil et al., 2020) and **b** statistical examination of the weight of evidence (WOE) and information value (IV) (Abuzied et al., 2020)

and a 30-year reservoir production. In addition, it was supposed that the geothermal reservoir contained hot solid rock and single-phase liquid water.

In Egypt, there are currently no installed geothermal power plants; nevertheless, several direct use applications have been installed. Thermal water has been used directly in ancient Egypt for thousands of years, with many ancient Egyptians using the warm waters from hot springs for medical and domestic purposes (Gianfaldoni et al., 2017). In Egypt's western desert, certain papyrus have been discovered that record such usage. Some direct low-grade geothermal applications have recently been implemented. District heating, fish farming, agricultural applications, and green houses are the most typical uses. Along the Gulf of Suez's eastern coast, some refreshment and swimming pools have already been built. These pools are mostly utilized for recreational and therapeutic purposes. The major source of

water for these pools is geothermal water from a hot spring (Kaiser & Ahmed, 2013). On the other hand, the low-enthalpy resource at the Gulf of Suez can be used to generate power using standard binary-cycle technology (Abdel Zaher et al., 2012). The generated electricity would be sufficient for desalination of water for both human and agricultural use. This might be put to good use in the Sinai Peninsula for long-term development.

According to Lashin (2013), downhole pumps can be employed to exploit the reservoir thermal waters of the Hammam Faraun region to provide a water that is over 85 °C. Thermal water can be used to run a simple design of a small Kalina cycle power plant. The surface thermal water from Hammam Faraun, on the other hand, can be utilized for various direct heat applications. Table 1 summarizes the usage of geothermal resources in direct heat use in Egypt (Lashin, 2015) and demonstrates that bathing and

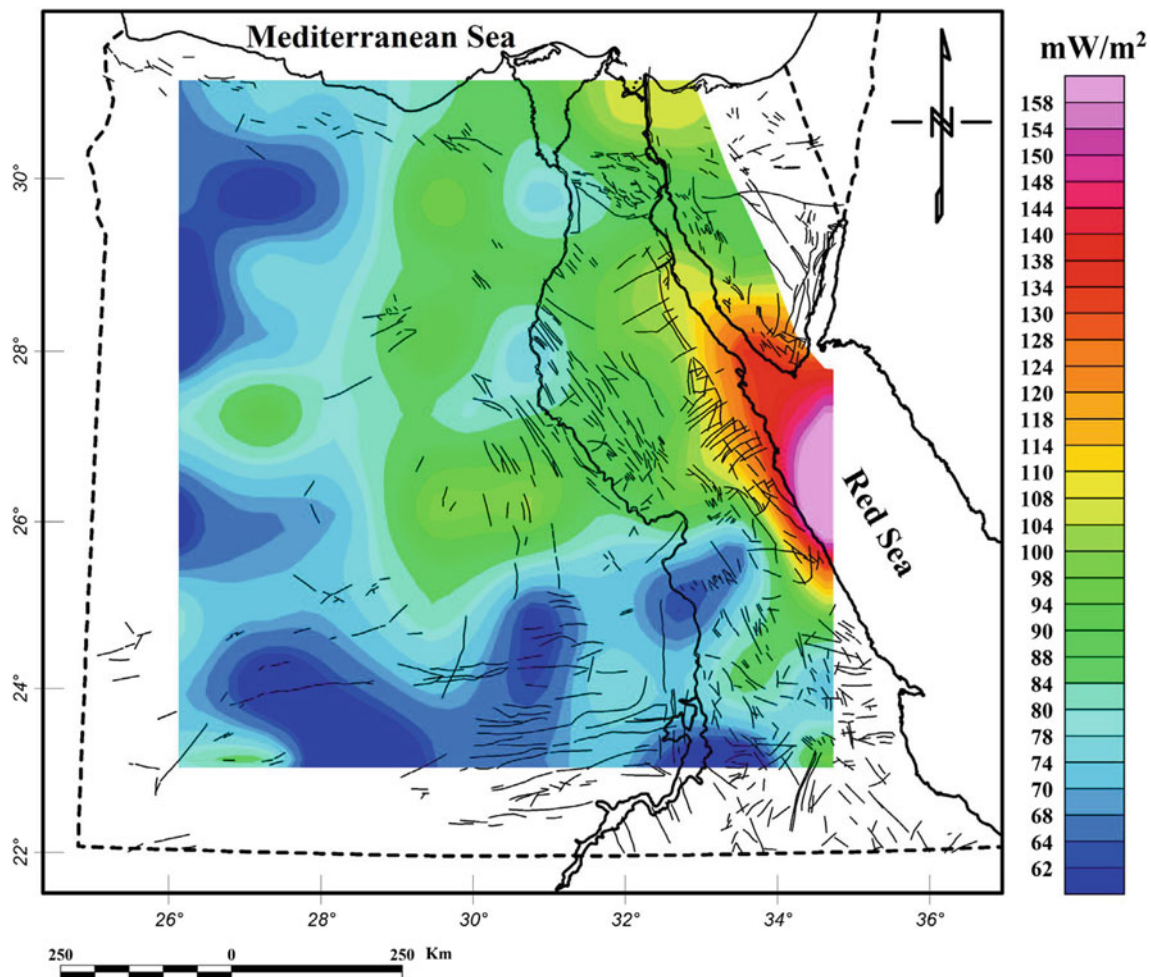


Fig. 10 Egypt's heat flow map, based on spectrum analysis of aeromagnetic data (Elbarbary et al., 2018)

swimming, greenhouses, and space heating are the most common direct heat uses. Aboulela et al. (2021) illustrated that the thermal water of Hammam Faroun hot spring can be exploited for probable energy generation employing low boiling water geothermal plants. A total of 19.68 MWt of geothermal energy may be produced.

7 Conclusions

According to the Ministry of Electricity and Energy's yearly reports, Egypt's installed generating power capacity is mostly dependent on oil and natural gas sources. The growing energy consumption has put a lot of pressure on the government's strategy to find alternative energy sources as a top priority for the country. In a nationwide appeal, the Egyptian Supreme Energy Council announced an ambitious aim to boost renewable energy's proportion of overall

demand to 20% by 2030 and geothermal energy is one of the most promising renewable energy sources.

Overall, Egypt has promising geothermal potential along the coasts of the Red Sea, the Gulf of Suez, and the Gulf of Aqaba which can be utilized to generate electricity. On the other side, the hot springs and thermal wells in the Western desert can be utilized as a direct application. Egypt's demand for clean, renewable, alternative energy, as well as the potential for collecting undiscovered geothermal resources, may fulfill internal electrical needs while also allowing Egypt to export electricity.

More in-depth research on geothermal resources is required for future work in order to fully assess Egypt's geothermal potential. The primary goal is to take a big step toward creating an ATLAS of Egypt's geothermal resources. This is accomplished by developing scientific and laboratory tools for geophysical and geothermal applications to assist government agencies, companies, and investors in better

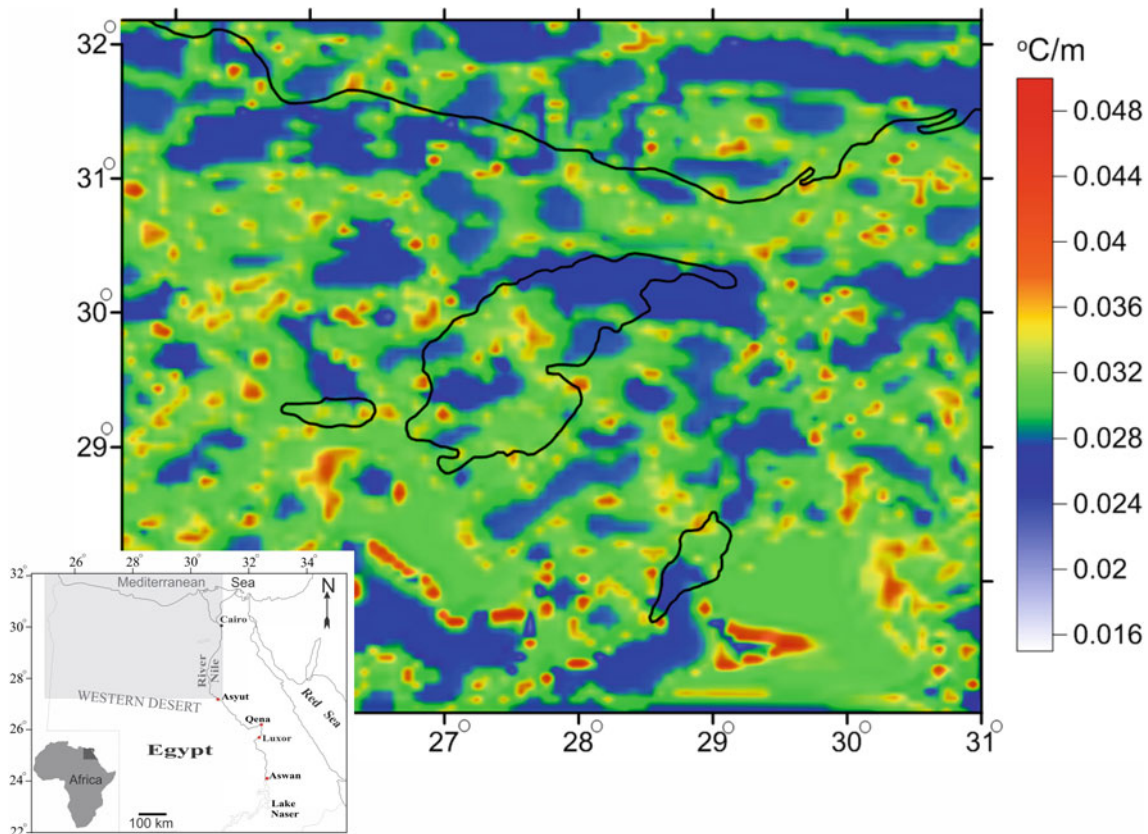


Fig. 11 Northern Western Desert temperature gradient map produced from gravity and BHT data correlation using ANN (Mohamed et al., 2015)

Table 1 Geothermal direct heat uses of Egypt (after Lashin, 2015)

Use	Installed capacity (MWt)	Annual energy use (TJ/yr = 1012 J/yr)
Individual space heating	0.3	3
District heating	1.5	15
Greenhouse heating	1	10
Bathing and swimming	4	60
Total	6.8	88

understanding the potential of geothermal energy in key and promising locations, as well as providing technical advice prior to the construction of a geothermal plant.

References

- Abdel Zaher, M., Elbarbary, S., El-Shahat, A., Mesbah, H., & Embaby, A. (2018). Geothermal resources in Egypt integrated with GIS-based analysis. *Journal of Volcanology and Geothermal Research*, 365, 1–12.
- Abdel Zaher, M., Nishijima, J., El-Qady, G., Aboud, E., Masoud, O., Soliman, M., & Ehara, S. (2011a). Gravity and magnetotelluric investigations to elicit the origin of Hammam Faraun hot spring, Sinai Peninsula, Egypt. *Journal of Acta Geophysica*, 59(3), 633–656.
- Abdel Zaher, M., Saibi, H., El-Nouby, M., Ghamry, E., & Ehara, S. (2011b). A preliminary regional geothermal assessment of the Gulf of Suez, Egypt. *Journal of African Earth Sciences*, 60, 117–132.
- Abdel Zaher, M., Saibi, H., Nishijima, J., Fujimitsu, Y., Mesbah, H., & Ehara, S. (2012). Exploration and assessment of the geothermal resources in the Hammam Faraun hot spring, Sinai Peninsula, Egypt. *Journal of Asian Earth Sciences*, 45, 256–267.
- Aboulela, H., Amin, A., Lashin, A., & El Rayes, A. (2021). Contribution of geothermal resources to the future of renewable energy in Egypt: A case study, Gulf of Suez-Egypt. *Renewable Energy*, 167, 248e265.
- Abuzied, S. M., Kaiser, M. F., Shendi, E. A. H., & Abdel-Fattah, M. I. (2020). Multi-criteria decision support for geothermal resources exploration based on remote sensing, GIS and geophysical techniques along the Gulf of Suez coastal area, Egypt. *Geothermics*, 88, 101893.
- Bosworth, W., Stockli, D. F., & Helgeson, D. E. (2015). Integrated outcrop, 3D seismic, and geochronologic interpretation of Red Sea

- dike-related deformation in the Western Desert, Egypt—the role of the 23 Ma Cairo “miniplume”. *Journal of African Earth Sciences*, 109, 107e119.
- Boulos, F. K. (1990). Some aspects of the geophysical regime of Egypt in relation to heat flow, groundwater and microearthquakes. In R. Said (Ed.), *The geology of Egypt* (pp. 61–89). Balkema.
- BP. (2021). *Statistical review of world energy* (70th ed.). <https://www.bp.com/content/dam/bp/business-sites/en/global/corporate/pdfs/energy-economics/statistical-review/bp-stats-review-2021-full-report.pdf>
- Ceicdata. (2021). *Egypt electricity consumption 1997–2021, Monthly, kWh mn*. Ministry of Electricity and Energy. <https://www.ceicdata.com/en/egypt/electricity-consumption/electricity-consumption>
- Chandrasekharam, D., Lashin, A., Al Arifi, N., Al Bassam, A., Varun, C., & Singh, H. K. (2016). Geothermal energy potential of eastern desert region, Egypt. *Environmental Earth Sciences*, 75, 697.
- Dahy, S. A. (2012). Seismic active zones and mechanism of earthquakes in northern Egypt. *European Journal of Applied Sciences*, 4(2), 65–71.
- Elbarbary, S., Zaher, M. A., Mesbah, H., El-Shahat, A., & Embaby, A. (2018). Curie point depth, heat flow and geothermal gradient maps of Egypt deduced from aeromagnetic data. *Renewable and Sustainable Energy Reviews*, 91, 620–629.
- El-Qady, G., Ushijima, K., & Ahmad, E. S. (2000). Delineation of a geothermal reservoir by 2D inversion of resistivity data at Hamam Faraun area, Sinai, Egypt. In *World geothermal congress* (pp. 1103–1108).
- El-Qady, G., Salem, A., Aboud, E., Khalil, A., & Ushijima, K. (2005). Geothermal reconnaissance study for Sinai Peninsula, Egypt. In *Proceedings world geothermal congress 2005*, Antalya, Turkey, 24–29 April 2005.
- El-Qady, G. (2006). Exploration of a geothermal reservoir using geoelectrical resistivity inversion: Case study at Hammam Mousa Sinai, Egypt. *Journal of Geophysics and Engineering*, 3(2), 114–121.
- El-Qady, G., Shanab, S., Omran, M., Embaby, A. A., & Aboelkhair, H. (2020). Hydrogeophysical study at an arid area: Case study at Ayun Musa hot springs Sinai, Egypt, NRIAG. *Journal of Astronomy and Geophysics*, 9(1), 16–29.
- El-Ramly, I. M. (1969). Recent review of investigations on the thermal and mineral springs in the UAR. In *Proceedings 23rd international geological congress* (Vol. 19, pp. 201–203).
- El Shazly, E. M. (1977). *The Ocean Basin and margins*. In A. E. M. Nairn, W. H. Kaner, & F. G. Stehli (Eds.), *The Eastern Mediterranean* (Vol. 4a).
- Enerdata. (2021). “Egypt” *contrary energy report*. <https://www.enerdata.net/estore/country-profiles/egypt.html>
- Fahil, A. S., Ghoneim, E., Noweir, M. A., & Masoud, A. (2020). Integration of well logging and remote sensing data for detecting potential geothermal sites along the Gulf of Suez, Egypt. *Resources*, 9, 109.
- Feinstein, S., Kohn, B. P., Steckler, M. S., & Eyal, M. (1996). Thermal History of the Eastern Margin of the Gulf of Suez, I. Reconstruction from borehole temperature and organic maturity measurements. *Tectonophysics*, 266, 203–220.
- Gianfaldoni, S., Tchernev, G., Wollina, U., Rocchia, M. G., Fioranelli, M., Gianfaldoni, R., & Lotti, T. (2017). History of the baths and thermal medicine. *Open Access Macedonian Journal of Medical Sciences*, 5(4), 566–568.
- GSE, Geological Survey of Egypt. (1981). *Geologic map of Egypt. Scale 1:2,000,000*.
- Hamimi, Z., El-Barkooky, A., Martínez Frias, J., Fritz, H., & Abd El-Rahman, Y. (2020). *The geology of Egypt* (p. 711). Springer. ISBN: 978-3-030-15265-9.
- Hussein, I. M., & Abd-Allah, A. (2001). Tectonic evolution of the northeastern part of the African continental margin, Egypt. *Journal of African Earth Sciences*, 33(1), 49–68.
- Kaiser, M. F., & Ahmed, S. (2013). Optimal thermal water locations along the Gulf of Suez coastal zones, Egypt. *Renewable Energy*, 55, 374–379.
- Lashin, A. (2015). Geothermal resources of Egypt: Country update. In *Proceedings world geothermal congress*, Melbourne, Australia, 19–25 April 2015.
- Lashin, A. (2020). Review of the geothermal resources of Egypt: 2015–2020. In *Proceedings world geothermal congress 2020*, Reykjavik, Iceland, April 26–May 2, 2020.
- Lashin, A. (2007). Evaluation of the geothermal potential around the coastal parts of the Gulf of Suez, Egypt, using well logging and the geothermometer data. *Journal of Applied Geophysics*, 6(2), 215–248.
- Lashin, A. (2013). A Preliminary Study on the Potential of the Geothermal Resources Around the Gulf of Suez, Egypt. *Arabian Journal of Geosciences*, 6, 2807–2828.
- Latin, D., Norry, M. J., & Tarzey, R. J. E. (1993). Magmatism in the Gregory Rift, East Africa: Evidence for melt generation by a plume. *Journal of Petrology*, 34, 1007–1027.
- Lashin, A., & Al Arifi, N. (2010). Some aspects of the geothermal potential of Egypt. Casestudy: Gulf of Suez-Egypt. In: *Proceedings world geothermal congress*, Bali, Indonesia, p. 7.
- Macgregor, D. S. (2020). Regional variations in geothermal gradient and heat flow across the African plate. *Journal of African Earth Sciences*, 171, 103950.
- Martin-Gamboa, M., Iribarren, D., & Dufour, J. (2015). On the environmental suitability of high- and low-enthalpy geothermal systems. *Geothermics*, 53, 27–37.
- Mohamed, H. S., Abdel-Zaher, M., Senosy, M. M., Saibi, H., El-Nouby, M., & Fairhead, J. D. (2015). Correlation of aerogravity and BHT data to develop a geothermal gradient map of the northern western desert of Egypt using an artificial neural network. *Pure and Applied Geophysics*, 72(6), 1585–1597.
- Morgan, P., & Swanberg, C. A. (1979). *Heat flow and the geothermal potential of Egypt* (Vol. 1 17). Pageoph, BirkNiuuser Verlag.
- Morgan, P., Boulos, F. K., & Swanberg, C. A. (1983). Regional geothermal exploration in Egypt. *Geophysical Prospecting*, 31(2), 361–376.
- Morgan, P., Boulos, F. K., Hennin, S. F., El-Sherif, A. A., El-Sayed, A. A., Basta, N. Z., & Melek, Y.S. (1985). Heat flow in eastern Egypt: The thermal signature of a continental breakup. *Journal of Geodynamics*, 4(1-4), 107–131.
- Nyblade, A. A., Owens, T. J., Gurrola, H., Ritsema, J., & Langston, C. A. (2000). Seismic evidence for a deep upper mantle thermal anomaly beneath East Africa. *Geology*, 7, 599–602.
- Riad, S., Abdelrahman, E. M., Refax, E., & El-Ghalban, H. M. (1989). Geothermal studies in the Nile Delta, Egypt. *Journal of African Earth Sciences*, 9(3/4), 637–649.
- Said, R. (1962). *The geology of Egypt* (p. 377). Elsevier Scientific Publishing Co.
- Youssef, M. M. (2003). Structural setting of central and south Egypt: An overview. *Micropaleontology*, 49(1), 1–13.



Mohamed Abdel Zaher is a professor at the National Research Institute of Astronomy and Geophysics (NRIAG), Egypt. He received a BSc degree in Geophysics (1999) and a MSc (2005) in applied geophysics from Assiut University (Egypt), and a Ph.D. (2011) from the Earth Resource Engineering Department, Kyushu University (Japan). The Academy of Science in Finland awarded him a one-year postdoctoral fellowship in 2012 to Oulu University. He is currently head of the Geothermal Energy and Well Logging Research Unit at NRIAG.

University of Science and Technology (E-JUST). He was the Cultural Attaché of Egypt in Japan from 2010 to 2013, and From 2013 to 2015, he was a JSPS visiting professor at Kyushu University (Japan), from where he also received a Ph.D. degree in 2001. He has been an active member of the Egyptian geophysical community since 2001, as well as the managing editor of the journal of the National Research Institute of Astronomy and Geophysics (NRIAG).



Gad El-Qady is a professor of applied geophysics and its applications in Environmental investigations, archaeological, geotechnical, groundwater and geothermal investigations. Since 2019, he has been the president of the National Research Institute of Astronomy and Geophysics (NRIAG) as well as the National Institute of Oceanography and Fisheries (NIOF), Egypt. He was previously coordinator of international relations at the Egypt-Japan



Samah Elbarbary is a researcher at the National Research Institute of Astronomy and Geophysics (Egypt). She received MSc (2011) and Ph.D. (2019) degrees from Damietta University (Egypt). Her Ph.D. project in applied geophysics was funded by a scholarship (2013-2019) from the Egyptian Academy of Scientific Research and Technology (ASRT). Her research interests focus on applied geophysics and geothermal explorations. She is currently a post-doctoral fellow at the Institute of Geophysics, University of Münster, Münster, Germany.



Petroleum Source Rocks of Egypt: An Integrated Spatio-temporal Palynological and Organic Geochemical Studies Within the Phanerozoic

Haytham El Atfy , Bandar I. Ghassal, and Ralf Littke

Abstract

This chapter evaluates the integration between optical and geochemical methods as one of the best ways to screen hydrocarbon source rock potential and its diagnostic impact on kerogen investigation, in addition to its consistent involvement in paleoenvironmental inferences. While those kerogen types are usually resulting from Rock-Eval data, palynofacies and organic petrographic data deliver additional and consistent information. Rock-Eval data for samples with low to moderate TOC are mostly non-reliable due to free hydrocarbons in the mineral matrix. Consequently, palynofacies analysis represents a valuable complementary proxy for investigating the petroleum generation potential of source rocks. This chapter presents the first comprehensive review of the application of palynofacies with respect to the framework of geochemical data and the interpretations of different spatio-temporal source rock windows in Egypt. This integrated palynofacies and geochemical approach provides an improved understanding of the paleoenvironmental and petroleum source potential studies of the Phanerozoic sequences in Egypt.

Keywords

Petroleum source rocks • Palynology • Hydrocarbons • Kerogen • Palynofacies • Paleoenvironment • Phanerozoic

1 Introduction

Egypt possesses five primary petroleum provinces located in various geographical regions, namely the Gulf of Suez, Red Sea, Nile Delta, North Western Desert, and Southern Egypt. These provinces comprise prolific petroleum basins of diverse Phanerozoic ages (Fig. 1) and represent diverse depositional environments (e.g., passive margin, rift, terrestrial, deltaic, and marine). The variable geological settings and ages resulted in complex petroleum systems that have required detailed investigations by advanced techniques. Some of these basins are better understood due to a long exploration history, a large number of drilled wells, and the availability of geological, geochemical, and seismic data. Furthermore, some of the basins are poorly understood with respect to the depth and age of the intervals (e.g., below the best-known reservoir rocks), such as the pre-Miocene in the Nile Delta and the pre-Jurassic in the Western Desert. In addition, few attempts have been made to assess unconventional petroleum resources in spite of the presence of source rock outcrops in several areas.

This chapter provides detailed insights into the principal petroleum systems in Egypt. It also addresses the possible overlooked geological intervals which may be relevant to petroleum systems using in-depth comprehensive exploration techniques, mainly palynology and organic geochemistry. Palynology was widely utilized in the petroleum industry during the mid-twentieth century as a standard tool for exploration. Since the 1980s, palynology has not solely meant the study of spores, pollen, and other organic-walled microfossils. It encompasses investigations of all categories

H. El Atfy (✉)

Department of Geosciences, University of Tübingen,
72076 Tübingen, Germany
e-mail: El-Atfy@daad-alumni.de

Geology Department, Faculty of Science, Mansoura University,
Mansoura, 35516, Egypt

B. I. Ghassal (✉)

Saudi Aramco, Dhahran, Saudi Arabia
e-mail: bandar.ghassal@aramco.com

R. Littke

Energy and Mineral Resources Group (EMR), Institute of Geology
and Geochemistry of Petroleum and Coal, RWTH Aachen
University, 52056 Aachen, Germany

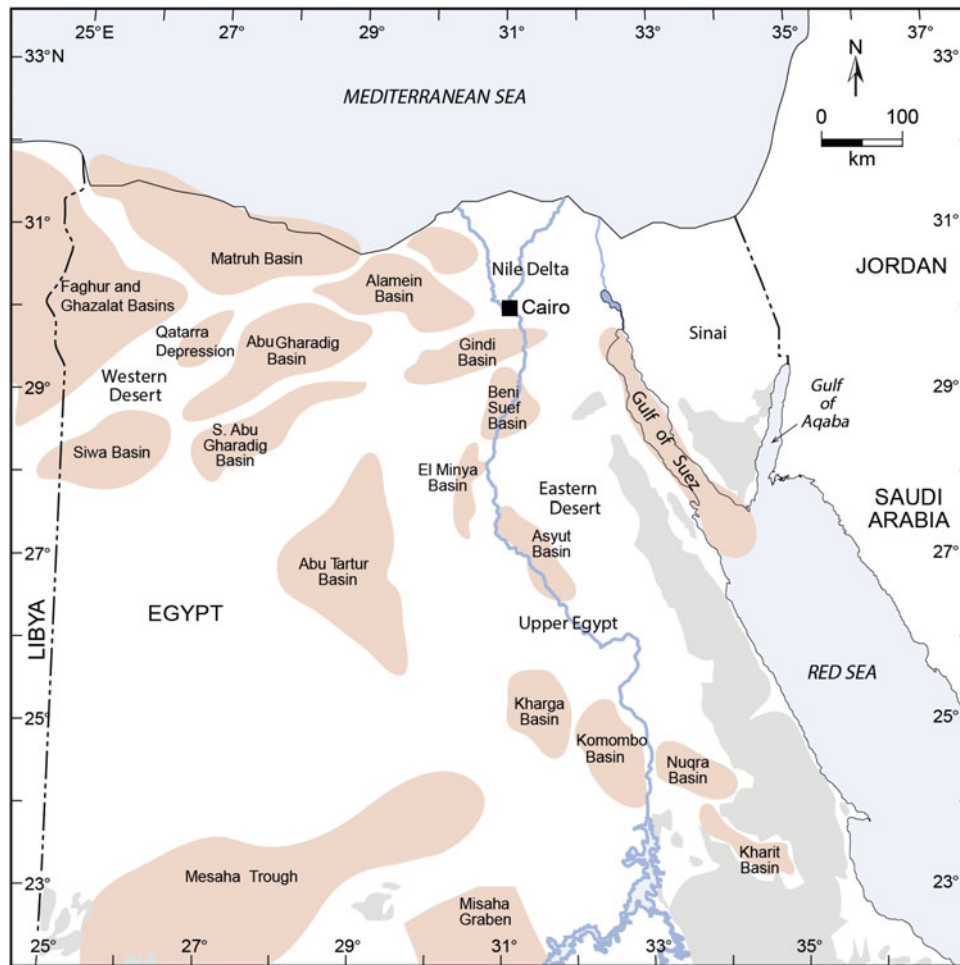


Fig. 1 Location map showing the sedimentary basins of Egypt (Dolson et al., 2000)

of microscopic organic particles ranging from objects with well-defined morphology, such as dinoflagellate cysts, wood particles and cuticles, structured and unstructured remains, and other tissues of indeterminate sources that are not easily categorized. Although palynology has a broad spectrum of applications in paleoenvironmental and paleoclimatic reconstructions, palynostratigraphy continues to be the most important for the majority of palynological research and is still the focus of most studies.

During the last few decades, more focus has been given to the wide variations in the composition of organic facies linked to different rock types, generating rapid growth of research in other non-biostratigraphic implications. The most important of these, because of their value to the petroleum industry, is the source rock evaluation in terms of quantity, quality, and maturation of organic matter (OM) recovered from sedimentary successions (Batten, 1982).

Palynofacies (*sensu* Combaz, 1964) analysis as a helpful proxy into the interpretation of depositional environments and petroleum source rock identification has been considered in detail by Tyson (1995) and Batten (1996a, 1996b), in

addition to some more recent publications (e.g., El Atfy, 2021; Ghassal et al., 2018; Zobaa et al., 2013), thereby aiding in the general evaluation of the hydrocarbon potential. In the oil and gas industry, there is a considerable emphasis on improving the recovery of hydrocarbons within producing fields; thus, there is a need for biostratigraphy to be applied on a very fine scale to determine both the reservoir architecture and provide answers to problems associated with petroleum production and development. Under such circumstances, the palynological effort usually relies largely on quantitative and semi-quantitative analyses of data and, hence, on palynofacies analysis from which local changes in depositional conditions may be inferred (Batten, 1999).

Although some efforts have been made to integrate both palynological and sedimentologic data dating back to the 1950s, only within the last few years, has a substantial effort in these fields considering this sort of work thoughtfully. From the standpoint of petroleum potential, especially important studies should be concerned with the occurrence and composition of source rocks. Many papers have been written on this topic, but only a few discuss their

palynological contents in satisfactory detail. The present chapter presents the first summary of the concept of palynofacies and its application within the context of geochemical data and interpretations of different spatio-temporal source rock windows in Egypt. Such an integrated approach undoubtedly enhances the understanding of the detailed paleoenvironmental and petroleum source potential studies in the Phanerozoic successions in Egypt.

It is also worth mentioning that, since the 1960s, researchers studying Egyptian palynology have focused on the classic aspects of palynology comprising taxonomy, palynostratigraphy, and paleoenvironmental deductions. Only recently have they started to give more consideration to the application of palynology for thermal maturation of organic constituents of sedimentary rocks (e.g., Hartkopf-Fröder et al., 2015) and source rock potential (El Atfy et al., 2014; Ghassal et al., 2018).

The integration between optical (i.e., palynofacies and organic petrology) and organic geochemical methods has a definite impact on determining kerogen types, petroleum source rock potential, and paleoenvironmental deductions. Kerogen types are traditionally assigned based on organic petrology and Rock-Eval pyrolysis. However, optical microscopic methods such as palynofacies and organic petrography can provide additional and reliable information. In particular, Rock-Eval pyrolysis data are mostly doubtful for samples with low to moderate TOC due to the retained hydrocarbons in the mineral matrix (e.g., Grohmann et al., 2018), in addition to unreliable readings of hydrogen and oxygen indices. Therefore, integrating geochemical and palynofacies methods is a valuable complementary technique for comprehensively investigating the petroleum generative potential of source rocks. Historically, this integration was first introduced for the Phanerozoic sediments in Egypt by El Beialy et al. (2010) for the Upper Cretaceous of the north Western Desert, followed by a series of contributions on different spatio-temporal stratigraphic windows, which will be discussed in depth subsequently in this chapter. The chapter employs integrated palynological and geochemical approaches to shed more light on selected case studies and examples and reviews the primary successions of the Phanerozoic sedimentary cover in Egypt.

2 Source Rock Deposition: Processes and Mechanisms

Source rocks are fine-grained carbonate or siliciclastic sedimentary rocks that are rich in organic matter and expected to generate hydrocarbons when subjected to high temperatures (Littke et al., 1997; Tissot & Welte, 1984). Organic matter productivity, preservation, and depositional settings are the key aspects that control the source rock richness and

quality (Ghassal, 2017). The origin of the organic matter in source rocks is either transported (allochthonous), mostly from terrestrial sources, or in-situ (autochthonous), (e.g., Bustin, 1988; Katz, 2012; Littke et al., 1997). Comprehensive investigations have been conducted to understand the productivity and preservation of organic matter, as well as kerogen formation under several depositional environmental conditions. This section reviews the common marine source rock depositional environments that mostly characterize the Egyptian source rocks.

The Nile Delta petroleum system represents one of the most challenging systems investigated in Egypt (Ghassal et al., 2016), especially because the depositional environment of deltas is transitional from terrestrial to marine settings. Deltas are characterized by high energy and sedimentation rates, the predominance of silicates, and the presence of abundant heavy minerals within low salinity waters (Ghassal, 2017). In such fluvial-deltaic settings, higher land plant tissues are common with a lower content of aquatic algae (Bustin, 1988; Littke et al., 1997; Tissot & Welte, 1984). Galloway (1975) classified deltaic environments into three chief types: river-dominated, wave-dominated, and tide-dominated deltas—primarily based on the supply and types of sediments. In addition, primary productivity and organic matter preservation are significantly different in these three types of deltas. Prominent examples of river-dominated petroleum systems are the Mississippi, Niger, and Mahakam deltas (e.g., Peters et al., 2000; Tuttle et al., 1999). Therefore, this delta type is probably the most well-understood system among the three types in terms of petroleum potential. However, the Nile Delta which is allocated as a wave-dominated delta (Coe et al., 2003), is still poorly understood (Ghassal et al., 2016). Rivers supply the inner shelf with terrestrial organic matter such as vitrinite, inertinite, and coal particles as well as fresh/brackish water algae (Ghassal, 2017; Ghassal et al., 2016). Mixing of freshwater and marine water can lead to changes in nutrient supply and thus primary productivity and bottom water oxygen supply. Moreover, the liptinite macerals possess low densities that make them selectively transported (Bustin, 1988). These effects lessen toward the distal settings as the interplay between fluvial and marine systems becomes minimal. Other factors such as tectonism, climate, and sea-level change play significant roles in the bottom water condition and, thus, the source rock quality and richness.

Rift basins usually host prolific petroleum source rocks in the pre-, syn- and post-rift sections. Typical examples are the Atlantic Ocean and Red Sea basins (e.g., Duarte et al., 2012; Ghassal, 2010; Katz, 1995). Small rift basins and failed rift basins also host source rocks but on a small scale, depending on the burial history, dimensions of the basin, sedimentation rates, and climate (Katz, 1995). Due to the tectonic complexities and rapid changes in sediment fill and water

chemistry in such basins, the source rock distribution, richness, quality, and thermal maturity are very heterogeneous within small distances (Ghassal, 2010; Katz, 1995). Note that there are two types of rift systems: marine and non-marine basins. The focus of this chapter is on the marine rift system as it represents the common type found in the various Egyptian basins (the Gulf of Suez Basin is the prominent example). In rift basins, the balance between primary productivity and preservation is the principal controlling factor of the source rock richness. These two factors are regulated by tectonic stability and sedimentation rates which change the oxygen contents and drive the nutrient availabilities (Katz, 1995 and references therein).

Apart from rift basins, sedimentation of marine petroleum source rocks occurs mainly in three settings, namely oxygen minimum zones on continental margins, upwelling zones, and silled/barred basins (Fig. 2) (e.g., Katz, 2012; Littke, 1993; Selley, 1998).

The biomass decay and the deficiency of circulation and photosynthesis in relatively deep and dark water consume the bottom water oxygen and inhibit its resupply, which causes anoxic conditions and creates oxygen minimum zones (Selley, 1998). Furthermore, water temperature and salinity determine the position of these zones (Katz, 2012). Upwelling zones reckon nearly half of the organic-rich source rocks worldwide (Parrish, 1987) and are characterized by high biological productivity that surpasses the

productivity of regular shelves by almost three-fold (Katz, 2012; Koblentz-Mishke et al., 1970; Ryther, 1969). During the predominant global greenhouse warming climate, winds move the shallow coastal warm water, which enables upwelling nutrient-rich water to substitute it (Bakun, 1990). The introduction of the nutrients increases bio-productivity, and later rapid deposition of organic matter (Bakun, 1990; Parrish, 1987). Additionally, the water oxygen level decreases, creating favorable conditions for organic matter preservation (Katz, 2012; Parrish, 1987). Climate also plays a significant role in intensifying the upwelling processes that are less prevailing during cold phases (Bakun, 1990; Parrish, 1987). Furthermore, the locations of the pronounced upwelling zones are usually along the western continental margins due to variations in wind direction and the Coriolis Effect ensuing from Earth's rotation (e.g., Katz, 2012).

In silled/barred basins, the bottom water anoxia evolves due to density-related stratification or thermal stratification. Density stratification forms when low saline and less dense water cover the more saline and denser deep water. Thermal stratification occurs when warm water rests on colder ones and no mixing takes place. Many barred basins are present in tropical and subtropical areas where minimum changes occur in the seasonal temperatures (Gluyas & Swarbrick, 2013; Katz, 2012).

3 Source Rock Distribution Through Time and Space—Egyptian Outlook

The Paleozoic source rocks in Egypt are poorly understood due to limited well penetrations and outcrop data. A generic overview of the geology and available source rock understanding is discussed in this section. Moreover, a global-scale glaciation event took place through the stabilization of the Gondwana supercontinent (~750–600) (Craig et al., 2009). There is no evidence of Infra-Cambrian source rock potential in Egyptian basins due to the lack of suitable climatic, tectonic, and marine and non-marine source rock development conditions (Bassett, 2009; Craig et al., 2009; Lučić and Bosworth 2019). Throughout the Paleozoic, a significant part of North Africa acted as the southern margin of the paleo-Tethys ocean, which received sediments from the hinterland from the south (Lučić and Bosworth 2019). The Paleozoic witnessed four global-scale glaciation events alternating with multiple marine transgressions, which resulted in siliciclastic-dominated tectonostratigraphy (Bassett, 2009; Beydoun, 1998; Craig et al., 2009; Lučić and Bosworth 2019). The lower Silurian hot shales constitute a major domain of the proven Paleozoic source rocks in northern Africa. These shales, which are rich in organic matter and uranium, are primary source rocks in North Africa and Arabia (Abohajar et al., 2015; Abu-Ali and

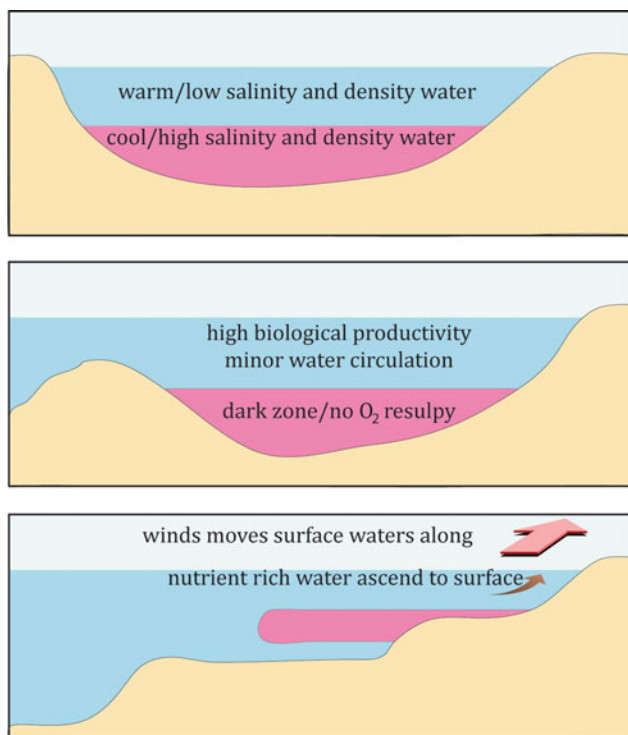


Fig. 2 A schematic diagram of common marine source rock depositional settings. Pink polygons are anoxic/oxygen minimum zones

Littke 2005; Belaid et al., 2010; Dolson et al., 2014; Lüning et al., 2000; Yahi et al., 2001). However, these successions have not been discovered in Egypt yet. Few studies reported siltstone dominated lithologies in various locations in Egypt but no organic-rich layers (El-Hawat et al., 1997; Keeley, 1989; Klitzsch, 1990; Lüning et al., 2000).

The source rock deposition of the Mesozoic to Cenozoic in Egypt was controlled by several tectonic and climatic events including the breakup of Gondwana, Jurassic rifting, the Red Sea opening, the Syrian Arc event, and the Messinian Salinity Crisis. Moreover, several global warming/cooling climatic phases prevailed, which triggered oceanic anoxic events and intensified the sea-level changes.

The extensional system in North Africa, in general, is largely attributed to the opening of the Central Atlantic and the drift of the Turkish-Apulian terrain (Guiraud et al., 1987). During the Middle Jurassic, East–West half-graben evolution occurred in an association with sea-level transgressions. Prolific source rock depositions span the Middle Jurassic, such as the Masajid Formation. However, some of these source rock successions were eroded throughout the Upper Cretaceous and Cenozoic inversions (Guiraud & Bosworth, 1999). Good to excellent source rock potential with variable qualities occurs in rocks in the Gulf of Suez, southern Nile Delta, and the Western Desert (see details in Sect. 4).

During the Early Cretaceous, active rifting occurred coevally with the separation of the Arabian-Nubian Block from the South American Plate (Guiraud et al., 2005). Rifting continued during the Aptian until the Santonian. Furthermore, warm climate and the highest recorded Phanerozoic sea transgressions occurred throughout the Middle to Late Cretaceous, which resulted in oceanic anoxic events (OAEs) (Berra & Angiolini, 2014; Guiraud et al., 2005; Haq et al., 1988). The OAEs represented periods of excessive organic carbon deposition and improved bottom water anoxia (Jenkyns, 2010). The best source rock quality intervals in Egypt were deposited during the Cretaceous in all the major Egyptian petroleum basins (e.g., El Atfy et al., 2019; Ghassal et al., 2018).

Large areas of North Africa witnessed major sea transgression during the Paleocene to Eocene, which was responsible for depositing shallow marine sediments (Guiraud et al., 2005). During the early Oligocene, high sea level coexisted with the NE-SW extensions in North Egypt, which started the Gulf of Suez and the Red Sea rifts (Dolson et al., 2014).

During the Miocene, extreme compressional and extensional tectonic events prevailed in Northeast Africa, including the rifting of the Red Sea and the Gulf of Aqaba, and the maturation of the River Nile (Bosworth et al., 2005; Dolson 2020). The Miocene witnessed the deposition of the primary source rocks in the Nile Delta, Gulf of Suez, and the Red Sea basins (El Atfy et al., 2014; Ghassal et al., 2016).

The Quaternary is characterized by extensive fluvial deposits (Guiraud et al., 2005). No source rock deposition was recognized during this time.

4 Phanerozoic Source Rocks—Examples and Evaluation

4.1 Paleozoic Source Rocks

The oldest recognized potential source rocks in Egypt are in the poorly studied Carboniferous basins in the Western Desert that are unseen underneath the Hercynian unconformity and, consequently, poorly understood. To the west, in Libya and Algeria, sub-Hercynian traps comprise stratigraphic and structural cessations often sourced by bulky glacially scoured valleys that were later infilled with Silurian and Devonian source rocks. It is possible that comparable settings occur across northern Egypt, but they have not been proven so far from seismic and well data (Dolson 2020 and citations therein).

To the authors' knowledge, the only published studies on the palynofacies of the Paleozoic of Egypt have been by Makled et al., (2018, 2021). They integrated palynofacies with Rock-Eval pyrolysis and organic petrography to assess the hydrocarbon generation potential of the Devonian strata within the Faghur-1, NWD-302–1, and Sifa-1X wells in the north Western Desert. Their palynofacies data generally revealed the occurrence of gas-prone kerogen Type III. TOC concentrations indicate poor organic richness with content not exceeding 0.9 wt.%. These sediments are mostly mature based on the TAI (2–3). Their burial history models showed that hydrocarbon generation started throughout the Cretaceous in the studied boreholes. From our perspective, the T_{max} and Production Index (PI) data are not reliable in this case due to the low quality and insufficient reactive kerogen contents. Moreover, the reported TOC values indicate insignificant volumes of generated hydrocarbon.

However, in their study of the Sifa-1X well, Makled et al. (2021) reveal that Devonian succession has organic matter content of varied kerogen, namely Type I, Type II, mixed types II/III, and Type III. This mixture of kerogen was also identified using organic elemental and pyrolysis gas chromatography data. Furthermore, maturity data from the well shows that the entire Devonian sequence belongs to the oil window, and hence, has the potential to generate oil and gas.

4.2 Mesozoic Source Rocks

4.2.1 North Western Desert

Within the north Western Desert, the Upper Jurassic-Lower Cretaceous sequences are among the most prolific

hydrocarbon plays in North Africa. Though, their source rock characteristics and depositional environments are still not well known (El Atfy et al., 2019). Palynologically, those subsurface Jurassic-Cretaceous strata were the subject of several palynological investigations that have chiefly focused on taxonomy, palynostratigraphy, and to a lesser extent paleoenvironmental interpretations. On the other hand, few efforts have been paid to examine the thermal maturity and source rock potential (e.g., Ibrahim et al., 1997; El Beialy et al., 2010 and references therein; Zobaa et al., 2013; Ghassal et al., 2018; Gentzis et al., 2018; El Atfy et al., 2019).

(a) Jurassic

Felesteen et al. (2014) introduced the first comprehensive palynofacies investigation supplemented with organic geochemistry that targeted the Jurassic deposits in the north Western Desert. However, a previous investigation carried out on the Masajid Formation by Zobaa et al. (2013) produced relatively similar palynofacies results, as was also the case for the studies by Hewaidy et al. (2014) and El Atfy et al. (2019). The palynofacies results of Felesteen et al. (2014) did not offer a clear separation between the different Jurassic rock units, resulting in their being lumped under one palynofacies group dominated by opaque phytoclasts and interpreted as mixed but gas-prone facies. El Atfy et al. (2019) suggest fair to good gas source rock potential, with possible minor oil potential within multiple intervals in the Jurassic formations (Fig. 3). Their TOC concentrations exceed 2.0 wt.% and HI values reach 240 mgHC/gTOC. The results of Felesteen et al. (2014) share the same conclusions. They reported marginal to very good source rocks with TOC and HI values up to 4.0 wt.% and 199 mgHC/gTOC, respectively, at low thermal maturity.

Gentzis et al. (2018) studied the hydrocarbon potential of the Jurassic succession in the Abu Tunis-1 \times well in the Matruh Basin, north Western Desert. Their multi-proxy approach identified two palynofacies associations for the studied material, both are AOM-dominated. The first association represented the Wadi Natrun Formation, the lowermost and the uppermost Khatatba Formation, and the Masajid Formation. The second palynofacies association from the upper Khatatba Formation. The Rock-Eval and organic petrological data reveal similar conclusions with relatively high TOC and HI index values and VRe values exceeding 0.9%. The evaluated Jurassic section possesses mixed Type II/III kerogen and attained thermal maturity within the peak oil window.

A recent investigation of the Khatatba and uppermost Ras Qattara formations in the Falak-21 borehole (Shushan Basin) by Mansour et al. (2020) tells that this

interval has a good–excellent generative potential (kerogen Type III). The maturity reached a mature oil window in the Khatatba and uppermost Ras Qattara formations. Based on the total sulfur (TS) versus TOC relationship, the uppermost Ras Qattara Formation and Yakout Member (of the Khatatba Formation) were formed under oxic circumstances, however, the middle and upper parts of the Khatatba Formation were mostly deposited throughout high paleoproductivity in dysoxic–suboxic and suboxic conditions, correspondingly.

(b) Cretaceous

The Cretaceous strata in Egypt comprise manifold generative source/reservoir intervals. Consequently, they are considered the chief deeply-seated exploration goals of working companies, especially in the north Western Desert. A closer view of the Cretaceous sedimentary successions demonstrates that they have been well explored in comparison with the pre- and post-Cretaceous layers. The Cretaceous strata in the north Western Desert are subdivided into a lower unit, made of clastics that have their place in the Lower Cretaceous Burg El Arab Formation (comprising from bottom to top: Alam El Bueib, Alamein, Dahab, and Kharita members), and an upper unit composed of carbonates of Upper Cretaceous age that represent from bottom to top, the Bahariya, Abu Roash, and Khoman formations.

Lower Cretaceous

In spite of the fact that the Upper Jurassic-Lower Cretaceous sequences in the north Western Desert are among the most productive hydrocarbon plays in North Africa, their source rock characteristics and depositional environments are still not well known. The study of El Atfy et al. (2019) which utilized an integrated palynofacies and organic geochemical approach for the Upper Jurassic Masajid Formation and Lower Cretaceous Alamein and Alam El Bueib members in the OBA. 3–1/1A and OBA. S-C wells yielded interesting results (Fig. 3). Two main organic facies types connected to depositional environments and kerogen types were established: palynofacies PF I in the Alamein and Alam El Bueib members and PF-II in the Masajid Formation. PF I is expressed by kerogen Type II and Type III, which is more confirmed by pyrolysis data that tell fair organic richness and gas generation potential in the Alamein Member, with TOC values ranging from 1.0 to 2.5 wt.% and HI from 64 to 112 mg HC/gTOC. The Alam El Bueib Member demonstrated better organic richness and quality with TOC ranging from 1.6 to 3.1 wt.% and HI from 121 to 318 mg HC/gTOC. The thermal maturity assessment indicates that the Alamein Member is immature, whereas the Alam El Bueib Member is early to oil-mature (Table 1). Furthermore, the APP ternary

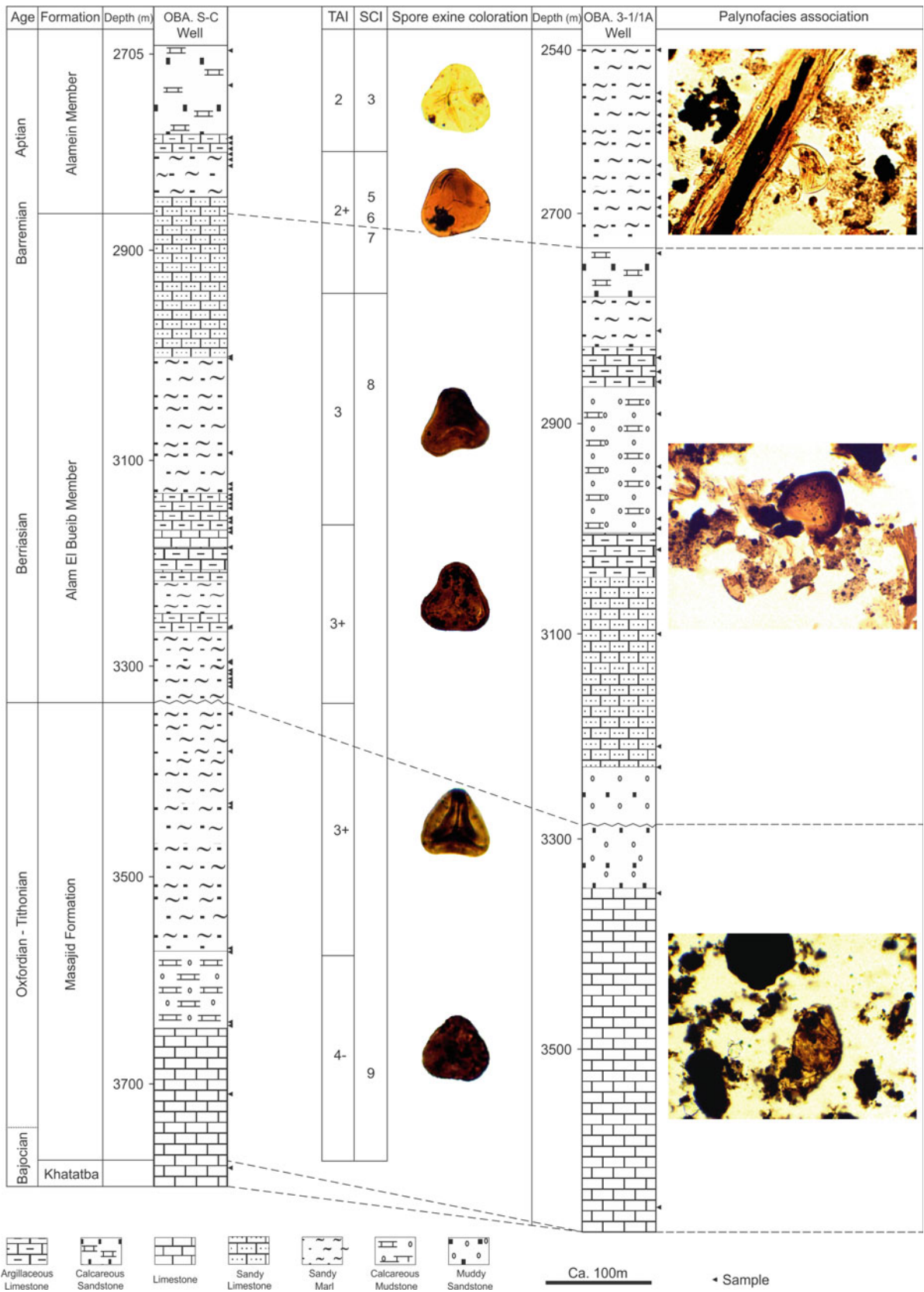


Fig. 3 Palynofacies, TAI, and SCI readings of the upper Jurassic-lower Cretaceous samples (BA. 3-1/1A and OBA. S-C wells), north Western Desert, Egypt (El Atfy et al., 2019). Spore colors follow the corrected scheme of Pearson (1984); SCI numbers per Marshall and Yule (1999) and TAI numbers after Batten (1982)

plot data suggest that both the Alamein and Alam El Bueib members were formed in a suboxic to anoxic basin (Fig. 4). While the Type III kerogen (gas-prone) interpretation for the Alamein Member by El Atfy et al. (2019) is similar to those previously described for the Sharib-1 × and Ghoroud-1 × wells (Zobaa et al., 2013), other authors, such as Ibrahim et al. (1997) and El-Soughier et al. (2010) stated that the Alamein Member was characterized by Type II kerogen (oil-prone).

It is worth noting here that the Late Jurassic and Early Cretaceous perceived the deposition of gas-prone source rocks as similar to those from the southern onshore Nile Delta Basin. These results have weighty inferences for the understanding of the types of source rocks in the northern onshore and offshore Egyptian basins and the future of gas exploration in the region (El Atfy et al., 2019). These source rock intervals were deposited in shallow marine environments based on geochemical and palynological assessments. Better source rock qualities are expected in deeper facies where optimum preservation of organic matter prevailed, but more work is needed to completely understand the source rock quality and distribution in this vital petroleum basin.

Upper Cretaceous

The integrated approach for studying the Upper Cretaceous successions in the north Western Desert was pioneered by El Beialy et al. (2010), who studied the subsurface Cretaceous units in the basin through a collective optical (spore coloration, palynofacies, and vitrinite reflectance) and organic geochemical (TOC and Rock-Eval pyrolysis) investigation. Their results appear to be valid for most north Western Desert regions and have been confirmed by other later contributions, such as Zobaa et al. (2011) and Mahmoud et al. (2017). In a detailed study, Ghassal et al. (2018) refined the results of these earlier studies to provide new understandings of the depositional environment from the Cenomanian to the Santonian (Table 2; Fig. 5), as well as the petroleum source rock potential of the Abu Roash “F” Member and residual hydrocarbons in the Abu Roash “C” and “D” members. Below, we highlight the results from all these studies.

1. The Abu Roash and Bahariya formations are comprised mainly of kerogen Type III, and thus gas-prone, except for the Abu Roash “F” Member which shows of an oil-prone facies (Fig. 6).
2. In contrast to the other Abu Roash members, the “F” Member shows a positive correlation between TOC and CaCO₃ as well as TS. It signifies an interval of anoxic or strongly oxygen-depleted bottom waters with improved preservation of organic matter, which is expressed in a

high proportion of amorphous organic matter (AOM), high TOC, and HI values. This organic-rich layer is interpreted to mark the short-term global oceanic anoxic event (OAE2). Three depositional phases (Figs. 7 and 8) have been recognized, as follows:

- a. Transgression phase-I is marked by anoxic bottom water conditions, generating sediments that are rich in TOC, carbonate, and S, and partially deprived in Fe and other detrital elements. This recommended sulfur amalgamation into organic matter. Sediments representing this phase seem to have been deposited in a more humid climate compared to the other intervals based on the illite/smectite ratio.
 - b. Regression phase has seen a fall in sea level and freshwater incursions, together with acidification of the waters and heavy mineral deposition, as construed from the abundance of siderite, rutile, detrital elements, and Mn.
 - c. Transgression phase-II is plentiful in TOC, characterized by suboxic conditions and fairly higher detrital element concentrations related to transgression phase-I, which hampered sulfur assimilation into kerogen.
3. The differences between the two transgressive phases of the depositional environment resulted in the formation of types of two source rocks, one, as well as the other, is immature relative to oil generative potential. Nevertheless, transgression phase-I source rock comprises kerogen Type IIS, which produces high sulfur oil, whereas transgression phase-II contains kerogen Type II/III, which expells sweet oil with negligible gas upon expulsion. Interestingly, Rock-Eval and biomarker maturity data reveal lower thermal maturity for the Abu Roash “F” source rock interval compared to the sediments beyond it. This conclusion advocates retardation/suppression of maturation courses in oil-prone source rocks, but may also be due to the existence of migrated bitumen of improved maturity, i.e., from deeper source rocks, in all rock units except for the Abu Roash “F” Member.
 4. The residual oils of the Abu Roash “C” and “D” reservoirs reveal two different partitions. The Abu Roash “D” residual oils are forced by either biodegradation or evaporation, whereas those from the Abu Roash “C” show a bi-modal *n*-alkane distribution with higher concentrations of low molecular hydrocarbons relative to the Abu Rash “D” residual oils. The different oil types may be indicative of more than one source rock charging the Abu Roash Formation.
 5. Quantitative and qualitative investigations of palynofloras and palynofacies show that the Abu Roash “A” and “C” Members, together of Coniacian-Santonian age,

Table 1 TOC and rock-eval pyrolysis results of the upper Jurassic-lower Cretaceous samples (OBA. 3-1/1A and OBA. S-C wells), north Western Desert, Egypt (El Afify et al., 2019)

Sample	Well	Rock unit	Depth (m)	Petroleum potential		Kerogen quality			Thermal maturity		OI (mg CO ₂ /g rock)	PI	S ₂ /S ₃	TIC (wt. %)	CaCO ₃ (wt. %)
				TOC (wt. %)	S ₁ (mg HC/g rock)	S ₂ (mg HC/g rock)	S ₃ (mg CO ₂ /g rock)	HI (mg HC/g TOC)	T _{max} (corr.)						
15/1321	OBA. 3-1/1A	Alamein member	2582	1.04	0.12	0.67	0.96	65	429	93	-	0.70	7.04	58.63	
15/1327	OBA. 3-1/1A	Alam El Bueib member	2860	-	7.85	3.39	0.27	-	-	-	-	-	-	-	
Ex1				2.11	0.27	2.55	4.00	121	427	190	0.09	0.64	0.13	1.08	
15/1328	OBA. 3-1/1A	Alam El Bueib member	3100	-	20.56	10.50	0.21	-	-	-	-	-	-	-	
Ex1				-	0.45	7.10	1.33	-	436	-	0.06	-	-	-	
Ex2				2.06	0.26	6.27	0.94	304	437	45	0.04	6.69	0.09	0.71	
15/1329	OBA. 3-1/1A	Alam El Bueib member	3210	-	28.63	15.48	0.21	-	-	-	-	-	-	-	
Ex1				-	-	-	-	-	-	-	-	-	-	-	
Ex2				3.01	0.24	9.59	1.41	319	437	47	0.02	6.83	0.06	0.51	
15/1330	OBA. 3-1/1A	Alam El Bueib member	3250-	-	28.13	12.01	0.21	-	430	-	-	-	-	-	
Ex1				-	0.55	6.46	1.77	-	-	-	-	-	-	-	
Ex2				2.25	0.15	4.92	1.27	218	434	56	0.03	3.87	1.19	9.95	
15/1331	OBA. 3-1/1A	Masajid formation	3400	-	23.56	0.20	-	-	-	-	-	-	-	-	
Ex1				2.40	0.52	5.65	1.81	236	427	75	0.08	3.13	1.82	15.14	
15/1343	OBA. S-C	Alamein member	2740	-	2.96	3.41	0.24	-	429	-	-	-	-	-	
Ex1				-	0.14	2.82	2.15	-	433	-	-	-	-	-	
Ex2				2.50	0.19	2.85	1.94	113	433	77	0.06	1.46	2.73	22.76	
15/1350	OBA. S-C	Alamein member	2800	-	1.22	2.11	0.19	-	-	-	-	-	-	-	
Ex1				-	0.07	1.35	1.71	-	-	-	-	-	-	-	
Ex2				2.04	0.08	1.46	1.34	71	433	66	0.05	1.09	0.60	4.98	
15/1352	OBA. S-C	Alam El Bueib member	3002	-	3.22	5.85	0.21	-	434	-	-	-	-	-	
Ex1				2.89	0.18	5.10	2.10	176	436	72	0.03	-	2.30	19.18	
15/1353	OBA. S-C	Alam El Bueib member	3160	-	3.85	5.33	0.21	-	432	-	-	-	-	-	
Ex1				-	0.19	3.90	2.33	-	434	-	-	-	-	-	
Ex2				2.76	0.09	3.53	1.99	128	434	72	0.03	1.78	0.03	0.25	
15/1357	OBA. S-C	Alam El Bueib member	3314	-	2.95	4.10	0.25	-	428	-	-	-	-	-	
Ex1				1.54	0.10	2.79	1.02	181	435	66	0.03	2.75	0.24	1.99	
15/1360	OBA. S-C	Masajid formation	3572	-	3.79	5.87	0.25	-	-	-	-	-	-	-	
Ex1				1.28	0.08	1.89	0.87	148	430	68	0.04	2.17	2.60	21.96	
15/1362	OBA. S-C	Khatatba formation	3782	2.43	0.36	5.80	2.42	239	431	100	0.06	2.40	3.71	30.92	

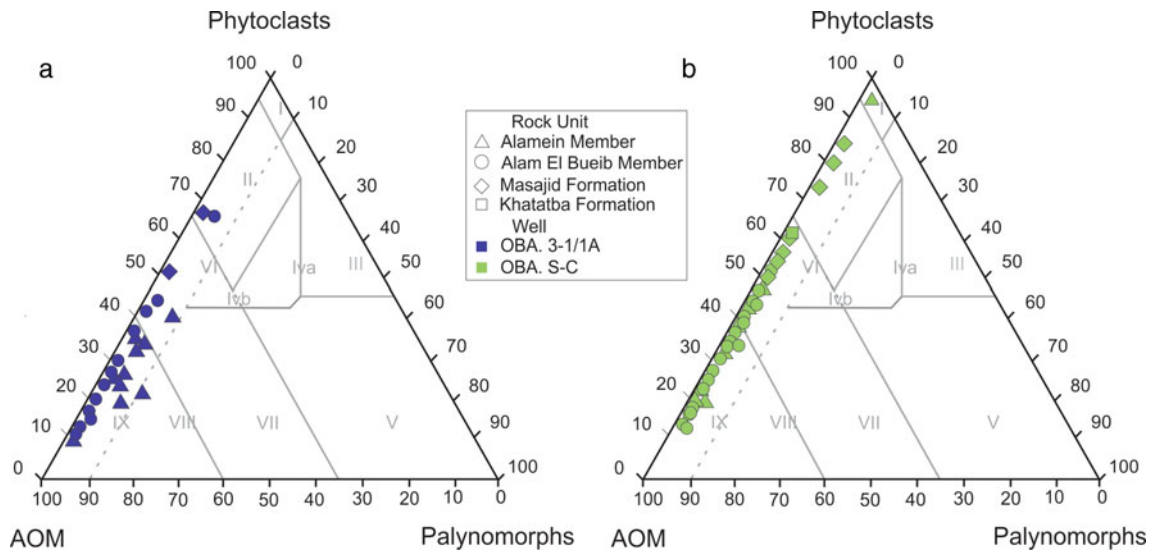


Fig. 4 APP ternary plot (Tyson 1993), A = OBA. 3-1/1A well, and B = OBA. S-C well. Field I = kerogen type III; field II = kerogen type III; field III = kerogen type III or VI; field IV = kerogen type III or II; field V = kerogen type III>IV; field VI = kerogen type II; field VII = kerogen type II; field VIII = kerogen type II>I

signify an oxic proximal and distal shelf environments, respectively. The Abu Roash “D” and “E” members, dated as Turonian, denote an oxic proximal shelf, whereas the Abu Roash “F” Member of the Cenomanian age was deposited in a distal suboxic–anoxic basin. The Abu Roash “G” Member and the Bahariya Formation, also Cenomanian in age, were formed in shallow marine and shallow marine to fluvio-deltaic environments, correspondingly. The integrated approach illustrates strong agreement between the palynological, organic, and inorganic geochemical interpretations.

4.2.2 Gulf of Suez

Petroleum exploration in the Gulf of Suez is relatively difficult since it is surrounded by many uncertainties. Due to huge sequences of evaporites, seismic data for the pre-salt are of very limited use and much of the Rock-Eval data are missing or unreliable. As discussed earlier, rift basins are very dynamic, and hence, the source rock quality, thickness, and distribution are highly variable. Also, approximately, all organic-rich intervals in the Gulf of Suez are drained in humic macerals while vitrinite particles are mostly absent, or show low reflectance (Mostafa & Ganz, 1990). Therefore, introducing palynofacies as an exploration tool, especially as a maturation detection parameter, will help to solve this problem.

El Diasty et al. (2014) introduced the first combined palynofacies and organic geochemical study that focused on the Upper Cretaceous-Eocene (Matulla, Brown Limestone,

and Thebes formations) within the central part of the Gulf of Suez. Palynofacies analysis (Fig. 9) indicated that the Thebes and Brown Limestone formations were both deposited under a distal suboxic–anoxic environment. Conversely, the Turonian-Santonian Matulla Formation supports the presence of variable depositional settings from a marginal marine under dysoxic–anoxic basinal to proximal suboxic–anoxic shelf environments. Rock-Eval pyrolysis and TOC results indicate that most of the formations are immature to slightly mature and have a good petroleum source potential. They are organic-rich, containing oil- and gas-prone Type II and III kerogens, preserved under marine reducing conditions satisfactory for hydrocarbon generation and expulsion.

4.2.3 Nile Delta

The Nile Delta Basin is well-thought-out one of the most prolific petroleum basins in Egypt and the eastern Mediterranean region, particularly for gas resources, and accounts for approximately 60,000 km² correspondingly onshore and offshore (Barakat, 2010).

Data for the source rocks within the Mesozoic strata in the Nile Delta Basin (sometimes referred to as the north Eastern Desert) based on an optical investigation (i.e., palynofacies) are available exclusively from Ibrahim et al. (1997). They applied the spore coloration index (SCI), which is equivalent to the thermal alteration index (TAI), in an attempt to deduce the thermal maturation of the sediments. They inferred that the Jurassic sequence in the Abu Hammad-1 well was generally thermally mature, while the overlying Lower Cretaceous sediments were immature. In their conclusion, Ibrahim et al. (1997) highlighted the

Table 2 Carbon, sulfur, and rock-eval data of the upper Cretaceous Bahariya and Abu Roash formations (GPT-3 well), north Western Desert, Egypt (Ghassal et al., 2018)

Sample no.	Sample type	Depth (m)	Formation	TOC (%)	CaCO3 (%) ^	TS (%)	S1*	S2*	S3**	T _{max} ***	PI	HI ****	OI *****
15/400	Cuttings	1413–1416	Abu Roash "A"	1.30	26.50	1.13	0.12	1.06	3.25	431	0.10	82	249
15/401	Cuttings	1422–1425	Abu Roash "A"	1.25	33.10		0.11	0.85	2.79	430	0.11	68	223
15/402	Cuttings	1431–1434	Abu Roash "A"	1.00	41.20		0.11	0.79	2.72	429	0.12	79	271
15/403	Cuttings	1440–1443	Abu Roash "A"	1.13	37.60		0.13	0.88	2.93	428	0.13	78	260
15/404	Cuttings	1449–1452	Abu Roash "A"	1.07	42.35	1.35	0.11	0.74	2.74	428	0.13	69	256
15/405	Cuttings	1458–1461	Abu Roash "A"	0.89	46.88		0.11	0.64	2.39	428	0.15	72	269
15/406	Cuttings	1467–1470	Abu Roash "A"	0.89	52.25		0.13	0.83	2.81	430	0.14	92	315
15/407	Cuttings	1476–1479	Abu Roash "A"	0.89	50.97		0.12	0.77	2.37	430	0.13	86	266
15/408	Cuttings	1485–1488	Abu Roash "A"	0.77	71.78	1.06	0.15	0.76	2.28	427	0.17	99	297
15/409	Cuttings	1494–1497	Abu Roash "A"	1.22	34.77		0.13	0.82	2.69	424	0.14	67	220
15/410	Cuttings	1503–1506	Abu Roash "A"	0.90	45.09		0.12	0.69	1.96	427	0.14	76	218
15/411	Cuttings	1512–1515	Abu Roash "A"	0.97	45.36		0.14	0.82	2.18	428	0.15	84	225
15/412	Cuttings	1521–1524	Abu Roash "A"	0.88	55.87		0.13	0.70	2.08	429	0.15	80	236
15/413	Cuttings	1530–1533	Abu Roash "A"	1.19	42.55		0.13	0.73	2.63	425	0.15	61	220
15/414	Cuttings	1539–1542	Abu Roash "A"	1.21	48.71	1.19	0.12	0.81	2.61	426	0.13	67	216
15/415	Cuttings	1548–1551	Abu Roash "B"	0.81	66.55	0.86	0.17	1.06	1.85	432	0.13	131	228
15/416	Cuttings	1557–1560	Abu Roash "B"	0.78	67.38		0.16	0.93	1.94	432	0.15		
15/417	Cuttings	1566–1569	Abu Roash "B"	0.78	90.01		0.39	1.62	1.79	430	0.20	209	230
15/418	Cuttings	1575–1578	Abu Roash "B"	0.96	78.78	0.66	0.45	2.12	2.19	430	0.18	222	229
15/419	Cuttings	1587–1590	Abu Roash "B"	0.78	90.30		0.33	1.48	2.04	431	0.18	189	261
15/420	Cuttings	1593–1596	Abu Roash "B"	0.80	92.55	0.36	0.71	2.34	1.94	428	0.23	294	244
15/421	Cuttings	1602–1605	Abu Roash "B"	0.85	74.73		0.17	0.91	2.06	430	0.16	107	244
15/422	Cuttings	1611–1614	Abu Roash "B"	1.06	81.21	0.94	0.20	1.25	2.35	433	0.14	118	222
15/423	Cuttings	1620–1623	Abu Roash "B"	0.79	73.70		0.14	0.90	2.42	431	0.14	114	306
15/424	Cuttings	1629–1632	Abu Roash "B"	0.78	87.08		0.22	0.95	2.53	430	0.19	121	324
15/425	Cuttings	1638–1641	Abu Roash "C"	1.01	50.31		0.13	0.80	2.28	430	0.14	79	226
15/426	Cuttings	1647–1650	Abu Roash "C"	1.36	29.53	1.52	0.15	0.89	2.92	428	0.14	66	214
15/427	Cuttings	1656–1659	Abu Roash "C"	1.24	23.69	1.54	0.13	0.86	2.81	427	0.14	69	226
15/483	Core	1670	Abu Roash "C"	0.37	12.39	0.73	0.45	0.64	0.45		0.41		
15/484	Core	1671	Abu Roash "C"	0.27	1.47		0.11	0.34	0.40	426	0.23	129	149
15/428	Cuttings	1674–1675	Abu Roash "C"	1.20	21.62		0.15	0.79	2.50	427	0.16	65	208
15/486	Core	1678	Abu Roash "C"	0.73	0.69		0.21	0.81	0.22	426	0.21	111	31
15/429	Cuttings	1692–1695	Abu Roash "C"	1.75	22.71		0.12	0.87	2.51	428	0.13	50	144
15/430	Cuttings	1701–1704	Abu Roash "D"	0.96	68.63		0.16	0.87	2.00	433	0.15	91	209

(continued)

Table 2 (continued)

Sample no.	Sample type	Depth (m)	Formation	TOC (%)	CaCO ₃ (%) ^	TS (%)	S1*	S2*	S3**	T _{max} ***	PI	HI ****	OI *****
15/431	Cuttings	1710–1713	Abu Roash "D"	1.03	52.81	1.01	0.15	1.04	2.05	433	0.13	101	199
15/432	Cuttings	1719–1722	Abu Roash "D"	0.79	59.33		0.13	0.76	1.95	431	0.15	95	246
15/433	Cuttings	1728–1731	Abu Roash "D"	0.89	52.16		0.12	0.72	1.81	432	0.14	81	202
15/434	Cuttings	1737–1740	Abu Roash "D"	0.99	56.51		0.10	0.80	1.95	433	0.12	80	196
15/435	Cuttings	1746–1749	Abu Roash "D"	0.77	60.39		0.12	0.92	1.95	433	0.12	120	254
15/436	Cuttings	1755–1758	Abu Roash "D"	0.74	77.47		0.16	0.94	1.69	434	0.15	127	228
15/437	Cuttings	1764–1767	Abu Roash "D"	0.90	63.49		0.14	0.93	1.90	433	0.13	103	212
15/487	Core	1771	Abu Roash "D"	0.53	1.12	0.06	0.27	0.88	0.35	433	0.24	167	66
15/488	Core	1772	Abu Roash "D"	0.32	96.08		0.12	0.38	0.63	433	0.24	119	198
15/438	Cuttings	1773–1774	Abu Roash "D"	1.21	34.73	1.31	0.15	1.03	1.79	431	0.13	85	148
15/490	Core	1777	Abu Roash "D"	0.32	112.00		0.15	0.50	0.26	432	0.23	157	81
15/491	Core	1781	Abu Roash "D"	1.37	110.50		5.94	12.18	0.44		0.33	887	32
15/439	Cuttings	1782–1783	Abu Roash "D"	1.70	20.26		0.09	0.84	1.95	432	0.10	49	114
15/492	Core	1785	Abu Roash "D"	1.19	113.99		5.82	5.24	0.33		0.53	442	28
15/493	Core	1787	Abu Roash "D"	1.57	110.31		5.82	7.03	0.62		0.45	447	39
15/440	Cuttings	1803–1806	Abu Roash "D"	0.88	39.49		0.09	1.02	2.26	436	0.08	116	255
15/441	Cuttings	1812–1815	Abu Roash "D"	1.06	54.12		0.13	1.21	2.20	433	0.09	115	208
15/442	Cuttings	1821–1824	Abu Roash "E"	1.26	39.23		0.11	1.07	2.36	434	0.09	85	187
15/443	Cuttings	1830–1833	Abu Roash "E"	1.41	27.32	1.75	0.12	1.03	2.81	431	0.11	73	199
15/444	Cuttings	1839–1842	Abu Roash "E"	1.39	14.94		0.09	0.83	2.85	433	0.09	60	205
15/445	Cuttings	1848–1851	Abu Roash "E"	1.32	5.74	0.96	0.10	0.91	2.46	435	0.10	69	186
15/446	Cuttings	1857–1860	Abu Roash "E"	1.25	27.55		0.12	0.89	2.13	434	0.12	71	170
15/447	Cuttings	1866–1869	Abu Roash "E"	1.06	25.35		0.09	0.66	2.56	432	0.11	62	242
15/448	Cuttings	1875–1878	Abu Roash "E"	1.30	16.24	1.04	0.10	0.79	2.34	434	0.11	60	179
15/449	Cuttings	1884–1887	Abu Roash "E"	1.17	29.91		0.11	0.76	1.84	432	0.13	64	157
15/450	Cuttings	1902–1905	Abu Roash "E"	1.08	32.84	0.87	0.09	0.63	2.13	431	0.12	59	197
15/451	Cuttings	1911–1914	Abu Roash "E"	1.40	11.35	1.34	0.11	0.82	2.90	428	0.12	59	207
15/452	Cuttings	1920–1923	Abu Roash "E"	1.46	4.09	1.20	0.17	0.89	2.07	428	0.16	61	142
14/1345	Cuttings	1929–1932	Abu Roash "E"	1.45	6.67		0.13	0.91	2.16	428	0.13	63	149
15/453	Cuttings	1938–1941	Abu Roash "E"	1.54	5.14	1.82	0.11	0.77	2.31	427	0.12	50	150
14/1344	Cuttings	1947–1950	Abu Roash "E"	1.55	9.38	1.65	0.13	1.12	2.44	428	0.10	72	157
15/454	Cuttings	1956–1959	Abu Roash "E"	1.84	18.62	1.44	0.11	0.96	2.27	431	0.10	52	123
15/455	Cuttings	1965–1968	Abu Roash "F"	1.79	30.66	1.26	0.21	2.83	2.27	430	0.07	158	127
15/495	Core	1974	Abu Roash "F"	4.00	100.87	0.27	2.43	26.21	1.53	424	0.08	655	38

(continued)

Table 2 (continued)

Sample no.	Sample type	Depth (m)	Formation	TOC (%)	CaCO ₃ (%) ^	TS (%)	S1*	S2 *	S3**	T _{max} ***	PI	HI ****	OI *****
15/456	Cuttings	1974-1975	Abu Roash "F"	2.82	46.01	1.05	0.36	7.12	2.30	427	0.05	252	81
15/496	Core	1976	Abu Roash "F"	0.32	2.22	0.54	0.10	0.40	0.34	425		127	109
15/497	Core	1977	Abu Roash "F"	6.63	55.87	0.32	0.08	0.33	3.40				
15/498	Core	1978	Abu Roash "F"	5.87	91.80	1.69	3.11	40.33	1.48	423	0.07	687	25
15/499	Core	1979	Abu Roash "F"	4.37	102.82	0.40	2.41	27.13	1.98	421	0.08	621	45
15/457	Cuttings	1983-1986	Abu Roash "F"	3.75	57.65	0.93	1.03	14.33	2.59	421	0.07	382	69
15/458	Cuttings	1995-1998	Abu Roash "G"	1.91	27.00	1.62	0.15	2.25	2.56	428	0.06	118	134
15/459	Cuttings	2004-2007	Abu Roash "G"	1.81	9.55	1.14	0.15	1.87	2.91	431	0.08	103	160
15/460	Cuttings	2015-2018	Abu Roash "G"	1.23	8.20		0.12	0.82	1.89	429	0.13	66	154
15/461	Cuttings	2023-2026	Abu Roash "G"	1.97	9.16	1.38	0.18	1.72	2.71	432	0.09	87	138
15/462	Cuttings	2043-2047	Abu Roash "G"	1.38	3.21	1.04	0.09	0.89	3.03	430	0.09	65	221
15/463	Cuttings	2061-2063	Abu Roash "G"	1.35	14.21		0.11	0.90	3.10	432	0.11	67	231
15/464	Cuttings	2070-2073	Abu Roash "G"	1.34	28.82		0.36	0.94	2.65	432	0.27	71	199
15/465	Cuttings	2079-2082	Abu Roash "G"	1.07	30.22		0.10	0.83	2.67	432	0.11	78	250
15/466	Cuttings	2088-2091	Abu Roash "G"	1.43	9.88	1.29	0.11	0.88	2.70	429	0.11	61	190
15/467	Cuttings	2097-2100	Abu Roash "G"	1.24	19.62		0.10	0.91	2.60	429	0.10	73	210
15/468	Cuttings	2106-2109	Abu Roash "G"	1.24	26.43		0.11	0.83	2.53	430	0.11	67	205
15/469	Cuttings	2115-2118	Abu Roash "G"	1.28	27.60		0.14	0.85	2.25	430	0.14	66	176
15/470	Cuttings	2124-2127	Abu Roash "G"	1.22	10.95	1.38	0.23	1.99	2.57	432	0.11	164	212
15/471	Cuttings	2133-2136	Abu Roash "G"	1.29	17.07		0.08	0.63	2.34	430	0.11	49	182
15/472	Cuttings	2142-2145	Baharyia	1.63	15.42		0.25	1.38	2.94	431	0.15	85	180
15/473	Cuttings	2151-2154	Baharyia	1.65	9.86	1.12	0.19	1.32	3.14	431	0.13	80	190
15/474	Cuttings	2169-2172	Baharyia	1.35	13.74		0.10	0.82	1.91	428	0.11	61	141
15/475	Cuttings	2178-2181	Baharyia	1.30	8.06	1.32	0.08	0.80	2.18	429	0.10	61	167
15/476	Cuttings	2187-2190	Baharyia	1.18	6.17		0.08	0.89	1.56	436	0.08	75	132
15/477	Cuttings	2196-2199	Baharyia	1.95	1.56	0.95	0.23	1.84	2.20	435	0.11	94	113
15/478	Cuttings	2205-2208	Baharyia	1.50	1.66		0.17	1.30	1.85	436	0.12	86	123
15/479	Cuttings	2214-2217	Baharyia	1.56	2.69		0.16	1.50	2.61	434	0.09	96	168
15/480	Cuttings	2223-2226	Baharyia	1.22	15.13	1.33	0.16	1.40	2.35	436	0.10	115	193
15/481	Cuttings	2232-2235	Baharyia	1.54	10.42		0.11	1.02	2.30	434	0.10	66	149
15/482	Cuttings	2235-2238	Baharyia	1.42	35.27	1.18	0.14	0.99	1.72	434	0.12	70	121

^ calculated from total inorganic carbon

* (mg HC/g rock)

** (mg CO₂/g rock)

*** (°C)

**** (mgHC/gTOC)

***** (mgCO₂/gTOC)

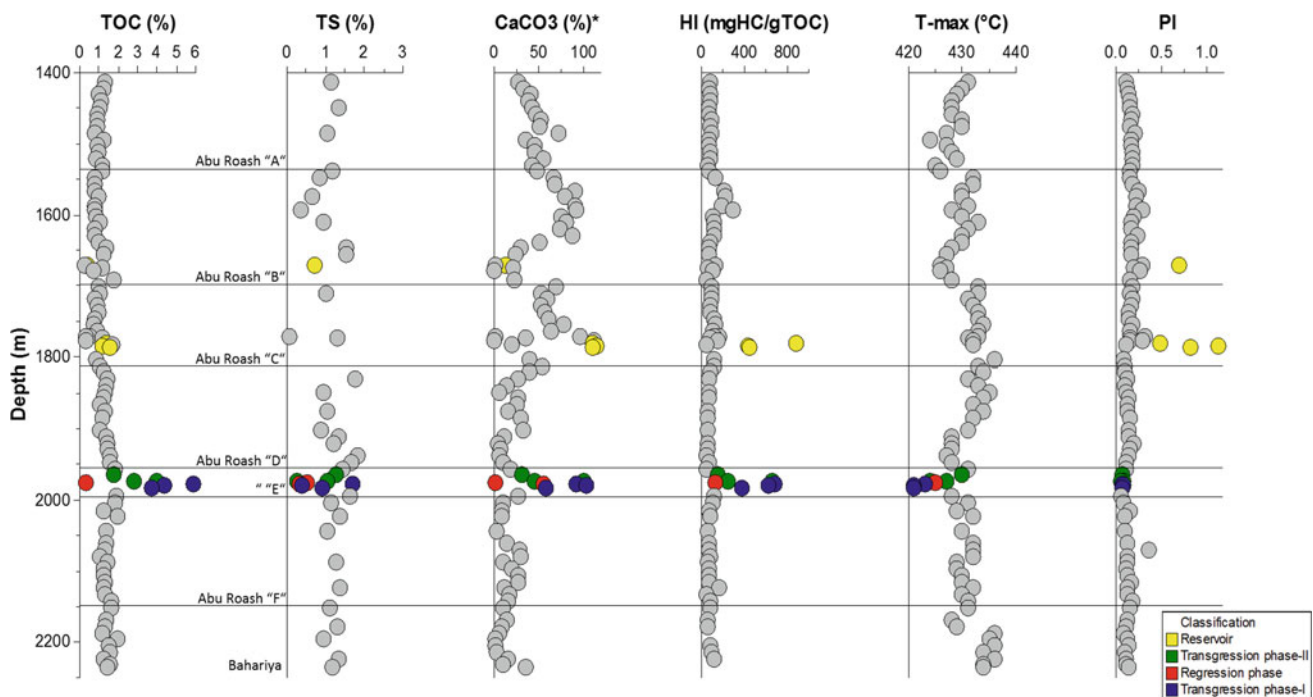


Fig. 5 Total organic carbon (TOC), CaCO₃, total sulfur (TS), and rock-eval data versus depth, Bahariya, and Abu Roash formations within the GPT-3 well, Abu Gharadig basin (Ghassal et al., 2018)

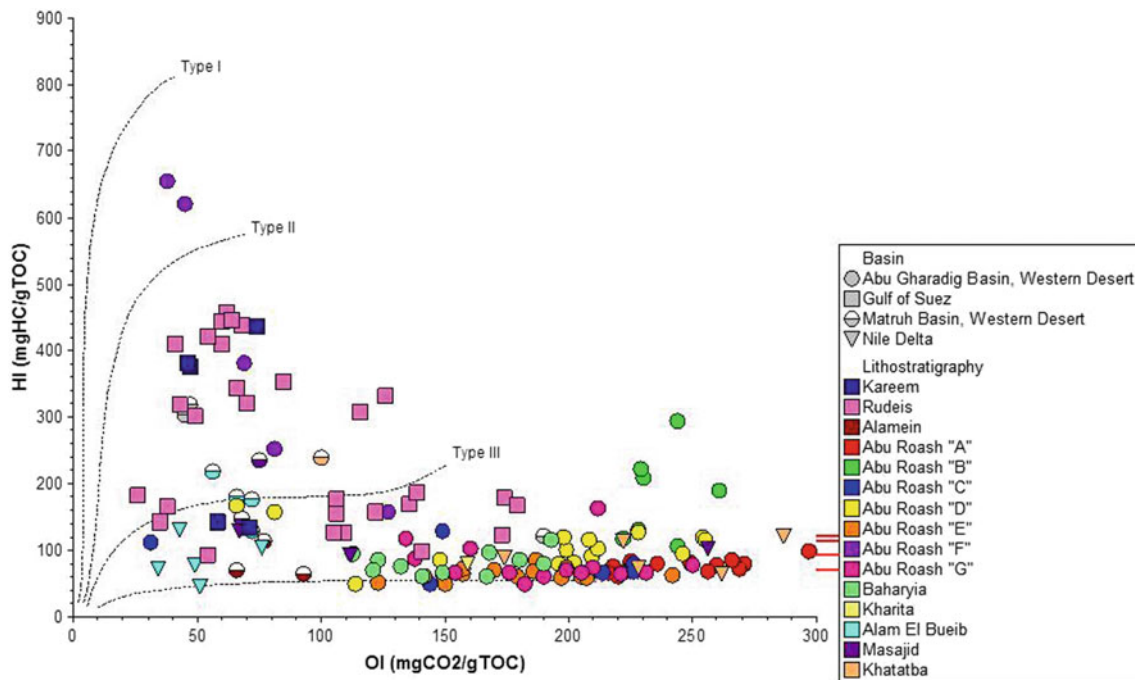


Fig. 6 Pseudo van Krevelen diagram covers most of the known source rock intervals within different basins in Egypt. Data are available in Tables 1, 2, 3, 4 and 5

nature of the source rocks for the Abu Hammad-1 well as follows:

1. Highly oil-prone and mature source rocks with amorphous organic matter in the lower Masajid, Khatatba, and middle Rajabiah formations.

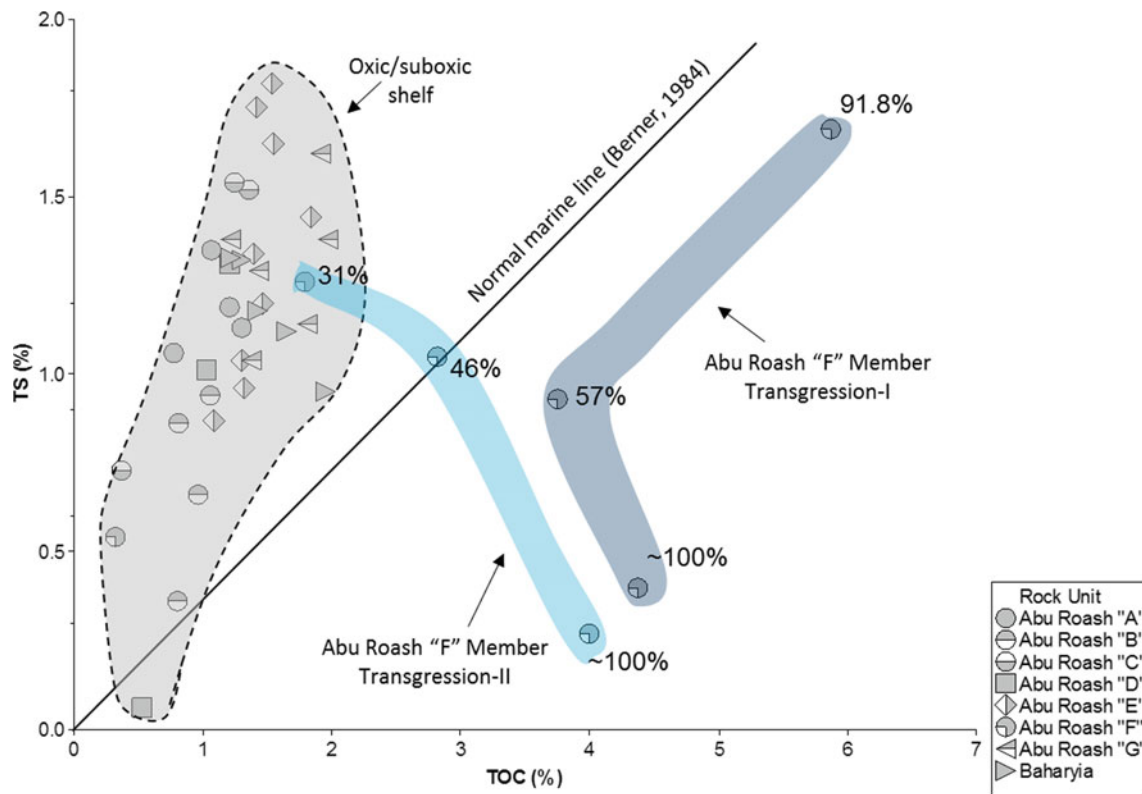


Fig. 7 TS versus TOC showing the characteristic signature of the Abu Roash “F” Member. The samples are classified into three groups, which are: (1) Abu Roash “F” Member transgression-I; (2) Abu Roash “F” member transgression-2; and (3) oxidic/suboxic shelf: the samples from the rest of the rock units. CaCO₃ was calculated from total inorganic carbon (Ghassal et al., 2018)

2. Highly oil-prone but immature source rocks with amorphous organic matter in the Alamein and Alam El Bueib formations.
3. Oil-prone, mature source rocks in the upper Masajid Formation.
4. Gas-prone, mature source rocks in the upper Rajabiah Formation.

However, geochemical investigation of the Abu Hammad-1 well by Ghassal et al. (2016) suggests that the Upper Jurassic Masajid and the Lower Cretaceous Alam El Bueib formations contain gas-prone source rock, with TOC up to 4.0 wt.% and HI ranging from 46 to 130 mg HC/g TOC (Table 3). Microscopic investigation reveals that these source rocks are dominated by vitrinite, inertinite, and coaly particles (Fig. 10). Furthermore, T_{max} and vitrinite reference (VRe) indicate low thermal maturity.

4.3 Cenozoic Source Rocks

Palynological studies dealing with the Cenozoic of Egypt are somewhat dispersed and few in comparison with those carried out on older strata. Moreover, among the relatively

limited number of publications, palynofacies studies targeting are even fewer. These studies are available only from the Gulf of Suez and the Nile Delta, and there is one case from the north Western Desert.

4.3.1 North Western Desert

From a palynofacies perspective, El Beialy et al. (2016) introduced the first study that dealt with the kerogen portion of the subsurface material (Amana-1X well) within the Dabaa Formation. They utilized palynofacies analysis to study the hydrocarbon potential of the organic matter and provided a comprehensive interpretation of the prevailing paleoenvironmental conditions (Fig. 11). As a result, they established two major marine palynofacies. The older palynofacies (palynofacies 1) contained Type II/III kerogen (mostly oil-prone), which was formed in an outer shelf to upper slope under suboxic to anoxic settings. Palynofacies 2 comprised Type III kerogen (largely gas-prone) that signifies shallower, more terrestrially influenced circumstances. However, SCI determination (spore coloration measurements) implied thermally mature conditions for both palynofacies. There was no verification by organic geochemistry.

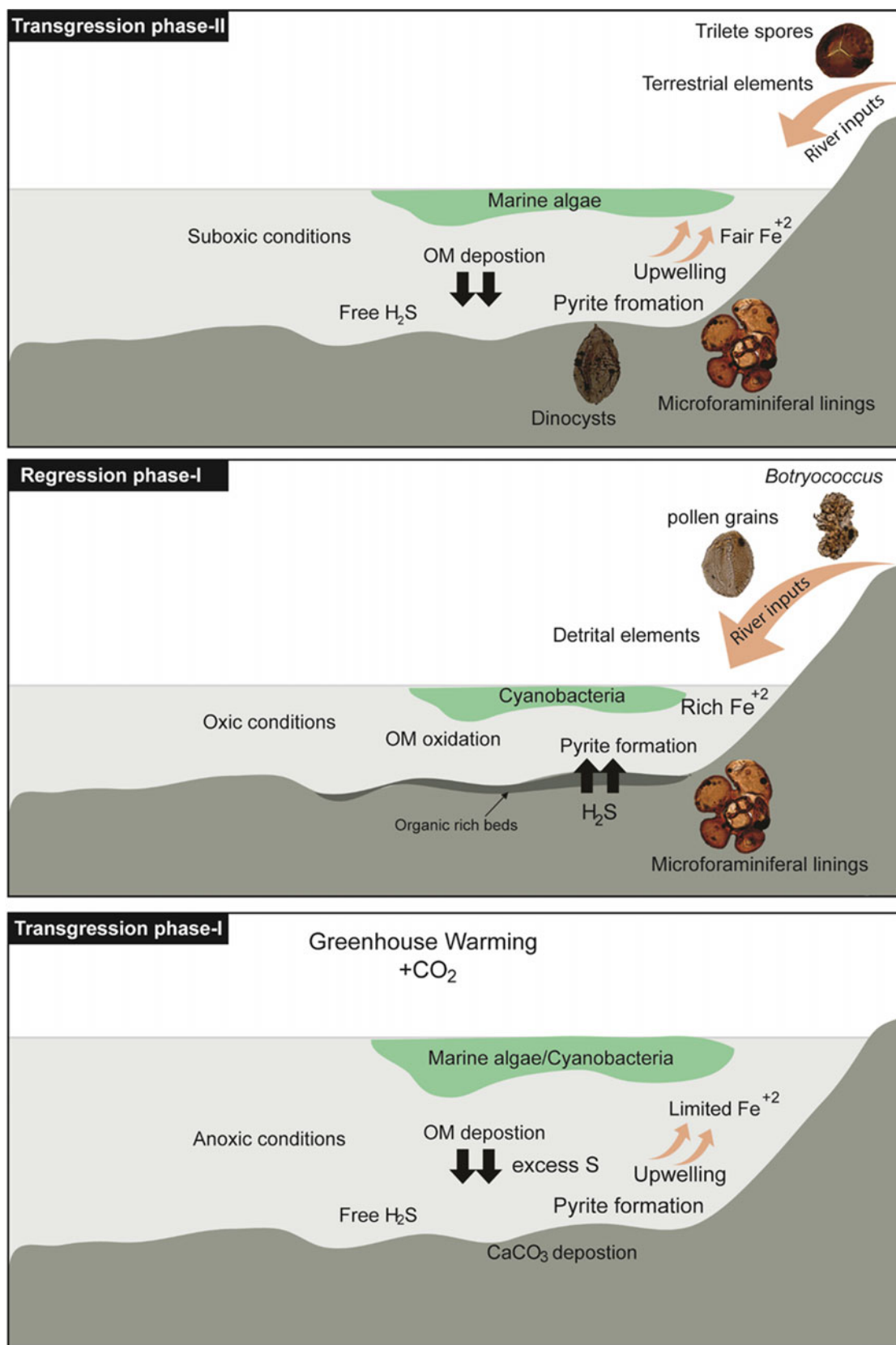


Fig. 8 Comprehensive depositional model of the Abu Roash “F” member, depended on an integrated geochemical and palynological interpretation of the Abu Gharadig Basin (Ghassal et al., 2018)

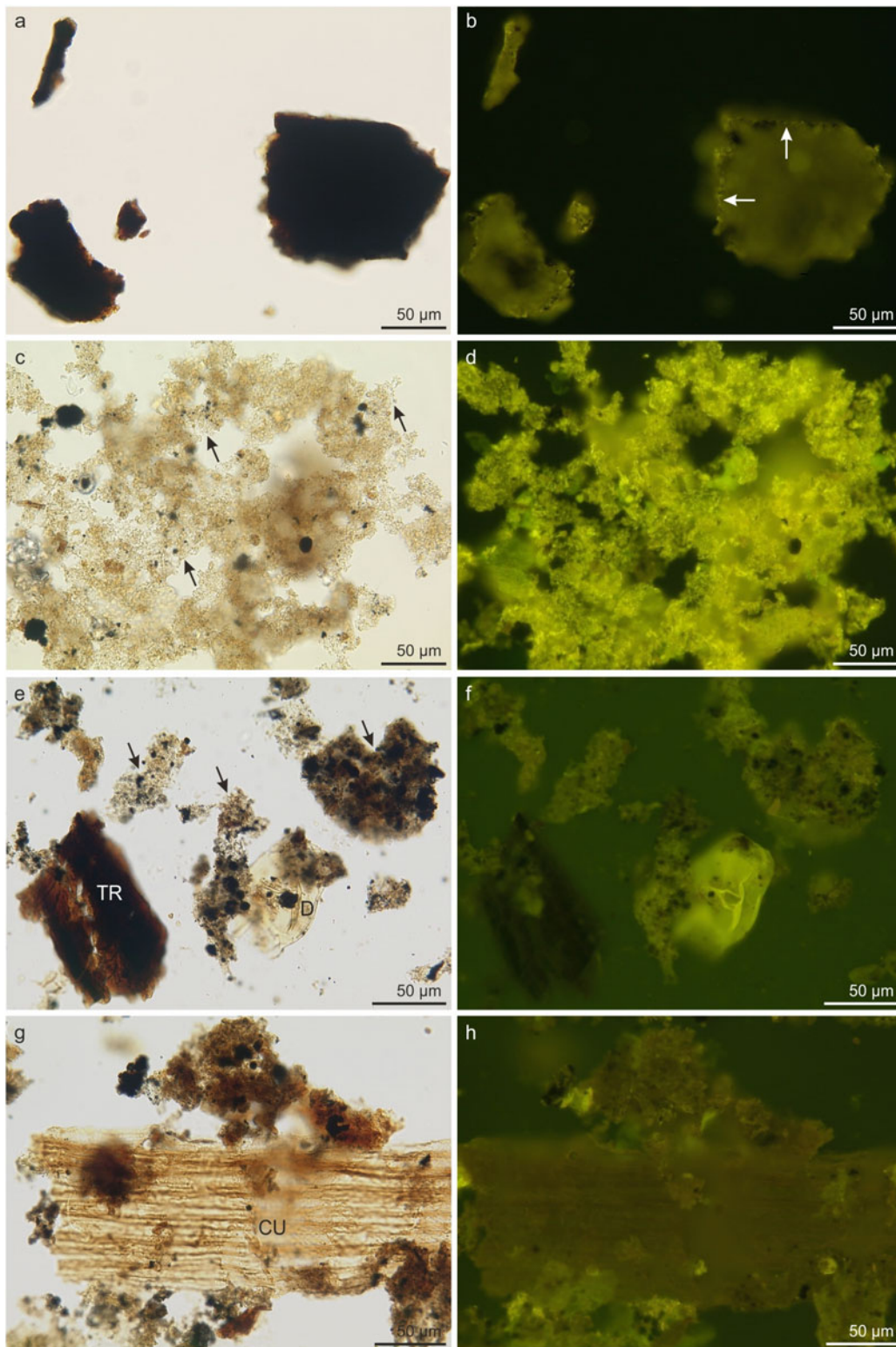


Fig. 9 Palynofacies assemblages from the central Gulf of Suez, Egypt (reproduced from El Diasty et al., 2014). **a** Non-marine AOM flakes may characterize amorphous biodegraded phytoclasts (Thebes Formation); **b** fluorescent AOM aggregates, a distinctly structured rim (arrows) might signify biodegradation or transformation of phytoclasts into AOM (Thebes Formation). **c** Fine granular, yellow to gray (arrows) marine amorphous masses, apparently of algal origin (Thebes Formation); **d** highly fluorescent AOM, may reflect an algal origin (Thebes formation). **e** A mixed palynofacies association comprised mainly AOM (arrows) with dispersed pyrites, tracheid phytoclast (TR) and dinoflagellate cyst (D) may represent *Isabelidium/Chatangiella* sp. (Matulla Formation); **f** a variable fluorescent potential among the different palynofacies components (Matulla formation); **g** a dispersed leaf cuticle (CU) phytoclast displays a regular, rectangular cellular structure bounded by AOM (Matulla formation); **h** a dispersed leaf cuticle shows very weak fluorescence (Matulla formation)

Table 3 TOC, rock-eval, elemental data, and vitrinite reflectance equivalent (VR_e) of the upper Jurassic Masajid and the lower Cretaceous Alam El Bueib formations (Abu Hammad-1 well), Nile Delta, Egypt (Ghassal et al., 2016)

Sample number	Well name	Depth (m)	Formation	Age	TOC (wt.%)	TIC (%)	CaCO ₃ (%)	TS (%)	TOC/TS	S ₁	S ₂	S ₃	T _{max} °C	HI	OI	VR (%)	
15/215	Abu Hammad-1	1212	Kharita	U. Cretaceous	0.36	11.56	96.34	0.78	0.47	0.09	0.26	1.21	428	70	331		
15/216		1242	Kharita	U. Cretaceous	0.79	3.02	25.15	0.70	1.13	0.11	0.63	1.25	421	80	159		
15/217		1362	Kharita	U. Cretaceous	0.58	10.95	91.28	0.99	0.59	0.24	0.36	1.09					
15/218		1461	Alam El-Bueib	L. Cretaceous	1.67	1.94	16.18			0.67	1.74	1.26	427	104	76		
14/1350		1605	Alam El-Bueib	L. Cretaceous	3.56	0.51	4.23	2.11	1.69	0.49	4.62	1.54	422	130	43	0.42	
14/1351		1794	Alam El-Bueib	L. Cretaceous	3.46	0.23	1.96	1.26	2.74	0.25	2.65	1.69	426	77	49		
15/221		1803	Alam El-Bueib	L. Cretaceous	3.88	0.31	2.62	0.98	3.96	0.52	2.78	1.32	429	72	34		
15/222		1947	Alam El-Bueib	L. Cretaceous	3.18	0.22	1.85	2.23	1.43	0.38	1.45	1.64	423	46	51	0.47	
15/223		1965	Masajid	U. Jurassic	1.74	3.14	26.17	1.18	1.47	2.44	2.22	1.17	428	128	67		
15/224		2016	Masajid	U. Jurassic	1.18	1.26	10.46	1.35	0.87	0.29	1.10	1.32	427	93	112		
14/1352		2034	Masajid	U. Jurassic	0.58	4.78	39.80	1.20	0.48	0.07	0.59	1.48	422	102	256		
15/226		2379	Khatatba	M. Jurassic	0.63	7.44	61.98			0.20	0.71	1.39	432	113	222		
15/227		2448	Khatatba	M. Jurassic	0.66	6.13	51.06	0.92	0.71	0.09	0.58	1.14	429	89	174		
14/1353		2502	Khatatba	M. Jurassic	0.53	3.02	25.14	0.82	0.65	0.07	0.65	1.53	426	121	287	0.63	
15/229		3306	Khatatba	M. Jurassic	0.57	3.99	33.25	0.84	0.68	0.05	0.41	1.29	434	73	228		
15/230		3537	Khatatba	M. Jurassic	0.51	5.27	43.93			0.04	0.33	1.33	433	64	262	0.71	

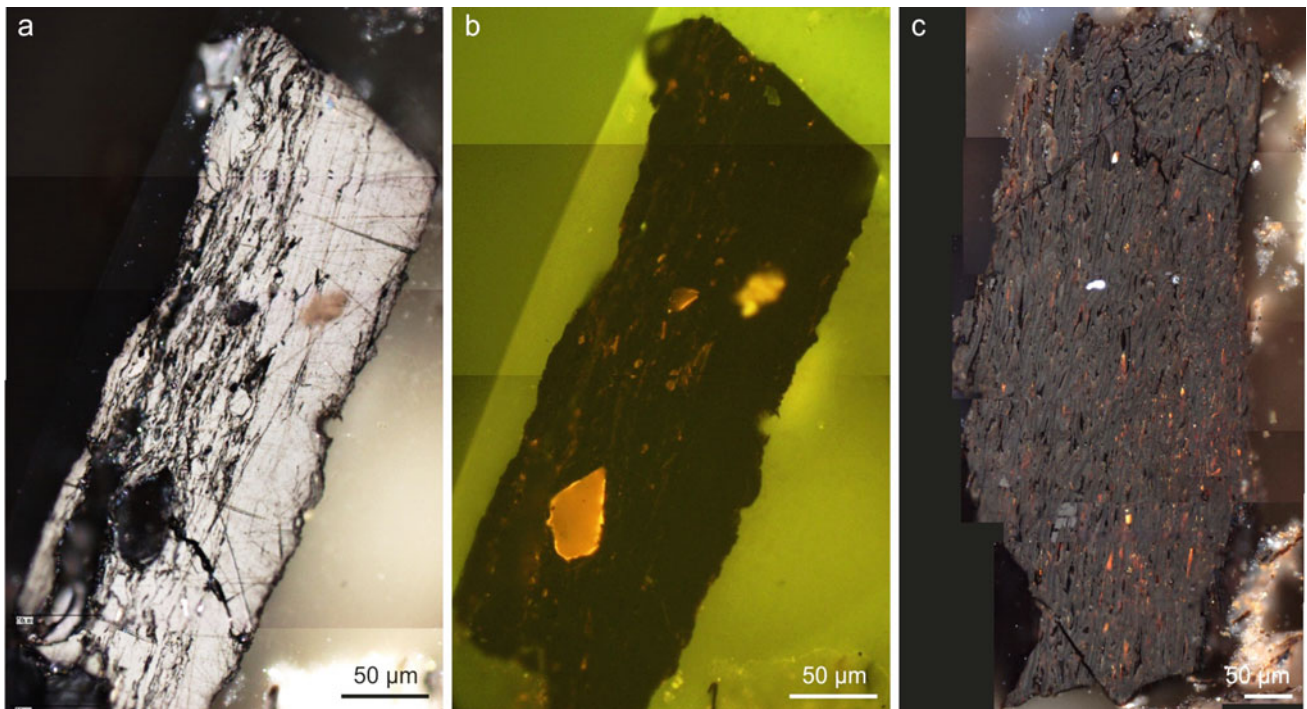


Fig. 10 Organic microscopy photographs from the Nile Delta source rock. **a b** Allochthonous coal particles under incident and fluorescent lights; **c** tellovitrinite under incident light

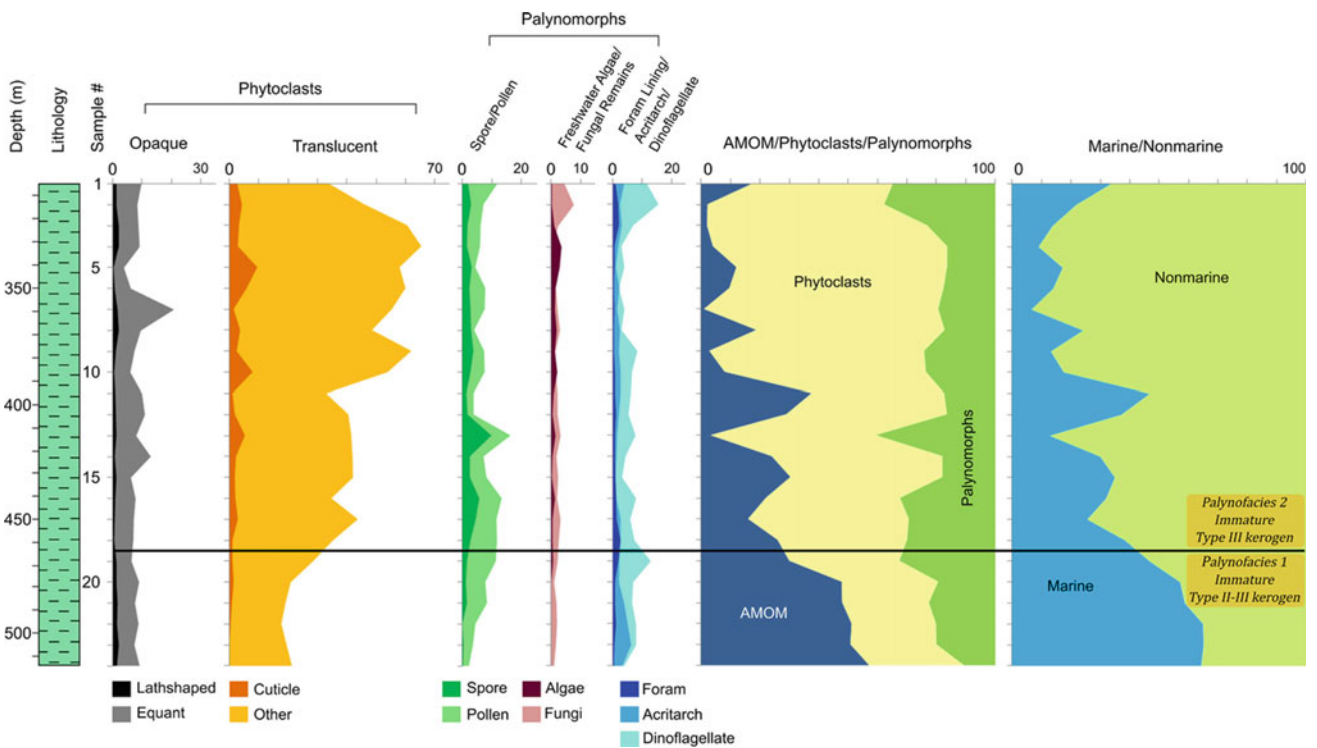


Fig. 11 Quantitative distribution of the different kerogen components of the Oligocene Dabaa Formation, AMOM represents amorphous marine organic matter (El Beialy et al., 2016)

Table 4 TOC and rock-eval pyrolysis results of the Miocene samples (GH 404-2A, GH 420-1, and SA-E6A wells), Gulf of Suez, Egypt (El Atfy et al., 2014)

Well name	Sample	Status	Depth [m]	Formation	TOC [wt.%]	S ₁ [mg HC/Rock]	S ₂ [mg HC/Rock]	S ₃ [mg CO ₂ /Rock]	T _{max} [°C]	PI S ₁ /(S ₁ + S ₂)	HI S ₂ *100/TOC	OI S ₃ *100/TOC	S ₂ /S ₃
SA-E6A	SA_013	Extracted	1405.1	Kareem	2.27		8.50	1.07	419		375	47	7.93
SA-E6A		Non-extracted			8.75		10.43	0.96	426				
SA-E6A	SA_015	Extracted	1466.1	Rudeis	2.69		11.01	1.62	425		410	60	6.81
SA-E6A		Non-extracted			8.96		16.03	1.27	420				
GH 404-2A	04_072	Non-extracted	2542.0	Kareem	2.26	0.99	3.03	1.60	432	0.25	134	71	1.90
GH 404-2A	04_076	Non-extracted	2578.6	Kareem	1.40	0.39	1.99	0.81	436	0.17	142	58	2.44
GH 404-2A	04_082	Non-extracted	2633.5	Rudeis	1.33	0.62	1.64	2.30	437	0.28	123	173	0.71
GH 404-2A	04_086	Non-extracted	2670.0	Rudeis	2.04	1.80	6.78	2.57	434	0.21	332	126	2.63
GH 404-2A	04_090	Non-extracted	2706.6	Rudeis	2.24	0.41	2.83	2.45	438	0.13	127	109	1.16
GH 404-2A	04_094	Non-extracted	2743.2	Rudeis	2.40	0.78	3.72	2.56	439	0.17	155	106	1.46
GH 404-2A	04_098	Non-extracted	2779.8	Rudeis	2.35	0.69	3.33	0.82	437	0.17	142	35	4.04
GH 404-2A	04_102	Non-extracted	2816.4	Rudeis	1.97	0.32	1.83	1.06	437	0.15	93	54	1.72
GH 404-2A	04_110	Non-extracted	2889.5	Rudeis	1.28	0.55	1.62	1.34	437	0.25	127	105	1.21
GH 404-2A	04_118	Non-extracted	2962.7	Rudeis	1.40	0.82	2.50	2.43	437	0.25	179	174	1.03
GH 404-2A	04_122	Non-extracted	2999.2	Rudeis	2.32	1.75	4.23	0.61	436	0.29	182	26	6.95
GH 404-2A	04_126	Non-extracted	3045.0	Rudeis	1.68	2.68	5.18	1.95	439	0.34	308	116	2.66
GH 404-2A	04_130	Non-extracted	3081.5	Rudeis	1.21	0.77	2.02	2.16	439	0.28	167	179	0.93
GH 404-2A	04_134	Non-extracted	3118.1	Rudeis	2.60	0.93	2.57	3.67	439	0.27	99	141	0.70
GH 404-2A	04_140	Non-extracted	3173.0	Rudeis	1.88	1.31	3.17	2.56	439	0.29	169	136	1.24
GH 404-2A	04_142	Non-extracted	3191.3	Rudeis	1.50	3.33	2.36	1.84	441	0.59	157	122	1.29
GH 404-2A	04_144	Non-extracted	3209.5	Rudeis	1.90	0.96	3.34	2.00	439	0.22	176	106	1.67
GH 404-2A	04_146	Non-extracted	3227.8	Rudeis	1.76	2.22	3.28	2.44	442	0.40	186	139	1.34
GH 404-2A	04_150	Non-extracted	3264.4	Rudeis	1.69	1.40	2.80	0.64	442	0.33	165	38	4.37
GH 420-1	20_048	Extracted	2200.7	Kareem	3.17		12.06	1.46	421		381	46	8.27
		Contaminated			7.16		12.82	1.70	428		436	74	5.93
GH 420-1	20_049	Extracted	2231.1	Kareem	2.18		9.50	1.60	422				
		Contaminated			6.49		9.45	1.42	432				
GH 420-1	20_052	Extracted	2258.6	Rudeis	2.45		11.21	1.51	423		458	62	7.43
		Contaminated			7.15		9.62	1.35	439				
GH 420-1	20_055	Extracted	2286.0	Rudeis	1.81		5.81	1.26	421		321	70	4.60
		Contaminated			7.62		15.11	1.34					

(continued)

Table 4 (continued)

Rock eval 6 data

Well name	Sample	Status	Depth [m]	Formation	TOC [wt.%]	S ₁ [mg HC/Rock]	S ₂ [mg HC/Rock]	S ₃ [mg CO ₂ /Rock]	T _{max} [°C]	PI S ₁ /(S ₁ + S ₂)	HI S ₂ *100/TOC	OI S ₃ *100/TOC	S ₂ /S ₃
GH 420-1	20_059	Extracted	2322.6	Rudeis	2.26		9.88	1.53	424		438	68	6.46
		Contaminated			7.29		10.52	1.46					
GH 420-1	20_063	Extracted	2359.2	Rudeis	3.36		10.15	1.66	433		302	49	6.10
		Contaminated			7.59		12.57	1.54					
GH 420-1	20_069	Extracted	2414.0	Rudeis	2.72		12.13	1.63	426		445	60	7.45
		Contaminated			8.43		11.04	1.42	432				
GH 420-1	20_075	Extracted	2468.9	Rudeis	2.82		11.87	1.53	421		421	54	7.76
		Contaminated			7.62		9.71	1.60	432				
GH 420-1	20_077	Extracted	2487.2	Rudeis	3.42		13.96	1.39	425		409	41	10.04
		Contaminated			9.37		12.43	0.45					
GH 420-1	20_081	Extracted	2523.7	Rudeis	3.20		10.17	1.39	426		318	43	7.33
		Contaminated			9.97		11.69	0.44					
GH 420-1	20_084	Extracted	2551.2	Rudeis	1.89		8.42	1.21	429		446	64	6.97
		Contaminated			8.95		15.94	1.49					
GH 420-1	20_090	Extracted	2606.0	Rudeis	1.58		5.59	1.34	428		353	85	4.17
		Contaminated			8.71		1.28	0.04	418				
GH 420-1	20_093	Extracted	2633.472	Rudeis	2.59		8.90	1.72	427		343	66	5.17
		Contaminated			7.06		10.31	1.83	429				

Table 5 TOC, rock-eval, elemental data, and VR_e of Miocene and Pliocene rock units (Matariya-1 well), Nile Delta, Egypt (Ghassal et al., 2016)

Sample number	Well name	Depth (m)	Formation	Age	TOC (wt.%)	TIC (%)	CaCO ₃ (%)	TS (%)	TOC/TS	S ₁	S ₂	S ₃	T _{max} °C	HI	OI	VR (%)
15/190	Matariya-1	2284	Kafr El Sheikh	M. Pliocene	0.51	0.42	3.49			0.06	0.30	1.21				
15/191	Matariya-1	2311	Kafr El Sheikh	M. Pliocene	0.29	0.53	4.42			0.07	0.27	1.15				
15/192	Matariya-1	2368	Qawasim	U. Miocene	0.57	0.37	3.09			0.06	0.36	1.28	416	63	225	
15/193	Matariya-1	2479	Qawasim	U. Miocene	0.59	0.41	3.42			0.06	0.37	1.27	424	64	215	
15/194	Matariya-1	2503	Qawasim	U. Miocene	0.50	0.24	2.01			0.04	0.33	1.29	412	65	258	0.48
15/195	Matariya-1	2590	Qawasim	U. Miocene	0.59	0.28	2.33			0.07	0.39	1.15	428	66	196	
15/196	Matariya-1	2629	Qawasim	U. Miocene	0.71	0.33	2.73	1.09	0.66	0.10	0.60	1.27	415	84	178	
15/197	Matariya-1	2659	Qawasim	U. Miocene	0.51	0.22	1.86			0.05	0.33	1.30	425	64	257	
15/198	Matariya-1	3113	Qawasim	U. Miocene	1.28	1.11	9.28	0.98	1.31	0.15	0.89	1.30	428	69	101	
15/199	Matariya-1	3293	Qawasim	U. Miocene	1.30	0.23	1.92			0.13	0.83	1.13	428	64	87	
15/200	Matariya-1	3362	Sidi Salem	M. Miocene	1.06	0.35	2.93	0.86	1.24	0.07	0.55	1.28	434	52	120	
14/1354	Matariya-1	3380	Sidi Salem	M. Miocene	0.99	0.26	2.16	0.90	1.10	0.06	0.59	1.45	426	60	146	
15/202	Matariya-1	3443	Sidi Salem	M. Miocene	1.03	0.28	2.32			0.15	0.63	1.22	428	61	119	
15/203	Matariya-1	3482	Sidi Salem	M. Miocene	1.35	0.36	3.03	0.80	1.68	0.12	1.04	1.13	426	77	84	
15/204	Matariya-1	3527	Sidi Salem	M. Miocene	1.59	0.42	3.48	0.96	1.66	0.08	0.66	1.27	428	41	80	
15/205	Matariya-1	3560	Sidi Salem	M. Miocene	1.17	0.29	2.38			0.07	0.61	1.28	429	53	109	0.53
15/206	Matariya-1	3593	Sidi Salem	M. Miocene	1.46	0.41	3.45			0.16	1.17	1.27	428	80	87	
14/1355	Matariya-1	3626	Sidi Salem	M. Miocene	1.32	0.64	5.34			0.09	0.84	1.53	425	64	116	
15/208	Matariya-1	3647	Sidi Salem	M. Miocene	2.08	1.23	10.25	1.24	1.68	0.31	1.71	1.50	433	82	72	
15/209	Matariya-1	3740	Sidi Salem	M. Miocene	2.88	1.14	9.52	1.09	2.65	0.77	3.04	1.38	430	105	48	
15/210	Matariya-1	3824	Sidi Salem	M. Miocene	0.95	0.41	3.39			0.77	1.31	1.44	416	139	152	
15/211	Matariya-1	4002	Sidi Salem	M. Miocene	1.70	0.88	7.32	0.89	1.91	0.95	2.31	1.11				
15/212	Matariya-1	4035	Sidi Salem	M. Miocene	1.11	0.71	5.93	1.10	1.01	0.36	1.29	1.13				
15/213	Matariya-1	4108	Sidi Salem	M. Miocene	1.65	0.76	6.37			0.66	1.76	1.26	420	106	76	
15/214	Matariya-1	4141	Sidi Salem	M. Miocene	1.38	0.62	5.20			0.92	2.52	1.25	423	183	90	0.66

4.3.2 Gulf of Suez

Mainly, the Miocene has been studied in the Gulf of Suez. In spite of the intense micropaleontologic efforts (mainly foraminifera and calcareous nannofossils) in the last years, few contributions have been published on the palynology of this region in comparison with other parts of Egypt. Until recently, there were few palynological studies (mainly biostratigraphic) on the Miocene deposits of the Gharandal and Ras Malaab groups, which are considered among the most important hydrocarbon-bearing sequences in Egypt. Therefore, introducing palynofacies herein especially as a maturation detection parameter covers such a niche.

To the authors' knowledge, El Atfy et al., (2013, 2014) introduced palynofacies research to the Miocene of the Gulf of Suez. These publications integrated palynofacies with organic geochemistry and organic petrography to attain the following results:

1. Palynofacies analyses discriminated the Nukhul Formation into three of two main palynofacies assemblages (PF-Ia, PF-Ib, and PF-II): PF-Ia and PF-Ib were the dominant facies within the Ghara Member, representing a suboxic–anoxic environment. Kerogen Type III was established for these two assemblages. PF-II mainly dominated the Shoab Ali Member, showing a composition of mixed Type III and Type II kerogen with more phytoclast input supporting a fairly continental suboxic–anoxic basin characterized by low AOM. These results were in great accordance with previous organic geochemical analyses (El Atfy et al., 2013).
2. TOC and Rock-Eval analyses suggested a fair to good organic richness for the Rudeis and Kareem formations (Table 4). According to palynofacies analyses and organic petrology, Type III or Type II/III kerogen were identified with a very limited terrestrial input. Furthermore, most of the sediments were deposited under oxygen-deficient, but not totally anoxic, conditions. Multi-proxy thermal maturation determination techniques indicated an immature to early mature level for the organic matter and a rise of maturation with depth.

4.3.3 Nile Delta

The study carried out by Ibrahim (1996) on core samples retrieved from El Qara-2 borehole in the north-central Nile Delta was the only attempt to employ palynofacies as an exploration proxy within the basin. SCI index enabled him to recognize three organic facies, immature, mature (Kafr El Sheikh Formation), and overmature (Abu Madi Formation).

The Miocene source rocks of the Nile Delta, on the other hand, were studied in more detail by organic geochemistry by Ghassal et al. (2016) who provided a comprehensive review of the regional source characteristics (Table 5). The

central Nile Delta Basin possesses higher source rock quality than the eastern part. The difference in quality is ascribed to the variation of the depositional setting. The eastern Nile Delta Basin was deposited in shallower water settings during the Middle Miocene time. For example, the highest reported HI values in the eastern part of the delta is 184 mgHC/gTOC, whereas it reaches 480 mgHC/gTOC in the western part of the basin (El Nady, 2007; El Nady & Harb, 2010; Ghassal et al., 2016; Keshta et al., 2012; Shaaban et al., 2006).

5 Conclusions

The integration of optical and geochemical techniques represents the best way to screen hydrocarbon source rock potential and has a distinguishing impact on kerogen analysis, besides its utilization in paleoenvironmental inferences. It is worth noting that while kerogen types are usually obtained from Rock-Eval data, palynofacies and organic petrographic data offer additional reliable information. For samples with low to moderate TOC, Rock-Eval data are mostly uncertain for the reason that the retained hydrocarbons in the mineral matrix (Grohmann et al., 2018). Consequently, palynofacies analysis is a valuable, complementary technique for investigating the petroleum generation potential of source rocks.

Acknowledgements The authors are also grateful to the Egyptian General Petroleum Corporation (EGPC) and the operating companies for the provision of samples and well logs during the past ten years during which this research was conducted. The first author acknowledges the financial support from the Alexander von Humboldt Foundation, Germany (EGY-1190326-GF-P). Insightful reviews by two anonymous referees enabled an improved presentation of this work.

References

- Abohajar, A., Littke, R., Schwarzbauer, J., Weniger, P., & Boote, D. R. D. (2015). Biomarker characteristics of potential source rocks in the Jabal Nafusah area, NW Libya: Petroleum systems significance. *Journal of Petroleum Geology*, 38(2), 119–156.
- Abu-Ali, M., & Littke, R. (2005). Paleozoic petroleum systems of Saudi Arabia: a basin modeling approach. *GeoArabia*, 10(3), 131–168.
- Bakun, A. (1990). Global climate change and intensification of coastal ocean upwelling. *Science*, 247(4939), 198–201.
- Barakat, M. K. A. (2010). Modern geophysical techniques for constructing a 3D geological model on the Nile Delta, Egypt. Dissertation, Technical University of Berlin. <https://doi.org/10.14279/depositonce-2627>
- Bassett, M. G. (2009). Early Palaeozoic peri-Gondwana terranes: New insights from tectonics and biogeography. *Geological Society, London, Special Publications*, 325, 1–2. <https://doi.org/10.1144/SP325.1>
- Batten, D. J. (1982). Palynofacies, palaeoenvironments and petroleum. *Journal of Micropalaeontology*, 1, 107–114.

- Batten, D. J. (1996a). Palynofacies and palaeoenvironmental interpretation. In J. Jansonius, D. C. McGregor (Eds.), *Palynology: Principles and applications 3* (pp. 1011–1064). AAPG Foundation
- Batten, D. J. (1996b). Palynofacies and petroleum potential. In J. Jansonius, D. C. McGregor (Eds.), *Palynology: Principles and applications 3* (pp. 1065–1084). AAPG Foundation
- Batten, D. J. (1999). Palynofacies analysis. In T. P. Jones & N. P. Rowe (Eds.), *Fossil plants and spores: Modern techniques* (pp. 194–198). Geological Society.
- Belaid, A., Krooss, B. K., & Littke, R. (2010). Thermal history and source rock characterization of a Paleozoic section in the Awbari Trough, Murzuq Basin, SW Libya. *Marine and Petroleum Geology*, 27, 612–632.
- Berra, F., Angiolini, L. (2014). The evolution of the Tethys Region throughout the Phanerozoic: a brief tectonic reconstruction. In L. Marlow, C. C. G. Kendall, L. A. Yose (Eds.), *Petroleum systems of the Tethyan region* (vol. 106, pp. 1–27). AAPG Memoir
- Beydoun, Z. R. (1998). Arabia plate oil and gas: Why so rich and so prolific. *Episodes*, 21(2), 1–8.
- Bosworth, W., Huchon, P., & McClay, K. (2005). The Red Sea and Gulf of Aden Basins. *Journal of African Earth Sciences*, 43, 334–378.
- Bustin, R. M. (1988). Sedimentology and characteristics of dispersed organic matter in Tertiary Niger Delta: Origin of source rocks in a deltaic environment. *AAPG Bulletin*, 72(3), 277–298.
- Coe, A. L., Bosence, D. W. J., Church, K. D., Flint, S. S., Howell, J. A., & Wilson, R. C. L. (2003). *The sedimentary record of sea-level change* (p. 2003). Cambridge University Press and the Open University.
- Combaz, A. (1964). Les palynofaciès. *Revue De Micropaléontologie*, 7, 205–218.
- Craig, J., Thurow, J., Thusu, B., Whitham, A., & Abutarruma, Y. (2009). Global Neoproterozoic petroleum systems: The emerging potential in North Africa. *Geological Society, London, Special Publications*, 326, 1–25.
- Dolson, J., et al. (2020). The petroleum geology of Egypt and history of exploration. In Z. Hamimi (Ed.), *The geology of Egypt* (pp. 635–658). Springer.
- Dolson, J. C., Atta, M., Blanchard, D., Sehimi, A., Villinski, J., Loutit, T., Romine, K. (2014). Egypt's future petroleum resources: a revised look in the 21st Century. In L. Marlow, C. Kendall, L. Yose (Eds.), *Petroleum systems of the Tethyan region, Memoir* (vol. 106, pp. 143–178). AAPG
- Dolson, J. C., Shann, M. V., Matbouly, S. I., Hammouda, H., & Rashed, R. M. (2000). Egypt in the twenty-first century: Petroleum potential in offshore trends. *GeoArabia*, 6(2), 211–230.
- Duarte, L. V., Silva, R. L., Mendonça Filho, J. G., Ribeiro, N. P., & Chagas, R. B. A. (2012). High-resolution stratigraphy, palynofacies and source rock potential of the Agua de Madeiros formation (lower Jurassic), Lusitanian basin, Portugal. *Journal of Petroleum Geology*, 35(2), 105–126.
- El Atfy, H. (2021). Palynofacies as a paleoenvironment and hydrocarbon source potential assessment tool: An example from the Cretaceous of north Western Desert, Egypt. *Palaeobiodiversity and Palaeoenvironments*, 101, 35–50.
- El Atfy, H., Brocke, R., Uhl, D. (2013). Age and paleoenvironment of the Nukhul Formation, Gulf of Suez, Egypt: Insights from palynology, palynofacies and organic geochemistry. *GeoArabia*, 18(4), 137–174
- El Atfy, H., Brocke, R., Uhl, D., Ghassal, B., Stock, A. T., Littke, R. (2014). Source rock potential and paleoenvironment of the Miocene Rudeis and Kareem formations, Gulf of Suez, Egypt: An integrated palynofacies and organic geochemical approach. *International Journal of Coal Geology*, 131, 326–343
- El Atfy, H., Ghassal, B., Maher, A., Hosny, A., Mostafa, A., & Littke, R. (2019). Palynological and organic geochemical studies of the upper Jurassic-lower cretaceous successions, Western Desert, Egypt: Implications for paleoenvironment and hydrocarbon source rock potential. *International Journal of Coal Geology*, 211, 103207.
- El Beialy, S. Y., El Atfy, H. S., Zavada, M., El Khoriby, E. M., & Abu Zied, R. H. (2010). Palynological, palynofacies, paleoenvironmental and organic geochemical studies on the upper cretaceous succession of the GPTSW-7 Well, North Western Desert, Egypt. *Marine and Petroleum Geology*, 27, 370–385.
- El Beialy, S. Y., Zobaa, M. K., & Taha, A. A. (2016). Depositional paleoenvironment and hydrocarbon source potential of the Oligocene Dabaa formation, North Western Desert, Egypt: A palynofacies approach. *Geosphere*, 12, 346–353.
- El Diasty, W. S., El Beialy, S., Abo Ghonaim, A. A., Mostafa, A. R., & El Atfy, H. (2014). Palynology, palynofacies and petroleum potential of the upper cretaceous-Eocene Matulla, brown limestone and thebes formations, Belayim oilfields, central Gulf of Suez, Egypt. *Journal of African Earth Sciences*, 95, 155–167.
- El Nady, M. M. (2007). Organic geochemistry of source rocks, condensates, and thermal geochemical modeling of Miocene sequence of some wells, onshore Nile Delta, Egypt. *Petroleum Science and Technology*, 25, 791–817.
- El Nady, M. M., & Harb, F. M. (2010). Source rocks evaluation of Sidi Salem-1 well in the onshore Nile Delta, Egypt. *Petroleum Science and Technology*, 28, 1492–1502.
- El-Hawat, A. S., Missallati, A. A., Bezan, A. M., Taleb, T. M. (1997). The Nubian sandstone in Sirt Basin and its correlatives. In M. J. Salem, A. J. Mouzoughi, O.S. Hammda (Eds.), *The geology of Sirt Basin* (vol. 2, pp. 3–30). Elsevier
- El-Soughier, M. I., Mahmoud, M. S., & Li, J. (2010). Palynology and palynofacies of the lower cretaceous succession of the Matruh 2-1X borehole, Northwestern Egypt. *Revista Española De Micropaleontología*, 42, 37–58.
- Felststeen, A. W., El-Soughier, M. I., Mohamed, M. S., & Monged, M. N. S. (2014). Hydrocarbon source potential of the Jurassic sediments of Salam-3X borehole, Khalda Concession, Northern Western Desert, Egypt. *Arabian Journal of Geosciences*, 7, 3467–3480.
- Galloway, W. E. (1975). Process framework for describing the morphologic and stratigraphic evolution of deltaic depositional systems. In M. L. Broussard (Ed.), *Deltas: Models for exploration* (pp. 87–98). Houston Geological Society
- Gentzis, T., Carvajal-Ortiz, H., Deaf, D., & Tahoun, S. S. (2018). Multi-proxy approach to screen the hydrocarbon potential of the Jurassic succession in the Matruh Basin, North Western Desert, Egypt. *International Journal of Coal Geology*, 190, 29–41.
- Ghassal, B., Littke, R., El Atfy, H., Sindern, S., Scholtysik, G., El Beialy, S., & El Khoriby, E. (2018). Source rock potential and depositional environment of upper cretaceous sedimentary rocks, Abu Gharadig Basin, Western Desert, Egypt: An integrated palynological, organic and inorganic geochemical study. *International Journal of Coal Geology*, 186, 14–40.
- Ghassal, B. I. (2010). Petroleum geochemistry and geology of the Midyan and Al Wajah Basins, northern Red Sea, Saudi Arabia (p. 231). M.Sc. Thesis, The University of Utah
- Ghassal, B. I., El Atfy, H., Sachse, V., & Littke, R. (2016). Source rock potential of the middle Jurassic to middle Pliocene, Onshore Nile Delta Basin, Egypt. *Arabian Journal of Geosciences*, 9, 744.
- Ghassal, B. I. H. (2017). Source rock depositional processes in different marine settings: Examples from North African basins. Ph.D. Thesis, Universitätsbibliothek der RWTH Aachen. <http://publications.rwth-aachen.de/record/696615/files/696615.pdf>
- Gluyas, J., & Swarbrick, R. (2013). *Petroleum geoscience*. Wiley.

- Grohmann, S., Fietz, S. W., Littke, R., Daher, S. B., Romero-Sarmiento, M. F., Nader, F. H., Baudin, F. (2018). Source rock characterization of Mesozoic to Cenozoic organic matter rich marls and shales of the Eratosthenes Seamount, Eastern Mediterranean Sea. *Oil & Gas Science and Technology/Revue d'IFP Energies nouvelles*, 73, 49
- Guiraud, R., Bellion, Y., Benkhelil, J., & Moreau, C. (1987). Post-Hercynian tectonics in Northern and Western Africa. *Geological Journal*, 22, 433–466.
- Guiraud, R., & Bosworth, W. (1999). Phanerozoic geodynamic evolution of northeastern Africa and the northwestern Arabian platform. *Tectonophysics*, 315, 73–108.
- Guiraud, R., Bosworth, W., Thierry, J., & Delplanque, A. (2005). Phanerozoic geological evolution of Northern and Central Africa: An overview. *Journal of African Earth Sciences*, 43, 83–143.
- Haq, B. U., Hardenbol, J., Vail, P. R. (1988). Mesozoic and Cenozoic chronostratigraphy and cycles of sea-level changes. In C. K. Wilgus, B. S. Hastings, H. W. Posamentier, J. van Wagoner, C. A. Ross, Kendall G. S. C. (Eds.), *Sea-level changes: An integrated approach* (pp. 71–108). Society of Economic Paleontologists and Mineralogists, Special Publication no. 42.
- Hartkopf-Fröder, C., Königshof, P., Littke, R., & Schwarzbauer, J. (2015). Optical thermal maturity parameters and organic geochemical alteration at low grade diagenesis to anchimetamorphism: A review. *International Journal of Coal Geology*, 150–151, 74–119.
- Hewaidy, A. A., Baioumi, A., Makled, W. A., El Garhy M. M. (2014). Integrated palynological and organic geochemical analysis of Jurassic rocks from BYX-1 Borehole, North Western Desert, Egypt. *Egyptian Journal of Paleontology*, 14, 157–188
- Ibrahim, M. I. A. (1996). Spore colour index and organic thermal maturation studies on the Pliocene sediments of the El Qara-2 borehole, Nile Delta, Egypt. *Qatar University Science Journal*, 16 (1), 167–172.
- Ibrahim, M. I. A., Aboul Ela, N. M., & Kholeif, S. E. (1997). Paleoecology, palynofacies, thermal maturation and hydrocarbon source-rock potential of the Jurassic-lower cretaceous sequence in the subsurface of the north Eastern Desert, Egypt. *Qatar University Science Journal*, 17(1), 153–172.
- Jenkyns, H. C. (2010). Geochemistry of oceanic anoxic events. *Geochemistry, Geophysics, Geosystems*, 11(3), 1–30.
- Katz, B. (2012). *Petroleum source rocks*. Springer Science & Business Media
- Katz, B. J. (1995). Petroleum source rocks—an introductory overview. In B. J. Katz (Ed.), *Petroleum source rocks* (pp. 1–8). Springer
- Keeley, M. L. (1989). The Palaeozoic history of the Western Desert of Egypt. *Basin Research*, 2, 35–48.
- Keshta, S., Metwalli, F. J., Al Arabi, H. S. (2012). Analysis of petroleum system for exploration and risk reduction in Abu Madi/Elqar'a Gas Field, Nile Delta, Egypt. *International Journal of Geophysics*. <https://doi.org/10.1155/2012/187938>
- Klitzsch, E. (1990). Paleozoic. In R. Said (Ed.), *Geology of Egypt* (pp. 393–406). A.A Balkema/Rotterdam/Brookfield
- Koblentz-Mishke, O. J., Volkovinsky, V. V., Kabanova, J. G. (1970). Plankton primary production of the World Ocean. In W. S. Wooster (Ed.), *Scientific exploration of the South Pacific* (pp. 183–193)
- Littke, R. (1993). Deposition, diagenesis and weathering of organic matter-rich sediments. In *Lecture Notes in Earth Sciences* (p. 216). Springer
- Littke, R., Baker, D. R., Rullkötter, J. (1997). Deposition of petroleum source rocks. In D. H. Welte, B. Horsfield, D. R. Bake (Eds.), *Petroleum and basin evolution* (pp. 271–333). Springer
- Lučić, D., & Bosworth, W., et al. (2019). Regional geology and petroleum systems of the main reservoirs and source rocks of North Africa and the Middle East. In A. Bendaoud (Ed.), *The geology of the Arab world—An overview* (pp. 197–289). Springer.
- Lüning, S., Craig, J., Loydell, D. K., Storch, P., & Fitches, B. (2000). Lowermost Silurian 'hot shales' in north Africa and Arabia: Regional distribution and depositional model. *Earth Science Reviews*, 49, 121–200.
- Mahmoud, M. S., Deaf, A. S., Tamam, M. A., & Khalaf, M. M. (2017). Palynofacies analysis and palaeoenvironmental reconstruction of the upper cretaceous sequence drilled by the Salam-60 well, Shushan Basin: Implications on the regional depositional environments and hydrocarbon exploration potential of North-Western Egypt. *Revue De Micropaléontologie*, 60, 449–467.
- Makled, W. A., Mostafa, T. F., Mousa, D. A., & Abdou, A. A. (2018). Source rock evaluation and sequence stratigraphic model based on the palynofacies and geochemical analysis of the subsurface Devonian rocks in the Western Desert, Egypt. *Marine and Petroleum Geology*, 89, 560–584.
- Makled, W. A., Gentzis, A., Hosny, A. M., Mousa, D. A., Lotfy, M. M., Abd El Ghany, A. A., El Sawy, M. Z., Orabi, A. A., Abdelrazak, H. A., & Shahat, W. A. (2021). Depositional dynamics of the Devonian rocks and their influence on the distribution patterns of liptinite in the Sifa-1X well, Western Desert, Egypt: Implications for hydrocarbon generation. *Marine and Petroleum Geology*, 126, 104935.
- Mansour, A., Geršlová, E., Sýkorová, I., & VoRoš, D. (2020). Hydrocarbon potential and depositional paleoenvironment of a Middle Jurassic succession in the Falak-21 well, Shushan Basin, Egypt: Integrated palynological, geochemical and organic petrographic approach. *International Journal of Coal Geology*, 19, 103374.
- Marshall, J. E. A., & Yule, B. L. (1999). Spore colour measurement. In T. P. Jones & N. P. Rowe (Eds.), *Fossil plants and spores: Modern techniques* (pp. 165–168). Geological Society.
- Mostafa, A. R., & Ganz, H. (1990). Source rock evaluation of a well in the Abu Rudeis area, Gulf of Suez. *Berliner Geowissenschaftliche Abhandlungen*, 120, 1027–1040.
- Parrish, J. T. (1987). Palaeo-upwelling and the distribution of organic-rich rocks. *Geological Society, London, Special Publications*, 26(1), 199–205.
- Pearson, D. L. (1984). Pollen/spore color “standard”. Phillips petroleum company exploration projects section (reproduction in traverse 2007). In *Paleopalynology*, Figure 19.2. Springer
- Peters, K. E., Snedden, J. W., Sulaeman, A., Sarg, J. F., & Enrico, R. J. (2000). A new geochemical sequence Stratigraphic model for Mahakam Delta and Makassar slope, Kalimantan, Indonesia. *AAPG Bulletin*, 84, 12–44.
- Ryther, J. H. (1969). Photosynthesis and fish production in the sea: The production of organic matter and its conversion to higher forms of life vary throughout the world ocean. *Science*, 166(3901), 72–76
- Selley, R. C. (1998). *Elements of petroleum geology* (2nd ed., p.470). Academic Press
- Shaaban, F., Lutz, R., Littke, R., Bueker, C., & Odisho, K. (2006). Source-rock evaluation and basin modelling in ne Egypt (NE Nile Delta and northern Sinai). *Journal of Petroleum Geology*, 29, 103–124.
- Tissot, B., & Welte, D. H. (1984). *Petroleum formation and occurrence* (p. 699). Springer.
- Tuttle, M. L. W., Charpentier, R. R., Brownfield, M. E. (1999). The Niger delta petroleum system: Niger Delta Province, Nigeria, Cameroon, and Equatorial Guinea, Africa. U.S. Geological Survey, Open-File Report 99-50-H
- Tyson, R. V. (1995). *Sedimentary organic matter—organic facies and palynofacies* (p. 615). Chapman and Hall.

- Yahi, A., Schaefer, R. G., & Littke, R. (2001). Petroleum generation and accumulation in the Berkine basin, eastern Algeria. *AAPG Bulletin*, 85(8), 1439–1467.
- Zobaa, M. K., El Beialy, S. Y., El-Sheikh, H. A., & El Beshtawy, M. K. (2013). Jurassic-Cretaceous palynomorphs, palynofacies, and petroleum potential of the Sharib-1X and Ghoroud-1X wells, North Western Desert, Egypt. *Journal of African Earth Sciences*, 78, 51–65.
- Zobaa, M. K., Oboh-Ikuenobe, F. E., & Ibrahim, M. I. I. (2011). The Cenomanian/Turonian oceanic anoxic event in the Razzak Field, north Western Desert, Egypt: Source rock potential and palaeoenvironmental association. *Marine and Petroleum Geology*, 28, 1475–1482.



Haytham El Atfy is an associate professor at Mansoura University (Egypt) from where he received a BSc degree in geology and an MSc in palynology. He received a PhD in geosciences (palynology and organic geochemistry) from Goethe University, Frankfurt (Germany) in 2014, and acquired experience in industrial palynology through work with GUPCO (BP), Egypt. Haytham has been a Research Fellow of the Alexander von Humboldt Foundation at the University of Tübingen (Germany) since 2019. He was

recently a visiting scientist at the Senckenberg Research Institute, Germany. His research interests span all aspects of palynology and its applications in dating, palaeoenvironmental and palaeoclimatical reconstructions, and hydrocarbon exploration, particularly of the Mesozoic and Cenozoic and, to a lesser extent, the Palaeozoic. He has more recently become involved in organic geochemistry. He is a member of the AASP – The Palynological Society, the Micropalaeontological Society (TMS), Arbeitskreis für Paläobotanik und Palynologie (APP), and the Paleontological Society of Egypt (PSE). He is a recipient of many awards, including the Bernd Rendel Prize from the German Science Foundation (DFG), Egyptian State Incentive Award, and the First-Class Excellence Concession that is provided by the Egyptian president.



Bandar I. Ghassal is a petroleum geochemist and supervisor at the Saudi Aramco EXPEC Advanced Research Center. He has 17 years of industry and academic experience in mineral resource and petroleum exploration fields. He obtained a BSc (2004) degree from King Abdulaziz University (Saudi Arabia), MSc (2010) from the University of Utah (USA), and a PhD (2017) from RWTH Aachen University, Germany. He has published several papers on various topics in petroleum geology and engineering.



Ralf Littke has been a professor of geology and geochemistry of petroleum and coal at RWTH Aachen University (Germany) since 1997. He graduated with a BSc degree in geology from Ruhr-University Bochum (Germany), where he also received his PhD degree in 1985 and Habilitation in 1993. From 1985 to 1997, he worked at the Federal Research Center Jülich, Germany, in the Institute of Petroleum and Organic Geochemistry. His research interests include (1) dynamics and numerical modeling of sedimentary

basins, (2) generation and storage of oil and natural gas, (3) transport and accumulation of petroleum fluids, (4) geology, petrology and geochemistry of petroleum source rocks and coals, and (5) unconventional fossil fuels. He is a member of the German National Academy of Science and Engineering (Acatech) and member of the Academy of Sciences and Arts, Northrhine-Westfalia. He is also a former chairman of the Board of Geologische Vereinigung (German Geological Union), former chairman of the Advisory Board of Deutsches Geoforschungszentrum (GFZ Potsdam), longtime editor-in-chief of *International Journal of Coal Geology*, and former coordinator of the German priority research program *Dynamics of Sedimentary Basins*.



Hydrocarbon Potential of Carbonate Rocks in Egypt

Mohammad Abdelfattah Sarhan

Abstract

Carbonate rocks in Egypt are characterized by a great variability in facies and complexity in deformational styles. Their role as hydrocarbon reservoir in Egypt is still associated with some remaining open questions. This chapter summarizes the whole carbonate rock units which have significant importance in petroleum exploration in Egypt rather than attempting to comprise everything that has been published on the carbonate deposits of Egypt over the past decades. Also, the current chapter provides a careful selection of case studies in hydrocarbon exploration from different carbonate fields in Egypt. Three major provenances in Egypt containing thick carbonate deposits varying from Mesozoic to Tertiary in age are extremely prospective for oil and gas as conventional or unconventional resources. These provenances are Western Desert, Gulf of Suez and offshore Nile Delta Basin. The continuous progress in the technologies of seismic and well logging data techniques resulted in the development of new approaches that can identify and accurately evaluate the hydrocarbon-bearing carbonate rocks in Egypt.

Keywords

Carbonate rocks • Gulf of Suez basin • Nile delta basin • Western desert • Hydrocarbon reserves • Egypt

1 Introduction

Carbonate rocks encompass approximately half of hydrocarbon reservoirs worldwide (Harbaugh, 1967). Studying carbonate reservoirs has drawn the consideration of numerous academic researchers and petroleum exploration companies (e.g., Vicentelli et al., 2015; Wei et al., 2015; Beigi et al., 2017; Liu & Wang, 2017; Nazari et al., 2019; Sequero et al., 2019).

Due to the difference in the carbonate facies and the complexity in their deformation styles, assessment of the carbonate reservoir is very difficult. Accordingly, several applications of different geophysical and geological techniques are required for characterizing the lithology and structure of carbonate reservoirs (Burchette, 2012; Cerepi et al., 2003). Moreover, in carbonate hydrocarbon reservoirs, pore networks are vital components controlling the fluid pathways, reservoir quality and production (e.g., Anselmetti & Eberli, 1999; Eberli et al., 2003; Hollis et al., 2010, 2017a, 2017b; Karimpouli et al., 2013; Worden et al., 2018). Because of the heterogeneity and the complicated relation between rock fabric and pore system in the carbonate deposits, modelling of petrophysical properties is challenging (e.g., Sha et al., 2019; Zhao et al., 2015). Accordingly, in order to adequately evaluate carbonate reservoirs, multiscale and integrated datasets are required together (Radwan et al., 2021). The subdivision of carbonate deposits into units called electrofacies (e.g., Euzen & Power, 2012; Torghabeh et al., 2014) led to categorize petrofacies based on their variation in physical properties and geological conditions (Radwan et al., 2021).

Carbonate rocks are susceptible to diagenesis which cause noticeable changes in pore size and shape, leading to either decrease or increase of the petroleum reservoir quality (e.g., Afife et al., 2017; Watney et al., 1999). The pore spaces, structures and petrophysical characterization of carbonate reservoir rocks can change through time or be affected by several factors such as diagenesis (e.g.,

M. A. Sarhan (✉)
Geology Department, Faculty of Science, Damietta University,
New Damietta, Egypt
e-mail: msarhan@du.edu.eg

Center of Space Research and Applications (CSRA), Damietta
University, New Damietta, Egypt

Ehrenberg & Nadeau, 2005; Ehrenberg et al., 2019; Nabawy et al., 2020; Salah et al., 2016a, 2016b), structural and sedimentological discontinuities (e.g., Ali et al., 2018; Baud et al., 2017; Heap et al., 2018; Michie & Haines, 2016; Rashid et al., 2017; Trippetta et al., 2017), presence of infilling materials (e.g., Trippetta & Geremia, 2019; Trippetta et al., 2020) and temperature/pressure settings (Anselmetti & Eberli, 1993).

Fractured carbonate reservoirs are significant in producing oil and gas in numerous giant fields such as Gachsaran Field in Iran and Kirkuk Field in Iraq. Several types of fractures may be developed and extremely increase the heterogeneity of the hydrocarbon-bearing rocks (Tavakoli, 2019). Based on their natural existences, fractures are divided into tectonic, regional, surface-related and contractional fractures, but also, they can be classified experimentally into extension, shear and tensile (Nelson, 2001). Open fractures increase the permeability of the hydrocarbon reservoirs; while, mineral-filled fractures may produce compartmentalization as they act as fluid barrier layers (e.g., Massaro et al., 2018). Even though all fractures are secondary in origin, they may be affected by lithologic characteristics and sedimentary facies (e.g., Korneva et al., 2018; Michie, 2015). Although fractures are very important in rising the permeability of the reservoirs, they are ignored in many reservoir studies. This is due to the complication in the interaction between fractures, matrix porosity and permeability and the overall deficiency of quantitative data covering fractures

(Nelson, 2001). In carbonates reservoirs, the value of cementation exponent “ m ” of Archie model (Archie, 1942) differs according to the type of porosity. In limestone of intergranular porosity, “ m ” equals two whereas in fractured porosity, “ m ” is less than 2, and for the vuggy porosity, “ m ” is larger than 2 (Asquith, 1985). For example, by applying m equal or exceeds two (i.e., $m = > 2$) in fractured carbonate reservoirs, a major error will be caused in the calculated values of “ S_w ”. Consequently, this mistake leads to the hydrocarbon zones which can be easily wasted as they appear as water zones. Also, if fractures are plane in nature, “ m ” can be as low as 1.0, while, if fractures are not plane, “ m ” is between 2.0 and 1.0 (Aguilera, 1980; Ransom, 1984).

In Egypt, the carbonate reservoirs represent a large portion of the remaining oil and gas reserves. Accordingly, this chapter aims to summarize the potential of the hydrocarbon-bearing carbonate rocks (source rocks and reservoirs) in different sedimentary basins in Egypt. The carbonate rock units are located in different three provenances; northern Western Desert, Gulf of Suez Basin and the recently explored in the offshore Nile Delta Basin (Fig. 1).

2 Western Desert

The petroleum potential in northern Western Desert is occurring preliminary within the thick Mesozoic-Cenozoic section. The folds related to the Late Cretaceous inversion

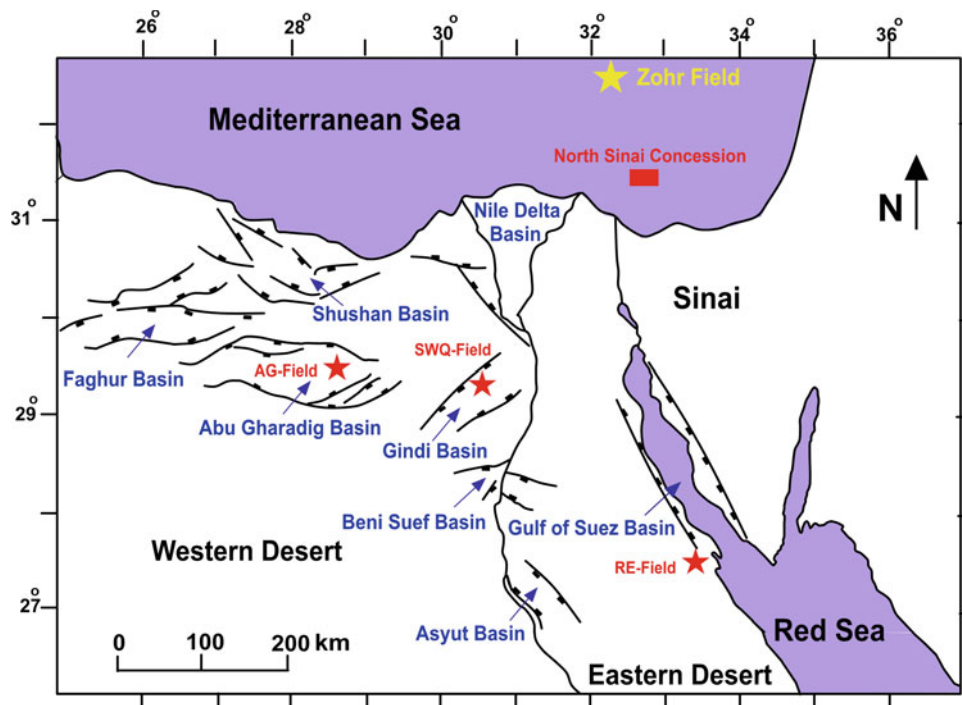


Fig. 1 Regional map representing the locations of different sedimentary basins in Egypt and the sites of several carbonates hydrocarbon fields presented in this chapter as case of studies

Table 1 Summary table displays the hydrocarbon potential for the carbonate rock units in the Western Desert Basins

Rock unit	Lithology	Age	Hydrocarbon potentiality		Fields examples	References examples
			Source rock	Reservoir		
Apollonia formation	Chalky limestone	Late Paleocene–middle Eocene	√	√	BED–JDT	Elmahdy et al. (2020)–Maky & Saad (2009)–Salah et al. (2016a, 2016b)–El-Bendary et al. (2016)–Sousa & Badri (1996)
Abu Roash D member	Limestone	Turonian–Coniacian		√	SW Qarun–Abu Gharadig	Sestini (1995)–Sarhan et al. (2017)
Abu Roash F member	Limestone		√		SW Qarun	Lüning et al. (2004)–Labib (1985)–Sarhan & Basal (2020)
Alamein formation	Dolomite	Aptian		√	Alamein–Razzak–Yidma	Abdel-Fattah et al. (2015)–El Shaarawy (1994)
Masajid formation	Limestone	Late Jurassic	√		Different fields in the western desert basins	Ramadan et al. (2014)–Peters (1986)

tectonic plus the tilted fault blocks of the Jurassic-Cretaceous rifting phase are the chief structural traps at northern Western Desert; although, numerous stratigraphic and combination traps are yet to be explored (Moustafa, 2008). The Mesozoic-Cenozoic megasequence in northern Western Desert classified into four major cycles each one completed by a marine transgressive phase (Sultan and Hahm, 1988) and contains alternations between siliciclastics and carbonate rock-units.

The carbonate rock units which have hydrocarbon potential in the Western Desert basins include as follows; the Late Jurassic Masjid Formation; the Aptian Alamein Dolomite, the late Cenomanian–Turonian Abu Roash Formation and the Eocene Apollonia Formation (Table 1).

2.1 Masajid Formation

The Late Jurassic Masajid Formation is composed of dense limestone section with no clastic intercalations reflecting the prevailed open marine nature during its deposition. It is variable in thickness due to the paleotopography and the tectonic activity during the Late Jurassic time (Ramadan et al., 2014). The total organic carbon content (TOC) of Masajid Formation ranges between 0.60 and 1.02 wt% (Ramadan et al., 2014) indicating that the organic richness for this formation is fair to good (Peters, 1986).

The Masajid limestones entered the initial stage of petroleum generation during the Early Cretaceous (90 MYBP) and reached the oil window through the Late Cretaceous (75 MYBP) to Oligocene time (35 MYBP), while it entered the gas window in the Eocene age (40 MYBP) till the present time (Ramadan et al., 2014).

2.2 Alamein Dolomite

The Aptian Alamein Dolomite has a prevalent lateral extension over most of the northern Western Desert. It is considered one of the important oil reservoirs in different fields such as Alamein, Razzak and Yidma fields (Abdel-Fattah et al., 2015).

The Alamein Dolomite reservoir in Razzak oil field was initially discovered in 1972 (El Shaarawy et al., 1992). The first exploratory well (RZK-1) was drilled to examine Alamein Dolomite high structure (El Shaarawy, 1994). This well produced from seven different oil-bearing zones within the Alamein Dolomite by perforating an interval varies between 7652 and 7704 ft. The cumulative oil production from this well reached 4.95 million barrels of oil in 1983, but after performing 3D seismic survey in 2004, new reservoir zones within Alamein Dolomite have been explored in north Razzak area (Abdel-Fattah et al., 2015).

On seismic profiles, Alamein Dolomite horizon is very clear and displaying strong, continuous and high amplitude seismic reflector due to the high contrast of the acoustic impedance between the dolomite and the overlain clastics. Usually, the top of Alamein Dolomite on seismic data picked and interpreted to show the development of structural elements affected the Cretaceous rocks in northern West Desert basins (e.g., Abdel-Fattah et al., 2015).

The trapped hydrocarbon within Alamein Dolomite reservoir usually migrated from the older rocks beneath and sealed by the overlying impermeable shales of Dahab Formation. The oil-producing horizons of Alamein Dolomite are restricted either in the topmost part of four-way closures where the extreme fractures occur or in three-way dip closures sealed by fault (Abdel-Fattah et al., 2015).

2.3 Abu Roash Formation

Abu Roash Formation represents the Turonian-Coniacian time span, and it superimposes the Cenomanian Bahariya Formation and underlies the Senonian Khoman Formation in Western Desert. It is distinguished into seven different members, (*A, B, C, D, E, F* and *G*) (EGPC, 1992). *B, D* and *F* are mainly carbonate members, where *A, C* and *E* are mainly clastic units.

Generally, Abu Roash Formation was deposited through shallow marine settings within high fluctuating sea levels (Sarhan, 2017a). The carbonate members were deposited in moderately high relative sea-level episodes; however, the clastic members (*C, E* and *G*) were deposited throughout comparatively low relative sea-level intervals (RRI, 1985; EGPC, 1992). Commonly, the clastic members of Abu Roash Formation are potential hydrocarbon reservoirs at different sedimentary basins in western Desert (El Gezeery & O' Connor, 1975). Moreover, Abu Roash *D* Member is also an oil-bearing reservoir in the Western Desert basins such as Abu Gharadig Basin (Sestini, 1995) and Gindi Basin (Sarhan et al., 2017).

The abundance of the normal faults (extensional regime) affected the entire limestone of Abu Roash *D* Member within Abu Gharadig Field (AG-Field) within Abu Gharadig Basin (Sarhan & Collier, 2018; Sarhan, 2017b) as shown in Figs. 2 and 3 increases the possibility of forming fractures, which may retain hydrocarbon and become suitable hydrocarbon

reservoirs. Also, the seismic explanation and the created structure map for the top of Abu Roash *D* Member in SW Qarun-Field show NE-SW anticline plunges toward NE and bounded by NE-SW reverse faults (Figs. 4 and 5). This anticline forms a distinctive structural closure for being suitable oil reservoir in the fractured limestones of Abu Roash *D* Member within Gindi Basin (Sarhan et al., 2017). This folding formed by the Late Cretaceous tectonic inversion ensuing the NW movement of the African Plate relative to Laurasian Plate (Moustafa, 2008). Moreover, the mud log description (Fig. 6) in addition to the well logging interpretation for the limestone of Abu Roash *D* Member in SW Qarun-Field evidenced the existence of fractures with relatively high porosity and low water saturation (Fig. 7) reflecting the high potential of these fractured limestone for being hydrocarbon reservoir within Gindi Basin (Sarhan et al., 2017).

Abu Roash *F* Member is the greatest potential source rock with total organic carbon content (TOC) which ranges between 1.5 and 6% (Labib, 1985; Lüning et al, 2004). In Southwest Qarun-Field (SWQ-Field) at Gindi Basin, Abu Roash *F* Member represents the maximum promising source rock in the whole members of Abu Roash Formation with calculated TOC content which ranges from 1.5 to 3.2% TOC (Fig. 8) indicating good to very good source rock (Sarhan & Basal, 2020). The calculated S2 values (which represents the amount of the released hydrocarbon from samples during pyrolysis process) for the carbonates of Abu Roash

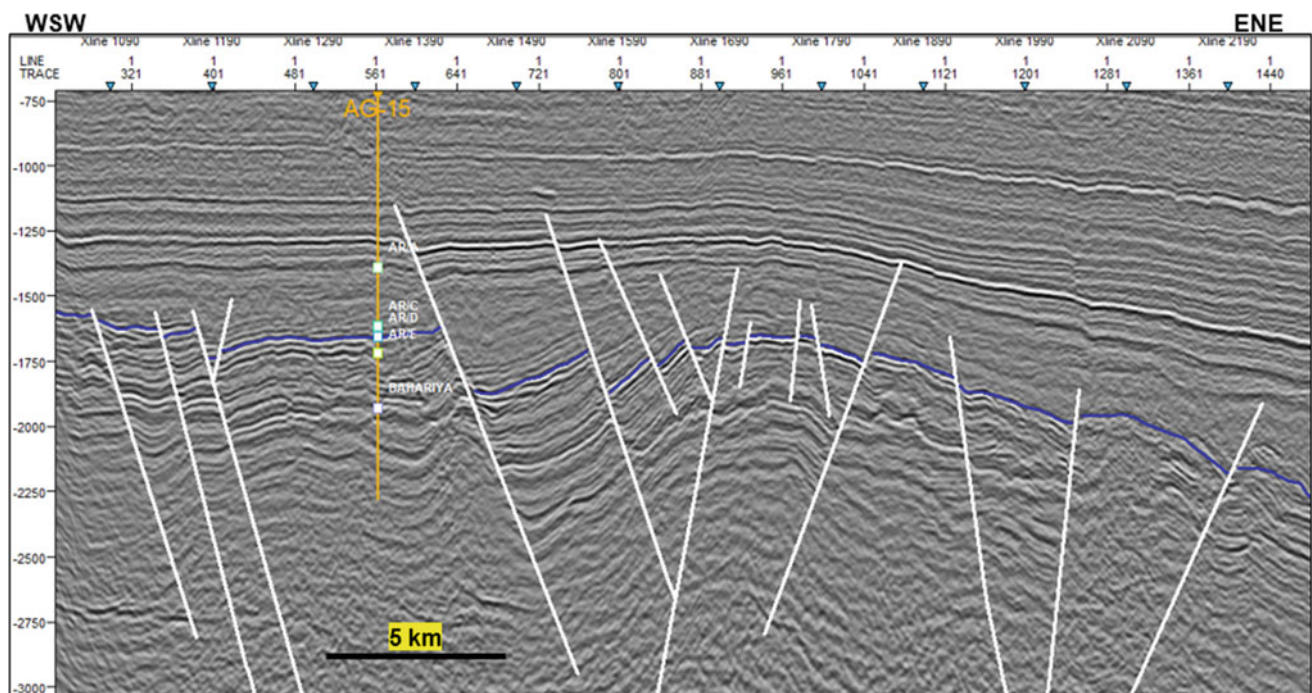


Fig. 2 Interpreted seismic line no. 5240 within Abu Gharadig Field (after Sarhan, 2021a) shows frequent normal faults (extensional regime) intersect Abu Roash *D* Member which increase the possibility of forming fractures within the Abu Roash *D* limestones

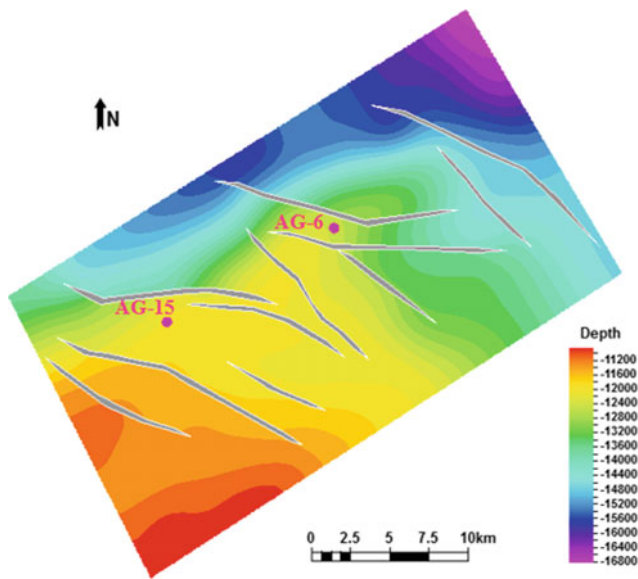


Fig. 3 Structure contour map (in depth unit) for the top of Abu Roash D Member in Abu Gharadig Field (edited after Sarhan, 2021a) displays the ENE-WSW asymmetrical anticline that plunges to NE and its fragmentation by abundant NW-SE normal faults indicating the effect of the Late Cretaceous dextral wrench tectonic in Abu Gharadig Basin

F Member in SWQ-Field are high and varying from 7.63 to 18.66 mg HC/G (Sarhan & Basal, 2020).

2.4 Apollonia Formation

Apollonia Formation corresponds the Late Paleocene to Middle Eocene age and overlain by the shale of the Oligocene Dabaa Formation and underlain by the chalky limestone of the Late Cretaceous Khoman Formation (Schlumberger, 1984, 1995). It has been subdivided into four units; A, B, C and D members but the most porous gas-bearing zones lie within A and C members (Elmahdy et al., 2020). Apollonia Formation is composed mainly of microcrystalline pelagic chalk with abundant planktonic foraminifera and intercalated with terrigenous clay. The pelagic chalk is subdivided based on the clay percentage into four different facies; clean chalk, slightly argillaceous chalk, argillaceous chalk and marl (Elmahdy et al., 2020).

The of Apollonia carbonates are characterized by high porosity (around 30%) and low permeability (less than 1 mD) (Elmahdy et al., 2018) with good live-source rock and low formation pressure (Maky & Saad, 2009; Salah et al., 2016a, 2016b). Accordingly, this chalk is an unconventional gas reservoir requiring different techniques such as hydraulic fracturing plus horizontal drilling to release the excessive amount of the entrapped hydrocarbon within this formation (Elmahdy et al., 2020; Salah et al., 2016a, 2016b).

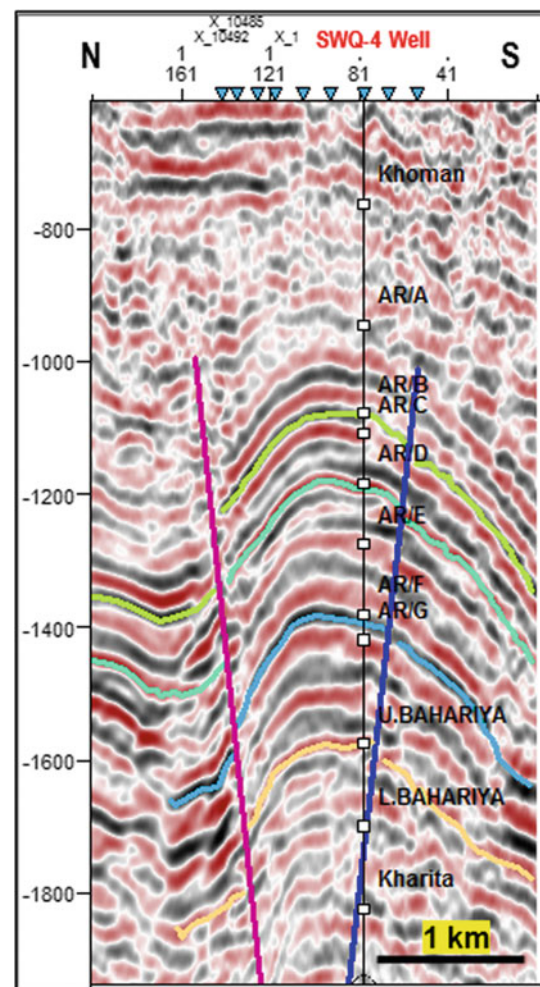


Fig. 4 Interpreted seismic line no. 4766 within the Gindi Basin showing its central anticline bounded by two reverse faults (edited after Sarhan & Collier, 2018)

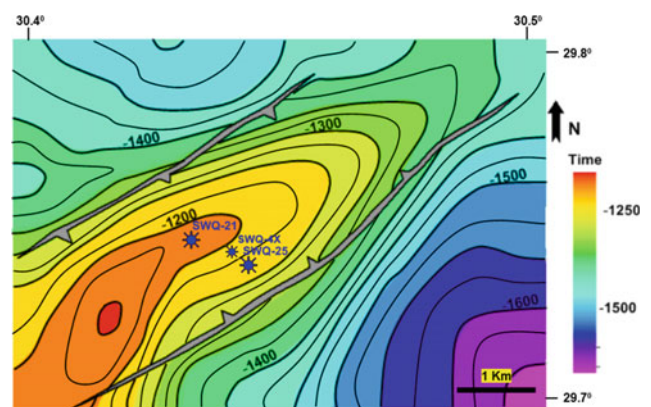


Fig. 5 Structure contour maps (in time unit) for the top of Abu Roash D Member in SW Qarun-Field in Gindi Basin characterizing the NE-SW anticline plunges toward NE bounded by two NE-SW reverse faults (modified after Sarhan & Collier, 2018)

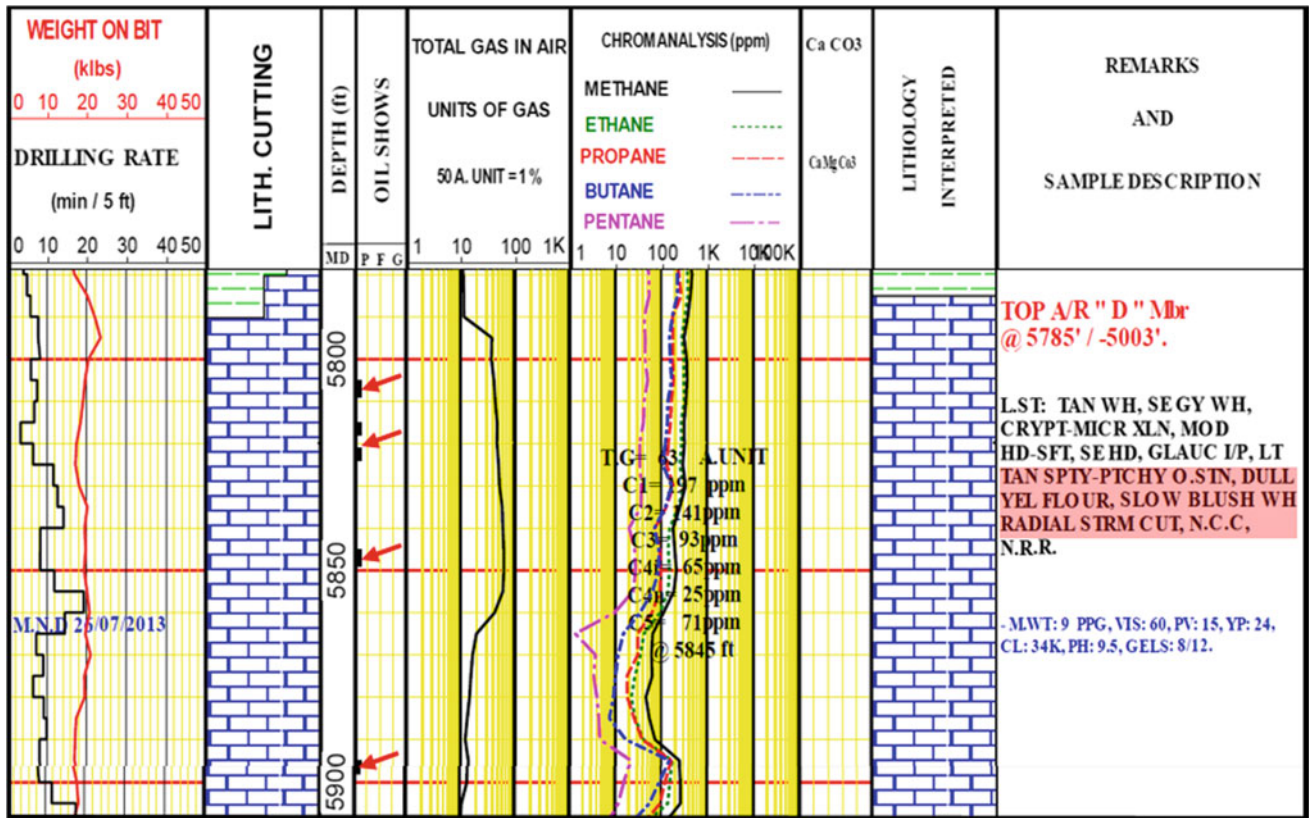


Fig. 6 Mud log of SWQ-21 well in Gindi Basin (modified after Sarhan et al., 2017) shows the topmost part of Abu Roash D limestone. Note the high value of total gas content with 97 ppm methane, 41 ppm ethane, 93 ppm propane, 65 ppm butane, 25 ppm pentane and 71 ppm hexane. The red rectangle in the lithologic description track highlights the presence of tannish (TAN), spotty (SPTY) and pachy (PTCHY) oil stains (O.STN) with dull (DULL) yellow (YEL) fluorescence (FLOUR) and slow bluish (BLUSH) with (WH) radial stream (STRM) cut. The red arrows display the existence of oil shows opposite the uppermost carbonate interval of Abu Roash D Member. Note the high drilling rate for the uppermost interval (6 min/5 ft) reflecting the presence of fractures rather than massive or tight limestone

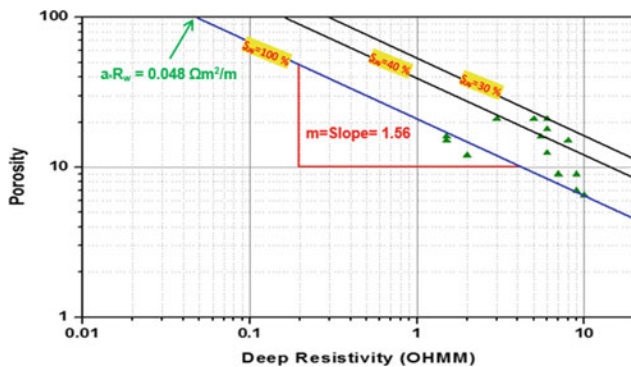


Fig. 7 Pickett cross plot for Abu Roash D reservoir in SWQ-21 well (redrawn after Sarhan et al., 2017). Note that: **a** $m < 2$ ($= 1.56$) revealing the occurrence of fractures; **b** points plotted between Sw lines; 30 and 40% represent the oil zone within Abu Roash D limestone

The first successful well in Apollonia Formation was drilled in 2007 by Shell (Elmahdy et al., 2018), and many fields in Abu Gharadig Basin such as BED and JDT are targeting the shallow gas in the chalk of the Apollonia reservoir, though most of the production fields in this basin concerns

with the deeper targets including; Cretaceous, Jurassic and Paleozoic hydrocarbon zones (Elmahdy et al., 2020).

The chalk of the Apollonia reservoir in Abu Gharadig Basin is described as a tight reservoir (Meckel & Thomason, 2008) as it has a vertical permeability fluctuating from 0.01 to 0.13 mD and horizontal permeability range from 0.03 to 1.1 mD. While, the porosity of this chalk ranges from 10 to 40% (Elmahdy et al., 2020). The application of foam-fracturing technique in Apollonia reservoir in the BED field at Abu Gharadig Basin improved the rate of hydrocarbon production 40 times greater than the normal production (El-Bendary et al., 2016). Therefore, the Apollonia chalk requires attention from petroleum exploration companies (Sousa & Badri, 1996).

3 Gulf of Suez Basin

The Gulf of Suez Basin is the most prospective and prolific oil province in Egypt. It is an intercontinental rift extending northward from Hurghada city in the south for about

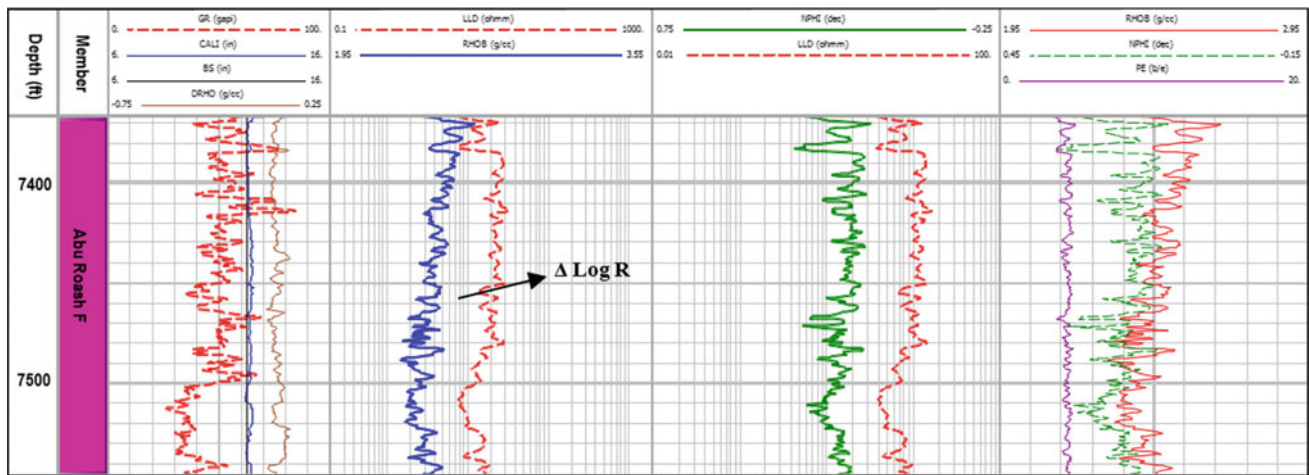


Fig. 8 Well log suite displays the resistivity-porosity logs overlay technique (Passey et al., 1990) for Abu Roash *F* carbonate in SWQ-25 well (edited after Sarhan & Basal, 2020). Note that: **a** the separation between porosity logs (density log “RHOB”; neutron log “NPHI”) overlays the deep resistivity log “LLD” reflects that the limestone of Abu Roash *F* Member is an organic-rich interval due to the existence of organic matter lead to low values for both density and velocity, whereas the resistivity log characterized by high values because of the presence of organic matter. **b** The wide separation between the resistivity-porosity logs ($\Delta \log R$) indicates the high degree of thermal maturity for the organic matter in Abu Roash *F* carbonate

325 km (El Nady et al., 2016). Its rifting was initiated in the Miocene age, both post-rift and pre-rift sequences hold potential source rocks and hydrocarbon reservoirs (EGPC, 1996; Shaheen & Shehab, 1984; Atta et al., 2002). To the west of Gulf of Suez Basin (Southern Galala plateaus), the Late Cretaceous carbonate platform-derived slope sediments intercalated with basinal chalk and calcareous shale farther south. However, during the Early Tertiary, carbonates were deposited within platform, slope and basin settings. The facies architecture of this platform–slope–basin transition reflects the evolution from a rimmed shelf (in the Late Cretaceous) to a distal steepened ramp (within the uppermost Cretaceous to Paleocene) and finally to a homoclinal ramp (during the Early Eocene age) (Kuss et al., 2000).

The potential pre-Miocene carbonates source rocks within the Gulf of Suez Basin includes the Late Senonian Brown Limestone in addition to the Eocene Thebes Formation (Table 2). These formations also represent vertical seals above the Cretaceous sandstone reservoirs. However, the carbonate reservoirs within the Gulf of Suez (Table 2) can be classified into pre-rift reservoirs, such as the fractured limestone of Eocene Thebes Formation; and syn-rift reservoirs, such as the Miocene carbonates of Nukhul Formation, Rudeis Formation, Kareem Formation, Belayim Formation and Ras Gharib Formation which usually sealed by Miocene evaporites (Alsharhan, 2003). These Miocene carbonates are also form some proven stratigraphic traps in the Gulf of Suez region such as in Ras El Bahar discovery, where the porous carbonate wedge is sealed laterally and vertically by dense carbonate (Alsharhan, 2003).

3.1 Brown Limestone

The Brown Limestone Formation represents the Late Senonian age which was deposited during the Tethyan transgression across the north-eastern portion of Africa (Alsharhan, 2003). It represents the primary and richest source rocks in the central and northern parts of the Gulf of Suez (Alsharhan & Salah, 1994, 1995; Rohrbach, 1982). The carbonate of this formation has average TOC of 3.5% and exhibits high hydrogen index (HI) with low oxygen index (OI) values of type I and type II kerogen.

The generated oil from the Brown Limestone Formation was formed within strong reducing marine conditions and characterized by low API gravity and high sulfur content such as in the oil fields of October, Ras Budran, Abu Rudeis, Belayim Marine and Belayim Land (Alsharhan, 2003).

3.2 Thebes Formation

Generally, the Eocene rocks in the Gulf of Suez Basin play a critical role in the development and evolution of the petroleum system, where they are representing self-source rocks or self-reservoirs or combination in several areas within the basin (Radwan, et al., 2020).

The entire carbonate of Thebes Formation was deposited throughout the Tethyan transgression over the NE of Africa like the Brown Limestone. It also represents a potential source rock with TOC equals 3.2% of type I/II kerogens, but the generated hydrocarbon has low API gravity, high sulfur content, high HI and low OI values (Alsharhan, 2003).

Table 2 Summary table shows the hydrocarbon potential for the carbonate rock units in the Gulf of Suez Basin

Rock unit	Lithology	Age	Hydrocarbon potentiality		Fields examples	References examples
			Source rock	Reservoir		
Ras Gharib formation	Limestone-dolomitic limestone	Miocene		√	Different fields in the Gulf of Suez basin	Alsharhan (2003)
Belayim formation	Reefal Limestone			√	Esh El Mellaha–Ras Fanar–Hareed–Felefel	Alsharhan (2003)
Kareem formation	Limestone			√	Felefel	Alsharhan (2003)
Rudeis formation	Limestone and Dolostone			√	Rabeh East	Sarhan (2020)–Sallam et al. (2019a, 2019b)
Nukhul formation	Reefal Limestone			√	Kareem–Al Ayun–Zeit Bay	Alsharhan (2003)
Thebes formation	Limestone	Eocene	√	√	Asal–Sudr–Ras Matarma–Kareem–Bakr–West Bakr–Issaran–Shoab Ali–Rahmi–Rabeh East	Radwan et al. (2020)–Alsharhan (2003)–Sarhan (2021b)
Brown limestone formation	Limestone	Late Senonian	√		October–Ras Budran–Abu Rudeis–Belayim Marine–Belayim Land	Rohrback (1982)–Alsharhan & Salah (1994, 1995)–Alsharhan (2003)

The fractured limestones of the Thebes Formation contribute about 1.1% of oil production in the Gulf of Suez provenance with 13% average porosity and net pay thickness of 15–17 m. It produces oil from many fields such as Asal, Sudr, Ras Matarma, Kareem, Bakr, West Bakr, Issaran, Shoab Ali and Rahmi fields (Alsharhan, 2003).

The thick Eocene carbonate of Thebes Formation in October oil field within the Gulf of Suez region (recently named Radwany Formation) has unique multiscale characterization as unconventional (tight carbonate reservoir) and conventional hydrocarbon resource in its basal part (Radwan et al., 2021). The pore system in these carbonates varies between mesopores and macropores and displays a combination of diagenetic and depositional processes with different porosity types including; fractures, inter-particles, intra-particles and moldic porosity (Radwan et al., 2021).

3.3 Nukhul Formation

The reefal limestone of Nukhul Formation yields oil from few fields in the Gulf of Suez provenance (e.g., Kareem, Al Ayun and Zeit Bay); however, it produces oil and gas from Felefel field. This limestone has porosity equals 16% with net pay thicknesses ranges from 20 to 60 m (Alsharhan, 2003).

3.4 Rudeis Formation

Rudeis Formation deposited under shallow to deep marine settings through Early Miocene age in the Gulf of Suez (Alsharhan & Salah, 1994). It is conformably overlying the Early Miocene Nukhul Formation and underlies the Middle Miocene Kareem Formation (Takasu et al., 1982). The included foraminifers within Rudeis Formation prove a Burdigalian age and represent intertidal lagoon; barrier shoals; and reef complex which reflects down-dip depositional profile of rimmed carbonate shelf under shallow marine conditions (Sallam et al., 2019b). It contains considerable oil and gas reserves, making it one of the most productive hydrocarbon reservoirs within the Gulf of Suez Basin (Sallam et al., 2019a).

The clastic sediments of Rudeis Formation represent hydrocarbon source rocks in the Miocene section in the Gulf of Suez province (El Sharawy & Nabawy, 2018; El Srogy et al., 2002). The sandstone intervals of Rudeis Formation are oil producing in several oil fields such as Sudr, Um El-Yusr, Belayim, Kareem, Feiran, Asl and October fields (Metwalli et al., 1978; Nabawy et al., 2018; Zaid, 2012).

The carbonates of Rudeis Formation are composed principally of vuggy/moldic, fractured/stylolitic, bioclastic coralline-algal dolostone and biogenic limestone. The diagenetic characteristics including cementation, com-

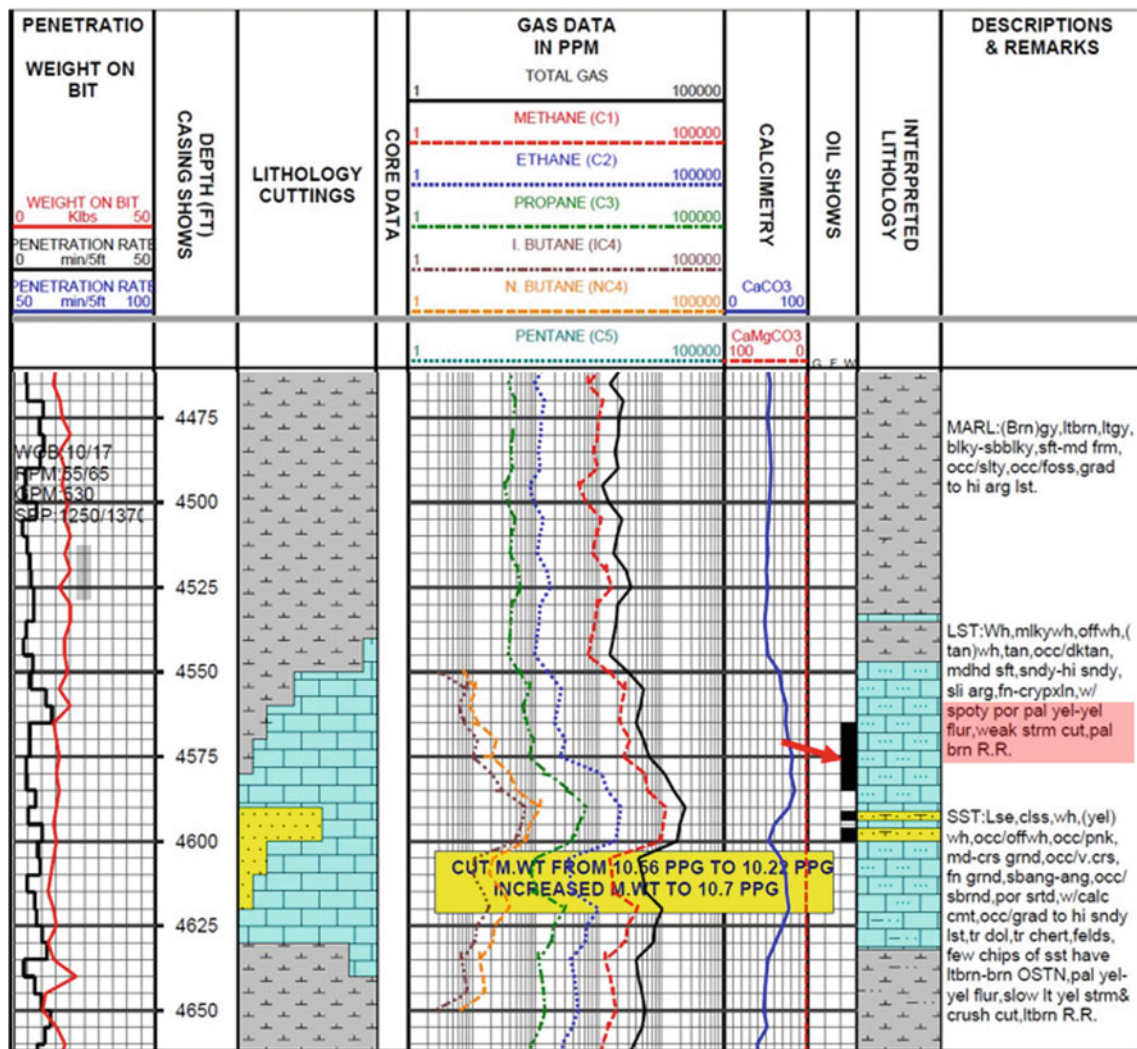


Fig. 9 Mud log of RE-22 well in Rabeh East Field (edited after Sarhan, 2020) displays the gas analysis and the lithology of Rudeis formation. The red arrow refers to the occurrence of oil shows in front of a thick limestone interval between depths 4550 and 4630 ft which based and sealed by marl with high values of gas analysis. The red rectangle in the lithologic explanation track highlights the presence of spotty oil stains with pale yellow to yellow fluorescence with weak stream cut

paction, micritization and anhydritization reduce the reservoir quality, while stylolitization, dissolution and microfracturing improved the production potential (Sallam et al., 2019a). These carbonate beds are also oil producers in the Bahr, Zeit Bay, Asl, Sudr and Matarma fields, whereas, in the Felefel field, it produces both oil and gas, with porosity of about 16%. These beds are principally well developed in the submerged high areas inside the Early Miocene basin, for example, in the North Bahar area (Alsharhan, 2003).

In Rabeh East Field (RE-Field) at the southwestern portion of the Gulf of Suez Basin, an oil-bearing limestone bed of 26 feet thick within Rudeis Formation (Fig. 9) forms a distinctive stratigraphic trap by vertical and lateral facies change to non-permeable marl. This stratigraphic trap extends for about 1.5 km in N-S direction and for 0.75 km

in E-W direction (Fig. 10). This interval displays hydrocarbon saturation above 50% (Fig. 11), shale volume of 21%, total porosity of 20%, effective porosity of 15% and bulk volume of water of 0.07 (Sarhan, 2020).

3.5 Kareem Formation

The carbonates of Kareem Formation display good secondary porosity and represent potential gas reservoir in several fields in the Gulf of Suez Basin such as Felefel Field (Alsharhan, 2003).

3.6 Belayim Formation

The Belayim limestones are more significant than the Belayim sandstones in the Gulf of Suez Basin. These

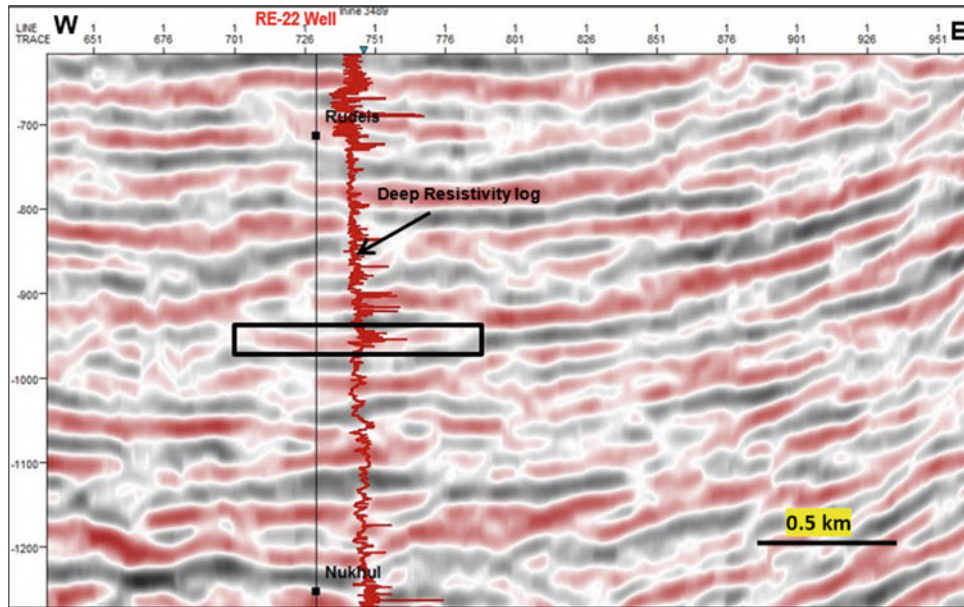


Fig. 10 E-W seismic line no. 789 tied to RE-22 well (edited after Sarhan, 2020) displays the entire seismic reflectors of Rudeis formation in in Rabeah East Field. The continuous seismic reflector outlined by the black rectangle represents a stratigraphic trap for the limestone interval between depths 4550 and 4630 ft in RE-22 well and extending for about 0.75 km. The black arrow displays the high deep resistivity value for the examined reflector approving the presence of hydrocarbon

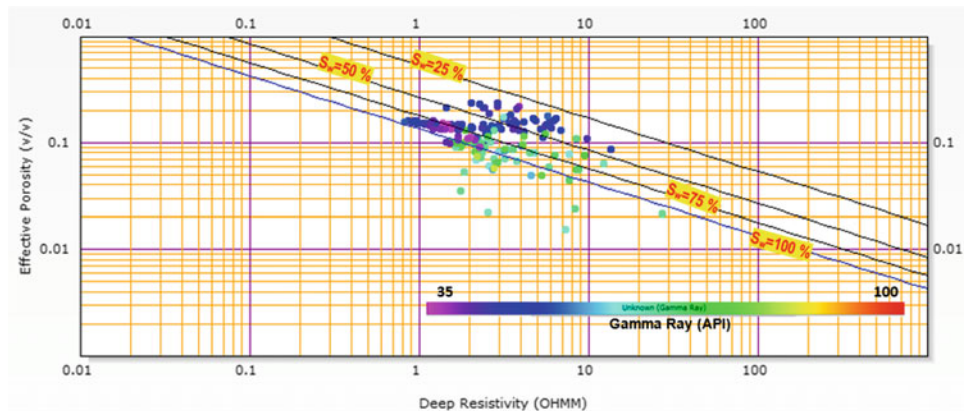


Fig. 11 Pickett cross plot for the limestone interval within Rudeis Formation in RE-22 well (edited after Sarhan, 2020). Note that plotted points situated between S_w lines; 25 and 50% characterize the promising oil-bearing reservoir

carbonates form reefal buildups on fault-controlled high areas and display porosity fluctuating between 10 and 19%. The net pay thickness of these limestone beds is around 9–12 m. These carbonates produce both oil and gas from Esh El Mellaha Field and oil from Ras Fanar Field. However, in Hareed and Felefel fields, yield only gas (Alsharhan, 2003).

3.7 Ras Gharib Formation

The limestone and dolomitic limestone interbeds within the evaporitic successions of Ras Gharib Formation produce oil

in different fields within the Gulf of Suez Basin (Alsharhan, 2003).

4 Offshore Nile Delta Basin

The Nile Delta Basin (NDB) is a huge clastic play province in the East-Mediterranean region. In the last years, numerous big gas fields have been discovered from stratigraphic sandy levels vary from Oligocene to Quaternary. NDB contains a reserve of around 223 trillion cubic feet of natural gas in more than 126 gas fields dispersed in the

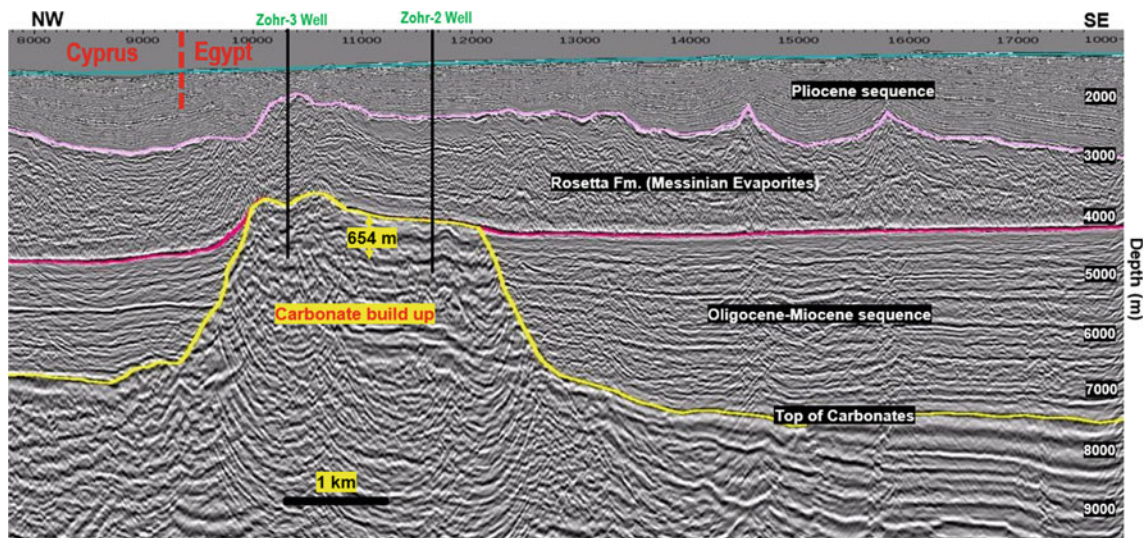


Fig. 12 NW-SE seismic profile (modified after Bertello et al., 2016) displays the giant Zohr prospect in the Shorouk concession close to the Egypt/Cyprus boundary with 654 m of gas column and 30 TCF of estimated gas reserve. Zohr Field is a huge Miocene carbonate buildup sealed by the Messinian evaporites (Rosetta formation) and charged by biogenic gas from Tertiary source rock

Nile Cone (Kirschbaum et al., 2010). These fields assumed to be sourced mainly from thermally mature source rocks corresponding to the Neogene deltaic sedimentary succession as well as the existence of a significant biogenic gas constituent (Vandre et al., 2007). The Messinian Abu Madi sandstones are the chief gas provenance in the onshore and offshore portions of the NDB (e.g., Abu El-Ella, 1990; Sarhan, 2021c). But also, the sandy levels of the Early-Middle Pliocene Kafr El-Sheikh Formation besides the Late Pliocene El-Wastani Formation are positive targets for gas exploration in NDB (Lashin & Mogren, 2012). The presence of thick evaporite deposits beneath the NDB due to the Messinian crisis when the Mediterranean was isolated from the Atlantic ocean and desiccated (Barber, 1981; Harms & Wary, 1990; Sestini, 1989) led to poor seismic imaging for the pre-Messinian section (Dolson et al., 2002).

In 2015, the Italian oil and gas company ENI discovered a giant carbonate buildup (Zohr Field) beneath the dense Messinian evaporites in the Shorouk Concession approximately 190 km north of Port Said City close to the Egypt/Cyprus boundary. Based on regional 2D seismic data interpretation, Zohr Field represents high structural feature in an area of 100 km² at a water depth of 1450 m. Zohr buildup is an incredible biogenic gas column of 654 m (Fig. 12) with 30 TCF of estimated gas in place (Bertello et al., 2016; Esestime et al., 2016). This huge carbonate buildup was deposited during the Early-Middle Miocene times under shallow water conditions confirming the occurrence of a basin locates north of the Nile Delta (Esestime et al., 2016).

The carbonate buildup features may be also found in other places within the offshore part of the Nile Delta Basin beneath the Messinian evaporites. In North Sinai concession, the seismic data shows possible carbonate buildup like those of Zohr Field in the Mesozoic succession (Fig. 13). It exhibits a great similarity and is expected to be new target for hydrocarbon exploration, but it should have the interest to be tested by new deep exploration wells.

5 Conclusions

The current chapter is an attempt to identify and collect different carbonate rock units which may have significant hydrocarbon potential in different sedimentary basins of Egypt. These units were grouped in three major districts: Western Desert, Gulf of Suez Basin and Offshore Nile Delta Basin.

The sedimentary succession of the northern Western Desert contains three carbonate intervals which exhibit hydrocarbon reservoir characteristics. These potential reservoirs are Alamein Formation (Aptian), Abu Roash *D* Member (Late Cretaceous) and Apollonia Formation (Tertiary). However, the main potential carbonate source rocks in the Western Desert include as follows; the Jurassic Masajid Formation, the Late Cretaceous Abu Roash *F* Member and the Apollonia Formation. However, the sedimentary section of the Gulf of Suez Basin comprises five Miocene carbonate reservoirs; Nukhul Formation, Rudeis Formation, Kareem Formation, Belayim Formation and Ras Gharib Formation. However, the limestone of the Eocene Thebes Formation displays source rock and reservoir characteristics. The late

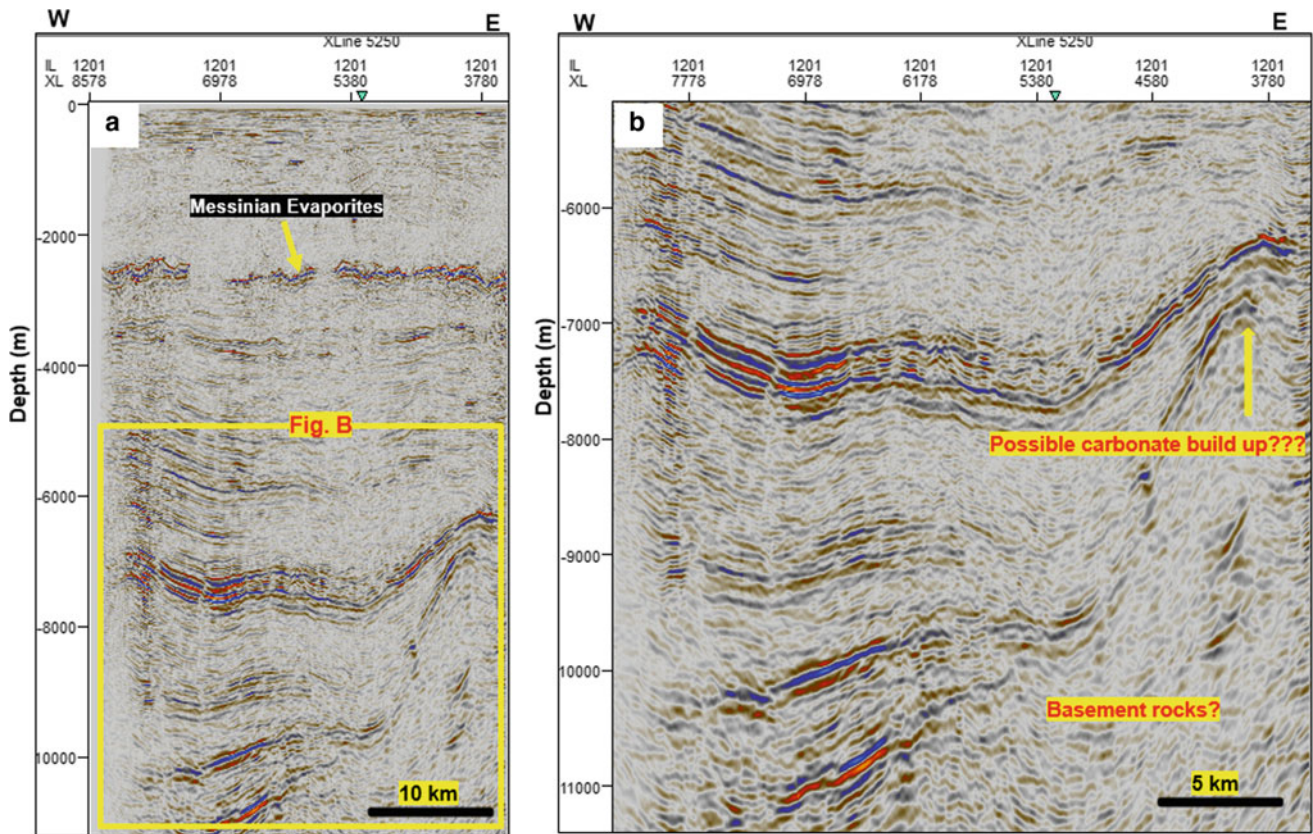


Fig. 13 E-W seismic section in North Sinai concession displays possible hydrocarbon prospect of carbonate buildup similar to those of Zohr Field in the Mesozoic succession, offshore Nile Delta basin

Cretaceous Brown Limestone Formation is also one of the most important carbonate source rock in the Gulf of Suez.

Recently, the offshore Nile Delta Basin contains important exploration in carbonate which builds up beneath the Messinian evaporites such as Zohr Field. These reef builds up may be also explored in the adjacent places in the offshore Nile Delta Basin which will provide extensive reserve replacements in the coming decades.

Discovering the hydrocarbon zones in carbonate succession is a challenge due to the carbonate reservoirs display several forms of primary and secondary porosity (intergranular, intracrystalline, vuggy, moldic and fractured). Also, the pore size in carbonate rocks varies from micro-to mega-pore based on the diagenetic processes plus the depositional environment. Accordingly, it is highly recommended to apply the advanced techniques in seismic acquisition, processing and visualization in addition to running the modern well log suit such as nuclear magnetic resonance (NMR), formation micro-imager (FMI), oil-based micro-imager (OBMI) to improve the identification and evaluation of the carbonate reservoirs.

Acknowledgements I really appreciate the help of the Egyptian General Petroleum Corporation (EGPC), Khalda Petroleum Company, North Sinai Petroleum Company (NOSPCO), Ganoub El-Wadi Petroleum Holding Company and Qarun Petroleum Company for providing the geophysical data presented in this chapter.

References

- Abdel-Fattah, M., Gameel, M., Awad, S., & Ismail, A. (2015). Seismic interpretation of the Aptian Alamein Dolomite in the Razzak Oil Field, Western Desert, Egypt. *Arabian Journal of Geosciences*, 8(7), 4669–4684.
- Abu El-Ella, R. (1990). The Neogene-Quaternary section in the Nile Delta, Egypt; Geology and hydrocarbon potential. *Journal of Petroleum Geology*, 13, 329–340.
- Afife, M. M., Sallam, E. S., & Faris, M. (2017). Integrated petrophysical and sedimentological study of the Middle Miocene Nullipore formation (Ras Fanar Field, Gulf of Suez, Egypt): An approach to volumetric analysis of reservoirs. *Journal of African Earth Sciences*, 134, 526–548.
- Aguilera, R. (1980). *Naturally fractured reservoirs* (p. 703). Petroleum Publishing Company.
- Ali, A., Wagreich, M., & Strasser, M. (2018). Depositional constraints and diagenetic pathways controlling petrophysics of Middle

- Miocene shallow-water carbonate reservoirs (Leitha limestones), Central Paratethys, Austria-Hungary. *Marine and Petroleum Geology*, 91, 586–598.
- Alsharhan, A. S. (2003). Petroleum geology and potential hydrocarbon plays in the Gulf of Suez rift basin, Egypt. *AAPG Bulletin*, 87(1), 143–180.
- Alsharhan, A. S., & Salah, M. G. (1994). Geology and hydrocarbon habitat in a rift setting: Southern Gulf of Suez, Egypt. *Bulletin of Canadian Petroleum Geology*, 42(3), 312–331.
- Alsharhan, A. S., & Salah, M. G. (1995). Geology and hydrocarbon habitat in rift setting: Northern and central Gulf of Suez, Egypt. *Bulletin of Canadian Petroleum Geology*, 43(2), 156–176.
- Anselmetti, F. S., & Eberli, G. P. (1993). Controls on sonic velocity in carbonates. *Pure and Applied Geophysics*, 141(2–4), 287–323.
- Anselmetti, F. S., & Eberli, G. P. (1999). The velocity-deviation log: A tool to predict pore type and permeability trends in carbonate drill holes from sonic and porosity or density logs. *AAPG Bulletin*, 83(3), 450–466.
- Archie, G. E. (1942). The electrical resistivity log as an aid in determining some reservoir characteristics. *Petroleum Technology*, 5, 54–62.
- Asquith, G. B. (1985). *Handbook of log evaluation techniques for carbonate reservoirs. Methods in exploration series, Member 5.* AAPG
- Atta, M. A., Shahin, A. N., Blanchard, D., & David, H. (2002). Petroleum potential of the Gemsa Basin, southern Gulf of Suez, Egypt. In *International petroleum conference and exhibition* (pp. 27–30)
- Barber, P. M. (1981). Messinian subaerial erosion of the Proto-Nile Delta. *Marine Geology*, 44, 253–272.
- Baud, P., Exner, U., Lommatsch, M., Reuschlé, T., & Wong, T. F. (2017). Mechanical behavior, failure mode, and transport properties in a porous carbonate. *Journal of Geophysical Research: Solid Earth*, 122(9), 7363–7387.
- Beigi, M., Jafarian, A., Javanbakht, M., Wanas, H. A., Mattern, F., & Tabatabaei, A. (2017). Facies analysis, diagenesis and sequence stratigraphy of the carbonate-evaporite succession of the Upper Jurassic Surmeh formation: Impacts on reservoir quality (Salman Oil Field, Persian Gulf, Iran). *Journal of African Earth Sciences*, 129, 179–194.
- Bertello, F., Harby, H., & Brandolese, S. (2016). Egypt: Zohr, an outstanding gas discovery in a new deep-water hydrocarbon play. In *8th Mediterranean offshore conference and exhibition* (pp. 1–10).
- Burchette, T. P. (2012). Carbonate rocks and petroleum reservoirs: A geological perspective from the industry. *Geological Society, London, Special Publications*, 370(1), 17–37.
- Cerepi, A., Barde, J. P., & Labat, N. (2003). High-resolution characterization and integrated study of a reservoir formation: The danian carbonate platform in the Aquitaine Basin (France). *Marine and Petroleum Geology*, 20(10), 1161–1183.
- Dolson, J. C., Boucher, P. J., Dodd, T., & Ismail, J. (2002). The petroleum potential of the emerging Mediterranean offshore gas plays, Egypt. *The Oil and Gas Journal*, 100(20), 32–37.
- Eberli, G. P., Baechle, G. T., Anselmetti, F. S., & Incze, M. L. (2003). Factors controlling elastic properties in carbonate sediments and rocks. *The Leading Edge*, 22(7), 654–660.
- EGPC (Egyptian General Petroleum Corporation). (1992). Western Desert, oil and gas fields, a comprehensive overview. In *11th Petroleum exploration and production conference* (pp. 1–431). Egyptian General Petroleum Corporation
- EGPC (Egyptian General Petroleum Corporation). (1996). Gulf of Suez oil fields (A comprehensive overview) (p. 387). EGPC
- Ehrenberg, S. N., & Nadeau, P. H. (2005). Sandstone versus carbonate petroleum reservoirs: A global perspective on porosity-depth and porosity-permeability relationships. *AAPG bulletin*, 89(4), 435–445
- Ehrenberg, S. N., Walderhaug, O., & Bjørlykke, K. (2019). Discussion of “Microfacies, diagenesis and oil emplacement of the Upper Jurassic Arab-D carbonate reservoir in an oil field in central Saudi Arabia (Khurais Complex)” by Rosales et al. (2018). *Marine and Petroleum Geology*, 100, 551–553
- El Gezeery, N. H., & O’ Connor, T. (1975). Cretaceous rock units in the Western Desert, Egypt. In *13th Annual Meeting of Geological Society of Egypt* (p. 2). Geological Society
- El Sharawy, M. S., & Nabawy, B. S. (2018). The role of gamma-ray logs in deciphering geochemical and geological aspects of the Rudeis Formation, Gulf of Suez, Egypt. *Arabian Journal of Geosciences*, 11(10), 242.
- El Nady, M. M., Mohamed, N. S., & Shahin, A. N. (2016). Source-rock potential of Miocene-Paleozoic sediments in GH-376 oilfield, South Gulf of Suez, Egypt. *Energy Sources, Part a: Recovery, Utilization, and Environmental Effects*, 38(1), 100–109.
- El Shaarawy, O. A., Abdel Aal, A., Papazis, P. (1992). Tectonic setting of the Razzak oil field, north Western Desert of Egypt. In *EGPC 11th Petroleum exploration and production conference* (pp. 1–20)
- El Shaarawy, O. A. (1994). *Zonation of the Bahariya formation and Alamein Dolomite reservoirs in the Razzak oil field, North Western Desert of Egypt*. Paper presented at the second international conference on The Geology of the Arab World, Cairo University (pp 22–26)
- El Srogy, S. A., Helal, I. H., Amer, E. I., & Mohamed, H. A. (2002). Hydrocarbon generation, expulsion and migration in the Geisum and Tawila oil fields-Southern Gulf of Suez. In *International petroleum conference and exhibition* (pp. 1–5)
- El-Bendary, A., Faraga, Y., Magde, M., Moukhtar, A., & Ramadan, H. (2016). Critical success factors identification to develop unconventional high porosity low permeability shallow limestone reservoir of Apollonia formation, Western Desert, Egypt. In *Abu Dhabi international petroleum exhibition and conference*. Society of Petroleum Engineers
- Elmahdy, M., Farag, A. E., Tarabees, E., & Bakr, A. (2018). Pore pressure prediction in unconventional carbonate reservoir. In *SPE Kingdom of Saudi Arabia annual technical symposium and exhibition*. Society of Petroleum Engineers
- Elmahdy, M., Tarabees, E., Farag, A. E., & Bakr, A. (2020). An integrated structural and stratigraphic characterization of the Apollonia carbonate reservoir, Abu El-Gharadig Basin, Western Desert, Egypt. *Journal of Natural Gas Science and Engineering*, 103317
- Esestime, P., Hewitt, A., & Hodgson, N. (2016). Zohr—a newborn carbonate play in the Levantine Basin, East-Mediterranean. *First Break*, 34(2)
- Euzen, T., & Power, M. R. (2012). Well log cluster analysis and electrofacies classification: a probabilistic approach for integrating log with mineralogical data. In *2012 CSPG CSEG CWLS Convention*
- Harbaugh, J. W. (1967). Carbonate reservoir rocks. In G. V. Chilingar, H. J. Bissell, & R. W. Fairbridge (Eds.), *Carbonate rocks, A: Origin, occurrence and classification* (pp. 349–397). Elsevier.
- Harms, J. C., & Wary, J. L. (1990). Nile Delta. In: R. Said (Ed.), *The Geology of Egypt* (pp. 329–344). Balkema
- Heap, M., Reuschlé, T., Baud, P., Renard, F., & Iezzi, G. (2018). The permeability of stylolite-bearing limestone. *Journal of Structural Geology*, 116, 81–93.
- Hollis, C., Vahrenkamp, V., Tull, S., Mookerjee, A., Taberner, C., & Huang, Y. (2010). Pore system characterisation in heterogeneous carbonates: An alternative approach to widely-used rock-typing methodologies. *Marine and Petroleum Geology*, 27(4), 772–793.
- Hollis, C., Lawrence, D. A., de Perière, M. D., & Al Darmaki, F. (2017a). Controls on porosity preservation within a Jurassic oolitic reservoir complex, UAE. *Marine and Petroleum Geology*, 88, 888–906.

- Hollis, C., Lawrence, D., Darmaki, F. A., Perriere, M. D. D., Foote, A., & Kostic, B. (2017b). Origin of complex carbonate pore systems and associated reservoir quality variations: An example from the Arab formation upper Jurassic, onshore United Arab Emirates. In *Abu Dhabi international petroleum exhibition and conference*. Society of Petroleum Engineers
- Karimpouli, S., Hassani, H., Nabi-Bidhendi, M., Khoshdel, H., & Malehmir, A. (2013). Application of probabilistic facies prediction and estimation of rock physics parameters in a carbonate reservoir from Iran. *Journal of Geophysics and Engineering*, 10(1), 015008.
- Kirschbaum, M. A., Schenk, C. J., Charpentier, R. R., Klett, T. R., Brownfield, M. E., Pitman, J. K., Cook, T. A., & Tennyson, M. E. (2010). Assessment of undiscovered oil and gas resources of the Nile Delta Basin Province, Eastern Mediterranean (No. 2010-3027). US Geological Survey
- Korneva, I., Bastesen, E., Corlett, H., Eker, A., Hirani, J., Hollis, C., Gawthorpe, R. L., Rotevatn, A., & Taylor, R. (2018). The effects of dolomitization on petrophysical properties and fracture distribution within rift-related carbonates (Hammam Faraun Fault Block, Suez Rift, Egypt). *Journal of Structural Geology*, 108, 108–120.
- Kuss, J., Scheibner, C., & Gietl, R. (2000). Carbonate platform to basin transition along an upper Cretaceous to lower Tertiary Syrian Arc uplift, Galala Plateaus, Eastern Desert of Egypt. *Georabia*, 5(3), 405–424.
- Labib, M. (1985). Contributions to the geology of upper Cretaceous with special emphasis on Turonian–Senonian sedimentation patterns and hydrocarbon potentialities in the Abu Gharadig area, North Western Desert, Egypt. Unpublished Dissertation thesis, Geology Department, Cairo University (p. 189)
- Lashin, A., & Mogren, S. (2012). Analysis of well log and pressure data of the gas-bearing sand reservoirs of Kafr El-Sheikh formation: Case study from the off-shore Nile Delta-Egypt. *International Journal of the Physical Sciences*, 7(35), 5353–5366.
- Liu, Y., & Wang, Y. (2017). Seismic characterization of a carbonate reservoir in Tarim Basin. *Geophysics*, 82(5), B177–B188.
- Lüning, S., Kolonic, S., Belhadj, E. M., Belhadj, Z., Cota, L., Barić, G., & Wagner, T. (2004). Integrated depositional model for the Cenomanian-Turonian organic-rich strata in North Africa. *Earth-Science Reviews*, 64(1), 51–117.
- Maky, A. F., & Saad, S. A. (2009). Kerogen composition and hydrocarbon potentiality of some cretaceous to middle Eocene rock units and their depositional environments at Abu El-Gharadig basin Western Desert, Egypt. *Australian Journal of Basic and Applied Sciences*, 3(4), 4675–4692.
- Massaro, L., Corradetti, A., Vinci, F., Tavani, S., Iannace, A., Parente, M., & Mazzoli, S. (2018). Multiscale fracture analysis in a reservoir-scale carbonate platform exposure (Sorrento Peninsula, Italy): Implications for fluid flow. *Geofluids*
- Meckel, L. D., Thomasson, M. R. (2008). Pervasive tight-gas sandstone reservoirs: an overview. In S. P. Cumella, K. W. Shanley, W. K. Camp (Eds.), *Understanding, exploring, and developing tight-gas sands—2005 Vail Hedberg conference: AAPG Hedberg Series* (vol. 3, pp. 13–27)
- Metwalli, M. H., Phillip, G., & Youssef, E. S. A. (1978). El-Morgan oil field as a major fault-blocks reservoir masked by the thick Miocene salt; a clue for deeper reserves of hydrocarbons in Gulf of Suez Petroleum Province, Egypt. *Acta Geologica Polonica*, 28(3), 314–389.
- Michie, E. A. H. (2015). Influence of host lithofacies on fault rock variation in carbonate fault zones: A case study from the Island of Malta. *Journal of Structural Geology*, 76, 61–79.
- Michie, E. A. H., & Haines, T. J. (2016). Variability and heterogeneity of the petrophysical properties of extensional carbonate fault rocks, Malta. *Petroleum Geoscience*, 22(2), 136–152.
- Moustafa, A. R. (2008). Mesozoic-Cenozoic basin evolution in the Northern Western Desert of Egypt. In: M. Salem, A. El-Arnauti, A. Saleh (Eds.), *3rd Symposium on the sedimentary basins of Libya, The geology of East Libya* (vol. 3, pp. 29–46)
- Nabawy, B. S., Rashed, M. A., Mansour, A. S., & Afify, W. S. (2018). Petrophysical and microfacies analysis as a tool for reservoir rock typing and modelling: Rudeis formation, off-shore October Oil Field, Sinai. *Marine and Petroleum Geology*, 97, 260–276.
- Nabawy, B. S., Mansour, A. S., Rashed, M. A., & Afify, W. S. (2020). Implementation of sedimentary facies and diagenesis on the reservoir quality of the Aquitanian-Burdigalian Rudeis formation in the Gulf of Suez, Egypt: A comparative surface and subsurface study. *Geological Journal*, 55(6), 4543–4563.
- Nazari, M. H., Tavakoli, V., Rahimpour-Bonab, H., & Sharifi-Yazdi, M. (2019). Investigation of factors influencing geological heterogeneity in tight gas carbonates, Permian reservoir of the Persian Gulf. *Journal of Petroleum Science and Engineering*, 183, 106341.
- Nelson, R. A. (2001). *Geologic analysis of fractured reservoirs* (2nd ed., p. 352)
- Passey, Q. R., Creaney, S., Kulla, J. B., Moretti, F. J., & Stroud, J. D. (1990). A practical model for organic richness from porosity and resistivity logs. *AAPG Bulletin*, 74(12), 1777–1794.
- Peters, K. E. (1986). Guidelines for evaluating petroleum source rock using programmed pyrolysis. *AAPG Bulletin*, 70(3), 318–329.
- Radwan, A. E., Kassem, A. A., & Kassem, A. (2020). Radwany Formation: A new formation name for the Early-Middle Eocene carbonate sediments of the offshore October oil field, Gulf of Suez: Contribution to the Eocene sediments in Egypt. *Marine and Petroleum Geology*, 116, 104304.
- Radwan, A. E., Trippetta, F., Kassem, A. A., & Kania, M. (2021). Multi-scale characterization of unconventional tight carbonate reservoir: Insights from October oil field, Gulf of Suez rift basin, Egypt. *Journal of Petroleum Science and Engineering*, 197, 107968.
- Ramadan, F. S., El Nady, M. M., Eysa, E. A., & Abdel Wahed, N. M. (2014). Subsurface geology and potential capability of oil generation of some Jurassic and Lower Cretaceous source rocks in North Western Desert, Egypt. *Middle East Journal of Applied Sciences*, 4, 300–317.
- Ransom, P. C. (1984). A contribution toward a better understanding of the modified Archie formation resistivity factor relationship. *The Log Analyst*, 25(02)
- Rashid, F., Glover, P. W. J., Lorinczi, P., Hussein, D., & Lawrence, J. A. (2017). Microstructural controls on reservoir quality in tight oil carbonate reservoir rocks. *Journal of Petroleum Science and Engineering*, 156, 814–826.
- Robertson Research International (RRI) (1985). Further evaluation of the Abu Sennan–Alam El Shawish area, Western Desert, the Arab Republic of Egypt, with emphasis on stratigraphic trapping potential
- Rohrback, B. G. (1982). Crude oil geochemistry of the Gulf of Suez: 6th Egyptian General Petroleum Corporation. In *Petroleum exploration and production conference* (vol. 1, pp 212–224)
- Salah, M. K., El Ghandour, M. M., & Abdel-Hameed, A. M. T. (2016a). Effect of diagenesis on the petrophysical properties of the Miocene rocks at the Qattara Depression, north Western Desert, Egypt. *Arabian Journal of Geosciences*, 9(5), 329.
- Salah, M., Orr, D., Meguid, A. A., Crane, B., & Squires, S. (2016b). Multistage horizontal hydraulic fracture optimization through an integrated design and workflow in Apollonia tight chalk, Egypt from the laboratory to the field. In *Abu Dhabi international petroleum exhibition and conference*. Society of Petroleum Engineers
- Sallam, E. S., Afife, M. M., Fares, M., van Loon, A. J., & Ruban, D. A. (2019a). Sedimentary facies and diagenesis of the Lower Miocene Rudeis Formation (southwestern offshore margin of the Gulf of Suez, Egypt) and implications for its reservoir quality. *Marine Geology*, 413, 48–70.

- Sallam, E. S., Afife, M. M., Fares, M., van Loon, A. T., & Ruban, D. A. (2019b). Depositional cycles of the lower Miocene Rudeis formation (southwestern offshore margin of the Gulf of Suez, Egypt): Implications for reservoir evaluation. *Marine Geology*, *415*, 105964.
- Sarhan, M. A. (2017a). Seismic-Wireline logs sequence stratigraphic analyses and geologic evolution for the upper Cretaceous succession of Abu Gharadig basin, Egypt. *Journal of African Earth Sciences*, *129*, 469–480.
- Sarhan, M. A. (2017b). Wrench tectonics of Abu Gharadig basin, Western Desert, Egypt: A structural analysis for hydrocarbon prospects. *Arabian Journal of Geosciences*, *10*(18), 399.
- Sarhan, M. A. (2020). Geophysical appraisal and oil potential for Rudeis Formation at West Hurghada area, southern Gulf of Suez: Detection of stratigraphic trap. *Arabian Journal of Geosciences*, *13*(6), 1–9.
- Sarhan, M. A. (2021a). Geophysical appraisal for the sandy levels within Abu Roash C and E members in Abu Gharadig Field, Western Desert, Egypt. *Journal of Petroleum Exploration and Production*, *11*(3), 1101–1122.
- Sarhan, M. A. (2021c). Assessing hydrocarbon prospects in Abu Madi formation using well logging data in El-Qara field, Nile Delta Basin, Egypt. *Journal of Petroleum Exploration and Production Technology*, *11*(6), 2539–2559.
- Sarhan, M. A., & Basal, A. M. K. (2020). Total organic carbon content deduced from resistivity-porosity logs overlay: A case study of Abu Roash formation, Southwest Qarun field, Gindi Basin, Egypt. *NRIAG Journal of Astronomy and Geophysics*, *9*(1), 190–205.
- Sarhan, M. A., & Collier, R. E. L. (2018). Distinguishing rift-related from inversion-related anticlines: Observations from the Abu Gharadig and Gindi Basins, Western Desert, Egypt. *Journal of African Earth Sciences*, *145*(2018), 234–245.
- Sarhan, M. A., Basal, A. M. K., & Ibrahim, I. M. (2017). Integration of seismic interpretation and well logging analysis of Abu Roash D Member, Gindi Basin, Egypt: Implication for detecting and evaluating fractured carbonate reservoirs. *Journal of African Earth Sciences*, *135*, 1–13.
- Sarhan, M. A. (2021b). Petrophysical characterization for Thebes and Mutulla reservoirs in Rabeh East Field, Gulf of Suez Basin, via well logging interpretation. *Journal of Petroleum Exploration and Production Technology*, 1–14
- Schlumberger (1984). *Well evaluation conference* (pp. 1–64). Geology of Egypt
- Schlumberger (1995). *Well evaluation conference* (pp. 58–66). Schlumberger Technical Editing Services
- Sequero, C., Aurell, M., & Bádenas, B. (2019). Sedimentary evolution of a shallow carbonate ramp (Kimmeridgian, NE Spain): Unravelling controlling factors for facies heterogeneities at reservoir scale. *Marine and Petroleum Geology*, *109*, 145–174.
- Sestini, G. (1989). Nile Delta: A review of depositional environments and geological history. *Geological Society, London, Special Publications*, *41*(1), 99–127.
- Sestini, G. (1995). Egypt. In H. Kulke (Ed.), *Regional petroleum geology of the world, part II: Africa, America, Australia and Antarctica* (vol. Beiträge zur regionalen Geologie der Erde, Gebrüder Bornträger Verlagsbuchhandlung, pp. 66–87)
- Sha, F., Xiao, L., Mao, Z., & Jia, C. (2019). Petrophysical characterization and fractal analysis of carbonate reservoirs of the eastern margin of the pre-Caspian basin. *Energies*, *12*(1), 78.
- Shaheen, A. N., & Shehab, M. (1984). Petroleum generation, migration and occurrence in the Gulf of Suez offshore, South Sinai: 7th Egyptian General Petroleum Corporation. In *Petroleum exploration and production conference* (vol. 1, pp. 126–152)
- Sousa, S. M., & Badri, M. A. (1996). Evaluation of the Apollonia carbonate reservoir in the Western Desert, Egypt, using surface and borehole geophysical methods. In *SEG technical program expanded abstracts 1996* (pp. 1830–1833). Society of Exploration Geophysicists
- Sultan, N., & Halim, M. A. (1988). Tectonic framework of northern Western Desert, Egypt and its effect on hydrocarbon accumulations. In *Proceedings of the EGPC 9th exploration and production conference, Cairo. Egyptian general petroleum corporation bulletin* (vol. 2, pp. 1–19)
- Takasu, Y., Ganoub, A. F., & Hirano, M. (1982). Exploration history and geology of west Bakr fields Eastern Desert, Egypt. In *Sixth exploration seminar* (pp. 7–10). GPC
- Tavakoli, V. (2019). *Carbonate reservoir heterogeneity: Overcoming the challenges*. Springer Nature
- Torghabeh, A., Rezaee, R., Moussavi-Harami, R., Pradhan, B., Kamali, M., & Kadkhodaie-Ilkhchi, A. (2014). Electrofacies in gas shale from well log data via cluster analysis: A case study of the Perth Basin, Western Australia. *Open Geosciences*, *6*(3), 393–402.
- Trippetta, F., & Geremia, D. (2019). The seismic signature of heavy oil on carbonate reservoir through laboratory experiments and AVA modelling. *Journal of Petroleum Science and Engineering*, *177*, 849–860.
- Trippetta, F., Carpenter, B. M., Mollo, S., Scuderi, M. M., Scarlato, P., & Colletini, C. (2017). Physical and transport property variations within carbonate-bearing fault zones: Insights from the Monte Maggio Fault (Central Italy). *Geochemistry, Geophysics, Geosystems*, *18*(11), 4027–4042.
- Trippetta, F., Ruggieri, R., Brandano, M., & Giorgetti, C. (2020). Petrophysical properties of heavy oil-bearing carbonate rocks and their implications on petroleum system evolution: Insights from the Majella Massif. *Marine and Petroleum Geology*, *111*, 350–362.
- Vandré, C., Cramer, B., Gerling, P., & Winsemann, J. (2007). Natural gas formation in the western Nile delta (Eastern Mediterranean): Thermogenic versus microbial. *Organic Geochemistry*, *38*(4), 523–539.
- Vicentelli, M. G. C., Contreras, S. A., de Castro, J. C., & Riffel, S. H. (2015). Albian Carbonates reservoir facies characterization on Campos basin, based on geophysical facies analyses. In *14th International Congress of the Brazilian Geophysical Society and EXPOGEF* (pp. 142–144, 3–6 Aug 2015). Brazilian Geophysical Society
- Watney, W. L., Guy, W. J., Doveton, J. H., Bhattacharya, S., Gerlach, P. M., Bohling, G. C., & Carr, T. R. (1999). Petrofacies analysis: A petrophysical tool for geologic/engineering reservoir characterization. *Memoir—American Association of Petroleum Geologists*, *71*, 73–90.
- Wei, C., Tian, C., Zheng, J., Cai, K., Du, D., Song, B., & Hu, Y. (2015). Heterogeneity characteristics of carbonate reservoirs: a case study using whole core data. In *SPE reservoir characterisation and simulation conference and exhibition*. Society of Petroleum Engineers
- Worden, R. H., Armitage, P. J., Butcher, A. R., Churchill, J. M., Csoma, A. E., Hollis, C., Lander, R. H., & Omma, J. E. (2018). Petroleum reservoir quality prediction: Overview and contrasting approaches from sandstone and carbonate communities. *Geological Society, London, Special Publications*, *435*(1), 1–31.
- Zaid, S. M. (2012). Provenance, diagenesis, tectonic setting and geochemistry of Rudies sandstone (lower Miocene), Warda Field, Gulf of Suez, Egypt. *Journal of African Earth Sciences*, *66*, 56–71.
- Zhao, H., Ning, Z., Wang, Q., Zhang, R., Zhao, T., Niu, T., & Zeng, Y. (2015). Petrophysical characterization of tight oil reservoirs using pressure-controlled porosimetry combined with rate-controlled porosimetry. *Fuel*, *154*, 233–242.



Mohammad Abdelfattah Sarhan is an associate professor of applied geophysics at Damietta University (Egypt). He received an MSc (2009) degree from Mansoura University (Egypt), and a PhD in 2013 from Channel Mission between Leeds University (UK) and Damietta University. He performed two post-doctoral studies at Leeds University's School of Earth and Environment, from February 2015 to August 2015 and from October 2016 to March 2017. His core research interests focus on interpreting seismic

and well logging data for hydrocarbon exploration and reservoir evaluation. Particular interests include sequence stratigraphic analysis to improve predictions of potential hydrocarbon distributions and reservoir quality in subsurface settings. He has received several prizes, including the Damietta University Prize for Scientific Creativity in Basic Sciences (2017), the Damietta University Prize for Distinguished Scientific Publishing in (2018, 2019, 2020, 2021), and the 'State Encouragement Award in Geology' from the Ministry of Higher of Education in Egypt (2019).



Western Desert Petroleum System: New Exploration Opportunities and Challenges

Ahmed E. Radwan

Abstract

The Western Desert province is one of Egypt's most productive hydrocarbon provinces, ranking second in terms of oil production after the Gulf of Suez province and second in terms of gas and condensate production after the Nile Delta. Over the last few decades, many discoveries and thousands of wells have been drilled to explore hydrocarbons in the organic-rich sedimentary basins of the Western Desert. This chapter aims to provide comprehensive studies on the Western Desert's total petroleum system, as well as the tectono-stratigraphic history control on petroleum system development across the basins. The dominant source rocks, conventional reservoirs, unconventional reservoirs, seals, and petroleum traps have all been thoroughly discussed in this chapter. This chapter also includes the major Western Desert sedimentary basins and their petroleum systems in detail. Furthermore, this chapter introduces new exploration opportunities as a means of achieving successful exploration and the discovery of new resources, such as stratigraphic traps, deeper targets, inversion structures and faulted traps, sequence stratigraphy application, and unconventional resources. Finally, the chapter discusses the challenges that could affect hydrocarbon exploration in the Western Desert, such as drilling, petroleum systems, and seismic imaging, as well as some mitigations.

Keywords

Western desert • Petroleum system • Unconventional resources • Conventional resources • Source rocks • Petroleum traps

1 Introduction

Understanding the petroleum system of hydrocarbon reservoirs in sedimentary basins is a critical factor in evaluating and simulating hydrocarbon reservoirs for better exploitation and development (Radwan et al., 2021a). Global energy consumption has increased significantly in the last few decades as a result of significant technological advancements and rising living standards. Thus, ongoing research developments in the energy sector aim to improve subsurface resource exploitation by increasing production (Radwan, 2022; Radwan et al., 2022). This can be accomplished by accurately modeling the characteristics of the petroleum system in subsurface basins in order to improve production efficiency and resource recovery (Radwan et al., 2021a). Furthermore, a better understanding of the petroleum system elements will lead to more discoveries and shed light on unconventional reservoirs, which will impact countries' economies and raise people's living standards. Northeast Africa sedimentary basins have been distinguished by their organic richness and multi-hydrocarbon-bearing reservoirs, including the Western Desert (WD), Nile delta, Gulf of Suez and Mediterranean sedimentary basins of Egypt. Intraplate rift basins, according to Guiraud et al. (2005) and Radwan et al. (2021a), are the most prolific hydrocarbon-bearing places in Northeast Africa. The Egyptian economy is heavily reliant on petroleum energy, and governments are focusing on attracting foreign and domestic companies to invest in Egyptian petroliferous basins. Egyptian oil and natural gas production is constantly expanding as a result of ongoing exploration and investment activities. According to BP's 2019 statistical report, Egyptian oil proved reserves reached 3.1 BBL in 2019, and natural gas proved reserves exceeded 75.5 TCF (Fig. 1). The daily production of oil, natural gas, and condensate is increasing year after year as a result of new discoveries in the three major petroleum provinces, which include WD, the Nile Delta, and the Gulf of Suez (Fig. 1).

A. E. Radwan (✉)
Faculty of Geography and Geology, Institute of Geological Sciences, Jagiellonian University, Gronostajowa 3a, 30-387 Kraków, Poland
e-mail: radwanae@yahoo.com; ahmed.radwan@uj.edu.pl

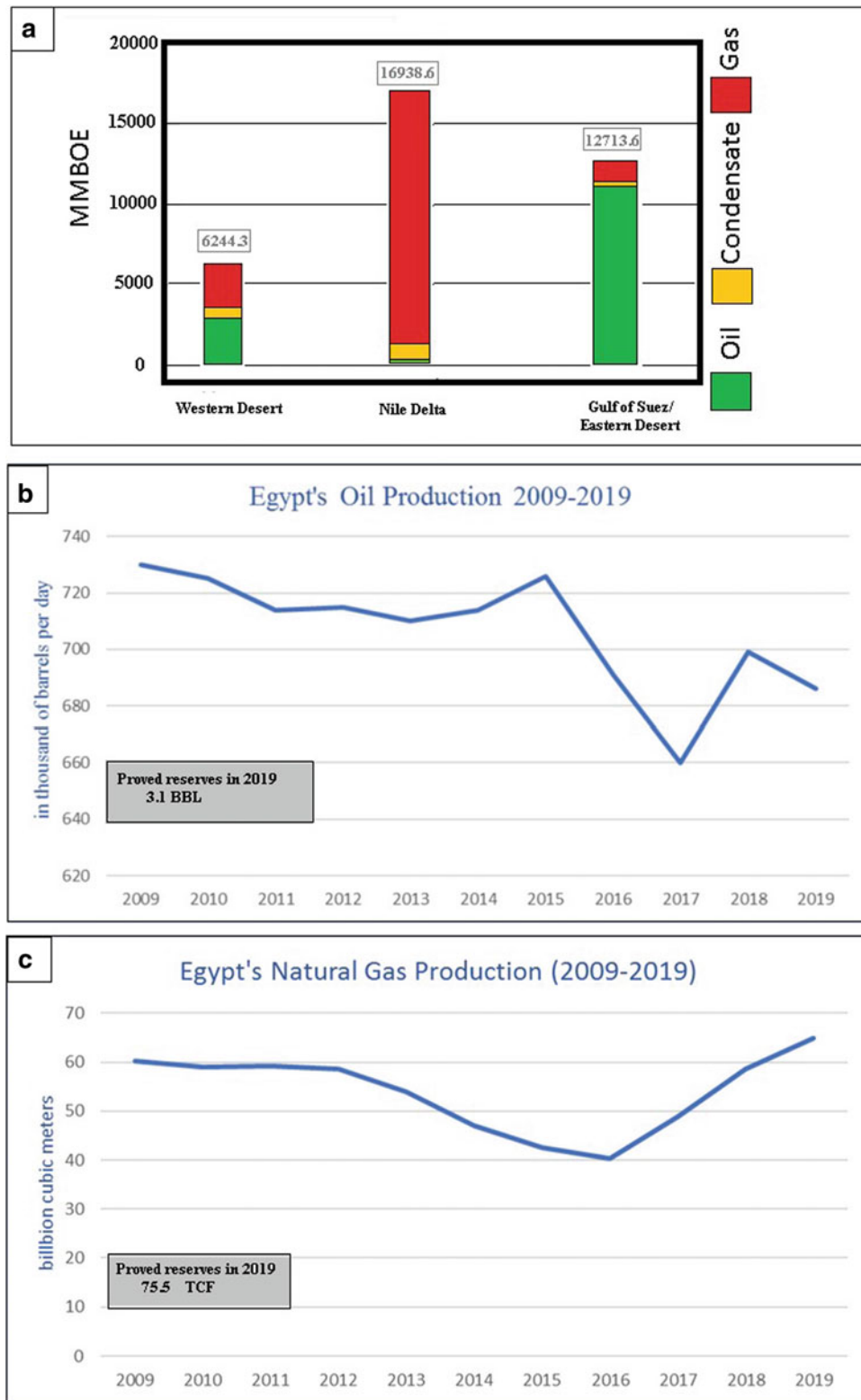


Fig. 1 Petroleum production sketch for Egyptian petroleum provinces, **a** summary of the discovered volume of fluids in Egyptian petroleum main provinces, updated to 2017 (Dolson, 2020); **b** Egypt's oil production from 2009 to 2019, with proven oil reserves until 2019; **c** Egypt's natural gas production from 2009 to 2019, with proven oil reserves through 2019 (BP Statistical Review of World Energy 2020)

The WD is Egypt's second most important petroliferous province in terms of oil, gas, and condensate production (Fig. 1). Over geological time, the WD sedimentary successions formed during complex tectonic regimes such as rifting, inversion, and deformation phases. The WD sedimentary succession is rich in reservoir intervals and organic-rich source rocks (e.g., Dolson et al., 2001a, 2001b; Katz, 1995; Leeder & Gawthorpe, 1987; Scherer et al., 2007). Rifting in WD begins in the Late Triassic, but the main rifting phase is mostly associated with the Middle Jurassic (Dolson et al., 2001a, 2001b; Garfunkel, 2004; Guiraud et al., 2005). These basins are formed by a southwestward thickening Paleozoic strata overlying the crystalline basement complex, which is followed by a northward thickening Mesozoic-Neogene sedimentary pile (Said, 1990; EGPC 1992). The north WD rift basins were formed during the Early Mesozoic continental breakup phase, following the opening of the Neo-Tethys Ocean (Bosworth et al., 2008; Garfunkel, 1998, 2004; Tassy et al., 2015). Throughout the Mesozoic, the WD coastal rift basins remained a broad shelf region near sea level.

They witnessed various transitions between continental and marine deposition, so facies changes are regular (Moretti et al., 2010; Said, 1990; Sultan & Halim, 1988). The North WD of Egypt (greater Western Desert basins) is a crucial component of Northern Africa's unstable shelf (Fig. 2). The North WD of Egypt has been subjected to various tectonic regimes since the Paleozoic Era, allowing the formation of multiple basins, sub-basins, ridges, platforms, and troughs. Most significant hydrocarbon accumulations have been encountered in Mesozoic rift basins of the WD. More than 3 (bnboe) were produced from the WD's overall reservoirs, with the Cretaceous and Jurassic reservoirs contributing significantly (IHS and WoodMac, online source). According to Dolson (2020), the estimated reserves of the WD as high as 5.6 billion barrels of oil equivalent (BBOE) recoverable to date, with additional reserves yet to be discovered that could reach 7 BBOE. This chapter will focus on the following: (1) the WD petroleum system, (2) the tectono-stratigraphic history control on petroleum system development, (3) exploration history of the WD hydrocarbons, (4) WD sedimentary basins and their petroleum system, (5) the development of innovative opportunities as a means of achieving successful exploration and the discovery of new resources, (6) challenges that could affect the hydrocarbon exploration in the WD.

2 General Lithostratigraphy of the Western Desert

The WD lithostratigraphy contains a variety of lithologies ranging from the Cambrian to more recent deposits that have been influenced by numerous tectonic events which

have formed its current sedimentary succession (Fig. 3). The WD's sedimentary succession was influenced by transgressive/regressive cycles that constrained its evolution. The Paleozoic succession in WD is characterized by coarse and fine clastics, as well as minor carbonate rocks that overlie the basement rocks (Fig. 3). Four major regressive cycles distinguished the WD sedimentary succession, each terminated by a marine transgression (Sultan & Halim, 1988). The Middle to Late Jurassic non-marine clastics (Ras Qattara formation) represent the earliest cycle, and the deposition continued by the marine deposits of the Khatatba formation. The earliest cycle was ended by the maximum transgression surface represented by the Late Callovian carbonates of the Masajid formation. The post-Paleozoic sedimentary succession consists of alternating clastic and carbonate strata from four major depositional cycles: The Jurassic, Lower Cretaceous, Upper Cretaceous, and Paleogene (Fig. 3; Sultan & Halim, 1988). The syn-rift sediments originate from the Jurassic and Lower Cretaceous cycles, whereas the post-rift strata belong to the Upper Cretaceous and Paleogene (Said, 1990; Sultan & Halim, 1988). The Lower Jurassic fluviolacustrine siliciclastics of the Yakout and Ras Qattara formations overlie the Paleozoic sandstones unconformably in the Jurassic cycle (Said, 1990; EGPC, 1992). The Middle Jurassic sediments comprise the Khatatba formation's coastal and shallow marine strata, which are followed by the Masajid formation's marine carbonate that represents the maximum extent of the Jurassic transgressive phase (Sultan & Halim, 1988; El Hawat, 1997).

The second cycle started during the Early Cretaceous and was separated by an unconformity surface that separated the carbonates mentioned above from the marine clastics of the Alam El Bueib (AEB) formation, Dahab shale, and Alamein dolomite (Moretti et al., 2010). The sediments of the second cycle lie unconformably on the Masajid carbonates, and began with the shallow marine siliciclastics and carbonates of AEB formation and ended by the Dahab shale deposition.

The third sedimentary cycle spanned the Middle Albian to Paleogene epochs. The post-rift Upper Cretaceous cycle is characterized by continental to coastal siliciclastic facies at the base (Kharita and Bahariya formations) changing upward into marine carbonates (Abu Roash and Khoman formations) (Fig. 3). The fourth cycle is composed of marine clastics, such as the Apollonia, Dabaa, and Moghra formations, which are capped by the flat-lying Marmarica limestone (El-Din et al., 2001). The Upper Cretaceous cycle is terminated by a major unconformity that marks the base of the Paleogene sediments of the fourth cycle, which are dominated by marine carbonate at the base (Apollonia formation), followed by marine siliciclastics of the Dabaa and Moghra formations (Sultan & Halim, 1988; EGPC, 1992).

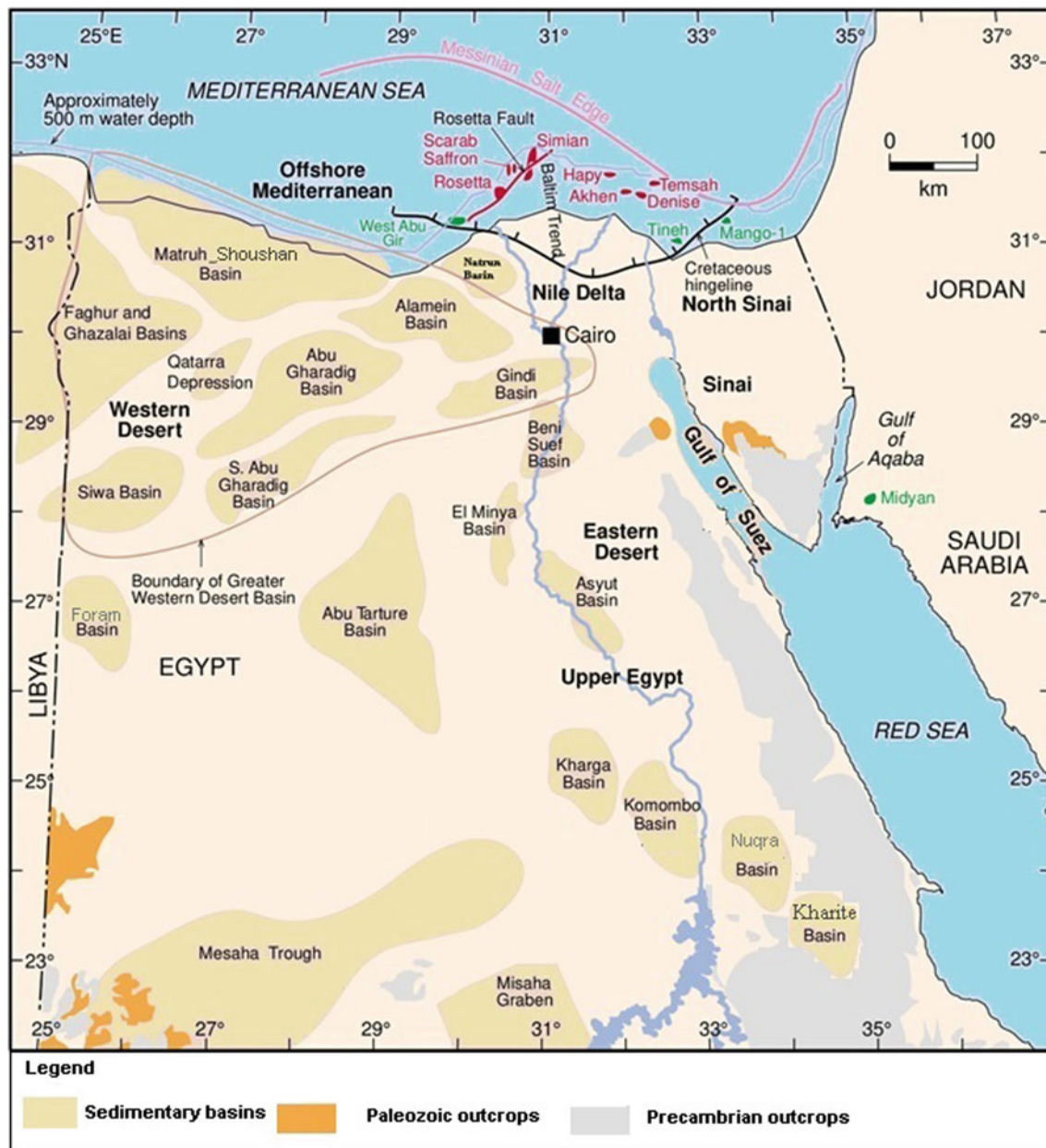


Fig. 2 Location map displays the main sedimentary basins of the WD, the basement rocks distribution and Paleozoic outcrops across Egypt (modified after Dolson et al., 2001a, 2001b)

3 Exploration History

Exploration efforts in the WD began in 1954, several decades after the exploration in the Gulf of Suez. The Sahara Petroleum Company conducted the exploration trial after signing an agreement with the Egyptian government at this time. The aforementioned company conducted geological and geophysical studies for four years, until 1958, and they also used aerial photography and surface mapping in their research. Later, in 1963, two foreign oil companies were awarded

exploration contracts: one (Phillips Petroleum) was given rights to explore areas north of latitude 30°N, and the other (Amoco) was given rights to explore areas east of longitude 27°E and south of latitude 30°N. Both companies have used aeromagnetic surveys in their ongoing efforts for ten years.

Phillips Petroleum Company conducted geophysical studies in 1966, on the Alamein field using 2D seismic profiles, which resulted in the identification of an anticline related to the Late Cretaceous inversion structure. Subsequently, this petroleum company has drilled Alamein-1X exploratory well which is considered the first producing well in the WD. The

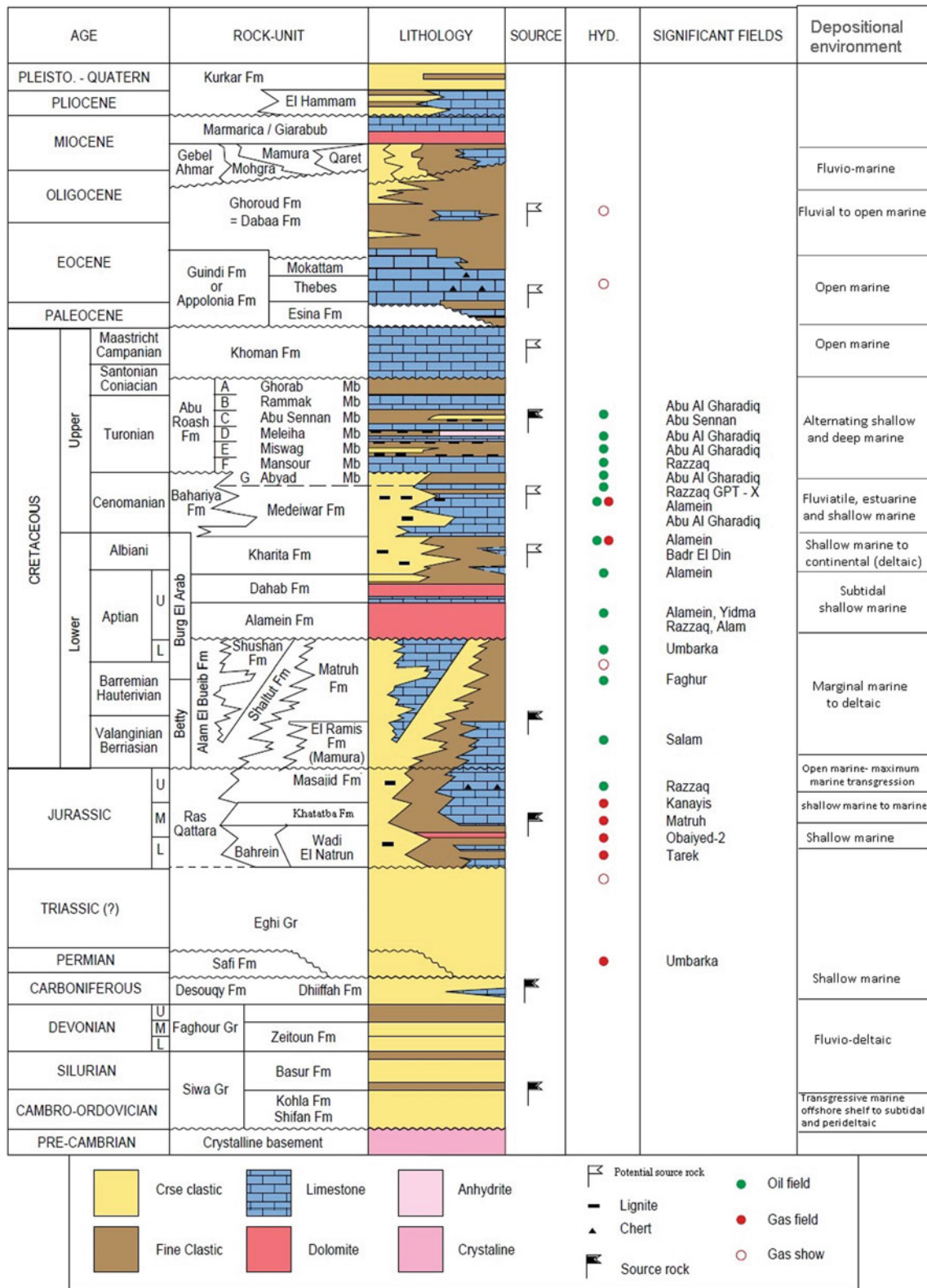


Fig. 3 General Lithostratigraphic column of the Western Desert display the dominant source rocks, reservoirs, and reservoir production in the significant fields from the Western Desert (modified from Schlumberger, 1984, 1995; EGPC, 1992)

initial oil production of Alamein-1 × was approximately 8000 barrels of oil per day (BOPD), with a very good quality of 34.5°API gravity oil. The Aptian reservoir's dolomitic limestone exhibits very good petrophysical characteristics, with permeability ranging from 30 to 2250 md and fracture and vugs dominating as secondary porosity.

The Alamein discovery brought attention to the WD's petroleum potential, and several petroleum companies conducted additional studies and drilled exploratory wells to maximize production. Egyptian companies have been conducting exploration trials in WD since 1969 when the General Petroleum Company (GPC) began exploration activities in the Siwa area. The gigantic Abu Gharadig field was discovered in 1969 by the Amoco Petroleum Company, one of the most important hydrocarbon finds in Egypt. Following the exploration of the Abu Gharadig field, many large to small fields were discovered within the WD sedimentary basins providing rewarding discoveries, particularly the northern greater WD basins (Table 1).

The ongoing exploration activities in the WD were continued, and various companies were involved in the explo-

ration activities; by 1985, approximately 20 fields had been discovered in the WD. In 1985, Phoenix Petroleum used the most advanced seismic techniques available at the time to explore previously unexplored areas, and they discovered oil and gas in the Jurassic sediments of the Salam field. Many exploration wells have been drilled across the WD basins in recent decades, with a focus on numerous localized "highs" within these rift basins, providing a variety of reservoir possibilities to date. The majority of petroleum fields have been discovered in Mesozoic basins that formed after the Permo-Triassic rifting of Neotethys. The estimated ultimate recovery (EUR) of some significant hydrocarbon fields in the WD is summarized in (Table 2).

4 Tectono-Stratigraphic History Control on Petroleum System

The geological framework of Egyptian lands has been dominated by major events (see Fig. 4). As a result, these episodes have influenced the hydrocarbon potentiality of each basin in

Table 1 Giant fields and significant discoveries examples located in the WD display the hydrocarbon type, exploratory well name, year, and reservoir ages

Fields	Discovery well name, year	Age	Hydrocarbon types	References
Abu Gharadig	Abu Gharadig-1,1969	Cretaceous	Oil and gas	Hegazy (1992)
Khaleda	Khaleda-1, 1971	Cretaceous	Oil and gas	Hegazy (1992)
Bed-2	Bed2-1, 1982	Cretaceous	Oil and gas	Hegazy (1992)
Bed-3	Bed3-1, 1987	Cretaceous	Oil and gas	Hegazy (1992)
Kanayes	Kanayes-5,1992	Jurassic	Oil and gas	IHS Energy Group (2006)
Obayeid	Obayeid-3, 1993	Jurassic	Oi and gas	IHS Energy Group (2006)
Qarun	El Sagha-3x,1995	Lower Cretaceous	Oil	Dolson et al. (2001a, 2021b)
Shams	Shams-2x, 1997	Jurassic	Oil and gas	IHS Energy Group (2006)

Table 2 Estimated ultimate recovery of significant fields that located in the WD display the operator company, EUR, year, and hydrocarbons field names. MMBOE is million barrels of oil equivalent

Fields	Company	Estimated ultimate recovery (EUR)	Year
Alamein	Phillips Petroleum Company	82 MMBOE	1966
Abu Gharadig	Pan American Oil Company/Amoco	320 MMBOE	1969
Meleiha	Wepco/Agiba	77 MMBOE	1972
Badr el Din complex (3 fields)	Shell Winning N.V	510 MMBOE	1982/83
GPAA	General Petroleum Company	190 MMBOE	1985
Obaiyed 1	Shell Egypt N.V	155 MMBOE	1992
Obaiyed 2	Shell Egypt N.V	270 MMBOE	1992
Qarun	Phoenix Resources Company	72 MMBOE	1994
Qasr	Khalda Petroleum Company/Apache	700 MMBOE	2003

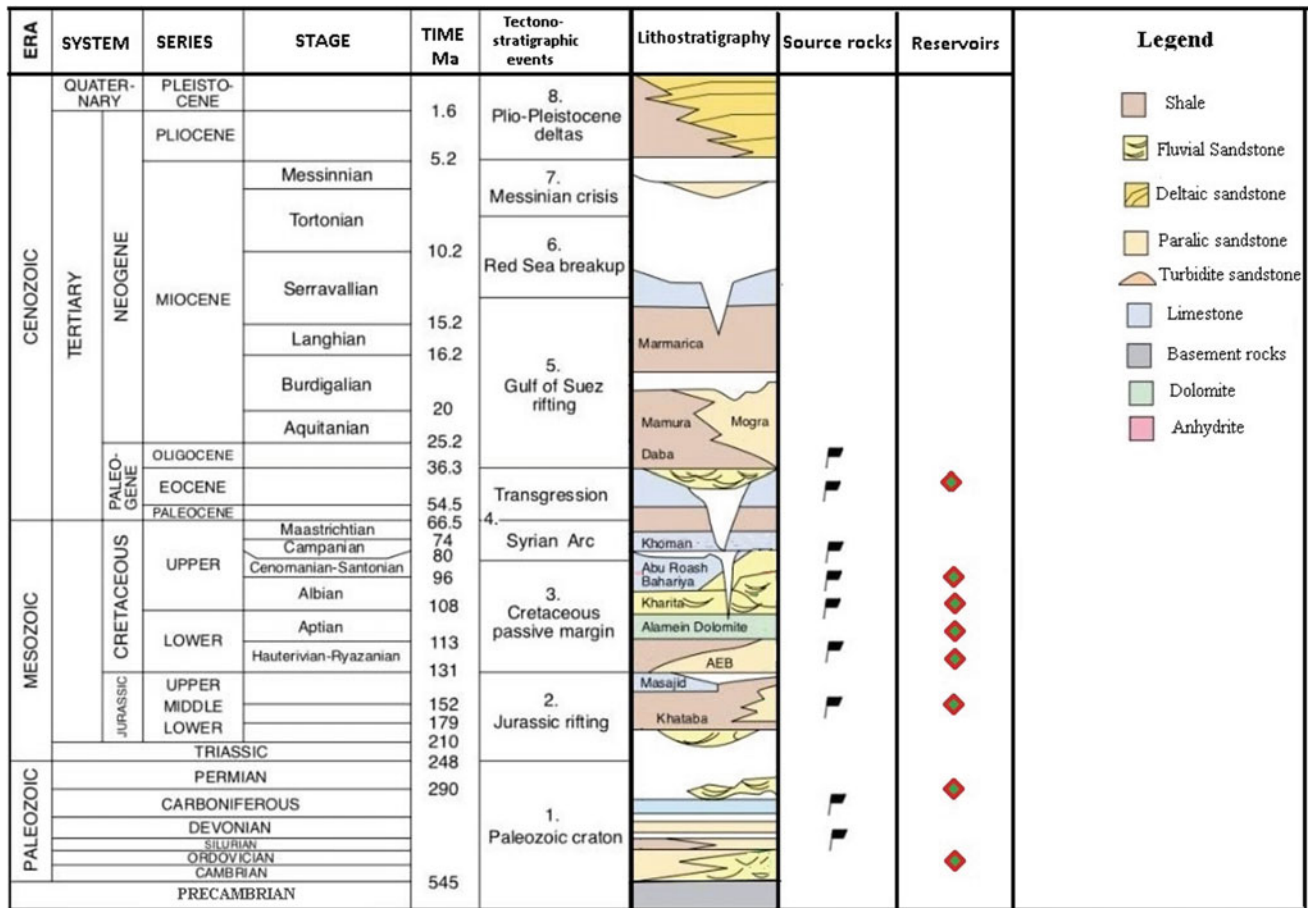


Fig. 4 General Tectonostratigraphic events of the Western Desert display the dominant source rocks, reservoirs (modified from Schlumberger, 1984; EGPC, 1992)

Egypt, where petroleum system elements were developed in relation to these tectono-stratigraphic frameworks.

4.1 Paleozoic Craton

During the Paleozoic Craton event, the WD was composed of a low relief alluvial plan dipping *N* along the (proto-Mediterranean) and *W* toward (cratonic sags, Libya), and it was dominated by shallow marine facies of carbonates and clastics in the north (Dolson et al., 1999). The southern area of the WD, on the other hand, was dominated by fluvial-alluvial lithofacies composed primarily of glauconitic sandstones and red shales. Furthermore, Silurian-age black shales were deposited in the WD, equivalent to an important source facies (Tenzuft Shales) in Libya (Dolson et al., 1999; Farooqui et al., 2012; Hegazy, 1992). The Paleozoic’s main source rocks are organic-rich Carboniferous and Silurian deposits; however, the Paleozoic petroleum system is not fully understood. The maximum thickness of Paleozoic strata in the WD is 2500 m in the Siwa area, with a general thickness increase trend toward the north. Strong erosion

events and onlap around pre-existing basement have affected the Paleozoic strata throughout Egypt during the Triassic and Jurassic rift, resulting in the absence of these strata along large areas of Egypt. Paleozoic sediments received little attention prior to the 2000s, in comparison to other Mesozoic facies. However, new Paleozoic discoveries (mainly Carboniferous) have drawn attention to Paleozoic deposits.

4.2 Jurassic Rifting

During Late Triassic through the Jurassic, several rift basins occurred across North Africa. These rift basins were formed during the Pangea breakup, which controlled the opening of the Neotethys (Dolson et al., 1999; Garfunkel, 2004; Stampfli et al., 2001). The Mesozoic rift basins affected the North WD areas, (e.g., Matruh-Shoushan, and Natrun) (Fig. 2). The Mesozoic rift basins of Northern WD are synchronous with other rift basins in Sinai-Levant, Algeria, and Libya forming a regional system that surrounds the Nubian Craton (Bosworth, 1994; Dolson et al., 1999; Guiraud et al., 2005; Morris & Tarling, 1996). On the other

hand, three rift basins have been reported in the Southern WD, namely the Komombo, Nuqra, and Kharit basins, in addition to other basins below the greater WD sedimentary basins (Fig. 2), but these basins do not appear to be linked to the larger WD basins (Dolson et al., 1999).

Prosser (1993) discusses the Jurassic strata sedimentary record as a typical example of three-phase rifting development. Non-marine and shallow marine sediments were developed at Late Triassic and Early Jurassic, which thinned southward. More carbonate and marine shale were formed north of the Tethyan margin, while sandstones and red shales were noticed south of the Tethyan margin (Dolson et al., 1999). During this time, the organic-rich deposits of the Khatatba formation formed by overlapping on paleostructural highs from the early rifting phase. Later, by the Middle Jurassic, fault blocks had fully developed, resulting in the deposition of deep marine facies of the Masajid formation.

The most well-preserved syn-rift deposition occurred during the Middle Jurassic (Bathonian-Callovian) and was subsequently culminated during the period of the Early Cretaceous (Bosworth, 1994). As a result, the Middle Jurassic Khatatba formation sediments provide a complete stratigraphic record and are mostly home to highly productive hydrocarbon exploration targets (e.g., Keeley et al., 1990; Alsharhan & Abd El-Gawad, 2008; Shalaby et al., 2011). Masajid formation is considered as carbonate-prone with some local black marine shales, while Khatatba formation is dominated by marine shale and grading into carbonaceous shales and coal toward the south. Both Masajid and Khatatba formed proven source rocks within the WD petroleum system. These rift basins host the most significant hydrocarbon fields of the WD province (e.g., Alamein, Safir, Abu Sennan, Meleiha, Badr El-Din, Aghar, Razzak, Khalda, Qarun, Um Barka, Salam, and Tut).

4.3 Cretaceous Passive Margin

Early Cretaceous time has witnessed the development of mixed siliclastic and carbonate systems across North Africa in response to thermal events associated with wide passive margin development (Dolson et al., 1999). During this period, the AEB formation was deposited overlying the Masajid formation, but some local unconformities were recorded and distinguished by lignite and carbonaceous shale prior to the deposition of this formation. According to Dolson et al. (1999), these deposits could indicate a local continuation of rift episodes during the Early Cretaceous. Extensional faulting have perhaps proceeded during the Early Cretaceous, and multiple unconformities were created locally as a result of horst block erosion. The AEB formation is characterized by mixed sandstone, shales, and carbonate, indicating sea level oscillations during deposition, and it is

similar to the Nubia formation. The marine carbonate of AEB formation is organically rich and proven source rock. The aforementioned formation is overlain by a dolomite facies known as the Alamein Dolomite, which dates from the Aptian period and reflects sea level rise, implying regional level oscillations during this era. Aptian age transgression was discovered in the Komombo basin (Fig. 3), indicating that it influenced southern Egypt. According to Dolson et al. (1999), the Aptian age transgression is used as a useful flooding surface marker horizon by many authors throughout the WD. Thermal subsidence has been accompanied by continued southward transgressions, which regulate the deposition of significant widespread source and reservoir rocks (Kharita and Bahariya formations). The aforementioned sediments are synchronous to the Nubia (fluvial) and Raha (shallow marine) formations in the Gulf of Suez, and they are dominated by a mixture of sandstones, shales, siltstones, and carbonates.

4.4 Syrian Arc Deformation and Foreland Transgression

The Tethys closure between the African and European plates has formed a series of northeast-southwest trending folds that occurred during the Cenomanian to Turonian periods. These cretaceous folds have affected the entire area from Syria to the northern part of the WD (Moustafa & Khalil, 1990). The aforementioned folds, known as the "Syrian Arc," have caused regional uplift in many areas, resulting in some rift basin inversion across the Northern WD (Ayyad & Darwish, 1996; Guiraud & Bosworth, 1997; Shahar, 1994). According to structural deformation events on these evolving highs, unconformities developed throughout the inverted structural crests.

The Syrian Arc continued through Turonian to Santonian, where carbonates of the Abu Roash formation were deposited on the flanks of inverted structural crests. The Abu Roash carbonate facies deposits exhibit cyclicity and they are important productive traps of the WD petroleum system, that influenced by the Syrian Arc related structural trends (ceased by Early Campanian). As a result of the subduction of the African and European plates, wide foreland has developed in the Northern WD beginning in the Cenomanian (Dolson et al., 1999). According to Haq et al. (1988), the early Campanian witness significant sea level rise, which resulted in the deposition of source-rich carbonate and shales deposits of the Khoman formation in the WD and their equivalent in the Gulf of Suez (Brown Limestone). Moreover, the Campanian-Maastrichtian important sediments have not been affected by Cenozoic Era uplift and erosion. The Paleocene and Eocene periods are distinguished by continued transgression, which formed widespread shales

and carbonates across Egypt including the WD, each with its different name. The Paleocene–Eocene sediments are considered top seals of the Cretaceous underlying reservoir, and they control the faults and folds structural geometries in some ways.

Other tectono-stratigraphic events have affected the sedimentary basins of Egypt of the Gulf of Suez, Nile Delta, and Mediterranean provinces, but with less significant control on the WD total petroleum system, these include (1) Gulf of Suez Rifting, (2) Red Sea Breakup, (3) Messinian Crisis, and (4) Plio-Pleistocene Delta Progradation.

5 Total Petroleum System in the Western Desert

The main hydrocarbons play that encountered in the northern WD basins are Cretaceous (mostly oil-prone), Jurassic (mostly gas-prone), and Paleozoic (mostly oil-prone) plays. The source rocks within the basins have mature and immature conditions with varying organic richness and are distributed in Paleozoic (Silurian and Carboniferous deposits), Jurassic (Khatatba, Masajid), Cretaceous (AEB, Alamein Dolomite, Kharita, Bahariya, Abu Roash, Khoman), Eocene (Appollonia), and Oligocene (Dabaa) deposits. Immature conditions exist in shallower organic-rich areas (Khoman, Appollonia, Dabaa). In some basins, the Kharita, Masajid, Alamein Dolomite, Abu Roash, and Bahariya formations have poor to fair source rock potential. However, the Jurassic Khatatba and AEB shales are the most common source rocks in most basins. The reservoirs are mainly porous sandstones that are distributed from the Paleozoic to Eocene, while the carbonates are restricted to the Jurassic Masajid, and Cretaceous Alamein dolomite and Eocene Apollonia carbonates. The trapping style is mainly structural with little contribution from combined and stratigraphic traps. The main seal rocks are the shales and carbonates across the sedimentary sequence from the Paleozoic to Miocene.

6 Western Desert Sedimentary Basins and Their Petroleum System

The sedimentary basins that are distributed across two-third of Egyptian lands (about 680,650 km²) can be classified into two categories: the first is the greater WD sedimentary basins which are located Northern the WD and have been subjected to the same geological and tectonic events and they are linked together. These basins include Matruh, Matruh-Shoushan, Abu Gharadig, Natrun, Alamein, Faghour, Ghazali, Siwa, and Guindi basin. The second is the southern basins which include distributed basins in the

middle and southern parts of the WD (Fig. 2). Over 10,600 wells have been drilled in the WD sedimentary basin, forming the current WD basin shapes and aiding in the discovery of numerous hydrocarbon fields. The following section will discuss some of these basins and some representative examples from their fields.

6.1 Northern or Greater WD Sedimentary Basins

6.1.1 Abu Gharadig Basin

The first significant discovery in the WD was the AG-1 well, which was drilled to Upper Cretaceous clastics in the Abu Gharadig field and yielded oil and gas. Despite the fact that the AG-1 well was discovered in 1969, oil production started in 1973 and gas production began in 1975. The basin is 330 km long and 50–75 km wide, and it is classified as an intracratonic rift basin with an *E-W* trend. The basin is defined as an asymmetrical sublatitudinal graben with flanks complicated by normal and strike-slip faults that form semi-graben structures, sometimes horsts, and buried linear inversion folds formed by wrenching dislocations during the Alpine tectonic epoch. The basin includes several oil and gas fields that reach more than 100 hydrocarbon fields. As a result of the Syrian Arc movement, the basin experienced inversion during the Late Cretaceous period (Abdel-Fattah et al., 2020; El Gazzar et al., 2016). As a result, an asymmetry anticline with a NE-SW orientation developed in the basin, which is bounded by inverted faults. Based on stratigraphic relationships and thickness changes, El Gazzar et al. (2016) concluded that the inversion began in the Santonian and continued to the Dabaa formation deposition period (Late Eocene). In terms of the petroleum system, the main reservoirs in the basin are hosted by sandstone facies of the Bahariya formation (Cenomanian) and the Abu Roash formation (Turonian). However, the carbonate facies of the Abu Roash *D*, *F*, and *G* members are also oil-bearing reservoirs in local areas within the basin (EGPC, 1992). According to EGPC (1992), the Bahariya formation sandstones have excellent porosity (up to 18–25%) and permeability (up to 500 mD). Locally, commercial hydrocarbon pools have been discovered in the Kharita (Albian) and Khoman formations. Oil and gas shows have also been reported from the sedimentary rocks of the AEB, Masajid, and Khatatba formations. In general, the hydrocarbon fields in the region are multipay and form producing trends along linear uplifts complicated by faults. The Abu Roash horizons yielded oil, while the Cenomanian Bahariya and Albian Kharita reservoirs yielded mostly gas (EGPC, 1992). Other Jurassic and Early Cretaceous reservoir potentialities of the sandstone facies of the AEB, Khatatba, and Ras Qattara formations have recently been confirmed. The sediments of the Abu Roash (*E*, *F*, *G* Members) and the Bahariya

formations contribute as source rocks in the basin. According to Lüning et al. (2004) and El Nady (2016), both formations are immature to mature source rocks with fair to good source potential for oil generation, which are still within the early stage of hydrocarbon generation till the present time. The Abu Roash “F” Member has oil-prone character (type I-II kerogen) with TOC values of 1.5–2.5 wt. % that reach to 6 wt. % or higher value at the central of the basin (EGPC, 1992; Lüning et al., 2004). The Abu Roash “G” Member has mixed Type II/III with marine and terrestrial origins with TOC values of 0.4–2.35 wt.% and has entered the early stage of hydrocarbon generation (Salama et al., 2021). The Bahariya formation has kerogen Type III of terrestrial origin and entered the early stage of hydrocarbon generation in Eocene time (Salama et al., 2021). On the other hand, the AEB, Masajid, and Khatatba formations are mature source rocks for generating both oil and gas. The AEB and Masajid formations entered the oil window between the Cretaceous and Miocene epochs and remain within oil and gas windows today, whereas the Khatatba formation entered the oil window between the Late Cretaceous and Eocene epochs (El Nady, 2016). The Khatatba formation sediments are a unique source rocks not only in the Abu Gharadig Basin, but all over the Northern WD sedimentary basins. For example, the TOC, Rock-Eval pyrolysis, and vitrinite reflectance in the northern area of the basin indicate mixed oil/gas-prone with fair to very good hydrocarbon generating potential in this mature source rock (1.0 to 5.36 wt.% TOC, S₂ yields 2.29–15.18 mg HC/g rock, and HI 225 to 332 mg HC/g TOC) (El Diasty, 2015). In addition, other kerogen types exist, such as oil-prone (1.02–21.32 wt. % TOC, S₂ yields 4.36–7.26 mg HC/g rock, and HI 368–687 mg HC/g TOC), and gas-prone (1.28–1.69

wt. % TOC, S₂ yields 2.31–2.40 mg HC/g rock, and HI 142–180 mg HC/g TOC). The basin contains multi-seal rocks of shales and carbonates that range in age from the Middle Jurassic to the Oligocene. The large proportion of hydrocarbons discovered in the WD basins, including the Abu Gharadig Basin, were discovered through the drilling of structural traps, either as three- or four-way closure structures or as fault block structures. The dominant trapping mechanisms are structural traps formed by compressional tectonics associated with the Syrian Arc tectonic event and extensional tectonics associated with rifting. The basin traps include the tilted fault block trap, the horst fault block trap, and the horst fault block with three faults trap that accompanied the extensional tectonic regime. On the other hand, other traps like folds related to the basin bounding fault trap, inverted, folded and faulted within the basin trap, reverse fault trap, strike-slip trap, and flower structure trap that formed due to the compressional tectonic regime. The main petroleum system elements of the basin are summarized in (Fig. 5).

6.1.2 Matruh-Shoushan Basin

The Matruh-Shoushan Basin is a Mesozoic rift basin that experienced three stages of development, including (Pre-Syn-Post-rift) (Fig. 2) (Shalaby et al., 2014; El Nady, 2013). The Matruh-Shoushan Basin was influenced by the Syn-rift phase of the basin, which occurred from the Jurassic to the Middle Cretaceous when rapid subsidence occurred due to crust stretching and was accompanied by the highest heat flow (Metwalli & Pigott, 2005). Later, during the Post-rift phase, the basin experienced thermal cooling subsidence from the Albian to the Coniacian epochs (113–88 Ma). The basin contains numerous reservoirs and source

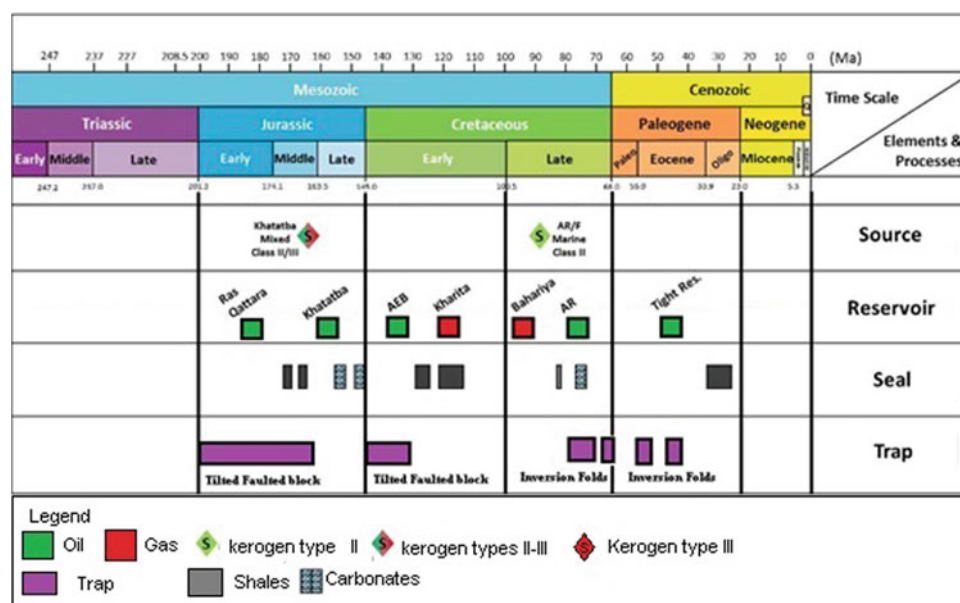


Fig. 5 Constructed petroleum system chart of Abu Gharadig basin. Legend is applied to all petroleum system charts in this chapter

rocks, and some horizons serve as both source and reservoir rocks. In terms of the petroleum system, the deltaic and shoreline facies of the Ras Qattara and Khatatba formations are recognized the source and reservoir rocks at the Jurassic depositional system level, while the inner carbonate platform of the Masajid formation is Seal rocks for the underling Khatatba (Shalaby et al., 2011). The TOC of Khatatba and Ras Qattara formations dark shale ranging from 1.8 to 46.9 wt. % and 2.23 to 53.71 wt. %, respectively (Shalaby et al., 2011). The source rock analysis indicated mixed kerogen types II-III as well as kerogen type III in both Khatatba and Ras Qattara formations (Fig. 6). TOC values and pyrolysis analysis of the aforementioned formations indicate excellent

source rock quality, and petroleum system studies indicate that these dark shales have reached the final maturation stage of the hydrocarbons generation window in the Late Cretaceous. The Lower Cretaceous sediments have significant reservoirs and sources, which are represented by the deltaic to shoreline facies of the AEB formation, which has reservoir and source rock intervals capped by the shallow water peritidal dolostone of Alamein Dolomite. The TOC of AEB formation shales ranges from 1.85 to 2.40wt. % and is characterized by mixed kerogen types II-III (Younes, 2012). TOC values and pyrolysis analysis indicate good source rock quality, and petroleum system studies indicate that these shales have reached the mid maturation stage of the

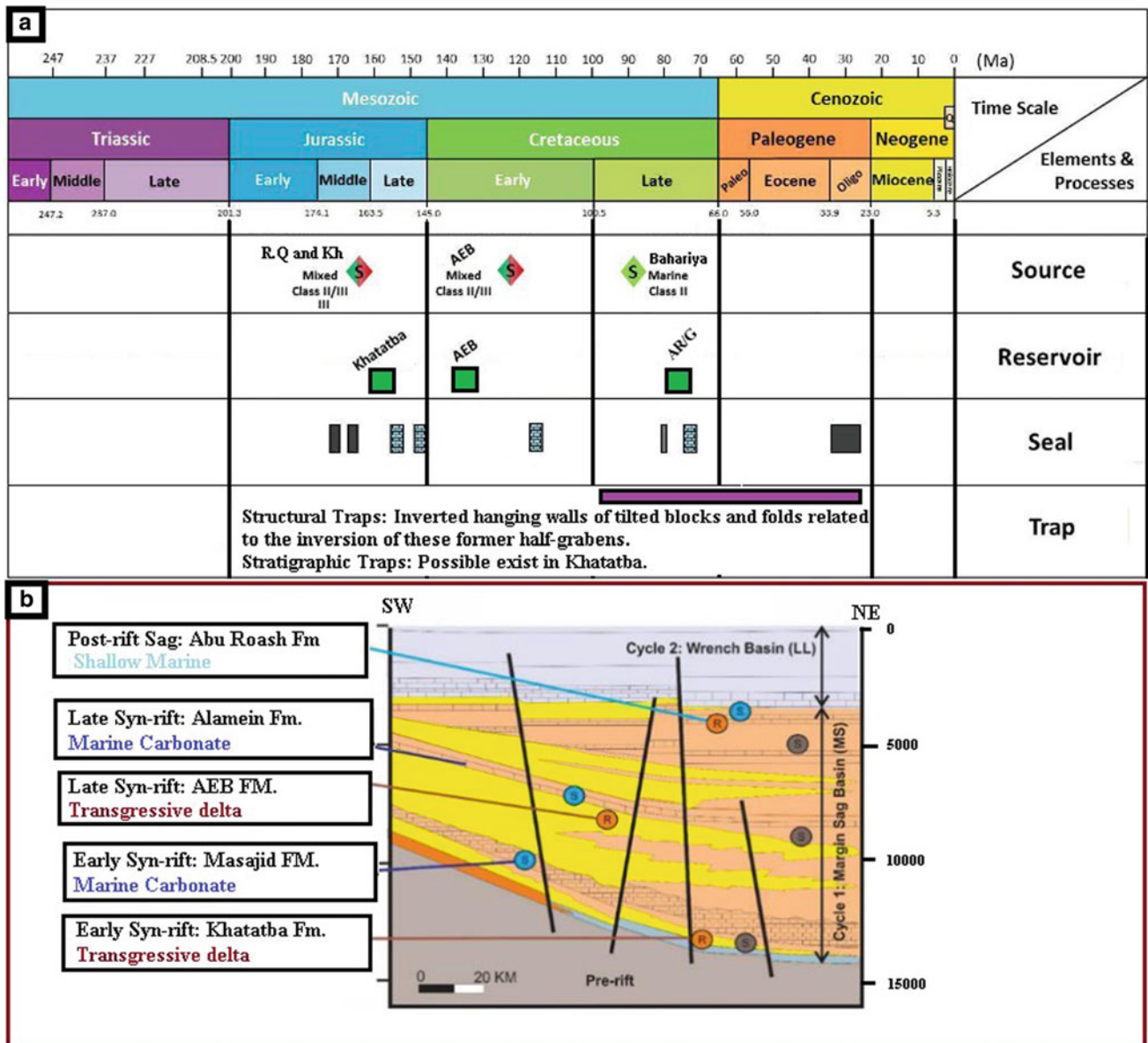


Fig. 6 a Constructed petroleum system chart of the Matruh-Shoushan basin, b schematic diagram showing the petroleum system types (PSTs) of the basin (adapted from Shalaby et al., 2014)

hydrocarbons generation window in the late Cretaceous. The shallow marine deposits of the Abu Roash formation, serve as a source and reservoir, while the upper carbonate of the Abu Roash Members serves as cap rock. The TOC of AR formation (AR/G Member) shales ranges from 1.10 to 1.50 wt. % and is characterized by mixed kerogen types II-III. TOC values and pyrolysis analysis indicate fair source rock quality, and petroleum system studies indicate that these shales have reached the mid maturation stage of the hydrocarbons generation window in the Late Cretaceous to Late Eocene. The Matruh-Shoushan basin produced both oil and gas fluids, and its hydrocarbon traps are dominant due to the structural type that formed during the Late Cretaceous period (Abdel-Fattah, 2015). Generally, the dominant trapping mechanism is structural traps formed by extensional and compressional tectonic regimes. The basin traps include the tilted fault block trap and the horst fault block trap that accompanied the extensional tectonic regime. On the other hand, other traps like inverted, folded and faulted within the basin trap, inverted and faulted trap that formed due to the compressional tectonic regime. The Khatatba formation, on the other hand, is stratigraphic due to facies change in these sediments. The reservoir characteristics of Khatatba Sandstones display measured permeability values range from 0.05 to 1000 mD and porosity values ranging from 1 to 17% (Cheng, 2020). The main petroleum system elements of the basin are illustrated in (Fig. 6).

6.1.3 Alamein Basin

The Alamein Basin was the source of the first hydrocarbon discovery in the WD, so it is an iconic basin, and it is known as the deeply buried basin. The Alamein basin is bounded on the Northeast by the Matruh-Shoushan basin, and it is separated from the Abu Gharadig basin by the Shareb-Sheiba high structural ridge (Fig. 2). The basin contains several oil-producing fields arranged in a belt of an ENE-WSW direction, including Razzak, Alamein, Horus, and others (Yousef et al., 2019). The basin is distinguished by an ideal inversion anticline that has been compartmentalized by several NW-SE trending faults (Abdine et al., 1993; Yousef et al., 2019). The basin includes a total of 33 hydrocarbon fields distributed across the basin. There are numerous reservoirs and source rocks in the basin, and some horizons serve as both source and reservoir rocks. From the petroleum system analysis in the basin, it has been inferred that the Jurassic rocks of the Khatatba formation are considered both source and reservoir rocks, and the expelled hydrocarbons migrated upwards to fill the Cretaceous reservoirs. The faults of the Alamein basin have a corridor nature, which aided oil drainage within the basin; however, it is unclear whether the formation of the

dominant structural traps occurred prior to or concurrent with hydrocarbon migration. The Abu Roash formation's shales and tight carbonates acted as the basin's ultimate seal rocks, while the Masajid formation's inner carbonate platform serves as the basin's seal rocks for the underlying Jurassic reservoirs. In terms of reservoirs, the basin is distinguished by numerous clastics sandstone reservoirs including Kharita, Bahariya, and AEB, as well as the dolomitic limestone of Alamein Dolomite and Abu Roash "G" Member (EGPC, 1992). In terms of hydrocarbon traps, Ayyad and Darwish (1996) argued that the structural traps are dominant in the Cretaceous plays of the basin (ex. inverted hanging walls of tilted blocks, tilted blocks, three-way dip closures, and inverted anticlines of former half-grabens). In terms of source rock potentiality, Younes (2012) reported that the major matured source rock of the Khatatba formation contained mixed kerogen types II-III. According to Yousef et al. (2019), the AEB is still in its early stages of maturation. Moreover, the Abu Roash formation ("F" Member) has potential as source rock (Fig. 7). Furthermore, the Lower Cretaceous Kharita and Bahariya formations have some source rock potential in the basin and WD. The Eocene Apollonia formation has good source potential as well, but it is still immature in most basins (Moretti et al., 2010). The Abu Roash "F" sediments have TOC measurements ranging from 2 to 2.50 wt.% and are characterized by mixed kerogen types II-III. TOC values and pyrolysis analysis indicate that the source rock is of good quality (Moretti et al., 2010). The AEB shales have TOC measurements ranging from 1 to 2 wt.% and are characterized by mixed kerogen types II-III too. TOC values and pyrolysis analysis indicate that the source rock is of fair to good quality, with more lipid-rich material. The TOC measurements of the Khatatba shales range from 1 to 64 wt. % and are characterized by mixed kerogen types II-III. TOC values and pyrolysis analysis indicate that the source rock is of fair to excellent quality, with more lipid-rich material. Moretti et al. (2010) point to the Paleozoic sediments (e.g., Carboniferous, Devonian, and Silurian) as having source rock potential, although it is still not understood. According to petroleum system studies by Moretti et al. (2010), the migration of oil and gas in the basin begins in the Oligocene-Miocene epoch. The dominant trapping mechanism is structural traps formed by compressional and extensional tectonic regimes. The basin traps include folds related to the basin bounding fault trap, and (inverted, folded and faulted within the basin trap) that formed due to the compressional tectonic regime. Also, the basin traps include the tilted fault block trap that accompanied the extensional tectonic regime. The main petroleum system elements and burial history of the basin are illustrated in (Fig. 7).

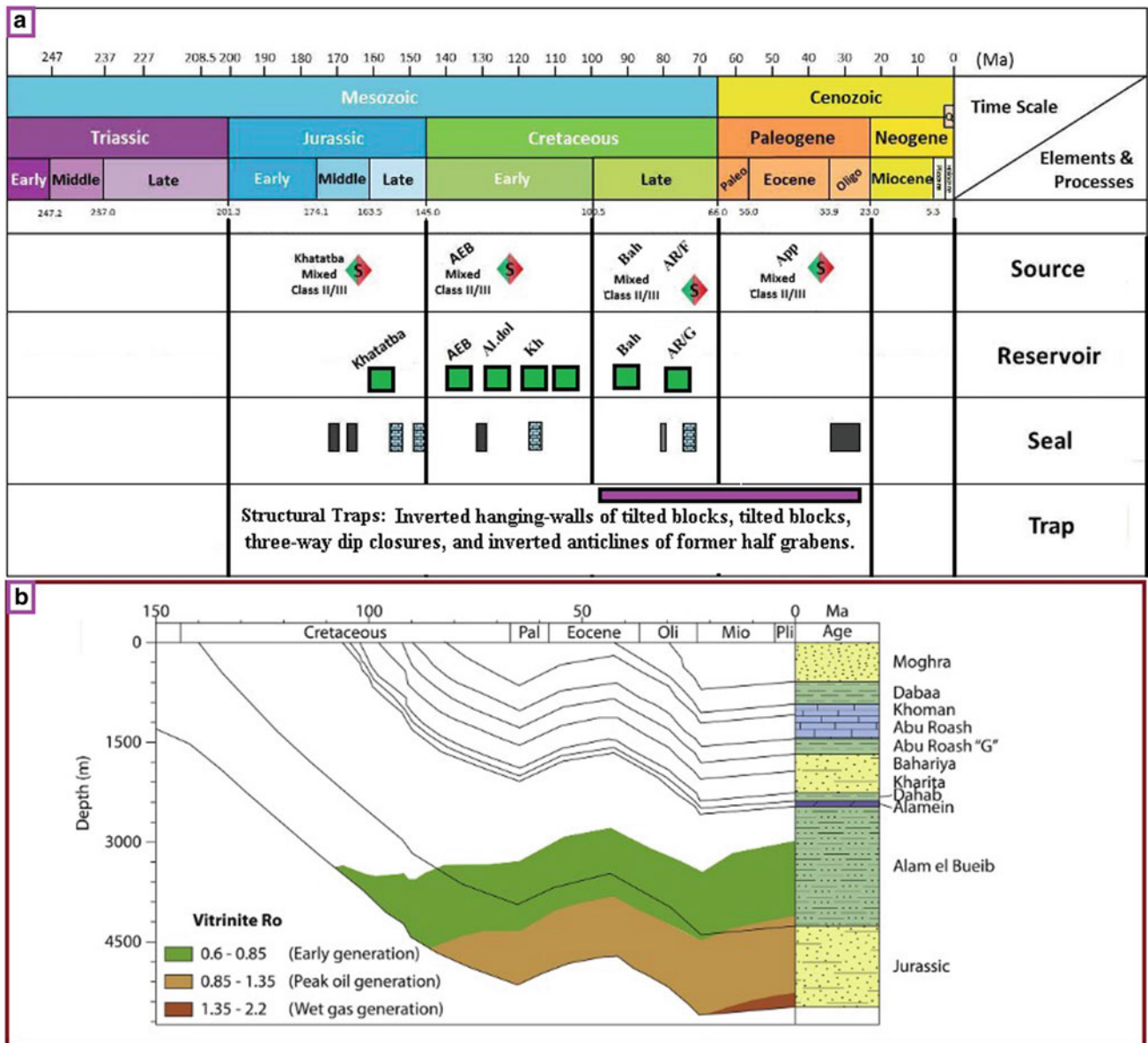


Fig. 7 a Constructed petroleum system chart of the Alamein basin, b burial history model of (PSTs) of the basin (after Yousef et al., 2019)

6.1.4 Faghur Basin

The basin is located near the borders of Libya in the western most of the WD rift system (Fig. 2). Although the hydrocarbons discoveries within the neighbor basins, the commercial discovery in Faghur basin commenced in 2006 (Bosworth & Tari, 2021; Bosworth et al., 2015a, 2015b). According to Bosworth et al. (2015a, 2015b), only the fluvial to estuarine Khatatba formation which deposited in the Late Jurassic first phase of rifting is the functioning source rock in the basin. The Khatatba was affected by extensional faults dip to the south that might reflect reactivation during the Hercynian according to Bosworth and Tari (2021). The TOC measurements of the Khatatba shales range from 0.1 to 80 wt.% (coals), with an average reading of 2.9 wt.%,

and are characterized by mixed kerogen types II-III (Bosworth et al., 2015a, 2015b). The basin is affected by the inversion at the very Early Cretaceous while the deposition of AEB, forming inverted anticline and four-way dipping unfaulted closures. The Aptian–Cenomanian rifting was very important for the basin petroleum system as it brought the Khatatba source rocks below the oil generating window. Bosworth et al. (2015a, 2015b) reported that the hydrocarbons migration in the basin started after the Late Cimmerian inversion structure. Abu Roash formation was affected by younger inversion resulted in forming small folds. Later, renewed NE-SW extension influenced Campanian and Maastrichtian sedimentation. It can be inferred that both Late Cretaceous NW-SE shortening and NE-SW extension

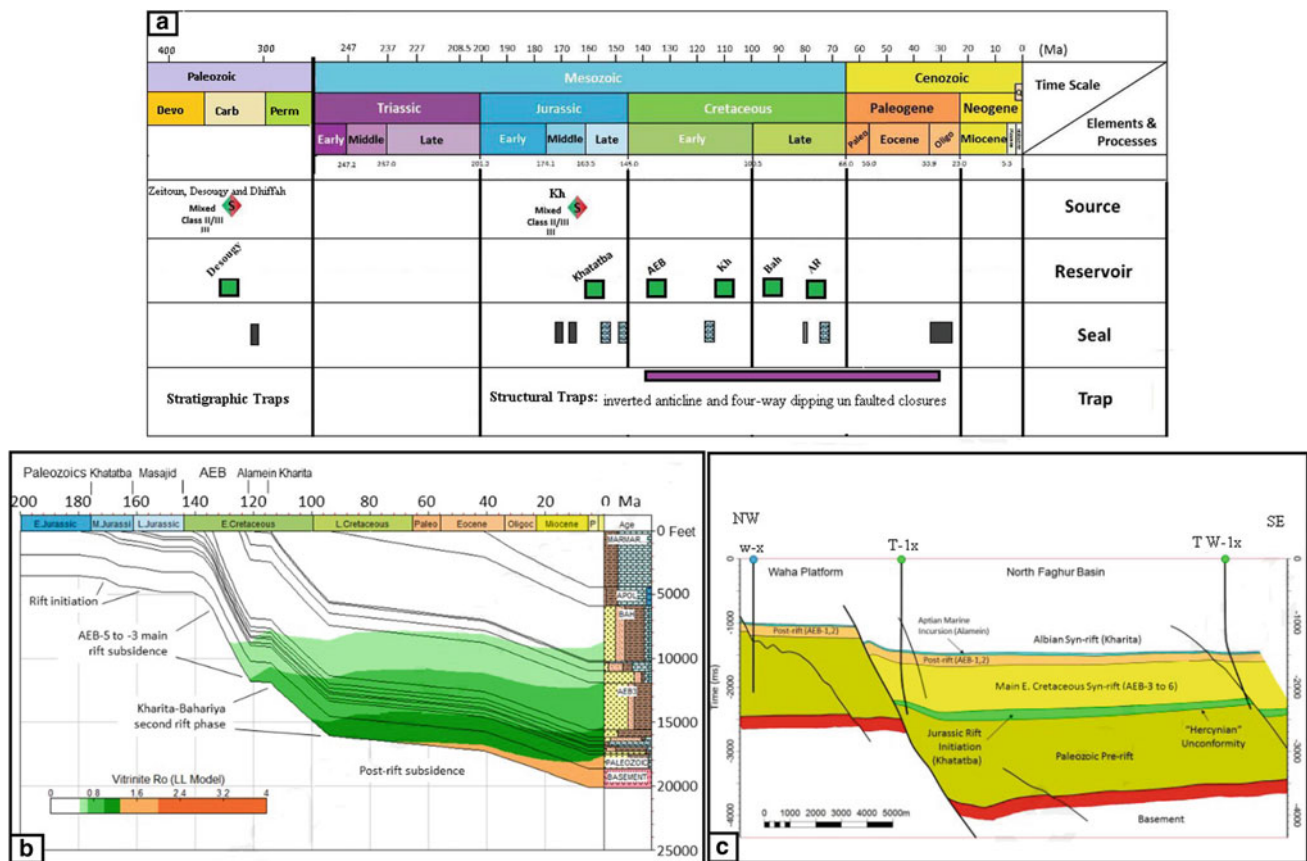


Fig. 8 a Constructed petroleum system chart of the Faghur basin, b burial history model of the basin, c representative cross section of the Faghur basin (after Bosworth & Tari, 2021)

influenced the basin, in turn, all these indicated the role of dominant structural traps in the Faghur basin. In terms of reserves, the porous sandstones in both pre and post-inversion time act as reservoirs, and the produced oil is characterized by variable wax content and a wide range of API gravities. Having fluvial sandstones interbedded with the actual source beds (Khatatba) also increases the robustness of the hydrocarbon system as vertical migration is not necessary in this case (source-reservoir). A recent study by Makled et al. (2018) and Abd el Gawad et al. (2019a, 2019b) studied the Paleozoic section in the Faghur basin and they inferred that Paleozoic Zeitoun, Desouqy, and Dhiffah are source rocks in the basin and they are characterized by kerogen type III and mixed type II/III (Fig. 8). Abd el Gawad et al. (2019a, 2019b) argued that the Paleozoic petroleum system mainly depends on stratigraphic traps that might form along the unconformity surfaces. The main petroleum system elements and burial history of the basin are illustrated in (Fig. 8).

6.1.5 Gindi Basin

The Late Cretaceous-Eocene basin is located 80 km southwest of Cairo and bisects the Nile in the easternmost part of

the WD rift system, south of the Alamein Basin (Fig. 2). The surface area of the basin is about 9500 km² and the main famous hydrocarbon field is Qarun, which was discovered in 1994 by the El Sagha-1A wildcat well. Other oil and gas fields include a total of 27 fields distributed across the basin. For example, Silah, North Silah, Ain Assillen, N. Silah deep, southwest Qarun, Tersa, NE Tersa, Kahk, West Auberge, and SE Gindi fields. The basin was affected by the Jurassic-Early Cretaceous rifting phase, followed by right-lateral wrenching in the Late Cretaceous, and ended by reactivation of the NW-SE oriented fault (El Ghamry et al., 2020). The stratigraphic column of the Gindi Basin is the same as other basins in the northern WD, but it is less thick, ranging between 4 and 6 km, compared to 9 km of sedimentary thick in the Abu Gharadig Basin. The E-W and ENE fault trends are dominant in the Gindi Basin and intersected by the youngest fault sets of the NW and NNW trends (EGPC, 1992). The Albian Kharita formation, together with the Aptian Dahab formation, has a very thick sedimentary succession of about 1000 m, while the Upper Cretaceous formations are composed of more than 1500 m of thick sediments (Mansour & Tahoun, 2018).

In terms of reserves, the porous sandstones in both pre and post-inversion times act as reservoirs, and the produced oil is

characterized by variable wax content and a wide range of API gravities. The Albian Kharita formation, deposited in a fluvio-deltaic to marginal marine environment, and the Early-Middle Cenomanian Bahariya formation, deposited in oxic fluvio-deltaic, marginal to inner neritic environments, are the dominant reservoirs in the Gindi Basin since they are composed of sandstones with intercalated siltstones and shales. The sandstones of the Albian Kharita formation are occasionally medium to fine-grained, fair porous with traces of glauconite, while the Bahariya formation sandstones are characterized by being fine to medium-grained with dominant calcareous cement. The shallowing and deepening depositional trend has exerted significant vertical and lateral lithologic control over the Abu Roash formation in the Gindi Basin. It is divided into seven members from base to top (*G–A*) like in other northern WD basins. The “*B, D, and F*” members are mostly carbonate-dominant, while the “*A, C, E, and G*” members are mostly fine clastics, and these have produced hydrocarbons and have potential reserves in the basin.

According to Hammad et al. (2010), the fluvial to estuarine Khatatba, AEB, Kharita, Bahariya, and Abu Roash formations are the basin’s source rocks. The TOC measurements of the Khatatba shales range from 1.29 to 4.64 wt. % and are characterized by mixed kerogen types II-III that are capable of producing oil and gas, with T_{max} ranging between 433 and 444 °C, forming mature source rocks. The III kerogen type is detected in the AEB, Kharita, and Bahariya formations with gas generation potential. According to Hammad et al. (2010), the Abu Roash sample analysis is characterized by mixed kerogen types II-III that are capable of producing oil and gas, while some samples belong to Abu Roash “*F*” indicate a capability of generating oil with OI and HI values of 51–72 mg/g and 212–472 mg/g. According to Hammad et al. (2010)’s analysis of the AEB and Kharita formations, T_{max} ranges between 417 and 436 °C, indicating an immature to marginally mature stage, as well as the Bahariya nad Abu Roash formation. The hydrocarbon expulsion started after the deposition of the Apollonia formation. El Ghamry et al. (2020) claimed that the Gindi’s inversion resulted in the deposition of a remarkably thick succession of Appolonia carbonate, which acted as a seal rock, and these carbonates have contributed to enhancing the hydrocarbon trapping of Cretaceous source rocks. They refer to quick subsidence of the fault’s down-thrown side as a result of concurrent activity on the Gindi fault (basement structure), which resulted in hydrocarbon migration in an up-dip direction and the formation of hydrocarbon traps. The dominant trapping mechanism is structural traps formed by compressional and extensional tectonic regimes. The basin traps include folds related to the basin bounding fault trap and (inverted, folded and faulted within the basin trap, reverse fault trap) that formed due to

the compressional tectonic regime. The basin traps include the tilted fault block trap and the horst fault block trap that accompanied the extensional tectonic regime. The main petroleum system elements and structural elements of the basin are illustrated in (Fig. 9).

6.2 Southern WD Sedimentary Basins

In general, the southern WD sedimentary basins have not gained the same importance and directed exploration activities as the greater WD sedimentary basins. Because of fewer exploration activities in the Upper Egypt and Red Sea regions, the Southern WD basins are poorly understood as a part of the Upper Egypt lands. The WD’s southern basins include Kharit and Komombo, El Minya, Abu Tarure, Beni Suef, Assiut, Foram, and Kharga (Fig. 2). Non-marine lacustrine sediments were identified in Upper Egypt and Sudan by Schull (1988) and Taha (1992). According to the former researchers, additional Mesozoic rift basins are not physically connected to the greater WD rift basins. In 1990, geophysical and geological studies were conducted by Repsol Petroleum Company to determine the geological characteristics and boundaries of the Nuqra, Kharit, and Komombo basins that are located in the Southern WD. The first three basins are distinguished by their NW-SE orientation, which may be due to rifting associated with the breakup of the Afro-Arabian plates. Although the Nuqra basin is located geographically in the eastern desert, some authors consider it part of the WD sedimentary basins because it is structurally aligned with the Komombo Basin. In 1997, the Komombo-1 well in the Komombo basin was completed, and the results were interesting for both the government and investors, as oil was produced from Jurassic reservoirs (Dolson et al., 2001a, 2001b). Elmaadawy and El-Ashmony (2021) investigated the Foram basin, which is close to the Libyan border. They used magnetic, gravity, basin modeling, and seismic methods, as well they indicate that the basin structure trend is NE-SW, with a thickness of 1.8–5 km of Paleozoic sediments and the remaining represent the Mesozoic-Cenozoic sediments. As a result, Elmaadawy and El-Ashmony (2021) identified the basin as a Paleozoic basin with the Silurian Kohla formation as the main source rock. Elmaadawy and El-Ashmony (2021) basin modeling and petroleum system analysis revealed that hydrocarbon generation is quite low and cannot facilitate oil expulsion. Recently, new discoveries in southward basins (for example, Komombo and Beni Suef) in Cretaceous reservoirs have demonstrated that hydrocarbon systems exist within those smaller basins, implying that the WD will remain an attractive exploration target in the future. To conclude, more research is required to confirm the hydrocarbon potential of

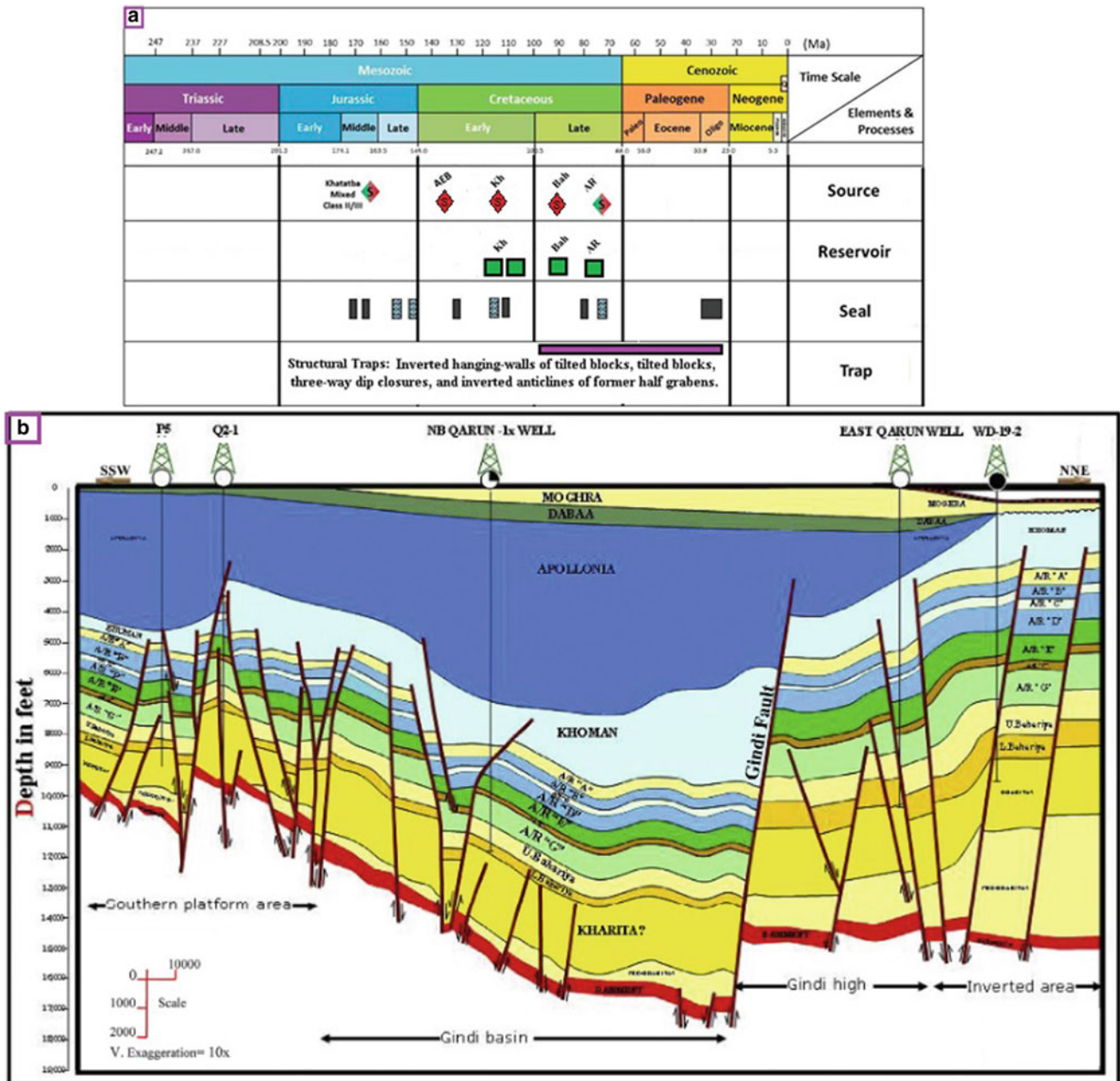


Fig. 9 a Constructed petroleum system chart of the Gindi Basin, b representative cross section of the Gindi Basin (after El Ghamry et al., 2020)

Upper Egypt basins, particularly the Southern WD basins, where additional studies can bring new ideas and exploration plans into Egypt's southern basins.

6.2.1 Beni Suef Basin

The Beni Suef basin is located south of the greater WD sedimentary basins and it belongs to the Southern WD basins (Fig. 2). The Beni Suef Basin bisects the present-day Nile Valley. The eastern side of the basin is located in the Eastern Desert, while the western side is located in the WD region. Although the hydrocarbon discoveries are within the neighboring Greater WD sedimentary basins, the

commercial discovery in this basin commenced in 1997 by the Seagull Energy Corporation (Makky et al., 2014). The basin includes many fields, namely Yusif, Beni Suef, Lahun, Azhar, Gharibon, and Sobha. The stratigraphic column of the basin is similar to the neighboring Greater WD sedimentary basins, where basement rocks through the Jurassic clastics followed by the Cretaceous sequence, the Eocene carbonates, Oligocene shales, and topped by Late Tertiary to recent deposition (Makky et al., 2014). According to Makky et al. (2014), several source rocks exist in the basin. They report fair to good source rock in the Abu Roash (E member) with 0.51 to 3.66 wt.%. The Abu Roash "F" member had

TOC content ranging from 1.27 to 4.46 wt.%, indicating good to very good source rock characteristics. The Abu Roash “G” member had TOC content ranging from 0.51 to 1.15 wt.%, indicating fair to good source rock. TOC content in the Kharita formation ranged from 0.58 to 1.16 wt.%, indicating fair to good source rock, while TOC content in the Betty formation ranged from 0.39 to 1.16 wt.%, indicating fair to good source rock. The Rock-Eval pyrolysis that were analyzed by Makky et al. (2014), point to the Abu Roash (*F* member) as oil-prone source rock with excellent generation potential, while Abu Roash “E” member have the potential to generate mainly oil with some gas.

On the contrary, the Abu Roash (*G* member) and Betty formation have mixed oil/gas-prone source rocks. Mainly gas-prone source rock is assigned for the shales of the Kharita formation. Later, Abdel-Fattah et al. (2017) studied the TOC and Rock-Eval pyrolysis data and concluded three main source rock (kerogen) types, where the Abu Roash “A, E, and F” members indicate strongly oil-prone (kerogen type II). They found kerogen mixed type II/III belongs to shale-rich intervals within the Abu Roash “A & G” members and the AEB formation. The third source rock type by Abdel-Fattah et al. (2017) is gas-prone (kerogen type III) sediments and belongs to the Abu Roash “E & G” members, Kharita, and AEB formations. In terms of reservoir rocks, the main reservoirs in the Bani Suef basin are sandstone reservoirs. Both the Kharita and Bahariya formations have excellent sandstone reservoirs and represent the main reservoirs. The clastic sandstones of the Abu Roash “A, E, and G” members might act as additional resources in the basin. Anticline, half-anticline, fault block, and anticline faulted structure are the dominant trap types in the Bani Suef basin. The aforementioned reservoirs in the basin are sealed by the Lower Cretaceous and Upper Cretaceous shales of the Kharita and Bahariya formations, as well as the fine-grained limestones of the Abu Roash formation, which act as seals too. The Early to Late Cretaceous rifting tectonics resulted in forming migration pathways for accumulated hydrocarbons. The later developed faults and anticlines assist in the secondary migration of hydrocarbons. According to Abdel-Fattah et al. (2017), the Cretaceous source rocks commenced oil generation during the Late Cretaceous period. The dominant trapping mechanism is structural traps formed by extensional tectonic regimes. The basin traps include the tilted fault block trap, the horst fault block trap, and the horst fault block with three faults trap that accompanied the extensional tectonic regime.

6.2.2 Komombo Basin

The Komombo basin is an intracontinental rift basin that is located in South Egypt; it belongs to the Southern WD basins (Fig. 2) and it lies 65 km northwest of Aswan. The

basin is defined by a normal fault that runs northwest to southeast, it is characterized by 70-km-long and 30-km-wide. This basin is a very significant basin in the petroleum system of the Southern Western Desert, where it is the most significant hydrocarbon resource in Upper Egypt to date. The basin includes two fields, namely Al Baraka and West Al Baraka fields. The stratigraphic column of the basin is about 4000 m of Cretaceous non-marine and shallow marine sequences (Abdeen et al., 2021; Hakimi et al., 2023; Ali et al., 2020). The formations in the Komombo basin are named from top to bottom: Dakhla, Qusier, Taref, Maghrabi, Sabaya, Abu Ballas, Six Hills, and Komombo formations (Fig. 10). Komombo formation is debated between authors, where El Nady et al. (2018) and Abdeen et al. 2021 add it in the stratigraphic column, while Selim (2016) and Ali et al. (2020) did not add this formation in their studies. Various sandstone layers are distributed across the stratigraphic column of the basin and can act as reservoirs (Fig. 10). The Albian/Cenomanian formations act as reservoirs deposited during the Albian/Cenomanian period and consist of shallow marine sandstone. As well, the Abu Ballas (Aptian) and Six Hills formations (Early Cretaceous) are reservoirs in the Al Baraka oilfield. In the flanks and depocenter of the basin, the Albian/Cenomanian thickness ranges from 137 to 411.5 m. Horst, graben, and half-graben are the dominant structures in the basin. The Albian/Cenomanian sandstones have good to very good reservoir quality. However, hydrocarbon saturation is restricted to some parts of the basin. The sandstone reservoirs in the basin are characterized by high amount of siliceous and argillaceous cement which control the reservoir tightness in some parts. According to Abdeen et al. (2021), the core data indicate poor to fair reservoir properties (average $\varnothing = 4.03\%$, FZI = 5.50 μm , and $k = 3.56$ md) in the siliceous sandstone samples. On the other hand, the argillaceous samples are characterized by tight to poor reservoir properties (average $\varnothing = 11.8\%$, FZI = 1.22 μm , and $k = 3.44$ md). The proven source rock belongs to the Early Cretaceous, represented by the Hauterivian–Early Barremian and Neocomian sediments. Ali et al. (2018) studied the Hauterivian–Early Barremian source rock and found the TOC content ranged from 1 to 3.36 wt.%, which indicates good to very good source rock characteristics. The Hauterivian–Early Barremian formation is dominated by Type II/III kerogen based on Rock-Eval pyrolysis and indicates oil–gas-prone (Ali et al., 2018). The structural traps are dominant in the basin. The pre-Cretaceous and Cretaceous shales act as a seal rock across the Komombo basin. El Nady et al. (2018) studied the source rock characteristics of the Sabaya and Abu Ballas formations and concluded that kerogen type III and mixed type II/III are dominant, which indicates fair to excellent source rocks. They found the in Sabaya and Abu Ballas formations. El Nady et al. (2018)

considered the Six Hills formation as poor to fair source rock in Komombo basin. They found that the kerogen type III and IV is dominant in the Six Hills formation. They concluded that the shales of Komombo formation (*B* member) have fair to excellent source rock with kerogen type II and mixed type II/III. El Nady et al. (2018), studied Quseir and Taref formations and indicate poor to fair source rock, on the other hand, they indicate very good to excellent source rock in the Maghrabi formation (III and II/III kerogen type). The Campanian-Maastrichtian sediments.

Indicate fair to excellent source rocks (II and II/III kerogen type). Both oil and gas are mainly the potential products of the Cretaceous formations based on the thermally transformed organic matters within these formations. According to El Nady et al. (2018) work the upper cretaceous sediments are immature to marginally mature source

rocks, except Maghrabi formation that entered the early stage of hydrocarbon generation. The Neocomian sediments are mature rocks based on thermal maturity ($R_0 = 1.25$), while sediments of the Sabaya and Abu Ballas formations are of marginally mature.

6.2.3 Nuqra Basin

The Nuqra basin is an intracontinental rift basin that is located in South Egypt. It belongs to the Southern WD basins. The basin is characterized by a NW-SW fault trend, but a younger fault set of NE-SW to the east of the Nile River (Abdeen et al., 2021). The basin includes two fields, namely Al Baraka and West Al Baraka fields. The stratigraphic column of the basin is about 2000 m. The formations in the Nuqra basin are named from bottom to top: Six Hills, Abu Ballas, Sabaya, Maghrabi, Quseir, and Duwi

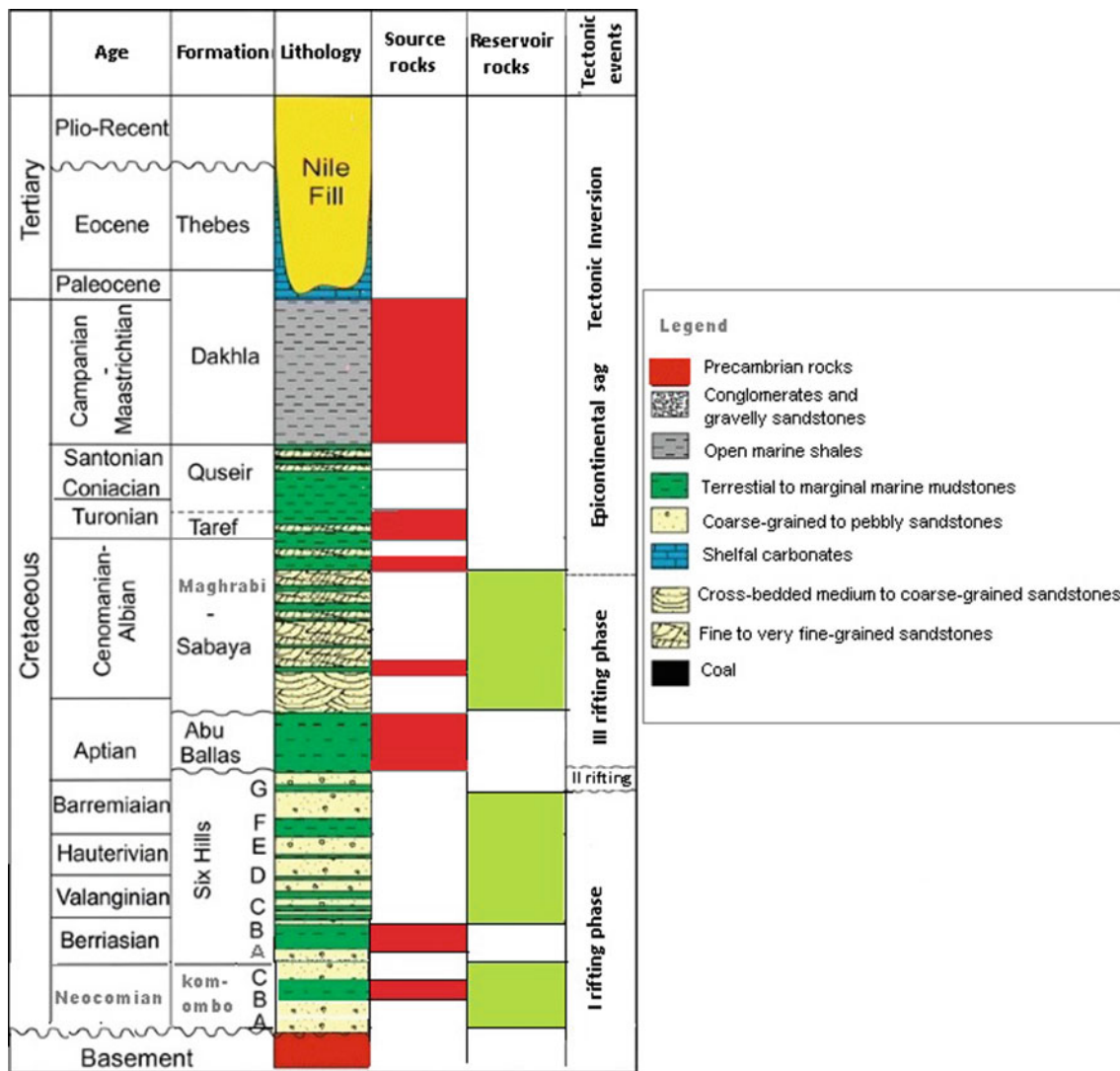


Fig. 10 a lithostratigraphic column of komombo basin (modified after El Nady et al., 2018)

formations. The aforementioned formation is of Late Jurassic, Cretaceous, and Paleocene succession. The Six Hills formation acts as the dominant reservoir deposited during the Early Cretaceous period and consists of porous sandstone. However, the water saturation is very high in these reservoirs, except in selected layers with low water saturation that might be prospective. The source rocks in this basin are from the Jurassic and Early Cretaceous periods, but the available information is not well documented. The structural traps are dominant in the basin. The pre-Cretaceous and Cretaceous shales act as a seal across the Nuqra basin. Further exploration is much needed in the Nuqra basin to better understand the petroleum geology and find economical quantities of hydrocarbon.

7 New Opportunities: Road to Successful Exploration and New Resources

Changes in exploration concepts and/or utilized technology are the most important factors in achieving significant development and increasing the extracted hydrocarbons from any basin (Dolson et al., 1999; Dolson, 2020; Radwan et al., 2021a). Moreover, governments can play a positive role in this by changing business terms in the energy sector, which may create trends and attract new companies to explore. In this regard, the Egyptian government has made ongoing efforts over the last several decades to facilitate the exploration agreement process and attract a number of new companies to work and explore in the WD sedimentary basins. The observed significant increase in WD petroleum reserves over the last two decades indicates a combination of evolving exploration concepts and technological advancement (ex. enhanced seismic imaging in particular deep horizons).

Although many discoveries have been made in the WD sedimentary basins over the last few decades, it is believed that the WD sedimentary basins have not yet revealed their maximum petroleum resources. Successive exploration and potential growth of WD basins can be achieved by employing an integrated approach that can deliver more refinement of the play, trap, or reservoirs. In order to achieve the maximum benefits, the former integrated studies should be supported with source, maturation and migration studies (Radwan et al., 2021a). According to Radwan et al. (2021a), source rock analysis is critical in both the exploration and development stages because it quantifies the expelled hydrocarbon volumes in each trend within a specific sedimentary basin to be traced in the basin or neighboring basins. Dolson et al. (1999) conducted statistical studies to predict potential unexplored fields in the WD, and they proposed about 30 new fields in the WD basins that have yet to be discovered. Dolson (2020) based their prediction on the assumption of new deeper objectives that must be traced

within the WD's large distributed basins. According to the distribution of source rock facies across the WD basins and the calculation of the expected recoverable hydrocarbons, it can be assumed that approximately 7–10% of the expelled hydrocarbons have migrated toward the basin traps (Dolson et al., 1999). The estimated migrated hydrocarbons by (Dolson et al., 1999) are very large (47.4 BBOE) when compared to the actual produced (1.15BBO and 3.2 BBOE) from the various basins in the WD. As a result, the yet-to-find discovered hydrocarbons in the WD sedimentary basins are very likely to be discovered by additional petroleum studies and exploration efforts.

According to Dolson et al. (1999), new discoveries in the WD petroliferous basins may contain more than 11 BBOE of additional resources. Finding such hidden hydrocarbons, however, necessitates long-term planning as well as significant technological investments. In addition, new ideas and a willingness to pursue more difficult targets (ex. deeper reservoirs). In this section, I summarize some of the new opportunities that should be pursued in further exploration within the WD sedimentary basins.

7.1 Stratigraphic and Combined Trap Concept

Exploration for stratigraphic and combined petroleum reservoirs has made significant progress around the world (Radwan et al., 2021a). The petroleum exploration strategy in the WD was primarily based on structural analysis of comparable petroleum provinces in Egypt and around the world (EGPC, 1992). Stratigraphic traps in hydrocarbon exploration have received increased attention in the WD basins over the last two decades, with consideration in both the exploration and development phases. The exploration of stratigraphic traps began in the 1990s, when over 250 m of Jurassic rocks in Obaiyed Field displayed pinch-outs due to rapid lateral facies changes (Fig. 11). Furthermore, (Abd El Gawad et al., 2019a, 2019b) reported a Paleozoic stratigraphic trap in the Faghur basin in response to an angular unconformity.

Apache Corporation announced the discovery of a stratigraphic trap by the Riviera SW-1X (Riviera field, Abu Gharadig Basin), with oil (5800 barrels) and gas (2.8 MMcf) production from reservoirs 24 feet thick of Lower Bahariya sandstones. Another stratigraphic trap (1000 acres) was discovered while drilling Narmer-1X to the east of the Neilos oil field in the Faghur basin. The Narmer-1 × well encountered about 85 feet net pay of Paleozoic-aged sandstones, with daily oil (1200 bbl) and gas production (400 Mcf). The former examples of explored stratigraphic traps highlight the significance of these types of traps, which may add additional reserves to the total hydrocarbon reserves across the WD sedimentary basins. In this regard,

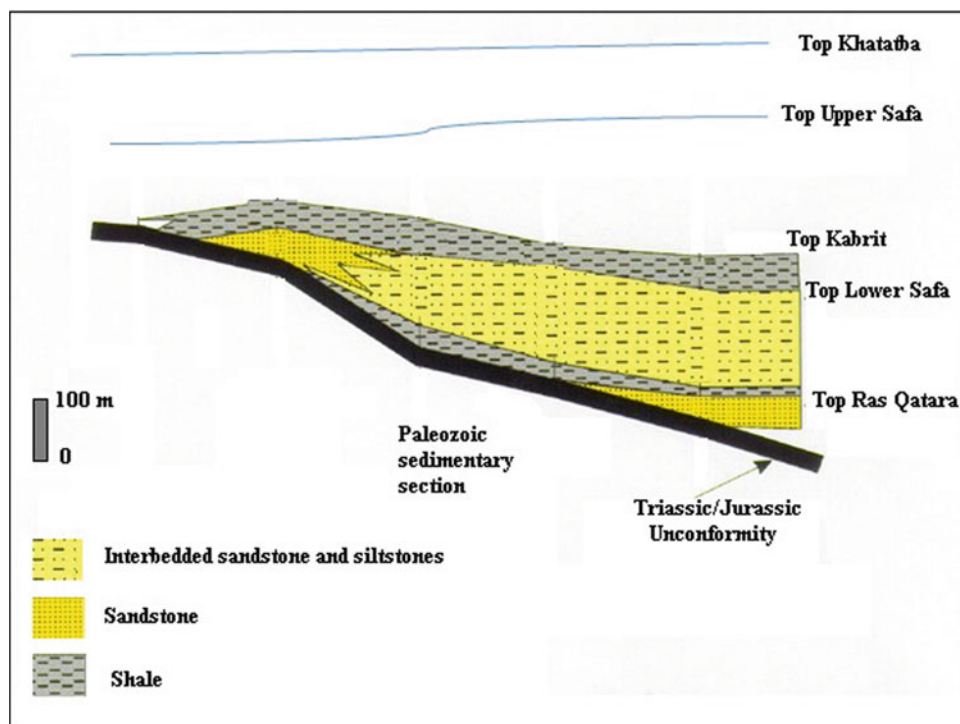


Fig. 11 Jurassic play of Obaiyed Field, Matruh Basin, WD. (modified from Mahmoud & Barkooky, 1998)

hydrocarbon accumulations may exist in the WD's deeply buried Mesozoic (half-graben basins) and Paleozoic sediments. More emphasis should be placed on the heterogeneous reservoirs found in the WD sedimentary basins (ex. Khatatba, Bahariya, AEB, Abu Roash, and Paleozoic formations). When looking for stratigraphic elements in the WD basins, the following characteristics are especially important: facies change, pinched-out sandstone bodies facies, truncation or erosion at unconformities, isolated sand bodies (channel) and diagenetic traps. The former stratigraphic elements can form perfect stratigraphic petroleum traps in all WD sedimentary basins. For example, the Khatatba formation is composed of sandstone channels that thin away from the channel axis in some regions and are surrounded by floodplain mudstone; tracing the channel axis could be advantageous and bring thick isolated reservoirs in new wells rather than thin sandstone drilled far from the channel axis. At the same time, it is not necessary to find a pure stratigraphic trap on its own; it could be accompanied by other structural elements, resulting in combined stratigraphic-structural traps, such as the Gulf of Suez trapping style (Radwan et al., 2021a).

7.2 Deeper Targets Reservoirs

The deeper Paleozoic and Jurassic targets are the treasure of WD sedimentary basins, and while some petroleum

companies have recently begun to explore deeper targets, additional resources are still under-exploration, and significant discoveries in these promising targets require extensive research. The OBA-A3 well was one of the wells drilled in 1996 to target deeper reservoirs in the Matruh Basin, and it produced Paleozoic oil. Later, as the importance of deeper targets becomes more widely recognized, Eni announces some new discoveries in the South West Meleiha Field (Faghur Basin). Aligning with Eni efforts to explore the WD's deep geological resources, particularly within the deeper Paleozoic and Jurassic sequences of the Faghur Basin.

Eni drilled several exploratory wells and announced new discoveries in the Faghur Basin; I will highlight some of the most recent new discoveries here. The SWM A-2X well (5090 m total depth) was drilled in the Faghur Basin and encountered an 18-m oil column of Carboniferous age sandstones, with an average production of 2300 BOPD. Later, the SWM B1-X well in the same basin made another discovery (7 km distance from SWM A2-X). The SWM B1-X well reached a total depth of 4523 m and encountered light oil (37° API) produced from deeper targets of Carboniferous sandstones with a thickness of 35 m and an average production rate of 5,130 BOPD. Another recent discovery was made while drilling the SWM-A-6X well (4815 total depths in meters), where a 130-ft oil column was discovered in the Dessouky formation (Carboniferous age) with an average production of 5000 BOPD.

In addition to Paleozoic source rocks, Khatatba source rocks appear to contribute significantly in the expulsion of

oil to both syn-rift and deeper Paleozoic reservoirs (Devonian and Silurian). According to Boote et al. (1998), the Devonian and Silurian deposits are important source rocks in Libya, but these deposits are thinning from Libya to the WD. Recent petroleum discoveries by petroleum companies in deeper targets have also discovered hydrocarbons in the AEB formation at deeper levels, indicating the additional resources that can be gained through deeper target exploration across the WD sedimentary basins. Exploring deeper targets, on the other hand, presents several challenges in terms of exploration and drilling, which will be highlighted in the challenge section.

7.3 Structural Play: Inversion Structures and Faulted Traps and Their Accompanied Fluid Migration

Inversion events influenced the structural regime of most WD sedimentary basins, reinitiating faults and forming folds in response to the unique structural features of each basin. More attention should be paid not only to the effect of such inversion events on structure features, but also to the accompanying “Tertiary” hydrocarbon migration. Inversion structures are common in the WD sedimentary basins, such as the Razzak Field, Mubarak Field, and Kattaniya High (Bevan & Moustafa, 2012).

Fluid leakage or Tertiary migration in a faulted trap, according to Sales (1997) & Bevan and Moustafa (2012), can be caused by gouge failure spill point juxtaposition spill point, or filled to seal capacity, which is known as “Cryptic” spill points. Bevan and Moustafa (2012) provided an example from Kattaniya High in the WD, where inversion events affected hydrocarbon accumulations on the inverted hanging wall half-graben anticline, causing the AEB formation to “switch off” to a shallower depth and influencing hydrocarbon migration (Fig. 12). More research into such phenomena could lead to new discoveries and unexpected reservoirs, but this will be dependent primarily on the petroleum system study in new prospect basins, which must be analyzed due to the uniqueness of each field.

7.4 Applying Sequence Stratigraphy Concept

The study of the spatiotemporal evolution of sedimentary basins is critical for fully understanding the geological and sedimentation conditions that control reservoirs and can lead to the discovery of new reservoirs (Catuneanu, 2006; Slatt, 2006; Radwan et al., 2021a; Shehata et al., 2021). Radwan et al. (2021a) emphasize the significance of sequence stratigraphy in hydrocarbon exploration in half-graben rift basins, which are similar to the WD half-graben basins.

According to Posamentier and Vail (1988), it is critical to investigate the spatial and temporal rock relationships within a surface boundary of erosion or non-deposition, as well as their correlative conformities. Several sedimentary cycles and sequence boundaries are recorded in the WD sedimentary succession; applying recent advances in sequence stratigraphy and tracing the output of these models will contribute to a better understanding of depositional sequences, which will improve our understanding of reservoir geometries and reservoir qualities at the pre-rift and syn-rift levels.

The use of sequence stratigraphy in WD sedimentary basins will lead to significant advances in predicting the lateral and vertical distribution of depositional sequences, including source, reservoir, and seal rocks. Furthermore, the sequence stratigraphy concept in hydrocarbons exploration can aid in the definition of component system tracts and facies, which will contribute significantly in the exploration and development of reservoirs, particularly clastic reservoirs. Using the sequence stratigraphy concept and the utility of correlating time-synchronous surfaces in heterogeneous clastics reservoirs of Cretaceous, Jurassic, and Paleozoic clastics deposits could lead to new discoveries and petroleum system geometries, specifically reservoir geometries.

7.5 Unconventional Resources

Recently, the development of unconventional resources has been one of the primary economic goals (Law & Curtis, 2002; Radwan et al., 2021b). Unconventional resources are becoming one of the ways to maintain domestic energy demand in Egypt and worldwide in order to replace declining conventional resources. The WD basins are not far from such unconventional resources and technology, and now some wells are already tested to discover and assess the predicted unconventional resources (Salah et al., 2017; Gomaa et al., 2019).

Unconventional resource evaluation necessitates the collection of a variety of integrated data, including geochemical, geomechanical, and petrophysical measurements. Because of the organic richness and widespread nature of Khatatba shales as the primary source of petroleum to conventional resources in the WD basins, it is of relative importance. The Apollonia and Khatatba formations are the most promising unconventional resource layers in the WD. In this regard, a series of horizontal and vertical wells were drilled in the WD to evaluate the Apollonia tight carbonate and Khatatba dark shales using multistage and one-stage hydraulic fracturing.

The open marine Apollonia Tight (Gas) Chalk formation, on the other hand, is spreading across the WD lands and is characterized by high porosity/low permeability soft chalky limestone. The Apollonia formation is divided into four

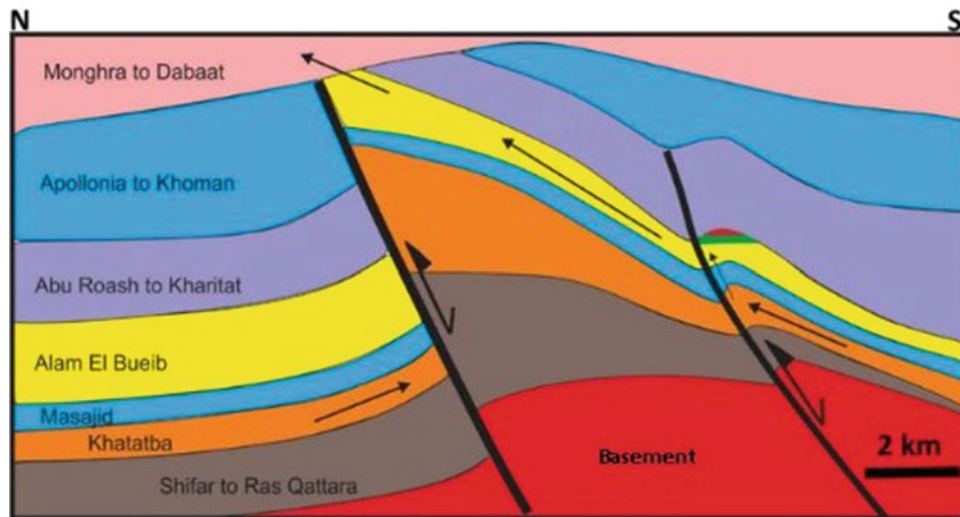


Fig. 12 Kattaniya high inversion structure and fault trap (after Bevan & Moustafa, 2012)

units: A, B, C, and D; the candidate's unconventional resources are massive chalky limestone (A) and glauconitic limestone (C). The Apollonia Tight Chalk and Khatatba formations in Egypt's Western Desert have been identified as potentially containing economically valuable gas accumulations. Salah and Ibrahim (2018) compared the Khatatba characteristics in the Matruh-Shoushan Basin to the well-known shale plays in the United States (Barnett and Marcellus) (Table 3). Accordingly, the WD Apollonia Tight Chalk and Khatatba formations have significant unconventional gas reserves, and developing these resources can help Egypt increase its natural resources. The tight sandstones in the southern WD should be evaluated economically for potential hydraulic fracturing for better hydrocarbon exploitation. More integrated work is required to better assess existing unconventional resources in the WD, as well as to improve exploration, characterization, and evaluation of WD sweet spots. More efforts are required to stimulate the unconventional gas industry, improve industry policy in the WD, and address development challenges.

7.6 Further Exploration in the Southern Western Desert Basins

More focus is needed to explore the hydrocarbon secrets of the southern WD sedimentary basins of Nuqra, Kharite, and Komombo basins. The exploration efforts in the Upper Egypt sedimentary basin during the last decades succeeded in presenting two commercial discoveries in the Komombo Basin, namely Al Barka and West El Barka oil fields. Petroleum companies were disappointed with high water saturation and low reservoir quality (tightness) in Nuqra and Komombo basin, however this because the less understanding of the structural setting and hydrocarbon system of these basins compared to other basins in the WD. The discoveries in Komombo basin indicate the potential of multi-pays across the sedimentary succession of these basins, therefore more structural, geophysical and geochemistry studies on the sedimentary succession of these basin studies has potential to bring new insights and better exploitation of these potential resources. According to El Nady et al. (2018), the source rocks of the Upper Cretaceous

Table 3 Comparisons of the Khatatba of the Matruh Shoushan basin with well-known shale plays (Barnett and Marcellus)

Shale plays	Khatatba	Barnett	Marcellus
Age	M. Jurassic	Mississippian	Devonian
Vertical depth (ft)	11,000–1300	6500–9000	4500–8000
Thickness (ft)	250–240	200–300	50–300
TOC (% wt.)	10-Feb	7-Mar	10-Mar
Vitrinite reflectance Ro	1.0–1.4	1.0–1.74	0.8–3
Pressure gradient (psi/ft)	0.55	0.45	0.4–0.6
Porosity (%)	12-Aug	10-Apr	6-Apr
Brittleness (%)	60–70	60–70	50–60
GIP (BCF/section)	100–200	100–300	70–150

formations range from immature to marginally mature, with the Maghrabi formation reaching only the early stages of oil generation. On the eastern side of the Komombo basin, there is a good chance of finding oil generated by the Abu Ballas, Dakhla, Maghrabi, Duwi, and Sabaya formations. Proven kerogen II source rock of up to 7wt. % TOC is exist in the Cretaceous sediments of Komombo Basin, the very good potential of source rocks to generate hydrocarbon shed the light for more exploration opportunities compared to the current minimal explored hydrocarbon traps. The presence of porous clastics throughout the stratigraphic section of these rift basins, as well as the seal capacity in the upper interval of the Senonian-Paleocene, indicate the presence of potential reservoirs somewhere in these basins. Furthermore, the formation of rotated fault blocks by the Early Cretaceous extensional rift and mildly inverted structures by a long period of Late Cretaceous to post-Early Eocene Syrian Arc compression in South Egypt indicate the potential for forming structural hydrocarbon traps and the presence of good hydrocarbon system elements. These rift basins are formed structurally as NW-trending rift basins with asymmetric fault-bounded half-grabens trending (oblique) to the Red Sea trend as a result of the reactivation of a major by the Neocomian, the Precambrian Pan African tectonic zone had been replaced by the Neocomian extensional tectonic. According to recent drilling and seismic interpretations, Neocomian-Barremian maximum subsidence might be exist and the Kharite, Nuqra of the eastern Nile River.

Advanced production techniques such as horizontal drilling and hydraulic fracturing might be the best option to enhance the productivity in tight sandstone reservoirs. Applying this technique has raised the reserves from 0.6 to 5.23 MMBO in the Al Baraka field (Mostafa et al., 2021). The produced oil from the southern basins is 37°API with a wax content that is similar to the oil in the neighboring Sudanese rift basins. The main risk is the absence of one of the hydrocarbon petroleum elements in the Komombo, Nuqra, and Kharite sedimentary basins. In terms of exploration risks, basin exhumation caused erosion of the basin roof and brought the maturity level to 1200 feet in the Nuqra basin. Moustafa et al. (2002) argued that the basin roofing was milder in the Komombo basin, with a maturity level of 2100 feet in the Komombo basin. The mildness of the inversion tectonics in the Nuqra and Kharite basins provides a good opportunity for hydrocarbon preservation, but the time of basin exhumation remains a risk. Further exploration is much needed in the Nuqra basin to better understand the petroleum geology and find economical quantities of hydrocarbon.

8 Challenges for Hydrocarbon Exploration in WD Basins

Although the WD's Mesozoic basins offer a variety of rewarding exploration opportunities, they are difficult to obtain and represent a difficult exploration opportunity. In general, the WD basins are distinguished by a complex geological history that has influenced their depositional setting and petroleum system elements. The structural regime of most basins in the greater WD sedimentary basins has been influenced by the Syrian Arc event's deformation and inversion. Furthermore, below the Alamein Dolomite, the quality of seismic imaging is very low.

Despite the numerous benefits of exploration in WD (for example, multiple reservoirs, onshore drilling, various traps, low cost, and conventional resources), it appears that exploration will continue to be active in WD for many years to come. However, challenges are arising at various levels of exploration and drilling. In this section, I will discuss some of the difficulties associated with hydrocarbon exploration in the WD sedimentary basins.

8.1 Drilling Issues Challenges

Quite apart from the geological and geophysical modeling of planned exploration and development wells, drilling obstacles have emerged as a major issue during the exploration and development phases (Radwan et al., 2019; Radwan, 2021). Drilling success is typically achieved through improved pore pressure prediction and geomechanical analysis (Radwan et al., 2020, Radwan and Sen, 2021a, 2021b). Drilling issues can arise during drilling into the carbonate of the Masajid and Alamein formations, resulting in partial or total losses.

According to, the main cause of these losses was that the former carbonates was karstified during the Jurassic period in response to tectonic uplift (Keeley et al., 1990). The difficulty in predicting the geometry and patterns of such phenomena is that the vugs are localized.

While drilling these sections, some mitigations, such as underbalanced drilling and Pressurized Mud Cap Drilling (PMCD), can be considered. The current depletion of conventional resources adds additional risks for losses while drilling, resulting in a stuck pipe and lost money which is matched with the current depletion status in gulf of suez according to (Radwan and Sen, 2021a, 2021b; Kassem et al., 2021; Abdelghany et al., 2021).

8.2 Petroleum System Challenges

Much of the deeper production from the Paleozoic across the WD is attributed to charge from Khatatba (Jurassic) or (AEB) Cretaceous shales via fault juxtaposition with the Paleozoic, raising questions about the role of the oldest Carboniferous source rocks, which are sometimes unknown. A comprehensive study that confirms the Paleozoic petroleum system has yet to be completed. Poor seismic images of the deepest source rocks (Carboniferous), contributing to poorly studied source rock. More research into the geochemical characterization of deeper resources, as well as biomarker analysis, are required to confirm the petroleum system in the deeper targets.

8.3 Seismic Issues

The number of 3D and 4D seismic surveys conducted across the WD basins is very limited, and the few conducted 3D seismic surveys are local in extent. In terms of seismic quality, seismic images beneath the Alamein dolomite horizon are low resolution, and thus deeper Jurassic and AEB horizons are poorly imaged.

Furthermore, human insight is still required in seismic imaging. In order to provide a precise interpretation. Improved seismic imaging could aid in the discovery of additional structural and combined traps. The majority of the new discoveries are based on 3D seismic imaging, demonstrating the importance of precise seismic imaging in increasing the resources in the WD basins. Furthermore, the deep basin geometries were not adequately defined and are still being unraveled, implying that seismic image quality will improve across the WD sedimentary basins.

Acknowledgements I am indebted to the reviewers for their constructive reviews which improved the chapter considerably. Special thanks to Prof. Zakaria Hamimi and co-guest editors for their invitation to contribute this Springer's book "The Phanerozoic Geology and Natural Resources of Egypt".

References

- Abd El Gawad, E. A., Ghanem, M. F., Makled, W. A., Mousa, D. A., Lotfy, M. M., Temraz, M. G., & Shehata, A. M. (2019a). Source rock evaluation of subsurface Devonian-Carboniferous succession based on palyno-organic facies analysis in Faghur Basin, North Western Desert of Egypt: A division of the North Africa Paleozoic Basins. *Arabian Journal of Geosciences*, 12(21), 1–20.
- Abd El Gawad, E. A., Ghanem, M. F., Lotfy, M. M., Mousa, D. A., Temraz, M. G., & Shehata, A. M. (2019b). Burial and thermal history simulation of the subsurface Paleozoic source rocks in Faghur basin, north Western Desert, Egypt: Implication for hydrocarbon generation and expulsion history. *Egyptian Journal of Petroleum*, 28(3), 261–271.
- Abdeen, M. M., Ramadan, F. S., Nabawy, B. S., et al. (2021). Subsurface structural setting and hydrocarbon potentiality of the Komombo and Nuqra Basins, South Egypt: A seismic and petrophysical integrated study. *Natural Resources Research*, 30, 3575–3603. <https://doi.org/10.1007/s11053-021-09898-2>
- Abdel-Fattah, M. I. (2015). Impact of depositional environment on petrophysical reservoir characteristics in Obaiyed Field, Western Desert, Egypt. *Arabian Journal of Geosciences*, 8(11), 9301–9314.
- Abdel-Fattah, M. I., Pigott, J. D., & Abd-Allah, Z. M. (2017). Integrative 1D–2D basin modeling of the Cretaceous Beni Suef basin, Western Desert, Egypt. *Journal of Petroleum Science and Engineering*, 153, 297–313. <https://doi.org/10.1016/j.petrol.2017.04.003>
- Abdel-Fattah, M. I., Pigott, J., & El-Sadek, M. S. (2020). Integrated seismic attributes and stochastic inversion for reservoir characterization: Insights from Wadi field (NE Abu-Gharadig Basin, Egypt). *Journal of African Earth Sciences*, 161, 103661.
- Abdelghany, W. K., Radwan, A. E., Elkhawaga, M. A., Wood, D., Sen, S., & Kassem, A. A. (2021). Geomechanical modeling using the depth-of-damage approach to achieve successful underbalanced drilling in the Gulf of Suez Rift Basin. *Journal of Petroleum Science and Engineering*. <https://doi.org/10.1016/j.petrol.2020.108311>
- Abdine, A., Meshref, W., Safi Wasfi, A., Aadland, A., Aal, A. (1993). Razzak field—Egypt, Dolson, J., Shann, M., Rashed, R. (2000). The petroleum potential of Egypt. In *Second Wallace E Pratt memorial conference 'petroleum provinces of the 21st century'*, San Diego (p. 37). Razzak-Alamein Basin, Northern Western Desert. AAPG special volumes: 29–56
- Ali, M., Darwish, M., Essa, M. A., & Abdelhady, A. (2018). 2D seismic interpretation and characterization of the Hauterivian-Early Barremian source rock in Al Baraka oil field, Komombo Basin, Upper Egypt. *Journal of African Earth Sciences*, 139, 113–119. <https://doi.org/10.1016/j.jafrearsci.2017.12>
- Ali, M., Abdelhady, A., Abdelmaksoud, A. et al. (2020). 3D Static modeling and petrographic aspects of the Albian/Cenomanian Reservoir, Komombo Basin, Upper Egypt. *Nature Resources Research* 29, 1259–1281. <https://doi.org/10.1007/s11053-019-09521-5>
- Alsharhan, A. S., & Abd El-Gawad, E. A. (2008). Geochemical characterization of potential Jurassic/Cretaceous source rocks in the Shushan Basin, northern Western Desert, Egypt. *Journal of Petroleum Geology*, 31(2), 191–212.
- Ayyad, M. H., & Darwish, M. (1996). Syrian Arc structures, a unifying model of inverted basins and hydrocarbon occurrences in North Egypt. In *Proceedings of the 13th Egyptian general petroleum corporation exploration and production conference* (21–24 Oct 1996, vol. 1, pp. 40–59)
- Bevan, T. G., & Moustafa, A. R. (2012). *Inverted rift-basins of Northern Egypt*. Elsevier.
- Boote, D. R., Clark-Lowes, D. D., & Traut, M. W. (1998). Palaeozoic petroleum systems of North Africa. *Geological Society, London, Special Publications*, 132(1), 7–68.
- Bosworth, W. (1994). A model for the three-dimensional evolution of continental rift basins, northeast Africa. *Geologische Rundschau*, 83, 671–688.
- Bosworth, W., & Tari, G. (2021). Hydrocarbon accumulation in basins with multiple phases of extension and inversion: Examples from the Western Desert (Egypt) and the western Black Sea. *Solid Earth*, 12(1), 59–77.
- Bosworth, W., El-Hawat, A. S., Helgeson, D. E., & Burke, K. (2008). 649 Cyrenaican "shock absorber" and associated inversion strain

- shadow in the collision zone of northeast Africa. *Geology*, 36(9), 695–698.
- Bosworth, W., Stockli, D. F., & Helgeson, D. E. (2015a). Integrated outcrop, 3D seismic, and geochronologic interpretation of Red Sea dike-related deformation in the Western Desert, Egypt—the role of the 23 Ma Cairo “mini-plume.” *Journal of African Earth Sciences*, 109, 107–119.
- Bosworth, W., Drummond, M., Abrams, M., & Thompson, M. (2015b). Jurassic rift initiation source rock in the Western Desert, Egypt—relevance to exploration in other continental rift systems. In *Petroleum systems in “rift” basins, 34th annual GCSSEPM foundation perkins-rosen research conference* (pp. 13–16).
- Catuneanu, O. (2006). *Principles of sequence stratigraphy*. Elsevier.
- Cheng, J. E. (2020). Petroleum system of Matruh-Shoushan Basin, Western Desert, Egypt. *Geological Behavior (GBR)*, 4(1), 1–8.
- Dolson, J. C., Shann, M. V., Matbouly, S. I., Hammouda, H., & Rashed, R. M. (2001b). Egypt in the twenty-first century: Petroleum potential in offshore trends. *GeoArabia*, 6(2), 211–230.
- Dolson, J. C., Shann, M. V., Hammouda, H., Rashed, R., & Matbouly, S. (1999). The petroleum potential of Egypt. *AAPG Bulletin*, 83(12).
- Dolson, C., Shaan, V., Matbouly, S., Harwood, C., Rashed, R., & Hammouda, H. (2001a). The petroleum potential of Egypt. In W. Downey, C. Threet, A. Morgan (Eds.), *Petroleum provinces of the twenty-first century* (vol. 74, pp. 453–482). American Association of Petroleum Geologists.
- Dolson, J. (2020). The petroleum geology of Egypt and history of exploration. In *The geology of Egypt* (pp. 635–658). Springer.
- Egyptian General Petroleum Corporation, EGPC (1992). WD, oil and gas fields (a comprehensive overview) (p. 431). Egyptian General Petroleum Corporation.
- El Diasty, W. S. (2015). Khatatba Formation as an active source rock for hydrocarbons in the northeast Abu Gharadig Basin, north Western Desert, Egypt. *Arabian Journal of Geosciences*, 8(4), 1903–1920.
- El Nady, M. M. (2013). Geothermal history of hydrocarbon generation of wells in the Northwestern Desert, Egypt. *Energy Sources Part A: Recovery, Utilization, and Environmental Effects*, 35(5), 401–412.
- El Nady, M. M. (2016). Timing of petroleum generation and source maturity of selected wells in Abu Gharadig Basin, North Western Desert, Egypt. *Energy Sources, Part a: Recovery, Utilization, and Environmental Effects*, 38(3), 391–401. <https://doi.org/10.1080/15567036.2013.78483>
- El Gazzar, A. M., Moustafa, A. R., & Bentham, P. (2016). Structural evolution of the Abu Gharadig field area, Northern Western Desert, Egypt. *Journal of African Earth Sciences*, 124, 340–354. <https://doi.org/10.1016/j.jafrearsci.2016.09.027>
- El Ghamry, M. N., El Amawy, M., & Hagag, W. (2020). The role of Late Cretaceous wrench tectonics in hydrocarbon endowment in El-Gindi Basin, northern Western Desert, Egypt. *Marine and Petroleum Geology*, 112, 104093. <https://doi.org/10.1016/j.marpetgeo.2019.10>
- El Nady, M. M., Ramadan, F. S., Hammad, M. M., Mousa, D. A., & Lotfy, N. M. (2018). Hydrocarbon potentiality and thermal maturity of the Cretaceous rocks in Al Baraka oil field, Komombo basin, South Egypt. *Egyptian Journal of Petroleum*, 27(4), 1131–1143.
- El Hawat, A. S. (1997). Chapter 4 Sedimentary basins of Egypt: An overview of dynamic stratigraphy. In *African Basins* (pp. 39–85). [https://doi.org/10.1016/s1874-5997\(97\)80007-x](https://doi.org/10.1016/s1874-5997(97)80007-x)
- Elmaadawy, K. G., & El-Ashmony, M. R. (2021). Tectonostratigraphic evolution of the new frontier Foram Basin and implications for hydrocarbon potential, Western Desert, Egypt. *Journal of African Earth Sciences*, 177, 104142.
- Farooqui, M. Y., Farhoud, K., Mahmoud, D., & El-Barkooky, A. N. (2012). Petroleum potential of the interpreted Paleozoic geoseismic sequences in the South Diyar Block, Western Desert of Egypt. *GeoArabia*, 17(3), 133–176.
- Garfunkel, Z. (1998). Constrains on the origin and history of the eastern Mediterranean basin. *Tectonophysics*, 298, 5–35.
- Garfunkel, Z. (2004). Origin of the Eastern Mediterranean Basin: A reevaluation. *Tectonophysics*, 391, 11–34.
- Gomaa, S., Attia, A., Abdelhady, A., Khaled, S., Elwageeh, M., Elhoshoudy, A. N., Omran, M., Essam, A., Osama, M., Ashraf, A., & Wagdy, C. (2019). Well testing analysis of unconventional gas reservoirs: real case study of tight gas carbonate reservoir, Apollonia formation, Western Desert, Egypt. *International Journal of Petroleum and Petrochemical Engineering (IJPPE)*, 5(1), 1–5.
- Guiraud, R., & Bosworth, W. (1997). Senonian basin inversion and rejuvenation of rifting in Africa and Arabia: Synthesis and implications to plate-scale tectonics. *Tectonophysics*, 282, 39–82.
- Guiraud, R., Bosworth, W., Thierry, J., & Delplanque, A. (2005). Phanerozoic geological evolution of Northern and Central Africa: An overview. *Journal of the African Earth Sciences*, 43, 83–143.
- Hakimi, M. H., Lotfy, N. M., El Nady, M. M., Makled, W. A., Ramadan, F. S., Rahim, A., Qadri, S.T., Lashin, A., Radwan, A. E., & Mousa, D.A. (2023). Characterization of Lower Cretaceous organic-rich shales from the Kom Ombo Basin Egypt: Implications for conventional oil generation. *Journal of Asian Earth Sciences* 241105459–S136791202200390X. <https://doi.org/10.1016/j.jseae.2022.105459>
- Hammad, M. M., Awad, S. A., El Nady, M. M., & Moussa, D. A. (2010). The subsurface geology and source rocks characteristics of some Jurassic and Cretaceous sequences in the West Qarun Area, North Western Desert, Egypt. *Energy Sources, Part a: Recovery, Utilization, and Environmental Effects*, 32(20), 1885–1898. <https://doi.org/10.1080/15567030701715955>
- Haq, B. U., Hardenbol, J., & Vail, P. R. (1988). Mesozoic and Cenozoic chronostratigraphy and cycles of sea-level change.
- Hegazy, A. (1992). WD oil and gas fields (A comprehensive overview). In *EGPC conference proceedings* (p. 4321). Egyptian General Petroleum Corporation.
- IHS, E. (2006). *Gulf of Suez Basin Monitor* (No. Iris21 ID:410900). IHS Energy.
- Kassem, A. A., Sen, S., Radwan, A. E. et al. (2021). Effect of depletion and fluid injection in the Mesozoic and Paleozoic Sandstone Reservoirs of the October Oil Field, Central Gulf of Suez Basin: Implications on drilling, production and reservoir stability. *Nature Resources Research*. <https://doi.org/10.1007/s11053-021-09830-8>
- Katz, B. (1995). A survey of rift basin source rocks. *Geological Society London Special Publications*, 80(1), 213–240.
- Keeley, M. L., Dungworth, G., Floyd, C. S., Forbes, G. A., King, C., McGarva, R. M., Shaw, D. (1990). The Jurassic system in Northern Egypt: I. Regional stratigraphy and implications for hydrocarbon prospectivity. *Journal of Petroleum Geology*, 13(4), 397–420.
- Law, B. E., & Curtis, J. B. (2002). Introduction to unconventional petroleum systems. *AAPG Bulletin*, 86(11), 1851–1852.
- Leeder M. R., & Gawthorpe R. L. (1987). Sedimentary models for extensional 784 tilt-block/half-graben basins. In M. P. Coward, J. F. Dewey, P. L. Hancock (Eds.), *Continental extensional tectonics. Geological Society London Special Publications*, 28, 139–152.
- Lüning, S., Kolonic, S., Belhadj, E. M., Belhadj, Z., Cota, L., Barić, G., & Wagner, T. (2004). Integrated depositional model for the Cenomanian-Turonian organic-rich strata in North Africa. *Earth-Science Reviews*, 64(1–2), 51–117.

- Mahmoud, A., & El Barkooky, A. (1998). Mesozoic valley fills incised in Paleozoic rocks: potential exploration targets in the North Western Desert of Egypt, Obaiyed area. In *Proceedings of the 14th Petroleum Conference*, Cairo (pp. 84–100). Egyptian General Petroleum Corporation
- Makky, A. F., El Sayed, M. I., Abu El-Ata, A. S., Abd El-Gaied, I. M., Abdel-Fattah, M. I., & Abd-Allah, Z. M. (2014). Source rock evaluation of some upper and lower Cretaceous sequences, West Beni Suef Concession, Western Desert, Egypt. *Egyptian Journal of Petroleum*, 23 (1), 135–149. <https://doi.org/10.1016/j.ejpe.2014.02.016>
- Makled, W. A., Mostafa, T. F., Mousa, D. A., & Abdou, A. A. (2018). Source rock evaluation and sequence stratigraphic model based on the palynofacies and geochemical analysis of the subsurface Devonian rocks in the Western Desert, Egypt. *Marine and Petroleum Geology*, 89, 560–584.
- Mansour, A., & Tahoun, S. S. (2018). Palynological and palaeoenvironmental analyses of the upper Albian-Cenomanian succession in Gindi Basin, Egypt: Implication for transgressive/regressive systems tracts. *Journal of African Earth Sciences*, 147, 603–622. <https://doi.org/10.1016/j.jafrearsci.2018.0>
- Metwalli, F. I., & Pigott, J. D. (2005). Analysis of petroleum system criticals of the Matruh-Shushan Basin, Western Desert, Egypt. *Petroleum Geoscience*, 11, 157–178.
- Moretti, I., Kerdraon, Y., Rodrigo, G., Huerta, F., Griso, J. J., Sami, M., Said, M., & Ali, H. (2010). South Alamein petroleum system (Western Desert, Egypt). *Petroleum Geoscience*, 16(844), 121–132.
- Morris, A., & Tarling, D. H. (1996). Palaeomagnetism and tectonics of the Mediterranean region: An introduction. *Geological Society, London, Special Publications*, 105(1), 1–18. <https://doi.org/10.1144/gsl.sp.1996.105.01.01>
- Mostafa, A., Sehim, A., El Barkooky, A., & Hamed, M. (2021). Structural setting and hydrocarbon potential of Kharite-Nuqra-Komombo Rift Basins, South Egypt: A prospective approach. *International Journal of Engineering Applied Sciences and Technology*, 6(3), 20–29. ISSN No. 2455-2143
- Moustafa, A. R., & Khalil, M. H. (1990). Structural characteristics and tectonic evolution of north Sinai fold belts. In R. Said (Ed.), *The geology of Egypt* (pp. 381–392). Balkema Publishers.
- Moustafa, A. R., El-Barkooky, A. N., Mahmoud, A., Badran, A. M., Helal, M. A., Nour El Din, M., & Fathy, H. (2002). Matruh basin: hydrocarbon plays in an inverted Jurassic-Cretaceous rift basin in the northern Western Desert of Egypt. In *AAPG International meeting, Cairo*. Abstract.
- Posamentier, H. W., & Vail, P. R. (1988). Eustatic controls on clastic deposition II—sequence and systems tract models
- Prosser, S. (1993). Rift-related linked depositional systems and their seismic expression. *Geological Society, London, Special Publications*, 71(1), 35–66.
- Radwan, A., & Sen, S. (2021a). Stress path analysis for characterization of In Situ stress state and effect of reservoir depletion on present-day stress magnitudes: Reservoir geomechanical modeling in the Gulf of Suez Rift Basin, Egypt. *Nature Resources Research* 30, 463–478. <https://doi.org/10.1007/s11053-020-09731-2>
- Radwan, A. E., & Sen, S. (2021b). Characterization of in-situ stresses and its implications for production and reservoir stability in the depleted El Morgan hydrocarbon field, Gulf of Suez Rift Basin, Egypt. *Journal of Structural Geology*, 104355. <https://doi.org/10.1016/j.jsg.2021.104355>
- Radwan, A. E., Abudeif, A. M., Attia, M. M., & Mohammed, M. A. (2019). Pore and fracture pressure modeling using direct and indirect methods in Badri Field, Gulf of Suez, Egypt. *Journal of African Earth Sciences*, 156, 133–143. <https://doi.org/10.1016/j.jafrearsci.2019.04.015>
- Radwan, A. E., Abudeif, A. M., Attia, M. M., Elkhawaga, M. A., Abdelghany, W. K., & Kasem, A. A. (2020a). Geopressure evaluation using integrated basin modelling, well-logging and reservoir data analysis in the northern part of the Badri oil field, Gulf of Suez, Egypt. *Journal of African Earth Sciences*, 162, 103743. <https://doi.org/10.1016/j.jafrearsci.2019.103743>
- Radwan, A. E., Trippetta, F., Kassem, A. A., & Kania, M. (2021a). Multi-scale characterization of unconventional tight carbonate reservoir: Insights from October oil field, Gulf of Suez rift basin, Egypt. *Journal of Petroleum Science and Engineering*, 107968. <https://doi.org/10.1016/j.petrol.2020.107968>
- Radwan, A. E., Rohais, S., & Chiarella, D. (2021b). Combined stratigraphic-structural play characterization in hydrocarbon exploration: a case study of Middle Miocene sandstones, Gulf of Suez basin, Egypt. *Journal of Asian Earth Sciences*, 104686. <https://doi.org/10.1016/j.jseae.2021.104686>
- Radwan, A. E., Wood, D. A., Mahmoud, M., Tariq, Z. (2022). Gas adsorption and reserve estimation for conventional and unconventional gas resources. In D. A. Wood, J. Cai (Eds.), *Sustainable geoscience for natural gas sub-surface systems* (pp. 345–382). Elsevier. <https://doi.org/10.1016/B978-0-323-85465-8.00004-2>
- Radwan, A. E. (2021). Modeling pore pressure and fracture pressure using integrated well logging, drilling based interpretations and reservoir data in the Giant El Morgan oil Field, Gulf of Suez, Egypt. *Journal of African Earth Sciences*, 104165. <https://doi.org/10.1016/j.jafrearsci.2021.104165>
- Radwan, A. E. (2022a). Three-dimensional gas property geological modeling and simulation. In D. A. Wood, J. Cai (Eds.), *Sustainable geoscience for natural gas sub-surface systems* (pp. 29–45). Elsevier. <https://doi.org/10.1016/B978-0-323-85465-8.00011-X>
- Said, R. (1990). North Western Desert. In R. Said (Ed.), *The geology of Egypt* (p. 729). Balkema
- Salah, M., & Ibrahim, M. (2018). Unconventional reservoir development in Egypt's Western Desert: Lessons learned from the first appraisal wells. In *Proceedings of the 6th unconventional resources technology conference*. <https://doi.org/10.15530/urtec-2018-2902739>
- Salah, M., Orr, D., ElSebaee, M., Kamar, A., Batmaz, T., Eldarawy, Y., & Salem, L. (2017). Integrated advanced workflows and heterogeneity analysis for planning unconventional horizontal wells in Western Desert of Egypt. In *Offshore Mediterranean conference and exhibition*. OnePetro
- Salama, A. M., Abd-Allah, Z. M., El-Sayed, M. I., & Elbastawesy, M. A. (2021). Source rock evaluation and burial history modeling of Cretaceous rocks at the Khalda Concession of Abu Gharadig Basin, Western Desert, Egypt. *Journal of African Earth Sciences*, 184, 104372. <https://doi.org/10.1016/j.jafrearsci.2021.1>
- Sales, J. K. (1997). Seal strength versus trap closure—a fundamental control on the distribution of oil and gas. In R. C. Surdam (Eds.), *Seals, traps, and the petroleum system*. *AAPG Memoir*, 67, 57–83
- Scherer, C. M. S., Lavina, L. E. C., Dias Filho, D. C., Oliveira, F. M., Bongioiolo, D. E., & Silva, E. (2007). Stratigraphy and facies architecture of the fluvial eolian lacustrine Sergi formation (upper Jurassic), Recôncavo Basin, Brazil. *Sedimentary Geology*, 194, 169–193.
- Schlumberger, (1984). In C. M. Smith (Ed.), *Well evaluation conference*, Cairo (vol. 1, pp. 19–43)
- Schlumberger, (1995). *Well evaluation conference*, Egypt (pp 72–87). EGPC Report
- Schull, T. J. (1988). Rift basins of interior Sudan: Petroleum exploration and discovery. *AAPG Bulletin*, 72(10), 1128–1142.


- Selim, S. S. (2016). A new tectono-sedimentary model for Cretaceous mixed nonmarine-marine oil-prone Komombo Rift, South Egypt. *International Journal of Earth Sciences*, 105(5), 1387–1415.
- Shahar, J. (1994). The Syrian arc system: An overview. *Palaeogeography, Palaeoclimatology, Palaeoecology*, 112(1–2), 125–142.
- Shalaby, M. R., Hakimi, M. H., & Abdullah, W. H. (2011). Geochemical characteristics and hydrocarbon generation modeling of the Jurassic source rocks in the Shoushan Basin, North Western Desert, Egypt. *Marine and Petroleum Geology*, 28(9), 1611–1624. <https://doi.org/10.1016/j.marpetgeo.2011.07.003>
- Shalaby, M. R., Hakimi, M. H., & Abdullah, W. H. (2014). Petroleum system analysis of the Khatatba formation in the Matruh-Shoushan Basin, North Western Desert, Egypt. *Arabian Journal of Geosciences*, 7, 4303–4320.
- Shehata, A. A., Kassem, A. A., Brooks, H. L., Zuchuat, V., & Radwan, A. E. (2021). Facies analysis and sequence-stratigraphic control on reservoir architecture: Example from mixed carbonate/siliciclastic sediments of Raha Formation, Gulf of Suez, Egypt. *Marine and Petroleum Geology*, 105160. <https://doi.org/10.1016/j.marpetgeo.2021.105160>
- Slatt, R. M. (2006). *Stratigraphic reservoir characterization for petroleum geologists, geophysicists, and engineers*. Elsevier Science Limited.
- Stampfli, G. M., Mosar, J., Favre, P., Pillevuit, A., & Vannay J. C. (2001). Permo-Mesozoic evolution of the western Tethys realm: The Neo-Tethys East Mediterranean Basin connection. *Anglais*, 186, 51–108
- Sultan, N., Halim, M. (1988). Tectonic framework of Northern Western Desert, Egypt and its effect on hydrocarbon accumulations. In *EGPC 9th petroleum exploration and production conference*, Cairo (pp. 1–19)
- Taha, M. A. (1992). Mesozoic rift basins in Egypt: their southern extension and impact on future exploration. In *Proceedings of the 11th petroleum exploration and production conference*, Cairo (pp. 1–19). The Egyptian General Petroleum Corporation
- Tassy, A., Crouzy, E., Gorini, C., Rubino, J., Bouroullec, J., Sapin, F. (2015). Egyptian Tethyanmargin in the Mesozoic: Evolution of a mixed carbonate-siliciclastic shelf edge (from Western Desert to Sinai). *Marine and Petroleum Geology*
- Younes, M. A. (2012) Hydrocarbon potentials in the Northern Western Desert of Egypt. In: M. Younes (Ed.), *Crude oil exploration in the world*, (pp. 23–46)
- Yousef, M., Yousef, M., & Sehim, A. (2019). Structural style and evolution of inversion structures of Horus field, Alamein Basin, Northern Western Desert of Egypt. *Marine and Petroleum Geology*, 110, 55–72. <https://doi.org/10.1016/j.marpetgeo.2019.07.009>
- Zein El-din, M. Y., Abd El-Gawad, E. A., El-Shayb, H. M., & Haddad, I. A. (2001). Geological studies and hydrocarbon potentialities of the Mesozoic rocks in Ras Kanayis onshore area, North Western Desert, Egypt. *Annals of the Geological Survey of Egypt* 24,115–134



Ahmed E. Radwan is an adjunct professor at the Institute of Geological Sciences of the Jagiellonian University (Poland). Dr. Radwan has academic and industrial experience, since he obtained his Ph.D. in geophysics at Sohag University, Egypt, besides his proficient work in the oil and gas industry as a section head at the exploration department of the Gulf of Suez Petroleum Company (Gupco), Egypt. As a post-doctoral research scientist, he attended Innsbruck University in Austria in 2019. In 2020, he joined the Jagiellonian University in Poland. Despite his youth, he has received numerous awards from international organizations such as the International Union of Geological Sciences (IUGS), the Geochemical Society (GS), the Clay Minerals Society (CMS), the Austrian Forschungsgemeinschaft (FG), the Narodowa Agencja Wymiany Akademickiej (NAWA), the Austrian Federal Ministry of Education, Science, and Research (BMBWF), and petroleum companies. Dr. Radwan has authored more than 90 papers in highly indexed international peer-reviewed journals, published three book chapters, presented at numerous international conferences, and invited to join the technical committees of many international conferences worldwide. Dr. Radwan serves as an editor in leading journals with the famous publishers worldwide such as *Asian Earth Sciences*, *Marine and Petroleum Geology*, *Petroleum Science and Engineering*, *Petroleum Exploration and Production Technology*, *the Geological Journal*, *Energy Geosciences*, and *Petroleum Research*, in addition to being an editorial board member of unconventional resources, besides his role as an associate editor in MPG. Dr. Radwan is a book reviewer and a research article reviewer for several publishers and journals, and he organizes many special issues in different journals with the leading publishers. His research interests focused on multidisciplinary research integrating geosciences (geophysics, geochemistry, and geology), petroleum engineering, and reservoir engineering, as follows: 1: Geology areas include: petroleum geology, reservoir characterization, sedimentology, facies analysis, depositional environment, diagenesis, paleo-environment interpretations, subsurface analysis, basin analysis, reservoir quality, fluid flow, fractures, formation evaluation, and unconventional and conventional resources; 2: petroleum engineering (petroleum geomechanics, drilling, fluids, and casing design); 3: reservoir engineering (reservoir geology and geophysics, reservoir damage, production optimization, water flooding, stimulations, fluid flow, and enhanced recovery); 4: the geophysics fields of study (e.g., formation evaluation, petrophysics, borehole geophysics, and rock typing); 5: geochemistry fields of study include geochemical characterization, basin modeling, petroleum systems, and isotope analysis; 6: petroleum geomechanics (pore pressure, wellbore stability, in-situ stress orientation, and magnitudes); 7: machine learning applications in the energy industry; and 7: energy storage.



A Review of the Offshore East Mediterranean Mesozoic-Cenozoic Petroleum Systems

Fadi H. Nader, Sebastian Grohmann, Bandar I. Ghassal, Haytham El Atfy , Maria F. Romero-Sarmiento, Samer Bou Daher, François Baudin, and Ralf Littke

Abstract

A geological overview on the East Mediterranean realm, featuring the tectono-stratigraphic evolution and associated depositional environments as well as the known petroleum systems, is provided in this contribution. The Levant Basin, the (northern) Western Desert, and the Nile Delta are the main focus of this review because they include significant oil and gas discoveries (a total of 63,000 MMBOE has been forecasted for these regions), providing a considerable amount of data. The onshore-offshore extension of the Northern Western Desert (to Herodotus Basin) is compared to that of the Eastern Levant Margin—both share similar tectono-stratigraphic evolutions until the establishment of the Levant Fracture System. The Upper Cretaceous source rocks distribution across the Western Desert margin is, nevertheless believed to be controlled by increased bio-productivity and

nutrients with sediment transport from nearby hinterland, contrasting an upwelling scenario for the same source rocks in the Levant Basin. The possibility of mixing hydrocarbon from these deeper kitchens with the known overlying microbial gas accumulated in the Oligo-Miocene interval has been proven by the Karish discovery in the Levant Basin and through modeling the probability for fracturing the Eocene sealing unit. This may well occur in offshore Western Desert. The Nile has been the principal sediment feeder of the East Mediterranean basins since the Late Miocene. The Nile Delta is characterized by Oligo-Miocene petroleum systems, while the deeper Mesozoic systems still need further studies. The presence of carbonate plays has already been demonstrated by the discovery of the giant Zohr field. Succeeding in finding similar prizes requires understanding the complexity of such heterogeneous, yet attractive carbonate reservoirs. The East Mediterranean realm remains a frontier hydrocarbon province with a considerable wealth of knowledge that will help in understanding sedimentary basins at the intersections of major plate boundaries and the association of deep lithospheric processes and major shallow and surface processes.

F. H. Nader (✉) · M. F. Romero-Sarmiento
IFP Energies Nouvelles, Earth Sciences and Environmental
Technologies, Paris, France
e-mail: fadi-henri.nader@ifpen.fr

S. Grohmann · R. Littke
Institute of Geology and Geochemistry of Petroleum and Coal,
Energy and Mineral Resources (EMR), RWTH Aachen
University, Aachen, Germany

B. I. Ghassal
EXPEC Advanced Research Center, Saudi Aramco, Dhahran,
Saudi Arabia

H. El Atfy
Institut Für Geowissenschaften, Eberhard Karls Universität
Tübingen, Tübingen, Germany

Geology Department, Faculty of Science, Mansoura University,
Mansoura, Egypt

S. B. Daher
Division of Global Solutions, Beicip-Franlab, Paris, France

F. Baudin
ISTeP, Sorbonne Université, Paris, France

1 Introduction

The Mediterranean coastline stretches over 46,000 km on the African, European and Asian continents, hosting around 480 million people whose growing energy demands need to be met with optimal development of georesources. The East Mediterranean region, where northern Egypt occupies a significant part, is located—from a geological perspective—at the triple junction point between the Eurasian Plate in the North, the African Plate in the Southwest, and the Arabian Plate in the East (Fig. 1). This region is characterized by an

older, thicker, cooler, and stronger lithosphere compared to the western part of the Mediterranean Sea (Fig. 1; Roure et al., 2012). It is also commonly believed that this region belongs to the southern, passive margin of the Tethys, including evidence of its associated rifting, post-rift subsidence, and inversion phases. Hence, deep mantle dynamics and the evolution of plate boundaries resulted in the specific subsidence and thermal histories of the East Mediterranean sedimentary basins that influenced local petroleum systems.

During the last decades, the East Mediterranean region has witnessed exceptional oil and gas exploration developments, demonstrated by significant discoveries (Figs. 1 and 2) and the opening of new frontiers and acreages. The industrial advances happened together with an impressive set of scientific achievements in various fields (geophysics, seismic data acquisition and interpretations, geodynamics and structural geology, tectono-stratigraphy and sedimentology, as well as petroleum systems analyses and geochemistry, e.g., Hawie et al., 2013; Ghalayini et al., 2014; Bou Daher et al., 2014; Tassy et al., 2015; Ghassal et al., 2016; Grohman et al., 2018; Papadimitriou et al., 2018a, 2018b; Symeou et al., 2018; Inati et al., 2018; El Hajj et al., 2019). Hence, a huge amount of data, viable concepts, and expertise have been made available for this region.

Egypt is situated in the southern part of the Eastern Mediterranean region, where the first hydrocarbon exploration and production operations occurred at the beginning of the previous century. In 2015, the discovery of the giant Gas Field Zohr, located south of the Eratosthenes Seamount between the Herodotus and Levant Basin (Fig. 1), sparked new interest in the overall region. Egypt's total oil and gas discoveries amount to 29,000 MMBOE in 2009, principally from three petroleum provinces (Dolson et al., 2014): Gulf of Suez (11,500 MMBOE), Nile Delta (11,200 MBOE) and the Western Desert (5,700 MBOE). Dolson et al. (2014) predicted an ultimate yet-to-find of 37,600 MBOE for Egypt resources (revised to 38,600 MBOE, Dolson, 2018) in agreement somehow with the USGS forecasts for the Nile Delta (223 TCF, or 38,000 MMBOE) and the Levant Basin (117 TCF, or 20,000 MMBOE) (Kirschbaum et al., 2010; Schenk et al., 2010 and 2012).

More than 70 TCF (around 12,500 MBOE; Fig. 2) of natural gas were recently discovered in the Levant Basin (East Mediterranean region), which lies offshore Cyprus, Egypt, Israel, and Lebanon (Fig. 1). New plays have been proposed, and new un-explored areas may yield additional significant discoveries (e.g., Ghassal et al., 2016; Montadert et al., 2014; Nader, 2011, 2014). Nevertheless, the East Mediterranean region is characterized by a general lack of published geological data, a complex geodynamic and tectono-stratigraphic evolution, and high exploration costs. It is one of the typical frontier exploration areas, where numerical solutions, such as stratigraphic forward modeling (SFM), complex burial/

thermal modeling (including petroleum systems modeling; PSM) (Barabasch et al., 2019; Grohmann et al., 2021), and uncertainty modeling with machine learning (Ducros & Nader, 2020), proved to be an excellent help for enhancing reservoir play fairways predictions.

In the last two decades, a significant amount of 2D and 3D seismic reflection data have been acquired throughout the East Mediterranean region. These activities generated a considerable amount of new data on the stratigraphic intervals below the Messinian salt, sparking the interest for academic and industry-led investigations. Recent seismic reflection acquisition offshore Egypt (Western Desert) also yielded invaluable information for a promising future exploration era. According to PGS (Petroleum Geo-Services; <https://www.pgs.com>), the exhaustive new 2D and 3D seismic data covering more than 80,000 km² confirm the viability of this new exploration frontier area. Hence, seismic data interpretations already showed the possible extension of the Pliocene sandstone play from the Nile Delta, potential for Zohr-type pre-salt carbonate and pre-salt sandstone plays. The offshore area is believed to be an extension of the prolific onshore Western Desert.

Recent research work, which focused on the Levant Basin and was based on such substantial new data, provided new concepts for better understanding the crustal, structural, and stratigraphic characteristics of this region, as well as its key petroleum systems (e.g., Bou Daher et al., 2016; Ghalayini et al., 2015; Grohmann et al., 2018, 2021; Hawie et al., 2017; Inati et al., 2018; Papadimitriou et al., 2018a, 2018b; Symeou et al., 2018). These contributions together with the previous work of Abdel Aal et al. (2001), Shaaban et al. (2006), Dolson et al. (2014), Tassy et al. (2015), and Ghassal et al. (2016) on the Nile Delta and the Western Desert, Gardosh and Druckman (2006) and Gardosh et al. (2008) on offshore Israel and Bowman (2011) on offshore Syria, to name a few, encompass the collective geological knowledge of the southern East Mediterranean region. Gvirtzman et al. (2014), Hawie et al. (2017), Nader et al. (2018), and Grohmann et al. (2021) have proposed 3D stratigraphic forward models for the Levant Basin and offshore Egypt (Nile Delta). Still, to date, no comprehensive regional stratigraphic model exists for the southern East Mediterranean region. The area stretching from the Sinai Hinge Zone and the Nile Delta in the South to the Cyprus Arc in the North, and from the inverted Palmyra Trough and the Levant Fracture System to the East to the Eratosthenes Seamount and Herodotus Basin to the West (Fig. 1) requires detailed local studies but also has to be investigated as a whole (e.g., Wood, 2015) in order to achieve an overall geological understanding.

This chapter aims to provide a general overview of the geologic settings, the tectonic history, the depositional evolution, and petroleum systems of the East Mediterranean region, focusing on the Levant Basin, the Western Desert,

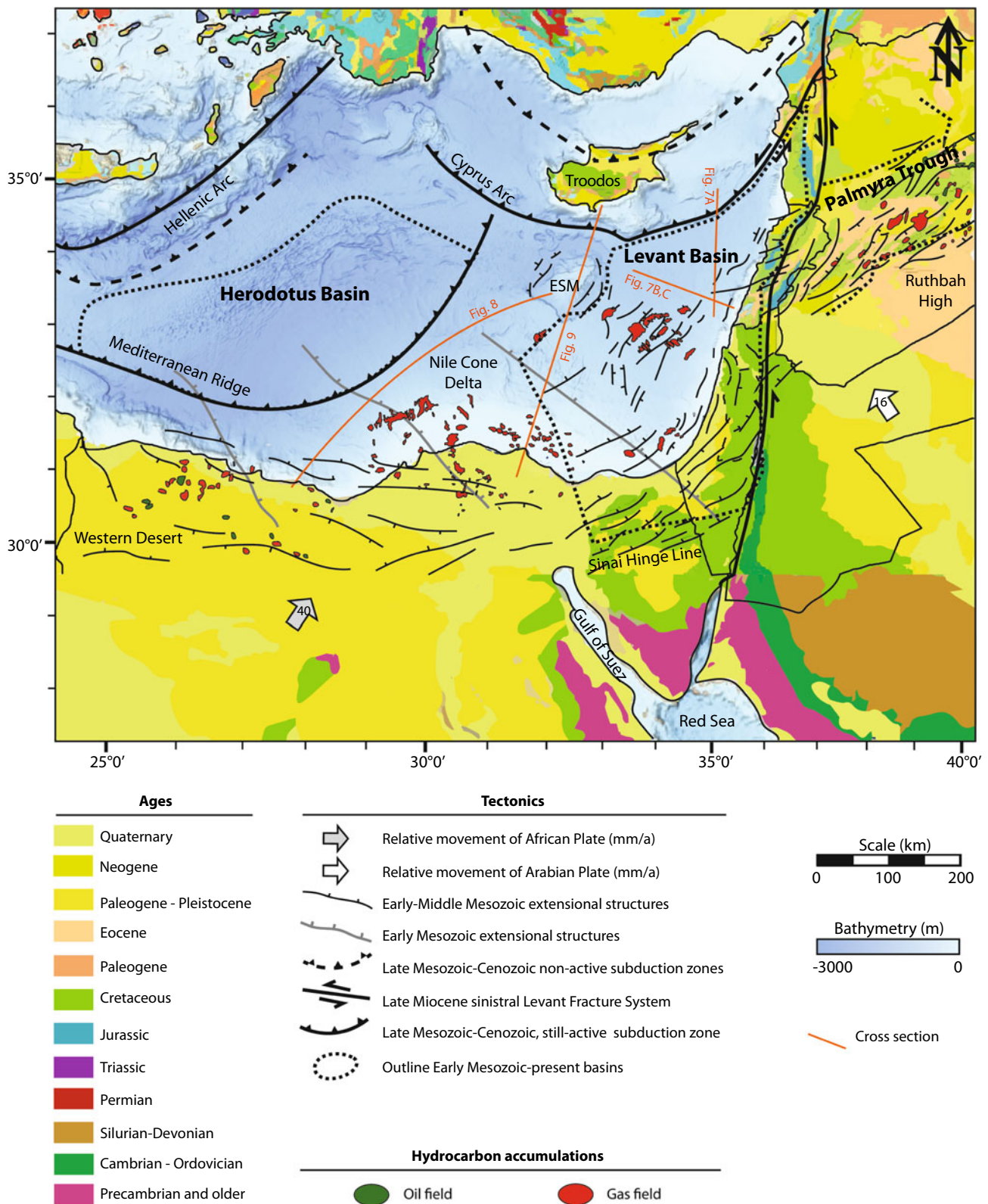


Fig. 1 Simplified geological map of the East Mediterranean region together with the main tectonic features as well as present-day oil and gas fields. In this work, the main focus lies on the regions representing the former northern margin of Gondwana, characterized by Early Mesozoic extensional structures that can be traced from the Western Desert in northeastern Egypt over Israel and Lebanon up to Syria as well as on their main adjacent sedimentary basins, the Herodotus Basin in the West, and the Levant Basin in the East. The orange lines indicate the location of regional cross-sections shown in Figs. 7, 8, and 9, respectively (Geological map based on data from Asch (2003) and Thiéblemont (2016); bathymetry taken from NOAA, 2022; tectonic features based on Dilek & Altunkaynak, 2009; Tassy et al., 2015; Ghalayini et al., 2018)

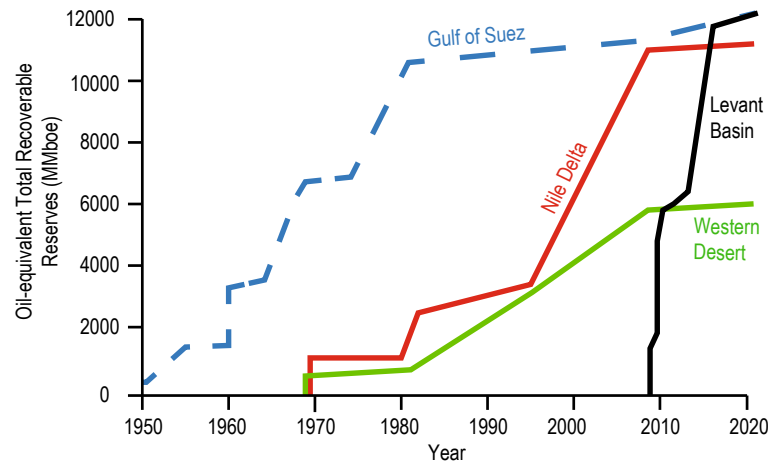


Fig. 2 Schematic creaming curves for the East Mediterranean region including the Gulf of Suez, Nile Delta, Western Desert, and Levant Basin (see text for references)

and the Nile Delta. This approach is made possible by integrating and synthesizing a great wealth of information from published data.

2 Geological Setting

2.1 Geodynamic Evolution

The East Mediterranean geodynamics are principally associated with the Pangea breakup in the Late Paleozoic, the interactions of the resulting separate plates, and the evolution of the Tethys Ocean (Fig. 3). The disintegration of Gondwana and the opening of the Tethys (Fig. 3a) led to the creation of major sedimentary basins in this region (e.g., Palmyra, Levant, Herodotus; Figs. 1 and 3) and their filling. By the Late Cretaceous (Fig. 3b), the overall extensional tectonics became compressional and initiated the closure of the Tethys ocean. The older Mesozoic basins started to be inverted in the East Mediterranean region. The Afro-Arabian plate moved northward, and a north-verging subduction zone evolved at the southern margin of Eurasia (Hawie et al., 2014, and references therein; Fig. 3b). There, slab pull-related forces resulted in new oceanic crust and the obduction of ophiolitic complexes (e.g., Lord et al., 2009; Swarbrick & Robertson, 1980). The Troodos ophiolites that are exposed in Cyprus mark the southern limit of the Tethyan Ocean and rest on Mesozoic platform carbonates, most probably belonging to the Afro-Arabian passive margin (Roure et al., 2012). Traces of basin inversions have been investigated primarily onshore, along the eastern and southern margins of the Levant Basin (cf. Syrian Arc structures in Palmyra Basin and along the Levant margin) and to a lesser extent offshore, e.g., the Cyprus Arc System (Symeou et al., 2018).

In the aftermath of the Tethys Ocean closure and the prominent Afro-Arabia collision with the Eurasian blocks, the Afar mantle plume contributed to the uplift and tilting of Afro-Arabia northern margins. Faccenna et al. (2013) applied mantle circulation computations to confirm the association of the Afar mantle upwellings with the Aegean slab pull (Fig. 4). The igneous province of Ethiopia demonstrates localized mantle upwelling about 30 Ma while rifting took place in the Red Sea and the Gulf of Suez (as of Late Eocene–Early Oligocene). The first phase of uplift of the Red Sea shoulders and the Levant margins are also ascribed to the Late Eocene–Early Oligocene (Faccenna et al., 2013). At almost the same time, the northern edge of the Arabian Plate collided with the Anatolian blocks. Zagros-Bitlis subduction took place as of Early Oligocene. During the Miocene (Fig. 3c), Africa’s motion slowed down as the rifting of the Gulf of Suez transferred to the Gulf of Aqaba, while Arabia kept its northward motion. This resulted in the initiation of the Levant Fracture System (Fig. 3d) from the Gulf of Aqaba, through the Dead Sea Fault northward through Lebanon and Syria (Nader, 2014). These events (Fig. 4) were contemporaneous with slab steepening and break off events (15–10 Ma, respectively), with the emplacement of mantle convection dynamics and northward flow from Afar to Anatolia (Faccenna et al., 2013). Thus, such mantle dynamics may be considered as the driving force for the observed increased subsidence and sedimentary filling of Herodotus and Levant basins together with the uplift of the surrounding margins. The significant inversion effects of the Levant Fracture System on the eastern margin of the Levant Basin (including the Lebanese mountains) continued in the Late Miocene and were followed by the tectonic westward escape motion of Anatolia, which has been well illustrated along the Cyprus Arc System (Montadert et al., 2014; Symeou et al., 2018).

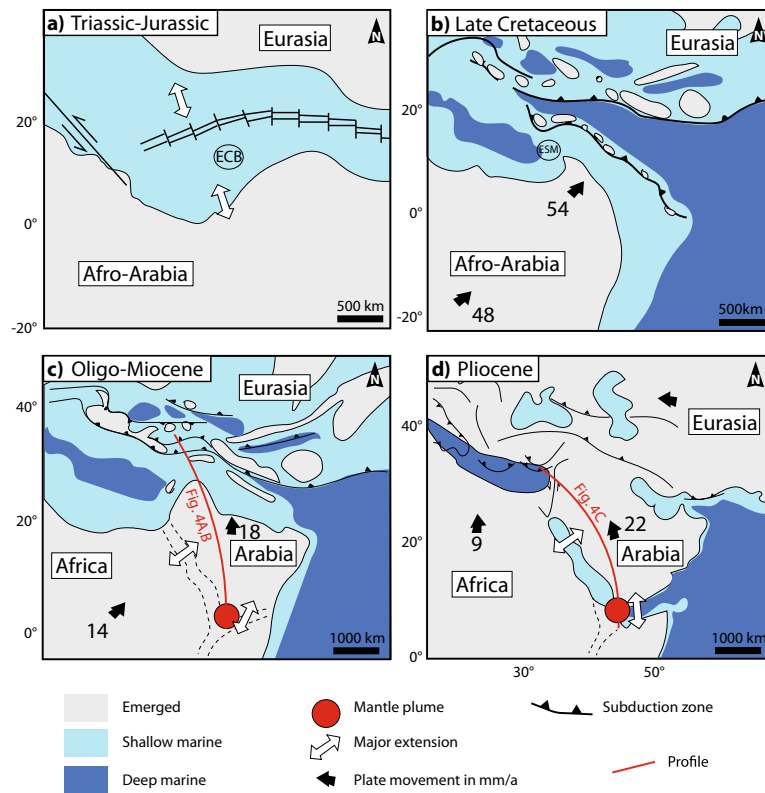


Fig. 3 Tectonic evolution of Afro-Arabian and Eurasian realm illustrating, **a** the Early Mesozoic rifting and disintegration of northern Gondwana, **b** the change from an extensional toward compressional tectonic setting with the subduction of the Afro-Arabian Plate below Eurasia, **c** the beginning of the separation of Arabia and Africa in the Oligocene caused by the Afar mantle plume and the opening of the Red Sea, causing further, **d** isolation of the Mediterranean Sea in the Late Miocene-Pliocene. Figure modified from Hawie et al. (2017) and Symeou et al. (2018)

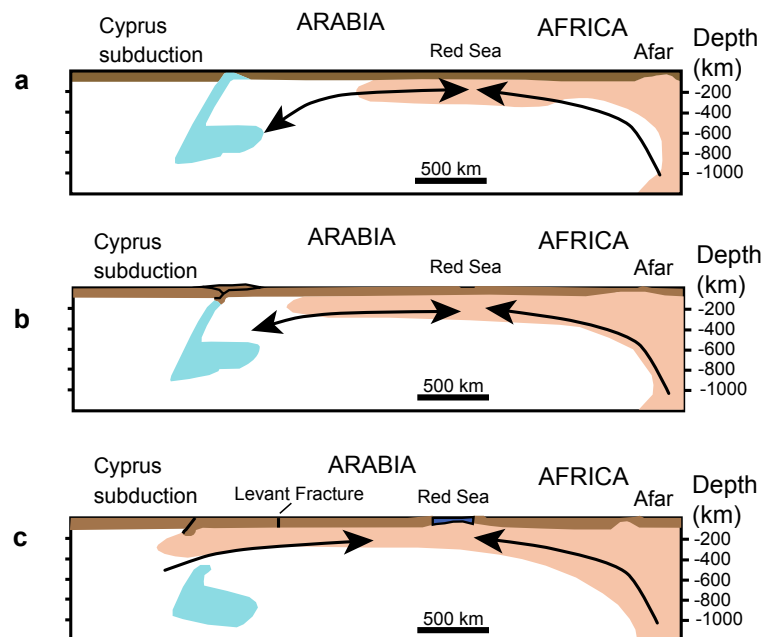


Fig. 4 Geodynamic evolution of the East Mediterranean illustrated by regional cross-sections for **a** 30 Ma, **b** 20 Ma, and **c** 10 Ma, showing the mantle flow (arrows) below the African, Arabian, and Eurasian plates. Note the mantle upwelling in Afar, the Red Sea opening, the collision, subduction, and slab break off in Cyprus (from Faccenna et al., 2013)

Moreover, the breakup of Afro-Arabia (through the rifting and opening of the Red Sea) with an accelerated northward drift of the Arabian Plate in the Oligocene (Fig. 3c) resulted in the ultimate isolation of the Eastern Mediterranean basins (remnants of Tethys oceanic domain). Hence, the uplifted hinterland provided a massive amount of eroded sediments, which were washed into the East Mediterranean basins. Due to the thin continental crust and oceanic crust, the Levant and Herodotus basins, respectively, subsided further, becoming major depocenters. At the same time, their margins were uplifted and affected by further tectonics associated with the opening of the Red Sea, the Levant Fracture System, escape tectonics of the Anatolian block, and the evolution of the Nile system (Inati et al., 2018). The Levant Fracture System led to the re-organization of the sediment input pathways (i.e., major rivers) into the Levant Basin (Hawie et al., 2017; Nader et al., 2018). The general settings were also shaped by the Miocene-Pliocene evolution of the Nile River and the Messinian Salinity Crisis. The latter resulted in drying up the Mediterranean Sea and the deposition of up to 2 km of evaporites between 5.96 and 5.33 Ma (Krijgsman et al., 1999), while the former brought an immense amount of sediments and disturbed the overall stratigraphic configuration of the East Mediterranean.

2.2 Tectono-stratigraphic Evolution

Rifting of the Tethys Ocean is believed to have occurred in two phases (late Early Carboniferous—related to the Variscan orogeny and Early Permian), with seafloor spreading following the second phase (Stampfli et al., 2001). Several major tectonic features concerning the East Mediterranean existed since that early time, such as the Palmyra and Dakhla basins, the Eratosthenes platform, and the Heletz high (Fig. 5a). The latter is defined as an uplifted rift shoulder of the Eastern Mediterranean Basin, with similar examples found in Egypt, Libya, and Tunisia (Roure et al., 2012; Stampfli et al., 2001).

By the end of the Middle Jurassic (Figs. 3a and 5a), active rifting ceased, allowing (post-rift) passive thermal subsidence in the Eastern Mediterranean basins (Fig. 5b). “Mesogean” oceanic spreading started, which refers to a new oceanic domain formed principally in the Cretaceous, extending from the Maghreb Ocean to the West to the Neo-Tethys to the East, and covering mostly the East Mediterranean region (Barrier et al., 2018; Dercourt et al., 1986). The end of the rifting and active extensional tectonic subsidence in the Eastern Mediterranean region is represented by the “breakup” horizon on seismic data (Montadert et al., 2014), regarded as a key surface that overlies the tilted blocks morphologies across the continental, marginal, and

basin domains. The Eratosthenes and Troodos carbonate platforms as well as the marginal domains prevailed, surrounded by slope–basinal deeper marine carbonates. By the end of the Jurassic, the Eastern Mediterranean basins were surrounded by flooded lowland, marginal marine, shallow mixed shelf to the South, the Rutbah and Mardin paleohighs to the southeast and the East, and the Mesogea Ocean to the North. Localized volcanic activities occurred as well.

In the Campanian, the collision and closure of Mesogea continued with the thrust belt advancing southward (Figs. 3b and 5b). The Troodos platform (in Cyprus) was consumed by thrusting. Uplift led to subaerial exposure and mountain ranges just north of Baer Bassit (northern Syria), which became sources for sediment influx. A regional foredeep basin prevailed to the South of the thrust faults (and accretionary tectonic melange) (Papadimitriou et al., 2018a, 2018b). Further south, Egypt hinterlands continued to supply Nubian sand sediments toward Dakhla Basin and the Mediterranean. By the Late Cretaceous (Fig. 3b), the Mesogea Ocean was almost closed due to the Alpine orogeny, encroaching the northern periphery of Afro-Arabia. The initiation of the “Syrian Arc,” a belt of intra-plate structural inversion affected the Egyptian through Syrian margins, coinciding with the start of ophiolite obduction on the passive margin of Arabia. In the Maastrichtian, most of the East Mediterranean basins became sites of deeper marine deposition (Fig. 5b). The southern margin was characterized by slope–basinal marine carbonates and the eastern margin by carbonate and terrigenous platforms (Nader, 2014).

In the Early Eocene, as the almost S–N extension switched from the Suez to the Aqaba and all along the eastern margin of the Levant Basin, major carbonate platforms covered the northern Mardin, southern Rutbah, and the Western Desert areas (Fig. 6). Localized carbonate platforms prevailed in Sinai as well. The eastern margin of the Levant Basin was the site of deeper marine carbonates (slope/basinal) passing to deeper marine clastics toward the West. In the Middle Eocene, further extension occurred along the eastern margin of the Levant Basin. The East Mediterranean basins were limited by deeper marine carbonates (slopes/basin) with carbonate platforms to the South and terrigenous platforms with clastics near the shoreline. Channel incisions and widespread slumping suggest syn-depositional differential relief and possibly tectonic instability (Ghalayini et al., 2014; Hawie et al., 2013). The advance of orogeny continued through the Eocene, with significant narrowing of the seaway between North Arabia and Eurasia (Anatolian block). The Taurides were affected by uplift and mountain building and associated erosion. In the Late Eocene, the marine domain retreated to the North. In Egypt, several delta fans prevailed with fluvio-lacustrine domains extending to the south and lowland erosional plains in the southeast and along the southeastern margin of the

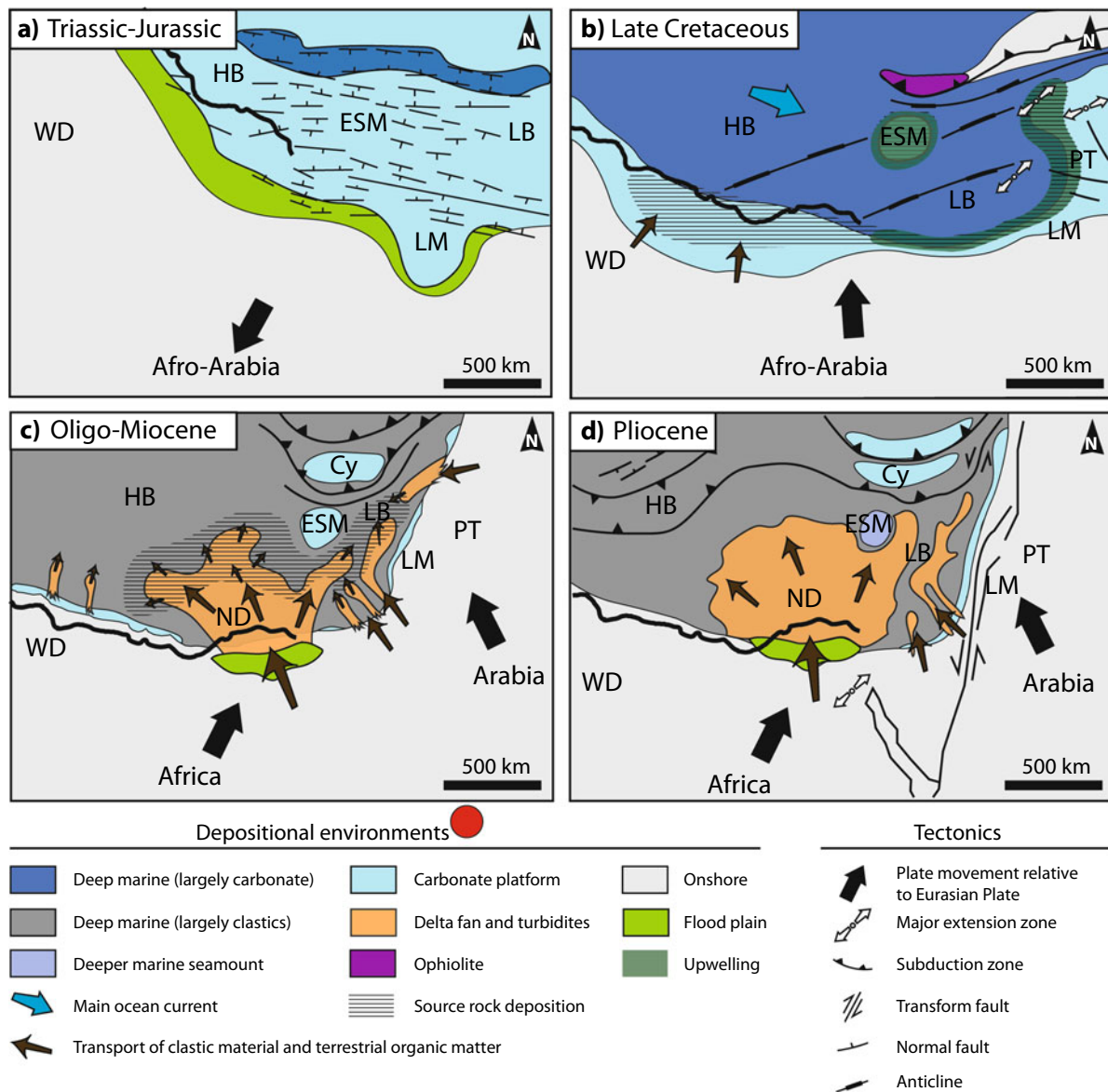


Fig. 5 Regional paleogeographic reconstruction of the East Mediterranean region together with the major tectonic and sedimentary depositional evolutions (maps based on Barrier et al., 2018 and modified after interpretations given in Bou Daher et al., 2015; Hawie et al., 2017 and Grohmann et al., 2018, 2021): **a** Triassic-Jurassic, **b** Late Cretaceous, **c** Oligo-Miocene, and **d** Pliocene. Used abbreviations: WD: Western Desert, HB: Herodotus Basin, ESM: Eratosthenes Seamount, LB: Levant Basin, PT: Palmyra Trough, Cy: Cyprus

Levant Basin, which became separated from the Palmyra Basin. The former contained deep-marine clastics, while the latter remained dominantly filled by carbonates. While Afro-Arabia moved northward, subduction along the northern margin of the Mesogea Ocean advanced closing the remnant seaway and starting a continent-to-continent collision at the northeastern part of the East Mediterranean region.

The main phase of continent-continent collision occurred in the Oligocene, coinciding with the Afar mantle plume activity (Fig. 3c). Afro-Arabia was tilted to the North, conveying considerable amounts of sediment to the Levant

Basin (Fig. 3c), resulting in the deposition of thick clastic Oligo-Miocene intervals in the Levant Basin (Fig. 6 and 7A). The Gilf-, El Bahr-, and Fayum deltas became the main Nubian sediment input sources from Egypt hinterland toward the North. As the thrust belt advanced southward, the Troodos platform was consumed (Papadimitriou et al., 2018a, 2018b). Uplift led to subaerial exposure and mountain ranges, which became sources for sediment influx. In the Early Miocene, continent-to-continent collision along northern Arabia was underway, resulting in major uplifts. The Cyprus Arc System is related to that collision, forming the southernmost thrust belt (Fig. 5c). To its North, a

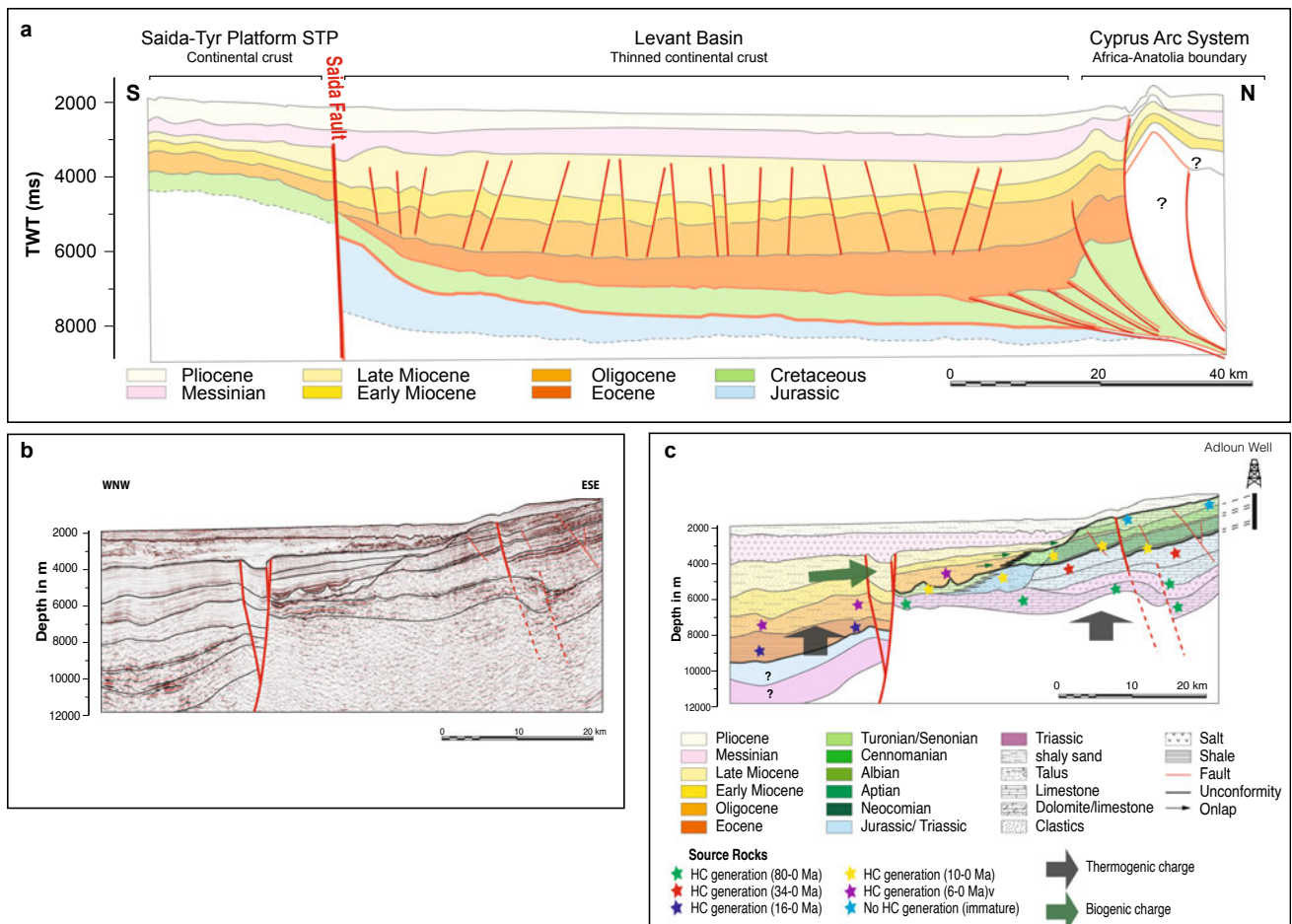


Fig. 7 Key Levant Basin cross-sections, based on seismic data (courtesy of Petroleum Geo-Services, PGS and the Lebanese Petroleum Administration): **a** S-N trending cross-section featuring the Saida-Tyr Platform (STP) part of the Levant Eastern Margin (LEM), the basin stratigraphic and structural characteristics and its northern limit with the Cyprus Arc System; **b** and **c** PSTM 2D Seismic profile and its structural, stratigraphic and petroleum systems interpretations. Locations of the cross-sections are indicated in Fig. 1. This figure is slightly modified from Nader et al. 2018

filled this foreland basin, while its depocenter migrated southward during the Cenozoic (Hawie et al., 2013). The Messinian drawdown may have accentuated the discharge of sediments locally from the hinterland (Fig. 5c and d).

Further collision occurred with major uplift along the eastern and southern margins. The Nile became the major basin feeder in terms of clastic sediments (Fig. 5c), while El Arish and Sinai deltas supplied important amounts of sediments too (Barrier et al., 2018; Dolson et al., 2014). From the North, sediments originated from the uplifted mountainous ranges and the Paleo-Euphrates river system and reached the Mediterranean through the Lattakiya Basin and Nahr el-Kabir (Hawie et al., 2017). In the Pliocene, the Levant Fracture was already in place, completely separating Arabia from Africa and cutting off most of the sediment supply from the Arabian plate toward the Levant Basin (Figs. 3d and 5d). Anatolia went through westward lateral tectonic escape (with

the Cyprus Arc system changing from S-N compressional to strike-slip dextral motion). A lateral slab tear has been documented below Anatolia (around the Antalya Basin). Compression associated with uplift dominated the northern part of the Levant Basin. No more input of sediments from the North was possible—except the Troodos ridge and the Lebanese mountains. The latter had accelerated uplift through transpressional tectonics (Nader, 2014).

An overview of the different stratigraphic units from the ESM, the Levant Margin and Basin over the Nile Delta toward the Western Desert is provided in Fig. 6. Further, Figs. 7, 8, and 9 show representative regional cross-sections—based on seismic interpretation—of the three main regions Levant, Western Desert, and Nile, respectively. The evolution of their depositional environments and their related petroleum systems will be discussed in detail in the following sections.

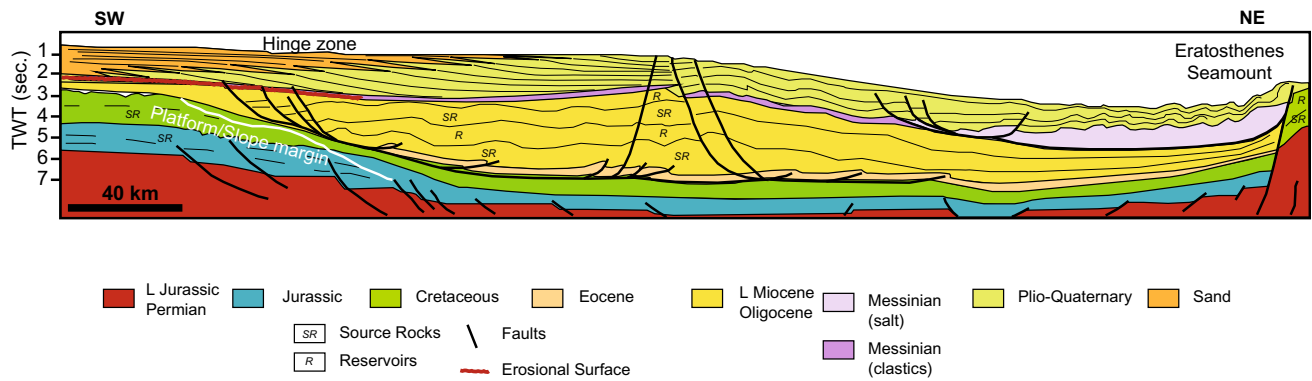


Fig. 8 Cross-section from offshore Western Desert passing by the Nile Delta toward the Eratosthenes Seamount. The Mesozoic platform/slope margin is delineated (white line) and can be also observed on the Eastern Levant Margin (see Fig. 7b) invoking similar configuration for the East Mediterranean margins from the Western Desert to the eastern Levant, prior to the Cenozoic tectonics and basin filling, particularly through the Nile (from Tassy et al., 2015)

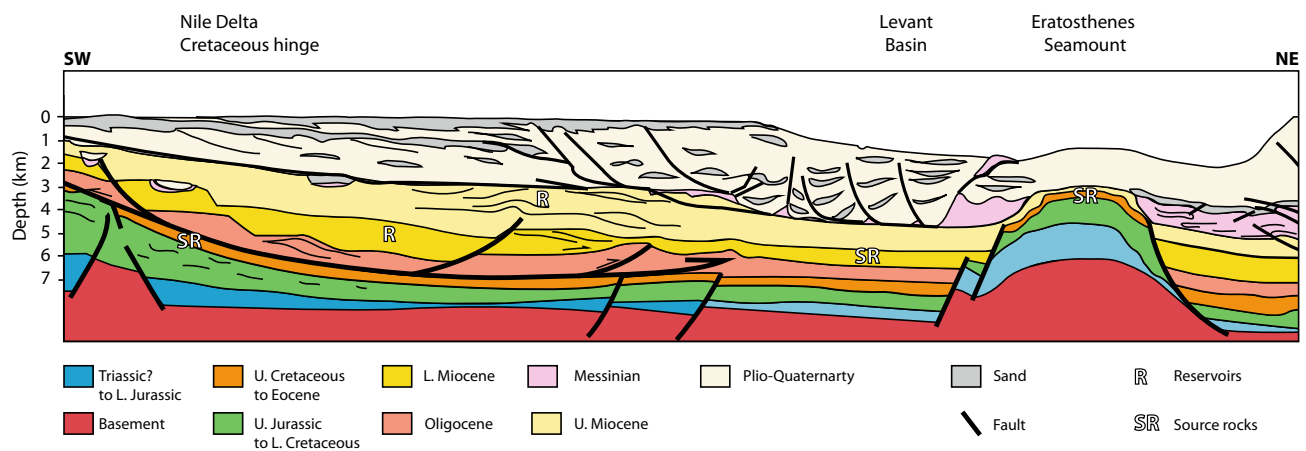


Fig. 9 Cross-section from the Nile Delta to Eratosthenes Seamount and Cyprus showing similar Mesozoic configuration underlying the complex Cenozoic basinal filling architecture governed by major supply of sediments from the Nile, margin instability and gliding tectonics toward the North (modified from Dolson et al., 2001 and Wood, 2015)

3 The Levant Basin

3.1 Depositional Environments

During Early Triassic times, the “Eastern Mediterranean Rift,” extending from Tunisia to Palmyra (central and North Syria), was filled by thick marine deposits, mainly present as dolomite (Nader, 2014; Fig. 6). In the shallow regions along the Eastern Levant Margin (ELM), as well as on top of the Eratosthenes Seamount, which always represented a bathymetric high since its disintegration from the Afro-Arabian margin in the Triassic (e.g., Ghalayini et al., 2014; Montadert et al., 2014; Robertson, 1998; Segev & Rybakov, 2010), sequences of evaporites, dolomites, as well as platform carbonates, developed during the Carnian between 237 and 227 Ma (e.g., Garfunkel & Derin, 1984, Fig. 6). The continuous rifting around the Triassic-Jurassic boundary led

to extensional subsidence of the whole area that prevailed together with the deposition of slope and deeper marine carbonates, promoting the accumulation of organic-rich facies (Fig. 6).

In the Late Jurassic and toward the Early Cretaceous, the open sea retreated with the evolution of rather shallow carbonate platforms along the ELM and in the southern part of the Levant Basin. In contrast, its northern part together with the ESM remained in a rather deep environment (Grohmann et al., 2021, and references therein). In the Early Cretaceous, post-rift thermal subsidence continued in the Levant Basin, which became filled by deeper marine clastics derived from Afro-Arabia (Nader, 2014). Along the ELM, these clastics are bounded by an unconformity to their top and base, the latter one comprising a slightly larger time span toward the South from the end of Kimmeridgian (152 Ma) to Valangian (140 Ma). The ESM and the Troodos platform, at that time, shrank but remained in a rather shallow environment

with the deposition of platform carbonates. In the late Aptian, the global settings remained the same with the development of a belt of carbonate platforms on the margins of the Levant Basin which was filled with slope–basinal and deeper marine clastics. Terrigenous clastic platforms also prevailed toward the onshore areas (Fig. 6). Active extension and thus tectonic subsidence occurred again in the Palmyra and Abu El Gharadig basins (Fig. 5c; Barrier et al., 2018), while the remaining area underwent passive thermal subsidence. The Mardin (Turkey) and Rutbah (Iraq) paleohighs became the major providers of continental sediments found mainly in the northern part of the Levant Basin (Nader, 2014).

The Cenomanian is associated with a major sea-level rise and transgression, which affected the eastern Mediterranean basins with the development of large carbonate platforms covering the entire Mardin and parts of the Rutbah paleohighs (Nader, 2014). The Levant Basin and the Palmyra Basin in the northern part of the ELM hosted deeper marine carbonates, whereas the southern ELM as well as the ESM developed shallower carbonate buildups (Fig. 5b). The transition toward these general shallower conditions is marked by the regional top Turonian (also referred to as Base Senonian) Unconformity along the ELM (Bou Daher et al., 2016).

The closure of the Mesogea Ocean in the Late Cretaceous, just before the collision of the Afro-Arabian and Eurasian Plates, was accompanied by a general sea-level rise together with post-rift subsidence. This resulted in the drowning of the whole Levant region leading to more deep-marine, pelagic carbonate sedimentation (e.g., Gardosh et al., 2008; Nader, 2014). Major inversion began especially on the margins of the Levant Basin (e.g., Syrian Arc structures, Cyprus Arc). At the same time, a large-scale upwelling system affected the whole Levant region forcing the deposition of Upper Cretaceous source rocks along the ELM (Almogi-Labin et al., 1993; Bou Daher et al., 2014, 2015), the ESM (Grohmann et al., 2018, Fig. 5b), and the Western Desert Basin (Ghassal et al., 2018). Similar upwelling processes might have occurred in the Nile Delta, southern Levant Basin, and Eratosthenes in the Eocene, resulting in the deposition of important source rocks.

In the Paleocene, the overall settings did not change considerably. The Sinai region became the domain of a terrigenous platform with deposition of clastics, while the anticlinal structures became uplifted and subaerially exposed—some surrounded by carbonates (Figs. 7b, c). The Azraq and Euphrate grabens witnessed passive thermal subsidence. Together with the Palmyra and Levant basins, these grabens became sites of sedimentation of deep-marine clastics, probably derived from the highlands (Baer Bassit, Mardin, Rutbah, and Sinai).

The uplift and tilting of the African and Arabian northern margins due to plate collision (with Eurasia) in the

Oligocene led to considerable denudation of the subaerially exposed hinterland and the rapid filling of the basins with siliciclastics (Gardosh et al., 2008; Nader, 2014; Figs. 5c and 6). The pathways for this sediment transfer were numerous ancient rivers and submarine canyons along the eastern and southern margins of the Levant Basin (Hawie et al., 2017). Today, the Nile River is the only major sediment source for the Levant Basin (Fig. 5d).

3.2 Petroleum Systems

During several periods, depositional conditions were suitable for the formation of petroleum source rocks of different qualities, which occur either throughout the whole East Mediterranean realm or rather localized in certain smaller regions. Based on Rock-Eval® data, Fig. 10 shows a comprehensive overview of the major source rocks of the East Mediterranean region.

Terrigenous clastic intervals of Early Jurassic age are among the oldest proven source rocks that can be found in the East Mediterranean. Such intervals are found in the southern Levant Margin (Figs. 5a and 6; Gardosh et al., 2008). Triassic to Mid-Jurassic organic-rich limestones are believed to provide potential source rocks with mixed marine-terrestrial Type II–III kerogen in Lebanon, based on regional correlation with the nearby Palmyra Basin (Ghalayini et al., 2018). El Hajj et al. (2019) investigated dysodiles and organic-rich facies from the Upper Jurassic and the Lower Cretaceous intervals surface exposed in Lebanon (ELM), revealing a very good to excellent source rock potential (Total Organic Carbon (TOC) contents 13–19 wt.%; hydrogen index (HI): up to 649 mg HC/g TOC; T_{\max} : 424–428 °C; vitrinite reflectance (VR) < 0.5%). During the Late Cretaceous sea-level rise, deposition of deeper marine source rocks took place throughout the East Mediterranean region (Bou Daher et al., 2014). The source rocks along the Levant Margin are related to a large-scale upwelling system (Almogi-Labin et al., 1993; Bou Daher et al., 2014 and 2015; Grohmann et al., 2018 and 2021; Fig. 5b). Along the Levant Margin, such source rocks can be found as fine-grained limestone intervals of Turonian to lower Maastrichtian age, showing good source rock qualities with TOC contents up to 11 wt.% in Lebanon (Bou Daher et al., 2014 and 2015) or as phosphatic shales and limestones of Maastrichtian to Paleocene age with even higher TOC contents up to 22 wt.% in Israel or Jordan (e.g., Almogi-Labin, 1993; Abed et al., 2005; Abu-Mahfouz et al., 2020). The thickness of these intervals can reach up to 200 m in Lebanon (Bou Daher et al., 2014) and Israel (Almogi-Labin et al., 1993), and up to 400 m in N-NE Jordan (Abed et al., 2005). As typical for upwelling systems, these source rocks are rather restricted

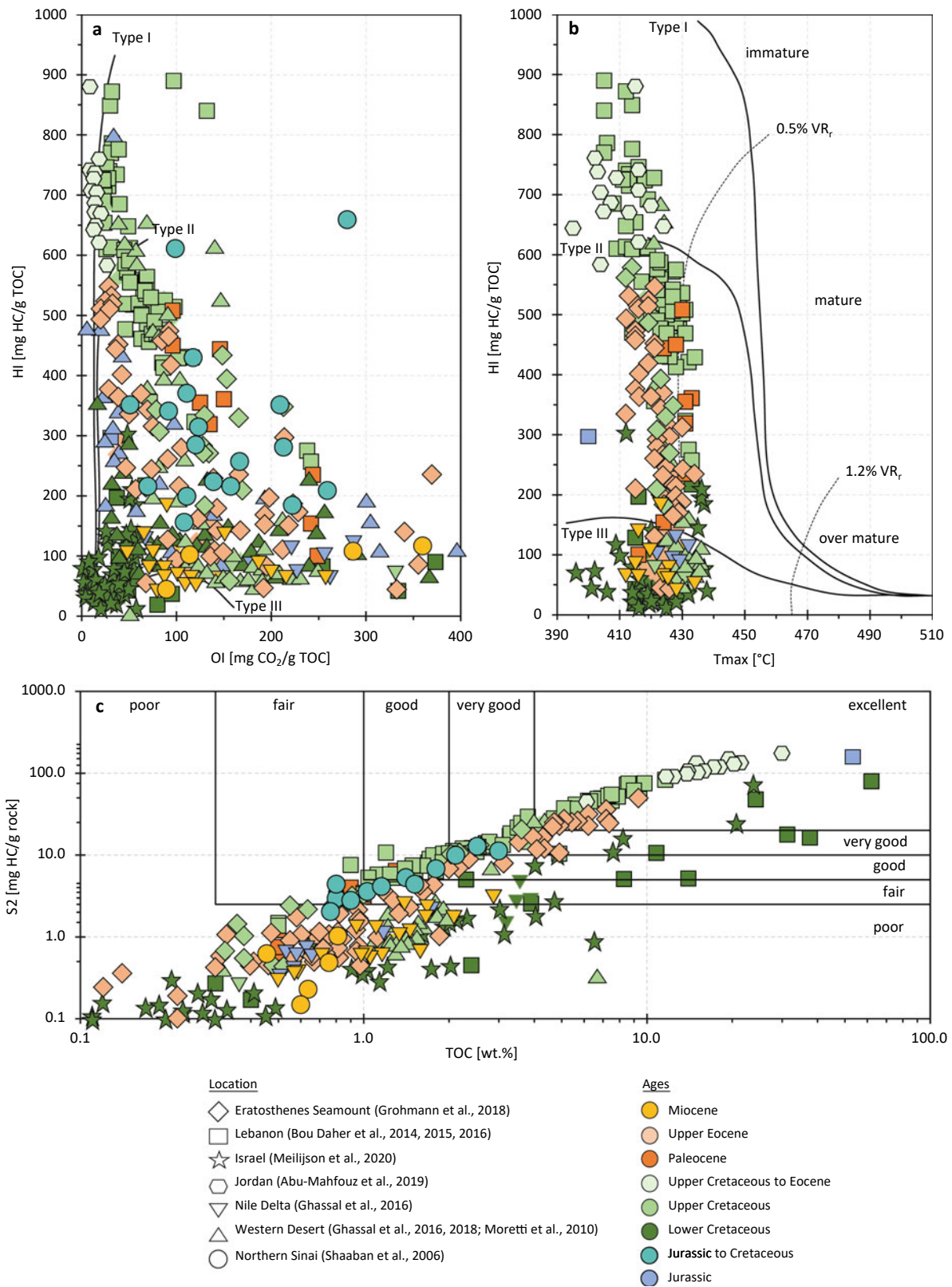


Fig. 10 A selection of various source rocks in the Eastern Mediterranean realm, based on Rock-Eval Pyrolysis data: **a** shows the kerogen classification based on hydrogen index (HI) and oxygen index (OI); **b** correlation of HI and the thermal maturity parameter Tmax; and **c** source rock quality classification based on the total organic carbon (TOC) content as well as the hydrocarbon generation potential (S₂)

to the paleo-shelf and upper margin regions, and it is unlikely that they extend into the deepest part of the basin. Further, all these intervals contain partly organic sulfur-rich Type II-S kerogen with high HI values generally ranging between 400 and 800 mg HC/g TOC classifying them good to excellent source rocks (Abed et al., 2005; Bou Daher et al., 2014 and 2015); Fig. 10a). Such Type II-S kerogen is expected to start generating petroleum at lower temperatures than a sulfur-lean kerogen type would do. Similar source rock intervals of Late Cretaceous and of Eocene age are found on the ESM, which are believed to be related to either the same or to similar upwelling processes in the area (Grohmann et al., 2018). Information on these source rocks was based on the interpretation of geochemical data from a few, mainly onshore locations. In a recent study by Grohmann et al. (2021), the depositional processes of these source rocks were numerically modeled. The results of this study support the geochemical interpretations and provide a numerical model of the spatiotemporal source rock distribution for petroleum system modeling, changing important source rock parameters from a user-defined choice to a model-based input. At the basin-marginal locations, where all studied samples originate from, these source rock sections are commonly thermally immature with VR values < 0.4% onshore Lebanon (Bou Daher et al., 2014, 2015) and < 0.3% in Jordan (Abed et al., 2005) and along the ESM (Grohmann et al., 2018). The integration of the numerical source rock models and petroleum system modeling increases the probability for finding thermogenic Late Cretaceous petroleum systems in certain offshore areas, such as offshore northern Lebanon or South and East of the ESM (Grohmann et al., 2021, Fig. 11).

Considerable amounts of terrestrial organic matter were most likely transported along with the clastic material that was shed into the Levant Basin upon the separation of the Afro-Arabian plate in the Oligo-Miocene and the strong uplift of the Levant margins (Hawie et al., 2013, 2017; Inati et al., 2018). In contrast to the upwelling-related Cretaceous source rocks, which are probably rather restricted to the shelf regions, the Oligo-Miocene source rocks might be much more widely distributed and can even occur in much greater thickness. The numerical simulations by Grohmann et al. (2021), for example, have shown that terrestrial organic matter might be accumulated to different extents in all the clastic fan and turbidite deposits in the Levant Basin. While TOC contents are generally low (<1 wt.%), cumulative thicknesses of moderately organic-rich rocks might reach more than 1000 m. All the Oligo-Miocene source rocks are mainly immature (VR < 0.5%), based on gas

shows in some wells rather close to the basin's margin (e.g., Feinstein et al., 2002). Within the deeper basin, however, thermal maturities might reach the early onset of the thermogenic oil window (Grohmann et al., 2021). Despite this, the high sedimentation rates during these periods, together with rather low geothermal gradients, provided perfect conditions for microbial gas generation (Schneider et al., 2016). Thus, these source rocks might be the primary source of microbial gas, which is present in almost all accumulations within the area, discovered during the last decades. Although gas makes up by far the most significant contribution in all these discoveries, some indications of a mixed oil-gas system are also available (e.g., Karish field; Ducros & Nader, 2020).

The highest generation of microbial gas can be expected below temperatures of about 45 °C (e.g., Katayama et al., 2022). Even at low geothermal gradients, such temperatures occur at depths, where compaction of the organic matter containing shale and marl deposits is still rather low; these rocks cannot act as proper seals yet. Thus, it can be expected that only minor amounts of the total generated gas were trapped (e.g., Barabasch et al., 2019). Next to the many, rather moderately filled clastic reservoirs, recently, shallow-marine carbonate reservoirs with rudist biofacies of Cretaceous age (e.g., Zohr field) were discovered hosting gas accumulations. Assuming that most generated gas was lost due to the lack of proper seals above the clastic reservoirs in the basin during the main generation phase, the entrapment within adjacent carbonate reservoirs seems reasonable. This assumption is also supported by statistics, where several rather small to moderate (clastic) reservoirs (1–16 Tcf) compete with one large (30 Tcf, Zohr) (and few minor) carbonate ones. Thus, the focus on carbonate-dominated regions adjacent to the main delta and turbidite deposits both along the Levant Margin as well as in the Western Desert might increase the chance for more and significant discoveries. The ultimate cap-rock in the East Mediterranean region, offshore (Levant and Herodotus basins), is the up to 2 km thick Messinian salt (or evaporite) interval. However, most clastic reservoirs appear to be sealed by the surrounding and overlying fine-grained siliciclastic facies (marls and clays). The Upper Cretaceous, rudist-carbonate reservoirs are either sealed by the overlying marl (a result of platform drowning in the latest Cretaceous) or ultimately by the Messinian evaporites. In addition, several Mesozoic and Cenozoic intervals of evaporites, marls, and shales may act as excellent sealing units for potential reservoirs (Fig. 6).

The turbidite systems may create their own sealing and trapping mechanisms, which, however, as described above, might not have been properly working in the early microbial as

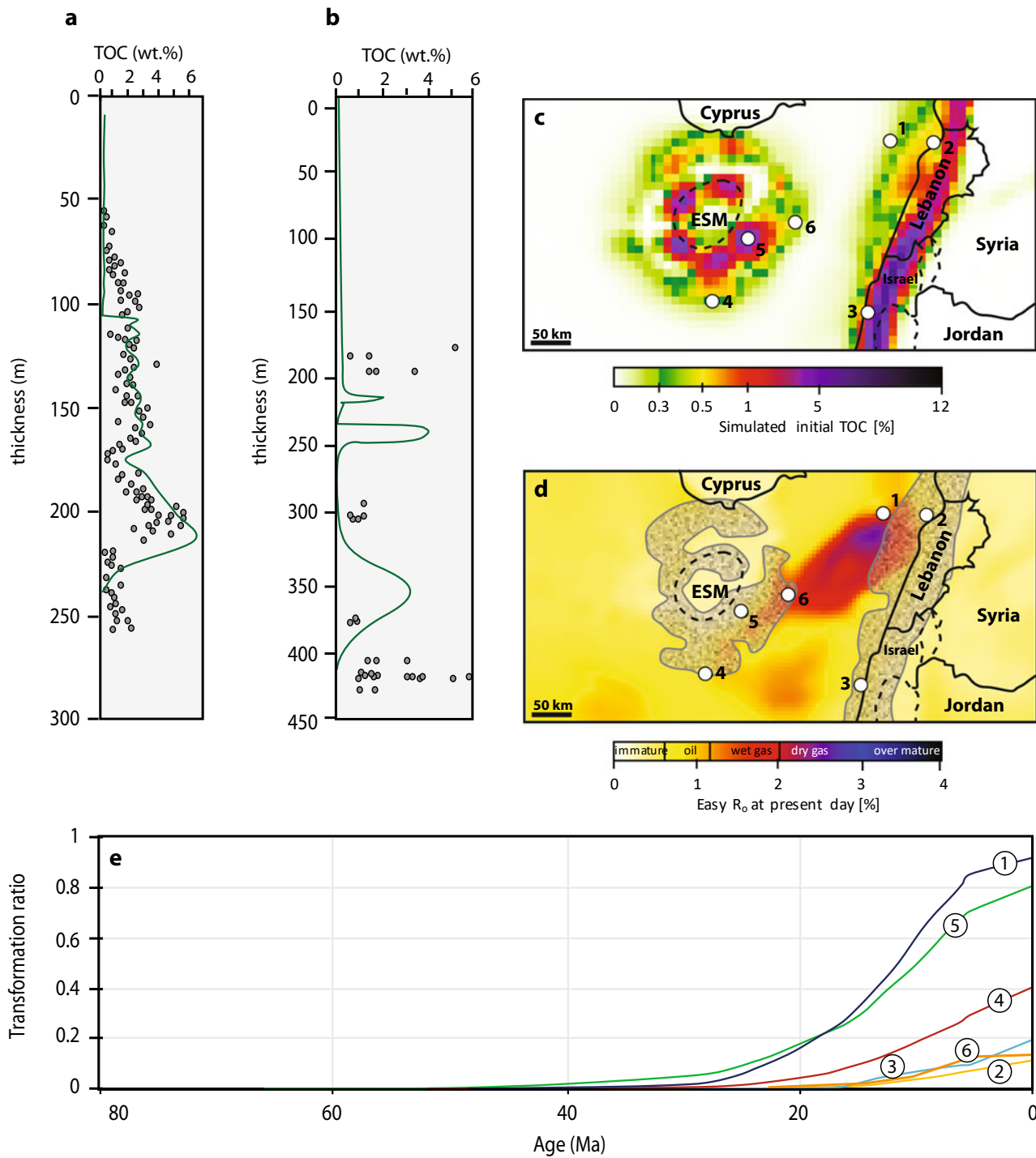


Fig. 11 Combined results of a simulated source rock distribution model (obtained from stratigraphic forward modeling) incorporated in a numerical petroleum system model: **a** and **b** comparison of measured and simulated total organic carbon (TOC) contents in the Upper Cretaceous source rocks onshore Lebanon and offshore Cyprus, respectively; **c** map showing the distribution of TOC contents obtained from the stratigraphic forward model incorporated as input parameter to the petroleum system model; **d** map showing the overlap of source rocks and thermal maturity windows; and **e** the evolution of Upper Cretaceous source rock transformation ratio for 5 selected locations with the highest likelihood for thermogenic hydrocarbon generation. Figure modified from Grohmann et al. (2021)

generation stages due to low compaction. Nevertheless, trapping is partly a result of paleoclimatic conditions and the evolution of source-to-sink sediment transfer. The tectonic evolution resulted as well in four-way closure features, trapping considerable hydrocarbon accumulations (Ghalayini et al., 2018; Symeou et al., 2018). The most significant tectonic event capable of such trapping is the inversion that resulted from convergence and ultimate collision of the Afro-Arabian and Eurasian plates, also termed as Syrian Arc deformations. This phase was followed by the breakup of Arabia and Africa and the evolution of the Levant Fracture systems, which led to transpression and major strike-slip faults and associated structures. The latter also shows excellent four-way closures on seismic data (Ghalayini et al., 2014).

4 The Northwestern Desert

4.1 Depositional Environments

The Western Desert of Egypt covers an area of approximately 700,000 km², which represents about two thirds of the total area of the country. The northern part of this area borders the Mediterranean Sea–West of the Nile Delta, including a continental shelf passing northward into the deep offshore Herodotus Basin (Fig. 1), where the sedimentary fill is likely to exceed 13,000 m (Schlumberger, 1984). Structurally, the Northwestern Desert formed a part of the southern margin of the Mesogea Ocean (Figs. 3 and 5) and was a tectonically active from the Paleozoic to the Early Cenozoic, when basin reconfigurations occurred (Fig. 8; Hantar, 1990; Said, 1962).

The sedimentary column of the Northwestern Desert comprises strata straddling from Cambrian-Ordovician to Quaternary, reaching a thickness of more than 10,600 m in the Abu El Gharadig Basin (Schlumberger, 1995). Within this section, four major sedimentary cycles occurred, with maximum, southward transgression in Carboniferous, Upper Jurassic, Middle and Late Cretaceous, middle Miocene and Pliocene times. However, maximum northward transgression phases occurred during the Permo-Triassic and Early Jurassic and continued in the Early Cretaceous, and again in the Late Eocene to Oligocene, with a final phase in the Late Miocene (Schlumberger, 1984; Fig. 6).

Onshore Western Desert, most of the known stratigraphic units alternate between carbonates and clastics with a basinward succession (shallow carbonate to deeper clastic turbidites; Fig. 6). This is probably due to both tectonics and sea-level fluctuations, as the onshore part of the Western Desert is located on the unstable shelf (Said, 1962) at the margin with the Herodotus Basin. The offshore Western Desert is characterized by Triassic–Lower/Middle Jurassic dolomite and evaporite sequences, overlain by thick

deep-marine clastics of Late Jurassic to Miocene age. Wood (2015) and Tassy et al. (2015) used offshore–onshore seismic and well data to illustrate the Jurassic and Cretaceous stratigraphic architecture and structural configuration across the Egyptian margin. Their results demonstrate a striking similarity between the Levant and Egyptian margins, with Jurassic carbonate platforms prograding toward the East Mediterranean basins and the overlying aggrading and retrograding Cretaceous carbonate platforms (Figs. 7 and 8). Tassy et al. (2015) further proposed that the varying Cretaceous shelf edge slope morphologies (abrupt to distally steepen) control the deposition of shallow-marine sediments and their export to the deeper basin. Similar slope morphologies have been observed on the Eastern Levant Margin (ELM) and the Eratosthenes Seamount (ESM), highlighting basin fill onlaps (Hawie et al., 2013; Papadimitriou et al., 2018a, 2018b). The basin sediment extension offshore the Western Desert is characterized by thick mass transport deposits (Tassy et al., 2015). Wood (2015) consider the basal Abu Roash shales (Late Cenomanian age) a detachment surface that was active during the margin uplift and steepening of the slope coinciding with the “Syrian Arc” inversions (Fig. 8). Turbidite systems are believed to occur in the Oligo-Miocene intervals similarly to those observed in the Levant Basin (Dolson et al., 2014; Nader et al., 2018; Figs. 5c and 6) and could be very attractive for future exploration.

4.2 Petroleum Systems

The Khatatba and Ras Qattara formations that are exposed in the Shushan Basin in the Western Desert include Early Jurassic source rocks of a mixed Type II-III, rather gas prone kerogen type with low HI values of 100–260 mg HC/g TOC; however, very high TOC contents of up to about 50 wt.% can be reached (Shalaby et al., 2011). With thermal maturities between 0.5 up to 3.5% VR, they cover the whole range from early oil to late gas window maturities, which were reached between the Late Cretaceous and Tertiary (Shalaby et al., 2011). Therefore, most of the hydrocarbon generation potential has already been transformed, and these source rocks are believed to be responsible for thermogenic oil and gas generation in the Western Desert and the Nile Delta (e.g., Shaaban et al., 2006; Wigger & Bailey, 1997). Similar source rocks containing mainly terrestrial organic matter can be also found in the Upper Jurassic as well as in the Lower Cretaceous sections of the Northwestern Desert. TOC contents of these intervals are rather low with maximum values of about 2.4–3.1 wt.%, while HI values are generally lower than 240 mg HC/g TOC (Fig. 10), emphasizing a strong contribution of terrestrial organic matter (El Atfy et al., 2019).

The Late Cretaceous source rocks found in the Western Desert are thought to be the result of increased bio-productivity caused by increased nutrient input via deposition of detrital material (Ghassal et al., 2018; Fig. 5b), in contrast to the source rocks along the ELM, which have been related to a large-scale upwelling system that affected the whole Levant Margin (see above).

The Triassic clastics in the onshore Western Desert host mainly oil accumulations (Fig. 6). The Lower and Upper Jurassic shallow-marine coarse clastics, in the same region, also host oil. The onshore Western Desert basins also include evaporite (and dolomite) oil reservoirs (Albian) and shallow platform carbonate oil reservoirs (Upper Cretaceous and Eocene). The common Cretaceous reservoirs in the Western Desert are within the Bahariya and Abu Roash formations (Ghassal et al., 2018). Previous interpretation of seismic data (onshore and offshore; e.g., Tassy et al., 2015) and newly acquired data suggest a continuity of the known onshore reservoirs (and generally the related petroleum systems) to the proximal shelf area. Further into the basin, the platform slopes may also host carbonate buildups with potential reservoirs as also observed on the eastern margins of the Levant Basin (Ghalayini et al., 2018). In the distal offshore, the Oligo-Miocene turbidite systems may as well provide potential reservoirs, especially for microbial gas accumulation. The turbidite systems may also provide trapping layers with finer sediments, which are ultimately sealed with the Pliocene shales and Messinian evaporites.

5 The Nile Delta

5.1 Depositional Environments

The Nile Delta is located between the Western Desert and the Levant Basin along the northern margin of the African Plate (Morgan, 1990; Fig. 1). The Nile Delta Basin was influenced by several tectonic events since the beginning of the Mesozoic (Tassy et al., 2015; Zaghoul et al., 1999a). The oldest known stratigraphic record in the Nile Delta Basin is assigned to the Middle Triassic; however, due to the lack of outcrop or well penetration in the Nile Delta Basin, the stratigraphy can only be inferred by regional paleogeographic interpretations. In the southern Nile Delta Basin, the Triassic sedimentary sequence was interpreted as a tidal flat deposit by Kerdany and Cherif (1990), whereas Guiraud and Bosworth (1999) suggest a carbonate platform depositional environment in the South and deep-marine environment in the North. Further opening of the Neo-Tethys in the Early Jurassic caused the expansion of a wide Jurassic-Cretaceous carbonate platform from the Western Desert to Sinai (Parisot et al., 1996; Tassy et al., 2015; Figs. 5a, b). The oldest sedimentary rocks penetrated are indeed these shallow-marine Early Jurassic

carbonates (Ghassal et al., 2016; Fig. 6). Various depositional environments were inferred for the better known Lower Cretaceous that could range from lagoonal to open shelf (Harms & Wray, 1990; Zaghoul et al., 1999b). The depositional environment changed from open marine in the Aptian to alternating marine and alluvial deposits in the Albian (Figs. 5b and 6) and again to open marine during the Cenomanian, lasting until the end of the Cretaceous (Guiraud & Bosworth, 1999).

During the Late Cretaceous–Early Eocene period, regional sedimentation was influenced by the Syrian Arc inversions, resulting in E-NE-trending structures occurring contemporaneously with the closure of the Tethys (Harms & Wray, 1990; Zaghoul et al., 1999a). The Syrian Arc event was responsible for regional erosion; thus, these rocks are not widely preserved (Ghassal et al., 2016). This is a plausible reason for limited penetration of the Upper Cretaceous to Eocene succession in most Nile Delta wells (Harms & Wray, 1990).

The opening of the Gulf of Suez and the Red Sea during the Chattian-Aquitainian produced dominant extensional NW-trending faults resulting as the African and the Arabian plates diverged (e.g., Bosworth, 1994; Patton et al., 1994). The rift reactivated Syrian Arc structures and developed coastal faults that enhanced the gravitational sliding of the Oligocene shales over the pre-Oligocene carbonate rocks in the hinge zone along with the extrusion of basaltic flows (Hussein & Abd-Allah, 2001). It triggered the formation of highs in southern parts and lows to the North of the delta area. Few wells penetrated the Oligocene, showing various lithologies from upper to middle slope deposits, open marine deposits, fluvial clastics, and basalt (Harms & Wray, 1990). The Oligocene deposits were derived from the South through a canyon (up to 300 m depth) with about 12 entry points, whereas the southern Nile Delta was subaerially exposed (Dolson et al., 2001) following an eustatic sea-level fall (Guiraud & Bosworth, 1999). Fluvio-deltaic sedimentation prevailed toward the Nile Delta, while shallow-marine and deepwater shales were deposited beyond the hinge zone (Dolson et al., 2001). The hinge zone created a paleo-topography in which the delta sediments were accumulated (Tassy et al., 2015). It is typified by a significant increase in dip rates north of seismically mappable Cretaceous-Eocene horizons and associated WNW–ESE-trending basement fault (Sarhan & Hemdan, 1994). The early Oligocene shoreline shifted rapidly northward, where fluvial and shallow-marine sandstone facies were deposited during the maximum highstand (Dolson et al., 2001). The tectonically induced lowstand continued during the upper Oligocene and is characterized by upper- to mid-fan deposits overlain by outer-fan clastics (El-Heiny & Enani, 1996). In addition, reactivation of the older listric normal faults (of Cretaceous-Eocene age) led to throws

sometimes exceeding 400 m and gravitational instability affecting the Oligo-Miocene strata, which probably generated fluid leakage to the seafloor (Tassy et al., 2015). Listric normal faults during the latest Cretaceous-Eocene period affected the whole Tertiary basinal argillaceous strata along the hinge zone causing spatial extensions (Fig. 9). An uplift, associated with the Gulf of Suez rift, took place during the Miocene and detrital clastic sedimentation prevailed. The Miocene sediments were mainly controlled by structures related to the opening of the Red Sea and Gulf of Suez (Zaghloul et al., 1999b). The sea level rose more prominently during the Middle Miocene. Thus, the thicknesses of the Middle Miocene sediments are greater than the Lower Miocene ones (Fig. 9; Harms & Wray, 1990; Zaghloul et al., 1999b). Throughout the middle-late Miocene, a prevalent uplift interrupted marine sedimentation conditions that prevailed during the Early Miocene (Farouk et al., 2014). A rapid sea-level fall occurred in the East Mediterranean region, affecting particularly the Nile Delta Basin (bounded by reactivated listric faults) and resulted in the development of a major unconformity (Hanafy et al., 2016). Regression occurred in the Late Miocene, especially during the Messinian salinity crisis (Guiraud & Bosworth, 1999). This is expressed by an abrupt sea-level fall resulting in fluvial incision on the delta plain and the transport of a large volume of deltaic sediments outboard (Dolson et al., 2001). Deposits of this time are nearly absent in the southern Nile Delta Basin, while sandy shale lithologies covered the eastern part of the basin (Zaghloul et al., 1999b). This also left a wide erosional surface and Grand Canyon scale incised valleys (Barber, 1981). During the Pliocene, marine transgression occurred and resulted in deposition of marine sediments that filled the Messinian incised valleys (Dolson et al., 2001; Ross & Uchupi, 1977). Then, fluvial and fluviomarine deposits prevailed (Zaghloul et al., 1999a). The Pleistocene is mainly composed of fluvial sandy facies (Zaghloul et al., 1999b).

5.2 Petroleum Systems

The oldest proven East Mediterranean source rocks of Early Jurassic age (found on the northern margins of the African and Arabian plates) are believed to be buried deeply below the Nile Delta (e.g., Shaaban et al., 2006). These source rocks, as mentioned above, comprise mainly a mixed Type II-III, rather gas prone kerogen (e.g., Shaaban et al., 2006; Wigger & Bailey, 1997).

With the separation of the Afro-Arabian plate in the Oligo-Miocene and the strong uplift of the Levant area, the pelagic, carbonate-dominated depositional environment changed and huge amounts of clastic materials were shed into the Levant Basin coming from both the Nile Delta as

well as from the Eastern Levant Margin (e.g., Hawie et al., 2013 and 2014; Inati et al., 2018; Fig. 5c). It is also likely that relatively high amounts of terrestrial organic matter were transported along with the clastic material. This fact is reflected in the type of source rocks, which were deposited during this time. Whereas Cretaceous and Eocene source rocks are mainly composed of Type II and Type II-S marine-derived kerogen (Fig. 10), the Oligo-Miocene sections are rather characterized by a mixed Type II-III kerogen. Consequently, source rock qualities are generally lower, with HI values often clearly below 200 mg HC/g TOC, as for example, in the Nile Delta (e.g., Ghassal et al., 2016; Fig. 10). Further, the idea of low TOC and low quality, but thick clastic source rocks, is supported by observations by Rasoul and Khaled (2019), who report thick (>1000 m) intervals of Oligocene sand and siltstones with low but rather homogenous concentrations of terrestrial organic matter in the Nile Delta.

Due to the limited penetrations, the pre-Paleogene reservoirs are poorly understood in the Nile Delta Basin. Most of the known reservoirs in the Nile Delta are Cenozoic in age (Oligocene, Miocene, and Pliocene/Quaternary) and primarily host thermogenic and microbial gas (e.g., Monir & Shenkar, 2016). The Nile Oligo-Miocene reservoirs are made up of deepwater slope channels as well as fluvial channels, while the Messinian and younger reservoirs are related to Nile turbidite and fan delta facies (Cross et al., 2009; Keong et al., 2014; Pigott and Abdel Fattah, 2014). The traps are mainly rotated-fault blocks, 4-way dip closures, and anticlines (Monir & Shenkar, 2016). The Nile Delta lithologies are very heterogeneous, including siliciclastics of variable grain sizes as well as argillaceous carbonates (Cross et al., 2009; Nabaway et al., 2018).

6 Discussion

The current geodynamic understanding of the East Mediterranean region comprises the Tethyan oceanic evolution, the associated lithospheric mantle upwelling within the Afro-Arabian plate and subduction slab pull and rupture at its boundary with Anatolia, the opening of the Red Sea and the establishment of the Levant Fracture System, and finally the westward escape tectonism of Anatolia. The Mediterranean margin of Egypt has been affected by the above geodynamic events whose imprints are recorded in the Herodotus and Levant basins (as well as their continental margins) and the Nile Delta Basin. In this chapter, the geodynamic driving forces, tectono-stratigraphic features, depositional environments and petroleum systems of the Levant Basin (and its ELM and ESM), the Western Desert (passing northward to the Herodotus Basin), and the Nile Delta are presented. The similarities along the East

Mediterranean southern and eastern margins are demonstrated since these areas were part of the Mesogea Ocean southern passive margin and underwent the same geodynamic history since the Paleozoic (break up of Pangea) until the Cenozoic (separation of Africa and Arabia). Therefore, the onshore–offshore extension that is relatively well known across the Levant Basin can provide clues for the new exploration frontier across the Northwestern Desert margin and the Herodotus Basin. Figure 6 illustrates in a simplified form these similarities in terms of lithostratigraphic successions, potential source rocks, and reservoir rocks. For example, the Lower Jurassic, Upper Jurassic/basal Cretaceous, Upper Cretaceous source rocks are equally found in the onshore ELM and the Western Desert.

Upon the convergence of the African and Arabian Plates with the Eurasian blocks, the first phases of inversion took place along the East Mediterranean margin, resulting in the “Syrian Arc” structures. Changes in the orientations of these structures and further deformation associated to the Levant Fracture System (Nader, 2014) result in different structural patterns along the ELM compared to the Egyptian margins as well as in distinct structural trapping mechanisms. The evolution of the Levant Fracture, leading to the complete separation of Arabia from Africa and cutting off all major eastern sediment pathways to the Mediterranean basins (including a northern Paleo-Euphrates source), left the Nile as the main sediment feeder to the East Mediterranean basins. The huge amount of sediments channeled through the Nile included complete petroleum systems with source rocks prone for microbial gas generation, turbidite sand reservoirs, and shale seals. The entire Nile Delta Basin system exists today, and sediments can be traced from source to sink. This contrasts with the older, Oligo-Miocene sediment pathways from the hinterland to the Levant and Herodotus basins, which are more difficult to define.

Based on the proposed correlation between the Eastern Levant Margin and the northern Western Desert, the potential of the Upper Cretaceous source rocks needs to be revisited. First, the onshore–offshore extension of these source rocks, where thermal maturities are expected to be high enough for thermogenic hydrocarbon generation, has been investigated (Ghassal et al., 2018; Grohmann et al., 2021). Two conceptual depositional environment models are proposed for the Late Cretaceous source rocks found in the Western Desert and the Levant Basin. While in the former area, the organic-rich intervals are thought to result from increased bio-productivity and nutrient input through deposition of detrital material sourced from the immediate hinterland (Ghassal et al., 2018); in the latter area, an upwelling model has been proposed limiting the organic-rich interval to a specific zone along the slope (Bou Daher et al., 2016). Without available well data in the offshore, a major uncertainty remains for any analysis of petroleum systems

confirming or rejecting any proposed concept. Recently, numerical simulations of depositional pattern over time, including source rock deposition, combined with basin and petroleum system modeling (Bou Daher et al., 2016; Grohmann et al., 2021), confirmed the upwelling model pertaining to the Levant Basin and suggested the two regions, where the source rocks and favorable thermal maturities co-exist. They are located about 50 km offshore northern Lebanon as well as about 50–100 km southeast of the ESM, where respective intervals might be present and lie within the oil-window thermal maturity since the Eocene. The latter region, southeast of the ESM, is close to the Zohr discovery which is reported to be charged by microbial gas. Hence, if more reservoir structures could be identified along the southern flank of the ESM, both thermogenic and microbially charged reservoirs should be taken into consideration.

Additionally, the occurrence of such an upwelling system during the Late Cretaceous along the eastern margin of the Levant Basin was prompted by a number of paleogeographic and paleoclimatic factors that have been more or less unchanged throughout the Late Cenomanian to Late Eocene period (Dercourt et al., 2000). Thus, during the Late Cenomanian to Late Eocene upwelling period in the East Mediterranean, petroleum source rocks were deposited on the shelf at times of high sea level, e.g., Campanian-Maastrichtian. At times of low sea level, some organic matter rich deposits were probably deposited along the slope with varying quantity and quality due to a shift of locations of high primary bio-productivity and changes of their lateral extent.

Numerical modeling, if coupled with suitable analog studies (Grohmann et al., 2021), may overcome the issues pertaining to the lack of control and calibration wells. In addition, the relatively recent development of seismic data processing and interpretation techniques appears to be attractive for revealing possible source rocks (Liu et al., 2007). Finally, regional correlation and robust structural geological interpretations based on state-of-the-art concepts remain essential. This type of petroleum geology requires complex regional efforts that cross over disciplines and state borders—something that remains difficult in this part of the world.

Bou Daher et al. (2016) and Barabasch et al. (2019) showed that hydrocarbons generated from the potential Upper Cretaceous source rocks in the eastern Levant Basin would migrate up dip through the margins toward the east. The authors suggested that unless the sealing Eocene marl and clay units are breached, the Oligo-Miocene microbial and the deeper Cretaceous thermogenic systems would not mix and not charge the same structures. Furthermore, Ducros and Nader (2020) proposed areas in the Levant Basin prone to fracturing of the Eocene equivalent sealing unit leading to mixing of thermogenic and microbial systems (Fig. 12) based on machine learning and uncertainty analysis. This is indeed demonstrated by the Karish discovery, offshore

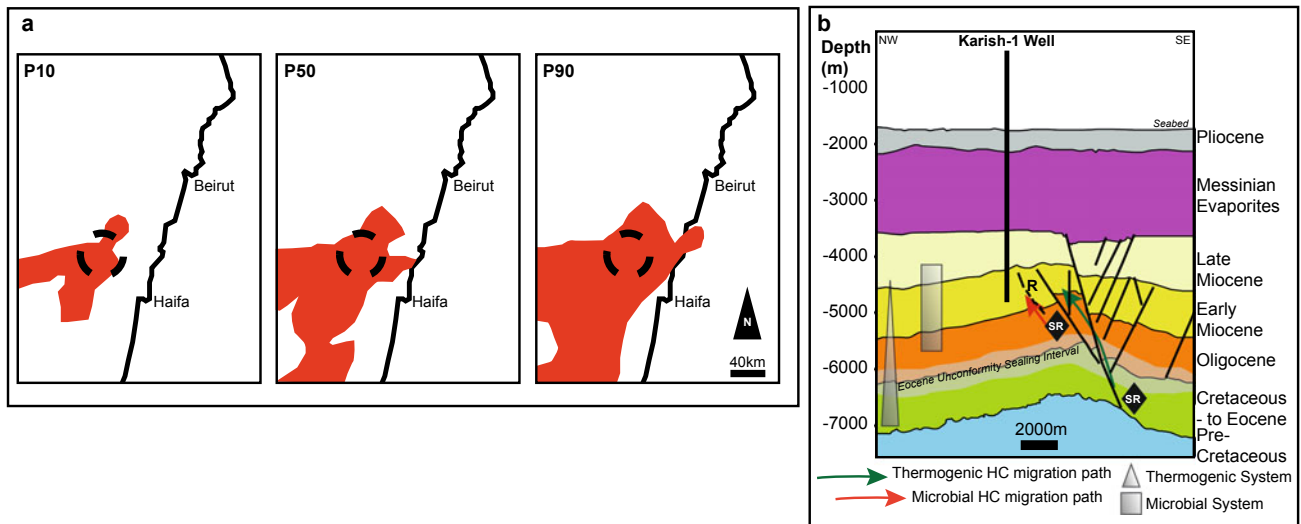


Fig. 12 Schematic illustrations of the probability of fracturing the Eocene marl unit in the Levant Basin (considered as a regional seal between the Mesozoic and Cenozoic petroleum systems): **a** maps showing the extension of the areas with a calculated index of fracturing $> 80\%$ (red areas on maps)—this index is defined as fluid pressure/geostatic stress, and calculated through uncertainty and sensitivity analysis over 50 simulations of the reference basin model (for more details, check Ducros & Nader, 2020); and **b** interpreted seismic profile crossing the Karish field, offshore Israel (location indicated with detached circles in **a**), based on Energean internet published reports, showing major fracturing and faulting across the Cretaceous–Cenozoic intervals. SR is source rocks, and R is reservoir

Israel, which contains a mixed oil-gas accumulation and is located along a major deep-rooted fault system. Based on the discussion above, particularly, in relation to the correlation between the margins of the Levant Basin and the northern Western Desert, similar mixing of petroleum systems can occur as well in offshore Western Desert.

The discovery of Zohr field is regarded as a game-changer in the exploration activities across the East Mediterranean realm. Such rudist-carbonate buildups of Cretaceous age are believed to be present in many locations, based on seismic data interpretation. They are surrounded by Oligo-Miocene shale and clastics and ultimately capped by the Messinian evaporites. Such isolated buildup or structure have been reported along the margins of the Levant (Eratosthenes flanks and eastern margin/Lebanon, Israel; Ghalayini et al., 2018; Papadimitriou et al., 2018a, 2018b) and Herodotus (offshore Western Desert) basins. These are ideal traps for any type of petroleum accumulation. Cemented carbonate reservoirs might also provide more optimal reservoirs with respect to the less compacted sandstones at the early stages of the microbial gas generation and entrapment. This might explain the huge amount of gas hosted in Zhor field (30 Tcf).

7 Conclusions

This chapter presents a general geological overview on the East Mediterranean realm integrating geodynamic evolution, tectono-stratigraphic features, and depositional environments as well as the known petroleum systems. The focus is

set on the Levant Basin, the Western Desert, and the Nile Delta, where major discoveries have been reported and a considerable amount of data exists. These regions within the East Mediterranean are believed to include more than 63,000 MMBOE (based on various previous studies, cited above). Their common geodynamic history until the separation of the African and Arabian plates entices correlated petroleum systems. The general onshore–offshore extension of the Northwestern Desert (to Herodotus Basin) is comparable to a certain degree with the Eastern Levant Margin—until the establishment of the Levant Fracture System. The Upper Cretaceous source rock distribution across the Western Desert margin is, nevertheless believed to be controlled by increased bio-productivity and nutrients with sediment transport from nearby hinterland, contrasting an upwelling scenario for the same source rocks in the Levant Basin. In addition, the possibility of mixing hydrocarbons from such deeper kitchens with the overlying microbial gas accumulated in the Oligo-Miocene interval has been proven through modeling the probability for fracturing the Eocene sealing unit and the discovery of Karish. The Nile Delta includes such Oligo-Miocene systems and is regarded as the principal sediment feeder of the East Mediterranean basins since the Late Miocene.

The presence of carbonate plays has been demonstrated by the discovery of the giant Zohr field. Though complex and challenging to predict, similar reservoirs are expected to be present and will need further geological concept development, numerical modeling, and integration of regional knowledge to be discovered.

Finally, the East Mediterranean realm remains a frontier hydrocarbon province with the potential to bring surprising discoveries that will support the region's societal development, but also a considerable wealth of knowledge that will help in understanding sedimentary basins at the intersections of major plate boundaries and the association of deep lithospheric processes and major shallow and surface processes.

Acknowledgements We appreciate the Editor's interest and proposal to produce this chapter. Haytham El Atfy acknowledges the financial support by the Alexander von Humboldt Foundation, Germany (EGY-1190326-GF-P). Insightful reviews by Isabelle Moretti, François Roure, and Moataz El-Shafey enabled an improved presentation of this work.

References

- Abdel Aal, A., El Barkooky, A., Gerrits, M., Meyer, H.-J., Schwander, M., & Zaki, H. (2001). Tectonic evolution of the Eastern Mediterranean and its significance for hydrocarbon prospectivity of the Nile Delta deepwater area. *GeoArabia*, 6(3), 363–383.
- Abed, A. M., Arouri, K. R., & Boreham, C. J. (2005). Source rock potential of the phosphorite-bituminous chalk-marl sequence in Jordan. *Marine and Petroleum Geology*, 22(3), 413–425. <https://doi.org/10.1016/j.marpetgeo.2004.12.004>
- Abu-Mahfouz, I. S., Cartwright, J., Idiz, E., Hooker, J. N., & Robinson, S. A. (2020). Silica diagenesis promotes early primary hydrocarbon migration. *Geology*, 48(5), 483–487. <https://doi.org/10.1130/G47023.1>
- Almogi-Labin, A., Bein, A., & Sass, E. (1993). Late Cretaceous upwelling system along the southern Tethys margin (Israel): Interrelationship between productivity, bottom water environments, and organic matter preservation. *Paleoceanography*, 8, 671–690. <https://doi.org/10.1029/93PA02197>
- Asch, K. (2003). The 1:5M International Geological Map of Europe and Adjacent Areas: Development and Implementation of aGIS-enabled Concept. *Geologisches Jahrbuch*, SA 3
- Barabasch, J., Ducros, M., Hawie, N., Bou Daher, S., Nader, F. H., & Littke, R. (2019). Integrated 3D forward stratigraphic and petroleum system modeling of the Levant Basin, Eastern Mediterranean. *Basin Research*, 31(2), 228–252. <https://doi.org/10.1111/bre.12318>
- Barber, P. M. (1981). Messinian subaerial erosion of the proto-Nile Delta. *Marine Geology*, 44, 253–272.
- Barrier, E., Vrielynck, B., Brouillet, J. F., & Brunet, M. F. (2018). Paleotectonic reconstruction of the central Tethyan Realm. Tectono-Sedimentary-Palinspastic Maps from Late Permian to Pliocene. CCGM/CGMW, Paris, Atlas of 20 maps (scale: 1/15.000.000)
- Bosworth, W. (1994). A model for the three-dimensional evolution of continental rift basins, north-east Africa. *Geologische Rundschau*, 83(4), 671–688.
- Bou Daher, S., Nader, F. H., Strauss, H., & Littke, R. (2014). Depositional environment and source-rock characterization of organic-matter rich upper Santonian-upper Campanian carbonates, northern Lebanon. *Journal of Petroleum Geology*, 37(1), 5–24.
- Bou Daher, S., Nader, F. H., Muller, C., & Littke, R. (2015). Geochemical and petrographic characterization of Campanian-Lower Maastrichtian calcareous petroleum source rocks of Hasbaya, South Lebanon. *Marine and Petroleum Geology*, 64, 304–323.
- Bou Daher, S., Ducros, M., Michel, P., Hawie, N., Nader, F. H., & Littke, R. (2016). 3D thermal history and maturity modelling of the Levant Basin and its eastern margin, Onshore Lebanon. *Arabian Journal of Geosciences*. <https://doi.org/10.1007/s12517-016-2455-1>
- Bowman, S. A. (2011). Regional seismic interpretation of the hydrocarbon prospectivity of offshore Syria. *GeoArabia*, 16, 95–124.
- Cross, N. E., Cunningham, A., Cook, R. J., Taha, A., Esmia, E., & El Swidan, N. (2009). Three-dimensional seismic geomorphology of a deepwater slope-channel system: The Sequoia field, offshore west Nile Delta, Egypt. *American Association of Petroleum Geologists Bulletin*, 93(8), 1063–1086.
- Dercourt, J., Zonenshain, L. P., Ricou, L.-E., Kazmin, V. G., Le Pichon, X., Knipper, A. L., Grandjacquet, C., Sbertshikov, I. M., Geyssant, J., Lepvrier, C., Pechersky, D. H., Boulin, J., Sibuet, J.-C., Savostin, L. A., Sorokhtin, O., Westphal, M., Bazhenov, M. L., Lauerh, J. P., & Biju-Duval, B. (1986). Geological evolution of the Tethys belt from the Atlantic to the Pamirs since the Lias. *Tectonophysics*, 123(1986), 241–315.
- Dercourt, J., Gaetani, M., Vrielynck, B., Barrier, E., Biju-Duval, B., Brunet, M. F., Cadet, J. P., Crasquin, S., & Sandulescu, M. (2000). Atlas Peri-tethys, Palaeogeographical Maps. 24 maps and Explanatory Notes I-XX. CCGM/CGMW, Paris, 269
- Dilek, Y., & Altunkaynak, Ş. (2009). Geochemical and temporal evolution of Cenozoic magmatism in western Turkey: Mantle response to collision, slab break-off, and lithospheric tearing in an orogenic belt. *Geological Society, London, Special Publications*, 311(1), 213–233.
- Dolson, J. C., Shann, M. V., Matbouly, S. I., Harwood, C., Rashed, R., & Hammouda, H. (2001). The petroleum potential of Egypt. In M. W. Downey, J. C. Threet, W. A. Morgan (Eds.), *Petroleum provinces of the twenty-first century* (vol. 74, pp. 453–482). AAPG Memoire
- Dolson, J. C., Atta, M., Blanchard, D., Sehim, A., Villinski, J., Loutit, T., & Romine, K. (2014). Egypt's future petroleum resources: a revised look into the 21st century. In L. Marlow, C. Kendall, L. A. Yose (Eds.), *Petroleum systems of the Tethyan Region* (vol. 106, pp. 143–178). AAPG Memoir
- Dolson, J. C. (2018). Have We Overlooked the Role of Deep Basin Hydrodynamic Flow in Flushing and Tilted Hydrocarbon Contacts in the Nile Delta and Gulf of Suez?, AAPG Search and Discovery, Article #11152.
- Ducros, M., & Nader, F. H., (2020). Map-based uncertainty analysis for exploration using basin modeling and machine learning techniques applied to the Levant Basin petroleum systems, Eastern Mediterranean. *Marine and Petroleum Geology*, 120. <https://doi.org/10.1016/j.marpetgeo.2020.104560>
- El Atfy, H., Ghassal, B., Maher, A., Hosny, A., Mostafa, A., & Littke, R. (2019). Palynological and organic geochemical studies of the Upper Jurassic-Lower Cretaceous successions, Western Desert, Egypt: Implications for paleoenvironment and hydrocarbon source rock potential. *International Journal of Coal Geology*, 211, 103207.
- El Hajj, L., Baudin, F., Littke, R., Nader, F. H., Gèze, R., Maksoud, S., & Azar, D. (2019). Geochemical and petrographic analyses of new petroleum source rocks from the onshore Upper Jurassic and Lower Cretaceous of Lebanon. *International Journal of Coal Geology*, 204, 70–84. <https://doi.org/10.1016/j.coal.2019.02.003>
- El-Heiny, I., & Enani, N. (1996). Regional stratigraphic interpretation of Neogene sediments, Northern Nile Delta, Egypt. In *EGPC, 13th petroleum exploration and production conference*, Cairo (vol. 1, pp. 170–290)
- Faccenna, C., Becker, T. W., Jolivet, L., & Keskin, M. (2013). Mantle convection in the Middle East: Reconciling Afar upwelling, Arabia indentation and Aegean trench rollback. *Earth and Planetary Science Letters*, 375, 254–269.
- Farouk, S., Ziko, A., Eweda, S. A., Said, A. E. (2014). Subsurface Miocene sequence stratigraphic framework in the Nile Delta, Egypt. *Journal of African Earth Sciences*, 91, 89–109
- Feinstein, S., Aizenshtat, Z., Miloslavski, I., Gerling, P., Slager, J., & McQuilken, J. (2002). Genetic characterization of gas shows in the East Mediterranean offshore of southwestern Israel. *Organic Geochemistry*, 33, 1401–1413.

- Gardosh, M. A., & Druckman, Y. (2006). Seismic stratigraphy, structure and tectonic evolution of the Levantine Basin, offshore Israel. *Geological Society, London, Special Publications*, 260(1), 201–227.
- Gardosh, M., Druckman, Y., Buchbinder, B., & Calvo, R. (2008). The Oligo-Miocene deepwater system of the Levant basin. *Geological Survey of Israel*, 33, 1–73.
- Garfunkel, Z., & Derin, B. (1984). Permian—Early Mesozoic tectonism and continental margin formation in Israel 710 and its implications to the history of the eastern Mediterranean. In J. E. Dixon, & A. H. F. Robertson (Eds.), *The 711 geological evolution of the Eastern Mediterranean* (vol. 17, pp. 18–201). Geological Society
- Ghalayini, R., Daniel, J.-M., Homberg, C., Nader, F. H., & Comstock, J. E. (2014). Impact of Cenozoic strike-slip tectonics on the evolution of the northern Levant Basin (offshore Lebanon). *Tectonics*, 33(11), 2121–2142. <https://doi.org/10.1002/2014TC003574>
- Ghalayini, R., Nader, F. H., Bou Daher, S., Hawie, N., & Chbat, W. E. (2018). Petroleum systems of Lebanon: An update and review. *Journal of Petroleum Geology*, 41(2), 189–214.
- Ghalayini, R., Homberg, C., Daniel, J. M., & Nader, F. (2015). Genesis and growth of the NW trending normal fault array of the Levant Basin. In *EGU general assembly conference abstracts* (p. 6144)
- Ghassal, B., Littke, R., El Atfy, H., Sindern, S., Scholtysik, G., El Beialy, S., & El Khoriby, E. (2018). Source rock potential and depositional environment of upper Cretaceous sedimentary rocks, Abu Gharadig Basin, Western Desert, Egypt: An integrated palynological, organic and inorganic geochemical study. *International Journal of Coal Geology*, 186, 14–40.
- Ghassal, B. I., El Atfy, H., Sachse, V., & Littke, R. (2016). Source rock potential of the Middle Jurassic to Middle Pliocene, onshore Nile Delta Basin, Egypt. *Arabian Journal of Geoscience* 9, 744–765
- Grohmann, S., Fietz, S., Nader, F. H., Romero-Sarmiento, M. F., Baudin, F., & Littke, R. (2021). Characterization of late Cretaceous to Miocene source rocks in the Eastern Mediterranean Sea: An integrated numerical approach of stratigraphic forward modelling and petroleum system modelling. *Basin Research*, 33, 846–874. <https://doi.org/10.1111/bre.12497>
- Grohmann, S., Fietz, S. W., Littke, R., Bou Daher, S., Romero-Sarmiento, M. -F., Nader, F. H., & Baudin, F. (2018). Source rock characterization of Mesozoic to Cenozoic organic matter rich marls and shales of the Eratosthenes Seamount, Eastern Mediterranean Sea. *Oil and Gas Science and Technology*, 73, 49. <https://doi.org/10.2516/ogst/2018036>
- Guiraud, R., & Bosworth, W. (1999). Phanerozoic geodynamic evolution of northeastern Africa and the northwestern Arabian platform. *Tectonophysics*, 315, 73–104.
- Gvirtzman, Z., Csato, I., & Granjeon, D. (2014). Constraining sediment transport to deep marine basins through submarine channels: The Levant margin in the Late Cenozoic. *Marine Geology*, 347, 12–26.
- Hanafy, S., Nimmagadda, S. L., Mahmoud, S. E., Mabrouk, W. M., & Farhood, K. (2016). Regional integrated interpretation of the hydrocarbon prospectivity of the Nile Delta, Offshore Egypt. *Arabian Journal of Geosciences*, 9, 376.
- Hantar, G. (1990). Northwestern desert. In R. Said (Ed.), *The geology of Egypt* (pp. 293–319). A.A. Balkema
- Harms, J. C., & Wray, J. L. (1990). Nile Delta. In R. Said (Ed.), *The geology of Egypt* (p. 329–343). A.A. Balkema
- Hawie, N., Gorini, C., Deschamps, R., Nader, F. H., Montadert, L., Granjeon, D., & Baudin, F. (2013). Tectono-stratigraphic evolution of the northern Levant Basin (offshore Lebanon). *Marine and Petroleum Geology*, 48, 392–410.
- Hawie, N., Deschamps, R., Nader, F. H., Gorini, C., Muller, C., Desmares, D., Hoteit, A., Granjeon, D., Montadert, L., & Baudin, F. (2014). Sedimentological and stratigraphic evolution of northern Lebanon since the late Cretaceous: Implications for the Levant margin and basin. *Arabian Journal of Geosciences*, 7(4), 1323–1349.
- Hawie, N., Deschamps, R., Granjeon, D., Nader, F. H., Gorini, C., Muller, C., Montadert, L., & Baudin, F. (2017). Multi-scale constraints of sediment source to sink systems in frontier basins: A forward stratigraphic modeling case study of the Levant region. *Basin Research*. <https://doi.org/10.1111/bre.12156>
- Hussein, I. M., & Abd-Allah, A. M. A. (2001). Tectonic evolution of the northeastern part of the African continental margin, Egypt. *Journal of African Earth Sciences*, 33, 49–68
- Inati, L., Lecomte, J.-C., Zeyen, H., Nader, F. H., Adelinet, M., Rahhal, M. E., & Surssock, A. (2018). Crustal configuration in the northern Levant basin based on seismic interpretation and numerical modeling. *Journal of Marine and Petroleum Geology*, 93, 182–204. <https://doi.org/10.1016/j.marpetgeo.2018.03.011>
- Katayama, T., Yoshioka, H., Kaneko, M., Amo, M., Fujii, T., Takahashi, H. A., & Sakata, S. (2022). Cultivation and biogeochemical analyses reveal insights into methanogenesis in deep subseafloor sediment at a biogenic gas hydrate site. *The ISME Journal*, 1–9
- Keong, O. S., Abdullah, A. L. B., Fuad, A. S. B. A. et al. (2014). The integration of petroleum systems elements for hydrocarbon prospecting in pre-Messinian stratigraphic section of the Offshore West Nile Delta, Egypt. In *International petroleum technology conference, IPTC-17970-MS*
- Kerdany, M. T., & Cherif, O. H. (1990). Discussion: Mesozoic. In R. Said (Ed.), *The geology of Egypt* (pp. 407–438). Balkema.
- Kirschbaum, M. A., Schenk, C. J., Charpentier, R. R., Klett, T. R., Brownfield, M. E., Pitman, J. K., Cook, T. A., & Tennyson, M. E. (2010). Assessment of undiscovered oil and gas resources of the Nile Delta Basin Province, Eastern Mediterranean. In *U.S. geological survey fact sheet 2010-3027* (p. 4). <https://doi.org/10.3133/fs20103027>
- Krijgsman, W., Hilgen, F. J., Raf, I., Sierro, F. J., & Wilsonk, D. S. (1999). Chronology, causes and progression of the Messinian salinity crisis. *Nature*, 400, 652–655.
- Liu, Z., Chang, M., Zhao, Y., Li, Y., & Shen, H. (2007). Method of early prediction on source rocks in basins with low exploration activity. *Earth Science Frontiers*, 14(4), 159–167.
- Lord, A. R., Harrison, R. W., Boudagher-Fadel, M., Stone, D. B., & Varol, O. (2009). Miocene mass transport sediments, Troodos Massif, Cyprus. *Proceedings of the Geologists Association*, 133–138
- Monir, M., & Shenkar, O. (2016). Pre-Messinian petroleum system and trapping style, Offshore Western Nile Delta, Egypt. In *AAPG search and discovery article #30489*
- Montadert, L., Nicolaidis, S., Semb, P. H., & Lie, Ø. (2014). Petroleum systems offshore Cyprus. In L. Marlow, C. Kendall, L. Yose (Eds.), *Petroleum systems of the Tethyan region* (pp. 301–334). AAPG special volumes memoir 160
- Morgan, P. (1990). Egypt in the framework of global tectonics. In R. Said (Ed.), *The geology of Egypt* (pp. 91–111). A.A. Balkema
- Nabawy, B., Basal, A., Sarhan, M., & Safa, M. (2018). Reservoir zonation, rock typing and compartmentalization of the Tortonian-Serravallian sequence, Temsah Gas Field, offshore Nile Delta, Egypt. *Petroleum Geology*, 92, 609–631.
- Nader, F. H. (2011). The petroleum prospectivity of Lebanon: An overview. *Journal of Petroleum Geology*, 34(2), 135–156.
- Nader, F. H., Souque, C., Lecomte, J. -C., Deschamps, R., Chauveau, B., Granjeon, D., Staples, R., Woon, E., Tricker, P., & Frascati, A. (2018). Advanced 3-D forward stratigraphic modeling of the East-Mediterranean frontier deepwater basins: An approach for enhancing reservoir fairways predictions. In *Search and discovery article #11133. AAPG 2018 annual convention and exhibition*, Salt Lake City, 20–23 May 2018. <https://doi.org/10.1306/11133Nader2018>
- Nader, F. H. (2014). Insights into the petroleum prospectivity of Lebanon. In L. Marlow, C. Kendall, & L. Yose (Eds.), *Petroleum systems of the Tethyan region* (vol. 106, pp. 241–278). AAPG Memoir

- NOAA. (2022). GEBCO_2022 Basemap (NOAA NCEI Visualization), National Ocean and Atmospheric Administration, National Centers for Environmental Information., A shaded-relief visualization of the GEBCO_2022 Grid
- Papadimitriou, N., Gorini, C., Nader, F. H., Deschamps, R., Symeou, V., & Lecomte, J. C. (2018a). Tectono-stratigraphic evolution of the western margin of the Levant Basin: (offshore Cyprus). *Marine and Petroleum Geology*, *91*, 683–705.
- Patton, T. L., A. R. Moustafa., R. A. Nelson., and S. A. Abdine. (1994). Tectonic evolution and structural setting of the Gulf of Suez rift, in S. M. Landon, ed., Interior Rift Basins: AAPG Memoir No. 59, Tulsa, Oklahoma, The American Association of Petroleum Geologists, p. 9–56
- Papadimitriou, N., Deschamps, R., Symeou, V., Souque, C., Gorini, C., Nader, F. H., & Blanpied, J. C. (2018b). The tectonostratigraphic evolution of Cenozoic basins of the Northern Tethys: The northern margin of the Levant Basin. *Oil and Gas Science and Technology*, *73*, 73. <https://doi.org/10.2516/ogst/2018085>
- Parisot, T., Verdier, P., Amaral, J., & Mounoury, M. (1996). Egypt Western Desert. Elf Aquitaine Production
- Pigott, J. D., & Abdel-Fattah, M. I. (2014). Seismic stratigraphy of the Messinian Nile Delta coastal plain: Recognition of the fluvial Regressive Systems Tract and its potential for hydrocarbon exploration. *Journal of African Earth Sciences*, *95*, 9–21.
- Rasoul, M. A., & Khaled, A. (2019). Integrated study on oligocene sediments and petroleum systems of the Offshore Eastern Nile Delta, Egypt. In *81st EAGE conference and exhibition 2019*
- Robertson A. H. F. (1998). Mesozoic-tertiary tectonic evolution of the easternmost Mediterranean area: Integration of marine and land evidence. In *Proceedings of the ocean drilling program. Scientific results* (vol. 160, pp. 723–782). Ocean Drilling Program
- Ross, D. A., & Uchupi, E. (1977). Structure and sedimentary history of southeastern Mediterranean Sea-Nile cone area. *AAPG Bulletin*, *61*, 872–902.
- Roure, F., Casero, P., & Addoum, B. (2012). Alpine inversion of the North African margin and delamination of its continental lithosphere. *Tectonics*, *31*, TC3006. <https://doi.org/10.1029/2011TC002989>
- Said, R. (1962). *The geology of Egypt* (p. 377). Elsevier
- Sarhan, M., & Hemdan, K. (1994). North Nile Delta structural setting and trapping mechanism, Egypt. In *12th EGPC petroleum exploration and production conference*, Egypt (pp. 1–18)
- Schenk, C. J., Kirschbaum, M. A., Charpentier, R. R., Klett, T.R., Brownfield, M.,E., Pitman, J. K., & Tennyson, M. E. (2010). Assessment of undiscovered oil and gas resources of the Levant Basin Province, Eastern Mediterranean. In *U.S. geological survey fact sheet 2010-3014* (p. 4). <https://doi.org/10.3133/fs20103014>
- Schenk, C. J., Kirschbaum, M. A., Charpentier, R. R., Klett, T. R., Brownfield, M. E., Pitman, J. K., & Tennyson, M. E. (2012). Assessment of undiscovered conventional oil and gas resources of North Africa. In *U.S. geological survey fact sheet 2012-3147* (p. 4). <https://doi.org/10.3133/fs20123147>
- Schlumberger, (1984). *Well evaluation conference* (p. 201). Schlumberger Middle East SA
- Schlumberger, (1995). *Well evaluation conference*, Egypt (p. 87). Schlumberger Technical Editing Services
- Schneider, F., Dubille, M., & Montadert, L. (2016). Modeling of microbial gas generation: Application to the eastern Mediterranean “biogenic play.” *Geologica Acta*, *14*, 403–417.
- Segev, A., & Rybakov, M. (2010). Effects of Cretaceous plume and convergence, and early tertiary tectonomagmatic quiescence on the central and southern Levant continental margin. *Journal of the Geological Society*, *167*(4), 731–749.
- Shaaban, F., Lutz, R., Littke, R., Bueker, C., & Odisho, K. (2006). Source-rock evaluation and basin modelling in NE Egypt (NE Nile delta and Northern Sinai). *Journal of Petroleum Geology*, *29*, 103–124.
- Shalaby, M. R., Hakimi, M. H., & Abdullah, W. H. (2011). Geochemical characteristics and hydrocarbon generation modeling of the Jurassic source rocks in the Shoushan Basin, North Western Desert, Egypt. *Marine and Petroleum Geology*, *28*(9), 1611–1624. <https://doi.org/10.1016/j.marpetgeo.2011.07.003>
- Stampfli, G. M., Mosar, J., Favre, P., Pillecuit, A., Vannay, J. -C. (2001). Permo-Mesozoic evolution of the western Tethys realm: The Neo-Tethys East Mediterranean Basin connection. In P. A. Ziegler, W. Cavazza, A. H. F. Robertson, & S. Crasquin-Soleau (Eds.), *Peri-Tethys memoir 6: Peri-Tethyan rift/wrench basins and passive margins*, *Mémoires du Muséum national d'histoire naturelle*, Paris (vol. 86, pp. 51–108)
- Swarbrick, R. E., & Robertson, A. H. F. (1980). Revised stratigraphy of the Mesozoic rocks of Southern Cyprus. *Geological Magazine*, *117* (6), 547–563.
- Symeou, V., Homberg, C., Nader, F. H., Darnault, R., Lecomte, J.-C., & Papadimitriou, N. (2018). Longitudinal and temporal evolution of the tectonic style along the Cyprus Arc system, assessed through 2-D reflection seismic interpretation. *Tectonics*, *37*, 30–47. <https://doi.org/10.1002/2017TC004667>
- Tassy, A., Crouzy, E., Gorini, C., Rubino, J. -L., Bouroullec, J-L., & Sapin, F., (2015). Egyptian Tethyan margin in the Mesozoic: Evolution of a mixed carbonate-siliciclastic shelf edge (from Western Desert to Sinai). *Marine and Petroleum Geology*, *68*, 565–581
- Thiéblemont, D. (2016). New edition of the 1:10,000,000 geological map of Africa, CGMW-BRGM, Geological Map of Africa
- Wigger, S., & Bailey, J. (1997). Ha’py field: A Pliocene bright spot example from the Nile Delta, Egypt. *The Leading Edge*, *16*, 1827–1829
- Wood, B. G. M. (2015). Rethinking post-Hercynian basin development: Eastern Mediterranean Region. *GeoArabia*, *20*(3), 175–224.
- Zaghloul, Z. M., Elgamel M. M., Shaaban F. F., & Yossef A. F. A. (1999a). Plates interactions and petroleum potentials in the Nile Delta. In Z. Zaghloul, M. El-Gamal (Eds.). Mansoura University, Deltas (ancient and modern) (pp. 41–53)
- Zaghloul, Z. M., Shaaban, F. F., & Yousef, A. F. (1999b). Mesozoic and Cenozoic sedimentary basins, Nile Delta, Egypt. In Z. Zaghloul, M. El-Gamal (Eds.). Mansoura University, Deltas (ancient and modern) (pp. 21–33)



Fadi H. Nader is currently a project leader and geosciences expert at IFP Energy nouvelles (IFPEN, France) and chair professor of “Multiscale Fluid-Rock Interactions” at Utrecht University (the Netherlands). He graduated from the American University of Beirut (Lebanon) in Geology (BSc 1994, MSc 2000), received a PhD in 2003 from the KU Leuven University (Belgium) and HDR (Habilitation de Direction de la Recherche) from the Paris-Sorbonne University (France) in 2015. He is an expert in sedimentology, characteri-

zation and modeling of sedimentary basins and reservoirs/aquifers (clastics and carbonate rocks, fluid flow, diagenesis), integrated stratigraphy, and seismic interpretation. He is very active in several international scientific and professional societies, such as the Geological Society, London (GSL), the American Association of Petroleum Geologists (AAPG, Europe and Middle East), and the International Lithosphere Program (ILP – IUGS-IUGG).



Sebastian Grohmann is currently working as a postdoctoral researcher at the Institute of Geology and Geochemistry of Petroleum and Coal, RWTH Aachen University (Germany). He graduated from RWTH Aachen University (BSc 2014, MSc 2016) and received a PhD in 2019 as part of a cotutelle collaboration between RWTH Aachen University, Paris-Sorbonne University (France) and IFP Energies nouvelles (IFPEN, France). His expertise is in the areas of organic and inorganic geochemical characterization of fine-grained organic-rich rocks, simulation of

associated depositional processes, and their thermal evolution in sedimentary basins. His recent studies have focused on the processes that occur during the primary migration of petroleum within and from source rocks. He is also involved in planning and directing a new federal research program to investigate the suitability of Early Jurassic mudstone formations as potential nuclear waste repositories.



Bandar I. Ghassal is a petroleum geochemist and supervisor at the Saudi Aramco EXPEC Advanced Research Center. He has 17 years of industry and academic experience in mineral resource and petroleum exploration fields. He obtained a BSc (2004) degree from King Abdulaziz University (Saudi Arabia), MSc (2010) from the University of Utah (USA), and a PhD (2017) from RWTH Aachen University, Germany. He has published several papers on various topics in petroleum geology and engineering.



Haytham El Atfy is an associate professor at Mansoura University (Egypt) from where he received a BSc degree in geology and an MSc in palynology. He received a PhD in geosciences (palynology and organic geochemistry) from Goethe University, Frankfurt (Germany) in 2014, and PD (Habilitation) from the University of Tübingen (Germany) in 2022. He acquired experience in industrial palynology through work with GUPCO (BP), Egypt. Haytham has been a Research Fellow of the Alexander von Humboldt Foundation at the University of Tübingen (Germany) since

2019. He was recently a visiting scientist at the Senckenberg Research Institute, Germany. His research interests span all aspects of palynology and its applications in dating, palaeoenvironmental and palaeoclimatical reconstructions, and hydrocarbon exploration, particularly of the Mesozoic and Cenozoic and, to a lesser extent, the Palaeozoic. He has more recently become involved in organic geochemistry. He is a member of the AASP – The Palynological Society, the Micropalaeontological Society (TMS), Arbeitskreis für Paläobotanik und Palynologie (APP), and the Paleontological Society of Egypt (PSE). He is a recipient of many awards, including the Bernd Rendel Prize from the German Science Foundation (DFG), Egyptian State Incentive Award, and the First-Class Excellence Concession that is provided by the Egyptian president.



Maria F. Romero-Sarmiento is a senior research scientist in organic geochemistry at the IFP Energies nouvelles (IFPEN, France). She holds a Ph.D. (2010) degree in organic geochemistry from the University of Lille (France). She also holds a HDR diploma to supervise research from Paris - Sorbonne Université (France, 2021). Her research mainly focuses on the following topics: (1) Characterization of the sedimentary organic matter, complex source rocks (including their geochemical and petrophysical properties), oils, geothermal

scales, corrosion inhibitors, lubricants, polymers, biogas, among others. (2) Physicochemical analysis of the sedimentary organic matter: organic extraction, kerogen isolation, open and closed pyrolysis, biomarkers (GC-MS), vitrinite reflectance, gas chromatography, stable isotopes, Raman, HRTEM, among others. (3) Developments of new models and methods for ROCK-EVAL® device and basin modeling software TEMISFLOW™. (4) Identification of potential source rock intervals: quality and thermal maturity including source rock kinetics (Canada, USA, Argentina, Africa, Eastern Mediterranean, Middle East, Venezuela).



Samer Bou Daher is a stratigraphic modelling specialist at the independent petroleum consultancy firm Beicip-Franlab where he has been involved in developing innovative integrated workflows tackling exploration and production challenges since 2019. He graduated from the American University of Beirut (Lebanon) in 2009 with a BSc degree in geology, obtained an MSc from Lund University (Sweden) in 2012, and a PhD from RWTH Aachen University (Germany) in 2016. For the PhD

degree, he worked on the East-Mediterranean Levant Basin, producing a substantial geochemical dataset and constructing a 3D petroleum system model in close collaboration with IFP Energies nouvelles (IFPEN, France). As a postdoctoral researcher at the University of Copenhagen (Denmark) (2016-2019), he further developed skills in geochemistry, basin modelling, sequence stratigraphy, and sedimentology.



François Baudin is a professor of sedimentology and petroleum geology at Sorbonne University – Paris (France). He received a PhD degree from Pierre and Marie Curie University (1989) and HDR (Habilitation à Diriger des Recherches) at the same institution (1998). His research is focused on the processes that control the preservation and distribution of organic matter in sedimentary rocks as well as recent sediments and soils. He has published more than 200 articles in international journals and several textbooks. His work has been

awarded a number of prizes (e.g. Académie des Sciences, 1993 and 2007; Bronze Medal from CNRS, 1999; Dumont Medal of the Geologica Belgica Society, 2017). François Baudin is active in some scientific societies, including the Geological Society of France, which he has chaired between 2020 and 2022.



Ralf Littke has been a professor of geology and geochemistry of petroleum and coal at RWTH Aachen University (Germany) since 1997. He graduated with a diploma (master) degree in geology from Ruhr-University Bochum (Germany), where he also received his PhD degree in 1985 and Habilitation in 1993. From 1985 to 1997, he worked at the Federal Research Center Jülich, Germany, in the Institute of Petroleum and Organic

Geochemistry. His research interests include (1) dynamics and numerical modeling of sedimentary basins, (2) generation and storage of oil and natural gas, (3) transport and accumulation of petroleum fluids, (4) geology, petrology and geochemistry of petroleum source rocks and coals, and (5) unconventional fossil fuels. He is a member of the German National Academy of Science and Engineering (Acatech) and member of the Academy of Sciences and Arts, Northrhine-Westfalia. He is also a former chairman of the Board of Geologische Vereinigung (German Geological Union), former chairman of the Advisory Board of Deutsches Geoforschungszentrum (GFZ Potsdam), longtime editor-in-chief of International Journal of Coal Geology, and former coordinator of the German priority research program Dynamics of Sedimentary Basins.



Correction to: The Phanerozoic Stratabound/Stratiform Ore Deposits of Egypt: Their Mode of Occurrence and Formation in Accordance with the Phanerozoic Geological Evolution

Mortada Mourad Taha El Aref

Correction to:

Chapter “The Phanerozoic Stratabound/Stratiform Ore Deposits of Egypt: Their Mode of Occurrence and Formation in Accordance with the Phanerozoic Geological Evolution” in: Z. Hamimi et al. (eds.), *The Phanerozoic Geology and Natural Resources of Egypt, Advances in Science, Technology & Innovation*, https://doi.org/10.1007/978-3-030-95637-0_18

The original version of the book was inadvertently published with incorrect words [paleo-karst] in chapter “The Phanerozoic Stratabound/Stratiform Ore Deposits of Egypt: Their Mode of Occurrence and Formation in Accordance with the Phanerozoic Geological Evolution”. The chapter and the book has been updated with the changes.

The updated version of this chapter can be found at https://doi.org/10.1007/978-3-030-95637-0_18

© The Author(s), under exclusive license to Springer Nature Switzerland AG 2023
Z. Hamimi et al. (eds.), *The Phanerozoic Geology and Natural Resources of Egypt*, Advances in Science, Technology & Innovation, https://doi.org/10.1007/978-3-030-95637-0_27